DTIC FILE COPY

AD-A228 834

Environment Induced Cracking of Metals

NACE-10

Editors: Richard P. Gangloff and M. Brian Ives

DTIC
ELECTE
NOV 19 1990
S D
D

DISTRIBUTION STATEMENT A
Approved for public release;
Distribution Unlimited

NACE
National Association of Corrosion Engineers
AN OFFICIAL NACE PUBLICATION

Available for $155 from National Association of Corrosion Engineers. P. O. Box 218340. Houston, TX 77218-8340.

VHG 11/16/90

Environment-Induced Cracking of Metals

DTIC COPY INSPECTED 6

Proceedings of the First International Conference on Environment-Induced Cracking of Metals

held in conjunction with

the First World Materials Congress

October 2-7, 1988
The American Club
Kohler, Wisconsin, USA

Accesion For
NTIS CRA&I ☑
DTIC TAB ☐
Unannounced ☐
Justification .....
By 155
Distribution/per call
Availability Codes
Dist | Avail and/or Special
A-1 | 21

Proceedings edited by R.P. Gangloff and M.B. Ives

Cosponsored by

ASM INTERNATIONAL

NACE National Association of Corrosion Engineers

TMS Minerals • Metals • Materials

Conference Organizing Committee

M.B. Ives (Chairman), McMaster University, Canada
R.P. Gangloff, University of Virginia, USA
R.H. Jones, Pacific Northwest Laboratories, USA
R.M. Latanision, Massachusetts Institute of Technology, USA
T. Murata, Nippon Steel Corporation, Japan
R.N. Parkins, University of Newcastle upon Tyne, UK
E.N. Pugh, National Institute of Standards and Technology, USA
H. Spaehn, BASF, Federal Republic of Germany

Financial Sponsors

Electric Power Research Institute U.S. Office of Naval Research
World Materials Congress Special Events Contributors

Published by the National Association of Corrosion Engineers
Houston, Texas 77218-8340

Published by
National Association of Corrosion Engineers
1440 South Creek Drive
Houston, Texas 77084

Production Artist
Sandy Cox

NACE Staff Editor
Laura A. Wagner

Typesetters
Teri J. Poldervaart
Rosa Flores

Neither the National Association of Corrosion Engineers, its officers, directors, nor members thereof accept any responsibility for the use of the methods and materials discussed herein. No authorization is implied concerning the use of patented or copyrighted material. The information is advisory only and the use of the materials and methods is solely at the risk of the user.

Printed in the United States All rights reserved. Reproduction of contents in whole or part or transfer into electronic or photographic storage without permission of copyright owner is expressly forbidden.

Library of Congress Catalog Card Number: 90–60186
ISBN 1-877914-07-X

Copyright 1990
National Association of Corrosion Engineers

INTERNATIONAL CORROSION CONFERENCE SERIES

Conferences and Volumes Published to Date

Volume Number	Title
NACE-1	*Fundamental Aspects of Stress Corrosion Cracking.* Conference held at the Ohio State University, September 11-15, 1967. Volume published in 1969. Editors: R.W. Staehle, A.J. Forty, and D. van Rooyen.
NACE-2	*Corrosion Fatigue: Chemistry, Mechanics, and Microstructure.* Conference held at the University of Connecticut, June 14-18, 1971. Volume published in 1973. Editors: O. Devereux, A.J. McEvily, and R.W. Staehle.
NACE-3	U.R. Evans Conference on *Localized Corrosion.* Conference held at Williamsburg, Virginia, December 6-10, 1971. Volume published in 1974. Editors: R.W. Staehle, B.F. Brown, J. Kruger, and A. Agrawal.
NACE-4	*High Temperature, High Pressure Electrochemistry in Aqueous Solutions.* Conference held at the University of Surrey, England, January 7-12, 1973. Volume published in 1976. Editors: D. de G. Jones, J.E. Slater, and R.W. Staehle.
NACE-5	*Stress Corrosion Cracking and Hydrogen Embrittlement of Iron Base Alloys.* Conference held at Unieux-Firminy, France, June 12-16, 1973. Volume published in 1977. Editors: R.W. Staehle, J. Hochmann, R.D. McCright, and J.E. Slater.
NACE-6	*High Temperature Corrosion.* Conference held at San Diego, California, March 2-6, 1981. Volume published in 1983. Editor: Robert A. Rapp.
NACE-7	*Corrosion Inhibition.* Conference held in Dallas, Texas, May 16-20, 1983. Volume published in 1986. Editor: R.N. Hausler.
NACE-8	*Biologically Induced Corrosion.* Conference held in Gaithersburg, Maryland, June 10-12, 1985, and cosponsored by the National Institute of Standards and Technology (formerly National Bureau of Standards). Volume published in 1986. Editor: S.C. Dexter.
NACE-9	*Advances in Localized Corrosion.* Conference held in Orlando, Florida, June 1-5, 1987. Volume in press 1990. Editor: H.S. Isaacs.
NACE-10	*Environment-Induced Cracking of Metals.* Conference held in Kohler, Wisconsin, October 2-7, 1988, and cosponsored by ASM International and The Metallurgical Society of the American Institute of Mining, Metallurgical, and Petroleum Engineers. Volume published in 1990. Editors: R.P. Gangloff and M.B. Ives.

TABLE OF CONTENTS

List of Conference Participants i

Editors' Summary
R.P. Gangloff and M.B. Ives v

SECTION I: Stress Corrosion, Hydrogen Embrittlement, and Metal-Induced Cracking
Co-Chairmen's Introduction vii

Stress Corrosion Cracking
R.N. Parkins 1

Mechanisms of Hydrogen-Related Fracture of Metals
H.K. Birnbaum 21

Metal-Induced Fracture
N.S. Stoloff 31

SECTION II: Corrosion Fatigue and High-Temperature Effects
Co-Chairmen's Introduction 43

Corrosion Fatigue Crack Initiation Processes: A State-of-the-Art Review
D.J. Duquette 45

Corrosion Fatigue Crack Propagation in Metals
R.P. Gangloff 55

Elevated-Temperature Creep-Fatigue Cracking in Relation to Oxidation Effects
A. Pineau 111

SECTION III: Fundamental Processes
Chairman's Introduction 123

Atomistic and Micromechanical Modeling Aspects of Environment-Induced Cracking of Metals
K. Sieradzki 125

The Crack-Tip System and Its Relevance to the Prediction of Cracking in Aqueous Environments
F.P. Ford 139

Environment-Induced Cracking of Metals, Fundamental Processes: Micromechanics
W.W. Gerberich and S. Chen 167

SECTION IV: Mechanistic Aspects of Environment-Induced Cracking in Metals and Alloys
Rapporteurs' Report on Poster Presentations 189

Relative Importance of Crack-Tip Charging and Bulk Charging in Hydrogen-Assisted Cracking in Aqueous Solutions
A. Turnbull and M. Saenz de Santa Maria 193

Flow-Enhanced Diffusion Transport in Corrosion Fatigue Cracks
C.J. van der Wekken 197

Hydrogen Entry and Trapping in High-Strength Alloys
B.G. Pound 203

Anodic Dissolution and Hydrogen Embrittlement During Mechanical Depassivation of the Ferritic Phase of a Duplex Stainless Steel in Chloride Solution Containing H_2S
R. Oltra and A. Desestret 207

Mechanical Condition Dominating Cyclic Stress Corrosion Cracking of a High-Strength Steel Under Combined Multiaxial Loads
K. Komai and K. Minoshima 213

Relationships Between Plasticity and Stress Corrosion Cracking
D.B. Kasul, C.L. White, and L.A. Heldt 219

Crack Initiation and Short Crack Growth During the Corrosion Fatigue of Steels in Saline Solutions
R.A. Cottis, A. Markfield, A. Boukerrou, and P. Haritopoulos 223

Low-Temperature Creep of Austenitic-Ferritic and Fully Austenitic Stainless Steels and a Ferritic Pipeline Steel
M.M. Festen, J.G. Erlings, and R.A. Fransz 229

Aqueous Environment Effects on Intrinsic Corrosion Fatigue Crack Propagation in an Al-Li-Cu Alloy
R.S. Piascik and R.P. Gangloff 233

Corrosion Fatigue of Alloy X-750 in Aqueous Environments
R.G. Ballinger, C.K. Elliott, and I.S. Hwang 241

Transgranular Stress Corrosion Cracking in Copper-Gold Alloys
B.D. Lichter, W.F. Flanagan, J.B. Lee, and M. Zhu 251

Surface-Mobility Stress Corrosion Cracking Mechanism in Silver Alloys
G.S. Duffo and J.R. Galvele 261

The Contribution of Localized Surface Plasticity to the Mechanism of Environment-Induced Cracking
D.A. Jones 265

SECTION V: Environment-Assisted Cracking of Nonferrous Metals
Co-Chairmen's Introduction 271

Environment-Induced Cracking of Copper Alloys
U. Bertocci, E.N. Pugh, R.E. Ricker 273

Environment-Induced Crack Growth Processes in Nickel-Base Alloys
R.H. Jones and S.M. Bruemmer 287

Environment-Induced Cracking of High-Strength Aluminum Alloys
N.J.H. Holroyd 311

The Environment-Induced Cracking of Hexagonal Materials: Magnesium, Titanium, and Zirconium
D. Hardie 347

SECTION VI: Environment-Induced Cracking in Nonferrous Alloys
Rapporteurs' Report on Poster Presentations 363

Stress Corrosion Cracking of Aluminum Alloys in Chloride Media
M. Elboujdaini, E. Ghali, A. Galibois 365

Pb-Induced Solid-Metal Embrittlement of Al-Mg-Si Alloys at Ambient Temperatures
Y.S. Kim, N.J.H. Holroyd, J.J. Lewandowski 371

The Stress Corrosion Cracking of Al-3.7wt%Zn-2.5wt%Mg and Al-4.7wt%Mg Alloys
C.-M. Liao 379

The Influence of Microstructure on the Stress Corrosion Cracking and Exfoliation of Commercial Al-Zn-Mg-Cu Alloys
W. Hepples, M.R. Jarrett, J.S. Crompton, and N.J.H. Holroyd 383

Effect of pH on the Stress Corrosion Cracking of 70/30 Brass in Fluoride Solutions
H.C. Shih and R.J. Tzou 389

An Analysis of Evidence to Support an Adsorption Model for Stress Corrosion Cracking in Alpha-Brass
U.K. Chatterjee and S.C. Sircar 397

Stress Corrosion Cracking of Nickel-Base Alloys in Room-Temperature HCl Containing H_2S
J. Kolts, C.C. Burnette, M.W. Joosten 401

Intergranular Attack Behavior and Mechanisms for Nickel-Base Alloys in Caustic Solutions at Elevated Temperatures
H. Nagano, K. Yamanaka, K. Tokimasa, and H. Miyuki 407

Threshold Stress and Crack Growth Rate Considerations Based on a Strain-Rate Damage Model of IGSCC for Alloy 600
Y.S. Garud and A.R. McIlree 415

Effect of Crevice Corrosion on Hydrogen Embrittlement of Titanium
C.F. Clarke, B.M. Ikeda, and D. Hardie 419

Crack Initiation Mechanism for Ti-6Al-4V in Acidic Methanol
X.G. Zhang and J. Vereecken 425

Stress Corrosion Cracking of Uranium-Silver Interfaces in Silver-Aided Diffusion Welds
R.S. Rosen, S. Beitscher, and M.E. Kassner 429

SECTION VII: Environment-Assisted Cracking of Iron-Base Alloys
Co-Chairmen's Introduction 435

Low-Alloy Iron-Base Alloys *(Abstract)*
T. Murata 437

Hydrogen Effects in High-Strength Steels
R.A. Oriani 439

Stress Corrosion Cracking and Corrosion Fatigue of Martensitic, Ferritic, and Ferritic-Austenitic (Duplex) Stainless Steels
H. Spaehn 449

Stress Corrosion Cracking of Austenitic Steels
R.C. Newman and A. Mehta 489

SECTION VIII: Environment-Induced Cracking in Ferrous Alloys
Rapporteurs' Report on Poster Presentations 511

Conceptual Model of Stress Corrosion Cracking of Low-Alloy Steels in High-Temperature Water
R.M. Rieck, A. Atrens, S. Ramamurthy, J.D. Gates, and I.O. Smith 513

The Initiation of Intergranular Stress Corrosion Cracking on Sensitized Stainless Steel in Dilute Thiosulfate Solutions
J. Stewart, B. Wells, and P.M. Scott 517

Correlating Sulfide Cracking Resistance with Hydrogen Uptake of 13% Chromium Martensitic Stainless Steel in Sour Environments
A. Turnbull and M. Saenz de Santa Maria 523

Strain-Rate Effects in Hydrogen Embrittlement of a Ferritic Stainless Steel
R.N. Iyer and R.F. Hehemann 527

Hydrogen Susceptibility of 2 1/4Cr-1Mo and 9Cr Steels: The Role of Trapping Effects
L. Coudreuse, J. Charles, R. Blondeau, and A. Cheviet 531

Liquid-Zinc-Induced Crack Propagation in High-Strength Steels
K. Nakasa and M. Suzawa 537

A Model for Transgranular Stress Corrosion Cracking in Austenitic Stainless Steel
S.C. Jani, M. Marek, R.F. Hochman, and E.I. Meletis 541

Stress Corrosion Crack Initiation and Slip Parameters in a Ferritic Stainless Steel
R.N. Iyer 545

Study of Transgranular Stress Corrosion Crack Propagation in Austenitic Steels by Load-Pulsing Method
V. Desai, F. Friedersdorf, and T. Shaw 549

Fractography of Environmental Cracking of C-Mn Steels in Anhydrous Methanol-Ammonia Environments
Z. Wenyue, R.C. Newman, and R.P.M. Procter 555

SECTION IX: Views of the Past, Present, and Future
Co-Chairmen's Introduction 559

Understanding "Situation-Dependent Strength": A Fundamental Objective in Assessing the History of Stress Corrosion Cracking
R.W. Staehle 561

SECTION X: Final Discussion Session
Co-Chairmen's Introduction 613

Author Index 617

Subject Index 619

CONFERENCE PARTICIPANTS

International Conference on Environment-Induced Cracking of Metals
The American Club
Kohler, Wisconsin
October 2-7, 1988

T. Angelio
University of Michigan
USA

A.I. Asphahani
Haynes International
USA

A. Atrens
University of Queensland
Australia

R.G. Ballinger
Massachusetts Institute of Technology
USA

U. Bertocci
National Institute of Standards and Technology
USA

H.K. Birnbaum
University of Illinois
USA

J.E. Bokelman
Cummins Engine Co. Inc.
USA

C.L. Briant
General Electric Corporation
USA

S.M. Bruemmer
Pacific Northwest Laboratory
USA

S.-C. Chang
National Tsing Hua University
Republic of China

P.D. Chase
U.S. Air Force
USA

S.H. Chen
University of Minnesota
USA

Y.-C Chen
Materials Research
Republic of China

L. Coudreuse
Creusot-Loire Industrie
France

B Cox
University of Toronto
Canada

D. Crawford
University of Michigan
USA

R.D. Daniels
University of Oklahoma
USA

M Danielson
Pacific Northwest Laboratory
USA

V.H. Desai
University of Central Florida
USA

G.S. Duffo
Comision Nacional de Energia Atomica
Argentina

D.J. Duquette
Rensselaer Polytechnic Institute
USA

M. Elboujdaini
Laval University
Canada

H.-J. Engell
Max Planck Institut fur Eisenforchung
Federal Republic of Germany

M.M. Festen
Koninklijke/Shell-Laboratorium
The Netherlands.

N. Flanders
Petro Canada Inc.
Canada

M.L. Foos
General Dynamics Ltd.
USA

F.P. Ford
General Electric Corporation
USA

F.J. Friedersdorf
University of Central Florida
USA

J.R. Galvele
Comision Nacional de Energia Atomica
Argentina

R.F. Gangloff
University of Virginia
USA

R. Garber
S.E.A. Inc.
USA

Y S. Garud
S. Levy Incorporated
USA

M.A Gelpi
Framatome
France

W.W. Gerberich
University of Minnesota
USA

L. Germeys
Avesta A B
Sweden

R.B Griffen
Texas A&M University
USA

M. Haim
N.R.C.N.
Israel

M.M. Hall
Westinghouse Electric Corporation
USA

D. Hardie
University of Newcastle Upon Tyne
UK

L.A. Heldt
Michigan Technological University
USA

W. Hepples
Alcan International Limited
UK

R. Hermann
The Open University
UK

E.T. Ho
Ontario Hydro
Canada

N.J.H. Holroyd
Alcan International
UK

J.-L. Horng
I.T.R.I.
Republic of China

B.M. Ikeda
Atomic Energy of Canada Ltd.
Canada

M.B. Ives
McMaster University
Canada

R.N. Iyer
Pennsylvania State University
USA

S.C. Jani
Georgia Institute of Technology
USA

M.R. Jarrett
Alcan International Limited
UK

R.H. Jones
Pacific Northwest Laboratory
USA

D.A. Jones
Desert Research Institute
USA

P. Jones
Dofasco Inc.
Canada

H. Kaesche
Friedrich Alexander Universitat Erlangen.—
Nurnburg
Federal Republic of Germany

D.B. Kasul
Michigan Technological University
USA

M.K. Hiroshima
Institute of Technology
Japan

Y.S. Kim
Case Western Reserve University
USA

J. Kolts
Conoco Inc.
USA

K. Komai
Kyoto University
Japan

C.M. Liao
China Steel Corporation
Republic of China

B.D. Lichter
Vanderbilt University
USA

J.T. Litwinski
Rockwell International Corporation
USA

J.L. Luo
McMaster University
Canada

J.P. Lynn
Westinghouse Electric Corporation
USA

M. Marek
Georgia Institute of Technology
USA

R.L. Martin
Petrolite Corporation
USA

F. Mazza
University of Milan
Italy

D.D. McNabb
Ontario Hydro
Canada

E.I. Meletis
Louisiana State University
USA

F. Miller
Westinghouse Electric Corporation
USA

A. Molander
Studsvik A B
Sweden

J.V. Monter
Babcock and Wilcox
USA

J.P. Moran
University of Virginia
USA

T. Murata
Nippon Steel Corporation
Japan

H. Nagano
Sumitomo Metal Industries Ltd.
Japan

K. Nakasa
Hiroshima University
Japan

A. Natori
Sumitomo Metal America Inc.
USA

H.G. Nelson
National Aeronautics and Space Administration
USA

R.C. Newman
University of Manchester Institute
of Science and Technology
UK

R. Oltra
Universite de Bourgogne
France

R.A. Oriani
University of Minnesota
USA

R.N. Parkins
University of Newcastle Upon Tyne
UK

R.M. Pelloux
Massachussetts Institute of Technology
USA

R.A. Piascik
University of Virginia
USA

A. Pineau
Ecole des Mines de Paris
France

B.G. Pound
SRI International
USA

R.P.M. Procter
University of Manchester Institute of Science and
Technology
UK

E.N. Pugh
National Institute of Standards and Technology
USA

S.-I. Pyun
Korean Advanced Institute of Science and
Technology
Korea

R.E. Ricker
National Institute o. Standards and Technology
USA

G. Rondelli
C.N.R.—I.T.M
Italy

R.S. Rosen
Lawrence Livermore Laboratory
USA

E. Ryan
Rocketdyne
USA

J.M. Sarver
Babcock and Wilcox
USA

J.M. Schluter
Union Carbide Corporation
USA

S.A. Shiels
Westinghouse Electric Corporation
USA

H.C. Shih
National Tsing Hua University
Republic of China

K. Sieradzki
Johns Hopkins University
USA

E.P. Simonen
Pacific Northwest Laboratory
USA

R.L. Sindelar
E.I. du Pont de Nemours & Co. Inc.
USA

S. Smialowska
Ohio State University
USA

H. Spaehn
BASF Aktiengesellschaft
Federal Republic of Germany

R.W. Staehle
University of Minnesota
USA

J. Stewart
Harwell Laboratory
UK

N.S. Stoloff
Rensselaer Polytechnic Institute
USA

K.E. Szklarz
Shell Canada Limited
Canada

M.D. Tseng
Materials Research Laboratory
Republic of China

A. Turnbull
National Physical Laboratory
UK

C.J. van der Wekken
Delft University of Technology
The Netherlands

W.S. Walston
Carnegie Mellon University
USA

J.-T. Wang
Taiwan Power Company
Republic of China

R.P. Wei
Lehigh University
USA

L.E. Willertz
Pennsylvania Power and Light Company
USA

K. Wrisley
Rensselaer Polytechnic Institute
USA

T.-L. You
Teledyne Wah Chang Albany
USA

CONFERENCE PARTICIPANTS
of the
International Conference on Environment-Induced Cracking of Metals



Photo: Ken Pannier, CPP, Plymouth, Wisconsin, USA

Environment-Induced Cracking of Metals
Editors' Summary

R.P. Gangloff
University of Virginia
Charlottesville, Virginia, USA

M.B. Ives
McMaster University
Hamilton, Ontario, Canada

Throughout the 1988 World Materials Congress in Chicago, we were reminded of how the scope of materials science and engineering has expanded over the few years of its identifiable existence as a discipline. Early studies emphasized the relationship between *structure* and *properties*. This was soon expanded to add a third component, *processing*. Problems with engineered components and a myriad of frontier challenges on earth and in space focus our attention on a fourth dimension, *performance*. It is this final element of the materials tetrahedron that underlies the importance and urgency of the topics covered in this First International Conference on Environment-Induced Cracking of Metals—"EICM-I"—held as a "satellite" event of the 1988 World Materials Congress. The predictable, reliable, and high performance of engineering materials under combinations of load and aggressive environment are without a doubt important challenges to the materials community.

Since it is, perhaps, folly to search for the unifying mechanism for all forms of environmental cracking, so it is ill-advised to summarize a conference of the scope of this one. In both endeavors, the considerations are legion, the biases of the observers are substantial, and many factors are beyond our current state of measurement and comprehension.

This volume provides the final written record of the Kohler conference. Here, we have worked to record the proceedings in a format that is inclusive of all invited and contributed papers, which have been peer reviewed and include substantial discussion contributions from a large proportion of the participants. The final discussion session is particularly interesting in that many of the participants offered their perspectives on consensus issues, uncertainties, and areas for future research and engineering.

Each reader of this volume must ultimately develop his or her own summary of the significant accomplishments and weaknesses of the first International Conference on Environment-Induced Cracking of Metals. Our opinions are offered as follows.

Consensus Issues

Identification of consensus issues is undoubtedly controversial. Many of the written comments from participants suggested that no true consensus was reached on any particular aspect of environmental cracking! This camp believes that while we may have progressed somewhat in our appreciation of the various environmental cracking phenomena since the Firminy meeting, we have not reached any true understanding of the phenomena as a whole. This view proposes that continued, often unsubstantiated and qualitative, debate on the details of a variety of mechanisms hinders our progress toward material and component performance predictions. This situation, more than anything else, makes for frustration within the engineering design community.

A second camp of participants concludes that substantial progress has been made since Firminy. Much of the speculation of the 1970s has been replaced by quantitative experimental evidence. Quantitative and testable models are emerging, with focus on specific embrittlement mechanisms that are relevant to classes of alloys and environments. Meaningful life predictions may be developed to include environmental cracking. The critical importance of crack chemistry and crack tip process-zone deformation and fracture has spawned new models and experimental probes. Those with this view do not believe that all problems are solved, but rather that the field is generally on the right track. Useful information is being made available for the user, but improvements and new ideas are, of course, still required.

Transgranular vs Intergranular Cracking

A major discussion topic was the significance of intergranular vs transgranular crack paths, and whether each type is indicative of a unique crack growth mechanism. R.N. Parkins, unarguably a significant contributor to the field of stress corrosion cracking over the years, is of the view that there is no overwhelming need for different mechanisms, although it was clear that his viewpoint, since it has not been conclusively proven, was not shared by all. More detailed microscopic analysis of fracture paths and whether the transitions of a single crack between these paths is a consequence of changes in micromechanics or electrochemical driving force remain to be determined.

Quantitative fractographic investigations of environmental cracking were not represented at the Kohler meeting. This approach has much to offer to mechanistic and failure analysis studies, and is worthy of renewed emphasis.



Photos: M.B. Ives

Relevance of Fracture Mechanics to Environmental Failure Mechanisms

Extensive debate on the application of fracture mechanics concepts (for example, using the stress-intensity factor to correlate the behavior of different alloys and environmental effects) pointed to an interesting dichotomy. The fracture mechanics approach has yielded significant mechanistic and component life-prediction gains since the Firminy Conference and provides a rational characterization of the mechanical driving force for environmental crack growth. No other approach has been developed quantitatively.

In contrast, many participants expressed difficulty in accepting that macroscopic mechanics parameters can describe the local mechanical driving force at a crack tip. Additional problems are associated with crack-geometry-dependent chemistry, phenomena not described by a purely mechanical approach. While clearly a critical problem requiring future research, recent successes in modeling crack-tip chemistry and crack-tip stress–strain-rate fields to within microns of the crack tip show the usefulness of the fracture mechanics approach. Perhaps the most important challenge is to relate continuum crack-tip deformation to microscopic events such as single-grain slip, grain-boundary sliding, and interface decohesion.

Any abandoning of the fracture mechanics approach would require that it be replaced by a mechanical method that is capable of quantitative prediction. Both mechanistic and component life-prediction issues must be served in this regard. No such approaches were offered at Kohler.

The "Film-Induced Fracture" Model

The recent work of Sieradzki and coworkers has quantified a thought-provoking model to explain the local brittleness exhibited by certain nominally ductile metals when stressed in corrosive environments. This has emphasized the possibility that cracks originate in brittle surface corrosion films and "overshoot" to propagate directly into the otherwise ductile substrate metal. Many are skeptical of this process for a variety of reasons, evidence of which was provided by the extensive discussions on this subject at the meeting. It appears that the model has now found some respectability, especially when coupled with newer concepts involving local dealloying that occurs, for example, in austenitic stainless steels as well as in brasses.

A statement by Parkins on this subject is particularly illuminating: "While I have no difficulty in accepting the concept of film-induced cleavage, I feel that there is still a need to show, by direct measurement, that the cracks do jump very rapidly. At present this is only inferred from experiments that may have other explanations. There are others who have difficulty in accepting the concept because of the considerable microplasticity associated with cracking. Some of this deformation may be involved in initiating the dealloying or dissolution that leads to other films that actually initiate the cleavage, so that emerging slip steps may play an integral part in the film-induced cleavage mechanism." This subject will undoubtedly be actively researched over the next decade.

Mechanisms of Environmental Embrittlement

An oft debated topic, that of "the mechanism" for environmental cracking, received significant a[ttention]. The emerging view appears to support the idea that each dis[crete] mechanism (hydrogen embrittlement by either decohesion or enhanced slip localization, film-induced cleavage and/or film rupture, and transient metal dissolution during crack tip repassivation) is a strong candidate for most material/environment systems. Moreover, these mechanisms are likely to contribute jointly to crack growth in many materials.

Elegant experimental evidence was presented to demonstrate the occurrence of these mechanisms in simple systems (e.g., pure metal in hydrogen gas). Unfortunately, elaborate analyses are required to preclude a specific mechanism and specific uncertainties remain for engineering alloys and complex electrolytes. Perhaps the correct view, as indicated by the discussions, is that these atomistic processes can and do operate in series or parallel for most important situations involving environmental cracking.

A New Material Property: "Situation-Dependent Strength"

The thought-provoking presentation made by Staehle at the final session reviewed the progress of the field since 1961 and introduced the term situation-dependent strength to emphasize the critical role played by the environment on the mechanical behavior of engineering materials. Specifically, Staehle noted that the strength of a material in a given engineering application depends on the specific situation as defined simultaneously by material, environment, stress, and geometry." Acceptance of Staehle's proposal by those present (although some sought a property other than strength for the definition) was significant. Some participants suggested that the concept, while useful for designer comprehension, does not address the complex factors that confront true predictions of strength.

Reduction to Practice

Whenever a group of researchers meets together for an extended period to discuss their 'life works,' a considerable amount of introversion can be expected, and this conference was no exception for most of the week. However, the final session included discussion of how we may better translate the mechanistic concepts of environmental cracking to engineering practice. Sparked by the banquet address on the significant environmental challenges to materials represented by the hypersonic U.S. National Aerospace Plane" (NASP) and the situation-dependent strength concept aimed at catching the interest of the design engineer, participants appeared sympathetic to improving the transition from theory to engineering practice. Assisted by the presence of delegates concerned primarily with the application of materials in aggressive engineering environments, it was agreed that the first move must come from the researchers.

Topics Not Discussed

Several important topics were not covered by any of the invited review papers, contributed papers, or discussions. These include the following:

(1) The environmental fracture behavior of advanced monolithic and composite materials.
(2) Applications of advanced optical and electron microscopic and surface spectroscopic techniques, particularly those capable of *in situ* application, to probe localized chemical reactions and mechanical damage.
(3) Descriptions of integrated and quantitative life-prediction methods for specific applications.
(4) Developments of environment chemistry and crack initiation/growth damage sensors for *in situ* laboratory and component applications.

These important topics are in an infant state and are likely to be the target of increased research interest in the near future.

Final Thoughts

Finally, our week in Wisconsin did not solve the environmental cracking problem nor did it provide a reliable blueprint for engineering success in the near future. We are now sure that there is no one unified theory of environmental cracking. But this review and analysis should help the corrosion research community assess the current state of knowledge and provide for more efficient research direction for the future.

This volume contains two types of paper. Eighteen world-renowned specialists were commissioned to critically review the state of the art and knowledge of all aspects and mechanisms in particular of environmental cracking. Additionally, 35 contributed papers are included. Each of these manuscripts was peer reviewed by a three-person panel according to international journal standards.

This conference, from its inception through the planning, running, reviewing, editing, and publication, was made possible through the enormous individual contributions of so many colleagues and a dedicated NACE staff. We extend our sincere thanks to everyone, but particularly to the authors, who ultimately determine the archival quality of this book.

Charlottesville, Virginia USA
and Lausanne, Switzerland
October 1989

SECTION I

Stress Corrosion, Hydrogen Embrittlement, and Metal-Induced Cracking

Co-Chairmen's Introduction

E.N. Pugh
National Institute of Standards and Technology
Gaithersburg, Maryland, USA

M.B. Ives
McMaster University
Hamilton, Ontario, Canada



Photos: M B. Ives

The first day of the conference was devoted to overview papers, describing the state of knowledge of the major phenomena of environment-induced cracking. The first session included reviews on stress corrosion cracking, hydrogen embrittlement, and metal-induced cracking. Each review was prepared by an author with worldwide recognition for his continuing contributions to the subject. As such, the three reviews in this session and the three in the following session represent a definitive exposition of the current scope of the conference topic.

Stress corrosion cracking was reviewed by Parkins in a paper that ably summarizes the critical considerations within an enormous field, and one that is constantly being added to in the scientific research literature. Parkins points out that the evidence now points against the existence of a single, all-embracing mechanism of stress corrosion cracking, and that a spectrum of different mechanisms is more likely. Thus, in the review, the proposed mechanisms are divided into two groups, one that considers that cracking involves embrittlement of the metal by interaction with the environment, and one that believes cracks grow by localized dissolution processes. The review, and much of the following discussion, compares and contrasts the processes involved in transgranular and intergranular cracking modes, since the fracture path is considered to be a principal indicator of operative mechanism, even if there is still considerable ambiguity about which precise mechanism might be appropriate in a given metal–environment system. Parkins also focuses on environmental aspects of stress corrosion cracking. It is noted that the earlier concept of specificity, e.g., ammonia for copper alloys, chlorides for stainless steels, and nitrates and hydroxides for ferritic steels, has become less relevant as the environments known to cause stress corrosion cracking in specific alloys grow in number. Attention is now being directed to the relevant environmental processes, such as film formation and breakdown, with environments considered more generically.

In his overview of hydrogen embrittlement, Birnbaum also emphasizes that a single, universal mechanism is unlikely. Rather, it is concluded that at least three types of fracture mechanisms can be operative, viz., hydride formation and cleavage, hydrogen-induced local plasticity, and hydrogen related weakening of bonds (decohesion). These and other viable mechanisms are discussed in terms of the experimental evidence, with particular emphasis on *in situ* transmission electron microscopy. The discussion is aided by the classification of metal–hydride systems on the basis of the stability of hydrides, including cases in which hydrides are stress induced. Despite the review of a large amount of data, Birnbaum concludes that there is still insufficient data to establish firmly the appropriate mechanism of hydrogen embrittlement in many systems.

Stoloff reviews a subject for which the scope of the phenomenon and the extent of its study is much less than the other two processes. Nevertheless, there is an increasing use of engineering systems involving metal–metal contacts, and it is likely that metal-induced fracture will become more important as time goes on. Indeed, Stoloff observes, "It is quite likely that virtually all higher melting solid metals can be embrittled by lower melting metals provided that the microstructural and environmental conditions are favorable." From a mechanistic standpoint, metal-induced cracking can be expected to provide insight into the processes operating in stress corrosion cracking and hydrogen embrittlement. Stoloff indicates that there are at least three mechanisms of crack nucleation involving metal–metal contact, involving any or all of surface diffusion, grain-boundary diffusion, and locally enhanced plasticity.

Newcomers to the environment induced cracking field would do well to review these papers in detail, since they represent an excellent overview of the current appreciation of some extremely complex phenomena.

Stress Corrosion Cracking

*R.N. Parkins**

Abstract

Mechanisms of stress corrosion cracking can be divided for convenience into those mechanisms that invclve embrittlement of the metal as a consequence of corrosive reactions or those in which the cracks grow by extremely localized dissolution processes. The arguments supporting and opposing such ideas are considered in the context of specific systems with particular emphasis upon the environmental requirements for cracking. Thus, the cracking domains for steels and for copper-base alloys are considered in relation to the relevant potential–pH diagrams, as are crack growth kinetics involving dissolution, film growth, and crack-tip strain rates as the controlling parameters. Brief consideration is also given to the phenomenon of crack coalescence as a matter that has implications for mechanistically oriented studies, as well as for its engineering implications in service situations.

Introduction

The early literature on the stress corrosion cracking (SCC) of metallic materials is associated with the earlier part of the present century, although it is probable that service failures were experienced before that, while the last three decades have seen a considerable increase in interest in this subject. Possible reasons for the latter are that as the problem of general corrosion has been overcome, by control of environmental factors and the development and use of inherently more corrosion-resistant materials, the probability of localized forms of corrosion occurring has increased. These trends have been accompanied by moves towards higher operating stresses, deriving from the more efficient use of materials, and the more extensive use of welding as a method of fabrication, resulting in relatively high residual stresses in structures, all of which may be expected to increase the incidence of SCC.

The earliest hypotheses offered by way of explaining such failures are still reflected in current thinking. Thus, Andrew[1] was one of the first to suggest that the embrittlement caused by the ingress of hydrogen into ferritic materials offered a possible explanation of the intergranular cracking of a boiler steel as reported by Stromeyer,[2] although the latter was the first of a number of workers to suggest that chemical heterogeneity at the grain boundaries was the cause, a mechanism subsequently developed in more detail by Dix[3] in relation to aluminum alloys The beginnings of oxide film rupture mechanisms are apparent in the early papers of Straub and Parr,[4] while mechanics occupies the dominant role in an explanation offered[5] for the caustic cracking of boilers, the stresses remaining in the boiler seams after riveting, together with the working stresses, being considered to be high enough to exceed the fracture strength of the steel. This rather simplistic view might have had more credence if it had invoked the concept of surface energy, but the classical work of Griffith[6] on the fracture of glass based on an energy argument was still about 20 years away The possibility of accounting for the caustic cracking of boilers on the basis of a fatigue mechanism was suggested by Wolff,[7] and McAdam[8] attempted an explanation based on his experience with corrosion fatigue, reflecting the more recent interest in the interface between stress corrosion and corrosion fatigue. In the discussion that the Faraday Society held in 1921, Fletcher[9] suggested that the problem might be explained by the corrosive attack being concentrated in regions that had suffered the greatest amount of cold work, which bears a similarity to the explanation offered by Straub and Parr[4] involving, *inter alia*, the suggestion that, under stress, grain boundaries will be seats of high energy and will therefore suffer enhanced corrosion, an offering frequently taken up subsequently by others.

These early ideas, dominated by physico-metallurgical considerations at the expense of electrochemistry, lacked the rigorous tests of critical experiments, an affliction not restricted to early papers in the field. Nevertheless, while consideration of the role of the environment rarely extended beyond the stage of writing chemical equations that showed reactions leading to the release of hydrogen or the formation of an oxide film, until the advent of the paper by Dix,[3] current ideas on the mechanistic aspects of SCC are not essentially different from those propounded more than half a century earlier. This is not to imply that understanding has not changed over that period, since some of the critical experiments not always available to early workers have now been conducted to test the early hypotheses and, as a consequence, some of these concepts have gained acceptance.

The problems to be considered in explaining environment-sensitive fracture are essentially twofold. The first problem concerns accounting for the fracture of normally ductile materials with little attendant deformation at relatively low stresses and the second with the role of specific environments, with its thermodynamic and kinetic overtones, in promoting such failure. The mechanistic options available would also appear to be essentially twofold. Thus, either the metal must become embrittled as a consequence of the corrosive reactions or the cracks propagate by extremely localized dissolution processes. The precise details may vary from one system to another, or even for the same metal exposed to different environmental conditions, since the variability of the mechanisms of fracture of metals in the absence of environmental influence by brittle, ductile, or fatigue fracture, and the variability of electrochemical reactions, according to potential and solution composition, would appear to preclude the possibility of some all-embracing mechanism of environment-sensitive fracture that accounts for all such instances.

Embrittlement Mechanisms

Embrittlement mechanisms are the detailed concerns of other papers[10,11] and so will be touched upon only briefly here. Since stress corrosion cracks propagate in an apparently brittle manner, albeit at low velocities, the Griffith approach[6] to brittle fracture has

*Department of Metallurgy and Engineering Materials, University of Newcastle upon Tyne, Newcastle upon Tyne, NE1 7RU England.

often proved attractive in the context of environment-sensitive fracture. Thus, the fracture stress (σ_c) to cause the spread of an elliptical crack, Length 2(c), is given by:

$$\sigma_c = \left(\frac{2E\gamma_s}{\pi C} \right)^{1/2} \quad (1)$$

where E is Young's modulus and γ_s is the surface energy Clearly, any process that lowers γ_s will reduce the stress for brittle fracture and γ_s may be lowered by the absorption of appropriate species at the fracture surface. Petch and Stables[12] have invoked such an approach in relation to the hydrogen embrittlement of steel, the initial Griffiths cracks, being likened to blocked glide planes, extending by the formation of a surface on to which hydrogen is absorbed

The "stress sorption cracking" hypothesis of Uhlig[13] is not essentially different from that indicated above, except that the chemisorbed species are effective at the surface of the crack tip rather than at some distance into the metal beyond the crack tip, as is often assumed in relation to hydrogen-induced cracking. There are various difficulties associated with the "stress sorption cracking" concept,[14] but the demonstration by many workers that small, although measurable, amounts of plastic deformation are involved in stress corrosion crack propagation creates a particular problem. Where plastic deformation is involved in fracture, Orowan[15] suggests that the surface energy term in Equation (1) needs to be modified to take into account the work done in plastic deformation, so that to γ_s should be added γ_p, the work for plastic strain. Now γ_p is greater than γ_s by a few orders of magnitude (5 kJ/m^2 as opposed to 5 J/m^2), and therefore any reduction in the latter by absorption will have a negligible effect on the fracture stress. Moreover, in some instances of hydrogen-related fracture of metals, evidence of the fracture mechanism involving enhanced local plasticity caused by the presence of hydrogen[10] has become apparent in recent years and, for those cases at least, the mechanism of crack growth is hardly consistent with an approach based on Equation (1).

Apart from hydrogen reacting with dislocations, vacancies, or larger voids to influence fracture behavior, there is another type of reaction into which it can enter and influence cracking, namely, the formation of hydrides in appropriate alloys. Scully and Powell[16] have developed earlier observations[17] on the formation of a brittle hydride phase in α-Ti alloys to explain the SCC of such materials, involving cleavage of the hydride as an important step in the cracking process. Pugh and his coworkers have extended these observations on the importance of hydride formation in the cracking of Ti alloys and have shown that the fracture planes correspond to the habit planes of the hydride, as well as showing that Mg/Al alloys may form hydrides.[18]

From the localized repetitive generation of brittle hydrides in advance of a crack tip, it is a short step to consider the possibility that embrittling films formed at exposed surfaces of metals may play a critical role in SCC. Film rupture has often been invoked as a mechanism of SCC since the early work of Straub and Parr,[4] the name of Logan,[19] in particular, frequently being mentioned in this context. Despite the fact that in many cases where it has been offered as a mechanism of crack growth, it has been no more than a rate-determining step, rather than the mechanism of growth *per se*, the concept has certain attractions, especially in the form that it has more recently been developed. Edeleanu and Forty[20] observed that the cracking of α-brass single crystals exposed to an ammoniacal solution occurred discontinuously, with short bursts of extremely rapid cracking followed by relatively long rest periods. It was suggested that truly brittle fracture was associated with the bursts, while the rate-controlling periods of nonpropagation were concerned with the corrosive processes that established the conditions for further crack bursts. The model requires that α-brass can support a free-running cleavage crack, albeit over short distances of the order of a few microns and this presented a major difficulty. Thus, while cleavage in a body-centered cubic (bcc) metal, such as α-iron, has been observed on a micro-scale, to reflect its well-known tendency for macroscopic cleavage in appropriate conditions, such cleavage of face-centered cubic (fcc) metals, as α-brass, has not been demonstrated in a like manner. However, relatively recent atomic modeling studies indicate the theoretical possibility of short-range cleavage of ductile metals from an initiating surface film of appropriate characteristics,[11,21,22] and there are claims for the apparent cleavage of fcc metals from electron microscopical studies of stressed thin foils.[22]

The attraction of a microcleavage-based mechanism for transgranular stress corrosion cracking (TGSCC) in a number of systems derives from fractographic observations[23] and the emission of discrete acoustic events and electrochemical current transients accompanying crack growth.[22] Thus, stress corrosion fracture surfaces are characterized by flat, parallel facets separated by steps, opposite fracture surfaces being matching and interlocking Arrest markings are sometimes observed, suggesting that crack growth is discontinuous, as observed in the experiments of Edeleanu and Forty.[20] Moreover, there is a strong correlation between peak amplitude acoustic emission events and electrochemical current transient peaks during the transgranular cracking of α-brass exposed to $NaNO_2$ solution.[22] Of course, it may be argued that such observations are not unequivocal demonstrations of crack growth by fast cleavage. Thus, arrest markings make no comment upon the processes occurring between successive markings, which simply indicate that the crack stopped. If, as is likely, the crack stops because of plastic deformation and crack yawning, the acoustic emissions and electrochemical current transients could be a consequence of such deformation. Attempts to measure possible cleavage events directly[24] by appropriately sensitive electrical resistivity changes during crack growth in fine α-brass wires exposed to $NaNO_2$ have not indicated rapid changes in resistance, despite the presence of cleavage-like features and arrest markings being observed on the wires after failure. Moreover, the expression used in the analytical modeling of cleavage initiated by films[22] appears to involve dislocation-crack interactions that are only likely to be valid under small scale yielding conditions. Yet, the initiation of stress corrosion cracks in α-brass exposed to $NaNO_2$ solution is associated with the onset of yielding and continues with general yielding.[25] The latter leads to extensive branching, which seems more likely to be related to shear strains being very effective in producing crack growth than to any dynamic effects, not least because crack branching in cleavage-type fracture only occurs at very high crack velocities

Despite these current difficulties, the film-induced cleavage model for TGSCC in some systems has advantages over the only realistic alternative, the so-called "slip-step dissolution model." Although the latter expression is often used incorrectly, it has its origins in the work of Hoar and his colleagues[26,27] on yield-assisted anodic dissolution, the expression that is usually more appropriate Slip step dissolution implicitly means dissolution at or along slip lines and, although such has been observed,[28,29] it does not appear likely to lead to the matching and interlocking fracture surfaces often observed in the transgranular cracking of fcc metals.[23] Nevertheless, Kaufman and Fink[30] consider that TGSCC of α-brass in ammoniacal solutions occurs by extremely localized ductile fracture, reflecting the recent interest in such a mechanism for hydrogen-related cracking in certain materials.[10] They suggest that the mechanism involves the following steps:

(1) Anodic dissolution of both Cu and Zn occurs preferentially along slip bands.
(2) As the preferential anodic dissolution continues to cause atom removal, the stress becomes concentrated locally, leading to dislocation activity in these regions.
(3) Corresponding to this enhancement in localized deformation, the rate of anodic dissolution is accelerated locally resulting in further increases in the stress.
(4) Deformation continues to be localized by the action of the anodic dissolution, and the material undergoes ductile fracture, albeit on a very local scale.
(5) The combined action of localized anodic dissolution and deformation continues leading to fractures that appear brittle macroscopically.

However, their arguments appear to be strongly dependent upon the observations of greater densities of dislocations very close to fracture surfaces, compared to relatively few such features about 1 mm from the fracture surfaces. This is hardly surprising in view of the facts that SCC is associated with macroscopically brittle fracture, but is accompanied by microplastic behavior in the crack-tip region, as are some other processes of fracture in which environments play no part. The proposals of Kaufman and Fink [illegible] an obvious resemblance to the ideas of Hoar and his colleagues, apart from the rather ill-defined differences in the relative contributions of dissolution and ductile fracture to the overall crack growth. Nevertheless, the paper should be read for a useful comparison of the arguments for and against the various preferred mechanisms for TGSCC.

Dissolution Mechanisms

Although these mechanisms relate to some of the oldest concepts offered by way of explanation of SCC, they are now applied mostly to instances of intergranular cracking, possibly because many workers believe that the fractographic differences between transgranular and intergranular cracking are so marked that different mechanisms must operate. However, the problem is not so simple because hydrogen-induced cracking can be intergranular as well as transgranular, and the cracking of α-brass in nitrite solutions, for example, is initiated at grain boundaries, and immediately becomes transgranular and sometimes reverts to intergranular after some transgranular propagation.[25] It is difficult to imagine that the essential features of the mechanism can change so dramatically as the crack path, especially in the brass system just mentioned. Moreover, the difficulty mentioned earlier in relation to explaining transgranular fractographies for some systems on the basis of the slip-step dissolution model, that the mating surfaces match and interlock to an extent that is difficult to relate to dissolution at two separated surfaces, may also be a problem in relation to intergranular cracking.

Nevertheless, there is one factor relevant to intergranular cracking that does not apply to transgranular failure and is the segregation of solutes or the precipitation of discrete phases that can occur at grain boundaries and that may result in electrochemical heterogeneity. It appears reasonable to expect that those combinations of metal and environment that show a propensity towards intergranular attack in the absence of stress may display intergranular stress corrosion cracking (IGSCC) in the presence of stress of appropriate magnitude. In the absence of stress, the initial penetration may not extend far before ceasing; whereas, in other cases, intergranular corrosion may continue, albeit at a slower rate than when stresses are present, e.g., in the weld decay of steels. For various environments that promote intergranular attack on ferritic steels, it has been shown that the same environments promote intergranular attack in the presence of appropriate stresses, even though the initial attack on unstressed samples may penetrate to much less than a typical grain diameter before filming prevents further penetration; similar observations have been made on other alloy-environment combinations.

Discussion of such phenomena is now largely concerned with the nature of the substances present at grain boundaries that induce such sensitivity to selective corrosion. The relatively recent advent of experimental and analytical methods[31] for assessing the extent of segregation to interfaces, including grain boundaries, has provided information that previously was largely inferred from indirect measurements. However, there are some possible problems in simply assuming that the demonstration of specific heterogeneity at grain boundaries is sufficient to indicate the causes of selective dissolution or cracking at such locations. As an example of the type of approach that is necessary, the work of Joshi and Stein[32] may be cited. They used Auger electron spectroscopy (AES) to determine the segregation effects in the vicinity of intergranular fracture surfaces in type 304 (UNS S30400) stainless steel (SS) and showed that Cr-depleted zones accounted for grain-boundary attack in a weakly oxidizing solution such as the H_2SO_4-$CuSO_4$ environment involved in the Strauss test. However, in the strongly oxidizing solution of the Huey test (HNO_3-K_2CrO_4), there was no correlation with Cr depletion, although the extent of grain-boundary attack in the solution did correlate with the segregation of S to the grain boundaries.

In relation to the IGSCC of ferritic steels in an NH_4NO_3 solution, Lea and Hondros[33] have defined susceptibility in terms of a *fragility index* (a product of the propensity of an element to segregate to grain boundaries and its relative harmfulness, atom for atom, once at the grain boundary) From tests on 11 ingots of mild steel to which different elements were added, the data are presented as

$$\text{fragility index} = 20\%P + 1.9\%Cu + 1\%Sn + 0.9\%Sb + 0.4\%As + 0.3\%Zn + 0.2\%Ni (+ 700\%S + 27\%Ca + 1\%Al) \quad (2)$$

It is claimed that since S, Ca, and Al will be present as precipitates, they would not, in general, be detected as grain-boundary segregants and their ineffectiveness is indicated by the brackets in Equation (2). The extent of segregation to the grain boundaries was determined by AES. Since such steels do not normally fracture intergranularly and in order to allow spectroscopic measurement on grain-boundary material, a stress corrosion crack was produced from a notch in the specimens by exposure to the nitrate solution, and then the remaining metal was fractured at liquid nitrogen temperature. The authors indicate that this produced short lengths of grain-boundary fracture beyond the stress corrosion crack before the brittle crack became transgranular, and it was upon this small area of grain-boundary fracture that the spectroscopy was conducted. The SCC data are shown in Figure 1 as fracture times in slow strain rate tests (SSRTs) for the mild steels in nitrate and paraffin, the latter as an inert environment. Clearly, P had the most deleterious effect, but only marginally so by comparison with S, while Al and Ca, the other elements, together with S, that are discounted in relation to Equation (2), also show significantly deleterious effects.

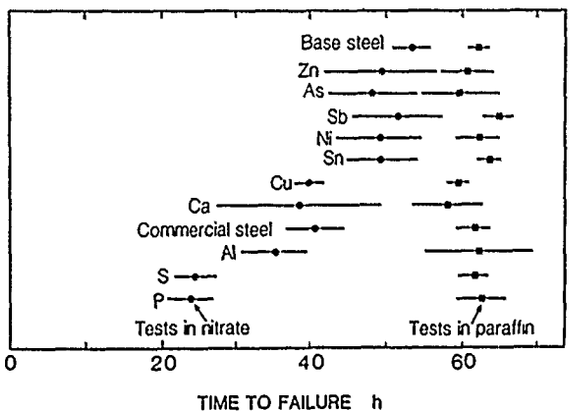


FIGURE 1—Failure times from replicated SSRTs in 5 N NH_4NO_3 and in liquid paraffin for a mild steel base to which various impurities were added (after Lea and Hondros[33]).

Lea[34] used a reduced form of Equation (2), involving only the first four elements, to compare the cracking susceptibilities of various steels that had failed in service in a variety of environments. The fragility indexes for steels that did and did not crack for similar exposure conditions are compared, and it is shown that the fragility index was nearly always higher in cracked than in the corresponding uncracked specimens Since the first four terms in Equation (2) are dominated by the high coefficient for P, Lea states that a similar correlation with cracking is obtained by considering P alone.

More recently, Krautschick, et al.,[35] have measured the cracking responses of iron-phosphorous alloys containing 0.003 to 2 wt% P in SSRTs with exposure to 5 N NH_4NO_3 at 75°C. Figure 2 shows

the work of fracture in the nitrate solution, relative to that for an inert environment, for what the authors describe as "carbon steels" with different P contents, the samples being heat treated at 940°C for 1 h followed by 48 h at 500°C, the latter to establish grain-boundary segregation of P. In the potential range from −300 to −100 mV, the resistance to cracking is somewhat greater for the low-P material than the corresponding values for the high-P steels and, for the latter, the relative work of fracture is reduced further by extended subcritical heat treatment. Unfortunately, although the authors refer to the materials as carbon steels, no chemical analyses other than for P are given, but the fact that the 0.003 wt% P steel shows appreciable susceptibility to cracking indicates that substances other than P could be involved in promoting susceptibility to cracking, despite the correlations with the grain-boundary P contents determined by AES analysis. Krautschick, et al., attribute the effects of P to impeding the formation of oxides in the grain-boundary regions, thereby stimulating selective corrosion at the boundaries. However, because of the absence of any influence of P at potentials above −100 mV, they conclude ". . . that P segregation is not necessarily the origin of IGSCC of mild steels in nitrate solutions and that special low P containing carbon steels could also show susceptibility to IGSCC in certain conditions."

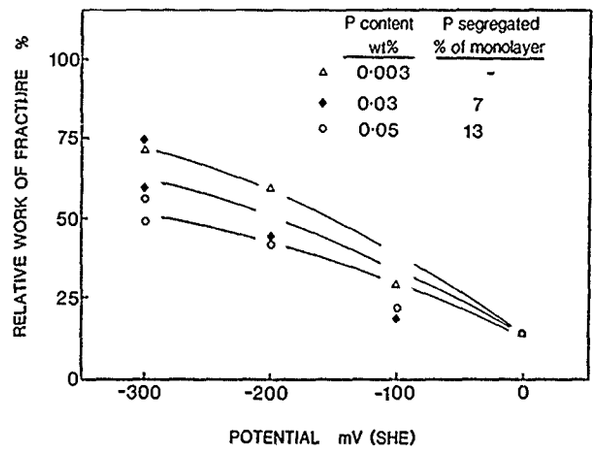


FIGURE 2—Results from SSRTs on C steels wih different P contents in 5 N NH_4NO_3 at various potentials (after Krautshick, et al.[35]).

While there are these indications of the possible importance of P in ferritic steels in promoting IGSCC, there are other data available[36,37] indicating that C and N are important in such materials in relation to nitrate-induced cracking. Moreover, attempts to reproduce the Auger measurements of Lea and Hondros,[33] by propagating intergranular stress corrosion cracks through brittle fracture at liquid nitrogen temperature to produce intergranular facets on which spectroscopy could be conducted, were not successful on a range of ferritic steels.[38] Consequently, a different approach was applied to the problem of determining the relative contributions of C, N, and P to the IGSCC of ferritic material This involved starting with pure iron (0.001 wt% C, 0.002 wt% P, and N not detectable), which was shown to be not susceptible to IGSCC in SSRTs with exposure to a carbonate-bicarbonate solution, and adding controlled amounts of C, N, or P by diffusion and subsequent homogenization. The addition of 0.03 to 0.231 wt% C, 0.0226 or 0.393 wt% N, or 0.03 wt% P all resulted in IGSCC, although such was not observed with 0.005 wt% P. Clearly, the conclusion of Krautschick, et al.,[35] that P segregation is not necessarily the origin of IGSCC of mild steels is confirmed, even in relation to a different environment.

Quite apart from ensuring that corrobatory experiments or measurements are undertaken to ensure that substances segregated to grain boundaries are involved in the cracking reactions, the question remains as to the mechanism whereby such segregants are operative in promoting cracking. The early work of Mears, Brown, and Dix[39] showed that the Mg_2Al_3 phase precipitated in Al-Mg alloys is ~0.2 V anodic to the matrix when the two phases are immersed in a $NaCl/H_2O_2$ solution. Several workers have subsequently shown similar galvanic effects at grain boundaries, using micro-electrodes to measure potential differences between grain-boundary regions relative to the bulk corrosion potential or by the preparation of substances in bulk representing the differences in composition between boundary and matrix materials. Lea and Hondros[33] have applied what they term a simplistic approach to their data for the IGSCC of steel in nitrate (Figure 1). They consider that the driving force for dissolution is related to the potential difference between the matrix and the segregant atoms forming a galvanic cell. They calculate this potential difference from the equilibrium potentials at pH 5 (taken from potential-pH diagrams and on the assumption that there is an ionic concentration of about 0.1 M of the dissolving species at the crack tip) for each segregant and for iron. Although there are obvious queries as to the validity of such an approach, especially for the elements S, P, As, and Sb, their plot of these potential differences between iron and the iron segregants, $|\Delta E_o| = E_o^{seg} - E_o^{Fe}$, against the normalized effect on SCC propensity shows a tendency for the potency of the segregant to increase as $|\Delta E_o|$ increases, as is apparent from Figure 3. While the use of such equilibrium potentials may be too simplistic for some to accept, Lea and Hondros claim that even with accepting Figure 3 just as an empirical indication, the trend is sufficient to be used predictively.

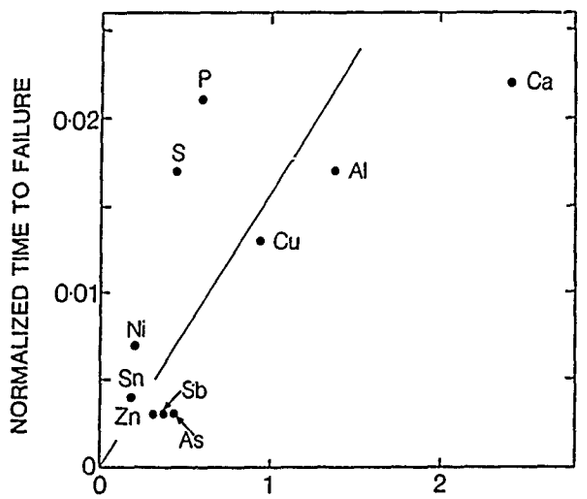


FIGURE 3—Normalized times to failure of the steels shown in Figure 1 as a function of the equilibrium potential between Fe and the segregant atoms at the grain boundaries (after Lea and Hondros[33]).

If that is done in relation to the effects of other alloying elements upon the cracking propensities of ferritic steels, but in a $NaNO_3$ solution, it is clear that precisely the opposite effect to that shown in Figure 3 is obtained. Tests upon some 45 steels containing various alloying additions were expressed in terms of a stress corrosion index (SCI) that not only reflected the normalized cracking susceptibility, as in Figure 3, but the variation of that parameter with potential.[40] The SCI for a given steel was, therefore, a measure of the area bounded by a plot of the normalized time-to-failure in SSRTs against potential. Regression analysis of such data for tests in a $NaNO_3$ solution produced:

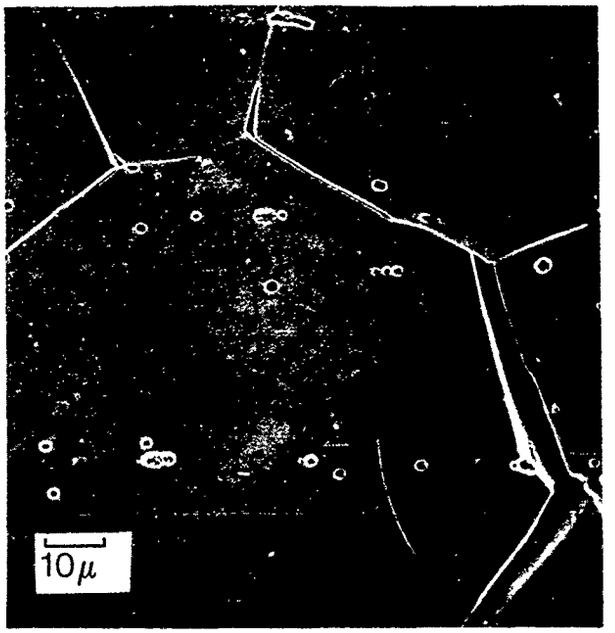
$$SCI = 1777 - 996\%C - 390\%Ti - 343\%Al\ (-132\%Mn) - 111\%Cu - 90\%Mo - 62\%Ni + 292\%Si \quad (3)$$

A negative coefficient indicates a beneficial effect in relation to cracking susceptibility, while the result in brackets for Mn indicates that the t ratio from the statistical treatment was small and the result, therefore, probably insignificant. If the $|\Delta E_o|$ values as defined by Lea and Hondros are calculated for these various elements, it will be seen that as $|\Delta E_o|$ increases, so does the coefficient in Equation (3), i.e., precisely the reverse of the effect indicated in Figure 3. There are available[40] equivalent equations to Equation (3) for tests in NaOH and a sodium carbonate-bicarbonate solution, and they also do not conform to the predicted trend suggested by Lea and Hondros on the basis of Figure 3. The effects of the alloying elements indicated in Equation (3) for these various solutions are more readily explicable on the basis of their filming tendencies than upon their tendency to segregate to grain boundaries, although their carbide-forming tendencies also probably have some influence.[40]

Apart from, or probably in addition to, simple galvanic effects arising from segregants located at grain boundaries, there is also the possibility that filming characteristics are modified in grain-boundary regions where segregants are present. The suggestions of Krautschick, et al.,[35] along these lines to explain the effect of P segregated to grain boundaries in steels has already been mentioned, but Flis[41] ascribes a similar role to segregated C in the IGSCC of Armco iron and other low C, iron alloys in a phosphate solution. It would appear inevitable that if enhanced dissolution occurs in grain-boundary regions because of the presence of segregants, then filming will be impaired in these regions and to offer the latter as an effective explanation of IGSCC simply restates the problem in different terms. Moreover, the evidence offered in support of such explanations is usually in the form of potentiodynamic polarization curves for alloys of different C contents, so the electrochemical behavior is that of a heterogeneous electrode and presumably reflects, at best, some averaged behavior of the phases exposed. The inadequacies of such approaches are readily apparent from the work of Cron, et al.,[42] who studied the distribution of attack in transmission electron microscopy (TEM) foils of a 0.45% C steel immersed in various environments at different potentials. Selective attack was upon the carbide, the iron-rich matrix or the interface between these phases depending upon the pH, potential, and anion present. Similar observations have been made in relation to the exposure of mild steel to the IGSCC environments, nitrates, hydroxides, and carbonate-bicarbonate solutions [43] There is need for more work of the type conducted by Cron, et al.,[42] and where associated polarization measurements are made it would be more appropriate that they be on single phase materials representing the different compositions and phases present in multicomponent alloys. Only by such approaches coupled with the identification of precipitates or segregates at grain boundaries will those aspects of the IGSCC mechanism in specific systems be removed from the realms of guesswork.

Apart from being preferred sites for the generation of localized electrochemical heterogeneity, there are other roles that grain boundaries may fill in cracking mechanisms. The association of IGSCC in aluminum alloys with the existence of precipitate-free zones near grain boundaries suggests that the relative ease of plastic deformation in such zones will facilitate crack growth. The well established role of grain boundaries, even in single phase materials, in providing obstacles to dislocation motion whereby pile-ups occur at boundaries has also been invoked in the context of the importance to cracking mechanisms of localized deformation in grain-boundary regions Certainly, there is evidence for grain-boundary sliding accompanying IGSCC [Figure 4(a)], but so also is there for transgranular cracking [Figure 4(b)], which is hardly surprising in view of the compatibility requirements of deformation in polycrystalline materials However, the precise role of plastic deformation in crack initiation or growth does not always conform to the apparent mechanistic requirements, especially of those that are dissolution related.

It has already been mentioned that dissolution at slip steps has been observed[28,29] in conformity with the slip step dissolution model. However, a further requirement of the latter is that for such a mechanism to operate, the slip-step height should exceed the thickness of the surface film if unfilmed metal is to be exposed to the environment. Measurements of film thickness and maximum slip-step heights, the latter dependent upon the grain size of the metal, have been measured for α-brass exposed to a $NaNO_2$ solution.[44]



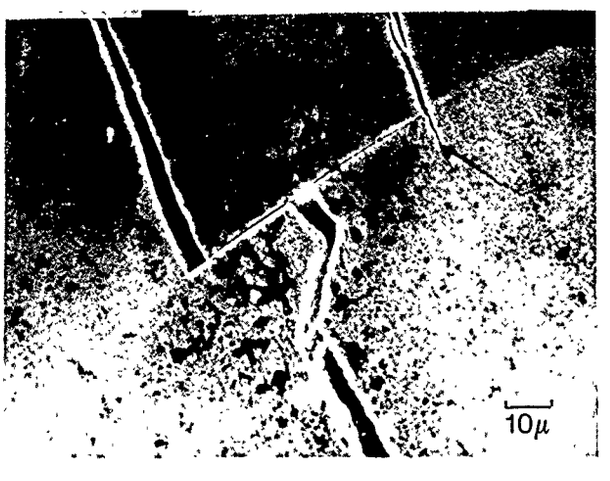


FIGURE 4—Evidence of grain-boundary sliding accompanying (a) IGSCC in an Al-Zn-Mg alloy exposed to a chloride solution and (b) transgranular cracking in α-brass exposed to $NaNO_2$ solution.

Figure 5 shows the film thicknesses, measured by different methods, as a function of potential together with the maximum slip-step heights for three different grain sizes, from which it is apparent that only for the 180-μm grain size material below about 0 V_{SCE}, and below about 0.1 V_{SCE} for the grain size of 35 μm, is slip-step emergence beyond the oxide film thickness likely. For the smallest grain size material shown in Figure 5, the maximum slip-step heights are always below the film thickness for any potential at which cracking occurs. These indications, especially for the smaller grain size brasses, that no crack initiation at emergent slip steps should occur were confirmed by metallographic observations on specimens strained in the $NaNO_2$ solution. What did occur was that cracks invariably initiated at grain or twin boundaries. Even in 180-μm grain size brass at −0.1 V_{SCE}, cracks initiated at grain boundaries before initiating at merging slip steps. However, although intergranular initiation was dominant, the cracks immediately propagated in a transgranular mode, behaviors also shown to be operative in the presence of other environments that promote transgranular propagation.

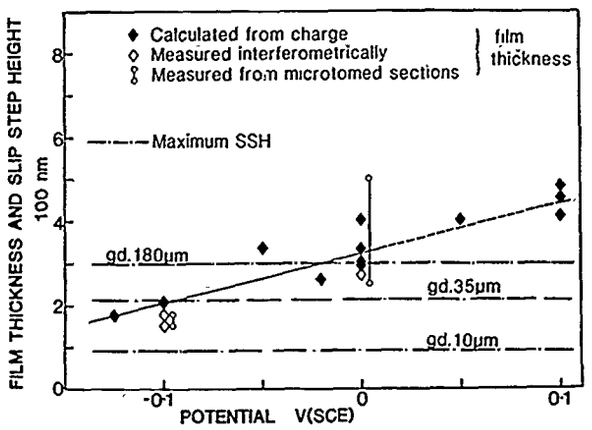


FIGURE 5—Measured and calculated film thickness as a function of applied potential for α-brass exposed to 1 M $NaNO_2$. The maximum slip-step heights, measured interferometrically after 2% strain for typical grain sizes, are also shown to indicate the condition for crack initiation by slip-step emergence.[44]

The protagonists of the slip-step dissolution model for SCC may find support in the result that transgranular crack initiation was only observed when the maximum slip-step height exceeded the film thickness However, such a result was obtained only for relatively coarse-grained brass, to maximize the slip-step height, and at low potentials, to minimize the film thickness; yet, SCC occurs in coarse- and fine-grained brasses where it would not be predicted to occur on the basis of such an approach It may be argued that the common factor throughout was crack initiation at grain or twin boundaries, and so the slip-step dissolution model for propagation is not reflected by such observations on initiation. But why should cracks prefer to initiate at grain or twin boundaries when the subsequent propagation is transgranular? It appears likely that this will relate to either chemical heterogeneity at the grain boundaries, mechanical phenomena concentrated in such regions, to some peculiarity of the overlying film at these locations, or to some combination thereof. Consideration of these alternatives suggests that filming characteristics at boundaries probably plays the dominant role. No evidence was obtained that the film thickness was essentially different at such sites from those at grain surfaces, although the fact that the strain to initiate cracking at boundaries is appreciably less than that to initiate transgranular cracks at emergent slip steps in coarse-grained material[25] may indicate that the mechanical properties of the film in such regions are different from those covering other parts of the exposed surfaces. The epitaxy that probably obtains at grain surfaces is likely to be perturbed in boundary regions and may account for a preference for fracture in such locations.

Of course, even such suggestions make no comment upon why cracks initiated at grain or twin boundaries should subsequently propagate transgranularly. Indeed, the problem is further complicated by the observation[25] for the brass-$NaNO_2$ system that, in some circumstances, the crack propagation reverts to intergranular after some transgranular growth. It is possible to speculate that the latter change may result from changes in the environment contained within the crack enclave, but there is, as yet, no evidence of such for this system. Interchanges between intergranular and transgranular cracking are not unique to the brass-$NaNO_2$ system and can result from small changes in applied potential, from changes in environment composition or from modifications to the structure or composition of an alloy Such phenomenology should not be ignored, as is so frequently the case, since it sometimes will constitute a test of mechanistically oriented models that might otherwise persist through default.

While the current fashion may be to invoke dissolution-controlled mechanisms primarily in relation to intergranular cracking, there remains a considerable body of evidence[45] relating transgranular cracking to localized dissolution processes. The localization of the dissolution in such cases is most often related to slip and particularly that which occurs with some fcc alloys having a low stacking fault energy or displaying short range order, where planar groups of dislocations are favored and cross slip made more difficult.[46] The observations of Swann and his coworkers[47-49] of dissolution associated with planar dislocation arrays in TEM foils led to the suggestion that arrays of fine corrosion tunnels form, which subsequently interconnect by the tearing of the remaining ligaments between the tunnels. The objections that have most frequently been raised to such transgranular dissolution models is that they have difficulties in accounting for the matching opposite fracture surfaces, and the fact that the planes on which tunneling and fracture occur are not the same. However, at about the same time that Swann was developing the tunneling model, Nielsen[50] was examining, by TEM, the corrosion products removed from stress corrosion cracks in austenitic SSs after exposure to chloride solutions. In general, these take the form of fans showing lamella markings (Figure 6), suggesting that crack growth was discontinuous. It may, of course, be argued that such oxide films are formed after the crack tip has advanced and that they are simply replicating the stress corrosion fracture surface. However, when Nielsen exposed samples of the steel to $MgCl_2$ solution for only a few minutes, oxide-filled corrosion tunnels developed, which, as Figure 7 indicates, were joined by lateral tunnels that increased in number on moving towards the original surface of the specimen, to produce a corrosion-product fan resembling Figure 6. Figure 7, in particular, shows features that appear more consistent with crystallographically related dissolution than with film-induced cleavage. Somewhat similar effects have been observed[51] in a copper alloy exposed to ammonia vapor and again suggest that localized dissolution processes cannot be ruled out as a contributing factor in the growth of transgranular stress corrosion cracks in some systems. Of course, one of the most important tests of any model is the extent to which it can predict the known or likely behavior of a system, and in this respect, some models are quite successful, especially in relation to the environmental requirements for cracking, the matter now considered.

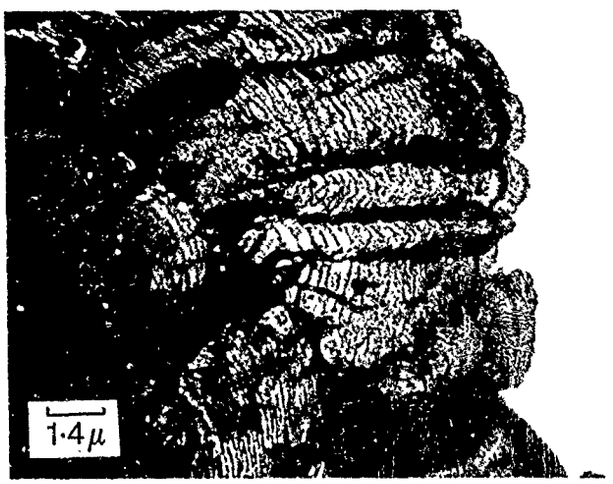


FIGURE 6—Corrosion product fans emanating from cracks in stainless steel (original magnification X7200).[50]

Environmental Aspects of Cracking

One of the most important problems in relation to avoiding service failures by SCC is concerned with predicting those environmental conditions that sustain this mode of failure. The specificity of solution conditions that promote SCC has sometimes been misleading in that it has engendered the thought that cracking only occurs in those almost classical environments that have long been known to promote this type of failure in specific alloys, e.g., nitrate and hydroxides in relation to ferritic steels, chlorides in relation to SSs, and ammonia in relation to brasses. While the concept of solution specificity remains in the sense that not all environments corrosive

towards a particular metal will promote SCC, nevertheless, the number of environments that are potent towards a specific alloy continue to increase with the passage of time.

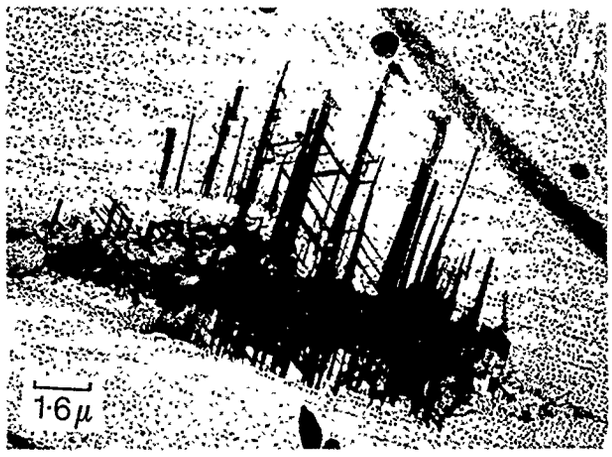


FIGURE 7—Oxide extraction replica of corrosion tunnels in 18Cr-8Ni-type SS (original magnification X6400).[50]

Assuming an alloy of appropriate composition and structure and a stress intensity factor or strain rate of suitable magnitude to promote SCC, what are the environmental requirements? If the crack growth involves dissolution, then, like any localized corrosion problem, stress corrosion requires some critical balance between active and passive behavior since gross activity is likely to promote general, rather than localized, dissolution, and passivity, by definition, will not be associated with any corrosion. More specifically, the geometry of a crack requires that the reactions that occur at a crack tip proceed at a considerably faster rate than any dissolution processes that occur at all other exposed surfaces of the metal, including the crack sides, so that there is not a requirement of complete passivation of all surfaces except for the crack tip, but merely that the relative rates of reaction are very different. Moreover, as the crack tip advances, those parts of the surface that at an earlier stage constitute part of the crack-tip region become incorporated in the crack sides, so that they must undergo an active → passive, or relatively inactive, transition. If this did not occur and the crack sides remained active, then they would spread laterally and the crack geometry would be lost.

The extent to which metal surfaces will exhibit active → passive transitions at rates appropriate to sustain SCC depends not only upon the nature of the environment, including its composition, temperature, and the potential that it engenders, but also upon the composition and the structure of the metal. Thus, the environmental requirements for cracking will vary from one alloy to another, as exemplified by the observations that those materials that are inherently more reactive, such as C steels and Mg-base alloys, require the passivating influence to be incorporated into the environment, hence the cracking of mild steels in nitrates, hydroxides, carbonates, phosphates, and the like, and the cracking of Mg-Al alloys in appropriate mixtures of chromate and chloride. On the other hand, those metals that are inherently less active, such as the Al and Ti base alloys and the SSs, because of the ease with which they form protective oxide films, crack most readily in the presence of aggressive halide ions. The highly specific nature of the solution composition requirements for crack growth by a dissolution-controlled mechanism are not so rigid in relation to crack growth resulting from the ingress of hydrogen into the metal, the primary requirement being that the environment provides a source of hydrogen that is released by appropriate electrochemical conditions.

There is an interesting distinction between stress corrosion and corrosion fatigue in relation to the environmental requirements for crack growth under nominally static and cyclic loading. Thus, with cyclic loading, those environments that promote stress corrosion will also promote corrosion fatigue, but so will many other environments that do not promote stress corrosion. The probable reason is that whereas with stress corrosion, the retention of crack geometry is dependent upon achieving an appropriate active → passive transition, with cyclic loading, mechanics retains the geometry of the crack. The consequence is that the environmental requirements for cracking are less specific for corrosion fatigue than for stress corrosion.

There are various methods available for measuring the propensity for active → passive transitions, all involving the observation of the current response of the metal surface for specific exposure conditions since the obvious implication of such a transition is that the current density should diminish at an appropriate rate with time.[52] The methods vary in relation to the technique used for creating the bare metal surface upon which the current response is monitored, and these range from cathodic reduction of the initial air-formed film, in those relatively few cases where such is possible, to scratching or otherwise mechanically rupturing surface films of the more electrochemically stable forms. Such methods will usually give at least an approximate indication of the potentials at which SCC is likely, and they can be useful in indicating probable upper-bound crack growth rates, matters which are considered below.

Various thermodynamic considerations

It is now well established that SCC only occurs over particular ranges of potential for a given metal-environment combination. Such potential dependence must be related to specific reactions whereby the environmental requirements for cracking are met. Probably the simplest situation in this respect arises with hydrogen-induced cracking, where the hydrogen derives directly from the bulk environment to which the metal is exposed, and in which circumstances the conditions for cracking would be predicted to be met where the potential is below that for hydrogen discharge at the relevant pH. Figure 8 shows a plot of the highest potentials at which hydrogen-induced cracking was observed in various ferritic steels exposed to different solutions.[53] Clearly, those potentials lie just below the calculated equilibrium potential for hydrogen discharge as a function of pH, so, there is reasonable agreement between the predicted and observed behaviors.

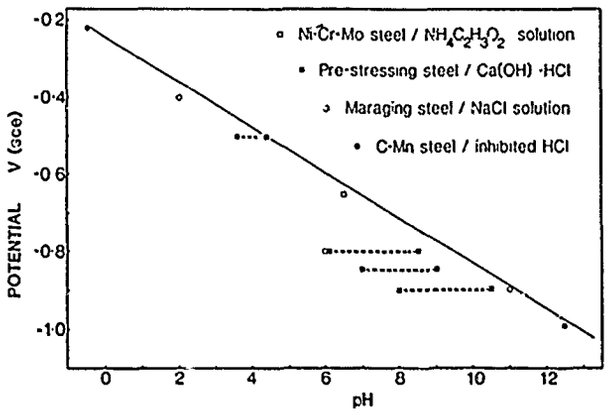


FIGURE 8—Highest potentials at which hydrogen-induced cracking was observed in various ferritic steels exposed to different solutions and subjected to SSRTs. The line represents the equilibrium potential for hydrogen discharge as a function of pH.[53]

Where crack growth is by dissolution associated with filming reactions to retain crack geometry, the potential dependence of cracking should reflect those requirements, again with some pH dependence because of the influences of that quantity upon the potentials at which the various reactions are possible. Where the necessary thermodynamic data are available for the species involved in a particular system, it should be possible to calculate the limits of the cracking domain. This has been done for the cracking of low strength ferritic steel exposed to phosphate solutions and the agreement between the observed and calculated boundaries of the

cracking domain is reasonable [54] For that system, as with ferritic steels in other environments, the upper boundary of the cracking domain is met when the stable phase becomes γ-Fe_2O_3, i.e., at potentials where only the latter forms cracking does not occur. While the potentials and pHs at which that phase can form will depend upon the phases formed within the cracking domain, it is interesting to consider the location of the potential-pH domains for cracking in various systems involving different ferritic steels in a range of environments at temperatures between 20 and 288°C. Figure 9 shows the various cracking domains together with the calculated equilibrium potentials for reactions between Fe_2O_3 and Fe_3O_4 and between Fe_3O_4 and Fe and for hydrogen discharge, all at 90°C as representing an average temperature for the various systems involved.[55] Clearly, each cracking domain is associated with the calculated Fe_3O_4/Fe_2O_3 line and, indeed, in all of these systems, Fe_3O_4 is observed to form under conditions where cracking occurs, although it is frequently associated with other phases, e.g., $FeCO_3$ in the case of cracking by carbonate-bicarbonate solutions and $Fe_3(PO_4)_2$ for cracking by phosphate solutions. Moreover, for most of the systems shown in Figure 9, only ductile failures occur in SSRTs conducted at potentials high enough to form Fe_2O_3 alone. While it is clear that the anions exert a significant influence upon the location of the cracking domains, the importance of Fe_3O_4 formation within the cracking ranges and Fe_2O_3 formation under conditions associated with ductile fracture appear well established, but the reasons for such are less so.

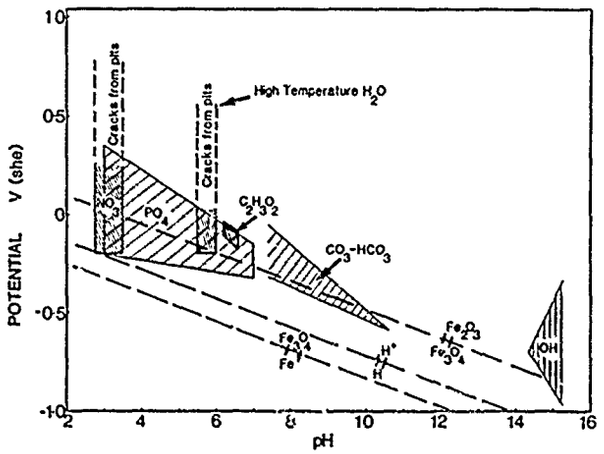


FIGURE 9—Potential and pH ranges for the SCC of ferritic steels in various environments, together with the pH-dependent equilibrium potentials for reactions involving Fe → Fe_3, H → H^+, and Fe_3O_4 → Fe_2O_3.[55]

The exceptions in Figure 9 to only ductile failure occurring at potentials high enough to form Fe_2O_3 involve nitrates and high-temperature water. In both of those systems, cracks grow from pits and within the pit crack enclaves, Fe_3O_4 forms, despite the external surfaces being covered with Fe_2O_3 films. The initiation of stress corrosion cracks from pits has been observed in a variety of systems and is usually taken as indicative of the local environment within the pit being potent and different from that of the bulk environment external to the crack. Where cracking does extend from pits, there is usually reasonable correlation of the onset of cracking with the pitting potential, as, for example, with ferritic steel exposed to nitrite-containing nitrate solutions.[56] The perturbation of the electrochemical conditions within pits has inevitably led to similar considerations being given to the conditions within crack enclaves and since the early pioneering work of Brown,[57] the subject has attracted much attention.[58,59] While there can be no doubt of the existence and importance of localized changes in environment composition and potential within crack enclaves in some systems, it is equally clear that such changes are negligible in other systems.

The latter point may be illustrated with data for a C-Mn steel immersed in a carbonate-bicarbonate solution involving a simulated crack that allowed measurements of the potential and current flow in the enclave.[60] Figure 10 shows the potential along the simulated crack at various times and indicates that although there was initially a steep potential gradient, it was approximately halved in 315 min and then disappeared, quite suddenly, at 360 min. The reason for this behavior is shown by the associated current measurements indicated in Figure 11. At the outset, there was a large current density gradient, but the current density at the entrance to the simulated crack soon began to form and the peak current density moved down the simulated crack. These changes continued with the passage of time, the entrance to the crack passivating and requiring little current so that more of the current could flow into the crack to extend the passivating process further from the mouth. When the peak current density reached the tip of the crack, that region finally passivated and the potential and current density gradients disappeared. Indeed, a visible film, largely of Fe_3O_4, could be observed progressing down the simulated crack as the potential and current density gradients changed, until the film reached the end of the crack and the gradients disappeared. Although the aspect ratio of the simulated crack to which Figures 10 and 11 refer was only 280, and, therefore, about an order of magnitude less than that for many real cracks, when the aspect ratio for the simulated crack was increased to exceed 1000, the only effect was to delay the disappearance of the potential and current density gradient. A criticism of that work is that it did not involve an actively growing crack tip having a continuing current requirement. Consequently, further experiments have been conducted involving, at the remote end of the simulated crack, a specimen that could be dynamically strained at various rates.[61] This latter work was conducted upon a Ni-Cr-Mo-V steel exposed to NaOH solution, which showed similar behavior to that shown in Figures 10 and 11. When SSRTs were conducted on specimens at the remote end of the simulated crack for various potentials applied at the entrance to the enclave, the maximum crack velocities were not essentially different from those obtained with specimens openly exposed, i.e., not exposed to the creviced condition of the simulated crack, for the same potentials. This is apparent from Figure 12 involving a simulated crack with an aspect ratio in excess of 1000.

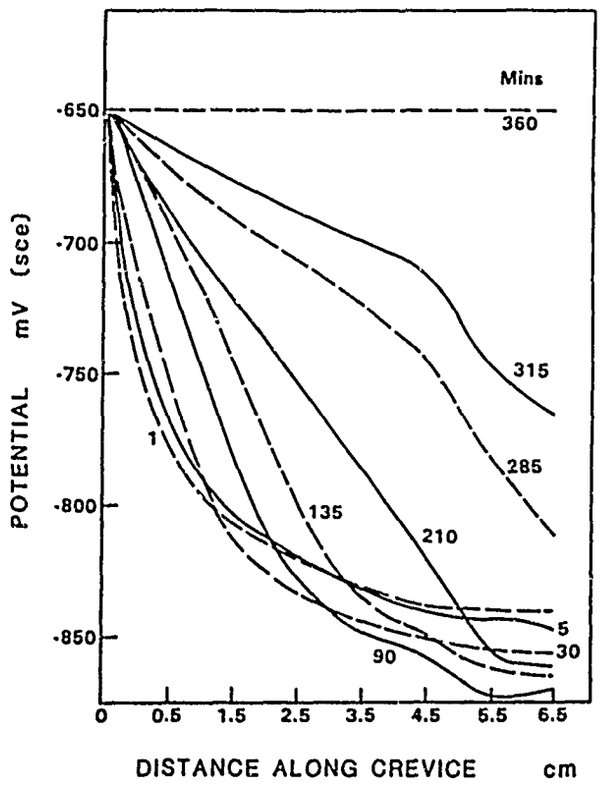


FIGURE 10—Potential-distance at various times for C-Mn steel surfaces exposed to CO_3/HCO_3 solutions in segmented crevices at 75°C. Well potential −0.65 V, crevice thickness 0.25 mm.[60]

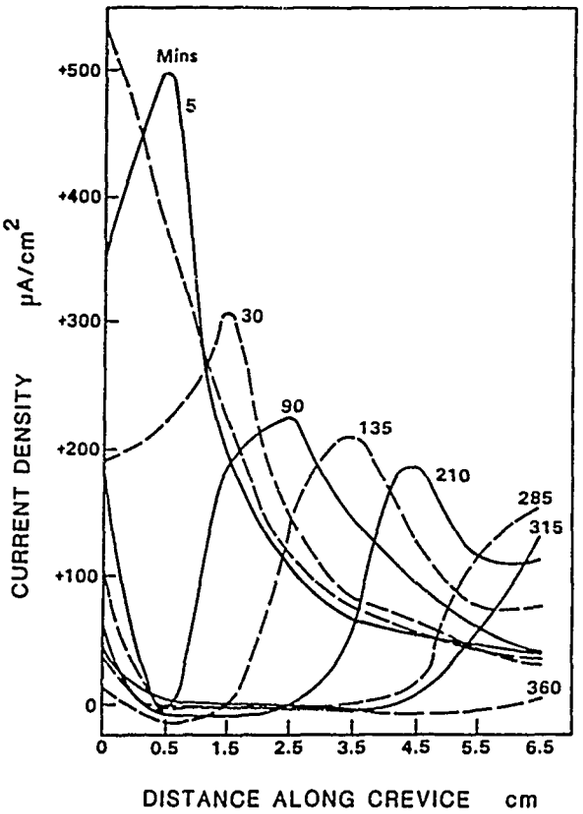


FIGURE 11—Current density-distance curves at various times for C-Mn steel surfaces exposed to CO_3/HCO_3 solution in segmented crevice at 75°C. Well potential −0.65 V, crevice thickness 0.25 mm.[60]

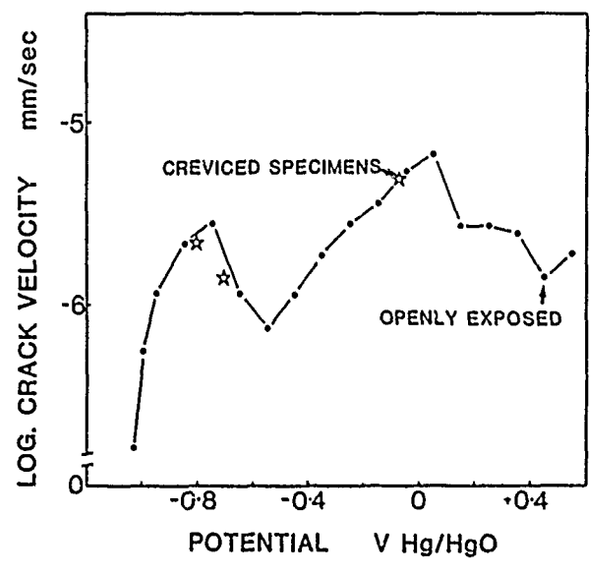


FIGURE 12—Crack velocities from SSRTs in openly exposed and creviced specimens, the latter to simulate crack-tip conditions, of a Ni-Cr-Mo-V steel in 10 M NaOH at 100°C and various potentials.[61]

Such results are, of course, relevant to the observed potential ranges for SCC If significant potential changes exist along cracks, then it may be expected that the potential range over which cracking is observed will be a function of whether precracked or initially plain specimens are used for determining the potential range in which cracking is observed. If results from both types of specimen are obtained, then the potential ranges for cracking may be expected tc be displaced by the amount of the potential drop along the precracks, assuming that the stress corrosion cracks are propagated over relatively short distances compared to the lengths of the precracks so that any change in the magnitude of the potential drop is small. Results are available[52] for the system to which Figures 10 and 11 refer and which show that the potential ranges for cracking in that system are not essentially different according to whether precracked or initially plain specimens are used in determining that range. The reason is clear from Figures 10 and 11 since if the crack-tip potential initially differs from the applied potential, that difference will disappear in a relatively short time compared to typical total test times; so that for most of the test, the crack-tip potential will be effectively at the applied potential. This is likely to be so for other systems in which the crack growth involves dissolution and the crack sides become filmed so that there is insignificant current drainage at the crack sides. Moreover, if, as is so for the systems to which Figures 10 through 12 refer, the environment is one that is essentially buffered and in which the dissolving metal has a very low solubility, then the chances of marked changes in the composition of the electrolyte in the crack enclave are remote. On the other hand, where these various conditions do not obtain then the potentials that will promote cracking for precracked and initially plain specimens can be appreciably different. Thus, with a maraging steel exposed to NaCl solution at initial pHs of 6 or 11, initially smooth specimens failed in two regimes of potential separated by a region, some 300 mV in extent, in which cracking did not occur.[62] However, precracked specimens did display environment-sensitive crack growth over the whole range of potentials, as indeed did smooth specimens that were pitted before exposure to those conditions that did not promote cracking in unpitted specimens.

This cracking of a maraging steel in two regimes of potential separated by a range of potentials in which cracking did not occur for initially plain specimens is indicative of cracking by two different mechanisms above and below the range of immune potentials. This has been observed in a number of different systems and the separation of hydrogen-induced and dissolution-related cracking in Figures 8 and 9 is not intended to imply that, for the systems involved, cracking is invariably by one or other of these mechanisms. The interrelation of these, and other failure mechanisms, in a potential-pH diagram for a single system may be illustrated by Figure 13, which refers to the exposure of Ni-Cr-Mo steel specimens to an ammonium acetate solution.[63] The experimental data have been superimposed upon part of the potential-pH diagram for the $Fe-H_2O$ system calculated for 90°C, but because the solution pHs were measured at 25°C, the scales have been adjusted for the latter temperature. Moreover, the calculated boundaries were moved, *en bloc*, relative to the experimental data until reasonable coincidence was obtained, that amount corresponding to an overpotential in effect and being about 100 mV, a reasonable value for overpotentials. The agreement between the experimentally observed modes of failure and the various domains of the potential-pH diagram is reasonable, with ductile failure in the presence of Fe_2O_3, intergranular stress corrosion when Fe_3O_4 formed and hydrogen-induced cracking at potentials where hydrogen discharge is to be expected.

While such approaches to identifying the potential ranges for SCC provide hope for predictive approaches to the study of other systems, the above all refers to ferritic steels and raises the question as to the extent that it is applicable to other metals. Figure 14 shows the cracking domains for α-brasses exposed to various nonammoniacal environments superimposed upon the $Cu-H_2O$, potential-pH diagram.[53] While the anions will have a significant influence upon the location of the cracking domains, as with those involved in the cracking of steels, there is a tendency for the cracking domains to be concentrated in regions where Cu_2O is likely to form, comparable to the role of Fe_3O_4 in the cracking of ferritic steels. If the indications of the importance of Cu_2O films in the SCC of brasses shown in Figure 14 is other than fortuitous, it is not immediately clear how this relates

to the apparent importance of dealloying and TGSCC in brasses.[64] Some of the cracking induced by the environments indicated in Figure 14 are intergranular, for which dealloying and film-induced cleavage are not claimed to be involved in the crack growth mechanism. Moreover, pure copper, in which dealloying clearly cannot be involved, can also be made to display TGSCC in nitrite solutions over essentially the same potential range as is shown in Figure 14 for α-brass.[65] It is difficult, therefore, to escape the conclusion that Cu_2O films are involved in the SCC of such materials in a variety of environments Congruently, the evidence suggesting that dealloying is associated with cracking by some environments cannot be ignored and there is an obvious need for these apparent conflicts to be resolved, the beginnings of which are apparent from recent work by Fritz, et al.,[66] By working with a Cu-Au alloy exposed to an acidified sulfate solution, they have shown that dissolution is necessary during crack propagation and not simply as a prerequisite for film-induced cleavage.

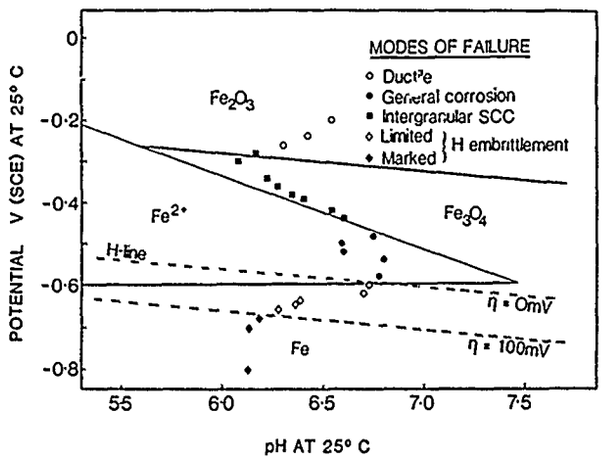


FIGURE 13—SSRT results showing the modes of failure of a Ni-Cr-Mo steel in 1 M $NH_4C_2H_3O_2$ at 90°C, superimposed upon part of the Fe-H_2O potential-pH diagram.[63]

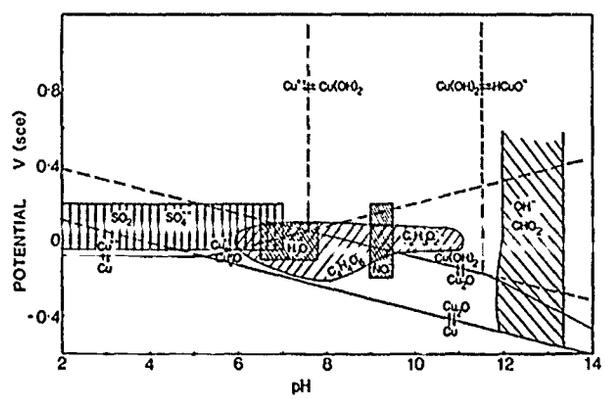


FIGURE 14—Potential and pH ranges for the stress corrosion of α-brass in various environments, together with the equilibrium potentials for various reactions.[53]

Various kinetic considerations

Where crack growth is by a dissolution-controlled process and the crack-tip strain rate is such that filming of the crack tip is prevented then the crack velocity may be expected to be related to the bare metal dissolution rate. Thus, writing Faraday's second law as a penetration rate, the crack velocity

$$CV = i_a \times \frac{M}{zFd} \qquad (4)$$

where i_a = anodic current density, M = atomic weight of the metal, z = valency of the solvated species, and F = Faraday's constant. Figure 15 shows a plot of the measured crack growth rates and dissolution current densities gathered from papers presented at a particular conference,[67] and to which much additional data could now be added, that indicates a reasonable correlation of these parameters, the line being that calculated from Equation (4) assuming a valency of 2. It is interesting to note that the two systems shown in Figure 15 which displayed significantly higher crack velocities than Equation (4) indicates, brass in ammonia and SS in $MgCl_2$ solution, are those most frequently offered as examples involving crack growth by short-range cleavage initiated in a brittle surface film.

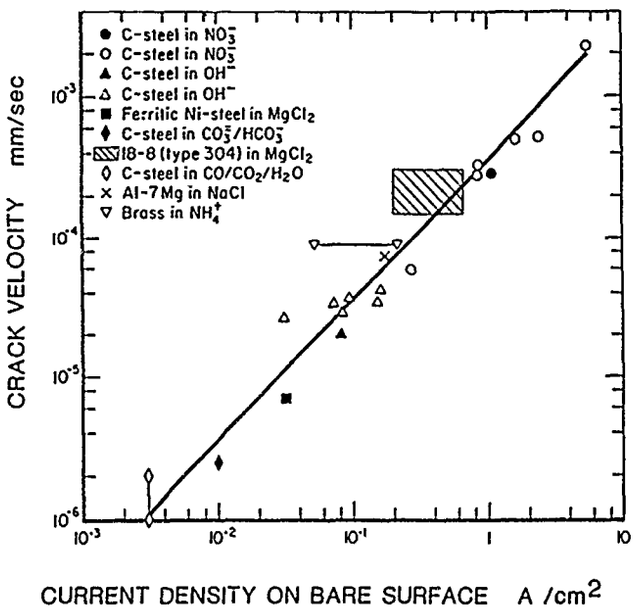


FIGURE 15—Observed stress corrosion crack velocities and measured anodic peak current densities for a variety of metal-environment systems. The line is that calculated from Equation (4) assuming a valency of 2 for all solvated species.[67]

Equation (4) represents an upper-bound crack velocity by continuous dissolution, requiring strain rates, and hence stresses or stress intensity factors, that probably do not exist in many service situations until the later stages of stress corrosion crack growth. The earlier stages of growth may involve appreciably lower crack velocities than those given by Equation (4), and even from laboratory tests, there is evidence of such. Figure 16 shows data from laboratory tests on initially plain specimens exposed to static or cyclic loads or to monotonic slow straining for various times and all show significant reductions in crack velocity with increasing test time. The reasons for such behavior most probably relate to the relative rates of film growth and bare metal creation at crack tips. Once a crack tip has become filmed, growth will cease, until the film is ruptured and dissolution can restart until film growth prevents it again, the frequency of such events depending upon the crack-tip strain rate and the dissolution and film growth kinetics. Integration of the current transients over an appropriate time interval will provide the relevant anodic charge (or charge density) passed (Q_f), which can then be incorporated into Equation (4) to reflect the fact that the crack is not propagating continuously at the upper bound, i.e.,

$$CV = \frac{Q_f}{\epsilon_f} \dot{\epsilon}_{ct} \times \frac{M}{zFd} \qquad (5)$$

where ϵ_f = strain to rupture the film and $\dot{\epsilon}_{ct}$ = crack-tip strain rate.

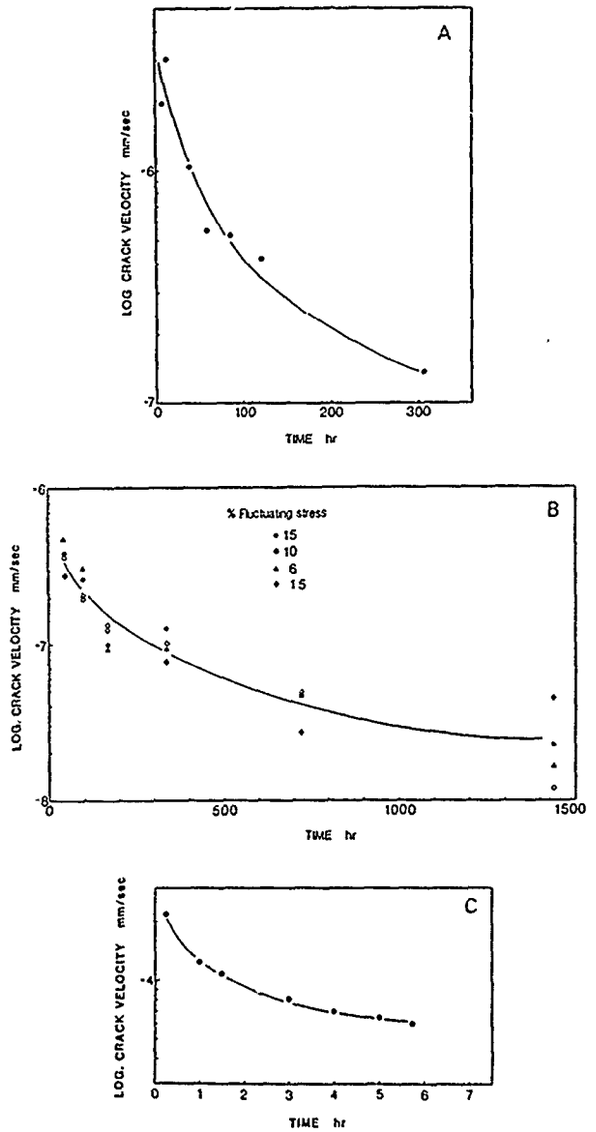


FIGURE 16—Effects of test time upon crack velocity in (a) constant-load tests on C-Mn steel in CO_3-HCO_3 solution; (b) cyclic loading tests (maximum stress = yield stress) on ferritic steel in CO_3-HCO_3 solution; and (c) SSRT below yield stress on C-Mn steel in NO_3 solution.[69]

The most obvious reason for the reductions in crack velocity with test time shown in Figure 16 is work hardening, accompanying the creep in the constant-load tests or the hysteresis in repetitive cyclic loading. There is, however, another factor, and probably that which explains the reduction in crack velocity with time in the SSRTs shown in Figure 16, which is concerned with the fact that in initially plain specimens, new cracks continue to be nucleated with increasing time. Figure 17 shows some results from tests on C-Mn steel specimens exposed to a carbonate-bicarbonate solution that indicate the marked effect of test time upon the number of cracks detected. Obviously, if a given applied strain rate is distributed over the cracks present in the gauge length, then as the number of cracks increases, the crack-tip strain rate will decrease. An expression is available[55] for the crack-tip strain rate as a function of the number of cracks in slow strain rate specimens and is:

$$\dot{\epsilon}_{ct} = \frac{75}{N} \times \dot{\epsilon}_{app} + \frac{CV}{5} \ln \frac{1000}{N} \qquad (6)$$

where N = the number of cracks along the gauge length and $\dot{\epsilon}_{app}$ = applied strain rate. [The constants in Equation (6) will depend on the material involved and test specimen size.]

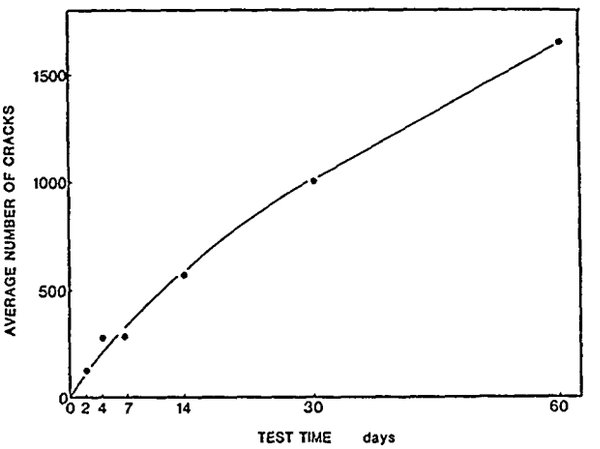


FIGURE 17—Average number of cracks along a 12.5-cm gauge length for specimens of a ferritic steel subjected to cyclic loading while exposed to 1 N Na_2CO_3 + 1 N $NaHCO_3$ solution at 75°C and −650 mV_{SCE} for various times.[70]

If some appropriate values for the applied strain rate, crack velocity, and number of cracks are put into Equation (6), the results can be expressed graphically, as shown in Figure 18. Because the first term in Equation (6) dominates at high applied strain rates and the second term at low applied strain rates, there is little effect of crack velocity at high applied strain rates; i.e., the crack growth contributes little to the crack-tip strain rate. However, at low applied strain rates, the stress corrosion crack growth maintains the crack-tip strain rate at values that are appreciably higher than would be obtained if the crack growth had been ignored. This probably explains why it is not always possible to find a lower limiting strain rate below which SCC does not occur.

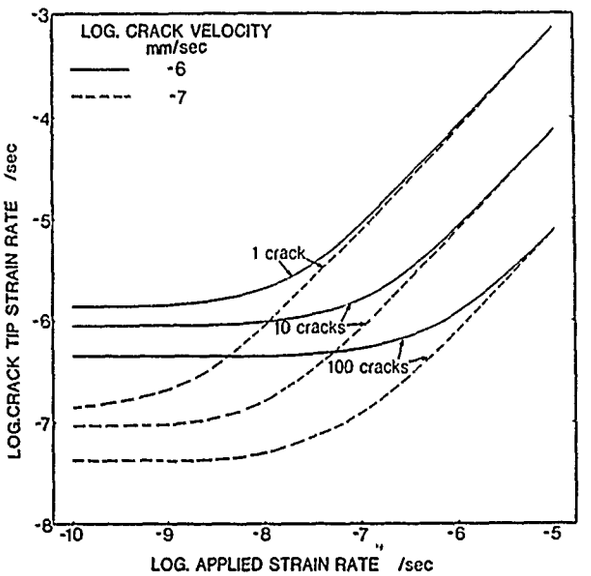


FIGURE 18—Effects of crack velocity and number of cracks on the crack-tip strain rate calculated from Equation (6).[68]

Equations (5) and (6) may be used to calculate the crack velocity as a function of applied strain rate for comparison with experimental data.[68] Figure 19 shows the results for tests involving a C-Mn steel exposed to a carbonate-bicarbonate solution and

indicates reasonable agreement between the observed and calculated values, except that the latter show the Faraday upper bound given by Equation (4) and this was not observed experimentally. This arises from a change in the number of cracks with applied strain rate and is considered in the source of Figure 19.

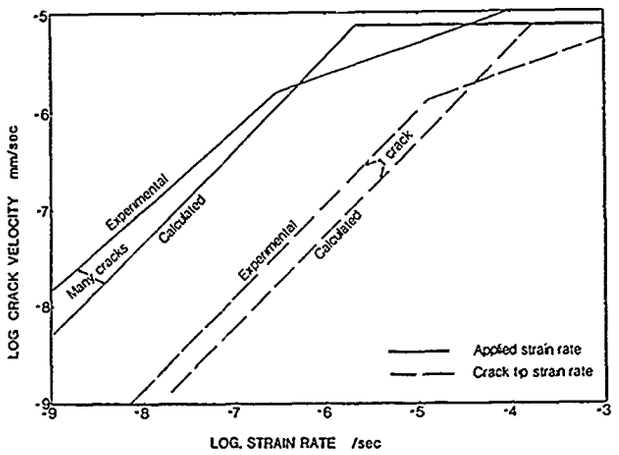


FIGURE 19—Comparison of calculated and experimental crack velocities as a function of strain rate for a ferritic steel exposed to 1 N Na_2CO_3 + 1 N $NaHCO_3$ at −650 mV_{SCE} and 75°C.[68]

Other workers[71-75] have applied Equation (5), or some modified version thereof, to SCC in other systems than that to which Figure 19 refers. Usually, some empiricism needs to be introduced to obtain reasonable agreement between observed and calculated behaviors, either because of difficulties in estimating the crack-tip strain rate or because of the crack enclave electrochemistry presenting problems. The same approach has been applied to the TGSCC of α-brass by $NaNO_2$ solutions, but without the agreement obtained for the cracking of C-Mn steels in carbonate-bicarbonate solution.[65] At relatively high strain rates, the observed and calculated crack velocities approximate one another for tests at 20°C, but at strain rates below $10^{-5}\cdot s^{-1}$, the calculated crack velocities reduce with decreasing strain rate much more markedly than do the observed values. At higher temperatures, the disagreement between the observed crack velocities and those calculated from Equation (5) is even more marked for this system. The reasons for this discrepancy are considered[65] in terms of the data used in performing the calculations, where, instead of the crack-tip strain rate, the engineering strain rate was used, simply because the numbers of cracks nucleated in the slow strain rate specimens were not determined. Data from other systems suggest that the number of cracks increases with decreasing strain rate, probably because the total test time increases, and if that is so for the brass/$NaNO_2$ system, the discrepancy between calculated and observed crack velocities will be decreased. Cole, et al.,[76] have criticized the method for determining the anodic current and charge densities used in manipulating Equation (5) for the brass/$NaNO_2$ system, claiming that the rapid straining of a filmed specimen to observe its current response is inappropriate because the surface film undergoes a gross mechanical failure when strained. It is surprising that those who have used the rapid straining method in studying this system[65,77] have not noticed this gross mechanical failure in the form of detachment of films during straining or upon subsequent examination of strained specimens. Cole, et al., prefer the method of obtaining current response by producing a scratch over a filmed surface, but the data from that approach leave something to be desired. Figure 20 shows the maximum current densities observed from various applied potentials by different workers using the straining and scratching electrode techniques on copper and α-brass exposed to $NaNO_2$ solutions. The two data sets from the straining electrode measurements on α-brass agree reasonably, but those from the scratching electrode measurements are markedly different at the higher potentials. With pure copper, the scratching electrode measurements are in agreement with the straining electrode measurements in the vicinity of + 100 mV, but the current densities remain at similar values for the scratching electrode measurements as the potential is reduced, whereas, the straining electrode measurements show a marked decrease in current densities with decreasing potential. The consequence is that the straining electrode measurements predict the lower limit of the potential range for cracking, whereas the scratching electrode measurements do not.

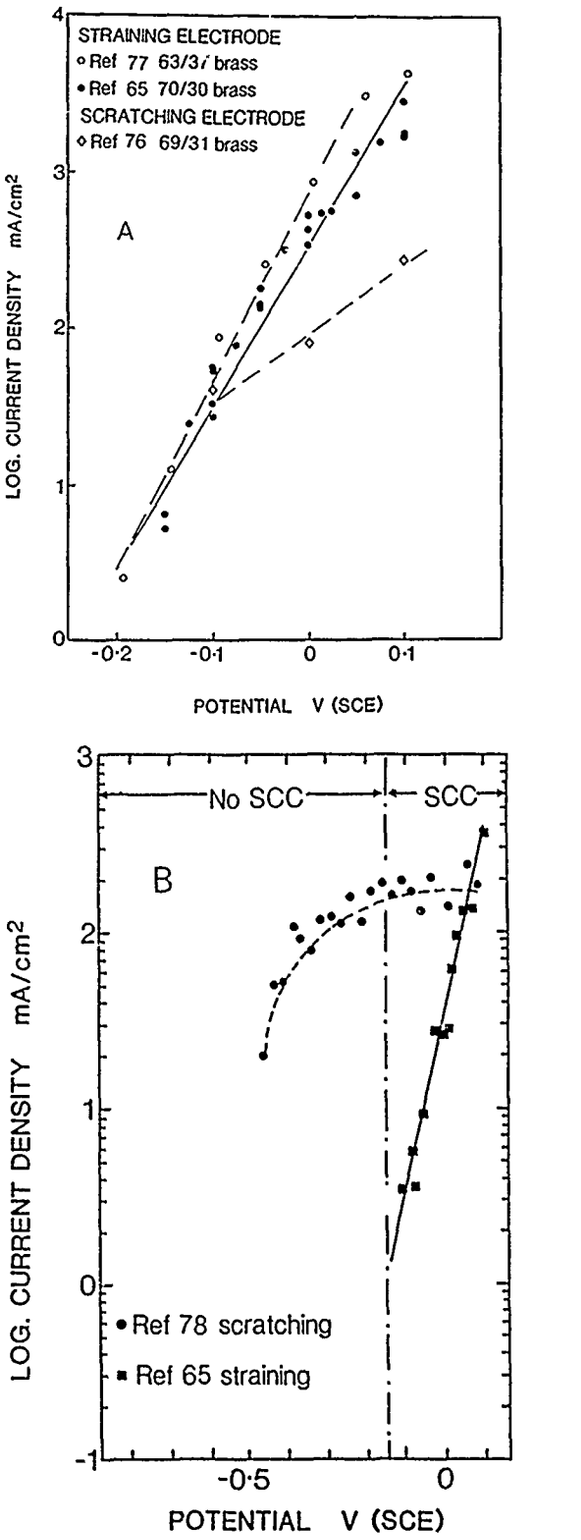


FIGURE 20—Comparison of maximum current densities at various controlled potentials from straining and scratching electrode experiments in $NaNO_2$ solution on (a) brasses and (b) pure copper.

Cole, et al ,[76] also criticize the low passivation rates involved in the measurements of Alvarez, et al.,[77] following the cessation of rapid straining, claiming that such low rates are indicative of the exposed surface area being much larger than that calculated from the amount of strain applied However, the repassivation rates for strained and nonstrained electrodes of α-brass in $NaNO_2$ solutions are not significantly different,[65] which does not appear to support the suggestion of gross mechanical failure of the surface film on straining, unless film detachment also occurs with unstrained specimens Although Cole, et al , conclude that "there is a surprisingly large area of new surface produced during the rapid straining tests," that is inferred rather than proven, and on the evidence currently available, it would be equally feasible to conclude that the effective area involved in scratching tests is appreciably less than is assumed from the measurements of the scratch size. Nevertheless, while the different methods of measuring the current responses of electrodes have been shown to give reasonably consistent results for some systems, this does not appear to be so for copper base materials and there is need for further investigation in this area.

The reason for the interest in such electrode kinetics in copper alloy systems comes from the mechanistic implications of such. Thus, the straining electrode measurements of Alvarez, et al.,[77] are claimed to predict crack velocities on the basis of a dissolution model that are in reasonable agreement with observed crack velocities. On the other hand, Cole, et al.,[76] claim that straining electrode measurements are not reliable and so they prefer scratching tests that do not predict crack velocities that are in good agreement with observed values. An alternative to the simple dissolution model is that involving film-induced cleavage.[11,21,22] A simple approach[65] to quantifying the crack velocity for a growth mechanism dominated by rapid mechanical jumps interspersed between periods of dissolution and film growth is as follows. The unit step in crack growth is the formation of a film, thickness (t), followed by a rapid jump over a distance (j) before arrest and repetition of these processes. The time interval between these repetitions may be taken as that required to reach the critical strain for crack initiation, ϵ_c, the time intervals being strain-rate dependent and equal to $\epsilon_c/\dot{\epsilon}$. The crack velocity may then be defined as:

$$CV = \frac{j + t}{\epsilon_c/\dot{\epsilon}} \qquad (7)$$

for the effect of strain rate upon crack velocity for α-brass in $NaNO_2$.[65] Film thicknesses at 20°C are 430 nm at 0.1 V, 300 nm at 0 V, and 180 nm at −0.1 V_{SCE}, and taking the distance between arrest markings, the jump distance, as 2 μm, the crack velocities calculated from Equation (7) as a function of engineering strain rate are in agreement with observed values at strain rates of about 10^{-4} s^{-1} for each of the potentials indicated above. However, the calculated velocities are about an order of magnitude too high at the strain rate of 10^{-3} s^{-1} and about an order of magnitude too low at 10^{-6} s^{-1}, and so this simple model is no better, nor worse, than the dissolution model in predicting crack velocities. However, Equation (7) would be more appropriately manipulated if crack-tip strain rates were used, and it is also possible that the strain to initiate a crack growth event and the jump distance are both functions of strain rate, all of which await the acquisition of appropriate data.

Cole, et al.,[76] take a somewhat different approach to that involved in Equation (7),because the film-induced cleavage model emphasizes a critical film thickness rather than strain increment. This requires Equation (4) to be modified to:

$$CV = \frac{Q_\tau}{\tau} \frac{M}{zFd} \qquad (8)$$

where Q_τ anodic charge density passed during the first τ seconds after scratching, and τ the interval between cleavage events calculated from the spacing between arrest markings divided by the crack velocity, reflecting the variation in the time to reach the critical film thickness at different potentials. Figure 21 shows a plot taken from the paper by Cole, et al., to which have been added additional data for the strain rates of 1.8×10^{-6} and 4.5×10^{-7} s^{-1}, which were not shown in the original version. Their argument that the difference between the predicted crack velocities and those obtained experimentally "epitomizes the concept of film-induced cleavage" because "nearly all the advance of the crack occurs by cleavage" clearly becomes less convincing as the applied strain rate is reduced. Indeed, the experimental results shown in Figure 21 indicate the need for a strain rate term in any expression that attempts to model crack velocity in this system. Moreover, the crack velocities predicted from Equation (8) and shown in Figure 21 on the basis of scratching electrode measurements are not markedly different from those calculated from measurements on a static electrode by rapidly switching potentials from a nonfilming value to that for which the current response is required.[65] This underlines the thought that the strain rate sensitivity of either SCC or the current response of α-brass in $NaNO_2$ solutions requires further study and that the distinction between the dissolution and film-induced cleavage mechanisms for this system on the basis of crack growth kinetics still leaves much to be desired.

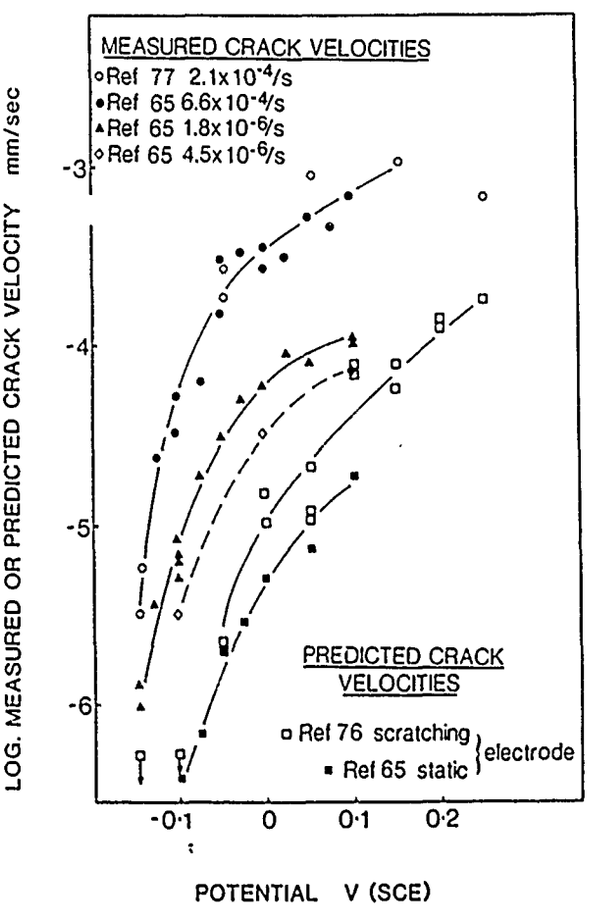


FIGURE 21—Measured and predicted crack velocities from various sources for brasses exposed to $NaNO_2$ solution.

Although previously a protagonist of dissolution models, Galvele[79] appears to have abandoned that position recently in favor of a mechanism based upon surface mobility. This change has been engendered by the view that available mechanisms are unable to predict new cases of environment-sensitive fracture (a view that is not consistent with some of the data given earlier) and by the observation, following others, that SCC, hydrogen embrittlement, and liquid metal embrittlement exhibit great similarities and, therefore, a single all-embracing mechanism must explain all of these phenomena. The model leads to an expression for crack growth rates in these various modes of failure on the basis of the surface diffusion of

atoms, as depicted in Figure 22, the equation for the crack velocity being:

$$CV = \frac{D_s}{L}\left[\exp\left(\frac{\sigma a^3 + \sigma E_b}{kT}\right) - 1\right] \quad (9)$$

where D_s = coefficient of surface self-diffusion of the metal, L = diffusion path length (10^{-8} m), a = atomic diameter, σ = maximum stress at the tip of the crack, E_b = hydrogen-vacancy binding energy, α = relative degree of saturation with hydrogen of a vacancy at the tip of a crack, k = Boltzmann's constant, and T = absolute temperature. There are problems in estimating D_s for contaminated metal surfaces, as will almost invariably obtain with SCC in aqueous environments, but Galvele concludes that a D_s value of 10^{-20} m^2 s^{-1} is a safe limit, below which surface diffusion and hence cracking are unlikely. Such a D_s value will be related to temperature, and the implication is that compounds having melting points below 1200°C, corresponding to the value of D_s quoted above at room temperature, will promote stress corrosion; whereas, compounds with higher melting points are protective. This appears to raise a difficulty in relation to, say, the cracking of iron-base alloys since, while predicting that nitrates would promote cracking because the melting point of iron nitrate is very low, it would predict that Fe_3O_4 is a protective compound, since its melting point is 1597°C. It has already been mentioned that in many instances of SCC in steels, the potential range for cracking is associated with Fe_3O_4 formation. Galvele surmounts this problem by invoking arguments relating to the breakdown of the film, chemically or electrochemically, so that active → passive transitions and potential dependence, for example, are expected to be involved in SCC. In that sense, the surface-mobility model is not essentially different from some considered earlier, with the essential difference being that the experimental determination of relevant electrochemical data is replaced to some extent by the properties of the salts involved.

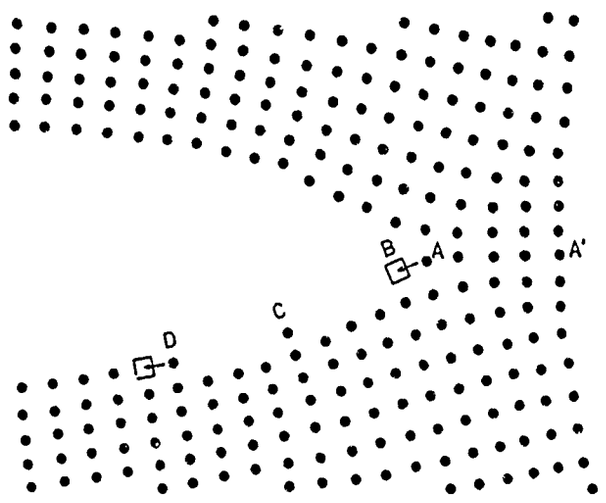


FIGURE 22 – Schematic illustration of the surface-mobility cracking mechanism. Stresses at the crack tip will favor the movement of an atom at A to position B, introducing a vacancy at the tip of the crack and advancing the crack one atomic distance. The rate-determining step will be the rate at which excess atoms are transported by surface diffusion from the tip of the crack to new lattice sites, B-C-D (after Galvele).[79]

Crack coalescence. There is a particular respect in which the various crack growth kinetics models referred to above are all deficient, and this is in relation to them ignoring crack coalescence. Measurement of the profiles of cracks suggests that crack coalescence occurs both at the microscopic and macroscopic levels and the observation of growing cracks at surfaces shows more direct evidence of cracks merging. Figure 23 shows the profiles of some small cracks in a C-Mn steel exposed to a carbonate-bicarbonate solution, while Figure 24 shows the fracture surfaces of a high-pressure gas transmission pipeline involving relatively large stress corrosion cracks and, in both instances, the shapes suggest that crack coalescence occurred. A common form of crack coalescence observed at external surfaces involves two slightly misaligned cracks initially propagating beyond one another and then their closest tips moving towards the opposite crack and joining the latter. The consequence is that a small island of metal is initially left within the crack but later may become detached, Figure 25 shows a typical example. Similar behavior has been reported by Kitagawa, et al.,[80] in relation to corrosion fatigue crack growth in a high-strength steel exposed to a NaCl solution. They consider the interactions in terms of stress intensity factors and show that because of decreasing K_I and increasing K_{II} values when two appropriately spaced cracks pass one another, the tips curve and approach one another to achieve coalescence, as in Figure 25.

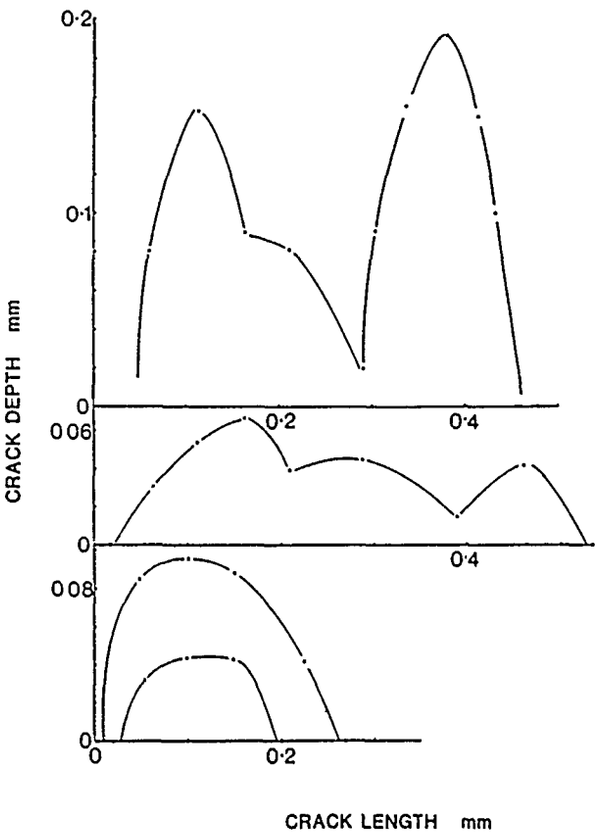


FIGURE 23—Typical small stress corrosion crack profiles from specimens of a ferritic steel subjected to cyclic loading while exposed to 1 N Na_2CO_3 + 1 N $NaHCO_3$ solution at 75°C and −650 mV_{SCE} for one week.[82]

If cracks are to coalesce in this manner, the lateral distance between the cracks would be expected to be important, since if the separation is too large for given sized cracks, the stress fields associated with the two cracks will not interact. Figure 26 shows a plot of the conditions under which cracks in a ferritic steel exposed to carbonate-bicarbonate solution did or did not coalesce[81] and makes the points that, at lateral separations greater than about 0 75 of half the crack lengths, merging is not likely and that coalescence is more likely after the nearest tips have passed one another (negative values of x/a) than before that situation has arisen. Obviously, the greater the lengths of the merging cracks, the higher the chances of coalescence for a given lateral spacing. An implication of such merging is that the length.depth ratio should increase beyond that for a single crack and that this occurs is suggested by the results shown in Figure 27, where the longest cracks have a length.depth ratio of about 15 and the shortest about 5. (It is possible that some of the



FIGURE 24—Matching surfaces of stress corrosion cracks in a high-pressure gas pipeline. (The outside surfaces of the pipe have been placed together.)[66]

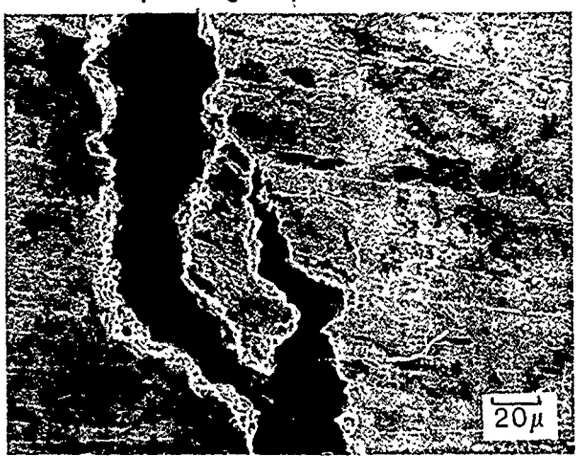


FIGURE 25—Scanning electron micrograph showing crack coalescence and the formation of a metallic island in a ferritic steel exposed to 1 N Na_2CO_3 + 1 N $NaHCO_3$ at 75°C and −650 mV_{SCE}.

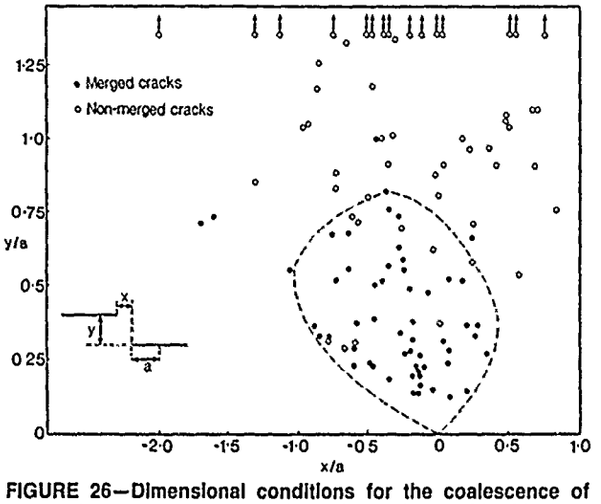


FIGURE 26—Dimensional conditions for the coalescence of adjacent stress corrosion cracks at the surfaces of ferritic steel specimens exposed to a CO_3-HCO_3 solution.[81]

The merging of cracks appears relevant to points made earlier about the time dependence of crack velocities (Figure 16) and of the numbers of cracks (Figure 17), all of which have considerable significance to service situations and the increasing interest in life prediction of structures containing growing cracks. It is likely that cracks nucleated at initially defect-free surfaces will grow at diminishing rates with the passage of time (Figure 16), with probably many cracks ceasing to propagate, but others reaching some low but essentially constant velocity when the crack-tip strain rate reaches a lower bound (Figure 18). However, new cracks continue to be nucleated (Figure 17) and the chances of such coalescing with

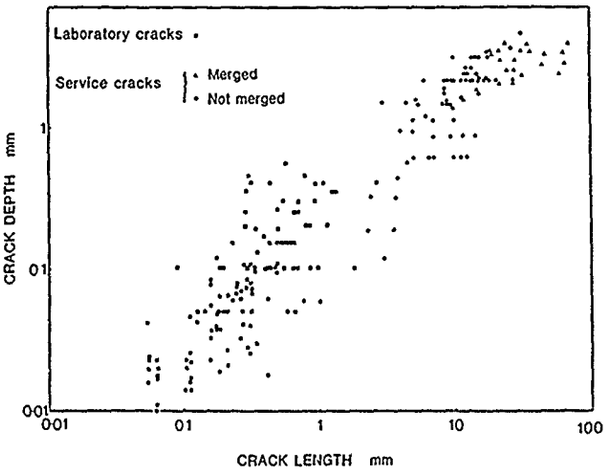


FIGURE 27—Maximum lengths and depths of stress corrosion cracks in ferritic steels that failed in service or in laboratory tests involving exposure to CO_3-HCO_3 solution.

previously existing small cracks (Figure 23) will increase until the critical crack size corresponding to K_{ISCC} is reached. The crack velocity will then increase to the upper bound for the exposure conditions involved, with further coalescence of relatively large cracks (Figure 24) until the critical crack size corresponding to K_{ISCC} is reached, as indicated schematically in Figure 28. It is possible to quantify the behavior shown in Figure 28 in a simple fashion and to compare the predictions with observed behavior.[82] Comparison with service behavior indicates the importance of crack coalescence, in the absence of which lifetimes would be markedly greater than sometimes experienced and a leak rather than a rupture would more often occur. Such indications of the very significant contributions of crack coalescence to service behavior indicates the need for its consideration in laboratory studies and especially to those where kinetic considerations are used for differentiating between mechanistic alternatives. Moreover, even in the context of the engineering implications of SCC, it suggests that less obsession with the events after K_{ISCC} is exceeded and more consideration of the circumstances whereby K_{ISCC} is reached in initially defect-free structures is justifiable.

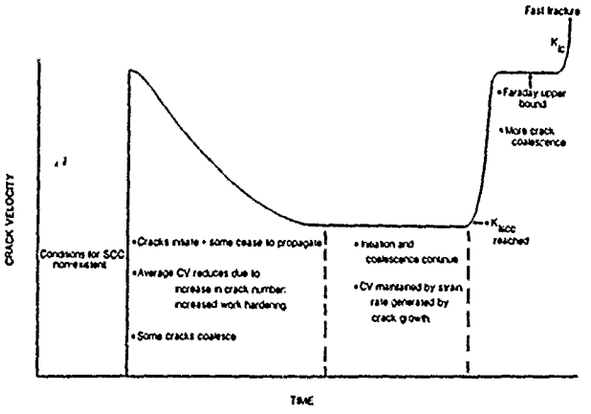


FIGURE 28—Schematic illustration of the effect of time of exposure upon stress corrosion crack velocity.

Conclusion

While statements will continue to be made to the effect that *the* mechanism of SCC is still not known or understood—the definite article implying some all embracing mechanism—considerable strides have been made over the last two or three decades towards a better understanding of this phenomenon. Certainly, predictability of potent metal-environment combinations is vastly improved, even if based upon experimental methods, but with the latter underpinned by a better understanding of the mechanistically oriented parameters. The search for some all-embracing mechanism to explain all instances of environment-sensitive fracture will continue to attract some investigators, despite the evidence to the contrary. But the concept of a spectrum of mechanisms,[83] despite its current limitations in defining the ingredients with precision or where particular systems fall in the spectrum, continues to have attractions, if only as a reminder that changes in the environmental conditions for the exposure of a given metal or change in the structure or composition of an alloy for constant exposure conditions may result in a change in the mechanism of cracking. Some of the areas in which more reliable and definitive experimental data are required have already been indicated but, in very general terms, it may be that a subject that was dominated by physico-metallurgical considerations in its early years is in need of a return to that area in the light of the markedly improved understanding in more recent years of the environmental and mechanics overtones to this mode of failure.

References

1. J.H. Andrew, Trans. Faraday Soc. 9(1913): p. 316.
2. C.E. Stromeyer, J. Iron Steel Inst. 79(1909): p. 404.
3. E.H. Dix Jr., Trans. Inst. Metals Div. AIME 137(1940): p 11
4. S.W. Parr, F.G. Straub, Univ. Illinois Bull. (1928): p. 177.
5. J.T. Milton, Trans. Inst. Nav. Arch. 47(1905): p. 359.
6. A.A. Griffith, Phil. Trans. Roy. Soc. A221(1920), p. 163.
7. E.B. Wolff, J. Iron Steel Inst. 96(1917): p. 137.
8. D.J. McAdam, Proc. ASTM (Philadelphia, PA, 1931), p. 259.
9. J.E. Fletcher, Discuss. Faraday Soc. 17(1921): p. 158.
10. H.K. Birnbaum, this proceedings.
11. K. Sieradzki, this proceedings.
12. N.J. Petch, P. Stables, Nature 169(1952): p. 842.
13. H.H. Uhlig, Fundamental Aspects of Stress Corrosion Cracking (Houston, TX: National Association of Corrosion Engineers, 1969), p. 86.
14. R.N. Parkins, Stress Corrosion Cracking and Hydrogen Embrittlement of Iron Base Alloys (Houston, TX: NACE, 1977), p. 601.
15. E. Orowan, Reports on Progress in Physics 12(1948-49), p. 185.
16. J.C. Scully, D.T. Powell, Corros. Sci. 10(1973): p. 719.
17. G. Sanderson, J.C. Scully, Trans. AIME 239(1967): p. 1883.
18. E.N. Pugh, Atomistics of Fracture, ed. R.M. Latanision, J R Pickens (Plenum Press, 1983), p. 997.
19. H.J. Logan, J. Research NBS 48(1952): p. 99.
20. C. Edeleanu, A.J. Forty, Phil. Mag. 5(1960): p. 1029.
21. K. Sieradzki, R.C. Newman, loc. cit. A 51(1985): p. 95.
22. K. Sieradzki, R.C. Newman, J. Phys. and Chem. of Solids, 48(1987): p. 1101.
23. E.N. Pugh, Corrosion 41(1985): p. 517.
24. A.S. Ahluwalia, R.N. Parkins, to be published.
25. J. Yu, N.J.H. Holroyd, R.N. Parkins, "Environment Sensitive Fracture: Evaluation and Comparison of Test Methods," ASTM STP 821, ed. S.W. Dean, E.N. Pugh, G.M. Ugianski (1984), p. 288.
26. T.P. Hoar, J.G. Hines, J. Iron Steel Inst. 182(1956): p. 124.
27. T.P. Hoar, J.M. West, Proc. Roy. Soc. A 268A(1962): p. 304.
28. G.M. Scammans, P.R. Swann, Stress Corrosion Cracking and Hydrogen Embrittlement of Iron Base Alloys, p. 166.
29. B.C. Syrett, R.N. Parkins, Corros. Sci. 10(1970): p. 197.
30. M.F. Kaufman, J.L. Fink, Acta Metall. 36(1988): p. 2213.
31. E.D. Hondros, M.P. Seah, Int. Met. Rev. 22(1977): p. 262.
32. A. Joshie, D.F. Stein, Corrosion 28(1972): p. 321.
33. C. Lea, E.D. Hondros, Proc. Roy. Soc. 377A(1981): p. 477.
34. C. Lea, Corrosion 40, (1984): p. 337.
35. H.J. Krautschick, J.H. Grabke, W. Diekmann, Corros. Sci. 28(1988): p. 251.
36. R.N. Parkins, J. Iron Steel Inst. 172(1952): p. 149.
37. H.H. Uhlig, J. Sava, Trans. ASM 56(1963): p. 361.
38. E. Belhimer, R.N. Parkins, to be published.
39. R.B. Mears, R.H. Brown, E.H. Dix Jr., ASTM-AIME Symposium on Stress-Corrosion Cracking of Metals (1945), p. 323.
40. R.N. Parkins, P.W. Slattery, B.S. Poulson, Corrosion 37 (1981): p. 650.
41. J. Flis, Corros. Sci. 25(1985): p. 317.
42. C.J. Cron, J.H. Payer, R.W. Staehle, Corrosion 27, 1(1971): p. 1.
43. R.N. Parkins, The Theory of Stress Corrosion Cracking in Alloys, ed. J.C. Scully (Brussels, Belgium: NATO, 1971), p. 167.
44. J. Yu, R.N. Parkins, Y. Xu, G. Thompson, G.C. Wood, Corros. Sci. 27(1987): p. 141.
45. R.N. Parkins, Met. Rev. 9(1964): p. 201.
46. P.R. Swann, Corrosion 19(1963): p. 102t.
47. H.W. Pickering, P.R. Swann, loc. cit. 19(1963): p. 373t.
48. P.R. Swann, The Theory of Stress Corrosion Cracking in Alloys, p. 113.
49. J.M. Silcock, P.R. Swann, Environment-Sensitive Fracture of 1966 Engineering Materials, ed. Z.A. Foroulis (Warrendale, PA: TMS-AIME, 1979), p. 133.
50. N.A. Nielsen, Second International Congress on Metallic Corrosion.
51. W.D. Robertson, E.G. Grenier, W.H. Davenport, V.F. Mole, Physical Metallurgy of Stress-Corrosion Fracture, ed. T.N. Rhodin (Interscience, 1959), p. 273.
52. R.N. Parkins, Corros. Sci. 20(1980): p. 147.
53. R.N. Parkins, "The Use of Synthetic Environments for Corrosion Testing," ASTM STP 970, ed. P.E. Francis, T.S. Lee, 1988, p. 132.
54. R.N. Parkins, N.J.H. Holroyd, R.R. Fessler, Corrosion 34 (1978): p. 253, p. 173.
55. J. Congleton, T. Shoji, R.N. Parkins, Corros. Sci. 25(1985): p. 633.
56. C.M. Rangel, R.N. Parkins, Proceedings of the 6th European Symposium on Corrosion Inhibitors (Ferra, Italy: Ann. Univ. 1985), p. 655.
57. B.F. Brown, The Theory of Stress Corrosion Cracking in Alloys, p. 186.
58. Embrittlement by the Localized Crack Environment, ed. R.P. Gangloff (New York, NY: AIME, 1984).
59. Corrosion Chemistry within Pits, Crevices and Cracks, ed. A. Turnbull (London, England: Her Majesty's Stationery Office, 1987).
60. R.N. Parkins, I.H. Craig, J. Congleton, Corros. Sci. 24(1984) p 709.
61. R.N. Parkins, Y. Liu, J. Congleton, loc. cit. 28(1988): p. 259.
62. I.H. Craig, R.N. Parkins, Brit. Corr. J. 19(1984): p. 3.
63. N.J.H. Holroyd, R.N. Parkins, Corros. Sci. 20(1980): p. 707.
64. K. Sieradzki, J.S. Kim, A.T. Cole, R.C. Newman, J. Electrochem. Soc. 134(1987): p. 1635.
65. J. Yu, R.N. Parkins, Corros. Sci. 27(1987): p. 159.
66. J.D. Fritz, B.W. Parks, H.W. Pickering, Scripta Metall. 22(1988): p. 1063.
67. P. Lacombe, R.N. Parkins, Stress Corrosion Cracking and Hydrogen Embrittlement of Iron Base Alloys, p. 521.
68. R.N. Parkins, Corrosion 43(1987): p. 130.
69. M. Henthorne, R.N. Parkins, Corros. Sci. 6(1966): p. 357.
70. J.A. Beavers, W.E. Berry, R.N. Parkins, Materials Performance 42, 6(1986): p. 9.
71. V.S. Garud, T.L. Gerber, ASME Conference on Advances in Life Prediction Methods (New York, NY: ASME, 1983).
72. T.L. Gerber, Y.S. Garud, S.R. Sharma, Thermal and Environmental Effects in Fatigue: Research Design Interface, PVP,

Vol. 71 (New York, NY: ASME, 1983), p. 155.
73. T.L. Gerber, Y.S. Garud, S.R. Sharma "IGSCC Damage Index. Application of IGSCC Damage Model to BWR Piping and Components," NP-2807-LD, Research Project T118-12, EPRI, Palo Alto, California, January 1983.
74. S.J. Hudak Jr., D.L. Davidson, R.A. Page, Embrittlement by the Localized Crack Environment, ed. R.P. Gangloff (New York, NY: AIME, 1983), p. 173.
75. F.P. Ford, CORROSION/86, paper no. 327 (Houston, TX. NACE, 1986).
76. A.T. Cole, R.C. Newman, K. Sieradzki, Corros. Sci. 28(1988). p. 109.
77. M.G. Alvarez, C. Monfridi, M. Giordano, J.R. Galvele, loc. cit. 24(1984): p..769.
78. R.C. Newman (Ph.D. diss., University of Cambridge, Cambridge, England, 1980).
79. J.R. Galvele, Corros. Sci. 27(1987): p. 1.
80. H. Kitagawa, T. Fujita, K. Miyazawa, "Corrosion Fatigue Technology," ASTM STP 642, 1978, p. 98.
81. P.M. Singh, R.N. Parkins, to be published.
82. R.N. Parkins, Proceedings of the Workshop on Mechanics and Physics of Crack Growth. Application to Life Prediction, Mater. Sci. Eng., in press.
83. R.N. Parkins, Brit. Corr. J. 7(1972). p. 15.

Discussion

E.N. Pugh (National Institute of Standards and Technology, USA): You have described both intergranular and transgranular failures and transitions between them. Do you favor the view that the mechanisms are different, or do you believe the path changes with no change in mechanism?

R.N. Parkins: Where the conditions of exposure remain the same, i.e , the crack-tip environment, potential, and strain rate do not change significantly but there is a change in crack path, I have difficulty in imagining that the mechanism of growth can change in any significant way. However, when the same material is exposed to different environmental or stressing conditions and there are morphological differences, the mechanism can be different for intergranular and transgranular cracking.

F.P. Ford (General Electric R&D Center, USA): With regard to the change in cracking morphology during the same test, surely the crack will follow the path by which it propagates the fastest. Thus the changes in morphology are related to changes in rate-determining step for the various systems available at the crack tip. For example, changes in mass transport, crack-tip plasticity, etc., will change with crack depth There is no need to invoke a change of mechanism.

R.N. Parkins: Obviously the crack path that is observed will correspond to the mechanism that has the most favorable kinetics, as is apparent from studies of the effects of cyclic loading on the cracking of carbon manganese steel in a nitrate solution where transitions fron intergranular to transgranular and vice versa occur, depending upon the relative velocities of the different modes [Greenwell and Parkins in Fatigue of Engineering Materials and Structures, vol. 5 (1982), p. 115]. However, that does not mean that a change in crack path will never be associated with a change in mechanism. For example, if a system displays an inherent sensitivity to grain boundary attack in the absence of applied stress, and the penetration rate is significantly enhanced in the presence of an appropriate stress to produce intergranular cracking, that sensitivity to intergranular attack is likely to be dependent upon solution composition and potential. If, after some intergranular growth, the crack tip environment and/or potential change to conditions that no longer favor intergranular cracking, then growth may still occur, following a transgranular path by a different mechanism.

H-J. Engell (Max Planck Institut fur Eisenforschung, Federal Republic of Germany): When considering the influence of alloying elements on the SCC susceptibility of iron and steel, I think we should distinguish among the following. (1) the direct influence of dissolved or segregated elements; (2) the elements influencing structure, e.g., carbon, (3) elements not dissolving but reacting with dissolved elements, e.g., calcium.

R.N. Parkins: I agree, and to your list I would add other factors that may be influenced by alloying, as indicated in the text of the paper. The important point is that the changes in alloy composition can influence structure electrochemistry and response to the application of stress in a variety of ways, and to ignore one or more of these influences in preference to another may lead to invalid conclusions.

J.R. Galvele (Comision Nacional de Energia Atomica, Argentina): I believe that the transition from transgranular to intergranular cracking is not a reason for rejecting the surface-mobility mechanism. In the case of brass in nitrites, we found that the change in the crack morphology was a result of a change in the environment composition. In the presence of pure sodium nitrite only transgranular cracks were found, while intergranular cracks were observed when the solutions were contaminated with ammonia [Rebak, Carranza, and Galvele, Corros. Sci. 28(1988): p. 1089]. On the other hand, with stainless steels in magnesium chloride, both types of crack are observed simultaneously [Manfredi, Meier, and Galvele, Corros. Sci. 27(1987): p. 887]. We believe that, when the low melting point compound is distributed on the whole surface, only intergranular cracks are formed (see Duffo and Galvele, this proceedings). However, when passivity breakdown is involved, as, for example, for brass in nitrite and stainless steel in magnesium chloride, a low melting point compound is formed on the slip steps, where the passive film is fractured, and transgranular cracking starts.

R.N. Parkins: I am not aware that I have said or written that a transition in crack path is a reason for rejecting the surface-mobility mechanism. I reject it on the same grounds as I reject any mechanism that attempts to explain all instances of environment-sensitive fracture in some all-embracing hypothesis. It is not usually accepted that the mechanisms of fracture, in the absence of environmental influences, by cleavage, fatigue, creep, or ductile failure are the same, nor is it usually accepted that the reactions that result in different forms of environment-induced degradation of materials are the same. If those statements are accepted, then I, for one, have difficulty in imagining that when materials are simultaneously exposed to appropriate stresses and environments, they suddenly begin to behave in ways very different from those experienced when stresses or environments are applied separately. The single-mechanism concept, whichever one is invoked, invariably has to ignore so much reliable phenomenological information that, so far, they have lacked the rigor to which they need to be subjected if they are to be acceptable.

J.R. Galvele: While we supported for several years the idea of anodic dissolution, we found that such a mechanism could not explain "specificity" in SCC. By "specificity," we mean not the susceptibility to SCC, but the different crack propagation rates found in various environments, as happens, for example, when we compare brass in nitrites to brass in pyrophosphates. These differences are easily explained by the surface-mobility mechanism.

R.N. Parkins. I have no difficulty in accepting the concept of the surface-mobility mechanism in explaining specific instances of environment-sensitive fracture, as in the solid-metal embrittlement of certain materials, where it has often been invoked. My objection is when it is invoked to explain everything in relation to environment-sensitive fracture. You may be correct in stating that the differences in crack velocities for brass in nitrites and pyrophosphates are easily explained by the surface-mobility mechanism, just as I am sure I could make the same statement if someone else were to claim that such differences are easily explained by some alternative suggestion. Just because dissolution may not explain the different crack velocities in brass exposed to nitrites or pyrophosphates is no reason for assuming that dissolution cannot explain any instances of environment-sensitive cracking.

R.C. Newman (University of Manchester Institute of Science and Technology, UK): I wonder if one can address the intergranular–transgranular transition problem in terms of alloy type. Would you agree with the view that the solid-solution type of alloys (brass, austenitic stainless steels) show the most facile transition with little or no change in rate, whereas in low-alloy ferritic steels, for example, the transition either never occurs (especially in statically loaded material) or involves a large change in rate? Maybe this tells us something, especially about transgranular cracking, and maybe about the role of dealloying.

R.N. Parkins: An interesting thought, but I am not sure that the premises on which it is based are valid, i.e., that single-phase alloys show little change in crack velocity with change in crack morphology, whereas ferritic steels show large changes in crack growth rate with change in crack path. For example, slow-strain-rate tests on α-brass in a formate solution can show an order of magnitude change in crack velocity between intergranular and transgranular cracking, the latter being slower [Parkins and Holroyd, Corrosion 34(1982): p. 245]. On the other hand, similar tests on a carbon-manganese steel exposed to an arsenic-containing potassium carbonate solution show virtually no change in crack velocity when a transition from intergranular to transgranular cracking occurs as a result of a small change in applied potential [Parkins, Alexandriou, and Majumdar, Materials Performance 25, 10(1986): p. 20].

H. Kaesche (Friedrich Alexander University Erlangen-Nurnburg, Federal Republic of Germany): Concerning the change from trans- to intergranular crack propagation, we have (Kessler and Kaesche, Werkst. u. Korros. 35(1984): p. 171] studied the case of type 304 (UNS S30400) stainless steel in HCl-$MgCl_2$ solution. Cracks start from micropits on repassivated slip steps filled with brittle chromium-rich oxides proceeding transgranularly into the material as long as the passage of dislocations across relatively soft grain boundaries is easily possible. Deformation of the specimen is, however, accompanied by hydrogen uptake from local corrosion at the crack tip, being transported by dislocations and eventually stopped at grain boundaries. With deformation increasing during the progress of cracking, dislocations will pile up at hydrogen-embrittled grain boundaries. Crack growth then turns to being intergranular, but apparently only at a relatively late stage of cracking.

R.N. Parkins: This is an interesting comment and underlines the suggestion, made in the text of the paper, that study of the localized deformation characteristics in the context of environment-sensitive cracking may well pay significant dividends.

R.L. Jones (Pacific Northwest Laboratory, USA): With regard to your figure showing crack velocity vs current density, how do you account for very high crack-tip current densities, such as those exceeding 1 A/cm²? Where do the cations go, and what is the rate-limiting step? How do we account for crack velocities exceeding the v–i curve shown?

R.N. Parkins: The current densities in excess of 1 A/cm² in Figure 15 of the paper relate to the cracking of C-Mn steel in nitrate solutions and were reported (by T.P. Hoar) at the conference to which Reference 67 refers. In that particular system, but involving a different nitrate solution from that used by Hoar and his coworkers, average intergranular penetration rates in the absence of stress of about 2×10^{-5} mm/s have been observed [Henthorn and Parkins, Brit Corros. J. 2(1967). p. 186], and that requires an average current density of about 0.1 A/cm². At strain rates that maintain the crack tip in an essentially bare condition, crack velocity increases by about an order of magnitude, and the current density measurements quoted by Hoar also show an order of magnitude increase. It is most likely that, in that particular system, there is appreciable acidification of the environment at the crack tip, and so I see no particular difficulty with the high current densities required. It should be remembered that the current requirements are very small at the crack tip, being of the order of 10^{-5} A for a typical stress corrosion crack in a slow-strain-rate test specimen some 10^{-3} mm wide at the tip, and propagating on a 1-mm front. The rate-limiting step, in relation to the crack velocity, is probably as indicated in Figure 19, being the rate of dissolution at strain rates high enough to keep the crack tip bare, and being the rate of film rupture at strain rates that permit crack-tip filming.

It is interesting in relation to Figure 15 that the two systems that show crack velocities consistently and appreciably above the v–i line are for type 304 stainless steel in chloride and α-brass in ammonia, both of which are strong candidates for a film-induced cleavage mechanism of crack growth. Obviously, where crack growth rates are in excess of any maximum current-density measurement, it is difficult to conclude other than that some purely mechanical component of crack growth is involved in making at least a partial contribution to growth.

S.M. Bruemmer (Pacific Northwest Laboratory, USA): I have a comment and a general question. The two empirical equations to estimate elemental effects on cracking propensity that you compared basically address two different conditions. Seah and Hondros's equation can only be valid for steels of a constant microstructure, and it indicates potential effects on grain-boundary chemistry, while the other deals primarily with alloying element effects on bulk and grain-boundary microstructures. The fact that these two equations do not agree with one another is not surprising.

My general question relates to our current understanding of dissolution-controlled intergranular SCC. We commonly refer to grain-boundary structure and chemistry controlling susceptibility to intergranular SCC, but most practical examples link only chemistry to cracking. Do you feel that grain-boundary structure has a primary or secondary effect on intergranular SCC?

R.N. Parkins: Your comment is fair, but the comparison was made to show that the claim of Lea and Hondros—that accepting Figure 3 of the text as an empirical indication that can be used predictively—is not valid.

Insofar as grain-boundary structure, as opposed to grain-boundary chemistry, may influence grain-boundary deformation (as indeed may grain-boundary chemistry), then I think it may have a significant role to play in intergranular cracking.

W.W. Gerberich (University of Minnesota, USA): A comment and a question on your observation that intergranular attack occurs without stress. If either chemical reaction products or chemical concentration gradients result, very large self-stresses may be induced. Have the magnitudes of these been measured?

R.N. Parkins: Reaction products formed within cracks as a source of self-stresses have been argued as occupying an important role, for example, by Nielson [in Physical Metallurgy of Stress Corrosion Fracture, ed. Rhodin (New York, NY: Interscience, 1959), p. 121] in relation to the cracking of austenitic stainless steel, but I am not aware of any measurements of such stresses. The issue is complicated by virtue of the fact that, in many cases, crack growth will be accompanied by crack opening and, just as with cyclic loading where crack-closure effects associated with corrosion products are much more prevalent with negative R values, the wedging open of stress corrosion cracks is only possible if the corrosion products grow faster in the appropriate direction than the crack-opening displacement rate.

R.W. Staehle (University of Minnesota, USA): The state of affairs at the crack tips might be clarified by considering more carefully the real chemistry inside the crack, i.e., the saturated solution with metal cations; the formation of compounds from grain-boundary species; the rush of ions into a saturated solution with these previous species.

R.N. Parkins: I agree A small amount of work along these lines has been performed for a few systems, usually by varying the pH of the bulk environment to reflect changes in the crack enclave, but much more needs to be done.

M.M. Hall Jr. (Westinghouse Corporation, USA): An understanding of the factors that determine mode of cracking (intergranular vs transgranular) is of engineering importance in that laboratory specimens may not always produce the mode of cracking experienced in the field. We find that slow-strain-rate tests reproduce the transgranular cracking of an austenitic stainless steel found in our application, but that compact-tension specimens do not. Is it possible that stress state is important, and do you know of examples in which this has been demonstrated?

R.N. Parkins: Clearly, laboratory tests must reproduce, as closely as possible, the mode of failure produced in a service situation that they purport to simulate. If they do not, they are of little value in that context. There are a number of possible explanations of the result that is quoted, one obvious one being that cracking in that system is strain rate dependent and that the compact-tension specimens did not achieve the minimum strain rate for cracking. Such may occur when specimens are loaded and not brought into contact with the test environment before the crack-tip strain rate has exhausted to below the minimum rate for cracking (see Parkins, in "Stress Corrosion Cracking—The Slow Strain Rate Technique," ASTM STP 665, ed. Ugianski and Payer, 1979, p. 5). Alternatively, it is conceivable that the environmental conditions within the enclave of the compact-tension specimens were not conducive to cracking. Those are the factors that I would tend to consider in explaining the differences between the results from the two different tests, rather than differences in stress state, because once cracking has propagated for an appropriate distance in a slow-strain-rate specimen, the stress state is not likely to be markedly different from that in a compact-tension specimen.

Mechanisms of Hydrogen-Related Fracture of Metals

*H.K. Birnbaum**

Introduction

The number of studies of hydrogen-related fracture in recent years is quite impressive both in the variety of systems studied and in the amount of materials characterization that has been obtained.[1-3] Despite this effort, there is still incomplete understanding of the mechanisms by which the hydrogen-related failures occur, and hence each material becomes a new and novel problem. The advantage of obtaining an adequate understanding of the failure mechanisms is that general rules of behavior can then guide the selection and application of new materials in aggressive environments.

In focusing on the understanding of the basic mechanisms of environment-related fracture, it is important to distinguish between those experiments and effects that are dependent on the kinetics of fracture and those that are mechanistically related. Kinetic studies can be applied to develop an understanding of the factors that determine the failure rates but should not be used to classify materials with respect to the mechanisms of failure. Thus, materials previously classified as insensitive to hydrogen effects, e.g. Al,[4] stainless steels (SSs), etc. have recently been shown to be highly susceptible to "hydrogen embrittlement" when exposed to a sufficiently high fugacity of hydrogen or tested at sufficiently low strain rates and the proper temperature range.[5,6]

There has been no shortage of suggested mechanisms,[1,2,7] but few have stood the test of critical examination, particularly as new experimental and theoretical methods become available. At present, several viable mechanisms remain, each of which can be supported by some experimental and theoretical evidence. The preponderance of evidence indicates that there are several hydrogen-related failure mechanisms rather than a single, dominant mechanism, and that even within one material system, several of these may be operative. In cases in which this is true, the particular mechanism leading to failure is controlled by kinetics. An example of this will be discussed subsequently. In the present paper, three mechanisms will be discussed: (1) embrittlement resulting from hydrogen-related phase changes, (2) hydrogen-enhanced plasticity-related fracture, and (3) the decohesion mechanism.

Hydrogen-Related Phase-Change Mechanisms

A number of metallic systems have demonstrated hydrogen embrittlement resulting from stress-induced formation of hydrides or other relatively brittle phases and the subsequent brittle fracture of these phases.[8-13] Several types of phases may take part in this failure mechanism, e.g. hydrides, martensitic phases,[14-17] etc. The basic requirements are that these phases be stabilized by the presence of hydrogen and the crack-tip stress field,[10,16,18] and that the phase that forms be brittle.[19,20] The typical system that exhibits failure by this mechanism forms stable hydrides in the absence of stress, and these hydrides, by virtue of their large $\Delta V_{formation}$, are thermodynamically more stable under the stress and hydrogen-fugacity conditions at the crack tip.[18] In some cases, hydrides can be shown to result from this stress stabilization even when they are not formed in the absence of the stress.[21,22] Among systems that exhibit hydride embrittlement are the group Vb metals (Nb, V, and Ta),[8-13, 23-25] Zr,[26,27] Ti,[28-30] and alloys based on these metals.

There are also a number of alloy systems that form "pseudo-hydrides" under high-fugacity conditions such as cathodic charging. These "pseudo-hydrides" are in fact high-concentration solid solutions formed in the presence of a miscibility gap.[31,32] These systems often exhibit embrittlement in the presence of this high-concentration solid solution (or by the stress-induced formation of this high-concentration solid solution), even though this phase is not a true hydride; i.e., it lacks the ordering of the hydrogen in the interstitial positions. Examples of these systems include Ni and its alloys;[32] Pd and its alloys;[33] the Group Vb metals Nb, Ta, and V at elevated temperatures;[31] and possibly SS, which forms a "pseudo-hydride" phase at high hydrogen fugacity.[16]

Hydrogen embrittlement by stress-induced formation of hydrides (or high-concentration solid solutions) is observed under conditions in which the hydrides can form at a rate sufficient to preclude other forms of failure. In these systems, ductile rupture can occur if the strain rate is increased or if the temperature is decreased,[34] since both cause ductile fracture prior to failure by hydride formation and cleavage. Similarly, if the temperature is increased, the stability of the hydride may be sufficiently decreased so that it can no longer be stress induced, and hence failure may again occur by ductile processes. The thermodynamics of the processes allow prediction of the conditions under which hydride-related embrittlement can be observed.[18] Establishment of this failure mechanism requires direct evidence for the formation of a hydride at the crack tip of a propagating crack.[11,12,23,30] In some cases, the stress-induced hydrides remain at the fracture surface and can be detected;[12,35] in others they disappear when the stress field of the crack tip is removed[23] and must be observed while under stress.

Another condition for hydride embrittlement is that the hydride be a brittle phase that undergoes "cleavage" fracture. In general, this is not a restrictive condition, since most of the hydrides exhibit very limited ductility because of restricted dislocation mobility resulting from the disordering of the hydrogen by dislocation motion.[19,20]

The embrittlement mechanism may be qualitatively described as follows. Under the applied stress, the chemical potential of the solute hydrogen and the hydride are reduced at tensile stress concentrations, such as crack tips. Diffusion of hydrogen to these elastic singularities and precipitation of hydrides at the crack tips then occur. The phase change is accompanied by a decrease in the critical stress intensity for crack propagation because the hydrides are generally brittle phases. The crack may propagate into the hydride, the formation of which is accompanied by a high, compressive local stress field resulting from the very large $\Delta V_{formation}$. This compressive stress field can give rise to "phase transformation toughening."[30] However, the greatly decreased K_{Ic} allows rapid crack propagation when the applied stress is only moderately increased, and the crack propagates by cleavage until the hydride-solid solution boundary is reached. At this point, the crack enters a

*Materials Research Laboratory, University of Illinois, Urbana, IL 61801.

ductile phase with a high K_{Ic} and the crack stops until more hydride is formed. The process repeats itself, resulting in discontinuous crack growth through the stress-induced hydride phase and with hydride formation along the flanks of the cracks.

The stress-induced hydride formation and cleavage mechanism can account for all of the observed characteristics of hydrogen embrittlement in those system in which it is observed.

(1) Hydride embrittlement occurs only over a limited temperature range with ductile behavior being observed at higher and lower temperatures.[9,11] The solvus temperature of the hydride-forming systems depends on the local stress at the crack tip and the local hydrogen concentration.[18] Therefore, above a critical temperature, the stress-induced increase in solvus is not sufficient to cause hydride formation before ductile failure intervenes. At the lower temperatures, previously precipitated hydrides crack under the applied stress. However, the hydrogen diffusivity and the rate of hydride formation are too low to allow re-precipitation of the hydrides, and ductile fracture intervenes.

(2) The extent of hydrogen embrittlement is decreased as the strain rate is increased.[34] Ductile fracture and stress-induced hydride formation and cleavage are competitive failure mechanisms. As the strain rate is increased, less time is available for the diffusion-controlled hydride formation at the crack tip, and ductile fracture intervenes. The temperature range over which hydrogen embrittlement is observed is increasingly restricted and the strain to failure increases as the strain rate decreases. A clear demonstration that the extent of hydride fracture is dependent on diffusivity-controlled hydride growth rate was provided by studies that used deuterium at low temperatures.[34] The deuterium diffusivity at low temperatures is very much lower than that of hydrogen (the diffusion is highly nonclassic[36]), and the metal-deuterium alloy behavior is correspondingly much more ductile during fracture.

(3) Pre-existing hydride precipitates do not necessarily cause severe embrittlement. In some systems, such as Zr-based alloys,[37] the presence of massive hydrides does not necessarily cause hydrogen embrittlement. While these pre-existing hydrides often crack under external stresses, the fracture proceeds between the hydrides in a ductile manner. The loss of ductility is then similar to that caused by other brittle phases. The solid solution in equilibrium with the pre-existing hydrides is inherently ductile and fails in a ductile manner unless new hydrides grow at the tips of the cracks formed by fracture of the hydrides. It is this stress-stabilized hydride that is responsible for the propagation of brittle cracks. A continued fracture by the hydride mechanism may not occur for several reasons. The hydrogen diffusivity may be too low to allow significant hydride growth prior to ductile failure. Alternatively, the temperature may be too high relative to the solvus of the solid solution to allow stress-stabilized hydride at the crack tip.

(4) Hydrides are not always observed at the fracture surfaces. Brittle fracture by a crack propagating through the hydride phase[11,12,30] will occur on the habit plane and/or the cleavage plane of the hydride. The presence of hydride at the sides of the cracks requires that the hydride be stable after removal of the crack-tip stress field. In some cases (e.g., Nb[11,12] and Ti,[30]), this is possible because of the large thermal hysteresis between precipitation and reversion, while in other cases (e.g., V[23]), reversion occurs behind the crack. In the case of Zr alloys, reversion of precipitated hydrides occurs in front of the crack to supply hydrogen to the crack tip,[38] and similar reversion of the stress-induced hydride behind the crack may therefore occur.

(5) Hydrogen embrittlement of metal hydrogen alloys is often seen at temperatures above the solvus temperatures. This observation is a natural consequence of the effects of stress on the solvus of the metal-hydrogen systems.[18] The shift in the hydride solvus can be appreciable since the solvus temperatures published in the phase diagrams correspond to precipitation of hydrides that are constrained by the surrounding solid solutions.[22] In some cases, embrittlement results at high temperatures because the stabilization of dihydrides[39] by the applied stress.

In a qualitative sense, all of the phenomena described above for hydride embrittlement can apply to the embrittlement caused by stress-induced formation of other phases.[40] These may be oxides, nitrides, etc., or may be phases stabilized by the enhanced hydrogen concentration at the stressed crack tips. In all cases, the important factors are the same. (1) the effects of stress on the stability of the precipitated phases (i.e., the requirement that the precipitated phase have a significant and positive $\Delta V_{formation}$), (2) the kinetics of phase transition, and (3) the mechanical properties of the precipitated phases. One significant difference between hydride embrittlement and that resulting from the formation of other phases is that the diffusivity of hydrogen is much greater than that of other solutes at any particular temperature.[36]

One important case of hydrogen-related second-phase embrittlement of some importance is the embrittlement of SSs. This matter is still quite controversial and the mechanism(s) unproven. In a number of cases, hydrogen embrittlement of metastable SSs [e.g., types 304 and 316 (UNS S30400 and S31600)] have been associated with hydrogen-enhanced transformation of the γ-fcc phase to the α'-bcc and ε-hcp martensites.[14-17,41-43] *In situ* transmission electron microscopy (TEM) studies have shown that these martensitic phases are formed in front of the crack tip and along the crack sides.[15,17] While the fracture surfaces of hydrogen-embrittled SSs (which show a quasicleavage aspect) are clearly different from the microvoid coalescence fracture seen in the absence of hydrogen, the actual structure of the surface is a controversial matter. There are several difficulties in making a definitive association of hydrogen embrittlement with the formation of these martensitic phases.

(1) The very presence of these phases along the hydrogen-embrittled fracture surfaces has been disputed.[44,45] In part, this may result from the fact that the martensitic phases occur only very close to the fracture surfaces (within 1 μm) and hence require detection techniques sensitive to surface phases.

(2) The martensitic phases are present near the fracture surfaces even in the absence of hydrogen because of deformation-induced martensites. The major difference is that the amount of transformation and the stress at which the transformation occurs is much less in the presence of hydrogen gas or hydrogen in solid solution.[17]

(3) While few studies have been conducted, it does appear that the M_s temperatures are not significantly affected by the presence of hydrogen in solid solution,[46] but the M_d temperature is markedly reduced by hydrogen.[16]

(4) While the presence of martensitic phases at the surface of hydrogen-embrittled metastable SSs has been established, it has not been shown whether or not these phases are a necessary condition for fracture or a consequence of the enhanced deformation caused by hydrogen.[17]

In addition to the hydrogen-enhanced martensitic phases, the metastable and stable SSs both exhibit formation of a "pseudo-hydride" phase[16,47] at high hydrogen concentrations. This γ'-phase has an expanded fcc structure and has been suggested to result from a miscibility gap in the Fe-Cr-Ni system.[16] The role of this γ'-phase in the fracture of the alloys is not known. While stable SSs generally do not exhibit hydrogen embrittlement, except possibly in very high hydrogen fugacities [embrittlement has been observed in type 310 SS (UNS S31000)[48]], these stable steels do form the γ'-phase during hydrogen charging, and it is possible that this high-hydrogen-concentration phase may be associated with the fracture.

Hydrogen-Enhanced Local Plasticity Mechanism

In many cases, the definition of hydrogen-related fracture as a "brittle fracture" is based on loss of macroscopic ductility and/or relatively low-resolution studies of the fracture surfaces. It was Beachem who first suggested,[49] on the basis of careful fractographic examination, that hydrogen embrittlement of steels was in fact associated with locally enhanced plasticity at the crack tip. This viewpoint received little attention for many years. In recent years, it has become evident that hydrogen "embrittlement" by means of

locally enhanced plasticity is a viable fracture mechanism, the term hydrogen-enhanced local plasticity (HELP) will be used as a descriptive phrase. While the concept of enhanced plasticity appears to be at variance with embrittlement, there is no contradiction when it is recalled that the distribution of hydrogen can be highly nonuniform under an applied stress Thus, locally the flow stress can be reduced, resulting in localized deformation that leads to highly localized failure by ductile processes, while the total macroscopic deformation remains small In fact, we are familiar with shear localization in many systems,[50-52] the HELP mechanism proposes shear localization resulting from hydrogen. From a macroscopic vantage point, this type of failure will appear "brittle." Strain-to-failure measurements made over a macroscopic gauge length will be greatly reduced despite the high degree of local plasticity. Examination of the fracture surfaces at low resolution will induce a conclusion of a "brittle" fracture surface because of the highly localized nature of the ductile failure.

In recent years, this point of view has been supported by the work of Lynch[3,53] and Birnbaum, et al.,[30,54-64] on a variety of systems. Using both fractographic evidence and *in situ* environmental cell TEM deformation and fracture studies, it has clearly been shown that the HELP mechanism is a viable failure mechanism for a large number of systems, both pure metals and alloys, based on Ni,[54,55,60] Fe,[57-59] In 718,[61,65] type 304,[17] A533-B (UNS K03005),[66] and 316 (UNS S31600)[17] SSs; Al,[64] 7075 (UNS A97075), and 7050 Al age-hardened alloys;[63] and α-Ti alloys.[30] The phenomenon is quite general, having been observed in pure metals, solid-solution-strengthened alloys, precipitation-hardened alloys, and in bcc, hcp, and fcc crystal structures. In addition to the direct studies of fracture cited above, there is a growing body of results that support the microscopic observation that the addition of hydrogen to a system can decrease the flow stress of that system[67-72] and lead to strain localization.[4,73] All of these points will be discussed below.

While there is agreement between Lynch and Birnbaum, et al., on the basic thesis that the presence of hydrogen increases the plasticity at the crack tip and leads to fracture, there are significant differences in that Lynch views the phenomenon as a surface effect, while Birnbaum, et al., consider the hydrogen effect to occur in the volume of the material as well as near the surface. Since the views of Lynch have recently been reviewed,[53] the following will primarily discuss the HELP mechanism proposed by Birnbaum, et al. The systems to which this mechanism appears to apply are principally those that do not form hydrides. The HELP mechanism is competitive with the stress-induced hydride mechanism, as shown by the studies of α-Ti[30] (and possibly the metastable SSs[17]) in which both failure mechanisms have been shown to apply in different regimes of crack velocities.

The HELP mechanism is operative for hydrogen in solid solution and for gaseous hydrogen environments. In both cases, the application of a stress results in a nonuniform distribution of hydrogen with a high concentration in front of an elastic singularity such as a crack or a precipitate. The high local stress field at the tip of a crack reduces the chemical potential of solute hydrogen,[74] and as a result of diffusion, the concentration is locally increased. The tip of the crack is also the most likely place for hydrogen entry from a gaseous atmosphere since it is the place where plastic deformation first occurs, and hence any surface barriers to entry are minimized. As will be discussed shortly, the resistance to dislocation motion, and thus the flow stress, is decreased by the presence of hydrogen. Thus, in the regions of high hydrogen concentration, the flow stress is decreased and slip occurs at stresses well below those required for plastic deformation in other parts of the specimen, i.e., slip localization occurs in the vicinity of the crack tip. This has been clearly shown for high purity Al[4] and Fe N alloys.[72] In addition to the local decrease in flow stress, hydrogen has been shown to result in serrated yielding (Portevin LeChatelier effect) in the temperature range in which hydrogen embrittlement is severe.[75] The region of serrated yielding is one of negative strain rate dependence ($d\sigma/d\dot{\varepsilon} < 0$), and shear localization is a consequence.[76]

Continued localization of shear is expected to lead to fracture by the various plastic-failure processes, although the exact mechanism by which shear localization causes fracture is not known.[73] In the *in situ* TEM experiments, void formation is observed along the intense slip bands,[58-60,63,66] and shallow microvoids have been observed along the fracture surfaces of macroscopic hydrogen-embrittled specimens.[53] The *in situ* TEM experiments show fracture occurs along slip planes in a saw-toothed morphology and 3-dimensional analogs, pyramidal features bounded by {111} slip planes, are observed on macroscopic fracture surfaces.[54,55] One consequence of the HELP mechanism is that the fracture surface is predicted to be that along which the shear localization occurs. In general, this is the slip plane, as has been observed,[53,54] but in cases where cross slip is prevalent or where special constraints are imposed by the stressing mode,[3,77,78] the fracture plane may differ from the slip plane.

The behavior of many systems observed during *in situ* environmental cell TEM experiments is consistent with the above description of the HELP mechanism. Deformation of the specimens in vacuum resulted in failure by plastic deformation in front of the crack tip with the region of deformation extending in front of the crack and being relatively broad. In general, the deformation occurred in several positions in the specimen, and ductile failure often occurred at several different points. Propagation of these ductile cracks generally was preceded by voids opening in front of the crack front as well as appreciable thinning of the material in front of the crack.

The effects of hydrogen on fracture in these TEM specimens were studied for static cracks under stress. On adding hydrogen gas to the environmental cell, dislocation sources began to operate and dislocations began to increase their velocities. Removal of the hydrogen gas resulted in a cessation of the dislocation motion, this cycle could be repeated many times. The effect of the hydrogen was to reduce the stress for dislocation motion.[56-66] Similar effects were seen for dislocations in parts of the specimen that were of uniform thickness and far from the cracks and that were in thick (several hundred nm thicknesses) and thin parts of the specimen. Enhanced dislocation velocities resulting from hydrogen were observed for screw, edge, and mixed dislocations and for dislocations that were in tangles, in slip bands, and far from other dislocations. Similar behavior was observed for dislocations in fcc, bcc, and hcp crystal structures and in alloys as well as in pure metals. In the case of a number of metals, the effects of hydrogen are enhanced by the addition of small amounts of solutes.[57,58] One of the remarkable features of this phenomenon is its generality, which suggests that the mechanism is not specific to a particular type of material or dislocation type The effects of hydrogen on fracture result from these effects on dislocation behavior. Fracture in hydrogen was similar to that in vacuum but with several very important differences. In the presence of hydrogen, the plastic deformation processes and the resulting fracture took place at greatly reduced stresses, and the plastic zones were more limited in extent. Thus, hydrogen caused enhanced plasticity and local plastic failure at lower applied stresses, i.e., "hydrogen embrittlement."

Decreases in the macroscopic flow stresses because of the addition of hydrogen into solid solution have been interpreted as resulting from enhanced dislocation motion. These effects have been observed for hydrogen introduced by cathodic charging of pure iron,[67-69] by plasma charging of iron,[71] and by gaseous charging of pure nickel.[70] Very significant decreases in the flow stresses were observed, particularly after cathodic charging of high-purity iron, and while these can result from dislocations introduced by hydrogen charging, the experiments were conducted carefully to avoid surface damage. Flow stress decreases in iron were interpreted based on decreases in the energy to nucleate kinks on dislocations, thus decreasing the Peierls-Nabarro lattice interactions.[67-69] However, observations of the phenomena in systems in which there are no strong dislocation lattice interactions suggest that this explanation is not correct. The generality of the phenomena suggests that an explanation must be based on interactions common to many systems, such interactions are the elastic interactions between dislocations and hydrogen solutes.

The reasons for the enhanced dislocation motion resulting from hydrogen are not yet established. One mechanism being studied is based on "elastic shielding" of dislocations and other elastic singularities by hydrogen atmospheres.[79] In this mechanism, the mobility of hydrogen allows it to diffuse to positions of lowest free energy and form high-concentration atmospheres around dislocations, solutes, and precipitates. The binding enthalpies for the hydrogen are typically of the order of 10 to 50 kJ/mole,[80] which allows the atmospheres to form and to move with the dislocations in the temperature ranges where embrittlement is observed. Thus, in contrast to other solute atmospheres, when the dislocations move, the hydrogen atmospheres can move with them. The significant interactions are therefore between dislocations and defects, which include the respective atmospheres. Furthermore, since the hydrogen remains mobile during the interaction, the concentrations and configurations of the atmospheres respond to the stress fields of all of the elastic defects participating in the interaction. Thus, for example, as two dislocations approach each other, their hydrogen atmospheres reconfigure themselves, and the hydrogen concentration at each point responds to the sum of the stress fields of both dislocations; a reconfiguration that reduces the energy of the entire system. Similarly, in calculating the force one dislocation exerts on a second, the contributions to this force must be summed over both dislocations and the hydrogen atmospheres.

Self-consistent elasticity calculations using finite element methods were performed to study the hydrogen atmosphere configurations, the interaction energies, and the forces between elastic singularities.[79] In general, the effects of hydrogen atmospheres at dislocations is to decrease the interactions of elastic defects at short range and to have no effect at large distances. This spatial dependence is a consequence of the result that the hydrogen atmosphere interactions vary as $1/r^2$, while the dislocation stress fields vary as $1/r$. The magnitude of this decrease of the interaction stress can be of the order of the dislocation stresses at distances of about 10 Burger's vectors for reasonable hydrogen concentrations.

The magnitude of the hydrogen effect increases as the concentration of hydrogen in the atmosphere increases, i.e., as the lattice hydrogen concentration increases and as the temperature decreases. As a consequence, the "elastic-shielding" effects are small at high temperatures in which the concentration of hydrogen in the atmospheres is small. These effects are also small at low temperatures in which the atmospheres are not mobile. In the intermediate temperature range and at low dislocation velocities, the effects are largest because the atmosphere rearrangements can occur in phase with the dislocation motion.

These shielding effects correspond well to the macroscopic softening that has been observed (e.g., the softening is greatest at temperatures around 200°K in Fe[67-69]) is largest at low strain rates and increases as the number of short-range obstacles such as solutes are increased.[58,59] In nickel and Ni-C alloys, the temperature range of hydrogen-enhanced dislocation motion is also that in which serrated yielding is seen, indicating that hydrogen atmospheres can move along with the dislocations. Direct elastic-shielding effects have been observed using the N anelastic relaxation in iron.[81]

The general dependence of hydrogen embrittlement on temperature and strain rates is similar to that observed for hydrogen softening of the resistance for dislocation motion. The *in situ* TEM studies directly show that the hydrogen-enhanced dislocation motion leads directly to fracture by slip localization, opening up of voids, and thinning of the material along slip bands. This slip localization also leads to fracture in macroscopic specimens, although the detailed mechanism is not established. A detailed connection between the hydrogen effects on dislocation behavior, slip localization, and hydrogen "embrittlement" is not well established and remains a major issue.

No distinction was made between transgranular and intergranular fracture in the above discussion. Many of the nonhydride forming systems exhibit primarily "intergranular" fracture, as observed by relatively low-magnification optical and scanning electron microscope (SEM) fractography. On observation with higher-resolution instruments, in many cases these "intergranular" fractures exhibit features that suggest the fracture paths are not confined to the grain boundaries. One of the important issues is whether or not the intergranular and transgranular fractures are in fact caused by different mechanisms or if they are variants of the same fracture mechanism. This cannot be answered with great certainty, because in many systems the intergranular fracture in hydrogen environments is intimately related to the segregation of other solute species to grain boundaries and interfaces. The synergistic effects of solute segregation complicate an already difficult situation. In the case of Ni and Fe, the interaction of H with segregants such as S and P has been studied,[82-84] and it has been shown that segregation of species such as S at the grain boundaries reduces the fugacity and amount of H required for intergranular fracture.

In Ni, the causes of intergranular fracture resulting from hydrogen have been extensively studied.[85-88] Transgranular fracture by the HELP mechanism is observed on slow-rate straining in a hydrogen atmosphere at temperatures in the vicinity of room temperature, while the same testing conditions lead to "intergranular" fracture when hydrogen is present as a solute.[55] The basis for this difference in behavior can be seen in experiments using secondary ion mass spectroscopy (SIMS) to determine the distribution of hydrogen in Ni[89] and in Nb-V alloys.[90] Very large segregation of solute H (D) was observed at external surfaces and at some grain boundaries. Furthermore, studies of "intergranular" fracture using *in situ* TEM straining techniques have shown that in the presence of hydrogen, the "intergranular" fracture was in fact fracture by the HELP mechanism that occurred in the vicinity of the grain boundaries and occasionally along the grain boundaries.[91] Furthermore, this hydrogen segregation occurred over appreciable regions (about 100 nm thick) adjacent to the surfaces and grain boundaries. Sulfur segregation at external surfaces had the effect of increasing the amount of hydrogen segregation in the vicinity of these surfaces.

These results are consistent with the view that in Ni, and perhaps in other systems, hydrogen-enhanced "intergranular" fracture is in fact transgranular fracture by the HELP mechanism that occurs in the vicinity of the grain boundaries. Localization of the enhanced dislocation mobility to regions near the grain boundaries and therefore localization of the fracture resulting from this enhanced dislocation mobility is a consequence of the hydrogen segregation in the vicinity of the boundaries. Fracture occurs near the grain boundaries because that is where the greatest extent of hydrogen softening occurs Under relatively low magnification, these appear as intergranular fracture, but with higher resolution examination, fractures on the fracture surfaces that are consistent with plastic failure adjacent to the grain boundaries are observed.

The importance of H segregation to grain boundaries was clearly shown in a study of the fracture of Ni-H alloys at 77°K.[85-88] Ni-H alloys in which segregation of the H to grain boundaries did not occur were completely ductile. As the extent of segregation increased, the amount of intergranular fracture increased until the specimens exhibited completely intergranular fracture at a critical grain-boundary hydrogen concentration. It was the achievement of this critical concentration that controlled the fracture at the grain boundaries rather than the overall concentration in the lattice. Achievement of this critical grain-boundary concentration was controlled by diffusion of H to the grain boundaries either before or during the tensile tests (if they were performed at temperatures at which H could diffuse) At any segregation temperature, the lattice H concentration determined whether or not this critical grain-boundary hydrogen concentration could be achieved by segregation. Synergistic effects of S and H segregation were observed similar to those observed by cathodic charging.[82,83] In the presence of S segregation, the amount of solute hydrogen required to achieve the critical grain-boundary concentration for fracture was greatly decreased.[87]

Hydrogen Effects on the Cohesive Energy

One of the oldest and most commonly referred to mechanisms of hydrogen embrittlement is the "decohesion" mechanism.[92-94] In

general outline, decohesion associates hydrogen embrittlement with a decrease in the atomic bond strength resulting from the local concentration of hydrogen. Thus, the fracture is cleavage, which occurs when the applied stress exceeds the "cohesive stress," a material parameter that is assumed to be decreased by the presence of hydrogen in solid solution. This cleavage fracture is generally accompanied by plastic deformation,[95] which greatly increases the total energy of fracture and hence the macroscopic K_{Ic}. In the systems in which fracture occurs transgranularly, failure is expected to be along the cleavage planes and to exhibit the fractography of cleavage, while intergranular fracture should occur directly along the grain-boundary surfaces. In intergranular fracture, the relevant parameters are the cohesive energy and cohesive force of the grain boundary, which are also postulated to be decreased by the presence of hydrogen as well as the segregation of many other solutes.

There are a number of "open issues" relating to the observational base on which the decohesion mechanism is founded. Intergranular fracture by decohesion resulting from hydrogen implies that the fractography should reveal the morphology of the grain interfaces, whereas most high-resolution fractography shows a great deal more structure on the hydrogen-embrittled intergranular fracture surfaces than is expected from brittle fracture along the grain boundaries. *In situ* TEM observations of the hydrogen-related intergranular fracture of a number of systems[91] show that the fracture occurs mostly along slip planes in the vicinity of the grain boundaries, often crossing the grain boundary to follow slip planes in the adjacent grains. In contrast to this behavior associated with hydrogen-assisted fracture, hydrogen-assisted failure in the Ni-S system with S segregated at the grain boundary does occur by crack propagation along the grain boundary, albeit accompanied by significant plasticity on both sides of the boundary.[87,96]

The fractography of transgranular fracture resulting from decohesion should be cleavage fracture, whereas most observations can be classified as "quasicleavage." This term, whose meaning is somewhat elusive, generally describes a fracture surface that shows evidence of significant local plasticity and fracture features that resemble those on cleavage fracture surfaces but that are considerably less crystallographic. The differences in true cleavage surfaces are often ascribed to plastic deformation, this explanation is somewhat specious, since plastic deformation is crystallographically conservative, at least on a local scale. Thus cleavage of a predeformed material should show similar crystallographic features to those seen in an undeformed specimen. This is not generally true of the fractures cited as evidence for the decohesion mechanism. The other observation cited as evidence for decohesion is that the fracture surface corresponds to what is believed to be the cleavage plane of the system rather than the slip plane. However, the actual macroscopic plane will reflect the nature of the macroscopic stress tensor and may reflect fracture on a combination of slip planes on a fine scale that sum to an overall fracture plane corresponding to the supposed cleavage plane. This can only be determined by careful high-resolution fractography, which generally has not been conducted.

The principal issue in determining whether or not the decohesion mechanism has any validity is whether or not hydrogen decreases the "cohesive energy" or the "cohesive stress." Evidence for a hydrogen-related decrease in the "cohesive energy" may be sought in the elastic constants, atomic force constants derived from phonon dispersion curves, surface-energy measurements, fracture-surface energies, and theory. Direct support for this postulated decrease does not exist except in the realm of theoretical calculations.[97] The elastic constants of Group Vb metals with hydrogen have been extensively determined,[98-100] in the case of Nb, up to compositions of the order of H/Nb = 0.8. The general result is that significant increases in C_{11} and the bulk modulus B and decreases in the shear modulus C are observed. For the same metal, the phonon frequencies and the corresponding atomic force constants are all increased by the addition of H to solid solution.[101] These increases in the elastic constants and phonon frequencies are all the more remarkable because they occur despite the very large volume increases that accompany H in solid solution; these volume increases normally cause decreases in the elastic and atomic force constants (as observed in the fcc metals). Both the elastic constants and the phonon frequencies correspond to "small-strain" parameters and describe the effect of hydrogen on the part of the lattice potential curve close to the equilibrium positions. Despite this limitation, the dependencies of these parameters on H concentration in bcc metals are not consistent with hydrogen-related decreases in the cohesive energy or the cohesive force. In fcc metals, the situation is somewhat different in that hydrogen decreases the elastic parameters,[101] principally as a result of the volume increase on adding H to solid solution.

Since the elastic and atomic force constants pertain to the initial part of the atomic force-displacement curves, an increase in these parameters does not necessarily imply an increase in the cohesive force, i.e., the maximum of the force-displacement curve. A direct measurement of this parameter is not yet possible. The area under the atomic force displacement curve is $2\gamma_f$ where γ_f is the fracture surface energy. This parameter has been measured in the brittle β $NbH_{0.8}$ hydride phase[19] and shown to be equal to the equilibrium surface energy of Nb. Thus, even at H/Nb = 0.8, there was no significant decrease in the surface energy because of hydrogen. A similar conclusion was drawn from measurements of the equilibrium surface free energy of Ni + 300 appm H.[102]

Recent theoretical discussions of this problem have suggested that H causes a significant decrease in the bonding of atoms, i.e., a decohesion during stressing. While these calculations, based on a cluster variational method[103] and on the embedded-atom method,[97] support the decohesion mechanism, they remain the only support for it in the absence of direct experimental measurements. What is required is a sounder basis for this fracture mechanism before it is accepted as a viable embrittlement mechanism.

Conclusion

Several theories of hydrogen-related fracture have been discussed in the context of critical experimental measurements. While the discussion of the voluminous literature was limited to those experiments designed to challenge and test the theoretical concepts, the evidence presented clearly shows support for two mechanisms of hydrogen embrittlement," "stress-induced hydride formation and cleavage," and "hydrogen-enhanced localized plasticity." A third mechanism, "hydrogen-induced decohesion," remains a *possible* failure mechanism, since no definitive support can be mustered nor can completely convincing counter evidence be adduced.

The existence of several "hydrogen-embrittlement" mechanisms is clearly established. In a sense, these are competitive with each other and with ductile (nonhydrogen-related) fracture. Several mechanisms may even operate in a single system. The observed fracture mechanism is controlled by the thermodynamics and kinetics of the various fracture processes.

All of the observed environmental fracture characteristics can be accounted for on the basis of the above three fracture mechanisms.

Acknowledgment

The above discussion summarizes the efforts of many of my students and research associates over the past years. I am extremely grateful for the privilege of working with them. I would like to particularly acknowledge my interactions with Professor Ian Robertson. Particular thanks are due to the staff of the Argonne National Laboratory Center for High Voltage Electron Microscopy and of the Illinois Center for the Microanalysis of Materials, at which much of the experimental work was carried out. I am particularly grateful for the patience and understanding of the staffs of the Department of Energy, Division of Materials Research, of the National Science Foundation, Division of Materials Research and of the Office of Naval Research, all of which supported various parts of the research summarized above.

References

1. H.K. Birnbaum, M. Grossbeck, S. Gahr, Hydrogen in Metals, ed. I.M. Bernstein, A. Thompson (Metals Park, OH: ASM International, 1973), p. 303.
2. H.K. Birnbaum, Environmentally Sensitive Fracture of Engineering Materials, ed. Z.A. Foroulis (Warrendale, PA: The Metallurgical Society of the American Institute of Mining, Metallurgical, and Petroleum Engineers, 1979), p. 326.
3. S.P. Lynch, Acta Metall. 36(1988): p. 2639.
4. F. Zeides, H.K. Birnbaum, to be published; F. Zeides (Ph.D. diss., University of Illinois, 1986).
5. R. Liu, N. Narita, C.J. Altstetter, H.K. Birnbaum, E.N. Pugh, Metall. Trans. 11A(1980): p. 1563.
6. C.L. Briant, Hydrogen Effects in Metals, ed. I.M. Bernstein, A.W. Thompson (Warrendale, PA: TMS-AIME, 1981), p. 527.
7. H.K. Birnbaum, Atomistics of Fracture, ed. R.M. Latanision, J.R. Pickens (New York, NY: Plenum Press, 1981), p. 733.
8. D.H. Sherman, C.V. Owen, T.E. Scott, Trans. AIME 242(1968): p. 1775.
9. C.V. Owen, T.E. Scott, Metall. Trans. 3(1972): p. 1715.
10. D.G. Westlake, Trans. ASM 62(1969): p. 1000.
11. S. Gahr, M.L. Grossbeck, H.K. Birnbaum, Acta Metall. 25(1977): p. 135.
12 M.L Grossbeck, H.K. Birnbaum, Acta Metall. 25(1977): p. 125.
13. D. Hardie, P. McIntyre, Metall. Trans. 4(1973): p. 1247.
14. R.B. Benson, R.K. Dann, L.W. Roberts, Trans. ASM 242(1968): p. 2199.
15. N. Narita, H.K. Birnbaum, Scripta Metall. 14(1980): p. 1355.
16. N. Narita, C. Altstetter, H.K. Birnbaum, Metall. Trans. A 13A(1982): p. 135.
17. P. Rozenak. I.M. Robertson, H.K. Birnbaum, Metall. Trans. A, in press 1989.
18. T.B. Flannagan, N.B. Mason, H.K. Birnbaum, Scripta Metall. 15(1981): p. 109.
19. S. Gahr, H.K. Birnbaum, Acta Metall. 28(1980): p. 1207.
20. H.K. Birnbaum, J. of Less Common Metals 103(1984): p. 31
21. B. Makenas, H.K. Birnbaum, Acta Metall. 28(1980): p. 979.
22. M.L. Grossbeck, M. Amano, H.K. Birnbaum, J. Less Common Metals 49(1976): p. 357.
23. S. Takano, T. Suzuki, Acta Metall. 22(1974): p. 265.
24. T.W. Wood, R.D. Daniels, Trans. AIME 233(1965): p. 898.
25. A.L. Eustice, O.N. Calson, Trans. ASM 53(1961): p. 501.
26. D O. Northrup, Environmentally Sensitive Fracture of Engineering Material, p. 451.
27. K Nuttall, Effects of Hydrogen on the Behavior of Materials, ed. A.W. Thompson, I.M. Bernstein (Warrendale, PA: TMS-AIME, 1975), p. 441.
28. N.E. Paton, J.C. Williams, Hydrogen in Metals, p. 409.
29 H G. Nelson, D.P. Williams, J.E. Stein, Metall. Trans. 3(1972): p. 469.
30 D Shih, I.M. Robertson, H.K. Birnbaum, Acta Metall. 36(1988): p. 111.
5 T. Schober, H. Wenzl, Hydrogen in Metals II, ed. G. Alefeld, J. Völkl (Berlin, Federal Republic of Germany: Springer-Verlag, 1978), p. 11.
32. B. Baranowski, Hydrogen in Metals II, p. 157.
33. E. Wicke, H. Brodowsky, Hydrogen in Metals II, p. 73.
34. S. Gahr, H.K. Birnbaum, Scripta Metall. 10(1976): p. 635.
35. M.L. Grossbeck, P.C. Williams, C.A. Evans Jr., H.K. Birnbaum, Physica Status Solidi (a) 34(1976): p. K97.
36. J. Volkl, G. Alefeld, Hydrogen in Metals I, ed. G. Alefeld, J. Volkl (Berlin, Federal Republic of Germany: Springer-Verlag, 1978), p. 321.
37. C.J. Beevers, D.V. Edmonds, J. Nucl. Mater. 33(1969): p. 107.
38. R. Dutton, K. Nuttall, M.P. Puls, L.A. Simpson, Metall. Trans. A 8A(1977): p. 1553.
39. S. Gahr, H.K. Birnbaum, Acta Metall. 26(1978): p. 1781.
40. H.K. Birnbaum, Scripta Metall. 10(1976): p. 747.
41. D. Eliezer, D. Chakrapani, C. Atstetter, E.N. Pugh, Metall. Trans. A 10A(1979): p. 975.
42. M.R. Louthan Jr., J.A. Donovan, D.E. Rawl Jr., Corrosion 29(1973): p. 108.
43. C.L. Briant, Metall. Trans. A 10A(1979): p. 181.
44. H. Hanninen, T. Hakarainen, Corrosion 36(1980): p. 47.
45. M.B. Whiteman, A.R. Troiano, Corrosion 21(1965): p. 53.
46. A. Thompson, O. Buck, Metall. Trans. A 7A(1976): p. 329.
47. P. Maulik, J. Burke, Scripta Metall. 9(1975): p. 17.
48. A.W. Thompson, Mater. Sci. Eng. 14(1974): p. 253.
49. C.D. Beachem, Metall. Trans. 3(1972): p. 437.
50. H.E. Deve, S.V. Haren, C. McCullough, R.J. Asaro, Acta Metall. 36(1988): p. 341.
51. R.J. Asaro, Adv. in Appl. Mechanics 23(1983): p. 1.
52. R.J. Asaro, A. Needleman, Scripta Metall. 18(1984): p. 429.
53. S.P. Lynch, J. Mater. Sci. 21(1986): p. 692.
54. T. Matsumoto, H.K. Birnbaum, Trans. Japan Inst. of Metals 21(1980): p. 493.
55. J. Eastrnan, T. Matsumoto, N. Narita, F. Heubaum, H.K. Birnbaum, Hydrogen in Metals, p. 397.
56. T. Matsumoto, J. Eastman, H.K. Birnbaum, Scripta Metall. 15(1981): p. 1033.
57. T. Tabata, H.K. Birnbaum, Scripta Metall. 17(1983): p. 947.
58 T Tabata, H K Birnbaum, Scripta Metall. 18(1984): p. 231.
59 T Tabata, H.K. Bimbaum, Japan Inst. of Metals 24(1985): p. 485.
60. I.M. Robertson, H.K. Birnbaum, Acta Metall. 3(1986): p. 353.
61. D Shih, H K Birnbaum, Modeling Environmental Effects on Crack Growth Processes, ed. R.H. Jones, W. Gerberich (Philadelphia, PA: ASTM, 1986), p. 355.
62. H.K. Birnbaum, I.M. Robertson, G. Bond, D. Shih, Proceedings of the 11th International Congress on Electron Microscopy (Tokyo, Japan: Japan Society of Electron Mic., 1986), p. 971.
63. Japan Soc. of Electron Mic., Tokyo, Japan, G. Bond, I.M. Robertson, H.K. Birnbaum, Acta Metall. 35(1987): p. 2289.
64. G. Bond, I.M. Robertson, H.K. Birnbaum, Acta Metall. 36(1988): p. 2193.
65. I.M. Robertson, H.K. Birnbaum, to be published.
66. I.M. Robertson, H. Hanninen, H.K. Birnbaum, to be published.
67. H. Matsui, H. Kimura, S. Moriya, Mater. Sci. Eng. 40(1979): p. 207.
68. S. Moriya, H. Matsui, H. Kimura, Mater. Sci. Eng. 40(1979): p. 217.
69 H. Matsui, H. Kimura, A. Kimura, Mater. Sci. Eng. 40(1979): p. 227.
70 J. Eastman, F. Heubaum, T. Matsumoto, H.K. Birnbaum, Acta Metall. 30(1982): p. 1579.
71. A. Kimura, H.K. Birnbaum, Scripta Metall. 21(1987): p. 53.
72. A. Kimura, H.K. Birnbaum, Acta Metall. 35(1987): p. 1077.
73 H E Deve, R.J. Aaro, N.R. Moody, Scripta Metall. 23(1989): p. 389.
74 J.C.M Li, R.A. Oriani, L.S. Darken, Zeits. Physik. Chemie. Neue Folge 49(1966): p. 271.
75 A. Kimura, H.K. Birnbaum, Acta Metall. (submitted).
76. P.G. McCormick, Acta Metall. 36(1988): p. 3061.
77. H. Vehoff, W. Rothe, Acta Metall. 31(1983): p. 1781.
78. H. Vehoff, C. Laird, D.J. Duquette, Acta Metall. 35(1987): p. 2877.
79 H K Birnbaum, P. Sofronis, R. McMeeking, to be published.
80. J.P. Hirth, Metall. Trans. A 11(1980): p. 861.
81. J.J. Au, H.K. Birnbaum, Scripta Metall. 12(1978): p. 457.
82. R.H. Jones, S.M. Breummer, M.T. Thomas, D.R. Baer, Metall. Trans. A 14A(1983): p. 1729.
83. S.M. Breummer, R.H. Jones, M.T. Thomas, D.R. Baer, Metall. Trans. A, 14A(1983): p. 223.
84. K.S. Shin, M. Meshii, Acta Metall. 31(1983): p. 1559.
85. D. Lassila, H.K. Birnbaum, Modeling of Environmental Effects on Crack Growth Processes, ed. R.H. Jones, W.W. Gerberich (Warrendale, PA: TMS-AIME, 1986), p. 259.
86. D. Lassila, H.K. Birnbaum, Acta Metall. 34(1986): p. 1237.

87. D. Lassila, H.K. Birnbaum, Acta Metall. 35(1987): p. 1815.
88. D. Lassila, H.K. Birnbaum, Acta Metall. 36(1988): p. 2821.
89. H. Fukushima, H.K. Birnbaum, Acta Metall. 3(1984): p. 851.
90. B. Ladna, C. Loxton, H.K. Birnbaum, Acta Metall. 34(1986): p. 988.
91. I.M. Robertson, T. Tabata, W. Wei, F. Heubaum, H.K. Birnbaum, Scripta Metall. 18(1984): p. 841.
92. E.A. Steigerwald, F.W. Schaller, A.R. Troiano, Trans. TMS-AIME 218(1960): p. 832.
93. R.A. Oriani, P.H. Josephic, Acta Metall. 22(1974): p. 1065.
94. R.A. Oriani, P.H. Josephic, Acta Metall. 25(1977): p. 979.
95. C.J. McMahon Jr., V. Vitek, Acta Metall. 27(1979): p. 507.
96. T.C. Lee, I.M. Robertson, H.K. Birnbaum, Acta Metall. 37(1989): p. 407.
97. S.M. Folles, M.I. Baskes, M.S. Daw, Phys. Rev. B 33(1986): p. 7983.
98. F.M. Mazzolai, H.K. Birnbaum, J. Phys F 15(1985): p. 507.
99. F.M. Mazzolai, H.K. Birnbaum, J. Phys. F. 15(1985): p. 525.
100 A. Mageri, B Bere, G. Alefeld, Phys. Stat. Sol. (a) 28(1975): p. 591.
101. T. Springer, Hydrogen in Metals I, p. 75.
102. E.A. Clark, R. Yeske, H.K. Birnbaum, Metall. Trans. A 11A(1980): p. 1903.
103. C.L. Briant, R.P. Messmer, Phil. Mag. 42(1980): p. 569.

Discussion

B. Cox (Atomic Energy of Canada Ltd., Canada): The stress-induced hydride precipitation mechanism for cracking of hexagonal metals is interesting because it is directly testable after the event by fractography. If this mechanism is operating, then the fracture surface must satisfy the crystallography of the hydride phase (tetragonal or cubic) and not the matrix (hexagonal). I have not seen any fractography for stress corrosion cracking (SCC) of α-Ti that is other than hexagonal—suggesting this hydride cracking mechanism is not operating in SCC Have you seen any such SCC fractures (i.e., with cubic or tetragonal symmetry)?

H.K. Birnbaum: Evidence for hydride on the fracture surface has been obtained in the Nb-H system where there is a large thermal hysteresis between the hydride formation and reversion. This thermal hysteresis depends on the volume change on forming the hydride and on the extent of plastic accommodation. It should be large in Ti and Zr alloys, and therefore hydride should remain at the fracture surface if care is taken to prevent loss of hydrogen after the fracture. Hydride at the fracture surface of macroscopic specimens has been reported by Paton, et al., and of course we have seen it in the transmission electron microscope for embrittlement of alpha-titanium The hydride layer may be rather thin because the hydride plates are thin I would look for its presence with electron or x-ray diffraction on the fracture surface. I am not sure that it would be expected to be seen with fractography The epitaxial relationship between the hydride and the alpha-solid solution is such that the fracture plane would have symmetry close to the hcp alpha-phase. Hence, it is not clear that examination of fractographic evidence would distinguish the hydride from the matrix.

D Hardie (University of Newcastle upon Tyne, UK): You showed an electron micrograph of a crack passing through stress-induced hydride precipitate in alpha-titanium. Re-solution of such precipitate after passage of a crack has been reported, and I wonder whether you have observed such a phenomenon. Whether or not such solution occurs is very relevant to the comment made by Brian Cox.

H.K. Birnbaum: In our case, the hydride is formed in a hydrogen atmosphere and is thermodynamically stable. Reversion of the hydride occurs in vacuum but rather slowly, because it depends on the loss of hydrogen through the surface.

D. Hardie: I would certainly support your contention that hydrogen produces localization of strain in materials such as aluminum alloys and steel, but I was surprised by your statement that an overall increase in hydrogen content (as opposed to a localized enrichment) would also give rise to a decrease in the macroscopic yield stress. We have certainly found that thermally charging stainless steel with about 50 wppm hydrogen results in a few percent increase in flow stress.

H.K. Birnbaum: Increases in flow stress of steels containing hydrogen have also been reported by C. Altstetter, in agreement with your result. Both decreases and increases in flow stress due to internal hydrogen have been reported, and we have observed both in a number of systems. Our view of the situation is that decreases in flow stress are observed at temperatures and strain rates (10^{-6} s^{-1}) where the hydrogen atmospheres exist and can move with the dislocations. Softening has been observed in iron, nickel, and aluminum by various groups, as well as our group. In addition to low strain rates (the range of strain rates depends on the hydrogen diffusivity) softening requires that the process of hydrogen introduction not introduce any stresses, dislocations, or second phases. (As an example, cathodic charging often causes high surface stresses, dislocation generation, etc.) In stainless steel, I would be concerned about the possibility of hydrogen-related phase transitions, which might harden the material.

D. Hardie: I would advocate caution in extrapolating observations from thin foils in the electron microscope (under plane-stress conditions) to the behavior of thicker sections. It is one thing to observe voids forming ahead of the crack in a thin foil in the presence of hydrogen, but quite another to have void coalescence in the plane-strain region of a fracture.

H.K. Birnbaum: I agree caution is necessary. We try to correlate our observations with careful fractography of macroscopic specimens and with mechanical property tests. As described in the paper, we observe features on the fracture surface that can be directly correlated with the electron microscope observations.

R.A. Oriani (University of Minnesota, USA): I believe that the effects of hydrogen on the phonon frequencies and the elastic constants of the host metal are irrelevant to a discussion of the validity of the decohesion model. This is because the decohesion model addresses how hydrogen affects F_m, the maximum cohesive force in the cohesive force–separation curve, but there is no necessary, or even probable, relation between F_m and the initial slope of the curve.

H.K. Birnbaum: If you believe in continuity in the lattice potential, then one can expect a relationship between changes in the maximum cohesive force and the initial slope as measured by phonon frequencies and elastic constants. I agree that the form of this relationship is not known. However, for most commonly used lattice potentials, a decrease in the initial slope of the cohesive force–separation curve requires a decrease in the maximum cohesive force. However, I also agree that we are badly in need of more measurements of the cohesive force–separation curve, even one measurement would be welcome.

R.A. Oriani: There may be another source of mechanical stress involved in the *in situ* electron microscope experiments that show that introduction of gaseous hydrogen enhances dislocation of activity. This source is that a hydrogen concentration gradient arising from the hydrogen injection can produce large stresses that can generate dislocations. Because the dislocations serve as sinks for the injected hydrogen, it is possible that concentration gradient, and therefore the stresses, are maintained beyond the initial time of hydrogen presentation.

H.K. Birnbaum: Concentration gradients certainly exist when hydrogen is added to the environmental cell. However, for the specimen thickness used and for the separation of dislocations, a steady-state hydrogen distribution is achieved in one second or less. The enhanced dislocation velocity continues for rather long times (depending on stress relaxation) compared to a second. Hence, I do not believe that the stress due to concentration gradients has any significant effect.

R.W. Staehle (University of Minnesota): To what extent can your ideas be generalized to other environmental species such as oxygen, chloride, fluorine, etc.?

H.K. Birnbaum: Many of the concepts developed for hydrogen-related fracture can be extended to other species such as oxygen, chlorine, fluorine. The major difference is that hydrogen has a much higher diffusivity. Stress-induced oxide formation and cracking should be observable, and I believe it has been observed in vanadium, as an example.

R.W. Staehle: Would you comment on Magnani's work [Advances in Corrosion Science, Vol. 6 (New York, NY: Plenum Press, 1976)] on uranium, which shows that cracks will propagate in precracked specimens without stress being applied?

H.K. Birnbaum: I am not familiar with that particular work. However, hydride precipitation results in high localized stresses as the hydride plates act as wedge-opening-load notches, and it is possible that as the hydrides form in uranium their stress fields will cause cracking in front of the hydride plates.

W.W. Gerberich (University of Minnesota, USA): You have admonished us to look for microplasticity in the SEM at 10,000X, much as Lynch has in the past, to see if hydrogen-induced cracking is really brittle. I would equally caution that, in those processes that we think are ductile, we should look for cleavage or some other brittle process. In {100} cleavage of Fe-Si single crystals, external hydrogen produces a ductile/ brittle switching when the crack is growing with many ductile ligaments and a small amount of cleavage to almost pure cleavage. This switches back and forth in dead-weight loaded sustained-load growth. I believe that both of these processes are controlled by the cleavage process as the extensive ductile ligaments fracture after microcleavage Do you have evidence in bulk samples where cracking on the cleavage plane is in fact *led* by microscopic ductile fracture?

H.K. Birnbaum: Yes, to the extent that you would accept *in situ* scanning electron microscope tensile observations as macroscopic experiments. In nickel (and in other observations on aluminum), we have seen hydrogen-localized deformation preceding the fracture *Your observations, the details with which I am not familiar, may* suggest that both localized plasticity and decohesion are viable mechanisms in your experimental conditions and that they are chosen according to the detailed crack-tip conditions I certainly do not argue for the existence of a single failure mechanism and certainly agree that an open mind is required when viewing fractographic observations.

R.P. Gangloff (University of Virginia, USA): Acknowledging the experimental difficulties, have you obtained *in situ* transmission electron microscopy evidence for interactions between initially uniformly dissolved hydrogen and crack-tip dislocations? I ask this question in order to pose the scenario in which external, high-fugacity hydrogen "reduces" surface films and adsorbates (oxides, vacuum system carbon) that would otherwise impede dislocation motion Would you comment on this concern?

Secondly, do hydrogen-dislocation interactions result in unique crack-wake, near-surface dislocation morphologies?

H.K. Birnbaum: Transmission electron microscopy studies of systems with internal (solute) hydrogen are possible only in systems having oxide films that prevent loss of hydrogen to the vacuum (e.g., Nb, V, Ta). The hydride fracture mechanism has been studied in these systems in the transmission electron microscope. Since we cannot measure the stresses in transmission electron microscope specimens, the hydrogen-dislocation interactions must be studied by "differential" experiments in which H_2 is added or removed and the response of dislocations at constant stress is observed.

We do not believe that these experiments are controlled by H_2 effects on surface films as qualitatively similar behavior is observed in a wide range of systems, viz., Al and Ti with stable oxides, Ni and Fe with less stable alloys, etc. The hydrogen effects are also observed for dislocations that are completely contained in the volume of the foil, e.g., Frank-Read sources.

Our work suggests that a very high dislocation density should exist below the fracture surface due to hydrogen-enhanced plasticity. It is difficult to distinguish this from the dislocation distribution that accompanies a crack in the absence of hydrogen.

T. Murata (Nippon Steel Corporation, Japan): My question is associated with cracking of bright annealed (annealed in $N_2 + 3H_2$) 304 (UNS S30400) stainless steels. We have noticed the effect of either gas (air, hydrogen, hydrogen sulfide) or nonaqueous solutions (oils of various nature) on the propagation of cracks related to phase-transformation-related hydrogen cracking. I wonder if we have to consider the role of surface tension or energy in explaining the cracking mechanism, since environmental effects cannot be explained only by the role of hydrogen entry.

H.K. Birnbaum: These results are interesting and require more consideration than I can give them at the moment. I do not believe that changes of surface energy are important for several arguments. For example, the observation that other elements that cause larger decreases in surface energies do not cause embrittlement.

E. Ryan (Rocketdyne, USA): I would like some elaboration on the subject of hydrogen-enhanced local plasticity. While the stress field around a dislocation can be reduced by an atmosphere, the more effective an atmosphere in stress relief, the more effective it should be in stabilizing the dislocation. If diffusivity is high enough for the atmosphere to follow the dislocation, would not the drag of the atmosphere dominate the "shielding" effect? Has this point been addressed quantitatively?

H.K. Birnbaum: Both qualitative and quantitative considerations support the "elastic-shielding" effect on dislocation interactions with other stress centers. As long as the atmosphere solutes have sufficient mobility to move with the dislocations and to rearrange to a minimum energy configuration, the stress field of the dislocation and the solute atmosphere must be considered in calculating elastic interactions. At lower temperature where the atmospheres lag behind moving dislocations, hardening (or increases in flow stresses) is observed.

M.M. Hall (Westinghouse Electric Corporation, USA): In your discussion you illustrated hydride precipitation at the macrocrack tip and concluded that crack extension occurs when the "local" stress-intensity factor exceeds the hydride toughness, K_{Ic}. In our delayed hydride cracking studies on zirconium alloys, we find that (1) hydrides precipitate at a distance from the crack tip and (2) ductile shear of the ligament between the hydride and macrocrack tip is required for crack advance. When we account for the additional strain energy required to shear this ligament, better correspondence with the observed threshold stress-intensity factor is obtained. Have you ever observed in the microscope this two-step process for crack extension, and if not, is it possible that plane-strain conditions may be a necessary requirement for this latter mechanism of hydride-assisted fracture?

As an added note, our observations, which were obtained in room-temperature tests of precracked compact tension specimens, suggested to us that we should be able to measure significantly large deformation rates in room-temperature constant-load tests of tensile specimens. We were able, in fact, to obtain sustained load ductile stress rupture of Zircaloy† tensile specimens in less than 24 h for stresses slightly greater than the engineering yield stress Thermal creep rates extrapolated to room temperature cannot account for this observation. Is it possible that hydrogen-enhanced plasticity can account for our observations?

H.K. Birnbaum: Since the hydride formation depends on the local stress conditions, it will differ in detail between plane stress (as in the transmission electron microscope) and plane strain conditions The hydride is expected to form at the region of maximum triaxiality that is in advance of the crack tip in a plane-strain specimen We observe a "field" of hydrides, some of which are separated from the crack tip by a volume of solid solution We have not observed ligament fracture between the crack tip and the hydride, but it seems to be perfectly reasonable.

I would expect to see hydrogen-enhanced plasticity in Zircaloy but we have not examined the zirconium-based systems.

S.M. Bruemmer (Battelle Pacific Northwest Laboratories, USA): Considerable work has been done in recent years on

†Trade name.

dislocation activity within grain boundaries and dislocation interactions with grain boundaries. What do we currently know concerning hydrogen effects on this behavior? Does hydrogen enhance dislocation movement in, emission from, and/or transmission through grain boundaries?

H.K. Birnbaum: We are currently studying just these effects, and it is clear that no simple answer can be given. In general, hydrogen increases dislocation activity near the grain boundaries as well as in the grain interior. The situation is complicated by hydrogen segregation in the vicinity of the grain boundaries, which has been shown using secondary ion mass spectrometry. In a number of systems we have seen hydrogen-related fracture by enhanced plasticity in the vicinity of the boundaries (within several hundred Angstroms) rather than in the grain-boundary plane itself This suggests that many hydrogen-related intergranular fractures are in fact predominantly transgranular fractures that parallel grain boundaries because of the enhanced hydrogen concentrations near the grain boundaries.

We have seen cases of true intergranular fracture associated with hydrogen in certain systems, e.g., Ni with S segregated at grain boundaries, Ni_3Al, and a few others.

R.H. Jones (Pacific Northwest Laboratories, USA): You illustrated the effect of stress on the alpha + hydride solvus that results from hydrostatic stress accommodating the volume expansion of the hydride. However, you proceeded to show hydrides in transmission electron microscope foils where the hydrostatic component was virtually zero. Were these results of high fugacity where the hydride was stable or is something else occurring in these tests?

H.K. Birnbaum: The interaction between a stress field and a hydride is with the hydrostatic stresses as well as with the deviatoric components:

$$E_{int} = \sum_{ij} \sigma_{ij} \epsilon_{ij}^{hydride}$$

In a thin film, the stress component σ_{22} will dominate the interaction but there will also be shear stress contributions The transmission electron microscope experiments we conducted on alpha-titanium were at high enough hydrogen fugacities to form hydrides

A. Atrens (University of Queensland, Australia): In the case of cracking due to hydrides, do the cracks stop at the hydride/matrix interface or do they propagate into the ductile matrix ahead of the hydrides? That is, have you seen any evidence of brittle cracks propagating into the ductile matrix ahead of the cracked hydride?

H.K. Birnbaum: We see the cracks stopping in the hydride or at the hydride interface. However, recall that we can only study relatively slow-moving cracks with our technique because these are the only ones we can follow and record.

A. Atrens: Would you like to comment/speculate what conditions produce hydrogen-induced plasticity in iron and iron alloys? That is, what are the controlling parameters/magnitudes?

H.K. Birnbaum: This question deserves more attention than can be provided in a short answer. We will be publishing our views on the subject shortly. Briefly, we believe the hydrogen-enhanced plasticity results from elastic shielding of the dislocation interactions with other stress centers such as other dislocations, solute atoms, or precipitates. The hydrogen atmospheres rearrange dynamically to minimize the energy of the system, and this rearrangement results in a decrease of the pinning of the dislocations. These effects will occur as long as the hydrogen mobility is high enough to allow the dynamic rearrangement of the hydrogen atmospheres at stress singularities.

Metal-Induced Fracture

*N.S. Stoloff**

Abstract

Metal-induced embrittlement encompasses a variety of phenomena, induced by both liquid and solid environments. Long-range diffusion is sometimes involved, but it is rarely necessary to cause fracture. Similarly, grain boundaries are sometimes the preferred sites for embrittlement, but they are clearly not necessary for embrittlement to occur. In view of the number and complexity of embrittlement phenomena, the scope of this paper is limited to a discussion of "classic" embrittlement, in which corrosion and/or long-range mass transfer are not involved. Also, effects limited to selective dissolution of grain-boundary precipitates (e.g., lithium interaction with carbides in steels) or to rapid grain-boundary penetration (liquid gallium on aluminum) are excluded. However, treatment of cases involving short-range diffusion are included. The primary thrust of the paper is to summarize developments in the field since the last international conference on the subject (1982), and to assess the work that needs to be done to further enhance understanding of mechanisms.

Introduction

Liquid metal embrittlement (LME) was first reported in the literature in 1874.[1] However, it was not until the late 1950s that experiments were reported that suggested that solid films (or inclusions) could also lead to embrittlement.[2,3] Neither author commented upon the possibility of solid metal-induced embrittlement; instead, Tiner[4] was the first to actually discuss the role of solid environments (mercury on copper and brass) in embrittlement. There are now numerous cases of solid or liquid metal-induced failures reported in research and from industry, so that metal-induced embrittlement is far from being a laboratory curiosity.

Further, the resemblance of many cases of metal-induced embrittlement to hydrogen-induced cracking has suggested to many researchers a commonality of mechanisms for both phenomena.[1,5-10] The principal features of "classic" metal-induced embrittlement have been summarized in several recent reviews,[6,9] and a brief synopsis of these findings follows.

(1) Embrittlement of crystalline metals requires the simultaneous application of tensile stresses (including residual stresses) and intimate contact between environment and substrate. The latter condition is obtained only when wetting is achieved; wettability is itself a function of the atmosphere around the embrittler.[11]

(2) Amorphous metals are severely embrittled by several low-melting liquid metals; for these materials, compressive stresses may be sufficient for embrittlement to occur.[12]

(3) Test conditions, particularly temperature, strain rate, the presence or absence of notches and embrittler composition, drastically alter susceptibility. The role of temperature is shown schematically in Figure 1,[13] while data for varying embrittler compositions on type 4140 steel (UNS G43400) are shown in Figure 2.[14]

(4) Microstructure exerts a substantial influence on environmental susceptibility. Most notable factors are grain size [large grains are usually, but not always, detrimental, (Figure 3)[10]], slip character, cold work, and precipitate size and spacing.

(5) Solid metal embrittlement is rarely observed at absolute temperatures of less than 75% of the melting temperature of the embrittler. However, in at least one case (silver or gold on titanium alloys), embrittlement occurred at 0.38 melting temperature.[15]

(6) Embrittlement may occur even when intermetallics or solid solutions are formed between substrate and metal film (e.g., zinc or tin on steels[16,17]), contrary to earlier suggestions.

(7) The enormous diversity in susceptibility caused by microstructural changes or altered test conditions requires very careful testing over a wide range of test conditions before it may be concluded that a particular environment does not embrittle a given substrate. Accordingly, the list of embrittlement couples is constantly expanding. Table 1 summarizes some recent additions to the list.[18-23]

(8) No single mechanism is generally accepted for metal-induced embrittlement. However, most cases of classic embrittlement may be explained either by a decohesion model[24,25] or by the mechanism of enhanced shear.[7,26] These are also the most widely accepted models for hydrogen-induced cracking. A third mechanism, based upon short-range diffusion of embrittler atoms along grain boundaries, resulting in the formation of a zone of high dislocation density,[27] is also capable of explaining some cases of embrittlement, particularly those involving delayed failure or solid metal environments. However, while this mechanism may be applicable to crack nucleation, it must be modified to account for crack propagation.[28]

Historical Review

Amalgamated zinc and zinc-coated iron were the first reported embrittlement couples (cited by Johnson[1] in 1874). During the early part of this century, mercury embrittlement of alpha-brass[29-31] and the embrittlement of plain carbon and alloy steels by various lower melting metals were reported.[32-35] In fact, by 1936 Austin[35] had concluded that virtually all steels used for general engineering purposes were susceptible to "penetration embrittlement" when immersed in solder. Van Ewyk[36] went so far as to suggest that soldering be avoided in assembling structural components. By the late 1950s, the literature on LME was extensive enough to warrant a comprehensive monograph on the subject, the classic book by

*Materials Engineering Department, Rensselaer Polytechnic Institute, Troy, NY 12180-3590.

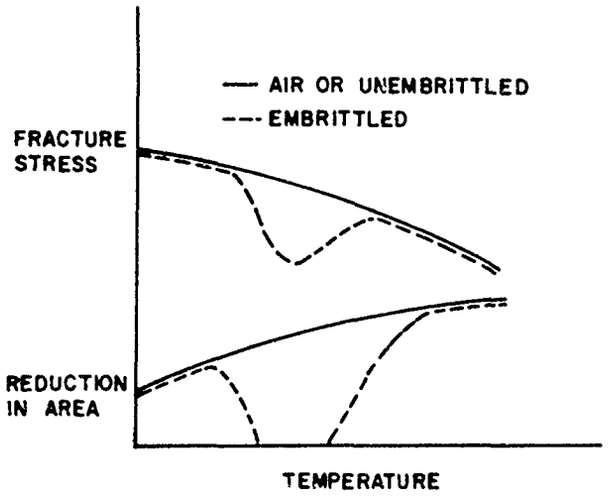


FIGURE 1—Effect of temperature on metal-induced embrittlement.[13]

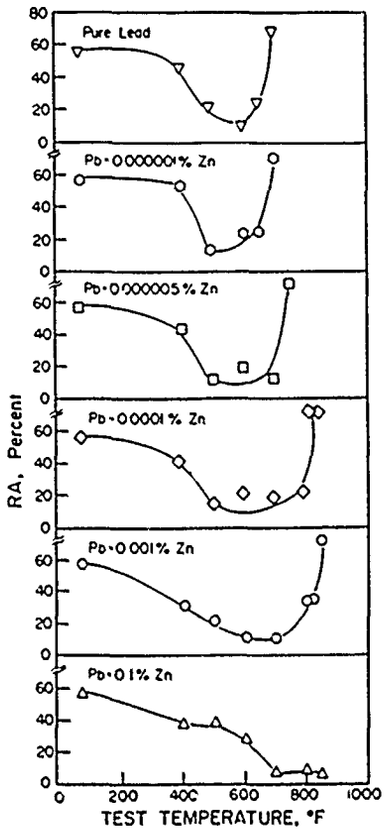


FIGURE 2—Influence of zinc additions to lead on embrittlement of type 4140 steel.[14]

Rostoker, McCaughey, and Markus.[37] This period coincided with great activity in the Soviet Union on LME, with numerous publications by the "Rebinder school."[38,39]

Studies of embrittlement under cyclic loading apparently were first reported in 1956.[40] To date, relatively little attention has been directed to fatigue phenomena in the presence of liquid metals, perhaps because there seems to be no significant difference in susceptibility under either cyclic or monotonic loading. A summary of fatigue data reported prior to 1979 appears in Reference 9.

Since the book by Rostoker, et al.,[37] was published, many examples of solid metal-induced embrittlement, noted mostly in the laboratory, were recorded; these have been admirably summarized (to 1982) in a review by Druschitz and Gordon.[41] Remarkably little

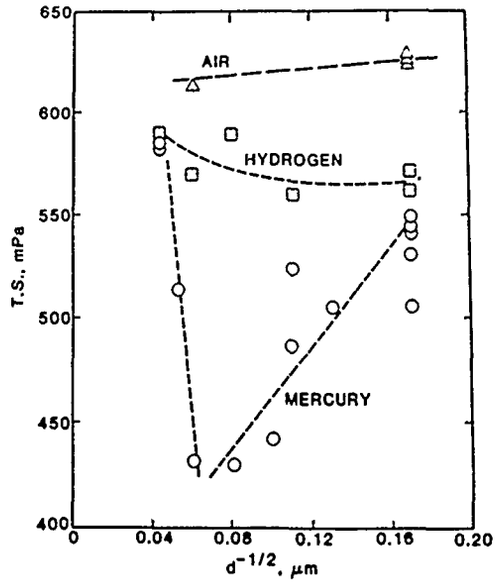


FIGURE 3—Influence of grain size on tensile strength of Monel 400 (UNS N04400) in mercury and in hydrogen.[10]

attention seems to have been focused upon metal-induced embrittlement as an important industrial problem until the Flixborough disaster in England in 1975 [which resulted in 28 deaths and was linked to cracking of stainless steel (SS) by zinc[42]] and the observation of reduced toughness in aircraft forgings containing lead impurities and in intentionally leaded steels[43] (to improve machinability).

Surprisingly, the nuclear fission and fusion industries, although dealing with alkali metal coolants in a number of reactor designs (including the fast breeder reactor), seem to have found few cases of classic embrittlement from these coolants. Apparently, alkali metals, with a few notable exceptions, do not cause such embrittlement at normal coolant temperatures. Nevertheless, alkali metals clearly do cause embrittlement of a number of metals and alloys. One may cite the recently noted cleavage of aluminum alloys in the presence of sodium[44,45] and the embrittlement of magnesium by sodium.[22] Nickel is severely embrittled by lithium[46,47] and moderately embrittled by sodium.[47] Also, the nuclear industry has had to deal with numerous examples of solid and LME of zirconium alloy fuel element cladding by cadmium[48,49] and cesium-cadmium[48] and type 316 SS (UNS S31600) by tellurium[50] environments. Solid cadmium embrittlement of Zircaloy† 2 is so severe that cracking can occur at stresses below the nominal yield strength of the alloy.[49] The most complete, recent review of specific embrittlement couples is by Nicholas.[51]

The importance of wetting as a precursor to embrittlement cannot be overemphasized. While most studies of embrittlement are conducted with the specimen *and* metal environment in air, several studies of embrittlement of iron by lead in vacuum have been reported in the Soviet literature.[52,77] The results show that although lead-iron is an immiscible system, when a vacuum surrounding iron permits good wetting by mercury, embrittlement is readily observed. On the other hand, in air, wetting of iron and steels by lead is very difficult, and embrittlement is usually observed only in medium- to high-strength steels, e.g., types 4340[20] (UNS G43400) and 4140.[17] The susceptibility of steels to lead is a function of both strength level and presence or absence of a precrack. Kamdar[20] has shown that precracking is necessary to see embrittlement at the 700 MPa level in a Cr-Mo steel, as described in more detail below.

An alternative to manipulating the gaseous environment to improve wetting is to use an intermediate layer between substrate and embrittler. For example, wetting of alloy steels by liquid lead is facilitated by precoating them with tin. Unfortunately, embrittlement

†Trade name.

TABLE 1
Recently Reported Embrittlement Couples

Substrate	Environment	Temperature (°C)	Test Conditions	References
Niobium	Sn	250	tension, drilling	Polukarova, et al.[18]
Al-Li	Na	RT	Charpy	Webster[19]
Al-Li	K	RT	Charpy	Webster[19]
Type 4340	Pb	350	tension, fatigue[A]	Kamdar[20]
IN718[B]	Hg	RT	HCF	Price and Good[21]
Cr-Mo steel	Pb	350	HCF	Kamdar[20]
Mg	Na	120	bend, tension	Trevena and Lynch[22]
A-286	Ag	500-600	delayed failure	Assayama[23]
Fe-Si	Li	210	tension	Trevena and Lynch[22]
7017-T651	In	10-150 (solid)	$\frac{da}{dt}$	Trevena and Lynch[22]

[A]Static and HCF.
[B]One of ten different Ni-base alloys.

revealed in subsequent tensile tests is not readily interpreted, since tin is itself an embrittler. Furthermore, many cases of grain-boundary penetration of steels by lead and lead-tin alloys have been reported [35,36] The influence of several lead-tin environments on a commercial low-alloy steel (ASTM A543) has been studied by Balaguer, et al ,[53] at two strain rates, and temperatures in the range 22 to 343°C Tensile tests in lead tin at 343°C resulted in severe embrittlement as measured by strain-to-fracture and true fracture stress. However, contrary to most observations on metal-induced embrittlement, increasing strain rate by 25 times decreased the degree of embrittlement Metallographic studies revealed grain-boundary penetration and secondary cracking in embrittled samples. Taken together with the anomalous strain-rate dependence, these results suggest a time dependent mechanism of intergranular cracking, perhaps akin to the solder induced embrittlement of steels reported by Austin[35] or to the Khristal[27] mechanism of grain-boundary penetration favored (with modifications) by Gordon and An.[28] An inverse embrittlement–strain rate relation has also been reported by Adamson, et al.,[50] for neutron-irradiated, cold-worked type 316 SS tested at 625°C in liquid cesium-tellurium in fatigue and by Price and Fredell[10] for Monel† 400 (UNS N04400) tested in mercury (Figure 4). These may be additional examples of grain-boundary penetration.

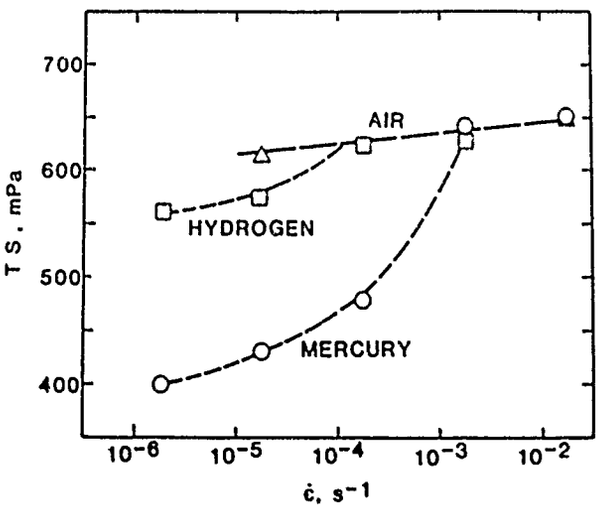


FIGURE 4—Effect of strain rate on fracture stress of Monel 400 (UNS N04400) in mercury and hydrogen.[10]

†Trade name.

Fractography

Fractography has played a central role in efforts to establish mechanisms of metal-induced embrittlement. Lynch,[7,26,64] in particular, has offered extensive fractographic evidence for an enhanced shear model of embrittlement (Figure 5) for both hydrogen and metal-induced failures. This point of view is based upon Beachem's[55] proposal that dissolved hydrogen facilitates dislocation motion in the plastic zone at crack tips, causing fracture by localized deformation to occur more readily. Birnbaum and coworkers[56] have shown direct evidence for enhanced dislocation activity in nickel and nickel alloys as well as several other alloys in the presence of hydrogen gas, therefore, no reason exists to doubt the basic premise that environmentally induced plasticity can cause fracture at reduced macroscopic strains. Specifically, Lynch[26] suggests that adsorption facilitates the injection of dislocations from crack tips, thereby promoting link up of cracks with voids ahead of cracks.

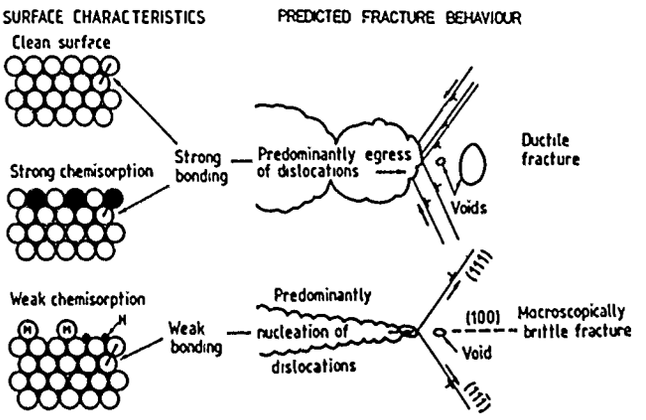


FIGURE 5—Schematic of adsorption-induced embrittlement, showing role of dislocations.[63]

Fractographic observations to support Lynch's dislocation injection mechanism in the presence of liquid metals (as well as aqueous and/or hydrogen environments) have been reported for the following substrates:[7,22,26,57,64]

(1) Aluminum and Al-Zn-Mg single crystals
(2) D6ac steel
(3) α-titanium alloys
(4) Pure magnesium
(5) β-brass single crystals
(6) Cadmium
(7) Nickel single crystals
(8) Iron-silicon single crystals

The principal components of the fractographic and metallographic evidence are as follows:

(1) Cleavage-like {100} cracks with fronts parallel to ⟨110⟩ slip directions in aluminum and nickel single crystals, as shown in Figure 6,[54] 110 crack fronts also were noted in β-brass,[26] although the usual slip vector in this alloy is of type 001 . This discrepancy has not been explained.

(2) Shallow dimples or tear ridges on fracture surfaces of embrittled D6ac, steel, iron-silicon, aluminum, cadmium, and nickel [22 63 64] For magnesium, fluted fracture surfaces parallel to pyramidal planes and cleavage-like basal facets were produced by liquid cesium, as shown in Figure 7 [22 26] Similar fracture surfaces have been noted in α-titanium alloys embrittled by liquid mercury.[22]

(3) Observations of large crack-tip opening displacements and enhanced dislocation activity in metal-coated aluminum and nickel single crystals.[26]

(4) Large shear band offsets with no major change in fracture appearance relative to air for amorphous metals tested in various liquid metals (Figure 8).[12]

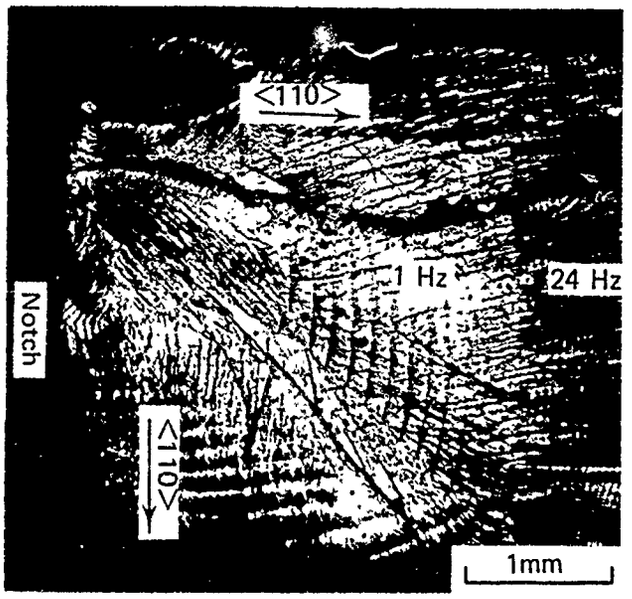


FIGURE 6 – Cleavage crack on {100} in aluminum single crystals cycled in liquid gallium.[7]

Soviet research on metal-induced embrittlement also provides some supporting evidence for the concept of enhanced shear. Popovich[52,77] has summarized a series of observations on adsorption-induced plasticity as follows: Shallow hardness measurements of steels in molten lithium and in vacuum as well as tensile tests in cadmium-coated Armco† iron indicate that plasticity is first facilitated by the environment, but that an increased work-hardening rate rapidly increases the flow stress in the medium to higher levels than that in vacuum, as shown schematically in Figure 9.[52] Although Popovich and Lynch agree, therefore, that dislocation activity is stimulated in the presence of an active medium, they differ in their conclusions as to the result. Popovich and coworkers[11 52 58 77] conclude that rapid hardening in surface layers after the initiation of plastic deformation leads to microcrack formation. These cracks are then proposed to propagate in bursts to the depth of the layer, crack origins formed in Armco iron samples of differing grain size were reported to correspond to the average grain size. Furthermore, serrated stress-strain curves of embrittled Armco iron, fractographic evidence of intermittent crack growth of zinc crystals in mercury and gallium, and acoustic emission measurements during crack growth in embrittled metals support the concept of repeated formation and fracture of hardened surface layers. Dmukhovskaya and Popovich[11] point out that the hardened layer concept is capable of explaining solid metal embrittlement, while the dislocation injection model, which requires molten metal to be present at the crack tip throughout crack propagation, does not. Also, this concept predicts a size effect on fracture, which was indeed noted.[11] However, the principal weakness of the Popovich mechanism, noted by Pickens and Westwood,[59] is the lack of metallographic and fractographic evidence to support the model.

Several recent fractographic studies of metal-induced embrittlement also support the decohesion model. For example, overaging 7075-T651 aluminum results in reduced susceptibility to embrittlement by mercury (Figure 10),[60] but in all heat-treatment conditions, a flat, cleavage-like fracture surface was observed. No dimples could be observed even at high magnification. Since the decreased strength is expected to enhance dislocation activity at any given stress-intensity level, the decreasing susceptibility to embrittlement with decreasing stress levels appears to offer support for the decohesion model.

Several investigators have reported the incidence of {001} fracture in mercury-embrittled aluminum single crystals[61 62] and polycrystals.[44,45] Recently, Fager, et al.,[44] have shown that cleavage along {001} and {110} of Al-Li alloys can be induced by sodium impurities. Furthermore, cleavage was produced in an Al-Li-Cu-Zr alloy and in type 2024 (UNS A92024) aluminum by placing liquid Na-K eutectic next to a propagating crack. Miller, et al.,[45] extended the observation of sodium-induced cleavage to a type 7075 alloy, as well as confirming the effect in an alloy similar in composition to that used by Fager, et al. Sodium was directly identified on the surfaces of the cleavage facets. These results also tend to support the decohesion model, since no dimples were observed on the fracture surfaces, although one could argue that the fractographic studies were not conducted with the sophistication of Lynch's work.

Finally, Lynch[63] has shown that the hardness (varied by tempering) of a D6ac steel has a profound influence on the proportion of intergranular (IG) failure noted in mercury or hydrogen environments (Figure 11). For tempering temperatures above 300°C, the proportion of IG fracture was nearly identical in both environments. For as-quenched material, transgranular (TG) fracture in both environments was mixed mode, with dimpled regions, quasi-cleavage facets, and martenite-lath boundary facets [Figure 12(a)]. For other heat-treatment conditions, TG facets were predominantly dimpled [Figure 12(b)]. Predominantly IG failure at tempering temperatures in the range 345 to 650°C was attributed to segregation of impurities to prior austenite grain boundaries. For nondimpled fracture modes, Lynch[63] concluded that crack growth occurred by either localized slip or a mixture of slip and decohesion. Lynch[64] also has attributed cracking of zinc in mercury to decohesion.

Cyclic Behavior

In most cases, metal-induced embrittlement can be observed under monotonic, cyclic, or static conditions in a susceptible substrate/environment system. However, a sharp fatigue crack often provides the most severe condition for embrittlement, as Kamdar[20] noted for a Cr-Mo steel in lead and Price and Good[21] noted for several nickel alloys tested in liquid mercury. A machined notch did not provide sufficient stress concentration to cause embrittlement of the steel by lead, yet a fatigue-precracked sample readily displayed embrittlement.[20] Similarly, Incoloy† 800 and 825 (UNS N08800 and N08825) were not embrittled by mercury in tensile tests, but displayed considerable reduction in life when cycled in mercury.[21] Price and Good[21 65] observed that ten widely differing nickel alloys were all susceptible under certain conditions (tension, fatigue, notched, unnotched) to embrittlement by mercury. Therefore, they concluded that similar effects would be found in most other nickel-base alloys.

Fatigue resistance in the presence of metal environments has usually been evaluated under high cycle conditions, with life measurements recorded rather than the rate of crack growth. Kapp, et

†Trade name.

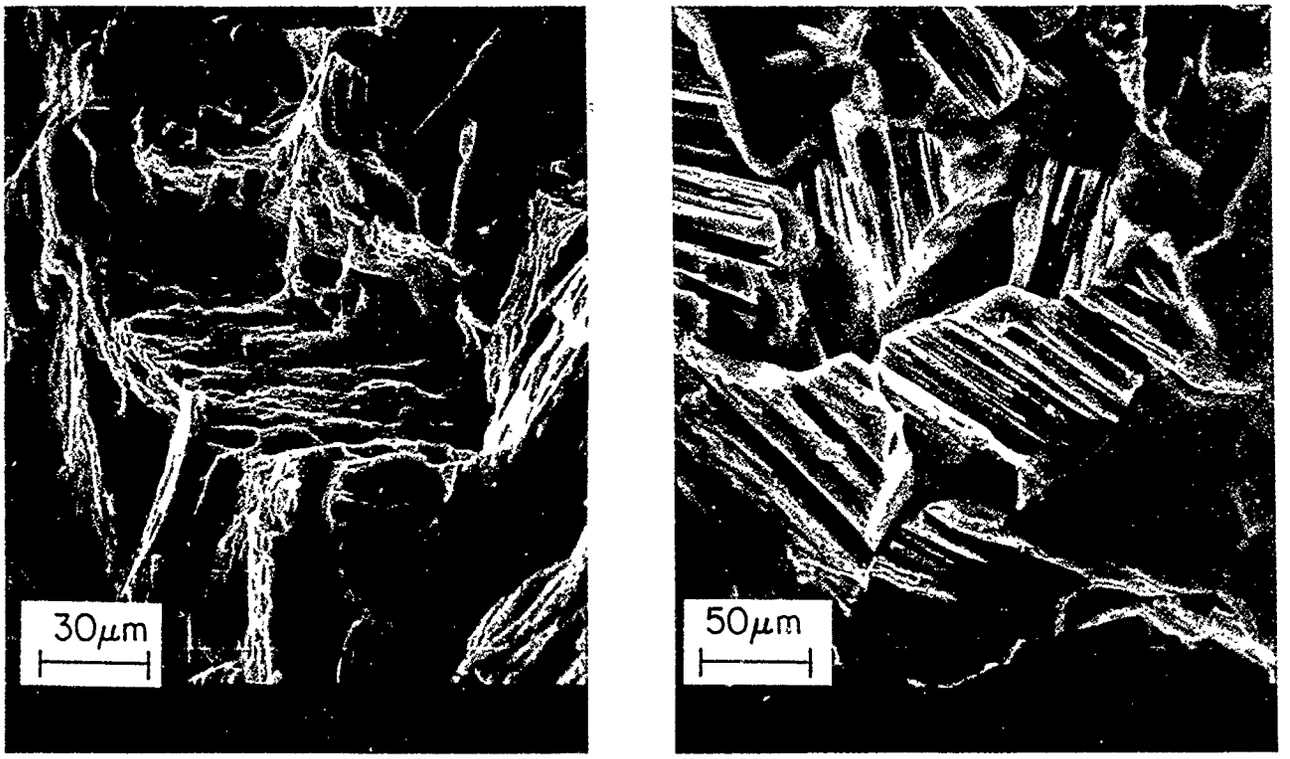


FIGURE 7—Fractographic features on magnesium tested at 50°C in (a) argon and (b) liquid cesium.[22]

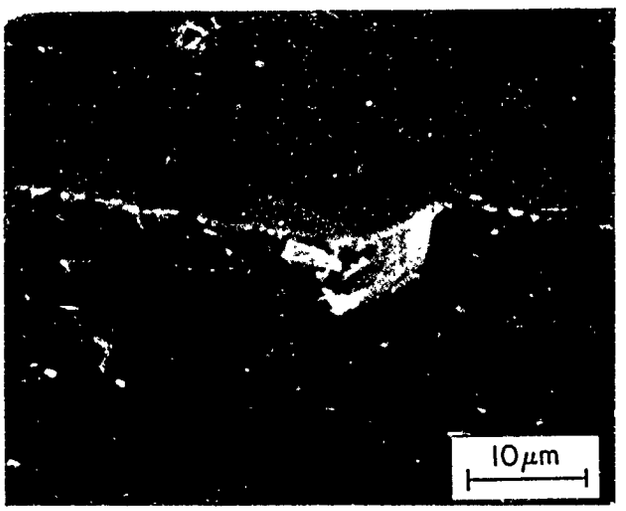


FIGURE 8—Fracture along shear bands in amorphous $Fe_{40}Ni_{38}B_{18}Mo_4$ tested in bending in lithium at 200°C.[12]

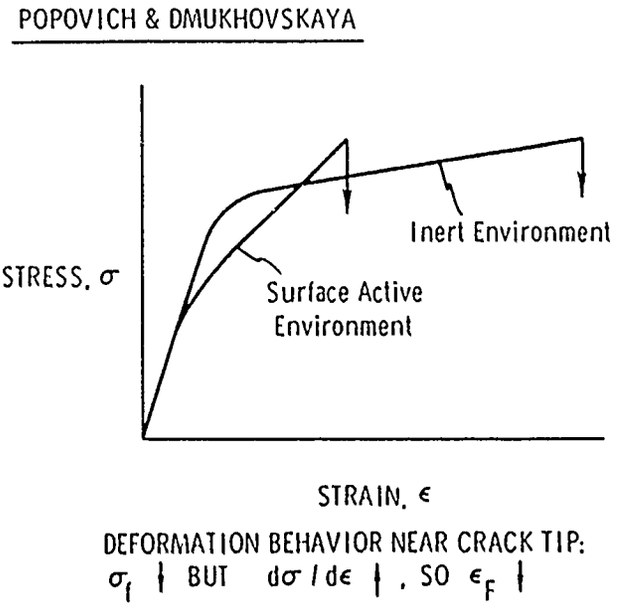


FIGURE 9—Popovich mechanism of enchanced shear coupled with rapid work hardening.[11]

al.,[66] have reported such measurements on three aluminum alloys: types 1100-0, 6062-T651, and 7075-T651, and compared the results with those from static loading under fixed loads or fixed displacements. Typical fatigue crack results are shown in Figure 13 for the 1100-0 alloy, tests were performed at 5 or 30 Hz at a constant R ratio ($R = K_{min}/K_{max}$) of 0.1. Note that more rapid cracking was noted in mercury, but only at high ΔK levels. Identical behavior was noted in type 6061-T651. However, limited data for type 7075-T651 revealed severe embrittlement at all ΔK levels. The data for the first two alloys resembled the behavior of hydrogen-embrittled steel[67] in that, below a certain minimum ΔK, the environment had no effect on crack growth. Once this level was exceeded, the crack growth rate rose rapidly with ΔK, however, at higher ΔK, the growth rate increased very little. Decreasing the frequency from 30 Hz to 5 Hz produced up to 100 times greater growth rates in type 7075 and 50 times greater growth rates in type 6061. Interestingly, the crack growth thresholds were nearly the same in both cyclic and static loading, with type 7075 embrittled the most and type 6061 embrittled the least by mercury. Fracture surface appearance did not change with the loading condition.

Critical Issues

A central feature of many early works on metal induced embrittlement was concern for "specificity," that is, whether only certain combinations of substrates and environments constituted embrittlement couples. There is now little doubt that virtually all solid

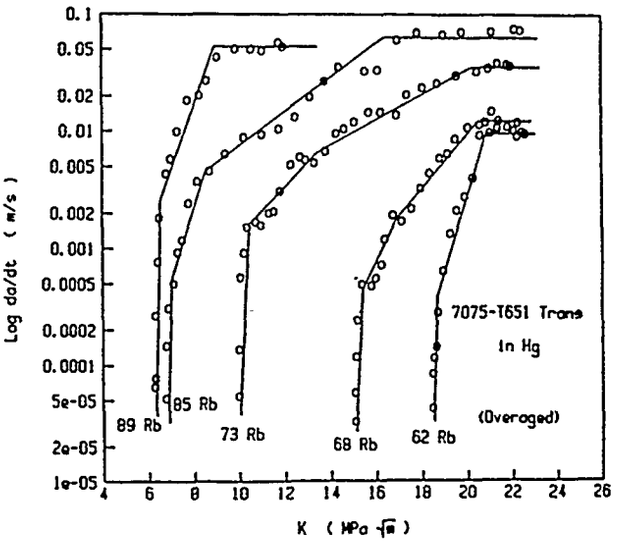


FIGURE 10—Influence of aging to alter strength on embrittlement of type 7075-T651 in mercury.[60]

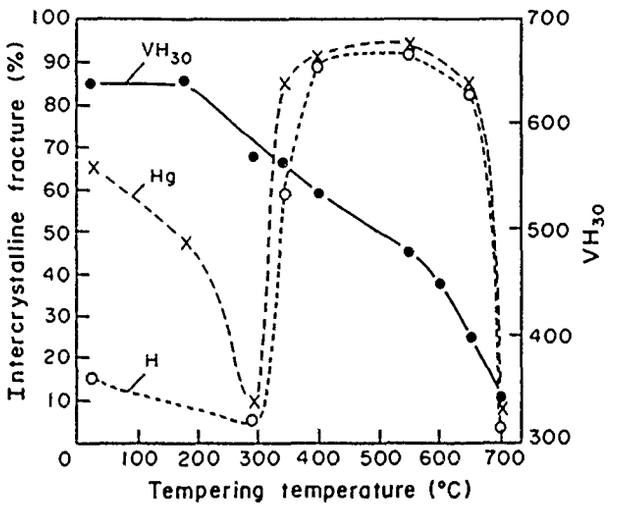


FIGURE 11—Influence of tempering temperature on hardness and crack path in D6ac steel in mercury and hydrogen.[63]

metals can be embrittled by some, if not most, lower melting point environments, provided that the experimental conditions are optimized. This point of view has also been adopted by others.[51] A list of recently discovered embrittlement couples is shown in Table 1; the list is constantly expanding. The most favorable conditions for classic embrittlement have been enumerated in the introduction and need not be repeated here. However, it is important to remind the reader that susceptibility to embrittlement of any given substrate can only be evaluated when a large number of experimental conditions have been examined. The mechanism of embrittlement in any given situation may then be deduced based upon the effects of critical variables such as strain rate and grain size on fractographic features. Furthermore, the strength level of the substrate can have a pronounced effect on susceptibility. For example, with type 7075-T651, increasing strength levels resulting from heat treatment cause a large decrease in the cracking threshold, accompanied by more rapid cracking at all stress intensity levels, as is shown in Figure 10.[60] Dislocation mobility is enhanced in low-strength alloys, so that correlations of degree of embrittlement with strength level can reveal the mechanism of fracture.



FIGURE 12—Fractographic features in D6ac steel:[63] (a) Hg, (b) H_2 (c) H_2, and (d) H_2.

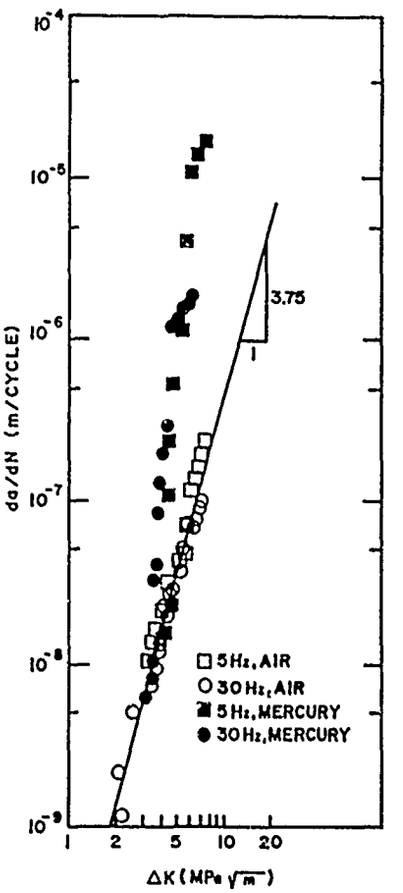
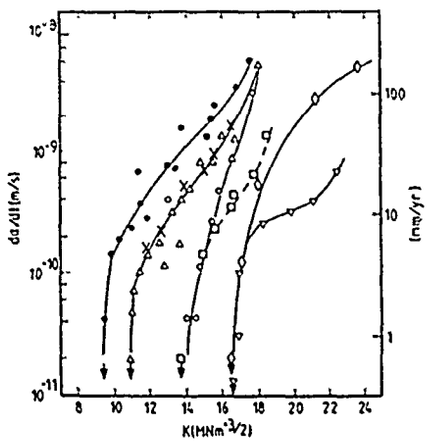


FIGURE 13—Effect of frequency on crack growth rates in 1100-0 aluminum, cycled in mercury.[66]

The second issue to be dealt with is the role of grain boundaries. Grain boundaries are not necessary for embrittlement to occur. Numerous single crystals and amorphous films have been embrittled by a variety of metals.[9,68] Furthermore, even face-centered cubic (fcc) metals, which usually fail intergranularly, are now known to display TG cracking in many instances (e.g., aluminum single crystals in sodium and nickel polycrystals fatigued in mercury or tensile tested in sodium). However, since grain boundaries are present in virtually all service applications, factors such as impurity segregation to grain boundaries, time of pre-exposure, and strain-rate changes can strikingly alter the degree of embrittlement observed. For example, internal lead-induced IG cracking of Al-Mg-Si alloys is observed only in slow-strain-rate tensile tests ($\dot{\epsilon} \leq 10^{-6} s^{-1}$) or in constant load tests (Figure 14), and only at temperatures high enough to permit transport of lead.[69] Embrittlement was not observed at high strain rates at room temperature or in slow-strain-rate tests at −196°C at any lead level. However, embrittlement was noted at temperatures as low as −4°C.[69] Thus, there is a complex interaction among test temperature, strain rate, embrittler composition, and substrate impurities that can change what appears to be a non-susceptible system to one in which severe embrittlement occurs.



Symbol	*Pb* (ppm)	*Homogenization treatment*	
		Time (h)	*Temperature* (°C)
●	550	2	550
×	120	2	550
△	60	2	550
○	30	2	550
□	<10	2	550
◇	30	12	450
▽	<10	12	450

FIGURE 14—Crack growth rates of Al-Mg-Si alloys at various lead levels.[69]

The third issue of concern is the influence of metallic environments on surface plasticity and the relationship, if any, between hydrogen- and metal-induced embrittlement. *In situ* transmission electron microscopy (TEM) experiments by Birnbaum and coworkers[56] have unequivocally demonstrated that hydrogen facilitates dislocation motion in nickel. Similarly, Kimura and Mitsui[70] have confirmed Beachem's[55] conclusions that hydrogen enhances plasticity in ferrous materials under certain specified conditions. However, while many similarities exist between metal- and hydrogen-induced embrittlement, significant differences have also been recorded, especially in the response of high-strength steels to mercury and hydrogen.[63,73] Much higher crack velocities and a greater proportion of IG cracking were noted in D6ac steel in mercury.[63] On the contrary, Price and Norman[73] found that on smooth samples of type 4142 steel, embrittlement by mercury was much less severe than hydrogen embrittlement, perhaps because of incomplete wetting by mercury. The degree of embrittlement was also a function of hardness, with increasing hardness leading to sharply reduced fracture stresses in hydrogen and relatively smaller effects in mercury (Figure 15).[73] A tenfold increase in strain rate had little effect on the flow curves in air or mercury, but it appreciably reduced the degree of embrittlement (in terms of fracture stress) in hydrogen With both D6ac steel and nickel alloys, cracks initiated more readily in hydrogen but propagated more easily in mercury Another difference between the two environments is that only IG cracking of the steel occurred in mercury, but a brittle TG fracture mode was also noted under dynamic charging with hydrogen. It was postulated that hydrogen could diffuse inward from the surface and promote subsurface dislocation nucleation and motion while the influence of mercury was limited to the surface.[63] Also note the difference in embrittlement with grain size for Monel 400 in mercury and hydrogen gas (Figure 3).[10] On the basis of these and other studies, it may be concluded that wetting problems, differing modes of embrittler transport, and different substrate strength levels can give rise to substantial differences in the response of metals to a given environment, and may lead to situations where hydrogen and a liquid metal cause strikingly different experimental results. *Indirect* evidence for enhanced plasticity in the presence of liquid or solid metals has primarily come from the Soviet literature.[11,52,58,77] Tensile and superficial hardness tests indicate lower critical flow stresses because of active environments, but rapid hardening is then observed. No such reports appear in the Western literature. Metallographic and scanning electron microscopy (SEM) studies on amorphous metals in our own laboratory also indicate that shear is facilitated by liquid metals, although no effect on macroscopic yield stresses was observed.[12] This may be a consequence of insensitivity of the tensile machine to changes in plasticity in the micro-yield region, although changes in flow stresses in the presence of hydrogen are very readily observed.[70] Clearly, more work is needed on direct measurements of flow stress in high surface/volume specimens to reconcile Soviet observations and negative results reported elsewhere.

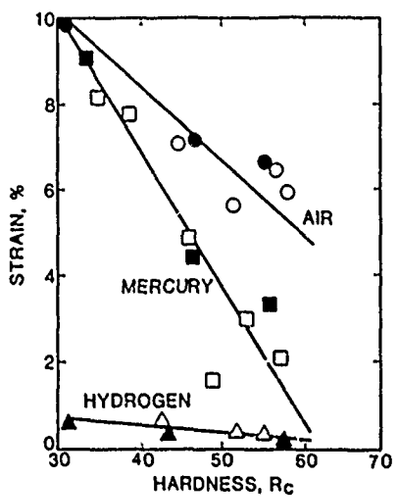


FIGURE 15—Influence of hardness on fracture strain of type 4142 steel in hydrogen and in mercury.[73]

Since the stress state at the tip of a crack is bound to influence susceptibility to metallic environments, tests under compression or torsion, as well as the almost universally used tensile tests, are necessary. Kapp[71] has used torsion tests (Mode III) on 70/30 brass in mercury to attempt to distinguish between shear- and tensile-dominated fracture modes. Unfortunately, the results shown in Figure 16 were inconclusive, since enhanced shear appeared to facilitate crack initiation, while crack propagation occurred along planes of maximum tensile stress, suggesting a decohesion mechanism.

Finally, with respect to the impact of metallic environments in industry, alloy steels present a series of problems with respect to basic understanding of embrittlement mechanisms. Attempts to correlate the embrittling effects of various low-melting liquid metals on steels with either composition, melting point, or vapor pressure of

the embrittler have not been successful.[14,17,72] For example, impurities or solutes in lead can drastically alter susceptibility to cracking, with zinc exhibiting the greatest effect (Figure 2) followed by antimony, tin, and bismuth.[14] The major influence of these solutes is on the recovery temperature (T_R) at which embrittlement is no longer observed (Figure 17).[14] It is highly unlikely that the properties of the substrate control this recovery; instead, the degree of wetting, of adsorption, or rate of surface diffusion more likely controls this transition. Of course, impurities in the substrate also can substantially alter fracture behavior. For example, small additions of sodium or potassium to Al-Li alloys reduce their impact toughness and ductility by forming discrete grain-boundary particles that are liquid at room temperature.[19] Careful control of both substrate and environment composition, as well as the gas surrounding the embrittler, is clearly required to accurately assess susceptibility to embrittlement.

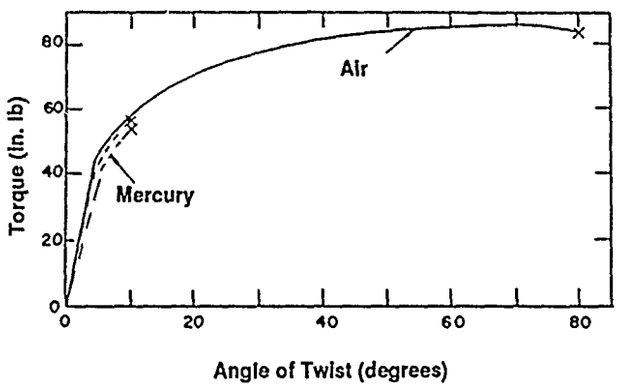


FIGURE 16—Torque–twist diagrams of 70/30 brass in air and mercury.[71]

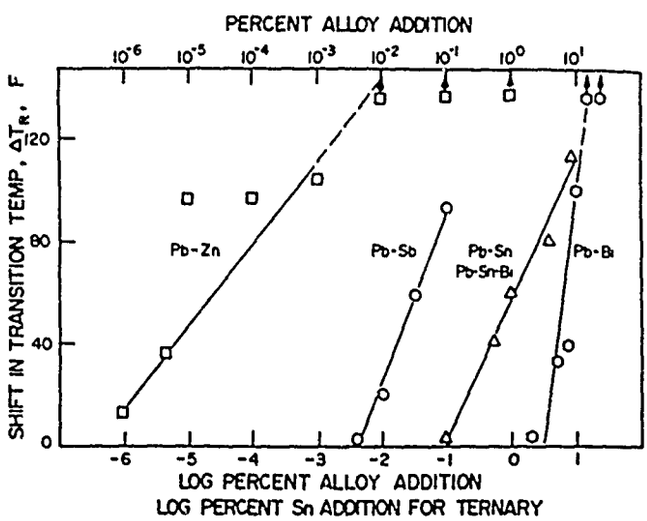


FIGURE 17—Influence of solutes in lead on recovery temperature (T_R) of ductility of type 4145 steel.[14]

Suggestions for Future Research

Table 1 illustrates the rapid expansion of observed embrittlement phenomena to new substrate/embrittler combinations. Data from these and earlier investigations have established those factors that tend to support each of the proposed theories of embrittlement (Table 2). Systems that have been identified with each of these mechanisms are summarized in Table 3. Most investigators continue to use polycrystalline substrates to examine new systems. For those substrates that usually fail intergranularly in the presence of metal environments, grain boundary chemistry is bound to play a significant role, as previously cited.[74-76] Therefore, mechanistic studies are best conducted either on systems exhibiting TG failure in polycrystals (listed in Table 4),[73] or on single crystals or bicrystals in which both orientation and chemistry of grain boundaries are carefully controlled. (Watanabe, et al., have already performed studies on well-characterized bicrystals and polycrystals, but they did not address the atomic mechanisms of fracture[74-76]). With such materials and suitable environments, the following experiments (some of which have been proposed earlier[68,76]) are suggested:

(1) Determine influence of surface/volume ratio (i.e., specimen size, cross section) upon cracking susceptibility. These experiments should be combined with examination for near-surface microcracks, as suggested in the Soviet literature.[11,77]

(2) Measure crack growth rates under cyclic and static conditions, and correlate these with diffusivities associated with likely transport mechanisms.

(3) Carry out experiments with metal environments applied in vacuum as well as in air to minimize spurious results due to inadequate wetting in air.

(4) Study response to cyclic loading with varying mean stresses; for a given stress intensity range (ΔK), enhancement of embrittlement at high R ratios (K_{min}/K_{max}) should be observed if decohesion is responsible.

(5) Study crack initiation in single crystals or bicrystals tested in compression, torsion, or bending; if enhanced shear is responsible for embrittlement, crack nuclei should be seen in compression or torsion as well as in tension. (Note, however, ambiguities in Kapp's results.[71])

(6) If possible, all sets of experiments should use strain rate as a variable to aid in distinguishing diffusion-controlled from adsorption-controlled embrittlement processes.

(7) Work should concentrate on a single substrate in each of a group of related potential embrittlers, so that differences in effectiveness of embrittlement might be correlated with physical or chemical characteristics of the environments. For example, nickel is severely embrittled by lithium, less so by sodium, and apparently unaffected by potassium, rubidium, or cesium. Nicholas and Fernback[47] have indicated that the nickel-lithium system is attractive for further study because it is relatively simple and able to be characterized; wetting characteristics and surface energies are well known.

TABLE 2
Mechanisms and Critical Factors for Embrittlement

Decohesion	Enhanced Shear	Penetration
instantaneous $\sigma_F \propto d^{-1/2}$ continuous cleavage or intergranular $\epsilon_F, \sigma_F \propto \dot{\epsilon}^{-n}$ tension only $\sigma_F \propto \sigma_{ys}^{-b}$	instantaneous $\sigma_F \propto d^{-1/2}$ continuous dimples $\epsilon_F, \sigma_F \propto \dot{\epsilon}^{-n}$ shear stresses $\sigma_F \propto \sigma_{ys}^{b}$	incubation time $\sigma_F \propto d^{1/2}$ discontinuous intergranular $\epsilon_F, \sigma_F \propto \dot{\epsilon}$ tension only $\sigma_F \propto \sigma_{ys}^{-b}$

TABLE 3
Mechanisms Identified

Decohesion	Enhanced Shear	Penetration
Zn/Hg[26] D6ac/Hg[63] α-brass/Hg (prop.)[71] 7075/Hg[60]	Ni/Hg[26] FeCBSi/Hg[12] D6ac/Hg[63] Al-Zn-Mg/Hg[7] α-brass/Hg (init.)[71]	Monel 400/Hg[(A),10] 4140/In-Sn[41]

[(A)]Contrary to authors' suggestions.

TABLE 4
Transgranular Embrittlement Couples[26]

Material	Liquid–Metal Environment								
	Hg (−39)[A]	Ga (30)	In (156)	Sn (232)	Li (179)	Na (98)	K (63)	Rb (39)	Cs (28)
Ni	E	N	N	N	E[A]	E	N	N	N
Al	E	E	E	E					
Cu/α-brass	N[B]	N[B]	N	N					
β-brass	E	E							
Fe-Si	E		E	E	E				
Mg	N	N				E	E	E	E
Ti	E	N							

[A]Mixed mode, predominantly IG.[22]
[B]Intercrystalline LME occurs in these and possibly other systems listed as not embrittled.

(8) *In situ* experiments in the TEM to observe the influence of metal environments on dislocation mobility would be very helpful in clarifying the role of enhanced shear. However, much care would be needed to avoid contamination of the microscope chamber.

In all experiments such as those described above, distinctions must be made between the mechanism of fracture and the rate-controlling steps in bringing metal embrittler atoms to the crack tip. Druschitz and Gordon[41] have pointed out that the local atomic mechanism of fracture at a crack tip may be either by tensile decohesion or enhanced shear. However, for crack nucleation, the rate-controlling steps will be grain-boundary diffusion (or other rapid diffusion paths in single crystals), and for crack propagation, transport of the environment to the crack tip, perhaps by surface diffusion. Lynch[79] has recently compared surface-diffusion coefficients obtained from solid-metal-induced embrittlement couples with value of surface self-diffusion coefficients obtained from other experiments and finds agreement within one order of magnitude. Nevertheless, the concept of a hardened layer susceptible to cracking at the surface[11,17] or along grain boundaries[27] as a precursor to embrittlement may be considered a distinct additional mechanism.

Summary

A brief history of metal-induced embrittlement has been presented. It is quite likely that virtually all higher melting solid metals can be embrittled by lower melting metals, provided that the microstructural and environmental conditions are favorable. However, there are at least three mechanisms of crack nucleation that have received support in the literature, at least one of which requires time-dependent, short-range diffusion. (Lynch[79] points out the importance of surface diffusion in solid-metal-induced embrittlement; Khristal's mechanism[27] requires grain-boundary diffusion.) Ways of distinguishing between the mechanisms on the basis of experimental data are described. Finally, several critical experiments to elucidate further the characteristics and mechanisms of embrittlement are suggested

References

1. W.H. Johnson, Proc. Roy. Soc. Lond. 23(1874): p. 168.
2. R. Eborall, P. Gregory, J. Inst. Met. 84(1955-56): p. 88.
3. E.M. Kennedy, The Effect of Cadmium Plating on Aircraft Steels in the Presence of Stress Concentrations at Elevated Temperatures, WADDTR40-4, September (1961), p. 468.
4. N.A. Tiner, Trans. TMS-AIME 221(1961): p. 261.
5. E. Coleman, D. Weinstein, W. Rostoker, Acta Metall. 9(1961): p. 491.
6. A.S. Tetelman, S. Kunz, Stress Corrosion Cracking and Hydrogen Embrittlement of Iron Base Alloys, NACE-5, ed. R. Staehle, J. Hochmann, R. McCright, J. Slater (Houston, TX: National Association of Corrosion Engineers, 1977), p. 369.
7. S.P. Lynch, Acta Metall. 29(1981): p. 325.
8. G.V. Karpenko, A.K. Litvin, V.I. Tkachev, A.I. Soshko, Fiz-Khim. Mekh. Mater. 9, 4(1973): p. 6.
9. N.S. Stoloff, Environment Sensitive Fracture of Engineering Materials, ed. Z A. Foroulis (Warrendale, PA. The Metallurgical Society of the American Institute of Mining, Metallurgical, and Petroleum Engineers, 1979), p. 486.
10. C.E. Price, R.S. Fredell, Metall. Trans. A 17A(1986): p 889
11. I.G. Dmukhovskaya, V.V. Popovich, Fiz.-Khim. Mekh. Mater 15, 4(1979): p. 64.
12. S. Ashok, T.P. Slavin, N.S. Stoloff, M.E. Glicksman, Proceedings of the MRS Symposium on Rapidly Solidified Amorphous and Crystalline Alloys, Vol. 8 (Pittsburgh, PA Materials Research Society, 1982), p. 309.
13. F.A. Shunk, W.R. Warke, Scripta Metall 8(1974). p 519
14. M. Landow, A. Harsolia, N.N. Breyer, J. Mater for Energy Systs. 2(1981): p. 50.
15. R.E. Stoltz, R.H. Stulen, Corrosion 35, 3(1979). p. 165.
16. J.C. Lynn, W.R. Warke, P. Gordon, Mater. Sci. Eng. 18(1975). p. 51.
17. M. Macek, "Liquid Metal Embrittlement of High Strength Steels by Tin and Tin Alloys" (Master's thesis, Illinois Institute of Technology, 1979).
18. Z.M. Polukarova, L.S. Bryukhanova, V.S. Yuschenko, E.D. Shchukin, Fiz-Khim. Mekh. Mater. 22, 5(1986). p. 39.
19. D. Webster, Metall. Trans. A 18A(1987). p. 2181.
20. M.H. Kamdar, Fatigue Life, Analysis and Predictions, ed. V.S. Goel (Metals Park, OH: ASM International, 1986), p. 333.
21. C.E. Price, J.K. Good, J. Eng. Mater. Tech. Trans. ASME 106(1984): pp. 178-183.
22. P. Trevena, S.P. Lynch, unpublished research.
23. Y. Assayama, Embrittlement by Liquid and Solid Metals, ed. M.H. Kamdar (Warrendale, PA. TMS-AIME, 1984), p. 317.
24. N.S. Stoloff, T.L. Johnston, Acta Metall. 11(1963). p. 251.
25. A.R.C. Westwood, M.H. Kamdar, Phil. Mag. 8(1963). p. 787.
26. S.P. Lynch, "Environmentally Assisted Cracking: Overview of Evidence for an Adsorption-Induced Localized Slip Process," Aircraft Materials Report 119, Aeronautical Res. Labs, Melbourne, Australia, AR-004-516, December 1986.
27. M.A. Khristal, Sov. Phys. Dokl. 15(1970): p. 614 (in English)
28. P. Gordon, H.H. An, Metall. Trans. A 13A(1982): p. 457
29. E. Heyn, J. Inst. Met. 12(1914): p. 3.
30. C.H. Desch, J. Inst. Met. 22(1919): p. 241.
31. A.K. Huntington, J. Inst. Met. 11(1914): p. 108.
32. R. Genders, J. Inst. Met. 37(1927): p. 215.
33. W.E. Goodrich, J.I.S.I. 132(1935): p. 63.
34. T. Swinden, J.I.S.I. 148(1943): p. 441.
35. G.W. Austin, J. Inst. Met. 58(1936): p. 173.
36. L.S.G. Van Ewijk, discussion to Ref. 35 (1936): p. 187

37. W. Rostoker, J.M. McCaughey, H. Markus, Embrittlement by Liquid Metals (New York, NY: Reinhold, 1960).
38. N.V. Pertsov, P.A. Rebinder, Dokl. Akad. Nauk SSR 123(1958): p. 1068.
39. E.D. Shchukin, B.D. Summ, Y.V. Goryunov, Dokl. Akad. Nauk SSR 167(1966): p. 155.
40. J.W. Martin, J.C. Smith, Metallurgia 53(1956): p. 227.
41. A.P. Druschitz, P. Gordon, Embrittlement by Liquid and Solid Metals, p. 285.
42. "The Flixborough Disaster," Report of the Court of Inquiry, Dept. of Employment, Her Majesty's Stationery Office, May 1975.
43. N.N. Breyer, P. Gordon, Proceedings of the Third International Conference on Strength of Metals and Alloys, Vol 1 (New York, NY: Pergamon Press, 1973), p. 493.
44. D.N. Fager, M.V. Hyatt, H.T. Diep, Scripta Metall 20(1986): p. 1159.
45. W.S. Miller, M.P. Thomas, J. White, Scripta Metall. 21(1987): p 663.
46. N.M. Parikh, Environment Sensitive Mechanical Behavior, ed. A.R.C. Westwood, N.S. Stoloff (New York, NY: Gordon and Breach, 1966), p. 563.
47. M.G. Nicholas, P.J. Fernback, "Some Tensile Properties of High Purity Nickel Stressed in Alkali Metal Environments," Harwell Lab, AERE-R13057, March 1988.
48. W.T. Grubb, Nature 256(1977): p. 56.
49. R.P. Gangloff, Embrittlement by Solid and Liquid Metals, p 485.
50. M.G. Adamson, W.H. Reineking, S Vaidyanathan, T Lauritzin, Embrittlement by Liquid and Solid Metals, p. 523.
51. M.G. Nicholas, Embrittlement by Liquid and Solid Metals, p. 27.
52. V.V. Popovich, V. Kalyandruk, G. Dumukhovskaya, M.A. Peresichanskaya, Fiz.-Khim. Mekh. Mater. 20, 5(1984): p. 84.
53. J. Balaguer, D.J. Duquette, N.S. Stoloff, B. Sikora, M. Motyl, unpublished research.
54. M.G. Adamson, W.H. Reineking, S. Vaidyanathan, Metall Trans. A 17A(1986): p. 2090.
55. C.D. Beachem, Metall. Trans. 3(1972): p. 437.
56. H.K. Birnbaum, Atomistics of Fracture, ed. R.M. Latanision, F.R. Pickens (New York, NY: Plenum Press, 1983), p. 733.
57. S.P. Lynch, Corros. Sci. 22(1982): p. 925.
58. I.G. Dmukhovskaya, N.Y. Yaremchenko, Y.V. Zima, V.V. Popovich, Fiz.-Khim. Mekh. Mater. 19, 5(1983): p. 66.
59. J.R. Pickens, A.R.C. Westwood, Embrittlement by Liquid and Solid Metals, p. 51.
60. D.A. Wheeler, R.G. Hougland, J.P. Hirth, Scripta Metall. 22(1988): p. 533.
61. C.F. Old, P. Trevena, Met. Sci. 13(1979): p. 591.
62. S.P. Lynch, Mater. Sci. Eng. 72(1985): p. 633.
63. S.P. Lynch, Acta Metall. 32(1984): p. 79.
64. S.P. Lynch, Embrittlement by Liquid and Solid Metals, p 105
65. C.E. Price, J.K. Good, J. Eng. Mater. Tech. Trans. ASME 106(1984): p. 184.
66. J.A. Kapp, D.J. Duquette, M.H. Kamdar, J. Eng. Mater. Tech. 108(1986): pp. 37-43.
67. R.P. Wei, ASTM STP 675, ed. J.T. Fong (Philadelphia, PA: ASTM, 1979), p. 816.
68. N.S. Stoloff, Embrittlement by Solid and Liquid Metals, p 3
69. J.J. Lewandowski, V. Kohler, N.J.H. Holroyd, Mater Sci Eng 96(1987): p. 185.
70. H. Kimura, H. Matsui, Scripta Metall. 21(1987). p. 319
71. J.A. Kapp, Embrittlement by Liquid and Solid Metals, p. 117.
72. M.W. Macek, N.N. Breyer, Embrittlement by Liquid and Solid Metals. p. 133.
73. C.E. Price, R.G. Norman, Acta Metall. 35(1987). p. 1639.
74. T. Watanabe, S. Shima, S. Karashima, Embrittlement by Liquid and Solid Metals, p. 161.
75. T. Watanabe, S. Shima, S. Karashima, Embrittlement by Liquid and Solid Metals, p. 173.
76. T. Watanabe, S. Shima, S. Karashima, Embrittlement by Liquid and Solid Metals, p. 183.
77. V.V. Popovich, Fiz.-Khim. Mekh. Mater. 20, 5(1984): p. 84.
78. N.S. Stoloff, Atomistics of Fracture, p. 921.
79. S.P. Lynch, Mater. Sci. Eng., in press.

Discussion

B. Cox (Atomic Energy of Canada Ltd., Canada): In your classification of mechanisms for metal embrittlement, I would like to point out that for HCP metals, the decohesion and perhaps the enhanced shear mechanisms can lead to discontinuous propagation because pseudo-cleavage occurs only on (or near) the basal plane, and crack propagation must then wait for slip on the prism planes to break those grains not oriented for cleavage. In practice (e.g., Zircaloy in mercury), discontinuous acoustic emission is observed and fracture surfaces consist only of basal pseudo-cleavage and prismatic slip (there is little or no evidence for pyramidal slip).

N.S. Stoloff: In all HCP metals, slip systems are fewer in number than in cubic metals. Nevertheless, the extensive literature on metal-induced embrittlement of zinc and cadmium, as well as recent unpublished work on embrittlement of magnesium, have not provided evidence for discontinuous crack growth. Similarly, cracking of cubic metals in liquid metal environments appears to be continuous. For these reasons, I listed adsorption-induced cleavage or enhanced shear as continuous processes. The case you cite seems not to be inherent in the embrittlement process, but I would need to know more about the experimental conditions in the Zircaloy/mercury experiments to provide a more complete answer.

B. Cox: The specimens were self-stressed double-cantilever beams from a Zircaloy-2 slab with mercury contained in the top of the specimen. Acoustic emission was massive over the plateau region of the V vs K curve but appeared to be discontinuous as the crack slowed down as K_1 (LME) was approached. Signals might have been discontinuous at higher velocities but could not be resolved by our acoustic emission system.

N.S. Stoloff: I reiterate that for most HCP single-phase metals, there is no evidence for discontinuous crack growth.

R.A. Oriani (University of Minnesota, USA): I would like to suggest that it would be valuable for the development of understanding of metal-induced fracture to establish experimentally whether or not there exists an equilibrium functionality between K and the activity of an embrittling species. This could be done by using various concentrations of embrittling species in an inert metal solvent. The old work by Westwood, et al., is a step in the right direction, but it is necessary to show that the K–a curve is not kinetically determined.

N.S. Stoloff: I agree with the desirability of such a set of experiments. However, it may be difficult to find an "inert" metal carrier to which an active species could be added. This is because many metals previously thought to be nonembrittling to a given substrate turn out to be susceptible under certain conditions. Therefore, considerable care would have to be taken to avoid a contribution to embrittlement from the carrier.

J.R. Galvele (Comision Nacional de Energia Atomica, Argentina): I would like to call your attention to some work we published in *Corrosion Science* [27(1987): p. 1] where we explained environment embrittlement by a surface mobility mechanism. The crack velocities calculated, for example, for aluminum in mercury, were very close to those published by Speidel. The same happened with crack velocities measured by Verns and Staehle for high-strength steels in chlorine.

N.S. Stoloff: I thank you for calling my attention to this work. Is it possible that your mechanism relates more to the kinetics of transport of the embrittling species than to the actual bond-breaking process that causes fracture? Note also that Figure 10 of my paper, showing the influence of aging of 7075 Al on crack velocity in mercury in both Stage I and Stage II, seems to be at variance with a surface mobility model.

R. Pelloux (Massachusetts Institute of Technology, USA): One of the examples you referred to was an Al-Mg-Si alloy embrittled by lead. The da/dt vs K data for this alloy suggest that it is a case of "creep crack growth" strongly dependent upon the amount (ppm) of lead at the grain boundaries. Could this be the case for many of the examples cited?

N.S. Stoloff: The work you refer to is shown in Figure 16 of my paper. It should be possible to distinguish between creep crack growth and metal-induced embrittlement by fractography and surface analytical techniques Although creep crack growth is possible at room temperature in aluminum alloys, the authors of that study provided substantial evidence in favor of lead-induced embrittlement. However, your point is well taken that creep crack growth and metal-induced embrittlement may occur in the same temperature range. Therefore, careful analysis of test data, especially as a function of temperature and including detailed fractographic analysis, is necessary to distinguish between the two cracking mechanisms.

K. Sieradzki (The Johns Hopkins University, USA): Over recent years, considerable theoretical modeling has suggested that surface energy reductions resulting from adsorption tend to favor or enhance cleavage processes over shear. What is your current thinking regarding mechanism(s) of enhanced shear processes resulting from pure surface effects?

N.S. Stoloff: Experimental evidence (metallographic, fractographic, and *in situ* transmission electron microscopy) for enhanced shear is quite convincing, both with respect to hydrogen and metal environments. The theoretical basis for enhanced shear is not well established. The interaction of hydrogen with dislocation cores very near the surface is probably more amenable to theoretical analysis than is similar interaction between metal environments and dislocation cores. I would welcome the attention of theoreticians to this problem.

SECTION II

Corrosion Fatigue and High-Temperature Effects

Co-Chairmen's Introduction

K. Komai
Kyoto University
Kyoto, Japan

R. Pelloux
Massachusetts Institute of Technology
Cambridge, Massachusetts, USA

The first two papers of this session are concerned with the mechanisms of crack initiation and crack propagation in corrosion fatigue. The last paper deals with the role of oxidation in high-temperature fatigue.

In the paper by D.J. Duquette, he discusses the effects of corrosion on the density and distribution of persistent slip bands during fatigue of copper single crystals. He shows that there is always a corrosion current generated by cyclic plastic strains. The persistent slip bands show preferential attack and grooving. In polycrystalline copper, corrosion fatigue cracking proceeds along the grain boundaries. It is shown that the near-surface dislocation density is usually dependent upon the corrosion rate. Duquette concludes by giving a list of research problems related to corrosion fatigue crack initiation.

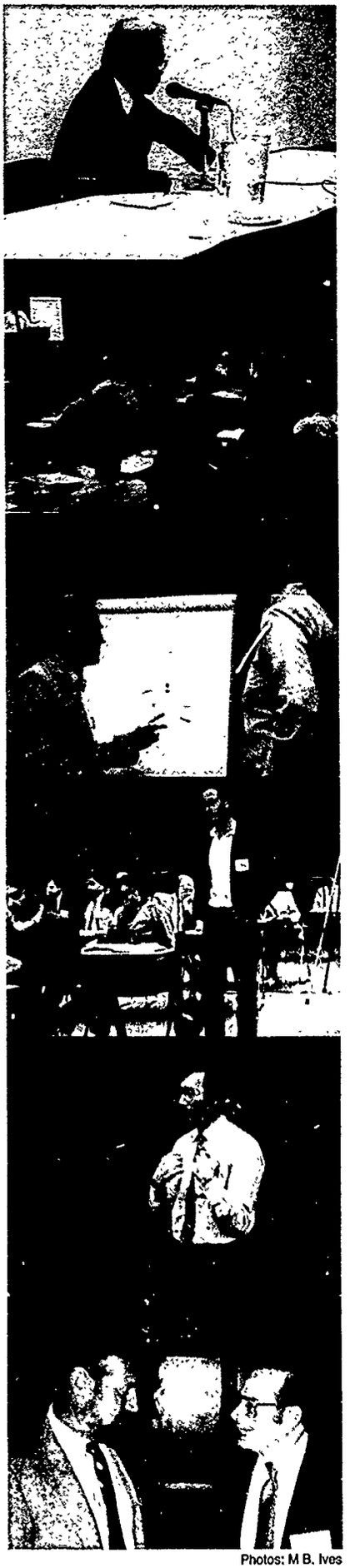
R.P. Gangloff first reviews the applicability of linear elastic fracture mechanics (LEFM) to report the fatigue crack growth data (da/dn) for long cracks in relatively inert environments. He then shows the sharp increase in the rates of crack growth that occurs in the presence of a corrosive environment with a strong effect of cyclic frequency. The roles of crack tip chemistry and crack closure are discussed. It is found that the principles of similitude, generally used in LEFM, do not work in the case of short cracks, where accelerated crack growth rates may lead to unconservative life prediction. Different models of corrosion fatigue crack growth based on hydrogen diffusion at the crack tip are available for steels. It is concluded that corrosion fatigue crack growth has a good database that needs better theoretical modeling.

The review by A. Pineau presents the mechanisms of creep fatigue–environment interactions in stainless steels and in nickel-base superalloys. He demonstrates the strong effects of loading hold times on the rates of fatigue crack growth as a result of oxidation embrittlement. The oxide layer can be either a spinel Fe(NiO) or Cr_2O_3. The latter oxide offers better resistance to grain-boundary embrittlement by oxygen.

Two types of oxidation damage are presented. Type A consists of an oxide film wedging the crack tip, Type B is related to diffusion of oxygen at grain boundaries ahead of the crack tip. The detrimental effect of oxidation is due to a reduction of fracture ductility at the tip of the fatigue crack. The acceleration of the crack growth rate because of oxidation can be modeled by including the oxidation effects in a damage rate equation. A large amount of detailed research work remains to be done to achieve a better understanding of the role of oxidation on fatigue crack growth rates.

In summary, there is a strong detrimental effect of corrosion and oxidation on fatigue crack initiation and growth. The corrosion and oxidation rates of freshly exposed microsteps at a free surface or at a crack tip are poorly understood and not quantified. Further research work on the micromechanisms of corrosion and oxidation is needed in order to derive sound life-prediction models.

These papers complete the overview of the phenomena of environment-induced cracking covered in the first phase of the conference.



Photos: M B. Ives

Corrosion Fatigue Crack Initiation Processes: A State-of-the-Art Review

*D.J. Duquette**

Abstract

This review attempts to define the areas of aqueous corrosion fatigue deformation processes that lead to crack initiation. It is apparent that there are three distinct corrosion situations under which cyclic deformation and crack initiation are affected. These situations are (1) under active dissolution conditions, (2) under electrochemically passive conditions, and (3) when bulk surface films, such as three-dimensional oxides, are formed on the surface. In the first instance, emerging persistent slip bands (PSBs) are preferentially attacked by dissolution. This preferential attack leads to enhanced mechanical instability of the free surface of a metal or alloy, and the generation of new and larger PSBs, which, in turn, lead to a localization of corrosion attack and, accordingly, crack initiation.

Under passive conditions, the relative rates of periodic rupture and reformation of the passive film appear to be the important phenomena that determine the extent to which fatigue resistance is lowered by the environment. Less is known about the surface deformation characteristics that are associated with passive metals or alloys, although it is known that changes in slip character have marked effects on the corrosion fatigue response.

When bulk oxide films are present on a surface, rupture of the film by PSBs leads to preferential dissolution of the fresh metal that is produced. However, little is known concerning the effects of such variables as film growth kinetics, film thicknesses, film plasticity, etc.

It is obvious that while a better understanding of corrosion fatigue deformation and crack initiation processes is being gained, there are still many areas that remain undefined.

Introduction

Fatigue processes can be divided into three principal mechanistic processes: (1) precrack deformation, (2) crack initiation, and (3) crack propagation. It should be noted that these divisions are essentially arbitrary and are only a convenience used in describing the phenomena, and that there is a continuity in behavior from one process to the next.

When metals or alloys are exposed to aqueous environments, it has been observed that each of these processes may be profoundly affected. The effects that are observed include changes both in microstructural development and electrochemical response. It is interesting to note that many of these changes have been observed for pure metals as well as for more complex alloys where second phases, grain boundaries, impurities, etc., can be expected to produce electrochemically inhomogeneous surfaces. These differences in microstructural evolution and electrochemical response that occur during fatigue in aqueous environments are observed under conditions of active dissolution or when a metal or alloy surface is in the passive state.

The purpose of this review is to examine the current state of understanding of precrack and crack initiation processes where "true" corrosion fatigue (CF) occurs. In this context, CF refers to the phenomena where surface dissolution or cyclic disruption of passive films results in an intrinsic sensible alteration in the conventional fatigue processes. Thus, corrosion-related phenomena such as hydrogen evolution or dissolution and their effect on fatigue behavior will not be discussed. Other effects such as precorrosion, which may result in surface roughening or pitting (and accordingly stress concentrations), will only be discussed in a historical context. Similarly, except where appropriate, the roles of metallurgical phase transformations, such as grain-boundary precipitation of carbides or other second-phase particles, which are known to have profound effects on localized corrosion resistance, will only be discussed in the context of crack initiation site preferences.

Prior to discussing the recent history of research on CF damage and crack initiation, it is interesting to note that, in contrast to some conventional fatigue processes, only a very small group of researchers is presently engaged in pursuing a basic understanding of CF crack initiation processes. This is in marked contrast to studies of CF crack propagation processes, which have been and are the subjects of numerous investigations. A review of that subject is included in the proceedings of this conference.[1]

The last comprehensive review of fatigue crack initiation processes that included CF processes was published in 1971.[2] Since then, several reviews of various aspects of CF have been published,[3-7] with the latest being published as part of a conference devoted to the chemistry and the physics of fracture, held in Bad Reichenhall, West Germany, in 1986.[8] In view of the number of reviews that has been published in the last few years, the purpose of this particular review will be to present a broad overview of the current state of understanding, to discuss some of the issues that remain unresolved, and to make suggestions for future work.

*Materials Engineering Department, Rensselaer Polytechnic Institute, Troy, NY 12180-3590.

Background

General fatigue behavior

The development of fatigue deformation, leading to crack initiation, particularly for pure metals, in the absence of aggressive environments has been extensively studied. (For more detailed discussions of the state of the art regarding general fatigue processes, see References 9 through 14.) It has been shown that the resultant deformation substructure that develops is a direct function of the microdeformational behavior of the specific metal or alloy. For example, single-phase, wavy slip metals or alloys, such as copper, copper-nickel, etc., form dense veins of dislocation tangles early in the fatigue life of the material. During the formation of these dislocation tangles, the metals or alloy cyclically harden until a saturation stress (under constant cyclic strain conditions) or strain (under constant cyclic stress conditions) is reached. At this time, the relatively uniform, veined dislocation structure begins to become unstable and bands of dislocation ladders and/or cells (ladders at low strains and cells at high strains) occur within the structure with specific crystallographic orientations (Figure 1).[15] These bands are generally glissile and their reverse slip action supports most of the cyclic plastic strain in the alloy. For many materials, the traces of these bands are readily observed at the external surface and are called *persistent slip bands* (PSBs). They were so named because it was observed that when certain metals were cyclically re-strained, after eliminating the visible slip bands by electropolishing, the glissile bands reappeared; whereas, monotonically induced slip bands, which were observed in the first quarter cycle of deformation, did not reappear. It is in these bands that fatigue crack initiation and early crystallographic crack growth occur.

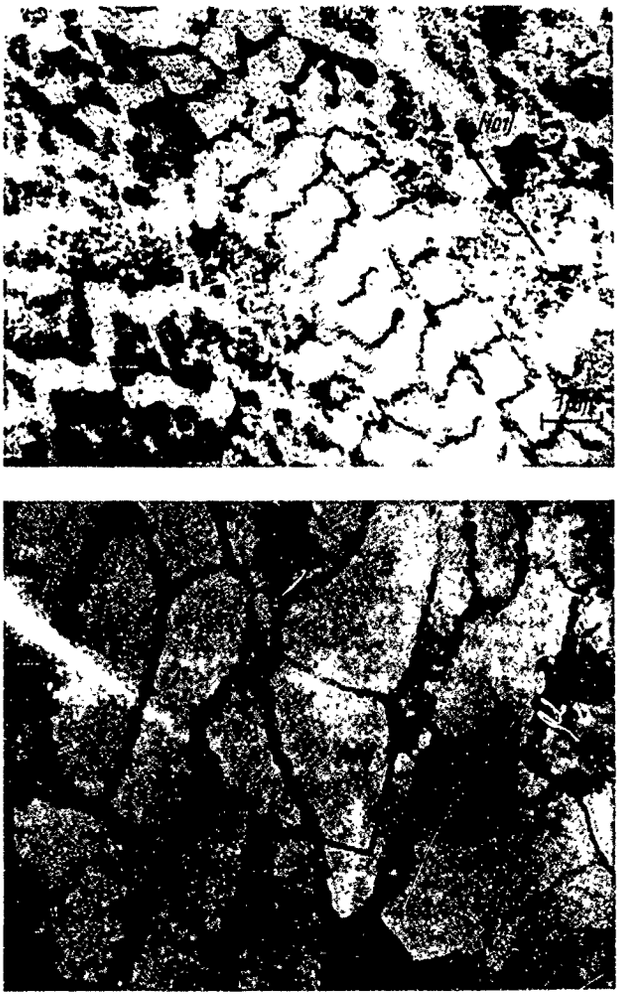


FIGURE 1—Dislocation structures in Cu single crystals: (a) ladder structure (PSB) and (b) cell structure.[15]

Planar slip alloys such as Cu-Al or Ni-Co and many precipitation-hardened alloys do not exhibit veinous or cellular dislocation structures, but rather retain their planar slip character. However, from a macroscopic point of view, they behave in a similar manner to wavy slip alloys in that they exhibit cyclic hardening, reach a saturation stress, and also generally exhibit PSBs.

Certain metals and alloys also exhibit a characteristic surface morphology known as extrusions, while still others exhibit both extrusions and intrusions. These surface-related substructures are clusters of slip bands that either erupt from the free surface (extrusions) or form notches in the surface (intrusions). While crack initiation is often associated with these structural discontinuities, they are by no means general, and many metals and alloys do not form either extrusions or intrusions; crack initiation being associated with either PSBs or, in the case of many engineering alloys, with second-phase particles that intersect the surface. Crack initiation, however, is virtually always a surface-related phenomena (barring large subsurface defects).

As has been stated, for most metals and alloys, crack initiation occurs as a crystallographic event, generally related to PSBs and/or to intrusion or extrusions. These initiated cracks are referred to as Stage I cracks and, for highly planar slip alloy, may progress for very large distances into the alloy; although for wavy slip materials, they may only progress for one or two grains. For most polycrystalline materials, the Stage I cracks eventually become approximately normal to the applied stress or strain direction, where they are referred to as Stage II cracks. It is at this juncture that fatigue crack propagation properly enters the realm of the fracture mechanician.

Corrosion fatigue behavior

Traditionally, CF crack initiation has been associated with pitting[16-19] or, alternatively, with enhanced electrochemical dissolution resulting from deformation.[20] There have also been some suggestions that the environment may lower the surface energy of a metal or alloy (the so-called "Rebinder effect"), resulting in enhanced deformation and possibly easy crack initiation.[21,22] When films are involved, rupture of the protective films by fatigue-generated deformation has also been implicated in crack initiation.[23,24] The general subject of CF was extensively studied in the 1930s and early 1940s, and then lay relatively dormant until the late 1960s when new scientific concepts related to fatigue processes as well as to electrochemical processes were evolving. There has been a marked acceleration of interest in the problem, beginning in the mid-1970s and extending to the present, particularly with the massive efforts that have coupled fracture mechanics principles to fatigue and environmentally assisted fatigue problems. In the area of corrosion-related fatigue deformation and crack initiation, however, only a small number of research efforts have been undertaken. These newer research efforts have begun to successfully couple modern fatigue concepts with electrochemical analytical techniques. In addition to the author's research efforts, significant advances have been achieved by Laird and his coworkers at the University of Pennsylvania,[31-33] by Magnin and his coworkers in France,[38-42] and somewhat earlier by Pyle and Robbins in the United Kingdom.[35-37] Much of the work of the latter two groups has been related to CF of passive alloys such as the stainless steels, whereas, the work of the former two groups has been primarily (but not exclusively) related to CF processes involving actively dissolving metals and have focused primarily on pure metals such as copper and nickel, although a considerable effort has also addressed aluminum, copper, and iron-based alloys.

Among other observations, it has been shown that controlled dissolution of a polycrystalline copper surface during cyclic deformation (under load control), results in broadening of the PSBs as well as enhanced growth of both the number and the height PSBs when compared to specimens cyclically deformed in laboratory air. In polycrystals, however, crack initiation and early propagation were, in general, primarily confined to grain boundaries (Figures 2 and 3).[24,25] When single crystals were tested, PSB formation was also enhanced, although the broadening of the PSBs (Figure 4) resulted in

a delay in crack initiation and fatigue lives that were even longer than for those observed in air.[26] These early experiments demonstrated that there is a significant interaction between the development and growth of PSBs and corrosion. PSB formation also resulted in marked electrochemical perturbations of the free surface. For example, it was shown that the dislocation-free zone, which occurs at the free surface in copper, was effectively removed (Figure 5) and that the PSBs are preferential sites for enhanced corrosion (Figures 6 and 7). Also, it was noted that the application of a cyclic load resulted in an almost reversible increase in current density when the potential of the copper was fixed (Figure 8).[27] The generality of these results was confirmed by a series of experiments conducted by Garcia and Duquette on polycrystals and on monocrystals of nickel.[28-30] These experiments were performed at constant strain amplitudes, almost exclusively with controlled electrochemical potentials. In these studies, it was shown that anodic dissolution of nickel surfaces resulted in a considerable redistribution and multiplication of PSBs when compared with the PSB morphologies obtained under cyclic deformation in air. The growth of the PSBs was, of necessity, inhibited since a larger number of PSBs accommodated the plastic strain of the metal. It was also noted that the rate of cyclic hardening appeared to be more rapid under corrosive conditions, although since the specimens were not cycled into saturation, there is still some question concerning the accuracy of this observation.[31] In fact, Laird and his coworkers have performed experiments on single crystals of copper, both unfilmed (actively dissolving) and filmed (corrosion resulting in a bulk oxide film).[32,33] For unfilmed specimens (active corrosion), an increase in the number of PSBs was reported, and the spacing of the PSBs was decreased and preferential dissolution of the PSBs was observed, which is in agreement with the results of Duquette and coworkers.[24-29] It was also reported, however, that an increase was noted in the maximum slip offset gradient, which is somewhat in disagreement and may be very significant for crack initiation processes.

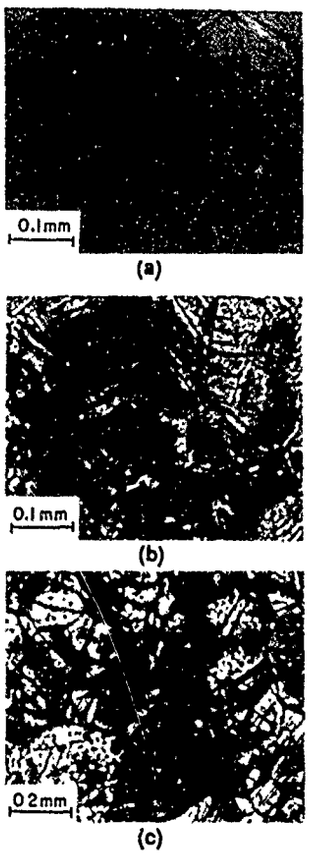


FIGURE 2—Surface characteristics of polycrystalline copper after 10^6 cycles of fatigue in[25] (a) air, (b) 0.5 N NaCl under free corrosion conditions, and (c) 0.5 N NaCl solution with an applied anodic current of 100 $\mu A/cm^2$.

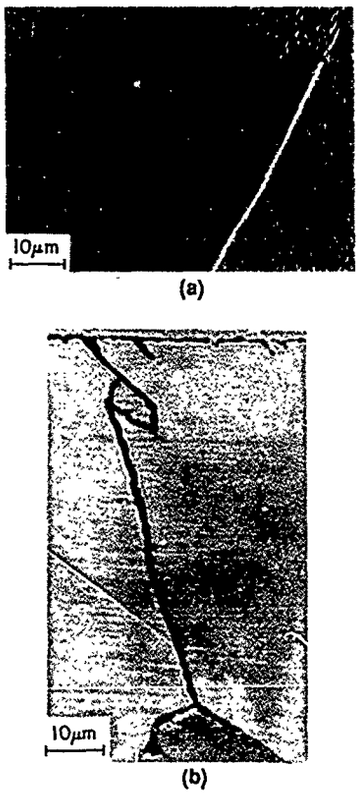


FIGURE 3—Cross sections through copper polycrystals (a) fatigued in air and (b) in 0.5 N NaCl solution with an applied current density of 100 $\mu A/cm^2$. In air, the initiated crack is entirely transgranular while under anodic dissolution conditions the primary failure crack is intergranular, although there is some transgranular initiation.[24] Enhanced deformation can also be observed at the specimen-free surface.

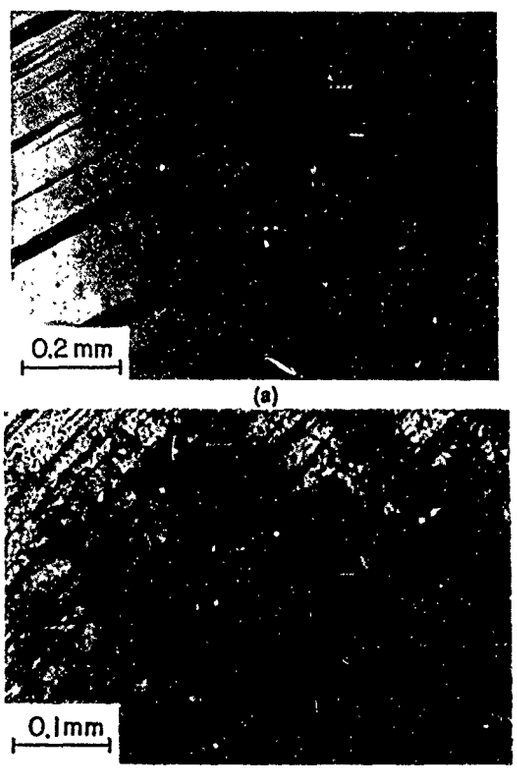


FIGURE 4—Surface slip characteristics of copper single crystals at 10^5 cycles (10% of Nf) in (a) air and (b) 0.5 N NaCl solution with an anodic current of 100 $\mu A/cm^2$.[26]

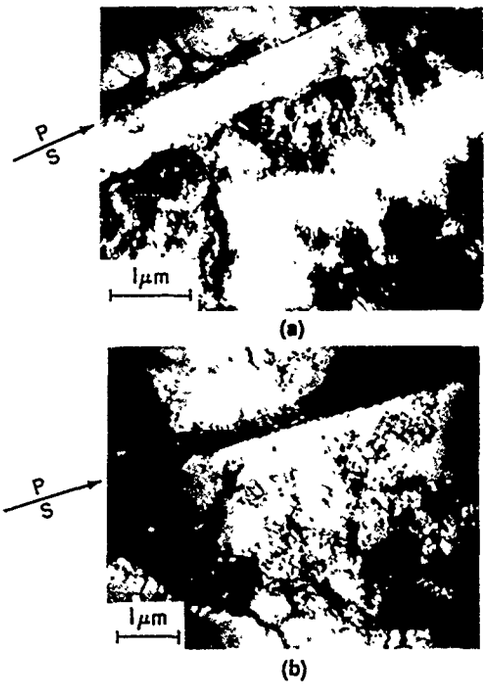


FIGURE 5—TEM micrographs of the fatigued surfaces of copper single crystals in (a) air and (b) 0.5 N NaCl solution with an applied anodic current of 100 μA/cm². P indicates deposited plate and S indicates specimen. Note that the surface-related dislocation free zone in (a) is not observed in (b).[26]

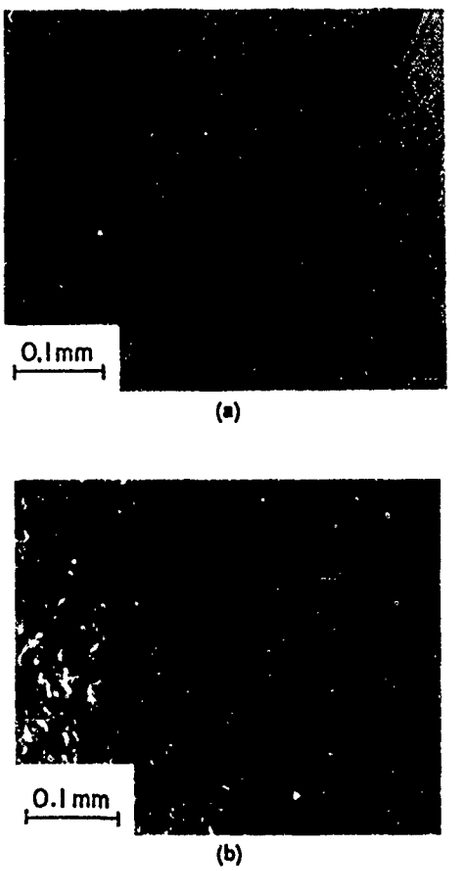


FIGURE 6—Surface deformation characteristics of similarly oriented single crystals of copper in (a) air and (b) 0.5 N NaCl solution with an applied anodic current of 100 μA/cm². The preferential corrosion attack of the PSBs is clearly shown.[26]

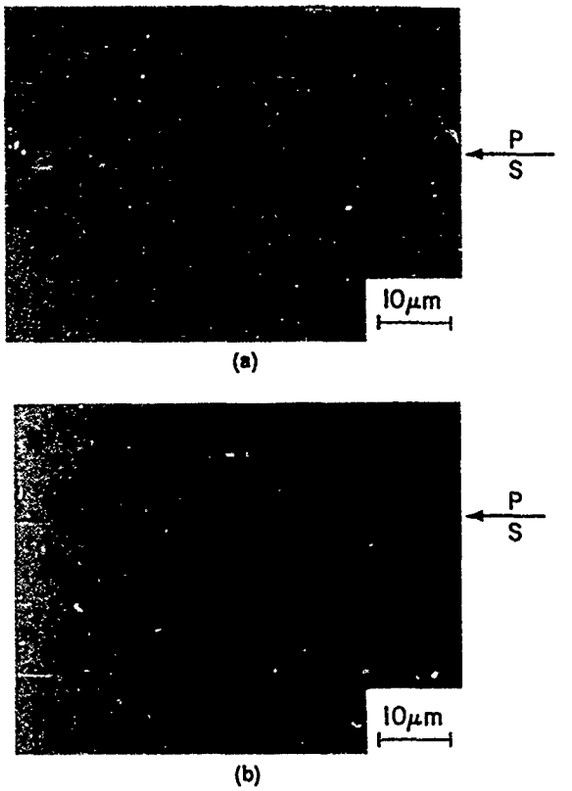


FIGURE 7—Cross sections of similarly oriented single crystals of copper in (a) air and (b) 0.5 N NaCl solution with an applied anodic current of 100 μA/cm². P indicates deposited plate and S indicates specimen. An extrusion and an associated Stage I crack are shown in (a), while the crystallographic orientation of corrosion in the same direction as the Stage I crack is shown in (b).[26]

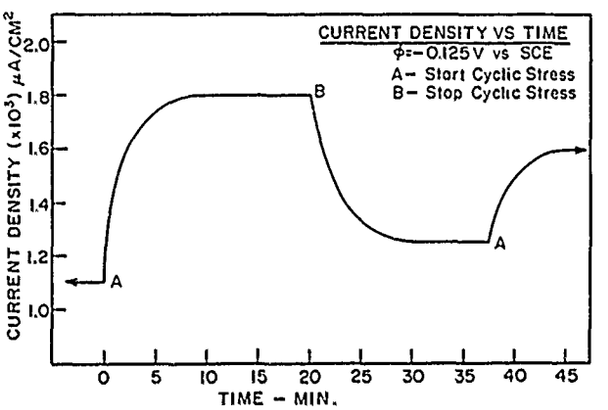


FIGURE 8—Measured current density as a function of applied cyclic stress for a copper single crystal held at a potential of −0.125 V vs SCE in 0.5 N NaCl solution.[27]

However, the work performed under oxidizing (but presumably not filmed) conditions showed no effect on the rapid hardening rate or on the cyclic stress-strain curve.[32] Results obtained on filmed specimens, on the other hand, showed some effect in that the hardening rate increased with a small "overshoot" in the stress prior to saturation, but no effect on the saturation stress itself.[31] The generality of these results remains to be determined.

In another study of the CF behavior of copper, Yan and Laird also demonstrated that there are strong interactions between simultaneous corrosion and cyclic straining in that enhanced corrosion was observed.[32,33] They confirmed the results of Duquette, et al.,[24-29] that enhanced dissolution is caused by the emergence of mobile dislocations, specifically, enhanced dissolution of metal

atoms associated with those dislocations that form the PSBs. This study also concluded that below a critical preferential corrosion rate, corrosion has no appreciable effect on fatigue resistance.[32] A similar result had been reported for carbon steels,[34] although Yan and Laird indicated that the critical corrosion rate was specific to PSBs rather than a general corrosion rate.

For filmed surfaces, Ortner[31] has reported that even thin films impede dislocation egress and increase the rate of rapid hardening. This makes PSB formation more difficult than in air and impedes intrusion/extrusion formation.[31] Upon penetration of the film by PSBs, the corrosion rate of the copper suddenly increases. This is in accordance with the results reported by Hahn.[27] A decrease in the rest potential was also observed by both investigators, and Hahn determined that it was virtually reversible; i.e., when cyclic loading of the metal was interrupted, the corrosion potential returned to the original rest potential (Figure 9). Thus, there is an implication that dynamic straining shifts the potential of anodic regions on the surface in the active direction. Whether this results from a physical shift in the reversible potential because of the strain energy or to a decrease in the anodic reaction kinetics because of the ease in removing unstable atoms (resulting from local strains) by electrochemical dissolution is not yet known.

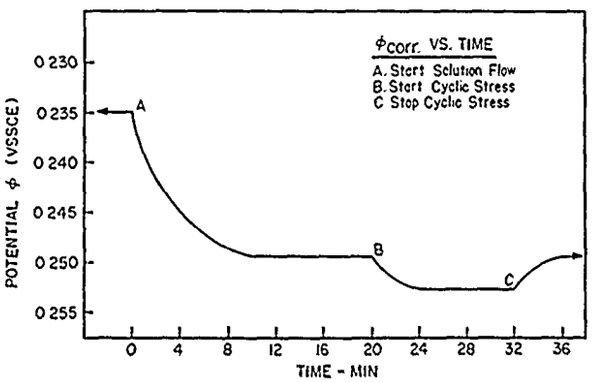


FIGURE 9—Measured potential as a function of applied cyclic stress for a copper single crystal under free corrosion conditions in 0.5 N NaCl solution.[27]

With reference to surfaces covered with ultra-thin films (passive), Rollins, Patel, and Pyle have pioneered some electrochemical studies relating cyclic deformation to current transients under electrochemical potential control.[35-37] By examining a diverse group of alloys, including mild steel, stainless steels, and aluminum alloys, they have demonstrated that there are significant current transients associated with each cycle of plastic strain. In general, current spikes associated with more or less rapid decays were observed in both tension and compression when the peak currents increased with increasing cycles, CF resulted; whereas, if peak currents decreased with increasing numbers of cycles, cracks were not initiated (Figure 10). These results suggested a definite relationship between cyclic plastic strain, repassivation rates after passive film rupture, and CF failures.

This type of experimentation has been considerably refined by Magnin and his coworkers.[38-42] In their work, the saturation peak stress for a 26Cr-1Mo stainless steel was shown to be identical in air and in aggressive solutions, confirming the generality of the result that had been reported for copper. It was also noted that the free corrosion potential decreased (moved in the active direction) during rapid hardening, increased at saturation, and decreased again at crack initiation. This suggests that newly exposed metal, resulting from cyclic slip-band generation, prior to crack nucleation, locally destroys the passive film. The film then attempts to repair itself when the stress level is constant (at saturation), shifting the potential in the noble direction, and is broken again at crack initiation. Thus, it appears that the rapid hardening portion of the cyclic stress–strain curve is very important to localized passivation and repassivation. It was also observed that the free corrosion potential cycled in parallel with the strain, reaching the largest negative potential at the maximum tensile applied strain. All of these effects were observed to be functions of the strain rate, with high strain rates leading to more intense local depassivation and dissolution (Figure 11). This is an interesting result since it had been widely believed that CF is not expected to be a problem at high frequencies. Obviously, frequency effects (and associated strain rates) are important parameters, and the amount of corrosion that occurs in each cycle must be compared with the repassivation rate (for alloys that show active-passive transitions). Table 1 indicates the effects of strain rate on the surface damage characteristics of 26Cr-1Mo stainless steels, at different levels of strain, and indicates the role of the deformation mode on the crack initiation mode in air and in 3.5% NaCl solution.[39]

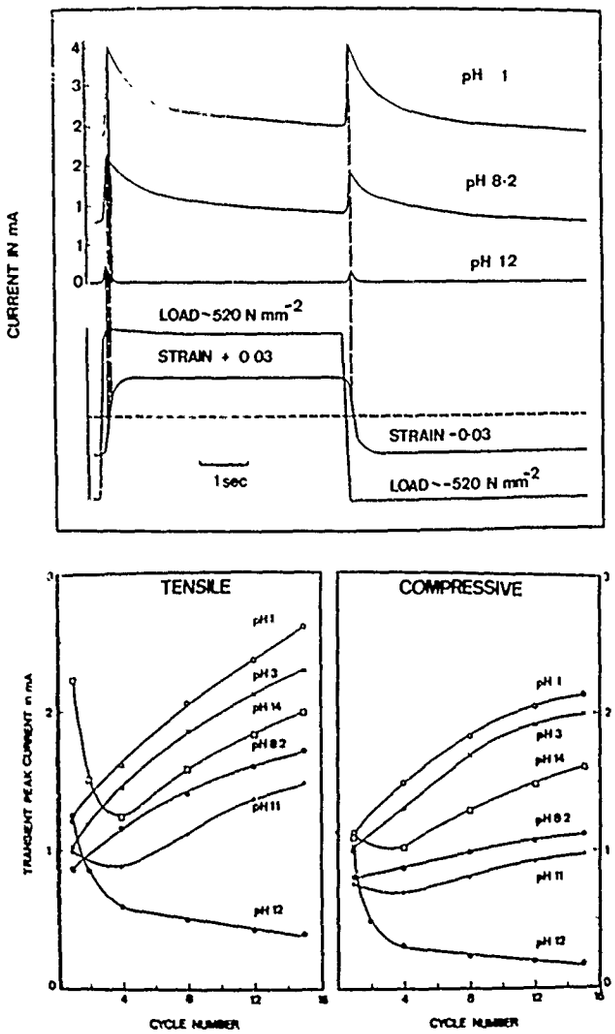


FIGURE 10—(a) Typical dissolution transients for mild steel fatigued in 3.5% NaCl solutions. (b) Variations of peak current densities associated with current transients and cyclic strains as a function of a number of applied strain cycles for mild steel in 3.5% NaCl. All pHs except pH 12 resulted in reductions in fatigue resistance when compared to laboratory air.[37]

Additionally, also using 26Cr-1Mo stainless steels, current transients under electrochemical potential control were observed. An example of these results is shown in Figure 12 where it is noted that in accordance with the work of Patel, Pyle, and Rollins, current transients are larger in tension than in compression. The total amount of metal that is dissolved is related to the area under the curve. However, the shapes of the current transient curves cannot be readily explained by single events rupturing the passive film. Rather, it is imagined that the curve is actually the sum of consecutive film ruptures by individual or groups of slip bands that are activated at

different stress or strain levels. A schematic diagram showing this sequence is shown in Figure 13.

Thus, it is apparent that there are at least three major electrochemical and/or environmentally related conditions that affect CF precrack deformation and crack initiation. These are under conditions of (1) active dissolution (unfilmed), (2) passivity (ultra-thin films), and (3) where a bulk oxide film either pre-exists or is formed during exposure to fatigue, on the surface.

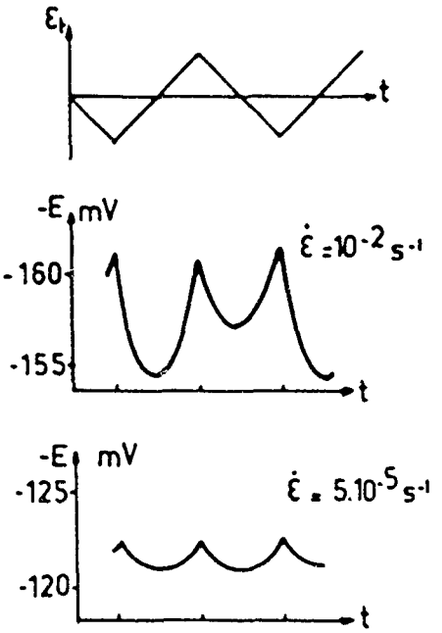


FIGURE 11—Influence of strain rate on the cyclic evolution of potential as a function of straining for an Fe-26Cr-1Mo alloy. The higher strain rate exhibits larger potential swings an assymetry in tension vs compression and more active potential shifts.[38]

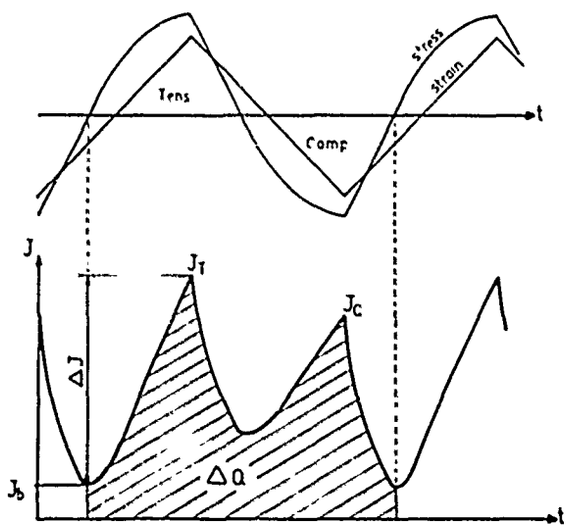


FIGURE 12—Current transient characteristics at constant electrochemical potential for Fe-26Cr-1Mo in 3.5% NaCl solution.[39]

In the first case, there is strong evidence that there is a definitive interactive reaction between the deformation induced by cyclic stresses or strains and the corrosive environment. This interaction is supported by the observation that the PSB distribution is altered by active dissolution of the surface, and by the observation that the geometry of the PSBs is also altered by the dissolution process. These observations have now been made on polycrystalline and monocrystalline pure copper as well as nickel, on high-purity polycrystalline Cu-Al alloys,[43] and on a commercial Cu-Ni-Cr-Fe alloy, both in the solutionized and in the aged heat-treatment condition.[25] There is also a strong implication that a similar rearrangement of intrusions and extrusions occurs in low-carbon steels.[34,44]

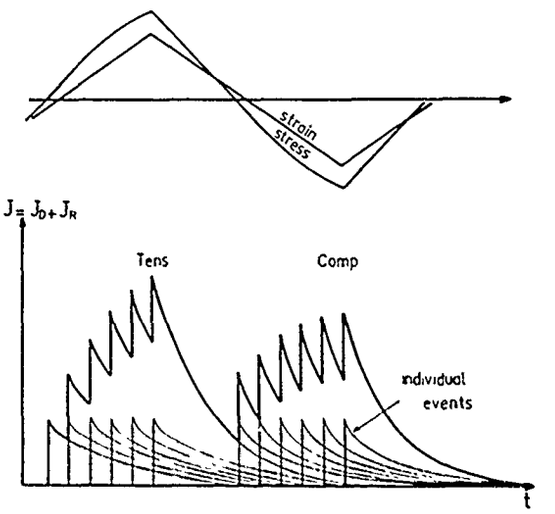


FIGURE 13—Schematic representation of the current transients at an applied electrochemical potential. The total current is made up of the sum of individual film-rupture events, the number of which is a function of the applied strain.[39]

It is the current belief of this investigator that the rearrangement of the surface deformation morphology occurs because of enhanced corrosion reactions of metal atoms that surround mobile dislocations and that are associated with the cyclic surface slip processes as they interact with the free surface. While it has been demonstrated that PSBs may form within a crystal when fatigue deformation occurs in air (in contrast to being observed only at the surface),[13,45,46] it is quite probable that the PSBs observed under active dissolution conditions are virtually all surface initiated. When fatigue occurs in nonaggressive environments, some slip bands become sessile (or nonpersistent) after the first one or at most few cycles, while others remain glissile and eventually become PSBs. When surface dissolution occurs, however, back stresses that may be generated because of surface-dislocation interactions are relieved,[31] and more slip bands become mobile, resulting in a higher density as well as a more uniform distribution of PSBs. This hypothesis is supported by the observation that the dislocation-free zone associated with the free surfaces of fatigued copper is eliminated under conditions of even mild dissolution.[15,26] Under strain control, the requirement for strain compatibility requires that if there are more PSBs, then the average slip offset height must, in general, be less, as is observed. Under load control, on the other hand, a form of low-temperature creep may actually occur, where more PSBs are generated and the removal of back stresses in the PSBs, by surface dissolution results in enhanced surface slip offsets, as well as a more uniform distribution of the PSBs. In this case, a saturation strain may not be observed for constant-load applications. While there is some limited evidence for such a phenomenon, further research must be conducted to verify this hypothesis.

TABLE 1
Influence of Strain Rate on the Crack Initiation Processes[39]

$\dot{\epsilon}$ (s^{-1})	$\Delta\epsilon_p/2$	Surface Damage	N_i(±5%)		Crack Initiation Mode	
			In air	In 3.5% NaCl	In Air	In 3.5% NaCl
5×10^{-5}	4×10^{-3}	Persistent slip bands	1200	1150 (pH6)	Transgranular in persistent slip bands	At persistent slip band–grain boundary intersections
10^{-3}	4×10^{-3}	Strain localization at grain boundaries	1490	700 (pH6) 350 (pH2)	Intergranular	Intergranular mixed
10^{-2}	4×10^{-3}	Strain localization at grain boundaries	1600	1200 (pH6)	Intergranular	Intergranular
10^{-2}	4×10^{-4}	Glide of edge dislocations	17,000	13,000 (pH6)	Transgranular	Transgranular
10^{-2}	10^{-4}	Glide of edge dislocations	95,000	60,000 (pH6)	Transgranular	Transgranular

With reference to the electrochemistry of the PSB/matrix couple when active corrosion is occurring, it appears that there is a partitioning of electrochemical potentials under open circuit (or free corrosion) conditions since there is a shift in the corrosion potential in the active direction.[27-31] This may result from an alteration in the reversible potential of anodic areas (the PSBs) or to a reduction in the activation energy for dissolution of the metal associated with the emerging PSBs. The latter suggestion is more likely since it has been shown that there is only a minuscule shift in the reversible potential even when a metal is heavily cold worked,[47] whereas, the shift in the corrosion potential for copper during cyclic loading is on the order of 10 mV in NaCl[27] and on the order of 100 mV in a strong oxidizing environment, $NaClO_4$, where a bulk film is formed on the surface.[31] In this case, the shift in potential also may be a measure of an alteration in reversible potential because of local destruction of the oxide film and the consequent exposure of bare, or unfilmed, metal. It is important to note that under active dissolution conditions, interruption of cyclic stressing causes the rest potential to return to the stable, more noble potential, which is measured prior to applying the cyclic load. Thus, the electrochemical shift in the rest potential upon cyclic loading must be associated with the emergence of fresh metal that is provided to the environment by the continued to-and-fro motion of the PSBs. It is further suggested that atoms associated with mobile dislocations in the PSBs are dissolved more readily than atoms that are only in the matrix. This is indicated by the preferential dissolution of the PSBs and, in particular of PSB/matrix interfaces under constant applied current conditions.[28] Under constant applied potentials, there is a partitioning of current between the matrix and the PSBs, which results in higher anodic current densities at the PSBs and, accordingly, preferential corrosion of the PSBs. This preferential corrosion accelerates further development of the PSBs or, if constant strain is imposed, results in the initiation of new PSBs. For very ductile single crystals, this sometimes results in a delay in the crack initiation process. However, for polycrystals, the enhanced deformation associated with grain boundaries results in preferential dissolution of metal associated with the PSBs that are generated by strain interactions with the boundaries. This, in turn, intensifies slip at the boundaries, with the result being total grain-boundary separation under CF conditions, whereas, transgranular crack initiation and propagation are generally observed in less aggressive media. Interestingly, a similar shift in the crack initiation site is also observed when large cyclic strains are applied to metal polycrystals.[48-50] Thus, the effect of surface dissolution may be equivalent to the local application of large strains. Accordingly, intergranular crack initiation is primarily observed in pure metals, where very significant slip processes are required to initiate fatigue cracks. For engineering alloys, enhanced slip associated with second-phase particles, or with nonmetallic inclusions, probably has an equivalent result except that transgranular CF cracking occurs. In every case, however, enhanced plasticity interacts with corrosion processes to further enhance local plasticity and accordingly affect fatigue crack initiation.

The observations that dissolution promotes surface plasticity, which, in turn, favors dissolution of the plastically deformed regions of a metal or alloy surface, also has important implications for both Stage I and II crack growths. The concept of environmentally affected plasticity has been suggested by the creep experiments of Revie and Uhlig,[51-53] and Lynch has suggested that aqueous environments may affect dislocation initiation processes at growing crack tips, resulting in crack surfaces that appear more "brittle."[50-56] In the first case, enhanced room temperature creep of copper was associated with divacancy injection into the metal surface by anodic dissolution of copper atoms, with the result that dislocation climb was believed to be enhanced. In the second case, chemisorption on the metal or alloy crack surface is believed to enhance dislocation generation (source activation) and accordingly increase the amount of shear associated with crack propagation. It is well known that fatigue intrinsically generates large concentrations of vacancies,[57] and it is likely that this excess of vacancies is primarily concentrated in the PSBs or at least at the PSB/matrix interfaces resulting from the dislocation dipoles in that interface.[13] Thus, it is unlikely that a small number of divacancies generated by surface dissolution could significantly alter the extent of surface slip. In the second case, chemisorption is credited with reducing the plastic zone size at a growing crack tip, rather than with an increase in plasticity. The results cited here, however, indicate a marked increase in local plasticity resulting from dissolution processes, and it is believed that this occurs because dislocation locking processes, i.e., tangles, sessile slip bands, etc., are effectively removed by dissolution, thus leading to surface destabilization. Accordingly, if surface plasticity is directly affected by active dissolution during cyclic stressing or straining, it is reasonable to assume that plasticity at a nucleated or growing crack (either Stage I or II) will be similarly affected. Thus, the enhanced growth rate often associated with CF (and sometimes modeled by superposition equations, which simply add fatigue crack growth rates to corrosion rates) may, in fact, be more rapid because of both enhanced plasticity and enhanced corrosion acting in concert. This is obviously a very interesting area for further research.

Future Work

Effects of passive films

With respect to CF crack initiation under conditions of electrochemical passivity, the bulk of the work to date has been associated with local breakdown and reformation of the passive films and has been primarily electrochemically related. As has been suggested for stress corrosion cracking, the rate of repair of the passive film relative to the rate of generation of fresh surface by deformation processes is apparently the key factor controlling precrack deformation and localized attack, leading to crack initiation. Interestingly, if this is correct, higher frequencies, or at least intermediate frequencies, may be more damaging than lower frequencies since repassivation is time dependent, and, in the absence of repassivation, active local attack of a fresh surface may dominate. There is some evidence for this behavior in the work of Magnin and coworkers, although they have attributed the decrease in crack initiation time to a change in the slip character for the alloy they have studied most extensively (a ferritic stainless steel). The roles of passivity and the cyclic, mechanical breakdown of passivity appear to be among the most fruitful areas for future study. In particular, it may be important to vary the amount of fresh metal provided to the environment by varying the strain levels in order to monitor the current transients as a function of such variables as the oxidizing power of the environment, the strain rate, strain orientation, frequency effects, and wave shape effects.

Effects of bulk oxide films

Surfaces covered with bulk oxide films appear to be an extension of the passive film situation with the added complication of the physically significant (and measurable) back stresses provided by the oxide. Ortner, for example, has shown that these back stresses can be a significant factor in reaching the saturation stress.[31] Thus, the rate of reformation of the oxide once it is ruptured by emerging slip bands is an important variable in determining CF deformation and crack initiation. Likewise, the nucleation of a bulk oxide on emerging slip steps may be very important to slip reversibility and thus may increase the rate of formation of PSBs. The physical and mechanical properties of bulk films formed during fatigue processes may also have profound effects on CF behavior. As with the effects of passivity, the roles of bulk oxide films on CF deformation and crack nucleation have only been cursorily examined.

Summary

To summarize the areas of research that could be fruitfully addressed in the future, it appears that reasonable concepts have been developed concerning CF behavior under actively corroding conditions, at least for pure metals and possibly for single-phase alloys. A great deal of work remains to be performed to refine the details of the models that have been proposed and to extend the models to alloy systems. The roles of passivity and of bulk oxide films are less well understood and should be addressed in the near future.

It should be noted that many other effects of environment on fatigue deformation and crack initiation have not been addressed in this brief discussion For example, the effects of hydrogen have been shown to be very important to fatigue resistance, and since hydrogen is readily dissolved by many metals and alloys, it can be expected to have significant effects on fatigue deformation and crack initiation. Likewise, elevated-temperature environmental interactions have also not been considered here, although they are certainly important in fatigue processes, and while some of the aspects of each of these cases have been addressed, particularly related to fatigue crack growth processes, there is even less known concerning their effects on fatigue deformation and crack initiation than there is in the area of aqueous CF.

References

1. R.P. Gangloff, "Corrosion Fatigue Crack Propagation in Metals," this proceedings.
2. C. Laird, D.J. Duquette, Corrosion Fatigue, NACE-2, ed. O. Devereux, A. McEvily, R. Staehle (Houston, TX: National Association of Corrosion Engineers, 1971), p. 88.
3. Corrosion Fatigue Technology, ASTM STP642, ed. H.L. Craig Jr., T.W. Crooker, D.W. Hoeppner (Philadelphia, PA: ASTM, 1978).
4. Conference Proceedings of the Influence of Environment on Fatigue (London, England: Institute of Mechanical Engineering, 1978).
5. Corrosion Fatigue: Mechanics, Metallurgy, Electrochemistry and Engineering, ASTM STP801, ed. T.W. Crooker, B.N. Leis, (Philadelphia, PA: ASTM, 1984).
6. Basic Questions in Fatigue, Vols. I and II, ASTM STP, ed. R.P. Wei, J.T. Fong, R.J. Fields, R.P. Gangloff (Philadelphia, PA: ASTM, 1988).
7. D.J. Duquette, Fatigue and Microstructure, ed. M. Meshii, (Metals Park, OH: ASM International, 1979), p. 339.
8. R.P. Gangloff, D.J. Duquette, Chemistry and Physics of Fracture, ed. R.M. Latanision, R.H. Jones (Dordrecht, The Netherlands: Martinus Nijoff, 1987).
9. A. Cheng, C. Laird, Mater. Sci. Eng. 51(1981): p. 111.
10. H. Mughrabi, Mater. Sci. Eng. 33(1978): p. 207.
11. N.Y. Yin, A.T. Winter, Acta Metall. 32(1984): p. 989.
12. A. Abel, Mater. Sci. Eng. 36(1978): p. 117.
13. J.M. Finney, C. Laird, Phil. Mag. 31(1975): p. 339.
14 A Cheng, C Laird, Fat. Eng. Mater. Struc. 4(1981): p. 331.
15 P Lukas, M Klesnil, J. Krejci, Phys. Stat. Srl. 27(1968). p. 545.
16. H.J. Gough, J. Inst. Metals 49(1932): p. 17.
17. D.J. McAdam, ASTM 28II, 1928, p. 117.
18. D.J. McAdam, G.W. Geil, Proc. ASTM 41(1928): p. 696.
19 J Congleton, R.A Olieh, R.N. Parkins, Metals Tech. 9(1984). p. 94.
20. D. Whitwham, U.R. Evans, J.I.S.I. 165(1950): p. 76.
21 E K. Venstrem, P.Q. Rebinder, Z. Fiz. Khim 26(1952). p. 12.
22 S P Lynch, Fatigue Mechanisms, ASTM STP675, ed. J.T. Fong (Philadelphia, PA: ASTM, 1979), p. 174.
23. K. Laute, Oberflachentech 10(1933): p. 281.
24 H N Hahn, D.J. Duquette, Metall. Trans. 10A(1979). p. 1453.
25. H. Masuda, D.J. Duquette, Metall. Trans. 6A(1975): p. 87.
26. H.N. Hahn, D.J. Duquette, Acta Metall. 26(1978): p. 279.
27. H.N. Hahn (Ph.D. diss., Rensselaer Polytechnic Institute, 1977).
28. C. Garcia, D.J. Duquette, Corrosion of Nickel Based Alloys, ed. R.C. Scarbury (Philadelphia, PA: ASTM, 1985), p. 127.
29. C. Garcia, D.J. Duquette, Modeling Environmental Effects on Crack Growth Processes, ed. R.H. Jones, W.W. Gerberich (Warrendale, PA: The Metallurgical Society-American Institute of Mining, Metallurgical, and Petroleum Engineers, 1986), p. 343.
30. C. Garcia (Ph.D. diss., Rensselaer Polytechnic Institute, 1982).
31. S.R. Ortner (Ph.D. diss., University of Pennsylvania, 1985).
32. B.D. Yan, G.C. Farrington, C. Laird, Acta. Metall. 33(1985): p. 1533.
33. B.D. Yan, G.C. Farrington, C. Laird, Acta Metall. (1985): p. 1593.
34 D.J. Duquette, H.H. Uhlig, Trans. ASM 62(1969). p. 839.
35 T. Pyle, V. Rollins, D. Howard, J. Electrochem. Soc. 122(1975): p. 1445.
36. C. Patel, Corros. Sci. 21(1981): p. 145.
37. C. Patel, T. Pyle, V. Rollins, Mechanisms of Environment Sensitive Cracking of Materials, ed. P.R. Swann, F.P. Ford, A.R.C. Westwood (London, England: The Metals Society, 1977), p. 390.
38. T. Magnin, L. Coudreuse, Fatigue 84, Vol. III, Birmingham, ed. C.J. Beevers (1984), p. 1447.
39. T. Magnin, L. Coudreuse, Mater: Sci. Eng. 72(1985): p. 125.

40. T. Magnin, L. Coudreuse, Acta Metall. 8(1987): p. 2105.
41. T. Magnin, J.M. Lardon, Mater. Sci. Eng. 76(1985): p. L7.
42. T. Magnin, L. Coudreuse, J.M. Lardon, Basic Questions in Fatigue, Vols. I and II, ASTM STP, ed. R.P. Wei, J.T. Fong, R.J. Fields, R.P. Gangloff (Philadelphia, PA: ASTM, 1988).
43. P. Andresen, "The Effect of Environment and Applied Current on Corrosion Fatigue of Cu-7.8% Al" (Master's thesis, Rensselaer Polytechnic Institute, 1972).
44. D.J. Duquette (Ph.D. diss., Massachusetts Institute of Technology, 1968).
45. R. Wang, H. Mughrabi, Mater. Sci. Eng. 65(1984), p. 235.
46. A.T. Winter, O.B. Peterson, K.V. Rasmussen, Acta Metall 29(1981): p. 735.
47. H.H. Uhlig, Physical Metallurgy of Stress Corrosion Fracture, ed. T. Rhodin (New York, NY: Interscience, 1959), p. 1.
48. D.S. Kemsley, Phil. Mag. 2(1957): p. 131.
49. C. Laird, G.C. Smith, Phil. Mag. 8(1963): p. 1945.
50. R.C. Boettner, C. Laird, A.J. McEvily, Trans. AIME 233(1965): p. 379.
51. R.W. Revie, H.H. Uhlig, Acta Metall. 22(1974): p. 619.
52. R.W. Revie, H.H. Uhlig, Corros. Sci. 12(1972). p. 669.
53. H.H. Uhlig, J. Electrochem. Soc. 123(1976): p. 1699.
54. S.P. Lynch, Atomistics of Fracture, ed. R.M. Latanision, J.R. Pickens (New York, NY. Plenum Press, 1983), p. 955.
55. S.P. Lynch, Mechanisms of Environment Sensitive Cracking of Materials, ed. P.R. Swann, F.P. Ford, A.R.C. Westwood (London, England: The Metals Society, 1977), p. 201.
56. S.P. Lynch, Fatigue Mechanisms, ASTM STP675, p. 174.
57. N. Thompson, N.J. Wadsworth, Adv. Phys. 7(1958). p. 72.

Corrosion Fatigue Crack Propagation in Metals

*R.P. Gangloff**

Abstract: Conclusions of the Review

The objective of this paper is to critically compile and evaluate experimental results and mechanistic models for corrosion fatigue (CF) crack propagation in structural alloys exposed to ambient temperature gases and electrolytes. Data and models are based on continuum fracture mechanics descriptions of crack-tip stress and strain fields, coupled with continuum modeling of occluded crack mass transport and chemical reactions. The aim is to inform the person seeking to broadly understand environmental effects on fatigue, to provide an experimental basis for life-prediction analyses and evaluations of mechanistic models relevant to specialists, and to define current uncertainties and worthwhile directions for CF research.

The second section ("Introduction") provides an introduction to CF crack propagation. The state of the art that emanated from the Storrs and Firminy conferences is summarized. Qualitative mechanisms for cracking are presented.

The third section ("The Fracture Mechanics Approach") assesses the fracture mechanics approach to CF, while the fourth section ("Experimental Procedures") considers experimental methods. The following conclusions are established:

(1) Fracture mechanics descriptions of CF crack propagation, viz., growth rate as a function of stress-intensity factor, provide an established and physically meaningful basis that couples alloy performance, damage mechanisms, and life-prediction studies through the concept of growth-rate similitude. Extensive databases have been developed for structural alloys over the past three decades.

(2) Experimental methods are developed for determinations of average crack growth rate as a function of continuum fracture mechanics crack-tip parameters, particularly ΔK. Nonsteady-state crack growth, unique to CF, and crack closure are not understood. Future procedures will incorporate precision crack-length measurement and computer control of stress intensity to develop quantitative and novel CF crack growth rate data, particularly near threshold. Advances have been recorded in measurements of small crack growth kinetics; however, such approaches are not easily adapted to controlled environments. The fundamental experimental problem is the lack of methods to probe mechanical and chemical damage processes local to the CF crack tip.

The fifth section ("Effects of Critical Variables") illustrates important variables that affect CF crack growth. The following is concluded:

(3) A plethora of interactive variables influences the CF crack growth rate–stress intensity relationship. The effects of chemical, metallurgical, and mechanical variables are well characterized and reasonably explained by qualitative arguments. Growth rates are affected by environment chemistry variables (viz., temperature; gas pressure and impurity content; electrolyte pH, potential, conductivity, and halogen or sulfide ion content); by mechanical variables such as ΔK, mean stress, frequency, waveform, and overloads; and by metallurgical variables including impurity composition, microstructure, and cyclic-deformation mode. Time, or loading frequency, is critical, complicating long-life component performance predictions based on shorter-term laboratory data. Limited studies show that yield strength is not a critical variable in cycle-time-dependent CF. Fractographic analyses of microscopic crack paths provide a basis for failure analyses and input to mechanistic studies.

The sixth section ("Quantitative Models of Corrosion Fatigue Crack Propagation") develops the mechanical crack-tip field and chemical mass transport and reaction components that are central to quantitative models of CF crack growth rates. Current predictions of crack growth rate, from both the hydrogen embrittlement and dissolution/film-rupture perspectives, are discussed.

*Department of Materials Science, University of Virginia, Charlottesville, VA 22903-2442.

(4) Micromechanical–chemical models of crack-tip driving forces and process-zone CF damage provide a sensible means to predict and extrapolate the effects of variables and to modify the fracture mechanics approach to account for compromises in similitude. Models have been formulated based on hydrogen embrittlement and film rupture/transient dissolution/repassivation. Fatigue damage due to crack surface films has not been considered quantitatively. Models successfully predict the time (frequency) dependence of CF and the effects of electrode potential, solution composition, and gas activity. All are, however, hindered by uncertainties associated with crack-tip processes and the fundamental mechanisms of environmental embrittlement. A process-zone model has not been developed for CF; as such, stress-intensity, yield-strength, and microstructure effects are not predictable. Furthermore, absolute rates of hydrogen-assisted crack growth are not predictable, and the film-rupture formulation is being debated. Successes to date indicate that a new level of mechanistic understanding is achievable.

The seventh section ("Complications and Compromises of Fracture Mechanics") reviews processes that compromise the fracture mechanics approach to CF.

(5) Fracture mechanics descriptions of CF and the similitude concept are complicated by the inability of stress intensity to describe the controlling crack-tip mechanical and chemical driving forces. The so-called closure, small crack, and high-strain problems in mechanical fatigue are relevant to CF. Data and analyses demonstrate that the unique relationship between da/dN and ΔK is compromised by mechanisms, including (a) premature crack-wake surface contact, (b) deflected, branched, and multiple cracking, and (c) time- and geometry-dependent occluded crack chemistry. Stress-intensity descriptions of elastic-plastic stresses, strains, and strain rates in the crack-tip plastic zone are uncertain within about 5 μm of the crack tip, within single grains that are not well described by the constitutive behavior of the polycrystal, and when deformation is time or environment sensitive. These limitations do not preclude the only quantitative approach developed to date to characterize subcritical crack propagation. Rather, they indicate the need for crack-tip modeling.

The eighth section ("Necessary Research") suggests necessary directions for future research in CF.

(6) Opportunities exist for research on CF: (a) to broaden phenomenological understanding, particularly near threshold, (b) to develop integrated and quantitative microchemical–mechanics models, (c) to develop experimental methods to probe crack-tip damage and to measure near-threshold cycle–time-dependent crack growth, (d) to characterize the behavior of advanced monolithic and composite alloys, and (e) to develop damage-tolerant life-prediction methods and *in situ* sensors for environment chemistry and crack growth.

A table of contents is provided in Appendix A.

Introduction

Corrosion fatigue (CF) is defined as the deleterious effect of an external chemical environment on one or more of the progressive stages of damage accumulation that constitute fatigue failure of metals, compared to behavior in inert surroundings. Damage results from the synergistic interaction of cyclic plastic deformation and local chemical or electrochemical reactions.

The cumulative damage processes for environmentally assisted fatigue are subdivided into four sequential categories: (1) cyclic plastic deformation, (2) microcrack initiation, (3) small crack growth to linkup and coalescence into a single short crack, and (4) macrocrack propagation. The mechanisms for these processes are in part common.

A goal of fatigue research is the development of an integrated mechanistic description of whole life. A sensible means to this end is to isolate and to characterize quantitatively each of the four regimes of fatigue damage. This approach is advocated because (1) the experimental and analytical methods necessary to study each regime are different, (2) variables may affect each regime uniquely, and (3) many applications are dominated by one of the fatigue regimes, for example, the behavior of crack like defected components in large structures. Environmental effects on cyclic deformation and micro crack initiation are considered separately in this volume by Duquette.[1] This paper reviews CF crack propagation; regimes 3 and 4 in the above hierarchy.

The development of an integrated and basic understanding of CF is hindered by several factors that are recurrent throughout studies of initiation and propagation. CF is influenced by a wide variety of mechanical, chemical, and microstructural variables that interact. It is necessary to investigate very slow rate deformation and cracking phenomena in a finite and realistic time. Model system studies on deformation and crack initiation have been conducted on relatively pure materials, often monocrystalline, while crack propagation studies are typically performed on complex structural materials, including steels and precipitation hardened aluminum or nickel based alloys. CF damage is highly localized at slip substructure and near the crack tip, direct experimental observations are not available, and behavioral interpretations must be based on indirect, averaged measurements. As the case for stress corrosion, CF is likely controlled by hydrogen-based, cleavage, and dissolution/passivation mechanisms, the atomistics of which are not known.

Scope of the review

The objective of this review is to critically summarize the phenomenology and mechanistic models of CF crack propagation and to identify current understanding and uncertainties that are principal to control of this failure mode in structural alloys. Results are emphasized that satisfy technological needs, including (1) quantitative mechanism-based predictions of long-term component life, derived from short-term laboratory data and describing the effects of interactive variables, (2) high-performance CF-resistant monolithic and composited alloys and chemically inhibited environments, and (3) a basis for nondestructive inspection procedures and sensors of environment chemistry and CF cracking damage.

In scope, this review emphasizes cycle–time-dependent CF crack propagation. Understanding of time-dependent fatigue above the threshold stress intensity (K_{ISCC}) for monotonic load stress corrosion cracking (SCC) follows from work summarized by Parkins.[2] Structural materials are discussed, including low carbon high strength low alloy (HSLA) and heat treated alloy steels, austenitic stainless steels, and precipitation hardened aluminum alloys in various embrittling gaseous and electrolytic environments for temperatures near 300°K. Spaehn discusses CF in ferritic and martensitic stainless steels, while Pineau reviews elevated temperature fatigue and

creep-fatigue interactions elsewhere in this volume.[3,4] There are similarities between low-temperature electrolytes and elevated-temperature gas environments.[5]

Despite important and controversial uncertainties, the fracture mechanics approach provides the foundation for this review of CF crack propagation data and predictive models. The issue considered here is the extent to which crack-tip modeling can extend the applied stress intensity and bulk-environment-based approach to CF.

State of the art: Storrs and Firminy Conferences

CF crack propagation has been the focal point for many international conferences[6-24] and major review papers.[5,25-39] Fatigue is described in a massive literature, with important symposia including discussions on environmental effects.[40-48] A foundation for the current review is provided by the proceedings of the seminal conferences held at Storrs, Connecticut, in 1971 and in Firminy, France, in 1973.[6,7] Several points emerged from these meetings.

Fracture mechanics characterization. The fracture mechanics description of CF crack propagation, presented as average crack propagation rate (da/dN) as a function of applied stress-intensity range ($\Delta K = K_{max} - K_{min}$), was embraced by many researchers. The schematics in Figure 1 indicate a variety of crack growth responses for embrittling environments, in sharp contrast to the power-law (Paris regime) relation between da/dN and ΔK coupled with a single crack growth threshold (ΔK_{th}) observed for alloys in vacuum and moist air.[25,(1)] The magnitude and pattern of CF cracking depend on SCC above K_{ISCC}, and a synergistic fatigue–corrosion interaction at lower stress intensities. The proportions of these events depend upon material and environment.

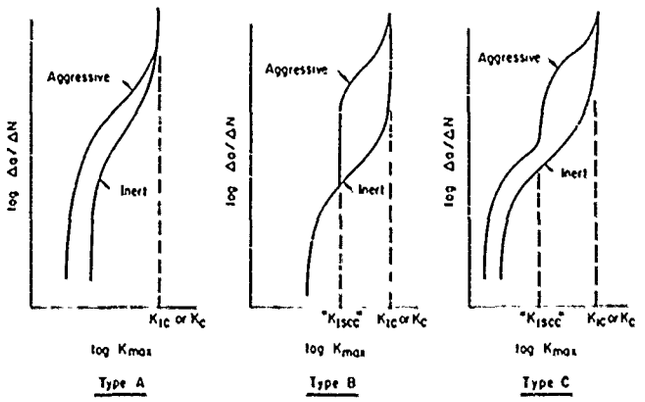


FIGURE 1—Schematic representations of corrosion fatigue crack propagation rate behavior; after McEvily and Wei.[25]

Classes of corrosion fatigue crack growth. Purely time dependent CF crack propagation is observed for materials and environments in which monotonic loading SCC occurs over a portion of the cyclic stress intensity loading wave (Type B in Figure 1). The cyclic character of loading and local plastic straining are not important. The fracture mechanics approach was launched by studies of subcritical fatigue crack propagation in high strength materials exposed to environments that readily induce stress corrosion crack growth. Type B behavior is prevalent for these systems, as is illustrated by data for high strength type 4340 (UNS G43400) steel in water vapor and argon (Figure 2).[49]

[(1)]The older representation in Figure 1, based on K_{max}, is equivalent to current growth rate data based on ΔK for fixed mean stress intensity. Two of these three parameters are independent variables in CF.

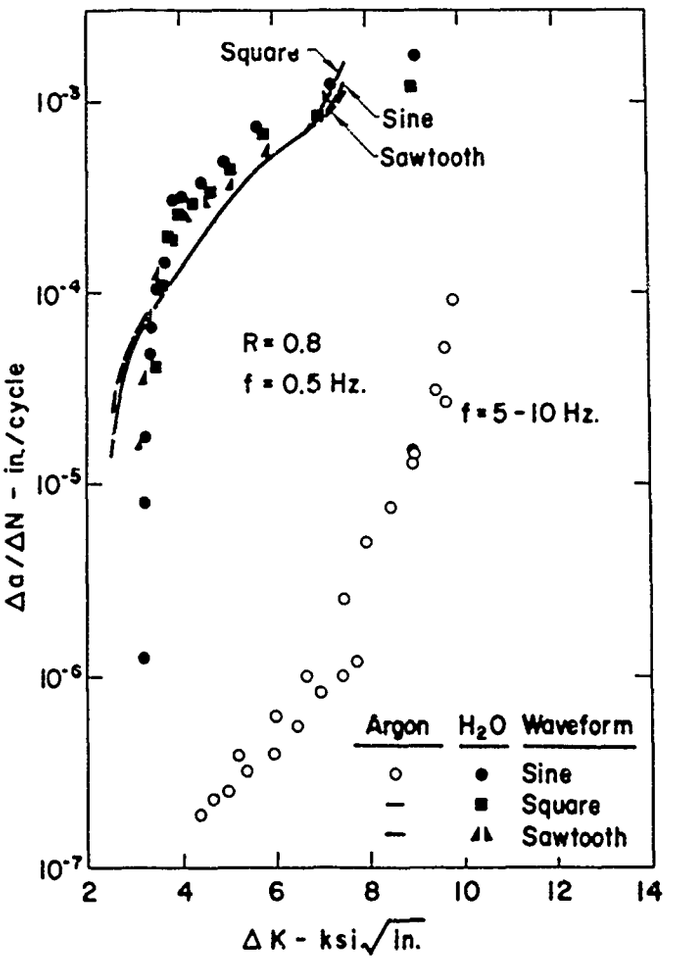


FIGURE 2—Time-dependent corrosion fatigue above K_{ISCC} for high-strength type 4340 (UNS G43400) steel in water vapor, modeled by linear superposition; after Wei, et al.[49,50] (1 in./cycle = 25.4 mm/cycle; 1 ksi√in. = 1.098 MPa√m)

The solid line in Figure 2 demonstrates that time-dependent CF crack growth rates are accurately predicted by linear superposition of stress corrosion crack growth rates (da/dt) integrated over the load–time function for fatigue.[50] Equivalent CF behavior is predicted and observed for sinusoidal, square, and asymmetric triangular load–time functions. Linear superposition modeling also predicts the effect of stress ratio.

A second class of CF behavior is based on synergistic interaction between cyclic plastic deformation and environment, which produces cycle- and time-dependent crack growth rates (Type A in Figure 1). Here, the environment accelerates fatigue crack growth below K_{ISCC}, a common scenario for low- to moderate-strength alloys that are either immune to SCC or exhibit high K_{ISCC} and low da/dt. This class of behavior was discussed by Barsom, based on data in Figure 3 for a maraging steel exposed to 3% NaCl.[51,52] Note the substantial CF effect below the static load threshold, but only for those loading waveforms that include a slow deformation rate to maximum stress intensity.

At the time of the Storrs and Firminy conferences, there were only limited data that showed an environment-induced reduction in ΔK_{th}, threshold measurements and concepts were in an infant state. Cycle–time-dependent CF below K_{ISCC} was further categorized based on observed frequency dependencies.

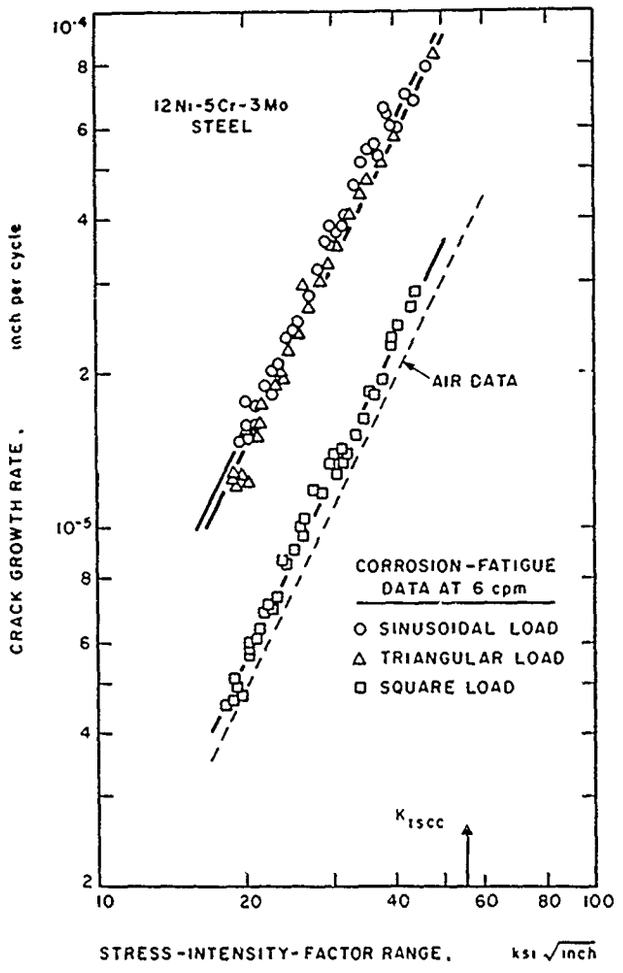


FIGURE 3—Cycle-time-dependent corrosion fatigue crack propagation below K_{ISCC} for 12Ni maraging steel in aqueous 3% NaCl; after Barsom.[51,52] (1 in./cycle = 25.4 mm/cycle, 1 ksi√in. = 1.098 MPa√m)

Frequency effects. Wei, Barsom, and Speidel independently emphasized the principal importance of loading frequency (f) for each class of CF, as typified by Figure 4 for aluminum alloy 7079 in aqueous sodium chloride and Inconel† 600 (UNS N06600) in hot sodium hydroxide solutions.[25,26,49-53] For time-dependent CF, da/dN due to environment is inversely proportional to f if the stress corrosion growth rate is constant with K, based on the assumptions that da/dN = (da/dt) × (1/f) and crack growth occurs throughout the loading and unloading portions of the fatigue cycle. This behavior is illustrated by the inclined dashed lines on the logarithmic plots in Figure 4. Superposition modeling (Figure 2 and Reference 50) predicts the effect of cyclic load period on time-dependent CF.

The frequency dependence of cycle-time-dependent CF is more complex. At low stress intensities, Speidel reported CF accelerations of da/dN for steels and nickel-based alloys that were independent of frequency.[5,26] This behavior was defined as "true" or cycle-dependent CF and is illustrated by horizontal lines in Figure 4 for air or the environments. A second behavior, that in which sub-K_{ISCC} CF growth rates increase with decreasing frequency, reflects the more general case of synergistic mechanically and chemically driven fatigue. This result is shown as the connecting region between time- and cycle-dependent da/dN in Figure 4 for those instances when da/dN calculated from da/dt and the vacuum rate sum to a value less than that measured for the environment. Speidel and others suggest that this behavior is best described as "cyclic SCC," where cyclic deformation lowers the susceptibility of the material to environmental cracking or "SCC." For the current review, all forms of CF below K_{ISCC} are viewed as cycle-time-dependent behavior.

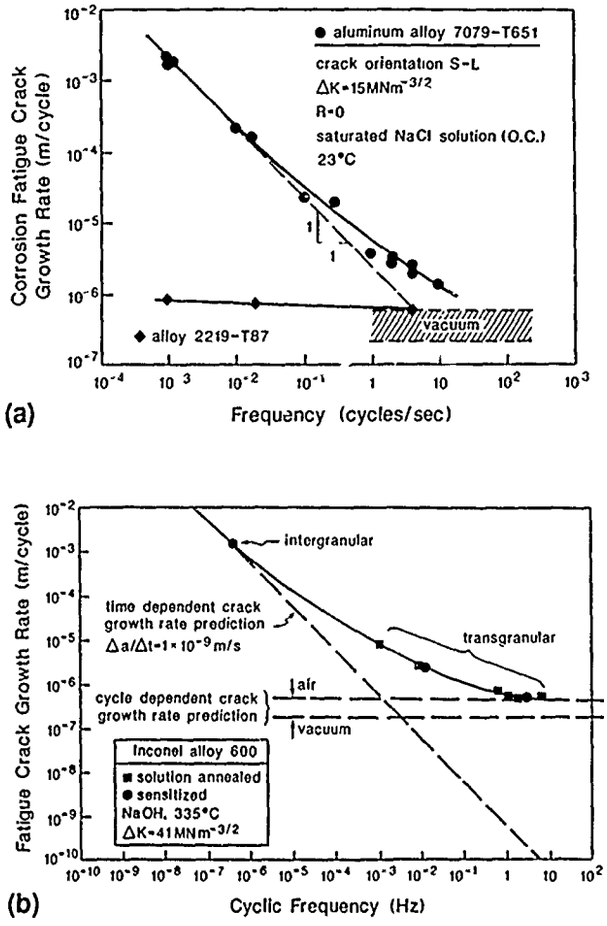


FIGURE 4—Frequency dependence of corrosion fatigue crack propagation illustrating time-dependent, cycle-dependent, and cycle-time-dependent behavior for (a) aluminum alloys in NaCl and (b) Inconel 600 (UNS N06600) in hot NaOH; after Speidel.[26,53]

From this discussion, the most general form of CF (Type C in Figure 1) involves cycle-time-dependent accelerations in da/dN below K_{ISCC}, combined with time-dependent cracking (SCC) above the threshold. ΔK_{th} may or may not be environment sensitive.

Principal variables. Extensive crack growth rate data presented at Storrs and Firminy demonstrate that mechanical, chemical, and metallurgical variables affect CF. The effects of ΔK, loading waveform, and loading frequency are illustrated in Figures 1 through 4. These conferences further established the important effects of environment chemistry, viz., temperature, gas pressure, electrolyte pH, electrode potential, dissolved oxygen, and environment composition. The effect of applied electrode potential on CF of a high-strength aluminum alloy in an aqueous halogen solution is shown in Figure 5.[5] The deleterious effect of low-pressure gaseous hydrogen and the associated beneficial poisoning effect of small O_2 additions on sub-K_{ISCC} CF in 4340 steel (σ_{ys} = 1240 MPa) are shown in Figure 6.[54] Note the mild frequency effect for pure hydrogen, consistent with cracking below K_{ISCC} and cycle-time-dependent embrittlement.

†Trade name.

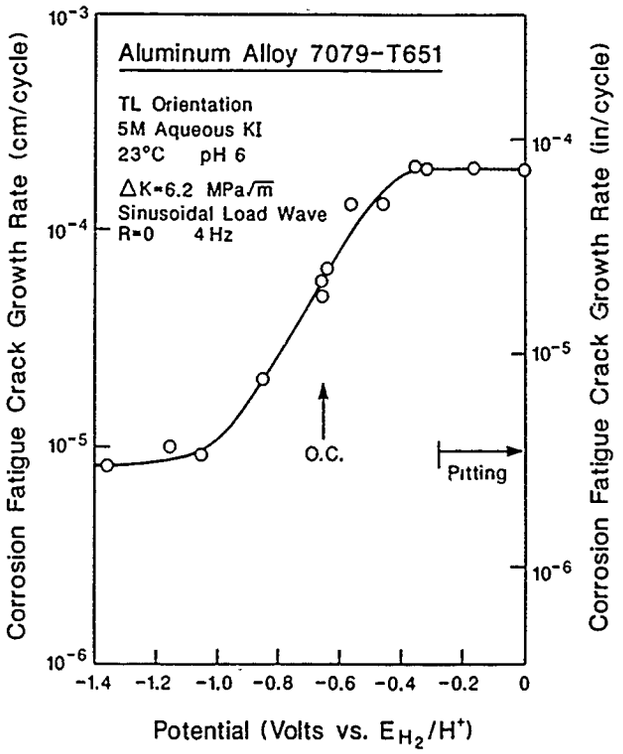


FIGURE 5—Effect of applied electrode potential on corrosion fatigue crack propagation in an aluminum alloy in aqueous potassium iodide; after Speidel, et al.[5]

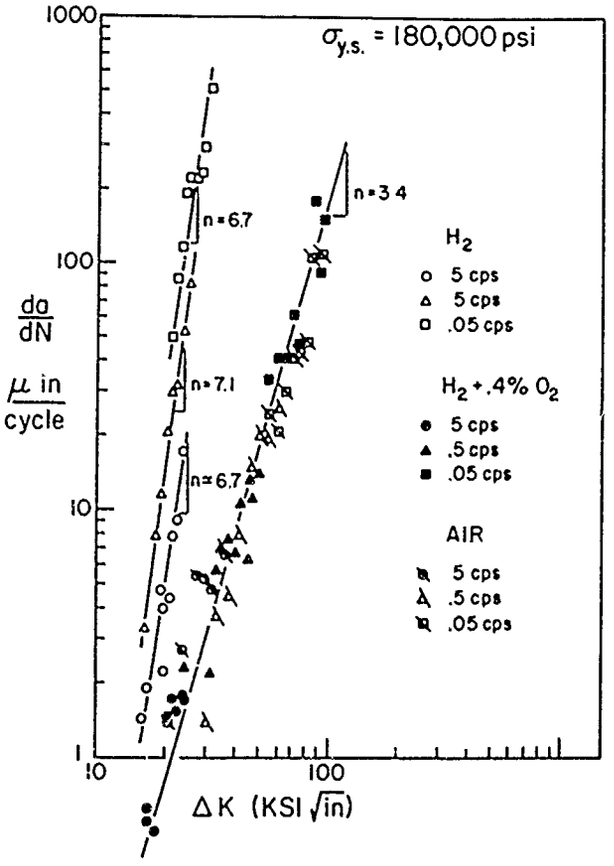


FIGURE 6—Effect of gaseous hydrogen and H_2 + O_2 mixtures on corrosion fatigue crack propagation in type 4340 (UNS G43400) steel (σ_{ys} = 1240 MPa); after Johnson.[54] (1 μin./cycle = 0.0254 μm/cycle, 1 ksi√in. = 1.098 MPa√m)

Mechanisms for corrosion fatigue crack propagation

Qualitative descriptions of the mechanisms for CF crack propagation provide a second foundation for this review. These mechanisms are the basis for understanding the CF crack propagation data presented in the third section, the necessary measurement methods discussed in the fourth section, the effects of critical variables in the fifth section, and quantitative models of CF cracking kinetics in the sixth section.

While debate continues on the microscopic and atomistic details of CF and while mechanisms are often specific to each material–environment system, several common concepts have been developed over the past 25 years. CF involves the synergistic interaction of cyclically reversed plastic deformation and local chemical or electrochemical reactions. Models differ based on the chemical damage mechanism.

Hydrogen environment embrittlement. Since hydrogen embrittles many alloys under static and dynamic monotonic loading,[55,56] this mechanism is invoked to explain CF crack propagation in a variety of alloy–gaseous or aqueous environment systems. Apart from occurring for many structural alloys in hydrogen gas, hydrogen embrittlement (HE) is proposed as the dominant mechanism for CF crack propagation of C-Mn and alloy steels in various electrolytes,[30,33,34,37,49,51,57-59] aluminum alloys in water vapor,[37,49,60-63] and titanium alloys in aqueous chloride.[37,64] While controversial, CF of aluminum alloys in aqueous chloride solutions has been ascribed to HE.[5,62,63,65,66]

In this view, atomic hydrogen chemically adsorbs on clean crack-tip surfaces as the result of dissociative gaseous H_2-metal reactions, of gas molecule (e.g., H_2O or H_2S) surface chemical reactions, or of electrochemical cathodic reduction reactions involving hydrogen ions or water. These reactions are catalyzed by clean metal surfaces and proceed to near completion in short times near room temperature. At higher temperatures, recombination of H to evolving H_2 greatly reduces HE.

Hydrogen production on crack surfaces follows environment mass transport within the crack and precedes hydrogen diffusion in the crack-tip plastic zone to the points of fatigue damage. Hydrogen atoms are often segregated or "trapped" at grain boundaries, precipitate interfaces, and dislocation cores. Trapping is detrimental if cracking occurs at such sites, but is beneficial if broadly distributed trapping reduces hydrogen transport kinetics and accumulation at fracture sites. Crack growth rates are likely to depend on the amount of adsorbed hydrogen produced per loading cycle by an environment. Crack growth will be rate limited by one or more of the slow steps in the crack environment mass transport, crack surface reaction, and plastic-zone hydrogen-diffusion sequence.

Major uncertainties exist. The location of hydrogen-enhanced crack-tip fatigue damage is not known. The atomistic processes by which hydrogen embrittles the metal, including bond decohesion and hydrogen-enhanced localized plasticity, are debated, as discussed in this volume by Oriani and Birnbaum, and elsewhere by Lynch.[67-69] The occurrence of HE for a given CF system is inferred based on circumstantial evidence, as discussed in the section "Justification for Hydrogen Embrittlement."

Quantitative HE models are discussed in the section "Corrosion Fatigue by Hydrogen Embrittlement."

Film rupture and anodic dissolution. Chemical damage based on film rupture, transient electrochemical anodic dissolution, and film reformation is invoked for several important CF problems, including carbon and stainless steels exposed to high-temperature water environments.[34,39,70,71] This mechanism was originally developed for SCC and was extended to CF based on the common role of crack-tip strain rate.[70] While controversial, film-rupture models have been applied to the aluminum–aqueous chloride system.[62,72]

In this view, localized plastic straining ruptures otherwise protective films at the crack tip. Crack advance occurs during transient anodic dissolution of metal at the breached film and while the surface repassivates. The amount of CF crack growth per fatigue

cycle depends faradaically on the amount of anodic current that flows and therefore on the kinetics of clean surface reaction (charge transfer) and on the time between film ruptures given by the crack-tip strain rate and film ductility The balance between sharp crack extension and crack broadening or blunting by general corrosion is important Quantitative film-rupture models are discussed in the section "Corrosion Fatigue by Film Rupture and Transient Dissolution."

Surface films. Early studies of CF, predominantly smooth-specimen whole life and crack initiation in gases, focused on the effects of environmentally produced thin surface films on slip-based damage processes. This work was reviewed by Duquette,[29,73] Marcus, et al.,[74] and Sudarshan and Louthan.[38] Over the past 20 years, these concepts have been advanced for CF crack initiation in electrolytes.[1 36] Film-based mechanisms have not been developed for crack propagation, however, recent advances in this regard were reviewed by Grinberg for moist air compared to vacuum.[75]

Films may affect crack extension by one or more processes, viz, (1) interference with reversible slip, (2) localization of the distribution and morphology of persistent slip bands and resultant crack damage, (3) reduction of near-surface plasticity and thus either reduced or enhanced fatigue crack growth rates, depending on the cracking mechanism, and (4) localization of near-surface dislocation debris and voids and thus enhanced fatigue crack growth.[1,29,36,38,73-76] These mechanisms have not been quantitatively developed nor experimentally tested.

Film effects on CF crack propagation are often speculatively considered. For example, Stoltz and Pelloux argue that crack-tip surface films minimize plasticity for aluminum alloys in aqueous NaCl, and thereby trigger local cleavage at high resulting stresses.[77] Others argue that crack-tip surface films reduce slip reversibility and thus increase damage and fatigue crack growth rates, at least for planar slip alloys.[78,79] A classic system here is aluminum alloys in vacuum compared to moist air. Faster crack growth in the latter occurs (hypothetically) by irreversible slip and crack blunting, which produces striations. Flat striation-free surfaces are observed for slowed crack propagation in vacuum, leading to the inference that slip is reversible because of the lack of an oxide film.[75,80,81] Others argue that crack-tip surface films minimize slip localization by preventing the emergence of slip bands, and thus homogenizing plastic deformation and decreasing da/dN relative to film-free environments such as vacuum.[61] Still others argue that crack-tip slip is homogenized, plastic-zone size at constant ΔK is increased, and fatigue damage is least in vacuum compared to air.[75]

Sieradzki and coworkers recently proposed that tens of Angstroms thick, environmentally produced crack-tip films fracture to promote cleavage in the adjacent alloy substrate, over a distance considerably larger than the film thickness.[82] The implications of this model to CF are important but have not been systematically considered.

The wide variety of film-based explanations for CF is possible because of a lack of direct observations of crack-tip damage processes and quantitative formulations of film effects. Controlled experiments in helium and film-forming gaseous environments such as O_2 are lacking; rather, effects of films are argued for complex electrochemical systems or for moist air in which several damage processes may be operative. This view is amplified in the section "Corrosion Fatigue by Surface Film Effects."

Adsorbed atoms. Adsorbed atoms may affect fatigue deformation and fracture by mechanisms similar to those of surface films, as reviewed by Marcus, et al.,[74] and Duquette.[29,73] A variety of processes are possible; however, none are modeled in detail for CF. For example, oxygen from the gas phase or a reduced cation from an electrolyte could adsorb on persistent slip sites at the crack tip, bind with dislocations, and reduce slip reversibility. Alternately, such species could form on slip-plane material to prevent rewelding on unloading. Presumably, these processes could lead to enhanced fatigue damage.

Reductions in surface energy by adsorption of an atom from the gas or liquid have long been proposed to reduce the associated work of fracture. For HE in gases or electrolytes, this mechanism is not viewed as sufficient.[67] For fatigue of aluminum alloys in O_2, this mechanism has been proposed but not proven convincingly.[74] Alternately, the chloride ion, oxidized from solution onto clean metal surfaces above a critical electrode potential, is held to embrittle austenitic stainless steels during SCC.[83] This concept has not been developed for CF.

Anodic dissolution and plasticity. CF crack propagation by localized anodic dissolution, the electrochemical knife, is generally not proposed Rather, Uhlig and coworkers[84-86] and more recently Jones[87] argue that anodic corrosion eliminates work-hardened material and stimulates localized plastic deformation to produce CF damage This model is based on the observation that smooth-specimen CF life is only degraded for electrode potentials that are noble to a critical value.[84] The idea is that CF crack initiation requires a critical anodic current to progress.

Anodic dissolution–plastic deformation processes have not been quantitatively modeled, particularly for CF crack propagation.

The Fracture Mechanics Approach

Conclusion

Fracture mechanics descriptions of CF crack propagation, viz., growth rate as a function of stress-intensity factor, provide an established and physically meaningful basis that couples alloy performance, damage mechanisms, and life-prediction studies through the concept of growth rate similitude. Extensive databases have been developed for structural alloys over the past three decades.

Stress-intensity similitude: inert environments

The fracture mechanics description of fatigue crack propagation illustrated in Figure 7 is traceable to the seminal work of Paris and coworkers for the case of moist air environments.[88] This evolution is chronicled by Hertzberg.[89]

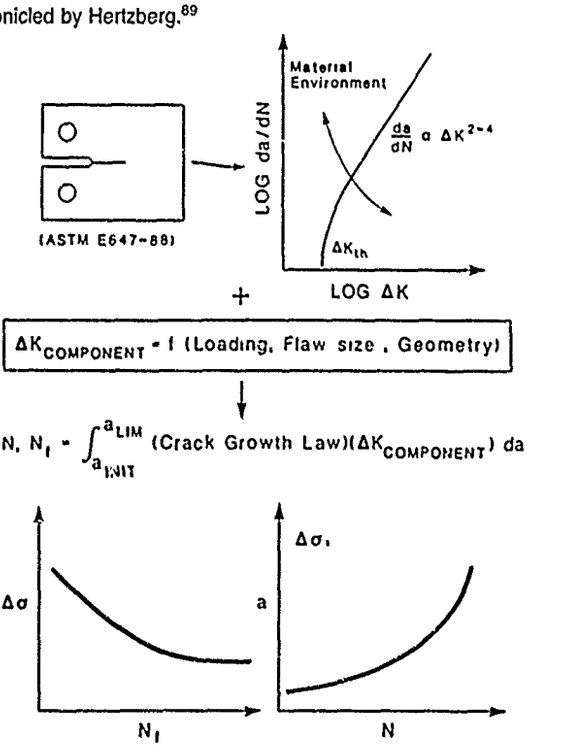


FIGURE 7—Fracture mechanics approach to corrosion fatigue crack propagation characterization and component life prediction.

Subcritical fatigue crack propagation is measured in precracked laboratory specimens according to standardized methods. Cyclic crack length data are analyzed to yield a material property averaged fatigue crack growth rate (da/dN) as a function of the applied stress-intensity range (ΔK). ΔK is the difference between maximum and minimum stress-intensity values during any load cycle.

Paris experimentally demonstrated the principle of similitude; that is, equal fatigue crack growth rates are produced for equal applied stress-intensity factors, independent of load, crack size, and component or specimen geometry. This da/dN–ΔK behavior is explained based on the fact that ΔK uniquely describes the magnitude and distribution of (1) elastic stresses, (2) elastic-plastic stresses, (3) plastic strains, and (4) plastic-zone and fracture process-zone sizes, all local to the crack tip (See the section "Models of Crack-Tip Mechanics .") The similitude principle enables an integration of laboratory da/dN–ΔK data to predict component fatigue behavior, in terms of either applied stress range–total life or crack length–load cycles, for any initial defect size.

Fatigue crack propagation rates for inert environments are reasonably approximated by a single function of applied stress-intensity range, normalized by the modulus of elasticity, for a variety of engineering alloys and microstructures tested in vacuum (Figure 8).[26] This result provides a basis for comparisons of environmental effects. Caution is, however, required. Crack propagation rates in vacuum may be influenced by surface welding during unloading, a more meaningful reference may be provided by ultra-high-purity helium or argon gas, where physically adsorbed molecules minimize surface welding.[74] Second, data in Figure 8 were obtained for near-zero stress-intensity ratio ($R = K_{min}/K_{max}$), where extrinsic crack closure can complicate the interpretation of mechanical cracking as discussed in the section Crack Closure." Data in Figure 8 are a useful guide, however, inert environment experimentation is a requirement for specific CF studies.

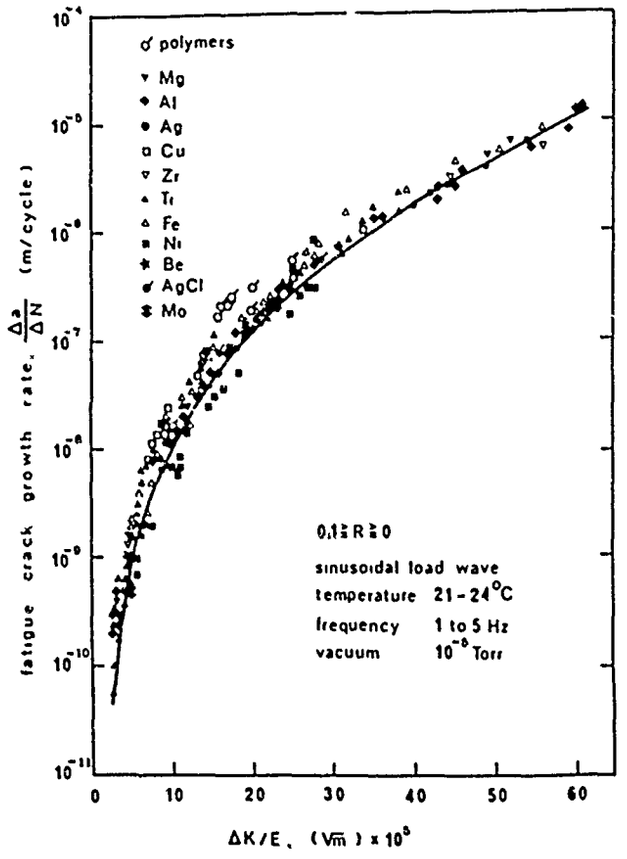


FIGURE 8—Inert environment fatigue crack propagation rate as a function of modulus normalized stress-intensity range for a variety of engineering alloys; after Speidel.[26]

Stress-intensity similitude: reactive environments

The application of fracture mechanics to subcritical stress corrosion and CF crack propagation progressed dramatically and in several periods over the past 25 years, as reviewed by Wei and Gangloff.[37]

The beginning: 1965-1971. Extension of the fracture mechanics method to stress corrosion and CF crack propagation was pioneered by Brown and by Wei[90,91] and was exploited by early experimentalists.[92-94] A highlight of this effort was the demonstration, following from the work of Paris on "K-increasing" remotely loaded and "K-decreasing" crack-surface-loaded specimens, that similitude is obeyed for CF crack growth. As shown in Figure 9(a), equal rates of CF crack growth are produced for equal ΔK, but for both increasing and decreasing net section stress specimens, demonstrating stress-intensity control.[95]

Phenomenological characterizations: 1970-1984. The fracture mechanics approach was broadly applied following these initial successes. High-strength materials were investigated in the early stages of work (1970-1976), while more recently (1976-1984), low-strength stress-corrosion resistant alloys were characterized

During this later period, concepts of premature crack surface closure were developed, significant understanding of near-threshold fatigue crack propagation emerged, and the small crack problem was intensively investigated, largely for benign environments.[41-47] Work on the implications of these problems to CF indicated cases in which the similitude concept was compromised. Data in Figure 9(b) show a wide range of CF crack growth rates for any constant ΔK for high-strength type 4130 (UNS G41300) steel in aqueous 3% NaCl.[96,97] Here, da/dN depends on varying short crack size and applied stress for the aqueous environment but is uniquely ΔK-controlled for benign moist air and vacuum. The origin of this effect is crack-size-dependent crack-tip electrochemistry, as detailed in the section "Crack-Geometry-Dependent Occluded Environment Chemistry."

Scientific studies: 1973-1987. Work during this period demonstrated that crack growth kinetics provide a basis for formulation and evaluation of CF crack propagation models.[30,33,34,36,39,49,98] Concepts of mass transport, chemical reaction rate, and diffusion control of da/dN were developed for gaseous and aqueous environments. Work in this period emphasized the complex cycle–time-dependent class of CF problems for the moderate ΔK regime but with limited studies on near-threshold phenomena. These models are discussed in the section, "Quantitative Models of CF Crack Propagation."

Applications to corrosion fatigue life prediction

Synthesis of life-prediction methods: 1983-1987. The fracture mechanics life-prediction method illustrated in Figure 7 was developed for complex structural applications in the energy, petrochemical, and transportation sectors as reviewed by Andresen and coworkers,[95] Tompkins and Scott,[100,101] and Novak and Barsom.[102] Vosikovsky and Cooke provide an example analysis for CF crack propagation in a welded carbon steel pipeline carrying H_2S-contaminated oil.[103]

As a further example, the damage-tolerant approach has been extensively investigated for welded carbon steel tubular components of oil and gas platforms operating in aggressive marine environments.[104-107] Here, classic design rules, based on smooth-specimen fatigue data and modified to account for complex time-dependent CF,[108] are being challenged by damage tolerant crack growth procedures.[99-101,109-111]

An example of the fracture mechanics framework and component life predictions are shown in Figure 10. An integrated approach includes fracture mechanics laboratory data, mechanism-based models to extrapolate the database, and stress/stress-intensity analyses of the component to predict cyclic life as a function of applied stress.[57,99] Such a prediction is represented by the band in

Figure 10.[111] Additionally, full-scale component tests are needed to verify the fracture mechanics analysis, the data points in Figure 10 resulted from extensive (and expensive) fatigue experiments with 0.5-m diameter, 1.6-cm wall thickness, welded carbon steel tubulars. Agreement is excellent. Note that the comparison in Figure 10 is for moist air. Predictions and tests are in progress for tubulars fatigued in actual sea environments with applied cathodic polarization.[104 107] The state of this development is, however, less than that represented for air.

Active sensors of environment chemistry and CF crack growth are important aspects of a life-prediction approach. Such devices have been successfully used in commercial nuclear power plants, piping systems, and offshore structures.[99 112-114]

Corrosion fatigue crack propagation databases

Extensive fracture-mechanics-based CF crack propagation databases were developed over the past two decades Examples are presented in Figures 11 through 15.

Carbon steels in hydrogen-producing environments. CF is significant for low-strength carbon-manganese steels of normalized ferrite-pearlite microstructures, stressed in a variety of gaseous and aqueous marine environments. Extensive data are represented in Figure 11.[115] Here, K_{ISCC} is well above 100 MPa$\sqrt{m}$; CF is cycle–time-dependent.

HE is implicated for these systems, as demonstrated by the two to three order of magnitude increase in da/dN for X42 steel in high-pressure, purified hydrogen gas (Curve 2).[117] Nelson reported similar results for gaseous HE of low-strength 1020 (UNS G10200) steel.[118] Considering aqueous environments, seawater produces enhanced fatigue crack growth relative to vacuum and moist air, with the magnitude of the effect increasing from free corrosion (Curve 4) to cathodic polarization (Curve 3) to H_2S additions at free corrosion (Curve 1). The strong effect of H_2S is further evidence for HE and is important to marine applications where biological reactions produce ionic sulfur-bearing products.[116,122]

The power-law regime of fatigue cracking observed for moist air and vacuum is altered by aqueous environments. A two-slope behavior is shown in Figure 11, where a strong ΔK dependence of rate at lower stress intensities transforms to a milder dependence at higher ΔK. For cathodic polarization, da/dN values within the latter regime are nearly independent of increasing ΔK; a plateau is sometimes observed. Environmental effects on near-threshold crack growth are less well characterized. For free corrosion, ΔK_{th} is reduced by seawater exposure, with the effect of stress ratio paralleling that reported for crack growth in benign environments. For cathodic polarization, high R thresholds are probably similar to those reported for free corrosion, but notably, very high ΔK_{th} values are reported for low R loading (Curve 5). Cathodic polarization produces calcium and magnesium hydroxide precipitates within the fatigue crack, causing corrosion product induced crack surface closure contact and increased ΔK_{th}. (See the section "Crack Closure in Aggressive Environments.")

The carbon steel–hydrogen environment system was reviewed in detail by Krishnamurthy, Marzinsky, and Gangloff[115] and by Jaske, et al.[32]

Precipitation-hardened aluminum alloys in aqueous chloride and water vapor environments. Extensive CF data have been produced for high-strength 2000 and 7000 series aluminum alloys in aqueous chloride and purified water vapor environments. Several conclusions are drawn from a tabulation of typical results (Figure 12).[5,60,61,65,79,95,125-131]

Both gaseous and aqueous environments produce significant CF crack propagation in aluminum alloys, relative to helium or vacuum for a wide range of stress intensities. Hydrogen production and embrittlement are implicated for these systems; however, the concurrent actions of anodic dissolution, passive film formation, and hydrogen production obscure the dominant mechanism.

For 3% NaCl, the large amount of data at moderate ΔK and low R generally describes CF below K_{ISCC} Here, aqueous chloride at typical free-corrosion potentials (about 800 mV_{SCE}) increases da/dN by between 4- and 100-fold relative to helium Distilled water also induces CF, Cl^- exacerbates but is not a requisite for cracking Moist air is an embrittling environment compared to helium, particularly for the 7000 series alloys. Wei and colleagues conducted extensive studies of the deleterious effect of pure water vapor on 7000 and 2000 series alloys at moderate stress-intensity levels.[61 129] The range of rates varies between an upper bound provided by moist air and a lower bound for inert gas. 7000 series aluminum alloys containing Zn, Mg, and Cu are more susceptible to CF compared to 2000 series alloys in the Mg-Cu and Li-Cu classes.

Only limited data have been obtained to describe near-threshold CF crack propagation in aluminum alloys.[60,125,126,132] Here, only high stress ratio results are reasonably interpreted, because the complicating extrinsic effects of crack closure are minimal. (See the section "Crack Closure.") As shown in Figure 12, water vapor, moist air, and aqueous chloride (either free corrosion or cathodically polarized) are embrittling relative to helium. The mechanism for this effect is speculative, with both HE and film-rupture/dissolution processes being possible. Notably, similar da/dN are reported for helium and oxygen, suggesting a minimal effect of surface oxide films. The 7000 alloy is more prone to CF compared to 2090, an advanced Al-Li-Cu alloy.

The transgranular CF sensitivity of 7000 series alloys (Figure 12) parallels the well-known differences in intergranular SCC resistance for these alloy classes,[133] the fundamental mechanism for the effect of alloy composition is, however, unclear. That a similar ranking is observed for aqueous chloride, moist air, and water vapor suggests that HE is central to the explanation. The systems represented in Figure 12 were reviewed by Speidel and Duquette.[5,62]

C-Mn and austenitic stainless steels in high-temperature water environments. An extensive database describes the stress corrosion and CF crack propagation kinetics for austenitic stainless and C-Mn pressure vessel steels in elevated-temperature, pressurized water environments.[134,135] Such data resulted from work over the past two decades aimed at guaranteeing the structural integrity of light water nuclear reactor plant materials and organized under the auspices of the International Cyclic Crack Growth Rate Group.[134,135] These fracture mechanics data, the hypothesized film-rupture mechanism, component life-prediction procedures, and new environment chemistry and crack growth damage sensors were reviewed by Ford, Andresen, and coworkers[39,70,71,99,136 138] and by Scott and Tompkins.[34,100,101]

CF crack propagation in nuclear reactor materials and environments is complex because of the interactive effects of many variables.[39] Typical data are presented in Figures 13 and 14. Da/dN vs ΔK data for normalized C-Mn steel in 288°C low-oxygen water (Figure 13) show a strong environmental effect relative to inert environment behavior.[39,136] Note the low loading frequency (0.017 Hz) and high mean stress (R = 0.7) conditions. Environmental cracking can exceed ASME Section XI criteria, such empirical guidelines have been increased as new results and heightened concerns on CF emerged from laboratory experimentation.[100,136]

The significant variability shown in Figure 13, further emphasized if a larger population of results are considered,[139] is traceable to a complex interaction between the MnS inclusions in the steel, the flow conditions of solution surrounding the fracture mechanics specimen in the autoclave, and the electrode potential of the specimen, largely established by the dissolved oxygen content of the solution.[39,139]

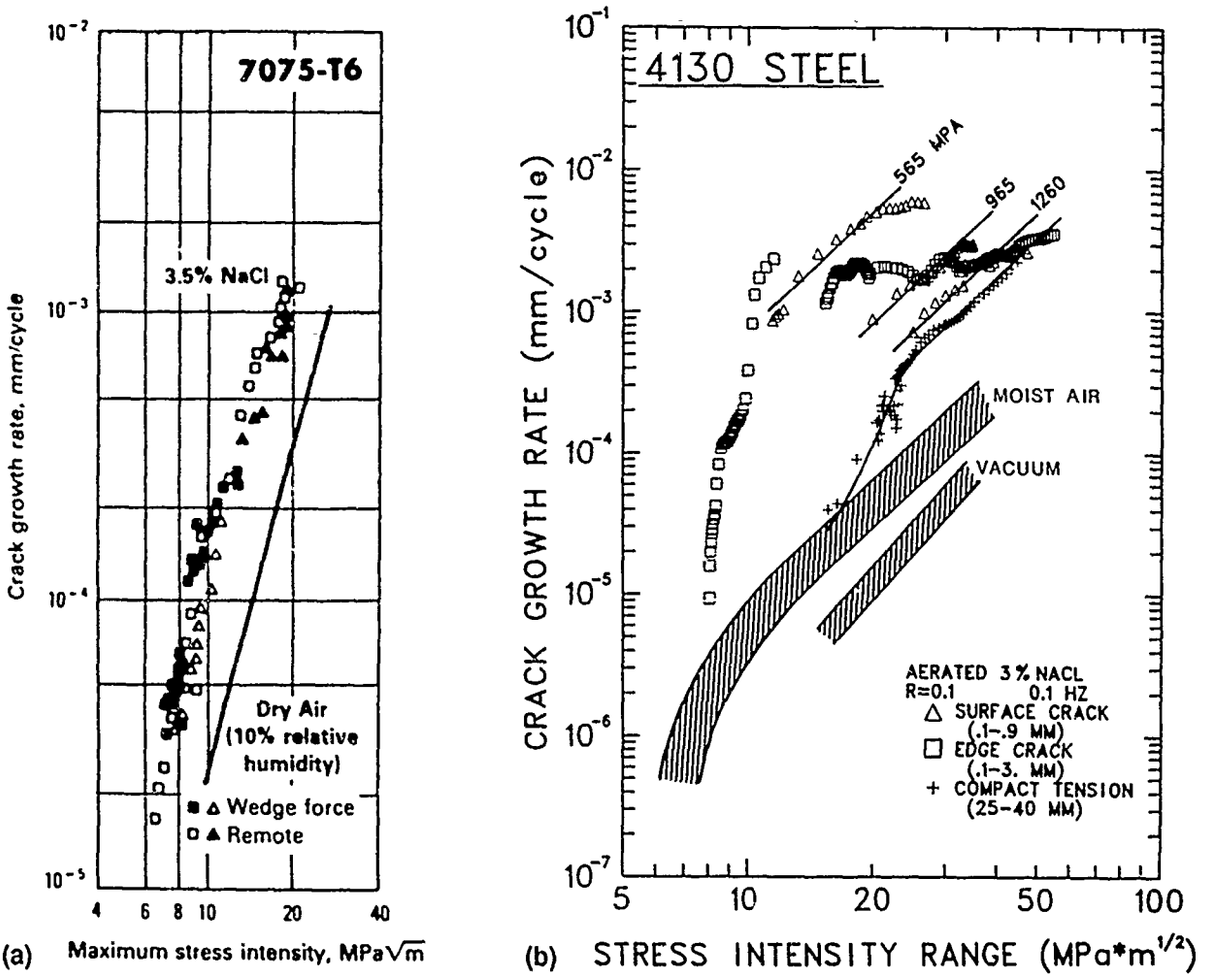


FIGURE 9—Effect of specimen geometry on corrosion fatigue crack growth demonstrating (a) similitude for remote and crack-surface loading; after Feeney, McMillan, and Wei;[95] and (b) a breakdown in similitude for short edge and surface cracks in aqueous 3% NaCl; after Gangloff.[96,97]

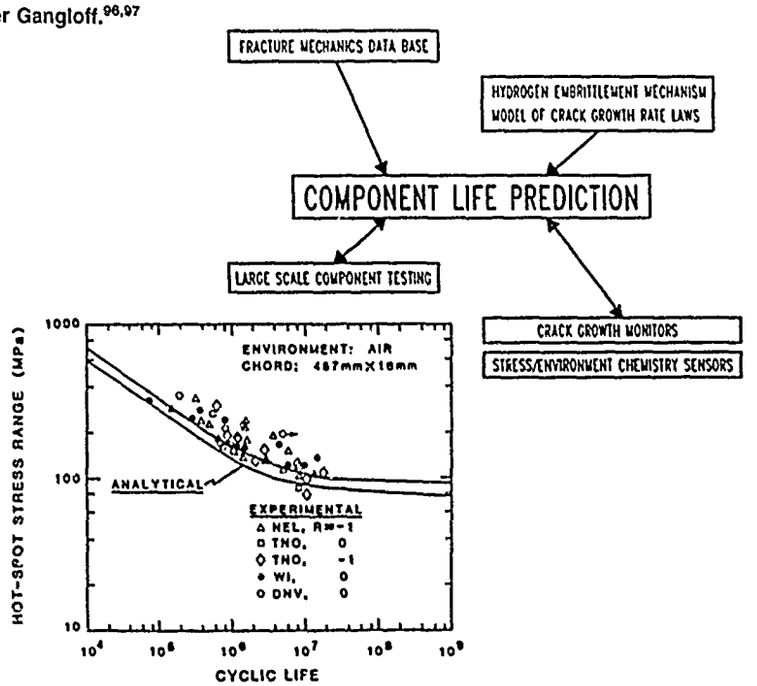


FIGURE 10—Integrated fracture mechanics method for fatigue life prediction; after Andresen, et al.,[99] with a comparison between predicted and measured cyclic life for welded carbon steel tubular joints fatigued in moist air; after Hudak, Burnside, and Chan.[111]

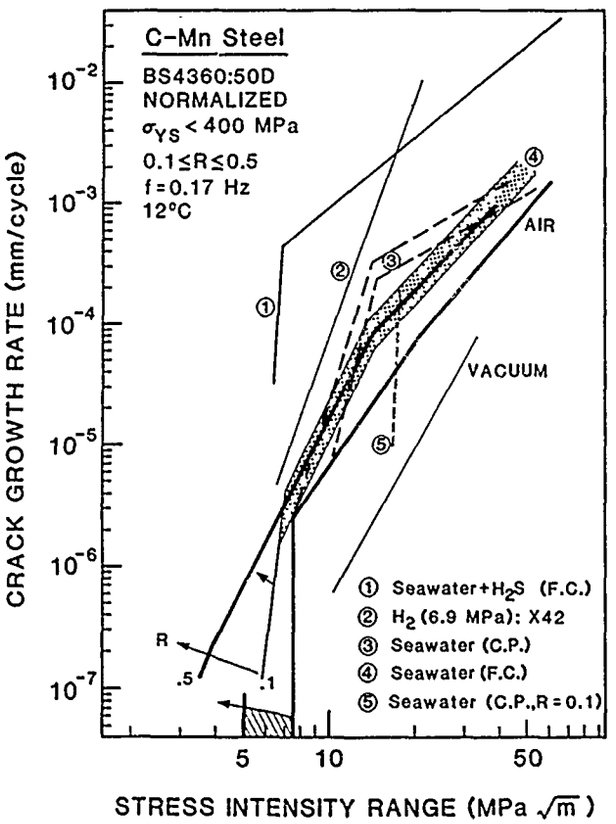


FIGURE 11—Corrosion fatigue crack propagation in low-strength, normalized carbon-manganese steels in hydrogen-producing environments: (1) seawater contaminated by H_2S;[116] (2) High-pressure H_2;[117] (3) seawater with cathodic polarization;[119-122] (4) seawater at free corrosion;[119-123] and (5) seawater with cathodic polarization at low R;[121] moist air, and vacuum.[58,115,124]

The strong effect of cyclic loading frequency is illustrated in Figure 14 by da/dN–ΔK data for sensitized type 304 (UNS S30400) stainless steel in oxygenated, high-temperature, pressurized water.[137] As typically observed, CF crack propagation rates increase with declining frequency, certainly for moderate levels of ΔK, with the near-threshold response unclear. Film-rupture models, including detailed treatments of crack electrochemistry, explain the distributed results shown in Figure 13 and predict the effects of a broad range of variables, including frequency.[39 71 99 136 138] Comparison between measured and predicted da/dN (Figure 14) provides an example of this predictive power.

Titanium alloys in aqueous electrolytes. Since the pioneering SCC work of Brown, which showed the sensitivity of precracked titanium alloys to aqueous chloride solutions,[140] many studies have investigated the CF behavior of this structural material.[5] Typical data are presented in Figure 15. Here CF crack growth rates are enhanced up to tenfold by cyclic loading in several halogen bearing solutions at the free-corrosion potential. A wide range of da/dN is likely, depending on solution electrochemistry, ΔK, frequency, and titanium alloy microstructure.[65,141,142]

Experimental Procedures

Conclusion

Experimental methods are developed for determinations of average crack growth rate as a function of continuum fracture mechanics crack-tip parameters, particularly ΔK Nonsteady-state crack growth, unique to CF, and crack closure are not understood Future procedures will incorporate precision crack-length measurement and computer control of stress intensity to develop quantitative and novel CF crack growth rate data, particularly near threshold. Advances have been recorded in measurements of small crack growth kinetics, however, such approaches are not easily adapted to controlled environments. The fundamental experimental problem is the lack of methods to probe mechanical and chemical damage processes local to the CF crack tip.

Fracture mechanics methods

Following from Figure 7, the procedure for laboratory measurement of fatigue crack growth rate as a function of ΔK is standardized by ASTM Committee E24 on Fracture Mechanics.[143] Additional details, specific to moist air, are provided by a summary chapter in the *Metals Handbook* and by user experiences.[144-145] Two aspects, environment control and crack-length measurement, are uniquely important to CF, as indicated by an annex to the ASTM standard and a U.S. Navy procedure for seawater.[143,146]

Control and characterization of the gaseous or aqueous environment that surrounds the specimen is of paramount importance to CF experiments. Particular emphasis must be placed on control and measurement of variables such as electrode potential, environment ionic and dissolved oxygen compositions, purity, flow rate, and temperature. Successful approaches have been reported for most environments, as reviewed by Gangloff, et al.[147] Detailed procedures are often complex, as illustrated by work on fatigue in high-temperature, pressurized water environments. Owing to the importance of slow loading frequency in exacerbating CF, experiments must often be maintained for weeks or months.

A wide range of crack-length monitoring methods are used in fracture mechanics studies of fatigue, as illustrated in Figure 16 after Marsh and Smith.[148] The indirect or remote methods are required for CF because the fracture mechanics specimen is immersed in an environmental chamber. Periodic interruption of loading or chemical exposure may introduce transient cracking. To date, successful applications have been reported for the compliance and electrical potential-difference methods. Procedures for each approach are reviewed in two volumes edited by Beevers.[149 150]

The electrical potential method has been widely applied to studies of CF (for example, References 50, 61, 97, 121,151) because of the simplicity of using simple wire probes in aggressive environments, and because the approach is applicable to through-thickness and surface-crack geometries. Typical data are presented in Figure 17, where computer acquisition and high-gain stable amplification produced hundreds of measured data points that merge to a continuous line. Here crack growth occurred at constant ΔK, with a single rate observed for air but not the aqueous chloride environment. The averaged resolution of the potential-difference approach varies between 2 and 30 μm, depending on circuitry and specimen geometry.

In all cases reported, the application of high (1 to 50 amperes) direct or alternating current has no effect on CF for gases or electrolytes. Presumably, the conductivity of the specimen is orders of magnitude higher than that of electrolytes, including conductive chloride, current leakage into solution at the crack tip is not significant. Possible drawbacks of the potential-difference method include specimen heating, crack-surface electrical contact (or shorting) when the crack surfaces are maintained clean and conductive, and a lack of information on crack-surface contact and mechanical load transfer.

Compliance measurements yield accurate determinations of crack length and provide an approximate indication of the extent of crack closure. (See the section "Crack Closure.") Crack-length resolution is on the order of 25 μm for typical long (25 mm) crack specimens. While the use of crack-mouth or back-face displacement gauges in gases and liquids is complex, the problems are not insurmountable, as indicated by specific applications.[60,123,130,136,139,142,152,153] The main issue associated with the compliance approach is the arbitrary character of the determination of an "effective" stress intensity to describe growth rates independent of crack closure. In this regard, the usefulness of crack-mouth opening and back-face compliance measurements is currently debated.

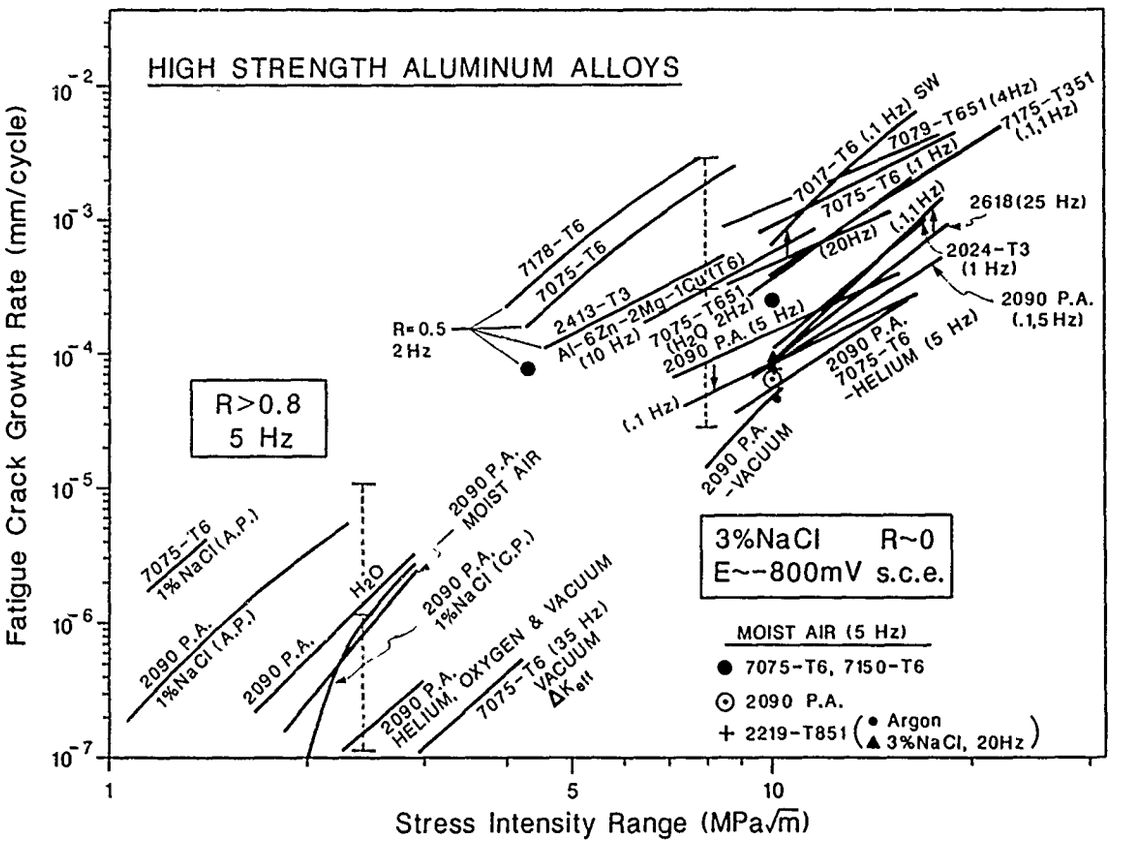


FIGURE 12—Corrosion fatigue crack propagation in high-strength 2000 and 7000 aluminum alloys for (1) Case A: high ΔK, low R; aqueous 3% NaCl near free corrosion;[21,95,61,64,79,125-130] and (2) Case B: near-threshold at high mean stress with aqueous chloride and gaseous environments.[60,125,126]

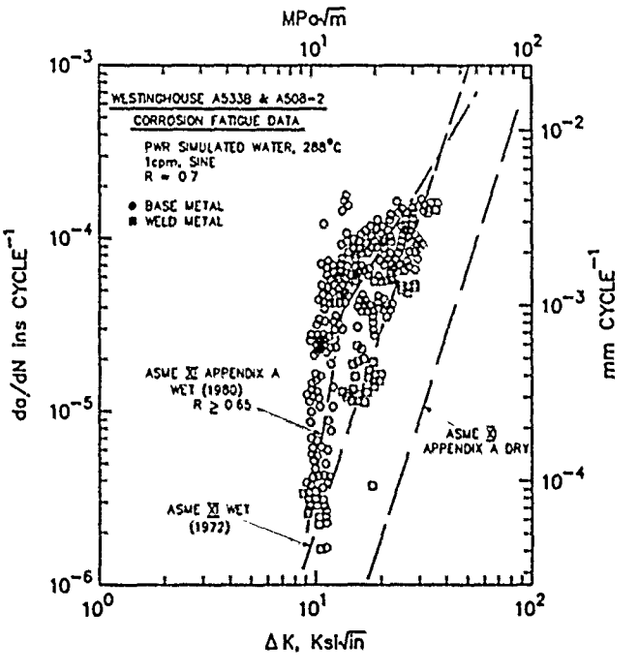


FIGURE 13—Corrosion fatigue crack propagation data for normalized C-Mn steel in elevated-temperature (288°C) pressurized water at low cyclic frequency and high R; after Jones.[39,136]

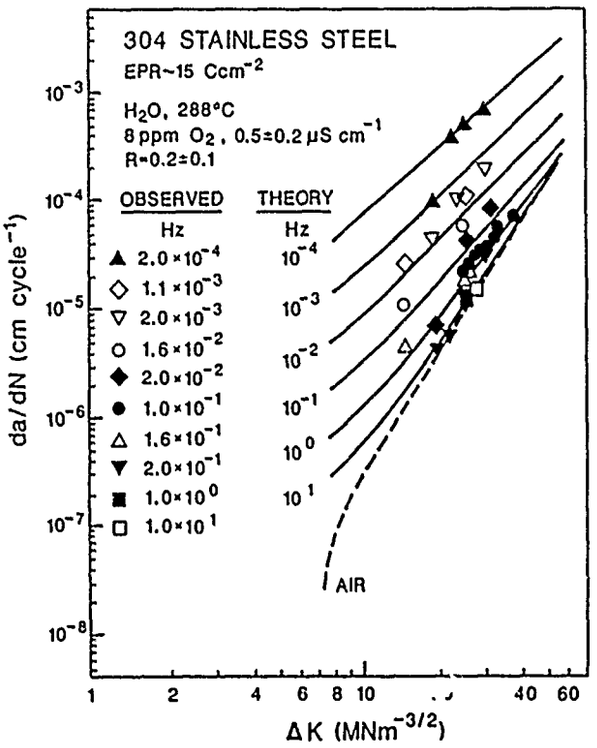


FIGURE 14—Corrosion fatigue crack propagation data for sensitized stainless steel in oxygenated, high-temperature water showing the deleterious effect of slow cyclic-loading frequency; after Ford, et al.[137]

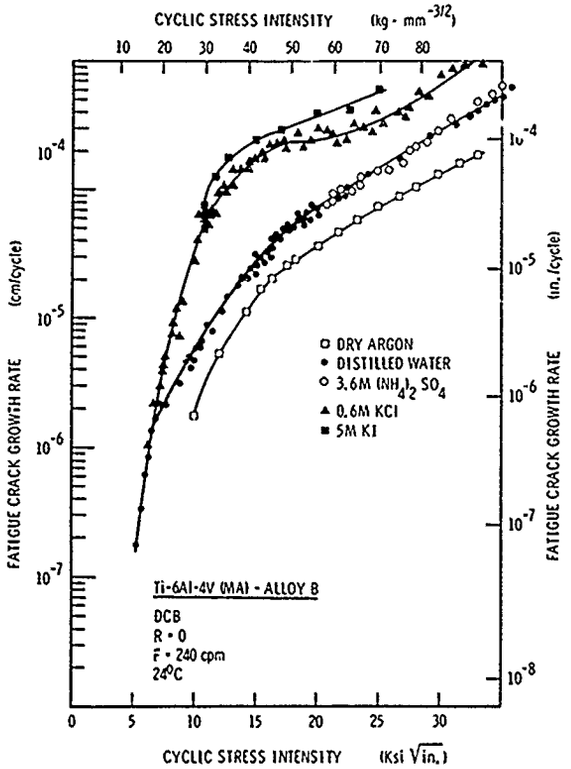


FIGURE 15—Corrosion fatigue crack propagation data for a high-strength titanium alloy in aqueous halide solutions, after Speidel, et al.[5] (1 ksi$\sqrt{in.}$ = 1.098 MPa$\sqrt{m}$)

It is critical to differentiate experimentally transient and steady-state CF crack growth rates, with the former dependent on time or equivalently loading cycles at constant applied stress intensity, as discussed by Hudak and Wei.[154] Crack geometries, programmed loading histories, and test interruptions, which are allowable under the ASTM standard and do not influence benign environment fatigue, can significantly influence CF crack propagation.[143] This complicating phenomena is attributed to time-dependent chemical contributions to fatigue damage. (See the section "Crack-Geometry-Dependent Occluded Environment Chemistry.")

New procedures

The data presented in Figures 11 through 15 were obtained by constant load, increasing ΔK, or by programmed, continuously decreasing ΔK methods.[155] That such rates represent steady-state conditions governed solely by ΔK is, however, generally not proven, and the effects of loading history and crack size are not understood.

The coupling of recent advances in remote crack-length measurement with the computer-controlled servohydraulic test machine enables meaningful characterizations of CF crack propagation rates. A useful procedure to supplement constant load or continuously decreasing ΔK cracking is represented in Figure 18 for the case of ferritic steel in aqueous chloride. Here, ΔK is maintained constant at selected levels labeled 1 through 7, and by either compliance or electrical potential measurements of crack length and computer-controlled load reductions. Steady-state crack growth and transient behavior will be indicated by the character of the crack length vs loading cycles data; viz., linear for the former and nonlinear for the transient case.

As a second sophistication, two regimes of crack growth can be probed by a procedure recently discussed by Hertzberg and coworkers.[158] For high ΔK and low R (points 1 to 3), stress ratio is maintained constant as increasing levels of constant ΔK are programmed. Subsequent tests are conducted at constant K_{max} and several levels of constant ΔK selected to decrease with increasing R (Points 3 and 4 through 7). In this way, near-threshold CF crack propagation is characterized without the complicating effects of delay retardation or crack closure. The possibility of closure effects at any combination of ΔK and R can be assessed by the linearity of cyclic crack-length data and by compliance measurements coupled with variations in K_{min} below the indicated crack-opening load.

The approach in Figure 18 has several advantages in addition to demonstrably steady-state kinetics. With constant ΔK and precision measurements of crack length, low values of da/dN can be obtained for low-frequency loading over a reasonable test time, because the crack growth increment for a meaningful rate determination is small. Secondly, environmental and loading-frequency variable effects are readily determined to within about ± 20% uncertainty, based on changing cyclic crack growth rate response at constant ΔK and R. Finally, the procedure in Figure 18 probes two important regimes of fatigue crack propagation, including conventional high-ΔK low R and high R near-threshold or "ripple" loading. This approach was successfully applied in an investigation of CF crack propagation in an aluminum-lithium alloy.[125,126]

The methods discussed above are based on small-scale yielding throughout the precracked specimen. Dowling extended this linear-elastic approach to describe fatigue crack propagation during large-scale yielding based on the J-integral characterization of the crack-tip stress and strain fields.[157] While established for moist air, this approach has not been applied to CF.

Novel measurements of corrosion fatigue cracking

The fracture mechanics approach is based on measurements of average crack growth rate and applied stress intensity for specimens containing single, large (> 25 mm) cracks. A second level of measurement probes mechanical and chemical damage processes local to the crack tip. Only limited successes have been recorded.

Electrical potential measurements can be used to monitor continuously the growth of single, defect-nucleated fatigue cracks sized above about 50 μm.[158] This method is applicable to aqueous (for example, Figure 17) and high-purity gaseous environments, and has been successfully used to monitor the growth of CF cracks in single, albeit large, grains of steels, nickel-based, and aluminum alloys.[97,125,126,159] Despite these successes, this method does not directly probe crack-tip damage processes.

Plastic-tape replication measurements are used to monitor the surface growth of small fatigue cracks in moist air.[157] This method requires periodic loading interruptions that may affect CF, it does not directly probe crack-tip damage, and it does not provide information on the crack perimeter. The only benefit over electrical potential monitoring is that replication methods characterize fatigue crack nucleation at natural microstructural features and defects such as inclusions.

Papers within this volume do not discuss experimental characterizations of crack-tip chemical and mechanical damage. This omission is traceable to the complexity of such endeavors. Gerberich, Davidson, and Lankford reviewed various microscopic techniques directed at crack-tip fracture observations.[160,161] The following methods yielded insights on fatigue crack propagation for vacuum and moist air:

(1) *In situ* scanning electron microscopy of a cyclically loaded specimen; stereoimaging analysis;
(2) Electron channeling pattern techniques;
(3) High-voltage transmission electron microscopy,
(4) X-ray diffraction and topographic techniques;
(5) TEM analysis of crack wake dislocation morphologies, and
(6) *In situ* Auger cracking and chemical analysis.

These methods have not been widely applied to CF.

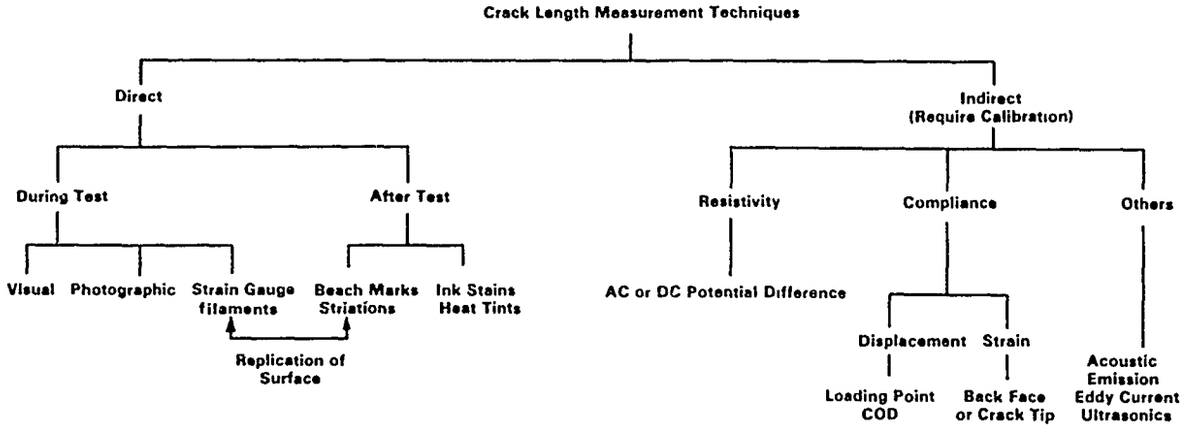


FIGURE 16—Methods for measurement of fatigue crack length; after Marsh and Smith.[148]

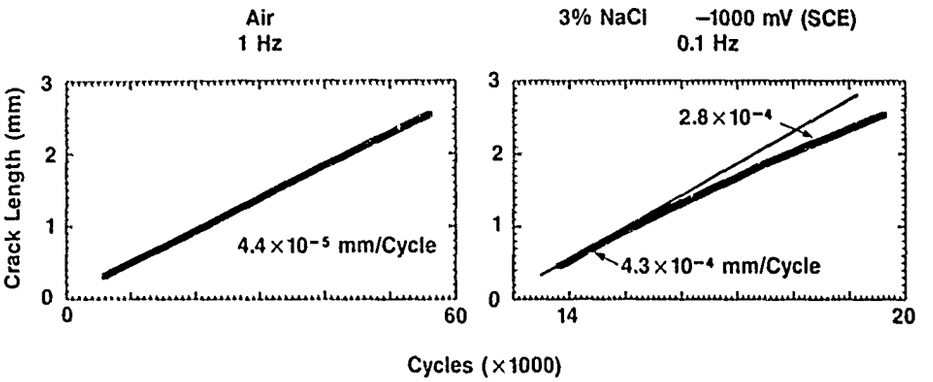


FIGURE 17—Cyclic crack-length data from automated dc electrical potential measurements of cracks in API-2H steel in moist air or aqueous NaCl with cathodic polarization and at constant ΔK; after Gangloff.[158]

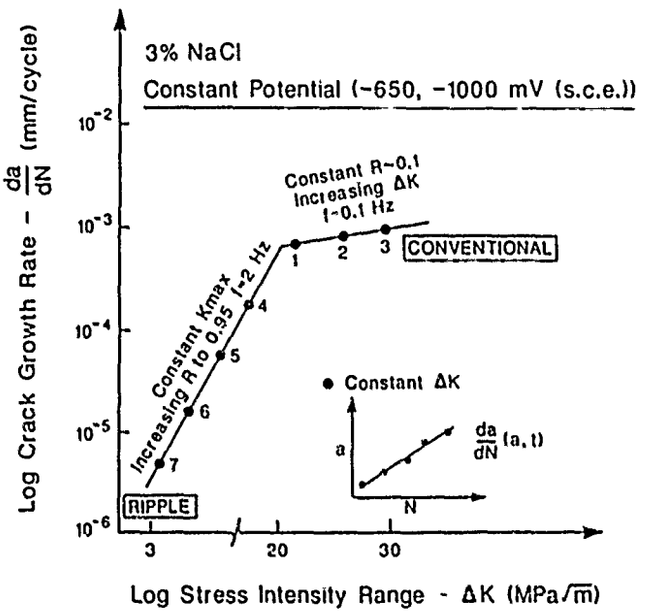


FIGURE 18—Programmed stress-intensity characterization of corrosion fatigue crack propagation for steel in chloride, based on constant ΔK segments at constant K_{max} and varying R.

As an example, Davidson and Lankford used stereoimaging to show that environment affects crack-tip plasticity and crack growth mode.[162-164] For constant applied ΔK, near-crack-tip-opening strain decreased for embrittling compared to inert environments. These studies were conducted with 1020 steel and 7075-T651 aluminum specimens that were loaded cyclically and observed in the SEM vacuum after prior fatigue cracking in either moist air or dry N_2. Additional work involved SEM analysis of crack-wake subboundaries formed by prior fatigue in moist air or dry N_2. *In situ* environmental cracking was not attempted. The mechanistic implications of this work are discussed in the section "Environment-Sensitive Microscopic Deformation."

Wei and coworkers used Auger spectroscopy to measure rates of water vapor and H_2S reactions with both polished and *in situ* fractured alloy surfaces.[37,66,129] These chemical kinetics were used to model rates of CF crack propagation.

Since the early work of Brown,[165] researchers have used electrochemical probes to define the crack environment. CF of a carbon-manganese steel in seawater has been extensively investigated by this approach.[166-168] Near-crack-tip pH, potential, and chloride ion concentration were measured for comparisons with mass transport and reaction model predictions. Detailed reviews of these experimental measurements are presented elsewhere.[138,169]

Effects of Critical Variables

Conclusion

A plethora of interactive variables influences the CF crack growth rate–stress intensity relationship. The effects of chemical, metallurgical, and mechanical variables are well characterized and reasonably explained by qualitative arguments. Growth rates are affected by environment chemistry variables (viz., temperature; gas pressure and impurity content; electrolyte pH, potential, conductivity, and halogen or sulfide ion content); by mechanical variables such as ΔK, mean stress, frequency, waveform, and overloads; and by metallurgical variables including impurity composition, microstructure, and cyclic deformation mode Time, or loading frequency, is critical, complicating long-life component performance predictions based on shorter-term laboratory data. Limited studies show that yield strength is not a critical variable in cycle–time-dependent CF. Fractographic analyses of microscopic crack paths provide a basis for failure analyses and input to mechanistic studies.

Introduction

Alloy development and life-prediction approaches to control CF are confounded by the many interactive variables that affect crack propagation beyond that expected based on benign environment fatigue Table 1 lists these variables for steels in marine environments The goal in CF is to develop da/dN–ΔK relationships, which include the effects of all such variables.

The variables in Table 1 influence fatigue crack propagation in most alloy systems Detailed analysis of each effect is not possible. Rather, the following discussion illustrates typical effects of the more important variables for ferrous, aluminum, and titanium alloys. Qualitative explanations for the experimental trends are provided. Quantitative models of fatigue crack growth rate response are outlined in the section "Quantitative Models of Corrosion Fatigue Crack Propagation."

Mechanical loading variables

Stress-intensity factor range. Figure 1 illustrates that applied stress-intensity range affects rates of CF crack propagation in a complex fashion compared to inert environments. Specific data are presented in Figures 3, 6, 9, 11, 13, 15, and 19.

TABLE 1
Mechanical, Environment Chemistry, and Metallurgical Variables Affecting Corrosion Fatigue in Marine Environments

Stress-intensity range	Mean stress
Crack size and geometry	Residual stress
Loading waveform and sequence	Loading frequency
Solution Cl^-,H^+,O_2,Mg^{++},Ca^{++}	Electrode potential
Hydrogen uptake promoters, $S^{=}$	Solution flow
Calcareous deposit formation	Exposure time
Steel yield strength	Specimen thickness
Steel composition and microstructure	

While a simple power-law response is typical for a limited range of ΔK (Figures 3, 6, and 11), the more general behavior is indicated in Figure 19 for Ti-6Al-4V; X65 controlled, rolled, microalloyed ferritic steel; and precipitation-hardened aluminum alloy 7017-T651, each in aqueous chloride (see also Figures 9, 13, and 15).[34,64,141,170] Such results are expected because inert environment fatigue is driven by crack-tip plasticity, which is simply related to ΔK, and compared to the conjoint plastic strain and chemical processes involved in CF.

At present, there are only limited analytical predictions of the stress-intensity dependence of CF crack propagation rates. Micromechanical–chemical models exist, as discussed in the section "Quantitative Models of Corrosion Fatigue Crack Propagation"; however, most are based on simplifying assumptions. It is useful to consider that three regimes of CF crack growth are possible, as represented schematically in Figure 1 for Type A cycle–time-dependent behavior.

Near-threshold ($da/dN < 10^{-6}$ mm/cycle) environmental effects may reduce ΔK_{th} and increase da/dN paralleling benign environment behavior. In Figure 19, rates for the titanium alloy are well above 10^{-6} mm/cycle, however, imaginative extrapolation suggests that the environment could lower ΔK_{th} and raise growth rates relative to moist air. For steels, indications of this effect were reported by Booth, et al.,[123] and by Bardal;[119] however, little difference is seen for near-threshold cracking in chloride vs moist air in Figure 19. In fact, near-threshold rates for the former are less than moist air kinetics and perhaps approach vacuum behavior. Near-threshold CF in aluminum alloys is largely unexplored, limited data are shown in Figure 12.[126]

Measurements of crack growth in the near-threshold regime are prohibitively time consuming owing to the low loading frequencies relevant to CF.[120,171] As such, environmental effects are poorly understood, as illustrated by models that predict HE may reduce ΔK_{th}, while corrosion blunting of the crack-tip may increase the threshold relative to an inert reference environment.[39,172] The experimental procedure outlined in Figure 18 provides a means of characterizing low-growth-rate CF.

A second regime of CF crack propagation is often observed for stress-intensity levels above the fatigue threshold. Here CF da/dN values increase rapidly relative to the reference environment and with a significantly stronger power-law dependence. This behavior is shown for each alloy in Figure 19 and may be interpreted as the intervention of cyclic-deformation-stimulated "SCC."[34,59,141] The steep slope is interpreted as evidence of mechanically rate-limited crack propagation in the presence of fast and sufficiently completed chemical reactions and mass transport.

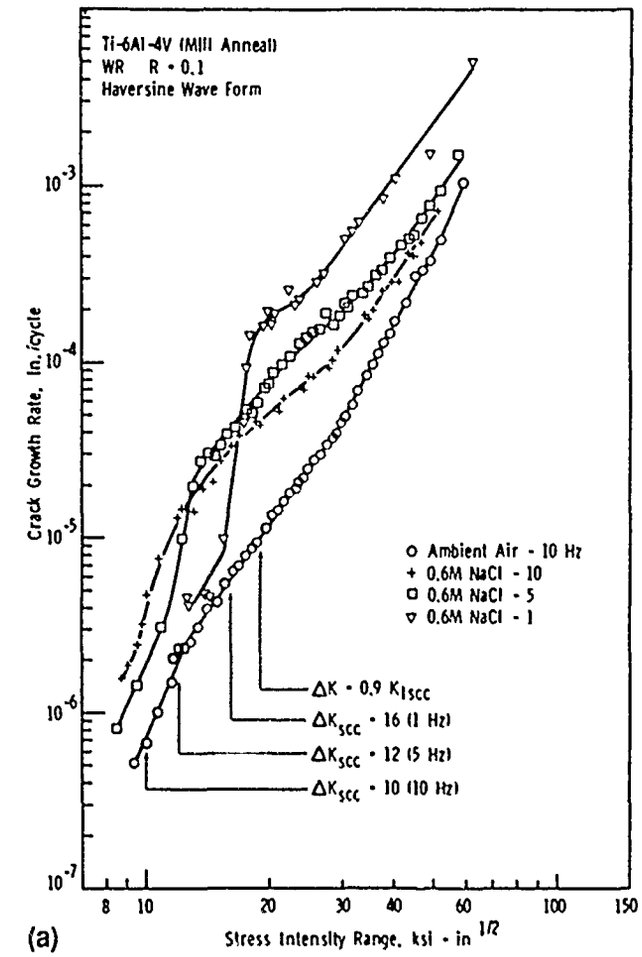
A third regime of CF response at higher ΔK is typified by so-called plateau (nearly) K-independent behavior, or more generally, by a reduction in the slope of the da/dN–ΔK dependence. This former behavior is indicated for the steel-NaCl system in Figures 11 and 19, while a reduced power-law relationship is observed for the titanium and aluminum alloys. The reduced dependence on ΔK is interpreted to result from a constant, K-independent, transport-limited "cyclic SCC" rate superimposed on a ΔK-dependent mechanical fatigue process. Stated equivalently, plateau behavior may be a result of chemically rate-limited environmental cracking that cannot respond to increasing mechanical driving force.

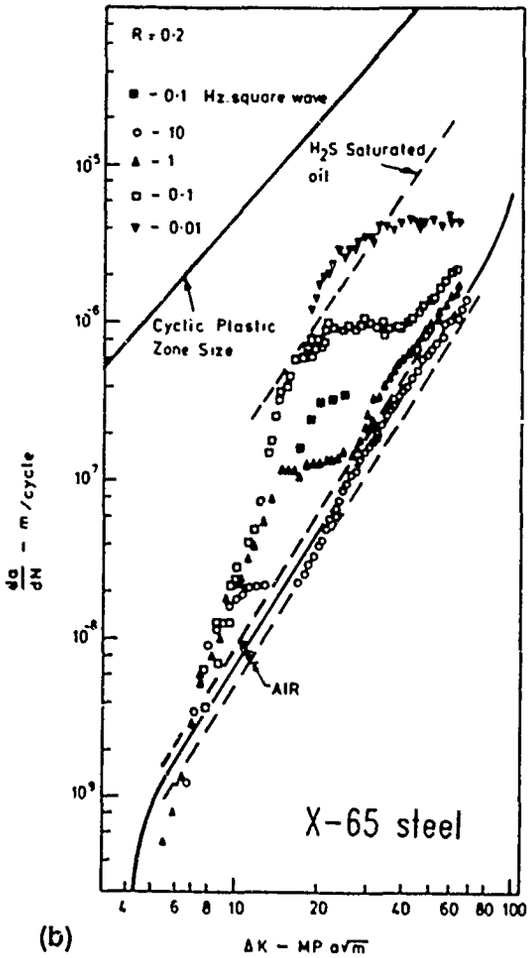
CF crack growth rates intersect and equal benign environment values at very high ΔK approaching K_{IC}. This regime is of little significance owing to the high levels of ΔK and fast crack growth rates involved.

The stress-intensity dependence of CF is typically characterized by a simple constant-load, increasing ΔK experiment. The data in Figure 19 were determined by this method. To date there have been no extensive studies of the load and crack-length history dependence of the da/dN–ΔK relationship for CF. That the results in Figure 19 are true material property laws that are independent of loading and geometry factors remains to be proven. This issue is particularly important when small crack and crack-closure processes occur, as discussed in the section "Complications and Compromises of Fracture Mechanics."

When characterizing the effects of variables on CF crack propagation and when developing models, it is important to recognize the various ΔK regimes.

Mean stress. Increasing mean stress intensity, as characterized by the "stress ratio" ($R = K_{min}/K_{max}$), generally increases rates of fatigue crack propagation, particularly for low growth rates ($< 10^{-5}$ mm/cycle) and inert or aggressive environments. For the former case and at temperatures where time-dependent plastic deformation is minimal, the casual mechanism is universally crack closure; see the section "Crack Mechanics."[153] Effects of increasing K_{max}, the monotonic plastic-zone size, and crack-tip mean strain on the da/dN–ΔK applied relationship are not well defined for intrinsic mechanical fatigue crack propagation.





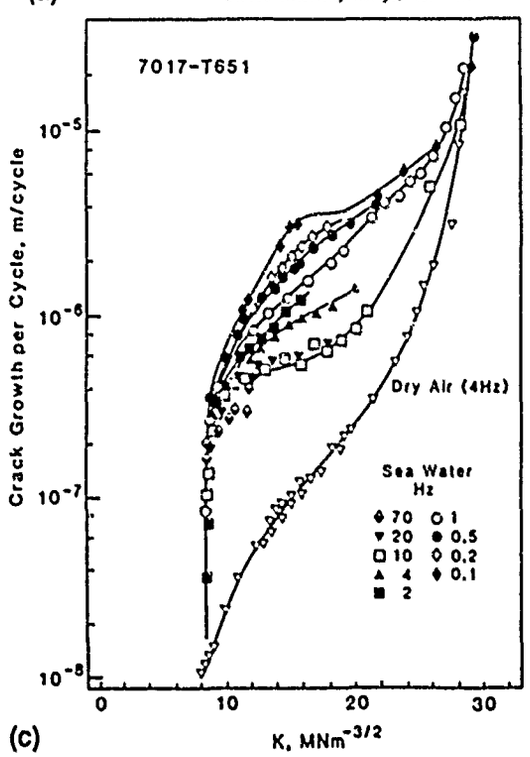


FIGURE 19—Effect of ΔK on corrosion fatigue crack growth rate at several frequencies for (a) Ti-6Al-4V in 0.6 M NaCl (after Dawson and Pelloux[141]); (b) X65 C-Mn steel in 3.5% NaCl with cathodic polarization (after Vosikovsky[34,170]), and (c) 7071-T651 aluminum alloy in seawater (after Holroyd and Hardie[65]). (1 in./cycle = 25.4 mm/cycle, 1 ksi√in. = 1.098 MPa√m)

For cycle-time-dependent CF, closure certainly contributes to the R-value effect; however, the magnitude of the maximum stress intensity could influence the cracking mechanism, as for example in HE. The relative contributions of crack closure and intrinsic mean stress effects have not been modeled. Dramatic stress ratio effects on CF above K_{Iscc} are well described by linear superposition modeling.[50]

Vosikovsky and coworkers demonstrated the deleterious effect of stress ratio on CF in carbon and heat-treated alloy steels exposed to NaCl.[173,174] For a specific frequency, single-crack growth rate laws of the type shown in Figure 19 were produced for air and for NaCl when ΔK was replaced by a function including the stress ratio; viz., (ΔK + 4R) for X70 C-Mn steel and (ΔK + 3R) for HY130 steel. The relative contributions of crack closure and R-sensitive environmental cracking were not defined. Given that the (ΔK + R) function equally correlates da/dN data for air and aqueous chloride and based on the relatively small effect of R on CF, it is likely that mean stress predominantly affected crack closure for this system. Indeed, Ewalds argued that these fatigue data are equally well correlated with an "effective ΔK" equal to (0.6 + 0.3R) × ΔK and based on Elber's physical notion of plasticity-induced crack closure.[175]

The need in this area is to define the effect of stress ratio on intrinsic CF crack propagation independent of crack closure. This aim is hindered by the complexity of measuring displacement in aggressive environments and by the lack of understanding of the relationship between such measurements, physical load transfer, and the relevant stress-intensity range.

Loading waveform and loading sequence. Two factors, constant amplitude loading wave shape and loading spectra, can influence CF crack propagation. The data presented in this review were obtained for constant amplitude, sinusoidal loading. Results on waveform and load-interaction effects in CF are limited.

Rates of CF crack propagation are well correlated by the root–mean square of the applied stress-intensity distribution for the steel-NaCl system under narrow-band random loading.[110 172 176 177] Complex overload and associated delay retardation effects in CF are beginning to be examined, for example, Reference 131. Hertzberg outlines a basis for such studies in benign environments.[89]

Several studies show that cycle–time-dependent CF crack growth rates are increased by waveforms that involve slow-rising load, compared to fast-rising–slow-falling or fast-rise–prolonged K_{max} hold periods for constant cyclic frequency. This trend was demonstrated by Pelloux and Selines for a type 7075 (UNS A97075) aluminum alloy,[128] by Barsom[51] for high-strength steel, and by Vosikovsky[170] for low-strength C-Mn steel, all exposed to aqueous NaCl. A typical example is presented in Figure 3.[51 52] Scott, et al., observed a modest reduction in da/dN for the low-strength carbon steel–seawater system when subjected to a fast-rise sawtoothed waveform and compared to equal CF for sinusoidal, triangular, and slow-rise sawtoothed loadings at constant frequency.[58] In contrast, Wei and Hudak reported that varying rise time had no effect on CF of 7075-T651 in distilled water (in Reference 51).

It is reasonable to expect that environmental effects are stimulated by slow strain and surface creation rates during rising loading. Nonetheless, the effect of waveform depends on the rate-controlling mechanism and will be material–environment specific. Changing rate of loading may have little effect on CF governed by fast surface reactions but a large effect on systems where hydrogen diffusion in the crack-tip plastic zone is rate limiting. The microscopic processes of surface creation on loading and of crack-tip shape change on unloading with varying convective mixing may also affect the waveform dependence.

Loading waveform effects on CF crack propagation above K_{Iscc} are well described by the integrated load-time history for each cycle.[50] Results suggest that crack growth only occurs on the loading portion of the cycle.[26]

Cyclic loading frequency

The time dependence of CF is arguably the most important aspect of this fracture mode. The general notion is that CF crack growth rates increase with decreasing cyclic loading frequency (f) because of increasing time per cycle available for increased chemical reaction and mass transport. This trend may be altered for cases in which increased frequency increases the rate of environmental cracking because of (1) enhanced mass transport by convective mixing, (2) enhanced crack-tip strain and surface creation rates, and (3) reduced crack-tip blunting by dissolution The frequency depen dence of cycle–time-dependent CF is accordingly complex.

To understand frequency effects, it is of paramount importance to identify the rate-limiting step in the transport, chemical reaction and fracture sequence for CF crack growth.[30 33 37 98] Additionally, the effect of stress intensity must be considered, the frequency depen dence may be specific to each of the three ΔK regimes.

ΔK_{th} and near-threshold regimes. Two unique frequency dependencies are reported for near threshold CF crack propagation, da/dN is constant with increasing f, or alternately, da/dN increases with increasing f. No data are available that show increasing near-threshold CF crack growth rates with decreasing frequency. More research is required, particularly at slow loading frequencies where test times are prolonged.

Frequency-independent CF crack growth was reported by Speidel for steels and nickel based alloys.[26] This "true" or cycle dependent CF behavior is illustrated by the horizontal dashed lines in Figure 4 for both moist air and NaOH. A similar frequency indepen dence of near threshold da/dN was reported by Meyn for Ti 8Al 1Mo 1V in 3.5% NaCl[65] and by Piascik and Gangloff for an aluminum lithium copper alloy exposed to 1% NaCl with anodic polarization.[126]

Frequency independent near threshold cracking is well estab lished for the steel aqueous chloride system. Vosikovsky reported da/dN independent of f for X65 and HY130 steels at low ΔK levels (Figure 19).[170 174] This effect was also observed by Gangloff for carbon and heat-treated alloy steels in 3% NaCl with cathodic polarization.[178] Specific data in Figure 20 were obtained for constant ΔK at a level within the steeply rising portion of the da/dN–ΔK dependence for each frequency. Note that crack growth rates in NaCl are independent of loading frequency, are about 3- to 4-fold greater than the value for moist air, and are 20 times the da/dN for vacuum. At very low ΔK, frequency-independent crack growth rates in aqueous chloride and moist air merge, as suggested in Figure 19.

In selected instances, low ΔK CF crack growth rates increase with increasing frequency. Specific examples were reported by Dawson and Pelloux for Ti-6Al-4V in NaCl (Figure 19)[141] and by Ford for an Al-7%Mg alloy loaded cyclically in 1 N Na_2SO_4 with cathodic polarization.[72] In the latter case, crack growth rates increased by an order of magnitude as f increased from 3 to 33 Hz, all rates were significantly faster than reference values for dry argon. This behavior was explained based on the film-rupture/repassivation model and the idea that environmental crack extension per unit time increases strongly with increasing crack-tip strain rate, equivalently increasing f, as discussed in the section "Corrosion Fatigue by Film Rupture/ Transient Dissolution."[72]

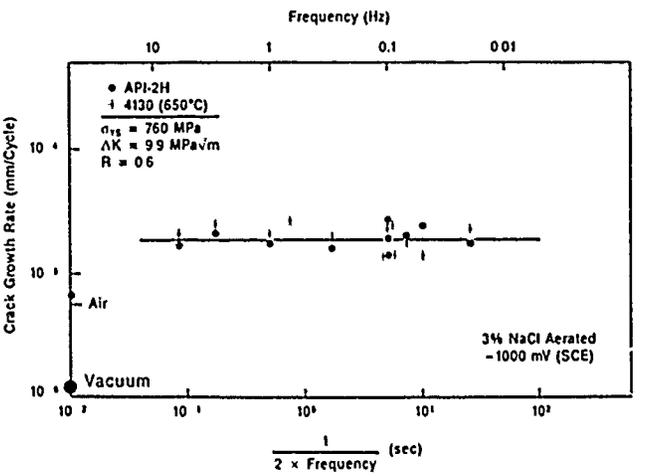


FIGURE 20—Effect of frequency on low-growth-rate corrosion fatigue crack propagation in the steel–aqueous chloride system; after Gangloff.[178]

Moderate ΔK "plateau" regime. For ΔK levels where the power-law dependence of da/dN is reduced and approaching plateau behavior, sub-K_{Iscc} CF growth rates generally increase with decreasing frequency. A saturation crack growth rate is often observed for low frequencies. Extensive data supporting these trends were reported by Vosikovsky [Figure 19(b)],[170 174] Scott, et al.,[58 121] Gallagher,[179] Gangloff,[37 99 180] and Hinton and Procter[181] for steels in aqueous chloride, by Wei and Shim[37 182] for steels in distilled water and water vapor, by Brazill, et al.,[151] for an alloy steel in gaseous H_2S, by Holroyd and Hardie,[64] for 7000 series aluminum alloys in seawater [Figure 19(c)], by Wei and coworkers[61 129 183] and Dicus[184] for 2000 and 7000 series aluminum alloys in purified water vapor, by Chiou and Wei[185] and Dawson and Pelloux [Figure 19(a)][141] for Ti-6Al-4V in aqueous NaCl, and by Ford and Andresen (Figure 14)[39 137] for austenitic stainless steels in high temperature purified water. Three cases are discussed, steel in aqueous chloride, aluminum alloys in water vapor, and stainless/ferritic C-Mn steels in high-temperature water.

Steels in aqueous chloride - The frequency dependence of the CF crack propagation rate in API-2H C-Mn steel exposed to 3% NaCl with cathodic polarization is shown in Figure 21.[180] These results were obtained by constant stress-intensity experimentation, with the specific ΔK level of 23 MPa$\sqrt{m}$ selected to be within the plateau region of CF cracking for this steel (see Figure 32). The logarithmic plot of environmental crack growth rate vs reciprocal frequency is suggested by mechanistic modeling, discussed in an ensuing section.

At frequencies above about 20 Hz, equal rates of fatigue crack propagation are observed for aqueous chloride and moist air, this value is about three times faster than crack growth in vacuum. Three regimes of behavior are observed with decreasing frequency. Initially, da/dN increases mildly, followed by a strong acceleration of CF for frequencies between 4 and 0.1 Hz, and leading to a third regime where da/dN is constant or mildly increasing as frequency declines to very small values.[2]

The trend shown in Figure 21 is general, as is indicated by the behavior of a variety of additional steels of varying yield strength but similar ΔK, R, and electrochemical conditions.[37,58,121,170,174,179-182,186] Results indicate similar behavior for the first two stages of the frequency response. Interestingly, the saturation behavior seems to be observed for the high-strength quenched and tempered steels (viz., API-2H and HY130 with σ_{ys} = 760 and 900 MPa, respectively) but not for lower-strength ferrite-pearlite BS4360 and X65 steels (σ_{ys} = 450 MPa). Additional experiments are required to explore this point.

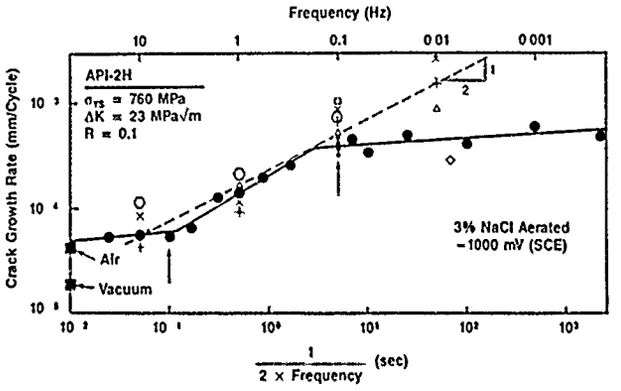


FIGURE 21—Effect of frequency on corrosion fatigue crack propagation in the "plateau" regime of ΔK for API-2H steel in 3% NaCl with cathodic polarization; after Gangloff.[180] Literature data: +, X, ⊡ X65, △, ◈ HY130, ⊙BS4360:50D.[50,170,174,181,186]

The frequency dependence in Figure 21 is explained by HE modeling reviewed in the section "Corrosion Fatigue by Hydrogen Embrittlement." The slope of the second regime is suggestive of the mechanism that controls CF, be it 1/2, indicating hydrogen diffusion control, or some other value, indicating hydrogen production (by surface reaction) rate control. The saturation behavior observed for the higher strength steels at the lower frequencies is also mechanistically significant. Similar results were reported for an aluminum alloy in seawater as indicated in Figure 19(c).[64]

Aluminum alloys in water vapor - While no one study has examined the frequency dependence of CF crack propagation in the high strength aluminum alloy-pure water vapor system, *in toto*, several investigations indicate that growth rates depend uniquely on environmental exposure, which is given by the product of load cycle period and water vapor pressure (P_{H_2O}) (viz., P_{H_2O}/loading frequency).[37,61,129] Data are presented in Figures 22 and 23 for two aluminum alloys, 2219-T851 and 7075-T651, in terms of environmental crack growth rate vs $P_{H_2O}/2f$ or P_{H_2O}. Several constant stress-intensity range levels are represented for a single frequency of 5 Hz and variable P_{H_2O}.[3]

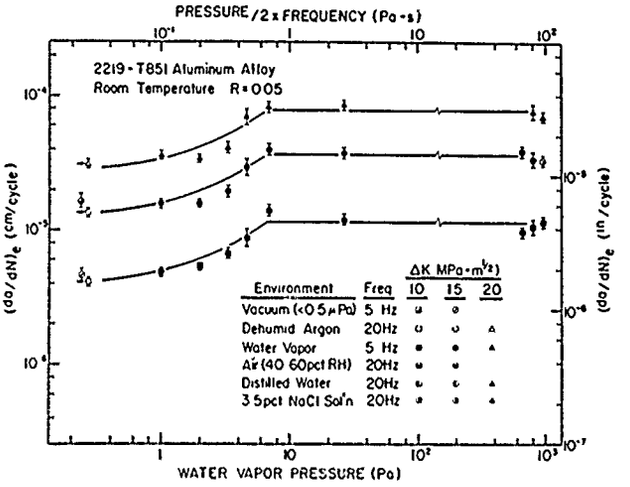


FIGURE 22—Effect of environmental exposure (water vapor partial pressure/frequency) on corrosion fatigue crack propagation in a precipitation-hardened aluminum alloy; after Wei, et al.[129]

The effect of frequency (water vapor pressure) on CF crack growth rates in the aluminum–water vapor system is similar to that exhibited by steel in aqueous chloride. Rates at high frequencies with water vapor are equal to values for inert environments. As frequency declines (or P_{H_2O} increases), da/dN values increase sharply to a saturation level. Some alloys such as 7075-T651 exhibit a second rate increase and saturation level.

Since frequency was not varied, the data in Figures 22 and 23 do not unequivocally establish the interchangeable influences of P_{H_2O} and frequency. The role of exposure to describe both frequency and water vapor pressure effects on crack propagation is better established when several studies are considered. Bradshaw and Wheeler examined an Al-Cu-Mg alloy (DTA 5070A) in water vapor at two frequencies (1 and 100 Hz) and a range of P_{H_2O}.[187] The pressure dependence at each frequency was equivalent to that shown in Figures 22 and 23, the levels of P_{H_2O} required to produce a given crack growth rate scaled with inverse frequency. Dicus concluded that frequencies between 1 and 10 Hz had no influence on CF rates for 7475-T651, only water vapor pressure controlled da/dN.[184] These results are consistent with the saturation behavior in Figures 22 and 23, at least for water vapor pressures up to the point of the second rise. Dicus found that this second rate transition occurred at a constant pressure for the two frequencies.

Theoretical modeling described in the sections "Gaseous Environments" and "Quantitative Hydrogen Embrittlement Models" supports the governing influence of the exposure parameter. Nonetheless, a complete characterization of the frequency dependence for selected constant P_{H_2O} levels would confirm this relationship.

The frequency dependence of CF in the aluminum–water vapor system has not been determined for near-threshold crack growth. Recent results for an Al-Li alloy suggest that the trends presented in Figures 22 and 23 are obeyed near ΔK_{th}.[125] Limited data by Niegel and coworkers show that ΔK_{th} for the onset of environmental fatigue cracking along high-angle grain boundaries in an Al-Zn-Mg alloy is reduced from the level for inert environment Stage II transgranular crack growth according to the reciprocal square root of P_{H_2O}.[132] Presumably, the exposure parameter would describe the effect of pressure and frequency.

[2] For perspective, the data point at a cyclic loading frequency of 0.0002 Hz required 12 days to produce a crack length interval of 0.10 mm during 250 load cycles.

[3] Environmental crack growth rate data are plotted for several constant stress-intensity ranges in Figures 22 and 23; however, experiments were conducted under constant load-increasing ΔK with several specimens cracked at a variety of frequencies or water vapor pressures. Data were cross plotted from complete da/dN–ΔK relations. Constant ΔK was generally not maintained over an interval of crack extension, in contrast to the results presented in Figures 20 and 21.

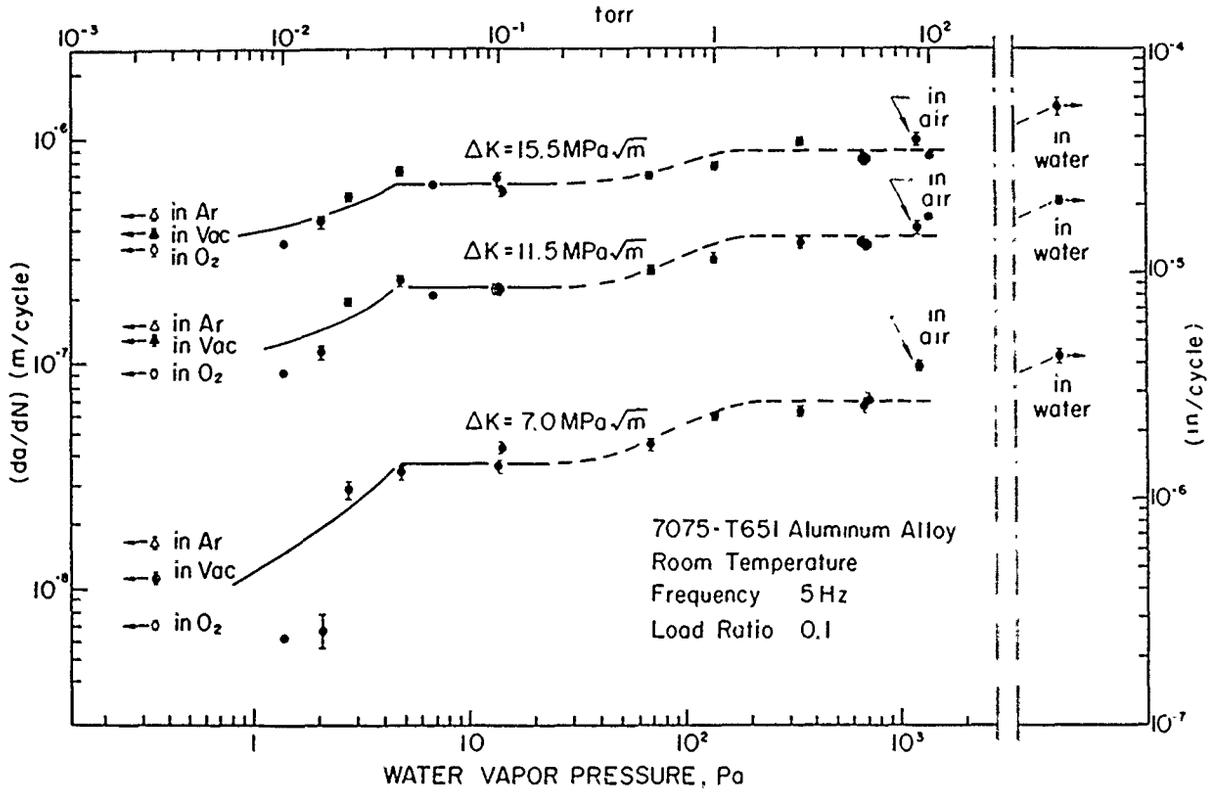


FIGURE 23—Effect of water vapor pressure on corrosion fatigue crack propagation in high-strength 7075-T651 at constant frequency; after Gao, et al.[61]

Mass transport and reaction rate modeling. hydrogen embrittlement—The essence of the mechanistic explanations for the aqueous and gaseous environment results contained in Figures 21 to 23 is equivalent. Crack growth per cycle is assumed to be proportional to the amount of hydrogen generated at the crack tip by chemical or electrochemical reactions. The frequency dependence is determined by the slow rate-limiting transport or reaction process, coupled with other fast steps in the CF sequence. This subject has been extensively investigated by Wei and coworkers.[37] For steel in aqueous chloride, hydrogen is produced by electrochemical reaction at the straining crack tip and in an amount proportional to the total charge passed per cycle. Electrochemical reaction on the clean crack surface is rate limiting. Measurements of the kinetics of these reactions demonstrate that the rise in the frequency response in Figure 21 is controlled by this slow surface-reaction step; lower frequencies result in longer exposure time per cycle, increased charge passed, and hydrogen produced.[37,182,188] At sufficiently low frequencies, the surface reaction per cycle is complete, with little additional hydrogen produced with further decreases in time; da/dN is constant. An alternate explanation based on hydrogen diffusion is described in the section "Corrosion Fatigue by Hydrogen Embrittlement."

For the aluminum-water vapor system, hydrogen is produced by water vapor oxidation of aluminum. This reaction is fast and not rate limiting Rather, the first rise to saturation in Figures 22 and 23 is due to slow water molecule transport along the crack, the rate-limiting process, and as influenced by crack wall-molecule interactions or impeded Knudsen flow. Da/dN increases with decreasing frequency because the amount of fast reaction at the crack tip is increased by increased transport supply and crack-tip pressure [61,129] Above a specific exposure, rates are insensitive to frequency (and pressure) because mass transport is sufficient for the surface reaction to reach completion; da/dN is constant. The second rise in Figure 23 is ascribed to slow chemical reaction between water vapor and magnesium that is segregated to grain boundaries in aluminum alloys.[183]

For both systems, the transport and reaction processes have been modeled as discussed in the section "Quantitative Models of Corrosion Fatigue Crack Propagation."[37 61 129 182 188] If the saturation growth rate is taken as an adjustable parameter, then the frequency dependencies shown in Figures 21, 22, and 23 are predicted A specific example is shown by the solid lines in Figures 22 and 23; these are model predictions.[61,129]

Steels in high-temperature water: film-rupture modeling—The strong effect of frequency on CF crack growth in "film-rupture" systems is illustrated by the behavior of stainless and ferritic C-Mn steels in elevated-temperature water.[39,71,136] Specific data and modeling predictions are shown in Figures 14 and 24. Here, moderate ΔK CF crack growth rates increase with decreasing frequency. Notably, however, ΔK_{th} decreases with increasing frequency, as seen in Figure 24(b). Film-rupture modeling, summarized in the section "Corrosion Fatigue by Film Rupture/Transient Dissolution," predicts that da/dN increases with decreasing frequency, as indicated by the predicted sets of power-law lines in Figures 14 and 24(a).

For a given crack-tip strain rate (equivalently, ΔK), a frequency exists below which brittle crack growth is replaced by crack-tip blunting by corrosion. This behavior is approximated by the shaded band in Figure 24(a). Crack growth rates cannot be sustained above this band, a threshold stress-intensity range is defined by the intersection of the blunting line and the film-rupture crack growth rate prediction. As shown in Figure 24(b), ΔK_{th}, defined in this manner, is predicted to decrease with increasing frequency, that is, with decreasing time for blunting.

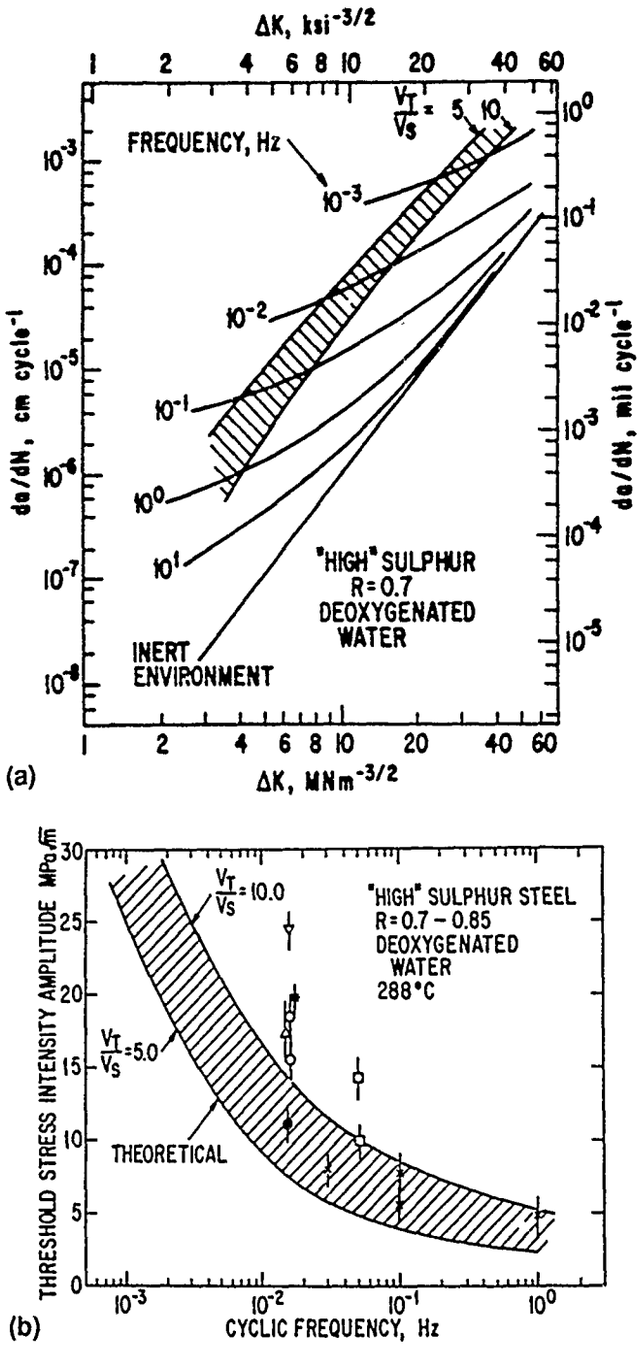


FIGURE 24—Effect of frequency on corrosion fatigue crack propagation in ASTM A508/A533-type steels in deoxygenated water at 288°C: (a) predictions of the film-rupture model and (b) predicted and measured threshold stress-intensity values; after Ford.[39]

Environment chemical activity

Environment chemistry variables including temperature; gas pressure and purity; and electrolyte pH, potential, flow rate, and halogen or sulfur ion content strongly affect rates of CF crack propagation. Understanding of these effects requires that a specific chemical variable be considered: (1) within each of the regimes of stress-intensity behavior, (2) as a function of loading frequency; and (3) uniquely for cyclic deformation, crack initiation, microcrack propagation and long crack growth. This task is formidable.

Three environment chemistry variables have been extensively investigated: (1) water vapor pressure for aluminum alloys, as discussed in the section "Aluminum Alloys in Water Vapor," (2) solution composition for stainless or carbon-manganese steels in high-temperature water, and (3) electrode potential for steels and aluminum alloys in aqueous chloride environments. A fourth case, gaseous hydrogen pressure and temperature effects on CF in steels, is not well understood.

Stainless and C-Mn ferritic steels in high-temperature water. Ford and Andresen broadly investigated the effects of electrolyte composition, oxygen concentration, solution flow, and electrode potential on stress corrosion and CF crack propagation in stainless and C-Mn ferritic steels exposed to high-temperature water environments typical of nuclear reactor and piping applications.[39,70,71,136,137] Many of these effects are explained by mass transport and electrochemical analyses of crack chemistry and transient repassivation reactions, coupled with the film-rupture model, as reviewed by Ford.[138]

Steels and aluminum in aqueous chloride: effect of electrode potential. Studies have been conducted on the effect of electrode potential on aqueous chloride CF crack initiation and propagation in low-strength C-Mn and heat-treated alloy steels and to a lesser extent in precipitation-hardened aluminum alloys.

C-Mn ferritic steels—For steels of yield strength below about 1000 MPa, fracture mechanics crack propagation experiments have emphasized the moderate ΔK "plateau" regime (> 18 MPa$\sqrt{m}$, Figure 11) and frequencies generally within the saturation range (< 0.2 Hz, Figure 21). CF in this ΔK–f regime is cycle-time-dependent below K_{ISCC}.

Results from several laboratories demonstrate that CF crack growth rates generally increase with increasing cathodic polarization.[58,115,122,170,173,174,178,189] Specific data in Figure 25 illustrate this trend for two carbon-manganese steels. Note, however, that "plateau ΔK" crack growth rates exhibit a minimum at about 200 mV cathodic to the free-corrosion potential.

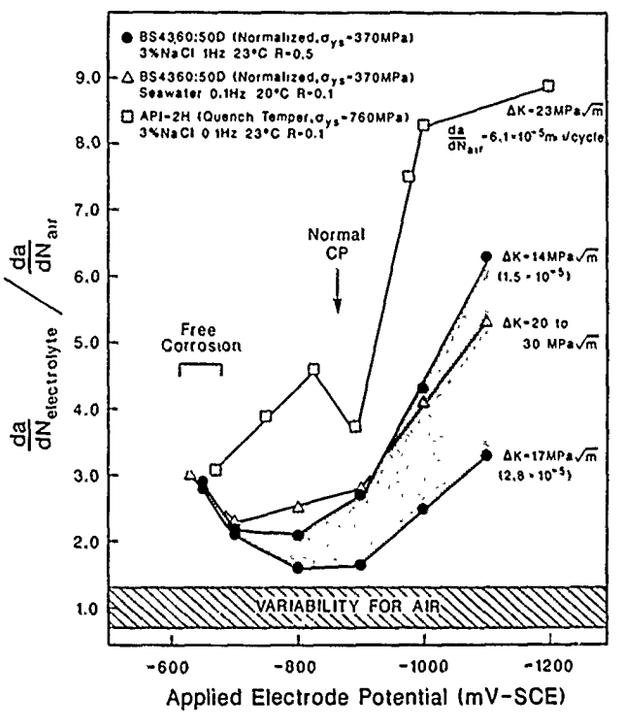


FIGURE 25—Effect of applied cathodic potential on corrosion fatigue crack propagation in C-Mn steel/aqueous chloride system,[115] BS4360:50D in 3% NaCl[122] or in seawater,[58] API-2H in 3% NaCl.[176]

The behavior shown in Figure 25 is explained based on HE and analytical modeling of crack chemistry. The notion is that da/dN increases with increasing crack-tip hydrogen production, as discussed in the sections "Models of Occluded Crack Chemistry and Transient Reactions" and "Corrosion Fatigue by Hydrogen Embrittlement." The minima is explained because crack-tip hydrogen is produced by both proton and water reduction; the former decreases with increasing cathodic polarization, while the latter increases in importance for potentials below about -800 mV_{SCE}.[190,191]

The correlation of CF crack growth rate with the amount of hydrogen produced at the crack tip and on surfaces exposed to bulk electrolyte is suggested by static-load HE models.[192] Turnbull developed analytical predictions of specimen surface and crack-tip hydrogen production as a function of bulk solution pH and applied electrode potential.[190,191,193] Gangloff correlated K_{ISCC} with hydrogen uptake from electrolytes and gases for static load cracking of high-strength steels.[194,195] Such information, coupled with *in situ* permeation measurements of hydrogen uptake in a component, provide a meaningful approach to control of cracking.[57,113] Yamakawa and coworkers and DeLuccia and Berman developed hydrogen permeation sensors.[113,114] Unfortunately, this integrated sensor, crack chemistry, and micromechanical cracking analysis has not been applied to CF.

Studies of the effect of electrode potential on CF illustrate an important distinction between crack initiation and propagation. Uhlig and coworkers reported that CF of polished specimens of types 1020 (UNS G10200) and 4140 steels, exposed to NaCl during high-frequency rotating-bending "S-N" conditions, only occurred if a critical anodic corrosion current was exceeded.[84-86] Typical data are presented in Figure 26 for 4140 steel in 3% NaCl at varying electrode potentials and loaded at stress levels above and below the moist air endurance limit of 379 MPa (55 ksi).[86] Mild cathodic polarization restores this air endurance limit and the number of cycles (4×10^5 for dry air) for fatigue failure at 448 MPa. Polarization noble to a critical value degrades both of these fatigue properties. A similar beneficial effect of cathodic polarization was reported by Rajpathak and Hartt based on measurements of CF crack initiation and early growth to a 1-mm depth at the root of a notch (see Figure 54).[196]

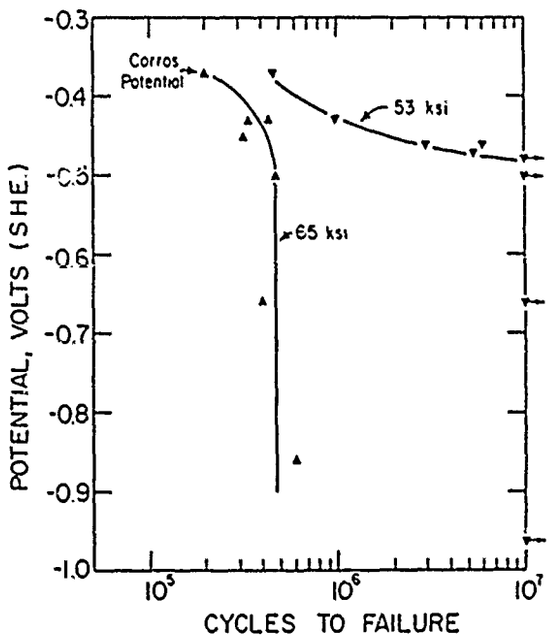


FIGURE 26—Effect of applied electrode potential on corrosion fatigue of smooth, rotating bend specimens of 4140 (UNS) steel (hardness = R_c 20) in 3% NaCl (free-corrosion potential = -610 mV_{SCE}). The dry air endurance limit is 55 ksi and cycles to failure in moist air at 65 ksi equal 4×10^5. (1 ksi = 6.89 MPa); after Lee and Uhlig.[86]

The opposite effects of cathodic polarization on smooth specimen life and crack propagation are readily understood. Presumably, anodic corrosion leading to either enhanced plastic deformation or localized pitting is required for CF crack initiation.[1,29,36,87] Here, hydrogen plays a secondary role, particularly for the moderate potentials, fast-loading frequencies and near-threshold stress intensities typical of the smooth-specimen studies. Anodic dissolution should similarly affect near-threshold crack propagation in steels; however, evidence in this regard is lacking. Cathodic polarization enhances moderate ΔK rates of CF crack propagation by the HE mechanism. Slow-loading frequencies, significant plastic straining and concentrated hydrogen production within the occluded crack provide the basis for HE as dissolution becomes less important.

Electrode potential effects on CF of steels in marine environments are critical because of the requirement to cathodically protect structures against general corrosion. Designers have debated the effects of cathodic potential on fatigue cracking.[104-107] From the above discussion and based on experiments with large-scale structural components, it is concluded that cathodic polarization can be either beneficial or deleterious to the CF resistance of a component.[99,100,110] The specific effect depends on the level of applied cathodic current, and the regime of fatigue that dominates component life, be it initiation or propagation.

Precipitation-hardened aluminum alloys—Applied electrode potential significantly affects CF crack propagation in precipitation-hardened aluminum alloys in aqueous chloride. In general, CF cracking occurs at the free-corrosion potential, is exacerbated by either anodic polarization or large cathodic polarization, and is mitigated by mild cathodic polarization. Mechanistic explanations are lacking.

As reviewed by Speidel and later Holroyd and Scamans, fracture mechanics stress corrosion crack growth rates and slow-strain-rate tensile ductility both indicate a maximum resistance to cracking at potentials that are mildly cathodic to the free-corrosion potential for 7000 series aluminum alloys in halogen-bearing solutions.[66,197] Data are limited for 2000 series alloys; however, anodic polarization appears to enhance SCC.[197] A similar trend could be expected for CF crack propagation above K_{ISCC}; data in Figure 5 for alloy 7079-T651 confirm this result.[5]

Two studies of cycle-time-dependent CF crack propagation indicate the detrimental effect of anodic polarization and the beneficial effect of mildly cathodic potentials.[77,126] Specific data are presented in Figure 27 for an advanced Al-Li-Cu alloy (2090).[126] Here, CF crack propagation is enhanced by loading in 1% NaCl with anodic polarization compared to growth rates for either moist air or high-purity helium. Cathodic polarization reduces crack growth rates to levels typical of moist air or lower. Similar results were reported for AA 7075 by Stoltz and Pelloux.[77] For the Al-Li alloy, the environmental effect is pronounced near ΔK_{th}; here, cracks growing at constant ΔK and R under anodic polarization were arrested by application of a cathodic potential. Prolonged cycling was required to reinitiate crack propagation upon a second application of the anodic potential.[126]

Duquette and coworkers reported that the fatigue lives of smooth specimens of Al-4Mg-2Li and 7075 aluminum alloys in NaCl were maximum at potentials mildly cathodic relative to free corrosion.[62,198] Anodic and high cathodic polarizations degraded CF life, much like the behavior of 4140 steel.[86]

The mechanism for the effect of electrode potential on CF in the aluminum alloy–chloride system is complex and unclear. Results can be speculatively interpreted in terms of anodic dissolution, HE, crack-tip blunting by corrosion, surface film/dislocation interactions, and surface film/reaction kinetics.[62,77,126,197,198] The problem in identifying the dominant mechanism is that both dissolution and hydrogen evolution occur on aluminum over a broad range of electrode potentials. Furthermore, the localized crack chemistry (viz., pH, potential, and ionic composition) changes with varying applied potential. These effects have not been separated and quantified; as

such, imaginative arguments can be constructed from each of the above perspectives. There is a strong likelihood that HE contributes to the behavior shown in Figure 27.[126]

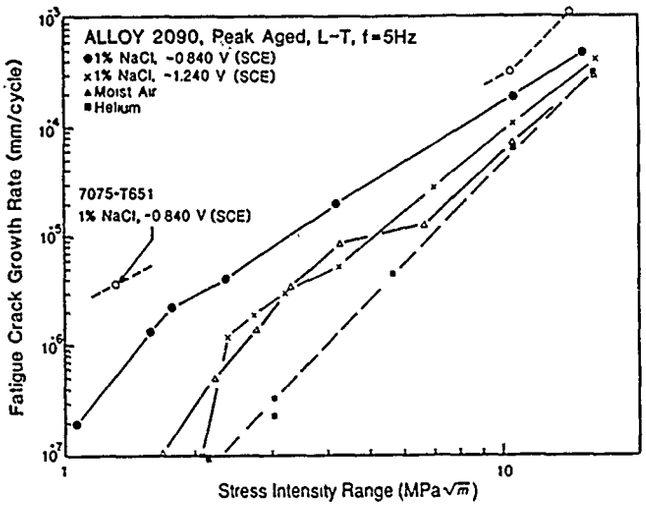


FIGURE 27—Effect of electrode potential on corrosion fatigue crack propagation in Al-Li alloy 2090 in aqueous chloride at constant ΔK and high mean stress; after Piascik and Gangloff.[126]

Corrosion fatigue of steels in gaseous hydrogen. Nelson and others demonstrated that purified gaseous hydrogen produces cycle-time-dependent CF crack propagation in low- to moderate-strength steels well below K_{ISCC}.[117,118,199] Typical data are shown in Figure 11. Ritchie and coworkers demonstrated that H_2 accelerated fatigue crack propagation in moderate-strength 2 1/4Cr-1Mo and in high-strength 300M steels for stress intensity ranges within the Paris regime.[200,202] While generally below K_{ISCC}, CF crack growth rates in this regime increased with decreasing loading frequency and with increasing R. A typical example is reproduced in Figure 28.[201]

Extensive data were reported for gaseous hydrogen effects on near-threshold CF crack propagation in steels.[200-207] As illustrated in Figure 28, ΔK_{th} is decreased and growth rates are increased by hydrogen, relative to cracking in moist air, for low- to moderate-strength steels, particularly 2 1/4Cr-1Mo.[200,202,204,205] Similar crack growth rates were reported for hydrogen and helium, and the environmental effect diminished for high mean stress loading, leading Ritchie, et al., to conclude that oxide-induced crack closure dominated fatigue. (See "Crack Closure.") In these experiments, H_2 pressure was low and loading frequency was high, the possibility for HE apart from reduced closure was not explored

An opposite hydrogen environment effect on ΔK_{th} was observed for high-strength steels; near-threshold growth rates in H_2 were decreased and ΔK_{th} was increased relative to moist air.[200,203,206,207] Hydrogen caused moderate embrittlement relative to inert environments. The mechanism for this effect is unclear, but may involve embrittlement in moist air because of a crack surface oxide film (see "Corrosion Fatigue by Surface Film Effects") or high-activity hydrogen production by oxidation and perhaps capillary condensation of water in moist air. Alternately, hydrogen could produce enhanced crack-tip plasticity and surface roughness, leading to a beneficial effect of crack closure, which dominates a chemical embrittlement effect.

There is a notable lack of data for moderate-strength steels below K_{ISCC} and that emphasize the effects of H_2 pressure, temperature, and environment impurities on CF. Such experiments and associated comparisons with surface reaction kinetics could lead to better understanding of the mechanisms for hydrogen effects in CF.[37]

Brazill and coworkers characterized the effect of hydrogen sulfide pressure (P_{H_2S}) on CF crack propagation in 2 1/4Cr-1Mo steel at room temperature for several relatively high-stress-intensity range levels.[151] Growth rates increased with increasing P_{H_2S} and reached a saturation plateau, analogous to that illustrated in Figure 23 for high-strength aluminum alloys in water vapor. The relationship between da/dN and pressure was predicted quantitatively based on a model of fast surface reaction–gas transport control at low P_{H_2S} and of fast transport–slow "second step" surface reaction control at high pressures of hydrogen sulfide.[151]

Several studies have shown that hydrogen environment composition critically affects rates of CF crack propagation in steels. Molecules such as CO or O_2 preferentially adsorb on clean crack surfaces, block or "poison" dissociative chemisorption of H_2, and accordingly reduce rates of CF crack propagation. This effect was demonstrated by the pioneering work of Johnson on 4340 steel (see Figure 6[54]) and later by Nelson[118] and Cialone, et al.,[117,199] for carbon-manganese steels.

Gangloff established that certain hydrocarbon molecules mitigate CF crack propagation in steels exposed to otherwise pure H_2.[208] Data are shown in Figure 29. Relative to helium, low-pressure gaseous hydrogen accelerates fatigue crack propagation in moderate-strength (σ_{ys} = 1030 MPa, R_c 36) type 4340 steel at constant ΔK and 1 Hz. The addition of equal partial pressures of saturated hydrocarbons such as methane (CH_4) and ethane (C_2H_6) had no effect on hydrogen-enhanced fatigue cracking rates. In contrast, ethylene (C_2H_4) with unsaturated double carbon bonding inhibited H_2-enhanced crack growth, albeit not completely relative to pure helium. Frandsen and Marcus reported a beneficial effect of acetylene (C_2H_2) on hydrogen enhanced fatigue of a high-strength steel.[209]

The mechanism for the beneficial effect of hydrocarbons on hydrogen cracking involves surface reaction between ethylene or acetylene and adsorbed hydrogen, where the concentration of the latter is reduced by the formation of inert methane The prerequisite for reactive gettering" of otherwise embrittling hydrogen is double or triple carbon-carbon bonds in the hydrocarbon that are catalytically split to combine with adsorbed hydrogen, a process likely for ethylene and acetylene at 300°K. Molecules such as methane or ethane have single (or saturated) carbon bonding and do not react with atomic hydrogen. Hydrocarbon molecules could also competitively chemisorb and reduce hydrogen uptake by a blocking mechanism

Data in Figure 29 show that pure environments embrittle steel according to the declining order of effect on da/dN:

$$H_2 > C_2H_4 > C_2H_6 > CH_4 = He$$

The embrittling potency of these gases is understood qualitatively based on the ease with which the molecule will dissociatively chemisorb to produce embrittling atomic hydrogen on the clean crack surface.

Yield strength

To date, no systematic fracture mechanics data have been reported to demonstrate an effect of yield strength, either monotonic or cyclic, on CF crack propagation below K_{ISCC}. This variable is not well understood.

For benign environmental conditions including moist air, experimental measurements indicate that yield strength has little effect on rates of fatigue crack propagation within the Paris regime. Threshold stress intensity is either constant or mildly decreases with increasing yield strength for high mean stress-intensity loading where crack-closure effects are minimal.[200,202] At low R, ΔK_{th} decreases strongly with increasing strength, largely because of strength effects on crack closure.[201]

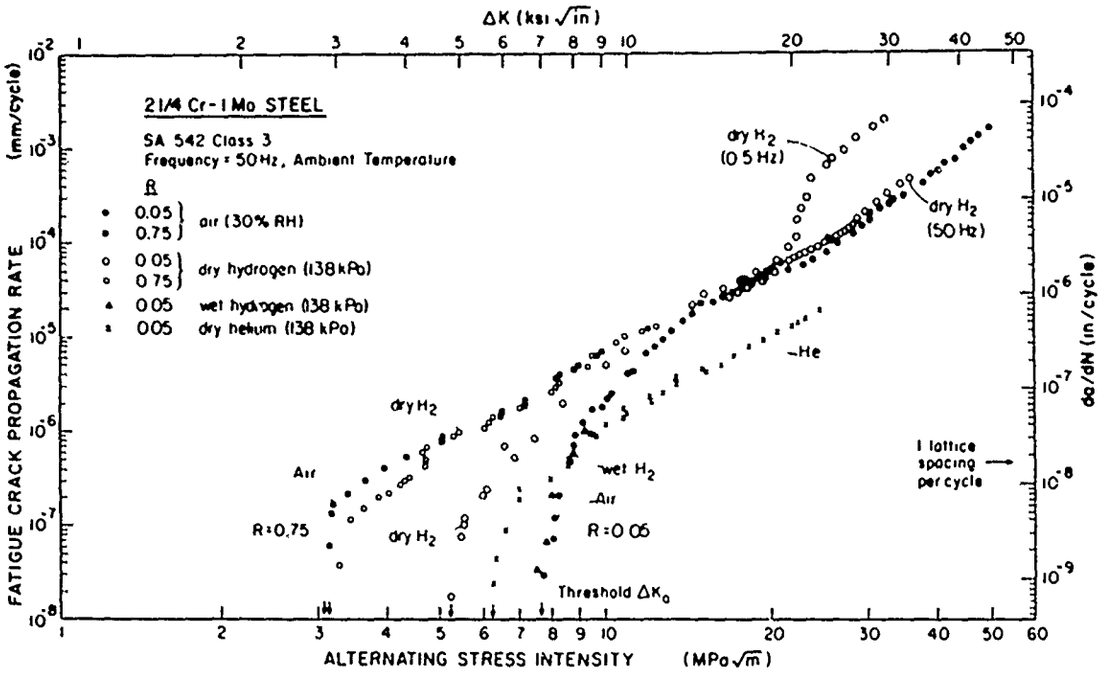


FIGURE 28—Corrosion fatigue crack propagation in 2 1/4Cr-1Mo steel in low-pressure gaseous hydrogen at room temperature; after Suresh and Ritchie.[201,203]

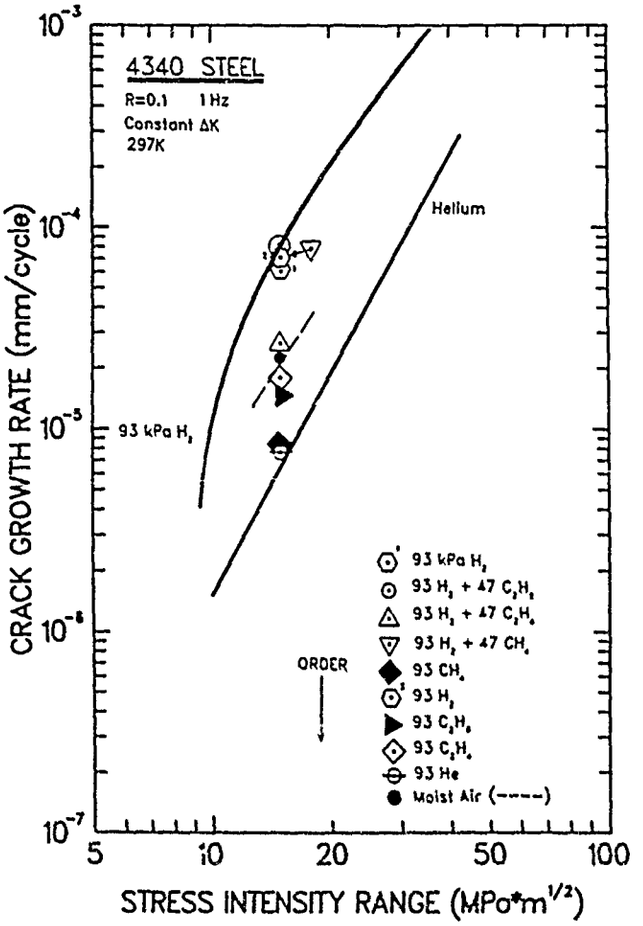


FIGURE 29—Fatigue crack propagation rate data for high-strength 4340 (UNS G43400) steel (R_c 36) in hydrogen-hydrocarbon gases at constant ΔK and frequency; after Gangloff.[208]

Micromechanical modeling (see "Models of Crack-Tip Mechanics . . .") indicates that the process-zone size and the cyclic plastic strain distribution within the crack-tip plastic zone decrease with increasing yield strength; fatigue crack extension by damage accumulation accordingly decreases and ΔK_{th} increases with increasing strength.[210,211] These effects are predicted to be small and may be dominated by microstructural changes (e.g., grain size), which are used to vary strength.

Yield strength is a primary variable that influences environmental cracking for monotonic loading. For many material-environment systems, for example, ferritic steels in hydrogen-producing gases and electrolytes, K_{ISCC} decreases and da/dt values increase with increasing strength.[195] CF crack propagation above K_{ISCC} will be accordingly exacerbated by increasing yield strength, as predicted by linear superposition.

A striking example of the lack of a strong yield strength effect on cycle-time-dependent CF crack propagation is shown in Figures 30 and 31 for ferritic steels in aqueous chloride with applied cathodic polarization and at low loading frequency. (The effects of these parameters are shown in Figures 21 and 25.) Since CF is attributed to HE, a yield strength effect could be expected. Rather, data in Figure 30 show an essentially constant environmental effect for steels that vary in monotonic yield strength from 390 MPa (BS4360:50D) to 1080 MPa (Ni-Cr-Mo).[115] Crack growth rates at a "plateau" stress-intensity range of 23 MPa$\sqrt{m}$ are plotted in Figure 31 for each steel in Figure 30. CF crack growth rates are five to eight times faster than the yield-strength-independent value for moist air; however, no trend is observed for cyclic yield strengths from 190 to 870 MPa. The data in Figures 30 and 31 were collected from the results of eight laboratories; differences in da/dN are reasonably attributed to interlaboratory variability. (Note the cross-hatched region for API-2H, which shows the range of CF crack growth rates determined by a single laboratory on five separate specimens. Similar replicate data are shown for X65. This variability is of the same order as the strength effect in Figure 31.)

While the data in Figures 30 and 31 suggest that yield strength is not a critical variable in CF, much work remains. For steels in chloride, no single study has been reported in which yield strength is systematically varied and CF characterized for constant chemical

and loading conditions within the threshold and "plateau" ΔK regions and as a function of frequency. Other alloy–environment systems must be investigated to examine strength effects for dissolution and film-rupture-based CF. A micromechanical damage model must be developed to predict the effect of yield strength and work-hardening behavior on CF crack growth rate. Finally, studies of yield strength effects must cope with concomitant variations in microstructure. For the steels in Figure 31, significant microstructural variations were necessary to develop the yield strength differences. Yield strength and microstructure effects on CF must be separated, to the extent possible.

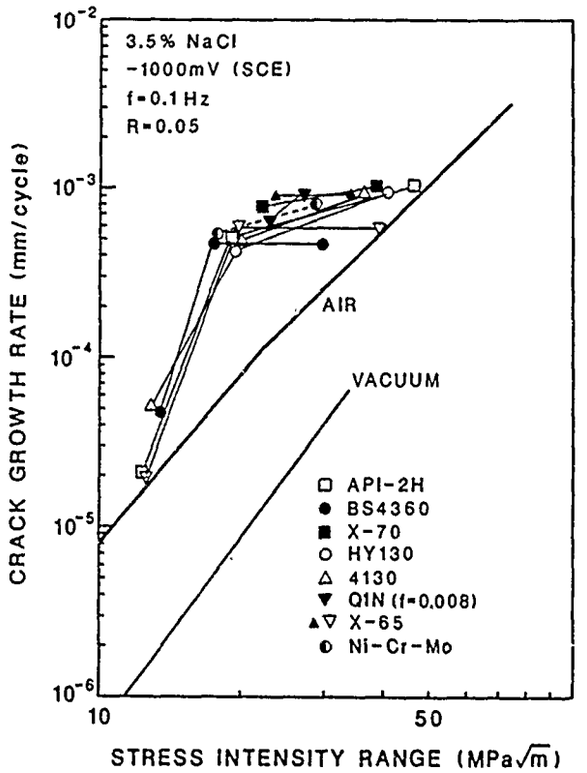


FIGURE 30—Corrosion fatigue crack propagation in steels of varying yield strength and microstructure in 3.5% NaCl at constant cathodic potential and low loading frequency; after Krishnamurthy, et al.[115]

Microstructure

Similar to yield strength, microstructural effects on CF crack propagation have received limited attention. Several examples are discussed, including steels in aqueous chloride and H_2, aluminum alloys in aqueous chloride, and stainless and carbon steels in high-temperature water.

Ferritic steels in aqueous chloride and gaseous hydrogen. For ferritic C-Mn and heat-treated alloy steels in aqueous chloride with cathodic polarization, data in Figure 31 indicate no systematic effect of microstructure on CF crack propagation. This conclusion is confirmed by an investigation summarized in Figure 32.[178] A C-Mn steel was heat treated to produce, in order of heat treatment on the figure, tempered martensite of two prior austenite grain sizes, upper and lower bainite, and dual-phase ferrite + martensite with two martensite volume fractions. These heat treatments produced a constant monotonic yield strength of 760 MPa, based on measured hardness of R_c 27 ± 2. These variations in microstructure have no effect on CF crack propagation for constant applied cathodic potential and low loading frequency. CF crack growth rates for these API-2H microstructures are in good agreement with the behavior of normalized BS4360:50D C-Mn steel of ferrite-pearlite microstructure. (The shaded band in Figure 32 represents CF in BS4360:50D reproduced from Figure 11.)

Jones reported that two quenched and tempered steels exhibit reduced CF crack growth rates compared to lower-strength normalized microstructures for seawater at the free-corrosion potential of −650 mV_{SCE}.[186] Literature results support this conclusion as shown in Figure 33.[115,186] Here, quenched and tempered HY130, EN5, and Q1N show CF at reduced rates compared to normalized or controlled rolled (ferrite-pearlite) EN5 and X65. Since the yield strengths of the ferrite-pearlite steels vary between 300 and 450 MPa, while the tempered martensitic steels are of strengths between 600 and 950 MPa, the contributions of yield strength and microstructure in Figure 33 are not understood.

Similar to aqueous chloride, only limited studies have been conducted on fatigue crack propagation in carbon or alloy steels exposed to gaseous hydrogen. Wachob and Nelson observed that ΔK_{th} increases with increasing yield strength and grain size for A516 steel in both moist air and high-pressure hydrogen.[212] These results may be explained based on extrinsic crack-closure effects (see "Crack Mechanics") and do not clearly indicate an effect of strength or microstructure on intrinsic HE. Cialone, et al., showed that CF da/dN in gaseous hydrogen decreases dramatically for high-carbon steels containing pearlitic carbide and compared to pure iron or low-carbon steel.[199] The authors speculated that carbide hinders hydrogen uptake, similar to the poisoning effect of CO discussed in the section "Corrosion Fatigue of Steels in Gaseous Hydrogen."

Temper embrittlement in steels, involving metalloid impurities segregated at prior austenite grain boundaries, is a well-known promoter of gaseous and aqueous environment HE for static loading.[213] Hippsley demonstrated a similar deleterious effect of this metallurgical variable for cyclic loading of 2 1/4Cr-1Mo steel in gaseous hydrogen.[214] Results in Figure 34 show that quenched and tempered steel with little or no impurity segregation (Material L; austenitized at 960°C, quenched, tempered at 600°C; monotonic yield strength of 510 MPa) exhibits a hydrogen environment effect compared to vacuum, particularly at higher ΔK. CF crack growth was along prior austenite grain boundaries. Notably, so-called reversible temper embrittlement due to 1000-h heating at 500°C of Material L (Material LE; monotonic yield strength of 530 MPa) caused a further increase in CF crack propagation rates, particularly near ΔK_{th} and for moderate Paris regime stress intensities. Temper embrittlement also affects fatigue crack propagation in moist air, with equivalent growth rates observed for each heat treatment stressed cyclically in vacuum. The magnitude of the hydrogen effect in CF was correlated with increased percentages of intergranular fracture and increased phosphorus segregation to prior austenite grain boundaries.

Hippsley also reported a strong deleterious effect of so-called one-step temper embrittlement, caused by low-temperature tempering at 300 to 500°C of material austenitized at 960°C and quenched.[214] H_2 increased rates of CF for as-quenched steel (yield strength of 960 MPa), but substantially higher rates of crack propagation were reported for the tempered steel (yield strength of 890 to 1000 MPa). Crack growth was transgranular and associated with precipitate effects on crack-tip plasticity and fracture.

This study of the H_2-temper embrittlement interaction during fatigue was limited to a single loading frequency (10 Hz), hydrogen pressure, and mean stress. Additional work is required to explore this metallurgical effect for slower frequencies that allow increased time for chemical effects, for higher hydrogen environment activities, and for higher stress ratios that eliminate the complicating effect of crack closure.

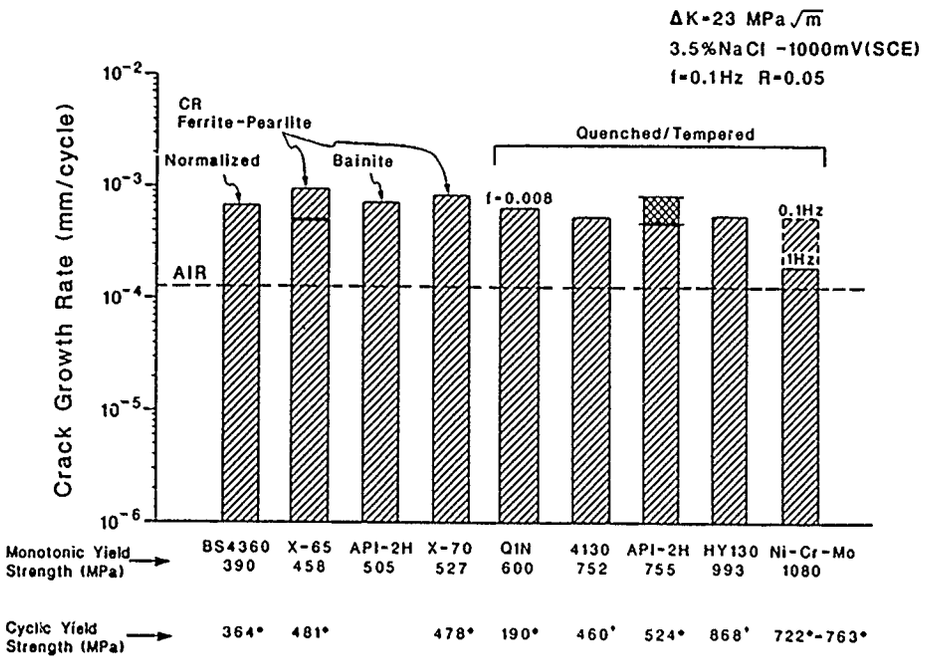


FIGURE 31—Effect of steel yield strength and microstructure on corrosion fatigue crack propagation rate at constant cathodic potential, ΔK, and frequency, from Figure 30; after Krishnamurthy, et al.[115]

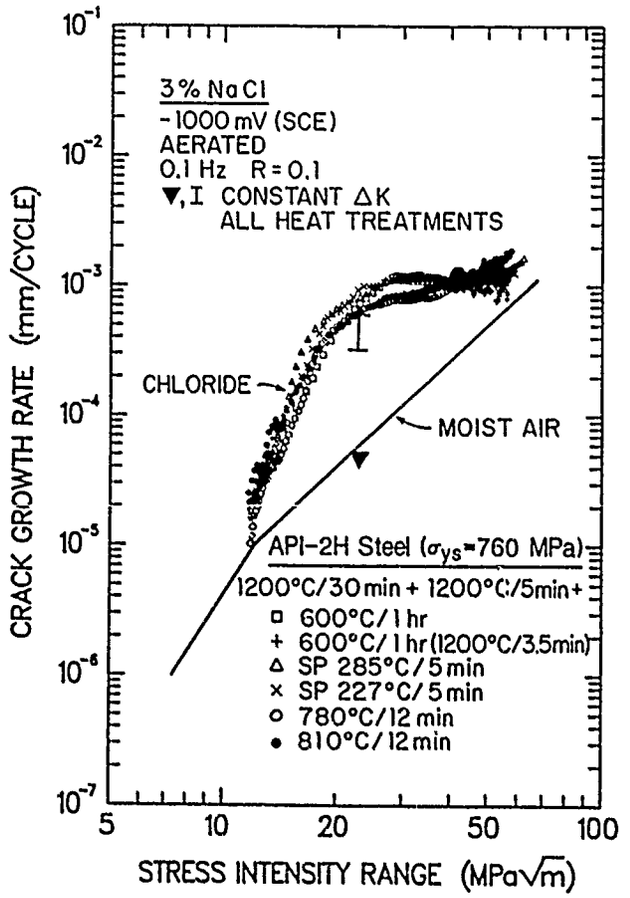


FIGURE 32—Effect of microstructure on corrosion fatigue in C-Mn steel heat treated for constant yield strength (760 MPa) and stressed at either constant ΔK or constant load in aqueous 3% NaCl with cathodic polarization; after Gangloff, Koo, and Marzinsky.[178]

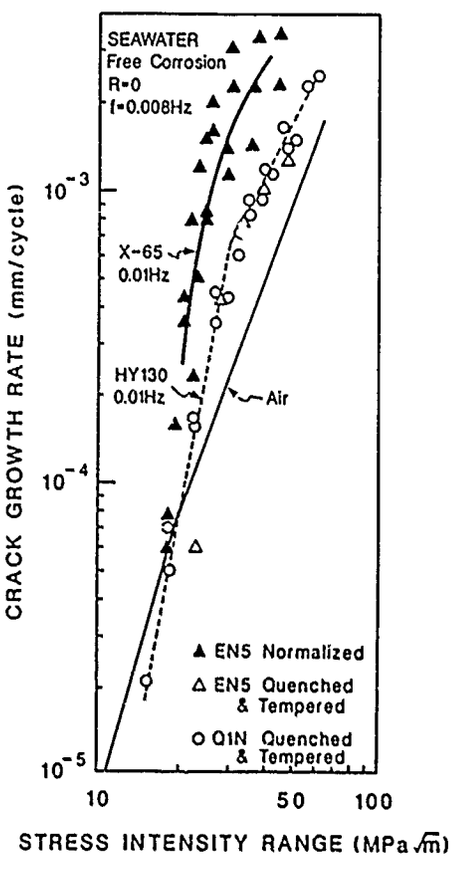


FIGURE 33—Effect of microstructure and yield strength on corrosion fatigue crack propagation in C-Mn and alloy steels in seawater, freely corroding at -675 mV_{SCE}; after Jones.[186]

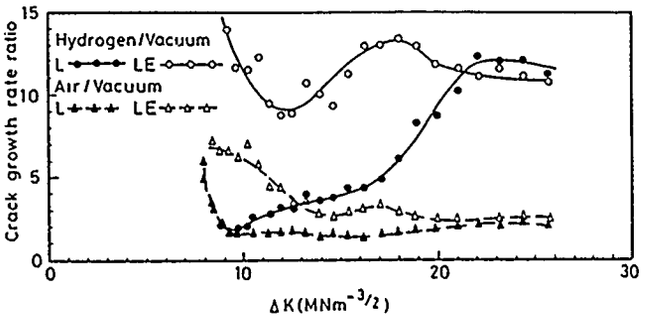


FIGURE 34—Effect of temper embrittlement on H_2-enhanced fatigue crack propagation in 2 1/4Cr-1Mo steel. Material L is not temper embrittled, while LE was heat treated for reversible temper embrittlement (10 Hz, R = 0.30); after Hippsley.[214]

Aluminum alloys in aqueous chloride. Despite extensive work on microstructural effects on SCC in precipitation-hardened aluminum alloys,[66] microstructure–CF properties relations have received limited attention. Lin and Starke demonstrated the effect of alloy copper content on CF crack propagation in four Al-6Zn-2Mg-Cu alloys, heat treated to either peak yield strength (T651, 480 to 550 MPa) or overaged (T7351, 400 to 460 MPa).[215] CF experiments were conducted in distilled water at a frequency of 10 Hz and R = 0.10. As shown in Figure 35, normalized CF growth rate decreased with increasing copper content, predominantly for the peak age condition and intermediate ΔK. These results were explained based on the damaging interaction between absorbed hydrogen and localized planar slip within the crack-tip cyclic plastic zone. Planar slip is eliminated by increased copper and by overaging, factors that both reduce precipitate coherency and increase precipitate looping by dislocations to homogenize plastic deformation. These authors did not consider the effects of copper and precipitate/precipitate-free zone sizes on the electrochemical activity of precipitates (presuming that distilled water is sufficiently impure to be an electrolyte), on crack chemistry, and on hydrogen uptake. Nonetheless, this work provides a hypothesis for the superior CF resistance of copper-bearing 2000 aluminum alloys compared to 7000 series materials (see Figure 12).

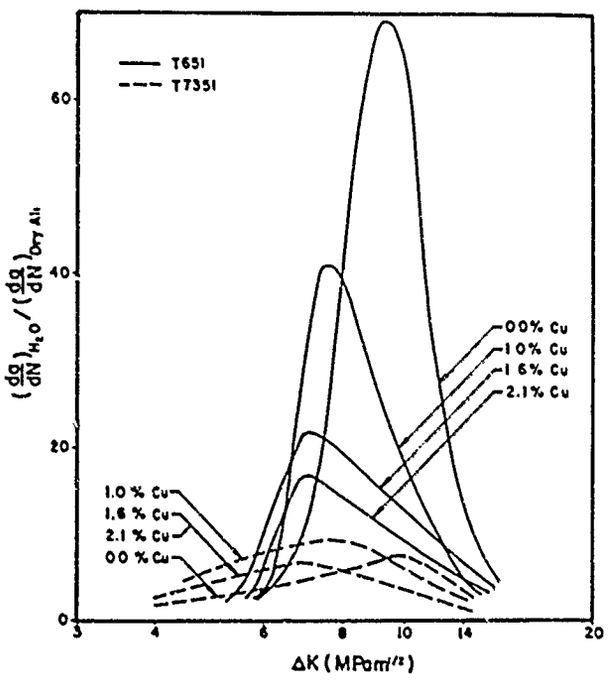


FIGURE 35—Effect of copper content and aging treatment on corrosion fatigue crack propagation in Al-6Zn-2Mg exposed to distilled water (10 Hz, R = 0.10); after Lin and Starke.[215]

Steels in high-temperature water. Two metallurgical variables are pertinent to CF crack propagation in ferrous alloys exposed to elevated-temperature pressurized water. Sensitization, that is, near-grain-boundary chromium depletion because of carbide precipitation, induces intergranular SCC in austenitic stainless steels. Sulfide inclusions affect environmental cracking of C-Mn ferritic steels.

For 304-type stainless steels, data and modeling show that CF crack growth rates are increased by sensitization. The da/dN–ΔK relationships in Figure 14 are reduced by up to a factor of five for annealed and quenched (EPR < 1 C·cm^{-2}) compared to sensitized (EPR = 15 C·cm^{-2}) stainless steel.[137] Other results show that sensitization enhances crack growth kinetics by up to 20 to 30 times for lower strain rates and more aggressive environmental conditions.[216]

High da/dN levels resulting from sensitization and aggressive environmental or mechanical conditions correlate with intergranular CF crack propagation. Slower growth rates for nonsensitized stainless steel correlate with transgranular cracking. If the environment is mildly embrittling, transgranular crack growth occurs independent of the degree of sensitization. Andresen and coworkers argue that these differences are predictable based on the decreased rates of transient repassivation and enhanced anodic dissolution for chromium-depleted regions of sensitized steels.

The sulfur content of ferritic pressure vessel steels is a critical metallurgical variable that influences CF crack initiation and propagation.[39] Data presented in Figure 36 demonstrate that high-sulfur content A533B or A508 steels crack in CF at over an order of magnitude faster rates than low-sulfur heats for stagnant, low-oxygen, pressurized water at 288°C. The mechanism for the deleterious effect of sulfur is based on dissolution of MnS inclusions intersected by the growing CF crack. Sulfur ions are introduced into the occluded crack solution and increase the amount of anodic current passed during repassivation of crack-tip surfaces. By the film-rupture concept, this chemical action increases rates of CF cracking.[39]

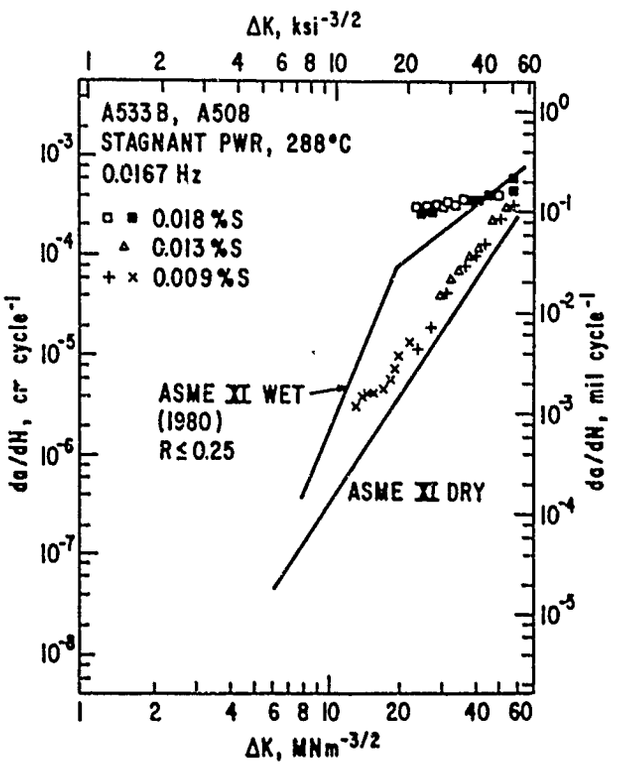


FIGURE 36—Effect of steel sulfur content on corrosion fatigue crack propagation in A533B and A508 in high-temperature, pressurized stagnant water with low dissolved oxygen (R = 0.20); after Ford.[39]

The deleterious effect of MnS inclusions is only observed for certain bulk environment chemistries that favor high levels of dissolved S^{-2} at the crack tip.[139] Ford argues that such conditions include either turbulent high dissolved oxygen water (BWR) or stagnant solutions of any O_2 level.[39] Sulfur ions are also concentrated at crack tips in low-sulfur steels exposed to stagnant, high-O_2 water but not to stagnant low-O_2 water. These relationships illustrate the complexities associated with unambiguous definitions of metallurgical effects on CF crack propagation.

Microscopic corrosion fatigue crack path. Determinations of CF crack paths through microstructures and associated surface features are critical to understanding cracking mechanisms and metallurgical effects. An example of this approach for the steel–moist air system was provided by Roven.[210] Such detailed study has not been applied to the CF problem. Nonetheless, two CF cases have been investigated: aluminum alloys in chloride or water vapor, and ferritic steels in aqueous chloride.

Aluminum alloys in water vapor and aqueous chloride— Fatigue-environment interactions produce a variety of complex fracture surface morphologies in aluminum alloys. Gudladt and coworkers demonstrated that hydrogen from water vapor–aluminum reaction causes intergranular cracking and promotes rates of Stage I fatigue crack growth along persistent slip bands and transgranular Stage II crack growth.[217-219] Since these studies were conducted on single and bicrystals of high-purity Al-Zn-Mg, the proportions and absolute rates of each fracture process were determined and demonstrated to depend on applied ΔK, water vapor pressure, grain-boundary orientation, and slip mode controlled by the extent of aging.

For sub-K_{ISCC} transgranular fatigue cracking in 7000 series aluminum alloys, Stoltz and Pelloux demonstrated the occurrence of "ductile" striations typical of crack propagation in inert dry air and certain benign aqueous environments, and "brittle" striations for fatigue in NaCl with anodic polarization, as first reported by Forsyth.[77,220] Ductile striations are attributed to crack advance by multiple shear and tip blunting, particularly in microstructures where planar slip was not localized. Brittle striations are attributed to environment-induced cleavage along {100} planes in the fcc aluminum lattice. Similar results were reported by Feeney, et al., for 7075-T6; intergranular CF cracking in 2024-T3 was also reported.[95]

Gao, Pao, and Wei reported crystallographic CF cracking parallel to {100} planes in 7075-T651 aluminum exposed to water vapor.[61] Brittle crack facets contained fine striations that were parallel to either <100> or <110> directions. This finding was correlated with the rate-limited and saturation regimes of the exposure parameter (Figure 23). At lower pressures of H_2O or for crack growth in gaseous oxygen, the fracture surface features were not crystallographic, but rather were flat and featureless with evidence of ductile tearing.

CF crack propagation in advanced Al-Li alloys (e.g., Figure 27) proceeds by a variety of microscopic mechanisms, as outlined by Piascik.[221] Crack growth in vacuum, helium, and oxygen occurs entirely by slip-plane cracking producing large facets parallel to {111} planes. For moist air, pure water vapor, and aqueous chloride, CF at moderate ΔK involves slip-band cracking and inter subgrain-boundary fracture. At low ΔK near threshold, CF is predominantly by cleavage along {100} planes. The change in environmental fracture mechanism with decreasing ΔK is attributed to reduced cyclic plastic zone size, cleavage is promoted when plasticity is contained within a single subgrain, while subboundary fracture occurs when deformation is distributed over several grains.

Ferritic steels in aqueous chloride - Procter and coworkers conducted quantitative fractographic analyses of CF in X65 steel exposed to 3.5% NaCl with cathodic polarization.[59] Crack growth rate data for this steel are equivalent to the results for API-2H steel in Figure 32 and BS4360.50D in Figure 11. Environmental cracking is characterized by a variety of microscopic processes, including intergranular separation, transgranular cleavage, brittle and ductile striation formation, and ductile tearing. The proportions of these features depend on ΔK and frequency (Figure 37).

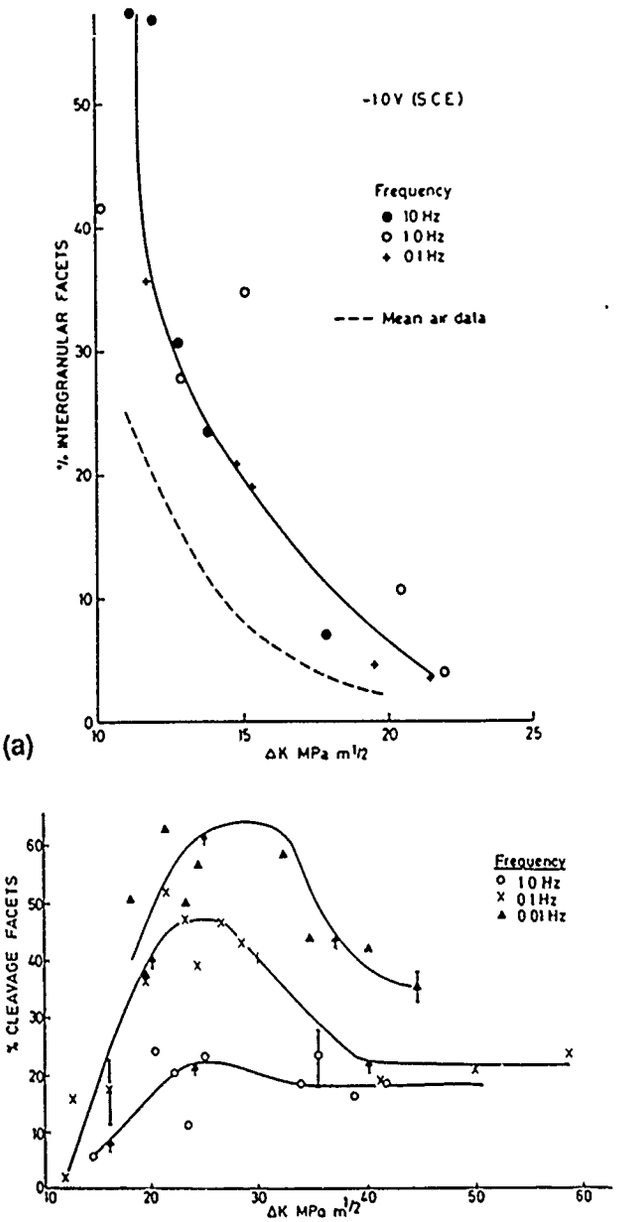


FIGURE 37—Quantitative fractographic results for corrosion fatigue in controlled rolled X65 steel in 3% NaCl (−1000 mV_{SCE}; R = 0.15). (a) intergranular cracking along ferrite grain boundaries, air and chloride, and (b) transgranular cleavage with brittle striations; after Hinton and Procter.[59]

Intergranular cracking along ferrite grains dominates CF in the low ΔK, steeply rising portion of the da/dN ΔK relationship. Fatigue crack propagation in moist air produces a reduced amount of intergranular separation at low ΔK. Crack growth in the plateau regime is largely by cleavage of uncertain crystallography but produces a facet about equal to the ferrite grain size. The proportion of cleavage increases with decreasing frequency and parallels increases in CF crack growth rate. Brittle striations are present on cleavage facets, indicating discontinuous crack propagation. Fatigue in air at plateau ΔK levels produces ductile transgranular striated fracture surfaces. Ductile fracture processes dominate at high ΔK levels.

Apart from usage in failure analyses, fractographic results of the type shown in Figure 37 provide important indications on the mechanisms for CF. For the steel-aqueous chloride system, intergranular and cleavage cracking were interpreted as a result of the entry of cathodically evolved hydrogen.[59] The ΔK induced transition

from intergranular to cleavage cracking may depend on increasing plastic-zone size beyond the ferrite grain size and on increasing deformation-based hydrogen production and transport. Alternately, intergranular cracking appears to dominate when sufficient hydrogen is available at the crack tip, while transgranular cleavage occurs for those ΔK and frequency conditions where da/dN is limited by the electrochemical production and mass transport of atomic hydrogen.

Miscellaneous

Additional variables often unexpectedly affect CF crack propagation. As suggested by Staehle, a material–environment system should be assumed prone to environmental fracture until proven otherwise.[222]

Temperature. Elevated-temperature environments are likely to promote rates of fatigue crack propagation by various oxidation and hot corrosion processes and by time-dependent plastic deformation. This important class of CF problems is reviewed by Pineau.[4] Moderate-temperature effects on aqueous or gaseous CF are considered here. Temperature should influence CF crack propagation through effects on mass transport and electrochemical or chemical reaction kinetics. It is surprising that the effect of temperature has received limited attention.

Marcus and coworkers demonstrated that fatigue crack growth rates in a high-strength steel and Nickel-200 exposed to low-pressure gaseous hydrogen increase with increasing temperature, exhibit a maximum near 300°K, and then decline at higher temperatures.[74,209] Specific data for steel are shown in Figure 38. This behavior is consistent with temperature–hydrogen-pressure effects on monotonic load crack growth rates for high-strength steels in H_2[223] and with the general maximum in a variety of hydrogen environment embrittlement phenomena near ambient temperature.[195]

The results in Figure 38 indicate that hydrogen uptake and transport through the plastic zone are maximized at a specific temperature. At very low temperatures, dissociative chemical adsorption to produce hydrogen atoms is rate limiting and is thermally activated. At higher temperatures, hydrogen entry may be reduced by enhanced recombination of hydrogen atoms to form desorbed H_2, by elimination of an adsorbed precursor to chemisorption of H, by a surface phase transformation, or by thermal detrapping of dissolved hydrogen.[223] While these processes are debated for monotonic loading, no substantial studies of the gaseous hydrogen fatigue crack propagation case have been reported.

Vosikovsky and coworkers reported that reduced temperature between 300 and 273°K resulted in up to a fourfold increase in CF crack growth rates for the ferritic steel–seawater system illustrated in Figure 11.[224] Nakai, et al., showed that CF crack growth rates for the Ni-Cr-Mo-V steel–0.3 N Na_2SO_4 system increased with increasing temperature.[188] This effect was explained based on temperature-enhanced rates of electrochemical reaction on clean crack surfaces to produce embrittling hydrogen.

Biologically induced corrosion. Biologically generated sulfur ions promote CF of steels in aqueous electrolytes. This result is consistent with a large body of literature that demonstrates the deleterious effect of sulfur bearing environments on HE systems.

Sulfur species enhance hydrogen uptake from electrolytes by adsorbing on metal surfaces to retard the recombination of hydrogen atoms to form molecules that would otherwise leave the surface. As a result, the proportion of cathodically produced hydrogen atoms that enters the metal increases. SCC of steels is exacerbated by sulfur ions in electrolytes and by H_2S additions to gaseous environments.[196] H_2S dissolved in seawater enhances CF crack propagation in steel, as shown in Figure 11.[116] A similar effect was demonstrated for H_2S dissolved in crude oil.[103,225] H_2S gas is a potent embrittler of low-strength alloy steels for fatigue loading.[151]

Biologically enhanced CF of C Mn steels in seawater was recently demonstrated by Thomas and coworkers and by Cowling and Appleton.[122,226,227] Typical data are presented in Figure 39. The steel, RQT 501 (σ_{ys} = 470 MPa, Fe-0.18C-1.5Mn), exhibits enhanced rates of fatigue crack propagation in seawater containing between 75 and 450 wt ppm of H_2S formed by bacterially stimulated decomposition of marine algae.[226] These results are indicated by the data points for fatigue loading at R = 0.7 and 0.167 Hz. The solid line represents crack growth in natural seawater, while the dashed line gives da/dN–ΔK for H_2S gas-saturated (520 wt ppm) seawater, see Figure 11. Cowling and Appleton reported similarly high levels of CF crack growth for BS4360:50D C-Mn steel in anaerobic artificial seawater containing a culture of sulfate-reducing bacteria harvested from the Lower Clyde Estuary in England.[122]

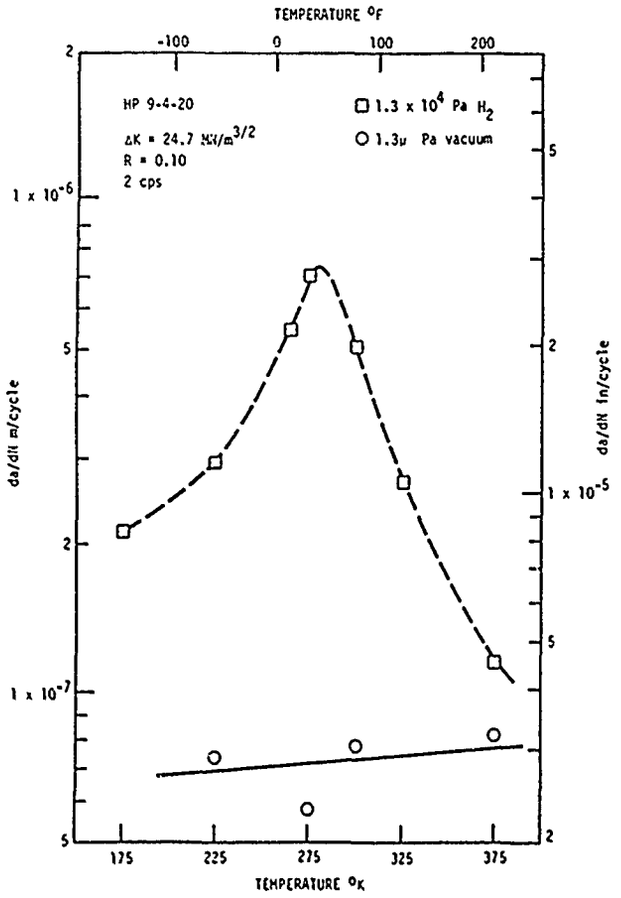


FIGURE 38—Temperature dependence of H_2-assisted fatigue crack propagation in high-strength HP-9-4-20 steel at constant ΔK and frequency; after Frandsen and Marcus.[209]

The effect of biologically generated H_2S should be quantitatively modeled based on hydrogen uptake characterized by permeation experiments. Dissolved hydrogen should be related to CF crack propagation rate and independent of the chemical or electrode potential stimulation of atomic hydrogen production. This approach will be complicated by crack chemistry effects of the type discussed in the Aqueous Electrolytes. Active Steels in Chloride–Crack Chemistry Modeling section and by biological effects on crack tip anodic dissolution and hydrogen recombination reactions. This possibility is indicated by the fact that higher crack growth rates are observed for H_2S gas-saturated chloride compared to biologically active solution at the same dissolved sulfide ion concentration.[122,226]

Biologically enhanced CF is an infant field. The rapid crack growth rates indicated in Figure 39 and the possibilities for organic species to be present in marine and industrial environments suggest that this problem will be more intensely researched in the future.

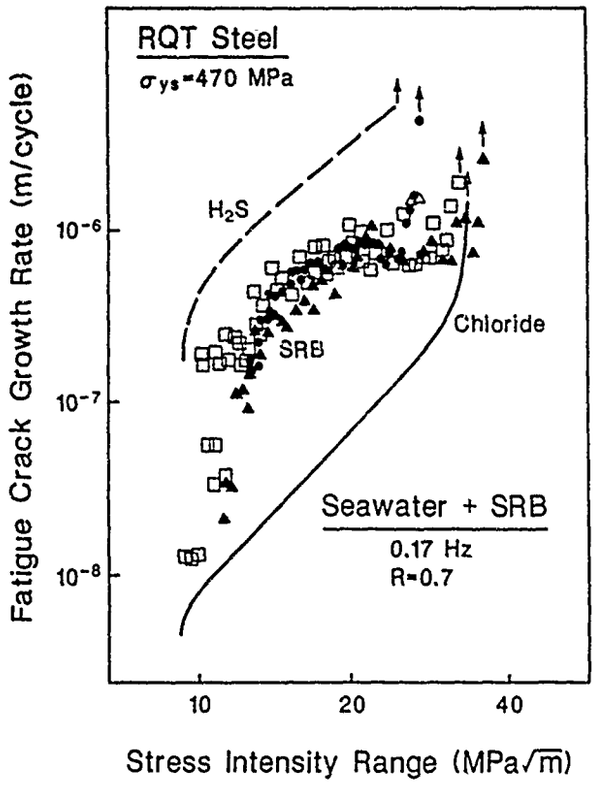


FIGURE 39—Biologically stimulated corrosion fatigue in a low-strength C-Mn steel, RQT 501, cycled at 0.167 Hz and R = 0.70. Solid line: cracking in pure seawater; data points: seawater with 75 to 450 wt ppm H_2S from decomposition of algae; and dashed line: gaseous H_2S saturated seawater (520 wt ppm); after Thomas, et al.[226]

Quantitative Models of Corrosion Fatigue Crack Propagation

Conclusion

Micromechanical–chemical models of crack-tip driving forces and process-zone CF damage provide a sensible means to predict and to extrapolate the effects of variables and to modify the fracture mechanics approach to account for compromises in similitude. Models have been formulated based on HE and film rupture/transient dissolution/repassivation. Fatigue damage due to crack surface films has not been considered quantitatively. Models successfully predict the time (frequency) dependence of CF and the effects of electrode potential, solution composition, and gas activity. All are, however, hindered by uncertainties associated with crack-tip processes and the fundamental mechanisms of environmental embrittlement. A process-zone model has not been developed for CF, as such, stress intensity, yield strength, and microstructure effects are not predictable. Furthermore, absolute rates of hydrogen-assisted crack growth are not predictable and the film-rupture formulation is being debated. Successes to date indicate that a new level of mechanistic understanding is achievable.

Introduction

Explanations for the effects of important variables on CF crack propagation (see "Effects of Critical Variables") were qualitative. Predictive models of crack-tip damage must be developed to expand limited databases. Recent conferences have focused on this theme for environmental fracture.[20,24]

A quantitative model of CF crack propagation, developed within the fracture mechanics framework, must contain the following elements:

(1) The rate of environmental fatigue crack propagation must be partitioned into mechanical and chemical–mechanical components. The former may be zero (environment dominant) or finite and described by slip-based or cumulative damage models. This issue is discussed in the section "Interaction of mechanical and environmental fatigue."

(2) The mechanical contribution to environmental cracking is described by relating applied stress-intensity factor to continuum crack-tip stress, strain, and strain-rate fields, and to microscopic deformation. The location of the fracture process zone is critical; see "Models of Crack-Tip Mechanics . . . ."

(3) The chemical contribution requires modeling of the local crack environment, which develops based on mass transport limitations within the occluded crack; see "Models of Occluded Crack Chemistry and Transient Reaction."

(4) The chemical contribution requires modeling of transient reaction kinetics for anodic dissolution, repassivation, and cathodic hydrogen production on straining clean crack-tip surfaces perhaps coupled to passivated flanks; see "Models of Occluded Crack Chemistry and Transient Reaction."

(5) The rate-limiting process must be defined. Either mass transport or chemical reaction will control CF crack propagation rates; see "Models of Occluded Crack Chemistry and Transient Reaction."

(6) The fracture process zone, a specific crack-tip damage process, and a failure criterion must be defined; see "Corrosion Fatigue by Hydrogen Embrittlement" and "Corrosion Fatigue by Film Rupture/Transient Dissolution" sections.

Each element of CF crack growth rate modeling is assessed in the following sections, within the frameworks of HE and film rupture. Substantial advances have been recorded in each area, however, no analysis has integrated the necessary chemical, mechanical, and microstructural components into a broadly predictive model of CF crack propagation.

Interaction of mechanical and environmental fatigue

Early attempts to model CF crack propagation linearly summed the contributions from inert environment fatigue and SCC, with the time rate of the latter integrated over a single loading cycle.[50] This model is, of course, not applicable to CF below K_{ISCC}. Here, several models have been proposed to combine mechanical fatigue and the chemical environment effect. An equation developed by Wei and coworkers provides a reasonable basis for modeling.

Superposition. Cycle–time-dependent rates of CF crack propagation were first described by a superposition concept championed by Wei and coworkers.[30,50,228] Considering da/dN–ΔK data for an alloy in inert and aggressive environments:

$$\frac{da}{dN_e} = \frac{da}{dN_m} + \frac{da}{dN_{cf}} \qquad (1)$$

where da/dN_e is the total measured crack growth rate for the aggressive environment, da/dN_{in} is the rate of plasticity-driven fatigue crack propagation for an inert environment, da/dN_{cf} is the incremental difference on the crack growth rate plot and represents the effect of interacting cyclic plastic deformation and chemical reaction.

This formulation follows directly from linear superposition of stress corrosion and inert environment fatigue cracking and is associated with the incremental environmental effect on a da/dN–ΔK plot. The question, however, is "Why should inert environment fatigue crack propagation influence da/dN_e for the case in which damage is entirely chemical–mechanical in origin?" That is, cracking in an environment may progress by a unique microscopic mechanism with no relationship to inert environment fatigue processes. It is important to recognize that unique fracture processes are involved in CF.

A more physically reasonable formulation states that the rate of fatigue crack propagation in an environment is produced by concurrent parallel processes. For two processes, the superposition concept is then given by the following:[228]

$$\frac{da}{dN_e} = \frac{da}{dN_m}(\theta) + \frac{da}{dN_c}(\Phi) \qquad (2)$$

where da/dN_c is the rate of "pure" CF crack propagation; θ is the fraction of the crack surface formed by mechanical fatigue; and Φ is the fraction of the crack surface formed by CF. Da/dN_c represents the rate of crack advance along those portions of the crack front that are solely environmentally affected. θ and Φ are measured by fractographic analysis. For two parallel processes, $\theta = (1 - \Phi)$.

Comparing Equations (1) and (2) demonstrates the following:

$$\frac{da}{dN_{cf}} = \left(\frac{da}{dN_c} - \frac{da}{dN_m}\right)\Phi \qquad (3)$$

That is, the phenomenological difference between inert and aggressive environment fatigue rates from the da/dN–ΔK relationship is equivalent to the difference between the rates of microscopic-process-driven chemical–mechanical and mechanical fatigue times the fractional occurrence of the former. This comparison relates the phenomenological difference in crack growth rates (da/dN_{cf}), and the underlying causes.

The rigorous basis for CF modeling is a derivation of da/dN_c and Φ as a function of chemical and metallurgical variables, as discussed in later sections, "Corrosion Fatigue by Hydrogen Embrittlement" and "Corrosion Fatigue by Film Rupture/Transient Dissolution." Only simplifications of this approach have been reported. For example, da/dN_{cf} is often assumed to be proportional to the amount of hydrogen produced at the crack tip or to the total electrochemical charge passed during multiple rupture events per load cycle. Alternately, from Equation (3) and for a specific material and environment, $(da/dN_c - da/dN_m)$ is assumed to be a constant that equals the maximum environmental enhancement (viz., $da/dN_c = da/dN_e$) due to complete chemical reaction in which Φ equals 1.0. Here Φ, but not da/dN_c, is equated to the extent of varying environmental reaction for either mass transport or reaction rate control. For values of Φ less than 1, the fatigue surface will be composed of fractions of mechanical and chemical–mechanical damage, with da/dN_{cf} given by Equation (3) or da/dN_e given by Equation (2).

Competition. Austin and Walker argue that CF crack propagation is modeled as a competition, rather than a superposition, of independent mechanical and chemical processes.[229] They assume that the measured environmental crack growth rate (da/dN_e) is determined by the dominant (faster) of two processes, including mechanical fatigue or cycle–time-dependent CF.

The competition model is a special case of Equation (2). Considering environment-dominant fatigue cracking, $\Phi = 1$ and $da/dN_m \ll da/dN_c$ in Equation (2); therefore, $da/dN_e = da/dN_c$. Here, the superposition and competition models are equivalent. If crack growth involves a significant amount of mechanical fatigue at comparable rates to CF, then the competition model is not adequate. Rather, analyses of θ, Φ, and the growth rate components in the superposition model [Equation (2)] provide an appropriate approach.

Other. Several models of CF crack propagation begin with the following assumption:[39,138]

$$\frac{da}{dN_{cf}} = \frac{da}{dt}\left(\frac{1}{f}\right) \qquad (4)$$

where f is the cyclic loading frequency and da/dt is the average time-based crack growth rate per loading cycle.

Austin and coworkers hypothesized that the CF crack propagation rate is given by the inert environment rate times a multiplicative factor that accounts for the aggressive environmental contribution.[230,231] This factor includes the accelerating effect of embrittling hydrogen and the mitigating effect of crack-tip blunting by anodic dissolution.

Models of crack-tip mechanics: relationships between ΔK and local plastic strain, strain rate, and stress

Crack-tip stress and strain, not stress intensity, control fracture processes, including CF As such, quantitative models of CF crack propagation require a description of crack-tip stress and strain fields, and microdeformation processes, explicitly defined as a function of the applied stress-intensity factor.

Regarding the success of the fracture mechanics approach to describe fatigue and environmental cracking, four points are critical. First, all analyses reported to date show that crack-tip mechanical quantities depend uniquely on applied ΔK. As such, it is reasonable to expect that stress intensity will uniquely characterize the growth kinetics of CF cracks. Second, precise analyses of crack-tip fields have not been conducted for growing fatigue cracks under cyclic loading, particularly for the region within several microns of the crack tip. Third, ΔK is derived based on continuum mechanics without consideration of microscopic deformation processes. This limitation does not mean that stress intensity is impotent to correlate processes such as slip density or morphology and grain-boundary strain localization. Rather, ΔK is analogous to "P/A" applied stress. The challenge is to develop experimentally or analytically the effect of stress intensity on noncontinuum deformation behavior. Finally, environment may modify crack-tip plasticity and thus alter the relationship between ΔK and local stress or strain. This complication does not void the fracture mechanics approach. Rather, it requires that time- and environment-dependent constitutive laws be determined for analyses of crack-tip fields.

The state of the art in crack-tip fields is summarized here and is reviewed in detail by Gerberich and by Sieradzki in this volume,[82,160] by Rice and McClintock at the Firminy conference,[7] and by Lidbury,[232] Ford,[39] and Knott.[233] While elastic-plastic analyses have been rigorously developed to within microns of the crack tip for monotonic loading and strain-hardening materials, the cyclic loading problem has received limited attention; only approximations have been developed.

One or more of the following quantities are necessary for CF crack propagation models. All results are for small-scale yielding and plane-strain crack-tip deformation.

Monotonic plastic-zone diameter (r_p):

$$r_p = \frac{1}{3\pi}\left(\frac{K}{\sigma_{ys}}\right)^2 \qquad (5)$$

Cyclic plastic-zone diameter (r_{pc}):

$$r_{pc} = \frac{1}{12\pi}\left(\frac{\Delta K}{\sigma_{ys}}\right)^2 \qquad (6)$$

Maximum blunted crack-tip-opening displacement in fatigue (δ_{max}):

$$\delta_{max} = \frac{0.5\,\Delta K^2}{(1-R)^2\,(2\sigma_{ys})\,E} \qquad (7)$$

Cyclic blunted crack-tip-opening displacement (δ_c):

$$\delta_c = \left(\frac{1+R}{1-R}\right) \frac{\Delta K^2}{4\sigma_{ys} E} \quad (8)$$

To approximate cyclic hardening or softening, the cyclic yield strength (σ_{ysc}) should be used in Equations (6) through (8) in place of monotonic yield strength (σ_{ys}).

For monotonic loading of a stationary crack, the maximum opening (normal) stress equals between 3 and 5 times σ_{ys}, depending on work-hardening behavior and independent of applied K. This maximum occurs at two crack-tip opening displacements ahead of the crack tip; stresses then decay within the plastic zone to merge with the well-known elastic stress distribution near the plastic-zone boundary.

Cyclic plastic strain, and perhaps mean strain, govern mechanical fatigue damage.

Crack-tip plastic opening strain (monotonic load, stationary crack) (ϵ_p):

$$\epsilon_p = \frac{\sigma_{ys}}{E} [(r_p/X)^{\frac{1}{n+1}} - 1] \quad (9)$$

The parameter (n) describes work-hardening according to the Ramberg-Osgood formulation, with an elastic-perfectly plastic material characterized by n = 0. X is distance ahead of the crack tip.

Crack-tip plastic opening strain (monotonic load, moving crack) (ϵ_{pm}):

$$\epsilon_{pm} = 5.5 \frac{\sigma_{ys}}{E} [\ln(r_p/X)]^{\frac{1}{1-n}} \quad (10)$$

The total monotonic strain includes an elastic component (σ_{ys}/E) added to Equations (9) and (10).

The cyclic plastic strain range ($\Delta\epsilon_p$) is estimated by substituting the cyclic plastic-zone size [Equation (6)] and cyclic yield strength and work-hardening parameters into Equations (9) and (10). As an example,

Crack-tip cyclic plastic strain range (n = 0, stationary crack) ($\Delta\epsilon_p$):

$$\Delta\epsilon_p = \frac{1}{12\pi} \left(\frac{\Delta K^2}{\sigma_{ysc} E}\right) \frac{1}{X} - \left(\frac{\sigma_{ysc}}{E}\right) \quad (11)$$

Crack-tip cyclic total strain range ($\Delta\epsilon_T$) may be measured experimentally by stereoimaging techniques (See "Novel Measurements of Corrosion Fatigue Cracking."). An example was reported by Hudak for CF cracks in type 304 stainless steel exposed to either moist air or an electrolyte at 363°K.[234,235]

$$\Delta\epsilon_T = \epsilon_0 \Delta K^\gamma [\Delta\epsilon_1 - m \ln (X + A)] \quad (12)$$

Here, γ, ϵ_o, $\Delta\epsilon_1$, m, and A are empirical parameters defined by curve fitting, with γ equal to between 2 and 5.5. This result is similar to Equation (11) based on cyclic plastic zone. Note, however, that the strain singularity is not observed experimentally.

Crack-tip total strain rate $(d\epsilon/dt)_c$ is a critical element of film-rupture models of CF.[39,234] While this parameter varies during a stress-intensity cycle and with crack growth [$d\epsilon/dt = (d\epsilon/dK \times dK/dt) + (d\epsilon/da \times da/dt)$], a per cycle average strain rate [$(\overline{d\epsilon/dt})_c$] is estimated by the following:

$$\left(\frac{\overline{d\epsilon}}{dt}\right)_c = \Delta\epsilon_{T\,@\,x=0}/t_{eff} \quad (13)$$

for the case where strain rate is dominated by the rate of change of crack-tip strain with respect to K; that is, where the rate of change of strain with crack growth is small. t_{eff} is given by reciprocal loading frequency times the fraction of the cycle where load is rising, times the fraction of the rising-load portion where the crack is opening above closure. (See "Crack Mechanics.") Several forms for the crack-tip strain rate have been published:

Empirical from Equations (12) and (13) (Hudak, et al.[234,235]):

$$\dot{\epsilon}_c = \alpha \epsilon_0 f \left(\frac{(\Delta K - \Delta K_{th})^\gamma}{1 - [\Delta K_{th}(1-R)/\Delta K]}\right) \quad (14)$$

Approximate analytical from Equations (11) and (13):

$$\dot{\epsilon}_c = \beta \frac{\Delta K^2}{\sigma_{ys} E} f \quad (15)$$

Analytical from time derivative of δ_c, *Equation (8)* (Atkinson[39]):

$$\dot{\epsilon}_c \alpha \frac{d\delta_c}{dt} = \phi \frac{\Delta K^2}{\sigma_{ys} E} f \quad (16)$$

Analytical based on crack-tip shear-band strain (Cole[39]):

$$\dot{\epsilon}_c = \theta \frac{\Delta K^2}{\sigma_{ys} E} f \quad (17)$$

Analytical based on crack-tip shear within r_{pc} (Lidbury[232]):

$$\dot{\epsilon}_c = \lambda \frac{\sigma_{ys}}{E} \left(\frac{\Delta K^2}{\Delta K_{th}}\right)^2 f \quad (18)$$

Analytical based on da/dt-dominated strain rate (Shoji[39]):

$$\dot{\epsilon}_c = (10 \text{ to } 100) \frac{da}{dt} = (10 \text{ to } 100) \ln \Delta K^{2 \text{ to } 6} \quad (19)$$

In these strain-rate equations, β, Φ, θ, λ, and n are unknown constants. In Equation (19), the ΔK and R dependencies are derived from inert environment fatigue crack growth rates stated in terms of time-based crack growth rates according to Equation (5).

Crack-tip strain rate measurements and predictions are shown in Figure 40.[39] Stereoimaging data [Equation (14)] are in reasonable agreement with the analytical predictions of Equations (17) and (18). Only the forms of the equations are supported because the constants in these models were adjusted to give best fits. The prediction based on growth-rate-dominated strain [Equation (19) and the lower solid line in Figure 40] is in poor agreement with the data.[234]

For CF modeling, it is reasonable to assume that crack-tip strain rate varies as

$$\dot{\epsilon}_c \alpha \left(\frac{1}{\sigma_{ys}}\right) f \Delta K^\gamma \quad (20)$$

with γ equal to 2.

These analyses demonstrate that crack-tip parameters that control CF crack propagation depend uniquely on stress-intensity range. Similitude is expected, at least from the mechanical perspective. Crack-tip field equations of the sort presented here have been successfully incorporated into micromechanical models for monotonic load fracture due to cleavage, HE, and ductile rupture.[57,160,192] Benign environment fatigue crack propagation kinetics have been similarly modeled based on crack-tip plastic strain coupled with a cumulative damage failure criterion.[210,211] Successes for CF crack propagation have been limited; additional work is required.

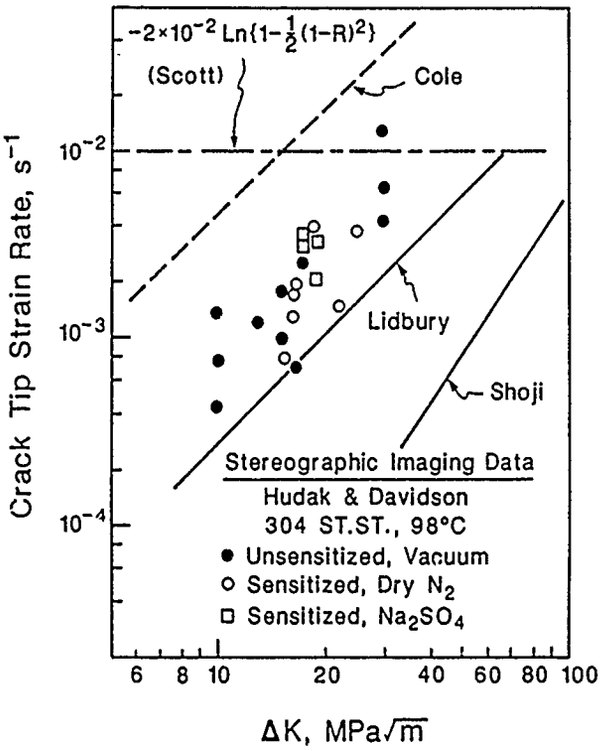


FIGURE 40—Measured and analytically predicted average crack-tip strain rates as a function of applied ΔK for R = 0.1 and f = 0.01 Hz. Data are described by Equations (12) and (14) and the predictions by Equations (17), (18), and (19); after Ford.[39]

Models of occluded crack chemistry and transient reaction

A model of CF crack propagation must recognize that significant differences can exist in the crack-tip environment compared to the bulk gas or electrolyte, and that rates of reaction on strained, transiently active surfaces are different compared to steady-state kinetics. Crack chemistry can be either more benign or more aggressive than the nominal environment. Mass transport and reaction modeling are required to define the specific conditions that drive crack propagation. While dissolution and film rupture are clearly crack-tip processes, embrittling hydrogen may be contributed from the crack tip and specimen surfaces in contact with the bulk environment. The relative importance of these hydrogen sources must be considered.

Detailed discussions of localized crack chemistry and reactions are beyond the scope of this review. Three international conferences were recently held to examine this topic.[17,19,236] Here, the conclusions of this work are assessed to provide a basis for discussions of CF crack propagation models in later sections.

Gaseous environments. For fatigue crack propagation in gases, the important consideration is that crack-tip gas pressure may be attenuated compared to the surrounding environment because of impeded molecular, or Knudsen, flow.[237] Here, gas transport within the crack is controlled by molecule collisions with crack walls, rather than by intermolecular collisions. Da/dN is reduced by this pressure reduction if crack surface reactions are rapid or on the same order as transport, as such, reaction is limited by gas supply.

The extent of the pressure decrease due to Knudsen flow depends on crack length and opening shape, molecular mean free path, and time determined by cyclic loading frequency and crack advance rate. As a generalization, impeded flow occurs when some multiple (about 10 to 100) of the mean free molecular path exceeds the crack-opening displacement.[238] Since the mean free path for low-pressure gases (water vapor, H_2, or O_2) is about 500 μm at 300°K and 20 Pa,[4] and since a typical blunted crack-tip opening displacement [Equation (7)] is about 4 μm, with the crack-mouth opening equaling 75 μm, impeded molecular flow is clearly important. The extent of the pressure attenuation must be calculated as a function of crack geometry. The approach to this problem follows from early treatments of simple slot geometries,[237] with the challenge being to account for the complex opening shape of a crack as a function of stress intensity and to define the crack length over which molecule-wall collisions dominate gas transport.

Impeded molecular flow effects in CF have been investigated, predominantly for the aluminum–water vapor system. Lawn demonstrated the important interaction of mass transport and reaction for environmental cracking under monotonic load.[238] He derived an approximate solution for the stress-intensity dependence of the gas "impedance factor" and related this term to static-load crack growth rate. The first considerations of Knudsen flow control in fatigue crack growth were by Snowden and Bradshaw.[239-241] Snowden argued that the pressure below which moist air ceased to reduce the smooth specimen fatigue life of lead was consistent with the onset of substantially impeded molecular flow of deleterious oxygen.[241] Bradshaw recognized the possibility of mass transport impedance for Al-Cu-Mg in water vapor but concluded that surface reaction kinetics are equally or more important.[239] Gangloff and Ritchie pointed out that crack-geometry-dependent gas pressure attenuation could lead to breakdowns in similitude if the local environment is controlled by stress and crack length, apart from a simple stress-intensity description.[203]

Bradshaw and Wheeler demonstrated that CF crack growth rates in the aluminum alloy–water vapor system decreased when a substantial pressure of inert gas was added to the low partial-pressure water environment.[187] The inert gas decreased molecular mean free path and caused a transition from impeded molecular transport to slower viscous flow governed by gas molecule–molecule collisions. This experimental observation is inconsistent with estimates of the gas mean free path for impedance by viscous flow, emphasizing the fact that Knudsen flow calculations and the criteria for molecule–wall vs molecule–molecule interactions are rudimentary.

Wei and coworkers coupled crack-tip gas–metal reaction kinetics with mass transport, controlled by molecule–wall interactions, to derive predictive relationships for CF crack growth rate.[129,242] This modeling was described qualitatively in the section "Mass Transport and Reaction Rate Modeling: Hydrogen Embrittlement"; quantitative relationships are presented in the section "Corrosion Fatigue by Hydrogen Embrittlement." Experimental observations (e.g., Figures 22 and 23) supported model predictions of fatigue crack growth rate vs bulk environment gas pressure/loading frequency for aluminum alloys in water vapor and steel in gaseous H_2.[61,129,151,242-244] This model predicts the bulk environment saturation pressure (P_o) below which gas transport limitations will reduce da/dN for the case in which surface reactions are fast:[61]

$$P_o = \{136\,(\beta/\alpha)\,f(R)\,[\frac{\sigma_{ys}^2\,l}{N_o\,kTE}]\,[\frac{T}{T_m}]^{1/2}\}^{-1} \qquad (21)$$

$$f(R) = 0.25\,\{[(1+R)/(1-R)]^2 + 0.5\}$$

T is temperature; M is the molecular weight of the gas; k is Boltzmann's constant; N_o is the number density of surface reaction sites; f is frequency; E is elastic modulus; σ_{ys} is yield strength; R is

[4]Mean free path is directly proportional to temperature, inversely proportional to gas pressure, and inversely proportional to the square of the molecular diameter.[237] As such, the mean free path of these molecules at atmospheric pressure (100 kPa) is about 0.1 μm.

stress ratio; and I, β, and α are parameters describing that portion of the crack geometry over which impeded flow occurs. These parameters largely relate to molecular mean free path and crack geometry.

Experimental results plotted in Figure 41 are in excellent agreement with the predicted stress ratio dependence of the saturation pressure [Equation (21)] for several aluminum alloys fatigued in pure water vapor[221] [(5)] This result and model emphasize the importance of the mean cyclic crack opening, rather than the maximum value, to gas transport and fatigue crack growth. Figure 41 explains why extremely small levels of water vapor are capable of enhancing rates of near-threshold fatigue crack propagation in aluminum alloys.[60,132,217,221] Specifically, the saturation pressure decreases strongly with increasing R value Near-threshold cracking is often conducted at high R, either by design or because of the effects of crack closure as described in the section "Crack Mechanics."

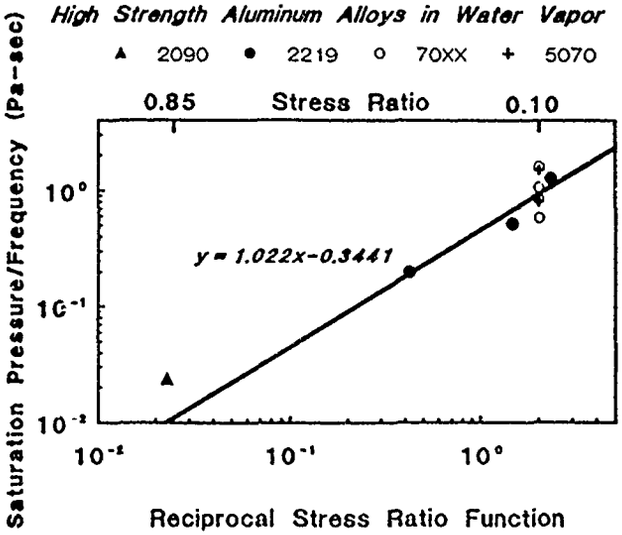


FIGURE 41—Effect of mean crack-opening shape, described by a function of R, on the saturation exposure (pressure/frequency) for corrosion fatigue crack propagation in aluminum alloys 2090,[125] 2219,[243] 70XX,[61,244] and 5070[184,187] in water vapor.

The main challenge to gas transport models is the uncertainty with the description of crack geometry, in fracture mechanics terms, and the crack length over which impeded flow occurs. As a result of this problem, the constants in Equation (21) are determined from crack growth rate data. Crack closure effects on Knudsen flow have not been investigated. Gas transport models are insufficient to predict absolute rates of CF crack propagation. Transport, surface reaction, and a crack damage criterion must be coupled as discussed in the section "Corrosion Fatigue by Hydrogen Embrittlement."

Aqueous electrolytes: active steels in chloride–crack chemistry modeling. From the pioneering work of Brown in the late 1960s, it is well recognized that impeded mass transport and localized reactions render the electrochemical conditions within occluded cracks unique, compared to bulk solution composition, electrode potential, and pH.[165] A quantitative approach to this problem requires solutions to the differential equations that describe coupled electrolyte transport and crack surface electrochemical and chemical reactions. Ideally, the kinetics of reactions on filmed crack flanks and the straining clean crack tip should be considered.

To date, localized crack chemistry has been modeled and probed experimentally for two systems, passive stainless and ferritic steels in high-temperature water, and active C-Mn and alloy steels in aqueous chloride solutions. The former topic is discussed extensively by Ford and Andresen elsewhere[39,136,138] and provides important input to film-rupture models of CF. Crack electrochemistry is reviewed here for steels in chloride and as a basis for a HE model.

For steels in aqueous chloride, crack growth is accelerated by adsorbed hydrogen produced electrochemically at the crack tip. As such, crack solution pH and electrode potential have been emphasized to calculate rates of crack-tip hydrogen production. It is critical to determine hydrogen production rate as a function of external electrode potential and to identify the contributions from the crack tip, the crack flanks, and specimen surfaces. Brown experimentally demonstrated that acidic conditions develop within cracks in steels exposed to neutral seawater for anodic polarization and free corrosion.[165] As the bulk potential was made more cathodic, the crack solution became more alkaline. Understanding of these trends has emerged from a series of papers by Turnbull and coworkers.[166,167,169,190,191,193,194,245-252]

The model of crack electrochemistry for CF in the steel–aqueous chloride system includes the following reactions:[165,190,249,252]

(1) Anodic dissolution of iron and major alloying elements, particularly chromium;
(2) Cation hydrolysis to produce hydrogen ions within the crack;
(3) Cathodic reduction of oxygen, both within the crack until depletion occurs and on external specimen surfaces;
(4) Cathodic reduction of hydrogen ions and of water, both within the crack and on external specimen surfaces.

Hydrolysis is rapid, while rates of the electrochemical reactions are determined by polarization methods and depend on pH and electrode potential in the standard way. The effect of straining on clean surface transient reactions was recently described by straining electrode measurements.[191] Reaction rates are coupled with descriptions of reactant supply and product removal through mass conservation. Mass transport by concentration gradient diffusion, ion migration, and convective mixing is modeled essentially one dimensionally in the direction of crack propagation. The differential equation that describes these terms is solved for the steady-state case. Appropriate boundary conditions and fracture mechanics descriptions of crack-opening shape complete the elements of the analysis.

The outputs of crack chemistry modeling include crack solution oxygen concentration, crack-tip pH, and electrode potential as a function of distance from the crack mouth to the crack tip. From pH and potential, it is possible to calculate the total rate of atomic hydrogen production and, from this, the concentration of adsorbed hydrogen on crack tip and external surfaces in equilibrium with the appropriate solutions. Each of these quantities is predicted as a function of applied potential, temperature, chloride composition (viz., seawater or NaCl), loading frequency, ΔK, R, crack length, and load waveform. These mechanical variables influence crack shape and hence mass transport.

Since the detail of this work is extensive, only those conclusions relative to CF crack propagation models are discussed.

(1) The concentrations of reactants and products in a pulsating fatigue crack depend on crack depth, mouth opening, loading frequency, ΔK, R, σ_{ys}, and specimen geometry. The interplay between diffusion and convection results in a minimum of reactant concentration and a maximum of products at a critical crack depth. Transport within cracks of varying length is controlled by different proportions of convection and diffusion. An example of specific calculations for crack-tip reactant oxygen concentration is shown in Figure 42.[248,252]

(2) CF cracks in bulk aerated chloride are deoxygenated for most solution and loading parameters owing to the rapid rate of oxygen reduction within the crack compared to diffusive and convective supply.[246,249] Without competition from oxygen, cathodic reactions solely produce adsorbed hydrogen. This result is controversial

[(5)]The regression line is calculated only for the data on alloy 2219. If all results are included, an excellent linear fit is achieved, as described by the equation: y = 0.8488 x - 0.5789. In either case, saturation pressure is nearly directly proportional to the reciprocal stress ratio function.

in the sense that crack surface contact will produce turbulent mixing and enhanced oxygen supply to the crack tip. In this case, Gangloff proposed that CF crack growth rates are reduced by oxygen reduction, which dominates cathodic reactions that otherwise produce embrittling hydrogen.[253] This hypothesis has not been proven by critical experimentation.[189,208]

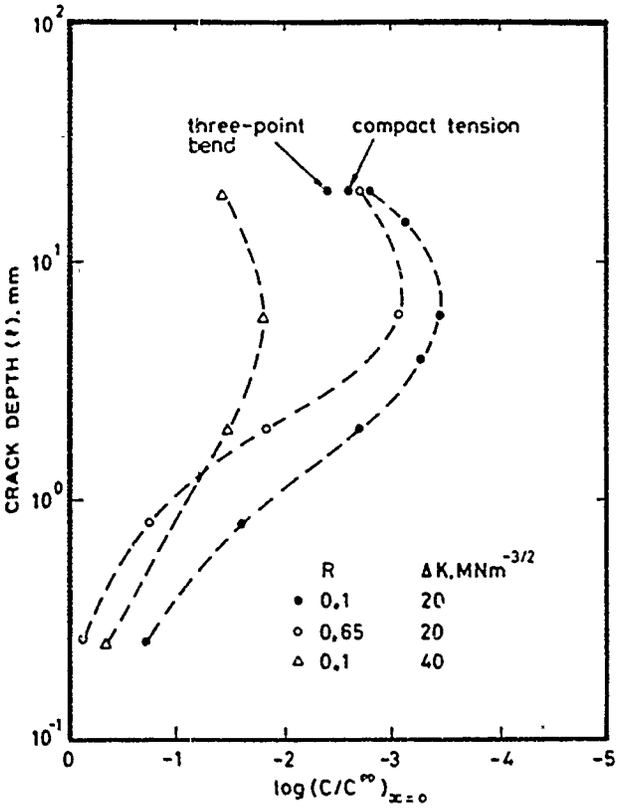


FIGURE 42—Model predictions of the effect of crack depth on dissolved oxygen concentration at the crack tip normalized to the bulk solution level for several specimen geometries, stress ratios, and ΔK levels; SEN, C-Mn steel, NaCl at −800 mV_{SCE}; after Turnbull.[248]

(3) For electrolytes such as NaCl or seawater, potential differences between the crack tip and bulk surfaces are less than 50 mV, with more cathodic values predicted for near-free corrosion and more noble values typical of cathodic polarization. Hydrogen bubbles, a tortuous crack path, or corrosion debris will increase IR drops" along the crack.[190,249]

(4) For neutral electrolytes, crack tip pH is mildly acidic (pH 6) for free corrosion potentials and basic for cathodic polarization. Crack acidification to pH 3 to 5 is only likely for applied anodic potentials, for cases where ferrous ions are oxidized to ferric, for short crack depths, or for steels containing strongly hydrolyzable specie such as chromium.[249]

(5) Near free corrosion or for anodic polarization, crack tip dissolution, cation hydrolysis leading to acidification, and H reduction dominate crack chemistry. Cathodic polarization promotes an alkaline crack with pH approaching 10, hydrogen production is predominantly through water reduction. Total crack tip hydrogen production rate and the adsorbed H concentration are substantial and are predicted to increase generally with increasingly cathodic polarization, as shown in Figure 43. Effects of frequency, R, ΔK, and waveform are of secondary importance.[191,250]

(6) For specimens cathodically polarized below about 900 mV_{SCE}, water and proton reduction on external surfaces are the dominant sources of hydrogen for crack growth, see Figure 43. Surface hydrogen supply is also dominant for acidic and H_2S bearing solutions.[191,193,250]

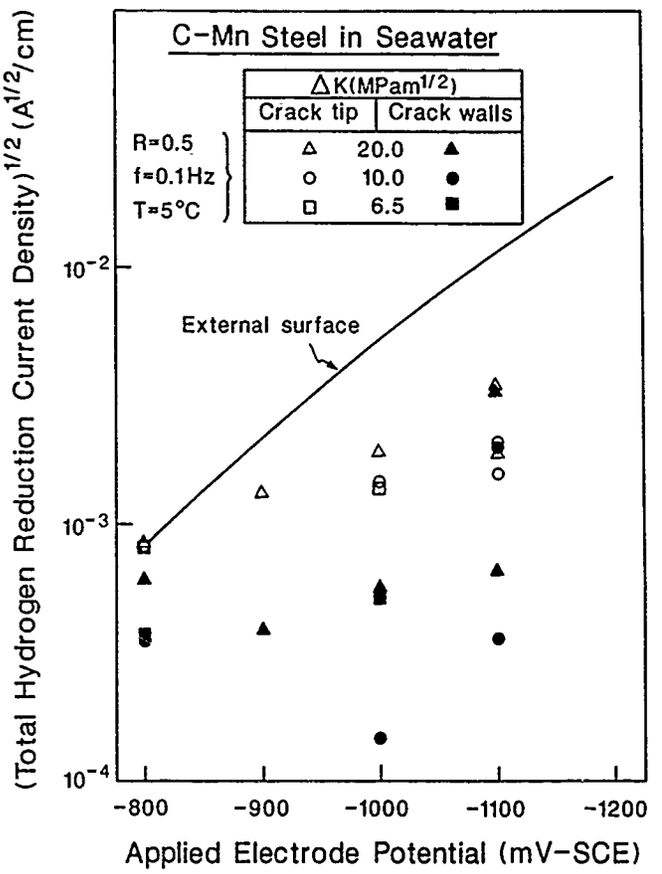


FIGURE 43—Model predictions of the effect of applied electrode potential on total atomic hydrogen production rate for various locations on a fatigue cracked specimen of C-Mn steel; after Turnbull and de Santa Maria.[191,250]

(7) Model predictions of crack-tip pH and electrode potential are in good agreement with measurements of local crack chemistry.[141,167,249]

(8) The effects of crack-tip straining, clean surface creation, and the associated reaction kinetics have not been broadly incorporated in crack chemistry models, additional work is required.[250]

These conclusions are important to interpretations of CF behavior in the steel–chloride system, however, modeling has been limited to predictions of crack electrochemistry and hydrogen production. No integrated model has been developed to relate crack chemistry calculations to da/dN by HE, as discussed in the section "Corrosion Fatigue by Hydrogen Embrittlement." Two initial results are noteworthy in this regard. Gangloff and Turnbull coupled crack chemistry modeling with an empirical HE failure criterion to predict K_{ISCC} as a function of crack geometry.[194] Such predictions were confirmed by experiment.

Following this simplified approach, it is reasonable to assume that CF crack growth rate is proportional to the amount of hydrogen produced at the crack tip. Hydrogen concentration, and therefore da/dN_e, should be proportional to the square root of the total reduction rate, particularly for the chemically limited plateau regime. Data on the effect of electrode potential on da/dN_e for API-2H steel in NaCl (Figure 25) were coupled with the calculated crack-tip hydrogen production rates shown in Figure 43 to yield the correlation in Figure 44. (The crack chemistry calculations and CF measurements were for identical material, ΔK, R, frequency, and electrolyte composition.)

Results in Figure 44 show that crack growth rate correlates reasonably with crack-tip hydrogen uptake, but the expected square root dependence is not observed. Rather, da/dN_e increases with

hydrogen production to the 1/4 power. If the dominant hydrogen concentration, either crack-tip or external surface, is used, then least squares analysis shows a similar good correlation. In this case, da/dN_c is proportional to total hydrogen production to the 0.14 power ($y = 0.1393 \cdot x + 1.8682$). Since no micromechanical model exists to relate hydrogen concentration to crack growth, the result in Figure 44 cannot be further explained. Additional work is required to pursue this approach; comparisons between electrolytes and gaseous H_2 would be particularly informative, as demonstrated for monotonic loading.[194]

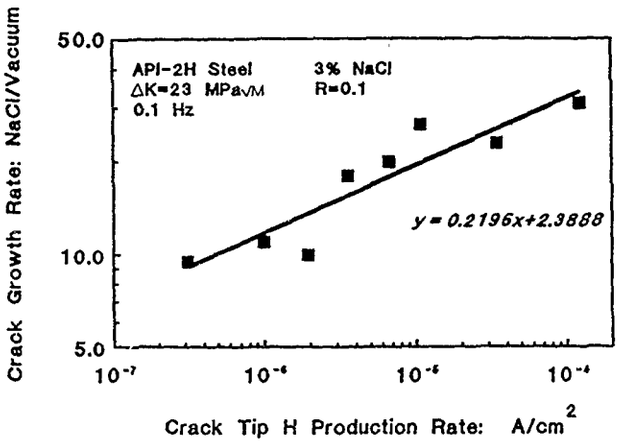


FIGURE 44—Corrosion fatigue crack propagation rates for API-2H in 3% NaCl from Figure 25, correlated with the crack-tip hydrogen atom production rate (Figure 43) to the 0.2 power.

Predictions of those conditions where specimen surfaces are the dominant source of hydrogen compared to the crack tip and vice-versa are particularly amenable to evaluation with coated specimens and with electrode potential/frequency transient experiments. Despite arguments to the contrary by Turnbull,[249] such existing evidence is weak.

The approach to crack chemistry modeling in steels should be applied to other systems in which CF is governed by HE. A notable example is high-strength aluminum alloys in distilled water and chloride (Figure 12) where limited crack chemistry measurement and modeling results have been reported to date. Hydrogen production by hydrolysis is likely; however, the system is complicated because both anodic dissolution of aluminum and hydrogen reduction occur simultaneously over a broad range of potentials.[254-256] Additionally, a variety of surface films are likely to form and complicate reaction kinetics.

Aqueous electrolytes: active steels in chloride-transient crack-tip reaction kinetics. The incorporation of transient reaction kinetics in crack chemistry and embrittlement modeling is controversial. Turnbull and coworkers replaced steady-state, filmed surface, polarization kinetics with similar results obtained with the straining electrode method.[191,250] Wei and coworkers have taken a different approach based on the idea that coupled and transient electrochemical reactions, which occur during each fatigue load cycle and as a cleaned surface refilms, control hydrogen production.[33,182,188,257,258] This work was recently reviewed.[37,259]

The essence of Wei's approach is that HE causes an increment of crack growth at maximum load. The resultant clean surface reacts anodically during the time to the next load maximum and produces an amount of cathodically generated adsorbed hydrogen near the crack-tip. The novel notion here is that rates of dissolution at the crack tip are controlled by the continuously changing (passivating) character of the reacting surface and as polarized by coupled, fully filmed crack flanks. The amount of hydrogen is assumed to be proportional to the integrated amount of current that passes during a load cycle; the environmental contribution to crack growth (da/dN_{cf}) is proportional to this quantity of hydrogen. The next increment of crack extension per load cycle is thus produced. For steel in aqueous electrolytes, it is hypothesized that electrochemical reaction rate limits fatigue crack propagation. These ideas follow from work on mass transport and reaction-rate-limited fatigue crack propagation in gaseous environments.[129,243]

From the "Models of Crack-Tip Mechanics . . ." section, crack-tip reaction-rate-controlled CF is described by the following:

$$\frac{da}{dN_{cf}} = \left(\frac{da}{dN_c} - \frac{da}{dN_m}\right)(q/q_s) \qquad (22)$$

where q is the charge transferred per loading cycle and q_s is the amount of charge required for completed reaction on the clean surface. q may be expressed as $[1 - \exp(-\tau/f)]$, where τ is an empirically determined reaction rate constant.

A new method was devised to measure the transient charge relevant to CF.[260-262] A notched specimen, coupled electrically to oxidized electrodes of the same steel, is fractured, and the current that is passed between the bare surface and the oxidized electrodes is measured as a function of time. This ensemble electrode is polarized to a fixed external potential by a counter electrode and with respect to a reference electrode, both contained in a separate solution coupled to the crack simulation by a salt bridge. In this way, the current transient can be measured for a constant applied potential, which will differ from the potential of the notch surface because of the IR difference across the salt bridge. In principle, the notch/oxidized electrode could be placed in an electrolyte that simulates crack solution pH and ionic concentration, however, such experiments have not been conducted.

Measurements of q/q_s, coupled with Equation (22), were used to predict the frequency dependence of CF crack propagation for ferritic steels in carbonate–bicarbonate, sulfate, buffered acetate, and NaCl solutions.[182,188,259,263] These predictions were in good agreement with crack growth rate measurements, supporting this approach. Several points are notable. First, the charge-transfer model predicts a frequency response that is qualitatively similar to that shown in Figure 21 for steel in chloride. Extensive charge measurements have not, however, been reported for this important system.[263] Second, the charge-transfer model has not incorporated crack environment changes into the analysis. Third, the charge-transfer model does not predict absolute values of crack growth rate because no micromechanical damage criterion has been included. Rather, charge transfer and crack growth kinetics are compared by multiplicative scaling factors. Finally, it is not clear how the charge-transfer model will deal with cathodic polarization. Here, crack growth rates increase (Figure 44) for applied potentials where crack-tip dissolution is not likely. While one can argue that polarization of the crack tip will allow transient dissolution for applied cathodic potentials, no evidence exists to support this reasoning. Crack chemistry modeling, albeit steady state, suggests only small IR differences along cracks in conductive electrolytes.

Advances in our understanding of crack-tip stress/strain fields, crack chemistry, and crack-tip transient reaction kinetics are outstanding. The challenge remains, however, to integrate these results into predictive models of CF crack propagation rate by either HE or film rupture.

Corrosion fatigue by hydrogen embrittlement

Justification for hydrogen embrittlement. That HE is the dominant mechanism for CF has been effectively argued for several systems; notably ferritic/martensitic steels in gases and electrolytes near 300°K,[34,37,51,57-59,116,122,170,174,189,194] and precipitation-hardened aluminum alloys in water vapor and halogen-bearing solutions.[37,60,62-64,125,126,132,133,217-219,264] This view is supported by extensive, but circumstantial, evidence:

(1) Pure gaseous hydrogen embrittles ferrous alloys under cyclic loading below K_{ISCC}.[54,117,118]

(2) Water vapor embrittles aluminum alloys under cyclic loading, but gases such as O_2, which produce surface films without releasing hydrogen, are inert; see Figures 12 and 27 and "Corrosion Fatigue by Surface Film Effects."[61,125,221]

(3) Water vapor embrittles aluminum alloys for stress intensity, frequency, and pressure conditions where crack-tip condensation and formation of an electrolyte are unlikely.[221]

(4) Hydrogen, introduced by chemical exposure prior to fatigue loading, increases inert environment rates of fatigue crack propagation in steels and aluminum alloys.[62,265,266]

(5) Plastic-zone damage, produced by fatigue deformation during crack growth in a hydrogen-producing environment, is evidenced by continued rapid fatigue crack propagation during loading in an inert environment. Damage is eliminated by heat treatment, albeit at high temperatures when atomic hydrogen is deeply trapped.[132,217-219]

(6) Crack growth rates vary with changes in frequency, stress intensity, and applied electrode potential in a manner consistent with HE of the cyclic plastic zone.[58,267] This point is controversial because of limited experimentation and because the fracture process zone may be within microns of the crack-tip-environment interface.

(7) Similar fatigue fracture surface features (viz., transgranular cleavage, intergranular separation, and interface cracking; see "Microscopic Corrosion Fatigue Crack Paths") are observed for pure H_2, water vapor, and electrolytes.[59,221]

(8) Chemical measurements and modeling elucidate the reaction sequence for environmental hydrogen production from water vapor and correlate CF crack growth rate data (viz., Figures 22, 23, and 41), including the deleterious effects of increasing P_{H_2O} and decreasing frequency.[61,98,129,221]

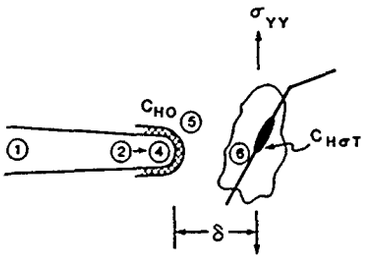
(9) Electrochemical measurements and modeling demonstrate environmental hydrogen production from electrolytes, and correlate da/dN data (viz., Figures 21, 25, 43, and 44), including the deleterious effects of increasing cathodic potential and decreasing frequency. CF in steels under cathodic potentials is only explainable by HE.[190,191,249,253,258,259]

The role of hydrogen has not been directly revealed. The difficulty is the lack of probes of crack-tip chemistry, surface reactions, and process-zone damage.

Quantitative hydrogen embrittlement models. Models of CF crack propagation rate are based on Equation (2). The pure CF crack growth rate and the proportion of CF depend on the rate and amount of hydrogen production by the reaction sequence for gases or electrolytes, combined with the local crack-tip field, most probably the cyclic plastic strain, and hydrostatic normal stress distributions. Microstructure determines the diffusion kinetics and distribution of segregated hydrogen through trapping processes. Local fracture will be determined by a damage criteria. The elements of these relations are shown schematically in Figure 45.[(6)]

The challenge in modeling is to derive equations that incorporate the processes shown in Figure 45 to predict da/dN_e as a function of ΔK, R, f, microstructural, and environmental variables. Quantitative HE models for CF are summarized in Figure 46[57] and are classed as either hydrogen-production-based (Scott, Gangloff, Wei, et al.) or hydrogen diffusion based (Holroyd and Hardie, Austin and Walker, Kim, et al.) Each model was developed from considerations of crack chemistry and to explain specific data. Some successes have been reported in this regard, however, generally predictive models are lacking.

The model by Scott assumes that the "plateau" CF crack growth rate, specifically for steels in aqueous chloride, is limited by hydrogen supply to the process zone.[58] Here, $da/dN_{eplateau} = da/dt \times 1/f$, and the time-based crack growth rate is assumed to be proportional to the rate of crack-tip electrochemical hydrogen production. Scott's original correlation with data was primitive. In fact, crack growth rates correlate with crack-tip hydrogen production current (Figure 44); however, the function is not the predicted linear dependence. This model is an extension of crack chemistry and is not based on a specific damage criterion.



GASEOUS HYDROGEN		ELECTROLYTE
MOLECULAR TRANSPORT	(1)	OXYGEN DEPLETION
PHYSICAL ADSORPTION H_2	(2)	CATION DISSOLUTION, HYDROLYSIS
H_2 MIGRATION, DISSOCIATION TO ATOMIC H	(3)	H^+ REDUCTION TO H
CHEMICAL ADSORPTION	(4)	WATER REDUCTION TO H
(5) SOLUTION TO LATTICE, TRAP SITES (5)		
(6) BULK DIFFUSION TO FPZ (6)		

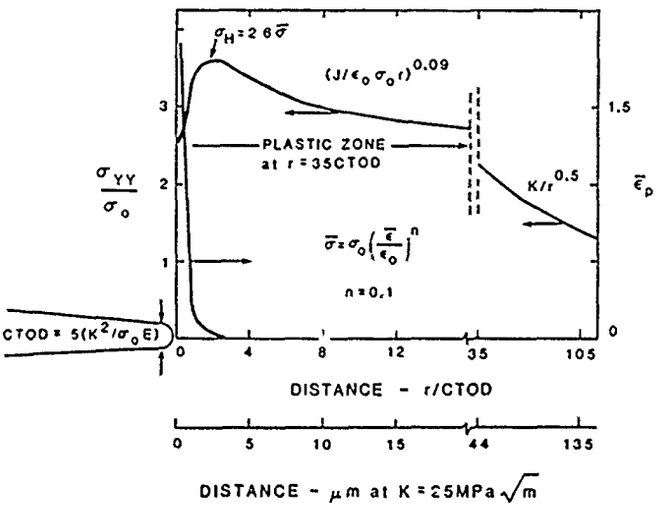


FIGURE 45—Transport and reaction sequences that produce adsorbed hydrogen for interaction with the crack-tip stress field and process-zone microstructure; after Gangloff.[57]

Gangloff assumed that the increment in growth rate for environmental cracking (da/dN_{cf}) is proportional to the amount of hydrogen produced per loading cycle by H^+ reduction at the crack-tip for steel in aqueous chloride.[208,253] Acidification was caused by the hydrolysis reaction sequence. Dissolved oxygen, supplied by convective mixing, is reduced within the occluded crack solution and competes to decrease the amount of cathodic hydrogen. The dependence of da/dN_{cf} on crack-opening displacement and oxygen reduction kinetics follows from an expression for perfect convective mixing and reaction. This da/dN dependence was confirmed by experiment; however, the beneficial effect of oxygen reduction at constant electrode potential was not demonstrated. The weaknesses of this model are similar to those discussed for the Scott model.

[(6)]The crack-tip stress and strain fields shown here are for the monotonically loaded, stationary crack. Less well-established results are available for cyclic deformation, see "Models of Crack-Tip Mechanics . . . ."

	CONTROL PROCESS	da/dN ASSUMPTION	GROWTH RATE PREDICTION
Scott	Crack Tip Cathodic Hydrogen Production	$\frac{da}{dN_{e,\ PLATEAU}} \alpha\ i_H$	$A(1/f)\ (\exp(-E/RT))$
Gangloff	Competition Between O_2 and H^+ Reduction	$\frac{da}{dN_{cf}} \alpha\ C_H$	$A'(V_{max})^{1/2} \exp(\alpha a_o / fV_{max})$
Wei et al.	Molecular Flow Gas Transport	$\frac{da}{dN_{cf}} \alpha\ C_H \alpha\ \theta$	$\frac{da}{dN_{cf,SAT}} \left(\frac{P_o}{f}\right) \Big/ \left(\frac{P_o}{f}\right)_{SAT}$
	Gas–Metal Reaction	$\frac{da}{dN_{cf}} \alpha\ C_H \alpha\ \theta$	$\frac{da}{dN_{cf,SAT}} (1-\exp(-kP_o/f))$
	Charge Transfer by Transient Reaction	$\frac{da}{dN_{cf}} \alpha\ C_H \alpha\ q$	$\frac{da}{dN_{cf,SAT}} (1-\exp(-\tau/f))$
Holroyd and Hardie	Hydrogen Diffusion in Plastic Zone	$\frac{da}{dN_e} \alpha\ \frac{\Delta x}{cycle}$	$4(\sqrt{D_H/f})$
Kim et al.	Hydrogen Diffusion in Plastic Zone	$\frac{da}{dN_{cf}} \alpha\ \frac{\Delta x}{cycle}$	$A''\ (\sqrt{P_o D_H / f})\ (\exp(-\Delta H/RT)) \Delta K^2$
Austin and Walker	Hydrogen Diffusion in Plastic Zone	$\frac{da}{dN_e} = \frac{da}{dN_m} X$	$\frac{(\Delta x - s)}{(r_p - s)} (\delta_{max} - s)$
			$\frac{da}{dN_{e,\ PLATEAU}} = 37.7\ \frac{\sigma_{ys}}{E} (\sqrt{D_H/f})$

E=Modulus
Δx=Hydrogen penetration distance = $4\sqrt{D_H/f}$
C_H=Hydrogen concentration
C_{H^+}=Hydrogen ion concentration
T=Temperature
θ=Fractional surface coverage
X=Environmental factor
q=Electrochemical charge
σ_{ys}=Yield strength
f=Frequency
i_H=H production rate
a_o,A,A',A'',R=Constants
ΔH=Binding energy of hydrogen to dislocation
s=Striation spacing
τ=Clean surface reaction rate constant
α=Oxygen reduction rate constant
V=Crack mouth opening
P_o=Nominal gas pressure
D_H=Hydrogen diffusivity
E'=Crack tip electrode potential
k=Reaction rate constant

FIGURE 46—Models for cycle–time-dependent corrosion fatigue crack propagation by hydrogen embrittlement. Scott, et al.,[58] Wei, et al.,[61,182,258,259] Gangloff,[253] Holroyd and Hardie,[65] Austin and Walker,[230,231] and Kim, et al.[258]

Wei and coworkers relate CF crack growth rate to the amount of hydrogen produced per loading cycle and proportionate to the extent of transient crack-tip surface reaction.[61,129,182,258,259] Quantitative relationships are derived for the cases of mass transport and surface-reaction-limited crack growth with the aim of predicting the time dependence of CF, as discussed for aluminum alloys in water vapor [see "Moderate ΔK (Plateau) Regime"] and steels in aqueous chloride (see "Aqueous Electrolytes: Active Steels in Chloride-Transient Crack Reaction Kinetics"). For gases at low pressures and with fast surface reactions, crack growth is limited by impeded molecular flow; the saturation exposure (P_o/f) is given by Equation (21). For gases at high exposures or with slow reaction kinetics, surface reaction is growth rate limiting. The expression for electrochemical reaction rate control by charge transfer was presented in Equation (22). The successes of these models in correlating CF crack growth rate data are significant (see Figures 22, 23, and 41 and References 61,129, 182, 258, and 259).

Several crack growth models are based on the assumption that da/dN_e is determined by the extent of hydrogen diffusion (Δx) within the plastic zone and during the time of a single loading cycle. Holroyd and Hardie argue that cycle–time-dependent crack growth in the aluminum–seawater system occurs by this process and at rates much greater than those of mechanical fatigue.[64] The mechanical contribution to fatigue is ignored and

$$\frac{da}{dN_e} = \frac{\Delta x}{1\ cycle} = 4\sqrt{D_H t} = 4\sqrt{D_H/f} \qquad (23)$$

with D_H being the diffusivity of hydrogen in steel and t the time per load cycle, 1/f. For an aluminum alloy in seawater, this relationship describes the frequency dependence of the maximum crack growth rate where environmental intergranular cracking was replaced by environmental transgranular cracking. A similar result was obtained for the environmental transgranular to mechanical transgranular fracture surface transition. Measured da/dN_e depends on the reciprocal of the square root of frequency; reasonable values of hydrogen diffusivity were calculated from the growth rate data

Holroyd and Hardie present no direct evidence to support the hypothesis that the growth kinetics are controlled by hydrogen diffusion. They further argue that the diffusion model reasonably describes the frequency dependence for CF in the steel–water vapor and steel–aqueous chloride systems that have been alternately described by crack environment mass transport and surface reaction rate models.

Austin and Walker postulate that CF crack growth rates are given by an enhancement of the mechanical propagation rate due to hydrogen diffusion within the plastic zone and countered by a reduction due to crack-tip blunting by corrosion [116,230,231] This model incorporates a rudimentary micromechanical description of fatigue based on the crack-tip-opening displacement approach after Tompkins.[233] Physically, da/dN_e is equated to the mechanical fatigue rate when the extent of hydrogen diffusion is less than one striation spacing (s). For diffusion distances that exceed the monotonic plastic-zone size [Equation (5)], da/dN_e equals the maximum fatigue crack-tip opening displacement per cycle [Equation (7)]. For intermediate Δx, CF crack growth rate is governed by the following equations:

$$\frac{da}{dN_e} = \left(\frac{\Delta x - S}{r_p - S}\right)(\delta_{max} - S) \quad (24)$$

$$S = C\Delta K^m \quad (25)$$

with the striation spacing described by the standard Paris expression with C and m as material constants.

The Austin and Walker model predicts ΔK-dependent plateau crack growth rates:

$$\left(\frac{da}{dN_e}\right)_{plateau} = 37.7\,\frac{\sigma_{ys}}{E}\sqrt{D_H/f} \quad (26)$$

for the case when ΔK, σ_{ys}, and f are small and R is large. The coefficient in Equation (26) was changed from the original value of 3.2 to be consistent with the best estimate for crack-tip opening displacement [Equation (7)] and the fact that hydrogen diffusion occurs throughout the entire loading cycle [Equation (23)]. With this change in coefficient, Equation (26) provides a reasonable prediction of absolute plateau velocities for the steel–seawater system. For X65 steel ($\Delta K = 21$ MPa$\sqrt{m}$, $R = 0.2$, $\sigma_{ys} = 450$ MPa, $f = 0.1$ Hz) with a trap-affected D_H value of 4×10^{-7} cm^2/s, a plateau velocity of 1.7×10^{-6} m/cycle is predicted from Equation (26) (and $S = 8 \times 10^{-5}$ mm, $\Delta x = 8 \times 10^{-2}$ mm, $r_p = 0.09$ mm, $\delta_{max} = 2 \times 10^{-3}$ mm). The measured da/dN in Figure 19 is 9×10^{-7} m/cycle. Data in Figure 25 suggest that the plateau crack growth rate for steel in chloride varies by two- to threefold depending on applied electrode potential. This factor is not predicted by the Austin and Walker model that relates da/dN to hydrogen penetration, without a concentration-based failure criterion and ignoring the level of crack surface hydrogen.

The Austin and Walker model describes the frequency dependence of CF similar to the Holroyd and Hardie model but at odds with the electrochemical surface reaction rate model of Wei and coworkers. The predicted inverse square root dependence of da/dN_e on f from diffusion is in good agreement with the measured frequency dependence of plateau crack growth rates for API-2H steel in 3% NaCl with cathodic polarization (Figure 21). Crack growth rates become independent of frequency below 0.1 Hz. At this point, Δx equals 0.08 mm compared to a maximum plastic-zone size of 0.09 mm. For a diffusivity of 5.1×10^{-7} cm^2/s, the penetration distance equals the plastic-zone size and growth rate is predicted to be constant at one δ_{max} per cycle, or 2×10^{-3} mm/cycle. The higher-frequency portion of the data is presumably described by that time in which the penetration distance becomes less than the striation spacing of 8×10^{-5} mm. The calculated frequency is 10^5 Hz; clearly this prediction is not consistent with the data in Figure 21.

Austin and Walker described the beneficial effect of corrosion blunting of the crack tip by scaling the applied stress intensity according to the following:

$$\Delta K_{Blunt} = \Delta K\,(\rho_s/\rho_c)^{1/2} \quad (27)$$

where ρ_s is the radius of a sharp fatigue crack and ρ_c is the enlarged radius due to corrosion. This reduced value of ΔK_B is used in Equation (24) for those cases in which anodic dissolution occurs.

While the Austin and Walker model reasonably predicts some experimental observations of CF for steels in aqueous chloride, the approach is not firmly established. The basis for Equation (24) is speculative, particularly the assumption that the environmental crack growth rate equals, or may be no faster than, the maximum crack-tip-opening displacement scaled by that proportion of the plastic zone penetrated by hydrogen.[58] No evidence is provided that hydrogen diffusion occurs over a substantial portion of the plastic zone to cause discontinuous crack propagation that rate limits CF. Regarding blunting, while the assumption that crack-tip stresses scale with the square root of radius is reasonable for notches with tip radii greater than about 0.05 mm,[89,158,231] it is not clear that such a relationship applies for radii on the size scale of a corroded crack tip. The extent of corrosion blunting and the associated effect on the crack-tip stress field remain to be established quantitatively.

While reasonable first steps, the models listed in Figure 46 are of limited use because none provide broad and absolute predictions of crack growth rate. Specifically, note that da/dN is *a priori* assumed to depend on hydrogen production or diffusion; no process-zone failure criteria are used. Without a damage criterion, models are unable to predict the stress-intensity dependence of CF.

The chemical and mechanical elements have been sufficiently developed to permit a next generation of CF crack growth rate models based on HE. For steels and aluminum and titanium alloys in electrolytes such as aqueous chloride, what is needed is (1) to build on the basis provided by damage accumulation models for mechanical fatigue,[210] (2) to establish crack-tip pH and electrode potential,[191] (3) to determine rates of clean surface dissolution and hydrogen production,[259] (4) to develop a hydrogen fracture criterion within an identified process zone, and (5) to partition the chemical–mechanical and mechanical components to crack growth.[228]

Corrosion fatigue by film rupture and transient dissolution

Over several decades, models of environmental fracture have been developed for both monotonic and cyclic loading based on a sequence of passive film rupture at the crack tip, oxidation and progressive repassivation of the exposed metal, and a new rupture of the freshly formed film. The elements of this approach include crack-tip strain rate, transient metal dissolution, film-formation kinetics, and film ductility. This model was extensively applied to ferritic and stainless steels in high-purity water over a temperature range of 300 to 600°K. Quantitative expressions for crack growth rate reasonably predict the effects of ΔK, frequency, metallurgical variables, and environment chemistry. This work was reviewed by Ford and coworkers[39,70,71,138] and is briefly discussed here for comparison with HE formulations.

For CF crack propagation, film-rupture models are based on two equivalent relationships for per cycle crack advance.[39,70,234]

$$\frac{da}{dN_{cf}} = \frac{da}{dr} \times \frac{dr}{dN} = \frac{1}{f}\frac{da}{dt} \quad (28)$$

Da/dr is the crack advance per film rupture plus dissolution event and dr/dN is the number of rupture events per load cycle (N). Both da/dr and da/dt are related by Faraday's Law to the amount of charge (Q_f) that passes during dissolution between rupture events. The time between rupture events (t_f) is given by the film-fracture strain (ϵ_f) to crack-tip strain rate [$(d\epsilon/dt)_c = \dot{\epsilon}_c$] ratio. The crack-tip strain range ($\Delta\epsilon_{CT}$) is given by the average crack-tip strain rate divided by loading frequency. Dr/dN is given by the crack-tip strain range to ϵ_f ratio. Combining these terms with Equation (28) leads to the following:

$$\frac{da}{dN_{cf}} = \frac{M}{\rho ZF}\left(\frac{\Delta\epsilon_{CT}}{\epsilon_f}\right)Q_f = \frac{1}{f}\left(\frac{M}{\rho ZF}\right)Q_f\left(\frac{\dot{\epsilon}_c}{\epsilon_f}\right) \quad (29)$$

where M and ρ are the atomic weight and density of the dissolving metal, Z is the number of electrons involved in oxidation, and F is Faraday's constant. Charge passed per rupture event is given by

$$Q_f = \int_0^{t_f = \epsilon_f/\dot{\epsilon}_c} i(t)\, dt \qquad (30)$$

where i(t) is the transient current associated with dissolution during reformation of the ruptured film. This treatment of film rupture is equivalent for static and cyclic loading, as described in Equations (28) to (30); only the crack-tip strain rate differs.

Hudak[234] and Ford and Andresen[71] have further derived the film-rupture model for type 304 stainless steel in sodium sulfate and high-temperature water, respectively. Hudak determined i(t) for a straining electrode in simulated crack-tip solution; calculation of Q_f for substitution into Equation (29) yielded the following:

$$\frac{da}{dN_{cf}} = \left(\frac{2\,M\,i_o}{\rho\,ZF}\right)\frac{1}{f}\left(\frac{t_o}{\epsilon_f}\right)^{1/2}\dot{\epsilon}_c^{\,1/2} \qquad (31)$$

where i_o is the bare-surface current density at the instant of film rupture, and t_o is the time for the initial decrease in the transient current. Equation (31) is based on the current decreasing according to the reciprocal square root of time between ruptures; more generally, current depends on time to the $-\beta$ power. Hudak determined the ΔK dependence of crack-tip strain rate for type 304 stainless steel; Equations (12) and (14). The total environmental crack growth rate was obtained by summing Equation (31) with an empirical result for inert environment mechanical fatigue:

$$\frac{da}{dN_o} = C\,(\Delta K - \Delta K_{th})^n + \left(\frac{2\,M\,i_o}{\rho ZF}\right)\left(\frac{t_o\,\epsilon_o}{\epsilon_f}\right)^{1/2}\Delta K\,\frac{1}{\sqrt{f}} \qquad (32)$$

C and n are material constants from the inert environment fatigue law, and ϵ_o is a constant from the measured $(d\epsilon/dt)_c$–ΔK relationship. This summation of rates is consistent with the superposition model, Equation (3).

Ford and Andresen previously derived an analogous expression for da/dN_o:[70,71]

$$\frac{da}{dN_o} = \frac{da}{dN_m} + \frac{1}{2F}\left[g(\beta)\,\dot{\epsilon}_c^{\,\beta}\right] = \frac{da}{dN_m} + \eta g(\beta)\Delta K^{\gamma\beta} f^{(\beta-1)} \qquad (33)$$

Here, $g(\beta)$ is stated generally to describe environment chemistry and metallurgical effects on CF crack growth kinetics. $\dot{\epsilon}_c$ is taken from Equation (20), with η as a constant.

Environmental effects on near-threshold cracking are modeled in terms of crack-tip blunting by corrosion.[39,234] The predictions of Equations (32) and (33) are extended to low growth rates and are truncated by the intersection with a blunting prediction. An example of this analysis is shown in Figure 24(a) by the intersection of the shaded band for blunting and the predictions from Equation (33). Blunting by dissolution of the crack flanks is not well described. As discussed in the section "Complications and Compromises of Fracture Mechanics," environment sensitive crack closure near ΔK_{th} introduces additional uncertainties.

The terms contained in Equations (32) and (33) are either known or are determined experimentally; modern film-rupture models are capable of predicting CF crack growth rates. Ford and Andresen report significant successes in predicting the effects of pertinent electrochemical variables (viz., temperature, solution conductivity, dissolved oxygen, electrode potential, bulk flow, radiation) and the effects of sensitization in type 304 stainless steels and soluble sulfide-bearing inclusions in ferritic pressure vessel steels in nuclear reactor environments.[39,70,71,99,138] Excellent agreement between predictions and measurements of time-based crack growth rates, for either monotonic or cyclic loading, indicates the potency of this approach; for example, see Figure 47.

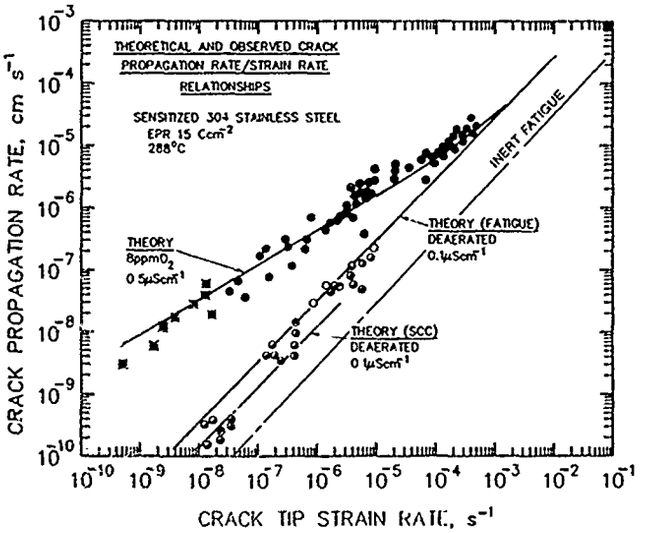


FIGURE 47—Film-rupture model predictions and measurements of time-based crack growth rates vs crack-tip strain rate for monotonic and cyclic loading of type 304 (UNS S30400) stainless steel in high-temperature water; after Ford and Andresen.[71]

On balance, however, controversy surrounds determinations of crack chemistry, crack-tip strain rate, the fracture behavior of a film of uncertain structure and adherence, and transient electrochemical reactions. Currently, judgment is used with reliance on adjustable parameters, a situation that has been improving rapidly.

Film-rupture predictions of the stress-intensity and frequency dependencies of da/dN_o are pertinent to this review. Crack-tip strain rate increases with increasing ΔK for fixed frequency, resulting in a linear dependence of da/dN_{cf} on ΔK. This dependence is weaker than the typical power-law relationship for mechanical fatigue and contributes little to total crack growth rates at very high ΔK, where rates of mechanical cracking are substantial. This prediction is in good agreement with crack growth rate data, as indicated in Figure 14.

The film-rupture model predicts a variety of frequency effects on CF. Physically, increasing frequency results in increasing crack-tip strain rate, and thus results in decreased time between ruptures, increased charge passed per film rupture, and increased crack advance per event. Crack growth per unit time (da/dt) is predicted to increase with increasing f, as indicated in Figure 47 and confirmed by extensive data for both monotonic and cyclic loading.[71]

For CF, the effect of frequency on da/dt is countered by the inverse effect of 1/f on time per load cycle [Equation (28)]. The net effect of f on da/dN_{cf} depends on alloy repassivation kinetics, particularly the β exponent. Typically, β equals 1/2 and da/dN_{cf} is predicted to increase with decreasing frequency, as indicated by the reciprocal square-root relationship in Equation (32). In the more general case, Equation (33) and Figure 24(a), da/dN_{cf} is predicted to increase with decreasing f provided that β is less than 1.0. This behavior is confirmed by the experimental results in Figures 14 and 47. In principle, the film-rupture model predicts that da/dN_{cf} could be independent of frequency ($\beta = 1.0$) or could increase with increasing frequency ($\beta > 1.0$). This behavior, while not typically observed, was recently reported for an Al-Li alloy in aqueous NaCl.[221] The predictions in Equations (32) and (33) are based on the assumption that mass transport is rapid and does not rate limit crack propagation.

Hudak recently demonstrated substantial differences in the predicted and measured frequency dependencies of CF for type 304 stainless steel in high-temperature water and in NaCl solution.[234] This comparison provides an important critique of quantitative film rupture and HE models. Specifically in conjunction with Equation (32), Hudak used reaction kinetics for type 304 stainless steel in

dilute sulfate to simulate crack solution for pure water and measured transient reaction kinetics for the chloride. Predicted and measured frequency dependencies of da/dN_{cf} are given in Figure 48. For the water environment, the agreement is of the same order of magnitude; however, a stronger (inverse square root) frequency response is predicted than is measured for several applied electrode potentials typical of the crack tip.

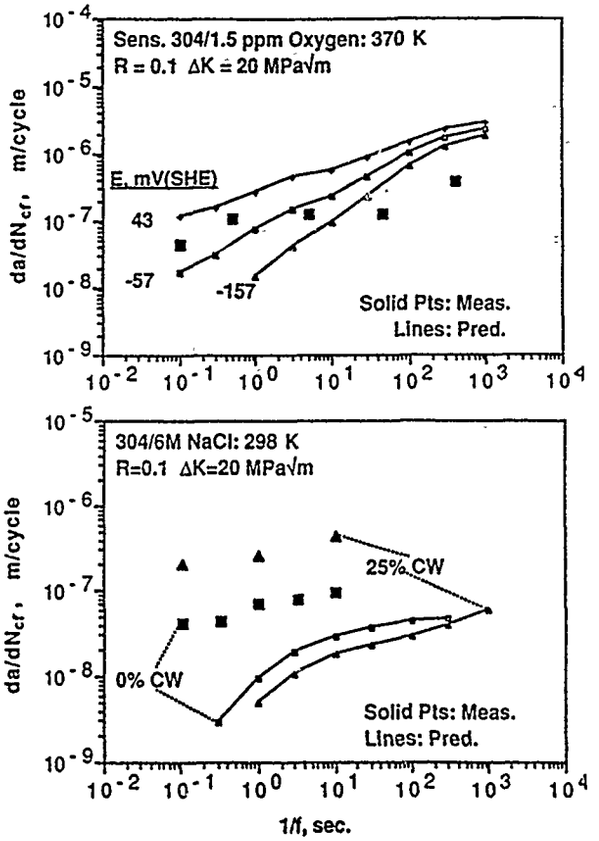


FIGURE 48—Film-rupture predictions and measurements of the frequency dependence of corrosion fatigue crack growth rate for type 340 stainless steel in two electrolytes; after Hudak.[234]

A dramatic underprediction of crack growth rates, by one to two orders of magnitude, is seen for ambient-temperature chloride. Hudak argues that these differences persist for wide ranges of values of the parameters used in Equation (32). The poor agreement is ascribed to a dominant HE contribution to CF. The data in Figure 48 were better described by the charge transfer-based HE model described in the section "Aqueous Electrolytes. Active Steels in Chloride-Transient Crack Reaction Kinetics."[7]

As transient reaction models for HE and film rupture are further developed and simultaneously applied to predict the frequency dependence of CF in model systems, mechanistic understanding will improve dramatically. Advances to date, and the likelihood for future refinements, suggest that in-depth mechanistic understanding of CF crack propagation is at hand. Predictive models will play a critical role in fracture-mechanics-based life-prediction procedures.

[7]The observed effect of cold work indicated in Figure 48 cannot be explained by the film-rupture model but may be rationalized in terms of hydrogen. Cold work, while not affecting electrochemical reactions, produces martensite, which reduces the amount of hydrogen required for a given crack extension. Unfortunately, the hydrogen model does not predict absolute rates of crack advance but scales a frequency response to the saturation rate (da/dN_c).

Corrosion fatigue by surface film effects

While environmentally produced thin surface films could accelerate fatigue crack growth rates by the plasticity mechanisms outlined in the section "Surface Films," such effects have been neither demonstrated by systematic experiment nor predicted analytically. This issue is important because crack-tip and flank films are produced by gaseous and electrolytic environments that are claimed to promote HE and film rupture. As an example for most metals, moist air is an aggressive environment relative to vacuum or helium. While atomic hydrogen production by water vapor oxidation is often cited as the mechanism for enhanced crack growth in moist air, the lack of a defined frequency dependence and the uncertain effect of surface films on deformation preclude a clear statement of mechanism.

The first question to address is the extent to which crack growth rate data demonstrate effects of surface films, apart from hydrogen and dissolution mechanisms. Gaseous oxygen provides an excellent environment in this regard. Data obtained in the author's laboratory are presented in Figure 49. For an Al-Li-alloy, equal crack growth rates are observed for vacuum, highly purified helium, and oxygen, while cracking is enhanced for water vapor and moist air.[125,221] In contrast, for a C-Mn steel, crack growth in oxygen is strongly accelerated compared to vacuum or helium and similar to that observed for gaseous hydrogen, moist air, and water vapor.[159] These data indicate that surface films produced by fatigue in oxygen lead to crack-tip damage for steel but not for aluminum. As such, the hydrogen mechanism is the sole cause of CF for the latter material in water vapor. For steel in moist air, the contributions of hydrogen and film formation cannot be separated.

The results contained in Figure 49 are consistent with literature data; however, some controversy exists. Oxygen has no effect on fatigue crack propagation in 7075-T651 and 2219-T87 alloys compared to vacuum.[61,268,269] Swanson and Marcus[268] and Piascik[221] used Auger spectroscopy and SIMS to show that substantial amounts of surface oxide were formed and that oxygen penetrated into the crack-tip plastic zone during fatigue. Nonetheless, crack growth rates were not affected. For three alloy and C-Mn steels, Frandsen and Marcus reported that crack growth rates were increased by up to a factor of two by loading in oxygen compared to vacuum.[209] In one of three cases, crack growth in O_2 was as rapid as that likely for moist air. Auger spectroscopy indicated that oxygen penetrated the steel during exposure to O_2.

A detailed study by Bradshaw and Wheeler demonstrated a strong CF action of O_2 on a 7000 aluminum alloy.[187] While oxygen either had no effect or slightly retarded crack growth rates compared to vacuum for ΔK levels above 6 to 8 MPa$\sqrt{m}$, this gas enhanced crack growth rates within the near-threshold regime, da/dN_o values exceeded vacuum levels by over an order of magnitude, and ΔK_{th} was reduced. A similar trend was observed for near-threshold cracking in alloy 5070, however, growth in O_2 was only twofold faster than that in vacuum. Extensive experiments with the 7000 series alloy further demonstrated that da/dN_o decreased with decreasing oxygen partial pressure at fixed frequency, analogous to the water vapor exposure effect illustrated in Figures 22 and 23. Oxygen affected a fatigue crack path transition. Growth in vacuum was faceted along slip bands for vacuum, while a flat "tensile" mode of unspecified morphology was observed for O_2. Piascik recently reported a similar result of O_2 accelerated near-threshold crack growth in 7075.[221]

Frandsen and Marcus reported four- to fivefold increases in crack growth rates for Monel† 404 and commercially pure titanium cycled in oxygen compared to vacuum.[209] Clearly, additional work is required to characterize the effects of oxygen and other film-forming environments on fatigue crack propagation. It is particularly important to characterize the effects of ΔK, loading frequency, environment activity, and temperature.

Given an effect of film-forming environments, it is important to question the causal mechanism. Those listed in the section "Surface Films" and the ideas on film-induced cleavage described by Sie-

†Trade name.

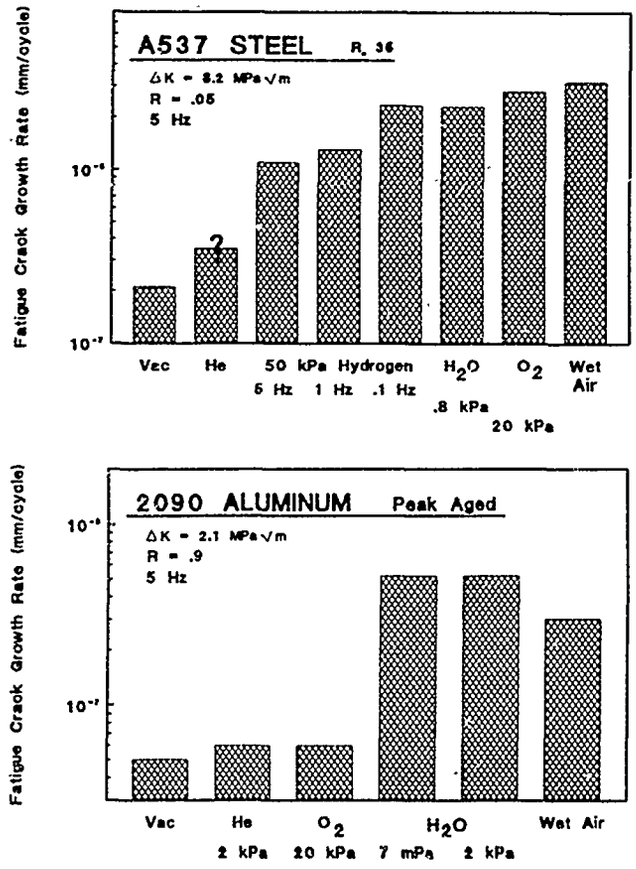


FIGURE 49—Fatigue crack propagation in a C-Mn steel and an Al-Li alloy as a function of the surrounding gas for constant ΔK and frequency.[125,159,221]

radzki in this volume[82] provide the basis for quantitative film-based models of CF. Bradshaw and Wheeler concluded that the results on cracking in O_2 give support for damage mechanisms based on surface films, however, no quantitative relationships have been derived to date. Surface film effects on crack-tip plasticity and dislocation morphologies must be considered.[75] A problem here will be to separate surface film effects from the influences of dissociated and dissolved solute.

Studies of surface film effects in CF are hindered by two problems. The rough crack surface typical of fatigue in vacuum and oxidation debris of thickness on the order of 0.1 to 1 μm can cause crack closure, which complicates analysis of intrinsic chemical damage mechanisms, as discussed in the next section. Indeed, the Bradshaw and Wheeler study can be interpreted based on oxide induced closure for O_2 at moderate ΔK and roughness induced closure for vacuum at low ΔK. Near-threshold faceted cracking and surface roughness could decrease, and da/dN_o could increase, with increasing oxygen pressure. Piascik provided a means to eliminate crack closure.[22] Second, the demonstration of an O_2 effect is only broadly established for alloy 7075, and perhaps steels, which are sensitive to HE. Recent data suggest that extremely small amounts of water vapor in O_2 affect crack propagation.[22] The purity of the oxygen environment must be carefully controlled.

Complications and Compromises of Fracture Mechanics

Conclusion

Fracture mechanics descriptions of CF and the similitude concept are complicated by the inability of stress intensity to describe the controlling crack-tip mechanical and chemical driving forces. The so-called closure, small crack, and high-strain problems in mechanical fatigue are relevant to CF. Data and analyses demonstrate that the unique relationship between da/dN and ΔK is compromised by mechanisms, including (1) premature crack-wake surface contact, (2) deflected, branched, and multiple cracking, and (3) time- and geometry-dependent occluded crack chemistry. Stress-intensity descriptions of elastic-plastic stresses, strains, and strain rates in the crack-tip plastic zone are uncertain within about 5 μm of the crack tip, within single grains that are not well described by the constitutive behavior of the polycrystal, and when deformation is time or environment sensitive. These limitations do not preclude the only quantitative approach developed to date to characterize subcritical crack propagation. Rather, they indicate the need for crack-tip modeling.

Crack mechanics

The fracture mechanics approach to fatigue crack propagation and the associated similitude concept are unambiguous if the applied stress intensity accurately describes local crack-tip stress and strain fields. Extensive work over the past 20 years on benign environment fatigue has demonstrated four situations in which the basic linear elastic formulation of applied ΔK must be modified to better define the governing driving force. These areas—crack closure, small crack size, large-scale yielding, and deflected cracks—are relevant to CF crack propagation. The environmental aspects of these issues have not been extensively investigated.

The fracture mechanics approach discussed in this review is based on the assumption that cracked specimens and components are loaded within the small-scale yielding regime.[88] Dowling conducted extensive studies on "high-strain" crack propagation and correlated growth rates with a nonlinear field parameter, the J-contour integral.[157] Unique geometry-independent crack growth rate laws are observed, and a variety of J solutions are available for various specimen and component geometries. This work has not been extended to crack growth in aggressive environments, but it is likely that many of the principles established for CF under small-scale yielding will be relevant.

Most stress-intensity analyses are derived for a single crack perpendicular to the applied load and growing in a nominally Mode I fashion. In CF, or with anisotropic microstructures, cracks may branch or deflect from this idealized geometry. In this case, growth proceeds under mixed Modes I and II. The governing stress intensity factor must be calculated to include a summation of the Mode I and II K levels for the deflected crack. Suresh has analyzed this problem and provided branched crack stress-intensity factors.[270] This analysis has not been broadly applied in CF, often the effect of deflection on ΔK is secondary, particularly within the Paris regime. Deflection effects on near-threshold environmental cracking, and the associated closure phenomena, are important and further study is warranted.

Crack closure. Premature crack-wake surface contact during the unloading portion of a fatigue cycle (viz., crack closure") reduces the applied stress intensity range to an effective value defined as $\Delta K_{eff} = K_{max} - f(K_{cl})$. Concurrently, the effective stress ratio increases to K_{cl}/K_{max}. When considered based on applied ΔK ($K_{max} - K_{min}$), fatigue crack growth rates decline as closure effects increase. Crack growth rate data, which are closure affected, are often referred to as extrinsic. Da/dN values that are obtained in the absence of closure, or are based on a closure-compensated ΔK level, are referred to as intrinsic. The topic of crack closure has been extensively reviewed for fatigue crack propagation in benign environments, particularly by Ritchie, McEvily, and their students.[41-43,47,202,271]

Overview for benign environments—Several mechanisms cause fatigue crack closure, including the following:

(1) Crack-wake plasticity;[272,273]
(2) Crack surface roughness or deflections with Mode II sliding displacements;[274]
(3) Crack corrosion debris;[205,275] and
(4) Crack fluid pressure.[276]

Quantitative models that estimate the degree of closure are provided in the indicated references.

Models and measurements of crack-closure loads by crack-mouth compliance or back-face strain-gauge techniques demonstrate that closure effects are exacerbated by (1) near-threshold loading, (2) low stress ratio loading, (3) tension dominated loading spectra or single overloads, (4) environments that produce corrosion debris within the crack, (5) anisotropic or planar slip materials which cause deflected and microscopically rough fatigue crack surfaces, and (6) environments that produce tortuous crack surfaces.

While the effects of closure on da/dN are clear, controversy exists as to the proper stress-intensity range that governs crack growth. The majority of studies have used an effective ΔK value ($\Delta K_{eff} = K_{max} - K_{cl}$), with K_{cl} determined from compliance measurements. Recent data indicate, however, that fatigue damage continues over a distributed range of loads below K_{cl}; ΔK_{eff} is too small.[277] A constant maximum stress-intensity procedure offers an alternate means of characterizing crack growth independent of closure as discussed in the "Novel Measurements of Corrosion Fatigue Cracking" section.[156]

When CF crack propagation data are obtained under the above conditions, it is likely that they are affected by crack closure. Such behavior has several implications for this review. It is necessary to assume that most of the results described here reflect closure influences. Given the complexities of making displacement measurements in aggressive environments, only limited work has been conducted to define closure in CF. An alternate approach is to design CF experiments that yield growth rates that are closure free; this approach with constant K_{max} and high R methods was taken by Piascik and Gangloff.[125,126,221]

In terms of crack growth mechanisms, it is reasonable to develop and evaluate models of the sort described in the section "Quantitative Models of Corrosion Fatigue Crack Propagation" in terms of intrinsic crack growth rates. As a separate problem, it is necessary to develop environmental mechanisms for crack closure. As an example, Hudak considered crack-closure contributions in film-rupture modeling of da/dN_o for stainless steels.[234] It is reasonable to question those studies that claim to have proved a specific CF model by crack growth rate measurements, if crack closure has not been accounted for.

In terms of life prediction under complex loading spectra, the crack growth rate law that describes the proper degree of closure for the component and loading history of interest is unclear. This problem has not been adequately dealt with for benign environment fatigue.

Crack closure in aggressive environments—Several mechanisms for closure are pertinent to CF.[35,60,196] For steel in aqueous chloride, Todd and coworkers demonstrated that grains, displaced or detached by environment-induced intergranular fatigue, act as wedges to hinder crack displacement.[152] Viscous fluids can exert closure forces on fatigue crack flanks.[276] Gangloff and Ritchie speculated that hydrogen may enhance plasticity and the extent of crack-wake-induced closure.[203] Environment-induced crack deflection is often encountered, but detailed closure analyses have not been applied to CF studies. Additional research is required to examine these environment-sensitive closure mechanisms.

Studies of closure have emphasized reductions in stress-intensity factor and hence crack-tip cyclic strain. It is also reasonable to suggest that crack closure will affect crack chemistry by influencing mass transport. Certainly the opening shape of the crack, varying with loading time, is an important factor in diffusion and convective mixing. (See the section "Aqueous Electrolytes: Active Steels in Chloride–Crack Chemistry Modeling.") As an example, Gangloff suggested that crack surface contact will transform an otherwise orderly mass flow situation into transport by turbulent mixing.[253] For this case, a perfect mixing model may be more accurate than detailed calculations based on slow laminar flow. Crack-closure effects on local environment chemistry have not been considered in detail.

Corrosion debris, the so-called oxide-induced closure mechanism, has a potent effect on fatigue crack growth rates. This process has been extensively investigated for low-strength alloy steels in moist gases and for C-Mn steels in seawater. Oxide-induced crack closure was broadly recognized by Ritchie for steels in various gas environments; for an example, see the data in Figure 28.[200-205] These and other results show that near-threshold crack growth rates are increased for all gases that prevent the formation of crack surface oxide, including pure H_2, He, and vacuum. For water vapor, wet H_2, and moist air, oxides of thicknesses on the order of the cyclic crack-tip-opening displacement and enhanced by a fretting mechanism cause reduced crack growth rates. This effect is observed for low stress ratios; equal crack growth rates are reported for all gases at R values above about 0.6, typical of closure.

Oxide-induced closure is not significant at higher stress intensities or for high-strength steels and precipitation-hardened aluminum alloys. For these materials in moist gases, oxide thicknesses are small, presumably because fretting is not an effective mechanism for accelerated oxidation.[278] More corrosive environments may, of course, cause debris-induced closure in these materials.

Crack closure of the sort illustrated in Figure 28 complicates mechanistic understanding of near-threshold cracking. The effect of closure must be eliminated or measured and growth rates adjusted to determine the extent of intrinsic environmental embrittlement. Since this is rarely done, data and models on near-threshold CF are lacking.

Suresh and Ritchie modeled oxide-induced closure in terms of the effect of a rigid wedge on the crack-tip stress intensity at the point of closure contact.[202,274]

$$K_{cl} = \frac{dE}{4\sqrt{\pi l}\,(1-\nu^2)} \qquad (34)$$

where d is the maximum thickness of oxide film and on the order of 0.01 to 0.1 μm; l is the distance behind the crack-tip to the location of maximum oxide thickness and on the order of several μm; E is the elastic modulus; and ν is Poisson's ratio. This analysis predicts K_{cl} levels on the order of 1.5 to 2 $MPa\sqrt{m}$ for steels.

Corrosion debris may promote crack closure for steels in aqueous chloride environments, as studied by Hartt, Scott, Bardal, van der Velden, and coworkers.[34,58,119,121,279-281] This phenomenon results in extremely low near-threshold growth rates and high levels of ΔK_{th} for environmental conditions that would otherwise promote HE. (See the section "Corrosion Fatigue by Hydrogen Embrittlement.") A typical example is shown in Figure 11. ΔK_{th} is increased markedly by seawater with cathodic polarization at low R (Curve 5) and compared to moist air, seawater with free corrosion (Curve 4), or seawater with cathodic polarization at high R (Curve 3). Closure during cathodic polarization is often sufficiently potent to cause crack arrest.

Corrosion-product-induced closure depends sensitively on the electrochemistry of the chloride environment, because this governs the precipitation of calcium- and magnesium-bearing salts, the offending corrosion debris.[279,280] These reactants are found in seawater, but not in pure 3% NaCl solution; as such, corrosion-product-induced closure only occurs in the former solution. As shown in Figure 44, cathodic polarization promotes CF crack growth in NaCl but greatly retards cracking in seawater. Here, precipitation of magnesium and calcium salts only occurs at electrode potentials below about $-850\ mV_{SCE}$, where the solubility product is sufficiently reduced. As such, calcareous-deposit-induced closure is likely for cathodic polarization but not for anodic potentials. This trend is clearly evident for crack growth in seawater in Figure 11. (Van der Velden reported that iron hydroxide can form on crack surfaces of steel in oxygenated 3% NaCl near free corrosion and can cause crack closure.[281] This observation is not general, as no evidence of crack closure has been reported in extensive studies of such steels in this environment.[115,170,173, 174,180,189,253])

It is likely that corrosion product deposition and crack closure are possible for other material–environment systems. The occurrence of this phenomenon is evidenced by time-dependent reductions in crack growth rates at constant applied stress intensity, by crack arrest at very high threshold stress intensities, and by compliance or back-face strain-gauge measurements of closure contact upon unloading. Crack chemistry modeling of the sort described in the section "Aqueous Electrolytes: Active Steels in Chloride–Crack Chemistry Modeling" predicts the occurrence of precipitation from occluded crack solution.[190,249,279]

The benefits of corrosion-product-induced closure to component life are unclear. The degree of product precipitation and the resulting effect on crack growth kinetics are possibly geometry and loading spectra dependent. For example, large compressive underloads may obliterate the corrosion product and reduce the closure effect compared to that expected from laboratory experiments with small specimens and simple tension loading. Application of the similitude concept in such cases is unclear;[100,101] additional work is required.

Environment-sensitive microscopic deformation. From the continuum perspective, crack-tip stresses and strains depend on the shape of the blunted crack tip and on material constitutive behavior through stress intensity. (See the section "Models of Crack-Tip Mechanics" and Reference 160.) Environment may influence these properties in a time-dependent fashion during CF crack propagation and thus influence the magnitude of the crack-tip fields. Crack-tip dissolution may affect blunting, and intergranular or transgranular fracture modes could produce unique crack-tip shapes compared to deformation blunting models. Hydrogen, dissolved in the plastic zone, could influence deformation mode and material flow properties. For these cases, stress intensity will describe crack-tip deformation; however, the appropriate crack shape and flow properties must be used in finite element models of the crack-tip. No work has been reported in these regards.

The influence of hydrogen on metal plasticity is controversial and has not been broadly demonstrated for materials subjected to the boundary conditions typical of a crack-tip plastic zone. No data have been presented to demonstrate alloy stress-strain behavior altered by dissolved hydrogen. Nonetheless, the possibility for such effects is strong based on (1) extensive evidence for hydrogen-induced plasticity in thin foils strained in the electron microscope,[68] (2) interpretations of fracture surface features,[69] and (3) electron microscope evidence for hydrogen-induced changes in the dislocation morphology within the crack wake.[282]

Information on environment-sensitive deformation at growing crack tips is provided by *in situ* fatigue loading in the scanning electron microscope coupled with stereoimaging analysis. (See the section "Models of Crack-Tip Mechanics . . . .") Lankford and Davidson[162-164] and Hudak[234] report that crack-tip-opening strain ranges are lower for aggressive compared to inert environments for any constant applied ΔK. These studies were conducted with 1005 steel and 7075-T651 aluminum in moist air or dry N_2 and with type 304 stainless steel in aqueous Na_2SO_4; an example of data for the latter material is presented in Figure 50.[232,(8)] Here, strain ranges are decreased by between a factor of four and eight for the sulfate; corresponding crack growth rates increased by between four- and twentyfold because of the environmental effect. Lankford and Davidson concluded that water vapor similarly lowered the crack-tip strain range for 7075; however, this point was obscured by substantial variability.[162]

The mechanism for the effect of environment on crack-tip strain is related to embrittlement of a fracture process zone on the order of 1 to 10 μm.[162,234] For the alloys examined, hydrogen is held to lower the "load bearing" or "accumulated strain" capacity of the process

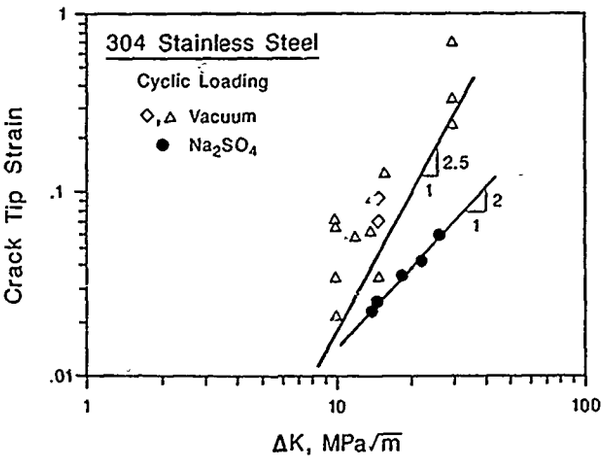


FIGURE 50—Measured fatigue crack-tip cyclic strain range as a function of applied ΔK for type 304 (UNS S30400) stainless steel cycled at 300°K in aqueous 0.1 M Na_2SO_4 or vacuum, and then characterized by *in situ* SEM loading and stereoimaging analysis; after Hudak.[234]

zone; the crack extends at a lower strain and after fewer cycles for any ΔK. Fatigue crack propagation progresses discontinuously, governed by a damage accumulation model for each environment.[162,210] For cyclic loading at constant ΔK, plastic strains build to a critical level, causing an increment of crack growth. The process-zone failure strain and measured crack-tip strains are reduced by environmental exposure consistent with Figure 50.

While crack-tip strains within the process zone differ with environment at constant ΔK and are therefore not well described by a continuum model, stress intensity provides the boundary condition that scales the magnitude of process-zone loading. Crack-tip strains, along with the near crack-tip opening shape, correlate with applied stress intensity as indicated in Figure 50. Stress intensity is not, however, capable of describing the cyclic evolution of the process-zone strain. A dislocation-hardening theory may be relevant.

Apart from the concept of a reduction in strain accumulation capacity, other factors could contribute to environment-sensitive crack-tip deformation. Varying process-zone strain, either hardening or softening, with cycling at constant ΔK is a critical assumption. Alternately, local plastic strain ranges may saturate at equal strains, independent of environment, for the same applied ΔK and at numbers of cycles well below the failure "life." An environmental reduction in a strain-life failure limit would then mean that fewer load cycles are required to cause an increment of crack extension and an increased growth rate, but measured crack-tip strains should be equal for aggressive and inert environments. The mechanism for the effect of environment on crack-tip strain may be more complex than indicated above. For example, if dissolved hydrogen homogeneously enhances plasticity, then crack-tip strains are expected to increase for environmental exposure at constant ΔK. Crack-tip strains will decrease, on average, if hydrogen promotes slip localization. Hydrogen effects on crack-tip shape, through an environmental fracture mechanism transition, could also alter the crack-tip strain distribution.

Experimental measurements of crack-tip shape, deformation, and dislocation configurations are critically needed as a function of applied ΔK and environment.

Small crack problem. The essence of the "small crack problem" is that stress corrosion, mechanical fatigue, and CF cracks propagate at unpredictably high rates when sized below a critical level and compared to the growth rates of long cracks. Small fatigue cracks propagate at stress-intensity ranges well below long-crack thresholds. The similitude principle breaks down; crack size and applied stress effects on growth kinetics are not uniquely described by a single parameter (ΔK). Extensive measurements and modeling indicate that crack size effects are important for crack depths below

(8)Note that the line indicated with a slope of 2:1 is incorrectly labeled. The data for Na_2SO_4 are not described by a ΔK squared dependence; rather, the slope of the data is somewhat lower.

about 1 to 5 mm. The definition of a small or short crack depends on the mechanism for the rapid growth rates.

Small cracks are technologically important because the early growth of cracks between 0.05 and 5 mm often dominates the fatigue life of components. An example is provided by CF crack growth in the weld of a pipe carrying H_2S-contaminated oil.[103] Here, 80% of the predicted life was involved with crack growth form 0.5 to 1.0 mm; cracking to failure required only 20% of life. Errors in the growth rates of small cracks have a large adverse effect on life prediction.

Small fatigue crack growth behavior has been extensively reviewed for benign environments by Ritchie, Lankford, Davidson, McEvily, Tanaka, Morris, and Hudak.[45,153,283,284] Gangloff, Wei, and Petit considered the behavior of small cracks in aggressive environments.[36,60,180,203,285]

Overview for benign environments—Several mechanisms have been established to explain small fatigue crack behavior, as summarized in Figure 51. Cracks are classified as short if they intersect many grains along the crack front and have a cyclic plastic zone much larger than the grain size but are of limited length dimension. A small crack and associated plastic zone are wholly contained within 1 to 5 grains. The absolute size of the small crack is microstructure dependent and may be quite large for a single crystal.

From the mechanical perspective, short cracks are poorly described by ΔK when small-scale yielding is violated by high net section stress, or when the crack size is less than 1 to 5 times the monotonic plastic-zone size. The J-integral approach may correlate cracking, as discussed in the section "Crack Mechanics." Microstructurally small cracks grow rapidly when the cyclic plastic zone is encased within a single grain because of abnormally large crack-tip opening strains compared to that expected based on applied ΔK. This effect appears to be related to single crystal and localized deformation mode effects on the crack-tip strain field.

Short and small cracks grow at accelerated rates because of a physical mechanism. Such cracks have reduced wakes and, as such, reduced levels of shielding crack closure. As the small crack propagates from the embryonic stage at constant applied ΔK, the crack wake develops, closure stress intensity rises, and crack growth rates decrease. Crack-length-independent cracking is achieved when closure reaches saturation or steady state above a specific crack size. Physical short/small crack behavior is correlated by stress-intensity approaches that account for closure, that is, either ΔK_{eff} or high stress ratio constant K_{max}.[156,277] Similitude is observed if rates are compared on a closure-free basis.

The mechanisms represented Figure 51 are important because they enable definitions of what constitutes a small crack, a question that has been posed for the past 20 years and that can now be reasonably answered for fatigue in benign environments.[283]

Aggressive environments—Chemical effects unique to the small crack geometry are an important aspect of CF behavior. The growth rates of small fatigue cracks (~ 5 mm) may be significantly faster than expected from longer crack da/dN-ΔK data for gases and liquids, while being predictable for benign environments. Aggressive environments play a role in mechanical and closure-based short small crack mechanisms. Additionally, the chemistry within such cracks may be uniquely embrittling (or benign), thus providing the basis for a chemical mechanism. These views are supported, albeit to a limited extent, by modeling and experiment as reviewed in detail by Gangloff and coworkers.[180,203]

Undoubtedly, experimental difficulties have hindered studies of small CF cracks. Surface replication techniques have been applied to fatigue in moist air; however, this tedious method with the necessity for test interruptions is not suited for aggressive environments. The electrical potential method (see the section 'New Procedures") was successfully applied to continuously monitor the growth of short cracks of length greater than 0.1 mm for a variety of materials and aggressive environments and under programmed applied ΔK.[158,159,221] Microstructurally small cracks have been monitored, provided that the grain size is enlarged above about 500 μm.[159] As developed, this method is not suited for naturally initiated CF cracks because the location of cracking must be precisely known for probe attachment. No measurements have been obtained on the closure behavior of small cracks in environments other than moist air.[159]

MECHANISMS FOR SMALL FATIGUE CRACK BEHAVIOR

	SHORT CRACK	MICROSTRUCTURAL SMALL CRACK
	• r_{pc} >> gs • Many grains @ front	• In 1 to 5 grains
MECHANICAL	SMALL SCALE YIELDING NOT MAINTAINED • High σ_{NET} • a < 1 to 5 r_p	ENHANCED CRACK TIP STRAIN • a < gs • r_{pc} < 1 to 2 gs
PHYSICAL	REDUCED CRACK WAKE CLOSURE • a < 1 mm	
CHEMICAL	CRACK SIZE DEPENDENT OCCLUDED CHEMISTRY • a < 5 to 10 mm	

r_p - monotonic plastic zone a - crack length
r_{pc} - cyclic plastic zone gs - grain size

FIGURE 51—Mechanisms for the unique behavior of small fatigue cracks.

The mechanical and closure mechanisms for crack size effects in CF have not been extensively investigated. Presumably, the ideas and results on closure in benign environments (see the section "Crack Closure") are relevant to CF cracks with limited wakes. As discussed by Piascik and Gangloff,[125,126,221] this situation provides for severe near-threshold CF crack growth effects and is worthy of additional study. Enhanced crack-opening strain for microstructurally small cracks should play an important role in CF by either film rupture or HE. No measurements exist to support this speculation, however, Hudak and Ford demonstrated the potency of this mechanism based on film-rupture model calculations [Equations (31) to (33)].[286] The prediction contained in Figure 52 indicates that enhanced crack tip strain and strain rate for the small fatigue crack enable propagation at high rates and well below the long-crack threshold for the stainless steel–high-temperature water system. This potential mechanism must be evaluated.

Experimental and analytical support for novel CF effects in the small crack regime exists for steels in aqueous chloride, a likely HE system.[180] A systematic study of short CF cracks was reported by Gangloff for a high-strength martensitic steel in 3% NaCl.[96,97] Typical data are presented in Figure 9. Note the one to two order of magnitude increases in the growth rates of short cracks (0.1 to 2 mm long, through-thickness and elliptical-surface cracks in a steel with 20-μm grain size) at any applied ΔK for the chloride and compared to compact-tension results. In contrast, crack growth in air and vacuum was uniquely correlated by applied stress intensity, independent of stress and crack size. This result demonstrates that crack closure and plasticity mechanisms do not explain the rapid growth of the short CF cracks.

A chemical mechanism must explain the short-crack effect in Figure 9, as detailed in the next section, "Crack-Geometry-Dependent Occluded Environment Chemistry." This point was reinforced by short-crack CF data that show that da/dN_e decreases with increasing initial applied stress range at constant R and with increasing R at constant ΔK.[97] A rapidly growing crack in NaCl was slowed by a stress range increase, in air or vacuum, increased stress caused increased crack growth rates, as expected from increasing

ΔK. These crack growth rate data correlated with the reciprocal of the maximum crack-mouth-opening displacement (V_{max}) at constant ΔK according to the following:[253]

$$\text{LOG}\left(\frac{da}{dN_{cf}}\right) = \Phi + \alpha\tau a^*/V_{max} \qquad (35)$$

Φ, α, τ, and a* are constants that characterize the chemical reactions controlling CF, as discussed in the next section $(V_{max})^{-1}$ decreases with increasing crack length and increasing K_{max}; particularly for crack lengths between 0.1 and 1 mm. For long cracks, changing crack length has only a small effect on V_{max}, indicating that ΔK would reasonably correlate CF crack growth rates.

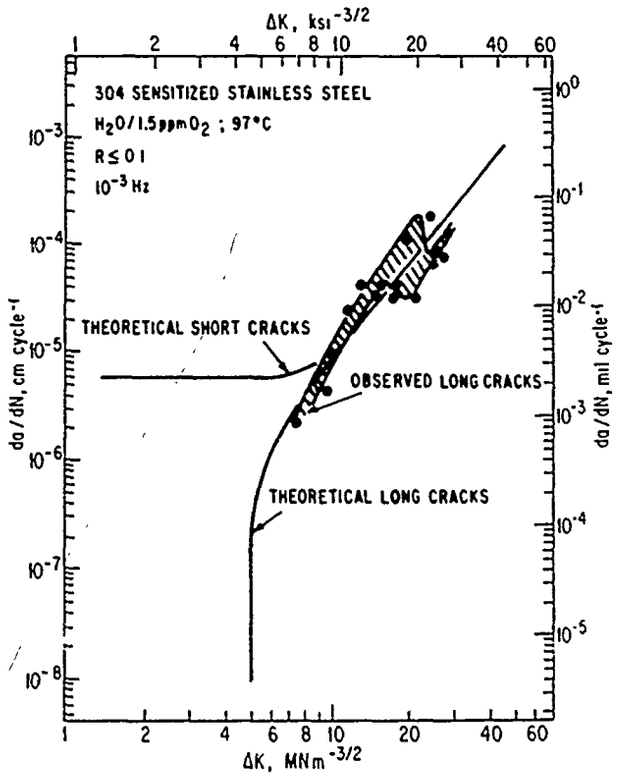


FIGURE 52—The predicted effect of small crack depth on corrosion fatigue crack propagation by film rupture for stainless steel in high-temperature water; after Hudak and Ford.[286]

Several points are relevant to the short crack results represented in Figure 9 and Equation (35). As the magnitude of the crack size effect increases, the fracture mechanism changes from brittle transgranular cracking associated with the martensitic microstructure to intergranular crack growth along prior austenite boundaries [97] In addition, K_{ISCC} equals between 24 and 30 MPa$\sqrt{m}$ for long cracks but declines to about 8 MPa$\sqrt{m}$ for the smallest cracks represented in Figure 9.[194] As such, it is likely that the result in Figure 9 is for time-dominant CF. A simple superposition model will not describe short-crack growth because of the effect of crack shape on local chemistry; for example, as indicated by the observation that da/dN_o decreases with increasing R. Finally, the "small" crack regime for this case extends to sizes on the order of several millimeters.

Cycle–time-dependent CF in the steel–chloride system is generally enhanced by reduced crack size; however, the magnitude of the effect decreases substantially with decreasing steel yield strength.[180] While systematic studies are limited, the data represented in Figure 53 show that da/dN_o is increased by between 1.5 to 2-fold for low-strength steels, comparing small crack kinetics to standard compact-tension data.[9] This result is further illustrated in Figure 17. As yield strength increases, short crack size becomes more important, for moderate-strength steels such as HY130, small cracks grow up to four times faster than long cracks.[180,287] This interaction between crack size and strength is consistent with the moderate effect of hydrogen for this class of steels. For high-strength steels, small CF cracks grow at unpredictably high rates, varying from long crack data by one to two orders of magnitude.

Small crack effects in CF have not been reported for nonferrous alloy and environment systems. A likely HE system, high-strength aluminum alloys in aqueous chloride, was examined by Piascik and Gangloff.[126,221] Similar CF crack growth rates were observed for through-thickness edge cracks sized between 0.2 and 5 mm and for 25-mm-long cracks in compact-tension specimens. While the high-angle grain size was large, no microstructure–environment interaction was observed. CF crack growth rates were consistent with the broad base of data presented in Figure 12.

Crack-geometry-dependent occluded environment chemistry

If occluded crack chemistry changes as a function of crack size, time, specimen geometry, or loading, then CF crack growth rates will not be steady state and will not be meaningfully described by applied ΔK. Crack chemistry effects are particularly important within the short- and small crack regimes.

Mathematical modeling provides a means to assess varying crack-tip electrolyte pH, potential, ionic composition, dissolution, and hydrogen-production rates, as discussed in the section "Aqueous Electrolytes: Active Steels in Chloride–Crack Chemistry Modeling." Such work for ferritic steels in aqueous chloride provides predictions of crack size and loading effects on local chemistry. Generally, reactant and product concentrations in a fatigue crack depend on crack depth and mouth opening, and thus on ΔK, R, load waveform, and specimen geometry.[248,252]

An example of crack-tip reactant oxygen concentration is provided in Figure 42; this specie is normally consumed by a reduction reaction within the crack that competes with hydrogen ion and water reduction. As crack length initially increases to 1 mm, the concentration of crack-tip oxygen declines because the diffusional supply of reactant O_2 from aerated bulk solution becomes increasingly difficult. This effect is offset by convective mixing supply, which becomes increasingly effective as crack length increases; a minimum in the oxygen level is predicted for a specific crack length. The relationship in Figure 42 depends on the rate of oxygen reduction, loading frequency, and crack surface area to occluded solution volume ratio.

The crack chemistry predictions in Figure 42 suggest that da/dN_o could either increase though a maximum or decrease through a minimum with increasing crack length at constant ΔK, the specific dependence would depend on the embrittlement mechanism. Only limited experimental evidence supports this prediction. For the steel–chloride system, Gangloff demonstrated the former trend, as expected from an inhibiting effect of dissolved oxygen on HE.[189] Experiments with variable O_2 but constant electrode potential and ΔK failed to confirm this chemical model.

Crack-geometry-dependent local chemistry is an important explanation for the small crack effect in the steel-chloride system. Initial modeling of the data in Figure 9 was based on a perfect mixing description of convection to supply oxygen to the crack-tip.[253] Those crack shape and loading conditions that reduce oxygen concentra-

[9] Subtle small crack effects are best characterized by constant ΔK experimentation with electrical potential monitoring. For example, in Figure 17, da/dN is constant with increasing crack length from 0.3 to 2.7 mm for moist air. Da/dN, while always higher than the air rate, decreases with increasing crack length for the chloride.[178] Surface replication methods would not indicate the behavior shown in Figure 17.

tion [slow loading frequency, large crack surface area to solution volume given by large $(V_{max})^{-1}$ and fast oxygen reduction kinetics] promote hydrogen production by cathodic reduction and hence crack propagation by HE. Equation (35) resulted from this modeling and explained how small crack size and low stress ratio enhanced da/dN_e.

Detailed modeling of crack chemistry further indicated that unexpectedly large and geometry-dependent adsorbed hydrogen concentrations develop at the tips of small CF cracks for steels in chloride. For monotonic loading, Gangloff and Turnbull demonstrated that crack-tip pH decreases with decreasing crack size because of enhanced hydrolysis. Here, cations are eliminated by diffusion from the tip of the short crack; dissolution is not transport limited.[194] Decreased pH dominated a slightly less cathodic crack-tip to produce increased amounts of adsorbed hydrogen for the short crack. Turnbull and Ferriss extended this work to cyclic loading with convective mixing and demonstrated a similar enhancement of hydrogen production for the short crack.[249] For this case, crack potential variation played a more important role than reduced acidification.

These calculations suggest an important effect of steel composition.[249] Chromium, present in alloy steels such as type 4130 (UNS G41300), hydrolyzes to produce acidic crack-tip conditions for electrode potentials near free corrosion. Cracks in C-Mn steels are less acidified, water reduction is an important source of embrittling hydrogen, and crack geometry appears to play a secondary role in local chemistry.

Crack chemistry modeling sensitizes the user of CF crack propagation data to possible problems with similitude. The use of laboratory specimens to predict the behavior of components can be questioned when crack chemistries differ because of geometry. This complex situation discourages the fracture mechanics approach to life prediction.

On balance, however, fracture mechanics studies of CF crack propagation demonstrate substantial steady-state and orderly material behavior. Applied stress-intensity control of da/dN_e is supported, perhaps because crack chemistry generally reaches constant conditions for most cracking situations, as suggested by modeling. The influences of specimen geometry, ΔK, R, waveform, and crack size above 1 to 5 mm are secondary. Note that time and specimen geometry effects on CF have not been examined systematically. Exceptions in this regard are the small crack issue,[97,180] predictions of surface crack CF behavior from compact-tension data,[121] and work on transient crack propagation preceding steady-state growth rates.[154]

Rapid progress over the past five years suggests that crack chemistry modeling will intensify and that similitude will be broadly tested for CF. There is no doubt that CF crack growth rate laws will be strengthened when necessary and applied to life predictions, despite the complexity of this endeavor.

Whole life

While the fracture mechanics approach emphasizes crack propagation, one must ultimately predict the whole life of components. A rational means to this end is to couple fracture mechanics studies of single small, short, and long CF cracks with work on environment-sensitive cyclic deformation and crack nucleation in homogeneous microstructures and near defects.[1,36] This can only be accomplished if each stage of fatigue deformation and fracture is isolated and characterized.

Fatigue crack initiation is correctly characterized by cyclic plastic strain amplitude, as reviewed by Dowling.[289] A fracture mechanics parameter [viz., applied ΔK divided by the square root of the notch-tip radius (ρ)] equals an elastic pseudo-stress range, which is a unique function of local plastic strain amplitude at the root of a notch; specifically for slender notches. This parameter is easily calculated for a variety of notched specimens and correlates notch-initiation data, as demonstrated for a variety of materials in benign air.[290] This approach has been successfully applied to CF crack initiation.

CF crack initiation in carbon and high-strength low-alloy steels is exacerbated by exposure to aqueous chloride electrolytes. An example is shown in Figure 54. Here, the load cycles required to produce a 1-mm-deep fatigue crack at the root of a notch are plotted vs $\Delta K/\sqrt{\rho}$ for the keyhole-notched compact-tension specimen.[290-293] A variety of modern steels (strengthened by microalloying, thermomechanical processing including controlled rolling, quench/tempering, and precipitation) were stressed in seawater and air. Classic endurance limit behavior is observed for fatigue in moist air, with the limiting stress range increasing with increasing steel yield strength.[290] In sharp contrast, exposure to either natural seawater or 3.5 wt% NaCl at free-corrosion potentials produced a dramatic reduction in initiation life. The endurance limit is eliminated by environmental exposure for each steel. Cathodic polarization up to about -1000 mV_{SCE} restores the majority of the air-fatigue performance; more cathodic polarization reduced initiation life.

Two points are notable in Figure 54 and are consistent with previous discussions of CF. First, notch crack initiation in the ferritic steel–chloride system is mitigated by mild cathodic polarization, despite the likelihood of HE. This behavior is analogous to that of smooth specimens but is in contrast to crack growth in precracked specimens, as indicated in Figures 25 and 26. An explanation for the effects of cathodic polarization on the initiation and growth stages of CF is given in the section "C-Mn Ferritic Steels."

Second, steel composition, microstructure, and strength have no resolvable effect on CF crack initiation and early growth, as indicated by the results for eight steels reported by Rajpathak and Hartt and for four steels by Novak (Figure 54). Apart from a variety of microstructures, monotonic yield strength varied from 275 MPa for normalized A36 steel to 1070 MPa for quenched and tempered V150. This conclusion is consistent with the lack of microstructure and yield strength effects on CF crack propagation in this system; see the sections "Yield Strength" and "Microstructure" and Figures 30 and 31.

The local strain approach to CF crack initiation, enabled by fracture mechanics solutions for stress intensity, provides an important complement to fatigue crack propagation studies. Additional work in this direction is warranted. Needs in this regard are for studies of additional materials and environments, for improved *in situ* measurements of notch-root crack initiation, and for the study of small notches typical of material and corrosion-produced defects. The results in Figure 54 were obtained by optical monitoring of large machined notches. The electrical potential method is well suited for high-resolution continuous measurement of crack initiation in complex environments.[158] The method was successfully applied to mechanically or spark-eroded defects as small as 75-μm semicircles. Crack initiation at pre-exposure corrosion pitting damage could be monitored by this approach.

Necessary Research

Conclusion

Opportunities exist for research on CF to (a) broaden phenomenological understanding, particularly near threshold, (b) develop integrated and quantitative micromechanical–chemical models, (c) develop experimental methods to probe crack-tip damage and to measure near-threshold cycle–time-dependent crack growth, (d) characterize the behavior of advanced monolithic and composite alloys, and (e) develop damage-tolerant life-prediction methods and *in situ* sensors for environment chemistry and crack growth.

Material	σ_{YS} (MPa)	Environment	Crack Size Type (mm)	da/dN Defined by ΔK?	$\frac{da/dN_{SMALL}}{da/dN_{LONG}}$	Limiting Small Crack Size (mm)	Comments	Reference	
AISI 4130 (.3C-.9Cr-.2Ni)	1330	3% NaCl	.1-40 Long 1.9 Wide Edge, Elliptical	Yes - Air, Vacuum No - NaCl	1.2 to 500	~2.5	Growth Retarded by Increased K_{max}, R, $1/\Delta_{max}$ Describes da/dN, 15 μm Grain Size	13, 21	High Strength
ASTM A289 B (18.2Mn 4.8Cr-.6C)	1120	655 kPa H_2 Sat. H_2O 80°C	1-40 Long 25 Wide Edge vs Notch	Yes - Air 23°C Yes - 10 Hz H_2 No - .02 Hz H_2	1.0 to 100	.8	Small Crack Growth Enhanced by Increased Initial ΔK and Loading Time, 100 μm Grain Size.	26	
HY130 (.1C-.5Cr-.5Ni)	930	3% NaCl	1-40 Long 1.9 Wide Edge	Yes - Air No - NaCl	~4	~1.0	Initial ΔK Not Important.	22	Medium Strength
	972	3% NaCl	4-40 Long 7.6 Wide Edge	Yes - Air No - NaCl	2	1.1	Limiting Crack Size Unaffected by Δσ, R.	18, 27	
	972	3% NaCl	.4-40 Long 7.6 Wide Edge	Yes - Air No - NaCl	1.0-1.8 Free Corrosion 0.8-1.3 Cathodic	0.9-1.4 5	Limiting Crack Sizes Up to 10 mm at Constant ΔK No Significant Crack Closure Measured	28	
	950	Seawater	~.5 Long 12.7 Wide Edge	Yes	1.0	.5	Limited Data.	29	
13 Cr (.03C-12.8Cr-.5Ni)	770	Water	?	No	4	?	High Frequency, Near Threshold Data. Magnitude of Small Crack Effect Enhanced at High R	25	
Q1N (.17C 1.2Cr 2.4Ni)	625	Seawater	.5-6 Long 12.7 Wide Edge	Yes - Air No - NaCl	4	2.0	No Crack Size Effect at R .05 or ΔK ~ 30 MPa√m, Limited Data for Air.	29, 30	Low Strength
BS4360 50D (.18C-1.2Mn)	370	Seawater	1-7 Long 23.5 Wide Edge	Yes - Air No - NaCl	3	1.0-3.0	Crack Size Effect Eliminated by Cathodic Polarization; da/dN Small to Large ~ 1.0	31	
EN5 (.3C-.7Mn)	300	Seawater	5-6 Long 12.7 Wide Edge	? - Air No - NaCl	2	2.0	Limited Data.	29	

FIGURE 53—Literature results on the effect of crack size on corrosion fatigue in the steel–aqueous chloride system. Reference numbers refer to the original paper; after Gangloff and Wei.[180]

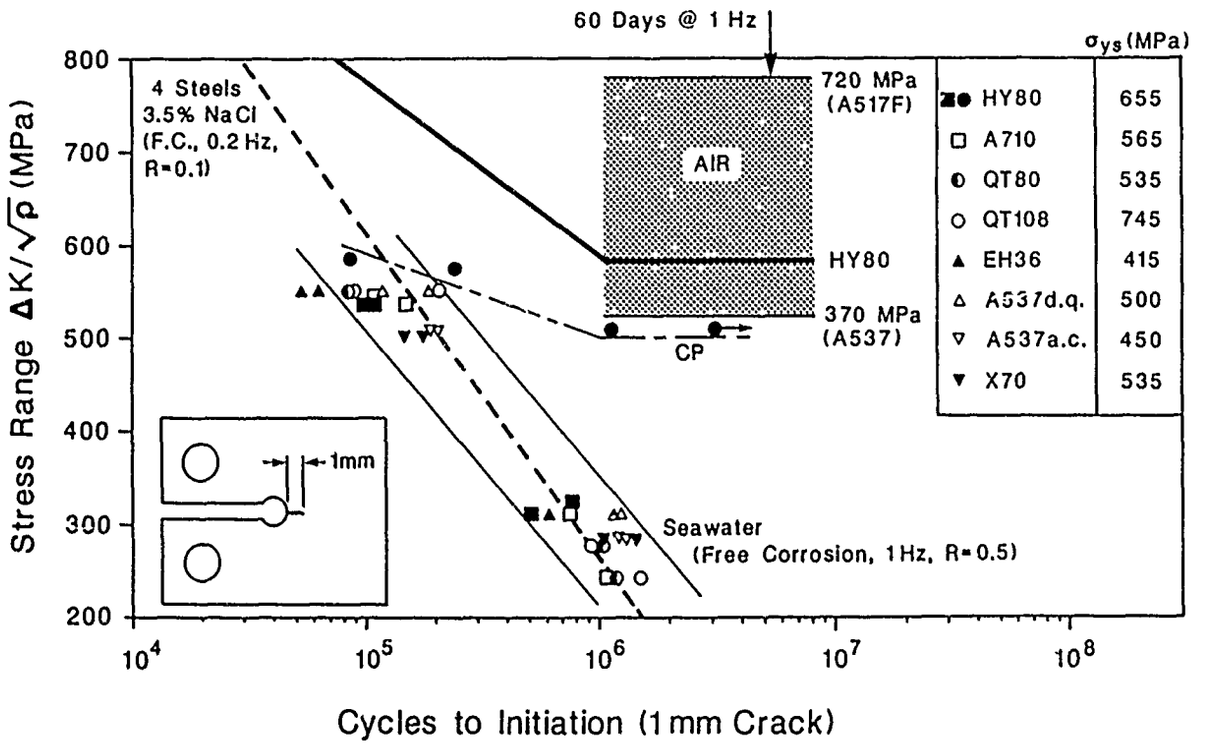


FIGURE 54—Corrosion fatigue crack initiation (Δa = 1 mm) at blunt notches in HSLA steels in seawater or NaCl. Local strain is approximated by elastic pseudo-stress from applied ΔK divided by the square root of the notch radius; after Hartt, et al.,[196,292,293] Novak,[291] and Rolfe and Barsom.[290]

Future research

The data and modeling studies presented in previous sections establish that the fracture mechanics approach can be exploited and extended to control CF crack propagation. Unresolved issues are listed for each of the main areas of this review.

Crack growth rate databases. Experiments must be conducted to determine the following:

(1) Environmental effects on near-threshold crack propagation, particularly as a function of cyclic loading frequency. Extrinsic closure and intrinsic environmental embrittlement must be separated.
(2) Yield strength and microstructural effects on CF crack propagation, with developments of reliable cracking-resistant alloys for extreme environments.
(3) Correlations between crack growth rates and environmental hydrogen uptake.
(4) CF crack propagation behavior of advanced alloys and composites. For the latter, the extent to which CF damage is distributed, and hence not described by continuum fracture mechanics, must be defined.
(5) CF crack propagation under complex spectrum loading, including the effects of single and multiple over/under loads and load history.

Experimental methods. New experimental methods are required for the following:

(6) Measurement of low growth rate CF crack propagation at low cyclic loading frequencies.
(7) *In situ* measurement of the early growth of microstructurally small CF cracks, without loading interruptions.
(8) Probes for crack-tip chemistry, surface reaction kinetics, and process-zone fatigue damage.

Fracture mechanics similitude. Work in this area is required for the following:

(10) Measurement and analysis of crack closure in aggressive environments.
(11) Determinations of the growth kinetics of short/small cracks, with associated chemical and mechanical mechanisms to extend similitude.

Micromechanical–chemical mechanism modeling. Modeling work must be expanded to include the following:

(12) Fractographic interpretations of the micromechanisms of CF crack propagation.
(13) Integrated occluded crack mass transport and transient straining surface reaction kinetics models.
(14) Integrated hydrogen production or film rupture and microscopic process-zone fatigue damage models.
(15) Understanding of the effects of crack surface films on cyclic plasticity and CF damage.
(16) Determinations of microscopic deformation and dislocation processes within the crack-tip process zone and as related to stress intensity.
(17) Environmental effects on material flow properties, incorporated into time-dependent crack-tip field models.
(18) Quantitative modeling of CF in aluminum, titanium, and nickel-based superalloys.

Life prediction. Applications of the fracture mechanics approach must include the following:

(19) Life-prediction codes that incorporate environmental effects on crack growth, extrapolated from short-term laboratory data and confirmed by component tests.
(20) Developments of sensors to monitor environmental conditions, hydrogen uptake, and fatigue crack propagation during component service.

Acknowledgment

Financial support for research on corrosion fatigue in structural alloys and for the preparation of this review was provided by the NASA-Langley Research Center under Grant NAG-1-745 with D.L. Dicus as monitor, by the Newport News Shipbuilding and Dry Dock Company under Grant POM-7671-R with G.M. Cobb as monitor, and by the Virginia Center for Innovative Technology under Grant CIT-TDC-88-01 with K. Blurton as monitor through the University of Virginia Center for Electrochemical Sciences and Engineering. This support is gratefully acknowledged.

References

1 D.J. Duquette, "Corrosion Fatigue Crack Initiation Processes," this proceedings.
2 R N Parkins, "Stress Corrosion Cracking," this proceedings.
3. H. Spaehn, "Stress Corrosion Cracking and Corrosion Fatigue of Martensitic, Ferritic, and Ferritic-Austenitic (Duplex) Stainless Steels," this proceedings.
4 A Pineau, "Elevated Temperature Creep-Fatigue Cracking in Relation to Oxidation Effects," this proceedings.
5 M.O. Speidel, M.J. Blackburn, T.R. Beck, J.A. Feeney, Corrosion Fatigue, Chemistry, Mechanics and Microstructure, ed. O. Devereux, A.J. McEvily, R.W. Staehle (Houston, TX: National Association of Corrosion Engineers, 1972), pp. 324-345.
6. O. Devereux, A.J. McEvily, R.W. Staehle, eds., Corrosion Fatigue, Chemistry, Mechanics and Microstructure (Houston, TX: NACE, 1972).
7. J. Hochmann, J. Slater, R.D. McCright, R.W. Staehle, eds., Stress Corrosion Cracking and Hydrogen Embrittlement of Iron Base Alloys (Houston, TX: NACE, 1977).
8. I.M. Bernstein, A.W. Thompson, eds., Hydrogen in Metals (Metals Park, OH: ASM International, 1974).
9. A.W. Thompson, I.M. Bernstein, eds., Effect of Hydrogen on the Behavior of Materials (Warrendale, PA: The Metallurgical Society-American Institute of Mining, Metallurgical, and Petroleum Engineers, 1976).
10. H.L. Craig Jr., T.W. Crooker, D.W. Hoeppner, eds., Corrosion Fatigue Technology, ASTM STP 642 (Philadelphia, PA: ASTM, 1978).
11. Proceedings, Conference on the Influence of Environment on Fatigue (London, UK: Inst. Mech. Eng., 1978).
12. Z.A. Foroulis, ed., Environment Sensitive Fracture of Engineering Materials (Warrendale, PA: TMS-AIME, 1979).
13. I.M. Bernstein, A.W. Thompson, eds., Hydrogen Effects in Metals (Warrendale, PA: TMS-AIME, 1981).
14. M.R. Louthan, R.P. McNitt, R.D. Sisson, eds., Environmental Degradation of Engineering Materials in Hydrogen (Blacksburg, VA: VPI Press, 1981).
15. J J Burke, V Weiss, eds., Fatigue: Environment and Temperature Effects (Watertown, MA: U.S. Army Materials Technology Laboratory, 1984).
16. T.W. Crooker, B.N. Leis, eds., Corrosion Fatigue: Mechanics, Metallurgy, Electrochemistry and Engineering, ASTM STP 801 (Philadelphia, PA: ASTM, 1984).
17. R.P. Gangloff, ed., Embrittlement by the Localized Crack Environment (Warrendale, PA: TMS-AIME, 1984).
18. R.A. Oriani, J.P. Hirth, M. Smialowski, eds., Hydrogen Degradation of Ferrous Alloys (Park Ridge, NJ. Noyes Publications, 1985).
19. A. Turnbull, ed., Corrosion Chemistry Within Pits, Crevices and Cracks (London, UK: HMSO, 1987).
20. R.H. Jones, W.W. Gerberich, eds., Modeling Environmental Effects on Crack Initiation and Propagation (Warrendale, PA: TMS-AIME, 1986).
21. M.R. Louthan, R.P. McNitt, R.D. Sisson, eds., Environmental Degradation of Engineering Materials III (University Park, PA: Pennsylvania State University, 1987).
22. Environment Sensitive Fracture of Metals and Alloys (Arlington, VA: Office of Naval Research, 1987).

23. T.W. Crooker, W.B. Lisagor, eds., Environment Assisted Cracking: Science and Engineering, ASTM STP (Philadelphia, PA: ASTM, in press 1989).
24. R.B. Thompson, R.O. Ritchie, J.L. Bassani, R.H. Jones, eds., Mechanics and Physics of Crack Growth: Application to Life Prediction (London, UK: Elsevier, 1988).
25. A.J. McEvily, R.P. Wei, Corrosion Fatigue: Chemistry, Mechanics and Microstructure, pp. 381-395.
26. M C. Speidel, Stress Corrosion Cracking and Hydrogen Embrittlement of Iron Base Alloys, pp. 1071-1094.
27. J.A. Moskovitz, R.M. Pelloux, Corrosion Fatigue Technology, ASTM STP 642, pp. 133-154.
28. R.N. Parkins, Metals Sci. July (1979): pp. 381-386.
29. D.J. Duquette, Environment Sensitive Fracture of Engineering Materials, pp. 521-537.
30. R.P. Wei, Fatigue Mechanisms, ASTM STP 675, ed. J.T. Fong (Philadelphia, PA: ASTM, 1979), pp. 816-840.
31. H.L. Marcus, Fatigue and Microstructure, ed. M. Meshi (Metals Park, OH: ASM International, 1979), pp. 365-383.
32. C.E. Jaske, J.H. Payer, V.S. Balint, Corrosion Fatigue of Metals in Marine Environments, Metals and Ceramics Information Center, MCIC-81-42 (1981).
33. R.P. Wei, G. Shim, Corrosion Fatigue: Mechanics, Metallurgy, Electrochemistry and Engineering, ASTM STP 801, pp. 5-25.
34. P.M. Scott, Corrosion Fatigue: Mechanics, Metallurgy, Electrochemistry and Engineering, ASTM STP 801, pp. 319-350.
35. K. Komai, Current Research on Fatigue Cracks, ed. T. Tanaka, M. Jono, K. Komai (Kyoto, Japan: Society of Materials Science, Japan, 1985), pp. 235-253.
36. R.P. Gangloff, D.J. Duquette, Chemistry and Physics of Fracture, ed. R.M. Latanision, R.H. Jones (The Netherlands: Martinus Nijhoff Publishers BV, 1987), pp. 612-645.
37. R.P. Wei, R.P. Gangloff, Fracture Mechanics: Perspectives and Directions, ASTM STP 1020, ed. R.P. Wei, R.P. Gangloff (Philadelphia, PA: ASTM, 1989), pp. 233-264.
38. T.S. Sudarshan, M.R. Louthan Jr., Intl. Metall. Rev. 32, 3(1987): pp. 121-151.
39. F.P. Ford, "Status of Research on Environmentally-Assisted Cracking in LWR Pressure Vessel Steels," J. ASME, in press (1989).
40. J.T. Fong, ed., Fatigue Mechanisms, ASTM STP 675 (Philadelphia, PA: ASTM, 1979).
41. D.L. Davidson, S. Suresh, eds., Fatigue Crack Growth Threshold Concepts (Warrendale, PA: TMS-AIME, 1984).
42. T. Tanaka, M. Jono, K. Komai, eds., Current Research on Fatigue Cracks (Kyoto, Japan: Society of Materials Science, Japan, 1985).
43. C.J. Beevers, ed., Fatigue 84 (West Midlands, UK: EMAS, 1984).
44. R.A. Smith, ed., Fatigue Crack Growth, 30 Years of Progress (Oxford, UK: Pergamon Press, 1986).
45. R.O. Ritchie, J. Lankford, eds., Small Fatigue Cracks (Warrendale, PA: TMS-AIME, 1986).
46. V.S. Goel, ed., Fatigue and Life Analysis and Prediction (Metals Park, OH: ASM International, 1986).
47. R.O. Ritchie, E.A. Starke Jr., eds., Fatigue 87 (West Midlands, UK: EMAS, 1987).
48. R.P. Wei, R.P. Gangloff, eds., Basic Questions in Fatigue, ASTM STP 924-2 (Philadelphia, PA: ASTM, 1988).
49. R.P. Wei, G.W. Simmons, Stress Corrosion Cracking and Hydrogen Embrittlement of Iron Base Alloys, pp. 751-765.
50. R.P. Wei, J.D. Landes, Mater. Res. Stds. 9(1969): pp. 25-28.
51. J.M. Barsom, Corrosion Fatigue, Chemistry, Mechanics and Microstructure, pp. 424-436.
52. J.M. Barsom, Intl. J. Frac. Mech. 7(1971): pp. 163-182.
53. M.O. Speidel, Unpublished research (1975), reported in J.C. Scully, Environment Sensitive Fracture of Engineering Materials, pp. 71-90.
54. H.H. Johnson, Stress Corrosion Cracking and Hydrogen Embrittlement of Iron Base Alloys, pp. 382-389.
55. R.A. Oriani, Corrosion 43(1987): pp. 390-397.
56. R.A. Oriani, Ann. Rev. Mater. Sci. 8(1978): pp. 327-357.
57. R.P. Gangloff, Mater. Sci. Eng. A103(1988): pp. 157-166.
58. P.M. Scott, T.W. Thorpe, D.R.V. Silvester, Corros. Sci. 23(1983): pp. 559-575.
59. B.R.W. Hinton, R.P.M. Procter, Metals Forum 5(1982): pp. 80-91.
60. J. Petit, A. Zeghloul, "Environmental Influence on Threshold and Near Threshold Behavior of Short and Long Fatigue Cracks," Environment Assisted Cracking: Science and Engineering, ASTM STP, in press 1989.
61. M. Gao, P.S. Pao, R.P. Wei, Metall. Trans. A 19A(1988): pp. 1739-1750.
62. D.J. Duquette, "Mechanisms of Corrosion Fatigue of Aluminum Alloys," AGARD Report No. AGARD-CP-316, 1981.
63. W. Gruhl, Z. Metallkde 75(1984): pp. 819-826.
64. D.A. Meyn, Metall. Trans. 2(1971): pp. 853-865.
65. N.J.H. Holroyd, D. Hardie, Corros. Sci. 23(1983): pp. 527-546.
66. M.O. Speidel, Metall. Trans. A 6A(1975): pp. 631-651.
67. R.A. Oriani, "Hydrogen Effects in High-Strength Steels," this proceedings.
68. H.K. Birnbaum, "Mechanisms of Hydrogen-Related Fracture of Metals," this proceedings.
69. S.P. Lynch, Atomistics of Fracture, ed. R.M. Latanision, J.R. Pickens (New York, NY: Plenum Press, 1983), pp. 955-963.
70. R.P. Ford, Embrittlement by the Localized Crack Environment, pp. 117-147.
71. F.P. Ford, P.L. Andresen, Advances in Fracture Research, ed. K. Salema, K. Ravi-Chandor, D.M.R. Taplin, P. Ramo Rao (Oxford, UK: Pergamon Press, 1989), pp. 1571-1584.
72. F.P. Ford, Corrosion 35(1979): pp. 281-287.
73. D.J. Duquette, Fatigue and Microstructure, pp. 335-363.
74. H.L Marcus, J.C. Williams, N.E. Paton, Corrosion Fatigue, Chemistry, Mechanics and Microstructure, pp. 346-358.
75. N.M. Grinberg, Intl. J. Fatigue April(1982): pp. 83-95.
76. J.C. Grosskreutz, Corrosion Fatigue, Chemistry, Mechanics and Microstructure, pp. 201-210.
77. R.E. Stoltz, R.M. Pelloux, Metall. Trans. 3(1972): pp. 2433-2441.
78. J. Lindigkeit, G. Terlinde, A. Gysler, G. Lutjering, Acta Metall. 27(1979): pp. 1717-1726.
79. K. Jata, E.A. Starke Jr., Metall. Trans. A. 17A(1986): pp. 1011-1026.
80. R.M.N. Pelloux, Trans. ASM 62(1969): pp. 281-285.
81. D.A. Meyn, Trans. ASM 61(1968): pp. 52-61.
82. K. Sieradzki, "Atomistic and Micromechanical Aspects of Environment-Induced Cracking of Metals," this proceedings.
83. H.H. Lee, H.H. Uhlig, J. Electrochem. Soc. 117(1970): pp. 18-22.
84. D.J. Duquette, H.H. Uhlig, Trans. ASM 61(1968): pp. 449-456.
85. D.J. Duquette, H.H. Uhlig, Trans. ASM 62(1969): pp. 839-845.
86. H.H. Lee, H.H. Uhlig, Met. Trans. 3(1972): pp. 2949-2957.
87. D.A. Jones, "Contribution of Anodically Attenuated Strain Hardening to the Mechanism of Environmentally Induced Cracking," this proceedings.
88. P.C. Paris, M.P. Gomez, W.E. Anderson, The Trend in Engineering, Washington State Univ. 13, 1(1961): pp. 9-14.
89. R.W. Hertzberg, Deformation and Fracture Mechanics of Engineering Materials, Ch. 13, 2nd ed. (New York, NY: John Wiley and Sons, 1983).
90. R.P. Wei, Fundamental Aspects of SCC, ed. R.W. Staehle, A.J. Forty, D. VanRooyen (Houston, TX: NACE, 1969), pp.104-112.
91. B.F. Brown, Met. Rev. 129(1968): pp.171-183.
92. F.J. Bradshaw, C. Wheeler, Applied Mater. Res. 5(1966): pp. 112-120.
93. A. Hartman, Intl. J. Frac. Mech. 1(1965), pp. 167-188.
94. R.P. Wei, P.M. Talda, C-Y. Li, Fatigue Crack Propagation, ASTM STP 415 (Philadelphia, PA: ASTM, 1967), pp. 460-485.
95. J.A. Feeney, J.C. McMillan, R.P. Wei, Metall. Trans. 1(1970): pp. 1741-1757.

96. R.P. Gangloff, Res. Mech. Let. 1(1981): pp. 299-306.
97. R.P. Gangloff, Metall. Trans. A. 16A(1985): pp. 953-969.
98. R.P. Wei, G.W. Simmons, Int. J. Fract. 17(1981): pp. 235-247.
99. P.L. Andresen, R.P. Gangloff, L.F. Coffin, F.P. Ford, Fatigue 87, pp. 1723-1751.
100. B. Tompkins, P.M. Scott, Metals Tech. 9(1982): pp. 240-248.
101. P.M. Scott, Mem. Etudes Sci. Rev. Metall. (1983): pp. 651-660.
102. J.M. Barsom, S.R. Novak, "Subcritical Crack Growth and Fracture of Bridge Steels," National Cooperative Highway Research Report 181 (Washington, DC: National Research Council, 1977).
103. O. Vosikovsky, R.J. Cooke, Int. J. Pres. Ves. and Piping 6 (1978): pp. 113-129.
104. Fatigue in Offshore Structural Steels (London, UK: Thomas Telford, Ltd., 1981).
105 Proceedings of the International Conference on Steel in Marine Structures (Paris, France: Comptoir des produits Siderurgiques, 1981).
106. Proceedings Institute of Mechanical Engineers Conference on Fatigue and Crack Growth in Offshore Structures (London, UK: Inst. Mech. Eng., 1986).
107. Steel in Marine Structures (Amsterdam, The Netherlands: Elsevier, 1987).
108. "Background to Proposed New Fatigue Design Rules for Steel Welded Joints in Offshore Structures" (London, UK: United Kingdom Department of Energy, HMSO, 1983).
109. W.D. Dover, Int. J. Fatigue 3(1981): pp. 52-60.
110. W.D. Dover, S. Dharmavasan, Fatigue 84, pp. 1417-1434.
111. S.J. Hudak, O.H. Burnside, K.S. Chan, J. Energy Resources Tech., ASME Trans. 107(1985): pp. 212-219.
112. W.D. Dover, F.D.W. Charlesworth, K.A. Taylor, R. Collins, D.H. Michael, Eddy Current Characterization of Materials and Structures, ASTM STP 722, ed. G. Birnbaum, G. Free (Philadelphia, PA: ASTM, 1985), pp. 401-427.
113. K. Yamakawa, T. Harushige, S. Yoshizawa, Corrosion Monitoring in Industrial Plants Using Nondestructive Testing and Electrochemical Methods, ASTM STP 908, ed. G.C. Moran, P. Labine (Philadelphia, PA: ASTM, 1986), pp. 221-236.
114. J.J. DeLuccia, D.A. Berman, Electrochemical Corrosion Testing, ASTM STP 727, ed. F. Mansfeld, U. Bertocci (Philadelphia, PA: ASTM, 1981), pp. 256-273.
115. R. Krishnamurthy, C.N. Marzinsky, R.P. Gangloff, Hydrogen Effects on Material Behavior, ed. N.R. Moody, A.W. Thompson (Warrendale, PA: TMS-AIME, in press 1989).
116. I.M. Austen, E.F. Walker, Fatigue 84, pp. 1457-1469.
117. H.J. Cialone, J.H. Holbrook, Metall. Trans. A. 16A(1985): pp. 115-122.
118. H.G. Nelson, Effect of Hydrogen on the Behavior of Materials, pp. 602-611.
119. E. Bardal, Fatigue Handbook, ed. A.A. Naess (Tapir, 1985), pp. 291-312.
120. E. Bardal, P.J. Haagensen, M. Grovlen, F. Saether, Fatigue 84, pp. 1541-1551.
121. T.W. Thorpe, P.M. Scott, A. Rance, D. Silvester, Intl. J. Fatigue 5(1983): pp. 123-133.
122. M.J. Cowling, R.J. Appleton, Proceedings Institute of Mechanical Engineers Conference on Fatigue and Crack Growth in Offshore Structures, pp. 77-92.
123. G.S. Booth, J.G. Wylde, T. Iwasaki, Fatigue 84, pp. 1471- 1484.
124. L. Bertini, Environment Assisted Cracking: Science and Engineering, ASTM STP, in press 1989.
125. R.S. Piascik, R.P. Gangloff, Advances in Fracture Research, pp. 907-918.
126. R.S. Piascik, R.P. Gangloff, "Aqueous Environment Effects on Intrinsic Corrosion Fatigue Crack Propagation in an Al-Li-Cu Alloy," this proceedings.
127. D. Aliaga, E. Budillon, "Corrosion Fatigue Behavior of Some Aluminum Alloys," AGARD Report No. AGARD-CP-316 ,1981.
128. R.J. Selines, R.M. Pelloux, Met. Trans. 3(1972): pp. 2525-2531.
129. R.P. Wei, P.S. Pao, R.G. Hart, T.W. Weir, G.W. Simmons, Metall. Trans. A 11A(1980): pp. 151-158.
130. P.S. Pao, M.A. Imam, L.A. Cooley, G.R. Yoder, Corrosion 45, 7(1989): pp. 530-535.
131. N. Ranganathan, M. Quintard, J. Petit, "Environmental Influence on the Effect of a Single Overload on the Fatigue Crack Growth Behavior of a High Strength Aluminum Alloy," Environment Assisted Cracking: Science and Engineering, ASTM STP (in press).
132. A. Niegel, H.J. Gudladt, V. Gerold, Fatigue 87, pp. 1229-1238.
133. N.J.H. Holroyd, G.M. Scamans, "Environment-Induced Cracking of Aluminum Alloys," this proceedings.
134. Proceedings of the First International Atomic Energy Agency Specialists Meeting on Subcritical Crack Growth I and II, US Nuclear Regulatory Commission Document, NUREG CP-0044 (1982).
135. Proceedings of the Second International Atomic Energy Agency Specialists Meeting on Subcritical Crack Growth I and II, US Nuclear Regulatory Commission Document, NUREG CP-0067 (1986).
136. P.L. Andresen, F.P. Ford, Mater. Sci. Eng. A103(1988): pp. 167-184.
137. F.P. Ford, D.F. Taylor, P.L. Andresen, R.G. Ballinger, "Environmentally Controlled Cracking of Stainless and Low-Alloy Steels in Light Water Reactor Environments," EPRI Report No. NP-5064M (Palo Alto, CA: EPRI, 1987).
138. F.P. Ford, "Crack-Tip Chemistry," this proceedings.
139. P.M. Scott, A.E. Truswell, S.G. Druce, Corrosion 40(1984): pp. 350-357.
140. B.F. Brown, Mater. Res. Stds. 6, 3(1966): pp. 129-133.
141. D.B. Dawson, R.M. Pelloux, Metall. Trans. 5(1974): pp. 723-731.
142. G.R. Yoder, L.A. Cooley, T.W. Crooker, Corrosion Fatigue: Mechanics, Metallurgy, Electrochemistry and Engineering, ASTM STP 801, pp. 159-174.
143. "Standard Test Method for Measurement of Fatigue Crack Growth Rates," ASTM Standard E647-88, ASTM Book of Standards 03.01 (Philadelphia, PA: ASTM, 1988), pp. 899-926.
144. D.A. Utah, et al., Metals Handbook: Mechanical Testing 8, 9th ed. (Metals Park, OH: ASM International, 1985), pp. 376-402.
145. S.J. Hudak Jr., R.J. Bucci, eds., Fatigue Crack Growth Measurement and Data Analysis, ASTM STP 738 (Philadelphia, PA: ASTM, 1981).
146. T.W. Crooker, S.J. Gill, G.R. Yoder, F.D. Bogar, Environment Sensitive Fracture: Evaluation and Comparison of Test Methods, ASTM STP 821, ed. S.W. Dean, E.N. Pugh, G.M. Ugiansky (Philadelphia, PA: ASTM, 1984), pp. 415-425.
147. R.P. Gangloff, et al., in Metals Handbook: Mechanical Testing 8, 9th ed. (Metals Park, OH: ASM International, 1985), pp. 403-435.
148. K.J. Marsh, R.A. Smith, Fatigue Crack Growth, 30 Years of Progress, ed. R.A. Smith (Oxford, UK: Pergamon Press, 1986), pp. 17-30.
149. C.J. Beevers, ed., Measurement of Crack Length and Shape During Fracture and Fatigue (West Midlands, UK: UMAS, 1980).
150. C.J. Beevers, ed., Advances in Crack Length Measurement (West Midlands, UK: UMAS, 1982).
151. R. Brazill, G.W. Simmons, R.P. Wei, J. Eng. Mater. Tech., Trans. ASME 101(1979): pp. 199-204.
152. J.A. Todd, P. Li, G. Liu, V. Raman, Environmental Degradation of Engineering Materials, pp. 533-541.
153. S. Suresh, R.O. Ritchie, Int. Metall. Rev. 29(1984): pp. 445-476.
154. S.J. Hudak Jr., R.P. Wei, Intl. J. Pressure Vessels and Piping 9(1981): pp. 63-74.
155. A. Saxena, S.J. Hudak Jr., J.K. Donald, R.W. Schmidt, J. Test. Eval. 6(1978): pp. 167-174.
156. W.A. Herman, R.W. Hertzberg, R. Jaccard, J. Fat. and Frac. of Eng. Mater. and Struc. 11(1988): pp. 303-320.

157. N.E. Dowling, Cyclic Stress-Strain and Plastic Deformation Aspects of Fatigue Crack Growth, ASTM STP 637 (Philadelphia, PA: ASTM 1977), pp. 97-121.
158. R.P. Gangloff, Advances in Crack Length Measurement, pp. 175-229.
159. F.H. Heubaum, "Propagation Kinetics of Short Fatigue Cracks in Low Alloy Steels" (Ph.D. diss., Northwestern University, 1986).
160. W.W. Gerberich, "Micromechanics," this proceedings.
161. W.W. Gerberich, D.L. Davidson, eds., Fracture. Measurement of Localized Deformation by Novel Techniques (Warrendale, PA: TMS-AIME, 1985).
162. D.L. Davidson, J. Lankford, Fat. Eng. Mater. and Struc. 6(1983): pp. 241-256.
163. J. Lankford, Fat. Eng. Mater. and Struc. 6(1983): pp. 15-31.
164. D.L. Davidson, J. Lankford, Intl. J. Frac. 17(1981). pp. 257-275.
165. B.F. Brown, Stress Corrosion Cracking and Hydrogen Embrittlement of Iron Base Alloys, pp. 747-751.
166. A.S. Dolphin, A. Turnbull, Corrosion Chemistry Within Pits, Crevices and Cracks, pp. 397-412.
167. A Turnbull, A.S. Dolphin, F.A. Rackley, Corrosion 44(1988). pp. 55-61.
168 T Hodgkiess, M.J. Cannon, Proceedings Institute of Mechanical Engineers Conference on Fatigue and Crack Growth in Offshore Structures, pp. 69-76.
169. A. Turnbull, Embrittlement by the Localized Crack Environment, pp. 3-48.
170. O. Vosikovsky, Trans. ASME, J. Eng. Mater. Tech. 97(1975). pp. 298-304.
171. E. Bardal, T Berge, M. Grovlen, P.J. Haagensen, B.M. Forre, Advances in Crack Length Measurement, pp. 139-158.
172. I.M. Austin, E.F. Walker, Steel in Marine Structures, pp. 859-870.
173. O. Vosikovsky, J. Test. Eval. 8(1980): pp. 68-73.
174. O. Vosikovsky, J. Test. Eval. 6(1978): pp. 175-182.
175. H.L. Ewalds, J. Test. Eval. 9 (1981): pp. 158-161.
176. J.M. Barsom, S.R. Novak, "Subcritical Crack Growth and Fracture of Bridge Steels," National Cooperative Highway Research Program Report 181, National Research Council, 1977.
177. O. Orjasaeter, A. Dragen, Fatigue 84, pp. 1553-1564.
178. R.P. Gangloff, J.Y. Koo, C.N. Marzinsky, unpublished research (Exxon Research and Engineering Company, 1986).
179. J.P. Gallagher, "Corrosion Fatigue Crack Growth Behavior Above and Below K_{ISCC}," Report No. NRL-7064, AD708377, Naval Research Laboratory, 1970.
180. R.P. Gangloff, R.P. Wei, Small Fatigue Cracks, ed. R.O. Ritchie, J. Lankford (Warrendale, PA: TMS-AIME, 1986), pp. 239-264.
181. B.R.W. Hinton, R.P.M. Procter, Hydrogen Effects in Metals, pp. 1005-1015.
182. G. Shim, Y. Nakai, R.P. Wei, Basic Questions in Fatigue, ASTM STP 924-2, pp. 211-229.
183. R.P. Wei, M. Gao, P.S. Pao, Scripta Metall. 18(1984), pp. 1195-1198.
184. D.L. Dicus, Environment Sensitive Fracture. Evaluation and Comparison of Test Methods, ASTM STP 821, pp. 513-533.
185. S. Chiou, R.P. Wei, "Corrosion Fatigue Cracking Response of Beta-Annealed Ti-6Al-4V in 3.5%NaCl Solution," U.S. Naval Air Development Center Report No. NADC-83126-60, 1984.
186. B.F. Jones, Embrittlement by the Localized Crack Environment, pp. 453-469.
187 F.J. Bradshaw, C. Wheeler, Intl. J. Frac. Mech. 5(1969). pp. 255-268.
188. R. Nakai, A. Alavi, R.P. Wei, Metall. Trans. A. 19A(1988). pp. 543-548.
189 R.P Gangloff, Critical Issues in Reducing the Corrosion of Steel, ed. H. Leidheiser Jr., S. Haruyama (Tokyo, Japan: NSF/JSPS, 1985), pp. 28-50.
190 A Turnbull, D.H. Ferriss, Corros. Sci. 26(1986). pp. 601-621.
191. A. Turnbull, M. Saenz de Santa Maria, Metall. Trans. A 19A(1988): pp. 1795-1806.
192. K.N. Akhurst, T.J. Baker, Metall. Trans. A. 12A(1981): pp. 1059-1070.
193. A. Turnbull, Scripta Metall. 20(1986): pp. 365-369.
194. R.P. Gangloff, A. Turnbull, Modeling Environmental Effects on Crack Initiation and Propagation, pp. 55-81.
195. R.P. Gangloff, Corrosion Prevention and Control, Proc. Sagamore Army Materials Research Conference 33, ed. M. Levy, S. Isserow (Watertown, MA. U.S. Army Materials Technology Laboratory, 1987), pp. 64-111.
196. S.S. Rajpathak, W.H. Hartt, "Keyhole Compact Tension Specimen Fatigue of Selected High Strength Steels in Seawater," Environment Assisted Cracking: Science and Engineering, ASTM STP, in press.
197. N.J.H. Holroyd, G.M. Scamans, Environment-Sensitive Fracture. Evaluation and Comparison of Test Methods, ASTM STP 821, pp. 202-241.
198. R.E. Ricker, D.J. Duquette, "The Use of Electrochemical Potential to Control and Monitor Fatigue of Aluminum Alloys," CORROSION/85, paper no. 354 (Houston, TX. NACE, 1985).
199. H.J. Cialone, N.J.H. Holbrook, M.R. Louthan, "Hydrogen-Enhanced Fatigue Crack Growth in Line Pipe Steels," presented at International Conference on Environmental Degradation of Engineering Materials III (University Park, PA: Pennsylvania State University, 1987).
200. R.O. Ritchie, S. Suresh, P.K. Liaw, Ultrasonic Fatigue, ed. J.M. Wells, O. Buck, L.K. Roth, J.K. Tien (Warrendale, PA. TMS-AIME, 1982), pp. 443-460.
201. S. Suresh, R.O. Ritchie, Metal Sci. 16(1982). pp. 529-538.
202. S. Suresh, R.O. Ritchie, Fatigue Crack Growth Threshold Concepts, pp. 227-261.
203. R.P. Gangloff, R.O. Ritchie, Fundamentals of Deformation and Fracture, ed. B.A. Bilby, K.J. Miller, J.R. Willis (Cambridge, UK: Cambridge University Press, 1985), pp. 529-558.
204. R.O. Ritchie, S. Suresh, C.M. Moss, J. Eng. Mater. Tech., Trans. ASME 102(1980): pp. 293-299.
205. S. Suresh, G.F. Zaminski, R.O. Ritchie, Metall. Trans. A. 12A(1981): pp. 1435-1443.
206. J. Toplosky, R.O. Ritchie, Scripta Metall. 15(1981): pp. 905-908.
207. P.K. Liaw, S.J. Hudak Jr., J.K. Donald, Fracture Mechanics: Fourteenth Symposium-Vol. II, ASTM STP 791, ed. J.C. Lewis, G. Sines (Philadelphia, PA: ASTM, 1983), pp. 370-388.
208. R.P. Gangloff, Basic Questions in Fatigue, ASTM STP 924-2, pp. 230-251.
209. J.D. Frandsen, H.L. Marcus, Metall. Trans. A 8A(1977): pp. 265-272.
210. H.J. Roven, "Cyclic Deformation and Fatigue Crack Propagation in a Low Alloyed Steel" (Thesis for Doctor Technique, Norwegian Institute of Technology, 1988).
211. E.A. Starke Jr., F.S. Lin, R.T. Chen, H.C. Heikkenen, Fatigue Crack Growth Threshold Concepts, pp. 43-61.
212. H.F. Wachob, H.G., Nelson, Hydrogen in Metals, pp. 703-711.
213. N. Bandyopadhay, J. Kameda, C.J. McMahon Jr., Metall. Trans. A. 14A(1983): pp. 881-888.
214. C.A. Hippsley, "Hydrogen and Temper Embrittlement Interactions in Fatigue of 2 1/4Cr-1Mo Steel," Harwell Laboratory (Oxon, England) Report AERE R 12322, 1986.
215. F.S. Lin, E.A. Starke Jr., Hydrogen Effects in Metals, pp. 485-492.
216. P.L. Andresen, General Electric Corporate Research and Development Center, Private Communication (1989).
217. A. Niegel, H.-J. Gudladt, V. Gerold, J. de Physique, Colloque C5 49(1988): pp. 659-663.
218. H.-J. Gudladt, A. Niegel, P. Liang, Proc. Mater. Res. Soc. 122(Boston, MA: MRS, 1988), pp. 405-409.
219. P. Liang, H.-J. Gudladt, V., Gerold, Low Cycle Fatigue and Elastic Plastic Behavior of Materials, ed. K.-T. Rie (London, UK.

Elsevier Applied Science, 1987), pp. 687-692.
220. P.J.E. Forsyth, C.A. Stubbington, D. Clark, J. Inst. Metals 90(1961-62): pp. 238-239.
221 R S Piascik, "Mechanisms of Intrinsic Damage Localization During Corrosion Fatigue: Al-Li-Cu System" (Ph.D. diss., University of Virginia, 1989).
222 R W Staehle, "Understanding 'Situation-Dependent Strength'. a Fundamental Objective in Assessing the History of Stress Corrosion Cracking," this proceedings.
223. R.P. Gangloff, R.P. Wei, Metall. Trans. A 8A(1977): pp. 1043-1053.
224. O. Vosikovsky, W.R. Neill, D.A. Carlyle, A. Rivard, Canadian Metall. Quart. 26(1987): pp. 251-257.
225. O. Vosikovsky, A. Rivard, Corrosion 38(1982): pp. 19-22.
226. C.J. Thomas, R.G.J. Edyvean, R. Brook, Biofouling 1(1988). pp. 65-77.
227. R.G.J. Edyvean, C.J. Thomas, R. Brook, I.M. Austen, Biologically Induced Corrosion, ed. S.C. Dexter (Houston, TX: NACE, 1986), pp. 254-267.
228. R.P. Wei, M. Gao, Scripta Metall. 17(1983): pp. 959-962.
229. I.M. Austin, E.F. Walker, Proc. Intl. Conf. Influence of Environment on Fatigue, pp. 1-16.
230. I.M. Austin, W.J. Rudd, E.F. Walker, Proceedings of the International Conference on Steel in Marine Structures, Paper ST 5.4.
231. I.M. Austin, "Quantitative Assessment of Corrosion Fatigue Crack Growth Under Variable Amplitude Loading," British Steel Company Report BSC FR S132-8/862 (Rotherham, England. Swinden Laboratories, 1987).
232. D.P.G. Lidbury, Embrittlement by the Localized Crack Environment, pp. 149-172.
233. J.F. Knott, Fatigue Crack Growth, 30 Years of Progress, pp. 31-52.
234 S.J. Hudak, "Corrosion Fatigue Crack Growth: The Role of Crack-Tip Deformation and Film Formation Kinetics" (Ph.D. diss., Lehigh University, 1988).
235. S.J. Hudak, D.L. Davidson, R.A. Page, Embrittlement by the Localized Crack Environment, pp. 173-198.
236. H.S. Isaacs, ed., Localized Corrosion (Houston, TX: NACE, in press, 1989).
237. S. Dushman, Scientific Foundations of Vacuum Technique (New York, NY: John Wiley, Sons, 1962), Chapters 1-2.
238. B.R. Lawn, Mater. Sci. Eng. 13(1974): pp. 277-283.
239. F.J. Bradshaw, Scripta. Metall. 1(1967): pp. 41-43.
240. K.U. Snowden, J. Appl. Phys. 34(1963): pp. 3150-3151.
241. K.U. Snowden, Acta Metall. 12(1964): pp. 295-303.
242. T.W. Weir, G.W. Simmons, R.G. Hart, R.P. Wei, Scripta Metall. 14(1980): pp. 357-364.
243 T H Shih, R.P. Wei, Eng. Frac. Mech. 18(1983). pp. 827-837.
244 P S Pao, M Gao, R P. Wei, Basic Questions in Fatigue, ASTM STP 924-2, pp. 182-195.
245 A Turnbull, J G N. Thomas, J. Electrochem. Soc. 129(1982). pp. 1412-1422.
246. A. Turnbull, Br. Corros. J. 15(1980): pp. 162-171.
247. A. Turnbull, Corros. Sci. 22(1982): pp. 877-893.
248. A. Turnbull, Mater. Sci. Tech. 1(1985): pp. 700-710
249 A Turnbull, D.H. Ferriss, Corros. Sci. 27(1987). p. 1323-1350.
250 A Turnbull, M Saenz de Santa Maria, "Relative Importance of Crack Tip and Bulk Charging in Hydrogen-Assisted Cracking in Aqueous Solutions," this proceedings.
251 A Turnbull, A.T. May, Brit. Corros. J. 22(1987). pp. 176-181.
252. A. Turnbull, D.H. Ferriss, Corrosion Chemistry Within Pits, Crevices, Cracks, pp. 397-412.
253. R.P. Gangloff, Embrittlement by the Localized Crack Environment, pp. 265-290.
254 N J H Holroyd, G.M. Scamans, R. Hermann, Embrittlement by the Localized Crack Environment, pp. 327-347.
255. A.H. Le, R.T. Foley, Corrosion 40(1984): pp. 195-197.
256 B.F Brown, C.T. Fujii, E.P. Dahlberg, J. Electrochem. Soc. 116(1969): pp. 218-219.
257. R.P. Wei, G. Shim, K. Tanaka, Embrittlement by the Localized Crack Environment, pp. 243-263.
258. R.P. Wei, Fatigue 87, pp. 1541-1560.
259. R.P. Wei, "Corrosion Fatigue Crack Growth and Reactions with Bare Steel Surfaces," CORROSION/89, paper no. 569 (Houston, TX: NACE, 1989).
260. A. Alavi, C.D. Miller, R.P. Wei, Corrosion 43(1987): pp. 204-207.
261. G. Shim, R.P. Wei, Mater. Sci. Eng. 87(1986): pp. 121-135.
262. R.P. Wei, A. Alavi, Scripta Metall. 22(1988): pp. 969-974.
263. J.P. Thomas, A. Alavi, R.P. Wei, Scripta Metall. 20(1986): pp. 1015-1018.
264. R.J. Jacko, D.J. Duquette, Metall. Trans. A. 8A(1977): pp. 1821-1827.
265 K.A Esaklul, G.A. Wright, W.W. Gerberich, Fatigue Crack Growth Threshold Concepts, pp. 299-326.
266 R E Ricker, D.J. Duquette, Metall. Trans. A 19A(1988): pp. 1775-1783.
267. P.S. Pao, W. Wei, R.P. Wei, Environment Sensitive Fracture of Engineering Materials, pp. 565-580.
268 J W. Swanson, H.L. Marcus, Metall. Trans. A. 9A(1978). pp. 291-293.
269. R.P. Wei, Intl. J. Frac. Mech. 4(1968): pp. 159-170.
270 S Suresh, Metall. Trans. A. 14A(1983): pp. 2375-2385.
271. R.O. Ritchie, Intl. Metall. Rev. 20(1979): pp. 205- 230.
272 W Elber, Damage Tolerance in Aircraft Structures, ASTM STP 486 (Philadelphia, PA: ASTM, 1979), pp. 230-243.
273 J C Newman, W. Elber, eds., Mechanics of Fatigue Crack Closure, ASTM STP 982 (Philadelphia, PA: ASTM, 1988).
274 S. Suresh, R.O. Ritchie, Metall. Trans. A. 13A(1982): pp. 1627-1631.
275. S. Suresh, R.O. Ritchie, Scripta Metall. 17(1983): pp. 575-580.
276. J.-L. Tzou, C.H. Hsueh, A.G. Evans, R.O. Ritchie, Acta Metall. 33(1985): pp. 117-127.
277. K T. Venkateswara, R.S. Piascik, R.P. Gangloff, R.O. Ritchie, "Fatigue Crack Propagation in Aluminum-Lithium Alloys," Proceedings, 5th International Aluminum-Lithium Conference, ed. E.A. Starke Jr., T. Sanders (West Midlands, UK: EMAS, in press 1989).
278. S. Suresh, A.K. Vasudevan, P.E. Bretz, Metall. Trans. A. 15A(1984): pp. 369-37.
279. W.H. Hartt, C.H. Culberson, S.W. Smith, Corrosion 40(1984): pp. 609-618.
280. W.H. Hartt, S.S. Rajpathak, "Formation of Calcareous Deposits Within Simulated Fatigue Cracks in Seawater," CORROSION/83, paper no. 62 (Houston, TX: NACE, 1983).
281. R. van der Velden, H.L. Ewalds, W.A. Schultze, A. Punter, Corrosion Fatigue: Mechanics, Metallurgy, Electrochemistry and Engineering, ASTM STP 801, pp. 64-80.
282. S.C. Jani, M. Merek, R.F. Hochman, E.I. Meletis, "A Model for Transgranular Stress Corrosion Cracking in Austenitic Stainless Steel," this proceedings.
283. R.O. Ritchie, J. Lankford, Mater. Sci. Eng. 84(1986): pp. 11-16.
284. S.J. Hudak, J. Eng. Mater. Tech. 103(1981): pp. 26-35.
285. A. Zeghloul, J. Petit, Small Fatigue Cracks, pp. 225-235.
286. S.J. Hudak, F.P. Ford, Small Fatigue Cracks, pp. 289-310.
287. K. Tanaka, R.P. Wei, Eng. Frac. Mech. 21(1985): pp. 293-305.
288. A. Turnbull, R.C. Newman, Small Fatigue Cracks, pp. 269-288.
289. N.E. Dowling, Fracture Mechanics, ASTM STP 677, ed. C.W. Smith (Philadelphia, PA: ASTM, 1979), pp. 247-273.
290. S.T. Rolfe, J.M. Barsom, Fracture and Fatigue Control in Structures (Englewood Cliffs, NJ: Prentice-Hall, Inc., 1977), pp. 213-222.
291. S.R. Novak, Corrosion Fatigue Technology, ASTM STP 642, pp. 26-63.
292. A.P. Badve, W.H. Hartt, S.S. Rajpathak, "Effects of Cathodic Polarization Upon Fatigue of Selected High Strength Steels in Sea Water," CORROSION/89, paper no. 570 (Houston, TX: NACE, 1989).
293. S.S. Rajpathak, W.H. Hartt, Proc. Offshore Mech. and Arctic Eng. III(1988): pp. 323-337.

Appendix A: Table of Contents

ABSTRACT: CONCLUSIONS OF THE REVIEW

INTRODUCTION

The scope of the review
The state-of-the art: Storrs and Firminy Conferences
- Fracture mechanics characterization
- Classes of corrosion fatigue crack growth
- Frequency Effects
- Principal variables

Mechanisms for corrosion fatigue crack propagation
- Hydrogen environment embrittlement
- Film rupture and transient anodic dissolution
- Surface films
- Adsorbed atoms
- Anodic dissolution and plasticity

THE FRACTURE MECHANICS APPROACH

Conclusion
Stress-intensity similitude: inert environments
Stress-intensity similitude: reactive environments
- The beginning: 1965-1971
- Phenomenological characterizations: 1970- 1984
- Scientific studies: 1973-1987

Applications to corrosion fatigue life prediction
- Synthesis of life-prediction methods: 1983- 1987

Corrosion fatigue crack propagation databases
- Carbon steels in hydrogen producing environments
- Precipitation-hardened aluminum alloys in aqueous chloride and water vapor environments
- C-Mn and austenitic stainless steels in high-temperature water environments
- Titanium alloys in aqueous electrolytes

EXPERIMENTAL PROCEDURES

Conclusion
Fracture mechanics methods
New procedures
Novel measurements of corrosion fatigue cracking

EFFECTS OF CRITICAL VARIABLES

Conclusion
Introduction
Mechanical loading variables
- Stress-intensity factor range
- Mean stress
- Loading waveform and loading sequence

Cyclic loading frequency
- ΔK_{th} and near-threshold regimes
- Moderate ΔK (plateau) regime
  - Steels in aqueous chloride
  - Aluminum alloys in water vapor
  - Mass transport and reaction rate modeling: hydrogen embrittlement
  - Steels in high-temperature water: film-rupture modeling

Environment chemical activity
- Stainless and C-Mn steels in high-temperature water
- Steels and aluminum alloys in aqueous chloride: effect of electrode potential
  - C-Mn ferritic steels
  - Precipitation-hardened aluminum alloys
- Corrosion fatigue of steels in gaseous hydrogen

Yield strength
Microstructure
- Ferritic steels in aqueous chloride and gaseous hydrogen
- Aluminum alloys in aqueous chloride
- Steels in high-temperature water
- Microscopic corrosion fatigue crack paths
  - Aluminum alloys in water vapor and aqueous chloride
  - Ferritic steels in aqueous chloride

Miscellaneous
- Temperature
- Biologically induced corrosion

QUANTITATIVE MODELS OF CORROSION FATIGUE CRACK PROPAGATION

Conclusion
Introduction
Interaction of mechanical and environmental fatigue
- Superposition
- Competition
- Other

Models of crack-tip mechanics: relationships between ΔK and local plastic strain, strain rate and stress
Models of occluded crack chemistry and transient reaction
- Gaseous environments
- Aqueous electrolytes: active steels in chloride-crack chemistry modeling
- Aqueous electrolytes: active steels in chloride-transient crack reaction kinetics

Corrosion fatigue by hydrogen embrittlement
- Justification for hydrogen embrittlement
- Quantitative hydrogen embrittlement models

Corrosion fatigue by film rupture/transient dissolution
Corrosion fatigue by surface film effects

COMPLICATIONS AND COMPROMISES OF FRACTURE MECHANICS

Conclusion
Crack mechanics
- Crack closure
  - Overview for benign environments
  - Crack closure in aggressive environments
- Environment sensitive microscopic deformation
- Small crack problem
  - Overview for benign environments
  - Aggressive environments

Crack-geometry-dependent occluded environment chemistry
Whole life

NECESSARY RESEARCH

Conclusion
Future research
- Crack growth rate databases
- Experimental methods
- Fracture mechanics similitude
- Micromechanical–chemical mechanism modeling
- Life prediction

Discussion

R.W. Staehle (University of Minnesota, USA): There is a large body of information on the properties of surfaces and their films, e.g., the large body of film growth work as measured ellipsometrically. Can such information be used to define critical experiments?

D.J. Duquette: At present, very few alloy systems have been investigated for corrosion fatigue (CF) crack initiation behavior. A large fraction of the available literature in film growth and stability does not relate to the alloy systems examined for CF resistance. One exception is the work of Magnin cited in this paper, but, even there, only gross electrochemical parameters, e.g., passive current density, repassivation kinetics, charge, etc., were measured. There is no question that attempts at correlating film growth and repair events under cyclic loading conditions will lead to significant advances in understanding CF crack initiation.

H. Kaesche (Friedrich Alexander University of Erlangen-Nurnberg, Federal Republic of Germany): Considering the two ways of describing corrosion cracking, namely, (a) atomistic physical chemistry and (b) continuum mechanical fracture mechanics, the important point is the "interface" where the two meet. This is the region of plastic deformation in front of the crack tip. The conventional linear-elastic fracture mechanical calculation must be modified to model fields within the plastic zone. This means going beyond the K_I concept, which is difficult, but can be done, as shown by Rice. The task is to calculate specifically the value of the crack-opening component of the stress tensor Σ_{yy} within the plastic zone up to the crack tip. It is Σ_{yy}, and not K_I, that affects the physics and chemistry of crack extension. K_I is useful only so long as Σ_{yy} can be expressed as a function of K_I. At the same time, the quantitative combination of physical chemistry and fracture mechanics appears to be the indispensable prerequisite for successful analysis of the matter in question.

D.J. Duquette: As far as corrosion-enhanced plasticity, which has been associated with crack initiation processes, is concerned, there has been little correlation of this observation with events occurring at crack tips. However, environment-enhanced plasticity has been described for hydrogen embrittlement [Birnbaum, in Atomistics of Fracture, ed. Latanision and Pickens (New York, NY: Plenum Press, 1983), p. 733] and for both hydrogen and liquid metal embrittlement (Lynch, ibid., p. 955). It will be interesting to see if such an effect is also observed under actively corroding conditions at crack tips.

R.P. Gangloff: I agree with Kaesche's observations, and hope that my review reflects the successes and remaining challenges in coupling crack-tip stress strain–strain rate field analyses with crack chemistry modeling. In this regard, Rice and colleagues [see, for example, J. Mech. Phys. Solids 30(1980): p. 447] have shown that K provides a reasonable single-parameter characterization of opening stress and plastic strain very near the crack tip, within the plastic zone, and in the elastic field for small-scale yielding. Clearly, local stress and strain control fracture; fortunately, such quantities scale with K. Additional research is required for moving cracks, very near-tip behavior, cyclic deformation, time-/environment-sensitive deformation, and noncontinuum microstructural effects. Gerberich reviews these advances and uncertainties in detail in his contribution to this conference.

F.P. Ford (General Electric R&D Center, USA): Is not the division between "initiation" and "propagation" purely arbitrary, and to a certain extent spawned by our preoccupation with fracture mechanics (which must break down as the crack depth approaches zero)? Is there a stress-related parameter that can be fundamentally related to the environmentally assisted component of crack advance? If so, surely this is the parameter that can be used to span the initiation/propagation semantic division.

D.J. Duquette: Unfortunately, most of the crack initiation research that has been recently reported was performed on single crystals, pure metals, or highly ductile alloys (with the exception of the effects of pits on initiation, as will be shown in Komai's paper in this conference) Accordingly, while links between initiation processes such as Stage I (crystallographic cracking) and the growth of moving cracks, which can be defined by fracture mechanics, may eventually be established, an attempt to do that now would be premature.

R.P. Gangloff: A major advance in fatigue over the past 20 years has been the recognition, separation, and quantitative characterization of cyclic deformation, crack initiation, microcrack growth, and long crack propagation. This separation is neither arbitrary nor based on preoccupation with a specific discipline. As we understand the individual processes, e.g., dislocation or fracture mechanics, we advance to the next stage of coupling the components into the obviously necessary description of whole life.

On the specific issue of fracture mechanics, the necessary modifications of common crack-tip field parameters and the point where alternative approaches are necessary as crack length decreases to zero represent one of the success stories recorded since the Firminy meeting. In my view, work on the so-called small crack problem replaces semantics-based arguments with reasonable mechanistic understanding that aims at merging the stages of cracking. For a growing crack, a hierarchy of deformation regions are identified, including applied load–remaining area, elastic crack-tip field, elastic-plastic zone, near-crack-tip process zone, and microstructural.

Depending on the environmental fracture mechanism, stress, strain, and/or strain rate in the near crack tip, microstructurally influenced process zone will govern crack advance. Fracture mechanics parameters such as K-, J-, or C-type integrals describe stress, strain, and strain rate for the middle three regions. These crack-tip field parameters must be modified to develop the stress and strain picture within single grains and local to grain boundaries or precipitates (The means to do this is not fully established, but some success has been reported; for example, in fatigue crack-tip damage accumulation models.) Just as we use P/A stress as a starting point in models of dislocation processes, it is reasonable to use K, J, or CT fields for descriptions of microstructural-scale deformation.

H.K. Birnbaum (University of Illinois, USA): I would support Ford's concern about using K as a parameter to correlate the behavior of materials in CF. The crack-tip plastic strain (and strain rate) depends on K and on the yield stress and work-hardening rate of the material. Yet Gangloff showed data indicating da/dN vs ΔK curves were the same for a wide range of steel microstructures in a corrosion environment At the same K, these should have large differences in crack tip ϵ and $d\epsilon/dt$, and yet they have the same da/dN!

R.P. Gangloff: It is true that sub-K_{ISCC} CF crack propagation in carbon-manganese and alloy steels appears to be independent of yield strength and microstructure, at least to within a factor of about two, due to measurement uncertainty. I do not believe that this finding indicates weakness in the stress-intensity characterization.

By analogy, Paris regime intrinsic crack growth in many material–inert environment systems appears to be independent of monotonic or cyclic yield strength and microstructure. Most agree that crack extension here is controlled by crack-tip cyclic plastic strain, the amplitude of which depends approximately on the ratio of ΔK_2 to the cyclic yield strength. Micromechanical damage accumulation models couple this strain field with low-cycle fatigue failure parameters and the microstructural distribution of strain to show that da/dN depends on ΔK_4 and (yield strength)-1. That is, yield strength has a second order effect on crack growth. (See, for example, H.J. Roven, Ph.D. diss., Norwegian Institute of Technology, 1988.)

The problem with interpreting the CF data is that we do not have a sufficiently predictive micromechanical and chemical model to describe strength and microstructural effects. When such a model is developed, I believe that fracture mechanics will play a central role in describing crack-tip plastic strain. As an aside, additional work is required to separate and systematically quantify strength and microstructural effects in CF crack propagation. Surprisingly, little work has been reported in this regard.

R.C. Newman (University of Manchester Institute of Science and Technology, UK): Duquette has referred to studies showing effects of both thick and thin films on crack initiation. I

wonder how important thick (hundreds to thousands of Angstrom) films can be, since they are normally precipitated, or at least contained a lot of precipitated material, when formed in aqueous systems. I should think that most precipitated films are poorly bonded to the metal, and therefore should not have much effect on deformation.

D.J. Duquette: There are only a few observations related to persistent slip band (PSB) interaction with "thick" films (S. Ortner, Ph.D. diss., University of Pennsylvania, 1986), and those films were more than likely not strongly interacting with PSB formation. However, when strain-controlled cyclic deformation experiments were performed in environments and at potentials where coherent bulk oxide films were formed, a readily definable and observable effect on PSB formation was observed. Moreover, a measurable back stress on PSBs, created by the bulk oxide, was measurable. Thus, at least in this system (copper in sodium perchlorate), a bulk oxide most definitely had an effect on surface deformation and subsequent crack initiation. Whether or not this can be stated as a general observation is still open to question, but will undoubtedly depend on the metal/environment systems.

R. Jones (Pacific Northwest Laboratory, USA): Are PSBs observed in short or long Mode I cracks? If not, and I strongly suspect that extensive PSB formation does not occur at crack tips, then results obtained with smooth-bar and precracked samples will differ significantly.

D.J. Duquette: It is, of course, very difficult to observe PSB structures at the tips of cracks. However, researchers who have long studied low-cycle fatigue processes have generally argued that plastic strain-controlled experiments on smooth-bar specimens in fact model events in the plastic zones of growing fatigue cracks. From a mechanistic (but not modeling) point of view, dissolution/deformation interactions should be similar. After all, a Stage I or crystallographic crack is only an extension of a PSB.

R.P. Gangloff: The common observation of crystallographic (Stage I) cracks, associated with single slip bands and produced at low stress-intensity ranges, is strong evidence for the operation of PSBs at crack tips. In fact, Starke and coworkers [in Fatigue Crack Growth Threshold Concepts (Warrendale, PA: TMS-AIME (1984), p. 43] model ΔK_{th} based on the K level that is necessary to exceed the threshold plastic strain required to form a PSB, as measured for smooth specimens. The similarity between smooth and cracked specimens is, perhaps, intuitively reasonable if the strong plastic strain gradient predicted from continuum mechanics is replaced by a series of discrete plastic strain levels averaged over a microstructural slip distance ahead of the fatigue crack.

S.C. Jani (Georgia Institute of Technology, USA): CF is a "synergistic" phenomenon, which implies that at least one of the processes (stress or corrosion) must be enhancing the other. I see no work that has addressed the effect of environment on the microdeformation process as a way of controlling and/or determining the crack-driving/initiation force.

The transition from PSB (initiation) to short crack is not necessarily due to a change of operating mechanism. Once again, the problem is one of getting a handle on the mechanics of the two processes. An energy-based parameter for correlating initiation time/crack growth rates is inherently more correct as opposed to a stress-based parameter (K or ΔK). Furthermore, once time-dependent processes (corrosion) modify the deformation behavior, K becomes a meaningless parameter, because although it still characterizes far-field Σ_{ij} and ϵ_{ij}, it has no relation to what is occurring in the process zone; i.e., similitude is nonexistent. Therefore, the linear-elastic fracture mechanics or elastic-plastic fracture mechanics concepts should be modified to account for the changed constitutive behavior in the process zone. The same comment applies to propagation behavior.

R.P. Gangloff: Jani makes an important point that is worthy of investigation. I agree that time-dependent environment-based changes in material deformation behavior will affect crack-tip stress, strain, and strain-rate fields, which ultimately control fracture. If this behavior occurs, then the crack field must be described by a parameter that incorporates the time-dependent (chemical) constitutive relationship. With the proper parameter, similitude is likely, as illustrated by C^* or CT descriptions of time-dependent (thermal) crack-tip fields. In the final analysis, however, the problem remains to demonstrate that environment alters material flow over the size scale of the process zone and to define the time-dependent flow rule. Without such evidence, the discussion is hypothetical. CF is a synergistic phenomenon that results from many interactions. It is not necessary, as envisioned by your first point, that stress enhance corrosion or vice versa.

R.P. Wei (Lehigh University): In discussing initiation vs propagation and short crack vs long crack, one must separate the contributions from mechanical and chemical factors. In assessing causes, it is necessary to recognize that the chemical environment may be quite different. For initiation and short cracks, the local environment is expected to be nearly identical to the external environment. For long cracks, on the other hand, the conditions at the crack tip are expected to be very different from that of the bulk.

With respect to mechanical forces, it is necessary to recognize the influence of loading modes (viz., predominantly Mode I for crack propagation vs mixed Modes I, II, and III for crack initiation along PSBs).

R.P. Gangloff: I generally agree with these observations. In our work on "chemical crack size" effects [Metall. Trans. A 16(1985): p. 953], we show that the geometry-sensitive contributions of wake closure and enhanced crack-tip plasticity are not important through measurements conducted with vacuum and air environments. Geometry-dependent crack-chemistry effects are therefore isolated. Second, it is an oversimplification to assume that short cracks are in total communication with the bulk environment, while long cracks are not. Turnbull [Corros. Sci. 26(1987): p. 601] has demonstrated that the effects of diffusion, convection, and the ratio of crack surface area to solution volume result in crack chemistries that differ from the bulk at intermediate crack depths (perhaps of the order of mm), with extensive diffusional exchange at shorter depths and enhanced convective mixing for deeper cracks.

R.W. Staehle: Is it possible to use more defined environments; for example, for aluminum use sodium hydroxide, which reduces film stability?

R.P. Gangloff: "More defined" is an elusive term. I believe that the most defined environments are those that have been extensively modeled and probed to characterize occluded crack electrochemistry and transient surface reactions. By this criterion, aqueous sodium chloride at constant bulk pH and applied potential is a reasonably well-defined system for ferritic alloys. I would not discourage the use of carefully selected environments (e.g., buffered); however, one must recognize the possibility for changes in crack-tip chemistry (e.g., depleted buffering capacity).

S.M. Bruemmer (Pacific Northwest Laboratories, USA): Duquette has indicated that CF crack initiation can change from transgranular slip band dissolution to intergranular. It is not clear why a deformed grain boundary would be more electrochemically active than a PSB. Why does this become the case and is this specific to copper or a general observation?

D.J. Duquette: For pure metals, the extent of deformation associated with grain boundaries is much greater than the deformation associated with PSBs (at least at large strain ranges). For example, in the absence of environment, both polycrystalline copper and nickel have been shown to exhibit intergranular fatigue crack initiation and propagation at either high cyclic loads or strains [Laird and Duquette in Corrosion Fatigue, ed. Devereux, et al. (Houston, TX: NACE, 1972), p. 88]. In fact, in our experiments, the observation of intergranular initiation and propagation under actively dissolving conditions at a stress range where transgranular cracking is observed in air supports a model in which preferential attack occurs at regions of highest deformation, and conversely, preferential deformation occurs at corroded sites. Thus, under conditions of active dissolution, the metal behaves as though it were actually at a much higher stress range.

M.M. Hall (Westinghouse Electric Corporation, USA): Gangloff's presentation and the resultant discussion has focused attention on the limitations of the stress-intensity factor for correlating environment-induced crack growth with microstructure and crack-tip chemistry For a normally ductile material in which the fracture process occurs in the crack-tip process zone, is it not possible that the cracking response can become independent of the stress-intensity factor whenever this process zone, the size of which is related to the stress-intensity factor, is significantly larger than the distance between the microstructural features that govern the micromechanical fracture event within the process zone? In a similar way, local chemistry effects may possibly be independent of stress-intensity factor when the embrittling effects on microstructural boundaries and influences on plasticity extend to a depth below the surface that lies entirely within the process zone. Can these concepts account for the example Gangloff provided?

R.P. Gangloff: I reject the implication that stress intensity is ill suited to correlate environmental crack growth. The stress-intensity-controlled process zone scenario that you describe is reasonable for threshold conditions but not for crack growth kinetics. I do not believe that this picture represents a limitation on ΔK correlations of microstructure and crack-chemistry effects, nor do I understand how it can explain the various data examples I presented. What you suggest is, of course, the basis for micromechanical modeling of cleavage, ductile fracture, and hydrogen embrittlement. In these monotonic fracture processes, the K level at which the process-zone stress or strain just exceeds a critical value over a characteristic microstructural distance is taken as an equilibrium K_{I_c} or K_{I_h} threshold Increased K will involve more "weak link" microstructural features in the fracture process zone, and growth rates will accelerate Kinetic models are not, however, available. For environmental cracking, rates will be defined by crack mechanical fields and by mass transport and reaction kinetics. A ΔK-independent cracking response may or may not develop, depending on the detailed driving forces and rate-limiting processes. The development of kinetic models is one of the important challenges facing the environmental fracture research community.

R.P.M. Procter (University of Manchester Institute of Science and Technology, UK): Gangloff has shown the excellent agreement that can be achieved between fracture mechanics life predictions and S-N data on full-size tubular joints in air. He then said that similar agreement could not be achieved in seawater and that he would return to this point later in the presentation. In fact, I do not think you did return to this point in your talk, and if it not dealt with in the written paper, would you please expand on your statement. Are you suggesting that the fracture mechanics life-prediction combined with appropriate CF crack growth rate data does not agree with the results of full-size tubular joint data in seawater, with or without cathodic protection? If not, why not? I believe that if you have good, reliable, and *appropriate* (i.e., appropriate frequency load spectrum, calcareous deposit) CF data, fracture mechanics life prediction will work well both in air and seawater.

R.P. Gangloff: Time prevented me from dealing with this important issue. I agree with your position. As detailed in a recent paper [see Fatigue 87, ed C.J. Beevers (Worley, UK: EMAS, 1987), p. 1723), I believe that the fracture mechanics approach is capable of predicting tubular joint life for fatigue in a marine environment. Results to date have, however, been limited in contrast to the air case for two reasons. First, low-frequency full-scale welded joint tests in seawater are few in number and only recently the focus of experimental work. Second, as I point out in the written paper, many interactive variables (viz., frequency, ΔK, closure, load spectrum, applied electrode potential, crack size, and organic content) greatly complicate identification of the appropriate crack growth law, particularly for rates below about 10^{-5} mm/cycle. The role of external surface hydrogen production is also unclear, and we are unsure as to how to deal with the conflicting effects of cathodic polarization on weld-defect-sensitive initiation and crack propagation. I suspect that major advances will be recorded over the next five years that will lead to reasonable fracture-mechanics-based life-prediction methods.

Elevated-Temperature Creep-Fatigue Cracking in Relation to Oxidation Effects

*A. Pineau**

Abstract

This paper is concerned with the effect of high-temperature fatigue on the cracking behavior of structural materials, especially austenitic stainless steels (SSs) and Ni- or Co-base superalloys. Both crack initiation and crack propagation are considered. In the introduction, it is shown that Ni-base superalloys are very sensitive to the effect of hold times on crack growth rates and that this behavior is directly related to oxidation damage. Moreover, large increases in crack propagation rates are observed when the failure mode changes from transgranular to intergranular. The mechanisms responsible for intergranular cracking are analyzed in the second section. Three types of mechanisms are successively discussed: (1) slip-induced intergranular cracking, (2) intergranular creep cavitation, and (3) oxidation-induced grain-boundary cracking. The results obtained on austenitic SSs are used to show the effects of bulk intergranular creep cavitation damage. The third mechanism is discussed more thoroughly. The results published in the literature on three specific materials, Cr-Mo-V steels, a Ni-base superalloy [Inconel† 718 (UNS N07718)] and a Co-base superalloy (MAR M 509) are reviewed. It is concluded that static oxidation data are not applicable to stressed material. Plastic strains can modify the type of oxide scale formed on the free surface of specimens. Moreover, the oxidation kinetics are largely dependent on the applied plastic strains. In the third section, an attempt is made to model creep-fatigue interactions with relation to environmental effects. Crack initiation is considered first. It is shown that a damage equation, in which the cyclic plasticity and the time-dependent oxidation components are simply added, provides satisfactory results. However, the limitations of this simple approach are underlined. Crack growth behavior of one specific Ni-base superalloy (Inconel 718) is considered. An upper bound for the crack growth rate under fatigue loading is suggested as being the sum of the time-dependent static component and the viscoplastic zone formed ahead of the crack tip. The difficulties encountered in the determination of the static component, which are probably related to environmental effects, are shown.

Introduction

Macroscopic cracks can initiate and propagate in metallic parts at elevated temperature under the combined influence of creep damage, fatigue damage, and/or environment-induced damage. In particular, fatigue is known to be a limiting factor affecting the useful life of aircraft turbine disks. In these components, where temperature can approach 650°C, time-dependent effects arising from creep-fatigue-environment interactions may aggravate the cracking problem. Similar examples can be found in the power-generating industry where the formulation of rational life-prediction procedures is still more essential in the sense that modern plants may be required to operate in aggressive or inert environments up to 30 years or more. In the creep range, the interaction of oxidizing, carburizing, or irradiation environment with creep and fatigue damage are potential areas for concern.

The major change between low-temperature and elevated-temperature fatigue is the occurrence of intergranular fracture. This change in fracture mode from transgranular at low temperature to intergranular at high temperature is a general rule observed in polycrystalline materials. Both crack initiation, which is usually investigated in high-strain, low-cycle fatigue and crack propagation (which is investigated using specimens tested under small scale yielding) tend to become intergranular in the creep range. This situation is illustrated in Figure 1, which refers to a disk material, Inconel 718 (UNS N07718), tested at a given ΔK (40 MPa$\sqrt{m}$) and at two temperatures, 550°C and 650°C by several investigators [1-6] A transition between transgranular and intergranular fracture is observed when the test frequency is decreased at a given temperature Figure 1 indicates that the critical frequency is increased by a factor of about 3 when the test temperature is increased from 550°C to 650°C. It is also worth noting that at 650°C and low frequency, the slope of the da/dN frequency curve is close to - 1 This suggests that in this regime the propagation rate is essentially time dependent This example is representative of the situation observed in other Ni-base superalloys, as shown in Figure 2, which compares the fatigue crack growth rates measured at 650°C under either continuous cycling at relatively high frequency (0.33 Hz) or under creep-fatigue conditions corresponding to the application of a 15-min dwell period at maximum load.[7] These materials were developed to achieve widely different mechanical properties (yield strength between 880 MPa and 1280 MPa) and metallurgical microstructures, such as grain size (between 5 μm and ~ 100 μm) and volume fraction of γ' precipitates (between 20 and 60%). The difference in crack propagation rates is less than one order of magnitude when the failure mode is predominantly transgranular [Figure 2(a)]. On the other hand, much larger differences are noticed (≃ 3 orders of magnitude) when the failure mode is predominantly intergranular [Figure 2(b)]. In Ni-base superalloys, the acceleration in crack propagation rate at low frequency is essentially related to the detrimental effect of oxidizing environment. In particular, this conclusion applies to Inconel 718 alloy. In this

*Centre des Materiaux, Ecole des Mines, BP 87, 91003 Evry Cedex, France, UA CNRS No. 866.

†Trade name.

material, the effect of microstructure and environment on the fatigue crack growth-rate behavior was investigated at 650°C under a fatigue cycle including a 5-min hold time at maximum load.[3] Three microstructures were investigated: a relatively fine grain size material (~ 40 μm), a coarse-grained microstructure (200 μm), and a necklace microstructure consisting of fine recrystallized grains (5 to 10 μm) surrounding hot-worked coarse grains (100 to 300 μm). Tests were conducted both under air environment and vacuum. The results reported in Figure 3 show that the strong microstructural effects observed under air environment no longer exist when these microstructures are tested under vacuum.

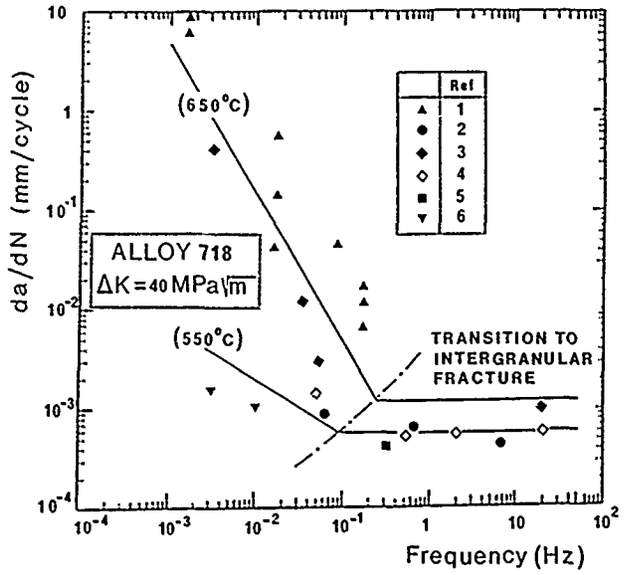


FIGURE 1—Inconel 718 alloy (UNS N07718): the effect of test temperature and frequency on the fatigue crack growth rate. Note that at 650°C and low frequency the slope of the da/dN-frequency curve is close to −1, indicating that the crack propagation rate is essentially time dependent.

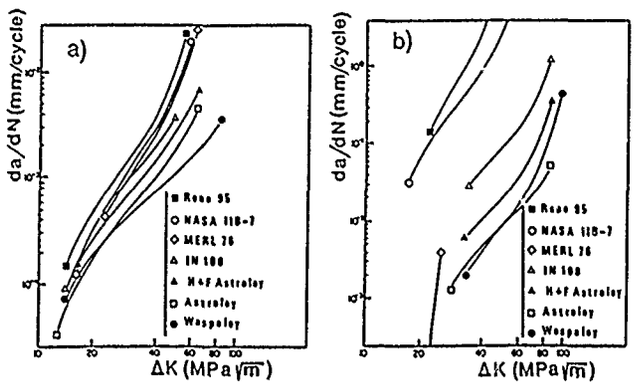


FIGURE 2—Fatigue crack growth rate as a function of ΔK range in various Ni-based superalloys tested in air, at 650°C: (a) 0.33 Hz triangular waveform, and (b) creep-fatigue tests with a 900-s dwell at maximum load.[7]

From this introduction, it should not be concluded that the transition in fracture mode is only associated with environmental effects. In other materials, other and/or additional forms of intergranular damage exist. As a rule, one can distinguish three types of microstructural damages that could explain the transition in fracture mode. They include (1) slip-induced intergranular cracking, which can take place even at low temperature, (2) grain-boundary creep cavitation, and (3) oxidation damage. These three types of damage are discussed successively, although the emphasis is upon environmental effects. Then an attempt is made to show how these studies devoted to the micromechanisms can be used as guidelines for the development of life-prediction methods. These methods have been reviewed recently by the present author.[8] This paper concentrates only on the methods in which environmental effects are taken into account.

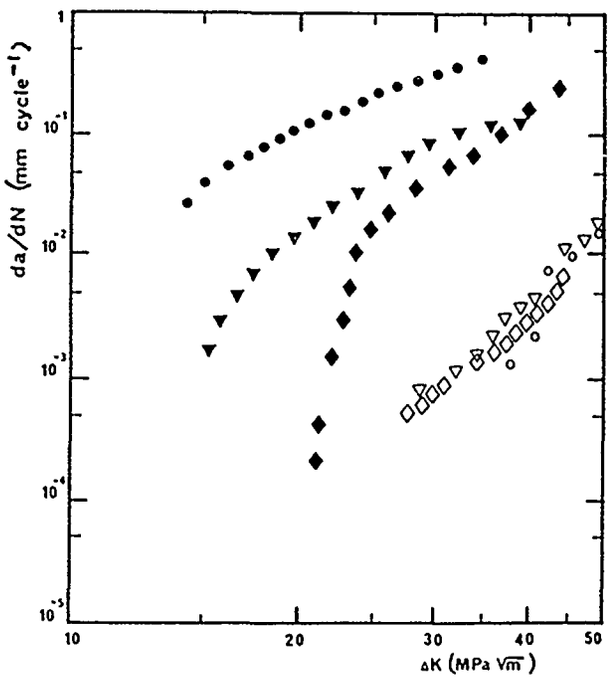


FIGURE 3—Inconel 718 alloy (UNS N07718) tested in air or under vacuum at 650°C: effect of microstructure on fatigue crack growth behavior under 10-300-10 cycling. Open symbols = vacuum; filled symbols = air:

◇ ◆ = necklace structure;
▽ ▼ = coarse-grained material;
○ ● = fine-grained structure.

Micromechanisms Responsible for Intergranular Cracking

Slip-induced intergranular cracking

At high strain amplitude, fatigue cracks in pure metals, such as Ni and Cu, nucleate preferentially along the grain boundaries at free surfaces. This mode of cracking can occur also in structural materials, such as Ni-base superalloys, at relatively low temperature ($T/T_f < 0.3$) and high temperature, as well. There is little fundamental work on this topic, especially at elevated temperature. It is usually recognized that crack nucleation at grain boundaries is promoted either by the notch effect at the grain boundaries, associated with rumpling of specimen surfaces, or by impinging slip bands at the surface.

In a given material, such as pure Ni, it has recently been shown that the factors influencing this mode of cracking are as follows.[9-11]

(1) The type of boundaries. High-symmetry Σ3 boundaries exhibit a better resistance. This has been rationalized in terms of the ease with which crystal dislocations can be transferred across the boundaries.

(2) The orientation of the grain boundaries. In push-pull tests, slip-induced grain-boundary cracking occurs more easily if the grain boundary plane makes a large angle with the stress axis and if the incompatibility in slip between adjacent grains is such that the out-of-surface component of the slip vectors is large.

(3) In structural materials, the slip character, which is related to both the chemistry of the material and the microstructure. Low stacking fault energy (SFE) promotes planar slip and the occurrence of mechanical twinning.[12,13] Austenitic SSs and some Ni base superalloys are materials exhibiting planar slip at room temperature. This mode of deformation may be responsi-

ble for intergranular cracking because of the high stress concentrations produced between a grain boundary and an impinging slip band.

The increase in temperature tends to promote a more dispersed or wavy slip. This tendency can be rationalized in terms of the increase in SFE with temperature, which is a general rule observed in most materials,[13] and in terms of the effect of thermal activation, which allows dislocations to cross slip and climb out of their original slip planes. This situation should reduce the occurrence of slip-induced intergranular cracking when the temperature is increased. Unfortunately, there are many exceptions to this rule. Many materials are used in a temperature range where dynamic strain aging can take place. This in turn favors planar slip character, which could be responsible for the reduction in fatigue life observed, e.g., in ferritic steels, over a temperature range close to 400°C.

In precipitation-hardened materials, slip character is directly related to the by-passing mode of particles by dislocations. Small precipitates are easily sheared by dislocations. They give rise to a concentration of the deformation into intense slip bands, while large particles that are by-passed by the Orowan process tend to disperse the deformation more homogeneously within the grains.[14] Recently, a model has been proposed in which large shearable particles led to coarser slip, which in turn produces intergranular fracture in age-hardenable Al-Li alloys.[15] In Ni-base superalloys, the fact that slip character plays an important role in the transition to intergranular fatigue fracture has been emphasized by many authors (for example, Reference 4). This was one of the viewpoints adopted in a detailed comparison of two Ni-base superalloys widely used for the fabrication of turbine disks, Waspaloy† (UNS N07001) and Inconel 718.[16-19]

The exact mechanisms by which slip-induced intergranular cracking is promoted by slip inhomogeneity are not yet fully established. The experiments performed on Nimonic† 80[20] and on Astroloy,†[,21] in which it was shown that a prior deformation at room temperature followed by a short anneal without any applied macroscopic stress was sufficient to induce the formation of grain-boundary cavities, clearly indicate that the large microscopic stresses associated with the intersection of a slip band with a grain boundary or a grain-boundary particle can be deleterious.

Intergranular creep cavitation

If oxidation appears to be the most damaging process in high-strength materials (such as Ni-base alloys) tested at intermediate temperatures (~ 650°C), in lower strength but highly ductile materials (such as austenitic SSs), grain-boundary cracking occurs by the nucleation and the subsequent growth of creep cavities. A large research effort has been made over the last ten years to improve the theoretical models (e.g., Reference 22). The applicability of these models to structural materials is somewhat questionable. In particular, they do not take into account the aging phenomena taking place in these materials, which can give rise to very strong effects. This is illustrated in Figures 4 and 5, which refer to the results obtained on two heats of type 316L (UNS S31603) austenitic SS.[23-25] These materials were tested at 600°C under low-cycle fatigue. A tensile hold time (t_h) was superimposed to the fatigue cycle at maximum strain. It is observed that the creep damage occurring during stress relaxation leads to a reduction in fatigue life (N_f).

This effect, noticed for relatively short hold times (t_h < 500 min) and thus relatively short test durations (t < 1000 h), is the basis of a number of creep-fatigue interaction models (for a review, see Reference 8) One of the difficulties with these models is that they are usually unable to predict the saturation effect observed for long times in both materials when tests as long as one year are performed at intermediate strain amplitude ($\Delta\epsilon_t \simeq 1\%$). These results, which have also been observed by other investigators (e.g., Reference 26), are of noticeable practical interest.

Qualitatively, they can be related to the complex variations in creep ductility associated with carbide precipitation during the tests

†Trade name.

The improvement in creep-damage resistance occurring for long hold times can be illustrated by the results of quantitative measurements of intergranular damage (D). The damage (D) was defined as the ratio between the cumulated length of cracked grain boundaries per unit area of a polished section (L_c) to the total length of grain boundaries on the same area (L_t).

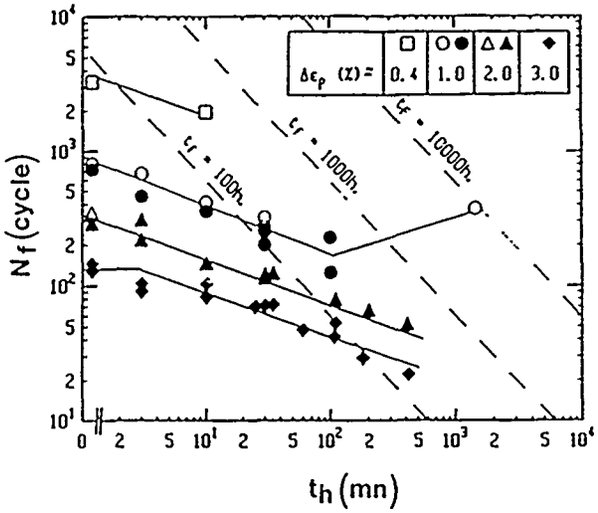


FIGURE 4—Austenitic SS tested at 600°C VIRGO heat: influence of dwell at maximum tensile strain on fatigue life. Note the saturation in hold time effect for very long test (~ 1 year).

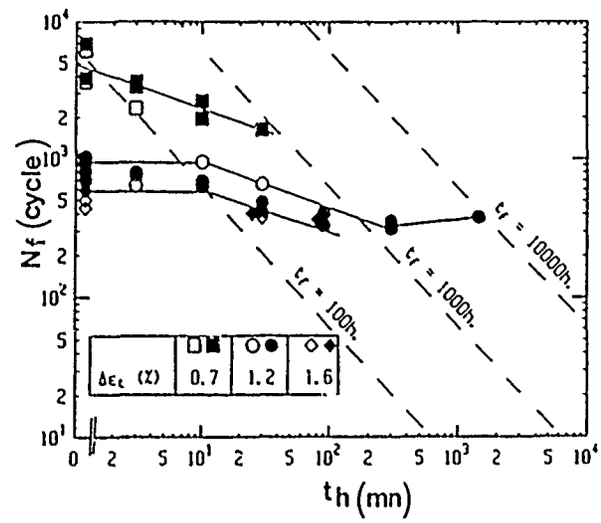


FIGURE 5—Austenitic SS tested at 600°C ICL heat: influence of a dwell at maximum tensile strain on fatigue life. Note also the saturation effect observed for long hold time (24 h).

In Figure 6, we have reported the variation of intergranular damage per cycle (D_c) (D_c = D/N) as a function of hold time. The results obtained by other authors are included.[29,30] As expected, for relatively short times, creep damage (D_c) is an increasing function of dwell period (t_h). However, for very long tests, the damage per cycle shows a saturation effect similar to the situation observed for the fatigue life in this material (Figure 4). These results were used to model the creep-fatigue interactions occurring in this type of material.[23-25] Briefly stated, this model is based on the accelerating effect of fatigue crack growth rate induced by creep damage. It was shown that even in these materials, which are strongly resistant to oxidation effects, oxygen attack largely reduced the crack initiation stage such that, within a first approximation, it can be assumed that for the tests

with a hold time the number of cycles to crack propagation (N_P^{CF}) is roughly equal to (N_F^{CF}). The reduction of the propagation stage can be measured by a parameter (i_c), which was defined as:

$$i_c = \frac{N_P^F - N_P^{CF}}{N_P^F N_P^{CF}} \quad (1)$$

where N_P^F and N_P^{CF} are the numbers of cycles to propagation in a pure fatigue test and a creep-fatigue test, respectively. N_P^F can be determined from conventional low-cycle fatigue tests provided the fatigue life to crack initiation (N_i^F) is known. Figure 7 shows that there exists a fairly good correlation between D_c and i_c, except for very short hold times (~ 3 mn) for which the assumptions made in this model are not valid. It is also worth noting that this correlation applies also to the tests corresponding to the longest hold times. This result is encouraging, since it suggests that the assessment of the remaining life of components subjected to creep-fatigue conditions could be made by using the results of metallographical observations similar to those used for a number of materials submitted to creep conditions.

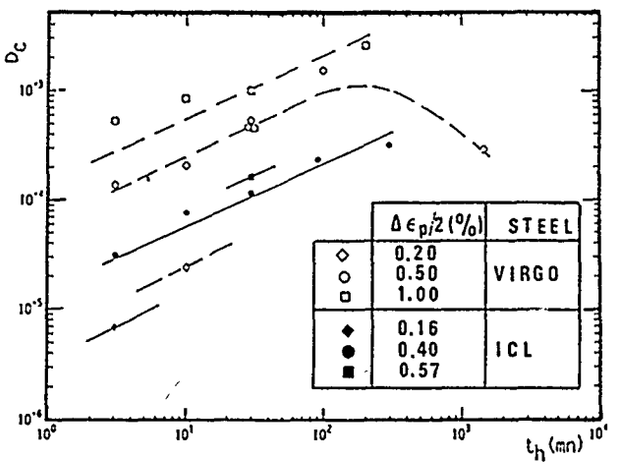


FIGURE 6— Austenitic SSs, heats VIRGO and ICL: variation of intergranular damage per cycle (D_c) as a function of tensile hold time (t_h). The saturation in the effect of dwell period on fatigue life correlates with the variation of intergranular damage (D_c) observed in VIRGO steel.

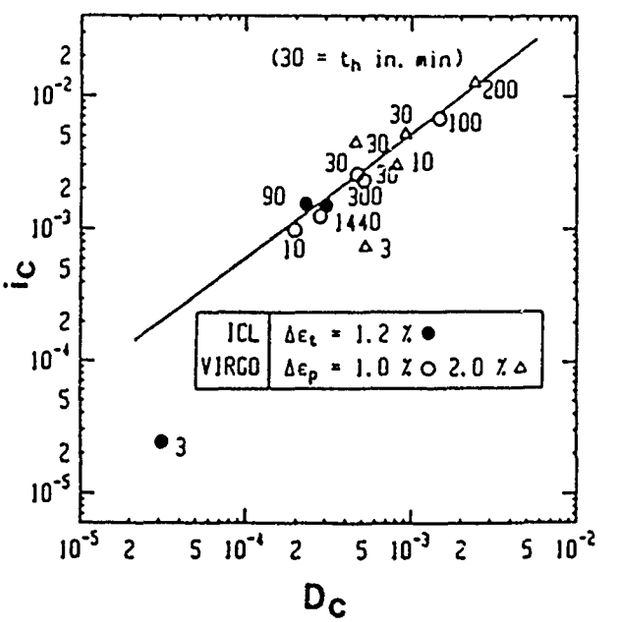


FIGURE 7—Correlation between the relative reduction in fatigue life, measured by i_c parameter and measured intergranular damage per cycle (D_c).

Oxidation

The extensive studies performed in particular by Coffin[31] have clearly shown that, in many materials, the reduction in fatigue life observed with an increase in temperature was closely related to a detrimental oxidation effect. In Ni-base superalloys, it is now well established that the environmental effect is mainly responsible for the degradation in endurance when these materials are tested in what is conventionally called "creep-fatigue" conditions. For a review, see Reference 32.

To simplify the discussion, we do not include the form of oxygen attack by simple absorption of oxygen at the crack tip. Two types of crack-tip situations are considered in Figure 8. In Type A, an oxide has formed at the crack tip. Cracking occurs in the oxide or at the matrix-oxide interface. In Type B, oxygen has diffused into the metal ahead of the main crack and promoted the formation of subsurface cracks that link to the main crack.

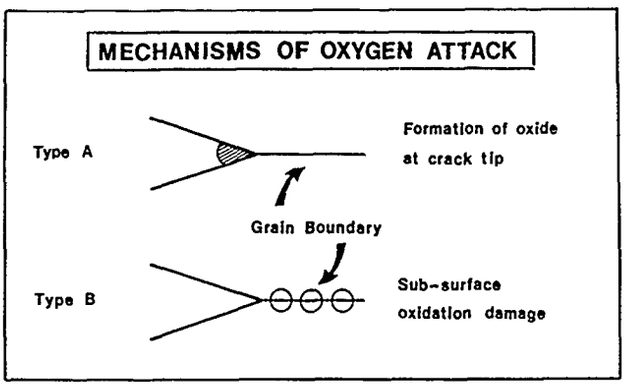


FIGURE 8—Mechanisms of oxygen attack.

Type A oxidation mechanism.

Oxide scale formation and preferential oxidation—One form of damage often reported in high-temperature fatigue is the formation of oxide wedges in grain boundaries. Grain boundaries are preferential sites for oxidation because of either more rapid intergranular diffusion or because the carbide particles commonly present in the boundaries are themselves preferred sites for oxidation. The fact that these grain-boundary wedges form preferential sites for crack initiation has been clearly shown by a number of investigators, in particular by Antolovich, et al.[33,34] These authors showed that the effect of prior oxidation with or without any applied stress was to reduce the fatigue life, the reduction being largest for stress-exposed specimens (Figure 9). It was also shown that in this material a crack initiation criterion based on the maximum stress (σ_{max}) and oxide depth (l_i) of the type:

$$\sigma_{max} l_i = \text{constant, with } p \simeq 4 \quad (2)$$

represented the data well.[33]

In this form of damage, the first factors are the alloy chemistry and the partial oxygen pressure. These factors control the preferential formation of one given species of oxide. In Ni-Cr alloys, it is accepted that Cr_2O_3-type oxide is more protective than a spinel-type FeNi-rich oxide.

To illustrate the variety of responses that can be observed in a given material, we refer to a recent study performed on a nickel-base superalloy containing about 18% Fe, Inconel 718.[35] This author used Auger spectrometry analysis to determine the type of oxide that was formed as a function of partial oxygen pressure and of the specimen preparation. All the oxidation tests were performed at 650°C. Electropolished specimens were observed first. The results given in Figure 10 show that, at low-oxygen partial pressure ($\lesssim 10^{-4}$ Torr), only Cr_2O_3 type was identified.

At higher oxygen partial pressure ($\gtrsim 10^{-2}$ Torr), both spinel type (FeNiO) and Cr_2O_3 oxides were observed. This suggests that the oxidation under air environment occurs in two stages, as indicated schematically in Figure 10(a), with the formation of FeNi-

rich oxide followed by that of the more protective film formed by Cr_2O_3 oxide. The transition time (t_p) was not measured. At atmospheric pressure, it is lower than a few minutes. Other results presented in the following suggest that the relative sensitivity of this nickel-base alloy to environmental effect might be related to the formation of the FeNi-rich oxide. Other factors, such as the Pilling-Bedworth ratio[36] associated with the volumetric expansion coefficient due to oxide formation and the difference in thermal expansion coefficients of base metal and surface oxide, are also important.

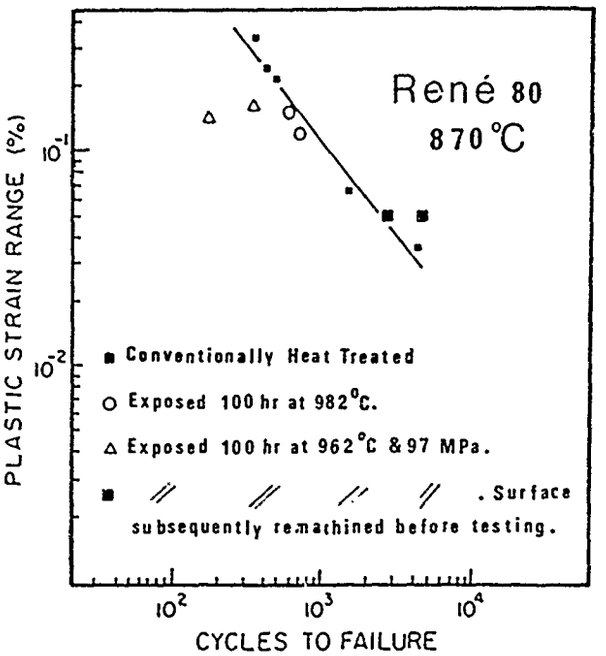


FIGURE 9—Rene 80 tested at 870°C: low-cycle fatigue life as a function of plastic strain range. Note the reduction in fatigue life on pre-exposed material and the effect of remachining before testing.[33]

Cyclic oxidation—There are still very few detailed studies devoted to the interactions between cyclic deformation and oxidation. Two main comments should be made: The first relates to the change in the type of oxide formed; the second relates to the dramatic change in kinetics.

The type of oxide film formed at the specimen surface can be strongly dependent on the specimen preparation, especially on the existence of cold-worked surface. The effect can occur when the material-atmosphere combination is such that several types of oxide scale can be formed. This is shown in Figure 11, which refers to Inconel 718.[35] In this material, it is observed that when the specimens are first submitted to a shot-peening treatment before being oxidized, only Cr-rich oxide is formed, whatever the partial oxygen pressure, which is different from the situation observed on electropolished specimens. In a study devoted to the interactions of low-cycle fatigue and oxidation, it was shown that the type of oxide scale formed on the surface of a 9.5Cr steel tested at 650°C was also strongly dependent on cyclic deformation.[37] In this material, the protective oxide scales on undeformed specimens are Cr rich. They cover a small surface area (~ 2%). On the other hand, low cycle fatigue deformation leads to a strong increase of the surface area covered by the nonprotective Fe-rich nodules that can reach 50%. The reason for this is the Cr depletion in the subsurface zone resulting from the formation of the Cr-rich oxide and oxide spalling due to cyclic deformation.

Quantitative studies devoted to the cyclic-deformation modification in oxidation kinetics are very scarce, except those by Skelton and Bucklow[38] on Cr-Mo-V steels and those by Reuchet and Remy[39] on a Co-base superalloy, MAR M 509. Both studies have clearly shown that stress and/or strain-free oxidation data are inapplicable to highly strained situations.

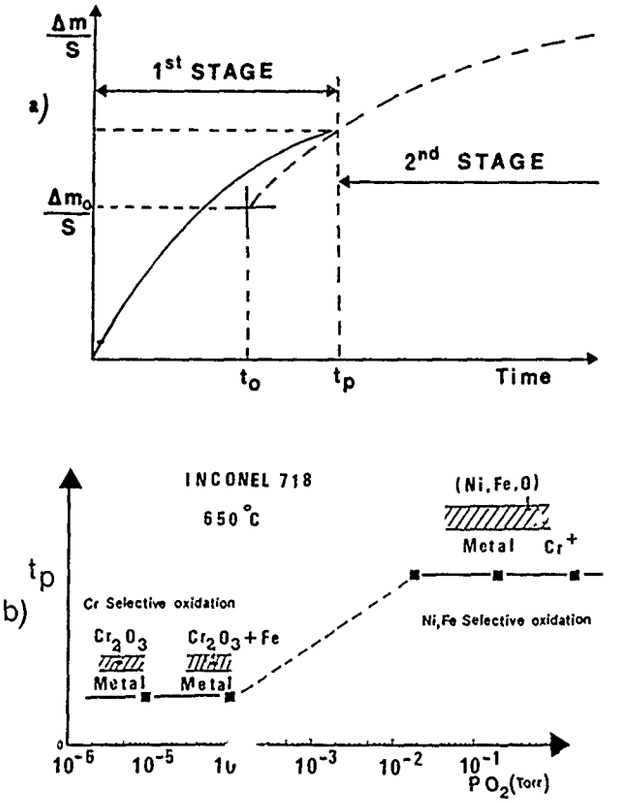


FIGURE 10—Results of oxide identification by Auger spectrometry on electropolished specimens of Inconel 718 alloy (UNS N07718): (a) sketch showing the variation in weight (Δm/S) as a function of time. Two stages are distinguished corresponding to FeNi-rich oxide and Cr-rich oxide formation, respectively; and (b) transition time (t_p) between both forms of oxides as a function of oxygen partial pressure.[35]

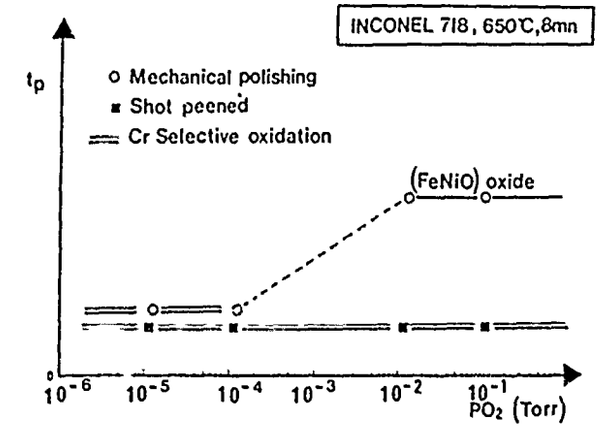


FIGURE 11—Inconel 718 alloy (UNS N07718): pre-exposure at 650°C. Influence of residual stresses on the transition in oxidation mechanism. Cr-rich oxide is preferentially formed on shot-peened specimens.[35]

Figure 12 shows the results of measurements of oxide growth per cycle obtained at 550°C by Skelton and Bucklow on a Cr-Mo-V steel.[38] It is observed, as noticed in other studies, that below some minimum strain (≈ 0.1%), the accelerating effects of cyclic deformation seem to disappear. This minimum strain is related to the fracture tensile strain of the oxide scale and to the residual stresses between the scale and the base material. In MAR M 509, Reuchet and Remy investigated both the matrix oxidation and the preferential oxidation of primary MC-type carbides.[39] In this cast material, the microstructure consists of a face-centered cubic (FCC) matrix plus primary MC carbides in a Chinese script morphology. At high temperatures,

cracks initiate at oxidized MC carbides and crack growth occurs through the matrix and along the carbides. The results of matrix oxide scale thickness measurements are shown in Figure 13, where it is observed that cyclic deformation increases the oxidation kinetics, the effect being an increasing function of applied plastic strain. These results were interpreted in terms of a classical equation for the kinetics of oxidation:

$$e_M = \alpha_M t^{1/2} \quad (3)$$

where e_M is the thickness of the oxide scale and α_M was found to be related to the plastic strain amplitude $\Delta\epsilon_p/2$ by a linear function:

$$\alpha_M = \alpha_M^\circ(1 + K_M \Delta\epsilon_p) \quad (4)$$

where K_M is a constant at a given temperature.

This equation applies to plastic strains larger than $3 \cdot 10^{-4}$. The preferential oxidation of MC carbides was measured by the depth of subsurface attack (Figure 14). The results can be expressed as:

$$l_{ox} = \alpha_c t^{1/4} \quad (5)$$

where the oxidation constant (α_c) is an increasing function of applied stress or applied strain. Expressed in terms of plastic strain, it was written as:[40]

$$\alpha_c = \alpha_c^\circ g(\Delta\epsilon_p) \quad (6)$$
$$\text{with } g = \Delta\epsilon_p/\Delta\epsilon_{po}, \text{ for } \Delta\epsilon_p > \Delta\epsilon_{po}$$
$$g = 1, \text{ for } \Delta\epsilon_p < \Delta\epsilon_{po}$$

These results can be used to model fatigue-environment interactions, as shown later. Skelton and Bucklow[38] were the first to suggest that at high temperature, the crack growth rate in an aggressive environment could be the sum of the fatigue component in an inert environment [pure fatigue, $(da/dN)_{Fat}$], plus the oxidation rate [$(da/dN)_{ox}$] at the crack tip, that is:

$$(da/dN) = (da/dN)_{Fat} + (da/dN)_{ox} \quad (7)$$

This approach is discussed in more detail in the following.

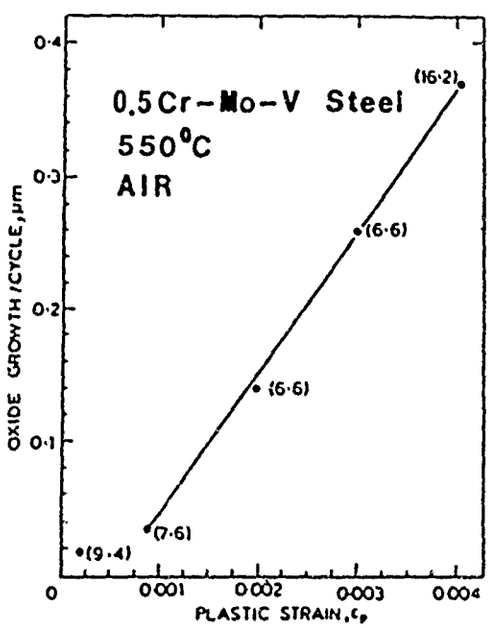


FIGURE 12—Cr-Mo-V steel tested in air, at 550°C. Influence of high-strain fatigue on oxidation rate.[38]

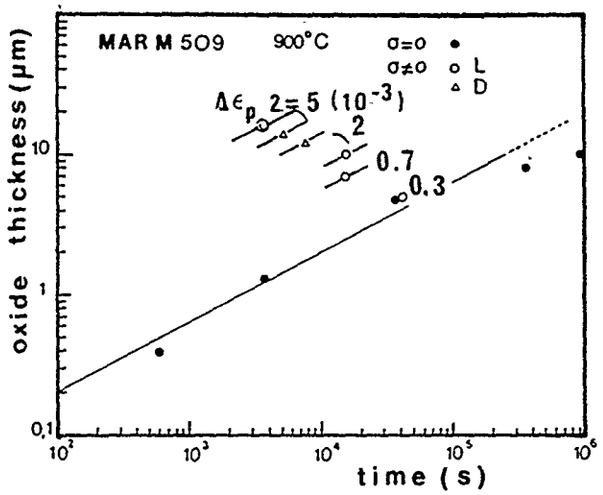


FIGURE 13—Co-base superalloy tested at 900°C. Variation of the matrix oxide scale thickness as a function of exposure time for stress-free specimens and for low-cycle fatigue specimens tested at failure.[39]

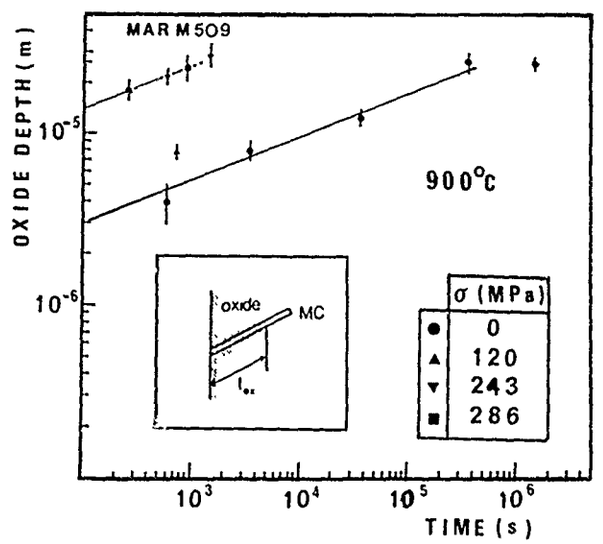


FIGURE 14—Co-base superalloy tested at 900°C. Variation of the average oxidized carbide depth as a function of exposure time for stress-free and low-cycle fatigue specimens. [39]

Type B oxidation. Subsurface environmental damage can also take several forms. It is extremely difficult to quantify these forms, essentially because of the absence of diffusion data.

Oxygen segregation along grain boundaries—No completely unambiguous experimental evidence exists of changes in cracking mode due solely to oxygen segregation along the grain boundaries. One is tempted to assume that oxygen penetrates and segregates along the grain boundaries and lowers the boundary energy. For instance, Woodford and Bricknell have speculated that oxygen segregated in the grain boundaries of Ni-base alloys could inhibit grain-boundary sliding and migration.[41-43] These phenomena in turn could reduce the ability of the material to relieve the local stresses built up during deformation.

It is worth noting that the oxygen concentration in the boundaries might also be related to the type of oxide that is formed on the free surface. In a material such as Inconel 718, the first oxide formed is an FeNi-rich compound, followed subsequently by the formation of the more protective Cr_2O_3 oxide scale, as shown earlier. The transition time (t_p) between the two corresponding parabolic laws is dependent on partial oxygen pressure [Figure 10(b)]. For short times, one can assume that the oxygen concentration in the boundaries in equilibrium with the oxide scale is larger when the FeNi-rich oxide is

formed instead of Cr_2O_3, as shown schematically in Figure 15, where Cr_2O_3 oxide appears to act as a passivation film. This two-step oxidation mechanism was compared by Andrieu[35] to the effect of a hold time at minimum load on the fatigue crack growth rate measured at 650°C.[44] The results reported in Figure 16 show a rapid effect of hold time since after only 30 s, a significant increase in crack growth rate is noticed. In these specific conditions, the fracture mode was intergranular. It is also worth noting that a saturation effect appears to occur for hold times longer than about 1000 s. This time is of the same order of magnitude as the critical time (t_P) determined in oxidation studies and corresponding to the formation of Cr_2O_3 type oxide beneath the FeNi-rich oxide scale (Figure 10).

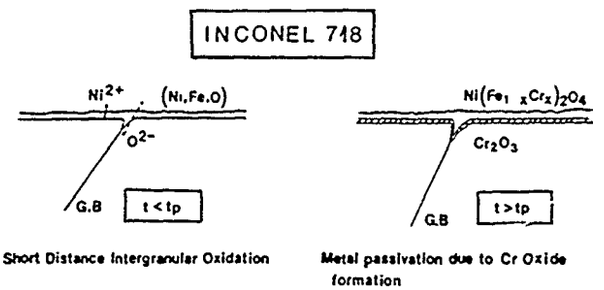


FIGURE 15—Inconel 718 alloy (UNS N07718): grain-boundary embrittlement resulting from short-distance intergranular oxidation for exposure times lower than the transition time corresponding to the formation of Cr-rich oxide scale.[35]

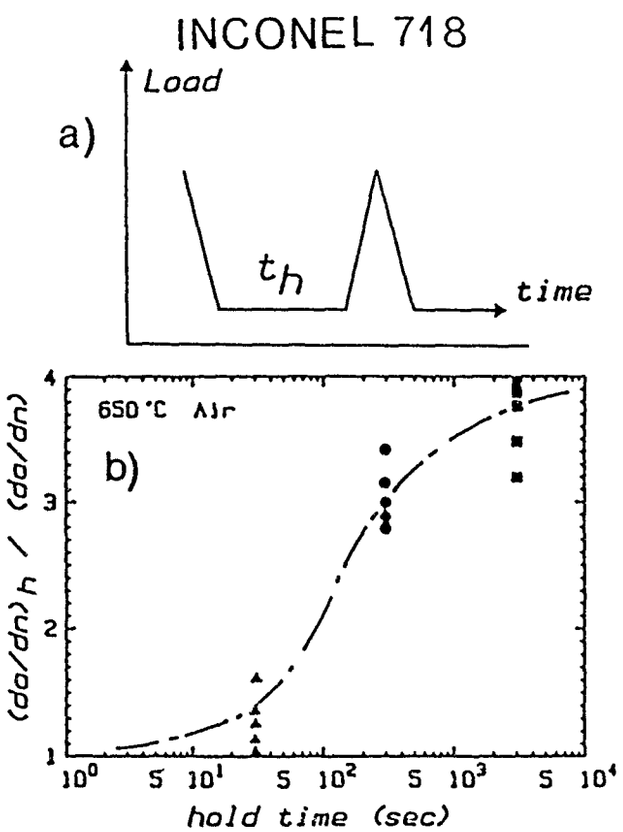


FIGURE 16—Inconel 718 alloy (UNS N07718) tested at 650°C: influence of a hold time applied at zero load on the fatigue crack growth rate: (a) waveform signal and (b) effect of hold time on the fatigue crack growth rate ratio, $(da/dN)_h/(da/dN)$.

Gas formation—Grain-boundary embrittlement of Ni produced by prior oxidation has been extensively investigated. At relatively high temperatures (~ 900 to 1000°C), this embrittlement is associated with the formation of grain-boundary cavities. Various suggestions have been made to account for their origin. Bricknell and Woodford concluded that the cavities were not voids by bubbles of either carbon monoxide or carbon dioxide gas.[45] These gases could result from a chemical reaction between carbon in solid solution and oxygen diffusing along the grain boundaries. Dyson, using thermodynamical calculations, showed that in Ni containing a small amount of carbon, the formation of carbon dioxide would take place preferentially to carbon monoxide.[46] This author also showed that gas bubbles could be nucleated with a high internal pressure. Moreover, he pointed out the fact that in Ni-base superalloys containing Cr, carbon dioxide formation is impossible when the oxygen potential is controlled by Cr_2O_3. In these materials, therefore, the deleterious effect of oxygen is likely only if the oxide scale is broken and fresh surface is exposed.

Experiments using mass spectrometry similar to the experiments of Bricknell and Woodford[45] were conducted by Andrieu[35] on preoxidized specimens of Inconel 718. This author did not detect the formation of gases when the specimens were broken. This does not mean that under cyclic deformation, gas formation ahead of the crack tip cannot also occur in this material, since simple static tests that preserve the oxide scale are not necessarily a good indication of environmental resistance under mechanical loading.

Modeling Creep-Fatigue Interactions

A life-prediction scheme applicable at high temperature should include several aspects: (1) crack initiation, (2) crack growth, and (3) calculation of local stress-strain fields in a component. In this part, we deal only with the first two aspects. Theoretically, fatigue life should be considered as divided into crack initiation and propagation phases, since their kinetics laws are known to be different. Experimentally, however, it is sometimes difficult to obtain separate and complete information on both phases. In particular, it is well known that there exists no universal definition of crack initiation, since this phase is very much dependent on the scale examined. In this part, unless otherwise stated, we adopt a "conventional" definition for crack initiation that corresponds to the formation of a relatively macroscopic crack or a physically short crack (0.5 to 1 mm), typical of those found at failure of conventional low-cycle fatigue smooth specimens. The number of cycles corresponding to the formation of this crack can also include a significant part associated with the nucleation of a microcrack. However, it can be assumed that, in the presence of strong environmental effects leading to a preferential oxidation damage of minor phases such as carbides, microcracks (~ 1 to 5 μm) are more easily formed at high temperature than at room temperature. Therefore, under these conditions, fatigue life is essentially reduced to the propagation of a small crack in a low-cycle fatigue specimen submitted to significant plastic strains. These are the conditions used to derive the kinetics of oxide formation shown earlier in Figures 12, 13, and 14. On the other hand, the crack growth phase refers to the propagation of a macroscopic crack (~ 10 mm), which is analyzed in terms of linear or nonlinear elastic fracture mechanics used at low temperature. At elevated temperature, the situation is far more complex because the constitutive equations are time dependent. This raises further problems related to the relevance of loading parameters. It is outside the scope of this paper to discuss these parameters. To simplify the discussion, we refer essentially to high-strength Ni-base superalloys for which the stress-intensity factor (K) should correlate the crack growth data.

The life-prediction methods applicable to high temperature have been reviewed by a number of authors.[8,47-52] The models are either phenomenological or physically based; in the part of this section devoted to crack initiation, we present only a model of the latter.

Crack initiation

Though air environment probably affects crack growth most, it also affects crack initiation. In particular, in Ni- and Co-base

superalloys, cracks initiate in oxidized grain boundaries. There is an especially strong stress corrosion effect on fine-grained alloys for tests in air at intermediate temperatures. Figure 17 shows the results obtained on a fine-grained powder metallurgy material (IN-100, grain size ≈ 5 μm) tested at low frequency and with 30-s or 15-min tensile dwells at the maximum tensile strain.[53] A dwell period of 15 min can reduce the fatigue life by a factor as large as one order of magnitude.

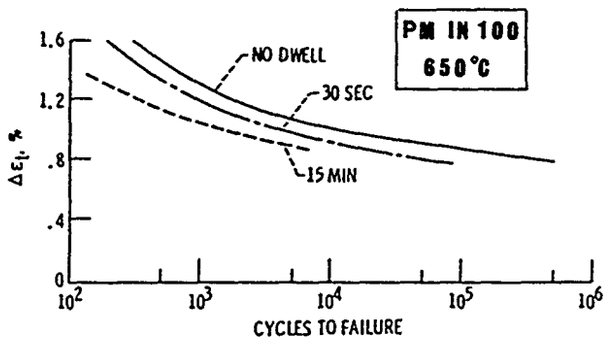


FIGURE 17—Powder metallurgy IN-100 with a small grain size (≈5 μm). Total strain-fatigue life relation at 650°C for 0.33 Hz tests and tests with 30-s or 15-min tensile dwells at the maximum tensile strain.[53]

Significant effects of test frequency and tensile or compressive hold times were also noticed for the Co-base superalloy presented in the preceding section.[39,40] An oxidation-fatigue interaction crack growth model applicable to low-cycle fatigue specimens was developed by Reuchet and Remy.[39] This model relies upon the results of metallographical observations shown in Figures 13 and 14. From these observations, a crack-growth damage equation was postulated [Equation (7)]. Though expressed in an additive form, this equation is not a simple linear damage summation rule, since, as discussed previously, the oxidation component is dependent on the inelastic-plastic strain amplitude ($\Delta\epsilon_p$), that is:

$$(da/dN)_{ox} = (1 - f_c)\,\alpha_M\,(1 + K_M\,\Delta\epsilon_p)\,\Delta t^{1/2} + f_c\,\alpha_c\,g\,(\Delta\epsilon_p)\,\Delta\,t^{1/4} \quad (8)$$

where f_c (0 12) is the effective volume of MC carbides on the crack path, and Δt is the cycle period. For the fatigue component [$(da/dN)_{Fat}$], an approximate expression derived from Tomkins's model was used:[54]

$$(da/dN)_{Fat} = 0.50\Delta\epsilon_p[\,1/\cos(\pi\sigma/2T) - 1]\,a \quad (9)$$

where σ is the peak tensile stress and T the tensile fracture stress. The number of cycles to initiation (N_R) is obtained by integrating the crack growth equation from an initial crack length a_o to a critical crack depth a_c. This leads to:

$$N_R = \frac{1}{B}\,\mathrm{Log}\,[1 + B\,a_c/(da/dN)_{ox}] \quad (10)$$

where $B = 0.50\,\Delta\epsilon_p\,[1/\cos(\pi\sigma/2T) - 1]$. This expression was shown to give results in good agreement with experimental data obtained under various frequencies and wave-form signals (Figure 18). It was also successfully applied to the results of thermal fatigue tests.[40]

This type of oxidation-fatigue interaction model is similar to those proposed for corrosion fatigue. It cannot be applied to all the situations that can be encountered when the environment plays a dominant role. The simple idea that assumes the oxidation crack growth component can be added to the fatigue component has strong limitations. It is only valid for high-temperature conditions when generalized Type A oxidation is the prevailing damage process.

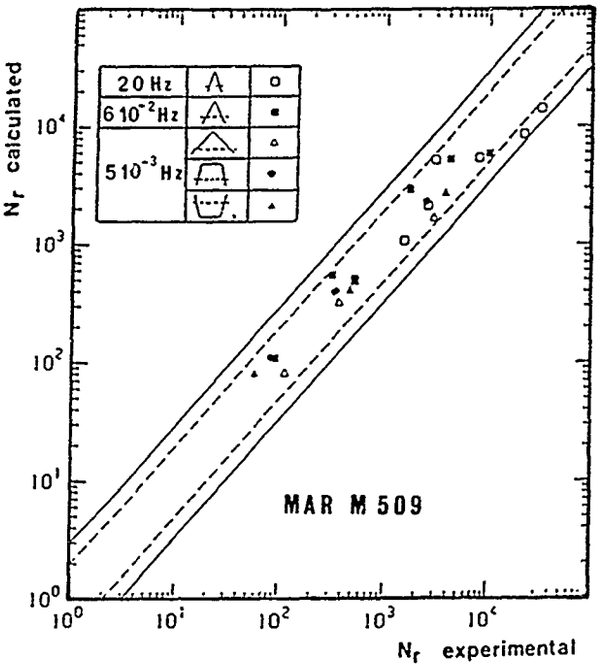


FIGURE 18—Co-base superalloy MAR M 509: results from a damage model based on strain-accelerated oxidation rate; comparison between calculated and experimental life for various waveform signals.[40]

Crack growth

Crack-tip oxidation during fatigue may produce effects other than those described above, even when Type A oxidation damage is taking place. Two effects can be mentioned: (1) Crack-tip welding or resharpening during unloading may be altered by absorbed atoms or films on the crack faces. With a greater amount of blunting, the crack tip cannot resharpen itself upon unloading and the growth rates will decrease. (2) Corrosion products at the crack tip can cause closure during unloading that will also decrease the effective stress-intensity factor range and thus retard cracking. Therefore, at low ΔK ranges and low stress ratios the crack growth rates in oxidizing environment may eventually be much smaller than those determined in inert environments. This behavior was observed, for example, by Skelton and Haigh[55] in fatigue crack growth tests on Cr-Mo-V steels at 550°C (Figure 19). In this figure, the apparent threshold increases when the test frequency is decreased, which is very unusual behavior. In this specific case, oxide build-up in the crack reduces the cyclic crack-tip opening displacement. It should be emphasized that these results or similar ones obtained on relatively long cracks (~ 10 mm) are not necessarily valid when applied to shorter fatigue cracks (<1 mm). Many studies over the last decade have shown that, even at room temperature, the fatigue crack growth rates data determined on long cracks are too conservative (see, for example, References 56 and 57). This is related to the fact that the effective crack driving force for long cracks is smaller compared to small cracks because the crack closure load is an increasing function of crack length (see References 58 and 59). It is expected that this crack-size effect is more pronounced when a large amount of oxidation debris is left along the crack faces.

In materials that are more resistant to oxidation, aggressive environments usually lead to detrimental effects, especially when Type B mechanism is taking place. This is probably the situation occurring in high-strength Ni-base superalloys. Figure 20 shows the results of fatigue crack growth rate tests conducted at 650°C on a fine-grained heat of Inconel 718 alloy.[60] In these tests, the frequency was decreased and a hold time was applied at maximum load. Figure 20 shows that the fatigue crack growth rates are increased by three orders of magnitude when a hold time of 5 min is applied, as compared to high frequency (20 Hz) tests. These crack growth rates

are plotted in Figure 21 on a time basis. In this figure, the static creep crack growth rates are also included. These data clearly indicate that the creep-fatigue crack propagation rates tend toward those measured under steady load as the hold time is increased. Similar results were obtained on other microstructures. This material is extremely sensitive to the effect of microstructural details, when tested at low frequencies and under air environment (Figure 22), as shown earlier (Figure 3). Figure 23 shows a similar behavior when these various microstructures are tested under static loading. Clearly, the crack propagation phase is essentially time dependent in this material, tested under these conditions.

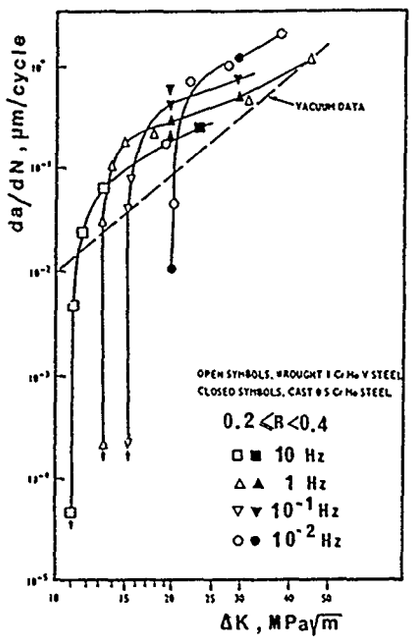


FIGURE 19—Crack growth rates in Cr-Mo-V steels at low stress ratios and low frequencies.[55]

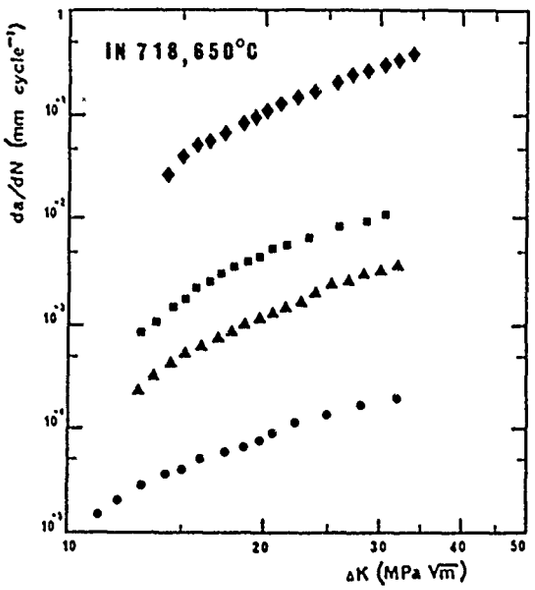


FIGURE 20—Inconel 718 alloy (UNS N07718) tested at 650°C: fatigue crack growth rate as a function of ΔK and wave-shape signal for fine-grained material:

- ♦ = 10-300-10
- ■ = 10-10-10
- ▲ = 10-10
- ● = 20 Hz.

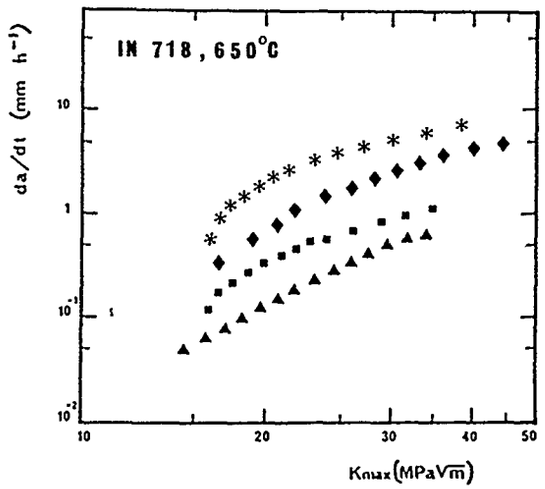


FIGURE 21— Results of fatigue crack growth rates (Figure 20) plotted on a time basis and creep crack propagation rate for fine-grained material:

- ★ = static creep
- ♦ = 300-10
- ■ = 10-10
- ▲ = 10.

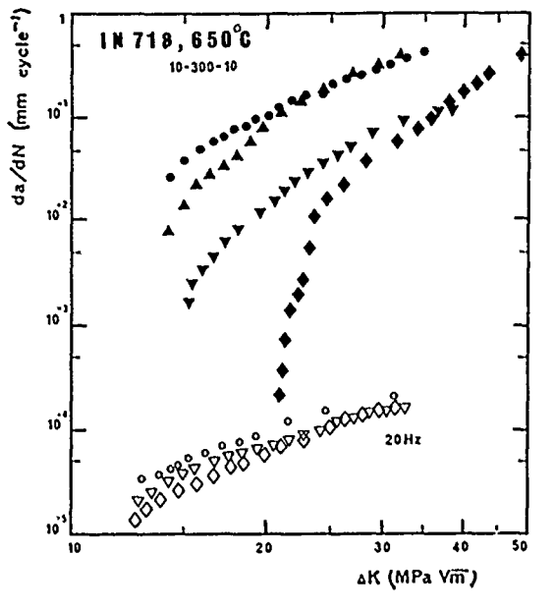


FIGURE 22—Effect of microstructure on the fatigue crack growth rate. Open symbols = 20 Hz; filled symbols = 10-300-10. ◇ ♦ = necklace microstructure; ▽ ▼ = coarse-grained structure (longitudinal direction); ▲ = coarse-grained material (short transverse direction); O ● = fine-grained structure.

Modeling crack growth behavior at high temperature under such conditions is extremely difficult. In previous studies, it was proposed that an upper bound for the crack advance during the cyclic loading could be as large as the viscoplastic zone (R_{vp}) formed ahead of the crack tip during the dwell period, t_h.[52] The size of this zone is related to K_{Max} and time (t) by:[61,62]

$$R_{vp} = A(K_{Max})^2 \, t^{2/n-1} \qquad (11)$$

where n is the exponent of the stationary creep Norton law, while A can be calculated from the theoretical expressions given by Riedel and Rice.[61] Using this assumption, an upper bound for the crack propagation rate can be written as:

$$(da/dN)_{CF} = a^{\bullet}\, t_h + R_{vp} \qquad (12)$$

where $a^{\bullet}$ is the creep crack growth rate measured under steady load at K_{Max}. Figure 24 shows the results obtained on one specific microstructure of Inconel 718, which is the large-grained material tested in the transverse direction. This figure shows that the application of Equation (12) is conservative over the whole range of crack propagation rates investigated in this study. It is worth noting that at high ΔK ($\geq$ 20 MPa $\sqrt{m}$), the measured crack growth rates are very close to the sizes of the viscoplastic zone (R_{vp}) calculated from Equation (11). This observation reinforces the soundness of the assumptions made in this model. However, it is clear that the strong environmental effects observed in this material cannot be explained only by assuming that $da/dN \simeq R_{vp}$ The creep-environment component, $a^{\bullet}\, t_h$ must therefore be taken into account.

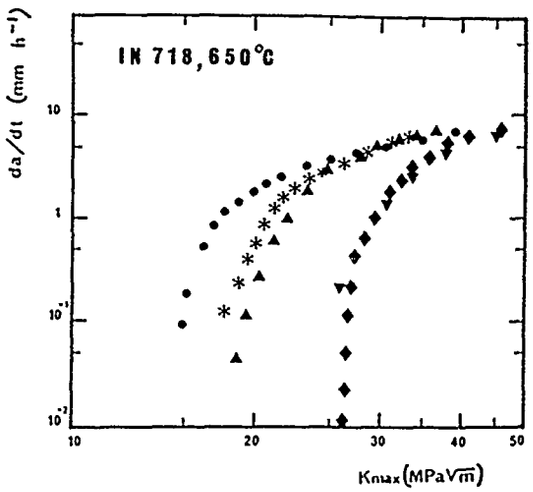


FIGURE 23—Creep crack growth rate as a function of microstructure: ♦ = necklace structure; ▼ = coarse-grained material (longitudinal direction); ▲ = coarse-grained structure (short transverse direction); ● = fine-grained structure; * = fine-grained material with β-phase precipitated along the grain boundaries.

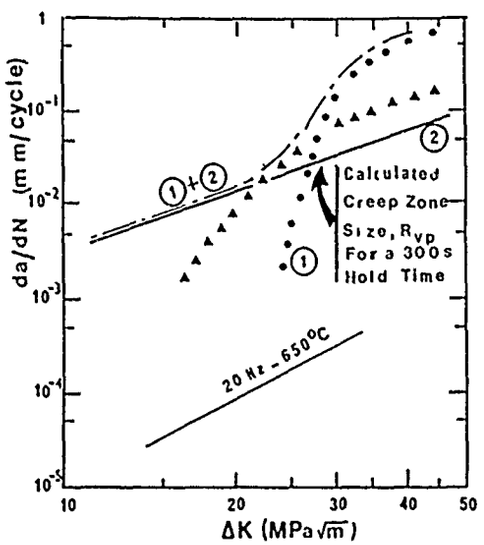


FIGURE 24—Inconel 718 alloy (UNS N07718) tested at 650°C; large-grained material. Fatigue crack growth rates at high frequency (plain curve); ▲ = measured crack growth rate with a 300-s dwell at maximum load; ● = creep crack growth rate on a cycle basis ($a^{\bullet}\, t_h$) [Curve (1)]; (——) calculated viscoplastic zone size [Curve(2)]; (– – – –) upper bound for the calculated crack growth rate corresponding to 300-s hold time.

The difficulty lies in the fact that a very clear procedure must be adopted to determine the time dependent crack growth component, since the creep-environment behavior may be largely dependent on the load history applied to the specimen. In this material, the static crack growth curves exhibit an apparent threshold at low K_{Max} (Figure 23). Two regimes of creep crack growth rates can be distinguished. The first regime (Stage I) corresponds to low growth rates with a steep slope in the da/dt-K curves. The second regime (Stage II) observed at higher crack growth rates corresponds to stationary conditions, while Stage I is only a transient effect. This was verified by using different specimen sizes and by testing the material under both increasing and decreasing stress-intensity factor.[44] The results of one of these experiments is shown in Figure 25. The specimen was first submitted to increasing K_{Max} until the expected onset of Stage II was reached. Then K_{Max} was decreased by changing the control mode from constant load to constant displacement. After this change in control mode, the crack growth rates decreased, first along a line located within the scatter band defined for Stage II, until an apparent crack arrest was observed at a lower value than the threshold measured initially under increasing K. The tests were continued under decreasing K by first applying a few fatigue cycles (~ 5). Crack reinitiation and transient crack growth were observed after the application of this loading. These results clearly indicate that Stage I is only a transient regime and strongly dependent on experimental procedures. Therefore, a more conservative approach to determine the creep crack growth component is obtained by extrapolating Stage II regime determined at relatively high crack growth rates, as shown approximately by the dotted line drawn in Figure 25. Figure 26 shows a better agreement between the fatigue crack growth rates and the extrapolated Stage II creep crack growth results compared to Stage I creep crack growth data. This reinforces the basis of the proposed model [Equation (12)], provided that the appropriate crack propagation time component is used.

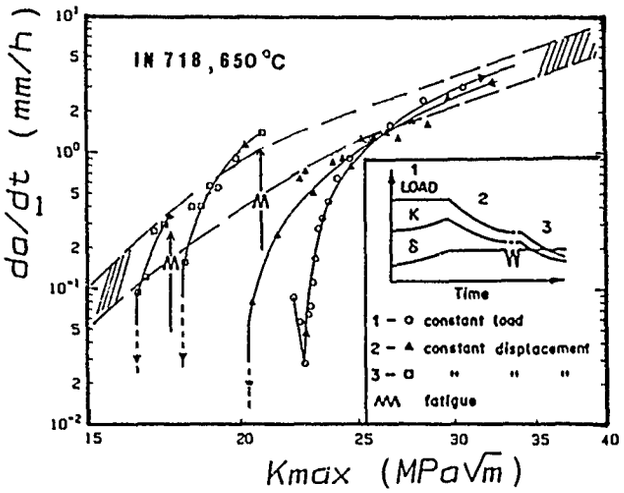


FIGURE 25—Results of creep crack growth rate tests under increasing or decreasing stress-intensity factor. The load history applied to the specimen is indicated schematically in the insert. A dotted line corresponding approximately to steady Stage II regime is drawn.

Transient Stage I is probably related to oxidation effects. In the preceding section, it was shown that in this material a very thin layer of FeNi-rich oxide was found on the free surface of the specimens before a more protective Cr-rich oxide scale was formed, depending on various factors, such as oxygen partial pressure, exposure time, and mechanical preparation. A similar behavior is expected in the vicinity of the crack tip, although it is much more difficult to investigate. The situation is therefore somewhat similar to that encountered in a number of stress corrosion or corrosion-fatigue studies when the time-dependence is related to the formation of a passive film. To model crack growth behavior observed under these conditions, a simple approach based on the theoretical stress-strain field for creeping cracked solids[61] and the ductility exhaustion concept was used.[44]

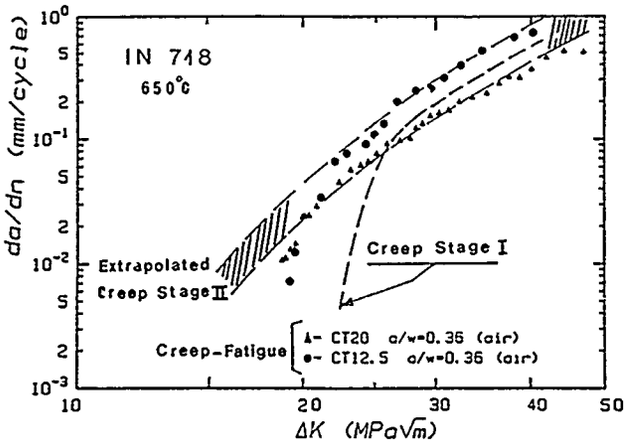


FIGURE 26—Fatigue crack growth rates with a 300-s dwell measured on two specimens. Comparison with creep crack growth data on a cycle basis. Note that the measured fatigue crack growth rates are close to the values extrapolated from those associated with creep Stage II regime.

This model provided satisfactory results by assuming that the creep ductility was time dependent because of environmental effects.

Summary and Conclusions

(1) At elevated temperature, both fatigue crack initiation and crack growth can be dramatically affected by oxidation. This effect is more pronounced when the failure mode is changed from transgranular to intergranular.

(2) Three forms of intergranular damage have been distinguished: (1) slip-induced intergranular cracking, (2) bulk intergranular creep cavitation damage, and (3) oxidation-induced damage.

(3) The high-temperature cracking resistance of Ni-base superalloys is largely dependent on microstructural details, such as the grain size and the grain-boundary microstructure. This behavior, illustrated for Inconel 718, is also closely related to oxidation effects.

(4) The application of plastic strains can largely modify the oxidation mechanisms by changing the type of oxide scale formed at the free surface of the specimen or by accelerating oxidation kinetics, as observed in Ni- or Co-base superalloys and in Cr steels. Stress-free oxidation data are inapplicable to highly strained conditions.

(5) Quantitative measurements of the effect of applied cyclic strains on oxidation rate can be used to model the time dependence observed in the crack initiation life of low-cycle fatigue specimens.

(6) In Ni-base superalloys, the application of a hold time at maximum load produces a large increase in fatigue crack growth rates. In Inconel 718, the fatigue crack growth behavior is similar to that observed under static load.

(7) Environmental effects are partly responsible for transient effects observed for creep crack growth. Special attention must be paid to the study of these transient effects to determine conservative crack growth rate measurements.

(8) An upper bound for high-temperature crack growth rates is proposed as the sum of the viscoplastic zone size ahead of the crack tip and the time-dependent component.

References

1 P Shahinian, K. Sadananda, Crack Growth Behavior Under Creep-Fatigue Conditions in Alloy 718, Creep-Fatigue Interactions, MPC 3 (New York, NY: ASME, 1986), p. 365.

2. L.A. James, Fatigue Crack Propagation Behavior of Inconel 718, Westinghouse Handford Engineering Laboratory Report HEDL-TME 7580 UC-79, 1985.
3. J.P. Pedron, A. Pineau, Effect of Hold Time on the Elevated Temperature Fatigue Crack Growth Behavior of Inconel 718 alloy, ICF 5, Vol. 5 (Oxford, England: Pergamon Press, 1981), p. 2385.
4. M. Clavel, A. Pineau, Metall. Trans. 9A(1978): p. 471.
5. A. Coles, R.E. Johnson, H.G. Popp, "Utility of Surface Flawed Tensile Bars in Cyclic Life Studies," General Electric Report TIS R 75 AE 6109, 1975.
6. H.G. Popp, A. Coles, Proceedings of the Air Force Conference on Fatigue and Fracture of Aircraft Structures and Material, ed. H.A. Wood, et al. (Dayton, OH: Wright-Patterson Air Force Base, 1970), p. 71.
7. G. Gayda, R.V. Miner, Int. J. Fat. 5(1983): p. 135.
8. A. Pineau, "Elevated Temperature Life Prediction Methods," Advances in Fatigue Science and Technology, NATO/ASI, ed. C. Moura-Branco, L. Guerra Rosa (Amsterdam, The Netherlands: Kluwer Academic Publishers, 1989), pp. 283-311 and pp. 313-338.
9. L.C. Lim, R. Raj, Acta Metall. 32(1984): p. 727.
10. L.C. Lim, R. Raj, Acta Metall. 32(1984): p. 1183.
11. L.C. Lim, Acta Metall. 35(1987): p. 1653.
12. L. Remy, A. Pineau, B. Thomas, Mater. Sci. Eng. 36(1978). p. 47.
13. L. Remy, A. Pineau, Mater. Sci. Eng. 26(1976): p. 123.
14. R.E. Stoltz, A. Pineau, Mater. Sci. Eng. 34(1978): p. 275.
15. J.M. Duva, M.A. Daeubler, E.A. Starke, G. Luetjering, Acta Metall. 36(1988): p. 585.
16. M. Clavel, A. Pineau, Scripta Metall. 16(1982): p. 361.
17. M. Clavel, A. Pineau, Mater. Sci. Eng. 55(1982): p. 157.
18. M. Clavel, A. Pineau, Mater. Sci. Eng. 55(1982): p. 173.
19. M. Clavel, "Fatigue plastique et fissuration de deux alliages durcis par des precipites coherents. Etude comparative des mecanismes" (Thesis, Universite de Technologie de Compiegne, 1980).
20. B. Dyson, M. Loveday, M.J. Rodgers, Proc. Roy. Soc. London A 349(1976): p. 245.
21. T. Saegusa, M. Uemura, J.R. Weertman, Metall. Trans. 11A(1980): p. 1453.
22. R. Raj, Flow and Fracture at Elevated Temperatures, ed. R. Raj, ASM Materials Science Seminar (Metals Park, OH: ASM International, 1983), p. 215.
23. C. Levaillant, A. Pineau, "Low Cycle Fatigue and Life Prediction," ASTM STP 770, 1982, p. 169.
24. P. Dabo, C. Levaillant, A. Pineau, J. Grattier, M. Mottot, Fatigue at High Temperature, International Spring Meeting of the French Metallurgical Society (Paris, France: French Metallurgical Society, 1983), p. 40.
25. C. Levaillant, J. Grattier, M. Mottot, A. Pineau, "Low Cycle Fatigue," ASTM STP 942, 1987, p. 414.
26. J. Wareing, Fat. Eng. Mater. Struc. 4(1981): p. 131.
27. M. Yoshida, C. Levaillant, A. Pineau, International Conference on Creep (1986), p. 327.
28. M. Yoshida, C. Levaillant, R. Piques, A. Pineau, Int. Seminar on High Temperature Fracture Mechanisms and Mechanics, held Oct. 1987 (Dourdan, France: 1987), p. I-1.
29. B. Rezgui (Thesis, Universite Paris XI, 1982).
30. Groupe de travail Materiaux, EDF-CEA Report no. 18, 1985.
31. L.F. Coffin, Fatigue at Elevated Temperatures, ASTM STP 520, 1973, p. 5.
32. S. Floreen, R. Raj, Environmental Effects in Nickel Base Alloys in Flow and Fracture at Elevated Temperatures, ed. R. Raj, Materials Science Seminar, held Oct. 1983 (Metals Park, OH: ASM International, 1983), p. 383.
33. S.D. Antolovich, P. Domas, J.L. Strudel, Metall. Trans. 10A(1979): p. 1859.
34. S.D. Antolovich, S. Liu, R. Baur, Metall. Trans. 12A(1981): p. 473.
35. E. Andrieu, "Influence de l'environnement sur la propagation des fissures dans un superalliage base nickel, l'Inconel 718" (Thesis, Ecole des Mines de Paris, 1987).
36. N.B. Pilling, R.E. Bedworth, J. Inst. of Metals 1(1923): p. 529.

37. J. Bardehon, A. Rahmel, M. Schutze, Low Cycle Fatigue and Elasto-plastic Behavior of Materials, ed. K.T. Rie, (Amsterdam, The Netherlands: Elsevier/Applied Science Pub., 1987), p. 371.
38. P. Skelton, J.I. Bucklow, Metal Sci. (1978): p. 64.
39. J. Reuchet, L. Remy, Metall. Trans. 14A(1983): p. 141.
40. L Remy, F Rezai Aria, R. Danzer, W. Hoffelner, "Evaluation of Life Prediction Methods in High Temperature Fatigue in Low Cycle Fatigue," ASTM STP 942, 1987, p. 1115.
41 D A Woodford, R.H. Brickne, Treatise on Material Science and Technology 25(1983): p. 157.
42. D.A. Woodford, Metall. Trans. 12A(1981): p. 299.
43. D.A. Woodford, R.H. Bricknell, Metall. Trans. 12A(1981). p. 1467.
44. A. Diboine, A. Pineau, Fat. Frac. Eng. Mater. Struc. 10(1987): p. 141.
45. R.H. Bricknell, D.A. Woodford, Acta Metall. 30(1982): p. 257.
46. B.F. Dyson, Acta Metall. 30(1982): p. 1639.
47. J.L. Chaboche, "Methods for Structure Calculations under High Temperature Fatigue, Present and Future Possibilities," in Fatigue at High Temperature, International Spring Meeting of the French Metallurgical Society, held June 1986 (Paris, France: French Metallurgical Society, 1986).
48. A.D. Batte, Fatigue at High Temperature, ed. R.P. Skelton (London, England: Applied Science Publishers, 1983), p. 365.
49. J.K. Tien, S.V. Nair, V.C. Nardone, Flow and Fracture at Elevated Temperatures, ed. R. Raj, ASM Materials Science Seminar, held Oct. 1983 (Metals Park, OH: ASM International, 1983), p. 179.
50. J. Wareing, B. Tomkins, I. Bretherton, Flow and Fracture at Elevated Temperatures, p. 251.
51. B.J. Cane, R.D. Townsend, Flow and Fracture at Elevated Temperatures, p. 279.
52. A. Pineau, Flow and Fracture at Elevated Temperatures, p. 317.
53. R.V. Miner, Fatigue in Superalloys II, High Temperature Materials for Aerospace and Industrial Power, ed. C. Sims, N. Stoloff, W. Hagel (New York, NY: J. Wiley and Sons, 1987), p. 263.
54. B. Tomkins, J. Eng. Mater. Technol. (Trans. ASME Series H) 97(1975): p. 289, 1975.
55. R P Skelton, J.R. Haigh, Mater. Sci. Eng. 36(1978). p. 17.
56 S Suresh, R.O. Ritchie, Int. Metall. Rev. 29(1984). p. 445.
57 A Pineau, Small Fatigue Cracks, ed. R.O. Ritchie, J. Lankford (Warrendale, PA: The Metallurgical Society, 1986), p. 191.
58. J.L. Breat, F. Mudry, A. Pineau, Fat. Eng. Mater. Struc. 6(1983): p. 349.
59 K Minakawa, M. Nakamura, A.S. McEvily, Scripta Metall. 18(1984): p. 1371.
60. J.P. Pedron, A. Pineau, Mater. Sci. Eng. 56(1982): p. 143.
61. H. Riedel, J.R. Rice, Fracture Mechanics, Twelfth Conference, ASTM STP 700, ed. P.C. Paris (Philadelphia, PA: ASTM, 1980), p. 112.
62. H. Riedel, J. Mech. Phys. Solids 29(1981): pp. 35-49.

Discussion

D.J. Duquette (Rensselaer Polytechnic Institute): If I understand your data, increasing plastic strain range, and presumably increasing ΔK, increase oxidation rates. Accordingly, superposition rules of da/dn cannot assume a constant advance rate. It seems to me that this will make modeling very difficult, and it will also strongly affect crack closure considerations.

A. Pineau: The data on a chromium steel and a cobalt-base superalloy clearly show that the cyclic plastic strains increase the oxidation rates. In the model proposed by Reuchet and Remy (Reference 39), which relies upon a superposition, the acceleration in oxidation rates due to cyclic deformation is taken into account. Crack closure explains the behavior observed by Skelton and Haigh (Reference 55) on long fatigue cracks. The modeling of these complex phenomena is certainly difficult. I have attempted to show that at least for the Type A mechanism, i.e., "oxide-assisted cracking," crack initiation can be modeled reasonably well, provided that data relating the oxidation kinetics to applied cyclic strains are available. Unfortunately, there are very few results published in the literature. This is certainly an area where much more work is needed.

R.A. Oriani (University of Minnesota, USA): How does one understand the effect of shot peening Inconel in producing Cr_2O_3 at 650°C, whereas, without shot peening, a spinel is produced?

A. Pineau: In Andrieu's work (Reference 35), no detailed explanation was given for this observation. One can only speculate that the lattice defects and/or the macroscopic residual stresses produced by shot peening favor the nucleation and growth of one species of oxide.

H.-J. Engell (Max Planck Institut fur Eisenforschung, Federal Republic of Germany): Did you also observe internal oxidation, and if so, did it have an influence upon the formation of cracks?

A. Pineau: In Inconel 718, no evidence of internal oxidation could be found. In particular, metallographic observations showed that all the primary carbides that were oxidized were in contact with either the main crack or with secondary cracks, linked to the main crack.

R. Pelloux (Massachusetts Institute of Technology, USA): What is known about the mechanical properties of the two oxide films (Ni,Fe)O and Cr_2O_3? How do these properties affect the overall crack growth rate?

A. Pineau: Very little is known about the mechanical properties of these oxides, in particular for the complex oxides formed on the surfaces of Inconel 718. However, a number of authors [for example, Barbehon, et al., Oxidation of Metals 30(1988): p. 80] have attempted to determine the critical strain at failure of various types of oxides. It is clear that the knowledge of these mechanical properties is important to model, as is, in particular, the cracking behavior of oxide films.

R. Pelloux: The Type A oxide can be beneficial or detrimental to the fatigue crack growth rate. Can you discuss this effect for short and long cracks?

A. Pineau: Type A mechanism is essentially detrimental to crack initiation and short crack propagation behavior. For the propagation of long cracks, this mechanism can be beneficial, as shown in the study performed by Skelton and Haigh on low-alloy Cr-Mo-V steels. (See Reference 55.) This beneficial effect is associated with the increase in crack closure produced by the accumulation of oxidation debris within the crack.

S.C. Jani (Georgia Institute of Technology, USA): Until now, time-dependent fracture mechanics parameters have been developed, but is there any drive to use them? Time relaxation of stress at the crack tip cannot be ignored and K and J are meaningless parameters unless they are conclusively shown to be able to be correct correlating parameters, e.g., in the case where the crack tip is moving faster than the zone of stress relaxation (creep), in which case K is a correct far-field parameter.

A. Pineau: In high-temperature environment-induced cracking, there are two time-dependent phenomena. You are referring to the time dependence of the crack-tip stress-strain field. The fracture mechanics of creeping solids has made significant progress over the past decade. The K parameter is able to describe the stress relaxation ahead of the crack tip only when the size of the visco-plastic zone remains small. The second time-dependent phenomenon is related to oxidation kinetics.

SECTION III

Fundamental Processes

Chairman's Introduction

A. Turnbull
National Physical Laboratory
Teddington, Middlesex, UK



Photos: M B. Ives

A general consideration of the fundamental aspects of environment-induced cracking raises some elementary questions. By what mechanism(s) does the metal/environment interaction lead to enhanced cracking? What type of metal/environment interaction can occur and what are the specific nature and kinetics of reactions at the crack tip in the crack advance process? To what extent can we model, qualitatively and quantitatively, crack development and growth?

The first of these fundamental questions is addressed by Sieradzki, who summarizes recent advances in modeling environmental fracture at the detailed atomistic level. Various atomistic models are described and their basic physical assumptions are discussed, viz., size effects, choice of interatomic potential, boundary conditions, and microstructural features. The micromechanisms of intergranular and transgranular fracture are discussed. Advances have been made in the understanding of the effect of impurities, such as sulfur and boron, on cohesive bonding and intergranular fracture. The most significant advance in relation to transgranular stress corrosion cracking has been the extensive work of Sieradzki and Newman on the role of surface films, particularly dealloyed layers, in inducing cleavage in normally ductile metals. There is a need for further studies in relation to the detailed kinetics of the processes involved.

The emphasis in Ford's paper is the development of models of crack growth as a basis for predicting environmentally assisted cracking in service. The various models of crack growth are reviewed and discussed in terms of the possible rate-determining steps. The local chemistry at the crack tip and mass transport processes within the crack are assessed, making use of recent mathematical modeling. Limitations exist in this modeling with respect to concentrated solution and multidimensional flow effects, but considerable progress has been made, and at the present time modeling provides the only method of characterizing the environment in "short" cracks. We are reminded that the key objective in determining the local chemistry at the crack tip is to quantify the kinetics of reactions and models of crack growth based on transient anodic reaction rates and strain rates. Quantitative models based on a hydrogen-assisted cracking mechanism remain more elusive.

The paper by Gerberich and Chen describes progress in understanding the micromechanisms of crack development. A number of topics are covered in relation to studies in notched specimens and the effect of varying loading mode and of biaxial loading. The crack extends in the environment in response to the local driving force. A description of the local stress and strain distribution at the crack tip is given and recent ideas concerning shielding effects in the process zone are discussed. The main emphasis is on statically loaded cracks rather than fatigue cracks, although there are common features. Clear evidence from acoustic emission studies of discontinuous cracking associated with hydrogen is presented. It is argued that cracking due to hydrogen is most probably associated with volume embrittlement, though this may include very near-surface sites.

Atomistic and Micromechanical Modeling Aspects of Environment-Induced Cracking of Metals

*K. Sieradzki**

Abstract

We critically review atomistic and micromechanical modeling work that relates directly to environment-induced cracking of metals. A brief introduction is given to molecular-dynamic and lattice-static modeling schemes and cluster calculations detailing the information that can be derived from each specific type of calculation and the shortcomings intrinsic to each calculation. Basic philosophies of atomistic modeling are described, and this provides considerable insight into the work that has been done in the area of environment-assisted fracture. Specific problems in atomistic modeling are addressed, including issues related to size effects, choice of interatomic potential, and boundary conditions.

Microscopic models that serve to couple atomistic aspects of environment-induced fracture to continuum aspects are discussed. These include variants of the Rice and Thomson (RT) model as applied to embrittlement phenomena, chemically assisted bond-rupture models, and various aspects of anodic-dissolution models. A new example of the application of the RT model to an environmentally assisted intergranular separation process is presented, and its predictions are compared with existing experimental data in the literature. The role of dealloyed layers in the film-induced cleavage model of transgranular stress corrosion cracking is discussed, and the predictions of the model are reviewed.

Introduction

We critically review recent atomistic and micromechanical modeling that directly relates to environment-induced cracking of metals. As a starting point, our review takes the International Conference on "Stress Corrosion Cracking and Hydrogen Embrittlement of Iron-Base Alloys," held in 1973 in Unieux-Firminy, France.[1] There were two papers presented at that conference that fall into the scope of this review "A Film-Rupture Model for Stress-Corrosion Cracking, by D. Vermilyea,[2] and "An Atomic Model of an Environmentally Affected Crack in BCC Iron," by A. Markworth, M. Kanninen, and M. Gehlen.[3] The paper by Markworth, et al., represents one of the earliest attempts to model an environmentally induced fracture process by an atomistic scheme. The Vermilyea paper was perhaps the first to incorporate fracture mechanics into a stress corrosion cracking (SCC) model. This represented a quantitative extension of the film-rupture notions of Logan[4] and Hoar.[5]

Markworth, Kanninen, and Gehlen used a hybrid molecular statics scheme to model hydrogen embrittlement of iron.[3] They modeled a centrally cracked panel of iron of thickness equal to the spacing (d) between two consecutive (100) planes, as shown in Figure 1. Atomic regions are embedded at the tips of the crack and a flexible boundary scheme is used to couple the atomistic region to the elastic continuum. The radius (t) of each of the atomistic regions is approximately 2 nm, which corresponds to between 7 and 8 layers. Within the atomistic region, the Fe-Fe interaction is modeled by a pairwise Johnson potential, and the Fe H interaction is modeled by a Morse potential. They examined the fracture toughness (K_c) of the intrinsic iron lattice and the effect of a single H atom placed at the tip of the crack on K_c, called K_{Th}. The subscript refers to a threshold-fracture toughness in the presence of hydrogen. The simulations are performed by placing an incremental load (P) at the sample boundaries, which results in a known continuum elastic field within a distance (r = t) from the crack tip, i.e., $\sigma_{ij} = K(2\pi r)^{-1} f_{ij}(\theta)$ where the $f_{ij}(\theta)$ are known trigonometric functions and K is the stress-intensity factor.[6] The atomistic regions are allowed to relax using an algorithm that minimizes the strain energy in the atomistic region while ensuring continuity at the atomistic-continuum interface. Figure 2 shows a simulation result for a run incorporating the hydrogen atom. The major results of this work are (a) $K_c \sim 2.78K_G$ and (b) $K_{Th} = 2.59K_G$, where K_G is the critical value of the stress intensity evaluated from the Griffith criteria, i.e., $K_G = (2E\gamma)^{1/2}$,[7] where E is Young's modulus and γ is the surface free energy for iron. Since $K_{Th} = 0.93K_c$, an embrittlement was observed that was probably a result of H-induced local distortions. It is important to note, as their result (a) indicates, that the simulations could not reproduce the intrinsic value of K_c ($= K_G$) for iron. This could result from either the inadequacy of the interatomic potentials used or the inability of the atomistic scheme (small size and the flexible-boundary method) to accurately model material behavior. It is likely that both of these issues contributed significantly to errors. In the last fifteen years, considerable progress has been made toward the development of more realistic interatomic potentials, as will be discussed in a later section. The remaining issue, i.e., that of coupling an atomistic region to a continuum, remains a difficulty. The problem is associated with finding an algorithm that properly accounts for the transmission of spatially discrete deformations (such as dislocations) into the continuum region. Most of the modern atomistic simulations are not hybrid and simply use large atomistic regions, avoiding this problem altogether.

During the late sixties and early seventies, Vermilyea developed a quantitative micromechanical model of SCC, and the paper he presented in Firminy[2] seems to be the culmination of that effort. Figure 3 is a schematic representation of the cyclic model he considered. A crack with a film covering its surfaces fractures, and dissolution of metal occurs over a time (t_L), advancing the crack by a length (L). The time (t_L) represents the time required to repassivate the crack surfaces, i.e., the time required for the film to reform. t_L is

*Department of Materials Science and Engineering, The Johns Hopkins University, Baltimore, MD 21218.

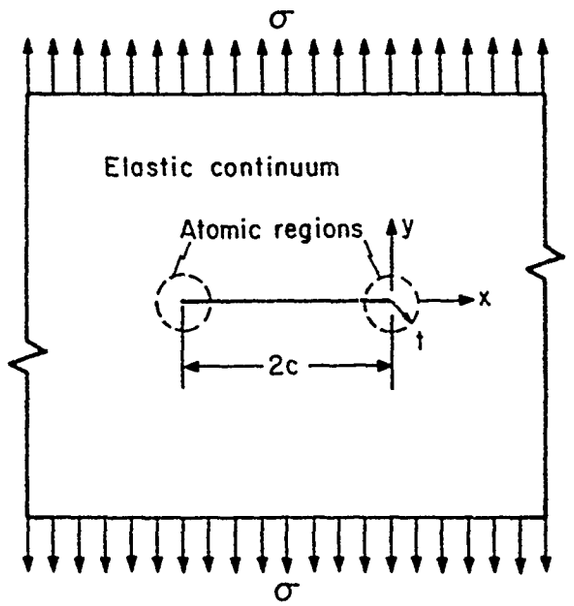


FIGURE 1—Location of atomic regions. The x and y axes are <100> directions, and the plane of the figure is a (100) plane. The stress σ is applied at infinity.[3]

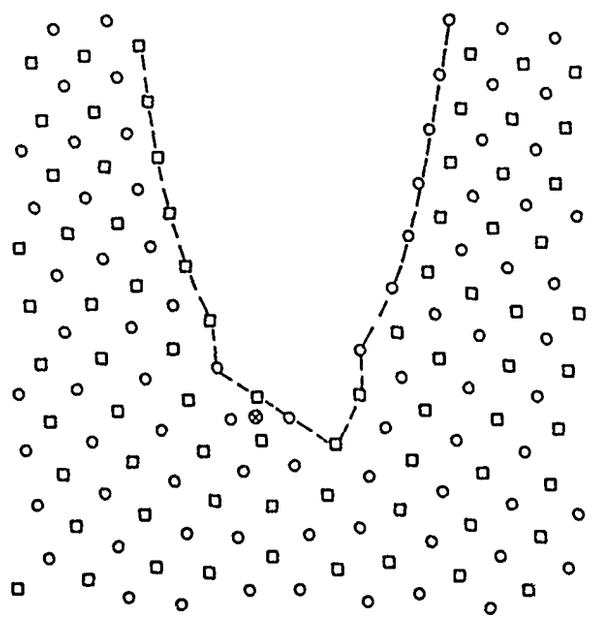


FIGURE 2—The atomic configuration around the crack tip for K = 2.59 K_a. Atoms in two consecutive (100) planes are represented by different symbols. Atoms linked by a dotted line have a separation distance larger than the cut-off distance of the interatomic potential and thus define the crack face within the context of the model. The H atom is indicated by X.[3]

considered to be short in comparison to the time scales associated with creep processes at the crack tip. Immediately following repassivation, the crack tip begins to experience a strain transient ($\Delta\epsilon$), as shown in Figure 3. After a time (t_c), enough strain accumulates so that $\Delta\epsilon$ equals the fracture strain of the film (ϵ_f), the film ruptures, and the cycle repeats. The strain gradient ($\partial\epsilon/\partial L$) drives the crack-tip strain accumulation, and the steeper $\partial\epsilon/\partial L$ is, the shorter L needs to be to allow such a mechanism to operate. Vermilyea examined the situation for two different elastic-plastic crack-tip continuum models: the plane-stress Dugdale model appropriate for thin specimens, and a plane-strain analysis appropriate for thick samples.

Figure 4(a) is a sketch of a Dugdale crack for which Vermilyea assumed the linear plastic-strain gradient.

$$\epsilon_r = \epsilon_{tip} - \frac{\epsilon_{tip} r}{R} \qquad (1)$$

where R is the extent of the plastic zone and ϵ_{tip} is the plastic strain at the crack tip. ϵ_{tip} is given by δ/T where δ is the crack-opening displacement and T is the sample thickness. For the mechanism to operate, Vermilyea calculates $L \geq \pi T \epsilon_f / 8\sigma_y$ where σ_y is the yield strength of the metal. Taking realistic values, $\epsilon_f = 10^{-3}$, $T = 10^{-4}$ m, $\sigma_y = 5.10^8$ Pa, and $E = 10^{11}$ Pa, yields a value for $L = 10^{-5}$ m. This penetration distance corresponds to a charge density under the repassivation current transient of ~ 10 coul/cm^2. Such charge densities do not usually occur in repassivating systems that undergo SCC.

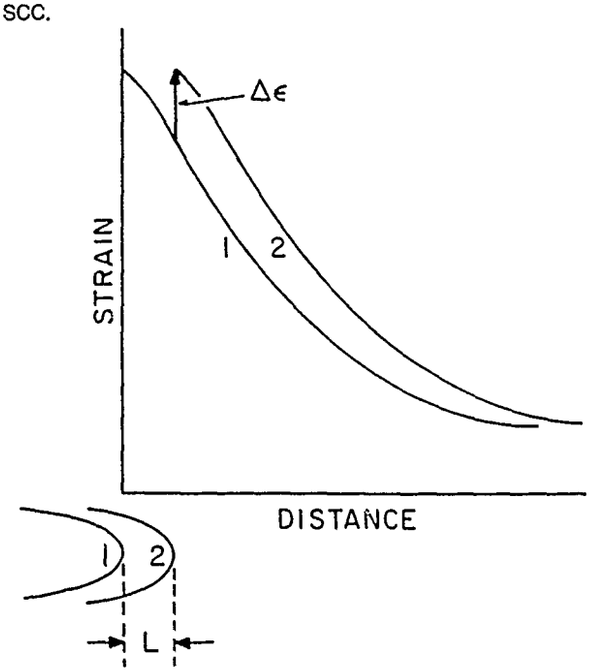


FIGURE 3—The relationship of the strain gradient to the requisite corrosion-advance distance (L). The strain gradient drives the crack-tip strain accumulation, and the steeper the gradient, the shorter L need be.

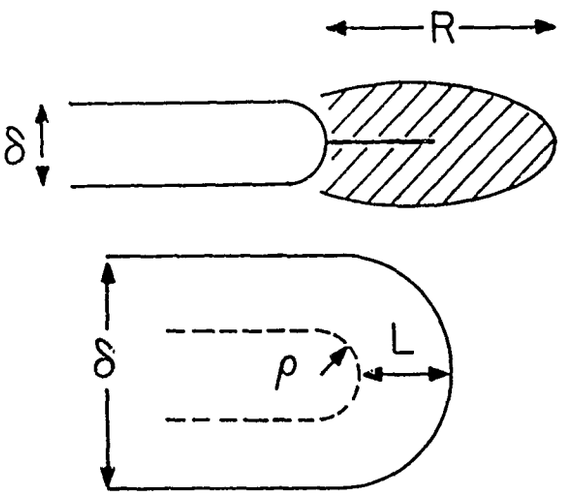


FIGURE 4—(a) The Dugdale plane-stress crack configuration, and (b) self-similar crack growth in Vermilyea's model for the case of plane-strain.

Figure 4(b) depicts the situation Vermilyea envisioned for the plane-strain case. He assumed a r^{-1} strain gradient, which is the steepest theoretically possible.[8] Crack advance occurs in a manner to maintain a self-similar geometry so that the crack advances a length (L) in a semicylindrical mode. The strain gradient is of the form $\epsilon = \epsilon_p (\rho/r)$, and he calculates $L = \epsilon_p \epsilon_f T/2(\epsilon_p - 2\epsilon_f)$, where ϵ_p is the strain at the crack tip. Note that for $\epsilon_f = \epsilon_p/2$, $L \Rightarrow \infty$. For $\epsilon_p \gg \epsilon_f$, $L = 1/2\epsilon_f T$, and for $\epsilon_f = 10^{-3}$ and $T = 10^{-3}$ m, $L \approx 10^{-6}$ m. This penetration distance corresponds to a charge density ≈ 1 coul/cm^2, which is quite large in comparison to the behavior relevant in experimental systems.

It is important to emphasize that the plane-strain calculation represents the *most optimistic* situation for the Vermilyea model. He assumes that $t_c \gg t_L$ so that no relaxation occurs during crack growth. However, it is more likely that $t_c \sim t_L$ so that some of the available creep strain required to fracture the film is wasted during the dissolution phase of the cycle. Additionally, continuum calculations for a moving crack predict that a logarithmic strain gradient exists at the crack tip, which would increase required values of L by many orders of magnitude. Our conclusions regarding the Vermilyea model of film rupture are as follows:

(1) Charge densities $\approx$ 1 to 10 coul/cm^2 (integrated under the repassivation current transient) are required for the operation of the Vermilyea model of the film-rupture mechanism.
(2) It is likely that "active paths" must pre-exist in those systems in which stress corrosion crack advance *does* occur by a pure anodic dissolution process.

In the next section, we briefly discuss various atomistic schemes and examples of work that have been used to model environmental fracture processes, and in Section 3 we discuss *selected* micromechanical models that serve to highlight the advances made during the last 15 years.

Atomistic Modeling in Environmental Fracture

Atomistic approaches to the fracture problem fall into one of the two following general categories:

Crack-modeling schemes. Various numerical techniques are used to solve a many-body problem that simulates various aspects of the continuum fracture problem. These approaches, briefly discussed below, require various degrees of simplification to result in a numerically tractable problem.

Quantum mechanical calculations on small clusters of atoms. These techniques use various quantum mechanical schemes to examine charge densities in the bonding of small clusters of atoms and cohesive energies of small clusters. They have been primarily applied to systems related to intergranular separation processes, e.g., S in Ni, H in Fe.

Crack-Modeling Approaches

Lattice-statics approach

The lattice-statics approach treats a large or infinite number of atoms interacting via a simple potential. The calculations are done on a two-dimensional or quasi one-dimensional (two semi-infinite chains of atoms bonded together by bendable and stretchable bonds) lattice, chosen because such models yield analytical solutions. The idea is to extract qualitative results from the simple model, which may be applicable to more complicated systems. These models allow us to separate effects related to the actual bond-breaking process from contributions associated with the whole lattice. For example, by the proper choice of coordinate system, Fuller, Lawn, and Thomson effectively decoupled the nonlinear crack-tip bond from the linearly connected atoms, which allowed for a detailed analysis of the energetics of an adsorption-induced separation process.[10]

They considered the atomistic model shown in Figure 5(a). The atoms are connected by horizontal bendable bonds of spring constant (β) and vertical stretchable (and breakable) bonds of spring constant (α). The manner in which the chemical reaction occurs is depicted in Figure 5(b), in which a diatomic molecule (A_2) adsorbs at the crack tip, forming two AB bonds, and bond failure occurs by breaking the weakened AA bond. The total potential energy of the loaded crack for the intrinsic BB system is

$$U = -2P\mu_o + 2\beta \sum_{j=1}^{\infty} (\mu_{j+1} - 2\mu_j + \mu_{j-1})^2 + nU_{BB} + \int_o^{2\mu_n} f_b \, d(2\mu_n) + 2\alpha \sum_{j=n+1}^{\infty} \mu_j^2 \qquad (2)$$

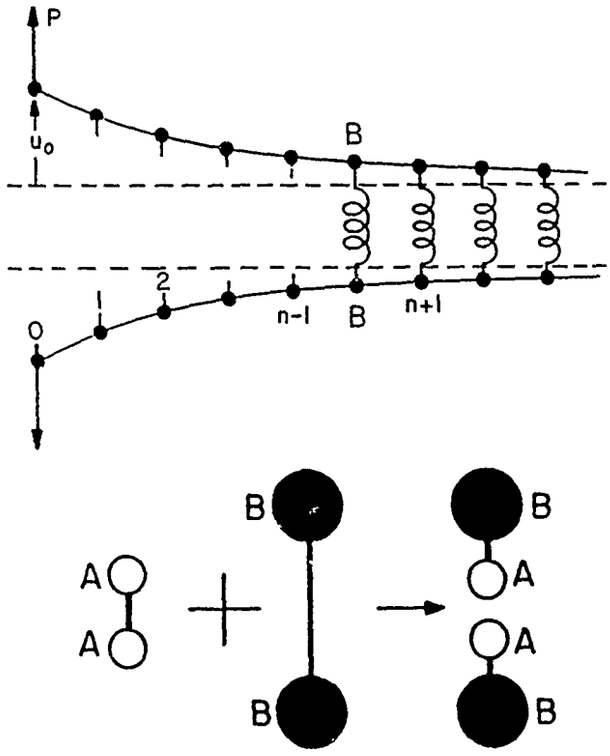


FIGURE 5—(a) Quasi-one-dimensional model of a crack. Atoms are linked longitudinally by bendable elements and transversely by stretchable elements; only the transverse element BB, representing the crack-tip bond, is considered to be displaced in a region of nonlinear response; and (b) schematic of chemically induced bond rupture. Extraneous molecule AA reacts with crack-tip bond BB to produce "terminal" bonds AB. (Reprinted with permission.[10])

The first term on the right-hand side is the potential energy of the loading system; the second term is the strain energy in the bendable bonds; the third term relates to the energy of the broken bonds; the fourth term is the energy of the nonlinear crack-tip bond; and the last term is the sum of the energy in the stretchable bonds ahead of the crack-tip bond. The bond-rupture energy is given by

$$U_b^r = \int_o^{2\mu_c} f_b \, d(2\mu_j) = U_{BB} \qquad (3)$$

i e , the energy of a BB bond. Here $2u_c$ represents a cut-off limit on the displacement Fuller, et al., show that a generalized force law for crack-tip bond rupture can be grouped into three terms.

(1) The applied driving force from external loads.
(2) The restoring force of the nonlinear creck-tip bond (BB).
(3) The restoring force exerted on the crack-tip bond by the remainder of the (linear) structure.

In effect, the crack structure in this model may be considered equivalent to a linear elastic continuum of an effective stiffness into which nonlinear separating atoms are embedded.

The adsorption of an A_2 molecule at the BB bond defining the crack tip alters the separation process shown in Figure 6. The total energy required to break the crack-tip bond is now given by

$$U_b^r \int_o^{2\mu_c} f_b \, d(2\mu_j) = U_{AA} + U_{BB} - 2U_{AB} \qquad (4)$$

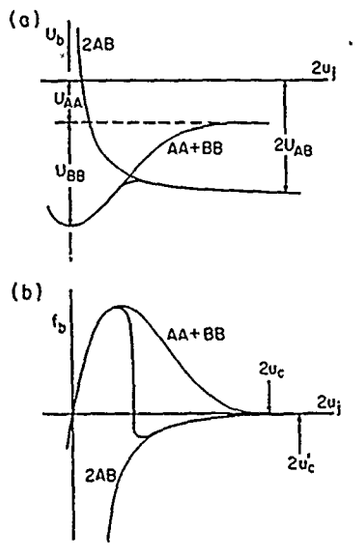


FIGURE 6—Potential energy (a) and force functions (b) for bonds subject to reaction in Figure 5(b). Heavy curves represent minimum energy state for any given BB bond displacement. Note crossover from AA + BB curve to 2AB curve at critical displacement (activated complex). Note also the reduction in bond-rupture energy (area under curve) resulting from the interaction. (Reprinted with permission.[10])

where U_{AA} is the energy required to break the AA bond bridging the crack tip. The chemically induced bond-rupture reaction

$$AA + BB \rightarrow 2AB \qquad (5)$$

is a function of μ_j, and [as shown in Figure 6(a)], for large enough μ_j, the reaction is favored. The crossover occurs for all $2U_{AB} > U_{AA}$, and [as shown in Figure 6(b)], as U_{AA} gets smaller, the crossover occurs at a smaller value of $2u_j$, so U_b^r is reduced. The model predicts that, although the area under the $f_b - 2u_j$ curve can change because of the environmental effect, the initial slope of the curve [$df_b/d(2u_j) = \alpha$] will not change. The lowering of U_{AA} has as its analogue a predissociated diatomic gas environment.

Hybrid models

Hybrid models involve two regions: an inner region, the region of interest, modeled as an atomistic region with a semiempirical potential, and an outer region, the elastic continuum in which the inner region is embedded. The Markworth, et al., paper discussed earlier is a good example.[3] The early work of the Sandia group, at the time headed by W.D. Wilson, also performed hybrid calculations of the properties of H in metals.[12] A molecular dynamic hybrid calculation for the H embrittlement of Fe was performed by Mullins and Dokainish.[13]

As discussed in the introduction, the major difficulties associated with the hybrid approach are in finding a good coupling scheme for the inner and outer regions. We do not know of any dependable technique developed to date in this regard and believe that new advanced coupling techniques need to be developed and tested. Researchers should be very careful in even using the qualitative predictions of *hybrid* calculations, as various spurious effects are introduced by the boundary schemes used.

Molecular dynamics

The molecular dynamic (MD) technique simulates atomic motion in solids.[14] "Atoms" are first placed at prescribed lattice positions corresponding to a two- or three-dimensional lattice structure. The atoms interact with one another according to an interatomic potential. External perturbations may be applied to this structure, or the structure may be allowed to relax to the minimum energy configuration for the system. The relaxation is accomplished dynamically by solving Newton's differential equations of motion by approximating them as difference equations. Paskin, et al., have used the form

$$\vec{r}_i(t+\delta) = -\vec{r}_i(t-\delta) + 2\vec{r}_i(t) + \sum_{j \neq i} \frac{\vec{f}_{ij}(\vec{r}_i, \vec{r}_j)}{m} \delta^2 \qquad (6)$$

where $r_i(t)$ is the position of the ith atom at time (t), and m is its mass, f_{ij} is the force exerted on the ith atom by the jth atom and is calculated from the interatomic potential (ϕ) by

$$\vec{f}_{ij} = -\nabla_i \phi(r_{ij}) \qquad (7)$$

The calculation of the force as a function of position using the embedded-atom method (EAM) potentials (described below) is accomplished by developing a table of neighbors and referring to it in the code. Molecular dynamic calculations are performed on a "finite" sample with free or periodic boundary conditions.[14] Depending on the "range" of the interatomic potential used (1st, 2nd, 3rd . . . nearest neighbor), the behavior of up to ~ 10^5 atoms can be simulated with the use of a computer such as a Cray. We will examine two molecular dynamic calculations relating to environmental effects on fracture: that of Daw, Baskes, Bisson, and Wolfer,[16] who used the EAM to study the H embrittlement of Ni and the calculations by Paskin, Sieradzki, Som, and Dienes[15] on the film-induced cleavage process.

Daw, Baskes, Bisson, and Wolfer examined the fracture of a slab of Ni periodic in the x and z direction with a central crack, as illustrated in Figure 7.[16] In the EAM, the energy of an atom (i) in the solid is given by

$$E_i = F(\rho_i) + 1/2 \sum_{j \neq i} \phi(r_{ij}) \qquad (8)$$

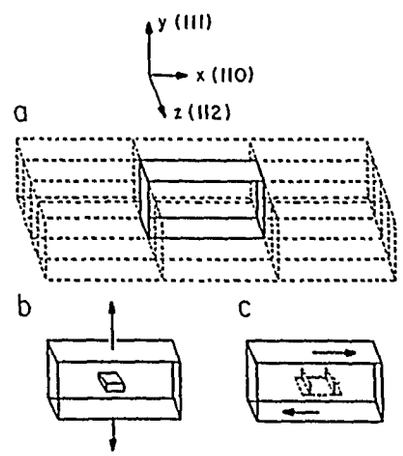


FIGURE 7—Illustration of the basic slab geometry used in the calculations of Reference 16. The crystallographic directions are as drawn. (a) The slab is finite in one direction and periodic in the other two. The finite direction is along the (111) axis, so the two-dimensional, periodic plane is the slip plane in nickel. The unit periodic cell is outlined in dark, with some of its neighboring identical periodic cells drawn in light. The top and bottom surfaces, shaded in the figure, are free (111) surfaces. The two periodic directions are chosen to be (110) and (112). Thus, the x-direction is the slip direction and the z-direction is along the axis of dislocation cores. (b) For the brittle-fracture calculations, a crack may be introduced in the material and forces are supplied normal to the free surfaces (normal to the slip planes). This produces a tensile stress. (c) For the dislocation dynamics calculations, a dislocation is introduced, and the forces are applied to the free surfaces along the slip direction. This produces a shear stress. (Reprinted with permission.[16])

ρ_i is the electron density at atom (i) because of the remaining atoms in the system and is assumed to be describable to accurate precision as a superposition of atomic densities:

$$\rho_i = \sum_{j \neq i} \rho_j^a (r_{ij}) \quad (9)$$

where the ρ_j^a is the atomic electron density contributed by atom (j) at a distance (r) from atom (i). $F_i(\rho_i)$ is the energy required to embed atom (i) into the electron density and is obtained by fitting to an empirical universal binding-energy curve such as

$$E_{univ} = -E_s (1 + a^*) e^{-a^*} \quad (10)$$

where $a^* = (a - a_o)/\lambda$; a_o is the lattice constant of the host (Ni), $\lambda = (9a_o K/4E_s)^{1/2}$, E_s is the sublimination energy for Ni, and K is the bulk modulus of Ni. The embedding function $[F(\rho_i)]$ for an element is universal in the sense that it is *independent of the source* of the electron density. They examined the fracture properties for the Ni slab shown in Figure 7 for the following cases: (a) the perfect material, (b) with a hydride (a H atom in every octahedral interstitial site), and (c) with H at full stoichiometry (a H atom at every octahedral interstitial site) *on the crack plane* in advance of the tip. They studied different slab widths in the (111) direction and various stressing rates and claim results independent of size-effect considerations. Their results are summarized together with our comments below.

(1) H moderately alters the fracture stress of "brittle" Ni by weakening the metallic crack-tip bonds. This is the embrittlement form discussed by Troiano[17] and results from a many-body effect.

(2) The H-dislocation interaction up to 300°K in temperature is elastic and weak.

(3) *In a system configured for slip,* H increases the nucleation rate of dislocations at 300°K. This does not mean that H transformed a brittle crack (orientation) in Ni into a ductile one, but rather that H tends to make a ductile crack (orientation) slightly more ductile.

(4) High H contents, ≈10 at% can pin dislocations in Ni.

We believe, based on our previous experience regarding size efforts in MD simulations of fracture processes, that several aspects of these EAM fracture results should be treated with caution. First, the brittle-ductile response of a solid can be greatly affected by the distance between the crack plane and the external boundary at which loads are being applied. Early results on Lennard-Jones (LJ) solids indicated that small samples using a constant-load boundary condition tended toward more ductile behavior than samples loaded by a constant-displacement boundary condition (see Reference 15 and references contained therein). This effect saturates for samples considerably larger than the 14-layer sample used by Daw, et al., in their calculations.[16] This means that even the qualitative nature of some of their results discussed above (i.e., those involving dislocations) are in question.

The embedded-atom potentials, which can be used in various computational simulation schemes, represent a significant advance over the pair-potential approach. The EAM, however, is yet to be exploited in a serious way for fracture problems, so this represents a fertile area of study for the future.

Paskin, Sieradzki, Som, and Dienes performed two-dimensional molecular dynamic simulations of environmental fracture processes in LJ solids.[15] The atoms were configured in a triangular lattice in centrally cracked" rectangular samples ranging in size from 608 atoms arranged in 19 rows to 10,680 atoms arranged in 79 rows. The samples were loaded in a quasi-static manner using a constant-load boundary scheme at the upper and lower boundaries. The crack surfaces were coated with thin films of varying thickness. The films represent the analogue of a reaction product for a metal-environment system. The thin films are composed of LJ material but with a different elastic modulus or lattice parameter from the host substrate material. Spectacular alterations of the fracture processes in the intrinsic host LJ material were observed in the situation for which the lattice parameter of the film differed from that of the substrate. Their results are summarized below.

(1) In situations such that the lattice parameter of the film is less than that of the substrate, coherency stresses act in a manner so as to embrittle the intrinsically ductile LJ material. For a large enough misfit, a cleavage crack is nucleated in the film and continues on into the substrate as illustrated in Figure 8. This effect was termed "dynamic embrittlement" and represents the computer analogue of film-induced cleavage. Figure 9 shows that as the number of film layers increase, the degree of embrittlement increases. This behavior is qualitatively similar to the gaseous Cl_2-induced cracking of a steel studied by Sieradzki.[15]

(2) In situations in which the lattice parameter of the film is greater than that of the substrate, coherency stresses inject dislocations into the substrate, as shown in Figure 10. The film-substrate interface serves as the source of the mobile dislocations, and the dislocation glide plane is different from what it is in the monolithic LJ material.

These authors speculated that film-induced dislocation injection may be a mechanism of liquid-metal-induced, enhanced shear processes.

Cluster Schemes

The Xα self-consistent field-scattered wave (SCF-Xα-SW) method

The so-called SCF-Xα-SW cluster method is based upon the combined use of Slater's Xα statistical theory of exchange correlation[19] and Johnson's multiple scattered-wave formalism.[20] This technique allows one to derive information on the electronic structure of small clusters of atoms. It has been applied to impurity-metal clusters of atoms that may be representative of impurity grain-boundary interactions leading to intergranular embrittlement. Such calculations were first performed by Briant and Messmer.[21] Recently, Eberhart, Johnson, Messmer, and Briant reviewed the application of this method to grain-boundary fracture processes.[22] The results of the calculations are represented in the form of energy-level diagrams and charge-density plots from which information regarding impurity effects on cohesion is inferred.

As representative of work in this area, we review calculations of Messmer and Briant on the effect of S and B impurities on binding in Ni clusters.[23] Ashby, Spaepen, and Williams have shown that the structure of a grain boundary in fcc solids can be described in terms of atoms at the vertices of Bernal deltahedra.[24] These are clusters containing 4 to 13 atoms. In this particular work, Messmer and Briant chose the tetrahedron shown in Figure 11. Figure 12 shows the energy-level diagrams for the Ni_4S and the Ni_4B clusters. The 1a and 1t wave functions describe the metal-impurity interaction. Figure 13 shows the charge-density plots for these clusters. Their results indicate the following characteristics of a strong embrittler:

(1) A heavy concentration of charge on the impurity atom.

(2) The impurity is electronegative with respect to the host atom, i.e., the formation of an ionic impurity–metal bond.

On the other hand, for a so-called cohesive enhancer, the metal-impurity bond is more equally shared, or covalent.

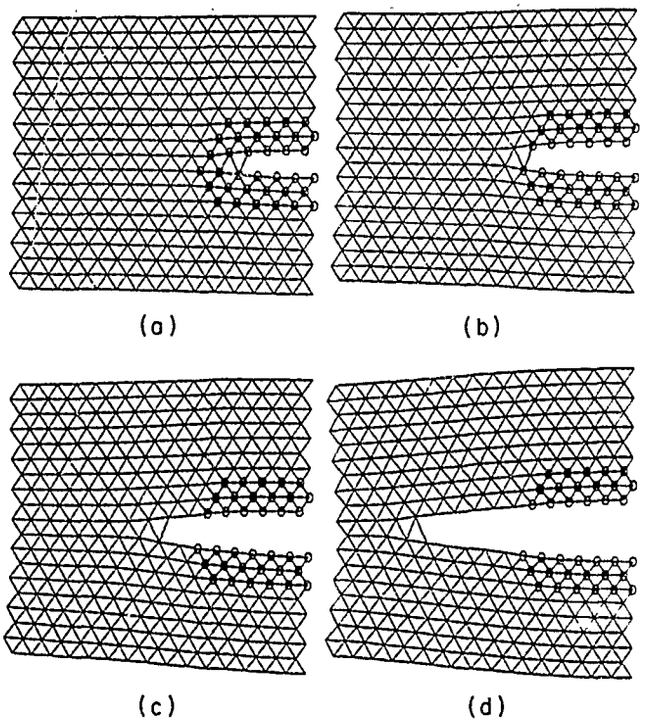


FIGURE 8—Brittle crack propagating with 3 layers of "small film atoms," d = 0.95 d_0. The external tensile load was increased from 1.25 to 1.31 at step number 400. Incipient breakage shown in (a) at step number 600. The film-film bonds are broken at step number 500 (b), clean brittle propagation is shown at step number 1000 (c) and 1200 (d), with no indication of any incipient dislocations. (Reprinted with permission.[15])

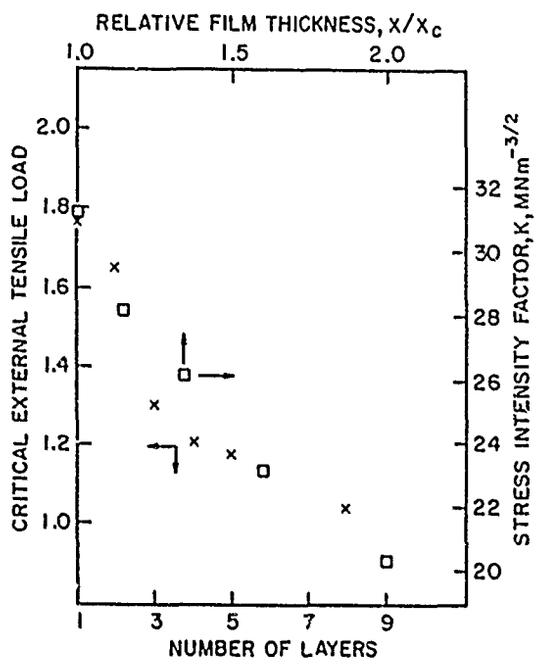


FIGURE 9—The critical external tensile load (X) required to cause brittle crack propagation as a function of the number of layers of "small film atoms" (d = 0.95 d_0). Large sample of half size 39 by 32. Some experimental data (□) are shown for comparison as stress-intensity factor vs relative film thickness (X/X_c) where X is the threshold film thickness. (Data from Reference 18. Figure reprinted with permission.[15])

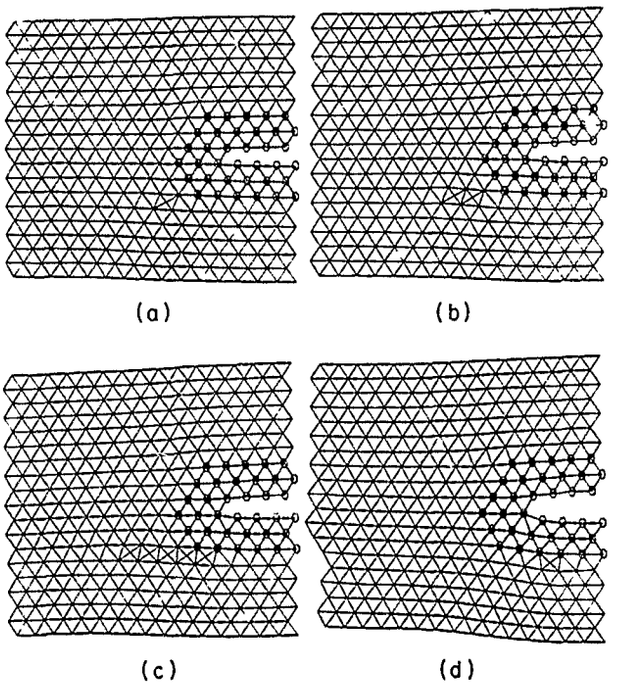


FIGURE 10—Three layers of "large film atoms" (d = 1.10 d_0) with a crack of 7 broken bonds. (a) External tensile load of 1.5—incipient deformation between Rows 6 and 7; (b) load increased to 1.65—increased deformation; (c) load increased to 1.50—incipient dislocation along X-direction between Rows 6 and 7; and (d) load increased to 1.95—dislocation moved out along X-direction forming a jog. (Reprinted with permission.[15])

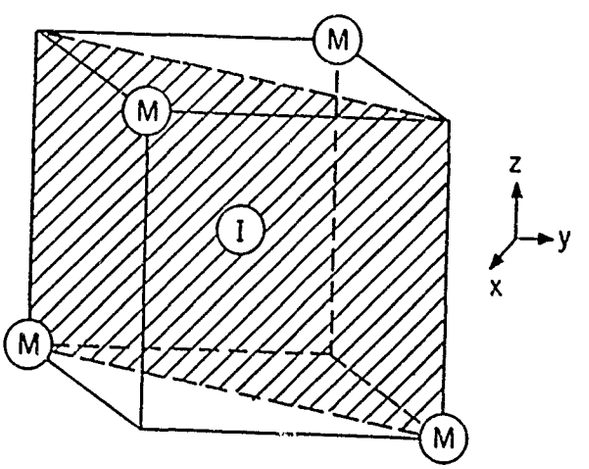


FIGURE 11—The tetrahedron used by Messmer and Briant. The metal atoms (M) are placed at the vertices and the impurity (I) in the center. The cross-hatched plane is the one used for the contour plots shown in Figure 13. (Reprinted with permission.[21])

Density-functional calculations

Various density-functional schemes have been used to model the effects of impurity bonding on grain-boundary embrittlement. These calculations offer quantum mechanical solutions for small clusters or cells of atoms using carefully chosen, approximate techniques to solve the many-body quantum-mechanical problems and yield information on the electronic structure and total energy of these clusters. We briefly review two examples of these calculation schemes below.

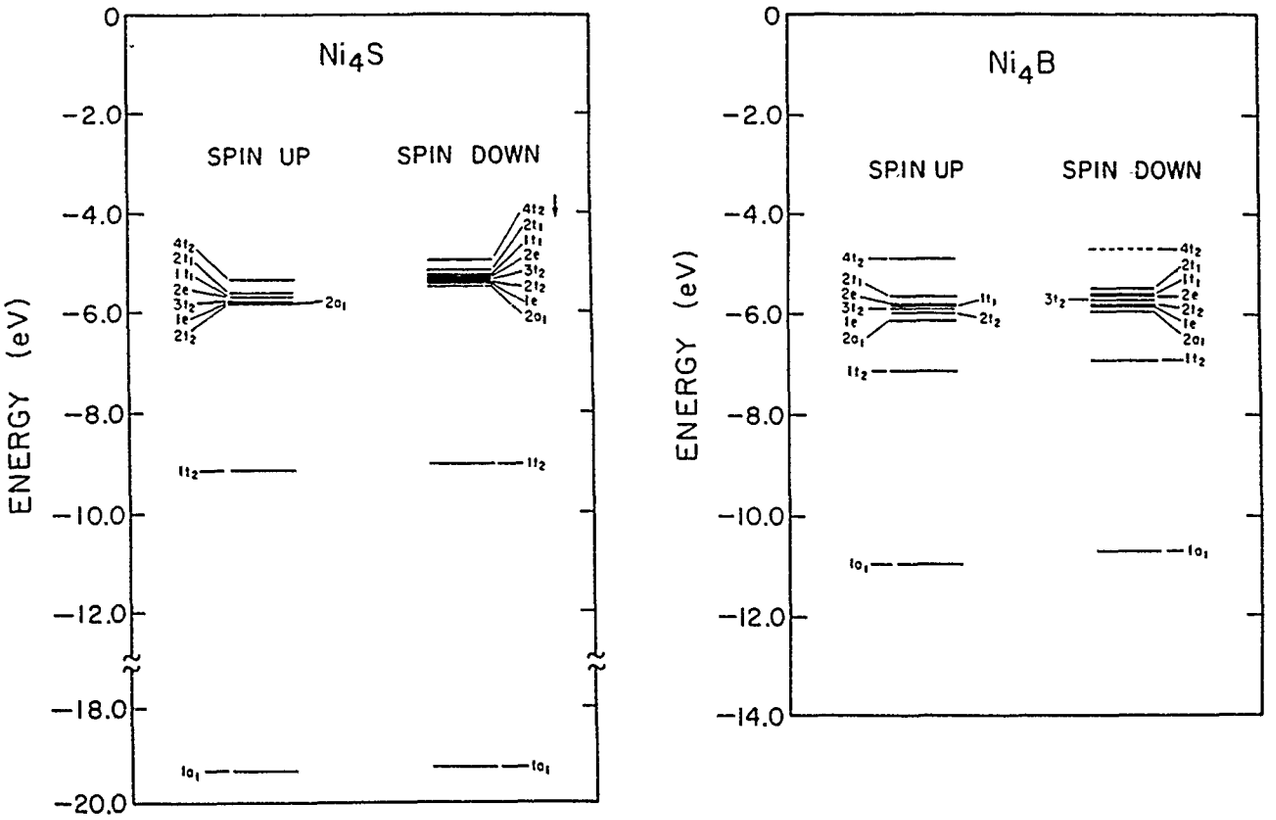


FIGURE 12—The energy-level diagram for the (a) NIS and (b) NIB cluster. (Reprinted with permission.[21])

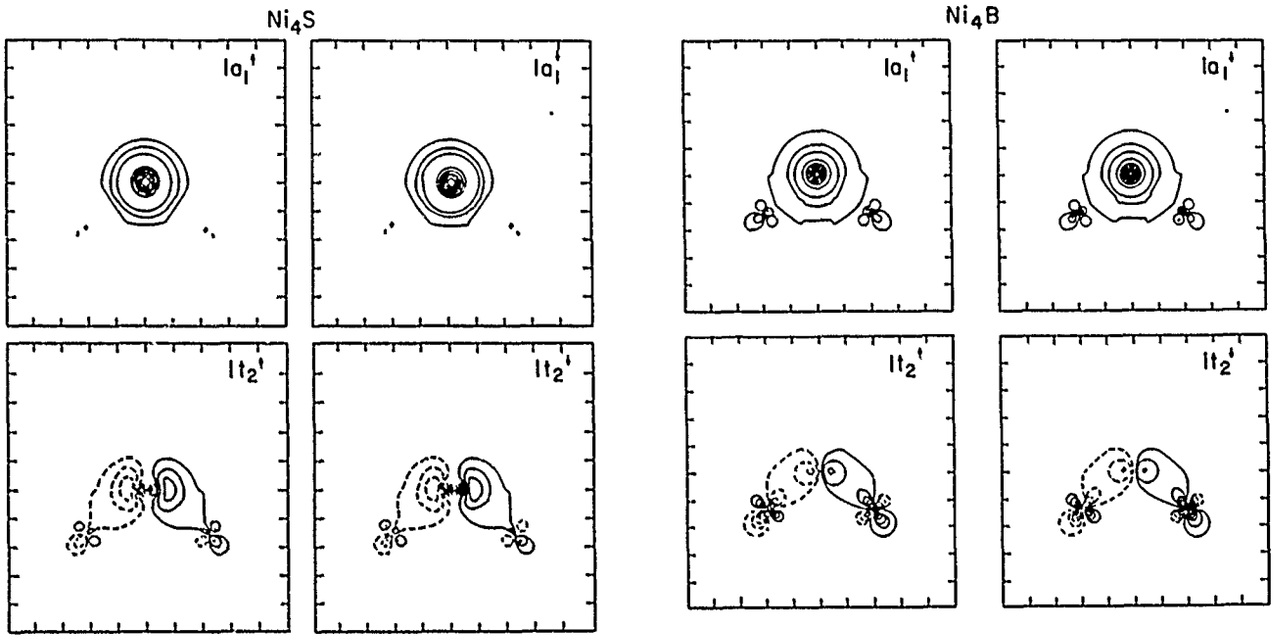


FIGURE 13—The orbital contour plots of the Ia and It orbitals (a) NIS and (b) NIB. (Reprinted with permission.[21])

Goodwin, Needs, and Heine examined the effect of Ge and As impurities on the fracture energy of a small cell of Al oriented for (111) fracture [25] Figure 14 is a schematic depiction of the cell for bulk and fractured Al with 6 (111) layers of 3 atoms per layer. The purpose of the simulation was to provide a test of two alternative views of embrittlement: (1) Embrittlement results from the formation of a weak metal-impurity bond, as first proposed by Troiano,[17] or (2) embrittlement results by the formation of a strong metal-impurity bond with the concomitant weakening of metal metal bonds, as proposed by Losch[26] and elaborated by Briant and Messmer.[21] The results of Goodwin, et al., are listed in Table 1, where the energies to fracture pure Al and impurity-doped Al both at the impurity-doped layer and one layer into the Al have been determined. These results indicated that the impurities caused small enhancement in cohesion, so they concluded that both the Troiano[17] and Losch[26] notions of embrittlement were not correct. They proposed that current ideas on embrittlement be replaced by a model proposed by Hadock.[27]

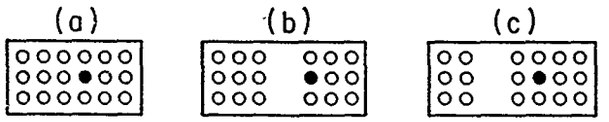


FIGURE 14—Schematic depiction of the supercells for bulk and fractured material with six (111) layers of three atoms per layer. The open circles are Al atoms and the filled circles impurity atoms. (a) Unfractured bulk material. (b) Fractured at the impurity-doped layer. (c) Fractured one layer distant from the impurity. (Reprinted with permission.[25])

TABLE 1
Energies of Fracture (E) for Pure and Impurity-Doped Al[(A)]

Impurity	E (eV)
Al	$E_a - E_b = 1.80$
As	$E_a - E_b = 1.94$
As	$E_a - E_c = 1.88$
Ge	$E_a - E_b = 1.82$
Ge	$E_a - E_c = 1.89$

[(A)]Calculated as the difference in energy between the unit cells of Figures 14(a), (b), or (c), where E_a denotes the total energy per unit cell of the structure shown in Figure 14(a), etc. Hence, E is the fracture energy to create a crack of area equal to 3 atoms, or 2.10 mm^2. (Reprinted with permission.[25])

The Goodwin, Needs, and Heine[25] calculation has been sharply criticized by Briant and Sieradzki[28] on the grounds that the authors chose to examine a system for which (experimental) embrittlement is not known to occur. Goodwin, Needs, and Heine have the misconception that the Troiano and Losch ideas predict that *all* grain-boundary impurities should lead to embrittlement. Briant and Sieradzki[28] have suggested that Goodwin, et al., repeat their calculations for a metal-impurity system, which is known to display embrittlement.

Using a density-functional approach, Painter and Averill examined the effect of a S and B interstitial on the stability of the octahedral Ni cluster shown in Figure 15.[29] They obtained rigorous results for the electronic structure, total energies, and restoring forces in atomic clusters Their results for the binding energy and local force as a function of the metal-impurity separation are shown in Figure 16. They found that B binds in the Ni host much more strongly (7.0 eV) than S (2.2 eV) and produces *less* of an expansion of the host cluster (12%) than does S (23%). Much of the difference in binding energy is a consequence of the larger Ni host strain energy (5.0 eV) required to accommodate S compared with B (2.0 eV). This means that for hole sizes close to the hole size of the stable Ni octahedral cluster, B is stable (3.0 eV), whereas S is unstable by more than 14 eV.

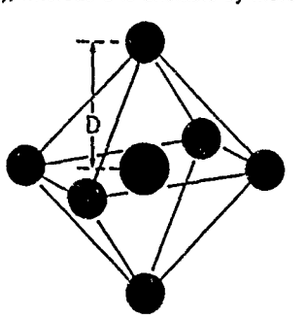
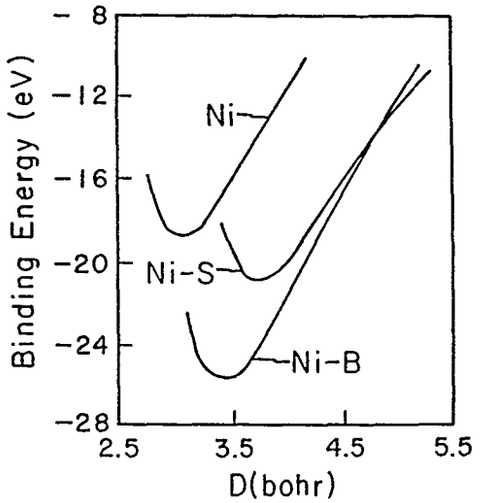


FIGURE 15—Octahedral Ni cluster used by Painter and Averill with interstitial impurity atom at center and host atoms a distance D away. (Reprinted with permission.[29])



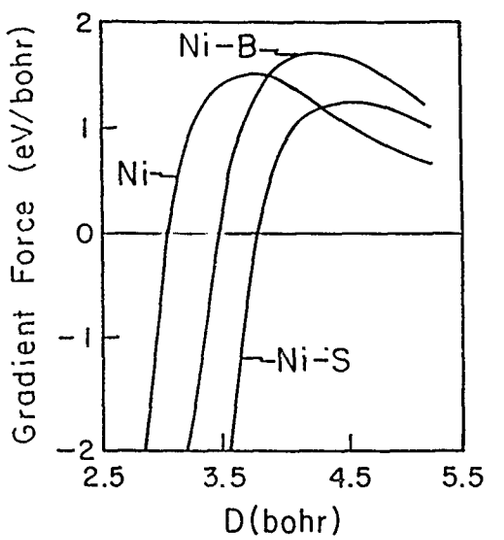


FIGURE 16—(a) Binding-energy variation with cluster radius D, the distance from the origin (impurity site) to one of the Ni atoms of the host octahedral cluster, for pure Ni and clusters containing boron (Ni-B) and sulfur (Ni-S). (b) Gradient force dependence on cluster radius (D) for pure octahedral nickel cluster (Ni) and clusters containing boron (Ni-B) and sulfur (Ni-S) in the octahedral interstice. Attractive forces on a reference nickel atom are negative and repulsive are positive.

These results are in qualitative agreement with the predictions of the Briant and Messmer[21] calculations discussed in the section on the SCF-Xα-SW method We believe that a coherent picture is beginning to emerge regarding the effect of impurities on interfacial separation processes. A thermodynamic analysis developed by Rice predicts that embrittling elements should segregate more strongly to free surfaces than internal interfaces (e.g., S in Ni),[30] whereas a cohesive enhancer should segregate more strongly to the internal interface than the free surface (e.g., B in Ni). Recent experimental results suggest that B does not segregate to free surfaces in Ni,[31] thus supporting the contention that B should act as a cohesive enhancer in Ni. The ductilizing effect of B on polycrystalline Ni_3Al is well known[32] and is in agreement with these concepts. The density-functional calculations[29] discussed above are also in qualitative agreement with these results, so a fundamental understanding of these processes is emerging. It is certainly unfortunate that Goodwin, Needs, and Heine chose to examine an irrelevant system.[25] Their approach applied to the Ni-B and Ni-S system would provide valuable insights into the actual separation process that other approaches have not addressed.

Micromechanical Modeling

Most of the micromechanical modeling of environment-assisted fracture has been directed toward the hydrogen-embrittlement problem.[33] Here we cannot possibly attempt to review the large quantity of literature on this topic; instead, we choose to discuss several new approaches developed in the last 15 years applicable to a wide range of problems associated with environmental effects on fracture.

In the early seventies, Rice and Thomson (RT) developed a model for predicting the brittle vs ductile response of a cracked solid.[34] They examined the nucleation processes associated with the emission of a dislocation from a crack tip within the continuum elastic sharp-crack model and the Peierls model of a dislocation core. Their work clearly demonstrates the conceptual fallacy regarding *simple* adsorption mechanisms of embrittlement. Consider the Griffith criteria relating the fracture stress (σ_G) to the reversible work to create two free surfaces. 2γ and $\sigma_G = (2E\gamma/\pi a)^{1/2}$, where γ is the surface free energy, E is Young's modulus, and 2a is the crack length. Adsorption processes occurring at constant temperature alter the surface free energy, according to the Gibb's adsorption isotherm, $d\gamma = -\Gamma d\mu$, where μ is the chemical potential of the adsorbate and Γ is the surface excess. The RT analysis shows that the alteration of the work to fracture by an adsorption process is not related to σ_G by a *simple* substitution of the Gibb's adsorption isotherm into the Griffith equation. They show that such an adsorption process may change the entire ductile-brittle response of a cracked solid; i.e., the alteration in the work to fracture could involve a fracture mode *transition*. An approximate criterion for predicting the ductile-brittle response of a solid resulting from their analysis is that brittle behavior is predicted for $\mu b/10\gamma > \xi_o$, whereas if the inequality is reversed, a ductile crack response is predicted. Here μ is the shear modulus, γ is the relevant surface or interfacial free energy appropriate for the surface created in the fracture process, and ξ_o is the dimensionless core cut-off distance for the dislocation in the solid.

Interfacial separation processes

We consider now in some detail the application of the RT model to interfacial separation processes following the analysis presented by Mason.[35] Figure 17 illustrates the problem analyzed by Mason, who considered the energetics of nucleating a dislocation loop at a crack tip in a solid. The activation energy (U_{act}) required to create a semicircular dislocation loop of radius (rb) in a crystal having a core cut-off radius ($\xi_o b$) for the dislocation is given by

$$U_{act} = \frac{2-\nu}{8(1-\nu)}\mu b^3 r \ln\frac{r}{\xi_o} + \frac{2}{\beta'}\gamma_{step} b^2 (r-\xi_o) - \frac{1.395}{\beta}\frac{b^2}{\sqrt{1-\nu}}\sqrt{\mu b\gamma_{int}}\,(r^{3/2}-\xi_o^{3/2}) \quad (11)$$

where β and β' are orientational factors, γ_{step} is the surface energy per unit area of the step formed by the nucleation of the dislocation at the crack tip, and $2\gamma_{int}$ is the energy associated with the reversible formation of the two free surfaces. The first term corresponds to the self-energy of the dislocation loop, the second term is associated with the energy of the ledge as the dislocation is nucleated, and the third term represents the energy decrement that results from introducing the dislocation into the stress field of the crack tip. Following Mason, we calculate the value of the stress intensity (K_{crit}) required to nucleate a semicircular dislocation loop of critical radius ($r_{crit}b$):

$$U_{act} = \frac{2-\nu}{8(1-\nu)}\mu b^3 r \ln\left(\frac{8}{e}\frac{r}{\xi_o}\right) + \frac{2\gamma_{step} b^2 r}{\beta'} - \frac{3(0.986)}{2\sqrt{2}} K b^{5/2} r^{3/2} \quad (12)$$

where $2\gamma_{int}$ has been replaced by $G = K^2(1-\nu)/2\mu$.

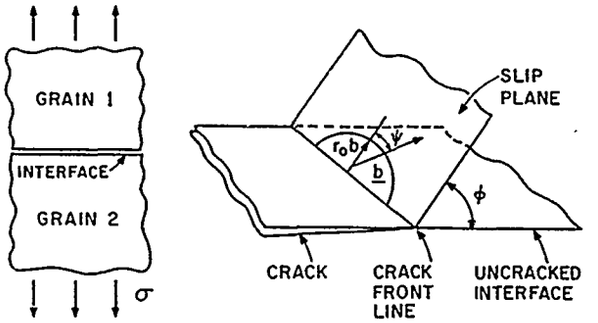


FIGURE 17—Grain-boundary model and crystallographic parameters. (Reprinted with permission.[35])

The force acting on the dislocation loop at equilibrium is given by the condition $dU/dr = 0$. The critical radius of the loop that corresponds to an instability condition is given by $d^2U/dr^2 = 0$. The following solutions are obtained:

$$r_{crit} = \frac{e^2\xi_o}{8}\exp(-5S) \quad (13a)$$

$$K_{crit} = \frac{2-\nu}{6(1-\nu)}\frac{\sqrt{2}\beta}{0.986}\frac{\mu b^{1/2}}{r_{crit}^{1/2}} \quad (13b)$$

where

$$S = -\frac{2\gamma_{step}}{\mu\beta\beta'}\frac{8(1-\nu)}{2-\nu} \quad (14)$$

Finally, taking the ratio of $G_{crit}/2\gamma_{int}$

$$G_{crit}/2\gamma_{int} = \frac{0.058}{R_o S}\exp(5S) \quad (15)$$

where

$$R_o = \left[\frac{16\beta'}{5(2-\nu)\beta^2}\right]\xi_o\frac{\gamma_{int}}{\gamma_{step}} \quad (16)$$

For $G_{crit}/2\gamma_{int} > 1$, brittle behavior is predicted as shown in Figure 18.

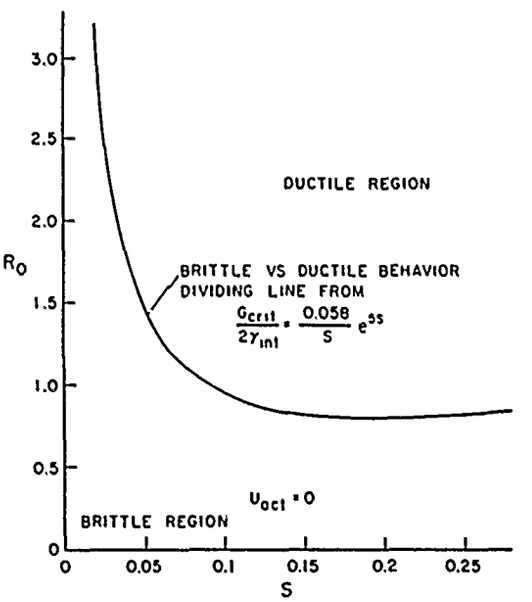


FIGURE 18—Regions of brittle and ductile behavior on R_o-S plane. (Reprinted with permission.[35])

Let us consider the application of this criteria to the well-known intergranular embrittlement of Fe by Sn. We choose this system because existing data of Seah and Hondros allows us to derive the grain-boundary and free-surface-adsorption isotherm for Sn in Fe.[36] Additionally, Kameda and McMahon have determined the K_{crit} values vs grain-boundary Sn coverage for a HSLA steel,[37] which allows us to compare our predictions with experiment.

For this system, we *approximate* $2\gamma_{int}$ as $2\gamma_{int} \approx 2\gamma_s - \gamma_{GB}$, where γ_s and γ_{GB} are the interfacial energies for the free surface and grain boundary, respectively. This expression represents the reversible work of separation while the surfaces are maintained at chemical composition equilibrium. It assumes a mobile segregant, which is not the case for the Sn-Fe system for a low-temperature separation process. For this case, the work to fracture, $2\gamma_{int} > 2\gamma_s - \gamma_{GB}$. We will examine the cases for which $\gamma_{step} = \gamma_s$ and $\gamma_{step} = \gamma_s^o$, where γ_s is the surface free energy of iron for an amount of Sn (θ_{Sn}) adsorbed or (segregated) at the surface, and γ_s is the intrinsic value of the surface free energy of Fe. The free-surface and grain-boundary adsorption isotherms derived from the Seah and Hondros data[36] are shown in Figure 19. γ_s ranges from the intrinsic value of $\gamma_s^o = 2.09$ to 1.2 Jm^{-2} for $\theta_{Sn} \approx 0.4$, and γ_{GB} ranges from 0.8 Jm^{-2} to 0.4 Jm^{-2} for $\theta_{Sn}^{GB} \approx 0.4$. Figure 20 is the plot for $R_o - S$ for the following three cases:

(a) Pure Fe; $\gamma_s^o = 2.09\ J\text{-}m^{-2}$, $\gamma_{GB} = 0.795\ J\text{-}m^{-2}$, $\gamma_{step} = \gamma_s^o$

(b) $\theta_{Sn}^{GB} = 0.4$, $\gamma_s = 1.28\ J\text{-}m^{-2}$, $\gamma_{GB} = 0.42\ J\text{-}m^{-2}$, $\gamma_{step} = \gamma_s$

(c) $\theta_{Sn}^{GB} = 0.4$, $\gamma_s = 1.28\ J\text{-}m^{-2}$, $\gamma_{GB} = 0.42\ J\text{-}m^{-2}$, $\gamma_{step} = \gamma_s^o$

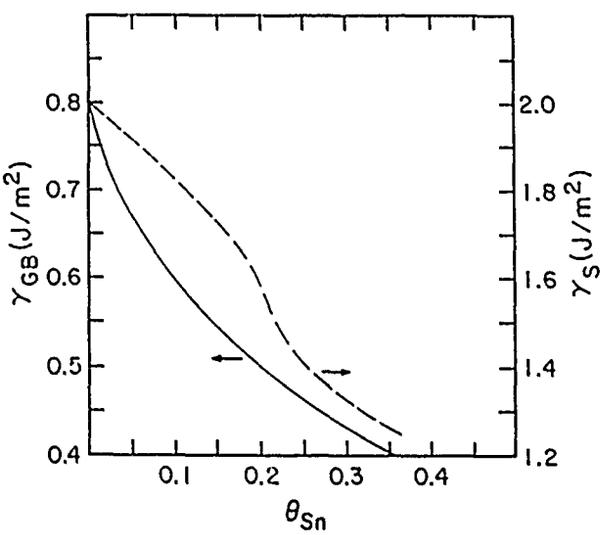


FIGURE 19—The grain-boundary energy and surface energy as a function of Sn coverage.

The results are in general agreement with the data of Kameda and McMahon;[37] however, our results are not sensitive enough for quantitative comparison with experiment. There is a trend of more brittle behavior, which is predicted for Cases (b) and (c) compared with the behavior of the intrinsic grain boundary, Case (a). Furthermore, consider the situation if a dislocation is nucleated at the sharp interfacial crack. The monotonic step that forms at the crack develops from the grain- boundary surface, and since the step width approximates the width of the grain boundary, $\gamma_{step} \approx \gamma_s$. What is the situation for the nucleation of the second (or third) dislocation? The next step that forms will require the formation of a surface not previously associated with the grain boundary, so that $\gamma_{step} \approx \gamma_s^o$ will represent the more appropriate value. Figure 20 shows that the analysis predicts more brittle behavior for Case (c) than Case (b), which indicates that a fracture-mode transition may occur, i.e., even if the system behavior is initially ductile, subsequent dislocation emission may not be energetically favored and brittle intergranular fracture could result.

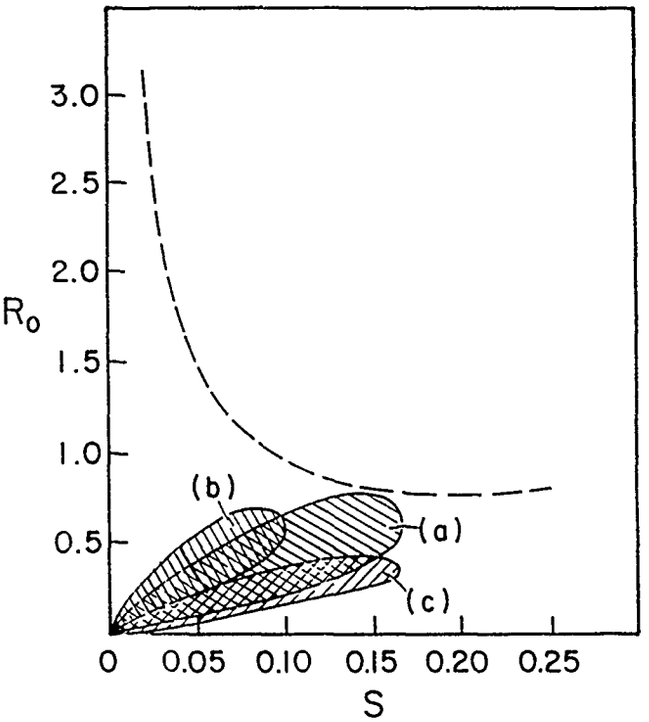


FIGURE 20—Drop-shaped regions represent points for crack-plane normals. Crack-plane normals are determined from points in (100) standard triangle. Uniform scatter within drop-shaped regions.

(a) Pure Fe

(b) $\theta_{Sn}^{GB} = 0.4$, $\gamma_s = 1.28\ J\text{-}m^{-2}$, $\gamma_{GB} = 0.42\ J\text{-}m^{-2}$, $\gamma_{step} = \gamma_s$

(c) $\theta_{Sn}^{GB} = 0.4$, $\gamma_s = 1.28\ J\text{-}m^{-2}$, $\gamma_{GB} = 0.42\ J\text{-}m^{-2}$, $\gamma_{step} = \gamma_s^o$

Film-induced cleavage

In a series of papers, Sieradzki and Newman developed a model for transgranular SCC.[38-40] The general features of the model are apparent in the atomistic simulations of Paskin, et al.[15] Brittle fracture initiates in a film formed by a reaction with the environment. Once brittle fracture has initiated in the film, Sieradzki and Newman discussed the conditions required for transmission of cleavage into the substrate and calculated arrest distances in the substrate.[40] We refer the interested reader to the appropriate references for the details of the calculations.[38-40] Here we discuss the predictions of the model and pay particular attention to films that may form by a dealloying process.

We consider a film to be intrinsically brittle or ductile depending on its behavior as predicted by the RT analysis.[34] If the film behavior is *intrinsically brittle*, the relevant analysis relates to the transmission of the dynamic crack across the interface, which is used to calculate crack arrest distances.[40] We believe that dealloyed layers that initiate a film-induced cleavage event are intrinsically brittle.[41] However, it is important to point out that because of coarsening processes operative during dealloying,[42] not all dealloyed layers are uniform enough, thick enough, or fine enough *vis à vis* size scale[43] to disply brittle behavior. For films that show intrinsic ductile behavior, brittle behavior of the film substrate composite is still theoretically possible, provided that the film is coherent with the substrate, the film has a smaller lattice parameter than the substrate, and the lattice parameter mismatch is large enough. Depending upon the magnitude of lattice-parameter misfit, film thickness, and $2\gamma_{int}$ of the substrate, SCC behavior is possible under vanishingly low applied

external loading If the lattice parameter of the film is greater than that of the substrate, film-induced cleavage is predicted only if the film is intrinsically brittle.

Conclusion

We believe that a clear and consistent picture is emerging regarding intergranular separation or embrittlement processes. There is good agreement between quantum mechanical, density-functional calculations, thermodynamics, and experiment. Future work in this area would profit from using realistic potentials and large cells in various atomistic schemes such as molecular dynamics. Transgranular SCC processes seem to be describable in terms of the film-induced cleavage process. Further experimental and theoretical work needs to be done in this area. Experimental work should focus on defining the kinetics of dealloying, the morphology of dealloyed layers, and the intrinsic mechanical properties of dealloyed layers. Additionally, actual measurements of the dynamic crack during a film-induced cleavage event would provide valuable information for the modeling. Finally, we believe that intergranular SCC is the least understood environment-assisted-fracture phenomenon. As we discussed, there are many difficulties with the Vermilyea model;[2] nevertheless, there can be little doubt that at least some intergranular SCC occurs by a pure electrochemical anodic dissolution process. The details regarding crack advance by such a process remain unclear.

Acknowledgment

The author would like to acknowledge D. Cubicciotti and the support of EPRI under contract No. RP2812-5 during the preparation of this manuscript.

References

1. Stress Corrosion Cracking and Hydrogen Embrittlement of Iron Base Alloys, NACE-5, ed. R.W. Staehle, J. Hochmann, R.D. McCright, J.E. Slater, held June 12-16, 1973, Unieux-Firminy, France, (Houston, TX: National Association of Corrosion Engineers, 1977).
2 D Vermilyea, Stress Corrosion Cracking and Hydrogen Embrittlement of Iron Base Alloys, pp. 208-217.
3 A.J Markworth, M.F. Kanninen, P.C. Gehlen, Stress Corrosion Cracking and Hydrogen Embrittlement of Iron Base Alloys, pp. 447-454.
4. H.L. Logan, J. Res. Nat. Bur. Stnd. 48(1952): p. 99.
5 T P Hoar, G. Hines, J. Iron and Steel Inst. 177(1954). p. 248.
6. P.C. Paris, G.C. Sih, Fracture Toughness Testing and its Applications, STP 381 (Philadelphia, PA: ASTM, 1965), pp. 30-76.
7. J.N. Goodier, Fracture, Vol. 2, ed. H. Liebowitz (New York, NY: Academic Press, 1966), pp. 2-66.
8. J.W. Hutchinson, J. Mech. and Phys. Solids. 16(1968): p. 13; J. R. Rice, G.F. Rosengren, J. Mech. and Phys. Solids, 16(1968): p. 1.
9. J.R. Rice, Fracture, Vol. 2, pp. 192-308.
10. E.R. Fuller Jr., B.R. Lawn, R.M. Thomson, Acta Metall. 28(1980): p. 1407.
11. G.J. Dienes, A. Paskin, Atomistics of Fracture, ed. R.M. Latanision, J.R. Pickens, Proceedings of the NATO Workshop, held May 1981, Corsica (New York, NY: Plenum Press, 1983), p. 671.
12 C F Melius, C.L. Bisson, W.D. Wilson, Phys. Rev. B. 18(1978). p. 1647.
13 M Mullins, M.A. Dokainish, Phil. Mag. 46(1982). p. 771.
14 D O Welch, G.J. Dienes, A. Paskin, J. Phys. Chem. Solids 39(1978): p. 589.
15 A Paskin, K Sieradzki, D.K. Som, G.J. Dienes, Acta Metall. 30(1982): p. 1781; 31(1983): p. 1258.
16. M.S. Daw, M.I. Baskes, C.L. Bisson, W.G. Wolfer, Modeling Environmental Effects on Crack Growth Processes, ed. R.H. Jones, W.W. Gerberich (Warrendale, PA: The Metallurgical Society of the American Institute of Mining, Metallurgical, and Petroleum Engineers, 1986), p. 99.
17. A. Troiano, Trans. ASM 52(1960): p. 54.
18. K. Sieradzki, Acta Metall. 30(1982): p. 973.
19. J.C. Slater, Advances in Quantum Chemistry, Vol. 6, ed. P.O. Lowden (New York, NY: Academic Press), p. 1.
20. K.H. Johnson, Advances in Quantum Chemistry, Vol. 7, ed. P.O. Lowden (New York, NY: Academic Press), p. 143.
21. C.L. Briant, R.P. Messmer, Phil. Mag. 42(1980): p. 569.
22. M.E. Eberhart, K.H. Johnson, R.P. Messmer, C.L. Briant, Atomistics of Fracture, p. 255.
23. R.P. Messmer, C.L. Briant, Acta Metall. 30(1982): p. 457.
24. M.F. Ashby, F. Spaepen, S. Williams, Acta Metall. 26(1978): p. 1647.
25. L. Goodwin, R.J. Needs, Volker Heine, Phys. Rev. Lett. 60(1988): p. 2050.
26. W. Losch, Acta Metall. 27(1979): p. 1885.
27. R. Hadock, J. Phys. C. 14(1981): p. 3807.
28. C.L. Briant, K. Sieradzki, Phys. Rev. Lett., in press 1989.
29. Painter, Averill, Phys. Rev. Lett. 58(1987): p. 234.
30. J.R. Rice, Effect of Hydrogen on the Behavior of Materials, ed. A.W. Thompson, I.M. Bernstein (Warrendale, PA: TMS-AIME, 1976), p. 455.
31. C.C. Koch, C.L. White, R.A Padgett, C.T. Liu, Scripta Metall. 19(1985): p. 963.
32. K. Aoki, O. Izumi, J. Jap. Inst. Metals 40(1979): p. 1190.
33. See for example, Hydrogen Damage, ed. C.D. Beachem, (Metals Park, OH: ASM International, 1977), and Effect of Hydrogen on the Behavior of Materials, ed. A.W. Thompson, I.M. Bernstein (Warrendale, PA: TMS-AIME, 1976).
34. J.R. Rice, R. Thomson, Phil. Mag. 29(1974): p. 73.
35. D.D. Mason, Phil. Mag. 39(1979): p. 455.
36. Seah, Hondros, Proc. Roy. Soc. London A335(1973). p. 191.
37. J. Kameda, C.J. McMahon Jr., Metall. Trans. 14A(1983). p. 903.
38. K. Sieradzki, R.C. Newman, Phil. Mag. A51(1985): p. 95.
39. K. Sieradzki, J.S. Kim, A.T. Cole, R.C. Newman, J. Electrochem Soc. 134(1987): p. 1635.
40. K. Sieradzki, R.C. Newman, J. Phys. Chem. Solids 48(1987). p. 1101.
41. R.C. Newman, T. Shahbari, K. Sieradzki, Scripta Metall. 23(1989): p. 71.
42. K. Sieradzki, R.R. Corderman, K. Shukla, R.C. Newman, Phil. Mag. 59(1989): p. 713.
43. R. Li, K. Sieradzki, in preparation.

Discussion

H. Kaesche (Friedrich Alexander University of Erlangen-Nurnberg, Federal Republic of Germany): How do you handle discontinuous crack propagation within the Sieradzki-type approach? Similarly, how can you model hydrogen-induced crack propagation by matrix-inclusion interfaces?

K. Sieradzki: This has been done and is described in Reference 38 of the paper. We have not attempted to model discontinuous interfacial separation processes.

J.R. Galvele (Comision Nacional de Energia Atomica, Argentina): You have shown a figure where a molecule from the environment reacts at the tip of an atomically sharp crack and produces crack propagation. I understand that such a mechanism works with glass in the presence of water. In the case of high-strength steels, a similar process could act in the presence of chlorine, but it certainly does not in the presence of oxygen. This could be explained by the surface mobility mechanism, because of the difference in the

melting points of the iron halides and the iron oxides. How could you explain this difference, based on any of the mechanisms you have just described?

K. Sieradzki: We have demonstrated [Sieradzki, Acta Metall. 30(1982): p. 973] that the intergranular embrittlement of a high-strength steel by chlorine is not related to monolayer adsorption processes. Bridging reactions, as discussed here, do seem to be responsible for glass embrittlement in water vapor.

R.P. Wei (Lehigh University, USA): In connection with your response to Galvele, regarding oxygen and chlorine, I wish to call your attention to the fact that there are ample data that show no enhancement of crack growth by oxygen in high-strength steels at "low" temperatures. The high-temperature effects discussed by Pineau last evening involve extensive oxides or internal oxidation and are not relevant to your model. The real issue here is that you need to consider the question of chlorine vs oxygen raised by Galvele under compatible sets of conditions and avoid bringing in data that are not directly relevant.

K. Sieradzki: There is a misconception that oxygen does not embrittle HSLA steels at low temperature. This notion is incorrect. See, for example, Frandsen and Marcus, Metall. Trans. 84(1977): p. 265.

H. Kaesche: With respect to the possible role of dry oxygen, I should like to note recent studies of fatigue crack propagation in a manganese-bearing low-alloy steel in dry hydrogen, water vapor, and oxygen at room temperature, with values of pressure between 10^{-8} and 10^{3} hPa [Popp and Kaesche, Proceedings of the Conference on Low Cycle Fatigue and Elasto-plastic Behavior of Materials, ed. Rie, Munich 1987 (Amsterdam, The Netherlands: Elsevier, 1987), p. 383]. In the first place, oxygen does increase the rate of fatigue crack propagation. However, while this rate continues to increase in both hydrogen and water vapor, at least at pressures up to 10^{3} hPa, the effect of oxygen levels off at $p(O_2) = 10^{-2}$ hPa, at a value of da/dN of approximately 2 nm/cycle. In both hydrogen and water vapor, the fatigue mechanism is probably affected by dislocation transport of atomic hydrogen into the crack-tip region. Oxygen will adsorb on the crack-tip surface but will not enter the lattice. The observed influence on the crack propagation must therefore be a surface effect caused by adsorbed oxygen and thus will saturate once the surface adsorption is saturated. This holds regardless of the actual mechanism of the effect, which may be surface pinning of dislocations.

B.D. Lichter (Vanderbilt University, USA): If your conclusions from molecular dynamic stimulation and the film-induced cleavage model are applied to the copper-gold system in a stress corrosion regime, it would seem that ductile behavior would be predicted on dealloying, because a(film) $>$ a(substrate) in this case. In fact, transgranular SCC readily occurs in this system. Do you anticipate that revised calculations involving other than the Lennard-Jones 6-12 potential would substantially alter the predictions of the model?

K. Sieradzki: Newman and I have clearly stated in earlier publications [see, for example, Sieradzki and Newman, Phil. Mag. 51(1985). p. 95] the following: If an intrinsically ductile film forms such that a(film) $>$ a(substrate), dislocation injection is predicted. However, if the film is intrinsically brittle, then regardless of the sign of the film–substrate lattice misfit, the tendency would be for more brittle behavior of the film-substrate system, i.e., film-induced cleavage. This is discussed in the "Film-induced cleavage" section of the paper.

B.D. Lichter: In your discussion of the failure of α-brass to undergo SCC in chloride media, you invoke Ostwald Ripening of dealloyed regions to account for the ductile behavior of large-pore and thickened-fiber structures, which would otherwise be "pseudo brittle," leading to transgranular SCC. Do you propose this as a mechanism for initial nucleation of a crack or is this process primarily being applied to the "renucleation" during discontinuous growth or both?

K. Sieradzki: These issues are expected to be important concerns for both.

B.D. Lichter: Do the "network coarsening" model and the "film-coated crack" model (as pursued through molecular dynamic simulations) constitute two distinctly different and alternative views of discontinuous cracking? If so, which in your view is the more promising picture?

K. Sieradzki: They are not different. It depends on the details of the system. Coarsening of a dealloyed network will tend not to favor a film-induced cleavage process. Dealloyed layers that retain uniform porosity will tend to serve as good "nucleators" of film-induced cleavage.

W.W. Gerberich (University of Minnesota, USA): You made the tantalizing suggestion that strains, analogous to those in epitaxial films, from liquid metals may ingest dislocations. You also showed that the external stress for this to happen is decreased for thicker films This is because the stored elastic energy increases with film thickness However, in liquid metals, the elastic strains would only be in the first layer, as the liquid would not support elastic strains. This leads to the suggestion that perhaps the liquid metal has to be incorporated into the substrate. Do you have any information as to whether a monolayer or some incorporation is required for such a process?

K. Sieradzki: In liquid metal embrittlement, we tend to think of initiation at flat surfaces when you are unlikely to get more than one or two layers of "film." However, it is possible that the liquid metal takes advantage of small fissures, thus effectively giving you a thicker film.

R.H. Jones (Pacific Northwest Laboratories, USA): Development of planar cracks in porous layers is conceptually and experimentally supported, but a key question regarding film-induced cleavage from dealloyed layers deals with the strain energy release rate Has it been demonstrated through calculation that the strain energy release rates of a crack propagating in a porous layer are sufficient to support crack growth in the substrate?

K. Sieradzki: The film-substrate relationships necessary for this process to occur have been described earlier [Sieradzki and Newman, J Phys Chem Solids 48(1987): p. 1101] and are applicable to porous dealloyed layers on intrinsically ductile substrates.

R.W. Staehle (University of Minnesota, USA): Regarding the oxygen controversy on crack growth, how do you interpret the observations of Hancock and Johnson [Trans. AIME 236(1966). p. 513] where oxygen additions to the hydrogen gas stops cracking?

K. Sieradzki: I agree with the arguments of Johnson. He suggests competitive adsorption and poisoning effects. However, this behavior does not exclude oxygen as a weak embrittler, as I noted in response to Wei's comments.

R.W. Staehle: With respect to the apparent difference between oxygen effects on cyclic stressing and static stressing, could it not be related to cycle frequency dependence and ΔK dependence?

K. Sieradzki: I don't know.

H.-J. Engell (Max Plank Institut fur Eisenforschung, Federal Republic of Germany): In my opinion, mathematical modeling is a powerful tool to understand the fundamentals of SCC processes. However, to understand phenomena of significant practical importance, other influences and variables must be considered.

As an example, in a growing crack, e.g., in mild steel in nitrate solutions, changes in the crack-tip chemistry may lead to a continuous active crack tip, and then SCC changes to crack-assisted intergranular corrosion, the surface layers only concentrating the electrochemical process at the crack tip. Thus, in cases like this, electrochemical parameters have also to be addressed. I am sure that considerations like that could be included into your modeling.

N.S. Stoloff (Rensselaer Polytechnic Institute, USA): You referred to a characteristic phase diagram type for the case of metal-induced embrittlement. I would like to have a clarification of that comment, since recent work has shown that criteria for embrittlement based upon solubility and intermetallic compound formation are invalid. Further, how do you account in your theory for the embrittling effects of both very small (lithium) and very large (mercury) embrittler atoms?

K. Sieradzki: We have demonstrated in our computer modeling that for films or layers that represent positive dilatational misfit, greatly facilitated dislocation injection is possible. In those cases where liquid metal embrittlement results from enhanced shear, such a mechanism could operate provided that a surface layer with the properties described above develops. You might also refer to my earlier response to the question from Gerberich.

H.K. Birnbaum (University of Illinois, USA): Is it not the case that oxygen effects on fatigue are only observed in the vicinity of the threshold stress intensity? If so, this differs from hydrogen effects, which increase da/dn over the range of stress intensities up to ductile overload. While it is true that oxide films (due to oxygen atmospheres) will influence slip behavior and thereby fatigue behavior, this differs from the atomistic effects you are discussing.

H. Sieradzki: No. I refer you to my earlier response to Wei.

S.C. Jani (Georgia Institute of Technology, USA): Can the crack growth rates in any of the atomistic models you reviewed be predicted? In the film-induced cleavage model, why should the crack continue on into the ductile matrix and why on specific planes for transgranular SCC?

K. Sieradzki: Newman and Sieradzki have discussed these issues in detail in several earlier publications. See, for example, Phil. Mag. A. 51 (1985) p. 95, and the proceedings of the NATO workshop, *The Chemistry and Physics of Fracture*, ed. Latanision and Jones, NATO ASI Series (1987), p. 597.

E.I. Meletis (Louisiana State University, USA): There is considerable evidence showing that transgranular SCC is crystallographic. How can the film-induced cleavage model explain that? Is there any element in the model to relate cracking direction in the dealloyed layer or "film" with cracking orientation in the ductile material?

K. Sieradzki: Newman and I have discussed and suggested possible explanations for (110) cleavage [see Sieradzki and Newman, Phil. Mag. A 51(1985): p. 95].

The Crack-Tip System and Its Relevance to the Prediction of Cracking in Aqueous Environments

*F.P. Ford**

Abstract

The underlying premise in this review is that the main reason for developing mechanistic knowledge of environmentally assisted cracking is to use it to solve the practical problem this phenomenon causes. The solutions may be both qualitative or quantitative and in both cases involve definition of the crack-tip system that is relevant to the crack propagation mechanism.

The crack propagation mechanisms considered are slip dissolution, film-induced cleavage, and hydrogen embrittlement, in which the common rate-controlling steps are as follows: mass transport rates in the crack enclave, oxidation and reduction reaction rates at the strained crack tip, and the anelastic behavior in that region. It is concluded that although the definition of some of these parameters may be imprecise, the extent of *qualitative* knowledge is enough to predict changes in cracking susceptibility that are of use to the design or operational engineer. These questions of system definition may be critical when deterministic, or probabalistic, life predictions are required. However, in some systems involving the slip-dissolution mechanism, usable *quantitative* definitions of the crack propagation rate are possible, and these can be used to formulate design or life-prediction codes.

Introduction

"No sooner knew the reason, but they sought the remedy"
From Shakespeare (1564-1616), *As You Like It*

Environmentally assisted cracking in the power generation, aerospace, oil, and chemical industries has led to severe economic and, sometimes, safety-related problems. Unfortunately, the solutions to these problems have been hampered by both practical and fundamental issues. For example, it is often difficult to define the actual material, stress, and environment conditions when the cracking occurs in inaccessible regions of the plant where complex environmental interactions occur. In addition, there is the intellectual problem of defining the dominant cracking mechanism when a combination of electrochemical, chemical, metallurgical, and mechanical factors is involved. Consequently, it is not surprising that mitigation actions and design or life-evaluation codes have been largely based on phenomenological and empirical observations on either smooth or precracked specimens tested under relatively simple laboratory conditions. A problem arises out of this procedure, because even if the cracking data are generated under "well-controlled" conditions, there may be large scatter in the results (see Figures 1 and 2 for stress corrosion and corrosion fatigue of low-alloy steels in 288°C water). Thus, empirical approaches have obvious limitations. Examples of such limitations include uncertain corrections to the life-prediction code if the *actual* system conditions change from those used originally in the code formulation; the question of predicting the plant integrity for design lives of 40 years, for instance, or even 1000+ years (for radioactive waste disposal), since this requires extensive extrapolation of data that were obtained over a short time period, etc.

In the last decade, significant advances have been made in understanding quantitatively the cracking mechanism pertinent to a particular alloy/environment system, and this offers the design and operating engineer the capability of validating the empirically derived remedial actions or operating specifications, developing realistic life-prediction methodologies for specific plant conditions,[3] etc. To develop quantitative, mechanistically based methodologies, it has been necessary to do the following:

(1) Define a working hypothesis for the cracking mechanism. Such a mechanism must account for the full spectrum of loading conditions expected in practice, e.g., stress corrosion and corrosion fatigue.
(2) *Independently* evaluate the relevant parameters in that mechanism.
(3) Validate the theoretical predictions of the cracking response by comparison with as wide an observed database as possible.

Inputs to such a logic path have accumulated from many sources over many years. It is the objective of this paper to review some of these advances, especially in terms of the definition of the crack-tip system, and to illustrate how these advances have helped in the evolution of a deterministic and probabalistic life-prediction methodology. Emphasis will be placed on the cracking of ductile alloys in aqueous environments, since the advances in these generic systems best illustrate (at this time) the strengths and weaknesses in the practical use of mechanistic knowledge.

The Initiation vs Propagation Debate

In the past, environmentally assisted cracking has been divided into the "initiation" and "propagation" periods. Consequently, remedies have been categorized in terms of "stopping crack initiation" or "slowing crack propagation." In this review, it is suggested that "initiation" is solely that time necessary to achieve a localized environment in any pre-existing defect on the specimen surface in which the defect may result from machining, scratches, pits, intergranular corrosion notches, etc. In engineering terms, this is often a short time in comparison to the design life, and, practically, one is concerned with the crack propagation from this initiating notch. The fact that one does not see the crack until it reaches a depth equal to

*General Electric Corporate Research and Development Center, Schenectady, NY, 12301.

the nondestructive testing (NDT) resolution limit is a practical matter that gives rise to an *arbitrary* division of nucleation and propagation periods; however, such a time allocation is of no fundamental importance.[4,5] Since the precise shape of the crack depth/operational time curve in Figure 3 is a quantifiable function of the specific material, environment, and stressing conditions, it follows that if there is a range in the *actual* system conditions, there will be a predictable range in the observed data. Thus, scatter in the observed data need not be a result of bad experimentation or random variations in the crack advance process, but is predictable (Figure 4) via the distribution of system conditions that affect the propagation process This thereby provides a bridge between deterministic and probablistic life-prediction methodologies.[6]

Thus, the relevant target for mechanistic analysis is the definition of the crack propagation rate and how this may accelerate or decelerate with changes in the crack-tip conditions. The sensitivity of these changes in crack propagation rate to changes in crack-tip conditions depends on the dominant crack propagation mechanism, as discussed below.

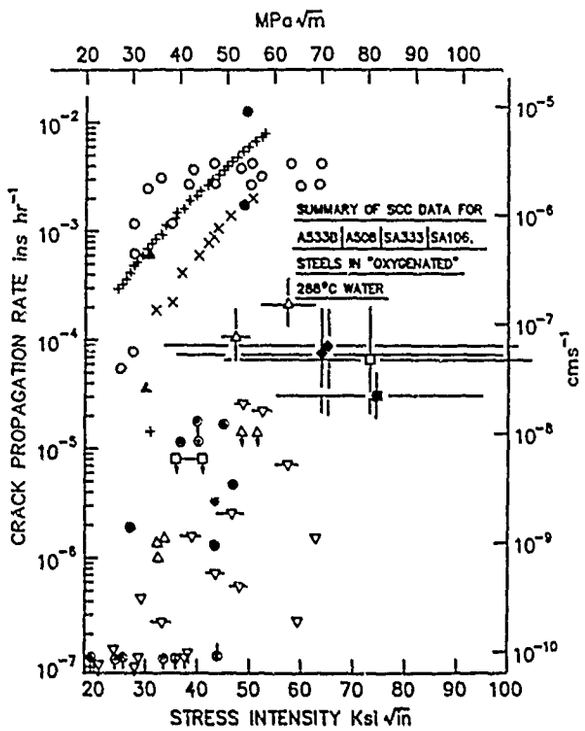


FIGURE 1—Summary of stress corrosion data for A533B, A508, SA333, and SA106 steels in oxygenated water at 288°C.[1]

Candidate Crack Propagation Mechanisms

"The great tragedy of science—the slaying of a beautiful hypothesis by an ugly fact"

From Thomas H. Huxley (1825-1895), *Collected Essays VIII, Biogenesis and Ablogenesis*

The basic premise for all of the proposed cracking mechanisms in aqueous solutions is that the crack tip must propagate faster than the corrosion rate on the unstrained crack sides, or the crack will degrade into a blunt notch.[4] Based on this criterion, the material/environment conditions for both intergranular and transgranular cracking to be possible may be defined based on the thermodynamic and kinetic requirements for the existence of a protective oxide, salt, or film on the crack sides.[7,8] For instance, the well-known cracking susceptibility of mild steel in hydroxides, carbonates/bicarbonates, nitrates, phosphates, and molybdates may be all predicted to occur in the specific potential/pH ranges where the protective oxide, salt, or compound is thermodynamically stable.[8] Very similar thermodynamic arguments may be made for other systems (e.g., brass/ammoniacal solutions[9]) and may be extended to kinetic arguments[10-12] that the electrochemical reaction rate (e.g., dissolution or oxidation) at the crack tip must be significantly higher than those on the crack sides for an "electrochemical knife" to operate.[10] Indeed, the suppression of both stress corrosion and corrosion fatigue in many systems may be explained in terms of blunting of embryo cracks during the early "initiation" stage because of the specific material/environment combinations. The cracking of mild steel and low-alloy steels in aqueous environments offer ideal examples of this criterion For instance, mild steels will not exhibit stress corrosion in acidic (such as citric or acetic) or concentrated chloride solutions unless the general corrosion/blunting effect is counteracted with chromium or nickel alloying additions.[8,13] Similar blunting explanations may be proposed for the ease of corrosion fatigue crack initiation of aluminum in chlorides in comparison to hydroxides,[14] the ease of stress corrosion initiation of carbon steels in 288°C water in comparison to < 100°C water,[4,7] etc.

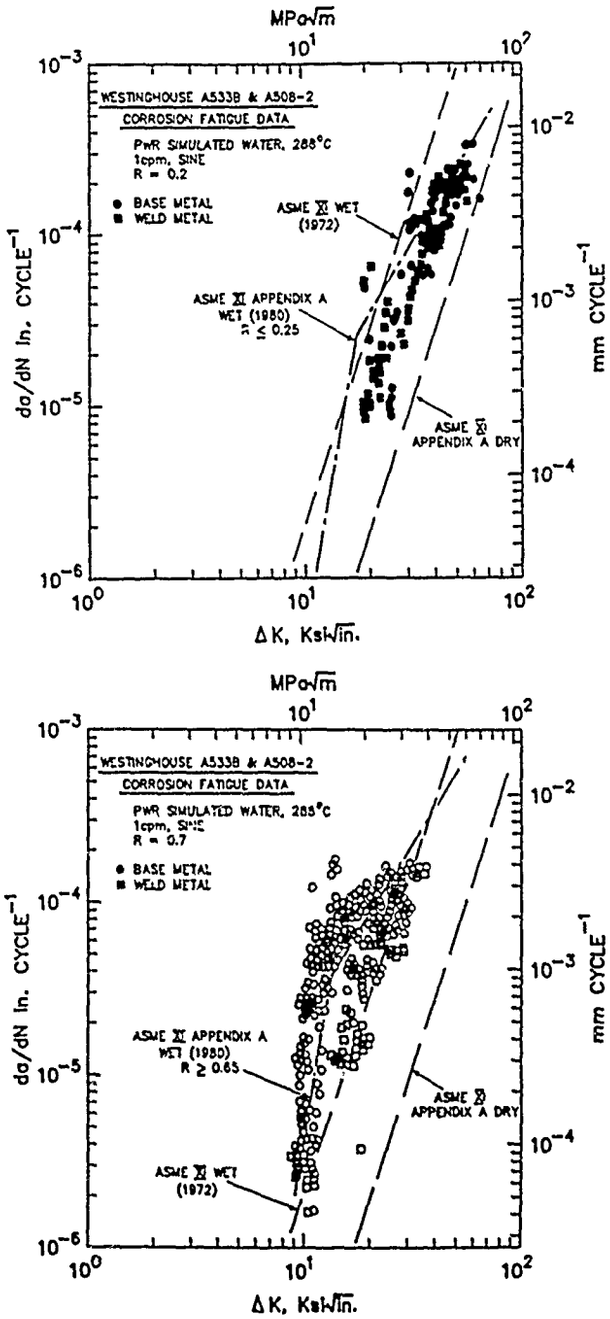


FIGURE 2—Summary of corrosion fatigue crack growth data for A533B and A508-2 steels in pressurized water reactor simulated water at mean stress (R) ratios of 0.2 and 0.7.[2]

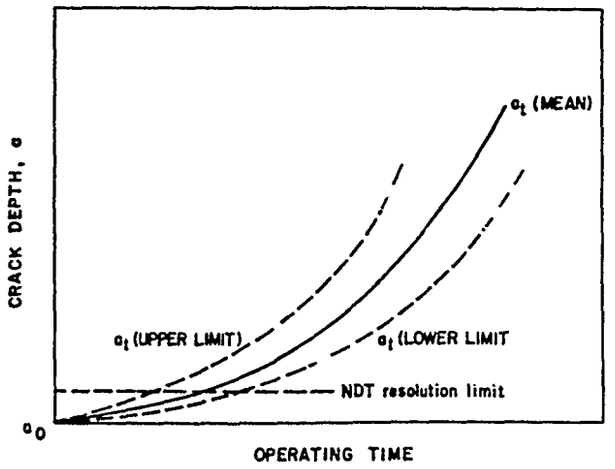


FIGURE 3—Schematic variation of crack length with time due to environmentally assisted cracking, showing the curves for the mean system condition (a_t) and the limiting values associated with extremes in material, environment, and stressing conditions.

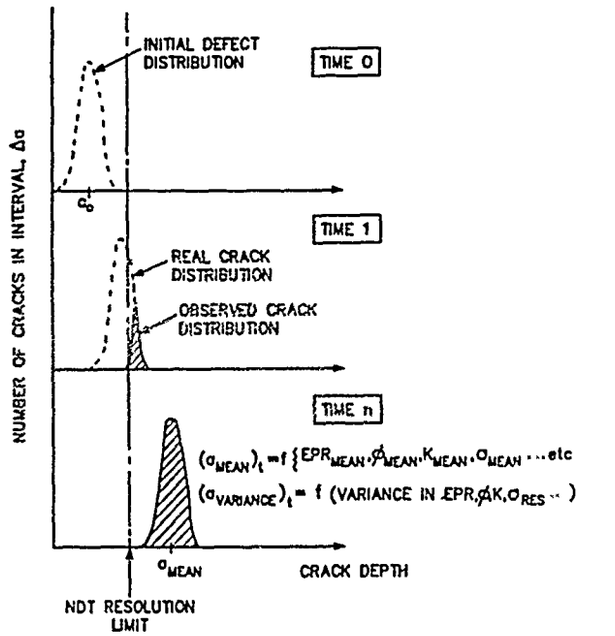


FIGURE 4—Schematic movement of the distribution curves of crack depth with operating time illustrating the influence of NDT resolution limit on the observed vs the actual distribution.

Provided a mechanism for preventing chemical blunting of the crack exists, numerous crack propagation mechanisms were proposed in the period 1965 to 1979,[15-25] ranging from the pre-existing active path mechanisms, through the strain-assisted active path mechanisms, to those depending on various adsorption/absorption phenomena [e g . hydrogen embrittlement (HE) mechanisms]. There was considerable debate concerning the dominant mechanism in a given material/environment system, promulgated in part by the fact that, until 10 years ago, few analytical techniques were available that would quantitatively test the various hypotheses. Parkins pointed out early on, however, that a "stress corrosion spectrum" probably existed that logically graded the cracking systems between those that were mechanically dominated (for instance, HE of high-strength steels) to those that were environmentally dominated (for instance, pre-existing active path attack in the carbon steel/nitrate system).[26] Indeed, it was suggested that two mechanisms may operate in one alloy/environment system with a dominant mode being determined by relatively small changes in the material, environment, or stressing conditions. Brown made the argument that changes in cracking susceptibility with applied potential (and how this altered the crack-tip environment) could be used to distinguish between dissolution-controlled and HE mechanisms.[27] The "stress corrosion spectrum" rationalization was followed by the suggestion (for example, see References 4, 5, 28) that a similar spectrum of behavior occurs between constant load (stress corrosion) and cyclic load (corrosion fatigue) conditions, with the *caveat*[29] that the definition of such a spectrum must be able to explain the general observation that the material/environment conditions for stress corrosion cracking seemed to be much more specific than those for corrosion fatigue.

With the advent of more detailed experimental examination capabilities, the candidate mechanisms for stress corrosion and corrosion fatigue crack propagation in aqueous environments have narrowed down to slip dissolution, film-induced cleavage, and HE. These are reviewed very briefly, since a discussion of the relevant crack-tip system depends on this understanding.

Slip-dissolution mechanism

Various theories for crack advancement have been proposed relating crack propagation to oxidation reactions at the crack tip and the stress/strain conditions in that region, and these have been supported by the good general correlation between the average oxidation current density on a straining surface and the crack propagation rate for a number of systems (Figure 5).[7,29] There have been various hypotheses for the precise atomistics at the crack tip; for example, the effect that the environment has on the ductile-fracture process;[30] the increase in the number of active sites for dissolution because of the strain concentration;[31] the preferential dissolution of mobile dislocations because of either the inherent chemical activity of the dislocation core or the solute segregation that can occur there;[32] etc.

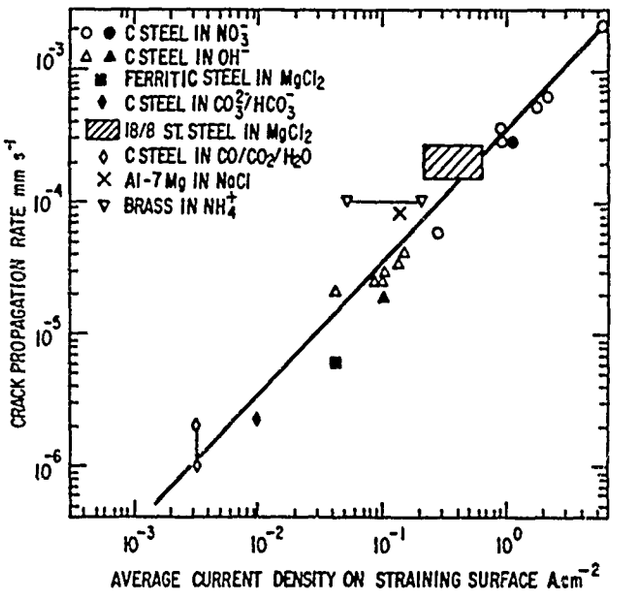


FIGURE 5—Relationship between the average crack propagation rate and the oxidation (i.e., dissolution and oxide growth) kinetics on a straining surface for several ductile alloy/aqueous environment systems.[7,29]

Experimentally validated elements of these earlier proposals have been incorporated into the current slip-dissolution model, which relates the crack propagation to the oxidation that occurs when the protective film at the crack tip is ruptured.[10,33-37] Different types of protective film have been proposed, including oxides, mixed oxides, salts, or noble metals left on the surface after selective dissolution of a more active component in the alloy. The increase in crack-tip strain necessary for the film rupture event may be related to a monotonically increasing or cyclic stress, or to creep process in the underlining metal matrix under constant stress. Once the film is ruptured, crack-tip advance is governed by oxidation on the bared surface, i.e., a mixture (depending on the thermodynamics and kinetics of the

system) of the dissolution of the exposed metal matrix and film reformation (Figure 6). This crack advance will be maintained provided the film-rupture process reoccurs because of the action of a strain *rate* at the crack tip. Thus, for a given crack-tip environment, potential, and material condition, the propagation rate over a given segment of the crack front will be controlled by both the change in oxidation charge density with time, and the frequency of film rupture at that segment of the strained crack tip. Therefore, by invoking Faraday's law, the average environmentally controlled crack propagation rate ($\bar{V}_t$) is related to the oxidation charge density passed between oxide rupture events (Q_f) and the strain rate at the crack tip ($\dot{\epsilon}_{ct}$) by

$$\bar{V}_t = \frac{M}{z\rho F} \times \frac{Q_f}{\epsilon_f} \times \dot{\epsilon}_{ct} \qquad (1)$$

where M, ρ = atomic weight and density of the crack-tip metal; F = Faraday's constant; z = number of electrons involved in the overall oxidation of an atom of metal; ϵ_f = fracture strain of the oxide at the crack tip.

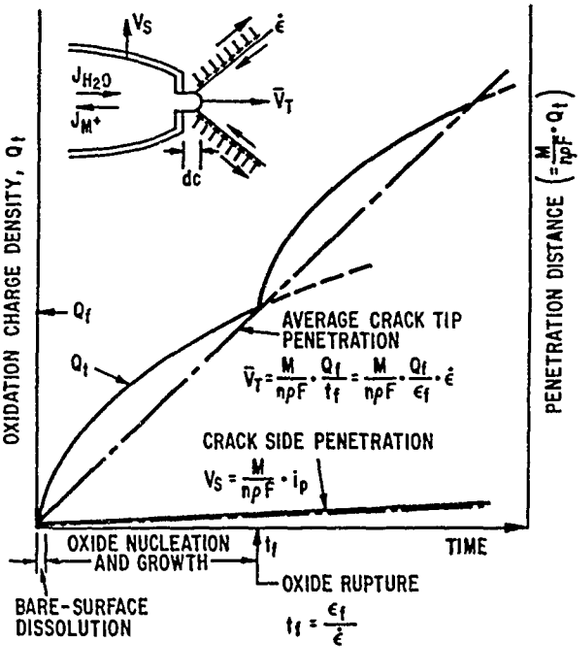


FIGURE 6—Schematic oxidation charge density/time relationships for a strained crack tip and unstrained crack sides.

Thus, the possible rate-controlling phenomena that can govern crack propagation by the slip-dissolution model[4] are as follows. liquid diffusion of either solvating water molecules or solvated cations to and from the crack-tip region, the overall oxidation (dissolution and oxide growth) rate, and the oxide or film-rupture rate at the crack tip itself. These fundamentally important parameters can be directly related to the stress, environment, and microstructure known from empirical observations to be the conjoint requirements for environmentally controlled cracking (Figure 7). In turn, these rate-controlling phenomena are functions of a myriad of system parameters such as dislocation morphology, solution viscosity, etc., this will be discussed later.

Because the oxidation charge density on a bare surface varies with time at a rate that depends upon the material and environment compositions at the crack tip, it follows (as will be discussed later) that Equation (1) may be reformulated in terms of a more general power law relationship:

$$\bar{V}_t = A\,\dot{\epsilon}_{ct}^{n} \qquad (2)$$

where A and n are constants depending on the material and environment compositions at the crack tip. There are limits to the validity of this relationship, however, that are observed at high and low crack-tip strain rates (Figure 8). At low crack-tip strain rates, the ultimate criterion is that sharp cracks cannot be maintained when the average crack-tip propagation rate ($\bar{V}_t$) approaches the oxidation rate on the crack sides (V_s); under these conditions, therefore, the crack propagation rate will decelerate with exposure time, and crack arrest will eventually occur because of blunting. At high crack-tip strain rates ($\sim 10^{-2}\ s^{-1}$), a bare surface is continuously maintained at the crack tip, and the environmentally controlled crack propagation rate becomes independent of $\dot{\epsilon}_{ct}$, since it cannot exceed the Faradaic equivalent of the bare-surface dissolution rate.

Under either constant or monotonically increasing load conditions, the stress corrosion crack propagation rate is defined by Equation (2) (within the limits discussed above). Under cyclic loading conditions, however, the crack is also moving forward by irreversible cyclic plastic deformation, e.g., fatigue striation formation. Since this mechanical crack advance is occurring independently of the crack advance by oxidation processes (i.e., the atom–atom rupture process is by two entirely different mechanisms), these two crack advance mechanisms, striation formation and oxidation, are considered additive, as shown by the dotted line in Figure 8, e.g.,

$$\bar{V}_{total} = A\,\dot{\epsilon}_{ct}^{n} + \dot{\upsilon}\left(\frac{da}{dN}\right)_i \qquad (3)$$

where $(da/dN)_i$ is the cyclic fatigue crack growth in an inert environment described, for instance, by a Paris law relationship, and $\dot{\upsilon}$ is the cyclic loading frequency. This simple coupling of environmental and inert components can, of course, be directly compared to the arguments proposed by Wei and colleagues,[38,39] who introduced further subcategories of environmental enhancement and considered different fractions of the crack front, which may be undergoing one failure mechanism or the other.

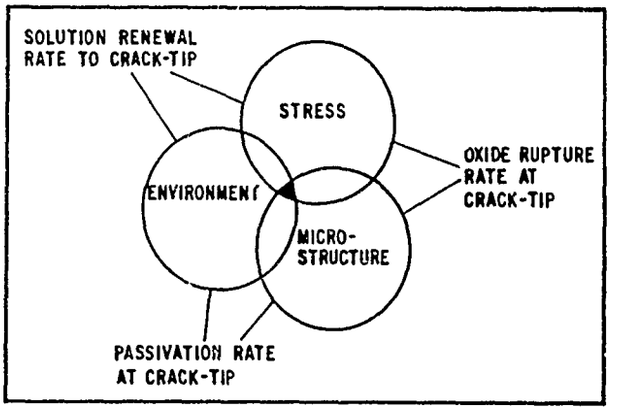


FIGURE 7—Interrelationship between the fundamental controlling parameters (mass transport rate, passivation rate, and oxide rupture rate) and the phenomenological parameters (stress, environment, and microstructure) known to affect environmentally assisted cracking.[4,7]

Film-induced cleavage mechanism

In some incidences of transgranular cracking, the Faradaic equivalent of the oxidation rate at a strained crack tip is insufficient to explain the observed crack propagation rate (see, for instance, the Cu/NH_4^+ data in Figure 5).[40] Moreover, the cleavage-like crystallographic features on the transgranular fracture surfaces are hard to rationalize convincingly in terms of a dissolution/oxidation model alone. Consequently, it has been proposed by several authors that transgranular environmentally controlled crack propagation can occur by a combination of oxidation-related (slip-dissolution) and brittle-fracture mechanisms.[40-45] Specifically, it has been suggested that, initially, the crack front moves forward by an oxidation process that is controlled by the same rate-determining steps as those in the slip-dissolution model, but when the film-rupture event occurs (because of an increment in strain in the underlying matrix), the crack

in the film may rapidly penetrate a small amount (a*) into the underlying ductile metal matrix (Figure 9) Thus, Equation (1) is modified as follows:

$$\bar{V}_t = \left(\frac{M}{z\rho F} Q_f + a^*\right) \frac{\dot{\epsilon}_{ct}}{\epsilon_f} \qquad (4)$$

The extent of the additional "film-induced cleavage" component of crack advance (a*) may be governed by the state of coherency between the surface film and matrix and the fracture toughness of the substrate.[40] Although the surface film may be considered an oxide, more recent investigations have refocused on the role played by dealloyed surface films; for example, the copper-rich film in Cu-Zn or the nickel-rich film in Fe-Cr-Ni alloys.

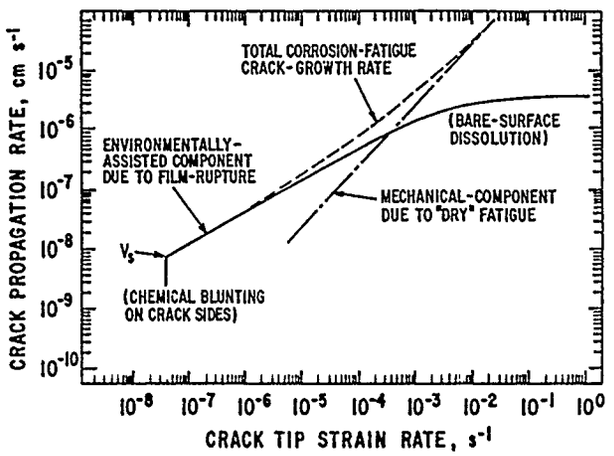


FIGURE 8—Illustration of the strain-rate dependence of the crack propagation rate due to the slip-dissolution model, and the additive properties of the mechanical and environmental components of crack advance during corrosion fatigue.[4]

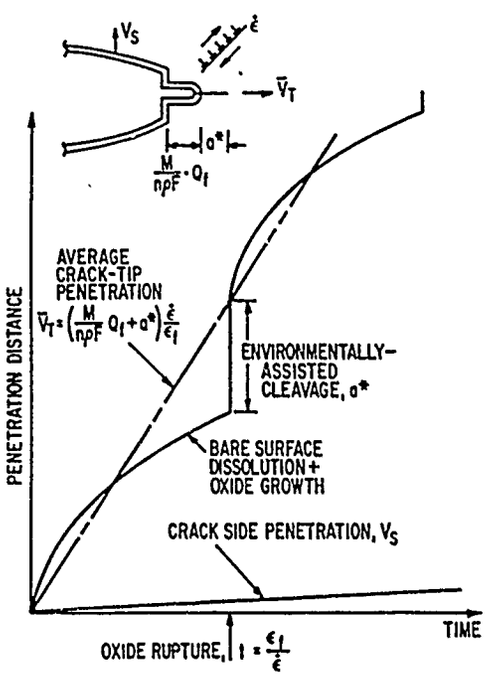


FIGURE 9—Schematic illustration of the elements of the film-induced cleavage mechanism of crack propagation. Note similarity to the slip-dissolution model (Figure 6) during initial stages of propagation cycle.

Factors of importance that control the effectiveness of the surface film in initiating the cleavage event in the metal substrate include the film-matrix misfit, the strength of bonding across the film-matrix interface, the film thickness and ductility, and the structure of, for instance, dealloyed layers.[40,44,45] It would be reasonable to suppose that absorbed hydrogen may also play an important role in such a limited cleavage process. The extent of the cleavage propagation into the matrix may be around 1 μ, the exact amount being a function of a combination of the various plasticity and microstructural factors mentioned above. Although qualitative evidence exists (based on computer simulaton of the atomistic bonding at the crack tip plus fractographic and acoustic emission observations) for such a mechanism in copper-base and austenitic nickel-base alloys and stainless steels (SSs) in low-temperature environments (i.e., < 115°C),[40,44] it has not been extensively tested so far for other alloy systems. Its attractiveness is, however, that it provides a rational basis for quantitatively explaining the interrelationships between the electrochemical parameters and the transgranular fractographic features.

Hydrogen embrittlement mechanisms

The general concepts and concerns behind the various HE models have been reviewed by Thompson and Bernstein,[46] Hirth,[47] Nelson,[48] and Birnbaum.[49] In brief, the subcritical crack propagation rate resulting from HE in aqueous environments depends on a sequence of events in the following order (Figure 10):

(1) Diffusion of a reducible hydrogen-containing species (e.g., H_3O^+) to the crack-tip region.

(2) Reduction of the hydrogen-containing ions to give adsorbed hydrogen atoms. Note that under open-circuit conditions, this reduction process must be accompanied by a corresponding oxidation reaction rate that, in high-resistivity electrolytes, will occur on an adjacent surface to that where the reduction process is occurring.

(3) Absorption of the hydrogen adatoms followed by interstitial diffusion of these hydrogen atoms to a "process" zone at a distance (X) in front of the crack tip. The extent of hydrogen adatom coverage (θ_H) on the crack-tip surface, which will be one driving force for hydrogen diffusion into the metal matrix, will be a function of the presence of films or other adsorbed species, and also the tendency of these hydrogen adatoms to undergo surface diffusion and recombination to evolve hydrogen gas. (Note that it is assumed that the amount of hydrogen being absorbed from the unstrained crack sides and specimen surface is relatively small).

(4) Once the hydrogen concentration in the process zone has reached a critical level (C_{crit}) over a critical volume (d_{crit}),[51] then localized crack initiation can occur within this zone followed by rapid propagation back to the main crack tip. Thus, disregarding the specifics of these localized fracture mechanisms for the present, it is apparent that HE models predict discontinuous crack propagation at an average rate ($\bar{V}_t$) given by

$$\bar{V}_t = \frac{X}{t} \qquad (5)$$

where X = the distance from the main crack tip to the process zone, which, in turn, is defined by the values of C_{crit} and d_{crit}, and t = time for the concentration of absorbed hydrogen ($C_{X,T}$) to reach a critical value (C_{crit}) over the volume (d_{crit}).

To evaluate the validity of Equation (5), quantitative data for X and t are needed. Unfortunately, these are difficult to obtain. For instance, even assuming that the criterion for the localized fracture phenomenon in the process zone was known, its evaluation is bedeviled with uncertainties about the interactions illustrated in Figure 10, and how the rate-determining step in this overall process is affected by, for instance, stress and dislocation-aided diffusion, the trapping and release of hydrogen at intermediate interfaces between the crack tip and process zone, the interaction between diffusion rates and changes in equilibrium hydrogen content because of hydrostatic stress, etc. Despite these uncertainties, however, the combination of these various diffusion paths and the sites for localized fracture leads to a qualitative explanation of different fracture morphologies observed (Figure 11) in many alloy/environment systems.[46]

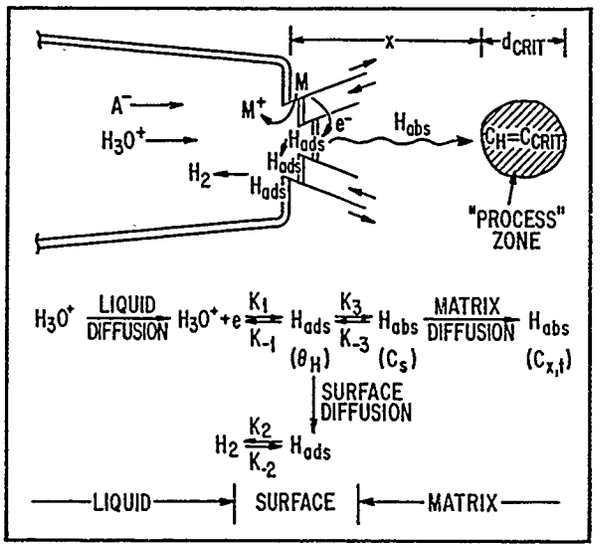


FIGURE 10—Schematic of various reactions at the crack tip associated with hydrogen embrittlement mechanisms in aqueous environments.[50]

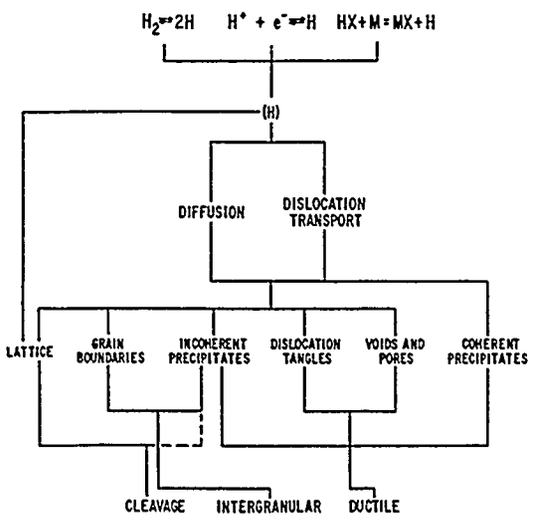


FIGURE 11—"Road map" of possible transport and trapping mechanisms for hydrogen embrittlement in ductile alloys.[46]

The evaluation of the values of X, C_{crit}, and d_{crit} all presume that the localized fracture mechanism in the process zone is known. Accordingly, various mechanisms for the localized fracture process have been proposed. For instance, it has been suggested that it is because of the build-up of gas pressure at internal interfaces,[52-54] this pressure may be associated with either the recombination of hydrogen atoms or the formation of either methane or hydrogen sulfide (because of the interaction of hydrogen with either carbide or sulfide inclusions). Alternatively, localized fracture may be related to the lowering of the atom-atom bond strength because of the modification of the electron d-band structure of the matrix by hydrogen,[55-59] or the localized fracture may result from fracture of brittle phases such as hydrides,[60-62] hydrogen- or strain-induced martensite,[63-66] etc. Finally, it has been proposed that the interaction of hydrogen atoms with the dilatational stress field around edge dislocations affects the degree of plasticity in the process zone, and hence, the localized fracture criteria.[67-69]

Much of the "evidence" for these mechanisms has been "after the fact" or "circumstantial," with very little first principles derivation of the crack propagation rate, in which all the constants are independently derived.[70] Great strides have been made in recent years, however, by *in situ* observations of cracking in high-energy electron microscopes, as reviewed by Birnbaum.[49]

The Rate-Controlling Parameters in the Crack-Tip System

"It is a capital mistake to theorise, before one has data"
From Sir Arthur Conan Doyle (1859-1930), *Scandal in Bohemia*

Various thermodynamic and kinetic criteria have been applied to determine which of the above candidate crack propagation mechanisms are valid. For instance, Bertocci indicated that at the tip of a static crack in the Cu/Zn/ammonia system[71] or a moving crack in the Cu/Au/chloride system,[72] hydrogen discharge had very little chance of occurring, and HE would therefore be very unlikely; thus, in these cases, the slip-dissolution or film-induced cleavage mechanisms would be more likely. However, it is comparatively rare that a candidate cracking mechanism can be categorically disallowed on such thermodynamic and crack-tip chemistry reasoning. Although equilibrium thermodynamic approaches have been used to calculate K_{ISCC} or K_{TH} for the slip-dissolution[73] and HE[74] mechanisms, the majority of quantitative validations of the candidate propagation mechanisms (up until ~ 1979) were based on analysis of either the *maximum* propagation rate allowed by each model or the observed sensitivity of the crack propagation rate to temperature, electrode potential, strength level, etc.[7] Each of these variables would give, supposedly, unique indications of the validity of a particular cracking mechanism. Although in some cases it was observed that the maximum observed crack propagation rate agreed with the maximum theoretical rate of, for example, the slip-dissolution model (e.g., Figure 12), in most cases, it was observed that the crack propagation rate was far lower than the maximum theoretical rates for any candidate cracking mechanism (e.g., Figure 13).[50] The reason for this is that the rate-determining step in all of the cracking mechanisms is not necessarily the atom-atom rupture process itself but is one or a combination of the following: mass transport of species to and from the crack tip, the oxidation or reduction reactions and dynamic strain processes at the crack tip.[4,7] Thus, *changes* in cracking susceptibility for most ductile alloy/aqueous environment systems with, for instance, *changes* in temperature (i.e., activation enthalpy), electrode potential, stressing mode (dynamic or static stress, plane-strain or plane-stress mode, dislocation morphology, etc.), or environmental composition, can be explained logically by movement over a reaction rate surface (Figure 14), regardless of the specific atom-atom rupture mechanism at the crack tip.[4,7] This may be interpreted in terms of the crack propagation rate/stress intensity [Figure 15(a)] or propagation rate/potential [Figure 15(b)] relationships for a given alloy/environment system subjected to different loading histories in which the limiting and rate-controlling reactions can be defined.[4] Although the arguments for the changes in rate-controlling parameters with, for instance, electrode potential and loading mode changes given above are for aqueous systems, similar approaches have been proposed by Wei and colleagues for corrosion fatigue of aluminum and high-strength steels in water vapor.[39,78,79]

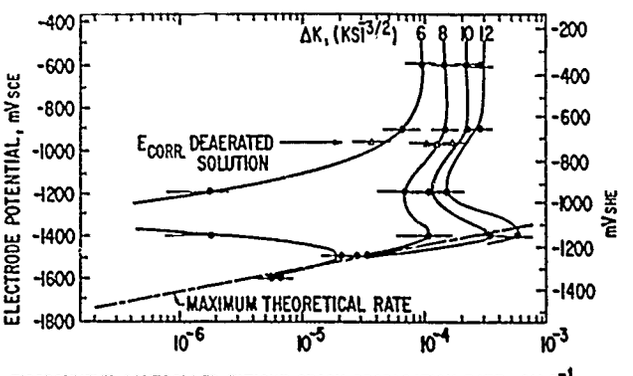


FIGURE 12—Comparison between the maximum theoretical crack propagation rates for the slip-dissolution mechanism and the observed environmental component in corrosion fatigue of an aluminum-7%magnesium alloy in IN Na_2SO_4, pH 2.0, 11 Hz.[50]

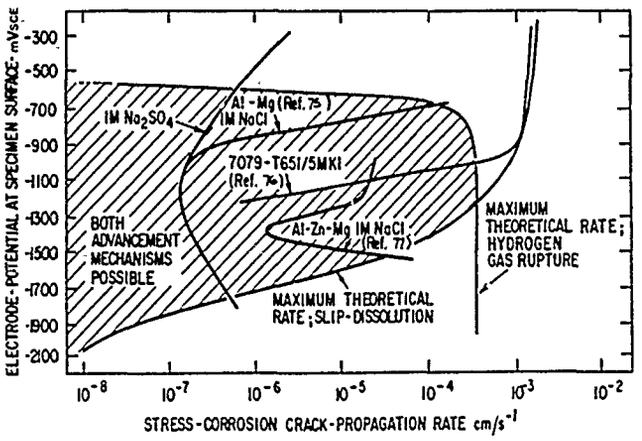


FIGURE 13—Relationship between the maximum[75-77] stress corrosion crack propagation rates for various aluminum alloy/aqueous environment systems and the maximum theoretical propagation rates for the slip-dissolution and hydrogen embrittlement (gas-rupture) theories.[50] Note the fact that in the potential range −1000 to −800 mV_{SCE} (covering the corrosion potential for aerated or slightly deaerated solutions), both advancement mechanisms are kinetically viable.

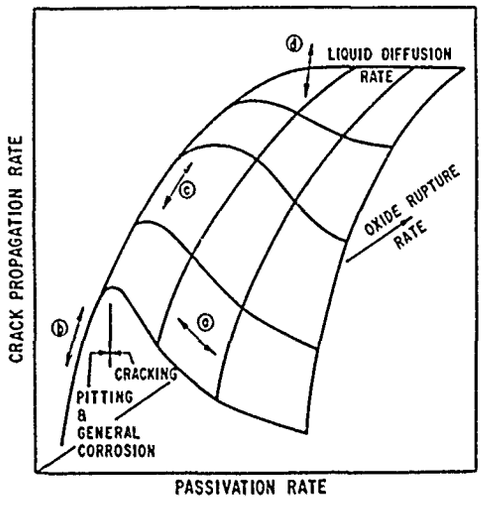
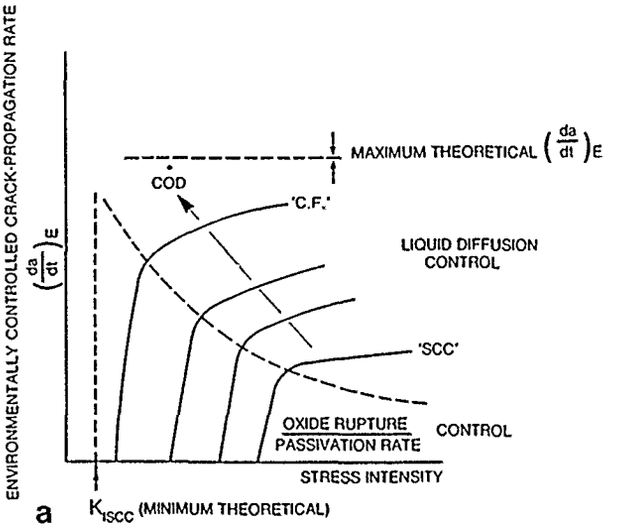


FIGURE 14—Reaction-rate surface illustrating the variation in crack propagation rate with the rate-controlling parameters in the slip-dissolution, film-induced cleavage, and hydrogen embrittlement mechanisms for environmentally assisted cracking in ductile alloy/aqueous environment systems.[4,7]

Knowledge of the *fundamental* importance of controlling mass transport, oxidation, or reduction rates and crack-tip strain rates has proven to be of great value in indicating to the design and operational engineer the system changes that are likely to reduce the extent of his particular environmentally controlled cracking problem, especially for cracking systems with "moderate" to "severe" cracking susceptibility (which may be defined as those with average crack propagation rates of $> 10^{-7}$ cm s^{-1}). For instance, the minimizing of the oxidation rate at the crack tip by control of the corrosion potential/anionic activity combinations, or the reduction in crack-tip strain rate (for a given imposed stress history) by attention to dislocation morphology, etc., all can be understood within a skeleton of fundamental logic (Figure 16).[4,7] However, in recent years, as economic and technical pressures dictate longer design lives, the emphasis has been on studying cracking in dilute environments where the relevant crack propagation rates are $\sim 10^{-7}$ cm s^{-1}, and on developing the quantitative prediction capability shown in Figure 3. The semiquantitative methodology described above is not capable of this. Thus, in the following section, the advances in quantifying the rate-determining reactions that occur at the crack tip and their influence in the life-prediction methodology are described.



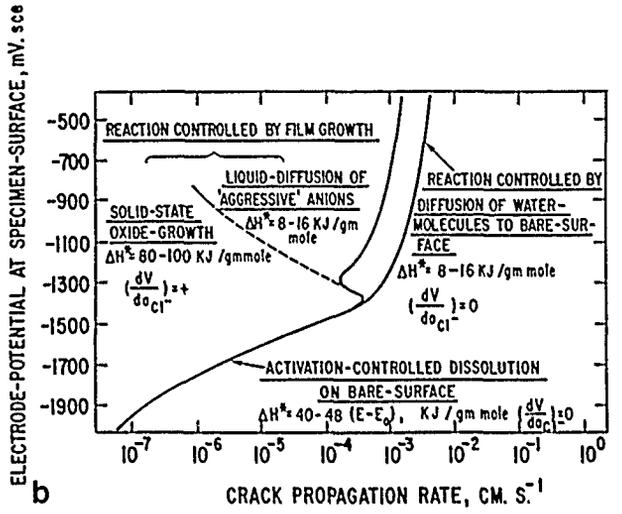


FIGURE 15—Suggested[4] variation in environment-controlled crack propagation rate with (a) stress intensity for various crack-tip deformation rates COD and (b) electrode potential. (Note the suggested rate-controlling parameters and the fact that these relationships should be bounded by a maximum crack propagation and a minimum theoretical K_{ISCC} or K_{TH}.)

Quantification of the Crack-Tip System

"But facts are chiels that winna ding an' canna be disputed"
From Robert Burns (1759-1796), *A Dream*

The purpose of this section is to review the present quantitative knowledge of the nature of the crack-tip system in aqueous environments, especially as it relates to the rate-controlling reactions for crack propagation.

Crack-tip solution composition

The parameters requiring definition in the crack tip solution are the electrode potential, anionic activity, and pH, since these can affect the metal oxidation and hydrogen ion or water reduction kinetics that are central to the candidate crack propagation mechanisms. In addition to the steady state composition at the crack tip, it is also necessary to know the rate at which the crack tip composition changes following abrupt alterations in the bulk (external) solution composition, such alterations in bulk solution chemistry occur in practice and lead to changes in propagation rate, which may be delayed because of mass transport considerations down the crack length.[5,80-82]

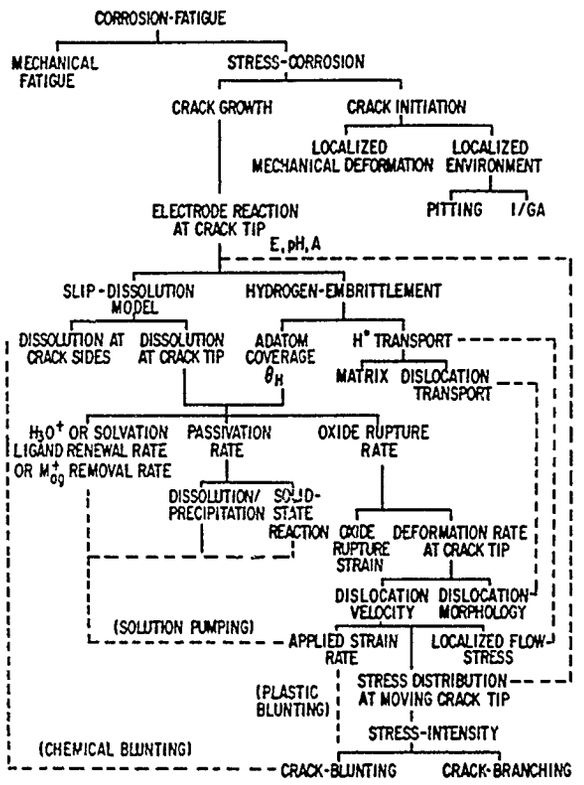


FIGURE 16—Suggested interaction paths between the modes and mechanisms of environmentally controlled fracture in ductile alloy/aqueous environment systems and the various rate-determining steps in crack propagation. Solid lines denote primary interactions, dashed lines denote secondary interactions.[4,7]

Advances in this area have been accomplished by an iterative process of modeling and experimental studies; these have been extensively reviewed by Turnbull.[83-85] In these reviews, discussion is given to the strengths and weaknesses of the various direct and indirect experimental techniques for determining the crack-tip solution composition. These aspects will not be repeated in the present review; however, modeling and experimental results will be covered and updated.

The electrode potential, pH, and ionic activity at the crack tip can be different from those values at the exposed crack mouth[86] because of the restricted mass transport in the crack enclave and the consequent separation of the main oxidation and reduction sites (Figure 17). All mass transport models are based on relationships between the flux of the various species and reaction rates that are occurring at various points down the crack,[87] and take into account the following:

(1) The flux of all species into and out of the crack may be controlled by Fickian diffusion, ionic migration, and convection.

$$J_i = -D_i\nabla C_i - Z_i\mu_i FC_i\nabla\phi + C_iV \quad (6)$$

where J_i is the flux of species i (mol/cm^2 s), C_i is the concentration of species i (mol/cm^3), ϕ is is the potential of the solution (volts) and V is the velocity field (cm/s) resulting from either natural (e.g., solution density) or forced (e.g., relative movement of the crack sides during cyclic loading) convection. D_i and μ_i are the diffusion coefficient (cm^2/s) and ionic mobility (cm^2 mol/J–s), respectively, and for dilute systems are related through the Nernst-Einstein equation:

$$D_i = RT\mu_i \quad (7)$$

It is important to note that these fluxes may be acting in different directions, giving rise to dynamic equilibria. For instance, if the crack mouth is at a more positive potential than the crack tip, anions will diffuse to the crack tip, but the steady-state anionic activity at that position will be governed by a Fickian diffusion flux of anions away from the crack tip; this point will be expanded upon later in this review.

(2) Mass conservation of species within the crack is obeyed:

$$dC_i/dt = -\nabla J_i + R_i \quad (8)$$

where R_i is the net production (or depletion) of species (i) per unit volume due to homogeneous reactions; i.e., this does not include the heterogeneous reactions such as electrode reactions occurring on the surfaces that are accounted for via (3).

(3) The relationship between the flux of a charged species and the electrochemical reaction rate:

$$i_d = \Sigma_i Z_i J_i \quad (9)$$

(4) Electroneutrality is conserved at all points down the crack length:

$$\Sigma_i Z_i C_i = 0 \quad (10)$$

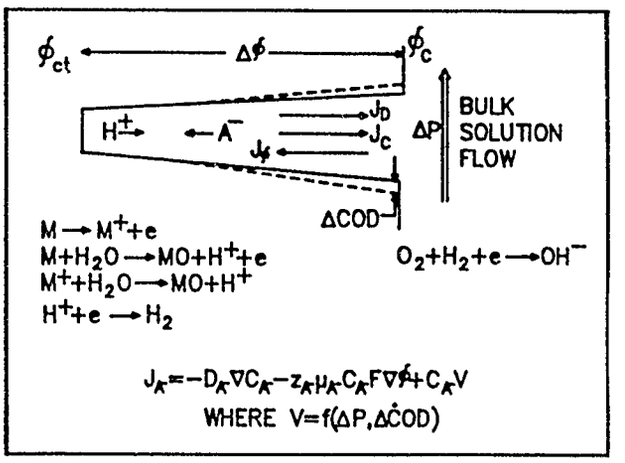


FIGURE 17—Schematic of a crack and the associated mass transport and thermodynamic criteria that govern the crack-tip environment.

These equations apply specifically to dilute solutions, and ignore solute–solute interactions, activity coefficient corrections, etc., that are necessary for more concentrated environments. Although corrections can be made,[87,88] the usual procedure is to use the above relations regardless of the solute concentration. The solution of these equations requires adequate knowledge of the relevant reaction rates, diffusion coefficients, convection effects in the complicated crack geometries encountered, etc. Since these data are not always readily available, simplifying assumptions are often used. For example, most modeling analyses confine mass transport to one-dimensional flow along the length axis of a parallel-sided or wedge-shaped crack and ignore the multidimensional aspects of concentration gradients between the walls of the cracks and across the specimen. Although such multidimensional flux aspects may account, for instance, for different crack-front shapes,[89] and more recent modeling[88,90,91] and experimental[92] studies can account for two-dimensional flow characteristics, Turnbull concludes that the present one-dimensional analyses can give usable predictions relevant to practical application.[83] Even so, further simplifying approaches have generally been made in modeling analyses, which have included neglecting one or two of the possible three mass transport processes in Equation (6). For instance,

(1) Analysis of Fickian diffusion alone in cracks,[93-94] pits,[95,96] and crevices;[97]

(2) Analysis of ionic migration alone in cracks,[98-103] pits,[104] and crevices;[105]

(3) Analysis of the combined effects of Fickian diffusion and ionic migration in cracks[71,72,106-109] and pits;[110,111] and
(4) Analysis of convection effects resulting from the movement of the advancing stress corrosion crack tip[112,113] or that associated with the relative movement of the crack sides during fatigue loading.[93,114-118]

The validity of these simplifications can be assessed[83] in terms of the actual operating conditions; for instance, the assumption of a dominant Fickian diffusion component may be valid for stress corrosion in stagnant, deaerated environments, etc. Thus, although significant problems remain for mathematical analysis[89,90,119] in addressing the combinations of the mass transport mechanisms and obtaining adequate input data to the mathematical solutions, the current modeling capabilities give good guidance as to the expected distribution of potential, pH, and anionic activity between the crack tip and exposed crack mouth.

The fact that the sites of the main oxidation and reduction reactions may be separated (e.g., because of the depletion of dissolved oxygen within the crack) leads to the possibility of a potential drop down the crack length, the extent of which will depend on the net ionic current and the solution resistivity. In relatively high-conductivity solutions (for example, 3% NaCl or seawater), the difference in potential between the crack mouth and crack tip may be minimal over an extended crack-mouth potential range (Figure 18).[85,120] At extreme negative potentials at the crack mouth, a potential drop down the crack length becomes apparent as the hydrogen-ion or water-reduction current density increases, or as hydrogen bubbles in the crack increase the resistive path.[108,121,122] At very positive crack-mouth potentials, a potential drop between crack mouth and tip is observed as the oxidation rate increases, with the limiting value of the crack-tip potential being associated with metal salt deposition. Although the data in Figure 18 are associated with carbon steels in an active state in chloride solutions, very similar relations are observed in, for instance, carbonate/bicarbonate solutions[123] and for SS,[108,124-126] titanium,[127] and aluminum[128,129] alloys in chloride solutions in which the increasing potential drops at the more positive potentials are exacerbated by the cell current increases associated with oxide breakdown. Although "high" potential drops may be experienced down the crack length if high oxidation currents are created at the crack tip because of, for instance, oxide breakdown, the potential drop in the high-conductivity media is still generally $\lesssim$ 150 mV. However, this is not the case for high-resistivity solutions, such as high-purity water. In this case, if the crack mouth is held at a positive potential by reduction of dissolved oxygen, then the potential drop down the crack may be around 500 mV (Figure 19).

The presence of a potential drop down the crack length can lead to ion migration and anionic concentration at the crack tip. If there are non-OH^- anions present, then this concentration will lead to an excess concentration of hydrogen ions in the crack-tip region to maintain solution electroneutrality. If the anionic activity is high enough to precipitate a metal salt, then the cationic activity will be fixed by the solubility product of the salt and anion activity. In turn, the maximum hydrogen ion activity possible at the crack tip will depend on the hydrolysis constant (K_H) of the metallic cation, e.g., for the hydrolysis reaction

$$2Fe^{3+} + 6H_2O \rightarrow Fe_2O_3 + 6H^+ \qquad (11a)$$

then

$$[a^*_H]^6 = K_H[a_{Fe^{3+}}]^2 \frac{[a_{H_2O}]}{[a_{Fe_2O_3}]} \qquad (11b)$$

The hydrolysis constant will vary with the metal cation,[132] being high for Cr^{3+}, Fe^{3+}, Al^{3+}, in comparison to Fe^{2+}, Mn^{2+}, or Ni^{2+}. Thus, if Cr^{3+} cations are introduced, either as a dissolved salt[134] or as a dissolution product[133] from the steel (Figure 20), a lowering of the crack-tip pH is expected.[84,85]

The steady-state potential/pH conditions at the crack tip are governed by the dynamic equilibrium associated with the metal oxidation and H_2O or H^+ reduction reactions. Thus, the steady-state potential/pH combinations at a crevice/crack tip in, for instance, iron-base alloys in reasonably concentrated chloride solutions[84] generally fall below the H^+/H_2 equilibrium line on a Pourbaix diagram and around the Fe/Fe_3O_4 equilibrium line (Figure 21),[84] with the minimum observed pH at the crack tip being associated with the reasoning given by Equation (11b). The crack-tip pH varies with potential drop down the crack, being acidic when the crack mouth is more positive, or alkaline when the crack mouth is more negative than the crack tip. An example of the former case for a SS crevice filled with 0.1 M sodium sulfate and exposed to 288°C oxygenated water is shown in Figure 22, illustrating the steady-state potential/pH conditions maintained under the indicated potential drop down the crevice, and the correlation between these potential/pH conditions and the Fe/Fe_3O_4 and H_2/H_2O equilibrium values.[5,135]

Acidification of the crack tip is not possible if there is no potential drop down the crack or if there are no non-OH anions to maintain electroneutrality.[5] This is illustrated in Figure 23 for crevices in several iron-base alloys exposed to deaerated water at 288°C in which the pH of the bulk water has been varied with LiOH additions.[131] In this case, no potential change is measured between the crevice tip and mouth and, consequently, there is no difference in pH between these two regions. A similar situation can occur in bulk *aerated* water (Figure 24)[5] for nickel-base alloys, because, although a potential drop may exist initially, the resultant acidification and increase in crevice-tip potential, according to the Ni/NiO equilibrium line, leads to a situation where there is *no* potential drop down the crevice after approximately two days of exposure, thus, the acidity of the crevice tip cannot be maintained,[5,136] and the crevice-tip pH approaches neutrality.

The criteria described above for the potential/pH conditions at the tip of an occluded cell apply equally well to cracks[137,139] or crevices, as indicated by the "crack" data in Figures 19 and 21. Interestingly, when cracks are advancing (i.e., $K > K_{ISCC}$), the crack-tip acidity may increase.[130,139] Such observations are in line not only with the model predictions[106] (i.e., the increased oxidation current at the crack tip leads to an increase in potential drop, anionic mass transport to the crack tip and hence, for electroneutrality reasons, an increase in hydrogen cation activity), but also with simulated crack experiments involving a strained crevice-tip region.[140]

If straining at the crack tip results from cyclic loading and the relative movement of the crack sides, then, theoretically, mass transport by convection may be affected.[93,114-117] Unfortunately, relatively few experimental investigations of these effects have been conducted. However, Charles, et al.,[141] and Andresen[5] have both indicated that appreciable cyclic frequencies and/or crack-mouth-opening displacements were required to enhance the *net* mass transport rate in the crack. Indeed, the magnitude of these two loading variables was enough to suggest that the changes in mass transport resulting from the relative movement of the crack sides were practically unimportant, since the time-dependent crack propagation rate under these extreme loading conditions would be dominated by the mechanical fatigue failure rather than the environmental component (Figure 8).[5] However, both of these experimental studies also indicated that the flow of the bulk solution past the mouth of the crack may have a significant effect in increasing the mass transport rate of species out of the crack; this effect could be either because of the flow-induced pressure drop across the mouth of the crack and the effect this would have on the near-crack-mouth hydrodynamics, or because the solution that was forced out of the crack mouth during the closure part of the cyclic loading period was swept away rather than getting drawn back into the crack during the subsequent crack-mouth opening.

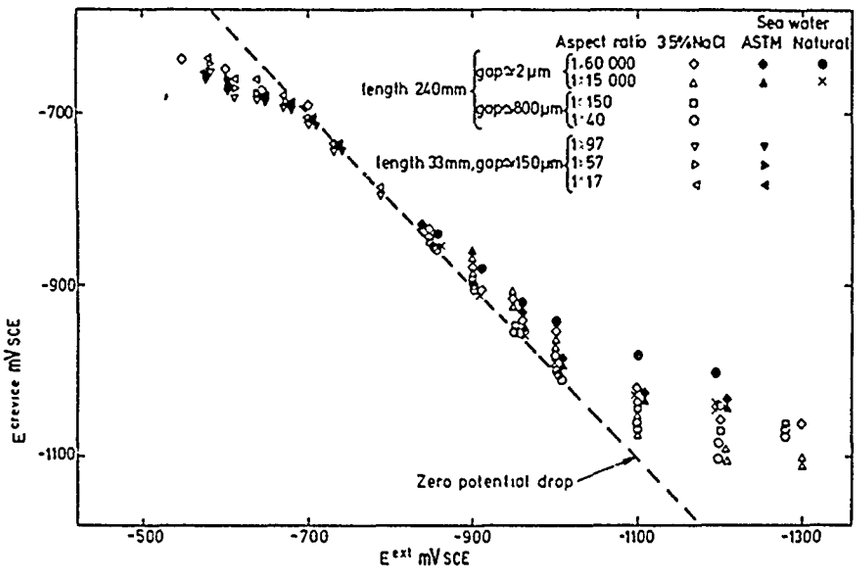


FIGURE 18—Variation of the potential in crevice with external potential for BS 4360 50D steel in 3.5% NaCl and in seawater.[85,120]

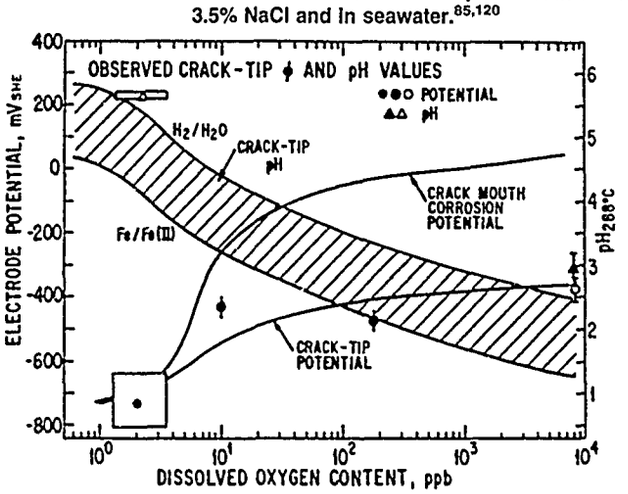


FIGURE 19—Crack-tip potential and pH variations as a function of dissolved oxygen content in water external to the crack. The observed data for crack-tip conditions at 288°C are for carbon steel (*);[131] A533B (●);[130] and stainless steel (Δ), (▲).[5] In this data, the carbon steel and stainless steel were in the form of tubular crevices and the A533B specimens were cracks.

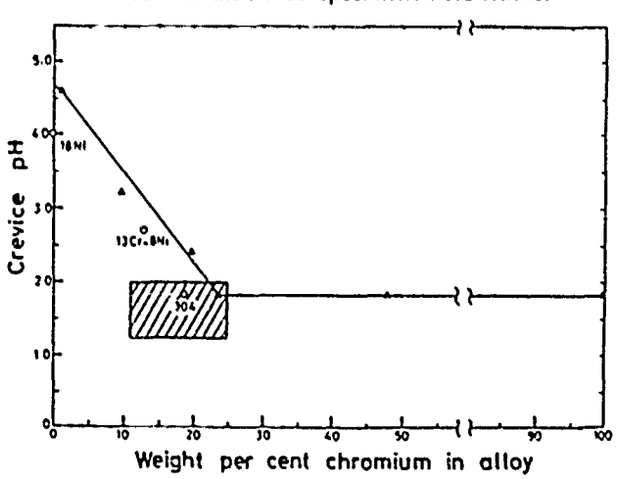


FIGURE 20—Crevice pH of Fe-Cr binary alloys as a function of the chromium content of the alloy.[133]

So far, discussion has centered around relatively concentrated non OH^- anionic concentrations in the crack enclave, that, under the appropriate potential conditions, allows the maintenance of low pH values at the crack tip (Figures 21 and 22). In higher purity environments, however, crack-tip pH values nearer neutrality are likely, with the value dictated by the crack-tip anionic activity that is governed by the dynamic equilibria among the various mass transport mechanisms. Andresen has systematically measured the contributions of Fickian diffusion, ionic migration, and natural and forced convection on the mass transport of anions in and out of a simulated crack.[5,80-82] Some of the experimental data have been analyzed in terms of one- and two-dimensional mathematical modeling.[90] For instance, when a potential field is applied between the crack mouth and tip, a time delay has been observed before a corresponding change in the anionic activity at various regions of the crack enclave. If the potential field causes an increase in anionic activity at the crack tip, this increase will be limited by the counteracting Fickian diffusion of anions *away* from the crack tip. Consequently, after a predictable time, a steady-state anionic activity (a_{ct}) at the crack tip is achieved (Figure 25), which, for cracks of sufficiently high aspect ratio, is governed by the following:

$$a_{ct} \sim a_b(316)^{\Delta\phi} \qquad (12)$$

where a_b is the anionic activity in the bulk system and $\Delta\phi$ is the potential drop down the crack.

The transients in crack-tip anionic activity resulting from, for instance, step changes in bulk solution anionic activity or from corrosion potential at the crack mouth are mirrored by the observed transients in the crack growth rate in, for instance, sensitized type 304 (UNS S30400) SS/water systems.[5] As noted in Figure 26, there are significant differences in the effects of rising and falling bulk solution anionic activity (conductivity) on the time to achieve a new steady-state crack growth rate[5] for SSs in oxygenated 288°C water. This is consistent with the theoretical predictions of the potential driven ionic migration, producing a rapid concentration of anions at the crack tip but providing a slowing down effect on the removal of anions by Fickian diffusion if the bulk solution anionic concentration is subsequently lowered.[5] It follows from Equation (12), therefore, that, in very dilute environments, the enhancement in crack-tip anionic activity over the bulk solution is limited to ≤ X100 (which occurs at the highest foreseeable potential drop in the crack of ~0.8 volts); thus, it is unlikely that salt precipitation would occur at the crack tip. For bulk solution anionic concentrations of the order of 10 to 35 ppb, the maximum anionic concentration at the crack tip would be in the range 1 to 3.5 ppm, which, from electroneutrality considerations, would correspond to minimum crack-tip pH_{25} values in the range 4 to 5 rather than ~ 2 expected in concentrated solutions/high-chromium alloy systems (see, for instance, Figure 20).

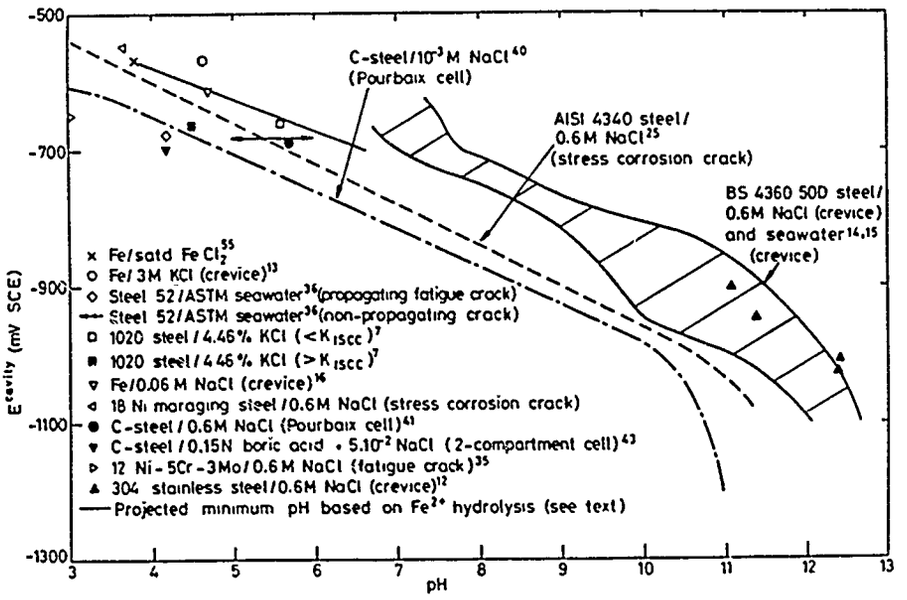


FIGURE 21—Variation of pH with potential in localized corrosion cavities for steels in the active state.[84] (Note that the reference numbers on the graph refer to data sources given in Reference 84 of the present review.)

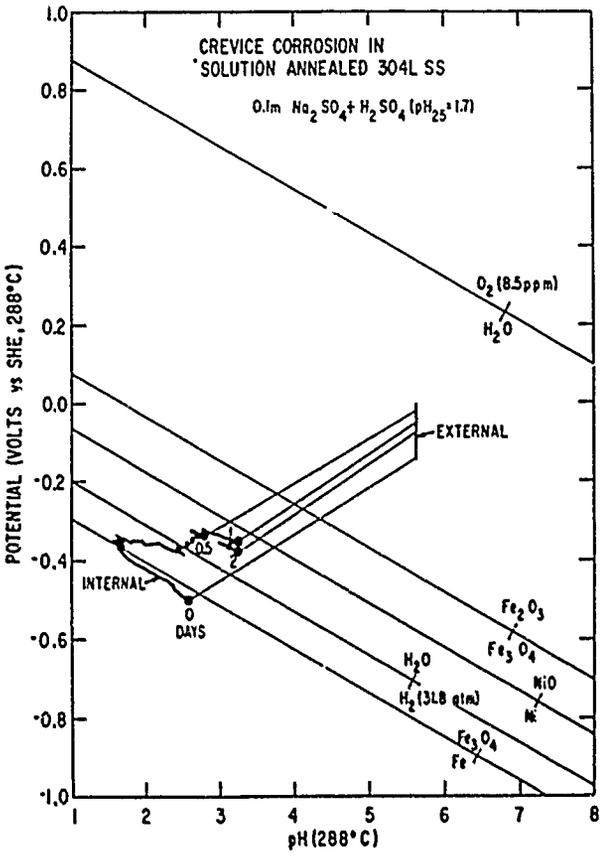


FIGURE 22—Time-dependent E/pH corrosion trajectory for solution-annealed type 304L (UNS S30403) stainless steel crevice containing 0.1 M Na_2SO_4 initially acidified to pH_{25} 1.7 with H_2SO_4. External solution is oxygenated water at 288°C.[5,135] Shown are the lines connecting the internal and external potential/pH values after various exposure times (indicated in days).

It should be stressed that the reasoning given above applies to the situation in which the source of anion is the bulk solution external to the crack. It is possible, however, that in some systems the alloy can be an anion source resulting from the dissolution of inclusions that intersect the crack enclave. This aspect has been addressed[1,5,131,142 145] for low-alloy steels in high-temperature water where MnS inclusions may dissolve;[146-148] the impact of this is that the sulfur-rich anion content at the crack tip is not solely a function of the mass transport criteria discussed above but is also a function of the dissolution rates of the MnS inclusions and the periodicity of introduction of fresh inclusions to the advancing crack tip (Figure 27).[1] Although preliminary modeling of such complex processes gives a sensible rationalization of the observed stress corrosion cracking[1] and corrosion fatigue[131,145,148,149] behavior of low-alloy steels in 288°C water, further analysis is required to account for inclusion size and orientation effects on these mass transport criteria.

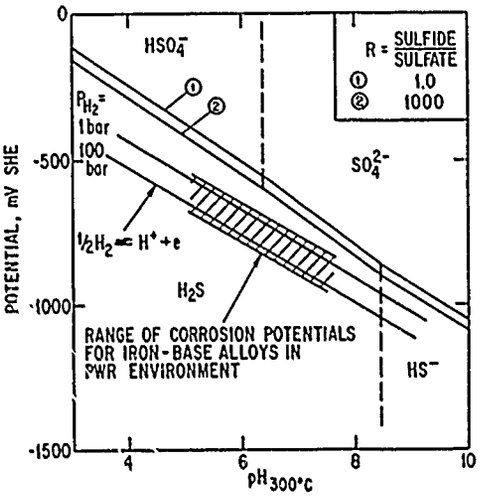


FIGURE 23—Range of corrosion potentials noted for iron-base alloys in simulated pressurized water reactor water at 288°C.[131] (Note it has been observed that, for such deaerated conditions, the crevice potential/pH conditions are within the hatched region.)

It is concluded that the basic mathematical analyses for defining the crack-tip solution composition are probably adequate to give a reasonable start in developing a quantitative life-prediction methodology for environmentally assisted cracking (Figure 3). this will be demonstrated later. These analytical capabilities, in conjunction with experimental verification, lead to thermodynamics and kinetics based definitions of the crack tip potential and pH (e g . Figures 21-24) and the crack-tip anion content [e.g., Equation (12)]. Obvi-

ously, there are many uncertainties behind this somewhat optimistic conclusion, and these may be associated with (a) extension of these mathematical modeling analyses [e.g., Equations (6-10)] to cover more concentrated solutions for multidimensional flow under all combinations of mass transport mechanisms, and (b) the accumulation of the low- and high-temperature data on diffusion coefficients, activity coefficients, reaction rates, etc., that are required for the solution of these mathematical analyses.

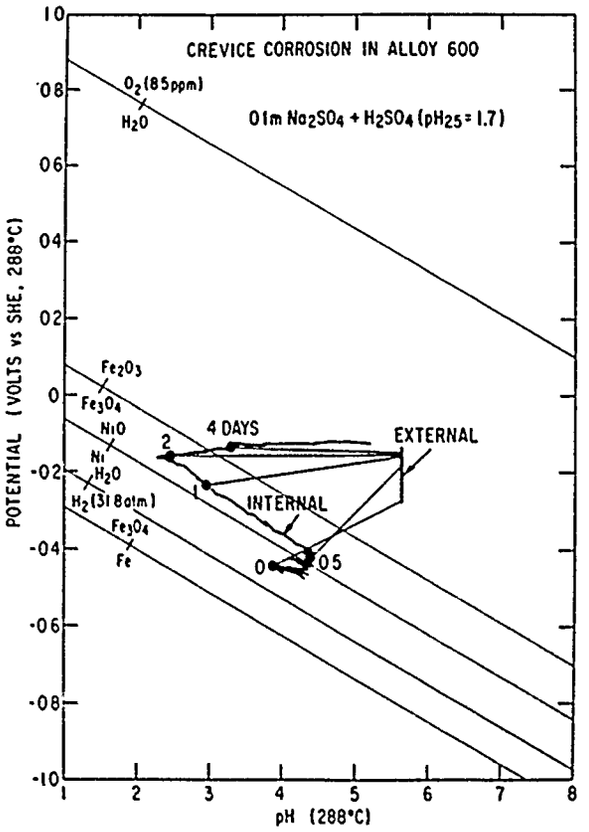


FIGURE 24—Potential/pH measurements on tubular Inconel 600 (UNS N06600) specimen when the tube bore initially contains acidified Na_2SO_4, and the external environment is water at 288°C, containing 8 ppm oxygen. Shown are tie lines connecting the internal and external potential/pH values after various exposure times (indicated in days).[5]

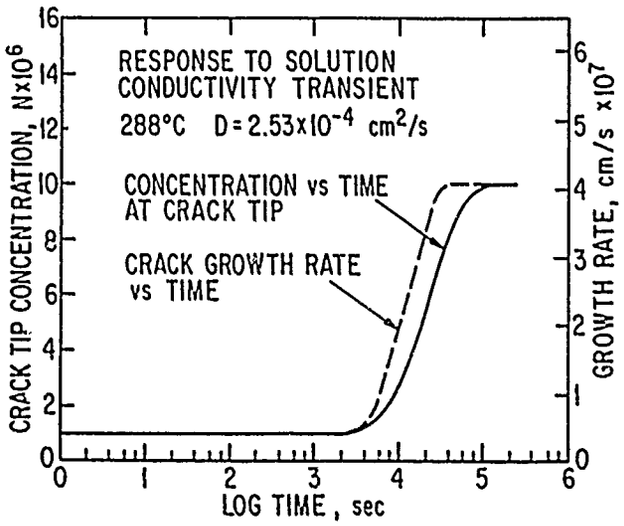


FIGURE 25—Comparison between the transients in anionic activity at a crack tip and crack velocity following a change in bulk solution anionic activity.[5] Crack growth data for sensitized type 304 (UNS S30400) stainless steel in 200 ppb oxygenated water, which undergoes a conductivity transient.

Perhaps the most practically pressing uncertainty about the current crack-tip solution analyses is the treatment of crack dimensions, especially for crack depths of metallurgical dimensions (e.g., $\lesssim$ 100 μm). Certainly, the mathematical modeling can be applied to these circumstances (e.g., pits), provided the correct boundary conditions are used, but the difficulty arises in experimentally verifying these analyses for propagating cracks. Preliminary unpublished measurements of crack propagation for very shallow cracks indicate that the "long crack" solution chemistry analyses may be applicable for crack depths $\geq$ 25 to 50 μm (for ductile type 304 SS in 288°C water),[150] but modification to these analyses are required for shorter cracks. Although such may be the case for situations where forced convection is not a dominant factor, current solution chemistry modeling for convection effects associated with cyclic loading indicates that, below a certain crack depth, the dominant mass transport mechanism at the crack tip changes from Fickian diffusion to forced convection.[118] This critical crack depth (1_{cnt}) depends on the diffusion coefficient (D), loading frequency (f), and mean stress ratio (R).[118] For instance, for parallel-sided cracks:

$$1_{cnt} = \frac{\sqrt{D/f}}{1-R} \qquad (13)$$

Such an analysis has been used by Gangloff[151] to explain "anomolous" corrosion fatigue propagation rates in short cracks (~ 1 mm) in relatively high-strength steels in NaCl, in terms of the ease of transport of oxygen to the crack tip and the effect this has on a HE mechanism of crack propagation. However, uncertainties persist in the treatment of physically and metallurgically short cracks in terms of both the definition of the crack-tip environment and the formulation of the crack-tip strain rate (discussed later).[152]

Crack-tip reaction rates

The electrochemical (and chemical) reaction rates can increase markedly when a protective surface oxide/film is ruptured, and these transients are central to crack propagation processes occurring at a strained crack tip (see the discussion of the candidate propagation mechanisms above). Therefore, to formulate a life-prediction methodology, such reaction rates must be measured in the relevant crack-tip material/environment system. The definition of the crack-tip system in terms of the solution composition and electrode potential was discussed in the previous section. The alloy composition at the tip of a transgranular crack is generally assumed to be that of the bulk alloy. In comparison, the alloy composition at the tip of an intergranular crack may be considerably different from the bulk composition if elemental segregation, or denudation, at the grain boundary occurs at rates controlled by, for example, thermally induced diffusion and/or irradiation-assisted damage. Discussion of these latter metallurgical aspects is outside the range of this particular review, but certainly there is adequate knowledge, backed up by extensive analytical electron microscope studies, to allow definition of the grain-boundary composition in terms of the thermal or irradiation history and the bulk alloy composition (see References 153-158).

The oxidation rates on a bare surface have a direct relationship to the crack propagation rate that is proposed by the slip-dissolution model (Figure 6). In many circumstances (as will be discussed later), the dissolution rate on a bare surface (i_b) can be maintained for a time (t_o) before the net oxidation current density decreases because of oxide formation; such a current density decay may occur by a power law of the general form:

$$i_t = i_b\left[\frac{t}{t_o}\right]^{-n} \qquad (14)$$

Integration of this relationship with respect to time to give the oxidation charge density leads directly to the expanded version of Equation (2). When the average periodicity of oxide rupture (t_f) ($= \epsilon_f/\dot{\epsilon}$) is significantly greater than t_o, then the average crack propagation rate is given by

$$\bar{V}_t = \frac{M}{z\rho F}\,\frac{i_b t_o^n}{(1-n)\epsilon_f^n} \times \dot{\epsilon}^n \qquad (15)$$

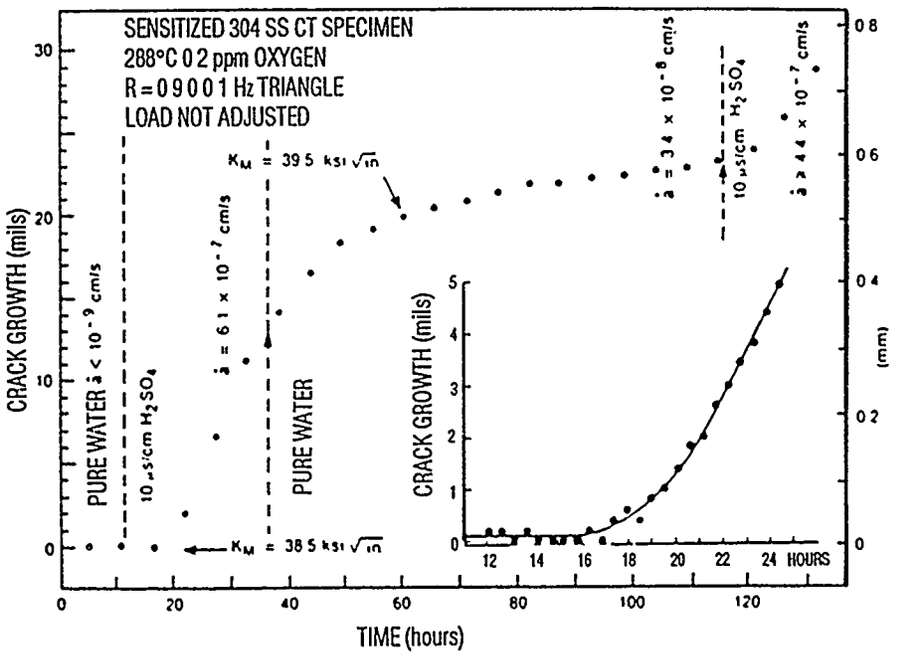


FIGURE 26—Crack growth rate responses for a cyclically loaded, sensitized type 304 (UNS S30400) stainless steel specimen in 288°C, 200 ppb oxygenated water, following changes in bulk water conductivity.[5]

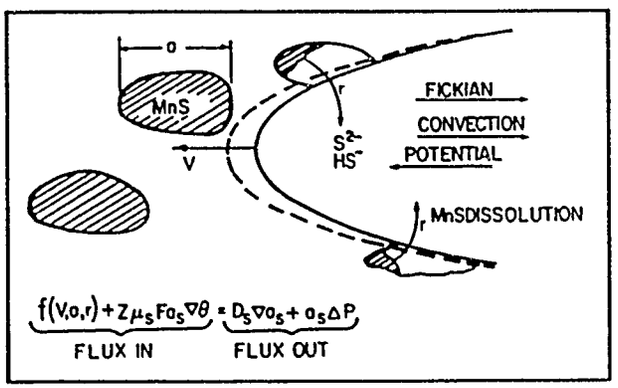


FIGURE 27—Schematic of advancing crack tip in mild or low-alloy steel showing the mass transport balance for dissolving MnS inclusions.[1,149]

However, the crack tip will be *maintained* in a bare-surface condition if the value of t_f is less than t_o, and under these high crack-tip strain-rate situations, the maximum crack propagation rate corresponds to the Faradaic equivalent of the bare-surface current density (i_b) (see Figures 5, 8, and 12):

$$\bar{V}_{t_{max}} = \frac{M}{z\rho F} \times i_b \qquad (16)$$

Thus, the measurement of the oxidation rate on a bare surface in the relevant crack-tip material/environment system gives a unique and fundamental prediction of the crack propagation rate. Unfortunately, such a clear-cut situation does not exist for HE mechanisms because the hydrogen-ion and/or water-reduction processes at a bared crack tip are not the atom-atom rupture processes pertinent to the crack advance. Increases in these reduction rates have been noted when a surface oxide is ruptured,[75,159,160] and this can lead to increases in the degree of hydrogen absorption and permeation into the underlying metal matrix.[161-164] Although such *changes* may relate to *changes* in crack growth rate by a specified HE model, the fundamental validity of these correlations is suspect without specific knowledge of the hydrogen adatom recombination kinetics, degree of dislocation-aided hydrogen diffusion, etc.

Various techniques have been used for creating the bare surface upon which the oxidation and reduction rates are measured. These have included mechanical methods to rupture the surface oxide such as slowly[75,160,165-170] or rapidly[171,172] straining the alloy; completely fracturing the specimen to create a bare fracture surface,[173-177] cyclic straining,[160,178] scratching the alloy surface,[159,179-189] or grinding.[174,190] Alternatively, electrochemical methods have been used that involve cathodically reducing the oxide (e.g., References 5, 191-193), then rapidly pulsing the potential to that of interest *vis-à-vis* the predicted crack-tip conditions. The experimental outputs may be either changes in corrosion potential (e.g., Reference 194), when the specimen has been strained under open-circuit conditions, or changes in cell current, when the strained specimen is connected galvanically to a large surface area of oxidized alloy.[176] More generally, however, the oxidation current density on the bare surface has been made under conventional three-electrode potentiostatic control with, in some cases, ellipsometric measurements of film growth.[193]

Recently, several comparisons have been made between the bare-surface reaction rates produced by the various experimental techniques.[5,195,196] Although all the techniques give the same general responses in terms of the changes in the bare surface reaction rates with, for instance, corrosion potential, pH, anionic activity, etc., questions have arisen about the *absolute* values of these reaction rates obtained by the various techniques. Such differences are usually related to the various aspects of experimental technique. For instance, uncertainty in the reaction rate analyses can arise for several reasons:

(1) Uncertainty concerning the bare surface area. Since it is the oxidation or reduction current *density* that is the important parameter, uncertainty in the reactive area leads automatically to uncertainty in the crack propagation rate predictions. Differences in reaction rate measurements between, say, straining and scratching electrodes techniques[195] may be related to uncertainties in the tensile fracture process of the surface oxide[197] or the surface roughness produced in the scratching electrode technique;[198] a similar surface roughness uncertainty also exists for experiments that involve the ductile fracture of the alloy specimen.

(2) Uncertainty concerning the surface condition of specimens cleaned by cathodic reduction of the oxide. In such cases, it is not always demonstrated that the oxide has been completely reduced before pulsing to the potential of interest,[199] and the contribution to

the subsequent oxidation current density on the "clean" surface resulting from the oxidation of adsorbed hydrogen is not always defined.

(3) Uncertainty concerning the IR correction, especially during the initial high-current pulse of the reaction rate transient. At small anodic overpotentials from the reversible potential for the metal oxidation reaction, the oxidation rates can follow an activation-controlled Tafel relationship,[159 200] and at overpotentials that are relevant to the crack-tip conditions, high current densities are possible. Thus, there is no question that, depending on the dimensions of the working electrode and the positioning of the reference electrode, high cell currents can give rise to "ohmic drop" deviations between the actual and measured potential. The saving grace is that, practically, this problem may not be as important *vis-à-vis* analysis of cracking phenomena, since it only exists for the time when a high cell current is passing, and this occurs for a time period (1 to 10 ms) that is short with respect to the time period of interest for most environmentally assisted cracking situations in which the periodicity of oxide rupture($= \epsilon_f/\dot{\epsilon}_{ct}$) is $> 10^2$ s.

(4) Uncertainty regarding the relative contribution to the measured oxidation current density transient due, for example, to oxide growth in two (i.e., surface coverage) dimensions, the dissolution rate in the intervening bare area, and, ultimately, the growth or thickening of the oxide. Although some of these questions may be cleared up by consideration of the charge density passed or by ellipsometric studies, this remains an analytical problem. Again, however, it may be of less importance practically since what is required to a first approximation is knowledge of the total oxidation charge density rather than its component parts, i.e., the movement of the metal/environment interface regardless of whether the "environment" is the solution or the converted oxide/film.

Although this latter statement is correct pragmatically, it does not alter the fact that knowledge of the precise atomistics of the oxidation (and reduction) reaction mechanisms on the bared surface[201,202] and how they are affected by the solution composition and electrode potential is of some importance. For instance, Burstein,[184] Lorenz,[203] Nobe,[204] Markus, et al.,[205] Ljungberg, et al.,[206] and Combrade[160] have all made arguments for the effect of adsorbed anions on the activation-controlled bare-surface dissolution rates. Ford and Andresen have argued that at higher anodic overpotentials for aluminum[200] alloys at low temperatures and for iron- and nickel-base alloys at 288°C,[5,80,81] the rate-controlling process for bare-surface dissolution may be diffusion of solvating water molecules to the oxidizing surface. They have also argued that this is affected by the "blocking effect" that results from precipitation of oxides adjacent to that surface. The common observation of a bare-surface dissolution rate of 0.5 to 5 A cm^2, regardless of the metal/environment system and the experimental procedures, seems to be a powerful argument for a common rate-controlling reaction, i.e., diffusion of solvating water molecules. For many systems, the bare-surface dissolution reaction is followed by a decay in the overall oxidation rate given by Equation (14),[5,171,173,185,186] or, in some cases,[75,167,187-189] by the following:

$$i_t = i_b \exp(-\beta t^n) \qquad (17)$$

In the limit, the value of n in Equation (14) approaches unity (see References 5, 75, 159, 200, 201), which would approximately correspond to the predictions of the place exchange[207] or high field-ion migration[208] mechanisms of oxide growth. Engseth and Scully have suggested that the law given by Equation (17) represents a summation of individual growth laws, each governed by Equation (14), which originate at different times on the strained surface.[167] Under certain combinations of material, composition, solution pH, electrode potential, and anionic type or activity, the value of n may decrease because of the breakdown of the growing oxide[5,75,159,200] as anions become incorporated into it (Figure 28).[5] The mean value of n over time periods of consequence to environmentally assisted cracking (i.e., $\sim 10^2$ s) may be related, therefore, to the crack-tip material composition, crack-tip potential and pH, and to the crack-tip anion concentration (Figure 29)[1] These latter parameters may, in turn, be related via the methodology given in the previous section to measurable bulk system parameters such as corrosion potential, anionic conductivity, degree of grain-boundary sensitization, etc (Figure 30).[5] Thus, there emerges a first principles methodology for relating n in Equation (14) to bulk system parameters and hence, via Equation (15), to the crack propagation rate.

The main conclusion regarding knowledge of the crack-tip reaction rates that are relevant to the candidate crack propagation mechanism is that the basic quantitative data for oxidation-related mechanisms (i.e., slip dissolution and film-induced cleavage) is either available or experimentally achievable. Although a similar statement could be made for the hydrogen-ion or water-reduction reactions that are pertinent to the HE mechanisms, it is still uncertain as to how these data could be used in the quantitative prediction of the crack propagation rate, since the first principles formulation of the crack propagation rate by these mechanisms [i.e., the counterpart to Equations (14) and (15)] have not yet been defined

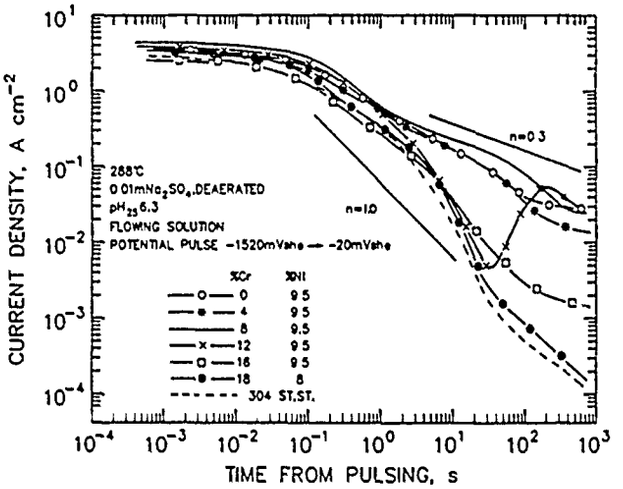


FIGURE 28—Oxidation current density/time relationships on a bare surface of various Fe-Cr-9.5Ni alloys in 0.01 M Na_2SO_4 at 288°C.

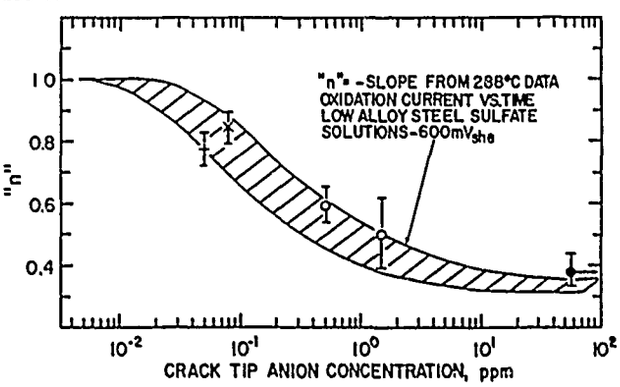


FIGURE 29—Variation of the parameter (n) in Equation (14) for various dissolved sulfur concentrations.[1] Data for mild and low-alloy steels in the initially bare conditions in sulfate,[5] borate,[160,209] molybdate,[5] and chloride solutions.[160]

Crack-tip strain rates

In the formulation of the candidate hypotheses for propagation, fundamental importance was placed on the periodicity of rupture of the thermodynamically stable oxide or protective film at the crack tip As shown schematically in Figure 16, this parameter will depend on the fracture strain of the oxide or protective film, and the various metallurgical and environmental parameters that affect the near surface deformation or strain rate. In this paper, the factors that affect the fracture strain of the surface oxide will not be reviewed, apart from commenting that this parameter can be independently measured and correlated with oxide thickness, slip morphology, etc. (For examples, see References 4, 5, 197, 210-216.)

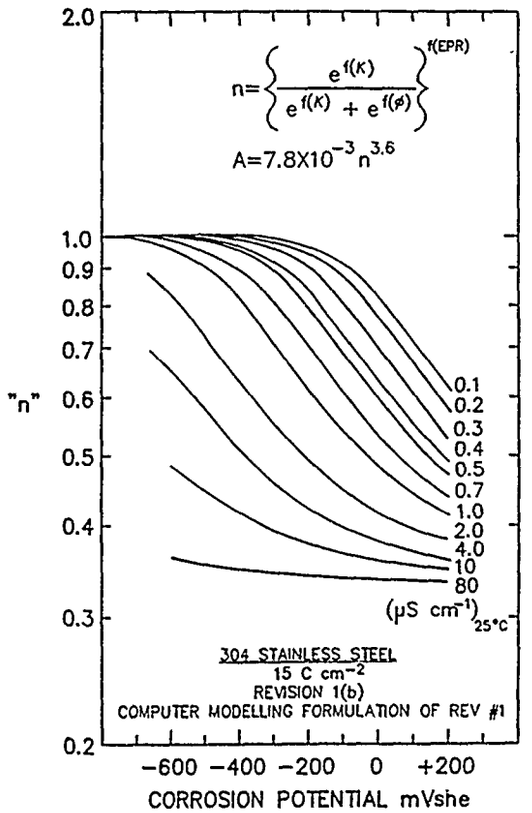


FIGURE 30—Relationships between n in Equation (14) and the corrosion potential and bulk solution conductivity for a sensitized (EPR = 15 Ccm^{-2}) type 304 (UNS S30400) stainless steel in water at 288°C.[5]

The oxide rupture prerequisite for crack advance may be associated with the interrelationship between cracking susceptibility and slip morphology, since coarse slip, rather than fine slip, will be more likely to rupture a brittle film of given thickness and thereby expose bare metal.[217] Such a relationship has been observed in both aqueous and gaseous environments (e.g., austenitic SS in aqueous[218,219] and hydrogen[68,69,220] environments) where the different dislocation morphologies are related to changes in stacking fault energy,[26,219,221] short-range order,[222-224] precipitate/matrix coherency, and precipitate distribution.[41,225-227] It should be emphasized, however, that although dislocation planarity may facilitate cracking, anomalies to the dislocation morphology/cracking susceptibility relationship exist, since rupture of the crack-tip film is not the *sole* requirement for subsequent crack propagation. Thus, the achievement of dislocation planarity per se is not a *sufficient* reason for environment-assisted cracking in ductile alloys.[219,228,229]

Despite these known effects of the microscopic heterogeneity of plastic flow at a crack tip on the cracking susceptibility, the main emphasis in formulating the periodicity of oxide or film rupture has been in terms of continuum parameters, such as strain rate. Previous reviews of the formulations for crack-tip strain rate ($\dot{\epsilon}_{ct}$) have been conducted by, for instance, Parkins, et al.,[230] Lidbury,[231] and Ford.[5,144] The following general equations have evolved.

For constant load:

$$\dot{\epsilon}_{ct} = A\dot{\epsilon}_{creep} + B\left(\frac{\bar{V}_t}{x^*}\right) \qquad (18)$$

For constant applied strain rates (SSRT):

$$\dot{\epsilon}_{ct} = C\dot{\epsilon}_{app} + D\left[\frac{\bar{V}_t}{x^*}\right] \qquad (19)$$

For cyclic load:

$$\dot{\epsilon}_{ct} = \left(\frac{\delta\epsilon}{\delta K}\right)_a \dot{K} + \left(\frac{\delta\epsilon}{\delta a}\right)_K \times \bar{V}_t \qquad (20)$$

In all of these equations, it is recognized that the crack-tip strain rate is a function not only of the applied stress, stress intensity (K), or strain rate ($\dot{\epsilon}_{app}$), but also of the crack propagation rate ($\bar{V}_t$). In other words, it is recognized that the movement (x^*) of the crack-tip stress field into the underlying metal matrix is activating new dislocation sources in a given time period, and thereby increasing the strain rate over and above that which would exist if the crack were stationary.

Constant-load conditions

Both Vermilyea[37] and Gerber and Garud[232] assigned prime importance to the creep component in Equation (18) when evaluating the crack-tip strain rate under constant-load conditions in SSs. At low homologous temperatures and under constant stress conditions, such a creep rate may be approximated by[233]

$$\dot{\epsilon}_{ct} = \gamma\sigma^m t^{-1} \qquad (21)$$

where σ = tensile stress, t = time, γ and m = constants. Such an analysis predicts that the crack-tip strain rate, and hence crack propagation rate, should decrease with time. Indeed, there is evidence for such a phenomenon of arresting cracks in several ductile alloy/aqueous environment systems,[234,235] and knowledge of creep relationships has been used to predict threshold stresses for environmentally enhanced cracking in systems in which a critical strain rate is required for the maintenance of cracking.[230] However, although such an approach may be correct in principle, the use of uniaxial creep data for the evaluation of the oxide rupture periodicity must be incorrect beyond "order of magnitude estimations," in view of the highly localized flow adjacent to the crack tip, the multiaxial stress conditions at the crack tip, the range of possible dislocation morphologies, and the known dependency of creep on surface dissolution,[236-239] adsorption,[240,241] surface films,[242,243] periodic stress relaxation,[244] etc. Indeed, a direct correlation has been observed between stress corrosion susceptibility and near-surface mechanical properties,[245] but such relationships have not been widely investigated.

Moreover, as intimated in Equation (18), a complication to the simple creep approach arises at faster propagation rates, because as the crack tip advances into the underlying matrix, it will activate new dislocation sources and thereby increase the creep rate for a given time increment. This process is shown in Figure 31, where it is conceived that as the crack propagates at a rate ($\bar{V}_t$), it will activate a number of new dislocation sources in a given time period. In an activation-controlled mechanism of creep, this is equivalent to decreasing the activation stress or increasing the applied stress. In other words, the steady-state creep rate at the crack tip will be governed by a dynamic equilibrium between the loss of dislocation sources by "exhaustion"[246] and the activation of new dislocation sources by the moving stress field associated with the advancing crack tip. Such a metallurgical concept is in accord with the "constant charge criterion" proposed by Scully,[247] Vermilyea,[248] and Newman,[249] who predicted that, for cracking to be sustained in certain alloy/environment systems, the crack had to advance a critical distance following the rupture of the oxide at the crack tip; i.e., a constant (oxidation) charge criterion had to be met. Moreover, it has been shown that such a constant charge criterion is applicable quantitatively to the cracking of stainless[172] and low-alloy steels[4,249] in aqueous environments at temperatures lower than 115°C.

Unfortunately, insufficient knowledge of the dynamics of creep processes exists to allow the relationship shown schematically in Figure 31 to be evaluated. Consequently, empirically based analyses have had to be used that, because of the design usefulness of fracture mechanics, have been formulated in terms of stress intensity.[1,3,5] For instance, for SS at 288°C, a *usable*[5] relationship for the crack-tip strain rate is

$$\dot{\epsilon}_{ct} = 4.1 \times 10^{-14} K^4 \qquad (22)$$

[where the stress intensity (K) is in units of $MPa\sqrt{m}$]. It must be emphasized, however, that this is an empirical formulation and must have limitations at high net section stresses and for short cracks when linear elastic fracture mechanics is invalid.

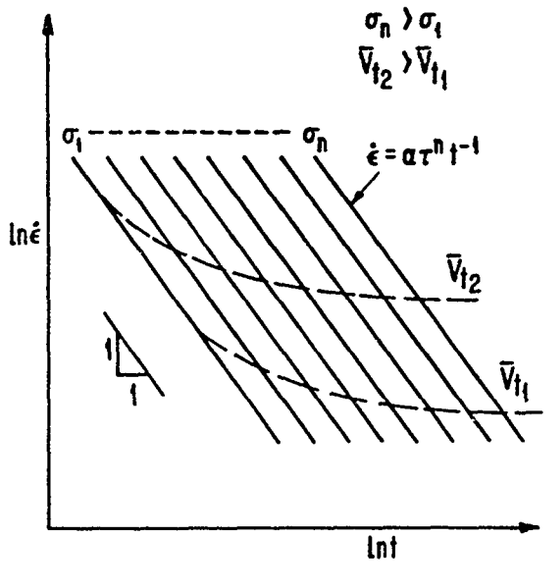


FIGURE 31—Schematic strain-rate/time relationships for various applied stresses (σ_n) illustrating how these may be changed at a crack tip because the crack is advancing at a velocity ($\bar{V}_t$).[5]

Slow-applied strain-rate conditions

Shoji and Congleton[250,251] and later Maiya[252] used as the basis of their calculations of the crack-tip strain rate under slow-applied strain-rate conditions the formula derived by Rice, Drugan, and Sham[253] for the rate of crack-tip-opening displacement ($\dot{\delta}$) at a distance (x) from a propagating crack tip in a fully plastic body:

$$\dot{\delta} = \beta \frac{J}{\sigma_Y} + \left(\frac{\sigma_Y}{E}\right) \bar{V}_t \ln\left(\frac{R}{x}\right) \qquad (23)$$

where x = crack length, σ_Y = yield strength, E = Young's modulus, β = constant, R = constant, approximately proportional to the plastic zone size, and $\bar{V}_t$ = average crack propagation rate (cm s^{-1}).

For the situation of a tensile specimen of gauge length L containing N cracks, Shoji and Congleton calculated the variation in $\dot{\delta}$ with an externally applied strain rate ($\dot{\epsilon}_{app}$) as follows.

$$\dot{\delta} = \sigma_Y \frac{L}{N} (\dot{\epsilon}_{app} - \dot{\epsilon}_{nc}) \qquad (24)$$

where $\dot{\epsilon}_{nc}$ = the strain rate in the intervening uncracked regions on the gauge length.

To translate the crack tip displacement rate to an average crack tip strain rate, it has been assumed that the appropriate gauge length" at the tip of the crack is the total width of the active flow bands, calculated to be 0.01 to 0.1 mm. By substituting these assumptions into Equation (23) and combining with Equation (24), an approximation for $\dot{\epsilon}_{ct}$ is

$$\dot{\epsilon}_{ct} = \frac{75}{N} \dot{\epsilon}_{app} + \frac{V}{0.50} \ln\frac{1000}{N} \qquad (25)$$

Thus as pointed out by Parkins,[254] the absolute value of the crack-tip strain rate depends on the number of crack initiation sites and the average crack propagation rate (which will be a function of the material/environment combinations). For instance, for the low-alloy steel/oxygenated water system at 288°C,[1,5] if the number of cracks is in the range 5 to 30 (commonly observed in slow-strain tests) and the applied strain rate is $> 10^{-7}$ s^{-1}, then for commonly observed crack propagation rates of 2×10^{-7} to 2×10^{-6} cm s^{-1}, the following approximate relationship may be used,

$$\dot{\epsilon}_{ct} = 10 \times \dot{\epsilon}_{app} \qquad (26)$$

Cyclic loading conditions

Calculations of the crack-tip strain rate under cyclic loading conditions have centered around separate evaluations of the parameters $(\delta\epsilon/\delta K)_a \dot{K}$ and $(\delta\epsilon/\delta a)_K \bar{V}_t$ in Equation (20).

Hudak, Page, and Davidson[255] have used a stereoimaging technique to measure directly the $(\delta\epsilon/\delta K)_a$ values on the surface of SS (and an aluminum alloy) specimens cyclically loaded in either vacuum, dry argon, or sodium sulfate. This technique relies on the comparison of the planar displacement of adjacent regions on the surface under loaded and unloaded conditions, and, since these measurements can be made under high magnification, the surface strain values can be measured close to the crack tip. Even though such measurements are taken under predominantly plane-stress (surface) conditions, the resultant $(\delta\epsilon/\delta K)_a$ measurements act as a "benchmark" for various calculations based on continuum fracture mechanics and finite element analyses; these approaches are reviewed briefly below.

Several investigators have calculated the average crack-tip strain rate during the full stress cycle by making the assumption that the use of linear elastic fracture mechanics is valid. The underlying assumptions have been, therefore, that the plastic zone strain and strain variations are treatable on a continuum basis, and that the system is subject to small-scale yielding. Scott and Truswell[256] assumed that (1) the crack-tip strain rate could be related to the time dependence of the crack-tip-opening displacement ($d\delta/dt$) and (2) the "gauge length" over which the strain was to be calculated was given by the instantaneous crack-tip-opening displacement (δ), i.e.,

$$\dot{\epsilon}_{ct} = \frac{1}{\delta} \times \frac{d\delta}{dt} \qquad (27)$$

When this relationship is averaged over a cyclic period (T), then for $R > 0$,

$$\dot{\epsilon}_{av} = \frac{-1}{T} \ln [1 - 1/2(1-R)^2] \qquad (28)$$

(where R = minimum load/maximum load).

Both Atkinson[257] and Gabetta[258] have questioned the use of the instantaneous crack-tip-opening displacement as the "gauge length." Gabetta suggested that this dimension should be a function of the distance between the crack tip and the bending hinge point on, for example, a compact tension sample. Atkinson, on the other hand, suggested that the gauge length should be a "characteristic" length (W). Regardless of the precise definition, the dissociation of this gauge length from the instantaneous crack-tip-opening displacement leads to a formulation of the form:

$$\dot{\epsilon} = \frac{1}{W} \frac{d\delta}{dt} = \frac{1}{T} \frac{\alpha \Delta K^2}{2WE\sigma_y} \qquad (29)$$

The advantage of these latter approaches is that they introduce a dependency of $\dot{\epsilon}_{ct}$ on ΔK that was missing from Scott's formulation. Alternatively, Cole, et al.,[259] argued that since the oxide rupture rate is governed by the movement of dislocations under shear, the appropriate strain rate should be the shear strain rate (γ) operating over a gauge length equivalent to the total width of the active flow bands. This would give a similar formulation to Equation (29), except that now the value of W can be related to a physical metallurgical parameter. Finally, Lidbury[260] related the average plastic shear strain rate to a function of the reversed plastic zone size at a given ΔK value, and the reversed plastic zone size at the threshold ΔK_O value. Such an approach led to the formulation of the *total* shear strain (i.e., elastic plus plastic strains) rate ($\dot{\gamma}_T$) in terms of the yield strain in shear (γ_o), the cyclic period (T), ΔK, and ΔK_o, as follows:

$$\langle \dot{\gamma}_T \rangle = \frac{2\gamma_o}{T} \left(\frac{\Delta K}{\Delta K_O}\right)^2 \qquad (30)$$

Since ΔK_o is known empirically to be a function of R via the work of Lindley and McCartney,[261] the effect of the R value also enters into this equation.

The validity of these various linear elastic fracture mechanics (LEFM) formulations for cyclic loading have been examined[5] by comparing their predictions with the experimental data produced by the stereoimaging technique.[255] This is shown in Figure 32, where the predicted $\dot{\epsilon}_{ct}$ vs ΔK relationships using the Scott,[256] Cole,[259] and Lidbury[260] formulations are compared to the observed data of Hudak and Davidson[255] for SS stressed at R = 0.1 and 10^{-2} Hz cyclic loading conditions. It is apparent from this comparison that the Lidbury and Cole formulations come closest to predicting the *trend* in the observed data. It is important, however, that the semiquantitative nature of this conclusion be noted, for the absolute values of the theoretical relationships are dependent on the unsubstantiated values placed on some parameters (such as the "gauge length"); further, the experimental results against which the theoretical relationships were compared were obtained under plane-stress surface conditions instead of the more relevant plane-strain conditions that will exist over the majority of the crack front on crack growth specimens.

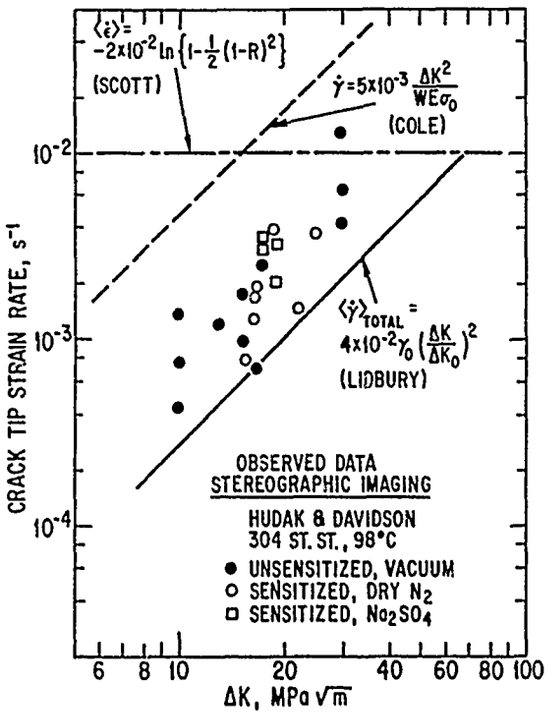


FIGURE 32—Comparison between the observed and calculated crack-tip strain-rate/stress-intensity amplitude relationships for R = 0.1, 10^{-2} Hz conditions.[5] Observed data obtained via the stereoimaging technique on stainless steel.[255] Calculated data on the basis of Scott, Cole, and Lidbury formulations [Equations (28), (29), and (30)].

Several authors have considered the restriction on the above analyses of small-scale yielding. Leis[262] and Mehta and Ranganath[263] applied elastic-plastic fracture mechanics to the analysis of corrosion fatigue. The conclusions from this preliminary work indicate that the use of such elastic-plastic analyses involving, for instance, J, are better able to formulate the crack tip strain and strain rate *vis à-vis* stress corrosion and corrosion fatigue than the LEFM approaches. Indeed, later work by Kawakubo and Hishida[264,265] indicated that stress corrosion crack propagation in the SS/water system for a variety of specimen geometries under monotonically increasing loads is normalized by the time differential of the J integral ($\dot{J}$).

The alternative (or additional) formulation of the crack-tip strain rate under cyclic loading is the $(\delta\epsilon/\delta a)_K\ \overline{V}_t$ term in Equation (20). The value of $(\delta\epsilon/\delta a)_K$ may be obtained from experimental data using the stereoimaging technique[255] or by finite element analysis. This latter approach has been used by Shoji,[266,267] who determined the change in the strain at a point in front of the crack as the crack tip moved toward it. When the crack tip coincides with the point, that point is exposed to the environment, and the value of $(\delta\epsilon/\delta a)_K$ at that instant is the appropriate value in calculating the crack-tip strain rate. Such approaches lead to a formulation of the crack-tip strain rate in terms of the time-base crack propagation rate in an inert environment ($\overline{V}_{it}$) of the form:

$$\dot{\epsilon}_{ct} = B\,\overline{V}_{it} \tag{31}$$

where the constant B depends on specimen geometry and alloy, and $\overline{V}_t$ may be defined in terms of the mean stress ratio (R), ΔK, and loading frequency. For instance, for SS at 288°C, the following relationship[5] has found extensive applicability:

$$\dot{\epsilon}_{ct} = 68.3\,\dot{\upsilon}\,A_R\,\Delta K^4 \tag{32}$$

where ΔK = stress-intensity amplitude (MPa$\sqrt{m}$), $\dot{\upsilon}$ = loading frequency (s^{-1}), and A_R = constant, which is a function of the mean stress ratio.

In conclusion, the positive aspect of the definition of the crack-tip oxide or film-rupture periodicity is that it is currently solvable, if only in a semiquantitative manner. As will be shown later, this state of the art is *usable* for current life-prediction requirements, but unanswered questions definitely remain in this analytical area. Perhaps the most pressing of these are the following:

(1) The uncertain validity of $\dot{\epsilon}_{ct}$ formulations that use linear elastic fracture mechanics parameters for ductile materials, and the possible desirability of using elastic-plastic approaches involving J, $\dot{J}$, or C*. Allied to this problem is the conceptual one of using a continuum fracture mechanics approach for localized plasticity phenomena in which, for instance, the dislocation motion and morphology are known to play a significant part in environmentally assisted cracking susceptibility.

(2) The formalism of accounting for the dynamic equilibrium between a decreasing logarithmic creep rate at a static crack tip and its increase with dislocation activation as the crack advances. Again, allied to this problem is the undefined effect of the crack-tip environment or its by-products (e.g., absorbed hydrogen) on the plasticity process itself.

(3) The problem of applying linear elastic fracture mechanics or elastic plastic formulations to metallurgically short cracks and to coalescing cracks.[254]

(4) The validity of the underlying assumption in all of the mechanics models that the whole crack front moves forward uniformly, rather than the (probably) more realistic notion that crack advance occurs at isolated points along the crack front and then links by lateral movement.

Validity of Candidate Propagation Mechanisms and Their Practical Use

"Even the best research is of little use unless it moves out of the laboratory and into the marketplace"
From *Business Week* (July 8, 1985, p. 87)

The validity of any crack propagation mechanism is demonstrated by its ability to predict quantitatively all the available data, even though that data may seem to exhibit a hopeless scatter (e.g., Figure 1) or when there seems to be little correlation between cracking incidents in a plant and, for instance, operational time (Figure 33).[268] Traditionally, such scatter would be tackled on a probabalistic basis but, as mentioned previously (Figures 3 and 4), it is suggested that (ignoring bad experimentation or measurement techniques) such scatter is not random but is predictable on a deterministic basis, provided the correct mechanistically based model is used. There have been comparatively few validation exercises for mechanistically based models, which have not had to make fairly major assumptions because of missing information about the definition of the crack-tip system. Some of these "missing information" problem areas have been discussed in previous sections. In this section, discussion is centered around a validation

exercise[5] in which the crack-tip system is comparatively well characterized in order to demonstrate[3] the practical use of this fundamental knowledge. The problem addressed in this exercise is that of intergranular stress corrosion cracking of SS in water at 288°C, which relates to the cracking of weld-sensitized piping in boiling water reactors (Figure 33). It was hypothesized[5] that the crack propagation mechanism was primarily slip dissolution, with intergranular cracking occurring because of (1) chromium denudation adjacent to grain-boundary $Cr_{23}C_6$ precipitates in the weld-heat-affected zone, (2) oxygenation of the water because of radiolysis in the reactor core, and (3) tensile residual stress from the welding procedure. Extensive investigations of the crack-tip solution composition, crack-tip reaction rates, and calculation of the crack-tip strain rate indicated that the appropriate crack propagation rate algorithms were

$$\overline{V}_T = f(n)\,\dot{\epsilon}_{ct}^{n} \tag{33}$$

where

$$f(n) = 7.8 \times 10^{-3}\, n^{3.6} \tag{34}$$

$$n = \left[\frac{e^{f'(\kappa)}}{e^{f'(\kappa)} + e^{g'(\phi_c)}}\right]^{g'(EPR)} \tag{35}$$

and the crack-tip strain rate ($\dot{\epsilon}_{ct}$) was given by Equation (22) and (32) for constant and cyclic loads. Thus, the crack propagation rate could be formulated on the basis of the bulk system parameters, κ (the solution conductivity), ϕ_c (the corrosion potential), EPR (measure of grain-boundary chromium denudation), stress intensity, etc., even though the model itself was based on crack-tip phenomena.

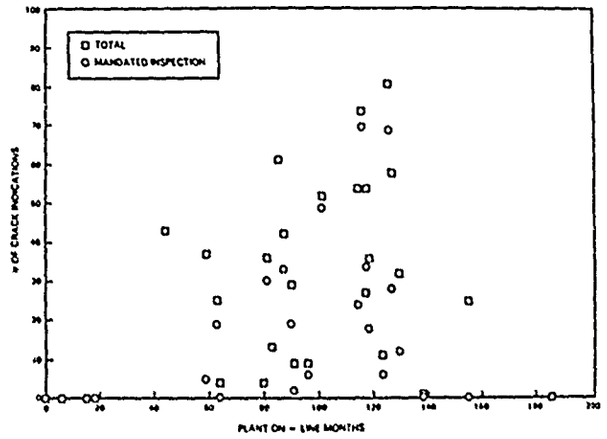


FIGURE 33—The relationship between the number of crack indications noted in stainless steel piping in a given boiling water reactor and the number of months that plant has been in operation.[268]

A comparison between the theoretical and observed crack propagation rate/strain-rate relationships is shown in Figure 34 for data obtained in 8 ppm oxygenated water under constant load, slow-applied strain-rate and cyclic load conditions. The agreement between theory and observation illustrates the utility of the mechanistically based model for both intergranular "stress corrosion" and "corrosion fatigue," which, at higher loading frequencies, is transgranular. Similar comparisons between observation and theory are shown in Figures 35 and 36 for the effects of corrosion potential and solution conductivity, respectively, on the propagation rate under the stated loading and grain-boundary sensitization conditions. The agreement between observation and theory for a very wide range of testing conditions is shown in Figure 37; in this example, the wide range in propagation rates was obtained via wide ranges in corrosion potential (deaerated to highly oxidizing in-core conditions), stressing (constant load to high-frequency fatigue), sensitization (solution annealed to furnace sensitized), etc. Further analysis of the data in Figure 37 indicated that the current model algorithms consistently over-predicted the mean observed data by approximately 17%, probably a result of assumptions in the crack-tip strain-rate calculations. Of equal significance, however, is the fact that the scatter in Figure 37 is predictable in terms of the high sensitivity of the crack propagation rate to corrosion potential and conductivity (Figures 35 and 36) and the fact that these parameters are not always adequately defined in the experimental test procedures. Thus, although assumptions have had to be made in all components of the crack-tip system definition, it is apparent that, for this system, a mechanistically based model can be formulated that *adequately* predicts a substantial amount of data observed in many laboratories.

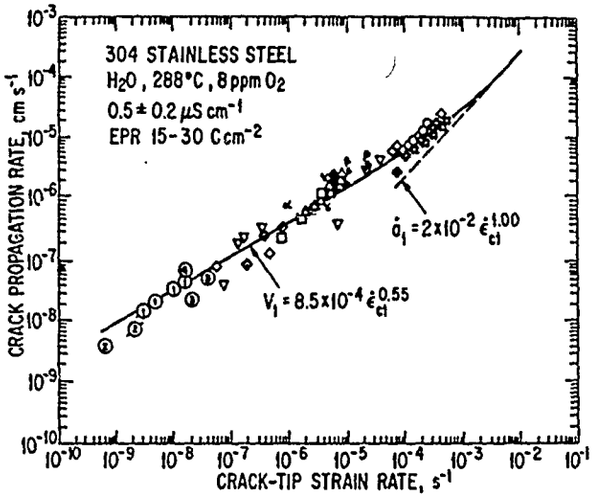


FIGURE 34—Observed and theoretical crack propagation rate/crack-tip strain-rate relationship for sensitized type 304 (UNS S30400) stainless steel in oxygenated water at 288°C.[5]

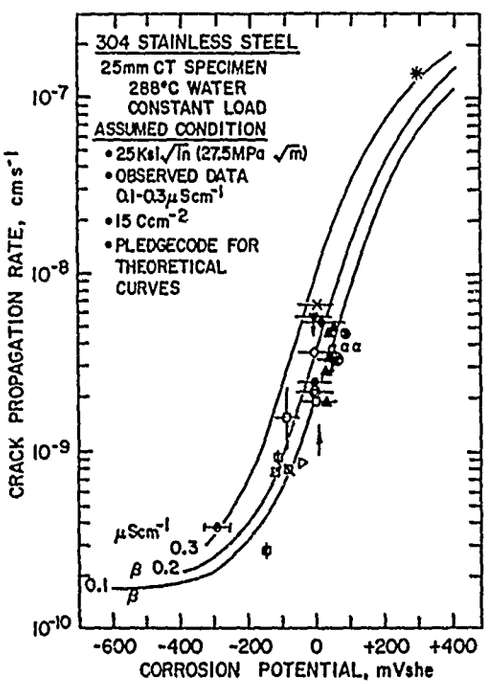


FIGURE 35—Observed and predicted relationships between the crack propagation rate and corrosion potential for sensitized type 304 (UNS S30400) stainless steel in water under constant load. Water conductivity in the range 0.1 to 0.3 μS cm^{-1}.[5]

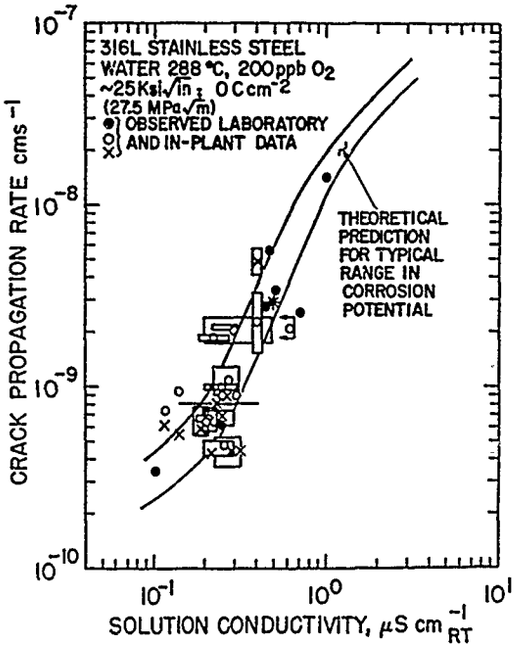


FIGURE 36—Observed and predicted relationships between the crack propagation rate and solution conductivity for type 316L (UNS S31603) stainless steel under constant load (25 ksi $\sqrt{in.}$) in water containing 200 ppb oxygen.[5]

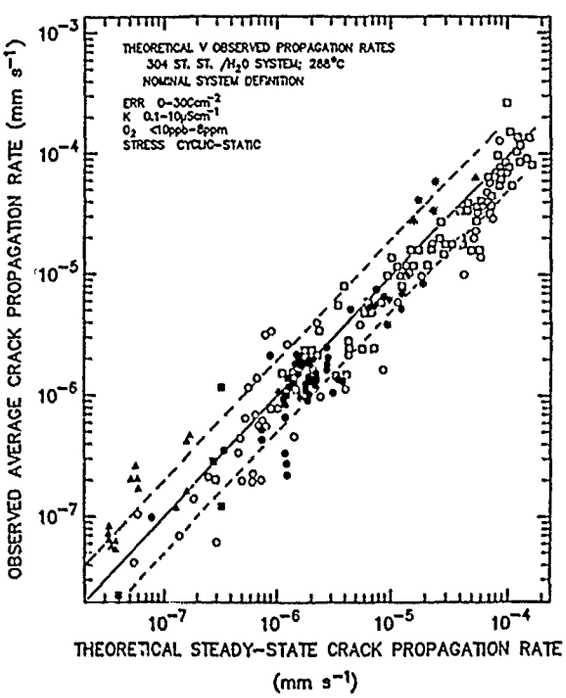


FIGURE 37—Relationship between the observed and theoretical steady-state propagation rates for stainless steel in water at 288°C for a wide combination of material, stress, and environment conditions.[5]

Such a validated mechanistically based model may be used practically,[5] preferably in combination with system monitors that define the actual (rather than the nominal) system conditions to solve practical problems.[6] Practical uses include[3,5]

(1) Validation of environmentally assisted cracking test methods,
(2) Validation of operating specifications and limits *vis-à-vis* environmentally assisted cracking;
(3) Validation of life-prediction and design codes, and
(4) Prediction of the effect of environment, material, and stress variables on the cracking susceptibility of plant structures.

An example of the latter application is shown in Figure 38 for the cracking of 10-in. (254-mm) diameter, schedule 80 weld-sensitized type 304 SS piping in 200 ppb oxygenated water at 288°C; in this example, the beneficial effect of improving the water purity in mitigating cracking is clearly predicted. These relationships are for well-defined conditions of residual stress, corrosion potential, grain-boundary sensitization, etc. It follows, therefore, that if there is a range of residual stress profiles, there will be a predictable range of cracking responses. This is illustrated in Figure 39, which shows that the minimum observed crack depth after a certain time at a given plant corresponds to the NDT crack resolution limit; the mean observed crack depth corresponds to the mean theoretical value appropriate for the average coolant conductivity; and the maximum observed crack depth corresponds to that predicted for the maximum observed residual stress profile for that classification of piping. From such predictions, it is apparent that there should be an inverse relationship between the coolant conductivity and the time for the crack depth to reach, for instance, a quarter-wall thickness. The precise relationship will depend on the material/stress/environment definition, as shown in Figure 40, for three such system definitions. Also shown in Figure 40 are observations from several operational plant indicating that the majority of observations are associated with the mean system definition, but the "outliers" may be explained in terms of a combination of a high degree of grain-boundary sensitization and a high residual stress from the welding process. Thus, the apparent scatter shown in Figure 33 may be analyzed mechanistically in terms of the knowledge of the specific system conditions, and, with this knowledge, predictions of future behavior may be made for specified operating conditions (Figure 41).

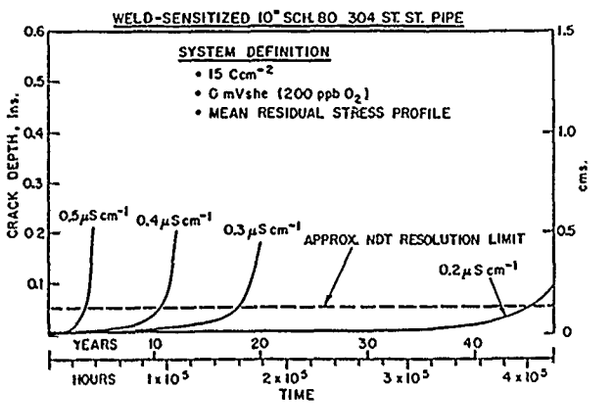


FIGURE 38—Theoretical variation in crack depth with operating time for weld-sensitized 254-mm-diameter Schedule 80 stainless steel piping in 288°C oxygenated (200 ppb) water as a function of solution conductivity.[5]

The development of the modeling and monitoring approach to life prediction of structures susceptible to environmentally assisted cracking has been detailed above for the austenitic SS/water system in the nuclear energy industry. The approach, lessons learned, and developments are directly applicable to numerous other cracking systems provided that the generic mechanisms of cracking discussed previously are assumed to be applicable. Indeed, preliminary assessments of such capabilities have been made for stress corrosion[1] and corrosion fatigue[5,148] of low-alloy pressure vessel steels in 288°C water and also nickel-base alloys.[269] There is no reason, in principle, why such practically helpful mechanistically based models cannot be developed for other cracking systems, provided the relevant crack-tip mass transport, reaction rate, and plasticity aspects are quantified. *If* there are common features, then it is attractive to think in terms of an environmentally assisted cracking diagram, akin to the Pourbaix diagrams or the deformation maps[270] for creep developed initially by Ashby.[271] Possible axes on such an environmentally assisted cracking diagram could be corrosion potential and temperature [Figure 42(a)], since these are both thermodynamically and kinetically significant to most of the candidate cracking mechanisms.[4,5,7] The main point is that iso-velocity lines are

predictable by quantifying the crack-tip processes associated with the cracking mechanism and can, in turn, be related to the corrosion potential/temperature regimes associated with the various component operating conditions [Figure 42(b)]. Thus, the stress corrosion and corrosion fatigue behavior of SSs in light water reactor environments is similar, in terms of the fundamental crack-velocity/crack-tip strain-rate relationship, to that for C-Mn steels in light water reactor environments and that for Ni-Cr-Mo-V steels in wet steam environments that are symptomatic of low-pressure steam turbine operations. Naturally, the constants in these relationships will change with system conditions and/or mechanisms of cracking, but, as shown in the previous sections, these changes can be predicted from first principles, and the resultant knowledge used for life-prediction purposes.

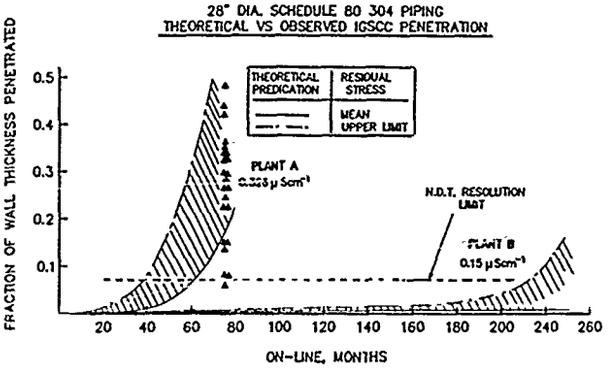


FIGURE 39—Theoretical and observed crack depth vs operational time relationships for 28-in.-diameter Schedule 80 type 304 (UNS S30400) stainless steel piping for two boiling water reactors operating at different mean coolant conductivities. Note the bracketing of the maximum crack depth in the lower-purity plant by the predicted curve that is based on the maximum residual stress profile and the predicted absence of observable cracking in the higher-purity plant (in 240 operating months).

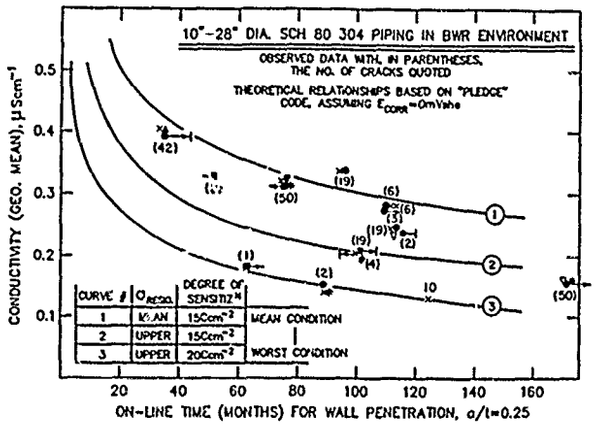


FIGURE 40—Observed and theoretical relationships between average boiling water reactor coolant conductivity and the operational time to achieve quarter wall penetration. Observed data from various operational boiling water reactors are shown with the number of cracks detected in parentheses beside each data point. Theoretical curves are for the quoted combinations of stress and degree of sensitization at the heat-affected zone.

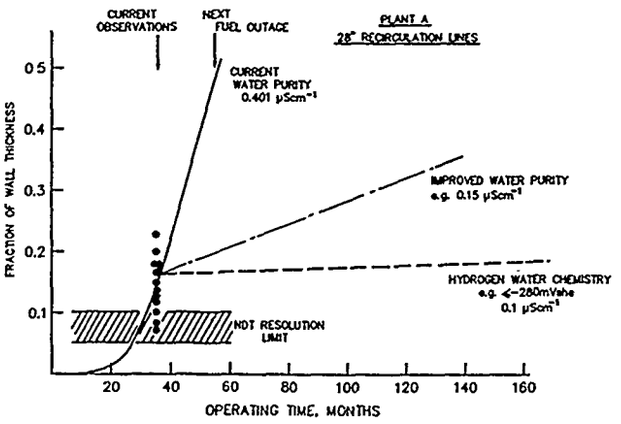


FIGURE 41—Use of modeling algorithms to explain the degree of current crack penetration in weld-sensitized type 304 (UNS S30400) stainless steel piping and to predict the future crack propagation characteristics for the defined operating conditions.

Conclusion

"He that will not apply new remedies must expect new evils; for time is a great innovator"

From Francis Bacon (1561-1626), *Essays II "of innovations"*

The underlying premise in this review has been that the main reason for developing mechanistic knowledge of environmentally assisted cracking phenomena is to use it to solve the practical problems they cause. Moreover, such a use of fundamental knowledge will become a necessary tool in life-prediction methodologies, since codes based solely on empirical data have become suspect as the operational systems become more and more complicated and the design lives are extended further. These mechanistically based solutions may arise out of both qualitative and quantitative knowledge of the mechanisms of cracking and, in both cases, involve definition of the crack-tip system. It was concluded that the main crack propgation mechanisms (slip dissolution, film-induced cleavage, and HE) were controlled by mass transport considerations between the crack mouth and crack tip, oxidation and reduction reactions at the crack tip, and the oxide rupture periodicity or strain rate at the crack tip. Qualitative knowledge of these rate-controlling parameters and how they affect *changes* in the crack propagation rate according to the candidate mechanism is enough in most systems to give invaluable advice to the design and operational engineer as to possible mitigating actions. However, problems persist in many of the details of the definitions of these rate-controlling processes, ranging from the mathematical and chemical validity of the assumptions made in the crack-tip solution definition to the calculation of crack-tip strain rate. These problems become especially significant when extending the qualitative prediction methodology to a quantitative deterministic or probabalistic capability that is necessary for defining extended operational times. It was demonstrated, however, that even for this imperfect state of the art (*vis-à-vis* the academic rigor of the analyses), a usable quantitative prediction capability is possible in a few selected systems and should, in principle, be able to be developed for other technically important systems. It is probable that this will be accomplished first for those systems in which the slip-dissolution or film-induced cleavage models are the relevant crack propagation mechanisms, since there are more severe fundamental problems still to be solved concerning the atomistics of the various HE mechanisms.

Acknowledgment

Acknowledgment is extended to the General Electric Company for permission to publish this paper and to my many colleagues at General Electric, NACE, EPRI, the International Cyclic Crack Growth Rate Committee, etc., with whom technical discussions over the years have made this review that much easier (or harder!) to write. In particular, acknowledgment is extended to P.L. Andresen, R.W. Staehle, and A. Turnbull, who kindly reviewed this paper.

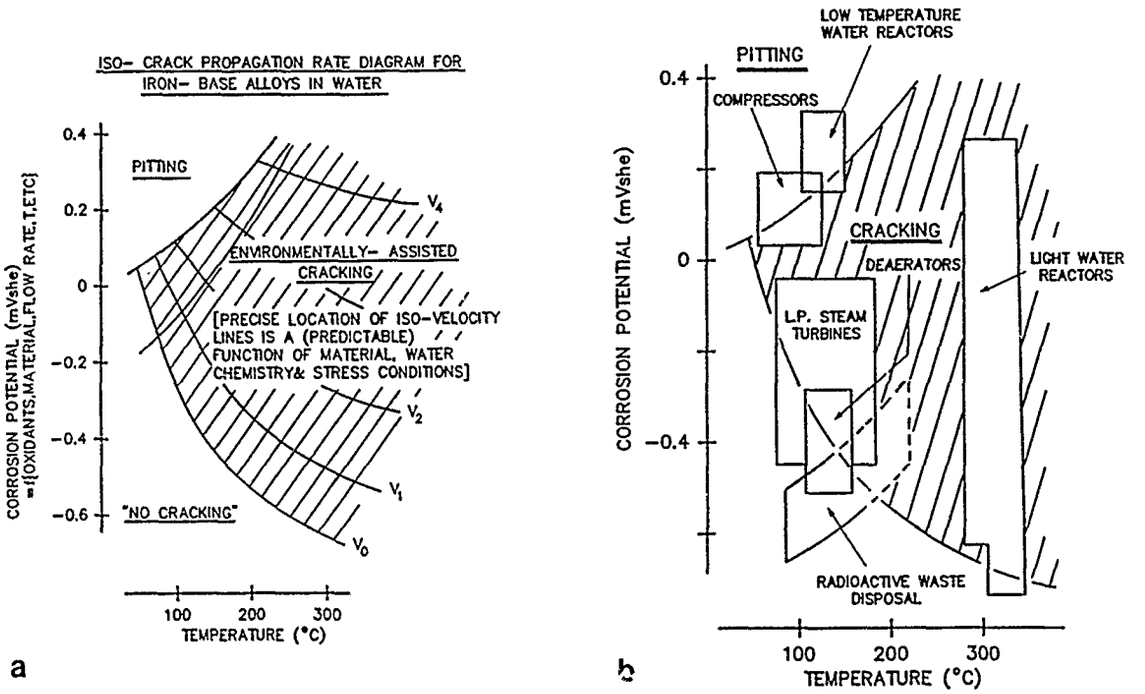


FIGURE 42—Iso-velocity diagram for iron-base alloys in water predicted from slip-dissolution model: (a) corrosion potential vs temperature and (b) operating conditions for various technologies.

References

1. F.P. Ford, P.L. Andresen, CORROSION/89, paper no. 498 (Houston, TX: National Association of Corrosion Engineers, 1989).
2. R.L. Jones, Proceedings of the 2nd International Atomic Energy Agency Specialists Meeting on Subcritical Crack Growth 1, 2, held May 1985, NUREG Report, NUREG/CP0067, Vol 1, pp. 1-9.
3. P.L. Andresen, F.P. Ford, Mater. Sci. Eng. A103(1988): pp. 167-184.
4. F.P. Ford, "Mechanisms of Environmental Cracking Peculiar to the Power Generation Industry," EPRI Report NP2589, September 1982.
5. F.P. Ford, D.F. Taylor, P.L. Andresen, R.G. Ballinger, "Corrosion Assisted Cracking of Stainless Steel and Low Alloy Steels in LWR Environments," EPRI Report NP5064S, February 1987.
6. F.P. Ford, P.L. Andresen, M.G. Benz, D. Weinstein, "On-Line BWR Materials Monitoring and Plant Component Lifetime Prediction," Proceedings of the Nuclear Power Plant Life Extension, held June 1988 (ANS), in press.
7. F.P. Ford, Corrosion Processes, ed. R.N. Parkins (London, England: Applied Science Publishers, 1982).
8. R.N. Parkins, N.J.H. Holroyd, R.R. Fessler, Corrosion 34, 8(1978): p. 253.
9. T.P. Hoar, G.P. Rothwell, Electrochim. Acta 15(1976): p. 1037.
10. T.R. Beck, Corrosion 30, 11(1974): p. 408.
11. C. Manfredi, I. Maier, J.R. Galvele, Corros. Sci. 27(1987): p. 887.
12. J.M. Sutcliffe, R.R. Fessler, W.K. Boyd, R.N. Parkins, Corrosion 28, 8(1972): p. 313.
13. B. Poulson, R. Robinson, Corros. Sci. 20(1980): p. 707.
14. J. Congleton, CORROSION/88, paper no. 284 (Houston, TX: NACE, 1988).
15. Environmental-Sensitive Mechanical Behavior, ed. A.R.C. Westwood, N.S. Stoloff (Gordon and Branch, 1965).
16. Fundamental Aspects of Stress Corrosion Cracking, ed. R.W. Staehle, A.J. Forty, D. van Rooyen (Houston, TX: NACE 1967).
17. Theory of Stress Corrosion Cracking, ed. J.C. Scully (Brussels, Belgium: NATO, 1971).
18. Corrosion Fatigue—Chemistry, Mechanics and Microstructure, ed. O. Devereaux, A.J. McEvily, R.W. Staehle (Houston, TX: NACE, 1972).
19. L'Hydrogene dans les Metaux, ed. M.P. Bastien (Science et Industrie).
20. Hydrogen in Metals, ed. I.M. Bernstein, A.W. Thompson (Metals Park, OH: ASM International, 1973).
21. Stress Corrosion Cracking and Hydrogen Embrittlement of Iron Base Alloys, ed. R.W. Staehle, J. Hochmann, R.D. McCright, J.E. Slater (Houston, TX: NACE, 1977).
22. Effect of Hydrogen on Behavior of Materials, ed. A.W. Thompson, I.M. Bernstein (New York, NY: American Institute of Mining, Metallurgical, and Petroleum Engineers, 1975).
23. Surface Effects on Crystal Plasticity, ed. R.M. Latanision, J.T. Fourie (Noordhof-Leyden, 1977).
24. Mechanisms of Environment Sensitive Cracking of Materials, ed. P.R. Swann, F.P. Ford, A.R.C. Westwood (London, England: The Metals Society, 1977).
25. Corrosion-Fatigue, Met. Sci. 13(1979).
26. R.N. Parkins, Brit. Corros. J. 7(1972): p. 15.
27. B.F. Brown, Stress Corrosion Cracking and Hydrogen Embrittlement of Iron Base Alloys, pp. 747-750.
28. R.N. Parkins, B.S. Greenwell, Met. Sci. 8(1977): p. 405.
29. R.N. Parkins, "Environment-Sensitive Fracture—Controlling Parameters." Proceedings of 3rd International Conference on Mechanical Behavior of Materials, Vol. 1, ed. K.J. Miller, R F. Smith (Elmsview, NY: Pergamon Press, 1979), pp. 139-164.
30. J.M. Kraft, J.H. Mulherin, Trans. ASM 62(1969): p. 64.
31. T.P. Hoar, Corrosion 19, 9(1963): p. 331.
32. P.R Swann, Corrosion 19, 3(1963): p. 102t.
33. H.L. Logan, J. Nat. Bur. Stand. 48(1952): p. 99.
34. R.W. Staehle, Theory of Stress Corrosion Cracking, p. 223.
35. J.C. Scully, Corros. Sci. 8(1968): p. 771.
36. T.P. Hoar, Theory of Stress Corrosion Cracking, p. 106.
37. D.A. Vermilyea, J. Electrochem. Soc. 119(1972): p. 405.
38. R.P. Wei, J.D. Landes, Mater. Res. Stand. 9, 7(1969): pp. 25-28.
39. R.P. Wei, G. Shim, K. Tanaka, Proceedings of Embrittlement by the Localized Crack Environment, ed. R.P. Gangloff (New York, NY: AIME/ASM, 1983), pp. 243-263.

40 K. Sieradzki, R.C. Newman, Phil. Mag. A 51(1985): pp. 95-132.
41. C. Edeleanu, A.J. Forty, Phil. Mag. 5(1960): p. 1029.
42 R.C Newman, K. Sieradzki, Scripta Metall. 17(1983): p. 621.
43. J.A. Beavers, E.N. Pugh, Metall. Trans. 11A(1980): p. 809.
44. K. Sieradzki, "Atomistic and Micromechanical Aspects of Environment Induced Cracking of Metals," this proceedings.
45. R.C. Newman, "Stress Corrosion of Austenitic Steels," this proceedings.
46. A.W. Thompson, I.M. Bernstein, "The Role of Metallurgical Variables in Hydrogen-Assisted Environmental Fracture," Rockwell Science Center Report SCPP-75-63, 1975.
47. J.P. Hirth, Metall. Trans. 11A(1980): pp. 861-890.
48. H.G Nelson, Treatise on Materials Science and Technolgy, Vol 25, ed C.L. Briant, S.K. Banerji (Academic Press, 1983), pp. 275-359.
49. H.K. Birnbaum, "Hydrogen Embrittlement," this proceedings.
50. F.P. Ford, Metal Sci. 7(1978): p. 326.
51 R. Raj, V.K. Varadan, Mechanisms of Environment-Sensitive Cracking of Materials, p. 426.
52 F. de Kazinsky, J. Iron Steel Inst. 177(1954). p. 85.
53. C.A. Zapffe, C.E. Sims, Trans. AIME 145(1941): p. 225.
54. A.J. Tetelman, W.D. Robertson, Trans. AIME 224(1962): p. 775.
55. A.R. Troiano, Trans. ASM 52(1960): p. 54.
56 R.A. Oriani, Berichte der Bunsenges fur Phys. Chem. 76(1972). p. 848.
57 R.A. Oriani, Stress Corrosion Cracking and Hydrogen Embrittlement of Iron Base Alloys, p. 351.
58. K. Yoshino, C.J. McMahon, Metall. Trans. 5(1974): p. 363.
59. W.W. Gerberich, Y.T. Chen, C St. John, Metall. Trans. 6(1975): p. 1485.
60. R.A. Gilman, Stress Corrosion Cracking and Hydrogen Embrittlement of Iron Base Alloys, p. 326.
61. D.N. Williams, J. Inst. Metals 91(1962): p. 147.
62. J.C. Scully, D.T. Powell, Corros. Sci. 10(1970) p. 719.
63 R.B. Benson, D.K. Dunn, L.W. Roberts, Trans. AIME 242(1968): p. 2199.
64. R.A. McCoy, Hydrogen in Metals, p. 169.
65. S.S. Birley, D. Tromans, Corrosion 27, 1(1971): p. 63.
66. C.L. Briant, Metall. Trans. 10A(1979): p. 181.
67. C.D. Beachem, Metall. Trans. 3(1972): p. 437.
68 M R Louthan, G.R. Gaskey, J.A. Donovan, D.E. Rawl, Mater. Sci. Eng. 10(1972): p. 357.
69. S.P. Lynch, Metall. Forum 2(1979): p. 189.
70. R.A. Oriani, "Hydrogen Effects in High-Strength Steels," this proceedings.
71. U. Bertocci, Embrittlement by the Localized Crack Environment, pp. 49-58.
72. U. Bertocci, "Modelling of Crack Chemistry in Cu-Au Alloys," submitted for publication in J. Electrochem. Soc.
73. J.M. West, Metall. Sci. 7(1973): p. 169.
74 W W. Gerberich, Y.T. Chen, Metall. Trans. 6A(1975). p. 271.
75. T.P. Hoar, F.P. Ford, J. Electrochem. Soc. 120(1973): p. 1013.
76 M.O. Speidel, Theory of Stress Corrosion Cracking, p. 289.
77 J. Berggren (Ph.D. diss., University of Erlangen-Nurnberg, 1973).
78. G.W. Simmons, P.S. Pao, R.P. Wei, Metall. Trans. A. 9A(1978): p. 1147.
79 T W Weir, G.W Simmons, R.G. Hart, R.P. Wei, Scripta Metall. 14(1980): p. 357.
80. P.L. Andresen, "The Effects of Aqueous Impurities on Intergranular Stress Corrosion Cracking of Sensitized Type 304 Stainless Steel," EPRI Project T115-3, Final Report NP-3384, November 1983.
81 P L. Andresen, Proceedings of the 3rd International Conference on Environmental Degradation of Materials in Nuclear Power Systems—Water Reactors (New York, NY: AIME, 1987), pp. 301-314. Also Report 87CRD221 (Schenectady, NY: GE Research and Development Center), February 1988.
82. P.L. Andresen, Proceedings of the 2nd International Conference on Environmental Degradation of Materials in Nuclear Power Systems—Water Reactors (Joint Sponsorship of American Nuclear Society, TMS-AIME, and NACE), held September 9-12, 1985, Monterey, CA.
83. A. Turnbull, Rev. Coat. Corros. 5(1982): pp. 43-171.
84. A. Turnbull, Corros. Sci. 23(1983): pp. 833-870.
85. A. Turnbull, Embrittlement by the Localized Crack Environment, pp. 3-31.
86. B.F. Brown, C.T. Fujii, E.P. Dahlberg, J. Electrochem. Soc. 116(1969): p. 218.
87. J. Newman, Electrochemical Systems (NJ: Prentice-Hall, 1973).
88. Ya.M. Kolotyrkin, Yu.A. Popov, Yu.V. Alekseev, Advances in Physical Chemistry—Current Development in Electrochemistry and Corrosion, ed. Ya.M. Kolotyrkin (Moscow, USSR: Mir Publishers, 1982), p. 11.
89. J.M. Barsom, Int. J. Fract. Mech. 7, 2(1971): p. 163.
90. R.G. Ballinger, et al., EPRI Report NP5064S.
91. A.J. Markworth, L.R. Kahn, "Mathematical Modeling of Electrochemical Conditions Within a Stress Corrosion Crack," EPRI Report RD4877, November 1986.
92. P.L. Andresen, et al., EPRI Report NP5064S.
93. A. Turnbull, Brit. Corros. J. 15, 4(1980): p. 162.
94. A. Turnbull, J.G.N. Thomas, NPL DMA Report No. A 11(1979).
95. J.W. Tester, H.S. Isaacs, J. Electrochem. Soc. 122, 11(1975). p. 1438.
96. J.R. Galvele, J. Electrochem. Soc. 123, 4(1976): p. 464.
97. J.W. Oldfield, W.H. Sutton, Brit. Corros. J. 13, 1(1978): p. 13.
98. J.G. Hines, Corros. Sci. 21(1961).
99. E.M. Gutman, Proceedings of the 3rd International Congress on Metallic Corrosion (Houston, TX: NACE, 1966), p. 377.
100. G.J. Bignold, Corrosion 28, 8(1972): p. 307.
101. P. Doig, P.E.J. Flewitt, Metall. Trans. A 9A(1978): p. 357.
102. P. Doig, P.E.J. Flewitt, Proc. Roy. Soc. London A357. p. 439.
103. P.H. Melville, Brit. Corros. J. 14, 1(1979): p. 15.
104. K. Nisancioglu, H. Holton, Electrochim. Acta 23(1978): p. 251.
105. D.A. Vermilyea, C.S. Tedmon Jr., J. Electrochem. Soc. 117(1970): p. 437.
106. A.L. Turnbull, J.G.M. Thomas, J. Electrochem. Soc. 129(1982): p. 1412.
107. T.R. Beck, E.A. Grens II, J. Electrochem. Soc. 116(1969): pp. 117-184.
108. H.W. Pickering, R.P Frankenthal, J. Electrochem. Soc. 119(1972): p. 1297.
109. B.G. Ateya, H.W. Pickering, J. Electrochem. Soc. 126(1979): pp. 15-22.
110. R. Alkire, D. Ernsberger, D. Damon, J. Electrochem. Soc. 123 (1978): p. 458.
111. R. Alkire, D. Siitari, J. Electrochem. Soc. 126(1979): p. 15.
112. J. Newman, W.H. Smyrl, Metall. Trans. 5(1974): p. 469.
113. W.H. Smyrl, J.J. Newman, J. Electrochem. Soc. 121(1974). p. 1000.
114. W.H. Hartt, J.S. Tenant, W.C. Hooper, Corrosion Fatigue Technology 5, ASTM STP 642 (Philadelphia, PA. ASTM, 1978).
115. T.W. Secom, J. Fluid Mech. 88(1978): p. 273.
116. R.J. Taunt, W. Charnock, Mater. Sci. Eng. 35(1978): p. 219.
117. R.J. Taunt, W. Charnock, Proceedings of the Conference on the Influence of Environment on Fatigue, held May 1977 (I. Mech. E 1977), pp. 43-50.
118. A. Turnbull, Corros. Sci. 22(1982): p. 877.
119. R.R. Shuck, J.L. Swedlow, Localized Corrosion, ed. B. Brown, J. Kruger, R. Staehle (Houston, TX: NACE, 1974).
120. A. Turnbull, M.K. Gardner, Brit. Corros. J. 16(1981): p. 140.
121. B.G. Ateya, H.W. Pickering, J. Electrochem. Soc. 122(1975): p. 1018.
122. H.W. Pickering, A. Valdes, Embrittlement by the Localized Crack Environment, pp. 33-48.

123. K. Landles, J. Congleton, R.N. Parkins, Embrittlement by the Localized Crack Environment, pp. 59-74.
124. G. Karlberg, G. Wranglen, Corros. Sci. 11(1971): pp. 499-510.
125. W.D. France, N.D. Greene, Corrosion 24, 8(1968): pp. 247-251.
126. T.J. Lennox Jr., M.H. Peterson, "Potential and pH Relationship in Cathodically Polarized Metal Crevices," EPRI Report, 1987, pp. 173-178.
127. T.R. Beck, J. Electrochem. Soc. 120, 10(1973): pp. 1317-1324.
128. R.A.H. Edwards, "Potential Drops and Concentration Changes in Stress Corrosion Cracks in 7075 Alloy in Halide Solutions," paper presented at a meeting on Control and Exploitation of the Corrosion of Aluminum Alloys, April 1983, Cranfield, UK.
129. A. Alavi, R.A. Cottis, Embrittlement by the Localized Crack Environment, pp. 75-87.
130. G. Gabetta, G. Buzzanaca, Subcritical Crack Growth, Vol. 2, pp. 219-230.
131. P. Combrade, M. Foucault, G. Slama, Subcritical Crack Growth, Vol. 2, pp. 201-218.
132. C.F. Baes, R.E. Mesmer, The Hydrolysis of Cations (New York, NY: J. Wiley and Sons, 1976).
133. F.D. Bogar, C.T. Fujii, "Solution Chemistry in Crevices on Fe-Cr Binary Alloys," NRL Report 7690, AD-778002, 1974.
134. J. Mankowski, Z. Szklarska-Smialowska, Corros. Sci. 15(1975): pp. 493-501.
135. D.F. Taylor, C.A. Caramihas, Embrittlement by the Localized Crack Environment, pp. 105-114.
136. D.F. Taylor, C.C. Foust, Corrosion 44(1988): pp. 204-208.
137. J.A. Smith, M.H. Peterson, B.F. Brown, Corrosion 26(1970). p. 539.
138. P. Bristol, European Offshore Steels Research, Welding Institute, Cambridge, 1978.
139. J.A. Davis, Proceedings of the 17th Annual Technical Meeting of the Institute of Environmental Science (1971), p. 117.
140. R.A. Page, A. McMinn, S.J. Hudak, Corrosion 44(1988) pp 623-631.
141. E.A. Charles, J. Congleton, R.N. Parkins, Corrosion 44(1988): pp. 599-605.
142. Proceedings of the 1st International Atomic Energy Agency Specialists Meeting on Subcritical Crack Growth, Vols. 1 and 2, held May 1981, Freiburg, Federal Republic of Germany, NUREG CP-0044.
143. Proceedings of the 2nd International Atomic Energy Agency Specialists Meeting on Subcritical Crack Growth, Vols 1 and 2, held May 1985, Sendai, Japan, NUREG Report, NUREG/CP0067.
144. F.P. Ford, J. Pressure Vessel Tech. 1(1988): p. 113.
145. P. Combrade, M. Foucault, G. Slama, Environmental Degradation of Materials in Nuclear Power Systems—Water Reactors, p. 276.
146. K. Torronen, M. Kemppainen, H. Hanninen, "Fractographic Evaluation of Specimens of A533B Pressure Vessel Steel," EPRI Report NP3483, May 1986.
147. J.H. Bulloch, Environmental Degradation of Materials in Nuclear Power Systems—Water Reactors, pp. 261-268.
148. F.P. Ford, P.L. Andresen, Proceedings of 7th International Conference on Fracture, held March 1989, Houston, TX (New York, NY: Pergamon Press, 1989).
149. P.L. Andresen, Proceedings of the 3rd International Conference on Fatigue and Fatigue Thresholds, held June 1987 (W. Midlands, UK: Eng. Matls. Advisory Services, 1987).
150. P.L. Andresen, I. Vasatis, unpublished work, 1988.
151. R.P. Gangloff, Embrittlement by the Localized Crack Environment, pp. 265-290.
152. R.P. Gangloff, R.O. Ritchie, Fundamentals of Deformation and Fracture, ed. K.J. Miller (Cambridge, UK: Cambridge University Press, 1984).
153. S.M. Bruemmer, L.A. Charlot, B.W. Arey, Corrosion 44(1988). pp. 328-333.
154. S.M. Bruemmer, L.A. Charlot, D.G. Atteridge, Corrosion 44 (1988): pp. 427-434.
155. K.L. Luthra, C.L. Briant, Metall. Trans. A 19A(1988): pp 1091-2108.
156. G.S. Was, V.B. Rajan, Corrosion 43(1987): p. 576.
157. T.M. Devine, Acta Metall. 36(1988): p. 1491.
158. D.I.R. Norris, ed., Proceedings of Symposium on Radiation-Induced Sensitization of Stainless Steels, CEGB (Berkeley, CA: Berkeley Nuclear Laboratories, 1986.
159. F.P. Ford, G.T. Burstein, T.P. Hoar, J. Electrochem. Soc. 127(1980): p. 6.
160. P. Combrade, "Prediction of Environmental Crack Growth on Reactor Pressure Vessels," EPRI Contract RP2006-8, UNIREC Report #1667, February 1985.
161. J.C. Scully, P. Moran, Corrosion 44(1988): pp. 176-185.
162. R. Jacko, Private Communication, 1984.
163. M.R. Louthan, R.G. Derrick, Corros. Sci. 15(1975): p. 565.
164. J.C. Sherlock, L.L. Shreir, Corros. Sci. 11(1971): p. 543
165. T. Hoar, R.W. Jones, Corros. Sci. 13(1973): p. 725.
166. J.J. Podesta, G.P. Rothwell, T.P. Hoar, Corros. Sci. 11(1971): p. 241.
167. D. Engseth, J.C. Scully, Corros. Sci. 15(1975): p. 505.
168. M. Keddam, J.V. da Silva, Corros. Sci. 20(1980): p. 167.
169. T. Zakroczmski, R.N. Parkins, Corros. Sci. 20(1980): p. 723
170. Y.S. Park, J.R. Galvale, A.K. Agrawal, R.W. Staehle, Corrosion 34(1978): p. 413.
171. R.B. Diegle, D.A. Vermilyea, J. Electrochem. Soc. 122(1975): p. 180.
172. F.P. Ford, M. Silverman, Corrosion 36(1980): pp. 558-565.
173. T.R. Beck, Corrosion 30(1974): p. 408.
174. T.R. Beck, Theory of Stress Corrosion Cracking, pp 64-85
175. T.R. Beck, J. Electrochem. Soc. 115(1968): p. 890.
176. A. Alavi, C.D. Miller, R.P. Wei, Corrosion 43(1987): pp 204-207.
177. R.P. Wei, A. Alavi, Scripta Metall. 22(1988). pp. 969-974.
178. C. Patel, Corros. Sci. 21(1981): p. 145.
179. T. Hagyard, W.B. Earl, J. Electrochem. Soc. 115(1968). p. 623.
180. J. Pagetti, D. Lees, F.P. Ford, T. Hoar, Comp. R. Acad. Sc. Paris 273(1971): p. 1121.
181. D.J. Lees, T.P. Hoar, Corros. Sci. 20(1980): p. 723.
182. J.F. Rimbert, J. Pagetti, Corros. Sci. 20(1980): p. 189.
183. R.C. Newman, G.T. Burstein, Corros. Sci. 21(1981). p. 119.
184. G.T. Burstein, D.H. Davies, Corros. Sci. 20(1980): p. 1143.
185. G.T. Burstein, P.I. Marshal, Corros. Sci. (1984): p. 449.
186. R.D.K. Misra, G.T. Burstein, Corros. Sci. 24(1984). p. 304.
187. A. Frignani, F. Zucchi, M. Zucchini, G. Trabanelli, Corros. Sci. 20(1980): p. 791
188. W.S. Rudd, J.-C. Scully, Corros. Sci. 20(1980): p. 611.
189. R.B. Diegle, D.M. Lineman, J. Electrochem. Soc. 131(1984): p. 106.
190. J.R. Ambrose, J. Kruger, Corrosion 28, 1(1972): p. 30.
191. Z. Szklarska-Smialowska, W. Kozlowski, J. Electrochem. Soc. 131(1984): p. 234.
192. B. McDougall, J. Electrochem. Soc. 130(1983): p. 114.
193. K.M. Goswami, R.W. Staehle, Electrochim. Acta 16(1971): 1895.
194. A.A. Adams, R.T. Foley, Corrosion 31, 3(1975): p. 84.
195. A.T. Cole, R.C. Newman, Corros. Sci. 28(1988): pp 109-118
196. M. Cid, M. Puiggali, H. Fatmaoui, M. Petit, Corros. Sci. (1988): pp. 61-68.
197. S.F. Bubar, D.A. Vermilyea, J. Electrochem. Soc. 113(1966): p 892.
198. R.C. Newman, G.T. Burstein, Electrochem. Acta 25(1980): p. 1009.
199. G.T. Burstein, G.M. Ashley, Corrosion 40, 3(1984): p. 116.
200. F.P. Ford, "Stress Corrosion Cracking and Corroson Fatigue of Aluminum 7% Magnesium" (Ph.D. diss., Cambridge University, 1973).
201. M. Barbosa, Corrosion 43(1987): p. 309.
202. M. Barbosa, Corrosion 44(1988), p. 149.
203. W.J. Lorenz, Corros. Sci. 5(1965): p. 121.
204. H.K. Kuo, K. Nobe, J. Electrochem. Soc. 125(1978): p. 853.

205. P. Marcus, A. Tessier, I. Olefjord, J. Oudar, Corros. Sci. 24(1984): p. 259.
206. L.J. Ljungberg, D. Cubicioti, M. Trolle, Corrosion 44(1988): p. 66.
207. N. Sato, M. Cohen, J. Electrochem. Soc. 111(1964): p. 512.
208. M. Cabrera, N.F. Mott, Rep. Prog. Phys. 12(1949): p. 163.
209. P. Hurst (UKAEA Risley), Private Communication, 1988.
210. R.A. Diegle, D.A. Vermilyea, Corrosion 32(1976): p. 411.
211. J.C. Grosskreutz, J. Electrochem. Soc. 116(1969): p. 1232.
212. J.C. Grosskreutz, Surf. Sci. 8(1967): p. 173.
213. J.C. Grossreutz, M.B. McNeil, J. Appl. Physics 40(1969): p. 355.
214. D.A. Bradhurst, J.S.L. Leach, J. Electrochem. Soc. 113(1966): p. 1245.
215. H.A. McCarthy, P.L. Harrison, Corros. Sci. 14(1974): p. 469.
216. O.F. Devereaux, et al., Corros. Sci. 15(1975): p. 361.
217. R.W. Staehle, J.J. Royuela, T.L. Raredon, E. Serrate, C.R. Morin, R.V. Ferrar, Corrosion 26(1970): p. 451.
218 G.M. Scamens, P.R. Swann, Stress Corrosion Cracking and Hydrogen Embrittlement of Iron Base Alloys, p. 166.
219 R.M. Latanision, R.W. Staehle, Fundamental Aspects of Stress Corrosion Cracking, p. 214.
220. A.W. Thompson, Hydrogen in Metals, p. 91.
221. A.W. Thompson, Mater. Sci. Eng. 14(1974): p. 253.
222. A.W. Thompson, I.M. Bernstein, Rev. Coat. Corros. 2(1975): p. 3.
223. R.R. Vandervoort, A.W. Ruotola, E.L. Raymond, Metall. Trans. 4(1973): p. 1175.
224. R.T. Ault, K.O. McDowell, P.L. Hendricks, T.M.F. Ronald, Trans. ASM 60(1967): ∩ 79.
225. M.O Speidel, Fundamental Aspects of Stress Corrosion Cracking, p. 561.
226. A. Kelly, R.B. Nicholson, Prog. Mater. Sci. 10(1963): p. 149.
227. S.M. Breummer, L.A. Charlot, C.H. Henager, Corrosion 44 (1988): pp. 782-788.
228. D.L. Douglass, G. Thomas, W.R. Roser, Corrosion 20, 1(1964): p.15t.
229. T. Smith, R.W. Staehle, Corrosion 23, 5(1967): p. 117.
230. R.N. Parkins, G.P. Marsh, J.T. Evans, Proceedings of EPRI Conference on Predictive Methods for Assessing Corrosion Damage to BWR Piping and PWR Steam Generators, ed. H. Okada, R. Staehle (Houston, TX: NACE, 1982).
231. D.P.G. Lidbury, Corros. Sci. 8(1986): pp. 149-172.
232. Y.S. Garud, T.L. Gerber, Advances in Life Prediction Methods (New York, NY: American Society of Mechanical Engineers, 1983).
233. Y.S. Garud, T.L. Gerber, "Development of an Engineering Model for Predicting IGCSS Damage-Particularly in Type 304 Stainless Steel in BWR Water Environments," Final Report on EPRI Contract T118-12, February 1982.
234. R.N. Parkins, ASTM-STP 665, ed. G.M. Ugiansky, J.H. Payer (Philadelphia, PA: ASTM, 1977), pp. 5-25.
235. W.R. Wearmouth, G.P. Dean, R.N. Parkins, Corrosion 29 (1973): p. 251.
236. H.H. Uhlig, J. Electrohem. Soc. 123(1976): p. 1699.
237. R.W. Revie, H.H. Uhlig, Acta Metall. 22(1974): p. 619; Scripta Metall. 8(1974): 1231.
238. E.W. Hart, Proceedings of the 14th Sagamore Army Materials Research Conference (Syracuse, NY: Syracuse Press, 1966), p. 210.
239. E.J. Duquette, H. Hahn, P. Andresen, Surface Effects on Crystal Plasticity, p. 469.
240. A. Pfutzenreuter, G. Mazing, A. Metallk 42(1951): p. 361.
241. R.M. Latanision, H. Opperhauser, A.R.C. Westwood, Science of Hardness Testing and Its Research Applications (Metals Park, OH: ASM International, 1973), p. 432.
242. G.E. Ruddle, H.G.F. Wilsdorf, Appl. Phys. Lett. 12(1968): p. 271.
243. V.K. Sethi, R. Gibala, Scripta Metall. 9(1975): p. 527.
244. J.T. Evans, R.N. Parkins, Acta Metall. 12(1976): p. 511.
245. I.R. Kramer, Corrosion 31(1975): pp. 383, 391.
246. A.H. Cottrell, Dislocations and Plastic Flow in Crystals (Clarendon Press, 1953), p. 199ff.
247. J.C. Scully, Corros. Sci. 15(1975): p. 207.
248. D.A. Vermilyea, Stress Corrosion Cracking and Hydrogen Embrittlement of Iron Base Alloys, pp. 208-217.
249. J.F. Newman, Corros. Sci. 21(1981): p. 487.
250. J. Congleton, T. Shoji, R.N. Parkins, Corros. Sci. 11(1970): p. 405.
251. T. Shoji, Proceedings of ASTM-PVP Symposium on Predictive Capabilities in Environmentally Assisted Cracking (Philadelphia, PA: ASTM, 1985), pp. 127-142.
252. P.S. Maiya, W.J. Shack, Embrittlement by the Localized Crack Environment, pp. 199-209.
253. J.R. Rice, W.J. Drugan, T.L. Sham, ASTM STP 700(1980): pp. 189-221.
254. R.N. Parkins, Corrosion 43(1987): p. 130.
255. S.J. Hudak, D.L. Davidson, R.A. Page, Embrittlement by the Localized Crack Environment, pp. 173-198.
256. P.J. Scott, A.E. Truswell, Structural Integrity of Light Water Reactor Components, L.E. Steele, et al. (London, England: Applied Science Publishers, 1982), pp. 289-309.
257. J.D. Atkinson, S.T. Cole, J.E. Forrest, Atomic Energy Agency Speicalists Meeting on Subcritical Crack Growth, Vol. 2, pp. 459-483.
258. G. Gabetta, Private Communication, 1984.
259. S.T. Cole, J.T. Atkinson, J.E. Forrest, Private Communication, 1982.
260. D.P.G. Lidbury, "The Calculation of Crack Tip Strain Rate Due to Cyclic Loading Under Conditions of Small Scale Yielding with Applications to the Characterization of Corrosion Fatigue Crack Growth," UKAEA ND-R-916 (R), 1983.
261. T.C. Lindley, L. McCartney, Developments in Fracture Mechanics-2, ed. G.G. Chell (London, England: Applied Science Publishers, 1981), pp. 247-322.
262. B.M. Leis, R. Rungta, J.T. Jentgen, Embrittlement by the Localized Crack Environment, pp. 211-228.
263. H.S. Mehta, S. Ranganath, "Environmental Fatigue Analysis Based on Elastic-Plastic Fracture Mechanics," ASME 82-PVP-23.
264. T. Kawakubo, M. Hishida, Corrosion 40(1984): p. 120.
265. T. Kawakubo, M. Hishida, Trans. ASME 107(1985): p. 240.
266. T. Shoji, et al., Trans. ASME, J. Eng. Mater. Techn. 103(1981): pp. 298-304.
267. T. Shoji, Proceedings of ASME Conference on Predictive Capabilities in Environmentally Assisted Cracking, ASME PVP, Vol. 99 (New York, NY: ASME, 1985), pp. 127-142.
268. D.A. Hale, C.W. Jewett, C.S. O'Toole, "BWR Coolant Impurities Program-First Annual Progress Report," EPRI Program NP2293, November 1985.
269. P.L. Andresen, CORROSION/87, paper no. 84 (Houston, TX: NACE, 1987).
270. J. Gittus, "Creep, Viscoelasticity and Creep Fracture in Solids," Chapter 6, Deformation Maps (New York, NY: J. Wiley & Sons).
271. M.F. Ashby, Acta Metall. 20(1972): pp. 887-898.

Discussion

J.R. Galvele (Comision Nacional de Energia Atomica, Argentina): We have been working on transport processes in pitting, and tried to apply those techniques to the intermediate strain-rate technique for predicting stress corrosion cracking (SCC) crack velocities. We found that while there was a considerable change in composition, no changes were observable on straining wires, so we had to conclude that the changes in crack composition were not relevant. Once you produce a low melting point (LMP) compound on the metal surface (CrO_3 in your case), cracks will start to propagate, and the changes in crack propagation will have no further effects, unless they change the nature of the LMP compound.

F.P. Ford: The main purpose of my review was to define the basic thermodynamic and kinetic criteria that dictate the nature of a crack-tip environment and then to question their relevance to crack propagation kinetics. In my view, that relevancy can only be demonstrated if the predictions of crack propagation agree quantitatively with observation For the specific cases of stainless and low-alloy steels in "high-purity" water, we do get a good agreement between observation and theory; thus, the logical conclusion is that, *for these systems*, the formalized ideas of mass transport in cracks and the resultant crack-tip chemistry are of relevance to crack propagation That is not to say that your observations and conclusions on your systems are wrong; that verdict depends on the outcome of a direct quantitative comparison of observed and predicted crack propagation rates over as wide a range of operating conditions as possible.

J.R. Galvele: The choice of an aluminum-copper alloy in sodium chloride solutions as a general example of intergranular SCC does not seem to be a very happy one. Eighteen years ago, we showed [Galvele and De Micheli, Corros. Sci. 10(1970): p. 795] that during intergranular corrosion this alloy acts as a three-phase system, and that intergranular corrosion starts at the pitting potential of the copper-depleted zone, along the grain boundaries. We also showed [Galvele, et al., Localized Corrosion, ed. Staehle, et al. (Houston, TX: NACE, 1974), p. 580] that intergranular SCC of this alloy also starts at the pitting potential of the copper-depleted zone. No such zones are detectable in other important cases of intergranular SCC, such as alpha-brass or the silver-palladium alloys we reported on in this conference.

As for the current densities required for the propagation of SCC by anodic dissolution (AD), those reported by Newman are not particularly high. Hoar and Galvele [Corros. Sci. 10(1970): p. 211] reported that current density values as high as 2 A/cm^2 were required to account for intergranular SCC of mild steel in calcium nitrate solutions, and Duffo and Galvele (Surface-Mobility SCC Mechanism in Silver Alloys," this proceedings) measured intergranular crack velocities of the order of 10^{-6} m/s on Ag-15Pd alloys, which, according to the AD SCC mechanism, would require current density values of 1 A/cm^2 at the crack tip.

In electrochemistry, the mechanism for the AD of metals are described at an atomic level [for example, H. Gerischer, The Surface Chemistry of Metals and Semiconductors, ed. H.C. Gatos (New York, NY: J. Wiley & Sons, 1960), p. 177]. One of the reasons why I abandoned the AD mechanism for SCC is that no such description could be found. As pointed out by various authors here, it is believed that intergranular SCC propagates by AD at the tip of the crack, but no attempts have been made to describe how such a process could take place at an atomic level, at the tip of the crack. In view of the high aspect ratios usually found in stress corrosion cracks, it is reasonable to expect that the tip of the crack will be almost atomically sharp. When modeling such a crack, two difficulties are found. The first one is that if all of the dissolution process is located at the tip of the crack, for high crack propagation rates, the cracks will be plugged by corrosion product, which will hinder the dissolution process. This can be easily shown with the simple calculations used for unidirectional pits [Galvele, J. Electrochem. Soc. 123(1976): p. 464]. The second difficulty is the explanation of how such a dissolution process takes place at the tip of the crack. Going back to Gerischer's descriptions, the electrochemical dissolution on a metal surface is located preferentially on surface steps, where the metal atoms are more exposed to the environment With high overpotentials, the dissolution of a flat surface could also be explained. Nevertheless, it is very difficult to visualize how the dissolution process will take place at the tip of a crack, where the atoms are shielded from the environment by the sides of the crack I believe that a more rational explanation is found in our model of surface mobility [Galvele, Corros. Sci. 27, 1(1987)]. This model assumes that an intermediate species, an adatom, is produced at the tip of the crack as a result of the simultaneous action of the stress and the environment. This adatom diffuses away from the tip of the crack, and eventually reacts with the environment by a conventional electrochemical mechanism. With this SCC mechanism, the anodic current density is not necessarily located at the tip of the crack and, in addition, the action of stress on the SCC process is accounted for.

R.C. Newman (University of Manchester Institute of Science and Technology, UK): Galvele suggests that very high current densities, of the order of 1 A/cm^2, are not possible in cracks. This seems to be refuted by Rota and Boehni [in Electrochemical Methods in Corrosion Research (Zurich, 1988)], who showed that intergranular corrosion of aluminum-copper alloys in sodium chloride could go at about 50 mA/cm^2 for a 1-mm crack depth; tiny stresses opened up these fissures and permitted 500 mA/cm^2. This seems to account for most cases of intergranular SCC, e.g., steel in nitrate solutions. Transgranular SCC, however, is another matter.

B.G. Pound (SRI International, USA): You propose that the diffusion limitation at the crack tip is associated with the transport of water to solvate the metal ions. An alternative interpretation is that the metal ions are exposed to sufficient water to become solvated and the rate of diffusion of the solvated metal ions from the surface provides the mass transport limitation (precipitation of oxide occurring when the concentration of dissolved species exceeds saturation). Is there evidence for control by water transport? If not, do you regard control by solvated metal ion transport in the crack environment as plausible?

R.C. Newman: Could you expand upon your suggestion that water transport can be rate controlling for crack growth? I would have thought that the solubility of metal salts or oxides is bound to intervene before water transport could become important. Please also clarify the portion of the i–t curve where you think this is relevant.

F.P. Ford: The reason for proposing that water diffusion to the bare surface may be a rate-limiting step in the initial oxidation reaction is based on circumstantial, rather than quantitative, evidence. For instance, many authors have observed that, although the oxidation reactions are activation-controlled at low overpotentials, the maximum oxidation current densities are generally in the range of approximately 0.5 to 5 A/cm^2. At higher overpotentials, the oxidation current density is relatively potential independent. We can assume that this transition is not *entirely* due to experimental problems (such as iR effects) since this limit is commonly observed in many alloy/environment systems, experimental procedures, cell geometries, etc. The suggestion that this limit is due to water diffusion is based on the following logic:

(1) Given the high driving force for oxidation on a bare surface (in most ductile alloy aqueous environment systems), it is possible for the free-water molecule concentration adjacent to the oxidizing surface to decrease as cation solvation proceeds. This would lead to a potential-independent water diffusion limiting step. Since water is common to all dissolution/oxide formation reactions, it is not surprising that the maximum oxidation current density range is similar for most systems so far studied, regardless of the cation involved In this respect, it should be noted that the upper end of this range (i.e., $\sim$ 5 A/cm^2) is usually observed in the high solution velocity/scratching electrode technique.

(2) Once the initial oxidation reactions have occurred, there is no question that oxides and salts may be precipitated as the metal cation concentration increases. The current suggestion is that this precipitation merely slows down the water diffusion rate even further. Admittedly, the proof of this is circumstantial, but reasonably complete. For instance, system changes, such as potential-driven diffusion of anions to the crack tip, which lower the crack-tip pH and hence increase the oxide solubility, should increase the crack propagation rate because the rate-limiting water diffusion is less impeded. Moreover, the crack propagation rate under these limiting conditions is generally observed to be governed by an activation enthalpy that is reasonable for liquid diffusion control (i.e., approximately 4 kcal/g.mol).

Certainly the diffusion of solvated cations away from the bare surface could be a possible controlling step, but I would have thought that this would be cation specific, and if true, this would contravene the *generality* of the 0 5 to 5 A/cm^2 bare-surface oxidation rate observation Obviously, more work is required in this area!

R.W. Staehle (University of Minnesota, USA): In addition to focusing on the precision of the model as it applies to the engineering context, it is possible to treat statistical variability with similar precision. This would be a valuable addition to your work. You might, for example, consider the work of Shibata, who is correlating data with Weibull parameters and doing parametric analysis on the Weibull fit parameters.

F.P. Ford: As you correctly point out, this approach to the prediction of crack propagation rates is strictly deterministic. That is, if you *know* the relevant bulk system parameters (e.g., flow rate, oxygen content, corrosion potential) and can relate these to the crack-tip conditions, then there is a *specific* crack propagation rate for that defined system. This automatically indicates a need to have monitors (e.g., pH electrodes, reference electrodes) in the system that give the required inputs to the prediction model. It follows that if there is a spread in the *nominal* system conditions, then there is a *predictable* spread in the crack propagation rate or crack depths. Moreover, the distribution of propagation rates, and hence crack depths, will mirror the distribution of operating conditions within the system. I illustrated this in Figure 4, with an example of the limiting conditions predictions in Figure 39.

We are currently tackling this deterministic to probabilistic prediction interrelationship for nuclear reactor components. Needless to say, it is not a trivial exercise to determine the spread in the relevant parameters in such a complex system. The alternative, as you suggest, is to use classical statistical approaches based on the past history of the plant. However, my initial feeling is that, apart from being scientifically less satisfying, such approaches may be less accurate in their predictive capabilities.

S.M. Bruemmer (Pacific Northwest Laboratory, USA): In addition to chemical and electrochemical differences in previous tests in "high-purity" water, the difference in material micrometallurgy promotes much of the observed data scatter in crack growth rates. Local microchemistry (which you estimate in the model) and microstructure will affect crack-tip dissolution/passivation rates and deformation processes. The need to input reasonably accurate microchemistries (e.g., chromium depletion minimum and widths, impurity segregation, and sulfides) and microstructure (e.g., carbide and inclusion distributions) appears to be critical for even semiquantitative predictions in *specific* cases.

F.P. Ford: I focused much of my review on the solution side of the crack-tip material/environment interface, but of course you are absolutely correct in saying that the microstructural variables are of equal importance The effects of these variables on, for instance, local crack-tip plasticity (e.g., dislocation morphology, hydrogen uptake) are the hardest to formulate *quantitatively*, although their qualitative effects have been recognized for a long time. Indeed, the need for quantitative relationships for crack-tip strain rate is, I think, becoming the rate-limiting step in developing upgraded quantitative life-prediction methodologies However, given the nature of the power-law relationship between propagation rate and crack-tip strain rate, we are allowed some uncertainty in the crack-tip strain rate before it adversely dominates the uncertainty in propagation rate values It has been our experience, so far, that this latter uncertainty is dominated by uncertainties in crack-tip water chemistry definition.

The question of the effect of local metallographic heterogeneities on the crack-tip chemistry is also very relevant. I mentioned the effect on cracking of grain-boundary chromium depletion in sensitized type 304 (UNS S30400) stainless steel, and manganese sulfide inclusions in low-alloy steels, but the absolute definition of these effects is still not perfect Your work on the inadequacies of the use of indirect measurements for the grain-boundary chromium depletion, for example, is germane to this, and there are many other examples (e g , metalloid segregation under fast neutron irradiation), where we are uncertain of the characterizing parameter that is relevant to the cracking process.

My main point, however, is that despite these warts in our understanding, we can make usable predictions of cracking behavior if we make reasonable assumptions of the material/microstructural contributions to cracking.

B. Cox (Atomic Energy of Canada Ltd., Canada): Whenever people rely on simulation experiments for part of their argument, I worry that the Heisenberg Uncertainty Principle is at work, and you change the factors you are trying to measure. From working with zirconium, we have learned that sufficient chloride leaches from silver chloride electrodes to cause pitting or SCC, and from the use of zirconium electrodes with sodium fluoride solid electrolytes that enough chloride leaches to cause SCC. So the question is what control experiments did you do to establish how much of the chloride in your simulated crack could have come from these two sources?

F.P. Ford: I should stress that these experiments you refer to were not mine, but Andresen's, which were reported in Reference 5. You are quite right that anions from, for instance, silver chloride electrodes or plastic tubing, etc., can introduce spurious effects. In the case of the experiments mentioned in this paper, however, these effects were minimal for the following reasons. (1) The experiments were conducted at room temperature, where the solubility of silver chloride is about 10^{-6} molar chloride. This is considerably less than the 10^{-3} molar chloride, which was the baseline concentration used in the experiments. (2) The tubing that was used as a membrane for selective hydrogen ion diffusion in some of the tests was washed well in boiling water before the tests to remove any soluble impurities.

H.-J. Engell (Max Planck Institut fur Eisenforschung, Federal Republic of Germany): Some newly developed grades of chromium and chromium-nickel steels containing up to 2 at% nitrogen exhibit unexpectedly good resistance to environment-induced fracture and pitting. Thermodynamic calculations using reasonable values of crack-tip pH and potentials indicate that ammonia may be formed during anodic dissolution. The change in crack-tip pH caused by the ammonia may be the reason for a stabilization of surface layers and/or reduction of hydrogen pick-up.

F.P. Ford: This is a most interesting observation and underlines the fact that relatively small alloying additions can alter crack-tip conditions and hence the crack propagation rate. This is most apparent for the case of metalloid segregation to grain boundaries and the effect this has on, for example, caustic embrittlement of low-alloy steels. This obviously has an impact on quality-control procedures in alloy production, but what I find exciting is that we now have a fundamentally based rationale for predicting the beneficial or deleterious effects of system changes (e.g., material composition) that were once regarded as "second order" phenomena. This is no longer a black art!

R.N. Parkins (University of Newcastle upon Tyne, UK): I suggest that any consideration of crack growth kinetics should consider the implications of crack coalescence. To show the implications of such in relation to life prediction, Figure A indicates the results of calculations for the lifetime of a pipeline in which SCC occurs due to the presence of a carbonate-bicarbonate solution. The figure shows the time dependence of the crack velocity for realistic loading conditions and temperature, and, most importantly, it shows the ways in which the numbers of cracks coalescing before and after the crack size corresponding to K_{ISSC} is reached influence the lifetime of a length of pipe. (The details are provided by R.N. Parkins, Corros. Sci., in press.) The time during which the cracks are below the size corresponding to K_{ISSC} is referred to as Stage 3 and the time after K_{ISSC} is exceeded is referred to as Stage 4. In Stage 3, relatively small cracks coalesce, having a marked effect upon the times spent in Stages 3 and 4, and hence upon the total time-to-failure, the latter indicated by the point at which each curve terminates. The important conclusions are that if crack coalescence does not occur, catastrophic failure will not occur before the crack reaches the size for fast fracture (the curves on the extreme right of Figure A). In addition, it is clear from the figure that it is the coalescence of small cracks before K_{ISSC} is reached that have the most marked effect on lifetime,

because the crack velocity increases markedly once K_{ISSC} is exceeded. I see no reason why similar considerations should not apply to other combinations of metal and environment, and indeed not only to predictions of the lifetime of structures, but to mechanistically oriented studies of crack growth kinetics.

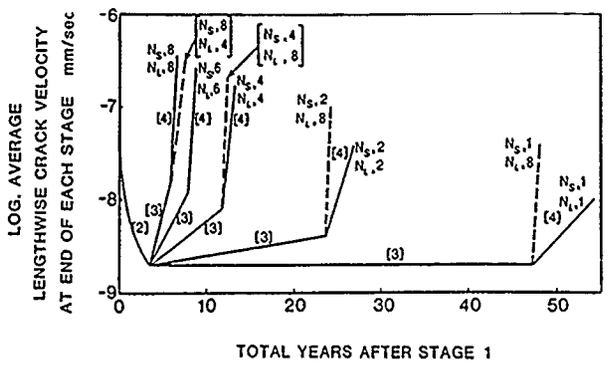


FIGURE A—Calculated crack velocities as a function of time after the start of cracking for various number of small cracks coalescing in Stage 3 and of large cracks coalescing in Stage 4. (The stages are indicated by the numbers in brackets appended to each line; the numbers at the end of each line indicate, in sequence, the number of small cracks, then the number of large cracks assumed to have coalesced in Stages 3 and 4. In Stages 3 and 4, the crack velocities have been calculated at the ends of those Stages and the points joined by straight lines).

F.P. Ford: I certainly agree about the practical importance of considering coalescence phenomena on the overall cracking susceptibility. Since the strain rate at the crack tip is fundamentally important to cracking in ductile alloy/aqueous environment systems, then intuitively I would think that the crack growth rate *should* increase when two adjacent cracks coalesce, because of changes in plastic constraint at the crack tip. In addition to your comment regarding the practical importance of crack coalescence, I think it is interesting to note that your data indicate crack propagation at stress-intensity values below K_{ISCC}. In other words, as has been discussed at other times this week, it is dangerous to ascribe anything more than engineering utility to fracture mechanics parameters in the environmentally assisted cracking of ductile alloy/aqueous environment systems.

S.C. Jani (Georgia Institute of Technology, USA): Congratulations on an excellent presentation, particularly your highlighting of the limitations of fracture mechanics and pointing out that they should only be used if shown to be valid. However, numerous participants have questioned the general validity of K, ΔK, J, etc., for correlating crack growth rates to eventually incorporate into a life prediction methodology. This is borne out by the scatter in the data you presented. Assuming that this scatter were narrower and data could be used with greater confidence, what would be the reasonable cut off level for ΔK or da/dN for components in service? Your data ranged in ΔK values from approximately 10 to 80 MPa $m^{1/2}$. Is this range representative of service from installation to replacement? If not, do you have any views on the confidence with which the scattered data can be extrapolated?

I would also appreciate any views you have about the utility of recently developed time-dependent fracture mechanics parameters, such as C^*, $C(t)$, C_t, etc., especially since these parameters incorporate, to varying degrees, time-dependent constitutive deformation behavior.

F.P. Ford: The question of the limit of application of linear elastic fracture mechanics (LEFM) to environmentally assisted cracking is a harder one to answer than it appears at first sight. For ductile alloy/aqueous environment systems, the fundamental parameter is the crack-tip strain rate $e\dot{\epsilon}_{ct}$ (or oxide rupture periodicity) and LEFM is used merely because *empirical* correlations between K, ΔK, etc., and $e\dot{\epsilon}_t$ may be formulated. This is useful since the engineer recognizes LEFM in his current codes. However, as pointed out, these correlations must break down at some point, either because of their *empirical* nature, or because of the inherent limitations of LEFM for short cracks, high stresses, etc. Thus, as pointed out by many people (e.g., Speidel, Leis, Parkins, Crooker), LEFM characterization of environmentally assisted cracking loses "similitude," and the point at which this occurs depends on the material/environment system. The replacement of K with J, $\dot{J}$, C^* may extend the similitude range, but it should be remembered that these new parameters are still *not* those of fundamental importance.

In answer to your direct questions concerning a representative range of K or ΔK, we have found that the empirical formulations in Equations (22) and (23) "work" in the range 15 to 45 ksi·in.$^{1/2}$ in austenitic stainless steels, and such a range is applicable to cracks that are resolvable by current nondestructive testing techniques in, for instance, welded piping.

J. Stewart (Harwell Laboratory, UK): Your predictive modeling of crack growth (for stainless steels in high-purity oxygenated water) takes no account of crack initiation. Assuming deterministic crack growth from time zero would seem to give an unduly pessimistic life prediction. Have you future plans to incorporate crack initiation into your models? How would you account for our observations; namely, many cracks initiate, most cracks arrest, cracks that grow do so by smaller crack coalescence. Should such factors be considered in your modeling?

F.P. Ford: Bear in mind that most of our thinking on this subject has been governed by problems in power generation equipment, and certainly I am not proposing that *all* cracking is governed by propagation alone. However, this is the easiest hypothesis to make, and, moreover, is supported by the agreement between observations and theory shown in, for example, Figures 39 and 40. Obviously, assumptions have had to be made and these have to be checked in the future. As I see it, the major problem in this area is experimental verification of the various hypotheses for the behavior of very short cracks. To do this, sensitive crack detection and crack-following techniques are required. Your technique, for example, of using electrochemical noise analysis to detect initiation could be a useful tool in this regard. The question as to why some of these very short cracks slow down, or possibly arrest, is understandable, *in principle*, in terms of logarithmic creep laws, crack coalescence, lack of continuous path of sensitized material (i.e., your percolation argument), etc., and how these individual phenomena control the *propagation* process. The problem is making the transition from these logical qualitative principles to quantitative predictions for short, multicracked structures. However, I think that now we understand what the analytical problem is, we can solve it.

Environment-Induced Cracking of Metals Fundamental Processes: Micromechanics

*W.W. Gerberich and S. Chen**

Introduction

The purpose here is to emphasize the interaction of stress and strain distributions from continuum approaches with thermodynamic, kinetic, and microstructural features of embrittlement phenomena. A further emphasis is the interaction of the environment with notches and cracks. By continuum, the definition is stretched to include not only classic applied-mechanic approaches but also dislocation approaches. These include both continuous distributions of dislocations or discrete arrays, in the context of a dislocation as a linear elastic-strain center. These may be used to describe elastic-plastic problems. How do such approaches lead to models capable of predicting time-to-failure or thresholds to failure? The micromechanical aspects of such models can cover a range of scales. That is, an understanding of the global stress distribution is essential to evaluate the probable nucleation site for some mechanisms. Within that scale, more local distributions of stress and strain may be required for an appropriate failure criterion. Thus, stress-state-controlled failure on the continuum scale such as plane stress vs plane strain and Modes I, II, and III will be covered at the macroscopic level. In addition, it will be shown that the load history is an important variable. On the more microscopic scale, some features of trapping and binding for crack nucleation as well as multiple crack nucleation for distributed damage will be discussed. Finally, on the finest microstructural scales concerned with discrete dislocation arrays, do shielding/blunting/anti shielding/dynamic instability/arrest concepts play a role in understanding the onset and growth of environment induced cracking?

To accomplish these goals, we start by reviewing several papers[1-9] from the Firminy Conference (1973) and four other more recent reviews[10-13] that address the "brittle" aspects of intergranular and transgranular environmentally induced fracture. As an overview, Table 1 summarizes much of the past emphasis on attempting to understand the micromechanics of environment-induced cracking. It is suggested that varying the macroscopic loading mode may lead to one of several mechanisms that may produce one of several microscopic failure modes. Although self explanatory in general, it should be pointed out under film mechanisms that these refer to passive film (5 nm) dissolution,[6] thick, brittle-film (100 nm) fracture[6] or film-induced (20 nm) substrate (1,000 nm) cleavage.[14] The 19 odd-loading and control variables, coupled with approximately 16 possible mechanism and local failure mode pairs, lead to more than one billion combinations, even when considering 13 at a time. As an example, the latter might consider an elastic plastic, Mode I crack in plane stress in a titanium alloy having a 100 GPa modulus, a 1 GPa strength, a strain-hardening exponent of 0.1, and so on. As this ignores microstructure, one appreciates the impossible task ahead. As such, microvoid coalescence will be de-emphasized in this paper, except where it has been proposed as an alternative mechanism or where it occurs concomitantly with more brittle-appearing modes. In addition, this paper will not extensively cover crack-tip chemistry, microstructural stability, hydrides, atomistic modeling, weak and deep traps for embrittling species, elevated temperature, or fatigue interactions, as these will be covered by others in this conference.

Reviewing the micromechanics aspects of selected papers from the Firminy Conference[1-9] shows that four deal with hydrogen embrittlement (HE),[1-4] two with film rupture,[5-6] three with stress corrosion cracking (SCC),[5-7] and three with continuum mechanics.[7-9] Approximately fifteen key micromechanics questions seemed to appear regularly in many of the papers[1-9] and subsequent reviews.[10-13]

(1) How does the state of stress affect environmental degradation?[1-5]
(2) Where is the site for embrittlement?[1,3,9,11]
(3) Can there be large local elastic stresses within the context of continuum descriptions?[1,8,10,13,14]
(4) Is crack propagation continuous or discontinuous?[2,6,8,11,12,14]
(5) Are incubation times for secondary cracking kinetically controlled?[1,12]
(6) Can blunt-notch samples assist in sorting out micromechanical aspects of crack initiation?[9,10]
(7) Is the porosity in the process zone in the advance of a decohering crack (or ligaments behind it) a significant aspect to growth or instability?[6,8,12,14]
(8) In those materials forming brittle films, can strain-induced film rupture by itself explain SCC?[5,6,12,14]
(9) Can dislocation shielding explain brittle/ductile switching in borderline materials such as iron?[9,13]
(10) Are there similarities between hydrogen and other embrittlement phenomena, for example, liquid metal embrittlement (LME)?[2]
(11) Does planar slip inducement by decreased stacking fault energies (SFEs) in fcc alloys and hydrogen additions to iron lead to similar sensitivities to embrittlement?[2,14]
(12) Is a modified Cottrell model viable for embrittlement onset?[2,11]
(13) What are the consequences of the stress and strain distributions for growing cracks?[5,8,9]
(14) What is the yield strength dependence of environmental degradation?[4,10]
(15) What are residual stress effects on environmentally induced cracking?[8]

To address these questions from a micromechanics view, it is first necessary to review continuum models of stress and strain distributions as well as stress states. We will then address most of these questions as several collective groups and see how the unanswered portions of these suggest future directions. Finally, by necessity, several concepts are proposed as to why many of the observed phenomena require a given micromechanical interaction.

*Chemical Engineering and Materials Science Department, University of Minnesota, Minneapolis, MN 55455.

Stress and Strain Distributions

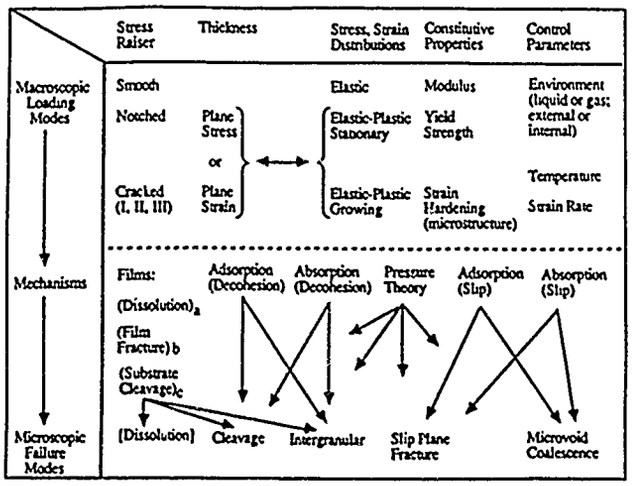
Regarding continuum theory, there are eight conditions of significance in isotropic, homogeneous solids. These are stationary and growing cracks, each of which may be in a material with or without strain hardening, furthermore, each of these four pairs may be under plane-stress ("thin-sheet") or plane-strain ("thick-plate") conditions. Note that anisotropic elasticity and plasticity and strain localization concepts substantially increase this set.

Current status

The stress distributions referred to above have been addressed in part in the two former reviews[8,9] and in more recent papers in the mechanics literature.[15-20] Thus, these will not be addressed in detail. It is important to note that continuum, small-scale yielding stress fields for growing and stationary cracks are very nearly the same. In Figure 1, it is seen that the values of σ_{yy}, σ_{xx}, and σ_{xy} normalized on the yield stress (σ_{ys}) are very similar for elastic, perfectly plastic conditions using a von Mises yield condition.[20] The analytical Prandtl field for the stationary crack, the finite element, and the Rice, Drugan, and Sham[17] models for the growing crack are very similar. However, the stresses *behind* the growing crack are lower and affect both the strain distribution and crack-opening profile. As such, recent modeling has been associated with crack tips and hole growth involving blunting[22,23] or shear banding.[24,25] Also, plastic instabilities from corner theory and the modification of steady-state stress intensities[21] for slow crack growth have been addressed and may have implications for modeling of subcritical crack growth. To the authors' knowledge, only a few applications of such models to environmentally sensitive cracking have been attempted.[21,26,27]

TABLE 1

Micromechanics of Environment-Induced Cracking



Regarding strain distributions, a recent review of the eight above conditions is summarized in Table 2. The plastic strain (ϵ_p) may be given as a function of the yield strain (σ_{ys}/E), the plastic zone diameter (R_p), and the distance from the crack tip (r). Here, the plane-stress and plane strain plastic zones are given reasonably well for both nonhardening and strain hardening conditions by the following:[18,28,29]

$$R_p\big|_{\text{plane stress}} \approx K_I^2/\pi\sigma_{ys}^2 \qquad (1.1)$$

$$R_p\big|_{\text{plane strain}} \approx K_I^2/3\pi\sigma_{ys}^2 \qquad (1.2)$$

$$R_p\big|_{\substack{\text{plane stress}\\ \sigma\to\sigma_{ys}}} \approx a\left[\sec\left[\frac{\pi\sigma}{2\sigma_{ys}}\right]-1\right] \qquad (1.3)$$

(1)

where σ and K_I are the applied stress and stress intensities, 2a is the crack length, and σ_{ys} is the yield strength. For Equations (2.2) to (2.9), $\alpha_1 \sim \alpha_2 \sim \alpha_3 \sim \alpha_3' \sim 1$ and $\beta \sim \beta' \sim 5.46$ are good first approximations. It should be mentioned that there is some controversy[30] about Equations (2.8) and (2.9) for elastic-plastic conditions with strain hardening[16] ($e \sim p^n$), and these may eventually need to be revised. While there has been a great effort in evaluating such models away from the crack tip, there have been few studies near the crack tip and almost none associated with environmental cracking, except for the corrosion fatigue work of Davidson and Lankford.[31] Such continuum models have been recently applied to the strains associated with fatigue cracks growing in one atmosphere of dry hydrogen at a ΔK of 13 MPa-$m^{1/2}$.[28,32] The strain distribution left by the growing crack was measured with the electron-channeling technique at the fracture surface, just below it by chemical polishing, and at large vertical distances below on a plane-strain section (a slice parallel to but well below the free surface). This gave the strain distribution for a growing "corrosion-fatigue" crack, in this case, hydrogen-induced fatigue crack growth on the {001} plane of an Fe-3wt%Si single crystal. As seen in Figure 2, neither the theoretical strain distribution for a stationary crack with strain hardening ($e \sim p^n$), nor the elastic, perfectly plastic distribution ($e \sim p$) for a growing crack fits very well. In the first, the singularity is too strong, meaning the strains are rising too rapidly, in the second, the singularity is too weak. In both cases, the strain magnitudes are generally well below those observed. The parameters used here were σ_{ys} = 296 MPa, $E_{[100]} = 1.32 \times 10^5$ MPa and n = 0.38 in Equations (1) and (2). Applying these same parameters with Equation (2.9) from Table 2 did give a good fit to the data, even to within about 1 μm of the crack tip.

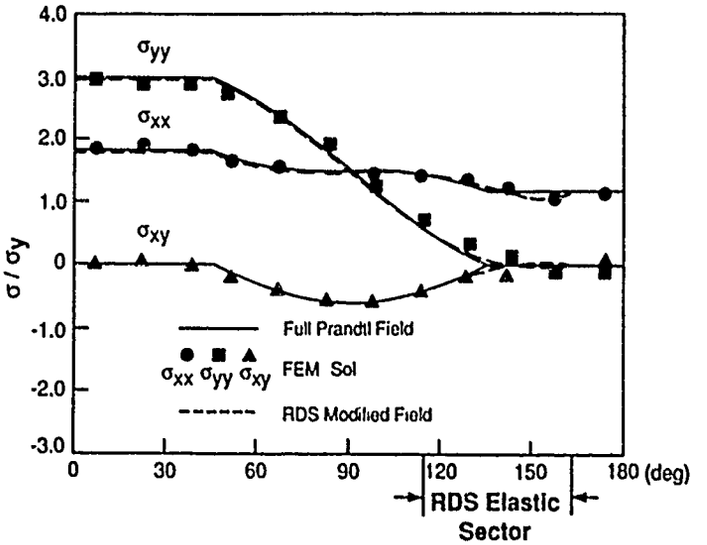


FIGURE 1—Stress field around a slowly growing crack in Mode I, plane strain. Elastic, perfectly plastic conditions with Poisson's ratio of 0.3 in a finite element[20] or small-scale yielding, RDS, model[17] compared to the Prandtl field for a stationary crack. [Copyright (c) 1987 Martinus Nijhoff Publishers.[21] Reprinted with permission from Kluwer Academic Publishers.]

Thus, what can be suggested is that current continuum solutions are on fairly firm ground and it is timely for both the mechanics and materials science community to ascertain the applicability of such approaches as a framework for micromechanical models.

Application of stress and strain distributions

It was originally suggested[9,10] that blunt-notch studies could help assess some of the critical issues in SCC and HE because the stress and strain distributions could be more precisely characterized. Since then, several studies[33-35] have addressed the blunt-notch case in high-strength steels. These were designed to address such issues as the site for embrittlement and whether or not there was a time for crack initiation. The first of these was a theoretical model that suggested there was a time to build up to a critical activity at a

distance (x^{cr}) in front of the notch.[33] This critical distance[33] was approximated by equating the hydrostatic pressures in the elastic and plastic regions.[33-36] While the elastic stresses do vary with notch-root radii, the hydrostatic pressure term along the direction of crack growth does not. This gives a first-order upper bound for the critical distance from the following:[33,34,37]

$$\frac{2(1+\nu)K_\rho}{3(2\pi x^{cr})^{1/2}} = \sigma_{ys}\left[ln\left(1+\frac{x^{cr}}{\rho}\right)+\frac{1}{2}\right] \quad (3)$$

Here ρ is the notch-root radius and K_ρ is the stress intensity calculated for the notch as if it were a crack. In terms of this distance (x^{cr}) and Fick's second law, they find an initiation time (t_i) given by

$$1-\text{erf}\left\{\frac{x^{cr}}{2(Dt_i)^{1/2}}\right\} = \exp\left\{\frac{\sigma_{ys}\overline{V}_H}{RT}\left[ln\left\{\frac{\rho+x_{th}^{cr}}{\rho+x^{cr}}\right\}\right]\right\} \quad (4)$$

Here D is a trapped diffusivity, x_{th}^{cr} is the critical distance at threshold, and $\overline{V}_H/RT$ is the partial molal volume term. This model may be tested if the effective diffusivity, critical distances, and initiation times can be measured, since x_{th}^{cr} can be determined from Equation (3) at threshold. Two such experimental studies give consistent results.[34,35] These were both on high-strength type 4340 (UNS G43400) steel, the first being cathodically charged with internal hydrogen and the second being tested in a 0.1 N H_2SO_4 solution. Note that these would be internal and external hydrogen cases. In the first case, an acoustic-emission technique was used to detect nucleation, while in the second, an electrical potential method was used. After detection, either metallographic sectioning[35] or fractographic analysis after liquid nitrogen fracture[34] was used to detect the initiation site. Crack initiation below the notch root is shown as a function of notch-root radius in Figure 3. The upper bound from Equation (3) gives a good accounting for the trend and magnitude of the critical distances. Note that both K_ρ and σ_{ys} were slightly different in the two studies with the shift in the two data sets reasonably consistent with Equation (3).

From these two investigations,[34,35] the time to crack initiation was also measured, the most complete set being shown in Figure 4. From this, a horizontal slice at K_ρ = 46.5 MPa-m$^{1/2}$ was taken to compare to the previous investigation that measured t_i at K_ρ = 54.9 MPa m$^{1/2}$. The comparison in Figure 5 shows a similar trend of t_i increasing with ρ. Modeling was attempted with Equation (4), but it was found to overpredict t_i by more than an order of magnitude. Part of this might be explained by the overprediction by Equation (3) of x^{cr}, but part of it is that Equation (4) implicitly assumes some critical concentration controls failure regardless of the stress-intensity level. However, it is now known that the fracture stress (σ_f^*) is a function of the hydrogen content (C_H), giving a σ_f^* C_H failure envelope.[38] If one uses this in the macroscopic sense,[39] it can be shown that[35]

$$t_i = \frac{C_1\rho^{1/2}}{K_\rho}\left\{\left[C_2\left(1-\frac{K_\rho}{2(\sigma_{ys}E\rho)^{1/2}}\right)\right]^2-1\right\}^{5/4} \quad (5)$$

For a given temperature and material, C_1 is a constant containing the diffusivity term and C_2 is a constant containing the σ_f^* $-C_H$ term. Taking C_2 to be 3.0, as used previously,[35] a single value of C_1 = 6.8 × 10^4 MPa-s predicts the initiation time in Figure 5 for the 500°C temper. Using the same value for C_1 and reducing C_2 to 1.8 gives a fit of Equation (5) to Hirose and Tanaka's data.[34] Here, a 40% drop in the failure envelope term for the more sensitive steel allows a fit. It is seen that the initiation times for cracking from a blunt-notch increase with notch-root radius and decreasing susceptibility to HE, i.e., higher tempering temperatures. The exact shift in Figure 5 is not meaningful since fugacities from prior charging and from SCC are not likely to be the same. It is emphasized that this simple model is incomplete and does not adequately cover the threshold regime. As shown in Figure 4, well-defined thresholds were demonstrated as a function of notch-root radius. Using a relatively involved continuous distribution of dislocations model for the hydrostatic pressure distribution and a Green's function approach to solve Fick's second law, Hirose and Tanaka were able to predict initiation times over the whole field of Figure 4.[34]

From this notch-root behavior, one might get the impression that issues such as critical distance and initiation times are convincingly settled. This is not true on the local scale. For example, the natural crack tip need not be blunt, and, as such, these findings may not be applicable to very high-strength materials containing natural cracks or perhaps not even to lower-strength materials containing "sharp cracks." One such "sharp crack" situation is the Fe-Si single-crystal case extensively investigated by Vehoff, et al.[40,41] Since these sharp cracks remained sharp while growing in hydrogen, even under general yield, it was of interest to assess the strain distribution associated with such cracks. Recently, it has been shown that sustained load crack growth is possible in Fe-3wt%Si in 1 atmosphere dry hydrogen at room temperature. For one sample with da/dt ~ 1.6 × 10^{-8} m/s at an effective applied stress intensity of 25 to 30 MPa-m$^{1/2}$, the strain distribution was determined with electron channeling patterns (ECPs), two of which are shown in Figures 6(a) and (b). The back-scattered channeling contrast in Figure 6(c) gives a sense of the iso-strain contours near the tip of the slowly growing crack. This terminated in rapid cleavage with much less plasticity, and thus the contours are representative of slow crack growth. From the ECPs in localized areas, individual strains were measured at a number of positions to give the strain contours in Figure 6(d). At positions of 640, 740, and 800 μm in front of the original crack tip, distributions at θ = 90° were taken and plotted in Figure 7. Also shown are the interpolated data from the iso-strain contours in Figure 6(d). Although incomplete, preliminary results indicate a reasonable prediction in the plane-stress regime with a calculated plastic-zone size of 20,000 μm from Equation (1.3) and the distribution from Equation (2.8). Additional work is in progress to assess this for samples with more constrained yielding. Still, from Figures 2 and 7, it appears that the growing crack-strain distribution is most appropriate to slow crack growth by HE of Fe-3%Si.

This applicability allows a threshold model to evolve following the original Cottrell and Petch ideas.[43,44] For environment-sensitive fracture, the idea was that the effective surface energy was reduced, and when a dislocation pile up nucleated a crack of sufficient size, unstable fracture resulted with $\sigma Nb \simeq 2\gamma_{off}^{envr}$. As derived in Appendix A, this idea can be coupled with Equation (2.9) to give a Cottrell-Petch type model for threshold stress intensity. For plane strain with strain hardening, this gives a result not too different from that derived by Smith[45] from other considerations,

$$K_{I_{th}}^2 \simeq 3\pi\sigma_{yr}^2 r_o \exp\left\{\left[\frac{K_{I_{th}}^2(1-\nu^2)}{\beta'\sigma_{ys}^2 L_s}\right]^{1-n}\right\} \quad (6)$$

With β' = 5.46, ν = 0.3, n = 0.38, and σ_{ys} = 300 MPa, all parameters are known except L_s and r_o. The former is the slip-band length and the latter is the distance from the crack tip where $\epsilon_\rho = \epsilon_f$, the "fracture strain." With r_o ~ 1 μm and L_s ~ 30 μm, one calculates a $K_{I_{th}}$ of 16.4 MP-m$^{1/2}$, which is close to the observed threshold. Since $\epsilon_f \sim K_{I_{th}}^2(1-\nu^2)/E\sigma_{ys}L_s$, the fracture strain may be calculated to be 0.21. This is reasonable comparing the theoretical plot of Figure 2 at r = 1 μm. Thus, the modeling is self-consistent. The ability to fit a threshold is not significant by itself, since there are two adjustable parameters (only one if ϵ_f is measured), r_o and L_s. It is the reintroduction of the old idea that γ_{off}^{envr}/L_s is a controlling parameter in embrittlement thresholds that has some merit. Having said that, the reader is cautioned on two points with regard to any implications on mechanism:

(1) First, the use of $2\gamma_{off}^{envr}$ in the derivation does not mandate a surface-energy mechanism, since any mechanism that reduces the effective work-of-fracture is appropriate.

(2) Second, the use of a strain distribution to describe the evaluation point does not necessarily mean this is a failure-strain criterion. This will become clear in the section on dislocation shielding/antishielding.

Besides Mode I, one must consider other states of stress for both sorting out macro- or micromechanism and the practical implications.

TABLE 2

Analytical Strain Distributions for Stationary and Growing Cracks

Conditions		Plane Stress	Plane Strain
Plastic zone size		(2.0) $R_p = \frac{K_I^2}{\pi\sigma_{ys}^2}$	(2.1) $R_p = \frac{K_I^2}{3\pi\sigma_{ys}^2}$
Stationary cracks	Elastic, ideally plastic (e–p)	(2.2) $\epsilon_p = \frac{\sigma_{ys}}{E}\left[\frac{R_p}{r} - 1\right]$	(2.3) $\epsilon_p = \frac{\sigma_{ys}}{E}\left[\frac{R_p}{r} - 1\right]$
	With strain hardening (e–p^n)	(2.4) $\epsilon_p = \alpha_1 \frac{\sigma_{ys}}{E}\left[\left(\frac{R_p}{r}\right)^{\frac{1}{n+1}} - 1\right]$	(2.5) $\epsilon_p = \alpha_2 \frac{\sigma_{ys}}{E}\left[\left(\frac{R_p}{r}\right)^{\frac{1}{n+1}} - 1\right]$
Growing cracks	Elastic, ideally plastic (e–p)	(2.6) $\epsilon_p = \alpha_3 \frac{\sigma_{ys}}{E}\left[ln\left(\frac{R_p}{r}\right) + \frac{1}{2} ln^2\left(\frac{R_p}{r}\right)\right]$	(2.7) $\epsilon_p = \beta \frac{\sigma_{ys}}{E}\left[ln\left(\frac{R_p}{r}\right)\right]$
	With strain hardening (e–p^n)	(2.8) $\epsilon_p = \alpha_3' \frac{\sigma_{ys}}{E}\left[ln\left(\frac{R_p}{r}\right) + \frac{1}{2} ln^2\left(\frac{R_p}{r}\right)\right]^{\frac{1}{1-n}}$	(2.9) $\epsilon_p = \beta' \frac{\sigma_{ys}}{E}\left[ln\left(\frac{R_p}{r}\right)\right]^{\frac{1}{1-n}}$

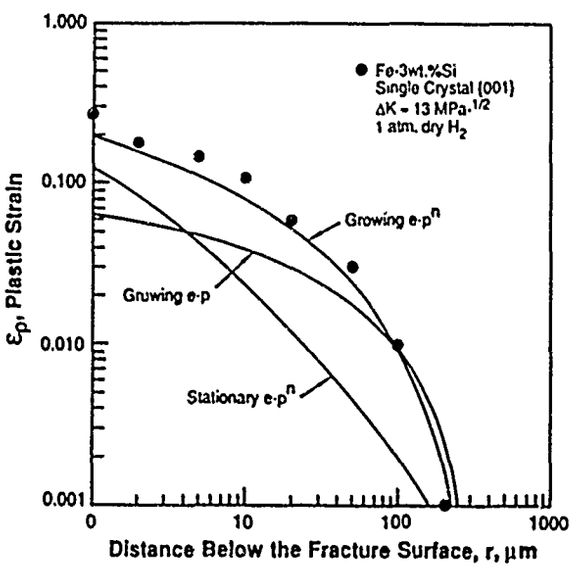


FIGURE 2—Plastic-strain distributions for subcritical crack growth in fatigue measured normal to the crack plane. Theoretical comparisons are for a stationary e-p^n crack, Equation (2), a growing e-p crack, Equation (2.7) and a growing e-p^n crack, Equation (2.9).

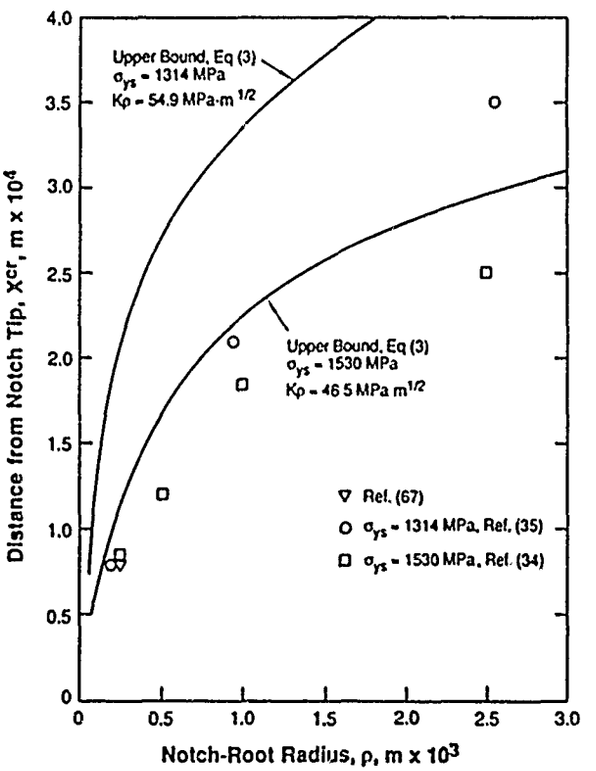


FIGURE 3—Crack nucleation site near a blunt notch as a function of notch-root radius. Two ultra-high-strength steels are represented with slightly different yield strengths and apparent stress-intensity factors (Kρ).

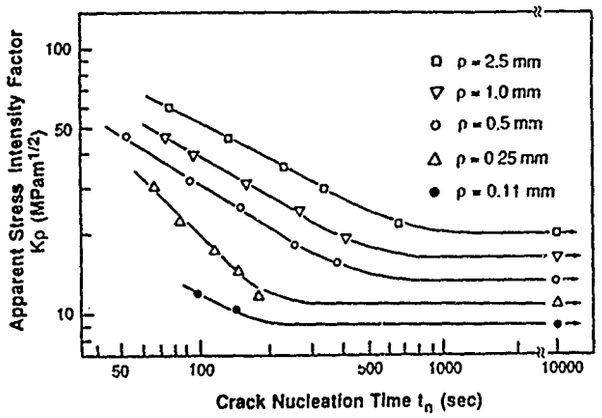


FIGURE 4—Effect of notch-root radius and applied stress intensity for time to nucleate a detectable crack. (Reprinted with permission from Pergamon Press plc.[34])

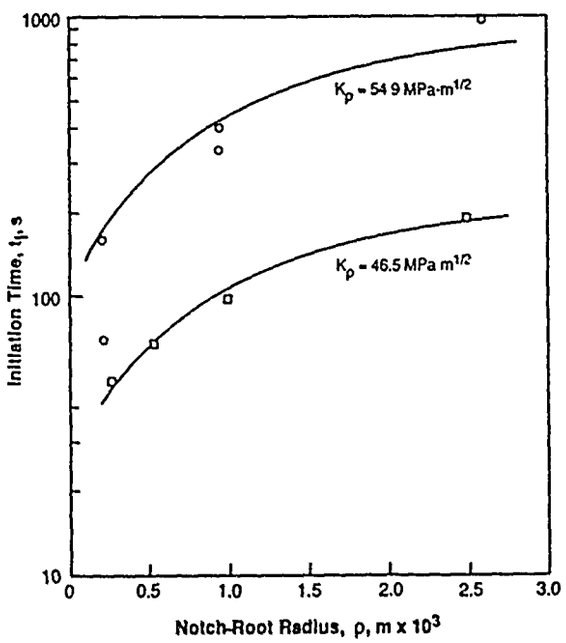


FIGURE 5—Crack initiation time as a function of notch-root radius for the two steels of Figure 3.[35] (Reprinted with permission from Pergamon Press plc.[34,35])

Loading-Mode Effects

Here, the classic Mode I, II, III loadings as well as degree of biaxiality and plane stress vs plane strain are included. Both stress and strain distributions can vary greatly in all of these loading-type groups. For that reason, a large number of investigations[46-66] have used these to sort out mechanisms. Since the stress distributions have been covered adequately,[8,9] these aspects will not be reviewed except where needed. The reader is reminded that these three groups are as depicted in Figure 8, and each of these will be addressed in sequence.

Modes I, II, III

To briefly review, it was originally suggested[67] that HE would more likely occur in a dilatant region or region of elevated hydrostatic tension stress (σ_{ii}). For the simple case of spherical strain centers in a dilute solution, Boltzman statistics give the following:[68]

$$C_H = C_o \exp\left\{\frac{\sigma_{ii}\bar{V}_H}{3RT}\right\} \qquad (7)$$

where C_o is the initial concentration. If σ_{ii} is large, as in Mode I, greater hydrogen is available but with $\sigma_{ii} = 0$, as in Mode III, HE should be difficult, if not impossible. Tests of Mode I and Mode III appeared to verify this argument.[66] There are three possible concerns in the way Equation (7) has been applied. First, if the hydrogen is collecting in a region where σ_{ii} becomes very large, then Fermi-Dirac statistics should be used. In the sense of a macroscopic process zone where stresses are no greater than $3\sigma_{ys}$, this would not be a problem except where C_o is initially large. Second, if hydrogen is nonspherical, additional off-diagonal terms must be considered, allowing Mode III to produce enhanced concentration levels.[61] Finally, a grain-boundary site with even a low binding energy near 25 kJ/mol concentrates on the order of 3000 times as much hydrogen as suggested by Equation (7).[70] It could then be argued that Mode I tensile stresses simply cause intergranular separation of boundaries greatly weakened by segregation that results from binding at trap sites, obviating the need for crack-tip dilation. Some of these same arguments could be applied to Mode II but will mostly be addressed below for Mode III.

Comparisons between Modes I and II have been relatively sparse, although the available information suggests that Mode II cracking is possible.[50,63-65] McGuinn and Aballe demonstrated that Mode II cracking did occur during SCC of steel coupled to a Mg anode in 3% NaCl solution.[63] This would produce a high hydrogen fugacity. Furthermore, the suggestion was that since the elastic hydrostatic stress tensor could not collect hydrogen in the near-tip region, HE did not require a significant bulk hydrostatic stress. It was later discussed that in using the Hutchinson, Rice, and Rosengten (HRR) stress field for an elastic-plastic material, a dilatational stress was possible for a Mode II crack.[64] Presently, it is not known whether SCC or HE of high-strength steels depends on the bulk hydrostatic stress for Mode II loading. Evaluations of lower-strength materials with greater resistance to embrittlement, such as iron or nickel with dispersed second phases, have been accomplished by Joosten, et al.[50] With U-notch bend tests, it was shown that precharged hydrogen promoted ductile plastic instabilities in Mode II for both type 1095 steel and thoria-dispersed nickel. However, under dynamically charged conditions, the failure mode switched from ductile Mode II to brittle Mode I. In a detailed study of Mode II cracking of highly textured Fe-Si, Zhang, et al.,[65] demonstrated that cleavage cracking was on the {001} planes regardless of the crystallographic orientation. As shown in Figure 9, the ratio of the initial applied Mode II stress intensity to the critical applied Mode II stress intensity (K_{II}/K_{II_c}) controlled the time-to-failure; however, the orientation also affected time-to-failure. With β being the angle between the load axis and the [001] rolling direction, and γ being the angle between the load axis and the crack-growth direction, they found $\beta + \gamma = 90°$ in all tests. They used these observations to disqualify the decohesion theory of HE. In addition, their observations of severe local plastic deformation reinforced their concept of a Cottrell mechanism with [001]-type dislocation pile ups and high internal hydrogen pressures leading to crack growth.

Three points are of note here. First, in Figure 7 it was seen that very large strains also accompany Mode I cracking of Fe-3wt%Si single crystals in hydrogen. Second, in a system where cleavage on {001} controls cracking, deviation from the maximum principal stress plane is to be expected for some orientations. Finally, the stress field in this anisotropic, double-notched specimen was unknown. Given this in perspective, our view is that these results do not disqualify a decohesion theory. Nevertheless, Zhang, et al.,[65] made an important contribution in identifying the strong crystallographic effect regardless of the loading angle and the fact that a critical number of dislocations may be involved in crack nucleation. While it would appear that the work of Vehoff and Neumann[41] negates the pressure-theory hypothesis, there is a possibility that a type of dislocation pile-up mechanism may be integrally involved with decohesion. This is discussed later.

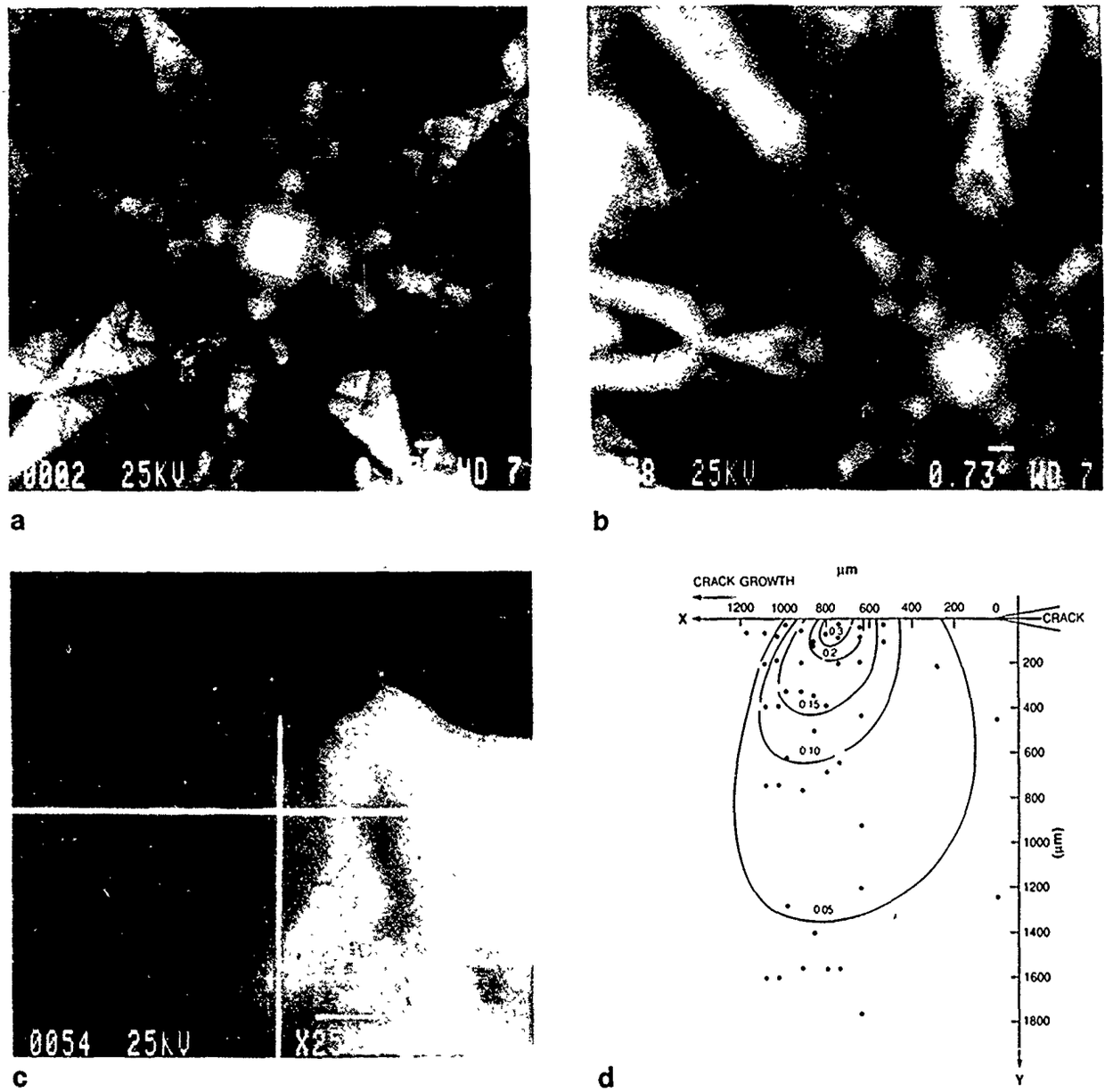


FIGURE 6—Electron channeling pattern (ECP) measurement of the iso-strain contours about a crack growing in an Fe-Si single crystal under 1 atmosphere of hydrogen: (a) and (b) ECPs at 0 and 30% strain; (c) back-scattered electron contrast; (d) iso-strain contours.

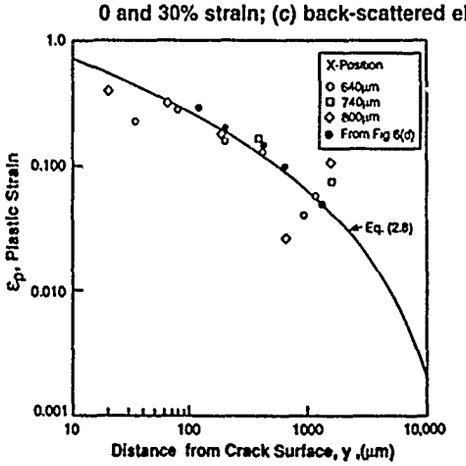


FIGURE 7—Comparison of theory [Equation (2.8)] to the measured plastic strains for the sample of Figure 6. The open symbols correspond to the points in Figure 5(d) at various x-y coordinate locations while the solid circles correspond to a vertical section through the iso-strain contours at x-800 μm.

There is some controversy in the literature[52,54,61,62,66] as to whether cracking occurs in Mode III as a pure Mode III crack. The original tests implied that cracking would not occur along the plane of the crack.[66] Later tests demonstrated that cracking could occur in such samples.[61,62] However, these cracks are really propagating as opening-mode cracks, since they propagate perpendicular to the maximum tensile axis, i.e., at about ±45° to the load axis. Just like brittle conchoidal fracture of chalk can occur in torsion, so can a smooth or notched steel bar fail along planes perpendicular to the normal stress by HE. The generally accepted observations are that microscopic Mode III cracking in the Mode III direction is very difficult to achieve. Results of Thompson, et al.,[52,54] and Green, et al.,[71] all suggest that susceptibility to cracking under SCC conditions was greater under Mode I loading. For example, Swanson, et al.,[52] demonstrated in aluminum alloy 7075-T6, that the time-to-failure was 2 orders of magnitude shorter, 100 min for Mode I and 10^4 min for Mode III, in constant-load tests at 323°K in a 3.5% NaCl solution. Additional evidence comes from Kapp[72] who evaluated notched bars of 70/30 alpha brass under LME conditions. In air, alpha brass required 70° of twist to initiate the crack. In liquid mercury, only 10°

of twist was required. After crack initiation for a short distance of 10 to 50 μm in Mode III, the crack switched to Mode I. The macroscopic fracture appearance showed 45° planes. To Kapp, this implied that while crack initiation may be strain controlled, decohesion had the largest effect on governing crack propagation along maximum tensile stress planes.[72]

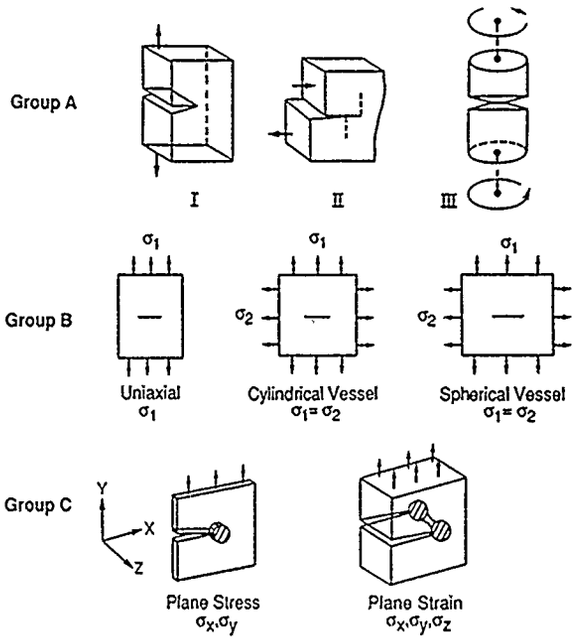


FIGURE 8—Three groups of state-of-stress effects resulting from loading or geometry: (a) opening Mode I, in-plane shear Mode II, and antiplane shear Mode III, (b) degree of biaxiality, and (c) degree of triaxiality or the thickness effect.

This leaves the possibility that Mode III and Mode II can initiate cracking, but Mode I dominates propagation. This still does not address whether the Mode III stress field initiates cracking because of a strain criterion, or in those cases where hydrogen is possible because of increased concentration due to nonspherical distortion.[61] With regard to the latter, considerable insight has been gained by Mode III and combined Mode I/III testing of smooth samples.[61,62] Chu, et al.,[61] had earlier shown that hydrogen-induced delayed cracking of ultra-high-strength steels was produced on 45 planes of torsion bars. This plane provided the largest magnitude (–) of the interaction energy between the strain field and the hydrogen atom. This is given by

$$U_{45^\circ} = -\frac{a^3\tau}{8}(\epsilon_1 + \epsilon_2 - 2\epsilon_3)\sin(2\alpha) = \frac{a^3\tau}{8}(\epsilon_2 - \epsilon_3) \qquad (8)$$

where α is the angle of the plane of the crack to the torsional plane. These planes have the maximum concentration of hydrogen in the macroscopic sense and lead to failure by intergranular fracture. Similarly, Takemoto provided evaluation of smooth bars of type 4135 steel but in Mode I, Mode III, and combined Mode I/III.[62] They demonstrated failure to occur on planes that made an angle (θ) with the specimen axis,

$$\theta = \frac{1}{2}\tan^{-1}(2\tau / \sigma_x) \qquad (9)$$

where the x-axis is the length of the bar. Thus a combined Mode I/III sample with the torsional stress equal to the tensile stress should fail at 31.7 and the observed macroscopic failure plane was 32°. Note here that α + θ is 90°. Takemoto observed that the θ plane also produces the largest magnitude of negative interaction energy between hydrogen and the elastic strain field.[62] He thus concluded that the critical combination of stress state and hydrogen concentration leads to HE. However, since in all of these tests, the θ plane is both the plane of maximum concentration and the plane of maximum principal stress, it could be argued that one of these is sufficient.

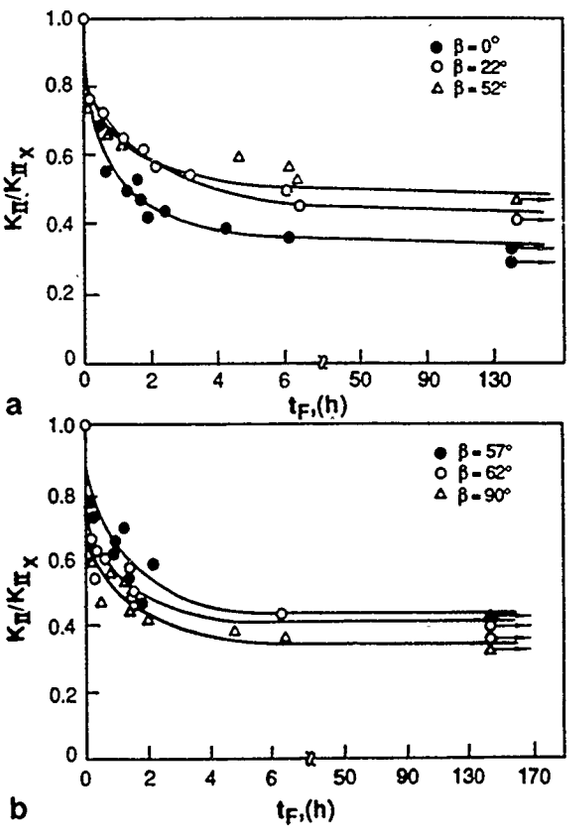


FIGURE 9—Variation of K_{II}/K_{IIx} with time-to-failure (t_f) for specimens with different orientations between the load axis and the [001] rolling direction in textured Fe-Si: (a) angles are 0, 22, and 52°, and (b) angles are 57°, 62°, and 90°.[65]

From the results on both notched- and smooth-bar specimens, the preliminary conclusion is that Mode I, II, and III crack growth favors those planes where the maximum principal stress is involved. For HE, these planes are generally also the planes of maximum hydrogen concentration. One exception is for strong crystallographic textures or single crystals where the cleavage plane controls rather than the macroscopic maximum principal stress. Although indirect, careful acoustic-emission or potential drop experiments would be useful to establish the existence of nucleation times under Mode III or combined Mode I/III loading. A similar set of Mode II or Mode I/II tests would assist in ranking the relative contributions of normal stress, dilational stress, and/or strain to crack initiation.

Biaxiality effects

To the authors knowledge, biaxiality effects have been exclusively addressed through crack initiation in uncracked specimens[48,55,56,59] rather than the precracked ones indicated in Figure 8, Group B. In 6.9 MPa hydrogen, Louthan, et al., demonstrated that biaxial loading (punched test on a clamped plate) was more detrimental than uniaxial loading (actually 4-point bending).[48] Holding untempered type 4340 steel with an ultimate strength of 2100 MPa for 120 h gave the results shown in Figure 10. Greater biaxial degradation was evident in both lower-failure stresses and more extensive intergranular cracking. Furthermore, there was a long incubation period prior to cracking, as evidenced by the lack of acoustic emission. During this long hold, it was assumed that dislocation activity became negligible in these sustained load tests Louthan, et al., concluded for HE of high strength steels that dislocation transport, internal pressure, slip softening, and hydrogen reduction of surface energy effects did not play a significant role, but that lattice dilation appeared to be important. They did not address the drop-off in failure stress with increased thickness of the bend samples, but this could be because of increased biaxiality effects in these "uniaxial" samples.

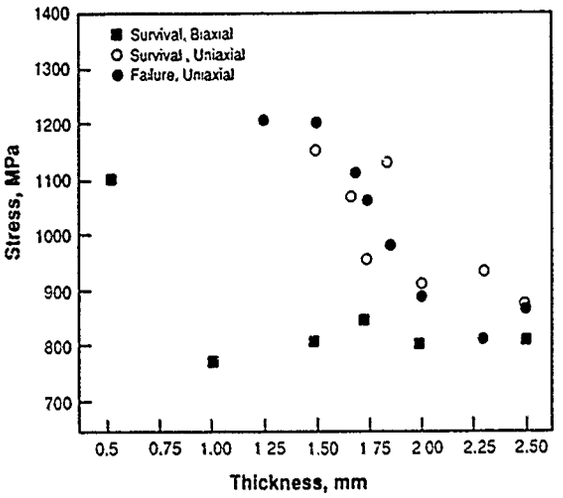


FIGURE 10—Minimum failure stresses and maximum survival stresses for type 4340 steel (UNS G43400) as affected by degree of biaxiality at various thicknesses. (Reprinted with permission.[48])

Blanchard, Koss, and Heldt[55,56] and Kampe and Koss[59] have shown nearly the same increased degree of biaxial degradation in both Admiralty brass in 0.1 M $CuSO_4$ and in pure nickel in 1 N H_2SO_4 charged at 100 A/m^2. Besides uniaxial and equibiaxial tension, a plane-strain Clausing[73] test was used. All three produced cleavage-like failures in Admiralty brass. First, note that the plane-strain condition for the Clausing test is not as severe a stress state as plane strain at a crack tip. The Clausing test gives a state of unbalanced biaxial tension with $\sigma_1 = \sigma_2/2$ and $\sigma_3 = 0$. Thus, the hydrostatic tension ($\sigma_{ii}/3$) increases in severity from tensile to unbalanced biaxial to equibiaxial tension. It may be of significance that the ratio of the load-to-failure in the environment to that in air (P_{env}/P_{air}) did scale inversely with the stress tensor. Since an internally dissolved species would be proportional to $\exp\left\{\alpha \frac{\sigma_{ii}}{3}\right\}$, a simple comparison in Table 3 shows that the increased availability of an embrittling species such as oxygen (?) or hydrogen (?) scales with the severity of the embrittlement. Whether this state-of-stress effect is associated with an internally dissolved species or some special dislocation mechanism is yet to be determined. Using the same set of tests, Kampe and Koss[59] have evaluated INCO 200 nickel containing 33 at. ppm sulfur. Hydrogen-produced intergranular fracture under all three conditions with equibiaxial tension again producing the severest degradation. They conclude that a critical normal stress criterion applies, as might be explained by either of the following:

(1) An increase in the local microscopic stress at grain boundaries because of plastic incompatibility between a hydrogen-softened boundary and the adjacent grains; or
(2) A decrease in the fracture stress of the boundary because of a hydrogen sweep-in process by dislocations.

One might add a third possibility, suggested by Table 3, that the equibiaxial condition would increase the local hydrogen availability most.

TABLE 3
Effect of Degree of Biaxiality on Failure Loads[A]

Test Type	Tension	Clausing	Balanced Biaxial
P_{env}/P_{air}	0.86	0.80	0.67
$\sigma_{ii}/3$	$\sigma_1/3$	$\sigma_1/2$	$2\sigma_1/3$
$[\exp(\alpha \frac{\sigma_{ii}}{3})]^{-1}$	0.85	0.78	0.72

[A] Specimens were of Admiralty brass in $CuSO_4$ and were initially crack free

Plane strain vs plane stress

Plane-strain vs plane-stress effects, and how to interpret them, go back more than two decades to B.F. Brown,[74] who showed thickness effects in the SCC and HE resistance of steel, titanium, and aluminum alloys. Gerberich, et al.,[36,75] also documented the increased resistance of thin-sheet plane-stress compared to thick-plate (plane-strain) conditions and explained them in terms of dilatational ($\sigma_{ii}/3$) and normal stress (σ_{yy}^{max}) effects. Later, Chu, et al.,[76,77] and Tien, Nair, and Bates[46] suggested that a dislocation sweep-in model was appropriate for crack growth. This was based upon observations of surface plasticity. Even though they describe extensive tunneling of the internal crack, which gives a ligament that undergoes surface plasticity, a time-dependent, plastic-zone growth model was invoked to explain growth kinetics. Alternatively, one could interpret this to mean that embrittlement kinetics leads the tunneled crack, and the plane-stress ligament that is holding on finally tears by a shearing mechanism. This is consistent with decreased kinetics being associated with decreased thickness, i.e., greater plane stress.[36,75]

There is additional evidence. Shaw and Johnson[47] have evaluated 2-1/4Cr-1Mo steels with an ultimate strength of 750 MPa in 50 psig H_2S gas. Without side grooves, these 75-mm-thick samples developed a large plastic zone with da/dt ~ 3.9×10^{-8} m/s at a stress intensity of 145 MPa-m$^{1/2}$. With side grooves, faster growth rates of 1.6×10^{-7} m/s occurred at lower K_I values of 25 to 50 MPa-m$^{1/2}$. Since the side grooves remove the plane-stress ligaments, this clearly indicates kinetics are favored by a plane-strain state of stress. It also suggests that microplasticity effects alone do not generally promote the severest degradation. Other, more recent evidence comes from hydrogen-induced fatigue and sustained crack growth on the {100} planes of single-crystal Fe-3wt%Si.[32,42] In samples 4.8-mm-thick, crack growth proceeded by a tunneling process. At ΔK 13 MPa-m$^{1/2}$, this occurred for macroscopic crack growth oriented in both the <001> and <011> directions.[32] These approached plane-strain conditions since the monotonic plane-stress plastic-zone diameter, Equation (1.1), was only 15% of the thickness. Under higher K_I values near 30 MPa-m$^{1/2}$, sustained crack growth still exhibited tunneling effects in the <011> growth direction. Since the microscopic crack front wants to be parallel to a <0$\bar{1}$1>, this deviation from a straight crack front appears to be driven by macroscopic plasticity considerations and not crystallographic ones. The crack-front curvature in Figure 11 clearly shows the surface lagging behind the center with the plane-stress surface being the slow step in the growth process. This suggests a strong plane-strain effect even in this 300 MPa yield strength single crystal.

In summary, the weight of the evidence is that strong state of stress effects exist in environmental degradation. Where brittle intergranular or cleavage modes are involved, it appears that Mode I, plane-strain cracking conditions are most severe for crack growth, and equibiaxial stresses are most severe for initiation in uncracked members. The fact that similar state-of-stress effects are at work in several classes of alloys subjected to different types of embrittlement phenomena suggests a common theme. This does not mean that a single mechanism exists, as that cannot be the case, however, it could mean that a common micromechanical condition is favorable for embrittlement onset.

Critical Questions

The fifteen questions posed in the first section are divided into three groups dealing with the micromechanics of the embrittlement site, the modification of stress or strain states associated with cracking, and other mechanics/microstructure interactions.

The embrittlement site

To summarize the first six questions, one could ask where this site is and what its character is. The position will depend upon its character, which includes local stress, local resistance, and the time to reach local instability.[1,3,6,8,9,13,46,56,78,104] Much of this has been reviewed for the blunt notch case in the section on the application of stress and strain distributions. Here, the site is subsurface where the

macroscopic stresses are highest. This, together with well-predicted initiation times, presents a consistent picture. In some ways, this might serve to confuse the real issues associated with sharp cracks, much controversy in the literature has evolved regarding this for two major reasons. First, there can be major similarities or differences in external vs internal sources of embrittling species. It all depends on the relative concentration of embrittling species in a given location, the relative velocity of the crack compared to the diffusivity of the species, and the relative stress or strain at that location. Second, there are embrittlement sites on the global scale and embrittlement sites on the local scale, what has been lacking is a consistent picture that includes both scales.

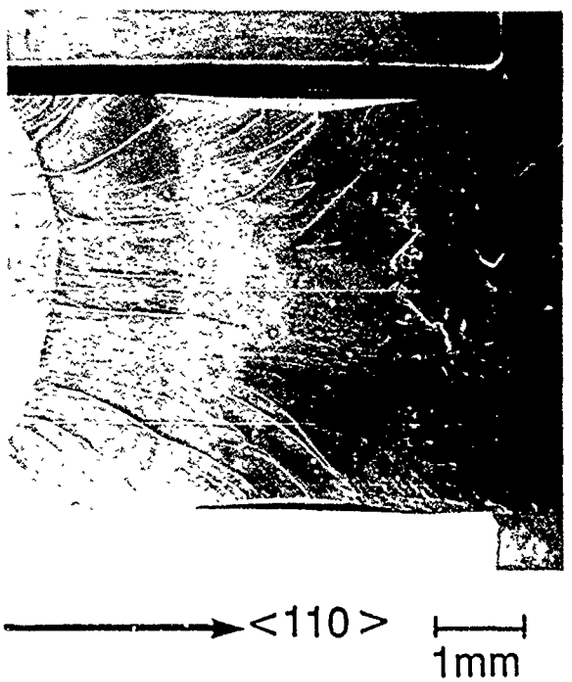


FIGURE 11—Crack-front curvature observed in a 4.8-mm-thick Fe-3wt%Si single crystal. Crack growth was in 1 atmosphere of dry hydrogen. [Reprinted with permission from Pergamon Press plc.[42]]

These ideas are summarized in Figure 12. Consider an internally distributed species as in Figure 12(a) for a high-strength material. While the species concentrates in the global sense because of the macroscopic stress gradient, it may initiate at an interface where the species segregate further. Because of crack initiation subsurface, there now exists a small microcrack that connects up with the macrocrack. The local stress field that governs this initiation and growth must be different in character and magnitude from the global stress field. More than an order of magnitude difference is implied with local stresses $\sim 10^4$ MPa being compared to macro-stresses near 10^3 MPa. This has been recognized by a number of investigators.[1 70 84 96] For external embrittlement of the same high-strength material, cracking most likely initiates very near or at the surface, since the combined local concentration and local stress is greatest there [Figure 12(b)]. Even though the macroscopic location is different, the local stress distribution and concentration of species may be very similar. This could lead to similar types of threshold and kinetic growth phenomena in some instances. The low-strength condition with a blunter notch leads to a similar macroscopic embrittlement site, but one that is displaced further from the crack tip for internal embrittlement, Figure 12(c). Still, the local stress required for crack advance might be nearly identical. Slower growth kinetics might be associated with either a modified stress field or a greater local resistance.

For the external case [Figure 12(d)], slower crack growth rates in the low-strength material allow for two embrittlement sites. The embrittling species diffuses in with a high-concentration gradient near the crack tip. This could be one site, but with time, this forms an additional concentration gradient near the macroscopic hydrostatic stress maximum. Although highly speculative, such a result can be inferred from the moving-line source[3] and quasistatic, elastic-plastic solutions.[34] Even if this stress maximum were not coincident with the concentration maximum, nucleation might still prefer a subsurface site. Again, the local stress and concentration differences between the external and internal case may or may not be large depending on the severity of the initial conditions. As will be shown, recent evidence indicates that these five scenarios do not comprise all the possibilities, which makes creating order out of this "site question" difficult.

Oriani[1] originally suggested that the embrittlement site in ultra-high-strength steels cannot be subsurface because of kinetic limitations, Figure 12(b). While this may be true, it is difficult to prove from growth rate alone, because the 1 μ distance involved to the stress maximum is easily transversed by hydrogen in 1 s. By contrast, Rice[9] suggested that embrittlement needs to be achieved over a microstructural-sized scale on the order of 1 to 30 μm, but there is no *a priori* reason for the initiation site to be coincident with the macroscopic stress maximum. For ultra-high-strength steels, Johnson,[3] Gangloff, and Wei[83,88] and Gerberich, et al.,[70] suggest that microstructural traps such as prior austenite grain boundaries, martensite laths, and sulfides at prior austenite grain boundaries are embrittlement sites, but there was not definitive proof of "volume embrittlement." By a special sustained-load, bake-out, fatigue sequence, Gao, Lu, and Wei[90] concluded that the fracture process zone is no greater than one prior austenite grain diameter. This would still be larger than the stress maximum predicted to occur at a distance of about two times the crack-tip displacements, 1.9δ, in front of the cracks. This is consistent with the observations of striations[70] along prior austenite grain boundaries in similar ultra-high-strength type 4340 steel, which were approximately 1 μm in size and, in this case, ~ 1.9δ as well. In such high-strength steels with the embrittlement site so close to or at the crack tip, separating out "surface" from "volume" embrittlement has not been successful.

In a similar steel, Elices, et al.,[81] did make a remarkable prediction of time-to-failure using a critical distance parameter of 100 to 400 μm. However, this distance was 2 orders of magnitude greater than 1.9δ and even a factor of 5 beyond the elastic-plastic boundary, reflecting the fact that the binding-energy term associated with the embrittlement site was neglected. Presumably, a good fit with a smaller critical distance parameter could result with slight modification.[70]

For all classes of steel, Thompson and Bernstein[49] have collected evidence to show that subsurface nucleation occurs at regions of highest triaxial stress. In HY 180 steel, Frazer and Metzbower[95] found discontinuous cleavage and secondary cracks at least 50 μm from the fracture surface. Here, 1.9δ was on the order of 28 μm, and thus the macro initiation site may have been slightly outside the highest stress region. In a similar high-strength Ti-30Mo alloy gas-phase-charged with hydrogen, cleavage initiation sites about 400 μm beyond the advancing crack were identified.[105 106] For this 900 MPa strength material, a K_I 50 MPa-m$^{1/2}$ gave a value of 1.9δ 30 μm and a plane-strain, elastic-plastic boundary of 330 μm. Moody, Stoltz, and Perra[98] concluded that the grain size establishes the minimum critical distance over which the fracture stress must be exceeded for cracking to occur. Note that this was not direct observation but was inferred from the threshold dependence on grain size in both IN 903, a superalloy, and type 4340 steel.

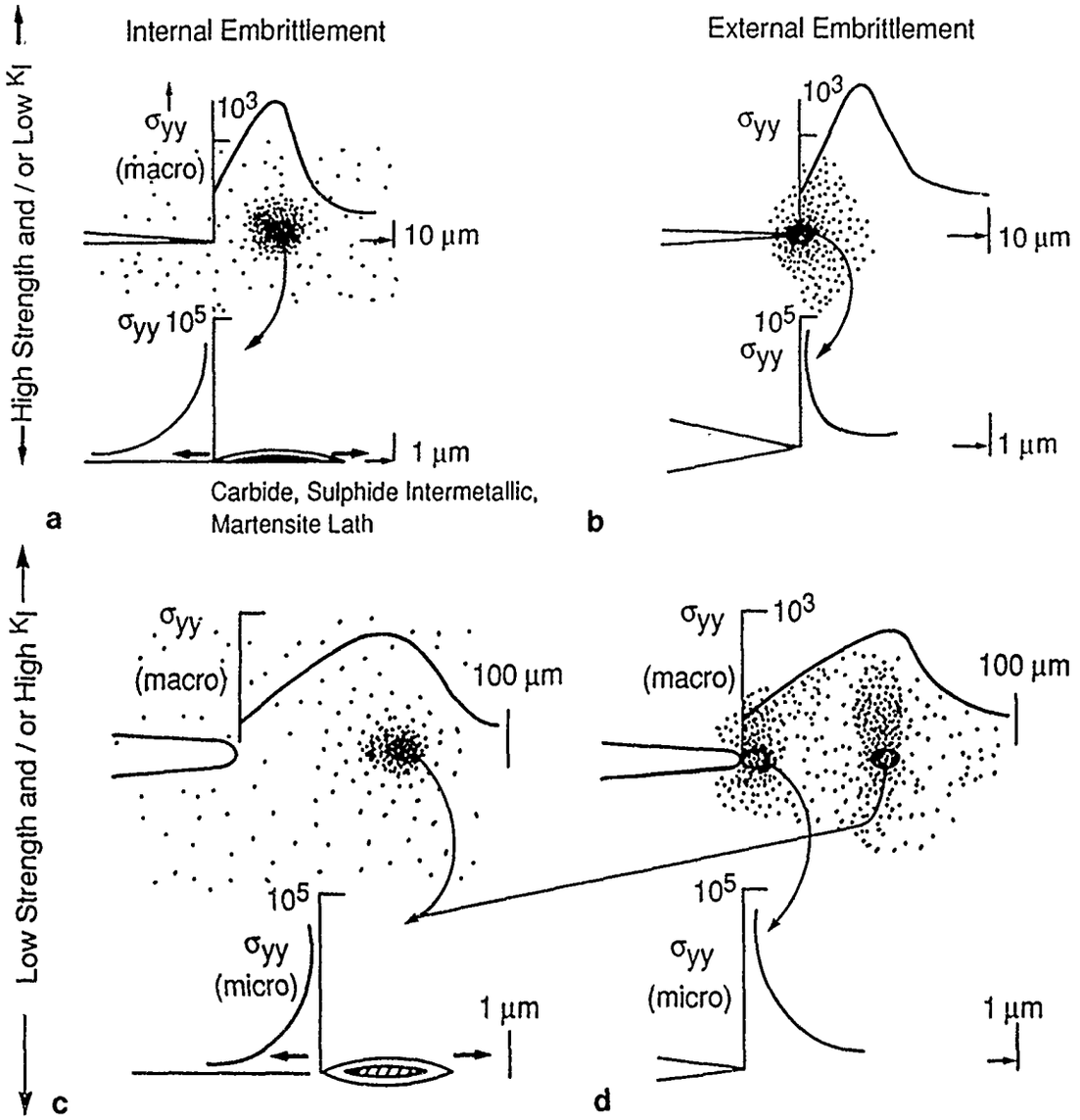


FIGURE 12—Schematic of possible crack-initiation sites for (a) and (c) internal, and (b) and (d) external environments.

In lower-strength materials, there is also a wide range of locations for the embrittlement site. Joosten, et al.,[50] indicated it was not clear whether hydrogen charging promotes brittle crack propagation or causes carbide/particle decohesion near the crack tip in a spheroidized type 1090 steel. Lassila and Birnbaum[79] identified a 300 Å grain boundary region rich in hydrogen to be responsible for embrittlement of nickel. Beggs, Hahn, and Pugh[86] have used a series of load-pulsing tests to demonstrate that Δx, the crack advance marked by the load pulse, does not decrease continuously as Δt decreases. They argued that this was fully consistent with a "volume embrittlement" model for type 310 (UNS S31000) SS tested in boiling $MgCl_2$ at 154°C. Here, the critical distance was found to be 0.5 μm, while Welch[107] found type 304 (UNS S30400) SS in water at 250°C to exhibit striations of 2.5 to 3 μm under sustained load. In Fe-3%Si single crystals, Vehoff and Rothe used high-resolution scanning microscopy to imply that the discontinuous crack advance is less than 0.1 μm.[40] Additional evidence from alternative exposure to H_2 and O_2 gaseous environments gave brittle crack stoppage within 1 second of the O_2 addition. Since the bulk was saturated with hydrogen to several microns, but the crack was calculated to stop within 0.1 μm, it was argued that the "volume embrittlement" could be not greater than 0.1 μm. Still, since Fe-3%Si is on the cusp between ductile/brittle behavior, it might only take a slight lowering of the hydrogen concentration to drop below this threshold. A 1-s cut-off from the external supply might be sufficient to accomplish this. In addition, the location of embrittlement site by itself does not guarantee the extent of a discontinuous crack advance. Neumann has suggested for the Fe-3%Si that although the extent of decohesion is not measurable, it is on the same order of magnitude as the embrittlement region, being 0.1 μm.[101] Finally, on low strength Fe and Fe + Sb polycrystals with σ_{ys} 100 MPa, Jones, Thomas, and Baer[108] found secondary cracks about 1000 μm away from a crack advancing under cathodic potentials of about 1.0 V_{SCE} in 1 N H_2SO_4. This embrittlement site of 1 mm is less than the 3 mm calculated plastic-zone size, but much greater than 1.9δ, which is estimated to be 100 μm. Even with external conditions, it appears as though susceptible grain boundaries may fail at distances beyond the stress maximum.

In summary to the questions about embrittlement site, there appear to be at least six very different material systems under cathodic over potential, open potential, and external and internal hydrogen conditions that exhibit embrittlement sites beyond the macroscopic crack. In materials with yield strengths ranging from 100 to 1000 MPa, these distances range from ≤ 0.1 μm to 1000 μm. Thus, it appears that the subsurface nucleation depicted in Figures 12(a), (c), and (d) is common to environmental degradation. How central this is to the actual extension process is still to be settled in

many cases, since cracking could be taking place at the main crack concurrently.

Alone, such subsurface nucleation sites do not make a case for "volume embrittlement." That is, cracking could initiate at a weak or highly segregated subsurface site and still grow several atom layers at a time back toward the macrocrack. Similarly, "volume embrittlement" and discontinuous cracking based upon crack-arrest marks for either internal or external embrittlement are complicated by other processes, such as substructural features, causing momentary arrest. For example, a crack could be growing smoothly by any dissolution or atom by an atom decohesion process, and the crack could stop because the external driving force is reduced or the internal local resistance increases. An arrest line would be left because of time-dependent, crack-tip plasticity, but this would not be associated with volume embrittlement.

Acoustic emission has been broadly used by a number of investigators to sort this process out. While there has been evidence of acoustic emission from discontinuous cracking,[85,86,92-94,109-111] much of this could be interpreted in two ways. First, it could be the usual interpretation as associated with the time between discontinuous cracking events. However, it could also be associated with a secondary fracture mode occurring behind the advancing stress-corrosion crack. That is, either quasicleavage or ductile rupture of ligaments behind an advancing intergranular crack could give acoustic events. In a recent paper, a strong correlation between the amount of acoustic emission and the amount of transgranular fracture occurring in ligaments behind the advancing crack was shown.[112] It is emphasized that these observations were under relatively low gain conditions of 80 dB. There are three studies that provide good evidence of acoustic emission correlating to discontinuous cracking at the advancing front. First, Beggs, Hahn, and Pugh[86] observed directly that an advance in crack position was coincident with an acoustic event in single crystals of Admiralty metal and Cu-30Zn. Second, Sieradzki, Sabatini, and Newman[113] demonstrated an acoustic event to be coincident with an electrochemical transient in the brittle cracking of copper. This oxide-induced cleavage process has been extended to other material systems and is further considered in the reviews of Oriani and Sieradzki in this conference volume. Third, recent results show that external HE in Fe-3%Si single crystals is discontinuous on the micron scale.[114] Well-defined arrest marks were observed 1 μ apart, as shown in Figure 13(a). Associated with each one of these were groups of acoustic events, whereas previous acoustic monitoring implied one advance was one emission.[86] In this single crystal, the crack front unzipped step-wise by nucleating at the apex and growing along the length of the front by a succession of events. As indicated in Figure 13(b), the local growth direction of the next step is unknown, but acoustic emission indicated that 40 to 70 of these local steps occurred in approximately 1 s. The fact that the individual event durations were only 5 μs and that there was a delay time of about 0.01 to 0.02 s between each event illustrates the discontinuous nature of the advance. Furthermore, between each group of events there was an approximate 12-s hold. This delay time divided into the 1-μ advance was consistent with the average macroscopic growth rate of 9×10^{-8} m/s. It seemed initially that this was irrefutable evidence of volume embrittlement. However, further discussions with Oriani, Sieradzki, and others,[1] suggested another possibility. A crack could initiate in less than a 0.1 μm region as suggested by Vehoff, Rothe, and Neumann,[40,41] and then arrest at 1-μ increments according to Sieradzki's exhaustion process[14,115] or some other stabilizing substructural influence. Of course, with Fe-3%Si in 1 atmosphere hydrogen, there is no oxide to cause unstable cracking. Nevertheless, other internal dislocation rearrangements can cause crack instability. How one such nucleation arrest renucleation process might occur is addressed in the section on dislocation shielding/antishielding.

[1]Private communication. See Acknowledgment.

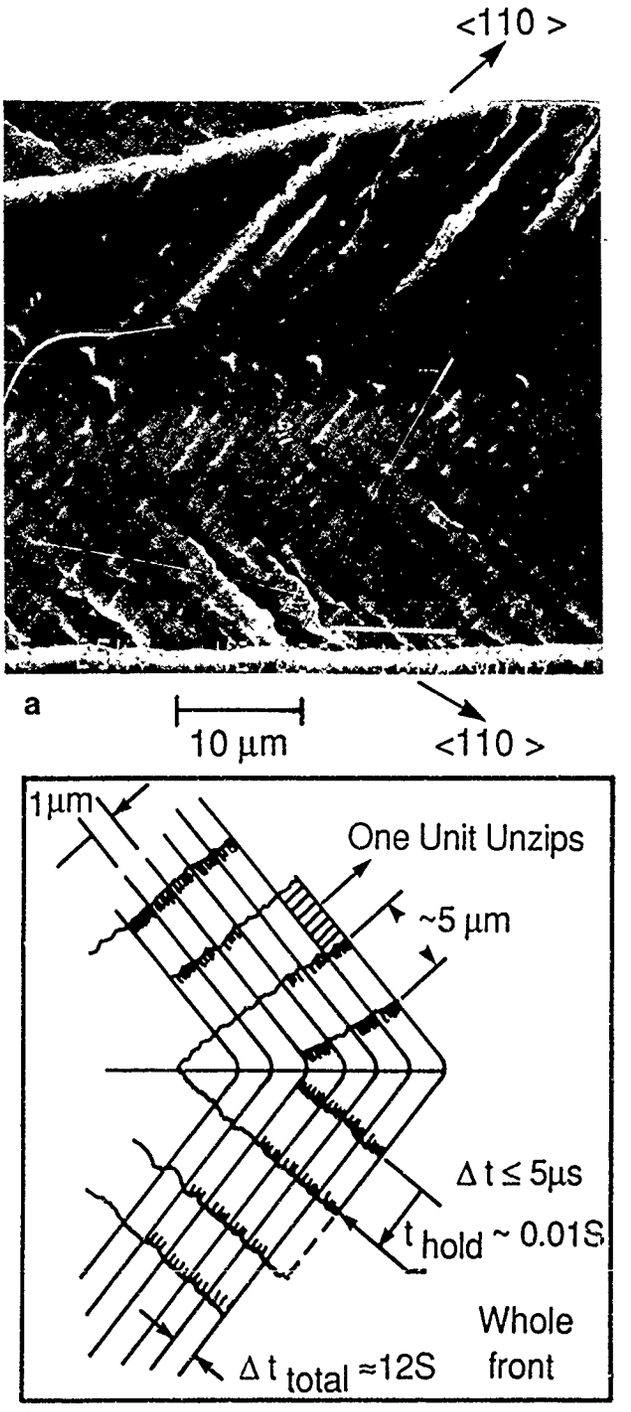


FIGURE 13—Slow crack growth by (001) cleavage of single crystal Fe-3wt%Si in 1 atmosphere H_2: (a) 1 μm arrest lines in two <110> directions, and (b) schematic from acoustic-emission analysis showing the additional discontinuous nature of the extension process along a single 1 μm advance; local growth is thought to be perpendicular to the macroscopic front but could be in either <110> direction in a given 5 μm unit. There is a hold time of approximately 0.01 s for each unit and a hold time of about 12 s after the whole front arrests.

The driving force

Anything that abruptly increases or decreases the local driving force for crack extension may cause initiation or arrest. The decision to detail this was prompted by questions seven through nine in the introduction. In micromechanical terms, porosity, or microcracks in the advance of a growing crack, ligaments behind it, dislocation shielding, or film-induced effects all could contribute to initiation or arrest. These three effects will be covered briefly:

(1) process zones,[8,12,39,58,105,124,125]

(2) film-induced cleavage,[5,6,12,14,86,103,104,110 111,113,115,134-136]

(3) dislocation shielding/antishielding.[9 13,118-123]

Process zones. Process-zone effects associated with environmentally induced discontinuous cracking have recently been reviewed[105] and will not be covered here. Two general aspects associated with macroscopic and microscopic scales are addressed. Macroscopically, process-zone effects can result in broadly fluctuating Stage II growth rates. Examples are shown in Figure 14 for two different heat treatments of type 4340 steel and a Ti-30Mo alloy all charged with hydrogen. Yield strengths are 1620, 1340, and 940 MPa, respectively. The process-zone sizes were estimated to be 10, 100, and 400 μm, respectively. In terms of the subsurface nucleation depicted in Figures 12(a) and (c), a larger discontinuous process zone would produce greater variations in microbranching or ligamentation, which would cause larger fluctuations in the local driving force.

McClintock[8] originally suggested that the time to achieve a given decohesion in front of an advancing crack will vary as given by the following:

$$t_n(x) = t_n[\,\delta(x), p(x)\,] \tag{10}$$

where δ(x), p(x) are the displacement and porosity or fraction cracked, which is a function of position This leads to a constituitive relation for microcracking,

$$\frac{dp(x)}{dt} = g\left\{\, p(x), \frac{d\delta(x)}{dt}, \text{chemistry}\right\} \tag{11}$$

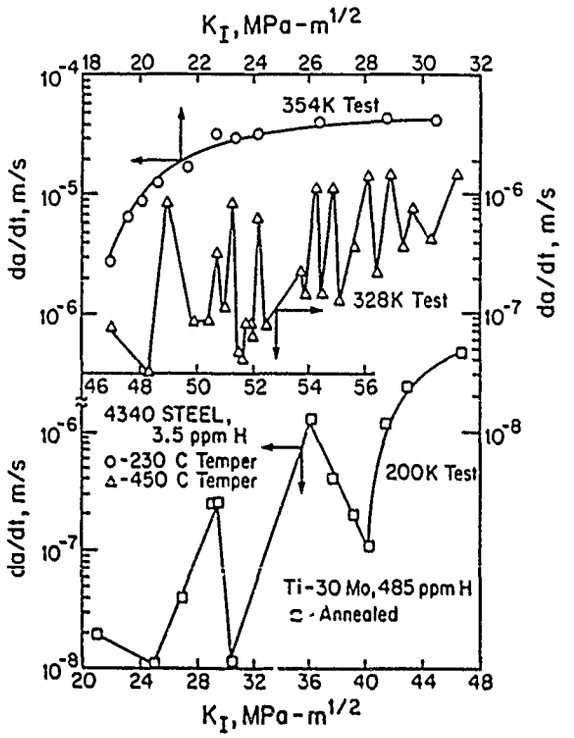


FIGURE 14—The degree of Stage II crack velocity fluctuations as affected by material condition. Process-zone sizes from top to bottom were estimated to be 10, 100, and 400 μm.

In principle, this could model crack-growth velocities, but it is difficult to include the proper interrelationships. McMeeking[24] and Tvergaard[74] have made some progress along these lines using finite-element modeling. Slightly more *ad hoc* modeling of the process zone in the context of a modified Dugdale model[29] has been applied by others.[24,45,97,103,124,125] Here, an assumption or measurement is made of the strength and size of the process zone and put into an analytical solution. Specifically, Rosenfield and Majumdar's ligament model[97] for brittle crack arrest is identical to the process-zone concepts applied to fatigue, SCC, and brittle fracture.[105 124 125] This is appropriate since both derive from the Dugdale,[29] Barenblatt,[126] and Bilby-Cottrell-Swinden[127] concepts of equilibrium. An approximate form for one such model, as given in Appendix B, leads to a reduced effective stress intensity (K_I^{eff}) given by the following.

$$K_I^{eff} \approx K_I \left[\, 1 - \frac{\Delta}{R_{P_I}} \,\right]^{1/2} \tag{12}$$

where Δ is the process-zone size and R_{P_I} is the plastic-zone size. For the type of zone modeled in Appendix B, one that is 75% of the plastic zone could reduce the effective stress intensity at the leading microcrack by a factor of two and arrest further growth. This led to complete arrest in repeated evaluations of coarse-grain Ti-30Mo,[106] since there was no evidence of a shear-lip effect, i.e., a plane-stress "ligament"; therefore, this latter restraining force was absent. This process-zone effect was also responsible for the large fluctuations in crack velocity noted in Figure 14.

Just as important may be process-zone effects on the more microscopic scale Consider a crack growing "smoothly" in the Stage II region. On a local time and size scale, there are still arrest and renucleation conditions in many material/environment combinations. Pugh[12] suggested that discontinuous cleavage arrests that result from step or ligament formation could be applied to μm-size cleavage advances in some CuZn, MgAl alloys, and in SSs. A first-order calculation, however, suggests that a generous process zone equal to the advance distance might only change the effective driving force by 0.1%. (See Appendix B.) Can a 0.1% drop in the driving force arrest a growing crack? In a continuum sense, it does not seem likely, since cracks grow in Stage II independent of the crack-driving force with large variations in the applied stress intensity. In a local sense, however, the K_I^{local} could be relatively small because of shielding dislocations, and an upset in the local picture could stabilize or destabilize the advancing crack front. A suggested experiment would be to use a very small fluctuating load on top of a "sustained" load to ascertain if the observed striation spacing is affected. Previously used[86] ΔP increments of 5% are too large to test such a hypothesis.

Film-induced cleavage. There are at least three types of film models for SCC. As earlier reviewed by Pugh,[6] film models consisted of two types. Together with the more recent proposal of Sieradzki and Newman,[14] they are summarized below:

(1) ~5-nm film → passivation film breakdown/dissolution: Champion[128] and Logan[129]
(2) ~100-nm film → tarnish film/film brittle fracture: McEvily and Bond,[130] Pugh[131]
(3) ~30-nm film → "brittle" film/substrate brittle fracture: Sieradzki and Newman[14,103]

The quotes around "brittle" signify application to oxide as well as dealloyed films. A number of papers have addressed these categories,[12,14,101,104] including several in this proceedings. It is emphasized here that there are several points of view even in similar material/environment combinations. Proponents of Faraday's second law believe that dissolution rates are adequate, while those favoring brittle-fracture mechanisms believe they are not. There is no question that cleavage occurs in a number of these systems undergoing transgranular SCC (TGSCC). Pugh[12] has reviewed these latter results and shows that discontinuous cleavage occurs in all three major crystal types: fcc, bcc, and hcp in a number of aqueous solutions. From a micromechanics view, it is important to understand how such cleavage takes place. Sieradzki[115] has produced the most quantifiable model in terms of a running crack growing into a ductile substrate. In a first order sense, this is most easily understood from Newman, et al.,[132] who give the stress corrosion crack growth rates by the following:

$$\frac{da}{dt} = (x_d + x_c)\frac{\dot{\epsilon}}{\epsilon^*} \approx \frac{x_c}{t^*} \quad ; x_c >> x_d \tag{13}$$

Here x_d and x_c are the increments of extension associated with dissolution and cleavage and t^* is the time associated with the critical strain (ϵ^*) to nucleate cleavage. This involves two points, the fact that there is a critical strain, and that the brittle-film fracture causes a

substrate cleavage (x_c) much greater than the dissolution increment. While the critical strain idea may be common to many models, the cleavage concept requires special comment.

First, there appears to be no disagreement that incoherent or coherent films may induce cleavage during SCC. What is of interest here is whether or not the brittle crack arrests at or near the interface. Sieradzki has recently reviewed possible mechanisms for crack arrest. Theoretically, he rejects the idea of ligaments, posed for macroscopic cracks, to play an important role at the micron scale.[97,125] As was discussed in the section on process zones, the authors tend to agree, but additional evidence is needed. Most attractive to date is the kinetic-energy argument, which implies that 30-nm film cracks growing at 400 m/s might grow into a ductile matrix to a depth of 2000 nm. The first question is how fast can a crack grow in a 30-nm-thick film. Consider epitaxial films with 4% elastic strains and an effective surface energy of $2J/m^2$. The Griffith crack would be on the order of 4 nm. By the time the crack emerged from the film it would be near terminal velocity, containing considerable kinetic energy. Based on the concept that a unit crack advance of one Burger's vector (**b**) required one dislocation to be emitted, or $\delta N \sim \delta l/b$, it was demonstrated that the velocity (v_c)—penetration (δl) profile could be calculated. This was done in terms of the Raleigh wave velocity (v_R) and the initial crack size (l_o). With $v_c \ll v_R$, one can approximate Sieradzki's analysis to show that the total incremental extension to arrest is

$$\delta l \Big|_{arrest} \approx \frac{l_o}{2[1 + \Gamma]} \left[\frac{Vc}{V_R}\right]^2 \qquad (14)$$

Here, Γ equals $\frac{\mu b}{4\pi\gamma}$ *ln* (r/r_o), with γ the surface energy and the rest of the term as associated with a dislocation energy. Reasonable values of $\Gamma \sim 3$ give additional increments of crack extension to range from about 1 to 6 μm for an initial 1000-μm-long crack growing with starting velocities of 300 to 700 m/s. This agrees with calculations by Sieradzki.[115] The problem arises when applying this to small cracks. If the crack starts out from a 30-nm brittle film, then it is initially 30 nm in length on a smooth sample. Following the above calculation, it would jump into the substrate less than 1 nm, much less than dissolution rates. Note that since v_c is always less than the Raleigh wave velocity for such problems, the additional crack increment can be no greater than its original size. The same conclusion is reached if some function for the stress distribution in an epitaxial film is used to analyze energy released into substrate crack extension Again, it was found that the added extension δl is some fraction of the original crack length. This is qualitatively consistent with Broek, who notes that the smaller the initial crack size, the smaller the additional crack growth will be prior to arrest.[133]

There also appears to be some controversy regarding the experimental observations.[104,113,134,136] In a recent study of dealloying, Fritz, Parks, and Pickering[136] showed that Cu 18%Au dealloyed to a depth of about 50 μm did produce 50-μm-size cleavage cracks upon subsequent bending. However, these cracks could not have propagated more than 0.5 μm into the ductile substrate. Here δl would be much less than l_o. On the other hand, Cassagne, et al.,[134,135] reported that Cu-25%Au produced cracks that ran 5 μm beyond the dealloyed layer.

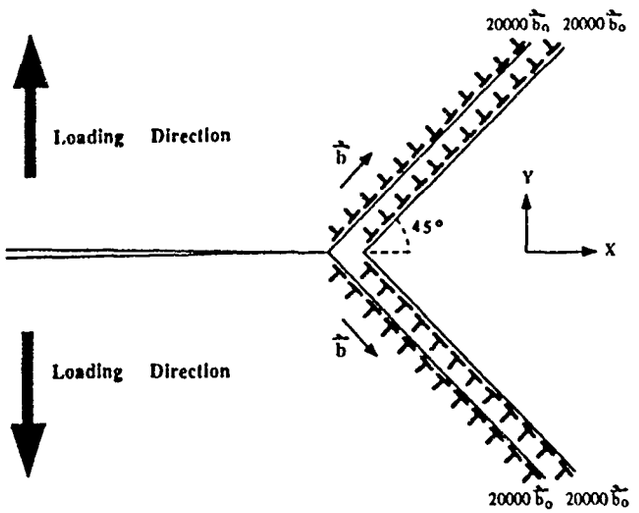
The authors of this paper do not reject the idea of film induced substrate cleavage but do suggest that a 30-nm film generating a 2000-nm substrate crack would be overstating the effect for small cracks. Additional theoretical and experimental work needs to be accomplished, since the most recent experiments imply that neither dissolution models nor the film-induced cleavage models alone account for the observed phenomena. For example, there is a real need for detailed, high-gain, acoustic-emission evaluations on single crystals with oxide or dealloyed films.

Dislocation shielding/antishielding. Rice and Thomson[117] originally suggested that a material such as iron is borderline ductile/brittle and that small changes in surface energy or core structure could trigger brittle fracture. During hydrogen induced slow crack growth, recent results[138] indicated that K_{IC} for cleavage of Fe-3wt%Si could be as little as 20 MPa-$m^{1/2}$ or as high as 100 MPa-$m^{1/2}$. This suggests that one or more shielding processes are accompanying subcritical cracking. One could then argue that an alternative to film-induced cleavage is a dislocation antishielding process that upsets the quasistatic equilibrium. This could periodically reform during subcritical crack growth in both ductile and brittle materials. In borderline materials, however, there is a good probability of this leading to total fracture.

Crack-tip stability criteria have been discussed by Lin and Thompson[118] in terms of dislocation emission from a crack tip. For a crack approaching an opposite sign source, dislocations emitted would form dipoles. This would subsequently cause hardening with regard to further emission, and the cleavage criterion would become favorable. They suggested that the crack could oscillate intermittently between emission and cleavage because of such antishielding and shielding influences. The authors agree on this general hypothesis, but the idea of emission being blocked by an opposite sign dislocation source is probably the exception rather than the rule. In most materials of interest, the cracks are not automatically sharp, so there are many emission planes that could be chosen to bypass an external source. Even at 20 MPa-$m^{1/2}$ in iron, the crack-tip opening displacement is on the order of 5 μm. With regard to blunting cracks, Sinclair[122] has shown that the effect on the dislocation emission criterion is almost unaffected. Thus, emission from many planes along the crack flank might be expected.

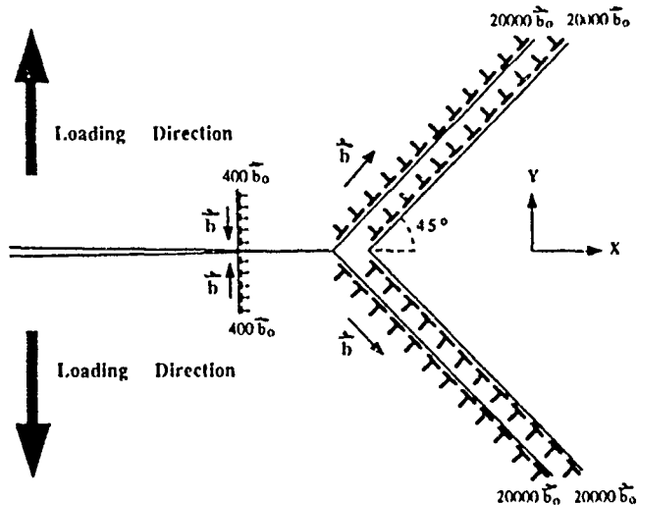
Observation of antishielding dislocations have been made by Narita, et al.,[119] and Ohr.[120] In SS foils, Ohr estimated that such dislocations decreased the effective shielding by 15%.[120] In such marginally stable materials as iron, a similar increase in the local driving force could trigger cleavage. As an added note, Ohr suggested that brittle fracture can be induced by crack-tip deformation producing antishields that reach the vicinity of the crack tip.[120] In addition, Narita, et al.,[119] found that the large shielding effect of 0.39 MPa-$m^{1/2}$ expected in NaCl at 77°K did not result. Because of antishielding dislocations, only 0.056 MPa-$m^{1/2}$ was achieved, a factor of seven difference. This would offer only marginal stability to such a brittle material. If such a mechanism is viable, it is important to consider the frequency of shielding/antishielding. Theoretical modeling of single-crystal deformation suggests that some slip patterns cannot be accomplished by crack-tip emission.[13] This requires a large number of external sources, which could result in antishielding. On the other hand, in silicon, Brede and Haasen[123] suggest that the only way to produce the necessary dislocations for the brittle-to-ductile transition is at the crack tip, contrary to other hypotheses.[121,137]

As this relatively new concept appears to be in a state of flux, the authors of this paper decided to add yet another version based partly upon observations in Fe-3wt%Si. With sustained load cracking in hydrogen, slip steps were observed emerging in the wake behind the advancing crack tip.[42] It was surmised that these were antishielding dislocations from external sources, since they were moving on an entirely different slip system in the direction of the crack tip. Using an approach suggested by the super dislocation model of Atkinson and Clements,[119] it had already been demonstrated that the stress tensor for an elastic-plastic field could be determined.[140] With a shielding dislocation array of 10,000 dislocations, depicted in Figure 15(a), the σ_{yy} stresses in this anisotropic, elastic crystal are shown in Figure 15(b). Note the near zero stresses up to about 2 μm from the crack tip. This equilibrium condition was then perturbed by an antishielding array. Based upon micron size emerging slip steps, it was considered that these 400 antishielding dislocations (10% of those required to form the slip step) could easily form during a short interval of the crack at rest. This situation is depicted in Figure 15(c). These relatively few antishields produce more than a two-order magnitude shift in the local maximum stress near the crack tip [Figure 15(d)]. Note that this was a plane stress calculation and that the stress distribution in the macroscopic regime from about 10 to 10,000 μm behaves as continuum plasticity might predict with $\sigma_{yy} \sim \sigma_{ys}$. This is discussed more fully elsewhere.[140]



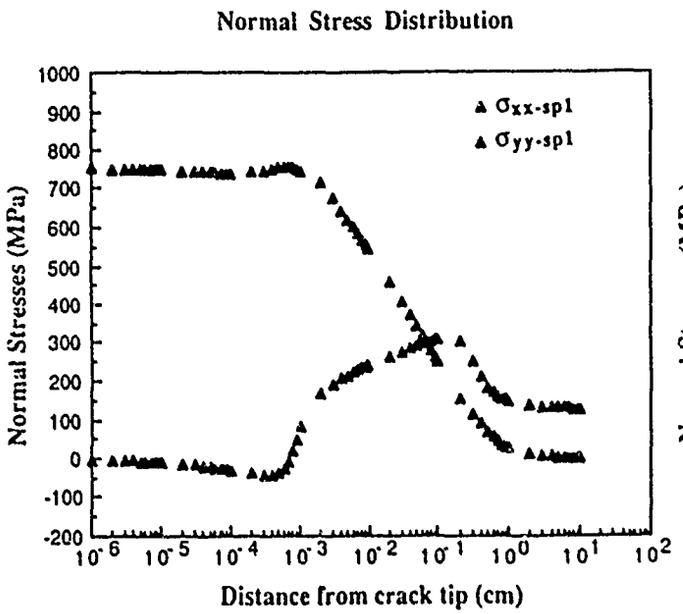
Crack Length c = 1.0 cm

a shielding array with

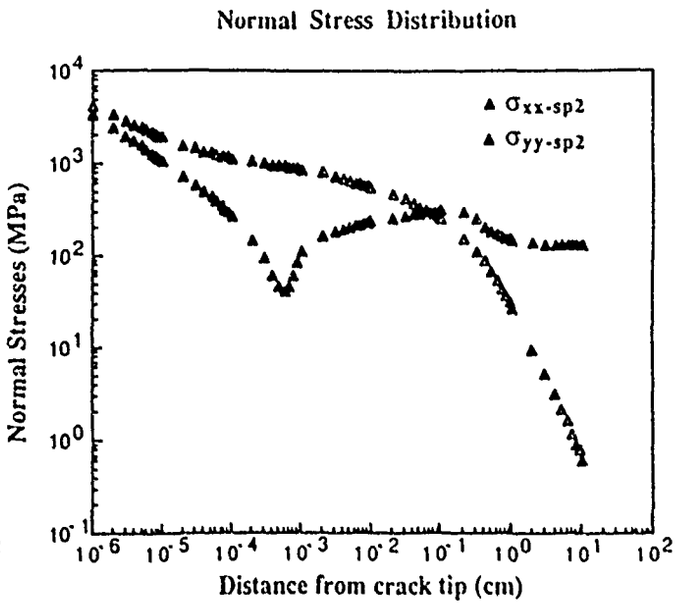


Crack Length c = 1.0 cm

c anti-shielding effect on



b normal stress distribution



d increasing the normal stress distribution

FIGURE 15—(a) and (b) The effect of shielding, and (c) and (d) subsequent antishielding on the stress distribution at a crack tip. Dislocation simulation on a Cray II supercomputer.

The remarkable result is that the theoretical stress is approached over a range of about 100 Å from the crack tip. As yet, this has not been considered in a step-wise computation, but the expectation is that the antishielding would extend with the subcritical crack until it ran into either more ductile, relatively hydrogen-free material or into a more stable dislocation situation. Thus, at least for relatively single-phase crystals, Orians' original suggestion for very large elastic stresses in the non-Hookean regime of the crack tip may be entirely consistent with the more macroscopic continuum theory. In fact, McClintock[8] originally acknowledged that such stresses might appear on a continuum scale that was about equal to the length between slip bands

Microstructural influences on the micromechanics of failure

In Table 1, the last two rows imply that different types of failure mechanisms may produce different failure modes. What is missing here is the microstructural influence. To summarize questions 10 through 15 in the introduction, one could ask how the magnitude, character, and time dependence of slip affects "brittle," subcritical crack growth. More specifically, what is the microstructural or substructural connection? Here, only a number of microstructural possibilities with regard to slip planarity[2,84,111-149] and yield stress[4,8,10,108,150-156] issues are referred to. A simple first-order model is then presented.

The planar-slip influence. Tetelman and Kunz[2] were among the first to point out the strong similarities between HE and LME. First, they pointed out that susceptibility in Fe-Si alloys increased with increasing yield stress. Second, the effect of SFE is similar, and the susceptibility increases as alloying elements are added that lower the SFE and promote planar glide. As taken from Tetelman and McEvily's book,[157] the effect of SFE on LME of Cu-base alloys, after Johnston, et al.,[158] is seen to vary the normalized fracture stress by a factor of eight (Figure 16). Later work and reviews suggested that hydrogen and/or LME was intimately connected to slip planarity,[2,46,84,157,159] slip-induced void formation,[141,142] or assisted slip-plane decohesion.[84,144] Only the slip-planarity effect is examined here.

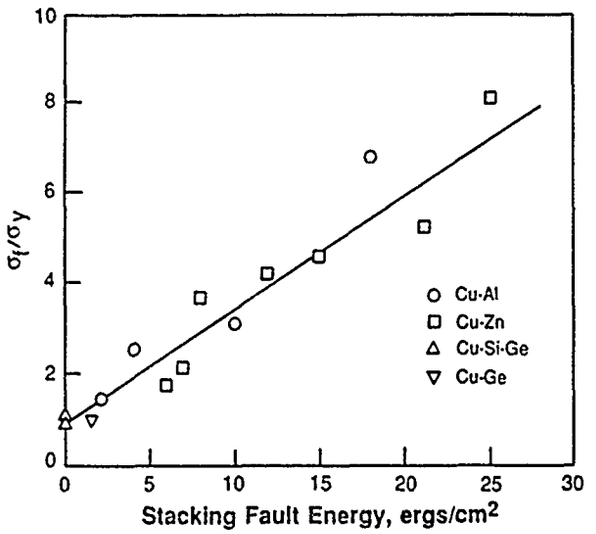


FIGURE 16—Normalized fracture stress as a function of the stacking fault energy for copper-base alloys tested in mercury. (Reprinted with permission.[157,158])

McMahon[84] reviewed much of the literature on how hydrogen affects the slip character in iron and concluded that hydrogen promotes planar slip by inhibiting the cross slip of screws. This results because screw dislocations control plastic flow. Later, Hwang and Bernstein[159] conclusively demonstrated this to be the case in hydrogen-charged Fe-Si single crystals. McMahon[84] emphasized how this might lead to strain controlled Mode II cracking, glide plane decohesion on {110} and {112} planes or {110} and {112} "quasi-cleavage" in iron and steel because of the blockage of dislocations at carbides. Still, Mode I cracking on {100} is most prevalent, and a slip planarity argument might also be valid here. In addition to BCC iron systems, there have been reviews of austenitic SSs[149] and γ'-strengthened superalloys to suggest that the hydrogen interaction with slip planarity reduces ductility. For example, in some austenitic SSs, higher nitrogen contents reduce the SFE promoting coplanar dislocation arrays and epsilon phase.[160] Whether it is the slip planarity or increased epsilon phase that then reduces ductility under 69 MPa of hydrogen exposure is not clear. In a more clear-cut observation, the effect of γ-γ' mismatch in superalloys was examined in terms of how it affected hydrogen-induced ductility loss.[149] As seen in Figure 17, the losses became large as the mismatch decreased. This was rationalized in terms of the local strain level at which particle matrix coherency is lost. With small misfits, large strains are required. This was associated with a larger amount of hydrogen at the particle matrix interface and hence larger ductility losses. However, it could just as easily be associated with a larger local strain in a slip band avalanche that could trigger fracture instability. Moody and Gerberich[148] demonstrated hydrogen induced failure at slip band intersections in an FeNiCo superalloy. With gas phase charging to 5500 appm, they showed that slip bands in charged samples were sharper than those in uncharged samples. This meant that the narrower slip bands would contain larger local strains and promote slip-band fracture.

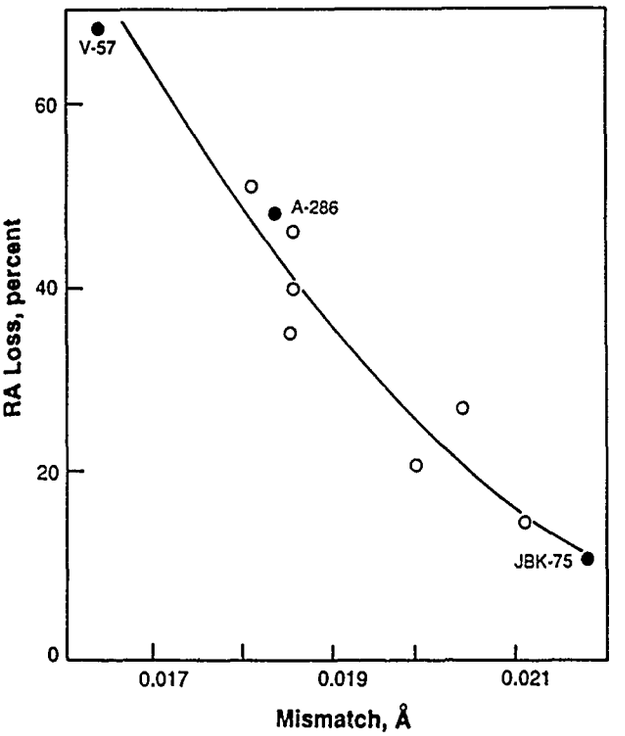


FIGURE 17—Ductility loss vs γ-γ' mismatch for several gamma prime alloys.[149]

Yield stress and residual stress implications. The more easily understood residual stress is discussed first. McClintock[8] pointed out the need to study residual stress effects, and in blunt-notch samples this has been accomplished.[34,35,154] Nakasa, et al.,[154] took a high-strength steel with a notch-root radius of ρ = 0.3 mm. They then overloaded the samples to $K_{I_{OL}}$, and then measured the time to initiate SCC (t_i) at a lower applied stress intensity of 78 MPa-m$^{1/2}$. The overload effectively puts the notch tip into residual compression. This residual compressive state is the macroscopic equivalent to dislocation shielding. A model has been generated to quantify the reduction of the local maximum stress, consistent with x-ray residual stress determinations. When combined with Equation (5), this gives the solid-line prediction in Figure 18. The important point is that this macroscopic residual compressive stress could produce an increase in delayed failure of more than an order of magnitude. Using the same residual stress model, one can show that a prior elevated-temperature overload can improve the cleavage resistance at lower temperatures. With the initial toughness being designated K_{IC_o} and the toughness after warm prestressing being K_{IC}^{WPS},

$$\frac{K_{IC}^{WPS}}{K_{IC_o}} = 1 + \beta' \left[\frac{K_{I_{OL}}}{K_{IC_o}} - 1 \right] \qquad (15)$$

where β' is 0.36. Specimens with two heat treatments of type 4340 steel were prestressed at room temperature and subsequently tested at 77°K. Observed values of K_{IC}^{WPS}/K_{IC_o} were 1.52 and 1.30 while calculated values were 1.54 and 1.35, respectively. An analogous interpretation of prior plastic overloads in silicon has been successful in predicting increases in cleavage fracture resistance.[162] Such overload effects are even more common in fatigue but have seldom been studied in SCC. In a study of environmental effects on fatigue crack growth, Katz and Bussiba[156] found strong overload effects on a U-Ti alloy tested in 80% relative humidity air. From the rate of change of the crack growth rate after the overload, it is apparent that the effect is much stronger at 1 Hz than at 30 Hz. In this case, it strongly implies that retardation in an environment is controlled largely by the sustained growth-mode phenomenon. It is suggested that overloads would have as strong a retardation effect on da/dt as they have on notched incubation times.

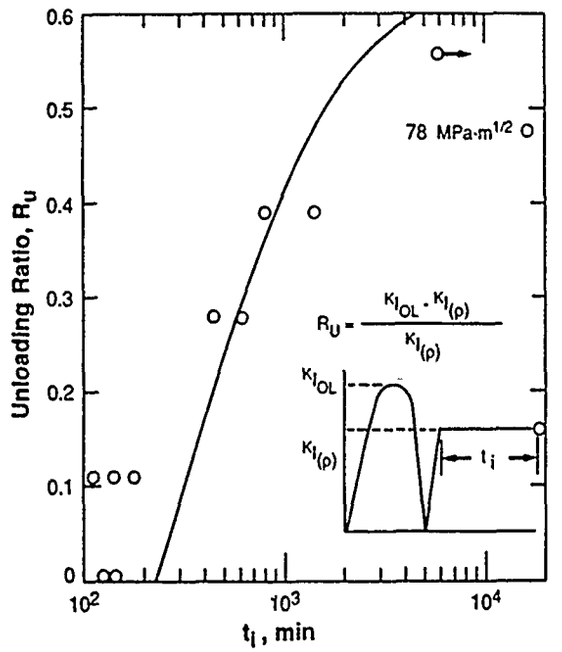


FIGURE 18—The effect of prior overloads on increasing the stress corrosion initiation times in sharply notched high-strength steels. (Data from Reference 154.)

There are other possible sources of strong crack-growth retardation besides residual compressive effects. Other types of shielding such as blunting, branching, and ligament formation cannot be discounted. For general application to a broad range of materials and microstructures, this retardation effect can be most easily understood in terms of dislocation shielding. It is important to note that a dislocation free zone is not essential, and that the only requirement is to have a net number of shielding dislocations in the vicinity of the crack tip The appealing nature of this is that it could apply to any crystalline material in a temperature regime where dislocation emission is possible. This type of model emerged when observing the startling comparison between two very different sets of data. Threshold studies have recently been reported on liquid mercury embrittlement of 7075-T651 aluminum subsequently overaged at 200°C for various times.[145] This produced hardnesses ranging from 69 to 82 R_B and $K_{I_{th}}$ values from 6 to 18 MPa·m$^{1/2}$. For the similar alloy of 7079-T651 overaged at 160°C for various times, Speidel[146] had measured SCC thresholds in saturated aqueous NaCl solutions under open-circuit potential. A similar result was obtained and in both cases the T-L orientation was evaluated. A comparison of the two types of test results is shown in Figure 19. Within experimental error, there is no difference between these two results, suggesting that the same micromechanical process is controlling threshold stress intensity.

Next, values of $K_{I_{th}}$ or $K_{I_{scc}}$ normalized on yield strength were compared to yield strength normalized on modulus. Besides keeping the aluminum correlations intact, this allowed SCC thresholds of medium- to high-strength steels[150] to be correlated. The steels, tested in 3.5 wt% NaCl aqueous solutions at room temperature, had yield strengths ranging from 700 to 1680 MPa. Normalized plots of $(K_{I_{scc}}/\sigma_{ys})^2$ vs σ_{ys}/E in Figure 20 essentially fall on the same curve. There is a *caveat* here since it is known that the SCC mechanism for such steels is HE, and a different fugacity of hydrogen through either potential change, pH, or pressure could shift the steel data up or down. Still, this comparison required further consideration.

In a macroscopic sense, this normalized plot was just the plastic-zone size at threshold vs the yield strain. This recalled the correlation in Figure 7 and Equation (2.8), which contains both plastic-zone size and yield strain. If appropriate, this means that a critical strain is associated with a critical distance at threshold. Based upon that, Appendix A shows the derivation of a simple relationship. The critical strain is related through the specific work-of-fracture ($2\gamma_{eff}$), and the critical distance (r_o) is associated with a macroscopic fracture strain (ϵ_f). As such, this is a microscopic work of fracture criterion within a continuum plasticity framework for growing cracks. This gave the following:

$$K^2_{I_{SCC}} \approx 3\pi\sigma^2_{ys} r_o \exp\left\{\frac{2E\gamma^{env}_{eff}}{\sigma^2_{ys}\,\alpha L_s \beta}\right\} \quad ;0 < \alpha \leq 1 \qquad (16)$$

With σ_{ys}, E, β, γ_{eff}, and $K_{I_{SCC}}$ known, the adjustable parameters are αL_s and r_o. As indicated in Appendix A, $0 \leq \alpha \leq 1$ implies that more planar slip materials would have a greater proportion of the plastic work directed toward fracture ($\alpha \rightarrow 1$), while materials with easy cross slip would have a smaller proportion ($\alpha \rightarrow 0$). There is also an implied slip-band length, subgrain, or grain-size effect here since L_s could be limited by a microstructural unit. This is extremely speculative and thus αL_s is treated as some microstructural fitting parameter. The other fitting parameter is the evaluation point (r_o), which is essentially the length scale over which the fracture strain is exceeded. A value in the range of 0.1 to 10 μm seems reasonable, since this encompasses the cell size, dislocation pile up, slip-band length types of scales typically observed. With the following reasonable parameters for the steels,

$\alpha L_s \sim 0.3\mu m$ $\qquad$ $E = 2 \times 10^5$ MPa
$r_o \sim 1\ \mu m$ $\qquad$ $\gamma_{eff} = 20$ J/m^2
$\qquad\qquad\qquad\quad$ $\beta = 5.46$ (plane strain)

one finds from Equation (16) that

$$ln\left[\frac{10^5 K^2_{I_{SCC}}}{\sigma^2_{ys}}\right] = \left[\frac{0.011E}{\sigma_{ys}}\right]^2 \qquad (16a)$$

This is the solid curve in Figure 20. However fortuitous this correlation is, it bears further investigation, as it would provide a common micromechanical basis for threshold stress intensities for many materials under environmental attack. While it would not apply to hydride formers, it could apply to those systems failing by cleavage or intergranular fracture. Environmental differences would affect γ_{eff} and differences between intergranular and cleavage failure would involve considerations of $\gamma_{eff}/\alpha L_s$ beyond the scope of this paper.

In summary to this last section on critical questions, it is clear that both near-crack-tip and subsurface embrittlement sites are possible because of microstructural, state-of-stress, and/or trapping effects elevating either local stress or embrittling species concentration. As to how the crack grows from these nucleation sites, recent acoustic-emission data demonstrate that discontinuous cleavage occurs on the micron scale. The growth process is not so clear for intergranular or microvoid coalescence processes. If the driving force is enhanced or diminished by thin-film, microplasticity, process-zone, or kinetic-energy phenomena, this may participate with the environmental degradation to produce initiation or arrest. Finally, microstructural features such as slip planarity and slip-band length may be combined with continuum strain distributions as a failure criterion. Such models may provide a common micromechanical basis for threshold stress intensities.

Conclusion and Recommendations

(1) Measured strain distributions for subcritical crack growth are reasonably consistent with continuum, small-scale yielding solutions. This is verified by two electron-channeling studies of hydrogen induced subcritical crack growth in Fe-Si single crystals. More information is required for fcc and hcp systems and in all materials for cracking under stress corrosion or liquid metal environments.

(2) The location and time dependency of crack nucleation from blunt notches is on reasonably firm ground for high-strength steels from both an experimental and a modeling viewpoint. While such results may give insight into lower-strength materials that blunt, they may be misleading with regard to very high-strength materials or even lower-strength ones with sharp cracks.

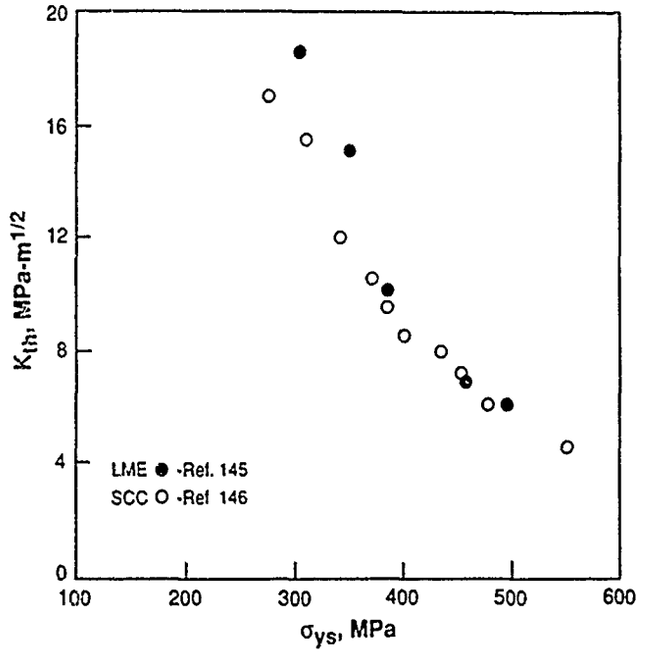


FIGURE 19—The similarity of threshold-stress-intensity variation with yield strength for LME and SCC. Two similar 7000 series aluminum alloys were aged to various strength levels.

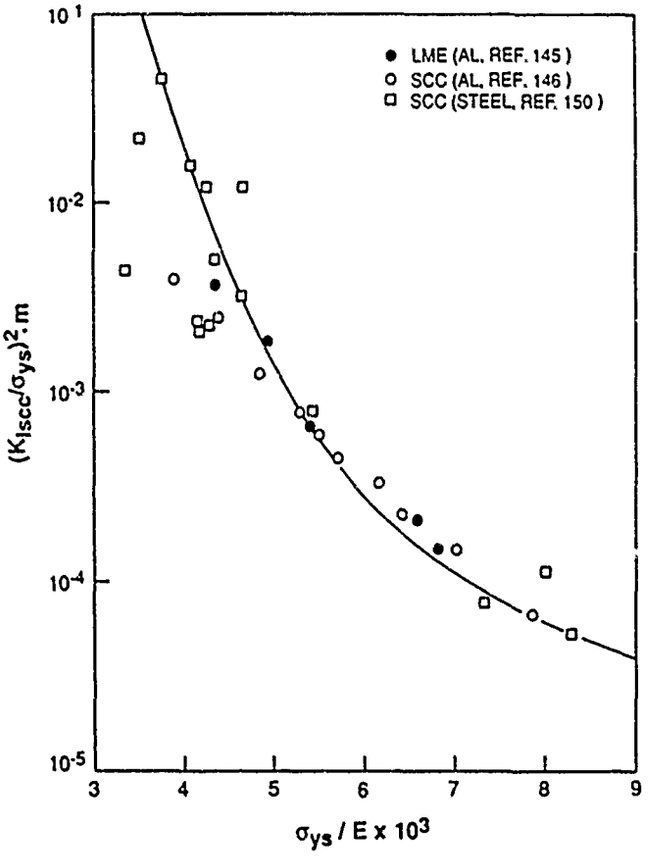


FIGURE 20—Comparison of normalized threshold (plastic zone) vs normalized yield strength (yield strain) to the theoretical model, Equation (16).

(3) In Mode I, II, and III tests, cracking favors growth on the maximum principal stress plane, even though cracking may initiate on a maximum shear plane. Additional Mode I/II or Mode I/III types of tests on all environmental cracking mechanisms are recommended with acoustic-emission or potential-drop detection of nucleation times.

(4) Other state-of-stress tests such as biaxiality or plane stress vs plane strain suggest that either a maximum stress or limited ductility criterion controls the material/environment response in materials as far ranging as Admiralty brass, nickel, and steel. Even low-strength single crystals of Fe-Si in hydrogen show a crack-front curvature state-of-stress thickness effect. The weight of the evidence favors a normal stress criterion.

(5) Embrittlement sites may range from less than 0.1 μm to as much as 1000 μm away from the crack tip. However, this still does not settle the issue of volume embrittlement vs surface or near-surface embrittlement.

(6) Recent acoustic emission and fractography of several alloy systems demonstrate that crack growth is discontinuous in both aqueous and gaseous environments. One study on Fe-Si single crystals demonstrates at least two levels of discontinuity as the whole crack front advances micron by micron on the cleavage plane. Understanding of how such discontinuities are both triggered and arrested requires additional theoretical modeling on the atomistic, dislocation, and macroscopic scales.

(7) Effects of microstructure on both the crack driving force and the resistance can be extraordinarily large, in some cases swamping more macroscopic state-of-stress effects. Process zones with discontinuous microcracks, for example, can change crack velocities by more than an order of magnitude. Computer simulations indicate that dislocation rearrangements within the near-tip region can increase the local stress by more than two orders of magnitude. *In situ* studies of bulk crystals, transmission electron microscopy studies of substructure, and additional dislocation-simulations are required for understanding.

(8) A remarkable similarity between normalized threshold and normalized yield strength for LME and SCC implies a common micromechanical basis. Addressing this or other types of models with overload effects and state-of-stress evaluations are important to separate microplasticity, dynamics, and decohesion aspects. Where possible, this should be accomplished on single crystals or specially fabricated bicrystals.

Acknowledgment

The authors would particularly like to thank a large number of their colleagues, D. Davidson, B. Flanagan, Y. Katz, N. Moody, D. Oriani, and K. Sieradzki, and several current students, X. Chen, T. Foecke, and M. Lii, for both stimulating discussion and release of information prior to publication. We would also like to acknowledge the Super-Computer Center of the University of Minnesota for use of their facilities. This work was supported by the Corrosion Center and the Department of Energy, Basic Energy Sciences, Materials Science Division, Grant DE-FG02-84ER45173 and the Division of Materials Research, National Science Foundation, Grant NSF/DMR 8400015.

References

1. R.A. Oriani, Stress Corrosion Cracking and Hydrogen Embrittlement of Iron Base Alloys, NACE-5, ed. R.W. Staehle, J. Hochmann, R. McCright, J. Slater (Houston, TX: National Association of Corrosion Engineers, 1977), p. 351.
2. A.S. Tetelman, S. Kunz, Stress Corrosion Cracking and Hydrogen Embrittlement of Iron Base Alloys, p. 359.
3. H.H. Johnson, Stress Corrosion Cracking and Hydrogen Embrittlement of Iron Base Alloys, p. 382.
4. H.G. Nelson, D.P. Williams, Stress Corrosion Cracking and Hydrogen Embrittlement of Iron Base Alloys, p. 390.
5. D.A. Vermilyea, Stress Corrosion Cracking and Hydrogen Embrittlement of Iron Base Alloys, p. 208.

6. E.N. Pugh, Stress Corrosion Cracking and Hydrogen Embrittlement of Iron Base Alloys, p. 37.
7. J.M. Krafft, H.L. Smith, Stress Corrosion Cracking and Hydrogen Embrittlement of Iron Base Alloys, p. 482.
8. F.A. McClintock, Stress Corrosion Cracking and Hydrogen Embrittlement of Iron Base Alloys, p. 455.
9. J.R. Rice, Stress Corrosion Cracking and Hydrogen Embrittlement of Iron Base Alloys, p. 11.
10. J.P. Hirth, H.H. Johnson, Corrosion 32, 1(1976): p. 3.
11 R.H. Jones, Advances in the Mechanics and Physics of Surfaces 3, ed. R. Latanision, T.E. Fischer (New York, NY: Scientific and Tech. Book Serv., 1985), p. 1.
12. E.N. Pugh, Corrosion 41, 9(1985): p. 517.
13. J.R. Rice, Chemistry and Physics of Fracture, ed. R.M. Latanision, R.H. Jones (Boston, MA: Martinus Nijhoff Publishers, 1987), p. 23.
14. K. Sieradzki, R.C. Newman, Philos. Mag. 51(1985): p. 95.
15. R. Dean, J.W. Hutchinson, Fracture Mechanics: 12th Conference, ASTM STP 700 (Philadelphia, PA: American Society for Testing Materials, 1980), p. 383.
16. Y.-C. Gao, K.-C. Hwang, Advances in Fracture Res., vol. 2, D. Francois (New York, NY: Pergamon Press, 1981), p. 669.
17. J.R. Rice, W.J. Drugan, T.-L. Sham, Fracture Mechanics: 12th Conference, p. 189.
18. W.J. Drugan, J.R. Rice, T.-L. Sham, J. Mech. Phys. Solids 30 (1982): p. 447.
19. A. Needleman, V. Tvergaard, Elastic Plastic Fracture Mechanics, ASTM STP 803, 1 (Philadelphia, PA. ASTM, 1983), p. 80.
20. P.S. Lam, R.M. McMeeking, J. Mech. Phys. Solids 32(1984): p. 395.
21. R.M. McMeeking, Chemistry and Physics of Fracture, p. 91.
22. J.R. Rice, M.A. Johnson, Inelastic Behavior of Solids, ed. M. F. Kanninen, et al. (New York, NY: McGraw-Hill, 1970), p. 641.
23. R.M. McMeeking, J. Mech. Phys. Solids, 25(1977). p. 357.
24. R.M. McMeeking, D.M. Parks, Elastic-Plastic Fracture, ASTM STP 668 (Philadelphia, PA: ASTM, 1979), p. 175.
25. V. Tvergaard, Int. J. Solids Structures 18(1982). p. 659.
26. R.D. Pendse, R.O. Ritchie, Modeling Environmental Effects on Crack Growth Processes, ed. R.H. Jones, W.W. Gerberich (Warrendale, PA: The Metallurgical Society of the American Institute of Mining, Metallurgical, and Petroleum Engineers, 1986), p. 321.
27. H. Kitigawa, Y. Kojima, Atomistics of Fracture, ed. R.M. Latanision, J.R. Pickens (New York, NY: Plenum Press, 1983), p. 799.
28. W.W. Gerberich, D.L. Davidson, M. Kaczorowski, J. Mech. Phys. Solids, in press 1989.
29. D.S. Dugdale, J. Mech. Phys. Solids 8(1960): p. 100.
30. J.W. Hutchinson, Private Communication, 1987.
31. D.L. Davidson, J. Lankford, Intern. J. of Fract. 17(1981): p. 257.
32 M. Kaczorowski, C.-S. Lee, W.W. Gerberich, Mater. Sci. and Eng. 81(1986): p. 305.
33. P. Doig, G.T. Jones, Environment-Sensitive Fracture of Engineering Material, ed. Z. Foroulis (Warrendale, PA, TMS-AIME, 1979), p. 446.
34. Y. Hirose, T. Mura, Eng. Fract. Mechan. 19(1984): p. 317.
35 R.A. Page, W.W. Gerberich, Metall. Trans. A 13A(1982). p. 305.
36. W.W. Gerberich, Y.T. Chen, Metall. Trans. A 6A(1975): p. 271.
37 R A. Page (Master's Thesis, University of Minnesota, 1976).
38 D R Baer, R.H. Jones, Chemistry and Physics of Fracture, p. 552.
39 W W Gerberich, A.G. Wright, Env. Degradation of Eng. Mater. Hyd. (Blacksburg, VA: Virginia Tech. Printing Dept., 1981), p. 183.
40. H. Vehoff, W. Rothe, Acta Metall. 31(1983): p. 1781.
41. H. Vehoff, P. Neumann, Hydrogen Degradation of Ferrous Alloys, R.A. Oriani, et al. (Park Ridge, NJ: Noyes Pub., 1985), p. 686.
42. X. Chen, J.A. Kozubowski, W.W. Gerberich, Scripta Metall. 22(1988): p. 245.
43. A.H. Cottrell, Trans. AIME 212(1958): p. 192.
44. N.J. Petch, Fracture, ed. B.L. Averbach, et al., MIT (New York, NY: J. Wiley, 1959), p. 54.
45. E. Smith, Res Mechanica 4(1982): p. 151.
46. J.K. Tien, S.V. Nair, R.C. Bates, in Env. Degradation Eng. Mater. Hyd., p. 147.
47. B.J. Shaw, E.W. Johnson, Hydrogen in Metals, ed. I.M. Bernstein, A.W. Thompson (Warrendale, PA. TMS-AIME, 1981), p. 691.
48. M.R. Louthan Jr., R.D. Sisson Jr., R.P. McNitt, P.E. Smith, Hydrogen in Metals, p. 829.
49. A.W. Thompson, I.M. Bernstein, Hydrogen in Metals, p. 291.
50. M.W. Joosten, T.D. Lee, J. Goldenberg, J.P. Hirth, Hydrogen in Metals, p. 839.
51. R.L. Schulte, P.N. Adler, N.E. Paton, Hydrogen in Metals, p. 176.
52. R.E. Swanson, A.W. Thompson, I.M. Bernstein, J.L. Maloney III, Hydrogen in Metals, pp. 459-466.
53. W.W. Gerberich, N.R. Moody, C.L. Jensen, C. Hayman, K. Jatavallabhula, Hydrogen in Metals, p. 731.
54. A.W. Thompson, I.M. Bernstein, Environ. Sensitive Fracture: Evaluation and Comparison of Test Methods, ASTM STP 821, ed. S.W. Dean, E.N. Pugh, G.M. Ugiansky (Philadelphia, PA: ASTM, 1984), p. 114.
55. W.K. Blanchard, D.A. Koss, L.A. Heldt, Corrosion 40, 3(1984). p. 104.
56. W.K. Blanchard Jr., D.A. Koss, L.A. Heldt, Metall. Trans. A 15A (1984): p. 1281.
57 N.R. Moody, M.W. Perra, S.L. Robinson, to appear in Scripta Metall.
58. L.-J. Qiao, W.-Y. Chu, C.-M. Hsiao, Scripta Metall. 21(1987). p. 7.
59. S.L. Kampe, D.A. Koss, Acta Metall. 34(1986): p. 55.
60. H.J. Maier, W. Popp, H. Kaesche, Acta Metall. 35(1987). p. 875.
61. W.-Y. Chu, T.-Y. Zhang, C.-M. Hsiao, Corrosion 40, 4 (1984). p. 197.
62. M. Takemoto, Corrosion 40, 4(1986): p. 585.
63. R.F. McGuinn, M. Aballe, Br. Corrosion J. 17, 1(1982): p. 18.
64. R. Magdowski, W.W. Gerberich, Scripta Metall. 17(1983). p. 421.
65. T.-Y. Zhang, W.-Y. Chu, R.-Y. Ma, C.-M. Hsiao, Corrosion 43, 2(1987): p. 70.
66. C. St. John, W.W. Gerberich, Metall. Trans. 4(1973): p. 589.
67. A.R. Troiano, Trans. ASM 52(1986): p. 54.
68. J.C.M. Li, R.A. Oriani, L.S. Darken, Z. Physik Chem. 49(1966). p. 271.
69. J.P. Hirth, Hydrogen Degradation of Ferrous Alloys, p. 131.
70. W.W. Gerberich, T. Livne, X.-F. Chen, M. Kaczorowski, Metall. Trans. A 19A(1988): p. 1319.
71 J.A.S. Green, H.W. Hayden, W.S. Montagne, Effects of Hydrogen on Behavior of Materials, ed. A.W. Thompson, I.M. Bernstein (New York, NY: TMS-AIME 1976), p. 200.
72 J.A. Kapp, Embrittlement by Liquid and Solid Metals, ed. M.H. Kamdar (Warrendale, PA: TMS-AIME, 1987), p. 117.
73. D.P. Clausing, Intern. J. Frac. Mech. 6(1970): p. 71.
74. B.F. Brown, SCC in High Strength Steels and in Titanium and Aluminum Alloys, ed. B.F. Brown (Washington, DC: Naval Research Laboratory, 1972).
75. W.W. Gerberich, Y.T. Chen, C. St. John, Metall. Trans. A 6A (1975): p. 1485.
76. W.-Y. Chu, C.-M. Hsiao, S.-Q. Li, Scripta Metall. 13(1979): p. 1063.
77. W.-Y. Chu, S.-Q. Li, C.-M. Hsiao, J.-Z. Tien, Corrosion 36, 12(1980): p. 475.
78. H. Vehoff, H.-K. Klameth, Acta Metall. 33(1985): p. 955.

79. D.H. Lassila, H.K. Birnbaum, Modeling Environmental Effects on Crack Growth Processes, ed. R.H. Jones, W.W. Gerberich (Warrendale, PA: TMS-AIME, 1986), p. 259.
80. C.-M. Hsiao, W.-Y. Chu, Hydrogen Effects in Metals, ed. I.M. Bernstein, A.W. Thompson (Warrendale, PA: TMS-AIME, 1981), p. 291.
81. M. Elices, V. Sanchez, I. Bernstein, A. Thompson, J. Pinero, Hydrogen Effects in Metals, p. 972.
82. H. Cialone, R.J. Asaro, Hydrogen Effects in Metals, p. 767.
83. R.P. Wei, Hydrogen Effects in Metals, p. 577.
84. C.J. McMahon Jr., Hydrogen Effects in Metals, p. 219.
85. P.W. Slattery, J. Smit, E.N. Pugh, Environment-Sensitive Fracture: Evaluation and Comparison of Test Methods, p. 399.
86. D.V. Beggs, M.T. Hahn, E N. Pugh, A.R. Troiano Honorary Symposium on Hydrogen Emb. and SCC (Metals Park, OH: ASM, 1984), p. 181.
87. M.B. Hintz, W.K. Blanchard, P.K. Brindley, L.A. Heldt, Metall. Trans. A 17A(1986): p. 1081.
88. R P. Gangloff, R.P. Wei, Fractography in Failure Analysis, ASTM STP 645, M.B. Strauss, W.H. Cullen Jr. (Philadelphia, PA: ASTM, 1978), p. 87.
89. M. Iino, Eng. Fract. Mech. 10(1978): p. 1.
90 M. Gao, M Lu, R.P. Wei, Metall. Trans. A 15A(1984). p. 735.
91. R.P. Gangloff, R.P. Wei, Metall. Trans. A 8A(1977): p. 1043.
92. R Padmanabhan, W.E. Wood, Metall. Trans. A 14A(1983). p. 2357.
93. R. Padmanabhan, N. Suriyayothin, W.E. Wood, Metall. Trans. A 14A(1983): p. 2357.
94. G. Green, Metal Science, 15(1981): p. 505.
95. F.W Fraser, E.A. Metzbower, Fractography and Materials Science, ASTM STP 733, L.N. Gilbertson, R.D. Zipp (Philadelphia, PA: ASTM, 1981), p. 51.
96. A.S. Tetelman, T.L. Johnston, Philos. Mag. 11(1965): p. 389.
97. A.R. Rosenfield, B.S. Majumdar, Metall. Trans. A 18A(1987): p. 1053.
98. N.R. Moody, R.E. Stoltz, M.W. Perra, Scripta Metall. 20(1985): p. 119.
99. R.A. Jones, D.R. Baer, Scripta Metall. 20(1987): p. 927.
100. S.P. Lynch, Scripta Metall. 20(1986): p. 1067.
101. P. Neumann, Chemistry and Physics of Fracture, p. 3.
102. J.P. Hirth, Chemistry and Physics of Fracture, p. 538.
103. R.C. Newman, K. Sieradzki, Chemistry and Physics of Fracture, p. 597.
104. T.B. Cassagne, W.F. Flanagan, B.D. Lichter, Chemistry and Physics of Fracture, p. 659.
105. W.W. Gerberich, Chemistry and Physics of Fracture, p. 419.
106. K.A. Peterson (Ph.D. Diss., University of Minnesota, 1983).
107. G.A. Welch (Ph.D. Diss., Ohio State University, 1978).
108. R.H. Jones, M.T. Thomas, D.R. Baer, Metall. Trans. A 16A (1985): p. 123.
109. W.W. Gerberich, C.E Hartbower, Fundamental Aspects of Stress Corrosion Cracking, ed. R. Staehle (Houston, TX. NACE, 1969), p. 420.
110. D.G. Chakrapani, E.N. Pugh, Metall. Trans. A 6A(1975): p. 1155.
111. J.A. Beavers, E.N. Pugh, Metall. Trans. A 11A(1980): p. 809.
112. R.H. Jones, M.A. Friesal, W.W. Gerberich, Acoustic Emission from Intergranular Subcritical Crack Growth, to be published in Metall. Trans. A 1989.
113. K. Sieradzki, R.L. Sabatini, R.C. Newman, Metall. Trans. A 15A (1984): p. 1941.
114. X.F. Chen, W.W. Gerberich, Scripta Metall. 22(1988): p. 1499.
115. K. Sieradzki, Chemistry and Physics of Fracture, p. 219.
116. H. Stenzel, H. Vehoff, P. Neumann, Modeling Environmental Effects on Crack Growth Processes, p. 225.
117. J. F. Newman, Environ. Sensitive Fract. of Eng. Mater., ed. Z. Foroulis (Warrendale, PA: TMS-AIME, 1979), p. 19.
118. J.H. Lin, R. Thomson, Scripta Metall. 20(1986). p. 1367.
119. N. Narita, K. Higashida, S. Kitano, Scripta Metall. 21(1987): p. 1273.
120. S.M. Ohr, Scripta Metall. 21(1987): p. 1681.
121. J.H. Lin, R. Thomson, Acta Metall. 34(1986): p. 187.
122. J.E. Sinclair, Computer Simulation in Physical Metallurgy ECSC, EEC, EAEC, Brussels, Belgium, and Luxembourg, Luxembourg (1986), p. 159.
123. M. Brede, P. Haasen, Chemistry and Physics of Fracture, p. 449.
124. W.W. Gerberich, N.R. Moody, Fatigue Mechanisms, ed. J. Fong (Philadelphia, PA: ASTM, 1979), p. 292.
125. W.W. Gerberich, S.-H. Chen, C.-S. Lee, T. Livne, Metall. Trans. A 18A(1987): p. 1861.
126. G.I. Barenblatt, Advances in Applied Mechanics, 7(1962). p. 55.
127. B.A. Bilby, A.H. Cottrell, K.H. Swinden, Proceedings Royal Society of London, A285(1965), p. 131.
128. F. A. Champion, Symp. on Intern. Stresses in Metals and Alloys, held in London, England (1948), p. 468.
129. H.L. Logan, J. Res. Natl. Bur. Stds. 48(1952): p. 99.
130. A.J. McEvily Jr., A.P. Bond, J. Electrochem. Soc. 112(1965). p. 131.
131. E.N. Pugh, The Theory of Stress Corrosion Cracking in Alloys (NATO, 1971), p. 448.
132. R.C. Newman, J.S. Kim, K. Sieradzki, Modeling Environmental Effects on Crack Growth Processes, p. 199.
133. D. Broek, Elementary Engineering Fracture Mechanics, 3d ed. (Boston, MA: Martinus Nijhoff, 1982), p. 155.
134. R.C. Newman, K. Sieradzki, Scripta Metall. 17(1983). p. 621.
135. T.B. Cassagne, W.F. Flanagan, B.D. Lichter, Metall. Trans. A 17A(1986): p. 703.
136. J.D. Fritz, B.W. Parks, H.W. Pickering, Scripta Metall. 22(1988). p. 1063.
137. J.R. Rice, R. Thomson, Philos. Mag. 29(1974): p. 73.
138. X.-F. Chen, Y. Katz, W.W. Gerberich, unpublished results.
139. C. Atkinson, D.L. Clements, Acta Metall. 21(1973): p. 5.
140. M. Lii, W.W. Gerberich, unpublished results.
141. S.P. Lynch, Environ.-Sensitive Frac. of Eng. Mater., p. 201.
142. S.P. Lynch, Environ. Degradation of Eng. Mater. Hyd. p. 229.
143. J. Eastman, T. Matsumoto, N. Narita, F. Heubaum, H.K. Birnbaum, Hydrogen in Metals, p. 397.
144. A.S. Argon, Chemistry and Physics of Fracture, p. 3.
145. D.A Wheeler, R.G. Hoagland, J.P. Hirth, Scripta Metall. 22 (1988): p. 533.
146. M.O. Speidel, The Theory of Stress Corrosion Cracking in Alloys, ed. J.C. Scully, NATO (Brussels, Belgium: 1971), p. 289.
147. M. Hashimoto, R.M. Latanision, Chemistry and Physics of Fracture, p. 505.
148. N.R. Moody, F. Greulich, Sandia Report SAND 85-8708 (1985).
149. G.R. Caskey Jr., Hydrogen Degradation of Ferrous Alloys, R. A. Oriani, et al. (Park Ridge, NJ. Noyes Pub., 1985), p. 822.
150. R. Kerr, F. Solana, ed. I.M. Bernstein, A.W. Thompson, Metall. Trans. A 18A(1987): p. 1011.
151. J.-G. Park, A.W. Thompson, Scripta Metall. 19(1985): p. 953.
152. Y.-B. Wang, W.-Y. Chu, C.-M. Hsiao, Scripta Metall. 19(1985): p. 1161.
153. H. Kimura, H. Matsui, Scripta Metall. 21(1987): p. 319.
154. K. Nakasa, M. Kido, H. Takei, Trans. ISIJ 22(1982): p. 106.
155. Y Katz, A. Bussiba, H. Mathias, Fatigue at Low Temperatures, ASTM STP 857, ed. R.I. Stephens (Philadelphia, PA: ASTM, 1985), p. 191.
156. Y. Katz, A. Bussiba, Environmental Effects On Cyclic Crack Extension, III, ECF 6, ed. H.C. Van Elst, A. Bakker (United Kingdom: UMAS, 1986), p. 1677.
157. A.S. Tetelman, A.J. McEvily Jr., Fracture of Structural Materials (New York, NY: J. Wiley and Sons, 1967).
158. T.L. Johnston, R.G. Davies, N.S. Stoloff, Philos. Mag. 12 (1965): p. 305.
159. C. Hwang, I.M. Bernstein, Acta Metall. 34(1986): p. 1001.

160. R.E. Stoltz, J.B. VanderSande, Metall. Trans. A 11A(1980). p. 1033.
161. W.W. Gerberich, T. Foecke, Y. Katz, unpublished data.
162. W.W. Gerberich, Fracture and Interactions Of Microstructure, Mechanisms and Mechanics, ed. J.M. Wells, J.D. Landes (Warrendale, PA: TMS-AIME, 1985), p. 49.

Appendix A: A Cottrell-Type Threshold Stress Intensity Model for Environment-Induced Cracking

Consider a semi-infinite crack in a body under plane-strain conditions. The plastic strain distribution for an elastic, perfectly plastic material is given by Equation (2.7) in Table 2. The plastic-zone size (R_{p_i}) is given by Equation (1.2). Let the plastic strain (ϵ_p) achieve the fracture strain to trigger environmental cracking (ϵ_f^{envr}) over a characteristic distance, $r = r_o$. With Equations (1 2) and (2.7), this gives a failure criterion at threshold, viz.,

$$K_{Iscc}^2 = 3\pi\sigma_{ys}^2 r_o \exp\left[\frac{E\epsilon_f^{envr}}{\beta\sigma_{ys}}\right] \qquad (A.1)$$

In a local sense, the fracture strain may be interpreted in terms of the work-of-fracture associated with subcritical cracking over the characteristic distance (r_o). With the work-of-fracture, mostly plastic deformation over a slip distance (L_s), this becomes

$$\alpha L_s \int_0^{\epsilon_f^{envr}} \sigma_{ys}\, d\epsilon = 2\gamma_{eff}^{envr} \;; 0 < \alpha \leq 1 \qquad (A.2)$$

with α some proportionality constant reflecting the fact that not all of the absorbed energy goes into resisting subcritial crack growth. Upon integration this gives

$$\epsilon_f^{envr} = \frac{2\gamma_{eff}^{envr}}{\alpha L_s \sigma_{ys}} \qquad (A.3)$$

Within the slip band, if there is concentrated planar slip, then the fracture strain may be relatively low, i. e., $\alpha \rightarrow 1$. On the other hand, for high SFE materials, cross slip and multiple slip could easily allow for a spreading of slip with large fracture strains, i.e., $\alpha \rightarrow 0$. An alternative way of viewing this is that slip-band triggering of crack growth is more difficult in high SFE materials. This would be in keeping with the observations on LME, where an increase in γ_{SFE} provided an increase in fracture resistance.[158] Combining Equations (A.1) and (A.3) gives

$$K_{Iscc}^2 \approx 3\pi\sigma_{ys}^2 r_o \exp\left\{\frac{2E\gamma_{eff}^{envr}}{\sigma_{ys}^2 \alpha L_s \beta}\right\} \;; 0 < \alpha \leq 1 \qquad (A.4)$$

which is Equation (16) in the text.

It was desirable to confirm whether or not Equation (A.4) could be a first-order model. There was some evidence on Fe-3wt%Si single crystals that, although incomplete, provided some physical reality. From Figure 7, there was confirmation that the plastic strain modeling was appropriate for hydrogen-induced growth in Fe-Si. Also, from fractography and acoustic emission, a characteristic distance of $r_o \sim 1$ μm was reasonable. For this single crystal with a high strain-hardening exponent, $n = 0.38$, the appropriate strain distribution for plane-strain threshold is Equation (2.9). With Equations (A.1) and (A.3), this gives

$$K_{I_{th}}^2 = 3\pi\sigma_{ys}^2 r_o \exp\left\{\left[\frac{2E\gamma_{eff}^{envr}}{\sigma_{ys}^2 \alpha L_s \beta'}\right]^{1-n}\right\} \qquad (A.5)$$

which is the square of the HE threshold. Recognizing that $2\gamma_{eff}^{envr}/\alpha = K_{I_{th}}^2(1-\nu^2)/E$, recasts Equation (A.5) into

$$K_{I_{th}}^2 = 3\pi\sigma_{ys}^2 r_o \exp\left\{\left[\frac{K_{I_{th}}^2(1-\nu^2)}{\beta'\sigma_{ys}^2 L_s}\right]^{1-n}\right\} \qquad (A.6)$$

which is Equation (6) in the text. Some observations on hydrogen affected slip morphologies in Fe and Fe-Si have been made by Hwang and Bernstein[159] and Kaczorowski, et al.[32] In Fe under monotonic loading, localized slip bands ~ 1 μm apart and slip-band lengths of at least 20 μm are shown.[159] It is suggested that hydrogen reduces the γ_{SFE} of bcc iron to enhance planar slip. In Fe-3wt%Si under fatigue loading in hydrogen, slip bands on the order of 10 to 100 μm in length and about 3 μm apart have been observed.[32] Thus, a value of $L_s \sim 30$ μm with $r_o = 1$ μm is used to calculate $K_{I_{th}} = 16.4$ MPa-m$^{1/2}$. This value compares to thresholds of 18 ± 3 MPa-m$^{1/2}$ observed in six determinations.[138] From the above definition of $2\gamma_{eff}^{envr}/\alpha$ and Equation (A.3), it follows that

$$\epsilon_f^{envr} = \frac{K_{I_{th}}^2(1-\nu^2)}{E\sigma_{ys}L_s} \qquad (A.7)$$

with the above values, this gives $\epsilon_f^{envr} = 0.21$. Although all of the calculated and input parameters are reasonable, a more precise interpretation of the physical process is required. One such interpretation[140] is given in the section on dislocation shielding/antishielding.

Appendix B

A previously used equation for ligament or process-zone models is given by Equation (A-1) of Rosenfield and Majumdar[97] or Equation (5) of Gerberich[162] to be

$$\pi\sigma - 2\sigma_\Delta \cos^{-1}\left\{\frac{C}{C+\Delta+R_{P_I}^{off}}\right\} - 2(\sigma_{ys}-\sigma_\Delta)\cos^{-1}\left\{\frac{C+\Delta}{C+\Delta+R_{P_I}^{off}}\right\} = 0 \qquad (B.1)$$

Here σ is the applied stress in an infinite plate containing a crack of 2C with a process zone (Δ) and an effective plastic zone ($R_{P_I}^{off}$) at the end of each crack tip. It is an elastic, perfectly plastic material with a yield strength (σ_{ys}) and a process-zone strength (σ_Δ). For simplification, the very approximate assumption is made that there are 50% ligaments (50% microcracks) in the process zone and that these have strain hardened to twice the yield strength. Clearly, this is not possible for a perfectly plastic material, but all that is desired here is an order of magnitude estimate. This is not physically unrealistic in low-yield-strength materials and leads to $\sigma_\Delta \sim \sigma_{ys}$, eliminating the last term from Equation (B.1). But the Dugdale model gives

$$\pi\sigma - 2\sigma_{ys}\cos^{-1}\left\{\frac{C}{C+R_{P_I}}\right\} = 0 \qquad (B.2)$$

By inspection, one sees that $C + \Delta + R_{P_I}^{off} = C + R_{P_I}$, as it should be for the strength of the process zone being equal to the yield strength. This leads to

$$\frac{R_{P_I}^{off}}{R_{P_I}} \approx 1 - \frac{\Delta}{R_{P_I}} \qquad (B.3)$$

which, on recognizing that $K_I \propto R_{P_I}^{1/2}$, gives

$$\frac{K_I^{off}}{K_I} \approx \left[1 - \frac{\Delta}{r_{P_I}}\right]^{1/2} \qquad (B.4)$$

This is Equation (12) in the main body. Applying this to an alloy single crystal of copper or iron with a yield strength of 200 MPa, an applied stress of 100 MPa and a crack length of 0.02 m, the plastic-zone size would be about 3000 μm. With a crack advance of about 5 μ, assume that a process zone equal to this could be maintained as the crack grew. With $\Delta = 5$ μ, Equation (A-4), gives $K_I^{off}/K_I = 0.999$.

Discussion

K. Sieradzki (The Johns Hopkins University, USA): Based upon "recent" continuum elastic-plastic solutions for crack-tip strain distributions, can you comment on the limits of applicability of the Vermilyea SCC and HE (Firminy, 1973) cracking model?

W.W. Gerberich: Since Vermilyea's model used a 1/r singularity rather than a logarithmic one, this would tend to throw his critical distance calculations off by a substantial amount. We did some rough calculations that suggested that his model, as posed, would not be compatible with the growing crack solutions.

R.P. Gangloff (University of Virginia, USA): Regarding your most interesting and important electron channeling results: (1) What is the quality of existing strain calibrations for single and polycrystals? (2) Is the spatial resolution of the method sufficient to distinguish grain to grain plasticity differences? If so, how do such results compare to continuum predictions? and (3) You compare fatigue crack-tip strain measurements to analytical predictions for monotonically loaded moving cracks. Isn't this a comparison of apples to oranges? What is the status of elastic-plastic crack-tip field models for cyclic deformation?

W.W. Gerberich: One must be careful in polycrystals to use the same channeling line and measure line widths at the same distance from the pole In this way, you can decrease the scatter to perhaps 1% for large strains and even less for smaller ones. This is even better for single crystals where the same channeling pattern is always present. With regard to your second point, the resolution is very good since you can obtain information from the top 100 nm. By using calibrated electropolishing rates of removals, we can depth profile at about 0.1 μm. Thus, 1, 2, 5, 10 μm sections are evaluated. You can do the same thing in polycrystals that have grain sizes on the order of 5 μm or greater since the selected area channeling pattern spot size is about 5 μm Concerning your point about comparing the growing crack strain distributions: In the paper we compare both monotonic and fatigue-induced strain distributions. Since this work. additional monotonic plane-strain measurements verify the goodness of fit to the theoretical distribution. I agree that the cyclic strain-hardening experiment and the reverse loading in fatigue makes such comparisons more speculative However, the cracks are growing relatively fast and the dislocation distribution observed in TEM is not that different, since cyclic stabilization is not achieved. Since the strain is accumulating at a material point in a "similar" way as the crack passes it either under monotonic or fatigue loading (at high ΔK) in this system, perhaps the comparison is not unexpected.

R.W. Staehle (University of Minnesota, USA): With reference to your Figure 13, what is the nature of the facet? Is it highly deformed or is it fully cleavage? What is, or would be, the effect of hydrogen pressure or, e.g., hydrogen sulfide molecules, on the 12-s delay and the 1-μm dimensionality?

W.W. Gerberich: I want to emphasize that we see very large strains accompanying fracture (about 0.1 to 0.5), but that the facets may be very flat with a few microligaments or may contain a more "ductile" appearance with many microligaments. Nevertheless, in this ductile/brittle switching, the cleavage facet still leads the growth process. On your second comment, Neumann and Vehoff at Max Planck Institute, Dusseldorf, have shown that increased hydrogen pressure increases crack velocity. I would expect this to decrease the 12-s delay with hydrogen sulfide producing an even greater effect Whether or not this would change the 1-μm spacing is an interesting question, since this would depend on the mechanism of arrest. If it is dislocation substructure controlled, this may not change, but if it is crack velocity exhaustion, it may. This is a good suggestion for further work.

F.P. Ford (General Electric R&D, USA): The critical stress-related parameter for the crack propagation rate in ductile alloy/aqueous environment systems may be the periodicity of oxide/salt rupture of the crack tip, that is, a function of the near-surface creep rate at the tip of a moving crack. What do you see as the major problems (and how soon can they be overcome) in developing algorithms between this creep rate and the fracture-mechanics-related parameters, such as K, ΔK, R, frequency, etc.?

W.W. Gerberich. Clearly, creep relaxation effects in moving cracks at elevated temperatures are more complicated, but there has been considerable progress in the last decade. There is the work of Riedel in Germany and C* concepts to describe stress-intensity fields in creeping solids How well these have been verified by experimental data is unknown to me, but this would be a fruitful area of research. My anticipation would be a 2- to 5-year time frame for developing good algorithms in this area if such work were funded.

B.D. Lichter (Vanderbilt University, USA). Regarding your observation of the need for a critical initial crack length required for discontinuous crack growth, there are a number of crack initiation mechanisms possible in SCC aqueous media. For example, we have observed that corrosion slots readily occur along slip bands under application of dynamic straining in an aqueous ammonia environment. These corrosion slots "etch out" crevices on {111} planes. At a critical point, nucleation of "true" discontinuous crack growth begins on the observed {110} fracture plane (Kim, Lichter, Flanagan, unpublished research, Vanderbilt University, 1986).

W.W. Gerberich: Your comment is a very informative one and does suggest one explanation as to why conflicting interpretations of such phenomena might arise. Considering that such observations have not been published, it would be important to have that information, with special attention to the length of the {111} slip-dissolution bands prior to the {110} cleavage. If this could be accompanied by fractography of any crack arrest lines in the cleavage region, it could be a good test of the crack arrest hypothesis, if reasonable variations in slot length (l_o) could be found and evaluated.

E.N. Pugh (National Institute of Standards and Technology, USA): Returning to the question of crack arrest during discontinuous propagation, I would like to bring up the possible role of unfractured ligaments trailing behind the crack front, corresponding to cleavage steps. We at NIST believe that they can exert restraining effects in fcc alloys (e.g., Cu-30Zn) sufficient to arrest the crack. What is your feeling about the role of these ligaments?

W.W. Gerberich: We had investigated large ligament effects in the dynamic cleavage of Fe-3%Si several years ago and concluded that these could have a significant effect on lowering the driving force. However, in the hydrogen cracking process, we see regions that are relatively free of large ligaments and only see a few smaller ones that appear to occur only 1 μm behind the tip. Even considering a large number of these, the driving force is only reduced by about 0.1%. If such ligaments are numerous and occur at 10 to 100 μm behind the tip, then this in fact could be a mechanism of crack arrest.

R.L. Jones (Pacific Northwest Laboratories, USA): Based on your observations of plasticity accompanying rapid crack growth (> 100 m/s) in Fe-Si, do you see any inconsistency with the film-induced cleavage model, which requires an absence of dislocation nucleation during the transition from film rupture to cleavage of the ductile matrix?

W.W. Gerberich: No, I see no particular inconsistency since I believe that dislocations can be ingested in that case as well. Perhaps Sieradzki could address the issue of the fine line between dislocation nucleation and cleavage advance as the velocity of the crack from the film entering the substrate is increased.

H.K. Birnbaum (University of Illinois, USA): As an added comment on the issue of dislocation generation at fast-moving cracks, TEM observations show significant dislocation generation at fast-moving cracks and retention of these dislocations along the crack flanks. This is true even for cracks moving in a "brittle" material such as MgO.

W.W. Gerberich: This is an interesting observation and we would be interested if you could quantify the relative crack velocity vs the relative dislocation velocity.

S.A. Shiels (Westinghouse Electric Corporation, USA): You showed that the use of notched specimens was a valid method of measuring incubation times and that the results can be predicted micromechanistically. Can the notched values be correlated well with precracked CT values and can precracked CT "incubation" times be used to predict incubation in notches of finite root radius also. What defines an incubated crack? 1 μm? 1 mm? 10 mm?

W.W. Gerberich: First, as to your last point, an incubated crack would be the first micron square area if we could detect it. But often it is difficult to do much better than 10 or 100 μm^2, so that it is conceivable that there is a scaling law depending on how good your instrumentation is. As is implied in the paper, there may not be any correlation between blunt-notch and precracked incubation times because of elastic plastic considerations, which can be very different for sharp cracks.

SECTION IV

Mechanistic Aspects of Environment-Induced Cracking in Metals and Alloys

Rapporteurs' Report on Poster Presentations

R.P. Wei
Lehigh University
Bethlehem, Pennsylvania, USA

S.M. Bruemmer
Pacific Northwest Laboratory
Richland, Washington, USA

Introduction and Background

This poster session was devoted to the mechanistic aspects of environmentally assisted cracking in metals and alloys. To put the various contributions into perspective, the processes that can control crack initiation and crack growth are briefly summarized, and some of the key issues are broadly outlined.

The processes that are involved in the enhancement of cracking in metals and alloys by aqueous environments (electrolytes) are as follows:

(1) Transport of the deleterious species to the crack tip.
(2) Reactions of the electrolyte with newly produced surfaces (e.g., slip steps and cracks) to effect dissolution, or to produce hydrogen.
(3) Transport of metal cations away from the crack tip to enable continued dissolution.
(4) Hydrogen entry (or absorption).
(5) Diffusion and partitioning of hydrogen to the various fracture (or embrittlement) sites.
(6) Embrittlement reaction (breaking of M-H-M bonds).

These processes operate in sequence. The overall rate is governed by the *slowest* of these processes, operating in conjunction with the mechanical driving force for cracking. The mechanical driving force is characterized by the crack-tip stress or stress-intensity factor and crack-tip strain rate, or indirectly through the applied stress or specimen extension rate.

The first step, or transport processes, really involves not only the transport of deleterious species to the crack tip, but also of the other species to and away from the crack tip. The transport processes in aqueous media include electromigration, diffusion, and convection. Coupled with reactions at the crack tip and along the crack flank, they define the local environment within the crack and at the crack tip. The near-tip region of interest may extend from 1 nm to 0.1 mm from the crack tip, and the overall crack depth may range from about 0.1 μm to tens of millimeters, to span crack initiation to crack growth.

The anodic processes (dissolution reactions) in the second step are directly responsible for crack initiation and crack growth enhancement, according to the various *dissolution mechanisms* for environmentally assisted cracking. To sustain dissolution-controlled crack advance, transport processes must be sufficient to maintain local crack-tip chemistries that promote dissolution. For the *hydrogen embrittlement mechanisms*, on the other hand, dissolution reactions function primarily as sources of electrons for the reduction of hydrogen.

The remaining processes are important only for the hydrogen embrittlement mechanism, and govern the rate of supply and distribution of hydrogen to the potential embrittlement sites and the rate of embrittlement. Distinction needs to be made, however, between the so-called surface embrittlement and volume embrittlement. For surface embrittlement, cracking results directly from the interaction of hydrogen with the metal–metal bonds at the crack tip, whereas volume embrittlement involves a region of material ahead of the crack tip. As such, the absorption, diffusion, and partitioning processes would play a part only in the case of volume embrittlement.

To make significant advances in the understanding of environmentally assisted cracking in metals and alloys, it is necessary to adopt a more rigorous and quantitative approach than those used heretofore. Specifically, analytical and experimental studies must be guided by well-posed questions that can be answered unambiguously. The concept of rate-controlling processes and how they impact test results must be well understood in the design of experiments, the development of models, and the interpretation of results. Test methods must be assessed with respect to their ability for providing quantitative results, *vis-a-vis* qualitative information. The papers in this poster session are to be viewed in this context.



Photos: M B. Ives

Paper Organization

Although the papers in this session touched upon some of the key issues, by and large they were narrowly focused. To provide focus for discussion, the papers were grouped into the following broad categories, recognizing that some overlap is inevitable.

(1) Crack/Crack-Tip Chemistry and Crack-Tip Processes: Papers by A. Turnbull and M. Saenz de Santa Maria; C.J. van der Wekken; B.G. Pound; R. Oltra and A. Desestret.
(2) Initiation and Loading Mode: K. Komai and K. Minoshima; D.B. Kasul, C.J. White, and L.A. Heldt; R.A. Cottis, A. Markfield, A. Boukkerou, and P. Haritopoulos; M.M. Festen, J.G. Erlings, and R.A. Fransz.
(3) Cracking Mechanisms. (a) Hydrogen Embrittlement. R.S. Piascik and R.P. Gangloff; R.G. Ballinger, C. Elliot, and I.S. Hwang; (b) Anodic Processes: B.D. Lichter, W.F. Flanagan, J.B. Lee, and M. Zho; G.S. Duffo and J.R. Galvele; D.A. Jones.

General Discussion of Issues Raised by the Poster Papers

In an attempt to develop a broader consensus among the international experts on key issues that require resolution, the rapporteurs proposed a series of questions for each of the topics to stimulate discussion in the full plenary session that followed the viewing period for the individual poster papers. Some significant issues surfaced; the major contributions are reproduced below.

Topic 1: Crack/Crack-Tip Chemistry and Crack-Tip Processes

This topic included consideration of models of crack-tip environments, measurement of local chemistries, criticality of crack-tip environments, and crack-tip processes. The question of the state of agreement between models and observations was also proposed.

M. Danielson (Pacific Northwest Laboratories, USA): One issue that I would like to point out and that may be a limit to the validity of current modeling efforts is the inability to consider the transport effects of porous deposits on the chemistry within cracks. Salt films, porous oxides, etc., are observed to form at sufficient thickness, they can isolate the crack tip from the external environment, and with their significant resistivity will strongly affect the concentration gradient across the film of all the ions (except those within the film). The film will change in concentration (through the migration relationship) at the metal/film interface in a manner that is much different from that when no film is present.

H.-J. Engell (Max Planck Institut fur Eisenforschung, Federal Republic of Germany): Salt films may or may not be precipitated at the high current densities at crack tips, even if thermodynamics would allow their formation. As observed experimentally in pits, instead of the (stable) salt layer, a supersaturated electrolyte film can form with high resistivity because of low water content, changing the crack-tip chemistry completely.

F.P. Ford (General Electric R&D Center, USA): In determining the theoretical stability of various species for modeling crack chemistry, are we in serious error in using Pourbaix diagrams that are based on, for example, free energies of formation of bulk compounds? Surely the fact that these compounds in cracks are either of atomistic dimensions or have high surface-to-volume ratios, puts into some question the use of bulk material properties.

H.-J. Engell: Pourbaix diagrams indicate what can happen according to thermodynamics, but not what must happen. As an example, the passivation of iron in sulfuric acid is a process not represented in an equilibrium potential–pH diagram, nevertheless, that it occurs is a matter of fact.

H. Kaesche (Friedrich Alexander University of Erlangen-Nurnburg, Federal Republic of Germany): Considering the conditions prevailing at interfaces, where anodic metal dissolution events may be discontinuously occurring at rates up to several tens of amperes/cm^2, leading to the transient stabilization of nonequilibrium compound layers, caution is clearly required in the application of the well-known and certainly very useful Pourbaix diagrams, which compile equilibrium data. Also, even if equilibrium calculations do apply, the thermodynamic activity of compounds in concentrated solutions may be known only very roughly, since activity coefficients may be far from close to unity. Tabulated diagrams generally refer to the low activity 10^{-6} concentrations of dissolved cations of the metal undergoing dissolution. The supposition that the crack-tip electrolyte is similar to a solution of the dissolving metal having a much higher equilibrium concentration of the metal salt formed with the anion of the solution is used by Pourbaix who, however, disregards nonequilibrium phase formation.

J.R. Galvele (Comision Nacional de Energia Atomica, Argentina): We published a transport model for pitting [J. Electrochem. Soc. 123(1976): p. 464] that could be applied to what happens at the tip of a crack. What is found is that, for cracks propagating at $> 10^{-7}$ m/s, the current densities should be so high that the cracks would end plugged by corrosion products. This points some doubts on mechanisms based on anodic dissolution. On the other hand, we know that anodic dissolution is localized on points like kink steps where the metal atoms are surrounded by water molecules. I find it very difficult to see how such a process could happen at an atomically sharp crack. We concluded that, as I said in a previous discussion at this meeting, the chemical composition inside the crack is not very relevant. What is critical is the nature of the surface compound present at the tip of the crack. We believe that the crack propagates by emission of adatoms from the tip of the crack, and if there is any anodic dissolution, it takes place a few atom distances away from the tip.

H. Kaesche: With regard to crack-tip solution chemistry, there is experimental evidence for discontinuous local metal dissolution events occurring at rates up to 30 amperes/cm^2. This applies to etch pitting and tunneling anodic dissolution from otherwise passive surfaces. It has not yet been established for tunneling metal dissolution during dealloying [see, for example, H. Kaesche, Advances in Localized Corrosion, NACE (in press 1990)]. At these rates of metal dissolution, deposition of salt films must be expected, as excess of hydrating water molecules becomes insufficient at the metal surface. Such films will be different from equilibrium hydrated salt deposits, and will be stabilized by, probably, high field ion transport.

Topic 2: Initiation and Loading Mode

The rapporteurs suggested discussion on a range of issues relating to crack initiation, including consideration of the relevance of testing methodologies. However, the resulting contributed discussion focused exclusively on the slow-strain-rate-test technique, for which the rapporteurs posed a number of questions (e.g., What does it measure? What does it tell/hide? How should test results be interpreted? Does it measure crack initiation or propagation? Is a single strain-rate test sufficient/meaningful?)

T. Murata (Nippon Steel Corporation, Japan): In contrast to slow-strain-rate testing in simulating stress corrosion cracking in a variety of environments, the use of fast-strain-rate testing should be addressed more in understanding crack-tip reactions in contact with crack-tip environments.

M.M. Hall (Westinghouse Electric Corporation, USA): Would not mechanical strain energy, or better yet, rate of mechanical strain-energy dissipation be a better test parameter for correlating results of slow-strain-rate tests? For smooth specimens, this quantity is readily obtained. Notched or precracked specimens require a more complicated analysis, but in principle the analysis can be made, given a knowledge of the material's constitutive behavior.

D.A. Jones (University of Nevada, USA): Slow-strain-rate testing forces film rupture under continuous strain, which is absent in service conditions of constant deformation or constant load. Thus slow-strain-rate testing is conservative. If an alloy does not show stress corrosion cracking in slow-strain-rate testing, it will probably not fail by stress corrosion cracking in service under identical conditions. However, if the alloy does show stress corrosion cracking

in slow-strain-rate testing, it may not fail in service because the continuous film rupture in slow-strain-rate testing is unrealistically severe.

R.N. Parkins (University of Newcastle upon Tyne, UK): I preface my remarks by repeating what I have said on many occasions, that if there were an ideal method of stress corrosion testing, we would all be using it in preference to any other. I believe that statement to be as valid in relation to slow-strain-rate tests as it is to tests on precracked specimens, or any other test. In any laboratory test, the objective is the acquisition of data in relatively short times compared to service lifetimes, that data then being used, empirically or otherwise, to predict service behavior. This acceleration of laboratory tests may be achieved by various routes, of which the introduction of precracks and/or the application of slow dynamic straining in the context of stress corrosion testing are two.

In relation to slow-strain-rate testing, although initially used as an *ad hoc* test, it is now clear that for many systems it has fundamental significance in that the time dependence of various reactions in the crack-tip region are related to the time dependence of strain in that region. The method is therefore as applicable to tests involving precracked specimens as it is to initially plain specimens. What it measures is the interrelation of the relative rates of filming (which may be rate controlling even with hydrogen-induced cracking) and bare metal by straining, as they influence crack growth. If the question as to what it measures needs to be answered in the context of engineering parameters, then it can be used to measure crack velocities or threshold stresses, or stress-intensity factors, all of which are functions of crack-tip strain rates in many systems. Thus, the determination of K_{Iscc} values, for example, without recognizing the strain-rate dependence of such, may result in misleading data.

As to the interpretation of slow-strain-rate test results, these can be by different routes depending upon the object of the exercise. In its simplest form, the specimen is taken monotonically to total failure, and if the objective is simply to decide whether or not the system displays sensitivity to stress corrosion, then fractography of the failed specimen will provide the answer If it is desired to quantify the answer, then there are various quantities that can be used for that purpose [See, for example, Parkins, Stress Corrosion Cracking – The Slow Strain Rate Technique, ASTM STP 665, ed. G.M. Ugianski and J.H. Payer (Philadelphia, PA. ASTM, 1979), p. 5.] That reference also indicates how the method can be modified to define the threshold conditions for cracking on initially plain or precracked specimens, for particular applied strain or deflection rates. The method does not hide anything. Only those who use it can decide upon such an outcome.

It has sometimes been claimed that slow-strain-rate tests are concerned with crack initiation, just as it has sometimes been claimed that precracked specimen testing is concerned with propagation. It appears to me that neither statement is valid. There is no agreed definition of stress corrosion crack initiation – it needs to be defined in the context of the measurements being made, essentially in terms of what constitutes a minimum detectable amount of growth, which statement indicates the irrelevance of such debate. But even if some arbitrary definition of initiation is agreed, if the cracks grow beyond that limit, they are presumably propagated, and in most slow strain-rate tests that is precisely what happens. By the same token, the claim that no initiation is involved in the growth of an intergranular stress corrosion crack from an initial transgranular fatigue crack, for example, ignores the important metallurgical and electrochemical influences in stress corrosion cracking because of an obsession with mechanics.

Where slow-strain-rate tests are used for mechanistic studies or for the measurement of crack velocities or threshold stresses, it appears to me to be necessary to conduct tests at various strain rates. Even if the method is to be used as an *ad hoc* sorting test, for example in the context of alloy development, the selection of inhibitors, or the study of other environmental factors, it is probably worthwhile to conduct tests at different strain rates, in view of the possible influence of these factors upon filming rates. Three or four tests spread over the range from about 10^{-7} to 10^{-4} s^{-1} will usually suffice, and even that range can be reduced on the basis of experience with various alloy/environment systems. Moreover, if the first test, which probably should be conducted at about 10^{-6} s^{-1} for iron, nickel, aluminum or copper alloys, or at about 10^{-5} s^{-1} for titanium or magnesium alloys, produces cracking, further tests may not be necessary. In other words, it depends upon the objective of the tests as to the extent to which variations in the strain rate is necessary.

It has often been stated in the context of slow-strain-rate tests, and indeed precracked specimen tests, that they promote cracking in systems in which, for apparently equivalent service situations, no cracking is observed. Similar statements may be made in relation to other types of test, and not just where variations in stressing conditions are involved, for example, where tests are accelerated by manipulation of the experimental conditions. Such results are not surprising for a variety of reasons, but the conclusion should not be divorced from the reasons for choosing a particular test method in the first instance. For example, it appears to me that if one is responsible for the design or operation of a pressure vessel containing some environment that may promote cracking and where the consequences of failure could be catastrophic, then it is important to use a relatively severe method of testing, such as slow-strain-rate testing. On the other hand, the situation may be very different if the consequence of cracking is no more than the seepage of some innocuous fluid. However, for any method to be used in assessing plant performance, then some value judgment is likely to be needed in attempting to relate the test results to service behavior.

Topic 3: Cracking Mechanisms

For this final topic, the rapporteurs asked "How are the observed cracking rates achieved through the various cracking mechanisms?" The main discussion concerned the relevance of the dealloying mechanism, about which Wei expressed his personal reservations.

D.A. Jones (University of Nevada, USA): I too share Wei's reservations about dealloying as the initiator for SCC. It is difficult to believe that a porous, dealloyed, and thus relatively pure surface layer can be more brittle than the parent substrate alloy. On the other hand, there is ample evidence of softening (attenuation of strain hardening) in many forms of environment-induced cracking. Revie and Uhlig [Corros. Sci. 12(1972). p. 669, Acta Metall. 22(1974). p. 619] demonstrated accelerated creep under anodic current, and others have seen creep prior to initiation of SCC.

I have suggested, in a poster paper at this conference (Jones, "The Contribution of Localized Surface Plasticity to the Mechanism of Environment-Induced Cracking," this proceedings), that high anodic current at film-rupture sites promotes localized softening or attenuation of strain hardening at the exposed plastically deformed slip-band surface. This softened material will crack in a brittle manner when constrained by the surrounding unsoftened alloy. A useful analogy might be two steel bars brazed together at their ends with a complete layer of pure soft lead. Although normally soft and ductile, the lead junction exhibits brittle fracture when sufficient tensile load is applied normal to the brazed joint. The surrounding undeformed steel constrains the small volume of lead, generating lateral stresses and a triaxial stress state in the lead. The triaxial stress state prevents the usual slip processes and the lead fails in a brittle manner by rupture of atomic bonds in lead, which are weaker than those in the adjacent steel.

Therefore, I still question the veracity and need for both surface dealloying and surface film embrittlement in the mechanism of SCC.

L.A. Heldt (Michigan Technological University): Evidence for the dealloying reaction is not found near the crack tip from Auger spectroscopy studies of stress corrosion cracking fracture surfaces in brasses [Hintz, Kass, and Heldt, Embrittlement by the Localized Crack Environment, ed. R.P. Gangloff (Warrendale, PA. TMS-AIME, 1984), p. 229]. The spacings between crack-arrest marks is seen to decrease with increasing K. This is not expected for film-induced cleavage but is consistent with arrest marks occurring when a crack is forced to move too rapidly for the embrittling environmental

reaction [Hintz, et al., Metall. Trans. A 17(1986): p. 681; Kaufman and Fink, Acta Metall. 36(1988): p. 2213].

B.D. Lichter (Vanderbilt University, USA): Our work has established that crack propagation occurs in the "passive" potential domain (below the critical potential, above which massive dealloying in copper-gold alloys rapidly occurs). We have evidence that cracking occurs discontinuously and are able to determine the local average crack growth rate by correlating crack-arrest markings with electrochemical transient current pulses. It is clear that these pulses are due to transient selective dissolution of copper and are likened to "repassivation" as gold atoms move to block further dissolution of copper. We have no direct evidence for the existence of "nanometer-sized" porous gold structures on the fracture surface, but may infer their existence from the current pulses during crack growth and from scratching experiments conducted in the same potential range. At the moment we accept the film-induced-cleavage hypothesis as the most plausible framework within which to interpret our data and to design further critical experiments. The copper-gold system continues to be the most fruitful system to test dealloying as a critical mechanism in transgranular stress corrosion cracking, in view of the possibility of excluding hydrogen involvement and oxide film formation processes.

R.C. Newman (University of Manchester Institute of Science and Technology, UK): Jones seems to have missed the importance of nano-porosity in determining the mechanical properties of dealloyed layers The purity of the material in the dealloyed layer is irrelevant. The brittleness (which, incidentally, is easily demonstrable using gold-silver alloys corroded in perchloric acid) arises from the extremely small ligament size in the layer. Such layers could not possibly have a softening influence. Perhaps there is a confusion with creep-inducing vacancy injection processes, which are not operative in dealloying of alloys with high melting points, where surface diffusion is clearly the means by which noblemetal atoms move around. The work of Revie and Uhlig [Corros Sci. 12(1972): p. 669] was interesting, but the correlation with dealloying was never established, and their experimental conditions probably did not cause dealloying to more than a few atom spacings in depth (in the cuprous ammonia solutions that cause SCC, the dealloying proceeds to several tens of nanometers.)

The last comment of Jones questions the "veracity" of dealloying and "surface film embrittlement." I doubt that he would question the role of dealloying in gold-copper alloys as just described by Lichter. The other systems, such as brass and stainless steel, are more subtle and require more subtle experiments. The correlation between dealloying and SCC was demonstrated by Sieradzki, et al. [J. Electrochem. Soc. 134(1987): p. 1635], for copper-zinc and copper aluminum, while film-induced cleavage in copper-zinc was demonstrated by Newman, et al [Scripta Metall. 23(1989): p. 71]. We have a long way to go in the stainless steel system, but everything looks the same so far.

Heldt's first comment has been addressed in detail by the work of Sieradzki, et al., quoted above. We believe that the fast dealloying only occurs at the crack-arrest positions. Thus, the Auger analysis would need very high spatial resolution to pick it up. The variation of crack jump distance with K has not been addressed by us in detail, but I disagree with the statement that this would be inconsistent with film-induced cleavage. At low K the crack jumps less frequently, so the film can grow thicker between jumps. This may well enable the crack to jump further, since an increase in film thickness may allow the crack to emerge from the film with a higher velocity.

Relative Importance of Crack-Tip Charging and Bulk Charging in Hydrogen-Assisted Cracking in Aqueous Solutions

A. Turnbull and M. Saenz de Santa Maria***

Abstract

An evaluation has been made of the relative importance of crack-tip hydrogen charging and bulk hydrogen charging in the corrosion-fatigue cracking of structural steel cathodically protected in seawater for a range of potentials and cyclic loading frequencies. At applied potentials more negative than about $-900\ mV_{SCE}$, at a frequency of 0.1 Hz, bulk charging becomes the dominant source of hydrogen atoms; this is further emphasized by reducing the frequency. Examination of the literature has shown that the contribution of bulk charging to cracking is significant for a range of steel/environment systems, particularly in solutions in which hydrogen sulfide is present. In relation to test methodology, factors such as time, thickness of specimen, specimen configuration (e.g., tubular or plate) and the application of paint coatings should be considered much more carefully if bulk charging is considered to be potentially significant.

Introduction

One of the complexities associated with interpreting hydrogen-assisted crack growth in steels under dynamic and static loading conditions in aqueous solutions is that the rate of generation of hydrogen atoms on the external and crack surfaces can vary significantly. The kinetics of hydrogen generation on the external surface are dependent on the bulk solution composition and electrode potential, while the kinetics within the crack depend on the solution chemistry and potential local to the crack enclave, and the rate of bare metal production by mechanical straining at the crack tip itself.

In a previous paper, a detailed model was developed to predict the rate of hydrogen generation during corrosion fatigue of a structural steel cathodically protected in marine environments.[1] The model enabled an assessment of the relative importance of hydrogen charging at the crack tip, crack walls, and external surface for this specific steel/environment system.

An outline of the essential features of this model is included in this paper, but the discussion is extended to include other steel/environment systems and to examine evidence in support of the basic predictions.

Model

Evaluation of the current density (CD) for production of hydrogen atoms on the crack walls and on the external surface can be made based on steady-state electrochemical measurements and knowledge of the solution composition and potential.[2-4] However, to calculate the CD at the crack tip, it is necessary to combine measurements of transient reaction kinetics on a bared metal surface with the kinetics of production of a new surface at the tip.

It was shown previously that the total current [I(t)] per unit thickness (B) flowing at time (t) during crack loading under fatigue conditions can be described by the following:[1]

$$\frac{I(t)}{B} = \int_0^t f(t-\tau)\,\frac{\partial CTOD(\tau)}{\partial \tau}\,d\tau \qquad 0 < t \leq 1/2f \qquad (1)$$

where τ is a dummy variable, f(t) represents the time variation of the CD, $\partial CTOD/\partial\tau$ is the rate of change of the crack-tip opening displacement equated to the rate of production of the new surface, and f is the cyclic frequency.

From scraping electrode experiments[5] on BS 4360 50D structural steel in 3.5%NaCl of varying pH, the relevant expressions for the time-variation of the CD are given by

$$i(t) = f(t), \text{ where } f(t) = i_o \text{ for } t \leq t_o$$
$$f(t) = i_o \left\{\frac{t}{t_o}\right\}^{-p} \text{ for } t > t_o \qquad (2)$$

where i_o is the maximum CD, t_o is the time prior to commencement of refilming and p is a decay constant. For cathodically protected steel in seawater, the pH at the crack tip is between 10 and about 12,[2] and the refilming kinetic parameters are as follows:

$$\text{pH 10}: \log_{10}\left[i_o t_o^p\right] = -7.635 \cdot E - 11.99; \quad \log_{10} i_o = -5.820 \cdot E - 7.398 \qquad (3)$$

$$\text{pH 11}: \log_{10}\left[i_o t_o^p\right] -6.989 \cdot E - 11.48; \log_{10} i_o = -7.030 \cdot E - 8.610 \qquad (4)$$

$$\text{and } p = 2.437 \cdot E + 3.059 \qquad (5)$$

where E is in V_{SCE}.

Calculation of the parameters at intermediate pH values was based on interpolation. Although the transient kinetic data for pH 12.0 were less complete, the results are consistent with values extrapolated from the above expressions.

*Division of Materials Applications, National Physical Laboratory, Teddington, Middlesex, England TW11 0LW.

**Chloride Silent Power Ltd., Runcorn, Cheshire, England, WA 1PZ.

The rate of change of the crack-tip opening displacement with time was expressed by

$$\frac{\partial CTOD}{\partial t} = \frac{\Delta CTOD}{(1/2f)} \quad (6)$$

where Δ CTOD is the range of opening during the fatigue loading cycle given by[6]

$$\Delta CTOD = \frac{(1+R)}{(1-R)} \frac{\Delta K^2}{4\sigma_f E'} \quad (7)$$

where σ_f is the cyclic flow stress, E' is Young's modulus, R is the stress ratio, and ΔK is the range of the stress-intensity factor. In the absence of specific data for σ_f, the value for the yield stress σ_y was used (340 MPa for BS 4360 50D steel).

During unloading, the time-dependence of the current depends on the extent of slip reversal and the contribution of brittle crack modes. However, when different possible mechanisms for unloading were assessed,[1] it was found that the additional contribution to the charge from the unloading process was less than 20% regardless of which mechanism was considered. In this paper, the calculated current densities at the crack tip represent the maximum values derived from the different unloading models.

Results and Discussion

Calculations have been made of the current density at the fatigue crack tip, crack walls, and on the external surface for a range of cathodic potentials. The CD at the crack tip is defined as the total current per unit thickness averaged over the crack-tip-opening displacement. The time-averaged value of this CD is compared with that on the adjacent crack walls and external surface in Figure 1. These calculations are based on BS 4360 50D steel in ASTM seawater (pH 8.0) at 5°C for a crack of 1.5 cm deep and loading frequency of 0.1 Hz. The square root of the CD has been used for comparison based on the demonstration by Bockris, et al.,[7] that the subsurface concentration of hydrogen atoms C_o and hence hydrogen permeation is dependent on $i^{1/2}$.

The most important conclusion from this figure is that for potentials more negative than about −900 mV_{SCE}, charging of the steel with hydrogen atoms is most effective from the external surface (the higher pH and increased potential drop making crack-tip conditions less favorable for hydrogen generation). The value of the potential at which bulk charging becomes the most important hydrogen source cannot be made too precise because of inherent uncertainties in the nature of the calculation, for example, with regard to the assumed model of crack-tip deformation. Nevertheless, from the viewpoint of experimentally testing these predictions, the corrosion fatigue studies should be directed at potentials of about −900 mV_{SCE} or more negative.

The proximity of the hydrogen-charging source at the crack tip to the actual location of crack advance may lead to the assumption that this hydrogen source must be the most important controlling crack growth, even if the CD is significantly lower. This will be true at short times; however, if the bulk-charging CD is greater, the concentration of hydrogen atoms along the crack front will be correspondingly greater provided sufficient time is allowed for steady-state charging to be attained. Indeed, at long times, the crack walls and crack tip may act as net sinks for hydrogen atoms.

The loading frequency also has a significant effect on the CD at the crack tip, as shown in Figure 2, for which the calculations are based on an external potential of −900 mV_{SCE}, ΔK = 20 $MPam^{1/2}$, R = 0.5 and crack depth of 1.5 cm. The increase in crack-tip CD with increasing frequency is associated mainly with the more rapid rate of production of bare metal maintaining the crack tip in a more active state on average. (The effect of changing frequency on crack-tip chemistry has a much less significant effect.[1]) Thus, charging of the steel through the crack tip is predicted to be more effective at the higher frequencies. Correspondingly, the potential at which bulk charging would become dominant is depressed to more negative values. The converse is predicted for decreasing frequency.

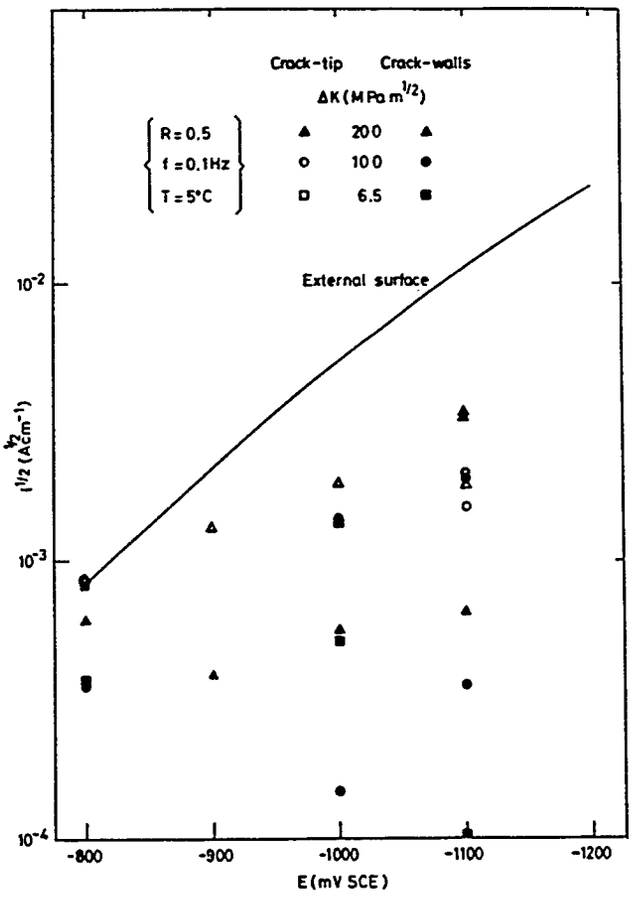


FIGURE 1—Comparison of current densities on the external surface, crack walls, and crack tip.

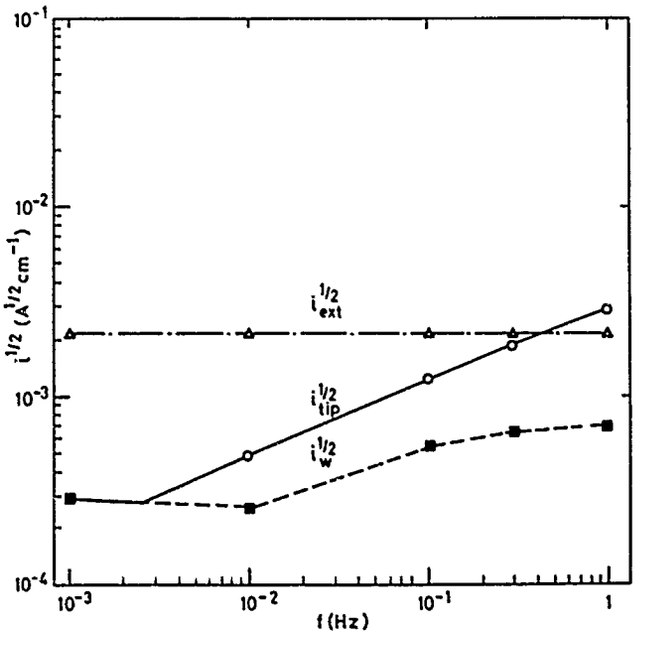


FIGURE 2—Effect of frequency on the square root of the CD for E^{ext} = −900 mV_{SCE} ΔK = 20 MPa $m^{1/2}$ and R = 0.5.

The calculations performed above are specific to seawater with a bulk pH of about 8.0. However, it would be expected that the relative importance of crack-tip charging can be altered not only by changing the potential and the loading frequency but also by changing the bulk environment. Thus, acidifying the bulk solution to values less than about three will significantly enhance the generation of hydrogen on the external surface.[4] However, changing the pH of the bulk solution is predicted to have only a very small effect on the pH at the tip of deep cracks (typically 1 cm)[3,8] Thus, bulk charging will become more dominant.

In environments containing H_2S, hydrogen uptake is dependent on the concentration of H_2S.[9] Detailed calculations of the hydrogen sulfide concentration in a crack have not been conducted, but, qualitatively, it would be expected that the concentration at the tip of a deep crack will be significantly depleted as a consequence of reaction within the crack, and thus, bulk charging will dominate the hydrogen supply.

A reason for the increased significance of bulk charging with increasing cathodic polarization of steel in marine environments is the increased potential drop within the crack, which means less negative potentials at the tip compared to the external surface. Decreasing the conductivity of the bulk solution while carefully controlling the surface potential would tilt the balance in hydrogen supply even more favorably toward the external surface.

These examples are used to illustrate that the relative importance of crack-tip charging to bulk charging is expected to be a sensitive function of the bulk environment, the applied potential, and the cyclic loading frequency. However, it is essential to inquire about the evidence for this proposition and the significance for the measured crack velocities. If bulk charging is controlling crack velocities, then several predictions follow naturally.

Time will have an important influence in relation to establishing steady-state hydrogen charging and thus crack velocities. In the same context, specimen size and configuration will also be important variables. For example, in a compact-tension specimen (CTS) the time constant for charging (arbitrarily defined as the time to charge the steel to 50% at half the thickness of the specimen). For a 25-mm-thick specimen with an effective diffusion coefficient of 10^{-7} $cm^2\ s^{-1}$ the time constant is about 69 days.

In addition, there will be differences in hydrogen distribution in fully immersed fracture mechanics specimens, such as the CTS, and in tubulars. This difference arises because tubulars are usually charged from one surface only leading to a hydrogen concentration gradient. In the case of sour oil or gas bearing pipes, charging will be from the internal surface of the pipe; for offshore jacket structures in the sea, cathodic protection will charge the external surface, but significant hydrogen generation is unlikely in the inhibitive solution used in the internal section of the tubulars.

Coating of the external surface should have a significant effect on cracking because of the decreased supply of hydrogen.

Evidence for certain of these predictions is dispersed in a number of studies. As early as 1971, Barsom[10] reported a distinct change in shape of the crack front from slightly concave to convex when fatigue testing 12Ni-5Cr-3Mo steel in 3% NaCl at an applied potential of $-1200\ mV_{SCE}$. The change in shape was attributed to the greater concentration of hydrogen atoms near the external surface enabling faster crack growth. The specimens used were 50 mm thick, and in the time scale of the experiments the hydrogen distribution along the crack front would be nonuniform. The potential in these tests was considerably depressed, but P.M. Scott of AERE Harwell also confirmed that the same change in shape of the crack front was observed in tests on structural steel in seawater at $-1000\ mV_{SCE}$.

Similar observations in relation to crack front shape have been reported by Kobayashi and Takeshi[11] in stress corrosion testing of a quenched and tempered steel in NACE solution (H_2S-saturated brine at pH 2.6) under free corrosion conditions. The K_{ISCC} value was observed to diminish with increasing thickness, consistent with a reduced concentration of hydrogen along the crack front because of the limited time-scale of the experiments. Nakasa, et al.,[12] also put forward an explanation based on limited hydrogen ingress for the effect of thickness on crack velocities in static loading of a high-strength steel in deionized water. Painting of the external surface of the specimen was used to confirm this interpretation.

Morgan, et al.,[13] investigated the effect of an organic paint coating on the corrosion fatigue crack growth of a structural steel cathodically protected in seawater and observed a long incubation period for the coated specimen. The subsequent crack velocities were similar to the unpainted tests. Interrante and Low[14] demonstrated that application of a surface wax coating reduced the crack velocity of a 2 1/4Cr-1Mo steel statically loaded in NACE solution.

In comparing the stress corrosion cracking of 13Cr martensitic stainless steel in NACE solution (H_2S-saturated brine at pH 2.6) and in H_2S-saturated seawater (pH 5.0), Saenz de Santa Maria and Turnbull[15] provided evidence for a change from bulk surface dominance of hydrogen supply at low pH, for which the steel is in the active state, to localized hydrogen generation at the higher pH, for which a degree of passivity is retained.

Although the number of studies quoted is relatively limited, there is clear evidence for an important role of bulk hydrogen charging in determining crack growth, which is dependent on the environmental conditions of the test.

Further investigations to assess the effect of pH and solution conductivity for a range of potentials are desirable. In the same context, attention to other parameters such as crack depth is important. The chemistry and potential within a shallow crack may be more favorable for hydrogen generation than for a deep crack under applied cathodic polarization.[2] Furthermore, the crack tip will also be more readily accessible with respect to bulk charging. In comparing shallow and deep cracks, these factors may contribute to an increased velocity of the shallow crack. However, it is important to isolate effects that are intrinsic and those that are a function of the test methodology. For example, when comparing data, the relevant crack velocity for the deep crack should be that under steady-state charging, which may require long-term testing.

Conclusion

In the corrosion fatigue cracking of steel cathodically protected in seawater, bulk charging is predicted to be the major source of hydrogen atoms at potentials more negative than about $-900\ mV_{SCE}$ (loading frequency of 0.1 Hz). The relative contribution of crack-tip charging is diminished further by decreasing the loading frequency.

The predictions of this study combined with evidence from the literature suggest that the contribution of bulk hydrogen charging to crack growth will also be a sensitive function of the bulk environment. When bulk charging is important, important considerations for test methodology are time, thickness of specimen, specimen configuration (tubular or plate), and the application of paint coatings.

The interpretation of crack-growth data has to be correlated with the hydrogen source and interpretation of variables such as cyclic frequency should be done with greater awareness of this aspect.

References

1. A. Turnbull, M. Saenz de Santa Maria, Metall. Trans. 19A(1988): p. 1795.
2. A. Turnbull, D.H. Ferriss, Corros. Sci. 26, 8(1986): p. 601.
3. A. Turnbull, D.H. Ferriss, Corros. Sci. 27, 12(1987): p. 1323.
4. A. Turnbull, A.T. May, Br. Corros. J. 22, 3(1987): p. 176.
5. D. Boomer, R. Hermann, A. Turnbull, submitted to Corros. Sci. (1988).
6. R.A. Smith, ed., Proceedings of the Conference on Fatigue Crack Growth-30 Years of Progress (New York, NY: Pergamon Press, 1984), p. 31.
7. J. O 'M. Bockris, J. McBreen, L. Nanis, J. Electrochem. Soc. 112(1965): p. 1025.
8. A. Turnbull, J.G.N. Thomas, J. Electrochem. Soc. 129, 7 (1982): p. 1412.
9. K. Kobe, I.M. Pearson, Y. Saito, Werkstoffe Korros. 31(1980): p. 763.

10. J.M. Barsom, Int. J. Frac. Mech. 7, 2(1971): p. 163.
11. J.I. Kobayashi, Y. Takeshi, Proceedings of the Conference on Predictive Capabilities in Environmentally Assisted Cracking, ed. R. Rungta (New York, NY: ASME, 1985), p. 223.
12. K. Nakasa, H. Takei, T. Saitoh, Eng. Frac. Mech. 16, 3(1982): p. 387.
13. H.G. Morgan, T.W. Thorpe, A. Rence, D.R.V. Silvester, P.M. Scott, "An Investigation of the Corrosion Fatigue Behaviour of Structural Steels in Seawater," Steel in Marine Structures, Paper 5.1 (Paris, France: IRSID, 1981).
14. C.G. Interrante, S.R. Low, Proceedings of the Conference on Hydrogen Effects in Metals, ed. I.M. Bernstein, A.W. Thompson (Houston, TX: National Association of Corrosion Engineers, 1981), p. 713.
15. M. Saenz de Santa Maria, A. Turnbull, Corros. Sci. 29, 1(1989): p. 89.

Flow-Enhanced Diffusion Transport in Corrosion Fatigue Cracks

*C.J. van der Wekken**

Abstract

Using a transparent Lucite† model of a corrosion fatigue crack, in which a dye was injected in the crack solution near the crack mouth, it was observed that the dye is transported in the direction of the crack tip at a strongly accelerated rate because of the cyclic movements. A theoretical model is presented showing that the transport in the crack occurs at a rate that is equivalent to the rate of a diffusion process in a static crack with an effective diffusion coefficient (D_{eff}), which can be calculated from the geometrical test parameters and the value of the normal diffusion coefficient.

Introduction

It was recently shown[1] that the electrochemical conditions, measured at the tip of corrosion fatigue (CF) cracks in steel specimens during external anodic polarization in a deaerated seawater environment, cannot be accounted for on the basis of a concept in which the crack-tip area is considered a "most occluded cell."[2] In the "most occluded cell" approximation, the crack-tip material is expected to be at the corrosion potential in the local-tip solution, the crack tip is not polarized as a result of the externally applied potential because of the large potential drop in the crack resulting from the high current densities on the crack walls. In this respect, the "most occluded cell" concept is expected to be applicable to CF cracks in cases in which the crack walls are not passivated. However, in contrast to the situation in static cracks (stress corrosion cracking), the local crack-tip solution composition in CF cracks will be strongly affected by interaction (mixing) with the solution from other parts of the crack. As far as the solution composition at the crack tip is concerned, the crack-tip region cannot, therefore, be considered "occluded" in the case of CF. In the earlier work mentioned above, the authors concluded that the acidification measured at the tip resulted from interactions between solution acidified in the crack mouth and the crack-tip solution.[1] It was suggested that this exchange is a result of the combined effects of cyclic laminar flow and diffusion in the direction perpendicular to the crack walls. In the present work, the interaction between the solution at the crack mouth and the tip solution is demonstrated by observations of the advancement of a colored dye injected in the crack-mouth region of a transparent model. It will be shown that the results can be interpreted quantitatively on the basis of a simple theoretical model in which the accelerated transport is taken into account by the use of an effective diffusion coefficient (D_{eff}) in a static crack, and the value of D_{eff} can be calculated from the geometrical test parameters.

Experimental

A model of a fatigue crack was made from 1-cm-thick transparent Lucite plate material (Figure 1). The short side of a 6-by-11.8-cm piece of this material (the top plate) was pressed onto a larger (bottom) plate using a rubber O-ring strip, which made it possible to rotate the top plate relative to the bottom plate and to obtain a triangular crack geometry. The crack sides were closed by means of silicon rubber seals, placed in slits that were machined in Lucite strips mounted parallel to the top plate. A sinusoidal movement, derived from a small electric motor coupled to a reduction gear box that was driving an excentrically mounted wheel, could be transmitted to the top plate, while the bottom plate was fixed in a transparent Lucite box. The frequency of the cyclic movements as well as the minimum and maximum opening of the crack could be varied.

The Lucite box was filled with the test solution to a level just above the crack, and dye was injected through a small hole in the top plate at 1.2 cm from the crack mouth while the crack was in the minimum opening position. The injected amount of dye solution was chosen such that a circular patch of 2.8-cm diameter was formed. The cyclic loading was then started after 1 min. To facilitate the observation of the distances reached by the dye at the moments of maximum and minimum crack opening, the crack model was placed on a diffusely lighted glass plate with a measuring scale. Three different dyes were injected in pure water. (1) a dark blue ink, Pelikan† 4001, (2) a bright red negative retouching dye, Neu-Coccin† (distributed by Agfa), and (3) a solution of $KMnO_4$. Finally, a concentrated solution of NaOH was injected into an aqueous suspension of phenolphthalein. The milky white solution containing the pH-indicator particles turns a bright red as the pH reaches values of more than 8.5, making it possible to follow the transport of OH^- ions.

A Quantitative Model for Flow-Enhanced Diffusion Transport

In an infinitely wide triangular crack under conditions of laminar flow, a parabolic velocity distribution between the crack walls causes the solution in the middle of the crack, located at a distance (L) from the tip at the moment of minimum crack opening, to travel up to within a distance (L_1) from the tip at the moment of maximum crack opening, which can be calculated[1] by equating the parabolically shaped volume (dV) of the solution flowing into the crack over a distance (dl) in the middle of the crack, at a distance (l) from the tip, to the increase in volume of a triangular crack of length (l), as the crack-opening angle (α) increases by $d\alpha$. It follows that for a unit width of the crack that $dV = \alpha\, l\, (-2/3\, dl) = 1/2\, l^2\, d\alpha$, or $dl/l = -3/4\, d\alpha/\alpha$. Integration yields $L_1/L = (\alpha_{min}/\alpha_{max})^{3/4} = R^{3/4}$, R being the ratio d_{min}/d_{max} between minimum and maximum opening.

If $r = d_{min}/d$, where d is the variable distance between the walls and d_{min} is the minimum distance at a distance (L) from the tip, the

*Laboratory of Metallurgy, Delft University of Technology, Rotterdamseweg 137, 2628 AL Delft, The Netherlands.

†Trade name.

distance traveled by the solution in the middle of the crack will be $L(1 - r^{3/4})$. If we start an experiment at the moment of minimal crack opening with a certain dissolved species having a concentration gradient (g) in the length direction of the crack, planes of equal concentration [e.g., C_1 and C_2 in the side view shown in Figure 2(a)] will, at this moment, be perpendicular to the plane of the crack. We now define flow profiles as planes that initially coincide with the planes of equal concentration, while their shape and position follow the laminar flow pattern in the crack under cyclic loading; the flow profiles change into curved planes (which, because of the wedge shape of the crack, are no longer parabolic in cross section for finite increments in the crack-opening angle) as the crack opens up, and as a result of the cyclic flow pattern, they will return their original position after each cycle. The volume of the solution between two flow profiles will remain constant. As an approximation, it will be assumed that the profiles can be represented by two flat planes intersecting at the calculated distance $(L \cdot r^{3/4})$ from the tip [see side view of the profiles in Figure 2(b)]. While the solution is flowing, there will be transport of dissolved particles because of diffusion in a direction perpendicular to the flow profiles There are two reasons why this diffusion transport is much more important than in a static situation: (1) The surface area of the profiles is highly increased, and (2) the laminar flow pattern will cause intense shearing to occur along the flow profiles. As a result, the concentration gradient in the direction perpendicular to the profiles will be increased. (The volume between profiles remaining constant, the distance between the profiles decreases.)

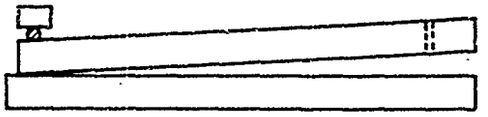


Fig. 1a. Cross section of the lucite crack model.

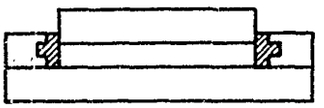


Fig. 1b. Front view of the crack.

FIGURE 1—(a) Cross section of the Lucite crack model and (b) front view of the crack.

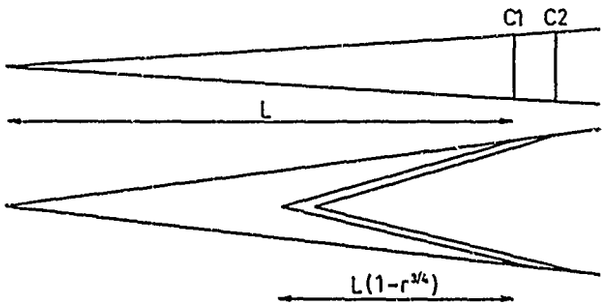


FIGURE 2—(a) Side view of flow profiles coinciding with planes of equal concentration, C1 and C2, at the moment of minimum crack opening, and (b) side view of flow profiles approximated by flat planes during the course of a fatigue cycle.

Let the surface area of the profiles be increased by a factor (f). The concentration gradients between the profiles will then be increased by the same factor (f), and the total diffusion flux across the profiles will be increased by a factor (f^2).

Since the crack-opening angle is always very small, the surface area of the profiles as drawn in Figure 2(b) will be, per unit crack width, approximately equal to two times the distance traveled by the solution in the middle of the crack. At the moment of minimum crack opening, the surface area of the profiles at distance (L) from the tip is equal to the local magnitude (d_{min}) of the crack-opening distance. Using the geometry shown in Figure 2, the ratio (f) of the surface areas can be expressed as a function of the variable r:

$$f = 2[L \cdot (1 - r^{3/4})]/d_{min} \quad (1)$$

The transport of a dissolved species during a cycle will be increased by a factor (F), where F can be obtained by calculating the average value of f^2 over the period (T):

$$F = 4(L/d_{min})^2 \times 1/T \int_0^T (1 - r^{3/4})^2 \, dt \quad (2)$$

(An analogous derivation yields a similar expression for outward transport of dissolved species, where d_{min} is replaced by d_{max}). The value of r in Equation (2) as a function of time depends on the wave form used.

Writing

$$F = 4(L/d_{min})^2 \cdot I \quad (3)$$

the factor I depends on R and on the shape of the cyclic waves used. Numerical calculation of I as a function of R for a sine wave, a linear saw tooth, and a square wave showed I to be nearly independent of the wave shape, except for very small R. For sinusoidal loading and $0.05 < R < 1$, a good approximation is

$$I = 0.66 - 2.5R + 3.5R^2 - 1.7R^3 \quad (4)$$

As expected, I decreases with R increasing and goes asymptotically to zero as R approaches the value of 1. An effective diffusion coefficient can now be defined that is based on the enhanced transport:

$$D_{eff} = D \cdot F \quad (5)$$

D is the normal diffusion coefficient. It follows from Equations (3) and (4) that the multiplication factor (F) will usually be of the order of $(L/d_{min})^2$ or $(\alpha_{min})^{-2}$ and can easily attain values of the order of 10^4.

Knowing the value of D_{eff}, which could be calculated on the basis of the above two-dimensional model, the enhanced diffusion transport of any species in the length direction of a CF crack under conditions of laminar flow can now be treated as a one-dimensional problem in a static crack. Since the value of D_{eff} is based on averaging the diffusion flux over a whole cycle beginning at the moment of minimum crack opening, the one-dimensional model where D_{eff} can be used applies to concentration distributions in the crack corresponding to the moments of minimum crack opening.

In the special case of the present tests, the model predicts that the front of a patch of dye injected in the crack mouth will move further in the direction of the tip after each cycle over a distance that depends on the period (T) and the value of D_{eff}. The solution of the diffusion equations for an infinite medium in which the diffusing species is initially concentrated in a plane is a one-dimensional Gauss distribution:[3,4]

$$C(x,t) = A(Dt)^{-1/2} \exp[(-x^2)/4Dt] \quad (6)$$

where A is a constant and x is the distance from the plane. We will now make the assumption that in the present tests, after a few cycles, the dye in the middle of the crack may be considered to be distributed according to a Gauss distribution, which at the beginning of the test

was concentrated in the plane where the dye was injected. Neglecting the effect of the wedge shape of the crack, the Gauss distribution expected to result after a whole number of cycles then has the form

$$C(x,t) = A(D_{eff}\, t)^{-1/2} \exp[(-x^2)/4D_{eff}\, t] \quad (7)$$

The observed distance traveled by the dye front is determined by the ability of the eye to detect the presence of small dye concentrations in a thin layer of the crack solution. Again neglecting the wedge shape and assuming now that the limiting observable dye concentration (C_L) during a test is constant, it follows that

$$C_L = A(D_{eff} nT)^{-1/2} \exp[(-x_n^2)/4D_{eff}\, nT] = A(D_{eff} mT)^{-1/2} \exp[(-x_m^2)/4D_{eff}\, mT] \quad (8)$$

where x_n and x_m are the observed distances traveled by the dye front after n and m cycles, respectively, and T is the period. From Equation (8), it follows that $(m/n)^{1/2} = \exp[(x_n^2)/4D_{eff}\, nT - (x_m^2/4D_{eff}\, mT]$, and

$$D_{eff} = (2T \ln m/n)^{-1} (x_n^2/n - x_m^2/m) \quad (9)$$

Experimental Results and Discussion

A few typical photographs illustrating the distribution of the dark blue ink during the course of a test at a frequency of one cycle per min, using a minimum crack opening of 0.67 mm and a R value of 0.36 at the place where the dye was injected, are shown in Figure 3. A rapid transport of dye towards the crack tip is evident from the pictures, which show the distribution of ink at successive moments of minimum and maximum crack opening during the first, fourth, and seventh cycles, respectively.

The effect of the frequency

The transport of the red retouching dye toward the crack tip under the influence of cyclic loading was measured, using similar geometrical test parameters as mentioned above, for the frequencies of 0.5/min, 1/min, and 2/min. The results are shown in Figure 4, where the observed distances (x_n), reached by the dye front after n cycles, are plotted as a function of *time*. The model presented above interprets the transport of dissolved particles in a fatigue crack as a process of accelerated diffusion, where the effective value of the diffusion coefficient is determined by geometrical factors and not by the frequency used. The data indicate that after 2 min, a similar rate of transport was found for the different frequencies, in agreement with the theoretical model.

The initial transport process was faster, however, at higher frequencies. A factor not taken into account in the present model is that the density of the solution in the crack increases with the dye concentration. (Dye flowing out of the mouth of the crack during a test appeared to flow from the bottom plane of the crack and was observed to collect at the bottom of the Lucite test cell.) Especially during the first stages of the tests, when the dye concentration is locally still very high, the dye will tend to collect near the bottom of the crack. While there is inward transport by the laminar flow, there will simultaneously be a downward flow of concentrated dye solution because of gravity. Dye particles near the bottom will flow back less far, the closer they have come to the crack wall. This may result in observed accelerated transport toward the crack tip, especially during the first cycle at relatively high frequencies, when the fast inward flow carries the concentrated solution far into the crack, and downward flow may occur around the point where the flow changes direction, at the moment of maximum crack opening. Tests in salt solutions of density equal to the injected dyes are planned to clarify this point.

The influence of the diffusion coefficient

The effect of the diffusivity of the dissolved species was investigated by comparing the results obtained for three different dyes in a series of tests at a frequency of one cycle per min and using the same geometrical test parameters mentioned above. In Figure 5, the values of $x_1^2 - x_n^2/n$ are plotted vs ln n. The linear part of the curves found after two cycles may be used to calculate D_{eff} using Equation (9). From D_{eff}, the normal diffusion coefficient (D) can be obtained using Equation (5), in combination with Equations (3) and (4). The magnitude of the factor (F) in Equation (5) was calculated to be 12,400 in this case. The resulting values for the diffusion coefficients are 5, 6.5, and 8×10^{-6} $cm^2\ s^{-1}$ for the permanganate, the negative retouching dye, and the sodium hydroxide solution, respectively. Comparing the calculated D value for $KMnO_4$ of 5×10^{-6} $cm^2\ s^{-1}$ with available data for the diffusion coefficients of various anions, such as nitrate or chloride ions, which are reported to be 1.8×10^{-5} and 1.9×10^{-5} $cm^2\ s^{-1}$,[5] it appears that the calculated diffusion coefficients are about a factor 3 to 4 lower than expected. The diffusion coefficient for NaOH is found to be a factor 1.65 higher than the value of D for $KMnO_4$, while a ratio of 2.0 is found between the average mobilities reported for the ions Na^+ and OH^-, and K^+ and MnO_4^-, respectively.[6] (Anions and cations are expected to diffuse together to maintain charge neutrality). The fair degree of correspondence between these results and literature data can be considered to support the basic validity of the proposed accelerated diffusion model.

The effect of the value of R

The negative retouching dye was used after having changed the minimum crack opening d_{min}, measured at the place of the dye injection, to 1.09 mm. The maximum opening being 2.36 mm, it follows that R = 0.46 and the factor (F) = 2500 in this case. Figure 6 shows the results obtained under these conditions at a frequency of one cycle per min and also shows the data obtained for d_{min} = 0.67 mm and R = 0.36, in which the value of F was calculated to be 12,400. As expected, D_{eff} is smaller for the wider crack. However, the ratio between the slopes of the linear part in the curves of Figure 6 is only 1.4, while a ratio of 4.4 would be expected from the values of F. Again, an explanation could possibly be associated with the higher density of the dye solution, which might affect the results more strongly in a wider crack.

Comparison of the present model with the literature

It is clear from the theoretical model, as well as from the above experimental results, that for similar concentration gradients, the effective value of the diffusion coefficient (D_{eff}) describing the diffusion transport of dissolved species in a crack during corrosion fatigue can easily be four orders of magnitude larger than in static cracks. Taking the effect of the electrical field in a CF crack into account quantitatively in the present static one-dimensional model would require the use of an average value of the field strength $(dE/dx)_{eff}$ experienced by a charged particle during a fatigue cycle. The transport of ions under the combined influence of an electric field and a concentration gradient can then be described by a modified form of the Nernst-Planck equation:

$$J = -D_{eff}\, dC/dx - D\, C\, nF/(RT)\, (dE/dx)_{eff} \quad (10)$$

where F is Faraday's constant and n denotes the valency of the ions. Because of the high ratio of D_{eff} over D, it can be concluded on the basis of this equation that the relative importance of electromigration, represented in the second term of Equation (10), will in general be much less in the case of CF than in a static crack. In other words, the flow-enhanced diffusion will result in strong solution mixing in the crack.

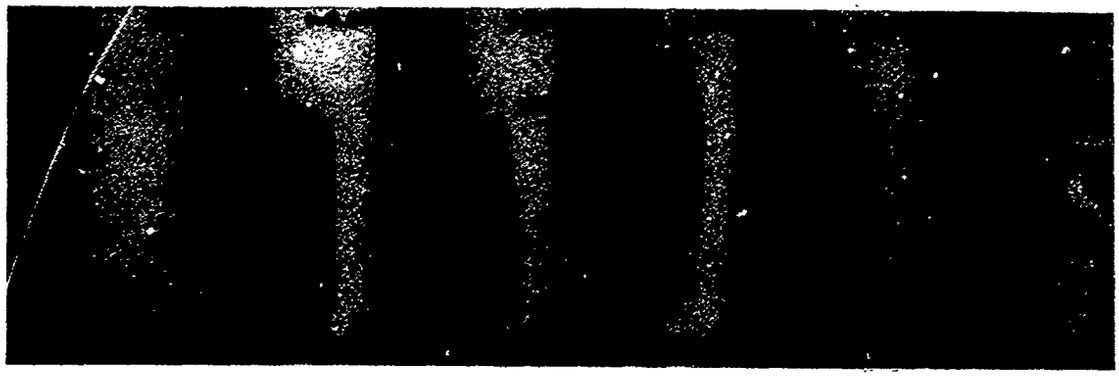


FIGURE 3—The distribution of a dye (Pelikan 4001 ink) at the moments of minimum and maximum crack opening, respectively, during the first, fourth, and seventh cycles: R = 0.36, d_{min} = 0.67 mm, ν = 1/min.

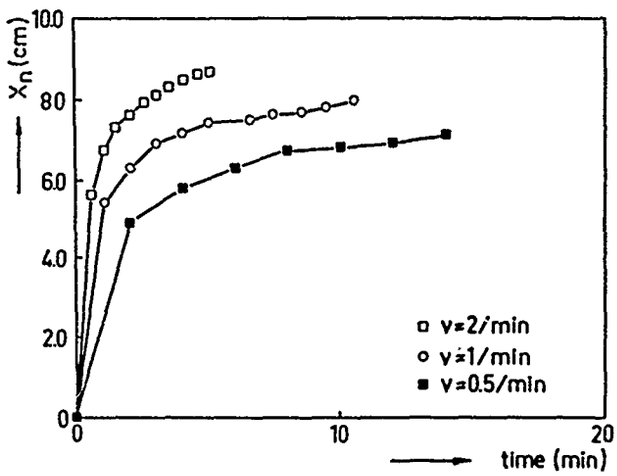


FIGURE 4—The distances X_n reached by the negative retouching dye, measured at the moments of minimum crack opening, for different frequencies: R = 0.36, d_{min} = 0.67 mm.

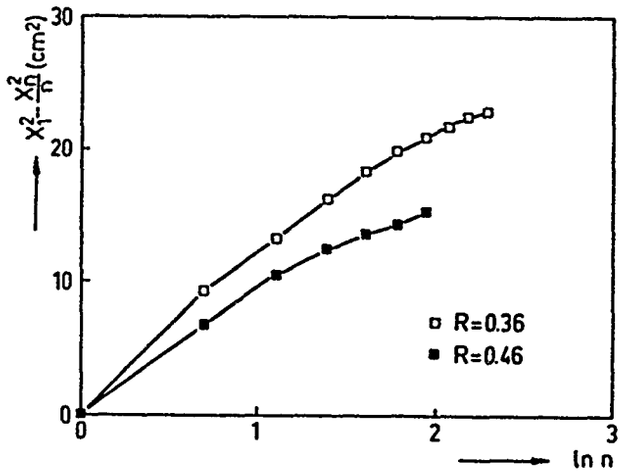


FIGURE 6—$X_1^2 - X_n^2/n$ plotted vs ln n for different crack geometries: R = 0.36, d_{min} = 0.67 mm, and R = 0.46, d_{min} = 1.26 mm, respectively; ν = 1/min.

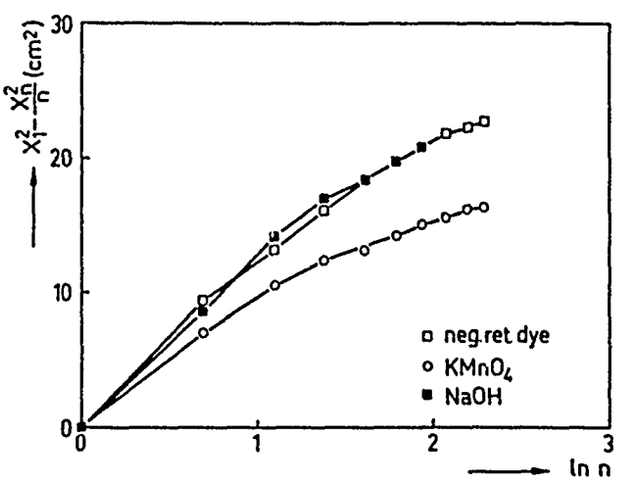


FIGURE 5—$X_1^2 - X_n^2/n$ plotted vs ln n for different dyes: R = 0.36, d_{min} = 0.67 mm, ν = 1/min.

The present results therefore provide support for the conclusions reached earlier,[1] where the low pH value measured in the crack-tip solution during CF of steel in deaerated seawater under conditions of external anodic polarization was ascribed to acidification of the solution in the anodically polarized crack mouth associated with the dissolution reaction and mixing of the solution in the crack. More direct evidence was provided by recent unpublished measurements in this laboratory. Using the same experimental crack model and similar conditions to those described above, a pH electrode was placed at the crack tip and a cylindrical piece of pipeline steel was mounted flush in the upper crack wall. The size of the steel sample corresponded to the size of the injected volume of dye in the present tests, and its location in the crack mouth was identical. The solution used was aerated 3.5% NaCl. The initial solution pH was 7.0. The pH measured and recorded at the crack tip was found to respond to the start of cyclic movements of the crack walls with a frequency of one cycle/min after about 10 min and then dropped rapidly from the initial value of 7 to a value of 6.0. The corrosion process at the crack mouth clearly affected the crack-tip pH within 10 min.

It is certainly relevant to attempt a comparison between the present model and the model as used by Turnbull, et al.[7,8] Assuming total solution mixing in the crack-opening direction and using averaged values for the velocity of the solution, his one-dimensional model served as a basis for extensive computer calculations concerning the electrochemistry in CF cracks. Considering a rela-

tively simple situation in which no reactions are occurring on the crack walls and in the absence of the effect of an electric field, as is the case in our experimental crack model, it is possible to indicate a significant difference between the approach used by Turnbull and the present analysis regarding the transport of dissolved species in the crack According to Turnbull's model, the contribution of diffusion is accounted for by the usual diffusion term (D dC/dx), which is added to the flux associated with the solution flow in the mass transport equation: J = C v − D dC/dx.

Based on this equation, the cyclic solution flow is not expected to contribute to the net mass transport after a whole cycle, while the diffusion process would in the case of our experiments be expected to result in an extension of the patch of dye at a rate similar to what would occur in a static situation. In other words, the experimental results for the extension of the dye front would be expected to follow Equation (6) instead of Equation (7). The flow-enhanced diffusion effect, which was experimentally established in the present tests and is accounted for in our model using the effective value for the diffusion coefficient (D_{eff}) is not represented in Turnbull's model. As a result, his computer calculations are expected to underestimate the importance of solution mixing in the length direction of CF cracks, and the actually occurring differences in the concentrations of the dissolved species in the crack are expected to be smaller than calculated.

Conclusion

(1) It has been shown that during CF, a strongly accelerated transport of dissolved species occurs in the length direction of the crack, which is a result of a combination of diffusion and the cyclic laminar flow of the crack solution.

(2) The resulting exchange between the solution at the crack tip and solution in other areas of the crack is much stronger than expected on the basis of recent computer calculations based on models where total mixing of the solution in the direction perpendicular to the crack walls is assumed.[7,8]

(3) The rate of accelerated transport can be calculated using the actual occurring electrochemical boundary conditions in a static model and using an effective value (D_{eff}) for the diffusion coefficient of the dissolved species. D_{eff} can be calculated according to Equation (5).

(4) The present results support the conclusions reached earlier, where the low pH value measured in the crack-tip solution during CF of steel in seawater under conditions of external anodic polarization was ascribed to acidification associated with the anodic reaction in the crack mouth.[1]

References

1. C.J. van der Wekken, J. Zuidema, Proceedings of the 10th International Congress on Metallic Corrosion, Vol. 3 (1957), p. 1571.
2 R.A.H Edwards (Ph.D. diss., Delft University of Technology, 1956).
3 H.S Carslaw, J.C. Jaeger, Conduction of Heat in Solids, 2nd ed. (Oxford, England: Oxford University Press, 1959), p. 259.
4 L D Landau, E.M. Lifshitz, Fluid Mechanics, Course on Theoretical Physics, 2nd ed , Vol. 6 (Oxford, England. Pergamon Press, 1957), p. 201.
5. CRC Handbook of Chemistry and Physics, 56th ed., ed. R.C. Weast (Cleveland, OH: CRC Press, 1975-76), p. F-60.
6. D. Dobos, Electrochemical Data (Amsterdam, The Netherlands: Elsevier Science Publishers, 1975), p. 90.
7. A. Turnbull, D.H. Ferriss, Corros. Sci. 26, 5(1956): p. 601.
8. A. Turnbull, Chemistry and Physics of Fracture, ed. R.M. Latanision, R.H. Jones (Dordrecht, The Netherlands: Martinus Nijhoff Publishers, 1957), p. 257.

Hydrogen Entry and Trapping in High-Strength Alloys

*B.G. Pound**

Abstract

Hydrogen ingress in three high-strength alloys [type 4340 (UNS G43400) steel, Monel† K-500 (UNS N05500), and MP35N† (UNS R30035)] was studied to obtain some insight into the differing resistances of these alloys to hydrogen embrittlement. A potentiostatic double-pulse technique was used to obtain current transient data for the alloys in 1 M HAc/1 M NaAc (Ac = acetate) with 15 ppm As_2O_3. The data were analyzed using a diffusion/trapping model, and in all cases the rate of hydrogen ingress was shown to be controlled by the interfacial flux. Values of the apparent trapping constant (k_a) and the ingress flux were obtained and used to calculate the trapped charge (q_T) from which the ingress charge (q_{in}) was evaluated. The value of q_T/q_{in} increases with charging time and potential, whereas the ratio of q_{in} to the cathodic charge is constant. The irreversible trapping constant (k) was also evaluated from k_a and was used to determine the density of irreversible traps for each alloy.

Introduction

The ingress of hydrogen into high-strength steels can lead to failure of these materials, whereas certain nickel-base alloys exhibit a much higher resistance to hydrogen embrittlement (HE). In this study, a potentiostatic double-pulse (PDP) technique was applied to a high-strength steel [type 4340 (UNS G43400)] and two nickel-base alloys [MP35N (UNS R30035) and Monel K-500 (UNS N05500)] to investigate their hydrogen ingress and trapping characteristics and thereby assist in understanding the differing susceptibilities of these alloys to HE. The principal objectives were to determine the following: (1) the rate-determining step for hydrogen ingress, (2) the irreversible trapping characteristics in terms of rate constants and density of traps, and (3) the relationships between hydrogen entering the metal, hydrogen formed on the metal surface, and trapped hydrogen.

The PDP technique is applied to a section of bulk metal charged with hydrogen at a constant potential (E_c) for a time (t_c), typically in the range 0.5 to 40 s.[1-3] The potential is then stepped to a more positive value (E_A) [5 to 10 mV negative to the open-circuit potential (E_{oc})], resulting in an anodic current transient with a charge q_a because of H-atom reoxidation at the same surface.

The data are analyzed using a model for the diffusion and trapping of hydrogen atoms in metals.[1,2] The effect of trapping on the diffusion of hydrogen is taken into account by modifying Fick's second law of diffusion to include a trapping term ($k_a c$):

$$dc/dt + k_a c = D_a(d^2c/dx^2) \qquad (1)$$

where k_a is an apparent trapping constant measured for irreversible traps in the presence of reversible traps and is given by $k/(1 + K_r)$; D_a is an apparent diffusion coefficient given by $D_L/(1 + K_r)$; D_L is the lattice diffusivity of hydrogen, k is the irreversible trapping constant; and K_r is an equilibrium constant for reversible traps.

Equation (1) has been solved analytically for two cases: (1) diffusion control in which the rate of hydrogen ingress is controlled by diffusion in the bulk metal, and (2) interface control in which the rate of ingress is controlled by the flux across the interface.[1] Thus, the PDP technique and associated model can be used to determine whether hydrogen ingress occurs under interface or diffusion control. In most cases, the interface control model is valid, so the trapping constant, the interfacial flux, and the amount of hydrogen irreversibly trapped can be obtained.

The analysis of the anodic current transients for the type 4340 steel and two nickel alloys has been reported elsewhere.[3] The diffusion-control model was not valid for any of the three alloys, but the data could be analyzed in terms of the interface control model to give the interfacial flux and apparent trapping constant for each alloy. In this paper, the hydrogen entry and trapping characteristics of these alloys are examined in terms of the hydrogen entering the metal compared to the total hydrogen generated during cathodic charging and the hydrogen that is trapped.

Experimental Procedure

Details of the alloys, electrochemical cell, and instrumentation have been given previously.[3] Briefly, the type 4340 steel was heat treated to Rockwell C hardness (HRC) values of 41 and 53, corresponding to yield strengths of 1206 and 1792 MPa (175 and 260 ksi), respectively. The heat treatments for the steel were as follows: austenitized at 830°C (HRC 41) or 850°C (HRC 53) for 45 min, oil quenched, tempered at 450°C for 60 min (HRC 41) or 180°C for 80 min (HRC 53), and water quenched.

The Monel K-500 (65%Ni-30%Cu) was used both in the as-received (AR) condition [HRC 26, yield strength ~758 MPa (110 ksi)] and age-hardened condition [HRC 35, yield strength ~1096 MPa (159 ksi)]. The aging was performed by heating for 8 h at 600°C and then cooling to 480°C at a rate of 11°/h. MP35N is a quaternary alloy with a nominal composition (wt%) of 35Ni-35Co-20Cr-10Mo. The alloy was used in the AR condition (cold-drawn and aged by heating at 590°C for 4 h and then air cooled) with a hardness and yield strength of HRC 45 and 1854 MPa (269 ksi), respectively.

The electrolyte was a deaerated acetate buffer (1 mol L^{-1} acetic acid/1 mol L^{-1} sodium acetate, pH 4.8) containing 15 ppm As_2O_3 as a hydrogen-entry promoter. The measurements were performed at 22 ± 2°C. All potentials are given with respect to a saturated calomel electrode (SCE). The time of data acquisition (t_a) for the anodic transient was made equal to that for the cathodic transient (t_c).

*SRI International, 333 Ravenswood Ave., Menlo Park, CA 94025.

†Trade name.

Results

Method of analysis

The anodic current transients for all three alloys, as noted above, could be analyzed in terms of the interface control model. According to this model, the total charge passed out is given in nondimensional form by the following:[1]

$$Q'(\infty) = \sqrt{R}\{1 - e^{-R}/\sqrt{(\pi R)} - [1 - 1/(2R)]\text{erf}\sqrt{R}\} \quad (2)$$

The nondimensional terms are defined by $Q'(\infty) = q'(\infty)/[FJ\sqrt{(t_c/k_a)}]$ and $R = k_a t_c$, where F is Faraday's constant, J is the ingress flux, and $q'(\infty)$ is the anodic charge corresponding to $t_a = \infty$. The charge $q'(\infty)$ is equated to q_a obtained by integration of the current transients.[3] For the model to be applicable, it must be possible to determine a trapping constant for which the ingress flux is constant over the range of charging times. The values of the trapping constant and flux can be used to calculate the irreversibly trapped charge given nondimensionally by

$$Q_T = [\sqrt{R} - 1/(2\sqrt{R})]\text{erf}\sqrt{R} + e^{-R}/\sqrt{\pi} \quad (3)$$

The dimensionalized trapped charge (q_T) is given by $Q_T FJ\sqrt{(t_c/k_a)}$.

The adsorbed charge (q_{ads}) was negligible for all three alloys;[3] thus, q_a was assumed to be associated entirely with absorbed hydrogen. Values of k_a, K_r, and k for each alloy are given in Table 1. The values of k for the steel and Monel were obtained from k_a by using hydrogen diffusivity data to evaluate K_r.

TABLE 1
Values of k_a, K_r and k

Alloy	k_a (s^{-1})	K_r	k (s^{-1})
Type 4340 steel	0.008	500	4
Monel K500	0.020	1	0.040
MP35N	0.026	n[A]	0.026

[A]n = Not available; k was approximated to k_a.

Type 4340 steel

The value of k_a is essentially independent of potential and is the same for the two heat-treated specimens. In contrast, the flux exhibits an exponential dependence on overpotential [$\eta = (E_c - E_{oc})$] as shown in Figure 1. The closeness in the slopes (m) suggests that the rate constant for the flux is determined primarily by electrochemical characteristics and not by alloy microstructure.

The trapping constant (k) can be related to the irreversible trap density (N_i) on the basis of a simple model involving spherical traps of radius (d):[2]

$$k = 4\pi d^2 N_i D_L/a \quad (4)$$

where a is the diameter of the metal atom. In the case of the steel, it has been found that if the irreversible traps are assumed to be MnS inclusions, the density of traps is 2×10^8 m^{-3}.[3] This value is in reasonable agreement with the actual number of inclusions, $2 \cdot 10^9$ m^{-3}, but is at least seven orders of magnitude smaller than the number of other possible irreversible traps such as Fe_3C and TiC interfaces.

The dimensionalized trapped charge (q_T) for type 4340 steel (HRC 53) was calculated using Equation (3), and the charge associated with the entry of hydrogen into the metal (q_{in}) was determined from the sum of q_T and q_a. The data for q_{in}, q_T, and the cathodic charge (q_c) were then used to obtain two ratios: (1) q_T/q_{in}, corresponding to the fraction of absorbed hydrogen that was trapped; and (2) q_{in}/q_c, representing the fraction of charge associated with hydrogen entry during the charging step.

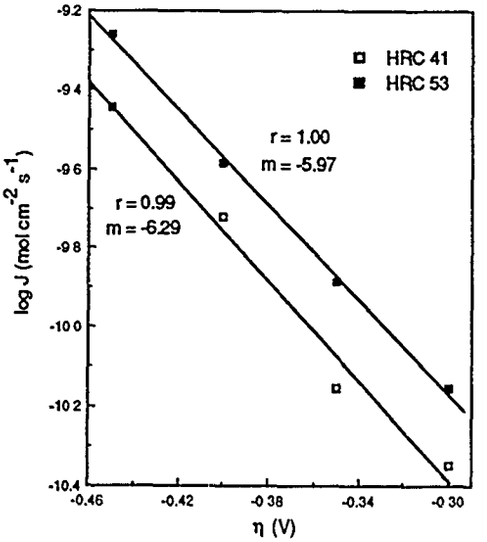


FIGURE 1—Dependence of flux on overpotential for type 4340 (UNS G43400) steel in acetate buffer.

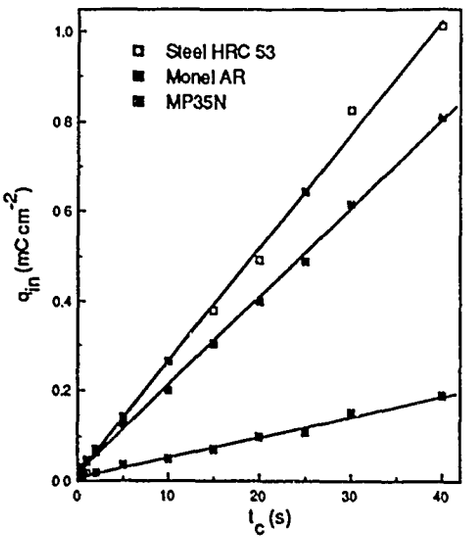


FIGURE 2—Dependence of ingress charge on charging time for type 4340 (UNS G43400) steel (HRC 53), Monel K-500 AR (UNS N05500), and MP35N (UNS R30035) in acetate buffer. E_c (SCE) = −0.985 V for steel; −0.905 V for Monel; −0.425 V for MP35N.

The dependence of q_{in} on t_c for the steel charged at E_c = −0.985 V is shown in Figure 2. As expected, q_{in} varies linearly with t_c.[1] The slope (FJ) is 25.3 μC cm^{-2} s^{-1}, which corresponds to the same value of J (0.26 nmol cm^{-2} s^{-1}) used to calculate q_T via Equation (3).

The ratio q_T/q_{in} has a small potential dependence and increases with t_c from between 1 and 2% at 0.5 s to between 35 and 42% at 40 s for E_c = −0.935 to −1.035 V. The increase with t_c shows that the *proportion* of hydrogen being trapped increases with the amount of hydrogen entering the metal. A change in q_T/q_{in} with t_c is predictable in view of the differing dependence of q_T and q_{in} on t_c, whereas q_{in} depends linearly on t_c, the relationship between q_T and t_c is more complex [see Equation (3)]. Despite the complex variation of q_T with t_c, q_T/q_{in} is found empirically to have an approximately linear dependence on $\sqrt{t_c}$, as shown in Figure 3.

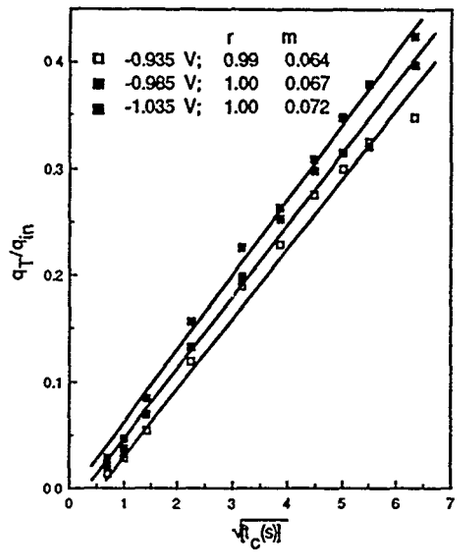


FIGURE 3—Dependence of trapped charge/ingress charge on charging time for type 4340 (UNS G43400) steel (HRC 53) in acetate buffer.

The ratio q_{in}/q_c is independent of potential and t_c, except at very short charging times (Figure 4). The invariance of q_{in}/q_c with potential implies that q_{in} and q_c share a similar potential dependence. The fact that this ratio lies between 0.02 and 0.03 ($t_c > 1$ s) indicates that only about 2 to 3% of the hydrogen atoms formed during charging enter the metal.

Monel K-500 and MP35N

The reduction of H^+ and the entry of hydrogen into these two alloys occurs on an oxide-covered surface, even up to relatively high overpotentials, and the film results in lower values of J than those for the steel As with the steel, k_a is essentially independent of E_c, and J increases with E_c The irreversible trap density was also determined for the Monel and MP35N using the simple model relating k and N_i.[3] The primary irreversible traps were assumed to be sulfur in the Monel and sulfur and phosphorus in MP35N. The values of N_i were found to be 2 6 × 10^{21} m^{-3} for the Monel and 8.2 × 10^{21} m^{-3} for MP35N, whereas the actual S and P concentrations were 1.6 × 10^{24} S atoms m^{-3} in the Monel and 8.1 × 10^{24} S and P atoms m^{-3} in MP35N.

The difference between the experimental and expected values of N_i was thought to result primarily from sulfur and phosphorus segregated at grain boundaries as clusters either in the elemental form or combined with metal components of the alloys. It is assumed that only the exposed outer atoms of the clusters would be available as H traps; the atoms under the exposed layer would be inaccessible to diffusing hydrogen, so that the effective trap density is much lower than the total number of S and P atoms.

Values of q_T, q_{in}, and the charge ratios were obtained also for the Monel and MP35N. The ingress charge for both alloys again conforms to the predicted linear dependence on t_c (Figure 2). The slopes of the q_{in}/t_c plot for the Monel (E_c = −0.905 V) and MP35N (E_c = −0.425 V) are 19.4 and 4.5 μC cm^{-2} s^{-1}, corresponding to fluxes of 0.20 and 0.047 nmol cm^{-2} s^{-1}, respectively. These values of J were the same as those used to calculate q_T via Equation (3).

As with the steel, q_T/q_{in} increases with t_c and q_{in}/q_c is essentially constant. In the case of the Monel, q_{in}/q_c decreases linearly with increasing overpotential from a mean value of 0.13 at E_c = −0.755 V to 0.03 at E_c = −0.905 V. The values of q_{in}/q_c (0.02 to 0.03) over the range 2 to 40 s at −0.905 V are similar to those for the steel, as shown in Figure 4. The ratio of q_{in} to q_c for MP35N also depends to some extent on E_c, but its values are up to an order of magnitude higher than those for the steel and Monel, suggesting that transfer of adsorbed hydrogen into MP35N is facilitated, possibly at grain boundaries. The similarity in the values of q_{in}/q_c for the steel and Monel at high overpotentials suggests that the higher interfacial fluxes for the steel compared with those for the Monel are associated with faster kinetics for H^+ reduction, rather than a higher rate constant for the entry of adsorbed H into the metal.

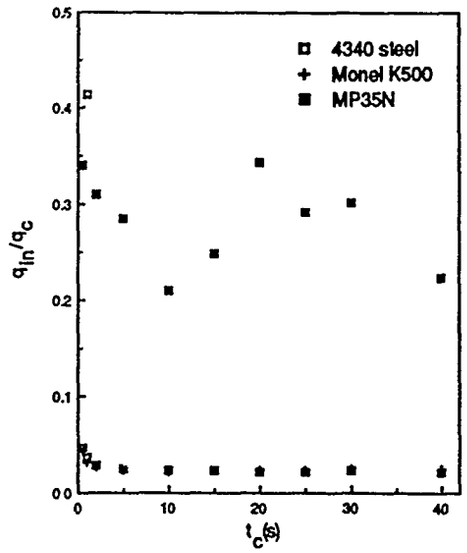


FIGURE 4—Dependence of ingress charge/cathodic charge on charging time for type 4340 (UNS G43400) steel (HRC 53), Monel K-500 AR (UNS N05500), and MP35N (UNS R30035) in acetate buffer. Potentials as given for Figure 2.

Conclusion

The charge ratios showed the following characteristics for hydrogen ingress on the basis of the interface control model:

(1) The proportion of hydrogen being trapped increases with the amount of hydrogen entering the metal.

(2) The more rapid increase in trapped hydrogen compared with absorbed hydrogen probably reflects the increasing number of trap sites available to the diffusing hydrogen with charging time.

(3) Only about 2 to 3% of hydrogen atoms formed during charging enter type 4340 steel, whereas the fraction of hydrogen entering Monel K-500 and particularly MP35N can be considerably higher, depending on the charging potential.

(4) The higher interfacial fluxes for the steel result from a higher coverage of adsorbed hydrogen rather than a higher rate constant for hydrogen entry.

(5) Hydrogen entry into MP35N appears to be facilitated, perhaps at grain boundaries, but the amount of hydrogen absorbed is restricted by the low interfacial flux for this alloy.

Acknowledgment

Financial support of this work by the Office of Naval Research under Contract N00014-86-C-0233 is gratefully acknowledged.

References

1 R. McKibbin, D.A. Harrington, B.G. Pound, R.M. Sharp, G.A. Wright, Acta Metall. 35, 1(1987): p. 253.
2. B.G. Pound, R.M. Sharp, G.A. Wright, Acta Metall. 35, 1(1987): p. 263.
3. B.G. Pound, Corrosion 45, 1(1989): p. 18.

Anodic Dissolution and Hydrogen Embrittlement During Mechanical Depassivation of the Ferritic Phase of a Duplex Stainless Steel in Chloride Solution Containing H_2S

R. Oltra and A. Desestret***

Abstract

This study has been conducted to further the understanding of the role of H_2S in the cracking process of duplex stainless steels in acidic chloride solutions bearing H_2S. Cracking is controlled mostly by the mechanical depassivation and cracking of ferrite, while H_2S can exert a significant influence upon the electrochemical processes, i.e., anodic dissolution and cathodic hydrogen discharge, which depend upon the surface film. A depassivation technique has been coupled with a hydrogen permeation cell instrumented with alternating current impedance measurements to follow simultaneously the effect of the mechanical depassivation on the anodic dissolution, and on the hydrogen discharge and entry on a ferritic alloy of the same composition as that of the ferrite phase of duplex stainless steels. This shows that both processes can be operative in the cracking of that steel, their relative importance depending upon the electrochemical conditions determined by H_2S. To improve the resistance to cracking of these steels, the sensitivity of ferrite must be considered to design the duplex alloy properly, balancing its composition to obtain the right amount of ferrite, and reducing the detrimental influence this phase may have after improper processing.

Introduction

Previous studies have shown that stress corrosion cracking (SCC) properties of duplex stainless steels (DSS) are related to complex electrochemical and mechanical interactions between the two phases, austenite and ferrite.[1] Regarding mechanical interaction, it was assumed that austenite can "protect" ferrite from straining and exerting mechanical protection because of its lower yield strength. It was indeed shown that, at low stresses, ferrite is not significantly strained, while austenite is plastically deformed.[1-3] When stress increases, ferrite can undergo depassivation either by discrete mechanical twinnings or by continuous slip, depending upon the composition and/or the previous metallurgical "history" of the duplex alloy.[2,3]

The better resistance of the DSS was then explained by considering not only this mechanical interaction between the two phases, but also the fact that ferrite was observed to be "anodic" in regard to austenite, at least in the environment investigated, i.e., a concentrated boiling solution of $MgCl_2$. This electrochemical coupling would thus prevent the attack of the slip steps, which can preferentially form at low stresses in austenite. When the stress applied to the DSS reaches the critical value for straining ferrite, the latter phase is locally depassivated and crack initiation occurs during this phase or at the alpha-gamma interface.[1] These studies highlighted clearly the important role of the depassivation of the ferrite phase in the cracking processes of the DSSs, and these processes could be operative in different corrosive environments.

Consequently, it appeared of great interest to study further the peculiar influence of H_2S upon the "electrochemical coupling" that may occur during mechanical depassivation of the two phases in the DSS. The electrochemical situation of the bare metal, especially that of the ferrite phase, has been investigated because it was observed to be the controlling step in the cracking mechanism.

To investigate the role of H_2S, experiments were conducted to determine the factors controlling the balance between anodic dissolution and hydrogen discharge and entry. The effect of mechanical depassivation on the electrochemical behavior of the ferrite phase was studied in the presence of H_2S. In the case of low-alloy, high-strength steels, it has been shown that hydrogen discharge and permeation into the metal were dependent both on the existence of a surface film and the presence of H_2S in the solution.[4] The aim of this paper was to determine whether similar processes could occur on DSS, the passive film of which is much more protective.

Experimental

Materials

Austenitic (AISI 316L) stainless steel (SS), austenitic-ferritic (duplex) SS (Cr 22%, Ni 6.1%, Mo 3%, Cu 1.5%), and laboratory alloys corresponding to the chemical composition of the ferrite phases of the DSS have been tested (Cr 25.2%, Ni 6 1%, Mo 3 5%, Cu 1.5%).

*Laboratoire de Recherches sur la Reactivite des Solides, U.A. 23 CNRS, Universite de Bourgogne, BP 138 21004 Dijon, France.

**Societe UNIREC, Centre Commun de Recherches, Groupe USINOR-SACILOR, BP 50 42702 Firminy, France.

Techniques

Tensile test experiments were conducted on smooth tensile specimens at elongation rates in the range 10^{-3} to 70^{-6} s^{-7}. Current-potential, potentiokinetic curves were plotted in acidic chloride solutions that did or did not contain H_2S. most of these tests were performed at slow scanning rates, e.g., -300 mV h^{-1}, from -1 V_{SCE}.

A depassivation technique has been coupled with a hydrogen permeation cell with AC impedance measurements to follow anodic dissolution and *in situ* changes in the nature of the surface films while these are continuously mechanically damaged (Figure 1). This device has been derived from an apparatus used for repassivation studies[5] or hydrogen permeation tests.[6]

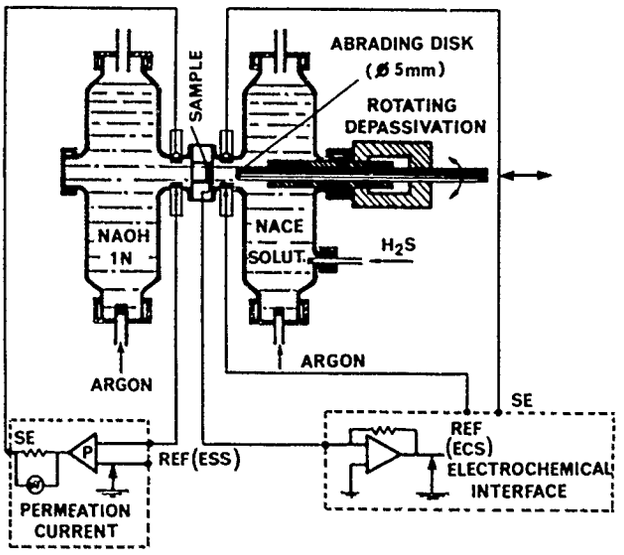


FIGURE 1—Schematic representation of the depassivated hydrogen-permeation-membrane electrode.

Electrolytes

Tests were conducted in different solutions based on the NACE Standard TM0177-86 ("Testing of Metals for Resistance to Sulfide Stress Cracking at Ambient Temperatures") test solution: (1) Solution A· the solution indicated in NACE Standard TM0177-86, NaCl 5% + CH_3COOH 0.5%, pH = 2.7/2.8, H_2S = 1 atmosphere, at 25°C, and (2) Solution B: the same solution as in A, but without H_2S, into which argon was instead bubbled continuously for deaerating to suppress the cathodic reduction of oxygen. Changes of electrolyte from Solution B to Solution A were made to investigate the role of H_2S upon the electrochemical behavior of the steels.

Results

Influence of H_2S upon the electrochemical coupling between austenite and ferrite

Considering the difference in the chemical composition of the two phases, an electrochemical coupling effect has been put forward to explain the better resistance of DSS in many corrosive environments.[1-3,7]

In the peculiar conditions to which NACE Standard TM0177-86 exposes SSs, the general concept of electrochemical coupling must, however, be investigated more precisely, particularly with regard to the behavior of the ferrite phase. On homogeneous materials, the two electrochemical half-reactions, cathodic discharge of hydrogen and anodic dissolution, are conjugate and occur simultaneously over the entire surface. On DSS, in passive conditions, anodic dissolution and/or cathodic discharge and entry of hydrogen proceed only at very slow rates. On the depassivated steel, both processes can be simultaneously active, but at varying rates on ferrite and austenite, depending upon the "free" corrosion potential, because of the different compositions and electrochemical properties of each (Figure 2). If mechanical depassivation occurs on one or the other, or both, phases, the situation can become variable and complicated, this could explain the difficulties encountered in investigating the cracking process of DSS in different environments in assigning it clearly either to hydrogen embrittlement or to localized dissolution along active paths.

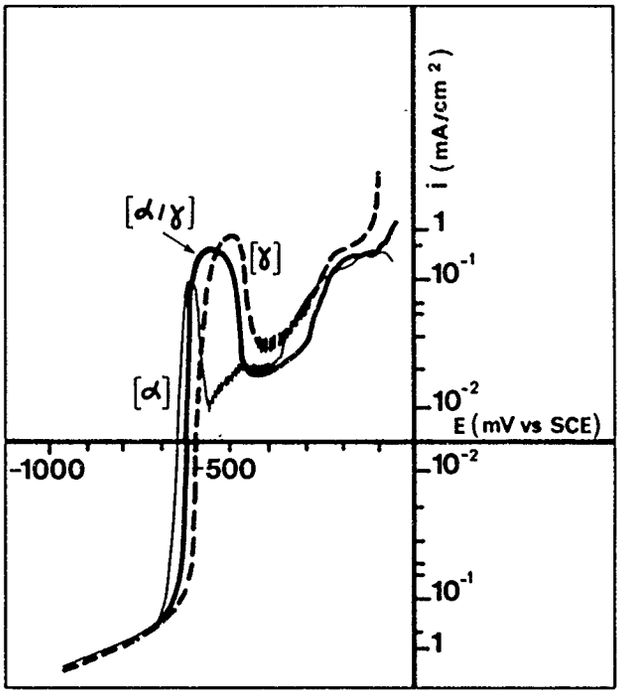


FIGURE 2—Polarization curves in Solution A.

Electrochemical and surface analysis were thus conducted on the separate phases and on DSS to try and clarify the influence of H_2S on the electrochemical interaction between the two phases and the mechanism that sets the potential of the DSS.

In Solution B, the potential of the DSS is set by the electrochemical reactions occurring on the austenitic phase in the range of its pitting potential, whereas presence of H_2S (Solution A) holds the electrochemical couple between the two phases in the range of potential -600 to -450 mV vs SCE.

In Solution A, anodic dissolution leads to the formation of a protective film of metallic sulfides, which will be shown to cause a decrease of the dissolution rate and of the entry of hydrogen. Surface analysis did not clearly bring to light any differences in the chemical composition of these films depending upon the nature of the metallic phase.[7] However, in the case of DSS, the formation of the film on either phase is dependent on the corrosion potential. Unfortunately, only few investigations with high-resolution surface analysis have been attempted to characterize the protective films on duplex steels.[8]

Role of H_2S during mechanical depassivation

Tensile tests were conducted on ferritic specimens that were simultaneously exposed to electrochemical and chemical conditions similar to those obtained during SCC in order to investigate the role of H_2S in promoting either hydrogen embrittlement or anodic dissolution.

Precharging experiment. In "free" corrosion conditions in the NACE solution, if the passive test-piece is not stressed, the potential falls down to about 500 mV vs SCE, at which potential hydrogen is discharged. Having been so exposed for 24 h, the specimen was removed from the electrolyte and strained in air at 10^{-3} s^{-1}. The mechanical behavior of the ferrite specimen is typically ductile, without any evidence of any effect of the hydrogen precharging during the 24-h immersion in the NACE solution.

Introduction of H_2S. In the course of plastic deformation in Solution B, that solution was replaced by Solution A. Whatever the mode of deformation, twinning or slip, the first event observed was an electrochemical one, i.e., exactly coincident with the introduction of H_2S, and before the drop in stress, a fall of the electrochemical potential occurred from about −200 mV down to −500 or −600 mV vs SCE (Figure 3). From this experiment, it can be concluded that the influence of H_2S on cracking is closely related to the electrochemical potential it imposes.

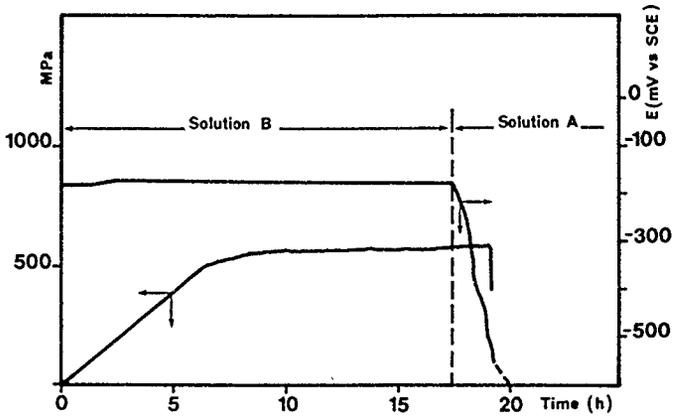


FIGURE 3—Tensile test on the ferrite phase with a change of solution during straining, strain rate = 10^{-6} s^{-1}. Stress (MPa) and potential (SCE) variations vs time.

Role of the potential. The same test was conducted throughout in Solution B, but the change in potential was controlled by a potentiostat (Figure 4). Comparing times-to-failure between both tests after the potential reached the range of −500 mV_{SCE} clearly demonstrates that failure either in Solution A or B results from hydrogen embrittlement of the specimen and that the presence of H_2S (Figure 3) decreases the time-to-failure. Nevertheless, in the light of these results alone, it cannot be concluded that this enhancement is related only to an increase of the hydrogen entry in presence of H_2S, as an important effect on the anodic dissolution cannot be ruled out in the domain of potential involved. In comparison with the first "precharging" experiment, this result shows that H_2S can readily exert an important influence only on a depassivated surface. This highlights the difficulty of understanding clearly the stress corrosion cracking processes occurring on strongly passive materials in presence of H_2S, contrary to what obtains on low-alloy steels, upon which surface films are much less protective, are more easily dissolved and reform much less rapidly, and are therefore less important to determine the behavior.[4]

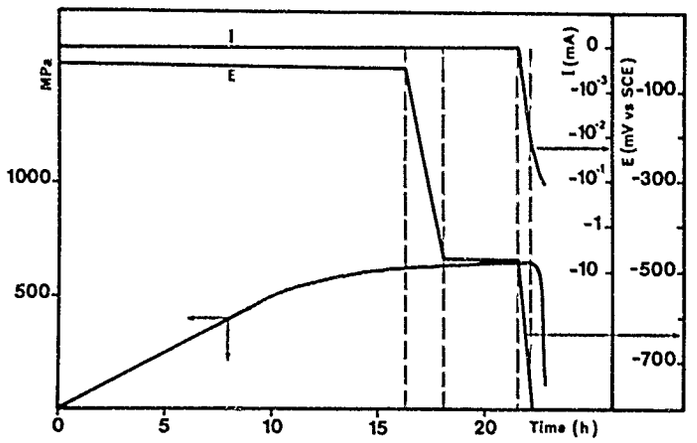


FIGURE 4—Tensile test on the ferrite phase with a change of potential during straining in Solution B. Stress (MPa), imposed potentials (SCE), and current (microamps) variations vs time.

Hydrogen permeation measurements on a depassivated surface

The protective role of passive films formed in the absence of H_2S (Solution B) and also of metallic sulfide films resulting from sulfidation of either austenite or ferrite has been shown to control the effect of H_2S in the cracking of DSS. The straining experiments described above do provide evidence for the sensitivity of ferrite to hydrogen without clearly demonstrating the role of H_2S. The main question to be answered now is relative to the effect of H_2S on the depassivated metal, on anodic dissolution or hydrogen entry.

At the corrosion potential. Using the permeation cell with a depassivated membrane (Figure 1), it has been possible to simulate the electrochemical changes resulting from the introduction of H_2S that was observed on a straining electrode (Figure 3). Typical permeation current transients can be recorded simultaneously with the changes of the potential induced by abrasion (Figure 5). Considering the breakthrough time[9] and the peak current transient it is found that the hydrogen permeation rate increases following mechanical depassivation, although the duration of the mechanical depassivation is limited.

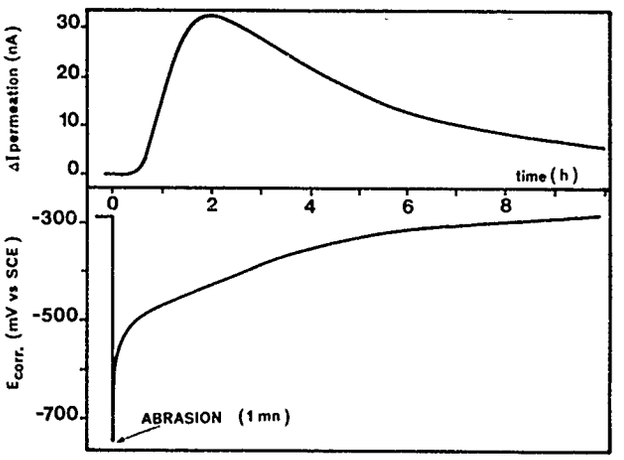


FIGURE 5—Effect of mechanical depassivation on the electrochemical behavior of the ferrite phase. Potential (SCE) and permeation current (nA) vs time after abrasion (1 mm) (Solution A).

In potentiostatic conditions. In addition, abrasion experiments have been conducted while maintaining the potential at a value relevant to the corrosion potential of ferrite in the NACE solution, i.e., around −600 mV vs SCE. But, before the depassivation experiments, the surface "oxide" layer was previously reduced at low potential, i.e., −1200 mV_{SCE}, in Solution B, and then a sulfide film was formed at the open-circuit potential in Solution A. As the main purpose of the experiment was to study the permeation transient during abrasion, the depassivation experiment was conducted after an immersion of about 24 h to obtain as low a residual permeation current as possible. To that aim, the specimen potential was maintained at −300 mV_{SCE}, at which potential impedance measurements showed that the sulfide film is not destroyed (Figure 2). The imposed change of the potential during the test, with or without abrasion, consisted in a potential step to −650 mV_{SCE} during 5 min, followed by a potential scan at high rate (1 V per h) to −300 mV_{SCE}. This test allows simultaneously measurement of the polarizing current (anodic or cathodic) on the corroding surface and the permeation current on the other face. The results are summarized in Figures 6 and 7. First, the anodic current transients observed during abrasion seem to be related to the discontinuous scratches on the filmed surface; they contrast with the lower constant cathodic current observed in the absence of abrasion. Following well-known data, it can be assumed that H_2S increases the rate of dissolution of the depassivated surface (Figure 6). On the other hand, the complementary effect of H_2S on the depassivated surface is outlined simultaneously by the transient permeation current arising on the abraded

specimen, the maximum peak of which is higher and the breakthrough time shorter than on the sulfide's filmed membrane (Figure 7).

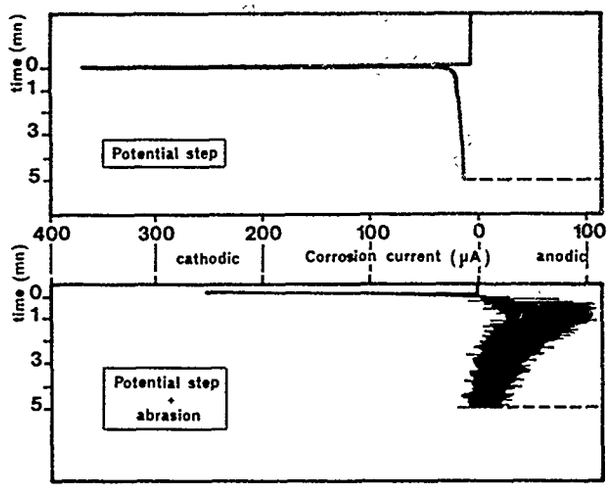


FIGURE 6—Change of the corrosion current after a potential step to −650 mV_{SCE} for a sulfide-film-covered electrode (Solution A): (a) potential step and (b) potential step and mechanical abrasion.

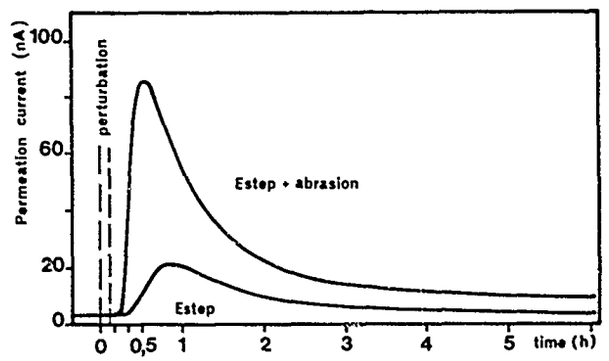


FIGURE 7—Change of the permeation transient for the experimental conditions described in Figure 6.

Discussion

The influence of H_2S on the several reactions that occur on a depassivated surface has been shown to cause simultaneously an increase of the dissolution rate with formation of sulfides and the enhancement of the entry of hydrogen. The permeation transient can be analyzed using mathematical models proposed by J. McBreen, L. Nanis, and W. Beck.[10] According to that treatment, as shown in Figure 8, significant differences can be observed between the diffusion coefficient on the filmed or on the mechanically depassivated surfaces. The enhancement of the entry of hydrogen into the depassivated surface can be interpreted as being dependent on an increase of the hydrogen concentration on that surface. H_2S would therefore seem to inhibit hydrogen recombination on the mechanically depassivated surface, permitting a greater proportion of hydrogen atoms to enter the metal. This assumption for a mechanically depassivated surface is totally in agreement with the conclusions drawn in the case of an anodically depassivated surface of a low-alloy steel.

Regarding the cracking behavior of the ferrite phase, the contribution of the anodic dissolution of the depassivated metal cannot be neglected, but both anodic and cathodic processes are active. The entry of hydrogen should be concentrated at the crack tip, as the walls of the crack are very probably covered by passive or sulfide films that have been found to form barriers to hydrogen.

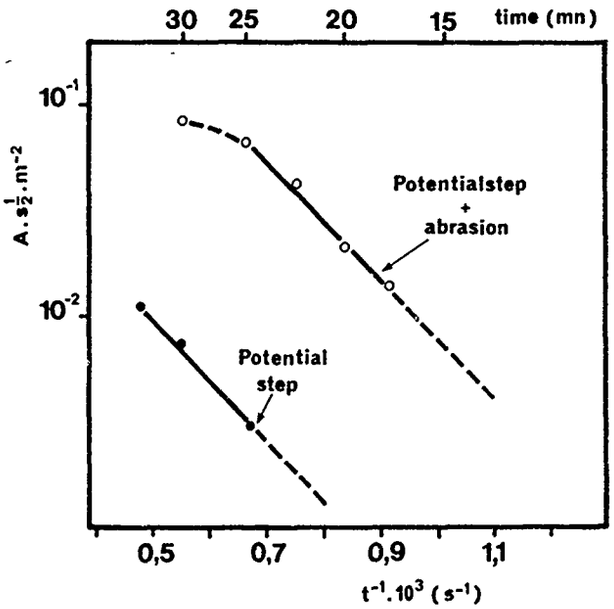


FIGURE 8—Analysis of the build-up of the permeation transients.

In case of strong, discontinuous, mechanical depassivation events, i.e., twinning, hydrogen embrittlement could be the more important process, as hydrogen has sufficient time to build up and embrittle the metal in front of the crack between the bursts of violent deformation that characterize mechanical twinning. Nevertheless, straining experiments (not reported here) on cathodically precharged specimens in a NaOH 0.1 N solution have shown that hydrogen does not affect the mechanical behavior of the ferrite phase in any way, i.e., twinning is not induced nor reduced by hydrogen. In case of slip, which is a more continuous process occurring by very small increments of deformation, the anodic dissolution (sulfidation) could be the controlling factor. Because of the less important local elementary depassivations, depassivation of ferrite takes place for much longer elongations. Twinning is more dangerous, as it occurs for smaller elongations, sometimes below yield.[3]

Conclusion

It has been shown that the metallic sulfide film formed on the ferritic SSs investigated in this paper acts as a barrier for both anodic dissolution and hydrogen entry; this is in contrast to what happens in low-alloy steels not protected by iron-sulfide films. But for a depassivated surface, the same effect of H_2S is found whatever the means of depassivation, i e , electrochemical in case of low-alloy steels or mechanical for the ferrite phase of the DSS.

These observations can help to explain the better resistance of the ferritic steels and of the DSS when the ferrite phase is not prone to twinning, and when the metallurgical processing of the alloy has been correctly controlled.[3,11,12,13] If the DSS has been so designed that the austenite phase is first strained and depassivated, because of its lower mechanical properties, it exerts mechanical protection on ferrite. This latter phase will not be depassivated, and hydrogen embrittlement, or anodic dissolution, will be very slight or negligible as the unruptured surface film (be it the so-called passive film or a film made up of sulfides) can protect ferrite from entry of hydrogen and from dissolution. In this situation, cracking of the duplex steel will be controlled mainly by the localized anodic dissolution of the austenite phase, which is not very sensitive to hydrogen embrittlement. For higher stresses applied to the austenite-ferrite duplex structure, after austenite has been significantly strained, ferrite will begin to undergo depassivation either by twinning or by slip, and the sensitivity to hydrogen of that phase, or the twinning-enhanced and localized anodic dissolution, can cause fast cracking. It should, however, be pointed out that such a situation will arise only for very high stresses, usually in excess of the yield point of the duplex steel. But this

highlights again the great importance of designing and processing correctly the DSSs, as regards their ferrite content and the solution-annealing treatment, to avoid the formation in ferrite of precipitates or phases that enhance mechanical twinning, like sigma or hardening phases, which are detrimental particularly when the environment can cause entry of hydrogen.

References

1. J. Hochmann, A. Desestret, P. Jolly, R. Mayoud, Stress Corrosion Cracking and Hydrogen Embrittlement of Iron Base Alloys, NACE-5, ed. R.W. Staehle, J. Hochmann, R.D. McCright, J.E. Slater (Houston, TX: National Association of Corrosion Engineers, 1977), p. 956.
2. A. Desestret, R. Oltra, Corros. Sci. 20(1980): p. 799.
3. T. Magnin, J. Le Coze, A. Desestret, Duplex Stainless Steels, ed. R. Lula (Metals Park, OH: ASM International, 1983), p. 535.
4. B.J. Berkowitz, H.H. Horowitz, J. Electrochem. Soc. 129 (1982): p. 468.
5. J.R. Ambrose, J. Kruger, Corrosion 28(1972): p. 30.
6. P.A. Kharin, G.E. Lazarev, V.D. Shipilov, L.A. Andreyev, 9th International Congress on Metallic Corrosion, held in Toronto, Canada (1984), p. 424.
7. R. Oltra, A. Desestret, E. Mirabal, J.P. Bizouard, Corros. Sci. 10-11(1988): p. 125.
8. K. Sugimoto, S. Matsuda, J. Electrochem. Soc. 130(1983): p. 2323.
9. M.A.V. Devanathan, Z. Stachurski, Proc. Roy. Soc. A270 (1962), p. 90.
10. J. McBreen, L. Nanis, W. Beck, J. Electrochem. Soc. 113 (1966): p. 1218.
11. A. Desestret, E. Mirabal, D. Catelin, P. Soulignac, "Special Stainless Steels for Application in Natural Sour Gas Exploitation Systems," CORROSION/85, paper no. 229 (Houston, TX: NACE, 1984).
12. A.P. Bond, H.J. Dundas, Stress Corrosion Cracking and Hydrogen Embrittlement of Iron Base Alloys, NACE-5, ed. R.W. Staehle, J. Hochmann, R.D. McCright, J.E. Slater (Houston, TX: NACE, 1977), p. 1136.
13. H.K. Kwon, A.R. Troiano, R.F. Heheman, Proceedings Conference on Solutions to Hydrogen Problems (Metals Park, OH: ASM International, 1982), p. 313.

Mechanical Condition Dominating Cyclic Stress Corrosion Cracking of a High-Strength Steel Under Combined Multiaxial Loads

*K. Komai and K. Minoshima**

Abstract

Cyclic stress corrosion (SC) cracking tests of smooth specimens under combined tensile and torsional loads have been conducted on a type 4135 high-strength steel in a 3.5% NaCl solution at 298°K. The stress wave form was triangular at a stress cycle frequency of 0.1 Hz. Two series of loading patterns were used: multiaxial cyclic-load tests under an in-phase cyclic tension and torsion [tensile stress ratio (R_σ) of 0 and torsional stress ratio (R_τ) of 0], and multiaxial cyclic–static tests where one of the two applied loads was cyclic and the other static (i.e., $R_\sigma = 0$, $R_\tau = 1$ or $R_\tau = 1$, $R_\tau = 0$). Combined stress ratios of τ_{max}/σ_{max} were selected as 0, 1/2, 1, 2, and infinity. In the case of multiaxial cyclic-load tests, a cyclic SC crack normal to the maximum principal stress is initiated at the bottom of a corrosion pit. In this case, the life of cyclic SC cracking is dominated by the maximum principal stress ($\sigma_{1,max}$), which equaled the maximum principal stress range ($\Delta\sigma_{1,max}$). In the case of multiaxial cyclic–static loads, a cyclic SC crack normal to the maximum tensile stress range is initiated at the bottom of a corrosion pit, provided that a static tensile load in the plane of the maximum tensile stress range is relatively small. In this case, the life of cyclic SC cracking was dominated by the maximum tensile stress range ($\Delta\sigma_{n,max}$). In either case, the mechanical condition dominating crack initiation at the bottom of a corrosion pit is determined by the stress-intensity factor range (ΔK_{IFSCC}) calculated on the assumption of a corrosion pit being a surface crack.

Introduction

High-strength materials are sensitive to environments. Their environmentally induced degradation, including stress corrosion (SC) cracking, poses serious problems. In high-strength materials sensitive to an environment, fracture modes dominated by SC cracking are often observed even under dynamic loads. For example, when materials sensitive to static SC cracking under a sustained load are subjected to dynamic loads such as a low frequency variation (stress ratio $R = K_{min}/K_{max}$ being near 0), the crack growth is greatly accelerated compared to fatigue in an inert environment,[1-5] which results from SC cracking promoted by dynamic loads. Therefore, such phenomena are termed "cyclic SC cracking"[1,2,4,5] and are differentiated from conventional corrosion fatigue. In this field, many investigations have been reported on the initiation and growth behavior of SC cracks under a uniaxial loading condition, though SC cracking behavior under multiaxial loading has rarely been reported.[6-9]

In the present study, cyclic SC cracking tests of smooth specimens under a combined tensile and torsional load were conducted on a type 4135 high strength steel sensitive to a hydrogen embrittlement type of SC cracking. Crack initiation sites were closely examined, and the mechanical condition dominating the initiation of SC cracks under a multiaxial load is discussed.

Experimental Procedures

The material tested was type 4135, a high-strength steel whose chemical composition, heat treatment, and mechanical properties are listed in Tables 1 to 3, respectively. Extruded rod materials were machined into smooth specimens in a longitudinal direction. Specimens shown in Figure 1 were finished with 2.5-μm diamond paste after polishing with #2000 emery papers. The corrosive environment was a 3.5 wt% NaCl solution at 298 ± 1°K, and it was circulated between a corrosion chamber and a corrosion reservoir at a flow rate of 12.5 mL/s.

An electrohydraulic tension (98 kN)-torsion (980 N m) fatigue testing machine was used. The stress wave form was triangular at a stress-cycle frequency of 0.1 Hz. Two series of loading patterns were used, multiaxial cyclic-load tests under in-phase cyclic tensile and torsional loads [tensile stress ratio (R_σ) of 0 and torsional stress ratio (R_τ) of 0] and multiaxial cyclic–static tests in which one of the two applied loads was cyclic and the other static (i.e., $R_\sigma = 0$, $R_\tau = 1$ or $R_\sigma = 1$, $R_\tau = 0$). Combined stress ratios of τ_{max}/σ_{max} were selected as 0, 1/2, 1, 2, and infinity.

Specimens' surfaces were closely examined, and depths of corrosion pits were measured using a defocusing method. The expected maximum pit depth in the exposed area was obtained by an extreme value analysis.[9,11] Doubly exponential distribution parameters were calculated by the minimum-variance linear unbiased estimator method.[11]

Experimental Results and Discussion

Initiation of cyclic SC cracks under multiaxial cyclic loads

S-t diagram and initiation sites of cyclic SC cracks. Figure 2 shows the relation between von Mises-type maximum equivalent stress ($\sigma_{eq,max}$) and time to fracture (t). The figure also contains the fatigue data in dry air under uniaxial loading ($\tau_{max}/\sigma_{max} = 0$) at $R_\sigma = 0$.

*Department of Mechanical Engineering, Kyoto University, Yoshida Honmachi, Sakyo-ku, Kyoto 606, Japan.

TABLE 1
Chemical Composition

C	Si	Mn	P	S	Cu	Ni	Cr	Mo
0.36	0.19	0.71	0.030	0.011	0.07	0.05	0.99	0.16

TABLE 2
Heat Treatments

Normalizing	Quenching	Tempering
1143°K 1 h AC	1128°K 1 h OQ	523°K 1 h WC

TABLE 3
Mechanical Properties

0.2% Yield Strength	Tensile Strength	Elongation
1380 MPa	1770 MPa	13%

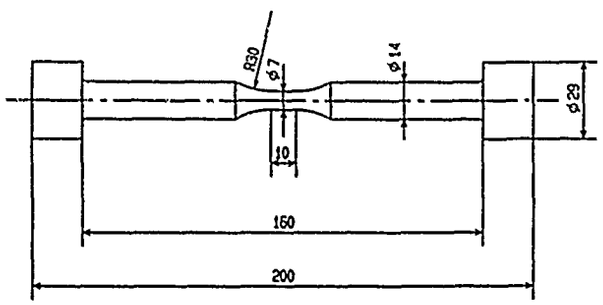


FIGURE 1—Shape and dimensions of test specimens. All dimensions are in mm.

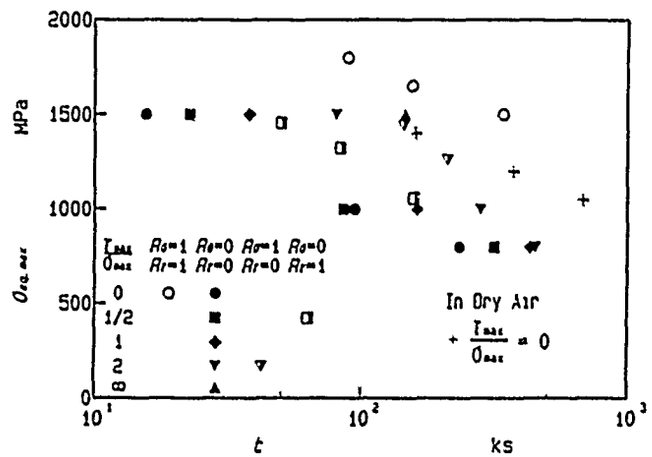


FIGURE 2—Relation between $\sigma_{eq,max}$ and time to fracture (t).

From the figure, it is clear that cyclic SC cracking life became longer with an increase in τ_{max}/σ_{max}, compared at a fixed value of the equivalent stress. Regardless of the loading condition, a cyclic SC crack normal to a maximum principal stress was initiated at the bottom of a corrosion pit and propagated as shown in Figure 3. The initiation behavior was quite similar to that of cyclic SC cracks under a pure bending or a pure torsional load, reported elsewhere.[12] The data in Figure 2 were replotted in terms of the maximum principal stress ($\sigma_{1,max}$). The results are shown in Figure 4. In the case of multiaxial cyclic loads, $\sigma_{1,max}$ is equal to maximum stress range of principal stress ($\Delta\sigma_{1,max}$) and also to maximum stress range of tensile stress ($\Delta\sigma_{n,max}$). It is clear that a single curve is obtained between $\sigma_{1,max}$ and time to fracture regardless of τ_{max}/σ_{max} value, and low-frequency variation caused a considerable decrease in cyclic SC cracking strength from those of static SC cracking under a sustained load as well as from those of fatigue in dry air.

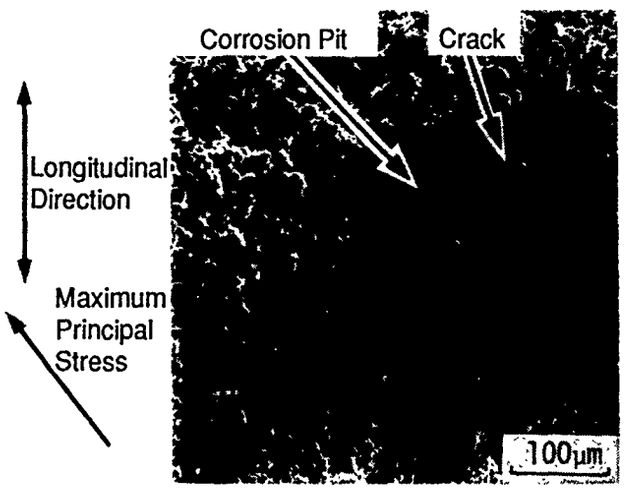


FIGURE 3—Crack initiated at the bottom of a corrosion pit (τ_{max}/σ_{max} = 2, σ_{max} = 222 MPa, τ_{max} = 444 MPa).

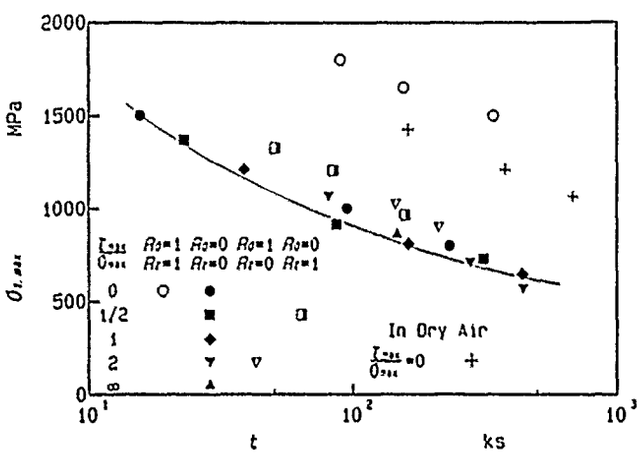


FIGURE 4—Relation between $\sigma_{1,max}$ and time to fracture (t).

Growth of corrosion pits and crack initiation. Similar to the initiation behavior of cyclic SC cracks under a uniaxial loading condition,[12] cyclic SC cracks under multiaxial cyclic loads were initiated at the bottom of a corrosion pit. Consequently, the most important parameter dominating the crack initiation is considered to be depth of a corrosion pit. Figure 5 shows the relationship between the extreme value of pit depth ($d_{p,max}$) and testing duration (t). Here, tests were interrupted at a duration of 25%, 50%, and 75% of time to fracture represented by a solid line in Figure 4. The data in Figure 5 show that growth rate of the corrosion pit was independent of τ_{max}/σ_{max} value, and a single relation ($d_{p,max}$) (μm) = $4.8t^{0.37}$ (ks)

was concluded, which is plotted by a solid line in the figure. Also, cracks at the bottom of corrosion pits were first observed at a duration of about 50% of total life, regardless of τ_{max}/σ_{max} value. This means that τ_{max}/σ_{max} value may not affect time to crack initiation and may not affect time to fracture either.

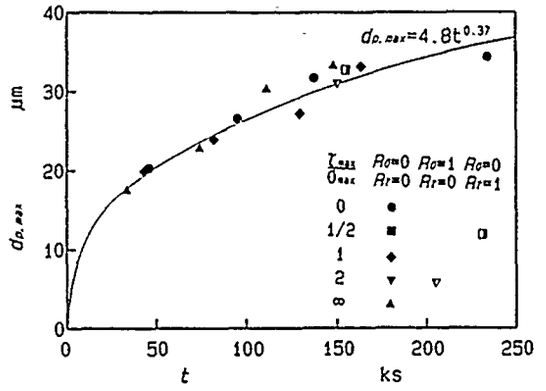


FIGURE 5—Relation between $d_{p,max}$ and testing duration (t).

Fracture mechanics approach to initiation of cyclic SC cracks. Figure 6 shows the relation between the maximum principal stress ($\sigma_{1,max}$) (= $\Delta\sigma_{1,max}$ = $\Delta\sigma_{n,max}$), and the pit depth with and without cracks. A cyclic SC crack was initiated when a pit depth exceeded a threshold value.

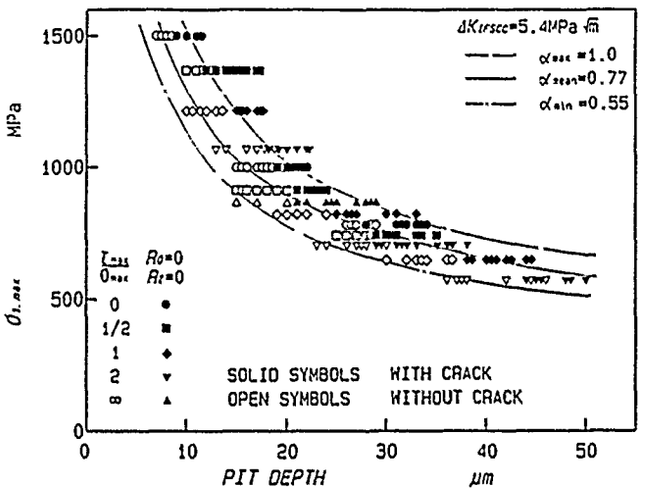


FIGURE 6—Relation between $\sigma_{1,max}$ and pit depth under multiaxial cyclic load.

Assuming a corrosion pit with cracks as a sharp semi-elliptical surface crack,[13,14] a Mode I stress-intensity factor range at the bottom of a corrosion pit (ΔK_I) (= $K_{I,max}$) was computed using the Newman Raju equation.[15] Here, the maximum principal stress range ($\Delta\sigma_{1,max}$) (= $\sigma_{1,max}$ = $\Delta\sigma_{n,max}$), was substituted for stress range. As for surface crack length, a projected pit width normal to the direction of maximum principal stress was adopted assuming a surface shape of the pit as an ellipse, and pit depth, including general wastage by corrosion, was substituted for the crack depth.[14] Most of the aspect ratios of corrosion pits (α) were smaller than unity. At high stress levels, however, some pits have values of greater than unity. The Newman-Raju equations used here are valid with α smaller than unity An aspect ratio α was thus assumed to be unity, when α . 1.

Ten pits, each with a crack, were randomly chosen in each fractured specimen and ΔK_I values were calculated, the relationship between the minimum values of ΔK_I in each specimen and $\Delta\sigma_{1,max}$ is shown in Figure 7. The data except at high $\Delta\sigma_{1,max}$ values were almost constant, and the average value of ΔK_I, ΔK_{IFSCC} was obtained at 5.4 MPa·m$^{1/2}$. The relationships between $\sigma_{1,max}$ (= $\Delta\sigma_{1,max}$) and the pit depth at ΔK_{IFSCC} are plotted in Figure 6 with an aspect ratio of 1.0, the maximum aspect ratio (α_{max}); 0.77, the average of the mean aspect ratio (α_{mean}); and 0.55, the average of the minimum aspect ratio (α_{min}). From the figure, it is clear that the threshold pit depth above which a crack was initiated at the bottom of a pit coincided with the line of ΔK_{IFSCC} = 5.4 MPa·m$^{1/2}$. At high stress levels, where the aspect ratios were close to unity, the threshold pit depth existed between the lines of α_{max} and α_{mean}, whereas at low stress levels, where the aspect ratios ranged from 0.77 to 0.64 on the average, the threshold pit depth existed between the lines of α_{mean} and α_{min}. These results support the idea that the mechanical condition dominating crack initiation at the bottom of a corrosion pit is the stress-intensity factor range calculated on the assumption of a corrosion pit being a surface crack.

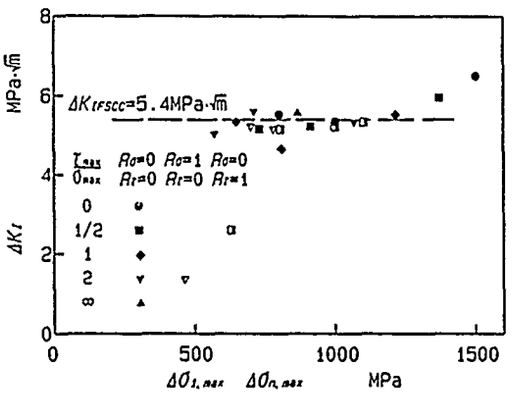


FIGURE 7—Relation between ΔK_I and $\Delta\sigma_{1,max}$ ($\Delta\sigma_{n,max}$).

Initiation of cyclic SC cracks under multiaxial cyclic–static loads

S-t diagram and initiation sites of cyclic SC cracks. Figures 2 and 4 also show the results under multiaxial cyclic–static loads. In Figure 2, the lifetime in terms of $\sigma_{eq,max}$ became longer than that under multiaxial cyclic loads shown by solid marks. The lifetime in terms of $\sigma_{1,max}$ was longer than that under multiaxial cyclic loads, though the scatter band was smaller than that in terms of $\sigma_{eq,max}$ (Figure 2). Figures 8 and 9 illustrate the initiation sites of cracks at R_σ = 0 and R_τ = 1 and at R_σ = 1 and R_τ = 0, respectively. At R_σ = 0 and R_τ = 1 with τ_{max}/σ_{max} = 1/2, a crack normal to the longitudinal direction of a specimen was initiated at the bottom of a corrosion pit, as shown in Figure 8, whereas at R_σ = 1 and R_τ = 0 with τ_{max}/σ_{max} = 2, cracks at an angle of 45 degrees against the longitudinal direction of a specimen were initiated as shown in Figure 9; these prove that the cracks were initiated in the plane where the tensile stress range took maximum, not in the plane of the maximum principal stress. Therefore, the data shown in Figure 4 were plotted in terms of the maximum tensile stress range ($\Delta\sigma_{n,max}$). The results are shown in Figure 10. Here, $\Delta\sigma_{n,max}$ under multiaxial cyclic loads equals $\sigma_{1,max}$ or $\Delta\sigma_{1,max}$, so the S-t diagram under multiaxial cyclic loads in Figure 4 is shown in Figure 10 by a solid line. The results under multiaxial cyclic–static loads coincided fairly well with the line under multiaxial cyclic loads, cyclic SC cracking life under multiaxial cyclic–static loads was proved to be dominated by $\Delta\sigma_{n,max}$.

Fracture-mechanics approach to initiation of cyclic SC cracks. Similar to multiaxial cyclic-load tests, the maximum pit depth in an exposed surface was estimated by an extreme value analysis. The results are shown in Figure 5 with those under multiaxial cyclic loads.

The maximum pit depth under multiaxial cyclic–static loads almost equaled the one under multiaxial cyclic loads, so differences of growth behavior of pits between multiaxial cyclic and multiaxial cyclic–static load tests were not observed, as long as the $\Delta\sigma_{n,max}$ was identical.

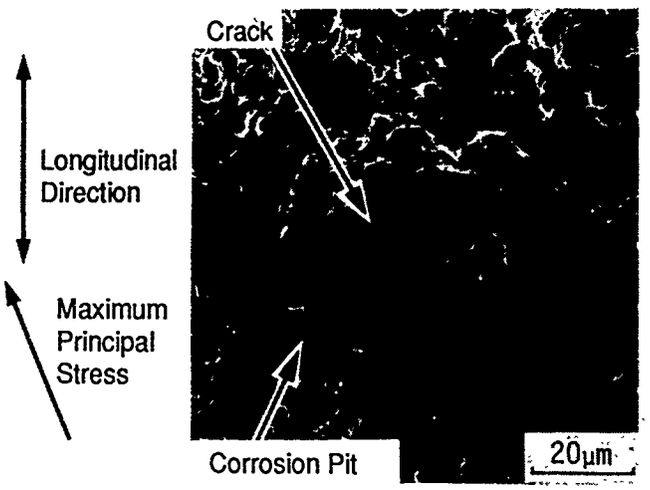


FIGURE 8—Crack initiated at the bottom of a corrosion pit under multiaxial cyclic-static loads (τ_{max}/σ_{max} = 1/2, τ_{max} = 800 MPa, Rσ = 0, τ = 400 MPa, R_τ = 1).

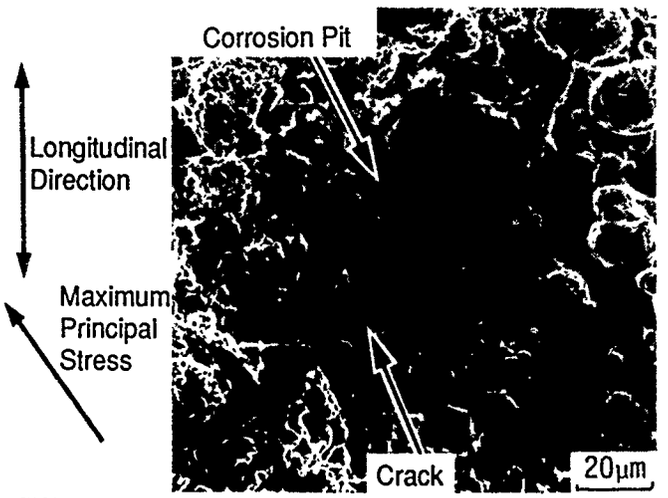


FIGURE 9—Crack initiated at the bottom of a corrosion pit under multiaxial cyclic-static load (τ_{max}/σ_{max} = 2, σ = 400 MPa, R_σ = 1, τ_{max} = 800 MPa, R_τ = 0).

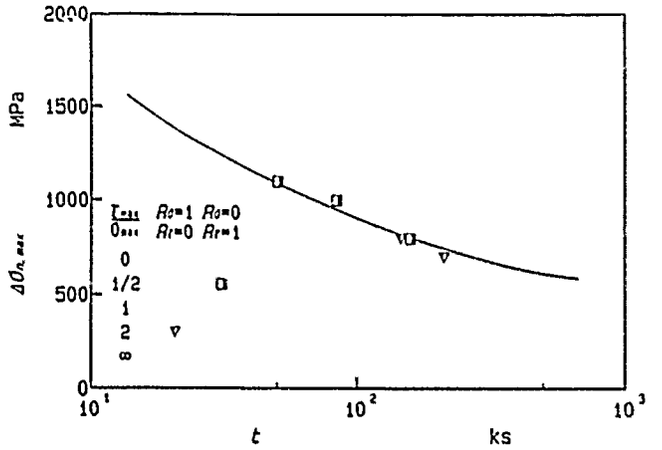


FIGURE 10—Relation between $\Delta\sigma_{n,max}$ and time to fracture (t).

Figure 11 shows the relationship between $\Delta\sigma_{n,max}$ and the pit depth with and without cracks. A crack was initiated when a pit depth exceeded a threshold value, in a similar way to the crack initiation behavior under multiaxial cyclic loads. Therefore, ΔK_I values at the bottom of a pit with cracks were calculated with the Newman-Raju equation by assuming a pit has the characteristics of a sharp crack, and the minimum values of ΔK_I in each specimen are plotted in Figure 7. Here, the maximum tensile stress range ($\Delta\sigma_{n,max}$) was substituted for the stress range instead of $\Delta\sigma_{1,max}$ and projected pit width normal to the direction of $\Delta\sigma_{n,max}$ for surface crack length. ΔK_I values under multiaxial cyclic-static loads equaled the ΔK_{IFSCC} value obtained under multiaxial cyclic loads. The three lines in Figure 11 represent the relation between pit depth and $\Delta\sigma_{n,max}$ at ΔK_{IFSCC} = 5.4 MPa·m$^{1/2}$ with the aspect ratios (α) of 1.0, 0.77, and 0.55, respectively. The threshold pit depth, above which a crack was initiated, lay in the zone between the lines of α = 1.0 and α = 0.55; whether or not a crack is initiated at the bottom of a corrosion pit under multiaxial cyclic-static loads is determined by the stress-intensity factor range deduced from $\Delta\sigma_{n,max}$, in the same manner as the crack initiation under multiaxial loads.

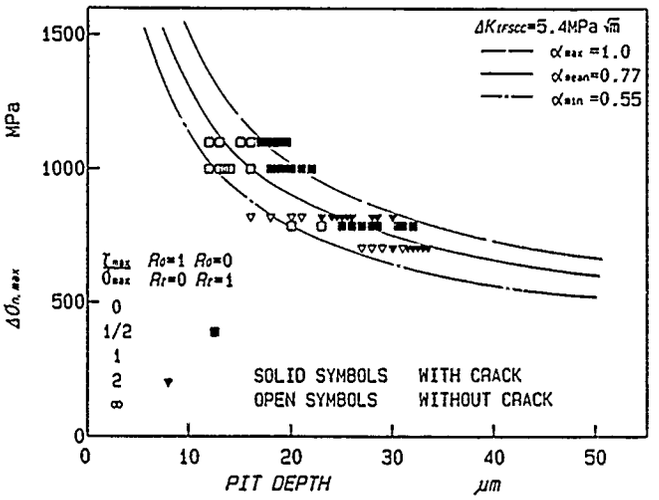


FIGURE 11—Relation between pit depth and $\Delta\sigma_{n,max}$.

We should note that the tensile stress ratio in the plane, where the tensile stress range is maximum, was rather small in the present experiment, ranging from 0 to 0.2. One author already reported that the threshold values of cyclic SC crack growth were strongly dependent on stress ratios, and that the linear relationship existed between stress ratios and the threshold values.[16] Therefore, one should also consider the effects of a maximum tensile stress or a mean value of stress variations in addition to the tensile stress range on crack initiation, when an applied tensile stress ratio is high. In fact, some cracks existed in the plane, where a tensile stress range was not maximum, as shown in Figure 12. In the plane, a maximum or a mean value of tensile stresses was larger than those in the plane where the tensile stress range reached the maximum. Figure 13 shows the relation between the number of cracks and crack angle (θ) defined by the angle between the longitudinal direction of a specimen and the normal direction of a crack. Most of cracks were dominated by $\Delta\sigma_{n,max}$ and θ equaled 0. However, some cracks existed that were affected by a maximum or a mean value of tensile stresses.

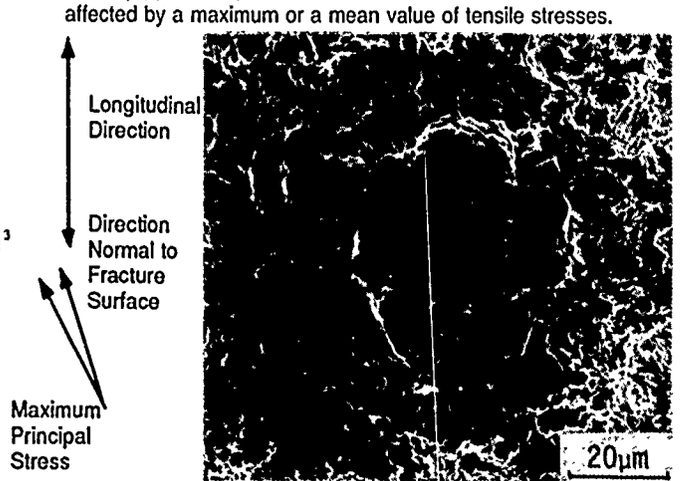


FIGURE 12—Crack initiated at the bottom of a corrosion pit under multiaxial cyclic-static loads (τ_{max}/σ_{max} = 1/2, σ_{max} = 1100 MPa, R_σ = 0, τ = 550 MPa, R_τ = 1).

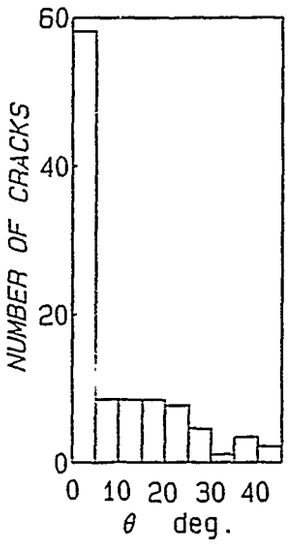


FIGURE 13—Distribution of cracks against crack angle (θ) (τ_{max}/σ_{max} = 1/2, σ_{max} = 1100 MPa, R_σ = 0, τ = 550 MPa, R_τ = 1).

Conclusion

Initiation behavior of cyclic SC cracks under multiaxial loading conditions were investigated in a high-strength steel, type 4135, sensitive to hydrogen embrittlement SC cracking, and the following were made clear.

(1) In the case of multiaxial cyclic-load tests, where in-phase cyclic tensile and torsional loads at a stress ratio of 0 were applied to specimens, a cyclic SC crack normal to the maximum principal stress was initiated at the bottom of a corrosion pit. In this case, the life of cyclic SC cracking was dominated by the maximum principal stress ($\sigma_{1,max}$), which equaled the maximum principal stress range ($\Delta\sigma_{1,max}$).

(2) In the case of multiaxial cyclic–static loads, where one of two applied loads was cyclic and the other static, a cyclic SC crack normal to the maximum tensile stress range was initiated at the bottom of a corrosion pit, provided that a static tensile load in the plane of the maximum tensile stress range was relatively small. In this case, the life of cyclic SC cracking was dominated by the maximum tensile stress range ($\Delta\sigma_{n,max}$).

(3) The mechanical condition dominating crack initiation at the bottom of a corrosion pit was determined by the stress-intensity factor range (ΔK_{IFSCC}) calculated on the assumption of a corrosion pit being a surface crack.

Acknowledgment

This study was performed through the Special Coordination Funds of the Science and Technology Agency of the Japanese Government for the fiscal year 1987 and through the Scientific Research Funds by the Ministry of Education of the Japanese Government for the fiscal years 1986 and 1987.

References

1. K. Endo, K. Komai, I. Yamamoto, Proceedings of the 22nd Japan Congress on Material Research (Japan: The Society of Materials Science, 1979), p. 199.
2. K. Endo, K. Komai, T. Fujimoto, Y. Matsuda, Bulletin Jpn. Soc. Mech. Engs. 23(1980): p. 807.
3. F.P. Ford, M. Silverman, Corrosion 36(1980): p. 597.
4. K. Endo, K. Komai, I. Yamamoto, Bulletin Jpn. Soc. Mech. Engs. 24(1981): p. 1326.
5. K. Komai, K. Minoshima, Advanced Materials for Severe Service Applications, ed. K. Iida, A.J. McEvily (Amsterdam, The Netherlands: Elsevier Applied Science Publishers, 1987), p. 373.
6. K. Komai, K. Minoshima, M. Yasumura, Proceedings of the 30th Japan Congress on Material Research (Japan: The Society of Materials Science, 1987), p. 77.
7. X. Chen, K. Nakasa, Trans. Jpn. Soc. Mech. Engs., 53A(1987): p. 935 (in Japanese).
8. M. Kido, H. Takei, K. Nakasa, Preprint of 35th Spring Meeting of Society of Materials Science (Japan: The Society of Materials Science, 1986), p. 52 (in Japanese).
9. Y. Ishikawa, T. Ozaki, N. Hosaka, O. Nishida, Boshoku-Gijutsu (Corrosion Engineering) 29(1980): p. 502 (in Japanese).
10. S. Takasaki, T. Kontani, J. Soc. Mater. Sci. 36(1987): p. 72 (in Japanese).
11. H. Imagawa, K. Matsuno, J. Soc. Mater. Sci. 36(1987): p. 76 (in Japanese).
12. K. Minoshima, A. Okubo, K. Komai, Proceedings of the 31st Japan Congress on Material Research (Japan: The Society of Materials Science, 1988), p. 39.
13. K. Komai, K. Minoshima, T. Fujito, Trans. Jpn. Inst. Metals 27(1986): p. 23.
14. K. Komai, K. Minoshima, S. Kinoshita, G. Kim, JSME Int. J. 31(1988): p. 606.
15. J.C. Newman, I.S. Raju, Eng. Frac. Mech. 15(1981): p. 185.
16. K. Endo, K. Komai, Y. Matsuda, Bulletin Jpn. Soc. Mech. Engs. 24(1981): p. 1885.

Discussion

R.P. Wei (Lehigh University, USA): Does stress corrosion (SC) cracking always initiate from corrosion pits?

K. Komai: Whether SC cracks initiate from corrosion pits or not depends upon the material–environment system, but in many cases corrosion pits play a dominant role in the initiation of SC or corrosion fatigue cracking. Our proposal is very simple and useful, which enables us to make life predictions of machines and structures operated in aggressive environments.

D.J. Duquette (Rensselaer Polytechnic Institute, USA): Quite often pitting is not observed on some alloys unless stress is applied. One of the difficulties of correlating pits with crack initiation is that cracks and pits are often associated, and pitting that precedes cracking cannot be treated independently. The relationship between pitting and cracking is still not well established.

K. Komai. In the case of aluminum alloys in sodium chloride solution, SC cracks under sustained load with small vibratory stresses superimposed were initiated at grain boundaries or hydrogen-induced {111} cleavages, and corrosion pits were not observed prior to the cracking (Komai, et al., Japan Soc. Mech. Eng Internat J 30(1987). p. 401]. On the other hand, in corrosion fatigue [Komai, et al., ibid. 30(1988): p. 606] as well as in cyclic SC cracking of high tensile strength steels in synthetic seawater, or in sodium chloride solution, corrosion pits always preceded cracking, and the mechanical condition dominating the crack initiation at the bottom of a corrosion pit was strictly determined by the stress-intensity factor range calculated on the assumption of a corrosion pit being a surface crack.

R.P.M. Procter (University of Manchester Institute of Science and Technology, UK): I would like to confirm and support the point just made by Duquette, but in a different alloy system. My colleague Cottis has shown that in carbon-manganese ferritic/pearlitic structural steels subject to corrosion fatugue in seawater, cracks initiate at pits that form around sulfide inclusions; however, the pitting around sulfide inclusions is much more severe in specimens that are subjected to cyclic loading than in static unstressed specimens. This is another example of a synergistic interaction between cyclic loading, pitting corrosion, and corrosion fatigue crack initation.

K. Komai: In corrosion fatigue, stress variation plays the most important role, and I agree with your opinion of a synergistic interaction between cyclic loading, corrosion pits, and corrosion fatigue crack initiation.

Relationships Between Plasticity and Stress Corrosion Cracking

*D.B. Kasul, C.L. White, and L.A. Heldt**

Abstract

Polycrystalline β-brass was prestrained various amounts in air or in an inhibiting environment (aqueous NaCl). The subsequent ductility in distilled water, which causes stress corrosion cracking (SCC), decreases linearly with prestrain.

SCC crack growth in large, single-crystal compact-tension specimens has also been characterized using crack velocity vs stress intensity and x-ray rocking-curve measurements. Rocking-curve results on a (100) SCC fracture surface indicate a high near-surface dislocation density that does not change appreciably with increasing stress intensity.

These results are consistent with models of SCC that are based on environment-induced dislocation activity.

Introduction

Several studies of stress corrosion cracking (SCC) have shown that a high density of dislocations develops in the near-surface region before cracking.[1-3] Kamachi, Otsu, and Obayashi used transmission electron microscopy and x-ray diffraction methods and found that for austenitic stainless steels, under otherwise identical conditions of stress and temperature, boiling $MgCl_2$ solution (an SCC environment) causes a much higher dislocation density to form in the near-surface regions than does an innocuous environment.[4] There are similar observations for other materials, including Naval brass[1] and titanium alloys.[2] These researchers have noted that stress corrosion cracks initiate when a critical dislocation density is reached. Similar behavior has been observed for materials undergoing fatigue cracking.[5-7] For example, Kramer, et al.,[1] have shown that cracking occurs in Naval brass when the dislocation density, as determined from measurement of microstrains by x-ray diffraction, reaches a value of approximately 6×10^{11} cm^{-2} for both SCC in a $CuSO_4$ environment and for fatigue in air.

With the above in mind, a series of slow-strain-rate experiments was designed to test the effects of prestraining in an innocuous environment on subsequent ductility in an SCC environment. β-brass polycrystals were prestrained various amounts in air or in 0.015 M aqueous NaCl and then strained to failure in distilled water. These alloys typically exhibit 55% elongation to failure in air and about 6% elongation in distilled water (an SCC environment). Tensile elongations in aqueous NaCl, an inhibiting environment, are comparable to those in air.

If there is, in fact, a critical dislocation density required for cracking, and if the rate at which that density is accumulated depends on the presence or absence of an SCC environment, then we expect a quantifiable relationship between the extent of prestrain in air or an inhibiting environment, and the subsequent strain exhibited in an SCC environment. We will show that such a relationship apparently exists for β-brass.

Measurements were also made of crack velocity as a function of stress intensity for β-brass single crystals. X-ray rocking curves[8] were taken from the fracture surface at two different locations in the Stage II cracking region to determine the near-surface strains associated with SCC.

Experimental Procedure

The materials used for study were single-crystal and polycrystalline β-brass containing approximately 49.0 wt% Zn. Polycrystal tensile specimens were produced by alternately swaging and annealing as-cast bars 20 mm in diameter down to 6.4 mm. Gauge sections 12.7 mm long and 3.2 mm in diameter were machined and the samples final annealed at 500°C for 1 h, which resulted in a grain size of approximately 250 μ. Single crystals of β-brass 37.5 mm in diameter and 23 cm long were grown parallel to [100] by the Bridgman method. A [100] seed crystal 6.4 mm in diameter and 5 cm long was used to initiate growth parallel to [100] in the larger crystal. Round compact-tension (CT) specimens[9] 5.6 mm thick and 37.5 mm in diameter were then obtained by slicing the crystal with a high-speed wafering saw. These were notched parallel to [100] with a slow-speed diamond saw using a 60° beveled blade. All specimens were electropolished in a cold bath of 33% nitric acid and 67% methanol prior to testing.

Polycrystal samples were tested at a strain rate of 1×10^{-5} s^{-1} in a nylon and polystyrene environmental cell. After prestraining in either air or a 0.015 M NaCl solution, straining was continued in distilled water until the onset of cracking was indicated by a drop in the measured load. For the air prestrain tests, distilled water was simply added to the cell once the desired extent of prestrain had taken place. For the 0.015 M NaCl prestrain tests, the solution was flushed from the cell and replaced with distilled water at the appropriate level of strain. In both cases, straining was continuous during the entire test. The single-crystal CT samples were tested in distilled water under constant load. Crack growth was monitored by a Krak-Gage† and the resulting fracture surfaces were examined by scanning electron microscopy (SEM). X-ray rocking curves were taken from the fracture surfaces, as shown in Figure 1. A Cu target with 0.1° beam slits was used for the x-ray source. The full-width half maximum (FWHM) of the (200) diffraction peak was measured for the fracture surface (B) and for an annealed specimen (b). The normal-

*Department of Metallurgical Engineering, Michigan Technological University, Houghton, MI 49931.

†Trade name.

ized rocking-curve breadth (B/b) was taken as a measure of the dislocation density in the sampled volume. Depth profiles were obtained by measuring B after electropolishing known thicknesses of material from the fracture surface.

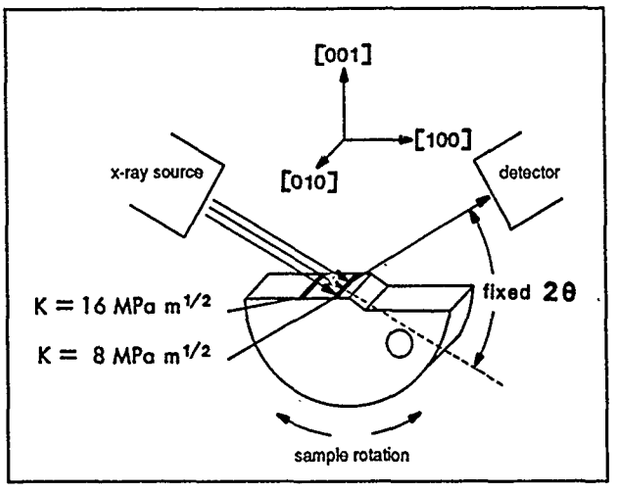


FIGURE 1—Schematic diagram of apparatus for obtaining rocking curves from (200) fracture surface of single-crystal compact-tension specimens. Fracture surfaces were incrementally electropolished to obtain a depth profile.

Results

Prestrain effects

As previously noted, ductility of the polycrystalline material is approximately 55% in air and failure is by ductile rupture, whereas in distilled water the value is about 6%. The SCC fracture of the polycrystalline samples is totally intergranular with zero prestrain; increasing prestrain increases the fraction of transgranular cracking. Figure 2 gives the effects of specific amounts of prestrain on subsequent deformation and fracture in distilled water. The plot of additional strain in distilled water vs prestrain in air has a constant slope of approximately −0.3. This indicates that straining in distilled water is approximately three times as effective in bringing the material to the point of crack initiation as is prestraining in air. This is also indicated by the plot (Figure 2) of [1/3 prestrain + strain in water], which is remarkably constant over the tested range of prestrain (0 to 21%). For specimens having the greatest amount of prestrain (21%), very little additional strain in water can be accommodated; fracture occurs within one minute.

Figure 3 shows the effects of prestraining β-brass polycrystals in a 0.015 M NaCl solution on additional strain in water. This NaCl solution is an effective inhibitor of SCC in brasses;[10] it causes the ductility of β-brass to be nearly that observed in dry air. Comparison of Figure 3 to Figure 2 indicates prestraining in the NaCl solution has a similar effect to prestraining in air.

Compact-tension specimen testing

Figure 4 shows the results of the crack velocity vs stress intensity for β-brass single crystals. The SCC cracks propagate on {100} planes in <110> directions[11] and have the macroscopic appearance of brittle transgranular cleavage fractures. K_{SCC} was found to be approximately 4.8 MPa·m$^{1/2}$. The Stage II crack velocity was found to be 1.4×10^{-4} mm s^{-1}.

The results of x-ray rocking-curve studies taken from a CT specimen fracture surface at two locations representing different stress intensities are shown in Figure 5. Figure 6 shows an example of the fracture surface in the Stage II region. Interpreted in terms of dislocation densities, these curves indicate relatively high densities within 20 to 30 μ of the fracture surface that are not strongly dependent upon the local stress intensity. The normalized peak breadths decrease to values comparable to those for annealed crystals upon removal of approximately 100 μ from the SCC fracture surface. Of particular interest in Figure 5 are the points corresponding to the as-fractured surface. The B/b ratios for the two locations are nearly the same (2.9 and 3.0 for the low and high K regions, respectively).

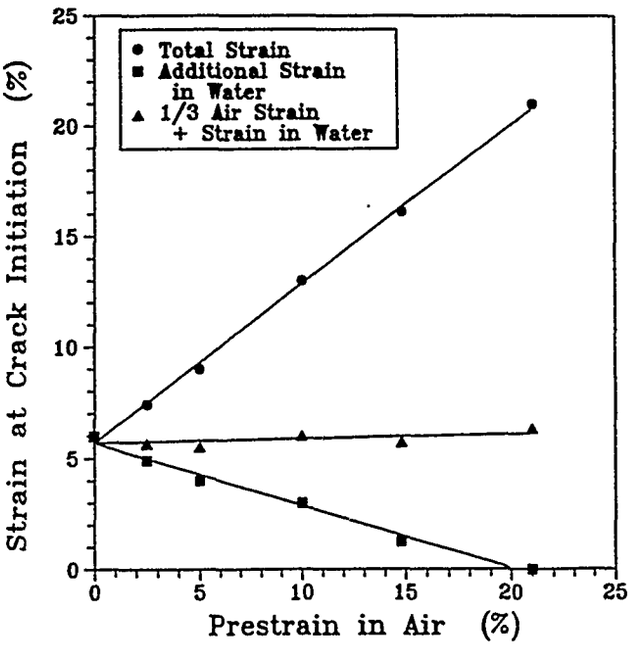


FIGURE 2—Prestrain in air vs ϵ_{total}, ϵ_{water}, and $(1/3\epsilon_{air} + \epsilon_{water})$.

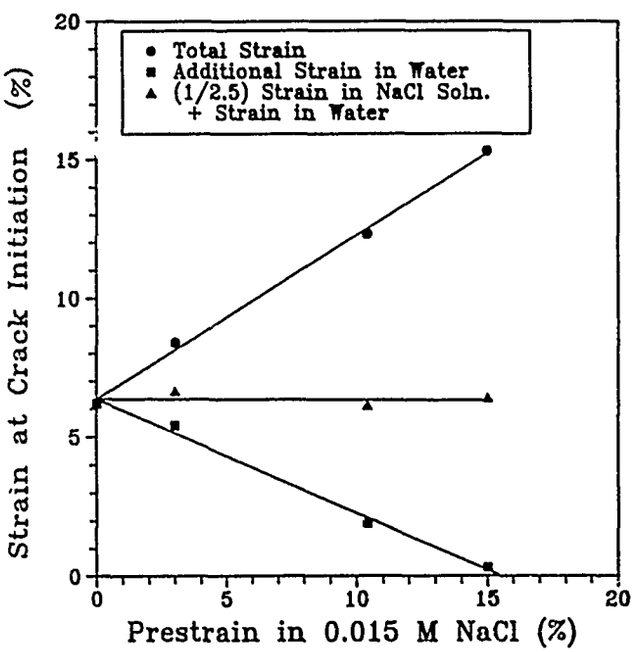


FIGURE 3—Prestrain in 0.015 M NaCl vs ϵ_{total}, ϵ_{water}, and $1/2.5\epsilon_{NaCl\ soln} + \epsilon_{water}$.

Discussion

According to the data presented in Figure 2, there is a linear relationship between the amount of prestrain in air and the additional amount of strain that can be accommodated by β brass in distilled water ($1/3\epsilon_{air} + \epsilon_{water}$ = constant). Kramer, et al.,[1] have shown that

an SCC environment for Naval brass, 0.1 M $CuSO_4$ at open-circuit potential, causes the observed average linear rate of dislocation accumulation with strain ($d\rho/d\epsilon$) for both the surface and the interior regions to be higher by a factor of two than the rate measured in air. This factor increases to nearly three when the samples are anodically polarized to +540 mV_{SCE} and goes to unity when the samples are cathodically protected.

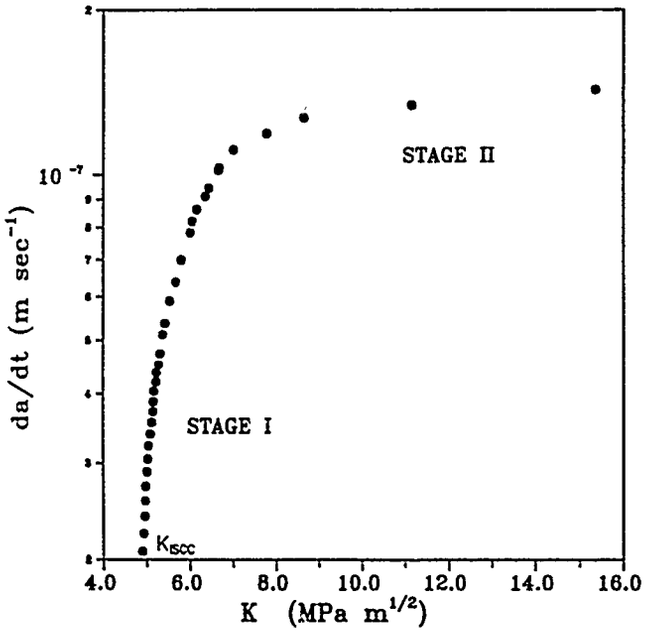


FIGURE 4—Crack velocity as a function of stress intensity for β-brass single-crystal compact-tension specimens. Specimens were oriented so that SCC occurred on (100).

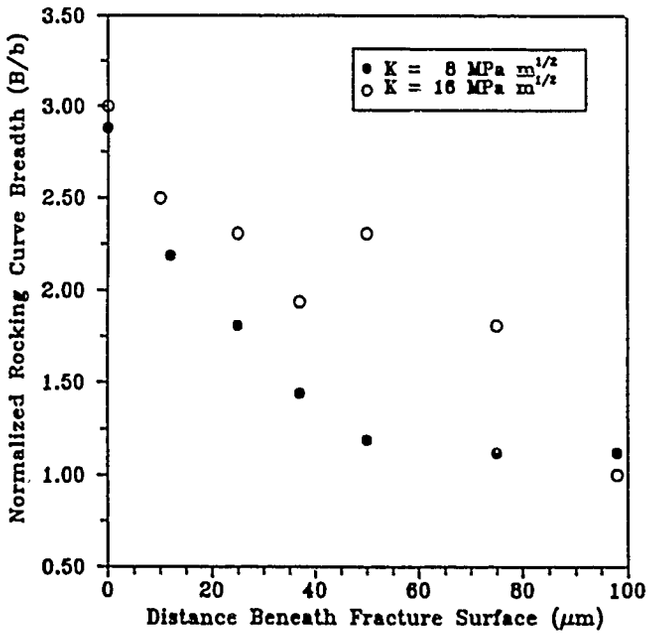


FIGURE 5—Ratio (B/b) (B = as-measured full-width half maximum (FWHM), b = annealed (FWHM) for rocking curves from (200) fracture surface of β-brass single-crystal compact-tension specimen.

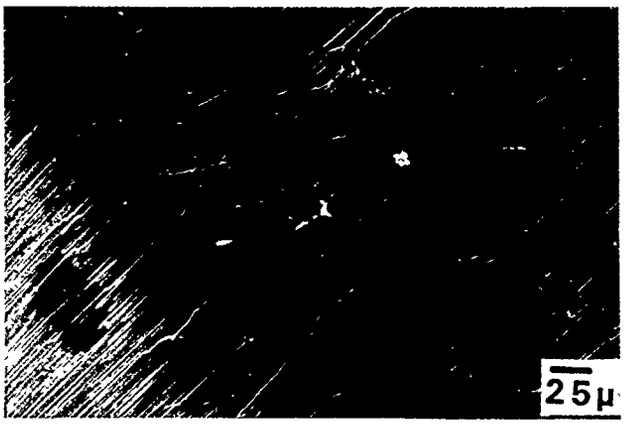


FIGURE 6—SEM micrograph from Stage II cracking region of (100) fracture surface from single-crystal compact-tension specimen. River lines are parallel to <110>.

If we assume that β-brass in distilled water (and perhaps other systems) behaves similarly to Naval Brass in 0.1 M $CuSO_4$, we can take the average rate of dislocation accumulation during tensile deformation in air [$(d\rho/d\epsilon)_{air}$] and the rate during deformation in water [$(d\rho/d\epsilon)_{water}$] to be constants. The work of Kramer, et al., suggests that

$$(d\rho/d\epsilon)_{air} \times \epsilon_{air} + (d\rho/d\epsilon)_{water} \times \epsilon_{water} = (\rho_{cnt})_{water} \qquad (1)$$

where $(\rho_{cnt})_{water}$ is the critical dislocation density required for crack initiation in water. Thus, based on a slope of approximately −0.3 for strain in water vs prestrain in air (Figure 2), our results suggest that

$$(d\rho/d\epsilon)_{water} \approx 3\,(d\rho/d\epsilon)_{air} \qquad (2)$$

Then from Equation (1),

$$1/3\epsilon_{air} + \epsilon_{water} = \frac{(\rho_{cnt})_{water}}{(d\rho/d\epsilon)_{water}} = \text{constant} \qquad (3)$$

The constancy of $1/3\epsilon_{air} + \epsilon_{water}$ for $0 < \epsilon_{air} < 21\%$ is seen in Figure 2. Similar results were obtained for β-brass prestrained in the inhibiting 0.015 M NaCl solution (Figure 3). Here the slope of the prestrain vs distilled water strain is ≈ −0.4, implying that

$$(d\rho/d\epsilon)_{water} \approx 2.5\,(d\rho/d\epsilon)_{NaCl\ soln} \qquad (4)$$

a value that is comparable to that for air prestrain. Accordingly, our results are consistent with the concept of environment-enhanced dislocation accumulation preceding crack initiation.

Environment-induced deformation is also invoked in the model proposed by Lynch for stress corrosion crack propagation.[12-16] Here, crack advance is accomplished by environment-induced slip in the crack-tip region. The nature of the necessary environmental interaction is not known. Lynch has postulated an adsorption process; and a model described by Hintz[17] takes into account that dissolution products may be active as adsorbates at the crack tip. Kaufman and Fink[18] suggest that dissolution and enhanced local plastic flow combine synergistically to cause crack propagation. Whatever the interaction, the present results indicate the response to the environment can be very rapid; samples prestrained in air 21% or more began to crack within one minute of exposure to distilled water.

The rocking-curve results (Figure 5) demonstrate the line broadening measured at two locations on the fracture surface in the Stage II cracking region (K = 8MPa·m$^{1/2}$ and K = 16 MPa·m$^{1/2}$) is nearly the same, with B/b ratios of 2.9 and 3.0 respectively. These FWHM ratios, indicative of the relative dislocation density, suggest that the final dislocation density at the fracture surface is insensitive to K in the Stage II cracking region where these data were taken.

Although the observed line broadening could result from dislocations generated either ahead of the crack tip or at the crack tip, the high dislocation density is uniform along the fracture surface. This also supports the previously reported concept that cracking in an SCC medium occurs at a critical dislocation density.

Summary

For β-brass, the additional strain that can be accommodated in distilled water (which causes SCC) decreases linearly with increasing prestrain in an innocuous environment (air or aqueous NaCl).

Rocking-curve measurements on a single-crystal SCC fracture surface indicate a relatively high dislocation density near the surface. The density does not change appreciably as the stress intensity increases.

The results support the concepts of environment-induced dislocation activity and cracking occurring at a critical dislocation density.

Acknowledgment

The authors gratefully acknowledge the assistance of Margaret E. Denomme. This research is sponsored by the U.S. Department of Energy, Grant No. DE-FG02-86ER 45255.

References

1. I.R. Kramer, B. Wu, C.R. Feng, Mater. Sci. Eng. 82(1986): p. 141.
2. R.M. Yazic (Ph.D. diss., Rutgers University, 1982).
3. C.F. Lo, W.E. Mayo, S. Weissmann, CORROSION/88, paper no. 282 (Houston, TX. National Association of Corrosion Engineers, 1988).
4. K. Kamachi, T. Otsu, S. Obayashi, Trans. Jpn. Inst. Met. 35(1971): p. 64.
5. I.R. Kramer, C.R. Feng, B. Wu, Mater. Sci. Eng. 80(1986): p. 37.
6. R.N. Pangborn, S. Weissmann, I.R. Kramer, Metall. Trans. 12A(1981): p. 109.
7. I.R. Kramer, S. Weissmann, Proceedings of the Symposium on Novel Non-Destructive Evaluation Methods for Materials (Warrendale, PA. The Metallurgical Society-American Institute of Mining, Metallurgical, and Petroleum Engineers, 1982), p. 141.
8. Metals Handbook, 9th ed., Vol. 10 (Metals Park, OH: 1986).
9. ASTM Designation E399-S3 (Philadelphia, PA: ASTM).
10. H. Uhlig, K. Gupta, W. Liang, J. Electrochem. Soc. 122(1975): p. 343.
11. W.K. Blanchard Jr., L.A. Heldt, Metall. Trans. 20A(1989). p. 1439.
12. S.P. Lynch, Dept. of Defence, Defence Science and Technology Organisation Aeronautical Research Laboratories, Aircraft Materials Report 119 (Commonwealth of Australia, 1986).
13. S.P. Lynch, J. Mater. Sci. 21(1986): p. 692.
14. S.P. Lynch, Scripta Metall. 20(1986): p. 1067.
15. S.P. Lynch, J. Mater. Sci. 20(1985): p. 3329.
16. S.P. Lynch, Corros. Sci. 22(1982): p. 925.
17. M.B. Hintz, Scripta Metall. 19(1985): p. 1445.
18. M.J. Kaufman, J.L. Fink, Acta Metall. 36(1988): p. 2213.

Discussion

W.W. Gerberich (University of Minnesota, USA): In your single-crystal [001], (001) orientation, the crack appears to be growing in a <110> direction. We also find this in hydrogen-induced or overload cracking in many body-centered cubic materials. Do you understand why cracking always occurs in the <110> direction?

L.A. Heldt: We have confirmed (Blanchard and Heldt, Metall. Trans., in press) that the direction of cracking is [110]. Ayres and Stein [Acta Metall. 19(1971) p. 789] assumed cleavage is a high-velocity process accompanied by plastic deformation at the crack tip. Although cleavage on the {011} is predicted on the basis of surface energy alone, they considered that the favored cleavage system would be that which caused minimum plastic deformation in front of the crack tip, i.e., the cleavage system that results in the lowest shear stress on the slip planes. Their analysis shows that cleavage on the {100} plane in the [110] direction is the favored system.

Crack Initiation and Short Crack Growth During the Corrosion Fatigue of Steels in Saline Solutions

*R.A. Cottis, A. Markfield, A. Boukerrou, and P. Haritopoulos**

Abstract

The initiation and early stages of growth of fatigue and corrosion fatigue cracks have been studied for two steels. The first of these was a quenched and tempered steel equivalent to HY80; the second was a ferritic-pearlitic structural steel to BS4360 grade 50D. Tests were performed in fully reversed four-point-bend loading at a frequency of 25 Hz. For both steels, cracks were found to nucleate primarily at inclusions and to propagate at stress-intensity factor ranges well below the threshold for long cracks. For tests conducted above the air fatigue limit, the effect of corrosion in 3.5% NaCl solution was to enhance the growth of the small cracks; at the same time, the cracks were seen to be significantly wider than those formed in air. The acceleration of crack growth in this regime is postulated to be associated with the effects of corrosion in assisting the growth of the crack through microstructural barriers such as grain boundaries. For tests performed below the air fatigue limit, the initiation process appeared to consist of pitting corrosion associated with sulfide inclusions, followed by fatigue crack growth when the crack length approached that required to achieve an appropriate threshold stress-intensity factor range. Once the cracks were growing in the "longer crack" regime (above about 1 mm in length), an acceleration due to corrosion was observed in these tests that was attributed to fully reversed loading conditions combined with crack broadening by corrosion. This reduced the effects of crack closure and increased the effective stress-intensity factor range.

Introduction

The initiation of corrosion fatigue cracks has frequently been associated with the development of pitting corrosion. Recently, understanding of the initiation and early stages of growth of fatigue cracks has been markedly enhanced by studies of the growth of cracks with dimensions on the order of the grain size (References 1 and 2) This work has demonstrated that fatigue cracks nucleate relatively easily, even in inert environments, and the fatigue behavior tends to be controlled by the ability of the cracks to cross the first few grain boundaries (or other microstructural barriers). This can be explained qualitatively in terms of the relative ease of slip on a single slip plane in a surface grain, compared to the much more difficult situation when the crack crosses into the next grain. This is repeated at subsequent grain boundaries and results in crack propagation of the form indicated in Figure 1. Small cracks also tend to grow under conditions in which the validity of linear elastic fracture mechanics breaks down, and, consequently, it becomes necessary to express the crack growth behavior in the form

$$da/dN = f(a, \Delta\sigma) \quad (1)$$

where a is the crack length, N is the number of cycles, and $\Delta\sigma$ is the stress range. Figure 2 attempts to present the typical form of this relationship, which is essentially a three dimensional representation of contour maps suggested by Brown.[3] Three regions can be seen on this diagram:

(1) Small a, low $\Delta\sigma$. No crack growth will occur, although it is not clear whether there is any threshold stress range below which no cracks will develop within single grains at the surface of the specimen.

(2) Small a, high $\Delta\sigma$. Crack growth occurs within single grains, and there is a marked reduction in growth rate as the crack approaches microstructural barriers such as grain boundaries. The crack growth rate in this regime is expected to be somewhat complex and probably requires statistical treatment to achieve a quantitative model. Thus, this region is only indicated schematically in Figure 2.

(3) Larger a, $\Delta\sigma$ sufficient to give $\Delta K \nearrow \Delta K_{th}$. The behavior will be defined by a crack growth law such as that due to Paris. For the shorter crack lengths and higher $\Delta\sigma$, the plastic-zone size may be sufficiently large that elastic-plastic fracture mechanics methods may be necessary to quantify the behavior.

The objective of the work presented here was to investigate the effects of corrosion on fatigue processes, with particular reference to the above views of the early stages of crack growth. Two materials have been investigated, a ferritic-pearlitic structural steel to BS4360 grade 50D and a quenched and tempered steel to specification Q1N. The latter specification falls almost entirely within the specification for HY80, and this material will be referred to as HY80 hereafter, as this specification is more widely known. The results obtained for the HY80 have been presented elsewhere.[4] This paper will concentrate on the results obtained for the structural steel, although the earlier results will be reproduced in sufficient detail to display their support for the models proposed.

*Corrosion and Protection Centre, University of Manchester Institute of Science and Technology, P.O. Box 88, Manchester, M60 1QD UK.

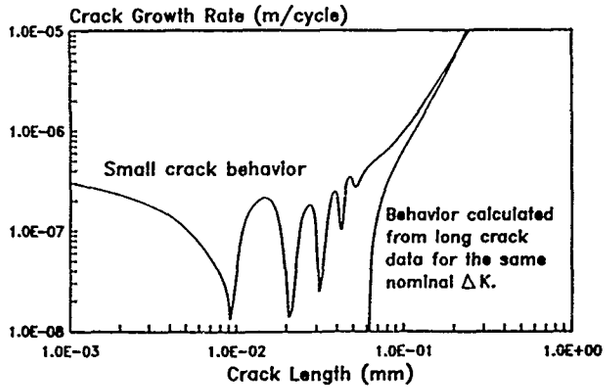


FIGURE 1—Propagation of a small fatigue crack, constant $\Delta\sigma$, crack length varying.

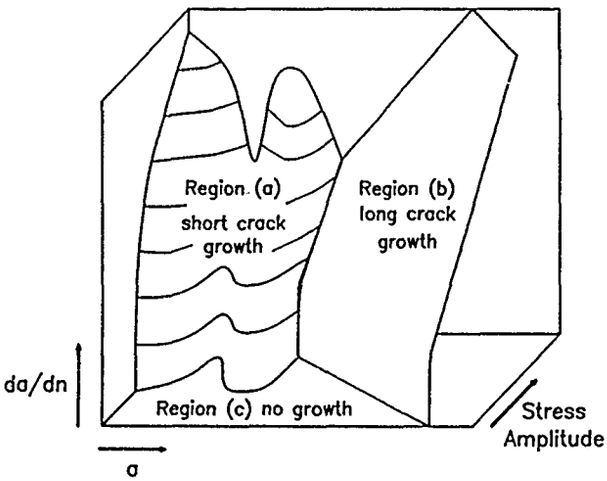


FIGURE 2—Schematic representation of crack growth as a function of a and $\Delta\sigma$.

Experimental

Materials

The composition and mechanical properties of the two materials that have been investigated are presented in Tables 1 and 2.

TABLE 1
Chemical Composition of Steels

Element	BS4360-50D	HY80
Carbon	0.16	0.15
Silicon	0.30	0.32
Manganese	1.44	0.35
Sulfur	0.011	0.007
Phosphorus	0.026	0.010
Nickel	0.03	2.61
Chromium	0.06	1.62
Molybdenum	<0.02	<0.05

TABLE 2
Mechanical Properties of Steels

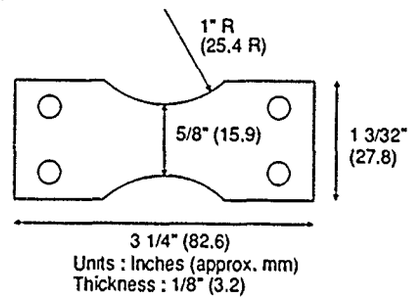
	BS4360-50D	HY80
0.2%Proof Stress (MPa)	378	610
Ultimate tensile stress (MPa)	522	730
Elongation (%)	30.5	23
Reduction of area (%)	69	69.5

Fatigue testing

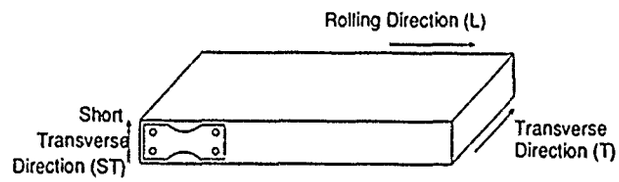
Fatigue tests were performed in an Avery-Denison† model 7803 testing machine. This uses a rather complex loading arrangement to provide a constant bending moment over the central region of the specimen (i.e., the loading is essentially four-point bend). The tests were performed at a frequency of 25 Hz, with a load ratio (R-value) of −1 (i.e., fully reversed bend). The test frequency was fixed by the design of the test machine. While it is high by comparison with recent crack growth studies on long cracks, it has been found to provide useful information for short cracks. An additional effect of the high frequency, fully reversed loading is that the flat surfaces of the specimen, in which the fatigue cracks initiate, are alternately exposed to tensile and compressive stresses. Thus, it seems unlikely that any accumulation of hydrogen to regions of triaxial stress can occur in the 20 ms tensile half-cycle, and it is considered improbable that hydrogen effects play a significant part in the results obtained in this work. For corrosion fatigue tests, the solution was placed in an open-topped silicone rubber cell surrounding the specimen. The vibration resulting from the fatigue cycling was presumed to ensure that the solution, which was in contact with the air, was fully aerated.

Specimen configuration

The specimen configuration is shown in Figure 3. Prior to testing, both surfaces and the edges of the specimen were polished to 1/4 μm diamond. It was necessary to polish all surfaces because any unpolished regions modified the corrosion behavior of the polished surfaces by virtue of their different corrosion potential. The specimen was clamped into the testing machine with steel bolts, and for the tests in solution, these were isolated from the solution by a thick coating of lacquer.



(a) Geometry of Bending Fatigue Specimen



(b) Specimen Orientation

FIGURE 3—Specimen configuration.

Crack growth measurements

The lengths of cracks developing on the surface were determined by optical microscopy. To achieve this, it was necessary to remove the specimen from the testing machine, and, in the case of the tests in solution, to clean the specimen to remove loose corrosion product and (probably more importantly) to remove the saline environment to restrict corrosion. While it is clear that this procedure will have modified the corrosion behavior to some extent, it is considered preferable to the alternative of taking plastic replicas from the surface, since there is evidence that the latter causes major perturbations in corrosion reactions.[5] Crack growth rates were computed directly from differences between individual crack lengths.

†Trade name.

Results

S-N curves

The curves of stress amplitude vs number of cycles to failure are presented in Figures 4 and 5. As expected, the effect of 3.5% sodium chloride solution is to reduce the fatigue endurance for both materials, with indications that the fatigue limit observed in air disappears in the corrosive environment.

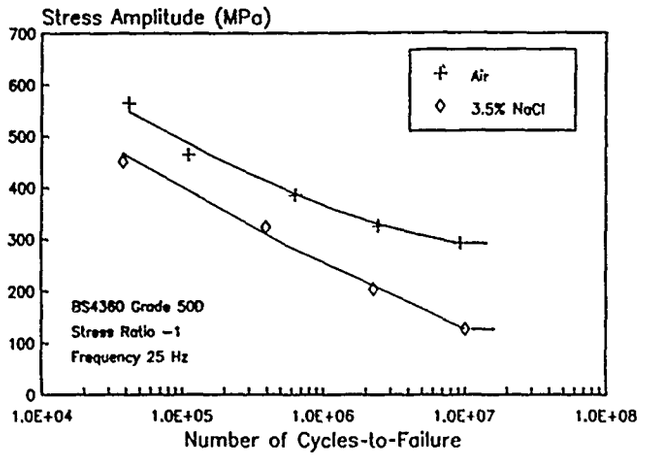


FIGURE 4—S-N curve for HY80.

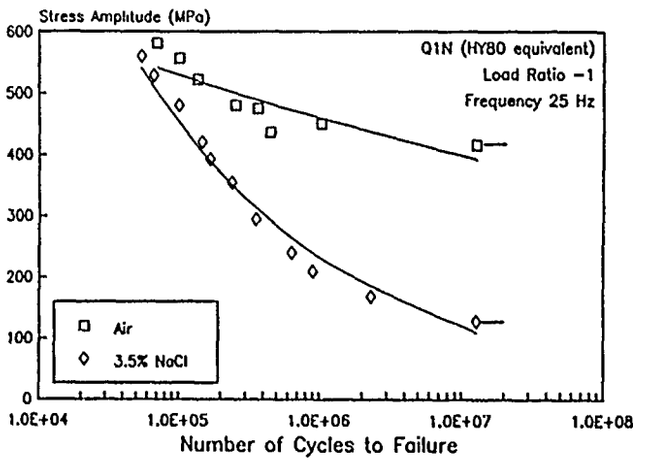


FIGURE 5—S-N curve for structural steel.

Crack growth behavior

The typical variation of crack length with time for the structural steel is presented in Figures 6 and 7 for air and 3.5% sodium chloride, respectively. To compare crack growth rates in the two environments, these tests were both performed above the air fatigue limit, and the extent of pitting associated with the tests in corrosion was very limited. Similar data for the quenched and tempered steel have been presented elsewhere.[4] Crack growth rates are plotted in Figure 8 as a function of crack length (for a constant stress amplitude of 350 MPa). Similar data for the quenched and tempered steel are presented in Figure 9, together with data obtained by other workers for long cracks (the latter have been converted from da/dN vs ΔK to da/dN vs a by assuming an appropriate K calibration, together with the actual stress amplitude of 540 MPa. As the crack is expected to be closed during the compressive half of the load cycle, only the tensile half of the cycle has been used in calculating ΔK). As all crack lengths in this work were measured at the specimen surface, the K calibration is based on a semielliptical crack with a c/a ratio of 0.75, which has been shown by other workers to be typical of small surface cracks.[7]

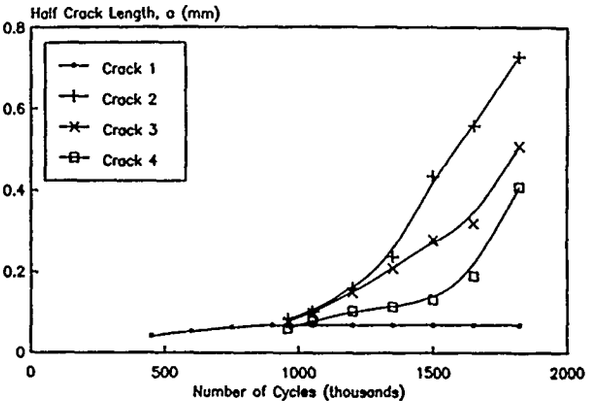


FIGURE 6—Crack length vs number of cycles for structural steel in air, stress amplitude 350 MPa.

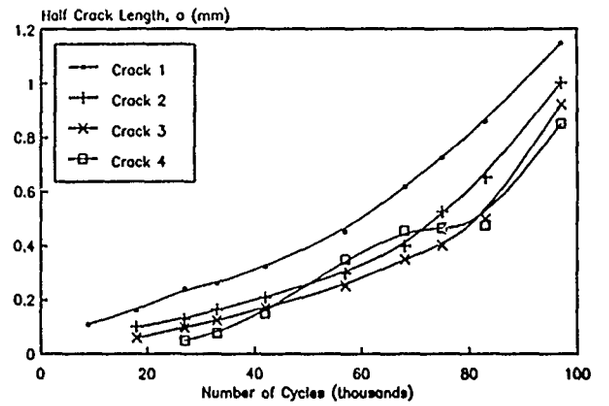


FIGURE 7—Crack length vs number of cycles for structural steel in 3.5% sodium chloride solution, stress amplitude 350 MPa.

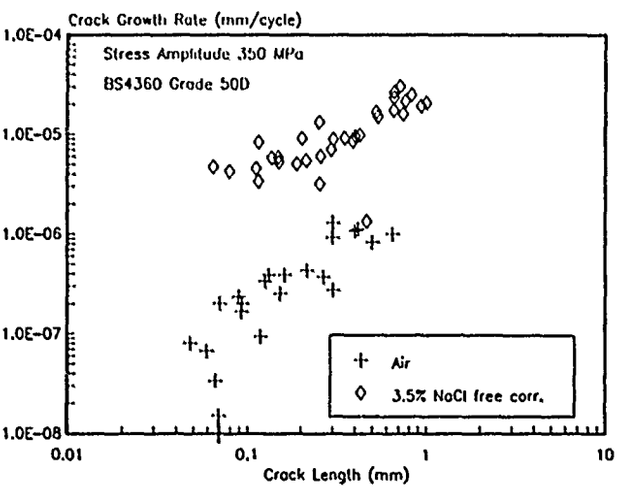


FIGURE 8—Crack growth rate vs crack length for structural steel determined by difference.

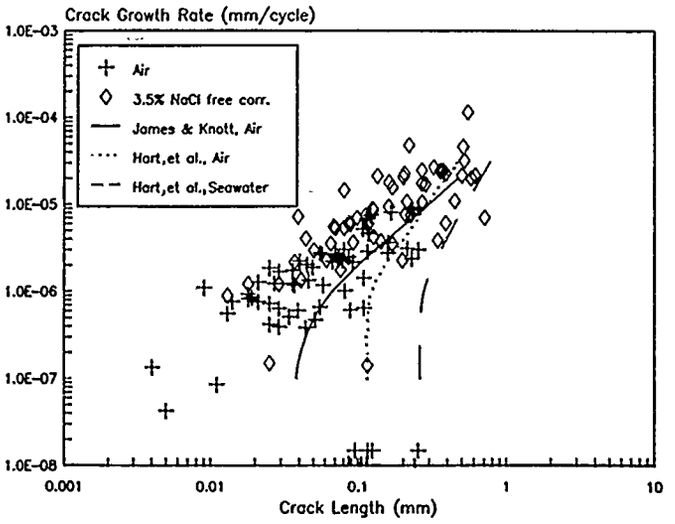


FIGURE 9—Crack growth rate vs crack length for quenched and tempered steel determined by difference.

Crack initiation sites

For both steels, the sites of crack initiation in air were primarily oxide inclusions, while in the corrosive environment, initiation moved to sulfur-containing inclusions, either plain sulfides or duplex inclusions.[4] At lower stress amplitudes, particularly below the air fatigue limit, crack initiation in corrosion was accompanied by pitting corrosion around the inclusions. As the applied stress range was reduced, the diameter of the pits found at fracture tended to increase, and the diameter of the largest pits found on failed specimens of the quenched and tempered steel are plotted on the Kitagawa diagram of Figure 10.

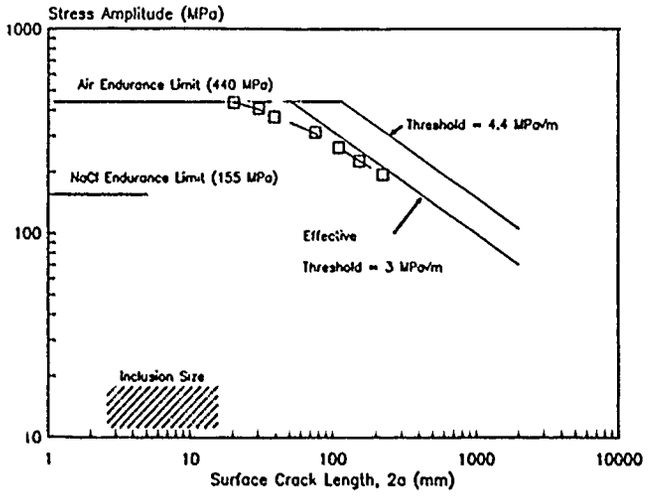


FIGURE 10—Pit depth at failure plotted on a Kitagawa diagram for quenched and tempered steel.

Discussion

Three regimes of behavior can be considered, according to the applied stress range and crack length:

(1) Low $\Delta\sigma$, small a. In this region, a fatigue crack would not be expected to grow in air (i.e., the stress range is below the air fatigue limit), although nonpropagating cracks may develop within individual grains. As indicated by Figure 10, it appears that cracks in corrosion fatigue initiate by pitting corrosion. Once the pits reach a sufficient size to attain the threshold stress-intensity factor range for crack growth, fatigue crack growth takes over. The pitting corrosion process may itself be influenced by the fatigue cycling, as pitting tests performed on static samples gave significantly lower pit densities than were observed on the fatigue samples, and the pitting on the fatigue samples tended to concentrate in the region of high cyclic stress. The mechanism of the pitting corrosion has been discussed elsewhere,[4] and it is considered to be associated with the enhancement of the anodic dissolution of the iron by the reduced sulfur species.

(2) High $\Delta\sigma$, small a: These have been described as microstructurally short cracks, and they will grow both in air and in the corrosive environment. For corrosion fatigue tests, relatively little pitting corrosion is observed over the time scale of the fatigue test. In this regime, it is notable that the fatigue cracks are much wider in the corrosive environment than in air. It is suggested that a primary role of corrosion in this situation is to assist in the propagation of the crack across microstructural barriers such as grain boundaries. To some extent, this may be considered simply a result of crack advance by a corrosion process. This would give a lower bound to the crack growth rate, which can be estimated from the pit growth rate. For the HY80, this may be estimated from Figure 10, which indicates that pits will grow to 200 μm in depth in the time required for a specimen to fail at an applied stress amplitude of about 200 MPa. From Figure 5, this implies a crack growth rate of 2×10^{-7} mm/cycle. It is difficult to test whether or not this minimum crack growth rate actually applies for the experiments presented here, as readings were taken rather infrequently, and the data obtained are averaged over a rather large number of cycles. However, it may be significant that the lowest crack growth rate observed in corrosion is on the order of 10^{-7} mm/cycle, whereas lower growth rates are observed in air.

Another aspect of the effect of corrosion of the crack tip in this regime is that corrosion will tend to blunt the crack tip. At first this might be expected to reduce the crack growth rate, and this process has been postulated to explain the increase in threshold stress-intensity factor range (ΔK_{th}) that is observed in some corrosive environments. However, further consideration of current views on the growth of microstructurally short cracks leads to a rather different conclusion. These cracks initiate easily within individual grains at free surfaces but tend to be arrested or delayed at microstructural barriers such as grain boundaries. Thus, a sharp crack at a grain boundary must be less damaging than an uncracked free surface. This is further demonstrated by the phenomenon of nonpropagating cracks that develop at notches but are unable to continue to propagate into the bulk material. This may be rationalized in terms of the effect of plastic constraint at the crack tip, which makes the reinitiation of the crack in the new grain more difficult than it is at the free surface, despite the stress concentration at the crack tip. Additionally, the slip planes in the new grain will usually be misaligned with respect to the crack tip, and the new crack will not be able to initiate on a single slip plane. By broadening the area of new grain exposed at a grain boundary, it is suggested that corrosion makes it easier for the crack to reinitiate in the new grain. In part this is because the reduction of plastic constraint will make slip in the new grain easier, and because the broader crack tip makes it easier to accommodate misalignment between the slip planes in the new grain and the plane of the crack as it approaches the grain boundary.

(3) High $\Delta\sigma$, larger a: In this work, the cracks in this region could be decribed as "chemically short," in that the crack length is larger than the grain size of the steel, but the chemical processes within the crack will be more markedly affected by the chemical conditions outside the crack than would be the case for longer cracks. In particular, it might be expected that the rate of corrosion at the crack tip will be much greater than would be the case for a long crack, which tends to be shielded from corrosion. This will be especially true for the results this work, which are based on measurements of surface crack length and will therefore be biased toward the effects of surface corrosion rates. In this region, cracks grow by essentially the same processes as long cracks.

For the test conditions studied in this work (in particular R = −1), broadening of the crack by corrosion of the crack walls leads to a reduction in the crack closure and a consequent increase in crack growth rate. At first sight, this effect is directly opposed to the concept of corrosion-product-induced crack closure postulated by Ritchie and others,[6] but these two phenomena can be reconciled by considering the site at which corrosion product is precipitated. If the corrosion product forms within the crack, it will probably act as a wedge and increase the closure load (since the corrosion product will almost inevitably have a larger volume than the metal from which it was formed). This is most likely to occur for longer cracks, particularly for cracks produced in humid air or low-conductivity electrolytes. In contrast, if the corrosion product precipitates outside the crack, as appears to be the case for the short cracks in the relatively concentrated chloride solutions used in this work, the closure load will be reduced, and crack growth rates will increase.

Summary of Proposed Mechanisms of Initiation and Early Growth of Corrosion Fatigue Cracks

The general behavior of fatigue cracks in corrosive environments is indicated in Figure 11. It is suggested that the crack growth rate is enhanced in all three regions (for the test conditions used in this work), although the detailed mechanisms may differ:

(1) Below the air fatigue limit, the main role of corrosion is to create pits that act as stress concentrators and cause the stress-intensity factor range to exceed the threshold. A secondary effect may be to reduce crack closure by corrosion of the walls of the crack and thereby reduce the effective threshold.

(2) Above the air fatigue limit, corrosion increases the growth rate of small cracks by corrosion of the crack tip, which allows the crack to cross the grain boundary more easily. This is partly because of the direct extension of the crack by corrosion, partly because of the reduction of constraint at the crack tip, which allows easier slip in the new grain, and partly because the broader crack tip makes it easier to accommodate the misorientation between the crack plane and the slip planes in the new grain.

(3) As the crack moves into the long-crack, Paris-law regime, the main effect of corrosion is to reduce closure by dissolution of the crack walls. For the fully reversed loading used in this work, this results in a doubling of the effective K, with a consequent increase in crack growth rate.

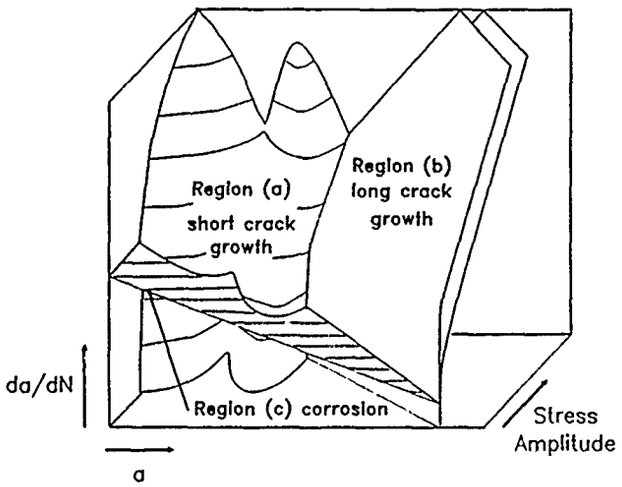


FIGURE 11—Effect of corrosion on the relationship between da/dN, a, and Δσ.

References

1. R.O. Ritchie, J. Lankford, eds., Small Fatigue Cracks (Warrendale, PA. The Metallurgical Society-American Institute of Mining, Metallurgical, and Petroleum Engineers, 1986).
2. K.J. Miller, E.R. de los Rios, eds., The Behaviour of Short Fatigue Cracks (Bury St. Edmunds, England. Mechanical Engineering Publications, 1986).
3. M.W. Brown, Fatigue of Engineering Materials and Structures, Vol. 1 (London, England. Institution of Mechanical Engineers, 1986), p. 93.
4. R.A. Cottis, A. Markfield, Proceedings of the Third International Conference on Fatigue and Fatigue Thresholds, Vol. 1, ed. R.O. Ritchie, E.A. Starke Jr. (Warley, England. Engineering Materials Advisory Services, 1987), p. 587.
5. R.A. Cottis, C.A. Loto, Materials Science Forum, Vol. 8, ed. M. Duprat (Aedermannsdorf, Switzerland: Trans Tech, 1986), p. 201.
6. R.O. Ritchie, R.M. Cannon, Acta Metall., in press 1989.
7. H. Kitagawa, Fatigue Thresholds, Fundamentals and Engineering Applications, Vol. 2, ed. J. Baecklund, J. Blom, C J Beevers (Warley, England: EMAS, 1982), p. 1051.

Low-Temperature Creep of Austenitic-Ferritic and Fully Austenitic Stainless Steels and a Ferritic Pipeline Steel

M.M. Festen, J.G. Erlings,** and R.A. Fransz****

Abstract

Low-temperature creep (LTC) behavior of duplex and type 316L (UNS S31603) stainless steels and API 5L X60 pipeline steel at 20°C has been determined at various stress levels below the yield stress ($\sigma_{0.2}$). It will be shown that even at these low stress levels, the LTC process may produce the plastic-straining conditions necessary for crack initiation in plastic-deformation-induced environmental cracking. Dynamic loading may pose an additional risk for stress corrosion cracking initiation as a result of a recurring LTC process.

Introduction

In many cases of stress corrosion cracking (SCC) and cracking that results from hydrogen embrittlement (HE), slow plastic deformation is a prerequisite for crack initiation and crack growth.[1-3] Careful test design is thus needed to acquire meaningful SCC/HE data. To this end, we previously developed a test procedure that permitted identification of the role of dynamic plastic deformation in SCC/HE cracking. This test procedure, based on various slow-strain-rate (SSR) tests, is explained in Figures 1 and 2.[2] The procedure is presently used for studies on SCC and HE mechanisms, for the assessment of environmental cracking susceptibilities under specific operating conditions, and for the generation of data for fitness-for-service analyses. For duplex stainless steel (SS), for example, in a variety of H_2S-containing environments, initiation of SCC was only observed when the material was subjected to slow plastic deformation.[3]

In constant-load tests, low-temperature creep (LTC) is known to result in significant amounts of plastic straining at tensile stresses above the yield stress.[4,5] Experimental confirmation that LTC at stress levels above the yield stress can result in SCC initiation was found in a cyclic loading experiment on carbonate/bicarbonate SCC of API 5L X60, a ferritic pipeline steel. Cyclic loading between 360 and 460 MPa (σ_{UTS} was 520 MPa and $\sigma_{0.2}$ was 382 MPa) at a strain rate of 7×10^{-7} s^{-1} and a frequency of 7×10^{-4} Hz, with the first cycles being performed at potentials outside the critical potential range for SCC initiation, resulted in severe cracking with a crack growth rate of 0.42 μm/cycle (2.1 μm/h). The stress-strain curve (Figure 3) clearly points to LTC during cyclic loading. In another test, no LTC was observed after prestressing of the specimen at σ_{UTS} prior to the same load cycling in the corrosive environment, and the SCC crack growth rate was an order of magnitude smaller.

Quantitative LTC data at stress levels below the yield stress, being of more practical importance, are scarce. In view of the dominant role of plastic straining for the initiation and propagation of environmental cracking in a number of cases, we investigated the occurrence of slow plastic deformation at stress levels below the yield stress ($\sigma_{0.2}$). In the present study, a strain rate between 10^{-5} and 10^{-9} s^{-1} is considered to be of practical significance for SCC initiation. The lower limit was chosen because of practical experimental limitations, because we observed SCC to occur at a strain rate in this order of magnitude,[2] and in view of realistic SCC crack propagation rates.

At low temperatures, creep is a transient process resulting from work hardening. The LTC strain (ϵ_{LTC}) generally obeys the equation $\epsilon_{LTC} = \epsilon_o \log(1 + \beta t)$, with t being time and ϵ_o and β being constants. Dynamic loading may cause additional creep after the creep by static loading has been exhausted.[5,6] This phenomenon can be explained as a special case of the Bauschinger effect, whereby the flow stress decreases as a result of unloading.[7] Since it was recently found that duplex SS is only susceptible to sulfide stress cracking in a sour environment if it is subjected to slow plastic straining, we performed LTC measurements with this material. API 5L X60 and type 316L (UNS S31603), an austenitic SS, were also examined.

Experimental

Solution-annealed duplex SS (UNS S31803), annealed type 316L SS, and API 5L X60 pipeline steel were tested for LTC in the as received condition. Tests were performed with dumbbell tensile specimens with a gauge length of 17.5 mm and a diameter of 3.5 mm for duplex SS and API 5L X60; for type 316L SS the dimensions were 31 mm and 4 mm.

LTC tests were performed in Mayes Unisteel† constant-load testing machines of 12 kN capacity, which were modified to enable gentle loading and load cycling. The LTC tests were done in a silicone oil bath at 20°C. Straining was measured with strain gauges of Hoettinger† Baldwin Messtechnik, a Vishay† 2110/2120 amplifier, and a Fluke† 8840A digital voltmeter. The load was measured with a load cell of Hoettinger Baldwin Messtechnik and recorded with a Hewlett Packard† 3955 digital voltmeter. The data acquisition and measurement control took place with a Hewlett Packard 86B computer. Constant load LTC straining was measured at several stress levels between the proportionality stress σ_p and $\sigma_{0.2}$. σ_p and $\sigma_{0.2}$ were measured at ambient temperature with a 50 kN tensile machine, built in-house. σ_p is strain rate dependent and was determined at a slow-strain rate. Dynamic loading LTC was measured on the same specimen after LTC by static loading had been exhausted. The load was cycled on/off between zero and the load used in the static test, at time intervals of 10 min.

*Koninklijke/Shell-Laboratorium, Amsterdam (Shell Research B.V.), Badhuisweg 3, 1031 CM Amsterdam, The Netherlands

**Shell Canada Limited, Calgary Research Centre, Calgary, Alberta T2P 356, Canada.

***Billiton Research B.V., Arnhem, The Netherlands.

†Trade name.

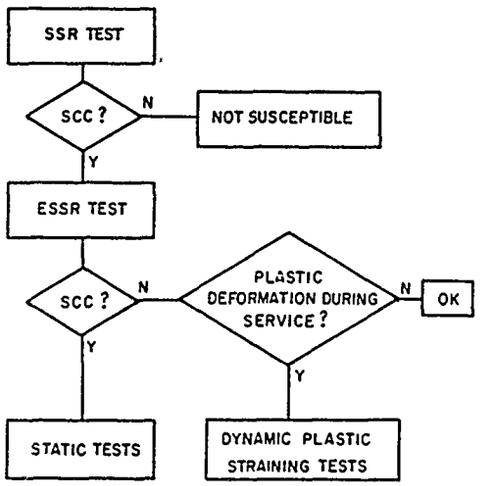


FIGURE 1—Stress corrosion cracking/hydrogen embrittlement test method selection procedure identifying the role of dynamic plastic straining. SSR = slow-strain rate; ESSR = elastic slow-strain rate; SCC = stress corrosion cracking.

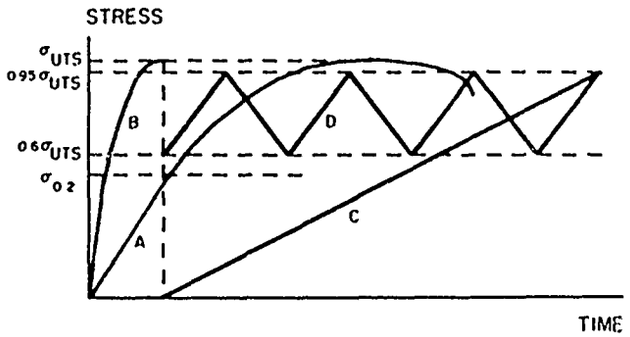


FIGURE 2—Schematic description of various test modes:
Mode 1 = A = monotonically rising load SSR test
Mode 2 = B + C = monotonically rising load ESSR test
Mode 3 = B + D = cyclic loading ESSR test

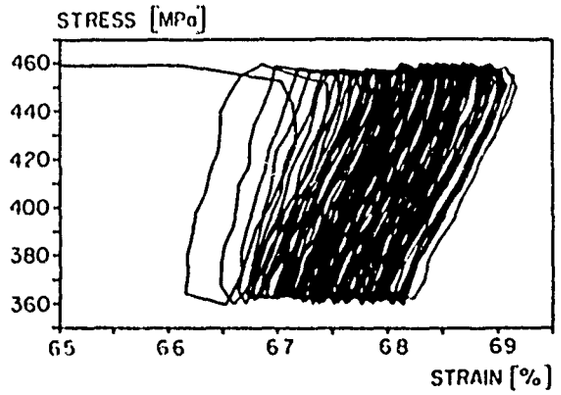


FIGURE 3—Stress-strain curve of API 5L X60 pipeline steel, showing low-temperature creep during cyclic loading at 75°C; σ_{UTS} = 520 MPa; $\sigma_{0.2}$ = 380 MPa.

Results and Discussion

The LTC straining during constant loading did obey the equation given in the introduction. The strain rate during load cycling was derived from a curve-fitting procedure applied to the envelope connecting successive individual cycles of loading using the same equation.

Duplex SS. Tensile testing revealed a $\sigma_{0.2}$ of 525 MPa, whereas an SSR test with a strain rate of 6×10^{-6} s^{-1} showed σ_p to be 265 MPa. Figure 4 gives the results of the LTC experiments with duplex SS Figure 4(a) shows the constant-load creep curves. Figure 4(b) shows the strain rate vs time for the constant-load test. At a constant stress level of 500 MPa, the specimen creeps with a strain rate larger than 10^{-9} s^{-1} for almost 3 days. Even at a constant stress level of 225 MPa, the creep rate is above this level for 1 h. The cyclic loading LTC strain rates are given in Figure 4(c); they show that, as a result of load cycling between 0 and 500 MPa—after the 500 MPa static load creep has been exhausted—the material still crept with a creep rate above 10^{-9} s^{-1} for approximately 1 day.

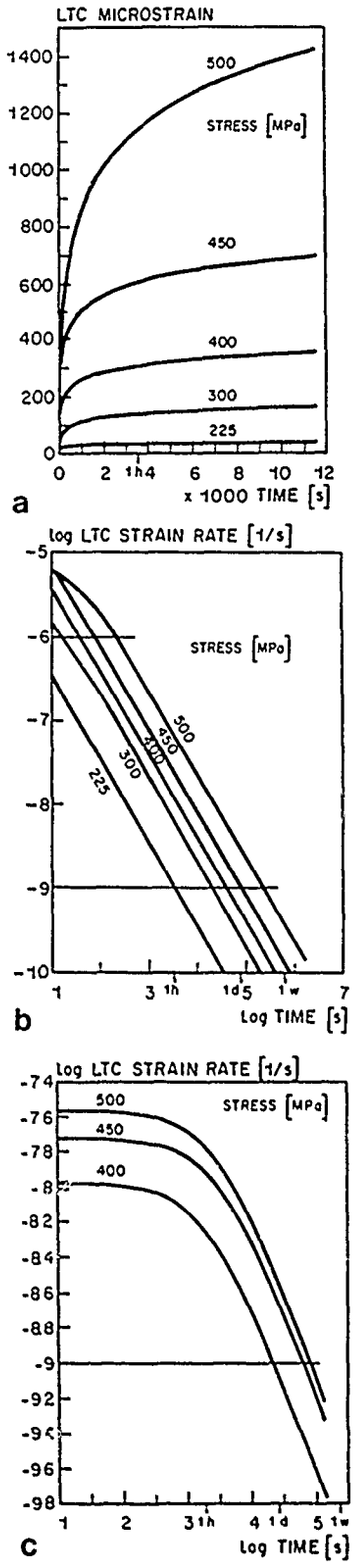


FIGURE 4—Low-temperature creep of duplex stainless steel at room temperature (yield stress is 525 MPa): (a) and (b) constant-load LTC strain vs time and (c) cyclic-load LTC (10/10 min) strain rate vs time.

Type 316L SS. SSR tensile testing at a strain rate of $7 \times 10^{-6}\ s^{-1}$ resulted in a σ_p value of 80 MPa and a $\sigma_{0.2}$ of 250 MPa. The experimental results, presented in Figure 5, show that LTC with a creep rate higher than $10^{-9}\ s^{-1}$ can be sustained during static loading for 1 h at σ_p and 1 day at 210 MPa. Cyclic loading between 0 and 210 MPa, at 10-min intervals, resulted in an LTC strain rate higher than $10^{-9}\ s^{-1}$ for 9 h after exhaustion of the static load LTC [Figure 5(c)].

API 5L X60 pipeline steel. SSR tensile sting with a strain rate of $1.3 \times 10^{-5}\ s^{-1}$ revealed a σ_p of 156 MPa and $\sigma_{0.2}$ of 485 MPa. The LTC results are given in Figure 6. The constant-load LTC strain rate is larger than $10^{-9}\ s^{-1}$ for 0.7 h at σ_p and 9.3 h at $\sigma_{0.2}$ The additional LTC straining with a strain rate above $10^{-9}\ s^{-1}$ lasts for 1.5 h during cyclic loading at σ_p and 6.7 h at $\sigma_{0.2}$ [Figure 6(c)].

The total constant-load LTC strains of the three materials as a function of the ratio of the constant-load stress over $\sigma_{0.2}$ is given in Figure 7. As a function of these relative stresses, the ranking of the materials, in order of decreasing LTC straining, is type 316L SS, duplex SS, API 5L X60; this is especially so at stress levels close to $\sigma_{0.2}$. Note that the $\sigma_{0.2}$ of duplex SS and X60 steel is a factor of 2 higher than that of type 316L SS. The period during which the material plastically strains—with a strain rate above $10^{-9}\ s^{-1}$—during application of a constant load below $\sigma_{0.2}$ is shown in Figure 8. At stress levels close to $\sigma_{0.2}$, the duration of LTC straining for X60 is considerably shorter than that of duplex and type 316L SSs.

The occurrence of LTC during constant-load tests may well be the cause of SCC/HE failures of duplex SS in sour environments during static testing and may explain the large scatter in these results in the literature.[3]

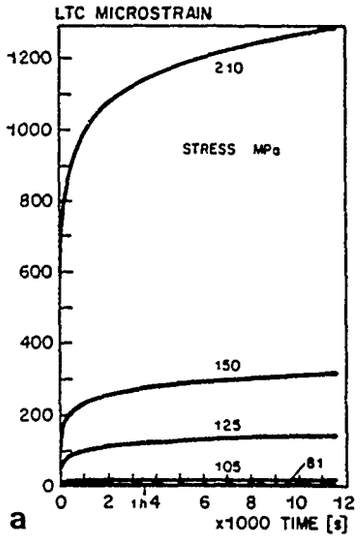
Under more realistic operating conditions, additional LTC straining may occur if the load fluctuates. Following SCC crack initiation, local LTC may be sustained at the crack tip because of the stress concentration. The continued plastic straining can then result in the propagation of SCC cracks.

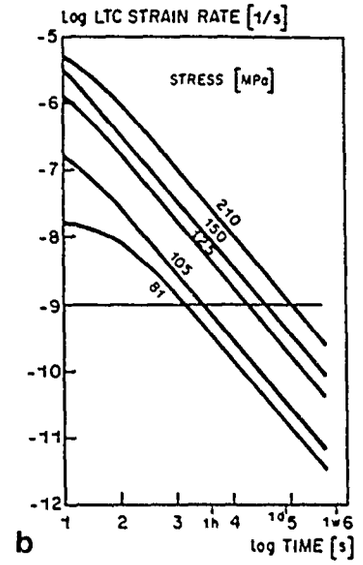
Conclusion

LTC measurements at 20°C have shown that at stress levels below $\sigma_{0.2}$, significant creep can occur in duplex and type 316L SSs, and to a lesser extent in API 5L X60 pipeline steel. The lower limit for the stress required to result in macroscopic LTC at constant load was found to be close to σ_p. Assuming a strain rate lower limit of $10^{-9}\ s^{-1}$ is required for the initiation of SCC/HE, these materials would be vulnerable as a result of constant-load LTC for a time period of approximately 1 h at σ_p, up to several days close to $\sigma_{0.2}$. Additional LTC straining, after exhaustion of the constant-load LTC, may occur if the load fluctuates.

References

1. R.N. Parkins, Stress Corrosion Research, ed. H. Arup, R.N. Parkins (Alphen aan den Rijn, The Netherlands: Sijthoff and Noordhoff, 1979), p. 1.
2. J.G. Erlings, H.W. de Groot, J. Nauta, Corros. Sci. 27(1987): p. 1153.
3. K. van Gelder, J.G. Erlings, J.W.M. Damen, A. Visser, Corros. Sci. 27(1987): p. 1271.
4. E.H. Jordan, A.D. Freed, Exper. Mech. (1982): p. 354.
5. J.T. Evans, R.N. Parkins, Acta Metall. 24(1976): p. 511.
6. P.S.G. Bennett, J.T. Evans, Mater. Sci. Eng. 38(1979): p. 111.
7. J Weertman, J.R. Weertman, Physical Metallurgy, ed. R.W. Cahn (Amsterdam, The Netherlands: North-Holland Publishing Company, 1977), p. 930.





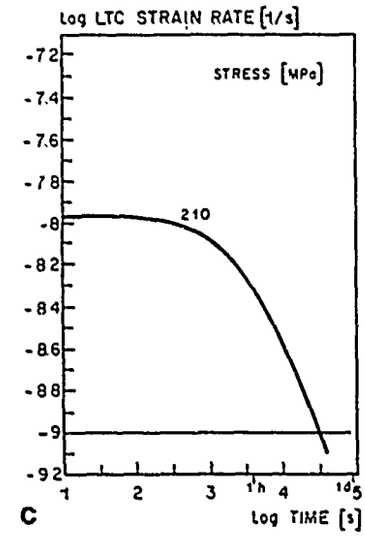
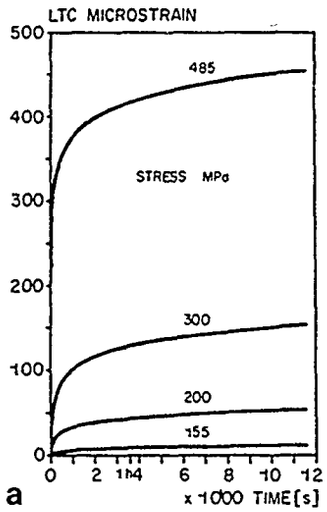
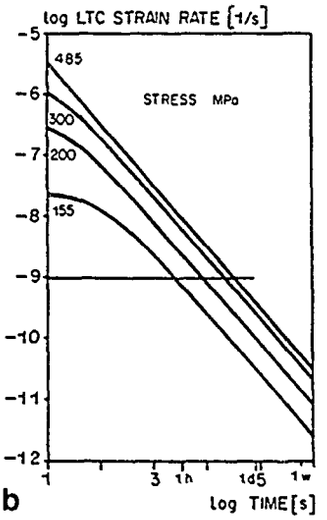


FIGURE 5—Low-temperature creep of type 316L (UNS S31603) stainless steel at room temperature (yield stress is 250 MPa): (a) and (b) constant-load LTC strain vs time, and (c) cyclic-load LTC (10/10 min) strain rate vs time.





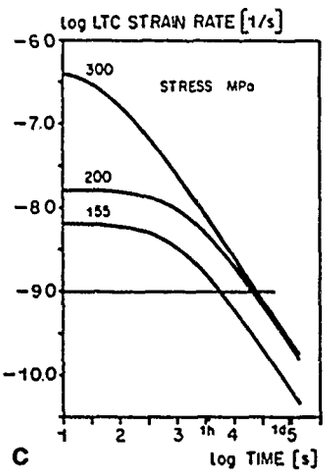


FIGURE 6—Low-temperature creep of API 5LX X60 pipeline steel at room temperature (yield is 485 MPa): (a) and (b) constant-load LTC strain vs time and (c) cyclic-load LTC (10/10 min) strain rate vs time.

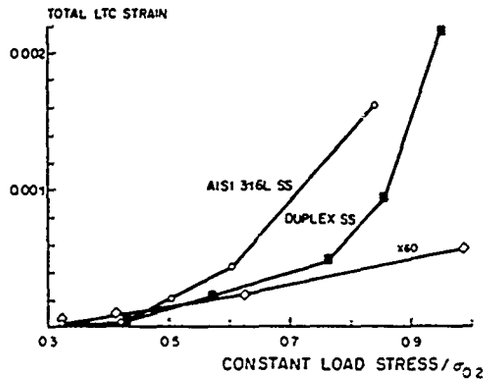


FIGURE 7—Total constant-load LTC strain for duplex and type 316L (UNS S31603) stainless steels and X60 pipeline steel as a function of the ratio of stress vs yield stress.

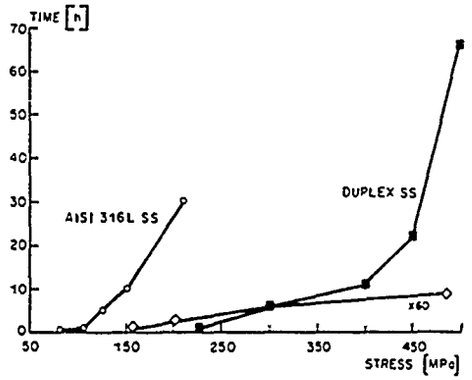


FIGURE 8—Duration of LTC straining in the critical strain-rate range for duplex and type 316L (UNS S31603) stainless steel and X60 pipeline steel while applying a constant load.

Discussion

F.P. Ford (General Electric R&D, USA): It is encouraging to see the relationship between creep rate and stress corrosion cracking (SCC) since this is fundamental to current cracking models. I would love to see, however, the relationship between stress (or stress intensity) and crack-tip creep rate, where the latter term is governed by the dynamnic equilibrium associated with loss of active dislocation sources (due to a logarithmic creep law) and introduction of new dislocation sources (due to the moving crack).

M.M. Festen: The low-temperature creep measurements done at the Koninklijke/Shell laboratory in Amsterdam have been performed with uniaxially stressed plain tensile specimens. Localized creep at a crack tip will be very difficult to determine experimentally. We intend to derive crack-tip rates from a model that translates uniaxial creep data into crack-tip creep data under the condition of a multiaxial stress state at a crack tip. For SCC-induced plastic straining, crack propagation should occur at such a rate that a sufficiently high creep rate is maintained at the crack tip.

We would be very pleased to learn more of your work in relation to this subject. Are there appropriate references?

F.P. Ford: The formulation of the crack-tip strain rate in terms of engineering "stress" parameters remains one of the hardest tasks in the overall objective of quantifying mechanisms based on life-prediction models, primarily because of the difficulty in experimentally verifying the various algorithms. References are given in my paper at this conference (Ford, "The Crack-Tip System and Its Relevance Prediction of Cracking in Aqueous Environments," this proceedings) on the crack-tip systems that tackle this problem. Realistically, I expect it will be several years before we have an unambiguous agreement between experiment and theory on this subject. The best we can do now is formulate empirically based algorithms. This is unsatisfactory from an academic viewpoint, but is usable!

Aqueous Environment Effects on Intrinsic Corrosion Fatigue Crack Propagation in an Al-Li-Cu Alloy

*R.S. Piascik and R.P. Gangloff**

Abstract

Intrinsic corrosion fatigue crack growth (FCG) in Al-Li-Cu alloy 2090 exposed to aqueous NaCl is examined by new fracture mechanics methods applied to short cracks of depth less than 5 mm. Two regimes of the environmental effect are studied: low mean stress–high cyclic stress-intensity range and high stress ratio–near-threshold or ripple loading. Within each regime, alloy 2090 exhibits accelerated transgranular FCG in an aqueous NaCl environment with anodic polarization, relative to moist air and inert helium. Corrosion FCG in the LT orientation exhibits a crystallographic "cleavage" morphology at low ΔK and highly deflected slip band cracking at high ΔK. Aqueous NaCl experiments reveal mildly increased FCG rates with increased cyclic frequency, strongly reduced da/dN with cathodic polarization, and a decreased environmental effect because of Li_2CO_3 addition. Hydrogen embrittlement is suspected, with surface films retarding crack-tip environmental reactions for hydrogen production and dissolution. Alloy 2090 is more resistant to aqueous corrosion FCG than Al-Zn-Mg-Cu alloy 7075 and behaves similarly to conventional 2000 series alloys such as 2219.

Introduction

The objective of this research is to characterize and understand intrinsic fatigue crack propagation in advanced aluminum-lithium-based alloys with emphasis on the damage mechanisms for environmentally assisted transgranular cracking. While the importance of complex extrinsic contributions (namely crack closure, delamination, and crack deflection) to the fatigue crack propagation (FCP) resistance of Al-Li alloys is established,[1] gaseous and aqueous environmental effects have not been examined.

Intrinsic corrosion fatigue crack growth (FCG) is that governed by crack tip microstructure and mechanical and chemical driving forces independent of the external influences of closure contact, crack deflection, and transient chemical factors that alter steady-state crack growth. We believe that it is fundamentally important for mechanistic interpretation to define intrinsic FCG rates that are constant with constant applied ΔK and with constant applied bulk environment conditions for any number of load cycles, crack size, or specimen geometry.

In this study, fracture mechanics experiments developed to characterize intrinsic FCP for benign environment exposure and based on short-crack, programmed stress-intensity methods[2] are extended to investigate the effect of aqueous sodium chloride. Emphasis is placed on electrochemical control of the environment and on high resolution measurements of fatigue crack length changes in response to chemical variations.

Experimental Procedure

A 3.8-cm-thick plate of an advanced Al-Li-Cu-Zr alloy (AA 2090) was studied in the rolled, unrecrystallized, peak-aged condition. Alloy composition, heat treatment, mechanical properties, and microstructure, defined by optical and transmission electron metallography, are summarized in Table 1. Results are compared to Al-Zn-Mg-Cu alloy 7075-T651 (6.4-cm rolled plate); chemical composition and mechanical properties are shown in Table 2.

Corrosion behavior was characterized by standardized potentiodynamic polarization experiments at a standard scan rate of 0.16 mV/s in helium deaerated, 1% aqueous NaCl at pH 8 and 297°K.[3] All scans were performed from the most cathodic to the most anodic potentials. Corrosion fatigue experiments were conducted with specimens fully immersed in flowing (30 mL/min), helium deaerated, 1% NaCl (pH 8) in a 1.5 L sealed Plexiglas† chamber. The electrode potential was maintained constant by a Wenking† potentiostat and platinum counter electrodes isolated from the solution through asbestos frits. Results are compared to FCG in moist air (30 to 60% relative humidity) and in purified helium contained in a bakable, metal bellows and gasket-sealed chamber capable of a dynamic vacuum of 1 μPa, as detailed elsewhere.[4]

Short crack fatigue propagation experiments were conducted with single-edge notched specimens (10.16 mm wide, 2.54 mm thick, 0.25 or 0.89 mm notch depth) machined in the LT orientation at the one-third thickness position in the rolled plate. Pinned, freely rotating grips were used, consistent with the stress-intensity solution.[5] The growth of short edge cracks, of total length (a) between 0.35 and 5 mm, was monitored continuously by a direct current electrical potential method including 8 to 12 amps current, 0.1 μv potential measurement resolution, and an analytical calibration relation.[6] This method was successfully applied to aluminum alloys, with better than 3 μm crack growth resolution and long-term (10-day) stability for near-threshold growth rate measurements.[2] Long-crack compact-tension (CT) experiments with compliance monitoring were conducted in accordance with ASTM E647.[7]

Intrinsic and transient or steady-state corrosion fatigue crack propagation rates were studied for both the high cyclic stress intensity (ΔK) Paris and near-threshold regimes. Edge-cracked specimens were stressed cyclically (sine waveform; 0.07 Hz < frequency < 20 Hz; 0.05 < stress ratio < 0.95) in a closed-loop

*Department of Materials Science, University of Virginia, Charlottesville, VA 22903-2442.

†Trade name.

TABLE 1
Alloy 2090 Material Properties[A]

Chemical Composition (wt%)											
Li	Cu	Zr	Fe	Si	Mn[B]	Mg	Cr	Ni	Ti	Na	Zn
2.14	2.45	0.09	0.05	0.04	0.00	0.00	0.00	0.00	0.01	0.001	0.01

Mechanical Properties (Longitudinal)	
Yield MPa	Ultimate
496 MPa	517 MPa

Microstructure					
Grain size	Subgrain size	Precipitates	Matrix phases	Subgrain boundary	High-angle grain boundary
3.3 mm (transverse)	15 μm (transverse)	δ' - Al_3Li	δ'	T_1	T_2
0.11 mm (short transverse)	5 μm (short transverse)	Θ' - Al_2Cu	T_1		
		T_1 - Al_2CuLi	Θ'		
		T_2 - Al_6CuLi_3			
		β - Al_3Zr			

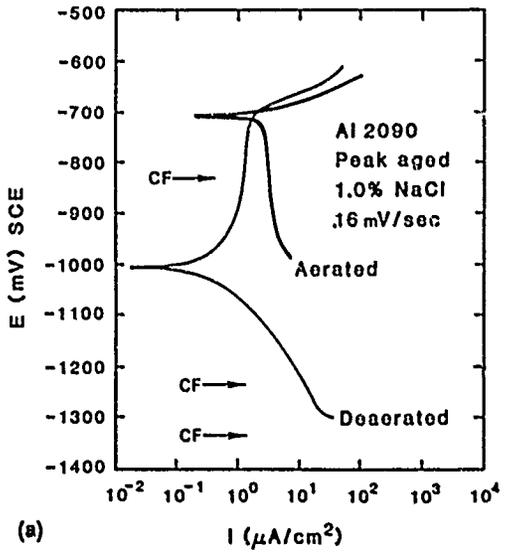
[A]Material condition: solutionized, water quenched, and stretched; peak aged 190°C for 4 h.
[B]Less than detection limit.

TABLE 2
Alloy 7075-T651 Material Properties

Chemical Composition (wt%)											
Zn	Mg	Cu	Cr	Zr	Fe	Si	Mn	Ni	Ti	Na[A]	Ca
5.74	2.31	1.58	0.20	0.01	0.26	0.10	0.05	0.01	0.05	0.000	0.0001

Mechanical Properties (Longitudinal)	
Yield	Ultimate
466 MPa	540 MPa

[A]Less than detection limit.



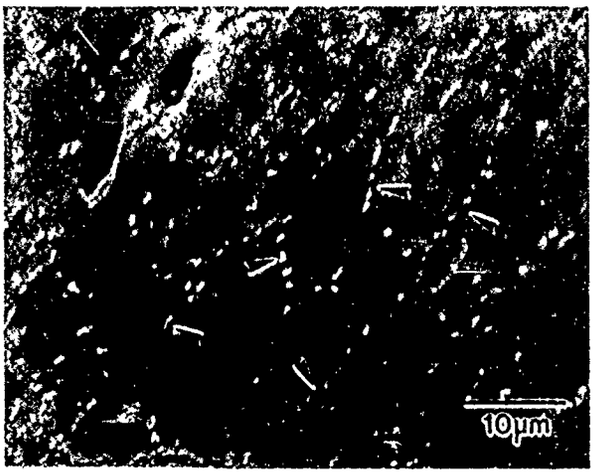


FIGURE 1—(a) Potentiodynamic polarization of alloy 2090 in aerated and deaerated 1% NaCl, and (b) photomicrograph of alloy 2090 exposed to deaerated 1% NaCl for 8 days at −0.840 V_{SCE}.

servohydraulic machine operated in load control. Using computer measurement and feedback control, ΔK was maintained constant over segments of growing crack length (about 0.25 to 1 mm), with step reductions (or increases) in ΔK at constant K_{max}, producing increasing (or decreasing) stress ratio (R). Crack growth rates (da/dN) were calculated by linear regression analysis of crack length (a) vs load cycles (N) data. For a single specimen, the load sequence initially probes high ΔK, low R cracking; followed by near-threshold ΔK, high R fatigue for deeper crack depths. Short crack length for the former and high stress ratio for the latter conditions minimize complicating extrinsic effects. Crack bifurcation was never observed. Continuous reduction in ΔK at constant K_{max} provides an effective characterization of intrinsic FCG.[8] Step changes in constant ΔK with increasing or decreasing R more effectively characterize transient to steady-state crack propagation associated with ΔK changes, electrochemical variables, and microstructure.

Results and Discussion

Corrosion characteristics

Potentiodynamic polarization data are summarized in Figure 1(a) for peak-aged alloy 2090 exposed to deaerated and oxygen-containing 1% NaCl solutions. In oxygen-containing aqueous NaCl, the open-circuit potential of alloy 2090 is near the breakaway potential, resulting in extensive surface pitting. Deaeration of the solution limits the oxygen reduction reaction and decreases the open-circuit potential in the cathodic direction, forming a passive region extending from −1.0 V to −0.7 V_{SCE}. At passive potentials, general corrosion and pitting are greatly reduced. Long-term (8-day) constant potential experiments (−0.760 V_{SCE}, deaerated 1% NaCl) nonetheless reveal that T_1 precipitates at sub-grain boundaries and constituent particles (Al_7Cu_2Fe) are sites of localized attack [Figure 1(b)].[2]

Corrosion fatigue experiments were performed in deaerated 1% NaCl to limit fracture surface corrosion and pitting, to reduce crevice corrosion at the electrical potential probes, and to minimize electrolyte IR-type errors in measured potential. Since the open-circuit potential of alloy 2090 varies by 100 to 400 mV during long-term exposure, fatigue experiments were performed at a constant anodic potential of 0.840 V_{SCE} and a cathodic potential of either −1 240 or −1.340 V_{SCE} [Figure 1(a)].

Intrinsic FCG in moist air and helium

The intrinsic FCG characteristics of alloy 2090 in moist air and purified helium are shown in Figure 2. The data points (Δ) for moist air were calculated from the linear a vs N responses shown in Figure 3 for seven constant ΔK levels obtained by step increases or decreases in R at a constant K_{max} of 17 MPa·m$^{1/2}$. Note that linear crack growth for the low ΔK region (ΔK = 1.7 MPa·m$^{1/2}$/R = 0.90) reveals no evidence of delay retardation, demonstrating that ΔK reductions at constant K_{max} do not induce overload effects, presumably because the maximum or forward loading plastic zone size is constant.

Results for short-crack, constant ΔK–step-changed R and long-crack, continuously decreasing ΔK constant K_{max} experiments are in excellent agreement. Figure 2 shows the results of a continuously decreasing ΔK experiment conducted with a large crack CT specimen (LT) and using two K-gradient parameters, C = 0.19 mm^{-1} for ΔK ranging from 13 MPa m$^{1/2}$ to 8 MPa m$^{1/2}$ and C = 0.39 mm^{-1} for ΔK from 8 MPa m$^{1/2}$ to threshold. Because the experiment was performed at constant K_{max}, the low K gradient parameter (ASTM E647 recommends C = 0.08 mm^{-1}) does not introduce overload effects, causing reduced da/dN. The data contained in Figure 2 are in excellent agreement with literature results for alloy 2090 and represent the intrinsic FCG behavior of this alloy for moist air.[1,2,8]

Accelerated transgranular FCG in moist air compared to helium reveals the damaging effect of water vapor, and suggests a hydrogen embrittlement mechanism for alloy 2090.[4] Figure 2 shows the results of FCG experiments performed in purified helium. At high ΔK, da/dN for helium and moist air are equivalent, revealing little environmental effect. At low ΔK and high R, moist air causes a factor of five increase in intrinsic FCG compared to that for helium. Crack growth rate data in purified He provide a mechanical basis for analysis of aqueous environmental effects. Moist air data in Figure 2 provide the customary base line.

Aqueous corrosion fatigue

Intrinsic corrosion fatigue characteristics. Figure 4 shows a comparison of the intrinsic transgranular corrosion FCG kinetics of alloy 2090 in helium, moist air, deaerated 1% NaCl (−0.840 V_{SCE} and −1.240 V_{SCE}) and deaerated 1% NaCl + 0.37% Li_2CO_3 (−0.840 V_{SCE}). All experiments were performed at a cyclic frequency of 5 Hz, using the constant $\Delta K/K_{max}$–step-changed R sequence similar to that shown in Figure 3. These results show that alloy 2090 exhibits a moderate environmental effect at high levels of ΔK where differences in crack growth rate are less than three-fold. Near threshold, considerable differences in FCG are observed, with a factor of fourteen increase in da/dN revealed by comparing 1% NaCl with anodic polarization and helium, the largest corrosion fatigue effect. In contrast, cathodic potential (−1.240 V_{SCE}) reduced FCG to a level slightly greater than that observed for moist air and produced crack arrest above the moist air threshold similar to fatigue in helium. The addition of Li_2CO_3 to 1% NaCl (−0.840 V_{SCE}) retarded crack growth; the reduction is not as dramatic as that produced by mild cathodic polarization.

Corrosion fatigue experiments performed in aqueous 1% NaCl at constant anodic potential (−0.840 V_{SCE}) show that alloy 2090 exhibits better transgranular corrosion FCG characteristics than alloy 7075-T651. Results for alloy 7075 are shown by the dashed line in Figure 4 for the high and low ΔK regimes. At high ΔK, alloy 7075 exhibits a factor of 1.5 to 4 increase in da/dN, and at low ΔK, 10-fold greater FCG rates are revealed compared to alloy 2090. Alloy 7075 growth rates are in agreement with previous findings by Stoltz and Pelloux, where accelerated FCG was observed for 3.5% NaCl with anodic polarization.[9]

For all cases in Figure 4, crack length increased linearly within the range from 0.35 to 3.5 mm and at constant ΔK. No evidence was obtained for crack-geometry-dependent increases or decreases in da/dN. While comparisons are limited, the corrosion fatigue effect shown in Figure 4 is similar to the behavior of 20- to 50-mm-long cracks in 2090 and 7075.[9,10] Experiments with short (0.1 to 3 mm) and long (20 to 50 mm) cracks for the steel-aqueous chloride system evidenced dramatic increases in corrosion FCG kinetics for the former and attributed to geometry-dependent crack electrochemistry.[11] Additional work is in progress to examine chemical crack-size effects on corrosion fatigue in high-strength aluminum alloys.

Frequency effects. The typical frequency effect on FCG propagation in 2000 and 7000 series aluminum alloys (viz., increased or constant da/dN with decreasing frequency) was not observed for alloy 2090 in 1% NaCl.[12-14]

In deaerated 1% NaCl solution (0.840 V_{SCE}), alloy 2090 exhibits mildly increased corrosion FCG rates with increased frequency at high cyclic stress intensity and little frequency effect at low ΔK. Figure 5 shows the comparison of average crack growth rate vs frequency at two levels of constant ΔK, 9.9 and 2.2 MPa m$^{1/2}$. For each frequency, the total variation in crack growth rate (calculated with a two-point secant method) and the least squares value are plotted. The numbers shown adjacent to each data point describe the sequence of experiments conducted on two specimens. At high constant ΔK, a factor of two decrease in FCG rate is observed when decreasing the cyclic frequency from 5 to 0.1 Hz. Similar results were reported by Yoder and coworkers for alloy 2090 in aerated 3 5% NaCl.[10]

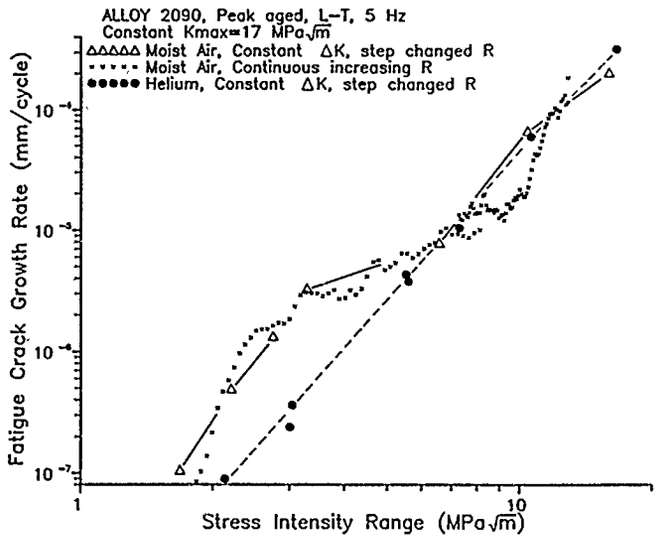


FIGURE 2—A comparison of constant $\Delta K/K_{max}$–step-changed R results with decreasing ΔK–constant K_{max} data showing the intrinsic fatigue crack growth behavior of AA 2090 in moist air and compared to helium.

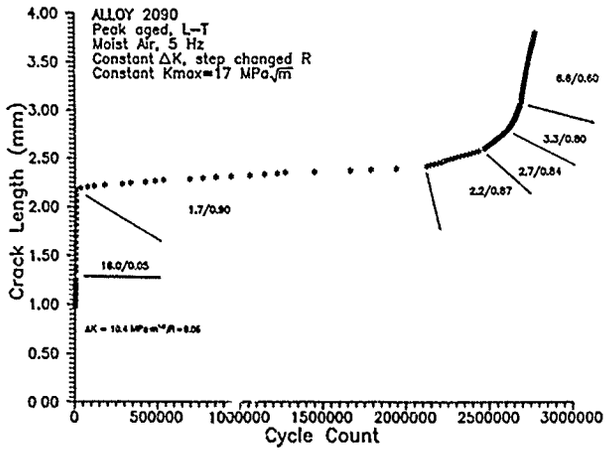


FIGURE 3—Crack length vs loading cycles data for the constant $\Delta K/K_{max}$–step-changed R results of Figure 2, moist air.

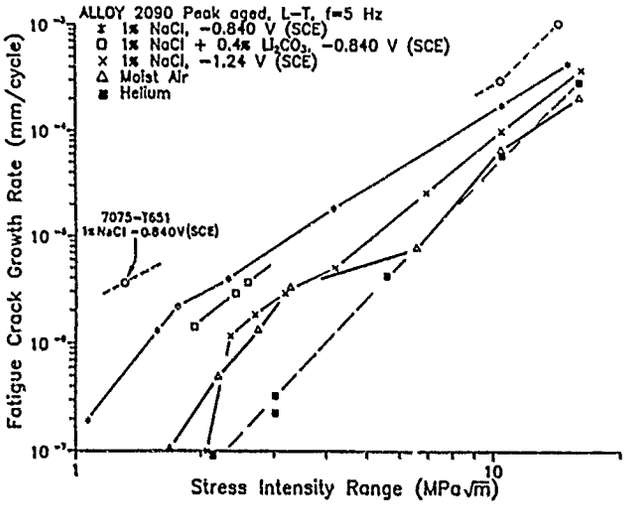


FIGURE 4—Corrosion fatigue crack growth behavior of alloy 2090 in deaerated 1% NaCl at constant anodic (−0.840 V_{SCE}) and cathodic (−1.240 V_{SCE}) potentials in 1% NaCl + 0.37% Li_2CO_3 (−0.840 V_{SCE}) and in moist air environments; and of alloy 7075 (UNS A97075) in aqueous 1% NaCl at constant anodic (−0.840 V_{SCE}) potential.

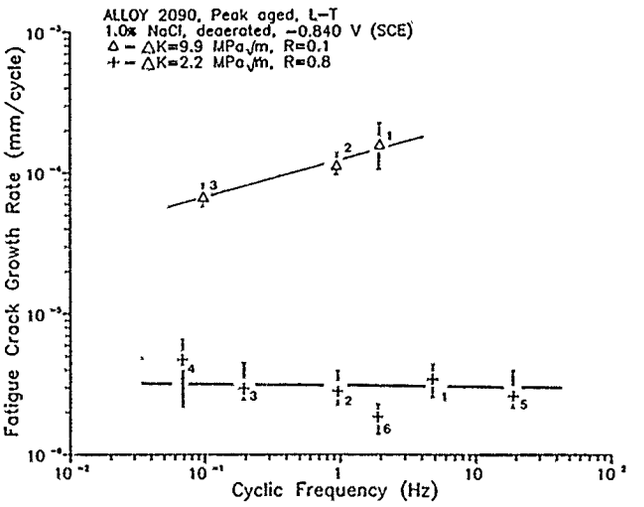


FIGURE 5—The dependence of corrosion fatigue crack growth rate on cyclic frequency at high and low constant ΔK; alloy 2090 in deaerated 1% NaCl with anodic polarization (−0.840).

At low ΔK, little difference in FCG rate is observed for cyclic frequencies between 0.07 and 20 Hz. Experiment 4, performed at 0.07 Hz, exhibits a slightly higher FCG rate compared to the mean da/dN at 2.2 MPa·m$^{1/2}$. The origin of this result is unclear. Fractographic analysis revealed evidence of increased dissolution for this long-term experiment (0.25 mm of crack extension in 8 days), possibly suggesting either an increased driving force for fatigue or simple crack-wake corrosion. Long-term electrical potential system variations may have contributed to the increased growth rate. The slight reduction in da/dN observed during Experiment 6 is attributed to a chemical or mechanical history dependence associated with crack length and shape.[15] These factors complicate characterizations of moderate frequency effects in corrosion fatigue.

The important point to be made for Figure 5 is that corrosion fatigue in alloy 2090 is not exacerbated by decreasing frequency; on the contrary, the opposite trend is likely, particularly at higher ΔK. The rate differences shown here are small but significant, as demonstrated by resolvable changes in a vs N upon a frequency change at constant ΔK for a single specimen.[2]

Polarization effects. The results of constant ΔK experiments show that corrosion FCG in 1% NaCl is mitigated by cathodic polarization. Cathodic polarization da/dN data are compared to the anodic case in Figure 4. Note the two-fold reduction in rate at high ΔK, increasing to a five-fold decrease at low ΔK and an increase in the approximate threshold stress intensity. Cracking under cathodic potential is similar to the behavior recorded for moist air and enhanced relative to inert He for all ΔK except the near-threshold regime.

The beneficial effect of cathodic polarization is clearly evidenced by cyclic crack length measurements at constant ΔK. Figure 6(a) reveals that, at low ΔK (2.2 MPa·m$^{1/2}$, R = 0.8) and anodic polarization (−0.840 V_{SCE}), a constant crack growth rate is maintained to a crack length of 2.1 mm. Here, a cathodic potential of −1.240 V_{SCE} was applied, resulting in crack arrest consistent with the threshold elevation shown in Figure 4. At 1 million load cycles, a potential of −0.840 V_{SCE} was again applied. Crack growth resumed after 76 hours or 2.2 million additional load cycles had elapsed, achieving a steady-state rate similar to the initial anodic condition. A second cathodic polarization of −1.240 V_{SCE} reproduced crack arrest. Cathodic polarization also reduced rates of corrosion fatigue at high cyclic stress intensity (9.6 MPa·m$^{1/2}$, R = 0.1), as shown in Figure 6(b). After initial cracking at −0.840 V_{SCE}, a small reduction in da/dN was produced by polarization to −1.240 V_{SCE}, and a significant, time-dependent retardation in crack growth was observed at a cathodic potential of −1.340 V_{SCE}. At a crack length of 3.1 mm, the applied stress-intensity range was decreased to 2.1 MPa m$^{1/2}$ at R = 0.9 with K_{max} maintained constant, and the electrode potential was

made anodic (−0.840 V_{SCE}). A slow recovery to a constant growth rate was observed. Crack growth arrest occurred because of cathodic polarization at −1.240 V_{SCE}, reproducing the results shown in Figure 6(a). The results of constant ΔK and R experimentation (Figure 6) are consistent with the single specimen constant ΔK–step-changed R results presented in Figure 4.

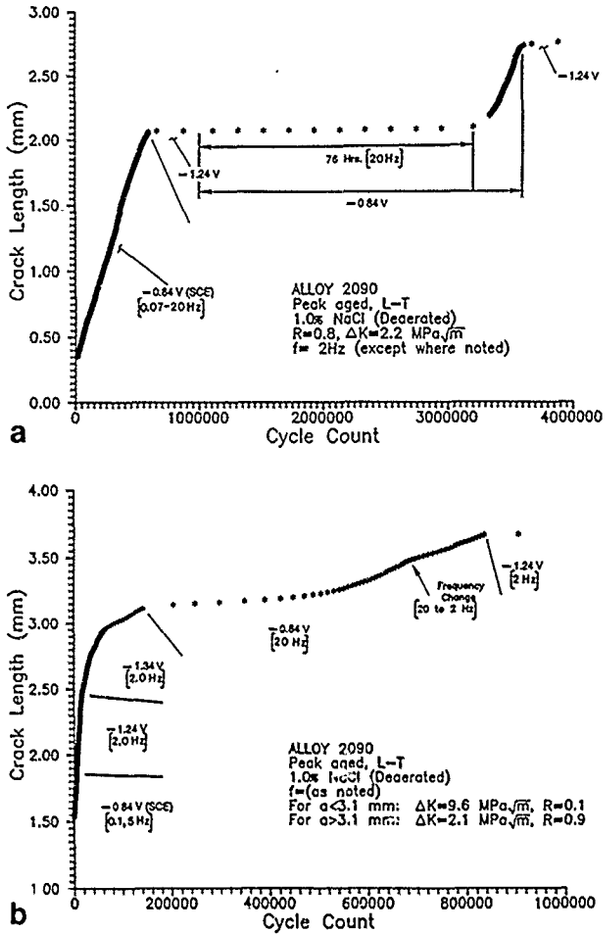


FIGURE 6—The effect of cathodic polarization on intrinsic corrosion fatigue crack growth in alloy 2090; deaerated 1% NaCl at constant ΔK levels of (a) 2.2 MPa·m$^{1/2}$ for high R and (b) 9.6 and 2.1 MPa·m$^{1/2}$ for low and high R conditions, respectively.

The reduction in corrosion FCG by cathodic polarization for alloy 2090 is consistent with the findings of other researchers. Cathodic polarization of alloy 7075 in aqueous 3.5% NaCl reduced corrosion fatigue crack propagation at ΔK = 11 MPa·m$^{1/2}$.[9] The enhanced stress corrosion cracking resistance of conventional 2000 and 7000 series alloys resulting from cathodic polarization is documented.[16] Consistent with data in Figures 4 and 6, although not conclusive, the smooth specimen fatigue life of an Al-4.2Mg-2.1Li alloy was increased by mildly cathodic potentials.[17]

Ion addition effects. The experimental results shown in Figure 7 demonstrate that a lithium carbonate (Li_2CO_3) addition to 1% NaCl reduces the rate of transgranular corrosion FCG at constant ΔK, pH, and electrode potential. At a cyclic stress intensity of 2.3 MPa·m$^{1/2}$ (R = 0.87) and an anodic potential of −0.840 V_{SCE}, a constant crack growth rate was initially established in deaerated 1% NaCl (pH = 8.1). No change in crack growth is observed as the solution pH is increased from 8.1 to 10.4 by addition of NaOH. At a crack length of 1.9 mm, the cell environment was changed by continuously pumping deaerated 1% NaCl + 0.37% Li_2CO_3 (pH = 10.4) solution from a separate reservoir. After purging the cell with flowing 1% NaCl + 0.37% Li_2CO_3, the experiment was resumed, resulting in a 30% reduction in the corrosion FCG rate. This beneficial effect was reproduced at two higher ΔK levels (Figure 4).

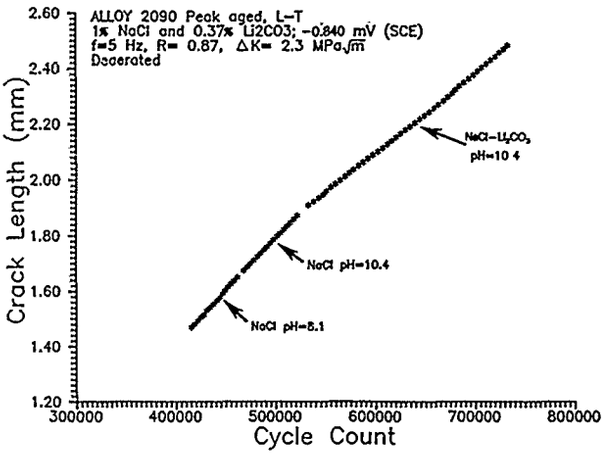


FIGURE 7—The effect of Li_2CO_3 addition and pH change on intrinsic fatigue crack growth in alloy 2090 exposed to deaerated 1% NaCl at constant anodic potential and constant ΔK.

Fractographic analysis

The fatigue crack surface morphologies for moist air and deaerated 1% NaCl (−0.840 V_{SCE}) environments exhibit similar components of microscopic fracture but in different proportions. At high ΔK (15 MPa·m$^{1/2}$), severe planar crack surface deflections resulting from decohesion or shear separation along intense slip bands and regions of inter-sub-grain-boundary fracture are observed for each environment. Results suggest that NaCl promotes increased sub-grain-boundary fracture and reduced crack deflections because of reduced slip-band cracking. The latter crack path is dominant for fatigue in moist air.[10]

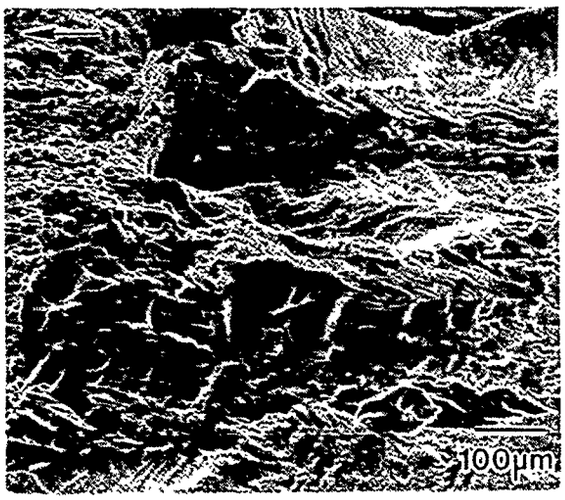
As the stress-intensity range decreases, the amount of crack-tip deflection is reduced and the fracture surface is characterized by increased areas exhibiting a flat, crystallographic "cleavage-type" appearance. A comparison of the fracture surfaces for moist air and deaerated 1% NaCl (−0.840 V_{SCE}) environments at low ΔK is shown in Figure 8. In moist air [Figure 8(a)], the transgranular fracture surface is crystallographic cleavage with intervening regions of deflected crack growth exhibiting a ductile appearance. The transgranular fracture morphology for 1% NaCl [Figure 8(b)] exhibits broad regions of cleavage fracture with little evidence of ductile tearing. Results suggest a greater proportion of crystallographic fracture for aqueous NaCl compared to moist air.

High-angle and sub-grain-boundary precipitates, T_2 and T_1, respectively, do not appear to be sites for crack-tip dissolution. Detailed examination of the corrosion fatigue crack–final overload fracture interface region reveals no evidence of corrosion. Behind this region, where crack surfaces are exposed to the occluded environment for longer times, small and widely dispersed regions of sub-grain-boundary T_1 precipitate corrosion, similar to that shown in Figure 1(b), were observed. No evidence was obtained for T_2 precipitate corrosion along high-angle grain boundaries. Secondary cracking along these generally low-strength, high-angle boundaries was not observed for the LT orientation. Corrosion fatigue was purely transgranular.

Mechanistic Implications

Many mechanisms have been proposed to explain rates of environmental cracking in aluminum alloys, including hydrogen embrittlement, adsorbate decohesion, film rupture/dissolution/repassivation, film-induced slip irreversibility, enhanced localized plasticity, and crack-tip blunting by corrosion.[9,12,13,15-18] In these studies, Paris regime corrosion fatigue has been emphasized, crack closure has not been accounted for, and aqueous environmental effects on near-threshold cracking have not been considered. For FCG at

moderate ΔK, the cleavage fracture morphology was linked to both hydrogen embrittlement and surface film effects without resolution of the cause. Hydrogen from cathodic reduction in electrolytes and chemical reactions in water vapor is believed to embrittle aluminum, with possible contributions from dislocation and grain-boundary transport processes. Alternately, surface films suppress plastic deformation by blocking the crack-tip emission of dislocations, the local normal stress is elevated, causing cleavage.



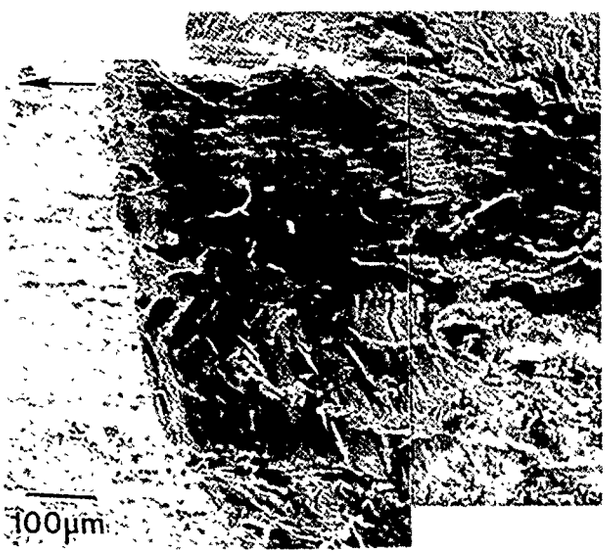


FIGURE 8—A comparison of the fracture morphology resulting from corrosion fatigue at low ΔK in (a) moist air at 2.5 MPa·m$^{1/2}$ and (b) deaerated 1% NaCl (−0.840 V_{SCE}) at 2.2 MPa·m$^{1/2}$. Crack growth is from right to left, with the fatigue crack–overload fracture interface shown.

Based on experimental observations of FCG rate response to ΔK, frequency, cathodic polarization, and Li_2CO_3 addition, and on the behavior of alloy 2090 in water vapor and oxygen,[4] we speculate that hydrogen embrittlement is likely, but that surface films and crack electrochemistry play an important role in crack-tip damage during transgranular corrosion fatigue. Faster crack growth is correlated with those environmental conditions that promote less protective crack-tip surface films and thus enhance hydrogen entry. This complex interplay and the effects of frequency and cathodic polarization are not consistent with surface reaction or transport limited hydrogen embrittlement, as suggested for steels and 7000 series aluminum alloys.[12,13,19,20]

Increased crack growth rate with increasing frequency suggests that time-dependent chemical reactions and mass transport within the electrolyte or crack-tip plastic zone are rapid and do not limit environmental crack propagation. Considering mechanical effects, crack-tip strain rate is, on average, proportional to loading frequency and stress-intensity range raised to a power on the order of 2.[21] At high ΔK, mechanical film disruption provides a plausible explanation for the small increase in crack growth with increasing frequency (Figure 5). Here, crack-tip strain rate increases with increasing frequency, the film is locally breached more frequently, and transient dissolution and hydrogen production progress to greater degrees. Crack extensions per unit time and cycle increase. The strong environmental effect for low ΔK may be ascribed to localization of crack-tip deformation and mechanical disruption of surface films. Since da/dN is independent of frequency, it is necessary to conjecture that film rupture by strain localization near threshold is not sensitive to frequency.

The frequency result is unique to the Al-Li alloy. Based on modeling and data for 2000 and 7000 series alloys in water vapor, Wei and coworkers argue for fast surface-reaction kinetics, which lead to da/dN independent of frequency and at a level that is governed by "saturation" surface reaction and hydrogen production.[13,19] (Low-frequency crack growth rates in 7000 series alloys may increase with decreasing frequency because of the intervention of a slow surface-reaction step.) Crack growth rates for aqueous chloride conditions increased with decreasing frequency for 7017, 7075, and 2618 alloys, for example, a factor of 250 decrease in frequency resulted in 7-fold, 3-fold, and 2-fold increases, respectively, in da/dN at ΔK = 15 MPa·m$^{1/2}$.[12,14]

Increased and decreased crack growth rates with anodic and cathodic polarization, respectively, could correspond to changes in the formation of crack-tip surface films. Reduced da/dN and the formation of a black corrosion product by cathodic polarization is evidence of a protective crack-tip surface film, possibly hydroxide based. [Under cathodic conditions, excess hydroxide ions are present within the crack to react with aluminum and lithium ions to form $Al(OH)_3$ + LiOH, resulting in a black surface film. A similar black surface film has been observed on the fracture surfaces of alloy 2090 specimens fatigued in pure oxygen, followed by exposure to moist air.[4] The reaction for LiOH formation during water vapor exposure is $Li_2O + H_2O = 2LiOH$.[22]] The formation of a surface film may limit hydrogen production by inhibiting the water reduction reaction, resulting in reduced hydrogen entry. The reduced cathodic effect on da/dN with increased ΔK is consistent with mechanical film rupture by intensified slip. Hydrogen production and entry are enhanced by increasing the area of reactive surface along slip steps. Increased da/dN is also observed for anodic potential, an environment that favors a less protective crack-tip surface film.

Reduced transgranular corrosion FCG, with the addition of Li_2CO_3, possibly results from the formation of a passive film, a result consistent with decreased da/dN associated with a cathodically formed surface film. Li_2CO_3 is thought to form a passive film on Al-Li alloys, which increases the susceptibility to intergranular stress corrosion cracking in aqueous NaCl.[23] The mechanism is unclear; Li^{+1} passivates aluminum,[24] and CO_3^{-2} affects surface film stability.[23]

The beneficial effect of a surface film is likely to be chemical in origin. Film- or corrosion-product-induced crack closure is not operative because the environmental influences are observed at stress ratios more than 0.85 and for short crack wakes. Also, there is no evidence that surface films promote irreversible dislocation damage.[4] Rather, we speculate that films interfere with crack-tip environmental reactions (hydrogen production or dissolution), resulting in a reduction in FCG rate. Once damaged by chemical or mechanical means, such as localized anodic pitting dissolution or slip step formation, the film no longer acts as a barrier, the alloy is rendered susceptible to brittle crack growth.

Although experimental evidence strongly suggests that surface films play a primary role in retarding crack-tip damage during transgranular fatigue of alloy 2090 in aqueous environments, further work must be performed to understand the roles of hydrogen and

transient localized anodic dissolution. Gaseous environment corrosion fatigue experiments and high-resolution fractographic analyses are being conducted in this regard.[4]

Conclusion

The high-resolution electrical potential difference technique, short-crack specimen geometry, and constant $\Delta K/K_{max}$–step-changed R approach successfully characterizes intrinsic FCG in complex aluminum–lithium-based alloys exposed to aggressive aqueous environments.

Al-Li-Cu alloy 2090, peak aged, is susceptible to corrosion fatigue crack propagation in aqueous 1% NaCl under anodic polarization. At low ΔK/high R, near-threshold crack growth rates are significantly increased, with growth occurring by a crystallographic cleavage process. High ΔK/low R growth rates are increased by the aqueous NaCl environment, with highly deflected slip-band cracking and sub-grain-boundary fracture the dominant microscopic modes. Environmental effects on alloy 2090 are less severe than those observed for high-strength alloy 7075, the new aluminum lithium alloy behaves similarly to conventional 2000 series alloys.

Crack-tip films play an important role in corrosion fatigue damage, as evidenced by (1) increased da/dN with increased cyclic frequency, particularly at high ΔK, (2) retarded crack growth due to cathodic polarization in NaCl, and (3) reduced da/dN due to Li_2CO_3 additions. Film formation hinders the hydrogen embrittlement process that is presumed to control environmental crack propagation.

Acknowledgment

The research support provided by the NASA-Langley Research Center, grant NAG-1-745 with D.L. Dicus as monitor, is gratefully acknowledged Alloy 2090 was provided by the Alcoa Technical Center and E.L. Colvin.

References

1. K.T. Venkateswara Rao, W. Yu, R.O. Ritchie, Metall. Trans. A 19A(1988): pp. 549-561, pp. 563-569.
2. R.S. Piascik, "Mechanisms of Intrinsic Damage Localization During Corrosion Fatigue: Al-Li-Cu System" (Ph.D. diss., University of Virginia, 1989).
3. ASTM G5-82, "Standard Reference Method for Making Potentiostatic and Potentiodynamic Anodic Polarization Measurements," 1985 Annual Book of ASTM Standards—Methods and Analytical Procedures, Vol. 3 (Philadelphia, PA. ASTM, 1985), pp. 123-133.
4. R.S. Piascik, R.P. Gangloff, Advances in Fracture Research, ed K Salema, K. Ravi-Chamdar, D.M.R. Taplin, P. Rama Rao (London, England: Pergamon Press, 1989), pp. 907-918.
5. H. Tada, P.C. Paris, G.R. Irwin, The Stress Analysis of Cracks Handbook (St. Louis, MO: Del Research Corp., 1985), pp. 2.10-2.11.
6. R.P. Gangloff, Advances in Crack Length Measurement, ed. C.J. Beevers (Wardley Heath, England: Engineering Materials Advisory Services, 1982), pp. 175-229.
7. ASTM E647-88, "Standard Test Method for Measurement of Fatigue Crack Growth Rates," Annual Book of ASTM Standards, Vol. 03.01 (Philadelphia, PA: ASTM, 1988).
8. W.A. Herman, R.W. Hertzberg, R. Jaccard, J. Fat. Frac. Eng. Mater. and Struc. 11, 4(1988): pp. 303-320.
9. R.E Stoltz, R.M Pelloux, Metall. Trans. 3(1972): pp. 2433-2441.
10. P.S. Pao, M.A. Imam, L.A. Cooley, G.R. Yoder, Corrosion 45, 7(1989): pp. 530-535.
11. R.P Gangloff, Metall. Trans. A 16A(1985): pp. 953-969.
12 N J.H Holroyd, D Hardie, Corros. Sci. 23, 6(1983). pp. 527-546.
13 M Gao, P S Pao, R.P. Wei, Metall. Trans. A 19A(1988): pp. 1739-1750.
14 D Aliaga, E. Budillion, "Corrosion Fatigue Behavior of Some Aluminum Alloys," AGARD Report No. AGARD-CP-316, 1981.
15. R.P. Gangloff, D.J. Duquette, Chemistry and Physics of Fracture, ed. R.M. Latanision, R.H. Jones, NATO Series E, No. 130 (Dordrecht, The Netherlands. Martinus Nijhoff Publishers, 1987), pp. 612-645.
16 N J H Holroyd, G.M Scamans, Environment-Sensitive Fracture, ASTM STP 821, ed. S.W. Dean, E.N. Pugh, G.W. Ugiansky (Philadelphia, PA: ASTM, 1984), pp. 202-241.
17. R.E. Ricker, D.J. Duquette, CORROSION/85, paper no. 354 (Houston, TX: National Association of Corrosion Engineers, 1985).
18. D.L. Davidson, J. Lankford, J. Fat. Eng. Mater. and Struc. 6(1983): pp. 241-256.
19. R.P. Wei, R.P. Gangloff, Fracture Mechanics. Perspectives and Directions, ASTM STP 1020, ed. R.P. Wei, R.P. Gangloff (Philadelphia, PA: ASTM, 1989), pp. 233-264.
20. R.P. Gangloff, "Corrosion Fatigue Crack Propagation in Metals," this proceedings.
21. S.J. Hudak Jr., D.L. Davidson, R.A. Page, Embrittlement by Localized Crack Environment, ed. R.P. Gangloff (Warrendale, PA: TMS-AIME, 1984), pp. 173-198.
22. C.E. Messer, The Alkali Metals, Publication No. 22 (London, England: The Chemical Society/Burlington House, 1967). pp. 183-198.
23 J.G. Craig, R.C. Newman, M.R. Jarrett, N.J.H. Holroyd, Environmental Degradation of Engineering Materials III, ed. M.R. Louthan, R.P. McNitt, R.D. Sisson (University Park, PA: Pennsylvania State University, 1987), pp. 313-320.
24. J. Gui, T.M. Devine, Scripta Metall. 21(1987). pp. 853-857.

Corrosion Fatigue of Alloy X-750 in Aqueous Environments

R.G. Ballinger, C.K. Elliott,** and I.S. Hwang****

Abstract

The corrosion fatigue behavior of alloy X-750 (UNS N07750) investigated in aqueous environments as a function of heat treatment over the temperature range 25 to 288°C. Variables studied were ΔK (12 to 45 MPa$\sqrt{m}$), R (0.1 to 0.6), and frequency (0.01 to 10 Hz). The investigation was conducted in high-purity deoxygenated water, air-saturated water, and 0.05 M Na_2SO_4 (pH 3 adjusted with H_2SO_4). Tests were performed at the free-corrosion potential as well as under anodic and cathodic polarization. The corrosion fatigue behavior is shown to exhibit two distinct temperature regimes: (1) a low-temperature regime below 200°C and (2) a high-temperature regime above 200°C. In the low-temperature regime, the behavior is characterized by a strong dependence of crack growth rate on frequency, temperature, heat treatment, and environment. In the high-temperature regime, crack growth rate increases gradually with temperature with minimal dependence on heat treatment, environment, and mechanical variables.

In high-purity water for microstructures containing γ' [$Ni_3(Al,Ti)$], intergranular crack growth is observed in the low-temperature regime for frequencies greater than 0.3 Hz. In this temperature range, the peak crack growth rate is approximately two orders of magnitude greater than that outside this region. Outside this temperature range, or below a frequency of 0.3 Hz, crack growth rate is transgranular. For other microstructures, the same effect is observed but to a much lesser extent and only for R values greater than 0.4.

The frequency-dependent intergranular crack growth regime is absent in 0.05 M Na_2SO_4 (pH 3.0 adjusted with H_2SO_4) solution unless the material is cathodically polarized. For the case of cathodic polarization, a gradual transition from transgranular to intergranular crack growth occurs with increasing degree of polarization. The maximum in crack growth rate for these conditions corresponds closely with the maximum observed in the high-purity water case.

It is proposed that a hydrogen mechanism is responsible for the behavior observed in the low-temperature regime. In the high-purity water case, it is proposed that the source of hydrogen is the galvanic couple between grain boundary γ' and the adjacent matrix, hydrogen reduction being highly localized because of the high IR drop in the solution. In the Na_2SO_4 solution, the local source of hydrogen must be augmented by cathodic polarization because of delocalization of the hydrogen-reduction process in the high-conductivity solution. In the high-temperature regime, the results are much less conclusive but suggest that competition between hydrogen recombination and absorption is dominated by recombination as the temperature increases. The results of this investigation demonstrate the importance of galvanic effects when considering a material for aqueous service.

Introduction

High strength nickel base alloys are used extensively in light water reactor (LWR) nuclear power systems because of their excellent corrosion resistance and strength in high-temperature aqueous environments. However, in spite of their excellent general corrosion resistance, this class of materials has been found to be susceptible to various forms of localized attack. These include stress corrosion cracking (SCC), corrosion fatigue (CF), and hydrogen-assisted cracking (HAC).[1] While the causes for failure have been the subject of considerable debate, it is well known that the fracture path is intergranular and strongly affected by the morphology and type of grain boundary precipitate and the composition of the adjacent matrix.[1]

Alloy X 750 (UNS N07750) is the most commonly used high-strength alloy in LWR environments.[2] Table 1 lists some of the heat treatments that are commonly used in service, Table 2 shows chemical composition. The HTH and AH treatments are used in aqueous environments. The primary strengthening phase in alloy X-750 is γ' [$Ni_3(Al,Ti)$], which is an ordered precipitate coherent with the matrix and precipitates as an ordered variant of face-centered cubic (fcc), $L1_2$ structure. Other phases of importance include (Ti,Nb)(C,N) carbonitride, $Cr_{23}C_6$ carbide, and $\eta(Ni_3Ti)$.

Unfortunately, for some heat treatments, alloy X-750 has been found to be susceptible to one or more forms of environment-assisted cracking (EAC), as mentioned above. In particular, the AH heat treatment has been found to be extremely susceptible to EAC in rising-load tests in 93°C water and in high-temperature aqueous

*Departments of Nuclear Engineering and Materials Science and Engineering, Massachusetts Institute of Technology, Cambridge, MA 02139.

**University of California, Department of Chemical and Nuclear Engineering, Santa Barbara, CA 93106.

***Department of Materials Science and Engineering, Massachusetts Institute of Technology, Cambridge, MA 02139.

environments.[3] On the other hand, the HTH heat treatment has been found to be much less susceptible.[4] In addition, the degree of susceptibility has been observed to be a strong function of temperature as well as frequency in fatigue.[5] Since accelerated cracking is intergranular and the heat treatments in Table 1 produce significantly different grain-boundary morphologies, it is likely that these factors play an important role. However, an exact mechanism has not been pinpointed.

Because of the technological importance of alloy X-750 and the uncertainty in knowledge concerning the mechanism(s) involved in EAC in this material, an investigation was conducted to determine the relationship(s) between heat treatment and EAC susceptibility in aqueous environments and to attempt to determine the fundamental mechanisms involved. The test technique selected to evaluate susceptibility was CF.

The CF behavior was investigated. The mechanical variables included in the program were (1) ΔK(12 to 45 MPa$\sqrt{m}$), (2) R (0.1 to 0.6), and (3) frequency (0.01 to 10 Hz). The electrochemical variables were (1) electrochemical potential, (2) the effect of polarization, and (3) the effect of electrolyte conductivity. The temperature range for the study was 25 to 288°C. The aqueous environments studied were (1) high-purity deoxygenated water, (2) air-saturated water, and (3) 0.05 M Na_2SO_4 (pH 3 adjusted with H_2SO_4).

Materials and Heat Treatment

Alloy X-750 for this study was procured in the form of 13- and 3.18-mm-thick hot-rolled plates. The chemical composition and heat numbers are listed in Table 2. The RPI[(1)] heat was obtained from D. Duquette at Rensselaer Polytechnic Institute in its final form. It is a typical commercial grade, although no processing information was available. The 13-mm-thick plates were processed from 10- by 10-cm length, electroslag-remelted forging stock. The billets were subsequently hot rolled to 13-mm-thick, 15-cm-wide plates. The rolling procedure consisted of heating the billet to 1121°C and reducing the thickness by 1.3 cm/pass to a thickness of 7.6 cm. On subsequent passes the thickness was reduced by 0.6 cm/pass to the final thickness of 13 mm. Reheats were performed when the temperature decreased to 954°C. Subsequently, the material was given the heat treatments listed in Table 1.

The heat treatments used in the investigation were intended to result in the precipitation of specific grain-boundary phases. The AH heat treatment was designed to produce grain boundaries characterized by a predominance of γ precipitation. The HTH heat treatment, on the other hand, was designed to produce a predominance of $Cr_{23}C_6$ grain boundary precipitation. The AH and HTH heat treatments represent commercial heat treatments that are highly susceptible (AH) and less susceptible (HTH) to EAC in LWR environments.[5]

Procedures

Microstructural characterization

Thin foils for transmission electron microscopy (TEM) examination were prepared by jet-polishing 3- by 0.5-mm-thick disks in a solution of 50 mL butycellosolve, 60 mL perchloric acid, 70 mL distilled water, and 350 mL of methanol at a temperature of −40 C at 35 V and a current of 40 to 60 mA. Foils were examined using a JEOL† JEM-200CX TEM with a LaB_6 filament.

Intermetallic phases were electrolytically extracted in a solution of 10% hydrochloric acid in methanol and identified using x-ray powder diffraction analysis, following the phase-identification procedures of Donachie and Kriege.[6] The composition of precipitated phases were analyzed using energy dispersive x-ray analysis of thin foils, extraction replicas, and extracted phases in a Vacuum Generators† HB 5 scanning transmission electron microscope (STEM).

(1)Rensselaer Polytechnic Institute, Troy, NY.
†Trade name.

TABLE 1
Typical Alloy X-750 (UNS N07750) Heat Treatments

Designation	Description	Treatment
AH	Double aged	Hot rolled 24 h/885°C/air cool + 20 h/704°C/air cool
HTH	Solution annealed and aged	Hot rolled 1 h/1093°C/air cool + 20 h/704°C/air cool

TABLE 2
Alloy X-750 (UNS N07750) Chemistries Composition (wt%)

Element	Heat 96457E6 (13 mm)	Heat 94501A2 (13mm)	RPI Heat (3.18 mm)
Ni	70.6 ± 1.5	73.2	71.4
Cr	15.0 ± 0.5	15.1	15.5
Fe	6.8 ± 0.1	6.9	7.5
Ti	3.9 ± 0.1	3.6	2.3
B	0.004 ± 0.002	0.004	—
Al	1.23 ± 0.05	1.13	0.67
Cb	1.36 ± 0.05	1.21	0.89
Ta	0.004 ± 0.002	0.002	0.037
Mn	0.15 ± 0.01	0.22	0.21
Si	0.09 ± 0.01	0.18	0.13
S	<0.002	<0.002	0.003
Cu	0.10 ± 0.01	0.10	—
C	0.058 ± 0.001	0.056	0.035
Co	0.08 ± 0.02	0.056	0.34
Zr	0.048 ± 0.002	0.032	—
P	0.003 ± 0.001	0.007	—

Corrosion fatigue tests

Corrosion fatigue tests were performed over the range of mechanical and environmental variables. Two specimen geometries were used, compact tension and single-edge notch. Figure 1 shows the physical characteristics of these specimens. Specimens were electrically isolated from grips and fixtures.

Tests were conducted at constant ΔK using a closed-loop servohydraulic fatigue machine adapted for use with a high-temperature, high-pressure titanium autoclave system that has been described elsewhere.[7] For single-edge notch specimens tested at temperatures lower than 65°C, a plastic cell was used.

Crack length was measured using either compliance or optical measurement techniques.[8,9] A fully automated system was used to measure and adjust all relevant parameters to ensure constant ΔK conditions in the former case. Electrochemical control was exercised, where necessary, with potential measured using an external Ag/AgCl reference electrode at a high temperature and a saturated calomel electrode a low temperature.[10]

Results

Microstructural characterization

A summary of the results of the microstructural characterization is given in Table 3. Figure 2 shows a TEM extraction replica of the microstructure that results from the AH heat treatment. The microstructure is characterized by (1) a grain size of approximately 10 μm, (2) a duplex γ' size in the matrix consisting of a coarse (0.1 μm) and

a fine (0.01 μm) fraction, (3) grain boundaries containing a third size fraction, slightly larger than the coarse matrix fraction, and (4) a region adjacent to the grain boundaries that is devoid of the large γ'-size fraction. The microstructure also contains occasional grain-boundary η-phase (Ni_3Ti) and large (1.0 μm) (Ti,Nb)(C,N) carbonitrides throughout the material. The coarse γ' precipitates during the 885°C heat treatment; the fine γ' fraction precipitates during the 704°C heat treatment. The narrow denuded zone results from the coarsening of the grain-boundary γ' at the expense of the matrix γ' adjacent to the grain boundaries during the 885°C age.

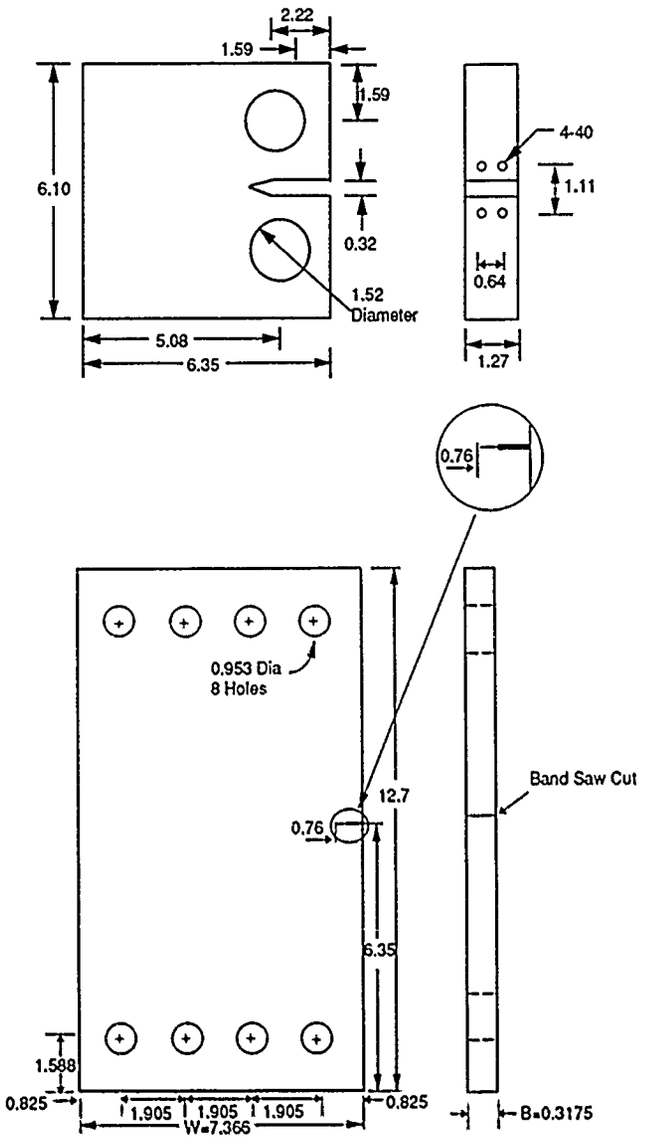


FIGURE 1—Fatigue crack growth specimen configurations.

Figure 3 shows a TEM micrograph of the HTH heat-treated material. The microstructure is characterized by (1) a grain size of approximately 100 μm, (2) extensive grain-boundary $Cr_{23}C_6$ precipitation, and (3) fine (0.01 μm) γ' precipitation throughout the matrix. Significant grain-boundary chromium depletion was observed (sensitization) by STEM analysis, which manifests itself as high weight losses in corrosion tests.

The results of the precipitated-phase analysis are summarized in Table 4. The γ is rich in titanium and dissolves a significant amount of chromium. This is especially true of γ' precipitated at lower temperatures. The means and standard deviations listed in Table 4 are based on analysis of a minimum of 10 particles for each phase, therefore, the totals may deviate slightly from 100%. The authors felt it more important to illustrate variability in individual concentrations than to force the sum of the mean values to equal 100%.

Corrosion fatigue

The crack growth data from the CF tests are shown in Figures 4 through 6. Figure 4 compares the data for the HTH heat treatment in 93°C water with helium data for both heat treatments at frequencies of 10 and 0.1 Hz and an R of 0.1. As the data shows, there is only a marginal effect of environment or frequency. The fracture path for both heat treatments is transgranular in helium. In water the crack path is also transgranular but, in this case, is crystallographic.

Figure 5 shows the data for both heat treatments tested in high-purity water at 288°C. The crack growth rate in the AH material is slightly higher than that for the HTH heat treatment. However, the difference is marginal. The crack path for both heat treatments is transgranular and, for the HTH treatment, crystallographic.

Figure 6 shows the data for the AH heat treatment in high-purity water at 93°C. There is little environmental effect but a strong dependence on frequency and stress ratio (R). The crack growth rate at 10 Hz is more than an order of magnitude greater than that at 0.1 Hz. The increase in crack growth rate is accompanied by a change in fracture path from transgranular to intergranular. Figures 7 and 8 show the fracture surfaces for material tested at 0.1 Hz and 10 Hz, respectively. Figure 9 shows the crack growth rate results plotted for a constant ΔK 25 MPa$\sqrt{m}$, and two temperatures, 60 and 93°C, for the AH treatment as a function of frequency. The threshold frequency for the transition to intergranular crack growth is approximately 0.3 Hz in 93°C water. The transition to intergranular crack growth is present at 60°C, but the increase in crack growth rate is much less.

All of the results presented to this point have been for an R of 0.1. Additional tests were conducted at a frequency of 10 Hz with R values of 0.4 and 0.6 for both heat treatments. Tests were conducted at a constant ΔK of 25 MPa$\sqrt{m}$ at 25°C intervals from 25 to 200°C. At R ratios of 0.4 and higher, both of the heat treatments showed a peak in crack growth rate at approximately 100°C. The crack growth rate for the AH heat treatment was in all cases much higher. Indeed, the crack growth rate for R = 0.6 was too high (> 1 mm/cycle) for the computer to maintain a constant ΔK.

The crack growth behavior in sulfate solution is entirely different from that in high-purity water. Figures 10 and 11 show results of tests conducted in sulfate solution [0.05 M Na_2SO_4 (pH 3)]. Also shown, for comparison purposes, is selected data from the high-purity water cases. Figure 10 shows results of tests performed under electrochemical control (galvanostatic). In a conductive electrolyte, cathodic polarization results in an increase in crack growth rate for both the AH and HTH heat treatments. A gradual transition from transgranular to intergranular crack growth is observed until, at a cathodic current density of 0.05 mA/cm^2, crack growth is completely intergranular. It is important to note that at the free-corrosion potential, the crack growth for the AH heat treatment is intergranular, while in the conductive electrolyte, it is transgranular and much lower. Also, the crack growth rates for both the AH and HTH heat treatments are comparable at the free-corrosion potential. Anodic polarization results in a decrease in crack growth rate for the AH heat treatment in the conductive electrolyte. On the other hand, the crack growth rate is high, intergranular, and independent of charging current density in high-purity water.

Figure 11 shows the data in sulfate solution as a function of frequency. While the data are limited, there is a clear inverse frequency dependence for cathodic polarization conditions.

TABLE 3

Grain-Boundary Phases in Alloy X-750[A] *Intragranular Phases in Alloy X-750[A]*

Treatment	Phase	Description	Treatment	Phase	Description
AH	γ'	Predominant phase, 0.3μm, cuboidal shape	AH	Fine γ'	Uniform distribution—0.01 μm
	(Ti,Nb)C	Rarely present, usually found at GB triple points		Coarse γ'	Absent near all grain boundaries, 0.14 μm
	η	Predominant phase in some regions, large, rod shaped		η	High concentrations in some regions of plate
HTH	$Cr_{23}C_6$	Predominant phase—several types, shapes, discrete and continuous	HTH	Fine γ'	Uniform distribution—0.02μm
	γ'	Usually present—0.04 μm, usually rod shaped			

[A]UNS N07750



FIGURE 2—Bright field TEM micrograph of the AH heat treatment showing a typical grain-boundary region. Note the three γ'-sized fractions and the region devoid of the large matrix-sized fraction adjacent to the grain boundary.

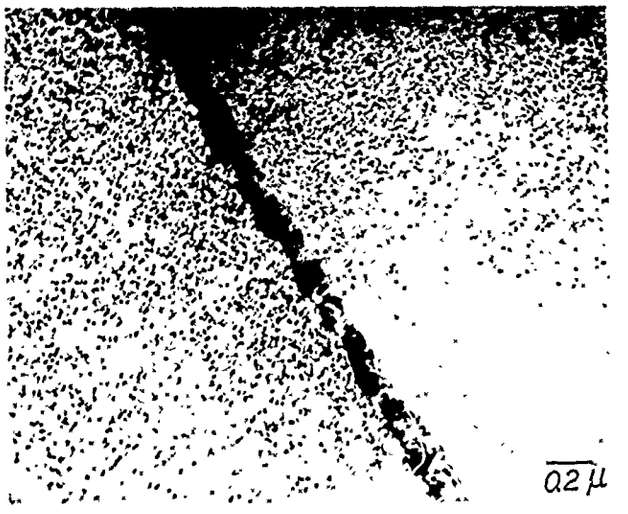


FIGURE 3—TEM extraction replica of the HTH heat treatment. Matrix contains fine γ'. Grain boundaries are decorated with $Cr_{23}C_6$ carbides.

TABLE 4

Compositions of Precipitated Phases in Alloy X-750 (UNS N07750) (wt%)

Element	Gamma Prime			$M_{23}C_6$ Carbides	Eta Phase
	AH-C[A]	AH-F[A]	HTH	HTH	AH
Al	6.4 ± 0.6	6.9 ± 0.6	6.4 ± 0.8	0.2 ± 0.2	3.0 ± 1.3
Ti	13.5 ± 0.3	13.9 ± 0.2	12.1 ± 0.4	0.4 ± 0.2	20.3 ± 0.5
Cr	1.9 ± 0.2	4.3 ± 0.6	2.3 ± 0.5	94.1 ± 3.7	2.6 ± 0.2
Ni	74.7 ± 0.8	71.1 ± 1.4	75.3 ± 1.0	5.0 ± 2.9	68.5 ± 0.8
Nb	0.7 ± 0.1	1.0 ± 0.1	0.4 ± 0.1	0.1 ± 0.05	1.6 ± 0.3
Fe	2.8 ± 0.1	2.9 ± 0.1	3.5 ± 0.4	2.7 ± 0.7	3.9 ± 0.2

[A]C = coarse; F = fine

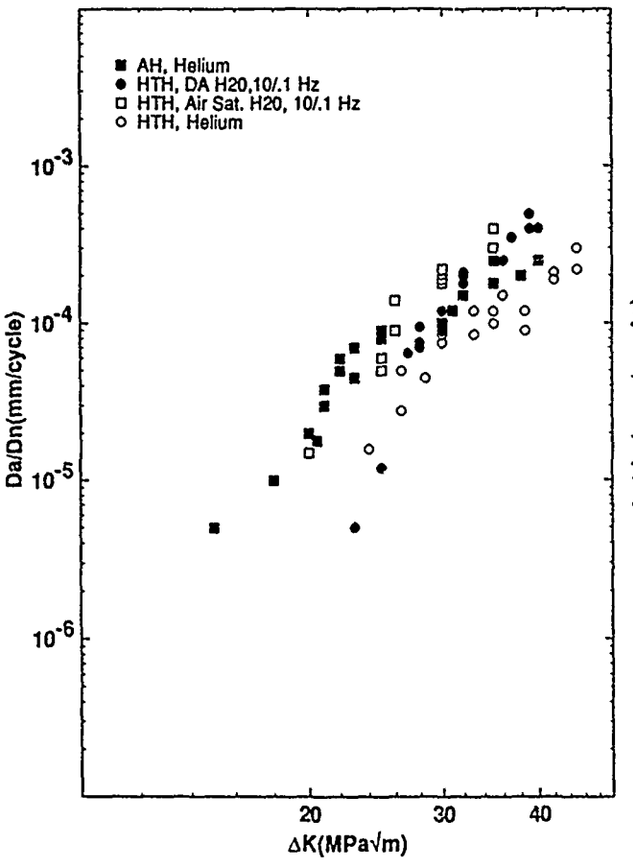


FIGURE 4—Fatigue crack growth for all heat treatments, including that for the AH heat treatment in helium at 93°C.

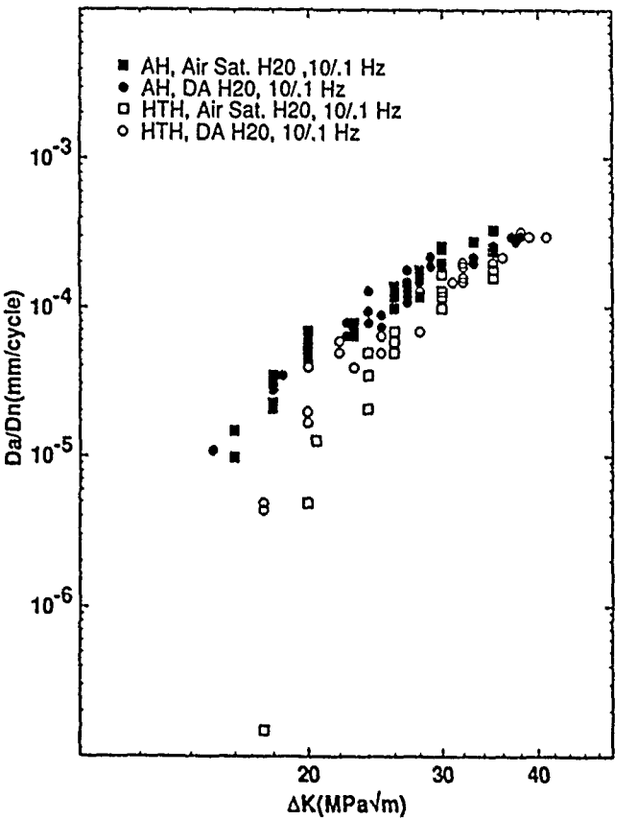


FIGURE 5—Fatigue crack growth for all heat treatments tested in high-purity water at 288°C.

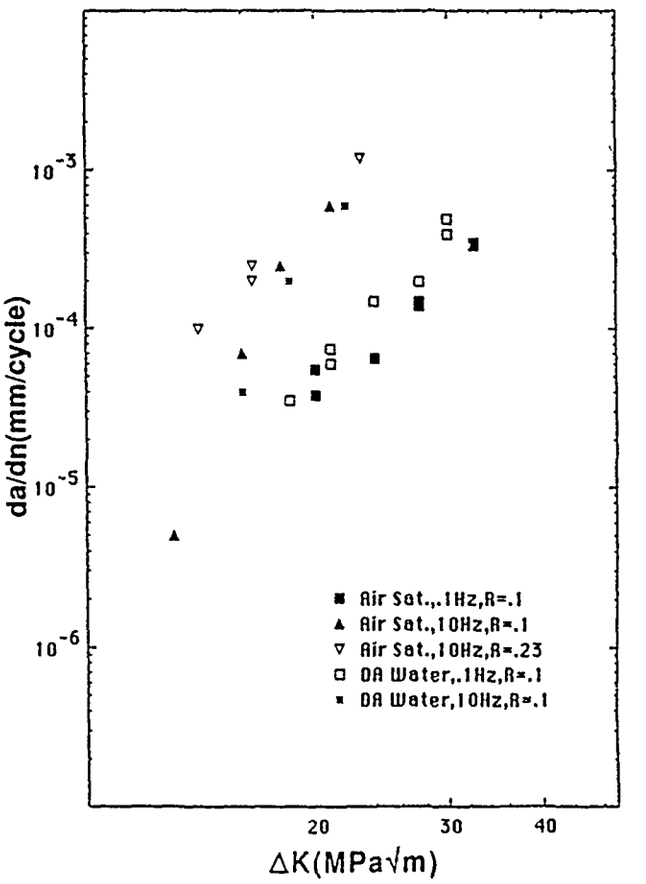


FIGURE 6—Fatigue crack growth data in air-saturated and deaerated high-purity water at 93°C for the AH heat treatment.

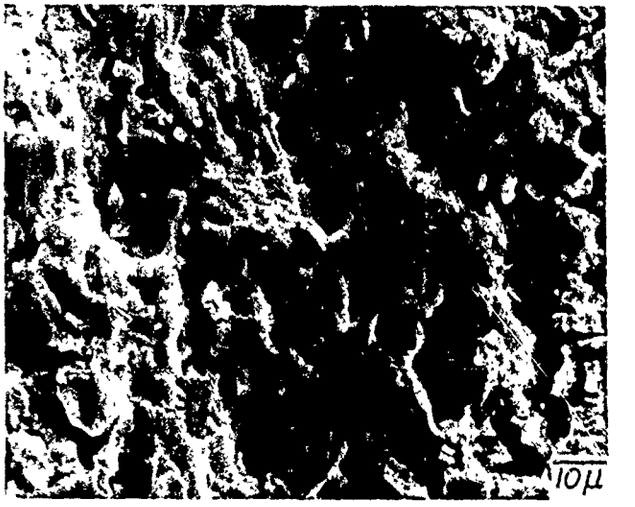


FIGURE 7—SEM micrograph of fatigue fracture surface in the AH heat treatment tested at 93°C in deaerated high-purity water at a ΔK of 25 MPa$\sqrt{m}$, frequency of 0.1 Hz, and an R ratio of 0.1.

To demonstrate clearly the effect of electrolyte type and cathodic polarization on the crack path, a test was conducted in which the same specimen was exposed to a series of different electrolytes and polarization conditions, after which the crack path was examined. Figure 12 shows a SEM micrograph for one of these tests. In this case, a stable crack growth rate was first established in high-purity water at a constant ΔK of 25 MPa$\sqrt{m}$, a frequency of 1 Hz, and an R ratio of 0.1. The test was then stopped and the solution drained from the cell. A solution of 0.05 M Na_2SO_4 (pH 3) was then

introduced and the test restarted. The crack growth rate was observed to decrease by approximately an order of magnitude. After ensuring a stable constant crack growth rate, the sample was cathodically polarized such that a constant current density of −0.5 mA/cm^2 was achieved. The crack growth rate was observed to increase to a value that was approximately the same as for the high-purity water condition. Figure 12 shows the fracture surface for this test. Upon introduction of the conductive electrolyte, the crack path changes immediately from intergranular to transgranular. Cathodic polarization results in an immediate transition to intergranular growth. This type of test was performed several times with identical results. However, for cases in which the test sequence consisted of high-purity water, sulfate (no polarization), and sulfate (polarization), the transition from intergranular to transgranular and back to intergranular was immediate. This is not the case when either high-purity water is introduced after a conductive electrolyte test or when cathodic protection is terminated in a conductive electrolyte test. In these cases, the transition in crack path is gradual and depends on the test frequency.



FIGURE 8—SEM micrograph of fatigue fracture surface in the AH heat treatment tested at 93°C in deaerated high-purity water at a ΔK of 25 MPa$\sqrt{m}$, a frequency of 10 Hz, and an R ratio of 0.1.

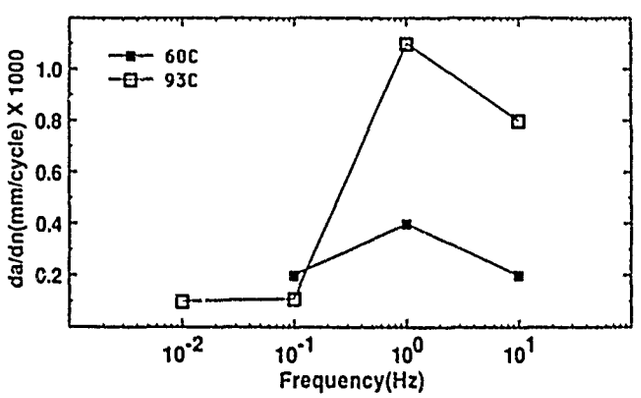


FIGURE 9—Fatigue crack growth rate at a ΔK of 25 MPa$\sqrt{m}$ and an R ratio of 0.1 as a function of frequency in deaerated high-purity water at 60 and 93°C for the AH heat treatment.

Discussion

The results of the experimental program show that the CF behavior is a strong function of microstructure and environment. Moreover, in the case of the low-temperature regime, the behavior would seem to be counterintuitive in that an increase in crack growth rate is observed with increasing frequency. The more common manifestation of an environmental effect is an increase in crack growth rate with decreasing frequency. This is indeed the case when a conductive electrolyte is present. However, the high-purity water case would appear to be anomalous. In light of this complex behavior, for the following discussion, it is appropriate to summarize the results of the investigation thus far:

(1) The crack growth rate in high-purity water is higher than that in helium for certain combinations of microstructure, mechanical, and environmental variables.

(2) There is a strong frequency effect that peaks at around 100°C. The AH heat treatment exhibits the strongest frequency effect, but the effect is present in all of the other heat treatments. The low-temperature regime (< 200°C) shows behavior distinct from the high-temperature regime (> 200°C).

(3) The high-growth-rate regime does not extend to higher temperatures for the conditions studied. At temperatures above 200°C, the crack growth rate exhibits a gradual increase with temperature for a given ΔK and is largely independent of heat treatment.

(4) There is no significant effect of oxygen or hydrogen concentration in high-purity water for any heat treatment.

(5) In the increased growth-rate regime, the crack path becomes intergranular for the AH heat treatment at an R value of 0.1. For the HTH heat treatment, intergranular fracture becomes noticeable only at higher R ratios.

(6) The threshold frequency for increased crack growth rate in the AH heat treatment is approximately 0.3 Hz at an R ratio of 0.1. The threshold frequency decreases with increasing ΔK and R.

(7) Cathodic polarization in a conductive electrolyte results in intergranular crack growth. Anodic polarization reduces the crack growth rate.

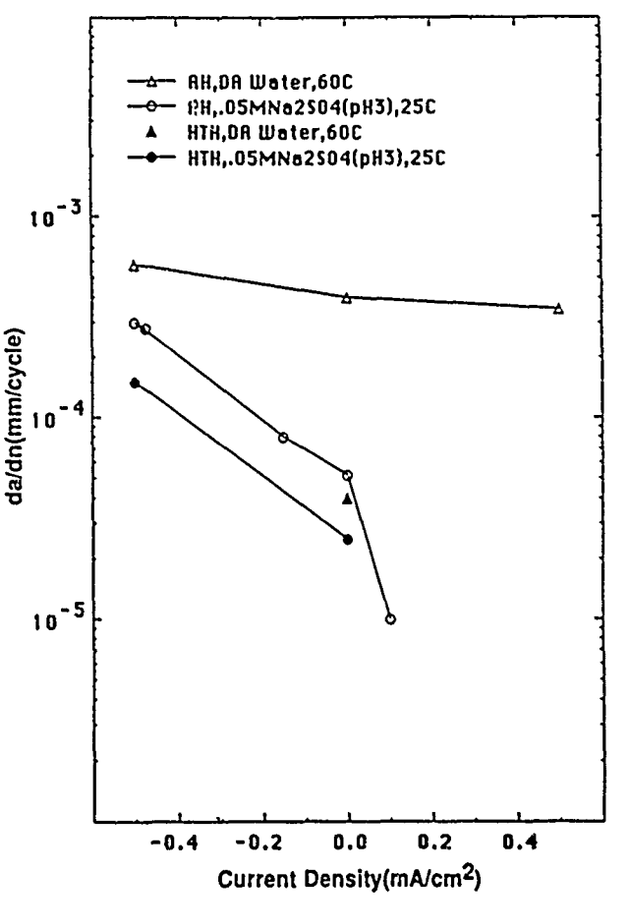


FIGURE 10—Fatigue crack growth rate of the AH and HTH heat treatments as a function of charging current density and environment. Tests conducted at a ΔK of 25 MPa$\sqrt{m}$, a frequency of 1.0 Hz, and an R ratio of 0.1.

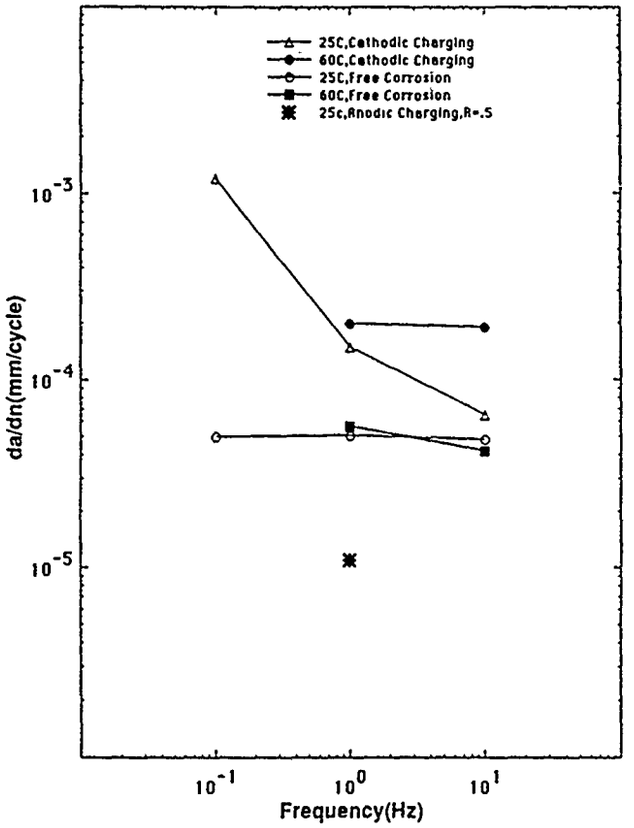


FIGURE 11—Effect of cathodic and anodic charging (current density = ± 0.5 mA/cm²) on the fatigue crack growth rate of the AH heat treatment in 0.05 M Na_2SO_4(pH 3) as a function of frequency at a ΔK of 25 MPa$\sqrt{m}$ and an R ratio of 0.1

The observed behavior at low temperature in high-purity water is consistent with a mechanism whereby the embrittling agent is produced by the material itself, as a result of crack propagation in sufficient quantity for the effect to manifest itself. Since one would normally expect that a rapidly propagating crack would eventually "out-run" the embrittling agent at some critical rate, there must also be a mechanism whereby the embrittling agent remains concentrated at the crack tip, independent of crack propagation rate.

Figure 13 shows a schematic of a typical crack tip in a precipitation-hardened alloy. If we consider only the environmental aspects of the propagation process, the major components of the system include the following: (1) fresh metal surface at the immediate crack tip, which for fatigue would be present even if crack propagation were not environmentally assisted; (2) grain-boundary and matrix chemistries that may be quite different; (3) grain-boundary precipitates that may be anodic or cathodic with respect to the adjacent matrix, grain boundary, or other precipitate; and (4) passivated or filmed crack flanks the nature and extent of which will depend on the stability and kinetics of film formation. As the crack propagates, these components are continuously being exposed to the environment. For these conditions, there will be competition between the exposure of fresh surface and the elimination of fresh surface because of film formation. The thermodynamics of a particular reaction, hydrogen reduction, and/or metal dissolution, for example, will determine if a reaction is possible. The kinetics of these reactions and/or their inhibition by film formation will determine the total charge transferred during the crack-extension increment.

For the γ'/Ni-Cr-Fe system, it has been demonstrated that a sufficient galvanic couple exists in these environments for the generation of corrosion currents of as much as of 0.5 mA/cm², with γ' being the anode and the matrix composition being the cathode.[11] In this case, the cathodic reaction was hydrogen reduction. Figure 14 shows the results of polarization studies on $(Ni\ Co)_3(Al)$ with variable titanium content in 0.05 M Na_2SO_4(pH 3 using H_2SO_4 additions) as a function of temperature.[11] The γ' in this study exhibited a transition from active/passive to active and back to active/passive behavior over the temperature range 50 to 150°C. As was discussed earlier, the AH heat treatment results in a predominance of γ' precipitation on the grain boundaries. It is interesting to note that the peak in critical anodic current density occurs at 100°C, the same temperature at which the peak in accelerated crack growth occurs in alloy X-750. It is thus proposed that the γ'/matrix couple, which will exist at the crack tip, can provide for local hydrogen generation during crack propagation.

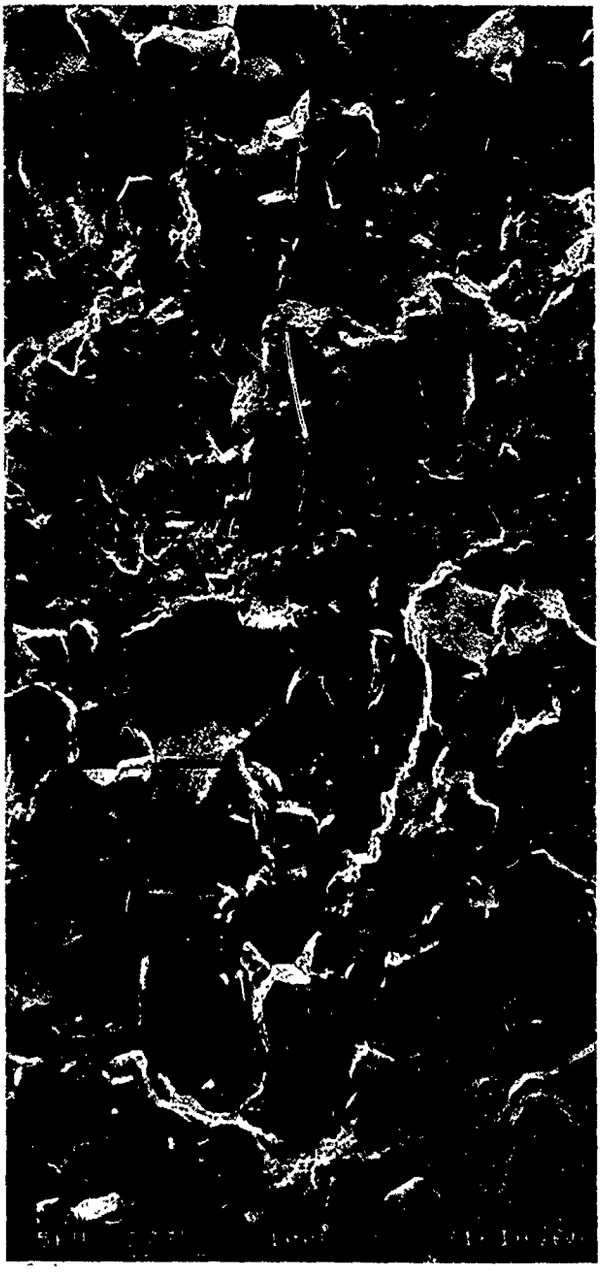


FIGURE 12—Transitions in fracture mode in response to environmental changes. Tests conducted at a ΔK of 25 MPa$\sqrt{m}$, a frequency of 1 Hz, and an R ratio of 0.1 (crack proceeded from top to bottom).

The discussion thus far has focused on the potential for significant galvanic effects in the material with γ' grain-boundary precipitation. However, the total charge transferred due to hydrogen reduction must equal the charge transferred during the anodic process. The critical anodic current density is a strong function of titanium concentration. The range of γ' titanium concentrations in this study was from 12.1 to 13.9 at%, which results in rapid passivation,

as shown by the results of potential jump experiments.[11] However, during the first second after a potential jump, the anodic current density of the γ' composition in alloy X-750 is comparable with that of titanium-free γ', which does not passivate. Thus, the potential exists for significant charge transfer on the time scale of approximately one second. For longer times, however, the anodic current density of the γ' in X-750 decreases to small values. This behavior allows for a partial explanation of the observed frequency effect in the low- temperature regime. At low crack propagation rates (da/dt), which would correspond with propagation at low frequency, the amount of hydrogen available for interaction at the crack tip will be limited both by metal exposure rate and film formation and its effect on the anodic half reaction.

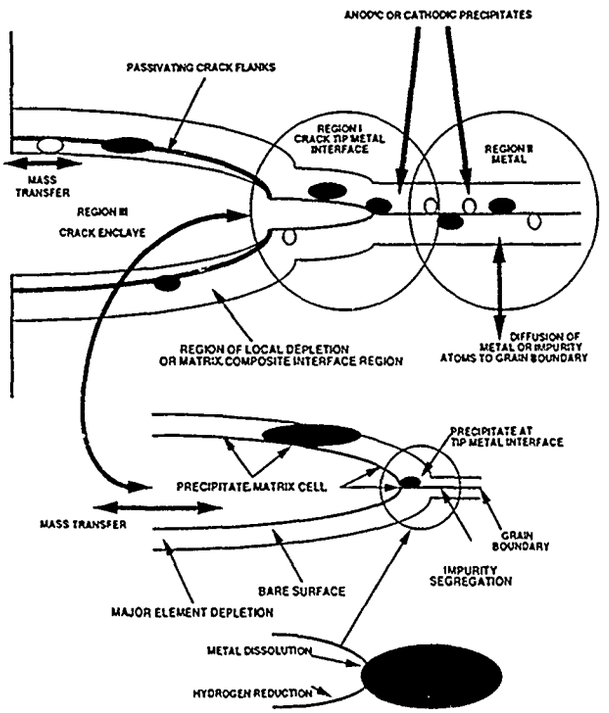


FIGURE 13—Model for intergranular crack propagation in precipitation-hardened materials.

For a complete explanation of the increase frequency effect, we must examine and compare the results of tests performed in the sulfate solution with those of tests performed in high-purity water. As shown in Figures 10 and 11, no acceleration in crack growth is observed for tests performed at the free-corrosion potential in the conducting electrolyte. In contrast, accelerated crack growth is observed, for some mechanical conditions, in high-purity water. In addition, cathodic polarization results in accelerated crack growth in a conducting electrolyte, and anodic polarization results in a decrease in crack growth rate. This is strong evidence that hydrogen is responsible for the accelerated crack growth rate—at least in the conductive electrolyte case. For the case of high-purity water, it is also proposed that hydrogen, this time self-generated because of the γ'/matrix couple at the crack tip, is also responsible for the accelerated crack growth rate. However, there still remains the task of explaining why, at the free-corrosion potential, accelerated crack growth occurs in the nonconducting (high-purity water) case and does not occur in the conducting electrolyte. As an explanation for this, it is proposed that the high IR drop present in the nonconducting electrolyte forces a severe localization of the hydrogen-reduction process to the immediate crack-tip region. The hydrogen-reduction process is thus forced to "follow" the crack tip. At a sufficiently high propagation rate, enough hydrogen is generated for an effect to manifest itself. In the conducting electrolyte, the localization of the hydrogen-reduction process is not possible. Thus, an insufficient amount of hydrogen is generated at the crack tip in spite of the same total hydrogen being generated by the γ /matrix couple. It is thus necessary to impose a local hydrogen-reduction process by cathodic polarization. As an additional note, Figure 10 shows that cathodic polarization has no effect on crack propagation rate in high-purity water. This is most likely because the high IR drop is making it impossible to polarize the crack tip sufficiently for additional hydrogen generation.

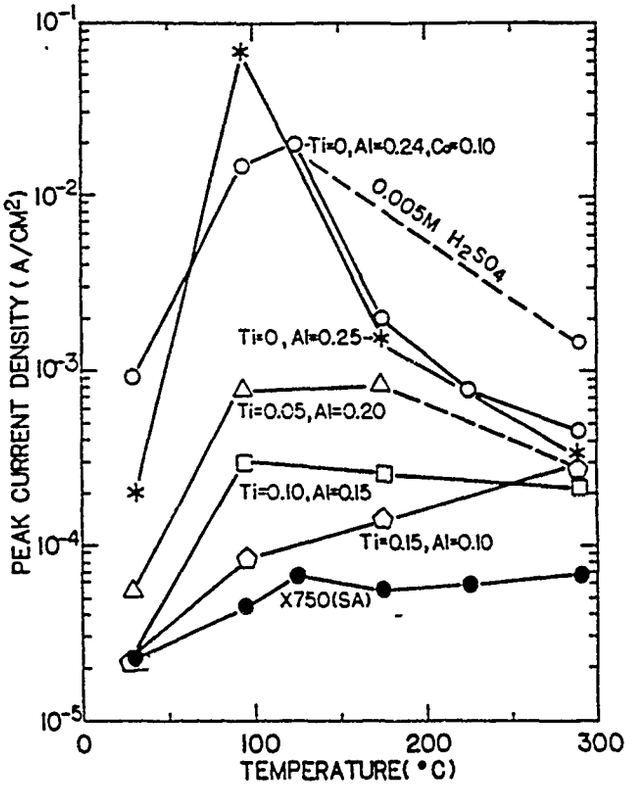


FIGURE 14—Effect of temperature on the active-dissolution peak density of Ni_3Al with various titanium contents in 0.05 M Na_2SO_4 (pH 3) compared with solution-annealed alloy X-750 (UNS N07750). Compositions are in atomic fractions.

The gradual transition between transgranular and intergranular crack propagation when high-purity water replaces the sulfate solution, and between intergranular and transgranular crack propagation after termination of cathodic polarization can be explained as follows. When the conductive solution is drained from the system, it is not possible to eliminate residual solution from the crack enclave; thus, some amount of pumping by the fatigue process is required to clean the crack. During this process, the conductivity of the solution in the crack decreases gradually, resulting in a gradual transition For the case after termination of cathodic polarization, one can hypothesize that some residual hydrogen remains either absorbed in the metal or adsorbed on the surface at the crack tip. Thus, the crack must propagate through this region or use up the remaining hydrogen during the transition period.

In contrast to the AH heat treatment, the HTH heat treatment grain-boundary microstructure is completely different In this case, the dominant grain-boundary phase is $Cr_{23}C_6$ carbide In contrast to γ', the carbide has been shown to be cathodic with respect to the matrix.[12] In addition, the fraction of grain-boundary carbide coverage is small, hence, the small cathode is coupled with a large anode For these conditions, it is unlikely that sufficient galvanic current can be generated to sustain an environmental effect for the conditions of this investigation. This does not mean that if an external source is available, as with the cathodic-charging case in the sulfate solution, accelerated cracking will not occur.

The behavior at high temperature clearly indicates that the low-temperature mechanism is not operative, or at least is not controlling crack growth. One would expect that as the temperature is increased, the hydrogen recombination reaction would become increasingly

rapid. This would result in a given amount of hydrogen being less effective as an embrittling agent. Since the crack path is transgranular for all heat treatments, grain-boundary morphology cannot be an important variable in this regime. However, the crack growth rate is significantly higher than that in helium, and the rate does increase with decreasing frequency for a constant ΔK. This would imply that an environmental component of crack growth is present. Thus, in this regime, we can hypothesize (with much less confidence, however) that crack growth rate acceleration results from crack-tip reactions in which the anodic process is dominant because of the generally increased reaction rates that arise as a result of the increased temperature.

Conclusion

The results of this analysis indicate that at least two mechanisms are responsible for the observed behavior in the temperature range 25 to 288°C: hydrogen embrittlement at low temperatures (< 200°C) and anodic mechanisms at high temperatures (> 200°C). The results of the investigation demonstrate that hydrogen plays a critical role in the CF process at low temperatures. It has also been shown that it is only necessary that a source of hydrogen be present in sufficient quantities for an effect to be observed. In the case of heat treatments that result in γ' precipitation on the grain boundaries, the source of hydrogen is provided by the γ'/matrix galvanic couple. For the HTH heat treatment, the grain-boundary couple between carbide and matrix is insufficient for the production of enough hydrogen except at high crack growth rates.

The results of this investigation demonstrate the importance of galvanic coupling between grain-boundary phases in multiphase alloys and their potential roles in the EAC process.

While a hydrogen mechanism is responsible for the observed behavior at low temperatures, this mechanism is not controlling at high temperatures. In this case, an anodic mechanism is more likely. Further work is necessary to confirm this.

Acknowledgment

The authors would like to express their appreciation to Dr. J.L. Nelson of the Electric Power Research Institute for providing funding for this research. We would also like to thank Dr. A. Turnbull of the National Physical Laboratory (UK) for providing a critical review that enhanced our understanding and forced us to tighten up the arguments in the paper. Professor R. Latanision's insight into the problem significantly helped in pinpointing the mechanistic understanding.

References

1. A.R. McIlree, Proceedings of the International Symposium on The Environmental Degradation of Materials in Nuclear Power Systems-Water Reactors (Houston, TX: National Association of Corrosion Engineers, 1984), pp. 838-850.
2. G.L. Garner, J.L. Smith, "Identification and Characterization of Commercial Nuclear Power Plant Components Fabricated from Age Hardenable Alloys X-750, A-286, and 718," EPRI Report RP2058-4, 1984.
3. M. Miglin, H.A. Domian, Proceedings of the International Conference on the Corrosion of Nickel Base Alloys (Metals Park, OH: ASM International, 1984), pp. 147-164.
4. C.A. Grove, L.D. Petzold, Proceedings of the International Conference on Corrosion of Nickel Base Alloys, pp. 165-180.
5. J. Prybylowski, R.G. Ballinger, "An Overview of Advanced High Strength Nickel Base Alloys for LWR Applications," presented at EPRI Workshop on Advanced High Strength Materials for LWR Internals, 1986.
6. M.J. Donachie, O.H. Krieg, J. Mater. 7, 3(1972). pp. 269 278
7. R.G. Ballinger, "Corrosion Fatigue in Nickel Base Alloys for Nuclear Steam Generator Applications" (Sc.D. Thesis, MIT, 1982).
8. W.C. Moshier, 'The Corrosion Fatigue Behavior of Alloy 600 in Steam Generator Environments" (Sc.D. Thesis, MIT, 1983).
9. I.S. Hwang, "Embrittlement Mechanisms of Nickel Base Alloys in Water" (Ph.D. diss., MIT, 1987).
10. D.A. Vermilyea, M.E. Indig, J. Electrochem. Soc. 119(1972). p. 39.
11. I.S. Hwang, R.G. Ballinger, J. Prybylowski, K. Hosoya, J. Electrochem. Soc. 136, 7(1989): pp. 1874-1883.
12. V. Cihal, A. Desestret, M. Froment, C.H. Wagner, Proceedings of the 5th Congress of European Federation on Corrosion (Paris, France: 1973), p. 249.

Transgranular Stress Corrosion Cracking in Copper-Gold Alloys

*B.D. Lichter, W.F. Flanagan, J.B. Lee, and M. Zhu**

Abstract

Transgranular stress corrosion cracking (TGSCC) was studied for disordered single crystals of Cu-25at%Au and Cu-50at%Au alloys in aqueous NaCl and $FeCl_3$ over the potential range 0 to 750 mV_{SCE}. In this domain, selective dissolution of copper occurs, and both anodic dissolution of gold and hydrogen generation are thermodynamically excluded. Under slow-strain-rate and constant-deflection loading, TGSCC readily occurs concurrent with rapid dealloying above a critical potential (E_c), which increases with increasing gold concentration in the alloy and decreasing chloride concentration in aqueous NaCl. However, embrittlement of Cu-25Au was also observed *below* E_c (where the steady-state dealloying rate is relatively low, $\sim 1 \times 10^{-6}$ amp/cm^2) under constant deflection in $FeCl_3$ and for slow-strain-rate loading in NaCl. The minimum average crack growth rate was found to be 1 to 3 orders of magnitude higher than the steady-state dealloying rate, indicating that although the dealloying process assists crack growth, it cannot account for the rate of crack propagation predicted by Faraday's law. Scratching experiments were conducted to determine the transient dealloying rates of Cu-25Au crystals in aqueous NaCl at potentials below E_c. Recurring current transients and associated load drops were also observed during slow-strain-rate testing, providing clear evidence for the discontinuous nature of crack advance. The time dependence of these current transients was similar to that observed during scratching. An attempt is made to interpret these results in the light of current theories of TGSCC.

Introduction

It is now believed that for many metal systems, transgranular stress corrosion cracking (TGSCC) occurs by discontinuous cleavage.[1-6] The evidence includes the following. (1) For face-centered cubic (fcc) systems in general and copper base systems in particular, the fracture surfaces generally occur as {110} facets rather than lying along {111} slip planes, as would be expected if the dominant mechanism were shear.[1,2] (2) observation of the fracture surfaces reveals that opposing faces are nearly matching and that the surfaces are cleavage like, displaying a distinctive 'facet-step morphology and "river markings",[1,3,4] (3) distinct crack-arrest markings are observed on the fracture surface;[2,5] and (4) discrete acoustic-emission pulses have been observed to correlate with electrochemical noise.[6]

Such results suggest that the processes leading to cleavage events must involve corrosion as well as deformation. This was discussed by Forty, who suggested that in brass, dezincification at the tip of an arrested crack leads to local embrittlement and resumed crack advance.[7] On the basis of two-dimensional computer simulation models, Sieradzki and Newman have proposed that surface modification, be it dealloying or film formation, could lead to embrittlement under the influence of the stress field of a crack tip.[8,9] In their model, the misfit stress arising from dealloying, for example, leads to the formation of a crack at the interface between the underlying matrix and the surface affected zone when the disparity between the atom sizes is sufficiently large.

Recent findings suggest that the initial nucleation step for TGSCC may differ from the continued reinitiation process associated with propagation of the crack. This initial step presumably develops the appropriate stress state and environmental conditions for TGSCC and involves the formation of a groove or crack, not necessarily of the same orientation as the ensuing transgranular crack.[10] For the case of brass in ammoniacal solutions, local dissolution of active slip planes provides the necessary nucleus for TGSCC.[11] In engineering alloys, pits, inclusions, intergranular cracks, etc., may serve as suitable nuclei for transgranular cracks. We have previously reported an alternative mechanism that occurs in copper-gold alloys in which a brittle gold sponge forms on the surface in both NaCl and ferric chloride solutions.[3] Under tensile loading, cracks form in this sponge and propagate into the underlying matrix, providing the nucleus for TGSCC.

Assuming that crack propagation in TGSCC occurs discontinuously, it must involve a succession of renucleation and rapid propagation events separated by finite time intervals during which the crack is momentarily arrested. A comprehensive theory must explain both the observed crack morphology (i.e., the crack orientation, the crack arrest markings, the details of the "river markings, etc.) and the observed kinetics (i.e., the effect of potential and crack-tip environment on the average propagation rate, which is the ratio of crack advance distance to time interval between microcracking events). Processes similar to those that lead to initial nucleation may be involved, such as selective dissolution (dealloying) leading to the formation of a sponge.[3,4] Alternatively, selective dissolution may lead merely to a depleted surface region ("film") or oxide at the crack tip.[8] A distinctly different process involves dissolution along slip planes intersecting the crack tip. This was suggested by Forty, but the detailed mechanism was unspecified.[7] For any of these mechanisms to be applicable, they must provide the necessary stress condition for crack renucleation. The subsequent arrest of the reinitiated crack has been explained by the activation of a slip band that absorbs the crack driving energy.[7,12] However, in some instances it could be the

*Department of Materials Science and Engineering, Vanderbilt University, Nashville, TN 37235.

consequence of a decaying crack driving force from a fixed crack-opening displacement, caused, for example, by the release of a dislocation pile-up.[13]

Rice has modeled the tensile crack-tip deformation fields in elastic, ideally plastic crystals and has shown that because of stress and displacement compatibility requirements, velocity discontinuities occur that are coincident with slip planes for a [110](001) crack but oblique to them for a [010](101) crack in an fcc lattice.[14] Despite the fact that the analysis considers only infinitesimal strains without lattice rotations, Rice concludes that fcc materials should be prone to {110} fracture. This is because for such {110} cracks, crack-blunting slip involves kink-like shear for which the required dislocation sources may not be available, leading to cleavage. This contrasts with the case for {100} cracks, in which crack-blunting slip could easily initiate at the crack tip. Such an analysis is moot for normally ductile materials in the absence of corrosion, but if TGSCC occurs, the role of corrosion becomes critical and must be included in the analysis. It might be that corrosion is capable of producing sharp cracks that could extend by cleavage according to the Rice mechanism; however, it is known that propagating cleavage cracks are blunted and therefore arrested by pre-existing active slip bands.[7] Therefore, our attention should be focused on the details of the arrest and (re)initiation of cleavage cracks, and the specific role of environment in this process.

From the foregoing account, the detailed mechanism for crack propagation remains unclear. Indeed, there may be more than one mechanism that could explain the process. However, anodic dissolution is certainly involved, and the study of transient currents associated with the initial nucleation and the subsequent discontinuous cracking events seems appropriate. The present work presents results for copper-gold alloys in aqueous NaCl, undertaken to elucidate some of the details of TGSCC. Results are presented for both steady-state and transient dealloying. In addition, results of slow-strain-rate tests are presented and compared with earlier bend-test results, and an attempt is made to interpret these based on the dealloying process. The copper-gold system was chosen because over the investigated potential range exclusive dissolution of copper occurs. Also, in this potential range, involvement of hydrogen in the cracking process can be discounted both on thermodynamic grounds and, more convincingly, because of the results of recent crack-chemistry modeling by Bertocci.[15]

Experimental Procedures

Experiments were performed on Cu-25Au and Cu-50Au single crystals produced using the Bridgman technique by co-melting copper and gold of 99.99% purity in a high-purity split graphite mold.[1] Samples with dimensions 3.5 by 0.3 by 0.03 to 0.1 cm were cut from single-crystal slabs. The crystals were wet-ground using 320- to 600-grit SiC paper, followed by fine polishing with a succession of suspensions of alumina powders, ending with 0.05 μm alumina particles, which resulted in bright and smooth surfaces. The specimens were then degreased with ethyl alcohol and acetone, vacuum sealed in quartz capsules, annealed at 850°C for 120 h to ensure homogenization and relieve any residual stresses, and brine quenched to obtain a disordered structure.

Steady-state (potentiostatic) anodic polarization was performed using platinum counterelectrodes in 0.006 to 0.6 M NaCl solutions, deaerated with hydrogen or helium, using PAR† Model 173/276 and Solartron† Model 1286 potentiostats. Electrode potentials were measured with respect to a saturated KCl calomel electrode (SCE).

[1]Gold was provided by Englehard Corporation through the assistance of Dr. Richard Lanam.

†Trade name.

Scratching experiments were performed on Cu-25Au samples in 0.6 M NaCl. One experiment was conducted to reveal the effect of scratching on dealloying below E_c. A sample was scratched in air, immediately submerged into the solution while polarized at 350 mV, and maintained at this potential for three days without an applied stress. The other experiment involved scratching crystals while they were submerged in the aqueous environment and anodically polarized to potentials between 100 and 30 mV, using a Thompson† Model 184 low-noise potentiostat. The transient current pulses following scratching were measured using a Nicolet† digital storage oscilloscope (Model 4094/4562.)

Slow-strain-rate tests were performed with Cu-25Au crystals in a specially constructed corrosion cell, controlled with the Thompson low-noise potentiostat and mounted on an Applied Test Systems† universal testing machine (ATS Series 1 102E). This is a relatively "hard" machine, so sudden extensions of the sample give rise to a load drop. This feature was useful in detecting initiation as well as renucleation during discontinuous crack propagation, as discussed below. The potential domain for TGSCC was established under slow-strain-rate loading using samples polarized between 300 and 430 mV_{SCE}, and the resulting data were compared with prior results[4] obtained under constant deflection in both aqueous NaCl and aqueous $FeCl_3$. During some of these tests, which were performed at a strain rate of 1.1 to 1.3 × 10^{-6}/s, current transients and associated load drops were observed and recorded with the Nicolet oscilloscope. In these instances, the sample area was masked with "Miccrostop,"† leaving only a small region along the edge containing the crack-initiation site exposed to the solution.

Microprobe observations were done using an Hitachi† X-650 scanning electron microscope (SEM) equipped to do electron microprobe x ray analysis using either energy or wave-length dispersion.

Results

Steady-state polarization studies

Effect of alloy composition. Figure 1 includes the results for anodic polarization for unstressed crystals of Cu-25Au and Cu-50Au in oxygen-free 0.6 M NaCl. A low-current plateau is observed up to a critical potential (E_c) (~ +430 mV for 25 Au and ~ +620 mV for 50 Au), above which a steep rise in current is noted. Similar behavior has previously been reported for this system[16] as well as for acid-sulfate solutions.[17] The phenomenon may be described as a "transpassive" transition, in which the dealloyed (gold-rich) surface layers are no longer protective above E_c, leading to formation of a gold "sponge" and rapid dissolution of copper.[4] The subject has been reviewed by Pickering[18] and more recently by Kaiser.[19] Figure 2 shows the appearance of the sponge formed above E_c.

Effect of Cl^- concentration. Figure 3(a) shows results for anodic polarization of Cu-25Au for different concentrations of aqueous NaCl and indicates a systematic variation of E_c with Cl^- activity. The dependence as shown in Figure 3(b) follows the relation

$$E_c = A + B \log_{10}(a_{Cl^-}) \quad (1)$$

where the constant B is found to be 0.05 V. These results are similar to those obtained by MacDonald, et al., in studies of the Cl^- dependence of the pitting potential in stainless steels,[20] suggesting possible relevance of their proposed model for the breakdown of passive films in chloride media. Thus, there exists the novel possibility of an oxide or salt film on the alloy surface, a condition that becomes more probable at higher potentials. The possible relevance of this situation to dealloying needs further consideration.

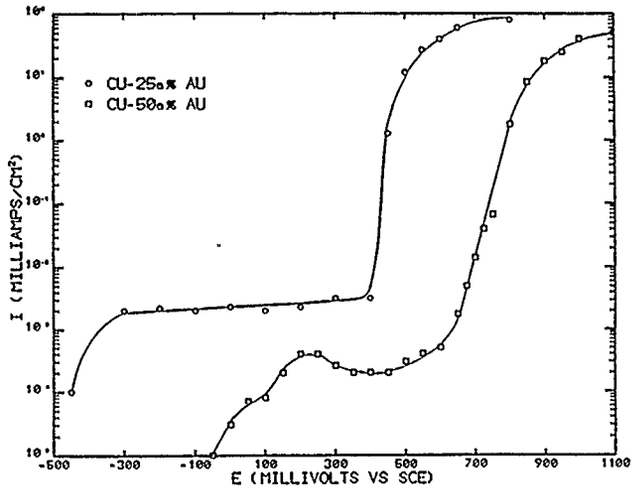


FIGURE 1—Steady-state anodic polarization for Cu-25Au and Cu-50Au single crystals in oxygen-free 0.6 M NaCl.

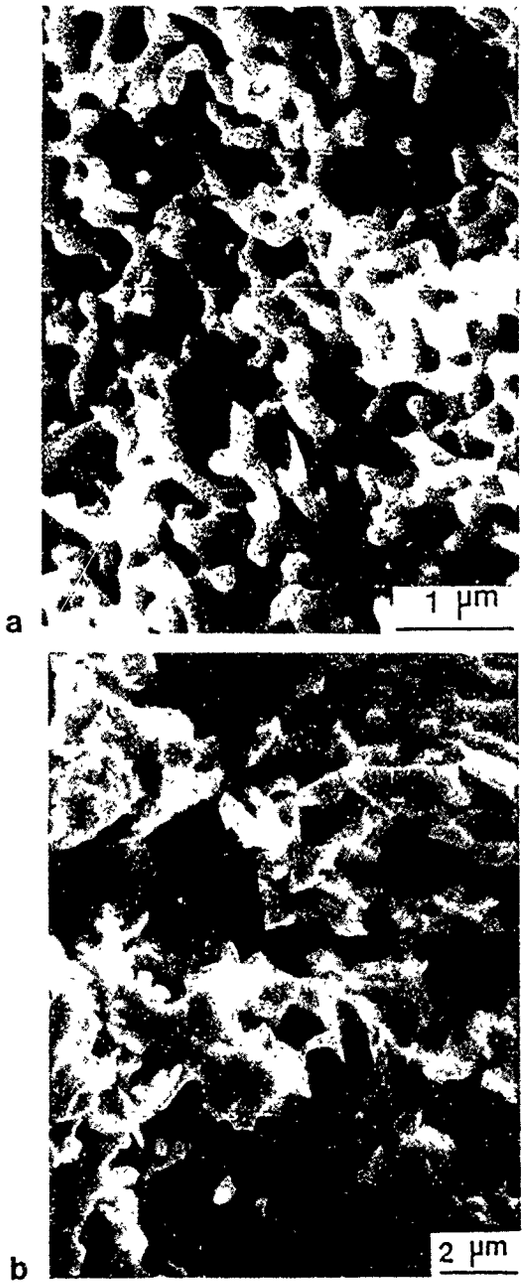
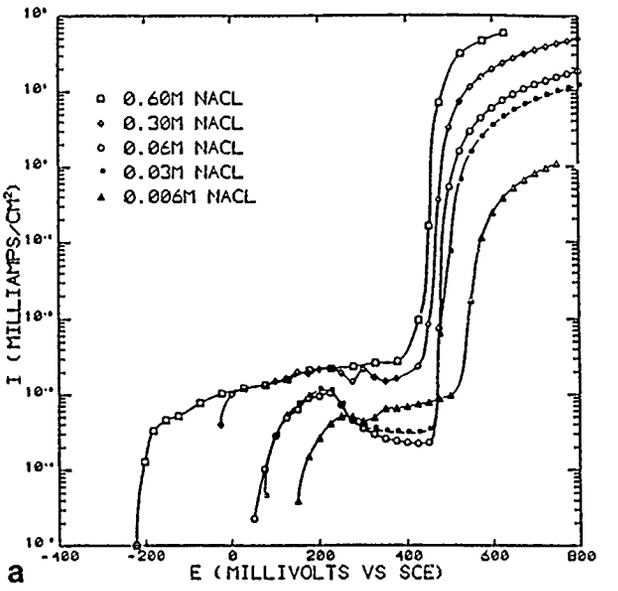


FIGURE 2—Gold sponge formed on surface of alloys polarized above E_c: (a) Cu-25Au[4] and (b) Cu-50Au.[23]



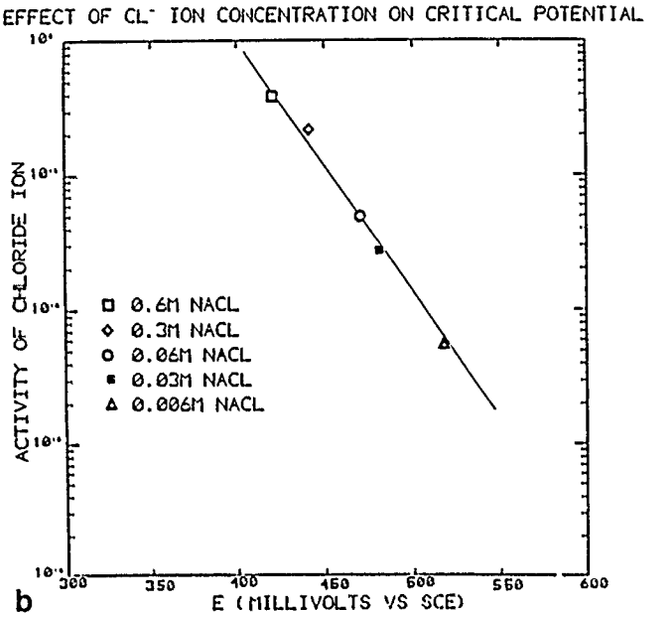


FIGURE 3—(a) Anodic polarization behavior of Cu-25Au for different concentrations of aqueous NaCl showing systematic variation of E_c; and (b) the dependence of E_c on chloride ion activity for Cu-25Au.

Scratching experiments

Samples scratched in air. Several authors have suggested that dealloying occurs only above the critical potential (E_c).[18,19] However, Cu-25Au crystals, scratched in air and immediately anodically polarized in 0.6 M NaCl solution at 350 mV_{SCE}, well below E_c, exhibited gold enrichment in the scratched region. This was confirmed by SEM microprobe analysis, which indicated extensive dealloying in the scratch, as can be seen in Table 1. More important, though, was the observation that cracks were formed in this dealloyed region perpendicular to the scratch, and that these cracks even extended into the unscratched region (Figure 4). No cracks were observed on crystals that were scratched but not immersed in the solution, nor was sponge or cracking detected in samples that were immersed unscratched, even after 17 days of exposure at 350 mV_{SCE}. Thus, it seems that in the proper environment, prior deformation caused by scratching can lead to an increased rate of steady state dealloying. This, in conjunction with residual stresses presumably caused by the surface deformation, can initiate TGSCC.

TABLE 1
Variation of Cu and Au Composition Between the Matrix and the Scratched Region

	Weight%		Atomic%	
	Cu	Au	Cu	Au
Matrix	49	51	75	25
Scratched Region	30	70	57	43

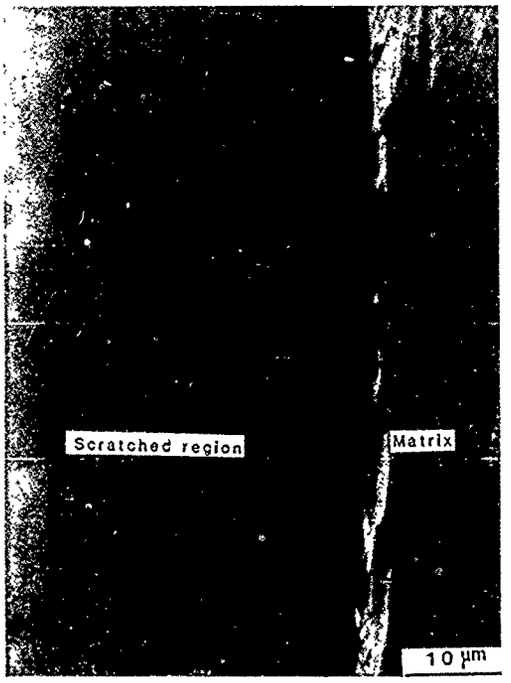


FIGURE 4—SEM micrograph of scratched region for Cu-25at%Au crystal scratched in air and immersed in 0.6 M NaCl for 3 days at 350 mV, well below E_c. Note cracks in scratched region, some of which propagate into the unscratched matrix.

Samples scratched while immersed. To study the scratching behavior more carefully, the corrosion current was monitored for Cu-25Au samples scratched while they were immersed in solution, as a function of imposed potential. A rapid rise in current accompanied the scratching followed by a current decay at a rate related to the imposed overpotential (Figure 5). The measured projected area of the scratch was 0.12 mm^2. The area exposed by scratching was not measured in each case, but the procedure was identical. This involved scratching across the entire specimen surface each time. The pressure exerted during the scratching was assumed to be the same, but variations in this pressure would lead to variations in exposed surface as well as in the related deformation and resulting residual stresses. A measure of such variation can be deduced from the measured transient peak heights, and since these varied linearly with potential with relatively little scatter (Figure 6), it was assumed that the variation in scratched area was not significant.

Slow-strain-rate experiments

Potential dependence of time-to-failure. Figure 7 shows the effect of the applied potential on the time-to-failure, which is seen to approach zero as E_c is approached for Cu 25Au samples in 0.6 M NaCl. A comparison is also shown with earlier results under constant deflection.[4] At potentials below 350 mV, the failure mode in the constant strain-rate tests is predominantly ductile, however, some environment-induced loss of ductility is still evident at 300 mV.[23] Typical fracture surfaces are shown in Figure 8. These show the characteristic morphological features associated with cleavage-like fracture, and they demonstrate the occurrence of TGSCC at potentials well below E_c.

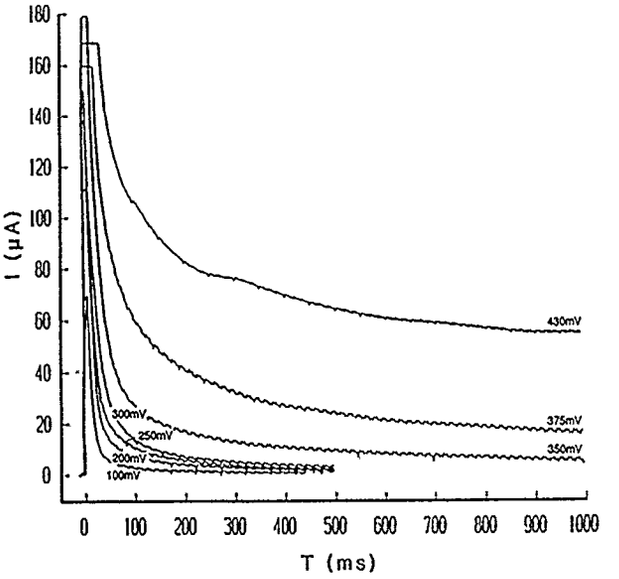


FIGURE 5—Current transients following scratching Cu-25at%Au crystals immersed in oxygen-free 0.6 M NaCl and anodically polarized to various potentials below E_c (background current of ~ 1 μA subtracted). The inverted periodic pips are instrumental artifacts.

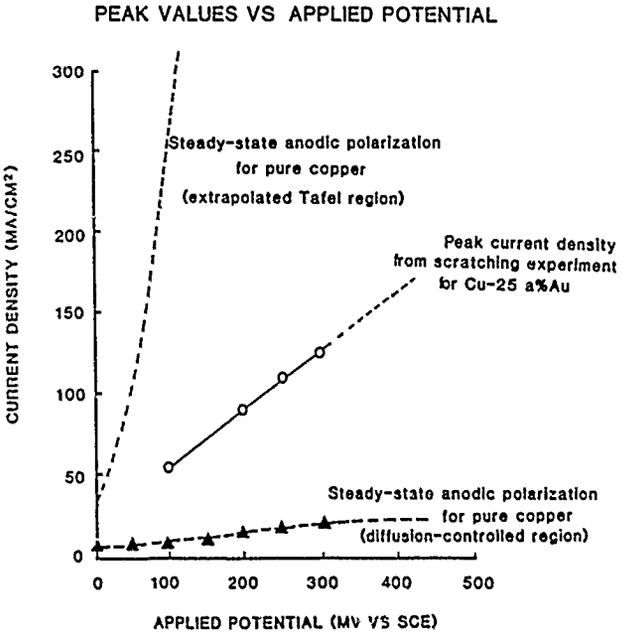


FIGURE 6—Potential dependence of transient current maximum shown in relation to steady-state anodic polarization curve for pure copper.

Observations of crack growth. In these tests, the sample was maintained at the rest potential (~ −100 mV) for 2 h and then anodically polarized in steps to a potential below E_c. Straining was begun, and the sample displayed an easy glide where serrated yielding was observed (nominal stress of 90 to 110 MPa.) Usually, a long induction period was observed prior to crack initiation, however, for the two tests reported below, initiation was promoted by polarizing the sample momentarily to 430 or 450 mV. The onset of cracking was detected by the appearance of a series of transient current peaks that coincided with drops in the measured load. Once the crack was nucleated, the potential was lowered to values below E_c. Subsequent

current transients and load drops continued to occur at regular intervals throughout the test, with a magnitude and frequency that increased with potential and decreased with increasing crack length.

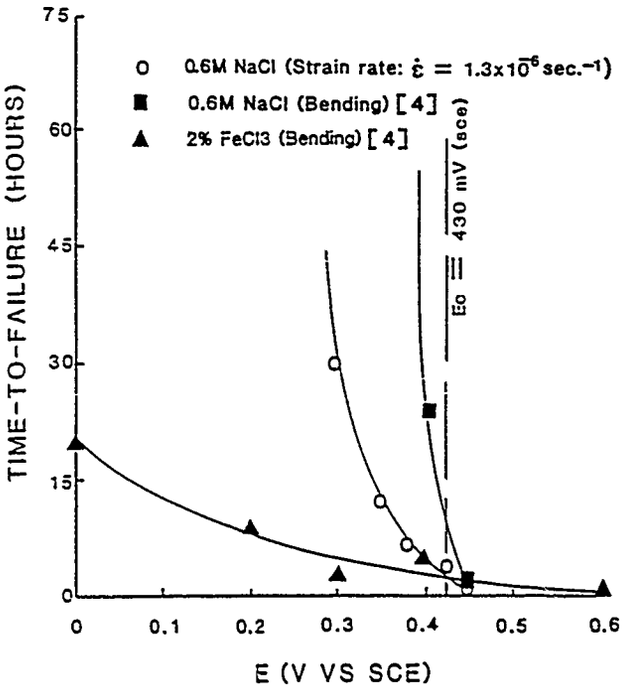


FIGURE 7—Effect of environment and loading mode on embrittlement of Cu-25Au single crystals in subcritical potential domain.[4,24]

Figures 9 and 10 show results from a single test in which nucleation occurred at 450 mV. After nucleation, the potential was reduced and changed successively to 400, 380, and 350 mV and then increased to 400 mV before fracture was completed. Figure 9(a) shows a single instance of coupled events observed at 380 mV. Figure 9(b) shows the series of events occurring shortly after the initial nucleation of cracking at 450 mV. In Figure 10, the current and load are shown for three potentials (all below E_c) following nucleation. These data were taken under constant average strain rate as the crack length increased (from ~ 0.5 mm to ~ 1 mm along the 3-mm fracture path) producing a decreasing average load at 400 and 380 mV but an increasing load when the potential was changed to 350 mV. The decrease, with decreasing potential, of both the magnitude and the frequency of occurrence of the transient current peaks and accompanying load drops is evident from Figures 9(b) and 10.

In a second test, initiation was affected at 430 mV, and then the potential was alternately varied (in ~ 10- to 20-min intervals) between 400 and 0 mV during the test until failure occurred. During the 0 mV intervals when the crack was stationary, load drops without associated current transients were observed under an increasing average load; during the 400 mV intervals, the average load decreased at an average rate of ~ 70 N/h, and both the magnitude of the load-drop/current transient events and the time interval between these events decreased as the crack length increased. A section of the fracture surface for a potential of 400 mV is shown in Figure 11. Crack arrests (five of which are shown) could be identified on the matching fracture surfaces, and an approximate correspondence could be made with the current transients and load drops. By summing the successive crack-arrest distances (Δx^*) and the corresponding time intervals between load-drop/current transient events (Δt^*), it was possible to ascertain the average velocity over this interval,

$$v = \Delta x^*/\Delta t^* = \sim 0.7\ \mu m/s \qquad (2)$$

An alternative method of estimating the velocity for this interval is discussed below.

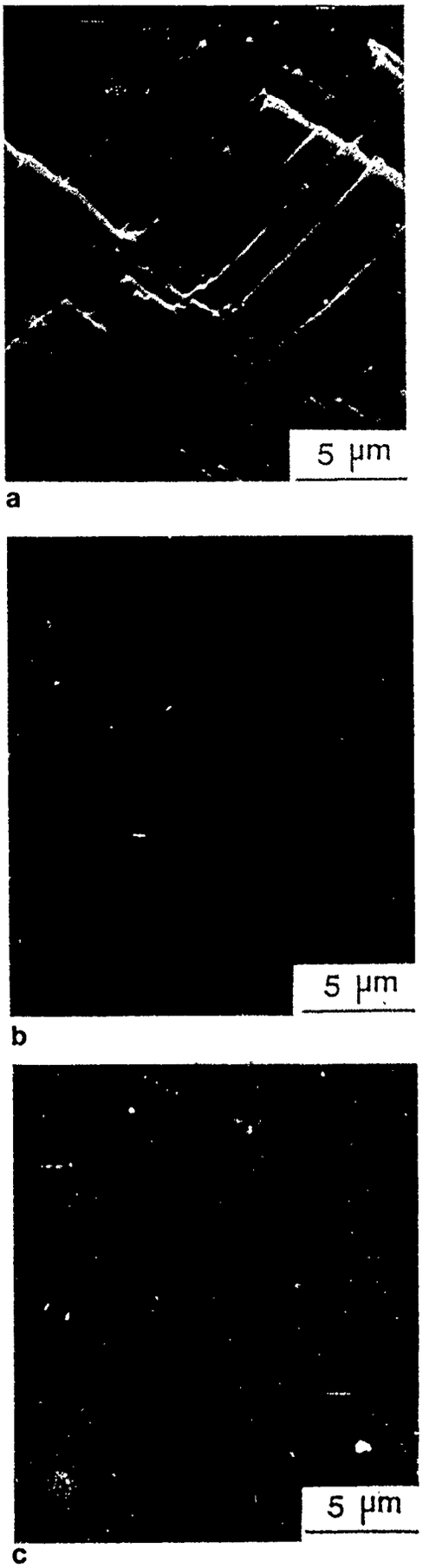


FIGURE 8—SEM micrographs showing fracture surfaces of crystals deformed under anodic polarization and slow-strain-rate (1.3 $\times 10^{-6}$/s): (a) 350 mV, (b) 380 mV, and (c) 430 mV.[23]

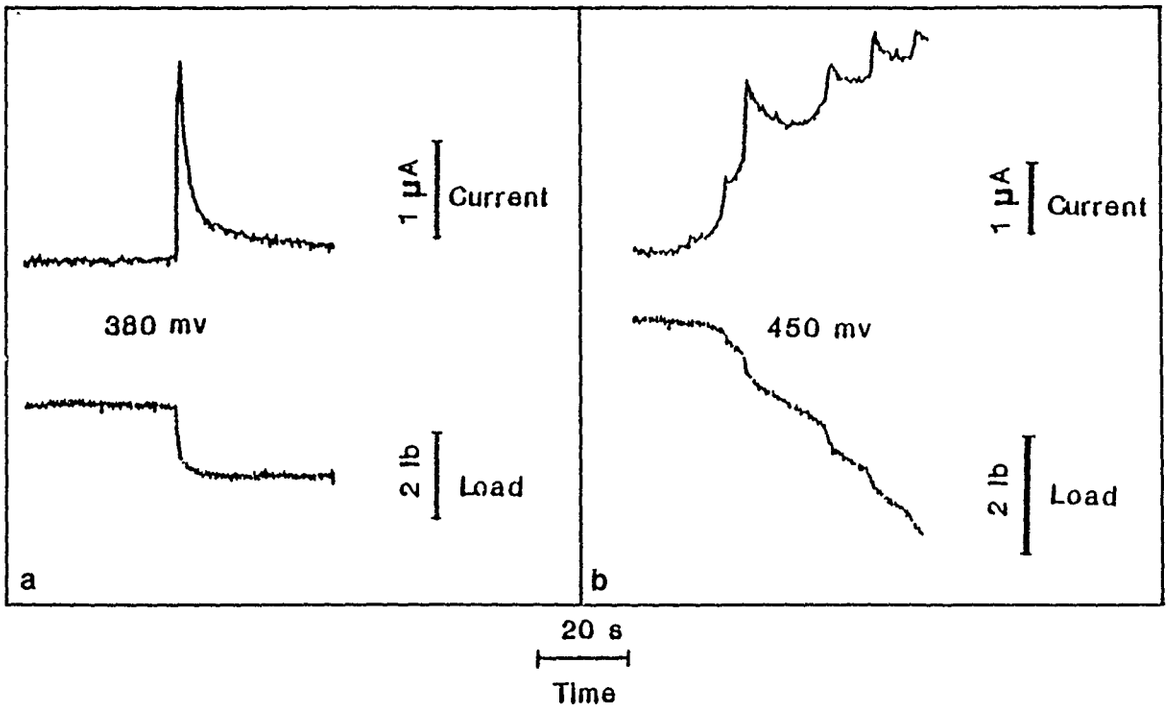


FIGURE 9—(a) Current transient and associated load drop observed during crack growth in Cu-25Au single crystal under slow-strain-rate loading (1.1×10^{-6}/s) in 0.6 M NaCl, anodically polarized to +400 mV; and (b) series of prior events observed at 450 mV, shortly after the initiation of discontinuous crack propagation.

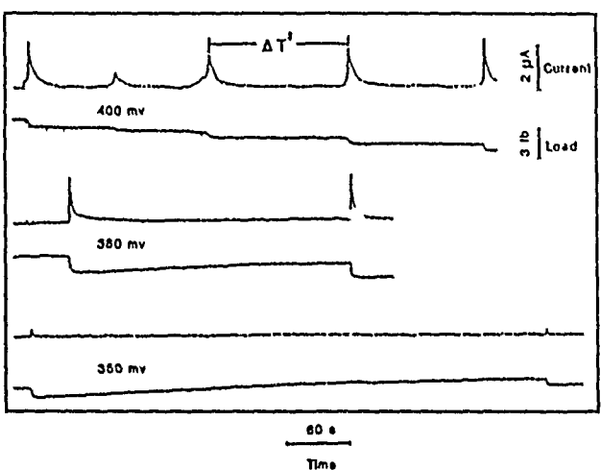


FIGURE 10—Potential dependence of current transients and associated load drops during crack growth in Cu-25Au.

Discussion

Discontinuous crack advance during TGSCC

To understand the above results, it should be noted that a current transient occurs as a consequence of a new surface created during crack advance, and this is associated with a simultaneous load drop resulting from the accompanying reduction in area. The magnitude of the load drop should be proportional to the magnitude of the crack advance under conditions in which the flow stress can be considered constant (i.e., in the "easy-glide" region of single-crystal deformation). Plastic flow of the crystal should be unaffected by this event, except for recovery of the elastic strain in the system, which is likely to be small. A complicating factor is the load drop associated with any accompanying slip. The continuous deformation associated with constant strain-rate testing has no effect, but sudden bursts generated at the crack tip when the crack is arrested, particularly if the arrest involves collision with an "active" slip band, could lead to load drops of the same order of magnitude as those resulting from crack advances. In this case, though, there is a recovery period, because a drop in stress accompanies the load drop (unlike the situation for the crack advance), and the stress–strain curve must recover to the flow stress for deformation to proceed as before. We have observed that the formation of such slip bands in samples deformed in air (or in solution prior to crack nucleation) are also accompanied by load drops, followed by just such a stress recovery. This presumably occurs in these alloys because of the presence of short-range order, which leads to coarse slip. For cases in which crack advance and shear bands occur together, these effects are superimposed. Normally (except when pre-existing shear bands arrest the crack), any slip generated from the arrested crack is relatively small and can be ignored. In preliminary straining-electrode tests with unmasked samples, the formation of such slip bands prior to crack initiation displayed both a load drop (which recovered with further straining) and a large current transient because of a new surface being created where the slip intersects the sample surface. For samples coated with Miccrostop, only the load drop without a current transient is seen on formation of slip bands prior to crack nucleation.

As mentioned above, over a 20-min interval at 400 mV, the average velocity of crack growth could be estimated from the approximate correspondence between the time interval between transient events and the spacing between crack-arrest markings on the fracture surface (Figure 11). The average velocity at a given potential can also be estimated for this case from the rate of change of the average load under the assumption that the load decreases at constant stress because of the decrease in cross section. Under these conditions, the load drop per unit crack advance is given by

$$(dP/dl) = w_o \sigma_{max} = P_{max}/l_o \qquad (3)$$

where w_o and l_o are the initial width and length of the fracture plane, and σ_{max} and P_{max} are the "easy glide" or flow stress and the corresponding load, respectively For the experiment described above, dP/dl = 33 N/m and dP/dt = ~ 70 N/h. The velocity is therefore given by

$$v = (dP/dt)/(dP/dl) = \sim 0.6\ \mu m/s \qquad (4)$$

in approximate agreement with the value obtained above. It should be noted that these velocities are "average" values, in that the crack is usually stationary while the corrosion renucleation process occurs. The actual velocity of the crack tip during the discontinuous motion is very high and may be estimated from the load-drop relaxation time (Figure 10).



FIGURE 11 – Fracture surface of Cu-25Au crystal showing crack-arrest markings formed in slow-strain-rate test at 400 mV. Arrest markings correlate with occurrence of current transients and associated load drops.

Steady-state dealloying and TGSCC

Steady-state dealloying varies with noble metal content in a manner expected from the treatment of Kaesche[2] and of Kaiser.[19] As seen in Figure 1, the polarization curve shifts downward and to the right for the higher-gold alloy, i.e., the rates in the subcritical potential domain are an order of magnitude lower for the higher-gold alloy, and, correspondingly, the critical potential is 170 mV higher. According to previous analyses,[19,21] above E_c, the large increase in copper dissolution rate occurs as a consequence of the activation of copper from the more plentiful terrace sites, distinct from kink sites of relatively limited effective concentration, which accounts for the extremely low dissolution rate below E_c. In the absence for this system of alternative mechanisms for TGSCC (e.g., hydrogen charging, oxide, or salt film formation), we presume that a critical amount of selective dissolution is required to nucleate cracks and sustain crack growth Generally, this will require terrace site dissolution, which can readily occur above E_c. However, we have shown (Figure 7) that for Cu 25Au, TGSCC occurs as low as 150 mV below E_c under slow strain rate in 0 6 M NaCl and as low as 450 mV below E_c under constant deflection in aqueous $FeCl_3$.[4] We suggest that once initiation has occurred, the required dissolution may occur as a high rate transient following discontinuous crack advance.

Transient dealloying and TGSCC

When a fresh surface is presented to the solution below E_c, as occurs on scratching or with the production of a cleavage crack, a high rate of copper electrodissolution occurs. This is followed by a decay to the steady-state value, as available kink sites are blocked by gold atoms. The process is phenomenologically analogous to the "repassivation" that occurs on reformation of passivating oxide films. The high mobility of gold adatoms assures a continuing low steady-state rate of copper dissolution In Figure 5, the total charge transfer (area under the current vs time curve) suggests a discontinuous change to lower values below a scratching potential of 300 mV. This may account for the fact that under slow-strain-rate loading, the ductility appears to be restored in 0.6 M NaCl as this potential is approached, as seen in Figure 7. It is also likely that the kinetics of transient dealloying are significantly influenced by solution composition, and this may account for the fact that in aqueous $FeCl_3$, even under the less severe condition of constant-deflection loading, embrittlement persists to a potential as low as 0 mV,[4] as shown in Figure 7 It would be of interest to explore the transient dealloying behavior in this solution, unfortunately, the measurements are hampered by the high background current resulting from the reduction of ferric ion. An alternative explanation for the persistence of embrittlement in $FeCl_3$ was offered by Newman,[22] who suggested that a more positive potential (400 mV) may exist near the crack tip, in view of the fact that in this instance the sample is cathodically polarized. According to recent modeling of this system by Bertocci,[15] a potential gradient of this magnitude is unlikely.

Figure 6 shows that the transient current density maxima observed during scratching experiments vary linearly with applied potential under anodic polarization between 300 and 100 mV. The peak values fall between the two limits of (actual) diffusion-limited and (extrapolated) charge-transfer-limited electrodissolution of pure copper, supporting the basic contention that the transient dissolution process is completely selective. The true instantaneous peaks are expected to be closer to the Tafel extrapolation and higher than the time-averaged recorded peaks, which represent a lower limit.

The similarity between the transient currents observed after scratching and those detected during crack growth can be seen by comparing results in Figures 9(a) and 10 with the scratching profiles in Figure 5. In a previous work, we showed that the kinetics of the transient dissolution process during TGSCC are the same as that for a surface newly exposed by scratching.[24] From this result, we can infer that the scratching experiments adequately model the events following cleavage, and the current transients during constant strain-rate tests reflect the sudden exposure of new surface to the corrosive environment. In other systems, dynamic straining markedly affects the dissolution process.[11] Thus, it is expected that the enhanced slip activity at the crack tip leads to high dissolution rates there, but the contribution of this strain-enhanced dissolution could be lost in the observed transients. The actual mechanism by which this enhanced dissolution leads to renucleation of the cleavage event is not yet known Observation of the details of current transients and load drops that coincide with cleavage events allows one to study the details of these events and their time sequence. Further work that attempts to distinguish among possible anodic dissolution mechanisms and to integrate these findings into a quantitative model is in progress.

Failure of the Faraday condition

In previous studies,[4] we showed that the average crack growth rate determined from time-to-failure measurements (which neglects the time for initial nucleation) is 1 to 3 orders of magnitude higher than the steady-state dissolution rate (expressed as a linear interface recession). This is illustrated by the results plotted in Figure 12. It can be argued that the average velocity so calculated is a lower limit, in view of the inclusion of an unknown initial nucleation time. Similarly, the calculated interface recession may be larger than that prevailing in a crack, in view of the tendency of the occluded environment to approach equilibrium in this instance, according to the modeling calculations of Bertocci.[25] Thus, the results in Figure 12 may

represent a "best-case" situation for the Faraday condition, which nevertheless fails to attain. This failure of the Faraday condition casts doubt on the general applicability of the slip-dissolution or film-rupture model, which is currently fashionable and forms the basis for much mechanistic modeling. As shown rather conclusively by the present results, TGSCC in the present system occurs as a series of discontinuous cleavage-like events with local "average" velocities as high as 28 μm/s, strongly dependent on potential (Table 2 and Figures 9 through 11) Finally, the interesting result obtained for an air-scratched sample after long-time immersion in the subcritical potential domain (Figure 4) supports our earlier observation of the propagation of cracks from a corrosion-affected domain into unattacked alloy.[3]

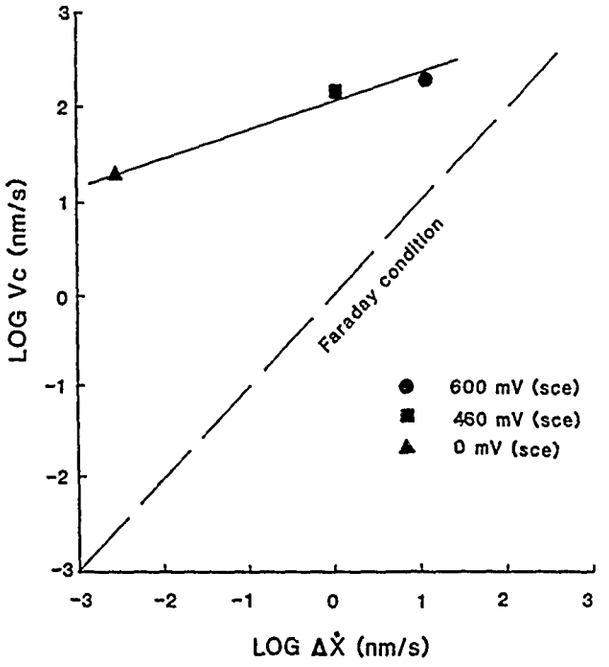


FIGURE 12—Evidence of failure of the Faraday condition when average crack growth rates (derived from bend tests) are compared with average rate of interface advance (derived from steady-state anodic dealloying currents.) Data taken from Table 3, Reference 4.

TABLE 2
Values of Crack Advance Distance, ΔX, and Time Interval Between Current Peaks, ΔT*, in 0.6 M NaCl at 400 mV*

Current Peak #	ΔX* (mm)	ΔT* (s)	V_c (μm/s)
1	144	5	28.8
2	92	12.1	7.6
3	126	24.6	5.1
4	81	123	0.7
5	58	161	0.4
6	63	101.4	0.6
7	95	14.8	6.4
8	104	177.5	0.6
9	78	10.4	7.5
10	75	98.4	0.8

Conclusion

(1) TGSCC occurs for disordered Cu-25at%Au and for Cu-50at%Au in aqueous NaCl at or above a critical potential (E_c), which increases with increasing gold concentration and with decreasing chloride ion activity.

(2) For disordered Cu-25at%Au, TGSCC also occurs below E_c, where the steady-state electrodissolution rate is vanishingly small. High rates of transient dealloying occur in this domain, and the kinetics of the transient current decay are similar to those observed during scratching experiments, however, neither the steady-state nor the transient dealloying rates can account quantitatively for crack propagation in a Faradaic sense.

(3) The discontinuous nature of TGSCC is further confirmed by the occurrence of current transients and load drops during crack growth; it was demonstrated that these events can be used to study cleavage events during TGSCC; in particular, the local average crack growth velocity can be determined.

(4) Enhanced dissolution is expected at the crack tip because of dynamic deformation, and this could lead to crack renucleation.

Acknowledgment

The authors gratefully acknowledge the support of the National Science Foundation (Grant No. NSF DMR 8420965).

References

1. E.N. Pugh, Atomistics of Fracture, ed. R.M. Latanision, J.R. Pickens, NATO Conference Series VI, Vol. 5 (New York, NY: Plenum Press, 1983), p. 997.
2. B.D. Lichter, T.B. Cassagne, W.F. Flanagan, E.N. Pugh, Microstruc. Sci. 13(1986): p. 361.
3. T.B. Cassagne, W.F. Flanagan, B.D. Lichter, Metall. Trans. 17A(1986): p. 703.
4. T.B. Cassagne, W.F. Flanagan, B.D. Lichter, Chemistry and Physics of Fracture, ed. R.M. Latanision, R.H. Jones, Proceedings of the NATO Advanced Research Workshop, ASI Series E, No. 130 (Dordrecht, The Netherlands: Martinus Nijhoff, 1987), p. 659; Metall. Trans. 19A(1988): p. 281.
5. M. Hahn, E.N. Pugh, Fractography and Materials Science, ASTM STP 733 (Philadelphia, PA: ASTM, 1981), p. 413.
6. R.C. Newman, K. Sieradzki, Scripta Metall. 17(1983): p. 621.
7. A.J. Forty, Physical Metallurgy of Stress-Corrosion Fracture (New York, NY: Interscience, 1959), p. 99; Fundamental Aspects of Stress Corrosion Cracking, ed. R.W. Staehle, A.J. Forty, D. van Rooyen (Houston, TX: National Association of Corrosion Engineers, 1969), p. 64.
8. K. Sieradzki, R.C. Newman, Phil. Mag. 51(1985): p. 95.
9. K. Sieradzki, Modeling Environmental Effects on Crack Growth Processes, ed. R.H. Jones, W.W. Gerberich (New York, NY: The Metallurgical Society-American Society of Mining, Metallurgical, and Petroleum Engineers, 1986), p. 187.
10. J.S. Kim (Ph.D. diss., Vanderbilt University, 1985).
11. J.S. Kim, B.D. Lichter, W.F. Flanagan (Vanderbilt University, Nashville, TN, unpublished research, 1987).
12. E.N. Pugh, Corrosion 41(1985): p. 517.
13. A.N. Stroh, Proc. Roy. Soc. A232(1955): p.548.
14. J.R. Rice, "Tensile Crack-Tip Fields in Elastic-Ideally Plastic Crystals," Mechanics of Materials (1987, in press).
15. U. Bertocci, J. Electrochem. Soc. 136(1989): p. 1887.
16. K. Hashimoto, T. Goto, Corros. Sci. 5(1965): p. 597.
17. H. Gerischer, H. Rickert, Z. Metallkunde 46(1955): p. 681.
18. H.W. Pickering, Corros. Sci. 23(1983): p. 1107.
19. H. Kaiser, Corrosion Mechanisms, ed. F. Mansfeld, Chemical Industries Series, Vol. 28 (New York, NY: Marcel Dekker, 1987), p. 85.
20. C.Y. Chao, L.F. Lin, D.D. McDonald, J. Electrochem. Soc. 128(1981): p. 1194.

21. H. Kaesche, Metallic Corrosion, English trans. by R.A. Rapp (Houston, TX: NACE, 1985), p. 194ff.
22. Discussion by R.C. Newman, Chemistry and Physics of Fracture, ed. R.M. Latanision, R.H. Jones, Proceedings of the NATO Advanced Research Workshop, ASI Series E, No. 130 (Dordrecht, The Netherlands. Martinus Nijhoff, 1987), p. 669.
23. D. Massinon (Master s thesis, Vanderbilt University, 1987).
24. W.F. Flanagan, J.B. Lee, M. Zhu, B.D. Lichter, Symposium on Environmentally Assisted Cracking. Science and Engineering, held November 9-11 (Philadelphia, PA. ASTM, 1987), in press.
25. U. Bertocci, Embrittlement by the Localized Crack Environment, ed. R.P. Gangloff (New York, NY: TMS-AIME, 1984), p. 49.

Discussion

J.R. Galvele (Comision Nacional de Energia Atomica, Argentina). If the yield point of the alloy is 100 MPa and the surface compound is Cu_2Cl_2, with a melting point of 430°C, the surface-mobility mechanism (SMM) predicts a crack velocity of 13 × 10 ^{6} m/s, which is very close to what was reported by the authors.

B.D. Lichter: This is an interesting observation, which requires further consideration. However, before accepting the SMM proposed by Galvele, we shall have to explain the discontinuous nature of crack advance. The actual crack propagation rate is considerably higher than that calculated in our paper, which is an average that takes into account the time during which the crack is locally arrested. (Actually, this value is closer to 1×10^{-6} m·s^{-1} than the value quoted by Galvele.) Furthermore, the potential range of observed transgranular SCC exceeds that for which we may expect stable surface chloride films to be present, according to the data and analysis of Nobo, et al., for pure copper. Direct observation of such films and correlation of their presence with the occurence of transgranular SCC in this system is needed.

S.C. Jani (Georgia Institute of Technology, USA): How do you explain the fact that there was no evidence of a dealloyed layer on the fracture surface?

B.D. Lichter: Once a crack has formed and is discontinuously propagating, the local environment differs considerably from the bulk solution. Near-saturation conditions may prevail, with a tendency for equilibrium to be approached and a consequent decrease in the overpotential for copper dissolution. Clearly some selective dissolution may occur on the fracture surface during the process of crack growth, but our observations indicate that the dissolution rate may be significant only in the vicinity of an arrested crack tip prior to renucleation. We are presently undertaking Auger spectroscopic studies of anodically polarized crystals, as well as of fracture surfaces.

E.I. Meletis (Louisiana State University, USA): Assuming that dealloying is responsible for transgranular cracking, can you deduce the length of the propagating crack, from the measured thickness of the dealloyed layer?

B.D. Lichter: It is clear from our measurements of the time interval between cracking events and the crack-arrest distances on the fracture surfaces that the dimensions of the dealloyed region formed while the crack is arrested are considerably smaller than this crack-arrest distance. Our present view of the process is that the crack-arrest distance is determined by 'mechanical' variables rather than electrochemical ones, while the time interval between renucleation events is determined by the extent of anodic dissolution occuring at the crack tip.

Surface-Mobility Stress Corrosion Cracking Mechanism in Silver Alloys

G.S. Duffo and J.R. Galvele***

Abstract

New experimental evidence supporting the surface-mobility mechanism for the embrittlement of metals was found. As predicted by this mechanism, (1) embrittlement of silver alloys in aqueous solutions occurred only at those electrode potentials where AgCl, AgBr, AgI, and Ag_2SO_4 were formed on the alloy surface, (2) crack velocities were higher as the melting point of the surface compound got lower, and (3) measured crack velocity values were very close to those predicted by the mechanism.

Introduction

According to the surface-mobility mechanism,[1] stress corrosion cracking (SCC), liquid metal embrittlement, and hydrogen embrittlement of nonhydride forming metals have a common mechanism at the tip of the crack. The surface-mobility mechanism states that crack propagation results from the capture of vacancies by the stressed lattice at the tip of the crack. The rate-controlling step is the rate of movement of adatoms along the surface of the crack, and the role of the environment is to change the surface self-diffusivity of the metal or alloy. This mechanism predicts that embrittlement should be observed on tensile stressed metals at temperatures below 0.5 T_m (T_m being the melting point of the metal, in °K) and in environmental conditions that allow high surface mobility.

Experimental evidence supporting this mechanism has been reported in four recent publications. Bianchi and Galvele[2] found embrittlement of high-purity copper in argon contaminated with CuCl at 200°C, where high surface mobility was previously measured.[3] Duffo and Galvele[4] reported SCC of Ag-Pd and Ag-Au alloys at the electrochemical potentials where compounds with a low melting point were formed on the alloy surface. Through this mechanism, Manfredi, Maier, and Galvele were able to explain the potential-dependent intergranular to transgranular SCC transition on type 304 (UNS S30400) stainless steel (SS) in $MgCl_2$ solutions.[5] Finally, Duffo, Maier, and Galvele reported that the dependence on temperature of SCC for type 304 SS in LiCl solutions was equal to that predicted by the surface-mobility mechanism.[6]

The aim of the present work is to test the capability of the surface-mobility mechanism to predict crack velocities for new systems quantitatively. As previously reported, silver alloys are of particular interest because of the high number of low melting point compounds they form.[1] For this purpose, the same alloys and environments used in a previous work were tested.[4]

Experimental Method

All the measurements reported in this paper were performed on 0.8-mm-diameter wires of Ag-15Pd (a/o) alloy. The environments used were 1 M KCl, 1 M KBr, 1 M KI, and 1 M Na_2SO_4 aqueous solutions. All the solutions were nitrogen deaerated and at room temperature. The samples were strained to rupture in a slow-strain-rate machine, with an initial strain rate of $2.6 \times 10^{-6}\ s^{-1}$. After straining, the wires were metallographically sectioned, the crack length was measured, and a mean crack velocity was calculated. Both the alloy composition and the experimental procedure were described in a previous publication.[4]

Results and Discussion

The surface-mobility mechanism predicts[1] that the crack propagation rate (CPR) will be given by the following equation:

$$CPR = \frac{D_s}{L}\left[\exp\left(\frac{\sigma \times a^3}{k \times T}\right) - 1\right] \qquad (1)$$

where $D_s (m^2 \times s^{-1})$ is the surface self-diffusion of the metal; L is the diffusion path, typically 10^{-8} m; a is the atomic diameter; σ is the maximum stress at the tip of the crack, k is the Boltzman constant; and T is the absolute temperature. While D_s values at the conditions of interest for SCC are not available, a rough estimate can be made with the following equation, based on the publications of both Gjostein[7] and Rhead:[8,9]

$$D_s = 7.4 \times 10^{-2} \exp{-(30\ T_m/RT)} + 1.4 \times 10^{-6} \exp{-(13\ T_m/RT)} \qquad (2)$$

where R is the gas constant (R = 1.987 cal.mole^{-1}·K^{-1}), T is the absolute temperature, and T_m is the melting point of the surface-adsorbed compound, both in °K. Equation (2) shows that a compound with a low melting point surface will induce high surface mobility and thus high SCC susceptibility.

The cases of silver and silver alloys in the above-mentioned environments are of particular interest. All of them belong to the family of the Ag/AgCl reference electrode; abundant literature is available on the electrochemically formed surface compounds, and the equilibrium potentials above which such compounds will begin to be produced are well known. The standard electrode potentials (E_o) for each of the silver compounds involved are as follows: E_o(Ag/AgCl) = 0.222 V; E_o(Ag/AgBr) = 0.074 V; E_o(Ag/AgI) = −0.150 V; and E_o(Ag/Ag_2SO_4) = 0.653 V. In addition, because of their low solubility, their presence during the SCC process can be confirmed *ex situ* by surface analysis techniques. Finally, their melting points are low (AgBr: 432°C, AgCl: 455°C, AgI: 558°C; Ag_2SO_4: 652°C), and according to Equations (1) and (2), they should lead to rather high CPR values.

*Comision Nacional de Energia Atomica, Depto. Quimica, Av. del Libertador 8250, 1429-Buenos Aires-Argentina.

**Comision Nacional de Energia Atomica, Depto. Materiales, Av. del Libertador 8250, 1429-Buenos Aires-Argentina.

Figure 1 shows the CPR values measured in the present work. The results were plotted as a function of the overpotential (i.e., the applied potential minus the standard electrode potential). As previously reported,[4] SCC was found only when the silver compounds became thermodynamically stable on the metal surface. At potentials below the standard electrode potential, where those compounds were absent, no SCC was found. Therefore, for Ag-15Pd alloys, the presence of AgCl, AgBr, AgI, or Ag_2SO_4 on the metal surface was concluded to be a necessary condition for SCC. Cracks were intergranular, as shown in Figure 2, and the presence of the silver compounds was observable under the scanning electron microscope. At low overpotentials, aside from the adsorbed monolayer of silver compound, isolated crystals were also present on the crack surfaces; at higher overpotentials, the silver compound crystals covered the entire surface. In every case, the nature of the compounds was confirmed by surface analysis.[10]

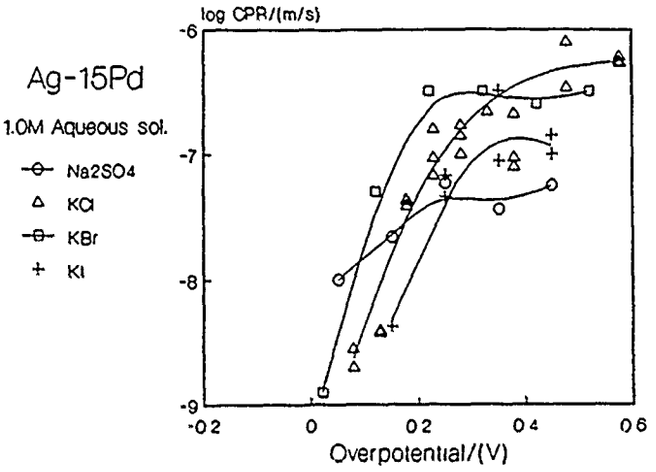


FIGURE 1—Crack propagation rates as a function of overpotential. Strain rate: 2.6×10^{-6} s^{-1}.



FIGURE 2—Typical intergranular fracture surface for Ag-15Pd strained in 1.0 M KCl, at 0.600 V_{NHE}. Deposits of AgCl are observed on the fracture surface. Dashes = μm.

The SCC process observed in the present work was not specifically related to the presence of Pd in the alloy, since Ag-15Au alloys have been shown to have a similar behavior.[4,10] Neither was it due to the presence of water in the environment, as shown in separate tests. Silver alloys are known to react chemically with free halogens, leading to the formation of silver halides. As reported separately,[10] SCC was found when Ag-15Pd wires were slowly strained in benzene or in toluene, both saturated with iodine. In the first case, the CPR measured was 6×10^{-8} m/s^{-1}, while in the second, it was 7×10^{-8} m/s^{-1}, both values falling within the range of maximum CPR values found in an aqueous 1.0 M KI solution in Figure 1.

Equation (1) does not explicitly show a dependence of CPR on the electrode potential. The surface-mobility mechanism only requires a compound with a low melting point to be present at the tip of the crack. The effect of the potential appears only in those cases, e.g., in aqueous solutions or in fused salts, where a charge transfer reaction is involved in the film formation process. In these cases, SCC will be observed either above the standard electrode potential for the formation of the compound, as in the present case, or above the passivity breakdown potential, as found by Rebak, Carranza, and Galvele[11] for brass in nitrite solutions. Figure 1 shows a dependence of CPR on the overpotential. This is due to the electrochemical processes taking place inside the crack, such as ohmic drop, diffusion overpotential, etc. The discussion of such processes falls outside the scope of the present work and will be discussed in a separate publication.[10] In the present work, only the maximum CPR values and their relation to Equation (1) will be considered.

Because of the very low strain rate used and the high crack velocities found, the fractured samples showed practically no plastic deformation. It seemed reasonable then to use for σ in Equation (1) the value of 0.2% proof stress, which, for the samples used in the present work, was found to be 62.4 MPa. The other values used were $a = 2.88 \times 10^{-10}$ m and $L = 10^{-8}$ m. In Figure 3, the maximum CPR values measured in the present work were compared with the predictions of the surface-mobility mechanism. As predicted by the mechanism, a low CPR corresponds to a high melting point of the surface compound. The predictions of the theory fit very well with the experimental results for KI and Na_2SO_4 solutions. A strong deviation was found in those solutions in which much higher CPR values were expected; it seemed as if the SCC rate had reached a saturation value. This was a result of the nature of the processes taking place inside a crack in aqueous solutions and called for separate analysis.

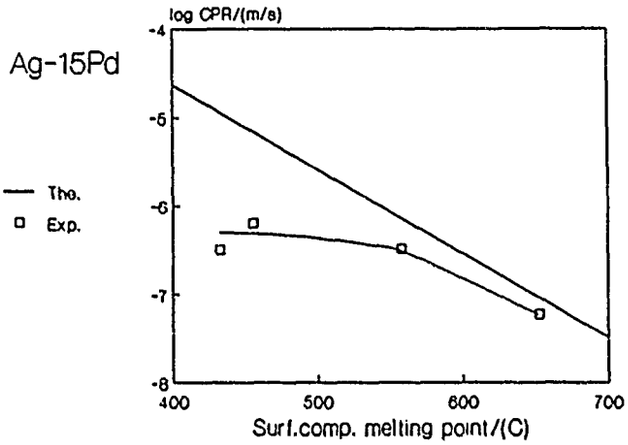


FIGURE 3—Maximum crack propagation rate values measured in the present work (Exp.), compared with the predictions of the surface-mobility mechanism (Theo.).[1]

As shown above, the presence of the silver compounds was a necessary condition for SCC of Ag-15Pd. In the aqueous solutions used in the present work, the production of those compounds was the result of reactions of the following type:

$$nAg + X^{n-} = Ag_nX + ne^- \qquad (3)$$

where X^{n-} stands for Cl^-, Br^-, I^-, or $SO_4^{=}$. As the crack propagated into the metal, bare metal was exposed to the environment, but at the electrode potentials used, this bare metal reacted according to the reaction in Equation (3). The result of this was an anodic current flowing through the crack. Simultaneously, by the same reaction, the anions X^{n-} were consumed at the tip of the crack and had to be transported from the bulk solution to the tip of the crack either by diffusion or by migration, provided convection inside a crack was negligible. Making a very conservative approach, a monolayer of Ag_nX was assumed to be formed along the crack walls. From this assumption, it was easy to calculate the current density flowing

through a crack at each CPR value, as well as the flow rate of the X^{n-} ions necessary to compensate those consumed by Reaction (3). The diffusion coefficient used, similar for most ions in aqueous solutions,[12] was 10^{-9} m^2/s^{-1}. A CPR value was found, above which the replenishment of ions by diffusion was insufficient for the SCC process to continue. This was equivalent to a limiting current density in electrochemistry that, when reactions of the type of Equation (3) were involved, led to what in electrochemical kinetics is called diffusion overvoltage.[13]

Using the equations developed for diffusion overvoltage in electrochemical kinetics,[13] a relation between the maximum CPR values allowed by diffusion vs overpotential was calculated. Figure 4 shows the results of these calculations as compared to the CPR values measured in KBr solutions. It was assumed that a monolayer of AgBr was formed on the crack surface, and that the diffusion path was of 0.01 cm. Under those conditions, it was found that for concentrations of 1.0 M of the active species, CPR values much higher than 10^{-6} m/s^{-1} were not possible in aqueous solutions because of the limitations introduced by ion diffusion in the liquid environment. The calculations were conservative, since accumulations of AgBr much thicker than a monolayer were observed on the crack surfaces. On the other hand, the diffusion path assumed was that of a stagnant solution[13] without allowance for the crack length.

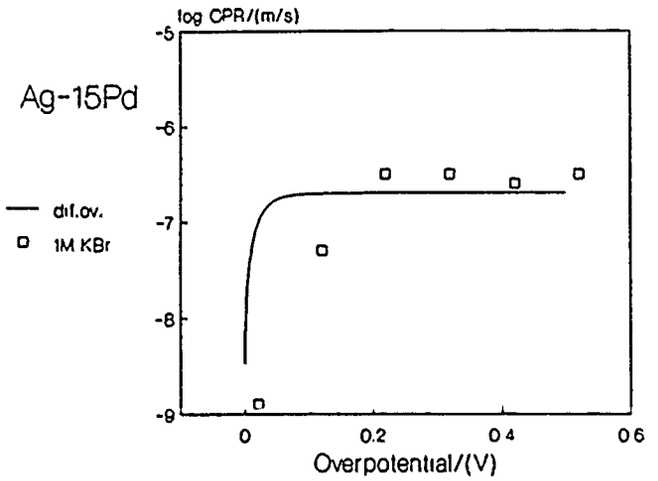


FIGURE 4—Maximum crack propagation rate values allowed by diffusion overvoltage compared to the values measured in KBr solution.

Thus, the deviation from surface-mobility mechanism (Figure 3) is concluded to be due to the presence of a volume diffusion rate-controlling step.

Conclusion

The conclusions from the present work are as follows: (1) Ag-15Pd alloys show intergranular SCC in KCl, KBr, KI, and Na_2SO_4 solutions, (2) SCC is observed only above the electrode potentials where the respective Ag_nX compounds are formed, and the presence of those compounds is a necessary condition for SCC; (3) the surface-mobility mechanism quantitatively predicts the CPR values expected in those environments; and (4) in aqueous solutions with 1.0 M active species, CPR values are limited to about 10^{-6} m/s because of bulk diffusion of the active species.

Acknowledgment

This research was supported by the Consejo Nacional de Investigaciones Cientificas y Tecnicas, Argentina, and by the Programa Latinoamericano de Lucha Contra la Corrosion OEA-CNEA.

References

1. J.R. Galvele, Corros. Sci. 27, 1(1987): p. 1.
2. G.L. Bianchi, J.R. Galvele, Corros. Sci. 27, 6(1987): p. 631.
3. F. Delamare, G.E. Rhead, Surf. Sci. 28(1971): p. 267.
4. G.S. Duffo, J.R. Galvele, Corros. Sci. 28, 2(1988): p. 207.
5. C. Manfredi, I.A. Maier, J.R. Galvele, Corros. Sci. 27, 9(1987): p. 887.
6. G.S. Duffo, I.A. Maier, J.R. Galvele, Corros. Sci. 28, 10(1988): p. 1003.
7. J.J. Burke, N.L. Reed, V. Weiss, eds., Surfaces and Interfaces-I (Syracuse, NY: Syracuse University Press, 1967), p. 271.
8. G.E. Rhead, Surf. Sci. 15(1969): p. 353.
9. G.E. Rhead, Surf. Sci. 22(1970): p. 223.
10. G.S. Duffo, J.R. Galvele, Corros. Sci., in press.
11. B. Rebak, R. Carranza, J.R. Galvele, Corros. Sci. 28, 11(1988): p. 1089.
12. J.R. Galvele, J. Electrochem. Soc. 123, 4(1976): p. 464.
13. K.J. Vetter, Electrochemical Kinetics (New York, NY. Academic Press, 1961), p. 170.

Discussion

R.A. Oriani (University of Minnesota, USA): Your model of stress corrosion cracking (SCC) is based on the idea that because of the different states of stress between the crack tip and the crack flanks, vacancies move from the crack flanks to the tips by surface diffusion, causing the crack to advance. I wish to point out that this idea is based on a misunderstanding of how stresses can affect the force, and hence the direction, of a diffusive flux.

A diffusive flux is motivated by a gradient or a difference in chemical potentials, and for lattice atoms (A) in a stress field, the relevant equation is that of Herring [Scripta Metall. 5(1971): p. 273], which is

$$u_A - u_V = u_A^\circ - V_A n \qquad (D1)$$

where u = chemical potential; V_A = partial molal volume of the species A; n = normal component of the stress at the interface, which can exchange atoms with a hydrostatically stressed surroundings, and V refers to the vacancy. The chemical potential of A and V in a nonhydrostatically stressed system can be defined only at an interface, not in the interior. This equation says that at constant volume concentration, $(u_A - u_V)$ decreases with increasing positive (i.e., tensile) normal stress on the interface. The flux equation becomes (again from Herring)

$$J_A = -\{D/kTV_A\} \times (u_A - u_v) \qquad (D2)$$

so that a flux of A atoms may be established toward the surface or interface having the larger tensile normal stress. This, of course, is in keeping with the direction of mass flux in Herring-Nabarro creep. The manner of how the transport of A species is accomplished, whether by volume diffusion or surface diffusion or by some other mechanism is here irrelevant, since I wish to discuss only the *direction* of the mass flux.

Now, to the extent that one can apply continuum concepts to the region of a crack tip, if one believes that atoms at the crack tip experience a component of stress normal to the "surface," whereas the atoms on the flanks of the crack surface clearly have zero normal stress, then the above equations would predict a force for transport of atoms from the flanks to the crack tip. If the crack tip is considered as more rounded because of plastic deformation, it is easier to see that the normal stress at the crack tip is zero, so that in either case one does not expect a flux of atoms away from the crack tip (i.e., of vacancies toward the crack tip) as your model demands.

That your model is based on how stress affects vacancy diffusion is clear in the reference to *Corrosion Science* [27(1987): p. 1], but it is mistakenly based. Therefore, I must regretfully conclude that whatever success you have had in making phenomenological correlations must have a different basis.

J.R. Galvele: I am sorry to say that the first statement made by Oriani ("Your model for SCC is based on the idea . . . causing the crack to advance.") is not correct, and consequently his further considerations do not apply to our work. Otherwise, we should be talking about intergranular creep cracks, growing by surface diffusion, a problem that was extensively discussed by Chuang, et al. [Acta Metall 21(1973): p 1625 and 27(1979): p. 265, and by Cocks and Ashby in Prog in Mater Sci 27(1982): p 189] Such a process should be present at temperatures well above 0 5 T_m, and, as I stated in the paper in *Corrosion Science* [27(1987): p. 1], we are only interested in what happens below 0.5 T_m.

As for the thermodynamic aspects of a SCC process based on surface mobility, these have already been treated by R.J. Asaro and W.A Tiller [Metall. Trans. 3(1972): p. 1789]. Our 1987 model is oriented to the kinetic analysis of the process at a molecular level, an aspect that had not been treated in any previous publication. The main idea on which our model is based is not about where vacancies move to, but what is the equilibrium concentration of vacancies at the tip of a crack, and how such equilibrium is reached It is based on very elementary metallurgical concepts. Let me quote, for example, J.P. Hirth and J Lothe [Theory of Dislocations (New York, NY: McGraw Hill, 1968), p. 458]: " . As an example, consider vacancies equilibrated at an external surface under hydrostatic pressure, P. Forming a vacancy by removing an atom from the interior and placing it on the surface leads to external work in the final step

$$W_e = P \times V_a \qquad [(D3)]$$

Thus, the vacancy concentration in equilibrium with the surface is

$$C_v = C_v^\circ \times \exp\{-PV_a/kT\} \qquad [(D4)]$$

where V_a is the atomic volume " [See also Franklin, Statistical Thermodynamics of Point Defects in Crystals, in Point Defects in Solids, Vol 1, ed Crawford and Slifkin (New York, NY: Plenum Press), p. 19.]

For the sake of simplicity, to reach the same equation, in my *Corrosion Science* (1987) paper, I quoted Nabarro's work. From Oriani's question, I see now that it was not a very fortunate choice, since it has led to confusing our mechanism with high-temperature creep fracture.

So far we have nothing new. Where I think originality lies in our model is in the analysis of the sources of vacancies with the crack propagation process Usually the sinks and sources of vacancies are surfaces, grain boundaries, and dislocations. When an excess of vacancies is produced in a metal, they will cause climbing of dislocations, or coalescence of dislocation loops (as shown by Smallman in the oxidation of metals), or alternatively they will diffuse to grain boundaries or external surfaces. An inversion of these processes is observed in the case of a depletion of vacancies.

In our model we assume that the temperature is below 0.5 T_m and that volume diffusion is negligible. This means that the usual sources of vacancies will be inactive. The other assumptions made in our *Corrosion Science* model are as follows.

(1) Under high surface-mobility conditions, the metal atoms close to the surface will be easily exchanged with those in the surface.
(2) The capture of vacancies from the tip of the crack will lead to a crack propagation process.
(3) The above reaction will lead to an injection of adatoms at the tip of the crack, and the rate-controlling step will be the rate at which this excess of adatoms is removed from the tip.

Incidentally, it is important to point out that, even if a stress-assisted anodic dissolution process were acting in SCC, adatoms must be emitted at the tip of the crack, in the same way as described in our model, and Parkins's rejection of our model should be reconsidered.

In conclusion, most probably the surface diffusion SCC mechanism, as described in our *Corrosion Science* (1987) paper, has some weak points that will have to be corrected in future versions, but as far as I can see, none of those points are addressed by Oriani's question.

R.A. Oriani: My understanding of Galvele's poster and the 1987 *Corrosion Science* paper is that the mass flux envisioned is between the surface at the crack tip and the surface of the crack away from the crack tip. His response implies that he envisions a mass flux between the crack-tip surface and the volume immediately below that surface. I therefore reshape my comments to this scenario. His reply in no way answers the basic point of my objections.

Following the sequence of his reply, I point out that his Equation (D4) presents equilibrium (i.e., equal chemical potential of the vacancies) between a compressed region of a lattice and a region not under compression. Hence, there will not result a vacancy flux between the two regions. Therefore, this equation is irrelevant to the question of the direction of the driving force for generating a vacancy flux or vacancy injection in the region of the crack tip. As I pointed out in Equation (D1) above, the driving force for mass flux is ? $(u_A - u_V)$, and of course the mass flux is equal, and oppositely directed, to the vacancy flux.

Galvele states that his model considers only cases for $T < 0.5$ T_m, so that volume diffusion is negligible and "the usual sources of vacancies will be inactive." In the previous paragraph, he states "Usually, the sinks and sources of vacancies are surfaces, grain boundaries, and dislocations." Hence, it is surprisingly inconsistent that in the first of the assumptions made in his model he assumes that metal atoms close to the surface (i.e., the volume close to the surface) will be easily exchanged with those in the surface. This must occur by vacancy exchange in the opposite sense, thereby negating his assumption. The most important aspect of Galvele's model for the present discussion is contained in his assumptions 2 and 3. Therein he suggests that the stressed lattice at the tip of the crack (presumably a tensile stress) captures vacancies from the crack surface (presumably at zero stress). Although in his response Galvele does not clearly state what he believes to be the driving force for the vacancy capture, his 1987 *Corrosion Science* paper indicates that he believes it to be a stress difference. However, the direction of the vacancy flux he assumes is wrong. The vacancies will flow from a region of tensile stress to one of smaller tensile stress or one of compressive stress. The mass flux will consequently go toward a region of larger tensile stress, in keeping with the thermodynamic driving force, and in keeping with the direction of mass flux associated with Herring-Nabarro creep. The last part of assumption 3, that the rate-controlling step is the rate at which injected adatoms move away from the tip, is irrelevant to this discussion.

I must reiterate that the basis of Galvele's model is incorrect.

J.R. Galvele: I am afraid this discussion is becoming unbearably long! However, before concluding, let me clarify a few of my points. Let us assume that we have a cracked, stress-free metal. The vacancy concentration at the tip of the crack will be $C_v o$. If we now apply a tensile stress to the metal, a stress concentration will be generated at the tip of the crack. In equilibrium, the new concentration of vacancies at the tip of the crack will be given by Equation (D4). As Oriani correctly points out, this is an equilibrium equation. The key point in our model is that at temperatures below 0.5 T_m, this equilibrium is never reached. Thus, the driving force in our model is the difference between the vacancy concentration the metal has at the tip of the crack, $C_v o$, and that it should have according to Equation (D4), namely C_v. Oriani is right about the direction vacancies should move in a stress field, but this does not apply to our work. Whenever we talk about movement of vacancies or adatoms it is on the stress-free surface Taking into account the contaminants that induce high surface mobility, liquid metals, or low melting point metals or salts, this surface must be stress free. Finally, Oriani misquotes me when he says there is an inconsistency in my assumption concerning the exchange of atoms with the surface. I assumed a condition of high surface mobility. Since such a surface behaves as if the metal were at a high temperature, it is reasonable to expect that some degree of exchange will take place between the surface and the first layer of atoms.

The Contribution of Localized Surface Plasticity to the Mechanism of Environment-Induced Cracking

*D.A. Jones**

Abstract

A comprehensive mechanism of environment-induced cracking (EIC) is described in which localized surface plasticity can induce brittle fracture in a surrounding alloy matrix. The key element in stress corrosion cracking (SCC) is the anodic attenuation of strain hardening at film-rupture sites, caused by galvanic coupling to adjoining passive surfaces. Anodic attenuation of strain hardening induces localized surface plasticity and provides a critical link between chemical and mechanical factors affecting EIC. The proposed mechanism explains numerous experimental factors affecting SCC. The mechanism of anodic attenuation of strain hardening is discussed, as well as common elements with corrosion fatigue and hydrogen-assisted cracking.

Introduction

Some degree of enhanced plasticity has been associated with the common forms of environment-induced cracking (EIC), including stress corrosion cracking (SCC), corrosion fatigue cracking (CFC), and hydrogen-assisted cracking (HAC). The objective of this paper is to further describe a mechanism whereby enhanced microscopic localized surface plasticity (LSP) can induce brittle cracking in a surrounding hard, strong alloy matrix.

The mechanism was previously introduced with emphasis on SCC and CFC,[1] in which anodic attenuation of strain hardening (AASH) can induce localized plasticity by anodic currents that result from coupling film-rupture sites with surrounding passive surfaces. Considerable discussion was devoted to the mechanism of attenuation of strain hardening involving corrosion-generated vacancies.

The emphasis in this paper is on the common element of increased plasticity in many forms of EIC, and the ability of the LSP mechanism to explain numerous experimental factors known to affect SCC. Common factors affecting CFC and HAC are discussed as appropriate and summarized later in the paper.

Enhanced Plasticity in Environment-Induced Cracking

Corrosion and anodic dissolution have been observed to increase primary creep under constant load in thin sheet and wire specimens. If conditions are favorable for SCC, cracking will ensue after an initial period of creep, as shown for type 304 (UNS S30400) stainless steel (SS) in Figure 1.[2] In the absence of SCC, creep will continue under conditions of general corrosion or anodic dissolution. Figure 2 shows that the creep rate for copper was enhanced by an impressed anodic current[3] where no surface film was present and no SCC could occur.

Normal primary creep in noncorrosive conditions is suppressed with time as strain hardening develops above the yield stress. However, Figures 1 and 2 show that corrosion and anodic dissolution, respectively, attenuate this strain hardening and allow creep to continue.

*Department of Chemical and Metallurgical Engineering, University of Nevada–Reno, Reno, NV 89557.

Careful examination of SEM fractographs reveals ductile serrations within larger areas of brittle cleavage in both SCC[4] and HAC.[5] SCC and HAC are enhanced in high-strength alloys in which dislocations are pinned by strain fields associated with solute atoms, nonequilibrium phases, and precipitates. Also, austenitic SSs are susceptible to HAC only after having been cold worked (strain hardened) to high strength levels because of strain fields created by dislocation tangles. Both anodic dissolution and dissolved or adsorbed hydrogen apparently act to increase dislocation mobility.

Fatigue in the absence of corrosion has also been observed to increase primary creep. Figure 3 shows recent data[6] for carbon-manganese steel in which primary creep was enhanced by low-cycle fatigue loading. Cyclic loading apparently also acts to attenuate strain hardening at persistent slip bands and again to increase dislocation mobility. It has been observed that a minimum corrosion (anodic dissolution) rate is necessary to cause corrosion fatigue.[7] Corrosion fatigue therefore includes enhanced dislocation mobility by both corrosion and cyclic loading.

Thus, corrosion-enhanced plasticity is a common feature of the major forms of EIC and may provide the key to a common explanation of many factors affecting these forms of metal failure.

Description of the LSP Mechanism

SCC must initiate with film rupture because a passive surface film is a prerequisite for virtually every system experiencing SCC. A dissolved oxidizer is usually required to form the film on the surface. Film rupture may be expected at the emergence of slip bands during yielding at the onset of plastic deformation. Exposed bare surfaces at the rupture sites have a transient rest potential that is considerably active to the passive surface potential. However, these bare surfaces are anodically polarized to the passive potential by coupling to the relatively large surrounding passive surfaces. The anodic current densities will be very high because of the high cathode/anode surface-area ratio and will cause a *localized* softening or plasticity by attenuation of strain hardening at the rupture sites, according to the data of Figure 2.

Straining electrode current transients in Figure 4 simulate conditions at the film-rupture sites during SCC.[8] The area under the current-transient curves are proportional to SCC susceptibility.[8] Potential was controlled potentiostatically at the original passive corrosion potential during the rapid-straining experiments, generat-

ing transient anodic currents. The potentiostat replaced the "chemical potentiostat," which results from coupling to large surrounding passive surfaces during usual SCC, and provided measurable anodic currents when rapid straining formed numerous film-rupture sites. Note that a current increase, evidence of film rupture, was not appreciable until yielding was apparent on the load–time curve. It should be noted that only ductile cup-and-cone rupture resulted from the rapid-straining experiments of Figure 4. Only the film-rupture conditions needed to initiate SCC were simulated. Strain rate was too rapid to permit actual initiation and growth of brittle SCC cracks.

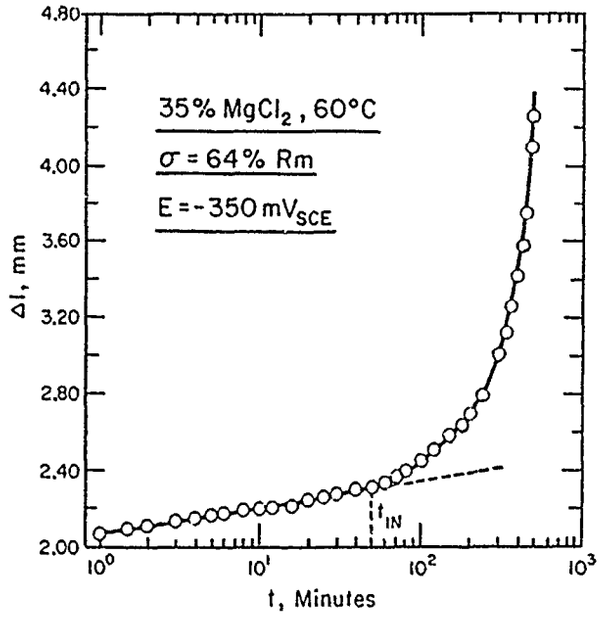


FIGURE 1—Creep followed by initiation of SCC in type 304 (UNS S30400) stainless steel loaded to 64% of the ultimate tensile strength in 35% $MgCl_2$ solution at 60°C. (Reprinted with permission.[2])

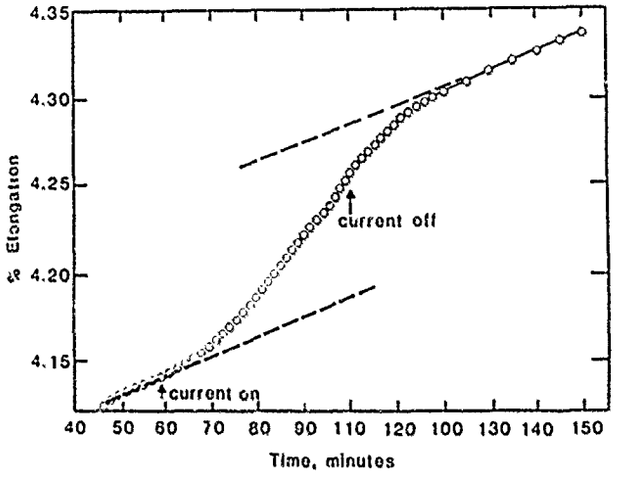


FIGURE 2—Creep of unfilmed copper wire resulting from imposed anodic dissolution current. (Reprinted with permission.[3])

A specific environment is generally required for SCC, although additional experience continually reveals new conditions that promote SCC in most alloy systems. In Figure 4, the maximum current transient coincident with maximum SCC occurs in the presence of an oxidizer, dissolved oxygen, and some critical aggressive species; in this case, nitrogen. The specific aggressive nature of Cl^- for SSs and NH_4^+ for brass is well known. It is thought that these critical species act to weaken the film by chemical interaction or adsorption to retard repassivation and sustain anodic dissolution at film-rupture sites.

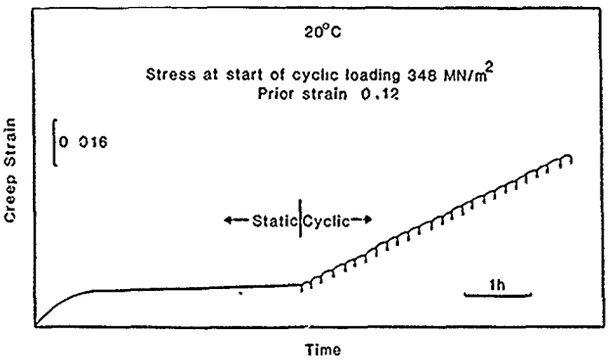


FIGURE 3—Creep of carbon manganese steel enhanced by low-cycle fatigue. (Reprinted with permission.[6])

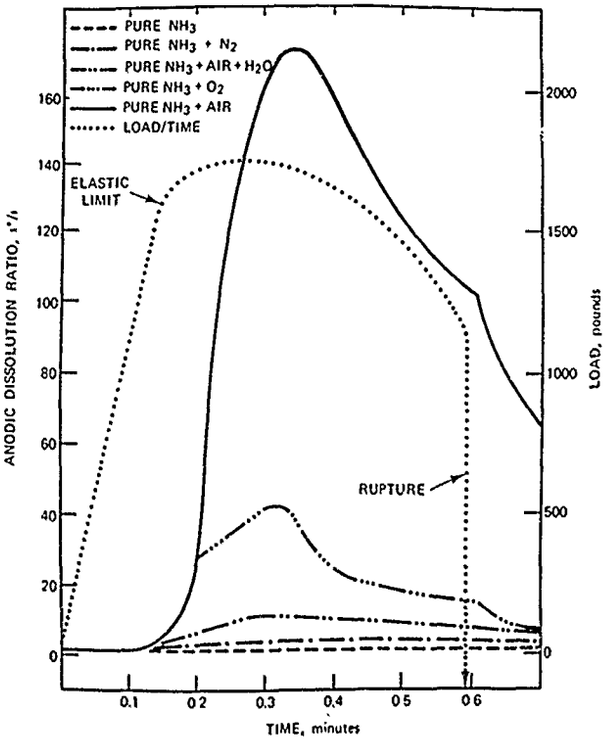


FIGURE 4—Current transients at straining steel electrodes potentiostated in liquid anhydrous ammonia solutions at the unstrained free-corrosion potential.[8]

As deformation progresses in a slip band emerging at the surface, lateral stresses (σ_1) normal to the primary tensile stress (σ_n) must develop to maintain continuity in the slip-band volume (Figure 5). A component of the lateral stress on the slip plane opposes the shear component of the tensile stress. A plane-strain condition with a triaxial stress results, and further slip is restricted in the slip band in which the material has been softened by localized attenuation of strain hardening.

Restrictions on slip become very severe in a small, thin volume of softened, plastic material embedded in surroundings that are at full strength and hardness. An analogous phenomenon has been described in an introductory text on materials science.[9] When lead solder is used to join the ends of two steel bars [Figure 6(a)], a sufficient tensile stress parallel to the common axis of the bars and perpendicular to the thin solder joint produces brittle cleavage fracture in the solder within the joint. Under conditions of severe triaxial stress, plastic slip is totally suppressed, and normally soft, ductile solder fractures in an entirely brittle manner. Similar conditions are present in the microvolume at a slip band [Figure 6(b)] in which the strain hardening has been locally attenuated by anodic current resulting from film rupture and galvanic coupling to the

surrounding passive surfaces. The softened slip-band material fractures by brittle cleavage that has resulted from restricted slip under severe triaxial stress conditions.

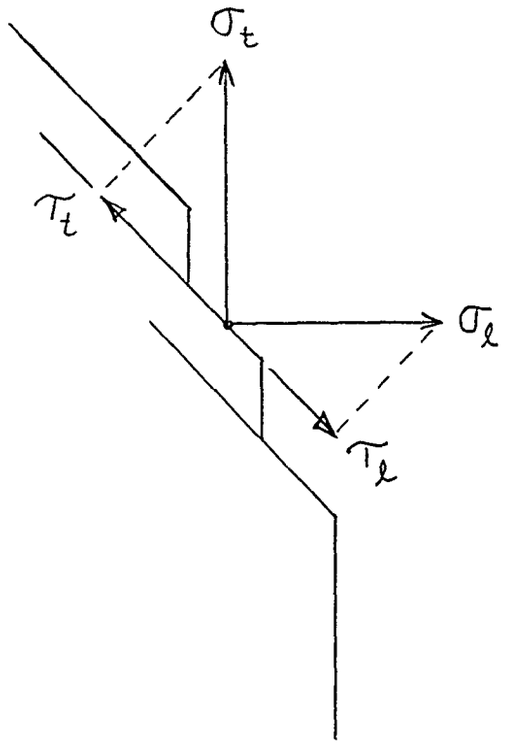


FIGURE 5—Lateral stress (σ_1) developed in a slip band to oppose usual shear stresses (σ_s) resulting from tensile stresses (σ_n).

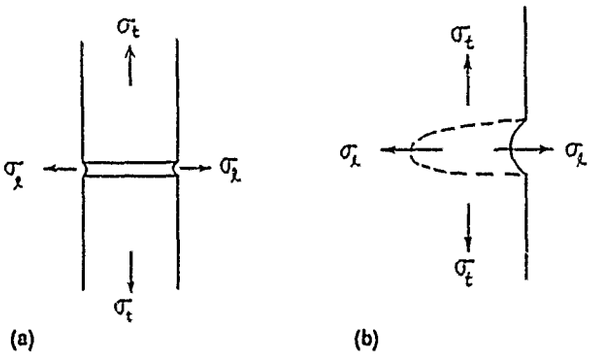


FIGURE 6—(a) Triaxial stress state developed in a thin layer of soft lead joining the ends of two steel bars and (b) similar triaxial stress state developed in softened slip-band material at a film-rupture site caused by anodic current.

With restricted plasticity, the localized relief of strain hardening at a film-rupture site is sufficient to trigger a brittle cracking "event" that then propagates the sharp crack from the softened region into the adjacent unaffected material at a rate higher than can be explained by either electrochemical dissolution or solid-state diffusion processes. As the crack grows into material that has been unaffected by corrosion, brittle fracture may be expected to slow or even stop. At the end of each such event, film formation and rupture, anodic dissolution, and attenuation of strain hardening must be renewed to initiate a new burst of brittle cleavage fracture.

The following list of steps summarizes the proposed LSP mechanism of SCC The steps, designated by ⟨ ⟩, are summarized schematically in Figure 7.

(1) Film rupture by initial plastic deformation at slip bands exposing underlying bare surface at the rupture sites.
(2) Anodic dissolution of bare metal at rupture sites from galvanic coupling to adjoining large passive surfaces.
(3) Chemical interactions or competitive adsorption of a critical dissolved species at the rupture sites to retard film healing and prolong localized anodic dissolution.
(4) Attenuation of the localized strain hardening in the surface slip-band volume and consequent softening of the alloy (LSP) at the rupture sites.
(5) Restriction of continued plastic flow at slip bands because of lateral stresses that develop normal to the imposed tensile stress and oppose the shear stresses on the slip plane.
(6) Crack initiation in the slip-step volume that becomes stressed triaxially by the developing lateral stresses from anodically stimulated attenuation of strain hardening. Brittle cracking is required to satisfy attenuation of strain hardening when plastic slip is restricted by the trivial stress state.
(7) Crack propagation in a brittle burst of cleavage fracture from the softened, triaxially stressed (plane-strain) volume at the initiated crack tip into the surrounding unaffected alloy, where it is temporarily arrested before continuing in a new cycle of film rupture, galvanically imposed anodic current, and LSP.

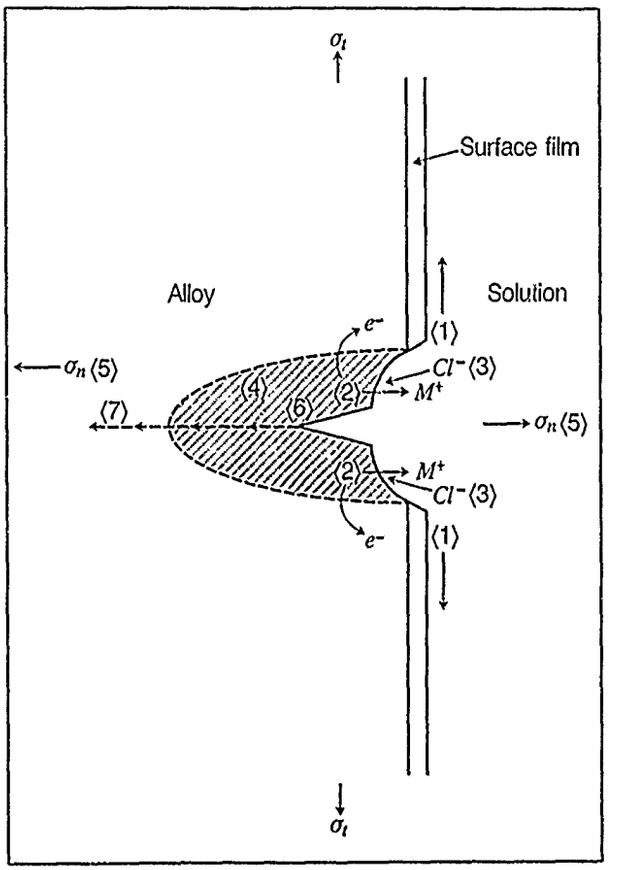


FIGURE 7—Schematic diagram of localized surface plasticity mechanism of SCC.

Explanation of Experimental Factors Affecting SCC

The following listed factors generally affect SCC in most alloy systems and are discussed relative to LSP. While isolated exceptions to these factors may be present, the LSP mechanism seems to explain the great majority of experimental information relating to SCC.

Film rupture. A common feature of alloys susceptible to SCC is the presence of a passive surface film that serves as a barrier to active and rapid general corrosion. Consequently, an oxidizer is often

required for film formation The application of mechanical stress with the attendant local deformation at slip bands is expected to rupture the surface film.

Film rupture of a passive surface film is required by LSP to concentrate anodic dissolution and attenuation of strain hardening at the slip band that underlies each film-rupture site.

Specificity of environment. Environments causing SCC are specific to the alloy. For example, hot chloride solutions cause SCC of SSs but few if any other alloys. The same can be said for carbon steel in hot nitrate and brass in ammonia solutions.

The LSP mechanism assumes that specific ions or environments for each alloy retard repassivation at film-rupture sites, maintaining localized anodic currents to attenuate strain hardening at underlying slip bands during initiation and at the crack tip during propagation of SCC.

Resistance of pure metals. Pure metals are almost universally immune or at least more resistant to SCC than alloys of the same metal. As alloying elements are added to a pure metal, the strain hardening and the ultimate tensile strength increase while the ductility decreases. On the other hand, during slow-strain-rate tests (Figure 8[10]), loss of ductility (embrittlement) by SCC is accompanied by *reduced* stress to produce deformation. Cracks are initiated during plastic flow above yield at stresses below those required for plastic flow in the absence of the SCC solution. Therefore, it is concluded that SCC causes an attenuation of strain hardening before initiation of cracks.

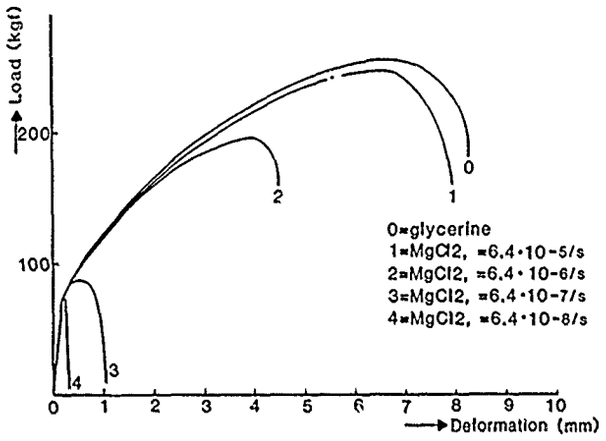


FIGURE 8—Slow-strain-rate curves for stainless steel in hot magnesium chloride solutions. (Copyright ASTM. Reprinted with permission.[10])

LSP requires some degree of strain hardening that is relieved or attenuated by anodic dissolution in an alloy. In the absence of extensive strain hardening in most pure metals, considerable deformation and ductility are permissible before strain hardening is sufficient to initiate brittle cracks, and pure metals are resistant to SCC.

Electrochemical dissolution at straining surfaces. It has been found that the rate of SCC crack growth is proportional to the anodic current density on a straining electrode surface of the same alloy in the SCC environment [11] Thus, cathodic polarization stops SCC by suppressing the causative anodic reaction in AASH.

Figure 9 shows a log-log plot of crack growth rate vs current density [11] The linearity indicates direct participation of anodic reaction in the SCC mechanism. It must be noted, however, that proportionality does not guarantee that the actual cracking process is electrochemical. The crack growth velocity is usually greater than can be accounted for by charge-transfer processes.[12]

In LSP local plasticity stimulated by anodic current at slip-band rupture sites may trigger those mechanical processes that account for the brittle, structure-dependent nature of SCC crack surfaces. The softened material at the slip band becomes brittle when embedded in the surrounding alloy, which is still at full strength and hardness (Figure 7). Brittle crack propagation through this softened material into the surrounding alloy is more rapid than any electrochemical dissolution or solid-state diffusion processes.

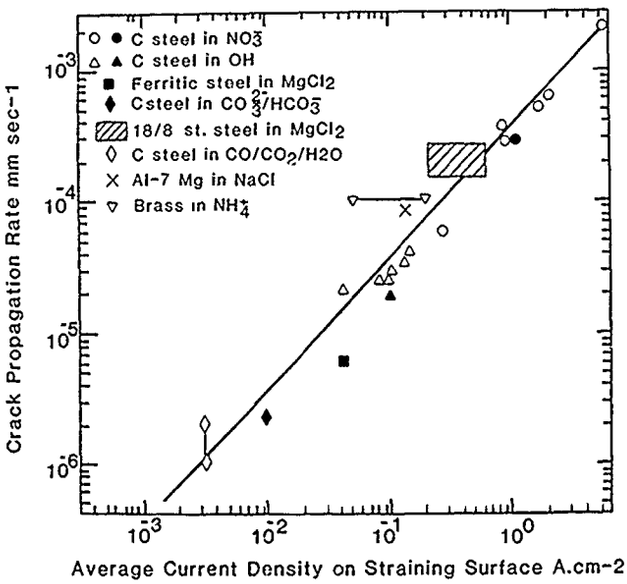


FIGURE 9—Proportionality between SCC crack growth rate and anodic current density at straining electrodes of ductile alloys.[4]

Sieradzki and Newman proposed that a dealloyed surface layer will initiate sharp, brittle cracks that can gain sufficient velocity to propagate into the adjacent ductile alloy.[13] Forty originally discarded this concept because of the unlikely continuity of the dealloyed layer with the substrate alloy.[14] Fritz and Pickering observed more recently that brittle cracks would propagate through the dealloyed layer into the substrate only in the presence of an anodic current.[15] Thus, it would seem that dealloying is probably a symptom rather than a cause of SCC.

Dealloying was found only on mechanically strained brass surfaces when exposed to a solution causing SCC.[16] Unstressed specimens showed no dealloying. These results are consistent with the LSP mechanism. Mechanical strain produces film rupture, and the resulting high anodic galvanic currents cause dealloying coincident with AASH at film-rupture sites.

Metallurgical effects. Effects of metallurgical parameters are varied depending on the alloy involved. No dominating metallurgical factors have emerged, and it is difficult to prevent transgranular SCC simply by changing the metallurgical structure or other features of a particular alloy. Grain-boundary composition can be adjusted to affect intergranular SCC. Higher-strength alloys are more susceptible than lower-strength alloys.

Explanations of these and other metallurgical effects often require considerable speculation, and LSP is no exception. However, strain hardening will be affected by most metallurgical factors, and AASH provides a unique link between chemical and mechanical parameters affecting SCC. Thus, the LSP mechanism readily accounts for the fact that highly strain-hardenable alloys such as brass and SS are susceptible to SCC, although both are ductile with relatively low yield strength. Similarly, pure metals with low strain hardening are resistant, as discussed above. High-strength alloys generally depend on dislocation pinning effects, and LSP can account for higher susceptibility by enhanced dislocation mobility on a localized microscopic scale.

Brittle fracture. Fractographic examinations of transgranular SCC fracture surfaces have shown cleavage planes of the type {100}, {110}, and {210} in otherwise ductile fcc alloys.[17] On the other hand, in the more frequent intergranular mode, SCC fracture surfaces often follow the grain boundaries rather closely. Facing halves of cracked

specimens exactly match one another, whether intergranular or transgranular, indicating a strong brittle-fracture component of the SCC mechanism.

In the LSP mechanism, slip is restricted by the triaxial stress state in the small softened volume at the film-rupture site. The softened material must fail by cleavage on {100}, {210}, and {110} planes with minimal opportunity to deform by slip. Such low index planes are weakest in cleavage because of their low atomic density, subsequent low density of atomic bonds, and maximum interplanar spacing.

Mechanism of Anodic Attenuation of Strain Hardening

The mechanism of attenuation of strain hardening by anodic dissolution and corrosion remains for study and speculation. Lynch proposed that adsorbed hydrogen increases plasticity by increasing dislocation mobility at the crack-tip surface.[18-20] As discussed above, cathodic processes, which stop most forms of SCC, are required to produce hydrogen. However, hydrogen is the acknowledged culprit for very high-strength steels and other nonferrous alloys when cathodic polarization enhances cracking.

One can speculate that other species such as chloride could adsorb or interact with surface films to stimulate anodic reactions and dislocation mobility at the crack tip. Surface dissolution has often been suggested to remove surface dislocation barriers[21] and thereby facilitate dislocation movements to the surface.

Revie and Uhlig proposed anodically generated vacancies to explain the increased creep resulting from anodic dissolution (Figure 2) in application to CFC.[3] Vacancies generated during corrosion were postulated to form divacancies, which have sufficient mobility to migrate to subsurface dislocations and facilitate movement of dislocations around obstacles by climb mechanisms. Apparently, they did not appreciate the possible importance of corrosion-induced relief of stain hardening in SCC as well as CFC.

The present author suggested that corrosion-generated vacancies are responsible for initial attenuation of strain hardening and subsequent embrittlement during SCC.[1] Divacancies can take an alternative role to enhanced slip or dislocation mobility to reduce strain hardening. As they accumulate in the plane-strain region at the crack tip, divacancies will randomly populate prismatic planes of low crystallographic indices. The cleavage stress across such planes will be reduced by displacement or weakening of bonds by the vacancies,[1] and a transgranular crack can initiate and grow. The fracture stress and ductility will be reduced as a result, in agreement with the slow-strain-rate results of Figure 7.

Diffusion calculations indicate that penetration of corrosion-generated divacancies may be up to a few thousand angstroms,[1] sufficient to trigger brittle cracking events and account for crack growth rates above that of simple electrochemical dissolution. While divacancy penetration is adequate to affect mechanical behavior, it is questionable whether divacancies are sufficient in number to cause such effects, since Pickering and Wagner estimated that the upper limit of lattice sites occupied by vacancies would be 1%.[22] However, anodic dissolution may create a supersaturation of vacancies that would produce a far higher concentration at the surface. At present, it is difficult to experimentally verify the presence of vacancies during anodic dissolution at a slip band or the crack tip.

Common Effects in SCC, CGC, and HAC

Several investigators have suggested that hydrogen acts to increase plasticity (or attenuate strain hardening) during HAC. Beachem proposed that hydrogen enhances dislocation mobility, leading to softening on a local microscopic scale at the crack tip.[5] Similar suggestions by Lynch have already been reviewed in this paper.[18-20] Finally, Birnbaum has shown considerable electron microscopic evidence of enhanced dislocation mobility by hydrogen charging.[23] Thus, hydrogen may act to cause cathodic softening and subsequent embrittlement in a small, localized near-surface volume in Figure 6(b) in a manner similar to AASH during SCC. Recently, published work has emphasized the importance of film rupture in HAC,[24] which would localize hydrogen penetration to such small volumes. The disturbed lattice in the slip-band volume may also be inherently more susceptible to hydrogen penetration.

For CFC, attenuation of strain hardening comes about by anodic dissolution as for SCC. Cyclic loading in CFC should inhibit repassivation at persistent slip bands and replace to some extent the function of a critical dissolved species in SCC. No specific environment is required for CFC or HAC. Both can occur in numerous solutions and require only a cyclic tensile stress and a source of hydrogen, respectively, in the presence of corrosion. For HAC, dissolved hydrogen generated by cathodic electrochemical processes apparently attenuates strain hardening, whereas anodic processes serve the same function for SCC and CFC. In any case, hydrogen may be generated from most aqueous solutions during corrosion and does not require any specific dissolved species.

Conclusion

(1) Some degree of enhanced plasticity has been associated with the common forms of EIC, including SCC, CFC, and HAC.

(2) For conditions of SCC, microscopic LSP can be introduced at emergent surface slip bands because of AASH by anodic currents from galvanic coupling between film-rupture sites and adjoining passive surfaces.

(3) LSP can result in brittle cleavage fracture of softened slip-band material constrained by the surrounding unsoftened, full-strength alloy resulting from restricted slip under a triaxial stress.

(4) The LSP mechanism of SCC explains (a) the need for a film-forming oxidizer with some critical aggressive species, (b) the resistance of pure metals and susceptibility of strain-hardenable alloys, (c) the proportionality of crack growth rate to anodic current on straining electrodes, (d) crack growth rates too high to be explained simply by electrochemical dissolution, (e) intermittent crack growth, and (f) brittle transgranular cleavage fracture on crystallographic planes of types {100}, {110}, and {210}.

(5) The mechanism of AASH may be related to removal of surface dislocation tangles or formation of a supersaturation of vacancies at the surface by anodic dissolution.

(6) Cyclic loading in CFC inhibits repassivation at persistent slip bands to maintain AASH at film-rupture sites and replaces the function of a critical dissolved species in SCC. Thus, CFC requires only an adequate corrosion rate and a cyclic tensile load with no critical aggressive species required.

(7) For HAC, hydrogen dissolved in the lattice from cathodic electrochemical processes apparently generates LSP at film-rupture sites, whereas AASH serves the same function for SCC and CFC.

References

1. D.A. Jones, Metall. Trans. A 16A(1985): p. 1133.
2. Z. Szklarska-Smialowska, J. Gust, Corros. Sci. 19(1979): p. 753.
3. R.W. Revie, H.H. Uhlig, Acta Metall. 22(1972): p. 69.
4. L. Engel, H. Klingele, An Atlas of Metal Failure (Englewood Cliffs, NJ: Prentice-Hall, 1981), p. 111.
5. C.D. Beachem, Metall. Trans. 3(1972): p. 437.
6. J.T. Evans, R.N. Parkins, Acta Metall. 24(1974): p. 511.
7. D.J. Duquette, H.H. Uhlig, Trans. ASM 61(1968). p. 449.
8. D.A. Jones, C.D. Kim, B.E. Wilde, Corrosion 33(1977). p. 50.
9. L.H. Van Vlack, Materials Science for Engineers (Reading, MA. Addison-Wesley, 1970), p. 446.
10. A.J.A. Mom, R.T. Dencher, C.J. van der Wekken, W.A. Schultz, ASTM STP 665 (Philadelphia, PA. ASTM, 1979), p. 305.
11. R.N. Parkins, Br. Corros. J. 14(1979). p. 5.
12. R.H. Jones, Metals Handbook, 9th ed., vol. 13, Corrosion (Metals Park, OH. ASM International, 1987), p. 145.
13. K. Sieradzki, R.C. Newman, Phil. Mag. A 51(1985). p. 95.

14. A.J. Forty, Physical Metallurgy of Stress Corrosion Fracture (Interscience, 1959), p. 99.
15 J D Fritz, B W Parks, H W Pickering, Scripta Metall. 22(1988). p. 1063.
16 N W Polan, J.M Popplewell, M.J. Pryor, J. Electrochem. Soc. 126(1979): p. 1299.
17. R. Liu, N. Narita, C. Alstetter, H. Birnbaum, E.N. Pugh, Metall. Trans. A 11A(1980): p. 1563.
18. S.P. Lynch, Hydrogen Effects in Metals, ed. A.W. Thompson, I.M. Bernstein (Warrendale, PA. The Metallurgical Society-American Institute of Mining, Metallurgical, and Petroleum Engineers, 1981), p. 863.
19. S.P. Lynch, J. Mater. Sci. 20(1985). p. 3329.
20. S.P. Lynch, Met. Sci. 15(1981): p. 463.
21. I.R. Kramer, Trans. Metall. Soc. AIME 227(1963). p. 1003.
22. H.W. Pickering, C. Wagner, J. Electrochem. Soc. 114(1967). p. 698.
23. H.K. Birnbaum, Environment Sensitive Fracture of Metals and Alloys, Office of Naval Research, ed. R.P. Wei, D.J. Duquette, T.W. Crooker, A.J. Sedriks (Arlington, VA: 1987), p. 105.
24. J.C. Scully, P.J. Moran, Corrosion 44(1986): p. 176.

Discussion

T. Murata (Nippon Steel Corporation, Japan): As a dominant factor of SCC, the idea of "anodic-dissolution-assisted localized deformation" is attractive, but we need to state it together with a competitive phenomenon such as film formation. To do this, I think, you should address the critical strain rate or slip formation above which you continually have localized straining.

D.A. Jones: Figure 4 shows that anodic current transients are present only after yielding when slip allows film rupture. An aggressive species such as chloride is often necessary to retard film healing and maintain anodic currents at the film-rupture sites. Slow-strain-rate tests are effective because they maintain film-rupture rate by continuous mechanical strain. The critical strain rate is often near 10^{-6}/s. Thus, anodically attenuated strain hardening must coincide with a number of other competing processes to cause SCC, as Murata suggests and as is summarized in our Figure 7.

SECTION V

Environment-Assisted Cracking of Nonferrous Metals

Co-Chairmen's Introduction

A.I. Asphahani
Haynes International
Kokomo, Indiana, USA

F. Mazza
University of Milan
Milan, Italy

The segment of the conference devoted to environmental effects on specific alloy systems was initiated with invited reviews of nonferrous systems. The review by Bertocci, et al., presented at the conference by Pugh, focuses on the alpha-brass/aqueous ammonia system. Intergranular and transgranular failure modes and crack propagation issues are discussed. The slip-dissolution concept (or "film-rupture" mechanism) is used to interpret observations related to intergranular stress cracking. For the transgranular stress cracking mode, experimental evidence of discontinuous crack propagation is shown to support the film-induced discontinuous cleavage model.

Jones and Bruemmer illustrate numerous cases of crack growth in nickel-base alloys in gaseous hydrogen and in acid and basic aqueous environments. Efforts are made to correlate the crack growth to microchemistry, microstructure, environmental parameters, and stress conditions. No *universal* theory is proposed, as it pertains to clarifying the roles of the critical factors controlling the SCC of various nickel-base alloys.

The review by Holroyd and Scamans provides a general update on advanced aluminum alloys and metal–matrix composites. The role of hydrogen embrittlement is discussed in terms of its applicability to "real life" conditions. Also, the aspect of combined effects of static stress and cyclic load is illustrated for actual service performance. Other issues, such as mechanical and thermo mechanical effects and weldment behavior, are covered along with a new "breaking load" test method for evaluating aluminum alloys.

The review paper on hexagonal metals by D. Hardie points out that the corrosion behavior of these metals is influenced by factors such as the very low nobility of these metals, the occurrence of protective passive films that are stable in aqueous media, the possibility of stable hydride formation at ambient temperature. The high reactivity and corrosivity is precisely what leads to the formation of protective oxide films that require a sufficient concentration of free water. When the free water concentration of the environment decreases (for example, in organic solutions or in concentrated ionic solutions at a crack tip), film breakdown can occur, leading to electrochemical conditions whereby loss of protection and possible hydride formation can produce cracking. It is pointed out that investigations of these conditions is difficult, and results are often inconclusive.

Overall, the four papers on nonferrous metals represent brief historical reviews of the basic phenomena of environment-induced cracking and the current state of knowledge in understanding these phenomena. The concept of a film-induced cleavage model for explaining transgranular SCC is an interesting one that provoked productive discussions. Thoughts for future research in the field of nonferrous metals should ensue.



Photos: M B. Ives

Environment-Induced Cracking of Copper Alloys

*U. Bertocci, E.N. Pugh, and R.E. Ricker**

Abstract

The path of stress corrosion cracking (SCC) in α-phase copper alloys can be intergranular (IGSCC) or transgranular (TGSCC), but there is no consensus as to whether these correspond to two different mechanisms. Since research into the mechanism(s) of environment-induced cracking of copper alloys has focused overwhelmingly on α-brass in aqueous ammonia and since both forms of cracking are observed in this system, this paper deals primarily with this system.

The characteristics of IGSCC in brass are consistent with cracking occurring by the film-rupture (or slip-dissolution) mechanism. TGSCC, on the other hand, is thought to proceed by discontinuous cleavage, with an average crack velocity on {110} planes of, typically, 10^{-7} ms^{-1}. The mechanism by which the environment induces brittle failure in the ductile face-centered cubic metal has not been established, but several have been proposed. Hydrogen embrittlement is an attractive mechanism in that it can account for the kinetics of propagation and for the repeated crack arrests. However, modeling of the chemistry within the crack indicates that hydrogen discharge is unlikely for copper-zinc in aqueous ammonia and impossible for copper-gold in ferric chloride. An alternative mechanism for TGSCC proposes that a thin epitaxial film, such as an oxide or dealloyed layer, forms at the crack tip and triggers brittle fracture. In terms of this model, it is not clear why the crack arrests, particularly under conditions in which the stress intensity increases with crack length. One approach involves unfractured ligaments at the crack front. Further, the shearing of these ligaments would be favored by coplanar glide and suggests an explanation for the correlation between TGSCC and stacking fault energy.

Introduction

The literature on the mechanisms of environment-induced cracking of copper alloys deals overwhelmingly with the stress corrosion cracking (SCC) of α-brass containing approximately 30% zinc in aqueous ammonia, therefore, this system is the focus of this paper, with work on copper, other α-brasses, copper-gold, other copper alloys, and other environments being described where it relates to the Cu-30Zn/aqueous ammonia system. As in other systems, there has been little recent work on the initiation of SCC in Cu-30Zn, and thus this review deals with crack propagation. Since one of the authors has previously reviewed this subject,[1,2] the present paper concentrates on work conducted since the publication of the last of these reviews.

In the last review,[3] it was argued that two basically different mechanisms for crack propagation operate in Cu-30Zn, corresponding to intergranular and transgranular failure (IG- and TGSCC). IGSCC was thought to propagate by the classic film-rupture model,[4,5] in which localized plastic deformation at the crack tip causes continual film rupture and preferential anodic dissolution. TGSCC, on the other hand, was considered to proceed by discontinuous cleavage, that is, by brittle mechanical fracture. It will be seen that this view remains tenable.

The mechanism of IGSCC in Cu-30Zn has received little attention since 1975, but there has been considerable activity on the transgranular form, both experimental and theoretical. New experimental results include the observation that pure copper can undergo this form of cracking,[6,9] that Cu-30Zn fails transgranularly in an ammoniacal solution that causes no detectable overall dissolution,[10] and that exposure of unstressed Cu-30Zn to such solutions leads to embrittlement.[11] Efforts on the theoretical side have centered on the concept that thin surface layers produced by reaction with the environment can initiate cleavage cracks, which then propagate for relatively large distances into the unaffected brass substrate.[12] The premise that cleavage can propagate in a ductile face-centered cubic (fcc) alloy has understandably generated controversy in the physical metallurgy community. There has also been some attention given to the related question of why a propagating cleavage crack should subsequently arrest.

In the second section, our understanding of the behavior of unstressed copper and α brass in aqueous ammonia is summarized. The phenomenology of SCC is then outlined in the third section, followed by a discussion of the proposed mechanisms of crack propagation.

Chemistry of the Brass/Ammonia System

Electrochemical reactions and complex equilibria

Practical cases of SCC of brass generally occur in moist air where a condensed moisture layer acquires ammonia and oxygen from the environment.[13] Since small amounts of water are involved in the condensed layer, the concentration of both ammonia, which is being absorbed in the film, and of copper ions, which are produced by anodic attack, can become quite large. This justifies the use of concentrated solutions in laboratory tests. Although early studies were conducted in the vapor phase, since the well-known work of Mattsson,[14] the general practice is to use bulk solutions of aqueous ammonia containing dissolved copper, e.g., ASTM G37-85. The corrosion behavior of Cu-30Zn in such solutions is illustrated in Figure 1(a), which shows the well-known relationship between corrosion rate and dissolved copper content.[15-17]

To understand this relationship, consider first the behavior of pure copper in aqueous solutions. Two reactions must be taken into

*Materials Science and Engineering Laboratory, National Institute of Standards and Technology, Gaithersburg, MD 20899.

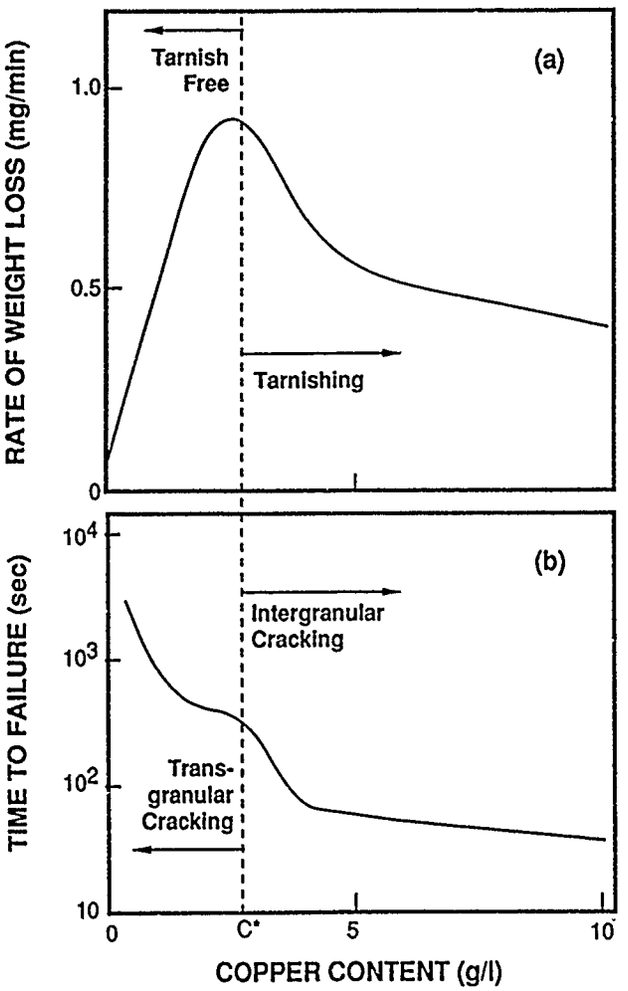


FIGURE 1—The relationship between the concentration of copper and (a) the rate of dissolution and (b) the time-to-failure for Cu-30Zn in 15 M aqueous ammonia. The critical copper concentration for the onset of tarnishing (C*) as determined from visual observations, is indicated by the broken line. (Based on data in Reference 5.)

account: a metal/solution transfer reaction

$$Cu = Cu^{+} + e^{-} \qquad (1)$$

and a redox reaction

$$Cu^{+} = Cu^{++} + e^{-} \qquad (2)$$

whose standard potentials are E_1° = 520 mV and E_2° = 159 mV vs NHE. In aqueous ammonia, the electrochemistry is dominated by the formation of very stable and soluble complexes. Two Cu^{+} and five Cu^{++}-ammonia complexes are known to exist;[18] in moderately concentrated ($NH_3 \geq 1$ M) solutions, cuprous ions are overwhelmingly present as $[Cu(NH_3)_2^+]$ complexes, while cupric ions are present either as $[Cu(NH_3)_4^{++}]$ or $[Cu(NH_3)_5^{++}]$, the second becoming the main species as the concentration of ammonia increases. No kinetic data are available for the complexation reactions, but on the basis of qualitative measurements of copper electrodes in these solutions, the homogeneous equilibria are very fast, so they don't seem to be rate determining.

Because of the high stability of these complexes, alkaline ammonia solutions can contain fairly large concentrations of copper ions before the solubility product for the precipitation of Cu_2O is reached. The solubility depends on pH as well as on ammonia concentration. For pH between 12 and 13, a few grams per liter of copper as cuprous complexes can be maintained in solution.

To account for the ammonia complexes, Reactions (1) and (2) must be rewritten in the following way:

$$Cu + (\beta+2\gamma)NH_3 = \alpha Cu^{+} + \beta Cu(NH_3)^{+} + \gamma Cu(NH_3)_2^{+} + e^{-} \quad (\text{with } \alpha+\beta+\gamma = 1) \qquad (1')$$

$$\alpha Cu^{+} + \beta Cu(NH_3)^{+} + \gamma Cu(NH_3)_2^{+} + \delta NH_3 = \epsilon Cu^{++} + \zeta Cu(NH_3)^{++} + \eta Cu(NH_3)_2^{++} + \theta Cu(NH_3)_3^{++} + \iota Cu(NH_3)_4^{++} + \kappa Cu(NH_3)_5^{++} + e^{-} \qquad (2')$$

$$(\text{with } \alpha+\beta+\gamma+\delta = \epsilon+\zeta+\eta+\theta+\iota+\kappa = 1 \text{ and } \beta+2\gamma+\delta = \zeta+2\eta+3\theta+4\iota+5\kappa)$$

The value of the various stoichiometric coefficients can be found, for a given ammonia concentration, by solving the system formed by (1), (2), and the stability constants of the complexes $K_{1n} = [Cu(NH_3)_n^+]/[Cu^+][NH_3]^n$ (n = 1 to 2) and $K_{2n} = [Cu(NH_3)_n^{++}]/[Cu^{++}][NH_3]^n$ (n = 1 to 5). Equilibrium for the corrosion reaction, in which cupric ions oxidize copper metal

$$Cu^{++} + Cu = 2Cu^{+} \qquad (3)$$

is reached when the ratio between the activities of the uncomplexed species, $[Cu^{++}]/[Cu^{+}]^2$, equals the equilibrium constant K, whose value at 25°C is 1.2×10^6.[19]

In uncomplexed solutions, if the concentration of Cu^{++} ions is 0.1 M, the Cu^{+} concentration is $[Cu^{+}] = ([Cu^{++}]/K)^{0.5} = 2.9 \times 10^{-4}$ M, and its equilibrium potential will be 310 mV. In aqueous ammonia, however, for example, 5 M, if the total copper in solution is 0.02 M, at equilibrium only about 5.5×10^{-7} M will be in the divalent form, and the concentration of the uncomplexed form, $[Cu^{++}]$, is 9×10^{-22} M, while $[Cu^{+}]$ is 2.7×10^{-14} M. Therefore, the equilibrium potential is 280 mV. One can see that Reaction (3) is completely shifted to the right: Copper immersed in a cupric-ammonia solution will corrode with the formation of cuprous ions.

Kinetics

Reactions (1) and (2) have been traditionally supposed to be very fast, so they have been assumed to be in equilibrium at the metal solution interface even when copper is rapidly corroding.[20] Such an assumption led to good agreement between experimental corrosion rates and those calculated on the basis of transport control.[21] However, for a more detailed understanding of the electrochemical processes, it would be desirable to have quantitative data on the charge-transfer kinetics of the two reactions. Unfortunately, published data on this are very sparse.[22]

In uncomplexed solutions, Reaction (2) is slower than (1), so as to be kinetically determining.[23] This is probably the case in aqueous ammonia as well, possibly because cuprous and cupric ions have a different number of ammonia ligands, and the redox reaction requires a rearrangement of the solvation shell. For Reaction (1), it is unlikely that the rate-determining step (rds) is the same as in uncomplexed solutions, involving only Cu^{+}, since its concentration is so small. The rds probably can be written as

$$Cu + nNH_3 = [Cu(NH_3)_n^+] + e^{-} \qquad (4)$$

but the reaction order, n, is unknown. We will mention here that some potentiodynamic measurements of the anodic current density of copper in pure aqueous ammonia of different concentrations have been conducted in our laboratory. Major obstacles to obtaining good results were the poor conductivity of the solutions and the difficulty in eliminating oxygen. The results showed that the rate of Reaction (1) was transport controlled in the range investigated, making it impossible to determine the reaction order of ammonia in the rds. Only a lower limit for the rate constant could be established. K cannot be less than 1 m/s, otherwise deviations from diffusion control would have

been detected. No kinetic data for Reaction (2) are available; however, considering that, at equilibrium, the ratio of the concentration of Cu^{++} to Cu^{+} ranges between 10^{-4} and 10^{-5}, even if the cathodic overvoltage at a corroding copper surface were, say, 120 mV, the Cu^{++} concentration at the interface would still be very low. This would affect the electrode potential

$$E_2 = E_2^0 + \frac{RT}{F} \ln \frac{Cu^{++}}{[Cu^{+}]} \qquad (5)$$

which depends on the Cu^{++}/Cu^{+} ratio, but not the corrosion rate, which depends on the concentration gradients. The concentration profiles during the corrosion of copper in cupric-ammonia solutions can then be schematized as in Figure 2, with the concentration of Cu^{+} at the metal surface roughly double that of Cu^{++} in the bulk and zero in the bulk solution, while the Cu^{++} concentration is close to zero at the metal surface.

Figure 2 illustrates the fact that the corrosion of film-free copper in the oxygenated solutions is under limiting current conditions, so the corrosion rate is proportional to the concentration of Cu^{++} in the bulk solution. This accounts for the linear portion of Figure 1(a). Figure 2 also illustrates the main role of oxygen in the process, which is to oxidize to Cu^{++} the Cu^{+} ions diffusing away from the metal surface. This reaction occurs within the diffusion layer, with the interesting consequence that oxygen, normally the cathodic reactant, does not contact the surface in solutions containing significant concentrations of Cu^{++}. It will be seen below that the presence of Cu^{+} within cracks eliminates oxygen in similar fashion. Note also in Figure 2 that the concentration of Cu^{++}, the primary cathodic species, can rapidly increase outside the diffusion layer during the corrosion process. Since the reduction of cupric ion generates two cuprous complexes, which in turn react with oxygen to generate the cupric complexes, the process has been termed autocatalytic.[24] It should also be noted that the concentration of the cupric complexes can attain values many times greater than that of oxygen, which is limited by its solubility in the aqueous phase.

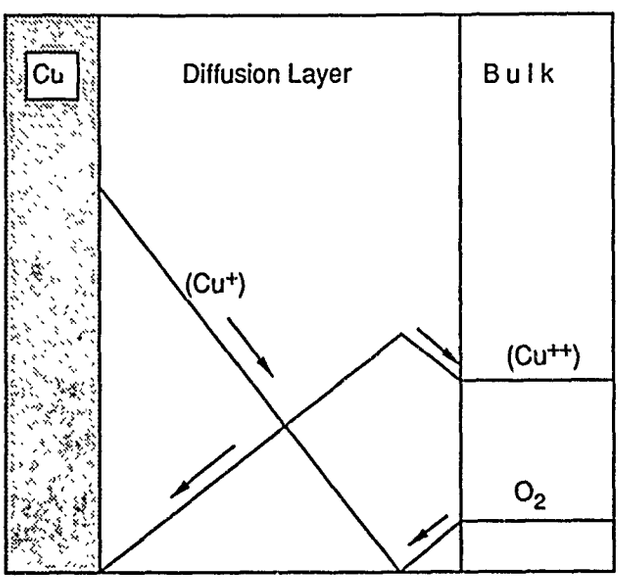


FIGURE 2—Schematic view of the diffusion layer for the corrosion of copper in oxygenated cupric ammonia.

Effects of alloying

The presence of zinc in α brass does not substantially change the description of the electrochemical behavior. Zinc also forms stable and soluble ammonia complexes; as far as solubility is concerned, only at pH around 13 may ZnO precipitate from solutions containing more than 10^{-3} M Zn^{++}. At pH = 12, the solubility of Zn^{++} is in the 0.1 M range. The electrode reaction should be written as follows:

$$Zn + (4\alpha+3\beta)OH^{-} + 4\gamma NH_3 =$$
$$(1-\alpha-\beta-\gamma)Zn^{++} + \gamma Zn(NH_3)_4^{++} + \alpha ZnO_2^{--} + \beta HZnO_2^{-}$$
$$+ (2\alpha+\beta)H_2O + 2e^{-} \qquad (6)$$

Given the low nobility of zinc and its relatively fast electrode kinetics in ammonia,[25,26] the generally held opinion that the corrosion of brass is qualitatively similar to that of copper is quite reasonable. The quantitative differences are mainly due to a smaller Cu^{+} concentration at the electrode than for pure copper for the same corrosion rate, as stoichiometry dictates.

Film formation

During the corrosion process, the Cu^{++} concentration will increase until the solubility of Cu_2O at the metal surface is exceeded and a film is formed. As illustrated in Figure 2, the concentration of Cu^{+} is greatest at the surface, approximately twice that of the Cu^{++} in the bulk. Studies have indicated that the tarnish formation process is a three-stage process:

(1) The formation of a thin (~ 20 nm) protective film of Cu_2O,
(2) Local breakdown of the thin film at anodic sites, leading to rapid attack at these sites and the growth by precipitation of a thick porous layer of Cu_2O (the "tarnish layer"); and
(3) The formation of an outer layer of CuO.

The first two steps of this process were originally suggested by Jenkins and Durham on the basis of film growth studies on copper and Cu-30Zn in 15 M aqueous ammonia.[27] However, the ellipsometry study of Green, et al., in 15 M aqueous ammonia with 8 g/L of dissolved copper did not indicate the formation of a thin protective layer as the initial step.[28] Later, Cheng[21] studied the kinetics of film growth on copper and Cu-Zn alloys in a 1 M aqueous ammonia solution, where the kinetics are slower, and he found that the original view of Jenkins and Durham[27] was essentially correct. That is, he found that (1) initially a thin protective film formed and grew to a limiting thickness of about 10 nm for pure copper and about 20 nm for Cu-Zn alloys, (2) the kinetics of film growth were faster for the Cu-Zn alloys, and (3) the rate of film growth and breakdown increased with increasing copper content of the solution. Prolonged exposure to the tarnishing solution results in the formation of an outer layer of CuO on the tarnish layer and eventually x-ray diffraction reveals the presence of CuO only in the tarnish layer.[29] During this process, the corrosion potential undergoes a noble shift, with the final values in the regions of stability of Cu_2O and CuO.[21] The thick layer, which is porous and relatively poorly protective, is commonly termed the tarnish. The onset of tarnishing causes the reduction in the corrosion rate, as illustrated in Figure 1(a), and results in the corrosion potential becoming more positive, indicating that the Cu^{++} activity at the interface has increased and that the corrosion process is no longer under transport control. The tarnish film was earlier believed to play a key role in the propagation of IGSCC,[30] but the work of Heidt and his colleagues[31] demonstrated that the thin passive film is present at the crack tip and that the thick tarnish is formed at some distance behind the advancing tip. While this observation eliminated any major role for the thick tarnish film in crack propagation, it does not preclude its role in crack initiation.

The difference between the structure of the tarnish film formed at a surface accessible to the cupric-ammonia complexes and that at the crack tip may be related to differences in the generation of cuprous ions. On the outside, Cu^{+} at the interface is provided both by Reaction (1') going anodically, possibly forming Cu_2O by a solid-state process, and Reaction (2') proceeding cathodically. The reduction of Cu^{++} might have a tendency to occur on the points of the oxide film protruding into the solution, where Cu^{++} transport is easier, rather than closer to the metal, since Cu_2O is a good electronic conductor. Therefore, during the growth of the tarnish

layer, the anodic and cathodic parts of the corrosion reaction might separate in space, occurring on the opposite sides of the oxide film, contributing to its loose and porous structure. Close to the crack tip, only the anodic process is available for film formation, since copper in solution is almost completely in the monovalent form.

It should be noted that the concentration of copper in laboratory test solutions at which the onset of tarnishing occurs depends on the method of preparation. The so-called preconcentrated solutions used in Figure 1 were prepared by dissolving copper powder in oxygenated ammonia. In such solutions, the only anion is OH^-, and their pH is higher than that of solutions prepared by dissolving a neutral salt such as $Cu(NO_3)_2$. In more alkaline solutions, the solubility product of Cu_2O is reached at lower Cu^+ concentrations. In solutions prepared with oxygen, saturation with respect to Cu_2O may be reached at concentrations 4 to 5 times lower than those prepared from $Cu(NO_3)_2$, since their pH can be 1 unit greater. To illustrate this point, Figure 3 shows, as a function of the total copper in solution, the total concentration of cuprous ions in equilibrium with the metal and the concentration of Cu^+ ions at saturation for the two methods of solution preparation: (1) dissolution of copper metal by oxidation with oxygen followed by equilibration with copper metal and (2) dissolution of half the copper as a neutral cupric salt, again followed by equilibration with the metal, both calculated for a 13 M aqueous ammonia solution. The maximum amount of copper in solution is quite different in the two cases. It should be pointed out that, in practice, the oxygen present in solution (or slowly leaking into the cell) is continually reduced, causing an increase of copper in solution as well as an increase in pH. Formation of Cu_2O, therefore, might be expected at concentrations intermediate between the two limiting values.

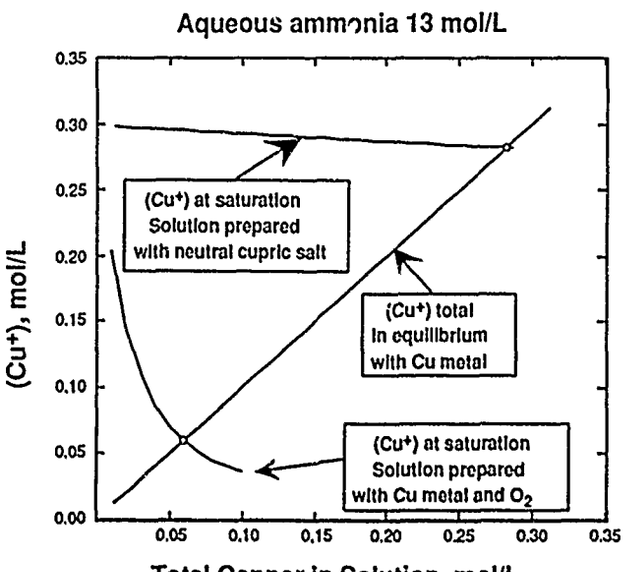


FIGURE 3—Total concentration of Cu^+ in equilibrium with copper metal and saturation lines with respect to Cu_2O, for different methods of preparation of the solution.

SCC Behavior of Brass/Ammonia System

This section is divided into two main parts. In the first, the status of our knowledge of SCC of Cu-Zn alloys in aqueous ammonia at the time of the most recent review of this subject by one of the authors (1979) will be surveyed briefly. For more details, the reader is directed to the earlier reviews.[1-3] In the second part of this section, the results of experiments that have been conducted since the time of the last review that have influenced our thinking on the SCC behavior of this system are presented. Then, the significance of these results on our understanding of the mechanisms of SCC of these alloys will be discussed in the section "Discussion."

Summary of earlier work

Experimental results reviewed previously showed the strong dependence of the SCC behavior on copper content in solution. For example, Figure 1(b) shows early data for thin sheet specimens of annealed Cu-30Zn, tested under constant load at open circuit.[15] These data indicate that (1) a minimum copper content is necessary for cracking, (2) time-to-failure decreases markedly with increasing dissolved copper, and (3) the path of cracking undergoes a transition from transgranular to intergranular at the onset of tarnishing. As noted above, copper was present in solution as cupric complexes, and observations (1) and (2) led understandably to the proposal that the complex ions play a major role in crack propagation.[32] However, later studies established that the complexes simply provide the cathodic reaction for the corrosion to run at a sufficient rate. Therefore, cracking can be produced in the absence of the cupric ions by applying an anodic current.[33] The simple correlation between crack path and the presence or absence of the tarnish assumed in (3) was found not to be totally valid. Failure of Cu-30Zn is transgranular in nontarnishing solutions, but cracking in tarnishing solutions can be either intergranular or transgranular, depending on factors such as crack length, stress intensity, strain rate, and grain size. Transgranular cracking has been observed in tarnishing solutions for heavily cold-worked samples,[34] in admiralty metal,[35-37] and a transition from intergranular to transgranular is observed with increasing crack length.[38-40]

In nontarnishing solutions, crack propagation can be either intergranular or transgranular depending on the zinc content of the alloy, being intergranular for zinc contents less than ~18% and transgranular for zinc contents above this value. The slip character of the alloy and the dislocation structure also varies with zinc content, with wavy slip and cellular dislocation arrays being observed at low zinc contents and planar slip with the formation of persistent slip bands being observed in the higher zinc content alloys, and this may be responsible for the change in crack path. However, recent evidence suggests that the percolation threshold for dealloying of Cu-Zn alloys is in the same range of zinc content; this may be a critical factor in this transition.[41]

Probably one of the most important observations made in the 1960s and 1970s was that the transgranular fracture surfaces were cleavage-like in appearance, with linear features resembling fatigue striations. McEvily and Bond examined replicas of fracture surfaces in the transmission electron microscope and found that these linear features were (1) parallel and remained so over dimensions much greater than the grain size, (2) were perpendicular to the direction of crack propagation, and (3) occurred at different stress levels.[30] They concluded that these features were the result of discontinuous crack propagation and plastic blunting of the crack when it arrests, in accordance with the earlier surface trace studies of Edeleanu,[42] and Edeleanu and Forty,[30] as illustrated in Figure 4. These investigators observed that the crack tip remained stationary for some time, as shown in Figure 4(a), after which a thin crack was observed to extend past the crack tip some distance, marked Δx^* in Figure 4(b), which then widened as the crack blunted, as shown in Figure 4(c). For an average time (Δt^*) between crack propagation events, the crack propagation velocity would be

$$da/dt = \Delta x^*/\Delta t^* \qquad (7)$$

Because of the importance of these observations to the understanding of the mechanisms of crack propagation, numerous investigators have examined transgranular fracture surfaces over the last 10 years; their results will be discussed below.

Results of recent studies

Characterization of the nature of crack propagation. Beggs, et al.,[44] confirmed the results of Edeleanu and Forty[43] on discontinuous crack advance and demonstrated that the crack advance observed optically corresponded to the detection of a discrete acoustic pulse. Beavers[37] reported that the acoustic activity that

accompanied transgranular crack propagation in admiralty metal consisted of discrete pulses of approximately 1 ms duration, including ringdown time, indicating discrete crack propagation events of approximately 1 μs duration. Newman and Sieradzki[45] showed that electrochemical current transients also occurred within 1 ms of the acoustic transients and that the magnitude of the transients was consistent with the crack advance distances measured on the fracture surfaces Finally, the application of load pulses to mark the location of the crack tip at discrete time intervals[40] confirmed the discontinuous nature of crack propagation and allowed the shape of the crack front to be determined This showed that the linear features originally reported by McEvily and Bond[42] are crack-arrest markings, as these authors postulated.

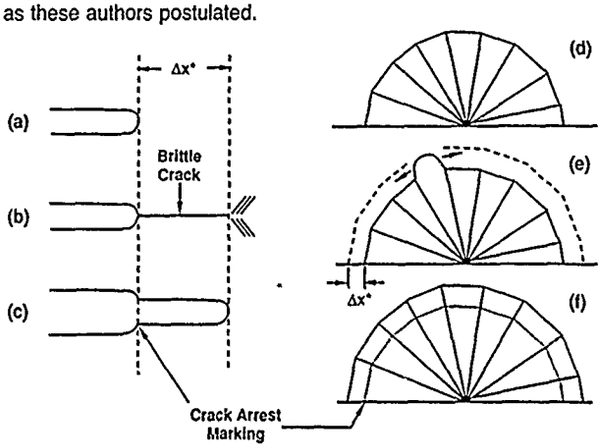


FIGURE 4—Schematic of the successive events that occur during the propagation of transgranular stress corrosion cracks: (a-c) section through crack tip, (d-f) plan view. (a) and (e) indicate crack advance distance per propagation event (Δx*).

The results of the fractographic studies have been reviewed recently[46,47] and will be summarized here. Transgranular fracture surfaces have been found to be cleavage-like in appearance, consisting of flat, parallel primary facets separated by steps that, at low stress intensities, are also crystallographic in nature. This is schematically illustrated in Figure 5, where the primary facets are {110} planes and the steps are {111} planes.[37,48] It has been shown also that opposite sides of the fracture surfaces match precisely, that the steps between the fracture facets are approximately perpendicular to the direction of crack propagation, that the steps radiate out from the initiation site as indicated in Figures 4(d) through (f), that river patterns form when the crack crosses a grain boundary, and that undercutting occurs at the steps.[46,47] Typically, the crack advance distances observed on the transgranular fracture surfaces of Cu-30Zn tested in aqueous ammonia are of the order of 1 μm, with a time interval of about 10 s between successive crack advance events.

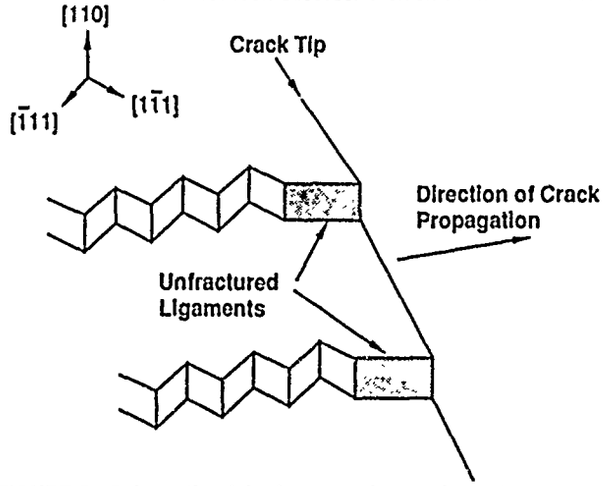


FIGURE 5—Schematic of the features observed on a transgranular SCC fracture surface.

SCC in equilibrated solutions. A recent development in SCC studies for brass has been the observation of TGSCC in solutions of equilibrium composition with respect to copper.[10,41] Since copper is not anodically attacked in these solutions, dissolution-based models of SCC would not predict cracking in these conditions. The solutions were prepared by adding excess copper powder and allowing it to react in the absence of oxygen until Reaction (3) reaches equilibrium. The justification for using such solutions is based on the realization that, because of the relatively fast kinetics of Reactions (1) and (2), the solution in contact with the bare metal is always close to equilibrium composition. It is then reasonable to assume that the same conditions exist inside a crack, where a small amount of solution is in contact with a large metal surface. Because of the relatively high resistance of the solution that electrically connects the tip of the crack to the exterior, the external conditions have only a minor influence on the electrochemical processes at the tip. Therefore, it is not surprising that cracking will occur in a similar fashion both in equilibrated and nonequilibrated solutions.

Kaufman and Fink have also conducted experiments in equilibrated solutions, but they were unable to observe TGSCC.[49,50] The solution used by these investigators was prepared from a 0.13 M cupric solution in nominally 15 M aqueous ammonia and after equilibration with copper metal should have contained at least 0.25 M copper. If some atmospheric oxygen had to be scavenged, the concentration of Cu^+-ammonia complexes might have been somewhat higher. Comparison with the curves in Figure 3 shows that the solution might have been saturated with respect to Cu_2O, particularly if the pH had become slightly higher than the value calculated, which does not account for the reduction of any oxygen. The formation of a thin Cu_2O layer might have been very difficult to detect (no thick tarnish would be expected in these marginal conditions) but might have prevented crack initiation or otherwise interfered with the cracking process.

More recently, Shahrabi[51] conducted constant-strain tensile tests in carefully controlled, copper-equilibrated solutions at various concentrations. By including sensor electrodes in his experiment, the cupric ion concentration could be measured, and it was demonstrated that the solutions were indeed at equilibrium. TGSCC was observed at potentials ranging from slightly anodic to slightly cathodic of equilibrium, but as the copper concentration of the solutions increased and approached those used by Kaufman and Fink, the time-to-failure and the load required to cause crack propagation increased, indicating that crack initiation and/or propagation is more difficult in these environments. These results have demonstrated that not only is dissolution of copper not required for crack propagation, but that crack initiation and propagation can occur under conditions of copper deposition, suggesting that the only anodic process contributing to cracking is dissolution of zinc from the alloy.

Experimental observations of embrittlement. Some of the recent advances have come from studies on alloys other than brass. An example is Cu-Au alloys, which have close structural similarities with α-brass. From the chemical point of view, copper is the base metal, corresponding to zinc in brass, while gold takes the place of copper as the noble metal. In the 1950s, Bakish and Robertson[52-54] studied various aspects of the corrosion behavior of Cu_3Au alloys. In the course of these studies,[55] thin slices of annealed Cu_3Au single crystals were exposed to a $FeCl_3$ solution for a month. When these samples were bent normal to the {110} plane in air, they exhibited brittle behavior, with what appeared to be cleavage on the {110} plane and cleavage steps that followed the {111} slip planes. Bakish concluded that the samples had become chemically embrittled by the dissolution of copper from the {110} planes and the formation of a gold-rich sponge on these planes. Renewed interest in this alloy system led Lichter and coworkers[56-59] to undertake a detailed study of the TGSCC of Cu-Au alloys. Their observations have contributed significantly to our understanding of the mechanism of TGSCC.

Lichter, et al.,[59] found that the transgranular fracture surfaces generated during SCC of ordered and disordered Cu-Au are essentially identical to those that form during transgranular cracking of brass in ammonia. The fractures appeared to occur by discontinuous cleavage with {110}-type cleavage facets, {111}-type cleavage steps, and crack-arrest marks perpendicular to the direction of crack growth. They found that, for the sample size and exposure time used

by Bakish,[55] copper had been completely removed by the $FeCl_3$ solution, so the entire sample had been converted to a dealloyed sponge. On bending, they found that, while the samples were macroscopically brittle, the facets formed were perpendicular to the loading axis and not crystallographic, that the steps on the surfaces of the fractures were not crystallographic, and that the fractures occurred by ductile failure of the remaining gold filaments in the sponge-like structure. More importantly, they exposed samples to the $FeCl_3$ solution for a shorter time, so that only a thin surface layer about 30 μm thick was dealloyed. On bending these samples, macroscopically ductile behavior was observed, but numerous "brittle" cracks perpendicular to the loading axis were observed. On cross sectioning through these cracks, it was found that most of them terminated at the boundary between the dealloyed sponge-like layer and the unattacked alloy; however, several of these cracks propagated up to 20 μm into the unattacked and normally ductile alloy. Careful microprobe analysis of cross-sectioned cracks indicated that dealloying had not occurred on the fracture plane beyond the 30-μm-thick surface dealloyed layer and that fracture did not occur along a dealloyed plane but penetrated into the unaffected matrix.

More recently, Fritz, et al.,[60] conducted SCC experiments on a Cu-18at%Au alloy in a 1 N Na_2SO_4 0.01 N H_2SO_4 solution, which had been shown to cause TGSCC of this alloy.[59] Fritz, et al., dealloyed unstressed samples at one potential, then switched to a second potential and applied a load to the sample. They found that cracks propagated beyond the dealloyed layer only if the second potential was in the range where copper dissolution occurs, and that the cracks always stopped before or at the dealloyed layer–unaffected matrix interface when the second potential was at a value where little or no copper dissolution occurs. They concluded that dissolution of the less noble metal, copper, is required for stress-corrosion crack propagation, and that the cracks observed to propagate beyond the dealloyed layer[56] were due to either (1) crack propagation in the $FeCl_3$ solution prior to bending because of residual stresses in the sample, (2) crack propagation during bending because of incomplete removal of the $FeCl_3$ solution from the sponge layer, or (3) a difference between the alloys examined (Cu-18at%Au vs Cu-25at%Au used by Lichter).

The recent experiments of Newman, et al.,[11] may help in reconciling the apparent discrepancies between the results reported above. These investigators tested samples of a 12.5-μm-thick brass foil by pulling them to failure in different environments after different pre-exposure treatments. They found that the pre-exposure and test environment influenced the fracture morphology. Figure 6 is a flow chart of the 7 different experiments conducted by these investigators, with the fracture morphology (ductile vs cleavage-like) that resulted from each experiment. First, these investigators demonstrated that the rapid straining of the brass foil in air at room temperature or at 77°K results in ductile fracture (experiments 6 and 7 in Figure 6) and that rapid straining in 15 M NH_3 + 0.04 M $Cu(NH_3)_2^{+}$ results in brittle cleavage-like fracture (experiment 1 in Figure 6). By analogy with the results of Lichter and his coworkers,[56-59] one would assume that pre-exposure to this solution, which causes dealloying and brittle fracture, followed by testing in air, would be all that is required to induce brittle cleavage, but this was not the case. Instead, after rinsing in methanol and drying in air at room temperature, the fracture behavior at both room temperature and at 77°K was ductile. This would seem to refute the role, if any, of a dealloyed layer in nucleating a fracture event that propagates into the unattacked matrix. However, these investigators took a sample out of the ammonia solution and immediately quenched it in liquid nitrogen and pulled it at 77°K. This sample failed by brittle cleavage (experiment 4 in Figure 6). Since earlier experiments had demonstrated that cooling at 77°K does not induce brittle fracture in this alloy (experiments 6 and 3 in Figure 6), and since the surface of the sample would not be wet at 77°K, Newman, et al.,[11] concluded that they had demonstrated that a dealloyed layer less than 100 nm thick could induce cleavage propagation over several μm, but, since cleavage was not observed in the room-temperature experiments (experiments 2 and 5 in Figure 6), they concluded that exposure at room temperature to conditions that do not cause dealloying results in room-temperature "aging" of the dealloyed film such that the film can no longer nucleate cleavage.

TGSCC of pure copper. One of the most important experimental results of the last 10 years is the observation of TGSCC in pure copper.[6-9] A thorough study of the conditions leading to SCC in pure copper was recently conducted by Cassagne.[8] He observed TGSCC in nitrite solutions, but also in acetate, confirming previous reports.[61] The presence of an oxide film was found to be necessary for cracking, so that in acetate solutions no SCC was observed at pH = 3, where no oxide forms. Cracking was also dependent on electrode potential and strain rate, indicating that when the strain rate is too fast (thus, decreasing the time available for film growth), and the potential is too negative (thus reducing the driving force for oxide formation), brittle fracture does not occur. Figure 7 shows potentiodynamic scans obtained in copper acetate at two pHs. Cracking was observed only in conditions where oxide formation was detected as indicated by the anodic current increase and by the existence of a reduction peak in the cathodic scan. The oxide growth process was investigated by ellipsometry in the two solutions in which TGSCC was observed, namely 0.1 M sodium acetate at pH = 5.5, and 1 M sodium nitrite at pH = 9. Initially, a thin Cu_2O film (1 nm or less) was found to form in both solutions, but subsequently the film breaks down by micropitting, and this is followed by the formation of a thick porous tarnish layer, several tens of nm thick. Based on his results, Cassagne concluded that it is not the formation of the initial thin film, but rather the breakdown of this film that is important for the initiation of the brittle crack.[8]

Modeling of crack chemistry. A possible explanation for the occurrence of TGSCC in otherwise very ductile alloys such as brass and Au-Cu could be hydrogen embrittlement. Such an explanation is attractive in that it can account for the observed kinetics of cracking. Thus, for Cu-30Zn, the diffusivity of hydrogen required to account for the embrittlement to a depth of 1 μm ahead of the crack tip in 10 s is 10^{-9} cm^2/s, a reasonable extrapolation from high-temperature diffusion data. One can speculate, therefore, that cathodically generated hydrogen is absorbed at the crack tip and produces a hydrogen-containing zone. The crack, once initiated, propagates through this zone and arrests when it emerges into the hydrogen-free lattice. The process is then repeated.

Hydrogen discharge is made credible because selective dissolution of the less noble metal at the fresh surface immediately following crack advance is expected to produce a transient decrease in potential, well below the values measured in steady-state conditions. The potential would then return to the prior value as dealloying becomes limited by solid-state diffusion. Evidence for periodic potential transients, correlated to the acoustic signals caused by the crack advance, has been reported.[45] Also, if 75Cu-25Au alloy is abraded with emery paper and rapidly immersed in $FeCl_3$, the potential shows an initial minimum of about 400 mV vs NHE and then, in less than a second, returns to its steady-state value of about 700 mV.[62]

When the crack advances, fresh, undealloyed surface is exposed to the solution. In the case of TGSCC of brass in aqueous ammonia, the cathodic reaction involves the deposition of copper according to Equation (1), while the surface zinc anodically dissolves according to Equation (6). In the case of Cu-Au alloys, copper is the base metal that is anodically oxidized to Cu^{+}, while gold is not attacked at the potentials of interest. Since the typical solution for TGSCC studies of Cu-Au alloys is acidic $FeCl_3$, copper dissolves according to the reaction

$$\begin{gathered} Cu + (\beta+2\gamma+3\delta)Cl^{-} = \\ \alpha Cu^{+} + \beta CuCl + \gamma CuCl_2^{-} + \delta CuCl_3^{--} + e^{-} \\ (\alpha+\beta+\gamma+\delta = 1) \end{gathered} \qquad (8)$$

In the presence of $FeCl_3$, which maintains the potential of the metal at a fairly high value, cuprous ions are further oxidized to Cu^{++}. As in ammonia solutions, the greater part of the copper ions are complexed. The cathodic reaction consists of the reduction of Fe^{+++} to Fe^{++}. Here, too, both ions are present mostly as chlorocomplexes. Electrochemical experiments have shown that TGSCC can occur under anodic oxidation in chlorides,[59] so that Fe^{+++} presence is not important, except for providing the cathodic reaction in the absence of an externally impressed current.

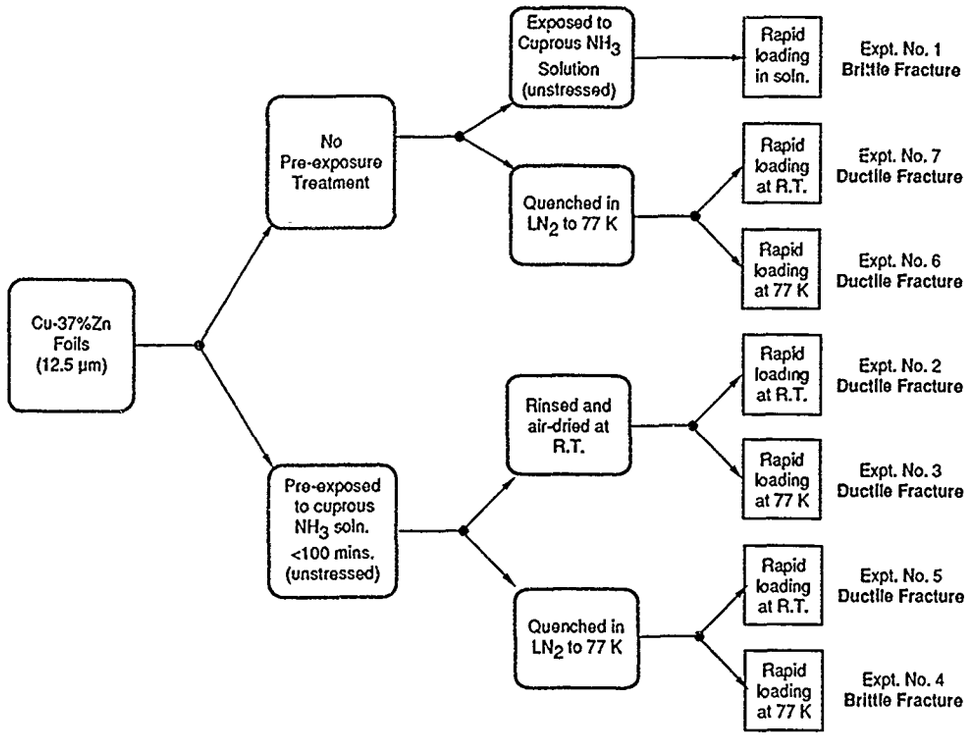


FIGURE 6—Chart of the experiments conducted by Newman, et al.,[11] which demonstrates the embrittlement of Cu-30Zn by pre-exposure (unstressed) to a cuprous ammonia solution.

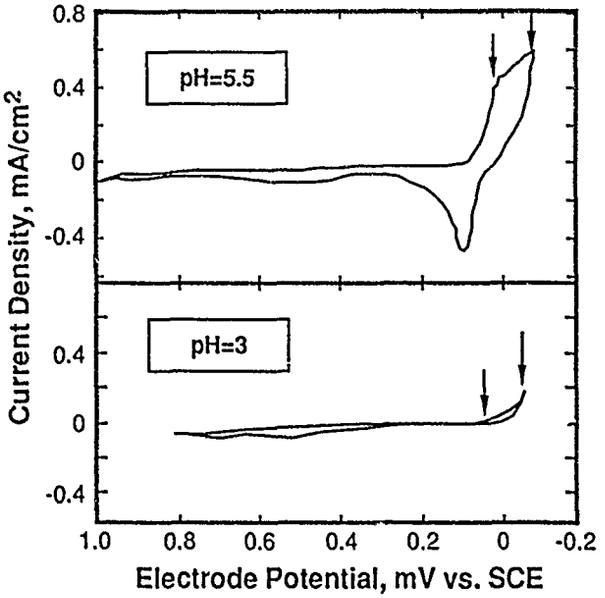


FIGURE 7—Potentiodynamic scans for copper in copper acetate at two different pHs. The arrows indicate the potentials at which the tensile tests were run.[8]

Since reliable measurements at the crack tip are difficult to achieve, modeling calculations of the transient minimum of the potential have been used to test the possibility of hydrogen discharge at the time of crack advance. The details of the calculations have been published.[62-65] In brief, to estimate the minimum in the electrode potential reached at the crack tip at the instant of the crack advance, it is necessary to calculate the ratio between the area where the anodic reaction occurs [either (6) or (8) for brass and Au Cu, respectively] and the cathodic area, which extends from the tip into the crack. This entails the treatment of an electrical circuit analogous to a transmission line. The calculation requires knowledge of the kinetic parameters of the reactions involved, and the results depend on solution composition as well as geometric parameters of the crack.

In the case of brass, the results are summarized in Figure 8, which compares the calculated minimum potential reached in solutions containing different amounts of ammonia, for a reasonable range of exchange current densities for the cathodic Reaction (1'), with the equilibrium potential for hydrogen evolution at pH = 12. Since some of the calculated potentials fall below the H_2/H^+ equilibrium line, hydrogen discharge at the crack tip cannot be categorically excluded on the basis of the modeling calculations. However, while H_2 evolution may occur in concentrated ammonia solutions, it is almost impossible in the more dilute ones. Since no changes in crack behavior or morphology have been observed as a function of ammonia concentration,[2] these results make hydrogen embrittlement as the cracking mechanism in brass very unlikely.

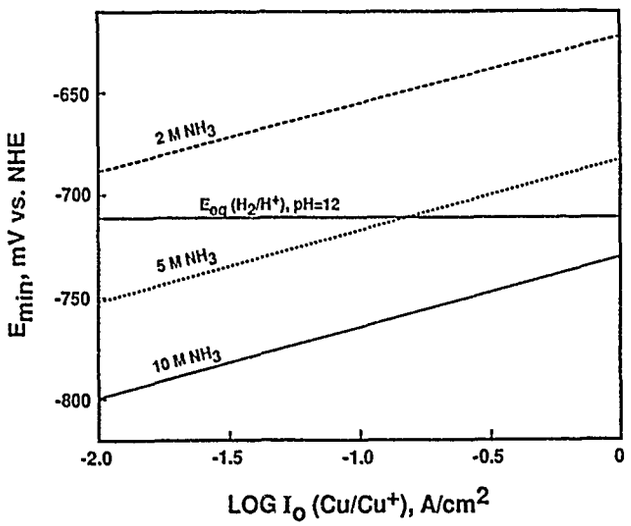


FIGURE 8—Minimum potential at the crack tip for Cu-30Zn as a function of the exchange current density of the cathodic reaction. Different lines valid for the ammonia concentration marked on them.

The results of the modeling for Au-Cu alloys in acidic $FeCl_3$ are summarized in Figure 9. Here there is no possibility for hydrogen

discharge at the minimum potentials calculated, even taking into account that on gold, H adsorption may occur about 100 mV more positive than the equilibrium potential for H_2 evolution.[66] The conclusion, therefore, is that hydrogen embrittlement can be ruled out as the cause of TGSCC in Au-Cu alloys, strengthening the belief that this is the case for brass also.

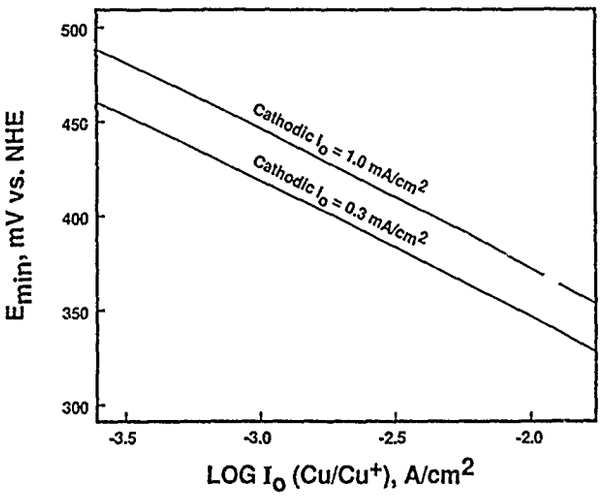


FIGURE 9—Minimum potential at the crack tip for 25Au-75Cu in acidified ferric chloride, as a function of the exchange current density of the anodic reaction.

Discussion

In a review of this subject published in 1971,[2] it was proposed that intergranular and transgranular cracking in nontarnishing solutions occurred by the same mechanism; preferential anodic dissolution at the crack tip. However, in a more recent review (1979),[3] this view was deemed to be inconsistent with the fractographic observations made in the 1970s, and as a result, it was concluded that the mechanisms of IGSCC and TGSCC were not the same, and that, while the mechanism of IGSCC still appeared to be preferential dissolution, there was convincing evidence that TGSCC occurs by discontinuous brittle mechanical fracture. Since no new data have appeared that would lead us to modify this conclusion, we will discuss each of these forms of crack propagation separately below.

Intergranular cracking

Relatively little recent work has been directed to studying the mechanism of intergranular crack propagation in the brass-ammonia system, and existing evidence continues to support the Logan-Champion[4,5] film-rupture model. The model has been modified by a number of workers,[67-69] but the basic concept remains that the crack propagates by preferential dissolution at the crack tip where the passive film is ruptured by localized plastic deformation. The evidence for this model in the Cu-30Zn/aqueous ammonia system is as follows:

(1) A thin passive film is known to exist at the crack tip.[31]
(2) The fracture surfaces are smooth, consistent with a dissolution process and exhibit no evidence of crack arrest or crack-front markings.[44]
(3) There is no evidence for discrete acoustic emissions of the type detected during the propagation of transgranular cracks.[44]
(4) The observed crack velocities, approximately 10^{-6} ms^{-1}, can be shown by a Faraday's law calculation to be fully consistent with a dissolution process.[3]

While these observations are consistent with the film-rupture model, they do not prove that it is operative, and it is possible that an alternative mechanism exists. In particular, they do not rule out a process based on dezincification. Such a process would be expected to be discontinuous, but observations (2) and (3) above would not rule out this possibility if the crack advance distance were small.

It should be noted that the film-rupture explanation leaves several details to be resolved. For example, the reason for the intergranular path is usually rationalized by postulating that repassivation is slower at the grain boundaries than in the grain interiors, presumably because of segregation,[3] but the nature of the segregant has not been established. There has also been debate over the question of whether the crack tip remains bare and active during propagation or whether it undergoes cycles of repassivation. The results of Loto and Cottis, who examined the electrochemical noise generated during IGSCC of polycrystalline Cu-30Zn in aqueous ammonia and detected transients, which they attributed to film-rupture events, would tend to support the latter viewpoint.[70]

Present treatments of the film-rupture model have been criticized for limiting consideration of the crack tips to two-dimensional representation. In particular, this oversimplified picture has led to the implication that a single film-rupture event can cause the entire crack front to become film free. However, if the crack is viewed in three dimensions (Figure 10), it can be seen that film rupture caused by slip would be expected to occur at a number of sites distributed along the crack front, each leading to independent anodic attack. Moreover, at each active site, the crack front would advance locally ahead of neighboring passivated sections, so that the stress on these sections would increase and this, in turn, would shield the propagating section from the externally applied load. In this way, the stress at the points where the crack is propagating will fall, and slip will no longer be able to keep them bare, except at high stress intensities. As a result, the crack tip should experience cycles of rupture and repassivation, with the percentage of the crack tip bare increasing with the stress intensity, and the probability of repassivation increasing for a section of the crack tip that deviates from the plane normal to the applied load. Crack propagation by the film-rupture mechanism can thus be viewed as the summation of a large number of almost independent events, each being influenced by their local environment and loading conditions.

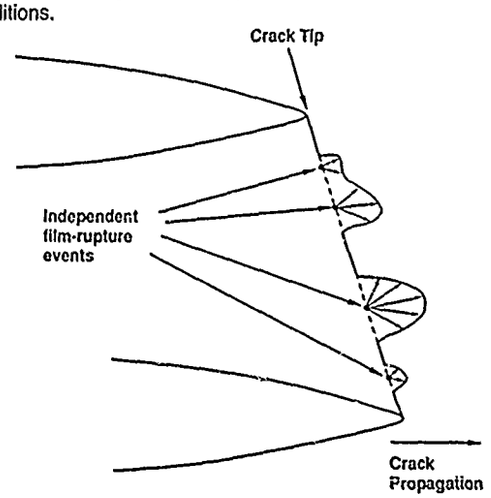


FIGURE 10—Schematic diagram of the film-rupture process in three dimensions.

Transgranular cracking

In contrast to IGSCC, over the past ten years a large amount of work has been focused on TGSCC of brass in aqueous ammonia, and considerable advances have been made in understanding its mechanism. The most significant experimental results were discussed in the preceding section, and the impact of these results on our understanding on the mechanism of TGSCC will be the subject of this subsection. The mechanisms that have been proposed for SCC fit into five basic categories: (1) dissolution (film-rupture and dissolution models), (2) adsorption, (3) hydrogen embrittlement, (4) dealloying or tarnish rupture (crack propagates in films only), and (5) film-induced cleavage.

In the last review,[3] it was concluded that dissolution models for TGSCC were not consistent with the fractographic evidence. At that time, there was no direct indication that dissolution of the noble component of the alloy was not required for TGSCC in brass, and the analogies with Au-Cu were not appreciated. Since then, experiments in cuprous ammonia, so-called equilibrated solutions, have shown that dissolution of copper is not a necessary condition for observing

TGSCC in brass [10,41,51] This conclusion has been challenged by Kaufman,[49,50] but, as previously discussed, there are sufficient reasons, in our opinion, to be skeptical of Kaufman's claims. Also, a dissolution-based mechanism cannot explain the embrittlement observed at 77°K by Newman[11] after a very short exposure to a corroding medium. These results demonstrate that, while dissolution of copper is not required, some dealloying is necessary to induce brittle cracking Mechanisms that do not involve mechanical fracture of a dezincified layer cannot explain these results. Circumstantial, but nonetheless significant, evidence for the role of dealloying in TGSCC is provided by the close correlation between the percolation limits for dealloying and the minimum concentration of the less noble component, for brass as well as for other alloy systems, necessary to observe cracking.[72]

Once it is concluded that crack propagation occurs by a mechanical fracture process, it is necessary to evaluate the environmental interactions that may cause this type of propagation. In the adsorption model, a chemical species is adsorbed from the environment on the bare metal, interacting with the interatomic bonds and inducing crack propagation by lowering the energy required to break these bonds This would explain SCC and liquid metal embrittlement by a single mechanism, and it could account for the influence of the electrode potential on cracking, at least for the case of adsorption of a charged species. However, it is unclear which species could play the critical adsorbing role. Uhlig, et al.,[32] suggested that copper-containing ammonium complexes could be responsible, and a similar proposal has been advanced recently by Hintz.[73] One of the problems is that it is hard to envisage how an adsorption mechanism would result in discontinuous crack advances. Hintz, et al.,[74] based on examinations of crack-arrest marks in α-β-brass, suggested that, at high stress intensities close to K_{crit}, the cracks propagate faster than the rate of transport can provide the damaging species to the crack tip, resulting in crack arrests and blunting. This would imply that crack-arrest markings are only present near the point of final ductile overload However, crack-arrest markings have been reported to be present throughout fracture surfaces, only being more difficult to observe at lower stress intensities.[30] The fact that acoustic emission and electrical potential transients are observed over the entire course of crack propagation cannot be easily explained by an adsorption process As a result, we conclude that while adsorption as a cause of TGSCC is an interesting hypothesis, it fails to account for all of the observations.

Hydrogen embrittlement may be considered a reasonable explanation for TGSCC in copper-base alloys, as it is in the case of other metal systems It would explain discontinuous crack propagation and the similarity between TGSCC fractures and the fracture surfaces generated by hydrogen charging of some fcc metals. However hydrogen solubility in copper alloys is generally considered very low Recently, Nakahara and Okinaka[75] reported damage as a result of electrochemical hydrogen charging of pure copper, but this was achieved only by poisoning the hydrogen-recombination reaction and lengthy exposures Also, as discussed above, modeling of the electrochemical conditions at the crack tip has indicated that, for brass in aqueous ammonia, hydrogen discharge is unlikely, and for Cu-Au in $FeCl_3$, impossible Therefore, while hydrogen embrittlement may be the cause of TGSCC of some alloys in some environments, it can be safely ruled out in the cases considered here.

In 1959, Forty[76] proposed that TGSCC of brass in aqueous ammonia resulted from the selective dissolution of zinc from the alloy, leaving a void-rich layer, which then fails in a brittle manner. According to this model, the crack blunts and stops when it reaches the end of the dealloyed layer As a consequence, the rate of crack advance would be limited by the rate of dealloying. Namboodhiri[77] has reported that dezincification of brass in ammonia is significantly accelerated by stress. If these results could be shown to be applicable to the crack tip, they might be able to account for the observed crack velocities, without requiring that the crack move ahead of the dealloyed layer Even if anomalously high dezincification rates are possible at the crack tip, a model based on brittle fracture of a dealloyed layer would have difficulties in explaining TGSCC of pure copper,[6-9] or the results of Lichter, et al.,[56-59] and Newman, et al.,[11] where the thickness of the dealloyed layer and the rate of its growth has been measured and shown to be less than the crack advance distance. We must conclude that, while dissolution of zinc from brass and of copper from Cu-Au alloys appears to be required for TGSCC, fracture of the dealloyed layer alone cannot explain the crack advance distances, the cleavage-like appearance of the fracture surface and the steps between the cleavage facets. The explanation of the cracking of pure copper, moreover, must be based on some different model.

At the time of the last review,[3] the only mechanistic possibilities for TGSCC appeared to be those discussed above, and each of them has been weakened, if not eliminated altogether, based on the experimental evidence obtained since. Recently, a new mechanism for TGSCC crack propagation has been proposed by Sieradzki and Newman[12] based on the experimental observations and the modeling work of these investigators and their coworkers.[78-82] According to this model, in the presence of a thin surface film at the crack tip, a fracture initiated in the film propagates in the normally ductile matrix. The critical difference between this film-induced cleavage model and the model proposed by Forty[76] is that, when the crack in the film reaches the film/matrix interface, traveling at a high velocity on an orientation favorable for cleavage, the ductile matrix cannot arrest crack propagation and blunt the crack tip until the crack has propagated for some distance into the matrix.

The critical questions in evaluating this mechanism are (1) what is the film, (2) can this film initiate brittle fracture, (3) can the brittle crack propagate in the ductile matrix, and (4) what, then, stops the crack. For brass in ammonia, the surface film at the crack tip is supposed to be the copper-rich dealloyed layer. The embrittlement experiments of Newman, et al.,[11] clearly demonstrate that the presence of a dealloyed layer on the surface of a Cu-30Zn sample can induce transgranular crack propagation for distances of about 12 μm. Similarly, Lichter and coworkers[56-59] have shown that the gold-rich layer in Cu-Au can initiate cleavage-like fracture. More recently, it has been reported that a dealloyed layer on Ag-Au can cause cracking.[83] In the case of the experiments of Newman, et al.,[11] on Cu-30Zn dealloyed in cuprous ammonia, since the measured thickness of the dealloyed layer was of the order of 100 nm, since the cracks propagated up to 12 μm at 77°K, where no adsorption or dissolution could take place, and since the cracks were identical to the transgranular cracks observed during SCC of Cu-30Zn in aqueous ammonia, we conclude that dealloyed layers can initiate brittle fracture that propagates beyond the dealloyed layer into the substrate. However, it should be noted that the presence of a dealloyed layer alone is not sufficient to cause brittle crack propagation. For example, brass dealloys rapidly in chlorides and, as yet, no SCC has been reported in this system. In the experiments discussed above, Newman, et al.,[11] found that aging the foils at room temperature resulted in the recovery of ductility. As a result, we must conclude that, although dealloyed layers can initiate brittle fracture that propagates into the alloy matrix, the ability of the layer to initiate brittle fracture depends on some property of the dealloyed layer, which, in turn, depends on the alloy and the environment. Obviously, more research is needed to help us understand this point.

The situation in brass is further complicated by the observation that pure copper undergoes TGSCC, also by discontinuous propagation on {110} planes. Clearly, a dealloyed layer cannot by invoked in this case. An alternative possibility was that the thin passive film represents the initiating layer in the pure metal. However, the studies of Cassagne,[8] discussed above, demonstrated that conditions that maintain the presence of the film do not lead to TGSCC, but rather the breakdown of the film by micropitting appears to be necessary for the occurrence of cracking. Cassagne has speculated that the pitting process can produce closely spaced, fine tunnels, which form a porous layer similar to that resulting from dealloying, and that this layer also initiates cleavage cracks.

From a scientific point of view, the elimination of all of the possibilities for crack propagation in the Cu-30Zn aqueous ammonia system other than film-induced cleavage is very important, and the

realization that brittle cleavage cracks can propagate in a ductile material will impact many areas of research outside of the corrosion research community. For instance, Lin and Thomson[84] addressed the issue of the ability of a high-speed brittle crack to propagate into a ductile matrix. This is a critical point, because previous theories on dislocation emission from moving cracks would predict ductile behavior for this case. These theorists used a time-dependent dislocation emission and cleavage treatment to predict that cleavage cracks can propagate in ductile materials if the crack velocity exceeds some critical value. For copper alloys, they estimated that a crack velocity of about half of the speed of sound would result in brittle crack propagation.

Once it is accepted that a brittle crack can propagate in a normally ductile matrix, the question becomes one of why does it stop. Two different mechanisms have been proposed. First, Sieradzki and Newman theorized that, as the crack propagates, it leaves dislocations in its wake that are then absorbed into the fracture surface as a result of image forces.[12] Using the simple assumption that the energy of the created dislocation is provided by the crack out of its kinetic energy,[85] these authors predict that the velocity of the crack will be reduced as it propagates and emits dislocations until the velocity drops below the critical value required to maintain brittle fracture. On the other hand, Pugh[46] suggested that arrest results from the existence of unfractured ligaments at the crack tip (Figure 5). It was postulated that these ligaments are produced because cleavage step formation, considered to involve plastic shearing, lags behind the cleavage crack front and that their lengths increase during crack advance. The ligaments thus become increasingly load bearing, eventually reducing the crack-tip stress below the level required for propagation. These are two different hypotheses, one based on the material's ability to nucleate dislocations during propagation and the other based on the morphology of the crack tip.

From an engineering viewpoint, the critical issue is to determine how we can use our understanding of the mechanism of crack propagation to improve the resistance of alloys to SCC. Equation (7) indicates that there are two approaches that can be taken to address this issue. One would be to alter the chemistry of the alloy or environment, influencing the films that form, so as to avoid the initiation of the brittle cracks or extend the time interval (Δt^*) between crack propagation events. The other would be to alter the alloy in such a way as to improve its ability to arrest the propagating crack, and thereby reduce the travel distance at each advance (Δx^*). Success in either of these options or both would result in the development of alloys that are more resistant to SCC.

Summary and Conclusion

The existing evidence continues to support the view[3] that IGSCC and TGSCC in the Cu-30Zn aqueous ammonia system occur by basically different mechanisms. There has been little recent work on the mechanism of IGSCC, and the film-rupture model remains the main contender. In the case of TGSCC, several important observations and conceptual advances have been made.

(1) Dissolution of copper is not required for TGSCC in this system.
(2) Hydrogen discharge at the crack tip is unlikely in the case of brass in ammonia and impossible for Cu Au in acidic chloride, ruling out hydrogen embrittlement as the cause of SCC in these systems.
(3) Computer modeling of the fracture behavior of film-covered surfaces showed that, once a brittle crack is nucleated in the film, it can continue to propagate in the matrix.
(4) Cleavage-like crack propagation can occur when brass is briefly exposed to aqueous ammonia, then quenched to 77°K and loaded in air, showing that crack propagation extends beyond the dealloyed layer.

Based on this evidence, we conclude that the film-induced cleavage mechanism is the only mechanism of those proposed so far that can explain all of the observations. The role that this mechanism may play in the cracking of other systems, in crack nucleation at inclusions, and in IGSCC remains to be determined by further research.

References

1. E.N. Pugh, J.V. Craig, A.J. Sedriks, Fundamental Aspects of Stress-Corrosion Cracking, ed. R.W. Staehle, A.J. Forty, D. Van Rooyen (Houston, TX: National Association of Corrosion Engineers, 1969), p. 118.
2. E.N. Pugh, The Theory of Stress Corrosion Cracking in Alloys, ed. J.C. Scully (Brussels, Belgium: NATO Scientific Affairs Division, 1971), p. 418.
3. E.N. Pugh, Stress Corrosion Research, ed. H. Arup, R.N. Parkins (Alphen aan den Rijn, The Netherlands: Sijthoff & Noordhoff, 1979), p. 177.
4. F.A. Champion, ed. (London: Institute of Metals, 1948), p. 468.
5. H.L. Logan, J. of Res. Natl. Bur. Stds. 48(1952): p. 99.
6. S. Pednekar, A.K. Agrawal, H.E. Chaung, R.W. Staehle, J. Electrochem. Soc. 126(1979): p. 701.
7. Y. Suzuki, Y. Hisamatsu, Corros. Sci. 21(1981): p. 353.
8. T.B. Cassagne (Ph.D. diss., The Johns Hopkins University, 1988).
9. T.B. Cassagne, J. Kruger, E.N. Pugh, ASTM STP 1049, 1989, in press.
10. U. Bertocci, F.I. Thomas, E.N. Pugh, Corrosion 40(1984): p. 439.
11. R.C. Newman, T. Shahrabi, K. Sieradzki, Scripta Metall. 23(1989): p. 71.
12. K. Sieradzki, R.C. Newman, Phil. Mag. A 51(1985): p. 95.
13. B.F. Brown, Stress Corrosion Cracking Control Measures, 2nd ed. (Houston, TX: NACE, 1981).
14. E. Mattsson, Electrochim. Acta 3(1961): p. 279.
15. E.N. Pugh, A.R.C. Westwood, Phil. Mag. 13(1966): p 167.
16. E N. Pugh, Environment-Sensitive Mechanical Behavior, ed. A.R.C. Westwood, N.S. Stoloff (New York: Gordon & Breach, 1966), p. 351.
17. U. Bertocci, E.N. Pugh, Proceedings of the 9th International Conference on Metallic Corrosion (Ottawa, Toronto: National Research Council, 1984), p. 144.
18. U. Bertocci, D.D. Wagman, Standard Potentials in Aqueous Solutions, ed. A. Bard, R. Parsons, J. Jordan (New York: M. Dekker, 1985), p. 287.
19. G.W. Tindall, S. Bruckenstein, Anal. Chem. 40(1968): p. 1402.
20. U. Bertocci, Electrochim. Metall. 3(1968): p. 275.
21. B.-C. Cheng, (Ph.D. diss., University of Illinois at Urbana-Champaign, 1975).
22. J.E.B. Randles, K.W. Somerton, Trans. Faraday Soc. 48(1952): p. 951.
23. E. Mattsson, J.O. Bockris, Trans. Faraday Soc. 55(1959): p. 1586.
24. E.N. Pugh, W.G. Montague, A.R.C. Westwood, Trans. ASM 58(1965): p. 665.
25. H. Gerischer, Z. Physik. Chem. 202(1953): p. 302.
26. H. Matsuda, Y. Ayabe, Z. Elektrochem. 63(1959): p. 1164.
27. L.H. Jenkins, R.B. Durham, J. Electrochem. Soc. 117(1970): p. 768.
28. J.A.S. Green, H.D. Mengelberg, H.T. Yolken, J. Electrochem. Soc. 117(1970): p. 433.
29. H. Gabel, J.A. Beavers, J.B. Woodhouse, E.N. Pugh, Corrosion 32(1976): p. 253.
30. A.J. McEvily, A.P. Bond, J. Electrochem. Soc. 112(1965): p. 131.
31. T.R. Pinchback, S.P. Clough, L.A. Heldt, Metall. Trans. A 6A(1975): p. 1479.
32. H.H. Uhlig, K. Gupta, W. Liang, J. Electrochem. Soc. 122(1975): p. 343.
33. E.N. Pugh, J.A.S. Green, Metall. Trans. 2(1971): p. 3129.
34. H.S. Tong (Ph.D. diss., University of Illinois at Urbana-Champaign, 1977).
35. B.C. Syrett, R.N. Parkins, Corros. Sci. 10(1970). p. 197.
36. M. Kermani, J.C. Scully, Corros. Sci. 18(1978). p. 883.
37. J.A. Beavers, E.N. Pugh, Metall. Trans. A 11A(1980). p. 809.
38. D. Tromans, J. Nutting, Corrosion 21(1965). p. 143.

39. L.P. Lee, D. Tromans, Environment-Sensitive Fracture of Engineering Materials, ed. Z.A. Foroulis (Warrendale, PA: The Metallurgical Society-American Institute of Mining, Metallurgical, and Petroleum Engineers, 1979), p. 232.
40. P.W. Slattery, J. Smit, E.N. Pugh, Environmental Sensitive Fracture: Evaluation and Comparison of Test Methods, STP-821, ed. S.W. Dean, E.N. Pugh, G.M. Ugiansky (Philadelphia, PA: ASTM, 1984), p. 399.
41. K. Sieradzki, J.S. Kim, A.T. Cole, R.C. Newman, J. Electrochem. Soc. 134(1987): p. 1635.
42. C. Edeleanu, Physical Metallurgy of Stress Corrosion Fracture, ed. T.N. Rhodin (New York, NY: Interscience Publishers, 1959), p. 79.
43. C. Edeleanu, A.J. Forty, Phil. Mag. 46(1960): p. 1029.
44. D.V. Beggs, M.T. Hahn, E.N. Pugh, Hydrogen Embrittlement and Stress Corrosion Cracking, ed. R. Gibala, R.F. Hehemann (Metals Park, OH: ASM International, 1984), p. 181.
45. R.C. Newman, K. Sieradzki, Scripta Metall. 17(1983): p. 621.
46. E.N. Pugh, Corrosion 41(1985): p. 517.
47. E.N. Pugh, Atomistics of Fracture, ed. R.M. Latanision, J.R. Pickens (New York, NY: Plenum Press, 1983), p. 997.
48. J.L. Nelson, J.A. Beavers, Metall. Trans. A 10A(1979): p. 658.
49. M.J. Kaufman, J.L. Fink, Metall. Trans. A 18A(1987): p. 1539.
50. M.J. Kaufman, J.L. Fink, Acta Metall. 36(1988): p. 2213.
51. T. Shahrabi (Ph.D. diss., University of Manchester, 1989).
52. R. Bakish, W.D. Robertson, Acta Metall. 3(1955): p. 513.
53. R. Bakish, W.D. Robertson, Acta Metall. 4(1956): p. 342.
54. R. Bakish, W.D. Robertson, Trans. AIME 206(1956): p. 1277.
55. R. Bakish, Trans. AIME 209(1957): p. 494.
56. T.B. Cassagne, W.F. Flanagan, B.D. Lichter, Metall. Trans A 17A(1986): p. 703.
57. T.B. Cassagne, W.F. Flanagan, B.D. Lichter, Chemistry and Physics of Fracture, ed. R.M. Latanision, R.H. Jones (Dordrecht, The Netherlands. Martinus Nijhoff Publishers. 1987), p. 659.
58. T.B. Cassagne, W.F. Flanagan, B.D. Lichter, Metall Trans. A 19A(1988): p. 281.
59. B.D. Lichter, T.B. Cassagne, W.F. Flanagan, E N Pugh, Micro Sci. 13(1985): p. 361.
60. J.D. Fritz, B.W. Parks, H.W Pickering, Scripta Metall 22(1988): p. 1063.
61. E. Escalante, J. Kruger, J. Electrochem. Soc 118(1971): p 1062.
62. U. Bertocci, J. Electrochem. Soc. 136(1989): p 1887
63. U. Bertocci, Embrittlement by the Localized Crack Environment, ed. R.P. Gangloff (Warrendale, PA: TMS-AIME, 1984), p. 49.
64. U. Bertocci, E.N. Pugh, Corrosion Chemistry Within Pits, Crevices and Cracks, ed. A. Turnbull (London, England: Her Majesty's Stationery Office, 1984), p. 187.
65. U. Bertocci, E.N. Pugh, Proceedings of the 10th International Congress on Metallic Corrosion, ed. K.I. Vasu V (New Delhi, India: Oxford & IBH Publishing Co., 1989), p. 213.
66. F.G. Will, C.A. Knorr, Z. Elektrochem. 64(1960): p. 271.
67. H.J. Engell, The Theory of Stress Corrosion Cracking in Alloys, p. 86.
68. R.W. Staehle, The Theory of Stress Corrosion Cracking in Alloys, p. 223.
69. D.A. Vermilyea, Stress Corrosion Cracking and Hydrogen Embrittlement of Iron Base Alloys, ed. J Hochmann, J E Slater, R.D. McCright, R.W. Staehle (Houston, TX: NACE, 1977), p. 208.
70. C.A. Loto, R.A. Cottis, Corrosion 43(1987): p. 499
71. A.J. Bursle, E.N. Pugh, Mechanisms of Environment Sensitive Cracking of Materials, ed. Z.A. Foroulis (Warrendale, PA. TMS-AIME, 1977), p. 18.
72. K. Sieradzki, R.R. Corderman, K. Shukla, R.C. Newman, Phil. Mag. A, 59(1989): p. 713.
73. M.B. Hintz, Scripta Metall. 19(1985): p. 1445.
74. M.B. Hintz, W.K. Blanchard, P.K. Brindley, L.A. Heldt, Metall. Trans. A 17A(1986): p. 1081.
75. S. Nakahara, Y. Okinaka, J. Electrochem. Soc. 136(1989). p. 1892.
76. A.J. Forty, Physical Metallurgy of Stress Corrosion Fracture, ed. T.N. Rhodin (New York, NY. Interscience Publishers, 1959), p. 99.
77. T.K.G. Namboodhiri, R.S. Tripathi, Corros. Sci. 26(1986): p. 745.
78. A. Paskin, D.K. Som, G.J. Dienes, Acta Metall. 31(1983): p. 1841.
79. A. Paskin, K. Sieradzki, D.K. Som, G.J. Dienes, Acta Metall. 30(1982): p. 1781.
80. A. Paskin, K. Sieradzki, D.K. Som, G.J. Dienes, Acta Metall. 31(1983): p. 1253.
81. G.J. Dienes, K. Sieradzki, A. Paskin, B. Massoumzadeh, Surf. Sci. 144(1984): p. 273.
82. K. Sieradzki, Acta Metall. 30(1982): p. 973.
83. R. Kelly, Private Communication (University of Manchester, Manchester, England, August 1989).
84. I.-H. Lin, R.M. Thomson, J. Mater. Res. 1(1986): p. 73.
85. N.F. Mott, Engineering 165(1948): p. 16.

Discussion

H.-J. Engell (Max Planck Institut fur Eisenforschung, Federal Republic of Germany): If there is some serrated yielding (Portevin-Le Chatelier Effect), the discontinuous yielding may contribute to the observed arrest of the cleavage cracks, through discontinuous blunting of the crack tip. What is your view?

E.N. Pugh: The idea that unpinning of dislocations ahead of the advancing crack could lead to blunting is reasonable. However, I am unaware of any evidence for serrated yielding in copper-zinc alloys, nor would I expect dynamic solute-dislocation interactions at ambient temperatures. Also, the occurrence of similar transgranular cracking in pure copper (i.e., discontinuous failure on {110} planes) would seem to preclude a major role for solute atoms in the cleavage process. As we have pointed out in the paper, the restraining effect of unfractured ligaments trailing behind the crack front seems a more likely cause of crack arrest.

B.D. Lichter (Vanderbilt University, USA): Regarding the existence of serrated yielding in systems undergoing transgranular SCC, this does occur in copper-gold alloys, and in certain instances in our laboratory we have seen that pre-existing slip bands serve as crack arresters. The orientation of the arresting slip band clearly indicates that the band formed prior to crack arrest and not as an adjunct to crack blunting.

E.N. Pugh: Presumably the occurrence of serrated yielding in copper-gold is related to short-range order effects and, as you know, the notion that the absence of short-range order at pre-existing slip bands promotes crack arrest was proposed for brass by Forty in his classic paper in *Physical Metallurgy of Stress Corrosion Fracture* (Interscience, 1959), p. 99. However, the evidence for crack arrest at such slip bands in both Forty's and your cases is based upon crack trace studies on single surfaces. In three dimensions, the crack front would have to lie in a <110> direction, that is, at the intersection of a {110} fracture plane with a {111} slip plane, for this proposal to be credible, and this is contrary to observation.

H.-J. Engell: Could you please address the question of whether or not, and how, short-range/long-range order affects the SCC mechanism in copper alloys? In the case of an ordered atom

distribution, dislocation movement may cause antiphase boundaries, which in turn can interfere with the glide process and cause discontinuous cleavage.

E.N. Pugh: As I indicated earlier, the failure of pure copper would seem to rule out the possibility that solute atoms, and hence ordering phenomena, play a necessary role in the inherent embrittlement process at the crack tip. However, in our paper it is argued that factors such as ordering and stacking fault energy, which promote coplanar glide, have a major effect on shearing of ligaments and on the ease of cleavage step formation, and therefore on crack propagation. Moreover, we speculate that this effect accounts for the correlation between restricted cross slip and susceptibility to transgranular SCC under static loading conditions.

B. Cox (Atomic Energy of Canada Limited, Canada): In the cracking of alpha-brass, if you can control the size of the crack-front jump distance by adjusting experimental conditions, and if there is always significant strain during the stationary phase of the crack front, then, if ligament tearing is controlling crack arrest, the strain accumulated during crack arrest should be proportional to the size of the jump (i.e., length of ligament). An accurate measure of this strain, using, for example, photoresist and a video camera, could provide useful evidence. Has anyone measured these crack-tip strains and strain rates and, if so, are they constant or proportional to jump distance, and how does the strain rate compare with identically loaded precracked specimens in air?

E.N. Pugh: You have put your finger on the major assumption in our hypothesis, that step formation by ligament tearing is unable to keep up with cleavage, so that the ligaments lengthen and increase the restraining force at the crack tip, and that the bulk of step formation occurs during the arrest stage. Experiments of the type you describe have not been performed in brass or in other cases of transgranular SCC but are essential to evaluate the hypothesis.

J. Kolts (Conoco, Inc., USA): In view of the fact that radiation can cause cleavage in face-centered cubic (fcc) metals, and since dissolution in specific environments can cause creep in alloys, have you considered the defect structure in front of the crack tip as being the cause of cracking? Also, can results from slow-strain rate and dealloying experiments be considered consistent with defect structure at the crack tip?

E.N. Pugh: In the early 1980s, I actively pursued the idea that the defect structure induced by the environment could initiate brittle cracks, specifically that vacancy injection caused by selective dissolution of zinc might cause hardening by interacting with dislocations. This view, first proposed by Forty in 1959 (see reference in my previous response, above), was encouraged by various observations of hardening of brass due to vacancy annihilation, for example, anneal hardening, but my attempts to embrittle foils by producing large vacancy concentrations by quenching or deformation, and straining at various temperatures and strain rates, were unsuccessful. The observation of cracking in pure copper caused me to abandon this approach.

Interestingly, recent results at our laboratory (see T.B Cassagne, Ph.D. diss., Johns Hopkins University, 1988) suggest that a micropitting process at the crack tip is necessary for cracking in pure copper. This may produce a structure similar to that of the porous dealloyed layer thought by Sieradzki and others at this conference to be responsible for crack initiation during transgranular SCC of copper alloys.

R.H. Jones (Pacific Northwest Laboratories, USA): I would like to make the observation that the porous structure produced by dealloying is similar to that found in irradiated materials. In copper and nickel at room temperature, radiation damage produces hardening by clusters of interstitials and vacancies.

A. Gelpi (Framatome, France): Is there any experimental evidence for the pores in front of the crack tip or in the dealloyed layer?

E.N. Pugh. I am not aware of any experimental evidence for the existence of the porous structure in front of crack tips or even on crack walls, but there are a number of papers that present transmission electron micrographs showing the characteristic sponge structure in specimens dealloyed in the absence of stress. An early paper by Pickering and Swann [Corrosion 19(1963), p. 373] illustrates the porous layer in several alpha-phase copper alloys and associates its occurrence with susceptibility to cracking.

M.M. Hall (Westinghouse Electric Corporation, USA): You discussed the difficulty in understanding how crack arrest may occur for transgranular SCC based on the assumption that crack advance occurs due to extension of the microcrack into the matrix by cleavage fracture initiated in a thin oxidized or dealloyed crack-tip layer. An alternative crack advance mechanism that does not require "crack arrest" is that crack advance occurs by, first, the nucleation of a cleavage crack at a distance *ahead* of the microcrack tip and, second, the extension of this microcrack *back* to the microcrack tip by fracture of the intervening ligament. Dislocation glide and blockage within the ligament could account for the cleavage crack nucleation, perhaps on hydrogen-embrittled cleavage planes, and would then accommodate microcrack opening and extension to the point of ligament rupture. Are not your experimental observations consistent with this alternative crack advance mechanism?

E.N. Pugh: The possibility that a subsurface crack is initiated ahead of the main crack and runs back to the tip has been suggested from time to time for copper alloys and other systems. However, existing experimental evidence does not permit this possibility to be distinguished from the more conventional view that the crack is reinitiated at the surface. Other details of the crack advance process remain unclear. For example, we assume that each propagating event is initiated at a point and that fracture then spreads laterally along the crack front. There is no direct experimental evidence for this view.

I should also comment on your suggestion that hydrogen embrittlement may play a role. In our paper, we conclude that hydrogen effects can be ruled out in alpha-phase copper alloys.

L.A. Heldt (Michigan Technological University, USA): There is increasing evidence [Kramer, Wu, and Feng, Mater. Sci. Eng. 82(1986): p. 141; Kaufman and Fink, Acta Metall. 36(1988), p. 2213, Kasul, White, and Heldt, "Relationships Between Plasticity and Stress Corrosion Cracking," this proceedings] that environment-induced local plastic flow is associated with, and may contribute to, stress corrosion of copper materials. Apparent cleavage may result in transgranular SCC from microscopic flow. The concept is promising for explaining (1) susceptibility of copper as well as alloys and (2) crystallography of observed fracture planes.

The nature of the environmental interaction is not known. Papers by Lynch [J. Mater. Sci. 20(1985), p. 3329, Scripta Metall. 18(1984): p. 321] and by Hintz, et al. [Metall. Trans. 17A(1986), p. 1081], have invoked adsorption, Kaufmann and Fink [Acta Metall. 36(1988), p. 2213] envision a dissolution–deformation synergism that is extremely localized. For the adsorption case, there are similarities to processes described for hydrogen embrittlement and metal-induced embrittlement, as discussed separately by Birnbaum, Gerberich, and Stoloff at this conference. For the dissolution case, a similar synergism has been described by Duquette for corrosion fatigue. A similar process may well contribute to intergranular SCC in the copper materials.

E.N. Pugh: The view that the propagation of transgranular stress corrosion cracks occurs by highly localized environmentally enhanced plastic flow rather than by discontinuous cleavage is legitimate and, as we state in the paper, merits further attention.

I agree that it offers an attractive and straightforward explanation for the observed orientation of the fracture surfaces in alpha phase copper alloys. Thus, it is plausible that coordinated slip on intersecting $\{111\}$ planes could result in macroscopic fracture on a bisecting $\{110\}$ plane, ligament shearing would then occur on the two $\{111\}$ planes that are perpendicular to the fracture plane and therefore in planes of maximum shear, as proposed in the paper. However, the case of type 310 (UNS S31000) stainless steel, also single-phase fcc, is not as straightforward, since failure occurs on $\{100\}$ rather than $\{110\}$. The $\{100\}$ plane also bisects intersecting slip planes, but in this case ligament shearing would occur on slip planes that are not perpendicular (actually approximately 55°) to the fracture plane. It is not clear why the two fcc alloys should behave differently

or why the steel should choose a less efficient option for ligament tearing.

It should also be noted that these crystallographic observations cannot be rationalized in terms of the cleavage model at the present time.

N.S. Stoloff (Rensselaer Polytechnic Institute, USA): The copper-bismuth experiment of Rice you described seems to be unconvincing support for a film-induced cleavage model. There are many instances in the literature of solid metal embrittlement of cracks extending well beyond initiating inclusions, often along transgranular paths. In the absence of detailed surface analytical experiments on the copper-bismuth fracture facets, you cannot rule out a simple metal-induced fracture model to explain the transgranular facets.

E.N. Pugh: I agree that the observation is not conclusive without surface analysis.

N.S. Stoloff: Cracking of pure copper in nitrite solutions seems to resemble metal-induced embrittlement as far as a transgranular cleavage-like crack path is concerned. Has high-magnification scanning electron microscopy been used to examine copper fracture surfaces, to determine whether localized plasticity is responsible for cracking?

E.N. Pugh: The nitrite solution causes considerable corrosive attack of the fracture surfaces, so that detailed fractographic studies are impossible. However, the failure in copper is similar in many respects to that of the alpha-brasses, and in that case there have been several high-resolution studies of the fracture surfaces. In particular, Lynch [Scripta Metall. 18(1984). p. 321] has used the replica technique with transmission electron microscopy to study cleavage-like fracture surfaces in Cu-30Zn produced at our laboratory in ammoniacal solutions under conditions in which corrosive attack is minimized. Fine markings were reported (not detectable with scanning electron microscopy), and these were claimed to be evidence for a propagation mechanism involving localized plasticity. However, I believe that further study is necessary to establish that the markings are slip traces rather than crack-arrest markings, and that they are not simply slip steps produced behind the crack front. More recently, Dixon, in unpublished work at Ecole Polytechnic, Montreal, Canada, 1988, has produced similar evidence in austenitic stainless steels tested in chloride solutions. As I indicated before in my response to Heidt, I agree that this possibility merits attention.

W.W. Gerberich (University of Minnesota, USA): This follows up on the comments of Stoloff, Heidt, Lichter, and Engell, concerning localized slip. If {111} slip along facets can shield with additional slip in the wake uncoupling the shield to produce high local stresses, this might be an alternative cleavage mechanism. Serrated yielding might enhance such a process, so this question addresses this aspect. Hydrogen is known to produce serrated yielding in nickel at low temperatures. Has anyone evaluated the stress–strain characteristics of copper-zinc during *in situ* electrochemical charging where large hydrogen fugacities are involved?

E.N. Pugh: I am not aware of such experiments in copper-zinc. Several workers, including Forty, Parkins [reported at an unpublished workshop on SCC of copper alloys, National Institute of Standards and Technology (formerly National Bureau of Standards), Washington, 1983] and myself, have attempted to produce transgranular cracking in Cu-30Zn by conducting slow-strain-rate tests while hydrogen was cathodically generated at the surface. These attempts were unsuccessful, so that the experiments were never reported. I do not know if the load–time curves showed evidence of discontinuous yielding. I should add that the occurrence of transgranular SCC in copper-gold alloys eliminates the possibility of a unique role for hydrogen, since hydrogen generation can be unequivocally ruled out in this case.

A. Atrens (University of Queensland, Australia): What environmental parameters govern SCC of copper and 70/30 brasses in other aqueous systems? Recent work has shown the possibility of cracking in sodium chloride, but there is a lot of confusion concerning the necessity of Cu^{+}, Cu^{++}, E, pH, Cu_2O, CuO. Is it possible to sort out these SCC-producing environmental conditions—perhaps in terms of E–pH diagrams? Can you specify what surface conditions are needed for SCC and then from these surface conditions predict environmental requirements?

E.N. Pugh: The situation is complicated by the fact that two forms of cracking occur—intergranular and transgranular—and that, in my opinion, they involve basically different mechanisms. In the intergranular case in brass, it seems likely that crack propagation occurs by the film-rupture mechanism, that is, by preferential anodic dissolution at the crack tip where a passive film is continually ruptured by localized slip. Several environments cause this type of failure in the laboratory, e.g., citrates, tartrates, acetates, and sulfur dioxide, in addition to ammonia. The governing parameters here are repassivation kinetics and anodic dissolution rates, so that thermodynamic data alone (E–pH diagrams) are not definitive. The use of potentiodynamic techniques of the type pioneered by Parkins [Corros. Sci. 20(1980): p. 147] offers the most promise for prediction at present.

In the case of transgranular cracking of brass, the mechanism of propagation is not established, but it seems that dezincification plays a key role. Clearly, the simple occurrence of dealloying is not a sufficient condition for cracking, since transgranular failure is not commonly observed in aqueous chlorides despite rapid selective dissolution. It appears that the rate of dealloying is critical, perhaps through its influence on the scale of the porous structure, so here again it is difficult to identify environmental parameters that have straightforward predictive value.

Of course, potential has a profound effect on both processes, and this is significantly affected by many extrinsic factors.

J.R. Galvele (Comision Nacional de Energia Atomica, Argentina): In a recent publication [Rebak, Carranza, and Galvele, Corros. Sci. 28(1988): p. 1089], we have shown that passivity breakdown is present in SCC of brass in sodium nitrite solutions. Cracking was only found at potentials above the pitting potential. Since the same happened in pure copper, I find it difficult to accept that two different mechanisms have to be applied for transgranular cracking—one for brass and another for pure copper.

E.N. Pugh: In our paper, we speculate that the basic mechanism for transgranular SCC is the same in both cases, namely, that it involves the formation of a zone containing pores or tunnels. In the case of copper, this obviously cannot result from dealloying, and it is suggested that micropitting may be responsible.

J.-P. Lynn (Westinghouse Electric Corporation, USA): The width of the crack at the crack tip must be on the order of the film thickness. As film grows, both internal (between film and matrix) and external stresses increase. Which force is the more likely to cause crack advance? Is there an optimum film thickness that cracks will not grow?

E.N. Pugh: In brass, two types of film are thought to be important; a passive film (oxide) and a dealloyed layer. Both are thin (approximately 1 nm) compared with the width of the crack at the tip (approximately 100 nm). Initially, the film-induced cleavage model proposed by Sieradzki and his colleagues [see, for example, Paskin, et al., Acta Metall. 31(1983): p. 1253] placed emphasis on the role of epitaxial stresses associated with both types of film, but, at this meeting, this view has been overshadowed by the idea that the porous layer is more likely to reinitiate cleavage.

J.-P. Lynn: If film is formed by the environment and is protective (at least thin film), why should the same environment cause pores to form?

E.N. Pugh: Depending on its composition, ammoniacal solutions can lead to film formation (tarnishing) in Cu-30Zn, or may cause active anodic dissolution in the absence of protective films. A quick answer to your question might be that passive film growth and dealloying (which leads to pore formation) are not considered to occur in the same environment, the latter taking place only in nontarnishing solutions. But this avoids an interesting issue. In tarnishing solutions, intergranular failure is widely believed to proceed by preferential anodic dissolution of bare metal at the crack tip, exposed by plastic deformation. However, it is legitimate to suggest alternatively that dealloying takes place during transient anodic dissolution and that crack advance is mechanical, as is believed to be the case for nontarnishing environments. There is no evidence for discontinuous propagation in intergranular SCC in tarnishing solutions, but this might be a result of small crack advance distance per event.

Environment-Induced Crack Growth Processes in Nickel-Base Alloys

*R.H. Jones and S.M. Bruemmer**

Abstract

Nickel-base alloys exhibit excellent corrosion resistance and are used extensively in corrosion applications, although environment-induced crack growth has occurred in several applications. Environment-induced crack growth in nickel-base alloys occurs in a number of environments, including water, acidic and basic solutions, and gaseous hydrogen. Factors controlling environment-induced crack growth are similar to those in other materials, namely, microstructure/microchemistry, environment, and stress. The critical factors controlling stress corrosion cracking of nickel-base alloys are generally known, but many of the details are not. In some cases, quantitative information is lacking with details limited to knowledge about general susceptibility. The crack growth mode is generally intergranular for aqueous environments and hydrogen-gas environments. A key difference between environment-induced crack growth in Fe-Cr-Ni alloys and nickel-base alloys is the susceptibility to cracking in hydrogen environments in nickel-base alloys, while Fe-Cr-Ni alloys exhibit cracking in hydrogen environments only under extreme conditions. This paper presents a comprehensive review of the literature on environment-induced crack growth of nickel-base alloys and covers both phenomenological observation and mechanistic interpretation.

Introduction

Ni-base alloys exhibit excellent corrosion resistance in a wide variety of environments This behavior, along with the high-temperature strength that can be developed in many Ni alloys, has prompted their extensive use in chemical, petrochemical, pulp and paper, food, and electric power industries. However, environment-induced cracking has been a continuing problem for certain material/environment conditions. It is important to keep in mind that even though cracking has been observed in service, Ni-base alloys have proven to be the most corrosion-resistant system for severe engineering applications.

Environment-induced cracking of Ni-base alloys in aqueous solutions will be reviewed, analyzed, and evaluated in this paper. Special interest will be given to the metallurgical variables that have been observed to influence susceptibility and on specific crack growth mechanisms. Stress corrosion cracking (SCC) and H-induced cracking (HIC) of solid-solution and precipitation-hardened Ni alloys will be examined to identify controlling parameters and crack growth processes. Transgranular and intergranular processes will be isolated and evaluated in relation to mechanistic models for environment-induced crack growth.

Environment-induced cracking of austenitic alloys has received considerable attention over the last 25 years and has been the subject of several reviews.[1-12] Most of these reviews have dealt primarily with austenitic stainless steels (SSs) and not directly with Ni-base alloys. The only Ni-base alloy that is often discussed is alloy 600 (UNS N06600), which exhibits many microstructural similarities to the unstabilized SSs. Other alloys ranging from simple binary systems (e.g., Monel† alloys) to complex systems (e.g., Hastelloy† alloys) have not been examined. Ni and a wide range of Ni-base alloys will be considered in order to develop a more comprehensive understanding of environment-induced cracking in this important alloy system.

FACTORS CONTROLLING ENVIRONMENT-INDUCED CRACK GROWTH

Environment-induced cracking can be defined similar to the classic definition of SCC Cracking occurs because of the combined presence of a susceptible material/microstructural condition, a sufficiently corrosive environment, and a sufficiently high stress. Each of these three components is required for cracking, and each will be described based on experimental observations in Ni-base alloys.

Metallurgical Aspects

Bulk effects

Ni is used for many corrosion-resistant applications without alloying Commercial-purity Ni has excellent resistance to attack in caustic environments. Numerous elements are added to Ni including C, Cr, Mo, Fe, Si, Cu, Al, Ti, Nb, and W. These elements can directly affect microstructural and microchemical development and impact material strength and deformation characteristics. Each of these metallurgical aspects can then affect cracking resistance, as will be discussed below A number of common Ni-base alloys are listed in Table 1 along with their nominal bulk compositions.

Bulk composition can have a controlling influence on environmental cracking. The effects of individual elements are a function of thermomechanical treatment and service environment. For example, the susceptibility of alloy 600 to intergranular (IG) SCC tends to increase with C content in oxidizing environments,[13-15] while the opposite behavior is found in deaerated, high-temperature water.[16-20] Thus, it is difficult to make generic conclusions concerning bulk effects without considering specific alloys, metallurgical conditions, and solution chemistries.

*Pacific Northwest Laboratory, Richland, WA 99352.
†Trade name.

TABLE 1

Nominal Compositions of Various Alloying Elements in Ni-Base Alloys, wt%

Alloy	C	Cr	Fe	Mo	Co	Cu	Al	Ti	Others
Ni 200	0.06	—	0.15	—	—	0.05	—	—	
Monel	0.15	—	1.5	—	—	30.0	—		—
Type 600[A]	0.08[C]	15.5	8.0	—	1.0[C]	0.5	—	—	
Type 625[A]	0.1[C]	21.5	5.0[C]	9.0	1.0[C]	—	0.4	0.4	Nb+Ta
Type 690[A]	0.08[C]	29	9.0	—	1.0[C]	0.5	—	—	
Type 718[A]	0.05	18	19.0	3.0	1.0[C]	0.1	0.5	0.9	Nb+Ta
Type X-750[A]	0.08[C]	15.5	7.0	—	1.0[C]	0.5	0.8	2.5	Nb+Ta
Type 825[A]	0.05[C]	21.5	29.0	3.0	2.0[C]	2.0	—	1.0	
Type C-276[B]	0.01[C]	16	5.5	16.0	2.0[C]	—	—	—	W

[A]Inconel alloy, INCO.
[B]Hastelloy alloy, Haynes International, Inc.
[C]Maximum concentration.

The addition of many minor alloying elements on IGSCC susceptibility has been examined for alloy X-750 (UNS N07750).[21,22] While there is some disagreement concerning the effects of Zr and B, other elements such as Cr, Mg, Cu, La, N, O, S, and P were found to have no significant influence on cracking. Floreen and Nelson reported beneficial effects of Zr and B additions,[21] while Hattori indicated B to be detrimental and Zr to have no effect on IGSCC.[22] Si was identified as being particularly detrimental to cracking resistance.[22] Again, it is important to keep in mind the complex interrelationship among composition, metallurgical condition, and solution chemistry on IGSCC susceptibility. Alloying and impurity elements tend to modify specific aspects of the material microstructure and microchemistry, which in turn impact SCC. Individual effects of certain elements will be explained during discussions of microstructure and microchemistry in Ni-base alloys.

Strength level can have a significant effect on cracking, particularly HIC. If all other parameters are kept constant, increasing material strength will increase HIC susceptibility. Cold work has been shown to accelerate cracking in many materials, including alloys 600,[23,24] X-750, 718 (UNS N07718),[25] 625 (UNS N06625), C-4 (UNS N06455), and C-276 (UNS N10276).[26] Precipitation-hardened alloys tend to exhibit an increased cracking susceptibility over solid-solution alloys of the same basic type. A good example of this is the comparison of alloys 600 and X-750, in which the higher-strength X-750 is much more prone to cracking in H and high-temperature deoxygenated water environments. However, higher strength need not involve increased HIC. Alloy 718 has shown excellent HIC and SCC resistance in several solutions, despite its high strength.[10,24,26,27]

Deformation characteristics have an important effect on SCC and HIC susceptibility. In particular, slip planarity can influence cracking susceptibility and fracture morphology. Planar slip leads to dislocation pile-ups and high local stresses. Crack nucleation at external and internal interfaces may be enhanced,[28] as well as H transport along planar arrays.[29] An example of these planar dislocation arrays (pile-ups) for alloy 600 is shown in Figure 1. Materials with relatively low stacking fault energies (SFEs) exhibit this behavior at small plastic strains because of higher stress requirements for cross slip to occur.

Short-range ordering (SRO) and long-range ordering (LRO) can also promote planar slip and increase susceptibility to HIC. While other factors influence HIC resistance, SRO and LRO appear to have an important effect on the cracking of alloy C-276.[30-36] Asphahani suggested that ordering prompted HIC through its effect on slip characteristics.[30] Dislocation substructures with planar arrays develop since dislocations move as coplanar groups and large stresses are needed for cross slip. As a result, ordering causes slip characteristics similar to low SFE metals even though the apparent SFE increases.[32]

Ordering also increases material strength level, which corresponds to the onset of HIC susceptibility. Results of Fiore and Kargol presented in Figure 2 illustrate this dependence as a function of aging time (i.e., degree of order) at 500°C.[32] The initial increase in hardness and decrease in time-to-failure is related to SRO, while the change after long-time aging is a result of LRO. It is not known at this time whether SRO or LRO is a sufficient condition to promote cracking or if P segregation is also required, as suggested by Berkowitz and Kane.[35] In the presence of cathodic H, Asphahani observed transgranular cracking in highly deformed and aged C-276,[30] so P segregation may not be a factor in heavily cold-worked material. P may have a complex effect on cracking since it also increases the rate of SRO.[32] In a more general sense, P[37,38] and N[38,80] have been shown to have the largest effect on slip planarity of all solutes in austenitic alloys. This is believed to result from SRO effects and not from changes in SFE.[7,38] Regardless, both elements are thought to increase environmental cracking susceptibility because of their influence on deformation characteristics.[8]



FIGURE 1—Transmission electron micrograph showing dislocation emission from grain-boundary carbides.

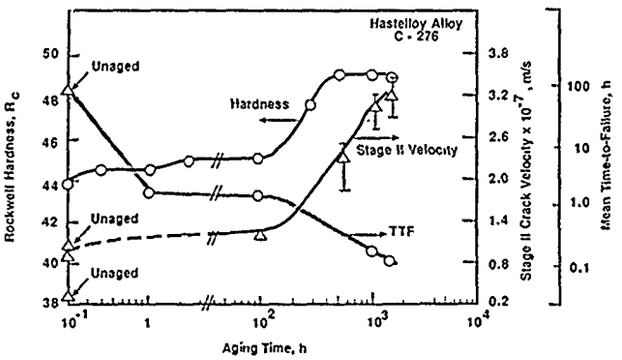


FIGURE 2—Comparison between hardness, Stage II crack velocity, and time-to-failure for Hastelloy alloy C-276 (UNS N10276).[32]

Microstructural effects

Environment-induced failure of Ni-base alloys is very sensitive to heat treatment. The most effective heat treatment often depends on the service environment (e.g., resistance to cracking can be markedly different in oxidizing vs nonoxidizing and low pH vs high pH solutions). Heat treatment impacts SCC and HIC through its effect on material microstructure and microchemistry. For many alloys, grain-boundary microcharacteristics control material behavior. Microstructure and microchemistry effects on environmental cracking are isolated (where possible) in this and the following section.

Carbide precipitation. C and Cr are primary alloying elements in many of the Ni alloys, particularly in Inconels,† as indicated in Table 1 This promotes the formation of Cr-rich carbides, typically M_7C_3 in alloy 600 and $M_{23}C_6$ in the more complex alloys. In addition, Ti carbides/carbonitrides and refractory-metal carbides are present in some of the precipitation-hardened alloys. Distribution and morphology of Cr-rich carbides in alloys 600 and X-750 have been shown to influence directly IGSCC resistance in high-temperature caustic and deaerated water environments.[3,16-20,40-50] Because these alloys are of critical interest in nuclear power plants and have been more extensively studied than other Ni alloys, carbide precipitation effects in alloys 600 and X-750 will be described in some detail.

Cr-carbide precipitation occurs readily because of the extremely low C solubility in most Ni-base alloys.[51] Mill-anneal temperatures below about 1000°C will not solutionize pre-existing carbides and result in predominantly intragranular carbides in the final structure. This combination of intragranular with no intergranular carbides appears to be very susceptible to SCC in high-temperature caustic or deaerated water. As mill-anneal temperatures are increased above 1000°C, carbides are dissolved so that C is available for intergranular precipitation during cooling or subsequent thermal treatment. If a large fraction of the bulk C is tied up in intragranular carbides, few intergranular carbides will form during cooling or thermal treatment.

The ability to produce a controlled carbide distribution is critical, since intergranular carbides tend to increase SCC resistance. Semicontinuous or continuous distributions have been shown to improve behavior in caustics and in deaerated water. Most evaluations have used U-bend specimens and have assessed susceptibility based on time-to-failure. As a result, crack growth data are very limited, and it is not known to what extent carbides influence crack initiation vs crack growth. Recent results suggest a relatively small effect on subcritical growth rates, while the larger effect of intergranular carbides appears to be on crack nucleation (or growth of very small cracks).[46,47] Unfortunately, a clear description of carbide effects on mechanistic aspects of environment-induced cracking of alloys 600 and X-750 in high-temperature deaerated water or caustics has not been established.

The presence of intergranular carbides does not indicate a more SCC resistant microstructure if alloy 600 or X-750 is tested in more oxidizing environments or in lower-temperature H environments. On the contrary, microstructures with a high density of intergranular carbides can be extremely susceptible to IGSCC. Carbide density effects on environment-induced cracking are illustrated by the results of Miglin and Domian in Figure 3.[49] The extent of cracking for alloy X-750 drops to low levels as intergranular carbide density increases in deaerated water tests, while the reverse is observed for tests in a H environment at lower temperatures. Cracking in H does not result solely from the presence of grain-boundary carbides. Cr depletion that develops adjacent to the growing carbides controls susceptibility in high-temperature oxidizing solutions[13-14,52] or in acidic sulfate environments.[53-55] Grain-boundary impurity segregation also promotes cracking, particularly in low-temperature H environments.[49,56-58] Cr depletion and segregation effects on environmental cracking will be discussed in a following section.

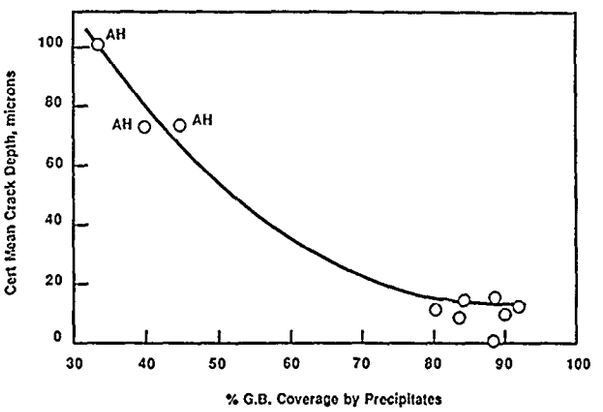


FIGURE 3—Average crack depth vs grain-boundary carbide coverage for alloy X-750 (UNS N07750).[49]

Intermetallic phases. A large number of intermetallic phases can form during aging of precipitation-hardening alloys (e.g., alloys X-750 and 718) including γ', $Ni_3(Al, Ti)$, γ'', $Ni_3(Al, Nb)$, η, Ni_3Ti, Δ, Ni_3Nb, and Laves (Fe_2Ti) phases. While many of these phases have an indirect impact on environment-induced cracking (by matrix strengthening), only γ' has been directly linked to the cracking process Hosoya and coworkers have suggested that preferential dissolution of γ' at grain boundaries of alloy X-750 generates H locally and prompts HIC in high-temperature deaerated water.[50] This proposal is based on electrochemical polarization work on single-phase compounds simulating intermetallics of interest. While γ may play a role in the mechanism of crack growth when present, the presence or absence of intergranular carbides remains the dominant microstructural feature influencing behavior in alloy X-750.

Intermetallic precipitates can also have an important effect on bulk deformation behavior. For example, exchanging γ (alloy X-750) for γ'' (alloy 718) as the matrix-strengthening phase sharply modifies resultant deformation structures. The γ' matrix phase in alloy X-750 promotes coplanar dislocation structures[61] and localized deformation behavior On the other hand, alloy 718 with γ'' as the matrix-strengthening phase exhibits a much more homogeneous dislocation structure [10] This difference in deformation characteristics may be a key aspect in the improved IGSCC resistance observed for alloy 718 vs X-750.

Dislocation density. Cold work has been noted to increase cracking susceptibility for many Ni-base alloys. Any prior working will lead to an increased dislocation density and residual stress in the material, and it will promote an overall increase in strength level. If the increased dislocation density is present before final aging treatments, elemental diffusivities and precipitation nucleation sites can be significantly modified For example, Hosoi, et al.,[43] reported a change from globular $M_{23}C_6$ carbides to cellular morphologies, and then to a fine scattered shape after final aging if cold work were present prior to heat treatment The fine distribution was the most resistant to cracking in high-temperature deaerated water.

Radiation damage. Core components in both boiling water reactors (BWR) and pressurized water reactors (PWR) have experienced IGSCC after a specific irradiation exposure. This cracking,

†Trade name.

termed irradiation-assisted stress corrosion cracking (IASCC), has been observed in austenitic SSs and Ni-base alloys.[10,60-63] The IASCC process is extremely complex, with radiation influencing material microstructure, microchemistry, and deformation behavior, and solution chemistry and electrochemistry.

From a microstructural point of view, radiation damage of austenitic SSs and Ni-base alloys at 300°C produces a large number of matrix defects including vacancies, interstitials, and clusters. Increases in cluster density with irradiation exposure produces a significant increase in material strength and a decrease in ductility. Local chemistry changes and second-phase precipitation or phase transformations can also be induced by radiation. The presence of a high density of clusters can lead to planar deformation behavior.[64,65] Dislocation activity becomes localized in narrow slip bands, which can promote large stress concentrations where these bands impinge on grain boundaries. Intergranular fracture has been observed in air for alloy X-750 after sufficient radiation damage, apparently because of this localized deformation behavior.[65]

While the majority of the data on IASCC has been obtained for austenitic SSs, observations of IASCC in Ni-base alloys have been made. Garzarolli, et al.,[66] reported on stress corrosion experiments with alloys 625, X-750, and 718 in the core of a BWR and PWR reactor. The samples were irradiated as cladding with mixtures of Al_2O_3 + B_4C pellets to induce various strain rates while being irradiated in the core and in contact with the reactor coolant. Two impurity concentrations of alloy 625 and variable heat treatments on a single heat of alloy X-750, given three different heat treatments, failed in both the BWR and PWR environments with strains of 1% or less. Alloy 718, heat treated at 954°C/1 h + 718°C/8 h + 621°C/8 h, has not exhibited IASCC up to strains of 1.5% in a BWR environment or 1.0% in a PWR environment; the same alloy heat treated at 1065°C/0.5 h + 760°C/10 h + 649°C/20 h exhibited IASCC at a strain of 0.5% in a PWR environment. An intergranular fracture mode was observed in all materials.

Microchemical effects

Environment-induced cracking of Ni-base alloys tends to be intergranular for many alloys and environments. This fact specifies a strong interest in grain-boundary characteristics for these alloys. Precipitation characteristics at grain interfaces were shown to be important in assessing cracking resistance in the previous section; in this section, grain-boundary microchemistry effects will be reviewed. Equilibrium and nonequilibrium processes can lead to critical enrichments of impurity elements or depletions in alloying elements that directly modify cracking resistance.

Impurity segregation. Ni and Ni-base alloys are very susceptible to intergranular embrittlement because of the grain-boundary segregation of certain trace impurities.[67-70] S has received the most attention, but other impurities such as Se, Te, Bi, and Pb have been shown to segregate and embrittle Ni-base alloys.[70] It is expected that this tendency for segregation-induced mechanical embrittlement indicates that these elements would also have a strong effect on environmental cracking and HIC in particular. Fortunately, these elements are carefully controlled in most Ni-base alloys, resulting in a bulk concentration low enough to minimize grain-boundary segregation.

S segregation has been shown to promote IG corrosion[71-74] and HIC[74-79] in Ni, but not SCC.[74,80,81] Bruemmer, et al., have documented direct correlations between the amount of S segregated to grain boundaries and susceptibility to IG corrosion[73] and HIC[76] in a low-temperature acidic solution (Figure 4). A transition in behavior is observed for both cases when grain-boundary S coverages increase from about 5% to 10% of a monolayer. This "critical" coverage to induce environmental degradation depends on electrochemical potential, as demonstrated by Jones, et al., for HIC at various cathodic test potentials.[79]

S has a very low solubility in Ni (100 appm at 973°K) and segregates to very high enrichment ratios at grain boundaries (10^5 times). As a result, an alloy with 1 ppm in the bulk can still reach levels of 10% at the boundary. The most effective method of limiting S segregation in Ni has been through additions of Mg or other strong sulfide-forming elements. Grain-boundary segregation in Ni-base alloys is typically quite small or not observed because of the presence of sulfide formers such as Mg, Zr, Hf, Ti, or Cr.[69,82-84] However, these elements do much more than simply tie up S in complex Ni-base alloys, and their effectiveness depends on alloy chemistry and thermomechanical processing.[84]

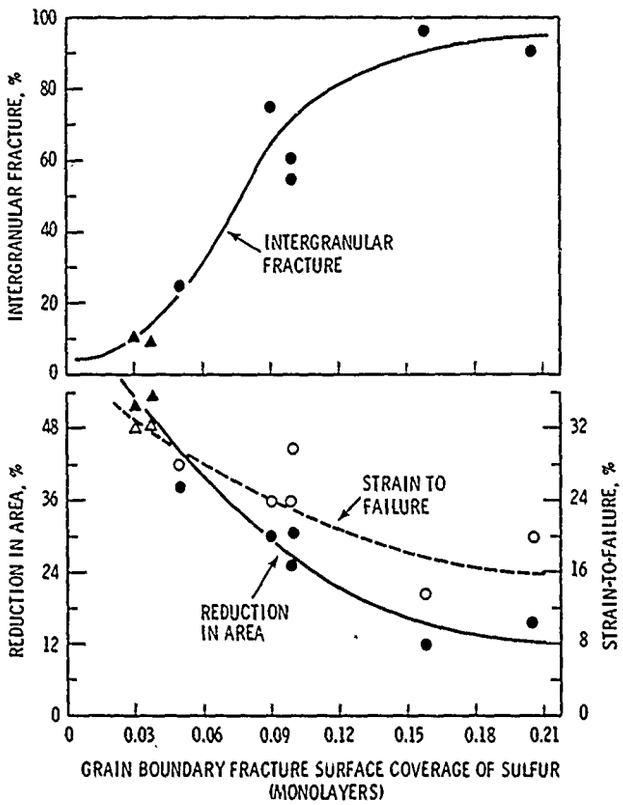


FIGURE 4—Percent intergranular fracture, strain to failure, and reduction of area vs grain-boundary S concentration for Ni tested in 1 N H_2SO_4.[76]

Grain-boundary segregation of S has been proposed to play an important role in the IGSCC of alloy 600 in deaerated water environments.[3,16] This appears to be unlikely based on the lack of significant S segregation measured in this system.[85-92] S levels enriched at grain boundaries are consistently below several percent of a monolayer, if observed at all. It is important to note that Andresen and Briant have shown that S segregation may enhance SCC of nonsensitized, austenitic SS in aerated, high-temperature water.[93] No comparable results have been documented in Ni-base alloys.

P also strongly segregates to grain boundaries in Ni and Ni-base alloys.[35,56,67-76,85-92,94] It is the primary impurity segregant in most Ni-base alloys and can achieve grain-boundary enrichment ratios comparable to those for S. Grain-boundary segregation data for Ni and several Ni alloys have been compiled and plotted in Figure 5 P enrichment increases with decreasing temperature consistent with the equilibrium segregation prediction shown as the solid line in the figure. The change in the predicted segregation behavior below about 700°C results from the solubility limit for P in Ni being exceeded. Thus, the amount of P available to segregate is expected to decrease as heat-treatment temperatures drop below this limit.

Unlike S, P segregation does not embrittle Ni in the absence of an environmental effect. P also appears to have a very small effect on HIC in low-strength Ni, certainly much less than that for S.[76] In higher-strength materials such as alloys 600 and X-750, HIC has been shown to depend on grain-boundary P composition.[56,85] However, the same heat treatments that produce high levels of P

segregation result in continuous grain-boundary carbide precipitation, which can influence the tendency for IG fracture. P segregation has been found to decrease the tendency for IG HIC in alloy 600[57] and Monel 400 (UNS N04400).[94]

Grain-boundary segregation of P has been shown to promote IG corrosion in oxidizing solutions for Ni[73,74,81,95] and Ni-base alloys.[87,89-91,96,97] P has also been implicated in the IGSCC of these same alloys. Bruemmer[74] and Jones and coworkers[80,81] demonstrated that P segregation to the grain boundaries in Ni causes IG cracking at passive and transpassive potentials in a low-temperature acidic solution. Evidence for a similar P effect in austenitic alloys has not been obtained. P segregation in alloys 600 and X-750 is almost always linked to IG carbide precipitation; i.e., both change concurrently. Was found that grain-boundary P did not promote IGSCC in a carbon-free, P-doped, alloy 600 heat when tested in high-temperature water.[98] This is consistent with recent results for type 304 (UNS S30400) SS.[93]

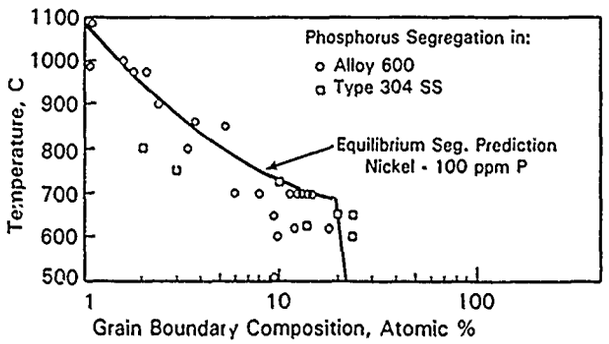


FIGURE 5—Grain-boundary P segregation in type 304 (UNS S30400) SS and alloy 600 (UNS N06600) as a function of temperature.

Several other impurities have been shown to become enriched in grain boundaries in Ni and Ni alloys. Carbon segregation leading to graphite precipitation has been observed in commercial-purity nickel,[99] which can result in poor mechanical and corrosion behavior. In most Ni-base alloys, C is essentially tied up in the form of carbides and is not considered to have an independent segregation effect on environmental cracking. B, on the other hand, appears to have at least an indirect influence on cracking susceptibility. Grain-boundary B segregation in alloy 600 has been documented by several authors.[86-88,90] B additions improve the HIC of pure Ni[100,101] and Ni-aluminide intermetallic compounds.[102] The effect of B on IG corrosion and SCC of alloy 600 appears to be related to Cr carbide-precipitation kinetics. Low bulk levels retard precipitation, while higher levels accelerate precipitation. Thus, B may affect SCC susceptibility in environments in which IG carbide precipitation and Cr depletion are instrumental in the cracking process.

Other potentially detrimental elements such as Se, Te, Bi, Pb,[70] and Sb,[52,78] which can segregate in Ni and Ni alloys, appear to do so only when the bulk concentration is significantly increased by doping. Enrichment ratios comparing segregated grain-boundary and bulk concentrations are too small for significant interfacial enrichment to occur in typical alloys. As a result, even though these elements can promote HIC, they probably do not play a role in environment induced cracking of commercial alloys.

Chromium depletion. The precipitation of Cr carbides along grain boundaries in the Ni Cr alloys, such as alloys 600 and X 750, promotes the formation of a Cr depleted region for certain time-temperature treatments. Because of C's low solubility and Cr's relatively fast diffusivity, this depletion or sensitization occurs much more rapidly in Ni-base alloy 600 than Fe-base alloy 304. A comparison of typical time–temperature–sensitization kinetics in alloy 600 and austenitic SSs of comparable C contents is shown in Figure 6 Because of the more rapid sensitization kinetics in the Ni base alloy, it is likely that moderate to high C heats will exhibit grain-boundary Cr carbides and some Cr depletion in the mill-annealed condition The extent of this depletion will depend on processing temperatures and cooling rates.

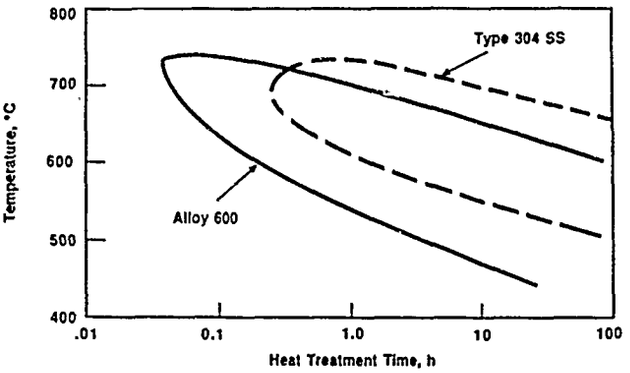


FIGURE 6—Comparison between grain-boundary carbide precipitation kinetics in type 304 (UNS S30400) SS and alloy 600 (UNS N06600) with comparable carbon contents.

Cr depletion becomes most significant during heat treatment in the temperature range 550 to 750°C. Desensitization occurs quite rapidly at higher temperatures, while Cr diffusion kinetics are too slow at lower temperatures for carbide nucleation and sensitization, as indicated in Figure 6. Another important difference between Cr depletion in Ni-base and Fe-base stainless alloys is the carbide-precipitation thermodynamics. Carbide thermodynamics specify the Cr concentration in equilibrium with the growing precipitate. Local grain-boundary Cr concentrations reach much lower levels than for SSs because of this difference. For example, minimum concentrations are typically about 10% at 600°C for alloy 304[103] and less than 6% for a comparable alloy 600 heat.[86]

Cr depletion controls IGSCC susceptibility in oxidizing environments for both Fe and Ni-base austenitic stainless alloys. The susceptibility of alloy 600 to IGSCC in aerated, high-temperature water environments directly depends on the extent of Cr depletion (degree of sensitization), as has been well documented for austenitic SSs.[104] This same correspondence can be noted for SCC tests in low-temperature sulfate solutions.[53,55] Was and Rajan determined that IGSCC susceptibility varied with the extent of Cr depletion and the minimum Cr concentration at the grain boundary in particular.[53] Intergranular cracking increased as Cr at the boundary was decreased below about 8 wt%. Bruemmer observed a similar IGSCC dependence on the minimum grain-boundary Cr concentration in type 304 during tests in aerated, high-temperature water.[104] These results (illustrated in Figure 7) point out the critical importance of sensitization and specific Cr-depletion characteristics on IGSCC in oxidizing environments.

The previous discussion was carefully limited to oxidizing environments because nearly the opposite behavior has been seen concerning carbide precipitation and Cr-depletion effects on IGSCC in high-temperature deaerated water and caustics. As noted in some detail earlier, this behavior results from the presence or absence of IG carbides. Any effect of Cr depletion is minor in comparison to the beneficial influence of the carbides in these environments.

Irradiation-induced microchemistry. Grain-boundary composition can be markedly changed during neutron, electron, or ion irradiation. Displacement damage produces a nonequilibrium concentration of vacancies that can enhance diffusion and segregation. Undersized solutes migrate to available sinks such as grain boundaries, while oversized solutes tend to migrate away from sinks. Most work has concentrated on SSs in which Si and P enrichment and Cr and Mo depletion have been measured at grain boundaries.[60,61,107]

The cause of IASCC in Ni-base alloys may be the same as in austenitic SSs, or there may be other contributing factors. Brimhall, Baer, and Jones evaluated the effect of irradiation on impurity segregation of Ni + 0.03% P and PE-16.[105] They found P segregation occurred at a rate similar to that observed in type 316 (UNS S31600), therefore, if impurity segregation is a factor in IASCC of these materials, it appears that it can occur at equal rates in Ni-base and Fe-Cr-Ni alloys. However, the effect of heat treatment on the susceptibility of alloy 718 suggests that the microstructure is a factor. Garzarolli, et al., observed large Ni_3Nb precipitates at the grain

boundaries of the unirradiated alloy 718, which they suggested contributed to this alloy's resistance to IASCC.[66] However, detailed microchemistry and microstructural examinations of irradiated material have not been conducted, so the role of segregation and grain-boundary microstructure in irradiated material is largely unknown.

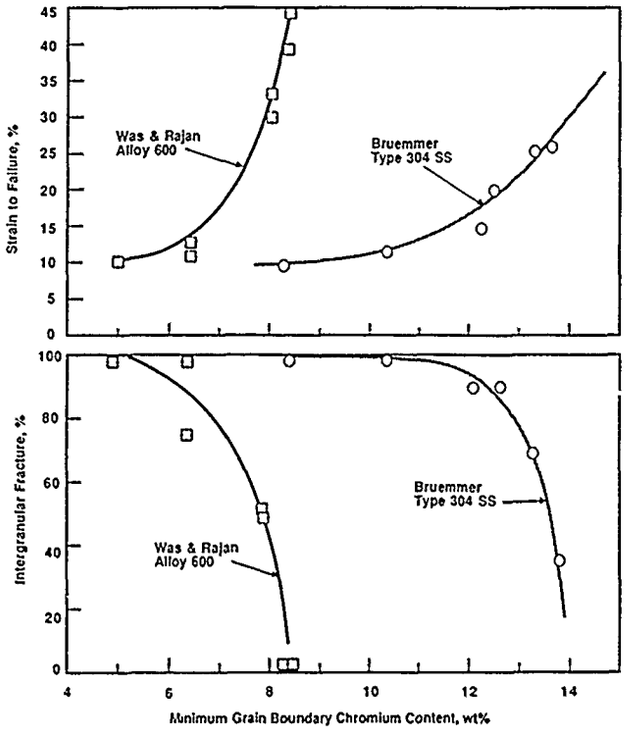


FIGURE 7—Comparison between the strain to failure and percent intergranular fracture vs grain-boundary Cr minimum for type 304 (UNS S30400) SS and alloy 600 (UNS N06600).

Environmental Aspects

SCC results when the environment, microstructure, and stress factors achieve critical conditions. Of these three controlling factors, the environment can assume greater importance than the microstructure and stress factors because it can change with time in service and is amenable to corrective actions. Microstructural and stress factors are established by fabrication procedures and design and do not change appreciably with time in service, while water purity, electrochemical potential, etc., can change appreciably in a short time period. Also, the environment is amenable to monitoring and alteration to minimize the potential for SCC.

Water environments

Ni-base alloys are susceptible to SCC in high-purity, high-temperature water, given that the material is in a susceptible condition and that the stress is sufficiently high. Alloys 600, 718, and X-750 have all exhibited crack growth in high-temperature water, although in general the crack velocities are slow (10^{-8} to 10^{-6} mm/s). In high-purity water, impurities such as Cl^-, $Na_2S_2O_3$, O, etc., enhance SCC of Ni-base alloys as they do with austenitic SSs. Material chemistry, microstructure, and heat-treatment effects dominate the SCC literature for Ni-base alloys, while there have been relatively few controlled water-chemistry studies.

Newman, et al., evaluated the effect of various concentrations of sodium thiosulfate and sodium tetrathionate on IGSCC of alloy 600.[106] Sodium tetrathionate induced crack growth at 22°C in U-bend tests at concentrations as dilute as 10^{-5} M in mill-annealed material, while sodium thiosulfate did not induce crack growth up to a concentration of 10^{-2} M and a temperature of 80°C. A reduction in the pH to 3 caused the sodium thiosulfate to be as effective as the sodium tetrathionate solutions with a threshold concentration of 10^{-6} M at 40°C in aerated solution with 1.3% boric acid. This concentration is 75 ppb of S, which is thought to be a critical species in causing IGSCC of Ni-base alloys. Was and Rajan also noted that sodium tetrathionate is especially effective in causing IGSCC of alloy 600.[53]

Oxygen concentration is a critical element in determining the SCC of austenitic steels and is also thought to be a factor in Ni-base alloys. Crack growth is more predominant in aerated solutions than in low-oxygen solutions, although crack growth has been observed in solutions with oxygen concentrations as low as 10 ppb at about 300°C.[49,107] An example of the effect of dissolved oxygen is shown by the results of Matsushima and Shimizu in Figure 8.[108]

Reduction in the dissolved oxygen content with H is sufficient to minimize SCC of austenitic SSs, but with Ni-base alloys, this approach was shown by Totsuka, et al.,[109] to induce crack growth by H uptake. This result suggests that the IGSCC of solid-solution Ni-base alloys can be H induced. Other results by Mager, who demonstrated crack growth in steam-plus-H environments, further corroborates this idea.[110] Matsushima and Shimizu also demonstrated a greater SCC susceptibility in alloy 600 at pH less than 4.[108]

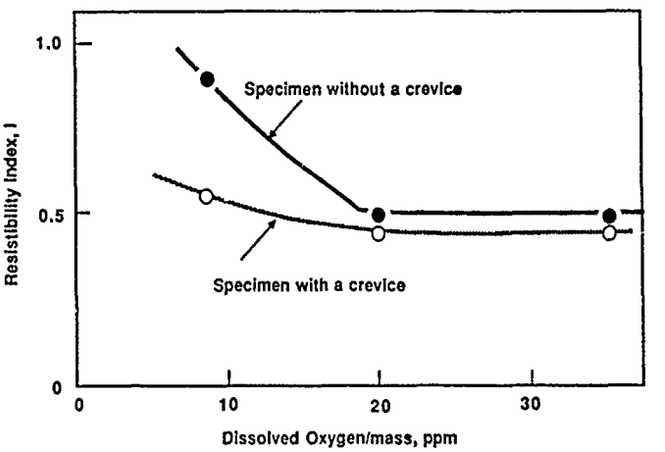


FIGURE 8—Effects of dissolved oxygen and a crevice on the resistibility index of solution-treated material in pH 4 water at 300°C.[108]

Concentrated solutions

Ni-base alloys are frequently used in applications involving highly corrosive solutions such as concentrated acids or alkali solutions. Considerable SCC work has been performed on alloy 600 in high-temperature caustic environments.[111-118] Caustics were thought to play a critical role in the SCC of steam generator tubing and have been used to accelerate cracking in laboratory tests. Alloy 600 has been shown to be particularly susceptible to cracking in NaOH solutions, illustrated by the data in Figure 9. Cracking was observed in NaOH concentrations as low as 4 g/L.

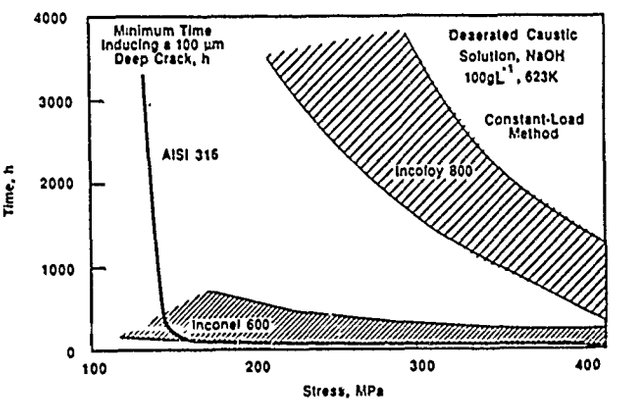


FIGURE 9—Comparison of SCC resistance of type 316 (UNS S31600) steel, Incoloy 800 (UNS N08300), and alloy 600 (UNS N06600) in NaOH solutions.[111]

Theus,[111] Cels,[114] Lee, et al.,[115] and Bandy, et al.,[116] all observed IGSCC of alloy 600 tested in caustic solutions with bend,[111] constant extension rate testing (CERT),[114,115] C-ring, and constant-load samples.[116] Other alloys such as Incoloy† 800 (UNS N08800) and type 304 exhibit transgranular cracking at or near the open-circuit potentials and intergranular crack growth at more oxidizing potentials. Theus concluded that IGSCC of alloy 600 occurred at electrochemical potentials in the active-to-passive transition, as shown in Figure 10. Lee, et al., found a similar potential dependence to cracking in mill-annealed and solution-annealed material.[115] Theus also observed that high-carbon material was less susceptible to IGSCC in NaOH, while Lee noted that high-carbon alloy 600 heat treated at 700°C was more resistant to IGSCC than the mill-annealed or solution-annealed material. Alloy 690, which has about twice the Cr concentration of alloy 600, was shown by Crum to be much more resistant to IGSCC than alloy 600 in both the annealed and 700°C heat-treated conditions.[117]

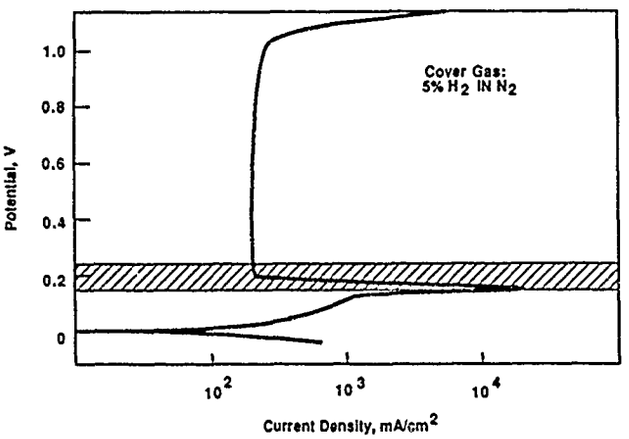


FIGURE 10—Cracking zone for alloy 600 (UNS N06600) shown with respect to an anodic polarization curve in 10% NaOH solution at 288°C.[111]

The beneficial effect of C relates to the dominant influence of grain-boundary carbides on SCC susceptibility of alloy 600 (and X-750) in high-temperature caustics and deaerated water. This behavior was discussed in some detail in the section on microstructural effects. The presence of carbides significantly improves SCC resistance in caustic or deaerated water but may indicate a microstructure susceptible to IG attack in acidic or oxidizing environments.

The severity of SCC in caustics is also a function of concentration and temperature. Several researchers have reported that a 10% NaOH solution was more aggressive than a 50% solution at 316°C.[45,112] Airey rationalized this concentration dependence by considering the electrochemical potential and corrosion rate in these tests.[87] Controlled potential tests (near the active-passive transition) showed faster crack growth with increasing NaOH concentration. Temperature has a large effect on caustic cracking. Significant increases in cracking have been reported in mill-annealed and thermally treated alloy 600 by increasing test temperatures to about 340°C.[87] Temperature effects on and activation energies for SCC will be discussed in a following section.

Ni-base alloys are resistant to SCC in concentrated chloride solutions. This resistance is controlled by the bulk Ni content itself. As Ni is increased above about 8% (in a SS alloy), SCC resistance increased continually. Ni additions shift the electrochemical potential to levels below the critical cracking potential in boiling $MgCl_2$ solutions.[8] Evaluation of the effect of Ni concentration on corrosion of a 17% Cr alloy by Coriou, et al. (Figure 11), illustrates that high Ni alloys do not exhibit desirable corrosion resistance in low-pH, highly oxidizing solutions.[118]

†Trade name.

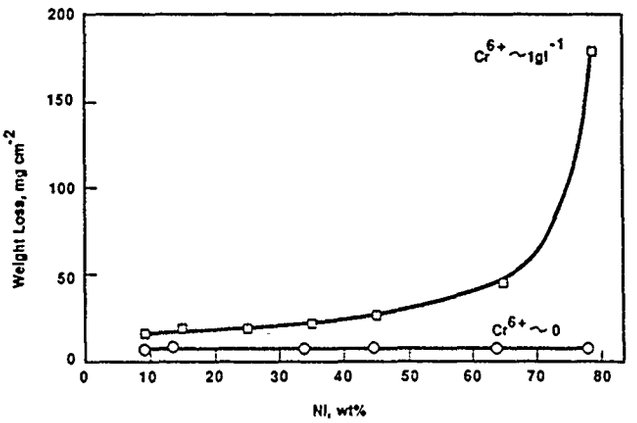


FIGURE 11—Effect of Ni content on corrosion of 17% Cr steel in boiling 5 N HNO_3 solution with and without Cr^{6+}.[118]

Hydrogen environments

Low-temperature acidic and gaseous hydrogen environments. Ni and Ni-base alloys have been shown to exhibit H-induced subcritical crack growth at 25°C under a variety of conditions including cathodic and gaseous H precharging and dynamic cathodic charging.[33,53,75-79,99,119-129] The results of these studies indicate that H has been shown to induce subcritical crack growth in "high-purity" and commercial-purity Ni, and in solid-solution and precipitation-hardened Ni-base alloys and Ni-Cu-Al alloys.

Ni tested under dynamic cathodic charging exhibits a reduced strain to failure and reductions of area, as shown by the data in Figures 12 and 13.[75,78] Latanision and Opperhauser demonstrated a reduced strain to failure and increased tendency for intergranular fracture with increasing cathodic potential and increasing grain size.[75] A loss of ductility and increased tendency for intergranular fracture with increasing cathodic potential was also demonstrated by Bruemmer, et al.[76,78] An enhanced H effect was demonstrated for Ni with grain boundaries enriched with S (Ni case in Figure 13) and Sb relative to P-enriched grain boundaries. Similar effects on the ductility of Ni are obtained whether H charging occurs simultaneously with the strain, as in a straining electrode test, or is precharged at cathodic potentials. Boniszewski and Smith demonstrated that the strain to failure is decreased from 30% for H-free samples to about 8% for samples charged with 87 cc [standard-temperature pressure (STP)] of H per 100 g of Ni and tested at 25°C and a strain rate of 8.33×10^{-3} s^{-1}. The reduction in the strain to failure was less for smaller H concentrations.[119]

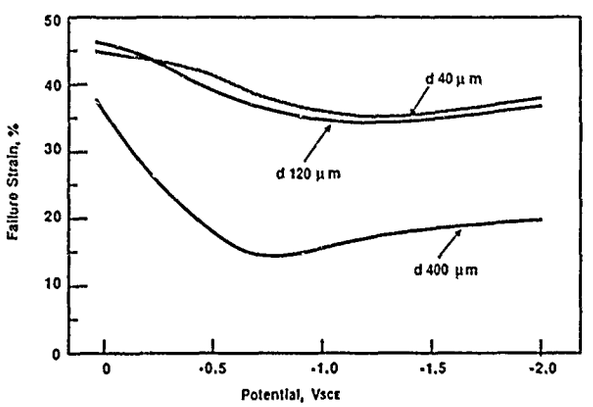


FIGURE 12—Fracture strain of polycrystalline Ni with grain sizes ranging from 40 µm to 400 µm tested in 1 N H_2SO_4 at cathodic potentials.[75]

H induces subcritical crack growth in Ni in a manner very similar to that observed in other materials. Examples of the subcritical crack growth of Ni and Fe with S-enriched grain boundaries tested at cathodic potentials are shown in Figure 14. The results of Jones, et

al.,[120] reveal that the stress-intensity threshold and Stage I crack velocities for Ni and Fe with S-enriched grain boundaries are very similar. Deviation occurred at higher stress intensities because the subcritical cracks in Fe become critical, while subcritical cracks in Ni do not become critical because of plastic-zone growth.

Ni tested under monotonic or cyclic loading is also influenced by the presence of gaseous H.[121-123] Wilcox and Smith[121] showed that thermally charging Ni with H was equivalent to the cathodic charging results of Boniszewski and Smith[119] for equivalent H concentrations. For instance, at 10 cc of H_2 per 100 g of Ni, thermally charged Ni had a strain to failure of 18%, and cathodically charged nickel had a strain to failure of 22%. In high-cycle and low-cycle fatigue tests of Ni in gaseous H, Verpoort, et al.,[124] demonstrated that the number of cycles to failure was decreased and the crack growth rate increased.

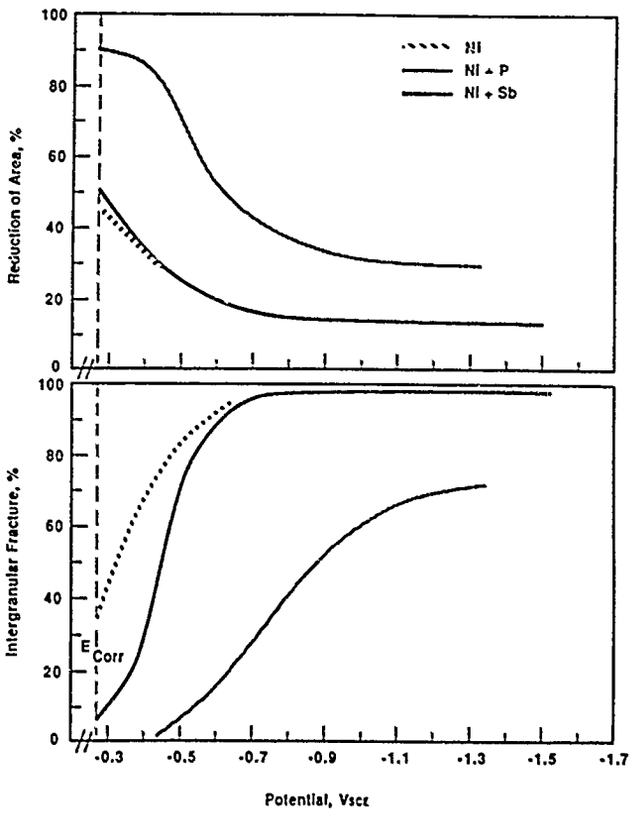


FIGURE 13—Percent intergranular fracture and reduction of area of polycrystalline Ni tested in 1 N H_2SO_4 at cathodic potentials.[78]

Grain-boundary segregation of elements such as S, Sb, P, and Sn[77-81,121,122] has been shown to contribute to the H-induced subcritical crack growth of Ni. H induces an intergranular fracture mode, and the evidence suggests that grain-boundary impurity segregation contributes to this transition from ductile to intergranular fracture.[130] H effects in commercial-purity Ni and Ni-base alloys are more complex than for "high-purity" Ni because of the additional effects of grain-boundary and matrix precipitation. For instance, Lee and Latanision concluded that precipitation of grain-boundary graphite particles at 425 to 650°C reduced the effect of H in Ni-200 (UNS N02200).[99] However, it should be noted that H changed the reduction of area from 70% for tests conducted in air to about 30% for tests conducted in H_2SO_4 at -1000 mV_{SCE}. The reduction of area of Ni-270 was only 15% for the same heat treatments and cathodic test conditions. Grain- boundary S segregation was noted to be the dominant factor contributing to the H-induced IG fracture mode.

Solid-solution alloys of Ni-Cr-Fe are also susceptible to H-induced intergranular fracture. Cornet, et al., demonstrated that intergranular fracture would occur in the absence of grain-boundary segregation for straining electrode tests conducted in 1.8 N H_2SO_4 and a current density of 50 mA/cm^2.[57] At a strain rate of 4×10^{-3} s^{-1}, the high-purity Ni-Cr-Fe material exhibited the same embrittlement as the material with Sb and Sn additions, while material with P and C additions were less embrittled. The authors presumed that the purity additions were segregated to the grain boundaries and that the high-purity material had clean grain boundaries, however, no direct Auger electron spectroscopy (AES) measurements were reported. Based on the AES results of Bruemmer, et al., for high-purity Ni, the high-purity Ni-Cr-Fe material may have had significant S segregation.[78] Therefore, the conclusion of Cornet, et al., that H induces intergranular crack growth along "clean" grain boundaries of IN600 is unproven.[57] In another solid-solution Ni-base alloy, C-276, Sridhar, et al., showed that the stress-intensity threshold was decreased, and the crack growth rates increased for material charged cathodically with H.[33]

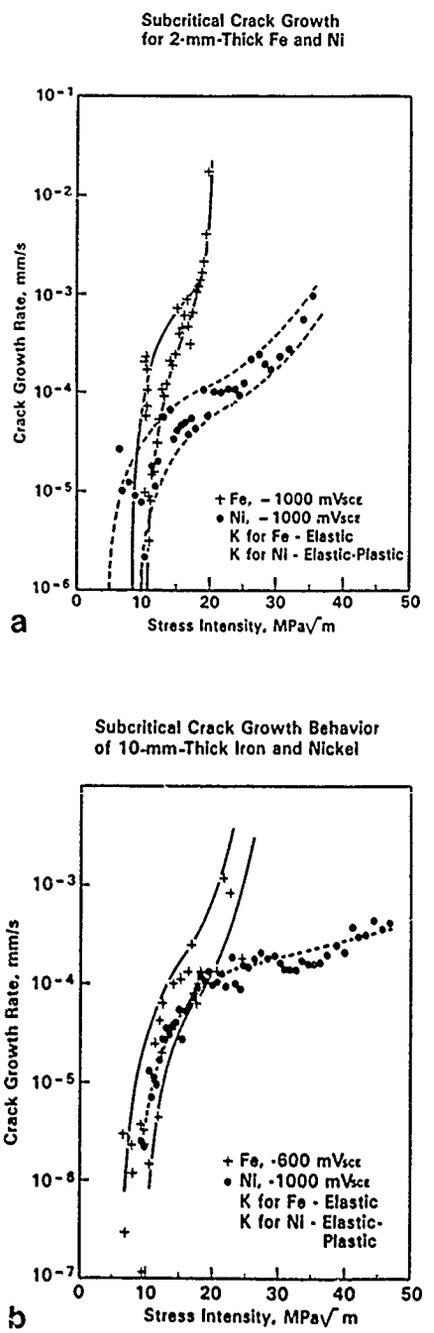


FIGURE 14—Subcritical crack growth (a) for 2-mm-thick Fe and Ni tested in 1 N H_2SO_4 at 25°C, and (b) for 10-mm-thick Fe and Ni tested in 1 N H_2SO_4 at 25°C.

Measurements of H-induced subcritical crack growth in two-phase Ni-base alloys have not been reported to the same extent as for Ni and solid-solution Ni alloys. Kekkonen and Hanninen reported on the time dependence for crack initiation in H-charged alloy X-750.[129] Small U-bend samples were cathodically charged with H at a current density of 5 mA/cm^2 and the time-to-failure was monitored. Failure times ranged from 8 to 140 min depending on solution-treatment temperature and aging conditions. Higher solution- treatment temperature increased the failure time, while samples given a single aging treatment had longer failure times than those given a double age.

Hydrogen-sulfide effects. The subcritical crack growth behavior of Ni-base alloys in aqueous environments with H_2S bears many similarities to their behavior in low-temperature acidic environments. Kolts and Sridhar have discussed the parallels between the H embrittlement and H_2S embrittlement (sulfide stress cracking) for ferritic steels and Ni-base alloys.[131] They concluded that the similarities include the effects of grain-boundary segregation, test temperature, strain rate, and applied stress, while some of the differences include less dependence on yield strength and the effect of ordering in Ni-base alloys. Both ferritic steels and Ni-base alloys are susceptible to cracking in H_2S environments. Kane[132] concluded that H_2S causes accelerated H charging of Ni-base alloys at temperatures lower than 200°C when these materials are cathodically coupled to steel. At temperatures higher than 200°C, he suggests that cracking results from anodically induced SCC.

Subcritical crack growth tests on Hastelloy alloys C-276, G, and X(LC) (UNS N10276, N06007, and N06002) in the NACE H_2O-5% sodium chloride-0.5% acetic acid solution saturated with H_2S[133] indicates that Ni-base alloys perform better than ferritic steels in H_2S-bearing environments. The stress-intensity thresholds for Ni-base alloys decreased with increasing yield strength with alloys X(LC) and C-276 having similar thresholds with higher yield strengths than alloy G. For instance, alloys X(LC) and C-276 had a threshold of 60 MPa$\sqrt{m}$ at yield strengths of 1300 MPa, while alloy G had a similar thresold at a yield strength of 1150 MPa. Crack growth occurred in an intergranular mode in all cases. Kane observed crack growth in alloys C-276, C-4 (UNS N06455), and 625 tested in the NACE solution and at temperatures ranging from 25°C to 149°C.[132] Cold work, aging time and temperature, sample orientation, galvanic coupling with steel and environment temperature, and composition were all evaluated. Failures were observed only in samples galvanically coupled to steel, which caused the Ni-alloy potentials to be cathodic. Aging was found to enhance crack growth, while the susceptibility to cracking decreased with increasing temperature. In a later evaluation, Berkowitz and Kane concluded that grain-boundary P segregation contributed to the intergranular subcritical crack growth of alloy C-276 in the NACE solution saturated with H_2S.[35] P segregation was correlated with aging treatment and the increased susceptibility of this alloy with aging treatment.

Hydrogen activity and temperature. H-induced subcritical crack growth is controlled by the microstructure or microchemistry of the material, the environment, and the stress. Grain-boundary chemistry is the dominant microchemistry issue, while grain-boundary precipitation effects have not been evaluated. Other transgranular effects were discussed in the previous section. H activity, as measured by H pressure, cathodic potential, or pH, depending on the environment, is the primary environmental parameter, although there are instances when active corrosion enhances H uptake. Also, stress, stress intensity, and strain rate are driving forces for H-induced subcritical crack growth.

Studies of the effect of H activity on H-induced subcritical crack growth are scarce Jones evaluated the effect of cathodic potential on the fracture mode transition of nickel as a function of grain-boundary S concentration [79] The results of this study are shown in Figure 15(b), where it can be seen that a given percent of intergranular fracture requires an increasing grain-boundary S segregation with decreasing cathodic potential By analyzing these results in terms of the Nernst equation, Jones, et al.,[79] were able to show that the shift in C_s could be described by a H-pressure dependence of $(P_{H_2})^{-1/2}$, which is consistent with crack growth being controlled by Sievert's law. This similarity suggests that the intergranular subcritical crack growth of Ni at cathodic potentials is dependent on H pressure similar to H uptake in gaseous H. Many studies have shown an increasing effect of H with respect to H concentration, cathodic potential, or H-charging time;[33,99,119,134] however, very few relate a crack growth parameter directly to H activity or pressure. Sridhar, et al., estimated the dependence of the Stage II crack velocity in alloy C-276 on H fugacity using cathodic current density.[33] They concluded that the velocity was proportional to the $f_H^{0.75}$, which is similar to that observed by Jones, et al.,[79] if da/dt is assumed to be inversely proportional to C_s. Both analyses suggest that the crack growth rate is controlled by the near-surface H activity, which is controlled by the H pressure or fugacity at the crack tip.

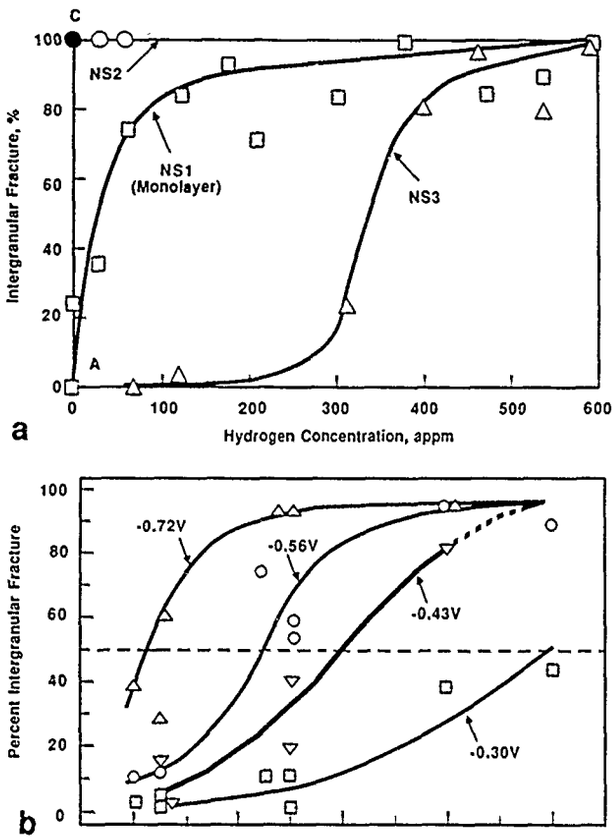


FIGURE 15—(a) Dependence of the fracture mode on the bulk H concentration for specimen series NS1, NS2, and NS3. Point A is for an NS1 specimen quenched from vacuum while Point B is for a similar specimen quenched from Ar gas containing some water vapor. Point C is for an NS2 specimen quenched from vacuum. (b) Fracture mode transition for Ni with increasing grain-boundary S concentration at various cathodic potentials.

Temperature is an environmental parameter that can have a strong influence on H-induced subcritical crack growth. This has been shown for ferritic steels,[135-138] but again, less information is available for Ni and Ni-base alloys. Wilcox and Smith found that the time-to-failure of charged Ni obeyed a 1/T dependence with an activation energy of 6.8 kcal/mol (Figure 16).[121] They concluded that the crack growth rate of precracked samples was controlled by H mobility at temperatures between 0 and −50°C. Activation energies for crack growth of alloy 600 in high-temperature water with variable water additions such as H_2 and H_3BO_3 have also been reported. Bandy and van Rooyen[139] reported a value of 33 kcal/mol and Totsuka and Smialowska[140] a value of 1 kcal/mol for tests conducted at temperatures of about 300 to 350°C and for high-purity water with H_2. Bandy and van Rooyen used both U-bend and CERT, Totsuka and Smialowska used a flat sample with a crimp that produced a stress concentration and stress gradients. Bandy and van Rooyen

have suggested that the large disparity in activation energy resulted from the fact that activation energy for Stage I crack growth was considerably larger than for Stage II. If this suggestion is correct, the wide difference in the activation energy obtained for alloy 600 could be explained by cracks initiated in the crimped sample used by Totsuka and Smialowska, propagated mostly in Stage II because of the high stress concentration, while those in the U-bend and CERT samples used by Bandy and van Rooyen produced data for cracks in Stage I. However, a variation in activation energy is also likely for a change in the crack growth mechanism such as H vs anodic dissolution. As noted, Wilcox and Smith observed an activation energy of 6.8 kcal/mol for H-charged nickel. While these tests were at a lower temperature (~ 0 vs 300°C), they suggest the possibility that the Totsuka and Smialowska results were related to a H mechanism and controlled by H transport, while the Bandy and van Rooyen results were more dependent on anodic dissolution.

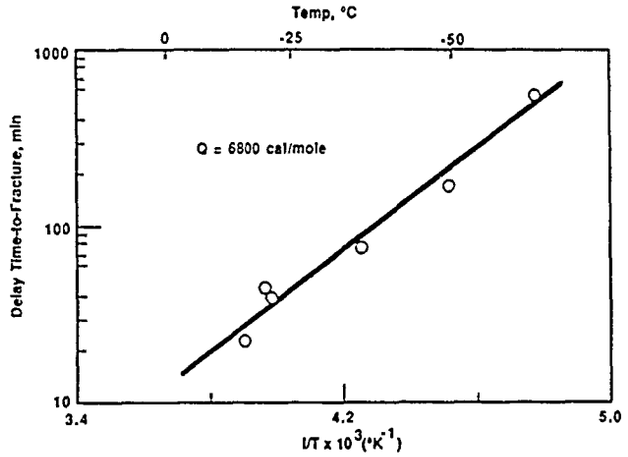


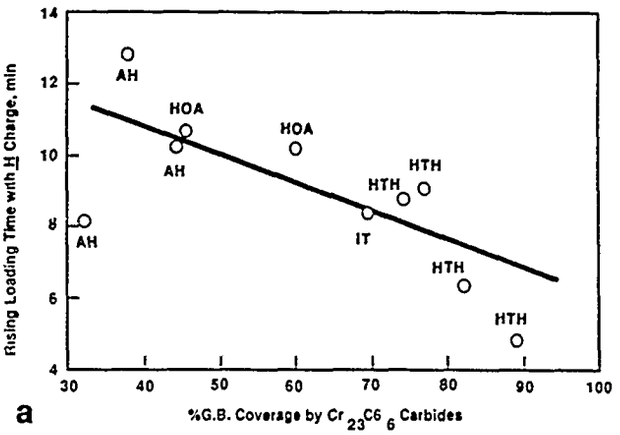
FIGURE 16—The temperature dependence of the delay time-to-fracture for H-charged Ni prestrained 15% at −80°C and $\epsilon = 3.3 \times 10^{-4}$/s.

Strain Rate, Stress, and Stress-Intensity Effects

High-temperature water environment

Strain rate, stress, and stress intensity are primary variables in determining whether subcritical crack growth will occur and at what rate it will occur. Strain rate can be an independent variable or a dependent variable controlled by the stress or stress intensity. Constant extension rate tests are frequently used to evaluate SCC of Ni and Ni-base alloys, although few results have been reported as a function of variable strain rate. Garud has suggested that the crack initiation rate for alloy 600 in high-temperature water can be described by $f(\dot{\epsilon}) = A\dot{\epsilon}^p$ where A and p are constants dependent on the material and environment.[141,142] A value of 0.65 for p was estimated for alloy 600 over a temperature range of 290 to 365°C.

Data on the crack velocity of Ni-base alloys as a function of strain rate have not been presented as for the case of type 304;[143] however, it has been clearly demonstrated that Ni[81] and Ni-base alloys[53,139] exhibit SCC at strain rates of 10^{-7} to 10^{-5} s^{-1}. The rising-load test using a notched Charpy-type sample is a variation of the CERT test, except that a sharp crack is dynamically strained throughout the rising-load test, while crack nucleation and propagation occur with the smooth CERT test. Examples of results from the rising-load test for alloy X-750 are shown in Figures 17 and 18. The data of Miglin and Domian in Figure 17(a) indicate that the rising-load time which increases with decreasing crack velocity, increases with increasing grain-boundary carbide coverage when tested in high-temperature water [49] In contrast, the rising-load time decreases with increasing grain-boundary carbide coverage when tested at cathodic potentials [Figure 17(b)] Results by Grove and Petzold (Figure 18) show that the rising-load time of alloy X-750 decreases with increasing P segregation [56] Therefore, the rising-load tests, which are equivalent to a notched CERT test, suggest that the crack growth mechanism in alloy X-750 supports a H induced subcritical crack growth mechanism that is enhanced by P segregation.



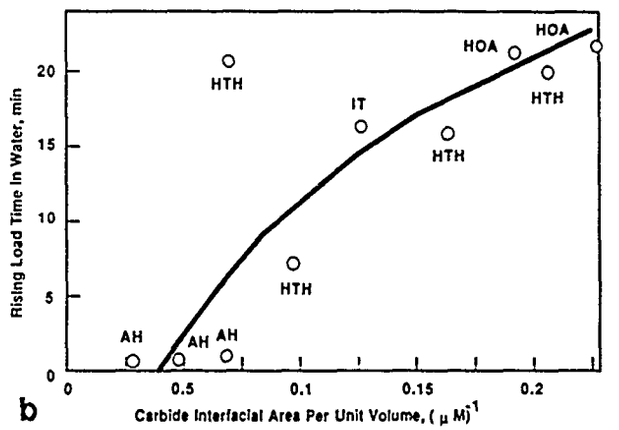


FIGURE 17—(a) Rising-load time in water vs carbide interfacial area per unit volume of material for alloy X-750 (UNS N07750) conditions (IT = No. 1 temper).[49] (b) Rising-load time during H charging vs percent grain-boundary coverage by $Cr_{23}C_6$ carbides for alloy X-750 (UNS N07750) conditions.[49]

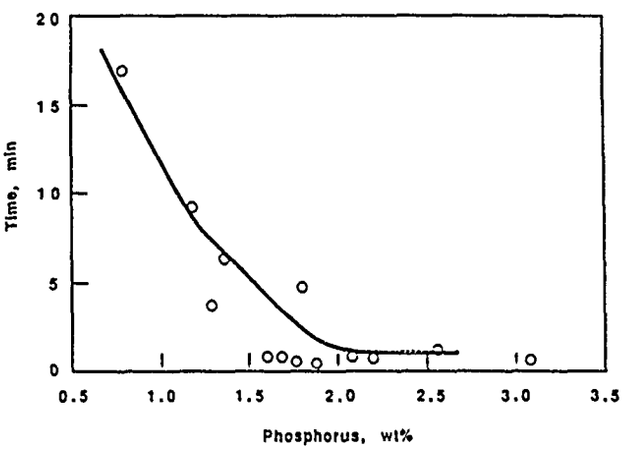


FIGURE 18—Effect of grain-boundary P concentration on rising-load performance of condition BH heats in 93°C water.[56]

Stress corrosion tests of Ni-base alloys have frequently been conducted at constant deflection or approximate constant-stress conditions. Tests using U-bend or reverse U-bend samples are common because they are compatible with samples removed from tubing, which is a common product form for Ni-base alloys. Results for U-bend samples of alloy 600 tested in deaerated high-temperature water are shown in Figure 19. Tests performed at a stress equal to the yield strength of alloy 600 failed in 100 days or less. A threshold stress is not indicated by these data. In NaOH solutions, alloy 600 was shown to exhibit crack growth to a stress of 100 MPa (Figure 9) substantially below the yield strength.[41] The behavior relative to other

alloys is also shown in Figure 9 and the poor performance of alloy 600 in high pH solutions is illustrated Results of constant-stress tests on alloy X-750 given various heat treatments and tested in high-purity water at 350°C are shown in Figure 20.[144] Solution treatment at 885°C resulted in a stress threshold of 700 MPa, while a higher-temperature anneal at 1093°C resulted in a threshold of 950 MPa. A two-step precipitation heat treatment was given to both sets of samples.

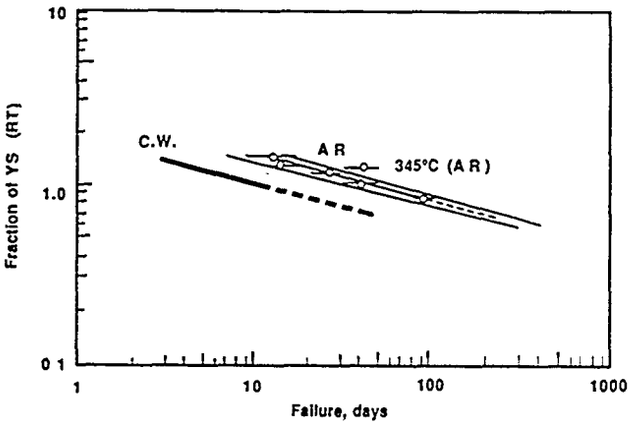


FIGURE 19—Effect of applied stress on failure time of as-received alloy 600 (UNS N06600) tubing, 365°C, pure H_2O.

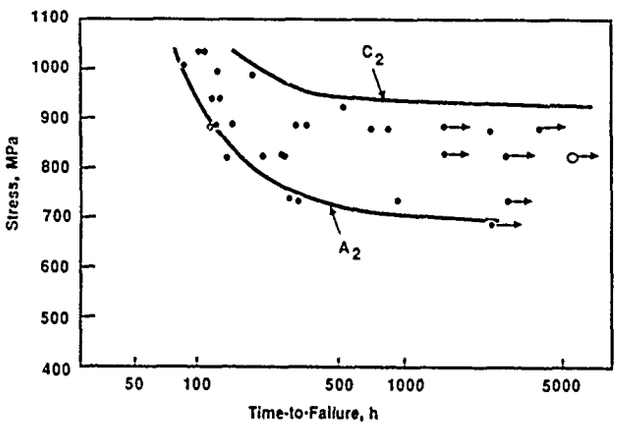


FIGURE 20—SCC of alloy X-750 (UNS N07750) with different heat treatments [solution anneal 885°C/24 h (A2) and 1093°C/1 h (C2) plus precipitation anneal 730°C/8 h and 620°C/8 h] in pure water [with H25/50 mL (STP)/kg] at 350°C.[144]

Subcritical crack growth tests are useful for defining the stress-intensity threshold at which an existing crack will begin to grow and for determining the steady-state crack velocity under known stress-intensity conditions. Crack velocity data can be obtained from CERT or U-bend tests, but the velocity is an average value determined from the time of crack initiation and propagation. Also, the stress-intensity cannot be accurately determined because the crack length is not known as a function of time. Subcritical crack growth data for Ni with 0.13 monolayers of P segregation tested at a low temperature at an anodic potential of +900 mV are shown in Figure 21. These data of Jones, et al., indicate that under these conditions Ni is very susceptible to SCC, because the stress-intensity threshold is low, 13 $MPa\sqrt{m}$, and the steady-state crack velocity is high, 2×10^{-4} mm/s.[81] Subcritical crack growth data for alloy 600 are not available; however, subcritical crack growth data for alloy X-750 are.[147,148] Figures 22 and 23 show a wide range in the threshold for crack growth but a similarity in the crack velocity. The results of Kawakubo and Rosborg[145] indicate a stress-intensity threshold of 70 $MPa\sqrt{m}$ (at 10^{-10} m/s), which is relatively independent of heat treatment, while the results of Vaillant[146] indicate a stress-intensity threshold of 10 $MPa\sqrt{m}$ at the same crack velocity. The material tested by Vaillant was solution treated at 885°C, while that of Kawakubo and Rosborg was solution treated at temperatures exceeding 982°C. A low solution-treatment temperature also coincided with a low stress threshold in constant-stress tests, shown in Figure 20, however, the crack velocity was relatively independent of solution-treatment temperature.

As discussed in a later section, the film-rupture model given in Equation (5) predicts a stress-intensity exponent of 2 to 4. While this equation has been applied primarily to austenitic SSs, it is informative to compare the stress-intensity exponent of the data shown in Figures 21 and 22 with that predicted by Equation (5). It is also worth noting that the accuracy of the exponent determined from the experimental data is very sensitive to the accuracy of the crack-length measuring system used for these tests. Since this is not generally known or given, it is difficult to assign a standard deviation or accuracy value to the experimental exponent values. For the data shown in Figure 21, n has a value of 41 in Stage I; for the data in Figure 21, n has a value of 5 in Stage I and 1 in Stage II. A relatively large stress-intensity-dependent Stage I and stress-intensity-independent Stage II is suggested by the data in Figure 23 in contrast to the linear dependence suggested by the results in Figure 22. Based on this relatively small database, it is not possible to determine whether Ni and Ni-base alloys can be described by Equation(5). Further testing with accurate crack-length measuring systems is needed to develop a model of the crack velocity stress-intensity dependence.

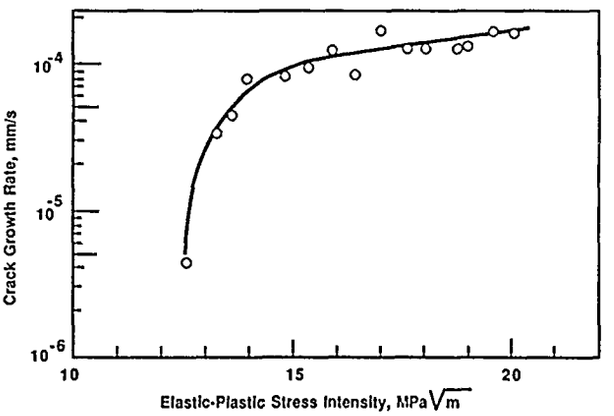


FIGURE 21—Crack growth rate vs elastic-plastic stress intensity for Ni+P a +0.9 V_{SCE}.

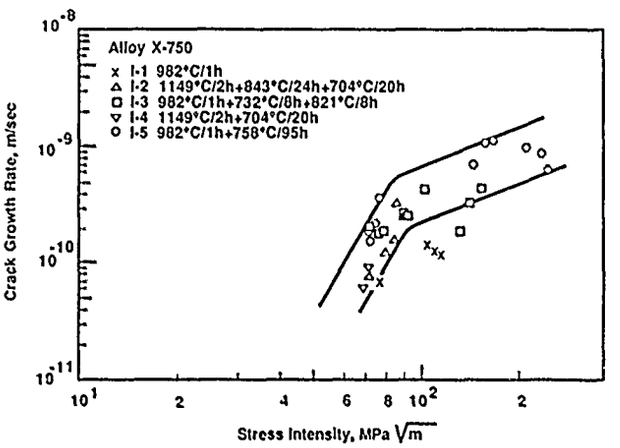


FIGURE 22—SCC growth rates of alloy X-750 (UNS N07750) in pure oxygenated water at 300°C.[145]

Hydrogen-induced crack growth

H-induced subcritical crack growth is dependent on microstrutural, environmental, and stress factors similar to anodic-dissolution-induced crack growth. Clearly, the specific conditions controlling crack growth in H and anodic-dissolution cases may differ, but the fact remains that crack growth varies with changes in these factors.

Of the three factors, the stress dependence of H and anodic-dissolution-induced crack growth are perhaps the most similar. For instance, the time-to-failure decreases with increasing stress with evidence for a stress threshold below which both H and anodic-dissolution crack growth ceases. This can also be expressed as a stress-intensity threshold in a crack velocity–stress-intensity plot, and both H and anodic-dissolution-induced crack growth exhibit a K_{th}. Also, three crack growth stages are evident in H-induced and anodic-dissolution-induced crack growth evaluations.

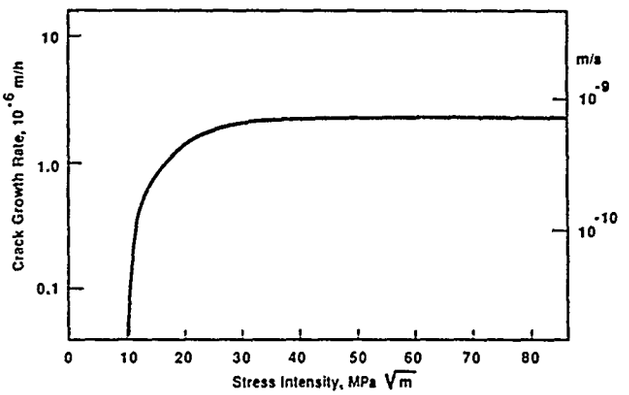


FIGURE 23—Stress corrosion crack growth of alloy X-750 (UNS N07750) given a solution heat treatment of 885°C/24 h and single-step precipitation treatment (704°C/20 h) in PWR primary water at 325°C.[146]

Evaluation of the stress or stress-intensity dependence of H-induced subcritical crack growth of Ni and Ni-base alloys is limited by a sparse database Many H-embrittlement studies have used CERT tests in H gas or at cathodic potentials or tensile tests of H-charged material Tests are frequently conducted at a single strain rate, and reduction of area or strain to failure are the primary properties reported from these tests; therefore, stress or strain-rate dependence is not established However, there are a limited number of subcritical crack growth tests that illustrate that H-induced subcritical crack growth of Ni and Ni-base alloys results in classical V–K relationships. Jones, et al , found that Ni tested at cathodic potentials (Figure 14) had a crack growth threshold of 10 MPa$\sqrt{m}$, a Stage I with a da/dt = AK^n dependence with n equal to 17 and a Stage II crack velocity of 10^{-4} mm/s [120] No Stage III was observed, presumably because of the large amount of plasticity in Ni and a large plastic zone. Sridhar, et al , also observed a classic V–K relationship for H-charged alloy C-276 [34] They evaluated the effects of H-charging current density and aging at 500°C following cold work. Stress-intensity thresholds (at 10^{-5} mm/s) decreased from 105 to 90 MPa$\sqrt{m}$ with charging current densities of 100 mA/cm^2 to 200 mA/cm^2 for material aged 100 h at 500°C Both aging and H-charging current decreased the threshold and affected the exponent n. For instance, values of n ranging from 41 for unaged material to 5 for material aged 1500 h at 500°C were observed, while the threshold decreased from 105 MPa$\sqrt{m}$ for cold-worked material without subsequent aging to about 65 MPa$\sqrt{m}$ for material aged for 500 h at 500°C. Likewise, the Stage II crack velocities increased with increasing H-charging current density and aging time Stage II crack velocities increased from 2 × 10^{-5} mm/s to 3 × 10^{-4} mm/s with 500°C aging up to 1500 h and from about 4 × 10^{-5} mm/s to 10^{-4} mm/s for current densities of 100 mA/cm^2 to 200 mA/cm^2. A Stage III was observed in alloy C-276, unlike in the Ni, presumably because the higher-strength alloy supported a higher local stress with increasing K, while increasing K in the Ni did not appear to increase the local stress, only the size of the plastic zone.

H has also been found to enhance the fatigue crack growth rate of Ni tested in H gas and cathodically charged with H.[147] Verpoort, et al., found a decrease in the number of cycles to failure and an increase in the crack growth rate when compared to tests in Ar gas.[147] Annealed Ni tested in H gas exhibited a crack growth rate of 10^{-4} mm/cycle at a ΔK of 10 MPa$\sqrt{m}$. Only Stage II crack growth behavior was evident with no threshold or Stage I or III. The fracture mode was predominantly intergranular in annealed Ni, while transgranular crack growth occurred during the early stages of crack growth with a transition to intergranular crack growth as the cracks lengthened in cold-worked Ni. Therefore, it appears that with cyclic load conditions, H can enhance transgranular crack growth, but that intergranular crack growth is predominant during static and dynamic monotonic tension loading modes.

MECHANISTIC UNDERSTANDING OF CRACK GROWTH PROCESSES

Hydrogen-Controlled Crack Growth Processes

Intergranular processes

Most of the experience with H-induced subcritical crack growth of Ni or Ni-base alloys reveals that the predominant growth mode is intergranular. Grain-boundary segregation was found to enhance the subcritical crack growth in H. There is also evidence that H affects the bulk properties of Ni and Ni-base alloys, which will be discussed in the next section.

The earliest data relating grain-boundary impurity segregation to H embrittlement of Ni were published by Latanision and Opperhauser.[75] In this study, the authors observed a decreasing ductility and increasing tendency toward intergranular fracture with increasing grain size and cathodic potential, as shown in Figure 12. Latanision and Opperhauser detected Sn and Sb on the intergranular fracture surfaces of the Ni-270 specimens that were fractured in the electrolyte and explained the tendency toward intergranular fracture by the presence of H recombination poisons in the grain boundaries. They postulated that the H-recombination poisons enhanced H absorption at the grain boundaries and therefore induced intergranular fracture.

The work of Latanision and Opperhauser identified a potentially new H-embrittlement process; however, their work also demonstrated the need for tests performed on Ni with a range of grain-boundary segregants and for AES analysis of samples fractured in high vacuum.[75] Jones and coworkers evaluated the fracture mode and ductility of Ni with several grain-boundary concentrations of S, P, and Sb.[78,79] The grain-boundary compositions were determined from samples fractured within the AES chamber and therefore excluded the possibility of contamination from the testing solution or air. The grain-boundary concentrations for the alloys tested by Jones, et al., are shown in the histograms in Figure 24. The distribution in segregation was the result of variations among individual grain faces, and hence, a variation in the range of grain-boundary energies and the dependence of segregation on grain-boundary energy. Jones, et al., used the straining electrode technique, an electrolyte of 1 N H_2SO_4, and strain rates and cathodic potentials similar to those used by Latanision and Opperhauser to evaluate the effect of S, P, and Sb on the intergranular fracture of Ni. The results of these tests demonstrated that S was the most effective in causing intergranular fracture of Ni in the presence of cathodic H, Sb was slightly less effective, and P was the least effective. The effectiveness of these impurities can be expressed by the following relationship:

$$C_s^{eq} = C_s + 0.5\,C_{sb} + 0.07\,C_p \qquad (1)$$

where C_s^{eq} is the equivalent grain-boundary S concentration and C_s, C_{sb}, and C_p are the S, Sb, and P grain-boundary concentrations. It can be seen from this relationship that Sb is 1/2 and P is 1/15 as effective as S. The effect of S, Sb, and P on the fracture mode and reduction of area of Ni as a function of cathodic potential is shown in Figure 2. Lee and Latanision[99] evaluated zone-refined Ni, Ni-270, and Ni-200 and found that intergranular fracture was promoted at cathodic potentials by the presence of grain-boundary S. It is important to note the small contribution of P segregation to the intergranular fracture of Ni as indicated by Equation (1). This result is

inconsistent with the recombination poison mechanism proposed by Latanision and Opperhauser, since P is known to be a recombination poison when added to the electrolyte.

Oxygen absorption from the annealing vacuum was claimed to have an effect on Ni tested in cathodic H by Ogino and Yamasaki.[101] They concluded, based on indirect evidence, that undoped, Sn-doped, and Sb-doped Ni were susceptible to H-induced crack growth because of oxygen absorption from the vacuum environment, while P- and B-doped materials did not exhibit susceptibility to H. They suggested that P and B impeded oxygen penetration along the grain boundaries Ogino and Yamasaki did not measure grain-boundary chemistries, therefore it is uncertain which mechanisms control this behavior.[101]

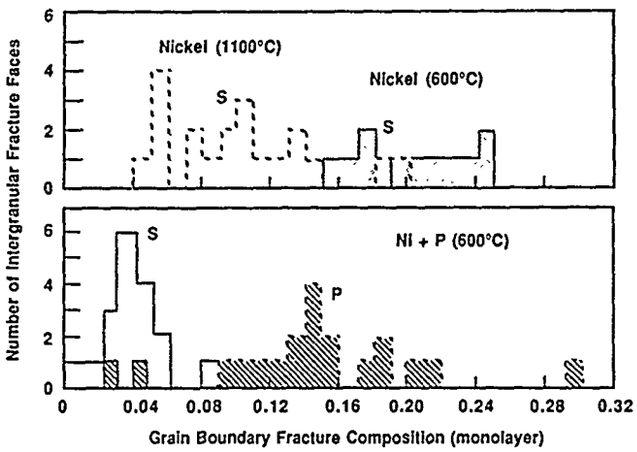


FIGURE 24—Distribution of S and P on intergranular fracture surfaces of Ni.[78]

The results of Cornet, et al.,[57] for alloy 600 strained at a cathodic current density of 50 mA/cm^2 in H_2SO_4 are consistent with those of Bruemmer, et al., for Ni.[78] They observed that alloys doped with P and C exhibited less embrittlement than those doped with Sn and Sb and less than the high-purity material without additions.

The observation that Ni tested in cathodic H is susceptible to intergranular fracture is similar to observations[121-123] made with Ni precharged with H or tested in H gas. In the precharged, charged Ni studies, the grain-boundary compositions were not measured, and therefore information about combined impurity plus H effects cannot be obtained from these results. However, according to the segregation results of Bruemmer, et al.,[78] the material used by Wilcox and Smith,[121] which contained about 20 appm S and was annealed at 1000°C, may have had as much as 0.1 monolayers of S at the grain boundaries. Therefore, it is quite possible that the results of Smith and coworkers were influenced by S segregation.[121-123] Smith and coworkers observed that the maximum embrittlement occurred at −50°C and was enhanced by the occurrence of serrated yielding and grain-boundary shear. However, Latanision and Opperhauer reported only a small serrated yielding effect in 400-μm grain size Ni tested at 20°C in external cathodic H and no measurable serrated yielding in smaller grain size material.[75] Latanision and Opperhauser observed grain-boundary shear ledges that were very similar to those reported by Windle and Smith.[123] Therefore, it would appear that serrated yielding, a temperature of −50°C, and the source of H are not major factors in the intergranular fracture of Ni, while grain-boundary shear and impurities (particularly S) may be important factors. In a recent study, Eastman, et al., observed the intergranular fracture of Ni in external gaseous H only when S was segregated to the grain boundaries.[148]

Lassila and Birnbaum[134] illustrated an interdependence between the grain-boundary concentration of S, the bulk H concentration, and the extent of intergranular fracture. They observed that less bulk H was necessary to produce an equal extent of intergranular fracture with increasing grain-boundary S segregation. Their results are very consistent with those of Bruemmer, et al.,[78] and Jones, et al.,[79] who demonstrated a relationship between the grain-boundary concentration of S and the cathodic overpotential for Ni tested at cathodic potentials in H_2SO_4. The results of Lassila and Birnbaum[134] and Jones, et al.,[79] are shown in Figure 15. The percentage of intergranular fracture is shown as a function of bulk H for various grain-boundary S concentrations in Figure 15(a) and as a function of grain-boundary S for various cathodic potentials in Figure 15(b). Lassila and Birnbaum show that intergranular fracture occurs in the absence of S segregation and the transition from transgranular fracture to intergranular fracture occurs at 300 appm of H. The lowest grain-boundary concentration of S examined by Jones, et al., was 0.04 monolayers, and a cathodic potential of −0.72 V_{SCE} was needed to produce 50% intergranular fracture. While Jones, et al., did not observe intergranular fracture with only H and no S segregation, significant intergranular fracture was observed at very low concentrations of S (0.04 monolayers) at a sufficiently high cathodic potential. Lassila and Birnbaum also concluded that the grain-boundary segregation of H was necessary for H to induce intergranular fracture and H-induced localized plasticity near the grain boundary.[134] They concluded that H-induced localized plasticity and S-induced decohesion were factors in the intergranular fracture mechanism.

In fatigue crack initiation tests of Ni-oriented bicrystals, Vehoff, et al., also observed that intergranular cracks nucleated when S was segregated to the bicrystal boundary, and the samples were fatigue tested in H.[149] No intergranular fracture was observed with only H or S. Persistent slip-band cracking occurred in bicrystals with clean grain boundaries when tested in H. Bicrystals with asymmetrical grain orientations crack more readily than those with symmetrical grain orientations. The bicrystal results are generally consistent with the polycrystalline Ni results, even though the bicrystals were loaded in fatigue, while the polycrystalline materials were loaded monotonically Intergranular crack growth induced by H along "clean" grain boundaries of Ni, as observed by Lassila and Birnbaum,[134] differs from that of Vehoff, et al.,[149] and to some extent from the results of Jones, et al [79] Although Jones, et al., observed intergranular fracture at 0 04 monolayers of S, the trend with decreasing S segregation, Figure 15(b), is toward decreasing or zero intergranular fracture with no S segregation.

Lassila and Birnbaum[134] tested Ni containing internal H and treated to intentionally allow H segregation to the grain boundaries, while Jones, et al.,[79] and Vehoff, et al.,[149] tested Ni in external cathodic and gaseous H, respectively. Samples tested in external H would have a concentration gradient ahead of the crack tip, while samples with presegregated H would have a uniform H concentration along the grain boundary ahead of the crack tip. Therefore, the ability of H to induce intergranular cracks along "clean" grain boundaries may be related to the concentration of H at the grain boundary within the large plastic zone ahead of the crack tip. Evidence for H enrichment at grain boundaries has been presented by Fukushima and Birnbaum using secondary ion mass spectroscopy techniques.[150] They concluded that H was enriched at grain boundaries and free surfaces of Ni and that S on the surface enhanced the H enrichment. In a similar study using electron-stimulated desorption, Jones and Baer evaluated the surface concentration of H on a type 4340 (UNS G43400) steel with a variable surface concentration of S (Figure 25).[151] They observed that H was enriched on S free and partially covered surfaces with a decrease in the H coverage at S coverages above 0.5 monolayers. Lee and Lee[152] reported a H grain-boundary binding energy of 20.5 kJ/mol for Ni, which is consistent with grain boundaries as strong traps for H. Therefore, H grain-boundary segregation is potentially a factor in H-induced intergranular fracture, as suggested by Lassila and Birnbaum.[134] The role that impurity segregation and H segregation play in H-induced intergranular fracture of Ni and Ni-base alloys could be to reduce the intergranular fracture energy or to other related effects on dislocation dynamics. H-induced intergranular fracture mechanisms are discussed in more detail in a later section.

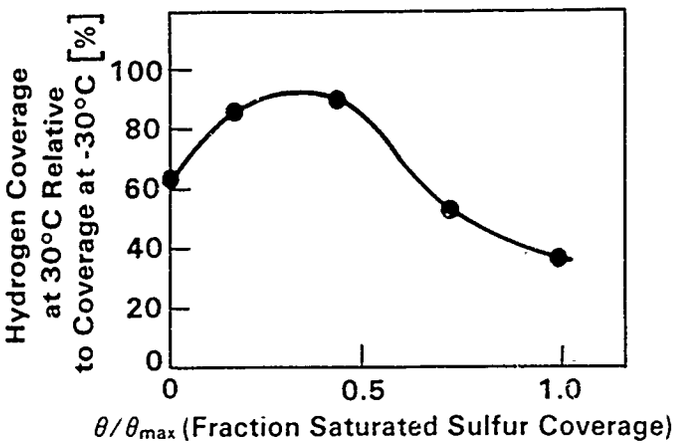


FIGURE 25—Hydrogen coverage on Fe vs S coverage.[151]

The critical distance that H penetrates ahead of a growing crack, the H-transport mechanism, and the rate-limiting step in H-induced subcritical crack growth of Ni and Ni-base alloys are key questions. Kimura and Birnbaum[153] concluded that intergranular crack growth of Ni in the presence of external H could be explained by the grain-boundary diffusion of H.[153] Using the following equation for the annulus area of grain-boundary fracture ratio (GBFR):

$$GBFR = 4b\,[\,a(Dt)^{1/2} - bDt]/a^2 \qquad (2)$$

where a is the sample radius, t is the charging time at 295 K, D is the diffusivity, and b is a constant taken to be equal to 2.0. Kimura and Birnbaum showed an excellent correlation with their experimental data, as shown in Figure 26. A diffusivity of 4×10^{-9} cm^2/s was used (Kumura and Birnbaum[156]). Data obtained from precharged samples showed the best fit with Equation (2), while samples charged during deformation gave results suggesting slower H transport.

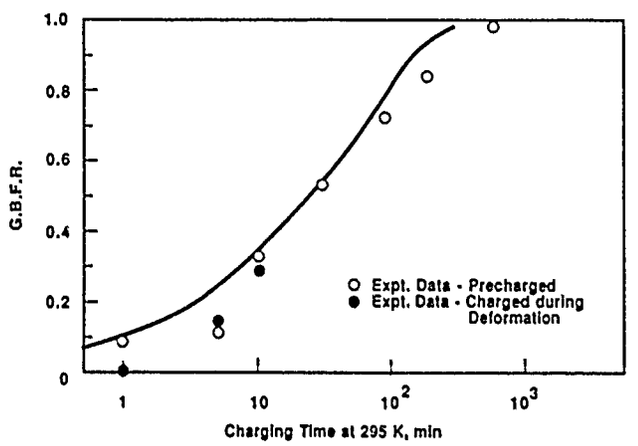


FIGURE 26—Calculated (solid line) and experimental grain-boundary fracture ratio vs cathodic charging time at 22°C.[156]

Transgranular processes

Hydrogen's primary effect in Ni and Ni-base alloys is to induce intergranular fracture, however, transgranular processes such as H transport and effects on dislocation dynamics and morphology are contributing factors. H transport is used here to include absorption from the environment in lattice diffusion and dislocation transport. Effects on dislocation dynamics include possible effects on dislocation mobility such as serrated yielding and H induced plasticity. Dislocation transport of H was first suggested by Bastien and Azou[155] and more recently by Tien, Thompson, and Bernstein.[29] H-induced serrated yielding,[119 123 156 157] strain-enhanced H release,[158] and autoradiographic evidence[159] are used to support the concept that dislocations assist hydrogen transport. The serrated yielding results clearly suggest an interaction between dissolved H and dislocations but do not indicate whether long-range transport occurs. Strain-enhanced H release could result from strain effects on surface processes and need not be due solely to dislocation transport. Frankel and Latanision reported on H-permeation measurements using single and polycrystalline Ni dynamically strained in an electrochemical permeation cell.[160,161] They concluded that enhanced permeation was observed only for single crystals strained in the easy-glide region and that H increased the easy-glide strain. The extent of enhanced permeation was small, on the order of a few percent increase, but their results support earlier observations of H-dislocation interactions. However, no evidence for dislocation transport of H was observed for polycrystalline material undergoing multiple slip. Frankel and Latanision concluded that dislocations are traps for H and under conditions of multiple slip, dislocation tangles reduce the transport distances such that H trapping dominates. Zakroczymski also evaluated the effect of strain on the H permeation through Ni and observed only a slight effect of plastic deformation on the effective diffusivity and permeation of H.[162] He also examined a low-carbon steel and austenitic SS and reached the same conclusion.

Therefore, the picture that emerges regarding dislocation transport of H is one in which H-dislocation interactions do occur, but long-range transport may occur only under selected conditions. In polycrystalline materials in which dislocation/dislocation interactions tend to confine dislocation glide distances and in which a net dislocation flux in the direction of crack growth is unlikely, it appears that dislocation transport of H is unlikely. Since intergranular fracture depths could be correlated with grain-boundary diffusion,[153] it would appear that this is the primary H transport mechanism in polycrystalline Ni and Ni-base alloys. Grain-boundary chemistry and structure would be expected to affect H transport and the critical grain-boundary concentration needed for crack growth. Kimura and Birnbaum[154] have evaluated the effects of S and C segregation in Ni on these parameters based on the kinetics of H charging to attain a GBFR of 0.5.

These results indicate that both S and C segregation decreases the grain-boundary diffusivity of H in Ni; they concluded that S decreased the critical concentration of H needed for fracture, while C had little effect or caused an increase in the critical H concentration. Therefore, grain-boundary impurity segregation can alter the kinetic response of Ni and probably Ni-base alloys to external H. Evaluation of the effect of other impurities such as P and B, which segregate to grain boundaries, on grain-boundary diffusivity and critical grain-boundary concentration of H has not been reported. Also, the effects of grain-boundary precipitates on these parameters would be useful for evaluating their role on crack growth. For instance, the effect of carbides in alloy 600 has been postulated by Bruemmer, et al., as being that of dislocation emission sources reducing the crack-tip stress;[92] however, the carbides may also reduce the grain-boundary H diffusivity or the dislocations emitted from the carbides may trap H. Either effect would increase the resistance to crack growth by H uptake. The crack growth mechanism of alloy 600 in high-temperature water has been suggested as a H-induced crack growth mechanism, although this needs further verification.

Evidence for a H-dislocation interaction in Ni also comes from H solubility studies and the observation of serrated yielding in H-charged Ni. Strong H-dislocation trapping has been suggested by the results of Louthan, et al.,[163] and Lee and Lee.[152] Louthan, et al., also observed an increase in permeation with cold work while Lee and Lee did not. Lee and Lee reported a H-dislocation binding energy of 7.5 to 13.4 kJ/mol and a H grain-boundary binding energy of 20.5 kJ/mol. These results support the contention of Lassila and Birnbaum that grain-boundary segregation of H is an important process in intergranular fracture because H grain boundary binding energy is sizable.[134] Also, H that enters along the grain boundary at the crack tip is not likely to be transported away by dislocation transport or bulk diffusion.

Serrated yielding of H-charged Ni has also provided significant evidence for a H dislocation interaction. These effects have mostly been observed at temperatures below 0 C. Boniszewski and Smith observed serrated yielding and yield points at 80 C in H-charged

Ni.[119] They determined the H-dislocation binding energy to be 7.7 kJ/mol, which is consistent with that reported by Lee and Lee.[152] Wilcox and Smith[121,157] also observed serrated yielding at −80°C and noted that each serration is associated with a dislocation-multiplication process. They also observed that fracture was intergranular and that the embrittlement was most severe under conditions that promoted serrated yielding. Windle and Smith[156] measured the flow properties of H-charged Ni single crystals and observed serrated flow at temperatures of 0 to −125°C, while in polycrystalline Ni,[123] serrated flow was observed at −30 to −130°C. They also concluded that intergranular fracture is enhanced under conditions that promote serrated flow and that H may reduce the SFE of Ni from 240 to 155 erg/cm^2.

While several authors observed that intergranular fracture is pronounced under conditions that promote serrated flow, intergranular fracture occurs under conditions in which serrated flow does not occur. Therefore, while the effects of H on the dislocation dynamics of Ni that cause serrated flow may contribute to intergranular fracture, these processes do not appear to be necessary. Wilcox and Smith concluded that the observed H-dislocation interactions contribute to intergranular fracture by dislocation transport of H to the grain boundaries.[157] The absence of long-range dislocation transport in the experiments of Frankel and Latanision[160,161] and Zakroczymski[162] suggest that only short-range transport occurs. In fact, the results of Frankel and Latanision showed dislocation transport of H in single crystals undergoing easy glide so that short-range transport from some distance within a grain to the grain boundary is quite feasible. Since Wilcox and Smith evaluated Ni with internal H, presumably short-range transport would significantly increase the grain-boundary concentration of H, and since the H grain-boundary binding energy exceeds the H-dislocation binding energy, H would be deposited at the grain boundary.

Increases in the strain-hardening rates of H-charged Ni have also been reported as evidence for a H-dislocation interaction.[119,121,123,156,157] Wilcox and Smith[157] concluded from etch-pit and transmission electron microscopy studies that the increased strain hardening in H-charged Ni resulted from an increase in the dislocation density. They suggested that each serrated yielding event was associated with a dislocation multiplication process that produced a greater dislocation density per unit strain than in the absence of H. A decrease in the strain-hardening rate for Ni deformed at cathodic potentials has been reported by Lunarska and Flis.[164] They concluded that the decrease was a result of redistribution of the subsurface stress and by the generation of new glissile dislocations. There is possibly a difference between the strain-hardening response of Ni with internal H and external H. For the internal case, H can redistribute and interact uniformly with the dislocations, while for the external case, the stresses associated with hydrogen uptake result in softening.

No increase in the yield strength was reported in early research on H-charged Ni,[119,121,123,156,157] although more recent work by Eastman, et al.,[165] indicated that H is a solid-solution strengthener in high-purity Ni. H also caused solid-solution softening in less pure Ni and especially in high-carbon material. Eastman, et al., suggested that the thermodynamics of C-C interactions may be affected by the formation of C-H pairs, or alternatively that H affects the strain field around C-C pairs. In any event, there is evidence that internal H can cause an increase, no change, or a decrease in the yield strength of Ni.

Wilcox and Smith[157] reported a factor of 2 increase in the dislocation density of H-charged Ni strained to 0.1; however, McInteer, et al.[166] and Robertson and Birnbaum[167] have reported no change in the dislocation cell structure or dislocation density. The latter observations were made on material strained at 25°C, while Wilcox and Smith evaluated material that was strained at −80°C and serrated yielding was prominent. Wilcox and Smith associated the increased dislocation density to the serrated yielding process. It appears that H has no effect on the dislocation density or structure of strained Ni at 25°C. H may cause a small increase in the dislocation density at −80°C.

H contributes to intergranular fracture by segregation to grain boundaries for H-precharged materials or by diffusion along grain boundaries for crack growth in external H. The contribution of H-dislocation interactions on intergranular fracture of Ni is more subtle. Wilcox and Smith concluded that dislocations transport dissolved H to the grain boundaries and thus increase the local H concentration and perhaps also the local stress. H causes solid-solution hardening in high-purity material and increased strain hardening. Either process could lead to increased local crack-tip stresses that promote fracture. However, Eastman, et al., observed that H causes solid-solution softening.[165,168] Deformation studies in a high-voltage electron microscope with a H-gas environment[168] indicated that this softening was associated with enhanced dislocation mobility along planes[109] ahead of the crack tip. In subsequent *in situ* studies, Robertson, et al., observed crack extension by planar slip adjacent to the grain boundaries.[169] They concluded that H in or near the grain boundaries promoted alternating planar slip adjacent to the grain boundaries and, ultimately, transgranular crack growth that propagated along the grain boundary. Robertson, et al.,[169] suggested that this is a H-induced intergranular crack growth mechanism; however, there is considerable evidence that impurity segregation enhances H-induced subcritical crack growth and that impurity effects are expected to be localized to the grain boundary.[78,79] Also, H-charging is used to promote intergranular fracture for *in situ* AES analysis, and this fracture is clearly along the grain boundary, not on alternating planes,[109] since the AES electron-escape depth for the elements of interest (S, P, Sb) is very small. Fatigue crack growth in single crystals of Ni tested in acidic solutions and H gas by Vehoff and Klameth[170] support the observation of Robertson, et al.,[169] of crack extension along slip planes,[109] although local brittle fracture along planes[100] was also observed by Vehoff and Klameth.

Formation of LRO in highly cold-worked alloy C-276 is an added feature to the H-induced crack growth of Ni-base alloys,[134] which is not a factor in Ni and solid-solution strengthened Ni alloys. It has been demonstrated that H permeation increases with the development of ordered zones[171] and that crack growth in H-bearing environments is related to H transport.[172] Alternatively, Berkowitz and Kane concluded that the H-induced crack growth of alloy C-276 was related to grain-boundary P segregation.[35] In studies of H embrittlement of a Ni_2Cr alloy, Berkowitz, et al.,[173] found that the disordered and 100%-ordered alloy were more susceptible to H embrittlement than the 40% to 50% ordered condition (Figure 27). An explanation for this effect was an increase in slip planarity with ordering and thus in H transported by dislocations. From the work of Frankel and Latanision[160] on H permeation in single-crystal Ni, increased slip planarity could contribute to dislocation transport of H. However, the increased permeation from this process is expected to be small. The effects of slip planarity on dislocation transport of hydrogen is more likely to influence the local redistribution of internal H to grain boundaries and not to uptake from the external environment. Mezzanote, et al.,[171] observed a factor of 2 increase in H permeation following aging for 100 h at 500°C. Whether this is sufficient to explain the susceptibility of alloy C-276 to H-bearing environments remains an open question.

Hydrogen-induced crack growth mechanisms

A comprehensive list of crack growth mechanisms includes the processes that affect the kinetics of crack growth as well as the critical processes that account for atomic separation. A summary of these secondary processes such as H uptake and transport, ordering, and segregation have been reviewed in the sections on intergranular and transgranular processes. In this section, the mechanisms that can account for atomic separation will be reviewed, and since the primary failure mode of Ni and Ni-base alloys in H is intergranular, those mechanisms dealing with intergranular separation will be emphasized. These mechanisms include (1) intergranular decohesion by H and impurity segregation; (2) enhanced planar slip and near grain-boundary shear failure; (3) reduced surface energy; and (4) formation of a brittle grain-boundary hydride.

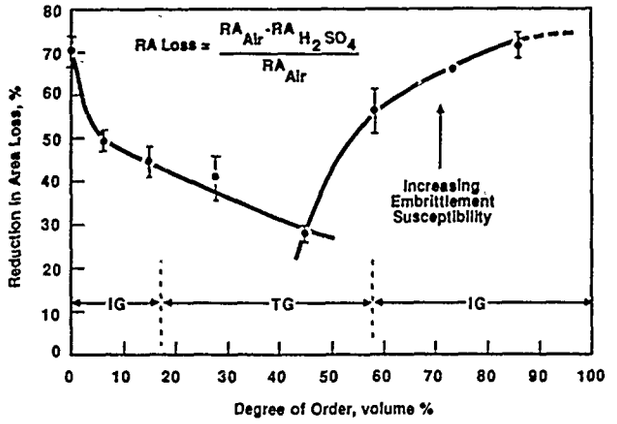


FIGURE 27—The effect of the degree of order on the embrittlement susceptibility of Ni_2Cr. Regions of intergranular and ductile transgranular failure are shown.[173]

Deuterium segregation to grain boundaries has been detected using secondary ion mass spectroscopy by Fukushima and Birnbaum[150] in support of the suggestion by Lassila and Birnbaum.[134] However, embedded-atom calculations by Baskes and Vitek indicate that H is not readily trapped at clean, defect-free grain boundaries of Ni [174] Differences in the experimental observation of Fukushima and Birnbaum and the theoretical calculations of Baskes and Vitek could result from the H binding energy between clean, defect-free grain boundaries being substantially different from grain boundaries with impurity segregation and defects. Also, the results of Fukushima and Birnbaum showed deuterium profiles extending 75 nm from the boundary, which is not consistent with equilibrium segregation, that are located within one or two atom layers of the interface. H atoms located several atom distances from the interface are not likely to contribute to intergranular decohesion but could alter dislocation behavior near the grain boundary. Therefore, that H can concentrate at grain boundaries and contribute directly to decohesion of Ni has not been demonstrated; however, there are theoretical calculations that suggest that segregated H would contribute to decohesion.

Daw and Baskes, using the embedded-atom method, concluded that when slip is constrained, H at the crack tip of Ni reduces the stress required to break Ni-Ni bonds.[175] When slip is allowed, these same authors found that H assisted dislocation emission from the crack tip of Ni and also reduced the brittle fracture stress.[176] A conclusion regarding the interdependence of these two processes was not possible with the embedded-atom method calculations. Molecular orbital calculations have indicated that it is possible for impurities such as S to reduce the intergranular fracture stress. Briant and Messmer, using detailed electronic structure calculations, concluded that S in the grain boundaries of Ni forms very strong bonds within the plane of the grain boundary while weakening the Ni-Ni bonds that run adjacent to the boundary.[177] Intergranular fracture was hypothesized to occur between Ni atoms adjacent to the grain boundary Eberhart, et al.,[178] performed molecular orbital calculations of a Ni-S cluster and concluded that there is a significant S-S interaction within the grain boundary when the S-S distances are less than 0.376 nm They concluded that at a critical grain-boundary concentration, the grain-boundary cohesive strength is decreased and the shear strength is increased. Both conditions were considered necessary for intergranular fracture Also, it was suggested that S and H in the grain boundary formed a bonding network that enhanced intergranular fracture Therefore, atomistic calculations suggest that H could contribute to intergranular fracture in Ni, and that this contribution is enhanced by impurity segregation. Birnbaum and coworkers[167-169] and Lynch[179] have suggested H-enhanced plasticity as a mechanism for H-induced crack growth. Robertson, et al., performed *in situ* high-voltage electron microscopy (HVEM) tensile fracture studies of Ni in a H-gas environment and observed that fracture occurred in the vicinity of the grain boundary but not along the grain-boundary interface.[169] Localized plasticity, which is thought to be enhanced by H, accompanied crack growth on planes vicinal to the grain boundary. Vehoff and Klameth[170] have reported H-induced crack growth along slip planes in fatigue tests on single crystals.[109] Therefore, it appears that H-induced shear fracture of Ni is feasible, but the relationship of H-induced plasticity and the transgranular fractures observed by Robertson, et al.,[169] to intergranular fracture in macroscopic samples remains uncertain. The lack of plastic constraint in thin (< 1 μm) HVEM samples appears to favor plastic-fracture processes over decohesion. It is conceivable that H-induced plasticity in slip planes adjacent to the grain boundary could enhance decohesion by increasing the local stress on the grain boundary. Many fractures reported as intergranular may indeed be mixed mode between decohesion along the interface and shear failure adjacent to the grain boundary with the proportion of decohesion increasing with grain-boundary impurity concentration.

Lassila and Birnbaum[134] observed extensive slip traces on the intergranular fracture surfaces of H-charged Ni and a lower density of slip traces on "brittle" intergranular fracture surfaces produced without H in samples with a thin grain-boundary sulfide. No change in the slip-line spacing was found with changes in the H concentration. However, Jones et al.,[81] found similar slip-line spacings on Ni + P samples that were cracked at anodic potentials in 1 N H_2SO_4, as those observed by Lassila and Birnbaum. Therefore, evidence for a mixed intergranular–transgranular H-crack growth process has not been presented at this time. A detailed study of fracture surface morphology as a function of grain-boundary S and H concentrations is needed to clarify whether such a mixed fracture process occurs.

A surface-energy argument to explain H-induced intergranular fracture has been suggested by the analysis of Rice,[180] who used the interfacial crack growth model of Rice and Thomson[181] and the solute segregation–interfacial fracture model of Mason.[182] The Rice and Thomson interfacial crack growth model considers the activation energy for dislocation emission vs brittle intergranular crack extension. Brittle intergranular crack extension is based primarily on the ideal work of fracture, which is a function of the grain-boundary surface energy in the absence of plastic deformation. Rice treated as a segregant and used the data of Petch[183] for the change in the surface energy of Ni with H. Using appropriate parameters for face-centered cubic (fcc) Ni, Rice concluded that the Rice-Thomson model predicts that intergranular fracture of Ni is favored if the surface energy is reduced by 750 ergs/cm^2.[180] The Petch data indicate that such a decrease is possible. However, the relevance of the Rice-Thomson model to intergranular fracture of Ni, which is preceded by significant plastic deformation, is not clear, because this model is based on an evaluation between dislocation emission from the crack tip and intergranular decohesion. Matrix dislocations would have to be sufficiently pinned to make crack-tip emission more difficult than bulk dislocation movement and both processes more difficult than intergranular decohesion.

Nickel-hydride formation has been an elusive mechanism that has been postulated to explain H-induced crack growth of Ni and Ni-base alloys. Convincing evidence that Ni hydride forms at high H fugacities during cathodic charging has been presented.[184-186] Wayman and Smith observed beta hydride in Ni and gamma hydride in Ni-20%Fe alloys with x-ray diffraction following cathodic charging at 1 A/cm^2 for 1 h.[184] Upon removal of the cathodic-charging current, the hydride decomposed with the beta hydride decomposing slower than the gamma hydride. Decomposition took several hours and was controlled by H transport. Hinotani, et al., observed beta hydride by x-ray diffraction of Ni-Cr-Fe alloys charged with H at a current density of 40 mA/cm^2 for 24 h,[185] although hydrides were observed in a 50%Ni-20%Cr-30% Fe alloy after 600 s at 10 mA/cm^2. Hydrides were observed in alloys with Ni concentrations ranging from 30% to 60%, with the loss in ductility being more severe with increasing Ni concentration. Surface cracks appeared at grain boundaries and the interfaces of microtwins after H charging ceased.[109] The authors concluded that the surface cracks occurred during the decomposition

of the hydride and that the tendency to intergranular fracture and concurrent loss in ductility with increasing Ni content resulted from the reduced microtwin formation and increased intergranular hydride-induced microcracking with increasing Ni content. In a recent study, Tseng, et al., observed surface hydrides in Ni following H charging at 10 mA/cm^2 for 5 h [186] They used a chemical method that relies on adsorbed, H-reducing Ag ions in a Ag-nitrate solution. A surface phase is clearly revealed with this technique, although no phase identification was made. A key feature in all of these studies[184-186] is the use of a H-recombination poison, that for a given H-reduction rate results in a much greater surface activity than in the absence of the poison.

Clearly, Ni hydrides can be formed by cathodic charging at current densities as low as 10 mA/cm^2 for 600 s when a H recombination poison is added to the electrolyte. A key question is whether hydrides are involved in the H-induced crack growth results of Ni and Ni-base alloys precharged cathodically with H or tested at cathodic potentials. In the study by Bruemmer, et al.,[78] straining electrode tests of Ni were conducted at current densities of 0.01 mA/cm^2 to 100 mA/cm^2 without a recombination poison. No effort was made to determine if hydrides had formed, although the results do not show a discontinuity across this wide current density range, suggestive of a change in crack growth mechanism. Since hydrides are not expected at current densities below 10 mA/cm^2, a discontinuity would have been expected in the results as a function of increasing current density.

Dissolution-Controlled Crack Growth Processes

SCC of Ni-base alloys is a complex process that may involve the simultaneous occurrence of several mechanisms such as active path dissolution, film rupture, and H embrittlement. Other intergranular and transgranular processes contribute to these mechanisms. For instance, the presence of carbides at the grain boundaries can cause localized deformation[187-189] that alters the grain-boundary stress, although the crack growth mechanism may not be affected. Also, the presence of precipitates that act as cathodes may contribute to crack growth by the generation of H A summary of the intergranular and transgranular crack growth processes is covered in the next two sections followed by a discussion of crack growth mechanisms.

Intergranular processes

Impurity segregation to grain boundaries is an intergranular process that has been demonstrated to affect IGSCC in Ni in low temperature environments, but a clear demonstration in Ni-base alloys has not been presented. S and P are the impurities most likely to be enriched at the grain boundaries of Ni-base alloys. Jones, et al., evaluated the effect of these impurities on the IGSCC of Ni in 1 N H_2SO_4 at 25°C and found that P induced IGSCC and IGC, but S did not induce IGSCC and produced only shallow IGC.[81] Evaluation of the effect of these two elements on the passivity of Ni revealed that a thin, implanted layer of P will inhibit passivity, but P is oxidized, and Ni passivates upon complete oxidation of P. S is somewhat more complex, it was shown to enhance the active corrosion rate and appeared to inhibit passivity similarly to the results of Marcus, et al.[190] However, if IR correction is used, the passivation potential of Ni is unchanged in the presence of S. Therefore, at a crack tip, an IR drop could shield the crack walls and tip from the applied potential, it was concluded that the crack walls and crack tip remained active. At high potentials, both the crack walls and crack tip could passivate. Either condition was shown to result in shallow IGC and a lack of IGSCC with a crack-tip corrosion model.

Evidence that impurity segregation induces IGSCC of Ni alloys in high-temperature water or at high pHs is not very convincing. As mentioned previously, S has been proposed as contributing to the IGSCC of alloy 600,[3 16] but direct evidence is lacking. In oxidizing environments, P has been shown to cause IGC of Ni-base alloys;[87,89-91,96 97] however, Was found that P segregation did not cause IGSCC in a low-carbon alloy 600.[100]

Cr-carbide precipitation at grain boundaries and Cr depletion have been shown to occur in alloy 600 in a manner analogous to austenitic SSs. However, carbide-precipitation effects occur at higher temperatures and lower C concentrations in Ni-base alloys relative to austenitic SSs. Also, overlapping crack growth mechanisms such as H-induced crack growth and carbide effects on microdeformation apparently complicate the relationship between Cr depletion and IGSCC. Bandy, et al., concluded that a sensitized structure was the cause of IGSCC of alloy 600 but that cracking was a combination of anodic dissolution and intergranular brittle fracture.[191] Was and Rajan found a specific relationship between the grain-boundary Cr content and IGC and IGSCC, where a grain-boundary Cr concentration less than 5% was found to promote rapid IGSCC and 12% gave complete protection in sodium tetrathionate solutions.[53] Therefore, it would appear that under some circumstances a sensitized microstructure contributes to the IGSCC of solid-solution Ni-base alloys.

The presence of carbides and intermetallic precipitates at the grain boundaries of Ni-base alloys can cause effects other than Cr depletion. It has been suggested by Bruemmer, et al., that grain-boundary carbides promote crack-tip deformation by acting as sources for dislocation emission.[187-189] Presumably, the localized deformation relaxes the crack-tip stress and the mechanical driving force for crack extension. This type of mechanism was proposed for alloy 600 in deaerated high-temperature water and caustic environments. In low-temperature sodium thiosulfate and sodium tetrathionate solutions, Bandy, et al., proposed that lamellar grain-boundary carbides assisted brittle intergranular fracture.[191] Evidence for an intergranular mechanical fracture was based on crack velocities exceeding those attributable to anodic current densities in an active path dissolution mechanism. A process in which intermetallic precipitates on grain boundaries contribute to local galvanic cells has been proposed for alloy X-750 by Hosoya, et al.[50] In this case, they determined that the Ni_3 (Al,Ti) phase was highly active relative to the matrix and did not passivate at temperatures around 100°C. Based on this observation, Hosoya, et al., concluded that crack growth of alloy X-750 at 93°C was by H embrittlement, but at higher temperatures the Ni_3(Al,Ti) phase was able to passivate so that the galvanic current was substantially less than at 93°C. Under these circumstances, it was concluded that crack growth was an anodic-dissolution mechanism.

Transgranular processes

There are several transgranular effects that have a bearing on SCC of Ni-base alloys These include bulk composition and general corroson resistance and slip planarity from low SFE or coherent precipitates Alloying elements that are added to Ni to increase its corrosion resistance include Cr for oxidizing conditions and Cu, Mo, and W in nonoxidizing acids. Cr reduces the stacking fault of Ni and can increase slip planarity, while ordering and coherent precipitates also increase slip planarity. Slip planarity has been identified as a factor in H-induced subcritical crack growth, but its effect on SCC of Ni-base alloys is not as well established. In austenitic alloys, slip planarity has been identified as contributing to transgranular stress corrosion through a slip-dissolution process. Transgranular stress corrosion of Ni-base alloys involving an anodic-dissolution process is uncommon, although Asphahani has observed TGSCC of alloy C-276 when tested in NaOH.[192] It is possible that planar slip could contribute to IGSCC by increasing the local grain-boundary stress. Bruemmer, et al , concluded that transgranular carbide precipitation, which promoted dislocation cell structures, contributed to IGSCC of alloy 600 because dislocation emission from grain-boundary carbides was impeded.[187,189] This led to less stress relaxation at the crack tip and increased IGSCC.

Anodic-dissolution crack growth mechanisms

Anodic-dissolution-controlled crack growth mechanisms are referred to as those in which the crack extension process results directly from anodic-dissolution processes. Included in this section

are active path and film-rupture mechanisms, as opposed to a H-induced crack growth process. However, also included are mechanical fracture processes that occur simultaneously with the anodic process or that may be induced by the anodic process. More than one of these processes may occur simultaneously.

In Ni or Ni-base alloys, active path stress corrosion occurs primarily along grain boundaries because of local microchemistry effects, such as segregation or depletion of specific elements, as discussed previously. For impurity segregation in Ni, Jones, et al., have shown that at low temperatures in low-pH solutions, P promotes IGSCC while S does not.[81] The crack velocity for an active path process is described in its simplest form below:[193]

$$da/dt = i\,M/zF^3 \qquad (3)$$

where i is the bare-surface current density, M is the atomic weight, z is the valence, and F is Faraday's constant and the material density. For a crack growing along a grain boundary enriched in a species that inhibits passive film growth such that the grain boundary remains in the "bared" condition, and there are no transport limitations within the crack, Equation (3) describes the maximum permissible crack velocity. Using Equation (3) and data on current density vs P-concentration data, Jones, et al., determined that the calculated crack velocity was about 10 times less than the measured velocity at high-stress intensities where crack transport limitations are minimal.[81] Potential processes that account for experimental crack velocities exceeding calculated velocities will be discussed below.

There are a number of processes that can retard crack velocities below those given by Equation (3). These processes include crack geometry and crack width effects on crack-tip chemistry and corrosion rate, salt or passive film formation, crack-tip shielding and crack deflection. Danielson, et al., evaluated the effects of crack length and width on the crack-tip corrosion rate for an active path corrosion process.[194] The results of crack-tip chemistry modeling are shown in Figure 28 for crack lengths of 0.25 mm to 3 mm and crack angles up to 3°. The crack length and angle effect results from the contribution of the crack-wall corrosion to the total metal ion concentration in the crack. Even though the crack wall was assumed to be passive and the tip was active, at small crack volumes, the crack-wall contribution is significant. Changes in crack angle result from sample stress; the angle increases with increasing stress. The results in Figure 28 show that the dependence of the crack-tip current density on crack angle decreases with decreasing crack length. For crack lengths of 0.5 mm or less, the crack-tip current density is independent of crack angle or stress–stress intensity. This is the regime in which IGC and IGSCC cannot be distinguished because there is no stress dependence; however, for longer penetrations there is a definite stress or stress-intensity dependence. The maximum current corresponds to the corrosion rate of the P-enriched grain boundary without any rate-limiting processes such as crack transport. Results in Figure 28 suggest that the K_{ISCC} and the transition from Stage I to Stage II cracking are crack-length dependent, as shown schematically in Figure 29. Experimental evidence for crack-length effects in anodic dissolution-controlled SCC is not presently available and represents a fruitful area of research.

Passive- or salt-film formation at the crack tip can retard the crack-tip corrosion rate and crack velocity to values lower than the active path values. A film-rupture model presented by Ford, as given below, expresses the crack velocity as a function of the time (t_f) between film-rupture events and the charge density (Q_f) passed between the time of film ruptures and re-forms:[143]

$$da/dt = M\,Q_f/z\,F\,t_f \qquad (4)$$

This model is an adaptation of a slip-dissolution model, originally presented by Vermilyea, which considers the corrosion that occurred on a slip plane following slip rupture of a passive film.[195] For active path dissolution retarded by film growth, crystallographic slip will only rarely produce a slip surface that coincides with the active path along the grain boundary. Therefore, the more general concept of crack-tip strain causing rupture of a passive or salt film is a more appropriate description. Ford has also expressed Equation (2) in terms of the crack-tip strain rate, film-rupture strain, and repassivation time, and more recently in terms of the applied stress intensity as given below.

$$da/dt = (7.8 \times 10^{-3}\,n3.6)(6 \times 10^{-14}\,K_4)^n \qquad (5)$$

where n is a function of the material condition, corrosion potential, and solution conductivity and K is the stress intensity. The value for n ranges between 0.5 and 1, which gives a K exponent between 2 and 4. Jones, et al., evaluated the stress-intensity dependence for crack growth of SSs and found that the exponent for K in Stage I ranged from 7 to 24,[196] which is considerably larger than the value given by Equation (5). Therefore, this equation describes more of a steady-state crack velocity, such as in Stage II, where the stress-intensity dependence is very small. Ford's analysis has been used for austenitic SSs and ferritic steels, but a detailed application to Ni-base alloys has not been made. Jones, et al.,[197] determined the crack velocity–stress-intensity dependence of Ni + P in 1 N H_2SO_4 at +900 mV_{SCE} and found that Stage I had a very large K exponent of 41. At cathodic potentials, Ni had an exponent of 17 and alloy C-276 had an exponent that ranged from 5 to 41 as discussed in the section on H effects. Based on these values, it is possible that Ni-base alloys exhibit the classic Stage I with strong K dependence and a Stage II with small K dependence, at this time, there are insufficient data to make such a conclusion possible.

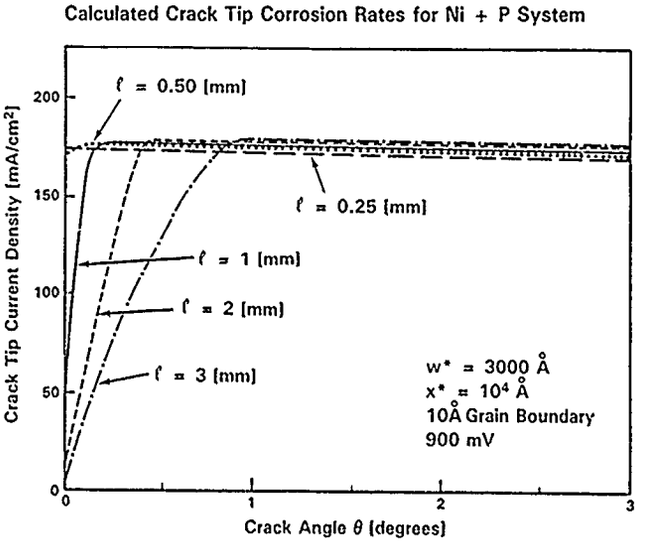


FIGURE 28 - Calculated crack-tip corrosion rates vs crack angle for Ni+P.[194]

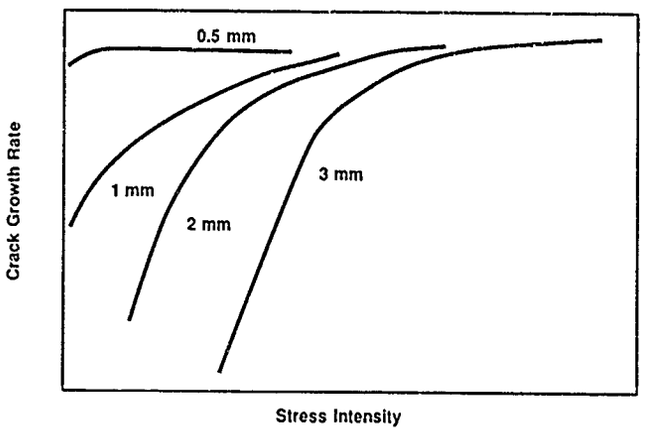


FIGURE 29—Schematic of crack growth rate vs stress intensity for various crack lengths, based on calculated crack-tip corrosion rate vs crack-angle results.

Mechanical fracture accompanying active path dissolution with or without film rupture has been suggested by Jones, et al.,[81] to explain the crack velocities of Ni+P and by Bandy, et al.,[191] to explain the crack velocity of alloy 600. Mechanical fracture during TGSCC of brasses has been presented as a stress corrosion mechanism by several studies.[198-207] Evidence for discontinuous crack advance includes a correlation between acoustic emission (AE) and current pulses and fractographic analysis.

Jones, et al., found that the measured crack velocity of Ni+P was about a factor of 10 greater than that determined by the active path mechanism, with no film formation and the grain-boundary current density determined with bulk Ni+P alloys.[81] Crack-tip corrosion-rate analysis also indicated that for crack angles corresponding to the high-stress-intensity Stage II crack growth regime, the crack-tip corrosion rate was not controlled by crack-transport limitations and the tip corrosion rate equaled that of a flat plate. The approach used by Jones, et al., is illustrated in Figure 10; it was suggested that active path dissolution along a P-enriched grain boundary could sharpen the crack, raise the local stress, and induce mechanic fracture. The geometry for a propagating (Ni+P) vs nonpropagating (Ni+S) crack [Figure 30(b)] was consistent with crack-tip shapes below and above the blunting line. The sequential process detailed in Figure 30(a) suggested that corrosion along a 1- to 2-nm-wide grain boundary enriched in an active element such as P could sharpen the grain boundary such that the crack tip is sharper than the tearing modulus for a radius p, and crack extension occurs to bring the crack into correspondence with a tearing modulus of p_2. Since some plastic deformation and crack blunting is likely to accompany the mechanical fracture, the crack-tip condition now corresponds to that of a blunter crack-tip radius such as p, but with a new crack length a_2. Resharpening of the crack tip by localized grain-boundary corrosion could resharpen the tip, which again induces mechanical fracture. Whether crack extension will occur by mechanical fracture or whether crack-tip sharpening by localized corrosion induces plastic flow without crack extension is a key question that has not been answered.

In an effort to detect mechanical fracture, Jones and Friesel[196] have monitored the AE emanating during subcritical crack growth of Ni+P. An AE event rate of 800 events/mm^2 of crack extension was detected; however, at present, the events detected appear to correlate with the fracture of ligaments such as transgranular ligaments or inclusion behind the crack tip. Detection of short 10-μm crack jumps was not feasible, and no conclusion could be reached regarding intergranular mechanical fracture. Bandy, et al., suggested that the high crack velocities of alloy 600 tested in thiosulfate and tetrathionate solutions correlated with the presence of large grain-boundary carbides.[191] Intergranular fracture extending beyond the grain-boundary carbides was considered a possibility, although no detailed mechanics or AE analysis was performed to verify the hypothesis.

In summary, evidence for identifying specific crack growth mechanisms in Ni-base alloys is sparse. There is some evidence that the crack growth mechanism in Ni with P-enriched grain boundaries can be described by active path dissolution with the possibility of mechanical fracture. For alloy 600, Cr depletion on activate path dissolution and Cr-carbide effects on crack-tip strain or mechanical fracture are processes that have been identified. Alloy X-750 has the additional effect of galvanic coupling between intermetallic phases and the matrix, which may contribute to crack growth.

Summary

Nickel base alloys exhibit environment-induced crack growth in a variety of environments. This cracking is controlled by the well-established stress corrosion parameters: (1) material microstructure/microchemistry, (2) environment, and (3) stress. Examples of microstructural effects include grain boundary carbide precipitation, slip planarity induced by LRO, grain boundary impurity segregation, and intermetallic phase precipitation. Sensitization occurs in Ni-base alloys but appears to promote cracking only in oxidizing environments, while grain-boundary carbide precipitation is beneficial in high-purity water environments. Slip-planarity effects contribute to hydrogen-induced crack growth by assisting local hydrogen transport to the grain boundaries and/or contributing to grain-boundary tensile stresses. Impurity segregation of elements such as P and S have been clearly related to hydrogen-induced crack growth but only implicated in crack growth in aqueous environments. It has been suggested that intermetallic phases such as gamma prime produce local corrosion cells at the crack tip and thus a high hydrogen activity.

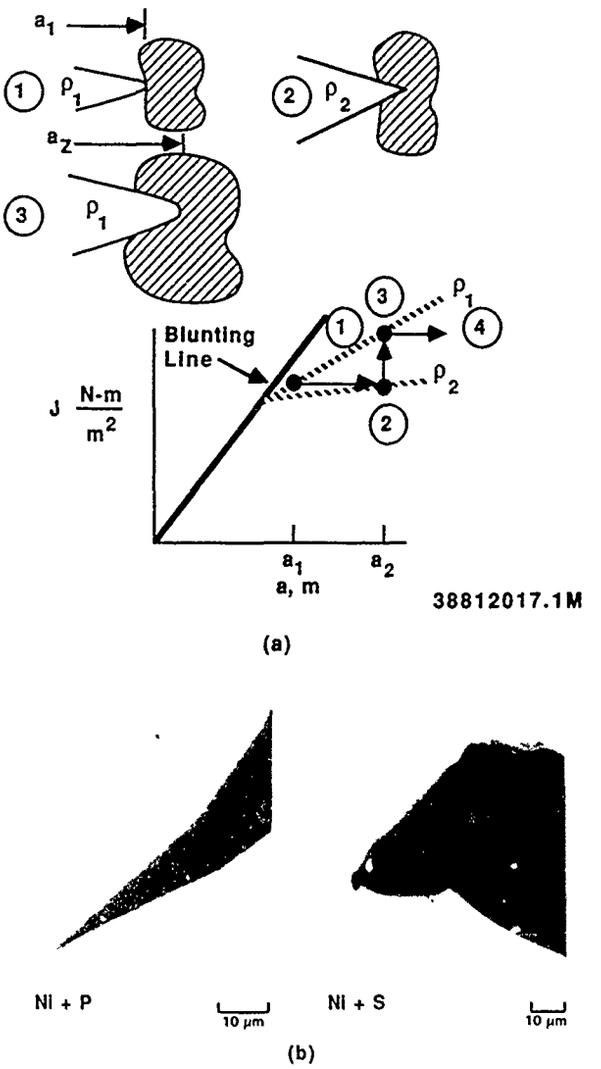


FIGURE 30—Schematic of a corrosion-assisted ductile intergranular fracure mechanism.[81]

Nickel-base alloys crack in high-purity water, although the crack velocities are relatively slow compared to austenitic SSs. Water impurities such as Cl, $Na_2S_2O_3$, O_2, etc., accelerate crack growth rates as they do in Fe-Cr-Ni alloys. Irradiation that produces an oxidizing environment induces cracking in nickel-base alloys and Fe-Cr-Ni alloys. Cracking occurs more readily in acidic environments and hydrogen gas in nickel-base alloys as compared to Fe-Cr-Ni alloys, and hydrogen has been implicated in the crack growth of alloy 600 in high-temperature water. Concentrated caustic solutions have been used to simulate some service environments, and crack growth has been observed in nickel-base alloys in the active-to-passive transition in these solutions.

Quantitative relationships between stress, stress intensity and strain rate, and crack growth rate are essentially unknown for nickel-base alloys. SCC tests have been primarily U-bend and CERT, which produce information on relative susceptibility but not

detailed relationships. Some information on crack growth rates and temperature dependence of crack growth rate has been obtained with these techniques, but the data needed to develop the stress and stress-intensity dependence of cracking are absent.

Improved understanding of the mechanisms of environment-induced crack growth of nickel-base alloys requires further research in the following areas:

(1) The role of grain-boundary carbides on crack growth in nonoxidizing environments;
(2) The role of intermetallic phases;
(3) The relationship between LRO and impurity segregation on crack growth in hydrogen-bearing environments;
(4) Grain-boundary hydrogen concentrations and critical concentrations for IG fracture;
(5) Grain-boundary hydrogen-transport rates, impurity trapping, disloction transport over short distances (cell diameter);
(6) Quantitative da/dt vs K in high-temperature water, and
(7) da/dt vs strain rate in high-temperature water.

This list may not be exhaustive, but it represents the most glaring unknowns encountered in writing this review.

Acknowledgment

The authors wish to express their appreciation to A.I. Asphahani, T. Harris, and I.S. Hwang for review of the manuscript and to M.I. Cochran for preparing the manuscript. Research support from the Office of Basic Energy Sciences, Division of Materials Sciences of the U.S. Department of Energy under contract DE-AC06-76RL0 1830, which made possible the research contributions and preparation of this review, is greatly appreciated.

References

1. R.M. Latanision, R.W. Staehle, Fundamental Aspects of Stress Corrosion Cracking, ed. R.W. Staehle, A.J. Forty, D. van Rooyen (Houston, TX. National Association of Corrosion Engineers, 1969), p. 214.
2. R.L Cowan, G.M. Gordon, Stress Corrosion Cracking and Hydrogen Embrittlement of Iron-Base Alloys, ed. R.W. Staehle, J. Hochmann, R.D. McCright, J.E. Slater (Houston, TX: NACE, 1977), p. 845.
3. J. Blanchet, H. Coriou, L. Grall, C. Mathieu, C. Otter, G. Turluer Stress Corrosion Cracking and Hydrogen Embrittlement of Iron-Base Alloys, p. 1149.
4. G.J. Theus, R.W. Staehle, Stress Corrosion Cracking and Hydrogen Embrittlement of Iron-Base Alloys, p. 1023.
5. A.J. Sedriks, J. Inst. Met. 101(1973): p. 225.
6 R.W. Staehle, J.J. Royuela, T.L. Raredon, E. Serrate, C.R. Morin, R.W. Farrar, Corrosion 26, 11(1970): p. 451.
7. A.W. Thompson, I.M. Bernstein, Rev. Coat. Corros. 2(1975). p. 5.
8. H.E. Hanninen, Int. Metals Rev. 3, 241(1979): p. 85.
9. R.M. Latanision, Corrosion of Nickel-Base Alloys, ed. R.C. Scarberry (Metals Park, OH. ASM International, 1984), p. 13.
10. H. Hanninen, I. Aho-Mantila, 3rd International Symposium on Environmental Degradation of Materials in Nuclear Power Systems—Water Reactors (1987), p. 77.
11. J. Kolts, N. Sridhar, Corrosion of Nickel-Base Alloys, p. 199.
12. A.W. Thompson, I.M. Bernstein, Advances in Corrosion Science and Technology, Vol. 7, ed. M.G. Fontana, R.W. Staehle (New York, NY: Plenum Press, 1980), p. 53.
13. C.L. Briant, C.S. OToole, E.L. Hall, Corrosion 42, 1(1986). p. 15.
14. H.R. Copson, G. Economy, Corrosion 24, 3(1968): p. 55.
15. R.C. Scarberry, S.C. Pearman, J.R. Crum, Corrosion 32, 10(1976): p. 401.
16. H. Coriou, L. Grall, C. Mathieu, M. Pleas, Corrosion 22, 10(1966): p. 280.
17. D. van Rooyen, Corrosion 31, 9(1975): p. 327.
18. R. Bandy, D. van Rooyen, Corrosion 40, 8(1984). p. 425.
19. H.A. Domian, R.H. Emanuelson, L.W. Sarver, G.J. Theus, L Katz, Corrosion 33, 1(1977): p. 26.
20. G.P. Airey, Corrosion 35, 3(1979): p. 129.
21. S. Floreen, J.L. Nelson, Metall. Trans. A 14A(1983), p. 133.
22. S. Hattori, Private Communication, reported in Reference 8.
23. D. van Rooyen, Predictive Methods for Assessing Corrosion Damage to BWR Piping and PWR Steam Generators, ed. H. Okada, R.W. Staehle (Houston, TX: NACE, 1982), p. 383.
24. P.W. Rice, Materials Performance 17, 9(1978): p. 16.
25. R.D. Kane, M. Watkins, D.F. Jacobs, G.L. Hancock, Corrosion 33, 9(1977): p. 309.
26. J. Prybylowski, R. Ballinger, CORROSION/86, paper no. 244 (Houston, TX: NACE, 1986).
27. M. Tsubota, Workshop on Advanced High Strength Materials for LWR Vessel Internal Applications (Clearwater Beach, FL. Electric Power Research Institute, 1986), p. 50.
28. N.S. Stoloff, R.G. Davies, Prog. Mater. Sci. 13(1966) p. 1.
29. J.J. Tien, A.W. Thompson, I.M. Bernstein, R.J. Richards, Metall. Trans. A 7A(1976): p. 821.
30. A.I. Asphahani, 2nd International Congress on Hydrogen in Metals, paper no. 3C-2 (New York, NY: Pergamon Press, 1977).
31. R.J. Coyle Jr., J.A. Kargol, N. Fiore, Proc. 11th Offshore Techn. Conference (Dallas, TX. OTC Committee, 1979), p. 1325.
32. N.F. Fiore, J.A. Kargol, 3rd International Conference on Hydrogen Effects in Metals, ed. I.M. Bernstein, A.W. Thompson (Warrendale, PA. The Metallugical Society-American Institute of Mining, Metallurgical, and Petroleum Engineers, 1981), p. 851.
33. N. Sridhar, J.A. Kargol, N.F. Fiore, Scripta Metall. 14(1980): p. 225.
34. N. Sridhar, J.A. Kargol, N.F. Fiore, Scripta Metall. 14(1980): p. 1257.
35. B.J. Berkowitz, R.D. Kane, Corrosion 36, 1(1980). p. 24.
36. R.D. Kane, B.J. Berkowitz, Corrosion 36, 1(1980): p. 29.
37. M. Kowaka, H. Fujikawa, Sumitomo Search 7(1972). p. 10.
38. P.R. Swann, Corrosion 19, 3(1963): p. 102.
39. P.E. Schremm, R.P. Reed, Metall. Trans. A 6A(1975). p. 1345.
40. R.E. Stoltz, J.V. VanderSande, Metall. Trans. A 11A(1980). p. 1033.
41. P. Berge, J.R. Donate, B. Prieux, D. Villard, Corrosion 33, 12(1977): p. 425.
42. G.J. Theus, Corrosion 33, 1(1977): p. 20.
43. K. Hosoi, et al., 1st International Symposium on Environmental Degradation of Materials in Nuclear Power Systems—Water Reactors (Houston, TX: NACE, 1982), p. 334.
44. T. Yonezawa, et al., 1st International Symposium on Environmental Degradation of Materials in Nuclear Power Systems—Water Reactors, p. 345.
45. I.L.W. Wilson, R.G. Aspen, Corrosion 32, 1(1976). p. 193.
46. J.R. Cels, J. Electrochem. Soc. 123(1976): p. 1152.
47. A.R. McIlree, H.T. Michels, Corrosion 33, 1(1977): p. 60.
48. E. Serra, EPRI Report No. NP-2114-SR, November 1981.
49. M.T. Miglin, H.A. Domian, Corrosion of Nickel-Base Alloys, p. 147.
50. H. Hosoya, R. Ballinger, J. Prybylowski, I.S. Hwang, CORROSION/87, paper no. 101 (Houston, TX: NACE, 1987).
51. R.C. Scarberry, Corrosion 32, 9(1976): p. 401.
52. L. Briant, E.L. Hall, Corrosion 43, 9(1987). p. 539.
53. G.S. Was, V.B. Rajan, Metall. Trans. A 18A(1987). p. 1313.
54. C.H. Samans, Corrosion 20, 8(1964): p. 256.
55. R. Bandy, K. Kelly, 2nd International Symposium on Environmental Degradation of Materials in Nuclear Power Systems—Water Reactors (1986), p. 93.
56. C.A. Grove, L.D. Petzold, J. Mater. Energy Syst. 7, 2(1985). p. 147.
57. M. Cornet, C. Betrand, M. Da Cunha Belo, Metall. Trans. A 13A(1982): p. 141.
58. C.K. Sheeks, W.C. Moshier, R.G. Ballinger, R.M. Latanision, R.M.N Pelloux, Proceedings of the International Symposium

on Environmental Degradation of Materials in Nuclear Power Systems—Water Reactors (1983), p. 702.
59. M. Igarashi, CORROSION/87, paper no. 287 (Houston TX: NACE, 1987).
60. R.H. Jones, Metall. Trans. A 13A(1982): p. 173.
61. K. Nakata, I. Masaoka, Y. Katano, K. Shiraishi, Annual Meeting of Japan Institute of Metals (1982), p. 12.
62. K. Nakata, J. Nucl. Mater. 133/134(1985): p. 575.
63. K. Fukuya, et al., Scripta Metall. 19, 8(1985): p. 959.
64. F.H. Huang, Int. J. Frac. 25(1984): p. 181.
65. W.J. Mills, Eng. Frac. Mech. 18, 3(1983): p. 601.
66. F Garzarolli, D. Alter, P. Dewes, Metall. Trans A 13A(1982): p. 131.
67. R.T. Holt, W. Wallace, Int. Metall. Rev. 22(1976): p. 1.
68. R.A. Mulford, Embrittlement of Engineering Alloys, Treatise on Material Science, Vol. 25, ed. C.L. Briant, S.K. Banerji (New York, NY: Academic Press, 1983), p. 1.
69. C.G. Bieber, R.F. Decker, Trans. AIME 221(1961): p. 629.
70. J.M. Walsh, N.P. Anderson, 3rd International Symposium on Superalloys: Metallurgy and Manufacture, ed. B.H. Kear, D.R. Muzyka, J.K. Tien, S.T. Wlodek (Baton Rouge, LA: Claitors, 1976), p. 127.
71. J. Oudar, P. Marcus, Appl. Surf. Sci. 3(1979): p. 48.
72. S. Smialowska, C.Y. Chao, H.E. Chang, R.W. Staehle, J. Electrochem. Soc. 126, 11(1979): p. 2038.
73. S.M. Bruemmer, R.H. Jones, M.R. Thomas, D.R. Baer, Environmental Degradation of Engineering Materials in Aggressive Environments, ed. M.R. Louthan Jr., R.P. McNitt, R.D. Sisson Jr. (Blacksburg, VA: 1981), p. 25.
74. S.M. Bruemmer, R.H. Jones, D.R. Baer, M.T. Thomas, CORROSION/81, paper no. 243 (Houston, TX: NACE, 1981).
75. R.M. Latanision, H. Opperhauser, Metall. Trans. A 6A(1975): p. 233.
76. S.M. Bruemmer, R.H. Jones, M.T. Thomas, D.R. Baer, Scripta Metall. 14(1980): p. 1233.
77. R.H. Jones, S.M. Bruemmer, M.T. Thomas, D.R. Baer, Scripta Metall. 14(1980): p. 369.
78. S.M. Bruemmer, R.H. Jones, M.T. Thomas, D.R. Baer, Metall. Trans. A 14A(1983): p. 233.
79. R.H. Jones, S.M. Bruemmer, M.T. Thomas, D.R. Baer, Metall. Trans. A 14A(1982): p. 1729.
80. R.H. Jones, M.J. Danielson, S.M. Bruemmer, D.R. Baer, M.T. Thomas, Embrittlement by the Localized Crack Environment, ed. R.P. Gangloff (Warrendale, PA. TMS-AIME, 1984), p. 419.
81. R.H. Jones, M.J. Danielson, D.R. Baer, J. Mater. Energy Syst. 8, 2(1986): p. 185.
82. W.C. Johnson, J.E. Doherty, B.H. Kear, A.F. Giamei, Scripta Metall. 8(1974): p. 971.
83. J.E. Doherty, B.H. Kear, A.F. Giamei, C.W. Steinke, Grain Boundaries in Engineering Materials, ed. J.L. Walter, J.H. Westbrook, D.A. Woodford (Baton Rouge, LA. Claitors, 1975), p. 619.
84. S. Yamaguchi, H. Kobayashi, T. Matsumiya, S. Hayami, Metall. Tech. (1979): p. 170.
85. M. Guttman, P. Dumoulin, N. Tan-Tai, P. Fontaine, Corrosion 37, 7(1981): p. 416.
86. G.S. Was, H.H. Tischner, R.M. Latanision, Metall. Trans. A 12A(1981): p. 1397.
87. G.P. Airey, EPRI Report No. NP-3051, July 1983.
88. G.P. Airey, Metallography 13(1980): p. 21.
89 G.S. Was, J.R. Martin, Metall. Trans. A 16A(1985). p. 349.
90 E.L Hall, C.L. Briant, Metall. Trans. A 16A(1985). p. 1225.
91 T S F Lee (Ph D diss., Massachusetts Institute of Technology, 1982).
92 S M. Bruemmer, L.A. Charlot, C.H. Henager Jr., EPRI Report No. NP-4465, Febrary 1986.
93 P L Andresen, C.L. Briant, 3rd International Symposium on Environmental Degradation of Maerials in Nuclear Power Systems—Water Reactors, p. 511.
94 A.W Funkenbusch, L.A. Heldt, D.F. Stein, Metall. Trans. A 13A(1982): p. 611.
95. P. Marcus, O. Oda, Mem. Rev. Sci. Metall. 11(1979): p. 715.
96. D.A. Vermilyea, C.S. Tedmon Jr., D.E. Broecher, Corrosion 31, 6(1975): p. 222.
97. A.R. McIlree, H.T. Michaels, P.E. Morris, Corrosion 31, 12(1975): p. 441.
98. G.S. Was, Private Communication.
99. T.S.F. Lee, R.M. Latanision, Metall. Trans. A 18A(1987): p. 1653.
100. Y. Ogino, T. Yamasaki, Scripta Metall. 15(1981): p. 821.
101. Y. Ogino, T. Yamasaki, Metall. Trans. A 15A(1984): p. 519.
102. A. Choudhury, The Intergranular Segregation of Boron in Substoichiometric Ni_3Al, ORNL/TM-10508 (Oak Ridge, TN: Oak Ridge National Laboratory, 1987).
103. S.M. Bruemmer, L.A. Charlot, Scripta Metall. 20(1986): p. 1019.
104. S.M. Bruemmer, Corrosion 44, 6(1988): p. 364.
105. J.L. Brimhall, D.R. Baer, R.H. Jones, J. Nucl. Mater. 122/123 (1984): p. 196.
106. R.C. Newman, R. Bandy, R. Roberge, Proceedings of 2nd International Symposium on Environmental Degradation of Materials in Nuclear Power Systems—Water Reactors, p. 636.
107. J.L. Nelson, S. Floreen, Metall. Trans. 14A, 1(1981): p. 133.
108. S.S. Matsushima, Y. Shimizu, Trans. Japan Inst. of Metals 24(1983): p. 149.
109. N. Totsuza, E. Lunarska, G. Cragnolino, Z. Szklarska-Smialowska, Corrosion 43, 8(1987): p. 505.
110 T.R. Mager, Fastener and Bolting Material for Westinghouse Design Internals, Advanced High Strength Materials Workshop (Clearwater Beach, FL: EPRI, 1986), p. 23.
111. G.J. Theus, Nucl. Technol. 28(1986): p. 388.
112. R.S. Pathania, "Caustic Cracking of Steam Generator Tube Materials," CORROSION/76, paper no. 98 (Houston, TX: NACE, 1976).
113. J.L. Nelson, S. Floreen, Proceedings of 2nd International Symposium on Environmental Degradation of Materials in Nuclear Power Systems—Water Reactors.
114. J.R. Cels, Corrosion 34, 6(1978): p. 198.
115. K.H. Lee, G. Cragnolino, D.D. MacDonald, Corrosion 41, 9(1985): p. 540.
116. R. Bandy, R. Roberge, D. van Rooyen, Intergranular Failures of Alloy 600 in High Temperature Caustic Environments, BNL-34595 (Long Island, NY: Brookline National Laboratory).
117. J.R. Crum, CORROSION/84, paper no. 178 (Houston, TX. 1984).
118. H. Coriou, L. Grall, C. Mathieu, D. Gay, Acad. Sci. 258(1984): p. 2566.
119. T. Boniszewski, G.C. Smith, Acta Metall. 11(1963): p. 165.
120 R.H. Jones, M.T. Thomas, D.R. Baer, Scripta Metall. 18(1984). p. 47.
121 B.A. Wilcox, G.C. Smith, Acta Metall. 13(1965). p. 331.
122. M. Hasegawa, M. Osawa, Trans. Iron Steel Inst. Japan 21(1981): p. 25.
123. A.H. Windle, G.C. Smith, Metal Sci. J. 4(1970): p. 136.
124 C.D Verpoort, D.J. Duquette, N.S. Stoloff, A. Met Mater. Sci. Eng. 64(1984): p. 135.
125. M. Hagiwara, J. Chene, Scripta Metall. 18(1984). p. 887.
126. R.E. Stoltz, A.J. West, Hydrogen Effects in Metals, ed. I.M. Bernstein, A.W. Thompson (Warrendale, PA. TMS-AIME, 1980), pp. 541-553.
127. R.J. Walter, W.T. Chandler, Mater. Sci. Eng. 8(1971): p. 90.
128. K.O. Efird, Materials Performance 24, 4(1985): pp. 37-40.
129. T. Kekkonen, H. Hanninen, Corros. Sci. 25, 8/9(1985). p. 789.
130. R.H. Jones, Advances in the Mechanics and Physics of Surfaces, Vol. 3, ed. R.M. Latanision, T.E. Fischer (New York, NY: Harwood Acadamic Publishers, 1986), p. 1.
131. J. Kolts, N. Sridhar, J. Mater. for Energy Syst. 8(1986). p. 306.
132. R.D. Kane, Intl. Metals Rev. 30(1985). p. 291.
133. E.P. Whelan, Hydrogen Effects in Metals, pp. 979-986.
134. D.H. Lassila, H.K. Birnbaum, Acta Metall. 35(1987). p. 1815.
135. D.P. Williams, H.G. Nelson, Metall. Trans. 1(1970), p. 63.

136. G.W. Simmons, P.S. Pao, R.P. Wei, Metall. Trans. A 9A(1978): p. 1147.
137. R.P. Gangloff, R.P. Wei, Metall. Trans. A 8A(1977): p. 365.
138. R.W. Pasco, K. Sieradzki, P.J. Ficalora, Scripta Metall. 16(1982): p. 881.
139. R. Bandy, D. van Rooyen, Nucl. Eng. Design 86(1985): p. 49.
140. N. Totsuka, Z. Szklarska-Smialowska, Scripta Metall. 21(1987): p. 45.
141. Y.S. Garud, Development of a Model for Predicting IGSCC of Alloy 600 Tubes in PWR Primary Water, Report No. EPRI NP-3791, January 1985.
142. Y.S. Garud, A.R. McIlree, CORROSION/85, paper no. 88 (Houston, TX: NACE, 1985).
143. F.P. Ford, Mechanisms of Environmental Cracking in Systems Peculiar to the Power Generation Industry, EPRI NP-2589, September 1982, pp. 3-5.
144. Y. Rouillon, Comportement de l'Alliage X 750 a la Corrosion Sous Tension Dans l'Eau: Influence des Traitments Thermique de Fabrication, HT/PV G 200 MAT/T 42 (France: Electricite de France, 1984), p. 47.
145. T. Kawakubo, B. Rosborg, Proceedings of the 2nd International Atomic Energy Agency Specialists' Meeting on Subcritical Crack Growth, Vol. 1 (USNRC Conference Proceeding NUREG/CP-0067, 1986), pp. 477-485.
146. F. Vaillant, Etude de la Corrosion Sous Contrainte en Milieu Primaire de l'Alliage X 750 Sur Eprouvettes Prefissurees: Influence du Traitment Thermique, HT/PV D 628 MAT/T 45 (France: Electricite de France, 1987), p. 22.
147. C.D. Verpoort, D.J. Duquette, N.S. Stoloff, A. Neu, Mater. Sci. Eng. 64(1984): p. 135.
148. J.T. Eastman, T. Matsumoto, N. Narita, F. Heubaum, H.K. Birnbaum, Hydrogen Effects in Metals, p. 397.
149. H. Vehoff, C. Laird, D.J. Duquette, Acta Metall. 35(1987): p. 2877.
150. H. Fukushima, H.K. Birnbaum, Acta Metall. 32(1984): p. 851.
151. R.H. Jones, D.R. Baer, Scripta Metall. 20(1986): p. 927.
152. S. Lee, J. Lee, Metall. Trans. A 17A(1986): p. 181.
153. A. Kimura, H.K. Birnbaum, Scripta Metall. 21(1987): p. 219.
154. A. Kimura, H.K. Birnbaum, Acta Metall. 36(1988): p. 757.
155. P. Bastien, P. Azou, C. Roy. Acad. Sci. 232(1951): p. 1845.
156. A.H. Windle, G.C. Smith, Metal Sci. J. 2(1968): p. 187.
157. B.A. Wilcox, G.C. Smith, Acta Metall. 12(1964): p. 371.
158. J.A. Donavan, Metall. Trans. A 7A(1976): p. 1677.
159. L.M. Foster, T.H. Jack, W.W. Hill, Metall. Trans. 1(1970): p. 3117.
160. G.S. Frankel, R.M. Latanision, Metall. Trans. A 17A(1986): p. 861.
161. G.S. Frankel, R.M. Latanision, Metall. Trans. A 17A(1986): p. 868.
162. T. Zakroczymski, Corrosion 41, 8(1985): p. 485.
163. M.R. Louthan, J.A. Donovan, G.R. Caskey Jr., Acta Metall. 23(1985): p. 745.
164. E. Lunarska, J. Flis, Scripta Metall. 18(1984): p. 889.
165. J. Eastman, F. Heubaum, T. Matsumoto, H.K. Birnbaum, Acta Metall. 30(1982): p. 1579.
166. W.A. McInteer, A.W. Thompson, I.M. Bernstein, Acta Metall. 28(1980): p. 887.
167. I.M. Robertson, H.K. Birnbaum, Scripta Metall. 18(1984): p. 269.
168. J. Eastman, T. Matsumoto, N. Narita, F. Heubaum, H.K. Birnbaum, Hydrogen Effects in Metals, pp. 397-409.
169. I.M. Robertson, T. Tabata, W. Wei, F. Heubaum, H.K. Birnbaum, Scripta Metall. 18(1984): p. 841.
170. H. Vehoff, K. Klameth, Acta Metall. 33(1985): p. 955.
171. D.A. Mezzanote, J.A. Kargol, N.F. Fiore, Scripta Metall., 14(1980): p. 219.
172. R.J. Coyle, J.A. Atrens, N.F. Fiore, Proceedings of the Conference on Environmental Degradation of Engineering Materials, ed. M.R. Louthan Jr., R.P. McNitt (Blacksburg, VA: Virginia Polytechnical and State University Printing Department, 1977), p. 411.
173. B.J. Berkowitz, M. Kurkela, R.M. Latanision, Hydrogen Effects in Metals, p. 411.
174. M.I. Baskes, V. Vitek, Metall. Trans. A 16A(1985): p. 1625.
175. M.S. Daw, M.I. Baskes, Phy. Rev. B. 29(1984): p. 6443.
176. M.S. Daw, M.I. Baskes, Chemistry and Physics of Fracture, R.M. Latanision, ed. R.H. Jones (Amsterdam, The Netherlands: Martinus Nijhoff Publishers, 1987), pp. 196-218.
177. C.L. Briant, R.P. Messmer, Phil. Mag. B. 42(1980): p. 569.
178. M.E. Eberhart, K.H. Johnson, R.M. Latanision, Acta Metall. 32(1984): p. 955.
179. S.P. Lynch, J. Mater. Sci. 21(1986): p. 692.
180. J.R. Rice, Effect of Hydrogen on Behavior of Materials, ed. I.M. Bernstein, A.W. Thompson (Warrendale, PA: TMS-AIME, 1976), p. 455.
181. J.R. Rice, R. Thomson, Phil. Mag. 29(1974): p. 73.
182. D.D. Mason, Phil. Mag. A 39(1979): p. 455.
183. N.J. Petch, Phil. Mag. 11(1956): p. 331.
184. M.L. Wayman, G.C. Smith, J. Phys. Chem. Solids 32(1971): p. 103.
185. S. Hinotani, Y. Ohmoir, F. Terasaki, Mater. Sci. Eng. 74(1985): p. 119.
186. D. Tseng, Q.Y. Long, K. Tangri, Scripta Metall. 22(1988): p. 649.
187. S.M. Bruemmer, L.A. Charlot, C.H. Henager Jr., Corrosion, in press.
188. S.M. Bruemmer, L.A. Charlot, C.H. Henager Jr., "Microstructural Effects on Microdeformation and Primary-Side Stress Corrosion Cracking Alloy 600 Tubing," EPRI NP-5192, 1987.
189. S.M. Bruemmer, C.H. Henager Jr., Proceedings of 2nd International Symposium on Environmental Degradation of Materials in Nuclear Power Systems—Water Reactors.
190. P. Marcus, A. Teisseier, J. Oudar, J. Corros. Sci. 24(1984): p. 259.
191. R. Bandy, R. Roberge, R.C. Newman, Corros. Sci. 23(1983): p. 995.
192. A.I. Asphahani, Slow Strain-Rate Technique and Its Application to the Environmental Stress Cracking of Nickel-Base, Cobalt Base Alloys in Stress Corrosion Cracking—The Slow Strain-Rate Technique, ASTM STP 665, ed. G.M. Ugianski, J.H. Payler (Philadelphia, PA: ASTM, 1979), pp. 279-293.
193. R.N. Parkins, Stress Corrosion Cracking and Hydrogen Embrittlement of Iron-Base Alloys, p. 601.
194. M.J. Danielson, C. Oster, R.H. Jones, Proceedings of Conference on Corrosion Chemistry Within Pits, Crevices and Cracks (United Kingdom: National Physical Laboratory, 1984).
195. D.A. Vermilyea, Stress Corrosion Cracking and Hydrogen Embrittlement of Iron-Base Alloys, pp. 208-217.
196. R.H. Jones, M.A. Friesel, Metall. Trans., in press.
197. R.H. Jones, M.J. Danielson, D.R. Baer, Microchemistry and Mechanics Issues in Stress Corrosion Cracking, 20th National Symposium on Fracture Mechanics, 1987.
198. C. Edeleneau, A.J. Forty, Phil. Mag. 46(1960): p. 521.
199. J.A. Beavers, E.N. Pugh, Metall. Trans. A 11A(1980): p. 809.
200. M.T. Hahn, E.N. Pugh, Corrosion 36, 7(1980): p. 380.
201. E.N. Pugh, Atomistics of Fracture, ed. R.M. Latanision, J.R. Pickens (New York, NY: Plenum Press, 1983), pp. 997-1010.
202. R.C. Newman, K. Sieradzki, Chemistry and Physics of Fracture, ed. R.M. Latanision, R.H. Jones (Amsterdam, The Netherlands: Martinus Nijoff Publishers, in press).

Discussion

S.C. Jani (Georgia Institute of Technology, USA): You mentioned the possibility of dislocation transport of hydrogen to the interior of a metal. It should be pointed out that although there is an interaction between dislocations and hydrogen in face-centered

cubic materials, the binding energies involved are relatively low (compared to body-centered cubic materials), and therefore transport of hydrogen by dislocations is unlikely.

R.H. Jones: I agree. The results of Frankel and Latanision (References 160 and 161 in the paper) on hydrogen permeation in nickel single crystals undergoing single slip suggests that long-range transport of hydrogen by dislocations occurs, but that the enhanced transport is only of the order of a few percent.

S.C. Jani: You questioned the relevance of the Griffith criterion for cracking (brittle transgranular or intergranular). The criterion has no inherent limitations. The real limitation is that the specific energy to form new surfaces is not easily determined because the energy imparted to a cracked body performs plastic work in addition to causing crack extension.

R.H. Jones: My point was that for materials in which dislocation nucleation and mobility is relatively easy, the balance between cleavage or decohesive fracture and slip tends to favor slip. Therefore, the use of the Griffith criterion is inappropriate, unless it can be shown that hydrogen reduces the surface energy of nickel sufficient for decohesion to be favored over slip.

A. Gelpi (Framatome, France): You mentioned briefly high-temperature stress corrosion cracking (SCC) of nickel-base alloys. In your opinion, can this cracking occur by an anodic-dissolution mechanism?

R.H. Jones: To my knowledge, an electrochemical reaction is not possible in steam without condensed water on the surface. Water can be stable in cracks or crevices at steam temperatures, so the absence of condensed water must be demonstrated before anodic-dissolution effects can be discounted.

J.M. Sarver (Babcock and Wilcox, USA): Can the work by Bruemmer be used to explain the intergranular and transgranular cracking of annealed and sensitized Inconel† 600 (UNS N06600) in the presence of lead?

R.H. Jones: Without more details about cracking of Inconel 600 in lead, it is not possible to correlate observations about the effect of grain-boundary carbides on microdeformation in high-purity water to the case in lead.

S. Szklarska-Smialowska (Ohio State University, USA): It is well established that by increasing the partial pressure of hydrogen in primary water, the intergranular SCC susceptibility of Inconel 600 is increased. It has also been found that a cathodically treated alloy is suceptible to intergranular SCC in high-temperature water [see, for example Totsuka and Szklarska-Smialowska, Corrosion 43(1987): p. 734] On the other hand, there are reports in the literature that high overpressures of hydrogen in water solution inhibit intergranular SCC of Inconel 600.

R.C. Newman (University of Manchester Institute of Science and Technology, UK): Smialowska appears to have lost confidence in hydrogen embrittlement (HE) as the mechanism of intergranular SCC of Inconel 600 in high-temperature borate solution. Yet in her papers with Totsuka [for example, Totsuka, et al., Corrosion 43(1987): p. 505], she shows a *continuity* in behavior between E(corr) and cathodic potentials as high as −1 V (I think). Surely this more or less proves HE is the mechanism, does it not?

S. Szklarska-Smialowska: Results of our experiments show that in dry hydrogen gas at high pressure, SCC does not occur, although hydrogen is absorbed into the alloy. However, there is no corrosion and no surface film formation. The totality of our results indicates that corrosion in hydrogenated water solution that is accompanied by oxide/hydroxide film formation is the necessary condition for intergranular SCC of Inconel 600. So, entry of hydrogen from water solution and oxide/hydroxide film formation both play important roles in intergranular SCC of Inconel 600 in primary water.

R.N. Iyer (Pennsylvania State University, USA): Is the presence of impurities a necessary and sufficient condition to cause HE? Oriani, in one of his review articles, has indicated that very clean metals and alloys (without nitrogen, phosphorus, and sulfur, etc.) do not embrittle in hydrogen, but in the presence of any one of these impurities, they do. Can we explain the impurity effect by solute pinning of dislocations by the impurities that increase hydrogen residence time sufficiently to cause dynamic trapping?

R.H. Jones: Based on our results and those of Birnbaum (References 134, 153, 154 of the paper), hydrogen-induced intergranular crack growth of nickel can occur with 0.04 monolayer or less of sulfur. Comparable Auger electron spectroscopy data for nickel-base alloys is not available, so similar conclusions cannot be made for these materials. Since impurities are not required for hydrogen-induced intergranular crack growth of nickel (and iron), your suggestion of impurity pinning of dislocations is not appropriate. However, there is some evidence that impurities in grain boundaries can alter the properties of grain-boundary dislocations, such as the critical stress for grain-boundary dislocation sources.

J. Kolts (Conoco, Inc., USA): The susceptibility to HE of various nickel alloys is very variable. For example, alloy C-276 (UNS N10276) requires strength levels beyond 150 ksi (950 MPa), while alloy 825 (UNS N08825) is almost immune even at its highest strength levels. How can these large variations be explained by impurity segregation to grain boundaries?

R.H. Jones: It is difficult to make correlations without knowing more about specific hydrogen uptake rates, grain-boundary microstructures and chemistries.

R. Griffin (Texas A&M University, USA): With regard to Kolts's comment on the lack of cracking in nickel alloys until very high-strength levels are achieved, I want to ask the following question. It seems that Kolts's comments would suggest that a critical strain, at or near the crack tip, would be an important parameter. Do you think this might be a useful way of approaching the problem?

R.H. Jones: It is difficult to generalize the role of crack-tip strain and stress, since different mechanisms will be activated by stress and strain. Decohesion at grain boundaries or particles such as carbides or hydrides is initiated by stress, while film rupture (passive, salt, or dealloyed layer), crack transport, and crack-tip plasticity effects are strain and strain rate related.

K. Sieradzki (The Johns Hopkins University, USA): It might be worthwhile to try to interpret some of the results you describe in terms of recently developed models for intergranular separation processes, which I reviewed yesterday. Do you have any plans to attempt this?

R.H. Jones: Our current emphasis is in anodic transgranular SCC processes and we are therefore not actively pursuing mechanisms of hydrogen-induced crack growth. However, our recent observations (Jones, et al., Corrosion, in press) of intergranular SCC in iron at crack growth velocities of 10^{-2} mm/s may require us to revisit these issues.

J. Stewart (Harwell Laboratory, UKAEA, UK): Your suggested explanation of acoustic emission during intergranular SCC tests is consistent with our findings during intergranular SCC propagation in sensitized stainless steels. We find that the corrosion current flowing during the early stages of crack propagation is somewhat cyclic, with each cycle corresponding to a crack advance of a grain-boundary facet length or less. However, cracks do not arrest during this period, but appear to be hindered. Perhaps you could consider using electrochemical techniques in conjunction with acoustic emission. Also, it appears to us that the propagating crack is hindered by "microstructural barriers" that will depend on the alloy and environment corrosivity, but that probably include grain-boundary triple points and precipitates. This is an important area requiring future research, with implications for alloy design. Would you comment please?

R.H. Jones: If your quiescent period results from ligaments behind the crack tip and further crack extension occurs when these ligaments fail, then acoustic emission should occur during your quiescent period and just prior to the next electrochemically active period. We are currently setting up an experiment to make these measurements.

†Trade name.

D.J. Duquette (Rensselaer Polytechnic Institute, USA): Just a comment. As has been pointed out, grain-boundary impurities are not required to cause embrittlement of nickel in hydrogen. In some cyclic loading tests we performed, rapid crack advance in grain boundaries of very pure nickel (no sulfur in the grain boundaries) was observed for annealed samples, while transgranular cracking was observed when the metal surfaces were shot peened. It appears that shot peening provides a large sink of dislocations for hydrogen and accordingly biases the crack path. In addition to enhanced fatigue crack propagation rates, enhanced cyclic hardening was also observed. Thus it appears that there is a strong link between dislocations and hydrogen.

R.H. Jones: Birnbaum and Lassila (Reference 134 in the paper) have also reported intergranular crack growth of nickel, with very little sulfur segregation, while we have also shown this for nickel with as little as 0.04 monolayers (this was zone-refined nickel) of sulfur on the grain boundary. Cold work has been shown to promote transgranular cracks in alloy C-276 and IN 600 in hydrogen-bearing environments. This may be evidence of hydrogen-enhanced shear along the planar dislocation arrays, causing a localized shear instability type of fracture. However, there has been little fundamental work performed on this issue.

Environment-Induced Cracking of High-Strength Aluminum Alloys

*N.J.H. Holroyd**

Introduction

Continual development of new generation aluminum alloys such as aluminum–lithium-based alloys, powder metallurgy products, 7090 and 7091, and new variants of existing alloys, e.g., 7010, 7050, and 7051, prompts a review of the current understanding of stress corrosion cracking (SCC) mechanisms. Excellent review papers summarize published information up until the mid-1970s,[1-6] and the reader is directed to these along with a recently updated general text[7] for background on the compositional, metallurgical, and mechanical details of aluminum alloys. Environment-sensitive fracture of aluminum alloys is almost exclusively intergranular (IG) unless the mechanical loading conditions are severe and/or the local grain boundaries (GBs) are unfavorably oriented. Although numerous detailed SCC mechanisms abound, two basic theories have evolved. One envisages cracking as highly localized anodic dissolution of GB regions under the combined influence of stress and environment, the other suggests embrittlement and loss of ductility is promoted after the ingress of an aggressive species (usually atomic hydrogen) onto or into the alloy. The Sprowls and Brown review[1] concluded in 1969 that the SCC of 2XXX (Al-Cu) and 5XXX (Al-Mg) series alloys occurs via an anodic dissolution mechanism, whereas mechanistic attributions for 7XXX [Al-Zn-Mg(-Cu)] series remain controversial.

Many authors favored anodic-dissolution-based SCC mechanisms for all aluminum alloy systems until the early 1980s, ignoring the pioneering work of Gruhl and coworkers in Germany on 7XXX series alloys (recently reviewed[8]) and the suggestions of Haynie, et al.,[9,10] until the work of Gest and Troiano[11] triggered numerous studies showing that hydrogen embrittlement (HE) generally has a role in the SCC of 7XXX series aluminum alloys[12,13] and may be involved for 2XXX[14] and 5XXX series alloys.[15] Despite the above, some authors still maintain the SCC of 7XXX series alloys propagates via purely anodic-dissolution-based mechanisms, with no role for HE.[16]

SCC of aluminum alloys is a complex process involving a multiplicity of time-dependent interactions that remain difficult to evaluate independently. SCC to date eludes a complete mechanistic interpretation. Nevertheless, considerable progress has been made over the last two decades, with most resulting from the availability of sophisticated experimental techniques involving high-resolution electron microscopy, electrochemistry, and the implementation of fracture mechanics.

The aim of this review is to present and discuss the experimental observations upon which the current understanding of the environment sensitive fracture of aluminum alloys is based. Discussion will focus upon published work for 7XXX series alloy plate material, and, where appropriate, results for other aluminum alloy systems will be highlighted. Important experimental observations and conclusions covering microstructural, environmental, and mechanical aspects of environment sensitive fracture of aluminum alloys are summarized in the following sections.

*Alcan International Limited, Banbury, Oxon, OX16 7SP England.

Microstructural Aspects

The influence of alloy microstructure upon the SCC of 2XXX (Al-Cu) and 5XXX (Al-Mg) is documented in detail elsewhere,[1-6] with SCC susceptibility being directly relatable to the development of local anodes and cathodes within GB regions. Notable exceptions are as follows Hardwick, et al.,[14] who suggested that an Al-Cu-Mg alloy, 2124, can suffer HE after being subjected to simultaneous straining and cathodic charging with hydrogen from an aqueous environment, and Higashi, et al.,[15] who reported the existence of pre-existing embrittled zones ahead of SCC crack fronts in precracked Al-8%Mg specimens, which are reversible and therefore associated with HE.

The general dependence of SCC susceptibility upon iso-thermal aging is well established for 7XXX series [Al-Zn-Mg(-Cu)] alloys,[5] 2XXX series alloys Al-Cu(-Mg),[1,6,14] and the Al-Li-Cu-Mg alloy 8090[18,19] (Figure 1):

Microstructure	Susceptibility
Solution Treated (No GB precipitation)	Immune
Underaged	Maximum
Peak Aged	Susceptible
Overaged	Decreases with aging

For 7XXX series alloys, numerous attempts to correlate susceptibility with microstructural features known to be influenced during thermal treatment include the following:

(1) Grain-boundary precipitate size and spacing;[20-34]
(2) Precipitate free zone (PFZ) width or preferential slip in the PFZ;[20,21,27,35-39]
(3) Matrix precipitate size/distribution and deformation characteristics;[40-44]
(4) Solute profiles in the PFZ;[7,29,45-54] and
(5) Grain-boundary segregation.[55-62]

Despite claims to the contrary (Figure 2), no single microstructural parameter has yet been identified that uniquely controls the SCC of 7XXX series alloys.[5] This conclusion is sustainable for the following reasons:

(1) In many studies, microstructural comparisons have been made without maintaining strength levels;
(2) It is almost impossible to vary independently the microstructural parameters listed above, for example, most parameters could change during aging of a solution-heat-treated and quenched alloy;
(3) Correlation of SCC susceptibility with one parameter need not exclude the possible dependence on other parameters and independence of the one associated with the apparent correlation; and
(4) Prior to the mid-1970s, SCC data was rarely considered in terms of initiation and propagation stages.

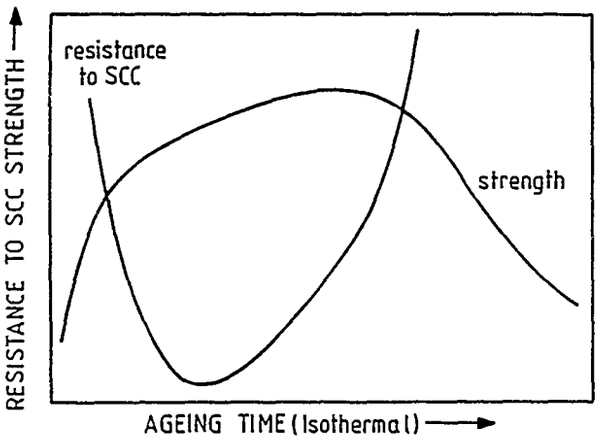
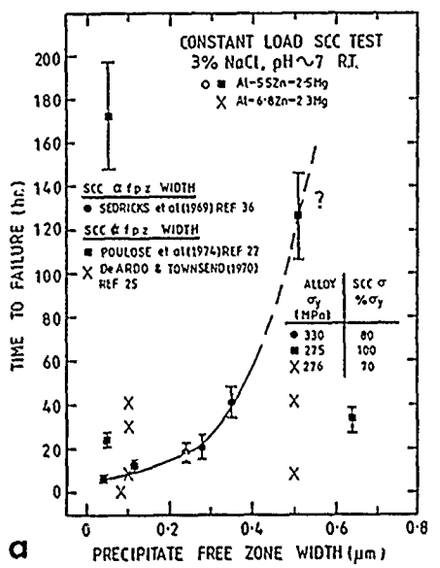
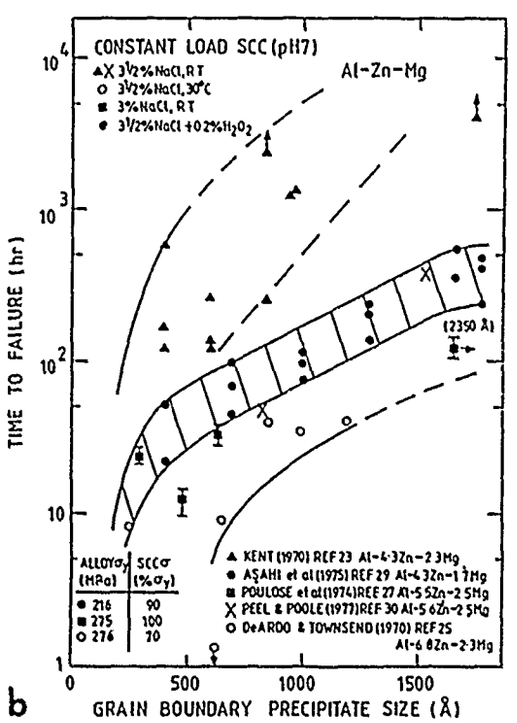


FIGURE 1—Typical dependence of SCC resistance upon thermal aging condition for precipitate-hardening aluminum alloys.[43]





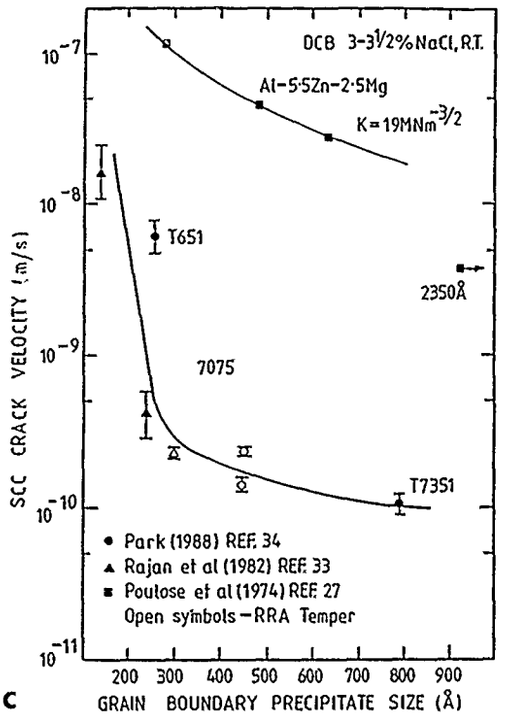


FIGURE 2—Implied relationships between alloy microstructure parameters and SCC performance for 7XXX series aluminum alloys in aqueous 0.5 to 0.6 M sodium chloride solutions: (a) influence of precipitate-free-zone width and (b) grain- boundary precipitate size upon failure time for Al-Zn-Mg alloys and (c) for the latter parameter upon crack growth rate in precracked specimens of Al-Zn-Mg(-Cu) alloys. (Reprinted with permission from Chapman and Hall Publishers.[33])

Further complications arise because, although it is well known that microstructural development during commercial thermal-mechanical practices almost inevitably differs from laboratory-based treatments, most published work involves, almost exclusively, either laboratory-cast and -processed alloys or commercial alloys subsequently subjected to laboratory-based heat treatments. In addition, many studies use high-purity analogue alloys that normally are completely recrystallized with isotropic SCC properties, whereas wrought products of commercial alloys (e.g., plate and extrusion) generally have elongated grain structures and potential SCC susceptibilities restricted to the short-transverse direction. The validity of equating the microstructural dependence of SCC for high-purity alloys with recrystallized GB structures with those of nonrecrystallized short-transverse pancake GB structures is not yet established. Many potentially important influences are thus ignored, for instance; grain refiners and dispersoids (e.g., Mn, Cr, and Ti), impurity elements (e.g., Fe and Si), trace element segregants (e.g., Pb, Bi, Sn, etc.), and the effects of GB shape and texture. Due care must therefore be exercised when generalizations are made for commercial alloys based upon noncommercial alloys and/or fabrication/thermal practices.

Experimental findings in which the above complications have been minimized are summarized in the following sections covering the various stages of thermal aging of precipitate age-hardening aluminum alloys.

Solution heat treatment

Pickens and Langan investigated the influence of solution heat-treatment (SHT) temperature upon SCC susceptibility of a high-purity Al-7Zn-3Mg laboratory alloy and attempted to eliminate other variables, such as recrystallization, grain growth, yield stress, and solute depletion, by carefully controlling alloy thermomechanical

processing and aging treatments.[59,60] Reported SCC crack growth rates increase with decreasing SHT temperatures, contrary to the trend reported by Shastry, et al.,[61] for the commercial Al-Zn-Mg-Cu alloy 7075-T651, but are in general agreement with the earlier data of Taylor and Edgar[46] for the Al-Zn-Mg alloy 7004 (Figure 3). Recrystallization, grain growth effects, and alloy yield stress could account for these differences It is interesting to note that the one result of Taylor and Edgar's that is contrary to the trend quoted by Pickens and Langan is for the highest temperature they tested, 575°C, the only one promoting significant grain growth.

All the above studies, which were principally aimed at assessing the influence of GB segregation on SCC, will be reviewed in a later section.

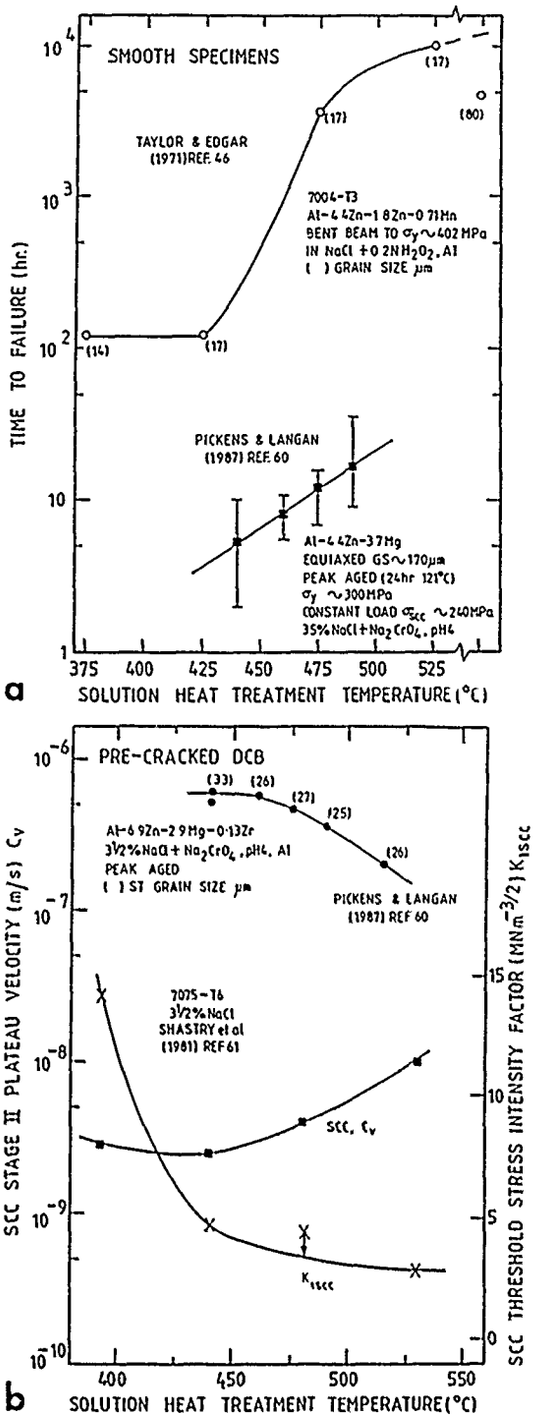


FIGURE 3—Influence of solution heat treatment upon the SCC performance of Al-Zn-Mg alloys in saline environments; (a) time-to-failure from smooth specimens and (b) Region 2 SCC plateaux crack velocities from precracked specimens.

Quench rate

The influence of quench rate upon IG corrosion and SCC susceptibility for 2XXX series alloys is considered to be well understood.[1,6,63] For alloys such as 2024-T3 and -T4, SCC susceptibility becomes marked when quench rates fall below around 500°C/s (Figure 4), and GB regions become sufficiently anodic with respect to grain interiors resulting from GB precipitation of Al_2CuMg.[1,6] If SCC occurs via a purely anodic dissolution mechanism, as is currently generally accepted for 2XXX series alloys, it may be possible to predict SCC susceptibility by integrating the effects of precipitation at intermediate temperatures during a quench.[63]

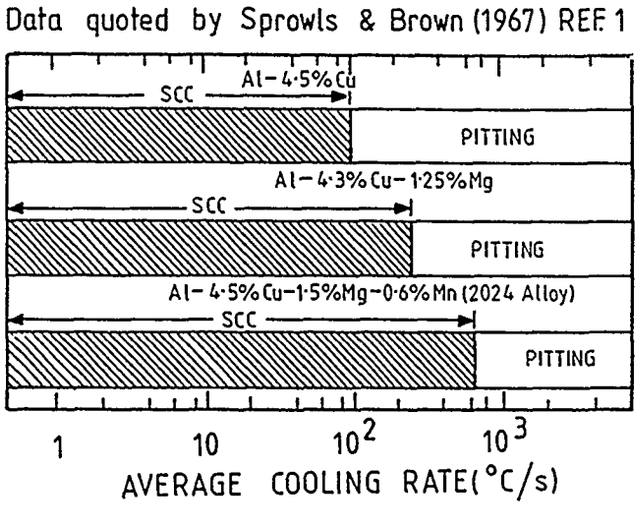


FIGURE 4—Effect of cooling rate during quenching between 315 and 400°C on the susceptibility of 2XXX series alloy to SCC.[1]

For 7XXX series alloys, the picture is less clear-cut, although there are undoubtedly microstructural changes occurring during quenching (such as precipitation on chromium-rich and to a lesser extent zirconium-rich particles[66] and precipitation near high-angle boundaries[20]) that influence subsequent aging responses.[2,65,66] Doig and Edington reported that rapid quenching promotes a local enrichment of magnesium on as-quenched grain boundaries for an Al-6Zn-3Mg alloy,[48] and Miller and Scott argued that this accounted for the SCC they observed in as-quenched Al-Zn-Mg alloys.[64] In hindsight, the latter explanation is improbable if, as is now thought, GB precipitation is a prerequisite for SCC.[62] A more plausible explanation is that GB precipitation occurred during their SCC testing at room temperature .

For 7XXX series alloys, it is generally believed that the influence of quench rate upon SCC is dependent upon an alloy's copper content. For copper-lean alloys, SCC resistance is progressively improved by reducing quench rates;[22] low rates (e.g., air cooling) offer practical immunity,[2,67] whereas the reverse is true for alloys containing more than about 1 wt% copper.[2,68] Sarkar, et al.,[69] attribute this to quench rates having to prevent dispersoid elements such as Cr and Mn acting as nucleation sites for copper-rich precipitation and the removal of copper from solid solution,[70] which they deem detrimental to SCC performance of Al-Zn-Mg-Cu alloys. Slower quench rates were considered beneficial for copper-lean alloys because more incoherent precipitation and homogeneous deformation characteristics are promoted that are well known to improve SCC performance.[22,43,71]

Thermal aging. For most commercial applications of high-strength aluminum alloys, precipitation hardening is of paramount importance. In general, the potential risk of stress corrosion prevents exploitation of the maximum strength offered, because although alloys are immune to SCC in the as-quenched condition (as long as GB precipitation is prevented[62]), they usually become susceptible with increasing precipitation hardening, reaching a maximum before peak strength (Figure 1).[43]

The influence of thermal aging upon the SCC of Al-Cu(-Mg) alloys generally reflects the electrochemical potential difference

between GB regions and the alloy matrix.[1,6] An example of this is given in Figure 5, comparing electrochemical data for Al-4%Cu with SCC data for 2024 during aging at 190°C.

For 7XXX series alloys, the beneficial effects that can result from overaging are strongly influenced by the presence of copper:[5] Alloys with copper contents below around 1 wt% require gross overaging before high resistances to SCC are obtained, whereas alloys with higher copper contents need only sacrifice 10 to 15% of the maximum strength, as is exploited in the commercial -T73 duplex aging practices developed during the 1960s[1] to minimize service problems (Figure 6).[5]

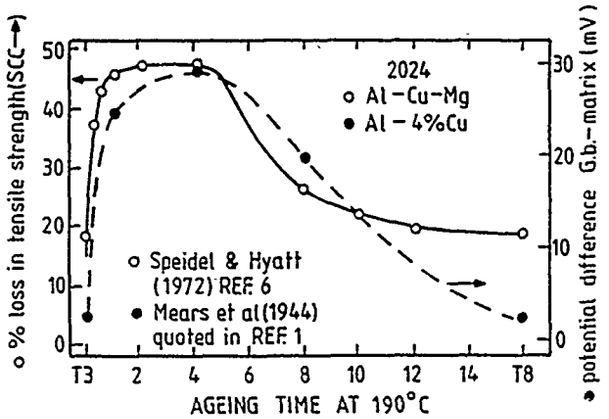


FIGURE 5—Comparison between measured potential difference between grain-boundary regions and the matrix and the SCC performance of 2XXX series alloys in 3.5% NaCl as a function of aging time at 190°C.

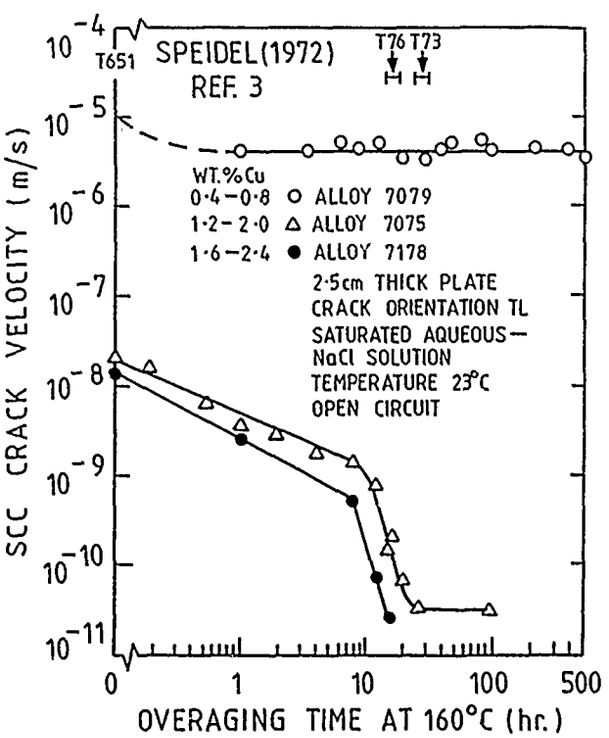


FIGURE 6—Influence of copper concentration on the improved SCC performance (Region 2 SCC plateau velocities) induced by overaging alloys at 160°C.[3]

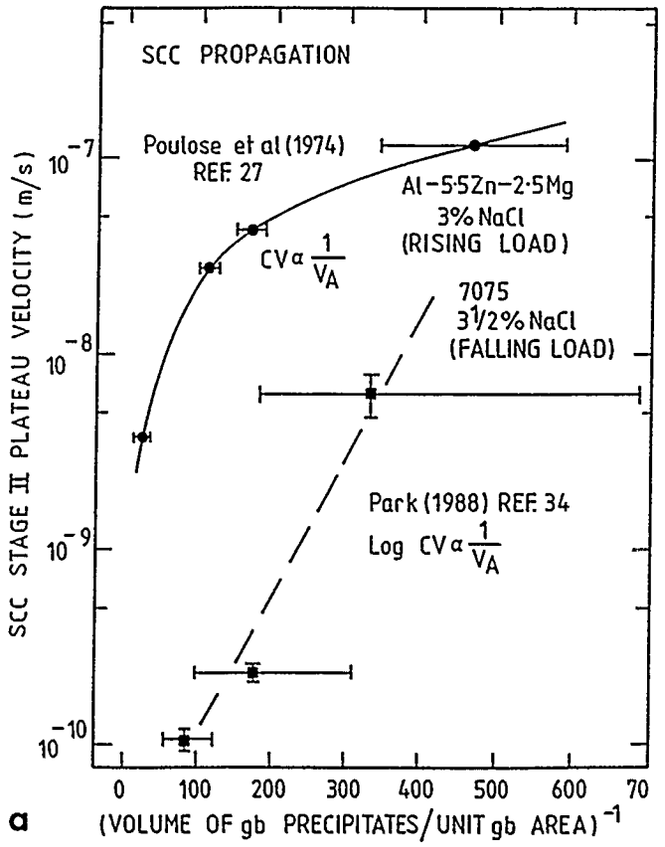
In the late 1960s, it was hypothesized that dislocation–precipitate interactions play an important role during the SCC of aluminum alloys.[5,39,69] Work by Thomas and Nutting[39] led to the proposition that preferential flow occurs in GB PFZs of SCC-susceptible Al-Zn-Mg and Al-Zn-Mg-Cu alloys, which facilitate localized corrosion along the regions subjected to plastic flow. This view was questioned by later work demonstrating that slip, even in the most susceptible alloys, concentrates in bands across grains,[40,41,71] thereby indicating the importance of the overall distribution and nature of precipitates within the matrix and their interaction with dislocations during plastic deformation. In view of this, Speidel suggested that SCC susceptibility is enhanced by precipitates being sheared during plastic deformation, with the effectiveness of particle shearing being determined by the particle size, volume fraction, and coherency.[43] Using the above, an argument can be generated explaining why overaging can improve the SCC resistance of Al-Zn-Mg-Cu alloys containing more than about 1 wt% copper without dramatic loss of strength, as found for Al-Zn-Mg alloys. The addition of copper to Al-Zn-Mg alloys not only increases the volume fraction of strengthening precipitates but also modifies the kinetics of the precipitation reaction. In the presence of copper, the development of η' from Guinier-Preston (GP) zones is accelerated and the semicoherent η' precipitate persists to longer aging times.[74] Consequently, precipitates in peak-aged Al-Zn-Mg alloys will be sheared and result in inhomogeneous planar deformation, whereas precipitates in Al-Zn-Mg-Cu alloys containing sufficient copper will develop dislocation loops and result in a more homogeneous deformation mode.

The dislocation–precipitate interaction hypothesis and the proposal of preferential deformation/corrosion of PFZ regions are at best incomplete, and most workers believe that a realistic model of SCC must include microstructural features of the GB region. PFZ width per se is unlikely to be a critical parameter. Most investigations have detected little or no effect upon SCC,[22-34,49,79] although reducing PFZ width has been claimed to increase[37] and decrease[36] SCC susceptibility. Evidence for SCC resistance increasing with increasing GB precipitate size and spacing is more convincing, although there are discrepancies here as well.

Middleton and Parkins's[76] indirect experimental evidence for the SCC in Al-Zn-Mg alloys generally being along GBs rather than within PFZs is supported by the later detailed fractographic evidence of Scamans,[77] although, as reported by Lynch,[78] cracking can in some instances involve microvoid-coalescence and therefore propagate within PFZs.

Middleton and Parkins[76] suggest SCC propagation in Al-Zn-Mg alloys occurs via $MgZn_2$ GB precipitates acting as an active path for corrosion, with creep preventing the formation of an effective passivating film over the crack tip and allowing dissolution of the material between the GB precipitates. Poulose, et al.,[27] modified these ideas by suggesting that GB precipitates act as sacrificial anodes and retard SCC and that crack growth rates (cv) in the K-independent domain (Region 2) are inversely proportional to the volume fraction of $MgZn_2$ GB precipitate (Figure 7). These authors held the alloy composition (Al-5.5Zn-2.5Mg) and strength level constant and conducted experiments to separate the microstructural variables of PFZ width and GB and matrix precipitate sizes. On the basis of their results, they maintain that rather than the number or the size of GB precipitates being critical, it is the volume fraction, and since the PFZ width, deformation mode, and matrix precipitation are not directly involved, their model is consistent with there being many apparently contradictory findings reported in the literature. Further work is needed to evaluate these ideas. Recent results quoted by Park for alloy 7075 (UNS A97075) in a 3.5% saline environment imply a logarithmic relationship between SCC plateau velocities and the volume of GB precipitates/unit GB area[34] (Figure 7).

Starke and coworkers used the above arguments, supplemented with ones based upon observed deformation and electrochemical behavior, to explain the influence of aging upon the SCC of commercially cast and fabricated Al-6Zn-2Mg-XCu alloys containing various levels of copper.[69,70,73-74] Homogeneity of slip was shown to be dependent upon an alloy's copper level[73] and the strengthening precipitate coherency, volume fraction, and the number of partially coherent and incoherent precipitates.[74] It was argued[69] that SCC crack growth rates in the stress-intensity factor (K) insensitive region (Region 2) were under electrochemical control, whereas those in the K sensitive region (Region 1) were influenced by the deformation mode.



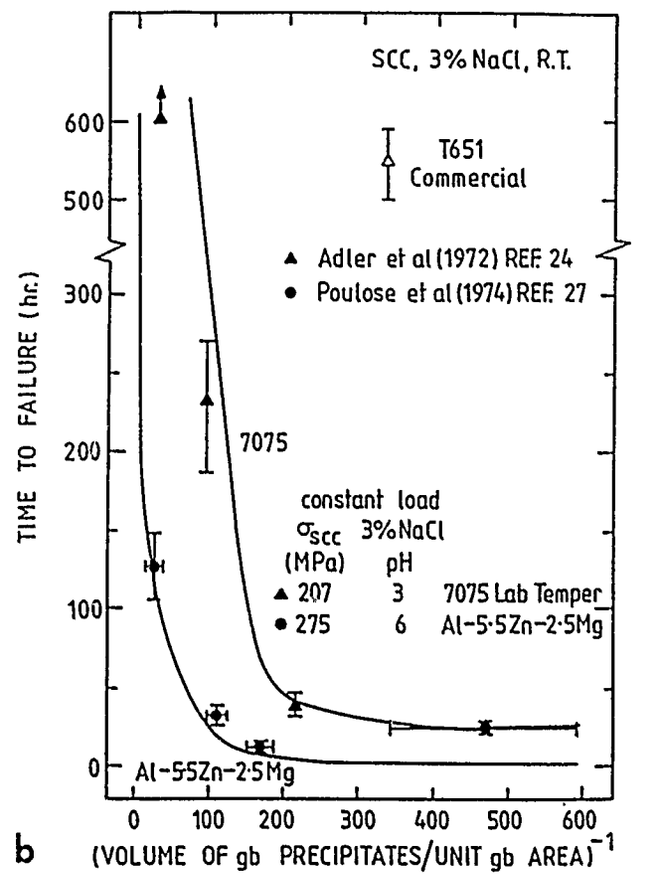
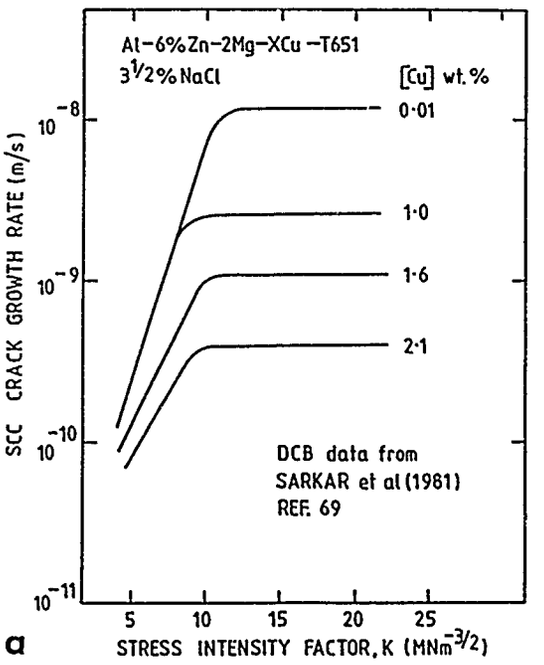


FIGURE 7—Implied relationships between SCC performance and the volume fraction of grain-boundary precipitates for 7XXX series alloys: in terms of (a) crack growth rate and (b) failure times for smooth specimens in 3 to 3.5% NaCl.

For alloys in the T651 temper (Figure 8), Sarkar, et al.,[69] suggested the following:

(1) In Region 1, copper levels up to 1 wt% had little influence upon either SCC crack growth rates or deformation mode, whereas for higher copper levels, slip homogeneity increased and crack velocities decreased; and

(2) In Region 2, the SCC crack growth rate progressively decreased with increasing copper level because copper entered hardening precipitates, making them more electrochemically noble and reducing local electrochemical differences in the crack-tip region. The beneficial effects of overaging copper-free alloys were primarily attributed to a deformation-mode transition from predominantly inhomogeneous (T651) to a homogeneous mode promoting reduced stress concentration at grain boundaries, whereas for copper-containing alloys, both copper enrichment of precipitates and homogenization of deformation were deemed important (Figure 8).



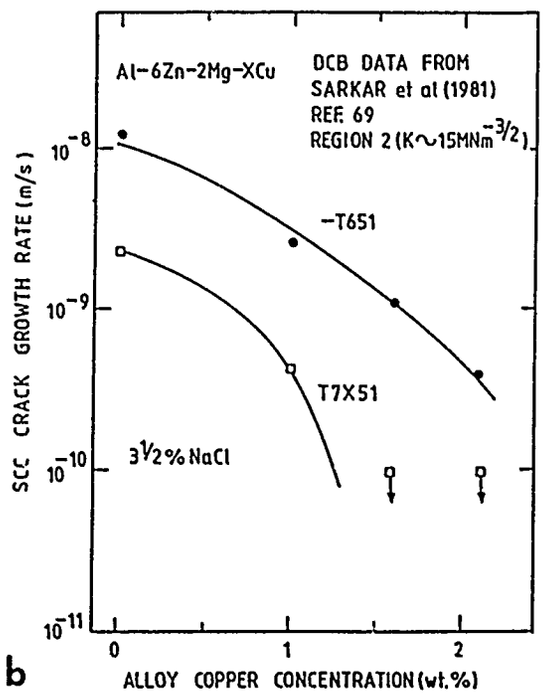


FIGURE 8—SCC of Al-6Zn-2Mg-XCu alloys in 3% NaCl; (a) SCC crack growth rate as a function of stress-intensity factor and (b) Region 2 plateau velocity at various copper concentrations.

Further development of the deformation-mode arguments should be possible now that it is appreciated that strain accommodation in precipitate-hardening alloys is strain-rate dependent, with GB deformation being favored by lower strain rates.[75]

Concurrent with attempts in the mid-1970s to characterize SCC in terms of deformation mode or GB precipitation, other workers focused attention upon the solute content of the GB region away from precipitates. Lorimer and Ryder suggested that the solute profiles within the PFZ may provide an electrochemical sensitive path.[80] Doig and Edington and Doig, et al., in a series of publications, reported solute concentrations across GBs for Al-Mg, Al-Zn-Mg, and Al-Zn-Mg-Cu alloys obtained using a range of electron-microscopy-based techniques.[50] Matrix and GB microstructural changes observed during the overaging of 7075 from a T6 to a T73 temper were minimal other than a twofold reduction in the Cu concentration within the PFZ. On the basis of this and electrochemical studies, they concluded that the SCC susceptibility of aged Al-Zn-Mg-Cu alloys, although independent of the GB PFZ width, are controlled by the width of a depleted copper zone within the PFZ, with improved SCC resistance associated with overaging being attributed to reduced cathodic polarization characteristics. Peel and Poole extended these arguments by observing that (1) Cu entered GB $MgZn_2$ precipitates during overaging leading to more positive electrochemical potentials in saline environments, and (2) cathodic polarization characteristics for Al-Zn-Mg-Cu solid solutions were insensitive to Zn and Mg depletion or reducing Cu from 1.5 to 0.7 wt% but were markedly decreased by the complete removal of copper.[30] Later work by Poole, et al., indicated that copper reductions from 1.5 wt% downward did significantly influence the cathodic polarization characteristics (Figure 9) and reinforced their belief that the beneficial effects of overaging retarding SCC of Al-Zn-Mg-Cu alloys is associated with crack blunting that results from preferential anodic dissolution of relatively wide GB regions with copper depletion.[72]

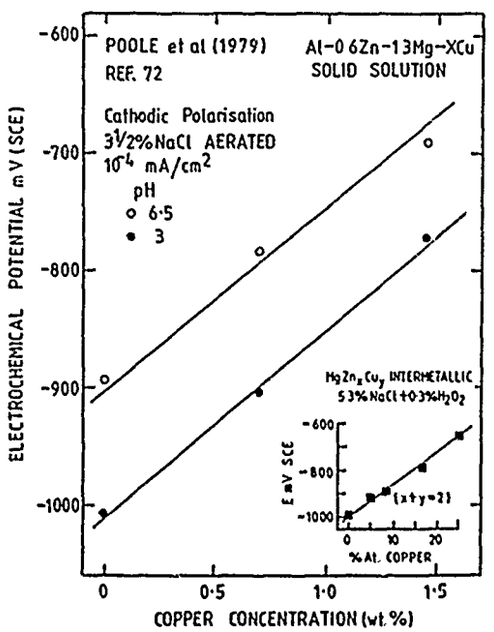


FIGURE 9—Electrochemical potential (vs SCE scale) for Al-0.6Zn-1.3Mg-XCu solid solutions and $Mg\text{-}Zn_x\text{-}Cu_y$ intermetallics at an anodic current density of 10^{-4} mA/cm² and the FCP, respectively, for various levels of copper in aerated 3.5% NaCl.

The failure of Doig, et al.,[50] to detect significant Zn or Mg solute level changes in GB regions during overaging 7075 must be attributed to a lack of measuring technique sensitivity, because more recent electron microscopy studies[32,81] report changes. For Zn, these changes are consistent with those expected, i.e., concentration decrease with overaging,[32,81] whereas those for magnesium are less clear, with increases,[32,81] decreases,[46] and minimal changes[55] all having been reported.

During the late 1970s and early 1980s, considerable effort was made to determine whether GB segregation of magnesium influenced the SCC of Al-Zn-Mg(Cu) alloys. Early work by Montgrain and Swann noted that magnesium oxide developed preferentially at GB surface intersections during solution treatment and was thought to be responsible for accelerated hydrogen entry and subsequent embrittlement under tensile stress (pre-exposure embrittlement).[12] This result led Viswanadham, et al., to propose that magnesium was also enriched in ambient oxide films adjoining GBs and that magnesium was segregated at GBs within Al-Zn-Mg(Cu) alloys.[58] A series of publications resulted, with spectroscopic and microscopic techniques being used to seek evidence of magnesium segregation at grain boundaries.

A research group at Martin Marietta Laboratories initiated work (recently reviewed in detail by Pickens, et al.[82]) using the enhanced surface sensitivity of Auger electron spectroscopy (AES) to obtain segregation profiles at grain boundaries in high-purity Al-Zn-Mg and commercial Al-Zn-Mg-Cu alloys. Initial segregation studies conducted by Green and coworkers involved fracturing several Al-Zn-Mg-Cu alloys *in situ* in an Auger chamber under ultra-high vacuum at around −194°C to produce IG fracture.[28,55,58] Segregation on the fracture faces was then measured using AES with information being obtained to a depth of 3 to 6 atomic layers from 6 to 8 grains under the electron beam. These workers concluded that both Zn and Mg atoms segregate to GBs with "free" magnesium existing in addition to $MgZn_2$. Further support for this was provided by plasmon-loss energies of the Auger spectra[56] which suggested that 60% of the magnesium existing on peak-aged 7075 GBs was 'free,' with all of the Zn being tied up as $MgZn_2$. Attempts to reproduce the latter findings have been unsuccessful[83] and several questions resulted. For instance, (1) does the IG microvoid coalescence fracture produced in the Auger chamber truly represent SCC fracture, which predominantly runs along GBs rather than in the associated PFZ, and (2) how significant are local compositional changes induced by the electron beam during analysis? Pickens and Langan have attempted to minimize the first problem by developing an embrittlement procedure capable of promoting the appropriate IG fracture morphology in ultra-high vacuum.[59,60] Three techniques were assessed using a high-purity laboratory Al-Zn-Mg alloy with a composition and temper known to give a high susceptibility to SCC: fracture at near liquid nitrogen temperatures without prior embrittlement and fracture at room temperature after pre-exposure to either liquid gallium or water-vapor-saturated air (WVSA) at 100°C. Fractographic evidence confirmed that the IG fracture promoted at liquid nitrogen temperatures was via microvoid coalescence, while that produced after the two pre-exposure procedures showed little evidence of ductile dimpling and was thought to be true GB fracture. Problems arose as Ga was found to react with the GB and lead to local Mg concentrations increasing with time, as was previously reported by Scamans.[84] Thus, by elimination, the WVSA pre-exposure method was deemed the most appropriate. However, the latter method also has drawbacks, because SCC for all alloys, save the most highly SCC sensitive in appropriate tempers, requires strain rates lower than those provided by impact fracture in the Auger chamber,[85] and if lower strain rates are used, sufficient time is now available for the vacuum to remove the pre-exposure effects, and ductile fracture will be promoted.[86]

The above spectroscopic work and parallel microscopic work (reviewed elsewhere[62]) present clear evidence for magnesium segregation on boundaries in the quenched condition in the absence of GB precipitation. The retention of segregation after precipitation remains a controversial point, although the weight of evidence for "free" magnesium on boundaries of aged alloys is growing.[60]

The importance of GB magnesium segregation during SCC of Al-Zn-Mg(Cu) alloys remains unresolved, since, on the one hand, the presence of magnesium at GBs is known to promote local activity and hydrogen entry into grain boundaries that can be detected by bubbles of molecular hydrogen discharged at suitable trap sites;[87,88] and, on the other hand, (1) the presence of GB magnesium is not a sufficient condition for SCC; (2) in the as-solution-heat-treated condition, when

GB segregation is maximized, alloys are immune to SCC; (3) experimental evidence suggests that magnesium concentrations at GBs can increase when SCC susceptibilities decrease, e.g., Al-Zn-Mg-Cu alloys being aged from T6X to T7X tempers (Figure 10).[32,81]

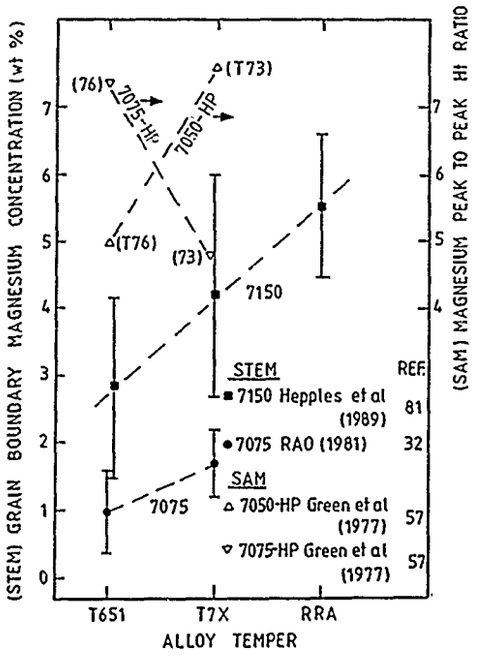


FIGURE 10—Influence of alloy temper upon the grain-boundary concentration of solid solution magnesium in various Al-Zn-Mg-Cu alloys.

Retrogression and re-aging

Although successfully minimizing SCC service problems for high strength Al Zn-Mg-Cu alloys, duplex aging prevents exploitation of an alloy's potential maximum strength.[5] Alternative heat treatment procedures known as retrogression and re-aging (RRA) have been claimed to provide SCC resistances equivalent to an overaged T73 temper while maintaining peak-aged strengths.[89] These heat treatments consist of a retrogression or reversion stage where peak or underaged material is heated in the temperature range 180 to 280 C followed by re aging at a lower temperature. Initial applications for RRA were restricted to thin sections[90] because it was not realized that retrogression temperatures below 220°C could be used for some Al Zn Mg Cu alloys. Use of these lower temperatures extend the required retrogression times from a few minutes up to over one hour (Figure 11) and has allowed thick sections to be successfully heat treated.[91]

Several papers have been published documenting the microstructural changes introduced during RRA[33,92] and the factors promoting improved SCC performance.[33,34] Work up until late 1986 has been reviewed by Thompson, et al.,[93] who conclude that there is general agreement on the final RRA microstructure but that two schools of thought exist on how it is obtained. Danh, et al.,[33] propose that the retrogression step promotes GP zone dissolution and η' nucleation within grains, whereas Park and Ardell[92] favor matrix nucleation of η and partial dissolution of η'. These differences may arise because Park and Ardell used a higher retrogression temperature (as suggested by Thompson, et al.[93]) or they may reflect microstructural differences in the initial plate material, which are known to be markedly sensitive to commercial fabrication practice. As yet, there is no general understanding of why the RRA microstructure offers a high resistance to SCC. Cina and Ranish's[94] initial explanation of the improved SCC resistance was based on the proposal of Jacobs[95] that SCC is due to concentrations of dislocations adjacent to undissolved $MgZn_2$ precipitates. The authors concluded that if the latter mechanism were operative, retrogression would be expected to reduce SCC susceptibility; however, they added the *proviso* that electron microscopy was needed for confirmation. More recent explanations have focused attention upon GB precipitates, some[33,93] have invoked ideas of Scamans,[87] Christodoulou and Flower,[88] and Pressouyre and Bernstein[96] that GB precipitates need to exceed a critical size before they act as preferential sites for hydrogen discharge or trapping, whereas others, who have also found SCC growth rates are related to GB precipitate size, believe further study is needed to describe quantitatively their results.[34] Data available to date suggest that the SCC rankings T6, T73, RRA are not linearly related to precipitate size, spacing, or volume fraction[34,81,97] (Figures 2 and 7), so, although there is a consensus that SCC resistance generally improves as GB $MgZn_2$ precipitate size increases, it seems probable that other factors are involved.

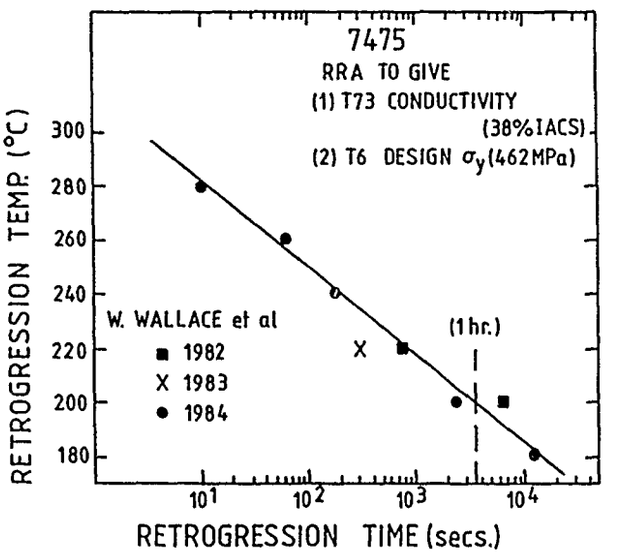


FIGURE 11—Retrogression times for peak-aged 7075-type (UNS A97075) alloys capable of providing retrogressed and re-aged properties with at least T6 design 0.2% proof stress, 462 MPa, and a T73 electrical conductivity, 38% IACS.[81]

A recent study on a Al-Zn-Mg-Cu alloy 7150[81,97] using ultra-high-resolution (2 nm) scanning transmission electron microscopy (STEM) has revealed that both RRA and duplex aging practices promote significant changes to GB segregation of zinc, magnesium, and copper These results, which are in close agreement with Rao s for 7075-T651 and T7351,[32] show that both duplex aging and RRA treatments promote increases in magnesium and decreases in zinc- and copper-segregation concentrations at grain boundaries (Figure 12). On the basis of these results, it seems unlikely that GB magnesium segregation controls SCC, and although the observed changes for zinc are consistent with the proposal of Schmiedel and Gruhl[54] that zinc controls SCC (Figure 13), the changes for copper are more striking (Figure 12) and have prompted a re-examination[97] of the proposals made by Doig, et al., in the mid-1970s that GB copper segregation controls SCC in 7075-type alloys.[50]

Transgranular SCC

Despite the SCC of aluminum alloys being almost exclusively IG,[1,5,6] transgranular (TG) SCC is well documented.[8,70,85,98-112] It occurs when factors such as grain shape/orientation,[99,103,109] crack-tip strain rate,[85,108] or local environmental conditions[85,113] are unfavorable for IGSCC, and the severe loading requirements for TGSCC may be established[88,112] without the onset of overload mechanical fracture. For example, albeit at very high stresses, TGSCC can occur in high-strength aluminum alloys: (1) across the fibrous grain structures often found in commercial plate and extrusions alloys, i.e., nonshort-transverse orientations that in general are highly resistant to IGSCC;[103,105] (2) in short-transverse precracked

specimens of 7XXX-T73 alloys loaded at stress-intensity factors approaching K_{1c};[104,109] or (3) in place of IGSCC if a critical crack-tip strain rate is exceeded and sufficient time is available prior to ductile overload failure.[85,108] The critical strain rate for the IG/TGSCC transition is microstructure sensitive, increasing with an alloy's SCC susceptibility and the aggressiveness of the environment/pre-exposure conditions.

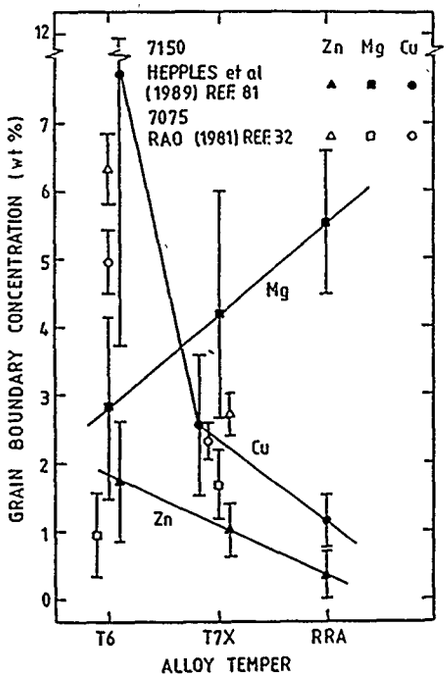


FIGURE 12—Influence of alloy temper upon zinc, magnesium, and copper concentration at grain boundaries for two commercial Al-Zn-Mg-Cu alloys, 7075 (UNS A97075) and 7150.

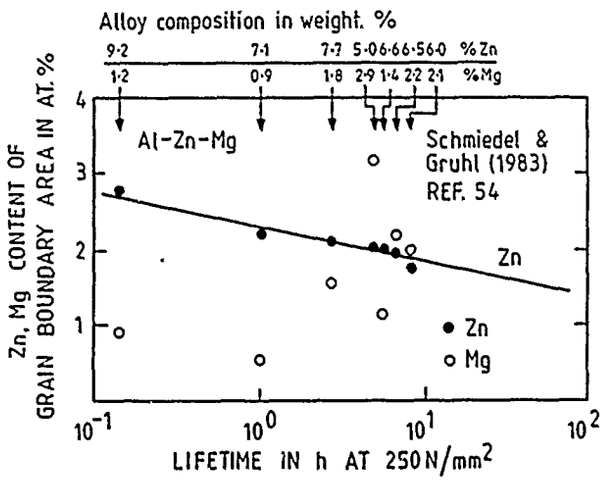


FIGURE 13—Relationship between zinc and magnesium content of grain-boundary regions and time-to-failure for Al-Zn-Mg alloys with varying Zn/Mg ratios in an aqueous saline solution.[54]

Hydrogen embrittlement

The most comprehensive study of microstructural effects upon HE of aluminum alloys is provided by Bernstein, Thompson, and coworkers,[14,114-118] who over the past decade have conducted systematic studies on Al-Zn-Mg-Cu alloys and have suggested that similar effects are operative for an Al-Cu-Mg alloy, 2124.[14] Initial studies[114] examined the influence of temper [underaged (UA), peak aged (PA), and overaged (OA)] upon the susceptibility of a laboratory-re-aged, commercially produced 7075 plate material, cathodically charged with hydrogen and fractured at temperatures between −196°C and room temperature. Their results confirmed the temperature-dependent HE previously reported by Gest and Troiano,[11] and demonstrated a microstructural sensitivity mirroring that known for SCC; i.e., HE and SCC susceptibility decrease UA > PA >> OA, despite the fact that in this work the principal fracture path is TG for HE, as opposed to IG for SCC. Albrecht, et al.,[115] in a later study obtained similar results using a commercially produced high-purity 7075 model alloy with Cr, Fe, and Si minimized and demonstrated that the fracture path for the HE (as with SCC) is primarily IG when grain structures are favorably oriented and the local hydrogen concentrations are sufficiently high. In this study, a test procedure known as SET (straining electrode test) was introduced, in which specimens were preloaded to about 70% of their yield stress and then continuously plastically strained to up to 2% total plastic strain using a low nominal strain rate of around 2×10^{-6}/s, while simultaneously cathodically charging with hydrogen at $-2000\ mV_{SCE}$ in a HCl environment with a pH of 1 prior to tensile testing in laboratory air using a nominal $\dot{\epsilon} \sim 3.3 \times 10^{-4}$/s. SET is an aggressive test for HE, often inducing greater embrittlement than static cathodic charging (Figure 14), an effect that has been attributed to the involvement of dislocation transport of hydrogen[115] via solute atmospheres being associated with mobile dislocations.[119-121] In view of this, Albrecht, et al.,[115] concluded that microstructural effects upon the HE of Al-Zn-Mg-Cu alloys were accountable in terms of the relative planarity of dislocation motion, the strain for slip-band segregation, and the effects of local slip-band softening.[114] Further evidence in support of these proposals was offered by concurrent studies[116,118] on commercially produced 7050-type alloys, Al-6Zn-3Mg-xCu, with and without copper. Here it was shown, as expected, that UA (80% PA strength) alloys were highly susceptible to HE, whereas the Cu-containing 7050 alloy when PA was highly resistant, unlike the copper-free version or 7075-type alloys,[114,115] which contain lower levels of Cu than 7050. The explanation offered was that matrix precipitates are sheared for 7050-UA, 7075-PA, and Al-6Zn-3Mg-PA,[73,74] which is often associated with a poor resistance to HE,[123] whereas for 7050-PA, they are looped[73,74] and thereby provide an improved HE resistance,[122] i.e., the same argument as previously used for SCC resistance improving with aging.[43,69,74]

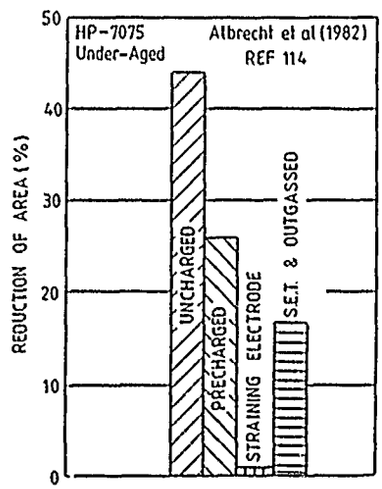


FIGURE 14—Comparison of ductility of uncharged, precharged and straining electrode test (SET) specimens for a high-purity 7075 (UNS A97075) analogue alloy in an underaged temper.[115]

A detailed examination of the microstructural dependence of the HE for the HP-7075 alloys previously used by Albrecht, et al.,[115] has been recently presented by Nguyen, et al.[117] These authors conclude for high-strength aluminum alloys in general that (1) matrix precipitates exercise the most control over HE through their influence on slip planarity, (2) GB precipitates play a secondary role, probably via hydrogen trapping providing localization of hydrogen and enhanced IG embrittlement, and (3) the presence and size of PFZs are of minor if any importance.

On the basis of the data obtained (Figure 15), it appears that a remarkably strong resistence to HE is obtained when the matrix precipitate size exceeds around 9.3 nm, which compares favorably to the 8.5 nm quoted by Jacobs[123] for high SCC resistance.

In the opinion of the reviewer, although the importance of matrix precipitation for transgranular SCC and HE is undoubtable, the case for matrix precipitation controlling the IG HE or SCC behavior is far from proven. The conclusions of Bernstein, Thompson, and coworkers are based upon observations for TG HE (IG HE in general being restricted to a maximum depth of a few grains). Plausible arguments for GB precipitation controlling IG HE can be made. For instance, it is interesting to note from the data of Nguyen, et al., given in Figure 15 that a high resistance to HE occurs when GB precipitate sizes exceed around 30 nm. This value has been quoted by several authors as a critical minimum size for good SCC resistance in 7075-type alloys, as used by Nguyen, et al.[117]

The most convincing evidence for the importance of GB precipitates during IGSCC is provided by Vasudevan, et al.,[124,125] who have manipulated the microstructures of Al-Li-Cu-Zr alloys using reversion and re-aging to provide microstructures maintaining PA GBs while varying the matrix structure. The SCC growth data for microstructures with PA GBs and an UA matrix closely resemble that of the PA rather than the UA material (Figure 16). This important observation questions the importance of matrix precipitation and the role of slip planarity during SCC.

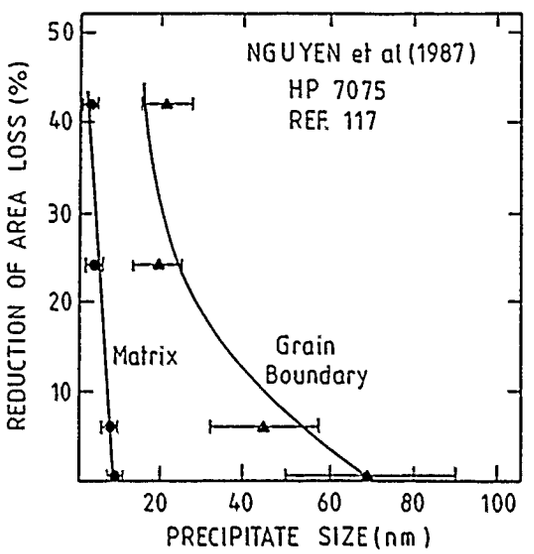


FIGURE 15—Ductility loss as a function of precipitate size, both in matrix and at grain boundaries.[117]

Clearly, more study is needed to clarify the role of microstructure during SCC and HE. It is interesting to note, however, that the dependence shows many similarities, a point that will be returned to in a later section.

Environmental Aspects

Almost all published SCC data for aluminum alloys (2XXX, 5XXX, 7XXX, and Al-Li-based alloys) involves cracking in aqueous saline environments. Some data is available for 7XXX series alloys in (1) various gases,[3,5,6] (2) aqueous environments containing halide anions other than chloride[1,3,5,6,126] or nonhalide anions,[3,5,6,126-131] and (3) nonaqueous organic environments.[3,5,6,132]

Gaseous environments

The influence of gaseous environments upon the SCC of Al-Zn-Mg(-Cu) alloys is summarized by Speidel as follows:[3]

(1) SCC neither initiates nor propagates in dry gases.
(2) SCC initiates almost immediately in wet gases when precracked specimens are subjected to stress intensity factors approaching K_{Ic}.
(3) SCC fracture morphology is IG with crack growth kinetics controlled by the humidity level and independent of gas composition (Figure 17).
(4) SCC is observed at sufficiently low humidity levels, e.g., below 30% relative humidity (RH), for condensation not to occur at propagating crack tips and therefore eliminate the possibility of anodic dissolution.

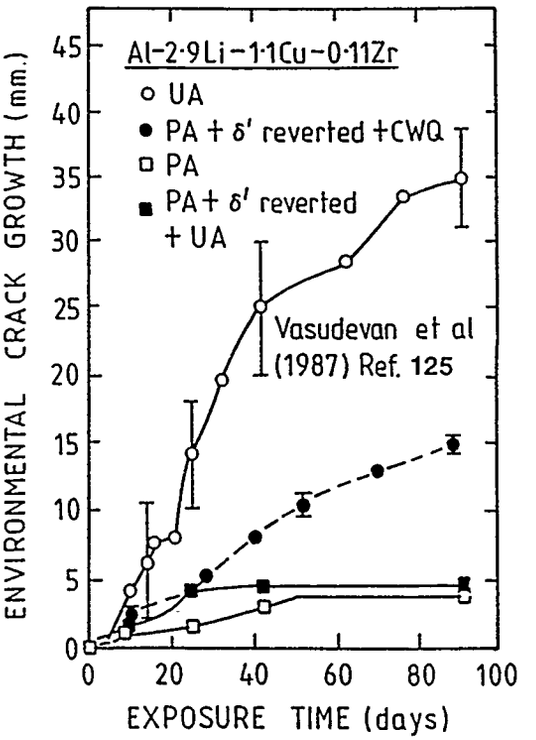


FIGURE 16—Variation in crack growth with exposure time for an under-, peak-, and peak-aged + reverted Al-2.9Li-1.1Cu-0.11Zr alloy exposed to drip-fed 3.5% NaCl aqueous solution.[125]

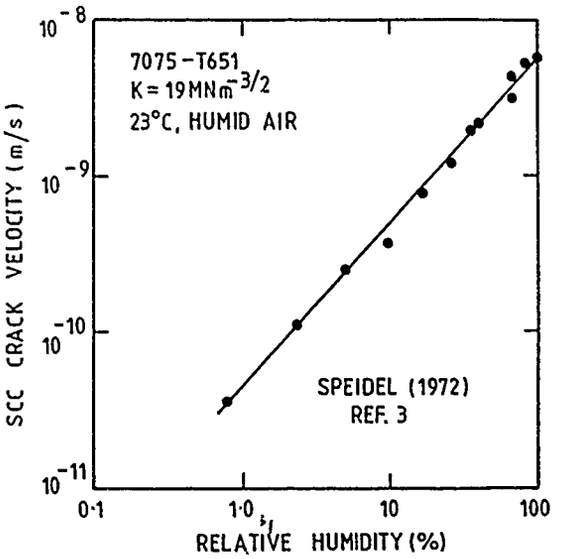


FIGURE 17—Effect of humidity upon Region 2 SCC crack growth rate in an Al-Zn-Mg-Cu alloy, 7075-T651.[3]

On the basis of the above, Speidel[3] argues that a HE mechanism must control the SCC of 7XXX alloys in moist, gaseous atmospheres.

SCC in moist environments has not been reported for 7090 or 7091 rapidly solidified powder alloys or ingot metallurgy (I/M) alloys other than 7XXX series, although 6XXX series alloys (Al-Mg-Si) are known to be potentially susceptible to nonenvironment-sensitive slow

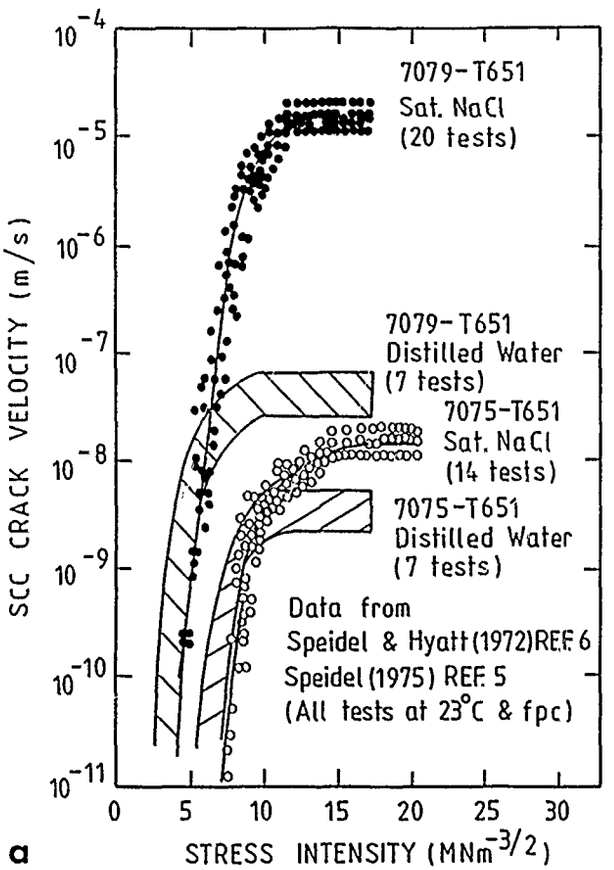
crack growth (SCG) when loaded to stress-intensity factors approaching K_{Ic}.[75] Further work is warranted to confirm these observations and to establish whether 7XXX series I/M alloys alone are susceptible to SCC in moist environments.

The inability of dry hydrogen to promote nucleation and growth of subcritical SCG in high-strength aluminum alloys has been used in the past as an argument against HE being a potential SCC mechanism. More recent work, however, now has demonstrated that this observation results from hydrogen-entry problems, as embrittlement has been promoted in dry hydrogen when (1) ionization occurs, e.g., during electrical discharge[105] or in the electron beam of a high-voltage electron microscope,[133] and (2) very. high gas pressures, e.g., 300 atmospheres, are combined with dynamic loading close to overload.[134]

Aqueous environments

Halide solutions. Published information on the influence of environmental parameters, such as solution composition, pH, temperature, viscosity, etc., and electrochemical potential, on SCC in halide solutions is limited, almost exclusively, to that available for 7XXX series alloys. Until a few years ago, all of the available information was based upon bulk solution conditions, despite it having being well known for the last twenty years that local environmental conditions within cracks generally differ significantly from bulk conditions.[135] The issue of bulk vs local environmental conditions will be returned to in a later section. Meanwhile, environmental effects will be discussed in terms of bulk conditions.

Speidel[3,5] and Speidel and Hyatt[6] have presented a wealth of data in the form of SCC crack velocity–stress-intensity factor curves. Unfortunately, most of this data is for 7079-T651 and is unlikely to be truly representative of 7XXX series alloys. SCC crack growth rates for 7079-T651 (1) are higher than for other 7XXX series alloys and (2) in 0 5 M sodium chloride are at least two orders of magnitude higher than those in distilled water (for other 7XXX series alloys the increase is less than an order of magnitude) (Figure 18).



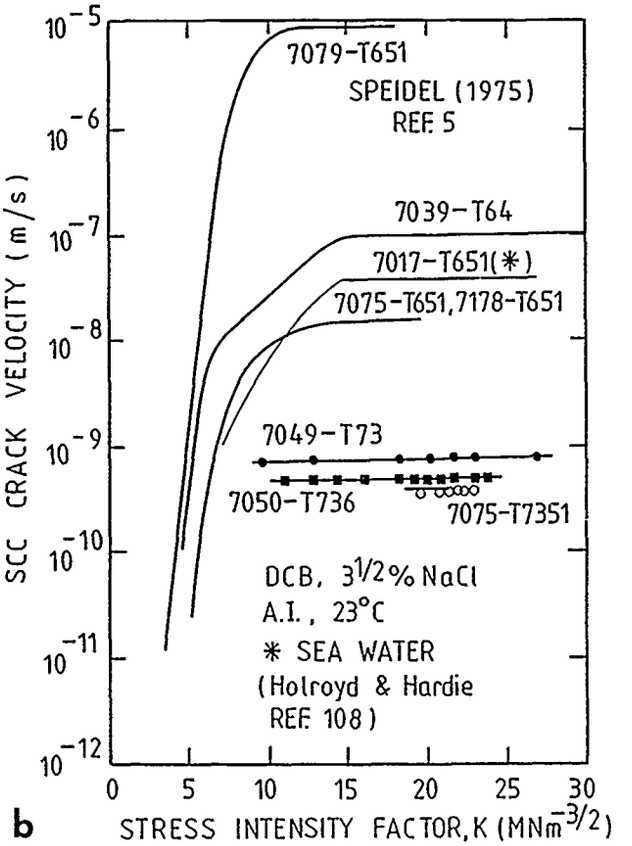


FIGURE 18—Stress corrosion crack growth rates in distilled water and aqueous sodium chloride solutions for commercial Al-Zn-Mg-Cu alloys; (a) comparison between crack growth rates in distilled water and saturated sodium chloride (note 7075-T651 shows a significantly smaller difference, more typical of 7XXX series alloys); and (b) crack growth rates in 3.5% NaCl for a range of commercial 7XXX series alloys.

Solution composition—Speidel[3] has proposed that the presence of cations other than Hg^{2+} and H^+, e.g., Li^+, Na^+, K^+, Rb^+, Al^{3+}, and NH_4^+, have little or no specific effect upon the SCC growth kinetics for 7XXX series alloys in neutral aqueous chloride solutions other than their influence upon solubility products and possible limitation on local concentration of specific ions.[6] Availability of Hg^{2+} presumably leads to the deposition of liquid mercury and the possibility of rapid cracking via liquid metal embrittlement. Similar arguments can be made for metallic ions of other low-melting-point elements that also tend to activate aluminum surfaces, e.g., Ga, In, Sn, and Pb.[136] The influence of H^+ ions will be discussed below in the section on solution pH effects.

A quantitative study of the SCC of 7XXX series alloys in aqueous solutions containing different halide ions is not available. From data given by Speidel and Hyatt[6] and Speidel[3] for 7079-T651, the following can be concluded: (1) F^- and the pseudo-halide ion SCN^- do not accelerate SCC like other halide ions and that F^- can act as an inhibitor, and (2) on the basis of the limited data available, SCC crack growth rates increase with increasing halide ion concentration above around 10^{-2} M and are not significantly different in Cl^-, Br^-, and I^- solutions of given anion concentration (Figures 19 and 20).

The extent to which the above is valid for 7XXX series alloys in general is debatable. The marked increase in Region 2 SCC growth rates reported for 7079-T651 in halide solutions[6] has not been observed for 7075-T651 in chloride solutions. For example, for a concentration increase 10^{-3} to 1 M sodium chloride, Le, et al.,[127] and deJong[137] report that crack growth rates for 7075-T651 increase by less than an order of magnitude, whereas for 7079-T651 in potassium iodide solutions, Speidel and Hyatt[6] observed an increase of three orders of magnitude (Figures 19 and 20). (Although deJong,[137]

like others,[104,128-140] failed to detect Region 2 SCC plateaux, his SCC crack velocity data for 7075-T651 are consistent with the plateaux data of Le et al.,[127] when assessed for stress-intensity factors associated with Region 2, Figure 20.)

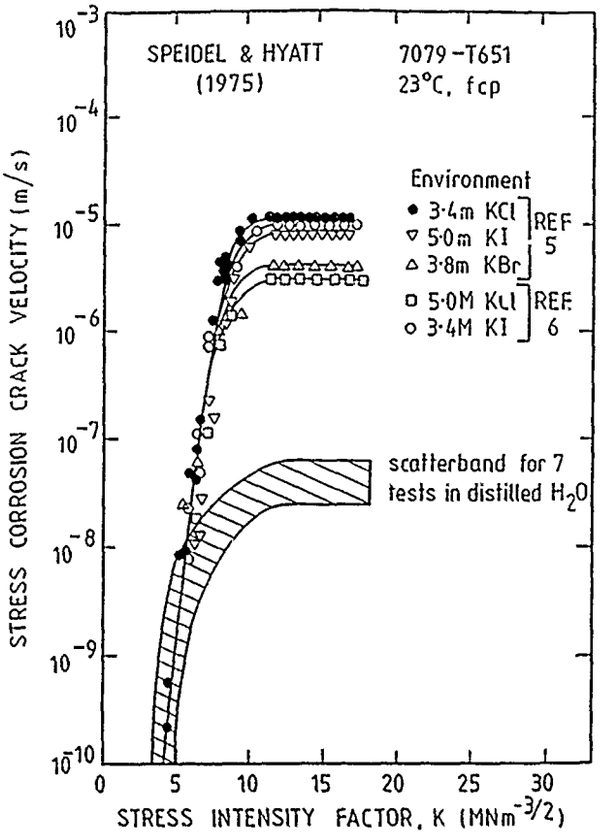
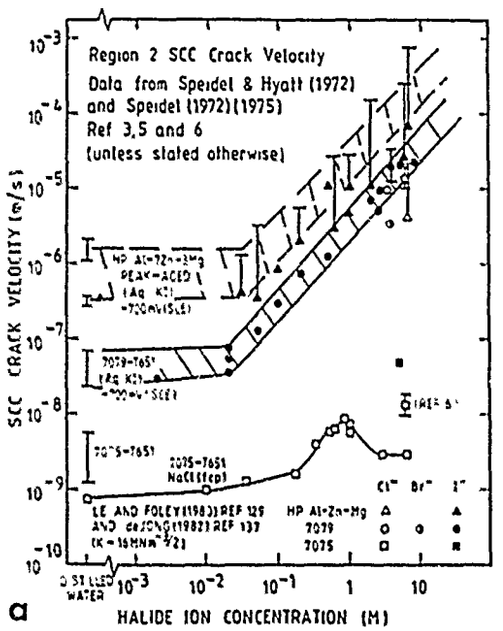


FIGURE 19—Stress corrosion crack velocities as a function of stress-intensity factor for 7079-T651 in distilled water and various aqueous halide ion solutions.



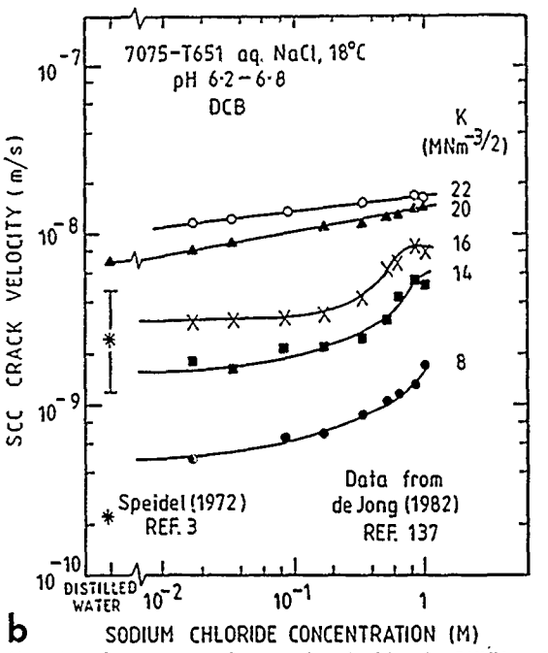


FIGURE 20—Stress corrosion crack velocities for 7XXX series alloys in aqueous solutions containing chloride and iodide ions; (a) Region 2 SCC plateau velocities for various alloys and (b) SCC crack growth rates as a function of sodium chloride concentration for a range of stress-intensity factors.

Detailed study of the influence of chloride ion concentration upon SCC initiation has not been reported. Available test data from smooth specimens involving SCC initiation and propagation suggest that increasing sodium chloride concentrations above 0.5 M (3 wt%) has little effect upon whether or not SCC crack initiation occurs. Crack propagation data, on the other hand, show that chloride additions up to around 0.1 M have a minimal effect upon SCC growth rates, whereas rates increase with further additions up to about 1 M chloride (Figure 20). Le, et al.,[127] noted that maximum crack growth rates for 7075-T651 occur for sodium chloride concentrations of around 1 M and suggested that this is probably associated with dissolved oxygen levels, which peak at similar chloride concentrations.

Additions of aqueous nonhalide anions to saline solutions can promote synergistic effects upon the SCC of aluminum alloys. These will be discussed in a later section.

Solution pH— There is general agreement that the occurrence of SCC in high-strength aluminum is reduced as saline solutions become more alkaline.[1,6] Constant-load SCC testing was used in the early studies of solution pH effects on the SCC of 7075-T651 in sodium chloride solutions. The results obtained suggested that SCC performance improves gradually with increasing bulk solution pHs up to 10, and then improves significantly at higher pHs (Figure 21).[141] In contrast, more recent data for 7075-T651 subjected to slow-strain-rate testing[142] in 3% NaCl suggest that SCC susceptibility increases significantly for pHs below 4 (Figure 21).[143]

Examination of the crack propagation data reveals that crack initiation and the development of local environments within cracks must influence the above trends. deJong's data for 7075-T651 suggest that crack growth rates increase logarithmically with bulk solution pH changes either side of 7 and that a discontinuity exists somewhere between pH 10 and 12 (Figure 22).[137] Further work is needed to establish whether these observations can be related to the stability of aluminum corrosion products such as $Al(OH)_3$, $Al_2O_3 \cdot xH_2O$, $Al(OH)_y(Cl)_z$, etc. (Figure 22).

In contrast to that reported by deJong for 7075-T651, Speidel and Hyatt[6] did not observe any influence of bulk solution pH (pH 0 to 11) upon Region 2 crack growth rates for either 7079-T651 in 5 M KI (-700 mV_{SCE}) or a high-purity Al-7Zn-3Mg alloy in 3.5% NaCl at room temperature. This probably reflects the very high SCC susceptibility of the alloys used by Speidel and Hyatt.

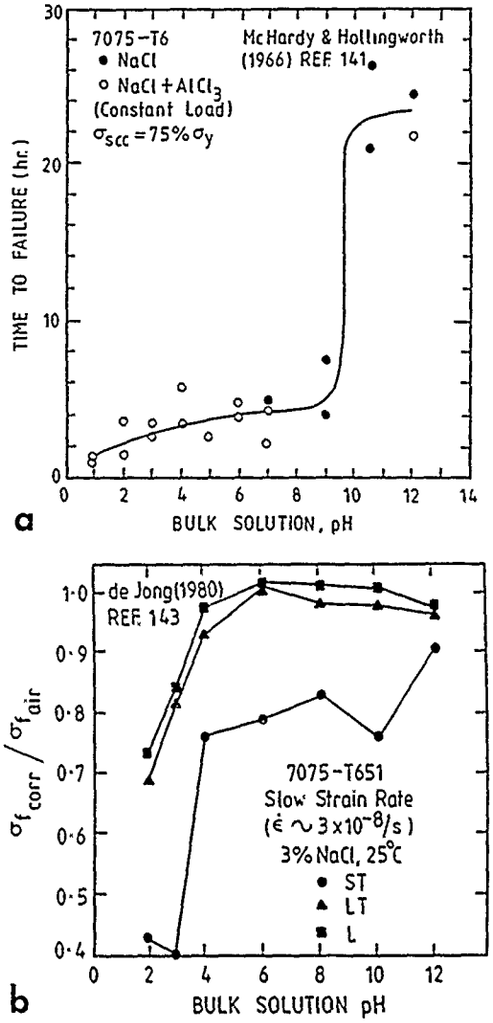


FIGURE 21—Influence of bulk solution pH on (a) failure times for constant tests on 7075-T651 in a saline solution[141] and (b) failure stress ratio after slow-strain-rate testing in 3% NaCl.[143]

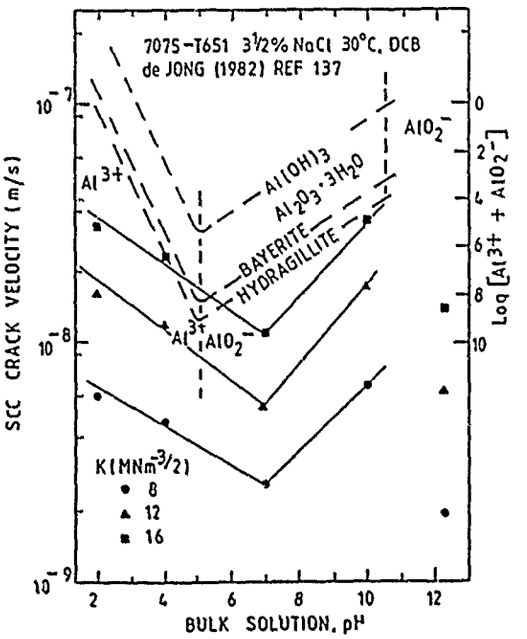


FIGURE 22—Crack growth rates as a function of bulk solution pH for 7075-T651 suffering SCC in 3.5% NaCl at various stress-intensity factors.

Solution temperature—The influence of temperature upon SCC has been assessed by several researchers in attempts to identify rate-controlling processes.[3,5,6,137,144-150]

In the early 1960s, Gruhl[145] reported that constant-load SCC tests, in a saline solution at temperatures in the range 25 to 70°C for a commercial Al-5Zn-3Mg sheet alloy in a highly SCC sensitive condition, yielded straight-line plots of applied stress against specimen life. Helfrich[147] obtained similar experimental results in 1 M NaCl for short-transverse C-ring specimens from 7039-T64 plate (Figure 23) and calculated activation energies and activation volumes using an approach developed by Hillig and Charles[151] that assumes SCC is a thermally activated process in which the rate of activation is dependent upon the local state of stress at or near the reaction boundary. Helfrich concluded that IGSCC of 7039 is a stress-activated and thermally activated process with the rate-determining step (RDS) involving anodic dissolution of GB $MgZn_2$ precipitates rather than a transport phenomenon such as diffusion of species to active GBs. He also suggested that factors such as minimum spacing of GB precipitates, low GB ductility, and a high yield stress would aid the mechanical aspect of SCC crack propagation.

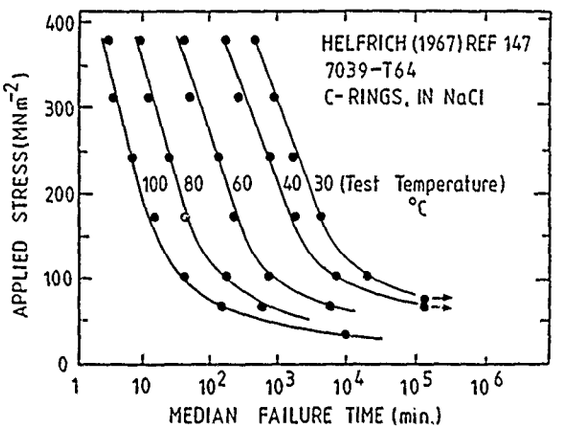


FIGURE 23—Effect of applied stress at constant temperature on failure time for constant strain SCC tests on 7039-T64 in 1 M NaCl. (Copyright ASTM. Reprinted with permission.[147])

Apparent activation energies (E_a) for 7XXX series alloys, calculated using time-to-failure data from SCC tests on smooth specimens tested in saline environments, are generally in the range 58 to 86 kJ/mole, with values depending on the SCC test method and stress level, in addition to alloy microstructure/composition and the test environment. Speidel and Hyatt suggest that the E_a values calculated from time-to-failure test data for smooth specimens will integrate Region 1 and Region 2 SCC behavior, with a bias toward that for Region 1, since these conditions generally prevail during most of the specimen life in these tests.[6] Data quoted by Helfrich[147] and Romans and Craig[148] is in qualitative agreement with Speidel and Hyatt's proposal in that E_a values are in the range 16 to 114 kJ/mole (see below), and they increase with decreasing initial load and/or the stiffness of the test-method loading system (Figure 24); i.e., E_a values increase as the Region 1 component increases.

Speidel and Hyatt reported that the activation energy (E_a) for SCC crack growth in 7079-T651 in 3 M potassium iodide under conditions of anodic polarization depends upon the operating stress-intensity factor (K): E_a ~ 113 kJ/mole for K values in Region 1 (stress-dependent region) and E_a ~ 16 kJ/mole for Region 2 (stress-independent region) (Figure 25).[6] Although most of their reported experimental data at temperatures above 25°C involved potassium iodide and anodic polarization, the above E_a values were also attributed to chloride solutions under free-corrosion conditions. On the basis of the above, Speidel and Hyatt propose that the rate-controlling step (RDS) during SCC crack propagation in 7079-T651 in aqueous halide solutions involves a chemical process in Region 1 and a mass transport process in Region 2. To explain why SCC crack propagation in Region 2 for 7039-T61 in 5 M potassium

iodide at the free-corrosion potential (FCP) has an apparent E_a of 85 kJ/mole and is contrary to the above, Speidel and Hyatt argue that SCC crack propagation for 7039-T61, unlike 7079-T651, can display two Region 2 crack velocity plateaux (Figure 26),[6] with the lower one being equivalent to SCC in distilled water and having an apparent E_a of ~ 85 kJ/mole (chloride-independent) and the higher one, existing at greater K values, being chloride-dependent with an apparent E_a of ~ 16 kJ/mole, similar to that found for 7079-T651 in Region 2.

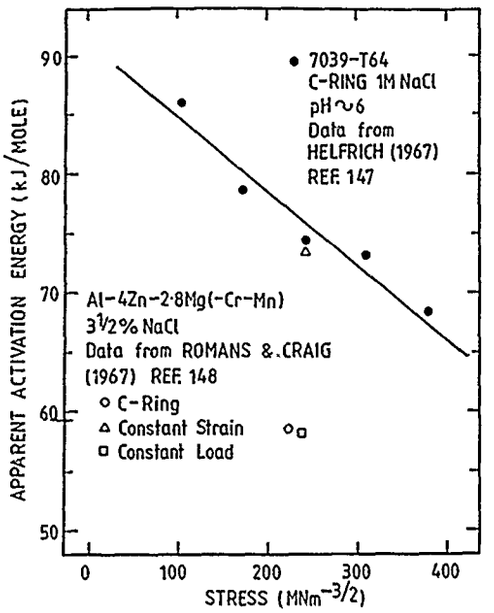


FIGURE 24—Apparent activation energies for 7039-T64 suffering SCC in 3% NaCl under various loading conditions.

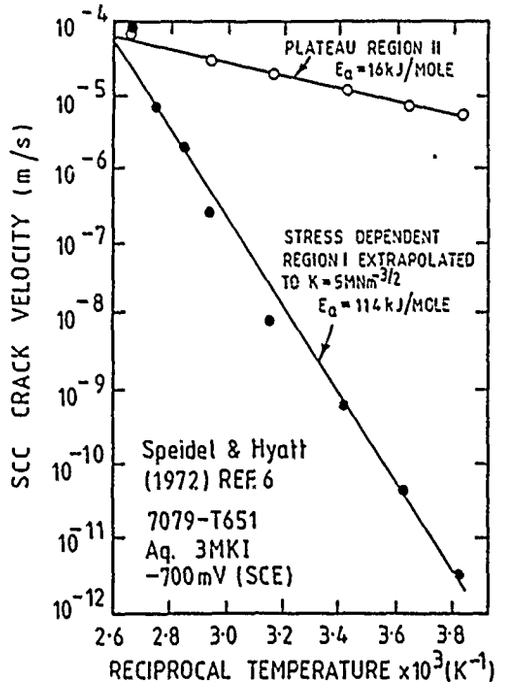


FIGURE 25—Apparent activation energies for thermally activated SCC crack growth under anodic polarization for 7079-T651 in an aqueous 3 M potassium iodide solution.

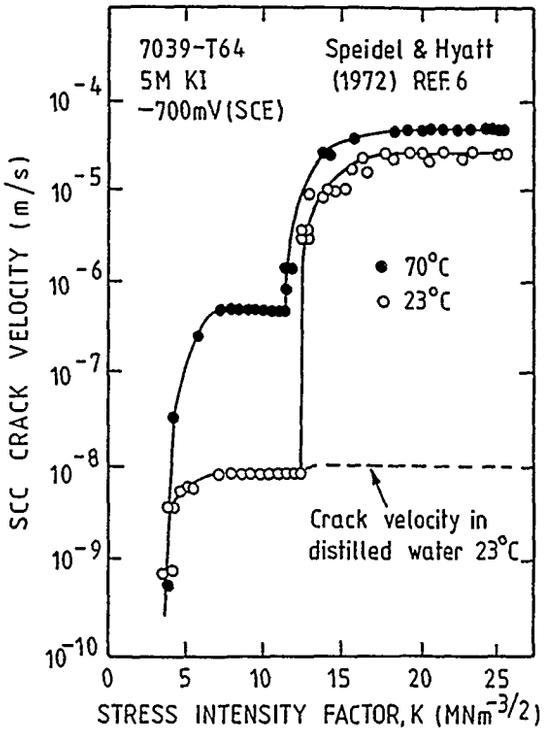


FIGURE 26—Stress corrosion crack velocity as a function of stress-intensity factor for 7039-T64 in distilled water at the FCP and under anodic polarization in an aqueous 5 M potassium iodide solution.[6]

Whether the above proposals are appropriate for the SCC of commercial 7XXX series alloys in saline solutions at the FCP is debatable. An alternative explanation for the E_a for 7039-T61 Region 2 SCC being too high to fit Speidel and Hyatt's proposal can be made if the low E_a values quoted above for Region 2 behavior, i.e., 16 kJ/mole, exist only when highly susceptible alloys such as 7079-T651 and 7039-T6X are subjected to sufficient anodic polarization. (Note that all Speidel and Hyatt's[6] and Speidel's[3,5] reported low E_a values were obtained using the above alloys or a high-purity Al-7Zn-3Mg alloy while being subjected to anodic polarization.) In other words, it is possible that it is the low E_a values that are unusual. Published E_a values from other authors favor this proposition, for example:

(1) All available E_a values for the commercial alloy 7075-T651 in saline solutions at temperatures below 40°C exceed 25 kJ/mole (E_a values with anodic polarization are not available);
(2) An E_a of 103 kJ/mole has been quoted by Landkof and Gal-OR[146] for Region 2 SCC in 7039-T63 cracking in a chromate-inhibited saline environment; and
(3) Pathania and Tromans[144] quote E_a values of 109 ± 26 and 109 ± 8 kJ/mole for SCC initiation in distilled water and a chromate inhibited 3.5% NaCl solution respectively, for a slightly overaged high-purity Al-6.3Zn-2.6Mg alloy.

Apparent E_a values calculated from the SCC crack growth data recently reported by deJong[137] for freely corroding 7075-T651 in a range of saline solutions are given in Figure 27 as a function of bulk solution pH and applied stress-intensity factor (K). deJong did not observe SCC crack growth rate plateaux, and the calculated E_a values are insensitive to K for the range 8 to 20 MNm$^{-3/2}$. The most striking observation from deJong's results is that the E_a values for solution temperatures above and below about 40°C fall into two sets: E_a values 55 to 80 kJ/mole for temperatures 40 to 55°C, and E_a values 27 to 47 kJ/mole for temperatures 25 to 40°C (Figure 27). The transition temperature of around 40°C is insensitive to solution pH (2 to 10) and decreases slightly with increasing K, i.e., ~ 40°C and 32°C for K values of 8 and 16, respectively (Figure 28). Because a change in SCC performance at temperatures around 40°C is a

common experience, it is tempting to speculate that this behavior is associated with surface filming characteristics, which also change significantly at temperatures around 40°C.[152]

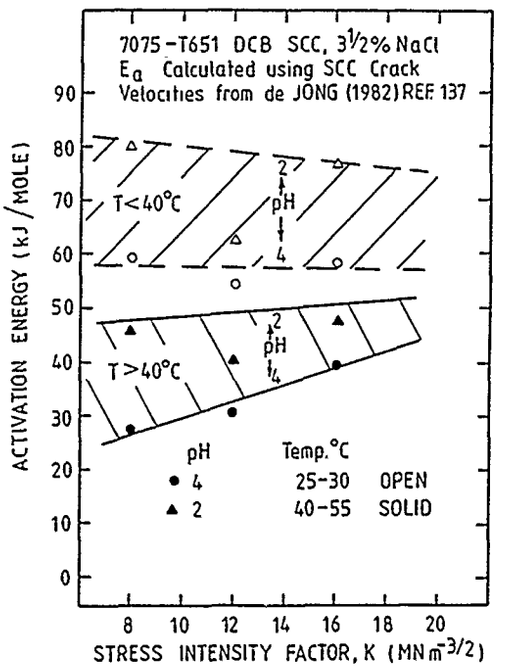


FIGURE 27—Apparent activation energies for 7075-T651 suffering SCC at various stress-intensity factors in an aqueous 3.5% NaCl solution.

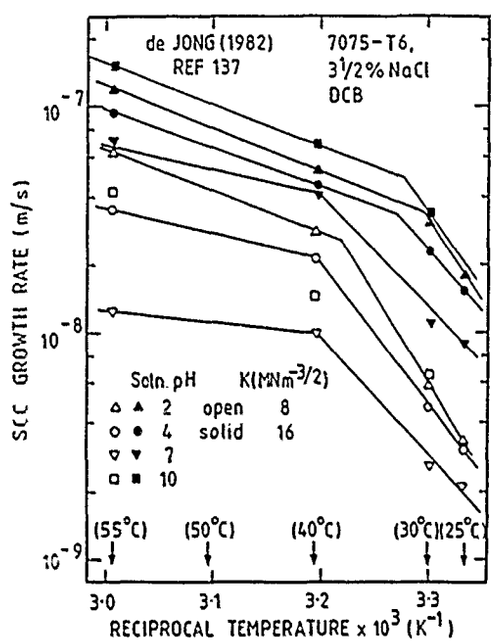


FIGURE 28—Arrhenius plots using SCC crack growth rates for 7075-T651 in 3 NaCl at various temperatures and solution pHs. (Note: Implied activation energies are not strongly influenced by stress-intensity factors being in Region 1 or Region 2.)

The dangers of attaching mechanistic significance to apparent activation energies are clear. Even when all experimental variables are removed (which is not always readily achieved) and apparent E_a values may be taken as actual E_a values, it must be remembered that several processes can have similar activation energies, and therefore generally only when strong independent evidence is available can a specific process be confidently selected. For example, E_a values of around 100 kJ/mole have been reported for (1) the anodic dissolution of aluminum alloys in aqueous solutions, 80 to 100 kJ/mole[153], (2) creep-deformation processes controlled by cross slip (103 to 117 kJ/mole[154]), and (3) the diffusion of hydrogen in the aluminum lattice (~ 90 kJ/mole[155]). E_a values of around 50 kJ/mole have been quoted for (a) anodic dissolution,[156] (b) grain-boundary sliding[150,157] and diffusion,[150,158] (c) creep-deformation processes controlled by intersection of dislocations,[159] (d) escape of dislocations from segregated atmospheres,[160] and (e) segregated yielding in Al-Mg alloys.[161]

In summary, the RDS during SCC of 7XXX series alloys awaits identification. Based on the evidence available, it is unlikely that the diffusion of species with aqueous environments controls SCC initiation or propagation other than under conditions of anodic polarization.

Electrochemical potential—Under appropriate anodic polarization conditions, all medium- and high-strength aluminum alloys can suffer SCC. Even commercial 6XXX series alloys (Al-Mg-Si) are susceptible,[162,163] although no failures have been attributed to SCC in more than 30 years of service experience, and cracking in the laboratory under freely corroding conditions only occurs for unconventional heat treatments.[1] As with solution composition, pH, and temperature, the available published data on the influence of electrochemical potential are almost exclusively limited to those available for 7XXX series alloys in halide solutions.

Speidel claims to have quantitatively investigated the effect of electrochemical potential upon SCC crack growth rates.[3] Typical crack velocity–stress-intensity factor (cv–K) curves for 7XXX series alloys in halide solutions is given in Figure 29. These data imply for a given K, a crack velocity in Region 1 decreases as anodic polarization decreases, while a Region 2 crack velocity remains constant at high levels of anodic polarization but decreases with decreasing potential below a critical value, with mild cathodic polarization promoting crack growth rate retardation compared to SCC in distilled water at the FCP.

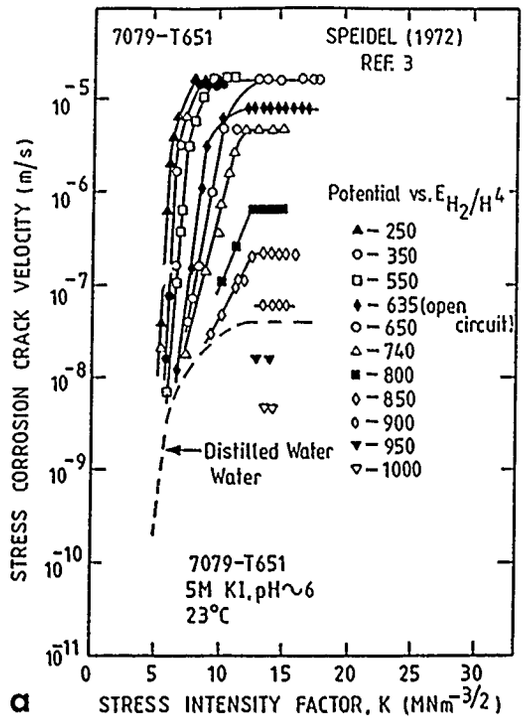
As with other environmental parameters assessed by Speidel[3,5] and Speidel and Hyatt[6] using cv–K curves, most of the reported data for electrochemical effects involve either 7079-T651 or a high-purity Al-Zn-Mg alloy in potassium iodide solutions. Limited data are available for these alloys in other halide ion solutions (SCC potency increases in the order $F^- < Cl^- < I^-$, Figure 30) and for 7075-T651 in a potassium iodide solution (Figure 29). Comparison of the data for 7075-T651 with that for 7079-T651 or the Al-7Zn-3Mg alloy once more demonstrates that the latter two alloys differ significantly from 7075-T651 and so do not provide characteristic behavior for 7XXX series alloys.

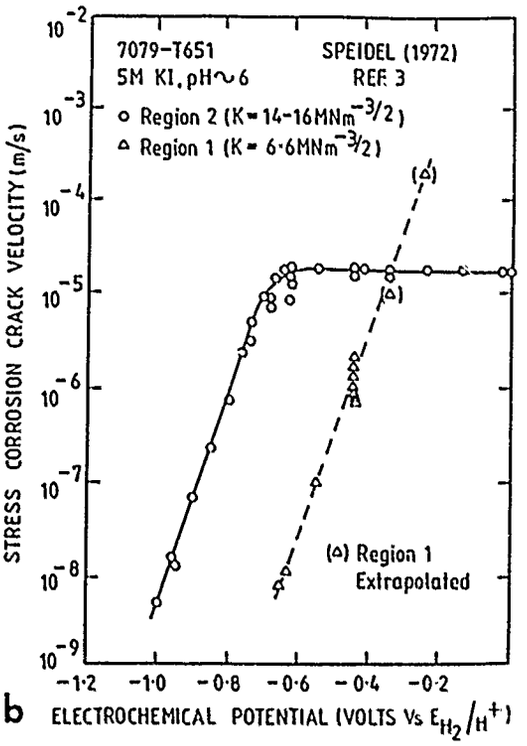
A major problem restricting interpretation of electrochemical potential effects upon SCC crack growth using the above data is that external electrode potential (i.e., potentials for DCB surfaces away from the crack) will only equal the crack-tip potential for potentials close to the FCP. Edwards measured electrode potentials within growing SCC cracks for 7075-T651 immersed in aqueous sodium chloride and potassium iodide solutions and published the relationships he obtained between impressed external potential and those developed within a SCC crack (Figure 31).[164] The data confirmed the earlier work of Davis[165] that external anodic or cathodic polarization becomes increasingly less influential upon crack-tip potentials as external potentials move away from the FCP, with limiting crack-tip potentials being 100 mV anodic and 300 mV cathodic to the FCP. Edwards[164] suggests that Speidel's[3,5] and Speidel and Hyatt's[6] data can be corrected to allow for the potential-drop effects, and when adjusted, their data show good agreement with his own experimental data (Figure 32).

The implication of the above is that the crack velocity plateaux shown in Figures 29 and 30 with SCC growth rates under increasing external anodic polarization are nothing more than crack growth rates at the limiting potentials attainable at the crack tip. In support of this proposal, it is interesting to note for 7075-T651 in potassium iodide that the potential (~ 550 mV_{SCE}) below which Speidel[3] found Region 2 SCC crack velocities started to decrease with decreasing anodic polarization corresponds to the limiting potential reported by Edwards[164] (compare Figures 29 and 31). Other authors,[11] including

the reviewer,[85,86] in the past have ignored potential drops when they are undoubtedly involved.

The influence of crack-tip potential on SCC is complex. Some researchers have used the observations that mild cathodic polarization retards SCC initiation and propagation rates in saline environments, while anodic polarization accelerates SCC to conclude or prove[166] that HE is not responsible for SCC of 7XXX series alloys in saline environments. The arguments presented do not exclude HE, and other experimental evidence, such as that provided by Ohnishi and Nakatani,[167] clearly demonstrates that hydrogen entry can be enhanced by anodic polarization. These issues will be returned to in a later section.





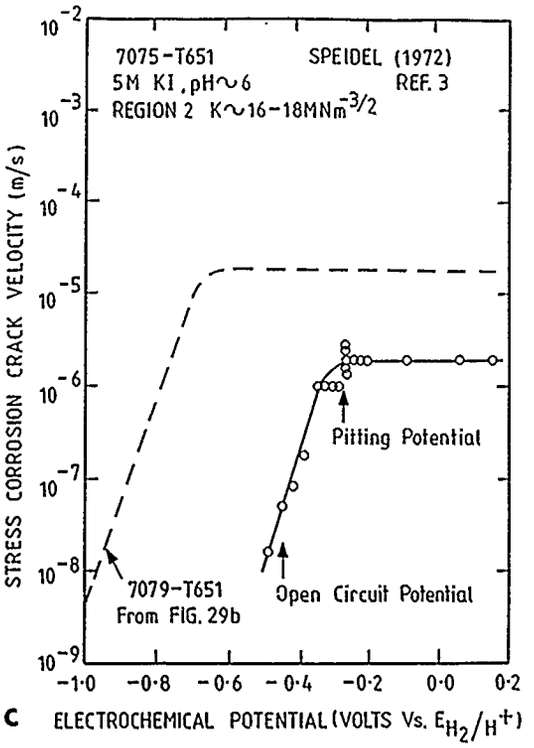


FIGURE 29—(a) The effect of imposed electrochemical potential and stress-intensity factor upon SCC crack growth rates for 7079-T651 in an aqueous 5 M potassium iodide solution; (b) data from (a) replotted as a function of electrochemical potential (see text for potential-drop effects) and (c) comparison of SCC data for 7079-T651 and 7075-T651 as a function of electrochemical potential.

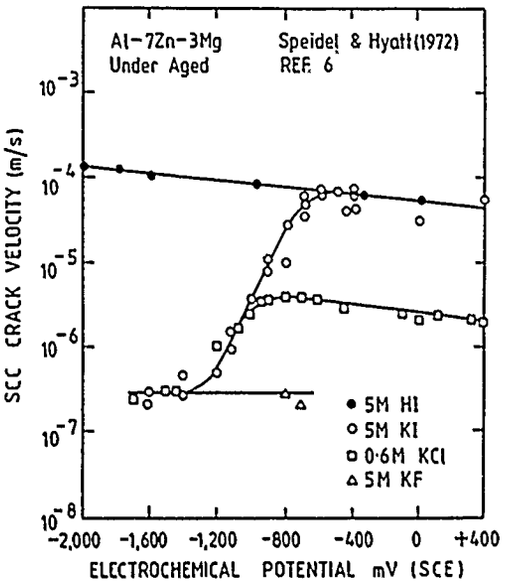


FIGURE 30—Effect of imposed electrochemical potential on SCC crack growth rates for an underaged high-purity Al-7Zn-3Mg alloy in various aqueous halide ion solutions.[6]

Solution viscosity—Published information on the influence of solution viscosity upon SCC is very limited. Speidel[3,5] and Speidel and Hyatt[6] provide cv-K data for 7079-T651 in a 2 M potassium iodide solution doped with various levels of glycerol to generate a range of solution viscosities (Figure 33). SCC crack growth involved an impressed external anodic potential of about 200 mV, and so the quoted linear relationship between Region 2 SCC crack growth rate and the reciprocal of solution viscosity probably reflects that SCC is under diffusion control for the specific test conditions investigated.

It has been reported that local conditions within SCC cracks are highly viscous, even for dilute bulk solution conditions, and so generally differ significantly from bulk solution conditions or freshly made-up simulated crack-tip solutions.[168] Further work is needed to establish the influence of solution viscosity upon SCC of aluminum alloys.

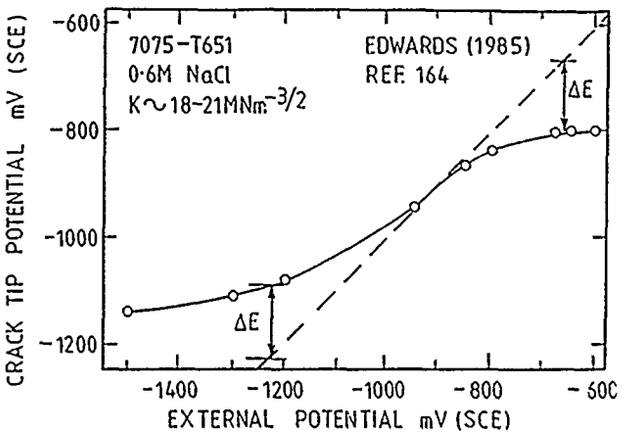


FIGURE 31—Crack-tip electrode potential measured as a function of externally applied potential for 7075-T651 in a 3% NaCl bulk solution.[164]

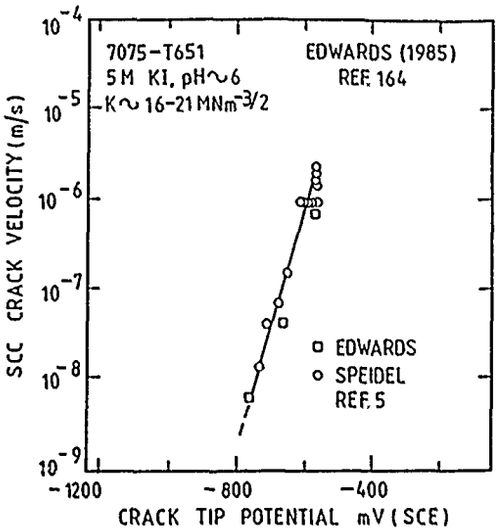


FIGURE 32—Region 2 crack growth rate as a function of electrochemical potential of the crack tip calculated taking into account potential-drop effects.[164]

Nonhalide solutions. Prior to the early 1980s, SCC data in nonhalide environments was scarce. Data quoted in the review articles by Sprowls and Brown in 1969[1] and Speidel and Hyatt in 1972[6] are limited to that published by Hunter[126,169] in the late 1960s. These data, reproduced in Figure 34, indicate the SCC initiation propensity for the alloys 2219, 7039, and 7075 in a range of aqueous environments of sodium salts. 7039-T63 suffered SCC in all of the solutions used; Cl^-, Br^-, I^-, F^-, NO_3^- and $CrO_4^{=}$ [169] and prompted Sprowls and Brown[1] to speculate whether 7039-T63 would resist SCC in any aqueous environment. 7075-T651, although generally more resistant than 7039-T63, eventually cracked in all the environments,[126] whereas 7075-T7351 and 2219-T87 showed no signs of SCC initiation during the test period adopted.

During the 1970s, Speidel[3,5] and Speidel and Hyatt[6] published cv-K data for 7079-T651 in various aqueous environments and reported that, for the anions assessed, only Cl^-, Br^-, and I^- accelerated SCC growth rates above the scatter band found for SCC in distilled water, irrespective of alloy temper or imposed electrochemical conditions.[3] More recent work by Le, et al.,[127] indicates that anions other than halides, such as perchlorate, carbonate, and benzoate, can markedly increase SCC crack growth rates for 7075-T651 in aqueous solutions. This apparent contradiction probably reflects the difference between 7079-T651 and 7075-T651 highlighted previously, and suggests that it is prudent to assume for 7XXX series in general that anions other than halides may potentially accelerate SCC crack growth rates relative to those in distilled water.

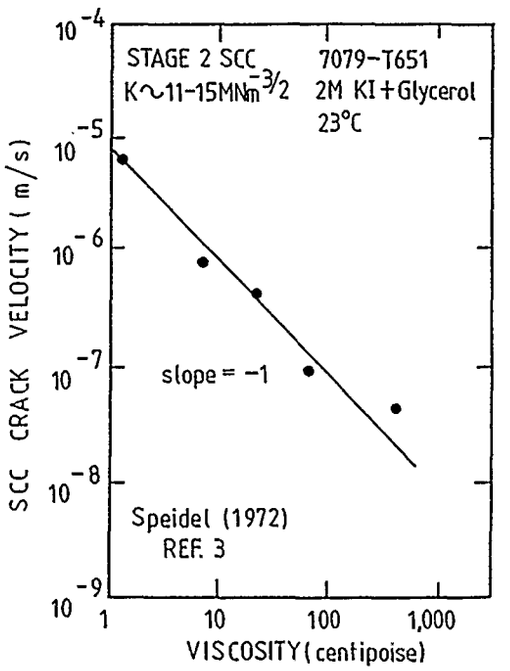


FIGURE 33—Effect of solution viscosity on Region 2 SCC crack velocity plateaux for 7079-T651 under anodic polarization in an aqueous 2 M potassium iodide solution.[3]

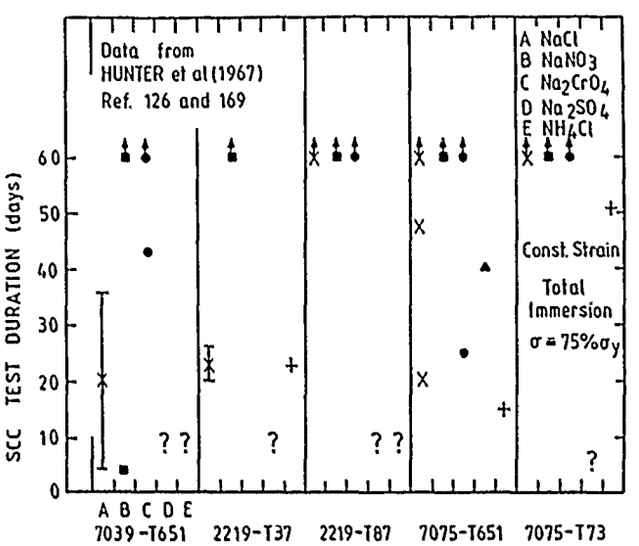


FIGURE 34—SCC test data for smooth tensile specimen of various aluminum alloys in a range of aqueous environments.[126,169]

Le and Foley[128] statistically assessed the reliability of SCC crack propagation data from DCB SCC testing and reported that their data for a given alloy heat of 7075 T651 generally were reproducible to about 5 to 10% at a 90% confidence level (6.7% and 8.6% for tests in 1 N NaCl and 1 N $NaClO_4$ solutions, respectively). On the basis of their data, it was suggested that sodium perchlorate solutions should be considered for use as standard test environments for SCC testing as, insofar as it is known, perchlorate ions do not form complexes with aluminum and thus should yield a test environment minimizing specific ion effects while providing a high conductivity and low chemical reactivity.

SCC crack growth rates quoted by Foley and coworkers[129-131] for 7075-T651 in aqueous sulfate, nitrate, chloride, and perchlorate solutions of sodium salts are reproduced in Figure 35. Growth rates increase in the order $SO_4^{=} < NO_3^{-} < ClO_4^{-} < Cl^{-}$ for SCC at the FCP or under anodic polarization, whereas the order is reversed for SCC under cathodic polarization, with significant SCC being promoted in both $SO_4^{=}$ and NO_3^{-} solutions. Foley and coworkers[129-131] also assessed the local environmental conditions developed within SCC cracks during crack growth in 7075-T651 in these aqueous environments; this work will be discussed in the next section.

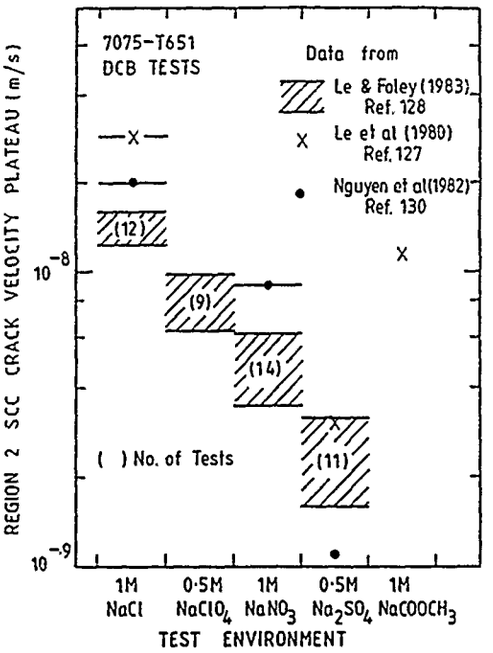


FIGURE 35—Region 2 SCC crack velocity data for 7075-T651 in various aqueous environments.

Environmental conditions within cracks. As mentioned earlier, it has been known for more than 20 years that the environmental conditions developed within cracks generally differ significantly from bulk conditions and that a detailed knowledge of these solution chemistries should help elucidation of the mechanisms of SCC in aluminum alloys.[135] A major restraint in obtaining such data is the limited solution volume available for analysis and its inaccessibility. Several attempts have been made to overcome these difficulties: (1) simulation of the local environmental conditions within a crack by immersing alloy shavings into restricted solution volumes,[170,171] i.e., minimizing the ratio of solution volume to alloy surface area, (2) monitoring local solution pH and electrochemical potential within real and artificial cracks using *in situ* microelectrodes,[164,165,172-173] (3) *ex situ* solution pH and chemical analysis of environments extracted from within SCC cracks using freezing and thawing,[129-131,135] direct extraction,[168,174] or a room-temperature "freezing" technique that uses specific solution gelling agents[175] and (4) post-fracture analysis of fracture surfaces using high-resolution electron microscopy[77] and surface spectroscopy techniques.[55,176]

Simulation of local environmental conditions using alloy shaving in restricted solution volumes at first seems a realistic approach to generate relatively large volumes of crack-tip environments. The results quoted by Sedriks, et al.,[170,171] for 7075-T651 alloy shavings immersed in highly acidified chloride environments are readily reproduced[168] with solution pH values of around 3.5, i.e., similar to those usually associated with SCC cracks. Holroyd, et al.,[168] observed that if the initial solution pH is above 3.5, the solution pH in the shavings becomes alkaline within a few minutes (Figure 36) and thus questions whether the "shavings approach" simulates conditions developing within SCC cracks that are not necessarily initially highly acidic. The rationalization of these observations is that the "shavings approach" is a reasonable simulation of a crack enclave region for 7XXX series alloys when the surface condition of the shavings is similar to the "oxide" composition of crack walls close to crack tips.[168] Evidence for this proposal is given by the observed pH–time behavior when shavings, prior to exposure to a limited volume of a neutral 3.5% NaCl solution, are given a short "wash" in dilute sodium hydroxide to replace the "as-machined" oxide layer with one formed in an aqueous environment. In this case, unlike that when shavings are only degreased, as for example in the previous studies,[170,171] solution pHs become acidic and approach values quoted for SCC cracks. (Figure 37).[168]

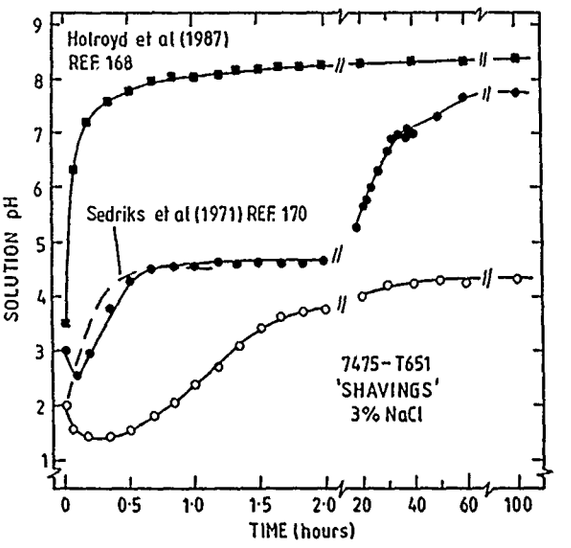


FIGURE 36—Solution pH as a function of time for 7475 shavings exposed to 3% NaCl solutions with various critical pH values.

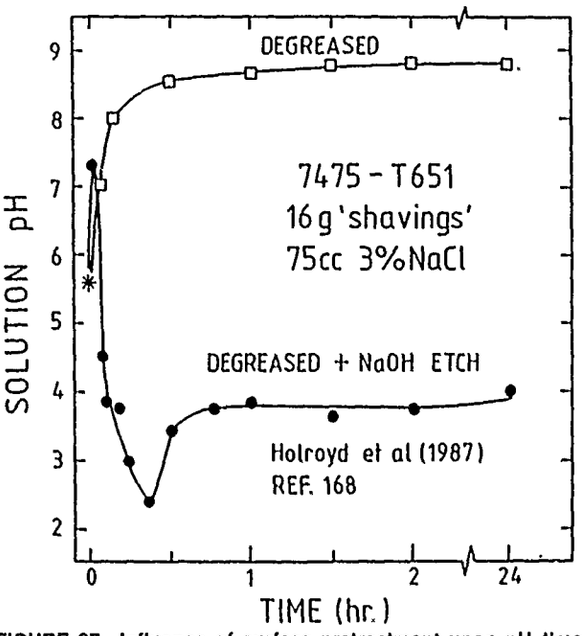


FIGURE 37—Influence of surface pretreatment upon pH–time behavior given by 7475 shavings exposed to 3%NaCl.[168]

Solution pH–time behavior in "shavings" experiments for aluminum–lithium-based alloys wetted by restricted volumes of neutral 3.5% NaCl differ significantly from those for 7XXX series alloys.[18] Identical behavior was observed for Al-Li, Al-Li-Zr, and Al-Li-Cu-Mg alloy shavings with solution pHs rapidly adopting values of about 9, irrespective of whether given an acid or alkaline pretreatment, and after a few hours displaying a sudden pH increase to 11, which was followed by a gradual decrease back to less alkaline pHs controlled

by CO_2 uptake and lithium carbonate generation (Figure 38).[18] On the strength of these results, it was suggested that solutions within SCC cracks for Al–Li-based alloys may be alkaline.[18] Further work has shown that saline solutions in long (> 1 mm) SCC cracks are acidic with pH around 4, slightly higher than those for 7XXX series alloys, as dissolved lithium as well as aluminum species are in solution. It appears that the Al–Li alloy "shaving" experiments are reflecting the behavior of cathodic regions, and their relevance to SCC initiation awaits clarification. Langan, et al.,[177] have recently conducted alloy "shavings" experiments for 7XXX series rapidly solidified powder alloys, 7090 and 7091, and have reported similar findings to those of conventionally cast direct chill 7XXX series alloys. These authors conclude that the improved SCC resistance of the powder alloys could not be attributed to oxides present in these alloys promoting more alkaline conditions within cracks, as speculated by Lyle and Cebulak,[178] and offered an alternative explanation that Co_2Al_9 precipitates act as cathodic reaction sites that enhance the kinetics of hydrogen recombination and evolution, thereby reducing that available to promote HE during SCC.

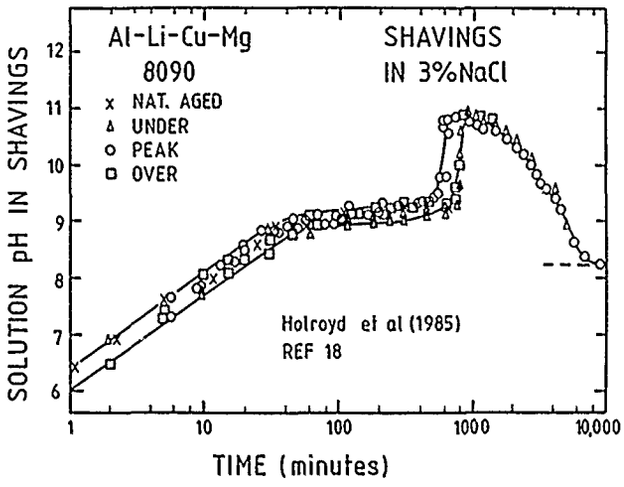
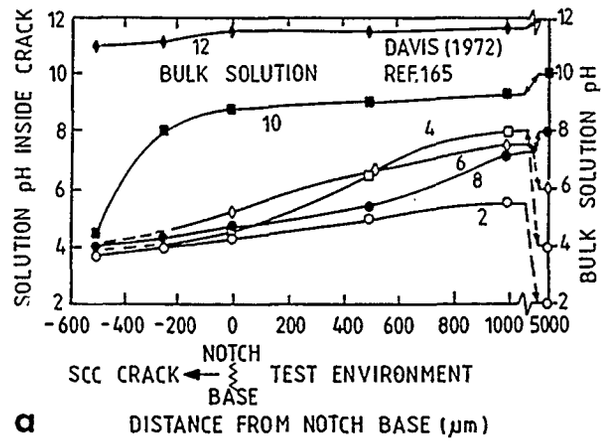


FIGURE 38—pH–time behavior given by 8090 alloy shavings in various tempers exposed to 3% sodium chloride solution.[18]

Direct *in situ* measurement of local environmental conditions within cracks is of course preferable to simulation or *ex situ* methods. In the early 1970s, Davis reported some elegant work using specially developed microelectrodes to measure solution pH and electrochemical potentials within SCC cracks for 7075-T651 exposed to a bulk 4.5% potassium chloride solution.[165] The data clearly demonstrate that environmental conditions within cracks can differ significantly from bulk conditions: solution pHs moved to values around 3.5 to 4 independent of bulk pHs in the range 2 to 10, and external polarization only significantly influenced potentials within cracks for potentials close to the FCP, with limiting crack-tip potentials being less than 100 mV anodic and 300 mV cathodic of the FCP (Figure 39). Davis only observed acidification when a sufficient stress was applied to his notched specimens and suggested this was related to the need for a minimum stress-intensity factor for SCC, K_{ISCC}.[165] This is not a valid assumption for aluminum alloys in general, because acidification readily occurs in cracks and crevices in the absence of stress when local geometries are sufficiently restricted.[168] Rationalization of Davis's observation is possible using the argument that the relatively wide open "V" notch at the start of his experiments had a local solution volume to surface area ratio (V/A ratio) too high to allow acidification to occur, i.e., local geometry not tight enough, and SCC initiation is needed to reduce the V/A ratio. The initial V/A ratio will be > 0.15 cm when Davis's notch is < 6 mm deep (assuming a 60° base angle), which, on the basis of data presented by Holroyd, et al.,[168] is too high to expect acidification to develop in the absence of a bulk solution (Figure 40).



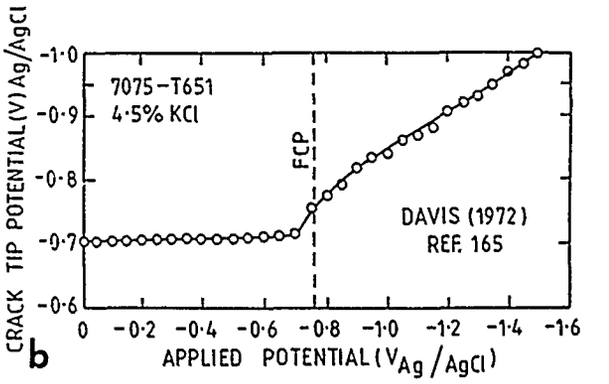


FIGURE 39—Environmental conditions within propagating SCC cracks reported by Davis[165] for 7075-T651 immersed in a 4% potassium chloride bulk solution; (a) solution pH in crack as a function of distance from the starter notch for a range of bulk solution pHs and (b) crack-tip electrode potential as a function of externally applied potential in a neutral pH 4.5%potassium chloride solution.

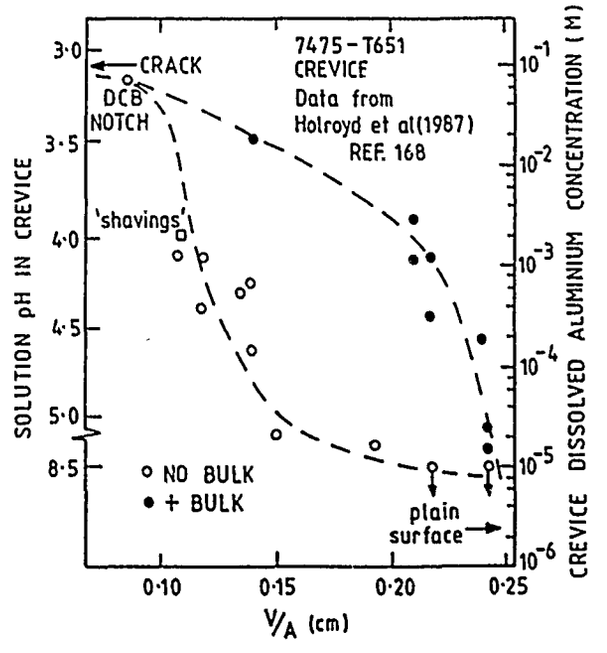


FIGURE 40—Solution pH and dissolved aluminum concentration in a range of cylindrical crevices geometries (V/A ratios) for 7475-T651 exposed to 3% sodium chloride with and without bulk solution above the crevice.[168]

Although other researchers using microelectrodes[164 172] have now confirmed the results reported by Davis[165] for solution pHs and electrochemical potentials within SCC cracks in 7075-T651, the only additional solution chemistry variable monitored using *in situ* microelectrodes is chloride concentration with silver/silver chloride electrodes.[179] These measurements show that a significant chloride accumulation can occur within cracks, and its magnitude is increased by anodic polarization (Figure 41). How much of the measured chloride is present as "free" chloride ions as opposed to aluminum hydroxychloride complexes awaits elucidation. All microelectrodes used to date (pH, potential, and Cl^-) are physically large compared to crack-tip dimensions, so all of the measurements quoted above apply to regions "close to" rather than "at" crack tips.

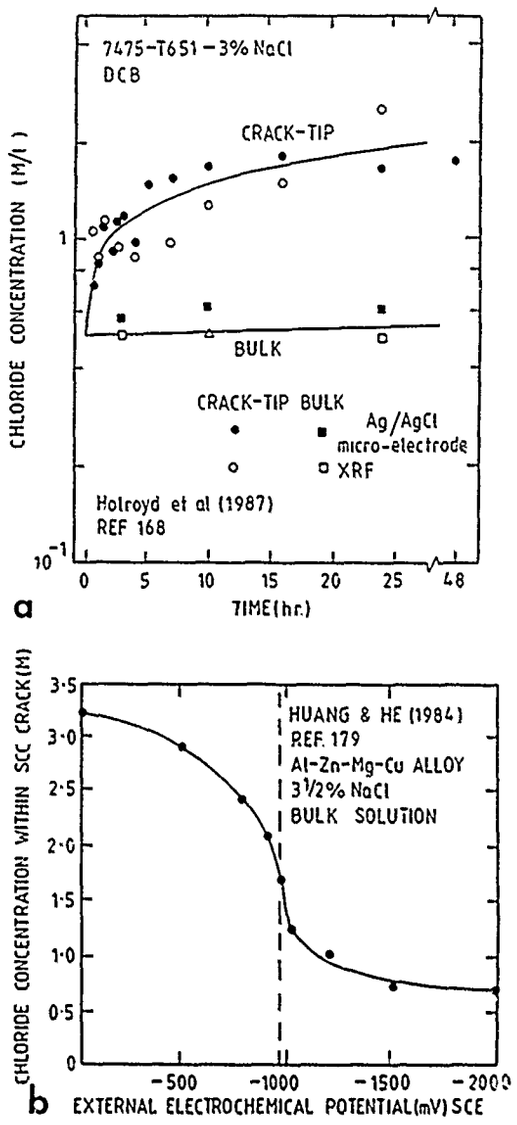


FIGURE 41—(a) Chloride concentration in a propagating SCC crack tip as a function of (a) time and (b) applied electrode potential, for 7075-T6 type alloys in neutral 3% sodium chloride.

Characterization of local solution chemistries associated with propagating SCC cracks, other than that quoted above, has involved solution-extraction techniques and *ex situ* chemical analysis, with work being conducted exclusively on 7075-type alloys. Until recently, little quantitative analytical or kinetic data has been published, and that available up until the mid-1980s indicated the presence of dissolved aluminum[135] and a semiquantitative estimate of its concentration.[130] More recent data obtained using the freezing-thawing technique developed by Brown, et al.,[135] and the extraction method of Holroyd, et al.,[169,174] have facilitated more quantitative characterization of the solution chemistries developed within SCC crack enclaves for 7075-type alloys exposed to 3.5% NaCl bulk environments.

During the initial stages of solution development within a crack, the local solution pHs are accountable in terms of the dissolved aluminum via the equilibrium reaction

$$Al^{3+} + H_2O = AlOH^{2+} + H^+ \quad (1)$$

For example, Le and Foley[131] measured a dissolved aluminum concentration of 2×10^{-2} M within a propagating SCC crack for 7075-T651 in a bulk 3.5% NaCl solution. Their measured solution pH of 3.0 to 3.2 compares favorably with the 3.4 predicted by Equation (1) After longer immersion times, the measured dissolved aluminum concentrations become too high and the chloride levels too low for pHs to be controlled by Equation (1) (even if "activity" is used rather than concentration to allow for solutions becoming relatively concentrated), and aluminum hydroxychloride complexes such as $Al(OH)_2Cl_2^-$ and gel products $Al(OH)_2Cl$ and $Al(OH)Cl_2$ promote the gelatinous solution conditions found within SCC crack-tip regions.[168]

Foley and Nguyen[180] argue that during the dissolution of aluminum in aqueous chloride solutions, high-energy aluminum metal ionizes rapidly to the Al^{3+} ion, which immediately hydrolyzes via Equation (1), and the two species Al^{3+} and $AlOH^{2+}$ react with chloride ions to yield

$$Al^{3+} + Cl^- = AlCl^{2+} \quad (2)$$

$$AlCl^{2+} + 2H_2O = Al(OH)_2Cl + 2H^+ \quad (3)$$

and

$$AlOH^{2+} + Cl^- = Al(OH)Cl^+ \quad (4)$$

$$Al(OH)Cl^+ + H_2O = Al(OH)_2Cl + H^+ \quad (5)$$

$$\text{and } Al(OH)_2Cl + H_2O = Al(OH)_3 + H^+ + Cl^- \quad (6)$$

$$Al(OH)_3 + H_2O = Al(OH)_3.H_2O \quad (7)$$
(amorphous)

An overview of the above reaction path provided by Foley and Nguyen[180] in the form of a schematic free-energy surface is reproduced in Figure 42. Based on these ideas and their own experimental measurements, Holroyd and Jarrett[181] suggested that the solution chemistries within SCC cracks for 7475-T651 exposed to 3.5% NaCl bulk solutions involve a range of aluminum species; with mainly simple Al^{3+} ions at the crack tip and then a series of complex aluminum hydroxychloride species with increasing hydroxide to chloride ratio moving away from the tip, e.g., $Al^{3+} \rightarrow Al(OH)Cl_2 \rightarrow Al(OH)_2Cl \rightarrow Al_2(OH)_5Cl \rightarrow Al(OH)_3$, leading to $Al(OH)_3$ associated with the crack mouth (Figure 43). Solution pHs are around 2.7 at crack tips and steadily increase to about 5.5 at crack mouths. The actual species present will be more numerate and complex than indicated as the local chloride concentration, solution temperature, and solution "aging" effects all influence the ratios of mononuclear and polynuclear ions and solids.[182] Substitution of chloride ions with sulfate ions dramatically reduces SCC crack growth rates in 7075-T651[130 131] (Figure 35) despite local solution conditions within cracks being similarly acidic[130 131] Foley and Nguyen[180] explained this by suggesting that the presence of sulfate ions modifies the reaction pathway for aluminum dissolution in aqueous solutions by introducing the processes

$$Al^{3+} + SO_4^{=} = AlSO_4^+ \quad (8)$$

and

$$AlOH^{2+} + SO_4^{=} = Al(OH)SO_4 \quad (9)$$

and providing low-energy intermediate species, $Al(OH)SO_4$ and $AlSO_4^+$, leading to the formation of basic aluminum sulfate with a lower energy than aluminum hydroxide (Figure 42) and an environment with an appropriate acidic pH and a low chemical reactivity.

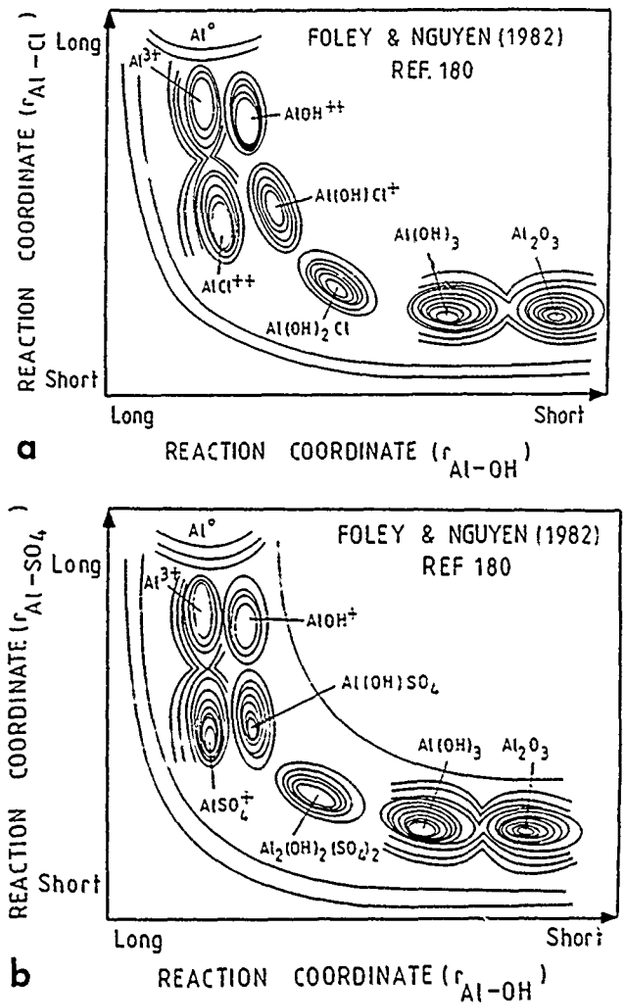


FIGURE 42—Schematic potential energy surface for (a) Al-chloride ion and (b) Al-sulfate ion constructed by Foley and Nguyen. (Reprinted with permission.[180])

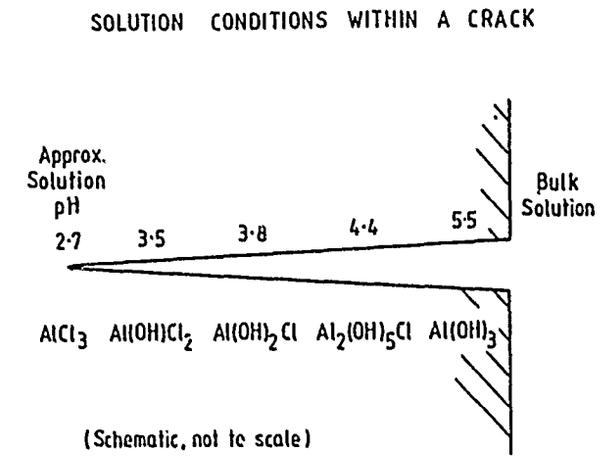


FIGURE 43—Schematic representation of aluminum hydroxi-chloride species existing within propagating cracks in high-strength aluminum alloys suffering SCC in a bulk saline environment.[181]

Le and Foley[131] developed these ideas to explain why aluminum chloride, nitrate, perchlorate, and sulfate all hydrolyze to give solution pHs in the range 2.6 to 3.8,[183] and yet within SCC cracks, only chloride and sulfate solutions adopt acidic pHs, and perchlorate and nitrate solutions remain at neutral pHs of 6 to 7. The controlling factor is thought to be the reaction pathway pursued during the earliest stages of aluminum dissolution, i.e., as cracks advance. For perchlorate and nitrate solutions (and distilled water), it is suggested that transient species, including hydroxide species produced during oxygen reduction, provide a direct pathway to $Al(OH)_3$ and thus prevent acidification. An additional complication can arise in nitrate solutions because "bare" aluminum at growing crack tips can promote ammonia formation via nitrate ion reduction within SCC cracks.[129] Under cathodic polarization, this process leads to the development of highly alkaline pHs and has been suggested to account for why cathodic polarization stimulates SCC for 7075-T651 in aqueous nitrate solutions but not in chloride solutions.[129,130]

Nonaqueous environments

Organic environments. Available data for the SCC of aluminum alloys in organic environments is limited to that quoted for 7075-T651 and 7079-T651.[5,6,132,184] Procter and Paxton[132,184] provided the earliest data and maintained that the IG and transgranular SCC promoted in their work was not due to traces of water. SCC was observed in 7075-T651 in a range of organic environments including methanol, ethanol, isopropanol, benzene, ethylene glycol, and carbon tetrachloride. Reported threshold stress-intensity factors were 6 to 10 MNm^{-2}, and Region 2 crack velocities were in the range 10^{-10} to 5×10^{-9} m/s with the highest being in ethanol and carbon tetrachloride and the lowest in benzene. Later work by Speidel and Hyatt[6] concedes that SCC may occur in very dry organic environments but suggests that SCC is controlled by moisture content when water trace levels exceed about 10^{-2} wt% (Figure 44), and thus SCC in re-agent grade organic environments will result from the presence of water for most practical situations.

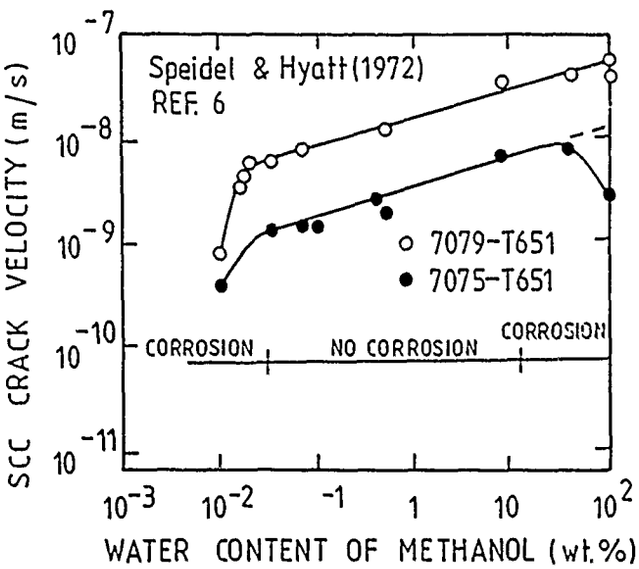


FIGURE 44—Velocity of SCC cracks in commercial 7XXX series alloys, 7075-T651 and 7079-T651, as a function of water content in methanol.[6]

Mechanical Aspects

The issue of whether the SCC of aluminum alloys occurs via a continuous process, driven by anodic dissolution of aluminum, or a discontinuous process involving mechanical and electrochemical components has been debated in the literature for at least the last three decades. Detection of SCC initiation from smooth surfaces remains difficult to resolve even with the high degree of sensitivity provided by state-of-the-art equipment.

To compound the problem, the definition of when SCC has initiated is not obvious. The position for crack propagation is more established, with published work generally suggesting that SCC propagation in age-hardening aluminum alloys is discontinuous with continual "reinitiation" via a mechanism probably differing from that of "true" SCC initiation from a smooth surface. Published SCC propagation data for ingot metallurgy alloys in saline environments is available in abundance for 7XXX series alloys, less so for 2XXX

series alloys, and is limited for aluminum–lithium-based alloys and rapidly solidified alloys Data available is generally in the form of crack-velocity/stress-intensity factor plots (cv–K curves) calculated from crack growth time data obtained using a coarse time scale of at best hours and normally days between crack length measurements, so short-term fluctuations in crack growth rates go undetected. Exceptions to the above will be discussed in the next sections.

Crack initiation

As implied above SCC, initiation is a poorly understood and loosely defined phenomenon necessitating further work for the development of a clear mechanistic interpretation. High-quality experimental data, as far as the reviewer is aware, is unavailable currently, but should be forthcoming with the use of a combination of modern techniques such as time-lapse video, acoustic microscopy, acoustic emission, and electrochemical noise spectroscopy.

Initiation smooth surfaces. About 25 years ago, Gruhl[185] suggested that SCC initiation in aluminum alloys involves a predominantly corrosion-driven process, whereas crack propagation requires a significant mechanical component. It is not clear whether this corrosion-driven process is strongly influenced by the development of local environmental conditions within tight crevices/flaws/cracks, because similar conditions develop whenever an appropriate local geometry is available, independent of stress level or an alloy's temper and inherent SCC susceptibility.[168 174] Attempts to mathematically model the development of environmental conditions within aluminum crevices look promising,[186-187] and with refinement and a further experimental input, they should be capable of accurately describing the overall process.

The critical process controlling SCC initiation probably involves the establishment of a sufficient stress raiser, located at an appropriate microstructural site within a susceptible microstructure, with the site of attack being dictated by the size and distribution of suitable anodic and cathodic reaction sites within an alloy's local microstructure. Experimental evidence in favor of this argument has recently been presented by Magnin and Rieux for crack initiation in a commercial weldable Al-Zn-Mg alloy, 7020 immersed in a saline environment.[188] These authors maintain that HE during SCC or corrosion fatigue in saline environments is only operative in the presence of a stress concentrator, so HE does not influence crack initiation from smooth surfaces unless a stress raiser is established by another process (e.g., corrosion or mechanical deformation). A universally agreed and consistent definition of SCC initiation is not available.

A reasonable definition of when the initiation process is complete is that the propagation stage starts when a SCC crack becomes self-sustaining and no longer a short crack/fissure, often referred to as "nonpropagating" in other alloy/environment systems, e.g., magnesium alloys[189] and ferritic steels.[190] Work reported to date on nonpropagating in aluminum-based alloys is very limited,[191] and considerably more work is needed to establish whether SCC initiation requires a critical stress raiser. Evidence in favor of this argument is given by an observed correlation between surface-attack morphology and SCC initiation behavior for a peak-aged Al-Li-Cu-Mg alloy, 8090. This alloy, as with aluminum–lithium alloys in general,[18] rarely suffers SCC initiation from smooth surfaces in neutral saline solutions under total immersion conditions but does so under alternate immersion conditions, as will other aluminum–lithium alloys containing sufficient copper,[18] if applied stresses are sufficiently high. Surface attack morphologies for polished sections exposed to 3.5% NaCl under total or alternate immersion conditions show that overaged tempers suffer general attack, i.e., limited stress raisers and SCC, whereas for peak-aged material, the mode of attack is more IG in nature and significantly more pronounced under alternate immersion conditions,[18] i.e., a greater stress raiser for the case in which SCC occurs more readily A similar situation probably exists for 2XXX series alloys such as 2014 T3 and 2024 T6, in which SCC tests using smooth specimens under total immersion conditions tend to show large batch to batch variations even with slow strain rate testing,[192] whereas SCC initiation under alternate immersion conditions is reasonably reproducible.

A recent experimental observation with relevance to SCC initiation is that strain accommodation in the Al-Mg-Si alloy, 6351, is strain rate dependent with grain-boundary accommodation of slip becoming more significant at lower strain rates.[75] An example of this is given in Figure 45, which shows the surface deformation of flat polished tensile specimens after straining to 0.4% using a fast (10^{-2}/s) or a slow (10^{-6}/s) nominal strain rate. As similar observations have now been made for other precipitate-hardening aluminum alloy systems, e.g., 2XXX, 7XXX,[193] and aluminum–lithium-based alloys,[194] it is reasonable to question the concept that the maximum strain rate for SCC initiation is dependent upon the availability of sufficient time for corrosion activity, as has been proposed for ferritic steels[195] aluminum,[108] and other nonferrous alloy systems.[189 196] The correct explanation for aluminum alloys is likely to be more subtle, with the maximum strain rate above which SCC fails to initiate (which will depend upon environmental and pre-exposure conditions) being related to those in which IG deformation becomes insufficient to sustain IGSCC Initial results suggest that the influence of alloy temper upon (1) SCC susceptibility and (2) the maximum strain rate for significant GB strain accommodation are in qualitative agreement and thus have the same microstructural dependence. Further work is needed to establish the importance of these observations and to determine whether IGSCC initiation in age-hardening aluminum alloys is controlled by GB precipitation, matrix slip characteristics, GB segregation, or some combination of these factors.

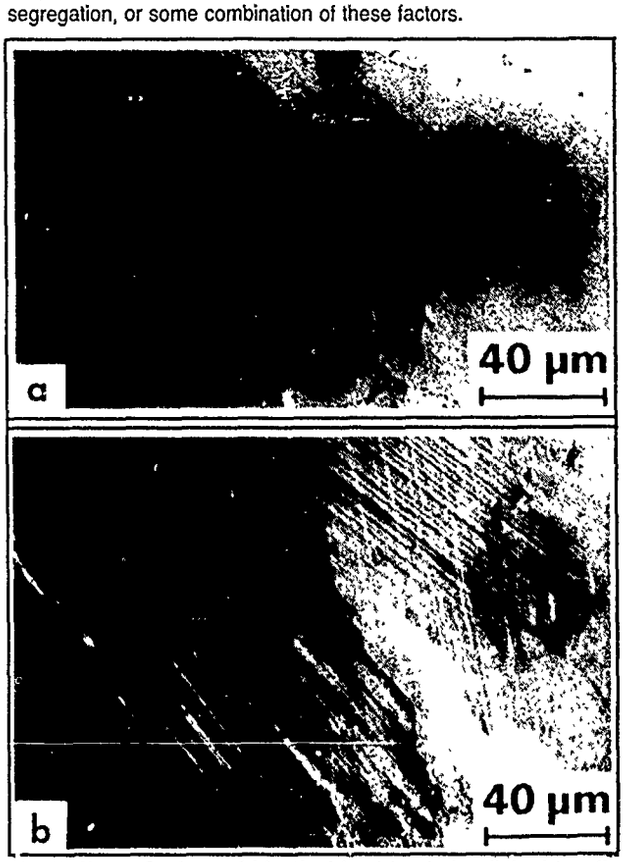


FIGURE 45—Surface of identical heat-treated polished tensile specimens strained to 0.4% plastic strain at strain rates of (a) 10^{-6}/s and (b) 10^{-2}/s.[75] Grain-boundary strain accommodation is more prevalent in the specimen tested at the slow-strain rate.

Initiation from notches/precracks. SCC "initiation" from notched or precracked specimens has been studied by many authors.[144 149 174 197 199] Pathoria and Tromans[144] report that SCC initiation times from mechanical-produced notches in high-purity Al-8.6Mg and Al-6.3Zn-2.6Mg alloys immersed under freely corroding conditions in aqueous saline or water-containing ethanol environments decrease with increasing solution temperature, stress-intensity factor, or hydrogen precharging times. Similar observations are quoted by Hermann and Holroyd[200] for a commercial Al-Zn-Mg-Cu alloy, 7475-T651, pre-exposed to saline environments prior to

testing in WVSA. Several proposals have been made describing SCC initiation from notches and precracks, Skoulikidis and coworkers, in a series of papers,[201 203] recently summarized[204] present experimental evidence for an Al-Mg alloy, 5052 (UNS A95052), from which they suggest that SCC initiation in aluminum alloys relies upon the generation of an "active path," by the fast solid-state diffusion of disordered mobile Al^{3+} during pit formation leading to local energy decreases and decohesion along the IG diffusion path. The latter studies have generated interesting results but further work is needed to substantiate the mechanistic proposals.

Holroyd, et al.,[174] observed local changes in the optical characteristics of the crack-tip region just prior to SCC initiation in the Al-Zn-Mg-Cu alloy, 7475-T651, immersed in a saline environment (Figure 46). These changes were detected using a technique known as the "shadow optical method of caustics,"[205-207] which can generate valid plane-strain stress-intensity measurements for aluminum alloy precracked specimens based solely on the diameter of the reflected caustic shadow from the external surface containing the crack-tip region (Figure 47). Environment-induced effects were found to influence results and the term "caustic shadow swelling"[174] was used to describe a phenomenon consistent with an internally driven process leading to higher stress-intensity factors without any change to the externally applied load or crack length. At first, caustic shadow swelling was thought to be uniquely associated with SCC initiation, but subsequent work showed it could be induced prior to SCC initiation if precracked specimens were loaded in laboratory air after pre-exposure to aqueous environments.[208] The controlling process has not been unambiguously defined; however, factors such as corrosion-product wedging, crack tunneling, and any nonreversible processes have been eliminated. Later work by Hermann[209] has shown that repeated loading/unloading can lead to caustic shadow swelling effects, invoking a role for plasticity effects and demonstrating that the phenomenon may be induced by more than one route. For the initial observation of the phenomenon, however, the precracked specimen (7475-T651) was only loaded once (under constant-strain conditions), and the "caustic shadow swelling" was observed after a few hours without any further changes to the external loading (Figure 46). In the opinion of the reviewer, the most plausible explanation of the "caustic shadow swelling" effect is that hydrogen uptake promotes a local elastic modulus increase in the crack-tip region. This would lead to increases in stress-intensity factors (K) without crack lengths or externally applied loads having to change. Independent evidence that environmental effects can induce K increases is provided by Domack,[210] who presented load–time data from strain-gauged bolts in a precracked DCB specimen during SCC testing of 7475-T651 in a saline environment. The reported load measurements under fixed strain conditions increased prior to detection of SCC initiation from the precrack (Figure 48). This observation is not readily explained, because even if SCC had initiated undetected the measured load levels would be expected to decrease rather than increase. An increase in elastic modulus would account for the observation, but how hydrogen ingress would achieve this is not clear. However, it is interesting to note that other elements with low atomic numbers such as lithium and beryllium are known to increase the elastic modulus of aluminum alloys,[7] and similar proposals after hydrogen uptake are being voiced for ferrous alloys.[211]

In the opinion of the reviewer, SCC initiation studies using notched or precracked specimens almost inevitably reflect crack propagation behavior, further discussion will continue in the next section.

Crack propagation

Although initial studies on the mechanical aspects of the SCC of aluminum alloys conducted in the early 1950s involved smooth test specimens, the then-available experimental techniques provided insufficient sensitivity to resolve "true" SCC initiation, so the reported results probably reflect the propagation of short SCC cracks. The electrochemical potential transients toward more negative potentials observed during SCC in saline solutions reported by Gilbert and Hadden[212] and Farmery and Evans[213] for Al-Mg and Al-Cu alloys, respectively, are significant nevertheless because they provide the first evidence that SCC propagation in aluminum alloys is a discontinuous process, probably involving a rapid micromechanical crack jump followed by a slower step involving corrosion prior to the next mechanical jump.

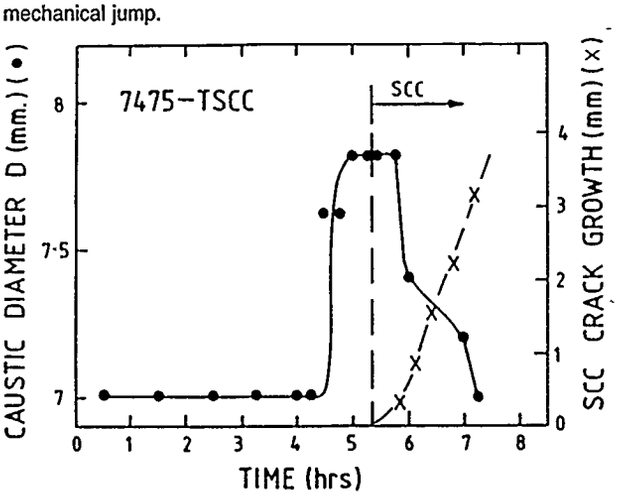


FIGURE 46—Swelling of the caustic diameter prior to SCC crack initiation.[174]

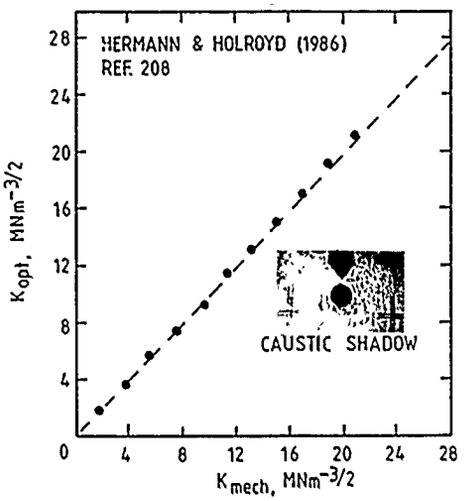


FIGURE 47—Stress-intensity factor (K) obtained by the shadow method of caustic (K_{opt}) as a function of K via conventional linear elastic fracture mechanics (K_{mech}).[208] (Insert shows a typical caustic).

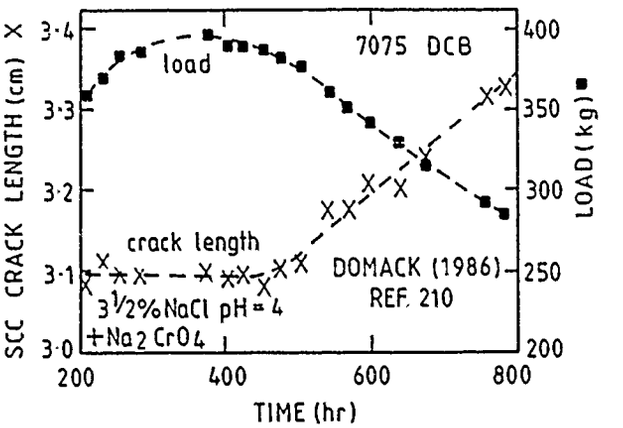


FIGURE 48—Load–time behavior from a strain-gauged bolt during a double-cantilever beam SCC crack propagation test on 7075-T651 in a 3.5% sodium chloride solution. (Note a load increase occurs under fixed displacement conditions prior to SCC initiation). (Reprinted with permission.[210])

In the early 1960s, van Rooyen[214] extended these ideas by observing that during SCC propagation in Al-7Mg and Al-4Cu alloys exposed to saline solutions, sound generation only occurred during the initial stage of the negative electrochemical potential transients, i.e., during the rapid 10 to 80 mV potential decrease, and not at other times, including those during the subsequent slower, yet still fast (~ 80% recovery within 1 s), potential rise region of the transient. These results are important because they complement data for Al-Zn-Mg(Cu) alloys[11 149 197 199 215 216] and provide quantitative evidence that SCC propagation generally is discontinuous for Al-Mg, Al-Cu, and Al-Zn-Mg(Cu) alloys, with one stage being rapid and mechanical in nature and the other being slower and probably involving a corrosion process. van Rooyen's[214] results generally are not reported in the context of the SCC of aluminum alloys because his results appear in papers principally dealing with the SCC of austenitic stainless steels in chloride environments. (The reviewer is indebted to Dr. R.C. Newman as the source of this reference.)

Work on Al-Zn-Mg(Cu) was initiated in the early 1960s by Gruhl and his coworkers in West Germany. Brenner and Gruhl[215] detected sudden deflection changes during SCC tests on an Al-5Zn-3Mg alloy in a saline solution and, as reported by van Rooyen, could not attribute the transients to a given crack but noted that crack jumps were obviously very fast. (Brungs and Gruhl estimated a crack velocity of around 0.2 m/s.[216])

Several authors have subsequently reported evidence for the discontinuous nature of SCC crack propagation in 7XXX series alloys: (1) Gest and Troiano observed intermittent rapid strain energy release rates;[11] (2) Scamans provided high-resolution fractographic evidence that face-matched IGSCC fracture surfaces can display striations fulfilling the requirements of "crack-arrest markings," and that regions between these striations show perfect face matching with minimal evidence of corrosion (Figure 49),[77] (3) others report repeated bursts of acoustic emission (AE) events,[149 198 199] and Martin, et al.,[198] correlated these AE signals with crack-arrest markings similar to the type reported by Scamans,[77] and (4) work on high-purity Al-Zn-Mg alloys in saline environments, currently in progress by the reviewer in collaboration with R.C. Newman and coworkers, identifies periodic electrochemical transients during SCC that show a 1:1 relationship with recorded load drops and striations on SCC fracture faces.

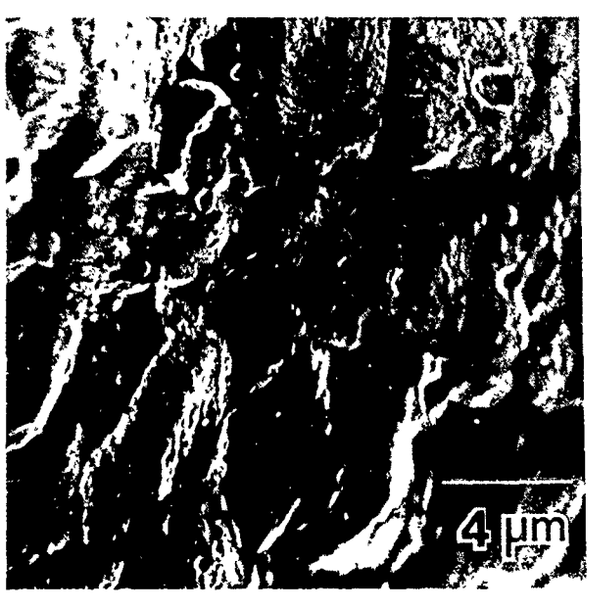


FIGURE 49—SEM fractograph of an IGSCC fracture face of an Al-Zn-Mg alloy, 7018-T76, stressed in an acidified inhibited saline environment (courtesy of G.M. Scamans).

The most systematic attempt to date to quantify the micromechanical contribution to the SCC of aluminum alloys is that presented by Wood and Gerberich[149 150] in the mid-1970s. These researchers designed a study based upon a commercial Al-Zn-Mg-Cu, 7075-T651, in which, to aid detailed definition of the mechanical component, they (1) re-heat treated the alloy to produce a recrystallized microstructure to provide a reasonable GB path, (2) used a pre-cracked specimen geometry to allow a good mechanical description during the SCC crack growth process, (3) selected an acidified saline environment and a peak-aged temper to provide a high SCC sensitivity, (4) ran tests at relatively constant stress-intensity factors as a function of temperature to permit apparent thermal activation energy determination, and (5) used AE to detect discontinuous crack jumps and scanning electron microscopy in an attempt to separate mechanical and chemical contributions to the crack growth process.

Remembering that the above study was conducted in the mid-1970s, it is a remarkable contribution. In hindsight, it is regrettable that the stress-intensity factors (K) used were generally too high and that the thermal aging practice used significantly reduced the alloy strength level and probably rendered the alloy temper unrepresentative of commercial 7XXX series alloys. The data obtained, however, clearly shows that IGSCC crack propagation is discontinuous and that at high K values, it involves a component of IG microvoid coalescence, as suggested by Jacobs,[44] who proposed that crack propagation in 7XXX series alloys occurred by a series of chemical-mechanical steps between $MgZn_2$ precipitates. In summary, Wood and Gerberich's experimental study and electrochemical-mechanical model[150] should be used as the basis of further study, capitalizing on the improved AE equipment now available and using a more appropriate alloy microstructure and loading orientation.

Martin, et al.,[198] detected "striations" on 7075-T651 IGSCC fracture faces promoted in 3.5% NaCl or humid air that closely resembled those reported by Scamans[77] for other 7XXX series alloys (7010, 7017, and 7079). The inferred crack jump distances, as reported by Scamans,[77] were insensitive to the applied stress-intensity factor (K) and the SCC crack velocity (cv). AE events recorded during SCC were consistent with the above, over the K range studied, in that the AE amplitude remained constant while the AE event count rate increased in proportion with SCC crack growth rates. This led to the conclusion that cracking occurs by a series of discrete crack jumps with a frequency depending upon the crack velocity and the characteristic jump distance for a particular alloy. The issue of whether SCC propagation occurs by a microscopically "brittle" or "ductile" fracture process remains unresolved. Lynch has consistently maintained that environmentally assisted cracking of a range of metallic alloys, including high strength aluminum alloys, can be described by a "chemisorption-induced localized slip" process, which he has recently reviewed with the experimental evidence.[217] Lynch concludes that environment-assisted cracking occurs because chemisorption facilitates the injection of dislocations from crack tips that promote coalescence of voids ahead of cracks. The reviewer believes the most likely SCC propagation mechanism for 7XXX series and probably for 2XXX series and aluminum–lithium-based alloys cracking in aqueous environments involves dissolved hydrogen concentrating in grain boundaries in high-stress regions ahead of crack tips and somehow reducing flow stresses locally and promoting a highly localized "reduced ductility" fracture.

Further detailed studies are needed to demonstrate if either or both of the above mechanisms operate. The information available is inconclusive in that (1) recent evidence from *in situ* high-resolution, high-voltage electron microscopy studies reported by Bond, et al.,[133] for commercial 7050-T651 plate and 7075-F sheet material can be used to support either mechanism, since the high strain rate and the unfavorable loading orientation used led to transgranular fracture, and (2) although the detailed high-resolution fractography of Scamans[77] and others[198 218] shows little evidence of the microvoids necessitated by Lynch's mechanism, it remains unproven that they are absent, as it is conceivable that they are too shallow to be resolved, or, as is more likely, that they are not easily recognized because they are only partially formed with the reduced ductility referred to above being a hybrid between classic grain-boundary decohesion and ductile microvoid coalescence.

Slow crack growth

Recently reported experimental observations indicate that IG slow crack growth (SCG) can occur in high- and medium-strength aluminum alloys in vacuum or dry air without any precharging with hydrogen.[75,193,194,219] SCG resembles SCC in several ways: Both are IG, except at at high stress-intensity factors, high strain rates, or unfavorable loading orientations, and the cracking susceptibility dependence upon thermal aging is identical for the two phenomena, i.e., OA $\ll$ PA $<$ UA.

SCG was first recognized in Al-Mg-Si alloys[75,219] because this alloy system is generally immune to SCC,[1] and when crack growth resembling SCC was observed in 6063 (UNS A96063) and 6082-T651 at room temperature, some other explanation was sought. Solid metal embrittlement was found to be promoted in susceptible microstructures by minute concentrations, e.g., > 20 ppm, of heavy metals such as lead and bismuth.[75,219] Further work has demonstrated that SCG is possible in other age-hardening aluminum alloy systems, e.g., 2XXX,[193] 7XXX,[193] and aluminum-lithium alloys,[194] and that SCG can be promoted by GB contaminants other than lead and bismuth, e.g., Lynch[220] has recently reported SCG in 7075-T651 induced by indium.

For the Al-Mg-Si alloy 6351, a detailed mechanistic study of the influence of lead on SCG is currently in progress.[221] Crack growth rate/stress-intensity factor relationships are sensitive to lead concentration (Figure 50). The apparent thermal activation energy for SCG in the temperatures in the range −4 to 80°C (~ 17 kJ/Mole) is consistent with control by GB lead self-diffusion and crack growth is predominantly internal and associated with the maximum stress region a small distance ahead of the crack tip.[222] The similarity between SCG and SCC in aluminum alloys is obvious, as is the mechanistic implication that a mechanical aspect of SCC propagation in aluminum alloys may have been overlooked. Further studies are needed to examine the latter possibility.

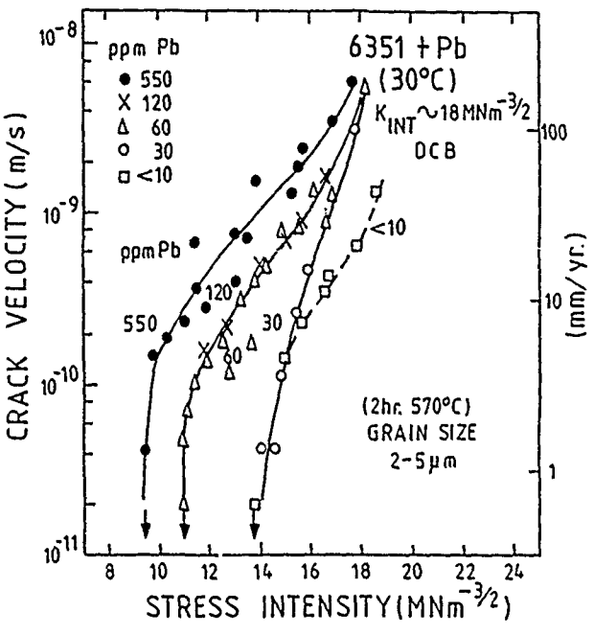


FIGURE 50—Influence of bulk alloy lead concentration upon slow crack rate in an Al-Mg-Si alloy, 6351-T6, as a function of applied stress-intensity factor.[75]

Hydrogen embrittlement and pre-exposure effects

As yet, no irrefutable evidence is available that proves the SCC of high-strength aluminum alloys in aqueous environments is controlled by HE. The nearest to this is that provided by Ratke and Gruhl[197] for a 7XXX series, Al-Zn-Mg alloy, suffering SCC in a saline environment. Their ingenious experiments involved loading externally notched hollow tubes in tension with the inside of the tube filled with a saline environment and the external surfaces carefully protected to prevent moisture access (Figure 51). Fractographic studies revealed that SCC crack growth initiation from the notches was internal and associated with a region ahead of the notch. These authors suggest that the only plausible explanation is that during the SCC test, hydrogen was generated via a cathodic electrochemical process in the aqueous electrolyte, with some diffusing into the alloy via GB diffusion to accumulate at sites of high stress ahead of the notch and lead to internal cracking. In the opinion of the reviewer, this is a true reflection of the events that occurred, and it is most unlikely that solid metal embrittlement was responsible for the subroot-notch cracking[222] and was mistaken for SCC.

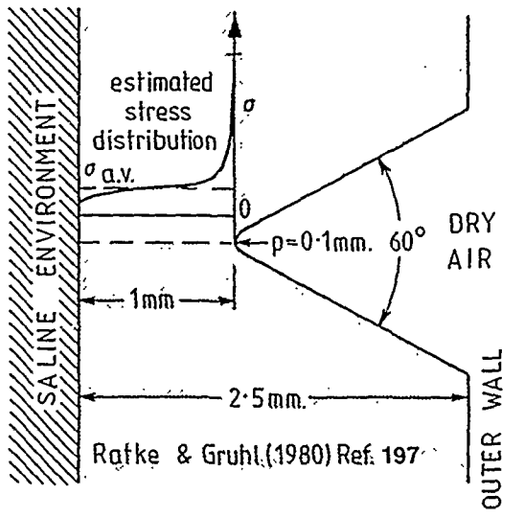


FIGURE 51—Notched hollow tube design used by Ratke and Gruhl[197] to show SCC initiation from a notch can occur internally.

The earliest suggestions that the SCC of 7XXX series alloys suffered HE during SCC in aqueous environments were made in the early 1960s by Gruhl and his coworkers in West Germany with their work on pre-exposure embrittlement (PE),[223] and Haynie, et al.,[9,10] in the United States who showed that stress increases the solubility of hydrogen at GBs in Al-Zn-Mg alloys exposed to aqueous environments. Little attention was paid to these studies until the work of Gest and Troiano[11] triggered a series of experimental studies worldwide, e.g., Scamans, et al.,[224] Christodoulou and Flower,[88] and Holroyd and Hardie[85] in the United Kingdom; Bernstein and Thompson and coworkers[114,115] in the United States; and Gruhl and coworkers,[54,197] who continued their studies in West Germany.

Gest and Troiano's work proposed that a high-strength Al-Zn-Mg-Cu alloy, 7075-T651, was susceptible to a strain aging type of reversible HE and that this played a major role during SCC in aqueous saline environments. They provided hydrogen permeation data ($D_0 \sim 2 \times 10^{-13}$ m^2/s) and related their internal friction and lattice parameter measurements directly to hydrogen uptake from the environment. Later work by Scamans, et al.,[224] on high-purity Al-Zn-Mg alloys and Holroyd and Hardie[85] on commercial Al-Zn-Mg-Cu alloys confirmed the observation of pre-exposure embrittlement reversibility. Scamans, et al.,[224] detected almost complete reversibility together with hydrogen out-gassing at low stresses during tensile testing of precharged specimens to failure in a vacuum chamber with a mass spectrometer attached. Holroyd and Hardie[85] observed complete recovery of PE when tensile specimens pre-exposed to aqueous environments were strained to failure at appropriate strain rates in dry air; for 7049-T651 pre-exposed to seawater for 30 days at room temperature, the degree of recovery increased with decreasing strain rates below ~ 10^{-3}/s (PE was not operative at higher strain rates) and was complete for strain rates below about 5×10^{-7}/s (Figure 52). These results are important because they demonstrate that HE of 7XXX series is a time-strain-dependent phenomenon and imply that hydrogen diffusion or some other process must occur during both crack propagation and HE recovery. Although it is only indirect evidence that SCC in aqueous

environments involves HE, it is interesting to note that a similar strain-rate dependence exists for pre-exposure embrittlement and SCC, and that the loss of ductility promoted by the two processes is additive.[85,112]

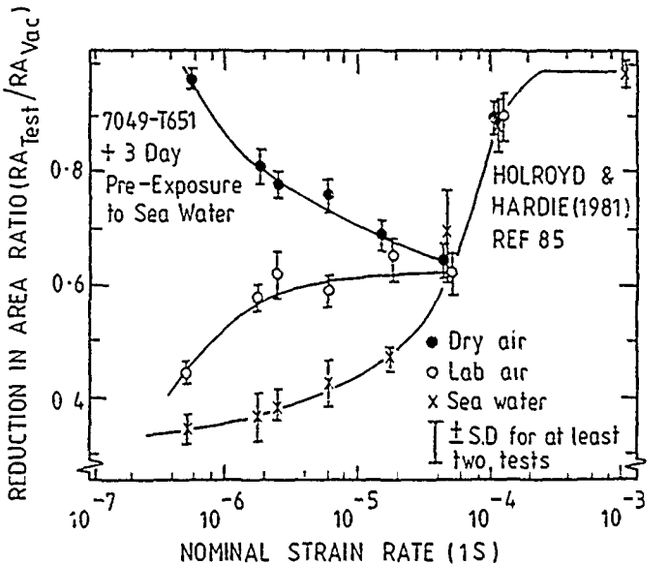


FIGURE 52—Variation in reduction in area ratio (test environment/vacuum) with strain rate for 7049-T651 tested in dry air, laboratory air and natural seawater after pre-exposure to seawater for 72 h at ambient temperature.[85]

Pre-exposure to aqueous environments at elevated temperatures can introduce complications. It appears that if an alloy's inherent susceptibility to SCC or PE is decreased during the pre-exposure period, then partial PE recovery occurs in laboratory air unstressed,[86] and the alloy adopts a sensitivity equivalent to that of the final alloy temper after pre-exposed at room temperature (Figure 53), and that further recovery requires sufficiently slow continuous straining in an inert environment.[85]

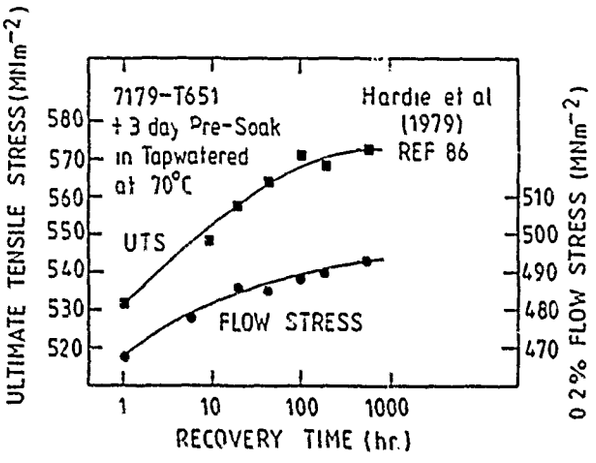


FIGURE 53—Recovery of 0.2% flow stress and ultimate tensile stress for 7179-T651 strained to failure at a nominal strain rate of 1.7 × 10^{-5}/s in laboratory air after immersion in tap water at 70°C for 72 h.[86]

Martin, et al.,[198] provided interesting indirect evidence that HE controls the SCC of 7XXX series alloys in aqueous saline environments During SCC propagation in 7075-T651 in 3.5% NaCl or humid air they detected identical AE signal count rates/unit crack advance and concluded that the same SCC mechanism must be operative in both environments If this assertion is correct and it is accepted that HE must be reponsible for SCC in humid air (David, et al., have stated that crack growth in moist air cannot be explained in terms of an anodic dissolution mechanism), then HE must also be occurring during SCC in aqueous environments.[199]

Loading mode effects. Although a common feature of most proposed HE mechanisms is the need for hydrostatic stresses,[225] it is not initially apparent why a triaxial stress state is a prerequisite for the HE of aluminum alloys, since hydrogen diffusion along GBs, in the absence of stress, can occur at sufficiently high fluxes to account for observed SCC crack growth rates in aqueous environments.[108] However, this issue is resolved by the recent results for 7XXX series alloys published by Magnin and Rieux, who showed that HE only operates in the presence of a sufficient stress raiser,[188] and those of Ratke and Gruhl,[197] who showed that SCC propagation generally initiated internally and was favored by highly stressed regions associated with stress raisers, i.e., a triaxial stress state; hence the assumption made by Green and coworkers[226] and others[227] that Mode III loading is not expected to promote crack growth by HE, whereas Mode I loading, with its high hydrostatic tension immediately ahead of crack tip, should promote HE of 7XXX series aluminum alloys is valid and Mode I/III loading experiments are an appropriate method to determine whether HE is involved during SCC in aqueous environments. These authors observed that SCC initiation and hydrogen-charging effects in notched 7075-T651 specimens immersed in saline environments occurred far more readily under Mode I loading (tensile) than Mode III loading (torsional) (Figure 54) and concluded that HE was involved during SCC in aqueous environments.

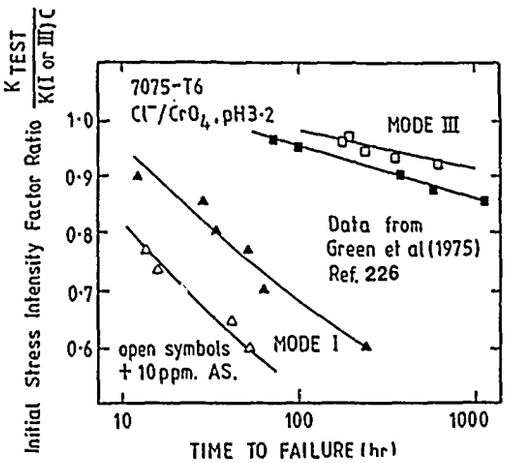


FIGURE 54—Influence of loading mode upon SCC susceptibility for 7075-T6 in an acidified inhibited saline solution with and without an arsenic addition to poison hydrogen recombination and hydrogen gas formation.[226]

Cyclic loading

Corrosion fatigue (CF) of aluminum alloys is covered in detail elsewhere in this volume, so discussion here will be restricted to the interfacial region between SCC and CF where IG environment-induced fracture processes are accelerated by cyclic loading. Limited research has been conducted in this area of environment-sensitive fracture of aluminum alloys,[108] and that published is restricted to 7XXX series alloys in saline solutions.

Based upon data obtained for 7079-T651 in a saturated NaCl solution, Speidel[228] showed that CF crack growth rates were predictable using a simple superposition model in which the observed CF crack growth rate $[(da/dn)_{CF}]$ is related to that occurring by fatigue in an inert environment $[(da/dn)_F]$ and the crack velocity resulting from SCC $[(da/dt)_{SCC}]$ by the relationship

$$(da/dn)_{CF} = (da/dn)_F + \int (da/dt)_{SCC} \qquad (10)$$

Unfortunately, this approach is inappropriate for other 7XXX series alloys,[108] in which SCC crack growth rates are two to three orders of magnitude slower (Figure 18), and the $(da/dn)_{CF}$ term is not controlled by the $(da/dt)_{SCC}$ term, as occurs for 7079-T651.

Holroyd and Hardie[108] addressed this issue by assessing the influence of loading frequency (0.1 to 70 Hz) upon crack propagation rates in the Al-Zn-Mg alloy, 7017-T651, immersed in natural seawater and characterizing CF fracture modes in terms of crack growth

rate, cyclic loading frequency, and ΔK (Figure 55). The data showed the following:

(1) IG CF, fractographically indistinguishable from SCC (other than possibly SCC "striations" details), was promoted at the highest loading frequency tested (70 Hz) as long as the ΔK values were sufficiently low;

(2) IG CF crack growth rates could be up to three orders of magnitude faster than the Region 2 plateau crack velocity;

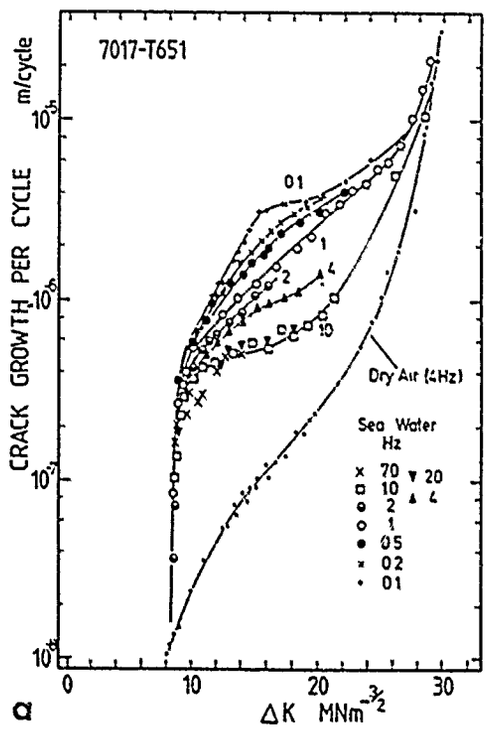
(3) The frequency dependence of the crack velocities associated with the transition from IG to TG shows a linear dependence upon the square root of the loading cycle period and an implied RDS consistent with GB diffusion of hydrogen during the loading cycle; and

(4) A simple superposition model is inappropriate for IG CF, and further work should be directed toward evaluating the influence of crack-tip strain rates upon CF (Figure 56). (Gao, et al., used a modified superposition model to describe TG CF.[229])

Magnin and Rieux[188] investigated the initiation of SCC and CF from smooth surfaces for an Al-Zn-Mg alloy, 7020, immersed in a saline environment. Their results demonstrate that HE only initiates and propagates when a sufficient stress raiser is made available by some other process. They observed that (1) under cyclic loading conditions, stress raisers may be promoted by either a mechanical or corrosion process, and so CF initiation and HE tend to occur at the FCP or under cathodic polarization conditions over a wide range of strain rates; and (2) under static loading, corrosion is generally the only available route, so SCC initiation from smooth surfaces occurs at the FCP at sufficiently low strain rates but is difficult or impossible under cathodic polarization conditions.

Environment-Induced Cracking of Welds

For weldable aluminum alloy systems other than medium-strength Al-Zn-Mg alloys, service failure resulting from environment-induced cracking is rare and is restricted to occasional instances for Al-Mg alloy welds[230] invariably associated with heat-affected-zone grain boundaries becoming decorated with an electrochemically active phase, β (Mg_2Al_3), and SCC occuring via a predominantly anodic dissolution mechanism that would occur in similarly sensitized parent plate material.[1]



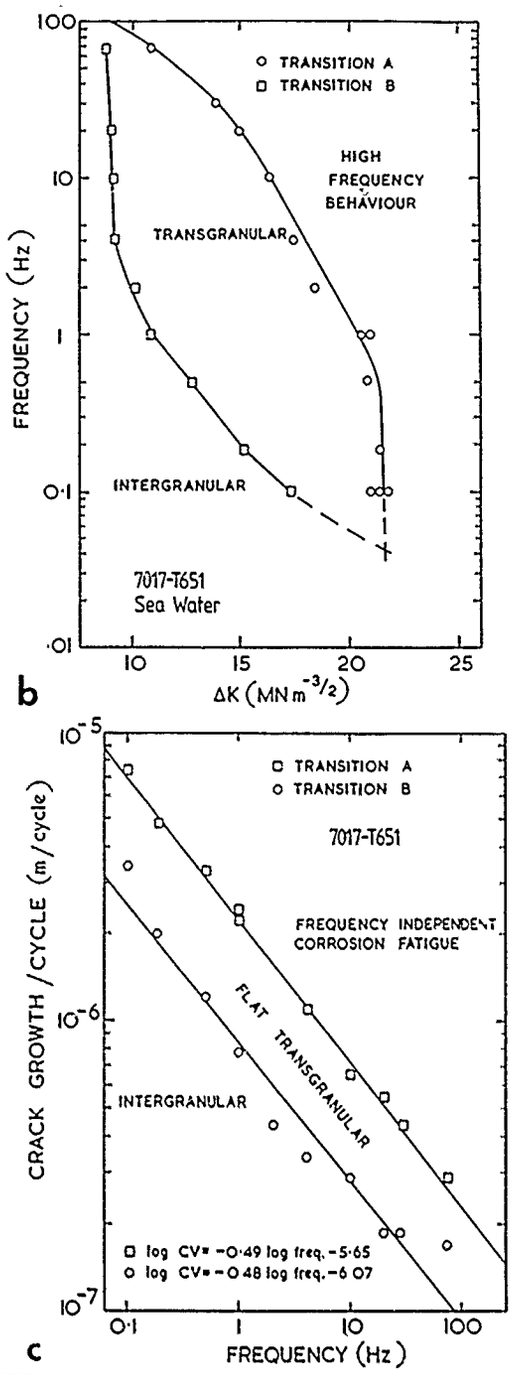


FIGURE 55—Corrosion fatigue of Al-Zn-Mg alloy, 7017 in natural seawater; (a) crack growth rate/cycle as a function of ΔK for a range of cyclic loading frequencies, (b) the dependence of corrosion fatigue fracture morphologies in terms of cyclic loading frequency and ΔK, and (c) fracture morphologies in terms of crack growth rate/cycle and cyclic loading frequency.[108]

Localized corrosion of welded Al-Zn-Mg joints has been observed in service[2,231-233] and laboratory experiments (see reference 234 for 27 references). It generally occurs as exfoliation corrosion within a heat-affected region a few millimeters from the weld bead or as a type of SCC, weld-toe cracking (WTC), which initiates at weld toes and propagates into the interfacial region between the weld bead and heat-affected zone (Figure 57), commonly known as the "white zone" because of its etching behavior in nitric acid.[235]

The reviewer has discussed WTC in Al-Zn-Mg welds in detail elsewhere.[234] It is a complex phenomenon that involves at least two processes; the first being separation of the mechanically weak/chemically reactive weld overlap region from the plate (the weld-toe region) and the second crack initiation and propagation in the white zone driven by HE.[232,236-237]

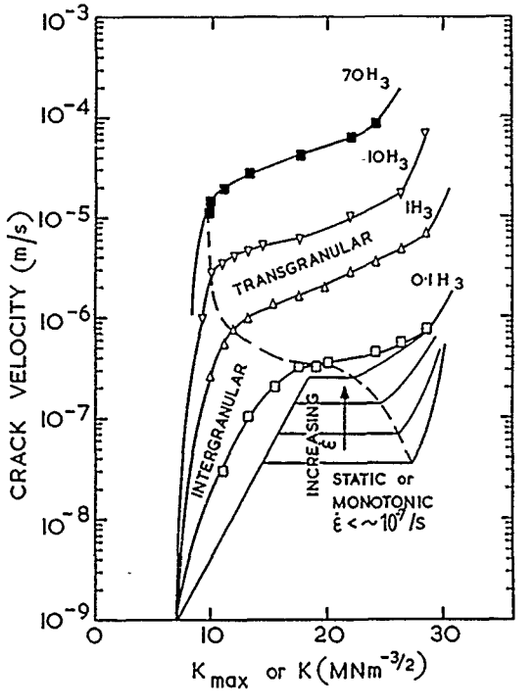


FIGURE 56—Schematic representation of the effect of crack-tip strain rate upon the relationship between crack velocity and stress-intensity factor.[108]

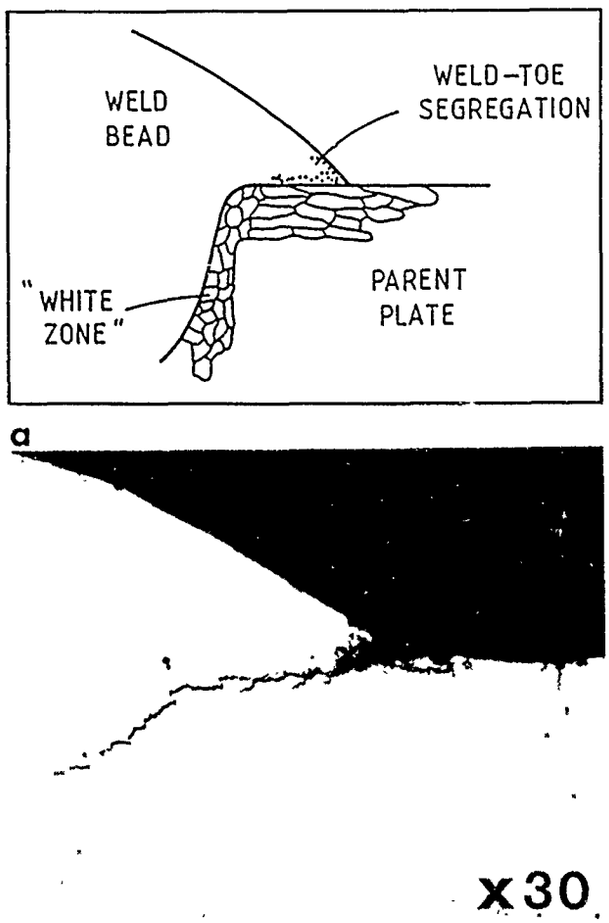


FIGURE 57 – (a) Schematic representation of the weld-toe region for a conventional aluminum alloy weld and (b) a weld-toe crack propagating in the "white-zone" region.

Considerable effort has been expended to prevent weld-toe cracking. Initial attempts concentrated upon copper[238-240] or silver[239-241] additions to the parent plate. This was followed by work involving silver additions to the filler wire.[235,242-245] Most of these studies revealed beneficial effects for Al-Zn-Mg weldments in both naturally aged and the otherwise highly susceptible post-weld aged condition. Encouraging as these results were, they have not led to a commercially viable solution. Silver additions, as well as being expensive, promote an increased quench sensitivity[239-241] and unacceptable strength losses in naturally or post-weld aged welds.[240] Copper additions, usually limited to around 0.15 wt% because of hot cracking limitations, and silver additions, typically 0.5 wt%, both can promote increased tendency toward exfoliation corrosion,[246-247] and recent observations indicate that the previously reported beneficial effects toward WTC are associated with crack initiation rather than propagation[247] and therefore do not offer a long-term solution.

More recent approaches have concentrated upon minimizing stresses in welded joints[233,248] and the development of protective coatings.[236,244,249] Di Russo and Abis[248] have shown that the use of weld gaps calculated using finite-element analysis can significantly reduce stress levels in welded joints, as can controlled peening.[233] These findings are encouraging, and such approaches should be incorporated into joint design since any reduction in stresses will be beneficial. They do not, however, provide a complete solution, because inevitably some joints will be highly stressed and therefore potentially susceptible to WTC.

The coatings approach, other than the passing reference to a "protective varnish" by Pirner and Bischel,[244] has been restricted to aluminum-based metal spray coatings that "cover up" weldments.[236] Although an aluminum-5wt%zinc flame-sprayed coating has been used with some success to prevent exfoliation corrosion in Al-Zn-Mg weldments in service conditions,[249] these coatings, whether flame- or arc-sprayed, do not provide complete electrochemical protection against weld-toe cracking in most service conditions unless the sprayed compositions are specifically tailored to do so using appropriate "activator additions."[234,250] In general, therefore, protection relies upon coatings acting as a physical barrier. This condition is rarely maintained long term in service because all secondary protection systems, e.g., paints, eventually allow moisture penetration and the sprayed coatings themselves are porous (Figure 58). In other words, to guarantee complete protection, it should be assumed sprayed coatings are breached, and the coating itself must provide controlled sacrificial protection preventing WTC and exfoliation. In view of this, some doubt must exist about the recent claims[251] made for arc sprayed aluminum–zinc coatings not containing the activator additions needed to generate sacrificial protection.

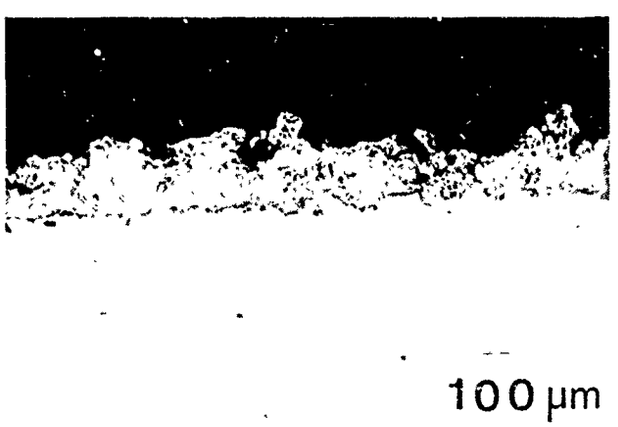


FIGURE 58—Scanning electron micrograph of a typical arc-sprayed aluminum-based coating on a medium-strength weldable aluminum alloy substrate.

Previous work by Holroyd, et al.,[236] outlined an approach to develop aluminum-based spray coatings that should provide immunity to WTC and exfoliation corrosion in service even when the coatings are mechanically or otherwise locally disrupted. The approach adopted was to identify first the local environmental conditions associated with propagating weld-toe cracks and then to define the electrochemical conditions providing immunity in these and the full range of environmental conditions expected in service. Worst-case laboratory testing indicates that immunity to all forms of localized corrosion is guaranteed if electrochemical potentials are maintained in the range −1130 to −1200 mV_{SCE}, irrespective of solution pH as long as general corrosion is avoided (Figure 59). A wider "safe" potential range will generally exist in service because the environmental and loading conditions will be less severe than those used in the above study.

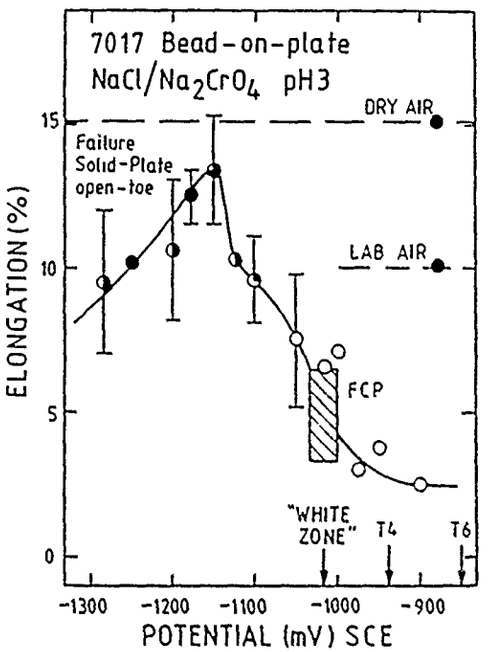


FIGURE 59—Influence of applied potential upon elongation and fracture mode for welded Al-Zn-Mg specimens slow-strain-rate tested (cross-head speed 2.5×10^{-5} mm/s) in 2% NaCl + 0.5% Na_2CrO_4, pH 3.[236]

Self-protecting welds. Analysis of the available published work describing electrochemical potential profiles across weldment cross sections during exposure to aqueous saline solutions reveals that a significant difference exists between Al-Zn-Mg alloys[252-254] and other weldable aluminum alloys such as Al-Cu,[252] Al-Mg,[252] and Al-Mg-Si.[255] Weld beads are electronegative with respect to the heat-affected zone and parent plate for all of the alloys other than Al-Zn-Mg (Figure 60). The potential data quoted by Shumaker, et al.,[252] for a 7039-T651 weld is representantive of Al-Zn-Mg alloys in general and corresponds closely to the data reported by Tuck[254] for the alloy 7017-T651, welded using similar welding conditions.

These observations are important because, when interpreted, they provide clear evidence for why Al-Zn-Mg alloys tend to suffer weld-toe cracking while other weldable aluminum alloys are generally immune. Holroyd, et al.,[234] asked the question, "why are Al-Mg and Al-Mg-Si welds immune to WTC while Al-Zn-Mg welds are susceptible even though, like the Al-Zn-Mg welds,[256] the Al-Mg and Al-Mg-Si welds also have white zones[257] with recrystallized microstructures and high concentrations of magnesium on the grain boundaries?" The answer proposed was that the potentially susceptible white zones are sacrificially protected by the weld bead in cases where WTC is not observed. To test this hypothesis, an attempt was made to reverse the weld-bead/white-zone potential couple for a 7017-T651 weld by using a super-purity-based Al-5Mg filler wire composition containing "activator" additions. Potentiokinetic polarization data in both 3% sodium chloride and an acidified saline solution indicated that the "activator" additions had promoted the desired potential shift toward more electronegative potentials, but unfortunately both the weld bead and the white zone were similarly effected, so the potential couple was not reversed. The reason for this is that parent plate melt-back during welding promotes up to a 50% dilution of the weld pool and promotes diffusion of "activator" elements into the white zone via partially liquated grain boundaries.

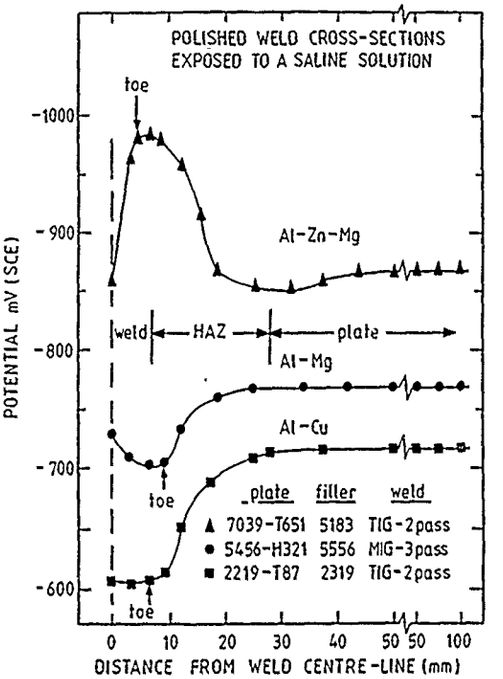


FIGURE 60—Electrochemical potential profiles across medium-strength weldable alloy weldments. (Data from Shumaker, et al.[252])

To overcome the problem of white-zone activation, a double-pass welding technique was developed in which the second pass involves the super-purity "active" filler wire,[258] and the first pass involves a commercial Al-5Mg filler wire that acts as a diffusion barrier preventing activator transfer in one direction and iron/silicon pick-up from the plate in the other (Figure 61).

Summary

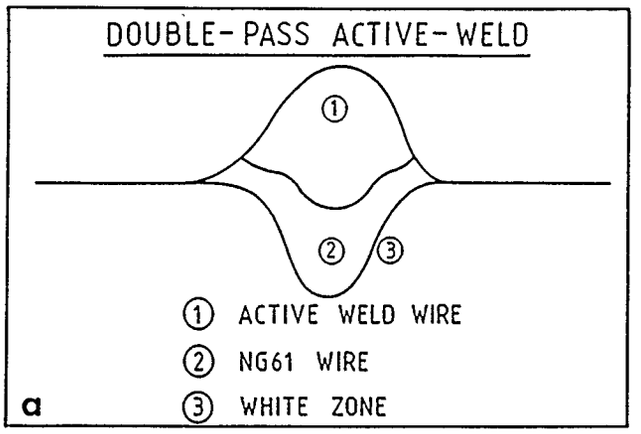
Evidence presented in the previous sections in this review clearly demonstrates that considerable progress has been achieved over the last 20 years in the quest to understand environment-induced cracking of aluminum alloys. Significant issues remain unanswered, and with the continual commercial drive toward using stronger alloys and less conservative designs for transport, structural, and other applications, the potential risk of environment-induced service failures will become more pronounced unless a greater predictive capability is established.

Some of the more important unresolved questions, in the opinion of this reviewer, are summarized below.

Alloy microstructure. Recent SCC crack velocity data[199] showing that long-term room-temperature aging of a peak-aged Al-Zn-Mg-Cu alloy can significantly influence crack velocity/stress-intensity factor (cv-K) behavior (Figure 62) indicate that the controlling microstructural features can be subtle, possibly involving GB segregation effects.

Work reported during the mid-1970s proposed that rapidly solidified powder metallurgy (PM) 7XXX series aluminum alloys offer an inherently better combination of strength and resistance to SCC initiation and exfoliation corrosion than conventional ingot metallurgy (IM) alloys, because for PM alloys, the number of heterogeneous corrosion sites available for SCC initiation, e.g., large iron-rich inclusions, are minimized and the corrosion attack is more uniform in

nature [5,178] While it is a fact that rapid solidification rates potentially offer castability for a wider range of alloy compositions and hence alloys with higher strength than IM alloys, it is not inevitable that PM alloys have superior SCC resistances compared to compositionally similar IM alloys. Published cv–K data for PM 7XXX series alloys 7090 and 7091[259-260] indicate that crack propagation characteristics can be matched by conventional IM alloys (Figure 63).



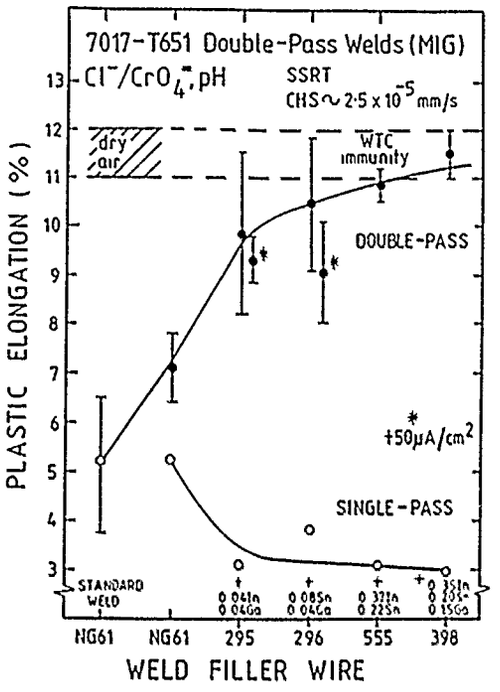


FIGURE 61—(a) A schematic representation of a double-pass self-protecting weld and (b) fracture elongation given by double-pass 7017-T651 welds after slow-strain-rate testing in 2% NaCl + 0.5% Na_2CrO_4, pH 3.[234]

Critical microstructural feature(s) controlling SCC (or CF) await identification. Attempts to achieve this need to augment those focused upon understanding the influence alloy microstructure has on fracture characteristics and other mechanical properties. The overall aim is to optimize the balance of properties offered by high-strength aluminum alloys.

Environmental conditions. Environment sensitive fracture studies for aluminum alloys in aqueous environments generally have been conducted in halide ion solutions, with some limited work in other solutions involving single anions. The significance of 'synergistic effects' needs to be established, as it is conceivable that a "new" aluminum alloy may be deemed insensitive to SCC (and CF) on the basis of laboratory testing using conventional test environments, when a significant susceptibility occurs in service because of a synergistic effect between various aqueous species. In hindsight, it is true that this situation has not promoted service problems for existing alloys, although synergistic effects are known to occur for (1) 7075-T651, where nitrate ion additions to saline solutions can accelerate SCC crack growth rates,[127] and (2) an Al-Li-Cu-Mg alloy, 8090, where sulfate ion additions to a 3% NaCl solution can promote SCC initiation in smooth specimens under total immersion conditions that otherwise would not have occurred.[261]

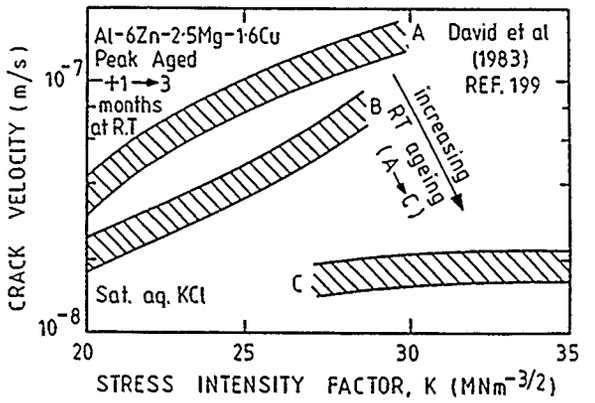


FIGURE 62—Stress corrosion crack velocity as a function of stress-intensity factor for a peak-aged Al-6Zn-2.5Mg-1.6Cu alloy after various storage time at room temperature after solution heat treatment and prior to SCC testing in a saturated aqueous potassium chloride solution.[199]

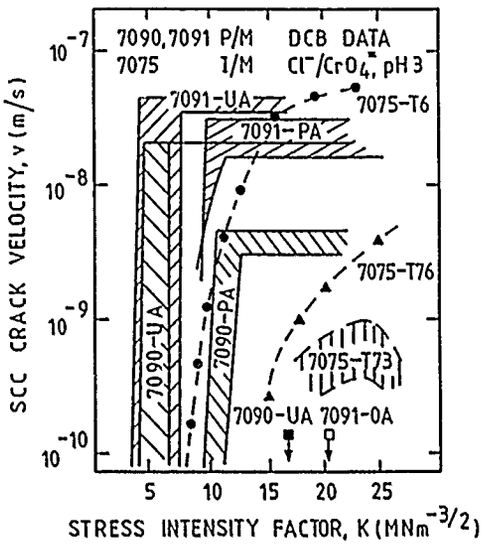


FIGURE 63—SCC crack propagation data for PM alloys 7090 and 7091[259-260] and IM alloy 7475[104] in an acidified inhibited saline environment.

Future work, of course, should be directed toward the development of alloy microstructures that minimize crack propagation; however, composition modifications, surface coatings, or novel processes that prevent the development of acidified conditions within pits/fissures/crevices and/or minimize potential stress raisers also offer major benefits if SCC and/or CF initiation can be significantly retarded or, ideally, prevented.

Mechanical aspects. Perhaps the least well-understood aspect of environment-induced cracking of aluminum alloys is the role of stress. Recently, two important observations were made for intergranular SCC. (1) SCC can involve internal fracture and (2) SCG in inert environments can occur in all precipitate-hardening aluminum alloys. It is possible that environment-induced cracking of aluminum alloys propagates by a similar mechanism to SCG somehow accelerated by the environment, e.g., by a HE mechanism that, like SCG, tends to involve crack propagation ahead of the crack tip. Further work is needed to establish this proposal.

In the past, it has been generally inferred that SCC crack-velocity–stress-intensity factor (cv–K) behavior provides a unique relationship independent of test procedure. Experimental[174 222] and theoretical evidence[262] now show that this assumption is often invalid with crack growth rates tending to be higher for increasing than decreasing K conditions[263 264] and/or different initial starter K values. In addition, now that SCC crack growth rates can be continuously monitored, using techniques such as potential-drop or compliance methods, it is evident that true "plateau velocities" rarely occur, but that crack velocity generally fluctuates with an overall tendency for the mean to increase with increasing K.[174]

Conclusion

A mechanistic interpretation of environment-induced cracking of high-strength aluminum alloys remains controversial. The wealth of experimental evidence that SCC propagation in these alloys is generally a discontinuous process indicates that a growth mechanism controlled solely by continuous anodic dissolution at the crack tip is impossible, and much systematic study is still required to achieve an adequate description.

To end on a positive note, (1) significant progress toward understanding environment-induced cracking of high-strength aluminum alloys should be possible over the next decade with the availability of novel experimental techniques and improved resolution and data capture/analysis capability for existing techniques, and (2) alloy microstructural "manipulation/optimization" offers a route to provide current and the new emerging high-strength aluminum alloys with inherently high resistances to environment-induced cracking.

References

1. D.O. Sprowls, R.H. Brown, Fundamental Aspects of Stress Corrosion Cracking (Houston, TX: National Association of Corrosion Engineers, 1969) p. 466.
2. K.G. Kent, Metall. Reviews 15, 147(1970): p. 135.
3. M.O. Speidel, Theory of Stress Corrosion Cracking in Alloys, ed. J.C. Scully (Brussels, Belgium: NATO, 1971), p. 289.
4. R.H. Brown, D.O. Sprowls, M.B. Shumaker, Stress Corrosion Cracking of Metals—A State of the Art," ASTM-STP518 (Philadelphia, PA: ASTM, 1972), p. 518.
5. M.O. Speidel, Metall. Trans. 6A(1975): p. 631.
6. M.O. Speidel, M.V. Hyatt, Advances in Corrosion Science and Technology, Vol. 2 (New York, NY. Plenum Press, 1972), p. 115.
7. Aluminium—Properties and Physical Metallurgy, ed. J.E. Hatch (Metals Park, OH. ASM International, 1984)
8. W. Gruhl, Z. Metallkde 75(1984): p. 819.
9. F.K. Haynie, W.K. Boyd, "Stress Corrosion Cracking of Aluminum Alloys," Battelle DMIC Report 228, July 1, 1966.
10. F.K. Haynie, D.A. Vaughan, D.I. Phalen, W. Boyd, P.D. Frost, Technical Report AFML-TR-66-267, U.S. Air Force, Jan. 1967.
11. R.J. Gest, A.R. Troiano, Corrosion 30(1974). p. 247, L'Hydrogene dans les Metaux, Editions Science et Industrie (Paris, France: 1972), p. 427.
12. L. Montgrain, P.R. Swann, Hydrogen in Metals, ed. I.M. Berstein, A.W. Thompson (Metals Park, OH: ASM, 1974), p. 575.
13. L. Montgrain, G.M. Scamans, P.R. Swann, Proceedings of the 3rd Tewkesbury Symposium on Fracture Processes (Melbourne, Australia: 1974), p. 194.
14. D.A. Hardwick, M. Taheri, A.W. Thompson, I.M. Bernstein, Metall. Trans. 13A(1982): p. 235.
15. K. Higashi, T. Ohmishi, Y. Nakatani, K. Okabayshi, J. Japanese Light Metals 31(1981): p. 386.
16. H. Kanematsu, M. Ohido, T. Oki, J. Japanese Light Metals, 36(1986): p. 125.
17. N.J.H. Holroyd, G.M. Scamans, Scripta Metall. 19(1985). p. 915.
18. N.J.H. Holroyd, A. Gray, G.M. Scamans, R.Hermann, Aluminium-Lithium III (London, England. Institute of Metals, 1985), p. 310.
19. R.C. Dorwood, K.R. Hasse, Corrosion 43(1987) p. 408.
20. A.J. Cornish, M.K.B. May, J. Inst. Metals 97(1967). p. 44.
21. P.N.T. Unwin, R.B. Nicholson, Acta. Metall. 17(1969). p. 1397.
22. K.G. Kent, J. Inst. Metals 97(1969). p. 127.
23. K.G. Kent, J. Aust. Inst. Metals 15(1970). p. 171.
24. P.N. Adler, R. De Isai, G. Geschwind, Metall. Trans. 3(1972). p. 3191.
25. A.J. De Ardo, R.D. Townsend, Metall. Trans. 1(1970). p. 2573.
26. A.J. Sedriks, J.A.S. Green, D.L. Novak, Localized Corrosion, NACE-3 (Houston, TX. NACE, 1974), p. 569.
27. P.K. Poulose, J.E. Morall, A.J. McEvily, Metall. Trans. 5A(1974): p. 1393.
28. J.A.S. Green, W.G. Montague, Corrosion 31(1975): p. 209.
29. T. Asahi, F. Yabusaki, K. Osamura, Y. Murakami, Proceedings of 6th International Conference on Light Metals (Lloben, Vienna: 1975), p. 64.
30. C.J. Peel, P. Poole, Mechanisms of Environmental Sensitive Cracking of Materials (London, England: The Metals Society, 1977), p. 147.
31. R. Hagg, J.E. Morrel, A.J. McEvily, International Conference Proceedings of the Environment Degregation of Engineering Materials (Blacksburg, VA: Virginia Polytechnic Institute, 1977), p. 19.
32. B.V.N. Rao, Metall. Trans. 12A(1981): p. 1356.
33. K. Rajan, W. Wallace, J.C. Beddoes, J. Mater. Sci. 17(1982): p. 2817. [Note misprint in Reference 33 acknowledged in Metall. Trans. 16A(1985): p. 2068.]
34. J.K. Park, Mater. Sci. Eng. A103(1988): p. 223.
35. P. Brenner, Aluminium 28(1952): p. 216.
36. A.J. Sedriks, P.W. Slattery, E.N. Pugh, Trans. ASM 26(1969): p. 238.
37. I.J. Polmear, J. Aust. Inst. Metals 89(1960). p. 193.
38. E.A. Starke, J. of Metals 22(1970): p. 54.
39. G. Thomas, J.J. Nutting, J. Inst. Metals 88(1959-60): p. 81.
40. H.A. Holl, Corrosion 23(1967): p. 173.
41. E. Hornbogen, Z. Metallkde 58(1967). p. 31.
42. N. Ryum, Acta Metall. 6(1968): p. 327.
43. M.O. Speidel, Fundamental Aspects of Stress Corrosion Cracking, p. 561.
44. A.J. Jacobs, Fundamental Aspects of Stress Corrosion Cracking, p. 530.
45. A.J. Cornish, M.K.B. Day, J. Inst. Metals 99(1971). p. 377.
46. I.T. Taylor, R.L. Edgar, Metall. Trans. 2A(1971). p. 833.
47. C.R. Shastry, G. Judd, Metall. Trans. 3A(1972): p. 779.
48. P. Doig, J.W. Edington, Brit. Corros. J. 9(1974). p. 220.
49. D.E. Ward, G.M. Lorimer, Proceedings 3rd Inst. Conference on Strength of Metals and Alloys, Vol. 1.1 (London, England: The Institute of Metals, 1973) p. 488.
50. P. Doig, J.W. Edington, Grain Boundaries in Engineering Materials (New York, NY. American Institute of Mining, Metallurgical, and Petroleum Engineers, 1974), p. 461, and P. Doig, P.E.J. Flewitt, J.W. Edington, Corrosion 10(1975). p. 347, Corrosion 33(1977): p. 217.
51. M. Raghavan, Metall. Trans. 11A(1980): p. 993.
52. M.S. Rahman, H. Cordier, I.J. Polmear, Z. Metallkde 73(1982). p. 589.
53. M.S. Rahman I.J. Polmear, Z. Metallkde 74(1983): p. 733.
54. H. Schmiedel, W. Gruhl, Z. Metallkde 74(1983). p. 777.
55. J.M. Chen, T.S. Sun, R.K. Viswanadham, J.A.S. Green, Metall. Trans. 8A(1977): p. 1935.
56. T.S. Sun, J.M. Chen, R.K. Viswanadham, J.A.S. Green, Appl. Phys. Lett. 31(1977): p. 580.
57. J.A.S. Green, R.K. Viswanadham, T.S. Sun, W.G. Montague, CORROSION/77, paper no. 17 (Houston, TX: NACE, 1977)
58. R.K. Viswanadham, T.S. Sun, J.A.S. Green, Metall. Trans. 11A(1980): p. 85.
59. J.R. Pickens, T. Langan, Progress Report on Contract N00014 83-C-0380, Martin Marretta Laboratories, June 1985.
60. J.R. Pickens, T. Langan, Metall. Trans. 18A(1987). p. 1735.
61. C.R. Shastry, M. Levi, A. Joshi, Corros. Sci. 21(1981). p. 673.

62. G.M Scamans, N.J.H. Holroyd, C.D.S. Tuck, Corros. Sci. 27(1985): p. 329.
63 J T Staley, Aluminium Technology '86, ed. T. Sheppard (London, England: Institute of Metals, 1986), p. 396.
64. W.S. Miller, V.D. Scott, Mater. Sci. 12(1978): p. 95.
65. R.R. Sawtell, J.T. Staley, Aluminium 59(1983): p. 127.
66 D S Thompson, B.S. Subramanya, S. Levy, Metall. Trans. 2(1971): p. 1149.
67 W.D Varnam, W.A. Anderson, U.S. Patent 3,171,760 (1965).
68. I. Taylor, Metals Progr. 84, 5(1963): p. 74.
69 B. Sarkar, M. Marek, E.A. Starke, Metall. Trans. 12A(1981). p. 1939.
70. E.A. Starke, Mater. Sci. Eng. 29(1977): p. 99.
71. W. Gruhl, H. Cordier, Z. Metallkde 55(1964): p. 577.
72. P. Poole, C.J. Peel, D.C.L. Greenfield, Royal Aircraft Establishment, Farnborough, UK, Technical Report 790077, June 1979.
73 F.S. Lin, E.A. Starke, Mater. Sci. Eng. 39(1979): p. 27.
74. T.H. Sanders, E.A. Starke, Metall. Trans. 7A(1976): p. 1407.
75 J J. Lewandowski, V Kohler, N.J.H. Holroyd, Mater. Sci. Eng. 96(1987): p. 185.
76. W.R. Middleton, R.N. Parkins, Corrosion 28(1972): p. 88.
77 G.M. Scamans, Metall. Trans. 11A(1980): p. 846, Hydrogen Effects in Metals, p. 467.
78 S P Lynch, Mechanisms of Environment Sensitive Cracking of Materials (London, England: The Metals Society, 1977) p. 201.
79. W. Gruhl, Aluminium 54(1978): p. 323.
80. G.M. Lorimer, D. Ryder, Engineering Practice to Avoid Stress Corrosion Cracking, NATO-AGARD, Conf. Paper 53 (1970).
81. W. Hepples, M.R. Jarrett, J.S. Crompton, N.J.H. Holroyd, "The Influence of Microstructure on the Stress Corrosion Cracking and Exfoliation of Commercial Al-Zn-Mg-Cu Alloys," this proceedings.
82 J R Pickens, T.J Langan, J.A.S. Green, Environment Sensitive Fracture of Metals and Alloys, Office of Naval Research, Washington(1988), p. 115.
83 J R Pickens, D Venables, G.D. Davis, J.R. Gordon, Progress Report, ONR Contract N00014-820C-0342, Martin Marietta Laboratories, Baltimore, MD (1982).
84 G M Scamans, Environmental Degredation of Engineering Materials (Blacksburg, VA: 1981), p. 153.
85 N J H Holroyd, D. Hardie, Corros. Sci. 21(1981). p. 129.
86. D. Hardie, N.J.H. Holroyd, R.N. Parkins, Metal Sci. 13(1979): p. 603.
87 G.M. Scamans, J. Mater. Sci. 13(1978): p. 27.
88. L. Christodoulou, H.M. Flower, Acta Metall. 29(1980): p. 481.
89 B. Cina, U.S. Patent, 3,865,584 December (1974).
90. R.S. Kaneko, Metal Progr. 117(1980). p. 41.
91. J.J. Thompson, E.S. Takins, V.S. Agarwala, Environmental Degradation of Engineering Materials III, ed. M.R. Loutham Jr., R P McNitt, R.D. Sisson Jr. (Pennsylvania State University, 1987), p. 329.
92 J.K Park, A.R. Ardell, Metall. Trans. 15A(1984). p. 1531.
93. J.J. Thompson, E.S. Tankins, V.S. Agarwala, Materials Performance 26(1987): p. 45.
94. B. Cina, B. Ranish, Aluminium Industrial Products, Pittsburgh Chapter (Metals Park, OH: ASM International, 1974).
95 A.J Jacobs, Trans. ASM 58(1965): p. 579.
96. G.M. Pressouye, I.M. Bernstein, Metall. Trans. 9A(1978): p. 1571.
97. J.S. Crompton, W. Hepples, M.R. Jarret, N.J.H. Holroyd, 10th International RISO Symposium on Metallurgy and Materials Science: Materials Architecture (Denmark. RISO National Laboratory. 1989), p. 313.
98. A.J. McEvily, J.B. Clarke, A.P. Bond, ASM Trans. 60(1966). p. 661.
99. J.C. Scully, Theory of Stress Corrosion in Alloys (Brussels, Belgium: NATO, 1971), p. 127.
100. J.L. Nelson, E.N. Pugh, Metall. Trans. 6A(1975). p. 1459.
101. Y. Kojima, T. Takahasi, J. Japanese Institute of Light Metals, 25(1975): p. 59.
102. A.J. Bursle, E.N. Pugh, Mechanisms of Environment Sensitive Cracking of Materials (London, England: The Metals Society, 1977), p. 471.
103. R.C. Dorwood, K.R. Hasse, Brit. Corros. J. 13(1978): p. 23.
104. R.C. Dorwood, K.R. Hasse, Corros. Sci. 19(1979): p. 131.
105. G.H. Koch, Corrosion 35(1979): p. 73.
106. R.C. Dorwood, K.R. Hasse, Corros. Sci. 22(1982): p. 251.
107. S.P. Lynch, Corros. Sci. 22(1982): p. 925.
108. N.J.H. Holroyd, D. Hardie, Corros. Sci. 23(1983): p. 527; ASTM-STP 821 (Philadelphia, PA: ASTM, 1984), p. 534.
109. D.O. Sprowls, J.W. Coursen, J.D. Walsh, ASTM-STP 610 (Philadelphia, PA: ASTM, 1976), p. 143.
110. S.P. Lynch, Corros. Sci. 24(1984): p. 375.
111. K.R. Hasse, R.C. Dorward, Corrosion 42(1986): p. 663.
112. N.J.H. Holroyd, D. Hardie, Third International Conference on Hydrogen and Materials (New York, NY: Pergamon Press, 1982), p. 659.
113. N.J.H. Holroyd, G.M. Scamans, R. Hermann, International Conference on Control and Exploitation of the Corrosion of Aluminium (Cranfield, UK: 1983).
114. J. Albrecht, A.W. Thompson, I.M. Bernstein, Metall. Trans. 10A(1979): p. 1759.
115. J. Albrecht, A.W. Thompson, I.M. Bernstein, Metall. Trans. 13A(1982): p. 811.
116. D.A. Hardwick, A.W. Thompson, I.M. Bernstein, Metall. Trans. 14A(1983): p. 2517.
117. D. Nguyen, A.W. Thompson, I.M. Bernstein, Acta Metall. 35(1987): p. 2417.
118. D.A. Hardwick, A.W. Thompson, I.M. Bernstein, Corros. Sci. 28(1988): p. 1127.
119. J.A. Donovan, Metall. Trans. 7A(1976): p. 1677.
120. J.K. Tien, A.W. Thompson, I.M. Bernstein, R.J. Richards, Metall. Trans. 7A(1976): p. 821.
121. J.P. Hirth, H.H. Johnson, Atomistics of Fracture, ed. R.M. Latanision, J.R. Pickens (New York, NY. Plenum Press, 1983), p. 813.
122. A.W. Thompson, I.M. Bernstein, Advances in Corrosion Science and Technology, Vol. 7, eds. M.G. Fontana, R.W. Staehle (New York, NY: Plenum Press, 1980), p. 53.
123. A.J. Jacobs, N. American Rockwell Corp., Rocketdyne Div., Report R-8173, 1970.
124. A.K. Vasudevan, P.R. Ziman, S.C. Jha, T.H. Sanders Jr., Aluminium-Lithium III (London, England: Institute of Metals, 1985), p. 303.
125 A.K. Vasudevan, J. Liu, R.E. Ricker, Environment Degradation of Engineering Materials III (Pennsylvania State University, 1987), p. 321.
126 M.S. Hunter, NASA Contract NAS 8-20396 Report, 1967.
127. A.H. Le, B.F. Brown, R.T. Foley, Corrosion 36(1980). p. 673.
128. A.H. Le, R.T. Foley, Corrosion 39(1983): p. 379.
129. T.H. Nguyen, B.F. Brown, R.T. Foley, J. Electrochem Soc. 129(1982): p. 780.
130. T.H. Nguyen, B.F. Brown, R.T. Foley, Corrosion 38(1982): p. 319.
131. A.H. Lee, R.T. Foley, Corrosion 40(1984): p. 195.
132. H.W. Paxton, R.P.M. Procter, Fundamental Aspects of Stress Corrosion Cracking, p. 509.
133. G.M. Bond, I.M. Robertson, H.K. Birnbaum, Acta Metall. 35(1987): p. 2289.
134. J.P. Fidelle, ASTM-STP543 (Philadelphia, PA. ASTM, 1974).
135. B.F. Brown, C.T. Fujii, E.P. Dahlberg, J. Electrochem. Soc. 116(1969): p. 218.
136. J.A. Hunter (Ph.D. diss., Oxford, 1989).
137. H.F. de Jong, Aluminium 58(1982): p. 526.
138. M.V. Hyatt, Corrosion 26(1970): p. 487.
139. R.C. Dorwood, K.R. Hasse, Corrosion 34(1978): p. 386.
140. L. Schra, R.J.H. Wanhill, Aluminium 59(1983): p 191.

141 J. McHardy, E.H. Hollingsworth, U.S. Navy Contract, Report NOW 65-0327f, 1966.
142. N.J.H. Holroyd, G.M. Scamans, ASTM-STP 821, p. 202.
143. H.F. de Jong, Brit. Corros. J. 15(1980): p. 118.
144 R.S Patharia, P. Tromans, Metall. Trans. 12A(1981). p. 607.
145. W. Gruhl, Z. Metallkunde 53(1962): p. 670.
146. M. Landkof, L. Gal-OR, Corrosion 36(1980): p. 241.
147 W.J. Helfrich, Stress Corrosion Testing, ASTM-STP 425 (Philadelphia, PA: ASTM, 1967), p. 21.
148. H.B. Romans, H.L. Craig, ASTM-STP 425, p. 363.
149 W.E. Wood, W.W. Gerberich, Metall. Trans. 5(1974). p. 1285.
150 W.W. Gerberich, W.W. Wood, Metall. Trans. 5(1974): p. 1295.
151. W.B. Hillig, R.J. Charles, General Electric Research Laboratory (Schenectady, NY), Report 64-RI 3756M, 1964.
152. R.S. Alwitt, J. Electrochem. Soc 121(1974): p. 1322.
153. F.P. Ford, Corrosion 35(1979): p. 281.
154 O.D. Sherby, J.L. Lytton, J.E. Dorn, Acta Metall. 5(1957). p. 219.
155 K Papp, E. Kovacs-Csetenyi, Scripta Metall. 11(1977). p. 921.
156. J. M. West, Electrodeposition and Corrosion Processes, 2nd ed. (London, England: D. Van Nostrand Co., 1970) p. 16.
157. T.G. Langdon, Phil. Mag. 22, 178(1970): p. 689.
158 H.B. Aaron, H.I. Aaronson, Acta Metall. 16(1968). p. 789.
159 F Gavofalo, Fundamentals of Creep, Creep Rupture in Metals (New York, NY: MacMillan, 1965), p. 74.
160 J Congleton, R.N Parkins, J. Inst. of Metals 97(1969). p. 134.
161. B. I. Brindley, P.J. Worthington, Acta Metall. 17(1969): p. 1357.
162 N.J.H. Holroyd, D. Hardie, Hydrogen Effects in Metals, p. 449.
163. K. Ebtehaj, D. Hardie, R.N. Parkins, Brit. Corros. J. 24(1989). p. 183.
164. R.A.H. Edwards, Predictive Capabilities in Environmentally Assisted Cracking (New York, NY: American Society of Chemical Engineers, 1985), p. 153.
165. J.A. Davis, Localized Corrosion, p. 168.
166. Y.C. Chu, S.M. Shu, S.Y. Pou, 8th International Congress on Metallic Corrosion, Vol. 1 (Federal Republic of Germany: Dechema, 1981), p. 499.
167. T. Ohnishi, Y. Nakatani, J. Japanese Inst. of Light Metals 27(1977): p. 224.
168. N.J.H. Holroyd, G.M. Scamans, R. Hermann, Corrosion Chemistry within Pits, Crevices and Cracks, ed. A. Turnbull (London, England: HMSO, 1987), p. 495.
169. M.S. Hunter, unpublished work at Alcoa Research Laboratories (1965).
170. A.J. Sedriks, J.A.S. Green, D.L. Novak, Corrosion 27(1971). p. 198.
171. A.J. Sedriks, J.A.S. Green, D.L. Novak, Localized Corrosion, p. 569.
172. O.V. Kurov, R.L. Melekhov, Zashch. Met. 15(1979): p. 314 (in Russian); English translation. Prot. Met. 15(1979). p. 244.
173. M. Marek, J.G. Rinker, R.F. Hickman, Proc. of 6th Int. Congress on Metallic Corrosion, held in Sydney (1975).
174. N.J.H. Holroyd, G.M. Scamans, R. Hermann, Embrittlement by the Localized Crack Environment, ed. R.P. Gangloff (Warrendale, PA. The Metallurgical Society-American Institute of Mining, Metallurgical, and Petroleum Engineers, 1984), p. 327.
175. J. Menys, M.R. Jarrett, N.J.H. Holroyd, work in progress (1989).
176. E.C. Pow, W.W. Gerberich, L.E. Toth, Scripta Metall. 15(1981). p. 55.
177. T. Langan, L. Christodoulou, D. Venables, J.A.S. Green, J.R. Pickens, Corrosion 44(1988): p. 165.
178. J.P. Lyle, W.S. Cebulah, Metals Eng. Quart. 14(1974). p. 52.
179 Z.X. Huang, Y D. He, Int. Congress on Metallic Corrosion, NRC, Toronto, 3(1984): p. 495.
180. R.T. Foley, T.H. Nguyen, J. Electrochem. Soc. 129(1982). p. 464.
181 N J H Holroyd, M.R. Jarrett, to be presented to Corros. Sci. (1990).
182. R.C. Turner, G.J. Ross, Canadian J. Chem. 48(1970): p. 723.
183. K. Sotoudeh, T.H. Nguyen, R.T. Foley, B.F. Brown, Corrosion 37(1981): p. 358.
184. R.P.M. Procter, H.W. Paxton, ASTM J. Mater. 4(1969). p. 729.
185. W. Gruhl, Metall. 19(1965): p. 206.
186. R.C. Alkire, D. Siitari, J. Electrochem. Soc. 129(1982). p. 488.
187. K. Herbert, R.C. Alkire, J. Electrochem. Soc. 130(1983). pp. 1001, 1007.
188. T. Magnin, P. Rieux, Scripta Metall. 21(1987). p. 907.
189. W.R. Wearmouth, G.P. Dean, R.N. Parkins, Corrosion 29 (1973): p. 251.
190. R.N. Parkins, Stress Corrosion Research, ed. H. Arupard, R.N. Parkins, NATO Advanced Study Series (The Netherlands. Sijthoff Noordhoff, 1979), p. 29.
191. W. Hepples (Ph.D. diss., University of Newcastle-upon-Tyne, 1988).
192. G.M. Ugianski, C.E. Johnson, D.S. Thompson, E.H. Gillespie, "Stress Corrosion Cracking. The Slow Strain Rate Technique, ASTM-STP 665 (Philadelphia, PA: ASTM, 1979), p. 254.
193. N.J.H. Holroyd, J.T. Evans, to be submitted to Scripta Metall. (1990).
194. N. Behnood, H. Cai, J.T. Evans, N.J.H. Holroyd, Mater. Sci. Eng. A 119(1989): p. 23.
195. R.N. Parkins, G.P. Marsh, J.T. Evans, Predictive Methods for Assessing Corrosion Damage to BWR Piping and PWR Steam Generators (Houston, TX: NACE, 1982), p. 249.
196. D.T. Powell, J.C. Scully, Corrosion 24(1968). p. 151, Corros. Sci. 10(1970): p. 719.
197. L. Ratke, W. Gruhl, Werkst. u. Korros. 31(1980). p. 768.
198. P. Martin, J.I. Dickson, J.P. Bailon, Mater. Sci. Eng. 69(1985). p. L9.
199. W. David, B. Stellwag, H. Kaesche, Aluminium 59(1983). p. E147.
200. R. Hermann, N.J.H. Holroyd, Mater. Sci. Tech. 2(1986): p. 1238.
201 Th. Skoulikidis, A. Karageorgos, G. Batis, Brit. Corros. J. 11(1976): p. 367.
202. Th. Skoulikidis, N. Kouloumbi, Brit. Corros. J. 14(1979): p. 216.
203. Th. Skoulikidis, G. Batis, N. Kouloumbi, Brit. Corros. J. 15(1980). p. 179.
204. Th. Skoulikidis, J.A. Colois, Aluminium 63(1987). p. 619.
205. J. Beinert, J.F. Kalthoff, Mechanics of Fracture, ed. G.C. Sih, The Hague, Vol. 7 (The Netherlands: Martinus Nijhoff, 1981' 281.
206. P. Manogg, Proceedings of the International Conference on Physics of Non-Crystalline Solids (Holland. North-Holland, 1965), p. 481.
207. P.S. Theocaris, J. Mech. Phys. Solids 20(1972). p. 265.
208. R. Hermann, N.J.H. Holroyd, Mater. Sci. Tech. 2(1986): p. 1238.
209. R. Hermann, Mater. Sci. Eng. A. 102(1988). p. 39.
210. M.S. Domack, Proceedings of the International Conference on Fatigue, Corrosion Cracking, Fracture Mechanics and Failure Analysis, ed. V.S. Goel (Metals Park, OH. ASM International, 1986), p. 191.
211. H.E. Hanninen, Private Communication (1988).
212. P.T. Gilbert, S.E. Haydon, J. Inst. Metals 77(1950). p. 237.
213. H.K. Farmery, U.R. Evans, J. Inst. Metals 84(1955-56). p. 413.
214. D. van Rooyen, Corrosion 16(1960). p. 421.
215. P. Brenner, W. Gruhl, Z. Metallkde 52(1961): p. 599.
216. D. Brungs, W. Gruhl, Metall. 24(1970). p. 217.
217. S.P. Lynch, Acta Metall. 36(1988): p. 2639.
218. R. Hermann, Corrosion 44(1988). p. 685.
219. M. Guttmann, B. Quantin, Ph. Dumoulin, Metal Sci. 17(1983). p. 123.
220. S.P. Lynch, Mater. Sci. Eng. A108(1989). p. 203.
221. J.J. Lewandowski, Y.S. Kim, N.J.H. Holroyd, work in progress at Case Western Reserve University, Cleveland, OH, 1989.
222. J.J. Lewandowski, Y.S. Kim, N.J.H. Holroyd, submitted to Metall. Trans. 1990.

223. W. Gruhl, Metall. 17(1963): p. 197; Z. Metallkde 54(1963): p. 86.
224. G.M. Scamans, R. Alani, P.R. Swann, Corros. Sci. 16(1976): p. 443.
225. A.W. Thompson, Environment-Sensitive Fracture of Engineering Materials, ed. Z.A. Foroulis (New York, NY: AIME, 1979), p. 379.
226 J.A.S. Green, H.W. Hayden, W.G. Montague, Effect of Hydrogen on Behavior of Materials, ed. I.M. Bernstein, A.W. Thompson (New York, NY: AIME, 1975), p. 200.
227 R.E Swanson, A.W. Thomspon, I.M. Bernstein, R.L. Maloney, Hydrogen Effects in Metals, ed. I.M. Bernstein, A.W. Thompson (New York, NY: AIME, 1981), p. 495
228 M O. Speidel, Stress Corrosion Research, ed. H. Arup, R.N. Parkins, NATO Advanced Studies Series (The Netherlands. Sijthoff and Noordhoff, 1979), p. 117.
229. M. Gao, P.S. Pao, R.P. Wei, Metall. Trans. 19A(1988): p. 1739.
230. D.N. Williams, Welding J. August(1983): p. 25.
231 L Chambers, D. Baxter, Engineer 223(1967). p. 518.
232 M C Reboul, B. Dubost, M. Lashermes, Corros. Sci. 25(1985). p. 999.
233 S.S Birley, Environmental Degradation of Engineering Materials III, p. 281.
234 N J H Holroyd, W Hepples, G.M. Scamans, Environmental Degradation of Engineering Materials III, p. 293.
235 H Cordier, I J Polmear, M. Schippers, Z. Metallkde 68(1977). p. 280.
236 N J H Holroyd, W Hepples, G M. Scamans, Corrosion Cracking, ed V S Goel (Metals Park, OH. ASM International, 1986), p. 291.
237 Y Kim, S Pyum, Aluminium 59(1983). p. 123, Brit. Corros. J. 18(1983): p. 71.
238 I Taylor, Metals Progress 84(1963): p. 74.
239 J Busby, J F Cleave, R.L. Cudd, J. Inst. Metals 99(1971). p. 41.
240 J M Truscott, V E Carter, H.S. Cambell, J. Inst. Metals 99(1971): p. 57.
241 J M Truscott, D S. Calvert, J. Inst. Metals 95(1967). p. 289.
242 P O Anderson, E. Lindstand, International Inst. Welding, Doc. IX-597-68 (1968).
243 R. Sunberg, J. Inst. Metals 95(1967). p. 95 (Discussion).
244. M. Pirner, H. Bischel, Metall. 29(1975). p. 275.
245. M. Pirner, Aluminium 53(1977). p. 674.
246. J.M. Truscott, J. Inst. Metals 95(1967): p. 94 (Discussion).
247 M.A. Reynolds, N.J.H. Holroyd, unpublished results (1984).
248. E. Di Russo, S. Abis, Z. Metallkde 78(1987). p. 157.
249. P.W. Jeffrey, unpublished work (1981).
250. N.J.H. Holroyd, G.M. Scamans, European Patent Application EP 0 282 174 A1 (1988).
251. P. Wylie, The Engineer 12, Sept.(1985): p. 24.
252. M.B. Shumaker, R.A. Kelsey, D.O. Sprowls, J.G. Williamson, ASTM-STP 425, p. 317.
253. R. Grauer, E. Wiedmer, Werkst. und Korros. 31(1980): p. 45.
254. C.D.S. Tuck, Corros. Sci. 23(1983): p. 379.
255. N. Kaekley, M. Levy, Computer Aided Acquisition and Analysis of Corrosion Data (Pennington, NJ: The Electrochemical Society, Inc., 1985), p. 237.
256. H. Schmiedel, W. Gruhl, Metall. 38(1984): p. 32.
257. M.S. Rahman, I.J. Polmear, Z. Metallkde 74(1983): p. 733.
258. N.J.H. Holroyd, W. Hepples, G.M. Scamans, European Patent Application, EP 0 261 969 A1 (1987).
259. L. Christodoulou, J.R. Gordon, J.R. Pickens, Metall. Trans. 16A(1985): p. 995.
260. J.R. Pickens, L. Christodoulou, Metall. Trans. 18A(1987): p. 135.
261. J.G. Craig, R.C Newman, M.R. Jarrett, N.J.H. Holroyd, J. De Physique, Colloque C3, Supplement 9, 9(1987): p. 825.
262. E. Smith, Res. Mechanica 9(1983): p. 237.
263 D O Sprowls, NASA Contract Report 172387, Phase 1 (1984).
264. J. Blain, J. Masounave, J.I. Dickson, Corros. Sci. 24(1984): p. 1.

Discussion

S.M. Bruemmer (Pacific Northwest Laboratories, USA): You discussed several methods to minimize weld heat-affected zone (HAZ) SCC but did not discuss optimization of welding technique itself In other SCC-susceptible materials (e.g., stainless steels) control of pass-by-pass welding parameters can produce SCC-resistant microstructures and controlled grain-boundary chemistries, in particular This has resulted from our ability to predict "quantitatively" temperatures and strains through the HAZ region and to predict microstructure and microchemistry development. Has research been performed in this area for these high-strength aluminum alloys? Could you comment on the ability to use such an approach for these alloys?

N.J.H. Holroyd: To my knowledge, the approach you outline for the welding of stainless steels has not been successfully applied to aluminum alloys, other than it being known that minimizing specific heat input during welding is beneficial [Kim and Pyun, Aluminum 59(1983). p. 123 and Brit. Corr. J. 18(1983). p. 71]. For weldable aluminum alloy systems other than the 7XXX series, weld beads generally provide sacrificial electrochemical protection to the potentially SCC-susceptible HAZs and thereby minimize service problems resulting from environment-sensitive fracture [Holroyd, et al., in Environmental Degradation of Engineering Materials III (Pennsylvania State University, 1987), p. 329]. For 7XXX series alloy welds the reverse is generally true, i.e., the weld bead is cathodic, and over the years various routes have been adopted attempting to prevent weld-toe cracking. These are reviewed elsewhere (Holroyd, et al., and Birley, ibid., p. 281) and include the following: (1) elemental additions to the parent alloy or welding wire, e.g., copper or silver; (2) various mechanical surface treatments or thermal/vibratory techniques to reduce residual stresses; (3) weld joint design using finite-element analysis, and (4) metallic coatings. It has been claimed that complete protection against weld-toe cracking is only provided when local electrochemical potentials are maintained within a "safe window," and the environmental conditions provide the alloy electrochemical stability, e.g., a pH in the range 4 to 9. Complete protection has been achieved on small-scale weldments in the laboratory, and scale-up and commercialization is now in progress [Holroyd, et al., European Patent Applications No. EP 0 261 969 A1 (1987) and No. EP 0 282 174 A1 (1987)].

Returning to your comment about the development of resistant microstructures in weldments, a unique advantage for the 7XXX series welds is that, unlike other alloys, the weld HAZ regains most of its strength via room-temperature age hardening [Kent, Metall. Reviews 147, 15(1970): p. 135]. This, coupled with the parent alloy's higher strength, potentially offers desirable mechanical properties. Unfortunately, the age hardening promotes SCC susceptible microstructures that are not readily removed by thermal treatment without either sacrificing strength or promoting SCC elsewhere in the structure. For example, post-weld heat treatments that successfully prevent exfoliation corrosion in HAZs generally exacerbate weld-toe cracking (Birley, as above).

E.I. Meletis (Louisiana State University, USA): Our experimental results show that aluminum-lithium-copper longitudinal specimens, pre-exposed in sodium chloride solution and then tested in air, fail under a transgranular mode. However, severe intergranular cracking also occurs. Since the effect is reversible, the only explanation is that hydrogen can cause transgranular cracking. This is in disagreement with your statement that anodic dissolution is necessary for intergranular cracking.

N.J.H. Holroyd: Similar experiments and results to those you describe were reported for 7XXX series alloys some years ago [Hardie, et al., Metal Sci. 13(1979): p. 603]. Transgranular, pre-exposure embrittlement is favored in commercial plate alloys when strained to failure in the longitudinal direction, although intergranular cracking also occurs. Further study showed that these alloys, after

pre-exposure to aqueous environments, did not suffer intergranular embrittlement when tested in vacuum or dry air, but did in laboratory air or aqueous environments when the test strain rates were sufficiently low [Holroyd and Hardie, Corros. Sci. 21(1981): p. 129]. These results imply that intergranular embrittlement requires anodic dissolution and/or hydrogen uptake during straining.

In my opinion, it is not yet established whether the SCC of aluminum-lithium alloys differs from 7XXX series alloys. The experiments you describe were conducted in laboratory air and so hydrogen pick-up during testing was not prevented. A further complication arises for aluminum-lithium-copper alloys, because the normal mode of nonenvironment-sensitive fracture is ductile intergranular failure [Suresh and Vasudevan, Aluminium 63(1987): p. 1020], which is difficult to distinguish from intergranular embrittlement because of the reactivity of fracture faces with laboratory air.

W.W. Gerberich (University of Minnesota, USA): The backface hydrogen entry experiment with the notch that Ratke and Gruhl [Werkst und Korros. 31(1980). p. 768] made is very convincing for hydrogen embrittlement (HE), but the amount of hydrogen that can be there in equilibrium with the mild stress effect of the notch is small. This implies that either slip-induced large stresses and/or binding to trap sites, such as precipitates, is required. Do you have a feeling for whether one or both of these is essential to produce HE?

N.J.H. Holroyd: It is presently impossible to answer your question unequivocally. It is known that atomic hydrogen enters unstressed aluminum alloys exposed to aqueous environments without the need for electrochemical stimulation [Scamans, et al., Corros. Sci. 27(1987). p. 329], and for some time this observation caused the authors to doubt the relevance of Mode I/III loading experiments for aluminum alloys. The work of Ratke and Gruhl provides strong evidence for HE occurring during the SCC of 7XXX alloys in aqueous environments and implies a role for triaxial stresses, thereby validating the Mode I/III approach adopted by several workers in attempts to determine whether SCC involved HE [Green, et al., Effect of Hydrogen on Behavior of Materials (New York, NY: AIME, 1975), p. 200; Swanson, et al., Hydrogen Effects in Metals (New York, NY. AIME, 1980), p. 459]. SCC, HE, and pre-exposure embrittlement of 7XXX series alloys all require the presence of grain-boundary age-hardening precipitation [Holroyd and Scamans, Scripta Metall. 19(1985). p. 915] and loading at sufficiently low strain rates [Holroyd and Hardie, Corros. Sci. 21(1981). p 129] Thus, grain boundary precipitation almost certainly has a role during intergranular environment-sensitive fracture. How the presence of hydrogen affects this is unclear. Several workers have observed during transmission electron microscopy studies that grain boundary precipitates above a critical size (250 to 300 nm) tend to act as hydrogen recombination sites and generate hydrogen gas bubbles [Scamans, J. Mater. Sci. 13(1978). p. 27, Christodoulou and Flower, Acta Metall. 29(1980). p. 481, Rajan, et al., J. Mater. Sci. 17(1982). p. 2817, note misprint acknowledged in Metall. Trans. 16A(1985). p. 2086] whereas smaller precipitates are thought to act as trap sites. The time dependency for environment-sensitive fracture, implied by the required slow-strain rates, has been interpreted as hydrogen having to move from a trap site to a site to do damage [Holroyd and Hardie, Hydrogen and Materials III (Pergamon Press, 1982) p 659] A possible role for hydrogen is that it somehow influences strain accommodation. Recent work on Al-Mg-Si alloys has shown that the strain accommodation mode is strain rate sensitive [Lewandowski, et al., Mater. Sci. and Eng. 96(1987): p. 185]. For small plastic strains, up to 2%, strain accommodation is via transgranular slip when strain rates are high but involves grain-boundary sliding/creep if strain rates are sufficiently low. In this work, solid lead was found to increase the maximum strain rate for intergranular strain accommodation. Could hydrogen have the same effect for 7XXX series alloys? If so, it would explain many experimental observations, e.g., maximum strain rate for pre-exposure embrittlement increases with pre-exposure time and/or availability of a hydrogen supply during testing. Further work is needed to clarify if the above could lead to slip-induced high stresses.

B. Cox (Atomic Energy of Canada Ltd., Canada): In the three-dimensional micrographs you showed, which were used to support your claim of a HE mechanism, there were undoubtedly many precipitates on the fracture face. However, there did not seem to be an equivalent number of holes. If the precipitates were there as the crack front passed, then (on the average) there should be equal numbers of precipitates and holes on each face. Since there appear to be very few holes, other origins for the visible features could be precipitation from solution after crack passage or extensive dissolution (greater than twice the mean precipitate size) during crack formation. Either route to the observed microscopy would seem to support a dissolution, rather than a HE mechanism.

N.J.H. Holroyd: Grain-boundary precipitates grow in coherent registry with one grain surface and have an incoherent interface with the opposing grain surface. On fracture, the fracture path tends to be along the incoherent interface, and hence an intergranular surface can show either a complete set of precipitates or a complete set of precipitate holes Equal numbers of precipitates and holes on one grain surface are, in fact, quite rare. This illustrates the need to examine both fracture surfaces at high resolution. This technique also demonstrates that the observed features are not formed by precipitation from solution, since the holes and the grain-boundary precipitates are fully matching. This would not be the case for particles deposited from solution. Fracture matched surfaces have been published by Scamans [Metall. Trans. 11A (1980): p. 846 and Aluminium 58(1982): p. 332].

E.N. Pugh (National Institute of Standards and Technology, USA): You concluded in your talk that intergranular SCC in 7XXX series alloys propagates by HE. I recognize that hydrogen absorption can lead to intergranular cracking, but it is not clear that HE, rather than the film-rupture (anodic dissolution) mechanism, is responsible. Could you summarize the main reasons for your conclusions? If the observation of crack-arrest markings on the intergranular fracture surfaces is considered important, I should add that it is generally not possible to detect such markings on intergranular SCC surfaces—indeed, their occurrence may be a special case.

N.J H. Holroyd: This question has been specifically addressed in the written paper, with a more detailed argument. Briefly, our conclusion is that the SCC of Al-Zn-Mg and Al-Zn-Mg-Cu (7XXX series) alloys occurs via a HE mechanism with sufficient anodic dissolution occurring during SCC to guarantee the required hydrogen generation Thus, crack propagation is principally via HE, and in the absence of anodic dissolution, intergranular SCC will be negligible. Evidence for subsurface SCC initiation, provided by Ratke and Gruhl [Werkst u Korros. 31(1980). p. 768] via notched, hollow tube experiments, taken together with the indirect evidence from acoustic emission, electrochemical noise, and load drops measured during cracking, provides strong evidence that SCC involves sudden bursts of crack growth followed by periods of crack arrest. This in my opinion demonstrates that, generally, a film-rupture mechanism is not operative during the intergranular SCC of 7XXX series alloys in aqueous saline environments. The situation is less clear for transgranular SCC.

The point you make concerning the fact that crack-arrest markings are not generally detected on intergranular SCC surfaces is accepted These markings are often difficult to identify and are easily obscured or destroyed by post-fracture corrosion.

H. Kaesche (Friedrich Alexander University of Erlangen-Nurnburg, Federal Republic of Germany): It seems that the essential mechanism of intergranular SCC of age-hardened aluminum-zinc-magnesium alloys, i.e., discontinuous crack propagation due to HE, is by now well established. An important point then is that the micropitting type of localized corrosion, apparently producing hydrogen at the crack tip, does occur at a value of electrode potential far below the potential for onset of either pitting or intergranular corrosion. The effect therefore appears to be one of crack triggering by stress- or strain-induced local crack-tip corrosion events. This also answers Pugh's question concerning the alternative possibility of crack propagation by continuous anodic metal dissolution, at least for

the particular case of aluminum-zinc-magnesium alloys, intergranular SCC, and chloride-containing aggressive environment

N.J.H. Holroyd: The proposal for micropitting occurring at potentials below the pitting potential is validated by your own work and that of others. [See Kaesche, Werkst. und Korros. 39(1988). p. 152, Baumgartner and Kaesche, ibid., p. 129, Foley, Corrosion 42(1986). p. 277.] The process of crack triggering is not well understood. Hydrogen entry into grain boundaries occurs without the need for stress-/strain-induced events. However, intergranular embrittlement for 7XXX series alloys precharged with hydrogen becomes difficult to initiate if anodic dissolution is prevented during straining and transgranular cracking generally occurs [Holroyd and Hardie, Corros. Sci. 21(1981): p. 129].

E.N. Pugh: I accept that anodic dissolution may be ruled out in the specific case Kaesche has described and that cracking corresponds to HE, but I am not sure that this is true in general for intergranular SCC of 7XXX series alloys in aqueous solutions.

N.J.H. Holroyd: SCC of 7XXX series alloys in aqueous environments can occur under electrochemical conditions where HE is improbable (Holroyd and Hardie, Corros. Sci. 21(1981): p. 129]. However, available experimental evidence strongly suggests that SCC at potentials close to the free-corrosion potential occurs via a HE mechanism requiring hydrogen generation and hence anodic dissolution during SCC propagation.

R.E. Ricker (National Institute of Standards and Technology, USA): In an aqueous environment, hydrogen evolution and metal dissolution will occur simultaneously at the tip of a propagating stress corrosion crack, regardless of the external environment, potential, etc As a result, you cannot use potentiostatic tests to discriminate between mechanisms, and that is why we [Ricker and Duquette, Metall Trans 19A(1988). p. 1775] elected to use water vapor as a hydrogen source in our corrosion fatigue and precharging experiments However, the debate over whether anodic dissolution, HE, or both are involved neglects the fact that both processes have a common step that can be rate limiting, and that is passive film breakdown As a result, it seems to me that the best way to improve the environmentally induced fracture resistance of these alloys is to improve the resistance of the passive films to breakdown at occluded sites and at the crack tip What, if anything, can be done to achieve this?

N.J.H. Holroyd: The inherent corrosion resistance of aluminum and its alloys relies upon the stability of a protective surface film. Upon immersion into aqueous saline environments, air-formed and anodized oxide films chemically react, with aluminum ions going into solution and chloride ions being adsorbed [see Nguyan and Foley, J. Electrochem. Soc 127(1980). p. 2563, Foley, Corrosion 42(1986). p. 277] Local geometric features, e.g., film defects or weak spots, can allow the local development of acidic solutions and provide potential initiation sites for localized corrosion. Hydrogen entry into 7XXX series alloys has been recorded even when corrosion rates are negligible, e.g., chromate inhibited saline environments [Scamans, et al , Corros. Sci. 27(1987). p. 326], and facilitates HE when an alloy temper is susceptible and loading conditions are appropriate.

To date no obvious approach has been identified offering self-repairing film generation that prevents hydrogen entry. Hence, the most effective route to minimize environment-sensitive fracture is to generate alloy microstructures that tolerate the presence of hydrogen, while providing maximum mechanical strength, ductility, and toughness in addition to good resistance to all forms of corrosion.

R.L. Jones (Pacific Northwest Laboratory, USA): A comment in response to Ricker's statement that crack growth occurs in aluminum alloys at conditions when anodic dissolution and hydrogen generation occur, and therefore a detailed understanding of the exact mechanism does not matter. I disagree. If we are striving to improve the performance of alloys in corrosive environments it is necessary to know the specific mechanism associated with the crack advance process. Even though anodic dissolution and hydrogen reduction are involved in the crack growth process, it may be necessary to add hydrogen traps or alter the sites at which hydrogen is collecting and causing crack propagation. Reductions in the crack growth rate can also be accomplished by reducing the corrosion rate and hence the hydrogen reduction rate, but there may be restrictions in the potential to reduce corrosion rates. Improving a material's tolerance for hydrogen can serve as a back-up to the reduced corrosion rate approach in the event that local corrosion causes a breakdown in the protective film.

R.P. Gangloff (University of Virginia, USA): I have four questions relating to SCC in aluminum alloys. (1) Are your results on copper segregation and retrogression aging sufficient to exclude the effects of planar slip on SCC in the 7000 series alloys? (2) What is the consensus mechanism(s) for the enhanced environmental cracking of 7XXX alloys, compared to the 2XXX series alloys? (3) What is the accepted mechanism for the beneficial effect of cathodic potential on stress corrosion and transgranular corrosion fatigue cracking in aluminum alloys? and (4) on a more modern note, do you have any results that indicate grain-boundary segregation effects in aluminum-lithium alloys?

N.J.H. Holroyd: Your first three questions are addressed in detail in the written paper, and I will not discuss them further here. On your last point, experimental work is now in progress to determine whether grain-boundary segregation effects are important in the environment-sensitive fracture of aluminum-lithium alloys [Gray, et al., Proceedings, Aluminum-Lithium V (Charlottesville, VA. University of Virginia, 1989, in press). Indirect evidence is consistent with copper segregation being important. For example, SCC initiation is difficult in alloys not containing copper, but generally occurs more readily as the copper content increases [Holroyd, et al., in Aluminum-Lithium III (London, England. The Institute of Metals, 1985), p. 310]. Surface analysis of intergranular fracture of Al-Li-Mg-Cu alloys produced by mechanical overload promoting grain-boundary microvoid coalescence has failed to reveal copper segregation [Wert and Lumsden, Scripta Metall. 19(1985). p. 205, Miller, et al., Mater. Sci. and Techn. 2(1986). p. 1210, Lewandowski and Holroyd, Mater. Sci. Eng., in press], so if segregation occurs, it is on and close to the grain boundary, i.e., within nanometers, as found for the 7XXX series alloys and described in our poster paper here (Hepples, et al., "The Influence of Microstructure on the Stress Corrosion Cracking and Exfoliation of Commercial Al-Zn-Mg-Cu Alloys," this proceedings).

J.-P. Lynn (Westinghouse Electric Corporation, USA): I would appreciate having more detail on your technique for measuring crack-tip chemistry. How close is the probe tip to the crack tip? If HE is reversible, what is the role of precipitates (S, Zn) on cracking?

N.J.H. Holroyd. Experimental details for the techniques used to characterize crack tip chemistry are published elsewhere [Holroyd, et al., Embrittlement by the Localized Crack Environment, ed. R.P. Gangloff (Warrendale, PA. TMS-AIME, 1984), p. 327, and Corrosion Chemistry within Pits, Crevices and Cracks (London, England. HMSO, 1987), p. 495]. During work on real, as opposed to simulated cracks, environment extraction techniques were used, and hence the issue of probe tip to crack tip does not directly arise. In the initial studies, we removed 5 or 10 μL solution samples from the crack-tip region, so even if all of the solution were removed from the crack tip, it would be diluted by solution associated with the initial few millimeters of the crack walls. Hence, solution chemistry characterization is that of the "crack tip region" rather than the "crack tip" itself Current work is aimed at addressing this by using a room temperature freezing technique using tailored gels containing pH and ion-specific indicators, which should provide good spatial resolution (Menys, et al., submitted to Corros. Sci.).

The doubt you express on the subject of reversibility of the HE in 7XXX series alloys should be balanced against the considerable weight of positive experimental evidence. Several roles have been envisaged for precipitates during SCC, these are discussed in the written paper for three types of precipitate. $MgZn_2$ hardening precipitates, Mn, Cr, or Zr dispersoids, and Fe-rich inclusions.

The Environment-Induced Cracking of Hexagonal Materials: Magnesium, Titanium, and Zirconium

*D. Hardie**

Abstract

An attempt has been made to present an overall picture of the environment-sensitive fracture of materials having a hexagonal crystal structure: particularly magnesium, titanium, zirconium, and their alloys. This does not include an exhaustive examination of the many specific environments that may induce such fracture in these metals, but rather presents a global view of the processes involved using particular examples of many systems to illustrate the points being made.

The three metals mentioned all adopt highly cathodic potentials when bare metal is exposed to aqueous environments; hence the influence of hydrogen uptake on their mechanical behavior becomes of great importance. The relevance of hydrogen embrittlement (HE) and hydrogen-induced cracking to failure mechanisms is therefore discussed.

Environment-sensitive fracture is very much influenced by the passive film that may develop on the metal surface under many environmental conditions, and the chemical and mechanical breakdown of such films is given appropriate consideration.

Since HE mechanisms do not offer a universal explanation of the failures observed, the competition between this and anodic dissolution is investigated.

The properties of the alloys based on these metals may be adjusted by suitable heat treatment, and the influence of the resultant microstructures on reaction to particular environments and their promotion of failure is of great importance. In this context, the occurrence of characteristic fractography may provide useful information.

Introduction

Only three of the metals having a hexagonal crystal structure appear to have been involved in industrial failures or have been the subject of a significant amount of laboratory investigation with respect to environment-induced failure: magnesium, titanium, and zirconium. The last two of these are exothermic occluders of hydrogen and form very stable hydrides, whereas magnesium hydride (MgH_2) will decompose rapidly at temperatures above 280°C,[1] unless high hydrogen pressures are sustained, and these make a considerable contribution to the major failure processes in these materials. The environments most involved in studies on these metals and their alloys reflect the particular applications for each.

Zirconium has a low neutron-capture cross section for thermal neutrons and hence has wide applications in the nuclear industry, mainly as alloys used for fuel sheathing and pressure tubes. As a result, most concern relates to its performance in high-temperature water, possibly with additions of halide that are relevant to contamination by fission products. But Cox found that zirconium alloys were susceptible to environment-sensitive fracture in most of the environments that produced failure in titanium alloys.[2] The restricted use of the magnesium appears to be attributable to undue concern about its inflammability, but it is generally believed[3] that only the aluminum-containing alloys show any appreciable tendency to stress corrosion cracking (SCC), with the susceptibility increasing with aluminum content up to 6%. Environment-induced cracking in such alloys has been widely reported since it was first observed by Althoff[4] in 1938. By far, the most extensively used hexagonal material is titanium, and many applications, particularly in the chemical industry, exploit its low density and excellent corrosion resistance. This is retained in a wide variety of potentially aggressive environments, largely because of the strongly adherent film of stable oxide that provides a protective layer on its surface. The metal and its alloys remain protected under most oxidizing, neutral, or inhibited neutral conditions, but, while they remain passive under mildly reducing conditions, they may be attacked by strongly reducing or complexing media. Although SCC of a titanium alloy in aqueous sodium chloride was first reported in 1966,[5] the first incidence of SCC in commercial purity (cp) titanium occurred in 1953 in red, fuming nitric acid.[6] The report of the latter included an extensive list of environments that did not induce such cracking.

If the surface film on passivated metals is removed or damaged in any way, then the underlying metal so exposed is extremely active. The standard potential of a bare magnesium metal surface is −2.69 V_{SCE} in acid and −2.93 V_{SCE} in an alkaline environment,[7] even though the steady-state potential in the presence of a passive film is usually about 1 V more positive.[8] Although not nearly so cathodic, the potential of titanium in the absence of an oxide film is still in the region −1.0 to −1.5 V_{SCE}.[9] Such potentials are well below the necessary potentials for hydrogen evolution on these metals in aqueous environments, and this inevitably introduces the likelihood of considerable hydrogen uptake under appropriate conditions. As a consequence, any consideration of environment-induced fracture in these metals invariably involves considerable discussion of hydrogen embrittlement (HE) effects, and most proposed failure mechanisms take account of the possible involvement of hydrogen at some stage.

Since hydrides may play a significant role in many fracture mechanisms, both the overall solubility of hydrogen and the terminal solubility in the hexagonal α-phase are very important. The overall

*Department of Metallurgy and Engineering Materials, University of Newcastle upon Tyne, NE1 7RU England.

solubility of hydrogen in solid magnesium is never very high, rising to a maximum of about 20 wppm at 640°C.[10] This is in marked contrast to that in both zirconium and titanium, in which the capacity for absorbing hydrogen is such that the amount taken up in the metal before precipitation of a hydride phase is considerably in excess of the total solubility in magnesium (Figure 1). Such a variation plays an important part in comparisons of the HE of these materials, and it is worth noting that extrapolation of high-temperature data indicates a terminal solubility of hydride in titanium[11] at 300°K of about 20 wppm, whereas that in zirconium[12] is less than 0.05 wppm.

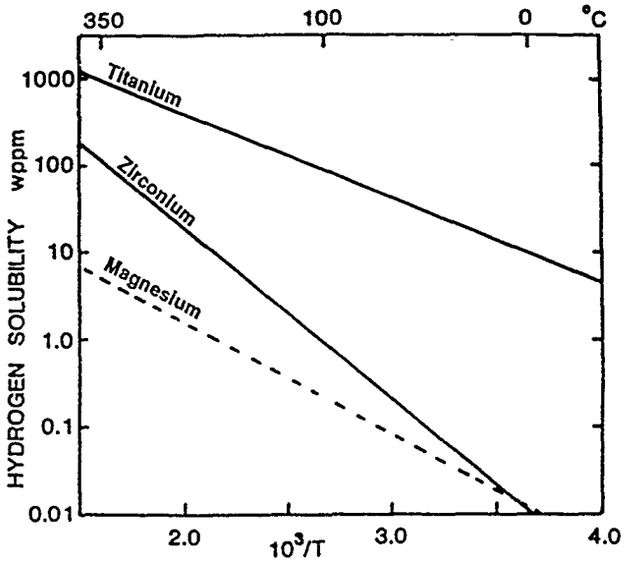


FIGURE 1—A comparison of the overall solubility of hydrogen in magnesium[10] with the terminal solubility of hydride in titanium[11] and zirconium.[12]

Hydride Cracking

Although normal tensile ductility is only significantly affected at relative high hydrogen concentrations, when large quantities of brittle precipitate are present, both titanium[13] and zirconium[14] are very susceptible to embrittlement by relatively small amounts of precipitated hydride at high strain rates or in the presence of triaxial stressing. With the latter, high strain rates are not essential but do increase the effect.[15] Since the solubility of zirconium and titanium hydrides is less than 20 wppm at ambient temperature (Figure 1), hydride precipitate is likely to be present in both in the as-received condition. Much more contamination would, however, be required to induce precipitation in titanium than in zirconium at temperatures above about 100°C.

The observation that the degree of embrittlement decreases rapidly with increasing temperature provoked various theories regarding the contributory factors. An early belief[16] that the decrease in the quantity of hydride in zirconium arising from the increasing hydride solubility at higher temperatures was responsible for the ductility transition was dispelled by solubility determinations.[17] The importance of twinning as a deformation mechanism in these hexagonal materials, particularly at lower temperatures and higher strain rates, together with the observation that twinning led to fracture of hydrides,[18] focused attention upon this as a cause of the transition, but such a position was later shown to be untenable.[19,20]

In fact, the two critical events in the fracture of hydride-containing materials are the initiation of cracking in the brittle precipitates and the propagation of these microcracks through an essentially ductile matrix from one hydride to the next. The first stage is strain dependent,[21] whereas the second appears to be stress dependent.[22] A study of seven samples of zirconium and Zircaloy†-2 in various conditions revealed that the temperature for transition from ductile to brittle behavior in notch-bend specimens hydrided to various levels up to 1000 wppm depended upon both the hydrogen content and the flow stress of the matrix. Although the variation of flow stress with temperature was very different for the different materials, the transition temperature for a particular hydrogen content invariably corresponded to the attainment of a specific value of the 0.7% flow stress in the material concerned. This immediately suggests that whether or not an unstable crack may readily propagate through the matrix from one brittle hydride to the next is determined by how much energy has been stored in the material by deformation before the hydride cracks (at something approaching 1% plastic strain) and thus releases the energy for crack propagation. The amount of energy required does, of course, also depend upon the distance to be traveled from one hydride to the next, and this explains the dependence of embrittlement upon the interhydride spacing.[15] In general, the occurrence of intergranular hydride introduces a dependence upon grain size as well as hydrogen concentration.

As the hydrogen concentration increases, so does the hydride concentration, up to a point, and the embrittlement becomes worse as a direct consequence of the decreasing interhydride spacing. The variation in the critical applied stress with hydrogen concentration for unstable fracture of a particular type of specimen (Table 1 shows results extracted from earlier work[22]) may be examined in terms of a simple energy model by equating the amount of energy stored up to the point of fracture with the amount of energy of the fracture surface produced. The elastic strain energy stored (S) in unit volume of material after deformation by a simple tensile stress is given by

$$S = \int_0^{\epsilon} \sigma \times d\epsilon = \frac{\sigma^2}{2E} \qquad (1)$$

where ϵ is the strain and E is Young's modulus of elasticity, although Griffith[23] has demonstrated that the presence of a crack of length (c) increases the strain energy of a sheet of unit thickness by an amount $\pi\sigma^2c^2/E$.

Assuming that a moving crack can draw energy from the volume surrounding the initiating hydride, the total energy available (S_T) will be related to the hydride spacing (r):

$$S_T = \frac{\sigma_2}{2E} \times Ar^3 \qquad (2)$$

where A is simply a geometric constant. The energy of fracture (F) will be related to the specific surface energy and the area of new surface created, which will depend upon the distance traveled from one fractured hydride to the next:

$$F = 2\gamma\, Br^2 \qquad (3)$$

where B is again a geometric constant.

The critical level of stress necessary to store sufficient energy to propagate an unstable crack when it is released (σ_c) can then be ascertained by equating Equations (2) and (3).

$$\frac{\sigma_c^2}{2E} \times Ar^3 = 2\gamma Br^2 \qquad (4)$$

when

$$\sigma_c^2 r^2 = \frac{4\gamma EBr}{A} \qquad (5)$$

where $B/A \approx 1$.

†Trade name.

TABLE 1

The Critical Stresses for Unstable Fracture in Slow-Bend Specimens[22,(A)]

Hydrogen Content wppm	Hydrides in Section /mm²	Average Hydride Spacing (r) 10^{-3}m	Critical Stress (σ_c) at Hydride Fracture MN/m²	Measure of Stored Energy $10^{-8}\sigma_c^2 r^2$
50	37	0.164	380	38.84
50	40	0.158	380	36.06
100	52	0.139	360	25.03
150	76	0.115	345	15.74
200	89	0.106	330	12.23
250	76	0.115	313	12.96
350	101	0.100	290	8.41
400	90	0.105	280	8.64
600	97	0.102	280	8.16
800	92	0.104	280	8.48
1000	90	0.105	280	8 64

(A)Related to the average distance between hydrides for various hydrogen concentrations in Zircaloy 2.

A simple plot of $\sigma_c^2 r^2$ against r should therefore produce a straight line of approximate slope 4γE For the results obtained from slow-bend specimens of Zircaloy[22] (Figure 2), there appears to be amazing agreement with such a simple relationship, and the slope obtained is 4.74×10^{13} N²/m³ For a Young's modulus of about 10^{11} N/m² (actually around $9\,5 \times 10^{10}$ N/m²), this would indicate a mean surface energy of 474 J/m² The testing of Charpy specimens of zirconium instrumented to provide a direct measure of the energy of fracture[24] gave fracture energies of about 50 ft-lb (about 68 J) in the ductile materials at room temperature, and this corresponds to a specific surface energy of 0.43 MJ/m². This implies, therefore, a significant lowering of the fracture energy of the matrix by hydrogen in solution It is interesting to note that when Beevers[25] applied a Griffith's criterion to the extension of hydride cracks in a ductile zirconium matrix, he obtained an effective surface energy of 200 J/m².

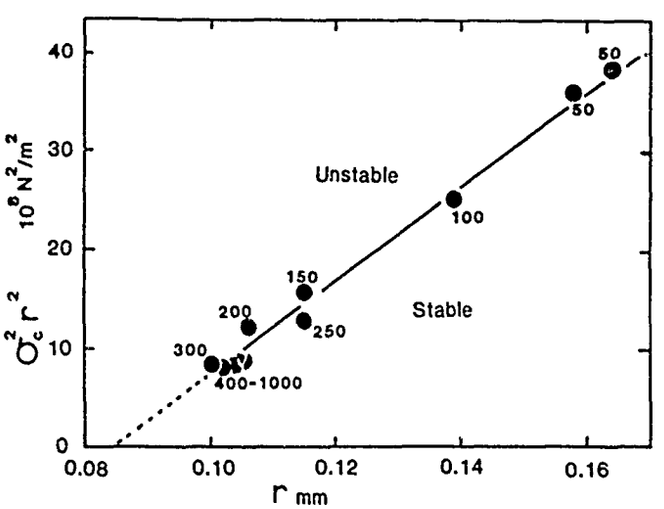


FIGURE 2—Plot of $\sigma_c^2 r^2$ indicating the critical stored energy required when hydrides crack for unstable fracture to occur in various hydrided bend specimens of Zircaloy-2. Hydrogen contents in wppm are noted against the points.

If the relationship of Equation (5) were still applicable for much closer hydride spacings, the plot should ultimately pass through the origin, which it obviously does not. However, it must be remembered that the model is greatly oversimplified and takes no account of the finite size of the hydrides themselves The latter varies considerably with grain size, even with slow cooling, and the prevalent length, which is always greater than the thickness, is about double the grain size.[26]

Similar mechanisms to those developed for the various hydride effects in zirconium might be expected to apply to hydride embrittlement of titanium, but the significant difference is that considerably higher hydrogen concentrations would generally be required in this material to produce similar hydride distributions to those found in zirconium.

Where hydride separates from solution on cooling in the form of rather coarse plates, it is obvious that the precipitate orientation has a considerable influence upon the fracture path and hence on the macroscopic ductility. The dependence of such orientation on the preferred orientation in fabricated zirconium alloy tubes and plates, and therefore upon the thermomechanical history, was recognized quite early.[27] Following a number of failures in Zircaloy fuel element tubes, Louthan and Marshall[28] conducted an extensive investigation of the control of hydride orientation in these materials when cooled under stress. Since the hydride has a lower density than zirconium itself, an expansion occurs on precipitation; hence, it is energetically favorable for precipitation of hydride plates to occur with the plane of the plate perpendicular to a tensile stress and parallel to a compressive stress. While the fabrication history[27] and the associated deformation were recognized as important factors in precipitation in unstressed materials, it was found that under stress, the texture[29,30] and stress[28,29] became of greater significance. Reorientation of precipitated hydride in zirconium-niobium alloy under stress was found to depend intimately upon solution of the hydride.[31] That is, the proportion of precipitate that became oriented perpendicular to an applied (or residual) stress on cooling was directly related to the amount dissolved during a heating cycle, and even then only occurred when the tensile component of stress was along a direction having a high concentration of basal poles, i.e., it was perpendicular to a high proportion of basal planes.

An equation based upon the nucleation relationship proposed by Ells[32] has been found[31] to provide a good representation of the results of reorientation under a stress (σ_t).

$$R_\sigma = R_o \exp(B\sigma_t) \qquad (6)$$

where R represents the ratio of hydride lying between 45 and 90° to the applied stress to that within 0 to 45°. (The subscripts σ and o

represent the presence and absence of stress, respectively.) R_o is indicative of the prevalent hydride orientation in the material in the absence of stress, and B is a factor appropriate to the nucleation process that is not particularly sensitive to the stressing temperature.

Stress-Induced Diffusion

Since the introduction of an interstitial solute into a metal lattice invariably introduces a localized distortion, the presence of a stress gradient would be expected to result in migration of the foreign atoms. The idea that hydride precipitation may be enhanced by stress in supersaturated titanium alloys was floated by Williams[33] as early as 1962, and Westlake[34] subsequently suggested that hydride precipitation in exothermic occluders could be induced by tensile stresses, particularly in the region of triaxial stress ahead of a crack tip or other stress concentration. As a result, stress-induced diffusion of hydrogen—up a stress gradient—was proposed[35] as the mechanism for delayed hydride cracking in the Zr-Nb alloy end-cap welds of an experimental nuclear fuel sheath after a period of two years. Earlier, Weinstein and Holtz[36] had investigated the susceptibility of zirconium and some of its alloys to delayed-failure effects when containing 500 ppm hydrogen. They reported no effects in either unnotched or notched specimens of zirconium and Zircaloy-2 at ambient temperature, but moderate susceptibility in Zr-2.5Nb and high susceptibility in a high-strength Zr-Al-Sn-Mo alloy. Lack of susceptibility was attributed not to lack of crack initiation but to subsequent stress relaxation by localized plastic yielding in the softer materials.

Waisman, et al., quoted the catastrophic delayed failure of a titanium pressure vessel that was the result of the build-up of hydride stringers during operation over a period of 1.5 years at room temperature, and they investigated the diffusion of hydrogen at 600 to 800°C resulting from composition, temperature, and stress gradients.[37] They concluded that the stress effect was a direct consequence of the lattice dilation required to accommodate the interstitial hydrogen atom, which corresponded to a partial molar volume $\bar{V}_H$ of 1.7 to 2.2 cm^3/mol. Wreidt and Oriani[38] had previously developed an equation for the effect of stress on the solubility of hydrogen in a solid and applied it to a palladium-silver alloy Dutton, et al.,[39] subsequently developed a general model for hydrogen-induced delayed cracking in hydride-forming materials that attempted to combine theories for the diffusion of interstitial solutes to stress concentrations[40,41] with ideas concerning stress-assisted precipitation. They calculated a rate of hydride growth from the anticipated hydrogen flux and compared calculated crack velocities expected from such precipitation in Zr-2.5Nb with those observed in earlier work.[42,43]

The temperature dependence of the crack velocity arising from their model was principally a consequence of the term involving the product of the hydrogen diffusivity and the terminal solubility for hydride, which varied by six orders of magnitude over the temperature range involved. The reasonable agreement of calculated and experimental results revealed at higher temperatures did not, however, apply at temperatures below 100°C.[42,43] Indeed, if the plateau velocities apparent from the reported results are plotted against the reciprocal of the testing temperature (in °K), the general trend toward higher crack velocities at higher temperatures can be seen to be unaffected by hydrogen content over the range studied (Figure 3), i.e., the variation can be explained by the activation energy for diffusion alone [taking a diffusivity $D_H = 2.17 \times 10^{-7} \exp(-4217/T) m^2/s$[44]]. This, of course, is hardly surprising when all of the specimens involved contained considerably more hydrogen than corresponded to the terminal solubility in zirconium C_a at the stressing temperature.

Although it has been suggested that the terminal solubility in Zr-2.5Nb could be higher by a factor of 5, Erickson[45] considered that the equilibrium value was unaffected by the presence of niobium, despite the increased hysteresis between heating and cooling results. While it is essential that the terminal solubility (under the appropriate stress) must be locally exceeded for precipitation of hydride to take place, it is not clear why the terminal solubility should exercise any other constraint on either precipitation or the crack velocity. Diffusion control of the crack velocity would seem to be more likely, and, indeed, an activation plot for diffusion does provide a good fit to the crack velocities quoted (Figure 3) (only deviating very slightly from the calculated line of best fit), bearing in mind the experimental scatter.

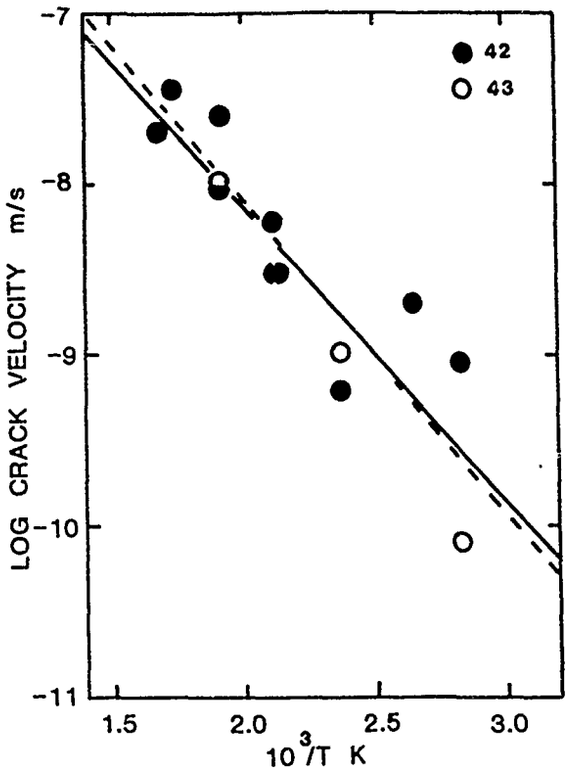


FIGURE 3—Reported results[42,43] for the velocity of sustained-load cracking of cold-worked Zr-2.5Nb compared with the rate of variation of diffusion with temperature (dotted line).[44]

On the other hand, Simpson and Cann[46] have produced evidence for a crack-velocity dependence upon the product $D_H C_a$ in Zr-2.5Nb hydrided to 200 wppm, with an activation energy of 65 5 kJ/mol compared with the 35.1 kJ/mol associated with diffusion alone. One factor that they discovered to have a considerable influence upon crack velocity was the distribution of the β-phase in the alloy. Higher crack velocities were observed in the as-received material, compared with the hydrided or annealed, and this they attributed to the continuous β-phase present in that condition

Thus, obvious points of conflict still exist, and carefully designed experiments will be necessary to unravel a complex situation that is further complicated by the influence of fabrication route and heat treatment on the inherent microstructure of alloys Whatever the controlling factors, there is no doubt that stress induced diffusion of dissolved hydrogen may take place The question that arises is how great a concentration gradient can be established as a consequence of stress gradients that may exist in the material The change in the solubility of hydrogen C_a under the influence of a hydrostatic stress (P) (which is equal to σ/3 where σ is a uniaxial applied stress) derives[12] from the work done against the external stress in expanding the metal lattice and is related to the solubility in the absence of stress (C_o) by the following:

$$C_a = C_o \exp(P\bar{V}_H/RT) \qquad (7)$$

and is increased under a tensile stress, i.e., where P is positive

The maximum enhancement of solubility will thus be related to the maximum stress that can be generated in the material In the

region of triaxial stress ahead of a crack tip, the maximum hydrostatic pressure can exceed the uniaxial yield stress (σ_y), but, even under plane-strain conditions, the enhancement factor is only about 2.4. Dutton suggests that the maximum increase in hydrogen concentration promoted by such conditions is given by the following.[47]

$$\frac{C_s}{C_o} = \exp\left(\frac{2.4\sigma_y \bar{V}_H}{RT}\right) \quad (8)$$

The enhancement thus depends exponentially upon the yield stress and the partial molar volume as well as the reciprocal of temperature. In their examination of titanium alloys, Waisman, et al., surveyed a large amount of data from previous literature and found quoted values of $\bar{V}_H$ from 1.1 to 2.2 cm^3/mol.[37] Taking a value of $\bar{V}_H$ = 2.0 cm^3/mol and a yield stress of 350 MN/m^2 (perhaps on the high side for cp titanium, for example) gives an enhancement factor of 2.0 at ambient temperature and 1.53 at 200°C (if the associated drop in yield stress is ignored). Doubling the yield stress by alloying would double the room-temperature enhancement.

It is immediately obvious that, although there is a definite effect of stress upon the hydrogen solubility in zirconium alloys, the effect is not particularly great and is only likely to significantly influence failure mechanisms if the terminal solubility is exceeded at some point. Under such circumstances, a steady flux of hydrogen to the stress concentration would inevitably lead to localized hydride growth. Coleman has pointed out that such processes may lead to catastrophic failures when zirconium alloys are used under conditions in which corrosion by high-pressure water or steam may lead to excessive hydrogen pick up.[48] Although Margolin[49] proposed a model for sustained-load cracking that was based simply upon the movement of hydrogen in solid solution between different interstitial sites, most of the mechanisms postulated involve strain-induced precipitation.[50]

It would seem, therefore, that even if the crack velocity in sustained-load cracking is essentially controlled by diffusivity, as suggested earlier, initiation of cracking is likely to be determined by the solubility limit for hydride and perhaps the degree of supersaturation. Under such circumstances, the susceptibility of a zirconium alloy with a particular hydrogen content at a particular temperature would be considerably greater than that of a titanium alloy under the same conditions simply because of the lower hydride solubility therein.

The situation is further complicated by alloys containing both α- and β-phases,[51] but Boyer and Spurr suggested that a hydride precipitation model fitted their crack growth data for Ti-6Al-4V: A reduction in temperature reinitiated crack growth in high-hydrogen-content materials and produced initiation in lower-hydrogen-content materials.[52] They reported that stress intensity did not play a major role in sustained load cracking beyond the minimum value required to induce hydrogen migration to the crack tip, which could, however, be very low (~ 12 $MPa \cdot m^{1/2}$). Moody and Gerberich[53] suggest that provision of hydrogen internally (38 wppm) in a Ti 6Al 6V 2Sn alloy results in an exponential dependence of crack growth on stress intensity. They also point out that the crack growth rates are dependent upon the diffusion of hydrogen through the β-phase. Increase in crack velocity up to a temperature of 300°K was attributed to the temperature dependence of diffusion and decrease at higher temperatures to problems of hydride nucleation. Subsequently, the same workers[54] extended their investigation to include the effect of plane-strain conditions on the threshold stress intensity and crack velocity. They found that the threshold approached a lower limiting value of 32 $MPa \cdot m^{1/2}$ as total plane-strain conditions were approached, but with increasing plane stress it moved toward immunity from hydrogen effects. A modified model was therefore developed that allowed for the stress state in the material and provided good agreement with observations. Where the ratio of the radius of the plane-stress plastic zone to the sample thickness was greater than 0.1, the threshold rapidly increased.

Integrity of the Passive Film

For a wide range of environments and conditions of exposure, titanium is protected by an adherent surface film of either rutile or anatase, which not only promotes passivity but may present a reasonably effective barrier to hydrogen absorption. In a similar way, a passive film that forms on the surface of magnesium when it is cathodically polarized in aqueous solutions[8] may prevent hydrogen uptake. Stampella, et al., suggest that rupturing this film by straining, even at 5.7×10^{-6}/s and −1500 to −2000 mV_{SCE}, is not sufficient to allow hydrogen absorption because of the rapidity of repassivation.[55] As a result of such effects, Blackburn, et al., went so far as to state categorically that SCC does not initiate in smooth specimens of titanium in aqueous environments.[56]

Under certain circumstances, however, the protective film may become disrupted and allow both localized corrosion and hydrogen absorption to occur. The requirements for such breakdown could prove quite critical. Such effects are believed to be involved in the SCC of titanium and zirconium when they are exposed to solutions containing chlorides, particularly in the presence of organic solvents that inhibit the repair of the passive film.[57] Very rapid cracking of both metals was observed when they were stressed in methanol containing more than 0.1% hydrochloric acid. The same authors pointed out the beneficial effect of the presence of water in the test environment and suggested that the addition of 1.5% of water was sufficient for the prevention of cracking in titanium, whereas double this quantity was necessary for zirconium. Such suggestions are consistent with the repassivation behavior of Ti-5Al-4V investigated by Buhl, who showed (Figure 4) that, although the amount of water present above 25% had little influence upon repassivation kinetics, as indicated by current decay, repassivation was prevented when the water level was only 0.05%.[58]

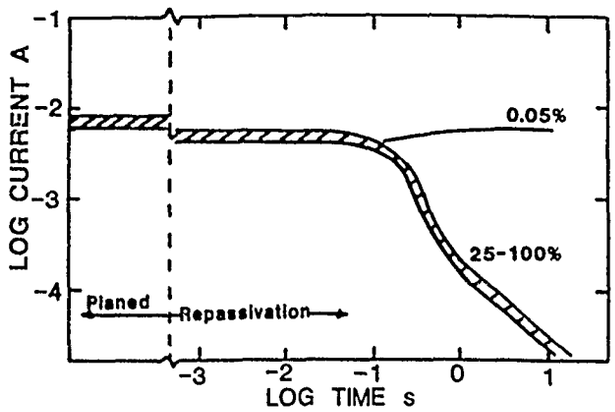


FIGURE 4—Influence of the water content of the solvent (methanol) on repassivation of Ti-6Al-4V after surface planing in 0.1 M sodium chloride, from the results of Buhl.[57]

Dawson[59] has drawn attention to the fact that the level of water or other inhibitor required to achieve substantial improvement in the corrosion fatigue behavior of Ti-6Al-6V-2Sn at 1 Hz and low ΔK is much greater than that needed to produce stable passivity in unstressed specimens or to prevent fracture under static loading. Chloride additions to the environment increase delay times for repassivation,[60] and even though titanium alloys exhibit passive behavior in pure methanol, a very small amount of chloride produces breakdown of passivity followed by pitting and intergranular attack. Depending upon both the alloy and the chloride concentration, the necessary water additions to restore passivity and inhibit intergranular attack vary from a fraction of 1% to more than 10% by volume.[61]

The importance of oxygen or water to prevention of hydrogen uptake at high pressures and temperatures has also been stressed in connection with the extensive use of titanium in oil refineries for process streams containing hydrogen.[62] However, such protection may be lost where cathodically impressed or galvanically induced currents generate atomic hydrogen directly on the surface of the

metal. The presence of > 1.34% water appears to introduce sufficient passivity to titanium when in contact with fuming nitric acid.[63]

The entry of hydrogen into magnesium is generally prevented by the passive $Mg(OH)_2$ film that forms on the metal surface in alkaline solutions As a result, pitting is a necessary precursor to HE and consequential cracking. The walls of a pit provide the bare, active, film-free magnesium surface that allows any hydrogen produced by local cathodic reaction to enter the metal. The corrosion potential of magnesium in aqueous solutions of sodium sulfate corresponds to the breakdown potential and hence pitting, with resultant hydrogen entry and embrittlement, can occur under open-circuit conditions.

Recent studies[64] of the effect of cathodic polarization on the ductility of titanium slowly strained in hot, deoxygenated aqueous chloride have confirmed the possibility of hydrogen uptake under the appropriate conditions Slow straining Grade 12 titanium (containing 1% nickel) revealed hydride formation at temperatures above 100°C and potentials below about $-730\ mV_{SHE}$ Where the time available for hydrogen dissemination was restricted and potentials were only slightly below the expected hydrogen evolution potential, the hydride appeared in the form of channels, which seemed to reflect the local mechanical breakdown of the oxide film (Figure 5), but with longer times and more drastic cathodic charging, a more continuous hydride layer developed Subsequent work using cyclic loading instead of straining to failure has indicated that plastic deformation makes an essential contribution to oxide film rupture and the consequent embrittlement by hydrogen.



FIGURE 5—Section of Grade 12 titanium strained in 3.5% aqueous sodium chloride at 200°C and a potential of $-908\ mV_{SHE}$. $\dot{\epsilon} = 2.8 \times 10^{-7}$/s.

At the temperature concerned, the diffusivity of hydrogen is adequate enough to promote extensive penetration of the specimen and therefore does not restrict crack growth once the surface film is disrupted. In fact, subsequent metallographic examination (Figure 5) indicates considerable general dispersion of hydride throughout the section, with precipitation of large hydride needles.

One surprising outcome of the investigation was that conditions giving rise to extensive hydride formation and consequential embrittlement in the Grade 12 material had no effect whatsoever upon Grade 2 samples, nor had a large variety of other combinations of temperature, cathodic polarization, and strain rate. This, despite the concurrent observation that application of a potential of $-750\ mV_{SHE}$ to the Grade 2 material promotes essentially the same cathodic current density as measured for the Grade 12 in deaerated solutions: 1 mA/cm^2 at room temperature and 10 mA/cm^2 above 100°C. If similar hydrogen fugacities are being developed at both surfaces, the obvious inference is that the hydrogen generated is being prevented from entering the Grade 2 titanium, presumably by the surface oxide. This implies that there is some subtle difference in the character of the surface film on the two materials. Leckie has suggested, from a study of the stress corrosion resistance of a Ti-Al-Nb-Ta alloy, that metallurgical structure plays a relatively minor role, but alloying affects the electrochemical stability of the oxide formed.[65] It has certainly been reported that the thermal oxide on Grade 12 does not constitute an effective barrier to hydrogen entry and that the presence of nickel in the alloy may be a contributory factor.[66] There is also some evidence that incorporation of nickel from the alloy in the passive film[67] or deposition of nickel on the metal surface[68] can greatly increase the efficiency of penetration by hydrogen. Sanderson and Scully also refer to the detrimental effect of alloying on the adherence of the protective film on Ti-6Al-4V when immersed in a methanol-hydrochloric acid mixture. [69]

The incorporation of iron particles into the surface oxide during abrasion likewise provides effective disruption of the passive film and greater hydrogen pick up.[70] On the other hand, galvanic coupling with iron in seawater does not result in hydrogen uptake unless hydrogen sulfide is present in the environment.[62]

The high chemical reactivity of magnesium greatly restricts its use in corrosive environments. The passive film of hydroxide that only forms under strongly alkaline conditions is readily destroyed by the presence of chlorides in the environment. Where the environmental conditions are such as to promote passivation, however, the environment-sensitive cracking that may occur exhibits many similarities to that occurring in titanium. Competition between the disruption of the surface film and repassivation thus constitutes an important factor in the SCC of magnesium-aluminum in a mixture of chloride and chromate.[71] The investigations conducted by Frankenthal established fairly conclusively that there is a relationship between SCC and pitting in magnesium alloys.[72] While the addition of chromate to less aggressive solutions prevents SCC, in more aggressive environments containing sodium chloride or sodium sulfite, it promotes a sharp increase in the rate of cracking. Chloride ions in the environment tend to disrupt the passive film by the formation of pits, but, although cracking may occur from the base of pits (Figure 6), the presence of another species such as potassium chromate is necessary to prevent excessive pitting and failure by more general corrosion rather than by stress corrosion.

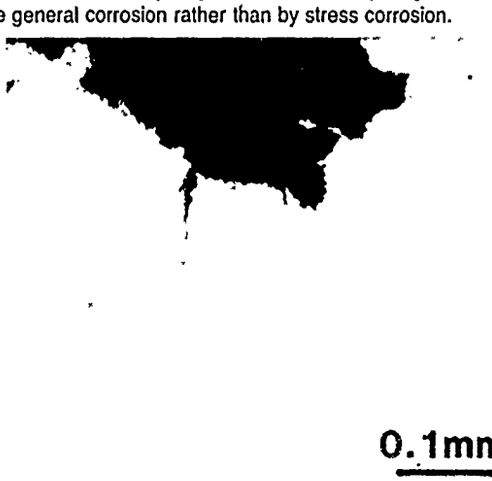


FIGURE 6—Cracking at the base of a corrosion pit in Mg-7Al strained to failure at 2.0×10^{-6}/s in an aqueous solution containing 35 g/L sodium chloride and 5 g/L potassium chromate.

SCC does not take place if either chloride or chromate are present on their own, but with both species present, a delicate balance may be set up that influences both the crack velocity (Figure 7) and the threshold stress.[73] The minimum threshold stress and the maximum crack velocity are promoted by solutions containing almost equal proportions (by weight) of both sodium chloride and potassium chromate. Excess chromate and excess chloride each result in a reduction in the cracking rate. The general relationship between the chloride/chromate ratio and the crack velocity does, however, appear to fall down at low ratios of chloride to chromate when the chloride concentrations are high (Figure 7), presumably because of the excessive pitting that then occurs and the inability of the chromate to localize the cracking process. The inhibiting effect of sodium nitrate on SCC[72] appeared to be associated with prevention of the breakdown by chloride of the passive film promoted by chromate.

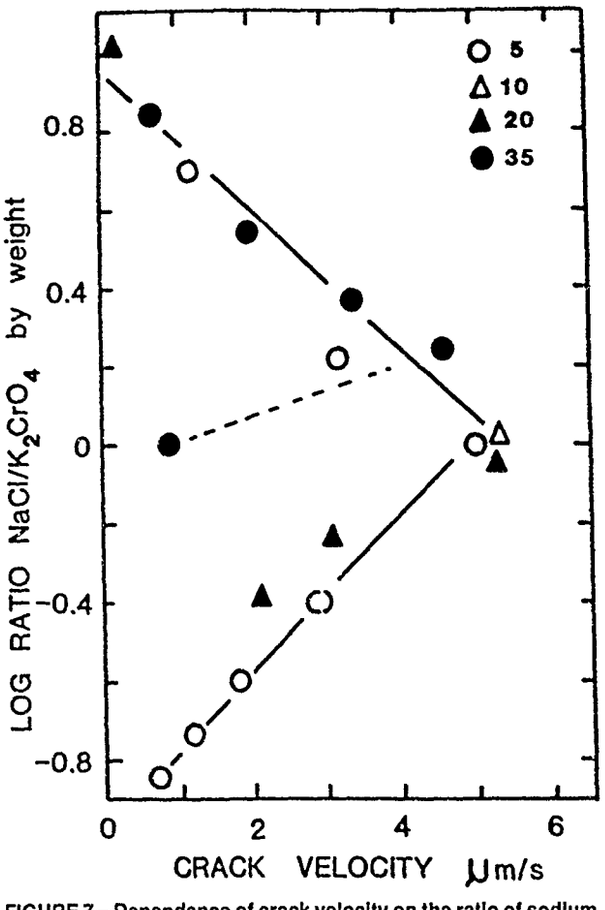


FIGURE 7—Dependence of crack velocity on the ratio of sodium chloride to potassium chromate (by weight) in aqueous solutions containing 5 to 35 g/L sodium chloride.

The question of film repair and maintenance is important even in the hot-salt cracking of titanium alloys.[74] Titanium and its alloys suffer from pitting when exposed to moist chlorine, and a critical level of moisture must be present to inhibit attack by repair of the protective film.[75]

The importance of strain rate and the consequential influence of creep on the progress of SCC has been highlighted by Parkins,[76,77] and it is interesting to compare such effects in magnesium[76] and titanium[73] (Figure 8), in which the data produced from constant strain tests on smooth tensile specimens, either stressed for 3 h (at the test stress or higher) prior to introduction of the test solution or stressed immediately after addition of the solution, show many similarities.

Whenever significant creep deformation occurred while the material was actually exposed to the corrosive environment, the lifetime was reduced compared to specimens in which stress relaxation was allowed to occur for a period before specimens were exposed to the solution, and the crack velocities were consequently higher. Both cp titanium and Mg-7Al therefore seem to be prone to environment-sensitive cracking at the slow-strain rates involved in the early stages of creep. Parkins suggested that such effects were related to the role played by deformation in the disruption of passive films and exposure of the underlying metal to the corrosive environment.[77] Naturally, the interplay between the creep properties of the material concerned and the critical strain rates for overcoming repassivation effects could be quite critical. Scully, for instance, has pointed out that the range of cross-head speeds over which cracking occurs in tensile straining of Zircaloy-2 is lower than that observed for Ti-O alloys.[78]

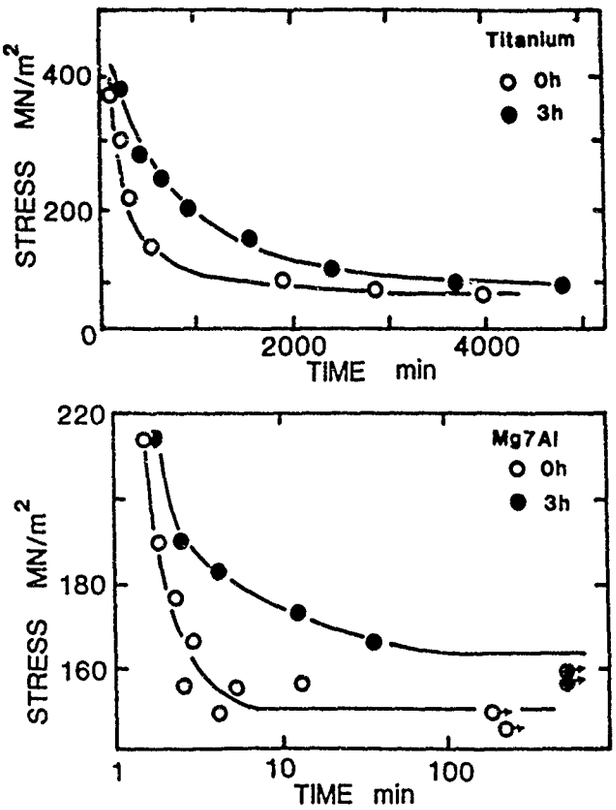


FIGURE 8—Effect of creep (stress relaxation for 3 h under load) prior to immersion in the test environment on time-to-failure for (a) commercial-purity titanium in methanol-hydrochloric acid[90] and (b) Mg-7Al (quenched from 350°C after 1 h) in a chloride-chromate mixture.[76]

Anodic Dissolution or Hydrogen Embrittlement

In many of the stress corrosion systems involving magnesium, titanium, or zirconium, extremely high crack velocities have been measured, and this has presented a considerable obstacle over the years to the identification of a cracking mechanism. When Scully considered the various objections raised to the proposal that hydrogen played a principal role in environment-induced cracking of titanium alloys, he took into account maximum reported crack velocities up to 10^{-3} mm/s for initially smooth specimens and considerably faster for precracked specimens.[79] Crack velocities as high as 10^{-2} mm/s have been quoted for specimens of a Mg-Al alloy,[73,76] for which Chakrapani and Pugh mentioned 10^{-4} mm/s for transgranular cracking of smooth specimens. On such a basis, Scully went on to point out that it was very unlikely that hydrogen could sustain such high propagation rates with a diffusivity of 10^{-14} m^2/s,

since this would mean that hydrogen would only penetrate a distance of about 10^{-4} mm in 1 s.[79] This general point concerning the necessary diffusivity has been discussed by Johnson, who stressed the importance of the ratio of crack velocity to diffusivity in connection with the penetration of hydrogen ahead of a propagating crack.[80] Mitigating circumstances quoted for the apparent discrepancy between crack velocity and diffusion rates tend to invoke an increased diffusivity produced by dislocation sweeping[81] or an alternative mechanism whereby cracks through embrittled material continue to propagate a certain distance into the unembrittled region before being arrested.[82]

On the other hand, many authors have firmly believed that the feasibility of producing these crack velocities by an anodic dissolution process was even less likely than by means of hydrogen-induced cracking. Beck considered the possibility of penetration of titanium by an "electrochemical knife."[83] If the current density (i_A) required for propagation by anodic dissolution is given by

$$i_A = \frac{zF\rho v}{M} \qquad (9)$$

where z is the valency of the metal, F the Faraday constant, ρ the density, M the atomic weight, and v the velocity of crack propagation, then a velocity of 1 mm/s[57] would require a current of 3×10^7 A/m^2. However, Beck did not believe that this was out of the question in view of his estimated current density at the mixed corrosion potential for bare metal surfaces. He also claimed that, since the average crack velocity in double-notched specimens of a duplex Ti-8Al-1Mo-1V alloy strained in aqueous chloride, bromide, and iodide solutions was directly proportional to potential (and current), the crack propagation process was intrinsically electrochemical.[84] Taken at its face value, of course, this statement does not exclude a hydrogen-induced mechanism.

The debate on the relative contributions of anodic dissolution and HE to the failure of titanium and its alloys in various environments has consequently continued over many years, particularly after Menzies and Averill[85] demonstrated that the preferential dissolution of grain boundaries that occurred when titanium was anodically attacked by methanol-hydrochloric acid mixtures was accompanied by entry of hydrogen into the grains to form hydride. The correct answer may well be that the relative contributions vary with the environment, and, in this context, the complementary results of different workers may shed considerable light on the subject.

Powell and Scully[80] showed quite definitely that unstressed titanium specimens could be embrittled by extended exposure to a methanol-acid mixture before straining to failure in air. Both grain-boundary failure and cleavage were reported. The dependence of the degree of embrittlement upon strain rate and the occurrence of failure at fast strain rates[87] eliminates the possibility that loss of ductility could be attributed to extensive anodic dissolution of grain boundaries during the period of pre-exposure, the extension of which nevertheless increased the initial loss in ductility. Sedriks, et al.,[88] had earlier drawn attention to the fact that cracking could be induced in Ti-5Al-2.5Sn by prior exposure to methanol, either as liquid or vapor, before stressing, but that vacuum annealing at 830°C before stressing completely eliminated embrittlement. This immediately suggests hydrogen-induced embrittlement. The effects are accelerated by the presence of halide ions, particularly bromine, in the environment, presumably because of their penetration of the protective surface film.

Following an extensive examination of the cracking of titanium and titanium alloys (containing aluminum, tin, and vanadium) in methanol-hydrochloric acid mixtures, Sanderson and Scully[74] deduced that two different processes might be operative in their stress corrosion failure: transgranular hydride formation and selective dissolution of the α-grain boundaries. They also observed that alloy specimens left in the mixture after fracturing or immersed unstressed for similar periods of time suffered extensive intergranular embrittlement. This did not occur when immersion was in methanol alone, presumably because of the essential part played by the chloride in penetrating the passive film. There was then a tendency[74,87,89] to attribute the intergranular cracking to anodic dissolution and the transgranular "cleavage" failure (with river patterns) to HE. Specimens pre-exposed to the methanol-acid mixture prior to straining tended to exhibit a three-zone fracture surface[89] in the early stages before complete embrittlement, where a central dimpled region was separated from an outer, intergranular region by a fluted "cleavage" region. The disappearance of the fluted region that resulted from aging up to 75°C before straining (but after exposure) was taken as further evidence of the involvement of hydrogen; i.e., the aging allowed more general dispersion of hydrogen from the transition zone between intergranular and dimpled failure. The authors therefore believed[89] that their experimental results were consistent with the proposal that transgranular cleavage is a direct result of hydrogen absorbed during the anodic dissolution that causes the intergranular fracture.

Later work has, however, demonstrated that such a model is an over-simplification of the true situation and that absorbed hydrogen may itself give rise to intergranular failure, whether or not anodic dissolution is also involved.[90] With less aggressive solutions, i.e., with a higher water content, the anodic dissolution process is retarded, and this allows more time during pre-exposure for penetration by hydrogen. Significant embrittlement is effected after only 48 h of immersion in a methanol-acid mixture (Figure 9) and, more significant still, considerable recovery of ductility occurs when specimens are held under vacuum at 200°C for two days before straining. Despite the lack of corrosive attack, except at the surface, during immersion, there was significant intergranular fracture to a considerable depth on subsequent straining.

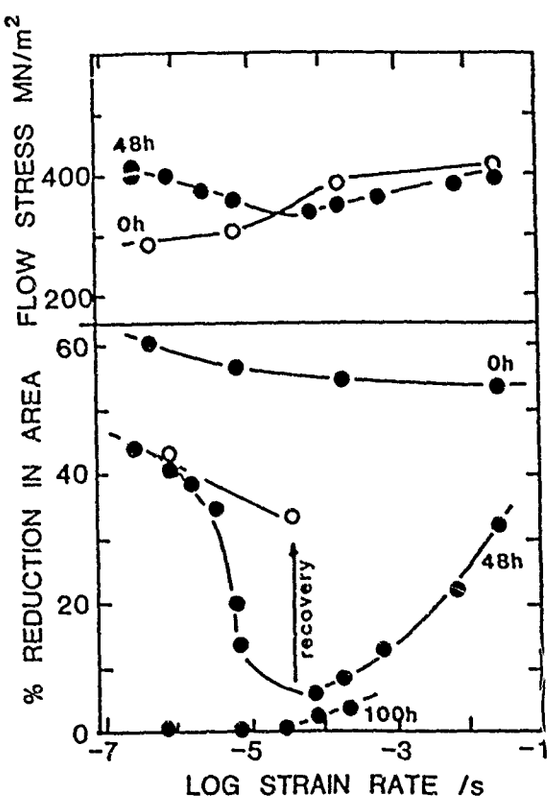


FIGURE 9—Variation of the ductility and flow stress with strain rate for commercial-purity titanium specimens strained in air after different periods of immersion in a methanol-acid mixture. The open points on the ductility plot represent specimens heated under vacuum for 2 days at 200°C, following 48-h exposure to the mixture, and then tested in air at ambient temperature.

Another interesting phenomenon associated with hydrogen uptake was also observed: the occurrence of dark-etching boundaries in polished sections removed from the pre-exposed specimens *after* straining at 3.2×10^{-5}/s (Figure 10). No such effect was observed when specimens were polished and etched without straining after immersion. That connection with hydrogen was further confirmed by the observation that no dark-etching grain boundaries were present in pre-exposed specimens that had been left for 60 days after straining to failure in air. The obvious inference is that hydrogen becomes concentrated at grain boundaries during straining after immersion but will disperse again within the grains on subsequent holding in air at ambient temperature. The introduction of the hydrogen to the titanium during prior exposure clearly provides a species that can become concentrated at grain boundaries during straining and so provide a susceptible path for brittle cracks (Figure 10). The variation of the depth of penetration (as assessed from the appearance of the dark-etching boundaries) with time of immersion in the methanol-acid mixture indicates[91] a hydrogen diffusivity of 1.4×10^{-13} m²/s, if hydrogen is indeed the cause. Although this is higher than the value of 5.2×10^{-15} m²/s obtained from extrapolation of high-temperature data,[92] Waisman, et al.,[93] have presented evidence in welded pressure vessels of a room-temperature diffusivity ($= 5 \times 10^{-9}$ cm²/s) more than an order of magnitude higher than that derived by such extrapolation.



FIGURE 10—Dark etching boundaries in a section from commercial-purity titanium specimen pre-exposed to a methanol-hydrochloric acid mixture for 73 h before straining to failure in air at 3.2×10^{-5}/s.

The possible involvement of HE in the stress corrosion failure of magnesium and Mg-Al has proved to be even more controversial over the years. HE was proposed, as is often the case, because of the difficulty of explaining the observed high crack velocities by anodic dissolution. The Mg 7Al alloy has, however, been embrittled in a similar fashion by cathodically generated and by dry gaseous hydrogen.[94] It was also discovered that embrittlement induced by immersion in a chloride-chromate mixture could be removed by vacuum annealing at 385°C. One of the obstacles to the acceptance of a mechanism involving HE was the effect of applied potential on the ductility of smooth specimens when slowly strained in tension (Figure 11); embrittlement is decreased by the application of more cathodic potentials. However, it now seems likely that, although high cathodic potentials support passivation of magnesium[8] and growth of a barrier to hydrogen ingress, anodic polarization not only causes breakdown of passivity but also hydrogen evolution because of the "negative difference effect."[95] It is therefore believed that disruption of the surface film on the metal by chloride pitting enables entry of the evolved hydrogen and initiation of brittle cracks at the base of pits (Figure 6).

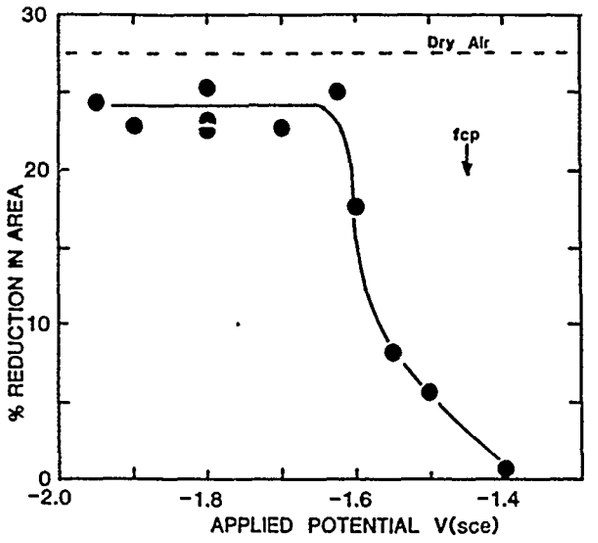


FIGURE 11—Variation of the reduction in area at fracture for smooth tensile specimens of Mg-7Al when strained at 2.0×10^{-6}/s while immersed in an aqueous solution containing 5 g/L sodium chloride and 5 g/L potassium chromate at various potentials.

Intergranular penetration of Zircaloy in a methanol-iodine mixture at room temperature and in a fused nitrate-chloride mixture at 300 to 450°C occurs even in the absence of applied stress and is thought to be governed by anodic dissolution.

Stress Concentration Effects

The very high rate of repassivation of cp titanium in the presence of water and the good resistance of the material to crevice corrosion led to the belief that it was immune to SCC in aqueous environments. Similar behavior has been reported for Ti-6Al-4V in halide solutions,[58,96] but such ideas are confounded by the discovery that specimens of this and Ti-8Al-1Mo-1V had a reduced resistance to crack propagation when prefatigued, notched bars were stressed in seawater.[5,97] Investigation of a duplex-annealed Ti-8Al-1Mo-1V in a wide range of environments[84] clearly demonstrated that, although precracking was not essential to the failure mechanism, there was a minimum notch radius above which SCC did not occur. However, the critical radius varied with the type of environment.

Scully and Adepoju[89] showed that titanium, even when it contained 0.37% oxygen, showed similar behavior to Ti-5Al-2.5Sn,[88] in that loss of ductility in smooth specimens occurred over only a very narrow range of strain rates (from 2×10^{-4} to 5×10^{-3}/s) in 3% aqueous sodium chloride (Figure 12), because ductile fracture pre-empted crack initiation at higher strain rates, and repassivation occurs faster than the creation of bare surface at slower strain rates. The reason for cracking at slower strain rates in the methanol-acid solution is that the presence of the methanol (in the absence of water) prevents repassivation.

Although it was believed that stress corrosion did not initiate in smooth specimens of α/β alloys in aqueous solutions,[56] precracked specimens showed a well-defined threshold stress intensity for cracking.[98]

It seems obvious that the protective oxide film on these materials introduces a very effective barrier to crack initiation. Since titanium does not suffer from pitting under the relatively mild conditions involving low chloride concentration at ambient temperature, some other agent for penetration of the film is required. One solution to the initiation problem is to use notched and/or precracked specimens, so that the high stresses developed at the notch root or crack tip can promote localized deformation. Smith, et al., were able

to deduce K_{ISCC} values for titanium alloys immersed in aqueous chloride in this way.[99] Competition between cyclic SCC and repassivation at the crack tip has been offered as an explanation of the ΔK_{SCC} transition observed under cyclic-loading conditions.[100] Cleavage of the grains in the Ti-6Al-6V-2Sn and Ti-6Al-4V examined was no longer suppressed by sufficient repassivation of the fresh surface exposed at the crack tip. It has also been discovered[96] that transgranular cracking of Ti-5Al-2.5Sn in acidified sodium chloride may be initiated by the brittle hydride layer produced on the surface during chemical polishing.

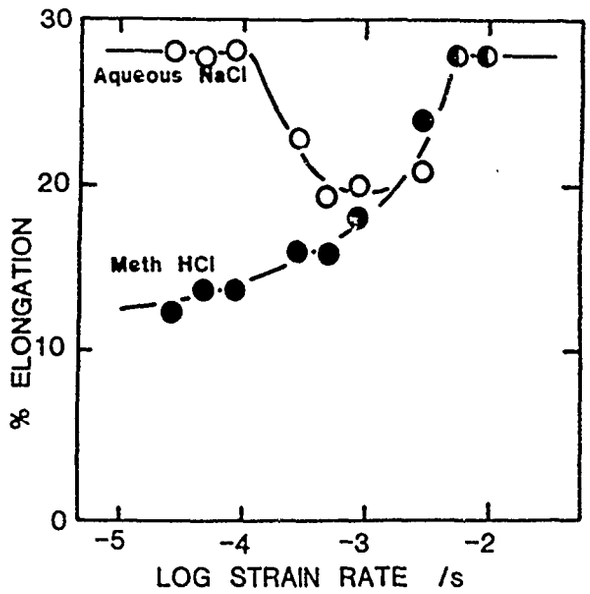


FIGURE 12—Variation of the ductility of Ti-0.34%O when strained in either 3% aqueous sodium chloride or a methanol-hydrochloric acid mixture at various strain rates.[89]

Straining of smooth Ti-6Al-4V tensile specimens at a variety of strain rates in aqueous chloride or acidified seawater revealed no significant change in mechanical properties compared with testing in laboratory air (Table 2). However, dead-weight loading of bend specimens produced a significant reduction in resistance to crack propagation in similar environments (Figure 13), with resultant crack velocities of about 10^{-6} mm/s. The performance of smooth specimens was not influenced adversely by heat treatment.

Initiation of environment-induced fracture by a brittle surface layer may also be achieved by heating titanium alloys in a "low" vacuum, to produce oxygen diffusion and develop a hardened α-case that suffers brittle cracking when specimens are strained. The stress concentrations and crevices so produced introduce a susceptibility to SCC (Table 2).

Microstructure and Heat Treatment

Alloying may influence the behavior of materials in a variety of ways with regard to their resistance to environment-induced fracture. The strengthening effect of any alloying additions may be important from the point of view of the manner in which the matrix reacts to the presence of brittle hydrides or the way in which creep properties interact with the integrity of any passive film under load. Accompanying variations in toughness may also have a major influence on crack propagation and ultimate failure because of the different reaction to the presence of initiated cracks. Where susceptibility to SCC is intimately connected with the properties of a protective surface film, incorporation of alloying elements or impurities in this film may promote both the initiation and, because of effects on the rate of repassivation, the propagation of cracks All of these factors have already been given some consideration here, but another very important aspect of alloying is its effect upon microstructure and the response of this to heat treatment.

Wearmouth, et al.,[76] demonstrated that the occurrence of transgranular or intergranular failure was a consequence of the inherent grain size and applied aging treatment in the stress corrosion of Mg-7Al; coarse grain leading to transgranular and fine grain to intergranular failure. On the other hand, Stampella, et al.,[55] deduced that the crack path in pure magnesium suffering from environmentally induced cracking in sodium sulfite was exclusively transgranular in the finer-grained, commercial metal and mixed mode, intergranular with transgranular, in coarse-grained, high-purity material.

Since titanium and zirconium each undergo a phase tranformation from hexagonal to body-centered cubic (at 882 and 862°C, respectively), the structure of their alloys and their response to thermal treatment are very susceptible to whether or not the alloying elements stabilize the hexagonal α or the body-centered cubic β. In practice, this aspect of alloy behavior has not always received the attention that it deserves and, worse, has even been ignored under certain circumstances. However, Curtis, et al.,[101] did conduct a comprehensive survey of the stress corrosion behavior of titanium alloys, both α and α+β, in 3.5% aqueous sodium chloride. They identified a dependence of susceptibility to cracking upon microstructure over a wide range of alloy compositions and thermomechanical conditions: Increasing the proportion of β-phase generally improved the resistance to failure, although stabilizing the β-eutectoid has a detrimental effect, and increasing aluminum (above 6%) and tin tended to make the alloys more prone to failure. It has been proposed[102] that transgranular stress corrosion fracture may be eliminated in certain alloys by (1) heat treatment in the β-range, (2) the introduction of a β-stabilizer, or (3) a decrease in aluminum content.

Heat treatments that produce a discontinuous network of the α-phase at least appear to decrease, and possibly even eliminate, susceptibility.[96] It has also been suggested[103] that martensitic conditions in Ti-6Al-4V and in Ti-8Al-1Mo-1V are not susceptible to stress corrosion. There is certainly no doubt that the behavior of alloys is very sensitive to the detailed distribution of the α- and β-phases in alloys with a duplex microstructure. Altering this distribution by high vacuum heat treatment (1 h at 800°C followed by furnace cooling) has been found to increase the crack velocity for bend specimens of the Ti-6Al-4V alloy subjected to dead-weight loading in aqueous sodium chloride by two orders of magnitude (Figure 13), despite the absence of any such effects from smooth tensile specimens treated in the same fashion.[104] This deterioration in stress corrosion resistance was associated with a general coarsening of the microstructure and an increase in the continuity of the β-phase (Figure 14). There was also an associated increase in the vanadium content of the β-phase, while the aluminum distribution did not change significantly.

The toughness of a Ti-5Al-4V alloy in three-point bending when surrounded by hydrogen at 0.9 bar has also been shown[105] to be markedly influenced by microstructure, but this was explained in terms of the relative hydrogen transport rates in the α- and β-phases. Those microstructures having a continuous α-phase with fine, dispersed β in the boundaries were least embrittled, whereas those with a β-phase throughout were most embrittled In the former, failure occurred by a transgranular cleavage mode; intergranular separation took place in the latter, as was reported in the early work on hydrogen-charged alloys.[33] This conclusion conflicts with some reported results for internal HE of a near α alloy,[105] where fine discontinuous films of β were associated with easy fracture The net effect will, of course, depend very much upon the specific role played by the β-phase, and creep deformation appeared to dominate the latter work. A long lifetime was obtained at 203°K where no creep effects were observed.

TABLE 2
Mechanical Properties of Smooth Ti-6Al-4V Specimens[A]

Heat Treatment	Test Environment	%Plastic Elongation	0.2% Flow Stress MN/m^2	UTS MN/m^2
As received	Air	12.1	843	918
As received	Aqueous 3.5% NaCl	11.9	848	918
As received	Seawater pH = 1	13.0	878	963
40 h at 250°C	Aqueous 3.5% NaCl	11.5	900	954
2 h at 650°C	Air	12.2	904	967
2 h at 650°C	Aqueous 3.5% NaCl	13.4	869	938
40 h at 650°C	Aqueous 3.5% NaCl	9.3	890	954
5 h at 800°C	Aqueous 3.5% NaCl	9.6	858	932
5 h at 800°C	Air	10.8	910	990
40 h at 250°C+	Aqueous 3.5% NaCl	11.5	900	954
40 h at 650°C+	Aqueous 3.5% NaCl	8.3	850	893
5 h at 800°C+	Air	10.8	910	990
5 h at 800°C+	Aqueous 3.5% NaCl	5.5	860	886

[A]Strained in tension at 3×10^{-5}/s in various environments, either in the as-received condition or after vacuum annealing. Specimens indicated by + were annealed in "low" vacuum.

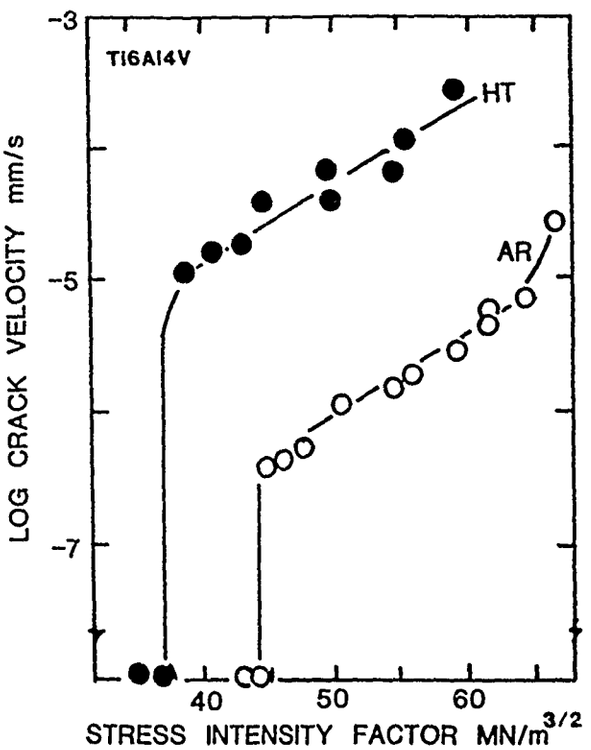


FIGURE 13—Variation of crack velocity with applied stress-intensity factor for Ti-6Al-4V specimens subjected to constant load in aqueous sodium chloride. The material was either in the as-received condition (AR) or had been vacuum annealed at 800°C for 5 h before testing (HT).

The consequences of alloying are not always predictable. This is amply illustrated by a comparison of the behavior of Ti-6Al-4V to that of cp titanium when tested in a methyl alcohol-hydrochloric acid mixture (1.13 vol% of 35.5% HCl) (Figure 15). The loss in ductility that the cp titanium suffered when pre-exposed to the mixture and then strained in air (Figure 9) was not exhibited by the alloy. By contrast, when the alloy was strained in the solution, so providing mechanical disruption of the passive film, it was more readily embrittled than the pure metal.

A comprehensive knowledge of the influence of microstructure on environment-induced cracking can, of course, be manipulated to advantage in developing a structure that is more resistant to failure in service. Work has been conducted on zirconium alloys[106] to this end: to help identify suitable manufacturing schedules for the production of pressure tubes that would resist delayed hydrogen cracking.

Fluted Fracture Surfaces

Over the years, it has become appreciated that the fluted fracture surfaces identified with stress corrosion or HE of these materials (Figure 16) are not, as initially believed,[107] a result of cleavage along particular planes of the hexagonal lattices involved. The observation of "pleated" failures in Mg-Al, which could be avoided by vacuum annealing, after immersion in a mixture of sodium chloride and potassium chromate was interpreted as a consequence of cleavage on $\{31\bar{4}0\}$ planes.[94] However, following investigation of analogous failures in titanium and zirconium, Aitchison and Cox[108] suggested the term "fluting" and emphasized the essentially ductile nature of such failures with complementary river patterns on mating fracture surfaces (ridge matching with ridge); i.e., the characteristic flutings resulted from necking between tubular voids and not cleavage. They also referred to the similar fractography associated with liquid metal embrittlement of zirconium alloys,[2] particularly with mercury at room temperature.

Knorr and Pelloux[109] observed fluted failures when studying the effects of texture and microstructure on the propagation of iodine stress corrosion cracks in Zircaloy and found a correlation with the orientation of the hexagonal structure.

Fracture surfaces presented from magnesium[110] and magnesium alloys[76] that had suffered stress corrosion failure in a mixture containing sodium chloride and potassium chromate and showed obvious fluting have frequently been referred to as cleavage, but appear to have a similar origin to analogous fractures in titanium and zirconium.

It has been proposed[108,111] that fluting, which appears to be peculiar to hexagonal materials, occurs because of the scarcity of active slip systems and is produced by the coalescence of tubular voids nucleated by the interaction of particular slip bands, or the intersection of slip bands with grain boundaries, ahead of crack tips.

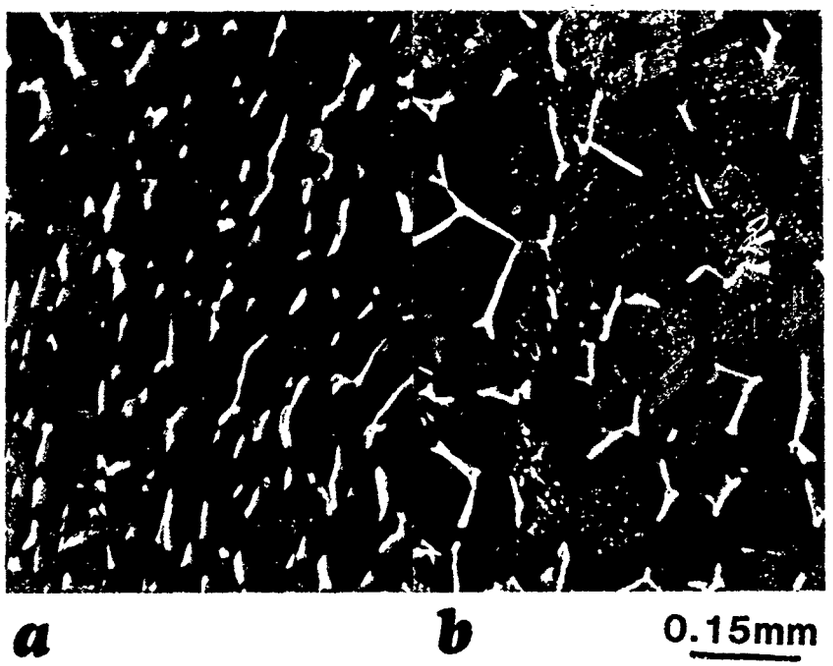


FIGURE 14—Microstructure of the Ti-6Al-4V alloy (a) in the as-received condition and (b) after vacuum annealing at 800°C for 1 h and furnace cooling.

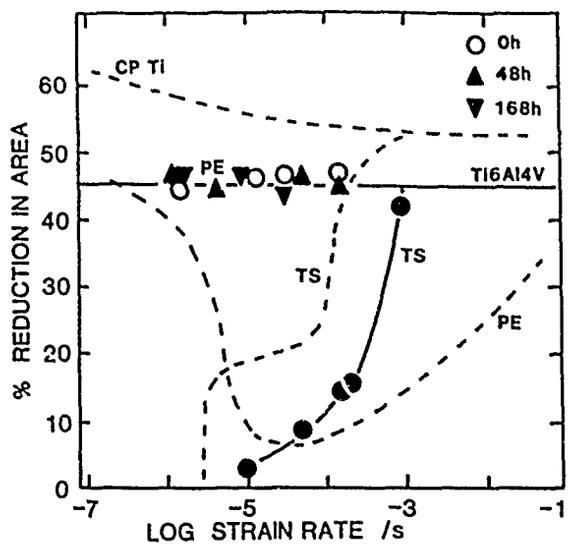


FIGURE 15—Effect pre-exposure (for 0, 48, or 168 h) to a methanol-hydrochloric acid mixture followed by straining to failure in air (PE), and straining in the same solution without pre-exposure (TS) on the ductility of Ti-6Al-4V. The curves for commercial-purity titanium (from Figure 9), tested in solution or after 48 h pre-exposure, are shown (dotted) for comparison.

After comparing the transgranular fractures of Zircaloy obtained in a methanol-hydrochloric acid mixture at room temperature with those induced by molten salts at 300 to 450°C and in liquid metals, Cox[108] believed that, despite certain obvious differences, they were all a consequence of the adsorption of some active species at the crack tip—the agent being hydrogen in both the methanol-acid mixture and the fused salt While it is always dangerous to base any failure model solely upon fractographic evidence, there does seem to be reasonable grounds for supposing that analogous mechanisms operate for both titanium and zirconium.

Conclusion

The three hexagonal materials concerned here exhibit many similarities in their susceptibility to environment-induced cracking, but there are also obvious essential differences. Although such failures in magnesium or its alloys have at times been attributed to hydride formation, it is only in titanium, zirconium, and their alloys that this plays such a major role in stress corrosion or corrosion fatigue. Since the hydride solubility is less in zirconium than titanium, the former suffers more obviously from hydride embrittlement, but both are prone to the more insidious delayed failure arising from stress-induced hydride formation.

Passive films, and particularly the tenacious oxide formed on both titanium and zirconium, play an important part, not only in protecting the metals from attack, but in preventing the ingress of hydrogen produced by ancillary cathodic reactions. The breakdown and repassivation of such surface films may be decisive factors in determining whether the materials remain immune to failure, undergo gross general attack or suffer from environment-induced cracking.

Once metal is exposed, there may be competition, as well as cooperation, between anodic dissolution and HE processes, and differentiation may at times prove difficult. The balance may also be very sensitive to environmental and material variables.

Introduction of brittle surface films, or embrittlement of the metal surface itself, and the occurrence of local stress concentrations may also introduce a susceptibility to failure that is notably absent from smooth specimens.

Alloying can have an important influence on the character and properties of passivating films. In certain circumstances, this may prove decisive, but in others the associated changes in microstructure and the way in which these may be modified by heat treatment may be of greater importance.

All these factors must be taken into consideration to make a realistic assessment of industrial performance or service failure.

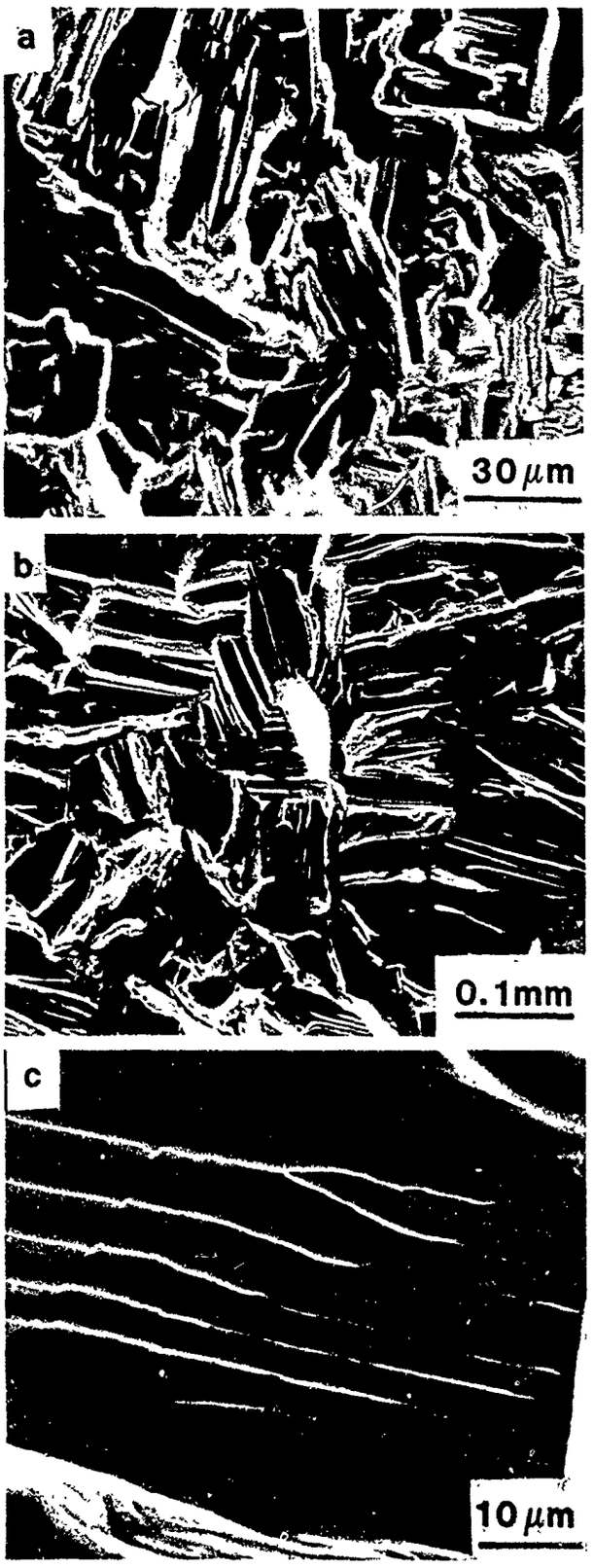


FIGURE 16—Characteristic fluted failures associated with the environment-induced failure of (a) a precracked specimen of Mg-7Al broken under constant load in an aqueous solution containing 35 g/L sodium chloride and 15 g/L potassium chromate, (b) titanium broken by cyclic loading at 0.05 Hz in 3.5% aqueous sodium chloride at −700 mV_{SCE}, and (c) commercial-purity titanium strained to failure in a methanol-acid mixture at 8.2×10^{-5}/s.

References

1. F.H. Ellinger, C.E. Holley, B.B. McInteer, D. Pavone, R.M. Potter, E. Staritzky, W.H. Zachariasen, J. Amer. Chem. Soc. 77(1955): p. 2647.
2. B. Cox, Corrosion 28(1972): p. 207.
3. E.F. Emley, Principles of Magnesium Technology (Oxford, England: Pergamon Press, 1966), p. 719 .
4. F.C. Althoff, Luftfahrt Forsch. 15(1938): p. 60.
5. B.F. Brown, Mater. Res. Stand. 6(1966): p. 129.
6. G.C. Kiefer, W.W. Harple, Metal Prog. 63, 2(1953): p. 75.
7. R. Glicksman, J. Electrochem. Soc. 106(1959): p. 457.
8. P.F. King, J. Electrochem. Soc. 110(1963): p. 1113.
9. N.D. Tomashov, P.M. Al Torskii, Corrosion and Protection of Ti, Government (USSR) Scientific-Technical Publication of Machine-Building Literature (Moscow, USSR: 1963).
10. Z.D. Popovic, G.R. Piercy, Metall. Trans. 6A(1975): p. 1915.
11. N.E. Paton, B.S. Hickman, D.H. Leslie, Metall. Trans. 2(1971). p. 2791.
12. J.J. Kearns, J. Nucl. Mater. 22(1967): p. 292.
13. G.A. Lenning, C.M. Craighead, R.I. Jaffee, Trans. AIME 200(1954): p. 367.
14. R.W. Dayton, A.D. Schwope, G.T. Muehlenkamp, H.A. Saller, R.F. Dickerson, C.M. Schwartz, M.W. Mallet, USAEC Rep. No. BMI-767 (1952).
15. C.E. Coleman, D. Hardie, J. Nucl. Mater. 19(1966): p. 1.
16. P. Cotterill, Prog. in Mater. Sci. 9(1961): p. 201.
17. W. Erickson, D. Hardie, J. Inst. Metals 93(1965): p. 444.
18. D.G. Westlake, Trans. ASM 56(1963): p. 1.
19. D.G. Westlake, Trans. AIME 233(1965): p. 368.
20. C.E. Coleman, D. Hardie, J. Less Common Metals 11(1966) p 168.
21. M.R. Warren, C.J. Beevers, Metal Sci. J. 1(1967): p. 173.
22. D. Hardie, J. Nucl. Mater. 42(1972): p. 317.
23. A.A. Griffith, Phil. Trans. Roy. Soc. A221(1921): p. 163.
24. G.D. Fearnehough, A. Cowan, J. Nucl. Mater. 22(1967): p. 137
25. C.J. Beevers, Electrochem. Tech. 4(1966): p. 222.
26. C.E. Coleman, D. Hardie, J. Nucl. Mater. 19(1966): p. 201.
27. R.P. Marshall, J. Nucl. Mater. 24(1967): p. 49.
28. M.R. Louthan, R.P. Marshall, J. Nucl. Mater. 9(1963). p. 170.
29. C.E. Ells, J. Nucl. Mater. 28(1968): p. 129.
30. E. Schelzke, J. Nucl. Mater. 30(1969): p. 324.
31. D. Hardie, M.W. Shanahan, J. Nucl. Mater. 55(1975): p. 1.
32. C.E. Ells, J. Nucl. Mater. 35(1970): p. 306.
33. D.N. Williams, J. Inst. Metals 91(1962): p. 147.
34. D.G. Westlake, Trans. ASM 62(1969): p. 1000.
35. C.J. Simpson, C.E. Ells, J. Nucl. Mater. 52(1974): p. 289.
36. D. Weinstein, F.C. Holtz, Trans. ASM 57(1964): p. 284.
37. J.L. Waisman, G. Sines, L.B. Robinson, Metall. Trans. 4(1973): p. 291.
38. H.A. Wreidt, R.A. Oriani, Acta Metall. 18(1970): p. 753.
39. R. Dutton, K. Nuttall, M.P. Puls, L.A. Simpson, Metall. Trans. 8A (1977): p. 1553.
40. H.W. Liu, J. Basic Eng. 92(1979): p. 633.
41. M.P. Puls, R. Dutton, R.W. Stevens, Acta Metall. 22(1974): p. 639.
42. L.A. Simpson, K. Nuttall, 3rd International Conference on Zirconium in Nuclear Industry, ASTM STP-633 (Philadelphia, PA: ASTM, 1977), p. 608.
43. C.E. Coleman, J.F.R. Ambler, Zirconium in Nuclear Industry, STP-633, p. 589.
44. A. Sawatzky, J. Nucl. Mater. 2(1960): p. 62.
45. W.H. Erickson, Electrochem. Tech. 4(1966): p. 205.
46. L.A. Simpson, C.D. Cann, J. Nucl. Mater. 126(1984). p. 70.
47. R. Dutton, Int. J. Hydrogen Energy 9(1984): p. 147
48. C.E. Coleman, Zirconium in the Nuclear Industry. Fifth Conference, ASTM STP-754 (Philadelphia, PA: ASTM, 1982), p. 393
49. H. Margolin, Metall. Trans. 7A(1976): p. 1233.

50. N.E. Paton, J.C. Williams, Hydrogen in Metals, ed. I.M. Bernstein, A.W. Thompson, (Metals Park, OH: ASM International, 1974), p. 409.
51. D.N. Williams, Mater. Sci. Eng. 24(1976): p. 53.
52. R.R. Boyer, W.F. Spurr, Metall. Trans. 9A(1978): p. 23.
53. N.R. Moody, W.W. Gerberich, Metall. Trans. 11A(1980): p. 973.
54. N.R. Moody, W.W. Gerberich, Metall. Trans. 13A(1982): p. 1055.
55. R.S. Stampella, R.P.M. Proctor, V. Ashworth, Corros. Sci. 24 (1984): p. 325.
56. M.J. Blackburn, J.A. Feeney, T.R. Beck, Advances in Corrosion Science and Technology, ed. M.G. Fontana, R.W. Staehle, Vol. 3 (New York, NY: Plenum Press, 1973), p. 67.
57. K. Mori, A. Takamura, T. Shimose, Corrosion 22(1966): p. 29.
58. H. Buhl, Corros. Sci. 13(1973): p. 639.
59. D.B. Dawson, Metall. Trans. 12A(1981): p. 791.
60 J R Ambrose, J. Kruger, J. Electrochem. Soc. 121(1974). p. 599.
61. M. Levy, D.W. Seitz, Corros. Sci. 9(1969): p. 341.
62. L.C. Covington, Corrosion 35(1979): p. 378.
63. L L Gilbert, C.W. Funk, Metal Prog. 70, 11(1956): p. 93.
64 C.F Clarke, D. Hardie, P. McKay, Corros. Sci. 26(1986). p. 425.
65. H.P. Leckie, Corrosion 23(1967): p. 187.
66. R.W. Schutz, L.C. Covington, CORROSION/81, paper no. 61 (Houston, TX. National Association of Corrosion Engineers, 1981).
67 V.H. Buchner, M.A. Gutjahr, K-D Bean, H. Saufferer, Z. Metallkunde 63(1972): p. 497.
68. T. Okada, Electrochim. Acta 28(1983): p. 1113.
69. G. Sanderson, J.C. Scully, Trans. TMS-AIME 239(1967): p. 1883.
70. J.B. Cotton, Chem. Eng. Prog. 66(1970): p. 57.
71 E.N. Pugh, J.A.S. Green, P.W. Slattery, Proceedings of the 2nd International Conference on Fracture (London, England: Chapman, Hall, 1969): p. 387.
72. R.P. Frankenthal, Corros. Sci. 7(1967): p. 61.
73. K. Ebtehaj, D. Hardie, R.N. Parkins, Corros. Sci. 28(1988): p. 811.
74. G. Sanderson, J.C. Scully, Corros. Sci. 8(1968): p. 771.
75 E E Millaway, M.H. Kleinman, Corrosion 23(1967): p. 88.
76 W R Wearmouth, G.P. Dean, R.N. Parkins, Corrosion 29 (1973): p. 251.
77 R N Parkins, Stress Corrosion Cracking – The Slow Strain Rate Technique, ed G.M. Ugiansky, J.H Payer, ASTM STP-665 (Philadelphia, PA: ASTM, 1979), p. 5.
78 J C Scully, Stress Corrosion Cracking – The Slow Strain Rate Technique, STP-665, p. 237.
79 J C Scully, Stress Corrosion Research, ed. H. Arup, R.N. Parkins (The Netherlands. NATO, Sijthoff and Noordhoff, 1979), p. 209.
80 H H Johnson, Stress Corrosion Cracking and Hydrogen Embrittlement of Iron-Base Alloys, NACE 5 (Houston, TX. NACE, 1977), p. 382.
81 J K Tien Effect of Hydrogen on the Behaviour of Materials, ed. A W Thompson, I M Bernstein (New York, NY. TMS-AIME, 1976), p. 309.
82 J C Scully, and D T Powell, Corros. Sci. 10(1970). p. 371.
83 T R Beck, Corrosion 30(1974): p. 408.
84 T R Beck, J. Electrochem. Soc. 114(1967). p. 551.
85 I A Menzies, A F Averill, Electrochim. Acta 13(1968). p. 807.
86 D T Powell, J C Scully, Corrosion 25(1969). p. 483.
87 J C Scully, D T Powell, Corros. Sci. 10(1970). p. 719.
88 A J Sedriks, P W Slattery, E.N. Pugh, Fundamental Aspects of Stress Corrosion Cracking (Houston, TX: NACE, 1969), p. 673.
89. J.C. Scully, T.A. Adepoju, Corros. Sci. 17(1977): p. 789.
90. K Ebtehaj, D Hardie, R.N. Parkins, Corros. Sci. 25(1985): p. 415.
91. D. Hardie, K. Ebtehaj, R.N. Parkins, Hydrogen and Materials Third Congress, ed. P. Azou (Paris, France: L'ecole des Arts et Manufacture, 1982), p. 815.
92. R.P. Marshall, Trans. TMS-AIME 233(1965): p. 1449.
93. J.L. Waisman, R. Toosky, G. Sines, Metall. Trans. 8A(1977): p. 1249.
94. D.G. Chakrapani, E.N. Pugh, Corrosion 31(1975): p. 247.
95. R. Tunold, H. Holtan, M.-B.H. Berge, A. Lasson, R. Steen-Hansen, Corros. Sci. 17(1977): p. 353.
96. G. Sanderson, D.T. Powell, J.C. Scully, Corros. Sci. 8(1968): p. 473.
97. B.F. Brown, C.D. Beachem, Corros. Sci. 5(1965): p. 745.
98. B.F. Brown, J. Material 5(1970): p. 786.
99. H.-R. Smith, D.E. Piper, F.K. Downey, Eng. Fract. Mech. 5(1968): p. 123.
100. D.B. Dawson, R.M. Pelloux, Metall. Trans. 5(1974): p. 723.
101. R.E. Curtis, R.R. Boyer, J.C. Williams, Trans. ASM 62(1969): p. 457.
102. I.R. Lane, J.L. Cavallaro, A.G. Morton, Stress Corrosion Cracking of Titaniun (Philadelphia, PA: ASTM, 1966), p. 246.
103. R.A. Sragué, D.L. Ruckle, M.P. Smith, Titanium Science and Technology, ed. R.I. Jaffee, H.M. Burte (London, England: Plenum Press, 1973), Vol. 1, p. 1731.
104. K. Ebtehaj (Ph.D. diss., University of Newcastle upon Tyne, 1984).
105. J.E. Hack, G.R. Leverant, Metall. Trans. 13(1982). p. 1729.
106. C.E. Coleman, S. Sagat, K.F. Amouzouvi, Atomic Energy of Canada Ltd. Report AECL-9524 (presented at Canadian Institute of Mining and Metallurgy Conference), 1987.
107. D.T. Powell, J.C. Scully, Corrosion 24(1968): p. 151.
108. I. Aitchison, B. Cox, Corrosion 28(1972): p. 83.
109. D.B. Knorr, R.M. Pelloux, Metall. Trans. 13A(1982): p. 73.
110. E.I. Meletis, R.F. Hochman, Corrosion 40(1984): p. 39.
111. R.H. Van Stone, J.R. Low, J.L. Shannon, Metall. Trans. 9A (1978): p. 539.

Discussion

E.N. Pugh (National Institute of Standards and Technology, USA): Do you consider that dealloying plays a key role in transgranular SCC of Mg-Al? In our work [Chakrapani and Pugh, Metall. Trans. 7A(1976): p. 173], we found that failure occurred by discontinuous cleavage on {3140}. Hydrogen embrittlement is attractive, but the fracture morphology and orientation is quite different in specimens tested in gaseous hydrogen and in precharged samples. Given the current interest in dealloying as the cause of transgranular SCC in other alloys and the early observation by Pickering and Swann [Corrosion 19(1963): p. 373t] that porous dealloyed layers are formed in Mg-Al, it is reasonable to suggest that transgranular SCC occurs by film-induced cleavage, the film being a dealloyed layer.

D. Hardie: A great deal of reference has been made to dealloying in this conference, and I feel that it is too frequently invoked in an apparent attempt to unify mechanisms. No dealloying has been detected in the Mg-Al alloys and, as shown by Proctor (Reference 55), identical features are observed on the fracture surfaces produced when pure magnesium suffers environment-induced cracking in an aqueous environment, where no dealloying can in fact occur. It should be noted that Pickering and Swann found dealloying, both in solutions that caused SCC and those that did not.

I would not dispute your point that transgranular fracture caused by hydrogen (both precharged and gaseous) may be of a different crystallographic character to that observed in aqueous environments, since we did not identify the crystal plane involved in cleavage of our Mg-Al. This does not in itself necessarily preclude hydrogen playing a role in the failures in aqueous environments.

R.P.M. Procter (University of Manchester Institute of Science and Technology, UK): In the work referred to, we showed that both commercially pure and high-purity magnesium are susceptible to hydrogen embrittlement when subjected to slow-strain-rate tensile

testing in 10^{-3} M sodium sulfate solution at pH 10. The source of hydrogen is the local action cathodic reaction. Atomic hydrogen can only enter the metal through bare, film-free pit walls. Cathodic polarization prevents pitting and therefore prevents hydrogen entry and embrittlement. On the other hand, anodic polarization promotes pitting and hydrogen entry and therefore results in more severe embrittlement. That the cracking was due to hydrogen was confirmed by the fact that specimens exposed unstressed to the environment and subsequently tested in air were embrittled. However, this embrittlement was eliminated by holding the pre-exposed specimens at room temperature for 24 h. The cracking was transgranular in commercial-purity magnesium and mixed inter- and transgranular in high-purity magnesium. We did not study the crystallography of the cleavage facets, but clearly the formation of a dealloyed layer cannot be involved in this cracking.

E.N. Pugh: I was not aware that pure magnesium undergoes {31$\bar{4}$0} cleavage-type failure in aqueous solutions. We have been unable to produce such failures. I believe it will fail by hydrogen embrittlement, as will Mg-7Al, but this is not equivalent to transgranular SCC of Mg-7Al in the aqueous Cl^-/CrO_4^{2-} solutions.

B. Cox (Atomic Energy of Canada Ltd., Canada): I thought I heard you say that titanium was more susceptible than zirconium to hydrogen embrittlement because of its high hydrogen solubility. The only way that would be true would be if both could be cracked in the absence of hydride precipitates. This is not so for zirconium and (despite the electron microscopy of Birnbaum) I know of no well-attested example of such a failure in a macroscopic titanium sample. In fact, most of the in-service failures of zirconium components by hydride cracking have occurred with the as-received hydrogen content, because that is inevitably above the low-temperature hydrogen solubility.

D. Hardie: If indeed I did say that, it was a slip of the tongue. The point that I intended making in Figure 1 was to emphasize that more hydrogen would be required to promote embrittlement of titanium than of zirconium under given conditions. At ambient temperature, the amount of hydrogen necessary to precipitate hydrides is certainly well below the normal level in as-received zirconium. Like you, I have not come across any reference to a service failure (due to hydrogen) in titanium that did not involve hydrides.

K. Sieradzki (The Johns Hopkins University, USA). A large number of models exist for the brittle-ductile transition in steels. [See, for example, Lin, Evans, and Ritchie, J. Mech. Phys. Solids 34(1986), p. 477.] These models incorporate many features that your simple model neglects. Have you investigated the applicability of some of these models to the brittle-ductile transition described in your paper?

D. Hardie: This idea would certainly be worth investigating, but it must be appreciated that the ductile-brittle transition in hydrided hexagonal metals is entirely different in character from that in carbon steels, i.e., it is not attributable to an intrinsic change in fracture mode in the matrix, but rather to the presence of brittle hydrides.

B. Cox: You choose between anodic dissolution and hydrogen embrittlement cracking mechanisms in zirconium or titanium, using the crack velocity as one criterion. Yet in zirconium the fastest transgranular cracking process is the "metal embrittlement" cracking, which occurs in metal vapor (as well as in liquid or solid metals) and is almost certainly an adsorption-induced cracking. The transgranular cracking of zirconium (and titanium) in dry halogen vapors is closely analogous to the metal vapor case and is also probably adsorption-induced, since neither anodic dissolution (no ionic solvent, the products are nonpolar) nor hydrogen embrittlement (hydrogen in solution) can be causing it. It seems possible that liberation of halogen at the crack tip could occur in methanol/hydrochloric acid and provide a third potential mechanism, with a velocity equal to or greater than that due to hydrogen embrittlement.

D. Hardie: I introduced the section on anodic dissolution vs hydrogen embrittlement by quoting the arguments that have been advanced with respect to the high crack velocities involved. My intention, however, was not to choose between the mechanisms on a velocity basis. There is obviously an even greater problem in reconciling high crack velocities with "diffusion" of metal or halide ions. I would therefore agree that the fracture mechanism in the latter environments must be entirely different and may indeed be attributable to surface adsorption. I see no fundamental objection, however, to invoking different basic mechanisms for differing circumstances. Your suggestion that halide embrittlement may be involved in cracking of titanium and zirconium in methanol/hydrochloric acid mixtures is interesting. This would mean there are three competitive mechanisms. There is no doubt, however, that the dark-etching boundaries to which I referred (Figure 10) provide unequivocal evidence for the involvement of hydrogen penetration.

R.A. Oriani (University of Minnesota, USA): You said that in the presence of stress concentrators, a titanium alloy needs more water in a mixed solvent to passivate than in the absence of stress concentrators. Would you explain this?

D. Hardie: I was referring to the corrosion fatigue results of Dawson (Reference 59) with respect to the need for high water levels to inhibit cracking in the presence of stress concentrations. I believe that the role of the stress concentrator in breaking down passivity is to promote local plastic strain.

T.-L. Yau (Teledyne Wah Chang Albany, USA): It seems that too much attention has been given to the hydriding tendency of these metals, and too little to the role of oxygen, which can greatly inhibit the hydriding tendency. For example, an environment with an oxygen/hydrogen ratio of 1.40 is sufficient to prevent hydriding of zirconium.

D. Hardie: Your comment relates to the effect of oxygen in the environment. This may indeed prevent hydrogen pick up in materials such as titanium and zirconium, which have a very high affinity for oxygen, particularly where it promotes a passive surface film. No mention of temperature is made in your question, but it should always be remembered that hydrogen may be driven out of exothermic occluders at high temperatures, unless a high hydrogen fugacity is maintained.

M.B. Ives (McMaster University, Canada): It is not clear to me what is unique, if anything, about the environmental cracking of hexagonal metals. What is the particular role of crystallography in these materials?

D. Hardie: Although I stated that crystallography does not provide a unifying factor in the environment induced cracking of hexagonal metals, the details of the specific failure mechanisms may indeed involve crystallographic considerations. One example from the literature is the relationship between deformation twin planes and the habit planes for hydride precipitation in the fracture of zirconium (Reference 18 in my paper). Others are the importance of basal pole concentration in stress induced hydride formation (Reference 31) and delayed failure (Reference 52) in zirconium and titanium.

R.C. Newman (University of Manchester Institute of Science and Technology, UK): I recall work by Latanision, Opperhauser, and Westwood [Scripta Metall. 12(1978)· p. 475] on zinc in sodium sulfate solution. They suggested that the effect of potential was to affect dislocation interactions with the surface, via the surface charge density (or maybe there was a film). Does this have any value in the discussion of magnesium cracking? Incidentally, the zinc cracking is really fun to study!

D. Hardie: I did not include zinc in my review, but I am grateful to you for bringing this work to our attention. Latanision, et al., do suggest that the effect of charge density on fracture behavior, where cracks initiate from the surface in contact with the environment, may be relevant to hydrogen embrittlement because of the electropositive absorbate. They certainly observed significant reduction in the time-to-failure of zinc crystals with an applied potential of -1200 mV_{SCE}.

SECTION VI

Environment-Induced Cracking in Nonferrous Alloys

Rapporteurs' Report on Poster Presentations

L.A. Heldt
Michigan Technological University
Houghton, Michigan, USA

B.D. Lichter
Vanderbilt University
Nashville, Tennessee, USA

This session included papers dealing with a variety of "nonferrous" materials. aluminum-, copper-, nickel-, and titanium-based alloys. It also included a paper on stress corrosion cracking of uranium-silver interfaces in silver-coated uranium/type 304 (UNS S30400) stainless steel weldments.

ALUMINUM ALLOYS: The paper by Elboujdaini, et al., presents data showing the relative differences in the stress corrosion cracking resistance of commercial aluminum-magnesium-silicon alloys at room temperature in chloride media. A strong relationship exists between pitting mode and susceptibility to stress corrosion cracking. Kim, et al., report interesting results for type 6351 that extend the concept of environment-induced cracking to consideration of lead-assisted failure. This work is interesting both from the variety of analytical techniques used and because of its relationship to solid metal-induced embrittlement reviewed earlier in the conference by Stoloff. During the plenary session, the following comments were made in relation to this paper:

Y.S. Kim (Case Western Reserve University, USA): We show in our paper that voids initiate by tensile separation at the interface between lead-containing particles on the grain boundaries and within the matrix in high lead-containing alloys. Low-ductility intergranular failure is promoted by lead, which is released from the cracked or decohered particle either in the matrix or at grain boundaries.

The contribution of Liao presents constant-deflection test results for 7000 and 5000 series aluminum alloys, including K_{Iscc} values, Stage II crack growth rates, and fractographic analysis The final paper in this group, by Hepples, et al., deals primarily with microstructural effects in alloy 7150, as affected by "retrogression re-aging," and shows the beneficial effects of this treatment in reducing copper segregation at grain boundaries.

COPPER ALLOYS Two papers are incorporated into the proceedings on alpha-brass, although only one was presented at the conference. The work of Shih and Tzou presented results of CERT'SSRT'SEXT (call it what you will!) tests in acidified fluoride solutions showing the effects of pH, strain rate, and potential on intergranular stress corrosion cracking. In response to several questions raised in the plenary discussion session following the poster viewing, the following statement was made by the author:

H.C. Shih (National Tsing Hua University, Republic of China): In our paper, we are dealing with brass in an environment containing fluoride and we have found that (1) there exists a critical pH value, at about 9, below which stress corrosion cracking will take place, but above which stress corrosion cracking is inhibited. The fracture mode is predominantly intergranular (2) Cathodic potentials prevent stress corrosion cracking, while anodic potentials promote it No hydrogen embrittlement was observed in this system. (3) X-ray diffraction showed the existence of cuprous oxide in alkaline environments. (4) The open-circuit potential changed to more negative values as solution pH was increased. OH ions in this system polarize the cathodic reaction and therefore can be considered as cathodic inhibitors (5) We are certain that the mechanism for the stress corrosion cracking of this system is the anodic dissolution at the crack tip. Cuprous oxide retards dezincification at solution pH greater than 9.

Additional concerns on this paper expressed by delegates are found in the discussion immediately following the paper in the volume.

One other paper on alpha-brass, by Chatterjee and Sircar, was not presented at the conference, and therefore was not discussed there. It is included in the proceedings without comment to provide a platform for the views of the authors.



Photos: M.B. Ives

NICKEL ALLOYS: The paper by Kolts presents a comparison of the susceptibilities to embrittlement of type 316 (UNS S31600) stainless steel and three nickel-base alloys [types 825 (UNS N08825), C-276 (UNS N10276), and C-22 (UNS N06022)] commonly used in deep-well environments. The test environments contained hydrogen sulfide and hydrogen chloride at room temperature and produced transgranular cracking, which was accelerated by anodic polarization and retarded by additive inhibitors. Nagano, et al., present an analysis of the factors that produce intergranular attack in type 600 (UNS N06600). This includes both intergranular corrosion, which serves as a crack initiator, as well as the ensuing intergranular stress corrosion cracking. The third paper in this group, by Garud and McIlree, develops a new model for the cracking of alloy 600. During the plenary session discussion, one of the authors of this paper led the following discussion exchange:

Y.S. Garud (S. Levy Incorporated, USA): In connection with the mechanisms of stress corrosion cracking (viz., metal dissolution vs hydrogen embrittlement), one is left with the impression, after reviewing the presentations on nickel-base alloys, that either one or the other mechanism prevails. As I have pointed out elsewhere (EPRI Report, NP-3057, 1983), it is likely that metal dissolution is essential for the intergranular stress corrosion cracking of type 600 in aqueous media, but that possibly hydrogen also influences the overall process. This may occur, for example, through the interaction of hydrogen with localized deformation, which in turn affects the film-rupture process. In effect, the two mechanisms need not be exclusive, and this may be particularly true for type 600.

R.H. Jones (Pacific Northwest Laboratory, USA): There are a number of combined anodic dissolution/hydrogen embrittlement processes that may act synergistically to cause stress corrosion cracking. These processes include corrosion crack-tip sharpening, hydrogen uptake during film-free corrosion, and hydrogen effects on the behavior of crack-tip dislocations.

TITANIUM ALLOYS: The poster paper by Clarke, et al., complements the review paper of Hardie, presented orally earlier in the session with a practical account of titanium alloy selection for possible application as a nuclear waste container material in which both crevice corrosion and hydrogen embrittlement may occur. One additional paper, not discussed during the conference, is authored by Zhang and Vereecken, and describes the behavior of Ti-6Al-4V in acidic methanol solutions.

A summary observation made at the end of the plenary session, returning to the question of whether anodic dissolution and hydrogen embrittlement are mutually exclusive mechanisms, is appropriate here:

D. Hardie (University of Newcastle upon Tyne, UK): I would like to link a comment on a point raised in this discussion with both a general observation made in my own presentation and the poster presentation on titanium. Although I introduced the topic of "anodic dissolution or hydrogen embrittlement" in my talk, I then continued by describing a particular situation where both were involved, and I believe quite firmly that this is frequently the case. A slight change in the prevailing conditions (such as the presence of water in the methanol-hydrochloric acid environment) may produce a pronounced change in the balance between dissolution and embrittlement. The dissolution itself may play a dual role by penetrating passive films and producing an embrittling species such as hydrogen. The crevice corrosion of Grade 2 titanium in the poster presentation by Clarke, Ikeda, and Hardie (this proceedings) provides a good example of such a situation, where localized dissolution results in penetration by hydrogen and the formation of embrittling hydrides. However, in these particular circumstances, penetration by crevice corrosion is so rapid that hydrogen embrittlement plays a minor role in the overall failure. Not only may both dissolution and hydrogen embrittlement be involved in a particular situation, but the one may actually depend on the other.

URANIUM-SILVER INTERFACES: The presentation by Rosen, et al., is concerned with the integrity of welds involving a uranium-silver interface when exposed to moist air. Under these conditions, stress corrosion cracking failures are observed at the interface. Specimens were stressed in Mode III loading, and subjected to long-term tests (four years) at a relatively small fraction of their ultimate strength. For short-term tests, specimens exhibited stress corrosion cracking within days when stressed to one-half their ultimate strength.

The individual papers submitted and presented as poster presentations now follow, along with specific discussion points where these are addressed primarily to specific papers.

Stress Corrosion Cracking of Aluminum Alloys in Chloride Media

*M. Elboujdaini, E. Ghali, and A. Galibois**

Abstract

Stress corrosion cracking (SCC) behavior of 5083 aluminum-magnesium (UNS A95083), 6061 (UNS A96061), and 6351 aluminum-magnesium-silicon alloys in 3% NaCl solutions was studied. Potentiokinetic determinations of the characteristic pitting potential (E_{pit}) and protection potential (E_{prot}) for a given sweep rate were made. Impressed potentials equal to or more positive than the pitting potential (E_{pit}) generated the maximum degradation of the mechanical properties, while at values lower than the protection potential (E_{prot}), no mechanical properties of aluminum alloys were altered. The mechanical and fractographic properties showed that the predominant features of SCC were pitting and anodic dissolution, attributed in some cases to the presence of precipitates at grain boundaries. The alloy 5083 showed a relatively better performance than alloy 6351, which demonstrated susceptibility to SCC with a clear intergranular path. A correlation between electrochemical behavior and SCC resistance of these alloys is discussed.

Introduction

When a metallic surface is not protected, it will suffer uniform corrosion. However, when the material is susceptible to the formation of a passive film, the latter corrosion phenomenon is replaced by a localized and more dangerous one resulting from the breakdown of this film, i.e., stress corrosion cracking (SCC). The transition from pitting attack to SCC has been noted in the literature.[1-3] The nucleation of stress corrosion cracks from corrosion pits has been observed in aluminum and some of its alloys.[4] Furthermore, the plastic deformation at a crack tip, resulting from the local stress concentration, could prevent the re-formation of the protective film. This leads, in an aggressive environment, to a localized and high rate of metal loss by dissolution, thus promoting crack growth.[5,6] The fundamental processes occurring in SCC have been the subject of several investigations reported and reviewed in the literature.[7-11]

Aluminum and aluminum alloys are materials falling into this class and are thus susceptible to the SCC phenomenon. However, because of their compatibility and their corrosion resistance to methane and hydrogen environments, aluminum alloys [except those of high mechanical properties, e.g., the series 7000 (Al-Zn-Mg) and 2000 (Al-Cu) series, which are in fact susceptible to hydrogen embrittlement[12,13]] are actually used to process, handle, and store these gases as well as natural gas. Indeed, aluminum is generally suitable for use with hydrogen under pressure both at high and low temperatures.[14] Tests conducted on aluminum and aluminum alloys (5000 and 6000 series) revealed that they represent one of the few classes of metals not embrittled by hydrogen.[15] In addition, aluminum is resistant to methane both in gaseous and liquid states.[16] The U S Department of Transportation (DOT) Exemption 6498 approves the use of Al 6351-T6 for the transportation of compressed methane.

Nevertheless, some problems are encountered in aluminum alloys with some of the contaminants either in commercial grade gases or from the environment. Therefore, performance of the more susceptible aluminum alloys to be used in different corrosion media should be fully examined for safety purposes. This paper deals with the SCC behavior of three such alloys, two from the 6000 series and one from the 5000 series, for comparison purposes.

Corrosion behavior, including pitting of different alloys, was studied by potentiodynamic techniques. Electrochemical control was maintained for a SCC test samples by galvanostatic or potentiostatic methods. Surface analyses and sample morphology were examined by x-ray diffraction analysis and scanning electron microscopy (SEM).

Experimental

Constant tensile load tests using smooth round-bar specimens were conducted in a 3 wt% sodium chloride environment to examine the influence of applied stress, alloying elements, current density (CD), and potential on the SCC behavior.

Materials

Plates of Al 5083 (UNS A95083) in the H321 temper condition, of Al 6351 (laminated) and of Al 6061 (UNS A96061) (extruded) in the T651 temper condition with the same thickness (13 mm) were obtained for this investigation. The chemical composition and mechanical properties of the tested material are summarized in Tables 1 and 2, respectively.

Test apparatus

The apparatus consisted of a solution tank (volume: 5 L) and five glass cells (volume: 50 mL), each containing a test specimen. The solution was circulated between the tank and each cell by a pump. The apparatus was constructed by ADAMEL.[(1)17] Each glass cell was provided with a counter electrode (Pt) and a saturated calomel reference electrode (SCE). A multichannel potentiostat (ESC† Model 440), interfaced with a computer for data acquisition

*Department of Mining and Metallurgy, Laval University, Quebec, Canada G1K 7P4.

(1)Irsid, France.

†Trade name.

and storage purposes, was used to impose the desired potential or current. Smooth-rod specimens with 5-mm diameters and 12.7-mm gauge lengths (2 cm^2) were used. The specimens were machined with long axes parallel to the rolling direction and were strained between 30 to 80% of the elastic limit during the anodic polarization and during the galvanostatic measurements.

Prior to exposure, each specimen was degreased, cleaned with acetone, and covered with Teflon† tape, except for its gauge portion, which was exposed to testing. The electrolyte was a 3% NaCl solution, deaerated by purging with argon for 60 min before and during the test. The pH measured at the beginning of the experiment was 5.5. The temperature was 21 ± 1°C. A Princeton Applied Research Laboratories† potentiostat (Model 173 plug-in) was used to study the linear sweep polarization behavior and to determine the characteristic pitting potential (E_{pit}) and protection potential (E_{prot}). Polarization curves were traced in the following sequence: (1) increasing the impressed potential in the positive direction at a rate of 17 mV/min, and (2) reversing the direction of potential scan after a CD of 1 mA cm^{-2} was reached.

Results and Discussion

The characteristic pitting potential (E_{pit}) and protection potential (E_{prot}) are shown in Figure 1. The scan speed was fixed at 17 mV/min and has been found to be relatively appropriate and representative for this study. In our experimental conditions, pitting corrosion initiates and propagates freely at potentials more positive than E_{pit}. In addition, existing pits propagate, but no new ones initiate, at potentials between E_{pit} and E_{prot}. The failure mechanism, which is attributed to SCC, was found at potentials approximately equal to or more positive than E_{pit}.

Galvanostatic studies

A galvanostatic study was conducted for the aluminum alloys 5083 and 6061 with and without different levels of external loads (30, 45, 60, and 80% of the elastic limit). The relationship between applied stress and time-to-failure is shown in Figure 2. The curves reveal that both alloys failed at much lower stresses than the material tensile strength, implying that both alloys exhibit SCC susceptibility in deaerated 3% NaCl solution.

For a CD of 3 mA cm^{-2}, the 5083 alloy displayed a much better corrosion resistance than Al 6061 under all applied loads. As shown in Figures 3 and 4, the alloy 5083 did not display any active shift of the potential as a function of imposed loads; however, an important systematic active shift was observed for alloy 6061 as a function of the stress level, and this shift reached 60 mV for the 80% elastic limit test. The results, shown in Figures 2 to 4, confirm the good stress corrosion behavior attributed to the alloy 5083.

The important observation for alloy 5083 is the presence of uniform pitting, numerous but shallow on the side surface, with predominant general corrosion [Figure 5(a)]. The fractographs show the side surface's flat appearance and shallow dimples, indicating poor ductility [Figure 5(b)], whereas, for alloy 6061, pits observed on the side specimens are accompanied with secondary cracks [Figure 5(c)]. Mixed failure modes are apparent, with about 20 to 30% intergranular cracking [Figure 5(d)]. Cracking of the Al 6061 initiates at oxide-filled pits that are probably associated with inclusions. Dissolution of stressed specimens begin at the particle–matrix interface; in some instances, mechanical rupture of the constituents occurred and SCC started at these interfaces. Therefore, the initial stage of SCC is caused apparently by localized corrosion or intergranular attack; when the stress intensity at the crack tip increases to a sufficiently high value, intergranular attack can no longer be sustained, and ductile failure ensues. Similar observations were supported by other authors.[18,19]

†Trade name.

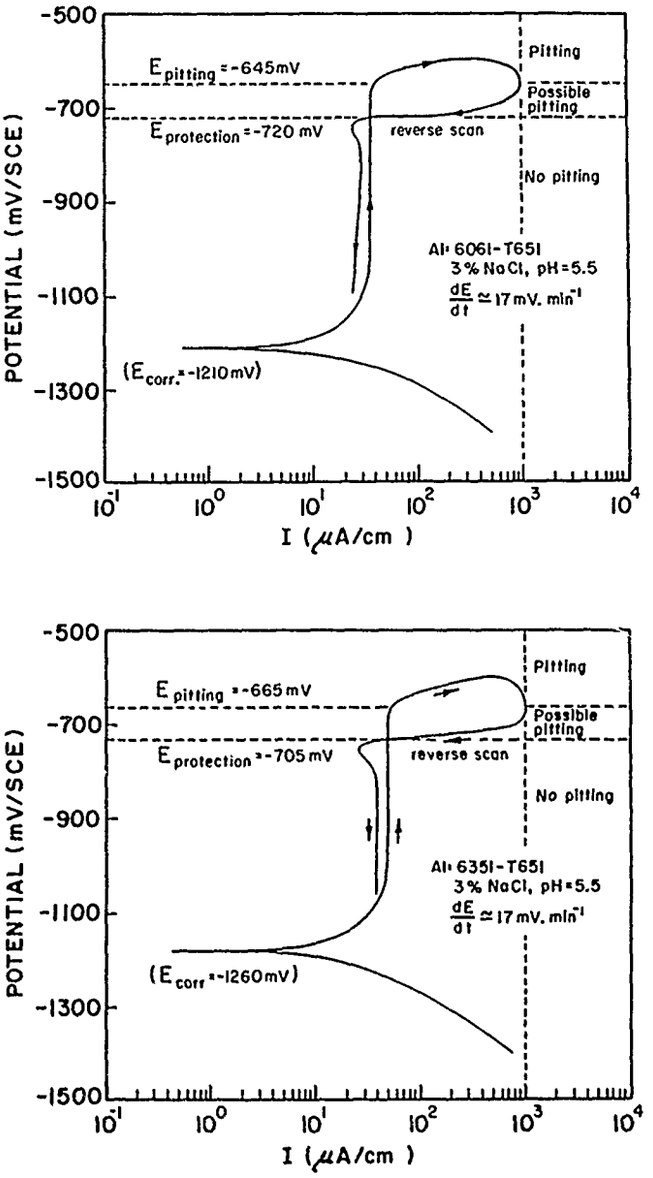


FIGURE 1—Polarization curves of aluminum alloys.

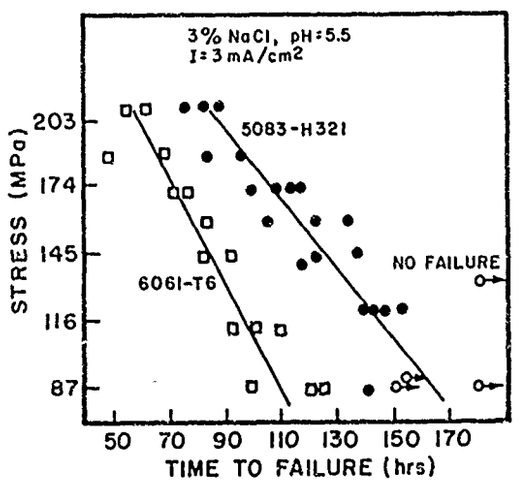


FIGURE 2—Relationship between applied stress and time-to-failure.

TABLE 1
Chemical Composition of Aluminum Alloys (wt%)

Al Alloys	Si	Fe	Cu	Mn	Mg	Cr	Zn	Ti	Others
5083-H	0.4	0.4	0.1	0.6	4.4	0.35	0.25	0.15	0.15
6061	0.6	0.7	0.27	0.15	1.0	0.25	0.25	0.15	0.15
6351	1.0	0.5	0.1	0.6	0.6	0.25	0.20	0.15	0.15

TABLE 2
Mechanical Properties of Aluminum Alloys

Al Alloys	Yield Strength (MPa)	Ultimate Strength (MPa)	Elongation (%)
5083-H321	248	367	10
6061-T651	293	335	15
6351-T651	315	341	12

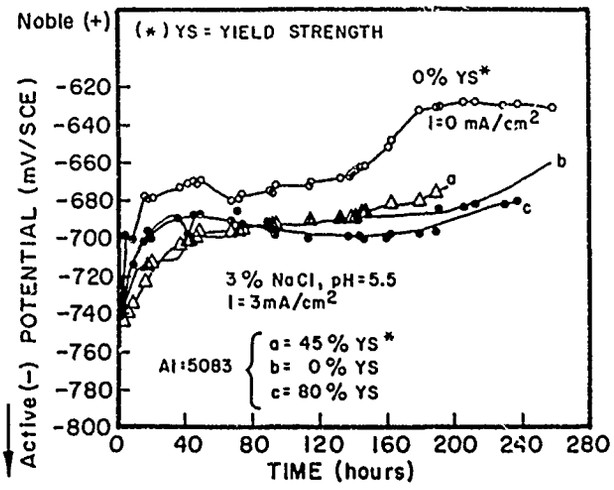


FIGURE 3—Potential evolution during galvanostatic studies of Al 5083.

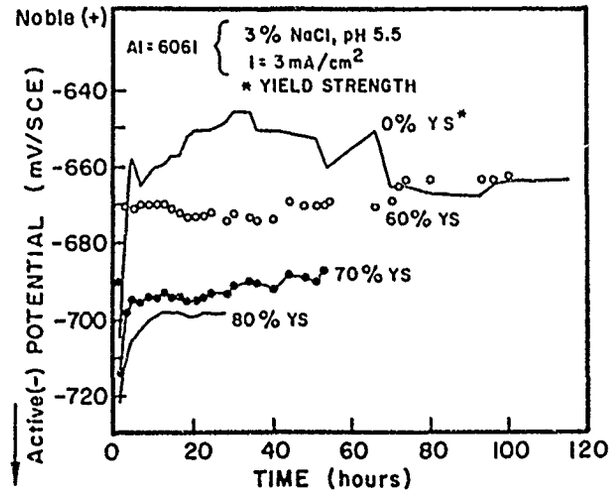


FIGURE 4—Potential evolution during galvanostatic studies of Al 6061 (UNS A96061).

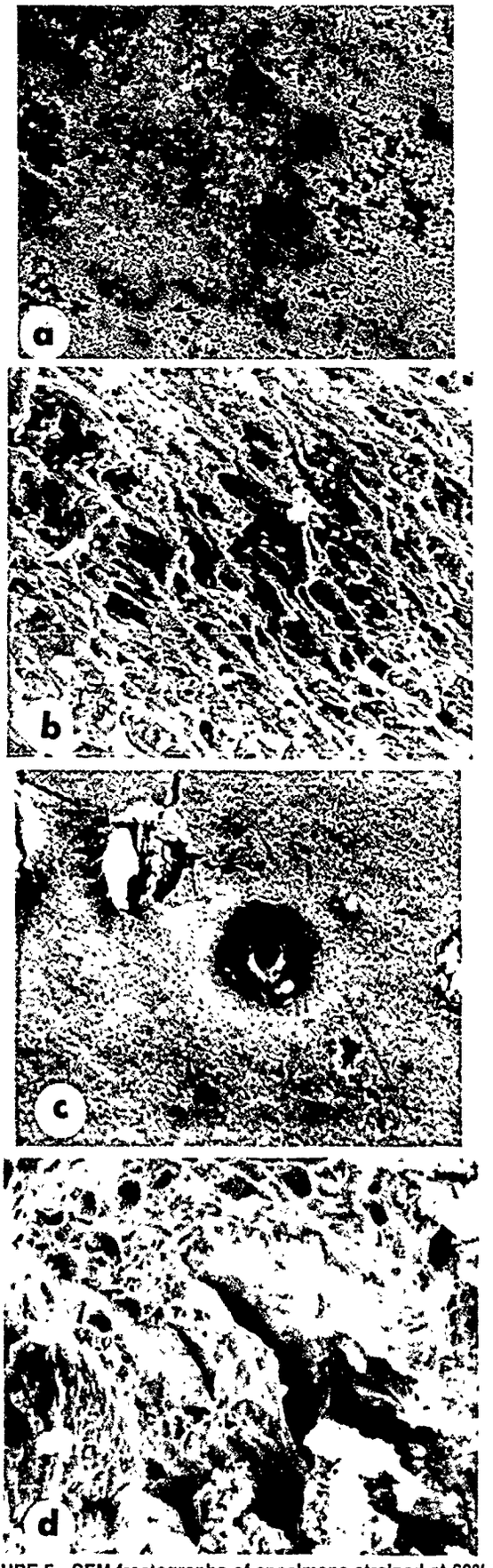


FIGURE 5—SEM fractographs of specimens strained at 60% of the elastic limit under current density (I = 3 mA/cm²) in a 3% NaCl solution: (a) shallow pits and general corrosion on side specimen of Al 5083, (b) fracture surfaces of Al 5083, and (c) propagation corrosion pits in Al 6061 (UNS A96061), and (d) fixture surfaces of Al 6061.

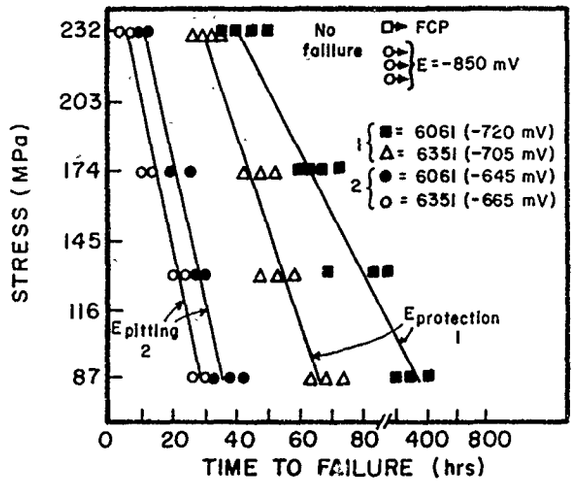


FIGURE 6—Relationship between applied stress and time-to-failure in 3% NaCl.

Potentiostatic Polarization

The influence of the applied potentials and stresses on SCC are shown in Figure 6. The characteristic pitting potentials (E_{pit}) were found to be −645 mV for Al 6061 and −665 mV for Al 6351, whereas the protection potentials (E_{prot}) were −720 mV and −705 mV for the above alloys, respectively (Figure 1).

In both aluminum alloys, when the applied potential was controlled at the pitting potential (E_{pit}) or at a more positive potential, failure occurred within a very short time after the stress was settled at 80% of the elastic limit. However, if that potential was more negative than the protection potential (E_{prot}), failure took longer to occur for the same stress level. The resistance of Al 6061 to SCC was about twice that of Al 6351 when the potential was set up between E_{pit} and E_{prot}, provided that the stresses were lower than 60% of the elastic limit. If the applied stress level was only 40% of the elastic limit, failure by SCC did not occur.

Anodic CD evolution

Figure 7 shows the evolution of the anodic current as a function of time for Al alloys of the 6000 series when either E_{pit} or E_{prot} was imposed. For the current evolution [E_{pit}, Figure 7(a)], two distinct regions are observed in each curve for the two alloys. (1) a rapid increase at the beginning (Part I), which may suggest a uniform attack of the reactive surface, and (2) a gradual current increase accompanied by a certain stabilization (Part II), which reflects the propagation of the pits. No efficient passivation is observed that can contribute to a decrease of the corrosion current. For E_{prot} [Figure 7(b)], the curve showed a noticeable decrease of current that is characteristic of a passivation phenomenon. The amount of current at E_{pit} was 30 times greater than at E_{prot} level, indicating the importance of the electrochemical attack, since SCC was observed at E_{pit}. Both potential levels show that the corrosion current for the Al 6351 alloy was always higher than that for the Al 6061 alloy.

Figures 8 and 9 show scanning electron fractographs of the specimens tested at the pitting potentials of −645 mV for Al 6061 and of −665 mV for Al 6351. The crack morphology on the specimens shows localized corrosion (pits) with secondary cracks [Figures 8(b) and 9(b) for alloys 6061 and 6351, respectively]. All of the specimens that underwent SCC exhibit the apparent mixed mode (intergranular and ductile failure) of fracture as seen in Figures 8(c) and 9(c). This can be explained as follows: Material degradation was brought about by electrochemical phenomenon, causing localized intergranular attack. This induced a weakening of the material, and led to a purely mechanical failure through overload, as shown by the typical dimple morphology.

A failure of the Al 6061 at the pitting potential (−645 mV), was observed on the side surface [Figure 10(a)]. General corrosion is also shown, in addition to the dominating preferential attack manifested by

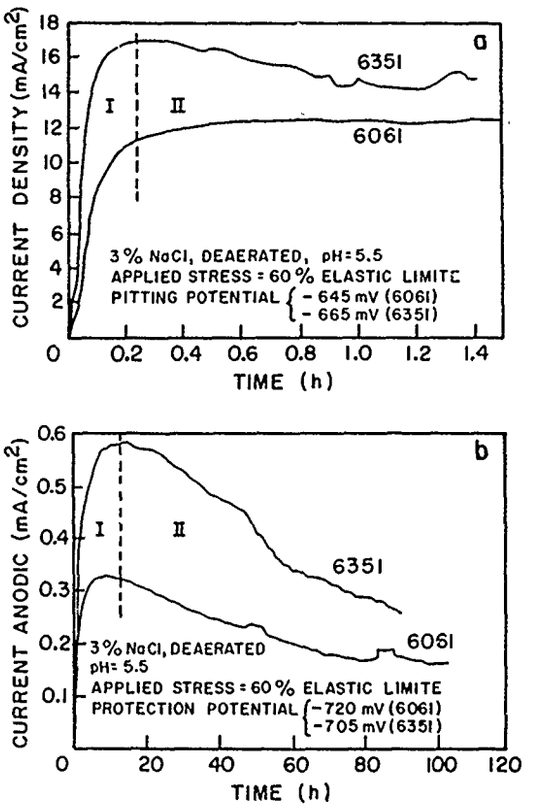


FIGURE 7—Current density as function of time at (a) the pitting potential and (b) the protection potential.

grooves at grain boundaries. In the passive region (−850 mV), the attack is much less than that at the pitting potential [Figure 10(b)], and the time-to-failure increases exponentially. The question that may arise now is whether the predominant SCC mechanism of the aluminum alloy 6061 and 6351 is hydrogen embrittlement or anodic dissolution. This work has shown that the stress corrosion behavior of these alloys is greatly affected by the load, and a large time-to-failure has been observed as a function of imposed potential.

A critical potential exists below which failure does not occur. It was also noted that the time-to-failure is dominated by the initiation period. This may suggest the existence of a critical potential for the initiation stage. The initiated crack can be arrested if the imposed potential is lower than the critical one, while at potentials more positive than the pitting potential (E_{pit}), localized and deep pits were formed. A morphological change has been identified previously[20] as an indication of the significant modification of the protective properties of the passive film that formed on aluminum alloys when the potential was increased above the protection potential (E_{prot}).

Experimental data suggests the main factor for SCC is polarization. If the potential is lower than the critical potential ($E < E_{pit}$), an aggressive environment cannot build up at the crack tip, and shallow cracks will remain inactive because of the formation of a protective film. However, if the potential is high enough, the rate of metal dissolution at the crack tip will be enhanced.

The electrochemical phenomena at the crack tip seem to control the potential that plays an important role in the Al alloys' resistance to SCC. The time-to-failure decreases with the increasing potential, indicating an increase in anodic dissolution. This is consistent with the results of other previous studies of the microscopic analysis of different aluminum alloys.[21,22]

Conclusion

(1) In a solution of 3% NaCl at a CD of 3 mA/cm², SCC in both alloys, i.e., Al 5083 and 6061, is strongly affected by the level of external loads. In spite of a large uncertainty in the time-to-failure vs stress relationship, the Al 5083 alloy appears to offer much better resistance to SCC than the Al 6061 alloy at ambient temperature.

(2) When the tests are conducted at the pitting potential, both the Al 6061 and Al 6351 alloys display ductile and intergranular cracks. SEM observations indicate that corrosion tunnels are formed occasionally at fracture planes, suggesting that propagation results from pitting. Prior to the protection potential (E_{prot}), the time-to-failure increases exponentially, and fractographs reveal a typical dimple morphology with shallow intergranular cracks.

(3) Results show that SCC susceptibility is increased by increasing anodic polarization. The better performance of Al 5083 alloy can be ascribed to its uniform type of pitting (numerous but shallow pits). The Al 6351 alloy, however, displays a more localized pitting pattern.

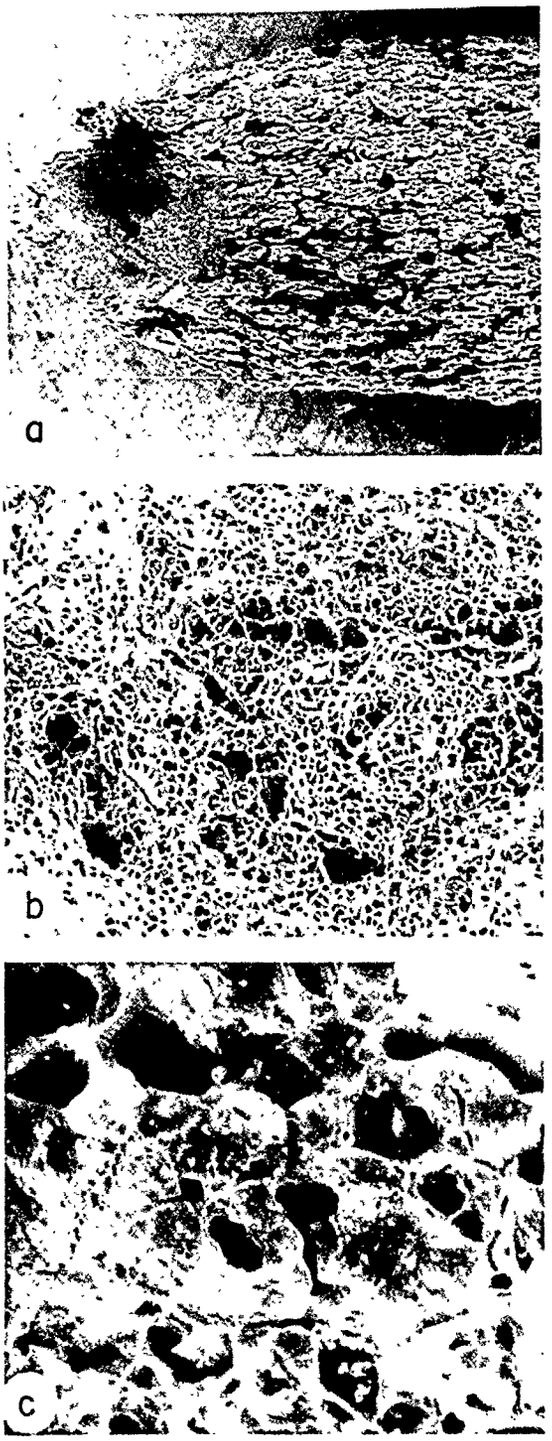


FIGURE 8—SEM fractographs of fracture surface of Al 6061 (UNS A96061) produced in 3% NaCl and tested at 60% of the elastic limit: (a) overall view, (b) intergranular and ductile failure, and (c) intergranular cracks.

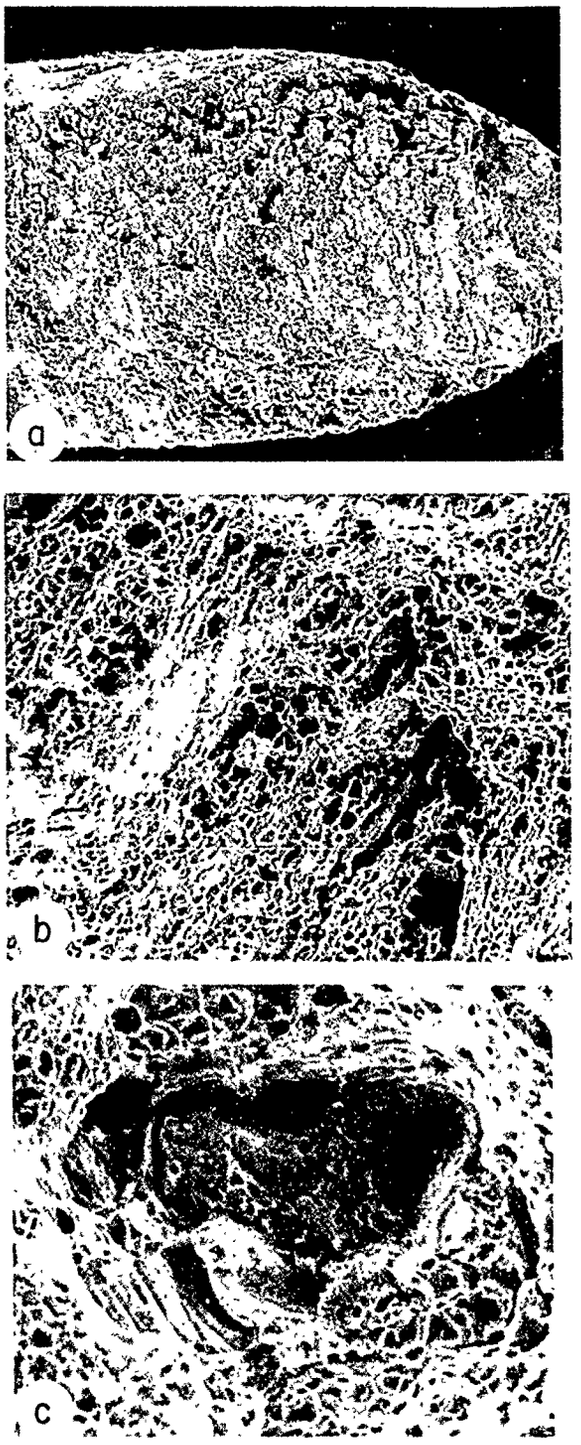


FIGURE 9—SEM fractographs of fracture surface of Al 6351 produced in 3% NaCl tested at 60% of the elastic limit showing (a) overall view, (b) intergranular and ductile failure, and (c) intergranular cracks.

Acknowledgment

The authors would like to thank the National Science and Engineering Research Council of Canada (NSERC) for providing financial support. The authors also thank Dr. M. Girgis of the Department of Chemistry at Carleton University of Ottawa for his helpful discussions.

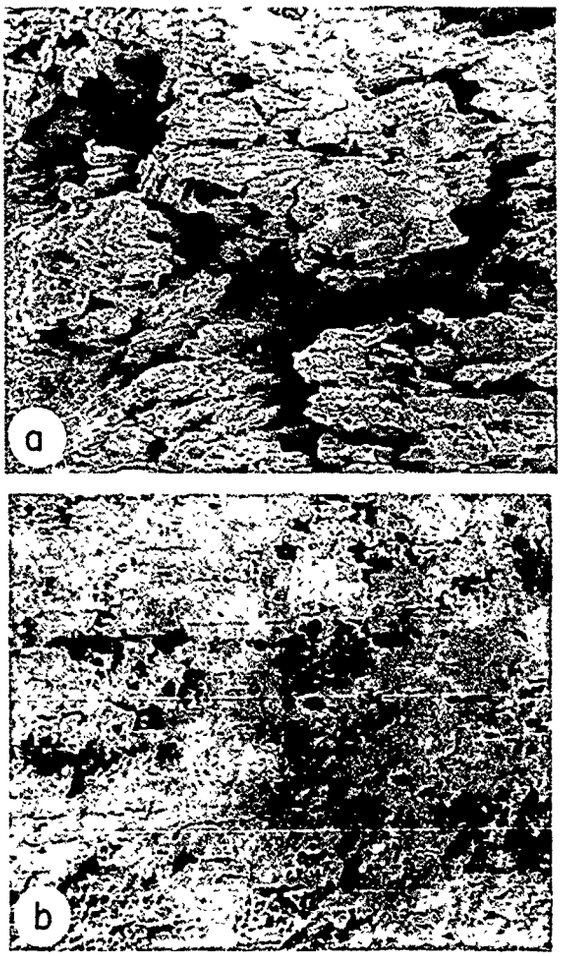


FIGURE 10—SEM fractographs of the lateral surface of Al 6061 (UNS A96061) in 3% NaCl at (a) E_{pit} = −645 mV and (b) E_{prot} = −850 mV.

References

1. J.E. Truman, Corros. Sci. 17(1977): p. 737.
2. J E Sotoudeh, T.H. Nguyen, R.T. Foley, B.F. Brown, Corrosion 37, 6(1983): p. 358.
3. B. Cox, Corrosion 29, 4(1973): p. 157.
4. C.J Semino, J.R. Galvele, Corros. Sci. 16(1976). p. 297.
5. H.L. Logan, J. Res. NBS 48, 99(1952).
6. T.P. Hoar, Corrosion 9, 10(1963): p. 331t.
7. T.G. Nguyen, B.F. Brown, R.T. Foly, Corrosion 38, 6(1982): p. 319.
8. R.A. Patterson, Corrosion 37, 8(1981): p. 455.
9. M.P. Mueller, A.W. Thompson, I.M. Bernstein, Corrosion 41, 3 (1985): p. 127.
10. J.R. Pickens, J.R. Gordon, J.A.S. Green, Metall. Trans. A 14A (1983): p. 925.
11. M.O Speidel, M.V. Hyatt, Advances in Corrosion Science and Technology, 2 (New York, NY: Plenum Press, 1972), p. 115.
12. J. Albrecht, A.W. Thompson, I.M. Bernstein, Metall. Trans. A 10A(1979): p. 1759.
13. B Sarkar, M. Marek, E.A. Starke, Metall. Trans. A 12A(1981). p. 1939.
14. B Cox, K D Williamson, Hydrogen. Its Technology and Implications (New York, NY: CRC Press, Inc., 1977).
15. Cambell, "Effect of Hydrogen Gas on Metals at Ambient Temperature," DMIC Report S-31, Battelle-Columbus, 1970.
16. Aluminum With Food and Chemicals (New York, NY. The Aluminum Company of America, 1967).
17. U.Q. Cabral (Master's thesis, Universite de Paris, 1968); fabricated by ADAMEL, Irsid, France.
18. S. Maitra, Corrosion 37, 2(1981): p. 98.
19. H. Buhl "SCC—The Slow Strain Rate Technique, ASTM STP 665" (Philadelphia, PA: ASTM, 1979), p. 333.
20. M. Elboujdaini, E. Ghali, A. Galibois, J. Appl. of Electrochem. 18 (1988): p. 257.
21. R.A. Patterson, Corrosion 37, 8(1981): p. 455.
22. M.P. Mueller, A.W. Thompson, I.M. Bernstein, Corrosion 41, 3 (1985): p. 125.

Pb-Induced Solid-Metal Embrittlement of Al-Mg-Si Alloys at Ambient Temperatures

Y.S. Kim, N.J.H. Holroyd,** J.J. Lewandowski**

Abstract

Minute amounts of Pb (i.e., 5 ppm to 500 ppm) are shown to induce embrittlement of Al-Mg-Si alloys at ambient temperatures. Transmission electron microscopy–energy-dispersive x-ray analyses and high-resolution scanning Auger microscopy of high-Pb alloys (i.e., 500 ppm) revealed that Pb was often associated with incoherent particles containing Si, Mn, and Fe, although isolated Pb particles were also found on the grain boundary and were associated with Fe in the grain. In the low-Pb alloys (i.e., 20 ppm), fracture surface analyses using backscattered electrons indicated that Pb was only found in association with Fe-containing particles. These sites of high-Pb concentration are preferential sites for crack initiation in a low-ductility intergranular mode (LDIGF). Sequential straining experiments revealed that grain-boundary accommodation of slip was more prominent with increased Pb level in alloys tested at a slow-strain rate. It was additionally shown that the nonuniform strain to failure was significantly reduced in Pb-containing alloys. Tensile interruption tests indicated that both increased Pb content and high holding temperature reduced the final tensile ductility, suggesting that Pb is mobile during tensile straining and that additional accumulation of Pb (i.e., internal) by diffusion promotes fracture in a LDIGF mode. It is proposed that locally segregated regions of Pb are preferential sites for cracking in a LDIGF mode either by decohesion or cracking of Pb-containing particles, with subsequent Pb-assisted crack propagation occurring along grain boundaries. Propagation of fracture in a LDIGF mode requires a continual supply of Pb to the crack-tip region, as supported by the tensile interruption tests, which conclusively showed that both the amount of LDIGF and the loss in nonuniform strain to failure increased with both increasing Pb level and increasing holding temperature.

Introduction

Pb is virtually insoluble in solid aluminum and is often intentionally added in the 1 to 3 wt% range to certain aluminum alloys to increase their machinability. In free-machining alloys, these low-melting-point additions enhance machinability by liquefying during machining, thereby aiding the formation of metal chips.[1] While enhanced machinability is achieved with these additions, it has recently been discovered that minute amounts of Pb (e.g., < 500 ppm) may be detrimental to the mechanical properties both at intermediate (e.g., 100°C)[2] and low (e.g., -4°C, 25°C)[3] temperatures.

Guttmann, et al.,[2] have indicated that small amounts of Pb may induce embrittlement of Al-Mg-Si alloys in creep conditions at elevated temperatures. Severely reduced creep-rupture lives of Al-Mg-Si alloys tested at 100°C were obtained by increasing the Pb content in the range < 10 to 165 ppm. However, there was little observable effect of Pb content on either the room-temperature Charpy impact toughness or smooth tensile behavior.

More recent work[3,4] on 6XXX series aluminum alloys has demonstrated the deleterious effects of Pb at ambient temperatures in sustained-load cracking tests and in slow-strain-rate testing. The schematic in Figure 1 illustrates the effects of Pb level and applied stress intensity (K) on the crack velocity in bolt-loaded double-cantilever beam (DCB) specimens.[3,4] Crack growth rates exceeding 100 mm/y were obtained at room temperature, with threshold values lower than 18 MPa $\sqrt{m}$ at room temperature. It was additionally shown in that work that the fracture morphology in the DCB specimens was affected by the Pb level and applied K.[3,4] Fracture occurred in a low ductility intergranular mode (LDIGF) for high-Pb alloys, while intergranular microvoid coalescence (IGMVC) was predominant in low-Pb alloys. LDIGF was also observed in smooth tensile specimens of high-Pb alloys tested at slow-strain rate (i.e., $\sim 10^{-6}$/s). It appeared that the rate of crack growth and the type of fracture mode was controlled by the availability of Pb.[3,4]

The present work was undertaken to identify the locations of Pb in the microstructure, in addition to performing experiments designed to elucidate the possible mechanisms of Pb-assisted failure of Al-Mg-Si alloys. A variety of analytical techniques were used in combination with sequential straining tests and tensile interruption tests, in addition to a grid technique adopted to enable local strain measurements as a function of total strain.

Experimental Procedures

Materials

Aluminum alloy 6351 containing Pb levels in the range 5 to 500 ppm were used in this study. The laboratory alloys were direct chill cast as 70 kg ingots by ALCAN International Ltd.[1] and were homogenized at either 570°C/2 h or 450°C/12 h. Additional processing details are summarized elsewhere,[3,4] and Table 1 lists the compositions. All specimens were tested in the peak-aged condition.

Tensile testing

Smooth, flat tensile specimens of gauge length 13 mm and thickness 2.54 mm were tested at room temperature at either 3.3 ×

*Department of Materials Science and Engineering, Case Western Reserve University, Cleveland, OH 44106.

**ALCAN International Ltd., Banbury, Oxfordshire, England.

[1]Banbury, Oxfordshire, England.

TABLE 1
Compositions of Alloys (wt%)

Mg	Si	Mn	Cu	Fe	Zr	Ti	Pb	Al
0.62	1.06	0.55	0.001	0.24	0.02	0.014	0.0005	Rem
0.62	1.01	0.59	0.007	0.25	0.02	0.013	0 002	Rem
0.62	0.99	0.58	0.007	0.23	0.02	0.017	0.005	Rem
0.62	1.00	0.55	0.007	0.24	0.03	0.012	0.01	Rem
0.62	1.02	0.56	0.007	0.23	0.03	0.016	0.05	Rem

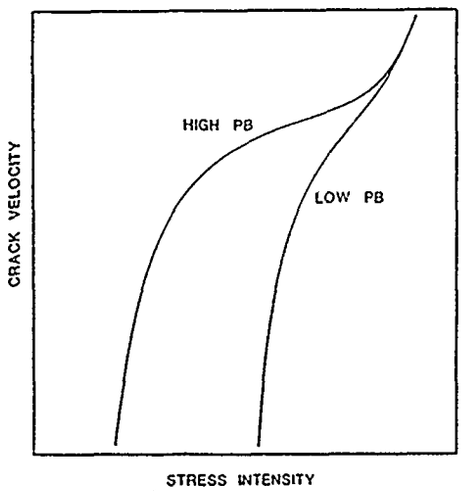


FIGURE 1—Schematic showing the effect of Pb level on crack growth.[3]

10^{-6}/s or 9.8 × 10^{-3}/s. Two kinds of tensile tests were conducted. (1) sequential straining tests and (2) tensile interruption tests. In the former, tensile specimens were sequentially loaded to higher strains in the uniform strain range, while the details of surface deformation were investigated using Nomarsky interference microscopy in combination with the use of a carbon grid deposited on the polished flat surfaces prior to testing. The grids were deposited on the specimens by placing a fine nickel mesh of 2000 lines/in. on a flat, polished tensile specimen, and vacuum depositing carbon onto the sample. Removal of the nickel mesh revealed a regular array of square carbon dots of 8-μm size and 6-μm spacing, as shown in Figure 2. The surface deformation was subsequently studied by photographing the displacement of the initially uniform grid, while the level of local strain was compared to the macrostrain, as Figure 3 illustrates. The change in the edge-to-edge distance of the dots (i.e., spacing of dots) in the tensile direction was used to monitor the local strains.

Tensile interruption tests were additionally conducted to determine the effects of Pb level on the nonuniform strain. The metallographically polished, flat tensile specimens were strained to the ultimate tensile strength (UTS), unloaded, and subsequently reloaded at the same rate after holding for 24 h at either room temperature or 80°C. Total elongation and reduction of area were measured at the UTS and at failure.

Electron microscopy

The polished surfaces and fracture surfaces of the sequentially strained tensile specimens were examined to elucidate the details of slip characteristics as a function of both Pb level and strain rate in a JEOL† 35CF scanning electron microscope (SEM).

Transmission electron microscopy (TEM) was used to characterize the microstructural features as well as the deformed tensile specimens, while energy dispersive x-ray (EDX) analysis was used to chemically analyze the features present. TEM foil preparation is described elsewhere.[3,4] Subsequent examinations of foils were performed in a Phillips† 400T analytical TEM at 120 kV.

†Trade name.

Surface analyses

High-resolution (i.e., 500 Å) surface analyses were obtained on polished, undeformed, and ion-sputter-cleaned specimens in a Perkin-Elmer† PHI 660 Scanning Auger Microprobe operated at 10 kV and at 110 μA, in an attempt to identify the source(s) and location(s) of Pb in the microstructure. Auger line scans were performed across grain-boundary regions in both high- and low-Pb alloys.

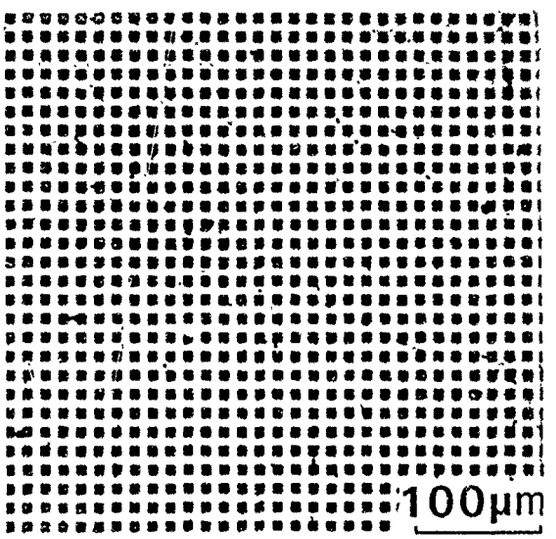


FIGURE 2—As-deposited carbon grid. Undeformed tensile specimen.

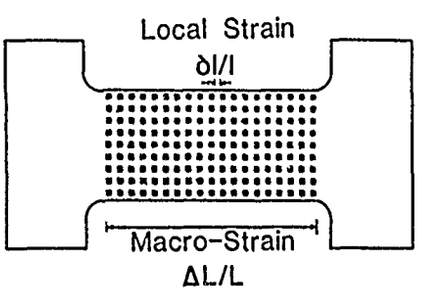


FIGURE 3—Schematic illustrating local and macrostrain measurement technique using deposited grid.

Results

Microstructure

Homogenization at 570°C/2 h produced grain sizes in excess of 1 mm, while homogenization at 450°C/12 h produced grain sizes below 30 μm. TEM foils taken from undeformed specimens containing various Pb contents revealed small (0.5 μm), slightly faceted particles in the matrix and at the grain boundary, as shown in Figure 4. In addition, large particles in excess of 1 μm were observed in the matrix. The former were identified by analyses of diffraction data and

the EDX spectra as being incoherent Al(Mn,Fe)Si phase or an Al-Mn-Si phase, while the latter contained Al, Fe, and Si. EDX analyses of the small-grained 100-ppm Pb alloy indicated that Pb was often associated with the small, faceted grain-boundary particles at the grain boundary,[4] and was also detected in association with the large Fe-containing particles both at the grain boundary and in the grain. Auger line scans across a grain boundary of the polished, ion-sputter-cleaned, undeformed, 500-ppm Pb-containing alloy is presented in Figure 5. Pb signals were detected both at the grain boundary and within the grain, as Figure 5 illustrates. Additional analyses revealed that the Pb was often associated with Mn, Fe, and Si, although isolated Pb signals were detected in the absence of these elements.[4] Analyses of low-Pb specimens (i.e., 20 ppm) have failed to locate the site(s) of Pb in the alloy. However, fractographic evidence indicates Pb association with Fe particles.[4]



FIGURE 4—TEM micrograph showing faceted particles (arrows) at the grain boundary in small-grained 100-ppm Pb alloy.

Tensile results

The local (i.e., micro-) strain as a function of macrostrain of the sequentially loaded flat tensile specimens, calculated via the technique shown in Figure 3, are presented in Figure 6, while Figure 7 shows deformed grids of specimen surfaces of (a) large-grained 500-ppm Pb alloy strained to 2.2% and (b) large-grained 20-ppm Pb alloy strained to 2% by slow-strain rate. Arrows indicate the deformed grain-boundary regions in (a) and the matrix slip lines in (b). Calculations of local strain were performed both across grain-boundary regions and within the matrix for the two strain rates. Figure 6(a) indicates a strong effect of Pb level on the microstrains obtained for a given macrostrain, when measured across grain boundaries in slow-strain rate tests. Direct comparison of the behavior of the 500 ppm (570°C) alloy and the 20 ppm (570°C) alloy is provided by the solid lines in Figure 6. Increased grain-boundary accommodation of deformation is evident in higher Pb materials [Figures 6(a) and 7(a)] and was more pronounced at the larger levels of macrostrain, while deformation by matrix slip was more prevalent for low-Pb alloys tested at the same rate [Figures 6(b) and 7(b)]. Figures 6(c) and (d) indicate that there was no measurable effect of Pb on the balance of deformation by grain-boundary or matrix slip for specimens tested at a fast strain rate (i.e., 9.8×10^{-3}/s). Arrows in Figure 6 indicate the strain at which grain-boundary failure was detected.

The nonuniform strain decreased with an increase in Pb content. As detailed earlier, additional specimens were unloaded at the UTS and were subsequently reloaded after holding in vacuum for 24 h at either room temperature or 80°C. The nonuniform strain to failure obtained after reloading, summarized in Figure 8, was strongly affected by both the Pb level and the holding temperature. Holding at room temperature for 24 h produced no measurable effect on the subsequent nonuniform strain to failure at either Pb level, whereas significant decreases were obtained for both low- and high-Pb specimens held at 80°C prior to reloading. Greater losses were obtained with higher Pb levels. The orientation of grain boundaries exhibiting failure was determined with respect to the tensile axis on the tensile interruption tests. Figure 9 summarizes the cumulative total of grain boundaries exhibiting fracture as well as their orientation with respect to the tensile axis. High Pb alloys exhibited a predominance of failure in boundaries oriented at 90° to the tensile axis, while grain-boundary failure for low-Pb alloys did not reveal any orientation preference.

Fractography

The fractography of failed specimens similarly revealed an effect of Pb level and holding temperature on the fracture mode. The high-Pb alloy (500 ppm) tested at slow-strain rate exhibited regions of LDIGF surrounding large (i.e., > 5 μm) voids, as shown in Figure 10(a). In contrast, the fast-strain-rate tests as well as the low-Pb alloys exhibited IGMVC or transgranular microvoid coalescence, as shown in Figure 10(b). SEM stereo pairs of the fracture surfaces revealed that LDIGF was typically present in regions normal to the stress axis.

TEM observations

TEM micrographs of tensile specimens strained various amounts revealed microvoid initiation both at the grain boundary and at cracked, large Fe-containing particles within the grain. The grain-boundary microvoids were typically associated with the small faceted particles shown earlier (i.e., Figure 4) at which Pb was detected. Figure 11 shows a TEM micrograph of a large-grained 500-ppm Pb specimen subjected to the tensile interruption test held at 80°C, and subsequently tested to failure. Pb was associated with the large particle shown in Figure 11, while the grain-boundary void shown was associated with a precipitate-free zone (PFZ). Cracks associated with the large Fe containing particles were observed at all Pb levels.

Discussion

The above results detailing Pb-assisted low-ductility failure at ambient temperatures exhibit a number of similarities to solid-metal-induced embrittlement (SMIE).[5,6] However, the present Pb embrittlement phenomenon was observed to occur at room temperature and below (i.e., −4°C),[3,4] while SMIE is typically observed to occur near the melting temperature of the embrittler.[5,6]

Although Pb exhibits some solubility in liquid Al, essentially zero solubility exists in the solid state. The present results indicate that the Pb distribution is affected by Pb level. In low-Pb alloys, Pb was only observed at Fe-containing inclusions, while high-Pb specimens exhibited a variety of locations. Isolated Pb peaks were detected at the grain boundary, within grains, and at incoherent particles [i.e., Al(Mn,Fe)Si or Al-Mn-Si] and inclusions (i.e., Al-Fe-Si). Pb was also detected at the boundary in the presence of Mn and Si.

TEM investigation of foils taken below the fracture surface revealed preferential crack initiation at Pb-containing grain-boundary particles. Figure 9 shows that the high-Pb alloys show a strong preference for grain-boundary failure by LDIGF for boundaries oriented normal to the stress axis. These cracks subsequently grow in a LDIGF mode by the continual supply of Pb from the process zone ahead of the crack. Thus, the Pb-containing Fe particles, in addition to isolated Pb globules at the grain boundary, are (internal) sources of Pb.[3,4]

The deleterious effects of Pb were particularly well demonstrated in the tensile interruption tests. While it appears that Pb is released either from cracking or decohesion of inclusions, or from decohesion of Pb globules from the matrix, the tensile interruption tests demonstrate the effect(s) of allowing additional Pb diffusion to the crack surfaces (i.e., internal). High-Pb alloys held at 80°C prior to retesting produced additional reductions in total elongation to failure. Low-Pb alloys as well as those held only at room temperature exhibited considerably less reduction in ductility. Therefore, the availability of Pb appears to be a major controlling factor in this embrittlement phenomenon.

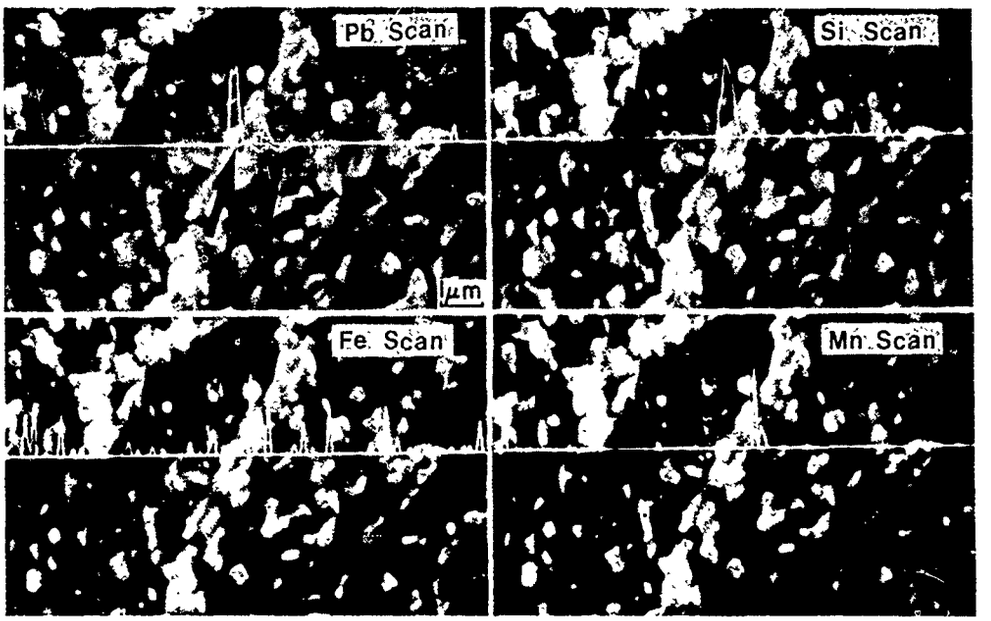


FIGURE 5—Auger line scans of the polished and ion-etched surface of large-grained 500-ppm Pb alloy. Pb is detected at the grain boundary (straight arrow) and in the matrix (curved arrow).

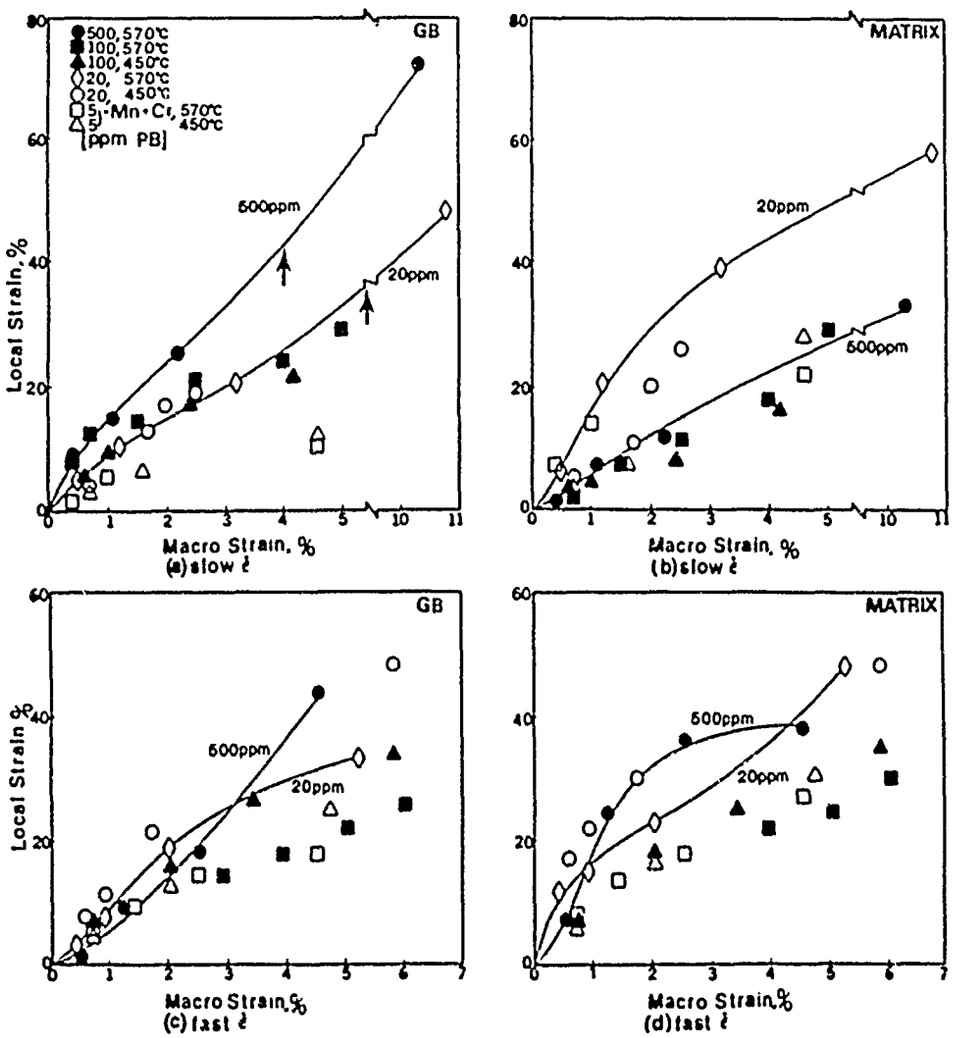


FIGURE 6—Local strain vs macrostrain measurements for different Pb levels at slow [(a),(b)] and fast [(c),(d)] strain rate. Solid lines compare data for the 500-ppm and 20-ppm specimens. Arrows indicate the strain at which grain-boundary cracks were noted.

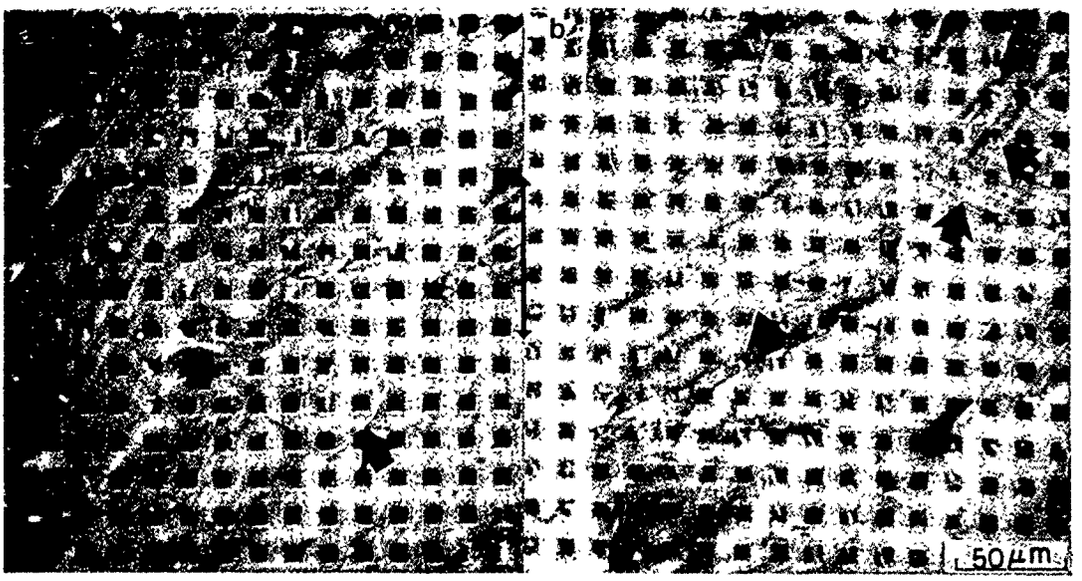


FIGURE 7—Deformed surfaces of (a) large-grained 500-ppm Pb alloy and (b) large-grained 20-ppm Pb alloy illustrating deformed grids by slow-strain-rate tensile test. A long arrow indicates the tensile direction.

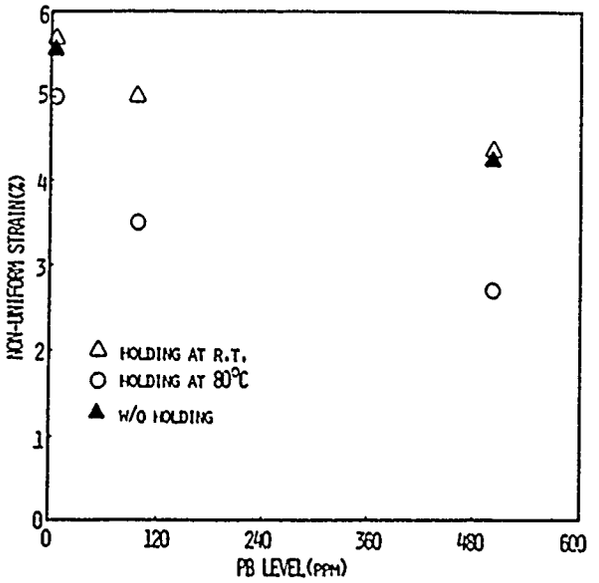


FIGURE 8—Nonuniform strain to failure vs Pb level. (Data obtained in the tensile interruption tests.)

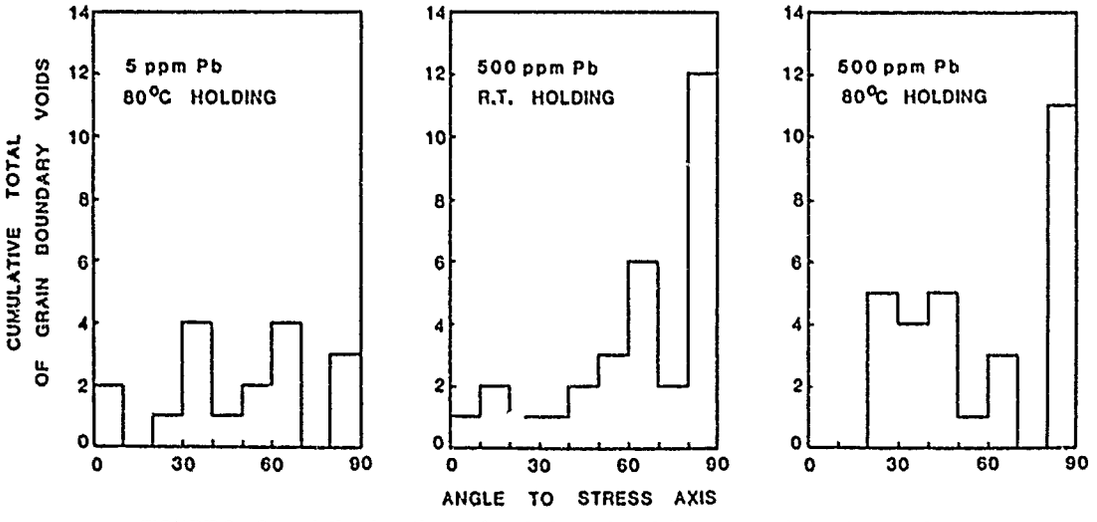


FIGURE 9—Cumulative locations of grain-boundary failure vs angle to stress axis.

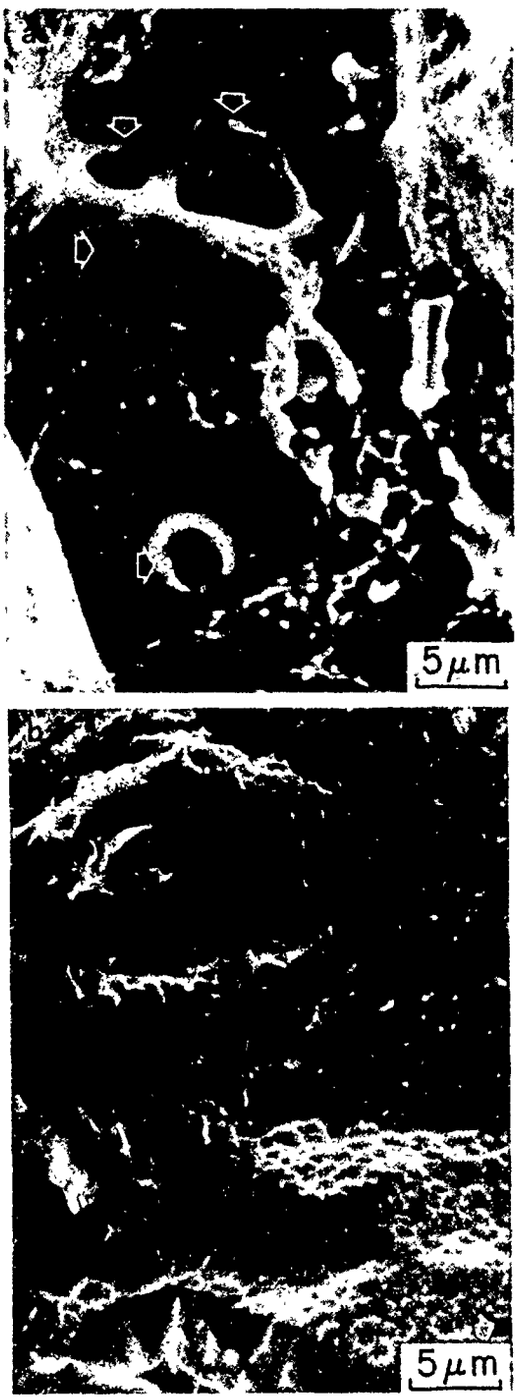


FIGURE 10—SEM fractograph of (a) low-ductility intergranular mode surrounding large (5 μm) grain-boundary voids (arrows) in large-grained 500-ppm Pb alloy and (b) intergranular microvoid coalescence in large-grained 5-ppm Pb alloy. Specimens were taken from tensile interruption tests held at 80°C.

In the absence of triaxial stress conditions, it is difficult to obtain LDIGF under *slow-strain-rate conditions* unless high-Pb levels (i.e., ~ 100 ppm) are tested. LDIGF is not typically observed in aluminum alloys tested under monotonic conditions. Although previous work has indicated that Mn removal may promote intergranular fracture of a dimpled nature in fracture toughness tests,[7,8] the present materials contain sufficient Mn to prevent low-ductility intergranular fracture at fast strain rates. It follows that Pb facilitates both crack initiation and propagation. Under slow-strain-rate conditions, the PFZs are preferred sites for deformation. In high Pb alloys, cracks will preferentially initiate at the interfaces of Pb-containing particles situated in these regions. In contrast, the stronger interfaces in the low-Pb alloys require additional stress and strain to decohere the interfaces. Thus, in the latter case, higher shear stresses along the grain boundary result, thereby promoting dimpled fracture. Once a crack has initiated, the crack will propagate with a continual supply of Pb (i.e., internal) to the crack tip. Therefore, the observation that LDIGF is not obtained in low-Pb or high-Pb alloys tested at fast strain rates can be rationalized as resulting from the mobility of Pb, which is insufficient to keep up with the growing crack. Although there is no unified mechanism that is generally accepted for SMIE, it has been suggested that crack propagation is controlled by surface self-diffusion of embrittler over embrittler.[9,10] The present results, although not quantitative, tend to support such a mechanism, since additional embrittlement as measured as loss in nonuniform strain was obtained in the tensile interruption tests, where it is expected that additional Pb diffusion may occur during holding at high temperature.

Many of the observations in the present work are similar to those made on specimens undergoing creep. However, conventional creep theories predict an increase in creep rate with decreasing grain size. The present work and previous work[3] have clearly demonstrated that large-grained material (i.e., high homogenization temperature) exhibited lower macroscopic strains to failure and faster crack growth rates in the presence of internal Pb than did the small-grained specimens. Unfortunately, the heat treatments used to obtain the two grain sizes tested in the present work may additionally change both the size and distribution of Mn dispersoids in the material,[11] which has also been shown to affect the deformation and fracture characteristics. Thus, an unambiguous determination of grain-size effects on fracture in the present work is difficult. Additional work on this subject is continuing.



FIGURE 11—TEM micrograph of grain-boundary voiding (v) along the precipitate-free zone in a large-grained 500-ppm Pb alloy. Specimen obtained from tensile interruption test where holding at 80°C was performed prior to reloading.

Conclusion

(1) LDIGF can be obtained in Al-Mg-Si alloys at ambient temperatures.
(2) The sources of Pb and LDIGF sites have been identified. In low-Pb alloys, Fe-containing inclusions provide the primary source of Pb, while a variety of sites were identified for the high-Pb material.
(3) Increasing the availability of Pb enhances the following during deformation. (a) grain-boundary accommodation of slip and (b) reduction of nonuniform strain to failure.

(4) Evidence for stress-driven mobility of Pb in producing and sustaining LDIGF was obtained in the tensile interruption tests.
(5) Although many of the observations obtained on Pb-induced LDIGF are similar to a creep mechanism, the observed grain-size effect is not consistent with conventional creep theories.

Acknowledgment

The authors would like to thank ALCAN International Ltd. for the provision of a research fellowship for one of the authors (YSK), and a Case Western Reserve University Research Initiation Grant for another (JJL). Collaborative work is also being supported by a N.A.T.O. Collaborative Grant.

References

1. F. Kutner, E. Nachtigall, Aluminum 45(1969). p. 641.
2. M. Guttmann, B. Quantin, Ph. Dumoulin, Metal Sci. 17, 3(1983): p. 123.
3. J.J. Lewandowski, V. Kohler, N.J.H. Holroyd, Mater. Sci. Eng. 95(1987): p. 185.
4. Y.S. Kim, N.J.H. Holroyd, J.J. Lewandowski, submitted to Metall. Trans. A, 1989.
5. A.P. Drushitz, P. Gordon, Embrittlement by Liquid and Solid Metals, ed. M.H. Kamdar (New York, NY: American Institute of Mining, Metallurgical, and Petroleum Engineers, 1984), p. 285.
6. M.H. Kamdar, Advances in Fracture Research—Proceedings of the 6th International Conference on Fracture, Vol. 6, ed. P.R. Rao, K.N. Raju, J.F. Knott, D.M.R. Taplin (Oxford, England: Pergamon Press, 1984), p. 3837.
7. B.J. Dunwoody, D.M. Moore, A.T. Thomas, J. Inst. Metals 101(1973): p. 172.
8. J.A. Blind, J.W. Martin, Mater. Sci. Eng. 57(1983). p. 49.
9. J.C. Lynn, W.R. Warke, P. Gordon, Mater. Sci. Eng. 18(1975). p. 51.
10. P. Gordon, H.H. An, Metall. Trans. 13A, 3(1982): p. 457.
11. W. Hepples, N.J.H. Holroyd, unpublished research (1987).

Discussion

B. Cox (Atomic Energy of Canada Ltd., Canada): It may be that the type of cracking you observe would be more common if the active metal were present in the metal lattice and so by-pass the protective surface film. A similar phenomenon occurred during an attempt we made to simulate fast reactor irradiation of zirconium in a thermal neutron reactor, by doping zirconium with boron to generate the required helium production during irradiation and annealing to form helium bubbles. When the samples were deformed to failure in tension, the observed fracture surfaces between the helium bubbles appeared brittle, characteristic of stress corrosion cracking (SCC). This was surprising, as no SCC environment was thought to be present. However, lithium is also a by-product of this neutron reaction. We concluded that failure had occurred by metal embrittlement due to its formation *in situ*, thus avoiding the surface barriers that prevent metal embrittlement of Zircaloy†-2 by an external source of lithium.

†Trade name.

The Stress Corrosion Cracking of Al-3.7wt%Zn-2.5wt%Mg and Al-4.7wt%Mg Alloys

C.-M. Liao

Abstract

The stress corrosion cracking (SCC) behavior of both Al-3.7wt%Zn-2.5wt%Mg and Al-4.7wt%Mg alloys in 3.5% NaCl solution has been studied using the double-cantilever-beam technique. Constant deflection tests for Al-3.7wt%Zn-2.5wt%Mg alloy in 3.5% NaCl solution were also conducted. The SCC resistance of Al-4.7wt%Mg is better than that of the Al-3.7wt%Zn-2.5wt%Mg alloy. The fracture morphologies of both alloys are intergranular along the elongated grains. In the constant deflection test of Al-3.7wt%Zn-2.5wt%Mg, SCC initiates from several different sites near the outer surface of the specimen and propagates toward the center.

Introduction

Both Al-Zn-Mg (7000 series) and Al-Mg alloys (5000 series) are high-strength aluminum alloys popularly applied in transportation, structural, and military equipment. Not only are the chemical compositions of these two kinds of alloys different, but also the strengthening mechanisms are not the same. The Al-Zn-Mg alloys are strengthened by precipitation hardening after the solution treatment, quenching, and aging processes. The Al-Mg alloys are strengthened by work hardening after the rolling process.

Although these two series of wrought alloys have high strength, they are susceptible to stress corrosion cracking (SCC), especially in the short transverse direction,[1] which corresponds to the plate thickness. In this work, tensile stress was applied in the short transverse direction of Al-3.7wt%Zn-2.5wt%Mg and Al-4.7wt%Mg alloys, and the SCC resistance of these alloys in this direction in 3.5 wt% NaCl solution was examined. The results are discussed.

Experimental Procedures

The chemical compositions of these two alloys are shown in Table 1. Double cantilever beam (DCB) specimens were chosen for the SCC testing; the dimensions of the DCB specimen are shown in Figure 1.[2,3] The length of the specimen corresponds to the rolling direction of the aluminum plates, and the thickness of the specimens corresponds to the short transverse direction. The specimen was stressed in the short transverse direction by bolt loading to pop-in crack and then placed in a vessel containing 3.5% NaCl solution.

The propagation of the crack was measured with a microscope (of 10 μm resolution) every two days on two surfaces of the specimen during the testing period. The crack-tip stress intensity value (K) ($MN \cdot m^{-3/2}$) was calculated by Equation (1):

$$K = \frac{E \cdot \delta \cdot h[3h(a+0.6h)^2 + h^3]^{1/2}}{4[(a+0.6h)^3 + h^2 a]} \qquad (1)$$

Where E = Young's modulus of the material ($N \cdot m^{-2}$), δ = the deflection at the load line (m) (i.e., between A and B in Figure 1), h = half of the thickness of the specimen (m), and a = crack length (m). The propagation velocity of cracking was plotted as a function of the crack-tip stress intensity (v–K curve) after testing.

In addition, a constant deflection SCC test was used for the Al-3.7wt%Zn-2.5wt%Mg alloy in the short transverse direction. Specimens were stressed by constant deflection[4] and then immersed in the 3.5% NaCl solution alternately.[5] 10 min immersed in solution and 50 min exposed to air. The specimen and the stressing frame are shown separately in Figure 2 before and after testing.

TABLE 1
Chemical Compositions of Alloys

Element (wt%)/Alloy	Zn	Mg	Mn	Si	Cr	Fe	Al
Al-3.7wt%Zn-2.5wt%Mg	3.66	2.48	0.29	0.062	0.22	0.17	bal.
Al-4.7wt%Mg	0.025	4.74	0.70	0.11	0.09	0.24	bal.

Results and Discussion

The resulting v–K curves for Al-3.7wt%Zn-2.5wt%Mg and Al-4.7wt%Mg alloys are illustrated in Figure 3. The shape of the curves for both alloys is quite similar. At the lower stress intensities, there is a strongly stress-dependent region called Region I. The SCC threshold stress intensity (K_{ISCC}) was defined by the stress intensity corresponding to a crack growth rate of 10^{-10} m/s.[3,6] At higher stress intensities, the crack velocity is independent of stress; i.e., the v–K curve has a plateau, and this region is called Region II or the plateau region. The K_{ISCC} values of Al-3.7wt%Zn-2.5wt%Mg and Al-4.7 wt%Mg alloys were measured to be 3 to 7 $MN \cdot m^{-3/2}$ and 28 to 32 $MN \cdot m^{-3/2}$, respectively. Crack growth rates at Region II are about 2×10^{-8} m/s and 3 to 4×10^{-9} m/s for Al-3.7wt%Zn-2.5wt%Mg and Al-4.7wt%Mg alloys respectively. Both K_{ISCC} and the Region II velocity are the indexes of the SCC sensitivity of materials.

The results show that the K_{ISCC} of Al-3.7wt%Zn-2.5wt%Mg alloy is lower than that of Al-4.7wt%Mg alloy, and the Region II velocity of

*China Steel Corporation, Lin Hai Industrial District, P.O. Box 47-29, Hsiao Kang, Kaohsiung 81233, Taiwan, Republic of China.

the former is faster than that of the latter. This indicates that the Al-3.7wt%Zn-2.5wt%Mg alloy is more susceptible to SCC compared to the Al-4.7wt%Mg alloy.

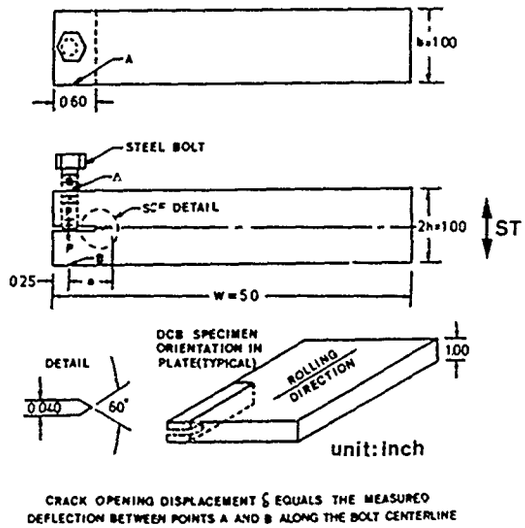


FIGURE 1—Dimensions and orientation of the DCB specimens.



FIGURE 2—The specimens and the stressing frames for constant deflection tests. (The right-hand specimen is before alternate immersion testing; the left one is after the test.)

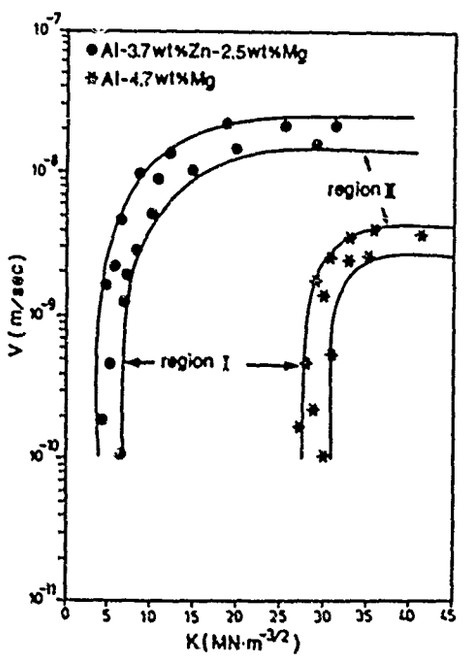


FIGURE 3—Effect of stress intensity on the velocity of SCC for Al-3.7wt%Zn-2.5wt%Mg and Al-4.7wt%Mg alloys.

The DCB specimens are fractured after testing, and the macrostructure of the fracture surface is shown in Figure 4. There are three regions on the surface. The first is the "pop-in region," which is caused by initial bolt loading. The second is the "stress corrosion cracking region," and the third is the fast fracture or "torn away" region, which results from tearing the specimen after SCC testing. The surfaces of both the pop-in and torn-away regions are rougher than that of the SCC region, which is smooth and contains some microbranches.

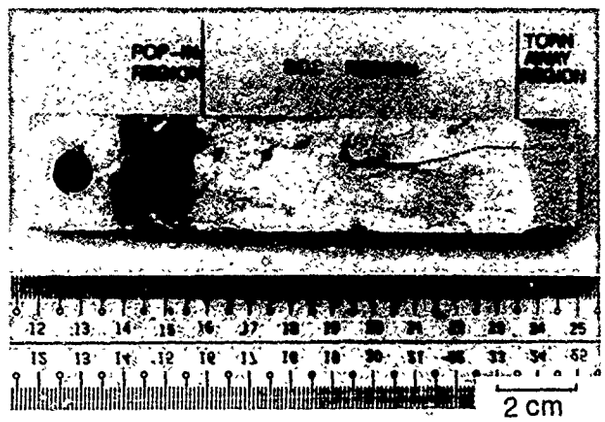


FIGURE 4—The macrostructure of the fracture surface of a DCB specimen after testing.

The fracture surfaces of the pop-in and torn-away regions are similar, as shown in Figure 5. The observed fiber-like and dimple structures are representative of ductile fracture, i.e., both these regions are ductile. The grains are elongated by rolling, as shown in Figure 6, and SCC of the wrought aluminum alloys is intergranular, so the propagation of the crack tip along the elongated grain boundaries makes the surface smooth. This SCC fracture shown in Figure 7 is similar to the work of Landkof, in which the SCC fracture morphology is smooth.[7] In the SCC region, several grains have been peeled off by microbranching;[8] this phenomenon can also be demonstrated in Figure 8, which shows several cracks in the specimen.

The fracture surface morphology of the Al-4.7wt%Mg alloy is similar to that of Al-3.7wt%Zn-2.5wt%Mg. It also has three regions: pop-in, SCC, and torn-away. The pop-in and torn-away regions are also ductile fracture, including fiberlike and dimple structures, while the SCC region shows intergranular SCC.

After the constantly strained specimens of Al-3.7wt%Zn-2.5 wt%Mg alloy failed during the alternative immersion test, the fracture surfaces were examined by optical microscopy and scanning electron microscopy.

The upper left side of Figure 9 illustrates a rough surface, while the lower right side is planar. When the magnification of the picture is increased, it is clear that the fiber-like and dimple structures are present in the upper region, and the smooth fracture morphology is present in the lower region. Compared to the fracture surface morphology of the DCB specimens, the lower region is the intergranular SCC region, and the upper region is the solely mechanical fracture region. This result indicates that SCC is initiated from the lower side, and the crack propagates toward the upper region until the cross section suddenly fractures.

Figure 10 shows another fracture surface for the constantly strained specimen of the Al-3.7wt%Zn-2.5wt%Mg alloy. There are three planar regions on different planes near the outer surface of the specimen, and the zone between each successive two planes is of the suddenly fractured morphology. This means that SCC initiates simultaneously at several sites on the outer surface and propagates

toward the center of the specimen When the cross section of the specimen is too small to sustain the force imposed by the frame, the specimens suddenly fracture and produce a surface containing both SCC and ductile fracture regions.

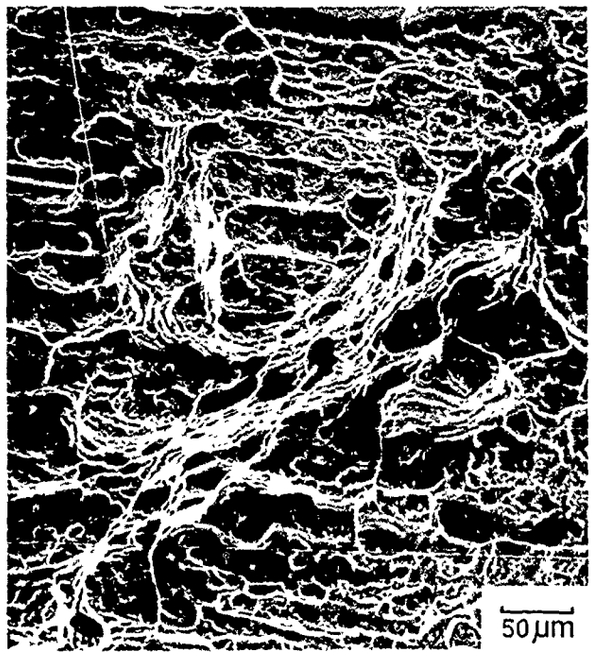


FIGURE 5—A scanning electron micrograph of the pop-in region of the Al-3.7wt%Zn-2.5wt%Mg alloy. (The morphology of the overload or torn-away region is similar to this.)

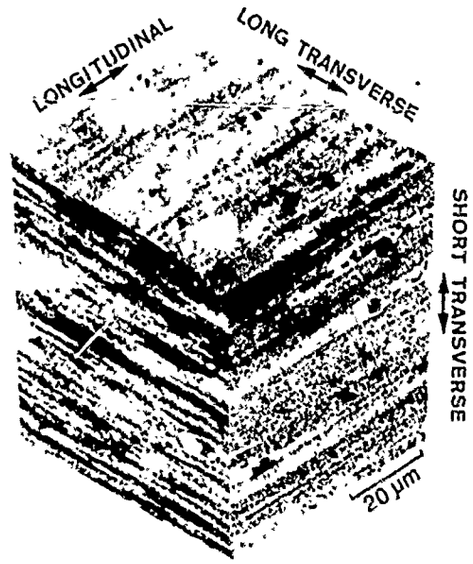


FIGURE 6—Micrographs of the elongated grains of the Al-3.7wt%Zn-2.5wt%Mg alloy after rolling.

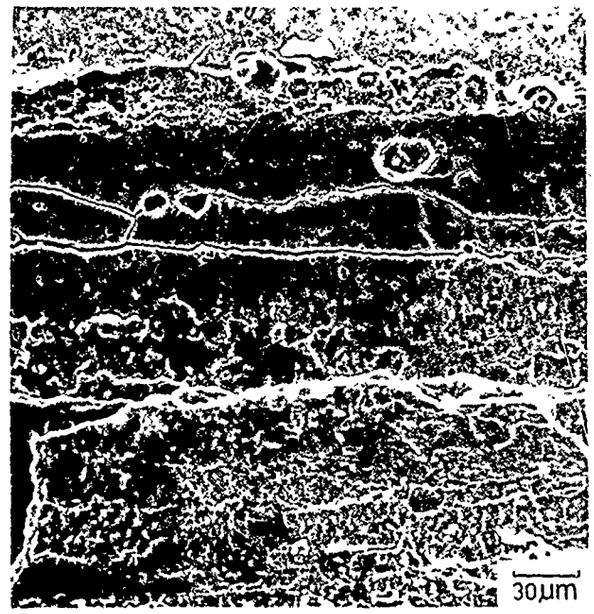


FIGURE 7—The morphology of the SCC region of a DCB specimen of Al-3.7wt%Zn-2.5wt%Mg. (That of the Al-4.7wt%Mg is similar.)

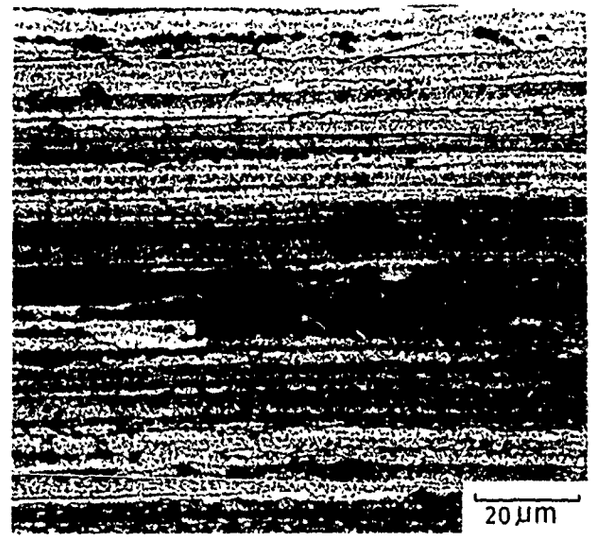


FIGURE 8—The microstructure of the Al-3.7wt%Zn-2.5wt%Mg alloy.

Conclusion

(1) The K_{ISCC} values of Al-3.7wt%Zn-2.5wt%Mg and Al-4 .7 wt%Mg alloys are about 3 to 7 $MN \cdot m^{-3/2}$ and 28 to 32 $MN \cdot m^{-3/2}$, respectively.

(2) The crack propagation velocities for Region II in the v-K curves are about 2×10^{-8} m/s and 4×10^{-9} m/s for Al-3.7wt%Zn-2.5wt%Mg and Al-4.7wt%Mg alloys, respectively.

(3) The SCC fracture morphologies of these two alloys are quite similar; the SCC regions are planar and intergranular, the pop-in and overload fracture regions are ductile, including fiber-like and dimple structures.

(4) The constant deflection test of the Al-3.7wt%Zn-2.5wt%Mg alloy in the short transverse direction shows that SCC initiates from several sites near the outer surface of the specimen and propagates toward the center of the specimen.

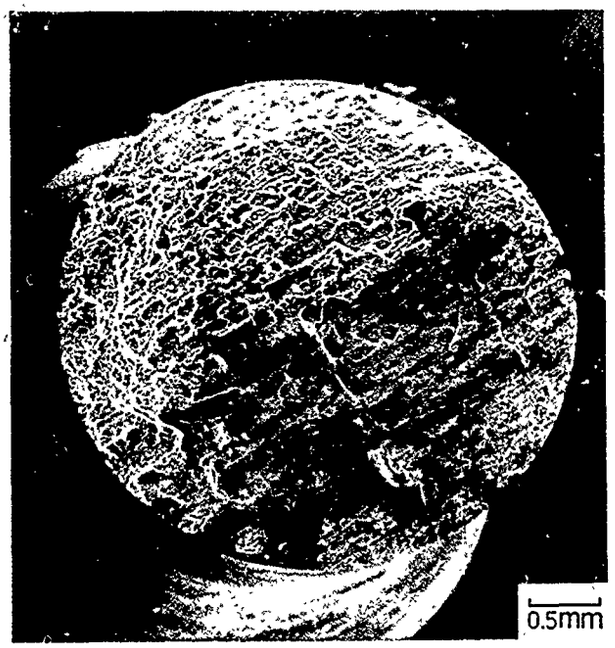


FIGURE 9—The fracture morphology of a constant strained specimen of Al-3.7wt%Zn-2.5wt%Mg.

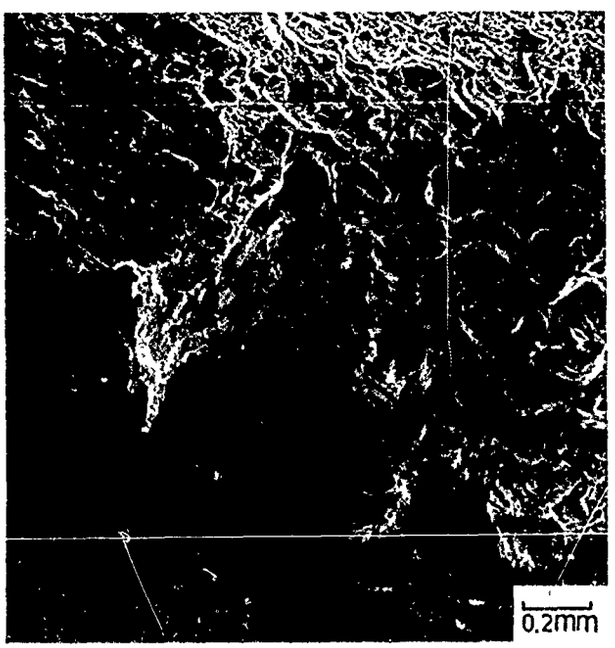


FIGURE 10—The fracture morphology of a constant strained specimen of Al-3.7wt%Zn-2.5wt%Mg.

References

1. N. Kackley, W. Czyrklis, M. Levy, CORROSION/85, paper no. 195 (Houston, TX: National Association of Corrosion Engineers, 1985).
2. M.V. Hyatt, Corrosion, 26, 11(1970): p. 487.
3 M.O Speidel, The Theory of Stress Corrosion Cracking in Alloys (Brussels, Belgium. North Atlantic Treaty Organization Scientific Affairs Division, 1979), p. 289.
4. ASTM Standard Recommended Practice G49-85 (Philadelphia, PA: ASTM, 1986).
5. ASTM Standard Recommended Practice G44-75 (Philadelphia, PA: ASTM, 1986).
6. M.O. Speidel, Metall. Trans. A 6A(1975): p. 631.
7. M. Landkof, Gal-Or, Corrosion, 36, 5(1980): p. 241.
8. M.O. Speidel, The Theory of Stress Corrosion Cracking in Alloys (Brussels, Belgium: NATO Scientific Affairs Division, 1979), p. 345.

The Influence of Microstructure on the Stress Corrosion Cracking and Exfoliation of Commercial Al-Zn-Mg-Cu Alloys

*W. Hepples, M.R. Jarrett, J.S. Crompton, and N.J.H. Holroyd**

Abstract

Retrogression and re-aging (RRA) Al-Zn-Mg-Cu alloy 7150 using commercially viable thermal process routes can provide material with peak strength and high resistance to stress corrosion cracking (SCC) and exfoliation corrosion. A correlation exists between alloy conductivity and the susceptibility to localized corrosion: If conductivity exceeds 38% of the International Annealed Copper Standard (IACS) exfoliation, corrosion and SCC resistance are high. Transmission and scanning transmission electron microscopy, along with very high-resolution chemical analysis, has enabled the characterization of grain boundaries in peak-aged, overaged, and RRA material. Significant differences in grain-boundary precipitation and segregation have been observed, but no simple relationships between SCC resistance and grain-boundary microstructure have been identified. The results of grain-boundary segregation profiles, however, indicate that segregation, particularly that of copper, can significantly affect the response to environmental attack.

Introduction

Commercial exploitation of high-strength Al-Zn-Mg-Cu alloys aged to peak strength is currently restricted by the potential risk of environment-sensitive cracking (Figure 1).[1] The commercial compromise uses duplex thermal aging practices developed during the 1960s[2] that minimize service problems[1] but introduce a 10 to 15% loss in strength. Alternative heat-treatment procedures known as retrogression and re-aging (RRA) have been reported[3] to provide stress corrosion resistance equivalent to an overaged T73 temper while maintaining the peak-aged strengths These heat treatments consist of a retrogression or reversion stage in which peak-aged material is heated for short times (i.e., a few min) in the temperature range 220 to 280°C, followed by re-aging at a lower temperature.[4] During retrogression, strength falls rapidly to a minimum, partially recovers after longer times, and finally decreases (Figure 2) [5] Re-aging after short retrogressing times can restore the strength to that of the peak-aged material, but extended retrogression times lead to a loss of the aging response.

The incorporation of these thermal practices into commercial production schedules for thick sections requires retrogression times of at least 1 h. Recent laboratory studies suggest beneficial RRA effects may be obtained under these conditions if the retrogression temperatures are below 200°C (Figure 3) [5-8] The aims of the present work are to examine commercially viable RRA practices that provide a peak strength of 7150 with a high SCC resistance and to identify the factors controlling localized corrosion.

Experimental Procedure

Alcan Plate Limited[(1)] supplied 7150 plates (12.7- and 32-mm thickness) in a W51 temper (solution treated, stretched, and naturally aged) with a nominal elemental composition (wt%) of 5.9 to 6.9 Zn, 2.0 to 2.7 Mg, 1.9 to 2.5 Cu, 0.08 to 0.15 Zr, and (Fe + Si) < 0.1.

Laboratory processing involved solution heat treatment for 1 h at 475°C followed by a water quench (ambient) and conventional or RRA aging treatments. RRA involved retrogression at 180 or 200°C for various times up to 180 min and re-aging at 120°C for a standard time of 24 h. Overaged microstructures (T73-Lab) involved aging W51 material 24 h at 120°C followed by 20 h at 160°C.

Electrical conductivity (measured as a percentage of the International Annealed Copper Standard, %IACS) and Vickers hardness (H_v) were monitored during heat treatment. Electrical conductivity measurements are a useful means of following changes in solute distribution. All known metallic additions to aluminum reduce its electrical conductivity, those in solid solution depress the conductivity to a greater extent than those out of solution. Since electrical-conductivity measurements can be made quickly and easily, this provides a convenient method for assessing an alloy's temper and stress corrosion susceptibility. Although it is unlikely that conductivity and intergranular SCC are directly related, it is well known for Al-Zn-Mg(Cu) alloys that the higher the conductivity, the greater the extent of alloying additions out of solution and the greater the resistance to SCC.[6,7] Exfoliation resistance for the T651 and RRA tempers was assessed using the ASTM EXCO[†] test, ASTM G34-86, with exposure times of 48 h on the t/10 surface. EXCO samples are rated on their degree of exfoliation after exposure to the EXCO solution. A rating of Ed indicates the least resistance to exfoliation corrosion, while resistance increases through Ed to Ea. P indicates a change in corrosion attack from exfoliation to pitting. SCC testing was conducted in an acidified saline environment (2%NaCl/0.5%Na_2CrO_4pH3) using displacement-loaded, double-cantilever beam specimens loaded in the short-transverse direction and oriented so that crack propagation occurred in the longitudinal direction.

Characterization of 7150 microstructures was achieved using a JEOL[†] 2000FX transmission electron microscope (TEM) fitted with energy dispersive x-ray analysis equipment. Chemical analyses of grain-boundary regions were obtained using a VG-HB501[†] scanning transmission electron microscope (STEM) with a probe diameter smaller than 3 nm.

*Alcan International Limited, Banbury, Oxon, OX16 7SP England.
(1)Alcan Plate Limited, Kitts Green, Birmingham, B33 9QR England.

†Trade name.

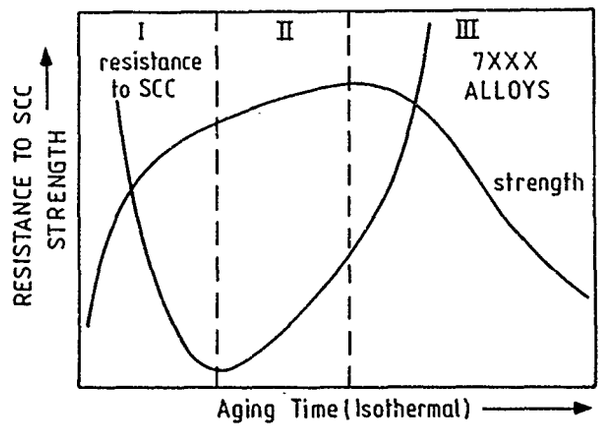


FIGURE 1—A schematic diagram illustrating the effect of isothermal aging on the strength and resistance to stress corrosion cracking of 7XXX series aluminum alloys.[2]

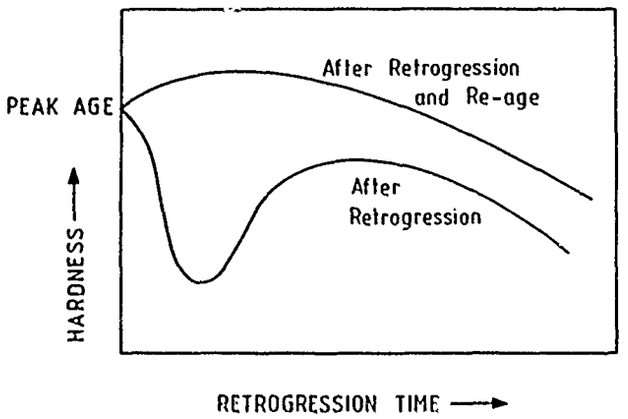


FIGURE 2—The effect of retrogression and re-aging on the strength of 7XXX series aluminum alloys.[5]

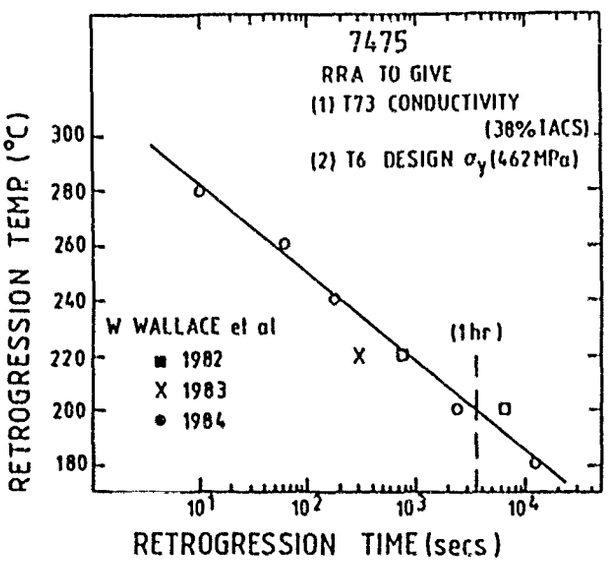


FIGURE 3—Retrogression conditions required to impart peak strength (T651) and high resistance to environment-sensitive cracking (T73), after subsequent re-aging, to 7475.

Results and Discussion

Mechanical properties

Commercially produced 7150-T651 had a hardness of 190 ± 2 H_v and a conductivity of 34.3 ± 1% IACS. These properties were evaluated for different retrogression treatments to determine the conditions under which improved properties could be obtained. The results indicated that the hardness and conductivity values of commercially produced T651 material can be achieved using RRA procedures (Figure 4) while maintaining strength and ductility (Table 1). The observed reduction in strength after retrogression has been discussed previously.[9,10] Two views prevail: Park and Ardell suggest that the initial loss in properties results from partial or complete dissolution of small η' precipitates,[9] whereas Danh, et al., conclude that the initial decrease is associated with the reversion of Guinier-Preston zones.[10] Both theories provide satisfactory explanations for loss of strength, and it is possible that both operate with retrogression treatment[8] and/or earlier commercial processing of the material dictating which mechanism predominates. Increases in strength associated with re-aging after retrogression are critically dependent on the retrogression time. If times are sufficiently short, strengths may be increased to T651 levels by re-precipitation of a fine distribution of η' during re-aging. During longer retrogression times, precipitate growth occurs and increases in strength after re-aging becomes less significant.

Optical metallographic examination of 7150 microstructures failed to distinguish between peak-aged, RRA, and overaged material. TEM studies, however, revealed differences reflecting the observed changes in corrosion performance. The matrix (η') precipitates of the RRA material were finer than those found for the peak-aged material, which, in turn, were finer than the matrix precipitates of the overaged material (Figure 5). In contrast, the mean grain-boundary precipitate size in the RRA (and overaged) material was larger than that in the peak-aged material (Table 2). Precipitate free zone (PFZ) width, as reported by others, was found to be independent of aging (Table 2).[11]

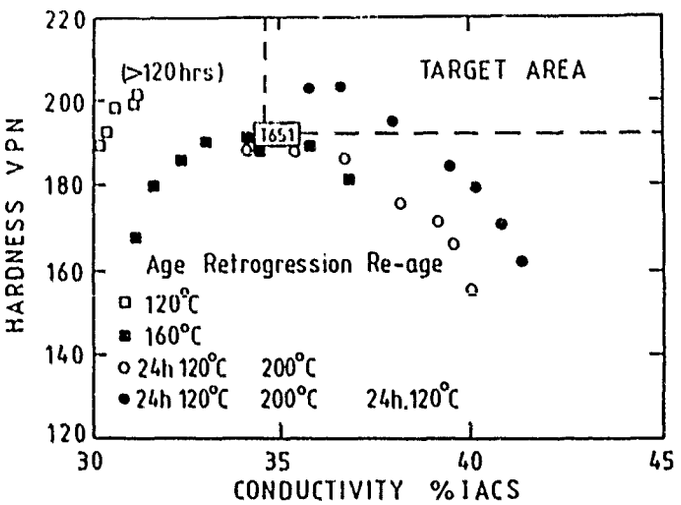


FIGURE 4—Effect of retrogression and re-aging on the hardness and conductivity of 7150.

Environment-sensitive properties

The EXCO performance of 7150 that was given RRA treatments providing T651 equivalent strengths with low and high conductivities was compared to that of the T651 material. T651 material suffered severe exfoliation, and RRA material behavior depended on the time of retrogression: For times < 30 min (conductivities < 36% IACS) intergranular attack predominated, whereas for times in excess of 45 min (conductivities > 38% IACS), localized pitting occurred, signifying a high resistance to exfoliation corrosion (Figure 6). Figure 6(b) shows that a critical conductivity exists (38% IACS) beyond which localized corrosion via an intergranular path is minimized.[6,7] On this basis, RRA-treated material can provide better corrosion resistance than the overaged material, which is, however, superior to the T651 material.

TABLE 1
Typical Mechanical Properties of 7150-T651 and a RRA Temper[A]

Temper	Hardness (Hv)	Conductivity (% IACS)	0.2% σy (MNm^{-2})	Ultimate Tensile Strength (MNm^{-2})	Elongation (%)
T651	192	34.3 ± 1	585	620	12
RRA	192	38 0	585	620	11

[A]Providing T6 strengths and T73 SCC and exfoliation corrosion resistance.

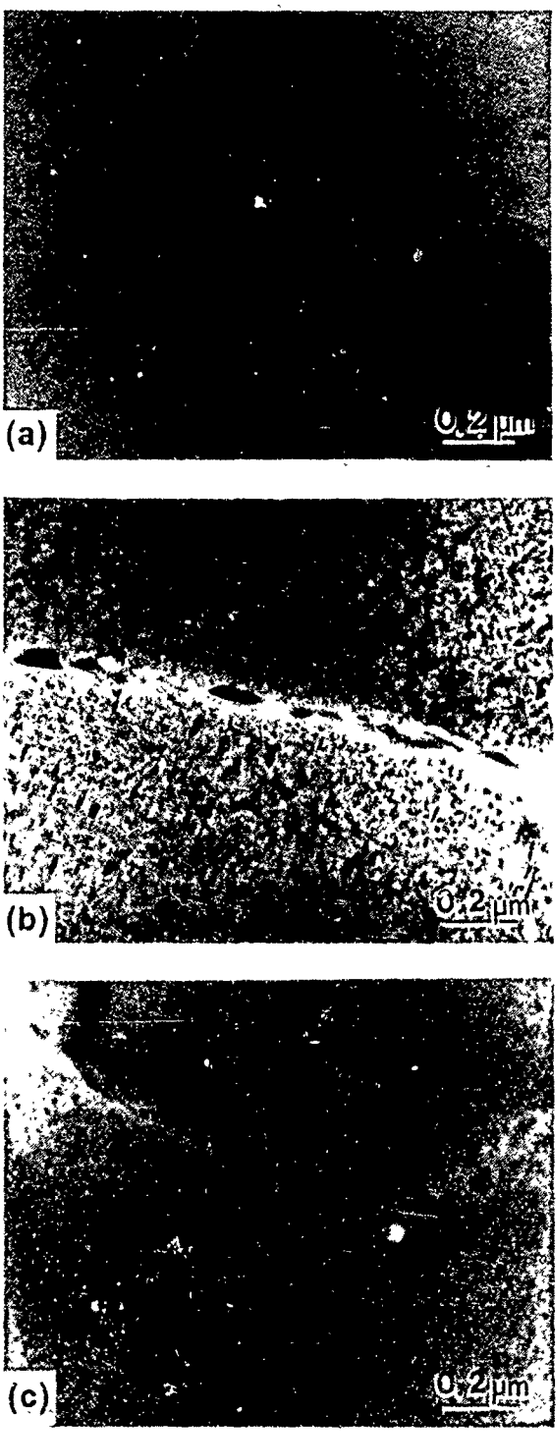


FIGURE 5—Bright field micrographs of grain-boundary precipitates in samples of 7150 after various heat-treatment conditions: (a) T651, (b) T73, and (c) RRA.

TABLE 2
Grain-Boundary Precipitate Sized for 7150-T651, T73, and RRA Tempers

Temper	Precipitate Size (nm) Length	Width	Precipitate Free Zone Width (nm)
T651	45.0 ± 16.5	16.1 ± 4.5	31.8 ± 4.9
RRA	72.0 ± 26.2	24.1 ± 5.7	32.4 ± 5.5
T73	88.0 ± 26.4	32.2 ± 8.5	37.0 ± 3.7

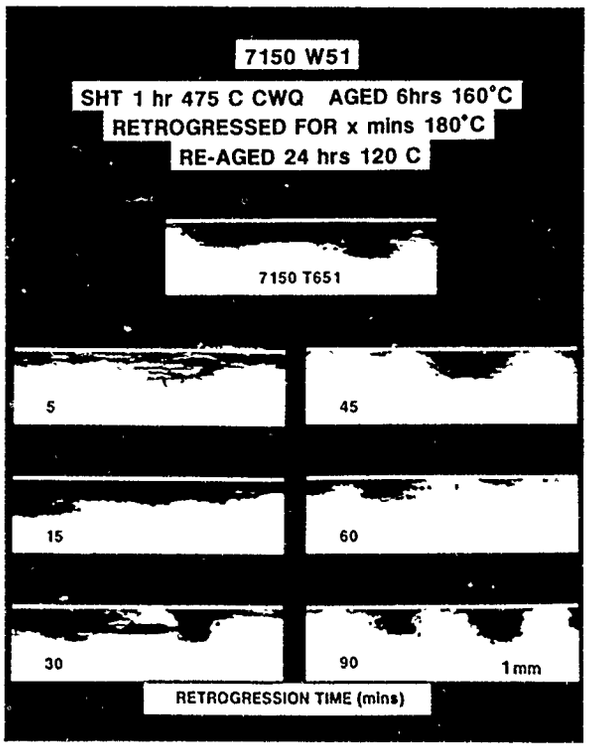
Similarly, SCC performance can be related to conductivity. 7150 shows the expected behavior:[12] laboratory peak-aged material (conductivity < 36% IACS) is susceptible to SCC, whereas material given suitable RRA treatments (conductivity > 38% IACS) displays lower crack propagation rates and higher threshold stress-intensity factors (Figure 7). Previous studies have linked improved SCC resistance to microstructural characteristics such as grain-boundary precipitate size and spacing,[13-16] PFZ width or solute content,[14-19] matrix precipitation and slip characteristics,[20-22] and grain-boundary segregation.[11,15,23-28] None of the evidence presented to date is unequivocal because it is impossible to interdependently vary the various microstructural parameters listed above. Nevertheless, the influence of alloy microstructure upon SCC has been discussed extensively in mechanistic terms and is reviewed elsewhere.[29,30]

Accepted SCC crack growth mechanisms fall into two generic categories: in one, crack propagation occurs via anodic dissolution (AD), and in the other, it is via hydrogen embrittlement (HE). Beneficial effects of RRA upon SCC susceptibility with respect to T651 material have been attributed to increases in grain-boundary precipitate size and spacing. Mechanistic interpretations encompass both AD and HE crack propagation mechanisms. For example, Thompson, et al.,[8] suggest that RRA reduces the dissolution kinetics of grain-boundary precipitates, thereby lowering local stress-raising effects, whereas, Rajan, et al.,[5] use the proposals of others that grain-boundary precipitates above a critical size act as hydrogen discharge sites and thereby reduce HE susceptibility.[31,32] Neither of these interpretations are complete since the observed SCC susceptibilities rankings (T651 >> T73 > RRA) do not match those of the grain-boundary precipitate size and spacing, for which T651 >> RRA > T73 (Table 2).

Grain-boundary segregation

Grain-boundary segregation is often cited as a factor influencing SCC of 7XXX series alloys. Available spatial resolution, i.e., with beam diameters of > 20 nm, has limited previous attempts to chemically analyze grain-boundary regions. In the present study, the use of improved spatial resolution, < 3 nm, has allowed a detailed investigation of Zn, Mg, and Cu segregation to within the PFZ and on grain boundaries (Figure 8). Grain-boundary Mg levels for T651 material were slightly above the matrix levels and increased with further aging, whereas zinc levels were below matrix levels and

decreased with aging, being highest for the T651 temper (~ 2 wt%) and least for RRA material (< 0.5 wt%). Copper segregation displayed similar trends to zinc with the influence of aging being more pronounced. Cu levels on T651 high-angle grain boundaries displayed considerable scatter, i.e., 4 to 14 wt% Cu compared to the overaged (T73-Lab) and RRA tempers with average concentrations of 2.5 and 1%, respectively. Similar data has been reported previously for 7075-T6 when overaged to a T7X temper (T6 + 24 h 160°C). Rao's data is in remarkable agreement, he quotes (wt%) magnesium increases, 0.97 (± 0.61) to 1.68 (± 0.50); zinc decreases 6.32 (± 0.52) to 2.72 (± 0.31); and copper decreases 4.96 (± 0.47) to 2.32 (± 0.26).[11] Earlier work by Doig, et al., detected a reduction of at least a factor of two for copper but failed to observe any changes in zinc or magnesium segregation.[2]



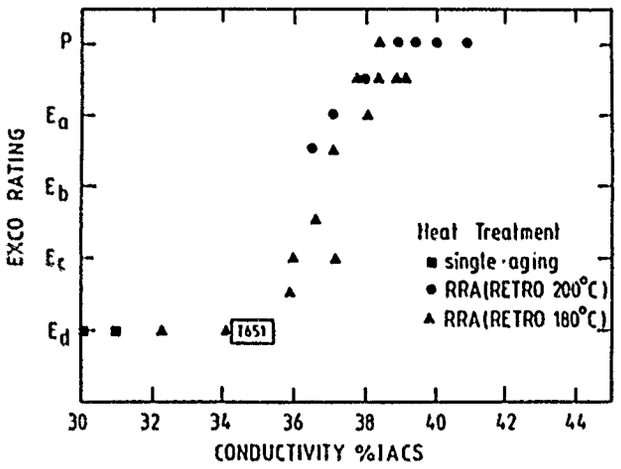


FIGURE 6—(a) Comparison of a cross section from a 7150-T651 sample with those of 7150-RRA samples after 48-h exposure to EXCO solution and (b) the relationship between the resistance to exfoliation corrosion and conductivity of 7150.

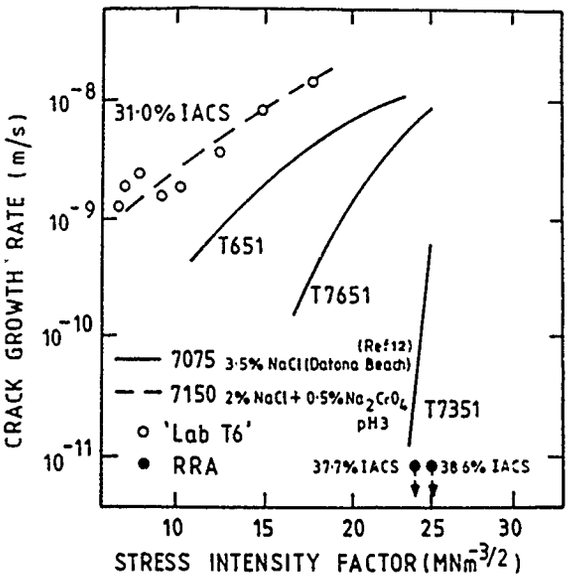
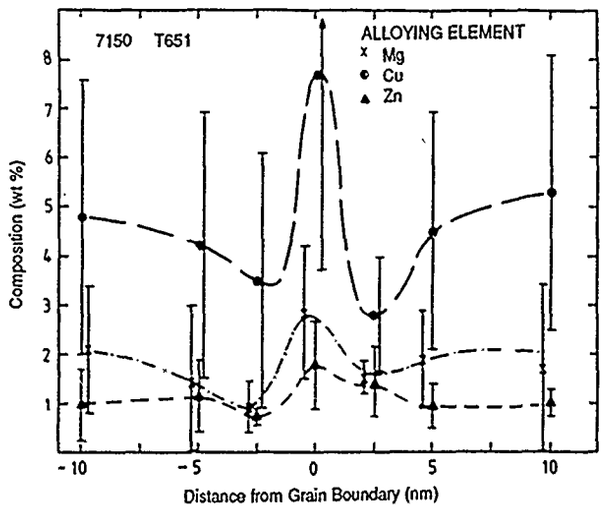


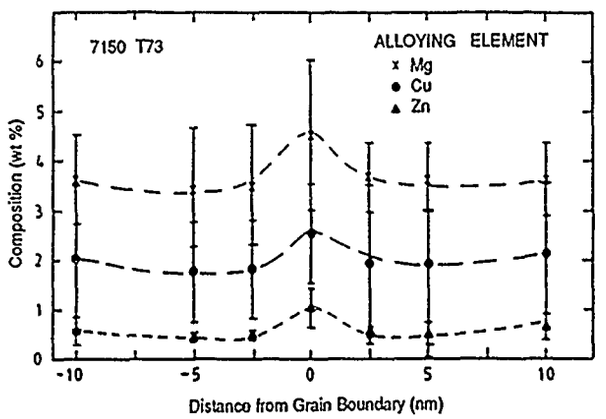
FIGURE 7—The resistance to stress corrosion cracking of 7150 and 7075 (UNS A97075) in various commercial and RRA tempers.

The role of magnesium segregation during SCC was recently reviewed by Scamans, et al.,[25] who conclude that, in itself, it does not induce SCC, but it promotes grain-boundary reactivity and the localized entry of hydrogen. Results obtained here showing that grain-boundary magnesium segregation increases with increasing SCC resistance (Figure 8) confirm that Mg segregation is not the dominant feature controlling SCC, despite free magnesium being present on grain boundaries.[25] Schmiedel and Gruhl suggest SCC of Al-Zn-Mg(Cu) alloys is independent of magnesium segregation and is controlled by grain-boundary zinc segregation,[26] which is inferred to induce increased hydrogen solubility and hence enhance SCC. This proposal is based on SCC time-to-failure data for a range of Al-Zn-Mg alloys that show a good correlation with measured grain-boundary region zinc concentrations but no relationship with the local magnesium concentrations (see figure in Reference 28). Doig, et al., on the other hand, attribute overaging's beneficial effects upon SCC solely to the reduced cathodic electrochemical kinetics of grain-boundary regions with lower concentrations of copper in solid solution.[23]

Clearly, further work is needed to elucidate the mechanisms controlling the SCC of Al-Zn-Mg-Cu alloys. Proposals that grain-boundary precipitate size and/or spacing control SCC are obviously incomplete since the SCC rankings (T651 >> T73 > RRA) do not match those of the grain-boundary precipitation (T651 >> RRA > T73). Similarly, grain-boundary segregation arguments are inadequate. Schmiedel and Gruhl's concept that zinc segregation controls SCC is not easily explained because zinc-hydrogen interactions are not expected to be strong,[30] and, as with magnesium segregation, the maximum concentrations occur for the as-solution-treated condition, which, in the absence of precipitation, is immune to SCC.[25,33] The copper-segregation-based arguments of Doig and Edington,[18] et al., also have limitations,[23] as highlighted by Rao,[11] since grain-boundary region electrochemistry will also be influenced by zinc and magnesium segregation levels.

Several factors may contribute to the improved SCC resistance of Al Zn Mg Cu alloys provided by retrogression and re-aging. These will include grain boundary precipitation (size, composition, morphology, and spacing) and copper segregation. A complete understanding of the relative importance requires further work.





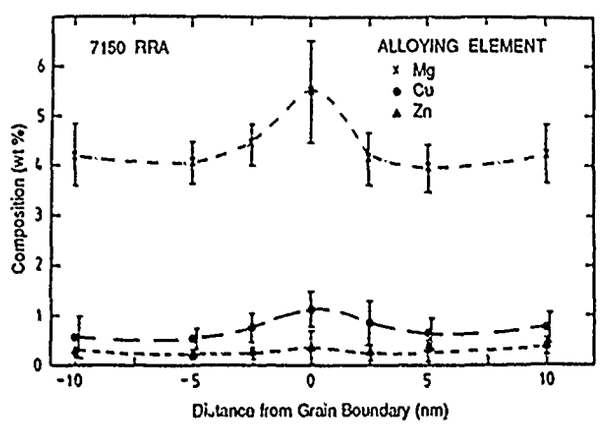


FIGURE 8 – High-resolution grain-boundary solute concentration profiles for various tempers of 7150: (a) T651, (b) T73, and (c) RRA.

Conclusion

(1) RRA thermal processing 7150 plate via a commercially viable process route provides a temper with T651 strengths, and SCC and exfoliation corrosion resistance superior to T73 material.

(2) The microstructure of this temper consists of a peak-aged matrix (mainly precipitates) and overaged grain boundaries.

(3) SCC and exfoliation corrosion resistances increase significantly when 7150 conductivities exceed 38% IACS.

References

1. M.O. Speidel, Metall. Trans. 6A(1975): p. 631.
2. D.O. Sprowls, R.H. Brown, Fundamental Aspects of Stress Corrosion Cracking (Houston, TX: National Association of Corrosion Engineers, 1969), p. 466.
3. W. Gruhl, Metall. 19(1965): p. 206.
4. B.M. Cina, U.S. Patent No. 3856584, Dec. 1974.
5. K. Rajan, W. Wallace, J.C. Beddoes, J. Mater. Sci. 17(1982): p. 2817.
6. M.U. Islam, W. Wallace, Metals Techn. 10(1983): p. 386.
7. M.U. Islam, W. Wallace, Metals Techn. 11(1984): p. 320.
8. J.J. Thompson, E.S. Tankins, V.S. Agarwala, Materials Performance 26(1987): p. 45.
9. J.K. Park, A.J. Ardell, Metall. Trans. 15A(1984): p. 1531.
10. N.C. Danh, K. Rajan, W. Wallace, Metall. Trans. 14A(1983): p. 1843.
11. B.V.N. Rao, Metall. Trans. 12A(1981): p. 1356.
12. R.C. Dorward, K.R. Hasse, Corros. Sci. 19(1979): p. 131.
13. P.K. Poulose, J.E. Morall, A.J. McEvily, Metall. Trans. 5A(1974): p. 1383.
14. K.G. Kent, J. Inst. Metals 97(1969): p. 127.
15. J.A.S. Green, W.G. Montague, Corrosion 31(1975): p. 209.
16. C.J. Peel, P. Poole, Mechanisms of Environment Sensitive Cracking of Materials (London, England: The Metals Society, 1977): p. 147.
17. A.J. Cornish, M.K.B. Day, J. Inst. Metals 99(1971): p. 377.
18. P. Doig, J.E. Edington, Corrosion 31(1975): p. 347.
19. G. Thomas, J.J. Nutting, J. Inst. Metals 88(1959-60): p. 81.
20. M.O. Speidel, Metall. Trans. 6A(1975): p. 561.
21. H.A. Holl, Corrosion 23(1967): p. 173.
22. A.J. Jacobs, Metall. Trans 6A(1975): p. 530.
23. P.E.J. Flewitt, J.W. Edington, Corrosion 33(1977): p. 217.
24. R.K. Viswanadham, T.S. Sun, J.A.S. Green, Metall. Trans. 11A(1980): p. 85.
25. G.M. Scamans, N.J.H. Holroyd, C.D.S. Tuck, Corros. Sci. 27(1987): p. 329.
26. H. Schmiedel, W. Gruhl, Z. Metallkde 74(1983): p. 777.
27. J.R. Pickens, T. Langan, Metall. Trans. 18A(1987): p. 1735.
28. W. Gruhl, Z. Metalle 75(1984): p. 819.
29. I.M. Bernstein, A.W. Thompson, Advances in Corrosion Science and Technology, Vol. 7 (New York, NY: Plenum Press, 1978), p. 235.
30. N.J.H. Holroyd, this proceedings.
31. G.M. Scamans, J. Mater. Sci. 13(1978): p. 27.
32. L. Christodoulou, H M. Flower, Acta Metall. 28.(1980) p. 481.
33. N.J.H. Holroyd, G.M. Scamans, Scripta Metall. 19(1985). p. 915.

Effect of pH on the Stress Corrosion Cracking of 70/30 Brass in Fluoride Solutions

*H.C. Shih and R.J. Tzou**

Abstract

The stress corrosion cracking (SCC) behavior of 70/30 brass has been studied in sodium fluoride solutions at 20°C using the slow-strain-rate technique. Under free corrosion conditions, the effect of strain rates on the SCC susceptibility was determined. It was found that the strain rate for the most severe SCC was at 1.1×10^{-5} s^{-1}. Using this strain rate, the effect of pH value on the susceptibility of SCC was assessed from a quantitative expression of maximum stress and reduction of area in this solution. The electrochemistry of the brass/fluoride/pH system is presented, and a correlation between SCC results and the electrochemical behavior is established. Results are summarized as follows: (1) SCC of 70/30 brass can occur in the fluoride; (2) the critical pH value was found to be 10; above this, SCC will be inhibited; (3) the application of a cathodic potential prevented SCC, while an anodic potential accelerated SCC of brass in fluoride solutions; and (4) the results are consistent with the concept that anodic dissolution initiates SCC, while a film formed on the surface of brass may be responsible for diminished SCC.

Introduction

Stress corrosion cracking (SCC) has proved to be one of the most frequent causes of failure of copper alloy equipment in industry. One technique particularly useful in determining the susceptibility of metallic materials to SCC is the slow-strain-rate test (SSRT).[1-4] The advantages and limitations of this technique have been discussed in depth.[5] The results of an SSRT are expressed in stress-elongation curves from which it is possible to obtain both the ultimate tensile stress (UTS) and reduction in area (RA) values. The lower these values are in comparison with those determined in an inert environment under the same experimental conditions, the more susceptible the material is to SCC. Among the advantages of this technique, as compared to those at constant load or total strain, are its high degree of reproducibility and its relatively short execution time.

70/30 brass has high strength and excellent hot-working properties and is widely used for heat exchangers, valve stems, and rivets because of its relative ease of fabrication and low cost. However, it usually exhibits somewhat poor resistance to SCC, which limits its applications. For many years, brass was thought to fail only in ammoniacal environments, but later work has shown cracking to occur in nonammoniacal environments as diverse as sulfate,[6-9] acetate, formate, tartrate, hydroxide,[10] acidic chloride,[11] mercurous nitrate,[12,13] and sodium nitrite solutions.[14,15] Little is known about the cracking susceptibility of 70/30 brass in applications involving fluoride solutions. For example, fluoride solutions are used to produce metal fluorides, such as cobalt fluoride, antimony fluoride, and particularly uranium hexa-fluoride in nuclear plants. It is also known that the addition of a few ppm of fluorine as sodium fluoride to drinking water can reduce tooth decay.

The purpose of the present work on 70/30 brass is to investigate, by means of the SSRT technique, the susceptibility and inhibition of SCC in this alloy in NaF solutions at various concentrations and pH levels.

*Department of Materials Science and Engineering, National Tsing Hua University, Hsinchu 30043, Taiwan, Republic of China.

Experimental

The chemical composition (wt%) of the commercial annealed brass plate used in these tests was 29.9% Zn, 0.02% Fe, 0.02% Si, and 0.007% Ni, with a balance of Cu, as analyzed by atomic emission spectrometry.

Round specimens fabricated from 4.76-mm-diameter rod had threaded ends and a 3.175-mm diameter by 12.7-mm gauge length, according to ASTM G49-76.[16] Prior to testing, the gauge length of the specimen was polished with alumina powder (3 μm) along the tensile direction to avoid a possible notch effect, then degreased in acetone, and dried in air. The chemicals used in this study were of extra pure grade; deionized water was used to prepare the test solutions.

The SSRT technique was used in this test, and the assembly is similar to that used elsewhere.[17] The driving mechanism consists of a moderately hard straining frame producing six crosshead speeds easily varied by gear changes. The use of a constant speed motor driving through reduction boxes, gear wheels, and chain sprocket drives gives a reliable positive drive. The load and elongation are monitored continuously by a load cell and a displacement transducer until fracture occurs. All tests were performed in aerated sodium fluoride solutions over a pH range of 2 to 12. The pH value was adjusted with either NaOH or HF. Experiments were performed under open-circuit conditions as well as at applied controlled potentials. The RA and UTS of the fractured specimen was then measured, and the fracture morphology was examined by means of scanning electron microscopy (SEM).

Potentiodynamic polarization was also studied for each alloy/environment system at a scan rate of 1 mV/s. The polarization apparatus is similar to the standard assembly used elsewhere.[18] The data were obtained using a Princeton Applied Research† Model 273 potentiostat/galvanostat interfaced to an IBM PC/AT for data processing, storage, and analysis. Potentials were measured against a saturated calomel electrode (SCE), as were all potentials in this investigation.

†Trade name.

Results

When the tensile tests were performed in air, the UTS was observed at 372 MPa and the corresponding RA was at 67.8%, the strain was at 82.7%. These data can be used as a standard for comparison.

Stress–strain curves at open-circuit potentials (OCPs)

Experiments were conducted to determine the most suitable conditions for producing SCC, both in terms of strain rate and fluoride concentration with various pH values. Figure 1 shows the stress-strain curves at various strain rates in 0.1 M NaF (pH 6.2). Both at the highest (5×10^{-5} s^{-1}) and lowest rates (2×10^{-6} s^{-1}) tested, the curves showed considerable SCC susceptibility, i.e., lower UTS, RA, and elongation values compared with the specimen failed in air. To produce strong evidence for cracking, it seemed necessary to use an intermediate strain rate of 1×10^{-5} s^{-1}. At this strain rate, not only the UTS values, but also the RA values of the test in fluoride solution were lower than those obtained from other strain rates, as shown in Figure 2.

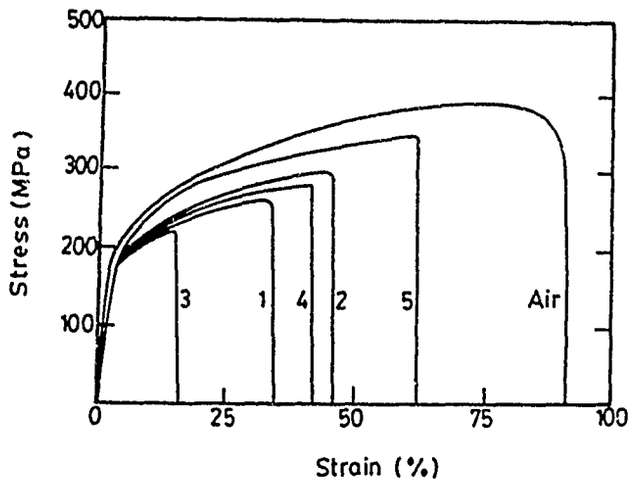


FIGURE 1—Stress–strain curves of 70/30 brass in 0.1 M (4200 ppm) sodium fluoride (pH = 6.2) at various strain rates: (1) 5×10^{-5} s^{-1}, (2) 1.2×10^{-5} $^{-1}$,(3) 1×10^{-5} s^{-1}, (4) 2.5×10^{-6} s^{-1}, and (5) 2×10^{-6} s^{-1}.

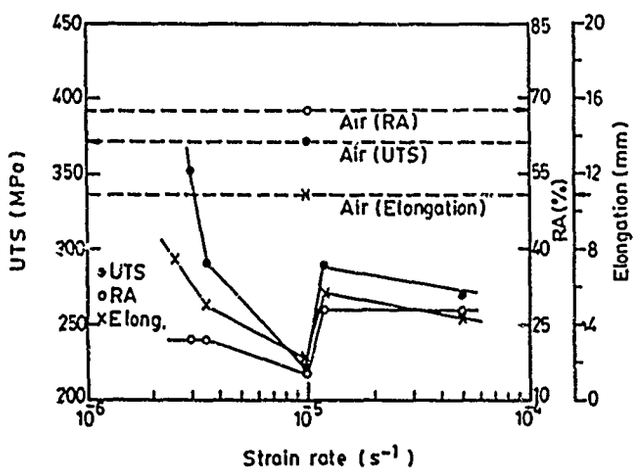


FIGURE 2—Effect of strain rates on the UTS, RA, and elongation of 70/30 brass in 0.1 M sodium fluoride solution (pH = 6.2).

The stress–strain curves, relating to a series of measurements performed to establish the pH range critical to SCC, are shown in Figure 3 From these results, it can be seen that there is relatively little difference between stress–strain curves between pH 10.0 and pH 11.2 fluoride solution (0.1 M). Furthermore, the tensile result of brass in solution pH 12.5 is similar to the ductile fracture of Specimen 4 tested in air. However, relatively severe decreases in elongation were observed in the solutions pH < 9.1. The effect of pH on UTS and RA is shown in Figure 4. Results indicate that significant recovery of ductility, as expressed by values of UTS and RA, occurs in solutions with pH > 10. On the contrary, the low values of both UTS and RA, indicating SCC susceptibility, are almost invariable with pH at < 9.1.

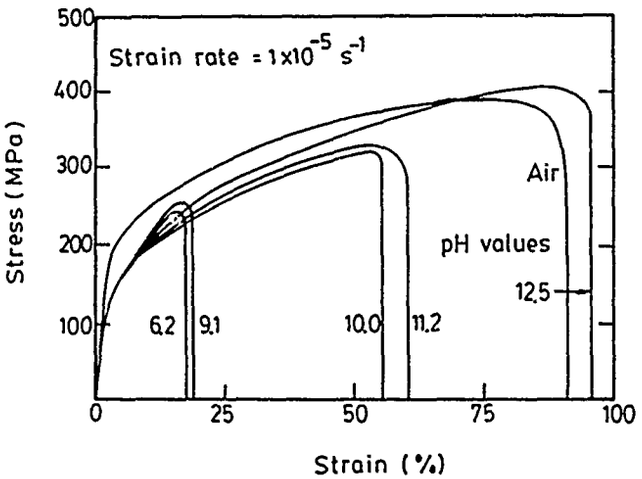


FIGURE 3—Stress–strain curves of 70/30 brass in 0.1 M sodium fluoride solution at various pH values.

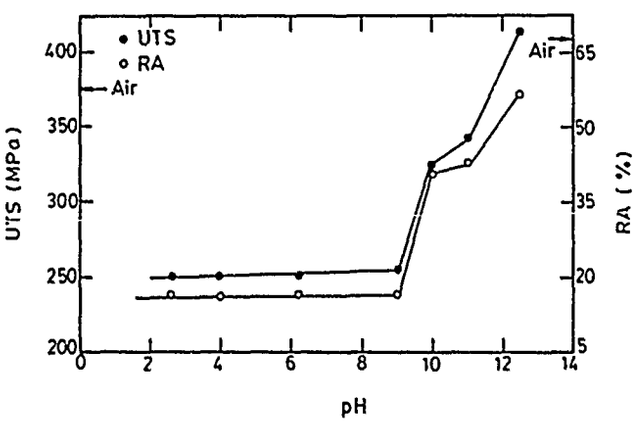


FIGURE 4—Effect of pH on the UTS and RA of 70/30 brass in 0.1 M sodium fluoride solution at the open-circuit potential. (Strain rate = 1.1×10^{-5} s^{-1}.)

Stress–strain curves obtained in various fluoride concentrations are shown in Figure 5. Apparently, there is little difference between stress–strain curves in fluoride-free solution and those in the solution containing 1 ppm fluoride. Moreover, a significant reduction in strain appears between 1 ppm and 10 ppm fluoride. Further decreases in strain were observed in the solutions containing 1000 ppm fluoride or more. Figure 6 shows the effect of fluoride concentrations on the UTS and RA, indicating that higher fluoride concentrations lead to greater SCC susceptibility.

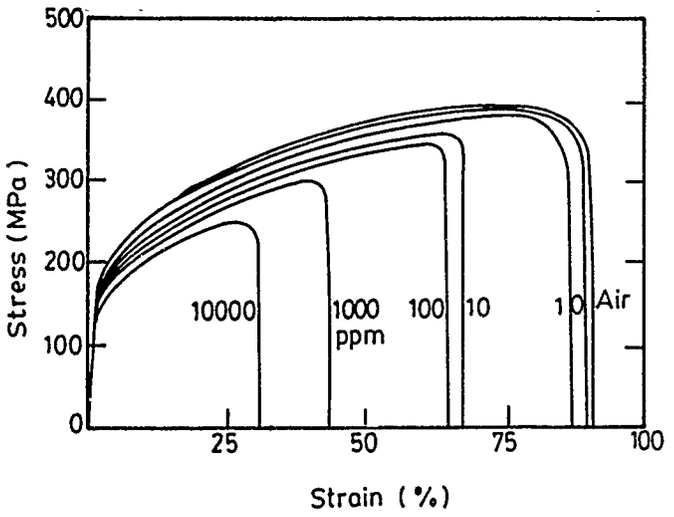


FIGURE 5—Stress–strain curves obtained in different fluoride concentrations at 20°C (pH = 6.2).

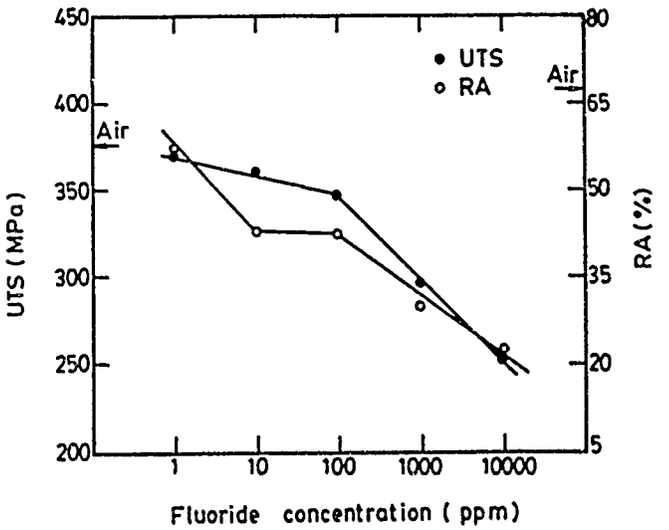


FIGURE 6—Effect of fluoride concentration on the UTS and RA of 70/30 brass at 20°C (pH = 6.2).

Stress–strain curves at the applied potentials

A series of tests was conducted at different potentials varying from −600 to +300 mV_{SCE} to investigate the effect of potential on the SCC behavior in 0.024 M (1000 ppm) fluoride solution. It was observed that no SCC occurred when the specimen was cathodically polarized at −300 and −600 mV_{SCE}, respectively. The OCP here was approximately −50 mV_{SCE}. On the other hand, when the applied potentials were set at 0 and +300 mV, respectively (i.e., anodically polarized), SCC did occur, as shown in Figure 7. The relationship between UTS, RA, OCP, and the applied potential in fluoride solution can be seen from Figure 8. It is clear that the severity of SCC increases with increasing applied potential.

Electrochemical analysis

Effect of pH. Polarization experiments were conducted with unstressed specimens in 0.1 M sodium fluoride for different solution pH, the results are shown in Figure 9. It is clear from Figure 9(a) that the anodic behavior of brass is almost indiscernible in solutions with pH < 8 and that no passivation takes place. Figure 9(b), however, shows apparent passivation of brass in solutions with pH > 10, which is probably a result of the oxide film on the specimen surface. A prominent peak showing at −360 mV_{SCE} on the cathodic curve, particularly at pH 11, signifies the intersection of the cathodic reaction on the passive range of the anodic reaction and belongs to a distinct transition from active to passive state. Therefore, the OCP of brass in this condition remains in the passive range of the anodic reaction.

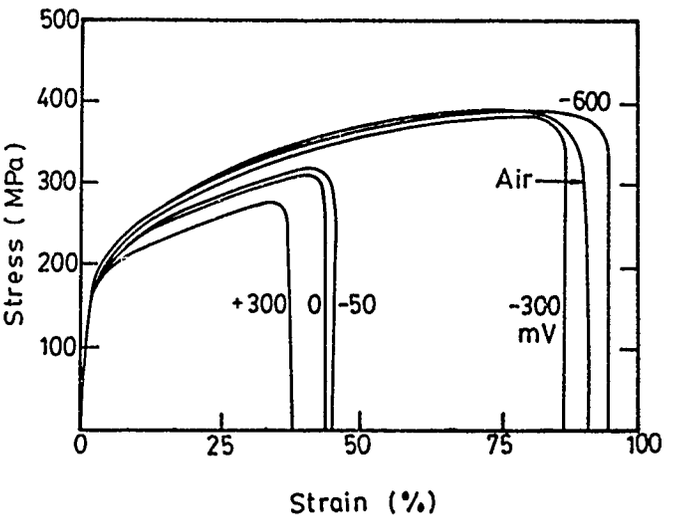


FIGURE 7—Stress–strain curves obtained in 0.024 M (1000 ppm) sodium fluoride solution (pH = 6.2) under various applied potentials.

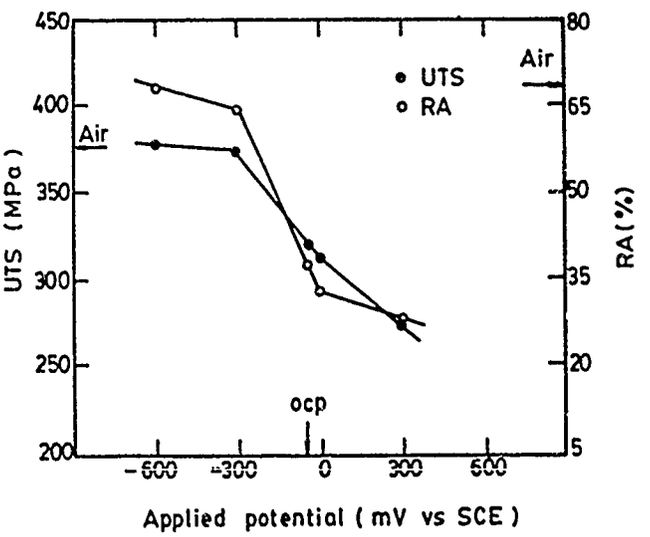


FIGURE 8—Effect of applied potential on UTS and RA of 70/30 brass in 0.024 M (1000 ppm) sodium fluoride solution (pH = 6.2).

A slight variation of the passive currents, as observed on the anodic curve [Figure 9(b)], is within a factor of 1.4. Figure 9(c) shows that the OCP of brass becomes much more negative as pH value increases. This suggests that hydroxyl ions may polarize the cathodic reaction substantially and thus act as a cathodic inhibitor for SCC. For instance, the OCP decreases from −10 to −280 mV_{SCE} as pH increases from 6 to 11. At pH 11, the measured OCP was found at −280 mV_{SCE} (−38 mV_{SHE}), which corresponds to the stable phase of Cu_2O according to the E-pH diagram[19,20] of Cu/H_2O a 25°C.

Effect of fluoride ion concentration. Polarization curves of unstressed specimens were also determined in solutions with various fluoride concentrations, and the results for neutral solutions (pH 6.2) are shown in Figure 10. It is clear from this figure that the more concentrated the fluoride, the higher the anodic and cathodic current densities. For instance, the polarization curves remain active even at the anodic potential up to +1000 mV_{SCE}, and the corrosion current increases as the fluoride concentration increases.

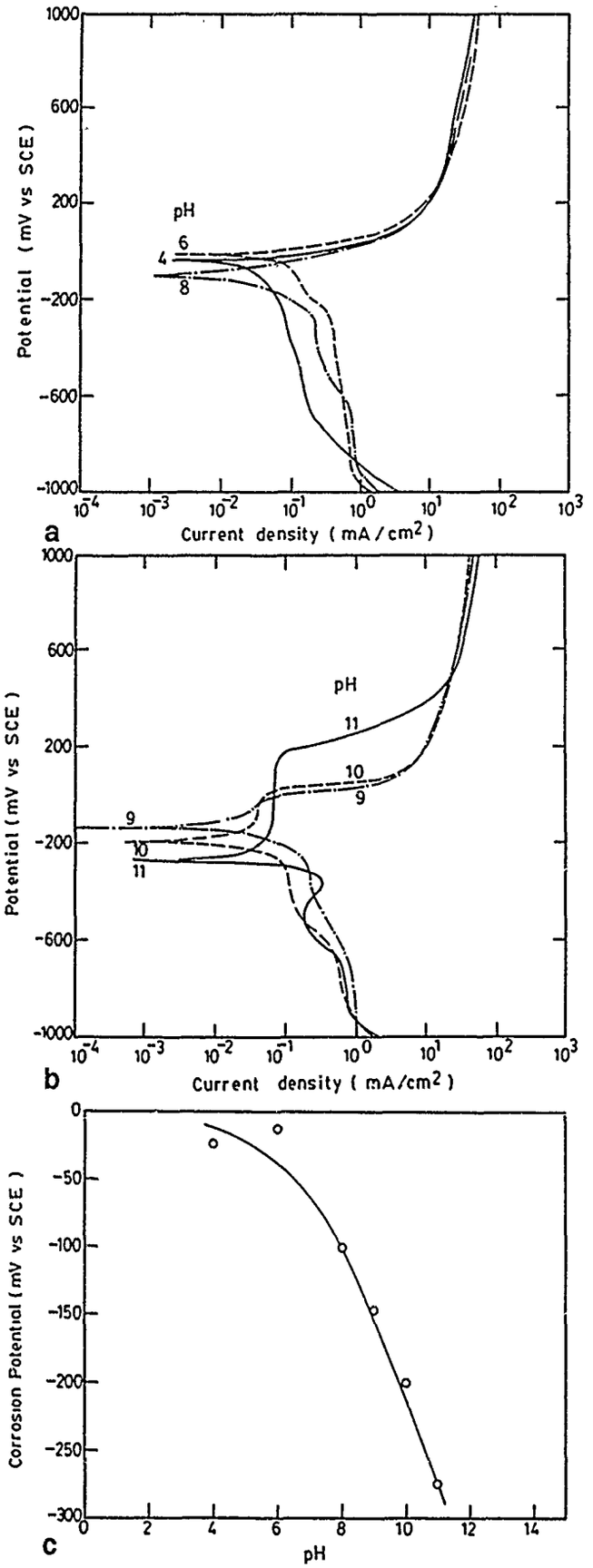


FIGURE 9—(a) and (b) Effect of pH on the polarization curves of unstressed 70/30 brass in 0.1 M (4200 ppm) sodium fluoride solutions (scan rate 1 mV/s) and (c) effect of pH on the corrosion potential of 70/30 brass in 0.1 M sodium fluoride solutions.

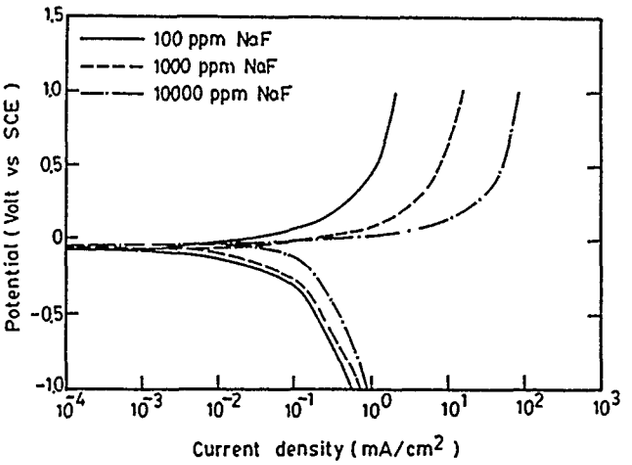


FIGURE 10—Polarization behavior of the unstressed 70/30 brass in different concentrations of fluoride solution (pH = 6.2).

Fractographic observations

As shown in Figure 11, the fracture morphology shows predominantly intergranular failure for the specimen tested at OCP in the 0.1 M sodium fluoride solution (pH 6.2). Photomacrographs show that secondary cracks are also clearly visible along the gauge length exposed to the solution containing different concentrations of fluoride, as shown in Figure 12. Almost no secondary cracks are visible on the gauge section of 70/30 brass in 1 ppm fluoride solution, whereas the secondary cracks are apparent in 10 ppm or more fluoride solution.



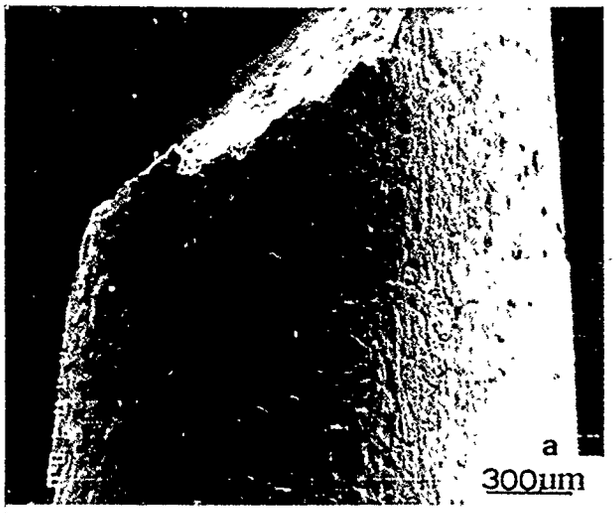
FIGURE 11—Intergranular SCC of 70/30 brass in 0.1 M (4200 ppm) sodium fluoride solution (pH = 6.2).

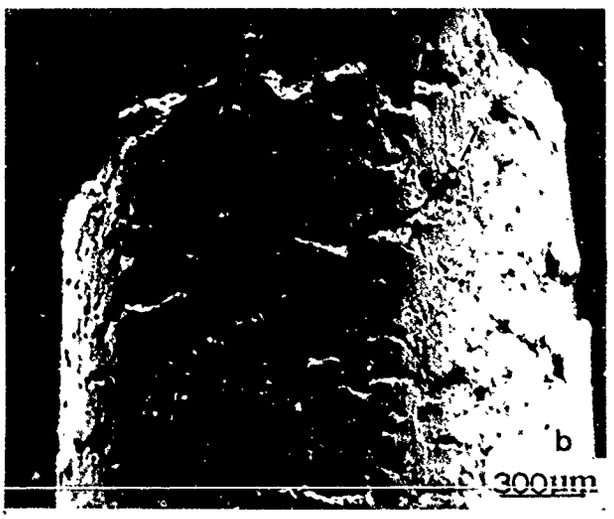
Discussion

A significant result of the present study is the clear susceptibility of 70/30 brass to intergranular SCC in aqueous fluoride solution at the OCP in the pH < 9.1.

The results indicate that the major factors that determine SCC susceptibility in 70/30 brass are the pH and the fluoride concentration of the solution. Specimens in solutions with pH < 9.1 were subject to general corrosion and were very susceptible to SCC, provided that the fluoride concentration exceeded 10 ppm. These effects of the pH and fluoride concentration on both the UTS and RA are consistent with the SCC mechanism involving stress-enhanced anodic dissolution. The formation of a cuprous oxide film protects the specimen

from corrosion and SCC. (See Figure 13.) The idea that anodic dissolution is the rate-controlling step in the SCC of copper alloys is not new. The work of previous investigators, which shows that anodic polarization generally accelerates SCC, while cathodic polarization retards it, can also be attributed to the enhancement of anodic dissolution.[7,21,22]





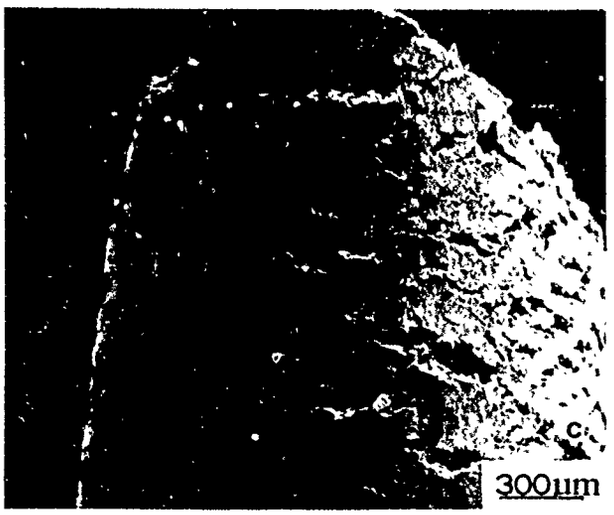




FIGURE 12—Photomacrographs showing secondary cracks on the side surfaces of 70/30 brass in (a) 1 ppm, (b) 10 ppm, (c) 100 ppm, and (d) 420 ppm sodium fluoride solutions.

Potentiodynamic polarization curves suggest that the specimen is generally corroded in the solution pH < 9.1, whereas the passive film is formed at solution pH > 10. Verink, et al.,[23] reported that cuprous oxide was found in the stable thin film corrosion products on brass and observed that this film was sufficient to reduce the extent of dezincification of brass. This result is consistent with the suggestion that anodic dissolution is responsible for the initiation of SCC, and the cuprous oxide film forms the protectiveness against the occurrence of SCC.

These results can be compared to those obtained when sodium sulfate is used as an SCC medium for admiralty brass.[8-11] Kawashima, et al.,[7] reported that maximum susceptibility to SCC in sodium sulfate solution lies in the pH range of 4 to 10, and the severity of SCC increases on applying anodic potentials of −27 to +238 mV_{SCE}. However, they did not observe SCC under open-circuit conditions. It is also interesting to note that some investigators have observed SCC of brass at the OCP in nonammoniacal solutions such as sodium nitrite, sodium chlorate, and sodium chloride.[14,15,22] These investigators also showed SCC of brass pH 4 to 9 at $1.5 \times 10^{-5}\ s^{-1}$, beyond which no SCC of brass was observed. The results of brass in F^- environments, however, indicated that SCC occurs in neutral and acidic F^- environments (pH < 9.1) and showed no SCC in an alkaline F^- environment (pH ~ 10). The major disagreement is that the SCC of brass in F^- environments can extend to a much more acidic environment (pH < 4) where no SCC was observed in Na_2SO_4, $NaNO_2$ and $NaClO_3$. It is well known that brass is susceptible to stress corrosion in hydrofluoric acid.[24]

Supporting data about the aggressiveness of fluoride ions have been published by many investigators.[25-27] Fluoride ions, even in a neutral sodium fluoride solution, could increase the critical and passive current densities of titanium and zirconium alloys during anodic polarizations.[25,26] Valand, et al.,[27] also provided evidence of the aggressiveness of fluoride ions on pure aluminum. It is worth noting that the fracture mode of 70/30 brass in sodium fluoride solution belongs to intergranular SCC, accounting for the fact that the grain boundary is more active and dissolves at a higher rate than the grain interior. In other words, the anodic sites are the grain boundaries, and the grain interiors act as cathodic sites. Thus, localized zinc dissolution takes place at the grain boundaries. These zones will crack readily in the presence of stress. Several workers favor the intergranular SCC mechanism for brass, which involves the dezincification at the crack tip.[12,22] Pugh, et al.,[28-30] and Bertocci, et al.,[31,32] indicated that an explanation can be made on the basis of the belief that dezincification plays a key role in the embrittlement process. The fact that pure copper did not fail in either copper-containing ammonia solution indicates that zinc plays a vital role and is thus consistent with the dezincification hypothesis.

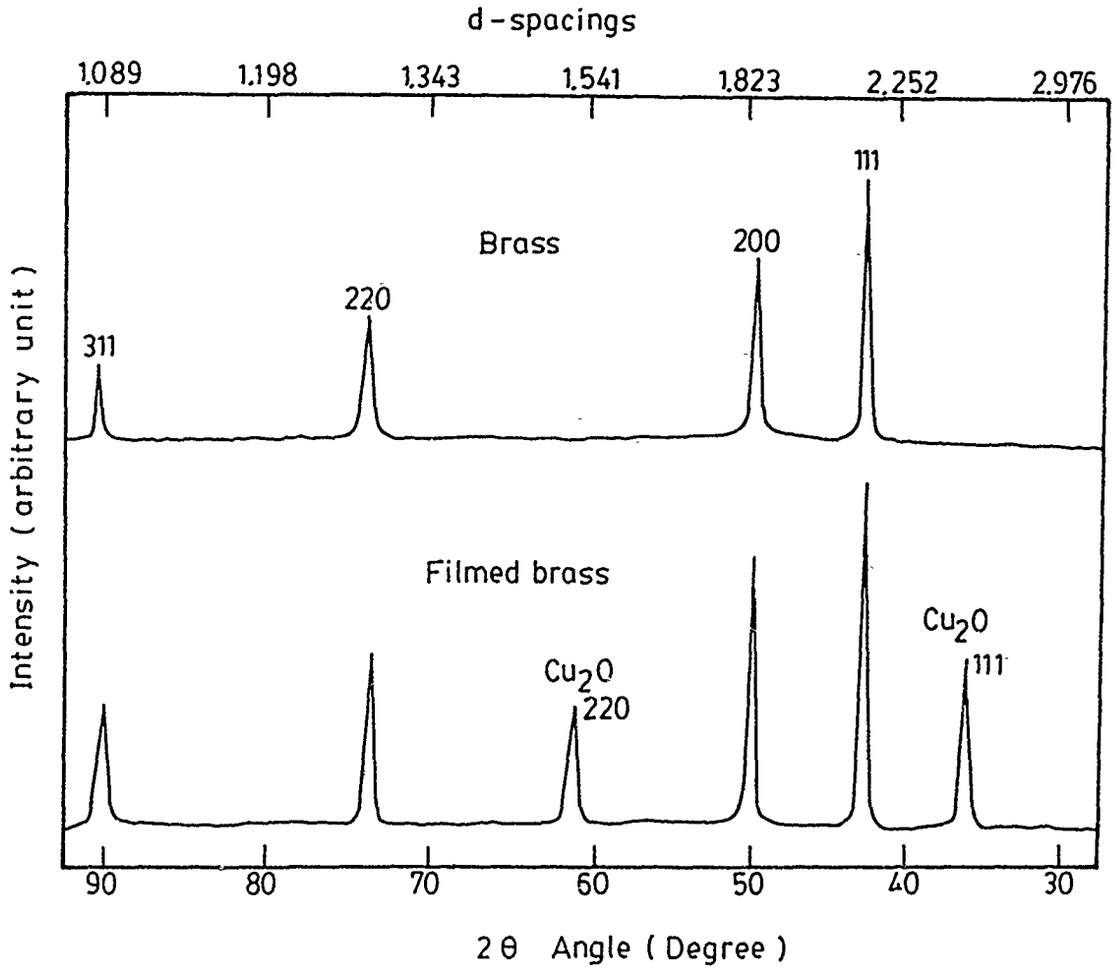


FIGURE 13—X-ray diffraction pattern of the surface on 70/30 brass immersed in 0.1 M sodium fluoride solution (pH = 12.5).

Analysis of the results obtained in the present research demonstrates that the SSRT constitutes a reliable method for studying SCC inhibition relatively quickly. Another significant feature of this study is that a good correlation between SCC susceptibility and the electrochemical behavior of the alloy/environment system has been developed from which a better understanding of the mechanism of SCC can be obtained.

Conclusion

From the results of the present study, the following conclusions can be drawn:

(1) 70/30 brass undergoes SCC in fluoride solution under free corrosion conditions for pH < 9.1. At pH greater than 10, SCC is inhibited. The fracture mode is predominantly intergranular.

(2) Application of cathodic potentials can prevent SCC, while anodic polarization can accelerate SCC of brass in fluoride solution.

(3) Evidence strongly suggests that anodic dissolution at the crack tip is the rate-controlling factor in SCC.

(4) SCC of brass in F^- environments can extend to a much more acidic environment (pH < 4) when no SCC was observed in SO_4^{2-}, NO_2^-, and ClO_3^-.

(5) Both x-ray diffraction for brass and the E-pH diagram for Cu/H_2O show the occurrence of a Cu_2O film.

(6) A good correlation between SCC susceptibility and the electrochemical behavior of the brass/fluoride/pH system has been obtained.

Acknowledgment

This work was supported by the National Science Council of the Republic of China under Contract No. NSC 76-0405-E007-22 to the National Tsing Hua University.

References

1. F. Mancia, A. Tamba, Corrosion 42(1986): p. 362.
2. F. Stalder, D.J. Duquette, Corrosion 33, 1(1977): p. 67.
3. T. Nakayama, M. Takano, Corrosion 42, 10(1986): p. 592.
4. M. Takano, Corrosion 30, 12(1974): p. 441.
5. G.M. Ugiansky, J.H. Payer, Stress Corrosion Cracking—The Slow Strain Rate Technique, ASTM STP 665, 1979.
6 T R Pinchback, S.R. Clough, L.A. Heldt, Corrosion 32, 12(1976): p. 467.
7 A Kawashima, A.K. Agrawal, R.W. Staehle, J. Electrochem. Soc., 124(1977): p. 1822.
8. S. Torchio, Corros. Sci. 26(1986). p. 1933.
9. H.W. Pickering, P.J. Byrne, Corrosion 29, 8(1973): p. 325.
10. R.N. Parkins, N.J.H. Holroyd, Corrosion 38, 7(1982): p. 245.
11. S. Torchio, Corros. Sci. 21(1981): p. 59.
12 ASTM B154-73 Annual Book of ASTM Standards, Part 6 (Philadelphia, PA: ASTM, 1974), p. 278.
13. S A. Bradford, T. Lee, Corrosion 34, 3(1978). p. 96.
14. J. Yu, R.N. Parkins, Y. Xu, G. Thompson, G.C. Wood, Corros. Sci. 27(1987): p. 141.

15. J. Yu, R.N. Parkins, Corros. Sci. 27(1987): p. 159.
16. ASTM G-49-76, 1982.
17. J. Congleton, H.C. Shih, R.N. Parkins, Corros. Sci. 25, 8/9(1985): p. 769.
18. N.D. Creene, Experimental Electrode Kinetics (Troy, NY: Rensselaer Polytechnic Institute, 1965).
19. R.J. Tzou, H.C. Shih, Corrosion, in press.
20. M. Pourbaix, Atlas of Electrochemical Equilibria in Aqueous Solutions (Houston, TX. National Association of Corrosion Engineers, 1974), p. 387.
21. H. Uhlig, K. Gupta, W. Liang, J. Electrochem. Soc. 122(1975). p. 343.
22. V.K. Gouda, H.A. El-Sayed, G.M. Sherbini, Br. Corros. J. 18(1983): p. 40.
23. J.E. Finnegan, R.E. Hummel, E.D. Verink Jr., Corrosion 36, 5(1981): p. 256.
24. M.G. Fontana, N.D. Greene, Corrosion Engineering (New York, NY: McGraw-Hill, 1976), p. 260.
25. M.J. Mandry, G. Rosenblatt, J. Electrochem Soc 119(1972): p 29.
26. D. Rettig, C. Voigt, K. Schwabe, Corros. Sci. 10(1970). p. 657
27. T. Valand, G. Nilsson, Corros. Sci. 17(1977): p. 449.
28. E.N. Pugh, A.R.C. Westwood, Phil. Mag. 13(1966): p. 167.
29. E.N. Pugh, J.A.S. Green, Metall. Trans. 2(1971): p. 3129.
30. E.N. Pugh, Atomistics of Fracture, ed. R.M. Latanision, J.R. Pickens (New York, NY: Plenum Press, 1983), p 997
31. U. Bertocci, F.I. Thomas, E.N. Pugh, Corrosion 40, 8(1984): p 439.
32. U. Bertocci, Proceedings of the Conference on Localized Crack Chemistry and Mechanics in Environment Assisted Fracture, ed. R.P. Gangloff (Warrendale, PA. The Metallurgical Society-American Institute of Mining, Metallurgical, and Petroleum Engineers, in press 1989).

Discussion

S.M. Bruemmer (Pacific Northwest Laboratory, USA): The results of slow-strain-rate (SSR) stress corrosion cracking (SCC) in fluoride show a very narrow strain-rate range over which cracking was observed. This narrow range, if true, is surprising when compared with SSR SCC test results usually observed for other materials. Can you explain this?

H.C. Shih: The evidence for this conclusion is based on observed changes in the ultimate tensile strength (UTS) and reduction in area of brass in the 0.1 M fluoride environment at the strain rate of 1×10^{-5}/s. For example, the reduction in area value reduces to one-third of the value attained when testing in air at this strain rate. Metallographic observations indicated little or no SCC at strain rates differing from this value.

R.N. Parkins (University of Newcastle upon Tyne, UK): I cannot recall seeing cracking only occurring over such a small range of strain rates as in the work of Shih and Tzou. Transgranular SCC of alpha-brass usually occurs in a wide range of environments, as indicated in Figure 14 of my paper (R.N. Parkins, "Stress Corrosion Cracking," this proceedings). Although not shown on that Figure, such cracking is promoted by 10^{-2} to 10^{-3} N sodium chloride, and also by brackish waters [R.N. Parkins, C.M. Rangel, and J. Yu, Metall. Trans. A 16A(1985): p. 1671].

However, it occurs to me that the range may be larger than suggested by Shih and Tzou, because at the fastest and slowest strain rates they used, the reductions in area (RA) were only in the region of 30%, which is low for ductile failure of alpha-brass. This suggests that if they were to conduct further tests at both faster and slower strain rates, their plot of RA vs strain rate would extend to higher RA values, thereby extending the strain-rate range over which cracking is observed.

H.C. Shih: Even both at the highest (5×10^{-5}/s) and lowest (2×10^{-6}/s) strain rates, the curves show considerable SCC susceptibility of brass in fluoride environments, i.e., much lower UTS (275 MPa) and RA (27%), compared with the one failed in air (UTS = 372 MPa; RA = 67.8%), as shown in our Figure 2.

The crosshead speeds of our SSR tests lie between 5×10^{-4} and 5×10^{-6} mm/s. The gauge length of the tensile specimens was 12.7 mm and the corresponding strain rates used in the system were 2×10^{-6}, 2.5×10^{-6}, 1.0×10^{-5}, 1.1×10^{-5} and 5×10^{-5}/s, respectively. Both at higher and lower strain rates than the range we have used, we believe our plot of RA and stress vs strain rate (Figure 2) should extend to higher RA and strain.

An Analysis of Evidence to Support an Adsorption Model for Stress Corrosion Cracking in Alpha-Brass

*U.K. Chatterjee and S.C. Sircar**

Abstract

The mechanism of stress corrosion cracking of alpha-brass in ammoniacal solutions has been studied from the viewpoint of a transition in the mode of cracking. A change in solution conditions or polarization causes this transition, which cannot be explained on the basis of structural changes in the material. The suggested model of adsorption of reacting species at the prevalent discrete anodic and cathodic sites can successfully explain these and other observations.

Kinetic studies involving the role of chemical variables and the effect of temperature lend support to the adsorption hypothesis and an electrochemical nature of the initiation and propagation stages of the cracking process. The effect of adding extraneous ions to the cracking media on time of cracking also supports this model.

Introduction

The mode of stress corrosion cracking (SCC) in alpha-brass in ammoniacal solutions has been found to be both intergranular and transgranular. A transition in the mode of cracking from intergranular to transgranular in polycrystalline alpha-brass has been reported to be caused by factors like cold work,[1-3] an increase in Zn content of the alloy,[4-7] an addition of a third element to the alloy,[7 11] and the condition of the corrosive medium.[12,13]

The pioneering work of Mattsson revealed the importance of solution pH in determining the mode of fracture.[12] In subsequent works by different authors, a solution-dependent transition in the mode of cracking was reported.[13-15] The reason for such transitions could not be attributed to structural changes in the material.

Shimodaira and Takano suggested a correlation between the physical properties of the surface film, viz., crystal grain size, thickness, porosity, hardness, strength, etc., and the mode of cracking and its transition.[16] Pugh[17] classified the ammoniacal solutions into two categories: tarnishing and nontarnishing, and attributed the intergranular cracking in tarnishing solutions to the tarnish-rupture model as postulated by Forty and Humble[18] and developed by McEvily and Bond.[19] In nontarnishing solutions, he explained the transgranular cracking on the basis of preferential dissolution at dislocations, based on the proposal of Tromans and Nutting,[20] without explaining why this preferential dissolution at dislocations should be absent in the same material when exposed to a tarnishing solution. Procter and Islam showed that while the tarnish fractured transgranularly, the metal cracked intergranularly, thus highlighting the discrepancy in the tarnish rupture mechanism.[21]

Pugh[22] subsequently replaced the tarnish rupture model with a modified film-rupture model,[23,25] that is, by preferential anodic dissolution of film-free metal at the crack tip where plastic deformation continuously ruptures the protective film. However, he suggested that transgranular cracking in a nontarnishing solution occurs by brittle mechanical fracture, rather than by dissolution, a view that has been reflected in a subsequent publication as well.[26] In a recent paper, Pugh[27] attributed this brittle fracture to environment induced cleavage and dwelt upon the importance of stacking fault energy and slip mode for the ease of cleavage step formation. While this may explain the propagation mode and crack morphology, the transgranular crack initiation step remains unexplained. Moreover, the role of chemical variables and their effect on time to fracture have been ignored. Based on the concept of Paskin, et al ,[28] and Sieradzki, et al.,[29] who showed that a brittle crack can initiate in a thin surface film and can attain a velocity sufficient to propagate as a cleavage crack for significant distances into the unaffected substrate, Pugh[27] proposed a film-induced cleavage model for crack initiation, but the feasibility of this model in reference to the SCC of alpha-brass remains to be established. Elsewhere, Bertocci, Thomas, and Pugh considered the embrittlement as a consequence of the adsorption of cuprous ammonium complex ions,[30] following the views of Lynch;[31] alternatively, they believed the cuprous ions provided the cathodic species with protection against a dezincification anodic reaction.

The overall picture of SCC of brass in ammoniacal solution remains unclear, particularly when considering the transition in the mode of cracking under the changed conditions of the solution.

The Effect of Polarization

The controversy was further aggravated when studies under applied potential conducted at our laboratory showed that in annealed samples, anodic polarization results in minimal cracking time accompanied by a transition in cracking mode from intergranular to transgranular (Figure 1).[32]

No ready-made explanation came from the existing theories for the rising part of the curves on the anodic side, as the anodic polarization is expected to bring about more dissolution, leading to a decrease in cracking time. An explanation based on blunting of the crack tip because of a high rate of dissolution, and hence a fall in the local stress intensity, which is unable to sustain the crack propagation, cannot account for the transition in cracking mode and the propagation of a transgranular crack. The minimum in cracking time can only be explained if an adsorption maximum at the most susceptible potential is assumed, followed by desorption at higher potentials. That the polarization leads to a change in the cracking pattern is an indication that the crack path is, after all, not dependent on the internal arrangements of defects or dislocations but on the situations existing at the surface or the interfaces of the corroding material and the environment.

*Department of Metallurgical Engineering, IIT, Kharagpur 721 302, India.

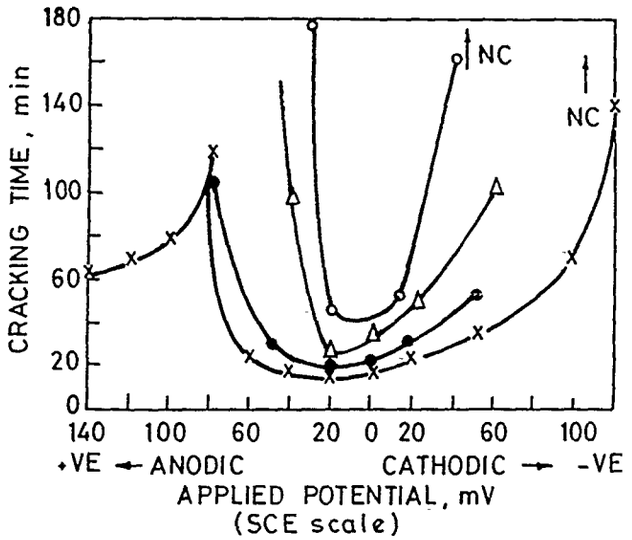


FIGURE 1—Effect of applied potential on the time of fracture of α-brass in Mattsson's solution of different compositions. (Reprinted with permission from Pergamon Press.[32])

NH^+ −1 g mol/L, pH = 7

X	X—0.03 g atom cu/L	V_{oc} = −50 mV
•	•—0.01 g atom cu/L	V_{oc} = −100 mV
Δ	Δ—0.005 g atom cu/L	V_{oc} = −150 mV
O	O—Cu-zero	V_{oc} = −250 mV

The explanation for these observations was as follows:[32] "If discrete sites of variable energies pre-exist on the surface, some of which are anodic and some cathodic in nature, then, on impressing an anodic potential, the cathodic sites become active anodic points, while on impressing a cathodic potential the anodic sites become active cathodic points. As we move away from the corrosion potential in either direction, the surface active points or regions change their nature, totally or partially, depending on the extent of polarization. During anodic polarization, the anodic reaction that initially occurs on the grain boundaries spreads to other areas in the grains. Therefore, the active centers are now more widely distributed in the grain boundaries as well as in the grain interiors, resulting in a mixed type of crack. Beyond the minimum, the grain interiors become more active than the grain boundaries, leading to a transgranular crack."

As a corollary to the mechanism proposed, it should be expected that where prior conditions for transgranular cracking prevail, i.e., where the susceptibility exists preferentially at the grain interior, as in the case of cold-worked materials, the changeover from transgranular to intergranular cracking should be possible if the active sites can be shifted from the grain interior to the grain boundaries. This was made possible with cathodic polarization of cold-worked samples.

The observation of a shift in the maximum susceptible potential range to more anodic values in cold-worked specimens compared to annealed specimens (and also in 80-20 brass compared to 70-30 brass) was successfully interpreted based on adsorption on discrete reaction sites.[33] The same idea was further supported by the occurrence of transgranular cracking and a shift in the open-circuit potential value toward more cathodic values when ammonia of the conventional Mattsson solution was substituted with butyl amine.[34]

Kinetic Studies

Having identified the role of discrete anodic and cathodic sites in determining the crack path, it became necessary to obtain more direct support for adsorption of reacting species and to understand the reactions involving these sites and the effect of compositional variations on these reactions. The basic question of whether or not the crack propagation is electrochemical or mechanical in nature was also asked. Since the SCC susceptibility is normally expressed in terms of time to fracture, an analysis involving the rate of crack growth as dependent on the environmental factors was likely to give better insight into the mechanism of SCC, particularly if effects on crack initiation and crack propagation stages were studied separately.

The variation of copper, ammonium ion, and hydrogen ion concentration in Mattson's solution on the rate of crack initiation and crack propagation yielded[35] rate equations conforming to a process where the Langmuir-Hinshelwood mechanism[36] operates through a competitive adsorption of these ions at specific sites. The overall chemical reaction involving the adsorbed species can occur in two ways:

$$2Cu(NH_3)^{2+}_{4(AD)} + 6H^+ + H_2O + 2e = Cu_2O + 8NH_4^+ \quad (1)$$

or

$$2Cu(NH_3)^{+}_{2(AD)} + 2OH^- = Cu_2O + 4NH_3 + H_2O \quad (2)$$

In the first reaction, the adsorbed species are cathodically reduced to Cu_2O. According to the second equation, the formation of Cu_2O occurs through a cuprous amine complex produced after a cathodic reduction step of

$$Cu(NH_3)^{2+}_{4(AD)} + e \rightarrow Cu(NH_3)^{+}_{2(AD)} + 2NH_3 \quad (3)$$

Thus, the copper oxide formed is a product of the cathodic reaction or electron-consuming reaction leading to a corresponding anodic reaction for attainment of a steady-state value. Copper oxide does not create a galvanic condition for the anodic reaction, but it can be viewed as a product that plays a minor role in the process of cracking.

Activation energy values for the initiation and propagation of cracks, as derived from the dependence of these two steps on temperature, were found to be the same (13 kcal/mol).[35] This shows that these two steps are chemically controlled processes and essentially the same. A more interesting observation was the dependence of activation energy on polarization (Figure 2), 6 kcal/mol for anodic and 21 kcal/mol for cathodic polarization, which indicates the electrochemical nature of the process and that the discrete energy sites facilitating the electrochemical reactions are influenced by electrical stimulation.

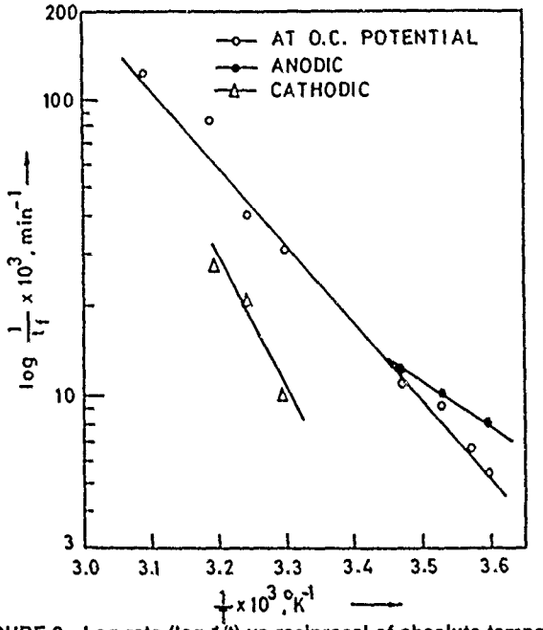


FIGURE 2—Log rate (log 1/t) vs reciprocal of absolute temperature plots for annealed brass under polarization conditions. (Reprinted with permission.[35])

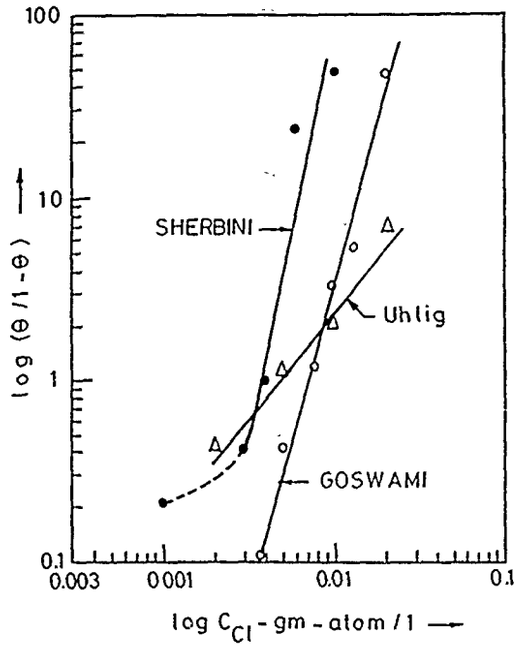


FIGURE 3—Log concentration of chloride ions added to test solution vs log θ/(1−θ) plots. (Reprinted with permission from Pergamon Press.[38])

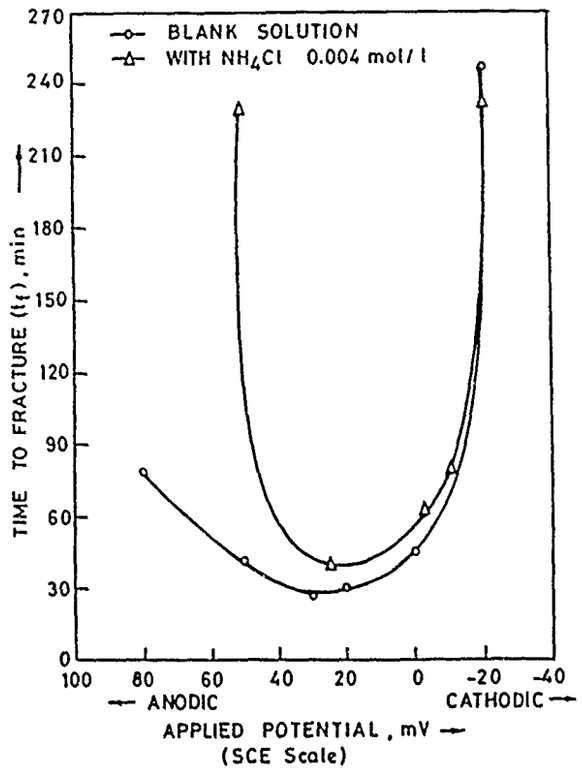


FIGURE 4—Effect of polarization on time to fracture of brass in test solutions with and without the addition of NH_4Cl. (Reprinted with permission from Pergamon Press.[38])

Effect of Extraneous Ion Additions

The ideas presented so far receive support from the observed effects of the addition of extraneous ions to conventional ammoniacal solutions. The addition of sodium chloride[37] or ammonium chloride to Mattsson's solution and ammonium sulfate to Pugh's solution[38] shows an inhibitive effect on SCC of brass and a transition in the mode of cracking from intergranular to transgranular.

An analysis has been made following the method proposed by Hoar and Holliday,[39] plotting a graph between log θ/(θ) and log concentration of the additive, where (1 − θ) corresponds to the fraction of protection affected by the addition of inhibitor, where the latter follows Langmuir's adsorption isotherm. The plots yield straight lines, a representative of which is shown in Figure 3 for the chloride addition, confirming the validity of the adsorption hypothesis. The plot also incorporates the analysis of results of Uhlig, et al.[40] Similar plot has been obtained for sulfate addition to Pugh's solution.[38]

The effect of polarization on time to fracture with or without the addition of chloride is shown in Figure 4. During anodic polarization, a sharp rise in cracking time has been observed in the solution containing chloride compared to the chloride-free solution. This can be explained as follows: In the normal cracking process at the open-circuit potential, the positively charged copper complexes get adsorbed to the cathodic sites in the grain interior. During anodic polarization, the negatively charged chloride ions will get a better situation for their attachment. They begin competing with the copper complexes, which were previously tightly adsorbed, and will try to dislodge some of them. As a result, the process goes through a transition in mode of cracking; the grain interiors lose their copper ions and become available anodic sites. The cathodic intensity decreases, leading to a fall in the intensity of the dislocation process. A similar observation has been made with phosphate addition to ammoniacal carbonate solution.[41]

The adsorption hypothesis put forward here can thus explain the preferential sites for crack nucleation as well as the preferred reduction reaction resulting from the absorbed species, either leading or not leading to a tarnish formation. The similar results reported by other authors can also be interpreted based on this model.[42-44]

Conclusion

(1) The SCC of brass in ammoniacal solution occurs as a result of the adsorption of various reacting species at discrete anodic and cathodic sites existing on the material surface and the subsequent electrochemical reaction at these sites.
(2) Film formation or the absence of it is a consequence of the prevailing electrochemical reactions and is not considered to be a deciding factor in the dissolution process.
(3) Factors like alloying, cold work, polarization, etc., cause a change in the distribution and activity of the sites, and a transition in the mode of cracking is thus explained.

References

1. F.C. Althof, Z. Metallk. 36(1944): p. 177.
2. W.D. Robertson, A.S. Tetelman, Strengthening Mechanism in Solids (Metals Park, OH: ASM International, 1960), p. 217.
3. A.K. Lahiri (Ph.D. diss., Banaras Hindu University, India, 1964).
4. D.H. Thompson, W.C. Tracy, Trans. AIME 185(1949): p. 100.
5. J.F. Klement, R.E. Maersch, P.A. Tully, Corrosion 15, 6(1959): p. 295t.
6. N.A. Leilsen, Corrosion 20, 3(1964): p. 104t.
7. J. Kopchik, Wire and Wire Products 37(1962): p. 475.
8. T.C. Wilson, G. Edmunds, E.A. Anderson, W.M. Pierce, Symposium on SCC of Metals (New York, NY: American Institute of Mining, Metallurgical, and Petroleum Engineers, 1945), p. 173.
9. W.B. Price, Symposium on SCC of Metals, p. 144.
10. G. Baumann, Brown Boveri Rev. 49(1962): p. 323.
11. L.E. Gibbs, Metal Prog. 45(1944): p. 881.
12. E. Mattsson, Electrochim. Acta 3(1961): p. 279.
13. E.N. Pugh, J.V. Craig, W.G. Montague, ASM Trans. Quart. 61(1968): p. 468.
14. W. Lynes, Corrosion 21, 4(1965): p. 125.
15. H.E. Johnson, J. Leja Corrosion 22, 6(1968): p. 179.

16. S. Shimodaira, M. Takano, Proceedings of the International Conference on Fundamental Aspects of Stress Corrosion Cracking, ed. R.W. Staehle, A.J. Forty, D. van Rooyen (Houston, TX: National Association of Corrosion Engineers, 1969), p. 89.
17 E.N. Pugh, The Theory of Stress Corrosion Cracking in Alloys, ed. J.C. Scully (Brussels, Belgium: NATO Scientific Affairs Division, 1971), p. 418.
18. A.J. Forty, P. Humble, Phil. Mag. 8(1963): p. 247.
19. A.J. McEvily, A.P. Bond, J. Electrochem. Soc. 112(1965). p. 131.
20. D. Tromans, J. Nutting, Corrosion 21, 5(1965). p. 143.
21. R.P.M. Procter, M. Islam, Corrosion 32, 7(1976): p. 267.
22. E.N. Pugh, Proceedings of the NATO Advanced Study Institute on Stress Corrosion Cracking (Brussels, Belgium: NATO, 1975).
23. F.A. Champion, Symposium on Internal Stresses in Metals and Alloys (London, England: Institute of Metals, 1948), p. 468.
24. H.L. Logan, J. Res. Natl. Bur. Stand. 48(1952): p. 99.
25. H.J. Engell, Proceedings of the NATO Advanced Study Institute on Stress Corrosion Cracking (Brussels, Belgium: NATO, 1975), p. 86.
26. A.J. Bursle, E.N. Pugh Environment-Sensitive Fracture of Engineering Materials (New York, NY: AIME, 1979), p. 18.
27. E.N. Pugh, Corrosion 41, 9(1985): p. 517.
28 A Paskin, K. Sieradzki, D.K. Som, G.J. Dienes, Acta Metall. 31 (1983): p. 1253.
29. K. Sieradzki, R.L. Sabatini, R.C. Newman, Metall. Trans. 15A (1984): p. 1941.
30. U. Bertocci, F.I.Thomas, E.N. Pugh, Corrosion 40, 8(1984): p. 439.
31. S.P. Lynch, Atomistics of Fracture (New York, NY. Plenum Press, 1983), p. 955.
32. S.C. Sircar, U.K. Chatterjee, M. Zamin, H.G. Vijayendra, Corros. Sci. 12, 3(1972): p. 217.
33. S.K. Narsaria, U.K. Chatterjee, S.C. Sircar, Trans. Indian Inst. Metals 28(1975): p. 127.
34 S.C. Sircar, U.K. Chatterjee, S.K. Roy, S. Kisku, Brit. Corros. J. (Quarterly) 1(1974): p. 47.
35. S.C. Sircar, U.K. Chatterjee, G.M. Sherbini, Proceedings of the 7th International Congress on Metallic Corrosion (Rio-de-Janeiro, Brasil: ABRACO, 1978, p. 964
36 K.J. Laidler, Chemical Kinetics (Bombay, India. Tata McGraw-Hill Publishing Co., 1950), p. 274.
37 U.K Chatterjee, S.K Goswami, S.C. Sircar, Trans. Indian Inst. Metals 33(1980): p. 76.
38. S.C. Sircar, U.K. Chatterjee, G.M. Sherbini, Corros. Sci. 23(1983): p. 777.
39. T.P. Hoar, R.D. Holliday, J. Appl. Chem. 3(1953): p. 502.
40. H.H. Uhlig, K. Gupta, W. Liang, J. Electrochem. Soc. 122 (1975): p. 343.
41. S.K. Narsaria (Ph.D. diss., IIT Kharagpur, India, 1972).
42. M. Kermani, J.C. Scully, Corros. Sci. 18(1978): p. 883.
43. T.P. Hoar, C.J.L. Booker, Corros. Sci. 5(1965): p. 821.
44. U.C. Bhakta, A.K. Lahiri, Proceedings of the 8th International Congress on Metallic Corrosion (Mainz, FRG: DECHEMA, 1981), p. 486.

Stress Corrosion Cracking of Nickel-Base Alloys in Room-Temperature HCl Containing H_2S

*J. Kolts, C.C. Burnette, M.W. Joosten**

Abstract

Nickel-base alloys were found to be susceptible to environmental embrittlement in room-temperature HCl + H_2S. The cracking was transgranular quasicleavage and was accelerated by anodic polarization. Cracking can be attributed neither to a film-rupture mechanism nor to classic hydrogen embrittlement. Commercially available acidizing corrosion inhibitors were effective in preventing cracking in nickel-base alloys. A new test sample configuration was developed for inexpensive evaluation of stress corrosion cracking performance. Notches machined at each end of two sheet samples have been used to stress the samples upon assembly without the use of fixtures, welding, or bolting.

Introduction

Recent reports show that about one third of present deep-well completions in the United States use corrosion-resistant alloys for corrosion control.[1] The term "corrosion-resistant alloys" is being used in the oil and gas industry to refer to alloys with corrosion resistance in deaerated production environments, which is at least an order of magnitude less than carbon and low-alloy steels. The term would include type 410 (UNS S41000) stainless steel (SS), duplex SS, and nickel-base alloys. Many of these deep wells will be acidized using either hydrochloric acid or mixtures that include HCl. Therefore, the likelihood of HCl contacting various corrosion-resistant alloys is quite high. Most of the experimental work on effects of acidizing environments on corrosion-resistant alloys has emphasized general corrosion, especially at elevated temperatures.[2,3] However, some evidence shows that stress corrosion cracking (SCC) can result with the presence of H_2S in room-temperature hydrochloric acids.[4-6] Since the dissolution of sulfide-containing scales during acidizing may provide a source of sulfide ions, this form of cracking must be considered in using corrosion-resistant alloys.

Corrosion inhibition can provide a method to mitigate SCC in HCl; however, only cursory examinations have been made on cracking behavior. This investigation therefore examined the effect of various inhibitors in their ability to prevent SCC. Furthermore, an attempt was made to better understand the mechanisms of cracking to help predict incidences of stress corrosion during acidizing.

Experimental Procedure

Because of the many requirements for SCC tests in HCl, a new testing sample configuration was developed. Testing fixtures sufficiently resistant to corrosion in HCl + H_2S to provide freedom from solution contamination and sufficient strength were not available to the authors. In addition, the time and cost needed to machine testing fixtures from exotic alloys was excessive. Therefore, a method was developed to stress the samples without the requirement for stressing fixtures. While there are stressing methods available that do not require fixtures, these methods are either not quantitative with respect to applied stress (i.e., U bends) or require welding. These restrictions were not acceptable.

The sample configuration developed is shown in Figure 1. Two slots are machined into each sheet sample. Fifty or more samples may be machined at one time, thus minimizing the cost and time to prepare samples. The cost of machining was approximately $1 per sample, thus coining our terminology for these coupons as "cheap specimen configuration."

The samples are easily assembled with pliers and a vice. The assembled coupons (Figure 2) were designed to provide a stress of 50% of the 0.2% offset yield strength at the regions with a full cross-section width. The stress at the reduced section was about the yield strength of the alloy.

Strain Calculations

Simple geometry was used to make the strain calculations for the samples, assuming that the stressed specimen conformed to the shape of an arc of a circle. The equation describing slot width for a given outer-fiber strain is

$$w = t\left[\frac{1}{\tan\frac{360\,\epsilon\,l}{\pi t}} + \frac{1}{\sin\frac{360\,\epsilon\,l}{\pi t}}\right] \quad (1)$$

where w = width of slot; t = thickness of sample, ϵ = desired strain; l = length of sample at midpoint of slot, the argument of the angle being in degrees. Appendix A details the derivation of Equation (1).

Materials and Environment Chemistry

Highly alloyed corrosion-resistant alloys considered for downhole equipment were selected for this investigation. Type 316 (UNS S31600) SS was also chosen for examination, since this alloy represents the standard by which industry compares corrosion resistance. All of the alloys except type 316 SS were high strength, and all of the alloys were solid-solution austenitic alloys. No second phases or precipitates were formed intentionally. Different methods of cold working will result in a range of mechanical properties for each respective alloy, these alloys were cold worked by cold rolling.

Table 1 presents the compositions of the alloys, while Table 2 gives the mechanical properties. Two lots of alloy C-276 (UNS N10276) were used. The sheet samples were high strength produced by cold work. The tubing samples used in the direct-tension tests were also cold worked but to a much lower strength level.

*Conoco Incorporated, P.O. Box 1267, Ponca City, OK 74603.

TABLE 1
Composition of Alloys (wt%)

Alloy	C	Si	Mn	P	S	Ni	Cr	Mo	Cu	W	Ti	Al	Fe	V	Cb	Co
Type 316	0.06	0.43	1.57	0.020	0.010	10.1	16.2	2 31	0.47	—	—	0.04	bal	—	—	—
Type 825	0.05	0.34	0.50	0.018	0.001	40.2	23.4	3.39	1.62	0.24	0.95	0.09	bal	—	—	—
Type C-276 Sheet	0.004	0.13	0.46	0.004	0.002	bal	16.1	16.5	0.17	3.24	—	0.45	3.45	0.08	0.14	0.27
Type C-276 Tubing	0.003	0.04	0.50	0.014	0.001	bal	16.0	15.9	—	3.63	—	—	5.2	0.19	—	2.0
Type C-22	0.008	0.10	0.22	0.003	0.002	bal	22.2	12.5	0.12	2.73	—	0.33	2.87	0.11	0.12	0.17
Type 718	0.022	0.08	0.06	0.003	0.001	52.3	17.6	2.87	1.85	—	0.96	0.46	20.2	—	5.09	—

TABLE 2
Mechanical Properties of Alloys

Alloy	Yield Strength MPa (ksi)	UTS MPa (ksi)	Elongation %
Type 316[A]	240 (35)	586 (35)	55
Type 825	1230 (179)	1270 (184)	3
Type C-276 Sheet	1140 (165)	1250 (181)	10
Type C-276 Tubing	785 (114)	1909 (158)	23
Type C-22	1230 (179)	1320 (191)	8
Type 718[B]	923 (134)	1240 (180)	29

[A]Nominal properties.
[B]Anneal 1024°C, 1-h water quench; age 788°C 6.5 h, air cool.

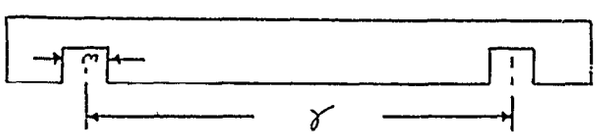


FIGURE 1—Sample configuration used in stress corrosion cracking evaluation.



FIGURE 2—Appearance of assembled sample.

Sheet samples were sheared, machined, degreased, washed, and stressed. The specimens were used as cold rolled and machined; no abrasion of surfaces was performed. These were placed in a solution containing 50% by volume of concentrated reagent-grade HCl and 50% by volume water to produce approximately 17 wt% HCl solution. The inhibitors were added as 0.5 vol% of the total solution and were dissolved in the concentrated HCl. The composition of the 938 inhibitor was not known. The HAI-75 and -85 inhibitors are a proprietary blend of acetylenic alcohols, quaternized heterocyclic amine dispersers, and inorganic salts containing cuprous iodide. The stressed samples were placed in the solution at room temperature, as shown in Figure 3. The solution was deaerated with nitrogen for approximately 2 h, then H_2S was used to saturate the acid.

The H_2S was intermittently purged, once every weekday for approximately 1 h over the total duration of 1 week of exposure. Some tests were conducted as controls with only nitrogen gas. After 1 week of exposure, the solution was purged with nitrogen, and the samples were removed, cleaned, and examined visually for cracking.

In another series of tests, 0.64-cm- (0.250-in.-) diameter tensile samples were stressed in commercially available proving rings to their yield strength. The solution in the cells contained either the NACE Standard TM0177-86 ("Testing of Metals for Resistance to Sulfide Stress Cracking at Ambient Temperatures") standard acetic acid, sodium-chloride-containing solution saturated with H_2S, or arsenic-poisoned (100 ppm) sulfuric acid (5% by weight) at room temperature. In the latter test, specimens were cathodically polarized with a galvanostat to different levels of current.

Polarization curves were obtained for coupons with areas of approximately 10 cm^2. Luggin capillaries and acid reservoirs not containing H_2S permitted the use of saturated calomel electrodes as potential references. Graphite or platinum counter electrodes were used as required.

In some SCC tests, stressed test samples were anodically or cathodically polarized in hydrochloric acid using a galvanostat. In these tests, one set of stressed samples was made the anode while the other set was the counter electrode (cathode). In this way, the effects of cathodic and anodic polarization could be assessed simultaneously in one test.

Results

Table 3 presents the results of the SCC tests. The type 316 SS samples did not crack in any of the test environments investigated, but this does not mean that it is a more resistant alloy than the nickel-base alloys examined. Type 316 SS was tested in the annealed condition and had a much lower yield strength than the other alloys. Consequently, this alloy was stressed to roughly one fifth of the stress of the other alloys.

In the uninhibited acid saturated with H_2S, all of the nickel-base alloys cracked. Cracking occurred primarily in the highly stressed area of the test specimen, although surface cracking was also associated with the sheared edge of the samples. The data from

Table 3 show that different inhibitors prevent SCC to varying degrees. Consequently, testing and selection of inhibitors are necessary for acceptable field service of corrosion-resistant alloys during acidizing.

One interesting feature was found on alloy 825 (UNS N08825) exposed for a short period of time in the uninhibited, H_2S-containing environment. Figure 4 displays SCC patterns that delineate the stress state of the assembled samples. Notice the high stress concentration at the corner of the machined, reduced cross section.

The slot width was chosen to stress the samples to 50% of the uniaxial yield strength in the region where the sample is full width At the location of the notch, the stress is approximately twice that, because the sample width is one half of the full section width. The stress concentration at the corner increases the stress even further; therefore, cracking is expected to occur in the reduced section locations. In spite of the high stresses at the corner, SCC also occurred in the full-width sections of the sample along the entire length of the stressed region. This demonstrates that SCC initiates and propagates at very low stress levels.

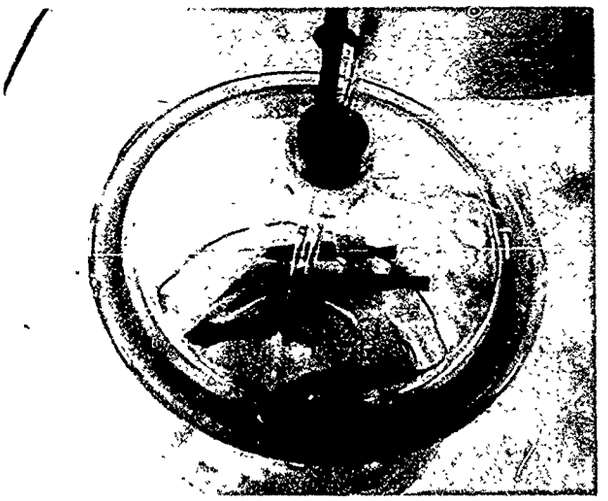


FIGURE 3—Photograph of experimental apparatus.

Since two stress states exist at the different locations of the same sample, the susceptibility to cracking could also be assessed by determining whether cracking occurred at only the highly stressed location or at both highly stressed and low-stressed locations. If the environment was not extremely aggressive from a cracking standpoint, cracks as in Figure 4 were found. However, in severe environments, cracking also occurred in the full-width sections.

The results of applied current on SCC revealed that anodic polarization increased cracking on alloy 825. In the absence of externally applied currents, alloy 825 cracked in HCl + H_2S, predominantly in the highly stressed region of the stressed samples. Only a few secondary cracks were noticed in the full-width section of stressed samples However, the application of anodic polarization corresponding to 20 $\mu A/cm^2$ greatly increased the incidence of cracking on the lower stressed portion of the samples. Correspondingly, the application of cathodic currents eliminated cracking on the lower stressed region of the samples when exposed to HCl + H_2S without inhibitors. However, cathodic polarization did not eliminate all of the cracking in the highly stressed locations of the samples.

Table 3 shows that acidizing inhibitors can reduce the incidence of cracking in HCl + H_2S. However, the application of anodic currents (200 $\mu A/cm^2$) on alloy 825 can overcome this inhibition, and cracking is again seen on this alloy even with corrosion inhibition. This demonstrates that coupling to steel would be beneficial in eliminating cracking in HCl The effects of cathodic polarization in the inhibited system containing the inhibitor HAI-85 have little meaning. This inhibitor contains cuprous ions as a component to enhance the inhibitor effectiveness. The application of cathodic polarization resulted in electroplating copper on the surfaces of the test samples of alloy 825.

Polarization curves of alloy 825 were obtained to help understand the effects of polarization and corrosion inhibition on SCC in HCl + H_2S. Figure 5 demonstrates the effect of inhibition on polarization behavior. The main effect of H_2S addition to HCl is the reduction of the free-corrosion potential to more negative values. Otherwise, only slight differences were noticed in the shape of the anodic polarization curve by the addition of H_2S or inhibitors. The anodic curves did not evidence passivity with or without inhibitors. Likewise, cathodic polarization showed differences only at highly negative potentials in inhibited environments. These effects are not expected to be of significance because of copper plating and decomposition of other inhibitor components at highly negative potentials.

The addition of corrosion inhibitors resulted in a positive shift in the free-corrosion potentials for all inhibitors examined. This shift can be partly accounted for by the cuprous/cupric redox potential. The potential measured on platinum showed a corresponding positive shift with inhibitor additions.

Table 4 shows the cracking response of alloys in a number of environments, based on round-bar tensile tests. Failures occurred in only the HCl + H_2S environment. Alloy C-276 samples did not crack in this test in the HCl/H_2S environment but readily cracked as sheet samples. This may be partly attributed to the test method. However, it is more likely that the higher strength of the sheet samples and the transverse instead of longitudinal orientation of the sheet of the tubing samples is responsible for cracking in the sheet and not tubing. Environments that cause severe entry of hydrogen into the alloys such as the TM0177-86 solution, especially when the alloys are coupled to steel or arsenic-poisoned sulfuric acid with cathodic charging of alloys at 10 mA/cm^2, did not cause cracking in the alloys tested. These tests further confirm that cracking in the HCl + H_2S environment is not a classic hydrogen embrittlement (HE) phenomenon found in steels or heavily cold-worked nickel-base alloys.

Discussion

The SCC of nickel-base alloys at room temperature is an unusual occurrence. The cracking is transgranular, typical of that found in environments at temperatures exceeding 204°C (400°F).[7,8] The cracking occurs only in the presence of H_2S. However, this cracking phenomenon is different from the classic type of HE found in some heavily cold-worked nickel-base alloys.[9,10] In the latter phenomenon, cracking is typically intergranular and is accelerated by cathodic polarization rather than anodic polarization. The higher iron-containing alloys, such as alloy 825, are more resistant to the classic HE than the alloys such as alloy C-276 or C-22 (UNS N06022). In the HCl + H_2S environments, the converse is true, and alloy 825 is more susceptible to cracking, as shown in Table 3. The presence of H_2S is required for SCC of nickel-base alloys in HCl. While the effect of sulfide ions on passivity of nickel has been studied, the corresponding effects in HCl may not have much relevance. The polarization curves in this work show that these nickel alloys in HCl do not exhibit the classic passivity found in less aggressive environments.

Crevice corrosion or crevice effects can often have accelerating effects in SCC. The use of the cheap specimen configuration places the highest stresses area near a crevice that is likely to increase the severity of the cracking. However, in HCl, the nickel-base alloys exhibit general corrosion, and crevice effects are not likely to affect the cracking since crevice corrosion does not occur in this solution.

Local yielding is very likely at the corners of this specimen. However, this does not negate the occurrence of SCC at stresses lower than the yield strength of the alloys. Cracking was also found on the middle of samples. Thus, cracking occurred at stresses lower than 50% of the 0.2% offset yield strength of the respective alloys.

TABLE 3
Stress Corrosion Cracking Results[A]

Alloy	Environment					
	Acid Only	Acid Visco 938	Acid H_2S Only	Acid H_2S HAI-75	Acid H_2S HAI-85	Acid+H_2S Visco 938
Type 316	NC[B]	NC	NC	NC	NC	NC
Type 316	NC	NC	C[C]	NC	NC	C
Type C-276	NC	NC	C	NC	NC	NC
Type C-22	NC	NC	C	NC	NC	NC

[A]Room-temperature tests 50/50 volume dilution of reagent-grade HCl—1-week exposure, sheet samples, inhibitors added as 0.5 vol%.
[B]NC denotes no cracking.
[C]C denotes cracking.

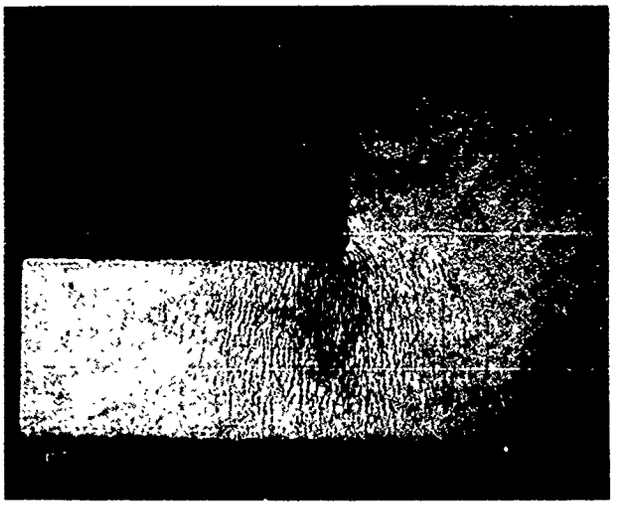


FIGURE 4—Appearance of stressed alloy 825 (UNS N08825) sample after exposure for a short period of time H_2S containing HCl at room temperature.

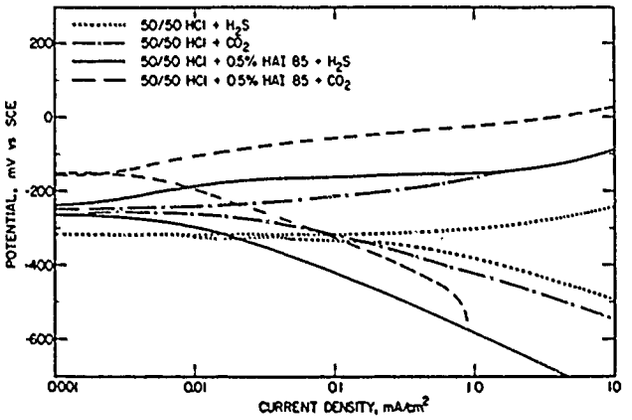


FIGURE 5—Polarization behavior of alloy 825 (UNS N08825) in various room-temperature environments.

The major effect of corrosion inhibitor additions was in increasing the free corrosion potential to more noble values. This shift is probably caused by the presence of Cu^{+} and Cu^{++} ions in the inhibitors. These additions to inhibitors are made to enhance the effects of the organic compounds in the inhibitor formulations for uniform corrosion resistance. The shift in corrosion potential to more noble values caused by inhibitor additions cannot account for the improved cracking resistance caused by inhibitor additions. The polarization experiments on stressed samples showed that a shift in potential in the positive direction actually increased the susceptibility of alloy 825 cracking. Also, even in the presence of corrosion inhibitors, a further positive shift in corrosion potential by use of a galvanostat increased the susceptibility of alloy 825 to SCC. It is likely that the inhibitor effects are related to competitive adsorption of sulfides and organic inhibitors on the metal surface. Possibly the inhibitor enhancers (copper ions) have little effect on the inhibition of SCC in HCl + H_2S environments.

TABLE 4
Proving Ring Stress Corrosion Cracking Tests[A]

Environment	Alloy	
	718 Bar	C-276 Tubing
TM0177-86 (5% NaCl + 1/2% acetic acid + H_2S)	NC[B]	NC
TM0177-86 Steel couple	NC	NC
5% H_2SO_4 + 100 ppm arsenite 0.1 mA/cm^2 cathodic current	NC	NC
5% H_2SO_4 + 100 ppm arsenite 10 mA/cm^2 cathodic current	NC	NC
50/50 volume dilution HCl + H_2S	28 h	NC

[A]Stress at 896 MPa (130 ksi); 758 MPa (110 ksi) minimum yield strength alloys; time-to-failure—h; 1-month exposure.
[B]NC denotes no cracking in 1 month.

The mechanism of cracking in the HCl solutions is not readily explained by existing theories of SCC. The polarization curves do not show regions of passivity, thus film rupture is probably not a mechanism. Much prior work has shown that the anolyte in pits, crevices, and cracks becomes acidic. However, none of the experimental work or theoretical treatments have shown that the acidity of solutions in pits or cracks can become more acidic than 17% HCl, which is the external environment. Thus, the environment on the surface is much more acidic and presumably more corrosive than the environment in the crack in the case of SCC of nickel alloys in HCl/H_2S solutions. Classic HE does not explain the results of the SCC found. In a large number of studies of nickel alloy applications for the oil and gas industry, the susceptibility of alloy C-276 to HE at high strength levels has been confirmed. Alloy 825 has been found to be relatively immune to cracking by HE. Yet in the HCl/H_2S solutions, this work and other work have shown alloy 825 to be more susceptible to cracking. Also, cathodic polarization has been shown to reduce the incidence of cracking, contrary to most expected trends in classic HE.

Conclusion

(1) Highly alloyed, corrosion-resistant nickel-base alloys are susceptible to SCC in ambient temperature H_2S-containing hydrochloric acid stimulation fluids. The cracking is transgranular and occurs only in the presence of H_2S.
(2) Hydrochloric acid corrosion inhibitors can prevent SCC in nickel-base alloys.
(3) Anodic polarization accelerates cracking in the nickel-base alloys in $HCl^+ + H_2S$, with and without inhibition.
(4) Cathodic or anodic polarization curves of the nickel-base alloys were not adequate to explain the inhibitor effects on cracking.
(5) A newly developed specimen configuration designed to offer an inexpensive and easy testing technique for assessing SCC resistance performed well.

References

1. R. McNally, J. Lindsey, Petrol. Eng. Intl. March (1988): p. 17.
2. M.L. Walker, T.H. McCoy, CORROSION/86, paper no. 154 (Houston, TX: National Association of Corrosion Engineers, 1986).
3. M.L. Walker, CORROSION/88, paper no. 189 (Houston, TX: NACE, 1988).
4. P.R. Rhodes, Shell Development Company, Private Communication.
5. J. Kolts, CORROSION/84, paper no. 217 (Houston, TX: NACE, 1984).
6. J. Kolts, CORROSION/86, paper no. 323 (Houston, TX: NACE, 1986).
7. A.I. Asphahani, J.C. Prouhezi, G.J. Petersen, Corrosion-Resistant Alloys for Hot, Deep Sour Wells: Properties, Experience, and Future Trends, Oct., 6067, Offshore Technology Conference (1989).
8. H.E. Chaung, M. Watkins, G.A. Vaughn, CORROSION/85, paper no. 227 (Houston, TX: NACE, 1985).
9. A.I. Asphahani, Hydrogen Cracking of Nickel-Base Alloys, 2nd International Congress on Hydrogen in Metals, held June 11, 1977, Paris, France (Elmsford, NY: Pergamon Press Inc., 1977)
10. J. Kolts, Environmental Embrittlement of Nickel-Base Alloys in Metals Handbook, Vol. 13, Corrosion (Metals Park, OH: ASM International, 1987), p. 647.

Appendix A
Derivation of Equation for Calculating Strain on Samples

Calculation of sample strain

The strain obtained by assembling the individual samples can be calculated from simple geometry if it is assumed that the radius of curvature remains constant throughout the stressed portion of the sample. Figure A1 displays the specimen configuration at the points of contact at each end of the specimens. In effect, the strain obtained is from four point contacts (two points at each end).

The width of the slot (w) from Figure (A1) is

$$w = a + b = \frac{t}{\tan\phi} + \frac{t}{\sin\phi} \qquad (A1)$$

Figure A1 represents the specimen configuration when stressed (arc of a circle). The strain on the outer fiber is given by

$$\epsilon = \frac{t}{2R} \qquad (A2)$$

The equation for the length of an arc of a circle is

$$l = \frac{\pi R\phi}{180} \qquad (A3)$$

Combining Equations (2) and (3), the angle in degrees is

$$\phi = \frac{360\,\epsilon\,l}{\pi t} \qquad (A4)$$

where w = width of slot, l = length of specimen between midpoints of slots, t = specimen thickness; ϕ = angle between samples at slots; and ϵ = outer-fiber strain.

Thus, using Equations (A1) and (A4), the slot dimensions for a desired strain can be calculated.

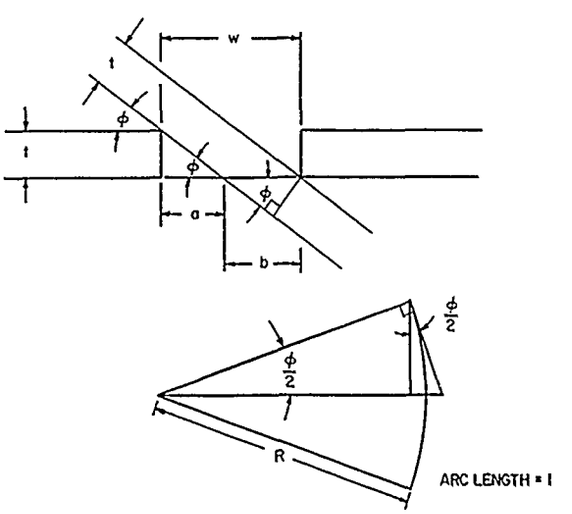


FIGURE A1—Schematic for calculating strain on samples.

Notice that stress is not a parameter in any of the above equations. To obtain a given stress, the strain corresponding to a given stress should be read from a stress–strain curve, and the samples should then be machined to obtain the corresponding strain. This is an advantage for austenitic alloys, since the stress–strain curves are not linear near the yield point of the alloys.

Intergranular Attack Behavior and Mechanisms for Nickel-Base Alloys in Caustic Solutions at Elevated Temperatures

*H. Nagano, K. Yamanaka, K. Tokimasa, and H. Miyuki**

Abstract

Intergranular attack (IGA) initiation and propagation processes, effects of environmental and material factors, and consideration of the selective grain-boundary dissolution mechanism of mill-annealed alloy 600 (UNS N06600) were studied in laboratory tests. The results obtained are as follows: (1) IGA is composed of intergranular corrosion (IGC) and intergranular stress corrosion cracking (IGSCC) following IGC. Experimentation has confirmed that IGSCC is initiated for a given applied stress when IGC depth reaches a threshold crack depth for initiation of IGSCC (a_{th}). Initiation may be defined in terms of a critical stress-intensity factor as $K_{ISCC} = \eta\sigma\sqrt{\pi a_{th}}$ (η = constant and σ = applied stress). (2) Environmental factors are more influential than material factors in the IGA of Alloy 600. IGA occurs in mixtures of NaOH solutions with pH higher than 10.3 and in metal oxide sludges such as Fe_3O_4 and CuO at high temperatures. Fe_3O_4 acts as a strong oxidizer in the caustic solution, as described by the following equation: $Fe_3O_4 + 2H_2O + 2e^- \rightarrow 3HFeO_2 + H^+$. (3) Concerning the mechanism of IGA, the segregation of dissolved elements such as C, B, and S at grain boundaries may be the cause of selective grain-boundary dissolution of mill-annealed alloy 600.

Introduction

Various instances of corrosion failures have occurred in the steam generators of pressurized water reactors (PWR), i.e., intergranular stress corrosion cracking (IGSCC) at the expanded parts and at severely U-bent parts of alloy 600 (UNS N06600) tubing in the primary side, and wastage, denting, and intergranular attack (IGA) in the secondary side.[1,2]

The occurrence of wastage and IGA is closely related to the accumulation of concentrated caustic solutions. Wastage has appeared on the tube surfaces in the crevices between tube and tube sheet in the steam generators that have been operated under phosphate treatment. IGA has occurred in the crevices between tube and tube sheet, and between tube and tube-support plate in the steam generators that have been operated initially under phosphate treatment and then under the all-volatile treatment (AVT), or that have been operated only under AVT. Another characteristic of IGA is that it appears after a longer time period than wastage.

Currently, remedial actions have been applied to steam generators with IGA, controlling environmental conditions

The objective of this study is to survey the effects on the IGA initiation and propagation process of environmental factors, such as NaOH concentration, potential (influenced by addition of oxide sludges), and hydrogen addition, as well as the effects of alloying elements. The mechanisms of IGA in nickel-base alloys are considered.

Experimental Procedures

Materials

Chemical compositions of alloys used are given in Table 1. Tubes and plates of alloy 600 (No. 1) were used for corrosion tests after they were mill annealed at 1050°C. The plate of alloy 600 containing 50 ppm boron (No. 2) was used to study the effect of boron segregation on IGA by the slow-strain-rate technique (SSRT)

Wires of 75% NiO to 15% Cr alloys (Nos. 3 to 5) were used to measure the repassivation rate of film by the straining electrode tests

Foils of rapidly solidified alloy 600 (Nos 6 to 14), supersaturated with C, S, P, N, and Si made by double-roller methods (cooling rate: 1.5×10^5 C/s), were used to study the effects of grain-boundary segregation of dissolved elements on IGA.

Specimens for C-ring tests and SSRT were cut from a tube of 22.23-mm diameter by 1.27-mm thickness, and specimens for electrochemical measurements and U-bend tests were cut from a plate of 4.9-mm thickness. Specimens for straining electrode tests were cut from a wire of 0.5-mm diameter, and rapidly solidified specimens for corrosion tests were cut from a foil of 50- to 100-μm thickness.

Procedures

Immersion tests. C-ring specimens loaded to a stress level of 15 or 30 kgf/mm^2 or U-bend specimens were put into a 40% NaOH solution or mixtures of 40% NaOH plus metal oxide sludges at 325°C for 200 h. Fe_3O_4, Cu, and CuO were mixed to simulate the sludge compositions forming on the surface of alloy 600 tubing at the crevices between tube and tube sheet or tube and tube-support plate. Reagent grade metal and metal oxides were used for the immersion tests. Particularly, Fe_3O_4 was rinsed in hot, pure water several times for the purpose of avoiding such impurities as chlorides and sulfates. The composition of the mixtures are as follows:

(1) 1 L 40% NaOH + 520 g Fe_3O_4
(2) 1 L 40% NaOH + 468 g Fe_3O_4 + 0.87 g Cu + 51 g CuO
(3) 1 L 40% NaOH + 0.5 g Cu + 300 g CuO

Specimens were covered with metal oxide sludges at 325°C during the test duration in autoclaves. Autoclaves are composed of

*Sumitomo Metal Industries, Ltd., Technical Research Laboratories, 1-3, Nishinagasu-hondori, Amagasaki 660, Japan.

TABLE 1
Chemical Compositions of Alloys (wt%)

No.	C	Si	Mn	P	S	Ni	Cr	Ti	Al	B	N	Fe	Shape of Material Used
1	0.027	0.33	0.31	0.008	0.001	74.45	16.45	0.20	0.11	0.0002	0.0073	8.10	Tube and plate
2	0.022	0.14	0.23	0.011	0.001	74.27	15.14	0.31	0.24	0.0050	0.0069	9.62	Plate
3	0.018	0.11	0.29	0.001	0.001	75.15	15 05	0.21	0.14	0.0001		9.02	Wire[A]
4	0.018	0.11	0.29	0.001	0.001	74.55	4.86	0.21	0.13	0.0001		19.82	Wire[A]
5	0.014	0.13	0.31	0.002	0.001	74.38	0.01	0 20	0.10	0.0001		24.85	Wire[A]
6	0.027	0.34	0.30	0.008	0.001	74.50	15.90	0.20	0.10	0.0001	0.0065	8.61	Foil[B]
7	0.10	0.34	0.30	0.008	0.001	74.50	15.90	0.20	0.10	0.0001	0.0065	8.54	Foil[B]
8	0.027	0.34	0.30	0 008	0.11	74.50	15.90	0.20	0.10	0.0001	0.0065	8.50	Foil[B]
9	0.027	0.34	0.30	0.008	0.50	74.50	15.90	0.20	0.10	0 0001	0.0065	8.10	Foil[B]
10	0.027	0.34	0.30	0.12	0.001	74.50	15.90	0.20	0.10	0.0001	0.0065	8.49	Foil[B]
11	0.027	0.34	0.30	0.53	0.001	74.50	15.90	0.20	0.10	0.0001	0.0065	8.08	Foil[B]
12	0.027	1.05	0.30	0.008	0.001	74.50	15.90	0.20	0.10	0.0001	0.0065	7.90	Foil[B]
13	0.027	5.10	0.30	0.008	0.001	74.50	15.90	0.20	0.10	0.0001	0.0065	3.85	Foil[B]
14	0.027	0.34	0.30	0.008	0.001	74.50	15.90	0.20	0.10	0.0001	0 52	8.09	Foil[B]

[A]0.5 mm in diameter for straining electrode tests.
[B]Foil is (50 to 100 μm) of rapidly solidified alloy 600 (UNS N06600).

stand-still type with alloy 600 lining with an internal volume of 3 L.

The SSRT tests. Specimens cut longitudinally from a tube were extended mainly at a strain rate of 4.17×10^{-6}/s or sometimes 4.17×10^{-7}/s in solutions of 4%, 0.4%, and 0.04% NaOH at 325°C at selected potentials against the Pt/Pt reference electrode. Potentials vs Pt/Pt electrode was converted into the standard hydrogen electrode scale (SHE) referring to the electrochemical data.[3]

The constant load tests. Specimens cut longitudinally from a tube were stressed at a constant load of 25 and 35 kgf/mm² in the solution of 4% NaOH in the autoclave at 325°C, at the potential 100 mV above the corrosion potential against the Pt/Pt reference electrode.

Electrochemical measurement. Anodic polarization curves for alloy 600 in NaOH solutions up to 40% at 325°C in an autoclave were measured against the Ag/AgCl reference electrode held in the NaOH solution of the same concentration at room temperature and high pressure in a separate autoclave, which had a liquid junction with NaOH at high temperature and high pressure.

Results

IGA process

Figure 1 shows the effect of stress on IGA of mill-annealed alloy 600 in 4% NaOH at 325°C and the constant potentials where severe IGA was indicated by content-load tests. Specimens with both 35 kgf/mm² and 25 kgf/mm² loadings show that IGA is composed of IGC plus IGSCC; specimens with 35 kgf/mm² loading show a smaller amount of IGC and a more significant amount of IGSCC.

It is suggested that IGA proceeds as IGC in an initiation period and then is converted to IGSCC in a propagation period, as shown in Figure 2. IGSCC is initiated when the IGC depth reaches a_{th}, which is a threshold crack depth for initiation of IGSCC and may be defined by the following equation:

$$K_{ISCC} = \eta\sigma\sqrt{\pi a_{th}} \quad (1)$$

where K_{ISCC} = critical stress-intensity factor (kgf/mm$^{3/2}$); η = constant, depending on the type of crack; σ = applied stress (kgf/mm²); a_{th} = threshold crack depth (mm).

From Equation (1), a_{th} becomes larger with decreasing σ because K_{ISCC} is constant under fixed material and environmental conditions. This relation is easily understood in referring to Figure 1, in which a_{th} is larger at 25 than at 35 kgf/mm². A lifetime for IGA (t_f) is shown by Equation (2) as the sum of the IGC period (t_{IGC}) plus the IGSCC period (t_{IGSCC}).

$$t_f = t_{IGC} + t_{IGSCC} \quad (2)$$

In general, the crack growth rate by IGC is very slow compared with the crack propagation rate by IGSCC, resulting in $t_{IGC} \gg t_{IGSCC}$, and Equation (2) is shown by an approximate equation of Equation (3).

$$t_f \simeq t_{IGC} \quad (3)$$

Equation (4) gives t_{IGC} using the terms of the average crack growth rate by IGC (V),

$$t_{IGC} = \frac{a_{th}}{V} \quad (4)$$

From Equations (1) through (4), Equation (5) can be obtained

$$t_f \simeq t_{IGC} = \frac{1}{\pi V}\left(\frac{K_{ISCC}}{\eta\sigma}\right)^2 \quad (5)$$

Therefore, it is necessary to obtain data concerning V, K_{ISCC} (a_{th}), and σ to evaluate the lifetime against IGA.

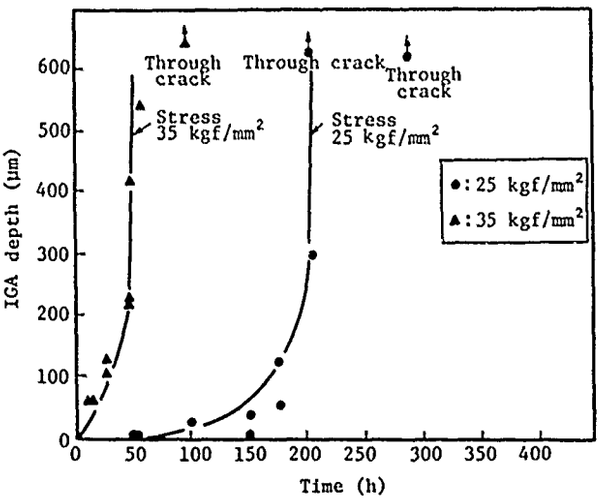
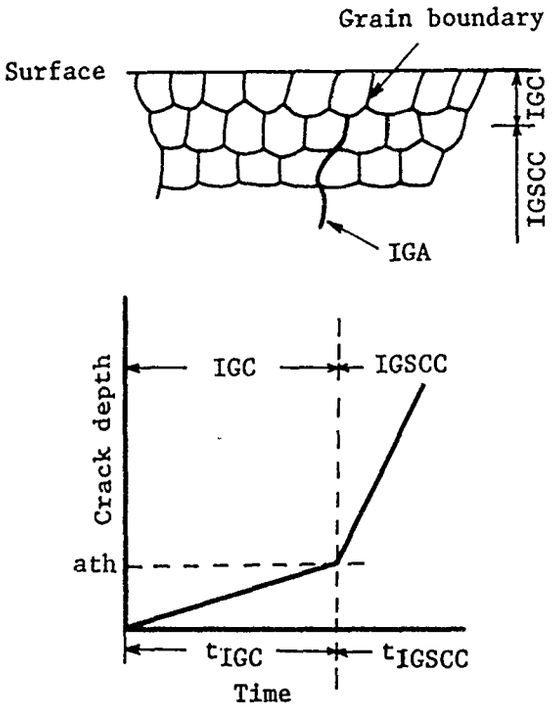


FIGURE 1—Effect of stress on occurrence of IGA of mill-annealed alloy 600 (UNS N06600) in 4% NaOH at 325°C at 100 mV above the corrosion potential.



a_{th}: Threshold crack depth for the initiation of IGSCC.

FIGURE 2—Development of IGA in alloy 600 (UNS N06600).

Effects of environmental factors on IGA

Effects of NaOH concentration and potential on IGA. Figure 3 shows the effects of NaOH concentration and potential on the occurrence of IGA for mill-annealed alloy 600 in caustic solutions at 325°C. IGA occurs in a particular region of NaOH concentration and potential, as can be seen in Figure 3. The shaded area for IGA occurrence begins at NaOH concentrations from 0.4% (pH = 10.3 at 325°C) up to higher values. IGA occurs in an active/passive, transient, potential region where the surface film of alloy 600 forms an unstable passive film (Figure 4).

In Figure 4, arrows indicate the corrosion potentials of mill-annealed alloy 600 that were increased at 325°C in mixtures of NaOH plus metal oxide sludges, such as Fe_3O_4 and CuO. IGA did not occur at the less noble potential region, as in 40% NaOH, or at the more noble region, as in 40% NaOH + Cu + CuO, as it occurred at the characterized potential region in the mixtures of 40% NaOH + Fe_3O_4 and 40% NaOH + Fe_3O_4 + Cu + CuO.

IGA occurs in an active/passive transition potential region in mixtures of concentrated NaOH plus metal oxide sludges at high temperatures, as shown in Figure 5.

Fe_3O_4 is one of the main components of sludges formed in PWR plants. It reacts with alloy 600 as an oxidizer in the caustic solution by the cathodic reaction described in the following equation. Because of its reduction, the corrosion potential of alloy 600 shifts to the active-passive transition potential, where alloy 600 is susceptible to IGA. The reaction is as follows:

$$Fe_3O_4 + 2H_2O + 2e^- \rightarrow 3HFeO_2^- + H^+ \qquad (6)$$

Inhibition of IGA by hydrogen addition. IGA may be inhibited when caustic concentration is sufficiently decreased or corrosion potentials are made less noble enough to shift the characterized potential region for IGA occurrence.

Figure 6 shows the effect of hydrogen addition on the corrosion potential of alloy 600 in the mixture of 40% NaOH + Fe_3O_4 + Cu + CuO at 325°C The corrosion potential decreases to the less noble side with increasing hydrogen pressure Shifting corrosion potential to the non-IGA potential region is made possible by the addition of hydrogen above 10^{-4} atm.

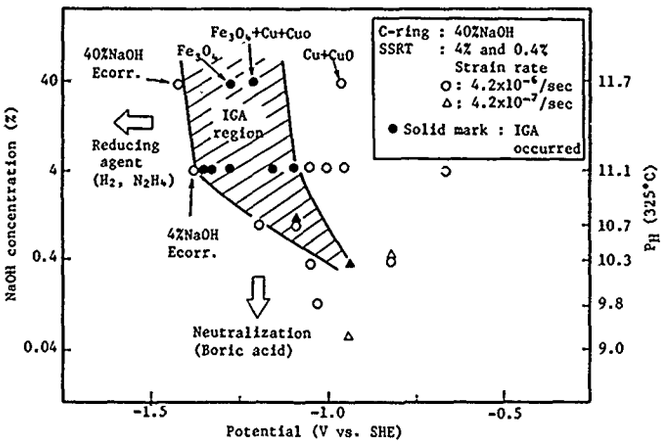


FIGURE 3—Effects of NaOH concentration and potential on the occurrence of IGA for mill-annealed alloy 600 (UNS N06600) in caustic solutions at 325°C.

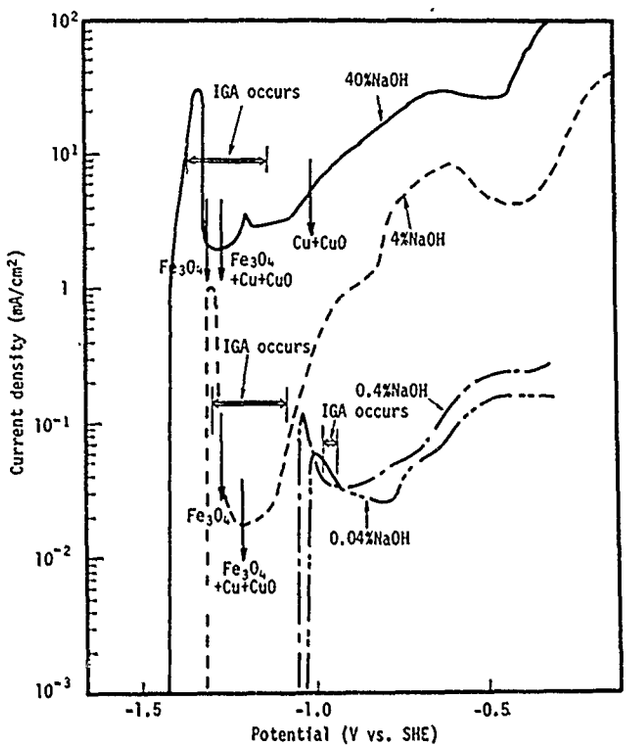


FIGURE 4—Potential ranges for occurrence of IGA in anodic polarization curves of mill-annealed alloy 600 (UNS N06600) in caustic solutions at 325°C.

Figure 7 shows that IGA initiation is inhibited by hydrogen addition greater than about 10^{-4} atm pressure from the immersion test results Furthermore, from the immersion test results using precracked C-ring specimens in the mixtures of 40% NaOH Fe_3O_4 + Cu + CuO at 325°C (Figure 8), it can be seen that IGA propagation is also inhibited by hydrogen addition above some 10^{-3} atm.

Consideration of selective grain-boundary dissolution mechanism. The mechanism of selective dissolution along grain boundaries is not clear yet for the IGA of mill-annealed alloy 600. Figure 9 shows a summary of proposed mechanisms for selective grain-boundary dissolution of Ni-base alloys. Among these mechanisms, it is thought that the grain-boundary segregation of dissolved elements such as C, B, and S can explain the experimental results of IGA of mill-annealed alloy 600.

Segregation of dissolved elements such as C, B, and S along grain boundaries seems to be detrimental to the resistance to IGA. For example, Figure 10 shows the corrosion test results for rapidly solidified alloy 600, supersaturated with C, S, P, N, and Si, immersed in the mixture of 40% NaOH + Fe_3O_4 + Cu + CuO at 325°C for 200

h. S and C accelerate the caustic corrosion in the mixtures of concentrated NaOH plus metal oxide sludges. In our experiment, samples of rapidly solidified alloy 600 supersaturated with more than about 0.1 wt% B could not be obtained by single- or double-roller methods because carbide precipitation could not be suppressed.

Chaung, et al.,[4] have reported that the segregation of sulfur along the grain boundaries of nickel 200 increases the anodic dissolution, e.g., grain-boundary attack within the sulfuric acid solution. The same behavior may also occur in alloy 600 in the caustic environments.

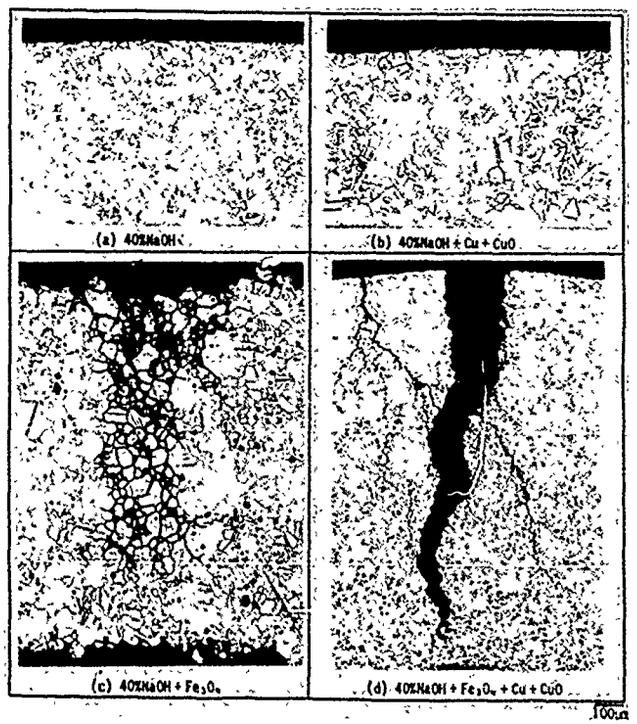


FIGURE 5—IGA morphology of mill-annealed alloy 600 (UNS N06600) in various kinds of mixtures of 40% NaOH plus oxide sludges at 325°C for 200 h using C-ring specimens.

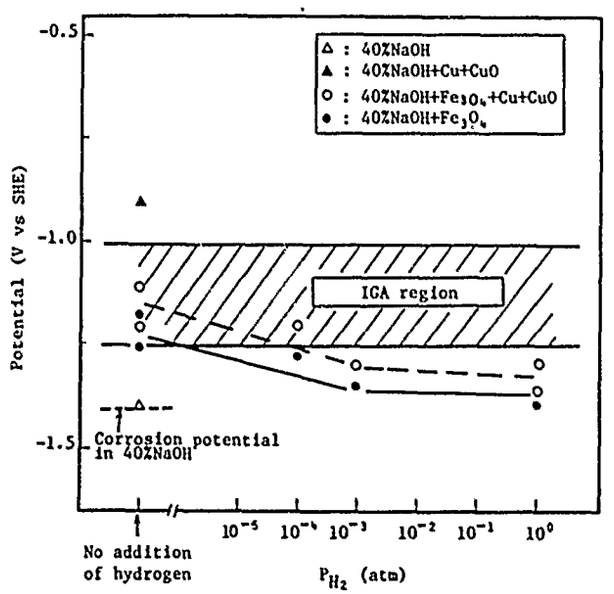


FIGURE 6—Effects of hydrogen pressure on the corrosion potential of mill-annealed alloy 600 (UNS N06600) in the mixtures of 40% NaOH plus oxide sludges at 325°C.

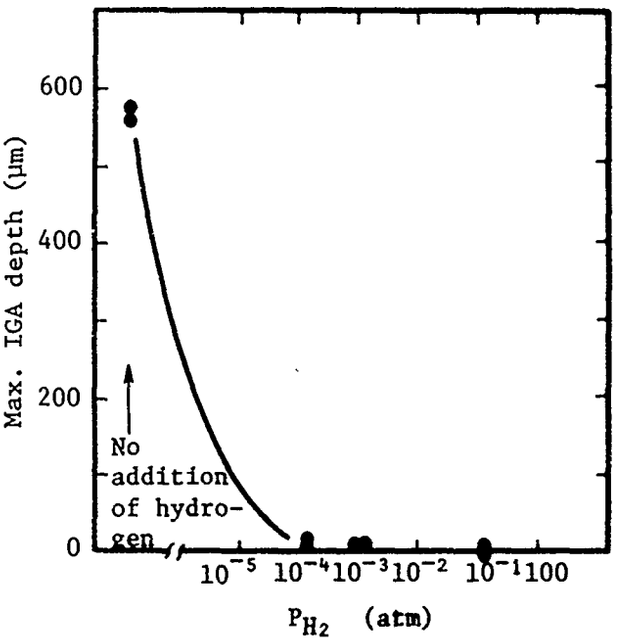


FIGURE 7—Effects of hydrogen pressure on IGA occurrence of mill-annealed alloy 600 (UNS N06600) in the mixture of 40% NaOH + Fe_3O_4 + Cu + CuO at 325°C for 200 h (C-ring specimen stressed at 30 kgf/mm²).

Figure 11 shows that the susceptibility to caustic IGSCC increases with the addition of very small amounts of boron in 50% NaOH solution at 350 C for 500 h using U-bend specimens.[9] On the other hand, the detrimental effect of boron is nullified by a thermal treatment at 700°C for 15 h.

Figure 12 shows that IGA is increased by segregated boron in mill-annealed alloy 600 in 4% NaOH at 325°C by the SSRT.

The grain-boundary segregation of boron in mill-annealed alloy 600 can be observed using the fission track-etching method shown in Figure 13.[9] Thus, the segregation of solute elements such as C, B, and S at the grain boundaries might cause the selective grain-boundary dissolution on mill-annealed alloy 600, but this does not preclude the other mechanisms shown in Figure 9.

Conclusion

(1) IGA is composed of IGC and IGSCC following IGC. It has been confirmed through experimentation that IGSCC is initiated when IGC depth reaches a_{th}, a threshold crack depth for initiation of IGSCC. It may be defined that K_{ISCC} is equal to $\eta\sigma\sqrt{\pi a_{th}}$ (η = a constant, σ = an applied stress).

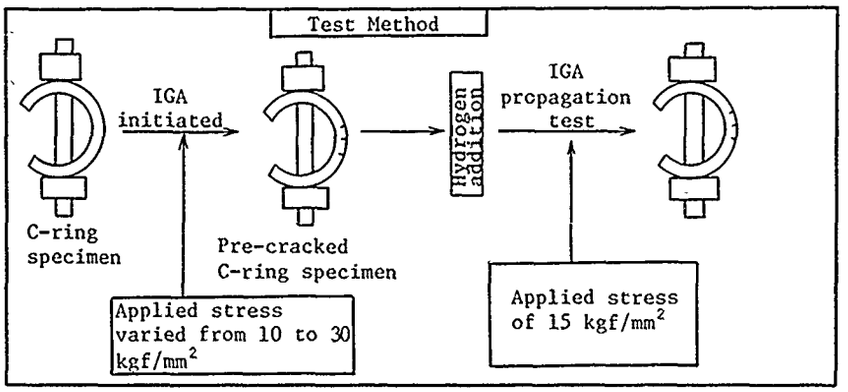
(2) Environmental factors are more influential on the IGA of alloy 600 than material factors. IGA occurs in the mixtures of NaOH solutions with pH above 10.3 and metal oxide sludges such as Fe_3O_4 and CuO at high temperatures. Fe_3O_4 is a main component of sludges formed in the plant and acts as a strong oxidizer in the caustic solution described in Equation (6):

$$Fe_3O_4 + 2H_2O + 2e^- \rightarrow 3HFeO_2^- + H^+ \qquad (6)$$

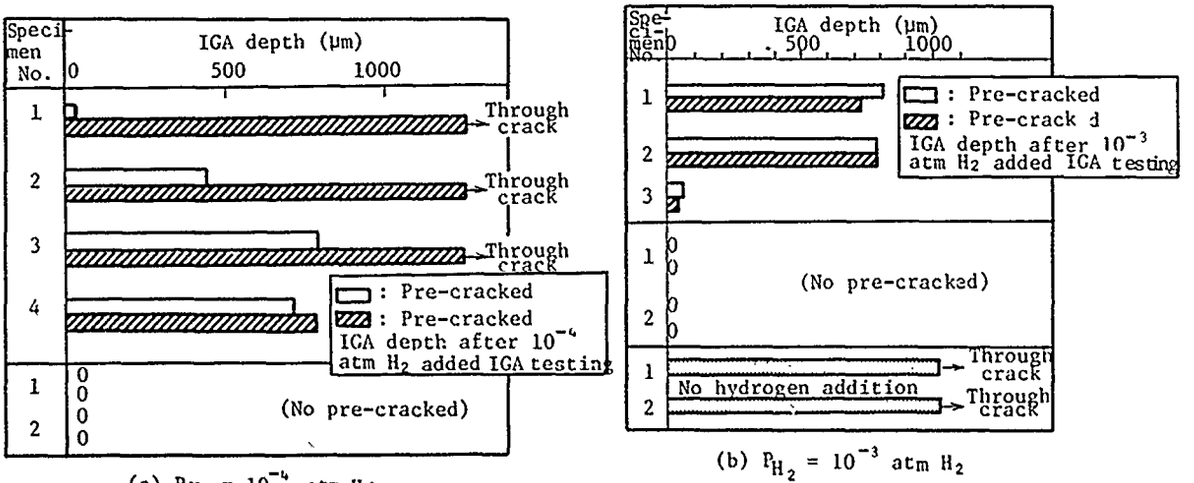
This shifts the corrosion potential of alloy 600 from an active potential region to an active-passive potential region, where IGA is initiated and proceeds.

(3) IGA initiation and propagation of mill-annealed alloy 600 can be inhibited by hydrogen addition above 10^{-3} atm in the mixtures of 40% NaOH and metal oxide sludges at 325°C.

(4) Concerning the mechanism of IGA, the segregation of dissolved elements such as C, B, and S at the grain boundaries may be the causes of selective grain-boundary dissolution for mill-annealed alloy 600.



* There is no suspicion of stress relaxation because strain gage is struck on the inner surface loaded at the maximum stress of the pre-cracked C-ring specimens.



(a) $P_{H_2} = 10^{-4}$ atm H_2 (b) $P_{H_2} = 10^{-3}$ atm H_2

FIGURE 8—Effects of hydrogen pressure on IGA propagation of mill-annealed alloy 600 (UNS N06600) in the mixture of 40% NaOH + Fe_3O_4 + Cu + CuO at 325°C for 200 h (C-ring specimen stressed at 15 kgf/mm²).

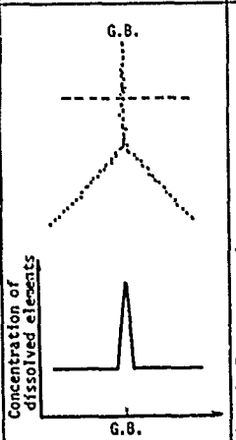
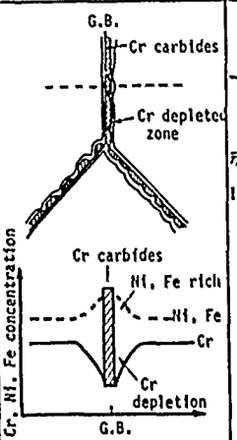
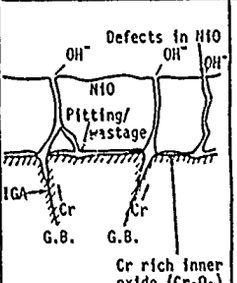
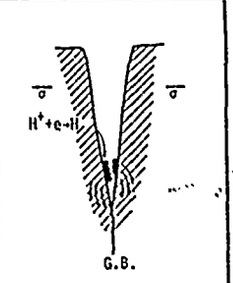
Theory	(a) Grain boundary Segregation	(b) Chromium Depleted Zone	(c) Chromium Enriched Zone	(d) Hydrogen Embrittlement
Description of Theory				
	Increase in the anodic dissolution by the segregation of dissolved elements such as C, B, S.	Active path corrosion (APC) along Cr depleted zone at grain boundaries	Preferential dissolution of Cr along grain boundaries in caustic solution	Weakening of grain boundary cohesion by hydrogen absorption
Proposer	K. Yamanaka et al.[5]	R.W. Staehle et al.[6]	B.P. Miglin et al.[8]	—

FIGURE 9—Summary of proposed mechanisms for selective grain-boundary dissolution or hydrogen embrittlement in Ni-base alloys.[5]

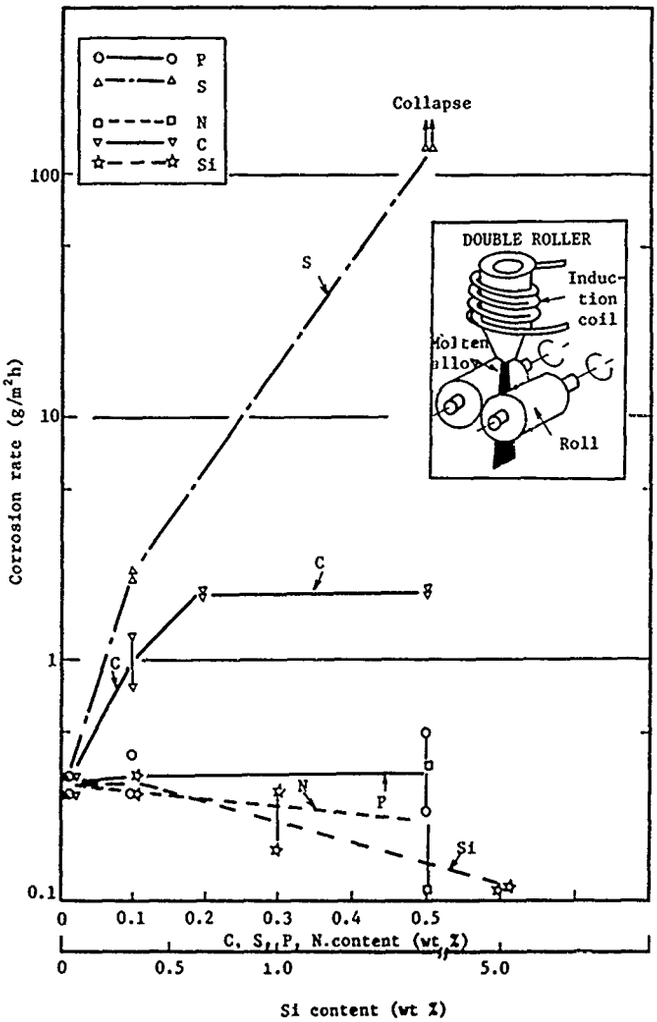


FIGURE 10—Effect of dissolved elements on corrosion rate of rapidly solidified alloy 600 (UNS N06600) in the mixtures of 40% NaOH + Fe_3O_4 + Cu + CuO sludges at 325°C for 200 h.

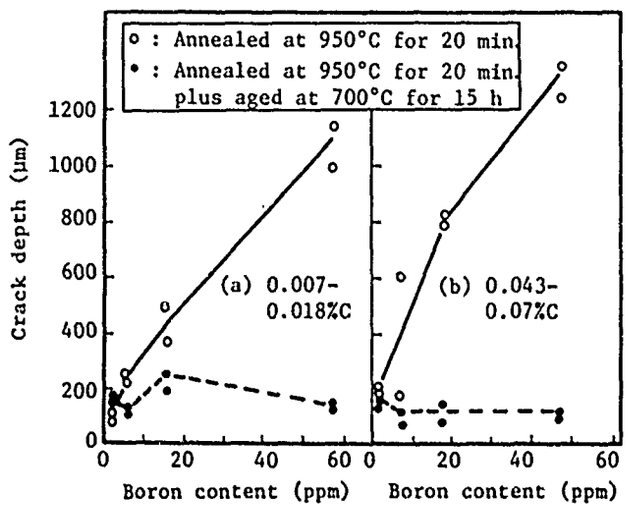


FIGURE 11—Effect of boron on the IGSCC of alloy 600 (UNS N06600) in deaerated 50% NaOH solution at 350°C for 500 h.[10]

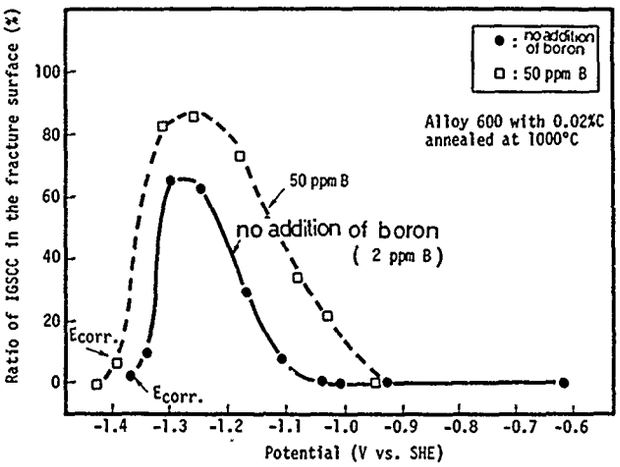


FIGURE 12—Effect of boron on the IGA of alloy 600 (UNS N06600) in 4% NaOH at 325°C by the SSRT.[7]

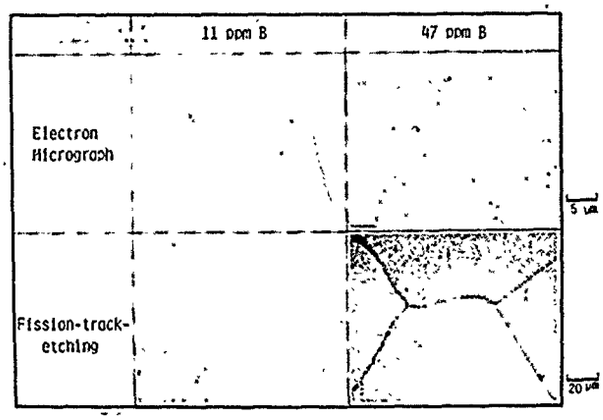


FIGURE 13—Electron micrographs and fission track etching of mill-annealed alloy 600 (UNS N06600) containing 11 ppm B and 47 ppm B.[9]

References

1. S.J. Green, J.P.N. Paine, Nucl. Tech. 55(1981): p. 10.
2. D. Van Rooyen, Corrosion 31(1975): p. 327.
3. D.D. Macdonald, A.C. Scott, P. Wentreck, J. Electrochem. Soc. 126(1979): p. 908.
4. H. Chaung, J.B. Lumsden, R.W. Staehle, CORROSION/77, paper no. 20 (Houston, TX: National Association of Corrosion Engineers, 1977).
5. K. Yamanaka, K. Tokimasa, H. Miyuki, H. Nagano, EPRI Meeting on IGA and Primary Water IGSCC Mechanisms (Palo Alto, CA: Electric Power Research Institute, 1987).
6. R.W. Staehle, ed., Proceedings of the Conference on Fundamental Aspects of Stress Corrosion Cracking (Houston, TX: NACE, 1969), p.1.
7. H. Nagano, K. Tokimasa, K. Yamanaka, H. Miyuki, EPRI Workshops on Remedial Actions for Secondary Side Intergranular Corrosion (Palo Alto, CA: EPRI, 1985).
8. B.P. Miglin, L.W. Sarver, CORROSION/85, paper no. 89 (Houston, TX: NACE, 1985).
9. H. Nagano, K. Yamanaka, T. Kudo, Sumitomo Search 31 (1985): p. 129.

Discussion

S.M. Bruemmer (Pacific Northwest Laboratory): Until now, the effect of carbide precipitates on the SCC of alloy 600 (UNS N06600) has not been studied too well. Nagano, et al., have given a good presentation regarding the action of carbides on the cracking behavior of alloy 600. It is very interesting that alloy 600, with continuous or discontinuous carbide precipitates, shows good SCC resistance in high-temperature pure water and caustic solutions, as compared with the performance of austenitic stainless steels. Carbide precipitation reduces the detrimental effect of dissolved carbon along grain boundaries, increasing SCC resistance.

However, you show a beneficial effect of intergranular carbides on the resistance to intergranular attack, apart from SCC. I can understand the effect of carbides on intergranular SCC, but how can we explain carbide effects on intergranular corrosion? Mechanistically, how can these carbides improve corrosion resistance?

H. Nagano: The details of the mechanism of intergranular corrosion remain obscure. In our paper we point out that environmental factors are generally more influential than material factors, such as the presence of carbides.

Threshold Stress and Crack Growth Rate Considerations Based on a Strain-Rate Damage Model of IGSCC for Alloy 600

Y.S. Garud and A.R. McIlree***

Abstract

An engineering model for quantitative evaluation of the intergranular stress corrosion cracking (IGSCC) of alloy 600 (UNS N06600) tubing material in high-purity water was recently presented by the authors. This paper deals with further applications of the IGSCC model. In particular, implications of the model with regard to (a) the possibility of a threshold stress for the IGSCC and (b) the crack growth rate evaluation are discussed with the objective of seeking some engineering correlations with the field data on the primary-side-initiated IGSCC in recirculating-type steam generators.

Theoretical estimates of the threshold stress are obtained as dependent on the temperature and material condition. It is shown that the threshold stress is related to the deformation characteristics of the material (such as the strain-rate sensitivity). Simplified correlations in terms of the room-temperature yield and ultimate strengths are presented for mill-annealed and thermally treated material conditions. The significance and limitations of the concept of threshold stress are discussed. Also, application of the IGSCC model to determine approximate (average) crack growth rates is illustrated, demonstrating the influence of stress and temperature on the pure-water cracking phenomenon. Failure times observed in the field are summarized, analyzed, and compared with the model results. Results presented in this paper lend further support to the utility and applicability of the strain-rate-based IGSCC damage model.

Introduction

The occurrence of intergranular stress corrosion cracking (IGSCC) in Ni-Cr-Fe alloy 600 (UNS N06600) tubing in the primary water-coolant environment of steam generators of pressurized water reactors (PWRs) has continued to adversely affect the availability of PWR power plants for over a decade.[1,2] Mainly because of increased costs of plant operation and maintenance, this has resulted in the need for quantitative and predictive modeling of IGSCC. An engineering model based on a detailed review of relevant data and mechanistic considerations[3] was presented in an earlier paper.[4]

The purpose of this paper is to provide estimates of threshold stress and average crack growth rate for alloy 600 in high-purity, high-temperature water by applying the model under simplified conditions of interest and to compare the results with service data.

Model Description

The strain-rate-based model for IGSCC of alloy 600 in high-purity water can be summarized by the following relations:[3,4]

$$D(t) = \int_0^t f(\dot{\epsilon})dt \quad (1)$$

$$f(\dot{\epsilon}) = A(\dot{\epsilon})^p \quad (2)$$

$$D(t_f) = a_f \quad (3)$$

Equation (1) states that the IGSCC damage (D) accumulated in time (t) is dependent on the strain rate ($\dot{\epsilon}$). The functional relation (f), as given by Equation (2), involves two parameters (A and p) that account for the material environment specific conditions. Equation (3) simply defines the failure condition for the occurrence of a small crack of engineering significance, and t_f is the time to reach that condition. Here, D and a_f are in units of length, A and f( ) have units of length/time, $\dot{\epsilon}$ has units of 1/time, and p is a dimensionless parameter.

Alternatively, the above relations may be combined as follows:

$$1 = \int_0^{t_f} (1/t^*)(\dot{\epsilon})^p \, dt \quad (4)$$

where $t^* \equiv a_f/A$, thus explicitly defining the time-to-failure (t_f). The strain rate used in the following discussion is taken equal to the total nominal strain rate accounting for nonelastic material response in the absence of any significant cracking.

Based on the material stress–strain data available for Ni-Cr-Fe alloy 600, the following formulation (referred to as the Bodner-Partom formulation[5]) was found suitable[3] to represent the strain-rate response for various material conditions of interest.

$$\dot{\epsilon} = \dot{\sigma}/E + \dot{\epsilon}_n \quad (5)$$

$$\dot{\epsilon}_n = (2D_0/\sqrt{3})\exp[-0.5(Z/\sigma)^{2n}] \quad (6)$$

$$Z = Z_1 - (Z_1 - Z_0)\exp(-mW_p) \quad (7)$$

$$Z_0 = (m_1T + C_1)Z_1 \quad (8)$$

$$m = m_0T + C_0 \quad (9)$$

$$n = a/T \quad (10)$$

*S. Levy Incorporated, 3425 S. Bascom Ave., Campbell, CA 95008-7006.

**Electric Power Research Institute, 3412 Hillview Ave., Palo Alto, CA 94304.

In these equations, D_0, Z_1, m_0, m_1, C_0, C_1, and a are material constants independent of temperature, E is Young's modulus of elasticity, and W_p is the cumulative work of nonelastic deformation (i.e., sum total or integrated value of the product of stress and incremental nonelastic strain), σ is stress, and T is absolute temperature. Here, E, Z, Z_1, Z_0, and W_p have units of stress,[1] m and C_0 are in units of 1/stress, $\dot{\sigma}$ has units of stress/time, $\dot{\epsilon}$, $\dot{\epsilon}_n$, and D_0 are in units of 1/time, and n is dimensionless. (Time is measured in seconds throughout this work.)

Values of the constants for four material conditions are given in Table 1 based on an analysis of stress–strain data. (For details of the data and analysis, the reader is referred to Reference 3.) The room-temperature yield strength and ultimate strength corresponding to the various heats of these materials are also listed in the same table for use in the subsequent correlations, these strength values are experimental data as gathered from various sources in Reference 3.

Comments on the Physical Basis and Material Parameters

Equations (1) through (4) constitute the IGSCC model that uses the strain rate as a key variable. Various mechanistic and phenomenological reasons for the strain-rate-based approach were discussed in the earlier work.[3,4] Very briefly, it allows one to interpret the SCC in terms of a film-rupture mechanism, because the periodicity of ruptures is expected to be related to the strain rate and also to influence the rate of progression of stress corrosion cracking. In addition, it is possible to relate the functional form f( ) [Equation (2)] and the two model parameters (A and p) to the current-density data from electrochemical strain-rate transient experiments.[3,4]

Equations (5) through (10) constitute the deformation mechanics formulation quite independent of the IGSCC model; i.e., any appropriate set of equations describing the stress–strain response of the material under consideration may be used to define the strain-rate input needed for the IGSCC model. The formulation selected in this work is essentially the one proposed by Bodner and Partom, who also discuss its physical basis in relation to the motion of dislocations.[5] For instance, the material parameter (n) is related to the intrinsic viscosity of dislocation motion and to the strain-rate sensitivity of the material (the lower value of n implies greater sensitivity).

D_0 also influences the strain-rate sensitivity and is related to a limiting (maximum) strain rate in shear. The parameter m relates to the rate of work-hardening (higher values of m imply higher rates). The variable Z is referred to as the hardness variable and represents the overall microstructural state of the material with respect to its resistance to the inelastic deformation; it is a type of scalar internal variable that accounts for the load-history dependence of the nonelastic deformation. The parameter Z_0 is the initial hardness corresponding to the reference state of the material from which the value of W_p is measured; Z_1 corresponds to a limiting saturation value of Z to ensure that the resistance to inelastic deformation is finite. It may be noted that the above formulation is applicable to steady as well as variable (uniaxial) loading of stress or strain, therefore, constant stress, constant deformation, and constant extension-rate conditions are only some of the particular cases of loading covered by the formulation.

Threshold Stress Evaluation

The concept of a threshold parameter (such as a stress or stress intensity) separating the regions of conditions for the occurrence and non-occurrence of a phenomenon is appealing to many engineers and researchers, and the phenomenon of IGSCC falls in this category. At the same time, however, it would be difficult to deny the elusive nature of the threshold, particularly when environmental influences on material degradation are important and when the loading is not one of uniformly constant intensity.[6] The Discussion section argues the validity and limitations of the threshold concept for IGSCC; the following is an attempt to estimate the threshold stress (under idealized conditions) as suggested by the above damage model.

[1]The SI unit for stress is MPa: 1 ksi = 6.895 MPa.

Starting with an ideally smooth surface (with no cracks) and under the condition of constant stress, the deformation mechanics formulation [Equations (5) through (10)] implies a steep decrease in the (nominal) strain rate at low (below-yield) nominal stresses, which, in turn, translates into an extremely slow rate of damage accumulation per the IGSCC model. Let $\dot{\epsilon}_{cr}$ denote the value of strain rate below which the damage accumulation rate is too slow to cause any significant degradation over the practical useful life of a component. To a first approximation, assuming conservatively that $Z = Z_0$ for $\dot{\epsilon}_n = \dot{\epsilon}_{cr}$, Equations (6), (8), and (10) result in the following expression for threshold stress (S_{th}):

$$S_{th} = Z_1(m_1T + C_1)\,[\,\ln(4D_0^2/3) - 2\ln(\dot{\epsilon}_{cr})\,]^{-T/2a} \qquad (11)$$

One estimate of $\dot{\epsilon}_{cr}$ may be obtained by equating it to the average strain rate needed to accumulate the strain equal to the rupture strain of a metal oxide in the practical life span for the component; e.g., a metal oxide ductility of 0.001 and a life of 40 years would imply the $\dot{\epsilon}_{cr}$ equal to 7.93×10^{-13} (1/s). Since the earlier work[4] permits an estimation of the accumulation of IGSCC damage for a mill-annealed alloy 600 condition at 365°C, this results in a more conservative value for $\dot{\epsilon}_{cr}$ of 7.09×10^{-18} (1/s). Based on the latter approach and allowing for some uncertainty, the value of $\dot{\epsilon}_{cr}$ is taken equal to 1.0×10^{-20} (1/s).

Using the above expression for the threshold stress and the conservative value of 1×10^{-20} (1/s) for $\dot{\epsilon}_{cr}$, the threshold estimates for various heats and material conditions of Table 1 were obtained for high-purity water in the temperature range of 500 to 680°F (260 to 360°C). Figure 1 shows these estimates.

The two material conditions for which data were available from multiple heats exhibited considerable heat-to-heat variations in the estimated threshold stress values, as can be seen from Figure 1. Note however, that the basic mechanical strength properties also show similar variation, as indicated in Table 1. Material constants in Bodner-Partom formulation are normally not available (and their determination requires more data and analysis) as compared with the readily available properties such as the room-temperature yield (S_y) and ultimate-strength (S_u) values. It is useful, therefore, to obtain alternative correlations for the threshold stress in terms of the latter values, if possible. The data from Table 1 and the model estimates from Figure 1 were analyzed and yielded the following regressions:

For the mill-annealed condition,

$$S_{th} = -48.050 + 0.8154S_y + 0.5440S_u - 0.01471F \qquad (12)$$

For thermally treated conditions,

$$S_{th} = -23.138 + 0.4496S_y + 0.4491S_u \quad 0.01578F \qquad (13)$$

Here, F is temperature in degrees Fahrenheit [500 to 680° (260 to 360°C)], and S_{th}, S_y, and S_u are in ksi. The goodness of fit is quite satisfactory, as can be inferred from Figure 2. The heat-to-heat variation is significantly accounted for, and most of the regression fitted values are within 5% of the model estimates.

Crack Growth Rate Estimates

As noted above, the IGSCC damage model was developed for the time-to-failure (t_f), with failure defined in terms of the initiation of a small crack of the order of 1 mm (a_f). Based on this definition, an average crack growth rate (or the average rate of IGSCC penetration) can be estimated as a_f/t_f.

Since the IGSCC damage model is based on the strain rate as a key mechanics variable, it becomes essential to obtain an estimate of strain rates acting in the critical locations of a service component. Such information is often not obvious nor readily obtainable; however, with the use of a reasonable constitutive relation (i.e., material stress–strain behavior), it is possible to relate strain rate to more readily available parameters such as temperature and stresses. As noted earlier, the Bodner-Partom formulation was found to be suitable for alloy 600 tubing material.

TABLE 1

Bodner-Partom Material Constants for Various Conditions and Heats of Alloy 600 (UNS N06600), Room-Temperature Yield (S_y), and Ultimate Strength (S_u)

No.[A]	D_0 1/s	Z_1 ksi[B]	a °K	$\dot{m}_0$ 1/(ksi °K)	C_0 1/ksi	m_1 1/°K	C_1	S_y ksi	S_u ksi
0.0	10	145.63	2868	1.307E-4	0.05826	−3.370E-5	0.41323	49.73	99.62
4.0	10	116.87	5950	0.703E-4	0.13393	−16.350E-5	0.42481	40.63	97.93
4.1	10	142.31	2541	1.402E-4	0 08167	−0.935E-5	0.35020	41.91	99.64
5.0	10	144.75	7319	0.723E-4	0.06842	−8.020E-5	0.45093	58.00	104.20
5.2	10	158.18	3507	1.251E-4	0.06435	−3.650E-5	0.40867	55.73	109.75
6.2	10	150.56	3287	0.991E-4	0.07888	−2.040E-5	0.36886	48.62	103.38
7.2	10	158.11	5240	0.521E-4	0.10173	−5.260E-5	0.41606	60.15	117.26
8.3	10	147.63	3689	1.327E-4	0.06974	−19.420E-5	0.67468	75.49	106.38
12.0	10	140.62	11141	0.0	0.10045	−10.370E-5	0.42225	53.77	107.84

[A]0.0, 4.0, 5.0, and 12.0 are mill-annealed heats (0.0 is average of 3 heats).
4.1 is mill-annealed and stress-relieved heat.
5.2, 6.2, and 7.2 are mill-annealed and thermally treated heats.
8.3 is mill-annealed and cold-worked heat.
[B]Note: 1 ksi = 6.895 MPa.

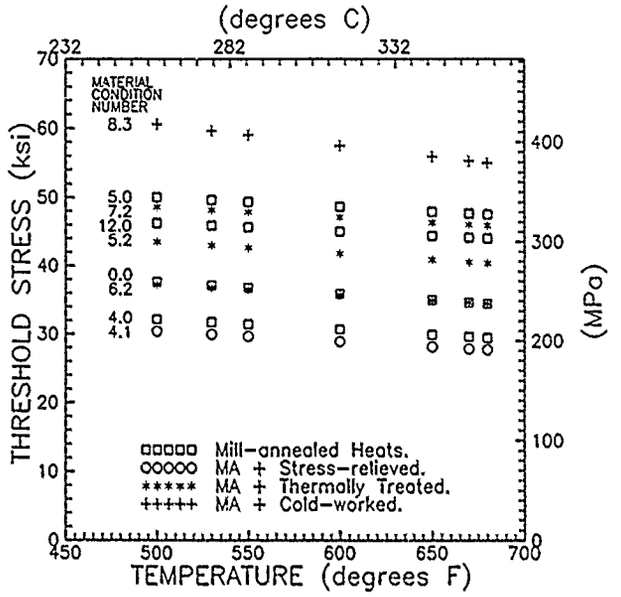


FIGURE 1—Model estimates of threshold stresses for IGSCC of various heats and material conditions of alloy 600 (UNS N06600).

For the U-bend steam generator tubing application, although the service temperature data is known fairly accurately, the acting (i.e., residual plus operational) stress values are generally unknown or reflect considerable uncertainty, particularly in the roll-transition (RT) zone and in the U-bend region, where fabrication histories and geometric complexities dominate the stress assessment. It is proposed here to use the engineering yield strength (for 0.2% plastic strain) as the uniform (effective) stress level acting in the critical location for purposes of estimating the average crack growth rate equal to a_f/t_i.

In our earlier work,[4] the model parameters were established for a mill-annealed condition (no. 4.0) of alloy 600 for the high-purity water environment between 290 and 350°C. In particular, the exponent p was estimated to be 0.65 and t* (in seconds) was 10.627 at 290°C (554°F), 6.05205 at 340°C (644°F) and 4.84027 at 350°C (662 F). In this work, the t* values were interpolated between 290 and 340°C (i.e., t* = 37.16171 − 0.091499T, where T is in °C). The corresponding parameters describing the material strain-rate response are listed in Table 1. To be consistent with the earlier work,[2]

[2]The authors would like to note a correction to the typographical error in Equation (4) of their earlier paper (Reference 4): The factor (1 p) (a_f/A) should read [(1 p) (a_f/A)]. Similar correction is warranted in Equation (3.3) of Reference 3 and in Equation (7) of Reference 7.

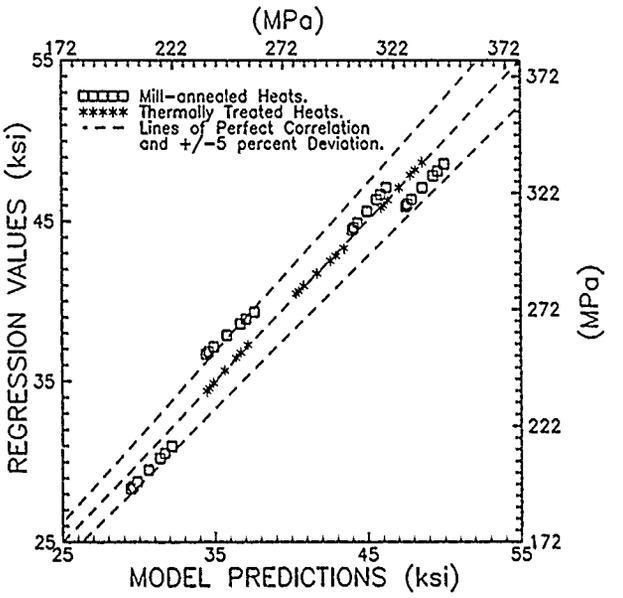


FIGURE 2—Comparison of estimated threshold stress with regression-fit calculations for mill-annealed and thermally treated heats.

the values of Z_s (in Equation A.7 of Reference 4) were estimated by linear interpolation between the stress range of 36 to 45 ksi and the temperature range of 290 to 340°C [The resulting linear relation was Z_s (ksi) = 1.1306639 + 1.0829918S + 0.0098T, where S is stress in ksi and T is temperature in °C].

Based on the above assumptions and model parameter values from the previous work (with a_i = 1 mm), the average rates of IGSCC penetration were calculated for the temperature range of 290 to 340°C (554 to 644°F) and stress levels of $0.90S_y$, S_y, and $1.10S_y$ (where S_y is the material yield strength at room temperature equal to 40.63 ksi for the material condition 4.0). The resulting model predictions are shown by the solid lines in Figure 3.

In addition, the field data[8,9] for reported IGSCC incidences at the two critical locations; namely, the first-row U-bend region and the RT zone (of mill-annealed alloy 600 tubing of the recirculating-type steam generators), are also shown on the same plot of Figure 3. Here, the average rate of IGSCC penetration was estimated (with appropriate unit conversions) by simply dividing the nominal wall thickness (50 mils or 1.27 mm) by the effective full-power days

estimate at which time each IGSCC incidence was reported. Note that the RT data includes three incidences of IGSCC in the cold-leg portion of the recirculating-type steam generators. All these field data have been reported for the IGSCC initiated from the primary-coolant side of the alloy 600 tubes.

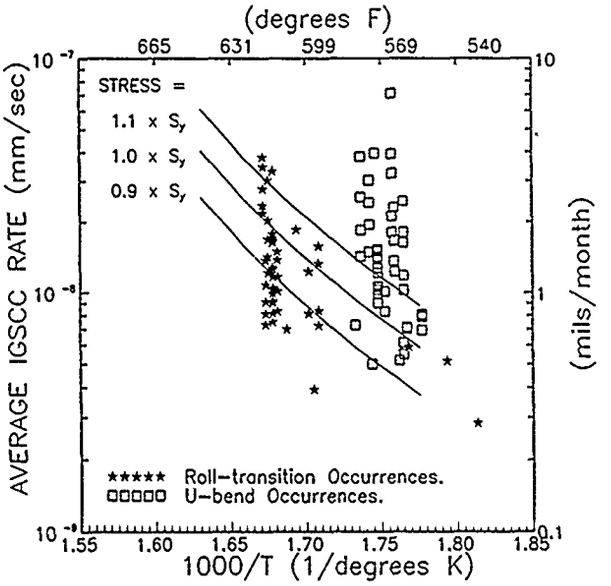


FIGURE 3—Temperature and stress dependence of penetration rate of IGSCC as estimated by the model and its comparison with field data.

Discussion

The IGSCC damage model suggests that the threshold stress as given by Equation (11) is dependent on deformation-related material parameters, in particular on n, which is related to the strain-rate sensitivity. Also, typical estimated threshold stresses at 600°F (316°C) range from about 70 to 84% of the material yield strength at room temperature. It is important to note an implicit assumption made in estimating the threshold stress. The material is assumed to be free of cracks just prior to the start of the holding period of the stress If this is not the case, the estimate would have to be lowered, depending on the severity of the cracking and of the environment. Note also that the value of $\dot{\epsilon}_{cr}$ (the critical strain rate) is expected to depend on the environment, thus, in principle, providing for the fact that these estimates would not be applicable to an aggressive environment such as the polythionic acid.

In view of the fact that the actual primary water environment is somewhat different from the high-purity water environments used in obtaining the model parameters, the correlation of Figure 3 might appear fortuitous The stress levels of Figure 3 are expected to be reasonable for the RT region; as such, the temperature dependence covering the hot-leg and the cold-leg transitions is very well represented by the model. Since the U-bend region is expected to be more highly stressed than the RT, the corresponding trend seen in Figure 3 appears to be in the right direction.

Concluding Remarks

Based on the strain rate IGSCC damage model for alloy 600 in high temperature, high purity water, the concept of threshold stress is evaluated for a smooth (uncracked) component under constant stress condition. It is shown that the threshold stress is related to the deformation characteristics of the material, and simplified expressions in terms of the room temperature yield and ultimate strengths are presented for mill annealed and thermally treated material conditions.

To a first approximation, the model implementation for estimating average crack growth rates for the IGSCC was presented. These estimates were shown to be in reasonably good agreement with data analyzed from the service tube failures. Results presented in this paper lend support to the utility and applicability of the strain-rate based IGSCC damage model.

Acknowledgment

The financial support for a major part of the work that forms the basis of this paper was provided by the Electric Power Research Institute (EPRI) (Palo Alto, CA) through the Steam Generator Owners' Group Program. The research and its presentation were facilitated by S. Levy Incorporated.

References

1. O.S. Tatone, P. Meindl, G.F. Taylor, Nucl. Safety 28, 3(1987): pp. 374-390 .
2. A.A. Stein, A.R. McIlree, eds., Proceedings: 1985 Workshop on Primary-Side Stress Corrosion Cracking of PWR Steam Generator Tubing, EPRI NP-5158, June 1987 (Palo Alto, CA: Electric Power Research Institute, 1987).
3. Y.S. Garud, "Development of a Model for Predicting Intergranular Stress Corrosion Cracking of Alloy 600 Tubes in PWR Primary Water," EPRI NP-3791, EPRI, January 1985.
4. Y.S. Garud, A.R. McIlree, Corrosion 42, 2(1986): pp. 99-105.
5. S.R. Bodner, Y. Partom, J. of Appl. Mech., Trans. ASME 42(1975): pp. 385-389.
6. M.O. Speidel, Design Against Environment-Sensitive Fracture, ICM 3, Vol. 1 (Oxford, England: Pergamon Press, 1979), pp. 109-137.
7. Y.S. Garud, 10th International Congress on Metallic Corrosion, paper no. 10.44 (Karaikudi, India. Central Electrochemical Research Institute, 1987).
8. Y.S. Garud, "Survey of Primary-Side IGSCC Events in Westinghouse Steam Generators of Pressurized Water Reactors," S. Levy Incorporated Report No. SLI-8508, Sept. 1985 (unpublished).
9. A.R. McIlree, Private Communication.

Discussion

M.M. Hall (Westinghouse Electric Corporation, USA): As I understand your strain-rate damage model of intergranular SCC, your damage function is the integral over time of the rate of mechanical strain-energy dissipation. Your threshold stress (for crack initiation) is then a critical strain parameter. Could you comment on the general applicability of this result? Do the current slow-strain-rate and static-loading test methods provide sufficient information for a rigorous test of the concept? If so, what data sets best illustrate this?

Y.S. Garud: Although the intergranular SCC damage D [Equation (1)] and the functional relation f [Equation (2)] are *related*—through the particular choice of material stress–strain law used in this study—to the time–integral of the work (per unit volume) of nonelastic deformation (W_p), the relation is neither obvious nor simple. It is difficult to see how either D or f is equivalent to W_p, as you suggest. However, the idea of a more explicit and direct relation between the two may be of some merit for further evaluation.

The threshold stress is actually related to a critical strain-*rate* parameter in this work. However, as indicated under Equation (11), it *may* be interpreted in terms of the rupture strain of a metal oxide expected to form under the conditions of interest. In this sense, and under the idealized conditions noted in the paper, the concept should be applicable to other alloy–environment systems [e.g., stainless steels such as type 304 (UNS S30400) in high-temperature aqueous conditions, as in a boiling water reactor] where the involvement of a film-rupture process is suspected.

The slow-strain-rate test and the static-load test do provide some information about the possibility of a threshold stress, but this information is only indirect and necessarily requires extrapolation (in time) of the test results. In other words, there are practical limitations of time and resources needed for an otherwise rigorous test program. We are not aware of currently available data (for the PWR tubing) generated specifically to test the threshold stress concept. However, recently, more specific data has been produced that might provide some (indirect) information on this issue, subject to further evaluation.

Effect of Crevice Corrosion on Hydrogen Embrittlement of Titanium

C.F. Clarke, B.M. Ikeda,* and D. Hardie***

Abstract

Titanium is a candidate container material for the disposal of nuclear fuel waste in Canada. A possible failure mechanism for titanium is hydrogen embrittlement (HE) caused by the hydrogen generated during crevice corrosion. Although Grade-2 titanium is less susceptible to HE than Grade-12 titanium, it is more susceptible to crevice corrosion, particularly at temperatures greater than 100°C. This paper describes the development of a crevice design in order to establish consistent crevice corrosion on Grade-2 titanium tensile specimens. Hydrogen entry into the metal does occur under the crevice. However, the material fails mechanically because of a reduction in its cross-sectional area brought about by crevice corrosion, not because of HE. The failure mode appears to be a competition between the rates of hydrogen uptake and metal wastage.

Introduction

Titanium is a candidate material for use as a nuclear waste container. In Canada, the design lifetime for such nuclear waste containers is 500 a at temperatures up to 100°C in saline ground waters that could approach saturation in chloride. Titanium owes its excellent corrosion resistance over a wide range of environments and conditions to a stable, adherent surface film of TiO_2, either in the form of rutile or anatase. Any assessment of its viability as a material for the long-term containment of radioactive waste must consider factors that may break down this protective film.

This passive film can be compromised by excessive cathodic protection or under crevice conditions, such as those created by surface deposits, metal-to-metal joints, or flanges containing gaskets. Commercial-purity titanium (ASTM Grades 1-4) is particularly susceptible to crevice corrosion in saline solutions at temperatures above 100 C. On the other hand, Grade-12 titanium, which contains small amounts of nickel and molybdenum, has been shown to have greater resistance to such attack.[1] However, it appears to have poorer resistance to hydrogen embrittlement (HE) when strained in neutral chloride solutions and cathodically polarized at temperatures greater than 100 C,[2] or when precharged with hydrogen under vacuum at elevated temperatures.[3] The results of Clarke, et al., suggest that at extremely negative potentials, the passive film on Grade-12 titanium is altered, rendering it more permeable to hydrogen.[2] Apparently, this alteration does not occur on Grade-2 titanium. The alloying elements in Grade 12 titanium, which are difficult to detect in the passive film, are thought to alter the properties of the oxide layer, making it more resistant to localized breakdown but more susceptible to hydrogen entry at negative potentials.

For free corrosion conditions (as opposed to cathodically polarized conditions), both Grade-2 and Grade-12 titanium have good resistance to HE. This behavior is believed to be a result of the effectiveness of the passive film as a barrier to hydrogen uptake. However, under conditions where the passive film can be altered or breached (e.g., crevice corrosion), hydrogen might enter the underlying metal. The question is whether or not embrittlement can arise from crevice corrosion and contribute to container failure.

Extensive studies have been conducted on the crevice corrosion behavior of Grade-2 titanium immersed in neutral saline environments under unstressed conditions.[1-4] During the active stage of crevice corrosion, the passive film in the crevice is absent. The loss of the passive film in the crevice provides an easy way for hydrogen entry into the bulk titanium. Therefore, more information is required concerning the relationship between HE and crevice corrosion.

Crevice corrosion behavior is dependent on alloy composition (even within the specification range) and on chloride and oxygen concentration, as well as on geometric considerations. In aqueous chloride solutions at temperatures up to 150°C, crevice corrosion initiates in both Grade 12 titanium, and Grade 2 titanium with an iron content 0.1 wt% but subsequently repassivates.[1,4,7] However, for a low iron containing Grade 2 titanium, active crevice corrosion proceeds until all the oxygen is depleted from the bulk environment.[1,4,5] Passivation does not occur. Since passive film formation in crevices does not occur for the low iron-containing titanium, this material is ideal for investigating the susceptibility of titanium to HE under crevice corrosion conditions.

At this point, it is important to distinguish between initiation, propagation, and passivation. Crevice corrosion can be initiated on titanium and then be followed by either passivation or propagation. Active crevice corrosion, or propagation, is limited by the supply of oxidant in the bulk environment, and repassivation does not occur as long as the oxidant is present. This behavior is usually observed for low iron containing Grade 2 titanium. When passivation occurs, the amount of corrosion is limited even in the presence of the oxidant, this behavior is characteristic of Grade 12 titanium. In this study, we are interested in active crevice corrosion, where the passive film is absent, and not in passivated crevices or the initiation event.

This paper discusses the influence of crevice corrosion on the susceptibility of ASTM Grade-2 titanium to hydrogen uptake in hot, aqueous, salt solution. Also, the development of a creviced tensile specimen will be described.

*Atomic Energy of Canada Limited, Fuel Waste Technology Branch, Whiteshell Nuclear Research Establishment, Pinawa, Manitoba, Canada R0E 1L0.

**Department of Metallurgy and Engineering Materials, University of Newcastle upon Tyne, England.

Experimental Procedure

The experiments were performed in Teflon†-lined titanium pressure vessels. The straining experiments were performed using tensile machines that have been previously described.[2] The data were collected using an LSI 11/73 computer system with a μMAC†-4000 multiplexer. The load cycling was achieved by computer control, but the strain rates were established manually.

Specimens were cut from plates of commercially available ASTM Grade-2 titanium (composition shown in Table 1). The tensile specimens used had a 2.54-mm gauge length, a 2.8-mm gauge diameter, and a 12-mm-long threaded shoulder at either end. All the metal specimens were machined with their long axes parallel to the rolling direction of the original plate.

TABLE 1
Composition of ASTM Grade-2 Titanium in wt%

Fe	0.024
Ni	<0.003
Cr	0.0026
Mn	<0.0008
Al	0.048
Mo	<0.002
Si	0.11
C	0.08
O	0.165

A galvanic coupling technique was used to electrochemically monitor the progress of the crevice corrosion reaction.[5] The artificially creviced electrode was coupled to a large surface area titanium counter electrode (a cathode) through a potentiostat used as a zero-resistance ammeter. The corrosion potential of the specimen was measured against an internal Ag/AgCl (0.1 mol/L KCl) reference electrode using a high-impedance voltmeter. The potential of this electrode is +200 mV vs the standard hydrogen electrode (SHE) at 150°C and, unless otherwise stated, potentials quoted in this paper are relative to the SHE. All the experiments were performed in 0.60 mol/L (3.5 wt%) NaCl.

The experiments were performed at 150°C to allow correlation with other crevice corrosion experiments that used unstressed specimens. This temperature is well above the expected maximum disposal vault temperature range of 90 to 100°C. Consequently, the experiment should be considered conservative, since the rates of electrochemical and diffusion processes involved will be accelerated compared with those expected in a disposal vault.

For tensile specimens, various stressing conditions were used in an attempt to distinguish crevice corrosion from HE effects. The specimens were strained at rates of 3 to 6 × 10^{-7} s^{-1} until a strain of ~2.5% (corresponds to 200 to 300 MPa) was obtained. The load was then cycled between ±10 MPa of the stress at this point. Cyclic loading was used for two reasons: (1) to extend the testing time for a given strain rate (i.e., to avoid straining to failure) and (2) to ensure that the geometry of the crevice was not unduly influenced by straining the specimen (i.e., necking) during the period of testing. If a constant extension rate was used, the specimens would fail, often before either hydrogen or crevice corrosion could influence the failure mode. To investigate the effect of strain rate on either crevice corrosion or HE, or to investigate the relationship between HE and crevice corrosion, it was important to apply the load cyclically.

After load cycling at 150°C for a given period, specimens were cooled to ambient temperature and inspected before straining to failure in air at a strain rate of 2 × 10^{-5} s^{-1}. Subsequent macroscopic and metallographic examinations noted (1) the depth and area of crevice corrosion and (2) the degree of embrittlement as indicated by the amount of brittle fracture surface observed. The elongation to failure provided a more reliable measure of the ductility under these conditions, because the attack within the creviced region precluded meaningful reduction-in-area measurements.

The hydrogen content of the samples was determined either chemically, by the hot gas extraction technique, or by metallographic examination following etching with Krolls reagent. On the whole, metallographic examination provided the more reliable indication of the variation in hydrogen content.

Surface analysis was performed using a SAM590A† scanning Auger microscope with a SIMS† II secondary ion mass spectrometer attachment, manufactured by the PSI electronics division of Perkin Elmer. The scanning Auger microscopy analyses were performed using an electron beam voltage of 3 kV and an electron beam current of 3 nA and an analyzer resolution of 0.6%.

Development of crevice design

The unstressed crevice samples were similar to those previously described.[5] A thin sheet of Teflon was sandwiched between two rectangular prisms of titanium (25 mm long by 11 mm wide by 6 mm thick) bolted together in the form of a cross by a 5-mm bolt passing through a central hole (Figure 1). The crevices were assembled while immersed in the solutions to be used. This procedure ensured that the crevices were wet at the beginning of the experiment and that crevice initiation was not delayed by lack of physical wetting of the crevice. Results were found to be reproducible when the fastening bolts were finger tightened.

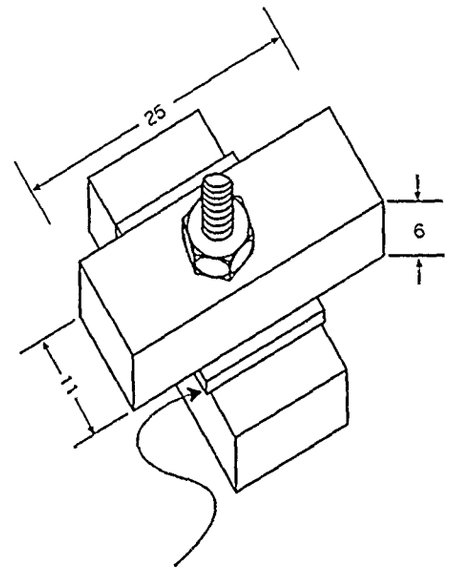


FIGURE 1—Schematic diagram of an unstressed crevice coupon.

Reproducible crevice corrosion was obtained using this unstressed sample geometry; however, it was more difficult to obtain reproducible crevice corrosion with artificial crevices formed on tensile specimens. It proved difficult to determine whether the differences in crevice corrosion behavior between stressed and unstressed samples were a result of the presence of the stress, resistance to crevice corrosion, or difficulties in producing the necessary crevice geometries. Therefore, a design was developed to reproduce a circumferential crevice around a portion of a tensile specimen having a gauge length of 25.4 mm, a creviced length of 14 mm, and a diameter of 2.8 mm. In an attempt to obtain reproducible data, the titanium containing low levels of iron was used for these experiments because it readily undergoes crevice corrosion in 0.6 mol/L NaCl at 150°C.[4]

†Trade name.

Under static (no strain) conditions, crevices are readily formed on titanium if (1) the crevices are very tight, and (2) there is sufficient access to the crevice to provide solution transport into the crevice. The latter condition is a geometry factor that is not well defined; however, it is important since, during crevice corrosion, the acidic environment that results from the hydrolysis of titanium must be balanced by anion transport into the crevice to maintain electroneutrality. The rate of anion transport may then limit the corrosion rate. The crevice tightness is also a poorly defined factor that can cause difficulties in forming reproducible crevices. This problem is mainly avoided by forming "wet" crevices as described above.

Initially, the crevice former was a split cylinder of Teflon extending over the entire gauge length of the tensile specimen. A 12.7-mm-diameter cylinder was drilled axially with a 3.175-mm-diameter hole. The cylinder was then cut in half lengthwise, and, while under solution, the tensile specimen was placed between the two halves. The assembly was held in place using chromel wire loops. The longitudinal slits on the sides of the crevice were each ~2 mm wide. Anodic polarization to -130 mV_{SHE} to initiate crevice corrosion, followed by cathodic polarization to -830 mV_{SHE} to induce hydrogen entry, demonstrated that crevice corrosion could be induced. Although no trouble had been experienced in initiating crevice corrosion in the simple unstressed (sandwich) design (Figure 1), reliable initiation was not achieved with this split cylinder arrangement, and modifications were therefore introduced.

Attempts to produce tighter crevices were made since the lack of crevice corrosion resulted from an insufficiently tight crevice. Drilling the central hole smaller and cutting the longitudinal slits so that the cuts were wider did not produce the desired reproducibility. Cutting the cylinder with only one longitudinal slit, so that the crevice former snapped tightly onto the tensile specimen, was equally ineffective.

With these designs, the solution contact between the crevice and the bulk solution was limited to the two ends of the crevice and the slits [Figure 2(a)]. This provided only a very small contact area and may have inhibited transport of solution (and chloride in particular) into the crevice. It was felt that environmental access to the crevice could be improved by exposing a larger portion of the gauge length. Hence, a modified crevice former was constructed by drilling a 12.7-mm-diameter by 14-mm-long Teflon rod axially to produce a 3.175-mm-diameter hole. One side of the holder was machined back in a plane tangential to the specimen's circumference until the inner hole had a 2-mm-wide access slot [Figure 2(b)]. This produced a long, wide crevice mouth and a completely accessible crevice. A 1-mm-wide slit was cut 3/4 of the way through the side diametrically opposite from the radial slot. The 1 mm wide slit provided sufficient spring in the Teflon to ensure that a tight crevice could be obtained around the specimen. The assembly was held tightly in place by circumferential loops of chromel wire. Crevice corrosion was still not consistently observed, but the situation was further improved by inserting a thin Teflon sleeve between the Teflon cylinder and the metal surface before tightening the wire loops.

Having addressed the difficulties normally encountered in producing stressed crevice coupons, we felt that the remaining irreproducibility may have been a result of the application of stress. The straining of the sample may have (1) disturbed the chemistry of the crevice during the initiation stage of the reaction or (2) caused sufficient slackening of the crevice to make it too wide for crevice corrosion. Consistency was further improved by delaying the initial straining until the potential of the specimen had decreased and stabilized in the region of -300 mV_{SHE}; i.e., until active crevice conditions had been established. Specimens were then either strained to failure or, more usually, loaded to an appropriate level for stress cycling.

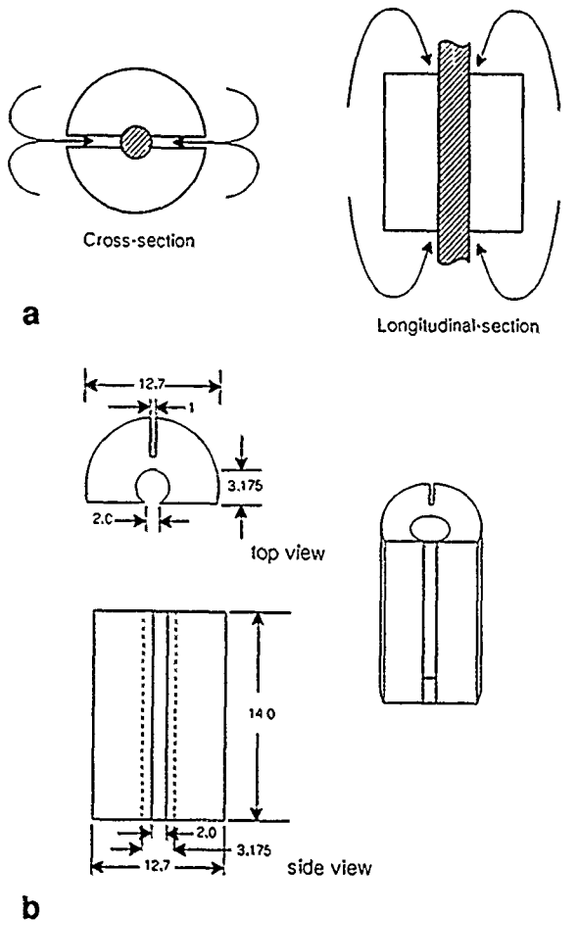


FIGURE 2—(a) Schematic views of basic (unsuccessful) crevice designs showing restricted access to the crevice region. (b) Schematic of the successful Teflon tensile crevice former developed. The dimensions are in millimeters.

Results and Discussion

Hydrogen entry in the absence of stress

During crevice corrosion, the local chemistry in the crevice is different from that of the bulk solution. The chemistry inside the crevice is complex and for a full discussion, the reader is referred to References 1 and 4 to 8. Briefly, it can be described as follows

Oxygen is depleted from the creviced region during the initial stages of crevice corrosion. This establishes a condition where different electrochemical processes can occur inside and outside the crevice. The overall anodic reaction

$$Ti \rightarrow Ti^{4+} + 4e^- \quad (1)$$

which occurs inside the crevice, is coupled to the oxygen reduction reaction

$$O_2 + 2H_2O + 4e^- \rightarrow 4OH^- \quad (2)$$

which occurs on the outer surface of the titanium coupon, i.e., the surface exposed to the free solution. As crevice corrosion proceeds, the pH in the crevice decreases (pH < 1)[1,5,8] because of hydrolysis of the dissolved titanium,

$$Ti^{4+} + 2H_2O \rightarrow TiO_2 + 4H^+ \quad (3)$$

Eventually, the pH is sufficiently low that the hydrogen evolution reaction

$$2H^+ + 2e^- \rightarrow 2H\cdot \rightarrow H_2 \quad (4)$$

can couple with the dissolution reaction [Reaction (1)], providing a self-contained reaction pathway inside the crevice. The entire process is limited by a complex interaction between Reactions (2) and (4) and diffusion of protons out of the crevice.

The hydrolysis reaction [Reaction (3)] leads to the precipitation of a voluminous, but nonpassivating TiO_2 layer inside the crevice. This precipitate appears to form its own tight crevice within the artificially formed crevice. The reaction

$$Ti + H_2O \rightarrow Ti\text{-}O + 2H^+ + 2e^- \quad (5)$$

which may be little more than oxygen adsorption on the bare titanium surface in the crevice, assists in blocking the dissolution reaction.

The hydrogen generated by Reaction (4) on the fresh titanium surface can rapidly diffuse into the metal. As we will show, oxygen produced by Reaction (5) also diffuses into the metal, but at a slower rate. The activity of the hydrogen developed by the electrochemical reaction is so high that, at 150°C, a hydride layer builds up on the metal surface immediately below the oxide in corrosion pits (Figure 3).

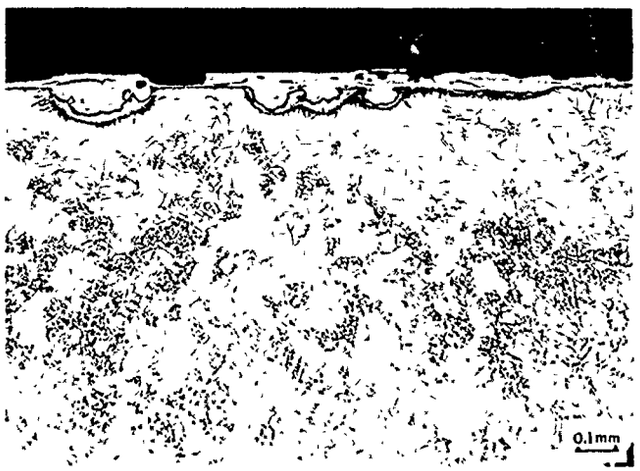


FIGURE 3—Micrograph of an unstressed crevice coupon after exposure for 3 days in 3.5 wt% NaCl showing the hydride layer under a pit inside a crevice. Note the oxide in the crevice. The surface of the coupon shown was entirely inside the crevice.

When unstressed crevice corrosion coupons were immersed in 0 6 mol/L NaCl for 36 h at 150°C, and cross sections of the samples were etched after this treatment, four distinct regions were observed. Proceeding from the top of Figure 4(a) one can see the following. (1) the greyish oxide layer filling the depression, (2) a layer extending from the black border of the oxide to the region with needle-like fingers extending into the metal, (3) a light-colored "halo" region of smooth metal; and (4) the bulk metal with distinct hydride needles. Comparison with unetched sections has confirmed that both the dark border forming the gap between the oxide and metal and the needle-like features are a result of etching, thus suggesting that this region actually consists of hydride prior to etching.

At a greater distance from the surface, this layer disappears and more distinct hydride needles are observed. In all cases, immediately below the corroded region there is a halo of metal (approximately the same thickness as the hydride) containing very little precipitated hydride The halo separates the surface hydride layer from the bulk material, where extensive hydride precipitation is visible [Figure 4(a)]. This effect is similar to the phenomenon observed in a hydrided zirconium specimen that had a "case" containing relatively high concentrations of oxygen [9] This observation was explained in terms of the increased hydride solubility promoted by higher oxygen content in solid solution (Figure 5) To test whether a similar effect could explain the microstructural observations in the present work, we annealed the sample in argon for 4 days at 400°C and then air cooled it to homogenize the oxygen and hydrogen concentrations in the sample This heat treatment eliminated both the surface hydride layer and the oxygen-rich halo [Figure 4(b)]. The absence of the region with needle-like fingers indicates that these needles were precipitated hydrides. If both sides of the halo region contain sufficient hydrogen to cause hydride precipitation, the halo region must also contain hydrogen. The absence of hydride precipitation indicates that the hydride solubility in the halo region is higher than in the bulk metal. A high oxygen content in this region could result in this increased hydride solubility. The hydride observed after the heat treatment was in the form of very fine needles on particular habit planes within the grains [Figure 4(b)]. Closer inspection of the original microstructure revealed a region of similar fine hydride precipitation at the interface between the clear halo and the metal. This represents a region where, even with the slower cooling rate involved with that specimen, i.e., slow cooling in the test solution, the effect of oxygen in reducing the diffusivity of hydrogen promotes a much finer hydride distribution than that in the bulk of the material.

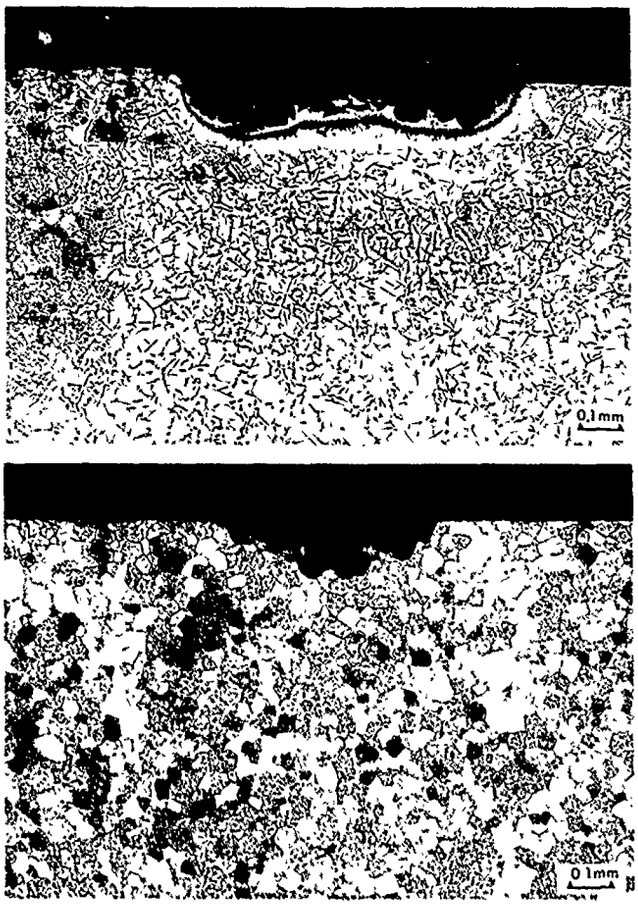


FIGURE 4—(a)Micrograph of the area under a crevice showing the four regions discussed in the text: (1) the oxide in the pit, (2) the region with the needle-like fingers, (3) the halo region, and (4) the heavily hydrided bulk metal; and (b) micrograph of the area under a crevice, as in (a), following heat treatment at 400°C for 4 days, then air cooled.

Microprobe analysis of a sectioned coupon suggested the presence of an oxygen gradient from the bulk metal through to the oxide. A sectioned coupon was used instead of sputtering through the film because of inaccuracies expected in sputtering to the necessary depth. The oxygen concentration in the halo region was 2 to 3 at%. The bulk material had an oxygen concentration of 1 to 2 at% with a detection limit of ~ 1 at%. Although the oxygen levels are close to the detection limit of the instrument, line scans using Auger, secondary ion mass spectroscopy, and electron-stimulated desorption spectroscopy across the halo region all indicate the presence of an oxygen gradient (Figure 6).

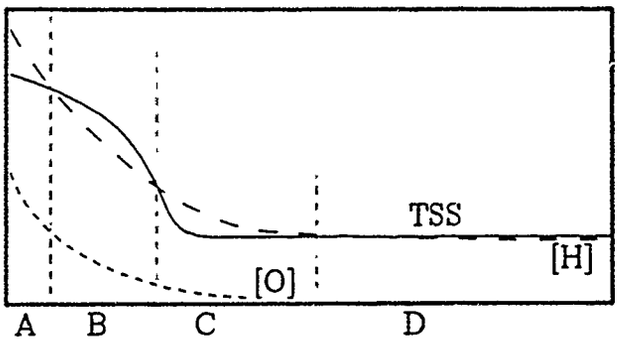


FIGURE 5—Schematic of the concentration profiles through the region beneath the crevice. The long dashed line is the hydrogen concentration; the short dashed line is the oxygen concentration; and the solid line is the terminal solubility limit for hydrogen. Region A is the heavily hydrided region directly below the crevice, Region B is the halo region, Region C is the hydrided region below the halo, and Region D is the bulk metal.

Chemical analysis for hydrogen in unstressed crevice specimens indicated an average level as high as 500 ppm in the first 1.5 mm below the creviced surface, compared with 30 to 40 ppm in the center of the plate. These observations provide direct confirmation that hydride and oxide were both produced by the acidic solution's reaction with the metal surface within the crevice.

Stress effects on crevice corrosion

The free-corrosion potential provides a means of monitoring the progress of the crevice corrosion reaction and, when galvanic coupling is used, the coupled current can also provide a measure of the corrosion kinetics. However, the coupled current is a measure of the coupling of Reactions (1) and (2) and is not a measure of the total corrosion, which includes coupling of Reactions (1), (2), and (4). Previous studies have determined that the electrochemical potential for active crevice corrosion falls below −300 mV and that most of the corrosion is caused by the coupling of Reactions (1) and (4).[1,4,5] The potential of −300 mV is considered a critical potential. As the crevice propagates, the potential becomes more negative and the reaction rate decreases. It has been suggested that the crevice remains active, but that its propagation is slow because of lack of oxygen.[1] It was shown experimentally that the further addition of oxygen leads to further current flow. It is also possible, however, that the slow propagation results from some form of surface coverage, e.g., via Reaction (5) or some similar process. If this is the case, then exposing fresh metal by straining the specimen may also increase the propagation rate.

Creviced specimens exposed to 0.6 mol/L NaCl at 150°C were electrochemically monitored. The load was not applied until after the potential was below −300 mV and the coupled current was zero (Figure 7). Once this stable condition was attained, the specimen was strained at a rate of 3 to 6 × 10^{-7} s^{-1} until a strain of 2.5% was obtained and then it was cycled between ± 10 MPa of the stress at this point. The potential increased as the load increased, but did not go above −300 mV_{SHE} and the current remained zero. The specimens failed either during cycling or after removal from the solution and straining to failure in air at room temperature. When extensive crevice corrosion occurred, the failure mode appeared mostly ductile, but there was some brittle nature to the fracture surface. These results suggest that when Grade-2 titanium is simultaneously subjected to active crevice corrosion and slow tensile deformation, failure occurs in a ductile manner because of reduction in area caused by a combination of crevice corrosion and tensile strain.

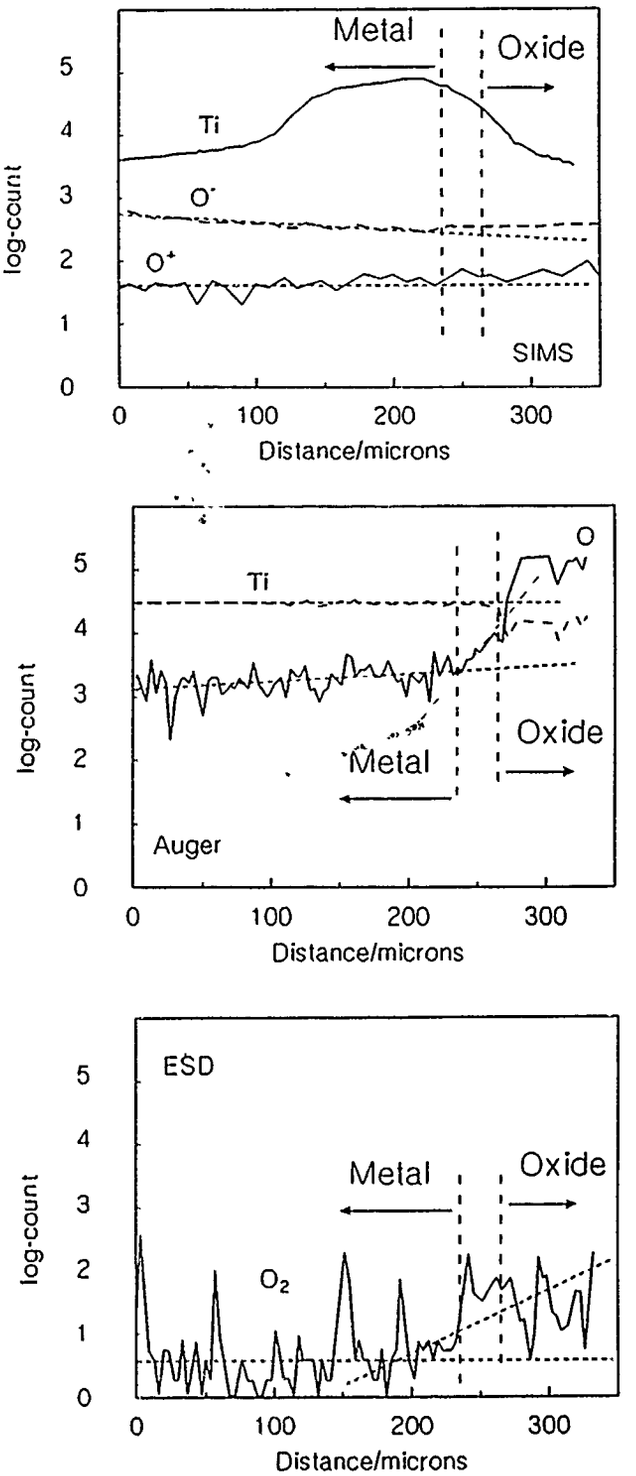


FIGURE 6—Auger, SIMS, and ESD line spectra for O and Ti taken from a cross section such as Figure 4. The vertical lines show approximately where the oxide layer is located. All line scans were taken from the same place on the sample.

Hydrogen embrittlement

Since considerable acidification occurs inside the crevice during crevice corrosion, a few tests were performed on specimens without a crevice to observe the effects of straining in an acidified environment. Slow straining (5.2 × 10^{-7} s^{-1}) in 0.6 mol/L NaCl acidified with HCl to pH 3 produced no measurable loss in ductility at either 150 or 175°C, even with cathodic polarization to −700 mV_{SHE}. On the other hand, when a concentrated HCl solution was injected into a Teflon

sleeve fitted tightly over the heads of a tensile specimen to provide a 6-mm internal diameter container around the gauge length, significant embrittlement occurred in a 0.48 mol/L HCl solution (4 vol%) but not in a 0.24 mol/L HCl solution during load cycling at 175°C. Difficulty was experienced in maintaining the load after about 13 h, probably because of the extension associated with the opening of cracks. This crack opening also serves to exaggerate the apparent elongation of the specimen during testing. Failure by localized necking occurred after cycling for 33 h, after general cracking had reduced the effective cross section. Examination of the fracture surface indicated that the specimen failed in a ductile fashion, although the outer surfaces of the specimens were visibly cracked. A subsequent metallographic examination of a polished section revealed the presence of a hydride layer about 60 μm thick on the surface, with only a very thin oxide layer (Figure 8). This is in marked contrast to the form of attack observed in the (unstressed) crevices, where the oxide is the predominant product in the pits and on the surface of specimens, with the hydride lying underneath (Figure 3).

These results indicate that hydrogen is unable to penetrate into the bulk material and completely embrittle the specimen. The corrosion reaction occurs rapidly enough that a dense, hydrided layer is formed near the surface of the specimen. This outer layer of the tensile specimen is embrittled and cracks, leaving a reduced cross section of material that contains little hydrogen and is therefore not embrittled The specimen appears to fail in a ductile fashion.

The situation in the creviced tensile specimens is different simply because the crevice corrosion reaction takes place more slowly and therefore, more time is available for hydrogen diffusion prior to failure. As a result, the hydride concentration in the bulk of the material is greatly increased, and, although the final fracture of the specimen was largely ductile, there was a greater degree of brittle nature to the fracture surface than was evident for samples exposed to the acidified environment. There is obviously a competition between the reduction of cross-sectional area caused by crevice attack that produces a ductile failure and the hydride penetration that produces embrittlement.

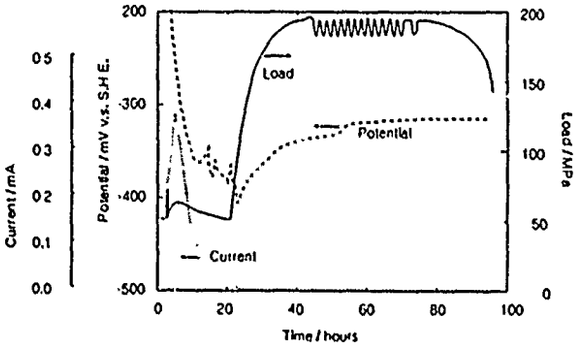


FIGURE 7—Electrochemical results from creviced tensile specimens exposed to 0.6 mol/L NaCl at 150°C. The coupled current, coupled potential, and applied load are shown.

Conclusion

When active crevice corrosion occurs on Grade-2 titanium, large quantities of hydrogen are absorbed into the metal under the crevice, especially in heavily corroded (pitted) regions. Extensive hydride precipitation is observed immediately below large oxide deposits. A hydride-free zone is observed between the surface hydride layer and the hydrides present in the bulk of the sample. This hydride-free layer corresponds with a high oxygen concentration, which increases the hydrogen solubility in titanium and thus decreases the hydride precipitation.

The generation of reproducible, active crevices on planar coupons is not difficult, but it is more difficult on round tensile samples. A crevice design has been devised to provide both the tight geometry required to initiate crevice corrosion on titanium and also the solution access necessary to maintain the crevice propagation reaction. Reproducible and active crevice corrosion has been obtained using this design.

The application of stress to active crevices appears to influence the propagation kinetics, possibly exposing more nonpassivated surface to the acidic environment of the crevice. The film then formed on the inside of the crevice may simply be a surface adsorbed layer and not a passive, or pseudo-passive, film. The hydride that produces embrittlement results from the hydrogen introduced by the crevice corrosion, but its penetration into the underlying metal depends upon the diffusivity. Thus, with fast rates of crevice corrosion, there is insufficient hydrogen diffusion for significant embrittlement to occur. However, if the corrosion process is slowed relative to the hydrogen uptake process, hydrogen uptake might then be important.

When titanium was exposed to acidic conditions where little surface oxide was observed, i.e., slow corrosion, the sample was grossly hydrided and underwent brittle failure. Obviously, the failure mechanism is a competition between the rate of hydrogen uptake, which leads to embrittlement, and the rate of reduction in area because of both crevice corrosion and tensile deformation, which leads to ductile failure.

Acknowledgment

The authors wish to acknowledge the assistance of W.H. Hocking and J.S. Betteridge for performing the surface analysis and to W.G. Hutchings for preparing the metallographic samples. Discussions with D.W. Shoesmith are also gratefully acknowledged.

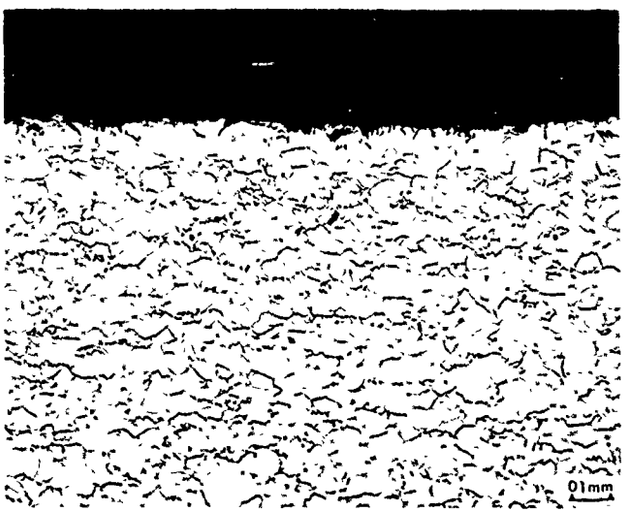


FIGURE 8—Micrograph of a cross section of a tensile specimen exposed to 0.48 mol/L HCl, strained at a rate of 5.08×10^{-6} s^{-1} with an applied load cycled between 220 and 228 MPa.

References

1. P. McKay, Proceedings of the Conference on Corrosion Chemistry within Pits, Crevices and Cracks, ed. A. Turnbull, held October 1-3 (London, England: Her Majesty's Stationery Office, 1984), p. 107.
2. C.F. Clarke, D. Hardie, P. McKay, Corros. Sci. 26, 6(1986): p. 425.
3. N.R. Sorensen, J.A. Ruppen, Corrosion 41, 12(1985): p. 560.
4. B.M. Ikeda, M.G. Bailey, C.D. Cann, D.W. Shoesmith, Advances in Localized Corrosion, held June 1-5, 1987, ed. H. Isaacs (Houston, TX: National Association of Corrosion Engineers, in press).
5. P. McKay, D.B. Mitton, Corrosion 41, 1(1985): p. 52.
6. E.J. Kelly, in Modern Aspects of Electrochemistry, ed. J.O'M. Bockris, B.E. Conway, R.E. White (New York, NY: Plenum Press, 1982), p. 319.
7. P. McKay, Proceedings of the 9th International Congress on Metallic Corrosion, Vol. 3, held June 3-7, 1984, p. 288.
8. J.C. Greiss Jr., Corrosion 24, 4(1968): p. 96.
9. A. Brown, D. Hardie, J. Nucl. Mater. 4, 1(1961): p. 110.

Crack Initiation Mechanism for Ti-6Al-4V in Acidic Methanol

X.G. Zhang and J. Vereecken***

Abstract

Stress corrosion cracking of Ti-6Al-4V in acidic methanol at anodic potentials has been studied. The specimen surface morphology was examined as a function of strain rate and heat treatment. Depending on the test conditions, two kinds of cracks can be formed: (1) cracks along the slip traces and (2) cracks perpendicular to the applied stress. A new model is proposed to explain the initiation of these cracks. The cracks along the slip traces result from preferential dissolution of moving dislocations. Rupture of the material between these cracks results in the perpendicular cracks.

Introduction

Stress corrosion cracking (SCC) of titanium alloys in acidic methanol has been studied for some time.[1-4] The detailed mechanisms of crack initiation and propagation, however, are not yet fully understood. It has been suggested that SCC of titanium alloys in acidic methanol may follow two paths, one involving anodic dissolution and another involving hydrogen embrittlement.[5,6] Whether anodic dissolution or hydrogen embrittlement dominates the cracking process depends on the solution composition, potential, and strain rate.

Understanding crack initiation is as important as understanding crack propagation, however, crack initiation has received little attention. Specifically, there has been little systematic information about the microscopic morphology of specimen surfaces reported in the literature. One possible reason is that most SCC experiments were conducted at slow-strain rate, and thus lasted for a quite long time. The specimen surface could be changed because of corrosion so that the surface features related to SCC could not be readily distinguished from those caused by corrosion.

This paper discusses the microscopic morphology of the surface of a titanium alloy, Ti-6Al-4V, tested in acidic methanol at an anodic potential. The effects of strain rate and heat treatment have been examined. A new model is proposed to describe the crack initiation process.

Experimental Method

The titanium alloy (Ti-6Al-4V) used in this study was received in the form of 12-mm-diameter bars. The chemical composition of the alloy is as follows. Al–6.5; V–4.4; Fe–0.21; C–0.01; O–0.13; N–0.01, H–0.002, and a balance of Ti (wt%). The material was in two heat treatment states, mill annealed and β annealed. Metallography of the mill annealed material showed equiaxed grains of α and transformed β with a grain size of about 1 μm, and that of the β-annealed material showed a basket-weave structure of α plates in a β matrix with a grain size of about 80 μm. Specimens for tensile testing were machined with a gauge diameter of 4 mm and a gauge length of 10 mm. Each specimen was coated with silicon paste except for a 3-mm length in the gauge section. The paste also served as the seal between the specimen and the cell. The exposed surface was polished with abrasive papers down to 1200 grade.

The solution was prepared by adding 8.5 mL of 37% HCl in 1 L of CH_3OH. The water content in the solution was adjusted by adding double demineralized water. The counter electrode was a cylindrical titanium plate, and the reference electrode was a saturated calomel electrode (SCE). The cell was constructed of Teflon.† The tests were performed at room temperature.

After polishing and washing, the specimen was installed in an Instron† tensile machine. The electrolyte was introduced into the electrochemical cell, and the electrode potential was kept at about 350 mV_{SCE} to avoid immediate corrosion. The solution was stagnant in the cell. The electrode potential was then shifted to the chosen value and straining of the specimen was started. During straining, the reaction current through the specimen was recorded. The straining continued until the specimen fractured. The imposed potential was immediately removed after the fracture. The surface morphology of the tested specimen was then examined with a scanning electron microscope.

Experimental Results

Figure 1 shows the surface morphology of the specimen tested at a strain rate of 8.3×10^{-3}/s (crosshead speed divided by gauge length) in CH_3OH + 1% H_2O at a potential of +300 V_{SCE}. The specimen failed with 14% area reduction. Numerous cracks were produced on the specimen surface in addition to the corrosion pits. There were generally two kinds of cracks. One type of crack was perpendicular to the applied stress and will be referred to as "perpendicular crack" in the following text. Another kind of crack was formed along slip traces, which were neither perpendicular nor parallel to the applied stress. Compared to the perpendicular cracks, these cracks, termed "oblique slip crack" hereafter, were narrow and sharp.

The two types of cracks were closely related. A perpendicular crack was generally associated with a set of oblique slip cracks. The oblique slip cracks were smooth while the perpendicular cracks were rough. Figure 2 shows that the slip blocks inside the big crack in the middle of the figure were disconnected from each other and protrusions were formed on the fracture surfaces. These protrusions were generally found on the fracture surface of perpendicular cracks and were oriented from the surface to the bulk of the specimen.

*Department of Electrical Engineering, Columbia University, New York, NY 10027.

**Department of Metallurgy, Electrochemistry, and Materials Science, Vrije Universiteit Brussel, Pleinlaan 2, 1050 Brussels, Belgium.

†Trade name.

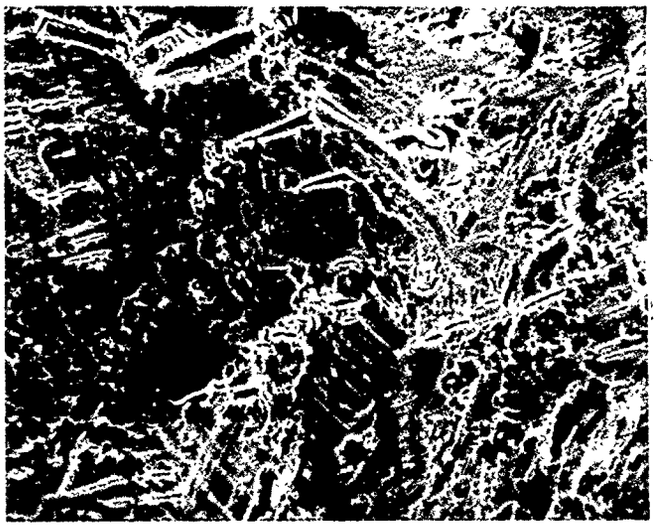


FIGURE 1— Surface morphology of the specimen strained until fracture at a strain rate of 8.3×10^{-3}/s (1% H_2O, +300 mV_{SCE}). The arrow indicates the applied stress direction (original magnification 300X).

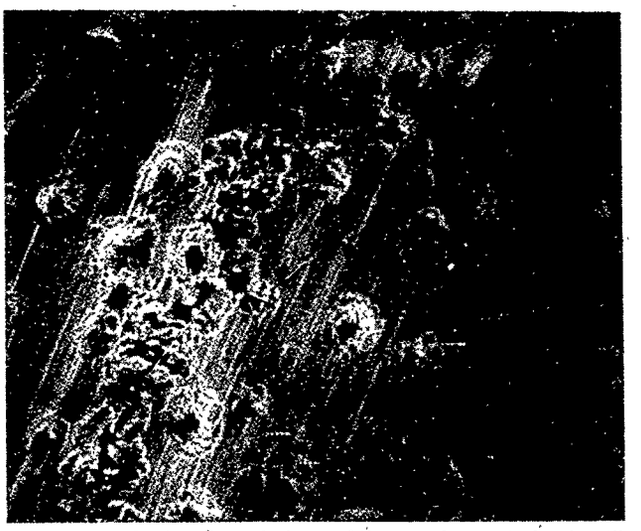


FIGURE 3—Surface morphology of the specimen strained until fracture at a strain rate of 8.3×10^{-5}/s in CH_3OH + 0.1 NHCl + 1% H_2O at a potential of +300 mV_{SCE} (original magnification 200X).

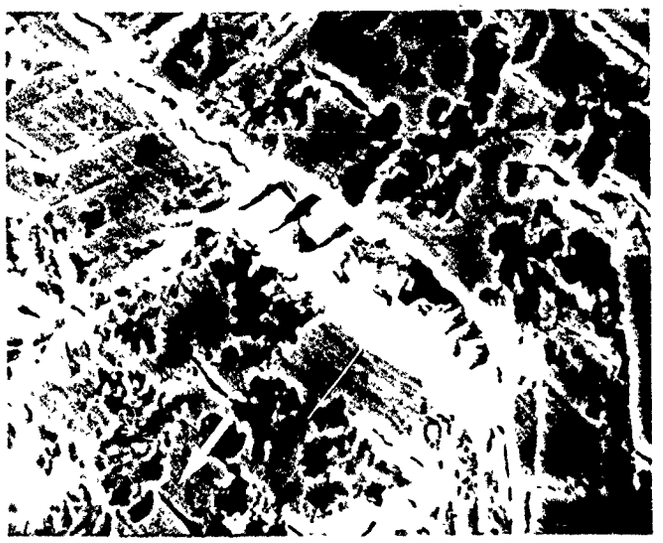


FIGURE 2—Inside the large crack at the middle of this photo, protrusions run from the specimen surface into the bulk; deep crevices developed between the slip blocks (8.3×10^{-3}/s, 1% H_2O, +300 mV_{SCE}) (original magnification 1000X).



FIGURE 4—Surface morphology of the specimen strained until fracture at a strain rate of 0.3/s. (1% H_2O, +300 mV_{SCE}) (original magnification 200X).

Figure 3 shows the surface morphology of the specimen tested at a slow-strain rate, 8.3×10^{-5}/s. No oblique slip cracks were produced. Cracks were all perpendicular to the applied stress. Compared to the previous case, the density of the cracks was reduced but the cracks were larger. The corrosion pits were also larger because the time to fracture is longer at slow-strain rate. The parallel lines in this figure were polish traces that had no influence on crack initiation. The specimen was broken with little plastic deformation (about 3% area reduction).

Figure 4 shows the surface morphology of a specimen tested at a high strain rate, 0.33/s. As opposed to that tested at a slow-strain rate, the specimen surface revealed no perpendicular cracks, but did reveal oblique cracks. The specimen was fractured with much deformation, 31% of area reduction, which was the same as that tested in air. Many corrosion pits were developed during the test, but compared to the cracks, the pits were shallow. It was observed that while corrosion pits could be formed with or without straining, cracks could only be formed by plastic straining. Some specimens were strained to fracture in air at different strain rates. No cracks were produced on the surface of these specimens.

Figure 5 shows the surface morphology of the mill annealed specimen. In contrast to the β-annealed specimens, no oblique slip cracks could be observed on the mill-annealed specimens. All cracks on the mill-annealed specimens were perpendicular to the applied stress. This kind of crack morphology did not change with the strain rate. In fact, when a mill-annealed specimen was fractured in air, no well defined slip traces could be observed on the specimen surface because the grain size was very small.

The size and number of cracks depended on the solution concentration and the electrode potential.[7] The number of cracks and the anodic current density increased with increasing potential. For a given strain rate and water content in the solution, there was a potential below which no crack could be produced. Water acts as a passivator in acidic methanol.[8,9] The number of cracks decreased with increasing water content, because the passivation rate was increased. No cracks could be produced for the potential and strain rate ranges tested when the water content was higher than 10%.[9]



FIGURE 5—Effect of strain rate on the surface morphology of the mill-annealed specimens (+300 mV_{SCE}, 1% H_2O, 8.3 × 10^{-3}/s (original magnification 200X).

Discussion

Both anodic dissolution and hydrogen embrittlement have been proposed as the SCC mechanism for titanium alloys in acidic methanol. It is probable that depending on the experiment conditions, one of the two processes is responsible for SCC. It is concluded that the SCC in the present case results from anodic dissolution for the following reasons. First, all experiments were conducted at 300 mV_{SCE}, which was far above the potential for hydrogen reduction. Second, the surface morphology of smooth specimens involved no local chemistry, i.e., the electrode potential and pH at all points on the surface were the same as measured during the experiment. Third, the oblique slip cracks were caused by shear stress. However, in hydrogen embrittlement, tensile stress is required to produce cracks.[10]

The formation of oblique slip cracks indicates that anodic dissolution occurs preferentially along the slip planes. This cannot be explained with the existing dissolution models. In these models, crack initiation and propagation are attributed to the successive processes of slip-step emergence, anodic dissolution, and repassivation of the steps.[11-13] However, the models are unable to explain the higher dissolution rate on slip steps than on other active surfaces such as inside corrosion pits. In addition, it is observed that the protrusions in the cracks were all oriented from the specimen surface to the bulk. According to the slip-step dissolution model, the protrusions, if there are any, should be parallel to the specimen surface. It does not seem possible that the sharp oblique slip cracks initiate and propagate through anodic dissolution on slip steps.

A new model for SCC

It was observed that cracking only occurred when there was plastic deformation. By contrast, oblique slip cracks could only occur at a high strain rate, indicating that the movement of the dislocations at a certain speed was a necessary condition for the preferential dissolution to occur along the slip planes. The only difference between the slip planes and other parts of the specimen during straining was that there were moving dislocations on these planes. This suggests that the oblique slip cracks formed because of the preferential dissolution of the moving dislocations along the slip planes.

The atoms along a dislocation line have a higher activity to chemical reactions such as dissolution, adsorption, etc., than do the surrounding ones.[14,15] These atoms will be more active when the dislocation moves. Therefore, when the material is strained in the solution, preferential dissolution occurs along the dislocation line during the movement of the dislocation. Figure 6 illustrates how the oblique slip cracks are initiated from such a preferential dissolution. Without straining, the oxide film on the surface protects the material, as shown in Figure 6(a). When straining is applied, the oxide film is broken because of the movement of dislocations. Thus, the intersection of the dislocation line with the specimen surface is exposed to the electrolyte. The preferential dissolution of the atoms around the moving dislocation line results in a crevice, i.e., the oblique slip crack as shown in Figure 6(b). The formation of the oblique slip cracks results in a reduction of the net section area, as shown in Figure 7. Thus the stress in the material left between the cracks is increased, and the material eventually ruptures, producing a perpendicular crack The rupture could be caused by cleavage, mechanical tearing, or preferential dissolution of moving dislocations in the net section area. Figure 2 clearly demonstrates such a crack feature.

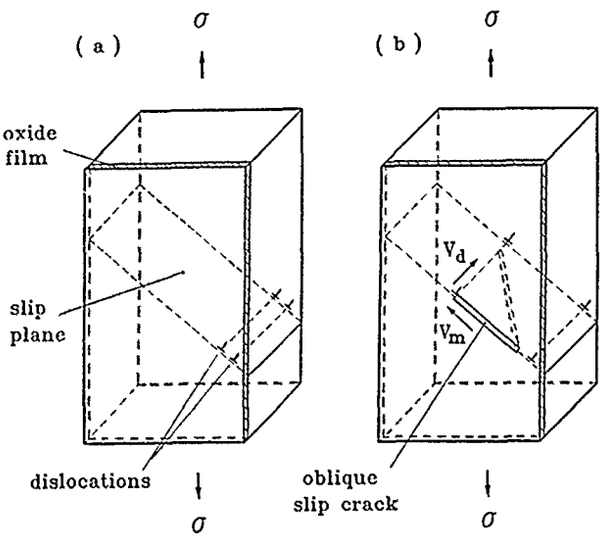


FIGURE 6—A scheme showing the formation of the oblique slip crack through preferential dissolution of moving dislocations: (a) a metal crystal before the movement of the dislocations; (b) movement of the dislocations breaks the oxide film, and the preferential dissolution of the moving dislocation produces an oblique slip crack. (V_m is the velocity of dislocation; V_d is the dissolution rate.)

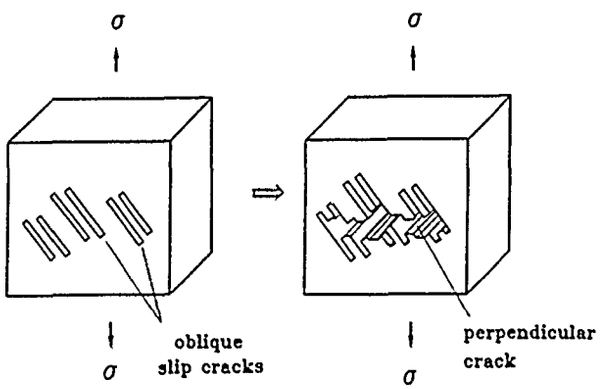


FIGURE 7—A scheme showing a perpendicular crack initiated through rupturing the material between the oblique slip cracks.

The dissolution rate (V_d) in Figure 6(b) is a function of potential and water content. [9] At a slow-strain rate, the dissolution rate (V_d) is much higher than the velocity of moving dislocations (V_m). Thus, perpendicular cracks are initiated from corrosion pits before any oblique slip cracks are formed. On the other hand, at a very high strain rate, the velocity of the dislocations is much higher than the preferential dissolution rate. Oblique slip cracks formed through

dissolution grow quickly in length and the specimen is broken before the formation of any perpendicular cracks. This means that the fracture is completely mechanical and is little influenced by the formation of the dissolution slip cracks. As a result, although there are many oblique slip cracks on the specimen surface, the strain to fracture is about the same as that tested in air (Figure 4). At a medium strain rate, both oblique slip cracks and perpendicular cracks are formed.

The grain size of the mill-annealed specimens was about two orders of magnitude smaller than that of the annealed specimens; hence the limiting slip length of a mill-annealed specimen was very small. No well-defined slip traces could be produced on the mill-annealed specimens by deformation. Therefore, oblique slip cracks were not observed on mill-annealed specimens. This model is proposed to explain the initiation of the oblique slip and the perpendicular cracks. It is conceivable that it could also be used to describe the crack propagation process under certain conditions.

Conclusion

The surface morphology of a titanium alloy (Ti-6A-4V), after straining to fracture in acidic methanol, was examined as a function of strain rate and heat treatment. Depending on the test conditions, cracks perpendicular to the applied stress (perpendicular cracks) and cracks along slip traces (oblique slip cracks) were produced. At slow-strain rate, only perpendicular cracks occurred, while at high strain rate, only oblique slip cracks occurred. Both perpendicular and oblique slip cracks could be produced at a medium strain rate. Oblique slip cracks only occurred on β-annealed specimens, not on mill-annealed specimens.

A new model is proposed to describe the initiation of SCC. Dislocations will move when the material is strained. The movement of dislocations has two effects: (1) It causes oxide film breakdown so that the material can react with the solution, (2) it increases the reactivity of the atoms along the dislocation lines. The preferential dissolution of these atoms along the moving dislocation lines results in the oblique slip cracks. Rupture of the material between these cracks leads to the formation of the perpendicular cracks.

References

1 M.J Blackburn, J.A Feeney, T.R. Beck, Advances in Corrosion and Corrosion Engineering, vol. 3 (New York, NY. Plenum Press, 1972).
2 C M. Chen, F H Beck, M.G. Fontana, Corrosion 27(1971). p. 77.
3 J. Spurrier, F.C. Scully, Corrosion 28(1972). p. 453.
4 K Ebthaj, D. Hardie, R.N. Parkins, Corros. Sci. 25(1985). p. 415.
5 A J Sedriks, P W Slattery, J.A.S Green, Trans. ASM 61(1968). p. 625.
6. J.C. Scully, T.A. Adepoju, Corros. Sci. 17(1977): p. 789.
7. X.G. Zhang, J. Vereecken, Corrosion, in press.
8. F. Mansfeld, J. Electrochem. Soc. 118(1971). p. 1412.
9. X.G. Zhang, J. Vereecken, Corrosion 45, 1(1989). p. 57.
10. R.M. Latanision, O.H. Gastie, C.R. Compeau, Environment Sensitive Fracture of Engineering Materials, ed. Z.A. Foroulis (New York, NY. American Institute of Mining, Metallurgical, and Petroleum Engineers, 1979), p. 48.
11. T.J. Smith, R.W. Staehle, Corrosion 30(1964). p. 117.
12. T.P. Hoar, R.W. Jones, Corros. Sci. 13(1973). p. 725.
13. E.I. Meletis, R.F. Hochman, Corros. Sci. 26(1986). p. 63.
14. W.G. Johnston, J.J. Gilman, Appl. Phys. 30, 2(1959): p. 129.
15. M.B. Ives, Localized Corrosion, ed. R.W. Staehle, B.F. Brown, J. Kruger, A. Agrawal (Houston, TX. National Association of Corrosion Engineers, 1974), p. 240.

Stress Corrosion Cracking of Uranium-Silver Interfaces in Silver-Aided Diffusion Welds

R.S. Rosen, S. Beitscher,** and M.E. Kassner**

Abstract

We have studied stress corrosion cracking (SCC) in weld specimens in which uranium and type 304 (UNS S30400) stainless steel were joined by an autoclave diffusion-weld method using silver as an intermediate layer. The specimens were placed in bend-test fixtures, which applied tensile stresses normal to the butt joints, in either laboratory air or in air saturated with water vapor. Those stressed in laboratory air at 1/2 of the ultimate strength exhibited ductile creep rupture predominately at the Ag-Ag diffusion-weld interface after more than 20 days, whereas those stressed in saturated water vapor at the same load exhibited cracking predominately at the U-Ag interface after only a few days. Similar specimens exposed to saturated water vapor for up to 37 days in an unstressed condition exhibited no evidence of interfacial corrosion. Other weld specimens were prestrained to establish residual shear stresses in the joints and then were stored for 4 years in polyethylene bags that were permeable to water vapor. Other unstrained specimens were stored in an identical environment. After 4 years, the prestrained specimens showed SCC at the U-Ag interfaces, whereas the specimens that had not been prestrained showed no evidence of interfacial corrosion. Thus, U-Ag weld interfaces have been demonstrated to be susceptible to SCC under both tensile and shear loading.

Introduction

Silver-aided diffusion welds have been successfully used to join otherwise nonweldable metals. The mechanical properties of silver-aided diffusion welds between uranium and stainless steel (SS) have been reported previously.[1,2] These joints have high tensile strengths (400 to 500 MPa), although they experience stress or creep rupture at stresses as low as half of the ultimate. These failures usually occur by ductile fracture within the silver (Ag-Ag failure). The purpose of the present study is to determine the susceptibility of U-Ag interfaces to stress corrosion cracking (SCC) in a water vapor environment.

Uranium is known to corrode in the presence of water or water vapor, generating uranium oxide and hydrogen as reaction products, and possibly forming uranium hydride as a by product.[3] The presence of oxygen has been shown to greatly retard the uranium-plus-water-vapor corrosion reaction.[4] The authors suggested that oxygen retards this reaction rate by forming a protective oxide layer that inhibits adsorption of water vapor and/or slows the diffusion of water vapor through the protective layer.

Hughes, et al.,[5] and Orman[6] reported that both the tensile strength and the ductility of uranium are reduced if the tests are performed in water vapor environments (or at temperatures below the dew point in air). The authors suggested that SCC or hydrogen embrittlement was responsible for the loss in ductility. Hughes, et al., showed that this reduction in ductility is essentially independent of temperature between 0 and 75°C, and that no loss in ductility occurs at temperatures above 100°C.[7] Hughes, et al., extended this study to include the effects of pH on tensile elongation at 20°C in water solutions.[8] The authors determined that embrittlement only occurs over the pH range of 5 to 10 and that normal ductility was observed for both high and low pH conditions. They concluded that the absence of embrittlement at low pH lends support to a uranium-plus-water-vapor SCC mechanism rather than hydrogen embrittlement by diffusion of hydrogen ions. This observation was additionally supported by tensile tests of prehydrided uranium by Hughes, et al.[9] The authors noted that hydrogen embrittlement occurred in the prehydrided uranium tested in vacuum or air but that a much larger reduction in ductility occurred when tests were performed in water. The amount of embrittlement in the presence of water vapor was found to be independent of hydrogen content. Therefore, uranium plus water vapor SCC rather than hydrogen embrittlement appears to be the more likely mechanism for the observed cracking of uranium.

Magnani tested precracked notch specimens of U-0.75%Ti alloy in oxygen, hydrogen, and 100% relative humidity (RH) atmospheres.[10] Results indicated that plain-strain threshold values for stress corrosion crack propagation were much lower in 100% RH air and hydrogen than in oxygen. Miller[11] studied the effect of RH on time-to-failure of precracked tensile specimens of U-7.5%Nb-2.5%Zr alloy. The results indicated that the time-to-failure decreases only slightly from 20 to 90% RH at constant initial stress intensities, but reduces by over 3 orders of magnitude from 90 to 100% RH.

Experimental Procedure

Materials and specimen preparation

Long term test specimens were machined from type 304 (UNS S30400) SS and depleted U 238 bars into right circular cylinders prior to coating. The machined specimen blanks were degreased, ion sputter-etched for 45 min (to remove the oxide), and coated with a 75-μm layer of nominally pure silver onto the faying surface. The coated specimens were then inserted into thin SS cans that were evacuated, welded closed, and isostatically compressed with gas to 207 MPa at a peak temperature of 600°C for 2 h. The bonded specimens were then machined into standard 6.35-mm-diameter reduced-section tensile specimens with the silver joint in the middle

*Lawrence Livermore National Laboratory, P.O. Box 808, L-355, Livermore, CA 94550.

**Rockwell International, Rockwell International, Rocky Flats Plant, Golden, CO 80401.

of the 25.4-mm-gauge section. A more detailed account of the specimen preparation procedures, including material properties, is given by Rosen, et al.[1]

Short-term test specimens were machined from type 304L (UNS S30403) SS and depleted U-238 circular plates after coating and bonding them together. The base-metal yield strengths were lower than those of the long-term specimens: 240 vs 296 MPa for the SS, and 240 vs 345 MPa for the uranium. Machining and degreasing procedures for the plates were similar to those of the long-term specimens, except that one plate of uranium had its oxide chemically etched prior to degreasing by immersion (pickling) in acid. Ion-sputter etching and coating of the circular plates for short-term tests were performed in a hot hollow-cathode coater very similar to the one used for the long-term specimens. Ion-sputter etch times for the SS were comparable with those of the long-term specimens but were varied at either 10, 60, or 120 min for the uranium plates for the short-term specimens. All plates were coated with a 75-μm layer of nominally pure silver, canned and bonded as before except that the bonding pressure was maintained at only 68 MPa (vs 207 MPa). Bend-test specimens were either cored from the plates by electrochemical machining (ECM) or machined conventionally to finished size (6.35-mm diameter by 25.4-mm length). Additionally, microtensile specimens (15.2-mm length by 2.54-mm diameter) were machined out of the bonded plates with the silver joint in the middle of the 11.4-mm-gauge section to determine tensile strength values for the joints.

Test methods

Ten tensile specimens fabricated during 1982-83 were used for the long-term study. First, the "as-fabricated" tensile strengths and stress-rupture times were determined by testing companion specimens fabricated during the same period. Next, six as-fabricated specimens were sealed in polyethylene bags (permeable to water vapor) and stored until 1986. Finally, four specimens were loaded in tension at 172 MPa for 2-1/4 months [approximately 16% of the stress-rupture time, based on extrapolations from stress- (creep-) rupture tests conducted at 207 MPa] and then unloaded, leaving residual stresses from plastic deformation at the Ag-U interface. These specimens were also sealed in polyethylene bags and stored until 1986. Tensile strength and stress-rupture tests were performed in 1986 to assess any environmental degradation of either the stressed or unstressed bonded specimens. Additionally, metallographic cross sections were prepared to identify any interface cracking that may have occurred during the 4-year period.

Short-term stress corrosion tests were performed using C-shaped (3-point) bend-test fixtures capable of maintaining a preset load in either laboratory air (40% RH, 22°C) or saturated water vapor environments (~ 100% RH, 22°C). A bending load was applied to the specimen through the fixture by torquing a lubricated bolt directly against the butt joint with the ends of the specimen supported (see Figure 1). First, tensile strengths were determined from microtensile specimen tests. Second, ultimate "torque bend strength" was measured by slowly applying torque with a calibrated torque wrench and noting the maximum torque at which the specimen fractured. Environmental effects were studied by torquing specimens to preset loads of either 1/2, 1/3, or 1/6 of the ultimate strength and then placing the specimen and fixture in laboratory air or saturated water vapor for various periods of time or until the specimen fractured. Additionally, control specimens were exposed to saturated water vapor in an unstressed condition. Saturated water vapor was achieved by using tap water at the bottom of a sealed glass jar containing air. The water level was not in contact with the specimen or fixture.

Results and Discussion

Table 1 shows the effects of 4 years of aging in sealed polyethylene bags on prestressed and unstressed specimens. The average as fabricated (1981 82) tensile strength of specimens produced from the same set from which prestressed specimens were selected was 392 MPa (SU-85 and 86). The average tensile strength of the 4 prestressed specimens was only 6 MPa when they were retested 4 years later, after having been successfully loaded to 172 MPa in 1982. One of the four specimens was noted to be fractured into two halves during storage. There was substantial cracking of these specimens, which reduced the load-carrying area by approximately 95 to 100%. The cracking appeared to occur almost exclusively at the U-Ag interface. All cracks appeared to initiate at the outer circumference of the specimens. A metallographic cross-sectional view of the unfractured specimen, SU-82, indicated that the oxide thickness along the crack tapered from 4 μm at the circumference to the detectability limit of 50 nm at the crack tip, with no oxide visible in the uncracked regions at magnifications up to 10,000X in the scanning electron microscope.

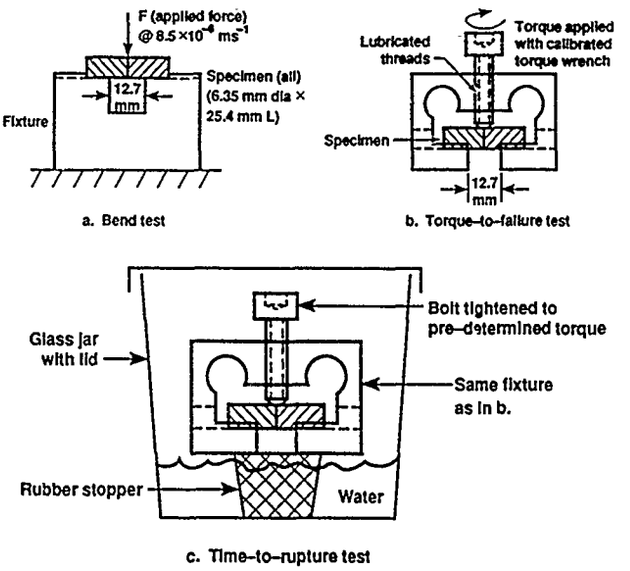


FIGURE 1—Schematic illustrations of bend-test methods and fixtures.

The average as-fabricated (1981-82) tensile strength of specimens produced from the same set from which unstressed specimens were selected for storage in bags was 330 MPa (SU 165 and 166). The average time for creep rupture at 276 MPa was 25 h (SU 167 to 169) Four years later, after storage in the same type of sealed polyethylene bags as the prestressed specimens, tensile strength and stress-rupture times showed no reduction from their original (1981-82) values. Tests conducted in 1986 resulted in an average tensile strength of 356 MPa, and an average rupture time of 15 h at 276 MPa No evidence of U-Ag interface corrosion was detected in any of the unstressed specimens.

It was found that the prestressed specimens plastically deformed (by creep) nearly 1% in the SS and silver, and approximately 0.1% in the uranium. Unloading of a plastically prestressed specimen would result in residual stresses at the bimetallic interfaces. The sources of these stresses would be twofold. First, plastic incompatibility occurs at the U Ag interface because of the larger strain in the silver and SS compared with that in the uranium (0.5% vs 0.05% lateral strain). Second, differences in elastic properties between silver, SS, and uranium result in residual stresses upon unloading even if the macroscopic plastic strain measurements in the uranium and SS are identical.

To approximate the interfacial residual stresses upon unloading of a plastically prestressed U Ag-SS specimen, finite-element method (FEM) analysis was conducted using the known elastic-plastic properties of the metals. The axial stresses vary from 21 MPa (3000 psi) tension at the outer diameter (right-hand side) to 6.9 MPa (1000 psi) tension along the bulk of the U-Ag cross section. The significant residual stresses are in-plane (bond) shear stresses. The typical shear stress along the U-Ag interface is approximately 41 MPa (6000 psi) or an effective (von Mises) stress of about 71 MPa, as shown in Figure 2. This computer model did not allow for time-dependent plasticity, therefore, stress relaxation is not considered.

TABLE 1
Results for Long-Term Specimens
(fabricated in 1982-1983 and tested or retested in 1986)

Specimen Number	1982-83 Prestress (% rupture time)	1982-83 Tensile Strength or $\sigma(t_r)$	1986 Tensile Strength or $\sigma(t_r)$
SU-81	16%		1.3 MPa
SU-82	16%		—[A]
SU-83	16%		15.2 MPa
SU-84	16%		O[B]
SU-85		395 MPa	
SU-86		388 MPa	
SU-165		328 MPa	
SU-166		331 MPa	
SU-167		276 MPa (68 h)	
SU-168		276 MPa (0.5 h)	
SU-169		276 MPa (6 h)	
SU-174	0		335 MPa
SU-175	0		276 MPa (1.3 h)
SU-176	0		276 MPa (48 h)
SU-177	0		276 MPa (3 h)
SU-178	0		276 MPa (8 h)
SU-179	0		377 MPa

[A]Specimen used for metallographic x-section
[B]Specimen noted to be fractured into two halves in 1986

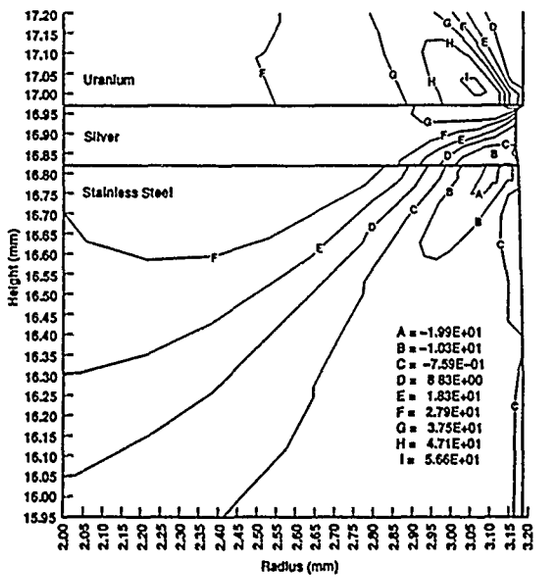


FIGURE 2—Residual (in bond plane) shear-stress contours (MPa) in prestressed U-Ag-SS specimen. Radius = 3.18 mm (0.125 in.)

Extrapolations based on the creep-rupture data reported by Rosen, et al.,[1] indicate that the residual stresses are much too low to cause creep rupture failure during this length of time. It should be noted that the outer circumference of the uranium surfaces of all specimens stored in sealed polyethylene bags was covered with a thick, flaking oxide consistent with a reaction of uranium and water vapor in a depleted oxygen atmosphere.[3,4] A comparison of the permeability coefficients of H_2O and O_2 through polyethylene indicates that H_2O permeates through at a rate 100 times greater than that of O_2 [12,13] Therefore, the prestressed specimens were simultaneously exposed to moisture and internal stresses for up to 4 years, and SCC is a likely explanation for degradation of the U-Ag interfaces It will be shown in the next section that the calculated equivalent uniaxial (von Mises) residual stress levels (1/6 ultimate strength) are sufficient to cause SCC .

Results of the short-term tests (ECM specimens) are listed in Table 2. Microtensile strengths of the 1- or 2-h ion-sputter-etched (uranium surface prior to coating) specimens are comparable to those of the long-term test specimens [386 to 393 (micro) vs 328 to 395 MPa]. The microtensile and torque bend-strength specimens tested in laboratory air all fractured at the Ag-Ag interface, as expected for plastic failures. No stress (creep) ruptures occurred in bend tests loaded to 1/2 ultimate strength in air for up to 22 days. Specimens loaded at 1/2 or 1/3 ultimate strength in water vapor, however, all fractured at the *U-Ag* interface in fewer than 20 days (two specimens fractured in less than 1 day). The specimen loaded to 1/6 ultimate strength in water vapor fractured after 13 days, also at the U-Ag interface. The control specimen (unloaded) was exposed to water vapor for 37 days and then exhibited normal bend-test strength, fracturing plastically at the Ag-Ag interface after being removed from the environment. Pickling of the uranium in acid prior to ion sputter-etching and coating did not affect the test results.

Microtensile strengths of the 10-min, ion-sputter-etched specimens were ~ 40% lower (221 MPa) than the previously discussed short-term specimen strengths. Creep rupture occurred in air at 1/2 ultimate strength after 22 days at load. Fractures occurred in water vapor at 1/2 or 1/3 ultimate strength in less than 1 day at load. The specimen loaded to 1/6 ultimate strength in water vapor fractured after 8 days. *All* fractures of the torque bend-test specimens from the 10-min, ion-sputter-etch group occurred at the U-Ag interface. Inadequate ion-sputter etching fails to remove the normal, pre-existing oxide on metal surfaces, causing reduced silver adhesion to the uranium. Therefore, the specimens show a corresponding reduction in rupture times in both air and water-vapor environments.

Results of the conventionally machined specimens are listed in Table 3. Microtensile strengths and torque bend-test strengths were slightly less than those of the adequately ion-sputter-etched specimens from the ECM batch. Fractures nearly always occurred at the Ag-Ag interface when experiments were performed in laboratory air. Stress (creep) rupture occurred in air at 1/2 ultimate strength after an average time of 31 days. Tests conducted in water vapor at 1/2 ultimate strength resulted in an average rupture time of only 8 days. *All* of the specimens tested in water vapor fractured at the U-Ag interface. The control specimen from this set that was removed from the water vapor environment after 9 days exhibited a normal bend-test strength and fractured exclusively at the Ag-Ag interface.

TABLE 2
Torque-Bend-Specimen Results
(electrochemical machining)

Fabrication Process	Environment	Load (N-m)	Fraction of Ult	Rupture Time (d)	Fracture Location[A]
U pickled, 2-h sputter etch[B]	Air	6.8	1	—[C]	Ag-Ag
	Air	6.3	1	—[C]	Ag-Ag
	Air	3.3	1/2	>22	—[D]
	Water vapor	3.3	1/2	1-20	Ag-U
	Water vapor	1.1	1/6	13	Ag-U
	Water vapor	2.3	1/3	1	Ag-U
	Water vapor	3.4	1/2	1	Ag-U
No pickle, 1-h sputter etch[E]	Air	7.7	1	—[C]	Ag-Ag
	Air	7.3	1	—[C]	Ag-Ag
	Air	3.7	1/2	>22	—[D]
	Water vapor	3.7	1/2	1-21	Ag-U
	Water vapor	3.4	1/2	6	Ag-U
	Water vapor	0	0	>37	—[F]
No pickle, 10 min-sputter etch[G]	Air	3.4	1	—[C]	Ag-U
	Air	3.7	1	—[C]	Ag-U
	Air	1.8	1/2	—[C]	Ag-U
	Air	1.8	1/2	22	Ag-U
	Water vapor	1.8	1/2	1-21	Ag-U
	Water vapor	0.6	1/6	8	Ag-U
	Water vapor	1.1	1/3	1	Ag-U
	Water vapor	1.7	1/2	1	Ag-U

[A]Tensile side given
[B]Microtensile specimen strength = 386 MPa (Ag-Ag)
[C]Ultimate strength test
[D]Unloaded before fracture
[E]Microtensile specimen strength = 393 MPa (Ag-Ag)
[F]Fractured at Ag-Ag interface at normal bend strength after removal from nonstressed/water vapor environment.
[G]Microtensile specimen strength = 221 MPa (Ag-Ag/Ag-U)

TABLE 3
Torque-Bend-Specimen Results
(conventional machining)

Fabrication process	Environment	Load (N-m)	Fraction of Ult	Rupture Time (d)	Fracture Location[A]
No pickle, 2-h sputter etch[B]	Air	5.4	1	—[C]	Ag-Ag
	Air	2.7	1/2	25	Ag-Ag
	Air	2.7	1/2	19	Ag-Ag
	Water vapor	2.7	1/2	<1	Ag-U
	Water vapor	2.7	1/2	<1	Ag-U
	Water vapor	0	0	>9	—[D]
No pickle, 2-h sputter etch[B]	Air	5.2	1	—[C]	Ag-Ag
	Air	2.6	1/2	47	Ag-U/Ag-Ag
	Water vapor	2.6	1/2	25	Ag-U
	Water vapor	2.6	1/2	7	Ag-U/Ag-Ag
No pickle, 2-h sputter etch[E]	Air	4.0	1	—[C]	Ag-Ag
	Air	1.9	1/2	41	Ag-Ag
	Air	1.9	1/2	25	Ag-Ag
	Water vapor	1.9	1/2	4	Ag-U

[A]Tensile side given
[B]Microtensile specimen strength = 366 MPa (Ag-Ag)
[C]Ultimate strength test
[D]Fractured at Ag-Ag interface at 4.6 N-m (Ag-Ag) after removal from unstressed/water vapor environment
[E]Microtensile specimen strength = 331 MPa (Ag-Ag)

It should be noted that the stress-rupture tests reported by Rosen, et al.,[1] and Elmer, et al.,[2] were performed in normal laboratory air averaging 40% RH. Even when specimens were stressed above 1/2 tensile strength for over 6 months, SCC at the U-Ag interface was not observed. This phenomenon is consistent with the effect of RH on the intergranular SCC behavior of uranium alloys.[11] Therefore, it is suggested that fracture times would most likely increase with decreasing relative humidity, possibly exhibiting a threshold below which SCC-type failures may not occur.

Summary

The torque bend-test results indicate that 100% relative humidity air causes SCC at U-Ag interfaces when they are simultaneously subjected to applied tensile stresses. Variations in coating and machining processes did not affect the observed SCC phenomenology. The results also suggest a trend of increasing time to fracture with decreasing applied stress. Specimens subjected to the same 100%-RH air in an unstressed state exhibited no loss in strength after lengthy exposure. These results are in agreement with the long-term specimen results, where residual shear stresses led to cracking in a humid air environment. Therefore, U-Ag interfaces are susceptible to SCC under both tensile and shear loading.

Acknowledgment

The authors thank G. Goudreau for the FEM analysis and W.L. Johns for the SEM analysis. This work was performed under the auspices of the U.S. Department of Energy by Lawrence Livermore National Laboratory under Contract W-7405-Eng-48 and by Rockwell International under Contract DE-AC04-76DP03533.

References

1. R.S. Rosen, D.R. Walmsley, Z.A. Munir, Welding J. 65, 4(1986): p. 83s.
2. J W Elmer, M.E. Kassner, R.S. Rosen, Welding J. 67, 7(1988). p. 157s.
3. M. McD. Baker, L.N. Less, S. Orman, Trans. Farad. Soc. 62(1966): p. 2513.
4. M. McD. Baker, L.N. Less, S. Orman, Trans. Farad. Soc. 62(1966): p. 2525.
5. A.N. Hughes, S. Orman, G. Picton, M.A. Thorne, J. Nucl. Mater. 33(1969): p. 99.
6. S. Orman, Corros. Sci. 9(1969): p. 849.
7. A.N. Hughes, S. Orman, G. Picton, J. Nucl. Mater. 33(1969). p. 159.
8. A.N. Hughes, S. Orman, G. Picton, M.A. Thorne, J. Nucl. Mater. 33(1969): p. 165.
9. A.N. Hughes, S Orman, G. Picton, Corros. Sci. 10(1970). p. 239.
10. N.J. Magnani, J. Nucl. Mater. 54(1974): p. 108.
11. A.R. Miller, Corrosion 30, 5(1974): p. 177.
12. J. Crank, G.S. Park, eds., Diffusion in Polymers (New York, NY: Academic Press, 1968), p. 276.
13. O.J. Sweeting, ed., The Science and Technology of Polymer Films, Vol. 2 (New York, NY. Wiley-Interscience, 1971), p. 94.

SECTION VII

Environment-Assisted Cracking of Iron-Base Alloys

Co-Chairmen's Introduction

H.-J. Engell
Max Planck Institut fur Eisenforschung
Dusseldorf, Federal Republic of Germany

F.P. Ford
General Electric Corporation
Schenectady, New York, USA

H. Kaesche
F. Alexander University of Erlangen–Nurnberg
Erlangen, Federal Republic of Germany

The topic of environmentally assisted cracking of iron-base alloys is reviewed in four papers, which address (a) the failure of low-alloy ferritic or pearlitic steels, (b) the embrittlement of high-strength steels by hydrogen gas or hydrogen precharging, (c) the failure of martensitic and duplex high-alloy steels, and, finally, (d) austenitic alloys in aqueous environments. The format for these papers ranges from the atomistics of the cracking mechanism (i.e., the hydrogen embrittlement and austenitic alloy papers) to the application of mechanistic knowledge to practical problem solutions (i.e., the ferritic and martensitic steel papers).

The review by T. Murata, the abstract of which is included here, dealt with the stress corrosion cracking of low-alloy ferritic steels in aqueous environments, which frequently can be observed under conditions in which a protective surface layer occurs and a film-rupture/anodic-dissolution mechanism operates. The original presentation concentrated on the conditions for film formation and stability, on the influence of chemical composition and structure of the steel, and on the influence of preceding cold work and welding. It stressed the operating mechanisms and made a number of recommendations for countermeasures. The author pointed out the importance of electrochemical attack of grain boundaries or pitting to initiate the cracks. He further dealt with failures in steels of higher strength level in coke oven gas, which are due to hydrogen-induced cracking. The pH of the solutions formed by condensation is the dominating effect in this case. Furthermore, the special conditions for corrosion of steel by very thin films of electrolytes (e.g., formed by condensation), were discussed and experiments related to this question described. The abstract of Murata's presentation, along with the discussion that followed, is included here in lieu of the paper

The paper by R.A. Oriani, "Hydrogen Effects in High-Strength Steels," is an update of previous reviews by the author covering the same subject. To make clear conclusions concerning the fundamentals of this cracking system and their application, the cases of stress corrosion cracking in aqueous environments and of fatigue of any kind are excluded from consideration, and the discussion is limited to hydrogen uptake from a dry atmosphere and to hydrogen-precharged material. The author clearly distinguishes between the thermodynamic aspects of embrittlement of steel by hydrogen, and the kinetics of embrittlement and crack propagation The first aspect deals with the weakening of cohesive forces in the lattice of the steel by absorbed hydrogen, which may lead either to metal–metal chemical bond weakening or to a lowering of the critical shear strength. The former possibility is the author's decohesion model, while the latter is Beachem's and Lynch's model of the pseudo-brittle crack propagation by localized slip resulting from hydrogen-induced dislocations emanating from the crack tip. Oriani presents the experimental and theoretical evidence available for the two models. He hypothesizes that both mechanisms may be potentially operative, subject to a number of conditions so far unspecified. He then proceeds to describe the various kinetic mechanisms of hydrogen embrittlement. The critical question is essentially that of the rate-determining step in the sequence of reaction steps going from, e.g., water molecules far away from the crack tip, to hydrogen generated at the surface, hydrogen crossing the interface and diffusing in the lattice, etc. One of the more significant findings to be explained is the "bell-shaped" relationship between the Stage II crack propagation rate and the temperature. The mechanistic suggestion brought forward by authors such as Simmons, et al.; Lu, et al.; Wei, et al.; Gerberich, et al., and others are presented. The author finally, and probably very correctly, points out that, to advance our fundamental knowledge further, it will be necessary to study the critical steps in the fracture processes in the absence of hydrogen, and then to establish the action of hydrogen on such steps.



Photos: M B. Ives

Whereas Murata dealt with the problem of cracking of steels that have a ferritic or ferritic-pearlitic structure, Spaehn addresses this problem in high-alloyed steels with a ferritic, martensitic, or ferritic-austenitic structure. All the materials he deals with are characterized by a chromium concentration ranging from 12% for the martensitic alloys up to 30% for the super ferrites. Together with chromium, the content of nickel and the interstitials carbon and nitrogen primarily determines the phases the steels are composed of, and the possibilities of precipitation reactions during welding and other heat treatments are discussed.

The aggressive media causing environmental cracking in these steels are numerous and different, depending on the steel composition and structure. With the duplex austenitic-ferrite steels, the anodic active path dissolution is assumed to prevail, whereas with the martensitic steel grades, hydrogen-induced cracking is the most frequent failure mode. This difference can be related to the different strength levels, to the physical metallurgy of plastic deformation, and to the stability of passivity in the metal-electrolyte systems in question.

A detailed discussion of corrosion fatigue leads to the conclusion that four different failure modes can be distinguished, which are related to the electrochemical behavior of the alloy-medium systems. A measurement technique is described correlating these different area modes with the local and electrochemical variables at developing cracks and the mechanical parameters in corrosion fatigue.

The final paper by R.C. Newman and A. Mehta addresses the problem of stress corrosion cracking of austenitic alloys, although the majority of this review centers on austenitic stainless steels, such as type 304 (UNS S30400), some attention is given to nickel-base alloys such as types 600 (UNS N06600), 690, X750 (UNS N07750), etc. The objective of this review was to examine the various crack propagation hypotheses for these alloy systems in, for example, high-temperature water, hydroxide, chloride, and sulfur-containing species such as sulfate. This examination centers primarily on the environment and reaction rates on the crack tip, rather than the metallurgical aspects (e.g., crack-tip plasticity, grain-boundary solute denudation/segregation). In particular, the likelihood of nickel-enriched layers at the tip of stainless steels is evaluated in the light of historical evidence, with the specific objective of analyzing the applicability of the film-induced cleavage mechanism of crack propagation. It was concluded that this was the most likely mechanism for transgranular cracking of austenitic stainless steels in chloride and, possibly, hydroxide solutions. An interesting hypothesis was introduced for the effect of nitrogen and phosphorous alloying additions on cracking susceptibility in terms of refining the porosity of the dealloyed layer and hence, the ease of film cleavage. The authors stressed that the evidence for a dealloyed (nickel-enriched) layer at the crack tip was not conclusive because of the masking effect of the corrosion product on its surface, however, some preliminary evidence for the existence of such a nickel-enriched film was presented based on analytical electron microscopy.

It is concluded that slip dissolution is the most likely mechanism for intergranular cracking of sensitized stainless steels and nickel-base alloys in oxygenated high-temperature water and sulfur-bearing solutions, with an additive grain-boundary mechanical fracture component in the latter case. The possibility of hydrogen embrittlement was acknowledged to be a possible mechanism for nickel-base alloys in, for example, hydrogenated high-temperature water.

The overall conclusion from this session on the environmentally assisted cracking of low alloy and ferritic, martensitic, and austenitic steels is that progress is continuing to be made not only on the validation of the mechanisms of cracking, but, just as importantly, on the practical use of such knowledge. Although some significant problems remain in the detailed quantification of the mechanisms (especially in the hydrogen embrittlement models), there is certainly sufficient knowledge available for the engineer to assess the relative danger of cracking in the given system, provided the relevant parameters in that system are defined. Indeed, in some systems (e.g., the austenitic stainless steel high temperature water system), this mechanistically based knowledge is sufficient to give specific quantitative predictions of plant performance.

Low-Alloy Iron-Base Alloys[A]

*T. Murata**

Abstract

Stress corrosion cracking (SCC) of low-alloy iron-base alloys was reviewed to make a clear picture of SCC in terms of initiation and propagation processes in which the operating mechanism changes with their progress. The emphasis was placed on (1) the stability of surface films as corrosion products, and (2) the role of stresses in localizing corrosion reactions, and also accelerating crack propagation through field failures of low-alloy iron-base alloys that covered, in the review, low-alloyed steels with tensile strength less than 50 kg/mm^2.

Issues involved in the evaluation of the susceptibility of low-alloy iron-base alloys in various environments were presented. (1) requirement for sample size, (2) surface of a sample to volume of a solution ratio in simulating field failures due to SCC, (3) stochastic approach to apparently random occurrences of localized corrosion and related SCC, (4) role of stress state and strains, (5) competitiveness of two basic mechanisms; active path corrosion (APC) and hydrogen-induced cracking (HIC) in certain alloy–environment systems, (6) local chemistry of a chosen environment, (7) interrelationships between SCC and corrosion fatigue.

The guidelines for designing the chemistry and microstructures of low-alloy iron-base alloys highly resistant to environment-induced cracking, which includes APC as well as HIC, were discussed.

Finally, the issues to be resolved were presented from the viewpoints of basic research, using for example the role of a thin water layer present at the reacting steel surface, and applied research such as the design criteria for attaining reliability of structures.

Discussion

F.P. Ford (General Electric R&D Center, USA): I would like to hypothesize that the instant the surface film is ruptured (i e , strain = 10^{-3}), crack propagation starts (at least in ductile alloy/aqueous environment systems). After all, most cracking mechanisms involve metal and water alone; aggressive anions are not required.

The time it takes for the crack to reach an observable depth is arbitrarily called the "initiation" time. Thus the effect of pits, for instance, is merely to create a localized environment that increases the propagation rate in this "initiation" period. Such an hypothesis, if correct, puts the semantic division between initiation and propagation into proper perspective and may reduce the amount of divisive effort applied to these two areas. Can you comment on this idea?

T. Murata: During field exposure tests of low-carbon structural steel to coke over gas-liquid for 24 months, the nucleation of localized corrosion and the initiation of cracks in relation to the localized corrosion have been studied with time. The results clearly indicate that no crack initiated before the size of localized corrosion (e.g., pits) met certain geometric conditions, suggesting not only the local solution but the localized strain rate of some level or stress intensity at the growing pits are key parameters for the initiation of cracks. The geometry of the pits in this case is not circular at free surfaces, but elongated with their major axes perpendicular to the tensile axis. As you hypothesized, it may not be wise to separate the process for strain-assisted pitting from that for cracking, since they are clearly different in their morphology, and the "acidified solution" is an insufficient condition for SCC to initiate.

R.P. Gangloff (University of Virginia, USA): I would like to comment on Ford's contention that an environmental fatigue crack begins to propagate at time or cycles equal to zero For corrosion fatigue of ferritic steels in aqueous chloride solutions, early work by Duquette and Uhlig [Trans. ASM 62(1969): p 839], coupled with our studies of micro-notch initiation, small crack growth, and conventional fracture mechanics specimens, leads to the conclusion that failure involves sequential cyclic deformation and crack propagation damage. Specifically, anodically stimulated surface deformation is attenuated by cathodic polarization below a threshold anodic current; failure life is greatly extended for smooth and micro-notched specimens; the latter simulating pits. In contrast, rates of propagation for cracks sized above about 25 μm are enhanced by cathodic polarization. This deleterious environmental effect is modeled based on hydrogen production and embrittlement, as discussed in my review at this conference.

While one is semantically safe in arguing for continued—but resolvable—crack propagation, I believe that it is more rational to examine the stages of initiation and small to long crack growth as separate processes. Eventually, a coupled model will emerge to properly connect each stage of failure. Pitting is a complication that can be viewed within this framework.

R.C. Newman (University of Manchester Institute of Science and Technology, UK): Your slides seemed to show data (or was this a prediction/extrapolation) indicating SCC of carbon steel in 50°C water. Is this not intergranular cracking of an alloy steel?

F.P. Ford: I would like to help answer Newman's question, since I think the data referred to are mine. These were obtained using slow-strain-rate testing in high-purity water on SA333 grade carbon steel (Ford, EPRI Report HD 2406, "Base Environmental Cracking Margins for Carbon Steel Piping," May 1982, p. 2-1). Transgranular cracking was observed in the higher-temperature regions (greater than 200°C). In the lower-temperature regime, this cracking was counteracted by pitting—especially with oxygen contents in waters of more than 1 ppm—that essentially prevented crack propagation at 50°C. This general trend of transgranular cracking susceptibility with oxygen/temperature combinations has been supported by other data of Indig (Indig, ibid., p. 1-1) and Mizuno and Pedneker (EPRI Progress Report on Project T115-5, December, 1980), for example.

T. Murata: The precise environmental conditions, such as the content of dissolved oxygen, are critical in addressing this type of question. So far, SCC in water has only been postulated under slow-strain-rate test conditions at high temperatures. I would expect shallow localized corrosion at 50°C rather than SCC

B. Cox (Atomic Energy of Canada, Ltd., Canada): In response to Ford's comment on pits nucleating cracks, I can offer an

---

[A]The written version of this presentation was not available for inclusion in the proceedings. The abstract has therefore been included, along with the discussion that followed the presentation.

*Nippon Steel Corporation, 6-3, Otemachi 2-chome, Chiyoda-ku, Tokyo, 100-71 Japan.

example of the reverse. In the iodine-induced SCC of the Zircaloys,† we deluded ourselves for a long time into the belief that cracks initiated at pits, because we commonly saw them in association. When we eventually sorted out the chemistry of crack initiation, we found that the transgranular cracks initiated immediately the stress was applied (no incubation time), and the crack in the protective oxide provided an ideal site for small pits to develop. Thus, in this system the crack initiates first and the pits form subsequently at the crack site, thus guaranteeing the observed association between pits and cracks.

R.W. Staehle (University of Minnesota, USA): It seems that there are four cases related to pitting and SCC: (1) pits, (2) cracks, (3) pits and cracks, and (4) pits initiate cracks. All four cases have been demonstrated. Next, there are two cases for stress/strain interaction to change the morphology One is Murata's demonstration of elongated pits influenced by strain. The second is Speidel's observation (private communication) that the stress causes pits to elongate and sharpen.

T. Murata: It may be important to observe the correlation between pitting and SCC in terms of the time scale, to clarify the mechanistic aspects. In dealing with multiple issues in localized corrosion within a given metal–environment system, we need to use a stochastic approach to connect micro-phenomena with macro-phenomena.

R.H. Jones (Pacific Northwest Laboratories, USA): Early work on intergranular SCC of iron in calcium nitrite indicated that carbides were necessary for crack growth. In recent work at our laboratories, we have observed rapid crack growth (10^{-2} mm/s) without carbides, but with both high sulfur and phosphorus segregation. I would appreciate your comment regarding the role of carbon in intergranular SCC of iron and your understanding of those processes that may account for such rapid crack velocities.

T. Murata: What we have observed is the preferential dissolution at high angle boundaries, including the interface between the matrix and pearlitic phase, where the segregation of interstitial elements (C,N) and solutes of low solubility are expected. However, the reason for preferential anodic dissolution due to those elements has not been clarified, except for the acceleration of proton discharge reactions by segregated phosphorus in acidified solutions. The very high propagation rate of cracks cannot simply be explained by anodic dissolution. I wonder if the steel had been heated by chance into the temperature zone where phosphorus can segregate to grain boundaries, weakening their cohesive strength. When the carbon steel has the propensity to temper embrittlement, cracks readily proceed in the presence of hydrogen, particularly in high-strength steels. In discussing intergranular SCC, deformation properties of grain and grain-boundary areas have to be considered, in addition to grain-boundary chemistry.

R.N. Parkins (University of Newcastle upon Tyne, UK): 99.999% iron, from which the carbon and nitrogen have been removed, will not fail by intergranular SCC in the slow-strain-rate test in carbonate/bicarbonate solution. However, the addition of carbon, nitrogen, or phosphorus, separately, to such iron all cause intergranular SCC to be displayed. So carbon is not necessary, and of those elements mentioned, nitrogen has the most deleterious effect for equivalent concentrations. I have difficulty in imagining that the effects of those three elements are all related simply to electrochemical effects and segregation to grain boundaries. Perhaps they influence grain-boundary deformation.

I also have a comment on the effect of phosphorus in promoting intergranular SCC in a nitrate solution at a crack velocity of about 10^{-2} mm/s, well beyond any crack velocity that could be explained by a dissolution-controlled mechanism. Assuming that phosphorus does not enhance the local dissolution rate beyond that measured for iron in that solution, I suggest that the dissolution-related crack growth is enhanced by some mechanical contribution.

R.H. Jones: I agree that mechanical fracture is a viable explanation for the fast crack growth observed in iron with impurity segregation to grain boundaries. However, for the iron with 0.3 monolayers (0.6 at grain boundaries) of phosphorus, intergranular crack growth could not be promoted at cathodic potentials in 1 N sulfuric acid. Therefore, some explanation other than impurity-induced decohesion or hydrogen-induced crack growth (the calcium nitrate tests were conducted at +750 mV—well above the hydrogen line) is needed to explain those results. A localized corrosion-produced sharp crack geometry may be a factor, but the conditions must be more severe than those produced by cathodic polarization.

R.A. Oriani (University of Minnesota, USA): Could you please describe in more detail the experiments with the Devanathan-Stachurski cell [Proc. Roy. Soc. A 270(1962): p. 90; J. Electrochem. Soc. 111(1964). p. 619] using thin electrolyte layers at the input side? Specifically, was the pH measured or only inferred from the permeation measurements? Was the chemistry of the corrosion products different in the thin-layer experiments, from that in ordinary deep-layer experiments? Did solid corrosion product prevent hydrogen input into the steel?

T. Murata: The local pH at corroding surfaces can be estimated from the steady-state hydrogen permeation rate and the relationship between pH and ΔJ, since the initial pH change is limited to electrolyte next to the iron surface. Corrosion products in a thin electrolyte film are much different from those formed in bulk electrolyte; they have a very fine morphology. The pH at the interface in a thin electrolyte deviates slightly from one place to another throughout the corroding surfaces, due primarily to the local hydrolysis of ferrous ions and the reduction reaction of dissolved oxygen. [See, for example, Sato and Murata, CORROSION/88, paper no. 192 (Houston, TX: NACE, 1988).]

The points to be made here are (1) acceleration of localized corrosion and, thereby, (2) acidification in the presence of a thin electrolyte or water layer.

A. Atrens (University of Queensland, Australia): You measured low pH values at the surface for iron corrosion in the water layers Would you tell us the implication of this observation for iron immersed in bulk water?

T. Murata: Quite often in engineering service conditions, thin water layers under deposits or equivalent stagnant environments exist where the distribution of solution chemistry different from the bulk prevails, and the propensity for localized corrosion is high. Our experiments also suggest that cyclic wet and dry conditions accelerate the local acidification, thereby indicating that the stimulation in the thin water layer accelerates localized corrosion.

B.G. Pound (SRI International, USA): Your hydrogen permeation experiments with the cotton cloth showed some delay time after wetting You attributed this delay to be associated with a decrease in pH on the side of the cotton cloth How do you distinguish this effect from the "normal" lag time required for hydrogen to appear on the oxidation side of the membrane?

T. Murata: We have conducted the hydrogen-permeation experiments using solutions with different pHs, identifying the lead time for permeation to be measured. Since we used a neutral solution, some time period was required in addition for acidification. Your point is well taken.

Y.-C. Chen (Materials Research Laboratories, ITRI, Republic of China): What was the temperature range of your coke oven gas (COG) runner system? To my knowledge, Prussian Blue is a very important corrosion product in the COG distribution line. I do not know why it is not listed in your test. Can you explain it? When taking a COG correlated test, I found hydrogen sulfide can ruin the passivity of the Prussian Blue film by the formation of SCN^-. Maybe this is the reason for pitting formation. What is your comment?

T. Murata: The temperature of our system was typically from 40 to 80°C. As to the corrosion products in this particular environment, we found a mixture of several compounds, including a variety of hydroxides and oxides of iron, with magnetite being dominant. At the later stages of COG treatment, where desulfurization is carried out, SCN^- becomes prominent. Generally speaking, the coexistence of hydrogen sulfide and chloride, or hydrogen sulfide and SCN^- depassivates the resistant steels, such as stainless steels, leading to pitting. However, Prussian Blue is negligible in our system, and pitting of low alloys is accelerated by chloride in this case. At temperatures higher than 60°C, sulfide formation becomes stifled.

It is important for us now to see the environmental variation from one site to another, depending on the kind of coal and process conditions, e.g., content of sulfur in coal and the desulfurization process. Please bear in mind that the pits discussed here are quite different from those observed in stainless steels, for example, in that the depth/opening ratio is rather small.

†Trade name.

Hydrogen Effects in High-Strength Steels

*R.A. Oriani**

Abstract

The full understanding of the embrittlement of high-strength steels by hydrogen, and indeed of any metallic alloy, may be subdivided into two parts: (1) understanding the basic mechanism(s) of the intrinsic embrittling action of hydrogen and how various microstructural features modulate that mechanism, and (2) formulating the kinetics of cracking to consider microstructure and alloy composition, stress state, temperature, and source of the hydrogen. This goal is still very distant. After distinguishing between thermodynamic arguments about the reduction of the driving force by adsorption and mechanisms that describe the path of the reaction, the decohesion and the localized plasticity models are described and the literature is examined for experimental and theoretical work in support of each. It is concluded that the two mechanisms are not competitive but complementary, both being manifestations of metal–metal bond weakening by hydrogen. The principal future task is to understand what circumstances control which manifestation will predominate in any one specific case. Recent kinetic models are examined to display their underlying assumptions. The majority of these models deal only with Stage II cracking and emulate the experimental dome-shaped curve of crack velocity vs reciprocal temperature by functions that represent a variety of temperature-dependent physical processes, but that do not incorporate any specific embrittling mechanism. The difficulties impeding a complete kinetic treatment are immense, not the least of which is posed by the bimodality of crack propagation.

Introduction

This review is concerned with the relatively small number of published investigations the aim of which is to shed light on the intrinsic action of hydrogen that embrittles a high-strength steel or on the mechanisms controlling the rate of crack propagation. It endeavors to bring up to date the earlier reviews of the author [1,2] It does not deal with stress corrosion cracking or with cyclic stress applied in hydrogenating environments, because the additional complexities of these phenomena render it extremely difficult to extract any insight from the measurements as to the basic embrittling mechanisms of hydrogen. The kinds of insight for which the literature is scrutinized are those that would allow one to calculate the rate of crack propagation (not curve fit) as a function of hydrogen fugacity in the environment or of precharged hydrogen content, and as a function of steel composition, microstructure, yield strength, and temperature. One would also like to understand the choice of crack path, as well as why hydrogen gas and chlorine gas[3] embrittle steel but oxygen gas does not. It is clear that these goals are far from being achieved.

In this paper, a brief review is presented of the current thought on the mechanisms by which hydrogen embrittles steels, as well as of the works that tend to support one or another point of view. A synthesis of mechanisms is presented. Various models for the kinetics of crack propagation for static or monotonic loading are then discussed. Finally, some remarks directing attention to fruitful approaches are offered.

*Corrosion Research Center, Department of Chemical Engineering and Materials Science, University of Minnesota, Minneapolis, MN 55455.

The Intrinsic Embrittling Action of Hydrogen in Steels

It should be abundantly clear that using high-fugacity hydrogen, such as is produced by cathodic charging from acid solutions, or by gaseous ionized or atomic hydrogen, is not the appropriate way to develop experimental information whereby to develop an understanding of the intrinsic or basic embrittling action of hydrogen. One reason is that such hydrogen precipitates within pre-existing microvoids and microcracks in the steel to produce molecular hydrogen at very high pressures, which generates not only internal stresses in addition to the externally applied and measured stress, but also much plastic deformation. This phenomenon is addressed by the Zapffe-Sims' idea[4] for the mechanism of hydrogen embrittlement. Another reason is that the input diffusion flux itself generates much plastic deformation and even cracking,[5,6] thereby changing the response of the steel. For the purpose of developing understanding, hydrogen should be applied that has a fugacity corresponding only to a pressure equal to a small fraction of the yield strength of the steel.

Two other points have been made in previous reviews[1,2] but appear to be worth repeating. The first point is that measurements of the time of delayed fracture or of the rates of crack propagation cannot by themselves provide information on the basic embrittling mechanism of hydrogen. In support of this statement, it should suffice to point out that kinetic measurements can at best give quantitative information relative only to the kinetically controlling step in the sequence of processes from the source of the hydrogen to the location of the critical embrittling action.

The second point has to do with the distinction between a thermodynamic argument and a mechanistic one. It is customary to use the rate of reduction of free energy of a system with unit advance of a process as a measure of the driving force for that process. The reduction of the surface free energy (γ) of a crack surface by adsorbed hydrogen is an example of the modification of the driving

force for a process, in this case for crack propagation. As such, this effect of hydrogen does not constitute a mechanism for crack propagation, because there is no specification of the path by which a region of a body becomes surface, nor of the role of hydrogen in that path. Couching[7] the reduction of γ in terms of the Griffith criterion (itself a thermodynamic argument) for the fully elastic body renders it somewhat more mechanistic because what is implied is the colinear separation of atoms, thereby excluding any other means for generating a surface. Nevertheless, it is still far short of a full-fledged mechanism because, by only comparing the postpropagation to the initial state, the Petch-Stables formulation does not attempt to describe the detailed role of hydrogen in facilitating the advance of the crack. Thus, it is incapable of addressing the question of why gaseous oxygen does not embrittle steel, whereas gaseous hydrogen and chlorine[3] do, recognizing that both oxygen and chlorine decrease γ of iron more than hydrogen does.

The decohesion model

The decohesion model[8-13] for hydrogen embrittlement of steels is consistent with the Petch-Stables formulation but is more mechanistic in that it specifies the role of hydrogen in reducing the stress necessary to drive a crack. It supposes that atomically dissolved hydrogen at high local concentrations, whether in normal lattice, grain boundaries, or interphase boundaries, lowers the local, maximum cohesive force (F_m) against the colinear separation of the metal atoms. In addition to the concentrating effect of energy-rich sites such as internal interfaces, the externally applied tensile force locally magnified by the intensification factor represented by the crack-tip geometry enhances the local dissolved hydrogen concentration via the dependence of the thermodynamic chemical potential on stress.[14] The crack-tip radius of curvature is controlled by the plasticity, itself modified by hydrogen,[12] of the region of the body near the crack tip. This is the point of view of the decohesion model for high-strength steels It was extended[1,15] to lower-strength steels by recognizing that very large stresses can be generated by the operation of inhomogeneous plastic deformation. The decohesive action of hydrogen will take place wherever sufficiently high tensile stresses occur, consistent with the local hydrogen concentration, such that the local tensile stresses rise to equal the hydrogen-decreased, maximum local cohesive force The decohesion model postulated that F_m is lowered by hydrogen but did not attempt to provide an explanation for that effect.

The localized-slip model

The localized-slip model is consistent with the lowering of γ by hydrogen, but not with the Petch-Stables-Griffith formulation. Beachem[16] first suggested, on the basis of metallographic observations, that hydrogen enhances localized plasticity and thereby lowers the energy required for crack propagation by slip. Lynch[17,18] later reinforced Beachem's idea, also on the basis of metallographic observations. He demonstrated the great similarity between the fractography of hydrogen embrittlement and that of liquid metal embrittlement (LME), from which, believing in the inability of the liquid metal to penetrate in the times involved beyond the surface at the crack tip, he argued that the deleterious action of hydrogen is also immediately at the crack tip. In this, the localized-slip model is similar to the decohesion model applied to high-strength steels subjected to external hydrogen supplied to the crack tip. The enhanced-slip model has not been made semiquantitative, so it is not possible to use it to describe an experimental curve of threshold stress-intensity parameter (K) vs hydrogen gas pressure, as has been done with the decohesion model.[19,20]

Phase transformation mechanisms

Hydrogen can take part in, or can cause to occur, various phase transformations in metals. Reference has already been made to the precipitation of molecular hydrogen gas of very high pressures within microcavities in steels from atomically dissolved hydrogen at very high activities. Hydrogen can also combine with many metals to form hydrides, especially in the tensile stress field ahead of a stressed crack.[21,22] The hydrides have metallic characteristics and are often brittle, which may be a manifestation of decohesion, so that the crack easily propagates by cleavage through the hydride. Whereas this occurs with metals such as niobium, vanadium, and zirconium, high-strength steels do not show hydride formation.

Unstable austenitic stainless steels can partially transform to brittle phases such as martensite and ϵ-phase.[23,24] Charging in of high-fugacity hydrogen causes lattice strains that induce such phase generation. Again, this is not a phenomenon that is found in high-strength steels.

Hydrogen can also react with other solutes in metals to produce mechanically deleterious results. Dissolved oxygen in copper can be reduced to water vapor at moderately high temperatures. Dissolved carbon and the carbon in carbides in steels can be converted by hydrogen to methane within pre-existing microvoids. The microvoids grow by grain-boundary diffusion of the iron atoms and weaken the steel [25] Because this "hydrogen attack" occurs only at moderately high temperatures (200 to 400°C), it is not considered hydrogen embrittlement in the sense used in this paper, and will not be discussed further.

Literature support for the decohesion mechanism

An immediate prediction of the decohesion model was[12] that there should exist, for a given high-strength steel, a threshold stress-intensity parameter (K) for any one hydrogen gas pressure, and also a threshold hydrogen pressure for any one value of K, below which a crack will not propagate. This prediction was confirmed for two kinds of high-strength steels,[26,19] and the curve of threshold p_{H_2}–K was very well fitted (Figure 1) by the quantitative development of the model. The main concepts that entered the model were the dependence of the concentration of hydrogen at constant thermodynamic activity upon the state of stress,[14] that an internal interface has a larger Sieverts law parameter (because of the binding energy) for hydrogen than does the normal lattice, that the crack is stressed in Mode I, that its tip radius is controlled by plasticity and affects the local stress through Gilman's[27] modification of the Inglis formulation, and that, consequently, the maximum stress state and hence the decohesive action of hydrogen occurs within a few angstrom units below the surface at the crack tip. From the fitting of the theoretical equation to the experimental data, the parameters of the model were evaluated and were found to be in reasonable agreement with the premises of the model. For example, the magnitude of the hydrostatic component of stress was calculated to increase from 1/30 to 1/12 of the Young's modulus with increasing K, the ratio of stress-induced to stress-free concentration attained values as large as 10^4, and the hydrogen-reduced F_m divided by the hydrogen-free maximum cohesive force turned out to be between 0.2 and 0.4 and increased with increasing K, as was to be expected.

Later work[20] modified the model to include the physically necessary increase of tip radius with increase of K. This enabled the model to describe a hysteresis found[20] experimentally. After a decrease of K that caused the crack to arrest under a specific hydrogen gas pressure, to restart the crack it was necessary to apply a larger hydrogen pressure than would have been required at the same K attained by monotonically increased loading. Furthermore, deductions from the model agreed with preliminary measurements of the temperature dependence of the threshold pressure–stress intensity curve. [20]

Following this initial semiquantitative success, many investigators have couched their thinking and interpreted their findings in terms of the decohesion model. Chief among these have been Gerberich[28,29] and MacMahon.[30,31] The former established threshold K values and based kinetic formulations on kinetic concepts for both static and cyclic loadings. The latter investigated the synergism between hydrogen and impurities segregated at grain boundaries and interpreted the results as additive decohesive phenomena.

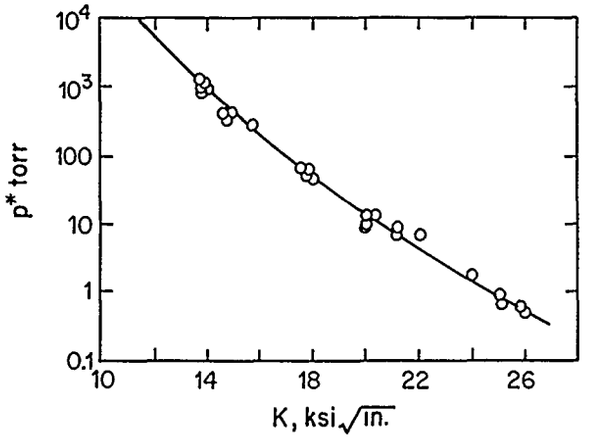


FIGURE 1—Experimental data (circles) and best fit (solid line) of decohesion theory[20] of threshold values of hydrogen gas pressure (p*) and stress-intensity parameter (K) for type 4340 (UNS G43400) heat treated to a yield strength of 1720 MPa. (Torr × 133 = Pa; ksi√in. × 1.10 = MNm$^{-3/2}$).[20]

Critical investigations that can be used to test the validity of the decohesion model for high-strength steels, and indeed for any alloy, are scarce. The most unambiguous work of which the author is aware is that of Vehoff and Rothe[32] using Fe-2.6%Si alloy and also nickel. With single crystals oriented with respect to the applied stress, so that a crack can propagate under monotonic loading by alternate activation of two slip systems intersecting along the crack front, the minimum crack angle is equal to the angle between the two sets of active slip planes when the crack propagates in a completely ductile fashion. Vehoff and Rothe found that the crack angle decreased below that minimum when the crack was propagated in a hydrogen gas. In a vacuum, the crack angle for the oriented Fe-Si single crystal was 71.4 , the minimum value for the orientation used for propagation by pure alternating slip. For propagation in 1 atm H_2 gas, the crack angle was only 9° (Figure 2). This considerable sharpening was accompanied by more rapid crack propagation, with the cracking rate increasing with increasing hydrogen pressure.

There are only two conceivable physical reasons why the crack can sharpen below the angle given by the intersecting slip systems. The additional fracture mechanism could be hydrogen-aided microvoid formation ahead of the crack tip or hydrogen-aided cleavage (decohesion) at the crack tip. Vehoff and Rothe,[32] and also Lynch,[33] carefully examined the fracture surfaces by scanning electron microscopy with and without replica techniques; evidence for microvoids was not found. In addition, with Fe-Si single crystals, the fracture surfaces always coincided locally with the {100} cleavage plane, even for cases when that plane was inclined up to 90 degrees from the tensile axis. Because there is no physical mechanism for microvoid formation on {100} planes, the microvoid mechanism for sharpening the crack angle was rejected. This leaves hydrogen aided decohesion as the only possible additional mechanism.

Thus, the general picture from this work is that in Fe-Si single crystals, both decohesion and alternating slip are responsible for the crack propagation in hydrogen, and that with increasing hydrogen pressure, the decohesion mechanism makes an increasing contribution. Furthermore, the results of suddenly introducing oxygen gas into the environing hydrogen gas enabled Vehoff and Rothe[32] to infer that the decohesive action of hydrogen occurs just below the crack tip at the highly elastically strained atomic bonds, and led them to doubt the mechanistic completeness of the Petch Stables adsorption idea[7] for understanding hydrogen embrittlement. They concluded that oxygen does not embrittle, although it adsorbs strongly, because its atoms are too large to enter into the highly strained region just below the crack tip surface. These investigations have reached conclusions identical with the postulates of the decohesion theory.[12,13] Later work by Vehoff, et al. (which will not be discussed in detail here),[34] on fatigue crack nucleation at grain boundaries in nickel bicrystals led the investigators to support the decohesion model, as extended by MacMahon, to segregated grain boundaries.[31]

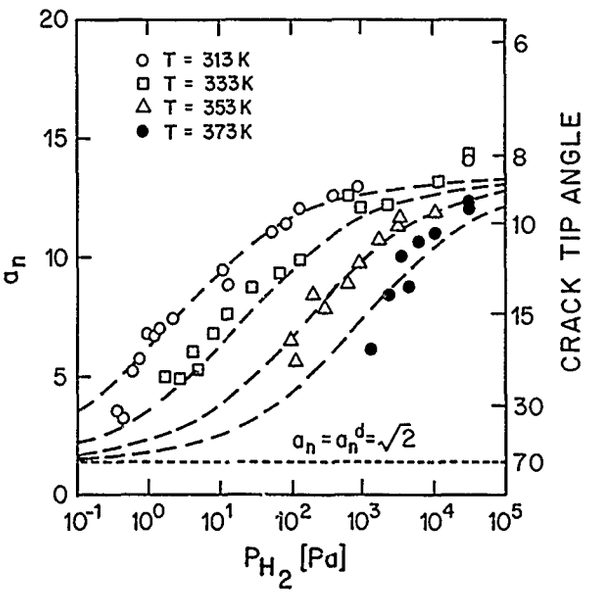


FIGURE 2—Crack-tip angle, α, right ordinate, and a_n (= cotan α/2), left ordinate, vs hydrogen gas pressure, P_{H_2}, for a crack advancing in a single crystal of Fe-2.6%Si alloy (Vehoff and Rothe[32]).

It is extremely difficult to test experimentally the basic postulate of the decohesion model, that F_m is decreased by large concentrations of hydrogen In this connection, it is important to realize that electronic interactions among metal atoms are functions of interatomic spacing For example, the cohesive force–interatomic distance relationship is known to be nonlinear. It should not be expected, therefore, that one can predict the effect of hydrogen in solid solution on the cohesive force at interatomic separations comparable to those related to F_m from experiments where the interatomic excursions from the normal lattice parameter are very small, such as by measurements of the effect of dissolved hydrogen on elastic moduli[35-37] or on phonon frequencies.[38,39] No one has yet been able to devise an unambiguous experiment to measure the cohesive force between iron atoms with which a very large hydrogen concentration (on the order of H/Fe ≈ 1/10) is dissolved. For this reason, we turn now to a consideration of theoretical work on this problem.

Markworth and Holbrook[40] used two-body potentials in computer simulations of hydrogen enhanced fracture from which they concluded that hydrogen facilitates the cleavage cracking of iron, i.e., the colinear separation of the iron atoms. An approach that avoids the use of unphysical two body forces is that of Messmer and Briant.[41] They have discussed theirs and others calculations with the quantum mechanical cluster method. This approach has demonstrated that the metal metal bonds are weakened by the hydrogen caused distortion of the interstitial site that is occupied. This quantum mechanical technique has so far been applied only to small clusters (14 or fewer) of atoms because of calculational difficulties.

A more generally applicable theoretical technique is the embedded-atom method.[42] This is a semiempirical, quantum mechanical approach, in the sense that experimental information is used to evaluate the parameters. It has been validated by its successes in calculating surface structure, grain-boundary configurations and energies, and dislocation dynamics. Calculations[42] have been conducted on a lattice of nickel containing a crack bounded by {111} planes, with and without dissolved hydrogen in its immediate neighborhood. By considering stress to be applied normal to the slip

directions on the (111) planes, the simulated fracture is constrained to be brittle, i e , to propagate by the colinear rupture of atomic bonds. The embedded-atom method clearly shows that hydrogen lowers the fracture stress of nickel (Figure 3). Although iron has not yet been explicitly investigated by these workers, there is no reason to expect a qualitatively different result for iron.

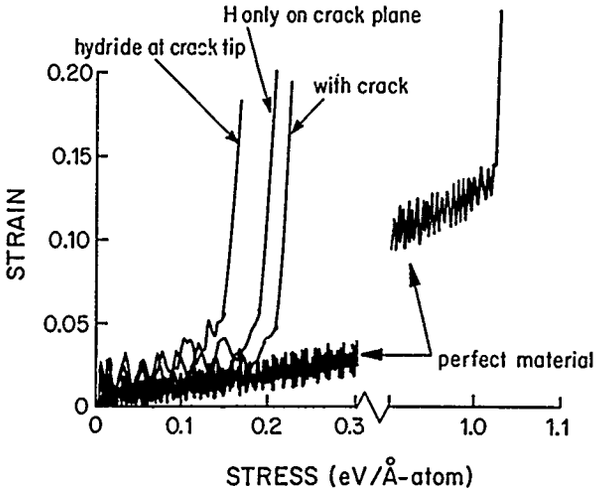


FIGURE 3—Stress–strain curves calculated by the quantum-mechanical embedded-atom method.[42] The curve labeled "perfect material" is crack free and without hydrogen. That labeled with "crack" is without hydrogen, whereas the adjacent curve is for material with a similar crack with dissolved hydrogen on the crack plane. Note that hydrogen lowers the applied stress to propagate the crack. Hydrogen as a hydride lowers the stress even more.

In contrast to Daw and Baskes,[42] who considered the effect of hydrogen on an already existing internal crack, McMullen and collaborators[43] consider the separation of a crystal into two halves by allowing interatomic spacing to vary at only one crystallographic plane. This is the same as the conceptual experiment by which the surface free energy is defined.[44] The calculation is conducted with and without a specified number of hydrogen atoms on the plane of separation. The metal atoms are not allowed to undergo surface relaxation (i.e., surface restructuring is not permitted), but the hydrogen atoms are permitted to seek positions of minimum energy as the interplanar separation is increased.

McMullen, et al., use the nonpairwise force model of Daw and Baskes for calculations on nickel, and that of Finnis and Sinclair[45] for iron that comes from tight-binding theory. They find that hydrogen reduces the maximum cohesive force between the metal atoms of Ca, Sc, Ti, V, Cr, Mn, Fe, Co, Ni, and Cu, but not of potassium. Specifically, a local hydrogen-to-metal ratio of 1/8 for nickel reduces the fracture stress by 12% from that of the pure nickel. For iron, the fracture [i.e., the maximum (F_m) of the cohesive force as modified by hydrogen] occurs at an increase of the interatomic separation of 0.05 nm, which is a strain at failure of about 25%. For this reason, McMullen, et al., remark, "It is not correct to interpret even completely brittle fracture using the simple (Griffith-like) criterion . . . ."[43] of reduction of the surface free energy. The present author notes that the manner of these calculations is very similar to the "gedanken experiment" used[12] to conceptualize the decohesion model. The only difference is that the calculations of McMullen, et al., use the unphysical restriction of a constant number of hydrogen atoms at the separating plane, whereas the decohesion concept is that, as the interatomic separation (and hence the cohesive force) increases, the number of dissolved hydrogen atoms at the separating plane increases by accepting hydrogen from the rest of the lattice or from a gas phase in order to maintain the chemical potential of hydrogen constant. It should be clear that the restriction of McMullen, et al., necessarily reduces the calculated decohesioning effect of hydrogen.

Masuda-Jindo has calculated the cleavage strength of vanadium and of body-centered cubic (bcc) iron with and without hydrogen.[46] He has applied the tight-binding quantum mechanical method to the force of separating the metal crystal to create two (001) crystal-plane surfaces without surface relaxation or reconstruction. If cleavage is forced to occur at a (001) plane immediately adjacent to a plane of hydrogen atoms in interstitial positions, it is found that the presence of hydrogen decreases the maximum force for the colinear separation of the vanadium or of the iron atoms.

I conclude that the basic concept of the decohesion model—that hydrogen decreases the cohesive force that resists the colinear (cleavage) separation of transition metal atoms—is amply supported by modern theoretical investigations.

Literature support for the localized-slip model

Both Beachem[16] and Lynch[17,18] were motivated toward the idea of highly localized (at the crack tip) slip by their fractographic observations, the former with steels and the latter with a variety of metallic alloys as well as with steels. Lynch was additionally motivated by the great similarity between the fractographic features caused by hydrogen and those caused by LME, coupled with the alleged inability of atoms in LME to penetrate into the subsurface region of the embrittled metal. In seeking accounts of critical experiments in support of the localized-slip mechanism of hydrogen embrittlement, one immediately encounters two serious difficulties in the case of steels. The first is that the majority of the information on the effect of hydrogen on the plastic behavior of iron alloys and steels has to do with the overall plasticity, not localized at a crack tip, and the effects are complex. Whether increased or decreased plasticity results from exposure to hydrogen depends on impurity level and temperature,[1] whereas the localized-slip model is presumed to be generally relevant to all ferrous alloys. The second difficulty is that in many of the literature experiments, hydrogen of high fugacity was unwittingly used, and it has been abundantly demonstrated that its introduction of itself, or its precipitation as H_2 molecules in microvoids, can cause much plastic deformation. These considerations seriously reduce the literature data relevant to the question of support for the localized-slip model.

Nakasato and Bernstein[47] observed that hydrogen charging of pure iron causes cracking along the {110} slip planes rather than along the usually preferred {100} cleavage planes. This observation may serve to support the Beachem-Lynch idea. The work of Inoue, et al.,[48] who examined the characteristics of cracks propagated in impure iron by transmission electron microscopy (TEM), does not support the localized-slip idea. In hydrogen-free metal, the crack was of zig zag configuration, with the straight segments along the traces of {110}, {112}, and {123} planes, which are slip planes in bcc iron. However, after cathodic charging, the crack lay along traces of {112} planes and was free of zig zag steps. These observations deviate from the requirements of Lynch's hypothesis that the crack plane bisect the angle subtended by two slip planes.

Birnbaum and collaborators,[49,50] using TEM with an environmental cell, have directly observed the effect of low-pressure gaseous hydrogen on dislocation activity in many metals, including iron. When gaseous hydrogen is admitted into the TEM, the velocity and the number of active dislocations suddenly increase in thin-foil specimens held under tension, with failure occurring by localized ductility in Mode III. These striking and beautiful results support the localized slip model of hydrogen embrittlement. What is open to question, however, is the general relevance of these results to hydrogen embrittlement in the multifarious conditions in which it arises.

Zhang, et al.,[51] investigated hydrogen-induced delayed fracture under sustained Mode II loading of a Cr-Ni-Mo steel of 1700 MPa tensile strength. By finite-element calculations, they established where at the notch surface the maximum principal stress, the maximum hydrostatic component of stress, and the maximum shear

stress are developed, as well as the directions of the maximum principal stress and maximum shear stress at these positions. When a Mode II specimen was strained in air, the first crack nucleated at the site of maximum shear stress However, with specimens that were hydrogen charged during testing, crack propagation began in the direction of the maximum shear stress from the site of maximum hydrostatic component of stress (which coincides with the site of maximum principal stress) Aside from the complications caused by the very high-fugacity hydrogen that was used by these investigators, the results indicate, but do not prove, that hydrogen facilitated crack propagation by slip The results also seem to indicate that the crack initiation was aided by the decohesive action of hydrogen.

It is to be expected that in metallic systems an electronic perturbation caused by dissolved hydrogen that reduces the force necessary to separate metal atoms colinearly should also weaken the shear-resisting forces of the lattice. This is indeed the result of the embedded-atom quantum mechanical calculations of Daw and Baskes[42] applied to nickel, qualitatively similar results are expected for iron Lynch[17] has pointed out that the localized-slip model of hydrogen embrittlement deviates widely from the usual concept[52,53] of competition between crack blunting by dislocation generation, and emission and crack propagation by cleavage. This is so because the postulated enhancement of slip by hydrogen is taken by Lynch to enhance propagation if it is alternating slip bocalized at the crack tip.

Conclusion

It is very obvious that the amount of critically developed experimental data relevant to the intrinsic embrittling effect of hydrogen on steels or iron alloys is pitifully small. The existing empirical information and theoretical considerations allow one to accept with confidence that dissolved hydrogen does decrease both the resistive force against the colinear separation of iron atoms and also that for the shear displacement. Which of these is the operative mode in any one particular experiment probably depends on the proportion[54] of Mode II loading, among other factors, and the examination of which mechanism is the important one in a specific instance remains one of the critical tasks for future investigations.

Because both the decohesion and the localized-slip models depend fundamentally on the bond weakening action of hydrogen, it is reasonable to regard the models as complementary. Both are really decohesion models, with one emphasizing the colinear and the other the shear mode of atomic separation. Although the localized-slip model has not yet been formulated semiquantitatively, it seems clear that its development must include the concept of a critical hydrogen concentration, which is itself a function of the local state of stress and that the action of hydrogen prior to the generation of the crack surface must be considered.

Kinetic Mechanisms of Hydrogen Embrittlement

Questions concerning the kinetics of hydrogen embrittlement of high-strength steels under sustained or monotonically increasing loading can take various forms. One may inquire how much time is required for the complete failure of an initially hydrogen-free, smooth steel specimen held under constant load under a constant hydrogen gas pressure and temperature, or under constant cathodic charging conditions This "delayed failure" mode will depend on the nature of the initial oxide on the specimen surface, on the plastic response of the steel (itself modified by the entering hydrogen), and on the transport of hydrogen from its source to the location of the intrinsic embrittling action of hydrogen. One may be interested in the "incubation time" for the initiation of observable crack propagation of a prenotched specimen in air and at a constant applied load, provided with an initially uniform, internal hydrogen concentration. The incubation time will depend on the manner in which the prior charging was done, the level of hydrogen attained, the nature of the initial notch put in, and the kinetics of the hydrogen transport within the steel. In both cases, the composition, microstructure, and strength level of the steel, the magnitude and character of the loading, and the temperature would be important determinative factors.

The above experimental scenarios involve the development of the crack process-zone geometry and the dislocation distribution within the latter, greatly complicating the modeling of the kinetics of the hydrogen embrittlement. An easier but still formidable task is the quantitative description of the rate of subcritical crack propagation at constant applied stress-intensity parameter, because one may consider the crack process-zone complex to have a steady-state configuration with respect to a coordinate system moving with the crack. If one considers a steel initially free of hydrogen in which the advancing crack is in contact with a time-independent source of hydrogen, another element of simplification is introduced. More difficult is the consideration of the crack propagation in precharged steel, since in this case, the critical action of hydrogen may not occur at the advancing crack tip but rather at some highly stressed microstructural feature that is ahead of the tip and that intercepts hydrogen diffusing toward the process zone from the rest of the specimen. In all of the cases described above, complete kinetic modeling needs complete knowledge of the mechanism of the embrittling action of hydrogen. Since this is not yet available, most ambitious kinetic modeling so far attempted avoids this problem by making an assumption, such as the necessity of attaining a critical hydrogen concentration at some location or over some linear dimension, which may have been inspired by a model of embrittlement but may not be uniquely related to that model. Following is a discussion of some recent approaches that are representative of the best work available.

Analysis of Simmons, et al.

It is clear that in the process of crack propagation, hydrogen must proceed from its point of origin, as H_2S molecules in the gaseous state, for example, to the adsorbed state on the crack surface (after crack propagation). Hence there are several sequential processes, any one of which can be kinetically controlling, and it is important to identify the controlling process. Simmons, et al.,[55] followed the kinetics of the reaction of water vapor with type 4340 (UNS G43400) steel surfaces by measuring the increase of the Auger electron peak intensity due to oxygen as a function of exposure (the gas pressure multiplied by the duration). The data of Auger peak intensity vs exposure at each of three temperatures were fitted with sigmoid-shaped curves (although monotonic curves fit just as well within the scatter of the data,) and it was inferred that the oxide formed by nucleation and growth with an activation energy of 36 ± 14 kJ/g mol. This means that the generation of hydrogen via the reaction $H_2O + Fe \rightarrow FeO + H_2$ proceeds with that activation energy. These investigators then measured, at various temperatures, the rate of crack propagation (v) in type 4340 steel of 1340 MPa yield strength. They found that v, in the stress-intensity-independent region of the v-K curve (where K is the stress-intensity parameter), exhibits an activation energy of 33 5 ± 5.0 kJ/g mol. The similarity of the two activation energies led the authors to conclude that the rate-limiting step in the hydrogen-induced cracking was the generation of the hydrogen at the input surface.

Analysis of Lu, et al.

Another investigation[56] from the same school followed the same coordinated approach, that of measuring both the surface reaction kinetics of gaseous H_2S with type 4340 steel and the crack propagation velocity as a function of temperature with the steel under various hydrogen sulfide pressures. The formation of metal sulfide at the surface was found to be rapid. At 1 Pa pressure, essentially complete reaction takes place in 1 ms, and the surface kinetics are virtually independent of temperature. On the other hand, in the temperature domain investigated, log v_{II} vs reciprocal temperature (where v_{II} is the rate of crack propagation in the K-insensitive region of the v-K curve) exhibits only a positive slope with H_2S pressure of 133 Pa, whereas the v_{II} (1/T) curve exhibits a weak maximum with H_2S at 2.66 kPa. Furthermore, under 133 Pa pressure, v_{II} is proportional to $pT^{1/2}$, where p is the gas pressure, which is the same functionality as that for crack propagation controlled by the rate of

suppiy by Knudsen diffusion of gas molecules to the crack surface. For this reason, Knudsen diffusion of the gas was identified as the rate-limiting process for crack propagation under low-pressure H_2S gas. Under higher pressures, at the lower-temperature side of the weak maximum, the log v_{II} (1/T) curve is characterized by an activation energy of 4.6 ± 3.6 or 6.7 ± 6.7 kJ/g mol, depending on which segment of the curve is considered. Because these numbers lie within the range (4 to 10 kJ/g mol) of the activation energy for hydrogen in bcc iron reported in the literature, Lu, et al.,[56] concluded that in the higher-pressure region, crack propagation is kinetically controlled by the diffusion of hydrogen in the steel. It must be remarked that this conclusion is on weak ground because a better value for the apparent activation energy for diffusion of hydrogen in a high-strength steel is about 32 kJ/g mol.[57]

Model of Pasco, et al.

Neither of the foregoing investigations concerned itself with the intrinsic mechanism of embrittlement, nor with the existence of a maximum in the plot of log v_{II} vs 1/T (see Figure 4), which has been observed by many investigators. One way of qualitatively understanding such a dome-shaped curve is that the kinetically controlling process at low temperature differs from the controlling process at higher temperatures. Another way depends on writing the rate of the kinetically controlling step as the difference between two exponential terms. The latter was done by Pasco, et al.,[58-60] who considered that v_{II} is proportional to the rate of adsorption at some critical value (θ_c) of surface coverage by negatively charged hydrogen species (H^-). The rate of adsorption is written as follows:

$$\dot{n} = (dn_H/dt) = k_1 p^{1/2} \exp(-E_a/RT) - k_2 \exp(-E_d/RT)$$

and

$$v_{II} = \frac{1}{C^*}[k_1 p^{1/2} \exp(-E_a/RT) - k_2 \exp(-E_d/RT)]$$

where $1/C^*$ serves as the coefficient of proportionality and C^* is defined as a critical volume concentration of hydrogen in the metal through which the crack advances once this concentration is attained. In the above expressions, p is the hydrogen gas pressure, E_a is an effective activation energy = $(2E_a + E_m + \Delta H_a)/2$, where E_a is the activation energy for dissociative adsorption, E_m is the activation energy for surface diffusion, and ΔH_a is the enthalpy of adsorption. E_d is the activation energy for desorption. The parameter k_1 is the rate of physisorption of H_2 molecules, and k_2 is the specific rate constant for desorption at coverage θ_c. Thus, the authors have divided a net rate of increase of coverage of an existing surface by a volume concentration to obtain a dimensionally correct rate of surface increase (crack propagation), but the operation is devoid of physical significance - or if there is one, it has yet to be elucidated by the authors. What is interesting is that this form of equation represents the experimental data of Wei and collaborators[61-64] for v_{II} (1/T) very well, and also $v_{II}(p)$ at the temperatures of the maxima of the log v_{II} (1/T) curves. The basic idea of Pasco, et al., is similar to that in the earlier work of Williams and Nelson,[63] who also considered that the rate-controlling step is at the gas-metal interface and developed an equation that successfully represented the dome-shaped log v_{II} (1/T) curve at constant stress intensity that they measured for a fully hardened type 4130 (UNS G41300) steel. Although their specific model has been criticized,[64,65] the probability that the adsorption step is rate-limiting was strengthened by the finding by Nelson, et al.,[66] that the use of dissociated hydrogen gas produces a straight-line plot in place of the dome-shaped curve obtained with the use of molecular hydrogen gas. It would therefore appear that the dissociation of the H_2 molecule must be one of the kinetically controlling steps at the higher temperatures.

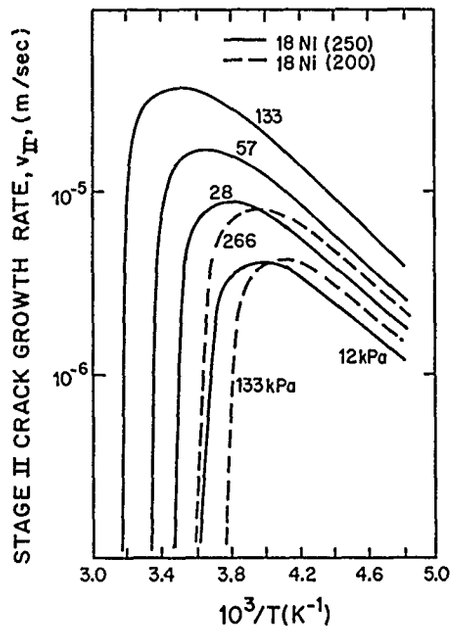


FIGURE 4—K-insensitive crack propagation rate vs reciprocal temperature for two-strength levels of maraging steel under various hydrogen gas pressures (Hudak and Wei[61]).

Model of Wei, et al.

Wei and collaborators[67-69] considered three possibilities for the kinetic control of the supply of hydrogen to the microstructural feature involved in cracking. These are as follows: (1) Knudsen flow of molecular gas in the narrow space between the walls of the crack (as discussed in a previous section), in which case the dependence of the flow upon gas pressure and temperature is as $pT^{-1/2}$. (2) Surface reaction control, expressed as $p^m \exp(-Es/RT)$ where E_s is an activation energy. Unlike the Pasco, et al., formulation, this control can only permit the hydrogen supply to increase with increasing temperature. (3) Diffusion control, expressed as $p^{1/2} \exp(-E_d/RT)$, in which E_d is an activation energy for diffusion of atomic hydrogen through the steel; again this term can only increase with increasing temperature.

Representing the three possible supply-control terms by $S_j(p,t)$, (j = 1,2,3), the central equations of Wei, et al., may be expressed as

$$v_{II} = \left[\sum_i (\alpha_i f_i k_i)\right] S_j(p,T),\ (j = 1, 2, \text{or } 3) \qquad (1)$$

in which the term in square brackets is the sum over the types of microstructure (grain boundaries, lattice, phase interfaces, etc.), the fracture of which contributes to crack propagation, and the argument of the summation sign is effectively the density of the hydrogen trapped at the i^{th} feature times the volume fraction (f_i) of that feature, times the "crackability" of that feature (α_i), i.e., its relative contribution to the rate of overall crack propagation (v_{II}) in the K-insensitive domain. In actual use, the summation is conducted only over two loci of cracking, grain boundaries (i = b) and lattice (i = l), so that the term in square brackets is written as follows.

$$\sum_i (\alpha_i f_i k_i) = \frac{\alpha_b f_b \tau\delta(a^3/n) N_x \exp(H_B/RT)}{1 + \tau\delta(a^3/n) N_x \exp(H_B/RT)} + \frac{\alpha_1 (1 - f_b)}{1 + \tau\delta(a^3/n) N_x \exp(H_B/RT)} \qquad (2)$$

in which a is the lattice parameter and n is the number of atoms per unit cell. In this relation, one need only note that H_B is the binding enthalpy of hydrogen to grain boundaries having a density N_x of trapping sites, and that τ deviates from unity if the trapped hydrogen is not in equilibrium with the lattice hydrogen.

It is clear that this formulation is not concerned with any specific embrittlement model, nor is there a critical hydrogen concentration or stress necessary for the cracking at a microstructural feature. Instead, the parameters (α_i) that should embody such concepts are evaluated, along with τN_x, by effectively curve fitting to experimental data of $v_{II}(T)$. In addition, a nonunity value of the parameter τ represents kinetic control other than that given by S_j, since the only way that lack of equilibrium among various populations of hydrogen can occur is through kinetic impediments. It is also clear that for S_j, representing either surface or diffusion control, Equation (1) can represent a dome-shaped curve of v_{II} (1/T) because S_j increases with increasing temperature and

$$\left[\sum_i (\alpha_i f_i k_i) \right]$$

decreases with increasing temperature.

For cracking under either of three pressures of hydrogen gas, the authors selected surface reaction control for S_j (p,T), for reasons that are not clear. They are therefore able to reproduce with Equation (1) their experimental v_{II} (1/T) data (see Figure 5). For cracking under H_2S gas (Figure 6), the authors selected Knudsen flow of gas as the controlling step at 0.133 kPa and in the higher-temperature domain at 2.66 kPa. At the latter pressure and at lower temperatures, hydrogen diffusion is taken to be the controlling step.

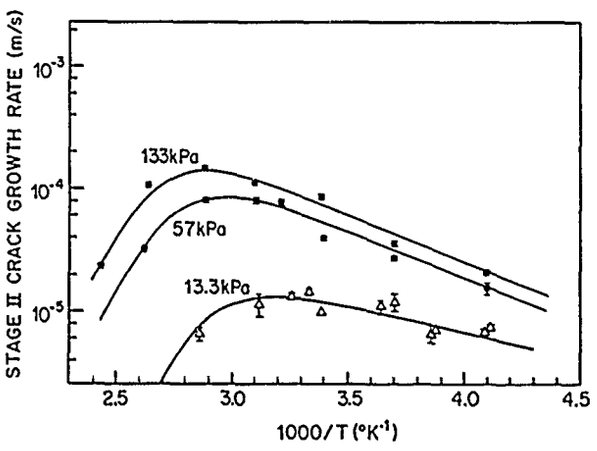


FIGURE 5—K-insensitive crack growth rate vs reciprocal temperature for type 4340 (UNS G43400) steel under hydrogen gas at each of three pressures. Points are experimental data, and the solid lines are best fit to the data of the analysis, assuming surface reaction control.[68]

Model of Gerberich, et al.

Gerberich and collaborators[70,71] have a similar approach for understanding the inverted-U shape of the log v_{II} (1/T) curve that they found for precharged type 4340 steel at two strength levels. Because their steels were cathodically precharged with hydrogen, followed by a baking treatment to distribute the hydrogen macroscopically uniformly, the controlling hydrogen supply kinetics was taken to be diffusion of atomically dissolved hydrogen in the steel. This yields a term that contributes to the increase of v_{II} with increasing temperature. The second term that contributes to the decrease of v_{II} with increasing temperature is, as with Wei, et al., that expressing the distribution between the microstructural features that serve as cracking locations (oxysulfide interfaces, martensite lath intersections with prior austenite grain boundaries) and the lattice. Because v_{II} is expressed as the product of these two contributions, Gerberich, et al., are able to reproduce their experimental dome-shaped log v_{II} (1/T) curves after evaluating the parameters of their equation by comparison with experiments.

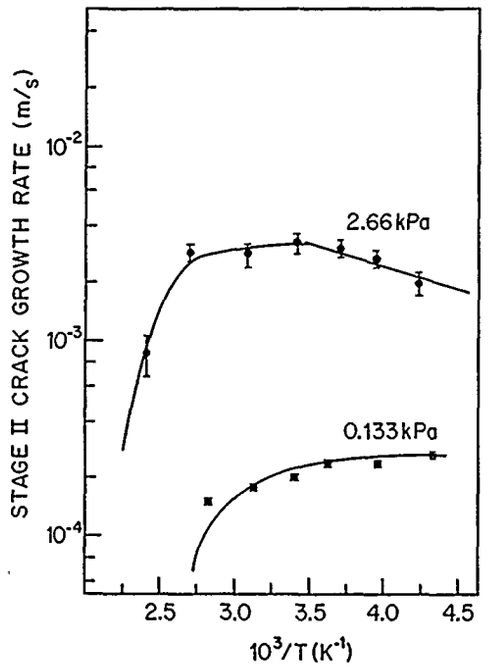


FIGURE 6—K-insensitive crack growth rate vs reciprocal temperature for type 4340 (UNS G43400) steel under each of two pressures of hydrogen sulfide gas.[68] The points represent experimental data. The solid lines are best fit to the data of the analysis, assuming Knudsen flow control at the higher pressure and higher temperatures, and also at the lower pressure. Hydrogen diffusion is taken as the controlling step at 2.66 kPa in the lower-temperature region.

Unlike Wei, et al., however, the approach of Gerberich is based explicitly on the decohesion model operating at one or the other of the microstructural features, depending on the temper of the steel, that are mentioned above. The concept is that the oxysulfide particle interfaces, for example, acquire a large population of adsorbed hydrogen that is enhanced by the tensile stress, and that the fracture stress (i.e., the interfacial cohesion) is reduced linearly by the thus-accumulated hydrogen. Cracking occurs locally when the maximum constrained flow stress, estimated via continuum mechanics, equals the hydrogen-reduced cohesion. The crack surfaces exhibit striations normal to the cracking direction that are convincingly deduced to be crack arrest markings; they have a fairly uniform spacing that is larger (~ 138 μm) for the lower-strength steel than for the higher-strength steel (~ 1 μm). This permits the development of an explicit relation for v_{II} by considering that the crack jumps a distance (X) equal to the striation spacing, beyond the hydrogen-enriched location, and that a time (t_i) is necessary for hydrogen to accumulate at the new crack front by diffusion with trapping, which is motivated both by concentration and by stress gradients. The crack is deemed to advance by this kind of intermittent decohesion at many localities at the crack front, leaving behind regions, or ligaments, that subsequently fail by ductile mechanisms.

There are difficulties in the details of the formulation and in the concepts. For example, the diffusion equation used is that of Doig and Jones,[72] which was developed for a point source and is therefore inappropriate for an initially homogeneous field of hydrogen. The stress field contributing to the diffusion is that of the continuum mechanical elastic plastic solution, which cannot yield stresses large enough to cause decohesion. The expression used for the effective (trapped) diffusivity is that of Ellerbrock, et al.,[73] which contemplates molecular hydrogen within microvoids. Nevertheless, it is satisfying that this kinetic model was couched in terms of the decohesion model and successfully represents the experimental results.

The most serious conceptual deficiency has to do with the intermittent nature of the crack advance. Within the framework of the decohesion model, there is no way that the crack front can get ahead of the hydrogen-enriched region;[12,19] the crack can advance at a given position only as fast as the critical concentration of hydrogen, consistent with the local stress, can accumulate there. Any intermittency in crack advance necessarily implies the intervention of another mechanism. One possibility is that the ligaments left behind between decohered regions, subsequently failing by plastic collapse, cause the local stress intensity to increase at the crack front so that, after the interval required for that failure, once again the decohesion criterion is satisfied at the crack front and decohesive advance can resume. Another possibility[(1)] is that crack inertia causes the decohered crack propagating in a hydrogen-rich region to continue into a hydrogen-poor region until arrested by energy loss mechanisms, as hypothesized by Sieradzki and Newman[74] for the stress corrosion cracking of copper. After the arrest, the crack must await the accumulation of enough hydrogen to satisfy the decohesion criterion.

Kameda's model

A purely thermodynamic analysis along the lines of the Petch-Stables idea is conducted by Kameda.[75] He calculates the work required to advance a crack along a grain boundary by considering the modification by hydrogen of the grain-boundary energy and of the crack surface energy He assumes that the crack-tip contour is that of two circular arcs intersecting at an angle controlled by the hydrogen-affected grain boundary and crack-surface energies, but does not permit plastic deformation that would be needed to achieve such a configuration The crack tip is shielded by a dislocation array ahead of the crack, which is carried along by the advancing crack. The energy balance includes elastic energy, which is a function of the crack-tip geometry, itself controlled by the hydrogen adsorption. Kameda considers two extremes, slow crack advance, so equilibrium partitioning of hydrogen to the interfaces is achieved, and rapid fracture, such that hydrogen is not partitioned but remains distributed as it was before the crack advanced.

The dependence of crack velocity (v) upon stress intensity (K) is formulated in terms of one-dimensional diffusion of hydrogen only along the grain boundary, neglecting volume diffusion, and precharged specimens are considered. For the kinetic analysis, Kameda restricts himself to steady-state, slow crack advance, considering stresses to be constant within any one region around the crack but different in different regions. The resulting log v(K) curves show approach to a threshold value and a domain of smaller positive slope; there is not a K-independent region. The dependence on temperature was not explored. Comparison with experimental data was not conducted.

Model of Lee and Unger

This analysis[76] is based upon the decohesion concept and attempts to deal with the entire v(K) curve as a function of temperature also. Unfortunately, it assumes that the cohesive force is independent of the interatomic separation; however, it is lowered by a hydrogen concentration in linear fashion. Hydrogen diffuses in response to concentration gradients; stress-gradient-induced diffusion is neglected A nonphysical criterion for crack propagation, a critical crack-opening displacement (δ_c) is introduced. Crack propagation is said to be accompanied by a diminution of the crack-opening displacement, but inconsistently the crack continues, even though $\delta < \delta_c$, until an arbitrarily introduced value (δ_A) is reached. In this way, the intermittent nature of crack propagation is unphysically built into the model, since diffusion must now occur to the new crack position.

The v(K) curves thus developed are shown in Figure 7. A Stage II of K-independent behavior is not generated. However, if the activation energy for diffusion is allowed to increase with increasing stress (or with crack length at constant load), then plateaus are obtained. It is clear that dome-shaped logs v_{II} (1/T) are not generated by inclusion of this unphysical assumption.

Conclusion

It is clear that despite the valiant efforts that have been exerted, much remains to be done in kinetic modeling. None of the models is complete in the sense of having incorporated all of the factors and phenomena that are known to be present in hydrogen-aided crack propagation All of the models are at best descriptive, not predictive, since they must use empirical information to evaluate parameters. Only one model, that of Gerberich, et al.,[70 71] is based solidly on an embrittlement mechanism One of the most difficult yet essential aspects to be incorporated in future modeling is the existence of more than one cracking mode during the overall advance of the crack, cleavage and plastic tearing, for example, both occur with the ratio of plastic failure to cleavage increasing with increasing stress intensity.[19,77] The fact of the sporadic advance of the crack is probably intimately involved with the mode not directly related to hydrogen-aided decohesion or to hydrogen-enhanced localized slip.

Future progress in elucidating hydrogen-aided cracking depends on further advancement in understanding fracture processes in the absence of hydrogen. For example, the magnitude of stresses built up at interfaces because of plastic incompatibility across the interface, stress gradients about the crack, dislocation dynamics and configuration, interfacial cohesion as a function of impurities, and the problem of crack inertia must be better understood. Following this, one must elucidate the effects of hydrogen on each of these phenomena separately. Finally, the synergistic interaction among the cracking modes must be understood and incorporated into a kinetic model of crack propagation.

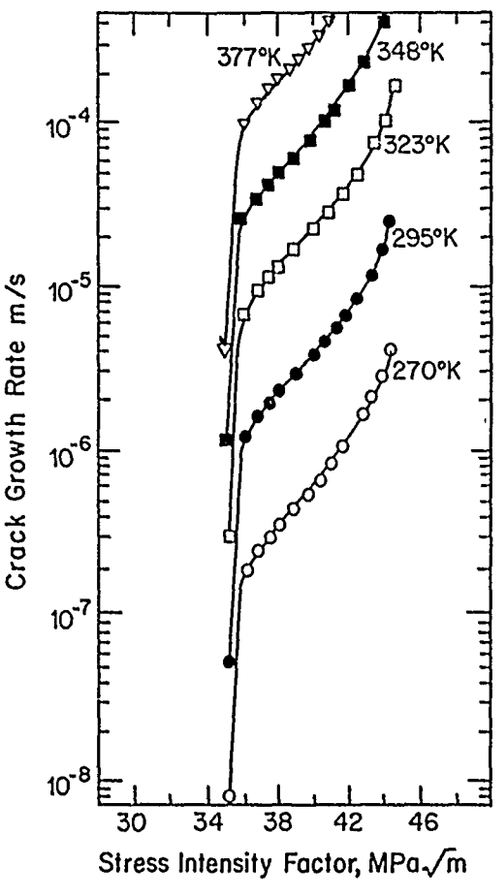


FIGURE 7—Crack velocity vs stress-intensity parameter. Modelistic calculations of Lee and Unger.[76]

[(1)]The idea of this possibility was mutually generated during an extended discussion with W.W. Gerberich.

References

1. R.A. Oriani, Ann. Rev. Mater. Sci. 8(1978): p. 327.
2. R.A. Oriani, Corrosion 43, 6(1987): p. 390.
3. G.E. Kerns, R.W. Staehle, Scripta Metall. 6(1972): p. 1189.
4. C. Zapffe, C. Sims, Trans. AIME 145(1941): p. 225.
5. A.S. Tetelman, W.D. Robertson, Trans. TMS-AIME 224(1962). p. 775.
6. M.E. Armacanqui, R.A. Oriani, Mater. Sci. Eng. 91(1987). p. 143.
7. N.J. Petch, P. Stables, Nature 169(1952). p. 842, N.J. Petch, Phil. Mag. 1 (Ser. 8) (1965): p. 331.
8. L.B. Pfeil, Proc. Royal Soc. (London) A112(1926). p. 182.
9. R.P. Frohmberg, W.J. Barnett, Trans. ASM 47(1955): p. 892.
10. P. Blanchard, A.R. Troiano, Mem. Sci. Rev. Metall. 57(1960): p. 409.
11. E.R. Slaughter, E.E. Fletcher, A.R. Elsea, G.K. Manning, WADC Tech. Report, p. 56, 1956.
12. R.A. Oriani, Ber. Bunsen Gesellsch. Phys. Chem. 76(1972): p. 848.
13. R.A. Oriani, Stress Corrosion Cracking and Hydrogen Embrittlement of Iron Base Alloys, NACE-5, ed. R.W. Staehle, J. Hochmann, R.D. McCright, J.E. Slater (Houston, TX: National Association of Corrosion Engineers, 1977), p. 351.
14. J.C. M. Li, R.A. Oriani, L.S. Darken, Z. Physik Chem. (N.F.) 49(1966): p. 271.
15. R.A. Oriani, Scripta Metall. 13(1979): p. 469.
16. C.D. Beachem, Metall. Trans. 3(1972): p. 437.
17. S.P. Lynch, Metals Forum 2(1979): p. 189.
18. S.P. Lynch, Scripta Metall. 13(1979). p. 1051.
19. R.A. Oriani, P.H. Josephic, Acta Metall. 22(1974): p. 1065.
20. R.A. Oriani, P.H. Josephic, Acta Metall. 25(1979). p. 979.
21. H.K. Birnbaum, M. Grossbeck, Hydrogen in Metals, ed. I.M. Bernstein, A.W. Thompson (Metals Park, OH. ASM International, 1974), p. 303.
22. S. Gahr, H.K. Birnbaum, Acta Metall. 26(1978). p. 1781.
23. G.R. Caskey Jr., Hydrogen Degradation of Ferrous Alloys, ed. R. A. Oriani, J.P. Hirth, M. Smialowski (Park Ridge, NJ. Noyes Publication, 1985), p. 822.
24. J.C. Swearengen, F.A. Greulich, J. Lipkin, Environmental Degradation of Engineering Materials in Hydrogen, ed. M.R. Louthan Jr., R.P. McNitt, R.D. Sisson (Blacksburg, VA. Virginia Polytechnic Institute, 1981), p. 303.
25. P.J. Grobner, V.A. Biss, Environmental Degradation of Engineering Materials in Hydrogen, p. 261.
26. R.A. Oriani, P.H. Josephic, Scripta Metall. 6(1972): p. 681.
27. J.J. Gilman, Plasticity, Proceedings of the 2nd Symposium Naval Struct. Mech. (Oxford, England: Pergamon Press, 1960), p. 43.
28. W.W. Gerberich, Y.T. Chen, Metall. Trans. 6A(1975): p. 271.
29. W.W. Gerberich, J. Garry, J.F. Lessar, Effect of Hydrogen on Behavior of Materials, ed. A.W. Thompson, I.M. Bernstein (New York, NY: American Institute of Mining, Metallurgical, and Petroleum Engineers, 1976), p. 70.
30. S.K. Banerji, C.J. McMahon Jr., H.C. Feng, Metall. Trans. 9A(1978): p. 237.
31. C.J. McMahon Jr., M.J. Morgan, Hydrogen Degradation of Ferrous Alloys, p. 608.
32. H. Vehoff, W. Rothe, Acta Metall. 31, p. 1781.
33. S.P. Lynch, Acta Metall. 31.
34. H. Vehoff, C. Laird, D.J. Duquette, Acta Metall. 35(1987): p. 2877.
35. H.A. Wriedt, R.A. Oriani, Scripta Metall. 8(1974): p. 203.
36. E. Lunarska, A. Zielinski, M. Smialowski, Acta Metall. 25(1977). p. 305.
37. A. Magerl, B. Berre, G. Alefeld, Phys. Stat. Sol. (a) 36(1976). p. 161.
38. T. Springer, Hydrogen in Metals, ed. I.G. Alefeld, J. Volke (New York, NY: Springer-Verlag, 1978), p. 75.
39. J.M. Rowe, N. Vagelatos, J.J. Rush, Phys. Rev. B12(1975): p. 2959.
40. A.J. Markworth, J.H. Holbrook, Hydrogen Degradation of Ferrous Alloys, p. 535.
41. R.P. Messmer, C.L. Briant, Hydrogen Degradation of Ferrous Alloys, p. 140.
42. M.S. Daw, S.I. Baskes, Phys. Rev. Lett. 50(1983): p. 1285; Phys. Rev. B29(1984). p. 6443, Sandia Report SAND 86-8863, Sandia Natl. Labs., Albuquerque, NM, NATO Adv. Workshop on Physics and Chemistry of Fracture, Bad Reichenhall, W. Germany, 1986.
43. T. McMullen, M.J. Stott, E. Zaremba, Phys. Rev. B35(1987): p 1076.
44. R.A. Swalin, Thermodynamics of Solids (New York, NY: J. Wiley and Sons, 1972).
45. M.W. Finnis, J.E. Sinclair, Phil. Mag. A 50(1984): p. 45.
46. K. Masuda-Jindo, Mater. Let. 5(1986): p. 45.
47. F. Nakasato, I.M. Bernstein, Metall. Trans. 9A(1978): p. 1317.
48. A. Inoue, Y. Hosoya, T. Masumoto, Tetsu-to-Hagane 65(1979): p. 535 in Japanese; Research Article 433 in English.
49. J. Eastman, T. Masumoto, N. Narita, F. Henbaum, H.K. Birnbaum, Conf. Proc. Met. Soc. (New York, NY. AIME, 1981), p. 397.
50. H.K. Birnbaum, Atomistics of Fracture, ed. R.M. Latanision, J.R. Pickens (New York, NY: Plenum Press, 1983), p. 1983.
51. T.Y. Zhang, W.Y. Chu, Y. Li, C.M. Hsiao, Metall. Trans. 17A(1986): p. 717.
52. A. Kelly, M.R. Tyson, A.H. Cottrell, Phil. Mag. 29(1974): p. 73.
53. J.R. Rice, R. Thomson, Phil. Mag. 29(1974): p. 73.
54. R. Thomson, Hydrogen Degradation of Ferrous Alloys, p. 454.
55. G.W. Simmons, P.S. Pao, R.P. Wei, Metall. Trans. 9A(1978): p. 1147.
56. M. Lu, P.S. Pao, T.W. Weir, G.W. Simmons, R.P. Wei, Metall. Trans. 12A(1981): p. 805.
57. P. Kedzierzawski, Hydrogen Degradation of Ferrous Alloys, p. 251.
58. R.W. Pasco, K. Sieradzki, P.J. Ficalora, Scripta Metall. 16(1982). p. 881.
59. R.W. Pasco, P.J. Ficalora, Acta Metall. 31(1983). p. 541.
60. R.W. Pasco, P.J. Ficalora, Hydrogen Degradation of Ferrous Alloys, p. 199.
61. S.J. Hudak Jr., R.P. Wei, Metall. Trans. 7A(1976). p. 235.
62. R.P. Gangloff, R.P. Wei, Metall. Trans. 8A(1977). p. 1043.
63. D.P. Williams, H.G. Nelson, Metall. Trans. 1(1970): p. 63.
64. R.A. Oriani, Metall. Trans. 1(1970): p. 2346.
65. V. Sawicki, H.H. Johnson, Metall. Trans. 2(1971): p. 3496.
66. H.G. Nelson, D.P. Williams, A.S. Tetelman, Metall. Trans. 2(1971): p. 953.
67. M. Gao, M. Lu, R.P. Wei, Metall. Trans. 15A(1984): p. 735.
68. M. Gao, R.P. Wei, Metall. Trans. 16A(1985): p. 2039.
69. R.P. Wei, M. Gao, Hydrogen Degradation of Ferrous Alloys, p. 579.
70. W.W. Gerberich, T. Livne, X. Chen, Modeling Environmental Effects on Crack Growth Processes, ed. R.H. Jones, W.W. Gerberich (New York, NY: The Metallurgical Society-AIME, 1986), p. 243.
71. W.W. Gerberich, T. Livine, X.F. Chen, M. Kaczorowski, Metall. Trans. 19A(1988): p. 1319.
72. P. Doig, G.T. Jones, Metall. Trans. 8A(1977): p. 1993.
73. H.G. Ellerbrock, G. Vibrans, H.P. Stuwe, Acta Metall. 20(1972): p 53.
74. K. Sieradzki, R.C. Newman, Phil. Mag. A 51(1985): p. 95.
75. J. Kameda, Acta Metall. 34(1986): p. 867.
76. S.L. Lee, D.J. Unger, Eng. Frac. Mech. 31(1988). pp. 647-660.
77. G.E. Kerns (Ph.D. diss., Ohio State University, 1973), V.R. Sawicki Jr. (Ph.D. diss., Cornell University, 1971), reported by G.E. Kerns, M T. Wang, R.W. Staehle, Stress Corrosion Cracking and Hydrogen Embrittlement of Iron Base Alloys, p. 700.

Discussion

K. Sieradzki (The Johns Hopkins University, USA): In your talk you mentioned that fracture mechanics may not be useful with regard to defining mechanical parameters important to the hydrogen embrittlement problem, owing to nonlinear crack-tip processes. Our recent molecular dynamic results [Sieradzki, Dienes, Paskin, and Massoumzadeh, Acta Metall 36(1988). p. 651] do not support your statement The results for our nonlinear elastic material indicate that linear elastic fracture mechanics (LEFM) solutions are approached within several atomic units from the crack tip. Additionally, LEFM descriptions of the energy balance during fracture are in excellent agreement with our molecular dynamic results.

R.A. Oriani: My understanding of fracture mechanics is that details such as the stress at the tip of a dislocation pile-up or the stress existing within a few angstroms of an atomically sharp crack are not calculable by that approach However, if recent developments of which I am not aware have enabled fracture mechanics to quantify such situations, I stand happily corrected.

K. Sieradzki: I believe that the effects you discuss can only be important if the hydrogen embrittlement mechanism operates within this nonlinear "core" region.

R.P. Gangloff (University of Virginia, USA): Given the limited experimental confirmations of decohesion, I suggest two areas for future research. We have previously discussed the importance of obtaining threshold local stress (or stress intensity) as a function of embrittler activity for solid or liquid metal systems. Here, the surface location of crack formation is reasonable and in contrast to the uncertain location of hydrogen-induced decohesion within a crack-tip process zone. I presume from your comments that such data have not been reported to date.

R.A. Oriani: I agree with the idea that curves of embrittler thermodynamic activity vs threshold stress intensity for liquid metal embrittlement (LME) should be experimentally determined. This is in fact the suggestion I made at the Firminy Conference and that I repeated earlier this week in a comment following Stoloff's paper. To my knowledge, such data for LME are nonexistent.

R.P. Gangloff: On another point, I suggest that the K-based decohesion derivation should be reformulated to reflect the three-dimensional character of hydrogen effects on microstructural weak links (high local hydrogen, strain incompatibility) throughout the process zone. The statistics for this analysis have been largely worked out by Lin, Evans, and Ritchie [J. Mech. Phys. Solids 34(1986). p. 477] and support the idea of hydrostatic and opening stresses over a critical microstructural distance.

R.A. Oriani: I would welcome a reformation of the decohesion model to incorporate the effects of microstructural features that are not only mechanically weak, but also are the loci of high hydrogen concentrations.

T. Murata (Nippon Steel Corporation, Japan): In practical high-strength steels, it is typical to have intergranular hydrogen embrittlement in proportion to the steel's strength level. How can we explain the competitive cracking between quasicleavage-type cracking and intergranular cracking?

R.A. Oriani: I am sorry to say that I have not thought about the correlation to which you allude, and that I cannot make any useful comments at this time.

R.E. Ricker (National Institute of Standards and Technology, USA): In the discussion section of his 1972 paper, Beachem [Metall. Trans. 3(1972): p. 437] pointed out that both his model and the decohesion model depend on the weakening of the interatomic bonding forces by hydrogen. The key difference between the models is in how this effect is manifested. That is, whether or not fracture results from alternate slip or cleavage. Can we make this distinction unambiguously and, if so, how?

R.A. Oriani: Your question echoes one of the points of my presentation, that a most important task for the future is to determine in specific cases the degree to which the two manifestations of bond weakening, alternate slip, and cleavage contribute to cracking. I have mentioned the work of Vehoff and Rothe as an example that was successful in demonstrating hydrogen-induced cleavage. I suspect that a fruitful approach may be through a controlled mixing of crack-opening modes.

Stress Corrosion Cracking and Corrosion Fatigue of Martensitic, Ferritic, and Ferritic-Austenitic (Duplex) Stainless Steels

*H. Spaehn**

Abstract

The stress corrosion cracking (SCC) and the corrosion fatigue (CF) of martensitic, ferritic, and ferritic-austenitic (duplex) stainless steels (SSs) are reviewed with emphasis on the influence of technologically important parameters such as alloy chemistry, heat treatment, strength level, and passivating properties of the environment.

The SCC susceptibility of martensitic SSs is related to a continuous chromium-depleted concentration profile around the prior austenite grain boundaries, full SCC resistance is regained by the industrially applied tempering temperatures that will level this gradient by overlapping diffusion fields from the coarsening effects of $Mo_{23}C_6$ precipitates in the prior austenite and martensitic interlath grain boundaries. The modern nickel martensitic SSs appear to follow a slip-step emergence/repassivation mechanism in anodic SCC. The cathodic mechanism seems to be complicated in sour gas environments where a pile-up of hydrogen at the martensite/retained austenite interphases and an interaction of hydrogen atoms with dislocations generated by the incompatible deformation of the two phases will lead to transgranular SCC at elevated strains in the double-tempered heat-treatment condition. These steels are more susceptible in the single-tempered condition; they fail in an intergranular mode that requires a shorter path and smaller fracture energy per unit crack extension. Straight Fe-Cr low interstitial ferritic SSs are immune to anodic chloride SCC if properly annealed. SCC initiation results from slip-step evolution by which film rupture and the formation of trenches is induced, thus starting an occluded cell mechanism.

Ferritic-austenitic SSs have found considerable application since 1973. Their SCC mechanism is closely coupled to an interplay of mechanical and electrochemical phenomena. Ferrite depassivation is determined by mechanical twinning at high strains and by glide processes in the austenite, the latter being cathodically protected by the ferrite. Therefore, in anodic SCC, crack propagation takes place in the ferritic phase at much higher threshold stresses than in austenitic SSs. Cathodic SCC of these steels appears to follow a chloride-induced mechanism in H_2S-containing solutions.

In CF, these SSs show essentially the same characteristic features. It can be classified in four modes.

Mode I. CF in the active state,
Mode II. CF in the stable passive state,
Mode III. CF under metastable passivity and endogenous activation, and
Mode IV. CF under metastable passivity and exogenous activation.

CF cannot occur under passive conditions if, under external cyclic loading, the plastic work becomes zero per cycle and per volume element as the most stringent condition, or if, in the course of cyclic deformation, any manifestation of plastic deformation at the surface (slip lines or bands, extrusions, intrusions) will be unable to penetrate the passive layer. Achieving the highest strength in Mode II CF requires a minimum passivation current density and the smallest difference between the air fatigue limit and the limiting stress at which critical dislocation-induced surface plasticity accrues.

Three steps can be discerned by an electrochemical transient measuring technique in Mode II CF of all SSs under potentiostatic conditions in rotating bending:

(1) Small stochastic current transients caused by the response of the passive layer to the alternating stress in an incubation period;
(2) Small sinusoidal current signals with a constant phase angle with respect to the spatially fixed plane of maximum bending moment; they determine the future position of a CF crack and are caused by emerging slip steps (initiation period); and

*BASF Aktiengesellschaft, Technische Entwicklung/Werkstofftechnik, D-6700 Ludwigshafen, Federal Republic of Germany.

(3) Steadily growing signals resulting from continuous repassivation processes at the crack tip (crack growth period).

By means of this technique, under potentiostatic conditions, the first interactions between cyclic slip processes and environment can be detected that establish crack initiation on a submicroscopic scale, determine the position of future cracks, and allow a differentiation between growing and dormant incipient cracks.

Introduction

Because of their corrosion resistance, steels of this kind are widely used in different process industries such as chemical and petrochemical industries, food processing, pulp and paper, gas and oil industries, steam generation, fossile, hydroelectric and nuclear power generation, etc. SCC is of concern to these industries and can be considered from different points of view. It is a process of highly localized (electrochemical) events that may produce losses in production, products, and equipment. The same holds true for corrosion fatigue (CF) Both of these types of environment-induced cracking also may pose certain hazards. For this reason, much work has been done in this area both for this class of SSs and the austenitic SSs to be dealt with in the subsequent contribution. SCC and CF can be regarded as electrochemically governed processes leading to an extremely localized form of corrosion. In fact, the finest cracks ever observed are those caused by CF in environments that put the steels in question into a state of stable passivity. Many factors exert an influence on both initiation and crack propagation under SCC and CF conditions, among them microstructure, alloy chemistry, nonmetallic inclusions, electrochemical conditions (like thickness and stability of passive films), sensitization, and, of course, mechanical loading conditions. From the fracture mechanics point of view, SCC and CF are specific sorts of subcritical crack growth leading to growth rates between 10^{-10} and 10^{-4} m/s in the former case, and a wide range of crack extension rates per cycle in the latter. SCC may be transgranular or intergranular, whereas in CF the transgranular mode prevails. The decisive electrochemical partial reaction in the corrosion process of CF is in most cases anodic. Many SCC systems are also anodic in nature ("active path mechanism"). However, there are many instances where the cathodic partial reaction in SCC is responsible for cracking; hardenable SSs, like martensitic SSs, are especially prone to cracking. This species of SCC may be termed "cathodic SCC" because of the decisive role played by the cathodic partial reaction. Synonyms are "hydrogen embrittlement," "sulfide stress cracking," "sulfide SCC," and "hydrogen-induced cracking," among others.

For both anodic and cathodic SCC, three conditions must be fulfilled in a SS/environment system to produce SCC:

(1) The steel must be susceptible to SCC, which can be, among other things, a question of its microstructure, hardness, or alloy chemistry Favoring anodic SCC are, for instance, an austenitic microstructure, nickel contents (though small) in ferritic SSs, or, in chloride-induced SCC, segregations of Cr or Mo that lower the pitting resistance locally Cathodic SCC is, among other factors, favored by high second-order residual stresses, produced in hardenable SSs in the heat-affected zone (HAZ) of weld seams when certain precautions are not taken.

(2) The environment must lead to some sort of corrosion causing anodic dissolution to induce an active path mechanism or hydrogen-ion discharge causing cathodic SCC especially in the presence of substances suppressing the recombination of H to molecular H_2 The anodic dissolution process must be localized. For this reason, a local breakdown of passivity is a specific feature of anodic SCC systems. By the same token, halides (except fluorides) play a major role in such systems because they are able to produce point defects in the passive layer.

(3) There must be sufficiently high tensile stresses resulting from external loading and/or internal tensile stresses.

CF differs in several respects from SCC. It is, of course, bound to the presence of tensile stresses in the load spectrum; purely compressive stresses will not produce CF cracks. In contrast to SCC, there are no other specific prerequisites. Thus, CF may occur under extremely low-cycle fatigue conditions on the one hand, and in the ultrasonic frequency range on the other. The load may be sinusoidal or stochastic and the corrosion system active or passive.[1]

Scope of Review

The following text will deal with the SCC behavior of martensitic steels, including precipitation hardening and maraging SSs and also ferritic and ferritic-austenitic SSs ("duplex steels"), with some paragraphs on the newer nickel martensitic SSs ("soft" martensitic SSs). Since the metallurgical and other features of these classes of steels have been comprehensively covered elsewhere,[2,3] they will not be dealt with in this context. The CF behavior in these alloy environment systems can be unambiguously classified in four modes,[4] allowing each to be reviewed in the same format. The alloys in question differ somewhat in their SCC behavior, and they will therefore be treated one after the other, distinguishing between anodic and cathodic SCC where it is pertinent or has been investigated.

Emphasis will be put on experimental findings and those mechanistic aspects that are of relevance to engineering applications.

SCC of Martensitic SSs

Because of their high yield strengths (YSs), this class of SSs finds wide application for highly stressed components. It comprises the straight 12% Cr steels from which the so-called Super 12% Cr steels evolved, and a second group based on 17% Cr that has found application in the machine-building industry for shafts, axles, pump parts, and valves. A specific domain of the 13Cr SSs are turbine running blades. Their spectrum of properties comprises the ability to be heat treated in large sections (which may be even larger for the Super 12Cr SSs), a high damping capacity (essential for turbine blades), good resistance against thermal shock, fatigue, and hot, pressurized molecular hydrogen.

Anodic SCC of martensitic SSs

Their SCC resistance is, in certain media, limited. For a type 410 (UNS S41000) SS in boiling 70% NaOH solution, it has been shown[5] that intergranular SCC will be produced in all heat-treatment states (as-received, annealed, quenched, tempered) and the YSs involved. Cracking occurred at stress levels from 10 to 100% of the yield stress, and time-to-failure increased under both cathodic and anodic polarization except for the quenched and tempered condition, where there was no increase under anodic polarization. The shortest time-to-failure was observed for quenched and tempered material. Since SCC occurred at -300 mV with respect to the corrosion potential, a value that lies in the immunity region of the Pourbaix diagram, hydrogen embrittlement evidently contributes to the cracking process.

This class of steels is susceptible to SCC in aqueous chloride solutions, too.[6] It has been shown[7] that, when heat treated to a strength level of 1380 MPa, these steels are susceptible in marine and semi-industrial atmospheres, the minimum stress for SCC being about 1200 MPa. In NaCl and NH_4Cl, the latter being more aggressive, these steels have been found to undergo SCC at YS levels between 175 and 600 MPa. Cathodic polarization decelerates SCC in NaCl solutions and accelerates it in NH_4Cl solutions, whereas

anodic polarization accelerates it in all chloride solutions. Cathodic polarization inhibits SCC in NaCl (pH 5.1), in which it is completely prevented at pH 6.2.

An influence of cations on SCC has been reported in other systems, for instance, in nitrate solutions, where NH_4^+ is more aggressive than $Ca(NO_3)_2$ or $Na(NO_3)$.[8-11] Figure 1 represents schematically the effect of anodic and cathodic polarization[5,6] on the time-to-failure in chloride solutions, from top to bottom. NaCl, pH 6.2, NaCl, pH 5 1, NH_4Cl, pH 5.1. The active path mechanism for NaCl had been noticed earlier.[12] The NH_4Cl results are in agreement with older work, too, where hydrogen embrittlement had been demonstrated as the underlying mechanism for SCC.[13] Figure 1 demonstrates that anodic polarization accelerates SCC in all chloride solutions, a change in pH having only a moderate effect.

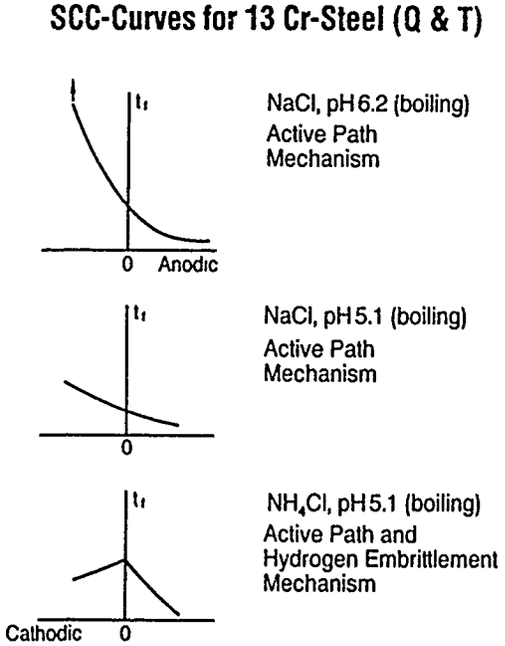


FIGURE 1—Active path and hydrogen embrittlement mechanisms in SCC systems (quenched and tempered 13Cr SS). Response of time-to-failure (t_f) to anodic and cathodic polarization, respectively. (Reprinted with permission.[6])

In more recent work,[14] SCC of such steels at high YS levels has been explained by a hydrogen embrittlement process at potentials more noble than the open-circuit potential: By hydrolysis of anodic dissolution products, the necessary conditions for hydrogen uptake by the alloy may be fulfilled.

The SCC behavior of quenched and tempered 12Cr SS has been investigated in other solutions, too. To recognize the effect of substituting Na^+ by NH_4^+, boiling solutions of 10% Na_2SO_4, 10% $(NH_4)_2SO_4$, 3% NaCl, 3% NH_4Cl, 70 % NaOH, and 60% Na_2S were used, respectively. A 410 SS, after solution heat treatment and air cooling, was tempered at about 600°C. Under such conditions, this steel is extremely sensitive to SCC in the above solutions and will fail at all stress levels between 10 and 100% of its yield stress. Again, with the exception of NH_4Cl, SCC is accelerated under anodic and decelerated under cathodic polarization.[15] In NH_4Cl, an active path and hydrogen embrittlement mechanism is operative as shown in Figure 1.

Early work indicated[13] that an optimum corrosion resistance will be obtained by simply quenching such steels from the austenite region, a heat treatment that is not applicable in practice because of the low toughness values obtained. Tempering leads to carbide precipitations at grain boundaries in martensitic SSs producing an almost continuing network of grain-boundary precipitations just above 500°C and a susceptibility to intergranular corrosion. In fact, SCC under the conditions described has been shown to be intergranular.[15]

An important result[16] is presented in Figure 2. Quenched, untempered martensite exhibits much faster crack growth rates and a definitely lower K_{ISCC} than the tempered material in a concentrated NaCl solution (22%). It can be expected that the industrially preferred tempering range between 700 and 750°C will improve the SCC resistance even more. This becomes evident[17] from long-time constant-load tests (Figure 3) with industrially heat-treated 13Cr- and 17Cr-2Ni martensitic SSs, Figure 3 points out a factual situation that will be dealt with later, i.e., the SCC immunity of low, interstitial ferritic steels in concentrated chloride solutions. It clearly exhibits a pronounced threshold stress for the 13Cr SS in 35% $MgCl_2$ (125.5 C). At the same time, the negative influence of nickel additions is displayed in Figure 3 showing the lowering of the SCC threshold stress.

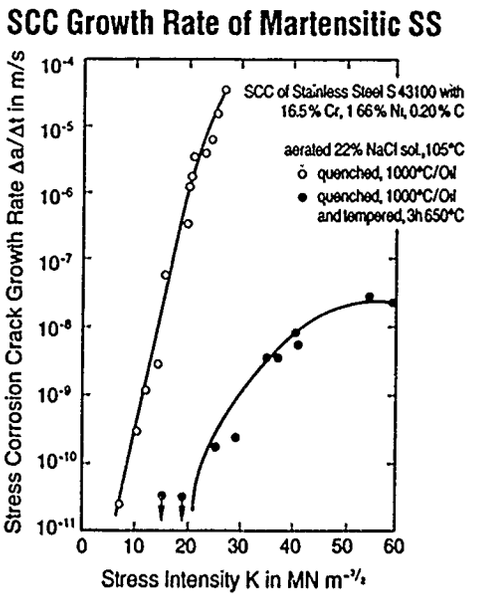


FIGURE 2—Influence of heat-treatment conditions on the subcritical stress corrosion growth rate of a nickel-bearing SS as a function of stress intensity. In the as-quenched condition, the steel shows much faster crack growth rates. (Reprinted with permission.[16])

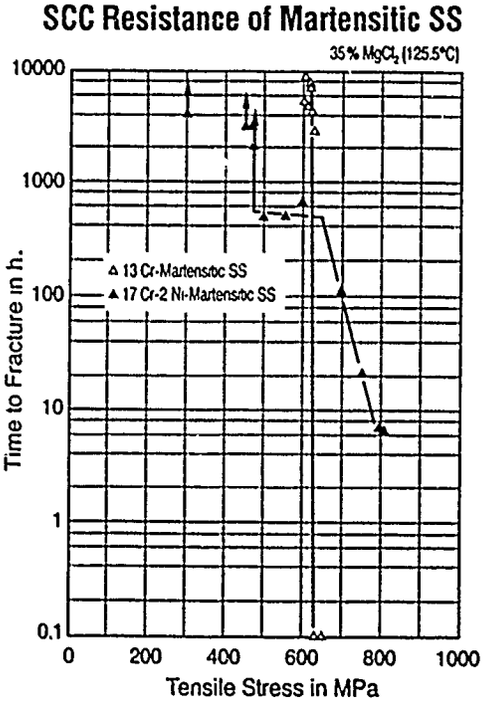


FIGURE 3—Long-time constant-load tests demonstrating a distinct SCC threshold stress in the case of a straight 13Cr martensitic SS as opposed to a nickel-bearing SS.[17]

The maximum effect of tempering on the growth rate of stress corrosion cracks is associated with the 475°C embrittlement. At higher tempering temperatures, up to 550°C, the crack growth rate is progressively reduced. It is interesting that, in fracture mechanics double-cantilever beam specimens, SCC occurs[18] with a velocity of $> 10^{-4}$ m/s in distilled water at 475°C tempering temperature (K about 50 MPa $\sqrt{m}$).

The striking fact that tempered martensitic Cr SSs can undergo intergranular SCC in sulfate solutions has been investigated for a tempered type 403 (UNS S40300) SS in 0.01 M Na_2SO_4 solution. Above some critical anodic potential at temperatures of 75 and 100°C, but not at 50 and 25°C, the steel suffers from SCC. Whereas the sulfur in the passive film increases with decreasing solution pH and is only weakly dependent upon temperature, the SCC susceptibility trend is in the opposite direction. Sulfur contaminations from the solution thus cannot be the prime cause of localized attack. It could be demonstrated[19] that a corrosion attack starts at the boundaries between nonmetallic inclusions of MnS and Cr carbide, respectively, and the passivated metal that leads to the formation of pits acting as sites for crack nucleation.

The foregoing findings and many others[20-24] have revealed clearly that martensitic SSs may be susceptible to intergranular SCC depending on environment and tempering temperatures. This susceptibility must be related to the development of nonequilibrium solute concentration profiles at the grain boundaries. They result from heterogeneous, intergranular precipitation reactions.[25-29]

Solute concentration profiles, usually much less than 1 μm in extent, have been investigated by means of scanning transmission electron microscopy (TEM) in combination with energy dispersive x-ray analysis.[30] Figure 4 shows instructive plots of hardness levels defining the boundary for intergranular SCC as a function of tempering temperature. The different curves correspond to different assumed values for critical diffusion-controlled chromium concentration profile widths of 35, 70, and 100 nm, respectively. These results refer to a Super 12% Cr-Mo-V martensitic SS and 0.01 M NaOH + 0.1 M NaCl solution (boiling). It has been demonstrated by the aforementioned technique that susceptibility is related to the existence of a continuous chromium-depleted concentration profile around the prior austenite grain boundaries. Destroying this profile by overlapping diffusion fields from the coarsening effects of $M_{23}C_6$ precipitates in the prior austenite and martensitic interlath grain boundaries removes the susceptibility[30] to intergranular SCC. This is equivalent, for this SCC system, to lowering its hardness by tempering at 1000 K to a level of less than 280 HV 10 for all three concentration widths. It should be emphasized, however, that the same criterion may not be applied to other systems. The permissible maximum hardness depends on the type of martensitic SS and, above all, the environment. In boiler feedwater, condensing steam, or boiler water, hardness levels up to 350 HV are deemed safe. In other environments, the maximum allowable hardness level may be different.[31]

Cathodic (sulfide) SCC of martensitic SSs

Cathodic SCC of martensitic SSs is a problem of technical importance. Figure 5 shows an example taken from an H_2S-containing soot water circuit. This failure resulted from the vendor using a type 410 SS tempered at too low a temperature, resulting in a hardness above 350 HV 10. A second example is illustrated in Figure 6; this figure shows a failed tube segment of a start-up heater coil with a fracture at the weld seam (left) and the fracture surface.[31] The material is a Super 12% Cr SS [German designation X 20 CrMoV 12 1, comparable to type 422 (UNS S42200), without tungsten]. In normal operation of the plant, the start-up heater was not fired but had the same pressure as the synthesis loop because there was only a gate valve upstream. This gate valve was slightly opened to avoid ammonia condensation in the coil from the downstream side. During the first year of operating the plant, the start-up heater had been fired for just about 1000 h in total when the failure occurred. A metallographic cross section through the crack initiation point (Figure 7) revealed that the crack path followed the HAZ, which showed high hardness values above 310 HV. Cracking was clearly hydrogen induced and resulted from condensing moisture on the outer tube surface during the time the start-up heater was not operated (practically none of the time). The coil was thus mostly below the dew point, so condensation of water (on the outer wall) and ammonia (on the inner wall, but of no importance to the failure) could not be prevented. The mechanism of such failures is straightforward and well known from hydrogen-induced cracking phenomena in low-alloy steels.

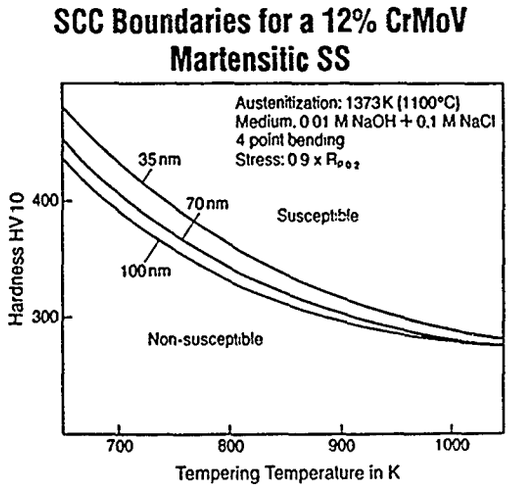


FIGURE 4—SCC boundaries as determined from different Cr concentration profile widths. (Reprinted with permission [30])

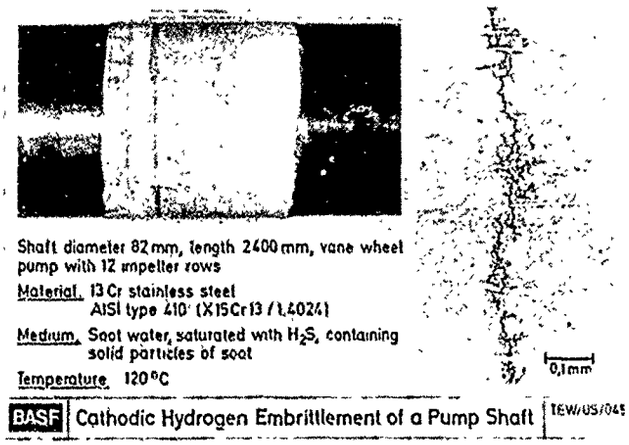


FIGURE 5—Cathodic hydrogen embrittlement of a pump shaft.

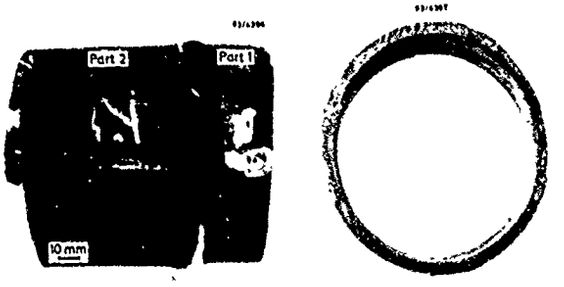


FIGURE 6—Cathodic SCC of a start-up ammonia heater coil. (Reprinted with permission.[31]) 12Cr SS similar to type 422 (UNS S42200) (X 20 CrMoV 12 1).

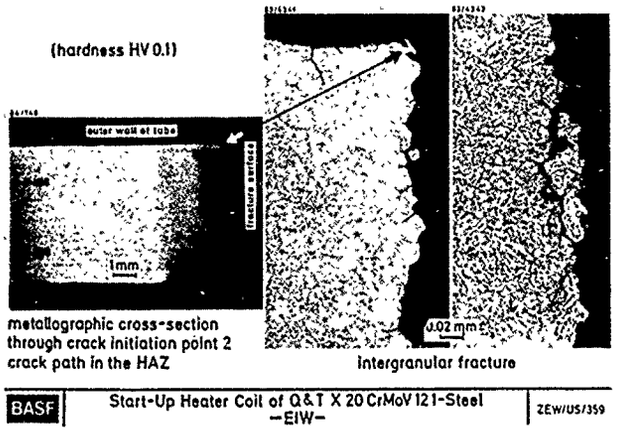


FIGURE 7—Metallographic cross section of coil (Figure 6).[31]

It is of paramount importance to avoid undue hardening by inappropriate welding procedures. Three working techniques avoiding this have been developed for the martensitic SSs in question:

(1) Austenitic welding by applying a preheat that keeps the temperature during welding at about 400°C;
(2) Martensitic welding with a preheat between 100 and 250°C;
(3) Partial martensitic welding keeping the temperature between 250 and 400°C.

In any case, the temperature of a welded component must be lowered to 80 to 100°C after welding to ensure the formation of martensite, which is mandatory for gaining the necessary toughness by a tempering treatment at about 750°C. Lowering the temperature to ambient will inevitably cause cathodic SCC as soon as condensation has set in, because the martensitic microstructure of such SSs is extremely sensitive to it, so tempering should immediately follow after cooling down to 80 to 100°C.

Low-Carbon Nickel Martensitic SSs

Martensitic steels with about 0.05% C, 12 to 17% Cr, and 3 to 6% Ni have several interesting properties:

(1) High YSs ($R_{p\,0.2}$ = 450 – 1200 N/mm²);
(2) Hardenability in heavy sections up to 250 mm;
(3) High toughness even in very high sections;
(4) Weldability;
(5) High resistance against cavitation, erosion; and
(6) Corrosion resistance under passive conditions, low corrosion rate in the active state.

They have been developed during the last 20 years based on the 13Cr steels, the main targets being

(1) To lower the carbon content to increase ductility and weldability;
(2) To compensate the lower carbon contents by higher Ni contents to avoid δ-ferrite;
(3) To choose Cr and Mo contents depending on the desired corrosion resistance; steels with 13Cr are close to the border of passivity. The 16Cr types with 1 Mo offer higher corrosion resistance (pitting and crevice corrosion resistance); and
(4) To add Cu for precipitation hardening and Nb to obtain fine-grained microstructures showing high YS.

Their metallurgical principles have been described in several review articles.[32-34]

The section through the ternary diagram Fe-Cr-C for 17% Cr[35] shows (Figure 8) that most of the alloys of this type solidify in the form of δ-ferrite. Upon further cooling, ferrite is more or less completely transformed in solid solution into austenite. In practice, the unwanted constituent δ ferrite may be present in 13Cr 4Ni, 16Cr 6Ni, and 17Cr 4Ni alloys. It will, among other effects, lower the fatigue strength and the corrosion resistance. The composition of type 16Cr-5Ni-1Mo can, however, be controlled in such a way that there is practically no ferrite present. The carbides to be expected at low temperatures are of type $M_{23}C_6$. These steels are usually air hardened and tempered or solution annealed.

The development of this modern type of steels, their production, mechanical properties, corrosion resistance, and application have been described in great detail elsewhere [37]

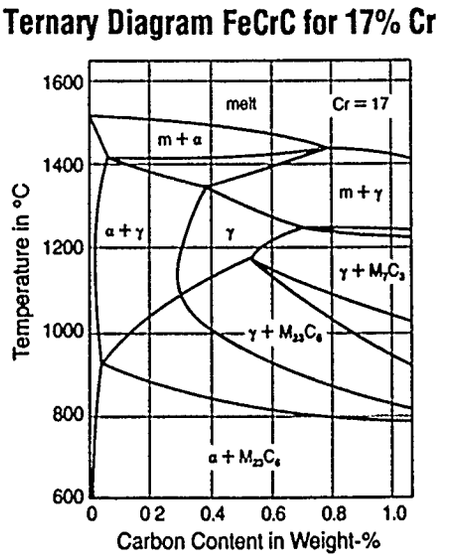


FIGURE 8 – Phase diagram helping to illustrate the solidification of low-carbon nickel martensitic SSs.[35]

Anodic SCC of nickel martensitic SSs

The anodic SCC behavior of the 16Cr-5Ni-1Mo martensitic SSs in boiling 35% $MgCl_2$ solution is compared to a 13Cr and 17Cr-2Ni martensitic SS and a standard 18Cr-10Ni austenitic SS in Figure 9. The constant extension rate tests[17] reveal that the normal heat treatment for this steel is yielding better results than a heat treatment, increasing its tensile strength. The 13Cr martensitic SS is remarkably resistant to anodic SCC. By way of comparison, the SCC resistance of the standard austenitic SS is very low and, according to this test, so is that of the 18Cr-10Ni (austenitic) SS. The negative effect of a deviation from the standardized heat treatment of 16Cr-5Ni-1Mo martensitic SSs aiming at higher strength levels also comes out clearly in constant-load tests, evidencing[17] a difference in threshold stresses of about 80 MPa (Figure 10).

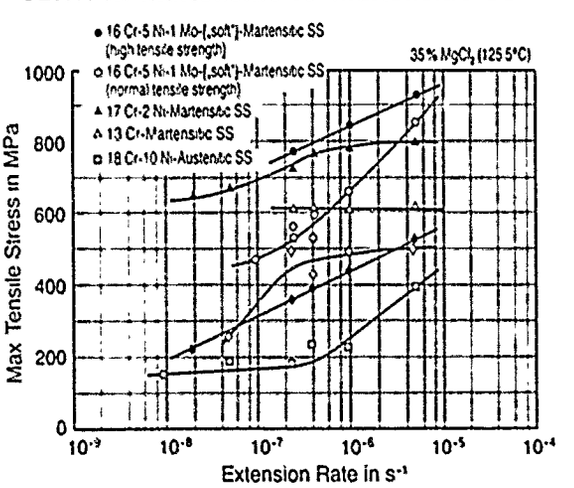


FIGURE 9—Constant extension rate tests comparing low-carbon nickel martensitic SS, martensitic SS, and austenitic SS in concentrated chloride solution.[17]

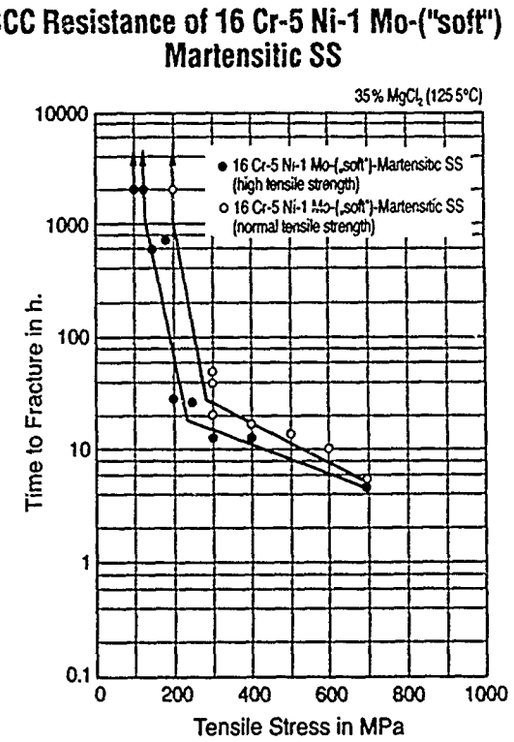


FIGURE 10—Influence of heat treatment (strength level) on the SCC resistance of a nickel martensitic SS.[17]

Cathodic SCC of nickel martensitic SSs

As low nickel martensitic Cr-Ni(Mo) SSs find application in various industries because of their excellent mechanical properties, e.g., in petrochemistry and in the oil and gas industries, H_2S in chloride-containing environments may trigger cathodic SCC (sulfide stress cracking, hydrogen embrittlement). NACE has therefore established a standard for testing steels under aggravated conditions.[38] Figure 11, left-hand side, represents[37] the stresses of various low-carbon nickel martensitic SSs as a function of their hardness and in comparison to a straight type 410 steel under NACE's test conditions. Results show that under such stringent testing conditions, no correlation between alloy chemistry, hardness level, and sustained stresses can be recognized. The chart on the right side gives the results on the basis of the 0.2% yield stresses, again, with no appreciable correlation except for the fact that, under cathodic SCC conditions, fracture at small fractions of R_p is possible. Many influencing factors like hardening temperature, cooling rate, and tempering conditions remain to be studied in detail. On the other hand, there is some information on the influence of strength, hardness and YS on the resistance against cathodic SCC of many nickel martensitic grades.[39-47] The general rule derived from field experience with low-alloy martensitic steels seems to hold true for the stainless grades, too: The lowest possible hardness will, in general, yield a relatively good performance.

Since the use of 13Cr-4Ni(Mo) SS at times involves applications where exposure to hot chlorides is required, the possible occurrence of anodic SCC must be considered. It has been shown[48] that tempered 13Cr martensitic alloys of CA-6NM composition are subject to SCC in mildly acidic or near-neutral solutions of boiling 25% NaCl after prolonged exposure. The effect of variation in tempering temperature appeared to have little effect on the resistance to cracking. Increasing the molybdenum content to 1.5% produced a substantial increase in resistance to anodic SCC. In fact, Figure 9 demonstrated a high resistance of 16Cr-5Ni-1Mo martensitic SS, and Figure 10 manifested the existence of a threshold stress under extreme conditions of chloride-induced anodic SCC.[17] In applying these laboratory results, it must not be overlooked that comparatively small partial pressures of H_2S will reduce[49] the pitting resistance and may thus be triggering anodic SCC. This becomes more critical the higher the H_2S concentration. Figure 12 shows a pertinent failure. This bolt had been given a hardness of 42 HRC (410 HV) by precipitation hardening, so that cathodic (sulfide) SCC was initiated in an aggressive chloride-containing sour gas environment (52% H_2S, 6.5% CO_2, 70°C) in which crack propagation proceeded intergranularly.

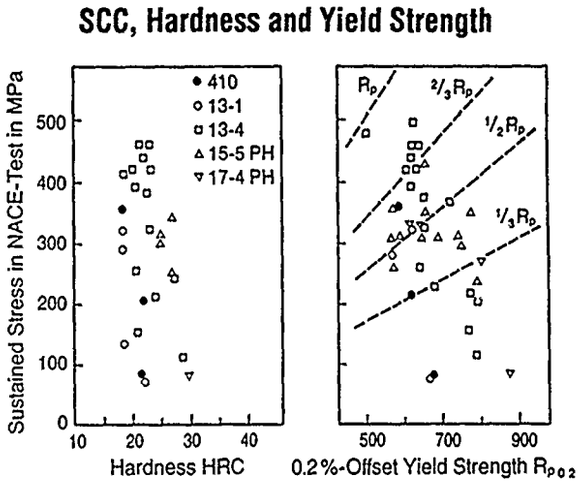


FIGURE 11—Cathodic SCC (sulfide stress cracking); comparison of martensitic, nickel martensitic, and precipitation-hardening steels, according to NACE Standard TM0177-86.[38] (Reprinted with permission.[37])

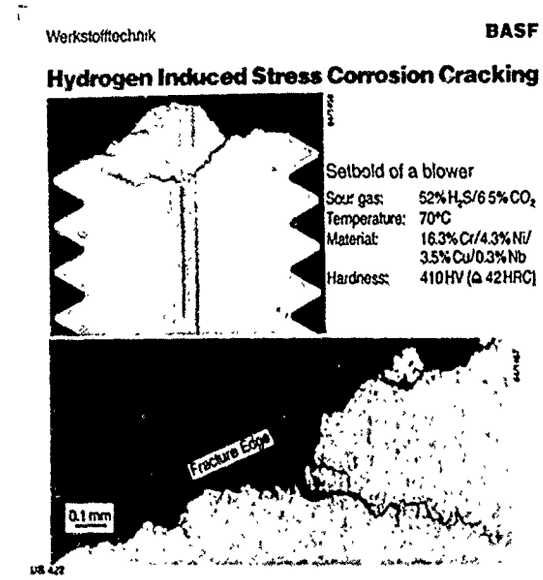


FIGURE 12—Case history: sulfide stress cracking of a setbolt of a blower in an aggressive sour gas environment.

Another example of the complicated interplay of parameters is that of double-temper treatment. It will increase the resistance to cathodic sulfide stress cracking via a change in the fracture mode from intergranular to transgranular quasicleavage cracking. However, double tempering impairs the resistance to pitting and thus to chloride SCC.[49] The improvement in cathodic SCC resistance by double temper is caused by a reduction in hardness of the martensite and an increase in the volume of retained austenite plus a change in fracture mode. Because of its face-centered lattice, the solubility of hydrogen in retained austenite is greater than in the matrix, whereas the diffusion coefficient is much smaller. This will lead to a pile-up of hydrogen at the martensite/retained austenite interfaces and an interaction of hydrogen atoms with dislocations generated in them on account of the incompatible deformation of the two phases, thereby

leading to transgranular cracking of double-tempered SSs at elevated strains. As opposed to this, single-tempered SSs failed by an intergranular cracking mode requiring a shorter path and perhaps smaller fracture energy per unit crack extension.[50] This appears to explain the inferior resistance of 13Cr-4Ni-Mo SSs in the single-temper heat treatment as opposed to the double temper, where the intergranular mode changes to transgranular quasicleavage cracking, resulting in a significant increase in the total fracture energy.[50]

Maraging Steels

The stress corrosion and hydrogen embrittlement behavior of maraging steels has been extensively treated in a previous publication [51] For this reason and because corrosion-resistant steels of this class are of limited use, this topic will not be dealt with in this review.

Low Interstitial Ferritic SSs

The development of modern metallurgical processes has made it possible to economically produce SSs with extra-low carbon contents of about 0.07% on a large scale. Figure 13 represents this development and shows the impact of secondary metallurgical processes like argon-oxygen decarburization (AOD) or vacuum-oxygen decarburization. It is further possible to obtain low-nitrogen concentrations because of the intensive refining reaction and to adjust them by modern rapid analytical methods via the gas phase.[52] One can make use of this by alloying steels with nitrogen or, for ferritic steels, by guaranteeing extremely low nitrogen contents. The latter is important to overcome cold brittleness (high-impact transition temperature) by either a very low concentration of carbon and nitrogen (C + N < 100 ppm) or by a sufficiently low concentration of these elements (C + N < 400 ppm) in the presence of stabilizing elements (Nb, Ti). These conditions must also be met to guarantee resistance to intergranular corrosion. The wall thickness of steels in the 400 ppm interstitial range nevertheless must not exceed certain limits. For one of the most important applications, heat-exchanger tubes, a wall thickness of 3 mm (0.12 in.) will seldom be exceeded anyway, and for this thickness (and up to about 12 mm), the (stabilized) 400 ppm level is adequate. Because of the extremely low solubility of the ferritic lattice for carbon and nitrogen at temperatures below 1000°C (1830°F) and the high diffusion rates of these elements, chromium-rich $M_{23}C_6$ carbides and nitrides can be formed on grain boundaries. The adjacent regions may thus become chromium depleted, causing a sensitization against intergranular corrosion. This demands the same metallurgical measures as before, i.e., lowering the concentration of interstitials and/or stabilization by Ti (e.g., Ti > 0.20 + 4 [C + N]) or Nb.[53]

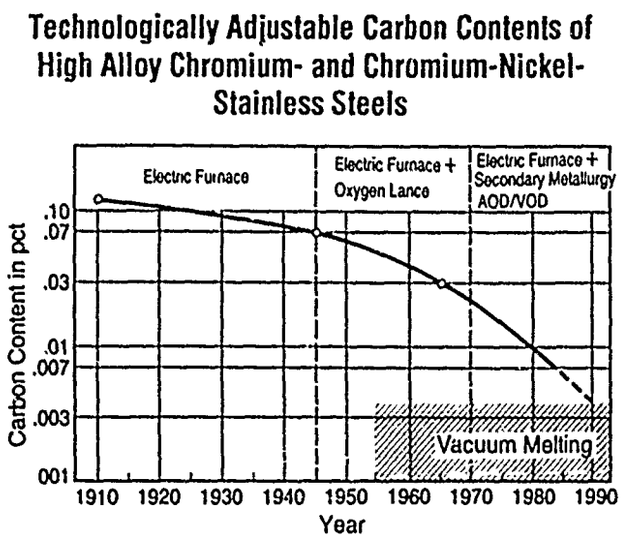


FIGURE 13—Technological development of steel-making processes.[52]

Anodic SCC

Low-interstitial ferritic Cr-Mo or Cr-Ni-Mo SSs have been engineered to resist anodic (chloride) SCC. Because of their aforementioned thickness limitation (at present, up to a maximum of 12 mm), no application in sour gas or other environments producing cathodic SCC seems to have been taken into consideration.

The resistance of such steels against chloride-induced SCC is remarkable, so they are used in heat exchangers. Even the straight 18Cr-2Mo ferritic SSs behave excellently in river water adjusted to an artificially high chloride content of 400 ppm (Table 1).[54]

Crack initiation in chloride environments. Higher-alloyed, high-purity, low interstitial Cr-Mo SSs are, if in the proper mill-annealed condition, immune to chloride SCC even in high chloride concentrations and at high temperatures under open-circuit conditions.[55] They may, however, become susceptible when their open-circuit potential is displaced in the active direction, which may happen under the following conditions:[55] (1) high-temperature annealing, and (2) high applied stress (in boiling 42% LiCl + thiourea, e.g., at stress values of 90% YS).

Ferritic SSs are very resistant to pitting corrosion. Initiation of SCC, therefore, depends on the evolution of slip steps that induce film rupture that will provide for the corrosion sites initiating cracking as soon as they have attained a critical size and geometry for starting an occluded cell mechanism. This induction period is characterized by transient creep processes (slip-step production), their rate decreasing towards the end of the induction period and by the current measured under potentiostatic control. The causes of this anodic current have been identified; transient creep produces an environmental attack where slip steps emerge, thereby forming distinct corrosion trenches.[55] Figure 14 shows the open-circuit potential response for the ferritic low interstitial 26Cr-1Mo SS, that is, in the as-received (mill-annealed) conditions, insensitive to SCC but undergoes SCC when heat treated (grain coarsened at 1050°C/30 min in air, followed by a water quench), or 5% prestrained. The total repassivation rates for the latter two conditions are slower than for the immune mill-annealed state. It could be demonstrated that both the logarithmic creep rates and the slip-step heights of low interstitial and higher interstitial 26Cr-1Mo SS are the same (Table 2). From this, it follows that the decisive difference is in the inherent corrosion and repassivation rates. The 26Cr-1Mo steel of lesser purity is bound to develop critical localized occlusion, thereby initiating cracks.

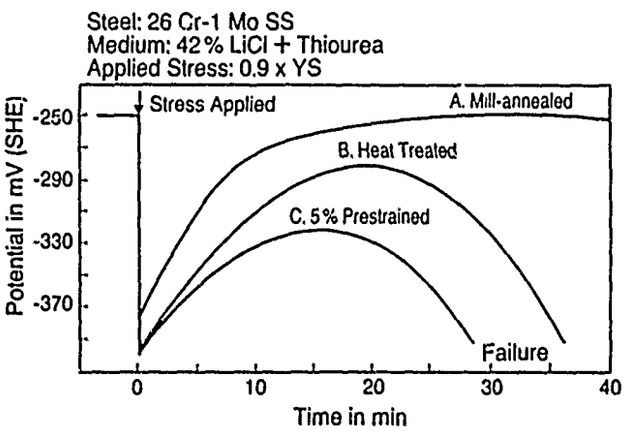


FIGURE 14—Open-circuit potential response of a low interstitial ferritic SS to different pretreatments.[55]

Effect of some alloying elements. The effect of various alloying elements has been studied but is not as well understood. In concentrated $MgCl_2$ solution, nickel[56,57] and copper[58] have adverse effects on SCC resistance. Although it withstood the NaCl wick test, 28.5Cr-4.2Mo ferritic SS cracked in the $MgCl_2$ test. On the other hand, a combination of small amounts of Ni and Cu will not impair the immunity of low interstitial ferritic SSs in concentrated boiling $MgCl_2$ solutions (Figure 15).[59] Figure 15 also illustrates the complete

immunity of purely ferritic steels containing Ni and Cu in a wider range of concentrations [60] Nickel additions (0, 0.5, 1.75, 4Ni) exert an influence upon the nominal tensile stress at fracture above one percent and at strain rates of the order of 10^{-6} s^{-1} in the ranges of total strains beyond 1% Under these conditions, a decrease of the fracture stress can be noticed [60] A straight 18Cr ferritic SS containing 1 5% nickel responds to potentiostatically applied potentials in a way[61] other than the high-purity, low interstitial, ferritic alloys of type 26Cr-1Mo or 28Cr-2Mo In contrast to those steels (and in 42% $MgCl_2$ solution containing no thiourea), SCC occurs at the open-circuit potentials and at more noble potentials (Figure 16).[61]

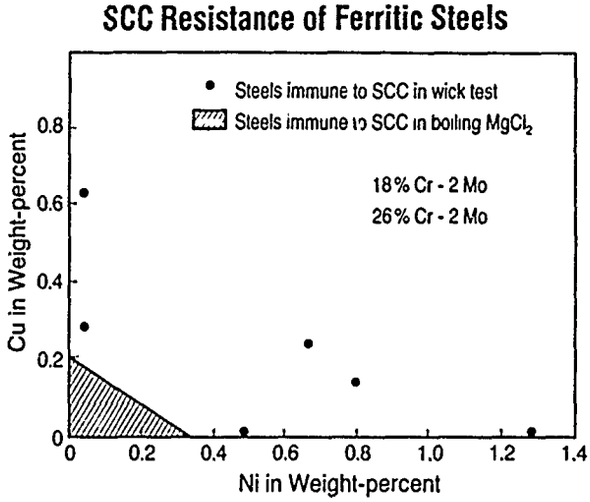


FIGURE 15—SCC resistance of low-interstitial ferritic SSs as influenced by copper and nickel contents.[59]

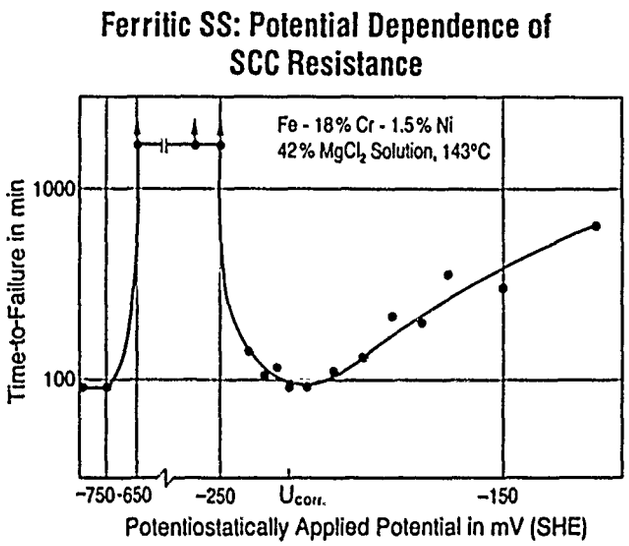


FIGURE 16—Potential response of a nickel-bearing ferritic SS showing a range of potentials below the open-circuit potential (U_{corr}), which provides cathodic protection. (Reprinted with permission.[61])

Research is still in progress to improve our understanding of the reactions of these steels exposed to environments and strains. In this context, the film-induced cleavage model should be mentioned,[62] and also the investigations into the properties of the passive films formed on ferritic SSs in Cl^- solutions.[63] It could be shown by Auger electron spectroscopy that the increased resistance of the passive films resulting from increased Cr concentrations in Fe-Cr and Fe-Cr-Mo ferritic SSs can be attributed to Cr enrichment, which, in turn resulted in this case in thinner films Figure 17 elucidates this for the ratio of Cr cations to iron cations in the passive film to that in the alloy.[63] For practical purposes, e.g., for heat-exchanger tubing in the chemical process industries, the observation that a solution passivation treatment leads to Cr enrich. ..nt is of immediate interest and so is the result that passive films formed at 260°C are much thicker, exhibit Cr enrichment, and increased pitting resistance. In accordance with findings for a ferritic, ferritic-austenitic, and austenitic SS in chloride-free sulfuric acid environments (see Figure 51),[100] molybdenum does not change the macrocharacteristics of the film much. Also, chloride is generally not incorporated into the film under pitting conditions and has no effect on passive film characteristics.[61]

In the practical application of these steels, Figure 18 should be kept in mind.[64] One warning of this constitution diagram pertains to thermal treatments during fabrication like welding and forming, which bear, at longer times in the critical temperature range, the risk of σ-phase formation accompanied by embrittlement. Another deterioration of ductility may occur in long-time service of components at temperatures higher than 280°C because of the 475°C embrittlement, which is caused by the miscibility gap leading to the decomposition of the Fe-Cr solid solution into the two phases indicated in Figure 18. Provided that such conditioning factors are taken into account, the immunity of low interstitial Cr-Mo steels to hot chloride and caustic solutions has been proven and also that of nickel-bearing "superferritic" steels in industrially important, concentrated chloride solutions.[65]

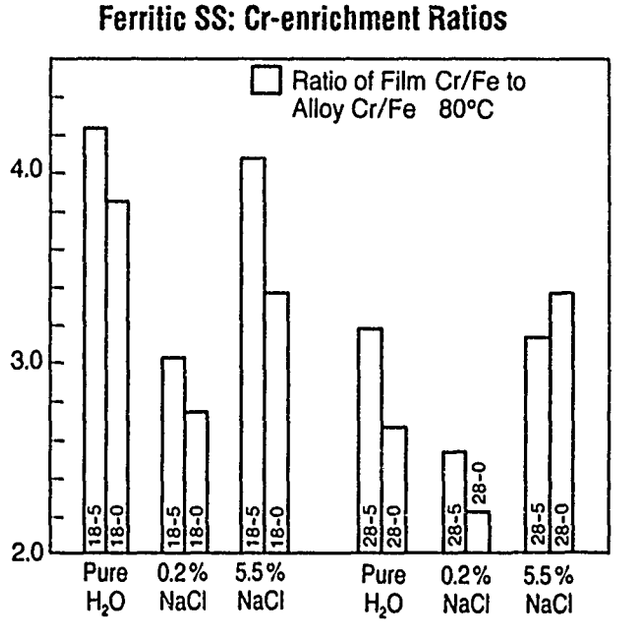


FIGURE 17—Auger electron spectroscopy results showing the ratio of Cr cations to iron cations depending on environment and alloy composition.[63]

Ferritic-Austenitic SSs

As in the previous cases, ferritic-austenitic SSs are used in environments that may produce anodic or cathodic (sulfide) SCC. The development of this class of steels was initiated by the chemical industry's demands for good corrosion resistance and higher strength than austenitic SSs. They have, however, found wide application in other areas, primarily in the oil and gas industry.

Anodic SCC

Duplex SSs have found many successful chemical engineering applications. This is in addition to their advantageous mechanical properties (see Reference 75), which result from two facts. (1) their pitting resistance (superior to austenitic standard grades) and (2) their high SCC threshold stresses. Figure 19 exemplifies this for three ferritic-austenitic SSs and an austenitic SS, in that the threshold stress of the latter is only about one-third that of the duplexes (boiling 35% $MgCl_2$ solution, 125°C).[66]

TABLE 1
Stress Corrosion Cracking in Rhine River Water[53,54]

Material Combinations: / Testing Time:	Rhine River Water Adjusted to a Chloride Content of 400 ppm: 80°C (176°F) Air (1 Bar) 5 Weeks	100°C (210°F) O_2 (2 Bar) 8 Weeks	130°C (265°F) O_2 (2 Bar) 8 Weeks
18Cr-2Mo/18Cr-2Mo	NC[A]/NC	NC/NC	NC/NC
18Cr-2Mo/type 321	NC/NC	NC/SCC[B]	NC/SCC
18Cr-2Mo/ 18Cr-10Ni-2.5Mo	NC/NC	NC/NC	NC/SCC
18Cr-2Mo (old)/ 18Cr-2Mo (old)	NC/NC	NC/NC	NC/NC
25Cr-25Ni-2.5Mo/ 18Cr-10Ni-2.5Mo	NC/NC	NC/NC	NC/SCC
Type 321/type 321	NC/NC	SCC/SCC	SCC/SCC

[A]NC = no cracking.
[B]SCC = stress corrosion cracking (transgranular).

TABLE 2
Slip-Step Height Measurements (Slip-Step Height in nm)[55]

Alloy	Low Interstitial 26Cr-1Mo Alloy (ASTM XM-27)[A]				High Interstitial Alloy 26-1 S (ASTM XM-33)[A]		
Condition	Mill annealed	5% Pretreatment	Grain coarsened	5% Prestrained 350°C–1 h–AC	Mill annealed	5% prestrained	Grain coarsened
Slip-Step Height	40 ± 2.5	210 ± 21	117 ± 12	60 ± 6	44 ± 5	220 ± 15	124 ± 12

[A]Samples were stressed at 90% of the yield strength for 1 h in silicone oil at 140°C.

Binary Fe-Cr Alloys α-,α'- and σ-Phase Domains

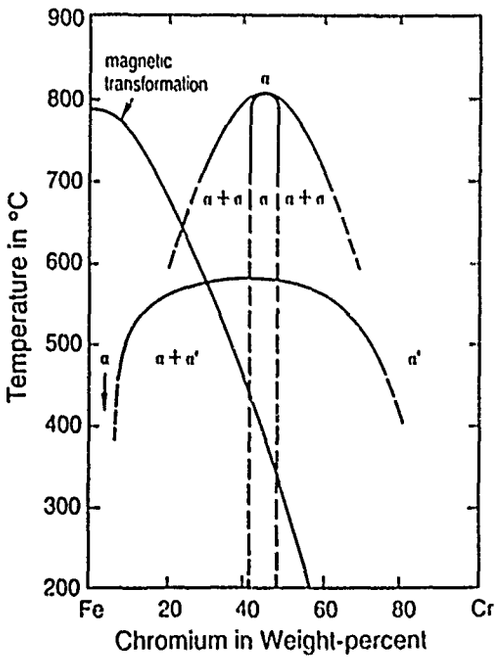


FIGURE 18—Binary constitution diagram Fe-Cr.[64]

SCC Resistance of Ferritic-Austenitic Steels

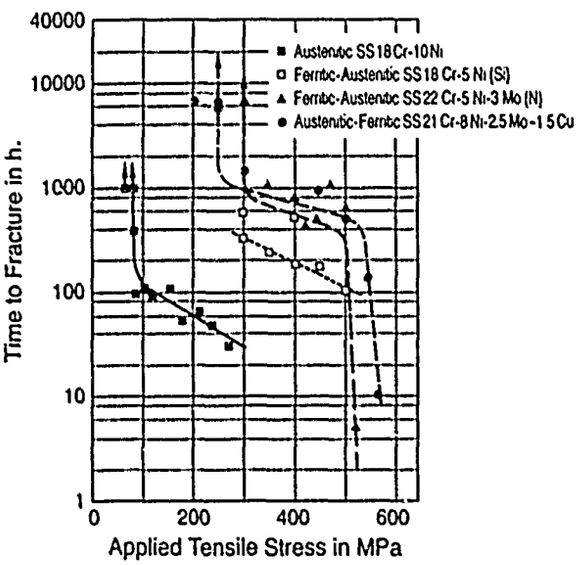


FIGURE 19—Constant-load SCC tests (ferritic-austenitic SSs vs austenitic SS).[66]

This high resistance can be explained by the fact that the formation of partial dislocations is necessary for twin nucleation.[67] It requires conditions of low thermal activation. At the temperature indicated, twinning and SCC susceptibility decrease.

Figure 20 reveals the existence of a cathodic protection potential.[66] It is interesting to note that the protection potentials for the duplex SSs and the austenitic SSs are close together despite the fact that the steels were stressed at a level corresponding to their widely differing room temperature YSs.

It is assumed, for copper-alloyed, ferritic-austenitic SS, that low strain rates will yield a particularly good resistance to SCC in $MgCl_2$ solutions.[68] For copper-free 22Cr-5Ni-3Mo SS, this result could not be confirmed in constant extension rate tests (Figure 21).[17,66] On the other hand, Figure 19 showed that the copper-bearing duplex steel has no higher threshold stress than the 22Cr-5Ni-3Mo(N) duplex steel. The question remains whether the reason for this is electrochemical or mechanical in nature.

Again, anodic SCC, like cathodic SCC in H_2S-containing chloride solutions, depends on the microstructure and is therefore influenced by thermal treatments. The formation of σ-phase will be detrimental, as in the case of sulfide SCC. Figure 22 indicates that exposing a duplex steel to 800°C for 1 h will lead to a reduction of threshold stress. Of much greater effect are inadequate welding procedures.[69] They may cause high-temperature ferritization (see Figure 29). Figure 23 shows the considerable loss in threshold stress by tungsten inert gas (TIG) welding, caused by high (tensile) welding stresses in the weld metal and the immediately adjacent HAZ. It is likely that the microstructural changes in the HAZ (see Figure 29) add to this dramatic loss in SCC resistance, which is less pronounced in the case of manual arc welding because it provides for a higher heat input, a longer characteristic cooling time $t_{12/8}$, and a sufficient retransformation of high-temperature δ-ferrite into austenite, respectively.

Figure 24 shows the influence of residual stresses on the SCC resistance. The circles refer to ground specimens, the triangles to those ground in the same way but thereafter pickled to remove a surface layer of 200 μm in depth. It had been proven by the $\sin^2\psi$–x-ray method that the internal tensile stresses resulting from grinding will be removed completely by pickling.[69] The two curves of Figure 24 differ by about 70 MPa, which is in good agreement with the internal stresses produced by the grinding procedure in question and measured by the $\sin^2\psi$ method.[69]

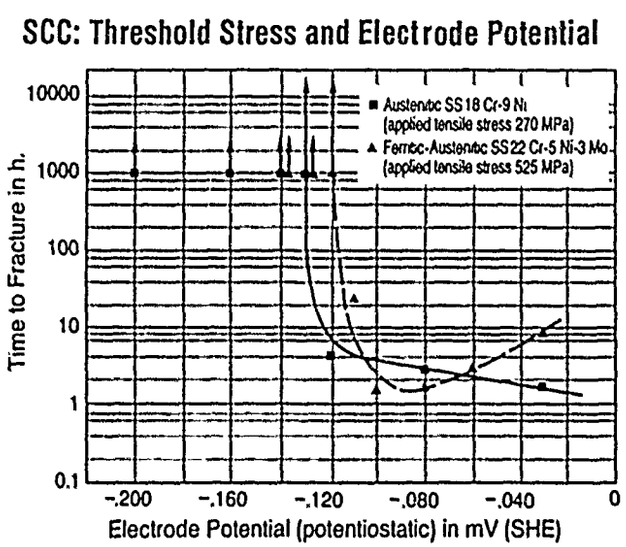


FIGURE 20—Threshold stress and electrode potential.[66]

Cathodic SCC in H_2S/chloride environments

The duplex (austenitic-ferritic) SSs are prime candidates for sour gas well applications in moderately aggressive environments [70-74] They combine high strength with good general corrosion resistance, resistance against pitting, SCC, and CF. YSs between 550 to 1100 MPa are needed for downhole tubular products, wellhead components, and other designs. The lower YS level can be covered by some annealed duplex alloys, whereas the higher strength range must be attained by cold working.

It has been shown that at elevated temperatures, a critical H_2S content exists above which cracking occurs.[71] The critical partial pressure of H_2S is in the 0.62 MPa (5 psi) range for stresses near the YS as shown in Table 3.[71]

The threshold stresses of newly annealed 25Cr-5Ni duplex steel are typically greater than 90% of the YS in the NACE Standard TM0177-86.[38] However, σ-phase embrittlement in the 800°C range causes short times-to-failure, even at stresses below 0.8 YS. Normal heat-treatment conditions like annealed, as-hot-worked, etc., seem to cause no major changes in susceptibility. These operations will not lead to such drastic changes in microstructure as may occur by welding.

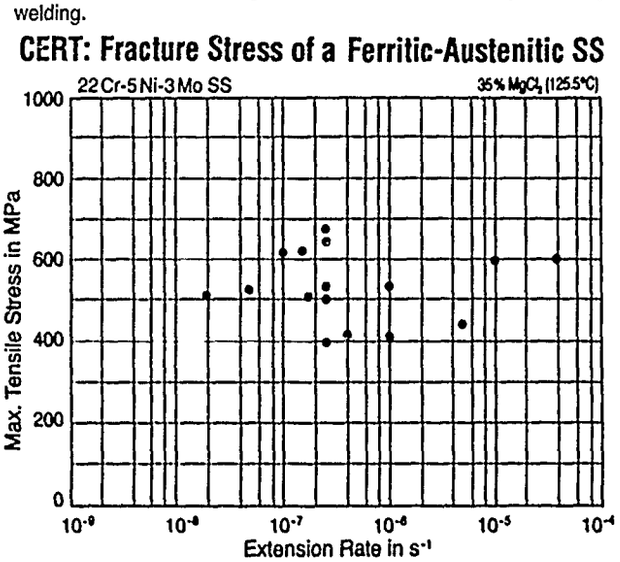


FIGURE 21—Copper-free, ferritic-austenitic SS: constant extension rate tests showing no rate influence.[17,66]

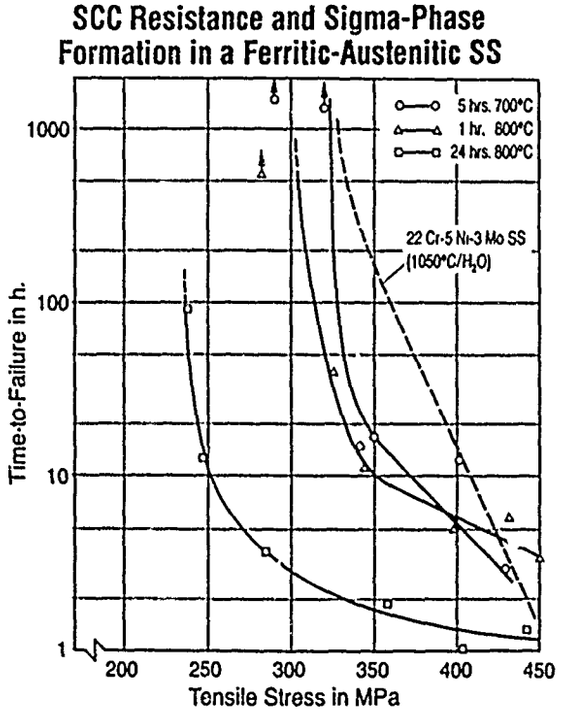


FIGURE 22—σ-phase formation and SCC resistance in a ferritic-austenitic SS.[69] σ-phase domains (Figure 18). Boiling 35% $MgCl_2$ solution (125.5°C).

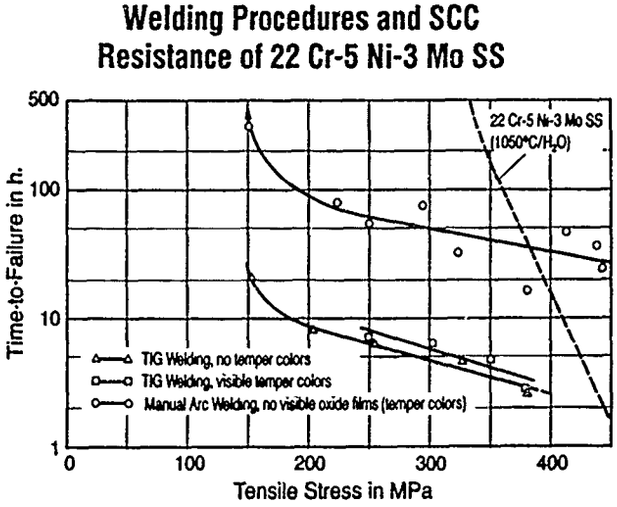


FIGURE 23—Welding procedures and SCC resistance of 22Cr-5Ni-3Mo ferritic-austenitic SS. Influence of welding procedures on time-to-failure.[69]

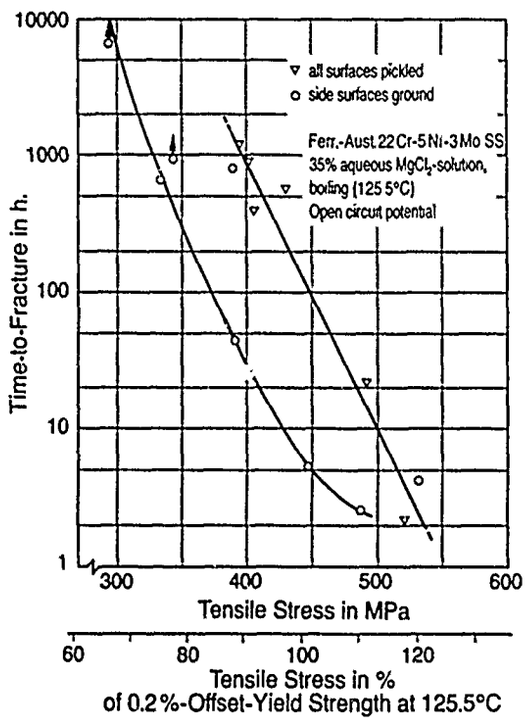


FIGURE 24—Influence of residual stresses on the anodic SCC resistance of a duplex steel. Internal stresses caused by grinding were removed by pickling, which resulted in a shift of the time-to-failure curve toward higher sustainable tensile loads.[69]

Changes in microstructure by welding

Constant-load tests at room temperature showed that TIG, metal inert gas (MIG), or electron-beam welding is not detrimental for the cracking resistance of duplex SSs in sections that are not too thick. Shielded metal arc (SMA) welding causes a slight decrease of the sulfide SCC resistance related to the particular pitting and crevice sensitivity of the weld. However, welding conditions must be carefully selected. Figure 25 exposes a section through the ternary system[75] Fe-Cr-Ni indicating that at usual Ni contents of, for example, 5.5% (dotted line), the δ-ferrite formed upon solidification will be partly transformed into austenite below around 1250°C. At slow cooling rates, the desired δ/γ ratio (50:50) will be acquired.[76] On the other hand, during welding, the formation of δ-ferrite is a speedy process, as Figure 26 demonstrates by the fact that there is no difference in δ-content between a 30-s flash annealing and long-time annealing. Slow cooling rates between 1200 and 800°C are necessary to allow sufficient time for the reaustenitization process. It has been shown that the minimum cooling rate requires a characteristic cooling time $t_{12/8}$ of at least 10 s for cooling from 1200 to 800°C.[77] The microstructure in the weld metal given (and certain prerequisites like minimum Ni content in the parent metal) will then contain at least 25% austenite (Figure 27). This demands, for different designs, a certain heat input and/or a preheat. Figure 28 displays examples demonstrating the criticality of spot-welding or arc strikes, built-up weld seams or repair welds that may be, because of too low an austenite content, extremely susceptible to SCC.[77] The welding process parameters are safeguarding proper microstructure,[78] and, by that, CF and SCC resistances as summarized in Figure 29.[77]

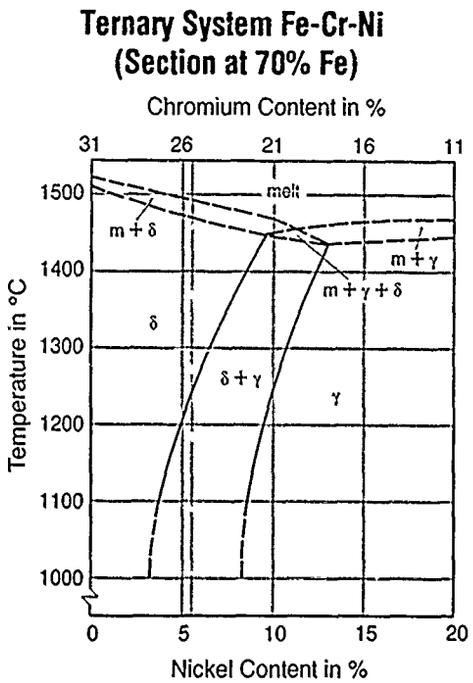


FIGURE 25—Constitution diagram Fe-Cr-Ni (section at 70% Fe).[76]

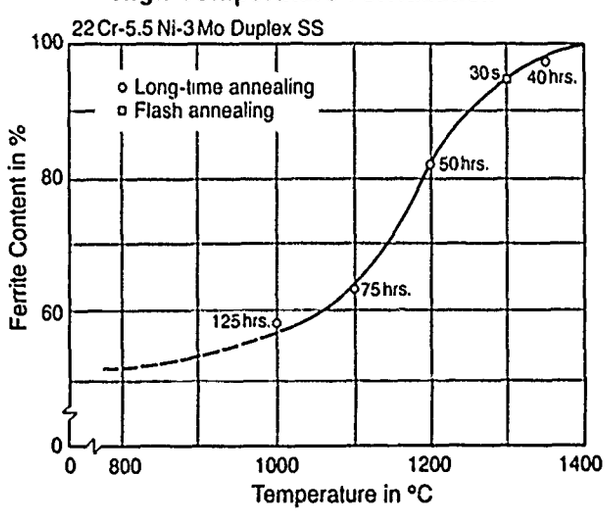


FIGURE 26—High-temperature ferritization of a ferritic-austenitic SS[77] by flash and long-time annealing.

TABLE 3

The Effect of H_2S Content and Temperature on Environmental Embrittlement 25% Cr Duplex SS C-Ring[71,(A)]

Temperature [°C (°F)]		% H_2S		
		0.04	1	10
25	(78)		NC[(B)]	C[(C)]
90	(195)	NC	NC	NC
121	(250)	NC	NC	C
149	(300)		NC	C
177	(350)	NC	NC	C
204	(400)	NC	NC	C
232	(450)		NC	NC
260	(500)		C	NC

[(A)]0.9 to 0.95 σ_y, like bolts $CO_2/H_2S/Cl^-$ environments, 1000-h exposure; initial pressure = 0.62 MPa (90 psia) at room temperature.[71]
[(B)]NC = no cracking.
[(C)]C = cracking.

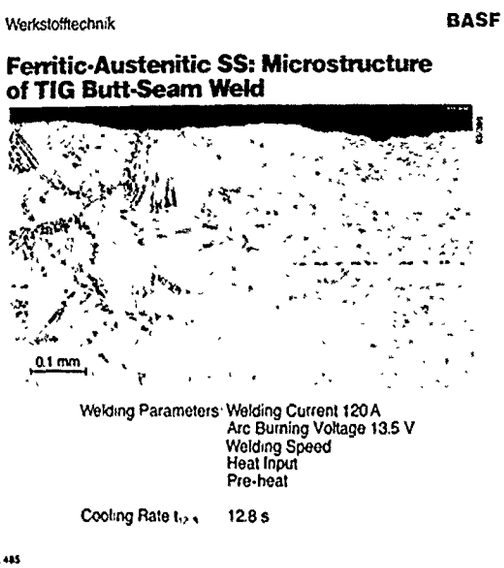


FIGURE 27—Microstructure of a TIG butt-seam weld of a ferritic-austenitic SS.

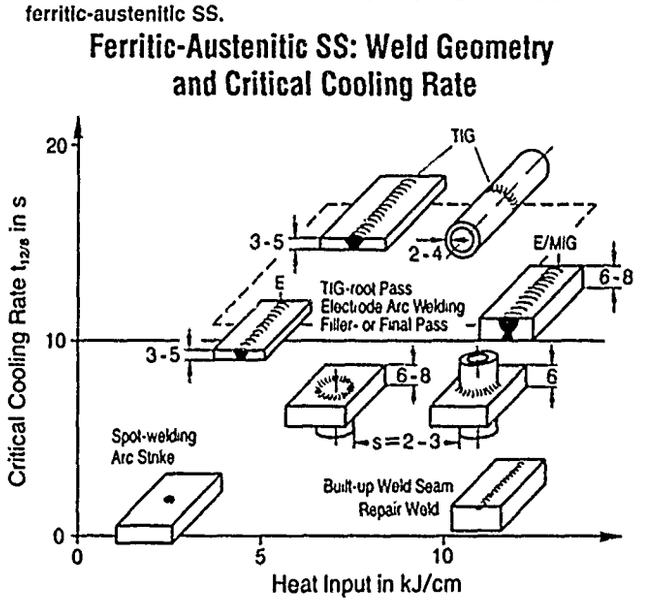


FIGURE 28—Influence of weld geometry and characteristic cooling time $t_{12/8}$ (indicative of the critical cooling rate) on the austenite content in weld metal and heat-affected zone. The geometries in the lower part ($t_{12/8}$ 10 s) are, without preheating, critical with respect to the minimum required austenite content and toughness.[78]

The resistance of duplex steels against sulfide SCC is, in addition to these microstructural changes, remarkably lowered by precipitations and hardening processes, respectively, in the ferrite, and also by precipitations at ferrite-austenite grain boundaries, e.g., chromium carbides or nitrides and, below 1000°C, σ-phase (700 to 850°C).

The alloying element nitrogen plays a beneficial role in the process of the reformation of austenite during cooling from welding temperatures. It has been shown that, depending on the cooling rate, precipitations of chromium nitrides (Cr_2N) or chromium carbonitrides will start to precipitate at grain boundaries and within the ferritic grains below around 1150°C. Depleting thereby their surroundings of Cr, austenite will start to form around such initiation points.[77] For a 22Cr-5.5Ni-3Mo duplex steel with about 0.15% N $t_{12/8}$ values 0 > 10 s (Figure 28) will safeguard a sufficient amount of reconverted austenite and a normally sufficient time for replenishing the Cr-depleted areas around precipitated nitrides. Low-nitrogen, duplex SSs behave in a different fashion.[79] In contrast to high-nitrogen alloys, they retain their α/γ structure upon annealing to temperatures up to 1260°C, whereas the high-nitrogen steels, upon cooling from 1350°C, for example, begin to precipitate Cr_2N well below this temperature.

There are other actions of nitrogen, too. It has recently been shown that the resistance against SCC in 20% NaCl solution with 1 bar H_2S drastically increases when the nitrogen content is increased from 0.04 to 0.14% N. From then on, in the investigated range up to 0.24% N, the alloys sustained 90% of the 0.2% YS (i.e., 441 MPa) in this test. This improvement appears to result from an increased resistance of the austenite phase by the dissolved nitrogen itself.[80]

Mechanistic aspects

The influence of temperature and H_2S pressure on the threshold stress that does not cause rupture after a 720-h period were studied by means of constant-load tests and constant extension rate tests. Results show that duplex grades withstand cathodic SCC up to 80 to 90% of the YS at room temperature. Increasing the temperature to the range from 60 to 90°C is detrimental, but at higher temperatures, up to 150°C, the threshold stress again becomes as high as at room temperature. This particular behavior is in contrast to that of 316L (UNS S31603) SSs. It seems to be related to the specific feature of the cracking process in duplex SSs consisting of local depassivation of the ferrite phase caused by a mechanical twinning in this phase. As twinning decreases with increasing temperature, duplex SSs exhibit a superior resistance in solutions that are hot according to NACE Standard TM0177-86.[81,82] The cracking process can be explained by the localized rupture of the passive film under the effect of both the chemical aggressiveness of the test solution and mechanical stresses. Table 4 shows the corrosion rates of 316L and a 22Cr-6Ni-3Mo 1.5Cu duplex SS to be increased by roughly 50% when a stress corresponding to 40% of the YS is applied. This anodic dissolution process is strongly accelerated when temperature in-

creases. The NACE Standard TM0177-86 solution at 60°C and 1 bar H_2S, for example, is so aggressive that austenitic 316L SS cannot repassivate. Duplex SSs are by far more resistant, having corrosion rates of 0.05 to 0.1 mm/year depending on their chromium content. This is another factor that accounts for their better SCC resistance.

The mechanism of SCC is closely coupled to mechanical and electrochemical phenomena:[83]

(1) In the ferrite, depassivation is essentially determined by mechanical twinning, whereas in the austenite, cracks initiate at glide steps. Gliding on the ferrite surfaces is, however, insufficient to cause localized depassivation occurring even for elevated temperatures (100 to 200°C) because of the more violent effects of mechanical twinning. This sensitivity to twinning disappears as soon as the ferrite contains no nickel, which is not the case in duplex steels (but is the case in straight 18Cr-2Mo, 26Cr-1Mo, or 28Cr-2Mo ferritic SSs) (see preceding paragraph).

(2) Cracking thus seems to be determined, in the lower stress region, by the localized depassivation of austenite caused by glide processes or, at higher stresses, by that of ferrite, twinning being responsible for crack initiation and propagation in most practical cases. Ferrite is anodic to austenite. At low stresses, ferrite, which is not yet plastically deformed, cathodically protects austenite, which is already plastically deformed. When the stress reaches the critical value for twinning, depassivation becomes possible in ferrite, initiating localized corrosion and cracking. This explains why (a) duplex steels are more resistant than austenitic steels and (b) why crack initiation takes place in ferrite containing Ni and at the α/γ interphases. It could be demonstrated that the stress at which twinning appears is lower than the yield stress in ferrite.[83] Damage from twins appears well before damage from slip. The SCC threshold stresses in duplex steels are directly related to the occurrence of twinning representing the critical strains at which twinning starts and promotes cracking at a certain fraction of YS. Twins constitute shared regions with a higher surface roughness as compared to slip. Consequently, the rapid rupture of the passive film upon the formation of twins will yield a stronger damaging depassivation effect compared to damage by slip steps.[84]

The observation that crack initiation seems to start frequently in the ferrite or the interphase ferrite-austenite underlines the close coupling of mechanical and electrochemical processes and the interrelationship between the two phases.[85] If the ferrite content is too high or too low, the cracking resistance may diminish. In the first case, cracks initiate and propagate in the ferrite or at the ferrite-austenite interphases. In the second case, the alloy behaves like an austenitic SS. The ferrite content therefore should be kept between certain limits, for example, 30 and 70%.

Regarding the cathodic (sulfide) stress corrosion in detail, there is still an open question: Is a chloride or hydrogen-induced cracking mechanism[56] prevailing? Table 5 does not clearly answer that question:

(1) If the chloride induced formation of pits would be the initial step of the cracking process, one cannot expect a marked increase in time-to-failure until a pH value nears the neutral point because the pitting potential depends little on pH in this range. A noticeable increase in time-to-failure would not be expected before weakly alkaline conditions are established.
(2) In the case of a hydrogen-induced cracking mechanism, the time-to-failure should markedly decrease with decreasing pH, and no cracks ought to be expected at pH > 6.

Table 5 hints more to a chloride-induced mechanism.[86]

A definitive distinction between these two mechanisms can be made on the basis of the dependency of time to failure on both test temperature and potential (Table 6). In this table, "free corrosion potential" means values at test start, "potential" refers to the potentiostatically impressed potentials relative to the free corrosion potential.

Under free corrosion conditions, the time to failure decreases markedly with an increase in temperature from ambient to 60°C, a metallographic examination reveals the formation of mostly branched cracks combined with preferential attack of the ferritic phase. Decreasing the potential potentiostatically by just 0.1 V relative to the free-corrosion potential increases the SCC resistance drastically. Increasing it by the same amount in the other (more noble) direction decreases it. In the latter case, cracks form in the initial stages of the corrosion process, whereas in the later stages their propagation rate seems to be exceeded by the growth rate of simultaneously formed pits. Again, the ferritic phase is preferentially attacked. Final failure is caused by cross-section reduction resulting from pitting.[86]

The preferential attack of the ferritic phase indicates a potential drop resulting from resistance polarization within the cracks, because in 1 M H_2SO_4 saturated with H_2S, this type of attack occurred only under complete active conditions The potential drop within pits is obviously lower than within the cracks, since within pits not only ferrite but also austenite can be attacked preferentially, the latter being possible only within the active-to-passive transition range in the corrosion rate vs potential curve.

The experimental findings that the time-to-failure increases when potentials become more negative, decreases when potentials become more positive, and decreases with increasing temperature can be explained in terms of a chloride-induced SCC mechanism. Hydrogen-induced cracking would result in a complete inverse dependence of time-to-failure on both potential and temperature.[86]

Cracking of the ferrite induced by hydrogen entry cannot be excluded,[87] especially in cases where the potential is rather negative, the pH is low, and the temperature is not too far above ambient. Figure 30 offers an example in which these factors came into play,[90] together with the formation of coarse grains because of the afore mentioned unfavorable welding parameters (Figures 26 and 28).

Measures for preventing SCC under the combined influence of chloride ions and H_2S in aqueous environments can be aimed at the following:

(1) Lowering the H_2S concentration. Table 7 shows that a decrease of the H_2S concentration from 1.8 to 1.0 g/L at ambient temperature and 1.1 to 1.0 g/L at 60°C have little influence on time-to failure. A further decrease to 0.1 g/L H_2S results in a pronounced rise in lifetime;
(2) Decreasing the stress level below the threshold stress; and
(3) Carefully selecting the welding parameters as mentioned above.

It should be noted that, at a high degree of high-temperature ferritization in the weld metal and HAZ, intergranular corrosion resulting from the well-known sensitization of ferrite after rapid cooling may occur.[88] The carbon not dissolved in the ferrite precipitates in the form of chromium carbides along the grain boundaries, these zones being attacked by acidified solutions in pits or, as observed earlier, in crevices.[89]

Corrosion Fatigue

All SSs show essentially the same characteristic features of CF. For this reason, it seems appropriate to mention the underlying common principles of this mechano-electrochemical type of loading, which is characterized by an unusually large number of parameters (see References 148-151).

Mechanical and electrochemical influencing factors

Figure 31 show some mechanical and electrochemical entities taking effect on the CF behavior of metals and alloys. CF comprises all the elements of fatigue from the engineering point of view (left part of Figure 31) beside those on the side of the corrosive medium. A mechanistic consideration ought to take into account an even greater number of fatigue parameters and their interplay with many characteristic materials properties (Figure 32).[91]

Of special importance for the CF of SSs is the initial stage in Figure 32 comprising a large or small number of cycles in the case of high- and low-cycle CF, respectively. In this stage, cyclic hardening, cyclic softening, or a combination of both will occur provided the stresses exceed the cyclic elastic limit. At the end of this stage, the formation of microscopic fatigue cracks can be observed, and along with that, the fatigue processes are moving more and more to the specimen or component surface where corrosion begins to come into play.

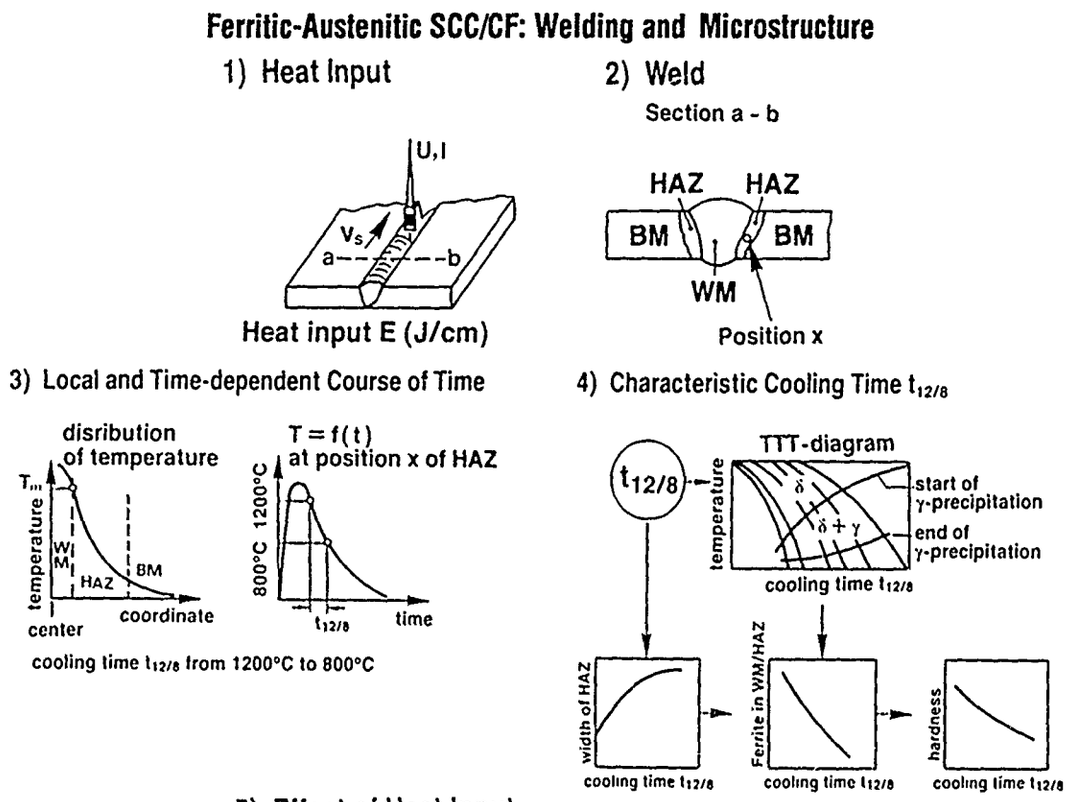


FIGURE 29—Influence of welding parameters (heat input), local and time-dependent course of time on microstructure in ferritic-austenitic weld metal and heat-affected zone, SCC, and corrosion fatigue resistance (schematic).[77]

TABLE 4

Influence of Stress on the Corrosion Rate of Austenitic and Ferritic-Austenitic SS in NACE TM0177-86[38] Solution at 60°C[82,(A)]

Grade	Stress (%yield strength)	Corrosion rate (mdd)
Austenitic type 316L SS	0	171
	40	241
Ferritic-Austenitic UR 45 N SS	0	25
	40	38

[(A)]Test duration = 200 h

TABLE 5

Effect of pH on Time-to-Failure of Tensile Specimens (S = 0.9 Yield Strength) in H_2S-Saturated NaCl Solution (4.3 M) Under Free-Corrosion Conditions[86]

Specimen Position	pH	Time-to-Failure (h)
longitudinal	3	62
longitudinal	4	38
longitudinal	5	55
longitudinal	6	147
longitudinal	7	166
longitudinal	8	519
transverse	3	48
transverse	4	31
transverse	5	29
transverse	6	55
transverse	7	155
transverse	8	720

TABLE 6

Effect of Temperature on Time-to-Failure of Stressed Tensile Specimens in H_2S-Saturated 4.3 M NaCl (pH 4)[86]

Temperature (°C)	Free-Corrosion Potential (V_{SHE})	Potential (V_{SHE})	Time-to-Failure or Testing Time (h)
Ambient	not measured	free corrosion (E_R)	38
40	not measured	free corrosion (E_R)	48
60	not measured	free corrosion (E_R)	4
Ambient	−0.16	E_R + 0.10	12
Ambient	−0.17	E_R − 0.10	1195, not cracked
Ambient	−0.23	E_R − 0.30	1030, not cracked
60	−0.23	E_R + 0.05	9
60	−0.23	E_R + 0.10	4
60	−0.23	E_R + 0.20	2
60	−0.18	E_R − 0.10	1097, not cracked

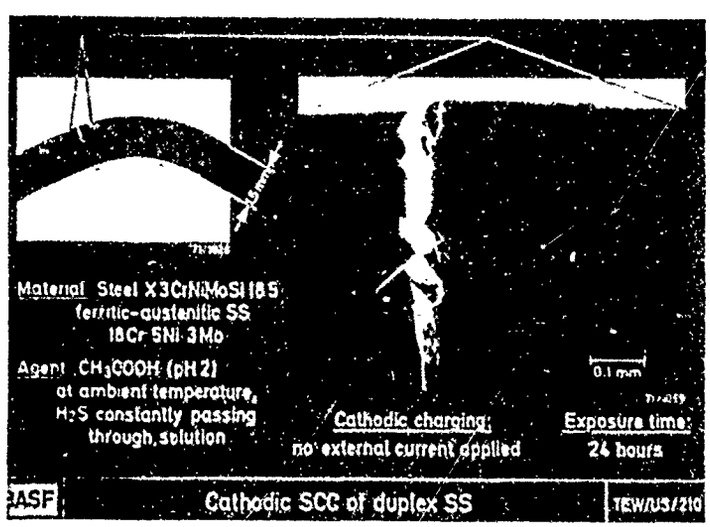


FIGURE 30—Cathodic SCC of a TIG-welded 18Cr-5Ni-3Mo SS in saturated, acidified H_2S solution.[87]

TABLE 7

Effect of H_2S Concentration on Time-to-Failure of Tensile Specimens (σ = 0.9 Yield Strength) in 4.3 M NaCl (pH 4) Under Free-Corrosion Conditions[86]

Temperature (°C)	H_2S Concentration (g/L)	Time-to-Failure (h)
Ambient	saturated (≈ 1.8)	38
Ambient	1.0	58
Ambient	0.1	471
60	saturated (≈ 1.1)	4
60	1.0	58
60	0.1	1007, not cracked

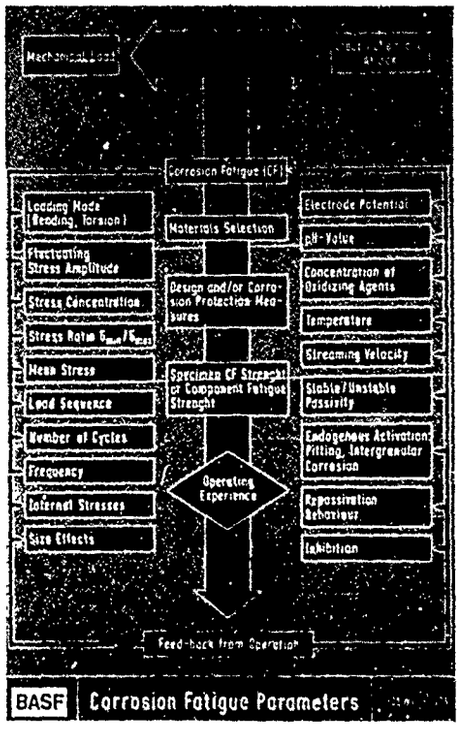


FIGURE 31—Some mechanical and electrochemical parameters in corrosion fatigue processes.

Another characteristic mechanical feature of CF is the initiation and propagation of cracks at stresses below the cyclic fatigue strength in an inert environment. Nevertheless, the CF strength of a SS at a given cycle number responds to many engineering parameters of Figure 31 and to many of those in Figure 32.

Electrochemical classification of corrosion fatigue—modes

Concerning corrosion on mechanical fatigue, the factual situation seems to be even more complex, and now the superposition of certain classification is desirable.[92,93] To this end, four electrochemical CF modes (Figure 33) have been identified:[92,93]

Mode I: CF in the active state;
Mode II: CF in the state of stable passivity;
Mode III: CF in the state of meta- or unstable passivity, endogenous activation being caused by mechanical (fatigue) processes, e.g., by the formation of active surface domains (persistent slip bands, slip lines, etc.) that exceed a critical area and thus cause, after a certain number of cycles, abrupt electrochemical activation; and
Mode IV: CF in the state of unstable passivity, exogenous activation being caused by processes like pitting, crevice corrosion, cavitation, etc.

These modes are detailed in the following sections.

Mode I corrosion fatigue

Using martensitic Cr steels (as well as the other steels in this contribution) in media in which they are active is confined to special boundary conditions under which it can, however, be very advantageous.

A martensitic Cr steel (0.2% C, 13% Cr) will, in contrast to an austenitic SS, become active at pH = 3 (20°C) and endure, for example, at pH = 2 (Figure 34), at the high nominal bending stress amplitude of $\pm S_r = 0.9\ S_f$, about 10^5 cycles (f = 50 Hz). Under practical circumstances, the amplitudes are much smaller, so that the sustainable number of cycles to fracture may become sufficiently high to make a component fit for application. Working under Mode I CF conditions in cases where the pH value is not much lower than the passivation pH obviously has the following advantages: (1) Mode IV CF, with its drastic reduction of CF strengths, can be excluded and (2) Mode III CF situations, with their wide scatter of endurance values because of fortuitous activation, are conservatively handled by the Mode I approach.

Based on mechanistic reasoning,[94] a model was developed[95] that aims at describing the influence of active corrosion on the cycle-dependent fatigue strength and crack propagation rate.

The premises are that active corrosion is occurring on locally limited surface sites, the stresses or strains resulting from external cyclic loading are constant in elements of length Δl (Figure 35), and, finally, there are no cyclic hardening or softening effects in those elements (i.e., cyclic plastic strains will only depend on external load and notch effects). One then has to consider two cases.

Case I. There are no external cyclic stresses or strains except those that, over an unlimited period of time, are so small that stresses/strains remain below the cyclic elastic limit. Under these premises, the linear corrosion rate $\Delta l_{corr}/\Delta t$ will depend solely upon the metal Me, the nature of the corrosive medium M, and local structural conditions S (primarily the actual corrosion depth). Accordingly, the partial linear corrosion depth $\Delta l_{corr,1}$ in a time interval Δt will be:

$$\Delta l_{corr,1} = k_1(Me, M, S) \times \Delta t \qquad (1)$$

$\Delta l_{corr,1}$ can also be expressed as a function of the cycle number N when introducing the frequency $\omega = \Delta N/\Delta t$:

$$\Delta l_{corr,1} = \frac{1}{\omega} \times k_1(Me, M, S) \times \Delta N \qquad (2)$$

Case II. An element of width Δl is stressed above the cyclic elastic limit $\Delta\epsilon_{el}$ by a sufficiently high external cyclic amplitude or by a low nominal amplitude, if $\Delta\epsilon_{el}$ is exceeded at a geometric discontinuity (e.g., a corrosion pit).

The plastic part $\Delta\epsilon_{pl} = \Delta\epsilon_{total} - \Delta\epsilon_{el}$ will then increase the corrosion rate in the considered element.[94] It seems reasonable to regard the plastic energy or work A_{pl} as a measure of the corrosion rate increment $\Delta l_{corr,2}$:

$$\Delta l_{corr,2} = k_2(Me, M, S, \omega, A_{pl})\Delta N \qquad (3)$$

with a limiting case:

$$k_2(Me, M, S, \omega, A_{pl} = 0) = \frac{1}{\omega} k_1(Me, M, S) \quad (4)$$

We assume, as a first approximation,[1] a linear relationship between corrosion rate and plastic energy A_{pl}:

$$\Delta l_{corr} = [\frac{1}{\omega} k_1(Me, M, S) + k_3(Me, M, S, \omega)A_{pl}]\,\Delta N \quad (5)$$

The plastic work A_{pl} can be expressed by the cyclic plastic strain ($\Delta\epsilon_{pl}$):

$$A_{pl} = c_1 \times \Delta\epsilon_{pl}^{\gamma} \quad (6)$$

so that in a shortened form

$$\Delta l_{corr} = [\frac{k_1^*}{\omega} + k_3^* \times c_1 \times \Delta\epsilon_{pl}^{\gamma}]\,\Delta N \quad (7)$$

Under the action of cyclic plastic strain $\Delta\epsilon_{pl}$, in the presence of medium M, the material will be corroded by Δl_{corr} after ΔN cycles (Element 1 in Figure 35).

After the same cycle number, the remaining part of volume Element 1 (not yet reached by the medium) has undergone fatigue, the mechanical crack growth being assumed to follow the Manson-Coffin Law:

$$\Delta l_{mech} = c_2 \times \Delta\epsilon_{pl}^{q} \times \Delta N \quad (8)$$

Volume Element 1 having failed means the formation of a notch whose notch factor K_t will increase the cyclic plastic strain in the neighboring Element 2, which, in turn, will accelerate the corrosion and crack propagation rate, etc. For the i-th volume element this means

$$\Delta l_i = \Delta l_{corr,i} + \Delta l_{mech,i} = [\frac{k_1}{\omega} + k_3^* \times c_1 \times \Delta\epsilon_{pl,i}^{\gamma} + c_2 \times \Delta\epsilon_{pl,i}^{q}]\,\Delta N_i \quad (9)$$

or

$$\frac{dl}{dN} = [\frac{dl}{dN}]_{corr} + [\frac{dl}{dN}]_{mech} = \frac{k_1^*}{\omega} + k_3^* \times c_1 \times \Delta\epsilon_{pl}^{\gamma} + c_2 \times \Delta\epsilon_{pl}^{q} \quad (10)$$

[c_1 and c_2: constant, Equations (6) and (8), respectively].

The above considerations have so far clearly resulted in a simple superposition model of mechanical and corrosion cracking.[95]

By a notch analysis, it is now possible to bring the geometric factor into play. The total strain range $\Delta\epsilon_{total} = \Delta\epsilon_{pl} + \Delta\epsilon_{el}$ in the notch root depends on (1) the strain-concentration factor $K_{t\epsilon}$, which is a function of notch depth l and notch radius r, and (2) the externally applied cyclic stress ΔS, (3) the elastic cyclic strain $\Delta\epsilon_{el} = \Delta S_{el}/E$.

Introducing $\Delta\epsilon_{pl}$ in Equation (10) yields (with $K = \epsilon_{pl}^{max}/\epsilon_{pl}^{min}$)

$$\frac{dl}{dN} = \frac{k_1^*}{\omega} + \frac{k_3^* \times c_1}{E^{\gamma}} \times [\Delta S \times (1 - c \times \kappa) \times K_{t\epsilon}(l, r') - \Delta S_{el}]^{\gamma} + \frac{c_2}{E^q} \times [\Delta S(1 - c \times \kappa)\,K_{t\epsilon}(1, r') - \Delta S_{el}]^{q} \quad (11)$$

Without integrating Equation (12), one can now discuss the two important cases (Figure 35).

[1] Under cyclic plastic straining, this relationship will be much more complicated.

Case A. There is no corrosion. Then the first two terms of Equations (10) and (12) drop out and Equation (12) gives the Woehler Curve with the air (inert-environment) fatigue strength S_f (Figure 36), with the conditions $\Delta\epsilon_{pl} = 0$ and $l = l_0$, $dl/dN = 0$:

$$\Delta S_f = \frac{\Delta S_{el}}{(1 - c \times \kappa)\,K_t(l_o, r')} \quad (12)$$

Case B. ΔS is below ΔS_f and cyclic loading takes place under Mode I CF conditions. Then the last two terms of Equation (11) drop out as per preposition no cyclic hardening or softening effects are to occur. For $k_1^* =$ constant (i.e., no changes in the corrosive medium during CF as well as in the metal), notch depth or crack length, as the case may be, increase proportionally to the cycle number N:

$$l - l_0 = \frac{k_1^*}{\omega} \times N \quad (13)$$

The notch factor increases, also. For surface notches that are not too deep, the Neuber-Notch factor is

$$K_t = 1 + \sqrt{\frac{l}{r'}} \quad (14)$$

The notch factor will, in this case, grow with N according to Equations (14) and (15):

$$K_t = 1 + \sqrt{\frac{\frac{Nk_1^*}{\omega} + l_0}{r'}} \quad (15)$$

This increase ends when the limit of elasticity is reached at the notch root, and cyclic plastic straining begins that marks the transition from static corrosion to true CF, in which the anodic dissolution is accelerated by increasing cycling plastic straining:[94]

$$\Delta S = \frac{\Delta S_{el}}{(1 - c \times \kappa)\left[1 + \sqrt{\frac{\frac{Nk_1^*}{\omega} + l_0}{r'}}\right]} \quad (16)$$

All three terms in Equation (11) are now operative, the second term being determinative for the increase in $\Delta\epsilon_{pl}$. The third term in Equation (11), crucial for a mechanically controlled crack propagation, is still small in this sequence of mechanisms. However, as the final fracture is drawing near and notch (crack) depth is advancing, this term finally contributes the largest share to crack propagation until fracture occurs.

The described regrouping is essentially governed[95] by the exponents γ and q in Equation (11).

Corrosion fatigue under stable conditions of passivity (Mode II corrosion fatigue)

Using high-alloy SSs in the active state undoubtedly offers advantages under specific circumstances, such as no risk of pitting, crevice corrosion, or SCC in chloride-containing environments, but it is an exception. These steels have been developed to offer corrosion resistance that they owe to passivity. For them, therefore, CF under stable passivity is the most important mode.

As in all cases of environment-induced cracking, a good insight into the mechanisms of Mode II is of great advantage for a successful application of SSs. As they are industrially subject, in practically all instances, to high-cycle fatigue regimes ($N > 10^5$), the following refers exclusively to this type of loading.

The potentiostatic results of Figure 37 indicate, from left to right, four ranges of CF resistance (at $S = 0.9\,S_{f,air}$): high resistance under cathodic protection, low resistance in the active state, high resistance by passivity (anodic protection), and low resistance in the transpassive range.

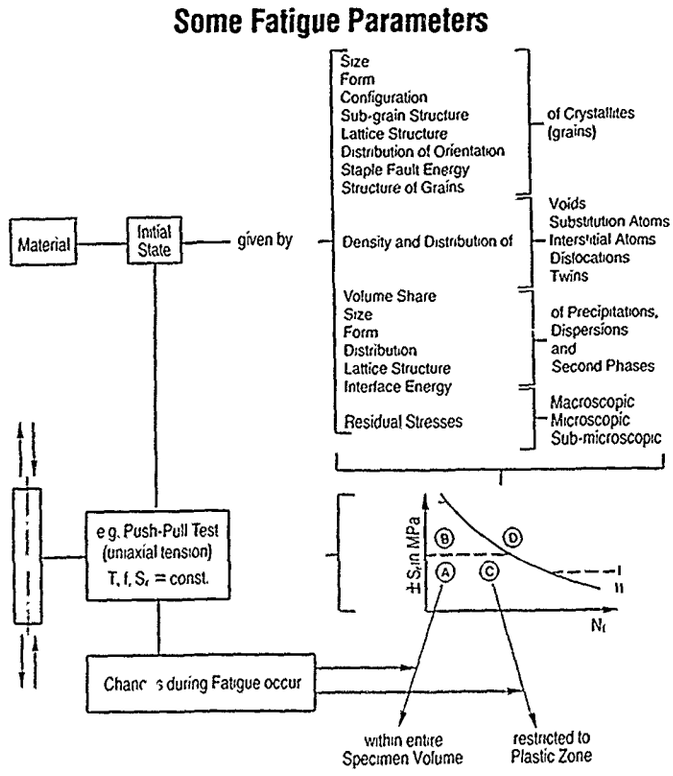


FIGURE 32—Schematic representation of fatigue processes and their parameters.[91]

CF Mode	Electrochemical Condition	Manifestation	Drop in Fatigue Strength
I Active State	I.1 Material does not show phenomenon of passivity I.2 Material does show phenomenon but $\varepsilon_m < \varepsilon_p$	„CF per se"—Corroded surface, many cracks filled with corrosion products	high (Corrosion Rate ↑, Notch Sensitivity ↑, Cycle Number ↑...)
II Stable Passivity	Material must show Phenomenon of Passivity, $i_c > i_p$ at $\varepsilon = \varepsilon_p$	Corrosion not detectable, few cracks	fair
III Unstable Passivity endogenous Activation	Material must show Phenomenon of Passivity, F-bands destroy Passivity, $i_c < i_p$ at $\varepsilon = \varepsilon_p$	similar to Mode I	fair to high
IV Unstable Passivity exog. Activ.	local Destruction of Passivity by Pitting, intergranular Corr., SCC	Superposition of CF and localized corrosion	very high

FIGURE 33—Corrosion fatigue modes.[92,93]

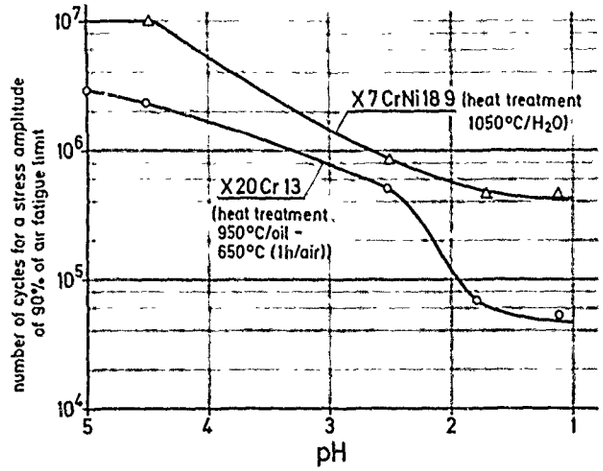


FIGURE 34—Influence of pH on the number of cycles endured for a stress range of 90% of AF limit comparing a martensitic 13Cr SS [type 420 (UNS S42000)] and an austenitic 18Cr-9Ni SS.

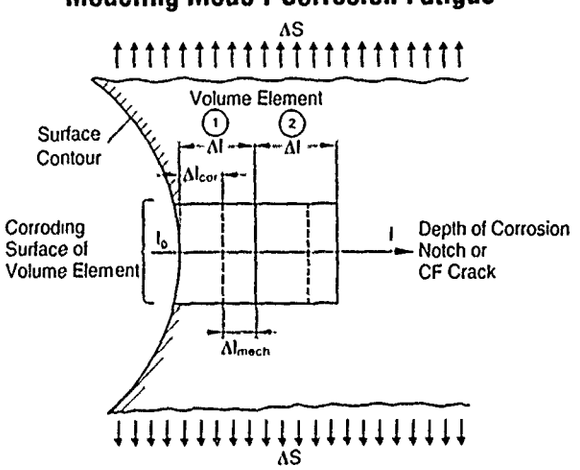


FIGURE 35—Mode I corrosion fatigue model based on localized straining and fracturing processes.[94,95]

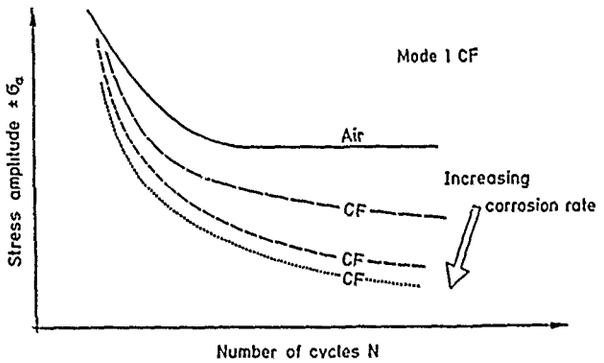


FIGURE 36—Stress range [± σa, ± S/cycle number (N)] relationship in air fatigue and corrosion fatigue (Mode I).

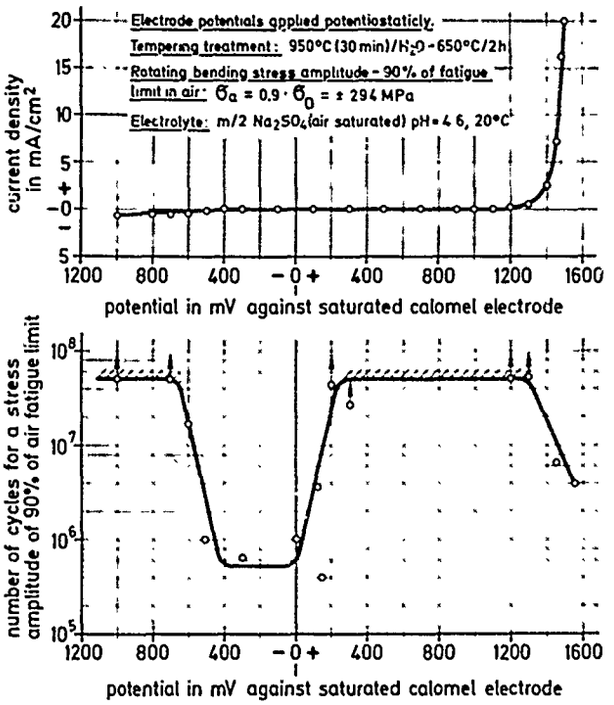


FIGURE 37—Potentiostatic corrosion fatigue tests in the active, passive, and transpassive range.

From both the practical and mechanistic point of view, the following findings should be kept in mind.[94]

(1) Passivity does not provide unlimited fatigue life except for amplitudes appreciably lower than $S_{f,air}$.

(2) The CF limit will be higher the less aggressive the corrosion conditions and, of course, the higher $S_{f,air}$.

(3) In environments for which the steels are engineered, the CF limit is lower (Figure 38) than $S_{f,air}$ even under the best conditions of passivity, viz., potentiostatic passivation at optimum potentials.[96] In cases where the CF limit seems to be higher[97] than the air fatigue (AF) limit (Figure 39), this results from experimental conditions, viz., evolution of heat during AF resulting in too low an endurance limit. Typical examples are austenitic SSs, with their high internal damping capacity that must be cooled by inert liquids in AF experiments.

(4) The physical appearance of passive CF differs widely from Mode I CF. Figure 40 illustrates the difference: one crack under ideal (i.e., potentiostatic) conditions or a few cracks under industrial circumstances (open-circuit potential, large surface areas); no recognizable surface nor crack-wall corrosion; smooth fracture surfaces in Mode II, as compared to many cracks starting from the bottom of shallow corrosion pits; heavy surface and crack-wall corrosion; and distinctly cleft fracture surfaces caused by cracks jumping to neighboring crack propagation planes in Mode I.

Mechanistic aspects

Early observations in potentiostatically controlled CF[94] brought insight into the mechano-electrochemical mechanisms by the striking fact that the anodic current necessary to maintain passivity remained low over nearly all the CF life of specimens cyclically loaded below the AF limit (Figure 41). It was only during the last 10% of life that it began to rise with increasing tendency. Incipient cracks could be detected under the optical microscope only in this final region of ascending current.

To explain this, two hypotheses seem possible: (1) The passive layer possesses an intrinsic fatigue strength and will be cracked in the course of cycling as other surface layers will be cracked, for instance, anodic conversion coatings on metals. At the bottom of such cracks repassivation will occur. (2) The passive layer will not be cracked. Instead, after a certain number of cycles, slip steps of sufficient height will emerge and pierce the passive film, whereupon repassivation will set in.

The first mechanism seems to be less likely for several reasons.

(1) Cracking of the passive layer should occur at the same strain amplitude independent of the base material's fatigue properties.
(2) Sets of conditions should exist where a steep current increase plus crack formation should occur early in life, and, again, this should happen independently, for instance, of a martensitic steel's tempering temperature (i.e., strength).
(3) For binary Cr-Fe alloys in particular but for other SSs, too, the passive films are so thin (0.5 to 10 nm) that the macroscopic concept of a fatigue limit no longer seems applicable to them.

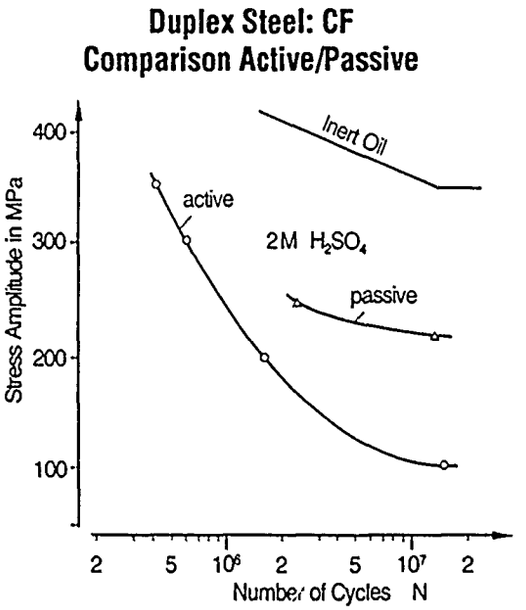


FIGURE 38—Typical Woehler Curves in air, in 2 M H_2SO_4 at open-circuit potential (Mode I corrosion fatigue) and under potentiostatic control (Mode II corrosion fatigue). Ferritic-austenitic SS (22Cr-5.5Ni-3Mo-0.2 N).[96] Ambient temperature.

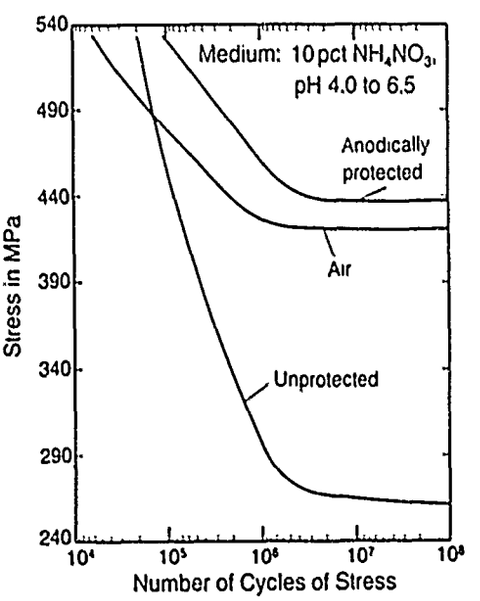


FIGURE 39—Increase of corrosion fatigue strength in Mode II above air fatigue strength resulting from the cooling action of the electrolyte.

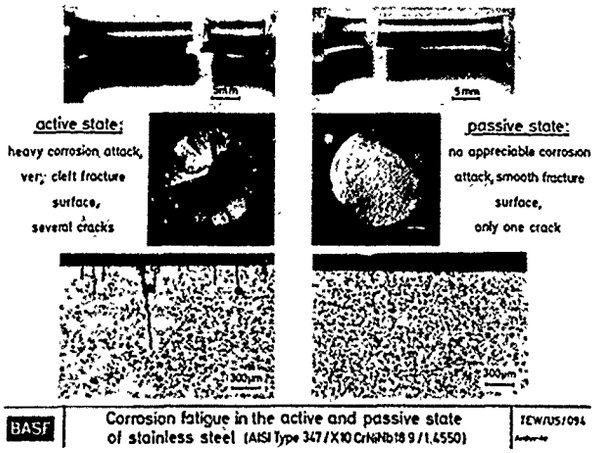


FIGURE 40—Phenomenological differences between Mode I and Mode II corrosion fatigue for an 18Cr-9Ni SS [type 347 (S34700)] in 6 M H_2SO_4 (rotating bending, stress range S = 0.8 × S_{air} = 243 MPa), ambient temperature.

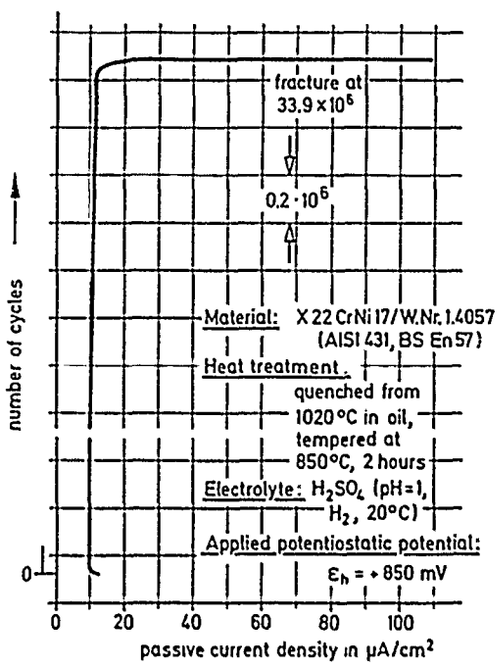


FIGURE 41—Current response of cyclically loaded specimens (rotating bending) under potentiostatic control in the passive range (Mode II corrosion fatigue).

The second mechanism was assumed to describe events as follows:[94] After a slip step of appropriate height pierces the passive film, a repassivation process will commence in which a certain charge will flow until passivity has been restored. According to Faraday's law a certain amount of metal will necessarily be dissolved before passivity has been restored and as a consequence, a small microscopic groove has been produced. This makes further plastic deformation at such a site likely [Equation (14)] because the stress has been locally increased. Slip steps will again protrude through the passive film and the interplay between repassivation, metal dissolution connected with it, strain concentration [Equation (15)], and triggering of further slip events continues. This process bears autocatalytic features and manifests itself, under potentiostatic conditions, in a gradual but finally steep increase of current (Figure 41). Current cycle characteristics of this type have been observed with all kinds of SS so far investigated. It seems likely that this mechanism of multi repassivation, caused by whatever type of dislocation induced microplastic deformation process, is responsible for CF in the passive state. One should recall that it takes a certain time until the process of repassivation is finished and passivity restored. During this time, a certain electrical charge ($\int I \times dt$) will flow. How much metal is dissolved in one elementary process, i.e., how deep the primary micronotch at the site will become where piercing of the passive layer has first occurred, depends on this quantity.

It has been shown that the charge necessary for repassivation is higher the higher the minimum CD for repassivation.[98] In other words, the higher this critical CD is, the more metal will be dissolved until passivity has been restored. Transferred to the case of CF, this means the primary micronotch becomes deeper and the stress concentration greater [Equation (15)] the higher the minimum CD for passivation. Steel/environment systems of this kind should have low CF strengths. We shall now exemplify the influence of acid concentration, alloy composition, and mechanical strength on this critical CD and CF strength or life, respectively.

Influence of acid concentration

The critical CD for passivation increases with acid concentration. To passivate a martensitic 13Cr steel [type 420 (UNS S42000), quenched and tempered at 650°C/2 h] requires about 6000 mA/cm² in sulfuric acid of pH 1, some 3 mA/cm² at pH 4.6. In the first case, this steel endures about 10^7 cycles to fracture, in the second, 5×10^7 cycles without fracture (rotating-bending stress S = 0.9 $S_{f,air}$/H_2SO_4, 20°C).

Another example is martensitic 17Cr-Ni steel [type 431 (UNS S43100), quenched and tempered at 675°C/2 h], rotating bending as above (50 Hz). The 5×10^7 CF strength values/minimum passivation CDs are, respectively,

(1) For pH 1: (H_2SO_4) 470 MPa/1800 mA/cm²; and
(2) For pH 4.6: 650 MPa/ < 1 mA/cm².

Influence of alloy composition

Alloying elements lowering the CD of passivation will increase the CF strength, keeping other factors constant. Among the alloying elements, chromium lowers that CD considerably and thus has a beneficial effect on CF life and strength, as shown in the above comparison between 13% and 17% Cr steels. However, any such comparison may be not unambiguous because of possible differences in AF strength.

Influence of mechanical strength

CF cannot occur under passive conditions if, under external cyclic loading, $A_{pl} = c_i \times \Delta \epsilon_{pl}^{\gamma}$ [Equation (6)] becomes zero per cycle and per volume element as the most stringent condition, or if, in the course of cyclic deformation, any manifestation of plastic deformation at the surface (slip lines or slip bands, extrusions, intrusions) will be unable to penetrate the passive layer. Conditions for repassivation being the same, the CF strength should, therefore, be higher the higher the AF limit. Figure 42 confirms this for the aforementioned martensitic 17% Cr steel whose AF strength was varied by tempering at different temperatures. The AF and CF curve take the same course.

Combining the findings of this and the preceding paragraph, the ideal combination of properties for achieving the highest CF strength in Mode II would be an alloy that has the lowest possible passivation CD in a given environment, the highest AF limit, and the smallest difference between the AF limit and the limiting stress range at which critical dislocation-induced surface plasticity accrues.

Crack initiation and propagation

Maintaining passivity potentiostatically will yield a typical response of the cell current to fatigue loading as shown in Figure 43 for rotating-bending loading.[94] The first feature is an induction Stage a, which is related to cyclic hardening. The DC signal information could yield only one event in these early investigations,[94] viz., crack growth being indicated by a steep rise of current. It could be shown by metallographic examination of specimens taken out toward the end of Stage b that cracks had initiated there. However, crack initiation was not recognizable in the DC signals.

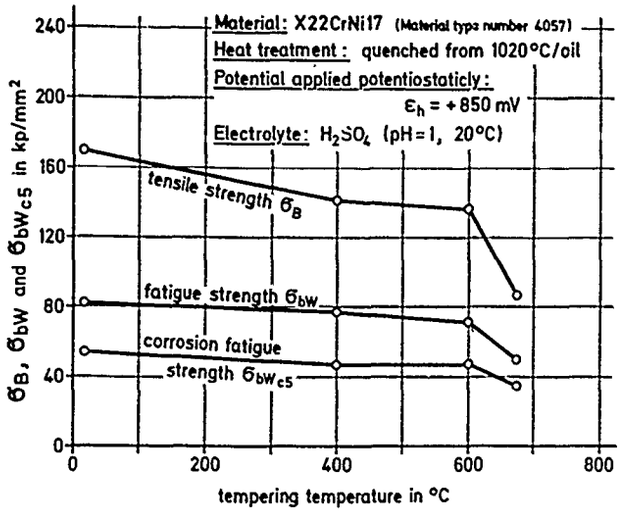


FIGURE 42—Tensile strength, fatigue strength, and corrosion fatigue strength (rotating bending) for a 17Cr-2Ni SS.

CF: Current Response of Passive Specimens (Potentiostatic Control)

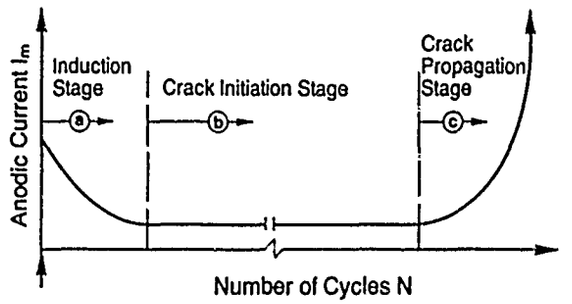


FIGURE 43—Current response during Mode II corrosion fatigue under potentiostatic control.

Further insight into the events during initiation and propagation has been gained by a special mechano-electrochemical measuring technique.[100]

Figure 44 shows the stress distribution over the specimen cross section under rotating bending and the direction of rotation. The specimen has a fixed marker triggering the transient recorder exactly in the spatially fixed plane of maximum bending moment. The distance between two subsequent trigger signals corresponds to one rotation of the specimen (0 to 360°), so the distance between trigger signal and maximum anodic current can be transformed into a phase angle. This angle indicates how many degrees the specimen has turned, after triggering the signal, until a specific feature of the cell current appears, e.g., when a sinusoidal cell current has reached its maximum.

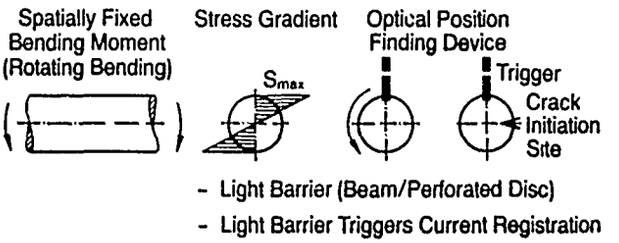
In detail, this has been accomplished by a light barrier/perforated disk installation. Under potentiostatic conditions, current signals could be recorded during each rotation and their origin located with respect to the reference line by means of a two-channel transient recorder. By careful electrical and magnetic shielding currents of some 10^{-9} A could be recorded together with the light barrier signal allowing to coordinate current transients and the sinusoidal mechanical stress. At the same time, the direct cell current was recorded (Figure 45).

Figure 46 shows three typical stages that can be discerned during the CF life of SS specimens under rotating-bending stresses.

Stage A. Stationary conditions with constant (DC) cell current and small stochastic current transients. Stage A begins when the induction Stage a of Figure 43, characterized by cyclic strain hardening processes, approaches its end. This induction Stage a is characterized by an initial high local slip activity that ceases because of cyclic hardening. It lasts only a small fraction of CF life and leads over to the Stage A in question (Figure 46).

Stage B. Stationary conditions with constant DC cell current and the appearance of small sinusoidal current signals that have a constant phase angle with respect to the light barrier signal (i.e., specimen reference line). These signals, with their phase angle, fix the future position of the CF crack. They are caused by emerging slip steps or, in the later stage, by persistent slip bands, their repassivation, renewed cyclic slip, repassivation, and so forth.

Device for Measuring Transient Currents under CF



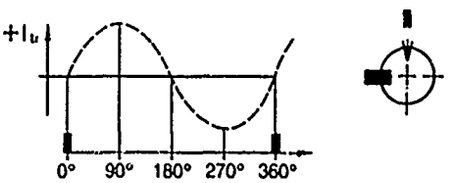


FIGURE 44—Device for measuring transient currents in rotating-bending corrosion fatigue experiments.[100]

Instrumentation for Measuring I-Transients under CF

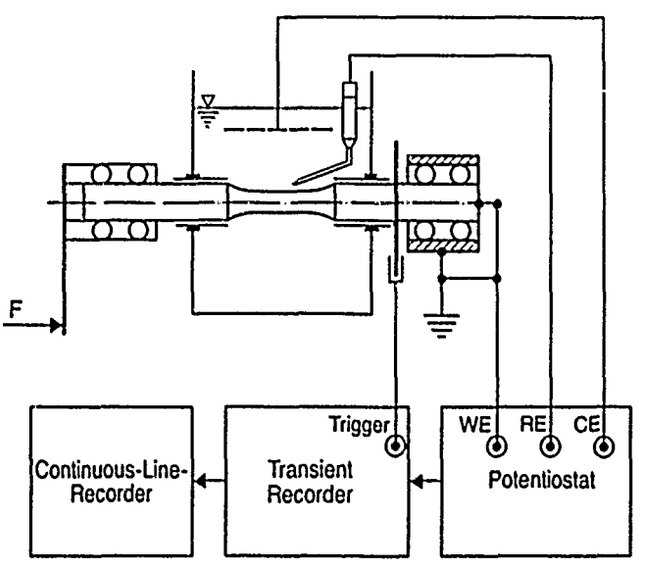


FIGURE 45—Instrumentation for measuring current transients under rotating-bending corrosion fatigue conditions.[100]

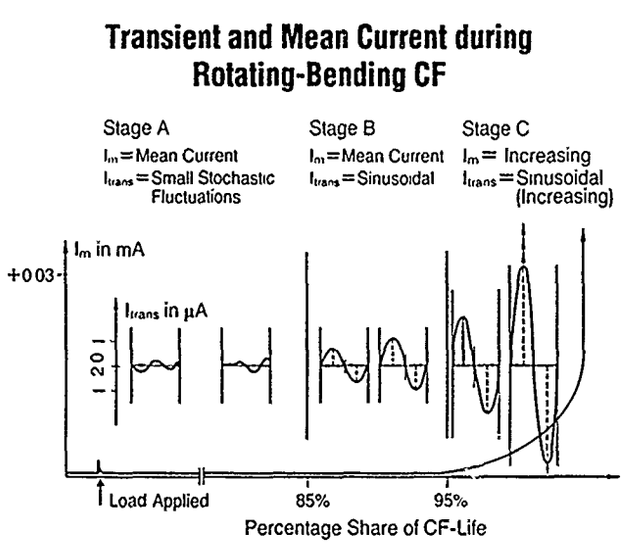


FIGURE 46—Transient and direct current during rotating-bending corrosion fatigue in three typical stages during the life of specimens (potential held potentiostatically in the passive region.)[100]

Stage C. Characteristics here are increasing cell current and steadily growing, sinusoidal current signals again showing a constant phase angle with resoect to the trigger signal stemming from the now very pronounced repassivation processes at the crack tip. Under potentiostatic passivation, as a rule, only one crack leading to fracture will develop (Figure 40).

Specimens taken out during Stage A and carefully inspected metallographically show no CF-induced surface defects whatsoever and may, therefore, be termed "incubation stage." The passive layer nevertheless responds to the alternating stress, shown by the drastic reduction of the transient current peaks immediately upon taking away the load. The remaining stochastic fluctuations were characteristic of the normal heal-up events in the passive film.

Applying the same procedure in Stage B reveals incipient cracks ("crack initiation stage"), which will start to grow in Stage C ("crack propagation stage"). It could be forecast from the phase angle between the trigger signal and the anodic maximum of the sinus half-wave on which surface line cracking initiated.

Figure 47 shows an example. A specimen removed from the rotating-bending machine during Stage B was tested in a rotary manipulator of an eddy current device. It was fixed in its zero position to the position of the trigger signal, its sense of rotation being the same as that of the rotating-bending machine. The phase angles of the cracks initiated on the specimen circumference are shown; they complied with the pertinent metallographic findings. The length of the cracks that were initiated correlated with the half-amplitude of the cell current signals. In addition, in systems where two cracks were initiated, it was possible to discern this by the appearance of two sinusoidal signals. The leading crack causing final fracture was identified by its fast-growing amplitude. Figure 48 shows the results for a two-crack specimen that had been taken out during the transition from Stage B to C and tested in the eddy current set-up mentioned. The crack that was longer and had a fast-growing amplitude, measured electrochemically (Figure 45), appeared at 95 to the reference line, the other appeared at 277°.

Similar investigations for other types of loading have so far not been conducted. However, the transient corrosion current behavior under pulsating tensile stresses of varying stress ranges was studied with the 22Cr 5.5Ni-3Mo duplex steel and in comparison to an austenitic SS (type 316). In sulfuric acid solutions at temperatures up to 70°C, it was found that the transient current is set by the alternating strain rate and is no function of the absolute value of stress. For unfractured specimen surfaces, the transient corrosion current describes the passive layer as a "mechanical impedance" and is therefore no function of experimental time. Crack initiation is marked by a typical deforming of the transient current signal, i.e., by a phase shift and increasing amplitudes. This indicated the state of starting cracks much earlier than any other signal and is thus an excellent help in studying CF initiation under this type of loading.[99]

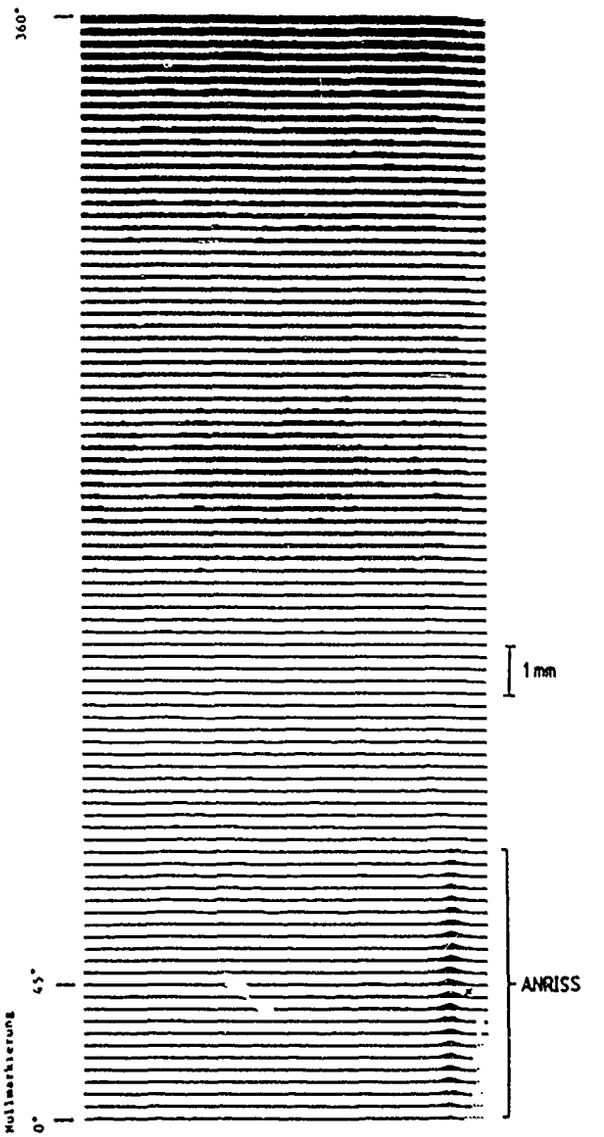


FIGURE 47—Scanning-type, computer-aided eddy current nondestructive test result. Specimen was removed from the machine during Stage B.[100] Anriss = incipient crack.

Crack initiation and alloy chemistry, a comparison of ferritic, austenitic, and ferritic-austenitic steels[100]

As mentioned, crack initiation starts at the transition from Stage A to Stage B, which is marked by a transition from stochastic current fluctuations to sinusoidal current signals. For practical purposes, it is useful to know at what percentage of cycles to failure this transition takes place. Crack initiation immediately before fracture is, for example, an unfavorable condition from the industrial safety point of view. It is, therefore, of interest to know more about the influence of alloy chemistry, protective value of passive layers, etc., on crack initiation.

Figure 49 compares the relative crack initiation ratio N_i/N_f of a ferritic 12% Cr steel with a ferritic-austenitic 22Cr-5Ni-3Mo steel and an austenitic SS (17Cr-12Ni-2Mo, Ti-stabilized) under constant relative alternating stresses (90% of the respective AF strength). The results indicate the following:

(1) The 12% Cr steel with the least protective passive layer undergoes crack initiation at N_i/N_f of about 0.38.
(2) The ferritic-austenitic steel with the most protective passive layer (because of increased Cr and Mo contents) undergoes initiation at N_i/N_f values between 0.8 and 0.85.
(3) Included for reasons of comparison, the austenitic SS has the same AF strength as the 12% Cr steel but higher N_i/N_f values, between 50 and 55%, because the higher Cr and Mo contents increase the protective value of the passive layer. The delay of crack initiation by improved passivity can also be seen in Figure 49 (dashed bars) when increasing the potential from U_H = 365 mV to 700 mV. This clearly leads to both higher fracture cycles and to an increase in N_i/N_f from 0.8 to 0.96.

The general term "protective value of the passive layer" comprises two factors: chromium content in the layer and its thickness. These factors were analyzed by ESCA on specimens of the aforementioned ferritic, ferritic-austenitic, and austenitic SSs that were potentiostatically held at U_H = 365 and 715 mV in 0.05 and 2 M H_2SO_4 showing an enrichment of the Cr-cation content in the passive film by a factor of 3 to 8. The highest contents were found in the ferritic-austenitic SS followed by the austenitic SS and the ferritic SS. Ni and Mo could also be detected in the film of the first two steels. Their concentration was much smaller than in the matrix. With increasing acid concentration, the Cr/Fe ratio decreases.

Figures 50 and 51 show the thickness of the passive layer in 0.05 M and 2 M H_2SO_4, respectively. The highest thickness (2.8 nm) is observed for the passive film of the ferritic-austenitic SS. The thickness is lowest for each steel at the lower potential and higher acid concentration. For the 12Cr steel in 0.05 M H_2SO_4/U_H = 0 mV, the monolayer thickness of 0.3 to 0.5 nm is reached.

The relations between these findings and those from rotating-bending CF tests can be summarized as follows:

(1) Increasing Cr contents in the steels lead to higher Cr-cation concentrations in the passive film and higher thickness and, on the other hand, to both higher N_i/N_f values and higher cycles to fracture under normalized alternating stresses (in the present case, for example, S_r = 0.9 $S_{f,air}$ and a fixed passive potential).
(2) Film thickness and chromium enrichment decrease as the potential in the passive region is decreased and so does the number of cycles to fracture under normalized stress amplitudes and the N_i/N_f values.

Influence of other system parameters on crack initiation[100]

Figure 52 demonstrates the influence of stress range on (nondimensional) crack initiation N_i/N_f for a ferritic-austenitic SS.

(1) The number of cycles-to-fracture decreases with increasing stress range.

(2) The (nondimensional) crack initiation starts sooner the higher the stress range.

(3) The stochastic cell current signals in Stage A change to sinusoidal amplitudes with a constant phase angle related to the light barrier signal (i.e., the specimen reference line) 5 to 7% before the direct cell current starts to increase. In other words, the crack initiation period constitutes, for this SS, about 6% of the total life. The dashed lines represent the relative percentage of life at which the cell current starts to increase; in other words, subcritical crack propagation begins.

(4) Below a stress range of S_r = 1.2 $S_{f(air)}$, just one crack initiates and leads to fracture; at S_r = 1.2 $S_{f(air)}$ several cracks can be found.

(5) Increasing acidity leads to earlier crack initiation. Examples for a ferritic-austenitic 22Cr-5Mo-3Ni SS at S_r = 0.7 $S_{f(air)}$: 0.05 M H_2SO_4: 91%/ 2 M H_2SO_4: 75%.

(6) The influence of the potentiostatically applied potential in the passive region is similarly pronounced· Increasing the potential within the useful range of passive potentials causes a significant retardation in crack initiation Example for a type 316 SS at S_r = 0.9 $S_{f(air)}$), U_H = +365 mV· 53%, U_H = +715 mV: 96% (even under the higher stress range of S_f = $S_{f(air)}$).

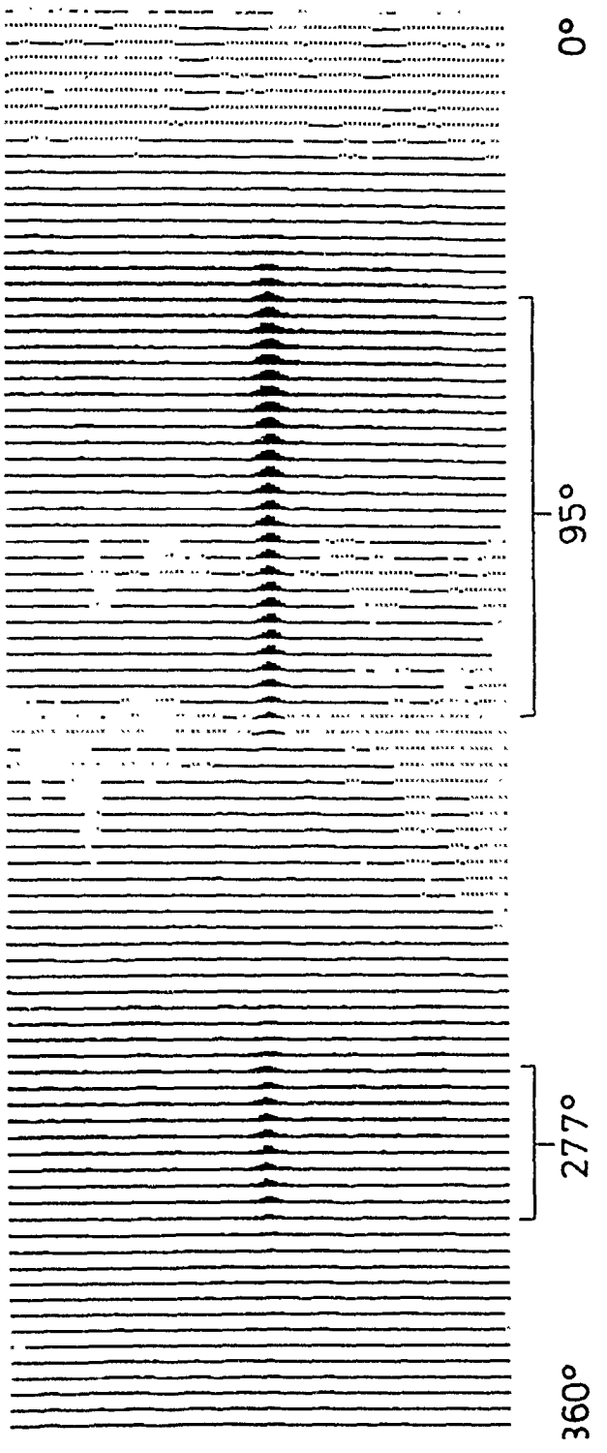


FIGURE 48—Same procedure as in Figure 47; however, specimen taken out during transition from Stage B (crack initiation) to Stage C (crack propagation).[100] Two cracks starting at 95 and 277°, respectively. Crack length at 277°: 2.7 mm.

The significance of stochastic cell current signals in Stage A[100]

Coming back to Phase A, in which no surface damage whatsoever could be detected, seems to be of little value. However, there are distinct processes that manifest themselves in stochastic peaks responding clearly to system parameters. Figure 53 manifests, for a type 316 austenitic SS, the peak heights of the transient current signals of potentiostatically controlled fatigue tests for three selected passive potentials clearly indicating lower values in the optimum passive range. Figure 54 demonstrates the difference when polariz-

ing slowly, under fatigue loading, from lower to higher potentials and vice versa. The upper curve should be compared with Figure 54 and demonstrates the higher peak heights of this 12 Cr steel, whose passive film is inferior to that of higher-alloyed SSs. This holds true for the lower ("reduction") curve, too.

Regarding the mechanical influence, Figure 55 evidences the fact that the transient currents in Stage A increase with increasing stress amplitude. Improved conditions of passivity (curve on the right-hand side) cause lower currents at higher stress ranges.

Figure 56 demonstrates the influence of alloy chemistry on the average peak height, again proving that steels forming "better" passive films respond to CF by lower transients in Stage A. Finally, Figure 57 shows the influence of acidity yielding the now expected result, viz., lower transients at lower acidity.

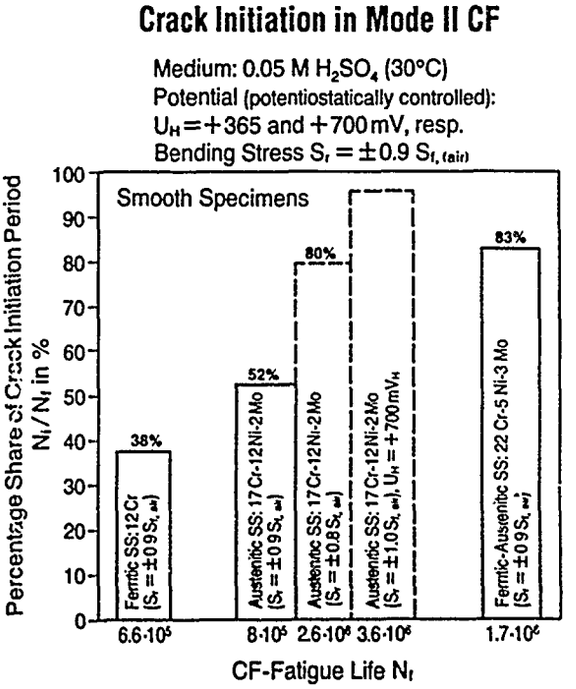


FIGURE 49—Crack initiation in a Mode II corrosion fatigue. Ratio of initiation cycles to fracture cycles for three SSs and dependence of N_i/N_f on stress range for an austenitic SS.[100]

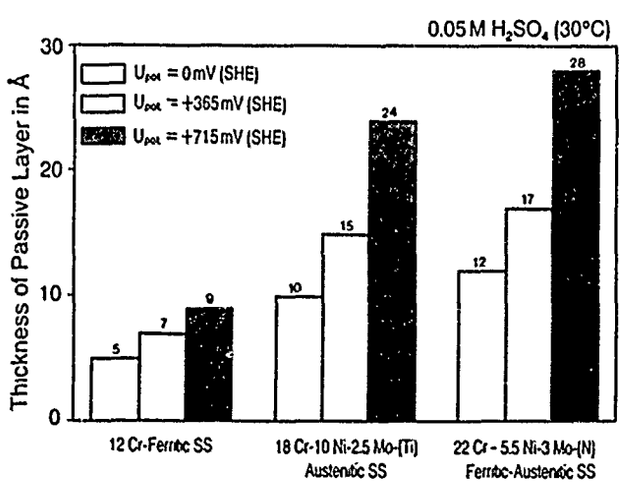


FIGURE 50 – Thickness of passive layer (Auger analysis) for three SSs at three potentials (potentiostatically) in 0.05 M H_2SO_4 (30°C).[100]

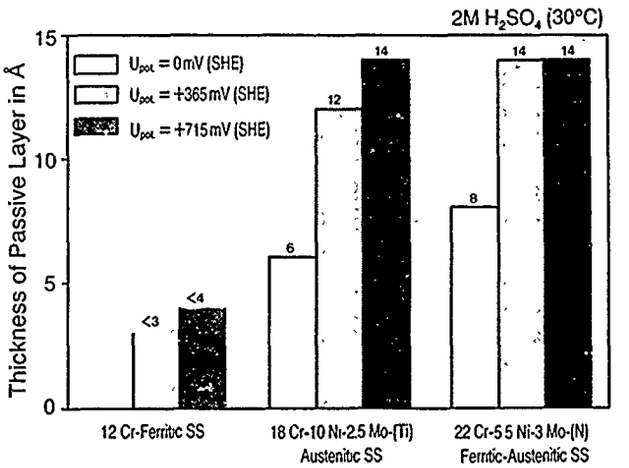


FIGURE 51—Thickness of passive layer (Auger analysis) for three SSs at three potentials (potentiostatically) in 2 M H_2SO_4 (30°C).[100]

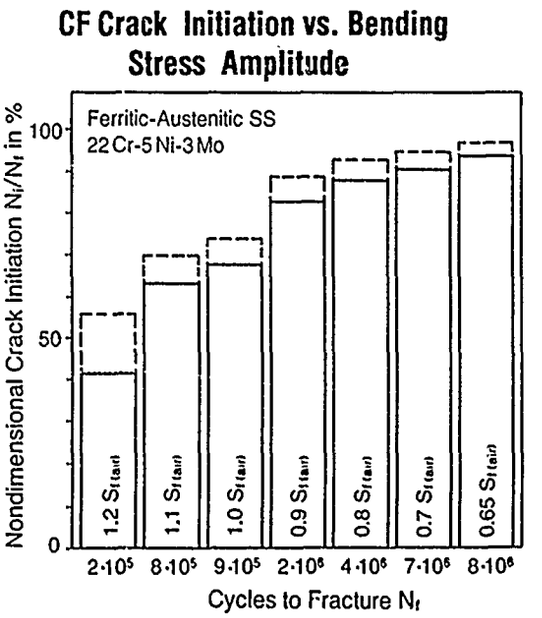


FIGURE 52—Dependence of nondimensional crack initiation N_i/N_f on rotating-bending stress range.[100] Potential (potentiostatic): +365 mV_{SHE}. Medium: 0.05 M H_2SO_4 (30°C). Dashed lines represent beginning of subcritical crack propagation.

Initial period of cyclic hardening

It was mentioned before that, after applying the fatigue load, there is a steep anodic increase of current under potentiostatic conditions. As cyclic hardening in this first fatigue period sets in, the current decays and reaches a low stationary value (Figure 43). As this is Mode II CF under stable passivity, such a current response is possible in no other way but by an initial, extremely localized damage of the passive film. This must be induced by some sort of near-surface bulk dislocation mechanism. As the current signals in the period indicate, there is some localized anodic dissolution that is weakening as cyclic hardening progresses. These signals seem to be caused by healing-up processes of the passive layer at sites where there is surface slip in the course of cyclic hardening. In fact, sinusoidal signals appear occasionally in the initial period of cyclic hardening in the same way as later on during the crack initiation Stage B. Thus, it is likely that slip/environment interaction during this period follows the mechanism of Stage B (slip-step emergence/passive film piercing/repassivation model[94]). Experimental observations support this view:

(1) The sinusoidal signals mentioned will decay as cycling hardening progresses in this period;
(2) All system parameters exert the same influence on the current transients in this period as on the sinusoidal signals in the crack initiation, Stage B, such as lower signals,
  (a) At potentials favoring improved passivity (signal amplitude at 900 mV ≅ 715 mV < 365 mV < 0 mV, Figures 53 and 55);
  (b) At lower stress amplitudes (Figure 55);
  (c) With alloys high in Cr and Mo (22Cr-5Ni-3Mo SS < 316 SS < 12Cr SS);
  (d) In less aggressive media (0.05 M H_2SO_4 vs 2 M H_2SO_4, Figure 57).

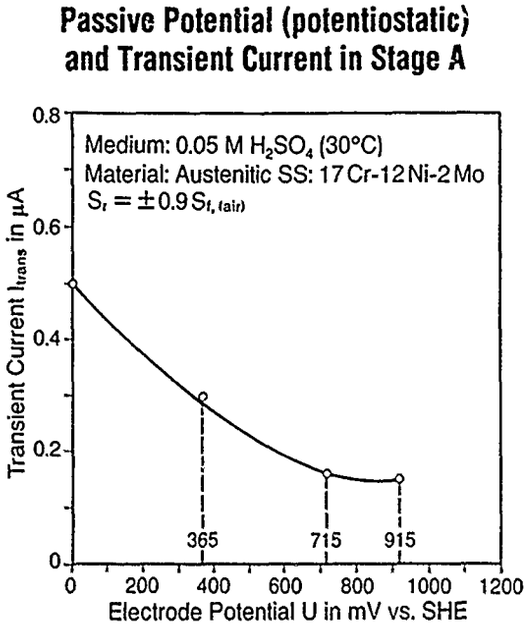


FIGURE 53—Dependence of transient cell current in Stage A on (potentiostatic) passive potential[100] in the incubation Stage A.

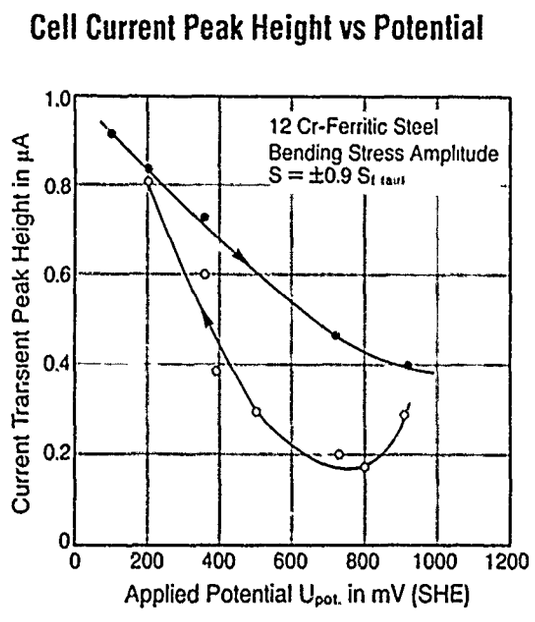


FIGURE 54—Dependence of cell current peak height on (potentiostatic) passive potential.[100]

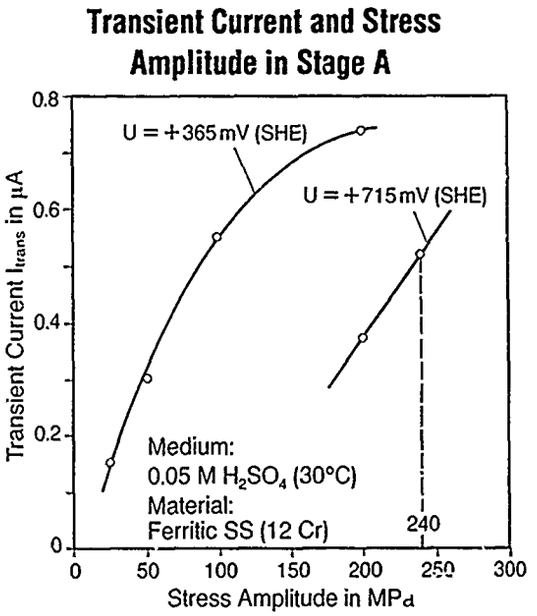


FIGURE 55—Dependence of transient cell current in Stage A on stress range.

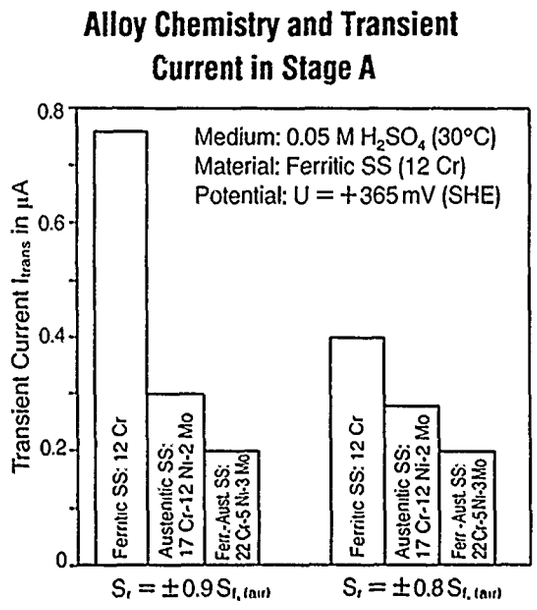


FIGURE 56—Dependence of transient cell current in Stage A on alloy chemistry.

It appears that, during the initial hardening period, local plastic strain events, limited both in time (cycle numbers) and extent, leave sites where microplastic processes are preferentially set in motion during the subsequent Stage A, where they manifest themselves in the aforementioned stochastic current transients. Those involving the highest charge transfer will be prime candidates for continued mechano-electrochemical reactions in Stage A until, at the transition from Stage A to Stage B, irreversible near-surface glide processes are induced at one or a few sites as manifested by the sinusoidal signals in Figure 46. They may be indicative of the appearance of persistent slip bands (PSBs). It has been demonstrated at PSBs that several processes can occur that all act toward depassivation:[101] the basic process of local rupture of a passive film by sufficiently extruded PSBs, surface roughening on PSBs, and stress raising at the matrix/PSB interface.

The answer to the question of whether one or a few cracks will initiate seems to be given already during the initial cyclic strain-hardening period. If sufficient strain localization and, as a consequence, preferential passivation/depassivation are possible there, it

is highly likely that only one crack will be initiated that will lead to fracture. Therefore, in favor of this are anodic protection, low acidity, high contents of passivating alloying elements in SSs, and low stress range. Figure 58 illustrates an example where all four parameters are in the adverse direction.

The limiting case where no cracks will initiate requires that PSBs be unable to form at all or, if they can form, that they have dimensions that are small compared to the thickness of the respective passive film.

It is for this reason that practical measures to counter Mode II CF aim at suppressing slip processes up to stress ranges as high as possible, e.g., by shot peening, hammering, autofrettage; using alloying elements that lower the electrical charge required for repassivation and, at the same time, assist in forming thick passive layers (Figures 50 and 51), applying redox systems, where feasible, that hold a favorable potential within the passive range (Figures 53 and 55), and designing for low stress ranges by eliminating geometrical and other stress raisers.

Résumé of the potential of the current transient measuring technique.[100] The signals that can be recorded during the CF life of specimens describe the corrosion system "stainless steels under fatigue loading and stable passivity."[100] They allow detection of the first interactions between cyclic slip processes and environment, discovery of crack initiation on a microscopic scale, determination of the position of growing cracks, at present for rotating bending, by measuring the phase angle between sinusoidal current signals and a reference line on the circumference of a specimen, and discrimination of whether one or more cracks develop and differentiation between growing and dormant cracks.

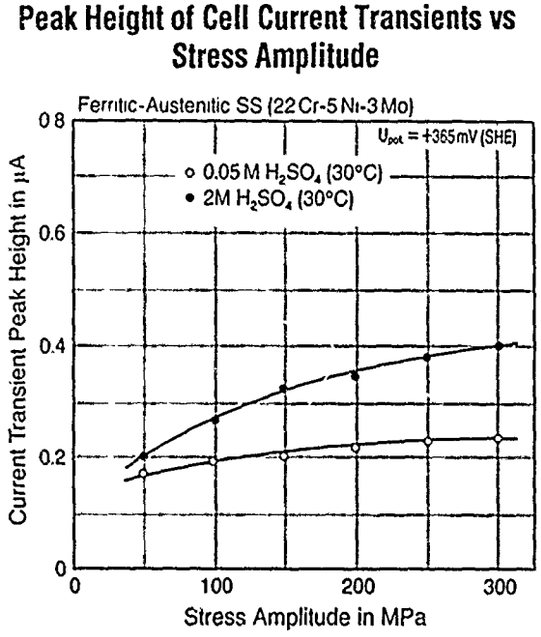


FIGURE 57—Dependence of cell current peak height on stress range and acid concentration in Stage A.

Peculiarities of ferritic-austenitic SSs[96]

These steels show all the salient mechanistic features dealt with in the previous paragraph. However, the duplex character of these steels causes some effects that result from the different chemical composition and lattice of the α- and γ-phase that are not observed in the aforementioned classes of monophase SSs. Figure 59 displays one of them. They may become passive after an appreciable lapse of time and high cycle numbers, e.g., 5×10^7, even under CF loading, if the system is not too far away from the active/passive borderline, as in the case of 2 M H_2SO_4 at ambient temperature.[96] The stress range is influential only insofar as it will limit the time-to-fracture and consequently the time available for self-passivation. Self-passivation occurs at $S_r = \pm 0$, too, indicating that the mechanism is purely electrochemical in nature. In fact, a microscopic and scanning electron microscope (SEM) investigation revealed a preferential corrosion attack on the austenitic phase, which is lower in Cr and Mo than the ferrite. This preferential attack produces trenches. In the plate-manufacturing process, the austenitic islands are stretched in the milling direction. Figure 60 shows the different configuration of the austenitic phase in the LT and TL directions,[(2)] respectively TL specimens, therefore, exhibit deeper trenches than LT specimens. By the selective dissolution of the austenitic phase during self-passivation, the surface will be steadily enriched in Cr and Mo until passivation becomes possible.

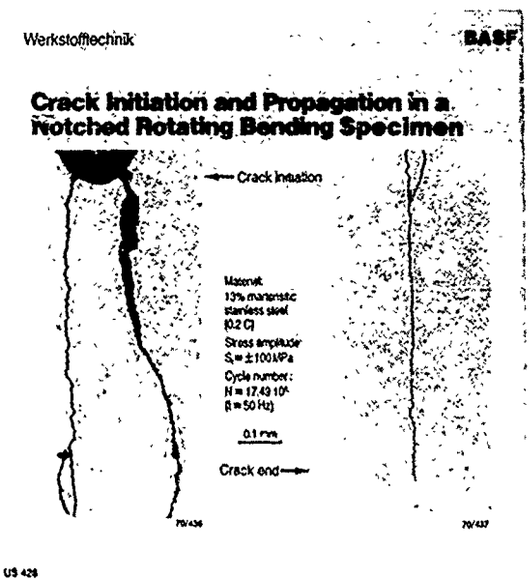


FIGURE 58—Crack initiation and propagation in a notched rotating-bending specimen under conditions favoring two cracks (and crack branching). Open-circuit potential, H_2SO_4 (pH = 3.3, 30°C, $S_r = 0.9\ S_t$(air).

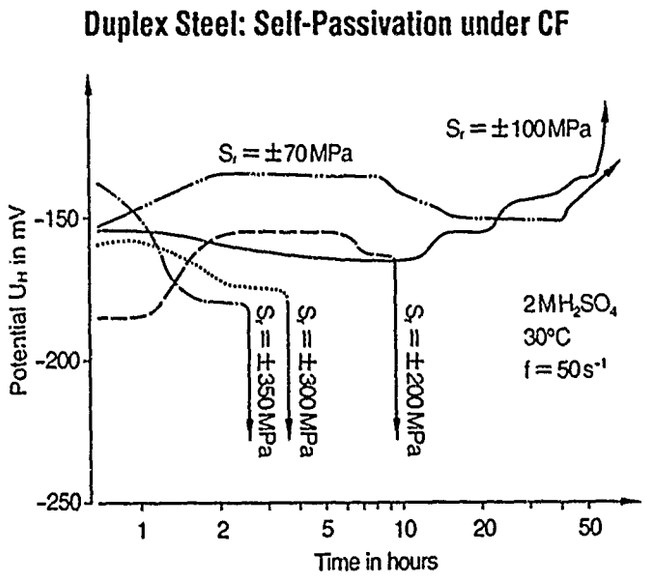


FIGURE 59—Self-passivation of a 22Cr-5.5Ni-3Mo ferritic-austenitic SS at open-circuit potential. Influence of stress range and time (number of cycles), respectively.[96]

[(2)]The first letter indicates the direction of principal stress; the second letter indicates direction of crack propagation direction.

Duplex Steel: Austenitic Phase in Ferrite Matrix

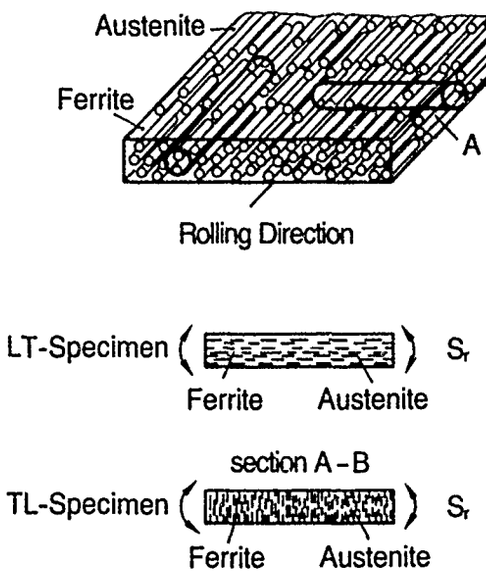


FIGURE 60—Milling texture of a ferritic-austenitic SS with the austenitic phase in the ferrite matrix.[96]

The process of self-passivation in these duplex SSs should be frequency independent in a range where the hydrodynamic conditions in the boundary layer are identical. This is brought out by comparing Figures 59 and 61 for stress ranges low enough to yield fracture times longer than the time for self-passivation ($\pm S_r < 100$ MPa).

The preferential dissolution of the austenitic phase should influence the fatigue life because of the surface notches formed. To demonstrate this,[96] specimens were self-passivated under the conditions of Figure 59 at $S_r = \pm 0$. In the first case, after passivity had been reached, the fatigue load ($S_r = \pm 200$ MPa) was applied (Figure 62). In the second case, again after identical self-passivation, the specimen was cathodically activated, and the load was applied. Despite the fact that trenches had been formed in the process of self-passivation in the first stage of the experiment ($S_r = \pm 0$), deepening of these notches and early crack initiation in the second case was responsible for a much lower fatigue life, compared to the first case where (stable passivity) Mode II CF conditions were maintained from the moment the load was applied.

Besides differences in the corrosion resistance of the two phases, an influence of rolling texture is noticeable even under optimum (potentiostatic) Mode II CF conditions. It becomes more so the longer the fatigue life. In an inert environment, the difference in fatigue strength between LT and TL specimens must remain constant because no electrochemical component is involved.

Maraging steels

The CF behavior of an 18Ni-7Co-5Mo maraging steel (R_m = 1780 MPa, $R_{p\,0.2}$ = 1700 MPa) has been studied in Mode II CF (pH = 4.62, M/10 acetate buffer, 20°C). The AF and CF results will be evaluated with respect to the notch sensitivity of this 18% Ni maraging steel after a few general remarks.

The reduction of fatigue strength is usually less than the theoretical stress concentration factor K_t indicates, which is the ratio of the greatest stress in the region of a mechanical notch or other stress concentrator, as determined by the theory of elasticity, to the corresponding nominal stress (S_n) (Figure 63). Theoretically, the stress at the tip of a notch should be increased by

$$S_{max} - S_n = K_t S_n - S_n = S_n (K_t - 1) \qquad (17)$$

Because of the formation of a plastic zone ahead of the notch tip, this increase is lower and determined by an "effective" stress concentration factor (termed fatigue notch factor K_f), which is the ratio of plane fatigue strength (S_f) to the notched fatigue strength (S_n):

$$K_f = \frac{S_f}{S_n} \qquad (18)$$

The real stress increase is therefore (Figure 63)

$$K_f \times S_n - S_n = S_n (K_f - 1) \qquad (19)$$

Introducing the notch sensitivity factor q will yield a measure of the degree of agreement between K_t and K_f:

$$q \times S_n(K_t - 1) = S_n (K_f - 1) \qquad (20)$$

$$q = \frac{K_f - 1}{K_t - 1} \qquad (21)$$

When $K_t = K_f$, i.e., $q = 1$, a material is said to be fully notch sensitive; if $q = 0$ ($K_f = 1$), it is notch insensitive.

Duplex Steel: Self-Passivation under CF

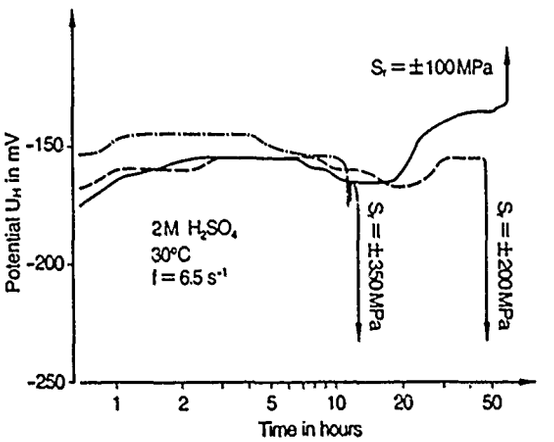


FIGURE 61—Self-passivation of a 22Cr-5.5Ni-3Mo ferritic-austenitic SS at open-circuit potential. Influence of stress range and time (number of cycles), respectively[96] (frequency 6.5 s^{-1} instead of 50 s^{-1} in Figure 59).

Duplex Steel: Life vs Self-Passivation/Activation

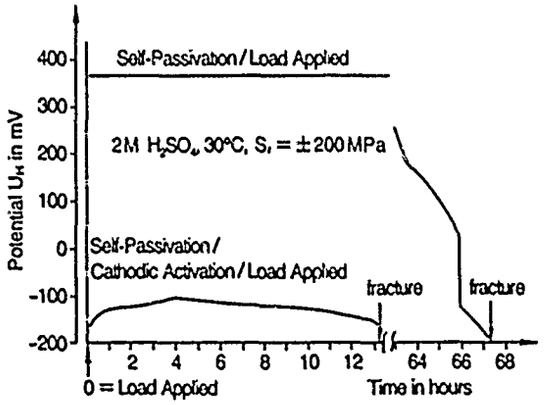


FIGURE 62—Corrosion fatigue life of a ferritic-austenitic SS (22Cr-5.5 Ni-3Mo) as influenced by self-passivation and cathodic activation, respectively.[95] Open-circuit potential.

The relationship between K_t and q is illustrated in Figure 63, which shows the stress distribution in a notched bar.[102] The left part illustrates the geometric influence on the notch effect [Equation (17)], whereas the right part of this figure expresses the influence from the side of the material [Equation (18)]. It should be noted, however, that the original assumption does not hold true: The notch sensitivity factor q is no material constant for a given material. Calculating q from Equation (21) is permissible provided q is determined under equal or at least similar conditions to which a component will be subjected. In addition, it has undoubtedly the advantage to be illustrative in the aforementioned sense: q = 1: extreme fatigue notch sensitivity; q = 0: no notch sensitivity.

Table 8 represents the results for the 18Ni-7Co-5Mo maraging steel in two heat-treatment conditions. For sharp notches (K_t = 4.80), the notch sensitivity factor in air is not too much different for push-pull or pulsating tension stresses, whereas q (on the basis of plane fatigue strength in air/notched CF strength) is falling, under such mild corrosive conditions, below the lowest q value in air in the age-hardened condition. On a CF basis (plane CF strength/notched CF strength), q is decreased to a very low value (0.19), demonstrating once more that mechanical notches, in their negative effect on fatigue strength, will be far surpassed by mechano-electrochemical notch effects.

Corrosion fatigue in the state of unstable passivity with endogenous activation (Mode III corrosion fatigue)

Among all SSs, martensitic 13Cr steels are especially prone to this type of CF[94] in little aggressive media because of their borderline composition for passivity. When passivated, for example, in a medium such as c_2 in Figure 64, an unstable passive potential ($_2\epsilon^{pass}$) will develop. In the course of fatigue loading, the aforementioned sequence of events will cause polarization as soon as a slip step (PSB) of critical height has penetrated the passive film. The open-circuit potential will become more and more negative until it falls below the passivation potential (ϵ_p) and total activation occurs. Corrosion proceeds in Mode I at the active open-circuit potential ($_2\epsilon^{act}$).

Failures resulting from this mode can occur when potential measurements in a medium show passive behavior and no potential–time curves after complete activation of test coupons (e.g., by touching them with Zn) were taken to prove stable passivity by repassivation.

Corrosion fatigue in the state of metastable passivity with exogenous activation (Mode IV corrosion fatigue)

The important case is that of a superposition of CF and pitting. Others concern CF with superposition of crevice corrosion, intergranular, and stress corrosion, respectively.

Superposition of pitting and corrosion fatigue. This mode has been studied first for austenitic SSs.[103] After an induction period, pitting is stabilized and cracks start from the anodic bottom of pits. Usually, cracking occurs in a number of pits so that a fracture surface full of fissures is formed that can be distinguished easily macrofractographically from Mode II but looks very much like Mode I fractures. However, all the surface except for the pits remains passive, acting as the cathodic area. With numbers of cycles increasing, the pitting area increases and the corrosion potential shifts toward less noble values. Figure 65 shows a SEM picture of the surface of a rotating-beam specimen. It gives an impression of the sequence of events underlining the fact that, because of the stress concentration in the ligaments between closely adjacent pits, the cracks tend to follow such paths. This figure also brings out the detrimental effect of pitting on CF strength. The low number of cycles (40×10^6) was endured at a stress amplitude of only ± 80 MPa.

An early practical example of the superposition of CF and pitting is given in Figure 66, illustrating the CF failure of a low-pressure turbine blade. Figure 67[104] shows a typical low-pressure turbine configuration.

Condensing reheat turbine blade failures. Such blade failures in condensing reheat turbines have, in the meantime, become a subject of wide interest. They usually occur after a long operating period (in Figures 68 and 69 after about 55,000 operating h).

Moving blades and guide vanes represent the highest number of single components in a turboset (e.g., 15,000 moving blades in a 1300 MW turbo set); two-thirds of all running blade failures[106,107] occur in the transition and condensating stages. As a high percentage of them is caused by Mode IV CF, it is understandable that great efforts have been untertaken to find ways to mitigate it, e.g., by EPRI,[3] BMFT/DECHEMA,[4] and others.

Figure 68 shows a running blade and its base after fracture. Many small, dark spots with a somewhat brighter ring can be recognized on both sides of the blade. The brighter rings surround the pits covered by tiny heaps of corrosion products. In the area of the bright rings, the cathodic partial reaction of pitting takes place. As is typical for Mode IV, several cracks (close to the blade base) combine in the final phase of fracture. This caused the fissured appearance of the fracture surface shown in Figure 69, which demonstrates that cracking started from the bottom of pits.

In this context, the origin of corrosive agents in condensing reheat turbines has been discussed,[92] because, after applying 100% condensate polishing, both the feedwater and the boiler water are very pure. However, traces of salts including chlorides may slip through the ion exchangers being carried along with the high-pressure steam in which they are soluble. It is a striking fact that CF failures in these turbines are restricted sometimes to only one or a few stages of running blades at which x = 1 ("Wilson Zone"). No CF failures occur in the first stages, where there is no condensation, and also in those where there is full condensation. It is in the range where condensation starts that one can observe CF cracks. This results from the fact that the front of condensation is not stable, thus causing alternate condensing and drying up in the Wilson Zone. This process leads to an accumulation of salts, among them chlorides that can induce pitting of 13% Cr turbine steels.

Heavy salt deposits do not represent the state of the art in modern power plants using 100% condensate polishing. Nevertheless, the problem remains that the first droplets of condensate may be enriched in ions, among them chlorides, because of the widely differing partition coefficients of substances in the steam/water system.

Mechanical and corrosive stressing of turbine blades. On the mechanical side, there are different and complicated loads that act on blades, for instance, centrifugal, steam bending, initial preload overspeed, and reactive loads resulting from thermal expansion.

Stress calculation and design put enough safety into the operational behavior of blades to avoid low-pressure steam turbine blade failures but could not take into account the loss of fatigue strength because of Mode IV CF. The significant reduction in fatigue strength of a typical 13Cr martensitic blade steel is plotted in Figure 70 and clearly reveals the following points:[105]

(1) The structural AF strength of a blade profile is lower than the plane-specimen AF strength;
(2) It is, however, conservative (in air) to take the notch fatigue strength as a basis for calculation if not for the environmental influence;
(3) The lowest strength is observed under CF conditions with notched specimens and blades coming down to the same level;
(4) It must not be overlooked that heavy pitting alone, e.g., provoked in stand-still periods, will lower CF strength considerably because of the notch effect alone, as the second lowest level of Figure 70 illustrates.

It thus becomes evident how important it is to test a steel under conditions sufficiently similar to reality.

[3]Electric Power Research Institute, Palo Alto, CA.
[4]Bonn/Frankfurt, FRG.

TABLE 8
Fatigue Notch Factor K_f and Notch Sensitivity Factor q (K_t = 4.80)[A]

Fatigue Mode ($N = 10^7$)	Solution Annealed, HV 30 = 330		Age Hardened (850°C, 30 min/475°C, 6 h)	
	K_f	$q = \frac{K_f - 1}{K_t - 1}$	K_f	$q = \frac{K_f - 1}{K_t - 1}$
Alternating stress (push-pull) (air) $R = \frac{S_{min}}{S_{max}} = -1$	3.31	0.61	3.60	0.68
Pulsating tension (air) $R = \frac{S_{min}}{S_{max}} = 0$	2.91	0.77	3.21	0.58
Pulsating tension 0.1 M acetate buffer, pH 4.62 R = 0	not tested	—	10.0[B]	0.42[B]
			1.71[C]	0.19[C]

[A]18% Ni-maraging steel (7.5 Co, 4.8 Mo, 0.4 Ti).
[B]Basis = plain fatigue strength (air)/notched CF strength.
[C]Basis = plain CF strength/notched CF strength.

Fatigue Notch Sensitivity

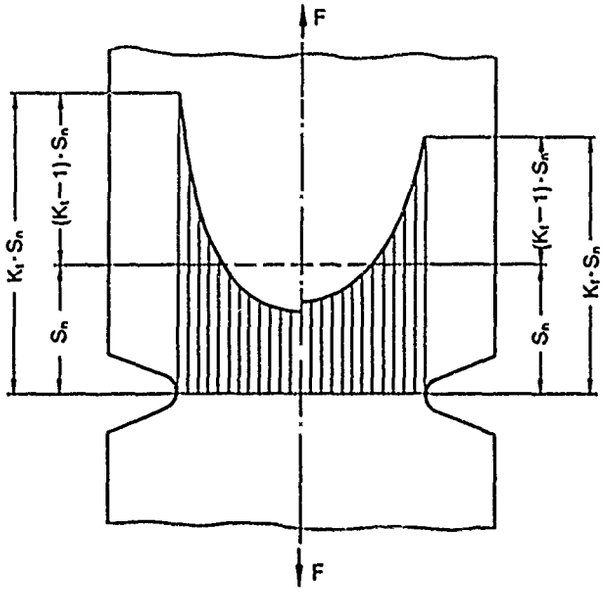


FIGURE 63—Illustrating fatigue notch factor (K_f), theoretical stress concentration factor (K_t), and notch sensitivity factor (q).[102]

As Figure 70 showed, condensate suffices to lower the fatigue strength. Fatigue data for 13% Cr steel tested at low frequencies in condensing steam have made this clear (Figure 71) in a more quantitative way.[108] The dashed line separates the pitted specimens from those in which the surface condition had remained unchanged, the full line encloses those with cracks. Data were obtained by repeated examination of the specimens by SEM at the intervals indicated by the data in Figure 71. After comparing them with published high-frequency data, it may be necessary to use notched fatigue data from high-frequency tests to model the reduction in fatigue strength that may occur when low cyclic loading is experienced in relatively innocuous environments. The low cycle CF side of the problem has thus been brought into focus and, with it, the events and effects under those 10^4 start-up conditions in the typical life of a turboset. On the other hand, Figure 71 shows that the pitting and cracking borderline under such conditions seems to be located at comfortably high stress levels. These data were obtained under continuous loading. Further research must demonstrate if and how far low-frequency load cycles intermittent with rest periods will yield results that differ from the continuous loading mode of Figure 71.

This picture changes dramatically when high chloride contents come into play as in blade stages near x = 1, i.e., at the (unstable) front of condensation, causing condensation and drying up. It is assumed, at least in Germany, that an aqueous solution of 26% NaCl by weight and 80°C will conservatively represent the real conditions. Figure 72 presents the results of the aforementioned BMFT research project in a complete Smith diagram.[109] The frequency chosen (50 Hz) was the rotary frequency, the cycles being limited to 3×10^7 or 5×10^7 for practical reasons. It displays the influence of oxygen in both deionized water and its extremely detrimental effect in the concentrated chloride solution. In deionized water, the decay of fatigue strength is nearly independent of pH between 5 and 9, whereas in concentrated NaCl solutions saturated with O_2, the CF strength between pH 7 and 9 is only a fraction of the AF limit. This dramatic drop is a result of Mode IV CF because, under such conditions, the open-circuit potential will be driven beyond the pitting potential.

Clearly, under such conditions, life will be limited. Aside from efforts to safeguard operational conditions that exclude events like an inrush of untreated water, faulty operation of condensate polishing units, etc., design measures to keep the fatigue load of running blades in the transition stages as low as possible and to damp vibrations, an intensive search for better blade materials and causes of failures was conducted.[110-128]

In addition to martensitic and ferritic-austenitic SSs, ferritic SSs were included in this search. In a classification,[129] ferritic-austenitic and high-chromium ferritic steels fall in one group with CF strengths of around 300 MPa, austenitic and martensitic SS in a second group with CF strengths around 100 MPa.

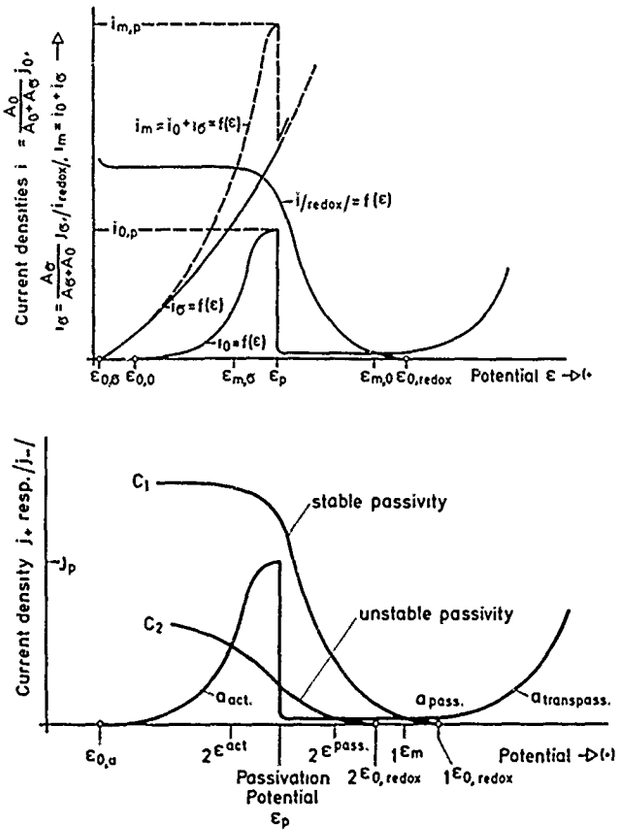


FIGURE 64—CD potential curves illustrating stable and unstable (metastable) passivity. Influence of the cathodic partial reaction.



Material: Steel X 10 CrNiNb 18 9
W.Nr. 1.4550
(AISI 347, BS En 58 F)

Surface Treatment: Grinding and electrolytic polishing (~500 µm/Φ)

Medium: Aqueous solution of 45 g/l NaCl, 22 g/l $FeCl_3 \cdot 6 H_2O$, 11 g/l $FeSO_4 \cdot 7 H_2O$ pH = 1,7

Stress Amplitude: ± 80 MPa

Number of Cycles: $4{,}08 \cdot 10^6$

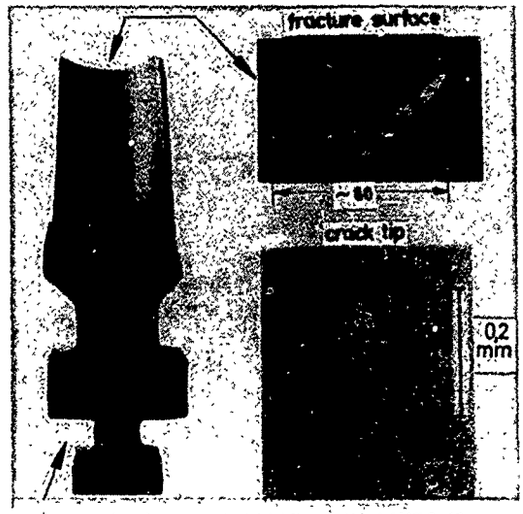
BASF | Corrosion Fatigue and Pitting Corrosion | TEW/US/054

FIGURE 65—Superposition of corrosion fatigue and pitting corrosion [Mode IV corrosion fatigue; material, steel X 10 CrNiNb 18 9; W.-No. 1.4550 [type 347 (UNS S34700); BS En 58 F)]. Original surface ground and electrolytically polished. Medium: aqueous solution of 25 g/L NaCl, 22 g/L $FeCl_3 \times 6 H_2O$, 11 g/L $FeSO_4 \times 7 H_2O$, pH 1.7. Stress range in rotating bending: ± 80 MPa. Number of cycles at fracture: 4.08×10^6).

From a practical point of view the following results shall be mentioned:

(1) Class 3 Super 12% Cr steels[130] were found to have rotating-bending CF strengths of around 350 MPa (artificial seawater, room temperature) as compared[111] to 335 MPa of a duplex 21Cr-6Ni-Mo SS.

(2) Adding 1% Mo to Class 1 13% Cr steels increases the uniaxial tension CF strength by about 80 MPa (S_m = 350 MPa, 10 Hz, 27% NaCl, pH = 7). This is caused by two effects: (a) shifting the pit initiation potential to more noble values; (b) formation of thicker passive layers.



Low-pressure turbine blade of steel X15Cr13 fractured in the range of beginning steam condensation

BASF | Corrosion fatigue of a steam turbine blade | TEW/US/032

FIGURE 66—Corrosion fatigue Mode IV failure of a low-pressure turbine blade.[92]

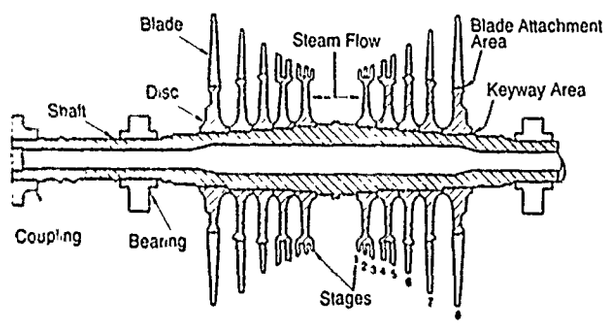


FIGURE 67—Typical low-pressure turbine configuration. (Copyright 1980 EPRI. EPRI WS-78-114. Reprinted with permission.[104])

(3) The damage ratio (CF limit divided by endurance limit in air) depends[119] strongly on the tempering temperature of martensitic 13 Cr steels (at 600°C the damage ratio was as low as 0.04 in 3% NaCl as compared to about 0.25 to 0.30 at 430 and 750°C). Especially large pits initiating CF were observed in specimens tempered at the critical temperature of 600°C. This is explained by precipitation of carbides M_7C_3 + $M_{23}C_6$ + $M_2(C, N)$ where martensite laths had been located.[131] Pitting seems to be favored under such heat-treatment conditions (quenching from 970°C in oil tempering at 450°C, 3 h/air cool). This is, once more, a hint not to deviate from long-established, heat-treatment procedures calling for a tempering temperature of at least 680°C. In contrast to the tempering temperature, the austenitizing temperature was found to have little influence.

(4) Choosing the proper heat treatment. The effect of heat treatments on the CF properties of 13Cr SSs in aqueous NaCl solutions has been studied in detail.[119] Whereas the austenitizing temperature (between 930 and 1100°C) has little influence, the tempering temperature is critical. The CF strength goes to a minimum at 600°C (as similarly shown in Figure 74). It is much smaller there than at 450 and 750°C. The former tempering temperature cannot be made use of as the mechanical properties, above all, the fracture toughness, are too small for practical purposes. The minimum at

600°C is explained by the fact that carbides of the type M_7C_3, $M_{23}C_6$, $M_2(C,N)$ are precipitated where martensite laths had been located.[111]

(5) An accelerated test procedure to determine quantitatively the propensity to CF could not be found.[110 120]

(6) The inhibiting effect of silicates and phosphates on the fatigue crack growth rates in type 403 SS is nil in 10 M NaOH (1 Hz, 100°C) They showed inhibiting effects, however, in 6 M NaCl at a concentration of 0.5 M Na_3PO_4 or Na_2SiO_3, respectively. At a concentration of 0.1 M, an accelerating effect was found enhancing the fatigue crack growth rates.[132]

(7) Of many types of coatings, only the anodic metallic deposits gave an improvement of type 403 SS CF strength.[113]

(8) The high-frequency CF strength (Figure 73) of type 403 steam turbine blade material (10^9 cycles) in 18 different environments is lower than that of the 17-4 pH and Ti-6Al-4V alloys.[133] 13Cr SS was tested over the broad range from 10^{-3} to 10^4 Hz by fracture mechanics fatigue crack growth methods showing that environmental crack growth rates decrease strongly at higher frequencies, demonstrating the possibility that ultrasonic tests allow the measurement of fatigue threshold stress-intensity ΔK_0 in short times.[134]

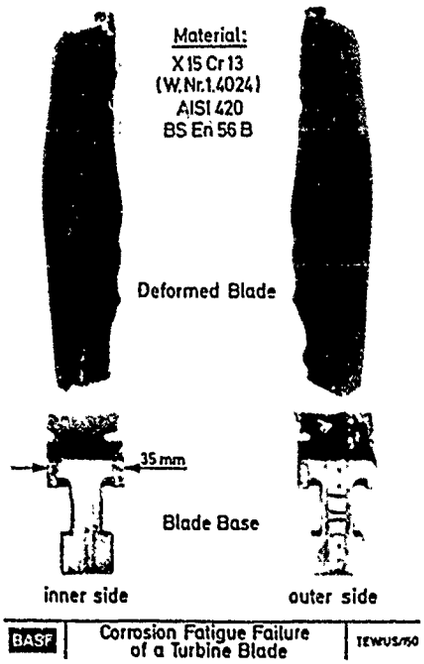


FIGURE 68—Superposition of corrosion fatigue and pitting corrosion (Mode IV corrosion fatigue: view of failed blade).

In a somewhat related field, type 410 SS compressor blades have been shown to gain considerably in their CF strength by residual magnetism. This improvement is attributed to a reduction in the rate at which dislocations cross slip to broaden slip planes, which are preferentially attacked by a synthetic seawater atmosphere.[123] It is interesting to note that the magneto-mechanical contributions to internal friction not only have a beneficial effect on fatigue by increasing the damping capacity of type 410 SS blades, they evidently act in a positive sense under CF conditions, too.

In an extensive study, the influence of microstructure on fatigue crack initiation in hot-neutral sodium chloride solution has been investigated.[115] Results showed that 3% sodium chloride solution (80°C) has a marked influence on the fatigue strength of tempered martensitic 12Cr and 17Cr-2Ni steels: Pitting corrosion started at sulfide inclusions at all stress ranges below the AF limit above which oxide-sulfide inclusions in the 12Cr steel and mixed-oxide inclusions in the 17Cr-2Ni steel become operative. It is interesting to note[115] that crack initiation in pure, extra-low carbon and low interstitial ferritic steels (18Cr and 28Cr-4Ni-2Mo) did not follow the Mode IV CF mechanism. Initiation was caused by the slip step emergence (Mode II mechanism[94]) because, in this environment, pitting will not be induced. CF cracks always pass along the interphase matrix/inclusion, the latter themselves not being cracked. Sulfide inclusions are less noble than the passive film[135] and have been identified as the preferential site of pit initiation.[136-139] Once attacked, they lead to an enhancement of local anodic dissolution not only on account of the galvanic effect but also by stimulating anodic dissolution in the presence of S^{2-} and SH^-. This stimulation is most effective, of course, in a crevice. Crevices between matrix and sulfide inclusions are likely because of the difference in the coefficient of thermal expansion leading to a stronger contraction for sulfide inclusions. This is one of the reasons for the close similarity between pitting and crevice corrosion.

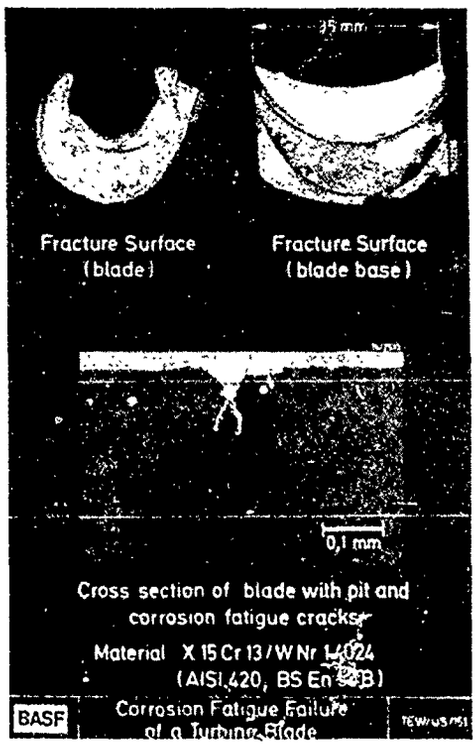


FIGURE 69—Fracture surface of blade, blade base, and cross section of blade with pit and corrosion fatigue cracks, respectively.

Fatigue and CF: Influence of Medium and Structure

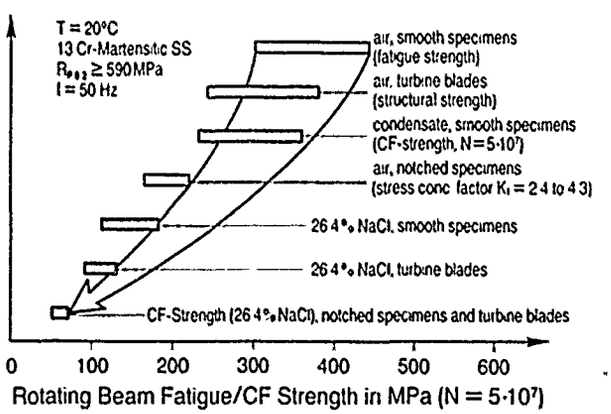


FIGURE 70—Fatigue and corrosion fatigue in connection with steam turbine running blades: Influence of medium and structure.[106]

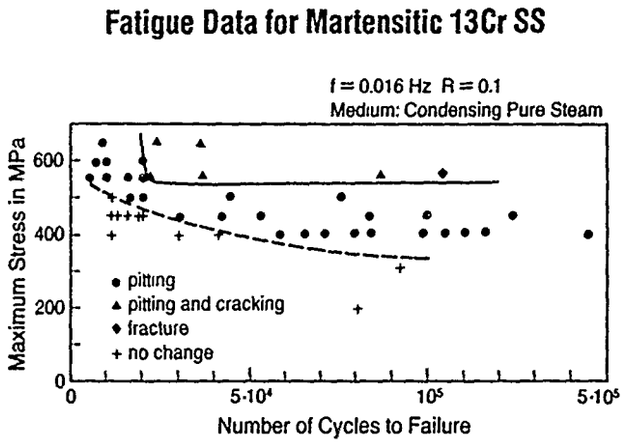


FIGURE 71—Tension–tension fatigue data for a 13Cr martensitic turbine blade steel.[106]

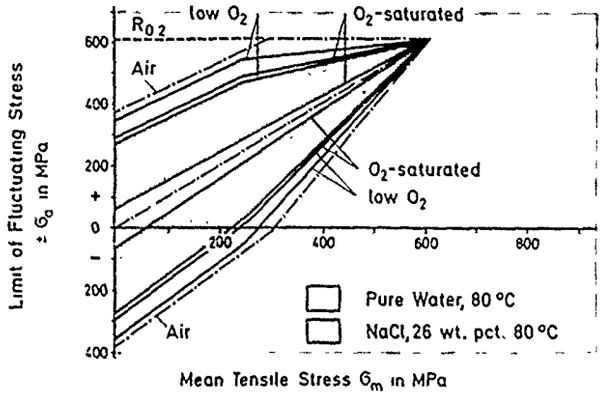


FIGURE 72—Smith diagram for air and corrosion fatigue showing the influence of oxygen.

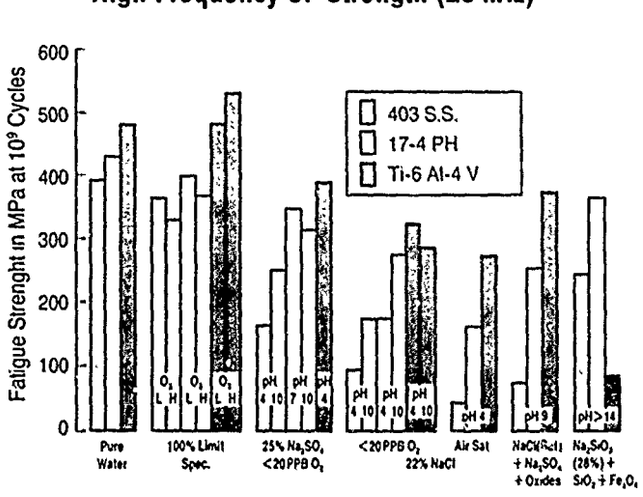


FIGURE 73—High-frequency corrosion fatigue strength of different materials. Influence of inhibitors.

Nickel martensitic and maraging steels

Because of their high tensile strength, this class of steels has higher fatigue strengths in air than austenitic SS. It is for this reason that they aroused interest and found application for Kaplan turbines in the form of heavy castings for runners, and as forgings for gliding planes. In the meantime, they are used in pumps for casings, runners, and shafts, and in compressors for similar components. The molybdenum-bearing qualities are used in seawater service and interest can be noted for using them as low-pressure turbine blade material.

Aqueous solutions. Nickel martensitic steels meet the requirements of hydro-turbine service, viz., strength, hardenability, weldability, and cavitation and CF resistance.

Water wheels for Pelton turbines and Kaplan runners are predominantly made of type 13Cr-4Ni currently. The reason for turning to these high-alloy materials was cracks in cast bucket wheels of Kaplan turbines that have been identified as caused by CF. As in the case of steam turbine CF blade failures (Figure 70), it is difficult and requires costly technical resources to obtain CF strength values representing the factual behavior of a steel in such components under service conditions. How problematic it is to determine a characteristic value meeting this requirement became evident.[140, 141] As emphasized in Reference 37, the S_f values of laboratory specimens can be much higher than the stress range endured by thick wall castings of type 13Cr-4Ni material applying test parameters closely related to practice.

The problem of how far the water quality influences the life of the components in question has so far not been resolved. In laboratory tests using different water qualities, no pitting was observed. It is not clear, however, whether or not the chloride concentrations in hydro-turbine service will induce Mode IV CF. On the other hand, the following parameters have been clearly identified:[37]

(1) The type of alloy and the chemical analysis have, except for impurities, little influence on CF;[140,141]
(2) Forgings have a higher fatigue and CF strength than castings, provided they are loaded in a favorable direction to the forging fibers. Weld metal has CF strengths at least as good as cast material;
(3) Heat-treatment conditions and strength, respectively, have, within wide limits, no influence on the CF strength. Even in small laboratory fatigue specimens, the fatigue strength increases only slightly with tensile strength.[37]

Seawater. For this service, grades on the basis 16Cr-5Ni-1Mo offer a good choice. As Figure 74[152] shows, the addition of about 1% Mo increases the CF strength in seawater considerably. Castings of 16Cr-6Ni (CA-6 NM) show a CF strength clearly below ±100 MPa, these values being considerably lowered at higher cycle numbers. In contrast to this, the curve drop of the 16Cr-5Ni-1Mo steel in seawater almost ceases, which is in agreement with results reported on wrought alloys of similar composition.[142] Figure 74 also indicates that a fatigue strength of at least ±200 MPa may be expected with respect to a tempering temperature of not less than 600°C under laboratory conditions.

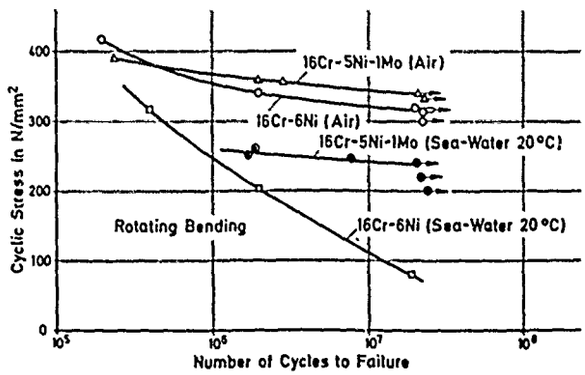


FIGURE 74—Rotating-bending fatigue strength of steel X 5 CrNi 13 4 (unpublished results by KSB Frankenthal, Federal Republic of Germany[152]), X 5 CrNiMo 13 6 and X 5 CrNiMo 16 5 1. Smooth specimens.[152] (Reprinted with permission.[142])

Chloride solutions at elevated temperatures. In connection with the aforementioned problem of low-pressure turbine blade failures by CF, extensive investigations were undertaken to compare the strength of nickel martensitic steels with those of standard martensitic grades in chloride solutions in a temperature range characteristic for low-pressure steam turbine stages in the critical condensation range. Results showed the CF limit decreases considerably with increasing temperature, whereas the chloride ion concentration is of minor importance. In the temperature range up to 80°C. Mode II CF was observed that was characterized by a plane crack path and no corrosion attack to the specimen surface. At a temperature of 150°C, Mode IV CF occurred.[143] CF fractures always pass along the interphase matrix/inclusion, the inclusions themselves not being cracked.

Compared to type 410 standard Cr steels, the CF strength of 16Cr-5Ni-2Mo nickel martensitic SSs was found to be appreciably higher under all conditions. Further improvements can be obtained by secondary metallurgical processing. An electroslag remelted 16Cr-5Ni-1Mo steel reached at $N = 3 \times 10^7$ in 22% NaCl at 80°C: $S_a = \pm 160$ MPa (mean stress $S_m = 350$ MPa) and at 150°C $S_a = \pm 60$ MPa (mean stress $S_m = 250$ MPa).

However, this positive effect on CF strength is not pronounced; if several melts are tested, the standard metallurgical grade and the electroslag remelting grade probably will fall within the same scatter band.

The highest CF strength under the aforementioned conditions were shown by the maraging 17-4 pH SS (e.g., $S_a = \pm 200$ MPa at $S_m = 350$ MPa in 22% NaCl of 80°C). However, there is a pronounced scatter of results, low values being obtained whenever copper-containing metallic inclusions (which quickly corrode away) are present in the surface or oxide inclusions containing Si, Mg Mn, and Ca.[146] The effect of microstructure on pitting and CF of 17-4 pH turbine blade steel in chloride environments was investigated in an EPRI research project.[145] Shot peening can cause changes in the microstructure of the surface layers by transforming the austenite to untempered martensite. As large amplitude cyclic voltammetry and pit propagation rate tests indicated, tempering temperature and shot peening have only minor effects on resistance to pit initiation and propagation in aqueous chloride environments. However, the susceptibility to CF in 6 wt% $FeCl_3$ was reduced by increasing the tempering temperature from 540 to 650°C, evidently by lowering the crack growth rates at lower strength levels, i.e., tempered at 650°C. At low stress levels, shot peening appears to have a slightly adverse effect on the CF behavior of specimens tempered at 650°C but has no effect on specimens tempered at 540°C.

Low interstitial ferritic SSs[125]

The dependence of CF crack initiation mechanisms on the corrosion behavior of a low interstitial ferritic 28Cr-4Ni-2Mo SS compared to a straight martensitic 12Cr SS (0.9Mo, 0.7Ni, $R_{p\,0.2}$ 730 MPa, R_m 890 MPa) has been studied in detail.[125] The microstructures to be compared were purely ferritic vs tempered martensite. Sulfide–oxide-type inclusions were found in both steels, the sulfide phase containing Mn and little Ca. The low interstitial ferritic steel contained Nb carbonitrides but no sulfide inclusions.

Crack initiation in air always started, in the case of the martensitic SS, at nonmetallic inclusions, mainly by a precracking process rupturing phase boundaries, or in some cases, decohesion of the boundary sulfide/metallic matrix. In the low interstitial ferritic SS, slip lines became visible and crack initiation in air thereafter commenced along the lines. Small (3 to 4 μm) Nb carbonitride inclusions were not involved in the initiation process.

Under CF conditions, the martensitic SS crack initiation was triggered by pitting at nonmetallic oxide-sulfide inclusions both in 0.5 and 4 M NaCl solutions. In contrast to this, the ferritic steel was fully passive, showing a kind of "fatigue limit" (in the technological sense) below which no more crack initiation occurred because the carbonitride inclusions did not crack below this fatigue limit. Above this limit, in 0.5 M NaCl, CF always initiated at slip lines. In spite of passivity, cracks initiated in the concentrated 4 M solution by cracking of Nb carbonitrides, which were leading to a local corrosion attack, and from there CF cracking started.

In assessing these findings,[125] a fatigue limit for the martensitic SS cannot exist because of the fact that its open-circuit potential is, in both NaCl solutions, more positive than the pitting potential, so pitting must occur. The crack initiation life is therefore reduced by all factors accelerating pitting.

In contrast, no pitting can occur in the case of the ferritic steel, because the corrosion potential is less noble than the potential for repassivating pitting in 0.5 M NaCl. Therefore, CF crack initiation under corrosion conditions follows the Mode II CF mechanism, i.e., slip steps, produced by cyclic plastic deformation of the bulk material rupturing the passive film on the metal surface followed by repassivation, etc.[148-151] This allows a prediction of the minimum value for the CF strength.[125] Below the cyclic YS, there is no plastic deformation and therefore no film rupturing. Several ferritic steels have a cyclic YS of about 70% of the static YS.[147] The 18Cr SS then is expected to have a cyclic YS of 230 MPa, a value that is about 30% lower than the fatigue limit observed in 0.5 N NaCl solution at 80°C. If, for the ferritic steel in question, the above relationship holds true, this difference may be explained by the presence of the passive film, which cannot be penetrated as long as the slip-step height under cyclic load remains lower than the passive film thickness and vice versa.

The mechanism in 4 M NaCl solution is straightforward. The steel is fully passive at stresses below the critical strain for cracking inclusions As soon as the latter occurs, crevices are formed at nonmetallic inclusions and pitting or crevice corrosion on account of this can be initiated following the Mode IV CF mechanism as explained above.[93]

Superposition of crevice corrosion and corrosion fatigue

Fittings and gasket elements of all kinds may provide the necessary electrolytic conditions for triggering crevice corrosion that will, when superimposed on fatigue, cause CF Mode IV failures. Microstructural changes produced by tempering have been shown to exert a characteristic influence[124] on the CF strength of martensitic 13Cr steels Figure 75 exhibits the results of flat-bending CF tests in a buffer solution of pH 4.62 in which the steel is, under crevice-free conditions, in a state of stable passivity at all tempering temperatures The insert of this figure illustrates the experimental set-up in which the seals of the corrosion chamber act as crevices. Under such conditions, there is a temperature range (500 to 550°C) of high susceptibility to crevice-corrosion-induced Mode IV CF, the reason for which appears to be chromium depletion. In the as-quenched condition, these steels contain untempered martensite, which may have minor precipitations of Fe_3C stemming from autotempering after cooling from the high martensite transition temperature of 270°C The amount of Fe_3C increases after tempering to about 300°C and diminishes until about 450 to 500°C, the Fe_3C has dissolved and Cr_7C_3 precipitates, mostly by formation of nuclei or, to a lesser extent, immediately from Fe_3C at 500 to 550°C. $(CrFe)_{23}C_6$ is finally formed containing up to 75% Cr in the equilibrium state. These precipitations cause a depletion of Cr in regions adjacent to grain boundaries. Besides the crevice effect, intergranular attack will thus be induced, too, which can be found in this critical temperature region on fracture surfaces by microfractography.

Much more aggressive conditions in crevices exist in the presence of chloride ions. Therefore, in contrast to the foregoing case, Mode IV CF is now possible in steels that have been quenched and tempered as usual. Figure 76 illustrates[118] the drastic reduction in CF strength for a type 403 13Cr martensitic SS under chloride crevice corrosion conditions that should be compared to the results of Figure 75. The fatigue strength under crevice corrosion conditions with methacrylic resin and copper fittings decreased to a level of 30 to 50 MPa (15% of the AF limit). In contrast, aluminum fittings provided, by galvanic coupling, cathodic protection, and therefore higher CF strength.

Typical components for which crevice-induced Mode IV CF is of importance are pump shafts where sleeves, nuts, keys, and impellers form fittings with narrow gaps.

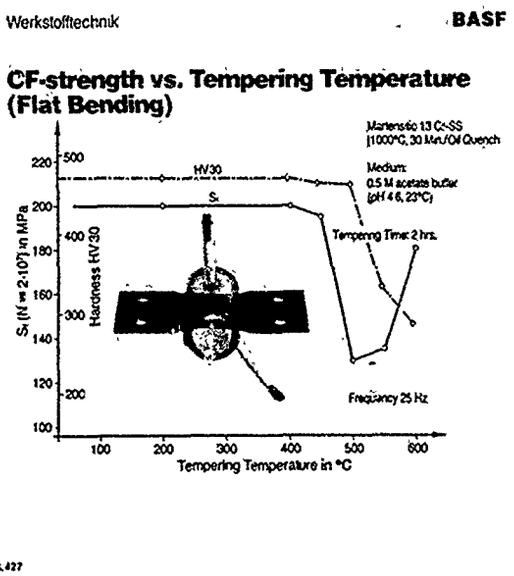


FIGURE 75—Bending corrosion fatigue strength (Mode IV, superposition of crevice corrosion) as influenced by tempering temperature.[121]

Summary

Since the Unieux-Firminy Conference[2] held in France in 1973, considerable metallurgical progress has been made by secondary metallurgy (argon-oxygen decarburization, vacuum decarburization, etc) or vacuum melting so that extremely low carbon and nitrogen contents have become technologically adjustable in high-alloy SSs. This development led to commercially available low interstitial ferritic steels of high resistance against anodic, halide-induced stress corrosion resistance Concurrently, the demand for SSs of improved tensile and fatigue strength has been the incentive for the development and production of low-carbon nickel martensitic Cr-Ni/Cr-Ni-Mo SSs The years after 1973 also brought the breakthrough for the ferritic-austenitic SSs, which owe their increasing application in many branches of industry to their anodic and cathodic stress corrosion resistance and their CF strength Finally, martensitic SSs have been given special attention after 1973 because of their extensive application as the preferred material for running turbine blades where CF resistance in condensing reheat turbines is of special concern.

To establish the technologically required data for the stress corrosion and CF behavior of these four groups of SSs, it was necessary to determine the influence of alloy chemistry, heat treatment, strength level, and microstructure on the one hand, and chemical composition as related to passivating properties of the environment on the other. This led to a wealth of information in the literature, some of which has been reviewed in this article.

Such data are indispensable, it is true. On the other hand, for the assessment of the effect of system parameters deviating from standard (test) conditions on stress corrosion and CF, an insight into the mechanisms involved is of great value. Some progress has been made in this respect since then, too.

Stress corrosion cracking

Martensitic SSs. (1) Cations in chloride solutions exert an influence NH_4^+, e.g., causing an active path (anodic) and hydrogen embrittlement (cathodic) mechanism, depending on the potential, as opposed to Na^+, which establishes an active path mechanism throughout.

(2) Heat treatment is of great influence. Tempering temperatures around 475°C are critical and will cause intergranular SCC even in distilled water. The SCC susceptibility is related to a chromium-depleted concentration profile around the prior austenite grain boundaries. At the industrially applied tempering temperatures (700 to 750°C), this Cr-concentration gradient will be destroyed by overlapping diffusion fields from coarsening $Mo_{23}C_6$ precipitates in the prior austenite and martensitic interlath grain boundaries thus removing the intergranular SCC susceptibility.

In the as-quenched state, such steels are insensitive to intergranular SCC because there is no such chromium-depleted zone around prior austenite grain boundaries, but this is of academic interest because of (a) the brittleness and (b) the extreme susceptibility to cathodic (hydrogen-induced) SCC of these steels in such a heat-treatment condition.

Nickel martensitic SSs. (1) The anodic SCC process appears to follow a slip-step emergence/repassivation mechanism.

(2) The cathodic SCC mechanism seems to be very complicated in sour gas environments. This clearly comes out in the influence of heat treatment. By double tempering, the resistance to cathodic SCC is increased by (a) a reduction of hardness and (b) a fracture mode change from intergranular to transgranular quasicleavage. The latter is brought about by an increase in the volume of retained austenite in which the solubility of hydrogen is greater than in the matrix, whereas the diffusion coefficient is smaller. This will cause a pile-up of hydrogen at the martensite/retained austenite interfaces and an interaction of hydrogen atoms with dislocations generated in them on account of the incompatible deformation of the two phases, thereby, at elevated strains, leading to transgranular SCC. As opposed to this, single-tempered SSs failed by the aforementioned intergranular cracking mode requiring a shorter path and perhaps smaller fracture energy per unit crack extension, thus explaining the inferior resistance of 13Cr-Ni-Mo SSs in the single-temper, heat-treatment condition.

Low interstitial ferritic SSs. These steels have been engineered to resist anodic (chloride) SCC. They are, in the proper mill-annealed condition, immune to chloride SCC even in high-chloride concentrations and at high temperatures under open-circuit conditions. They may, however, become susceptible when their open-circuit potential is displaced in the active direction, which can be caused by high-temperature annealing or in specific solutions (e.g., boiling 43% LiCl + thiourea) at high-applied stresses. As these steels are very resistant to pitting corrosion, SCC initiation depends on the evolution of slip steps inducing film rupture, which, in turn, will provide for the corrosion sites. As soon as they have attained a critical size and geometry, they will start an occluded cell mechanism. Transient creep thus produces distinct corrosion trenches. SCC then depends on the inherent corrosion and repassivation rates. Steels of lesser purity or low interstitial ferritic SS improperly heat treated or heavily prestrained are thus bound to develop critical localized corrosion, thereby initiating cracks.

Effective of Crevice Corrosion on CF

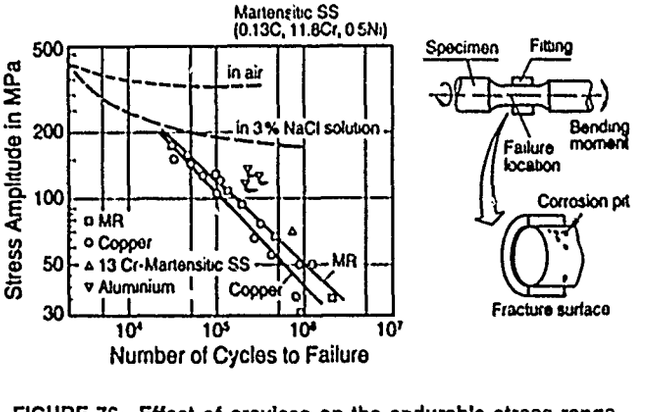


FIGURE 76—Effect of crevices on the endurable stress range (Mode IV corrosion fatigue). (Reprinted with permission.[118])

Ferritic-austenitic SSs

These steels have found considerable application in various industries They combine high strength, good corrosion resistance, and high fatigue/CF strength with good SCC resistance. As in the case of austenitic SSs, there is a cathodic protection potential. In concentrated chloride solution, the protection potentials for these steels and the austenitic SSs are close together. σ-phase formation lowers the resistance against anodic SCC. Welding may impair the SCC resistance when the cooling rate between 1200 and 800°C is too high As a rule of thumb, welding parameters should be chosen just in the opposite direction as with austenitic SSs, i.e., preheating, safeguarding a high heat input and, in critical instances, solution annealing followed by rapid cooling. Because of the high cooling rate, spot-welding or arc strikes, built-up weld seams or repair welds may be susceptible to SCC because of the high cooling rate involved that suppresses the reformation of austenite from high-temperature δ-ferrite.

The SCC mechanism is closely coupled to mechanical and electrochemical phenomena. In the ferrite, depassivation is essentially determined by mechanical twinning, whereas slip on the ferrite surfaces is insufficient to cause localized depassivation. This sensitivity to twinning disappears as soon as the ferrite contains no nickel (e g in low interstitial ferritic SSs). SCC of ferritic-austenitic SSs seems to be, in the lower stress region, determined by localized depassivation of austenite, caused by glide processes, or, at higher stresses, by that of ferrite twinning being responsible for crack initiation and propagation in most practical cases. Ferrite is anodic to austenite At low stresses, ferrite, which is not deformed, may cathodically protect austenite that, in turn, is plastically deformed. When the stress reaches the critical value for twinning, depassivation becomes possible in ferrite, initiating localized corrosion and cracking This explains why such steels are more resistant than austenitic ones and crack initiating takes place in the ferritic phase containing Ni.

Cathodic SCC of ferritic-austenitic SSs appears to follow, in chloride-containing H_2S solutions, a chloride-induced mechanism. This results from the finding that time-to-failure increases when potentials become more negative and increases with increasing temperature Cracking induced by hydrogen entry cannot be excluded in cases where the potential is rather negative, the pH low, and the temperature not too far above ambient, a combination sometimes encountered in practice.

Corrosion fatigue

All SSs show essentially the same characteristic features of CF that can be classified electrochemically into four modes:

Mode I: CF in the active state.
Mode II: CF in the state of stable passivity.
Mode III: CF in the state of meta- or unstable passivity, endogenous activation being caused by mechanical (fatigue) processes, e.g., by the formation of active surface domains (persistent slip bands, slip lines, etc.) surpassing a critical area share and leading, after a certain number of cycles, to activation.
Mode IV. CF in the state of unstable passivity, exogenous activation being caused by processes like pitting, crevice corrosion, cavitation, etc.

Mode I corrosion fatigue. Based on mechanistic reasoning, a model has been developed that aims at describing the influence of active corrosion on the cycle-dependent fatigue strength and crack propagation rate under the premise that active corrosion is taking place on locally limited surface sites, the stresses result from external cyclic loading are constant, and there are no cyclic hardening or softening effects. Mode I CF inevitably leads to a detrimental loss in fatigue strength.

Mode II corrosion fatigue. CF under stable conditions of passivity differs phenomenologically from Mode I CF in that, under potentiostatic conditions, only one crack (under ideal conditions) or a few [under industrial circumstances (e.g., open-circuit potentials, large surface areas)] will originate. There will be no recognizable surface nor crack-wall corrosion and the fracture surfaces will be smooth in contrast to distinctly cleft fracture surfaces caused by cracks jumping to neighboring crack propagation planes in Mode I.

From the mechanistic point of view, it appears to be less likely that passive films on SSs possess an intrinsic fatigue strength and will be cracked in the course of cycling. Instead, it must be assumed that the first slip step of sufficient height will pierce the passive film. A repassivation process will then commence in which a certain electrical charge will flow until passivity has been restored. Necessarily, a certain amount of metal has to be dissolved before passivity can be restored, by which process a microscopic groove will be produced Acting as a stress raiser, this makes further plastic deformation at such a site likely. Ongoing slip processes will again pierce the passive film and the interplay between repassivation, metal dissolution connected with it, and strain concentration, and triggering of further slip events will continue. This process manifests itself, under potentiostatic conditions and toward the end of CF life, in a gradual but finally steep increase of current. Current cycle characteristics of this type have been observed with all kinds of SSs so far investigated. It seems likely that this mechanism of multi-repassivation caused by whatever type of dislocation-induced microplastic deformation process is responsible for CF in the passive state. It has been shown that the charge necessary for repassivation is higher the higher the minimum CD for repassivation. The higher this critical CD is, the more metal will dissolve until passivity has been restored. This means that the primary micronotch becomes deeper and the stress concentration greater, the higher the minimum CD for passivation. Steel/environment systems of this kind show low CF strengths. Alloying elements lowering the CD of passivation will increase the CF strength, among them predominantly chromium.

CF cannot occur under passive conditions if, under external cyclic loading, the plastic work becomes zero per cycle and per volume element as the most stringent condition or if, in the course of cyclic deformation, any manifestation of plastic deformation at the surface (slip lines or bands, extrusions, intrusions) will be unable to penetrate the passive layer. Therefore, repassivation conditions being the same, CF strength will be higher the higher the AF limit. The optimum combination of properties for achieving highest Mode II CF strength requires a minimum passivation CD and a maximum AF limit and, at the same time, the smallest difference between the AF limit and the limiting stress at which critical dislocation-induced surface plasticity accrues. Based on DC signal information, only one event, crack growth, is indicated by a steep rise of current under potentiostatic conditions as mentioned above. Further insight into the events during initiation and propagation has been gained by a special mechano-electrochemical measuring technique using a light barrier/perforated disc installation by which current signals, under rotating-beam fatigue loading, can be recorded and their origin located. Three stages can be discerned:

(1) Stage A (incubation period): Small stochastic current transients are caused by the response of the passive layer to the alternating stress.
(2) Stage B (crack initiation period): Small sinusoidal current signals appear that have a constant phase angle with respect to a specimen reference line. These signals fix the future position of the CF crack. They are caused by emerging slip steps producing the mechanistic events described above.
(3) Stage C (crack growth period). Characterized by an increasing cell current and steadily growing sinusoidal current signals caused by the repassivation processes at the crack tip.

This transient measuring technique allows the detection of the first interactions between cyclic slip processes and environment, establishing crack initiation on a submicroscopic scale, determining the position of growing cracks, discriminating whether one or more than one crack develops and differentiating between growing and dormant cracks.

Mode III corrosion fatigue. Under an unstable passive regime, polarization will take place as soon as a slip step of critical height and surface area has penetrated the passive film. The open-circuit potential will finally become so negative that it falls below the passivation potential and total activation occurs. Corrosion then proceeds in Mode I at the active open-circuit potential.

Mode IV corrosion fatigue. The most important case of CF in the state of metastable passivity with exogenous activation is that of a superposition of CF and pitting. Condensing reheat turbine blade failures have been identified as being caused by this conjoint action that may occur in one or a few stages of running blades in the Wilson Zone. Because of its practical importance, many investigations have been conducted including the standard 12% Cr steels, ferritic-austenitic SSs, and ferritic SSs in chloride solutions at temperatures from 80 to 150°C. In tempered martensitic 12Cr and 17Cr-2Ni steels, pitting started at sulfide inclusions at all stress ranges below the AF limit, whereas low interstitial ferritic steels of type 18Cr and 28Cr-4Ni-2Mo CF did not follow the Mode IV mechanism. Instead, initiation was caused by the slip-step emergence (Mode II mechanism) as long as these steels are pitting resistant under the conditions given. CF cracks will pass along the interface matrix/inclusions, the latter not being cracked. Sulfide inclusions have been shown to be less noble than the passive film and have been identified as the preferential site of pit initiation.

Once attacked, they lead to an enhancement of local anodic dissolution not only because of the galvanic effect but also by the stimulated anodic dissolution in the presence of S^{2-} and SH^{-}. Crevices between matrix and sulfide inclusions are likely because of the difference in the coefficient of thermal expansion leading to a stronger contraction for sulfide inclusions. This is one of the reasons for the close similarity between the fatigue strength reducing action of pitting and crevice corrosion. Like pitting, the superposition of crevice corrosion and CF causes drastic reductions in CF strength, resulting in sustainable fatigue loads as low as 15% of the AF limit for a type 403 martensitic SS. Typical components for which crevice-induced Mode IV CF is important are pump shafts where sleeves, nuts, and impellers form fittings with narrow gaps.

References

1. H. Spaehn, U. Steinhoff, Werkst. u. Korros. 20, 9(1969): p. 733.
2. Stress Corrosion Cracking and Hydrogen Embrittlement of Iron Base Alloys, NACE-5, ed. R.W. Staehle, J. Hochmann, R.D. McCright, J.E. Slater (Houston, TX: National Association of Corrosion Engineers, 1977).
3. R.Q. Barr, ed., Stainless Steel '77, Climax Molybdenum Company (London, England: Amax Nickel, 1977).
4. H. Spaehn, Subcritical Crack Growth Due to Fatigue, Stress Corrosion and Creep (London, England: Elsevier, 1984), p. 275.
5. H.A. El-Sayed, K.M. El-Sobki, V.K. Gouda, Surf. Techn. 16 (1981): p. 245.
6. V.K. Gouda, H.A. El-Sayed, Surf. Techn. 18(1983): p. 327.
7. E.H. Phelps, A.L. Loginow, Corrosion 16t, 7(1960): p. 325t.
8. R.N. Parkins, R. Usher, Proceedings of the 1st International Congress on Metallic Corrosion (London, England: Butterworths, 1961), p. 289.
9. M. Smialowski, T. Ostrowska, Corros. Anticorros. 5(1957): p. 76.
10. E. Houdremont, H. Benneck, H. Wentrup, Stahl u. Eisen 60 (1940): p. 757.
11. R.A. Davis, Corrosion 19, 2(1963): p. 45t.
12. H.J. Bhatt, E.H. Phelps, Corrosion 17t, 9(1961): p. 430t.
13. H.H. Uhlig, Corrosion and Corrosion Control (New York, NY: J. Wiley & Sons, 1971), p. 299.
14. B.E. Wilde, Corrosion 27, 8(1971): p. 326.
15. H.A. El-Sayed, V.K. Gouda, Corros. Prev. and Control 12(1986): p. 142.
16. M.O. Speidel, Metall. Trans. A 12A, 5(1981): p. 80.
17. K. Bieh! (Ph.D. diss., Technische Hochschule Darmstadt, 1988).
18. M.O. Speidel, Corrosion Problems in Energy Conversion and Generation (Pennington, NJ: The Electrochemical Society, Inc., 1974), p. 359.
19. B Bavarian, Z. Szklarska-Smialowska, D.D. MacDonald, Corrosion 38, 12(1982): p. 604.
20. J E Trumann, R. Perry, G.N. Chapman, J. Iron and Steel Inst. 202(1964): p. 745.
21. B.E. Wilde, Corrosion 27, 8(1971): p. 326.
22. E.H Phelps, Metals Engng. Q. 5(1917): p. 44.
23. P Hewitt, B.S. Hockenhull, Corros. Sci. 16(1971) p. 47.
24. A.E. Durkin, Metal Progr. 64(1971): p. 72.
25. R.N. Parkins, Brit. Corr. J. 7(1972): p. 15.
26. P Doig, J W Edington, Proc. Roy. Soc. Lond. A339(1974): p. 37.
27. R P Frankenthal, H.W. Pickering, J. Electrochem. Soc. 120 (1973): p. 23.
28. C S Pande, M Suenage, B. Vyas, H.S. Isaacs, Scripta Metall. 11 (1977): p. 681.
29. B. Poulson, Corros. Sci. 18(1978): p. 371.
30. P Doig, D.J. Chastell, P.E.J. Flewitt, Metall. Trans. A 13A (1982): p. 913.
31. W Rall, H. Spaehn, Ammonia Plant Safety Symposium (New York, NY: AIChE, 1985), p. 17.
32. E. Zink, Th. Geiger, Schweizer Arch. 3, 4(1957): p. 3,
33. K Irvine, D.J. Crowe, F.B. Pickering, J. Iron and Steel Inst. 195, 4(1960): p. 386.
34. K. Irvine, D. Llewellyn, F.B. Pickering, J. Iron and Steel Inst. 192, 3(1959): p. 218.
35. K. Bungardt, E. Kunze, E. Horn, Arch. Eisenhutten. 29(1958): p. 193.
36. P. Brizina, Harterei-Techn. Mitteil. 38, 5(1983): p. 197.
37. P. Brizina, Harterei-Techn. Mitteil. 38, 6(1983): p. 251.
38. NACE Standard TM0177-86, "Testing of Metals for Resistance to Sulfide Stress Cracking at Ambient Temperatures" (Houston, TX: NACE, 1986).
39. H. J. Niederau, Stahl u. Eisen 98, 8(1978): p. 385.
40. W. Knorr, H. J. Kohler, Werkst. u. Korros. 32, 10(1976): p. 73.
41. J.E. Trumann, Met. and Mater. 2, 7(1968).
42. E.E. Levin, B.M. Gugelev, B.M. Idelchik, Sov. Mater. Sci. 9, 2 (1973): p. 242.
43. T.G. Gooch, Welding J., Res. Suppl. 53(1974): p. 287.
44. A.I. Radkevich, V.P. Koval, T.N. Kalichak, I.I. Vasilenko, Korroz. i Zashchita 11(1974): p. 3.
45. V G Starchak, A.B. Kuslitsky, Protsesach Russian Collection (Leningrad, USSR: 1974), p. 73.
46. A. Baus, J.C. Charbonnier, H.P. Lieurade, B. Manderet, L. Roesch, G. Sanz, Circ. Inform. Techn. 33, 7/8(1976): p. 1703.
47. H.L. Craig Jr., ASTM Spec. Techn. Publ. (Philadelphia, PA: ASTM, 1976), p. 610.
48. H.J Dundas, CORROSION/79, paper no. 173 (Houston, TX: NACE, 1979).
49. Y Yoshino, A. Ikegaya, CORROSION/84, paper no. 210 (Houston, TX: NACE, 1984).
50. Y. Yoshino, A. Ikegaya, Corrosion 41, 2(1985): p. 105.
51. Stress Corrosion Cracking and Hydrogen Embrittlement of Iron Base Alloys, p. 798.
52. W. Wessling, Stahl u. Eisen 106, 13(1986): p. 739.
53. R.Q. Barr, ed., Stainless Steel '77, Climax Molybdenum Company (London, England: Amax Nickel, 1977), p. 171.
54. K. Faessler, H. Spaehn, Z. Werkstofftech. 13(1982): p. 8.
55. I.E. Locci, J.K. Kown, R.F. Hehemann, A.R. Troiano, Corrosion 43, 8(1987): p. 465.
56. A.P. Bond, H.J. Dundas, Corrosion 24, 10(1968): p. 344.
57. Stress Corrosion Cracking and Hydrogen Embrittlement of Iron Base Alloys, p. 1136.
58. M.A. Streicher, Corrosion 30, 4(1974): p. 115.

59. R.F. Steigerwald, A.P. Bond, H.J. Dundas, E.A. Lizlovs, Corrosion 33, 8(1977): p. 279.
60 Stress Corrosion Cracking and Hydrogen Embrittlement of Iron Base Alloys, pp. 1136, 1003, loc. cit. 2.
61. S. Matsushima, T. Ishihara, Trans. Nat. Res. Inst. Met. 17(1975): p. 14.
62. E.N. Pugh, Corrosion 41, 9(1985): p. 517.
63. W.R. Cieslak, D.J. Duquette, Corrosion 40, 10(1984): p. 545.
64. H.H. Ettwig, W. Pepperhoff, Arch. Eisenhutten. 41(1970): p. 471.
65. H. Brandis, et al., Thyssen Edelstahl, Techn. Berichte 5, 1(1979): p. 7.
66. H. Krauss (Ph.D. diss., Technical University Darmstadt, 1982).
67. S. Mahajan, D.F. Williams, Int. Met. Rev. 18(1973): p. 43.
68. A. Desestret, R. Oltra, Corros. Sci. 20(1979): p. 799.
69. H. Wehner, "Zum Ausscheidungs- und Korrosionsverhalten eines ferritisch-austenitischen Chrom-Nickel-Molybdaen-Stahles nach kurzzeitiger Gluehbehandlung unter besonderer Beruecksichtigung des Schweissens" (Ph.D. diss., Technical University Darmstadt, 1982).
70. A.I. Asphahani, Corrosion 37, 6(1981): p. 329.
71. J. Kolts, A.I. Asphahani, CORROSION/81, paper no. 99 (Houston, TX: NACE, 1981).
72. S.O. Bernhardsson, J. Oredsson, M. Tynell, CORROSION/80, paper no. 14 (Houston, TX: NACE, 1980).
73. C. Herbsleb, R.K. Poepperling, CORROSION/80, paper no. 13 (Houston, TX: NACE, 1980).
74. J. Oredsson, S. Bernhardsson, CORROSION/82, paper no. 126 (Houston, TX: NACE, 1982).
75. J. Hochmann, A. Desestret, P. Jolly, R. Mayoud, Stress Corrosion Cracking and Hydrogen Embrittlement of Iron Base Alloys, p. 956.
76. R. Grundmann, P. Gumpel, R. Ortmann, P. Roth, Thyssen Edelstahl, Techn. Berichte 14, 1(1988): p. 57.
77. R. Spaehn, Schweisstechnische Studienarbeit (Technical University of Darmstadt, 1982).
78. R. Spaehn, H. Fiehn, H. Zuern, Welding of Ferritic-Austenitic Stainless Steels, Grosse Schweisstechnische Tagung (Deutsch-Franzoesiche Gemeinschaftstagung., Karlsruhe, 1987), DVS 105, p. 29.
79. N. Sridhar, J. Kolts, Corrosion 43, 11(1987): p. 647.
80. H. Zsuga, Y. Tarutani, T. Kudo, Corrosion 5(1988): p. 305.
81. J.P. Audouard, A. Desestret, D. Catelin, Proceedings of the International Conference on Duplex Stainless Steel, Paper 41, (The Hague, The Netherlands: Netherlands Institut voor Lastechniek, 1986).
82. T. Magnin, J. Le Coze, A. Desestret, Proceedings of the International Conference on Duplex Stainless Steels, ed. R.A. Lula (Metals Park, OH: ASM International, 1983), p. 535.
83. T. Magnin, J. Le Coze, A. Desestret, Proceedings of the ASM Metals Congress 1982, Paper 8201-027 (Metals Park, OH: ASM International, 1982).
84. A. Desestret, J.C. Colson, E. Mirabel, R. Oltra, 9th International Congress on Metallic Corrosion (Ottawa, Canada: National Research Council of Canada, 1984).
85. A. Desestret, R. Mayoud, Rev. de Metallurgie-CIT 4(1984): p. 321.
86. G. Herbsleb, U.R. Poepperling, Corrosion 36, 11(1980): p. 611.
87 H. Spaehn, G. Wagner, Conf. Int. Arts Chimiques (Paris, France: 1974).
88 J Olsson, S. Nordin, International Conference on Duplex Stainless Steel, Paper 48 (The Hague, The Netherlands: Netherlands Institut voor Lastechniek, 1986).
89 G H Wagner, "Failure of a Duplex Steel Spiral Heat Exchanger Originating at Sensitized Spot Welds With Crevices Causes Intergranular Corrosion Followed by Corrosion Fatigue," Case History Report, 1971.
90 H. Spaehn, CHEM + TECH Congress, Paper 22 (Bombay, India: 1978).
91. E. Macherauch, VDI-Berichte 268(1976): p. 11.
92. H. Spaehn, G.H. Wagner, Bruchuntersuchungen und Schadensklaerung (Muenchen, Federal Republic of Germany: Allianz-Technische Information, 1976), p. 59.
93. H. Spaehn, Subcritical Crack Growth Due to Fatigue, Stress Corrosion and Creep (London, England: Elsevier, 1984), p. 275.
94. H. Spaehn, Metalloberfl. 16, 10(1962): p. 299.
95. K. Kloeppel, T. Seeger, Ein Konzept fur den Dauerbruchmechanismus auf der Grundlage oertlicher Beanspruchungs- und Bruchvorgaenge (Inst. Statik und Stahlbau, TH Darmstadt: 1986), p. 85.
96. G. Bluemmel (Ph.D. diss., Technical University of Darmstadt, 1986).
97. W.E. Cowley, F.A. Robinson, J.E. Kerrich, Brit. Corros. J. 3(1968): p. 223.
98. U.F. Franck, Halbleiterprobleme II, Friedr. Vieweg, Braunschweig (1955), p. 214.
99. R. Spaehn, G. Bluemmel, H. Speckhardt, Z. Werkstofftech. 17, 4(1986): p. 154.
100. R. Spaehn (Ph.D. diss., Technical University of Darmstadt, 1988).
101 U. Essmann, U. Goesele, H. Mughrabi, Phil. Mag. A 44, 2(1981): p. 405.
102 K Wellinger, H. Dietmann, Festigskeitsberechnung (Stuttgart. Kroner Verlag, 1976), p. 136.
103. H Wiegand, H. Speckhardt, H. Spaehn, Arch. Eisenhuetten. 40(1969): p. 685.
104 EPRI Workshop Proceedings, Low Pressure Steam Turbine Blade Failures, prepared by Failure Analysis Associates (Palo Alto, CA: EPRI, 1980).
105 U Schieferstein, F Schmitz, VGB Kraftwerkstechnik 58, 3(1978). p. 193.
106 L Hagn, AZT-EPRI-Workshop, held June 21, 1979, in Ismaning, Federal Republic of Germany.
107 R C Bates, J.W. Cunningham, "Corrosion Fatigue of Steam Turbine Blading," Annual Report EPRI RP 912-1.
108 J Congleton, T P. Wilks, Conference on Environmentally Induced Cracking, Fatigue Fract. Eng. Mater. Struct. 11, 2(1988): p. 139.
109 H.J. Bohnstedt, P.H. Effertz, P. Forchhammer, L. Hagn, Maschinenschaden 51(1978): p. 73.
110 U Schieferstein, F Schmitz, VGB Kraftwerkstechnik 58(1983). p. 198.
111. M. Truchon, P. Rabbe, Mem. et Etudes Scient, Rev. Met. 3(1983): p. 117.
112 Kh G Schmidt Thomas, W.D. Haubenberger, H. Meisel, Werkst. u. Korros. 27(1976): p. 775.
113 K G Schmidt-Thomas, H. Meisel, W. Sessler, Werkst. u. Korros. 37(1985): p. 36.
114. K.G. Schmidt-Thomas, H.M. Tensi, A. Leidig, R. Schmid, Arch. f.d. Eisenhuetten. 46, 3(1975): p. 223.
115. M.P Mueller, Met. Tech. 9, 6(1982): p. 235.
116. M. Muller, Korrosionsermuedungsrissbildung an Werkstoffen im System Fe Ni-Cr, Brown Boveri Forschungsbericht KLR 81-66 C, BBC-Forschungszentrum, CG-5401, Baden, Switzerland.
117. H.-J. Lipp, Werkst. u. Korros. 26, 11(1975): p. 825.
118. K. Kasai, S. Kawai, Corrosion Fatigue Behavior under Crevice Corrosion Conditions in NaCl Aqueous Solutions (Ysuchiura, Ibaraki, Japan. Mechanical Engineering Research Laboratory, 1978).
119. H. Ishii, Y. Sakakibara, R. Ebara, Metall. Trans. A 13A, 8(1982): p. 1521.
120. K. Detert, W. Bertram, H. Buhl, Werkst. u. Korros. 31(1980): p. 439.
121. D. Wagner, J.-P. Chavaillard, A.Y. Meyzaud, M. Bonningue, R. Cozar, G. Baodry, Proceedings of the Conference on New

Developments in Stainless Steel Technology (Metals Park, OH. ASM International, 1985), p. 221.
122 P H Effertz, L Hagn, Maschinenschaden 55, 2(1982). p. 67.
123. J.D. Collins, Corrosion 32, 3(1976): p. 109.
124. H. Spaehn, G.H. Wagner, Mem. et Etudes Scient. Rev. Met. 74, 10(1977): p. 615.
125. M.P. Mueller, Corrosion 38, 8(1982): p. 431, Metals Techn. 9(1982): p. 235.
126 R Ebara, M Mihara, H Kino, T. Kai, K. Katayama, K. Shiota, Mitsubishi Tech. Bulletin 129(1978): p. 1.
127 V.G. Protsik, V.I. Pokhmurskii, G.V. Karpenko. Fiz.-Rim. Mekh. Mater. 4, 5(1968): p. 608.
128 W Betram, P.-H Effertz, L Hagn, K.H. Mayer, K. Schleithoff, F Schmitz, K. Schneider, FEKKs-Projekt Nr. 2.4/2, 1981.
129 M O Speidel, Influence of Environment on Fracture, Proceedings of the 5th International Conference on Fracture (New York, NY: Pergamon Press, 1981).
130 J Z Briggs, T D Parker, The Super 12% Cr Steels (New York, NY: Climax Molybdenum Company, 1965).
131 G V Prabhu Gaunkar, A.M. Huntz, P. Labombe, Metal Sci. 14(1980): p. 241.
132 W -T Tsei, A Study of Corrosion Fatigue Crack Growth in Fe-Cr-Ni Alloys (Ph D diss , Ohio State University, 1983).
133 L E Willertz, T.M. Rust, V.P. Swaminathan, Proc. Int. Conf. Fat. Corr. Fat., Ultrason (New York, NY: AIME, 1981), p. 333.
134 M O Speidel, S E. Stanzl, E. Tschegg. Z. Werkstofftech. 11(1980): p. 305.
135. M. Sato, Electrochim. Acta. 11(1966). p. 361.
136. V. Cihal, Protection Met. 8(1977): p. 14.
137. G. Eklund, Jernkontorets Ann. 155(1971): p. 637.
138. M. Janik, Brit. Corros. J. 7(1972): p. 90.
139 Z Szklarska, Corrosion 28, 10(1972). p. 388.
140 E Gassner, H. Ostermann, Water Power and Dam Constr. 32(1980): p. 27.
141. E. Gassner, Werkst. u. Korros. 30(1979). p. 723.
142. M. Grounes, S. Rao, Trans. ASM 62(1969). p. 902.
143. K.H. Schmidt-Thomas, R. Mathies, H. Meisel. Arch. Eisenhuetten. 54, 3(1983): p. 117.
144. K.G. Schmidt-Thomas, T. Happle, R. Wunderlich, Corrosion and Corrosion Protection, BMMFT-Research Program, Project B 2.5/9, Final Report, 1988.
145. B.C. Syrett, S.S. Wing, J.E. Wettig, RD-2284-SR, Special Report, EPRI, 1987.
146. K.G. Schmidt-Thomas, T. Happle, R. Wunderlich, "Corrosion and Corrosion Protection, BMMFT-Research Program, Project B 2.5/9, Final Report, 1988.
147. S. Usami, S. Shida, Fat. Eng. Mat. Struct. 1(1979): p. 471.
148. H. Spaehn, Metallobertl. 16, 9(1962): p. 267.
149. H. Spaehn, Metallobertl. 16, 11(1962): p. 335.
150. H. Spaehn, Metallobertl. 16, 12(1962): p. 369.
151. H. Spaehn, Z. Phys. Chemie 234, 1(1967): pp. 1, 234.
152. H.J. Niederau, Stahl u. Eisen 8(1978): p. 385.

Discussion

F.P. Ford (General Electric R&D Center, USA): You show a relationship between the thickness of oxide and the "initiation" time during corrosion fatigue (CF) If this is physically related to rupture of the oxide, then, if the fracture strain is independent of oxide thickness, your observed relationship must be due to changes in the angle between the slip plane and the tensile axis and how this affects exposure of bare surface to the environment. Do you know of any such relationship and can it be applied to your data?

H. Spaehn: This kind of damaging mechanism might well be operative in the manner you envisage, assuming experimental verification could be provided by single-crystal CF tests. However, I am not aware of any experimental work done in this respect. It seems to me that such a sequence of destructive events would most probably apply to relatively thick oxide films. There are limits, of course. In my last slide, I showed the results of XPS (ESCA) thickness measurements on a simple 12% chromium steel. The passive layer here is so thin that it becomes a matter of semantics whether it should be regarded as a monolayer of oxygen or an "oxide" film.

R. Oltra (Universite de Bourgogne, France): Have you studied the passive film grown on duplex stainless steel? In particular, with regard to the composition of the film, do you think it would be possible to describe the continuity of the film by taking into account the difference in composition of each alloy phase?

H. Spaehn: The average composition of the passive film on a nitrogen-alloyed duplex stainless steel X2 (nominal composition: 21/23Cr 4.5/6.5Ni 2.5/3.5Mo 0.08/0.2N < 0.03C) in sulfuric acids has been studied by XPS (ESCA). The results confirm the findings of Hochmann, et al. [Stress Corrosion Cracking and Hydrogen Embrittlement of Iron Base Alloys, NACE-5, ed. Staehle, et al. (Houston, TX: NACE, 1977), p. 956], based on microprobe analysis. That showed a strong enrichment of chromium and molybdenum in the film over the ferrite phase and an enrichment of nickel and depletion of chromium and molybdenum over the austenitic phase. The fact that excellent passivity can be achieved on duplex stainless steels is proof of the continuity of the passive film formed over adjacent ferrite and austenite grains. I have no difficulty in looking at the thickness of the passive films as measured by XPS (ESCA), as shown in Figures 50 and 51 of the paper.

R. Oltra: As regards the electrochemical coupling between the two phases, could you comment on the effect of the nature of the environment upon this coupling and its consequence on the SCC resistance of duplex steels?

H. Spaehn: The nature of the environment has a great influence on the relative electrochemical behavior of the two coupled phases, ferrite and austenite. A cast ferritic-austenitic alloy of 24Cr-6Ni-2.5Mo-0 2Cu will suffer from a selective corrosion attack on the ferritic phase in sulfuric acid in a concentration range between 20% and 96%. [See Horn, Z. Werkstofftechn. 14(1983). p. 350.] This selective effect takes place in a narrow potential range of between U_H = -150 and 200 mV. At 25 mV, both phases are attacked, whereas the austenite phase is preferentially attacked at +25 mV. (All results are quoted at 95°C) The attack on the ferrite takes place below the steep rise of the i-U curve, that of austenite at potentials slightly more noble than the peak current density of the potentiostatically determined passivation curve. A preferential attack on the ferrite has also been observed with less corrosion-resistant Cr-Ni-(Mo) duplex steels. [See Faingold and Shatowa, Zashchita metallov. 17(1981): p. 372.] In the passive range, no preferential attack on either one of the phases has so far been observed. Nevertheless, in Mode II CF, the orientation of the rolling direction to the tensile stress influences CF strength (see Figure 60 of the paper) simply for mechanical reasons. Transverse specimens show both lower fatigue and Mode II CF values in sulfuric acid.

As for the consequences of ferrite-austenite coupling for SCC resistance of duplex steels, mechanisms that have been proposed by Desestret and colleagues (see References 81 to 85 of the paper) and in your own poster paper at this conference (Oltra and Desestret, "Anodic Dissolution and Hydrogen Embrittlement During Mechanical Depassivation of the Ferritic Phase of a Duplex Stainless Steel in Chloride Solution Containing H_2S," this proceedings) are, in my opinion, viable and can immediately be applied in practice. Your observation that crack initiation in chloride solutions starts in ferrite or at the ferrite-austenite interface underlines the close coupling of mechanical and electrochemical processes in stress corrosion phenomena.

R.A. Oriani (University of Minnesota, USA): Within the picture of slip rupture of a passivating film for the initiation of CF, there is another characteristic besides the thickness that should be considered. This is the mechanical stress already existing within the passive film as a result of the growth mechanism and other factors about which we are still learning. We now know that extremely large stresses exist within passive films. If the stress is tensile, less strain will be needed to rupture the film.

H. Spaehn: A good example of films for which we know the internal stresses very well are thin electroplated films (e.g., chromium on steels) Here, extremely high tensile stresses have indeed been measured At a thickness of, for instance, 0.5 μm, they become so high that the coatings will crack At lower thicknesses the films will not crack Instead, the full magnitude of the first order internal stresses will be maintained They must be regarded, under fatigue loading, as positive mean stresses As can be understood from (macroscopic) fatigue strength diagrams, high positive (tensile) mean stresses reduce the sustainable stress amplitudes considerably. Therefore, your line of reasoning is appropriate for passive films, provided they are under positive internal stresses.

A. Atrens (University of Queensland, Australia): Could you discuss the industrial relevance of anodic protection against CF ? I would imagine that very careful process control would be required whenever there is the possibility of the presence of chlorides.

H. Spaehn: You are absolutely right. In the presence of chlorides of a critical concentration, anodic protection would shift the potential in regions above the critical pitting potential, inevitably leading to a massive loss of fatigue strength due to Mode III CF. The paper deals extensively with this failure mode, which has turned out to be of concern to running turbine blades, impellers, and stirrers, for example. To sustain sufficiently high cyclic stresses in Mode IV CF of stainless steels requires an appropriately high pitting index (P = %Cr + 3.3% Mo).

Stress Corrosion Cracking of Austenitic Steels

*R.C. Newman and A. Mehta**

Abstract

The stress corrosion cracking (SCC) of austenitic steels is reviewed with emphasis on the fundamental processes occurring within cracks. Crack-tip interactions are discussed in the context of the altered local environment. It is concluded that neither the slip-dissolution nor the hydrogen embrittlement models can be satisfactorily applied to chloride-induced SCC, but the film-induced cleavage model (where the film is a dealloyed, metallic layer) has considerable promise. Such a model is also attractive for caustic SCC of nonsensitized steels. Sensitized steels appear to crack by a slip-dissolution mechanism. The SCC of nickel-base alloys is briefly reviewed. In an appendix, recent surface analytical data are presented that support the view that metallic, nickel-rich, dealloyed layers are formed on susceptible steels in SCC environments.

Introduction

The stress corrosion cracking (SCC) of austenitic stainless steels (SSs) has produced an immense literature that at times has grown by more than 50 publications annually. To review this subject, it is necessary to extract significant scientific advances from this mass of material, including raw data that may be revealing but uninterpreted

Most of this review will deal with the chloride-induced SCC of austenitic SSs, but other related phenomena will be introduced as appropriate. These include gaseous or cathodic hydrogen embrittlement (HE), caustic SCC, high-temperature water SCC, and SCC of sensitized alloys, which will be mentioned only briefly, because there is little controversy regarding the mechanism (slip dissolution) of crack growth in these materials.[1]

Earlier reviews have dealt with the literature prior to about 1979. Latanision and Staehle,[2] Theus and Staehle,[3] and Staehle[4] favored variants of the slip-dissolution model (SDM) to explain chloride SCC, while Hanninen summarized the evidence for HE.[5] We shall conclude that the information on this subject can be rationalized by a film-induced cleavage model.[6-8] The film responsible for the cleavage is believed to be a nanoporous, metallic dealloyed layer, as in the ammonia SCC of copper alloys.[9] Evidence for the existence of such layers is presented in Appendix A.

Latanision and Staehle[2] analyzed the ability of various models to explain the alloying dependence of chloride SCC. They showed that the effect of nickel or other relatively noble metals (e.g., Cu) was consistent with protection of the crack walls by a noble metal layer, while active dissolution was maintained by slip-step emergence at the crack tip. This had been suggested earlier by Hines and Hoar[10] and could have formed the basis for a research program on chloride SCC using new surface analysis techniques in the 1970s. Unfortunately, the nickel-enrichment concept was abandoned in favor of a passive film-rupture model in which scant attention was paid to the acidity of the solution (and absence of a conventional passive state) inside a crack. As late as 1986, one can find studies of transient electrochemistry using neutral solutions, with no indication that this might not simulate the situation inside a crack.[11] Latanision and Staehle made the following points in support of their nickel-enrichment model:[2]

(1) Nickel enrichment would be expected on an actively dissolving SS surface.

(2) Copper or nickel at less than 1% can promote SCC of ferritic SS in boiling $MgCl_2$ solution, i.e., the austenitic structure is not necessary.

(3) The disappearance of SCC with increasing noble metal (Ni) content parallels observations of Graf[12] on alloys such as Cu-Au. The Ni or Au content required to prevent SCC is about 40%, as shown in Figure 1.

In reading Latanision and Staehle's paper, one is struck by the number of observations that could be interpreted using modern knowledge of crack chemistry;[13] e.g., the evolution of hydrogen from cracks in boiling $MgCl_2$ solution, as observed by Barnartt and van Rooyen,[14] is cited as evidence for deviation from ideal thermodynamic behavior but is easily interpreted using the knowledge that the crack pH is less than 2.[15] As in the work of Hines and Hoar,[10,16] there is uncertainty regarding the relative importance of repassivation and nickel enrichment, which is resolved if one recognizes that a passive film on the external alloy surface does not require one near the tip of an acid crack.[17]

Latanision and Staehle[2] referred several times to the cracking that occurs in bulk solutions of low pH, at both low and high temperatures. Although they were not explicit, it appears that they recognized this as being the same phenomenon as normal high-temperature, neutral-pH cracking, emphasizing the unimportance of conventional passivity in the crack propagation process.

The mechanistic importance of caustic SCC in austenitic SSs was also recognized by Latanision and Staehle.[2] They pointed out that water reduction was much less likely within caustic cracks than within chloride cracks and that this might provide some discrimination between possible models of the cracking process. This point will be discussed later.

The period between the Latanision/Staehle[2] and Theus/Staehle[3] reviews coincided with the proliferation of important practical problems in nuclear power plants, and hence an increased interest in the properties of sensitized steels and nickel-base alloys, but there was also extensive activity in chloride SCC. Important advances during this period included the use of electrochemically controlled SCC testing and crack simulation procedures, and the use of the SEM to study fracture surfaces. Staehle[4] favored a slip-dissolution concept

*Corrosion and Protection Centre, University of Manchester Institute of Science and Technology, P.O. Box 88, Manchester, M60 1QD UK.

for chloride SCC in which a passive film is periodically ruptured at the crack tip. Transient straining experiments in boiling $MgCl_2$ solutions were backed up by extensive room-temperature studies in various solutions including simple buffers. Despite the impressive variety of insights provided by Staehle's work, he would have benefited from attention to the crack acidification arguments of Baker, et al.,[15] and Marek and Hochman.[18]

One clear change from the Latanision and Staehle review was the abandonment of the nickel-enrichment concept, which has only occasionally resurfaced[17] despite its possible profound importance; according to Latanision,[(1)] attempts were made using Auger electron spectroscopy (AES) to analyze fracture surfaces, but no evidence for nickel enrichment was found. Appendix A summarizes our efforts in this area.

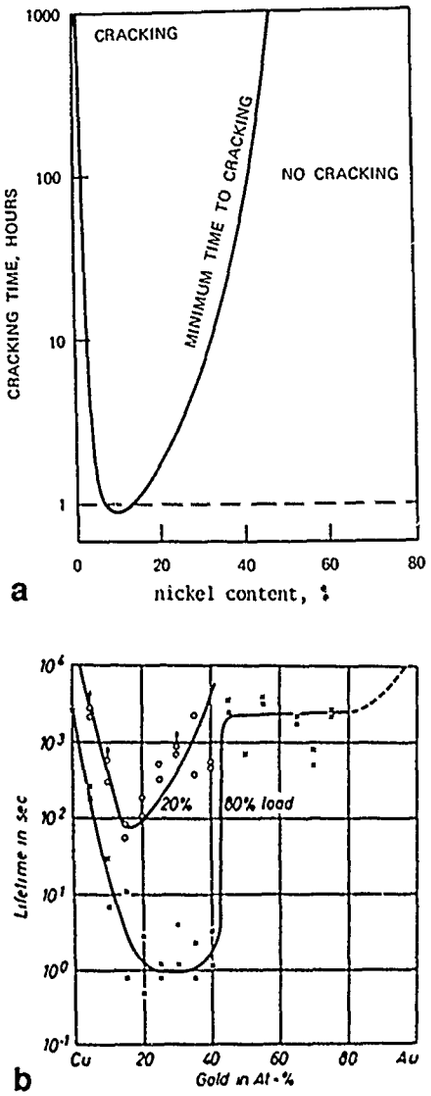


FIGURE 1—Compositional dependence of SCC in (a) Fe-Cr-Ni alloys in boiling $MgCl_2$ solution, the "Copson curve";[2] and (b) Cu-Au alloys in *aqua regia*.[12] Note: (1) Behavior at low Ni contents is complicated by the appearance of the ferrite phase, and (2) finite failure time of high Au alloys is a result of general corrosion.

[(1)]Private communication.

Crack Chemistry

Crack chemistry is part of the science of chemistry and electrochemistry of metals within cavities, as reviewed by Turnbull.[13] In particular, SCC of austenitic SSs in chloride solutions involves an active (or at least not conventionally passive) state within the crack, where the pH is between 1 and 2.[15,18]

Baker, et al.,[15] showed that SCC in hot $MgCl_2$ solutions gave rise to crack pH values between 1.2 and 2.5, and that the characteristic pH of a crevice in this system, freely corroding, is about 1.5 for concentrated $MgCl_2$ at 125°C. A dark or straw-colored film, much thicker than any passive film, was formed in acidified solutions and was found to be of low electrical conductivity (this could be a result of chromium hydroxide precipitation). Analysis of the solution indicated that the film was strongly Cr enriched; this does not necessarily address the question of dealloying (Ni enrichment), but it does show that any dealloying must be subtle in nature. The authors conducted an experiment designed to dissolve the dark film, predicting that this would lead to blunting of incipient cracks and hence no SCC. They added a large concentration of glycerol to an acidified $MgCl_2$ solution in which rapid film formation and SCC would normally occur and showed that SCC no longer occurred. They attributed this to dissolution of the film, especially complexing of chromium ions by the glycerol, leading to a corrosion rate too high to permit crack initiation. This result offers something of a challenge to a dealloying model of SCC in this system and needs further investigation; e.g., it is possible that the porous Cr-rich oxide both conceals and protects a dealloyed layer.

The pseudo-passive films found by Vaccaro, et al.,[19] and the corrosion sponges studied by Scamans and Swann[20,21] and Silcock[22] are the same as the films of Baker, et al.[15] In neutral solutions, the films form preferentially along slip bands (Figure 2) and are mostly composed of porous chromium hydroxide. We contend that this may conceal a dealloyed metallic layer, as hinted by Scamans and Swann (see Appendix A). Honkasalo[23] and many others have shown that similar films form in already acidified solutions at room temperature, one more piece of evidence that the low- and high-temperature cracking are the same as regards crack-tip interactions. An interesting observation was made by Jones,[24] who described the initiation of cracking as pitting leading to filiform corrosion; this, in slightly different words, resembles the tunneling nomenclature of Scamans and Swann.[20,21]

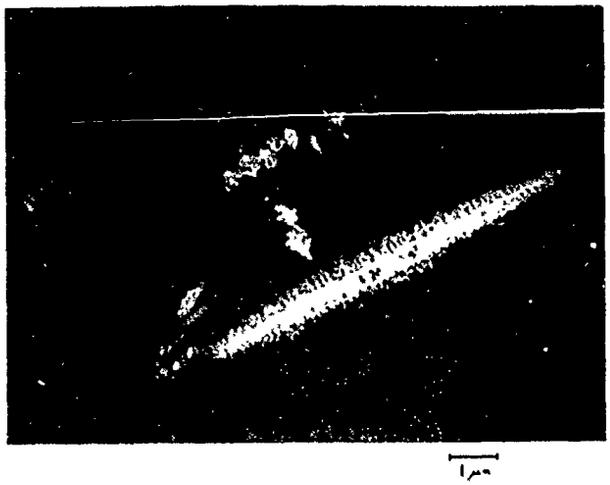


FIGURE 2—Transmission electron micrograph of corrosion sponge formation along slip traces, leading to stress corrosion crack nucleation in miniature specimens of type 304 (UNS S30400) SS exposed to concentrated LiCl solution at 150°C and pH 2.5. (Reprinted with permission from Pergamon Press.[21])

The difficulty of accepting ideas about crack chemistry that are now taken for granted is illustrated by Hoar.[25] The likelihood of crack acidification was clear in the original paper of Hoar and Hines[16] and is implicit in Figure 3, but in 1977, one had to read between the lines

to detect any reference to it. Hoar makes a careful argument about the existence of a passivating film in boiling $MgCl_2$ solution, within an "extremely limited" potential range, then states that this film is responsible for the protection of the crack sides near the apex and, by implication, removes the necessity for a nickel-enrichment model of the protection of the crack walls. Similar arguments were made by Wilde.[26] Presently, one would say that a passive film of such limited stability would be destroyed completely in a crack, and indeed this is easily seen by simulating the acid crack solution found by Baker, et al.[15] Passivity is only relevant in the initial stage of SCC in neutral solutions; propagation in neutral solutions, or initiation in already acidified solutions, is associated with the dark film.

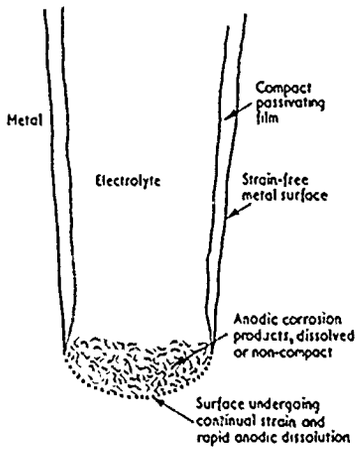


FIGURE 3 – Schematic view of crack propagation for austenitic stainless steel in hot $MgCl_2$ solution, according to Hoar and Hines.[16]

Much of the confusion about the role of oxygen and the existence of a passive state in chloride SCC can be traced to the use of boiling $MgCl_2$ solutions. When freshly prepared, these solutions are somewhat acidic, and the steel is transiently in an active state in which intergranular (IG) SCC predominates.[27] When well-aged, there is a passive state, but the chloride activity is so high that the "pitting potential" (in this case, virtually a general breakdown potential) is nearly coincident with the corrosion potential in deaerated solution, as shown by Hines and Hoar.[10] However, if one uses a milder solution, such as 9 molar LiCl below the boiling point, then the cathodic action of oxygen and the passive state of the steel are both obvious [26] Less obvious is the state of the metal inside the crack, and this is the important problem to be addressed.

In a series of papers using various acidified solutions, Galvele and others[27-30] showed that there was a film-formation process within the range of active potentials where cracking occurs (Figure 4) and applied and tested a conventional SDM to account for the crack velocities. This superceded the simplistic picture of a film-free active state given by Bianchi, Mazza, and Torchio.[31] The dark film, also discussed by Vaccaro, et al.,[19] and by Smialowska and Lukomski[32] (Figure 5), almost certainly conceals a dealloyed metallic layer,[33] and we believe that this has an important role in the cracking, in fact, there is some evidence for dealloying in Figure 4. However, the Galvele data show a close correlation between predicted and actual crack velocities that must be taken seriously. Apparently, Galvele[34,35] has abandoned this approach, implying that he regards the *kinetic* correlations as accidental, we find this extraordinary and propose another interpretation. The crack growth occurs by film induced cleavage, and the crack tip dissolution rate (though inhibited by the mass transport and ohmic restrictions) follows the trend with potential shown by the free surface electrochemistry of the system. A related argument has been developed in detail for brass in nitrite solution.[36] Recent data on intergranular corrosion and SCC of Al Cu alloys suggest that Galvele may have overestimated the diffusional limitations within a crack, since anodic current densities of 0.5 A/cm² were readily achieved.[37]

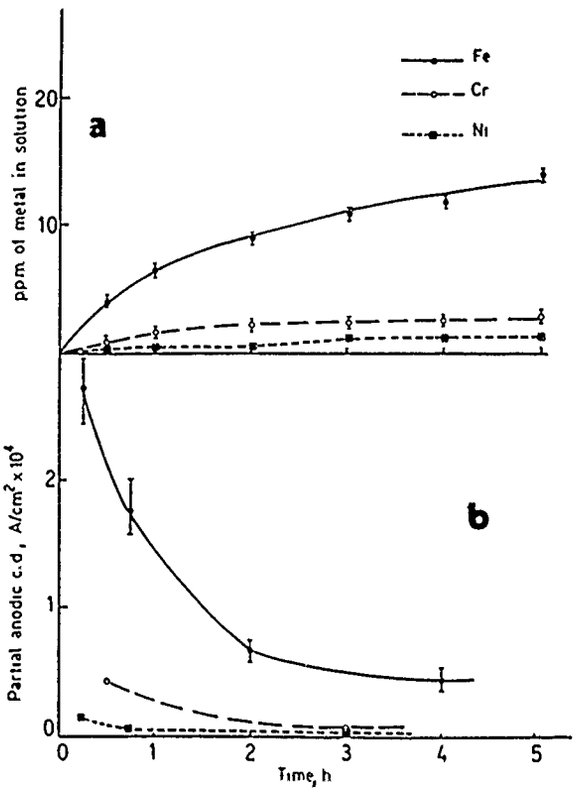


FIGURE 4—Dissolution rates and corresponding (calculated) partial anodic CDs for Fe, Cr, and Ni during immersion of type 304 (UNS S30400) SS in 5 N H_2SO_4 + 0.5 N NaCl solution at −0.16 V_H and 25°C.[29] Note the evidence for selective retention of nickel from 0 to 2 h.

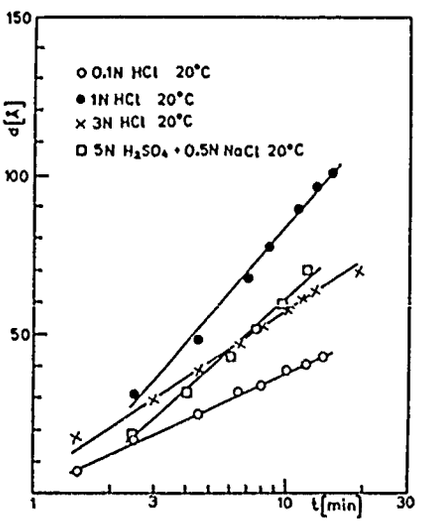


FIGURE 5 – Ellipsometrically measured film thicknesses during immersion of austenitic stainless steel in various acid chloride solutions.[32]

The problem of acid vs neutral, low vs high temperature has been elegantly addressed by Tsujikawa and others.[38,39] They showed that crevices on austenitic SSs would initiate cracks readily at 80°C in very dilute, neutral chloride solutions such as 0.03 wt% (0.005 M) NaCl. The cracking resembled conventional chloride SCC and was clearly initiated in an acidified crevice solution. From the practical point of view, this work is important as failures at less than 100°C generally occur in creviced regions. The interpretation is simple. The crevice environment of about pH 1 to 2 generates the same active or semiactive state as occurs in already acidified solutions or within slip-step grooves or pits in high-temperature,

high-chloride solutions. These authors also give a simple interpretation of the critical potential for SCC in terms of crack chemistry (Figure 6): The critical potential is the repassivation potential (minimum potential for the maintenance of acidity) of the steel in the acidified crack environment. For deep cracks and concentrated solutions, the repassivation potential approaches the corrosion potential in the crack environment; i.e., localized acidification cannot be maintained if there is a net cathodic current in the crack.[40] Crack chemistry arguments also provide a transparent explanation of the effects of many inhibitors in altering the critical potential, replacing the adsorption argument of Uhlig.[41]

Similar arguments regarding the critical potential can be found in other work, e.g., by Torchio,[42] Salvago, et al.,[43] Shamakian, et al.,[44] and Mancia and Tamba.[45]

The role of pitting in crack initiation has often been considered obscure, but in fact the literature permits a fairly easy rationalization of this point. Conventional pitting (and eventually crevice corrosion) becomes necessary as the chloride concentration and/or temperature are reduced, as shown by Smialowska and Gust.[46] In extreme conditions, such as boiling $MgCl_2$ solution, the passive state is so fragile that a trenching type of corrosion at slip steps can occur; the high chloride activity lowers the amount of local hydrolysis of chromium ions required to give a passive-to-active transition. In lower Cl^- concentrations, conventional pitting becomes necessary to generate the acidity, and eventually the Tsujikawa type of crevice corrosion is the only way of holding the right pH with a low enough dissolution rate to trigger the cycle of dealloying and cleavage that we believed to be necessary for cracking.

This subtle interplay of temperature and chloride concentration has been explored by Shamakian, et al.[44] They showed that the corrosion potential of type 304 (UNS S30400) SS in neutral, aerated LiCl solutions was independent of LiCl concentration at a given temperature, but the critical cracking potential (which is just below a pitting potential) increased with decreasing LiCl concentration. Thus, at some LiCl concentration, cracking no longer occurs at the free-corrosion potential but may occur with artificial anodic polarization. There must eventually come a point where cracking cannot be achieved by anodic polarization of a smooth specimen (even though pitting readily occurs) but requires the more restricted geometry of a crevice; the nature of this transition has not yet been carefully defined but presumably relates to the anodic current density (CD) in the pit or crevice, which (according to a dealloying model) must fall low enough for dissolution to become selective, triggering SCC. For a given pit geometry, lowering the chloride activity or temperature means that the critical pit chemistry eventually becomes so concentrated that it cannot be retained without passing local CDs that are too high to permit the transition from blunt pit (nonselective dissolution) to sharp crack (selective dissolution).

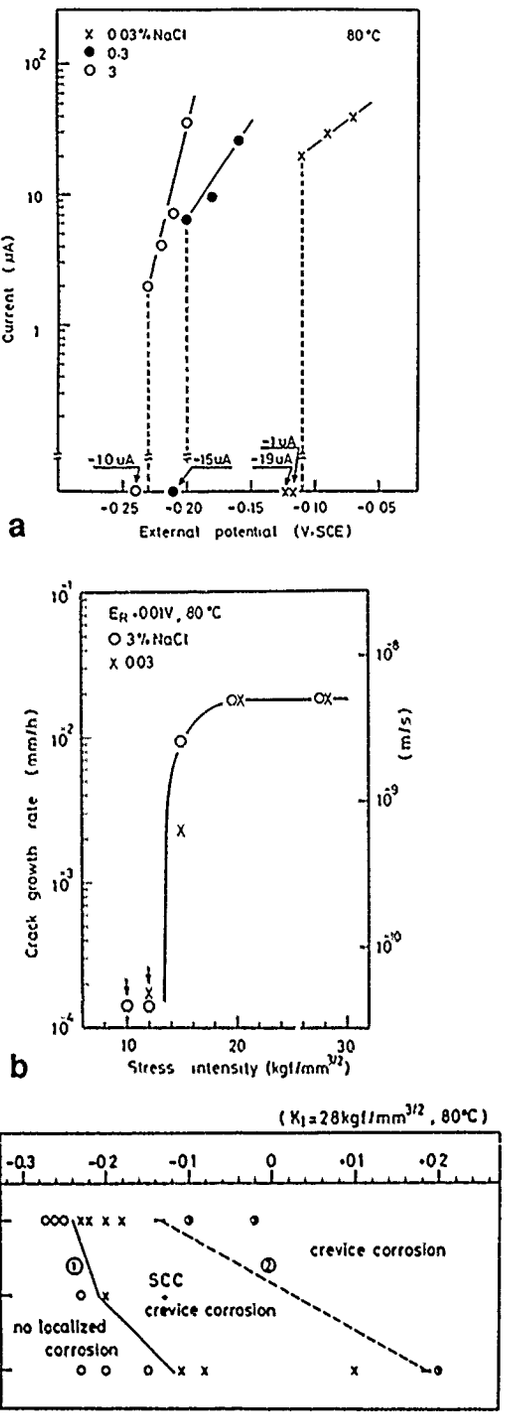


FIGURE 6—Crevice corrosion and SCC of type 316 (UNS S31600) SS in dilute NaCl solutions at 80°C:[38,39] (a) determination of crevice repassivation potentials (E_R); (b) v–K curves for creviced, tapered, double-cantilever-beam specimens showing superimposition of results for two NaCl concentrations by holding potentials at just above E_R, and (c) summary of results.

Kinetics of Chloride SCC in the Context of a Slip-Dissolution Model

Attempts to relate anodic kinetics to chloride SCC date to the pioneering work of Hoar and West.[47] West used a galvanostatic rapid straining method in conjunction with rapid solution flow to show that sufficient anodic CDs existed to explain (via Faraday's second law) the crack velocity at the corrosion potential (Figure 7). Hoar and Scully repeated the work using a potentiostatic method and obtained broadly similar results,[48] although Hoar states that Slater could not reproduce West's results.[25] Both West and Scully used the whole specimen area to calculate CDs, as the metal was not regarded as passive, thus, West's CDs were generally several times higher than Scully's, as his galvanostatic polarization gave him a more complete breakdown of passivity prior to determining the anodic CD. In view of this, one can see that small variations in experimental procedure, particularly with regard to cell geometry, could lead to different results and explain Slater's problems.

Once it was realized that SSs were passive in hot $MgCl_2$ solutions and filmed in cold, acidified solutions, it became appropriate to use the equation of Bubar and Vermilyea[49] to calculate the fraction of bare surface area created during a rapid straining test. This immediately increased the anodic CDs that could be deduced from such tests, and good agreement between these CDs and transgranular SCC velocities was obtained for acidified solutions at room temperature (Figure 8)[28,30] and for hot, concentrated chloride solutions (Figure 9).[27,50] Nakayama and Takano[11] (Figure 10)

showed that rapid-straining experiments on type 304 SS in unstirred 42% $MgCl_2$ at 143 °C gave sustained anodic CDs sufficient to account for the Region II velocity of transgranular SCC, e.g., 400 mA/cm^2 (160 nm/s) at the corrosion potential of −0.34 V_{SCE}. (Apparently they were unaware of the prior work of Hoar and West.) Doubts arise because their anodic current transients are very prolonged (e.g., about 12 μm dissolved in 100 s at −0.34 V), so the equation of Bubar and Vermilyea[49] cannot remain valid as dissolution at slip steps proceeds; there must be a large magnification of the corroding area and hence a reduction in the true CD.[51] Also, it is obvious that such depths of corrosion do not occur within cracks; it is not obvious how such results can be harmonized with the depth of chemical attack observed on fracture surfaces, generally around 0.1 μm, which is less than the corrosion during the first second in the straining experiment.

Whatever arguments one advances against the anodic kinetics shown by Nakayama and Takano,[11] the trend of SCC velocity with initial CD (over a few seconds) remains strikingly in accord with the slip-dissolution concept despite the use of a neutral solution. (This is not necessarily bad, because with the CDs quoted, the bare surface exposed must be quite acid and is presumably undergoing a trenching type of pitting corrosion.)

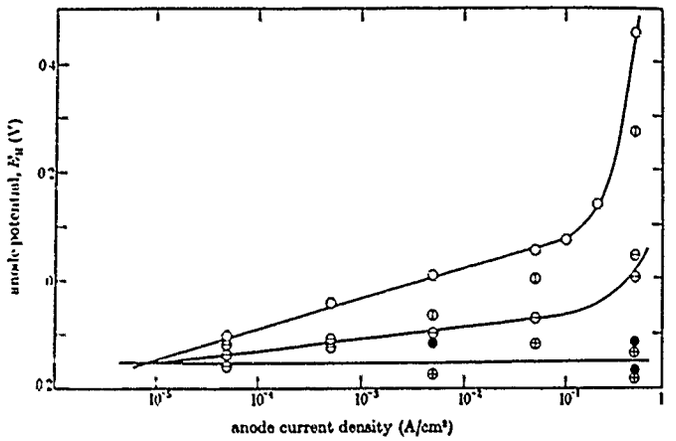


FIGURE 7—Reduction in anodic polarization by straining and solution flow for 18-8 SS in 42% $MgCl_2$ solution at 154°C: O = static metal in stationary solution; Θ = static metal in flowing solution; Φ = straining metal in stationary solution; ⊕ = calculated result for straining metal in flowing solution, assuming O and Φ are additive; ● = experimental result for straining metal in flowing solution. (Reprinted with permission.[47])

Nakayama and Takano understood the time scale of events (seconds) relevant to a repetitive film-rupture process at the crack tip.[11] In contrast, Rimbert and Pagetti[52] used peak anodic CDs or very short (10 ms) measurement times to interpret the SCC behavior in neutral $MgCl_2$ solutions. Such very short time scales are no longer believed to be relevant to SCC growth, because they imply impossible crack-tip strain rates of up to 1000%/s. The best that can be achieved in such an experiment is an indication of a pitting or breakdown potential that may correlate with SCC. Rimbert and Pagetti actually achieved *lower* CDs on their scratches than Maier, et al.,[50] achieved on strained electrodes, probably because the hydrodynamic disturbance of the scratching process does not permit establishment of the acid environment as readily as the comparatively tranquil straining method. If a scratching method is to be used, a simulated crack solution is necessary.

The diffusional and/or ohmic difficulties associated with the SDM, cited by Galvele,[34] were anticipated by Tromans and Swiniarski,[53] who prepared artificial active-passive cracks by sandwiching iron sheet between SS plates in hot $MgCl_2$ solution. They achieved penetration rates between 1 and 10 nm/s, which were too low by a factor of 5 to 50 to account for SCC rates. Various comments come to mind, e.g., real cracks are wedge shaped, some dissolved metal may be re-precipitated, etc., and judgment must be reserved on this matter until systems such as steel in hot nitrate solution have been re-examined. Most authorities agree that an anodic process is responsible for IGSCC in this system, yet the crack velocity is very high (up to 1 μm/s) and diffusionally impossible on a slip-dissolution basis, according to Galvele. Again, we draw attention to recent data showing very high anodic CDs during stress-assisted intergranular corrosion of Al-Cu alloys, where crack opening under stress was shown to exert a simple geometrical influence on the ohmic resistance within the crack.[37]

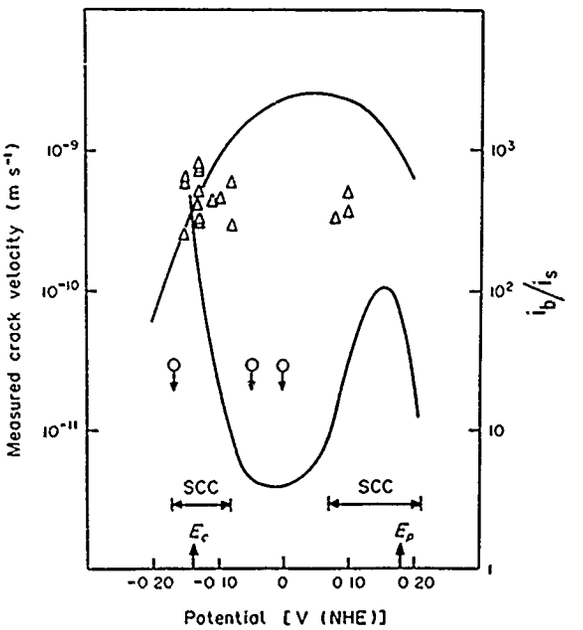


FIGURE 8—Correlation of SCC velocities with rapid-straining tests for type 304 (UNS S30400) SS in 0.5 M HCl + 0.5 M NaCl solution at room temperature. The upper solid line represents the predicted SCC velocity from the rapid-straining tests, and the lower line is the ratio of bare-to-filmed metal CDs (i_b/i_s). The triangles are the SCC velocities; the circles represent detection limits where no cracks were found. Cracking occurs near the corrosion potential and the pitting potential. (Reprinted with permission from Pergamon Press.[30])

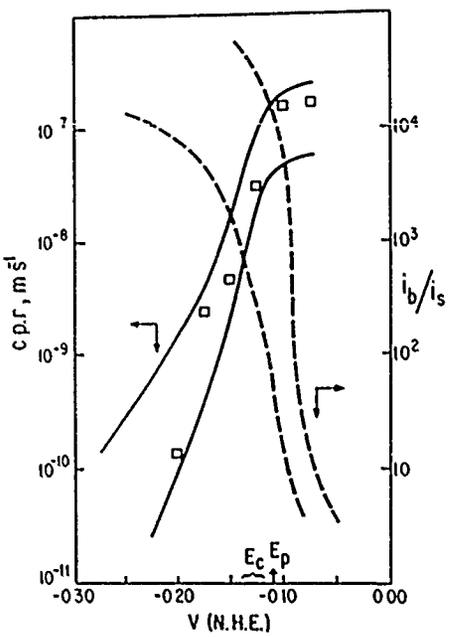


FIGURE 9—Similar plot to Figure 8, for *transgranular* SCC in 40% $MgCl_2$ solution at 100°C. *Intergranular* SCC did not correlate with the kinetics on strained electrodes (Figure 20), and the authors consequently proposed that crack growth did not result from anodic dissolution. (Reprinted with permission from Pergamon Press.[27])

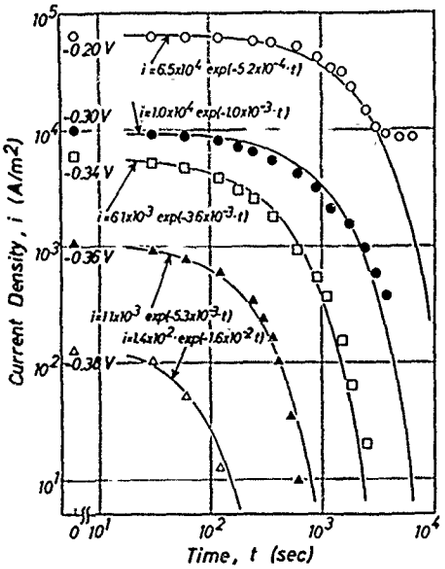


FIGURE 10—Anodic CD decays deduced from interrupted rapid-straining tests on type 304 (UNS S30400) SS in 42% $MgCl_2$ solution at 143°C.[11] Potentials are on the SCE scale; surface areas were calculated assuming the Bubar and Vermilyea equation[49] was applicable.

Inhibition of Chloride SCC

Buffers, such as acetate or silicate, and electroactive anions, such as nitrate, alter the potential dependence of SCC as reviewed by Uhlig.[41] This is partly an effect on the local electrochemistry within the crack or crack nucleus. Uhlig argued in discussion that he was studying crack initiation, and crack acidification was therefore irrelevant (probably an untenable argument, as all these inhibitors affect crack growth, and all cracks develop from acid nuclei). Inhibitors may be effective, even in boiling $MgCl_2$, as long as the crack is unable to acidify, i.e., if the corrosion potential on the external surface is lower than the crevice repassivation potential in the (now altered) crack solution.[39] Cracking resumes if the potential is raised above this critical potential, which may vary with crack length. If the temperature is made extremely high in the presence of nitrate, the inhibiting effect of this ion is not apparent as it begins to act as an oxidant and promotes SCC under free-corrosion conditions.[54]

High concentrations of NaI inhibit SCC in hot $MgCl_2$ solution, and this has been proposed to be a cathodic inhibition effect.[55] Various organic inhibitors have been shown to inhibit crack initiation in hot $MgCl_2$ solutions using either static or slow-strain-rate tests.[56,57] These effects deserve more study, especially with regard to the local environment of a crack nucleus, and the ability of such inhibitors to arrest crack growth. It would also be of interest to study milder conditions of chloride concentration and temperature, where most practical instances of SCC occur.

Analysis of Surface Films

We have already seen that the work of Baker, et al.,[15] decisively laid emphasis on the dark films formed in the acid crack environment in order to understand chloride SCC. Thus, it is unlikely that there is more than a fortuitous correlation between SCC and the compositions of films on external, passive surfaces, as studied by da Cunha Belo, et al.,[58] and Gluszek and Nitsch.[59] If the work of Baker, et al., had been heeded, great advances could have been made with UHV surface analytical techniques; we have tried to remedy this situation recently. (See Appendix A.)

Unusual Austenitic Alloys

Useful mechanistic insights can be obtained by examining data on austenitic cast irons, where there is no Cr,[60] or Fe-Mn-Al alloys, where there is neither Cr nor Ni.[61,62] It is difficult to assess the role of hydrogen in SCC of Fe-Mn-Al alloys, where the potential is very low, but for cast irons the similarity to austenitic SSs is striking. More basic work in this area would be very useful.

Fracture Mechanics Studies

The first study of chloride SCC using fracture mechanics methods and thick specimens was that of Speidel,[63] who demonstrated the low K_{ISCC} value in hot $MgCl_2$ solution [Figure 11(a)]. He also studied sensitized steel in 288°C solutions [Figure 11(b)]. Later, he showed that the "Copson curve" of SCC life vs nickel content could be recast in terms of K_{ISCC} (Figure 12).[64] Outstanding work was reported by Russell and Tromans,[65,66] who demonstrated that the Region II crack velocity in hot $MgCl_2$ solution varied with alloy composition but not with potential above the critical potential (Figures 13 and 14). Cold rolling to form strain-induced martensite could have a kinetic effect but was not fundamental to the cracking process. Depending on the method used, a weak dependence of K_{ISCC} on potential above the critical potential may be detectable (Figure 15),[67] but this is of little practical importance.

A detailed electrochemical rationalization of the variation of Region II velocity across types 304, 316 (UNS S31600), and 310 (UNS S31000) is not available. Probably a reasonable result could be obtained by using rapid straining in neutral $MgCl_2$ solutions, but a more interesting prospect is to study the kinetics in acidified solutions despite the difficulties of being near the free-corrosion potential.

Whatever model of SCC one favors, the independence of SCC velocity on potential above the critical potential and the very sharp cutoff below it can be interpreted on the basis of crack chemistry and IR considerations; i.e., the acid crack can only be maintained above the critical potential, which is the repassivation potential in the crack environment, but further anodic polarization rapidly generates an active state that severely restricts the polarization that can be achieved at the crack tip.

SCC in Dilute Chloride Solutions at Elevated Temperatures

At temperatures above 200°C, transgranular SCC of annealed austenitic SSs occurs with very low chloride concentrations and above a critical potential (Figure 16).[24,68-71] This has sometimes been considered different from cracking in boiling $MgCl_2$ and similar solutions but only because crack chemistry has not been considered. There is a close correlation between the cracking and the onset of pitting corrosion, and since the latter is known to require a high chloride concentration within the pit and a low pH because of Cr^{3+} hydrolysis, the crack environment is clearly analogous to that achieved at lower temperatures and higher chloride concentrations. The reduction with increasing temperature of the chloride concentration required for SCC reflects a less acidic crack environment required to achieve an active state and probably also the faster kinetics of the anodic reactions. Spongy corrosion products have been reported for high-temperature, low-chloride SCC that are very similar to those reported for hot $MgCl_2$ solutions.[24]

The usual finding with regard to sensitization is that the critical cracking potential drops abruptly at a particular level of sensitization, whereupon the cracking becomes intergranular (Figure 17). This cracking is less sensitive to the presence of chloride ions, occurring almost as readily in sulfate solutions.[72-75]

Recently, a complicating observation was made by Congleton, et al.,[76] who found two zones of SCC for annealed type 316 SS in dilute chloride solutions with oxygen at 265°C (Figure 18). One zone was as found by Andresen and Duquette (Figure 16),[68-70] while the other lay at very low oxygen contents (potentials). Congleton, et al., implied that the low-potential cracking was relatively severe, not a minor surface effect as found by Andresen and Duquette in type 304 SS; possibly, this has to do with the alloy composition or the degree of cold work. The crack chemistry aspects of the low-potential cracking are unexplored, but it appears improbable that there can be significant acidification. Congleton, et al., suggested a film-induced cleavage interpretation in which the film was a dealloyed layer at low potentials and a passive film at high potentials; in fact, it is the high-potential cracking that is unambiguously associated with an acid crack and therefore likely to involve dealloying. More work is required on the crack chemistry in this system.

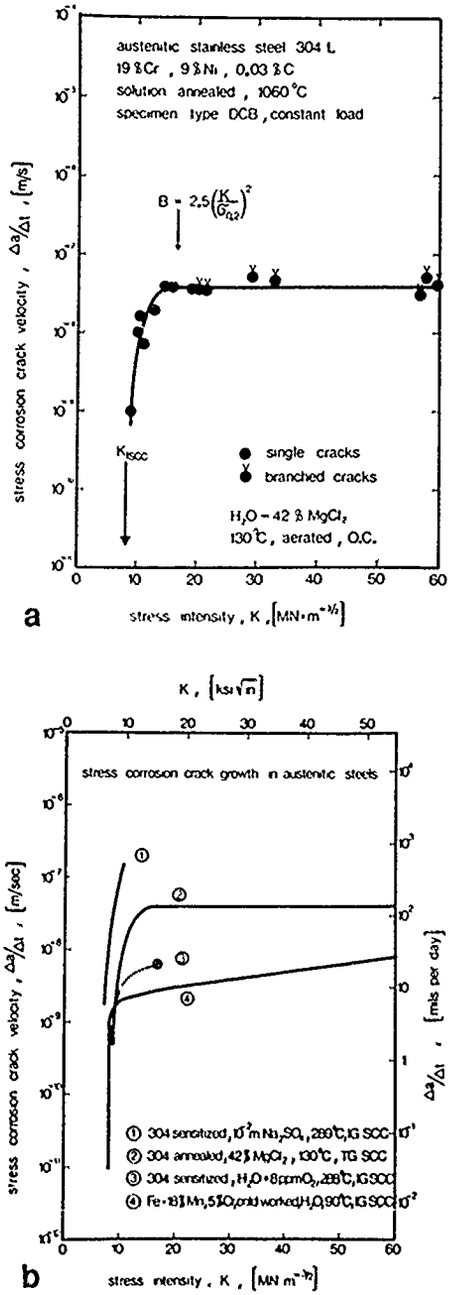


FIGURE 11—(a) Speidel's first v-K curve[63] for type 304L (UNS S30403) SS in 42% $MgCl_2$ solution at 130°C and (b) smoothed data for several systems showing very similar K_{ISCC} values.[63]

When cracking occurs near the pitting potential and the latter is much higher than the normal corrosion potential, an IR drop ensures that the potential at the root of the crack is depressed to an active value, which is necessarily near the corrosion potential in the crack environment. In certain combinations of HCl and NaCl at room temperature, this shows up particularly well because there are two zones of cracking: one near the corrosion potential and the other near the pitting potential.[30] (See Figure 8.) The crack conditions will differ only slightly with respect to potential and pH between these two free-surface conditions.

Under extreme conditions (Na_2SO_4-H_2SO_4, pH 2.5, 290°C), rapid transgranular SCC of type 304 SS can be obtained without chloride ions.[77,78] More research on this would be useful, as most work related to nuclear power plants avoids these unrealistically aggressive conditions that may yield more useful mechanistic information.

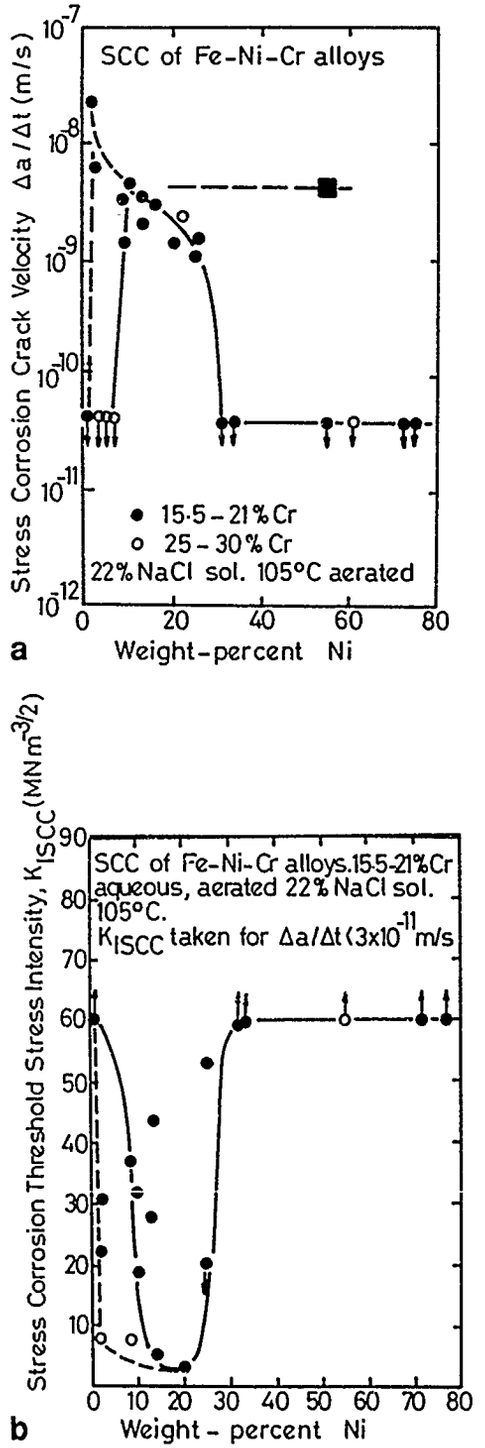


FIGURE 12—Speidel's reproduction of the Copson curve (Figure 1) using fracture mechanics: (a) in terms of "plateau" (Region II) velocity and (b) in terms of K_{ISCC}. (Reprinted with permission.[64])

Effect of Alloyed Phosphorus or Nitrogen

Nitrogen and phosphorus in solid solution are both detrimental to the chloride SCC resistance of austenitic SSs. Mozhi, et al.,[79] reviewed information related to the effect of solid-solution nitrogen and presented new data on sensitized material where nitrogen affects the sensitization process. Many authors agree that N and P affect the electrochemistry of SCC, but disagree on the sign of the effect. Staehle[4] suggested that nitrogen slows down repassivation, while Hoar[25] and Bednar[80] suggested that pure alloys were not

passive enough to show SCC. Silcock[81] suggested that phosphorus changed the morphology of slip-step corrosion but not necessarily its rate; if slip-step corrosion is a dealloying process, this could be a very significant observation. Cihal has clearly shown the effects of P and N using high-nickel alloys (25 to 40%) on the borderline of susceptibility to SCC in boiling $MgCl_2$;[82] these alloys are quite corrosion resistant, which tends to argue against Hoar's and Bednar's suggestions. N and P are particularly influential at relatively low temperatures and chloride concentrations, e.g., in crevice tests of the type used by Tamaki, et al., where it is again difficult to argue that the alloy is too corrodible.

We suggest a speculative interpretation of the effects of N and P. We have observed that ammonia actively inhibits aging (thought to be coarsening of porosity by surface diffusion) of thin dealloyed layers on brass,[83] so that a layer is only able to nucleate cleavage if it is still in contact with the ammonia solution or if the latter is quick frozen in contact with the alloy surface (by immersion of a thin foil in liquid nitrogen without rinsing). We have proposed that alloyed arsenic acts the same way in chloride environments, pinning the surface diffusion process that normally leads to a coarse porosity.[84] It is therefore possible that the role of P or N (or other Group VB elements[2]) is to maintain the dealloyed layer in the extremely fine (nanoporous) state required for cleavage nucleation, by enriching at critical surface sites in the elemental or partially oxidized state. Such a suggestion is not easy to test, but one possibility is to use AC impedance methods to follow the development of the porosity as attempted by Newman and Mehta.[33]

Further comments will be found in the section on hydrogen effects.

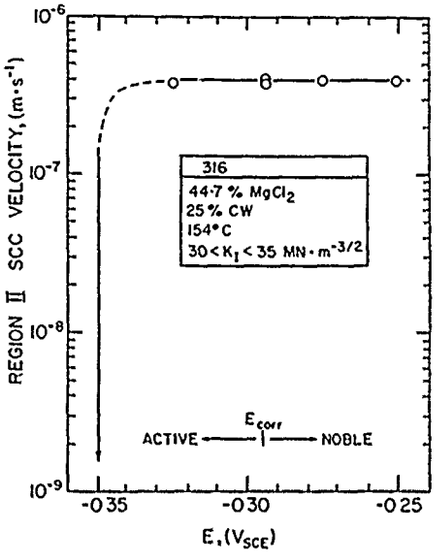


FIGURE 13—The effect of potential on the Region II crack velocity for type 316 (UNS S31600) SS in 44.7% $MgCl_2$ solution at 154°C. (Reprinted with permission.[65])

Intergranular Cracking of Annealed Alloys

Some IGSCC is invariably seen when austenitic steels are tested in hot chloride solutions over a range of potentials or mechanical parameters, and contradictory conclusions have been drawn depending on the exact conditions used. One clear observation is that transgranular SCC predominates at high potentials where there is a strong acidification; possibly corrosion can only be localized to grain boundaries when the potential is low and there is less acidification. The effect of raising the stress intensity or strain rate (Figure 19) is to promote intergranular cracking,[11,65,66] a result at variance with experience from α-brass.[85] It is not clear whether this is related to hydrogen or to austenite stability, but in either case one could rationalize the difference. Muraleedharan, et al.,[86] showed that prior cold work enhanced IGSCC in unstable steels and suggested that this was mechanistically analogous to the effect of stress intensity on annealed material.

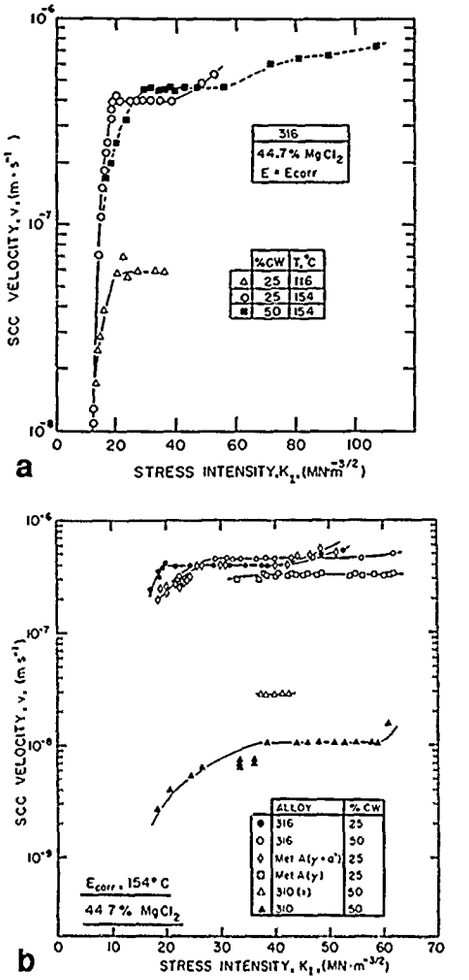


FIGURE 14—The effect of alloy composition, cold work, and temperature on v–K curves for austenitic stainless steels in 44.7% $MgCl_2$ solution at 154°C: (a) data for type 316 (UNS S31600) SS showing a large effect of temperature but small effect of cold work;[65] (b) Region II data showing relative resistance of three steels[66] (Metal A = metastable steel with 11Cr, 9Ni, 3.7Mo, 2Mn, 0.2C, 1Si). (See Figures 19 and 27 for more details on the effect of cold work and incidence of intergranular cracking.) (Reprinted with permission.[65,66])

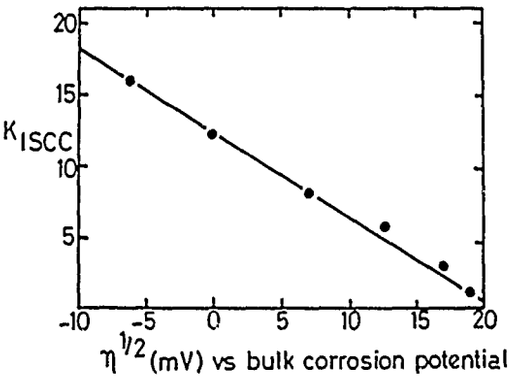


FIGURE 15—The effect of displacement of the potential from its natural value (in hot LiCl solution) on the K_{ISCC} value for 18-10-0.5Ti steel. (Reprinted with permission from Pergamon Press.[67])

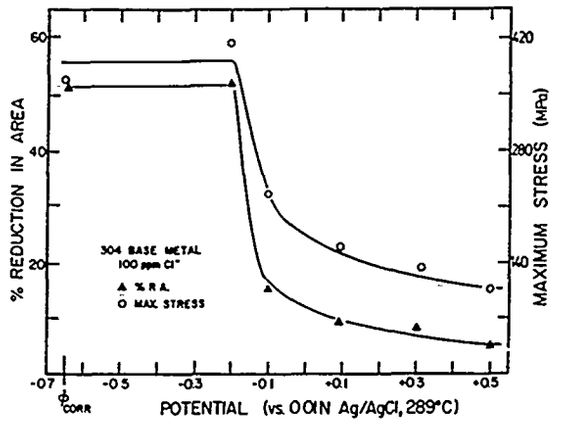


FIGURE 16—Results of slow-strain-rate tests (10^{-6}/s) on non-sensitized type 304 (UNS S30400) SS in 100 ppm Cl^- solution at 289°C, showing the critical potential.[68]

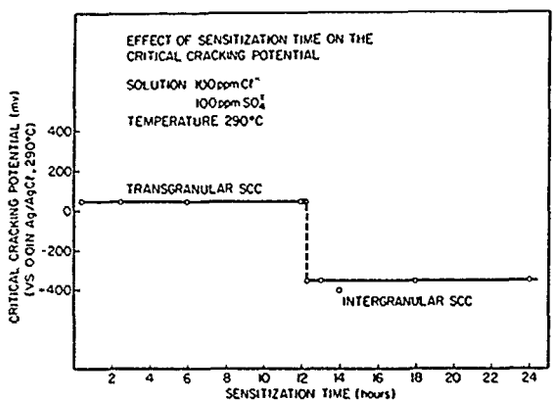


FIGURE 17—Variation of the critical SCC potential with sensitization time at 620°C for type 304 (UNS S30400) SS with 0.058% carbon, tested under slow-strain rate (1.1×10^{-5}/s) in 100 ppm Cl^- + 100 ppm SO_4^{2-} solution at 289°C.[75]

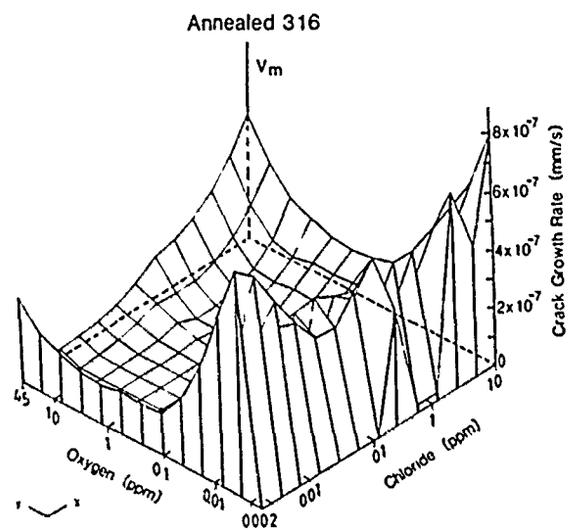


FIGURE 18—Variation of cracking tendency with oxygen and chloride concentration for slow-strain-rate testing (2×10^{-6}/s) of annealed type 316 (UNS S31600) SS at 265°C. Note the zone of cracking at low oxygen contents. (Reprinted with permission from Pergamon Press.[76])

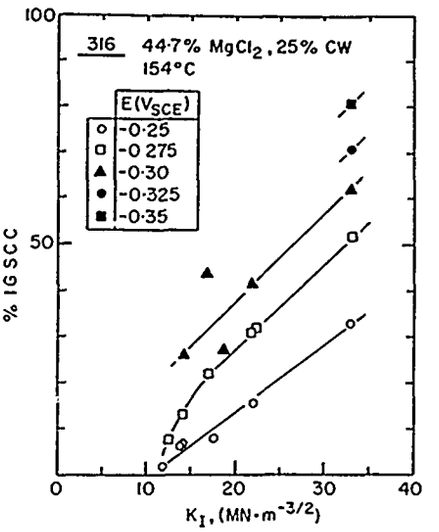


FIGURE 19—Incidence of IGSCC for the tests on type 316 (UNS S31600) steel shown in Figure 14, showing that high K values promote intergranular cracking. (Reprinted with permission.[65,66])

Manfredi, et al.,[27] showed that fresh $MgCl_2$ solutions (where type 304 SS is close to an active state because of the low pH of 3 to 4) tend to cause IGSCC at very low potentials (Figure 20), below the conventional critical potential determined in aged solutions (where transgranular SCC predominates). The results for fresh $MgCl_2$ solution resemble those obtained in room-temperature NaCl/HCl solutions,[30] where cracking occurred both in the active state and near the pitting potential. According to Manfredi, et al.,[27] the intergranular cracking cannot result from a slip-dissolution mechanism because there is insufficient anodic activity to sustain cracking at the rate observed, but on a dealloying perspective this observation is readily interpretable: A rate of dealloying that could sustain cracking by film-induced cleavage or brittle intergranular separation would not be sufficient to grow a crack by itself. Dealloying at low potentials would require an acid solution to maintain an active state. Manfredi, et al.,[27] consider that the results argue for the surface-mobility model of Galvele,[34,35] but this model is probably untestable in this system.

When the film-induced cleavage model was elaborated,[6] it was felt that intergranular and transgranular SCC differed in that only the latter involved brittle fracture of unattacked material. This view was influenced by the observations of Beggs, Hahn, and Pugh[87] on α-brass, where microscopic observation showed discontinuous transgranular but continuous intergranular cracking. However, recent observations on pre-exposed brass foils show abundant brittle intergranular cracking,[83] and we now believe that both forms of cracking are brittle *in systems where both forms occur in the same conditions of environment, potential, etc.* In systems showing only IGSCC, the SDM or HE models normally apply.

Using hydrogenated high-temperature water and a special tensile specimen with a cold-pressed hump, Totsuka, et al.,[88] have shown that intergranular hydrogen-induced SCC is possible in nonsensitized SSs. No cleavage-like cracking was reported. It is not clear whether this is the same phenomenon observed by Congleton, et al.,[76] or by Kuniya, et al.[99] (See Figures 18 and 21.)

Fractography, Discontinuous Cracking, and Crystallography

Throughout the Firminy conference proceedings (1977), there are references to the feathery, brittle appearance of SCC fracture surfaces in austenitic SS (e.g., Uhlig, p. 206, and Pugh, p. 1019). Proponents of SDMs still argue that this is the result of an extremely narrow dissolution front.

The basic fractography of chloride SCC was well established around 1970 by scanning electron microscopy (SEM) studies. Despite the brittle appearance of the transgranular fracture, the SDM

survived the 1970s more or less intact and is still widely accepted.[11] However, around 1977, Pugh and others began to question the view that such surfaces could be produced by dissolution processes. This was not a new departure (Edeleanu and Nielsen in the 1950s had proposed that cracking was discontinuous), but the combination of techniques and insights was new. Pugh's work ranged over a variety of face-centered cubic (fcc) systems, including brass and aluminum alloys as well as SSs, and this program enabled similarities and differences to be identified. The basic features of transgranular SCC are shown in Figure 22.

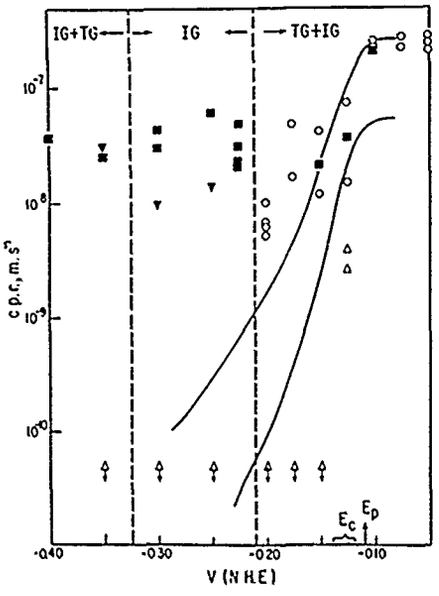


FIGURE 20—SCC velocities for slow-strain-rate tests (1.5×10^{-5} or $1.5 \cdot 10^{-6}$/s) of type 304 (UNS S30400) SS in 40% $MgCl_2$ solution at 100°C. Open triangles denote the results for a preboiled (near-neutral) solution, showing no cracking at low potentials. Other symbols denote results for fresh, or boiled and reacidified, solutions, showing extensive cracking at low potentials. This cracking was mainly intergranular. (Reprinted with permission from Pergamon Press.[27])

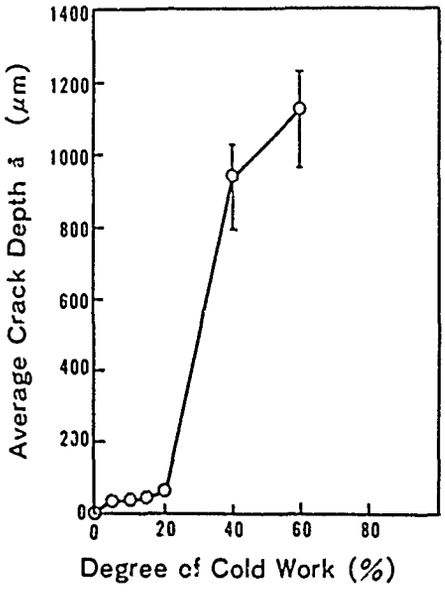


FIGURE 21—The effect of prior cold work on the occurrence of IGSCC in 500-h tests of crevlced bent-beam specimens of nonsensitized type 304 (UNS S30400) SS in oxygenated pure water (8 ppm O_2) at 288°C.[99]

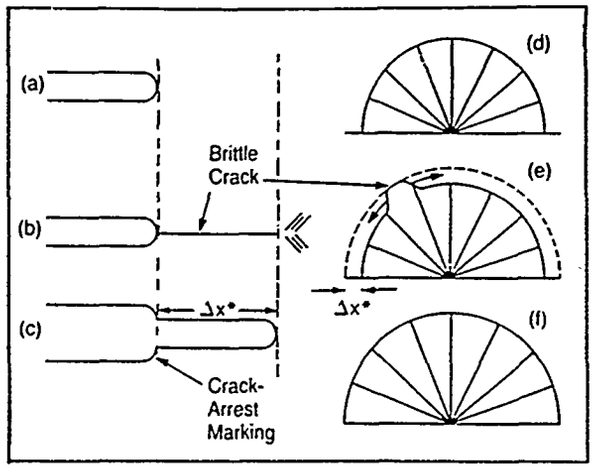


FIGURE 22—Schematic side view of a growing transgranular stress corrosion crack [(a) through (c)] and appearance of a fracture facet [(d) through (f)], according to Pugh.[92]

A key development in the understanding of SCC fracture surfaces was the use of load pulsing to identify the position of the crack front.[87,89-92] This front proved to be surprisingly smooth, crossing many steps (river lines) of varying height. By applying small load pulses at various frequencies, it was shown that there was evidence for a loss of correspondence between markings and pulses at high frequencies, and this was interpreted as evidence for discontinuous crack advance in units of about 0.5 μm (in type 310 SS). HE was suggested as the microscopic mechanism of crack advance, and approximate correspondence with hydrogen diffusivity was suggested. These results are shown in Figure 23.

The fracture surfaces in type 310 SS are of {100} orientation.[93,94] There is good agreement on this crystallography in type 310 SS but disagreement in type 304 SS where {100}, {111}, and {110} planes have all been reported, as reviewed by Meletis and Hochman.[95] (See Figure 24.) Possibly this reflects the formation of strain-induced martensite in the 304 steel and consequent disruption of the crack crystallography. A particularly thorough study of SCC fractography was done by Dickson, et al.,[96] on type 310 steel; they showed that the cracking on {100} had a preferred <110> direction, using an etch-pitting technique to measure the fracture-surface orientation. Dickson, et al., detected striations parallel to the crack front and favored a discontinuous mode of cracking, but in other work on corrosion fatigue of type 316 SS,[97] it has been proposed that cleavage-like fractures can be produced by purely plastic processes. This remains an area of controversy, but most likely both of Tromans's statements are correct; i.e., slip can produce seductively cleavage-like surfaces, but most cases of transgranular environmental cracking also involve genuine cleavage. Particularly convincing crack-arrest striations were displayed by Andresen and Duquette.[70]

Electrochemical Studies to Test the Dealloying/Cleavage Concept

There are a number of apparent difficulties in applying the film-induced cleavage model to chloride SCC. The presence of a dealloyed layer has not been demonstrated, but good progress is being made in that direction;[98] see Appendix A. One difficulty is the low percentage of nickel required to promote SCC; if the dealloyed layer is pure nickel, it is hard to see how it could be space filling. However, surface analyses show that thin dealloyed layers are normally porous alloys of continuously varying composition,[98] which solves this problem.

Experiments on binary Fe-Ni alloys in chloride and sulfate solutions at 80°C and pH 1 provided an opportunity to test a speculation regarding the role of the chloride ion in SCC.[33] Remarkable inhibiting effects of chloride on dissolution of Fe-Ni alloys were observed as shown in Figure 25. Dark tarnishes were formed near the corrosion potential in the presence of chloride ions; these are

clearly dealloyed layers, since Cr is not present to form an oxide and neither Fe nor Ni oxides could possibly form at pH 1 and −400 mV_{SCE}. AC impedance spectra of these surfaces showed evidence for porous conducting film formation, as shown in Figure 26. We believe that these observations are close to the heart of the SCC problem in this system: Chloride affects the relative dissolution rates of Fe and Ni, and/or surface diffusion of the latter, such that dealloying is promoted. It coincidentally favors the development of acidified crack solutions and the initial breakdown of passivity in neutral solutions, but these are essentially details from the fundamental viewpoint; the fundamental action is seen in Cr-free alloys and acid solutions, where these complications are eliminated.

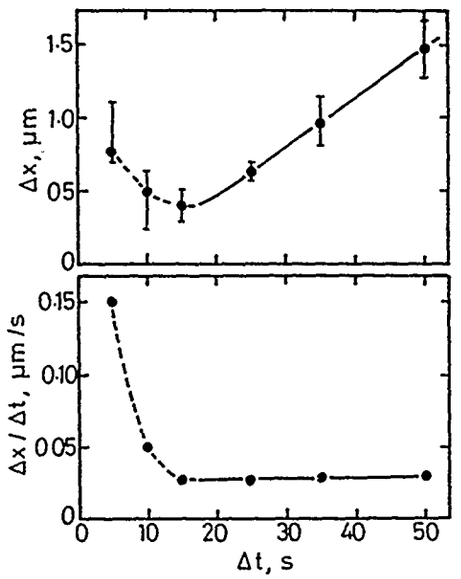


FIGURE 23—The results of load-pulsing experiments on polycrystalline type 310 (UNS S31000) SS in boiling $MgCl_2$ solution at 154°C.[89,90] Δt is the interval between overloads and Δx is the spacing of the corresponding markings on the fracture surface. Below a Δt value of 15 s, there is a loss of correspondence between markings and load pulses, indicating discontinuous crack growth.

Deformation-Induced Transformations and the Hydrogen Problem

The role of austenite stability in chloride SCC has been debated for 30 years. It is important to distinguish arguments related to cold rolling, where α' martensite is produced and is not removed by heating at SCC test temperatures,[99] from arguments related to the formation of α', ε, etc., *during* SCC. The work of Vaccaro, Hehemann and Troiano;[100] Russell and Tromans;[65,66] and Dickson, et al.,[100] shows that the effect of preformed α' phase is a kinetic one and is not required for SCC; e.g., cold rolling of type 316L (UNS S31603) steel caused a marked increase in Region II SCC velocity, from 50 to 500 nm/s, while type 310 SS showed no noticeable increase.[101] (See Figures 14 and 27.) The normal interpretation of the velocity increase in type 316 SS would be that hydrogen is assisting crack advance, but film-induced cleavage also copes with this readily by suggesting that a cleavage crack (or brittle intergranular crack) nucleated in a dealloyed layer propagates further in α' than in γ before arresting. If this is correct, the distance between crack-arrest marks should be greater in rolled than in annealed material. It is also possible that the dealloying is different in the two phases, in which case electrochemical measurements should be able to detect differences in dealloying response of α' and γ. Certainly there is a selective spongy attack of martensite in cold-worked austenite exposed to low-temperature acid chloride solutions, as shown by Honkasalo.[23] Another complicating factor is that cold work tends to promote intergranular cracking.[86]

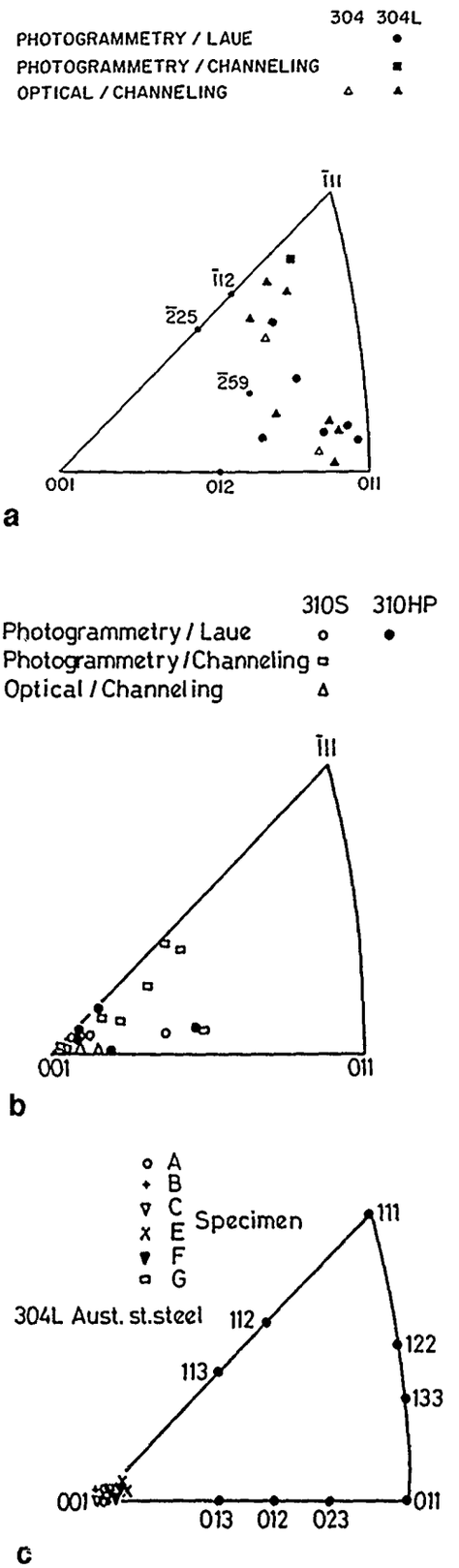


FIGURE 24—Stereographic triangles showing the poles of stress corrosion facets for austenitic stainless steels cracked in hot chloride solutions: (a) and (b) from Liu, et al., showing {100} orientation for type 310 (UNS S31000) SS but varying orientation for types 304 and 304L (UNS S30400 and S30403). (Reprinted with permission.[93]); (c) from Meletis and Hochman showing {100} orientation for type 304L (UNS S30403) monocrystals. (Reprinted with permission from Pergamon Press.[95])

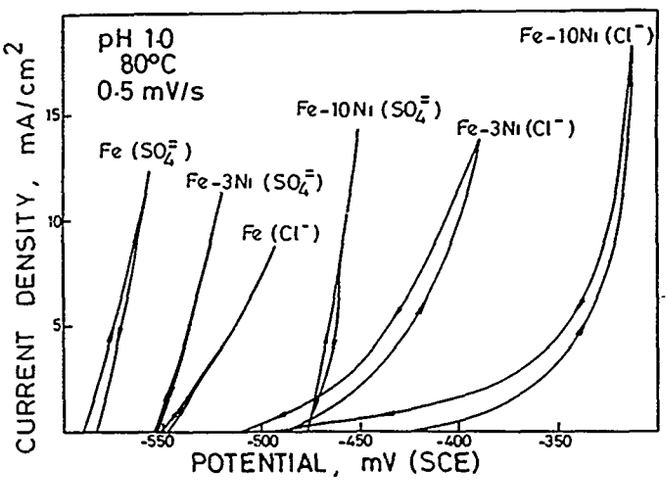


FIGURE 25—Anodic portions of cyclic potentiodynamic scans for Fe, Fe-3Ni, and Fe-10Ni alloys in Na_2SO_4/H_2SO_4 and NaCl/HCl solutions at pH 1.0 and 80°C. (Reprinted with permission from Pergamon Press.[33])

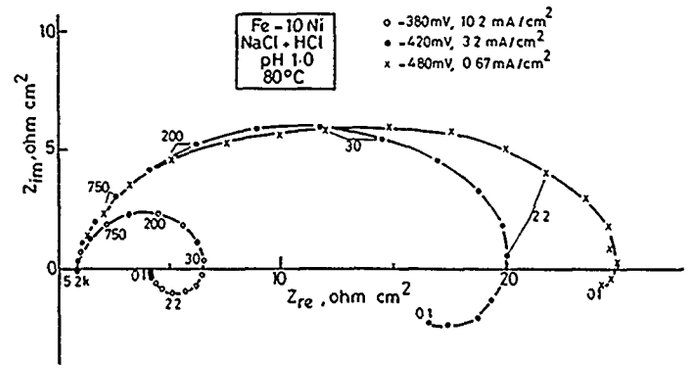


FIGURE 26—Nyquist impedance spectra for Fe-10Ni in NaCl/HCl solution at pH 1.0 and 80°C, showing a highly flattened response near the corrosion potential that correlated with the appearance of a tarnish (dealloyed layer) on the alloy surface. Such a response is indicative of a porous conducting film, equivalent to an electrical transmission line. (Reprinted with permission from Pergamon Press.[33])

Hydrogen can affect the stability of austenite, even in the absence of stress and around pits in neutral solutions, where small amounts of hydrogen are absorbed from corrosion in the acid pit solution.[102] Several authors have followed Asaro, et al.,[103] in proposing that hydrogen induced phase transformations (to α' and ε martensite) are associated with chloride SCC. According to these authors, the effect of prior cold rolling does not give information on the role of phase transformations or hydrogen in crack growth.

Cleavage-like transgranular fractures can be readily obtained in unstable austenitic steels using gaseous hydrogen or cathodic charging. These surfaces resemble SCC fractures (Figure 28), as argued by Hanninen and others,[5,104-107] but detailed differences have been reported by Nakayama and Takano,[108] Chu, et al.,[109] and Qiao,[110] who studied the effect of loading mode. These differences do not necessarily invalidate the hydrogen argument, but there are other problems with it. One is that stable austenitic steels exhibit SCC but show only superficial, cleavage-like cracking in gaseous hydrogen or under cathodic polarization, even at room temperature.[111] Another problem is that the trends of SCC with alloy composition and temperature are inconsistent with a hydrogen model; e.g., cleavage-like SCC occurs vigorously at very high temperatures such as 350°C, and nitrogen or phosphorus alloying enhances SCC while decreasing HE in line with the increase in austenite stability (Figure 29).[112] Most of the observations of hydrogen-induced phase transformations in otherwise stable austenitic steels have been made at room temperature, e.g., by Tahtinen, et al.,[113,114] who point out that martensite phases are found on some SCC fracture surfaces, but they have not demonstrated that these can form at temperatures relevant to chloride SCC even in type 304 SS, let alone in "stable" steels such as type 310 SS. In fact, Eliezer, et al.,[111] reported that type 304 SS did not undergo gaseous HE above its M_D temperature of about 110°C, while Liu, et al.,[93] showed that martensite phases were not detectable at the fracture surface of type 304, which had failed by transgranular SCC at 289°C; this bodes ill for a hydrogen model in unstable, not to mention stable, steels. Mehta and Burke[115] reported some hydrogen effects at 150°C in types 304L (UNS S30403) and 310 steels, but they did not obtain cleavage-like fractography. Finally, Wilde and Kim showed that more hydrogen was absorbed by SS under cathodic polarization, where no cracking occurred, than under SCC conditions[116] (but since neutral solutions were used, this does not necessarily address crack-tip hydrogen entry).

We expect HE to be abandoned as a model for chloride SCC within the next few years.

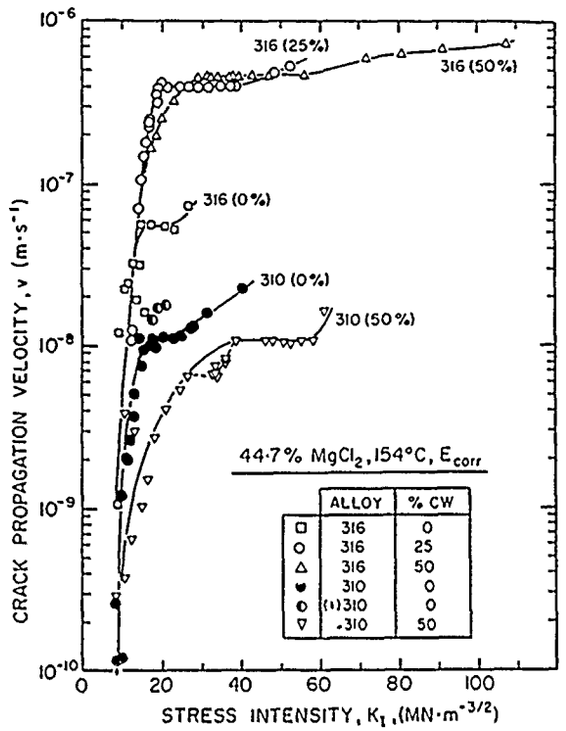


FIGURE 27—The effect of cold work on v-K curves for types 316 and 310 (UNS S31600 and S31000) SSs in 44.7% $MgCl_2$ solution at 154°C. This is an extension of Figure 14. (Reprinted with permission from Pergamon Press.[101])

Caustic SCC of Stainless Steels

Caustic cracking of SSs and nickel-base alloys has been an important practical problem in the nuclear power industry and is also of considerable scientific interest. In particular, Crowe and Tromans have argued that fractographic comparisons between caustic and chloride-induced SCC can give information on the probable role of hydrogen in the latter.[117,118] Since the caustic cracking can occur at somewhat oxidizing potentials and does not involve crack acidification, one can be fairly confident that water reduction does not occur within the cracks, however, the fractography of transgranular SCC in chloride and caustic is very similar. Crowe and Tromans argued that this supported a dissolution mechanism of crack advance with preferential (transpassive) dissolution of chromium. Obviously, one could also propose a film-induced cleavage concept, though this would be difficult to test in this system.

The transpassive potentials used by Crowe and Tromans are not often encountered in practice, practical instances of caustic SCC occur in the active or just-passive condition.[3,119-123] Depending on

the alloy composition, temperature, and potential, both intergranular and transgranular cracking can be obtained, but for our purposes it is sufficient to note that cleavage-like transgranular SCC occurs both in the active/active-passive and transpassive conditions. In the active state, a film-induced cleavage model based on dealloying is very attractive, and massive dealloying has been reported by Santarini and Boos[124] in type 304 SS at 150°C. The response of the cracking to nickel content has been stated to be different from that of chloride SCC,[3] but this may reflect the very high temperatures used for work related to nuclear power systems, so that IGSCC becomes a problem at the Ni-rich end. *Transgranular* caustic SCC seems to have a nickel dependence very similar to that of chloride SCC; i.e., it occurs up to around 40% Ni.[119,125] This supports a dealloying model, with or without cleavage, for the transgranular form of SCC, but after our earlier experience with SCC of brass,[83] we are reluctant to propose different mechanisms for inter- and transgranular cracking. Both are possibly a result of dealloying.

With regard to dealloying, it is interesting to note that Isaacs, et al.,[126] (Table 1) and Lumsden and Stocker[127] (Figure 30) report metallic nickel layers on alloy 600 (UNS N06600) (75% Ni) after exposure to caustic solutions at > 300°C. At these high temperatures, dealloying seems to be a much easier process than at the normal temperatures used for chloride SCC studies (but transgranular SCC is rarely, if ever, seen in Ni-rich alloys, so possibly the layer is formed in a different way, or else its porosity may coarsen too readily to enable it to nucleate transgranular cleavage).

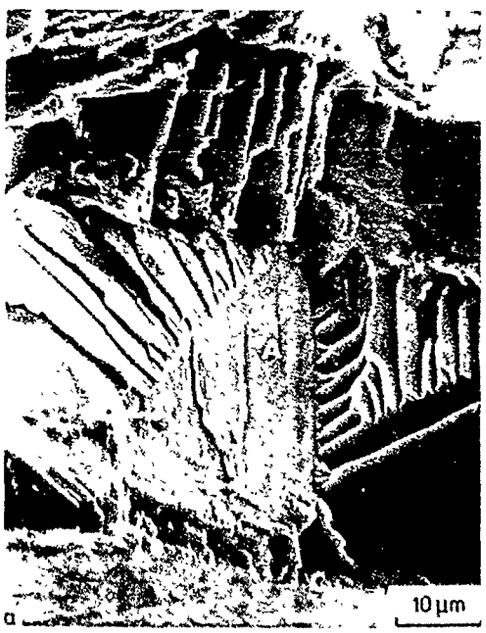


FIGURE 28—Typical cleavage-like fractography of cathodic hydrogen embrittlement in unstable austenitic stainless steels at room temperature. (Reprinted with permission.[105])

Sensitized Alloys

One of the more ambitious projects in modern corrosion science has been the attempt, initiated by Ford, to produce a predictive model for environmental cracking of nuclear alloys based on slip dissolution (Figure 31).[1,128,129] This approach has had fair success in accounting for the IGSCC of sensitized type 304 SS in pure water or dilute sulfate solutions, and few authors have questioned the applicability of the slip-dissolution concept for this type of system, despite the strong sensitivity of sensitized steels to hydrogen cracking at room temperature.[130] The main area of discussion is now the environment and potential inside a crack, and how this depends on the bulk environment, a situation familiar from other, more easily studied, forms of SCC Our discussion will focus on recent work, research up to 1979 to 1981 is reviewed by Szklarska-Smialowska and Cragnolino[131] and Cragnolino and MacDonald.[132]

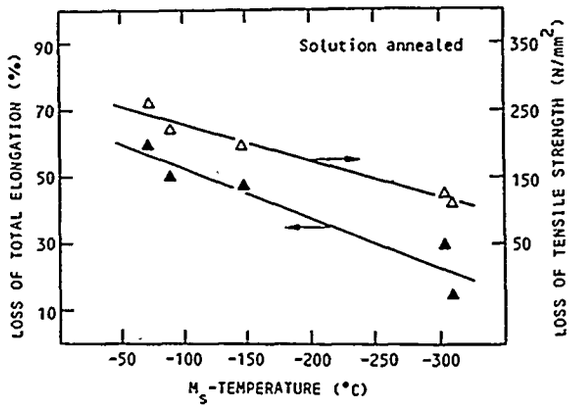


FIGURE 29—The effect of austenite stability, expressed as the M_s temperature, on cathodic hydrogen embrittlement of type 304 (UNS S30400) steels with various nitrogen additions up to 0.21%. Shows a trend opposite to that of SCC in hot chloride solution. (Reprinted with permission.[112])

TABLE 1
Surface Analyses by Rutherford Backscattering[(A)]

	AE	−90 mV	0 mV	70 mV[(B)]	170 mV[(B)]	225 mV[(B)]
Cr	14	0	0	15	15	14.5
Fe	10	4	0	17	14	6.5
Ni	76	96	87	68	73	77.4

[(A)]In mol%, for alloy 600 (UNS N06600) (Ni-15Cr-9Fe) specimens exposed to 1% NaOH + 1% Na_2CO_3 solution at 315°C with H_2/N_2 overpressure for 10 days. Potentials are relative to a nickel reference electrode. The results show almost complete dealloying of Cr and Fe at potentials of 0 and −90 mV. Thicknesses of the dealloyed layers were given as 100 nm (−90 mV) and 50 nm (0 mV).[126]

[(B)]Observable surface oxide present.

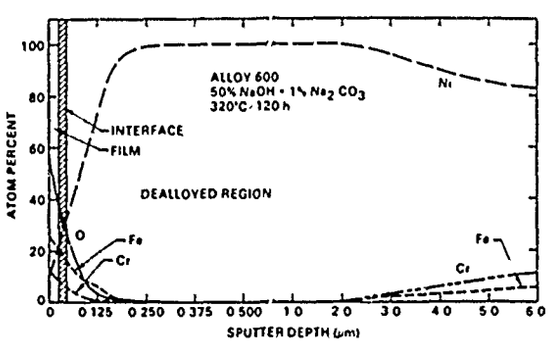


FIGURE 30—Auger depth profile analysis of the dealloyed surface of alloy 600 (UNS N06600) (Ni-15Cr-9Fe) after exposure to 50% NaOH + 1% Na_2CO_3 with H_2/Ar overpressure at 320°C for 120 H.[127] Shows several microns of dealloying.

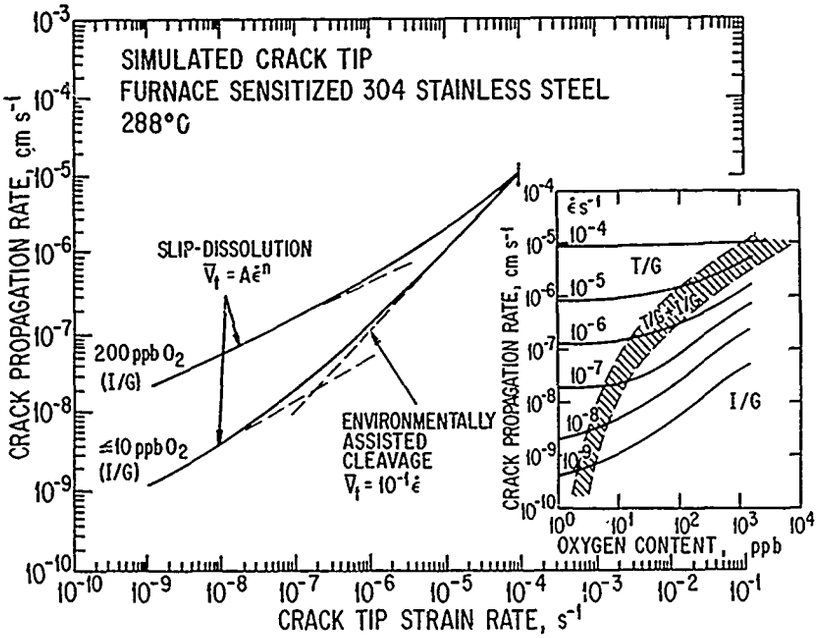


FIGURE 31—Illustration of the complex predictions made by Ford and Andresen[1] from transient straining tests on bulk alloys or simulated grain-boundary alloys in (partly) simulated crack environments for sensitized type 304 (UNS S30400) SS in oxygenated high-temperature water.

Recently, crack chemistry has become a concern in high-temperature SCC, especially the ability of cracks to acidify when oxygen and sulfate or chloride ions are present.[133] The role of crevices in crack initiation has also been studied.[99,134] In pure water, soluble sulfur species may be produced by the dissolution of manganese sulfide inclusions, early work assumed that the product would be sulfate, but with the recognition of large IR potential drops down cracks,[135] it seems more probable that sulfide is the product. Some authors have argued that sulfate in the bulk solution can be reduced to sulfide within a crack and hence catalyze anodic reactions;[136] no definite evidence exists for this interpretation, but it is consistent with the observation that sulfate is more aggressive, mole for mole, than chloride. Even at quite high sulfate concentrations, it is improbable that the crack-tip potential can be as well controlled from the external surface as assumed by Ford in his early work. This leads to a situation in which the potential primarily affects the crack chemistry rather than the kinetics of reactions at the crack tip.[40] Some of the most experimentally difficult work ever conducted on stress corrosion crack growth has been done in this system by Andresen,[137] who followed transients in crack growth rate resulting from changes in external environment, load, or potential. His latest thinking seems similar to that of Edwards,[40] with emphasis on crack chemistry and diffusional or ohmic control of dissolution reactions. Similarly, Weeks, et al.,[138] have tried to relate the temperature dependence of SCC to solubility data for magnetite.

Critical potentials for SCC in dilute chloride or sulfate solutions at high temperatures drop abruptly when type 304 SS is sensitized and become less sensitive to the nature of the anion.[72-75] (Compare Figure 32 to Figures 16 and 17.) This demonstrates that the intergranular cracking of sensitized alloys is a different process from normal chloride SCC in annealed alloys and is consistent with the view that the latter is a brittle process specific to chloride.

Research on SCC in flowing high-temperature water is exceptionally difficult, and mechanistic insights have flowed more easily from studies of sensitized alloys at ambient temperatures. "Polythionic acid" SCC of sensitized SSs was known in the 1950s[139] and correlated with sensitization tests in the 1960s.[140] Electrochemical studies by Matsushima established that cracking occurred over a range of potentials and was most likely associated with a localized dissolution process at the grain boundaries.[141] Zucchi, et al.,[142] showed that concentrations of tetrathionate as low as 3×10^{-5} molar would cause SCC. Around 1979, it was recognized that some nuclear power plants were experiencing low-temperature SCC of sensitized components, and this was ascribed by Isaacs, et al.,[143] to thiosulfate from emergency building spray systems. In the laboratory, concentrations as low as 6×10^{-7} molar were shown to cause SCC. Cragnolino and MacDonald reviewed the available information on low-temperature SCC and emphasized the catalysis of anodic dissolution by elemental (adsorbed) sulfur from decomposition of thiosulfate.[132]

Electrochemical kinetic studies by Newman, et al.,[144] and Newman and Sieradzki[145] showed that thiosulfate SCC could be closely related to the transient electrochemistry of simulated grain-boundary material in a simulated (acidified) crack environment (Figure 33). Simulation of the crack solution was assisted by the buffering action of the thiosulfate decomposition (disproportionation) products, which holds the pH near 3. The actual crack velocities in a furnace sensitized, 0.07% carbon type 304 steel were up to 50 times higher than predicted using reasonable CDs from the scratching electrode experiments [Figure 33(b)]. This finding was believed to result from intermittent brittle grain boundary fracture, confirmed by the much lower crack velocities seen in less extremely sensitized material. No evidence for HE was observed.

Sensitized nickel-base alloys are, if anything, more sensitive to thiosulfate than SSs. Following a major failure of steam-generator tubing, work on sensitized type 600 showed that cracking occurred at concentrations of thiosulfate as low as 10^{-6} molar (Figure 34).[146,147] Crack velocities in concentrated thiosulfate solutions were again very high (up to 0.4 μm/s), and, again, it is thought that there may be a contribution of mechanical failure.

The polythionic acid cracking phenomenon was clarified in an important contribution by Ahmad, et al.,[148] who showed that of all the polythionic acids, only tetrathionic acid ($H_2S_4O_6$) was a potent SCC environment. This is presumably because it is kinetically more readily reduced to adsorbed sulfur on the metal surface, a suggestion that could be tested by examining dissolution of model alloys in acid solutions with inoculation of various polythionates. The later work of Ahmad, et al.,[149] was curious in that thiosulfate SCC was not referred

to, as though it were a totally different phenomenon from "polythionic acid" SCC. The only difference we have been able to detect is that tetrathionate is much more stable in acid solutions than thiosulfate; otherwise, their action is transparently similar.

Thiosulfate solutions have been used in recent work related to a percolation model of IGSCC in sensitized alloys.[150] Essentially, this model states that a continuous path of susceptible grain boundaries must be present for a crack to propagate macroscopic distances, and the percentage of sensitized grain-boundary facets required to achieve this can be derived from a percolation model. A percolation threshold (p_c) of about 24% was derived for a model lattice of boundaries, and approximate correspondence to this was achieved in slow-strain-rate tests of material heat treated for various lengths of time. Below p_c, small cracks initiated but ran out of susceptible grain boundaries. Such a percolation concept is likely to form part of a new test methodology for SCC resistance in sensitized material. A percolation model may explain the extremely abrupt onset of SCC with increasing sensitization time seen by Poznansky and Duquette (Figure 17),[75] whose micrographs suggested the alternative (improbable) explanation of a sudden carbide precipitation on most of the grain boundaries.

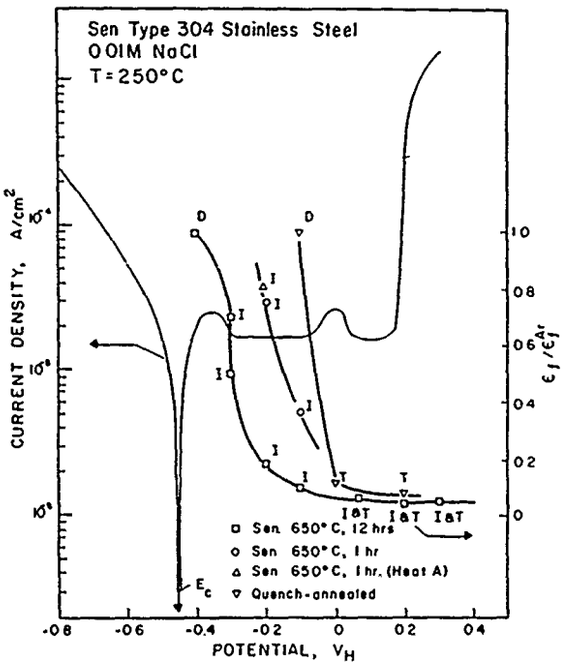
Nickel-Base Alloys

We have already briefly mentioned the IGSCC of nickel-base alloys in hot caustic solutions. Most practical instances of SCC have occurred in type 600 (Ni-16Cr-10Fe) in the primary water of pressurized water reactors (PWRs) (a deoxygenated, dilute boric acid/lithium borate buffer) or in boiling water reactors where the environment is oxygenated pure water. The cracking in PWR steam generator tubes is almost certainly the same phenomenon as the low-potential (active state) cracking seen in caustic solutions. Reviews by van Rooyen[151] and Bandy and van Rooyen[152] show that the cracking severity in PWR primary water increases with increasing temperature (up to 365°C) and with hydrogen additions to the water. Carbide precipitation on the grain boundaries, with or without chromium depletion, seems to prevent the cracking for practical purposes, and "thermally treated" (carbide-precipitated) material is now to be used in some new PWR steam generators.

Until recently, it was widely assumed that some form of anodic SCC mechanism was operating in the type 600 failures, but the effect of potential (as influenced by hydrogen overpressure) has forced a re-evaluation of the problem. Totsuka, et al.,[153-155] have shown that tensile specimens with a cold-pressed hump (and not conventional slow-strain-rate specimens) crack below a critical potential in simulated PWR primary water (Figure 35). The evident continuity of the behavior between anodic and cathodic potentials seems to show conclusively that the cracking results from hydrogen, and extraction of hydrogen from the cold-pressed regions showed that significant concentrations could be absorbed in cold-worked, strained material. Obviously, there was a significant IR potential drop in the tests performed at very negative potentials, so it is conceivable that some residual anodic reaction was occurring, but this is probably insignificant. The observations of Lumsden and Stocker[127] on dealloying (nickel enrichment) in reducing caustic solutions no longer seems to have much bearing on the cracking mechanism in the PWR primary water, though they are of importance in the intergranular corrosion and SCC that sometimes occurs in the tube-tubesheet crevices of PWR steam generators.

The embrittlement of type 600 persists in hydrogenated steam (Figure 36).[156] Thermal treatment to give grain-boundary carbides continues to be effective in this environment, and there is no reason to believe that the mechanism of cracking is different from that in water (see Figure 35).

Normally, intergranular HE is strongly influenced by grain-boundary segregation, but there does not seem to be a solution to the type 600 problem based on impurity control or heat treatment (other than heat treatment to produce carbides). The embrittlement seems to be intrinsic to grain boundaries in this material.



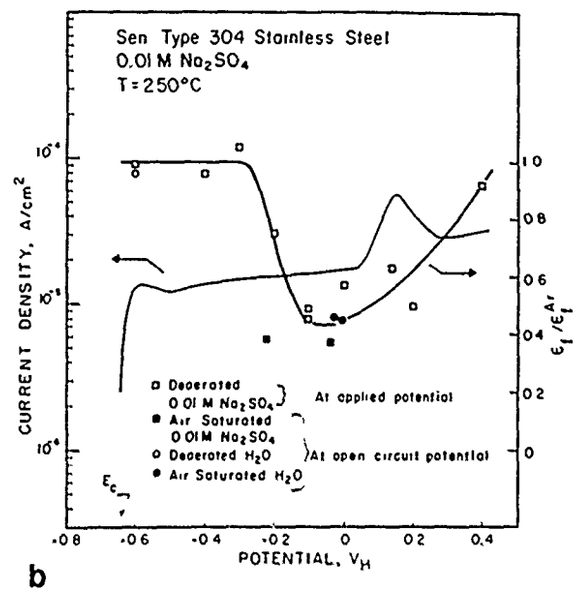


FIGURE 32—Results of slow-strain-rate tests (10^{-6}/s) on type 304 (UNS S30400) SS at 250°C: (a) potentiostatic tests in 0.01 M NaCl solution showing the fall in critical potential with sensitization [I = intergranular; T = transgranular; D = ductile]; and (b) potentiostatic or free-corrosion tests in 0.01 M Na_2SO_4 solution and pure water, showing the behavior of the sensitized steel (annealed steel does not crack in these environments unless cold worked). Potentiodynamic anodic polarization curves are also shown.[73] (See also Figures 16 and 17.)

Type 600 and related alloys, such as alloy 690 (Ni-28Cr-9Fe), are susceptible to IGSCC at relatively oxidizing potentials such as those obtained in oxygenated pure water or dilute sulfate solutions.[157] The alloy 690 is distinctly superior and requires sulfate to show any evidence of SCC. It is conceivable that this cracking occurs by a different mechanism from the low-potential cracking seen in water with hydrogen overpressure; e.g., sensitization of type 600 now accelerates cracking.

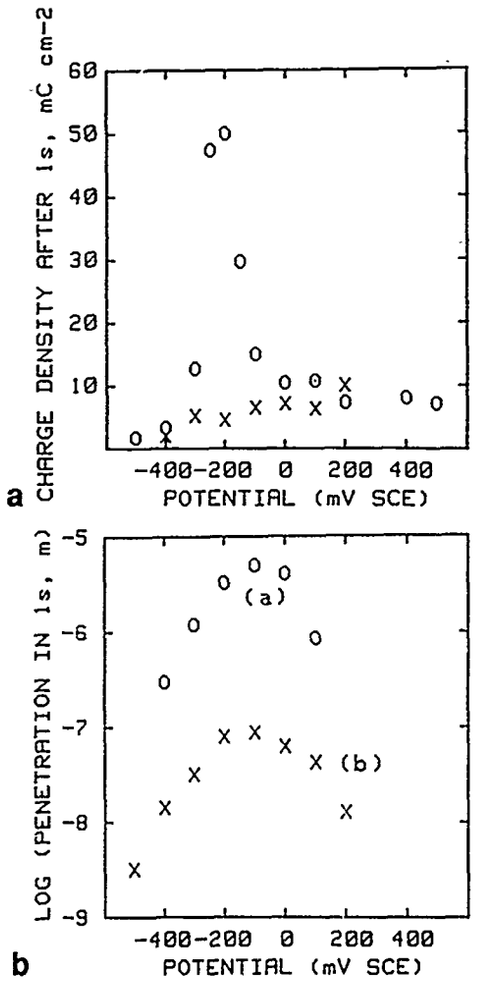


FIGURE 33—Results of scratching electrode experiments and comparison with SCC velocities for furnace-sensitized type 304 (UNS S30400) SS (0.07% C) in 0.5 M $Na_2S_2O_3$ solution at room temperature: (a) scratch tests on Fe-9Cr-10Ni (O) and Fe-19Cr-9Ni (X) alloys in neutral solution, showing the range of potential where transient activation of simulated grain-boundary material occurs; and (b) predicted SCC velocities from similar tests in pH 3 solution (X) compared to actual SCC velocities (O) showing evidence for brittle fracture as well as slip dissolution. (Reprinted with permission.[144])

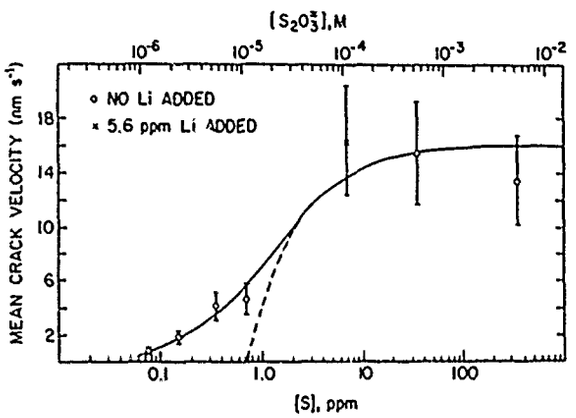


FIGURE 34—SCC velocities for slow-strain-rate tests (3×10^{-6}/s) of furnace-sensitized alloy 600 (UNS N06600) (0.04% C) in naturally aerated boric acid solution with sodium thiosulfate and lithium hydroxide additions at 40°C.[146,147]

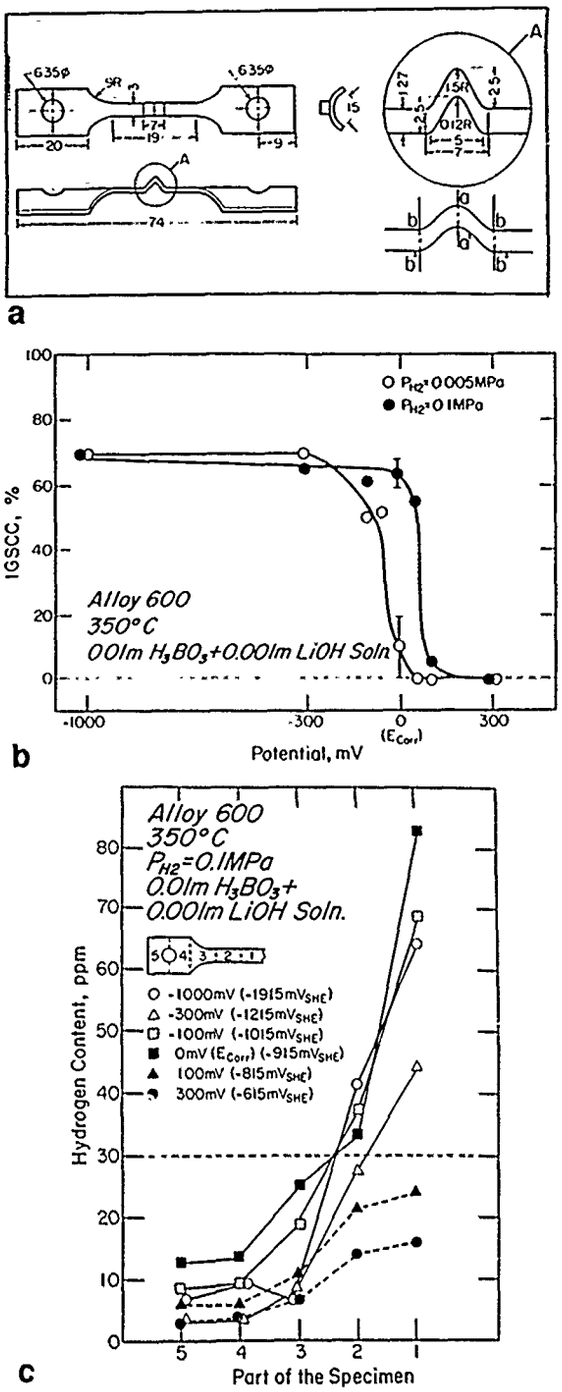


FIGURE 35—Hydrogen-induced SCC of mill-annealed, cold-worked alloy 600 (UNS N06600) in boric acid/lithium borate buffer solution at 350°C with hydrogen overpressure: (a) specimen design with cold-pressed hump; (b) evaluation of slow-strain-rate tests at two H_2 pressures for various potentials; and (c) extraction of hydrogen from the specimens.[155]

Intergranular SCC and traces of transgranular SCC can be obtained in precipitation-hardened (γ') nickel alloys such as Inconel† X-750 (UNS N07750).[158] Generally, the cracking is related to sensitization or other grain-boundary precipitation processes and is enhanced by oxygen in the water; thus, it probably belongs with the cracking of sensitized SSs in the category of SDMs. In contrast, iron-rich alloys containing γ' crack in boiling $MgCl_2$ solution, provided that the matrix Ni level is low enough.[159]

The SCC of alloys used in nuclear power plants has been comprehensively reviewed by Scott.[160]

†Trade name.

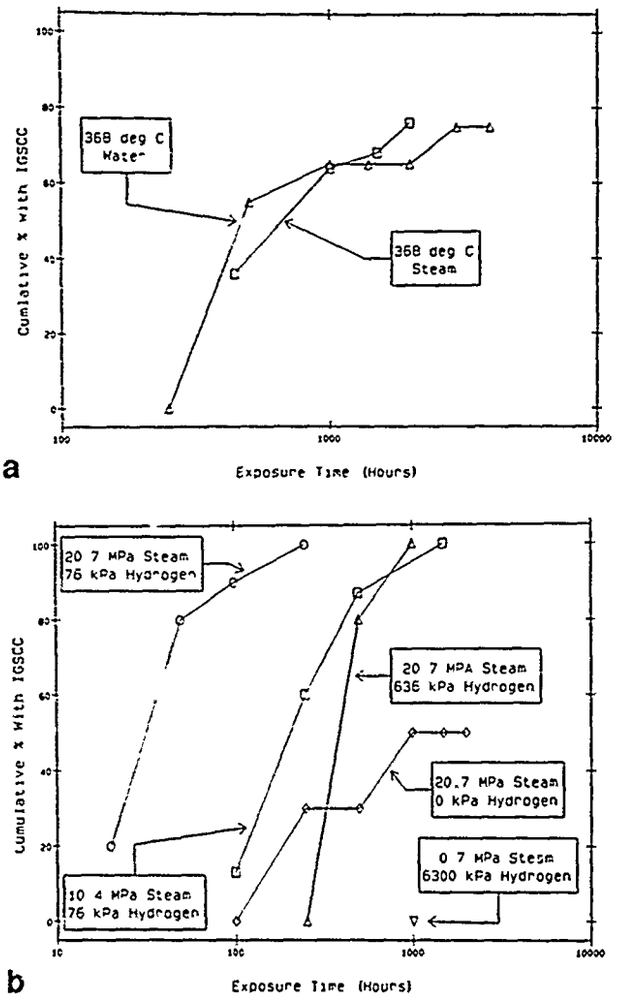


FIGURE 36—SCC of mill-annealed alloy 600 (UNS N06600) in water and steam:[156] (a) results of reverse U-bend tests on tube segments in water and steam at 368°C with 2.8 kPa hydrogen and (b) tests in steam at 400°C with various pressures of steam and hydrogen.

Acknowledgment

The contribution of A. Mehta to this review was made possible by a grant from British Gas. The authors are grateful to Dr. A.J. Jickells for his interest and support.

References

1. F.P. Ford, P.L. Andresen, CORROSION/87, paper no. 83, (Houston, TX: National Association of Corrosion Engineers, 1987).
2. R.M. Latanision, R.W. Staehle, Fundamental Aspects of Stress Corrosion Cracking, ed. R.W. Staehle, A.J. Forty, D. van Rooyen (Houston, TX: NACE, 1969), p. 214.
3. G.J. Theus, R.W. Staehle, Stress Corrosion Cracking and Hydrogen Embrittlement of Iron-Base Alloys, ed. R.W. Staehle, J. Hochmann, R.D. McCright, J.E. Slater (Houston, TX: NACE, 1977), p. 845.
4. R.W. Staehle, Stress Corrosion Cracking and Hydrogen Embrittlement of Iron-Base Alloys, p. 180.
5. H. Hanninen, Int. Met. Rev. 24(1979): p. 85..
6. K. Sieradzki, R.C. Newman, Phil. Mag. A 51(1985): p. 95.
7. K. Sieradzki, R.C. Newman, J. Phys. Chem. Sol. 48(1987): p. 1101.
8 R.C. Newman, K. Sieradzki, Chemistry and Physics of Fracture, ed. R.M. Latanision, R.H. Jones (Dordrecht, The Netherlands: Martinus Nijhoff, 1987), p. 597.
9. K. Sieradzki, J.S. Kim, A.T. Cole, R.C. Newman, J. Electrochem. Soc. 134(1987): p. 1637.
10. J.G. Hines, T.P. Hoar, J. Appl. Chem. 8(1958): p. 764.
11. T. Nakayama, M. Takano, Corrosion 42, 1(1986): p. 10.
12. L. Graf, Fundamental Aspects of Stress Corrosion Cracking, p. 187.
13. A. Turnbull, Corros. Sci. 23(1983): p. 833.
14. S. Barnartt, D. van Rooyen, J. Electrochem. Soc. 108(1961): p. 222.
15. H.R. Baker, M.C. Bloom, R.N. Bolster, C.R. Singleterry, Corrosion 26, 10(1970): p. 420.
16. T.P Hoar, J.G. Hines, J.I.S.I. 182(1956): p. 124.
17. K. Hashimoto, Corrosion 32, 10(1976): p. 398.
18. M. Marek, R.F. Hochman, Corrosion 26, 1(1970): p. 5.
19. F.P. Vaccaro, R.F. Hehemann, A.R. Troiano, Corrosion 36, 10(1980): p. 530.
20. G.M. Scamans, P.R. Swann, Stress Corrosion Cracking and Hydrogen Embrittlement of Iron-Base Alloys, p. 166.
21. G.M. Scamans, P.R. Swann, Corros. Sci. 18(1978): p. 983.
22. J.M. Silcock, Corrosion 38, 2(1982): p. 122.
23. A. Honkasalo, Corrosion 29, 6(1973): p. 237.
24. R.L. Jones, Corrosion 31, 12(1975): p. 424.
25. T.P. Hoar, Stress Corrosion Cracking and Hydrogen Embrittlement of Iron-Base Alloys, p. 1016.
26. B.E. Wilde, J. Electrochem. Soc. 118(1971): p. 1717.
27. C. Manfredi, I.A. Maier, J.R. Galvele, Corros. Sci. 27(1987): p. 887.
28. J.R. Galvele, S.B. de Wexler, J. Gardiazabal, Corrosion 31, 10(1975): p. 352.
29. I.A. Maier, J.R. Galvele, Corrosion 36, 2(1980): p. 60.
30. I.A. Maier, C. Manfredi, J.R. Galvele, Corros. Sci. 25(1985): p. 15.
31. G. Bianchi, F. Mazza, S. Torchio, Corros. Sci. 13(1973): p. 165.
32. Z. Szklarska-Smialowska, N. Lukomski, Corrosion 34, 5(1978): p. 177.
33. R.C. Newman, A. Mehta, Corros. Sci. 28(1988).
34. J.R. Galvele, J. Electrochem. Soc. 133(1986): p. 953.
35. J.R. Galvele, Corros. Sci. 27(1987): p. 1.
36. A.T. Cole, R.C. Newman, K. Sieradzki, Corros. Sci. 28(1988): p. 109.
37 A Rota, H. Boehni, Electrochemical Methods in Corrosion Research III, ed. B. Elsener (Zurich, Switzerland. Trans. Tech. Pubs., in press 1989).
38. S. Tsujikawa, T. Shinohara, Y. Hisamatsu, Corrosion Cracking, ed. V.S. Goel (Philadelphia, PA: ASTM, 1985), p. 35.
39. K. Tamaki, S. Tsujikawa, Y. Hisamatsu, Advances in Localized Corrosion, ed. H.S. Isaacs (Houston, TX. NACE, in press).
40 R.A.H. Edwards, Advances in Localized Corrosion, in press.
41. H.H. Uhlig, Stress Corrosion Cracking and Hydrogen Embrittlement of Iron-Base Alloys, p. 174.
42. S. Torchio, Corros. Sci. 20(1980): p. 555.
43. G. Salvago, G. Fumagalli, D. Sinagaglia, Corros. Sci. 23 (1983): p. 507.
44. R.L. Shamakian, A.R. Troiano, R.F. Hehemann, Corrosion 36, 6(1980): p. 279.
45. F. Mancia, A. Tamba, Corrosion 44, 2(1988): p. 88.
46. Z. Szklarska-Smialowska, J. Gust, Corros. Sci. 19(1979): p. 753.
47. T.P. Hoar, J.M. West, Proc. Roy. Soc. (Lond.) A268(1958): p. 304.
48. T.P. Hoar, J.C. Scully, J. Electrochem. Soc. 111(1964): p. 348.
49. S. Bubar, D.A. Vermilyea, J. Electrochem. Soc. 113(1966): p. 892.
50. I.A. Maier, E. Lopez Perez, J.R. Galvele, Corros. Sci. 22(1982): p. 537.
51. R.C. Newman, Corrosion Chemistry Within Pits, Crevices and Cracks, ed. A. Turnbull (London, England: Her Majesty's Stationery Office, 1987), p. 317.
52. J. Rimbert, J. Pagetti, Corros. Sci. 20(1980): p. 189.
53. D. Tromans, R.P..Swiniarski, Can. Met. Q. 23(1984): p. 471.
54. R.L. Jones, Corrosion 31, 12(1975): p. 431.

55. D. Itzhak, D. Eliezer, Corros. Sci. 23(1983): p. 1285.
56. F. Zucchi, A. Frignani, M. Zucchini, G. Trabanelli, Annali di Chimica 68(1978): p. 15.
57 A. Frignani, G. Trabanelli, F. Zucchi, Corros. Sci. 24(1984): p. 917.
58. M. da Cunha Belo, J. Bergner, B. Rondot, Corros. Sci. 21(1981): p. 273.
59. J. Gluszek, K. Nitsch, Corros. Sci. 22(1982): p. 1067.
60. M. Miyasaka, N. Ogure, Corrosion 43, 10(1987): p. 582.
61. S.C. Chang, T.S. Sheu, C.M. Wan, Strength of Metals and Alloys, ed. H.J. McQueen (New York, NY: Pergamon Press, 1985), p. 1081.
62. S.C. Chang, J.J. Chan, Corrosion 44, 4(1988): p. 209.
63. M.O. Speidel, Corrosion 33, 6(1977): p. 199.
64. M.O. Speidel, Metall. Trans. A 12A(1981): p. 779.
65. A.J. Russell, D. Tromans, Metall. Trans. A 10A(1979): p. 1229.
66. A.J. Russell, D. Tromans, Metall. Trans. A 12A(1981): p. 613.
67. B. Eremias, V.V. Maricev, Corros. Sci. 20(1980): p. 307.
68. P.L. Andresen, D.J. Duquette, Corrosion 36, 2(1980): p. 85.
69. P.L. Andresen, D.J. Duquette, Corrosion 36, 8(1980): p. 409.
70. P.L. Andresen, D.J. Duquette, Corros. Sci. 20(1980): p. 211.
71 W M.M Huijbregts, Corrosion 42, 8(1986): p. 456.
72. G. Cragnolino, L.F. Lin, Z. Szklarska-Smialowska, Corrosion 37, 6(1981): p. 312.
73. L. Lin, G. Cragnolino, Z. Szklarska-Smialowska, D.D. MacDonald, Corrosion 37, 11(1981): p. 616.
74 D J Duquette, A. Poznansky, Corrosion 39, 11(1983). p. 425.
75 A Poznansky, D.J. Duquette, Corrosion 40, 7(1984). p. 375.
76 J Congleton, H C Shih, T. Shoji, R.N. Parkins, Corros. Sci. 25, (1985): p. 769.
77 D.A. Vermilyea, Corrosion 29, 11(1973): p. 442.
78 D.A Vermilyea, J. Electrochem. Soc. 121(1974). p. 1190.
79. T.A. Mozhi, W.A.T. Clark, B.E. Wilde, Corros. Sci. 27(1987): p. 257.
80. L. Bednar, Corrosion 33, 9(1977): p. 321.
81 J.M. Silcock, Br. Corros. J. 17(1982): p. 301.
82. V. Cihal, Corros. Sci. 25(1985): p. 815.
83. R.C. Newman, T. Shahrabi, K. Sieradzki, Scripta Metall. 23(1989): p. 71.
84 R C Newman, T Shahrabi, K Sieradzki, Corros. Sci. 28(1988). p. 873.
85 M Kermani, J.C Scully, Corros. Sci. 19(1979). p. 489.
86 P Muraleedharan, H.S Khatak, J.B. Gnanamoorthy, P. Rodriguez, Metall. Trans. A 16A(1985): p. 285.
87 D V Beggs, M.T. Hahn, E.N. Pugh, A.R. Troiano Hon. Symposium on Hydrogen Embrittlement and SCC, ed. R. Gibala, R. Hehemann (Metals Park, OH: ASM International, 1984), p. 181.
88 N Totsuka, Z Szklarska-Smialowska, Corrosion 44, 2(1988). p. 124.
89 M.T Hahn, E.N. Pugh, Corrosion 36, 7(1980). p. 380.
90. M.T. Hahn, E.N. Pugh, Fractography and Materials Science, ed. L.N. Gilbertson, R.D. Zipp, ASTM STP 733 (Philadelphia, PA: ASTM, 1981), p. 413.
91. E.N. Pugh, Atomistics of Fracture, ed. R.M. Latanision, J.R. Pickens (Brussels, Belgium. NATO, 1983), p. 997.
92. E.N. Pugh, Corrosion 41, 9(1985): p. 517.
93. R. Liu, N. Narita, C. Altstetter, H. Birnbaum, E.N. Pugh, Metall. Trans. A 11A(1980): p. 1563.
94. M. Ahlers, E. Riecke, Corros. Sci. 18(1978): p. 21.
95. E.I. Meletis, R. Hochman, Corros. Sci. 24(1984): p. 843.
96. J.I. Dickson, D. Groulx, L. Shiquiong, D. Tromans, Mater. Sci. Eng. 94(1987): p. 155.
97. C.W. Fong, D. Tromans, Metall. Trans. (in press).
98. R.C. Newman, R.R. Corderman, K. Sieradzki, Br. Corros. J. 24(1989): p. 143.
99. J. Kuniya, I. Masaoka, R. Sasaki, Corrosion 44, 1(1988): p. 21.
100. P. Vaccaro, R. Hehemann, A.R. Troiano, Corrosion 38, 10(1982): p. 549.
101. J.I. Dickson, A.J. Russell, D. Tromans, Can. Met. Q. 19(1980): p. 161.
102. A.A. Seys, M.J. Brabers, A.A. van Haute, Corrosion 30, 2(1974): p. 47.
103. R.J. Asaro, A J. West, W.A. Tiller, Stress Corrosion Cracking and Hydrogen Embrittlement of Iron-Base Alloys, p. 1115.
104. H. Hanninen, Mechanisms of Environment Sensitive Cracking of Materials, ed. P.R. Swann, F.P. Ford, A.R.C. Westwood (London, England: The Metals Society, 1977), p. 168.
105. H. Hanninen, T. Hakkarainen, Metall. Trans. A 10A(1979): p. 1196.
106. H. Hanninen, T. Hakkarainen, Corrosion 36, 1(1980): p. 47.
107. H. Hanninen, T. Hakkarainen, Advances in Fracture Research, ed. D. Francois (Oxford, England: Pergamon Press, 1980), p. 1881.
108. T. Nakayama, M. Takano, Corrosion 38, 1(1982): p. 1.
109. W.-Y Chu, H -L. Wang, C.-M. Hsiao, Corrosion 40, 9(1984). p. 487.
110. L.-J. Qiao, Corrosion 43(1987): p. 779.
111 D Eliezer, D G Chakrapani, C.J., Altstetter, E.N. Pugh, Metall. Trans. A. 10A(1979): p. 935.
112. S.P. Hannula, H. Hanninen, S. Tahtinen, Metall. Trans. A 15A(1984): p. 2205.
113. S. Tahtinen, P. Nenonen, H. Hanninen, Scripta Metall. 20(1986): p. 153.
114. S. Tahtinen, P. Nenonen, H. Hanninen, Chemistry and Physics of Fracture, p. 568.
115. M.L. Mehta, J. Burke, Corrosion 31, 3(1975): p. 108.
116. B.E. Wilde, C.D. Kim, Corrosion 28, 9(1972). p. 350.
117. D.C. Crowe, D. Tromans, Can. Met. Q. 23(1984). p. 99.
118. D.C. Crowe, D. Tromans, Metallography and Corrosion (Houston, TX: NACE, 1986), p. 175.
119. I.L.W. Wilson, R.G. Aspden, Stress Corrosion Cracking and Hydrogen Embrittlement of Iron-Base Alloys, p. 1189.
120. J.R. Cels, Corrosion 34, 6(1978): p. 198.
121. Y.S. Park, J.R. Galvele, A.K. Agrawal, R.W. Staehle, Corrosion 34, 12(1978): p. 413.
122. Y.S. Park, A.K. Agrawal, R.W. Staehle, Corrosion 35, 8(1979): p. 333.
123. N. Pessall, Corros. Sci. 20(1980): p. 225.
124. G. Santarini, J.Y. Boos, Corros. Sci. 19(1979): p. 261.
125. A.J. Sedriks, S. Floreen, A.R. McIlree, Corrosion 32, 4(1976). p. 157.
126. H.S. Isaacs, H.W. Kraner, A.L. Hanson, Environmental Degradation of Materials in Nuclear Power Systems—Water Reactors (Houston, TX: NACE, 1984), p. 675.
127. J.B. Lumsden, P.J. Stocker, CORROSION/88, paper no. 252 (Houston, TX: NACE, 1988).
128. F.P. Ford, M. Silverman, Corrosion 36, 10(1980). p. 558.
129. F.P. Ford, D. Taylor, P.L. Andresen, R.G. Ballinger, "Environmentally-Controlled Cracking of Stainless and Low-Alloy Steels in Light-Water Reactors," Final Report on EPRI Contract RP 2006-6 (1986).
130. C.L. Briant, Metall. Trans. A 9A(1978). p. 731.
131. Z. Szklarska-Smialowska, G. Cragnolino, Corrosion 36, 12(1980): p. 653.
132 G. Cragnolino, D.D. MacDonald, Corrosion 38, 7(1982). p. 406.
133. K. Tanno, S. Ishizuka, S. Higuchi, N. Ohnaka, Corrosion 42, 9(1986): p. 559.
134. D. Taylor, C.C. Foust, Corrosion 44, 4(1988): p. 204.
135. G. Gabetta, E. Caretta, Corrosion Chemistry Within Pits, Crevices and Cracks, p. 287.
136 L G Ljungberg, D Cubicciotti, M. Trolle, Corrosion 44, 1(1988). p. 66.
137. P.L. Andresen, Corrosion 42, 3(1986): p. 169.
138. J.R. Weeks, B. Vyas, H.S. Isaacs, Corros. Sci. 25(1985): p. 757.
139. A. Dravnieks, C.H. Samans, Proc. American Petroleum Institute 37(1957): p. 100.
140. C.H. Samans, Corrosion 20, 8(1969): p. 256t.
141. I. Matsushima, Boshoku Gijutsu 22(1973): p. 141.
142. F. Zucchi, A. Frignani, M. Zucchini, G. Trabanelli, La Metallurgia Italiana 11(1979): p. 49.

143 H.S Isaacs, B Vyas, M.W. Kendig, Corrosion 38, 3(1982). p. 130.
144 R.C Newman, K. Sieradzki, H.S. Isaacs, Metall. Trans. A 13A(1982): p. 2015.
145 R C Newman, K Sieradzki, Corros. Sci. 23(1983). p. 363.
146 R C Newman, R Roberge, R. Bandy, Corrosion 39, 10(1983). p. 386.
147 R C Newman, R. Roberge, R. Bandy, Environmental Degradation of Materials in Nuclear Power Systems—Water Reactors, p. 636.
148 S Ahmad, M.L Mehta, S.K. Saraf, I.P. Saraswat, Corrosion 38, 6(1982): p. 347.
149 S Ahmad, M.L Mehta, S.K. Saraf, I.P. Saraswat, Corrosion 41, 6(1985): p. 363.
150 J. Stewart, P.M. Scott, D.B. Wells, A.W. Herbert, CORROSION/88, paper no 289 (Houston, TX: NACE, 1988).
151 D. van Rooyen, Corrosion 31, 9(1975): p. 327.
152 R Bandy, D van Rooyen, Corrosion 40, 8(1984). p. 425.
153 N Totsuka, E Lunarska, G. Cragnolino, Z. Szklarska-Smialowska, Scripta Metall. 20(1986). p. 1035.
154 N Totsuka, E Lunarska, G. Cragnolino, Z. Szklarska-Smialowska, Corrosion 43, 8(1987): p. 505.
155 N. Totsuka, Z Szklarska-Smialowska, Corrosion 43, 12(1987): p. 734.
156 G Economy, R J Jacko, W Pement, Corrosion 43, 12(1987): p. 727.
157 A McMinn, R.A. Page, Corrosion 44, 4(1988): p. 239.
158 M Tsubota, K Hattori, T Kaneto, Corrosion 44, 2(1988): p. 73.
159 J.M. Silcock, Br. Corros. J. 18(1983): p. 132.
160. P.M. Scott, Corros. Sci. 25(1985): p. 583.
161 J Laurent, D. Landolt, Electrochemical Methods in Corrosion Research III, ed B Elsener (Zurich, Switzerland: Trans. Tech. Pubs., in press 1989).

APPENDIX A

Auger Electron Spectroscopy of Austenitic Stainless Steels Exposed to Hot, Acidified Chloride Solutions; Comparison with Dealloyed Layers on Au-Ag Alloys

This work[98] was undertaken to test the idea that chloride SCC of austenitic SSs proceeds by the same mechanism as ammonia SCC of α-brass monocrystals,[9] i.e., periodic cleavage events of ~ 1 μm, each nucleated by a dealloyed layer some tens of nm in thickness. In this case, the dealloyed layer is expected to be nickel enriched,[2,10,17] but the surface is also expected to have a spongy, chromium-rich corrosion product,[15,20-22] which may obscure any dealloyed layer that might be present.

The environment used for this work was a 15 M LiCl solution at 90°C acidified to pH 1.0 with HCl to simulate a crack-tip environment.[15,18] Three commercial austenitic steels (types 304, 316, 310) were used in the complete study;[98] here, we report only the result for the type 304 steel surface and compare it with a 90Ag-10Au (atom percent) alloy dealloyed at 30 mA/cm^2 for 5 s in 0.4 M $HClO_4$ solution at room temperature. After some experimentation, the following procedure was used to prepare surface films on SS specimens for Auger electron spectroscopy:

(1) Immerse specimens, alumina-polished to a 1-μm finish, in 15 M LiCl solution at 90°C, acidified to pH 1.0 with HCl.
(2) Polarize for 30 s at −1000 mV vs SCE immersed directly in the solution. The counterelectrode was a graphite rod.
(3) Remove the polarizing potential and tap the specimen to remove hydrogen bubbles and permit dispersion of the alkaline solution near the surface (about 5 s).
(4) Step the potential to −400 mV_{SCE} for 60 s.
(5) Remove the specimen and rinse with warm distilled water for at least 30 s (to remove soluble ions from the porous surface film).
(6) Dry with an air jet and place in the spectrometer.

This procedure gave visually uniform dark or yellowish films after the 60-s immersion time, with little or no patchiness visible after the first 20 to 30 s of immersion. The surfaces were analyzed with a PHI Model 600 Auger electron spectrometer. The analyses used a 0.5-μm electron beam with a target current of 20 nA, with etching by a rastered beam of 2 keV Ar^+ ions. Spectra were recorded in the N(E) mode, but the results are presented as peak-to-peak heights from digitally differentiated spectra. All the experiments were repeated several times on different specimens and gave reproducible results.

Figure A1 shows the depth profile for the Ag-Au alloy. After the first 30 s of sputtering, only Ag and Au were detected. At first, it was thought that the surface might be a mixture of dealloyed and unattacked material, since the gold enrichment was so subtle, but repeated analyses using various sizes of electron beam always produced essentially the same result. The maximum gold concentration is no more than two or three times its bulk level of 10%, and there is evidence for porosity in the reduction of total signal intensity at the surface. This layer is probably about 250 nm thick rather than the 150 nm that would be deduced from the anodic charge density. Laurent and Landolt[161] have also reported that thin dealloyed layers are far from pure noble metals.

Figure A2(a) shows the depth profile for type 304 in the acidified LiCl solution, while Figure A2(b) omits carbon and enhances the nickel profile to display the similarity to Figure A1. Such a result does not conclusively demonstrate the presence of a metallic dealloyed layer; however, one can infer this with some confidence, as the oxygen level was much lower than in films produced by passivation or high-temperature oxidation.[98] With identical sputtering conditions, an air-formed oxide film was removed in less than 30 s, demonstrating the considerable thickness of the layer. X-ray photo-electron analyses are expected to show that the enriched nickel is predominantly metallic.

These data are a promising preliminary confirmation of the dealloying/cleavage model and are supported by electrochemical studies showing that chloride causes dealloying of binary Fe-Ni alloys, which would not occur in a sulfate solution at the same temperature and pH.[33] (See Figures 25 and 26.) It is increasingly plausible to propose that chloride causes SCC because it causes dealloying, and combining this with evidence for discontinuous brittle cracking[89] gives us a typical film-induced cleavage phenomenon.

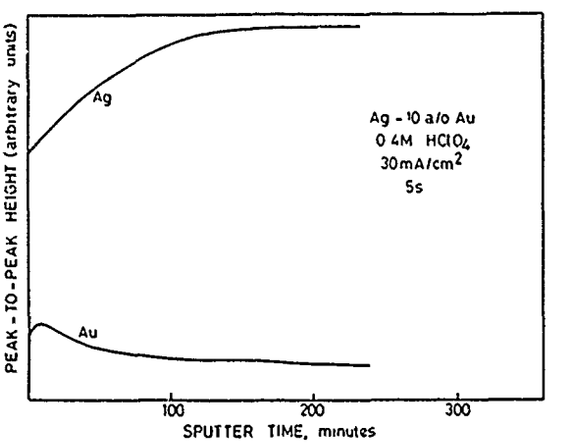


FIGURE A1—Auger depth profile of the dealloyed surface of a silver-10at%gold alloy[98] after passing an anodic charge density of 150 mC/cm^2 in 0.4 M $HClO_4$ solution at room temperature. The peak-to-peak heights displayed are those of Ag (351 eV) [1X] and Au (2024 eV) [10X].

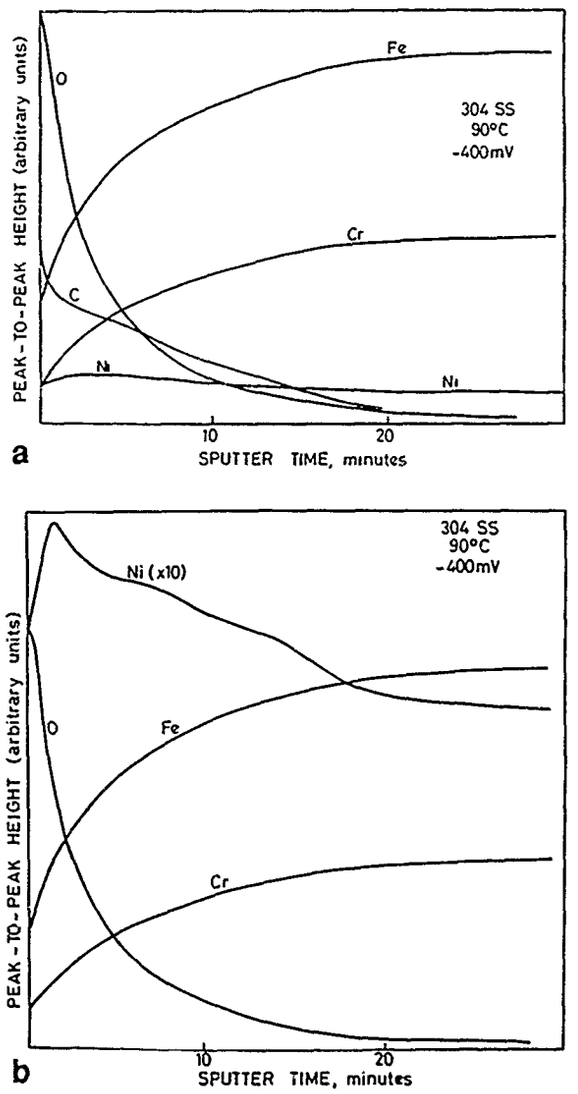


FIGURE A2—Auger depth profile of the surface of type 304 (UNS S30400) SS after a 60-s exposure to 15 M LiCl solution, pH 1.0, at 90°C and ~400 mV_{SCE}:[98] (a) all peak-to-peak heights 1X and (b) with carbon omitted and Ni 10X to display the similarity to Figure A1.

Discussion

H.-J. Engell (Max Planck Institut fur Eisenforschung, Federal Republic of Germany): I wonder whether the dealloyed layer is the reason for cracking or only a product of crack formation resulting from active path anodic dissolution.

R.C Newman: In the austenitic stainless steel case, we do not have the very strong evidence for the dealloying/cleavage mechanism that exists in α-brass [Sieradzki, Kim, Cole, and Newman, J. Electrochem Soc. 134(1987): p. 1635; Sieradzki and Newman, J. Phys. Chem. Solids 48(1987): p. 1101; Newman, Shahrabi, and Sieradzki, Scripta Metall. 23(1989): p. 71] or gold-copper alloys. However, the more we learn about the crack-tip reaction, the more it resembles these cases. The slip-dissolution model seems to fail on account of the demonstrable discontinuities in cracking (as shown, for example in the work of Desai, et al., "Study of Transgranular Stress Corrosion Crack Propagation in Austenitic Steels by Load-Pulsing Method," this proceedings). The hydrogen model still has life in it, but I personally believe that the transgranular cracking at high temperatures is unassisted by hydrogen, for the reasons we give in the paper.

S.C. Jani (Georgia Institute of Technology, USA): I would like to list some "againsts" for the film-induced cleavage model for transgranular stress corrosion cracking (SCC) of austenitic stainless steels: (1) crack branching, (2) specific cracking planes, (3) low-nickel alloy behavior, and (4) sponge (dealloyed layer) not observed on fracture surface. When these are addressed, I am willing to accept the idea.

R.C. Newman: (1) Cracks may nucleate anywhere where there is a (not very high) tensile stress. I do not understand this part of your question. (2) Cleavage of macroscopically brittle metals occurs on specific planes. Why should this not be the case for microscopic cleavage? (3) Low-nickel alloys will have difficulty forming a strong, connected dealloyed layer. Obviously the phase transformations complicate the issue, although, as I pointed out, similar behavior is seen in gold-copper, where there is complete solid solubility. (4) Not true Scamans and Swann [Corros. Sci. 18(1978): p. 983], and later Silcock [Corrosion 38(1982): p. 122], and more recently ourselves, have found plenty of sponge formation. In α-brass, the dealloying is much more superficial, and we do need to do more work on that system. We are currently doing cross-sectional transmission electron microscope studies.

S.M. Bruemmer (Pacific Northwest Laboratories, USA): Would you comment on the dealloyed-layer-induced cleavage concept as it applies to intergranular SCC of austenitic alloys? In particular, since dealloying may occur preferentially along grain boundaries, can this region induce brittle intergranular cracking?

R.C. Newman: We have recent data on gold-silver alloys, anodically polarized in perchloric acid, showing brittle intergranular events (beyond the dealloyed layer) generated by impact bending. We do not draw much distinction between transgranular and intergranular SCC in dealloying systems, but obviously more needs to be done in this area in view of Pugh's observations of low acoustic emission rates in intergranular SCC. I suppose you are particularly thinking of the alloy 600 (UNS N06600) system—I am not sure we have brittleness there, because the layer seems to be qualitatively different.

R.P. Gangloff (University of Virginia, USA): Would you please clarify the explanation for the critical (SCC) potential within the context of your dealloying and cleavage-jump model. Is this potential simply related to the attainment of a necessary level of crack acidification?

R.C. Newman: Yes. There has to be a net anodic reaction in the crack/crevice to maintain the acidity. The limiting crevice repassivation potential for an infinitely deep/tight crevice would be essentially the corrosion potential in the crevice environment.

R.P. Gangloff: Is the crevice repassivation potential, reported by the Japanese workers (Tanaka, et al., Advances in Localized Corrosion, ed. Isaacs and Bertocci (Houston, TX: NACE, in press)], sufficiently independent of crevice geometry and scan rate/time to be mechanistically useful, as you implied in your talk?

R.C. Newman: The crevices were not particularly tight or deep. The main point was that they were the same in the cracking experiment as the crevice-only experiment. However, the repassivation potentials were determined under ultra-low scan rate conditions, so they are limiting values for the particular crevices used. I would not expect more than a few mV change on going to tighter crevices.

T. Murata (Nippon Steel Corporation, Japan): As shown recently by Mueda and Yamamoto [J. Surf. Sci. Soc. Japan 9(1988). p. 218], you can make an instantaneous dealloyed layer in type 304 (UNS S30400) stainless steel, to a depth of 10 nm, by irradiating in nitrate solution, using a pulsed YAG laser.

R.C. Newman: I suppose this is a solid-state vacancy diffusion process, so it is not quite the same thing as dealloying; nevertheless, I would be interested in seeing the work.

T. Murata: More than ten years ago, the use of 42% magnesium chloride for duplicating chloride SCC of type 304 stainless steel was found to be misleading, because it did not simulate chloride cracking in service conditions at all. Kowaka and Kudo [Tetsu-to-Hagane 62(1976): p. 390; and ibid. 63(1977): p. 328] clarified the dependence

of SCC behavior on the concentration of magnesium chloride, either in intergranular or transgranular modes, with or without pitting. This turned out to be most interesting work, indicating where future work should be done. Following that report, a joint program of chloride SCC was conducted between university and industry in Japan. One of the major accomplishments was the recommendation that 20% sodium chloride solution (either boiling or at lower temperatures) be used to replicate SCC initiated from pitting or crevice corrosion. This is the reason why Tsujikawa used this particular solution [see Tsujikawa, et al., Tetsu-to-Hagane 66(1980): p. 2067 and Advances in Localized Corrosion, ed Isaacs (Houston, TX: NACE, in press)].

R.C. Newman: Thank you for this interesting history, which I think is an outstanding application of corrosion science to engineering practice, taken with the exceptionally elegant work of Tsujikawa and colleagues.

M. Marek (Georgia Institute of Technology, USA): Why do you find the film-induced cleavage model so attractive for this system, when the experimental evidence is limited to the presence of the dealloyed layer, which may or may not be involved in the mechanism?

R.C. Newman: I admit that we are not doing as well in this system as α-brass. However, I think you may be underrating the breadth of our approach to this problem. Perhaps my presentation was at fault in this respect. For example, the dealloying vanishes in type 310 (UNS S31000) stainless steel as you lower the temperature through the value where SCC becomes very difficult to achieve. I hope we are keeping an open mind on this topic, but since the cracking is demonstrably discontinuous and the hydrogen model seems to fail, I think it is very significant to demonstrate a similar dealloying reaction to that seen in brass where the film-induced cleavage model is so convincing.

R.L. Sindelar (Savannah River Laboratory, USA): What is the role of bulk aqueous impurities on intergranular SCC propagation? In addition to chloride, do other aqueous impurities such as nitrite or sulfate lower crevice potentials or act in some synergistic manner to effect propagation?

R.C. Newman: At relatively oxidizing potentials, these ions will concentrate in cracks Some authors think that sulfate is special because it is electro-reduced sulfide (see for example, Ljungberg, et al., Corrosion 44(1988): p. 66]. I think Ford's paper at this conference addresses these issues in detail.

F.P. Ford (General Electric R&D, USA): What is your working hypothesis to assert that the effect of cold work in increasing the intergranular SCC susceptibility of unsensitized stainless steel in high-temperature water is due to hydrogen embrittlement?

R.C. Newman: I was especially impressed by Totsuka and Smialowska's work [Corrosion 44(1988): p. 124] in borate solutions with hydrogen overpressure, including the cathodic polarization studies they made earlier on alloy 600 [Corrosion 43(1987): p. 734]. I find strong similarities between that and the Kuniya work [Corrosion 44(1988): p. 21] in oxygenated water. More speculatively, I could suggest that the increase in intergranular SCC with cold work in hot chlorides may involve hydrogen, but I am not too happy with the implications in terms of multiple mechanisms. Certainly the cold work effect in hot chlorides is limited to unstable steels.

E.N. Pugh (National Institute of Standards and Technology, USA): I certainly agree with you that transgranular SCC of stable austenitic stainless steels, such as type 310 in aqueous chloride, is unlikely to involve hydrogen. However, unstable steels such as type 304 may be different. Thus, it might be argued that cracking is due to hydrogen embrittlement at temperatures below M_D, changing to the stress corrosion process at temperatures higher than M_D. Have you come across any evidence for such a transition in your review of the literature?

R.C. Newman: I have not found any data that look like this, but I do wonder if the switch from trans- to intergranular cracking at high K values [Russell and Tromans, Metall. Trans. 10A(1979): p. 1229] is a hydrogen effect confined to unstable steels. Certainly, the effect of prior cold work (which also promotes intergranular cracking) is confined to unstable steels. I think monocrystal studies would be useful here, to isolate the transgranular cracking. One observation that tends to counter your suggestion is the rapid SCC seen in type 304 stainless steel at temperatures greater than 300°C, which is fractographically indistinguishable from that seen at 100°C to 150°C.

SECTION VIII

Environment-Induced Cracking in Ferrous Alloys

Rapporteurs' Report on Poster Presentations

C.L. Briant
General Electric Company
Schenectady, New York, USA

R.P.M. Procter
University of Manchester Institute of Science and Technology
Manchester, UK



Photos: M B. Ives

The papers given in this poster session, the written versions of which follow this rapporteurs' report, can be divided by topic into three general areas. (1) mechanisms of intergranular corrosion and stress corrosion cracking (also included here is the single paper on liquid metal embrittlement), (2) hydrogen embrittlement, and (3) mechanisms of transgranular stress corrosion cracking.

Let us first consider intergranular stress corrosion cracking of iron-base alloys. The paper by Atrens, et al , sought to provide a model for intergranular stress corrosion cracking in low-alloy steels in high-purity water. They proposed that at low temperatures the cracking might be a result of hydrogen embrittlement, while at high temperatures the cracking might occur as a result of anodic dissolution. They further suggested that, at least in the anodic dissolution regime, crack-tip strain rate would play an important role in determining the rate of cracking. This idea led to considerable discussion after the posters were presented. Most of the discussion focused on whether or not this strain rate could be measured experimentally and whether it could be incorporated into the analytical models. No strong consensus was reached on these points.

The other paper that came under the heading of intergranular corrosion was that of Stewart, et al , on crack initiation of sensitized austenitic stainless steels. They presented results showing that at the beginning of a slow-strain-rate tensile test, many cracks are initiated in a sensitized sample. There is then a period in which these cracks are rather dormant as the strain increases, and then one or two cracks begin to propagate through the sample. There was some discussion as to why the cracks go through this dormancy at intermediate strains. No complete explanation was found. Both Stewart and Atrens expressed the feeling that, although their respective papers did not directly address this issue, the grain-boundary composition was also very important in the problems they were investigating and must be included in complete models of intergranular corrosion and stress corrosion cracking.

The next topic that we wish to consider is hydrogen embrittlement. Three papers considered trapping of hydrogen in some way. Turnbull and Saenz de Santa Maria measured permeation transients in a martensitic stainless steel. They found that in the initial transient many traps were filled, and with additional runs the hydrogen passed through the sample more rapidly. They also found that in hydrogen sulfide solutions, the time-to-failure could be directly correlated with the internal hydrogen concentration as measured from the permeation transients. Iyer and Hehemann found that the time-to-failure during hydrogen charging was dependent on the amount of load relaxation the sample was allowed to have prior to charging. If the load was relaxed for a long time, the time-to-failure in hydrogen charging was also increased. A complete mechanism was not discussed, but it would appear that as dislocation activity subsides with longer relaxation times, hydrogen moves more slowly into the sample. Coudreuse, et al., showed that vanadium additions appear to enhance trapping in both 2.25Cr-1Mo steels and ferritic stainless steels. This trapping is thought to occur because of vanadium carbide precipitation in these steels. This trapping is reflected in somewhat improved resistance to hydrogen embrittlement.

In the discussion of these papers, it was pointed out that there are many measurements of hydrogen trap strengths in the literature, and that it would be instructive to interpret some of the results found in these papers in terms of these measured strengths. It was also pointed out that there are now a variety of models for hydrogen embrittlement that involve hydrogen transport by dislocations, enhanced dislocation mobility as a result of the presence of

hydrogen, crack-tip blunting by mobile dislocations, crack initiation by dislocation pile-ups, etc. It is not obvious how all of these observations and models fit together, and it was felt that some effort should be directed at trying to incorporate all of the experimental observation into a general coherent model.

The paper on liquid metal embrittlement by Nakasa and Suzawa concerned liquid zinc cracking of a high-strength steel. The authors showed that cracking occurred extremely rapidly in this steel, although there was some dependence on temperature. They also pointed out that crack branching occurred quite frequently and must be considered in reporting velocities.

The paper by Meletis, et al., forms a convenient link between those papers that deal explicitly with hydrogen embrittlement and those that consider other mechanisms. These authors have confirmed that cracking of type 304L (UNS S30403) stainless steel single crystals in boiling 45% magnesium chloride solution is crystallographic and occurs by microcleavage, primarily along {100} planes. However, their new observation is that the deformation mode is inhomogeneous and coplanar close to the stress corrosion fracture surfaces but homogeneous elsewhere. They attribute this difference to hydrogen from the cathodic reaction entering the steel and reducing the stacking fault energy of the austenite in the region of high triaxiality ahead of the crack tip.

Their suggestion that this results in the formation of Cottrell-Lomer locks, which in turn result in cleavage, provoked some discussion In a somewhat related paper, Iyer showed that the effects of various thermomechanical treatments on the stress corrosion susceptibility of 26Cr-1Mo ferritic stainless steel in boiling 42% lithium chloride solution also correlate well with changes in the deformation mode. In particular, when coplanar slip occurs, greater slip-step heights and densities result in increased stress corrosion susceptibility. The author concluded from these results that slip dissolution is the mechanism of stress corrosion crack initiation in this alloy/environment system. The paper by Kido, et al., also presented results that are relevant to the slip dissolution model of cracking. Specifically, they have used alternating current impedance techniques to study the effects of static tensile stresses on the dissolution and repassivation of type 304 (UNS S30400) stainless steel in pH 1.2 sulfuric acid They concluded from changes in the relevant time constants that elastic stresses suppress dissolution and promote film formation. On the other hand, plastic stresses have the reverse effect and promote dissolution during rather slow repassivation.

Finally, in a particularly elegant and painstaking piece of research, Desai, Friedersdorf, and Shaw have used load-pulsing techniques to study stress corrosion crack propagation in type 316 (UNS S31600) stainless steel in boiling magnesium chloride and lithium chloride solution. They have very clearly demonstrated the discontinuous nature of environmentally induced cracking in this alloy/environment system and have produced accurate values for the crack arrest time and the crack advance distance. Their results are of particular importance and significance, since they appear to be fully consistent with the film-induced cleavage model of environmental cracking.

In the general discussion following the poster viewing period, a number of delegates made what they felt were convincing arguments in favor of film-induced cleavage and against hydrogen embrittlement as the mechanism of stress corrosion cracking of austenitic stainless steels in a chloride-containing environment. In response to this, a more or less equal number of different speakers presented what they felt were equally convincing arguments in favor of hydrogen embrittlement and against film-induced cleavage. To say that no consensus was achieved considerably understates the passions that these discussions aroused!

Indeed, it is difficult to portray in this written report the flavor of the active discussions that took place in this session. Quoting various comments out of the full context of what was said trivializes them. However, it seems fair to say that in discussions on mechanisms, there is still a great deal of confusion. Most of this confusion stems from the fact that many of the mechanisms have not been verified experimentally. In some cases, it may not even be possible to verify the models with experiments, and this situation makes arguments even more tenuous and fuzzy. It is very difficult to take stress corrosion data in the variety of ways that is normally obtained and jump to an atomistic model of cracking, and because adequate information is not present, the same data can be used to support a variety of models. It therefore seems important for researchers to evaluate carefully what they can learn from an experiment, and if other techniques could provide more information that would help establish a particular model over another one, to redirect their work accordingly. The written versions of the individual papers follow, with specific discussion comments following the appropriate paper.

Conceptual Model of Stress Corrosion Cracking of Low-Alloy Steels in High-Temperature Water

R.M. Rieck, A. Atrens,** S. Ramamurthy,** J.D. Gates,** and I.O. Smith**

Abstract

This paper presents a conceptual model for the stress corrosion cracking (SCC) of quenched and tempered low-alloy steels in high-temperature, high-purity water. The model is based on the cracking mechanism of anodic dissolution. It is based on the postulate that the crack-tip strain rate is the controlling parameter, with the crack velocity increasing with an increase of crack-tip strain rate. Furthermore, it is assumed that the relationship between crack velocity and crack-tip strain rate is valid up to very high crack velocities resulting from strain-assisted dissolution. Following Parkins, the authors propose that K_{1SCC} is defined by a critical crack-tip strain rate, $\dot{\epsilon}_{cr}$. That is, the proposed model of SCC explains K_{1SCC} as being the stress intensity at which significant dislocation motion starts to occur to give significant crack-tip creep.

Introduction

This paper presents a conceptual model for the stress corrosion cracking (SCC) of quenched and tempered low-alloy steels in high-temperature, high-purity water. The model is based on the cracking mechanism of anodic dissolution (AD)[1,2] and the experimental observations[3-5] that crack-tip plasticity is an integral part of crack propagation, with there being considerable experimental evidence[5] contrary to crack advance by a mechanism of brittle mechanical fracture assisted by corrosion processes.

For the system of low-alloy steels experiencing SCC in high-purity water, recent work by Magdowski and Speidel[1,2] has indicated that the cracking mechanism is different at high and low temperatures; they suggested that AD occurred at high temperatures and hydrogen embrittlement (HE) occurred at low temperatures. A review of the literature by Atrens, et al.,[6] supports this view. The critical data are as follows.

In high-temperature water, the threshold stress intensity for SCC, K_{1SCC}, is independent of the yield strength of the steel, σ_y;[1,2,7] whereas, the threshold stress intensity for cracking in hydrogen, K_{1H}, increases as σ_y decreases.[8] These different trends of K_{1SCC} and K_{1H} with strength indicate that HE is not the cracking mechanism. This is reinforced by the fact that the crack velocity in Region II under Mode I loading, $v_{Mode\ I}$, is the same as under Mode III loading,[3] $v_{Mode\ III}$.

In contrast, in low-temperature water, the threshold stress intensity for SCC (K_{1SCC}) increases as the yield strength of the steel (σ_y) decreases,[1,2] and the threshold stress intensity for cracking in hydrogen (K_{1H}) increases as σ_y decreases.[8] These observations are in agreement with HE being the cracking mechanism. This is reinforced by the fact that the crack velocity in Region I under Mode I loading ($v_{Mode\ I}$) is greater than under Mode III loading[9] ($v_{Mode\ III}$).

Creep experiments[3,4] have demonstrated that crack-tip plasticity is an integral part of crack propagation; if primary creep is exhausted in a benign environment, then no SCC occurs in a cracking environment, despite an applied stress intensity four times K_{1SCC}. Moreover, the detailed examination of the fracture surfaces[6] indicates traces of crack-tip plasticity on the intergranular fracture surface with there being considerable experimental evidence[5] contrary to crack advance by a mechanism of brittle mechanical fracture assisted by corrosion processes. In addition, Ramamurthy, et al.,[10] have measured the crack velocity as a function of applied stress rate using the newly developed linearly increasing stress test (LIST)[11] Typical data are given in Figure 1,[10] which shows crack velocity as a function of applied stress rate at crack initiation. This test uses a smooth un-notched tensile specimen. Crack initiation is in the elastic region, and consequently, it is valid to discuss crack velocity also as a function of applied strain rate at crack initiation.

Much study[6] has gone into the system of interest and several attempts have been made to propose crack growth models None to date have been able to explain the observations of Speidel,[7] who showed that the crack velocity increases exponentially with increasing strength, increasing from a crack velocity of 1.0×10^{-11} m/s at a yield strength of 700 MPa to a crack velocity of 1.0×10^{-4} m/s at a yield strength of 1700 MPa.

The purpose of this paper is to present a conceptual model for this system that can provide a qualitative explanation of the experimental observations. It indicates where there are large gaps in the knowledge, which thereby provides a focus for research The model is conceptual and not mathematical because of these gaps in knowledge.

The Model

General principles

The proposed model of SCC is based on the following postulates:

(1) Crack-tip strain rate is the controlling parameter up to the maximum velocity observed experimentally for this system.

(2) There is a relationship between crack velocity and crack tip strain rate that is valid up to the maximum velocity observed experimentally for this system.

(3) The relationship between crack-tip strain rate and the applied stress intensity is as shown in Figure 2.

There is good experimental evidence for Postulate 1.[3-5] Postulate 2

*CRA Advanced Technical Development, P.O. Box 347, Cannington, W.A. 6107 Australia.

**Department of Mining and Metallurgical Engineering, University of Queensland, St. Lucia, Q. 4067 Australia.

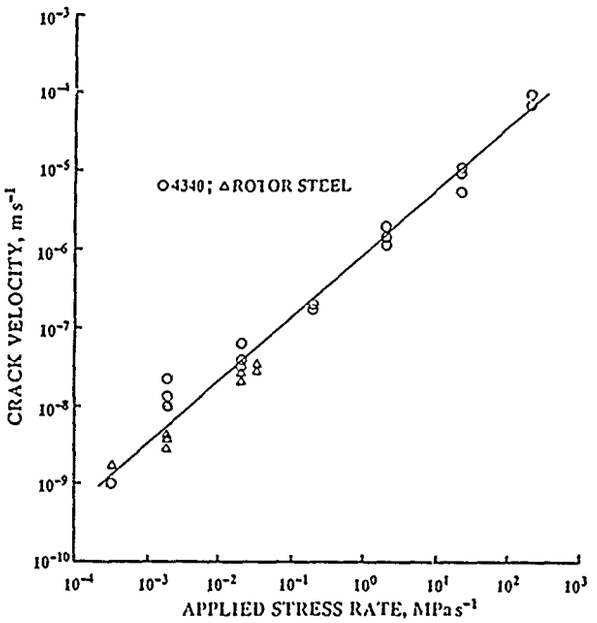


FIGURE 1—Crack velocities measured with the LIST test[8] as a function of applied stress rates for both as-quenched type 4340 (UNS G43400) steel and rotor steel in aerated distilled water at 90°C.

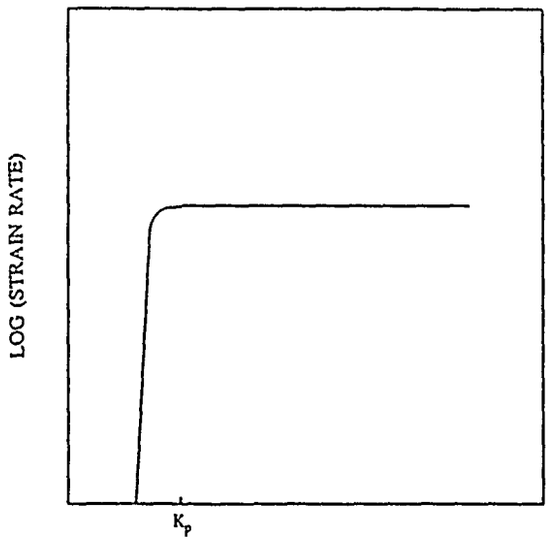


FIGURE 2—Expected relationship between crack-tip strain rate and applied stress intensity.

is a plausible generalization of Postulate 1. It is central to this conceptual model. If Postulate 2 is correct, then there is good evidence for Postulate 3.

Importance of crack-tip strain rate

The experimental evidence[3-5] in support of the crack-tip strain rate was summarized in the introduction.

Crack-tip strain rate vs K

For loading so that there is zero stress or zero stress intensity, the crack-tip strain rate must be zero. For reasons given below, there is a a critical stress intensity, termed K_p after Speidel,[12] above which the strain rate is independent of the applied stress intensity. Figure 2 reflects the above, joining the two extremes with a region wherein the the crack-tip strain rate increases very quickly, even exponentially, with stress intensity.

Crack tips above K_p

Above K_p, the crack tip has a well-developed plastic zone with the maximum stress in this plastic zone being $3\sigma_y$.[13] Higher stress intensities increase the size of the plastic zone at the crack tip, but do not affect the stress within the zone. Consequently, it is a plausible inference that above K_p, the creep rate is independent of stress intensity because the deviatoric stress that drives creep is independent of stress intensity.

It is important to emphasize that crack-tip strain rate or creep rate at the crack tip are being dealt with under conditions of full plasticity in precracked specimens with the additional factor of constraint. As pointed out previously, this produces a higher stress at the crack tip for a higher-strength steel.[13] High-strength steels also have much smaller zones of plasticity, so that dislocation motion will be more concentrated at the crack tip. These two factors combine to produce a higher strain rate at the crack tip in high-strength steels under conditions of full pasticity.

On the assumption that there is a relationship between stress corrosion crack velocity and crack-tip strain rate, this gives a region of crack velocity independent of applied stress intensity, but dependent on the yield strength (σ_y) of the material, as illustrated in Figure 3 and in agreement with the experimental results of Speidel and coworkers,[1,2,7] who showed that the crack velocity increases exponentially with increasing strength, increasing from a crack velocity of 1.0×10^{-11} m/s at a yield strength of 700 MPa to a crack velocity of 1.0×10^{-4} m/s at a yield strength of 1700 MPa.

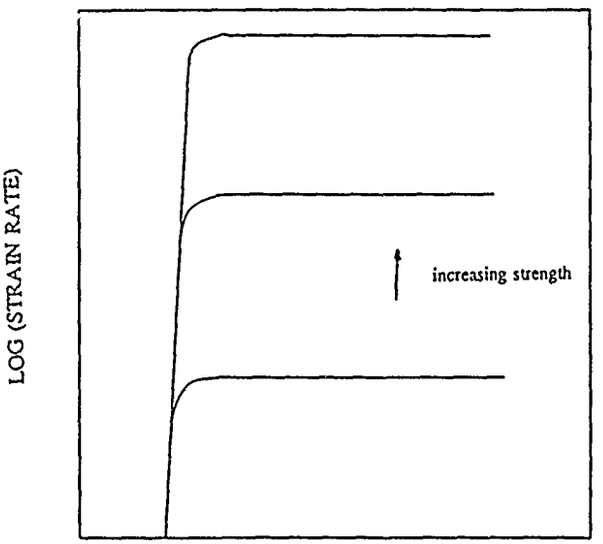


FIGURE 3—Expected effect of metal yield strength on the relationship between crack-tip strain rate and stress intensity.

Creep data, as described by conventional creep experiments, refer to steady-state creep; whereas, it has been shown that SCC is controlled by primary creep.[4,14] Primary creep in newly stressed metal occurs at a faster rate than secondary creep. An experimental program on the primary creep of low-alloy steels would be required to test this proposal since experimental results are not presently available.

K_{1SCC}

Following Parkins,[14] the authors propose that K_{1SCC} is defined by a critical crack-tip strain rate ($\dot{\epsilon}_{cr}$). That is, the proposed model of SCC explains K_{1SCC} as being the stress intensity at which significant dislocation motion starts to occur to give significant crack-tip creep. The process that limits plastic deformation such that a significant strain rate is only found above K_{1SCC} has not been identified. The observation that K_{1SCC} is independent of σ_y and temperature implies that these parameters have no effect on the processes limiting strain at the crack tip.[1,2,7]

Discussion

Strain-assisted dissolution

A crack velocity of 10^{-4} m/s requires a crack-tip anodic current density of 300 A/Cm^2 for cracking by AD Such high current densities have not been observed in scratching electrode tests. Lacombe and Parkins[15] report a maximum bare surface current density of 3 A/cm^2, correlating with a crack velocity of 10^{-6} m/s. The problem for AD models of SCC is accounting for crack velocities higher than 10^{-6} m/s. This requires a mechanism for accelerating the dissolution rate occurring at the crack tip.

This acceleration could be provided by strain-assisted dissolution at a bare crack tip. The large stress concentration at the crack tip ensures that dislocation motion is concentrated at the crack tip itself. Each dislocation that impinges upon the crack tip produces a ledge of bare metal in contact with the cracking solution. The atoms on the ledge so produced can dissolve very quickly because of a number of effects. Clean metal (i.e., without any films) is in contact with the solution. Atoms on the ledge are not strongly bound to the bulk metal because of the missing bonds on the two free faces of the ledge. These features cause the metal on the ledge to dissolve much more quickly than would occur on a film-free surface. Moreover, the dissolution rate is strain rate controlled through the rate of production of ledges by dislocation motion.

Moreover, there is also a small anodic area (active crack tip) in contact with a large cathodic area (crack sides), resulting from the geometry of the crack,[16] which increases the rate of reaction. The likelihood of such an effect being important cannot be assessed directly because of the unknown nature of the crack-tip electrochemistry. However, an area effect cannot account for the effect of strength on v_{II}, since the analysis of Doig and Flewitt,[17] which included strength defining the area of dissolution, could not account for the exponential relationship between σ_y and v_{II}. The independence of cracking kinetics on metal composition also makes it unlikely that area effects are important to SCC since the composition controls the corrosion potential and areas of anodic and cathodic reaction Variations in these parameters should change v_{II} and the lack of such change in v_{II} makes it unlikely that area effects are important to SCC This indicates that strain assisted dissolution may be the only feasible method of accounting for the high crack velocities found in the high-strength steels.

Prior creep influence

Rieck, et al.,[4] have shown that prior creep in a noncracking environment can inhibit cracking when a specimen is subsequently placed in a cracking environment, even if the applied stress intensity is well above K_{1SCC}. On loading above K_ρ, into Region I of SCC, the crack-tip strain rate will be that shown in Figure 2, unless subcritical cracking does not occur; in which case, this metal will undergo primary creep. Primary creep results in work hardening of the metal at the crack tip and a decreasing creep rate with time to such an extent that it is less than that required for the initiation of SCC, i.e., the crack-tip strain rate fails below $\dot{\epsilon}_{cr}$.

The value of $K_{1SCC} = 8$ MPa$\sqrt{m}$ measured by Speidel[7] for low-alloy steels cracking in pure water is only applicable to metal freshly stressed in the cracking solution, or metal that has cracked from a higher stress intensity down to K_{1SCC} with the stress intensity decreasing as the crack extends. This ensures that the strain-hardened metal at the crack tip is continuously removed by dissolution.

Intergranular nature of SCC

The intergranular nature of SCC has normally been attributed to segregation effects, with phosphorus being the major species.[18-20] Recent work by Magdowski and Speidel[1] has shown that for low-alloy steels in high-temperature water, segregation has no effect on SCC. Therefore, a new explanation is needed for the crack path. In low-alloy steels, wavy slip ensures that slip cannot concentrate on any one plane, nor at any obstacle within the grains. In the early stages of deformation, the most significant obstacle is the grain boundary so that dislocation motion will be concentrated in the grain-boundary region. This causes cracking to be intergranular. In the quenched and tempered steels, the prior austenite grain boundaries remain high-angle boundaries and, as such, are a more significant barrier to dislocation motion than the lower energy twin boundaries found in martensite. Thus, cracking occurs along the prior austenite grain boundaries. Such a result also explains the importance of slip morphology to SCC.

Critical Tests for the Proposed Model

The proposed model of SCC depends upon a number of assumptions, the validity of which, and consequently of the model itself, could be tested.

One critical assumption is that of the effect of stress intensity on crack-tip creep The fact that the creep rate at the crack tip is exponentially dependent on the stress at the crack tip is the most important assumption made This is very difficult to test since it is creep at the crack tip, rather than the region of general yielding, that is important to SCC. Creep tests on double-cantiliver beam specimens measuring only the crack opening displacement are unable to define the creep rate at the crack tip since the crack opening displacement is defined mainly by the size of the plastic zone at the crack tip. It is this problem with measuring crack-tip creep rate that makes the model difficult to test.

Strain-assisted dissolution was invoked to explain the very high crack velocities found in the high-strength steels. It may be possible to test this assumption using electrochemical measurements on straining samples. However, to simulate the crack-tip conditions of creep, it is necessary to localize the straining region, while keeping the rest of the sample passive.

The easiest test of the proposed model is a stress analysis of a precracked sample loaded in Mode III. The result of comparable crack velocities in Modes I and III indicates similar crack-tip creep rates in the two loading modes. A stress analysis of the Mode III loading should allow a comparison of the deviatoric component of stress at the crack tip in both loading modes. The experimental results indicate that this stress should be similar in the two loading modes.

References

1. R.M. Magdowski, M.O. Speidel, Metall. Trans. 19A(1988): p. 1583.
2. R.M. Magdowski, Ergebnisse der Werkstoff-Forschung—Moderne, ed. R. Staehle, P.J. Uggowitzer (1987), p. 107.
3. R.M. Rieck, "The Mechanism of Stress Corrosion Cracking of Quenched end Tempered Low Alloy Steels in Water" (Ph.D. diss., University of Queensland, 1988).
4. R.M. Rieck, A. Atrens, I.O. Smith, Metall. Trans., accepted for publication.
5. R.M. Rieck, A. Atrens, I.O. Smith, submitted to Materials Forum.
6. A. Atrens, R.M. Rieck, S. Ramamurthy, J.D. Gates, I.O. Smith, International Metal Review, accepted for publication.
7. M.O. Speidel, Corrosion in Power Generating Equipment, ed. M. O. Speidel, A. Atrens (New York, NY: Plenum Press, 1984), p. 85.
8. H.G. Nelson, D.P. Williams, Stress Corrosion Cracking and Hydrogen Embrittlement of Iron Base Alloys, NACE-5, ed. R. Staehle, J. Hochmann, R. McCright, J. Slater (Houston, TX: National Association of Corrosion Engineers, 1977), p. 390.
9. W.Y. Chu, C.M. Hsiao, S.Y. Ju, C. Wang, Corrosion 38(1982): p. 446.
10. S Ramamurthy, R.M. Rieck, A. Atrens, R.M. Rieck, J.D. Gates, I.O. Smith, ASIA CORROSION'88, paper no. 21 (Houston, TX. NACE, 1988).
11. A. Atrens, C. Brosnan, S. Ramamurthy, I.O. Smith, submitted to J. Phys. E.: Sci. Inst.

12 M.O. Speidel, The Theory of Stress Corrosion Cracking in Alloys, ed J.C Scully (Brussels, Belgium: NATO, 1971), p. 345.
13 J.F. Knott, Fundamentals of Fracture Mechanics (1973).
14. R.N. Parkins, Brit. Corros. J. 14(1979): p. 5.
15. P. Lacombe, R.N. Parkins, Stress Corrosion Cracking and Hydrogen Embrittlement of Iron Base Alloys, p. 521.
16. D.A. Vermilyea, R.B. Diegle, Corrosion 29(1973): p. 26.
17. P. Doig, P.E.J. Flewitt, Corrosion in Power Generating Equipment, ed. M.O. Speidel, A. Atrens (1984), p. 133.
18. N. Bandyopadhyat, C.L. Briant, Corrosion 38(1982): p. 125.
19. N. Bandyopadhyat, C.L. Briant, Metall. Trans. 14A(1983): p. 2005.
20. G.T. Burstein, J. Woodward, Met. Sci. 17(1983): p. 111.

The Initiation of Intergranular Stress Corrosion Cracking on Sensitized Stainless Steel in Dilute Thiosulfate Solutions[1]

J. Stewart, B. Wells,** and P.M. Scott**

Abstract

The initiation of intergranular stress corrosion cracking on sensitized type 304 (UNS S30400) stainless steel has been studied at room temperature using dilute, naturally aerated sodium thiosulfate solutions. Electrochemical techniques are used to detect anodic current transients during slow-strain-rate experiments at the free-corrosion potential. These anodic current transients are caused by the initiation, metastable propagation, and repassivation of microstructurally short cracks. The effect of thiosulfate concentration and strain rate on the initiation of cracks has been studied. A low-strain region (elongation < 5%) was identified in which the crack initiation frequency and electrochemical activity were at a maximum in dilute thiosulfate solutions. The transition to sustained crack propagation was clear and generally occurred at higher strains, where the metastable crack initiation frequency and electrochemical activity were very low. The variation in strain to failure values could be accounted for in the period required to initiate a crack. Crack propagation was shown to be a minor proportion of the total test period.

Introduction

Detailed studies of the mechanisms of initiation of stress corrosion cracks have usually been restricted to post-test examination of fractured specimens, and *in situ* measurements have not generally been available The experiments reported here have investigated the feasibility of using electrochemical current transients (electrochemical noise) for studying the early stages of crack nucleation and growth. The model system chosen for this investigation was sensitized type 304 (UNS S30400) stainless steel (SS) in thiosulfate solutions in which intergranular stress corrosion cracking (IGSCC) occurs readily.[1-4] Three specific topics have been examined: the effect of electrode potential on crack initiation; the relationship between electrochemical noise and multiple crack initiation and intermittent growth (metastable cracking); and the formation of sustained propagating cracks.

Experimental

The type 304 SS used in this study had the following composition (in wt%). 0.059 C, 17.8 Cr, 9.07 Ni, 1.5 Mn, 0.035 S, 0.38 Mo. Tensile specimens were machined from 6.25-mm-diameter rod to produce a smooth 19 mm gauge length of 3-mm diameter. The specimens were solution annealed at 1070°C in vacuum for 30 min, argon quenched, and then soaked at 650°C for 24 h under argon to produce a fully sensitized material (normalized ASTM EPR, Pa = 75 C cm^{-2},[5] and Pa = 10 C cm^{-2} using a quantitative image analysis method.[6]) The minimum chromium content in the sensitized grain boundary was measured at 10.3 wt% using a STEM-EDS system (analytical resolution approximately 2 nm).[7] The grain size was typically 80 μm, the 0.2% offset yield strength 190 MPa and the elongation to failure about 70% in air. Specimens were abraded to a 600 grit finish, cleaned in acetone and distilled water, and then coated with a resin-reinforced synthetic rubber to leave a 5-mm gauge length exposed. Slow-strain-rate (SSR) tests were conducted on a 100 kN servoelectric tensile testing machine.

Open-circuit potential experiments

The technique used to detect current transients during the SSR tests has been described in detail elsewhere.[8] The specimen was coupled through a high-resolution "zero resistance ammeter" to a large isolated cathode (30 cm^{-2}), and the current–time record was stored on a digital tape recorder. The apparatus is shown in Figure 1. The specimen potential was monitored using a platinum reference electrode and standardized against a saturated calomel electrode (SCE). A minimum of eight experiments were performed for each set of conditions studied.

Preliminary experiments were performed to correlate current transients with observed cracks in 1000 ppm (9×10^{-3} M) thiosulfate solutions at an extension rate of 10^{-6} s^{-1}. Two experimental parameters were then studied in detail. The effect of strain rate (nominally 5×10^{-7} s^{-1}, 10^{-6} s^{-1}, and 2×10^{-6} s^{-1}) was examined in 10 ppm thiosulfate solution (conductivity 22 μS cm^{-1}). The second parameter studied was thiosulfate concentration in the range 10 to 10,000 ppm (9×10^{-5} M to 9×10^{-2} M) at a nominal strain rate of 10^{-6} s^{-1}.

Controlled potential experiments

Potentiostatically controlled SSR experiments were performed in the range −350 mV to +100 mV_{SCE} in 0.5 M thiosulfate solutions at a nominal strain rate of 10^{-4} s^{-1}.[1] A series of experiments was stopped after applying 3.5% strain and the number of cracks evaluated using a scanning electron microscope (SEM) at 1000X magnification.

---

[1] This paper is reprinted with permission from the copyright holder, United Kingdom Atomic Energy Authority (UKAEA).

*Materials Development Division, Harwell Laboratory, Oxfordshire 0X11 0RA, England.

**Department of Metallurgy and Science of Materials, University of Oxford, England.

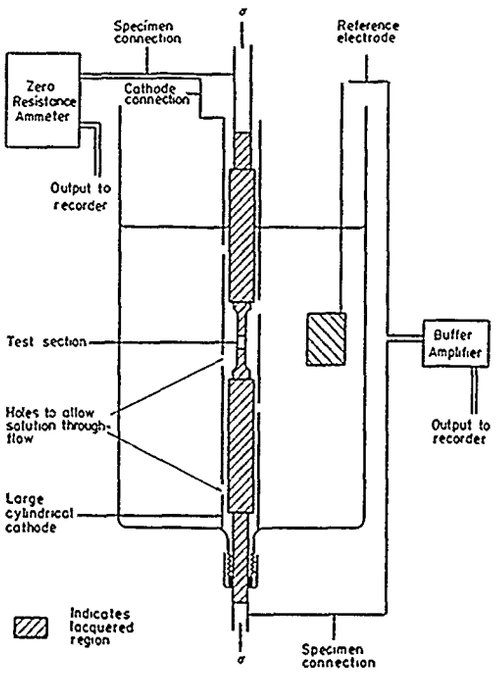


FIGURE 1—The test cell.

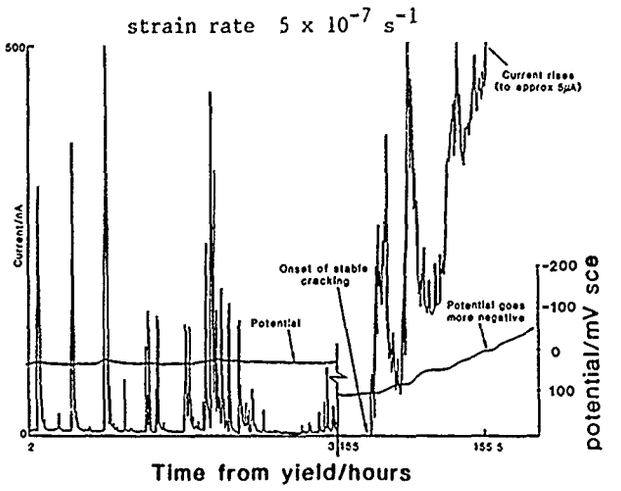


FIGURE 2—Typical current transients observed during slow-strain-rate tests at open-circuit potential (schematic).

Experimental Results

Open-circuit potential experiments

Current transients. Discrete current transients were first observed in the constant extension rate experiments shortly after the nominal yield point. Figure 2 shows typical transients measured on a specimen strained at $5 \times 10^{-7}\ s^{-1}$ in 10 ppm thiosulfate solution. The transients are characterized by peak currents of < 500 nA, an initial rise time of 5 to 20 s, and lifetimes of 30 to 1000 s. Marked fluctuations in the current were observed and were consistent with crack initiation, intermittent growth, and reinitiation of localized corrosion at the same noise source. The current remained low during the intervals between transients, typically 20 nA.

It was concluded that these current transients were caused by the nucleation, metastable propagation, and repassivation of short cracks from the following observations. In SSR control experiments, no transients or cracks were observed when an inert electrolyte (1000 ppm SO_4^{2-}) was used, or when solution-annealed material was tested in thiosulfate solutions. Detailed SEM examination of the gauge length from tests terminated after the observation of electrochemical transients indicated a direct correspondence between the number of cracks and the number of transients.

Application of Faraday's law incorporating representative materials parameters[6] indicated that the electrochemical measurement technique could resolve short cracks of considerably less than one grain-boundary facet in length. (The estimated resolution of the technique was 2 to 5 μm penetration.)

The frequency of crack nucleation in 10 ppm thiosulfate solution was found to be highly strain dependent; the maximum crack nucleation rate occurred between 2% and 5% strain (Figure 3). At higher strains, the incidence of crack nucleation decreased significantly. The average charge passed per transient was also greatest in the strain range of 2% to 5% and declined at higher strains (Figure 4). These observations were similar for the three strain rates studied. The effect of increasing the thiosulfate concentration was to increase the charge passed of the individual current transients (Figure 4).

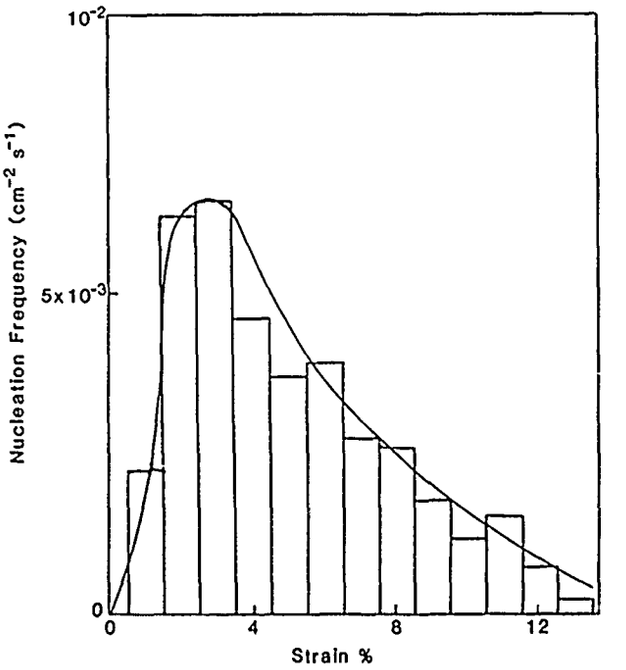


FIGURE 3—Frequency of current transients vs strain during slow-strain-rate tests at $10^{-6} s^{-1}$.

Crack propagation. The formation of a visually observed, sustained propagating crack was marked by a rapid increase in the anodic current of 3 to 5 μA (Figure 2), the high current level was sustained until the specimen fractured. Most current–time records showed considerable cyclic behavior during the early period of crack propagation. The charge passed during each increment of crack growth was on the order of a grain-boundary facet. In 10 ppm and 100 ppm thiosulfate solutions, sustained crack propagation often occurred at strain levels considerably higher than the region of maximum nucleation frequency (Figure 5). Crack propagation was rapid and the measured time-to-failure was concluded to be dominated by the period of crack initiation. At higher thiosulfate concentrations, the probability of nucleating a propagating crack increased, and fracture usually occurred at lower strains. Figure 5 summarizes the effect of thiosulfate concentration, in which survival probability [defined as $n/(N+1)$, n = specimens surviving, N = total number of specimens] is plotted against engineering strain to failure. Figure 6 summarizes the effect of strain rate on survival probability. The variance in survival probability decreased with respect to strain-to-failure for decreasing strain rate.

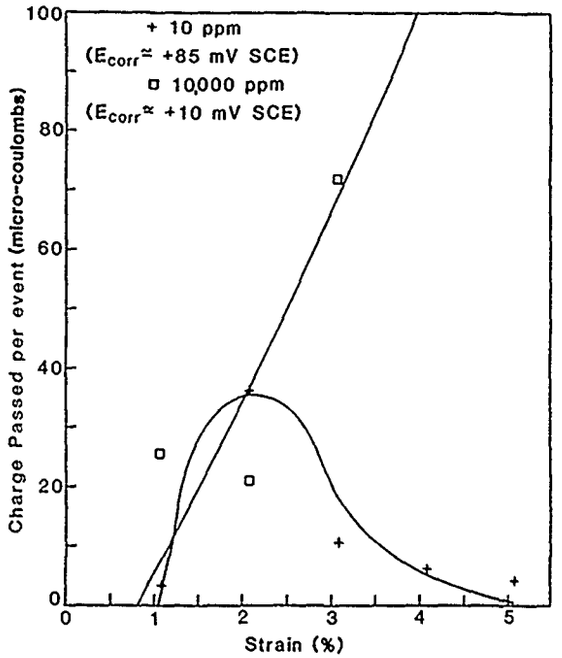


FIGURE 4—Charge passed vs % strain in 10 ppm and 1000 ppm thiosulfate solutions at open-circuit potential strain rate $10^{-6}s^{-1}$.

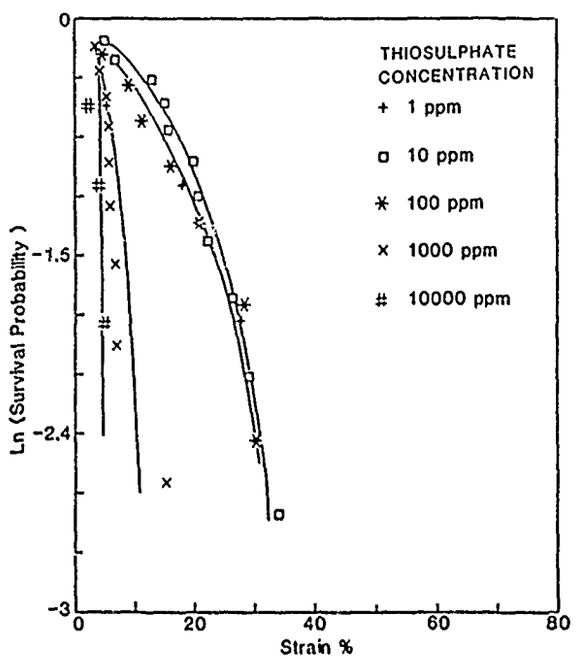


FIGURE 5—Effect of thiosulfate concentration of survival probability.

Controlled potential experiments

The current measured during potentiostatically controlled SSR tests is displayed in Figure 7 for the range of potentials −300 mV to +50 mV_{SCE}. Experiments in the range −100 mV to +50 mV_{SCE} showed a marked decrease in corrosion current at higher strains, which was consistent with the electrochemical noise data found in the open-circuit potential experiments. Further investigation of the reduction in electrochemical activity by stopping SSR experiments in the quiescent period and recording the relaxation in load suggested cracking had stopped. An examination of specimens from experiments terminated between 2% and 10% strain showed that the maximum current corresponded to the maximum crack nucleation rate, and that cracking had occurred in less than 1% of the grain boundaries.

The dependences of crack-initiation frequency and elongation to failure on electrode potential are exhibited in Figure 8. The severest cracking corresponded to the maximum initiation rate, at −150 mV_{SCE}. The "anodic protection potential" was found to be between +50 mV and +100 mV_{SCE}.

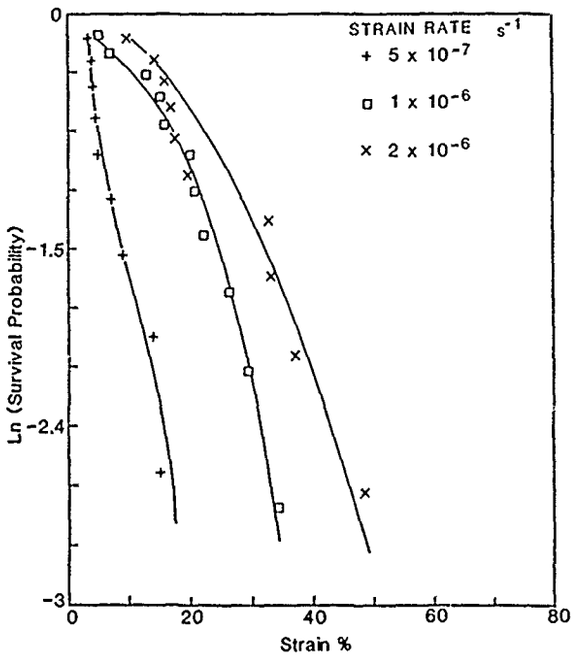


FIGURE 6—Effect of strain rate on survival probability.

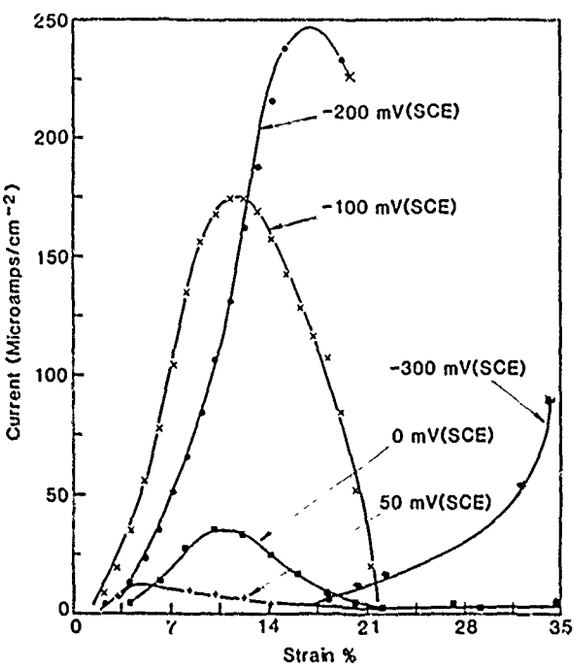


FIGURE 7—Corrosion current measured during slow-strain-rate tests at different electrode potentials.

Discussion

The interpretation of electrochemical transient measurements can provide detailed information on the process of stress corrosion crack initiation. The large variation in the strain to failure values, which was observed in less aggressive solutions (Figures 5 and 6), was concluded to be a result of the inherent randomness of crack initiation. Crack propagation generally did not represent a significant proportion of the test period.

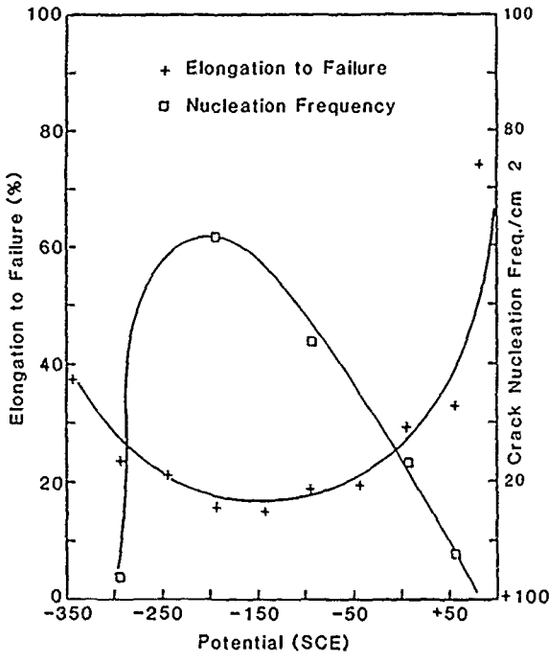


FIGURE 8—Elongation to failure vs potential in slow-strain rate at $10^{-4}s^{-1}$ (+). Crack initiation vs E at 3.5% strain (□).

Correlation analysis of the time interval between current pulses indicates that the occurrence of a current transient (made up of a number of current pulses) was consistent with the activity of an individual crack. The charge–time behavior during the early stages of crack propagation was noticeably periodic; each charge increment was on the order of one grain-boundary facet penetration. Although the total charge passed by some metastable cracks was sizable (i.e., greater than the penetration of one grain-boundary facet), the current flowing did not exceed 500 nA. Similarities are noted between these measurements and the metastable propagation and arrest of microstructurally small defects in pitting corrosion and fatigue, where (respectively) the generation[9] of localized acidity and the influence of microstructure on localized deformation[10] are important.

Crack initiation was found to be more probable at higher thiosulfate concentrations in the open-circuit potential experiments. The proximity of the maximum cracking potential to the potential at which reduction to adsorbed sulfur occurs provides some indication to the mechanism of anodic dissolution.[1] Indeed, the sensitivity of cracking propensity to electrode potential suggests that ohmic potential drop in dilute solutions may move the crack-tip potential below the maximum cracking potential, thereby impeding crack growth.

A rapid decline in the nucleation and propagation of cracks at higher strains was evident at potentials approaching the anodic protection potential, shown in Figures 3, 4, and 7. Interpretation of these results is more speculative. The potentiostatic experiments that were performed between −100 mV to +75 mV_{SCE} showed a significant reduction in current at larger strains, and an apparent reinitiation of cracking occurred shortly before fracture. Further examination of this period of quiescence supported the conclusion that crack propagation had ceased. These observations were also made in the open-circuit potential experiments and are noteworthy because of the large variation in extension rate. The open-circuit potential experiments were performed close to the minimum strain rate to initiate cracking, although crack nucleation and transient propagation has been observed at lower strain rates. It is suggested that preferential strain hardening of the grain boundaries impedes crack initiation. This is the subject of further investigation.

The potential dependence of the results presented in this study support those of Newman, et al.,[1] and Dhawale, et al.,[4] although the potential range for cracking susceptibility in the material used here was more restricted. The grain-boundary chromium-depletion minimum of the material has been measured as 10.3% Cr.[7] A computer model developed by Bruemmer[11] based on the thermodynamics of carbide precipitation and kinetics of chromium diffusivity predicted the chromium depletion to be approximately 10%.[12] A similar prediction for the sensitized material used by Newman, et al., predicted a minimum of about 9% Cr.[1] Repassivation experiments reported by Newman, et al., show that a significant increase in the charge passed before repassivation correlates with a decrease in chromium content in the range 12 to 9 wt%. The cracking behavior of the material used in this study was consistent with the predictions of those repassivation experiments.

Conclusion

(1) Electrochemical techniques have been used to detect current transients during SSR tests on sensitized type 304 SS in dilute thiosulfate solutions. The transients were caused by the initiation, metastable propagation, and repassivation of microstructurally short intergranular stress corrosion cracks.

(2) The current transients were characterized by an initial rise time of 5 to 20 s, and lifetimes of the order of 30 to 1000 s. They typically represent a crack advance of less than one grain-boundary facet in length.

(3) A low-strain region was identified in which both crack-initiation frequency and the associated current-transient frequency were at a maximum. This region persisted up to about 5% elongation.

(4) The large variations in strain to failure values measured in less aggressive solutions could be accounted for in the period required to initiate a crack. Crack propagation was shown to be a minor proportion of the test period.

(5) The formation of a sustained propagating crack (visually confirmed) was marked by a rapid increase in the anodic current of 3 to 5 μA. The high current level was sustained until the specimen fractured.

Acknowledgment

The authors wish to acknowledge the UKAEA underlying research program, the Electric Power Research Institute (contract number RP 8002-1), and the Department of Scientific and Industrial Research of New Zealand for financial support. The authors wish to thank R. Newman of UMIST, whose expertise in this subject area and comments on this work are much appreciated, and to D. Williams of Harwell for his helpful comments.

References

1. R.C. Newman, K. Sieradzki, H. Isaacs, Metall. Trans. A 13A (1982): p. 2015.
2. H.H. Horowitz, Corros. Sci. 23(1983): p. 353.
3. R.C. Newman, K. Sieradzki, Corros. Sci. 23(1983): p. 363.
4. S. Dhawale, G. Cragnolino, D.D. MacDonald, EPRI Project RP 1166-1, Final Report, August 1982.
5. W.L. Clarke, R.L. Cowan, W.L. Walker, Comparative Methods for Measuring Degree of Sensitization on Stainless Steel, ASTM STP 656, ed. R.F. Stiegerwald (Philadelphia, PA: ASTM, 1978), p. 99.
6. D.B. Wells, J. Stewart, A. Herbert, P.M. Scott, D.E. Williams, "The Use of Percolation Theory to Predict the Probability for

Failure of Sensitized Austenitic Stainless Steels by Intergranular Stress Corrosion Cracking," CORROSION/88, paper no. 289 (Houston, TX: National Association of Corrosion Engineers, 1988).
7. S. Ortner, unpublished work.
8 J Stewart, D B Wells, P M Scott, D.E. Williams, "The Development of Electrochemical Techniques to Study Initiation of IGSCC in Sensitized Stainless Steels," CORROSION/88, paper no. 285 (Houston, TX: NACE, 1988).
9 U Bertocci, Y Yang Xiang, J. Electrochem. Soc. 131(1984). p. 1011.
10 K J Miller, Fatigue Fract Eng. Mater. Struct. 10, 2(1987).
11 S M Bruemmer, L.A Charlot, D G. Atteridge, submitted for publication in Corrosion.
12 S.M. Bruemmer, Private Communication, May 1988.

Discussion

R.H. Jones (Pacific Northwest Laboratories, USA): As I commented in our discussion yesterday, your observation of current transients associated with crack growth (beyond the initiation stage) may be associated with ligament formation behind the crack front and subsequent crack-tip-opening displacement and ligament fracture, allowing further crack growth.

J. Stewart: Measurements of current transients resulting from nonpropagating cracks (i.e., cracks that arrest) show cyclic behavior, which we associate with a hindrance of crack advance due to microstructural barriers. Dissipation of the low pH environment (in 1 to 10 s), which is essential for crack propagation, contributes to crack arrest. Sustained crack propagation generally does not occur until much higher strain (and stresses), where mechanical constraints can be overcome. Again, the anodic current behavior is cyclic.

Correlating Sulfide Cracking Resistance with Hydrogen Uptake of 13% Chromium Martensitic Stainless Steel in Sour Environments

A. Turnbull and M. Saenz de Santa Maria***

Abstract

An evaluation has been made of the cracking resistance of 13% Cr martensitic stainless steel in 5% NaCl of varying pH and H_2S content. In solutions of pH ≤ 3.6, the steel is in the active state, and a correlation has been observed between time-to-failure in a slow-strain-rate test and the measured hydrogen uptake determined from permeation measurements. Complementary tests were also conducted in ASTM seawater saturated with H_2S at pH 5.0. In contrast to the behavior in the solution of lower pH, cracking in this environment is associated with hydrogen generated through localized pitting rather than general attack, and the correlation between hydrogen permeation measurements and cracking is no longer valid. In addition, delocalization by diffusion of the hydrogen absorbed from the pit gives rise to less severe cracking than would be predicted from the environmental conditions predicted within the cavity.

Introduction

Materials used in oil extraction must resist both corrosion and cracking associated wth the aggressive nature of the extracted fluid, which contains mixtures of salts, CO_2, and H_2S, and temperatures up to about 150°C. 13% Cr martensitic stainless steels (SSs) are commonly used for production tubing for relatively sweet environments (low H_2S), but there is insufficient information regarding the range of environmental conditions, e.g., H_2S concentration, pH, and temperature, within which this steel can be reliably used. In North Sea fields, the H_2S concentration is generally low, but there is recognition of the potential problem of environment-assisted cracking if wells follow the normal practice of becoming sour with increasing age At temperatures near ambient, failure is associated with hydrogen cracking Accordingly, a study was made of the hydrogen uptake of this steel as a function of environmental conditions,[1] and a broad correlation with cracking resistance was established.[2] The slow-strain-rate technique was used for assessing cracking resistance as a preliminary to more specific fracture mechanics tests, because it provides a rapid assessment of the relative severity (in terms of induced cracking) of varied and complex environments. In this paper, the key features of this work are described, and improved characterization of the hydrogen distribution in lattice and trap sites is reported.

Experimental Method

Full details of the test techniques used have been described elsewhere,[1,2] only the essential details are included herein.

The material used was a type 410 (UNS S41000) SS supplied in a quenched and double-tempered condition with composition and heat treatment as specified in Table 1. The microstructure was tempered martensite with globular carbides and the average prior austenitic grain size was 24 μm (ASTM No. 7.5).

The slow-strain-rate method was used to assess cracking resistance using conventional specimens of gauge length 12.7 mm and diameter 2.54 mm. The nominal strain rate was 1.7×10^{-6} s^{-1}. The specimen was mounted in a Perspex† or PTFE test cell through which the solution was circulated from a 20-L aspirator at a volumetric flow rate of about 0.4 L/min^{-1}. A gas control panel was used to obtain the required mixture of gases in the reservoir.

The test solutions were prepared from Analar† grade chemicals and distilled water. Most of the test solutions were based on NACE Standard TM0177-86[3] and consisted of 5% sodium chloride acidified to pH 2.5 and 3.6 using glacial acetic acid. Some tests were also conducted in ASTM seawater saturated in H_2S (pH ≈ 5.0) correspondingto NACE Standard TM0284-84[4] and in 3.5% NaCl acidified to an equivalent pH of 5.0. The solution temperature for all tests was 23 ± 1°C.

Determination of the hydrogen uptake of the steel was made using an adaptation of the conventional Devanathan-Stachurski cell.[2,5] The solution composition was kept constant by circulating the prepared solution from a large reservoir in a manner identical to that for slow-strain-rate testing. The oxidation current was measured by polarizing the "exit" side of the specimen to +300 mV_{SCE} in 0.1 M NaOH. For both slow-strain-rate testing and permeation studies, the solution flow rate past the specimen was approximately 0.1 cm s^{-1}.

To characterize hydrogen trapping in the steel, repetitive permeation transients were measured. The usual method of conducting these tests is by interrupted cathodic polarization, but, for this steel, the retention of the passive film (which is not completely reduced) and evidence that the surface film was retarding hydrogen entry[6] rendered this method unsuitable. Further studies indicated that the key to obtaining meaningful transients was to ensure that the steel remained in the active state at all times.[6] The method adopted involved obtaining the first transient in a solution of pH 2.6 (3.5% NaCl) with very low H_2S content (< 1 ppm by wt). The solution in the cell was then flushed with a deaerated 3.5% NaCl solution of pH 3.6 (after sealing off the reservoir). This pH was chosen because the steady permeation current density is low and the steel is just in the

*Division of Materials Applications, National Physical Laboratory, Teddington, Middlesex, TW11 0LW England

**Chloride Silent Power Ltd., Runcorn, Cheshire, WA7 1PZ England.

†Trade name.

active state. The anodic polarization curve in Figure 1 confirms the active behavior. However, at this pH, the balance between activity and partial passivity is very fine. With stirring to maintain consistency of pH at the surface and in the bulk, the steel remains active but a reduced stirring rate can cause partial repassivation.

TABLE 1
Composition of type 410 (UNS S41000) Stainless Steel (mass%)[A]

C	Si	Mn	S	P	Cr	Ni	Cu	Mo	Ti	Fe
0.14	0.32	0.46	0.007	0.02	13.5	0.71	0.15	0.05	<0.01	Bal

[A]Heat treatment included austenization temperature of 980°C (oil quench), first tempering temperature of 700°C (air cooling), and second tempering temperature of 630°C (air cooling).

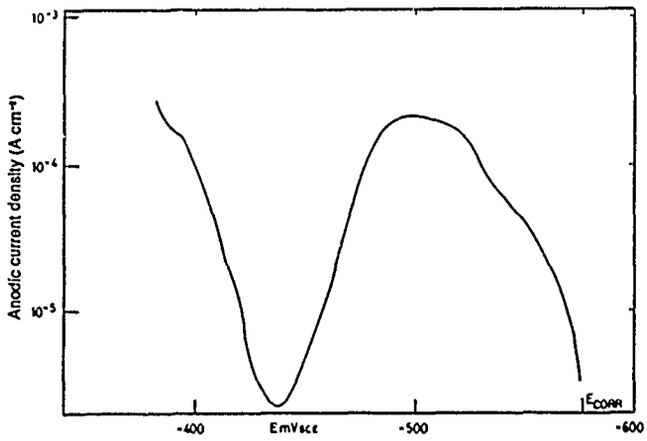


FIGURE 1—Anodic polarization curve for 13% Cr martensitic SS in vigorously stirred solution of 3.5% NaCl at pH 3.6. Polarization scan rate was 0.3 mV/min.

The H_2S content also has a significant effect on active-passive behavior, and a marked change in potential from about −590 mV_{SCE} to more negative values, Ω −660 mV_{SCE} occurs at about 1 ppm. To ensure active behavior in the repetitive permeation experiments, a magnetic stirrer was used during the current decay stage, and this stirring, combined with the presence of residual H_2S, maintained the potential between −660 mV and −670 mV_{SCE}.

During current decay, the reservoir was saturated with H_2S, and after sufficient time for the oxidation current to drop to its minimum value the reservoir solution was then pumped through the cell. Flushing was again conducted when the permeation current had reached steady state and the process repeated to obtain a third transient.

In the slow-strain-rate and permeation tests, determination of the H_2S content of the solution was made by the API electrometric titration method.[7] H_2S content and pH were measured at regular intervals during testing to ensure constancy of conditions. All tests were conducted under freely corroding conditions and the electrode potential of the specimen was monitored continuously. For solutions of pH 2.6 and 3.6, the values were in the range −650 mV_{SCE} to −700 mV_{SCE} for H_2S contents greater than 1 to 2 ppm with the more negative values being associated with the pH 3.6. At lower H_2S contents, the potential tended toward −600 mV_{SCE}. For H_2S saturated seawater (pH 5.0), the corrosion potential was about −612 mV_{SCE}. In the more acid solutions a slight shift in potential (usually ~ 20 mV) to more positive values occurred during straining, while in the seawater tests, the potential drifted about 20 mV more negative. The corrosion potentials in both slow-strain-rate and hydrogen permeation tests were broadly similar, though the final potentials in the slow-strain-rate tests were slightly less negative.

Results and Discussion

Characterization of hydrogen diffusion and trapping

Evaluation of the distribution of hydrogen in the steel was made by combining theoretical modeling[8] of hydrogen diffusion and trapping with experimental measurement of repetitive permeation transients.[6] During the first transient, all irreversible traps are filled, and thus the second transient relates only to reversible hydrogen trapping. The similarity of the second and third transients in Figure 2 (plotted in the form of normalized flux vs dimensionless time, where a is the membrane thickness) indicates that there is no significant void growth or trap development as a consequence of the permeation process. Figure 2 also shows the theoretical curves derived from fitting the model to the experimental data. The relevant parameters determined in this way are as follows.

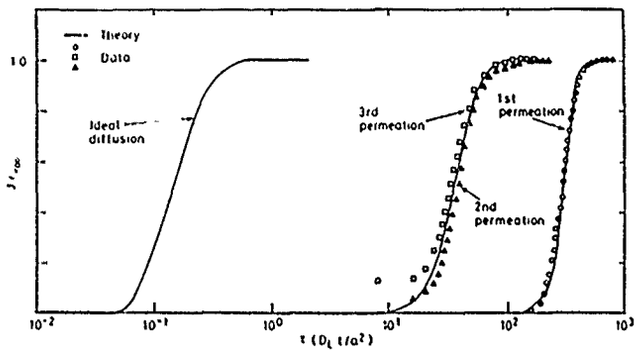


FIGURE 2—Repetitive permeation measurements on type 410 (UNS S41000) SS (see text).

The densities of reversible and irreversible trap sites were (3.0 ± 1.0) × 10^{19} sites cm^{-3} and about 1.5 × 10^{19} sites cm^{-3}, respectively. These values are consistent with the observation by Oriani[9] that the density of trap sites in undeformed steels is about 10^{19} sites cm^{-3}. The capture rate constant for the irreversible traps was (4.8 ± 1.3) × 10^{19} cm^{3} s^{-1}, and assuming a similar value for the reversible traps, the release rate constant of the reversible traps is evaluated to be (3.4 ± 1.6) × 10^{-2} s^{-1}. The binding energy of the reversible trap sites was determined to be (38.7 ± 1.0) kJ mol^{-1}, which is fairly close to the binding energies associated with dislocations and possibly grain boundaries.[10,11] Experimental evaluation of the lattice diffusion coefficient is not possible for this steel because of the large extent of trapping[6] and the literature value of 7.2 × 10^{-5} cm^2 s^{-1} at 23°C, from the data compiled by Kiuchi and McLellan,[11] was used in appropriate calculations.

The effect of trapping in concentrating the diffusing hydrogen atoms is exemplified in Figure 3, which is based on calculations for H_2S-saturated 5% NaCl at pH 2.6. The C_o value is about 2.5 × 10^{-7} mol cm^{-3} (1.5 × 10^{17} atoms cm^{-3}), and the corresponding concentration in trap sites is about two orders of magnitude greater. Hence, trapping provides the means of accumulating significant quantities of hydrogen atoms, which will be a factor in accelerating crack initiation and propagation.

No attempt has been made to describe the diffusion and trapping behavior in terms of effective diffusivity because the concept has no theoretical validity and quantitatively can be erroneous when fractional occupancy of sites is significant, this is always true when irreversible trapping is important, as in this 13% chromium steel.[6]

The calculated values of C_o (subsurface hydrogen concentration) derived in acid solutions of varying H_2S content are shown in Figure 4, and, as expected, the C_o value increases with increasing H_2S content and decreasing pH. The value for seawater was very low, despite the high H_2S level, and was associated with the retardation of hydrogen entry by the passive film with only localized pitting acting as a significant source of hydrogen atoms.[2]

Very recent results (which are not shown in Figure 4) from tests conducted in a CO_2-saturated salt solution (pH = 3.6) also gave rise

to a permeation current indiscernible from the background level; this suggests $C_o \leq 2.7 \times 10^{-10}$ mol cm^{-3}). At the low flow rates used, it is likely that $FeCO_3$ would have formed and limited significant corrosion and hydrogen entry Increasing the flow rate by use of a magnetic stirrer increased the C_o value to about 8.2×10^{-9} mol cm^{-3} Parallel slow-strain-rate tests have not been conducted as yet, but the results do suggest a probable effect of flow rate on the time-to-failure.

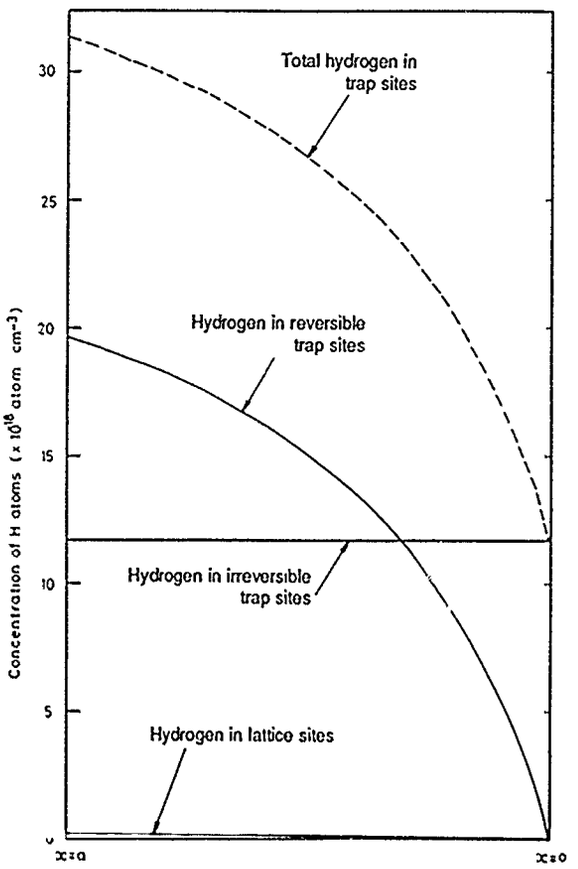


FIGURE 3 – Distribution of hydrogen atoms through membrane thickness at steady state.

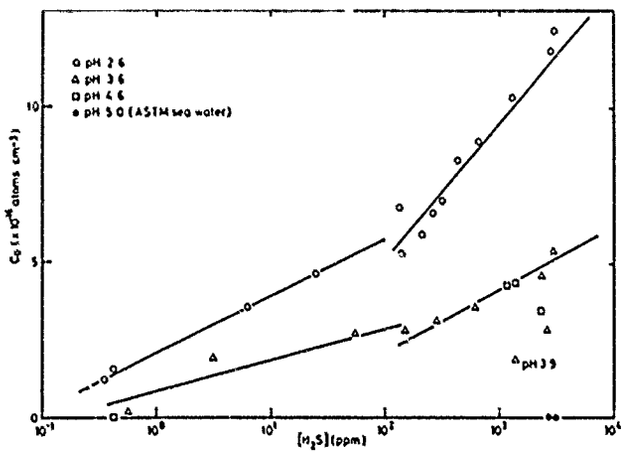


FIGURE 4—Variation of subsurface hydrogen concentrated (C_o) with H_2S concentration and pH.

Slow-strain-rate results

In analyzing the slow-strain-rate data for this system, it was shown previously that the time-to-failure provides the parameter most sensitive to changes in environmental conditions at this specific strain rate.[2] The effect of pH and H_2S concentration on time-to-failure is shown in Figure 5. The steel is highly susceptible to cracking in these aggressive environments, which is consistent with the conclusion of other workers.[12,13] Several of the specimens were pre-exposed to the solution for varying periods prior to loading to assess the influence of charging time, and this caused a slight reduction in the time-to-failure as shown in Figure 5, though the effect is only apparent for the less aggressive environments. In the more aggressive environments, generating higher C_o values, the traps effectively fill up more quickly, and thus their retarding influence on hydrogen transport is reduced. The results of Figure 5 indicate that cracking susceptibility is greatest at low pH and high H_2S concentration; under these conditions, hydrogen uptake is enhanced. Indeed, a direct correlation between the time-to-failure and C_o can be seen from Figure 6. However, this correlation exists only when the steel is in the active state (pH $\lesssim$ 3.6) and the steel surface is corroding uniformly.

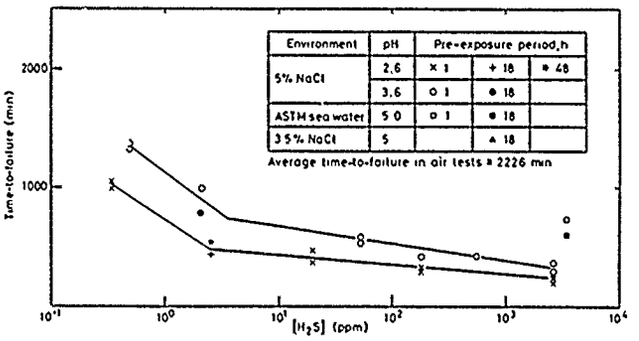


FIGURE 5—Time-to-failure of type 410 (UNS S41000) SS specimens in slow-strain-rate tests in 5% NaCl solution of varying pH and H_2S concentration. Strain rate $\dot{\epsilon} = 1.7 \times 10^{-6}$ s^{-1}.

The relationship between time-to-failure and C_o suggests that cracking depends on the hydrogen produced by *bulk* charging. Any hydrogen produced at the tips of cracks is evidently swamped by the hydrogen generated on the surface external to the crack. Extrapolation of this conclusion to fracture mechanics specimens must be done carefully. Nevertheless, it is very likely that in a solution that conforms to NACE Standard TM0177 86, charging will be predominantly from the external surface of fracture mechanics specimens, particularly if the precrack is deep, enabling partial consumption of H_2S within the crack (by reaction to form iron sulfide and by cathodic reduction). This has implications for test methodology with regard to factors such as time, specimen thickness and configuration (plate or tubular), surface condition, and application of coatings.[14] Derivation of a relationship between threshold stress-intensity factor and C_o, similar to that suggested for high-strength steels,[15] must consider the conditions of testing, and further investigation is planned.

In H_2S-saturated seawater, the permeation current was very small, yet significant cracking was observed with a time-to-failure much shorter than would be predicted based on Figure 6. In this environment, the attack on the steel is localized and significant amounts of hydrogen are generated only within pits, which then lead to accelerated failure. Calculations[1] have shown that the H_2S concentration will remain close to saturation in the pit solution and the pH must be less than or about 3.6. Hence, despite the smaller time-to-failure predicted from permeation, the observed time-to-failure is still significantly longer than suggested by this local evironmental condition (i.e., H_2S saturation at pH $\leq$ 3.6). The most probable explanation is associated with the localized nature of hydrogen generation. Dissipation of the absorbed hydrogen by diffusion to the region surrounding a pit will reduce the hydrogen content local to the pit or crack site. Consequently, the hydrogen content available for cracking will be less. In contrast, when the *bulk* solution is H_2S

saturated at pH 3.6, the steel is in the active state and hydrogen charging occurs uniformly over the surface with a consequent reduced time-to-failure.

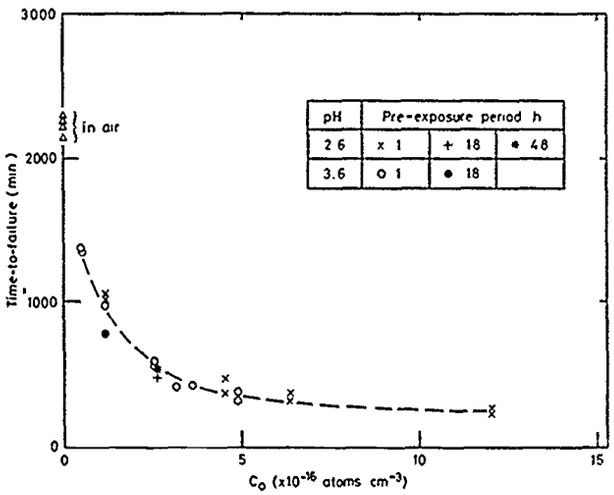


FIGURE 6—Variation of time-to-failure in slow-strain-rate tests for type 410 (UNS S41000) SS specimens with subsurface hydrogen concentration (C_o) (calculated from permeations tests) in 5% NaCl of varying pH and H_2S concentration. Strain rate $\dot{\epsilon} = 1.7 \times 10^{-6}$ s^{-1}.

For fracture mechanics tests in H_2S-saturated seawater, the supply of hydrogen will be predominantly from localized reaction within the crack, though crack size, in relation to H_2S consumption, may have a significant role.

Conclusion

In acidified brine solutions of pH ≤ 3.6 with varying concentrations of H_2S, 13% Cr martensitic SS is actively corroding, and a correlation between cracking resistance and hydrogen uptake of the steel can be identified. At higher pH values, the hydrogen uptake is considerably reduced by the presence of the passive film, and significant hydrogen entry occurs via pitting corrosion induced by the presence of H_2S.

However, delocalization of the hydrogen absorbed from reaction in the pit solution is considered to reduce the severity of cracking that otherwise would be expected, based on the environmental conditions within the pit.

Acknowledgment

M.W. Carroll, a "sandwich" course student from Coventry Polytechnic, contributed to the experimental studies of hydrogen permeation.

References

1. A. Turnbull, M. Saenz de Santa Maria, N.D. Thomas, Corros. Sci. 29, 1(1989): p. 89.
2. M. Saenz de Santa Maria, A. Turnbull, Corros. Sci. 29, 1(1989). p. 69.
3. NACE Standard TM0177-86, "Testing of Metals for Resistance to Sulfide Stress Cracking at Ambient Temperatures" (Houston, TX: National Association of Corrosion Engineers, 1977).
4. NACE Standard TM0284-84, "Evaluation of Pipeline Steels for Resistance to Stepwise Cracking" (Houston, TX: NACE, 1984).
5. M.A.V. Devanathan, Z. Stachurski, Proc. Roy. Soc. A270(1962): p. 90.
6. A. Turnbull, M.W. Carroll, D.H. Ferriss, "Analysis of Hydrogen Diffusion and Trapping in a 13% Cr Martensitic Stainless Steel," NPL (National Physical Laboratory) Report DMA(A)158, 1988, accepted for publication in Acta Metall.
7. API Recommended Practice for Analysis of Oil-Field Waters, API RP 45 (2d ed.) (Washington, DC. American Petroleum Institute, 1968).
8. D.H. Ferriss, A. Turnbull, "Analysis of Reversible and Irreversible Hydrogen Trapping in Metals," NPL Report DMA(A)154, January 1988.
9. R.A. Oriani, Acta Metall. 18(1970): p. 147.
10. J.P. Hirth, Metall. Trans. 11A(1980). p. 861.
11. K. Kiuchi, R.B. McLellan, Acta Metall. 31, 7(1983). p. 961.
12. A.K. Agrawal, W.N. Stiegelmeyer, J.H. Payer, CORROSION/86, paper no. 169 (Houston, TX: NACE, 1986).
13. F. Mancia, Corros. Sci. 27, 10/11(1987): p. 1225.
14. A Turnbull, M Saenz de Santa Maria, Metall. Trans. 19A(1988). p. 1795.
15. R P Gangloff, A Review and Analysis of the Threshold for Hydrogen Environment Embrittlement of Steel, Corrosion Prevention and Control, Proceedings of the 33rd Sagamore Army Materials Research Conference, ed. S. Isserow (Waterton, MA. U.S. Army Materials Technology Laboratory, in press 1986).

Strain-Rate Effects in Hydrogen Embrittlement of a Ferritic Stainless Steel

R.N. Iyer and R.F. Hehemann***

Abstract

A 26Cr-1Mo ferritic stainless steel was tested for severity of hydrogen embrittlement with respect to transient strain-rate effects. Tests were conducted at room temperature using a uniaxial constant-load fixture, incorporating appropriate cell assembly. After giving different amounts of creep exhaustion for the alloy, hydrogen was charged electrochemically using 5% sulfuric acid solution containing small amounts of arsenic trioxide as a poison for hydrogen evolution reaction. Results from creep exhaustion experiments showed that the time-to-failure by hydrogen embrittlement depended on the strain rate, but not on the total strain undergone by the specimen. The mode of failure also changed from intergranular/cleavage to cleavage/ductile rupture with increasing creep exhaustion time or decreasing peak transient strain rates. These effects are explained on the basis of strain localization by hydrogen.

Introduction

The transport of hydrogen to traps inside a material can occur by diffusion and dislocations and can lead to hydrogen embrittlement (HE).[1] Typically, dislocation transport of hydrogen is about 10^4 times faster than that by diffusion.[1] Both the transport behavior and trap behavior are intimately related to the strain rate of a material susceptible to HE.[2] A previous study[3] showed that 26Cr-1Mo steel (26-1S), a ferritic stainless steel (SS), was susceptible to HE, especially under grain-coarsened and prestrained conditions. The focus of this investigation was on the effect of transient strain rates on the severity of HE in a ferritic SS (26-1S) by electrochemical (cathodic) charging of hydrogen. Decreasing transient strain rate decreases the severity of HE.

Experimental

Materials and preparation

26Cr 1Mo ferritic SSs, designated 26-1S, were used for this study, the chemical analysis is presented in Table 1. The alloy was obtained as annealed strips 0.05 in. (1.27 mm) thick. Specimens 0 5 n (12.7 mm) wide and 11 in (280 mm) long were cut from the strips parallel to the rolling direction and were grain coarsened by heat treating them at 1050°C for 1 h in an atmosphere of nitrogen and subsequently water quenching them Test specimens were prepared by milling the heat treated specimens to gauge lengths of 2 in (50 8 mm) and widths of 1/8 in. (3.18 mm). They were then prestrained to 5% elongation (in air), using an Instron† tensile tester. The final preparation of the specimens involved sequential sanding with 240-, 320-, 400-, and 600-grit papers, degreasing with acetone, washing with distilled water, and drying with methanol. The prepared specimens were mounted in a rubber stopper with R.T.V.† silicone rubber and masked with the silicone rubber (to avoid failure at and above the liquid-vapor interface), leaving a 5-cm-gauge-length portion unmasked. The mounted specimens were allowed to cure for a day in a desiccator.

Table 2 shows the tensile strength, 0.2% offset yield strength and percent elongation determined using the Instron tensile tester after the above treatments of the specimens.

Test procedures

Hydrogen-charging experiments were performed at ambient conditions, in a glass cylindrical cell, with the tensile specimen uniaxially loaded by a cantilever arrangement.[3,4] Variation in the experimentation consisted of obtaining different amounts of creep exhaustion by loading in air *in situ* (in the cell) prior to the hydrogen charging. In this way, the specimen would be under different initial transient strain rates during hydrogen charging. The loading was uniaxial, corresponding to 90% of the 0.2% offset yield strength of the heat-treated alloy. The choice of this level of stress is based on the fact that dislocations become mobile, but bulk yielding will not occur, and the alloy can withstand this level of constant load for years under pure mechanical loading conditions. Elongation vs time was monitored using a dial gauge and an appropriately designed timing device. The dial gauge measured deflection of the cantilever beam, and from the ratio of the arms of the cantilever, the specimen elongation was determined.[3] Since specimen elongation was uniform throughout the gauge length during creep exhaustion, strain and strain rate were directly determined from the gauge length and elongation of the specimen.

The specimen was hydrogen charged galvanostatically at a current density of 100 mA/cm^2, with a cylindrical platinum gauze serving as the counter electrode. The charging solution was 5% sulfuric acid with additions of 2 g/L of arsenic trioxide acting as a promoter of hydrogen entry into the specimen. The solution was deaerated by bubbling nitrogen gas continuously.

The time-to-failure was recorded by a timing device and the failed specimens were fractographically examined with a scanning electron microscope (SEM).

*Department of Materials Science and Engineering, Pennsylvania State University, University Park, PA 16802.

**Deceased. Formerly Professor, Department of Metallurgy and Materials Science, Case Western University, Cleveland, OH 44106.

†Trade name.

TABLE 1
Chemical Composition of 26-1S (wt%)

C	N	Cr	Mo	Ni	Cu	Ti	Nb
0.02	0.068	26[A]	1[A]	0.25	0.07	0.49	0.003

[A]Indicates nominal composition.

TABLE 2
Mechanical Properties (Longitudinal) of 26-1S

Property		Mill Annealed	1050°C/1 h—Water Quenched[A] + 5% Prestrained
YS	(ksi)	55	61
(0.2% offset)	(MPa)	(379)	(421)
TS	(ksi)	76	78
	(MPa)	(524)	(538)
Elongation (%)		26	12

[A]Exposed for 1 h at 1050°C and water quenched.

Results

The decay of the specimen creep (strain) rate as a function of time at the constant load (corresponding to 90% of the yield strength) is shown in Figure 1, exhibiting the normal room-temperature (logarithmic) creep behavior. Increasing amounts of creep exhaustion prior to hydrogen charging provided lower initial transient strain rates during hydrogen-charging conditions. Figure 2(a) shows the time-to-failure as a function of the initial strain rate (i.e., the peak strain rate at the instant of hydrogen charging). It is obvious that the time-to-failure by HE was enhanced with decreasing initial strain rate. For example, the specimen having an initial strain rate of about 10^{-5} s^{-1}(i.e., without any creep exhaustion prior to hydrogen charging—see also Figure 1) failed in fewer than 3 h in a brittle manner, whereas the specimen having an initial strain rate of about 7×10^{-10} s^{-1} (after creep exhaustion for 100 h) failed after 13 h. However, at strain rates below about 2×10^{-10} s^{-1} (corresponding to 500 h of creep exhaustion), additional creep exhaustion did not improve the failure time any further [Figure 2(a)]. It is interesting to note that although the cumulative strain increased with increasing amounts of creep exhaustion, the time-to-failure did not decrease as would be expected; rather, the time-to-failure increased [Figure 2(b)].

To obtain an understanding of how the creep exhaustion is increasing the time-to-failure, fractographic analysis was performed. Figures 3(a) through (d) show the change in the failure mode with increasing amounts of creep exhaustion (or decreasing peak transient strain rates). When there was no creep exhaustion, i.e., when the loading and hydrogen charging commenced simultaneously (corresponding to the highest peak transient strain rate of about 10^{-5} s^{-1} shown in Figure 1 for almost zero time of creep exhaustion), the failure mode was predominantly intergranular fracture, as illustrated in Figure 3(a). That the hydrogen embrittlement cracks in 26-1S originate at the grain boundaries was shown before and was attributed to the trapping of hydrogen by segregated nitrogen and TiC precipitates at or near the grain boundaries.[5] With increasing creep exhaustion time (i.e., with prior loading in the cell in air for a period of time before the commencement of hydrogen charging corresponding to a lower peak transient strain rate, for example, of about 10^{-9} s^{-1} shown in Figure 1 for 50 h of creep exhaustion), the failure mode progressively changed from intergranular/cleavage [Figure 3(b)] to cleavage/ductile rupture [Figures 3(c) and (d)].

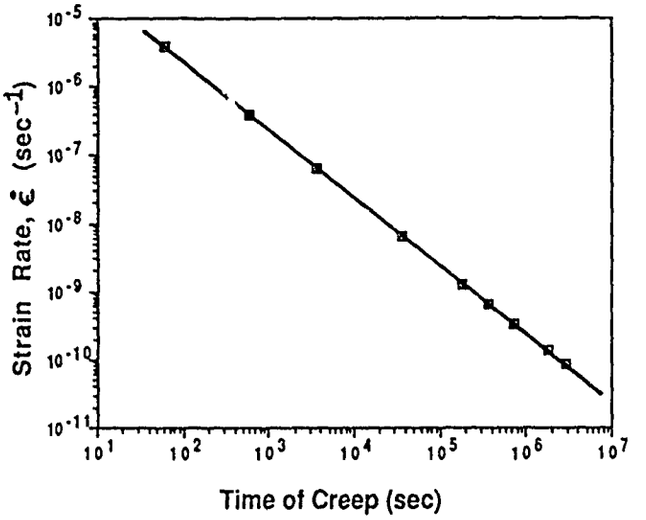


FIGURE 1—Transient strain rate as a function of time of creep for 26-1S (1050°C/1 h-water quenched + 5% prestrained) at room temperature.

Discussion

During transient creep (under constant load), strain rate decreases steadily as a function of time (Figure 1) as a result of strain hardening (or strengthening) effects offsetting recovery processes (i.e., as moving dislocations encounter obstacles such as grain boundaries and are immobilized). The peak strain rate (i.e., the strain rate at the commencement of hydrogen charging) is therefore varied with different amounts of prior loading or creep exhaustion. Both the time-to-failure plot (Figure 2) and the fractographs [Figures 3(a) through (d)] clearly indicated the beneficial effects of creep exhaustion on HE resistance. The occurrence of a particular fracture mode and transition in that mode depend on the stress intensity (K). With increasing K, the fracture path will change from intergranular to transgranular and to ductile rupture.[6,7] Several factors may be involved in determining the fracture path. For transgranular cracking, the availability of activated slip systems plays an important role.

Cross-slip processes can be inhibited[8] (i.e., strain can be localized because of hydrogen trapped by segregated impurities at various defects, such as P and S segregated to grain boundaries[7,9-11]), which will then make intergranular fracture (which can occur at low K values) possible. This is clearly demonstrated in the fractograph shown in Figure 3(b), where islands of intergranular fracture are interspersed with cleavage and ductile rupture areas. The mixed mode behavior (i.e., cleavage and ductile rupture) is also apparent in Figures 3(c) and (d) and is a clear indication of the phenomenon of strain localization by hydrogen. It should be kept in mind that the fast-fracture process is ductile rupture, as in pure mechanical failures, and intergranular failure occurs because of hydrogen embrittlement. Presence of interstitials such as nitrogen, which traps hydrogen well,[12] increases hydrogen absorption at grain boundaries and thus increases susceptibility to HE in 26-1S.[5]

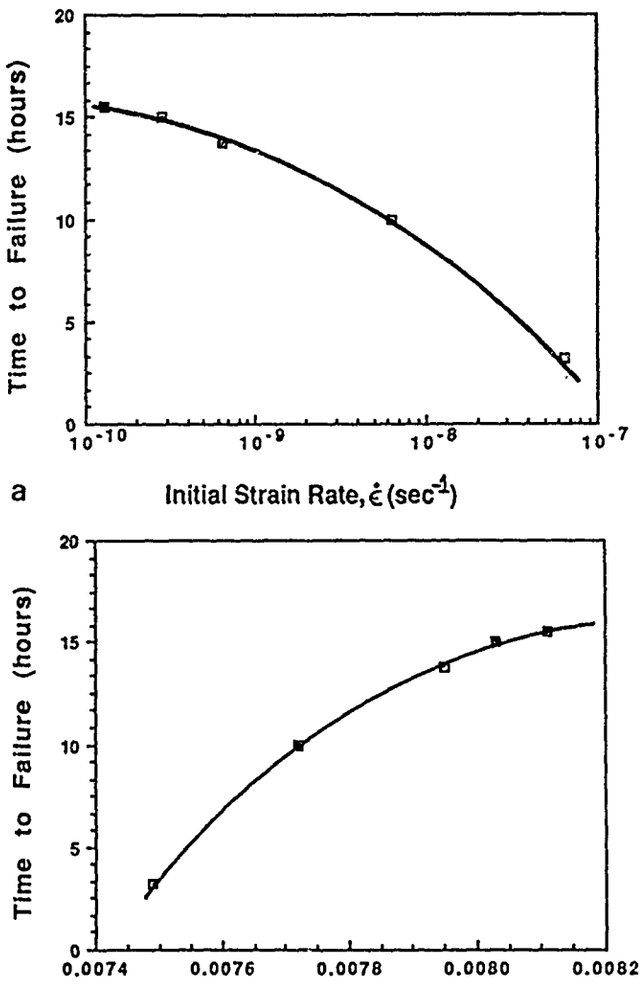


FIGURE 2—(a) Time-to-failure as a function of initial strain rate (i.e., the peak strain rate at the instant of hydrogen charging under stress, just after creep exhaustion) at room temperature for 26-1S (1050°C/1 h—water quenched + 5% prestrained), and (b) time-to-failure as a function of initial cumulative strain (i.e., the total strain at the instant of hydrogen charging under stress, just after creep exhaustion) at room temperature for 26-1S (1050°C/1 h—water quenched + 5% prestrained).

While the peak transient strain rate was very important in determining the time-to-failure by HE, the total strain did not seem to affect it. With increasing creep exhaustion, the total strain accumulated in the specimen increased, but the severity of HE did not. This is somewhat contradictory to what is simplistically expected but does not necessarily rule out a strain effect. Perhaps increased strain and associated dislocation morphologies may be beneficially mitigating hydrogen cracking. Certainly, the peak transient strain rate operating at the commencement of hydrogen charging was the important factor, and since it decreased with increasing creep exhaustion, the severity of HE also decreased. Since the strain rate controls slip processes and dislocation motion, one could rationalize that the strain rate and hydrogen concentration at a specific location combine to cause strain localization and local plastic instability, causing cracking to occur.[13,14]

Summary and Conclusions

(1) Various amounts of creep exhaustion were given to grain-coarsened and prestrained 26-1S alloy specimen, by loading *in situ* at 90% of the yield strength prior to exposure to sulfuric acid solution under cathodic charging conditions. Increasing amounts of creep exhaustion increased the time-to-failure of the specimen by HE.

(2) Analysis of the creep exhaustion results shows that the time-to-failure by HE depended on the strain rate, but not on the total strain undergone by the specimen; thus, it is the peak transient strain rate that is important in HE. However, strain effect cannot be ruled out since increased strain and dislocation morphologies may have some beneficial effect on hydrogen cracking, which is not simplistically expected.

(3) The HE fracture modes of the specimens changed from intergranular/cleavage to cleavage/ductile rupture with increasing creep exhaustion, i.e., decreasing peak transient strain rates.

(4) A critical factor in HE was the peak transient strain rate, in addition to the concentration of hydrogen at the embrittling sites. The fractographs suggested that strain localization and local plastic instability because of hydrogen were the causes of HE.

Acknowledgment

The first author is very grateful to Professor Howard Pickering of Pennsylvania State University for his helpful comments and financial arrangement for the poster presentation based on this paper and to the National Science Foundation for financially supporting the project. The authors acknowledge their gratitude to Case Western Reserve University, where the experiments were conducted.

References

1. J.K. Tien, Effect of Hydrogen on Behavior of Materials, Conference Proceedings, ed. A.W. Thompson, I.M. Bernstein (Warrendale, PA: The Metallurgical Society-American Institute of Mining, Metallurgical, and Petroleum Engineers, 1976), p. 309.
2. M. Taheri, J. Albrecht, I.M. Bernstein, A.W. Thompson, Scripta Metall. 13(1979): p. 871.
3. T.W. Mohr (Ph.D. diss., Case Western Reserve University, 1979).
4. M. Smialowska, M. Rychik, Corrosion 23, 7(1967): p. 218.
5. R.N. Iyer, R.F. Hehemann, A.R. Troiano, Thermomechanical Treatments and Hydrogen Embrittlement of Ferritic Stainless Steels with Different Interstitial Contents, International Symposium on Environmentally-Assisted Cracking: Science and Engineering, Special Technical Publication 1049, ed. W.B. Lisagon (Philadelphia, PA: ASTM, in press 1989).
6. C.D. Beachem, Metall. Trans. 3(1972): p. 437.
7. R A Oriani, Hydrogen Embrittlement of Steels, Annual Review of Materials Science 8(1978): p. 343.
8. C J McMahon Jr., Hydrogen Effects in Metals, ed. I.M. Bernstein, A.W. Thompson (Warrendale, PA. TMS-AIME, 1980), p. 219.
9. B.J. Berkowitz, R.D. Kane, Corrosion 36, 1(1980): pp. 24, 29.
10. C.L. Briant, S.K. Banerji, Int. Met. Rev. 23, 4(1978): p. 164.
11. S.K. Banerji, C.J. McMahon, H.C. Feng, Metall. Trans. 9A(1978): p. 237.
12. B.J. Makenas, H.K. Birnbaum, Acta Metall. 28(1980): p. 979.
13. A.W. Thompson, I.M. Bernstein, Proceedings of the Hydrogen in Metal Congress, Vol. 3 (Elmsford, NY: Pergamon Press, 1977), p. 3.
14. O.A. Onyewuenyi, J.P. Hirth, Metall. Trans. 13A(1982): p. 2209.

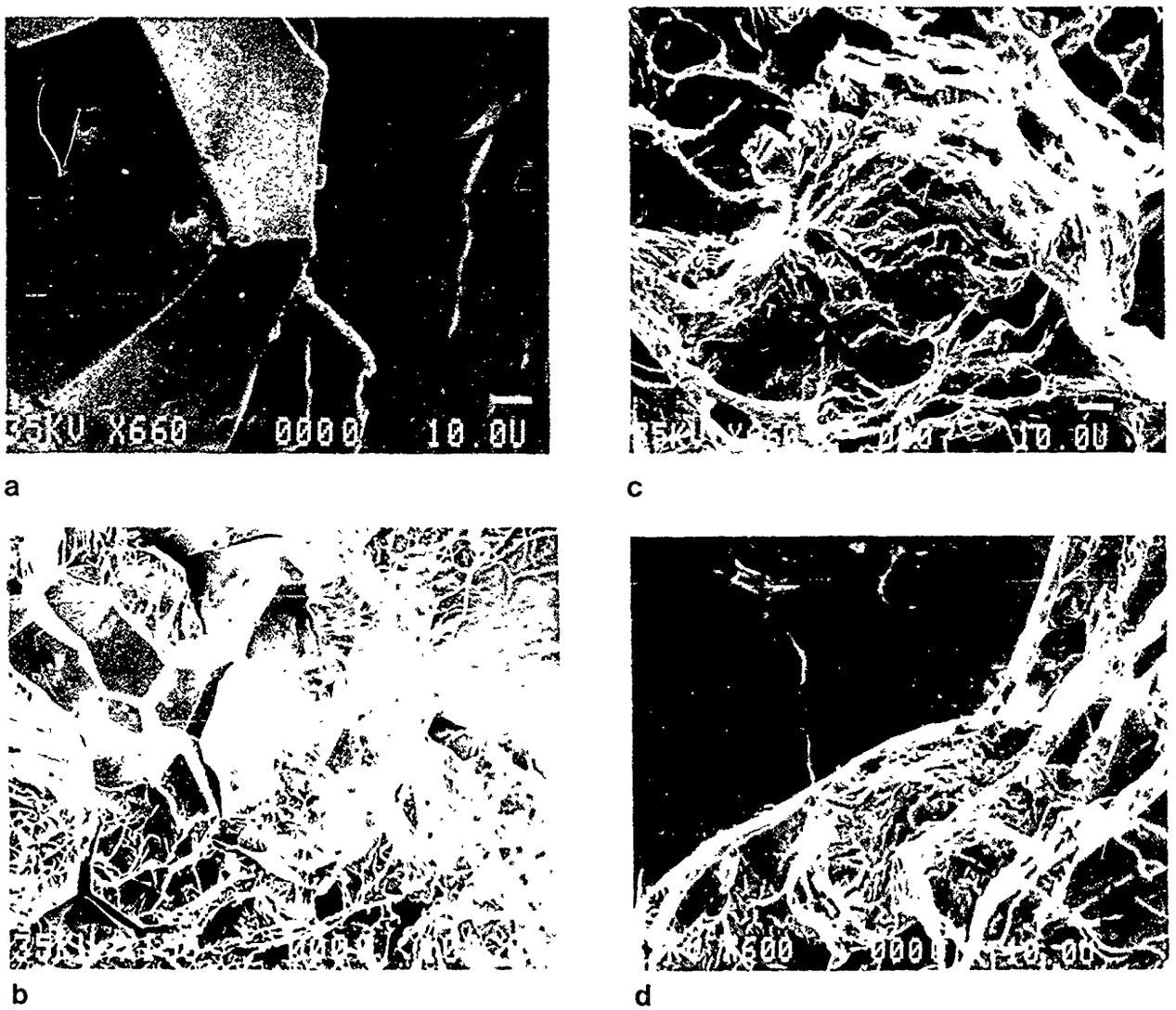


FIGURE 3—SEM fractographs of 26-1S (1050°C/1 h—water quenched + 5% prestrained) hydrogen charged under stress after creep exhaustion for a period of time: (a) 0 h, (b) 10 h, (c) 100 h, (d) 225 h.

Discussion

C.L. Briant (General Electric R&D, USA): Does the nitrogen at grain boundaries act as a trapping site for hydrogen? Why are impurities such as nitrogen, phosphorus, or sulfur necessary for hydrogen embrittlement?

R.N. Iyer: Hydrogen by itself cannot act as a sole embrittling agent, by, for example, pinning dislocations. Also, pure grain boundaries are not, by themselves, very effective hydrogen traps. But the presence of impurities such as N, P, or S can trap hydrogen by acting as an effective solute pinning agent for dislocations, for example. Thus, solute impurities can concentrate hydrogen when they are present at grain boundaries, causing hydrogen embrittlement.

Hydrogen Susceptibility of 2 1/4Cr-1Mo and 9Cr Steels The Role of Trapping Effects

L. Coudreuse, J. Charles,* R. Blondeau,* and A. Cheviet***

Abstract

The hydrogen embrittlement susceptibility of Cr-Mo steels proposed for use in future generation of hydrotreating reactors has been studied. Tensile tests and fracture mechanics tests have been performed on hydrogen-charged specimens of (1) standard 2 1/4Cr-1Mo steel, (2) vanadium-modified 2 1/4Cr-1Mo steel, and (3) modified 9Cr steel (SA 387 grade 91). The influence of hydrogen content has been analyzed. It is shown that vanadium-modified 2 1/4Cr steel and 9Cr steel present an improved behavior compared to the standard 2 1/4Cr-1Mo steel. For the latter, a decrease of the tempering has been found beneficial. The results obtained are discussed, and the role of hydrogen trapping is underlined: the higher the trapping, the better the hydrogen embrittlement resistance. Trapping is increased by elements such as vanadium and is influenced by the heat treatment.

Introduction

Cr-Mo steels are commonly used for the fabrication of hydrotreating reactors, which work under high hydrogen pressure at elevated temperature For these steels, good creep resistance and a resistance to hydrogen attack is required.[1] On the other hand, large quantities of hydrogen may be introduced during service. A part of this hydrogen remains in the steel after shutdown operations, giving rise to the risk of hydrogen embrittlement (HE).[2]

Future generations of reactors will require higher service pressure ($P \geq 200$ bar) and higher temperature ($T \geq 450°C$) and greater plate thicknesses. Therefore, the standard 2 1/4Cr-1Mo steel will have to be modified to yield thick plate material with higher creep resistance and higher hydrogen attack resistance. Several ways to meet this requirement were investigated. (1) decrease the tempering temperature of the standard 2 1/4Cr-1Mo steel, (2) use of 2 1/4Cr-1Mo steel modified by microalloying with (V, Nb, Ti, etc.) to increase creep and hydrogen attack resistance,[3] or (3) use of a steel enhanced by Cr + Nb and V addition, such as SA 387, grade 91, 9Cr steel.[4-7] In this paper, HE susceptibility of different Cr-Mo steels is investigated. Fracture mechanics tests and tensile tests have been performed on hydrogen-precharged specimens.

Experimental Procedure

Material

Tests were performed on four Cr-Mo steels. These comprised two heats of 2 1/4Cr-1Mo steels called A and B, a modified 9Cr steel (C), and a modified 2 1/4Cr-1Mo steel (V addition, Steel D). The chemical compositions were given in Table 1. Steels A, B, and C were industrial heats, while Steel D was a laboratory heat. The steels have been studied for different tempering temperatures (or PWHT), which are reported in Table 2 with the mechanical characteristics obtained.

*Creusot-Loire Industrie, CRMC, BP 56, 71202 Le Creusot, France.

**Creusot-Loire Industrie, Chateauneuf plant, BP 68, 42800 Rive de Gier, France.

Evaluation of Hydrogen Embrittlement Susceptibility

The effect of hydrogen on ductility has been studied by tensile tests on smooth specimens. Reduction of the area of hydrogen-charged specimens (RA_C) is compared to the reduction of the area of uncharged specimens (RA_{UC}). The susceptibility is given by the following index:

$$F\% = [(RA_{UC} - RA_C)/ RA_{UC}] \times 100 \quad (1)$$

The higher the F value, the higher the susceptibility of the steel to HE.

The threshold for crack propagation (K_{IH}) was obtained using the slow rising load technique on hydrogen-precharged specimens.[8]

Fatigue precracked specimens with side grooves were charged in an autoclave Conditions for hydrogen charging were 450°C for 16 h under variable hydrogen pressure to yield different hydrogen concentrations After charging, the specimens were rapidly cooled to room temperature, and the fracture mechanic test immediately performed The test procedure was automated with the loading rate fixed at 5 μm/min The test was stopped when the maximum of the strain–displacement curve was obtained. The specimen was then fractured at low temperature, and the hydrogen content was measured using part of the specimen. The threshold for crack propagation (K_{IH}) was computed from the comparison of the curve of the charged specimen with a reference curve for an uncharged specimen (Figure 1). The J_{MAX} value was measured at the maximum load; this value can be correlated to the tearing resistance of a hydrogen-charged material. The signification of J_{MAX} is the same as the CTOD values measured on flexion specimens (BS 5762).

Results and Discussion

Effect of hydrogen on ductility

The effect of hydrogen on the loss of ductility is shown in Figure 2, where the evolution of the F% index is plotted against hydrogen content for Steels B and D and for several tempering conditions. For a given hydrogen content, the F values are lower for Steel D (0.25 V steel). This shows the positive influence of a 0.25% V addition. Effect

of tempering treatment has also been investigated; it appears that the loss of ductility is less important for the steels with the lower tempering temperature.

TABLE 1
Chemical Compositions of Steels Studied (wt%)

Steel	A $t^{(A)}$=300	B t=55	C t=300	D
C	0.141	0.135	0.105	0.132
S	0.002	0.003	0.0025	0.002
P	0.006	0.007	0.009	0.0035
Si	0.207	0.255	0.43	0.218
Mn	0.565	0.515	0.38	0.659
Ni	0.144	0.250	0.13	0.225
Cr	2.28	2.30	8.26	2.32
Mo	1.04	1.0	0.95	0.97
V	—	—	0.20	0.247
Al	0.019	0.017	0.024	0.033
Cu	0.092	0.055	0.08	0.080
Sn	0.006	0.005	0.008	0.01
	—	—	+0.020 Nb	+Ti-B

$^{(A)}$t: thickness (mm)

TABLE 2
Heat Treatments and Mechanical Characteristics

Steel	Tempering	YS (MPa)	UTS (MPa)	El%	RA%
	650°C-20 h	553	688	22	75
A	670°C-20 h	496	639	26	77
	690°C-20 h	413	572	27	76
	635°C-7 h	634	741	20	77
B	670°C-7 h	550	670	22	78
	700°C-7 h	471	602	26	77
C	750°C-8 h	509	674	20	68
	635°C-7 h	980	1076	16	66
D	685°C-7 h	595	700	20	75
	700°C-7 h	570	675	21	77

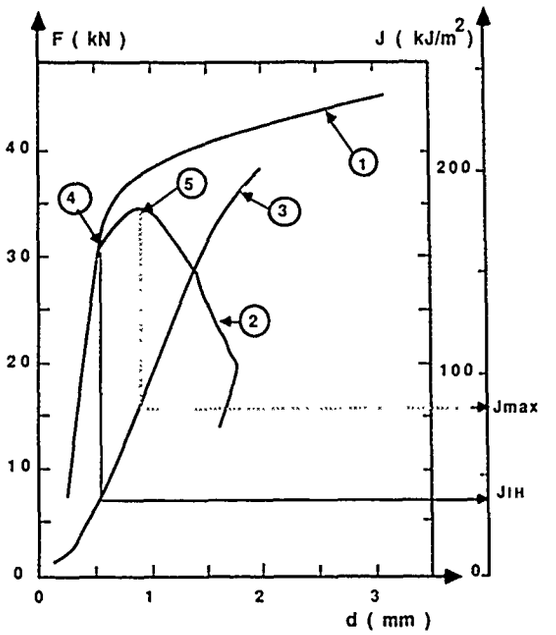
Effect of hydrogen on crack propagation

Steels A, B, and C. Results of fracture mechanics tests for Steels A, B, and C are shown in Figures 3 and 4, where the evolution of the parameters K_{IH} and J_{MAX} vs the hydrogen content are reported. The following points can be noted:

(1) The K_{IH} and J_{MAX} values decrease with increasing hydrogen content.

(2) K_{IH} and J_{MAX} values are higher for the 9Cr steel (steel C). Crack propagation in the presence of hydrogen is more difficult in the 9Cr steels than in the standard 2 1/4Cr-1Mo steels.

(3) For Steel A, no significant difference exists between the 670°C and 690°C tempering treatments, while a tempering at 650°C seems to have a beneficial effect. A large scatter is observed in K_{IH} values (Figure 3) This can be due to the experimental technique and to the fact that the experimental conditions at the fatigue crack tip are not well known.



(1) Reference curve , uncharged specimen.

(2) Stress/displacement curve for the hydrogen charged specimen

(3) J=f(d) curve computed from curve 2

(4) Point when K_{IH} is computed

$$K_{IH} = \sqrt{\frac{EJ_{IH}}{1-\upsilon^2}}$$

(5) Computation of J_{MAX}

FIGURE 1—Determination of K_{IH} and J_{MAX}, principle of the experimental technique.

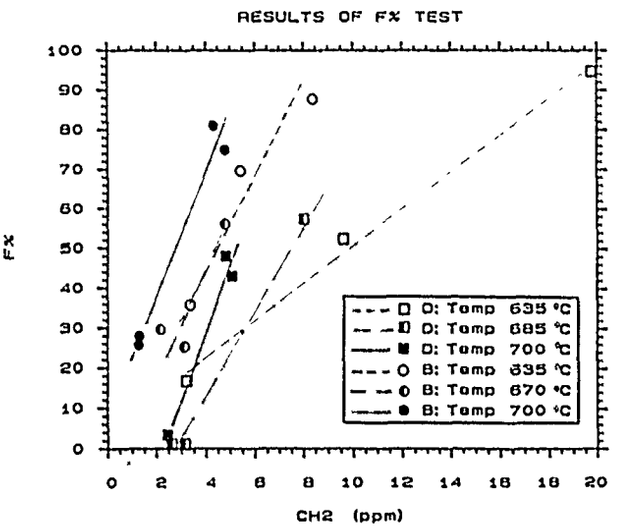


FIGURE 2—Results of tensile tests on hydrogen-charged specimens (Steels B and D).

Steel D. The behavior of Steel D (2 1/4Cr-1Mo-0.25 V) is different from the other steels. The uncharged reference specimens fractured in a brittle mode, the initial toughness of the steel was low, and the behavior of Steel D was not affected by the presence of hydrogen. There is no difference between the curve of the reference sample and the curve of the hydrogen-charged sample (Figure 5). The J values measured at fracture are given in Table 3, where it can be seen that there is no correlation between J and hydrogen content because of the brittle fracture of the specimens.

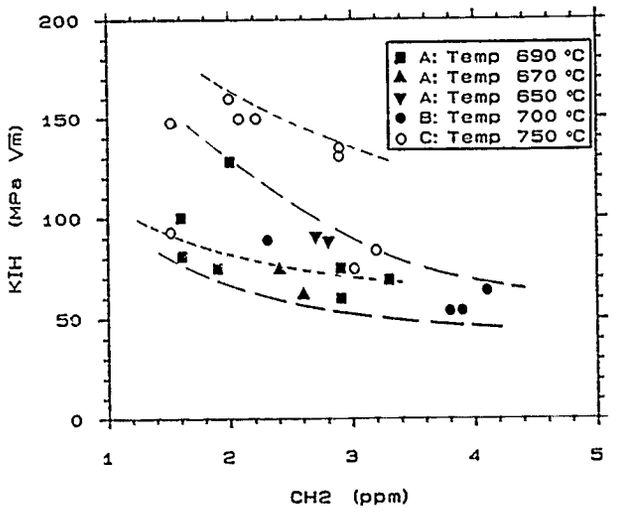


FIGURE 3—K_{IH} values vs hydrogen content.

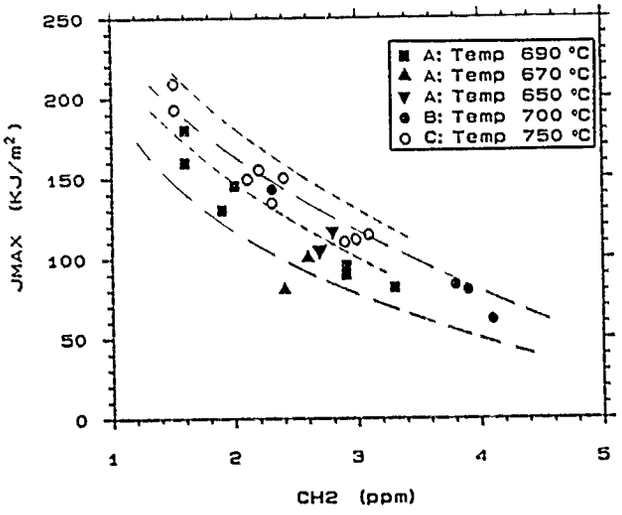


FIGURE 4—J_{MAX} values vs hydrogen content.

Fracture surface observations. Fracture modes were found to depend on hydrogen content and on the steel (Figure 6). For Steels A and B, a quasicleavage mode of fracture is dominant at low hydrogen contents, the proportion of intergranular fracture increasing with increasing hydrogen content. For Steel C, most of the fracture surface is ductile with only some areas of quasicleavage in evidence. A small zone of quasicleavage is observed near the fatigue crack tip. On Steel D, only a small zone of ductile fracture is observed before the final brittle fracture. For the latter, there is no difference between the mode of fracture of hydrogen-charged specimens and uncharged specimens.

Discussion—The Role of Trapping Effects

It is generally accepted that the HE susceptibility of steels increases with increasing mechanical strength and that brittle materials are more susceptible than ductile materials to HE. The present results are at variance with this criteria. The 2 1/4Cr-1Mo-0.25 V steel, which was the most brittle of the steels, was not affected by hydrogen during fracture mechanics tests. The steels tempered at low temperature with the higher mechanical strength showed lower ductility losses during tensile tests. In fact, the results are not contradictory. In this study, steels are compared at a given hydrogen concentration, while steels usually are compared at a given external hydrogen activity. Hydrogen content of the steel depends on trapping capacity of steels. For example, trapping capacities of different Cr-Mo steels are compared in Figure 7. To obtain this data, small specimens (10 by 10 by 20 mm^3) were exposed in an NACE solution[9] saturated with H_2S for 24 h. Diffusible hydrogen was then determined by performing a degassing at 45°C in a glycerin bath. The residual hydrogen (i.e., trapped hydrogen) was determined by vacuum degassing at 650°C. Results show that both diffusible hydrogen and trapped hydrogen depend strongly on the composition and the heat treatment of the steel. Trapping is more important for the highly alloyed materials and for the low-temperature tempering treatment. The question arises whether hydrogen susceptibility must be compared at a given hydrogen concentration or at a given hydrogen activity. In the present case, steels must be compared for a given hydrogen concentration, since during service, hydrogen is introduced at elevated temperatures (≥ 450°C), where trapping effects do not occur.

Results presented in this paper can be explained by considering the trapping capacities of the different steels. From Figure 7 it can be seen that trapping is more important in Steel D than in Steel B. Figure 8 shows degassing rates for Steels A and D (tempering temperature 685°C).

Degassing is very slow for Steels C and D, whereas for Steel A, the degassing rate decreases when the tempering temperature decreases. These degassing curves were obtained by measuring the hydrogen content of hydrogen-charged specimens held for different times at room temperature. From this experiment, it can be concluded that trapping is higher for the 9Cr and the vanadium containing 2 1/4Cr-1Mo steels than for the standard 2 1/4Cr-1Mo steel. For the latter, trapping decreases as the tempering temperature increases. This can be associated with the changes in the number, distribution, and nature of precipitated carbides as tempering temperature increases. For a given total hydrogen concentration, the HE susceptibility is lower for a material with higher trapping capacities. Hydrogen introduced at elevated temperatures is soluble hydrogen. During cooling, part of that hydrogen is trapped at the defects (inclusions, carbides, etc.), while the other part remains in solid solution in the steel (mobile hydrogen). Thus,

$$CH_2 \text{ (Total hydrogen concentration)} = C_T \text{ (Trapped concentration)} + Cm \text{ (mobile concentration)} \quad (2)$$

During testing, it can be assumed that only the mobile hydrogen participates in the embrittlement by interaction with dislocations Therefore, for a given total amount of hydrogen, it is not surprising that steels with higher trapping capacities are less susceptible to crack propagation in the presence of hydrogen.

Conclusion

Tests have been performed on hydrogen-precharged samples to study the influence of chemical composition and tempering treatment on HE susceptibility of Cr-Mo steels. It has been shown that (1) an improvement in HE resistance is obtained with the 9Cr steel and with the vanadium-modified 2 1/4Cr-1Mo steel, and (2) a decrease of tempering temperature leads to an increase in HE resistance. These results have been explained by hydrogen trapping effects. For a given hydrogen concentration, steels with the higher hydrogen trapping capacities show an improved resistance toward HE.

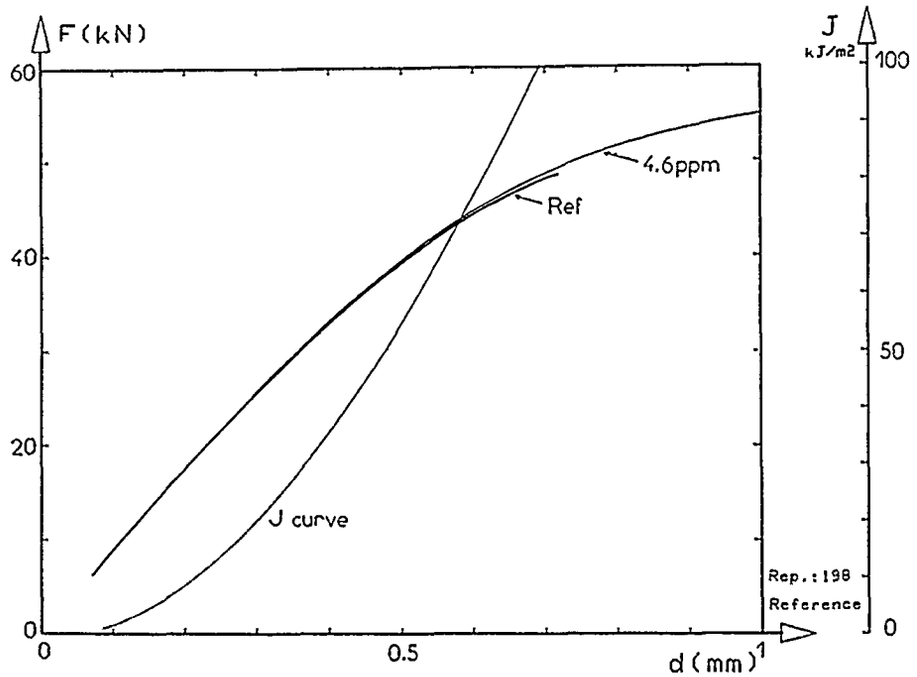


FIGURE 5—Steel D: fracture mechanics test. Comparison of hydrogen-charged specimen (H_2 = 4.6 ppm) and uncharged specimen.

TABLE 3
Results of Fracture Mechanics Tests on Steel D

Tempering	C_{H_2} (ppm)	$J_{FRACTURE}$ (kJ/m^2)
635°C-7 h	0	9→K_{IC} = 45 MPa$\sqrt{m}$
	5.7	8→ K_{IC} = 40 MPa$\sqrt{m}$
685°C-7 h	0	105
	6.8	208
	4.6	264
	3.4	378
700°C-7 h	0	148
	4.4	258

References

1. API Publication 941, Steels for Hydrogen Service at Elevated Temperatures and Pressures in Petroleum Refineries and Petrochemical Plants, 3rd ed (Washington, DC. American Petroleum Institute, 1983).
2. T Iwadate, T. Nomura, J Watanabe, CORROSION/87, paper no 193 (Houston, TX. National Association of Corrosion Engineers, 1987).
3. J Watanabe, T Ishiguro, T Iwadate, K. Uhnishi, Hydrogen Embrittlement of 2 1/4Cr 1Mo and 3 Cr 1Mo 1/4V Ti-B Pressure Vessel Steels, API/MPC Meetings (Washington, DC. API, 1987).
4. A. Cheviet, J. Burlat, R. Blondeau, Journees d'Automne de la Societe Francaise de Metallurgie (Paris, France. la Societe Francaise de Metallurgie, 1987).
5. D.A. Canonico, Ferritic Steels for High Temperature Applications, ed. K. Ashok (Metals Park, OH: ASM International, 1983) p. 31.
6. V.K. Sikka, C.T. Ward, K.C. Thomas, Ferritic Steels for High Temperature Applications, p. 65.
7. Proceedings of Topical Conference on Ferritic Alloys for Use in Nuclear Energic Technologies (New York, NY: American Institute of Mining, Metallurgical, and Petroleum Engineers, 1983), p. 413.
8. J.D. Landes, D.E. McCabe, Application of 2 1/4Cr-1Mo Steel for Thick-Wall Pressure Vessel, ASTM STP 755 (Philadelphia, PA: ASTM, 1982), p. 68.
9. NACE Standard TM0177-86 (Houston, TX: NACE, 1986).

Discussion

B. Pound (SRI International, USA): The effect of strong traps on hydrogen embrittlement (HE) is based on the rationale that fine, well-dispersed traps are beneficial and large traps are detrimental. The results of Coudreuse, et al., show that carbides of elements such as vanadium, which are fine and uniformly distributed in the steel used by these workers, improve the resistance to HE and so are consistent with this rationale. The detrimental aspect of this rationale was illustrated by the results of my work on type 4340 (UNS G43400) steel, also presented at this conference, showing large inclusions to be the principal irreversible traps in this highly HE-susceptible alloy.

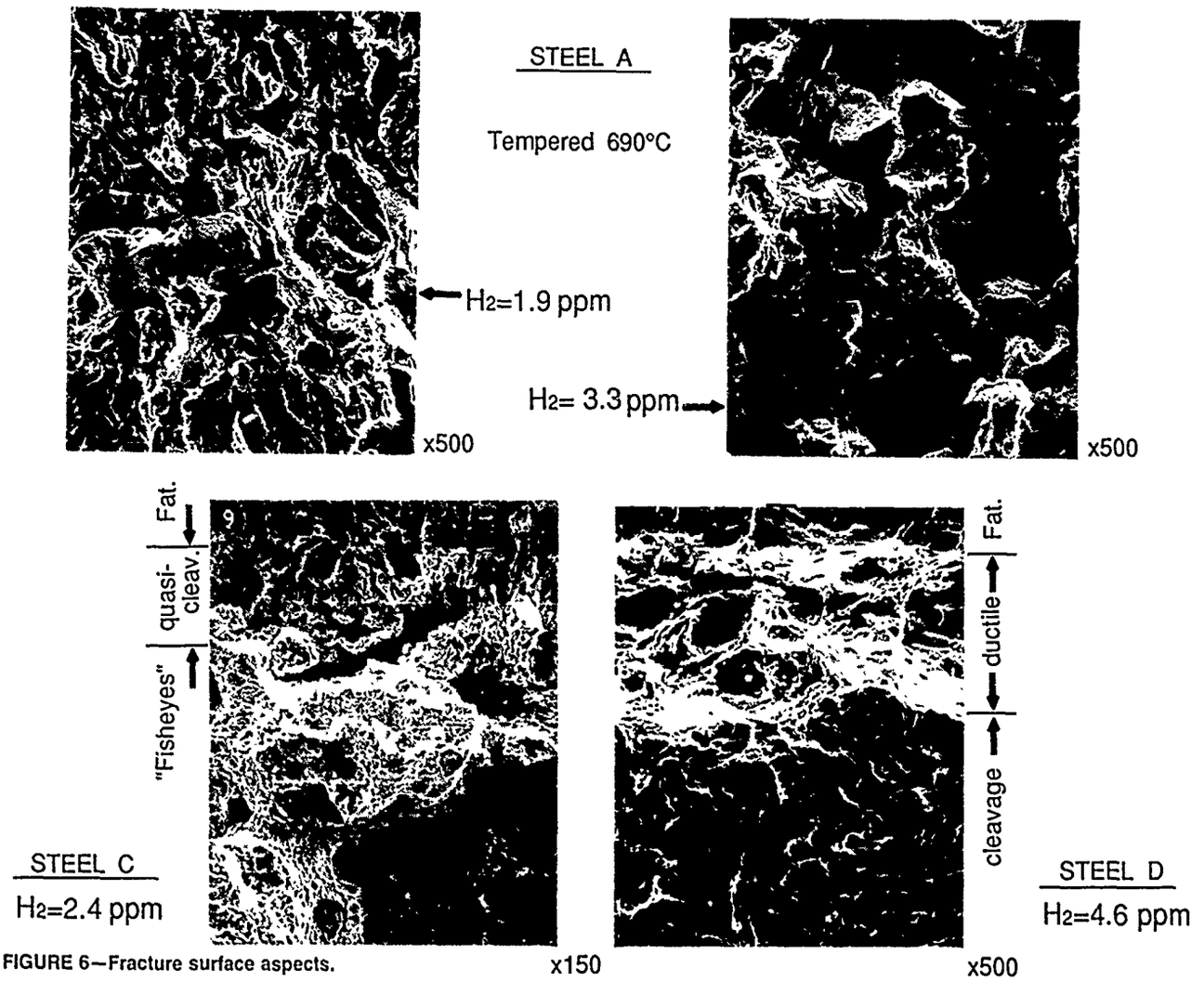


FIGURE 6—Fracture surface aspects.

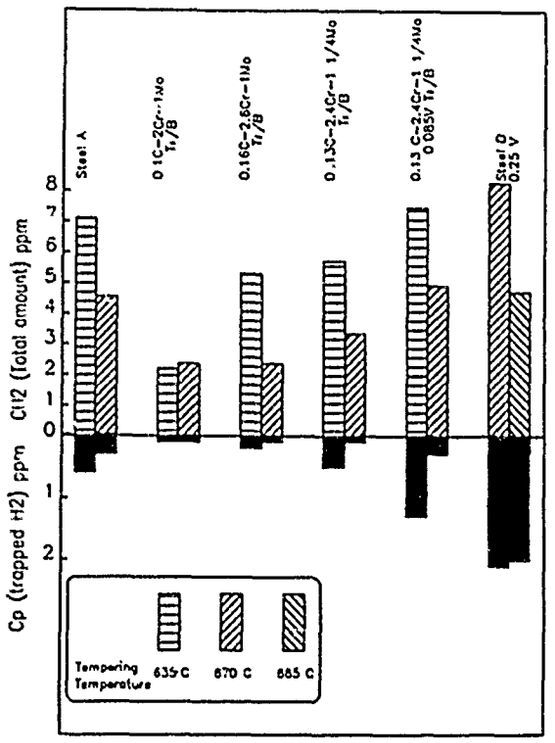


FIGURE 7—Comparison of trapping capacities of different Cr-Mo steels.

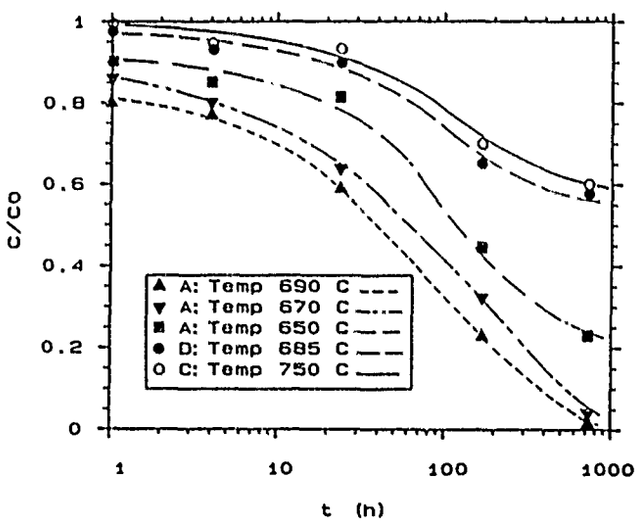


FIGURE 8 – Comparison of degassing curves for Steels A and C (at 20°C).

Liquid-Zinc-Induced Crack Propagation in High-Strength Steels

K. Nakasa and M. Suzawa***

Abstract

To investigate the crack propagation mechanism in liquid zinc embrittlement of high-strength steels, tensile tests with constant cross-head velocity were performed on precracked specimens of type 4340 (UNS G43400) and H11 steels in liquid zinc and in air. Unstable crack propagation occurred at much smaller loads in liquid zinc than in air at all testing temperatures for H11 steel and at 713°K for type 4340 steel. The crack propagation velocity of H11 steel showed a minimum at intermediate temperature. The specimen tested in liquid zinc revealed grain-boundary fracture, and fine zinc particles were observed on the fracture surface, which suggested that the adsorption of zinc vapor to the crack tip or tips was the reason for the unstable crack propagation. The existence of a minimum in the crack propagation velocity vs temperature relation was explained by the decrease in the sticking coefficient of zinc vapor, the driving force for crack propagation, and the increase in the frequency of zinc adsorption with increasing temperature.

Introduction

Liquid zinc coating or galvanizing has often been used to prevent the corrosion of steel structures. During the galvanizing process, however, crack propagation can occur from stress concentrators such as sharp notches and surface cracks in weldments because of the cooperation of thermal stresses or residual stresses with surface chemical reactions between the steel and liquid zinc. Recently, high-strength steels have been used to decrease the weight of structures and machine parts, but the sensitivity to liquid zinc embrittlement (LZE) increases with increasing strength levels of steels.[1,2] In the present study, the crack propagation mechanism in LZE of high-strength steels was investigated.

Experimental Procedure

The materials tested were low-alloy Ni-Cr-Mo steel [type 4340 (UNS G43400)] and Cr-Mo-W-V steel (H11). The type 4340 steel was quenched from 1123°K and tempered at 923°K for 3.6 ks. The H11 steel was quenched from 1323°K and tempered at 923°K for 5.4 ks or 9.0 ks, which resulted in Rockwell hardness (HR_C) of 47 or 43, respectively. The tensile strength (σ_B), yield strength (σ_{ys}), and fracture elongation (φ) at 753°K were 585 MPa, 529 MPa, 14% for type 4340 steel, and 911 MPa, 735 MPa, 14% for H11 steel tempered for 5.4 ks, respectively. Figure 1 shows the testing apparatus. The compact-tension-type specimen (72.5-mm width, 5-mm thickness, 38-mm precrack length; refer to Figure 6) was dipped into liquid zinc (99.9% purity) in an alumina crucible for 1.2 ks, and the load was applied with constant cross-head velocity (the deflection velocity of the actuator), $\dot{x}_1$ of 2×10^{-5} m/s. The load P, measured by a load cell, and the deflection between pins (Δx_2), measured by a clip gauge, were output to an X-Y recorder. Especially in the H11 steel, after the load reached maximum, the crack or cracks propagated throughout the specimen width with very high speed, so the load vs time curve was recorded using a digital memory. The average crack propagation velocity was calculated from the time for load to go to zero and the crack propagation length (specimen ligament width, 34.5 mm). Because the small scale yielding condition at the crack tip was satisfied in liquid zinc, the stress-intensity factor[3] at maximum load (K_{max}) was calculated.

Results

Some examples of load (P) vs deflection between pins (Δx_2) curves in liquid zinc and in air are shown in Figure 2. The crack growth occurred at much smaller loads in liquid zinc than in air for both steels. In addition, unstable crack propagation occurred in liquid zinc at 713°K for type 4340 steel, although stable crack propagation occurred at the temperatures higher than 753°K. For H11 steel, however, unstable crack propagation occurred at all the testing temperatures in liquid zinc.

When unstable crack propagation occurs in liquid zinc, the maximum stress-intensity factor (K_{max}) corresponds to the stress-intensity factor at which crack growth occurs because the $P - \Delta x_2$ curve is almost linear. The relations between K_{max} and testing temperature (T) obtained for H11 steel tempered for 5.4 ks or 9.0 ks are shown in Figure 3. The K_{max} in liquid zinc decreases monotonically with increasing temperature. Figure 4 shows the relations between temperature (T) and the crack propagation time after the unstable crack propagation has occurred. The crack propagation time in liquid zinc shows a maximum at an intermediate temperature. The crack propagation time in air is much shorter than that in liquid zinc, and the temperature dependency of the crack propagation time is very different from that in liquid zinc. The crack propagation time in air is short when K_{max} is large (see Figure 3). Moreover, shear fracture occurred in air at all temperatures; i.e., the crack propagated obliquely to the specimen surface with large plastic deformation.

Discussion

Relationship of crack propagation velocity, crack-branching pattern, and temperature

Macroscopic crack branching was observed at all the testing temperatures for the H11 steel, and only at 753°K for the type 4340

*Department of Engineering, Hiroshima University, Higashi-Hiroshima, 724 Japan.

**Graduate School, Hiroshima University, Higashi-Hiroshima, 724 Japan.

steel. Figure 5 shows the histogram of crack branching types examined for the H11 steel tempered for 9.0 ks. At a lower temperature range, the higher frequency of crack branching is recognized, and the well-developed crack branching (type A or B) that starts directly from the precrack [shown in Figure 6(a) or (b)] is often observed.

From Figure 4, the relations between crack propagation velocity (v) in liquid zinc and temperature (T) were obtained. The result is shown in Figure 7, where the crack branching patterns are classified with different marks. The crack propagation velocity reveals a minimum near 850°K. Because such fast crack propagation and crack branching have never been observed for low-strength steel under experimental conditions similar to those in the present experiment,[4,5] the unstable crack propagation at very small loads and the crack branching seem to be typical characteristics for LZE of high-strength steels only.

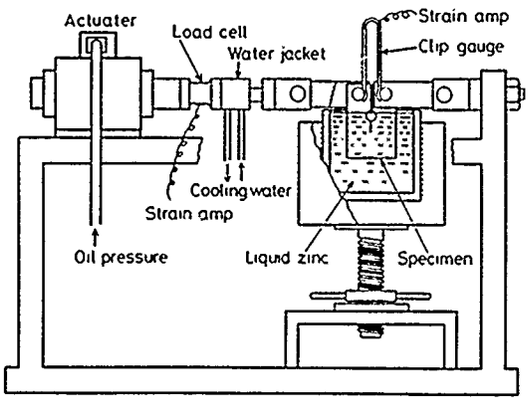


FIGURE 1—Experimental apparatus.

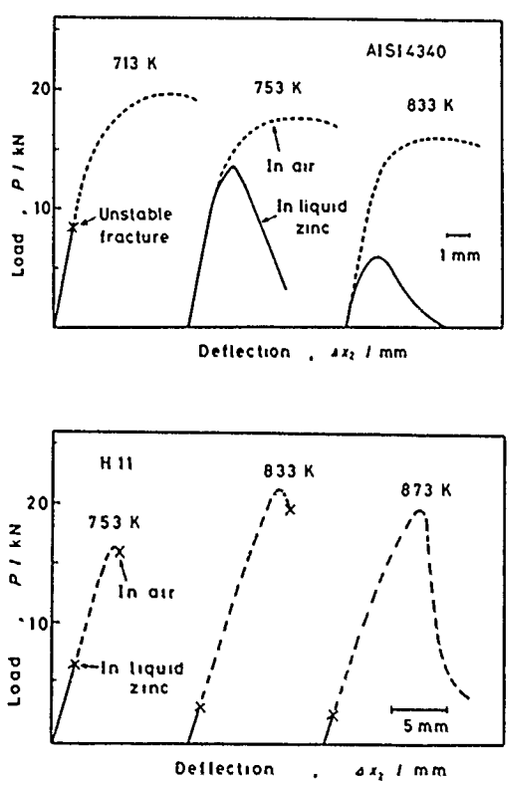


FIGURE 2 - Relationship between load and deflection between pins.

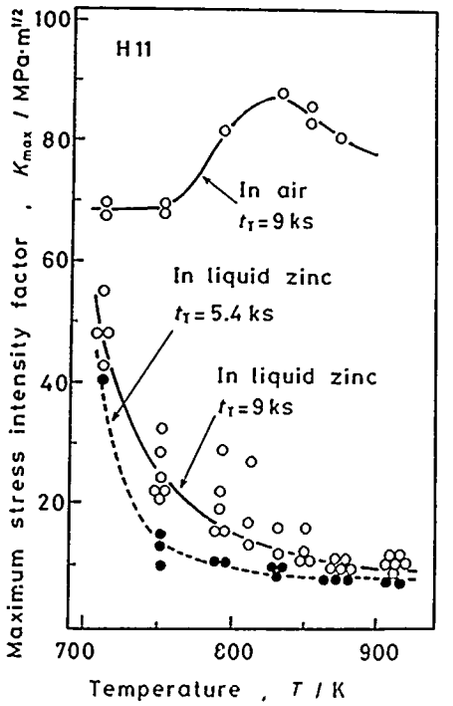


FIGURE 3—Relationship between temperature and maximum stress-intensity factor.

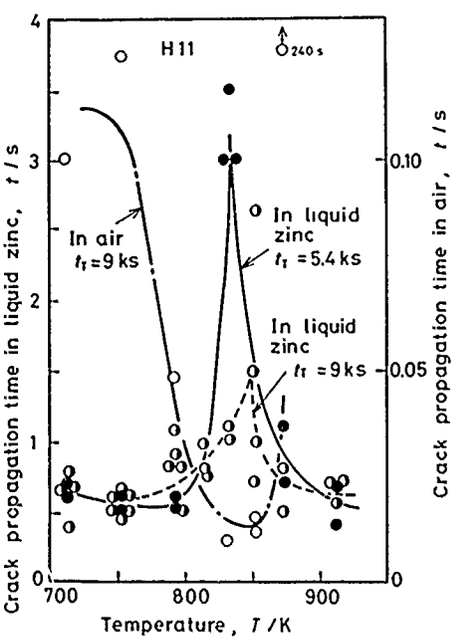


FIGURE 4—Relationship between temperature and crack propagation time.

Fractography at the crack tip

The crack propagation of type 4340 steel and H11 steel in LZE occurs along preaustenite grain boundaries.[1] Figure 8 shows an example of a fractograph at the tip of stopped branch crack of H11 steel (tempering time: t_T = 9.0 ks). There are many particles on the grain boundaries. These were determined to be zinc using an energy dispersive x-ray (EDX) analysis. Gordon[6] has already suggested that a vapor space exists at the crack tip because liquid zinc cannot penetrate into the crack tip because of its surface tension. Once the crack tip is opened during the test, it cannot be perfectly closed after the test because the crack opening caused by plastic deformation cannot be perfectly compressed by the elastic region around the plastic region. It was possible, therefore, that the zinc vapor at the crack tip was cooled after the test and adhered to the fracture surface

as many particles. In addition, the zinc particles were large when the testing temperature was high, which corresponded to the fact that the zinc-vapor pressure is high at high temperature. For low-carbon steel, which reveals slow, stable crack propagation in liquid zinc, the crack propagation occurs by grain-boundary diffusion of zinc,[2,4,5] because a smooth intergranular fracture surface exists in front of the surface on which the zinc particles adhere.[2] For H11 steel, where fast crack propagation occurs in liquid zinc, such a smooth grain-boundary fracture surface was not observed. Thus, the crack propagation mechanism of H11 steel in liquid zinc seems to be that the zinc vapor adsorbs on the crack tip and reduces the cohesive strength of the grain boundary. There seems to be no fundamental difference in the mechanism between the regions above and below the temperature at which the v vs T curve reveals a minimum because the fracture surface appearances are the same.

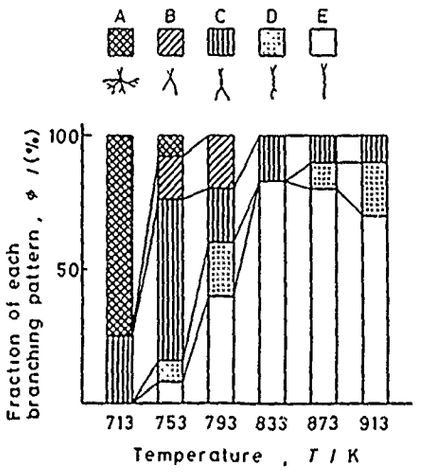


FIGURE 5—Relationship between temperature and fraction of branching pattern.

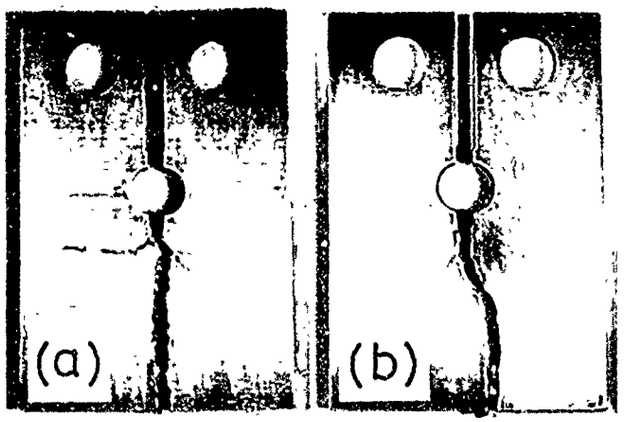


FIGURE 6—Crack branching patterns of H11 steel in liquid zinc, (a) T = 713°K and (b) T = 753°K.

Temperature dependency of crack propagation velocity

Such high crack propagation velocity as is observed in liquid zinc at all of the temperatures for H11 steel and at T = 713°K for type 4340 steel has been reported on other liquid metal-solid metal systems,[7] e.g., solid aluminum alloy in liquid mercury.

According to Figure 3, the crack-initiation load, or the maximum stress-intensity factor (K_{max}) of H11 steel in liquid zinc decreases monotonically with increasing temperature. The reason for this decrease is that the increase in temperature causes an increase in the probability of zinc adsorption because of the high vapor pressure, and because of the destruction of the protective film on the crack tip by eased plastic slip. The temperature dependency of crack propagation velocity is, on the other hand, greatly different from that of K_{max} (see Figure 7) There are two factors that affect the crack propagation velocity (v) in liquid zinc; one is mechanical and another is environmental Because K_{max} decreases with increasing temperature (T) (Figure 3), the driving force for crack propagation decreases with increasing T. In addition, the sticking coefficient of zinc vapor decreases with increasing T. By these effects, v decreases with increasing T. On the other hand, the zinc-vapor pressure increases in proportion to about the fourth power of T with increasing T. This effect increases the chance of zinc adsorption and increases v rapidly with increasing T. Thus, the interaction of the three factors brings out the appearance of a minimum in the v vs T curve. The crack propagation velocity (v) is almost constant and not so large at the lower temperature range, although the driving force for crack propagation (K_{max}) is large (see Figure 3). The reason seems to be that the limited adsorption frequency of zinc vapor causes the crack branching, which decreases the effective stress-intensity factor at the crack tip; i.e., there exists a "rate-limiting process" also in LZE, as has been reported on the crack branching in stress corrosion cracking and hydrogen-assisted cracking.[8,9]

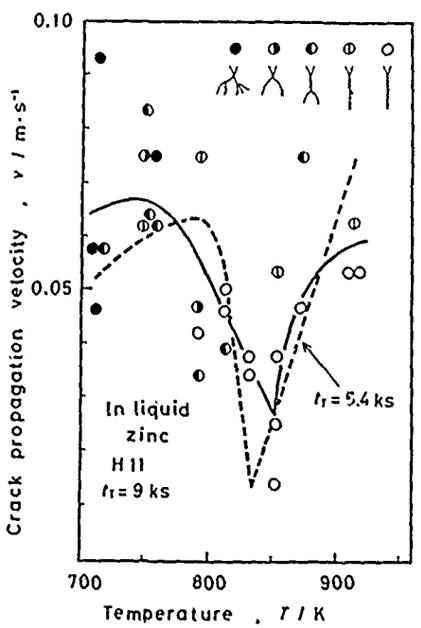


FIGURE 7—Relationship between temperature and crack propagation velocity.

Conclusion

To investigate the crack propagation mechanism of high-strength steels in LZE, tensile tests with constant cross-head velocity were performed in liquid zinc and in air on precracked specimens of type 4340 and H11 steels quenched and tempered at 923°K. The results obtained follow.

(1) Unstable crack propagation occurred at much smaller loads in liquid zinc than in air at all of the testing temperatures for H11 steel. For type 4340 steel, unstable crack propagation occurred only at 713°K, and stable crack propagation occurred at higher temperatures.

(2) Grain-boundary fracture occurred in liquid zinc, and fine zinc particles were observed on the fracture surface, which suggested that the adsorption of zinc vapor to the crack tip or tips was the reason for unstable crack propagation along grain boundaries.

(3) For H11 steel, the stress-intensity factor at the initiation of crack growth decreased with increasing temperature of liquid zinc, while the crack propagation velocity in liquid zinc decreased to a

minimum near 850°K and increased with increasing temperature T. The large v at lower T seemed to result from the high sticking coefficient of zinc vapor and the high driving force for crack propagation. The large v at higher T seemed to result from high zinc-vapor pressure, which resulted in a high frequency of zinc-vapor adsorption.

(4) Crack branching was often observed during crack propagation in liquid zinc. Well-developed crack branching occurred when T was low, which suggested an upper limit of frequency of zinc-vapor adsorption even if the driving force for crack propagation is high.

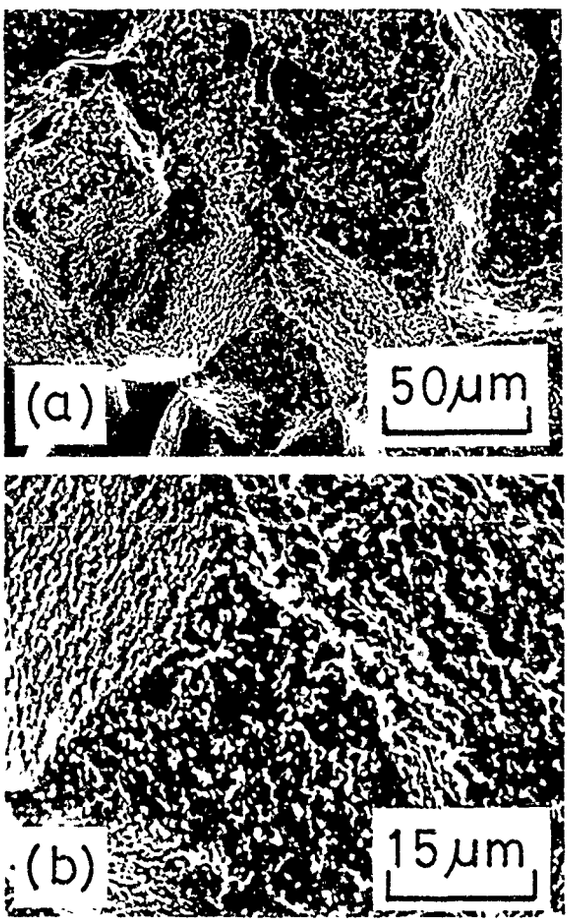


FIGURE 8—Fractograph of H11 steel near crack tip (T = 793°K).

References

1. K Nakasa, H. Takei, S. Takemoto, M. Matsuda, J. Soc. Mater. Sci. Jap. 34, 376(1985): p. 76.
2. K Nakasa, H. Takei, M Matsuda, Proceedings of the International Conference on the Role of Fracture Mechanics in Modern Technology, ed. G.C. Sih, H. Nishitani, T. Ishihara (Amsterdam, The Netherlands: Elsevier Science Publishers, 1987), p. 515.
3. W.F. Brown Jr., J.E. Srawley, "Plane Strain Crack Toughness Testing of High Strength Metallic Materials," ASTM STP410 (Philadelphia, PA: ASTM, 1967), p. 14.
4. K. Nakasa, H. Takei, S. Takemoto, J. Soc. Mater. Sci. Jap. 33, 372(1984): p. 1193.
5. K. Nakasa, H. Takei, M. Matsuda, J. Soc. Mater. Sci. Jap. 37, 413(1988): p. 166.
6. P. Gordon, Metall. Trans. 9A(1978): p. 267.
7. M.H. Kamdar, "Embrittlement of Engineering Alloys," Treatise on Materials Science and Technology, Vol. 25, ed. C.L. Briant, S.K. Banerji (New York, NY: Academic Press, 1983): p. 361.
8. M.O. Speidel, The Theory of Stress Corrosion Cracking in Alloys, ed. J.C. Scully (Brussels, Belgium: NATO Scientific Affairs Division, 1971), p. 345.
9. K Nakasa, H. Takei, S. Takemoto, Eng. Frac. Mech. 18, 4(1983): p. 879.

A Model for Transgranular Stress Corrosion Cracking in Austenitic Stainless Steel

S.C. Jani, M. Marek,* R.F. Hochman,* and E.I. Meletis***

Abstract

Electron channeling studies show that the transgranular stress corrosion cracking (TGSCC) of type 304L (UNS S30403) austenitic stainless steel in $MgCl_2$ is crystallographic, with brittle crack propagation occurring primarily on {100} planes with some secondary cracking on {110} planes. Transmission electron microscopy investigations show that the deformation mode at small distances (a few μm) from the fracture surface is entirely coplanar (inhomogeneous), while at large distances the slip morphology becomes homogeneous. It is widely recognized that hydrogen may be the embrittling species in chloride cracking in austenitic stainless steels, and an atomistic hydrogen-induced cleavage model is proposed in light of the experimental results of this investigation. The model is based on the reduction of the stacking fault energy in the hydrogen affected region in front of the crack tip and the formation of Lomer-Cottrell supersessile locks in this region. This model is consistent with many phenomenological observations of TGSCC in the austenitic stainless steel–chloride stress corrosion system.

Introduction

A great deal of research has been devoted to determining the mechanism(s) of stress corrosion cracking (SCC) in engineering alloys. However, no one model can account for the phenomenological observations of all known instances of SCC, and the mechanism of cracking may vary from system to system.

Transgranular stress corrosion cracking (TGSCC) of face-centered cubic (fcc) metals and alloys has posed a serious challenge, because SCC in these otherwise ductile alloys has shown brittle fracture characteristics. Austenitic (fcc) stainless steels (SSs) are notorious for their susceptibility to TGSCC in the presence of the chloride ion (Cl^-) containing environments.[1] As a result, a major thrust in recent years has been to characterize the crystallography of TGSCC of austenitic SS because it offers a unique opportunity to evaluate the mechanisms of the phenomenon. These studies have shown that crack propagation occurs primarily on {100} planes by a microcleavage process, i.e., crack propagation is mechanically driven as opposed to chemically driven.[2] However, this is not to say that the electrochemical processes occurring at an advancing crack tip play no role in the crack propagation events. This will be further amplified in a later section.

The onus then is for workers in this area to determine the exact mechanism that can account for the phenomenological observations of cracking. To this end, the present study was conducted to characterize the dislocation substructure of TGSCC of type 304L (UNS S30403) SS in $MgCl_2$, which would provide an insight into the micromechanisms of the phenomenon.

Experimental

Cylindrical single crystals of type 304L SS were tested for TGSCC in 45 wt% $MgCl_2$ at 155°C as described previously.[2] The testing was conducted under static tension of 15 ksi (103 MPa), which was below the nominal yield stress of 16 ksi (110 MPa). The chemical composition of the steel was 18.7 wt% Cr, 9.43% Ni, 1.56% Mn, and 0.025% C, with the balance being Fe. The pH of this solution is about 4.5.[3] The corrosion potential was not monitored in this study.

The deformation substructure was characterized by transmission electron microscopy (TEM). Thin foils of the tested alloys were obtained from the fracture surfaces and at various known depths under the fracture surfaces. To prepare electron-transparent thin foils, 0.127 mm thick wafers were initially cut at various distances from the fracture surfaces. A slow cutting rate (0.25 mm/min) and continuous water cooling were used to minimize deformation induced during cutting.

Disks of 3 mm diameter were punched from the wafers using a punch and die set. The disks were then thinned to electron transparency by electropolishing in a solution containing 92.5 vol% glacial acetic acid and 7.5 vol% perchloric acid at a temperature of 15°C and a voltage of 25 V. Electropolishing was conducted on a Tenupol† 2 (Struers) using both the 1 jet and the 2 jet techniques. Thin foils of the fracture surface were prepared using the 1 jet technique, electropolishing from the surface opposite the fracture, while foils from the interior of the sample were prepared by the 2-jet technique. TEM of these samples was performed at 100 KeV in a JEOL† TEM 100C microscope.

Results and Discussion

The deformation substructure observed at the fracture surface and at various depths under the fracture surface varied considerably. Only coplanar deformation was observed at the fracture surface (Figure 1). The deformation in foils made 2 mm under the fracture surface was completely homogeneous, as seen in Figure 2. Martensitic features, ε-martensite [hexagonal closed packed (hcp)] and α-martensite [body-centered cubic (bcc)], were observed at intermediate depths of about 1 mm under the fracture surface (Figures 3 and 4, respectively).

The logical conclusion that can be drawn from the observed deformation modes at various locations in reference to the crack

*Georgia Institute of Technology, School of Materials Engineering, Atlanta, GA 30332-0245.

**Louisiana State University, Mechanical Engineering Department, Materials Engineering Group, Baton Rouge, LA 70803.

†Trade name.

plane is that the stacking fault energy (SFE) immediately ahead of the crack tip is much lower than at larger distances further from the crack front, because a low SFE promotes coplanar slip. Further, it has been shown that all early deformation in austenites is coplanar, and a transition to cellular arrays occurs only at larger strains.[4] Since the largest strains would be expected at the crack tip, the SFE must have been lowered there to produce the results observed.

The SFE in a small region in front of the crack tip appears to have been lowered below the nominal value by the presence of the environment. An environmental species that has been reported to reduce the SFE of austenite is hydrogen.[5,6] Since hydrogen formation and discharge occurs readily in TGSCC of austenitic SS,[7-9] it is logical to conclude that hydrogen from the corrosion reaction participates in the cracking process. A model of the process by which hydrogen affects TGSCC follows.

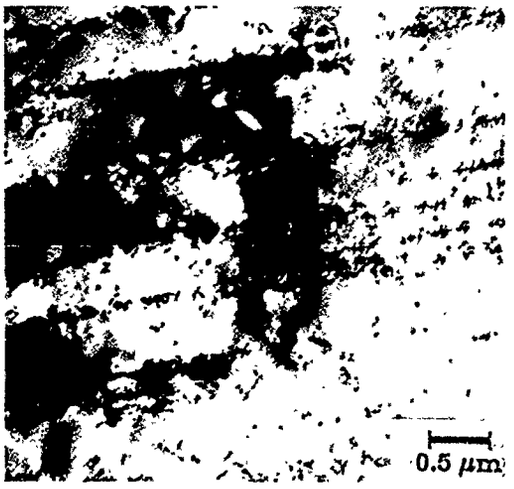


FIGURE 1—Parallel slip traces showing planar deformation at the fracture surface.

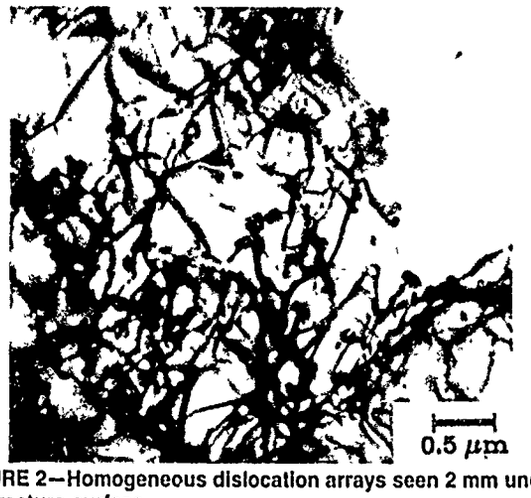


FIGURE 2—Homogeneous dislocation arrays seen 2 mm under the fracture surface.

A model for crack propagation

The model proposed here for TGSCC of austenitic SS is based on the effect of hydrogen on the SFE of austenite. The idea that TGSCC susceptibility is linked to the SFE of the alloy dates back to the work of Robertson and Tetelman reported in 1962.[10] The present model is essentially a modification of their original idea.

It is proposed here that atomic hydrogen from the cathodic reduction reaction diffuses to a small region ahead (a few μm) of an existing crack tip, creating a "hydrogen affected region" (HAR) where the SFE is lowered [Figure 5(a)]. Since cross slip is restricted in low SFE austenites, only planar slip occurs on intersecting {111} planes in the HAR [Figure 5(b)] and results in the formation of Lomer Cottrell (L-C) supersessile dislocations. L-C locks that lie on {100} planes [Figure 5(c)] act as obstacles to further slip, resulting in high stresses directed normal to the {100} plane. At a critical value of stress, the {100} plane within the ligament between the obstacle and the existing crack tip will cleave as shown in Figure 5(d). After the extension, the same series of events will be repeated again.

As stated earlier, the model for transgranular crack propagation presented here is a variation of the Robertson and Tetelman[10] model. They considered that crack propagation is associated with enhanced chemical reactivity of L-C locks, which leads to the formation of cylindrical cavities along the L-C lock dislocation lines. They postulated that these cavity dislocations act as traps for dislocations gliding on the original slip planes, thereby creating a crack nucleus. They concluded, as we do, that this process is most favored in low SFE materials. The novel aspect of the model proposed in the present work is that the SFE is lowered by an environmental species, specifically hydrogen, which further aids in the formation and stability of L-C locks. It should also be noted that since our model does not consider the chemical reactivity of L-C locks, these barriers do not have to originate or terminate at an external surface in physical contact with the environment.

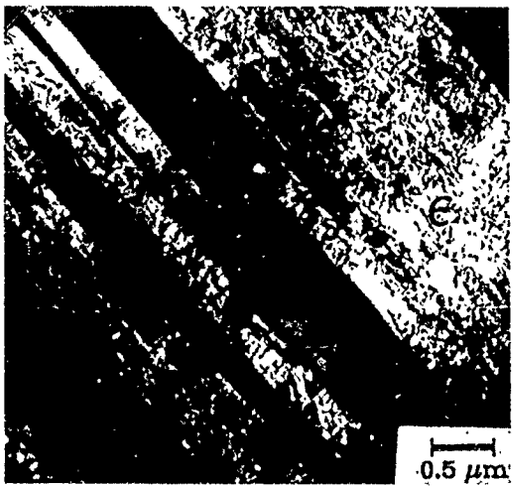


FIGURE 3—Dark field: (0111) micrographs of ε-martensite needles in foil prepared 0.5 mm under the fracture surface.

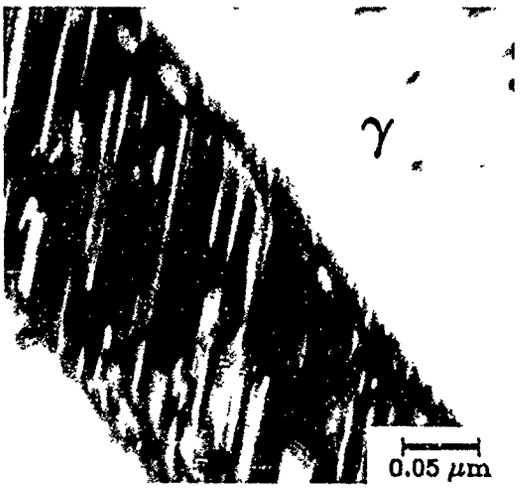


FIGURE 4—High-resolution micrograph of twinned α'-martensite seen in foil prepared 1 mm under the fracture surface.

Evaluation of model

This model predicts crystallographic, cleavage-like cracking that has been widely observed for austenitic SS.[2,4,6,11] The cracking plane predicted in such a model would depend on the number of dislocations piled up against the L-C lock on each of the two {111} planes, and, if an equal number are piled up, the fracture plane would be {110} or {100}. This is in excellent agreement with observed cracking planes.[2,4,6,11] The model also predicts discontinuous crack propagation, as has been the general observation[11-14] in most SCC of 300 series SSs.

In this model, the rate-determining step is the diffusion of atomic hydrogen, produced by the cathodic reduction of hydrogen ions. The activation energy for hydrogen permeability in austenitic SS approximately 60 kJ/mol,[15] which compares favorably with the activation energy of 65 kJ/mol for Stage II cracking of type 316 (UNS S31600) SS in boiling $MgCl_2$.[16] In addition, Pugh has shown that the bulk diffusivity of hydrogen accounts for hydrogenation to a depth that corresponds to the observed crack advance distance, Δx per cracking event, for a discontinuous crack propagation process.[13,17] The model predicts Δx to be on the order of the spacing between slip traces on the fracture surface. This study showed the mean slip trace spacing to be approximately 0.5 μm (Figure 1). This is in excellent agreement with the observed values for Δx of 0.5μm[12] and 0.3 μm for the near- threshold region and 1 μm for Stage II cracking[18] in type 310 (UNS S31000) SS.

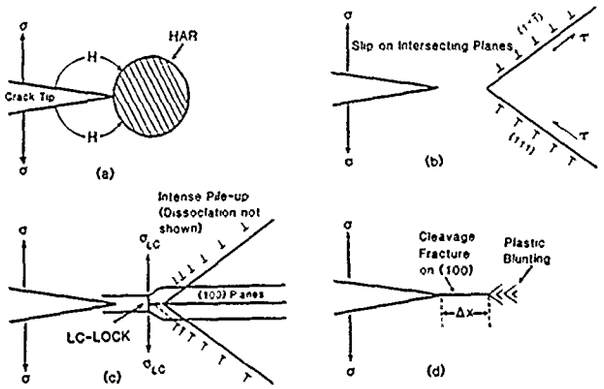


FIGURE 5—Physical presentation of the "hydrogen-induced cleavage" model: (a) hydrogen diffusion to areas of high triaxial stress and formation of a hydrogen-affected region; (b) slip on intersecting slip planes in front of the crack tip; (c) dislocation pile-up at the Lomer-Cottrell lock; and (d) cleavage crack joining the main crack front.

Crack branching is frequently observed in this SCC system[2] and can be readily accounted for by this model as follows. Crack extension proceeds microscopically in the opposite direction to the macroscopic extension by the joining of L-C lock sites with the pre-existing crack. This coalescence can very well occur in the wake region of the crack if the L-C lock is not formed directly in front of the crack tip, resulting in the formation of a branched network.

Increasing the nickel content of SS has been shown to impart higher resistance to TGSCC.[19] For this model, these observations can be explained on the basis of the tendency of nickel to increase the SFE of austenite.[20-22] Since the mechanism of the formation of L-C locks requires glide of pure edge or edge components of dislocations, cracks nucleated at emergent screw dislocations are not expected to propagate. This has been verified in the work of Silcox and Swann.[7]

It should be noted that some anodic dissolution on freshly exposed crack surfaces (passivation) is necessary, since it is directly associated with the production of atomic hydrogen. The rate of repassivation of the slip steps is still expected to play an important role, as discussed by Scully.[5]

Although the corrosion potential was not monitored in this study, published data on this system[23] show that the corrosion potential of strained specimens was below the hydrogen equilibrium, considering the acidic solution at the crack tip.[3] The fresh metal surface of the emerging slip steps tends to be polarized anodically by the surrounding filmed surfaces, but an IR drop would maintain the local potential below the hydrogen equilibrium, even if the specimen were anodically polarized. Observations of hydrogen gas evolution from stress corrosion cracks confirm that hydrogen ions are reduced at the crack tip.[6-8]

Any model of SCC of austenitic SS in chlorides that depends on hydrogen entry seems to be in conflict with the reports showing crack arrest by cathodic polarization[24] or the existence of a minimum potential for cracking.[25] However, the observed effect of polarization may be attributed to the changes in the repassivation kinetics. It has been shown that susceptibility to SCC is often at maximum in narrow potential regions of surface-film instability.[26] The propagation of stress corrosion cracks in this system thus may require a specific combination of conditions, including the strain rate at which fresh metal surface is exposed at a certain rate, local solution chemistry of high acidity and chloride concentration, and a potential at which both hydrogen ions are reduced and the repassivation occurs at a critical rate.

Conclusion

Based on the observed damage substructure of TGSCC of type 304 SS in boiling $MgCl_2$, it is proposed that the hydrogen from the cathodic reduction reaction diffuses into the area of high triaxial stress in front of a pre-existing crack tip (a few μm), creating a hydrogen-affected region (HAR). The hydrogen in the HAR lowers the SFE of the austenite. The formation and stability of Lomer-Cottrell supersessile locks will be favored in this low SFE region. Under the influence of stress, a microcrack is nucleated in the HAR at the head of a dislocation pile-up associated with a L-C lock, with subsequent cleavage occurring on a {100} or {110} plane. The cleavage crack for each cracking event will join up with the main crack front and the process will be repeated. This model is consistent with many phenomenological observations of TGSCC in this system.

References

1. R.M. Latanision, R.W. Staehle, Fundamental Aspects of Stress Corrosion Cracking (Houston, TX. National Association of Corrosion Engineers, 1969), p. 214.
2. E.I. Meletis, R.F. Hochman, Corros. Sci. 24(1984): p. 843.
3. M Marek, R F. Hochman, Corrosion 26, 1(1970). p. 5.
4. D.J. Burr, Corros. Sci. 5(1965). p. 733.
5. J C Scully, The Theory of Stress Corrosion Cracking in Alloys (Brussels, Belgium. North Atlantic Treaty Organization, 1971), p. 127.
6. M.R. Louthan, M.L. Holzworth, Fundamental Aspects of Stress Corrosion Cracking (Houston, TX: NACE, 1969), p. 303.
7. J.M Silcox, P.R. Swann, Mechanisms of Environment Sensitive Cracking of Metals (Warrendale, PA. The Metallurgical Society, 1977), p. 66.
8. D. Eliezer, D.G. Chakrapani, C.J. Altstetter, E.N. Pugh, Metall. Trans. A, 10A(1979): p. 935.
9. J A Honkasalo, H.E. Hanninen, Mechanisms of Environment Sensitive Cracking of Materials (Warrendale, PA. TMS, 1977), p. 83.
10. H D Robertson, A.S. Tetelman, Strengthening Mechanisms in Solids (Metals Park, OH: ASM International, 1962), p. 217.
11. A J Bursle, E N Pugh, Mechanisms of Environment Sensitive Cracking of Materials (Warrendale, PA. TMS, 1977), p. 471.
12. M T Hahn, E.N. Pugh, Corrosion 36, 7(1980). p. 380.
13. E.N. Pugh, Corrosion 41, 9(1985): p. 517.
14. N. Nielson, J. of Mater. 5(1970): p. 794.
15. M.R. Louthan, R.G. Derrick, Corros. Sci. 15(1975): p. 567.
16. A.J. Russel, D. Tromans, Metall. Trans. A 12A(1981): p. 613.
17. E.N. Pugh, Atomistics of Fracture (New York, NY: Plenum Press, 1983), p. 997.
18. J I Dickson, D. Groulx, L. Shigiong, D. Tromans, Mater. Sci. Eng. 94(1987): p. 155.
19. H R Copson, Physical Metallurgy of Stress Corrosion Fracture (New York, NY: Interscience, 1959), p. 247.
20. P.R. Swann, Corrosion 19, 3(1963): p. 102.
21. D.L. Douglass, G. Thomas, W.R. Roster, Corrosion 20, 1 (1964): p. 15.
22. C.J. Novak, Handbook of Stainless Steels (New York, NY: McGraw-Hill, 1977), p. 4.1.
23. T P. Hoar, J.M. West, Proc. of Roy. Soc. A 268(1962): p. 304.
24. B.E. Wilde, C.D. Kim, Corrosion 28, 9(1972). p. 350.
25. R L Shamakian, A.R. Troiano, R.F. Heheman, Environment-Sensitive Fracture of Engineering Materials (Warrendale, PA: TMS-American Institute of Mining, Metallurgical, and Petroleum Engineers, 1979), p. 116.
26. F.P. Ford, Corrosion Processes (London, England: Applied Science Publishers, 1982), p. 271.

Stress Corrosion Crack Initiation and Slip Parameters in a Ferritic Stainless Steel

*R.N. Iyer**

Abstract

Hot chloride stress cracking (HCSC) of a 26Cr-1Mo ferritic stainless steel (E-Brite†) was studied using a uniaxial constant-load fixture, incorporating an appropriate corrosion cell assembly. The slip-dissolution mechanism (SDM) was involved in the stress corrosion crack initiation stage. The rate of slip-step evolution that was responsible for the breakdown of the protective film as well as the repassivation rate were critical parameters in the SDM. Results showed that thermomechanical treatments altered HCSC susceptibility drastically as a result of changes in slip-step height and slip-step density. A low-temperature annealing treatment partly restored immunity to a HCSC susceptible alloy. Analysis showed that the reduction in slip-step height and slip-step density, a result of recovery processes during the low-temperature treatment, assisted in the amelioration.

Introduction

One of the most aggressive environments experienced by alloys, such as 26Cr-1Mo ferritic stainless steel (SS), is the hot chloride salt solution encountered in paper industries and chemical process industries.[1,2] Previous studies on a high-purity 26Cr-1Mo alloy (E-Brite) indicated that this alloy is highly sensitive to thermomechanical treatments toward hot chloride stress cracking (HCSC) susceptibility.[3] Also, the failure by HCSC of the ferritic SS E Brite has a crack initiation stage, which was shown to occur by a slip-dissolution mechanism (SDM).[4] The SDM has been studied in detail;[5] SDM occurs by the rupture of the protective film on the alloy surface as a result of emerging slip steps when the alloy is stressed. The film rupture exposes fresh metal to the aggressive solution, and this bared metal dissolves until that region is repassivated by the corrosion products, viz., oxide or hydroxide film. The slip and dissolution events have to repeat several times before a local occluded cell is formed,[5] which may be determined by the attainment of a critical IR drop at the bottom of the cell.[6,7] Coplanarity of the slip seems to be important for stress corrosion cracking (SCC) by SDM.[8] Since SDM is involved in the SCC initiation of the ferritic SS in hot chloride solutions, slip-step parameters will be important in determining SCC susceptibility. In the present investigation, the effect of low-temperature annealing on HCSC has been studied with a view toward understanding the importance of slip-step parameters on the SCC initiation.

Experimental

Materials and Preparation

26Cr 1Mo ferritic SS, designated E-Brite, was used for this study. Table 1 shows the chemical analysis for this alloy obtained as annealed strips 0.05 in. (1.27 mm) thick. For details of specimen preparation, see Reference 9. Here, the tensile specimens of the as received E Brite were prestrained to 5% elongation (in air), using an Instron† tensile tester.

Table 2 shows 0.2% offset yield strength determined using Instron after each treatment, the average grain size was 20 μ in all cases.

Test Procedures

HCSC experiments were performed in a glass cylindrical cell, with the tensile specimen uniaxially loaded by a cantilever arrangement and having facilities for heating the solution (by means of heater coils wound outside the glass cell).[4] The loading was uniaxial, corresponding to 90% of the 0.2% offset yield strength of the heat-treated alloy. The choice of this level of stress is based on the fact that dislocations become mobile, but bulk yielding will not occur, moreover, the alloy can withstand this level of constant load for years under pure mechanical loading conditions. Also, this level of stress assisted in accelerating the test and in obtaining a high enough creep rate and detectable slip steps. Elongation of the specimen was monitored as a function of time using a dial gauge (after magnifying the elongation by the cantilever assembly) and an appropriately designed timing device.

Slip-step parameters were determined by loading a polished tensile specimen of E-Brite to 90% of the appropriate yield strength in an inert environment of silicone oil at the temperature of the SCC test, i.e., at 140°C for 1 h. A high-resolution scanning electron microscope (SEM) (JEOL†-35CF) was found to be well suited to observe and photograph the slip steps, since the specimen stage could be tilted up to 60° with great accuracy. Thus, the determination of slip-step height and the estimation of slip-step density was greatly facilitated, especially since a large fraction of the total area could be scanned.

The solution used for HCSC experiments was 42% lithium chloride with additions of 2 g/L of thiourea (added as a poison for hydrogen evolution reaction). SCC tests were conducted at freely corroding conditions, just near the boiling point of this solution (140°C) and the solution was deaerated by bubbling nitrogen gas continuously. Electrode potentials (at open circuit) were measured with respect to a saturated calomel reference electrode (SCE) connected through a salt bridge with Luggin capillary arrangements. Prior to loading, the mounted specimen was exposed to the boiling solution for 15 h, to achieve a steady-state corrosion potential.

*Department of Materials Science and Engineering, Pennsylvania State University, University Park, PA 16802.

†Trade name.

TABLE 1
Chemical Composition of E-Brite (wt%)

C	N	Cr	Mo	Ni	Cu	Nb	Mn	Si
0.002	0.004	25.88	1.05	0.23	0.01	0.12	0.08	0.22

TABLE 2
Yield Strength, SCC Initiation Time, and Slip Parameters for E-Brite

Property	Mill Annealed	5% Prestrained	5% Prestrained + 250°C/1 h-AC[A]	5% Prestrained + 350°C/1 h-AC[A]
Yield strength (0.2% offset)	55 (ksi) (379 MPa)	73.5 (507)	70 (483)	67 (462)
SCC Initiation time, t_i (min)	No failure (up to 15 days)	14	2738	3239
Slip-step Height[B] (nm) (±10)	40	150	70	50
Slip-step density[B] (#steps/mm) (±1)	1	16	6	2
Slip-step height[C] (nm) (±1)	40	200	80	60

[A]Annealed at the indicated temperature for 1 h and air cooled.
[B]Measured with a high-resolution SEM.
[C]Measured with a TEM using gold-shadowed carbon replica.

SCC initiation time (t_i) was determined, as in previous experiments,[4] from the elongation vs log(t) plot by noting the time at which the plot becomes nonlinear, i.e., when the plot shows deviation from the (normal room temperature) logarithmic creep behavior. An independent check of t_i is the time at which the corrosion potential (E_{corr}) moves negatively,[4] corresponding to the maximum in E_{corr} vs time plot. These two independent determinations of t_i have been validated by microscopical observations[4] of the cross sections of the E-Brite specimens at various stages of HCSC experiments.

Results

Both the mechanical behavior and the electrochemical behavior were monitored for HCSC of E Brite as a function of the low-temperature annealing process. Figure 1 shows the elongation vs time plots and Figure 2 shows the corrosion (open-circuit) potential as a function of time for various annealing treatments. These plots and Table 2 indicate that the 5% prestrained E-Brite was fully susceptible to HCSC (under freely corroding conditions), failing in about 26 min, and the SCC crack initiating in about 14 min after loading the specimen in the hot chloride solution. The as-received E-Brite was immune under similar conditions of the experiment and no failure occurred even after 15 days of exposure to the HCSC environment. When the 5% prestrained E-Brite was annealed at temperatures between 200 and 350°C, some of the resistance to the HCSC was restored, with a dramatic effect occurring between 200 and 250°C of annealing (Figures 1 and 2). This large effect reflected mainly on the SCC initiation time (t_i) and not on the propagation time, evident from Table 2; but, between 250 and 350°C of annealing, t_i did not improve much, although the failure times increased slightly further with increasing temperature of annealing between 250 and 350°C. Increasing the annealing time also improved HCSC resistance, as Figure 1 shows for a 12-h 350°C anneal.

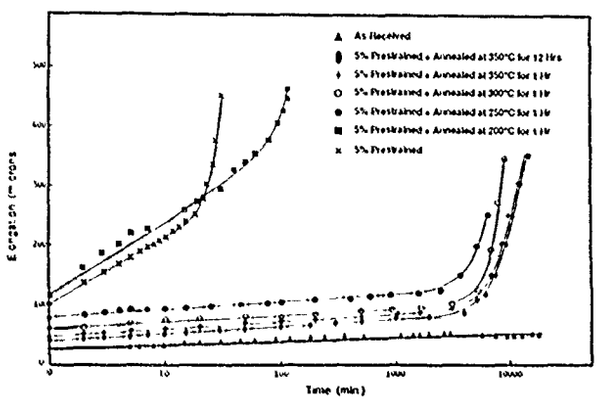


FIGURE 1—Elongation vs time behavior during hot chloride stress corrosion of E-Brite specimens given various treatments.

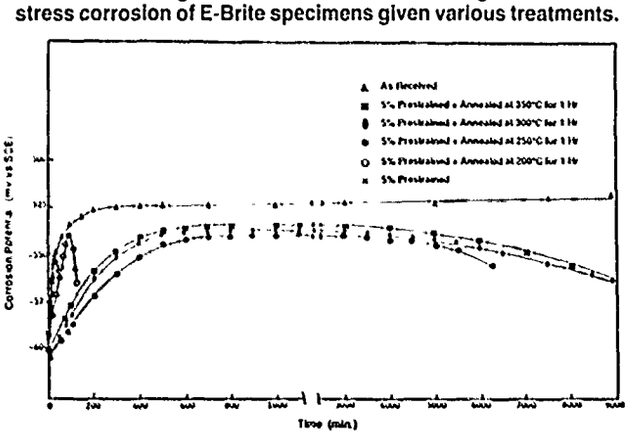


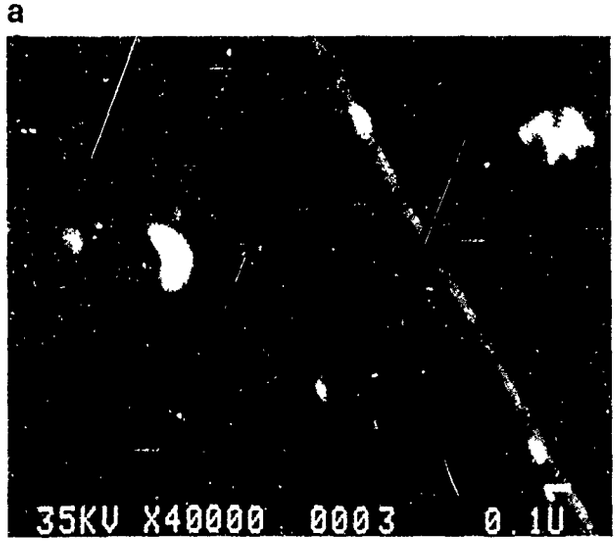
FIGURE 2—Change in open-circuit (corrosion) potential vs time behavior during hot chloride stress corrosion of E-Brite specimens given various treatments. Initial corrosion potential = −500 mV_{SCE}.

Analysis and Discussion

It is now clear that the SCC initiation in E-Brite under HCSC conditions occurs by a SDM, and that annealing at temperatures between 200 to 350°C increases the SCC initiation time toward that of the mill-annealed alloy, with a drastic change in t_i occurring between 200 and 250°C (Table 2) Therefore, one might suspect that the slip-step parameters involved in the SDM could have altered considerably when the 5% prestrained E-Brite was annealed in the low-temperature regime Independent determinations of the slip-step parameters (i e , slip-step height and density) by loading polished tensile specimens in hot silicone oil and examining them with the high-resolution SEM show the slip steps for the 5% prestrained E-Brite [Figure 3(a)] and that for slip steps subsequently annealed at 350°C for 1 h [Figure 3(b)]. As noted earlier, these conditions exactly simulated the mechanical factor of HCSC and eliminated the corrosion factor. Slip-step densities were estimated by statistical examination of the slip steps at different a eas of the specimen and using the intercept method commonly employed in the estimation of dislocation densities.



a



b

FIGURE 3—SEM micrographs showing slip steps, obtained by the application of constant load (90% of the yield strength) for 1 h in silicone oil at 140°C, of E-Brite specimens, given various treatments: (a) 5% prestrained and (b) 5% prestrained + 350°C anneal for 1 h.

Table 2 displays the values of slip-step height and density after various treatments of E Brite Slip step heights measured with the high resolution SEM agreed well with independent determinations using the well-known replica technique, which involves carbon-coating and gold-shadowing procedures to observe slip steps with a transmission electron microscope (TEM),[10] these values are also given in Table 2. Observations of the slip steps with the SEM and with the TEM indicated that the slip steps are fairly coplanar.

The relationship between the slip-step parameters and the SCC initiation time (t_i) is shown in Figure 4. The observations of the drastic change in t_i correlate well with the large reduction in slip-step height and density at 250°C of annealing vs the 5% prestrained E-Brite. Figure 4 thus shows that critical values of the slip-step parameters may be involved for the SCC initiation by SDM.

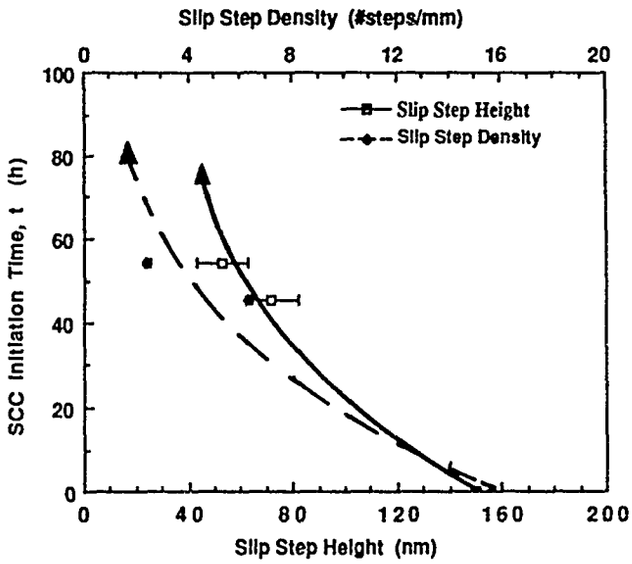


FIGURE 4—SCC initiation times as functions of slip-step height and density for hot chloride stress corrosion of E-Brite specimens given various treatments (as in Table 2).

For the SDM to operate for SCC initiation, the process of slip and dissolution events must repeat consecutively several times.[5] This process has been observed in a previous investigation of HCSC of E-Brite.[4] Thus, once the protective film is ruptured by a slip event, continued evolution of slip steps is necessary to counteract repassivation that occurs after each dissolution event. Staehle has concluded that SCC will occur by SDM only for an intermediate repassivation rate of the alloy, since at rapid repassivation no significant penetration can occur, and at negligible repassivation the extent of dissolution will be so great as to be essentially a pitting phenomenon.[5] Thus, the rate of slip-rupture process and the repassivation rate are critical parameters in SDM, and the slip steps must emerge continuously to keep up with the repassivation process. In Figure 5, the continuous emergence of slip steps resulting from creep of the alloy is clearly demonstrated. Thus, a mechanism exists by which the film can be ruptured continuously to counteract the process of repassivation after each dissolution event.

The repassivation of the local active regions of the alloy will depend on the electrochemical process of film reformation, occurring as a result of corrosion products adhering to the walls of the cells, and would be a function of the applied anodic potential, solution chemistry, etc. When the alloy is polarized anodically from the freely corroding potential, the repassivation rate would be much less, so the required rate of slip-step emergence (for SDM to operate) would also be less These are corroborated by the previous results on HCSC of E-Brite, showing faster SCC initiation at more anodic potentials.[3,4] Thus, a critical condition for SCC initiation to occur by the SDM could be written as follows: $(dh/dt)_{min} = (dR/dt)$, where $(dh/dt)_{min}$ = the minimum required rate of slip-step evolution and (dR/dt) = the repassivation rate at a particular applied potential. The importance of slip coplanarity has also been pointed out for SDM.[8]

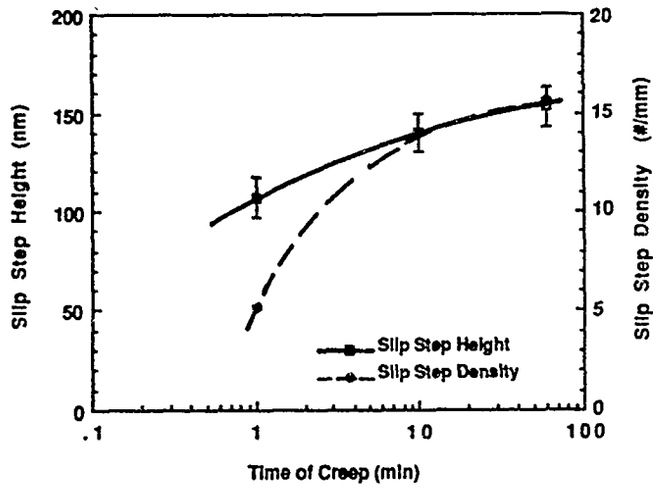


FIGURE 5—Slip-step height and density as functions of time of creep for 5% prestrained E-Brite loaded to 90% yield strength in silicone oil at 140°C.

In light of the foregoing discussion, the plots in Figure 4 can be understood in terms of the prevailing repassivation rate at the freely corroding condition For example, SCC will not occur if the slip-step heights are less than 40 nm when the alloy is subjected to freely corroding conditions in the hot chloride solution (Figure 4). However, if the alloy is anodically polarized in the hot chloride solution, smaller slip-step heights would be sufficient to cause SCC by SDM. So, even the mill-annealed alloy (having a slip-step height of 40 nm) will become susceptible to HCSC; this result is supported by previous observations.[3,4]

Thus far, we have seen that the rate of (coplanar) slip-step evolution and the rate of repassivation both control the SCC susceptibility as far as initiation by SDM is concerned. But, the role of slip-step density as a provider of (statistically) enough sites for SCC initiation, and thus a multiple number of cracks, should not be ignored This is apparent from the observed involvement of multiple cracks in SCC,[4] with the final failure occurring by the linking of these multiple cracks At present, however, the actual role of slip-step density and the importance of multiple cracks for failure by SCC are not fully understood.

Summary and Conclusions

(1) Low-temperature annealing in the range of 200 to 350°C and increasing annealing times in this temperature range improved the SCC initiation time of E-Brite in the HCSC environment. The most significant improvement occurred for annealing temperatures between 200 and 250°C.

(2) Slip-step parameters, i.e., slip-step height and density, were determined using a high-resolution SEM, and the trends of these parameters correlated quite well with the observations of improved SCC initiation time, including the result showing that the major improvement of SCC initiation time, occurring between 200 and 250°C of annealing, is because of the decrease in slip-step height and density.

(3) The critical parameters for the SDM, causing SCC initiation, were rationalized to be repassivation rate and the rate of slip-step evolution.

Acknowledgment

The author is grateful to Professor Howard Pickering of Pennsylvania State University for his expert comments and financial arrangements for the poster presentation based on this paper; the late Professor Robert Hehemann for providing constant guidance; the Department of Metallurgy and Materials Science, Case Western Reserve University, Cleveland, OH, where the experiments were conducted, and the National Science Foundation for its financial support.

References

1. J. Hochmann, A. Desestret, P. Jolly, R. Mayoud, Stress Corrosion Cracking and Hydrogen Embrittlement of Iron Base Alloys, NACE-5, ed. R.W. Staehle, J. Hochmann, R.D. McCright, J.E. Slater (Houston, TX: National Association of Corrosion Engineers, 1977), p. 956.
2. O.E. Moller, Corrosion Source Book, compiled by S.K. Coburn (Metals Park, OH: ASM International and Houston, TX: NACE, 1984), p. 266.
3. T.W. Mohr, A.R. Troiano, R.F. Hehemann, Corrosion 37, 4(1981): p. 199.
4. H.S. Kwon (Ph.D. diss., Case Western Reserve University, 1983).
5. R.W. Staehle, Stress Corrosion Cracking and Hydrogen Embrittlement of Iron Base Alloys, NACE-5, ed. R.W. Staehle, J. Hochmann, R.D. McCright, J.E. Slater (Houston, TX: NACE, 1977), p. 180.
6. H.W. Pickering, R.P. Frankenthal, J. Electrochem. Soc. 119(1972): p. 1297.
7. H.W. Pickering, Corrosion 42, 3(1986): p. 125.
8. R.M. Latanision, R.W. Staehle, Fundamental Aspects of Stress Corrosion Cracking, NACE-1, ed. R.W. Staehle, A.J. Forty, D. van Rooyen (Houston, TX: NACE, 1969), p. 214.
9. R.N. Iyer, R.F. Hehemann, "Strain-Rate Effects in Hydrogen Embrittlement of a Ferritic Steel," this proceedings.
10. K.C. Thompson-Russel, J.W. Eddington, Electron Microscope Specimen Preparation Techniques in Materials Science (Surrey, UK: The Gresham Press, 1977), p. 15.

Study of Transgranular Stress Corrosion Crack Propagation in Austenitic Steels by Load-Pulsing Method

*V. Desai, F. Friedersdorf, and T. Shaw**

Abstract

The load-pulsing method was used to study transgranular (TG) stress corrosion crack propagation in austenitic stainless steels exposed to boiling aqueous magnesium chloride (154°C) and aqueous lithium chloride (130°C). Small overload pulses were periodically superimposed on an otherwise constant load during crack propagation, which results in plastic blunting of the crack front. The time interval between pulses (Δt) varied from 2 to 200 s, and the corresponding spacing between crack-front markings (CFMs) (Δx) was measured by scanning electron microscopy. The spacing (Δx) decreased linearly with decreasing time interval (Δt) from 200 to 5 s. The slope of this line gave the velocity of crack propagation as 6.5×10^{-8} m/s in magnesium chloride at 154°C. For time intervals below 5 s, the smallest spacing between CFMs of 0.4 μm was recorded. These results were taken to indicate that the TG crack propagation in this alloy is discontinuous with the crack-arrest time of 5 s and a crack-advance distance of 0.4 μm per event. Similar tests in the lithium chloride environment at 130°C indicate a crack-arrest time of 5 s and a crack-advance distance of 0.3 μm per event. It is concluded that the load-pulsing method can provide accurate information about TG crack propagation.

Introduction

The transgranular (TG) stress corrosion crack is widely believed to propagate discontinuously by environment-induced cleavage.[1,2] The mechanism by which environmental interaction causes cleavage-type fractures in ductile alloys is not well established yet, and several possible mechanisms are being put forward.[1] The objective of this investigation was to delineate and define the TG crack propagation parameters. Periodic overload pulses on an otherwise constant load during TG crack propagation have been found to delineate crack-front positions on the fractured surface by plastic blunting of the crack tip.[3] These crack-front markings (CFMs) are discernible under the scanning electron microscope (SEM).

The load-pulsing technique was first used by Beavers and Pugh[3] to study the TG cracking of Admiralty metal in aqueous ammonia. It was observed that the CFMs were perpendicular to the serrated steps (also known as river or fan patterns) separating the primary cleavage facets, as would be expected in conventional cleavage. A one-to-one correspondence between the CFMs and load pulsing was also observed, leading to the calculation of crack propagation rate. In a later detailed study on the same system by Slattery, Smit, and Pugh,[4] it was found that the Stage II velocity deduced by the load-pulsing technique was higher than that deduced by conventional techniques. This was explained on the basis that the retarding effect of grain boundaries on crack propagation would not be a factor in the load-pulsing method, because the velocity is deduced from the parallel CFMs within a single grain.

Pulsing experiments have also been conducted on type 310 (UNS S31000) austenitic stainless steel (SS) by Hahn and Pugh[5] in boiling aqueous magnesium chloride at 154°C. Results from this study indicated that the spacings between CFMs decreased linearly with the decrease in pulsing intervals until Δt reached 15 s. Below a Δt of 15 s, linearity between Δx and Δt was not observed. Another significant finding was that for Δt below 15 s, there were fewer markings than pulses. This was taken to indicate that the natural crack arrest time (Δt^*) is about 15 s, so that more than one pulse was applied to the crack front while it was waiting to advance. Such a breakdown in one to one correspondence was not observed in Admiralty metal even at 2 s pulsing intervals.[5] Earlier work at the National Institute of Standards and Technology[(1)] on type 316L (UNS S31603) SS has also failed to establish a breakdown in the one to one correspondence between CFMs and pulses at pulsing intervals of 5 s.[6] However, the linearity between the CFM spacings (Δx) and the time interval between pulses (Δt) was lost below Δt of 25 s. At the point of linearity breakdown, the spacing between CFMs was minimum (0.7 μm). These values were taken to indicate the natural crack advance distance (Δx^*) and crack-arrest time (Δt^*), respectively. The crack advance distance (Δx^*) was in good agreement with the spacing of 0.9 μm observed between crack-arrest markings (CAMs) obtained by the slow-strain rate (SSR) test. CAMs are produced because of natural crack blunting during the arrest periods of a discontinuously propagating crack and are more discernible on fracture surfaces produced by SSR tests. It therefore appeared that the value of the natural crack-advance distance could be determined by the load pulsing method even though the one-to-one correspondence between pulses and CFMs does not break down.

The present work was conducted on type 316 (UNS S31600) austenitic SS in boiling aqueous magnesium chloride at 154°C and aqueous lithium chloride at 130°C. The primary objective of this work was to study the efficacy of the load pulsing method in establishing Δt^*, Δx^*, and the Stage II crack propagation rate in TG stress corrosion cracking.

*Department of Mechanical Engineering and Aerospace Sciences, University of Central Florida, Orlando, FL 32816-0993.

(1)Gaithersburg, MD.

Experimental Procedure

Specimens used in this study were prepared from annealed type 316 austenitic SS. The composition of the steel is given in Table 1. The mechanical properties are listed in Table 2. The smooth cylindrical tensile test type specimens were prepared by turning 0.79-cm (5/16-in.) bar stock to 0.63-cm (1/4-in.) bar stock with a gauge length of 1 in. (2.54 cm) and gauge diameter of 0.42 cm (0.165 in.).

TABLE 1
Chemical Composition of Type 316 (UNS S31600) SS

Element	Weight Percent
C	0.052
Mn	1.68
P	0.027
S	0.024
Si	0.60
Cr	17.07
Ni	12.96
Mo	2.01
Fe	Balance

TABLE 2
Mechanical Properties of Type 316 (UNS S31600) SS

Yield Strength (0.2% offset)	262 MPa (38,000 psi)
Ultimate Tensile Strength	572 MPa (83,000 psi)
% Elongation (2 in.)	61%
% Area reduction	75.2%

Load-pulsing tests

The load-pulsing tests were performed in boiling aqueous magnesium chloride at 154°C and aqueous lithium chloride at 130°C. The tests were conducted in a custom-designed corrosion cell made from a glass cylinder with Teflon† (PTFE) end plates at the top and the bottom. The top plate had openings for a temperature sensor and the addition of the solution. A heating tape wound around the glass cylinder maintained the required temperature within ± 1°C. An aluminum clamp kept the two Teflon end plates pressed against the glass to avoid any leakage. The salt concentrations were kept constant by condensing the vapors back into the corrosion cell.

A base load of 2700 N (600 lb) was applied through a hydraulic servoloop universal testing machine (MTS) and a 178-N (40-lb) overload pulse was applied at regular time intervals. The time interval between pulsing was varied from 2 to 200 s in the case of magnesium chloride solution and from 2 to 25 s in the case of lithium chloride solution. A signature pulse consisting of two values of Δt grouped together in a regular sequence was applied to several specimens to ascertain whether or not a one-to-one correspondence existed between CFMs and pulses for the selected Δt values.

The failed specimens were quickly removed from the corrosion cell, rinsed with water, ultrasonically cleaned in acetone and dried with hot air. The fracture surfaces were observed with a SEM (JEOL* model T-300).

Slow-strain-rate tests on type 316 steel in $MgCl_2$

SSR tests were independently conducted in boiling aqueous magnesium chloride at 154°C. The specimen geometry and the corrosion cell set-up were identical to those used in the load-pulsing tests. The purpose of running the SSR tests was to identify CAMs on stress corrosion facets so that comparisons could be made with Δx^*, determined by the load-pulsing method. Several specimens were tested under SSR conditions in the range of 5×10^{-7} to 2×10^{-6} per second. Fractured specimens were examined using the SEM to detect CAMs.

Results

Tests in magnesium chloride

Examination of the fracture surface under SEM indicated several separate stress corrosion cracks running inward, leading to final overload fracture. The CFMs were clearly visible at a number of locations, and they ran approximately perpendicular to the "river pattern." A typical fracture surface is illustrated in Figure 1. The fracture was predominantly TG exhibiting a typical cleavage-like morphology.

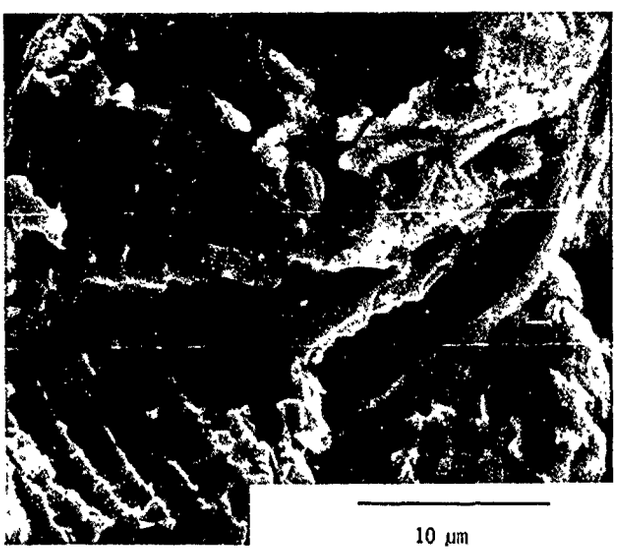


FIGURE 1—Scanning electron photomicrograph of the transgranular stress corrosion fracture surface with parallel crack-front markings produced by load pulsing in a type 316 (UNS S31600) steel specimen exposed to aqueous magnesium chloride.

The spacing between CFMs was measured from micrographs of single cleavage facets positioned approximately normal to the electron beam. The CFMs were predominantly found close to the overload fracture region. However, the spacings appeared fairly constant, indicating a Stage II behavior. Figures 2 and 3 illustrate characteristic CFMs on TG stress corrosion fracture surfaces for Δt values of 3 s and 50 s, respectively. To determine the Δx vs Δt variation, two to six areas with clear CFMs were photographed from two to four specimens for every value of Δt. The value of Δx was calculated for each Δt by simply measuring the length of the fractured facet showing clear CFMs and dividing it by the number of CFMs contained within that length. The values of Δx with standard deviations corresponding to each Δt are tabulated in Table 3. The resulting Δx vs Δt variation is plotted in Figure 4 using linear regression analysis. A linear relationship seems to hold for Δt < 5 s. Below a 5 s time interval, Δx seems to rise a little and then fall or plateau out at about 0.4 μm, as shown in Figure 5. This behavior seems to indicate that Δt^* is 5 s and Δx^* is 0.4 μm for type 316 steel in aqueous magnesium chloride at 154°C. The velocity of crack propagation measured by the slope of the Δx vs Δt above Δt of 5 s is 6.5×10^{-8} m/s.

The results of the signature pulsing indicated that one-to-one correspondence between the CFMs and number of pulses does not break down even at Δt equal to 2 s. Figure 6 shows a micrograph of signature pulsing that grouped 2 pulses at 20 s each and 4 pulses at

†Trade name.

4 s each. One-to-one correspondence between pulsing and CFMs is clearly evident. This is consistent with at least two previous studies, in which the one-to-one correspondence seemed to hold for $\Delta t < \Delta t^*$. It is conceivable that each pulsing leads to a crack-advance event prematurely, so that the breakdown in one-to-one correspondence with CFMs is not observed. The velocity of crack propagation deduced by the load-pulsing technique would still be very accurate because many crack-advance events occur during large Δt, and one premature advance would not significantly change the spacing between CFMs.

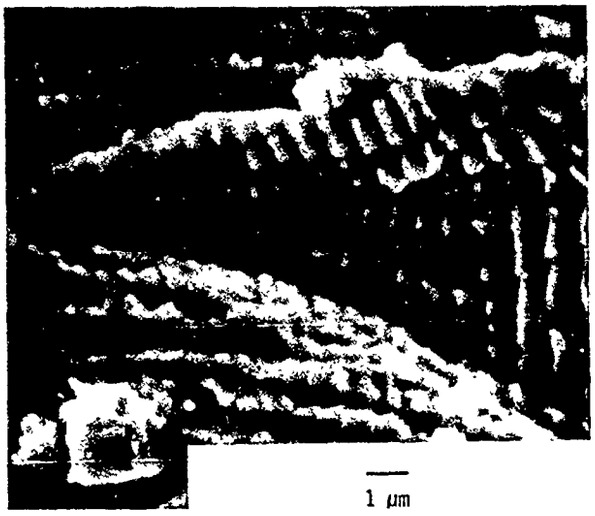


FIGURE 2—Scanning electron photomicrograph illustrating crack-front markings on a transgranular stress corrosion fracture surface for pulsing interval of 3 s in magnesium chloride at 154°C.

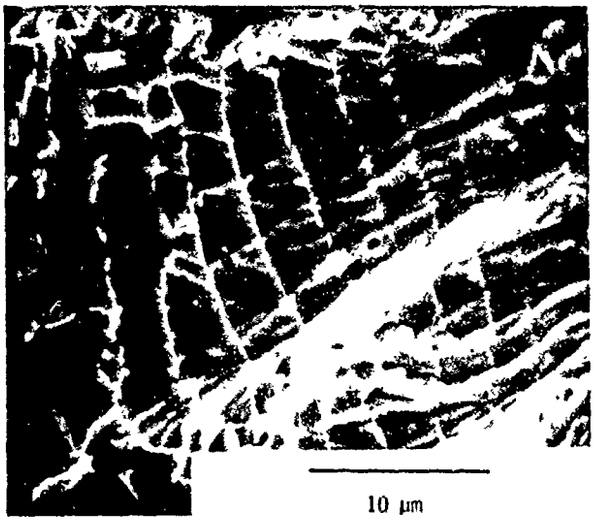


FIGURE 3—Scanning electron photomicrograph illustrating crack-front marking on a transgranular stress corrosion fracture surface for a pulsing interval of 50 s in magnesium chloride at 154°C.

TABLE 3
Relationship Between Pulsing Intervals and Crack-Front Markings Produced by Pulsing in $MgCl_2$ Environment

Time Between Successive Pulses Δt(s)	Spacing Between CFMs on Fractured Surface, Δx(μm)	Standard Deviation (μm)
2	0.39	0.01
3	0.62	0.07
4	0.45	0.01
5	0.59	0.07
10	1.04	0.10
15	1.49	0.08
25	2.03	0.22
50	2.92	0.48
75	4.82	0.22
100	6.78	0.35
150	11.62	2.35
200	12.93	0.98

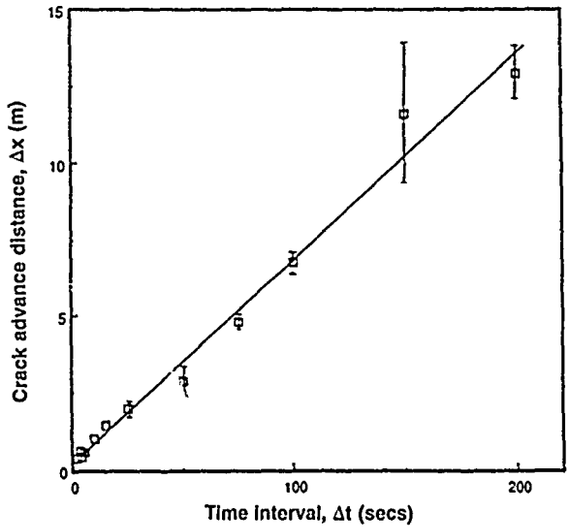


FIGURE 4—The relationship between the load-pulsing intervals and the spacing between crack-front markings on type 316 (UNS S31600) SS in boiling $MgCl_2$ at 154°C. The points indicate average values and the bars represent standard deviation.

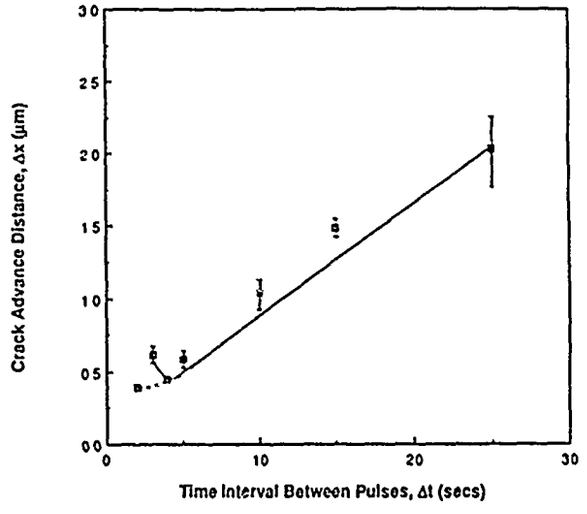


FIGURE 5—The relationship of the time interval between load pulses and the spacing between crack-front markings on type 316 (UNS S31600) SS in boiling $MgCl_2$ at 154°C, with an expanded scale for pulsing intervals shorter than 25 s.

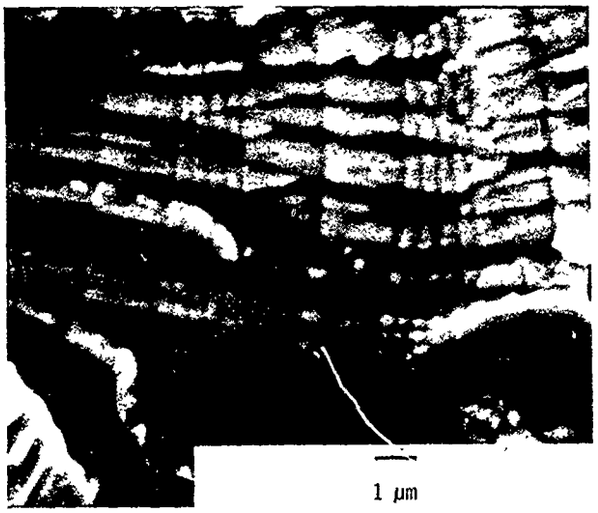


FIGURE 6—Scanning electron photomicrograph illustrating the existence of one-to-one correspondence between the crack-front markings and load pulsing by a signature pulse that grouped 2 pulses every 20 s and 4 pulses every 4 s.

Good agreement was found when the observed spacing between CFMs was compared to that calculated from the values determined for Δx^* and Δt^*. The SSR tests showed a few distinct CAMs on a couple of specimens. Figure 7 shows a representative micrograph of the TG stress corrosion fracture surface obtained under SSR conditions. The straight markings on the left side of the fractured facet are the slip steps; the markings on the right that follow the contour of the fractured surface are the CAMs. The spacing between CAMs in this figure is 0.8 μm. This is about twice the value of Δx^* deduced from the load-pulsing results. As indicated in Table 4, the spacing between CAMs measured from SSR tests is consistently larger than Δx^* deduced by the load-pulsing method. It is possible that more severe conditions in SSR testing (such as the continuous pulling) may cause the TG stress corrosion crack to propagate a longer distance at every cracking event.

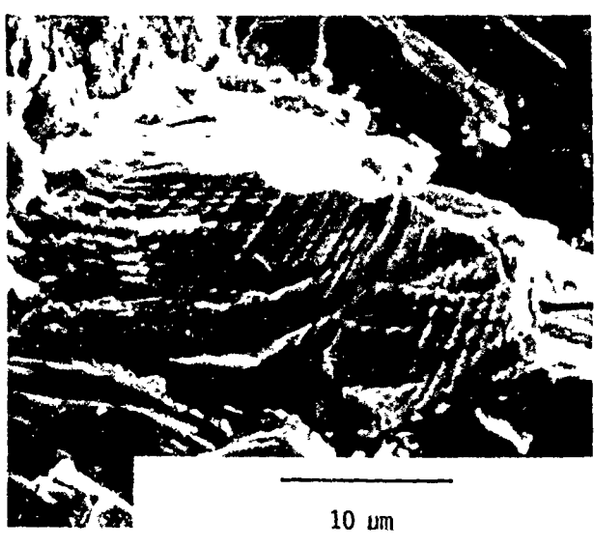


FIGURE 7—Scanning electron photomicrograph of transgranular stress corrosion fracture surface produced by slow-strain-rate conditions at the strain rate of about 10^{-6} per second in magnesium chloride at 154°C. Crack-arrest marks that follow the contour of the fracture surface are clearly visible on the right; the straight markings on the left are produced by slip steps.

TABLE 4
Comparison of Transgranular Stress Corrosion Cracking of Different Austenitic Stainless Steels

Alloy	Environment	Crack Velocity ($\times 10^{-8}$ m/s)	Δt^* (s)	Δx^* (μm)	Spacing Between CAMs (μm)
310[5]	$MgCl_2$ at 154°C	2	15	0.4	0.8[(A)]
316L[6]	$MgCl_2$ at 154°C	3	25	0.7	0.9[(A)]
316	$MgCl_2$ at 154°C	6.5	5	0.4	0.8[(A)]
316	LiCl at 130°C	—	5	0.28	0.27[(B)]

[(A)]Measured from slow-strain-rate test photomicrographs.
[(B)]Measured from load-pulsing photomicrographs (Figure 10).

Tests in lithium chloride

The load-pulsing tests on type 316 steel in lithium chloride were performed at 130°C. Examination of the fracture surface in the SEM revealed TG cracking in most specimens. However, a few specimens showed considerable evidence of intergranular cracking. CFMs perpendicular to river patterns were discernible on the TG fracture facets, shown in Figure 8. "Crack-front-like" markings were also observed on the intergranular fracture facets. This is an important finding, and a recent study at the National Institute of Standards and Technology supports the observation of CFMs on intergranular fracture facets.[7] The resulting Δx vs Δt behavior for TG stress corrosion cracking is represented in Figure 9, which indicates a Δx^* of 0.28 μm and Δt^* of 5 s. The most significant finding in lithium chloride tests was that, in at least two specimens, faint CAMs were observable between the more pronounced CFMs. The spacing between these CAMs from both specimens was measured to be about 0.28 μm. Figure 10 illustrates one such area where CAMs are observable. This is in exact agreement with Δx^* deduced from Δx vs Δt behavior. The value for crack propagation rate is not reported because tests were not run at sufficiently higher values of Δt to calculate the velocity with reasonable accuracy.

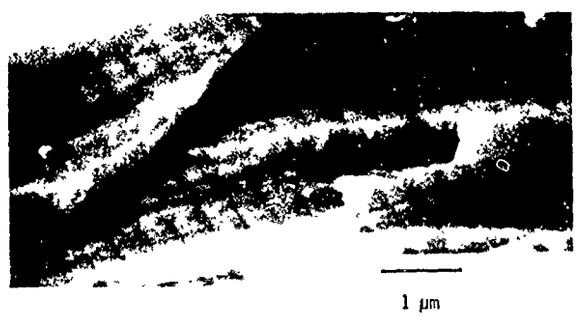


FIGURE 8—Scanning electron photomicrograph illustrating crack-front markings on transgranular stress corrosion fracture surface produced by load pulsing at intervals of 5 s in lithium chloride at 130°C.

Conclusion

From this study on the propagation of TG stress corrosion cracking, the following general conclusions can be drawn.

(1) The TG stress corrosion crack propagation in austenitic SSs occurs by a discontinuous cleavage fracture.
(2) The load-pulsing method yields value for TG stress corrosion cracking velocity, which is free from the complicating effects of grain boundaries.
(3) The overload pulse can trigger premature crack advance so that one-to-one correspondence between the CFMs and pulses may not break down even at $\Delta t < \Delta t^*$.

(4) The two fundamental parameters of TG stress corrosion cracking, crack-advance distance (Δx^*), and crack-arrest time (Δt^*) can be accurately determined from the load-pulsing tests. The crack jump distance measured as the spacing between CAMs from SSR tests is likely to be higher because of the severity of the test.

Acknowledgment

The authors are grateful to Dr. E.N. Pugh and Dr. R. Ricker of the National Institute of Standards and Technology for their invaluable support. The help of A. Hutchinson in running the tests is also acknowledged.

This research was partially supported by a National Association of Corrosion Engineers seed grant.

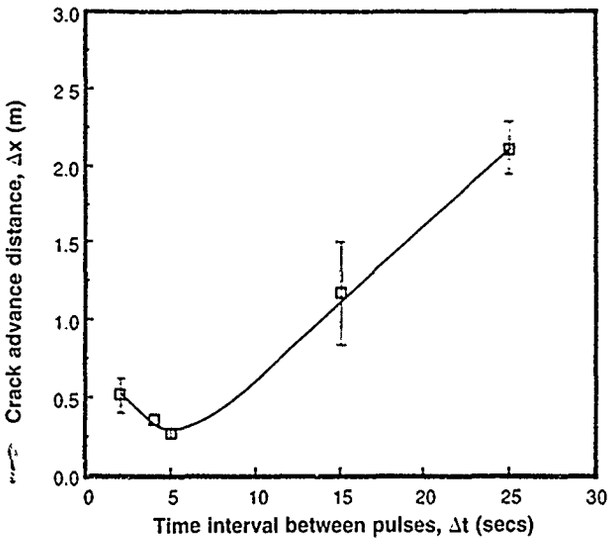


FIGURE 9—Relationship between the load-pulsing time interval and the spacing between crack-front markings on type 316 (UNS S31600) SS exposed to lithium chloride at 130°C.



FIGURE 10—Scanning electron photomicrograph illustrating the existence of crack-arrest markings between the more pronounced crack-front markings on a transgranular stress corrosion fracture surface produced by load pulsing in lithium chloride.

References

1. E.N. Pugh, Corrosion 41(1985): p. 517.
2. K. Sieradzki, R.C. Newman, Phil. Mag. A 51(1985): p. 95.
3. J.A. Beavers, E.N. Pugh, Metall. Trans. A. 11A(1980): p. 809.
4. P.W. Slattery, J. Smit, E.N. Pugh, Environment-Sensitive Fracture: Evaluation and Comparison of Test Methods, ASTM STP 821, ed. S.W. Dean, E.N. Pugh, G.M. Ugiansky (Philadelphia, PA: ASTM, 1984), p. 399.
5. M.T. Hahn, E.N. Pugh, Fractography and Materials Science, ASTM STP 733, ed. L.N. Gilbertson, R.D. Zipp (Philadelphia, PA: ASTM, 1981) p. 413.
6. V.H. Desai, M.J. Kaufman, E.N. Pugh, unpublished work at the National Institute of Standards and Technology, Gaithersburg, MD, 1984.
7. E.N. Pugh, Private Communication, 1988.

Fractography of Environmental Cracking of C-Mn Steels in Anhydrous Methanol-Ammonia Environments

*Z. Wenyue, R.C. Newman, and R.P.M. Procter**

Abstract

Cleavage-like transgranular stress corrosion cracking (SCC) occurs in iron or low-strength steels exposed to anhydrous ammonia environments. The experimental difficulties associated with the use of pressurized liquid ammonia can be avoided by dissolving ammonia in methanol at atmospheric pressure; environmental variables such as oxygen, water, and carbon dioxide content have very similar effects in ammonia and methanol-ammonia systems. Apart from the fracture appearance, the cracking has none of the characteristics of hydrogen embrittlement.

The fractography of methanol-ammonia SCC has been studied using a C-Mn steel, heat treated to grow the ferrite grain size to ~ 95 μm. The fracture surfaces are typical of transgranular SCC and exhibit a characteristic river-pattern morphology. Crack advance occurs on a smoothly curved front across each grain, and crosses many cleavage steps of different heights. Sets of striations visible on the surfaces were identified as crack-arrest markings using detailed scanning electron fractography. In particular, the striations were shown to be perpendicular to the local crack growth direction and to match on opposing fracture surfaces.

The mechanism of SCC in this system is believed to be film-induced cleavage. The role of oxygen and potential is to induce electrochemical oxidation of ammonia on the iron surface, producing a passive film that does not contain oxygen; this has been speculated to be a nitride.

Introduction

Stress corrosion cracking (SCC) of a ferritic-pearlitic C-Mn steel in anhydrous methanol containing about 20 wt% ammonia was first reported to have occurred in service in a large methylamine plant in 1978.[1] Since then, several studies of environmental cracking in this alloy/environment system have been published.[2-5] The results of these earlier studies may be briefly summarized as follows:

(1) Environmental cracking of low-strength, ferritic-pearlitic C-Mn steels only occurs in methanol-ammonia solutions under free corrosion conditions if the environment is anhydrous and contaminated with oxygen and carbon dioxide. The cracking is accelerated by the presence of nitrogen as a contaminant but inhibited by the presence of water.[2,3]

(2) The role of oxygen in the environment is to act as a cathodic reactant that raises the free corrosion potential of the steel from active values (about $-0.5\ V_{SCE}$) in oxygen-free methanol-ammonia into the passive region (about $-0.3\ V_{SCE}$) in oxygen-contaminated solution.[2,3] However, the oxygen apparently plays no other essential role in the cracking mechanism, since identical cracking also occurs in carbon-dioxide contaminated but oxygen-free methanol-ammonia solutions if the potential of the steel is held potentiostatically within the passive, cracking range.[4,5]

(3) It is probable that the role of carbon dioxide in the environment involves the formation of ammonium carbamate ($NH_2CO_2NH_4$). This subsequently dissociates with the formation of NH_4^+ ions, which effectively lower the pH of the environment and increase the conductivity from 0.17 mS/cm to 1.1 mS/cm.[2,3]

(4) Susceptibility to cracking appears to be critically dependent on the nature of the passive film. In anhydrous environments, the passive film is thought to be a nitride-like compound,[4,6] which accounts for the accelerating effect of nitrogen contamination of the environment. However, in solutions that contain additions of about 3000 ppm water, the passive film is oxygen based.

(5) Cracking is completely prevented by low levels of cathodic protection; no cracking occurs over the potential range $-0.4\ V_{SCE}$ to $-1.2\ V_{SCE}$, which suggests that hydrogen embrittlement is not involved in the mechanism of cracking.

(6) This view is strengthened by the facts that statically loaded "tuning-fork" specimens will crack in methanol-ammonia environments and that during slow-strain-rate tensile testing, cracking occurs as soon as the yield strength is exceeded.[2,3] These results are in marked contrast to hydrogen cracking of steels with very similar microstructures and strength levels in synthetic seawater under various levels of cathodic protection. In this case, statically loaded specimens do not crack, and in slow-strain-rate tensile tests, cracking only occurs once necking has started and high triaxial stresses are present in the specimens.[7,8]

(7) The above observations appear to suggest that environmental cracking of C-Mn steels in contaminated, anhydrous methanol-ammonia solutions occurs by a classic slip-dissolution mechanism; however, the following two observations argue strongly against this conclusion.

(8) The rate of crack propagation is relatively high, typically of the order of 5×10^{-8} m/s.[2,3] To sustain this growth rate by anodic dissolution would require a crack-tip anodic current density of more than $10^4\ A/m^2$, which would be very difficult to sustain in a relatively low-conductivity environment such as methanol-ammonia.

(9) The cracking generates a transgranular, cleavage-like fracture,[2,3] which would not normally be expected to result from cracking by slip dissolution.

In summary, therefore, neither hydrogen embrittlement nor slip dissolution is consistent with, or can satisfactorily account for, the

*Corrosion and Protection Centre, University of Manchester Institute of Science and Technology, Manchester, UK.

experimentally observed features and characteristics of cracking of C-Mn steels in anhydrous methanol-ammonia On the other hand, all aspects of the cracking phenomenology appear to be consistent with a film-induced cleavage mechanism.[9] In an attempt to test this hypothesis, a detailed fractographic examination of relevant fracture surfaces was undertaken and is reported here.

Experimental Procedure

The material used was basically a steel to British Standard 1501 containing 0.13% C and 0.89% Mn. In the as-received (cold-rolled) condition, this steel had a fine, banded, ferritic-pearlitic microstructure and a yield strength of 360 MN/m^2. However, to facilitate the detailed fractography, this material was vacuum heat treated as follows to coarsen the grain size:

(1) Anneal at 1200°C for 1 h;
(2) Furnace cool from 1200° to 840°C;
(3) Cool from 840° to 640°C at 8°C/h;
(4) Furnace cool from 640°C to room temperature.

This heat treatment resulted in a steel that had a yield strength of 215 MN/m^2 and a coarse ferritic-pearlitic microstructure with grain size of about 95 μm.

Cylindrical tensile specimens (gauge length 16.0 mm and gauge diameter 2.6 mm) of the as-received and heat-treated steel were subjected to conventional slow-strain-rate tensile testing at a crosshead speed of 35×10^{-5} mm/s under potential control in anhydrous methanol-ammonia contaminated with nitrogen and carbon dioxide. Preparation of and slow-strain-rate testing in this environment require rather complex and specialized procedures that have been described in detail elsewhere and will not be repeated here [2-4] Briefly, the methanol-ammonia solution contained about 18 wt% NH_3, less than 500 ppm H_2O, about 1000 ppm CO_2, and an N_2 partial pressure of 6 psig, the tests were performed at a potential of 0 3 V_{SCE}. In addition to monotonic straining, load-pulsing experiments were also undertaken, after Hahn and Pugh,[10] the magnitude of the load pulses was 4% of the ultimate tensile strength of the steel and each pulse was completed in 2 to 3 s. After stress corrosion testing in this environment, the fracture surfaces were subjected to a detailed fractographic examination using scanning electron microscopy.

Results and Discussion

After testing in air, both as received and heat-treated specimens showed typical ductile cup and cone fractures and about 70% reduction in area, the fracture surfaces exhibited dimples characteristic of fracture by microvoid nucleation, growth, and coalescence.

Figure 1 shows an as-received specimen after slow-strain-rate testing and failure by SCC in methanol-ammonia solution. The reduction in area is reduced to about 40%. Figure 2 is a polished and etched metallographic section through the gauge length of a similar specimen well away from the fracture surface. Note multiple secondary cracking along the gauge length well away from the primary fracture, and the transgranular, relatively unbranched crack morphology. Figure 3(a) is a scanning electron micrograph of the stress corrosion fracture surface of a specimen similar to that shown in Figure 1, note the characteristic brittle, cleavage morphology. At higher magnifications [Figure 3(b)], parallel bands are visible crossing the fracture surfaces; these correspond to the pearlite bands in the microstructure, as shown in Figure 2. Also visible are sets of parallel striations on a number of the individual cleavage facets. Apparently, similar striations have been reported on the transgranular stress corrosion fracture surfaces of α-brass in aqueous ammoniacal solutions[11,12] and of γ-stainless steel in hot, chloride-containing environments [13,14] Fracture surface striations may be either slip lines, which emerge from behind a moving crack tip, or crack-arrest markings produced by plastic deformation during temporary crack arrest in the course of discontinuous crack propagation. Crack-arrest markings, but not slip lines, are necessarily perpendicular to the local crack growth direction and are matchable on opposing fracture surfaces. However, using these characteristics to determine whether the striations observed in the present case were crack-arrest markings, which in turn would be evidence of discontinuous crack growth, or slip lines, required the use of heat-treated, coarse-grained steel to produce correspondingly large cleavage facets.

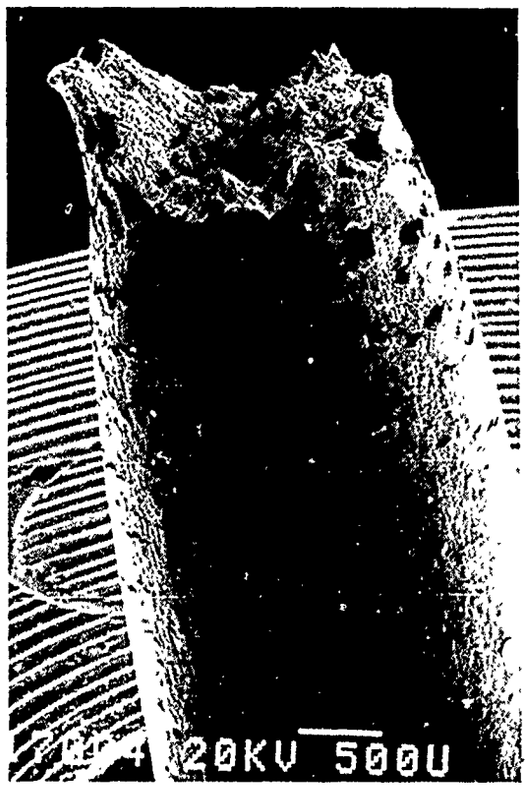


FIGURE 1—Micrograph of an as-received C-Mn steel specimen after failure by SCC in methanol-ammonia; X22.



FIGURE 2—Polished and etched metallographic section through the gauge length of an as-received C-Mn steel specimen after failure by SCC in methanol-ammonia; X170 (original magnification).

Figure 4 shows the matching opposing fracture surfaces of a heat-treated specimen after failure by stress corrosion cracking in methanol-ammonia. Figure 5 is a higher magnification matching pair taken from the area arrowed in Figure 4. It is clear from Figure 5 first that the striations are locally perpendicular to the cleavage steps (river markings), and second that there is precise, one-to-one matching between striations on opposing fracture surfaces. Taken together, these observations provide evidence that the striations are in fact crack-arrest markings rather than merely slip lines. It is also clear from Figures 4 and 5 that it is not only the striations that match

on opposing fracture surfaces; the river patterns and other detailed features on the fracture surfaces also match precisely. These observations are clearly inconsistent with the slip-dissolution mechanism of crack propagation, but they are fully consistent with a discontinuous mechanism of crack propagation involving repeated, film-induced cleavage.



a



b

FIGURE 3—Scanning electron micrograph of the stress corrosion fracture surface of an as-received C-Mn steel specimen after failure in methanol-ammonia; (a) X450 (original magnification) and (b) X1300 Note the parallel bands on the fracture surface, which correspond to the pearlite bands in the microstructure and also the parallel sets of striations on individual cleavage facets.

Figure 6(a) shows a relatively low-magnification micrograph of the fracture surface of a specimen that was pulse loaded at intervals of 200 s. Figure 6(b) is a higher magnification micrograph of a region when the load pulses were applied at intervals of 7.0 s or 3.5 s. Instead of the complete loss of correspondence between pulses and crack-front markings below 15 s reported by Hahn and Pugh,[10] continued one-to-one correspondence was observed. However, stereoscopic examination at higher magnification than Figure 6(b) showed that a flat cracking plane was maintained with pulse intervals of 7.0 s, whereas reduction of the pulse interval to 3.5 s resulted in a steep deviation from the flat cracking plane. The displacement of the crack tip therefore apparently occurs by a stretching (slip) process for pulse intervals of 3.5 s but continues as a cleavage process on the main crack plane for pulse intervals of 7.0 s. This result suggests that the characteristic arrest time between film-induced cleavage events in C-Mn steels in methanol-ammonia environments may be between 3.5 s and 7.0 s.

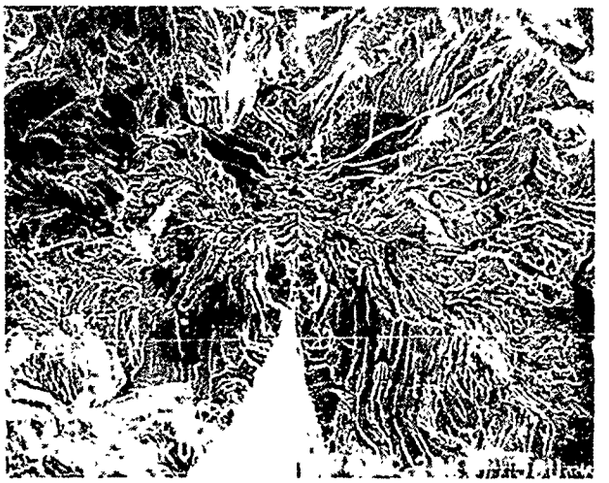


FIGURE 4—Scanning electron micrographs showing the matching opposing fracture surfaces of a heat-treated C-Mn steel specimen after failure by SCC in methanol-ammonia; X310 (original magnification).



FIGURE 5—Scanning electron micrographs showing the one-to-one matching of striations and other features on opposing fracture surfaces of a heat-treated C-Mn steel specimen after failure by SCC in methanol-ammonia; X4000 (original magnification).

It is clear from the summary of earlier investigations presented above that there are many similarities between cracking in anhydrous methanol-ammonia and the important engineering problem of stress corrosion cracking of steels in anhydrous ammonia.[15-18] It therefore seems reasonable to speculate that stress corrosion cracking in this alloy/environment system may also be due to repeated microcleavage induced by a nitrogen-containing passive film.



a



b

FIGURE 6—Crack-front markings produced by load pulsing during slow-strain-rate stress corrosion testing of a heat-treated C-Mn steel specimen in methanol-ammonia; (a) X680 and (b) X11,000.

Conclusion

Parallel striations have been observed on the transgranular stress corrosion fracture surfaces of a ferritic-pearlitic, C-Mn steel after failure in anhydrous methanol-ammonia environments. Using detailed scanning electron fractography, these striations have been identified as crack-arrest markings, they are perpendicular to the local crack growth direction and they exhibit precise, one-to-one matching on opposing fracture surfaces. On the basis of this and other published evidence, it is suggested that stress corrosion crack propagation in the C-Mn steel/methanol-ammonia system is discontinuous and occurs by repeated film-induced cleavage. The film involved is thought to be based on the Fe-N system.

Acknowledgment

Z.W. acknowledges with thanks financial support from The British Council.

References

1 J.A. Richardson, M.E.D. Turner, Private Communication, 1980.
2 M V E Omideyi, R.P M Procter, Proceedings of the Ninth International Congress on Metallic Corrosion (Ottawa, Canada. National Research Council, 1984), pp. 174-186.
3 M V.E. Omideyi (Ph.D. diss., UMIST, 1986).
4 Z. Wenyue (Ph.D. diss., UMIST, 1988).
5 R C Newman, W. Zheng, C.R. Tilley, R.P.M. Procter, CORROSION/89, paper no 568 (Houston, TX. National Association of Corrosion Engineers, 1989).
6 M Ahrens, K E. Heusler, Werkst. und Korros. 32(1981). p. 197.
7. B.R.W. Hinton (Ph.D. diss., UMIST, 1980).
8 B.R.W. Hinton, R.P.M. Procter, Corros. Sci. 23(1983). p. 101.
9 K. Sieradzki, R.C. Newman, Phil. Mag. A 51(1985): p. 95.
10 M.T. Hahn, E.N. Pugh, Corrosion 36(1980). p. 380.
11 M.B. Kermani, J.C. Scully, Corros. Sci. 19(1979). p. 489.
12 R C Newman, K Sieradzki, Scripta Metall. 17(1983). p. 621.
13 A J Bursle, E N Pugh, Environment Sensitive Fracture of Engineering Materials, ed. Z.A. Foroulis (New York, NY. American Institute of Mining, Metallurgical, and Petroleum Engineers, 1979), pp. 254-269.
14 V Desai, F Friedersdorf, T. Shaw, this proceedings.
15 T.J. Dawson, Welding J. 35(1956). p. 569.
16 A W Loginow, H. Phelps, Corrosion 18(1962). p. 299.
17 A Cracknell, Advances in Petrochem. Technology, Inst. of Chem Eng Symposium, no. 50 (London, England. 1977).
18. B.E. Wilde, Corrosion 37(1981): p. 131.

SECTION IX

Views of the Past, Present, and Future

Co-Chairmen's Introduction

R.P. Gangloff
University of Virginia
Charlottesville, Virginia, USA

M.B. Ives
McMaster University
Hamilton, Ontario, Canada

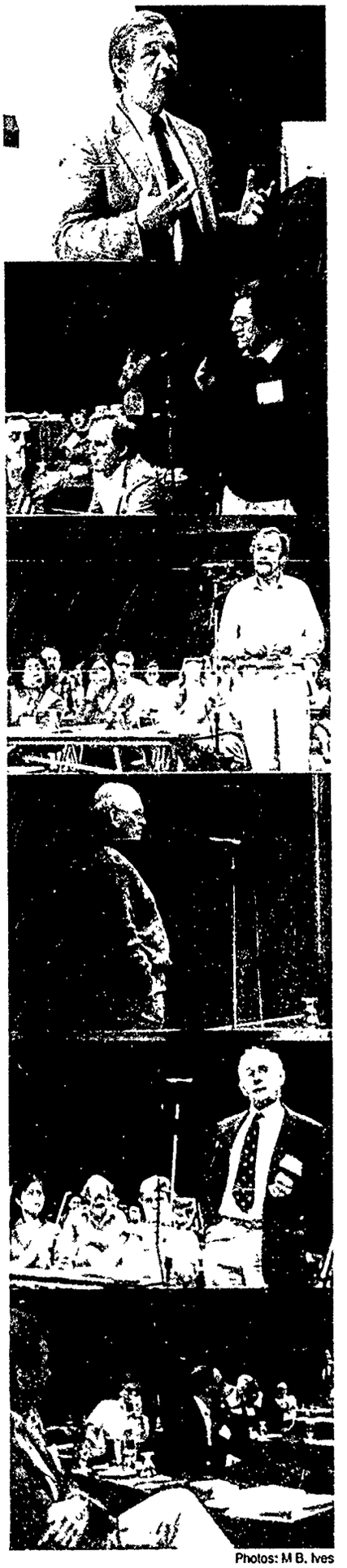
On the final morning of the conference, the topics changed from specific environmental cracking phenomena and mechanisms to important issues on information transfer and application in performance predictions. Discussion focused on fertile ground for future research.

As the architect of the seminal Firminy conference and an international leader in research and engineering on environmental fracture, R.W. Staehle was invited to assess the state of the field. He framed his presentation with the new concept of situation-dependent strength and the adage that a material should be presumed guilty of environmental fracture sensitivity until it is proven otherwise. This approach emphasizes the fact that a myriad of mechanical, metallurgical, and chemical variables affect environmental fracture strength.

While admittedly not breaking new mechanistic ground, this notion communicates to design and materials selection engineers the effects of important variables through computer represented plots of environment sensitive strength. In this way, those regimes in which cracking is mitigated may be identified with minimum confusion to the user of such information.

The success of deformation, fracture, and processing maps in materials science indicates that Staehle's approach will have important technological impact. This view in no way minimizes the importance of continuing to search for mechanistic understanding of environmental cracking. It is only with such information in hand that we will be able to predict quantitatively the effects of important variables, enabling extrapolations from the limited databases provided by laboratory research. Indeed, situation dependent strength and mechanistic laboratory studies are inextricably intertwined.

The second part of this session was devoted to a "wind-up" discussion by all participants. Here, lively interchanges focused on gaps in understanding and on problems in translating the results of laboratory studies to engineering applications. Two conclusions were obvious. First, significant uncertainties remain and are worthy of research. Many of these problems exceed our current capabilities to measure and model. Second, the interfaces between the laboratory and the application, the scientist and the practicing engineer, are generally fraught with difficulties, our field is no exception. The essence of these discussions is captured in the ensuing sections.



Photos: M.B. Ives

Understanding "Situation-Dependent Strength": A Fundamental Objective in Assessing the History of Stress Corrosion Cracking

*R.W. Staehle**

Introduction

I undertook this review to determine what has been accomplished in developing a quantitative and useful understanding of the science and engineering aspects of what is generally included in the term, "stress corrosion cracking" (SCC).

By the term "quantitative," I intend a reasonably good scientific description of the effects of material, environment, stress, geometry, temperature, and time on the initiation and propagation of SCC for systems of alloys and environments. By the term "useful," I am concerned with the application of this quantitative understanding to "design" as related to the design of components that can be expected to operate for their intended life avoiding failures by SCC. These ideas of "quantitative" and "useful" can be somewhat defined also by what has been done in science and in engineering, respectively, to understand SCC.

In general, I am taking the subject of SCC to include all of those phenomena in which the combination of stress, environment, and material interact to lower the load-carrying capacity below that in inert environments. Such phenomena are described by a range of terms such as anodic SCC, hydrogen embrittlement, liquid metal embrittlement, corrosion fatigue, environmentally affected cracking, and many others.

Undertaking such a review at this time responds to several needs. First, the ranges of temperatures, times, and environments in which commercial equipment must operate are expanding Second, there needs to be a more quantitative and relevant product of the scientific studies of SCC.

In the commercial arena, the length of time for reliable performance has been greatly extended by the need to store radioactive waste for times in the range of 1000 to 10,000 years. Maximum temperatures for a new class of materials have been increased by the program to develop a hypersonic plane. The envelope of long time and intermediate temperatures has been increased by the need to extend the life of nuclear power plants. Reliable performance of loaded structures for several hundred years are required for civil engineering. The size domain in computing and communications hardware has decreased to microscopic and virtually atomic dimensions. Finally, new environmental conditions are becoming important, including bactericides, chemical processing fluids, bacteria, and gaseous hydrogen These expanded domains of temperature and time are illustrated in Figure 1.

As these boundaries of temperature, time, and geometry are being extended, it does not appear that the understanding of SCC has kept up. One has only to look at the nuclear industry that failed to use well-established existing information with the result of extensive SCC over the 1970s and 1980s In the previous decade, the design of the military cargo plane, the C5A, neglected what was known about the SCC of high-strength aluminum; the design of other military equipment neglected what was known about the SCC of high-strength steels. Whether a similar pattern of disregard will apply as new boundaries are pushed to the limit is within our hands to influence.

For me to assess progress in the scientific and engineering work on SCC, it was necessary to define a framework within which to judge progress. For this framework, I chose six factors: material, environment, stress, geometry, temperature, and time. These are summarized in Figure 2. Thus, as I evaluated proposed theoretical propositions from various investigators, I asked whether their theories could explain the observed phenomenology of various metal–environment systems with respect to dependencies upon material structure and chemistry; physical and chemical features of the environment, stress in its various time-dependent modes; geometry as it affects local chemistry; and stress intensification, temperature, and time of exposure.

It is not surprising that I could find no theoretical models that provide quantitative rationalization of my six factors on an *a priori* basis, although some impressive progress has been made, as I describe in the section on the scientific status.

As I considered why so little progress had been made on developing quantitative models, I realized that we are still, to some extent, bound by misleading ideas of the past, including the following

(1) Materials have inherent strengths that designers can use without consideration of the circumstances of operation of a component.
(2) SCC failures are premature rather than an expected part of the performance of materials in environments.
(3) SCC is caused by "specific ions" rather than being a regular response to changes in the chemical continuum to which a material is exposed.
(4) A material may be "susceptible" or "not susceptible" to SCC rather than the "intensity" of SCC varying over an environmental continuum.
(5) There is a single universal mechanism of SCC rather than a multiplicity of microprocesses by which the inherent reactivity of materials leads to deterioration.

Of course, another reason for the lack of achieving the desired quantitative progress is the inherent complexity of SCC and the need for a number of disciplines to participate in developing useful theories.

The phenomenon of SCC is inherently related to the design and performance of engineering components and systems. However, there are, as has been pointed out by Westwood and Pickens,[1] applications for SCC in machining of materials and possibly in understanding earthquakes. Removal of snow, via weakening the ice, is another application. In this review, I am primarily concerned with SCC as it relates to the performance of engineering components and systems, and I have not considered these other applications.

*Department of Chemical Engineering and Material Science, University of Minnesota, Minneapolis, MN 55455.

Further, I have confined this review to the performance of metals, and I have not included other solids such as polymers, ceramics, or ice, for which many of the ideas here can be directly applied.

Since considering SCC relative to design is a primary concern of this review, I need to identify what kinds of questions the materials community must answer for the data to be useful in design. In addition to assessing progress in terms of the six factors of Figure 2, I also assess progress relative to what the materials community should furnish to the design community. Such information is at least the following:

(1) Means of organizing a performance envelope for components and systems in the framework of strength of materials that is situation dependent.
(2) Means of specifying the strength available for design under the conditions identified in Figure 2.
(3) Means to interpolate and extrapolate from existing information to specifically defined design conditions.
(4) Definition of environmental features that influence SCC.
(5) Means by which SCC can be incorporated into codes.

These needs suggest that a more regular framework is required both for communicating and for organizing data.

To develop this more orderly framework for describing SCC, a new means of thinking and of organizing data is required instead of the present, which is mostly "bits and pieces." This does not imply the need for a unified model of stress corrosion; rather, it implies the need for a flexible but orderly framework Further, one feature of such a framework should be that it not be so "on and off," as implied by terms such as "susceptibility" and "specific ions," but rather a continuum of "intensity" of SCC over some coordinates of independent variables such as the factors of Figure 2. Such an approach is discussed in the section "Engineering Status."

Such a more orderly framework should provide an improved capability for extrapolating and interpolating from existing data to new and untested circumstances Further, such an orderly framework should provide bases for predicting very long time behavior of the type defined in Figure 1.

There are other reasons for needing a more orderly framework for organizing data on SCC One is to increase the comparability of results from experimental programs The comparability of data for slow-straining experiments and reverse U-bend is questionable, the data taken under open-circuit conditions often does not specify oxygen and pH.

Building a database that is self-consistent, orderly, and uses comparable approaches would advance both scientific and engineering progress. An example of an orderly framework for organizing data is the various heat transfer and flow correlations used in chemical engineering Here, many different experimentalists can obtain data that can be integrated into a coherent, if somewhat scattered, set.

Another reason for developing a more orderly framework is to link theory and experiment Present theories speak only to a very small part of any of the continua to which they might apply. As the scientific workers seek to test their hypotheses, a more orderly picture of the phenomenological continuum would define a better target With such a framework, the interaction between theory and phenomenology could become more productive.

To assess the state of SCC in this review, I first define the criteria for my assessment. Next, I discuss historical landmarks and the steps by which improved understanding has developed. This includes a description of the state of affairs as of about the year 1955, which I use as a starting point From this starting point, I identify the events that caused a change in thinking; I describe the steps by which the various communities contributed to the changes. Next, I examine the status of scientific and engineering work The latter section on the status of engineering work is the longest of this review because I summarize the important features of what I consider to be useful ideas.

In the next-to-last section, I have a short section on what needs to be done Finally, I include a bibliography with the topics arranged to be useful to the reader.

In preparing the figures for this review, I intended to integrate many of the ideas that have been developed by many different authors. I have taken some liberties with the original graphics in order to show how the respective data answer questions or fit patterns. Also, I have omitted some information.

Situation-Dependent Strength and the Intensity of SCC

Approach

In the introduction, I identified my intention to develop a set of criteria by which I could judge progress in the development of models for SCC. I identified in Figure 2 six factors that I planned to include in such a ranking process.

As I attempted to use these factors for assessing the progress of developing models of SCC, I realized that I was being too severe of a critic. None of the theoretical models for SCC provides more than a qualitative description of critical dependencies, although many of these models provide insightful bases for thinking. The fact that none of these models provides the hoped-for quantitative description of the six factors in Figure 2 does not diminish the importance and creative accomplishments of the modeling work.

However, in developing these six factors for assessing progress, it became clear that these factors are, in fact, the coordinates for the orderly arrangement of data of SCC. Thus, the factors of Figure 2 are the independent variables, and the dependent variable or result is the "intensity" of SCC. This "intensity" of SCC may be some combination of crack velocity, initiation time, the time-dependent endurance limit (K_{Iscc}) or a similar parameter. Figure 3 shows the schematic relationship between the independent variables from Figure 2 and the intensity of SCC, which is the dependent variable of Figure 3.

The most profound implication of the dependence of SCC "intensity" upon the six factors of Figure 2, as shown in Figure 3, is that the strength of materials depends totally upon their situation. Unlike thermodynamics, strength is a "situation-dependent" quantity. In the past, this was partially acknowledged by noting that strength properties are "history dependent", i.e., strength depends on every previous step in fabrication. In this review, the "history dependence" applies only to the metallurgical factor of Figure 2. There are five other factors that define the "situation." Thus, the strength of an alloy cannot be defined except as it is defined in the total six-factor situation in which it operates.

Since Figure 3 implies that strength depends upon the situation in which the material finds itself, one might say that the strength is "situation dependent." The capacity of a material to handle loads is its "situation-dependent strength" (SDS).

Figure 4 illustrates the relationship among SCC, SDS, and strength as determined in inert environments. SDS is what is left from the inert environment strength after being altered by SCC. SCC is one of the most important processes by which strength is degraded. There is some question as to whether the inert environment strength is even a legitimate reference since it sets such a misleading standard. For now, it is useful to relate this review to existing information.

This implication of SDS is important relative to the presentation of materials properties in handbooks. So far as I am aware, there are no *caveats* in handbooks that the properties, as listed, apply only to inert and dry environments.

The discussion in this review considers only one mode of corrosion, SCC. Many features of the discussions in this review can be applied to other modes of corrosion such as general corrosion, pitting, intergranular corrosion, and parting. Such an approach would be important in the comprehensive assessment of a major commercial component.

In this section, I define each of the factors of SDS as applied to metals.

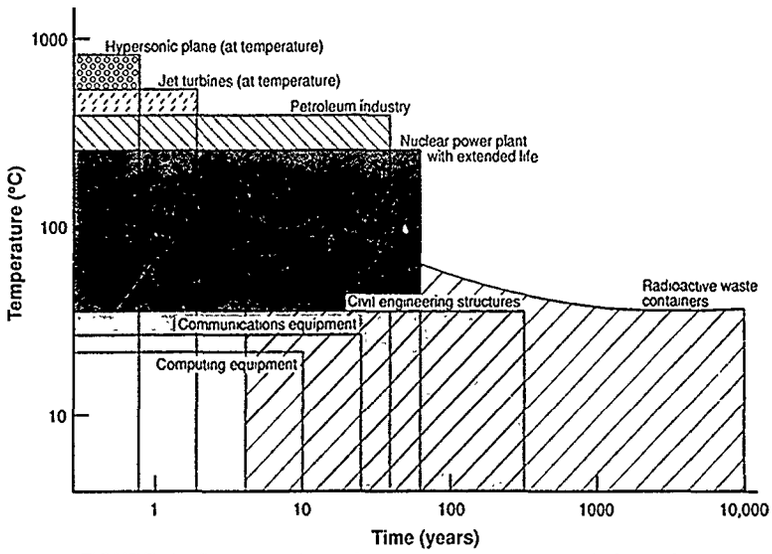


FIGURE 1—Ranges of maximum temperatures and times in which materials and components need to perform reliably in important industries.

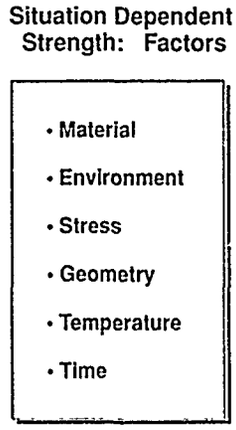


FIGURE 2 – Six factors for assessing scientific and engineering progress in SCC.

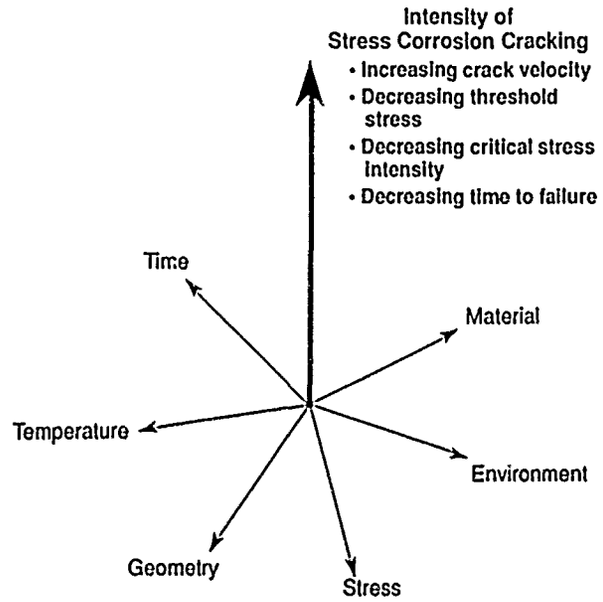


FIGURE 3—Schematic view of the independent variables that affect the dependent variable, the intensity of SCC. The dependent variable of intensity may be expressed as several different quantities depending upon whether the surfaces are smooth or initially defective.

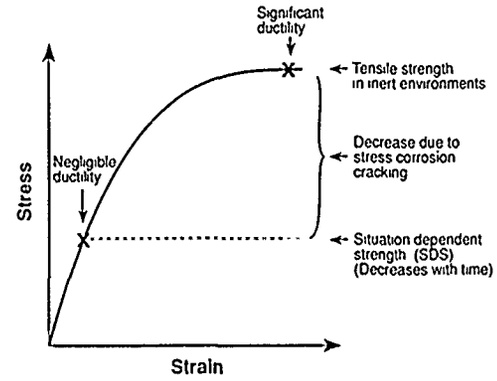


FIGURE 4—Relationship among situation-dependent strength, SCC, and strength as determined in inert environments. SCC reduces the effective strength from the strength determined in inert environments to the residual useful strength: the "situation-dependent strength."

In this review, I place emphasis upon the dependent variable for SDS being "intensity" rather than the term "susceptibility." The term "intensity" relates to such already well-established measured quantities as crack velocity, initiation time, K_{ISCC}, crack growth rate, and the time-dependent endurance limit. The reason for using the term "intensity" of SCC is to emphasize that SCC is not an erratic or episodic quantity as implied by the term "susceptibility." By using the term "intensity," I intend to imply that SCC varies more or less regularly according to reasonable expectations based on physical law. Thus, topologically, reasonable contours would be expected for the independent variable of intensity as a function of the independent variables as defined in Figure 3.

The use of the concept of intensity and the regularity implied also suggests that accounting for SCC in design can be performed on a more rational basis. It may be necessary, for example, to use a material in which the intensity of SCC is significant if the residual stress is high but is not significant when these stresses are relieved. It is not uncommon also to use designs in which SCC can occur but where the intensity is so low that further progress of SCC can be monitored in subsequent inspections.

I suggest that the term "susceptibility" should be eliminated from the vernacular of materials science and design in reference to SCC.

My intentions in defining these factors of SDS are the following: First, I want to identify for those who undertake mechanistic work what has to be explained and what dependencies have to be

accounted for; further, these factors are useful for those who are assessing progress of mechanistic work. Second, these six factors are the coordinates of the independent variables that determine the intensity of SCC. Such a pattern is illustrated schematically in Figure 3. Third, these factors provide a "check-off list" for designers who engineer with materials. Such a check-off list provides a framework for decision making; it also provides a framework for minimizing SCC.

The actual use of these independent variables will inevitably take the form of correlation equations where the multidimensionality may be more accessible. However, I show in the section "Engineering Status" that smaller sets of these factors can be used in graphical presentations where, for example, the "intensity" of SCC is shown in Figure 73 to depend on pH and potential for the alloy (Inconel† 600) at a given temperature and heat treatment.

The material factor of SDS

The principal features of the "material" factor are identified in Figure 5. Transgranular SCC is determined primarily by composition and structure.

For intergranular SCC, the composition of the grain boundaries is an additional critical factor. Figure 6 illustrates possible distributions of chemical species at grain boundaries in the case of (a) adsorption at the grain boundary and (b) precipitates. The distribution of species in Figure 6(a) covers only a few atom distances or in the range of a nanometer. The distribution of species in the case of precipitates shown in Figure 6(b) includes a larger range covering micrometers.

The numerous avenues by which the structure and composition of grain boundaries influence SCC at the grain boundaries are illustrated in Figure 7. The details of each of these are not discussed here; however, Figure 7 indicates there are many avenues by which SCC can proceed depending on the six factors of SDS in Figure 2. This multiplicity of avenues for intergranular SCC suggests that the propagation of any intergranular SCC could easily depend on several different atomic processes acting simultaneously.

It is shown in the section "Engineering Status" that every material will sustain SCC in every condition of heat treatment. However, the intensity of SCC for a given heat treatment in a given environment may be negligible.

The environment factor of SDS

Much of the description of environments relative to SCC has involved the terms "specific ions" or "cracking environments." This approach, while in the past well meaning, is misleading. Virtually all environments to which metals are exposed will produce SCC of some intensity under some circumstances, with changes in such variables as pH and potential for aqueous environments and vapor pressure for gaseous environments.

Important features of the environment factor of SDS are summarized in Figure 8. Each of the features of Figure 8 is a special circumstance to which a metal may be exposed and that may provide important conditions affecting the intensity of SCC. The features of Figure 8 are more indicative than inclusive, for nonmetals, other features may be important.

In Figure 8, I have distinguished the "chemical definition" from the "circumstance." The chemical definition is concerned with the chemical situation that the environment brings to the surface of a metal and its chemistry. Since SCC at the surface is largely a chemical process, this chemical definition is the central environmental consideration. However, the physical circumstances that bring the environment to the metal surface greatly affect the outcome from an engineering point of view. For example, such processes as wetting and drying, build-up of surface deposits, and flow greatly affect the chemistry at the surface. However, if this same concentrated chemistry were placed next to the surface in a more controlled manner, as one might develop by wetting and drying, the same result would be obtained.

†Trade name.

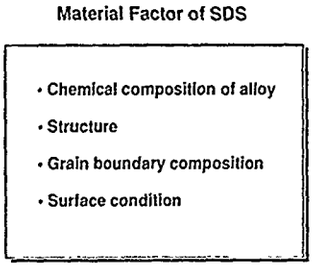


FIGURE 5—Principal features of the materials factor of situation-dependent strength.

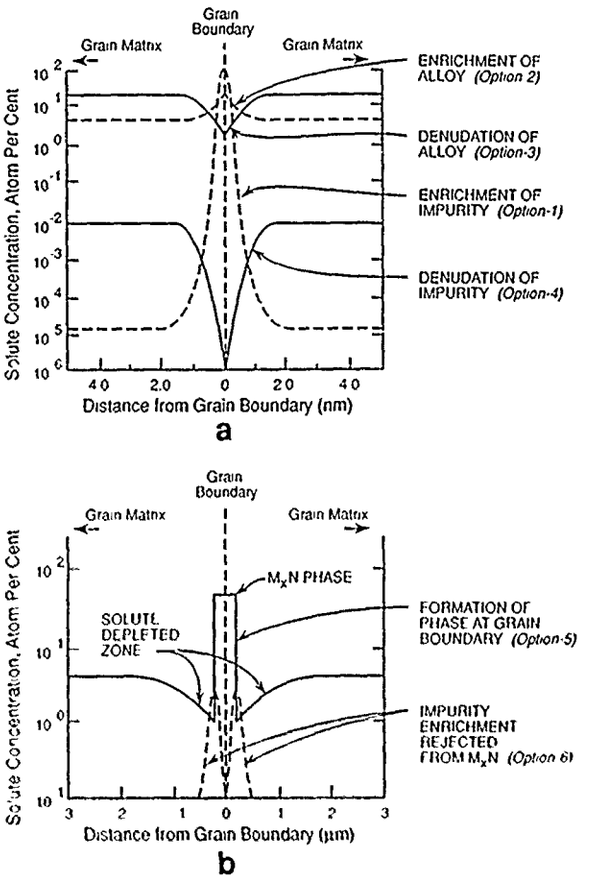


FIGURE 6—Distribution of chemical species at grain boundaries for the case of adsorption (a) and precipitate formation (b). Various options for distributions of species are identified.

I have distinguished the "chemical definition" and "circumstance" in Figure 8 also because it serves to identify features important to both science and engineering. Scientific studies are mostly interested in the former while engineering is interested in both. This differentiation is also a pattern I use for several of these SDS factors.

An important point of view implicit in the environmental factor of SDS as portrayed in Figure 8 is the difference between nominal and non-nominal environments. Generally, when components are designed they are designed for some nominal environment specified by the application. Often the testing for compatibility emphasizes only the nominal environment, although sometimes with minor variations. However more important are the non-nominal conditions, which are also included in Figure 8. Thus, crevices, deposits, wetting and drying, and thin moisture layers often provide more aggressive conditions. On the other hand, many of the nominal environments are often aggressive but are not perceived as such. A good example is the effect of pure water on the SCC of Inconel 600.

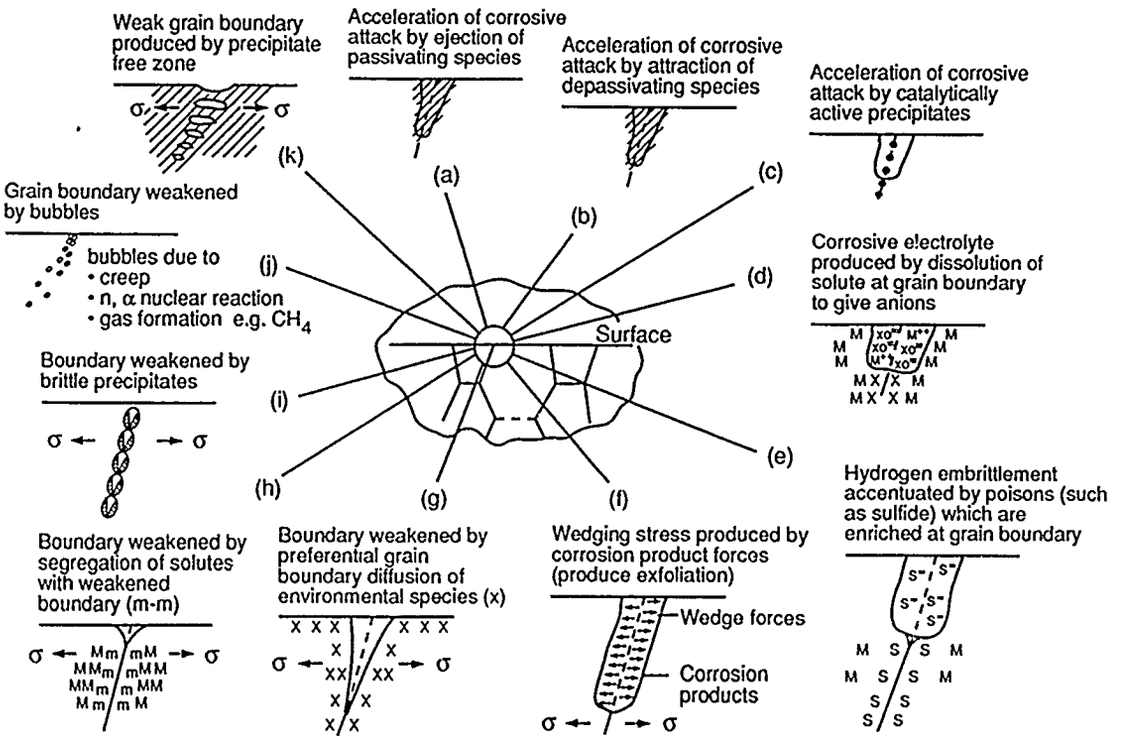


FIGURE 7—Different processes by which grain boundaries could lead to SCC.

Environmental Factor of SDS

Chemical Definition
- Type
- Chemistry
- Concentration
- Phase
- Conductivity

Circumstance
- Velocity
- Thin layer in equilibrium with relative humidity
- Wetting and drying
- Heat transfer boiling
- Wear and fretting
- Deposits

FIGURE 8—Principal features of the environmental factor of situation-dependent strength. Chemical definition is distinguished from circumstances that affect chemistry at the metal surface.

There are more details that apply to each of the features in the environment factor. For example, such features as pH and potential greatly influence SCC in aqueous solutions and would belong to the feature "chemistry." Also, pH and potential are important to thin moisture layers because their composition is affected by the solution of atmospheric gases.

This factor of environment merits more attention that I give it here. However, the purpose of this section is to identify key features of the SDS factors and describe their significance rather than to explore them. More thorough consideration of this environment factor awaits a definitive text. I believe that the problem of defining engineering environments is one of the major unexplored arts in the design and materials disciplines. Often, the response of a metal to SCC is reasonably well defined, what is not defined is a non-nominal but readily achievable environmental situation that coincides with a known vulnerability of the material.

The stress factor of SDS

Key features of the stress factor are identified in Figure 9. In this figure, I distinguish two ideas: first, the definition of stress, and second, the circumstances of stress. For example, the effect of stress on the intensity of SCC is independent of the origin of stress. However, residual stresses and stresses from corrosion product expansion are important in assessing the life of components.

Stress Factor of SDS

Stress Definition
- Mean stress
- Maximum stress
- Minimum stress
- Constant load / constant strain
- Strain rate
- Plane stress / plane strain
- Modes I, II, III
- Biaxial
- Cyclic frequency
- Wave shape

Sources of Stress
- Intentionally applied
- Residual
- Reaction products
- Thermal cycling

FIGURE 9—Principal features of the stress factor of situation-dependent strength. Features defining the stress as well as those that produce important circumstances are identified.

In the early years of considering SCC, it was common to distinguish between SCC and corrosion fatigue. It is now clear that there is a continuum between these phenomena; however, the lack of an obvious analytic relationship between SCC and corrosion fatigue in many metal–environment systems may mean that the full range of paths connecting the two phenomena has not been defined nor explored.

There are bases for distinguishing between corrosion fatigue at high cyclic frequencies and at low cyclic frequencies, since the crack growth rate ($\Delta a/\Delta n$) is well known to increase in some environments as the cyclic frequency is reduced to the range of 1 Hz. This pattern is the basis for poor predictions based only on high cycle fatigue. This pattern leads some to conclude that accelerated crack growth at high cyclic frequencies is different from what occurs at low cyclic frequencies. The lack of consistency between what happens at high cyclic frequencies and low cyclic frequencies may simply indicate the lack of an appropriate continuum for analysis.

It is also known that small cyclic ripples superimposed on a constant stress greatly increase the SCC intensity beyond any prediction based on usual interaction of the mean stress and R value. Such an apparent discontinuity results from an inadequate definition of continuum of environment and stress.

The geometry factor of SDS

Important features of the geometry factor of SDS are illustrated in Figure 10. The geometry factor is more of an engineering consideration than a scientific one, and I was originally uncertain as to whether or not it should be a part of the SDS factors.

Generally, the features of the geometry factor will not find their way directly into any correlation equations or a topological dependences; however, as with the consideration of residual stresses in Figure 9 for the stress factor, such features as galvanic effects are not only important, they may determine entirely the intensity of SCC. On the other hand, any galvanic effect may be understood fundamentally in terms of an electrochemical potential on the surface, independent of how the potential was produced.

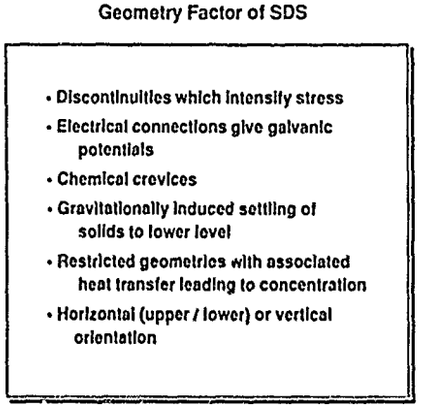


FIGURE 10—Principal features of the geometry factor of situation-dependent strength.

The fact that galvanic effects can be decisive identifies the necessity for the designers to determine the existence of possible galvanic couples.

The importance of intensifying stress by sharp geometries is more important to the stress factor. However, identifying such geometries and avoiding them is important enough to consider explicitly. Further, such geometries interact with other processes that influence the intensity of SCC. For example, tight geometries produce occluded regions where the environmental chemistry may differ greatly from the nominal bulk environments. Corrosion products accumulate in tight geometries and produce stress. Also, tight geometries sometimes involve materials of sufficiently different chemistry that local galvanic processes operate.

The temperature factor of SDS

Temperature is generally a standard factor to include in any consideration of fundamental chemical and physical processes. It is thus appropriate to include here. However, temperature affects the individual processes identified by the SDS factors in different ways. For example, the temperature dependence of creep strain at a crack tip differs from the effect of temperature on chemical reaction rates associated with film formation or with the diffusion of hydrogen inside a metal. Thus, while a given correlation equation for SCC intensity may depend on temperature, such a temperature dependence may not have a temperature–independent activation energy.

Features of the temperature factor of SDS are identified in Figure 11.

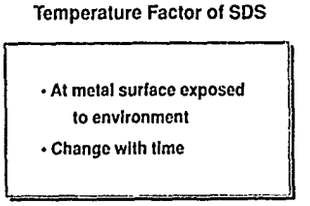


FIGURE 11—Principal features of the temperature factor of situation-dependent strength.

Since physical processes generally increase in intensity as the temperature increases, it is tempting to ascribe the same pattern to SCC. However, SCC in most metal groups occurs readily at room temperature and below with sufficient rapidity to be considered in design.

Temperature is also a trade-off with other factors. For example, in the SCC of nonsensitized stainless steels, temperatures in excess of 100°C are usually required for SCC in neutral chloride solutions. However, when the pH becomes more acidic, the temperature at which SCC becomes significant is reduced to room temperature and below.[2]

The temperature of interest to SCC is the temperature of the metal surface exposed to an environment as opposed to the bulk temperature of the environment. Such a provision is especially important in considering the performance of heat-transfer surfaces where deposits accumulate or where the flow of the cooling medium is inhomogeneous.

The time factor of SDS

To some extent, time is a dependent variable in the sense of "time-to-failure" or "initiation time." In this sense, it is part of the separate consideration of the dependent variable, "intensity," in the introduction to this section.

Time as an independent variable relates primarily to factors that may change with time to affect the intensity of SCC. For example, with increasing time, deposits on metal surfaces build up and change surface stresses, electronic conductivity, and surface chemistry. Important features of this factor of SCC are summarized in Figure 12.

As a layer of reaction products builds up on the surface, as, for example, in aqueous environments, the potential of the surface may change to move into a region where the SCC intensity increases or decreases. Changes in surface deposits with time will also influence galvanic processes.

Over the extended times suggested in Figure 1, the structure and local composition of the metal may change. One such change is "*in situ* sensitization," which is of interest to stainless steels. Also, grain-boundary chemistry sensitive to movements of atoms over a few nanometers would be affected by long exposure times.

Another kind of change with time is the development of surface defects that, at some point, reach a critical size for SCC crack growth. Such defects are produced in turbine blades by erosion and in high-strength steels by pitting. Here, the SCC will not initiate until a defect of the requisite size is reached and K_{ISCC} is exceeded.

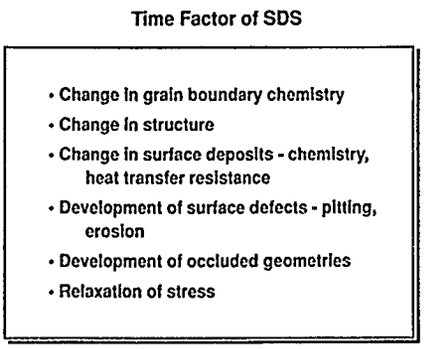


FIGURE 12—Principal features of the time factor of situation-dependent strength.

A still different time dependence is associated with the formation of occluded geometries. Here, an initially narrow but adequate dimension would permit adequate communication between a potentially occluded geometry and the bulk environment. Later, such a narrow region may become filled with deposits or corrosion products and then become occluded to the extent that the local chemistry will differ greatly from the bulk.

Initially clean surfaces are changed by the formation of deposits. Such deposits are often related to gravity effects where particles collect at the bottom of storage vessels and sometimes produce layers many inches thick. Such deposits may also form in regions of low flow in piping. In any case, these deposits may alter electrochemical and chemical conditions on the surface sufficient to change the intensity of SCC.

Time is important also with respect to the cyclic rates of temperature and stress changes. These cyclic processes are generally included in the stress factor.

Starting Point for Assessing Progress: Approximately 1955

It would not be useful to conduct a detailed assessment of the entire historical literature, since my primary purpose was to assess the scientific and engineering status of SCC. However, it is useful to view today's status relative to some reference in order to rationalize the present understandings. Therefore, I decided to take "approximately 1955" as the starting point. Taking "approximately 1955" as a starting point also provides a useful foil for developing a more orderly description of SCC.

Using 1955 as a starting point seemed reasonable since there was a literature of several hundred important papers at the time covering a range of alloys and scientific and engineering studies. There are some liberties I take with 1955 as the starting point in terms of what I include. From a personal point of view, 1955 is also the time when I started my M.S. program under M. Fontana at Ohio State. Thus, this review is something of a personal chronicle.

To identify the state of publications in 1955, Figure 13(a) shows a plot of published articles from the 1956 book edited by Robertson.[3] Here, the articles cited in both the 1956 volume and in the 1944 AIME-ASTM volume are summarized.

To determine whether the predicted rate of publication from Figure 13(a) continued, I counted the total number of publications used as references in the 1967 Ohio State volume and the total number used as references in the 1974 Firminy volume, only on iron-base alloys, together with two reviews on titanium and aluminum.[4,7] The results are plotted in Figure 13(b), which shows the cumulative number of articles published by a given year and suggest that 53,000 articles on all of SCC would have been published by 1988, the year of the Kohler conference.

After I define the state of affairs in 1955, in the next section, Events that Stimulated Change, I identify important events that indicated a need for greatly improving our understanding of SCC. This is followed in the next section, 'Response, by the main historical themes of the quest for improved understanding. These three sections, taken together, constitute the history. They also provide context for understanding the present scientific and engineering status of SCC. Finally, these three sections demonstrate first that a greatly improved framework is needed, and second that one is possible as identified in the section "Engineering Status."

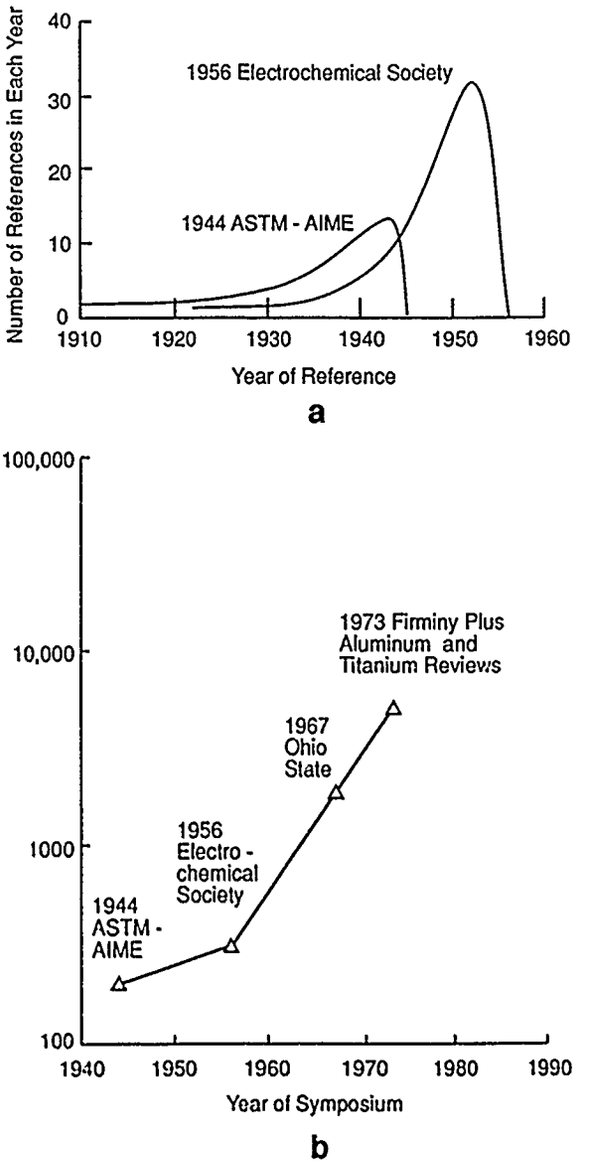


FIGURE 13—(a) Articles published on SCC vs time as determined from the proceedings of 1944 and 1954 meetings. Adapted from Reference 3; (b) cumulative articles published through 1973 based on the 1944 and 1954 data plus data from 1967 Ohio State meeting and 1973 Firminy meeting, including contemporary reviews on titanium and aluminum.

Prior to 1955, the following quote from Scheil[8] seems to describe the engineering view of SCC:

> Fortunately, the necessary corrosion conditions for SCC of the austenitic alloys are not too common and we believe that when these conditions do occur, an alloy can be selected to prolong the life of the equipment or an inhibitor may be added to the process to protect the stainless surfaces.

By 1955, some significant events had occurred. In 1945, ASTM published proceedings of the first major conference held in 1944 on SCC where most of the major alloy systems were discussed.[9] Later, in 1962, Smialowski published his book, *Hydrogen in Steels*.[10] The landmark article by Troiano on delayed failure was published as his 1959 Campbell Memorial Lecture for the American Society for Metals.[11] By 1955, Fontana had classified SCC as one of the "Eight

Forms of Corrosion,"[12] and discussions of 9 and 35 pages, respectively, were given in handbooks by Uhlig and Evans, respectively [13,14]

I have identified below 16 ideas that seem to characterize the understanding of SCC in "approximately 1955."

Metals have inherent strength. As engineering materials, metals have predictable and controllable mechanical properties, especially strength and toughness, that permit them to be used in a wide variety of service applications and environments. SCC is relatively rare and can be avoided by proper selection of materials.

The occurrence of SCC in various alloys was caused by specific ions. The reviews of SCC around 1955 usually described SCC with a table showing the important alloy systems and the specific ions or environments that "caused" SCC.[15,16] Such tables usually noted, for example, that chlorides and caustics caused SCC in stainless steels, nitrates and caustics caused SCC in mild steels, and ammonia caused SCC in brasses.

Certain alloys, crystal structures, and heat treatments were "susceptible" and others were not. It was thought, for example, that the bcc crystal structure was not susceptible to SCC in chloride environments based on the data of Copson.[17] It was also thought that the high nickel alloy Inconel 600 was not susceptible to SCC based on the Copson work, despite suggestions to the contrary.[18]

Pure metals are resistant to SCC. It was widely thought that pure metals were resistant to SCC, a materials system, Alclad,† was developed based on that idea. This was an effective material since the very high-strength aluminum alloys in the core of the Alclad sandwich were so prone to SCC and the pure aluminum on the outside was so resistant. However, it has yet to be proven that pure aluminum is resistant to SCC in the wide range of environments once imagined.

For many years, it was assumed that pure copper and pure iron were resistant to SCC, although the possibility of intergranular SCC was allowed because of "impurities." Today, the transgranular SCC of pure copper and iron is well established.[19]

Pure environments do not cause SCC. Similar to the assumption that pure metals are resistant to SCC was an assumption that pure environments do not cause SCC. This assumption followed from the second idea in this series that specific ions were required to cause SCC. This was later disproven by Coriou's work in 1959, which showed that SCC of Inconel 600 could easily occur in pure water.[20]

SCC and corrosion fatigue are different. In Fontana's eight forms of corrosion, corrosion fatigue and SCC were differentiated.[21] Such a differentiation persisted until at least 1970, when the corrosion fatigue conference at Storrs[22] attempted to find a continuum between these phenomena. Work by Wei and others[23] identified the fact that many phenomena called corrosion fatigue were simply the integral of SCC taken over the cyclic stress pattern. On the other hand, the work of Duquette and Uhlig pressed for differentiation.[24]

It appears to me that, even in those corrosion fatigue phenomena where the fatigue strength is reduced by environments when tested at high cyclic frequency but where the integral does not correspond to SCC crack velocity, we are seeing an incompletely defined system. If the coordinates for the environment and stress were extended, it is likely that what appear to be different phenomena would become parts of the same continuum.

The major difference between corrosion fatigue data that can be intergrated into SCC and that cannot, seems mainly to be associated with effects observed at high cyclic frequencies. I believe that any discontinuities in the possible continua between SCC and corrosion fatigue may be due more to inadequate conceptions of the continuum.

SCC and hydrogen embrittlement are different. Considerable effort was spent to differentiate SCC from hydrogen embrittlement with the implication that the former was clearly an anodic process. Such distinctions are now less clear. Further, it is not clear that SCC at the low potentials is directly associated with hydrogen. Species such as sulfur, phosphorus, and carbon at grain boundaries can react at low potentials to produce soluble species. Further, there is evidence that what was once thought to be SCC in pure water[20] is actually some type of hydrogen embrittlement.[25]

Further, to differentiate SCC by anodic and hydrogen embrittlement is simplistic, since there are so many atomic processes, besides these two, that have been shown to propagate SCC. Some processes that clearly do not involve hydrogen also do not involve dissolution in aqueous solution, the iodine SCC of zirconium alloys and the chlorine SCC of high-strength steels are good examples.[26,27] On the other hand, to exclude hydrogen entry from participating in processes at external potentials above the hydrogen equilibrium is also under question.

An endurance limit describes the stress below which failure will not occur. It was common to take data at different stresses and determine a stress below which SCC would not occur. Such a stress below which SCC would not occur was analogous to the endurance limit in fatigue. It is now clear that many such tests did not last long enough and that the stress below which SCC does not occur after long times may be relatively low.

Constant-strain specimens. Most testing prior and during the 1955 period used constant strain achieved either by 3- or 4-point loading or by a U-bend arrangement. Such testing was useful but not conservative. At high temperatures, such specimens tended to relax. At lower temperatures, such constant strain did not duplicate the frequent load changes in engineering systems.

Constant-strain testing has now been largely replaced by slow-strain-rate tests where serious experimental work is concerned, although the constant-strain tests in the form of U-bends or "reverse U-bends" are sometimes used. An interesting comparison between constant strain and constant load is seen in comparing Coriou's 1959 and 1965 papers where the latter at constant load produced more pronounced cracking and indications of the dependence of stress on time-to-failure.[20,28]

Constant-strain testing should not be used where any serious dependencies need to be obtained. Such testing might be useful to check out changes in industrial processes, but the results should be considered with caution.

Smooth specimens. For many years, smooth specimens were the standard for SCC studies. In some cases, the specimens were notched for good measure, however, for the most part specimens were smooth. Despite the present interest in precracked geometries, smooth geometries are not necessarily useless since it is the geometry of millions of square feet of heat exchanger tubing in many industries.

There were three deficiencies in using smooth specimens. First, such specimens did not relate to the engineering situation for thick sections where surface defects were inevitable. Second, data from testing specimens with smooth surfaces tended to be widely scattered. Third, it was difficult to distinguish time to initiate SCC from the time for it to propagate.

B.F. Brown at the Naval Research Laboratory urged that testing for SCC be done with precracked specimens so that the uncertainties in initiation could be minimized.

It should be noted that testing with smooth surfaces is still important, since many applications, such as heat transfer tubing, have wall dimensions that are too thin to qualify for the application of data from testing precracked specimens.

"The" mechanism of SCC. In the time range of 1955, there was a major effort to find "the" mechanism of SCC. This quest produced strong words between the people who studied what they thought was hydrogen embrittlement and those who studied what they thought was anodic SCC. Furthermore, the search for "the mechanism" led to some interesting ideas that could not be related to any predictive capability in the sense of the SDS coordinates described in Figures 5 and 8 through 12.

The general idea that there was such a thing as "the mechanism" led many investigators, who conducted quite useful engineering studies, to conclude that their work supported one or the other of the range of mechanistic ideas of the day. Unfortunately, there was usually little real support for any of their conclusions concerning such

†Trade name.

mechanisms except the ones that summarized the trends of their direct data.

Synergistic interaction of stress, material, and environment. There was a time when I, as well as many others, characterized SCC as a synergistic phenomenon. However, such a characterization suggests that there is something magical about SCC and that the origins of the often great reduction in strength are surprising and arcane.

This term, synergy, as applied to the combined action of stress, environment, and material, has not been useful. It needs to be replaced by a more orderly and accessible concept. Such approaches are described in the section "Engineering Status."

Pitting is required for SCC. In 1955, engineers thought pitting was a prerequisite for SCC; unfortunately, there are those who still believe this. Those who have studied initiation processes have shown that prior pitting is not required for many alloy–environment systems and that SCC can initiate and propagate from an absolutely smooth surface.

For example, it has been shown that the range of potential for pitting is generally different from that for SCC.[29]

There are some cases, generally for high-strength alloys, where prior pits are required. When the local stress intensity associated with such pits exceeds K_{ISCC}, SCC can initiate.

"Classic" SCC could be defined. For some time in the mid-1950s, as well as the present, it has been common for people to refer to "classic" SCC. I suppose that this means the transgranular SCC of stainless steel. Such a term, used by both by experts and novices on occasion, is misleading. There is nothing "classic" about any type of SCC.

The only reason that a particular type of SCC may be "classic" is that extensive information has been published on it or that the morphology of the SCC is particularly interesting as for the extensively branched transgranular SCC of austenitic stainless steel exposed to chloride environments.

The term classic is often used to distinguish what some think is anodically controlled SCC from what others think is hydrogen embrittlement.

Intergranular corrosion and intergranular SCC. It has been customary to differentiate intergranular corrosion, or intergranular attack (IGA), as it is erroneously called in the nuclear industry, from intergranular SCC. This distinction was generally made in the mid-1950s, as it is today, in terms of the former occurring through an extensive network of corroded grain boundaries with much grain dropping during specimen preparation, and the latter having a relatively confined attack, as illustrated in Figure 14.

While the morphological distinction is generally regarded as useful, it is also misleading. For example, in the case of sensitized stainless steels, they sustain SCC in the neutral range of pH. However, the same materials in oxidizing acidic solutions undergo extensive intergranular corrosion. Thus, in both cases the metal is the same with the same heat treatment. Only the pH is changed. Thus, distinguishing between intergranular corrosion and intergranular SCC may be more a matter of environmental definition than of material definition.

Assumption of severe environments. One of the most well-known experiments in the history of studies of SCC was that of Copson, where he determined the time-to-failure as a function of nickel concentration for Fe-Cr-Ni alloy exposed to boiling $MgCl_2$ solutions[17] and reported the results in 1959. His results, shown in Figure 15(a), showed that the worst composition was the most widely used industrial composition of stainless steel; these alloys would be largely immune to SCC above 50% of nickel, and that ferritic alloys would not sustain SCC. His results were subsequently repeated numerous times by others.[30]

When one considers the boiling $MgCl_2$ environment with its pH in the range of 2 to 4 and the high concentration of chloride, it is hard to imagine that any other environment can be more severe. However, the work of Copson proved to be misleading on several counts. First, the work of Coriou on Inconel first published in 1959 showed that Inconel 600 (77% nickel) would indeed sustain SCC but in absolutely pure water. His data compared with those of Copson are shown in Figure 15(b). This comparison means that pure water can be more aggressive than the boiling $MgCl_2$ solution. The explanation for such an apparent anomaly is given in the section "Engineering Status." Second, the idea that SCC would not occur in ferritic alloys was shown to be incorrect by the work of Bond and Dundas.[31] They showed that the SCC structure for these alloys did not determine intensity of SCC; rather, the chemical composition primarily determined SCC.

While the lesson of erroneously assuming the severity of environments should have been apparent, it should be recognized that such assumptions still need careful scrutinizing

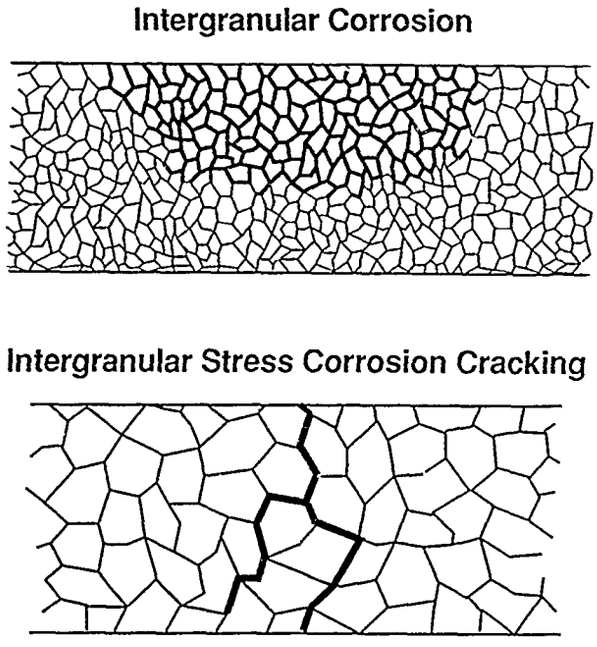


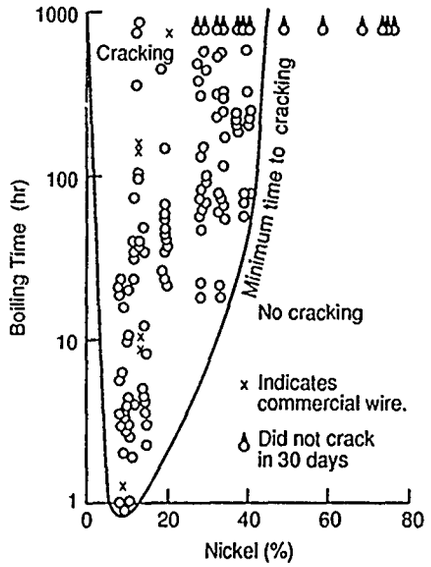
FIGURE 14—Schematic views of intergranular corrosion and intergranular SCC. Adapted from Copson[17] and from Coriou, et al.[205]

Events that Stimulated Change

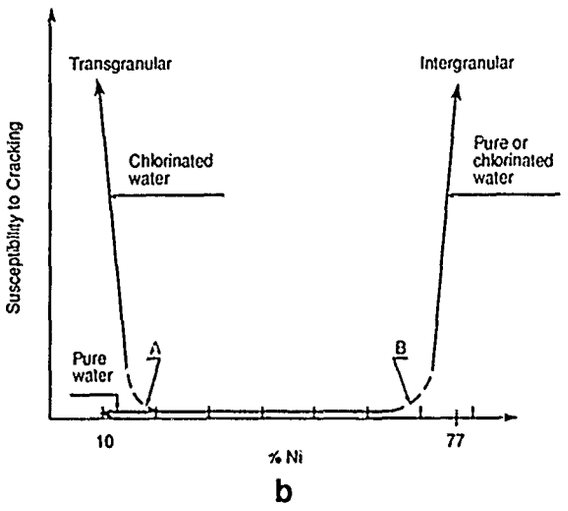
In 1955, it was possible to engineer with some confidence with the phenomenon of SCC in a few metal–environment systems. Certain guidelines were quite clear. The specific ion idea, while not fundamentally based and providing little basis for extrapolation and interpolation, furnished useful guidelines that could minimize failures and ensure reliable operation.

However, after 1955, failures by SCC in commercial equipment increased and occurred under circumstances that were not predicted from the relatively simple framework of 1955. I have outlined below 18 events that occurred after 1955 that required the 1955 view be substantially changed. These events are generally in four categories. First, new liquid environmental circumstances existed, including pure water, alcohol, anhydrous ammonia, and dinitrogen tetroxide. Second, there were new gaseous environments including hydrogen, iodine, and chlorine. Third, there were new physical conditions of testing. Fourth, there were instances of SCC in commercial applications that called for new insights.

SCC of Inconel 600 in pure water. In 1959, Coriou[20] published a paper describing the SCC of Inconel 600 in pure water. He found that the SCC required 90 to 120 days and progressed slowly. This finding caused great controversy partly because of vested interests in high-nickel alloys used for steam generator tubes in the nuclear industry and partly because the then existing wisdom was based on the 1959 results of Copson in boiling $MgCl_2$, shown in Figure 15(a), which showed that higher nickel alloys would not sustain SCC.



a



b

FIGURE 15—Effect of nickel on the SCC of Fe-Cr-base alloys as determined in (a) boiling $MgCl_2$ and (b) pure water environments. Adapted from Copson[17] and from Coriou, et al.[205]

Totsuka and Smialowska[25] would later show that pure water can be just as severe as boiling $MgCl_2$ when the electrochemical potential is lowered below the one atmosphere hydrogen equilibrium.

Main early criticisms of Coriou's work related to the possibility of contamination, galvanic effects, and specimen preparation; such questions were reasonable except that, had his work produced more conventional results, there would have been less resistance.

It was not until 1965[26] that his findings were unequivocally established. His 1965 experiments used constant load, rather than the constant strain of the 1959 experiments, and the resulting failure time was 90 days.

Coriou's findings were important because they established the fact that SCC would occur in pure water and that no specific ions were required. These results were further significant because Inconel 600 had been shown to be so resistant to SCC by the previous testing in the apparently more severe boiling $MgCl_2$. These results were even more important because the SCC of Inconel 600 occurred in completely deoxygenated water as opposed to work in chlorides, where it was thought that some oxidizing capacity was required for SCC to occur.

The quality and importance of Coriou's results were so well established that they provided the basis for the use of Incoloy† 800 for steam generator tubing in German pressurized water nuclear reactors.[32] This alloy exhibited less intensity of SCC in the chloride environments and no SCC in the pure water environments, as determined by Coriou.

Intergranular SCC of nonsensitized stainless steel in pure water. In a program to assess the maximum thermal output of nuclear fuel in tubular geometries, General Electric conducted a series of experiments during the early 1960s using stainless steel tubes containing uranium dioxide that received high burn-up exposure. These specimens sustained extensive intergranular SCC when exposed to boiling water reactor (BWR) water.[33] These results were particularly surprising because the stainless steel was not initially sensitized and because the SCC was so extensive.

These results prompted a major study of SCC in Fe-Cr-Ni alloys by General Electric and included work to define the composition and reactivity of grain boundaries in these alloys. Much of this work is summarized in the reviews by Cowan and Tedmon,[34] Cowan and Gordon,[35] and Armijo and coworkers.[36]

These results were significant in that they called attention to the role of compositionally changed grain boundaries that did not relate to effects of sensitization. The composite of grain boundaries and their relationship to corrosion had been analyzed previously in a review by Aust, et al.[37]

SCC of sensitized stainless steels. While the nature of sensitizing and the associated intergranular corrosion of stainless steels in oxidizing environments was well defined in 1933 by Bain and Aborn,[38] a number of SCC failures of piping in nuclear plants occurred in sensitized stainless steels in the 1960s. This sensitization was produced either by welding or by furnace heat-treatment processing.

The rate of such failures increased substantially in the 1970s as more plants were built and started to operate.[39] These SCC failures occurred in BWRs manufactured in the United States. The sensitized stainless steel piping in such plants was particularly at risk because of the oxidizing conditions resulting from the oxygen produced from the radiolytic action of the radiations in the nuclear plant. The progress of SCC in the U.S. BWR plants was summarized first in a General Electric publication in 1975; Figure 16 shows the occurrence of SCC in various BWR nuclear plants over time. As SCC progressed in these nuclear plants, additional articles chronicled the progress. Figure 17 summarizes incidents of additional SCC after the 1975 summary.[40]

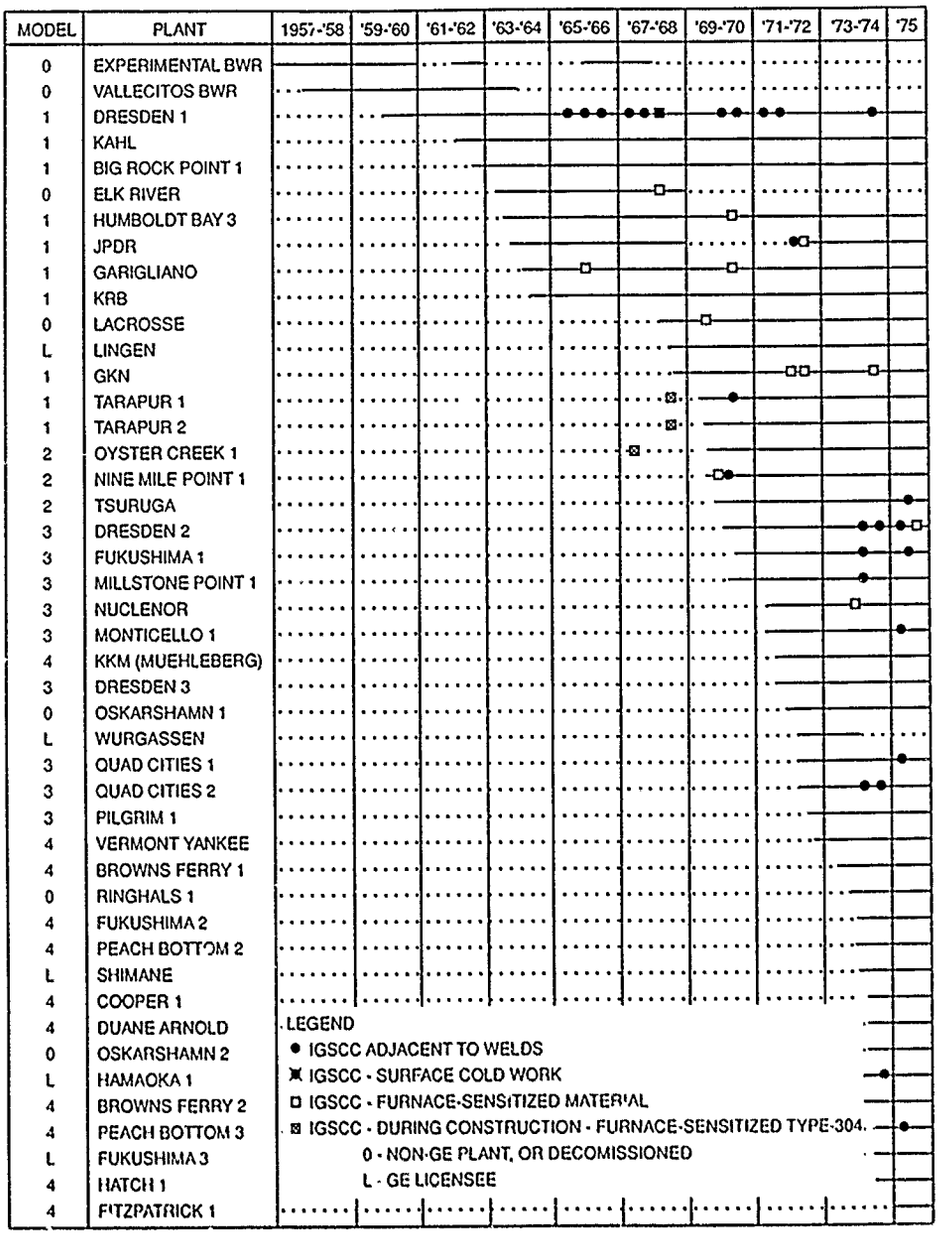
This pattern of proliferation of SCC in sensitized stainless steel piping was arrested by changing the alloy to type 316L (UNS S31603) and by applying residual compressive stresses to the inside surface of pipes.[41-44]

The potential for SCC with the sensitized stainless steel in oxidizing environments caused manufacturers of similar boiling water nuclear systems early to switch to low carbon or stabilized grades of stainless steel in Sweden and Germany, respectively. Such an action was not taken in the United States until later. The interesting question here is why the combined existence of sensitization and oxidizing conditions did not alert one company while others understood such implications and acted accordingly.

SCC of carbon steel in $H_2O/CO/CO_2$. During the late 1960s, observations in both Japan and the UK indicated that transgranular SCC could occur in carbon steel in gaseous environments containing critical ranges of combinations of H_2O, CO, and CO_2. These results and others were reviewed by Brown, et al.,[45] and by Kowaka and Nagata.[46]

These results were interesting because carbon steel had previously been observed to sustain SCC only intergranularly and because this environment differed greatly from the nitrate and caustic one in which intergranular SCC had been well established. Further, it was sufficient that the environment be gaseous rather than single-phase liquid.

†Trade name.



NOTE MORE THAN ONE CRACKING INCIDENT MAY HAVE OCCURRED AT A SYMBOL

FIGURE 16—Incidents of SCC in boiling water reactor nuclear plants manufactured by the General Electric company as occur in sensitized stainless steel through 1975. Adapted from Reference 39.

SCC of Inconel 600 within aqueous lead solutions. In an effort to understand the possible effects of impurities that led to the SCC of Inconel 600 in the work of Coriou, Copson and Dean conducted experiments with environments containing, among other additions, small amounts of lead in the water and published their work in 1965.[47]

Lead, as a liquid metal, had already been shown to embrittle nickel-base alloys. Thus, adding lead compounds to aqueous environments was a reasonable approach to searching for effects of contaminants on the SCC of Inconel 600. Additives of lead to aqueous solutions produced both transgranular and intergranular SCC in Inconel, subsequent results that Copson and Dean obtained together with later work by others showed clearly that the presence of lead in an aqueous environment greatly accelerated SCC.

Despite the transgranular nature and high intensity of SCC in Inconel exposed to aqueous environments containing lead, no serious study has yet been conducted to rationalize the role of lead or the broader implications of such environments. What was apparent in 1965 and what is more apparent today is that the lead, as an addition to water, may be incidental relative to the electrochemical conditions it establishes. It is more likely that the lead simply places the surface of Inconel into a region of potential and pH where the alloy sustains both intergranular and transgranular SCC at high rates. Such results could be achieved as easily by controlling the pH and potential by artificial means.

SCC of titanium alloys in alcohol. To avoid the SCC of titanium alloys that might occur in aqueous environments, NASA at point decided to hydrotest titanium alloy vessels in alcohol environments, owing to the assumption that alcohol would be an inert environment. The SCC that resulted in the alcohol solvent was a surprise.[48]

During subsequent testing, the SCC was found to be accelerated by contamination of water and chloride in the alcohol. It should be noted that experiments showed that SCC could occur in either pure water or pure alcohol as well as mixtures of the two. However, alcohol plays an important role here, and the type of alcohol was

shown later by Blackburn, Smyrl, and Feeney.[48] The combined effects of pure water and pure alcohol together with intermediate mixtures of the two is shown in Figure 18.

SCC of titanium alloys in N_2O_4. A Ti-6Al-4V alloy was selected by NASA for constructing pressure vessels to contain the N_2O_4 oxidizing agent for the Apollo vehicle. During pressure testing of the fabricated vessels in 1964, it was found that the Ti alloy sustained SCC.[48] This SCC was extensive, rapid, and transgranular.

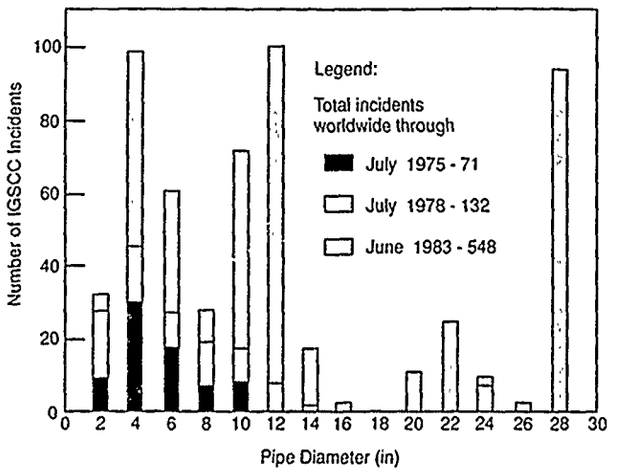


FIGURE 17—Incidents of SCC in boiling water reactor nuclear plants manufactured by the General Electric company through 1983.[40]

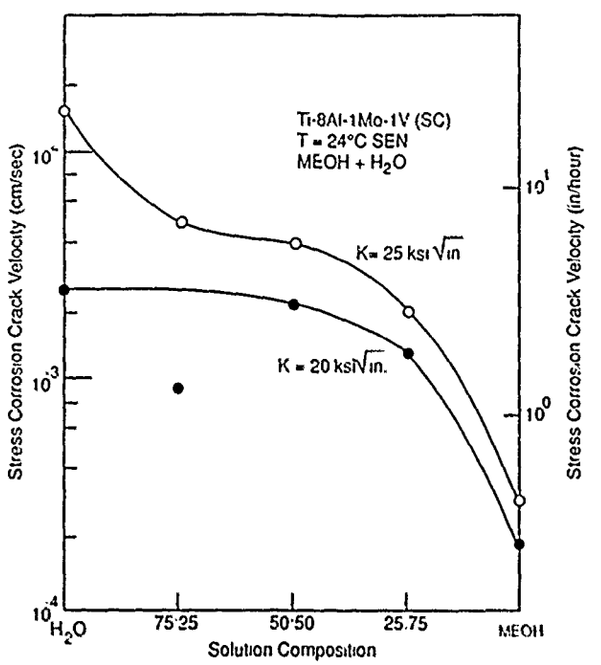


FIGURE 18—Effects of alcohol and water on the SCC of titanium alloys from work by Blackburn, et al. Adapted from Reference 48.

Aside from the SCC in fuming nitric acid,[49] there was nothing in the literature to suggest such a result. Many investigators were certain that a chloride impurity was responsible. However, none was found to be necessary. The SCC of the Ti-6Al-4V alloy in N_2O_4 was found to relate more to ratios of small quantities of oxygen and water. A high ratio of oxygen to water seemed to favor SCC and a low ratio prevented it. In fact, it was the low ratio that was used when the titanium alloy had been qualified. The higher ratio used later when the pressure testing was conducted resulted from slight changes in the processing procedures.

These results were important because they established the basis for a broader set of liquid environments in which SCC could occur. Further, these results showed that neither chloride nor hydrogen was required for SCC of titanium and that the intensity of SCC in titanium was based on broader, although not well-defined, considerations. This environment-alloy system is still not well defined.

SCC of steel in anhydrous NH_3. In about 1962, steel vessels containing anhydrous liquid NH_3 were reported by Loginow and Phelps to sustain predominantly transgranular SCC.[50] This SCC was accelerated by the addition of oxygen but could be inhibited by the addition of water. That SCC could occur in such an environment was surprising. Further, the past experience, especially in aqueous caustic environments, was that mild steel sustains primarily intergranular SCC, and finally, the fact that adding water inhibited SCC rather than promoting SCC was counter to conventional wisdom.

Work on SCC of steel in anhydrous NH_3 was extended by Wilde and Deegan and others,[51,52] who showed that oxygen and nitrogen as gaseous contaminants were responsible for cracking in otherwise pure ammonia. Figure 19(a) shows a potential vs time plot for different concentrations of oxygen. With no oxygen, there was no SCC. However, even with oxygen as low as 0.9 ppm, SCC occurred. In Figure 19(b), the effect of water additions to anhydrous ammonia shows that SCC can be inhibited above approximately 1000 ppm.

The SCC of steel in anhydrous NH_3, like that of titanium in N_2O_4, showed clearly the generality of SCC in different liquid environments.

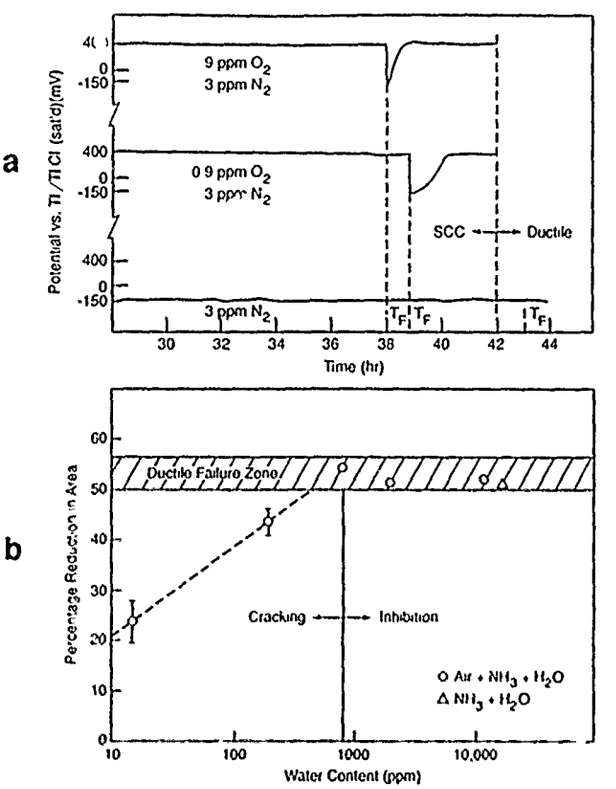


FIGURE 19—Effects of oxygen and water on the SCC of mild steel in anhydrous ammonia from work by Deegan, et al. (a) Effect of oxygen addition on the SCC as shown by potential transients occur corresponding to the occurrence of SCC, and (b) effect of water on SCC. From work of Deegan, et al.[51,52]

The hydrogen gas SCC of high-strength steel and its oxygen inhibition. From the work of Smialowski and Troiano[10,11] as well as many others starting early in the 1900s, it has been clear that hydrogen plays a major role in the SCC of steel as well as other materials. Before 1955, it was clear that the thermodynamic pressure alone, in principle, was quite high and greatly exceeded anything that would be normally available from ambient gas.

Further, it was well known that poisons such as sulfide and arsenic were effective in accelerating hydrogen entry owing to their property of reducing the rate of combination of hydrogen on the surface.[53]

The equilibrium pressure of hydrogen at the corrosion potential during typical corrosion processes may greatly exceed one atmosphere. However, such equilibrium pressures are not achieved, since the hydrogen combines quickly and leaves the surface as gas; the possibility of relatively high pressures in bubbles inside the metal in equilibrium with the effective hydrogen pressures on the surface can be reasonably explained.

A detailed model for SCC resulting from such pressures has been developed by Tetelman.[54] However, the experiments of Johnson showed that gaseous hydrogen even at ambient pressure caused SCC to propagate more rapidly than in water at ambient pressure and showed that the hydrogen pressure bubble model was not necessary.[55] Johnson's experiments were also interesting because they showed that introducing gaseous oxygen stopped the SCC. Such a result never occurred in aqueous environments where dissolved oxygen and oxygen from the reduction of water were readily available.

The chlorine gas cracking of high-strength steel. The doctoral work of Kerns in the early 1970s showed that SCC would propagate in high-strength steels in chlorine gas.[27] It was also shown that this SCC was not related to the presence of hydrogen. Kerns showed that the velocity of SCC in chlorine gas at ambient temperature was two orders of magnitude greater than in ambient pressure hydrogen.

Kerns's work showing that gaseous chlorine as well as gaseous hydrogen would produce SCC in high-strength steels was one of the most important changes in the established momentum of SCC phenomenology after Coriou's work. This result suggests that many other gaseous as well as liquid species might accelerate SCC in steels. These possibilities have yet to be pursued.

SCC of zirconium alloys in iodine gas. The initial development of zirconium-base alloys for cladding the uranium fuel in nuclear reactors concentrated on the compatibility between zirconium alloys with water on exterior surfaces at temperatures in the range of 200 to 400°C from the point of view of general oxidation and hydriding. Enormous efforts were expended on this project by laboratories throughout the world.[56] As a result of these efforts, zirconium alloys were brought rapidly to commercial use.

However, as these zirconium-clad uranium-containing tubes operated in reactors, it became clear in 1968 from the work by Cox that the iodine gas, produced inside the cladding by fissioning of uranium, could produce failures in addition to those, usually by hydriding, which were instigated on the outer surface.[26] Figure 20 shows results of the work of Cox and others on the SCC of precracked Zircoloy[1]-2 specimens tested in iodine gas at room temperature and 300 C.

Subsequent iodine-induced failures of uranium-containing zirconium alloy tubes in nuclear plants became well known as pellet-clad interaction (PCI) failures.[57] As the UO_2 pellets expanded because of an increase in volume due to the formation of fission products, the zirconium tube was stressed sufficiently to cause SCC.

The iodine-instigated SCC of zirconium alloys was important for many reasons. First, the environment contained neither water nor hydrogen; the SCC of zirconium was purely related to gaseous nonreduced iodine. Second, the SCC of zirconium was transgranular and independent of the chemistry of grain boundaries. Third, there is no potential drop or other feature of aqueous chemistry to raise questions concerning conditions at the crack tip.

Wedging action of corrosion products. Fontana had suspected for many years that the formation of corrosion products inside stress corrosion cracks was a main contributor to their propagation. The work of Pickering in 1961 demonstrated this effect by quantitative measurements of stress produced by expanding corrosion products.[58] These results also provided an explanation of the results of Nielsen in 1970, who found that SCC could initiate and propagate in nonstressed single crystals of stainless steels.[59]

These results were significant because they defined quantitatively the stresses that could be produced by corrosion products. However, the idea that corrosion or reaction products could produce stress had been studied over the period of 1905 to 1920 by workers investigating the effects of corroding reinforcing bars on the fracture of concrete.[60,61]

The results of Pickering and Fontana anticipated the occurrence of denting in the Westinghouse pressurized water reactor (PWR) steam generators.[62]

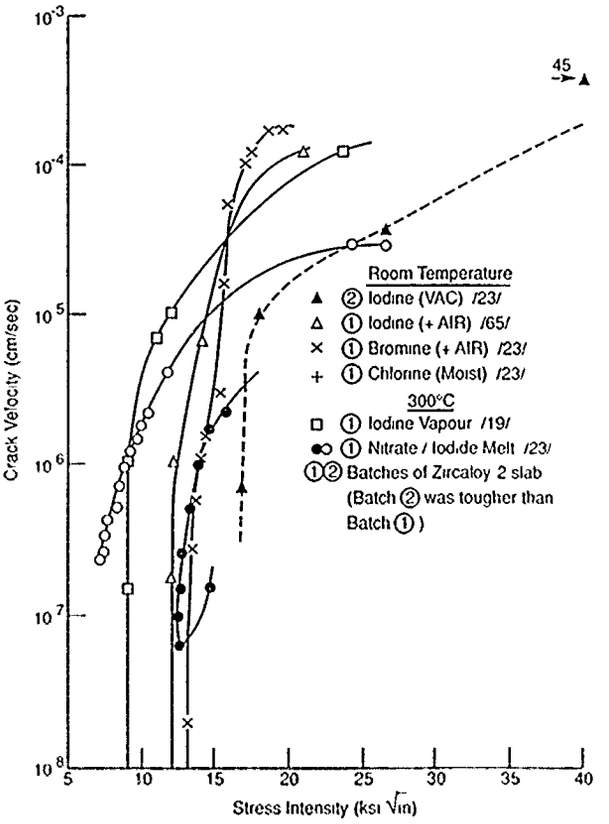


FIGURE 20—Crack velocity vs stress intensity for zirconium-base alloys exposed to halide environments. Adapted from the work of Cox.[26]

SCC of uranium alloys. Alloys of uranium were investigated at Sandia Laboratories in the late 1960s primarily by Magnani.[63] He found several interesting results. First, the velocity of SCC was very high. Second, these cracks could propagate in the complete absence of stress owing to the volume expansion of the corrosion products. Third, SCC could occur in water vapor only. Aside from Magnani's contribution to the knowledge of SCC in uranium alloys, his observation of high crack velocities in fracture mechanics type specimens in the absence of applied stress was consistent with Fontana's work on the wedging action of corrosion products.

Crevice effects on SCC. In 1968, Copson and Economy studied the behavior of Inconel 600 in simulated reactor water using a creviced specimen fabricated by using a double U bend. They found that SCC did not occur on the outside of the U bends but only inside the crevices.[64]

Such a finding supported work reported by dePaul[18] in 1957, which noted that intergranular corrosion may occur on Inconel surfaces in crevices but not on exposed surfaces for tests in simulated reactor waters.

The accelerated action of crevices on corrosion was first defined in the 1924 text of Evans.[65]

The Copson work received little direct interest because of the presumed aggressive conditions produced by high concentrations of oxygen added. However, in the mid-1970s, accelerated SCC of Inconel 600 in crevice geometries was indeed observed in the tube

[1]Trade name.

support plate regions of steam generators of pressurized water nuclear reactors designed by one company in the United States. On the other hand, other manufacturers in the United States and abroad designed their steam generators without such crevices and the possibility for crevice-accelerated SCC was minimized. In addition to SCC in these crevices, similar SCC of Inconel was observed in safe-end crevices of BWR plants. The first such observation reported publicly occurred in 1978 at the Duane Arnold nuclear plant in Iowa [66]

SCC of high-strength aluminum alloys on the C5A. The initial design of the C5A transport aircraft assumed that a high strength of the 7075 (UNS A97075) type of aluminum alloys would be available. It was found that this was not so and that these alloys were very prone to SCC, especially in the short transverse stressing situation. As a result, this aircraft had to be de-rated.

This result served to emphasize the importance of heat treatment and anisotropy in the SCC of high-strength alloys in the early 1960s. The review by Sprowls and Brown in 1967 and Speidel and Hyatt helped to place these properties into perspective.[67,68]

Hinkley Point. In 1967, a catastrophic failure occurred in a turbine at the fossil-fired Hinkley Point power station in the UK.[69] Initial hypotheses suggested that caustic-forming species had gotten into an internal keyway although, subsequently, no indications of sodium could be found.

It has more recently become clear that such cracking could be easily produced only by the action of water alone as a result of the work by Speidel and Magdowski.[70] The fact that pure water can cause the SCC of low-alloy steels even in relatively lower-strength conditions where the toughness is high is equivalent to the early finding of Coriou.

The Silver Bridge. In 1967, the Silver Bridge across the Ohio River failed catastrophically owing to the SCC of a single link.[71]

The bridge was a suspension bridge, however, the suspension elements were not wire rope as is widely used today, but rather solid metal links. Unlike the wire rope, if one link fails, the whole suspension structure fails. The suspension was, in that sense, nonredundant.

The important implication of this failure at the time was the confirmation of the fracture mechanics approach to improving the quantitative description of SCC. Further, this failure emphasized that relatively innocuous environments, the southern Ohio industrial atmosphere, was quite adequate to support SCC. From an inspection point of view, this failure indicated the need for careful inspection of high-strength materials for small defects. Finally, from a design point of view, this failure emphasized the need for redundancy and for a means to stop propagating SCC cracks short of their reaching a critical length for fast fracture.

SCC of the condenser at the Palisades Nuclear Plant. In 1974, about 7000 of the approximately 28,000 tubes of admiralty brass in a condenser at the Palisades nuclear plant suffered SCC in a time as short as about one week.[72] While ammonia was naturally suspected as the environmental accelerator, none was found.

This major failure stimulated work at Ohio State that led to results showing that a number of oxyanions would produce SCC in copper-base alloys and that pure copper would sustain transgranular SCC.[73] Contrary to previous trends, the work done at Ohio State showed that ammonia was not required for the SCC of copper-base alloys and that the idea of pure metals being resistant to transgranular SCC was not true.

Response

Introduction

The events described in the previous section greatly disturbed the 1955 view that I defined. These events did not suggest the need for merely further refinement but rather the need for a major change in thinking. The purpose of this section is to describe this response and the avenues that were followed. The substantive parts of this response started in 1955 and have continued until the present—a period of 33 years. In fact, one of the purposes of this review is to suggest what these efforts mean when taken together, and this overview is summarized in the "Engineering Status" section.

Setting the agenda

The beginnings of change were marked by three meetings from 1954 through 1965 and the proceedings that followed The first meeting, chaired by W.D. Robertson[3] and sponsored by The Electrochemical Society, Inc. was held in 1954 with the proceedings published in 1956. The second meeting, appropriately, sponsored by the AIME and chaired by T. Rhodin,[74] was held in 1958 with the proceedings published in 1959. The third meeting was organized by B. Westwood and N. Stoloff in 1965 with the proceedings being published by Gordon and Breach in 1966.[75] Taken together, these three meetings defined fundamental perspectives from the materials and environmental points of view, defined the range of materials in which such phenomena occur, and defined an agenda At this point, fracture mechanics had not become a serious consideration for SCC.

Generally, these meetings demonstrated that SCC was a more general phenomenon than the 1955 status was prepared to accept SCC was shown to be a phenomenon that occurred in all engineering solids, in a wide range of environments, and in a wide range of compositions and solid-state structures within the material classes These meetings also showed the need for serious interactions among the disciplines in environments and materials as well as the need for integrating the scientific and design communities Finally, these meetings indicated the need for studies at levels of atomistic science owing to the complexity of the SCC phenomena

With the agenda defined by these three meetings, a second set of meetings was held to define comprehensively the state of SCC phenomenology over the range of engineering materials and environments. The first of these meetings was held in 1967 at Ohio State.[4] Here, SCC in all major alloy systems was reviewed comprehensively and the beginning efforts to define improved mechanisms were identified.

This 1967 meeting was appropriately followed by a second 1971 meeting more focused on fundamental issues pertaining to each of the alloy systems. This meeting, held at Ericiera, Portugal, in 1971, under the sponsorship of NATO and admirably organized by J Scully of Leeds University, was an experts' meeting and focused attention of mechanisms as they were interpreted in each of the major alloy systems.[76]

A third meeting was held in 1971 in Storrs, Connecticut, to focus attention on corrosion fatigue and its interaction with SCC [22]

Also, in 1971, a fourth meeting was held in Williamsburg, Virginia, on localized corrosion processes[77] and an ASTM symposium, focusing more on failures caused by localized corrosion, was held during the same year.[78]

A sixth meeting was held in 1973 in Firminy, France, to focus attention on the similarities and differences of what was then perceived as the different processes of SCC and hydrogen embrittlement as applied to iron-base alloys This meeting was a collaboration between NACE and the Creusot-Loire steel company in France.[5]

Together with these six meetings, extensive work was underway at Boeing Scientific Laboratory by Speidel, Blackburn, Hyatt, Feeney, Smyrl, and Beck and their collaborators; this work defines the state of affairs of SCC of high-strength aluminum, steel, and titanium alloys. Extensive reviews on these alloys were published [6,7,48] This work of the Boeing people and the meetings from 1967 through 1973 defined the phenomenological state of affairs in SCC of all major alloy systems. Taken together, this body of work is still the classic collection of understanding of phenomenology of SCC.

Atomistic definitions

One of the clear mandates from the Robertson-Rhodin-Westwood/Stoloff meetings covering 1954 to 1965 was to approach SCC from an atomistic point of view. This work was undertaken along two avenues.

One avenue was taken by the Advanced Research Projects Agency (ARPA). The head of its materials program, R. Thompson, who was also a physicist and interested in fracture, started a summer meeting program where the outstanding contributors to solid-state physics would meet for a month every summer to discuss important

questions affecting solid-state physics. One of the topics that occupied these meetings was SCC. Such outstanding people as J. Gilman, J. Hirth, M. Cohen, J. Rice, and others who came as visitors devoted some time each year to atomistic questions on SCC. Results from these discussions showed up in technical papers over the subsequent years.[79,80]

Another avenue was taken by Latanision and his collaborators in organizing expert seminars sponsored by NATO where atomistic questions were explored by outstanding contributors from the various disciplines that could contribute to understanding SCC and related phenomena. These meetings were a natural outgrowth of the ARPA summer meetings but also benefited greatly from Latanision's personal commitment to attracting the fullest range of talent to look at SCC and related phenomena. These meetings spanned the period 1975 to 1986.

The first meeting organized by Latanision and Fourie held in Hohegeiss, Germany, considered the subject "Surface Effects in Crystal Plasticity." The second meeting, organized by Latanision and Pickens, held in Calcatoggio, Corsica, in 1981, considered "Atomistics of Fracture." The third meeting, organized by Latanision and Jones, was held in Bad Reichenhall, Germany, in 1986, and considered the topic "Chemistry and Physics of Fracture." The set of volumes that resulted from these meetings constitutes the classic description of atomistic processes of SCC.[81-83]

Hydrogen questions

Aside from the set of 1967 to 1973 meetings on SCC, another agenda was set by Thompson and Bernstein, as well as by Bastien and his colleagues in France, who considered that the role of hydrogen in metals in general and in SCC had not been fully described. They set about to rectify this imbalance and organized three meetings. The first one was held in Champion, Pennsylvania, in 1973, and considered the subject "Hydrogen in Metals" from a descriptive and phenomenological standpoint. The second meeting, held in Moran, Wyoming, in 1977, "Effect of Hydrogen on Behavior of Materials," focused on experimental approaches to hydrogen phenomena and mechanistic ideas. A third conference, "Hydrogen Effects in Metals," was held in Moran, Wyoming, in 1980, and expanded upon the groundwork set in the earlier conferences.[84-86]

In addition, Thompson and Bernstein wrote a review that summarized the role of environmental variables in hydrogen-assisted environmental fracture.[87] Also, several important meetings were organized by European workers who had been investigating the role of hydrogen in metals.[88,89]

Fracture mechanics

While understanding was expanding in both the atomistics and phenomenology of SCC, another important avenue concerning the mechanics of fracture was being explored. For many years, Irwin at the Naval Research Laboratory had considered fundamental aspects of fracture and fracture mechanics.[90,91] It became apparent to his colleague, F. Brown at the Naval Research Laboratory, that Irwin's approach to the fracture of metals in general would be a useful framework for considering SCC except that the velocity of SCC would be slower than the near speed of sound associated with dry fracture.

To focus the emphasis that Brown considered the fracture mechanics approach deserved, he worked with ARPA to organize an interdisciplinary and interinstitutional program to study SCC. Collaborators in this project included Lehigh University, Boeing Scientific, NRL, and Carnegie Mellon University. This highly focused emphasis, together with funding already available at the participating institutions, produced major advances and excellent work. Most importantly, this work enabled fracture mechanics to become an integral part of both testing and design with respect to SCC. This work in the ARPA-sponsored coupling program focused mostly on high-strength steels, aluminum alloys, and titanium alloys. Essential findings of this work are summarized in the report by Brown.[92]

Aside from the work committed directly to fracture mechanics, the general subject of fracture began to receive increased emphasis in the late 1960s and 1970s and continuing through the 1980s. This avenue of development embraced both micromechanisms and mechanics. Those who organized these efforts also were perceptive enough to include environmental effects. From 1968 to 1979, meetings were held to explore fundamental aspects of fracture.[93-95] The subject of SCC was an integral part of many of these programs. These meetings as a group provide the basic collection of the fracture-oriented phenomenology and mechanisms. Other meetings were sponsored by ASTM[96,97] that concentrated mostly on fracture testing methods.

Institutional initiatives

In this period from 1955 through the present, the initiatives of institutions were important. The work of ARPA was already mentioned with respect to their summer solid-state meetings and their support of the SCC coupling program. The Materials Laboratory at Wright Patterson Air Force Base under the leadership of Colonel L. Standifer supported a coupling program similar to that of ARPA's through a collaboration of the Ohio State University, Georgia Tech, Lockheed Marietta, and WPAFB. This program operated more or less contemporaneously with the ARPA program but emphasized more of the fundamental processes associated with surfaces and solid state.

The electric power industry, first through the Edison Electric Institute (EEI) and later through the Electric Power Research Institute (EPRI), supported extensive work on SCC as it related to both fossil and nuclear power. They supported extensive work at Ohio State, Westinghouse, General Electric, Babcock and Wilcox, and Combustion Engineering associated with SCC in piping, steam generators, and turbines. EPRI also organized special efforts when corrosion problems in BWRs and PWRs became especially troublesome. Owners groups were organized that focused on steam generators for PWRs and piping for BWRs. EPRI also convened a Corrosion Advisory Group that integrated efforts of the world leaders in corrosion research.

Extensive corrosion programs were organized by the Central Research Institute for the Reactor Industry in Japan and by the Central Electricity Research Laboratory in the United Kingdom.

Other initiatives were taken and encouraged by the Office of Naval Research, the Air Force Office of Scientific Research, and the Office of Basic Energy Sciences in the Department of Energy.

During this time, extensive work on SCC was underway at many institutes in the Soviet Union and Eastern Europe.[98-100]

Texts

Finally, several useful texts and overviews have been prepared. The first major text on SCC was sponsored by the Corrosion Division of The Electrochemical Society, Inc. and was prepared by H. Logan.[16] Logan's book was published in 1966. It does not, owing to the time period, deal with fracture mechanics, but it is a good summary of phenomenology.

The second important text was prepared by Brown.[69] This text incorporates fracture mechanics but is aimed at being succinct and relevant to engineering solutions. It addresses preventive methods as well as descriptions of the phenomena. This text, in a sense, was the pedagogical outcome of the ARPA coupling program.

There are good texts on SCC that have been prepared for several different handbooks. One appears in the comprehensive handbook of Schrier.[101] A second was prepared by an ASM committee and is in the 8th edition of the ASM handbook.[102] There is an excellent review by Jones in Volume 13 of the 9th edition of the ASM handbook.[103]

SCC has been treated in several of the well-known corrosion textbooks written during this period, in particular in the texts by Fontana and Uhlig and Revie.[104,105] From the point of view of fracture, SCC was nicely integrated in the fracture text by Tetelman and McEvily.[106]

This brings us to the Kohler meeting. The intention of this meeting was to regroup and reassess. What has 30 years of research meant?

One intention of this review was to examine the 33 years since 1955 and assess what it seems to have all meant. I do this in the next two sections. "Scientific Status" and "Engineering Status."

Scientific Status

I originally planned to assess each of the proposed mechanisms for SCC relative to how well they predicted SCC in the SDS terms described in Figure 2. As I began this task, I realized that none of the available mechanisms approached such quantitative predictability. However, excellent work has been done by many workers. Thus, my perspective here is to assess the potential utility of proposed mechanisms as possible frameworks for quantitative predictions in various metal–environment systems. A detailed assessment of each of the mechanisms for SCC would be more extensive than I need here to accomplish my objectives.

There are several perspectives I would like to introduce into the consideration of mechanisms. One is that some of the mechanistic work is more of definition than of mechanism. This category includes the study of electrochemistry inside SCC in aqueous solutions. This work has been useful but has little to do with the explanation of mechanisms of advancing SCC. Likewise, the study of grain-boundary chemistry, while valuable, again does not address the atomic processes of crack advance. Thus, there is a category of important definitional work that helps explain the behavior of metal–environment systems but does not, per se, define mechanistic unit processes.

A second perspective is that I refer to the various mechanistic processes as "mechanistic unit processes." Such a mechanistic unit process may be the hydrogen-induced decohesion defined so well by Oriani,[107,108] slip dissolution, which has been nicely refined by Ford and Andresen;[109,110] and brittle film rupture, first defined by Forty and Humble and later considered in detail by Pugh and by Newman.[111–113]

A third perspective is that SCC may propagate by a combination of the mechanistic unit processes with either separate ones, or several at a time, being dominant in various regimes of alloy and environmental compositions. These unit processes or their combinations also depend on inputs or modifications from the various definitional factors such as grain-boundary composition.

While I was not able to find any of the unit processes that could provide anything quantitative in the frame of reference of the SDS factors identified in Figure 2, I believe that useful and creative progress is being made conceptually. Progress is also occurring because theory and experiment are converging at the atomic level while at the same time such results are being integrated into the work of those who think about the phenomenology.

Definitional processes

The purpose of this section is identify the status of investigations into aspects of materials and environments that influence SCC but may be differentiated as not being critical to mechanisms of SCC progress itself.

Grain-boundary chemistry and structure. The chemistry of grain boundaries is especially important in intergranular SCC. The schematic diagram of Figure 6 showing the various options for the distribution of species at grain boundaries is the basis for describing the results of progress.

The composition of grain boundaries associated with sensitized stainless steel has been extensively studied and little has changed since the 1933 paper of Bain and Aborn except that the availability of more sensitive techniques have made it possible to measure grain-boundary compositions directly. The current situation is best described in the review papers by Cowan and Tedmon.[34]

There appears to be no other alloy system outside the Fe-Cr-Ni alloys where the formation of a grain-boundary compound and the associated depletion of the adjacent region is so well defined or the intergranular SCC so clearly associated with such a circumstance.

The situation depicted in Figure 6(a) where impurity species accumulate at the grain boundary and occupy a width of only several atom thicknesses has been a more difficult situation to predict. This situation differs materially from that associated with the compound formation shown in Figure 6(b). Also, in an alloy where several impurities are present and compete for adsorption, the eventual outcome is not easy to predict and measure. Finally, considering the many options for the progress of SCC in grain boundaries as shown in Figure 7, it is not clear how such compositionally changed grain boundaries will support SCC.

The first serious effort to assess the relationship between grain-boundary composition and SCC started with the review by Aust, et al., in 1966.[37] Much of this work was stimulated by the observation that intergranular SCC occurred in nonsensitized stainless steel. The composition at grain boundaries was reviewed by Aust and Iwao.[114]

The first studies that correlated direct measurements of composition of grain boundaries with the occurrence of SCC was published by Smialowska, et al.,[115] for pure nickel. Here, they measured the composition of the boundaries and found that sulfur segregated according to a reproducible heat-treating schedule. The materials were then exposed to room-temperature environments over a range of pH; potentials and morphology of SCC were noted. These results are shown in Figure 21, which shows that despite the adsorption of sulfur to the grain boundary, SCC does not always occur. This is not unlike the behavior of Inconel 600, in which being sensitized actually diminishes SCC at neutral and higher pHs; on the other hand, at lower pHs, the sensitized Inconel 600 is increasingly prone to SCC.

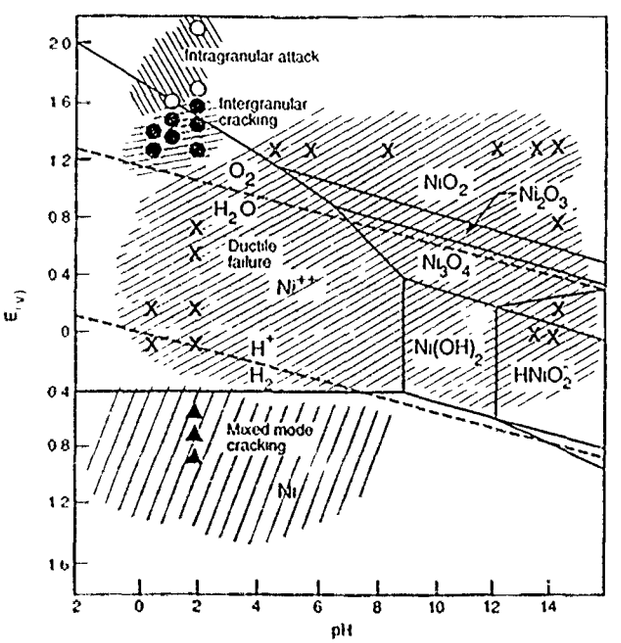


FIGURE 21—Failure morphology for relatively pure nickel with sulfur segregated at grain boundaries compared with the potential–pH diagram for nickel at room temperature. Zones over which these morphologies might occur are suggested by my shading. Adapted from Smialowska, et al.[115]

Electrochemistry inside stress corrosion cracks. Since many metal–environment systems where SCC occurs involve aqueous environments, the electrochemistry inside stress corrosion cracks is relevant. Beck made the first serious attempt to consider electrochemical conditions inside a stress corrosion crack.[116] Brown approached the same problem experimentally by measuring the pH inside SCC cracks directly and obtained the results in Figure 22.

comparing the external pH and potential with that on the inside of the stress corrosion cracks.[117]

Turnbull has reconsidered the question of chemistry in restricted geometries and published extensive and definitive studies on the subject.[118-120] His work supports Brown's early work but provides much-improved rational bases to effects of chemistry and configuration.

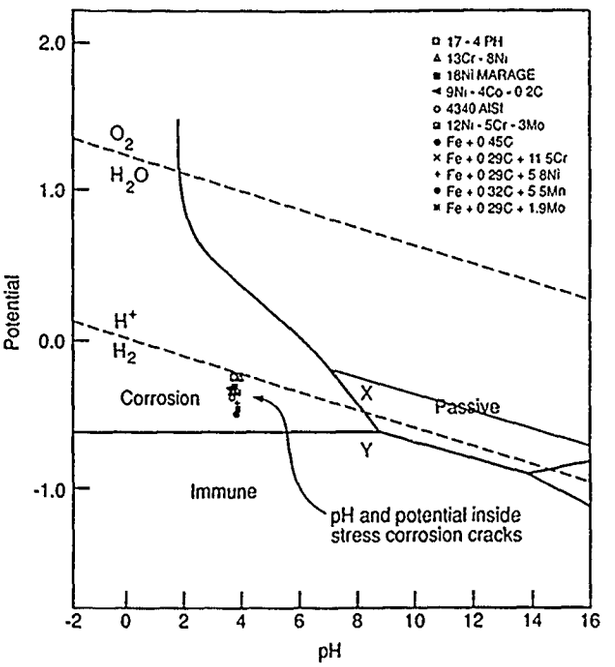


FIGURE 22—Plot of pH and potential inside stress corrosion cracks for various steels showing the results that occur regardless of the external pH. The crack tip is about pH 4 regardless of whether the bulk environment is made alkaline at pH 10 by NaOH or acidic at pH 2 by HCl. Adapted from the work of Brown.[117]

Slip processes. With respect to slip on atomic planes, the critical questions are associated with the degree of coplanarity. The more coplanar the slip, the more likely are stresses to concentrate internally at obstacles and the more likely are sharply defined slip-step emergences. These ideas were originally proposed by Swann and others as providing a virtually complete explanation of the metallurgical dependencies of SCC.[121,122] However, there were so many inconsistencies that this idea as a complete explanation was found not to be useful. Nonetheless, essential features of this idea remain useful in explaining some of the influences of alloy composition and structure.

Mechanistic unit processes

The purpose of this section is to assess the status of the individual unit processes by which SCC advances. I do not compare any of the mechanistic unit processes with the criteria that I originally defined in Figure 2, since none of the unit processes has been developed sufficiently to predict behavior from fundamental bases, although some of the unit processes do provide excellent bases for correlating data.

Strain-accelerated dissolution. In strain-accelerated dissolution, the crack is hypothesized to advance because the straining process at the crack tip activates the metal and it dissolves preferentially at the crack tip. This was originally suggested by Mears, et al.,[123] but it fails to discriminate between many of the simplest environmental and metallurgical considerations.

This unit process has been abandoned and is no longer considered useful. The lack of discrimination by this model of metallurgical and environmental conditions that support SCC of various intensities suggest that this mechanistic unit process, which relies totally on crack-tip strain rate, is not sufficiently inclusive to be useful.

Stress sorption cracking. In this unit process, it was hypothesized that the attractions of crack-tip atoms to species in the environment would be reduced in favor of attractions to atoms adsorbed on crack walls. This idea was largely proposed by Uhlig,[124] but little direct evidence was ever developed to support this idea and it too has been largely abandoned.

Slip dissolution. In this unit process, slip is hypothesized to break the protective film either in the initiation or propagation process with the result that a dissolution transient occurs of sufficient magnitude and with sufficient frequency that a stress corrosion crack propagates. Here, the major advance of the SCC occurs via the dissolution process. The essential idea for this process was originally suggested by Logan.[16] It was refined in work by Murata and Staehle[125] and Shibata and Staehle[126] and has received its most extensive application in the work of Ford and Andresen on SCC in sensitized stainless steels.[109,110]

The unit process of slip dissolution is conceived of as a break of the protective film followed by a transient dissolution process that consumes sufficient material to advance the SCC. This is illustrated in Figure 23, adapted from Shibata and Staehle.[126,127] The magnitude of the dissolution event depends on those factors that tend to retard the formation of a new protective film such as low pH, low chromium, certain ranges of electrochemical potential, and others. In situations where SCC does not propagate, the individual transient following the breaking of the film consumes a minimal amount of material and no SCC progresses. At the other extreme, breaking the film accelerates general corrosion.

Shibata and Staehle[126] studied the individual transients associated with the breaking of protective films. An example of the transients is illustrated in Figure 24. The event here shows a peak current density of 0.5 A/cm^2 and total material reacted of about 4.5 mC/cm^2.

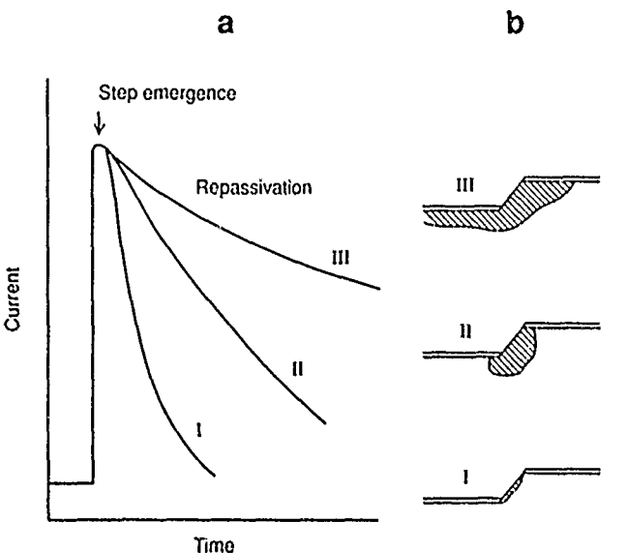


FIGURE 23—Schematic view of the processes associated with the initial stages of slip dissolution. The general shape of the individual current transient is shown (a) as associated with the morphologies of corrosion associated with slip events (b).

The transients such as the one in Figure 24 then occur rapidly and produce what amounts to an average current, which is the time-averaged result of many events occurring simultaneously and sequentially.

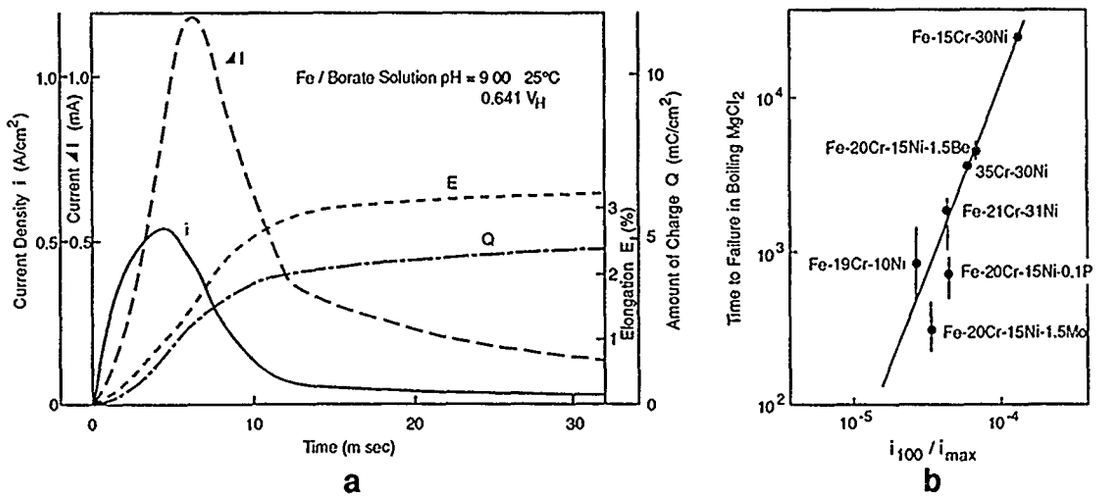


FIGURE 24—(a) Transient behavior of both the reaction current measured at constant potential and the strain vs time. Total current, instantaneous current density, strain, and total reaction vs time for iron in a borate buffer at room temperature. (b) Correlation of time-to-failure of Fe-Cr-Ni alloys in boiling $MgCl_2$ solutions as a function of the ratio of steady-state current at 100 s to the peak current observed in an experiment of (a). Adapted from the work of Shibata and Staehle.[126]

Ford and Andresen[109,110,128] have formulated this slip dissolution process as it propagates through a metal by a relationship that correlates the advance of the SCC with the electrochemical current as follows:

$$V_t = \frac{M}{n\rho F} \times \frac{Q_f}{t_f} = \frac{M}{n\rho F} \times \frac{Q_f}{\epsilon_f} \dot{\epsilon} \qquad (1)$$

Where M, ρ = atomic weight and density of the crack-tip metal; F = Faraday's constant; n = number of electrons involved in overall oxidation of 1 mole of metal; Q_f = oxidation charge density passed between rupture events; t_f = oxide rupture plasticity; ϵ_f = fracture strain of the oxide at the crack tip; and $\dot{\epsilon}$ = strain rate at the crack tip.

In practice, a relationship of the form,

$$V_t = A\dot{\epsilon}^n \qquad (2)$$

Where n = 1 to 1.5 and A = constant is used to correlate data.

The slip dissolution process as formulated by Ford and Andresen does not predict the occurrence of SCC *a priori*. It provides a useful method for correlating data around a mechanistic hypothesis. The model in this sense is not predictive but is rather "correlative."

There is an assumption in this model that does not correspond to the three-dimensional description of advancing SCC. The model epitomized in Equation (1) assumes that the SCC progresses uniformly along an advancing front. It is more likely that it goes in "fits and starts" with separate transients occurring along the front at random points, as illustrated in Figure 25. It is quite likely that the individual events could have a much higher peak current than the average of Equation (1) and would correspond more to the peak shown in Figure 24. However, the approach taken by Ford and Andresen has been productive, and it appears that the success of the correlations built around the slip dissolution hypothesis support the validity of the model.

In earlier work,[129] I had suggested that the passivating film in stainless steels was associated with the enrichment of nickel. Later, I abandoned that idea.[127] Recently, Newman[112] has suggested that there is indeed evidence for nickel enrichment playing a crucial role. However, the work of Bond and Dundas on Fe-Cr alloys containing molybdenum suggest that the enrichment of a more noble material may not be so crucial.[130]

Brittle film rupture. The unit process of brittle film rupture differs significantly from slip dissolution. In the latter, the major progress of SCC through the metal occurs via a dissolution processes. In the former, progress occurs via successive ruptures of weakened or embrittled layers of thicknesses that greatly exceed those of passive films. However, it should be noted that these films associated with brittle film rupture are formed by direct corrosive interaction with the environment.

Brittle film rupture was first suggested by J. Forty at Bristol as a means of explaining the SCC of copper.[111] He hypothesized that a reaction product film was first formed that was subsequently broken in a brittle manner. The advance of SCC was then conceived as a succession of such events as illustrated in Figure 26. The advance of SCC in this model as presented in Figure 26 occurs mainly by the breaking of a reaction product film that was formed by the reaction between the environment and the metal. This model has been extensively applied by Pugh to the explanation of SCC in copper alloys.[131,132]

While the breaking of a reaction product film, such as an oxide, provides one mode for propagating SCC by brittle film rupture, a second means for forming a brittle film is through parting or dezincification. Such a film could readily achieve thicknesses on the order of those necessary to rationalize the propagation of SCC. Such arguments have been advanced in the past by Pickering for explaining the SCC of noble metal alloys.[133]

A third variation of the brittle film-rupture model is one that hypothesizes that some action at the tip of the SCC prevents slip and causes a region under the crack tip to be brittle with the advance of the SCC occurring via cracking of successive embrittlements. The fact that surface processes of relatively minor dimension could resist slip was originally shown by Latanision.[134,135]

A final variation on modes of crack advance by brittle film rupture is associated with embrittlement by dissolved hydrogen at the crack tip. Rather than embrittling by decohesion, one version of hydrogen embrittlement is hypothesized as the hydrogen being trapped at dislocations, thereby immobilizing them and embrittling the metal at the crack tip. The crack thus progresses by successively embrittling and rupture of these regions where hydrogen is trapped in dislocations.

A second version of hydrogen embrittlement involves the formation of brittle hydrides in the hydride-forming metals to give the successive embrittlement shown in Figure 26.

One of the arguments in support of the brittle film-rupture process has been the fractography associated with transgranular SCC. The argument is that the cleavage-like features of the surfaces of transgranular SCC in copper alloys and Fe-Cr-Ni alloys cannot be

rationalized by a dissolution process and that a brittle cleavage process fits the observations better. This argument is carefully drawn by Pugh.[113]

Arguments in support of a brittle film-rupture process are also supported by acoustical emissions that are sometimes measured from such alloys during SCC.

While the brittle film-rupture process continues to be an attractive model, it predicts little on an *a priori* basis except for possibly the noble metal alloys with the variation of the brittle film-rupture model involving parting.

While there is, without question, fractographic appearance that strongly suggests cleavage as the mode of primary advance for some alloys such as copper base and stainless steels in the transgranular mode, the environmental dependencies strongly suggest that the advance of SCC in these alloys is dominated by chemically critical processes. The cleavage features do not rule out a local dissolution process.

There continues to be uncertainty here between the cleavage and dissolution processes as accounting for most of the crack advance, although it appears that the overall advance of SCC is controlled by electrochemical processes.

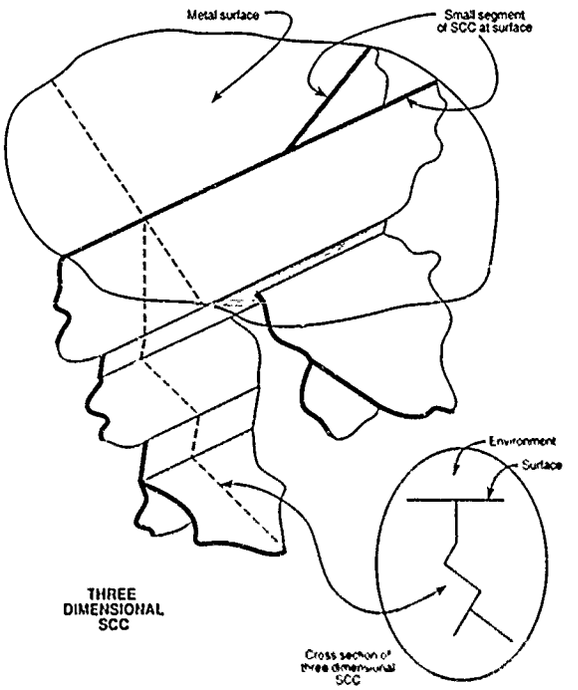


FIGURE 25—Schematic view of a stress corrosion crack proceeding through a metal. Note the unevenness of the SCC front and the patterns of branching. This contour is based on direct observations of SCC.

Enhanced atomic mobility at the crack tip. Galvele[136] has proposed that the advance of stress corrosion cracks may be modeled by a process that involves surface diffusion of species from a stressed cracked tip. Key features of his model are identified in Figure 27. The essential feature of his model that controls the rate of SCC is related to the rate at which atoms can leave crack tip. This rate at which atoms leave the crack tip is controlled by their surface mobility.

Galvele has demonstrated that the surface mobility is primarily affected by environmental combinations with the alloy composition where low melting compounds are formed. He hypothesizes that compounds with low melting points are the most likely to support SCC. He identified environmental species that have the highest likelihood of causing SCC in different alloys.[136] An important feature of Galvele's model is its capacity to rationalize many different combinations of environment and alloy where the intensity of SCC is likely to be high.

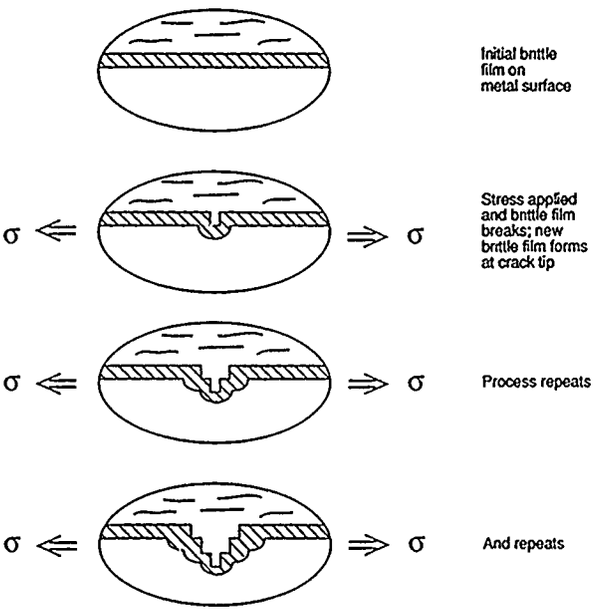


FIGURE 26—Schematic view of brittle film rupture as it progresses through a metal to produce SCC. The brittle film is first formed and then broken. More reaction product forms at the tip of the first break. This newly formed brittle layer breaks again with more reaction product forming at the tip. This process continues. Such brittle layers can be formed by reaction products, dealloying, hydrogen pinning of dislocations, or purely surface events that restrict slip.

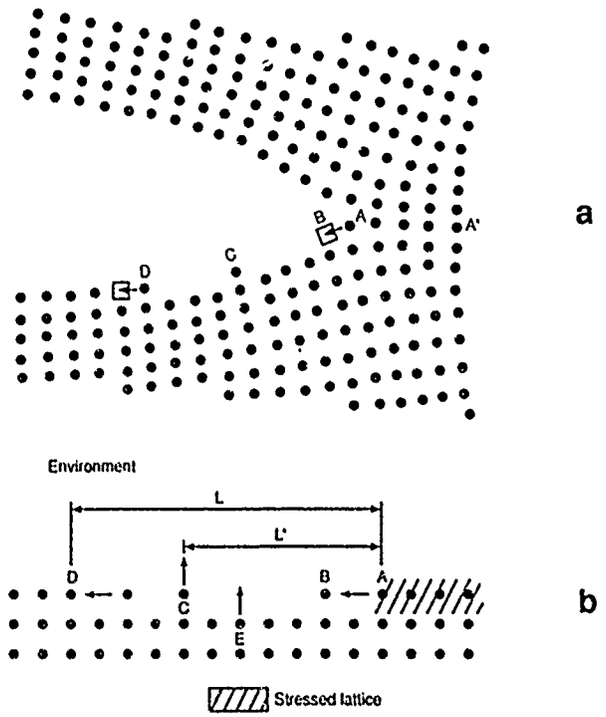


FIGURE 27—Schematic descriptions of atomic processes associated with the surface mobility model of SCC: (a) stresses at the crack tip favor the a-b exchange introducing a vacancy at the tip of the crack and advancing it one atomic distance. The rate-determining step is the rate at which excess atoms (C) are transported by surface diffusion to a new lattice site, b-d; and (b) distance (l) is the distance excess atoms must travel from the tip of the crack to a kink site on the crack surface. Distance will be smaller (l') if the excess atoms are dissolved by a reaction with the environment, or (c) if selected dissolution of the alloy is taking place (e). Adapted from the work by Galvele.[136]

Decohesion. Troiano, in his early considerations of hydrogen embrittlement, proposed that the role of hydrogen was to reduce the metal–metal bond strength.[12] A quantitative model was later developed by Oriani.[107,108]

In the model developed by Oriani, he proposed that the increased elastic strain at the crack tip would attract and stabilize a high concentration of hydrogen. The presence of this hydrogen would decrease the metal–metal bond strength and lead to SCC. This model rationalized the role of increased alloy strength in accelerating SCC since the increased yield strength would lead to higher elastic strains that would, in turn, attract more hydrogen.

The decohesion model seems to fit many of the observed patterns in high-strength steels. It seems also to fit some of the patterns in other alloys.

Enhanced ductility of the SCC tip. Another approach to rationalizing the SCC advance is a unit process that depends on the environment to increase the ductility at the tip of the advancing stress corrosion crack. This would either increase the rate of void formation or allow for additional deformation of the tip itself. Such a process has been suggested by several authors, including Hirth and Johnson and Birnbaum, et al.[79,137] This is somewhat similar to a suggested model for the advance of SCC in aluminum alloys, in which a softer precipitate-free zone was hypothesized to be the location of SCC advance.

This mechanistic unit process seems particularly applicable to hydrogen-related SCC in the lower-strength and tougher alloys, where the decohesion model is less appropriate.

Hydrogen bubble formation. The formation of internal hydrogen bubbles that would raise the internal stress and lead to premature failure has been a popular unit process, especially for hydrogen in steel. There is support for this process from well-known and directly observed hydrogen blistering that occurs in the presence of poisons that increase the effective pressure for hydrogen entry.[53]

Tetelman developed a model for the propagation of SCC involving hydrogen bubbles with associated high internal pressure.[54] While the hydrogen blister model is attractive from the direct evidence for hydrogen blistering, there is no evidence that it is the basis for SCC from, for example, the fractography. Another experimental observation that disputes the applicability of this model is Johnson's observation that one atmosphere of hydrogen gas pressure is sufficient to support the propagation of SCC. His result shows that the higher hydrogen fugacities that can be achieved in aqueous solutions are not necessary for explaining SCC.

Except for rationalizing blistering, which is not a part of SCC, the hydrogen pressure unit process does not seem to be useful for any system being studied. However, this process cannot be entirely neglected since evidence for such an action does exist in blistering.

Grain-boundary bubbles by chemical reaction. The mode of hydrogen embrittlement epitomized by the Nelson Curve shown in Figure 28 is different from those rationalized either by the decohesion or the enhanced ductility models.[138] The principal characteristics of this phenomenology are the increase in embrittlement with increasing hydrogen pressure and temperature and the decrease in embrittlement as the carbon activity in the alloy is reduced. These patterns have suggested to many that the unit process for SCC here involves the formation of bubbles of methane at the grain boundaries with a resulting decrease in strength of the grain boundary.

Shewmon has rationalized this process and shown convincingly that the methane bubbles do form and are directly related to this mode of SCC.[139] His model is sufficiently based upon fundamental principles and sufficiently quantitative in its prediction of the effects of the SDS variables so that it qualifies as one of the most quantitative models available.

Direct dissolution of compositionally modified grain boundaries. The work on grain-boundary composition has shown that as much as 50 to 100% of the atoms at the grain boundary could be impurities that are not part of the nominal alloy composition. Such impurities, unlike most of the alloy species, are highly soluble in aqueous solutions over a wide range of pH and potential. For example, sulfur is soluble at positive potentials as sulfate and at negative potentials as hydrogen sulfide or bisulfide. Carbon at high potentials is soluble as CO_2 or carbonates and at low potentials is soluble as methane or methanol. Such reaction products for carbon were identified by Payer and Staehle during the dissolution of iron carbides.[140]

This wide range of solubilities for species such as sulfur and carbon is the same for phosphorus and nitrogen.

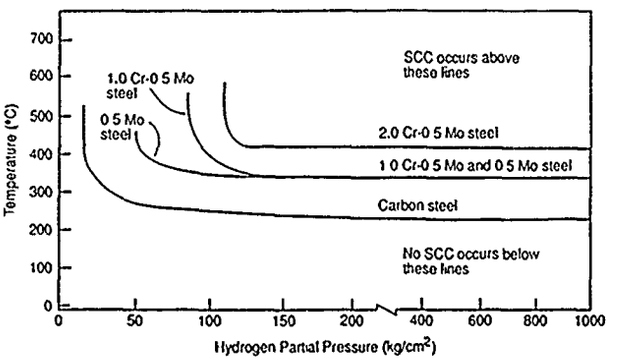


FIGURE 28—SCC as a function of temperature vs pressure for several alloy steels exposed to hydrogen. This curve was adapted from Nelson to show only the processes that are hydrogen embrittlement and not those that show decarburization. Adapted from the work of Nelson.[138]

The results of the sulfur segregation studies in Figure 21 show that the mere existence of such species at the grain boundaries does not lead to SCC. It appears that the residual passivity conferred by the alloy acts to prevent penetration along grain boundaries unless this passivity at weakened at lower or higher pH. However, when this inherent passivation is weakened, as with nickel in acidic solutions, then the effect of the highly soluble impurity species dominates. This suggests that there is some SCC that is effectively "active path dissolution" and does not even require the more sophisticated interpretation of slip dissolution.

Thus, the dissolution process is inherent when and if the impurity species aggregate at the grain boundaries. The occurrence of such SCC seems to depend, after the aggregation, on the range of passivity of the matrix material.

While this unit process has not been extensively explored, it appears to be viable.

Tunneling. Swann and Pickering[122] suggested that the formation of tunnels associated with slip dissolution could be the critical process for advancing SCC. Tunnels would form and mechanical processes would break the remaining ligaments.

Tunnel formation has been observed by Swann and Pickering in noble metal alloys,[122] by Neilsen for stainless steel[141] and by Long, et al., on a range of Fe-Cr-Ni alloys.[142]

It has been verified by electron metallography that tunnels do form. Long showed that the extent of tunnels in Fe-Cr-Ni alloys decreases with increasing nickel, just as the SCC in chloride solutions does.

Tunneling does not appear to have any present advocates. However, it does not seem to be extensively investigated. It may also be a variation of the slip dissolution process.

Synthesis

The unit processes outlined above, together with the definitions, combine to produce SCC. There may be other as yet unidentified processes.

None of the models for the unit processes satisfies the need for quantitative description in the SDS coordinates of any SCC phenomena in any metal–environment systems.

The unit processes outlined in this section are much improved in conceptual quality over the ones available in previous years. However, these need to be greatly refined if they are to provide explanations of existing phenomenology.

It is quite likely that the SCC in various metal–environment systems does not depend on a single unit process but rather

depends upon several of these operating simultaneously. The possibility that several of these processes operate simultaneously has not been investigated. Such work should be undertaken.

Engineering Status

"Engineering Status" is intended to imply "to what extent and how can we confidently design components for their intended life considering the effect of SCC?" It is refreshing to know that good engineering can be confidently undertaken without quantitative predictive models for some specific cases. Good engineering can be accomplished using well-established inferences from experimental data, i.e., "don't use austenitic stainless steels above 100°C with even small amounts of oxygen and chloride." However, such engineering is always suboptimum and often misses, wholesale, regimes of failure.

Generally, the difference between what could be done with quantitative models and with less quantitative inferential information is accounted for the safety factors used in engineering.

Before discussing the engineering status of SCC, I define what is needed, or at least should be needed, by designers.

In principle, the designer is the "impresario" who designs the entire system using the following principles (defined in Figure 29).

Factors of Comprehensive Design

- Performance to objectives
- Balanced interaction of component parts
- System performs reliably at maximum conditions
- Manufacturable
- Low cost
- Inspectable and repairable
- Performs reliably in nominal and non-nominal internal and external environments
- Materials perform reliably in as-manufactured condition
- Mean time between failure exceeds inspection interval
- Failure is not catastrophic
- System designed to work for its intended life

FIGURE 29—Factors of comprehensive design that include considerations of environmental effect on the strength of materials of construction.

(1) Performance of the intended purpose; i.e., the pump delivers so many gallons per minute.
(2) The components of a system work together harmoniously; i.e., the cooling water to the pump does not cause it to fail by corrosion; the pump delivers adequate fluid for the reaction vessel to produce at a desired rate.
(3) Performance conditions have been defined in terms of nominal and maximum expected: pressures, stresses, cyclic behavior.
(4) Manufacturability: The device can be made by available techniques by qualified contractors.
(5) Low cost: The device can be sold at a profit.
(6) Inspectability and repairability: Critical components can be periodically inspected and replaced if necessary.
(7) All features of design perform reliably in all nominal, expected, and accidental chemical/physical environments on both the process side and nonprocess side.
(8) Materials used for manufacture have been analyzed for performance in their actual as-manufactured conditions of heat treatment, fabrication, joining, and design configuration (including crevices).
(9) The mean time between failure (MTBF) is longer than the inspection interval with a high degree of confidence.
(10) Failure, if it does occur, does not produce catastrophic results; i.e., design for leak before break.
(11) The system will work reliably for its intended life.

In complex systems, it is usually necessary to conduct prototype and scale up testing as well as additional laboratory testing to ensure that these design principles are properly considered. When these tests are conducted, it is crucial that they be as close to design conditions as possible and that they be evaluated with respect to the principles outlined above and in Figure 29. It is the responsibility of the designer, in his role of impresario, to ensure that such tests are conducted and that the evaluations are meaningful. While the extent of such work naturally depends on already available prior experience, it is dangerous to make unproven assumptions for the following reasons:

(1) All engineering materials are reactive chemicals; the surprise is not that they fail, the surprise is that they work.
(2) In considering the possibility of failure, the operating maxim is the opposite of justice, guilty until proven innocent.

The above provides a framework in which the engineering status of SCC should be assessed.

This framework identifies established principles describing SCC that can be incorporated into design. While the theoretical modeling described in the section "Scientific Status" needs a great deal of work to become satisfyingly predictive, the engineering situation has progressed substantially.

Testing

Two important physical methods of testing have been developed and have greatly improved the quality of data available for design as well as interpretation of fundamental physical processes.

The slow-strain-rate testing method developed and refined by Parkins and many coworkers[143] provides a method for avoiding the uncertainties of initiating SCC. It has the advantage of determining whether SCC will occur under any circumstance in a given environment. It is a characteristic of these experiments that strain rates that are too rapid fail, as in tensile tests by mechanical overload; the strain rates must be sufficiently slow, usually less than 10^{-6}/s, so that the SCC processes can operate. Figure 30 shows some typical results in a plot of reduction in area vs log strain rate.[144] At high strain rates, ductile fracture generally occurs. For strain rates in the range of 10^{-7} to 10^{-5} s^{-1}, SCC processes operate and reduce the ductility according to the severity of cracking.

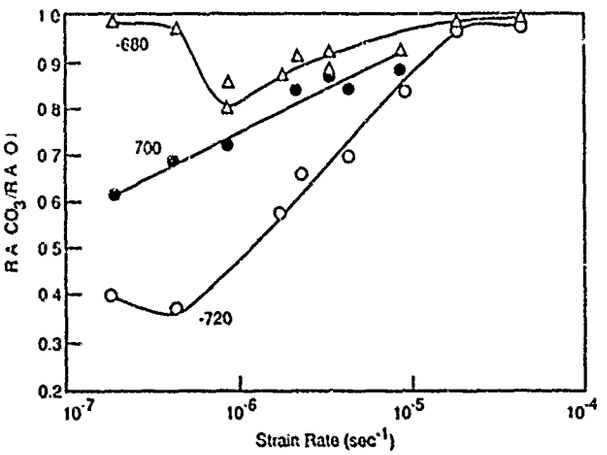


FIGURE 30—Ratio of reduction in areas of specimens in carbonate solution to those in oil vs strain rate for three applied potentials for line pipe steel at 79°C. Adapted from the work of Berry.[144]

Slow-strain-rate testing is now widely used. It has been the subject of several symposia and reviews.[145,146]

The output from these slow-strain-rate experiments, i.e., the dependent variable, may be an area or percent of fracture surface with SCC, time-to-fail, load at failure, or SCC velocity (length of SCC propagation divided by time-to-failure). These results are generally equivalent. Where SCC velocity is determined, it is usually inferred that this is the "plateau velocity" by analogy with the fracture mechanics testing discussed subsequently.

Slow-strain-rate testing provides mainly a qualitative indication of SCC intensity but does not give directly useful information on design stresses, initiation, and the part of the SCC velocity profile that is actually operating.

Fracture mechanics testing for SCC provides more direct information on the velocity of SCC under known conditions of stress and defect depth. Essential features of fracture-mechanics-type testing have, by now, been well defined, and such testing is in widespread use.[147,148] This is the method of testing that was encouraged by Brown[146] and emphasized in the ARPA-sponsored program in the late 1960s.

A typical fracture mechanics specimen is illustrated in Figure 31. The depth of the crack is determined as a function of time and the stress intensity is known from the crack depth and the load. The data are then plotted as crack velocity (m/s) vs stress intensity (ksi$\sqrt{\text{in.}}$). The resulting data usually take the form shown in Figure 32 where there are often well-defined Stages 1, 2, and 3.

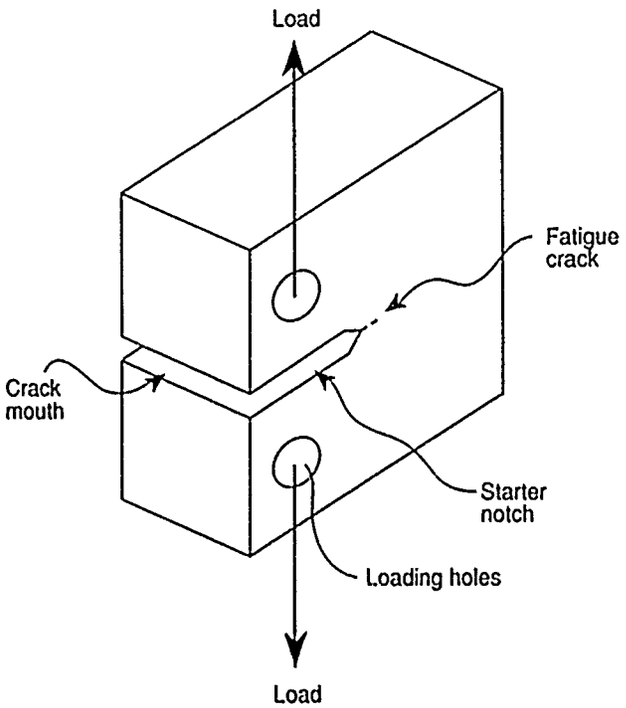


FIGURE 31—Typical configuration of specimens used for fracture-mechanics-type testing where crack velocity vs stress intensity is obtained.

In general, most testing is performed in the opening mode, which is designated as Mode I, although some work has been done using Modes II and III.[177]

Of great interest to design with SCC from the fracture mechanics point of view is the stress intensity below which SCC will not initiate. This is usually designated as K_{ISCC}, meaning that it is the stress intensity in the opening mode below which SCC will not initiate. It is presumed that once SCC starts, it will propagate at increasing rates following first the Stage I curve and then the Stage 2 curve until stress intensity is sufficiently great that K_{Ic} is reached and catastrophic failure is reached. This is illustrated in Figure 32.

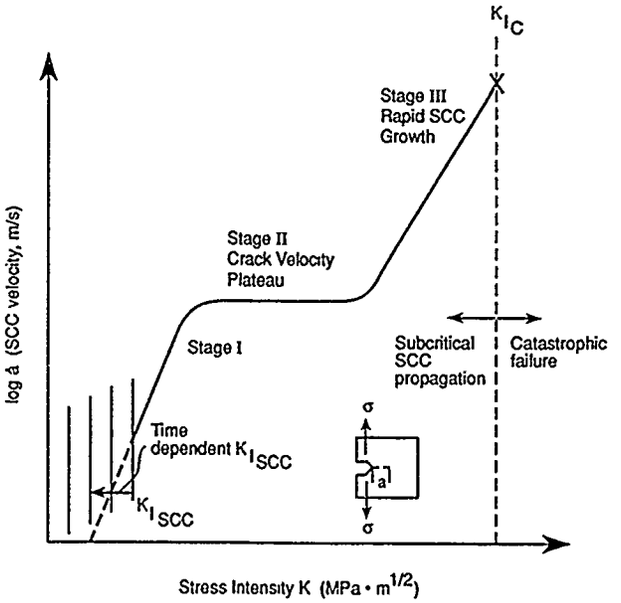


FIGURE 32—Schematic plot of data from fracture-mechanics-type testing where the log of crack velocity is plotted vs log of stress intensity. Above the value of K_{Ic} fast or catastrophic fracture occurs. The minimum stress intensity below which SCC does not occur is shown by K_{Iscc}. Here, K_{Iscc} is shown to depend on time.

There are several problems in using the fracture mechanics approach. One is that the minimum stress intensity below which SCC does not occur (K_{Iscc}) is often time dependent, so that over the lifespan of a component, there may never be a stress low enough to avoid SCC in certain environments. Such a concern is noted by Speidel.[149] This concern does not relate to the validity of the method of testing but rather to the conclusions that are reached from the data.

Another problem in applying fracture mechanics methodology concerns the analysis of thin wall tubing where SCC failure is more related to initiation time on smooth surfaces than to the rate of propagation. In thin wall tubing, the stress required to initiate SCC is the most important question. The times required for initiation and perforation are virtually the same. Thus, the data for thin-walled tubing needs to be obtained in the "endurance limit" or "threshold stress" format as shown in Figure 33. However, as with Speidel's concern for fracture mechanics testing, this threshold limit of Figure 33 may also decrease with time.

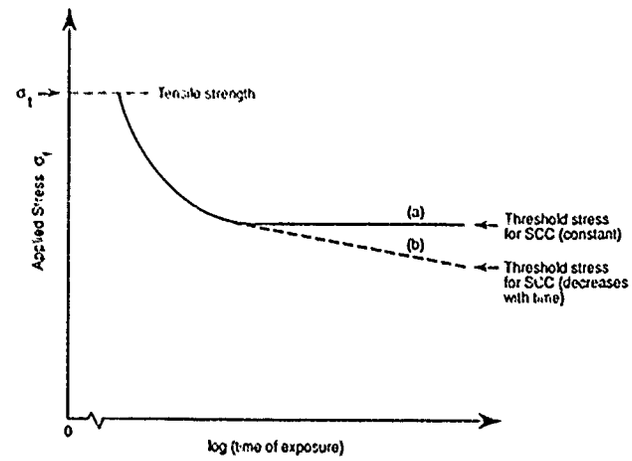


FIGURE 33—Schematic plot of stress to fail vs time for static-loaded SCC experiments showing both a constant stress below which SCC does not occur and a lower limit that decreases with time. Curve (a) shows no time dependence of the lower limit, Curve (b) does.

The problem of testing for application to thin sections such as tubing has been an interesting one and is sometimes misunderstood. Many in fracture mechanics insist that SCC cannot start without a pit or a grain-boundary crevice or other initial perforation by mechanical or chemical means. In fact, SCC usually initiates from absolutely smooth surfaces in either transgranular or intergranular modes and propagates by the same microprocesses as produced initiation. Thus, there is a great need for a method of testing that is sensitive to the surface stresses that initiate SCC.

It is also clear that any approach to defining threshold stresses of the type defined in Figure 33 (Curve a) should be sensitive to the effect of environments and time as shown in Figure 33 (Curve b). To illustrate this point, Figure 34(a) shows the results from testing of Totsuka and Smialowska[25] where they determined the effect of potential on the SCC of Inconel 600 at 350°C. Their open-circuit potential lies essentially on the hydrogen equilibrium line of the Pourbaix diagram. This figure shows where their open-circuit potential lies with respect to the hydrogen equilibrium potential in Figure 34(b). An important implication of their work is the effect of potential on the expectation for endurance limit curves of the type shown schematically in Figure 33. The general pattern here is implied in the effect of potential in Figure 30 for the slow-strain-rate work. Figure 34(c) implies that high stresses are required to produce SCC at the open-circuit potential; much lower stresses produce SCC at lower potentials. Such potentials can be reached in practice by galvanic coupling of the Inconel 600 with actively corroding carbon steel.

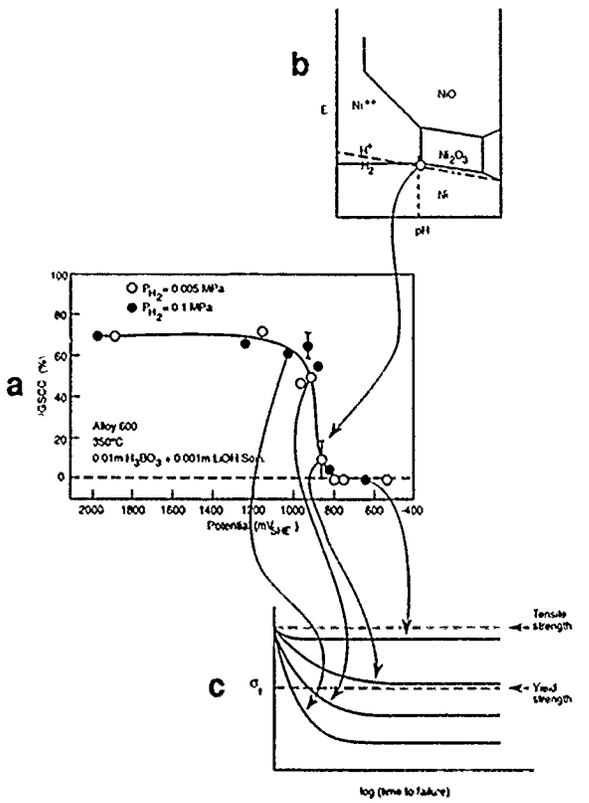


FIGURE 34—(a) Experimental data adapted from Totsuka and Smialowska[25] showing percent of area with intergranular SCC vs the applied potential for two hydrogen pressures using Inconel 600 (UNS N06600) at 350°C from slow-strain-rate testing. (b) These data are compared with a schematic view of the Pourbaix diagram for nickel. (c) Hypothesized stress vs time behavior is shown for failure of smooth specimens as might occur if held at constant potentials indicated.

For the smooth-surface, initiation-controlled situation, fracture mechanics data are more relevant to the point when K_{Ic} is reached for either circumferential or longitudinal SCC, as illustrated in Figure 35.

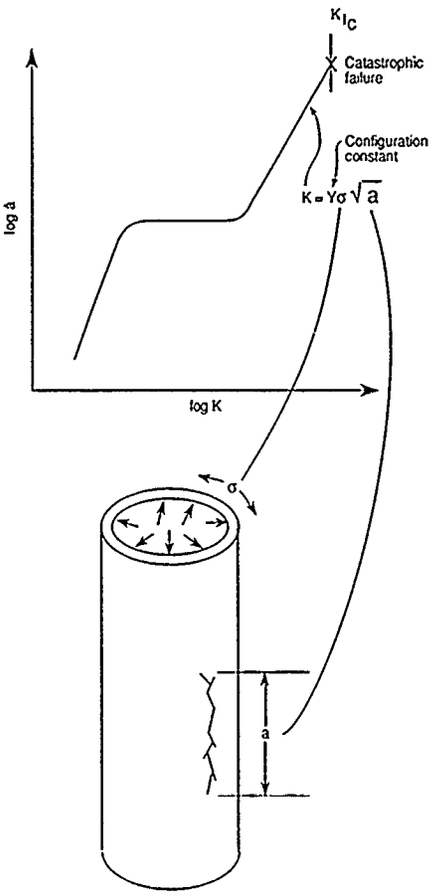


FIGURE 35—Schematic view of how longitudinal SCC in a smooth surface tube of a tough material may connect to produce a critical size defect in the presence of internal pressure.

Another advance in testing has been the increased control of environmental variables. The data of Indig and McIlree[150] in Figure 36 show the effect of oxygen concentration on the open-circuit potential of stainless steel in water at 288°C. These data show that a change from 10 ppb to 100 ppb corresponds to a change of almost 600 mV. Such a change should be compared with the data in Figure 34(a) for Inconel. It is probably this lack of control of oxygen that explains why Copson initially missed reproducing the SCC of Inconel found by Coriou.[20 47]

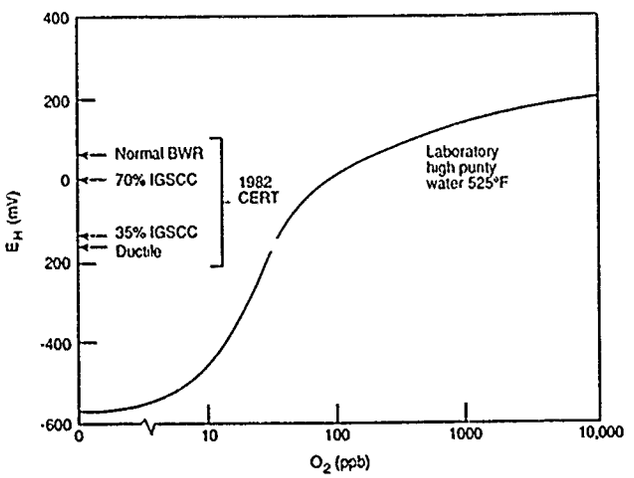


FIGURE 36—Open-circuit potential for stainless steel in pure water as a function of oxygen concentration at 288°C. SCC tests also shown for comparison. Adapted from the work of Indig.[150]

The use of controlled potential for testing in aqueous environments as indicated by Figure 34(a) from Smialowska and in Figure 30 from Berry has greatly improved the quality and the interpretability of results. Naturally, different methods of control are required for gaseous environments. Here, the control of partial pressure as done by many[48,51,151] has provided additional information for mechanistic interpretations.

The discussion above concerns static, albeit constant load vs constant strain, stressing. The more general case and more applicable to engineering circumstances is cyclic loading usually referred to as fatigue testing. Cyclic testing and the results of specimens with smooth surfaces is the subject of older work. Traditional studies produce data of the type shown in Figure 37,[152] where cyclic stressing of specimens in deaerated water produces an "endurance limit" effect, shown in Curve a of Figure 33. When testing is performed in more aggressive environments, the endurance limit decreases with increasing time, as shown for Curve b, which corresponds to aerated salt water in Figure 37. These effects of environments in cyclic stressing, especially when performed at high frequencies, often do not correlate with effects of environments in constant-load testing, and this area lacks any useful theoretical explanation.

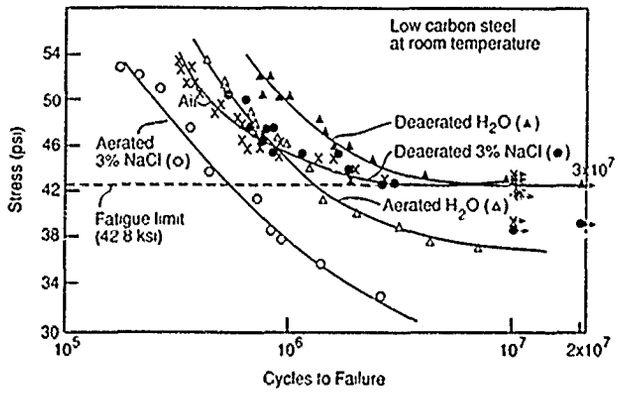


FIGURE 37 – Cyclic stress vs cycles to failure for low-carbon steel at room temperature for environments containing only water and then modified by additions of NaCl and oxygen. From the work of Duquette and Uhlig.[152]

Cyclic testing using fracture mechanics definitions produces data of the type shown in Figure 38,[153] where the crack advance per cycle ($\Delta a/\Delta n$) is a function of the magnitude of the cyclic stress intensity (ΔK). Effects of environments are measured as shown in Figure 39.[154] There is a critical K_{I_F} corresponding to the $K_{I_{SCC}}$ below which corrosion fatigue will not propagate, although such a value may decrease with time.

There are some testing techniques now in use that should be questioned and re-evaluated. One of those is the so-called reverse U-bend or RUB specimen illustrated in Figure 40.[155] This specimen is often used so that as fabricated industrial tubing material can be evaluated directly. However, this specimen provides a difficult geometry on which to apply controlled potentials and the stresses are generally irrelevant to those in use. What is needed is the kind of data shown already in Figures 32 and 33 where the stress below which failure will not occur can be determined. Such data can then help assess the importance of residual and applied stresses. For example, if the combined stresses are below some value at a selected life, SCC would not occur. The RUB specimens do not obtain such data.

Advances in techniques of mechanical testing to determine effects of environments have greatly improved the capacity to obtain data that can be used directly in design. Deficiencies still exist in methods for defining SCC that is initiation dependent and in defining the environments of testing. Further, there are some testing procedures, unfortunately widely used, e.g., RUBs, that provide useless data and should be abandoned just as constant strain testing has been largely abandoned for obtaining useful design data.

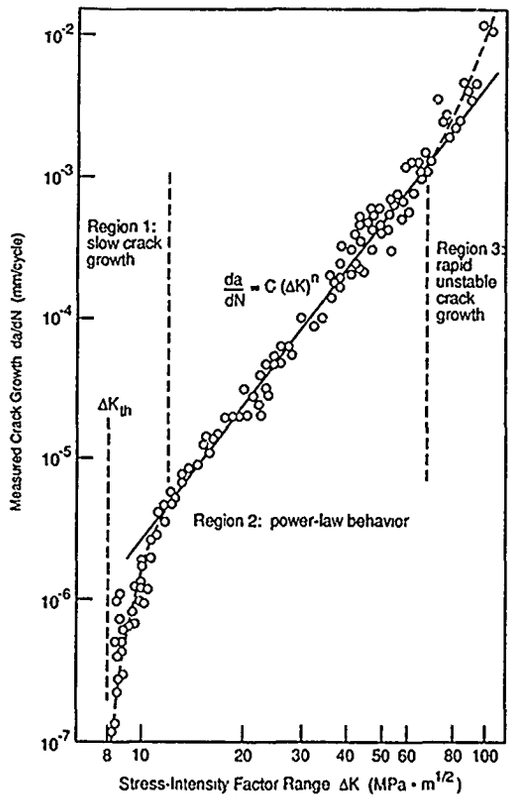


FIGURE 38—Crack growth rate vs stress-intensity range for a ASTM A 533 B-1 steel with a yield strength of 470 MPa. R = 0.1; ambient room air; 24°C. Adapted from the work by Campbell, et al.[153] This curve shows the ideal behavior expected in inert environments.

Status of understanding the six SDS factors

I do not attempt to review the situation on each material system since this has been done by other authors in this conference. However, there are certain general patterns that have emerged and characterize the engineering status.

Material factor of SDS. Figure 5 identified the important considerations in the materials factor of SDS. In this section, I consider the effects of purity, heat treatment, crystal structure, strength, and grain-boundary composition. Important general patterns are emerging, except that such general patterns depend greatly on the environmental composition, stressing, and temperature.

First, pure metals sustain SCC transgranularly. While intergranular SCC has also been observed in the same materials, the purity of the grain boundaries cannot be verified, thus the transgranular SCC is more significant.

Transgranular SCC of pure metals has been observed of pure materials in copper.[19,156,157] It has not been observed in other metals only because the proper experimental work has not been conducted. Further, while the rates of SCC in some of the pure metal studies have been lower generally that in some of the alloys, it is quite likely that different environmental definitions would alter this situation.

Second, all materials sustain SCC regardless of heat treatment. There is no such condition as a heat treatment that renders an alloy immune from SCC. Some heat treatments reduce or eliminate the intensity of SCC in some environmental conditions but do not prevent the alloy from sustaining SCC in all environments. Such different environments do not need to be as drastically changed as, for example, from aqueous to liquid metals, rather, slight changes in pH or in electrochemical potential may be sufficient to increase substantially the intensity of SCC for a heat treatment that had previously been considered immune. There are many cases of such patterns but the interaction of sensitization and pH for the SCC of Inconel 600 is a good example.[32,158]

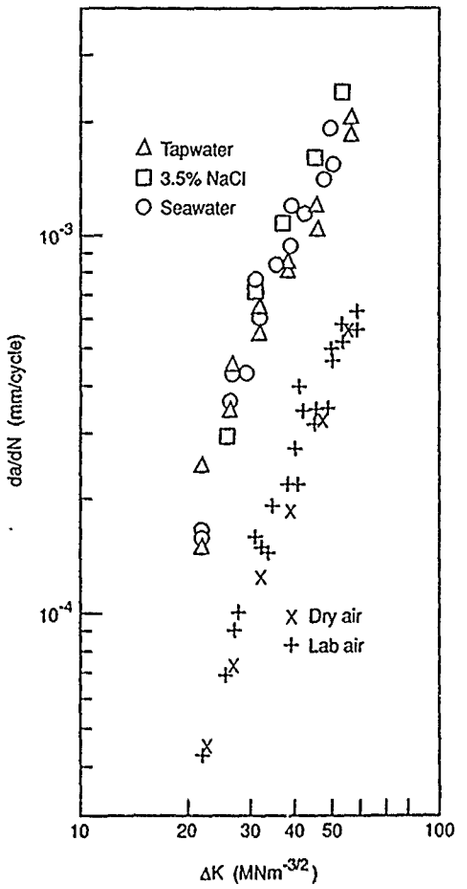


FIGURE 39—Crack growth rate vs stress-intensity range for a Q1N steel in dry air, laboratory air, aerated-recirculating tap water, 3.5% sodium chloride, and natural seawater with a test frequency of 30 cph and R = 0. Adapted from the work of Jones.[154]

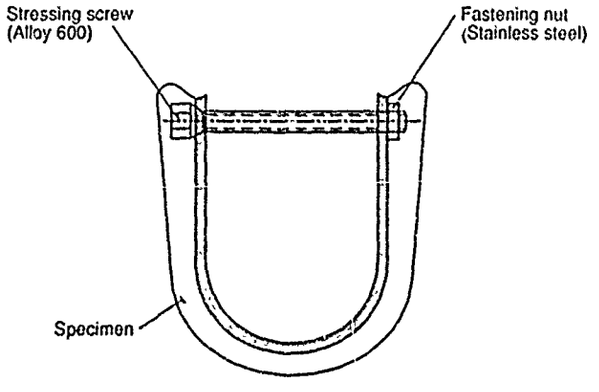


FIGURE 40—Schematic view of reverse U-bend specimen fabricated from tubing. Adapted from the work of Airey.[155]

Third, equilibrium crystal structure, per se, does not seem to be so dominating as chemistry in some alloys. For example, the change from fcc to bcc structures in Fe-Cr-Ni alloys produces no effect on the intensity of SCC as indicated by the work of Bond.[31,130]

Fourth, the distribution of microstructure seems to produce a great difference, as indicated in the work of Wang and shown in Figure 41.[158] Here, he produced the same strength material but by substantially different heat treatments that produced correspondingly different structures.

Fifth, the composition of alloys affects the intensity of SCC quite differently depending upon the environmental chemistry and the electrochemical potentials used. Figure 42 is a schematic composite showing the effect of alloy chemistry as assessed in different environments and at different electrochemical potentials. The patterns of Figure 42 suggest that there is not a composition that does not sustain SCC; the intensity simply depends on the environment as defined by its composition and electrochemical potential. It should be noted here in Figure 42 that these schematic SCC intensities apply only to generally well-known trends under open-circuit conditions. When the potentials are changed or substantial changes in pH are made, this behavior is greatly altered.

Figure 43 shows that the effects of stress on different alloys in different environments can be quite different, indicating that the environment, alloy, and mechanistic unit processes conspire to produce quite different results even in ductile alloys.[159,160]

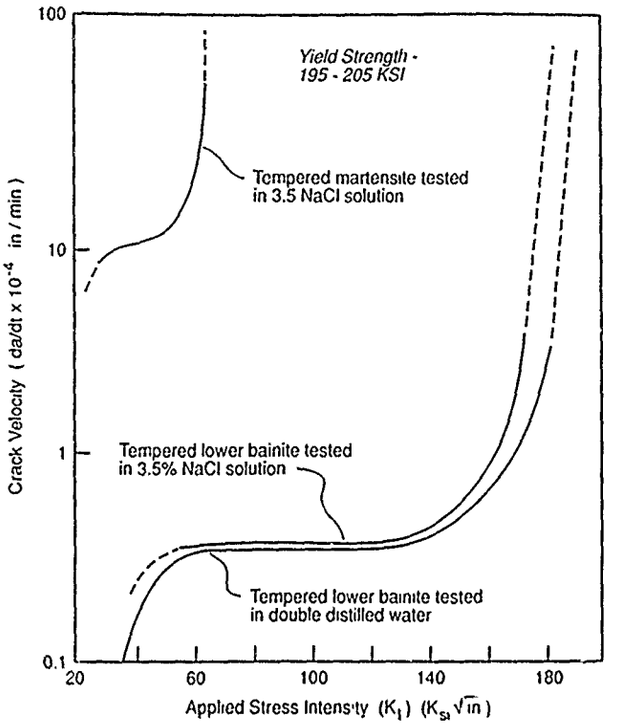


FIGURE 41—Crack velocity vs K for two different heat treatments of a type 4340 (UNS G43400) steel with martensitic and bainitic structures exposed in a 3.5% NaCl solution of pH 6.0 and a double-distilled water solution. Adapted from the work of Wang and Staehle.[158]

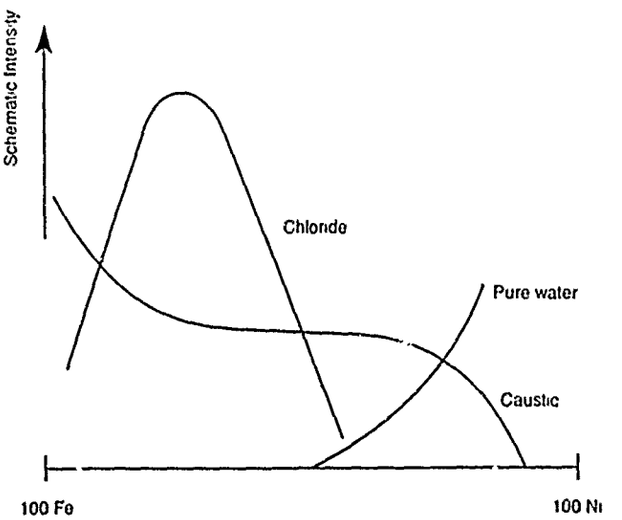
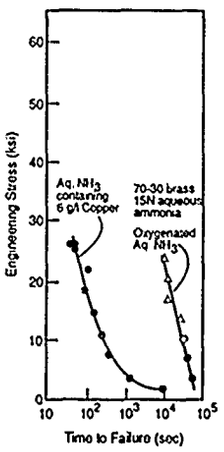
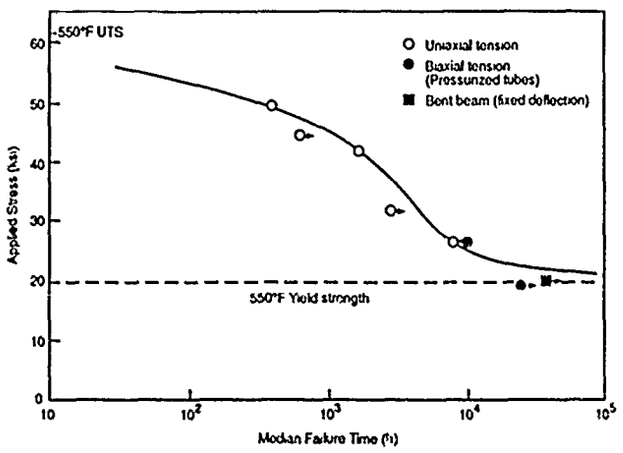


FIGURE 42—Schematic composite showing the effect of Fe-Ni alloys on the intensity of SCC for various environments in their usual open-circuit conditions.

Sixth, effects of alloy strength, in the range above about 100 ksi, seem to dominate both the fracture toughness and SCC of high-strength materials In general, increasing strength increases the intensity of SCC; increasing strength also decreases K_{Ic}. These patterns seem to be ameliorated, but not eliminated, by using more pure materials, often achieved by vacuum melting. This effect of increasing strength increasing the intensity of SCC seems to persist in many alloys despite the basic composition or how the high-strength is achieved; e g , whether the strength is achieved by transformations or by precipitation hardening, and whether, at least in the Fe-Ni system, the material is iron base or nickel base. This general pattern of increasing strength increasing the sensitivity to SCC and decreasing K_{Ic} also follows generally in titanium- and aluminum-base alloys. A further pattern in this class of alloys is that SCC may be sustained in pure water and also at low relative humidities. The effect of strength on fracture toughness is shown in Figure 44(a) and on the SCC velocity in Figure 44(b) from the work of Speidel.[161]



a



b

FIGURE 43—Effect of alloy composition and environment on the relative behavior of specimens with smooth surfaces for 70-30 copper (a) and sensitized stainless steel (b). Adapted from the work of Pugh, et al.,[159] and Clarke and Gordon.[160]

Seventh, when alloy strength is increased by cold working, the intensity of SCC seems also to be generally increased. Such effects are observed in cold-worked bolts of austenitic stainless steel exposed to pure water However, it appears that where cold working is very anisotropic, as with cold-drawn wire, much of the strength is preserved regardless of the environment unless there is extensive pitting, which simply reduces the cross section of the metal. This pattern is analogous to the beneficial effects of the longitudinal structure on the intergranular SCC in high-strength aluminum alloys.

Eighth, the composition of grain boundaries, especially those of the adsorption type indicated in Figure 6(a), has become a particularly important consideration in SCC for the following reasons: (1) The predictability of such compositions is not good; (2) such compositions are so sensitive to cold work and heat treatment; (3) such compositions can change easily with time owing to the short distances involved, (4) the results of competitive action of different species are unclear, and, finally, (5) there are numerous processes by which these compositions facilitate SCC, as shown in Figure 7.

Ninth, with respect to surface condition, such factors as pickling, machining marks, and surface contamination continue to be important to engineering performance For example, the Rentler and Welinski paper of 1970,[162] which looked at pickled surfaces of Inconel 600, showed that pickling greatly increased the intensity of SCC In retrospect, it is not clear whether the resulting effect was due to roughness of the surface, grain-boundary grooving, or the emergence of hydrogen that consequently controlled the potential with respect to the implications of Figure 34(a). While there is little of a quantifiable nature in these considerations of surfaces, the work of Cochran and Staehle[163] shows that different surface finishes produce significant changes in SCC and careful attention to surface preparation in both laboratory experiments and in application of components remains important.

In general, relative to the status in 1955, there is no longer any justification for the concept of "susceptibility" or "alloys or heat treatments susceptible to SCC"; all alloys and heat treatments sustain SCC. However, it is a fortunate circumstance that the intensity of SCC is negligible or minor in some circumstances, so that designs in some materials–environment systems can be expected to perform without failure.

Environment factor of SDS. It is now clear that SCC is a more general phenomenon with respect to environments in which SCC occurs and that the intensity of SCC in a single alloy varies regularly with changes in composition of the environments.

Such considerations as "specific ions" no longer apply. An excellent demonstration of this result is the montage by Congleton, et al.,[164] showing SCC of mild steel as affected by different environments overlaid on the Pourbaix diagram for iron as shown in Figure 45. Here, it is clear that SCC is more related to the location on the diagram than to the ionic species. For example, these results show that SCC is negligible in the range of pH where iron has its least solubility. At least for SCC processes that depend on slip dissolution, such a pattern is quite reasonable. Parkins's correlation shows that the role of any environmental species is more related to the range of pHs and potentials produced by the chemistry of the ion than to its "specificity."

This diagram as developed by Parkins does not define the effect of potentials lower than the hydrogen equilibrium and it would be reasonably expected that a wide range of SCC would occur here by analogy to observations such as those of Totsuka and Smialowska.[25] However, such a correlation is not presently available.

A second pattern that is now clear is that pure aqueous environments without any ionic contamination or intentional ionic content produce SCC whether the potentials are above or below the hydrogen equilibrium. For cases below the hydrogen equilibrium, it might be expected that hydrogen-related SCC would occur in pure water owing simply to the availability of hydrogen from the electrochemical reduction of water. However, SCC occurs in pure water above the hydrogen equilibrium potential in sensitized stainless steels as shown in Figure 36.[150]

A third pattern that is now well established is that hydrogen is not unique as an environmental species in producing SCC in high-strength steels as well as in other alloy systems. At least chlorine, if not other species, can support SCC in high-strength steels.[7] Hydrogen is further not unique in its supporting SCC in zirconium alloy as shown by the extensive work by Cox for SCC in iodine gas.[26,57] It is quite likely that this broadening pattern will continue, possibly along the lines suggested by Galvele.[136]

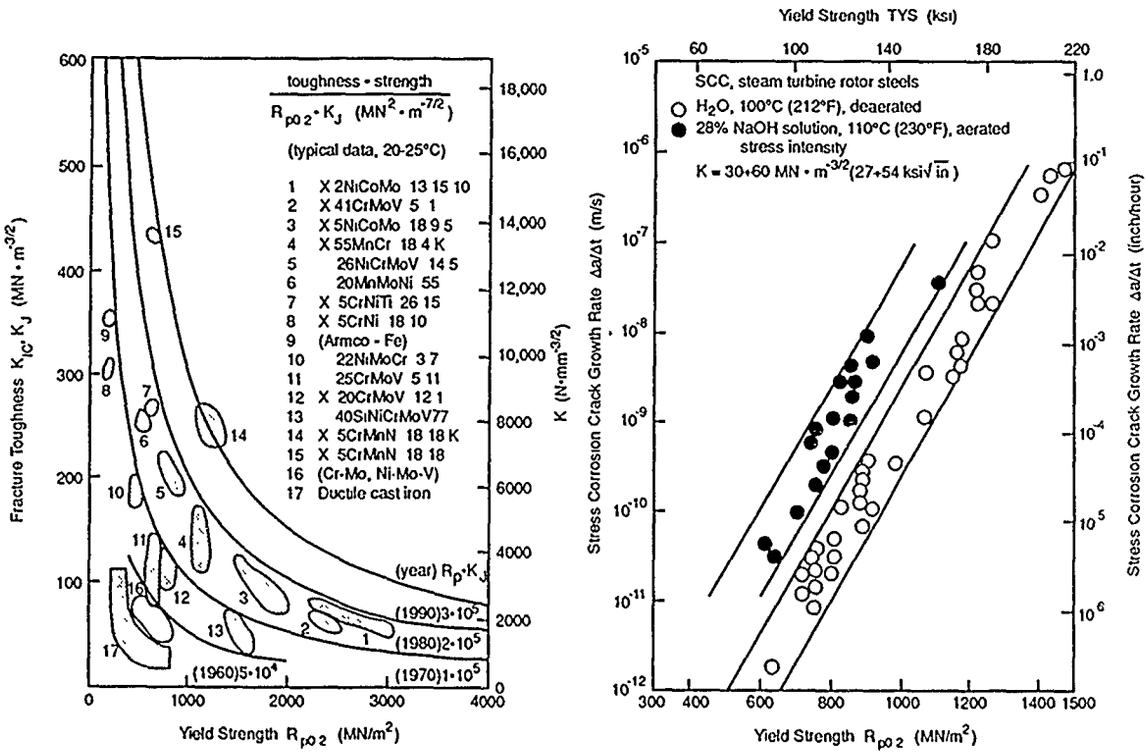


FIGURE 44—Effects of strength of steels on their toughness (a) and SCC velocity (b). Adapted from the work of Speidel.[161]

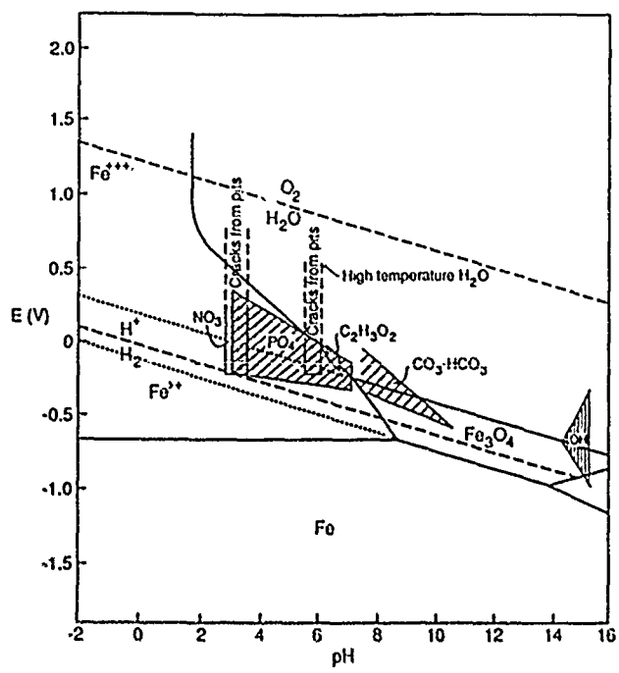


FIGURE 45—Data for SCC of mild steels as a function of pH and potential as affected by environmental chemistry. Ranges of SCC are compared with the Pourbaix diagram for iron determined at 25°C. Adapted from the work of Congleton, et al.[164]

A fourth pattern in environmental effects is the array of liquid types in which SCC occurs. These include at least alcohols, N_2O_4, molten salts, and anhydrous ammonia. There are, no doubt, many others that have yet to be investigated. It must be assumed, and it is quite likely, that SCC of some alloys can occur in a much wider range of liquids than has been tested to date.

A fifth pattern is that relatively low concentrations of gaseous species can support SCC as demonstrated by Kerns for H_2S.[151] In his experiments, he showed that 0.2 torr of H_2S was sufficient to produce SCC velocities of 10^{-3} in./s.

A sixth important pattern has been observed in copper-base alloys where transgranular SCC can be produced by two widely different environments in two different ranges of potential. The older, more traditional environment of ammonia produces SCC at potentials that relate clearly to the formation of copper ammonia complexes. The more recent environmental conditions that support SCC are oxidizing species such as nitrate, nitrite, and hypochlorite as studied first by Pednekar, et al.,[19] and later by others.[165,166]

Seventh, work on nonsensitized Inconel 600 has shown that SCC or IGA is readily produced in aqueous solutions in at least six different zones by what are probably five different mechanistic unit processes. In one zone, SCC in the alkaline oxidizing region occurs above the hydrogen equilibrium and has been reproduced by Nagano,[167] Kishida, et al.,[168] Economy, et al.,[171] and Bandy and van Rooyen.[170] In a second zone, alkaline and slightly above and below the one atmosphere hydrogen line, IGA occurs in the absence of stress according to the work of Bandy and van Rooyen.[170]

In a third zone, mildly alkaline and slightly oxidizing, intergranular and transgranular SCC occur when lead impurities are added according to the work of Copson and Dean.[47] In a fourth zone, SCC occurs below the one atmosphere hydrogen equilibrium line and over a broad range of pH based on work of Coriou, et al.,[205] Economy, et al.,[171] and Totsuka and Smialowska.[25] SCC occurs in a fifth zone that is mildly oxidizing and mildly acidic based on the work of Newman.[172] Finally, a sixth zone is defined by Kishida, et al.,[168] in their work in the mildly acidic but highly oxidizing region.

The occurrence of SCC in both intergranular and transgranular modes in these different ranges of pH and oxidizing potential suggests that the mechanistic unit processes are indeed different and that testing in one of these regimes cannot predict SCC in another. This array of regimes of pH and potential in which there are different mechanistic unit processes is probably the same as that suggested earlier for copper-base alloys.

An eighth pattern is based on the work of Stoloff showing that liquid metal embrittlement does not need to depend on the "environmental" metal being liquid. He has observed "solid metal embrittlement." Here, the vapor pressure of the solid metal adjacent to the metal of interest is sufficient to produce SCC. His work is summarized at this conference. The low vapor pressures at which "metal" SCC occurs is a situation similar to the low H_2S pressures for the SCC of high-strength steel studied by Kerns.[27]

For aqueous environments, it is becoming increasingly clear that the response of SCC under a given set of open-circuit environmental conditions can be reproduced by an equivalent applied electrochemical potential. A good example of this is the comparison of the data from Smialowska in Figure 34(a) with the earlier results of where Blanchet, et al., used galvanic couples.[206] This result is similar to the patterns identified by Congleton, et al., in Figure 45. The same pattern easily rationalizes the effect of noble metal additions in the SCC of Fe-Cr-Ni alloys in boiling $MgCl_2$ where SCC occurs as soon as a critical range of potentials is reached, regardless of the alloy addition. The addition of the noble metals ensures that this range of potentials is reached early with the result that SCC occurs almost instantaneously, as shown in the work by van Rooyen[173] and Royuela.[2] Another indication of the equivalence of open-circuit and applied potentials is the work of Uhlig on critical potentials for SCC in Fe-Cr-Ni alloys.[174] Cowan and Tedmon identified this equivalence in open-circuit and applied potential conditions for stainless steels in polythionic acids for stainless steel but noted that some adjustments were required for Inconel 600.[34]

In general, the patterns implicit in the above suggest that SCC in a single alloy exposed to a variety of environmental conditions within a single type of environment, e.g., aqueous, may incur SCC by many mechanistic unit processes. Second, there is a very broad range of environmental types, compositions, and concentrations that can support SCC. Third, the patterns followed by many of the regimes of SCC can be correlated with well-known and simple processes such as the formation of protective films, the availability of hydrogen, or the pressure of gas.

Figure 8 suggests that there are other environmental factors that influence the environmental circumstances rather than fundamental chemical processes. These circumstances, from an engineering point of view, are equally important because they often conspire to produce the chemistry adjacent to the surface that is necessary to produce SCC. Such considerations are crucial to designers.

The stress factor of SDS. The stress factor of SDS is identified in Figure 9. The effects of stress on SCC follow somewhat more obvious patterns, although there are some new and open issues.

First, stress affects different metals differently when tested as smooth specimens. For example, the effect of stress on copper alloys is compared with stainless steels in Figure 43 The copper sustains SCC at much lower stresses even at room temperature These results suggest quite different mechanistic unit processes

Second, the patterns of velocity vs stress-intensity curves vary greatly among and between alloys and among and between environments for a single alloy. Figure 46 illustrates these variations. Generally, the pattern of three stages shown in Figure 32 seems to persist.

Third, similar patterns for cyclic stressing in environments seem to follow as illustrated in Figure 47 when smooth specimens and fracture mechanics specimens are compared.[175,176] Certain environments decrease the threshold stress for cyclic stressing of smooth specimens; for fracture mechanics testing, certain environments increase the crack growth rate, $\Delta a/\Delta n$ for a given ΔK. The patterns due to the stress for Figures 46 and 47 are, more or less, expected. The effects of metallurgical structure and composition and environmental composition are more differentiated.

Fourth, Wei has demonstrated that, for some environment–metal systems, the fatigue crack growth rate as a function of ΔK and the crack velocity as a function of K can be directly related; i.e., the same mechanistic unit process operates sometimes, but not always, in both cases.[177] While this correlation has been observed to apply in some cases, it does not apply in others. However, in making such comparisons, it is not clear that the correct continuum has been used

Fifth, in addition to this continuum between static loads and cyclic loads defined for some circumstances by Wei, there is another continuum along the coordinate of cyclic frequency Wei has shown that the crack growth rate ($\Delta a/\Delta n$) increases as the cyclic frequency decreases as illustrated in Figure 48.[178] This pattern, from an engineering point of view, suggests that predictive testing in many environments cannot be performed at high cyclic frequencies if life at low cyclic frequencies is desired Such an engineering application might be propellers for ocean-going ships. This pattern does not mean that environments do not affect fatigue at high cyclic frequencies, it just means that there are differences in how the environments influence $\Delta a/\Delta n$ in the different ranges of frequency It is quite clear that environments do reduce the threshold stress for fatigue at high cyclic frequencies, as shown in Figure 39. However, such data do not discriminate between initiation and propagation processes

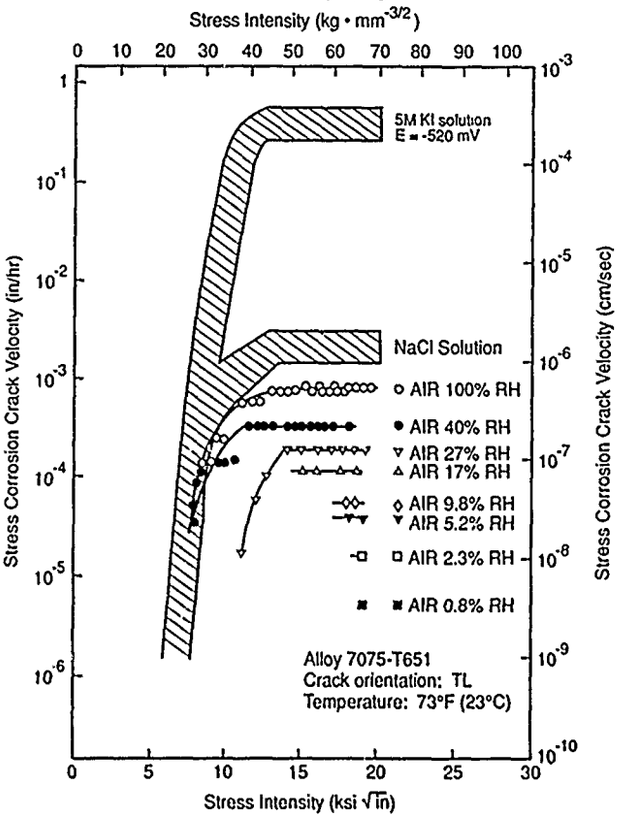


FIGURE 46—Stress corrosion crack velocity vs stress intensity for a high-strength aluminum alloy exposed to varying relative humidity and salt solutions. Adapted from Speidel and Hyatt.[7]

Sixth, since 1955, engineering results have shown that there is little question that constant-strain testing does not provide data that can be readily applied to design. At high temperatures, such specimens relax. Further, engineering structures can always expect slight increases and decreases in stress. Such persistent activity in stressing seems to accelerate SCC. Testing at constant load but superimposing a small load ripple greatly accelerates SCC, as shown in Figure 49.[179]

Seventh, the slow-strain-rate testing method has also alerted designers to the accelerating effects of such loading conditions when they occur in practice. Such a situation occurs in the case of the "denting" phenomenon.[62] The general pattern for the extent of SCC depending on strain rate is illustrated in Figure 50. There seems characteristically to be a strain rate above which little SCC occurs, in the range of 0.01/s. SCC effects seem to be fully developed in the range of 0.00001 to 0.000001/s. This pattern of strain-rate dependence may relate to the effect of decreased cyclic frequency increasing the crack growth rate.

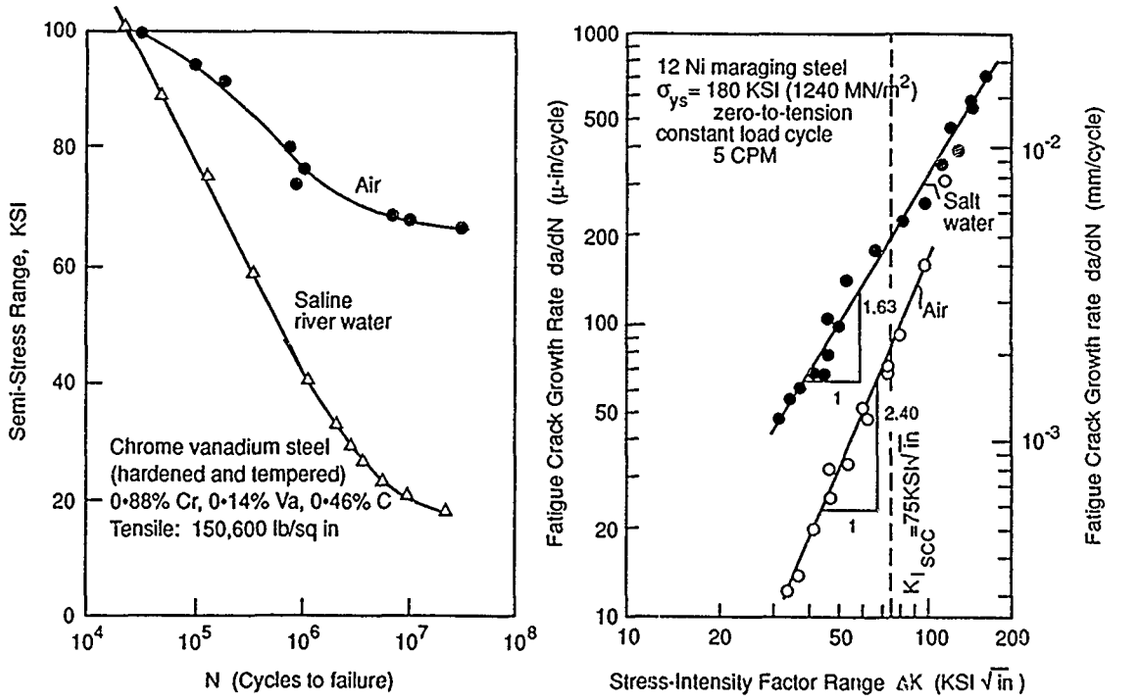


FIGURE 47—Corrosion fatigue results compared for smooth surface and fracture mechanics testing. (a) Stress range cycles to failure for air and saline river water, chromium-vanadium steel. Adapted from the work of Evans[176]. (b) Fatigue crack growth rate vs stress-intensity range for maraging steel exposed to air and saltwater. Adapted from the work of Crooker and Lange.[175]

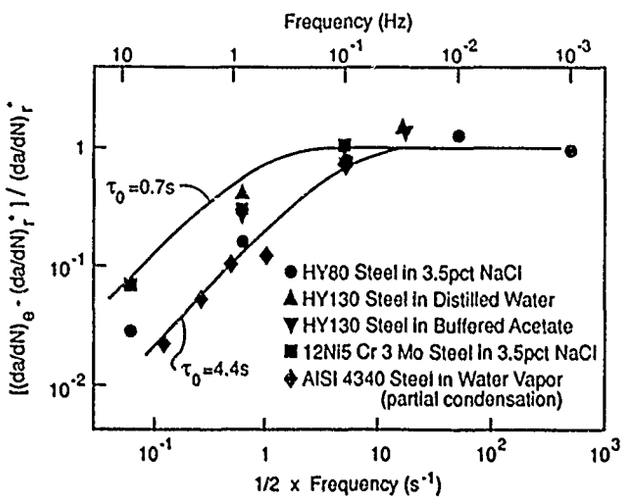


FIGURE 48—Effect of cyclic frequency on crack growth rate at room-temperature in high-strength steels in water vapor and aqueous environments. Adapted from the work of Wei.[178]

Eighth, in considering the role of stress in SCC, it is important to distinguish between applications that have relatively thin cross sections where perforation may occur after SCC proceeds for distances of half to one millimeter, from one with a relatively thick cross section. In the former case, results from smooth-surface specimens are more relevant; in the latter, testing in the fracture mechanics geometries are more relevant. These two circumstances may be integrated in a plot such as shown in Figure 51(a) where stress is plotted vs defect size. Such a diagram is called a "stress–defect" diagram. The relationship of the lines to the type of testing are indicated. This diagram shows that for small defects, the smooth surface tests may be more pertinent, while for larger defects, the fracture mechanics tests may be more pertinent.

Figure 51(a) shows schematically the different effects of SCC and corrosion fatigue on performance of both smooth and precracked specimens. Figure 51(b) shows the stress–defect plot as applied to sensitized stainless steels exposed to high-temperature oxygenated water. This case is a good example of a stress–defect diagram for a tough material. These data are based upon an analysis by Speidel.[181] Figure 51(b) shows a stress–defect diagram applied to a electric generator retaining ring steel, which has very high strength and little toughness and therefore very little capacity to sustain defects in aqueous environments. Figure 51(c) is also based on work of Speidel.

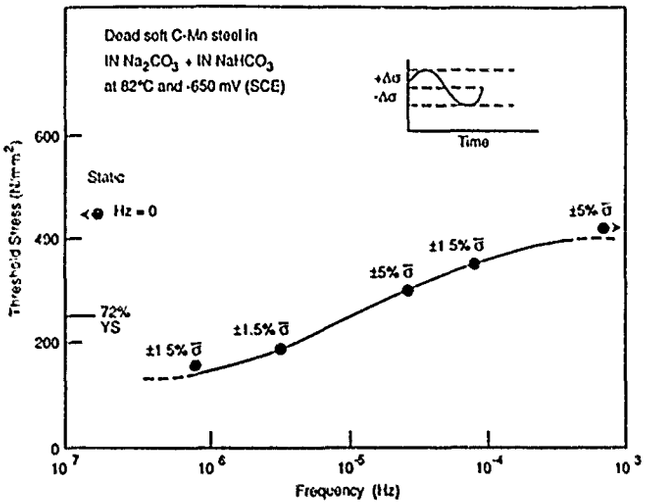


FIGURE 49—Threshold stress for intergranular cracking vs cyclic frequency for a carbon manganese steel exposed to 1 N Na_2CO_3 + 1 N $NaHCO_3$ solution at 82°C and −650 mV_{SCE}. Amplitude of cycle ripple shown at each data point. Adapted from the work of Fessler.[179]

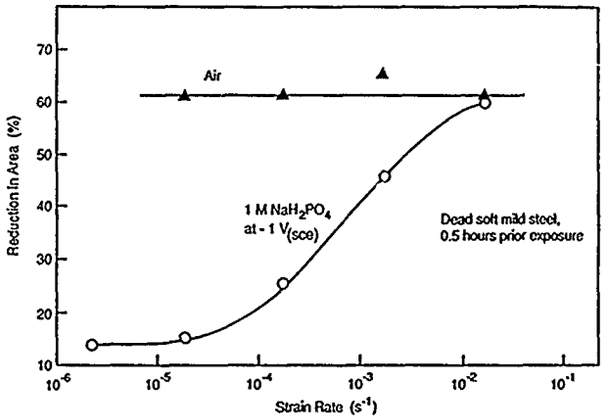


FIGURE 50—Reduction in area vs strain rate for dead soft mild steel in air and 1 M NaH_2PO_4 at −1 V_{SCE} as a function of initial strain rate. From the work of Parkins.[180]

The stress–defect diagrams shown in Figure 51 indicate that such an approach can readily integrate the considerations of smooth and precracked specimens in a single presentation. There are several important *caveats* constructing various lines on these diagrams. One is that the various threshold stresses or threshold stress intensities are assumed to be independent of time. Second, in these diagrams, other dependencies such as effects of environment and electrochemical potential are not shown.

Ninth, in this consideration of the stress factor in SDS, I have not considered effects of the modes other than the opening Mode I. Gerberich has looked at such effects and has concluded that only the opening mode (Mode I) is significant for SCC.[182]

Finally, there is an important unresolved issue at what is considered the interface between SCC and corrosion fatigue where it appears that Wei's approach does not lead to a continuous relationship. It is concluded by some that this indicates a difference between corrosion fatigue and SCC. Such apparent discontinuities suggest to me that the continuum has not been carefully evaluated and other continuum variables of potential, pH, and cyclic frequency should be more carefully considered. Also, the contributions of initiation and propagation need to be separated.

While the above deal with specific effects of stress, regardless of the source, the engineering status of SCC requires that we consider the source of stresses. As defined by Spaehn, et al., approximately 80% of all SCC failures are related to residual stresses.[183] Almost all of the SCC in the nuclear industry today is related to residual stresses,[184] except for that produced by the expansion of corrosion products in denting.[62]

It should also be noted that the stresses produced by corrosion products can (a) be substantial and sufficient to cause surrounding materials to exceed their yield strengths, and (b) often produce continuous, inexorable straining of the kind analogous to the slow-straining SCC test.

The geometry factor of SDS. The factors of geometry as identified in Figure 10 pertain to the following:

One important geometrical factor is that which intensifies the stress as indicated in Figure 51. Such intensifications may occur through the formation of pits from directly chemical effects or erosive effects as with turbine blades. They may also occur with defects in welds or in weld overlays in vessels used for chemical processes. Regardless of the source, whatever produces sharp geometries intensifies the stress and increases the likelihood of initiating SCC. The effects of such intensifications are already considered in the stress-factor discussion. However, this section is more concerned with how such geometries may develop.

The analytical understanding of how such geometries affect the stress intensity is well established.[185-187] The present understanding of how such geometries occur is better understood than in 1955; however, such geometries continue to develop and failures continue to occur. This circumstance needs more appreciation by the design community.

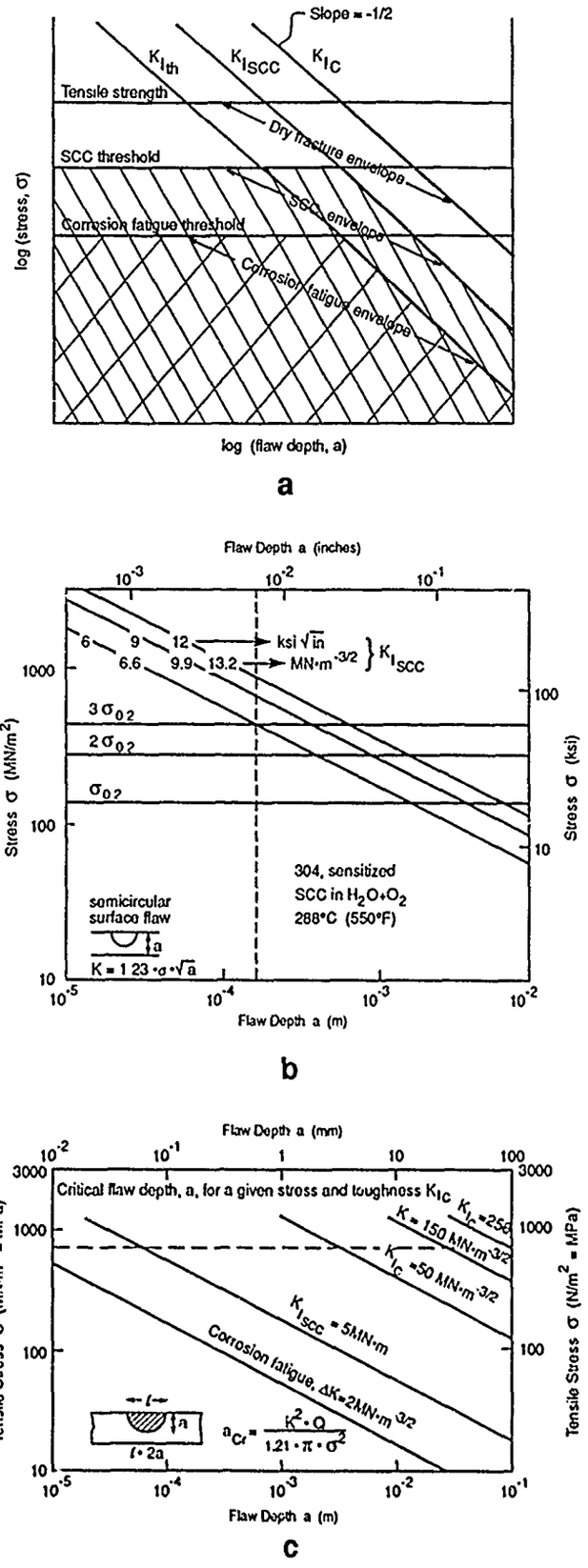


FIGURE 51—Stress–defect diagrams: (a) schematic diagram showing design envelopes for dry fracture, SCC, and corrosion fatigue, as defined by data taken from smooth-surface specimens and fracture mechanics specimens; (b) stress–defect diagram for type 304 (UNS S30400) stainless steel exposed to oxygenated water at 288°C; (c) stress–defect diagram for electric generator retaining ring steel with service stress of 700 MN/m^2. Adapted from the work of Speidel.[181]

A second important geometrical factor is that associated with the formation of crevices Metal surfaces inside crevices realize differences in pH and electrochemical potential depending on the compositions of the metals, composition of the bulk environment, geometry of the crevice and the external flow.[117-120] These differences in pH and potential on the metal surfaces inside the crevice relative to those in the external environment may easily be sufficient to increase the intensity of SCC substantially. Such effects may occur regardless of whether the crevice is formed by a metal-to-metal joint or by a deposit such as sludge in a steam generator.

Severe SCC of Inconel 600 occurred in a crevice at the Duane Arnold nuclear plant (a BWR in Iowa) in 1978.[66] The geometry of the crevice is shown in Figure 52. Penetration of the wall by SCC was extensive in depth and occurred almost all around the circumference. While Inconel 600 resists SCC in noncreviced circumstances unless the stresses are too high, the creviced situation reduces the threshold stress for SCC, as shown schematically in Figure 34. Similar circumstances occur in steam generators of PWRs where there are crevices.[62]

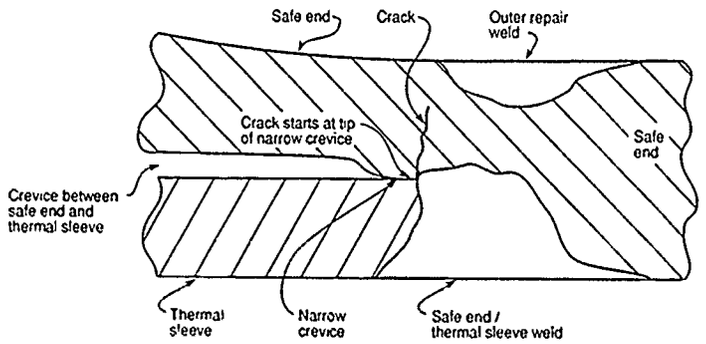


FIGURE 52—Cross section of safe end from Duane Arnold Nuclear Plant showing location of stress corrosion crack at tip of crevice formed between safe end and thermal sleeve. Adapted from the work of Pasupathi, et al.[66]

Galvanic couples lead readily to changes in potential, small changes, as shown in Figure 34(a), may substantially change the intensity of SCC Designers should be alert to any actions of galvanic couples that shift the potential into regions where corrosion modes or rates are changed Such situations may occur, for example, where a tube of relatively noble alloys is connected to tube sheets of less noble compositions such as steel. Blanchet, et al., investigated the SCC velocity of galvanic couples. Their data are discussed in a later section and shown in Figure 60. These data show that decreasing the potential by galvanic connection with increasingly less noble materials accelerates SCC.

Gravitational influences favor the formation of deposits and sludge piles These effects, too, are well known and can be avoided by knowledgeable designers.

The temperature factor of SDS. There is little really new about effects of temperature. Temperature produces well known effects on rate processes The only subtlety here is the difference in effects of temperature on the flow process of the metal as opposed to the effect of temperature on chemical processes such as the reduction of oxygen to water. However, this situation has not changed significantly since 1955.

The time factor of SDS. There is also little new about the effects of time The factors as laid out in Figure 12 still apply. There are two trends of major importance that relate to the time factor. One is the decrease in the endurance limit or K_{Iscc} with time. A second is the change in grain boundary composition with time at elevated temperatures.

The new pattern: intensity, modes, and situation-dependent strength

Figures 2 and 3 suggested schematically that the six factors of SDS, illustrated in Figures 5 and 8 through 12, act together to affect the intensity of SCC Also, it is now clear that the concepts of "susceptibility," "specific ions," and even "synergism" are no longer useful, as they suggest more of magic and chance than of knowable and regular physical processes.

My review of the status of the six factors of SDS in this section also suggests that the industrial occurrence of SCC has expanded substantially beyond the limits known at the 1955 reference.

To develop a framework for portraying regular dependencies of SCC on the independent variables of SDS, I review first some known patterns.

Certain patterns are relatively clear. For example, some crack velocities are proportional to the pressure of a particular gas or to regularly varying metallurgical conditions, this is illustrated from the work of Nelson in Figure 53.[188]

More complex patterns occur in electrolytes like water, and since this is such an important environment and so much work has been conducted in water, I concentrate my discussion on SCC processes in this environment.

Modes of reaction of nonstressed metals in electrolytes have been shown by Hoar[189] to follow a pattern of Figure 54. An array of modes of corrosion for stainless steel in sulfate and chloride solutions has been determined by Mazza and Greene, as shown in Figure 55,[190] where these modes were identified under open-circuit conditions. Murata has examined modes of corrosion also for stainless steel where his experiments were conducted at controlled potentials. For specimens that were stressed he showed a transition from complete passivity to SCC to pitting. He also observed that pitting and SCC occur in different ranges of potential.[191]

Agrawal conducted experiments similar to those of Murata but on stainless steel in alkaline solutions.[192] Figure 56 shows three simultaneous measurements for specimens held at constant potential. First, he shows the simple polarization curve for current as a function of potential. This shows prominent but not large active current densities. Similarly, it shows well-defined passive and transpassive regions, although none of these features in the alkaline environment is as prominent as usually observed in acidic environments. Second, the time-to-failure is plotted for specimens held at various potentials. Since the specimens are wires, they fail easily regardless of the mode of corrosion. However, most prominent is the long (not determined in the time available) failure time in the range of potentials corresponding to passivity. Third, Agrawal identifies the modes of corrosion that occur in the various ranges of potential. Considering that all of the specimens are stressed to the same magnitude, it is most interesting that passivity can be preserved and that the time-to-failure exceeded the duration of the test.

The array of modes of corrosion from the experiments of Agrawal and Murata as well as those of Greene and Mazza suggest that there are regular transitions among the modes of corrosion as a function of either chemical or electrochemical variables. Thus, the open-circuit situation for one environment may produce passivity, while another may produce pitting, SCC, or intergranular corrosion.

The data in Figure 56 show that the modes of corrosion of a given material can be determined regardless of open-circuit potentials. Then, whatever open-circuit potential occurs naturally will place the metal in a region where a given corrosion mode operates. An example of such a situation was illustrated by Agrawal,[193] who investigated the inhibition of SCC by chromate additives in the same alkaline system as shown in Figure 56. He showed that the role of the chromate was to place the potential in the passive region, the range of −650 to −350 mV, where no SCC occurs.

The process of defining modes of corrosion by experiment and then arranging environmental circumstances intentionally, or unintentionally, to be in a given region is illustrated schematically in Figure 57. Here an array of modes is first determined, in this case as a function of potential. This produces a diagram of Figure 57(a). The open-circuit potential may be adjusted intentionally to be in a region of stable passivity; or an open-circuit potential corresponding to an aggressive mode of corrosion may occur unintentionally according to one of several avenues suggested on Figure 57(b). In practice, the various avenues of Figure 57(b) may be achieved in either nominal or non-nominal conditions for example in crevices or under deposits.

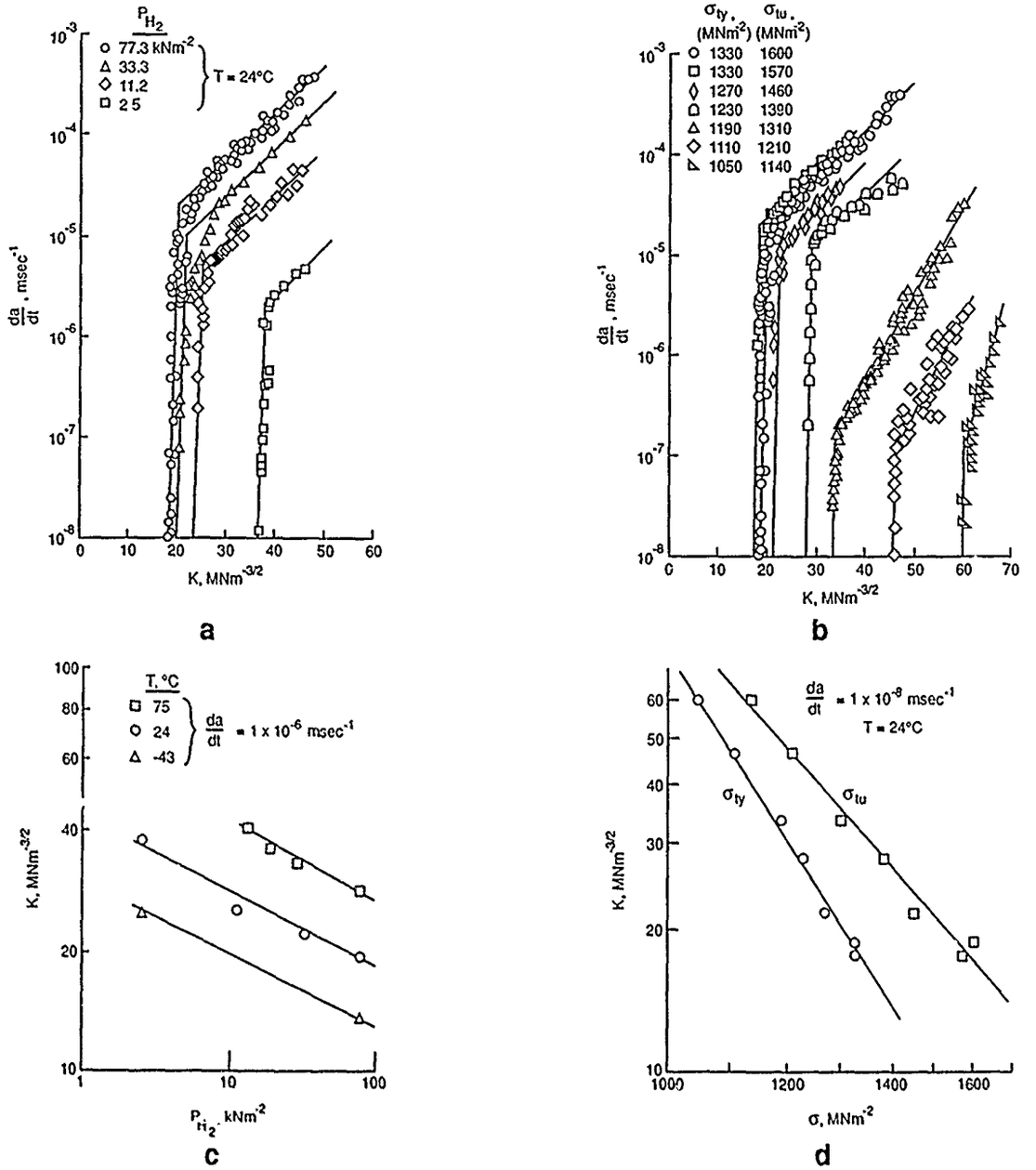


FIGURE 53—Effect of hydrogen gas pressure and strength for a type 4130 steel (UNS G41300): (a) Effect of hydrogen pressure vs stress intensity and temperature, and (b) effect of strength on stress intensity. Summary curves for effect of hydrogen and strength are shown in (c) and (d). Adapted from the work of Nelson.[188]

The pattern of Figure 57 can apply to any metal–environment system. For example, a similar pattern might be developed for the interaction of hydrogen and oxygen gases in the SCC of high-strength steels following the experiments of Johnson.[55]

Another example of the distribution of modes is given in Figure 45 from Congleton, et al. This figure shows that SCC in stressed materials may be avoided by staying out of the ranges of potential where SCC occurs. SCC can also be avoided here by lowering stress, although the magnitude of such lowering is not identified.

To explore this concept of regular patterns more extensively, I examined data for the SCC of Inconel 600 in the nonsensitized condition for the "low-temperature mill-annealed heat treatment" in aqueous solutions in the temperature range of 300°C. First, I collected data from various investigations in different ranges of pH and potential. An extensive study has been conducted by Kishida, et al.,[168] covering the full range of pH but only at potentials above the hydrogen equilibrium, their results are shown in Figure 58. Newman[172] had conducted a study in the mildly acidic and slightly oxidizing region and showed that SCC velocity decreased with increasing pH; his results are shown in Figure 59.

Blanchet, et al., conducted a study of galvanic couples in neutral and alkaline solutions and showed that the intensity of SCC increased with decreasing potentials as inferred from the nature of the galvanic couples, their results are shown in Figure 60.[206] Two other studies have been conducted in the same range of potentials. Totsuka and Smialowska[25] studied the same range of potentials but extended it to more negative values using controlled potentials as shown in Figure 34(a). A similar set of experiments was conducted by Economy, et al.,[171] but they achieved negative potentials by increasing the hydrogen pressure as shown in Figure 61. Unfortunately, he did not measure his open-circuit potentials and I infer his range of potentials.

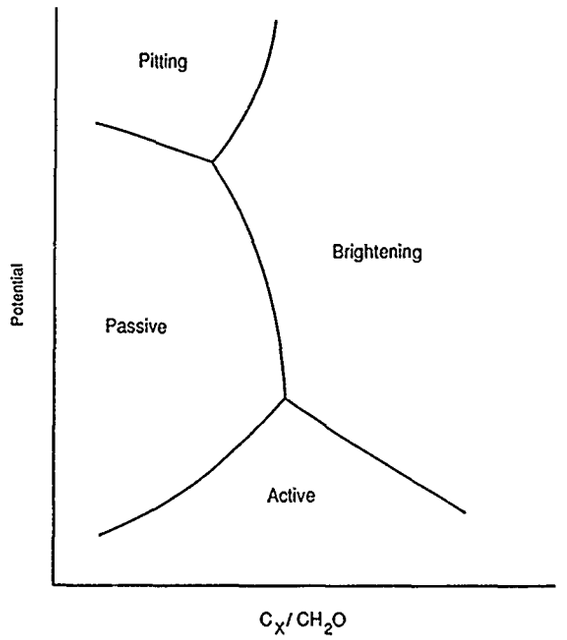


FIGURE 54—Schematic view of modes of surface reaction for metals as a function of electrochemical potential and concentration of ionic species. Adapted from Hoar.[189]

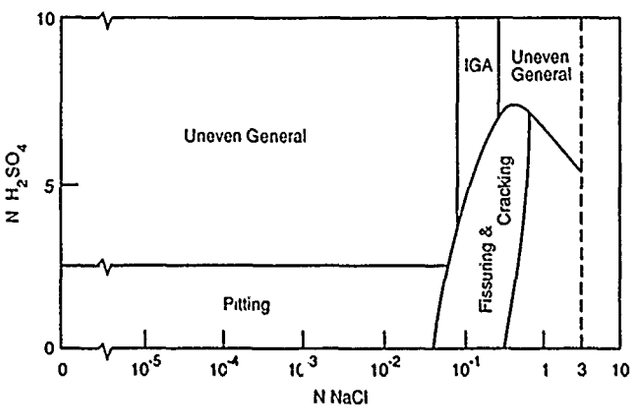


FIGURE 55—Corrosion morphologies observed for U-bend specimens of type 304 (UNS S30400) stainless steel in H_2SO_4-NaCl solutions and no applied potential. Adapted from work by Mazza and Greene.[190]

SCC of Inconel 600 has been studied in the alkaline region by many investigators partly because of direct interest in this region and partly as a presumed accelerating environment for understanding SCC in pure water. For the purpose of this illustrative discussion, I use the work of Nagano, et al.,[167] Pessall, et al.,[169] Kishida,et al.,[168] and Bandy and van Rooyen[170] to describe SCC in the alkaline region. Their data are shown in Figures 62, 63, and 64.

At this point, I construct a diagram that integrates work on SCC from numerous authors and plot their data on the framework of the Pourbaix diagram for nickel determined at 288°C. In making this plot of experimental data that are inherently based on kinetic processes but that are shown in a thermodynamic framework of an equilibrium diagram, I am not implying that the kinetic work is thermodynamically controlled. However, it should be noted that the same variables of pH and potential enter directly into equations that control the rate of chemical reactions. Therefore, plotting kinetic results on a thermodynamic framework is reasonable.

The direct relationship between electrochemical thermodynamics and kinetic measurements is illustrated in Figure 65 where polarization measurements are shown to be bounded by thermodynamic definitions.[194] The relationship between the Pourbaix diagram and the kinetic curves is similar to the well-established relationship in metallurgy between the binary equilibrium diagram and the time–temperature–transformation curves.

Another feature of organizing data for various kinetic mechanisms has been developed by Ashby and Tomkins,[195] as shown in Figure 66. Here, he plots stress vs temperature and identifies the different mechanisms of fracture for pure nickel. This diagram shows that different mechanistic processes can be mapped within a framework of thermodynamic parameters to reveal patterns that are important both for fundamental studies and for design.

I used the conceptual framework implied in Figure 65 for electrochemical kinetics and Figure 66 for mechanisms of fracture to develop analogous diagrams for modes of corrosion and its intensity. In particular, I considered the performance of Inconel 600.

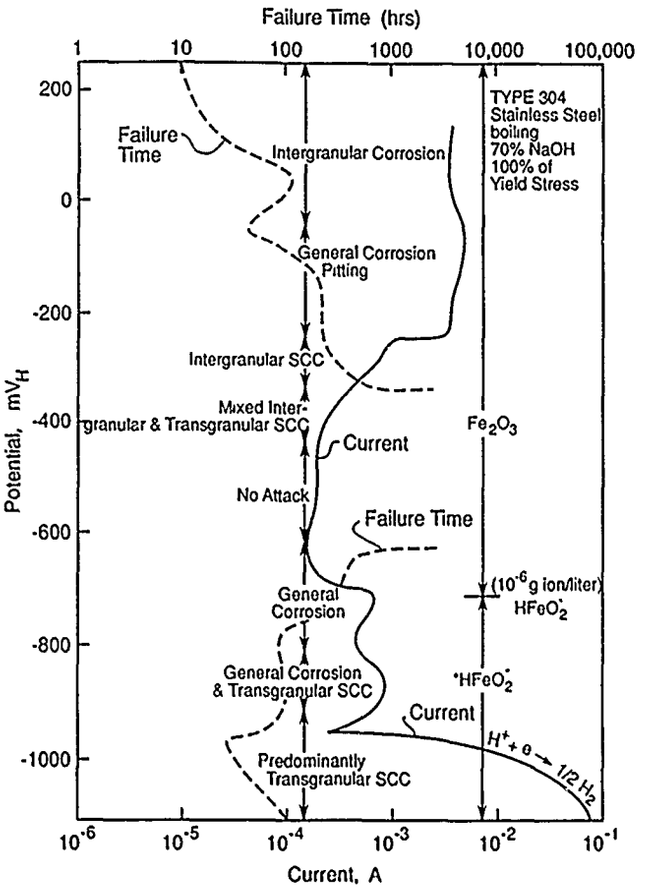


FIGURE 56—Effect of electrochemical potential on polarization current time-to-failure and mode of corrosion for type 304 (UNS S30400) stainless steel stressed at 100% of the yield stress in boiling 70% NaOH. Adapted from the work of Subramanyam, et al.[192]

I collected the data of Figures 34 and 58 through 64 and organized their data in the framework of the Pourbaix diagram for nickel as determined by Chen[196] for 288°C in Figure 67. I have illustrated this process in Figure 68. I also placed the data from the lead-related SCC of Inconel 600 according to my estimates of where it goes, since open-circuit potentials were not given. The placement of these data as shown in Figure 68 leads to a two dimensional plot as illustrated in Figure 69. This two-dimensional plot shows that there are clearly defined regimes of SCC as well as passivity.

Zone 1 - Alkaline, Oxidizing. SCC occurs in the caustic oxidizing range, although intergranular corrosion seems to occur at lower potentials. The Nagano, et al., data[167] does not distinguish intergranular SCC from intergranular corrosion, but the Bandy and van Rooyen[170] and Airey[169] data do.

Zone 2 - Alkaline, Slightly Oxidizing, and Reducing. Here, SCC does not occur but intergranular corrosion does. This intergranular corrosion seems to be focused on the hydrogen equilibrium line with the range of intergranular corrosion equally above and below the hydrogen line.[170]

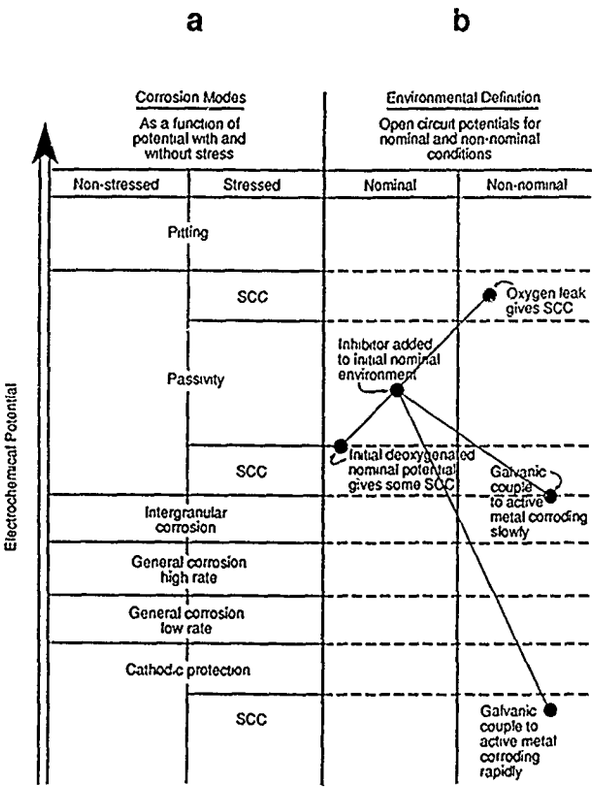


FIGURE 57—Schematic view of relationship between modes of corrosion and environmental definition as a function of increasingly oxidizing electrochemical potential. (a) Corrosion modes as a function of potential with and without stress. (b) Environmental definition as possible open-circuit potentials that might occur in nominal and non-nominal environments. All conditions here are hypothetical.

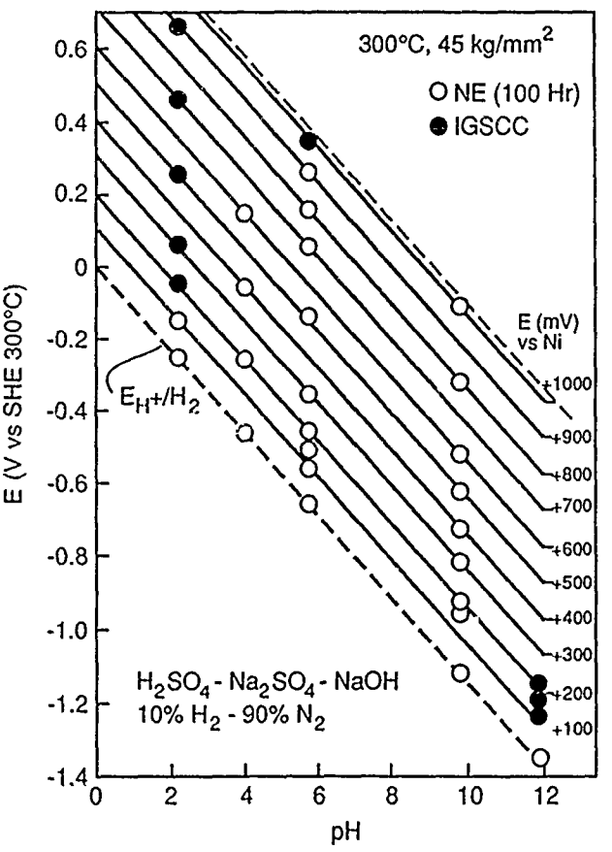


FIGURE 58—Applied potential at 300°C vs pH of Inconel 600 (UNS N06600) (1050°C or 0.5 h air-cooled heat treatment) exposed to aqueous sulfate solutions with a hydrogen/nitrogen overpressure. Specimens tested at 45 kg/mm². Locations of intergranular SCC failure shown in black dots and locations where no failure occurred in 100 h shown in open circles. Adapted from the work of Kishida, et al.[168]

Zone 3—Mild Alkaline, Oxidizing: The SCC that occurs when lead is added to aqueous solutions must occur at about the hydrogen line and in a mildly alkaline pH region. The fact that both intergranular SCC and transgranular SCC occur suggests that the intergranular SCC may be part of the intergranular SCC region from the Nagano, et al., data, and the transgranular SCC occurs in a slightly different, but adjacent, range of pH and potential.

Zone 4—Broad pH, Reducing: This is the range defined by Blanchet, et al.,[206] Totsuka and Smialowska,[25] Economy, et al.,[171] where the intensity of SCC decreases with lowering the potential. Such lowering may be achieved either by galvanic coupling, adding hydrogen, adding hydrazine, or by applying potentials.

Zone 5—Mild Acidic, Oxidizing: This is the region defined by Newman[172] that shows decreasing intensity as the pH increases.

Zone 6—Acidic, Oxidizing: This is the region defined by the Kishida, et al.,[168] data that extends to relatively high potentials. These may be achieved, for example, in nitric acid environments.

Zone 7—Broad pH, Oxidizing: In this range, Inconel 600 seems to exhibit passivity and negligible SCC intensity, although the details of this range need to be further defined.

Zone 8—Very Acid, Oxidizing: In this range, nickel will dissolve and would be of no use from a structural point of view.

Figure 69 is a useful chart from both an engineering and scientific point of view. First, it shows that the various data from the literature may be aggregated and, as such, can be combined to produce coherent patterns. Further, the data from many different investigations seem to be reasonably complementary and reproducible despite the many different types of experiments that were conducted.

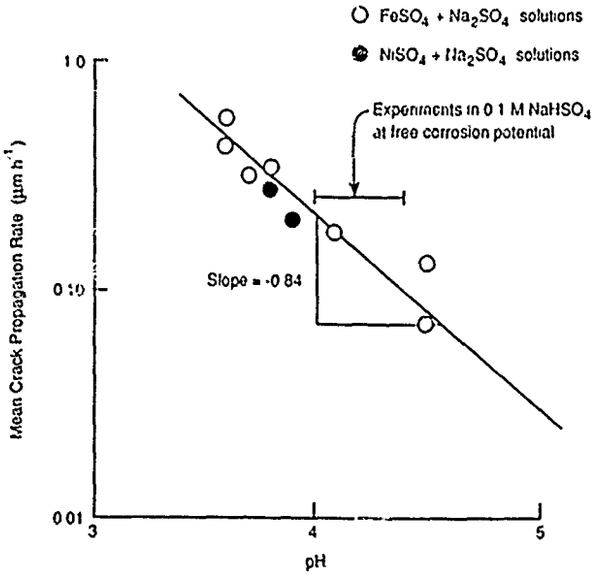


FIGURE 59—Mean crack propagation rate vs pH for Inconel 600 (UNS N06600) at 305°C in sulfate solutions. Adapted from the work of Newman.[172]

		Number of samples cracked after 12,000 Hours (examined by optical microscopy)	
		Water	LiOH at pH = 10.5
Inconel 600	Uncoupled	0/9	0/9
Inconel 600	Coupled to gold	0/9	0/9
Inconel 600	Coupled to platinum	0/9	0/9
Inconel 600	Coupled to 18/10 stainless steel	1/10	0/9
Inconel 600	Coupled to mild steel	4/10	2/10

FIGURE 60—Frequency of SCC for Inconel 600 (UNS N06600) in galvanic couples of various compositions exposed to neutral and alkaline pH environments. Adapted from the work of Blanchet, et al.[206]

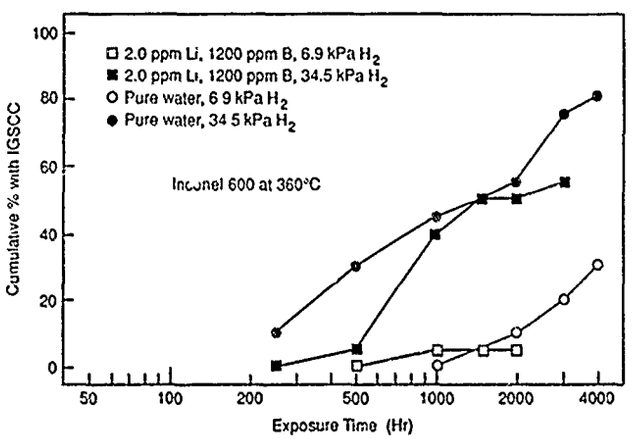


FIGURE 61—Cumulative percent failure specimens with intergranular SCC vs exposure time for Inconel 600 (UNS N06600) at 360°C as affected by hydrogen overpressure and lithium and boron additions. Adapted from the work of Economy, et al.[171]

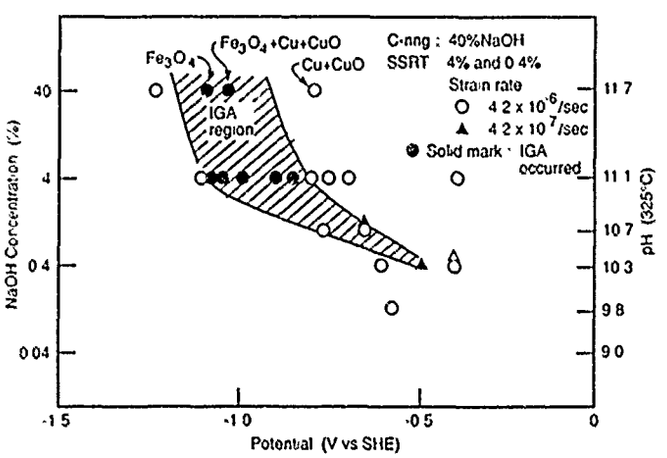


FIGURE 62—NaOH vs electrochemical potential showing region where intergranular attack occurs for Inconel 600 (UNS N06600) in alkaline solutions at 325°C. Adapted from the work of Nagano, et al.[167]

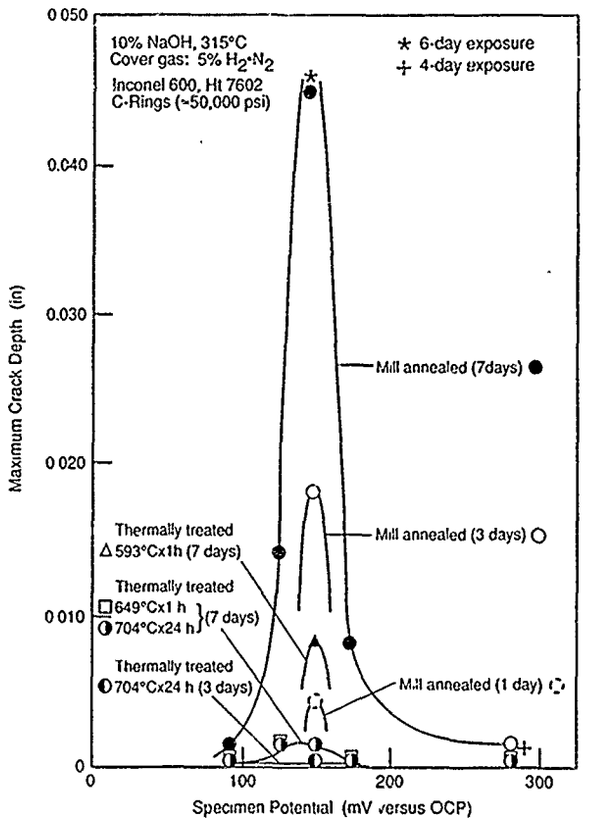


FIGURE 63—Stress corrosion crack depth vs applied potential for Inconel 600 (UNS N06600) exposed to 10% sodium hydroxide solutions at 315°C for different heat treatments. Adapted from the work of Pessall, et al.[169]

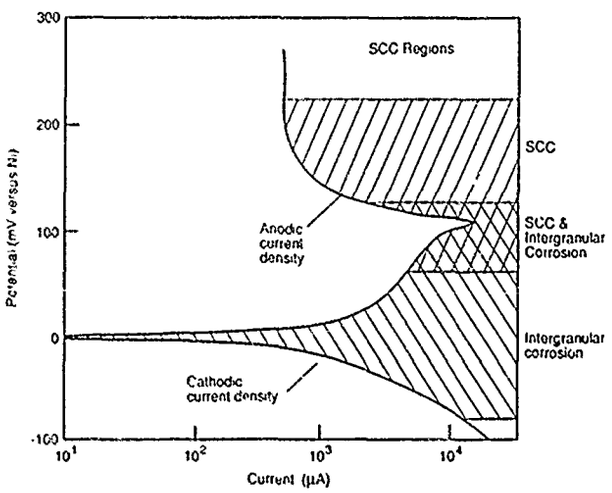


FIGURE 64—Effect of applied potential on the polarization current and mode of corrosion for Inconel 600 (UNS N06600) exposed in 10% NaOH + 1% Na_2CO_3 at 300°C. Adapted from the work of Bandy and van Rooyen.[170]

Second, Figure 69 shows that there are five distinguishable zones where SCC occurs. Although little serious mechanistic work has been conducted in any of these zones, it appears that the mechanistic unit processes for each of the zones is different. Certainly, the "Broad pH, Reducing" range in Zone 4 follows a mechanistic pattern different from the others, and the transgranular SCC of Zone 3 differs from the others. As a minimum, the patterns of Figure 69 show that presuming that the mechanistic unit processes of intergranular SCC of Zones 1 and 4 are the same is incorrect.

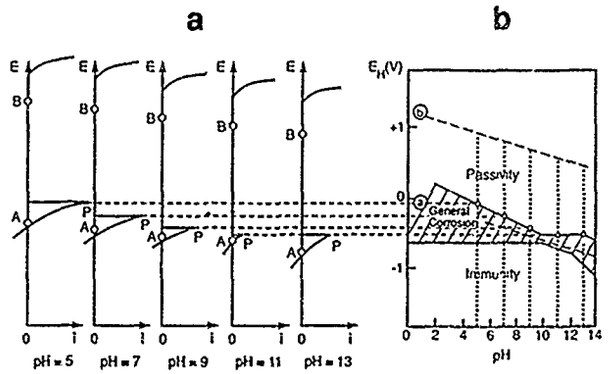


FIGURE 65—Correlation between a potential–pH diagram and electrochemical kinetics for iron at room temperature. Adapted from the work of Pourbaix.[194]

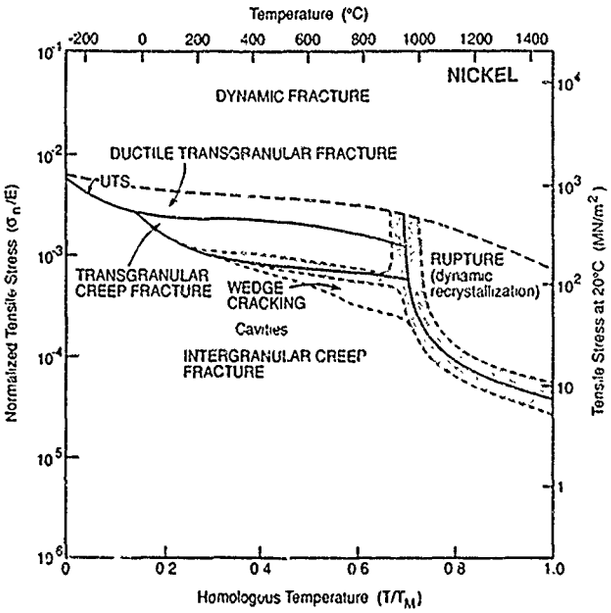


FIGURE 66—Diagram for fracture mechanisms of pure nickel as a function of temperature and stress. Adapted from the work of Ashby and Tomkins.[195]

Third, while SCC that occurs in five zones (1, 3, 4, 5, 6) can be avoided by reducing or eliminating stress, Figure 69 shows that in Zone 2 intergranular corrosion will still occur in the absence of stress.

However, Figure 69 does not show any indication of the intensity of SCC At one extreme, SCC will not occur if there is no stress, so that the occurrence of SCC in the various zones is meaningless and only those modes of corrosion that occur in the absence of stress are pertinent In this zero stress situation, the intergranular corrosion in Zone 2 is pertinent, as is the general dissolution in Zone 8 I suspect that there is also a region of intergranular corrosion in the mildly acidic region, but I have no information However, when there are stresses, SCC will occur depending on the magnitude of these stresses and on the intensity of SCC in the different zones

To establish a pattern for intensity of SCC as affected by the environmental variables of pH and potential, I developed a three-dimensional diagram shown in Figure 70 The potential–pH base of this diagram is the same as Figure 69. However, the vertical coordinate is an indicator of the intensity of SCC. To make this diagram useful for designers, I used effectively the "inverse intensity" and developed an ordinate called "useful strength", "useful strength" is that available to a designer after the environment takes its toll through SCC, intergranular corrosion, or general corrosion. Thus, in Zone 7 the useful strength is 100% of the strength determined in inert environments. I have taken the "useful strength" as the "flow stress," or the average of the yield and tensile strength. In Figure 71, I illustrate the meaning of "useful strength" and its relationship to the SCC intensity.

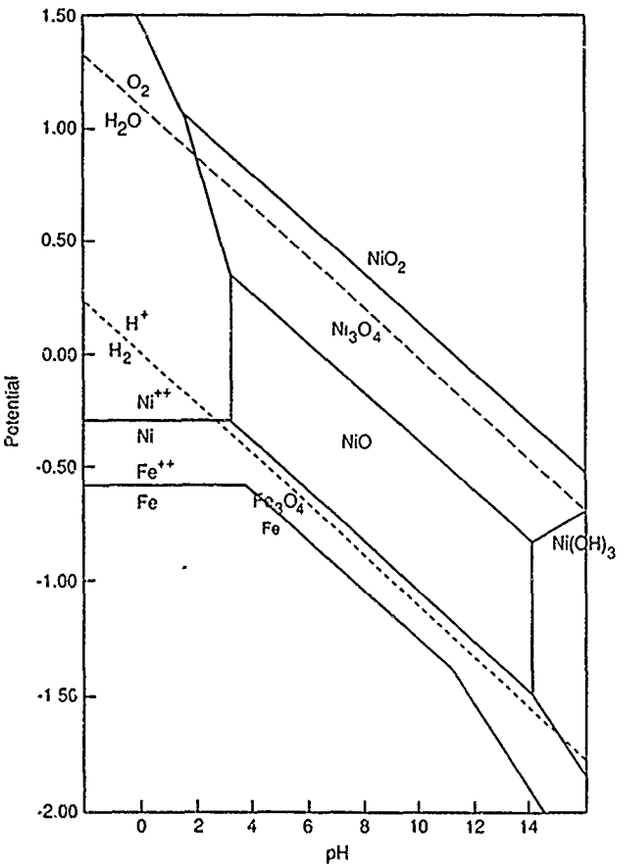


FIGURE 67—Pourbaix diagram for nickel at 288°C with some corresponding equilibria for iron. Adapted from the work of Chen.[196]

The approach I use in Figure 70 is most pertinent to thin wall tubes and may be less useful for thicker sections, since the most pertinent part of SCC for thin wall geometries is really initiation, which is essentially defined by an endurance limit approach to testing and plotting. As I continue to consider this matter of "intensity" of SCC, it is quite likely that a more useful and broadly based parameter can be developed.

To give Figure 70 reference, I have made the one atmosphere hydrogen line into a plane. I show the intersections of this plane with the topology of the useful strength as solid dots.

Figure 70 is then a three-dimensional plot of the data from Figure 69 but with the intensity (inverse intensity) indicated in the third dimension. To obtain the values of intensity for Figure 70, I used considerable license. The stress effects in each of the experiments used to make up Figure 70 were determined by the respective investigators differently. Further evaluation of the data as well as using data from many other investigators will improve the veracity of the contours. However, I suspect that the patterns as already shown are, at worst, good and semiqualitative.

Figure 70 shows that the various modes of SCC for Inconel 600 at about 300°C in the low-temperature mill-annealed heat treatment can be described by a three-dimensional plot where the various modes of SCC as well as other modes of corrosion can be characterized by smoothly varying contours. This surface could be called the "topology of SCC" or the "topology of corrosion," depending on what modes of corrosion are included.

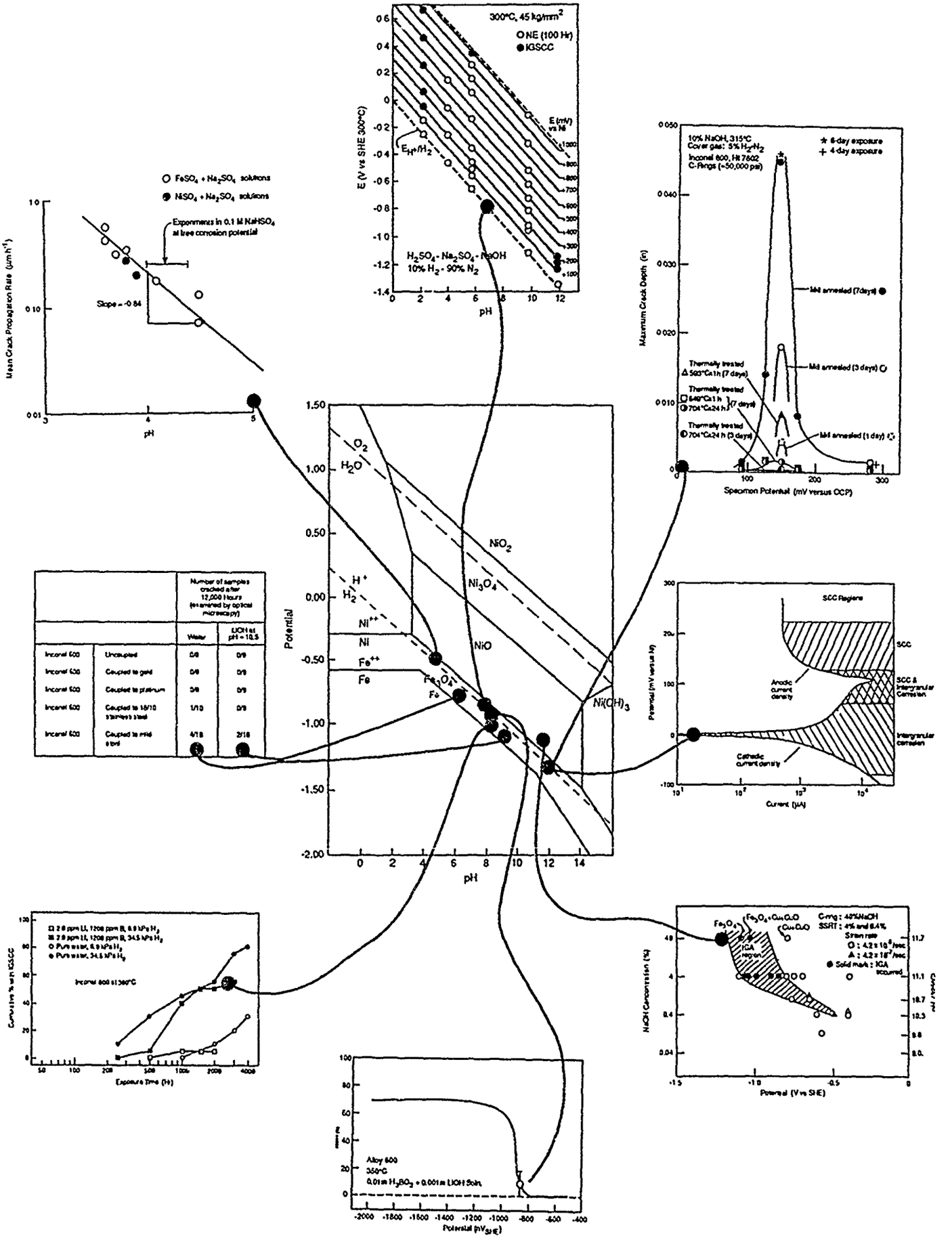


FIGURE 68—Montage showing location of experimental results of SCC studies for Inconel 600 (UNS N06600) with respect to pH and potential on Pourbaix diagram of nickel and iron at 288°C.

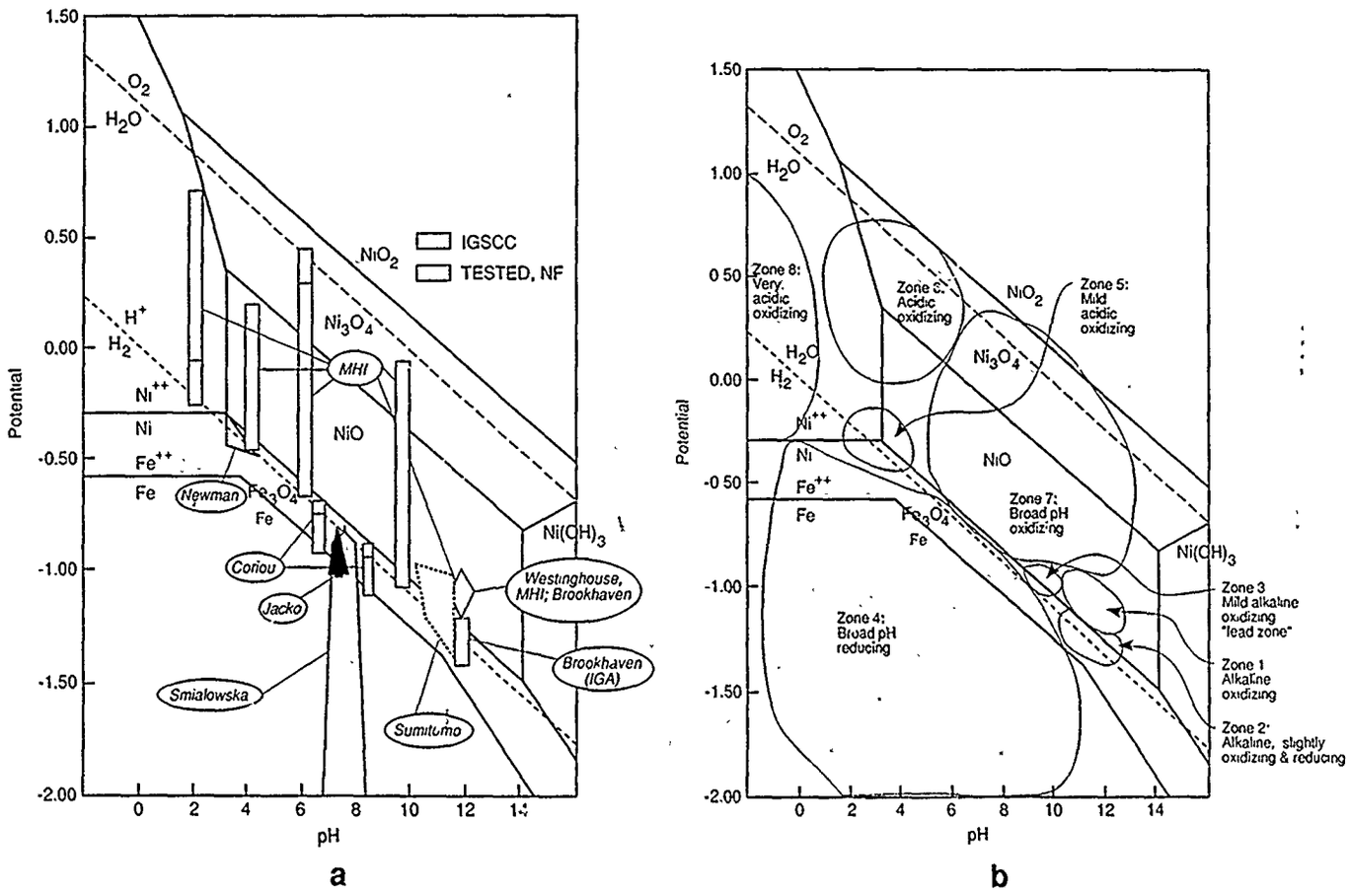


FIGURE 69—Results of plotting data from SCC investigations for Inconel 600 (UNS N06600) on Pourbaix diagram for nickel. (a) Schematic view showing location of data. (b) Suggested locations of zones for different modes of corrosion.

The topology plot in Figure 70 now presents to both the scientific investigator and to the designer important and useful information. To the investigator of mechanistic unit processes Figure 70 defines contours in stress-pH-potential space that must be rationalized. To the designer, Figure 70 shows what regions are to be avoided or what actions, i.e., lowering the stress, must be accomplished for reliable performance to be achieved.

The topology of Figure 70 is one approach to the schematic view of Figure 69(b), which suggested that the intensity of SCC should be a smoothly varying function of key independent variables.

While Figure 70 provides an interesting three-dimensional visual overview of the topology of various corrosion modes, certain important features are hidden. It is possible, using the appropriate software, to view Figure 70 from other perspectives. Figure 72 shows the result of viewing Figure 70 from different directions. Figure 73 shows the result of taking two-dimensional slices through the three-dimensional diagram. With such slices it is possible to obtain a detailed view of critical dependencies such as the effect of potential on the useful strength at selected pHs.

Figure 70 does not include such important independent variables as heat treatment, temperature, cyclic stressing, and other environmental species not accounted for by the normalizing effects of pH and potential. However, such variables can be incorporated as this approach becomes more sophisticated, possibly by using an expert system or by using contour plots in place of three dimensional ones where successive plots of other variables can be shown.

While the topology of intensity for the corrosion of Inconel 600 is defined in Figure 70, this figure does not define where the surface of the metal is with respect to environmental variables, i.e., Figure 70 says that "if the pH and potential are located at a given point, then the intensity of SCC is defined." However, it does not define what pH and potential can be expected.

To complete this discussion of corrosion mode diagrams, it is necessary to demonstrate how the environment is defined in the same framework as the mode-intensity diagram

Since Inconel 600 is widely used as a tubing material for steam generators in nuclear power reactors, the environments of such systems furnish a useful framework for discussion Starting again from the Pourbaix diagrams for the 300°C region developed by Chen,[196] Figure 67 shows key features of the nickel diagram with some important lines from the iron diagram. These are shown because Inconel 600 is often adjacent and electrically connected to mild steel, the minimum galvanic potential of an iron-nickel couple is defined by the iron equilibria. Figure 74 starts with Figure 67 and shows the effects of different nominal and non-nominal environments. Various environmental circumstances that can occur in these steam generator environments are depicted on Figure 74 as follows:

Environment 1a,b—deoxygenated with hydrogen: In completely deaerated solutions, the electrochemical potential lies on the hydrogen equilibrium line as modified by the hydrogen pressure at the metal surface according to the Equation (3):

$$E = E_o - k_1(pH) - k_2 \log P_{H_2} \qquad (3)$$

Where, E_o, k_1, and k_2 are temperature-dependent constants

The precise location on this line depends on the pH additives of lithium or ammonia depending on whether the focus is on the primary or secondary side of the Inconel 600 tube

Environment 2—oxygen added: If oxygen is added to the environment, the potential will increase according to the pattern of Figure 36 and may increase 500 to 600 mV above the hydrogen equilibrium potential in the range of 0 1 to 10 ppm of dissolved oxygen.

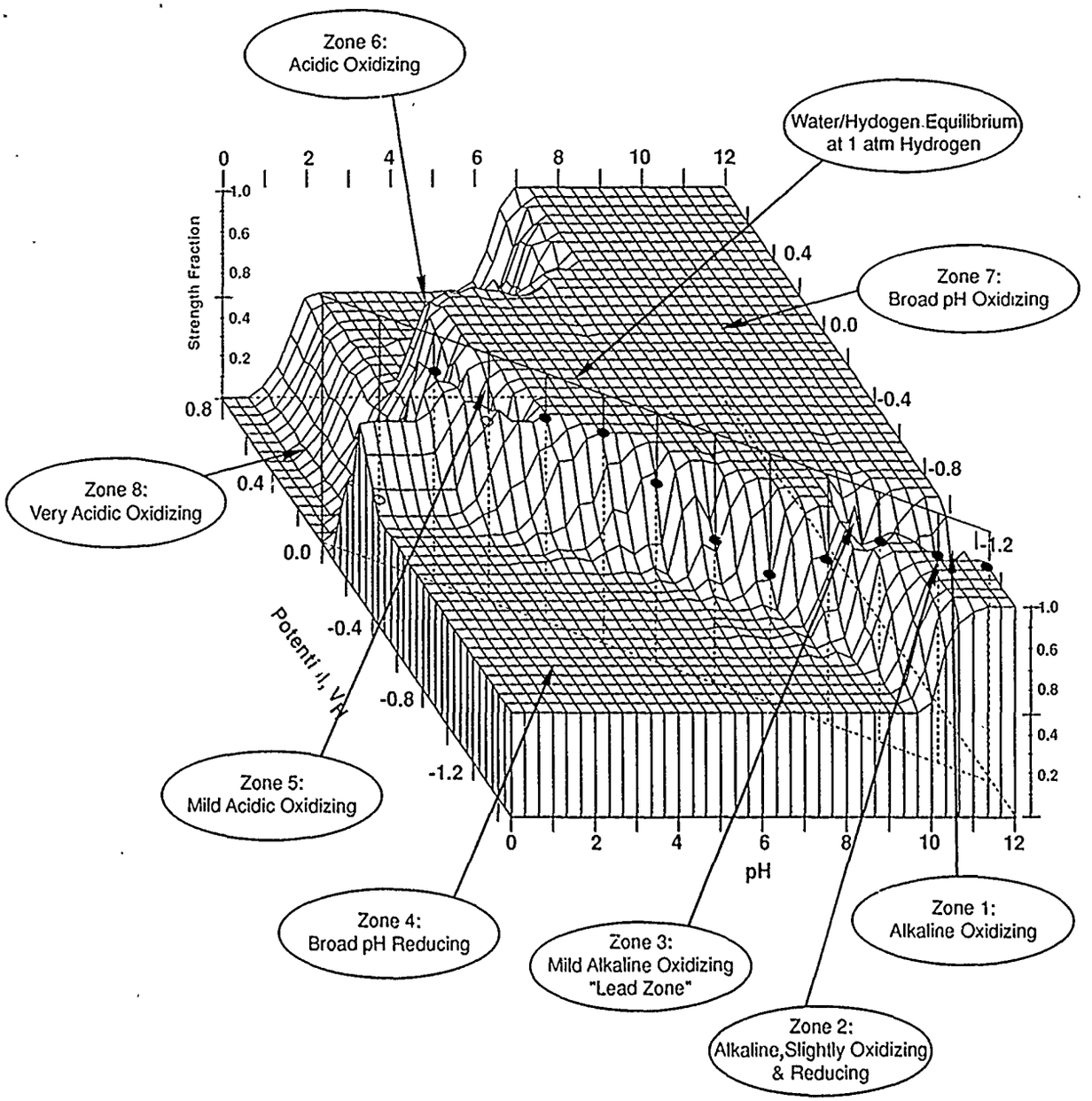


FIGURE 70—Three-dimensional diagram for intensity of SCC and other modes of corrosion for Inconel 600 (UNS N06600) in the range of 300°C for low-temperature mill-annealed Inconel 600. Useful strength plotted vs environmental parameters of electrochemical potential and pH. One atmosphere hydrogen equilibrium line shown as a vertical plane and indications shown where hydrogen plane intersects surface topology. Zones for various corrosion modes designated.

Environments 3a,b; 4a,b—alkaline and acidic crevices with and without oxygen: If species are concentrated in crevices or in sludge, the pH at the metal surface will depend on whether these species are acid or alkaline forming. If such environments develop in deaerated conditions, the potential is defined by the hydrogen line. If oxygen is present above about 0.01 ppm, the potential in these regions will increase according to the general pattern of Figure 36. Since some hydrogen will be generated locally, the potential may drop in these regions according to the prediction of Equation (3).

Environment 5—galvanic connection to steel. If Inconel 600 is galvanically connected to mild steel, the potential of the couple will approach that of the iron electrode. This approach will be closer as the corrosion rate of the steel increases, with the result that the potential on the Inconel surface will decrease.

Environment 6—hydrogen added. If hydrazine is added to the water, the potential on the surfaces will be decreased, although this is complicated, since hydrazine decomposes at 300°C and the potential on the surface also depends on the concentration of hydrazine and pH of the environment in ways that are not defined

Using Figure 74, the electrochemical conditions on the surface of the Inconel 600 tubes can be estimated even in the absence of direct measurements. These results can be compared with the intensity–mode diagram of Figure 70 to determine what modes of corrosion can be expected on smooth and creviced surfaces

The topology of corrosion modes defined by Figure 70 epitomizes what is meant by situation-dependent strength This figure shows that the strength that may be used by a designer depends on the environmental situation.

This approach, epitomized by comparing the mode–intensity diagram of Figure 70 with the environmental definition diagram of Figure 74, identifies what is now possible in engineering with SCC from a point of view that integrates considerations of material,

environment, stress, design, and temperature. This capacity now exists and should form the basis for future developments in applying SCC and its broad dependencies to engineering design.

Not every alloy–environment system nor every application will find the specific approaches in Figures 70 and 74 applicable. However, analogous mode–intensity and environmental definition diagrams can be developed.

In the future, such ideas of susceptibility, specific ions, and synergy will cease to have meaning in favor of the orderly description of SCC described in this section.

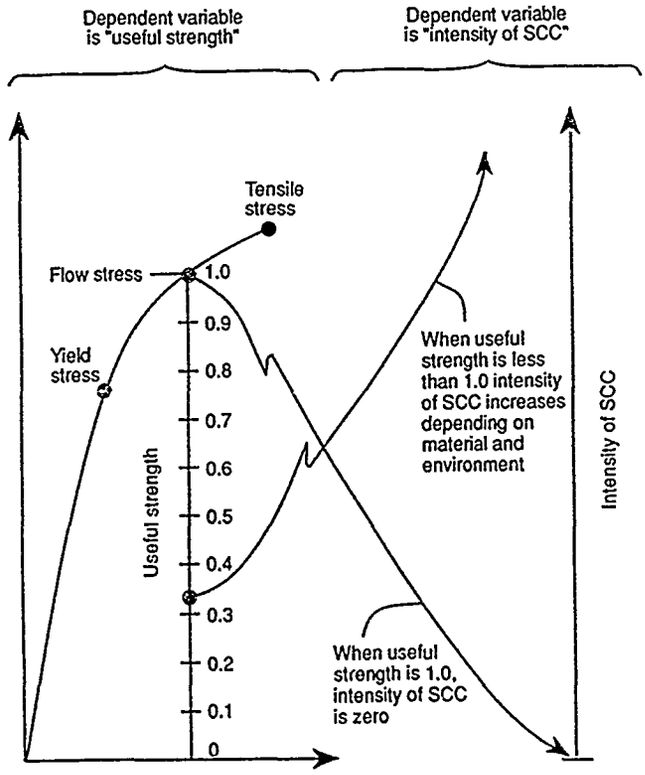


FIGURE 71—Schematic view showing useful strength related to stress–strain diagram and intensity of SCC.

Statistical description of SCC

The mode–intensity diagram of Figure 70 is one view of SCC that provides an overview of the averaged intensity of SCC at each environmental point. In reality, SCC data, like all data describing properties of materials, can only be described by a distribution function that gives frequency of occurrence vs an independent variable of stress, time, or other similar quantity. It is well known that the simple tensile properties of yield strength, tensile strength, elongation, and similar material properties are statistically distributed about some mean or characteristic value, and further that such descriptions have inherent scatter described by a parameter that is a characteristic of the scatter.

Generally, SCC data have not been taken from a statistical point of view. Consequently, the data for intensity or "inverse intensity," as shown in Figure 71, are only the best guess of the investigator. Such data as used for Figure 70 are not even proper mean values as well as not being described by a distribution function in the original published papers. Note that a least squares fit also does not provide any useful statistical information except to give some assurance that the line drawn through the data is the best available line.

When data such as that from SCC or similar testing is characterized statistically, several distribution functions are available as described in several texts.[157-161] The most frequently considered distributions are the normal, log normal, Weibull, extreme value, and Gumbull. The Weibull function has been widely used because of its flexibility in dealing with distributions of widely different shapes. The normal distribution is somewhat restrictive, since it implies symmetrical distribution about the mean, and log normal is similarly restrictive, although it has been useful in describing results from testing mechanical properties.

Generally, statistical data are presented in two formats. In the first, the frequency of occurrence is plotted vs an independent variable, i.e., the frequency of the yield stress measured in a given interval is plotted vs yield stress. This plot is illustrated in Figure 75(a). The Weibull distribution function is used as an example to illustrate these different functions. A second form of this plot is the "cumulative distribution function," which is the integral of the frequency plot. The cumulative function gives the fraction of all events that have occurred at a particular value of the independent variable. The cumulative distribution function is shown in Figures 75(b) and (c).

An early attempt to define SCC data from a statistical point of view was used by Cochran and Staehle[163] in which they differentiated among the effects of surface preparations for type 310 (UNS S31000) stainless steel stressed and exposed to boiling $MgCl_2$.

Recently, Shimada and Nagai have described the SCC of zirconium alloys used for nuclear fuel tubes exposed to gaseous iodine.[202] They took data at various stresses and plotted their data as cumulative distribution functions. An example of their data is shown in Figure 76(a) for a single stress. They also determined the effect of stress on the adjustable parameters of the Weibull function; these data are shown in Figure 76(b). The equations associated with the plots are also shown in Figure 76.

The data in Figure 76(b) show that the adjustable constants follow generally expected patterns in their dependence on applied stress; i.e., the characteristic value of Θ decreases with increasing stress much as its analog, the mean value, would in Gaussian statistics; the initiation time (t_o) decreases with increasing stress, also an expected result; and the slope (b) increases with increasing stress, indicating that the range of data is progressively narrower, which is also expected.

The data of Shimada and Nagai show both that their SCC data can be described accurately by a cumulative distribution function and that the adjustable parameters follow qualitatively expected patterns. This latter result suggests that these adjustable constants could be linked to the factors of SDS as described in Figures 5 and 8 through 12. Once this is accomplished, the distribution function can be applied over a wide range and interpolations and extrapolations would be greatly facilitated. In fact, it is reasonable that the distribution functions could be interconnected with the topology of the mode–intensity diagrams.

Shibata has also started significant work to consider the statistical properties of SCC and of pitting.[203,204] An example of his data is shown in Figure 77.

I have taken data from a paper by Blanchet, et al.,[206] in which the cumulative failures of Inconel 750 were determined in 350 C water, and plotted his data using the two-parameter [using the characteristic value (Θ) and the slope (b)] Weibull statistics to obtain Figure 78(a). I then determined the effect of stress on both the characteristic value and slope. These data are plotted in Figures 78(b) and 78(c). The slope determined for Θ of 4.3 corresponds to the well-established exponent of about 4.0 for creep. The values for the Weibull slope were bimodal and decreased significantly below the yield stress. This is in accord with the reasonable expectation that the scatter will increase at lower stresses.

These values for the dependence of Θ and b on stress shown in Figures 78(b) and 78(c) can be inserted directly into the distribution function. Further, the effects of other parameters such as temperature, pH and potential could also be determined and likewise inserted into the distribution function through the adjustable parameters.

The statistical description of SCC data provides the designer with an important tool. Using data such as those in Figure 70 and Figure 78, the designer can then determine what fraction of his total population will sustain SCC failure by a predetermined time.

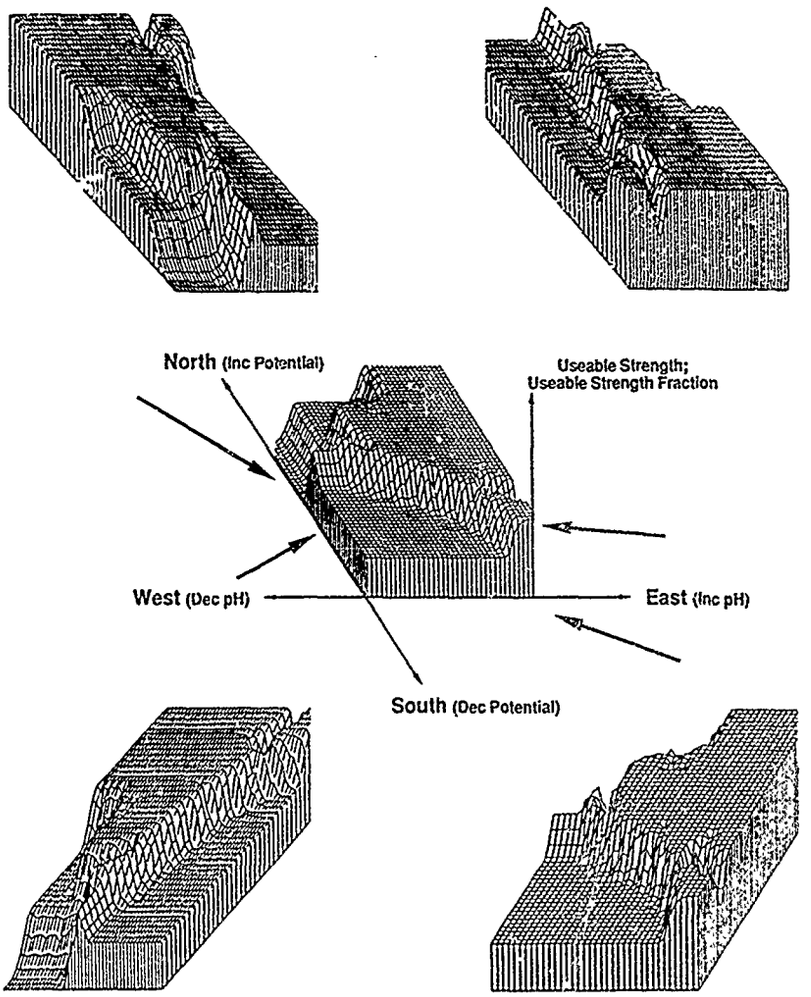


FIGURE 72—Corrosion mode–intensity diagram for Inconel 600 (UNS N06600) at 300°C shown from different perspectives.

While good work is underway in this area, statistical methods are greatly under-used by the materials community in organizing and characterizing data. These analytical tools could provide an important bridge between the materials and design communities.

Environmental definition

The discussion on the engineering status of mode–intensity diagrams considered environmental definition as epitomized in Figure 74. This subject is important in considering the engineering status of SCC because it is the environment that determines the mode and the intensity of SCC; i.e., the environmental coordinates must be located first before the likely mode and its intensity can be determined. At that point, the minimum stress or stressing conditions below which SCC will not occur can be determined. Despite the importance of defining engineering environments, it is usually badly done.

Generally, designers define the environment to which their materials of construction are exposed as the nominal ones or ones that are predisposed to make their components and materials perform ideally. While this may sound like a caricature, it has been my general experience in reviewing failed designs.

In this section on the engineering status of SCC, environmental definition is important because it determines whether SCC actually occurs. It is necessary to define both the mode–intensity diagram shown in Figure 70 and the environment on the metal surface to determine whether SCC can occur.

To illustrate the interaction of mode–intensity diagrams with environmental definition diagrams, I use some simplified examples from Figures 34 and 69 for Inconel 600 in high-temperature water. Note that in the discussion that follows, my use of the potential scale is schematic. From Figures 34 and 69, a simple view at a single pH of a mode–intensity diagram is shown in Figure 79(a). This shows that SCC, at a selected pH, is negligible above the hydrogen equilibrium and has a high intensity below. Figure 79(b) shows schematically the distribution of open-circuit potentials as affected by hydrogen pressure, galvanic coupling, oxygen concentration, and hydrazine.

Figure 79 shows that when the hydrogen is very low or there is a small amount of oxygen, the potential shifts positive out of the region where SCC is significant. On the other hand, when the potential is reduced by increasing the hydrogen, galvanic connection, or adding hydrazine, the zone of increasing SCC intensity progressively intersects with the range of open-circuit potentials.

To determine the proper view of the environment from the point of view of fixing locations on the mode–intensity diagram, it is crucial that realistic definitions of both nominal and non-nominal environments are developed. In addition, there is a third category of reasonable accident conditions that needs to be evaluated. Important features of nominal, non-nominal, and accident conditions are illustrated in Figure 80.

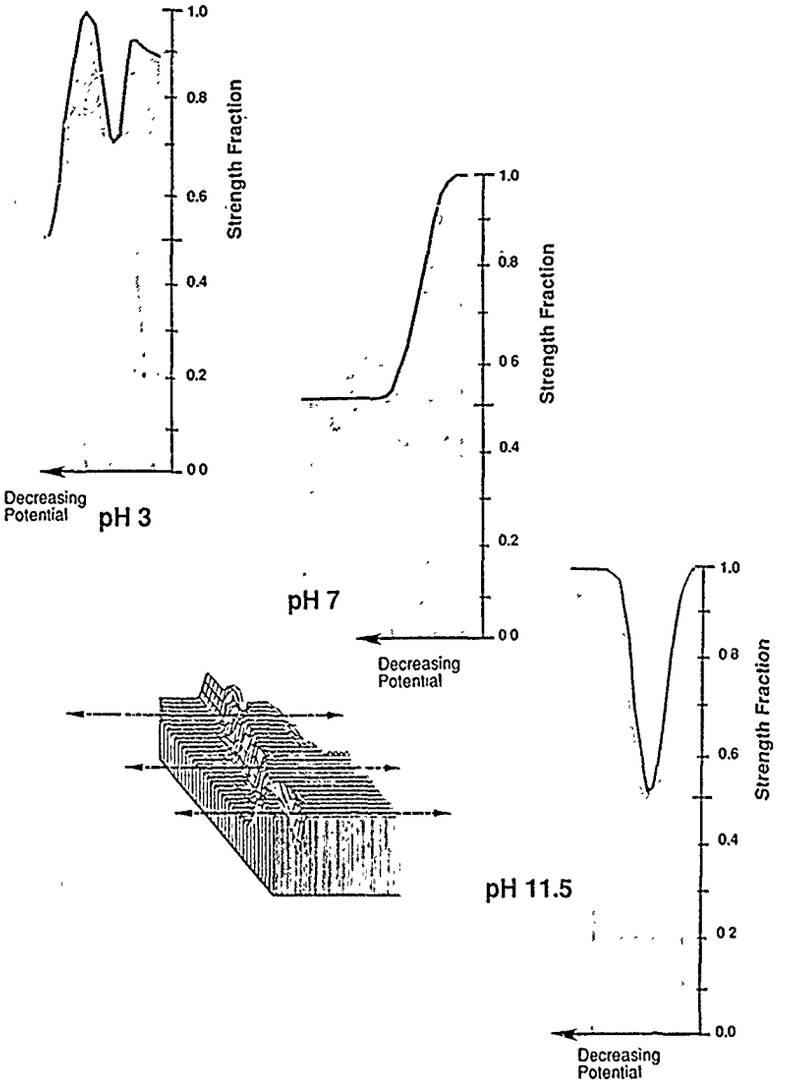


FIGURE 73—Cross-sectional views of useful strength vs electrochemical potential taken at three values of pH from corrosion mode-intensity diagram for Inconel 600 (UNS N06600) in 300°C temperature range.

The nominal condition is generally that environmental circumstance that results from the nominal environmental composition of the process fluid at its nominal flow on nominal surfaces. However, even here there is considerable opportunity for variation because of changes in species such as oxygen, hydrogen, chloride, reduced sulfur, mildly acidifying and mildly alkalizing species. Further, the rates of such interactions with the metallic surface are affected significantly by variations in the local flows.

The non-nominal condition involves the same nominal chemistry but as modified in crevices, deposits, heat-transfer surfaces (with and without crevices), zero flow, flow eddies, and wetting and drying or other concentrating processes. Such conditions usually produce environments on the surface that are vastly different from the nominal conditions.

The category of accident environments I introduce as part of the nominal condition to the extent that a given design of a component is prone to ingesting species from the surroundings through well-known leak paths such as inherently leaky condensers, leaky valve seals, leaking seals of rotating machinery, or the transfer of impurities from one component to another such as copper from condensers or sulfate from deionizing systems. These accident conditions must be included in the design and the possible effects on the corrosion modes and associated intensity evaluated.

The view summarized in Figure 80 is that from the point of view of the process environment, usually on the inside of piping or the inside of vessels. This is the "inside" or nominal system. In addition, there are environments that must be defined on the exterior of the system. These might result, for example, from leaching chloride from asbestos insulation and causing SCC of stainless steel on the outside of a pipe. There is a rigor that can be applied to such situations but it is rarely done, and such a discussion would occupy more space than required here to make the point.

I have introduced this section to illustrate that much of what occurs in SCC and corrosion failures generally results from inadequate definition of the nominal environments as described in Figures 74 and 79. Lack of such definition either prevents work from being done to develop pertinent mode-intensity relationships or leads designers to believe that they have no problem with existing mode-intensity relationships.

I consider rigorous approaches to developing environmental definition diagrams are as important as developing the data for defining mode-intensity diagrams. I recognize that much of this discussion on environmental definition belongs more in a text than in this review. However, the lack of a rigorous approach to defining the array of nominal conditions as described in Figure 74 is a major deficiency in the engineering status of SCC.

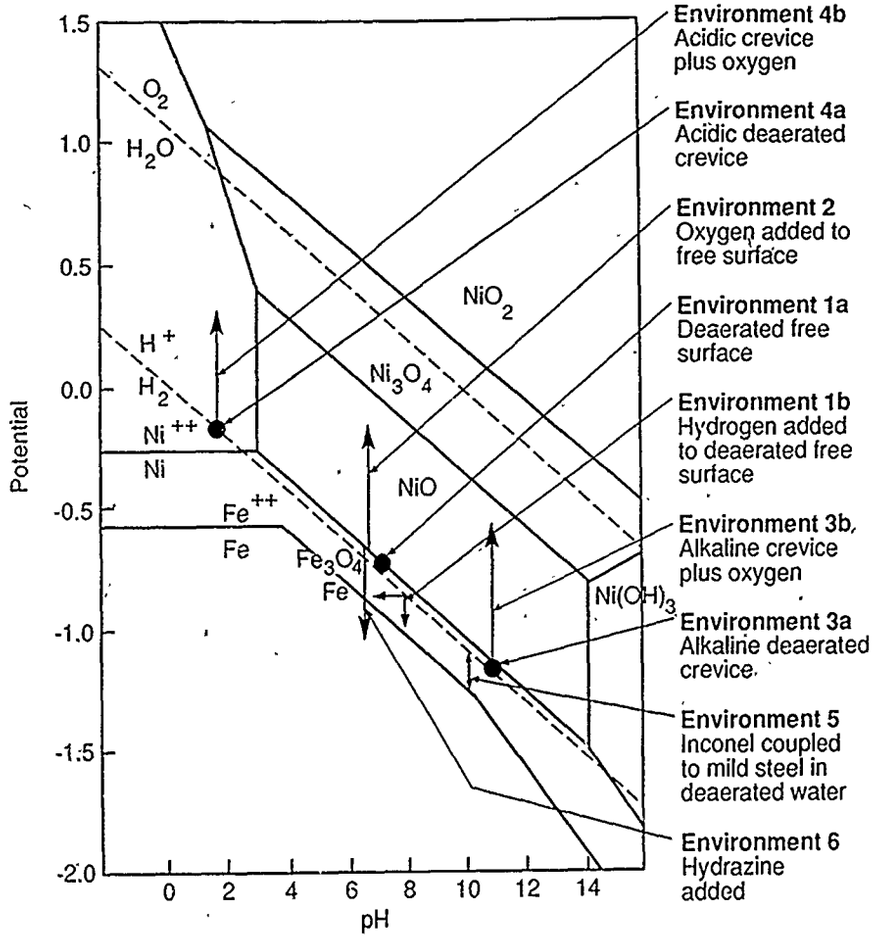


FIGURE 74—Environmental definition diagram for nickel-base alloys using nickel Pourbaix diagram at 288°C with some iron lines added as basis and effects of environmental changes for nominal and non-nominal conditions shown. Specific cases of environmental changes are noted.

The "multiplicative" nature of SCC

As correlation equations emerge from the development of the SDS approach as defined in Figures 5 and 8 through 12, as well as from the development of equations to describe the topology of the mode–intensity diagrams, it will become clear that SCC may be thought of as multiplicatively dependent upon the SDS factors of material, environment, stress, design, temperature, and time. This means that the intensity parameters as defined in Figures 2 and 3 will be the product of various expressions that characterize the six SDS factors.

In the simplest terms, the intensity of SCC increases generally with the stress. If the stress is zero, SCC does not occur. If the intensity as a function of environment is zero, then SCC does not occur, as for Zone 7 of Figure 70. If the intensity as a function of alloy at designated environmental coordinates is zero, the SCC is zero. Thus, SCC can be prevented if any of these SDS factors is zero, it is reasonable to conclude that the intensity of SDS is multiplicative.

However, the functionality of the environmental, material, and stress parameters is not usually monotonic so that increasing magnitudes of any of these independent SDS variables do not necessarily increase the intensity of SCC, with stress being the only exception. While the interaction is multiplicative, it is also complex. The quantitative and interactive product of the combined SDS parameters, even for a few simple ones, has not been approached either from scientific or engineering points of view. Such resulting information would be helpful in both predicting and preventing SCC. Achieving reliable prevention of SCC requires a greatly improved understanding of both the functionality of the SDS factors as they influence intensity as well as a similarly improved capacity to define the nominal environments.

Congruence of SDS factors

If the intensity of SCC depends on the six SDS factors, it also depends on their being at the same place at the same time. This is the principle of "congruence." Congruence is intuitively understood by those who are intimately familiar with SCC; however, the idea has never by clearly formalized and defined.

Identifying congruence and the need for the simultaneous occurrence of critical factors is a part of the present engineering status. A practical element of implementing congruence is to place a surface into compressive stress when exposed to an environment that produces high-intensity SCC when the stresses are tensile.

Nomenclature and appearances

Many of the leaders in this field have struggled to develop a suitable name for phenomena that are embraced by this review. I have opposed the idea of distinguishing what were once differentiated as hydrogen embrittlement and anodic SCC because it makes the nomenclature mechanism dependent and mechanisms change. Further, hydrogen may play some role in what has been called anodic SCC, conversely, it is known that some stress corrosion processes that occur at negative potentials possibly proceed by chemical dissolution.

In addition, it is increasingly clear that hydrogen may not only embrittle the material but also make it more ductile.

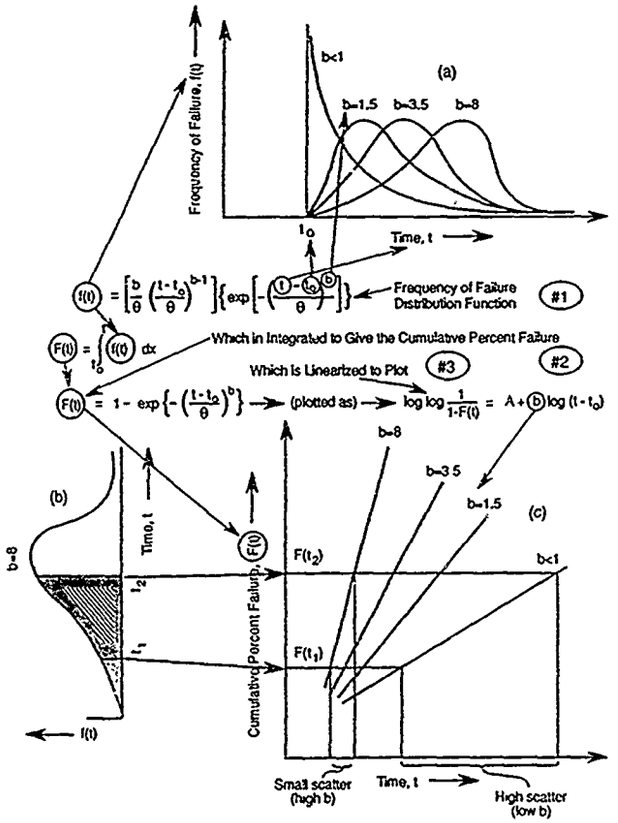


FIGURE 75—Schematic diagram showing relationships of graphics and equations between frequency of failure and cumulative percent failure based on Weibull statistics.

Terms like "environmentally reduced strength," "environmental embrittlement," or "environmentally accelerated cracking" lose sight of the fact that the metal is not embrittled in most cases nor is the inherent strength lost by some magic process. Further, the result is not so much a crack but rather a very narrow process of degradation or corrosion that is accelerated or incited by stress.

The term "stress corrosion cracking" is still a useful one because it identifies the important factors of stress and an interaction between the environment and material to produce degradation with the final "appearance" of a "crack."

If any change were to be made, it would be to shorten the term to simply "stress corrosion." The possible conflict with any general dissolution that is accelerated by stress is not serious, and such corrosion is usually called something else, as in the case of cyclic stresses breaking the thick oxide films in high-temperature oxidation.

I am concerned with the word "cracking" since it implies inherently to the design and most of the materials community that a mechanical crack has somehow occurred. While this problem of appearances causes little difficulty for the knowledgeable professionals, it is often a confusing term for lay persons. Further, it is a misstatement of what actually occurs.

The engineering status of terminology is one of confusion, and efforts should be made to make the generic term simple, direct, and inclusive. Thus, there should be one constant in the system as mechanisms continue to change. My choice is "stress corrosion."

I believe that "stress corrosion" should include what have in the past been called such names as hydrogen embrittlement (and there are a number of subsets here), anodic SCC, liquid metal embrittlement, and similar terms. Also, I urge that professionals in various industries drop such variations as PWSCC (primary water SCC), since the same process occurs in other environments. Such a confusing term could simply be replaced with "stress corrosion" as it occurs at a particular location.

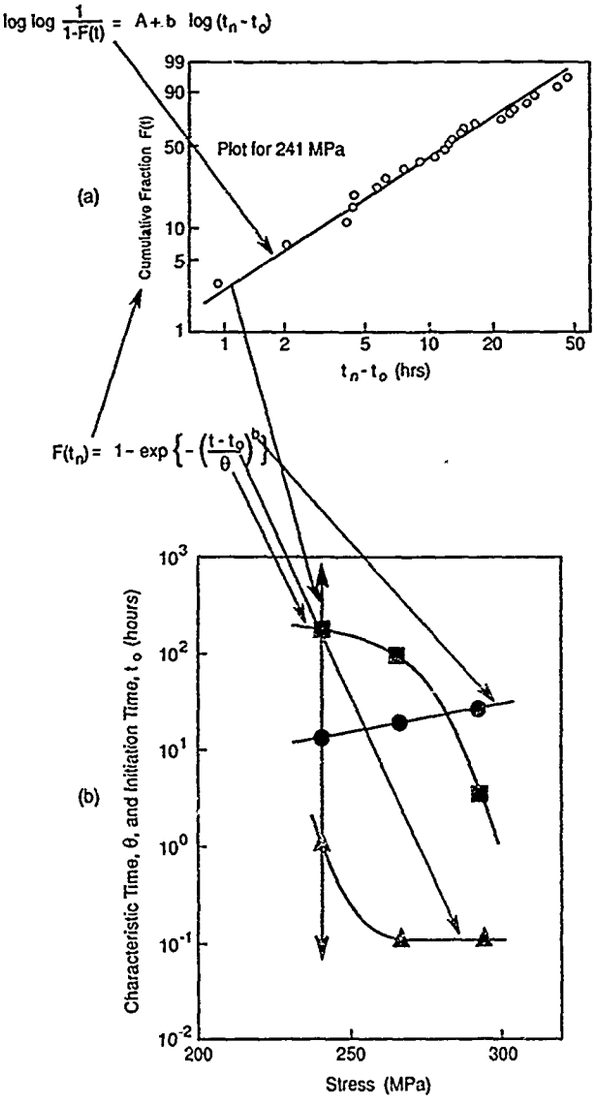


FIGURE 76—Statistical interpretation of SCC of Zircaloy-2 exposed to iodine gas: (a) Cumulative fraction failed vs time for a stress of 241 MPa, and (b) effect of stress on adjustable constants in Weibull correlation equation. Adapted from the work of Shimada and Nagai.[202]

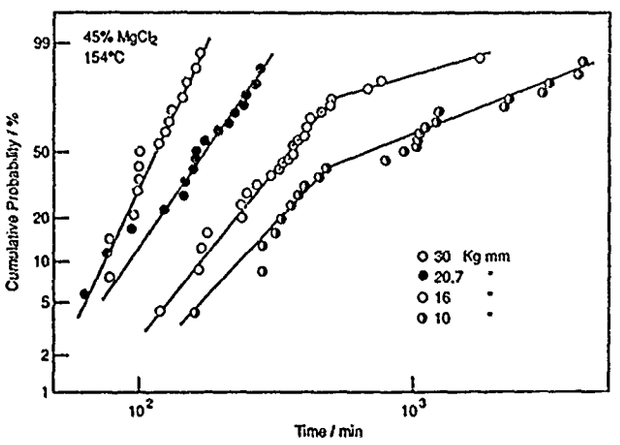


FIGURE 77—Cumulative fraction of specimens failed vs time using Weibull statistics for a Fe-17Cr-11Ni alloy exposed to boiling 45% $MgCl_2$. Adapted from the work of Shibata.[203]

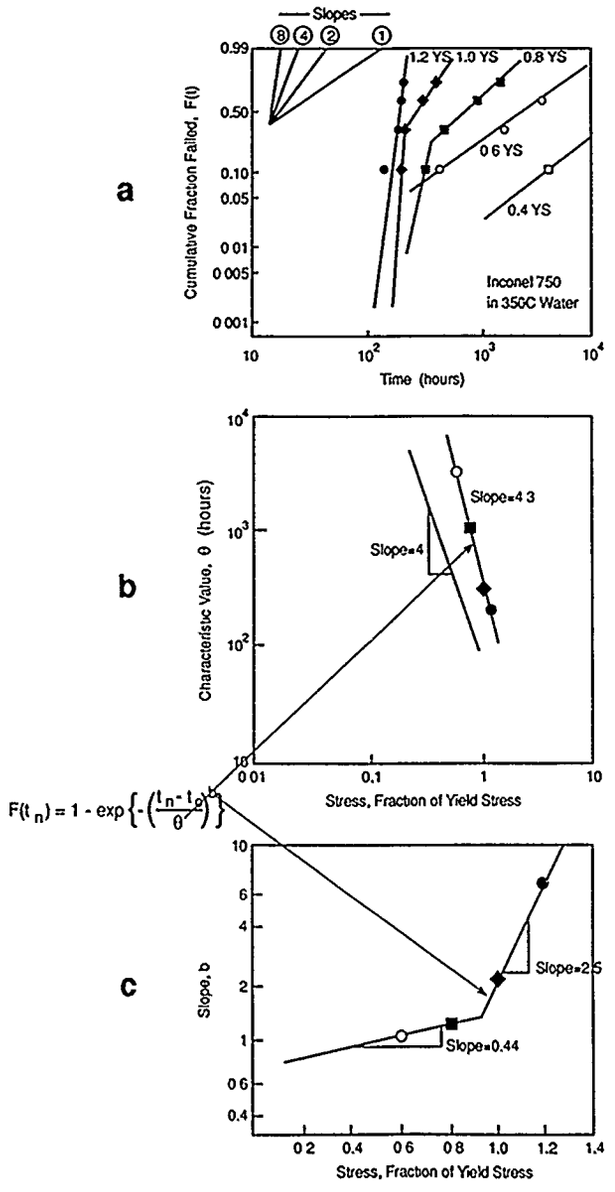


FIGURE 78—Statistical analysis of SCC failure of Inconel 750 exposed to 350°C water. (a) Cumulative fraction failed vs time for different magnitudes of yield stress plotted with Weibull statistics. Different values of Weibull slopes shown for comparison. (b) Characteristic value plotted vs stress. Data compared with slope of four. (c) Weibull slope plotted vs stress. Adapted from the work of Coriou, et al.[205]

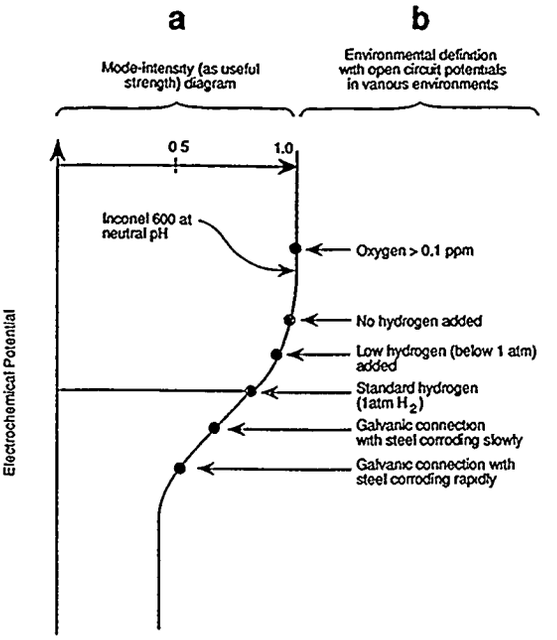


FIGURE 79—Comparison between mode–intensity diagram and environmental definition diagram shown schematically for Inconel 600 (UNS N06600) in high-temperature water with electrochemical potential increasing in the oxidizing direction. (a) Mode–intensity diagram shown for Inconel 600 at neutral pH with useful strength plotted vs potential. (b) Location of open-circuit potentials on the surface of Inconel 600 as affected by various environmental conditions.

Overall Nominal Condition

Nominal	Non-Nominal	Accident
• Open surface	• Crevices	• Leaks
• Bulk composition	• Deposits	• Exterior environments
• Standard flow	• Heat transfer	
	• Low flow	
	• Impurities from other components in system	
	• Excessive velocity	

FIGURE 80—Overall nominal conditions of environment shown including nominal, non-nominal, and accident conditions.

What Needs To Be Done

It is tempting at this point to define a catalog of all those actions that should be undertaken. However, what needs to be done is already defined in the sections Scientific Status and Engineering Status."

As a broad general approach, I suggest that emphasis be placed upon finding ways to increase the extent and quality of communication between the materials and design communities. I believe that such communication will be improved if approaches suggested by the mode–intensity diagrams and the environmental definition diagrams are emphasized. Then, whatever research funds are required to meet such objectives will be forthcoming as encouraged by an enlightened design community and a materials community that "has its act together."

Acknowledgment

First, I would like to thank Brian Ives and Rick Gangloff, the chairmen of this meeting, for arranging for me to present this paper.

Second, I am enormously grateful to Mary Elizabeth Berg and Dennis Deegan, without whose help I would not have completed this work. I also appreciate the careful work of Carolyn Swanson, who did the graphic illustrations.

Third, I want to recognize my deep gratitude to the late Mars Fontana for his support of my work while at Ohio State as a student and later as a member of the faculty. There are so many ways he influenced the course of my professional career beyond his ordinary duty of advisor that I only note: "Let me count the ways."

It is clear that this review represents, at least for me, a "paradigm shift" in thinking about stress corrosion cracking. In this era where paradigm shifts are commonplace in many arenas of society, one in stress corrosion cracking should not be out of place. However, my contribution to identifying such a shift has been greatly influenced by many others with whom I have sometimes agreed and at other times did not. I know that I will leave a few people out, but those whose ideas have helped me in this arena of stress corrosion cracking include some who are no longer here, such as Floyd Brown and Sam Hoar, as well as "Font " Those still living include Marcel Pourbaix, Herb Uhlig, Al Troiano, Dick Oriani, Michael Smialowski, John Hirth, Bert Westwood, Jack Westbrook, Redvers Parkins, Nev Pugh, John Scully, Markus Speidel, Jerry Kruger, Peter Swann, and Dan van Rooyen. I am sure that I am indebted to many others without knowing it.

This review also represents a bringing together of many of the ideas that developed from 33 years of research and thinking about this subject During that time, I have been greatly assisted by a number of outstanding students and associates, many of whose works are referred to in this review. Also, I greatly appreciate those who have supported my research with such great confidence and financial support In particular, Julius Harwood at the Office of Naval Research supported the research for my M.S. I am greatly indebted to Andy Van Echo, then of the Atomic Energy Commission, who gave me my first research contract while I was still a graduate student. Later, Gene Bailey of Commonwealth Edison and the Edison Electric Institute and Ed Zebroski and Tom Passel of the Electric Power Research Institute provided major funding to continue my work. Later, my work at Minnesota was supported by Don Stevens and Lou Ianniello of the Department of Energy.

References

1. A.R.C. Westwood, J.R. Pickens, Atomistics of Fracture, ed. R.M. Latanision, J.R. Pickens (New York, NY: Plenum Press, 1983), pp. 65-91.
2. R.W. Staehle, J.J. Royuela, T.L. Raredon, E. Serrate, C.R. Morin, R.V. Farrar, Corrosion 26, 11(1970): pp. 451-486.
3. W.D. Robertson, ed., Stress Corrosion Cracking and Embrittlement (New York, NY: Wiley, 1956).
4. R.W. Staehle, A.J. Forty, D. van Rooyen, eds., Fundamental Aspects of Stress Corrosion Cracking (Houston, TX: National Association of Corrosion Engineers, 1969).
5 R W. Staehle, J. Hochmann, R.D. McCright, J.E. Slater, eds., Stress Corrosion Cracking and Hydrogen Embrittlement of Iron Base Alloys (Houston, TX: NACE, 1977).
6 M.J Blackburn, J.A. Feeney, T.R. Beck, Advances in Corrosion Science and Technology Volume 3, eds. M.G. Fontana, R.W. Staehle (New York, NY. Plenum Press, 1973), pp. 67-292.
7. M.O. Speidel, M.V. Hyatt, Advances in Corrosion Science and Technology Volume 2, ed. M.G. Fontana, R.W. Staehle (New York, NY: Plenum Press, 1972), pp. 115-335.
8. M.A. Scheil, Stress Corrosion Cracking of Metals (New York, NY ASTM-American Institute of Mining, Metallurgical, and Petroleum Engineers, 1945), p. 410.
9. Stress Corrosion Cracking of Metals (New York, NY: ASTM-AIME, 1945).
10 M Smialowski, Hydrogen in Steel (New York, NY. Pergamon Press, 1962).
11 A.R. Troiano, Trans. ASM 52(1960): pp. 54-80.
12 M G Fontana, N D. Greene, Corrosion Engineering (New York, NY: McGraw-Hill, 1967), p. 91.
13. H.R. Copson, Corrosion Handbook, ed. H.H. Uhlig (New York, NY: Wiley, 1948), pp. 569-578.
14 U R Evans, The Corrosion and Oxidation of Metals. Scientific Principles and Practical Applications (London, UK. Edward Arnold, 1960), pp. 665-700.
15 M G Fontana, N D Greene, Corrosion Engineering (New York, NY: McGraw-Hill, 1967), p. 100.
16 H L Logan, The Stress Corrosion of Metals (New York, NY. Wiley, 1966), pp. 5-7.
17. H.R. Copson, Physical Metallurgy of Stress Corrosion Fracture, ed. T. Rhodin (New York, NY. Interscience, 1959), pp. 247-267.
18. D.J. DePaul, ed., Corrosion and Wear Handbook for Water Cooled Reactors (Washington, DC. USAEC, 1957), p. 165.
19. S.P. Pednekar, A.K. Agrawal, H.E. Chaung, R.W. Staehle, J. Electrochem. Soc. 126, 4(1979): pp. 701-702.
20. H. Coriou, L. Grall, Y. LeGall, S. Vettier, Third Metallurgy Conference on Corrosion, Saclay, France, 1959 (Amsterdam, Holland. North Holland, 1959), pp.161-169.
21. M.G. Fontana, N.D. Greene, Corrosion Engineering (New York, NY: McGraw-Hill, 1967), pp. 107-109.
22. O. Devereux, A.J. McEvily, R.W. Staehle, eds., Corrosion Fatigue. Chemistry, Mechanics and Microstructure (Houston, TX: NACE, 1972).
23. R.P. Wei, G.W. Simmons, Stress Corrosion Cracking and Hydrogen Embrittlement of Iron Base Alloys, pp. 751-765.
24. D.J. Duquette, Environmental Degradation of Engineering Materials in Aggressive Environments (Blacksburg, VA. Virginia Tech, 1981), pp. 131-139.
25. N. Totsuka, S. Szklarska-Smialowska, Proceedings of the Third International Symposium on Environmental Degradation of Materials in Nuclear Power Systems—Water Reactors, held August 30-September 3, 1987, ed. G.J. Theus, J.R. Weeks (New York, NY. AIME, 1988), pp. 691-696.
26. B. Cox, Stress Corrosion Cracking, ed. J. Yahalom, A. Aladjem (Tel-Aviv, Israel: Freund, 1980), pp. 162-172.
27. G.E. Kerns, R.W. Staehle, Scripta Metall. 6, 12(1972): pp. 1189-1194.
28. H. Coriou, L. Grall, C. Mahieu, M. Pelas, Corrosion 22, 10(1966): pp. 280-290.
29. R.W. Staehle, The Theory of Stress Corrosion Cracking in Alloys, ed. J.C. Scully (Brussels, Belgium: NATO, 1971), p. 255.
30. R.W. Staehle, J.J. Royuela, Revista Met. July-August (1971): pp. 281-289.
31. A.P. Bond, J.D. Dundas, Corrosion 24(1968): p. 344.
32. J. Blanchet, H. Coriou, L. Grall, C. Mathieu, C. Otter, G. Turler, J. Nucl. Mater. 55(1975): pp. 187-205.
33. W.H. Arlt, S.R. Vandenberg, "Fuel Failure Examinations and Analyses in the High-Power Density Program," GEAP-4360 (September 16, 1963).
34 R L Cowan C.S. Tedmon, Advances in Corrosion Science and Technology Volume 3, ed. M.G. Fontana, R.W. Staehle (New York, NY: Plenum Press, 1973), pp. 293-401.
35 R L Cowan, G M Gordon, Stress Corrosion Cracking and Hydrogen Embrittlement of Iron Base Alloys, pp. 1023-1070.
36. J.S. Armijo, Corrosion 24, 10(1968). pp. 319-325.
37 K T. Aust, J.S. Armijo, J.H. Westbrook, ASM Trans. Quart. 59(1966): pp. 544-567.
38. E.C. Bain, R.H. Aborn, J.B. Rutherford, Trans. Amer. Soc. Steel Treating 21(1933): p. 481.
39 Investigation of the Cause of Cracking in Austenitic Stainless Steel Piping, Volume 1, NEDO-21000, General Electric Company, Nuclear Energy Division, July 1975.
40. J.C. Danko, Proceedings of the 8th International Brown Boveri Symposium Corrosion in Power Generating Equipment (New York, NY: Plenum Press, 1984), p. 236.
41. "Investigation and Evaluation of Cracking in Austenitic Stainless Steel Piping of Boiling Water Reactor Plants," Technical Report NUREG 75/067, U.S. Nuclear Regulatory Commission, October, 1975.
42. "Investigation and Evaluation of Stress-Corrosion in Piping of Light Water Reactor Plants," Technical Report NUREG-0531, U.S. Nuclear Regulatory Commission, February, 1979.
43. "Investigation and Evaluation of Cracking Incidents in Piping in Pressurized Water Reactors, Technical Report NUREG-0691, U.S. Nuclear Regulatory Commission, September, 1980.
44. Proceedings of Seminar on Countermeasures for BWR Pipe Cracking, EPRI WS-79-174, 3 Volumes, 1980.

45. A. Brown, J.T. Harrison, R. Wilkins, Corros. Sci. 10(1970): p. 547.
46. M. Kowaka, S. Nagata, Corrosion 24(1968): p. 427.
47. H.R. Copson, S.W. Dean, Corrosion 21, 1(1965): pp. 1-8.
48. M.J. Blackburn, W.H. Smyrl, J.A. Feeney, Stress-Corrosion Cracking in High Strength Steels and in Titanium and Aluminum Alloys, ed. B.F. Brown (Washington, DC: NRL, 1972), pp. 245-363.
49. M.G. Fontana, N.D. Greene, Corrosion Engineering (New York, NY: McGraw-Hill, 1967), p. 246.
50. A.W. Loginow, E.H. Phelps, Corrosion 18(1962): p. 229t.
51. D.C. Deegan, B.E. Wilde, Stress Corrosion Cracking and Hydrogen Embrittlement of Iron Base Alloys, pp. 663-670.
52. D.C. Deegan, B.E. Wilde, R.W. Staehle, Corrosion 32, 4(1976): pp. 139-143.
53. R.D. McCright, Stress Corrosion Cracking and Hydrogen Embrittlement of Iron Base Alloys, pp. 306-325.
54. A.S. Tetelman, Hydrogen in Metals, ed. A.W. Thompson, I.M. Bernstein (Metals Park, OH: ASM International, 1974), pp. 17-49.
55. H.H. Johnson, Stress Corrosion Cracking and Hydrogen Embrittlement of Iron Base Alloys, pp. 382-389.
56. B. Lustman, F. Kerze, eds., The Metallurgy of Zirconium (New York, NY: McGraw-Hill, 1955).
57. B. Cox, J.C. Wood, Corrosion Problems in Energy Conversion and Generation, ed. C.S. Tedmon (New York, NY: The Electrochemical Society, Inc., 1974), pp. 275-321.
58. H.W. Pickering, M.G. Fontana, F.H. Beck, Corrosion 18, 6(1962): p. 230t.
59. N.A. Nielsen, 1970 Gillett Memorial Lecture, ASTM, Toronto, Canada.
60. G.F. Becker, A.L. Day, Amer. J. of Sci. VII (1905): pp. 283-288.
61. S. Taber, Amer. J. of Sci. XXXVII (1916): pp. 532-556.
62. D.D. Malinowski, W.D. Fletcher, Nucl. Tech. 37(1978): p. 105.
63. N.J. Magnani, Advances in Corrosion Science and Technology Volume 6, ed. M.G. Fontana, R.W. Staehle (New York, NY: Plenum Press, 1976), pp. 89-161.
64. H.R. Copson, G. Economy, Corrosion 24, 3(1968): pp. 55-65.
65. U.R. Evans, The Corrosion of Metals (London, UK: Edward Arnold, 1924), pp. 72-80.
66. V. Pasupathi, J.S. Perrin, D.R. Farmelo, G.P. Smith, S. Weiss, Trans. Amer. Nucl. Soc. 34(1980): pp. 232-233.
67. D.O. Sprowls, R.H. Brown, Fundamental Aspects of Stress Corrosion Cracking, pp. 466-512.
68. M.O. Speidel, M.V. Hyatt, Advances in Corrosion Science and Technology Volume 2, ed. M.G. Fontana, R.W. Staehle (New York, NY: Plenum Press, 1973), pp. 115-335.
69. B.F. Brown, Stress Corrosion Cracking Control Measures (Houston, TX: NACE, 1981), p. 52.
70. M.O. Speidel, R.M. Magdowski, Proceedings of the Second International Symposium on Environmental Degradation of Materials in Nuclear Power Systems—Water Reactors, held September 9-12, 1985 (LaGrange Park, IL: ANS, 1985), pp. 267-275.
71. B.F. Brown, Stress Corrosion Cracking Control Measures (Houston, TX: NACE, 1981), p. 2.
72. S.D. Reynolds, F.W. Pement, Materials Performance 13(1974): p. 21.
73. A. Kawashima, A.K. Agrawal, R.W. Staehle, Stress Corrosion Cracking—The Slow Strain Rate Technique, ASTM 665, ed. G.M. Ugiansky, J.H. Payer (Philadelphia, PA: ASTM, 1979), pp. 266-278.
74. T. Rhodin, ed., Physical Metallurgy of Stress Corrosion Fracture (New York, NY: Interscience, 1959).
75. A.R.C. Westwood, N.S. Stoloff, ed., Environment Sensitive Mechanical Behavior (New York, NY: Gordon and Breach, 1966).
76. J.C. Scully, ed., The Theory of Stress Corrosion Cracking in Alloys.
77. R.W. Staehle, B.F. Brown, J. Kruger, A. Agrawal, eds., U.R. Evans Conference on Localized Corrosion, held December 6-10, 1971 (Houston, TX: NACE, 1971).
78. M. Henthorne, ed., Localized Corrosion—Cause of Metal Failure, symposium held June 27-July 2, 1971, ASTM STP 516 (Philadelphia, PA: ASTM, 1972).
79. J.P. Hirth, H.H. Johnson, Atomistics of Fracture, pp. 771-787.
80. J.R. Rice, Stress Corrosion Cracking and Hydrogen Embrittlement of Iron Base Alloys, pp. 11-15.
81. R.M. Latanision, J.T. Fourie, eds., Surface Effects in Crystal Plasticity (Leyden, The Netherlands: Noordhoff, 1977).
82. R.M. Latanision, J.R. Pickens, eds., Atomistics of Fracture (New York, NY: Plenum Press, 1983).
83. R.M. Latanision, R.H. Jones, eds., Chemistry and Physics of Fracture (Dordrecht, The Netherlands: Martinus Nijhoff, 1987).
84. A.W. Thompson, I.M. Bernstein, eds., Hydrogen in Metals (Metals Park, OH: ASM International, 1974).
85. A.W. Thompson, I.M. Bernstein, eds., Effect of Hydrogen on Behavior of Materials (New York, NY: AIME, 1976).
86. A.W. Thompson, I.M. Bernstein, eds., Hydrogen Effects in Metals (New York, NY: AIME, 1981).
87. A.W. Thompson, I.M. Bernstein, Advances in Corrosion Science and Technology Volume 7, ed. M.G. Fontana, R.W. Staehle (New York, NY: Plenum Press, 1980), pp. 53-175.
88. P. Bastien, ed., L'Hydrogene dans les Metaux (Paris, France: Editions Science et Industrie, 1972).
89. E. Wicke, ed., Proceedings of the Julich Symposium, Hydrogen in Metals, Ber. Bunsenges. Physik. Chem. 76(1972).
90. G.R. Irwin, J.A. Kies, H.L. Smith, Proc. ASTM 58(1958): p. 640.
91. F.A. McClintock, G.R. Irwin, Fracture Toughness Testing and its Applications (Philadelphia, PA: ASTM, 1965), pp. 84-113.
92. B.F. Brown, "ARPA Coupling Program on Stress-Corrosion Cracking," NRL Report 7168, September 21, 1970.
93. P.L. Pratt, ed., Fracture 1969, Proceedings of the Second International Conference on Fracture, held in April 1969 (London, UK: Chapman and Hall, 1969).
94. Third International Congress on Fracture, held April 8-13, 1973 (Dusseldorf, FDR: V. Deutch. Eisenhuttenleute, 1973).
95. K.J. Miller, R.F. Smith, ed., Mechanical Behaviour of Materials, Proceedings of the Third International Conference, held August 20-24, 1979 (Oxford, UK: Pergamon, 1980).
96. G.M. Ugiansky, J.H. Payer, eds., Stress Corrosion Cracking—The Slow Strain-Rate Technique, ASTM STP 665.
97. L.E. Raymond, ed., Hydrogen Embrittlement Testing, a symposium held June 25-30, 1972, ASTM STP 543 (Philadelphia, PA: ASTM, 1974).
98. V. Cihal, Intergranular Corrosion in Stainless Steel, English translation by J.M.A. Van der Horst.
99. G.V. Karpenko and I.I. Vasilenko, Stress Corrosion Cracking of Steels (Tel-Aviv, Israel: Freund Publishing House, 1979).
100. E.M. Gutman, Mechano Chemistry of Metals and Protection from Corrosion (Moscow, USSR: Moscow Metallurgia, 1981).
101. L.L. Shreir, ed., Corrosion (London, UK: Newnes-Butterworths, 1965).
102. H.E. Boyer, ed., Metals Handbook, 8th Edition, Volume 10 (Metals Park, OH: ASM International, 1975), pp. 205-229.
103. J.R. Davis, ed., Metals Handbook, Ninth Edition, Volume 13, Corrosion (Metals Park, OH: ASM International, 1987), pp. 145-171.
104. M.G. Fontana, N.D. Greene, Corrosion Engineering (New York, NY: McGraw-Hill, 1967).
105. H.H. Uhlig, R.W. Revie, Corrosion and Corrosion Control, Third Edition (New York, NY: Wiley, 1985).
106. A.S. Tetelman, A.J. McEvily, Fracture of Structural Materials (New York, NY: Wiley, 1967).
107. R.A. Oriani, Fundamental Aspects of Stress Corrosion Cracking, pp. 32-49.
108. R.A. Oriani, Stress Corrosion Cracking and Hydrogen Embrittlement of Iron Base Alloys, pp. 351-358.
109. F.P. Ford, Embrittlement by the Localized Crack Environment, proceedings of a symposium held October 4-5, 1983, ed. R.P.

Gangloff (New York, NY: AIME, 1984), pp. 117-148.
110. P.L. Andresen, F.P. Ford, Mater. Sci. Eng. A103(1988): pp. 167-184.
111. A.J. Forty, P. Humble, Phil. Mag. 8(1963): p. 247.
112. R.C. Newman, K. Sieradzki, Chemistry and Physics of Fracture; R.H. Jones, Stress Corrosion Cracking and Hydrogen Embrittlement of Iron Base Alloys, pp. 597-611.
113. E.N. Pugh, Atomistics of Fracture, pp. 997-1010.
114. K.T. Aust, O. Iwao, Localized Corrosion, pp. 62-77.
115. S. Szklarska-Smialowska, H.E. Chaung, C.Y. Chao, R.W. Staehle, J. Electrochem. Soc. 126, 11(1979): p. 2038.
116. T.R. Beck, Fundamental Aspects of Stress Corrosion Cracking, pp. 605-619.
117. B.F. Brown, The Theory of Stress Corrosion Cracking of Alloys, pp. 186-204.
118. A. Turnbull, Embrittlement by the Localized Crack Environment, pp. 3-31.
119. A. Turnbull, Rev. on Coatings and Corros. 5(1982): pp. 43-171.
120. A. Turnbull, Corros. Sci. 23, 8(1983): pp. 833-870.
121. P.R. Swann, J.D. Embury, High Strength Materials, ed. Zackey (New York, NY: Wiley, 1965).
122. H.W. Pickering, P.R. Swann, Corrosion 19(1963): p 363t
123. R.B. Mears, R.H. Brown, E.H. Dix, Stress Corrosion Cracking of Metals (New York, NY: ASTM-AIME, 1945), p. 323
124. H.H. Uhlig, Physical Metallurgy of Stress Corrosion Fracture, ed. T. Rhodin (New York, NY: Interscience, 1959), pp. 1-17.
125. T. Murata, R.W. Staehle, Proceedings 5th International Congress on Metallic Corrosion, ed. N. Sato (Houston, TX: NACE, 1974), pp. 513-518.
126. T. Shibata, R.W. Staehle, Proceedings 5th ICMC, pp 487-492
127. R.W. Staehle, The Theory of Stress Corrosion Cracking in Alloys, p. 273.
128. F.P. Ford, EPRI Report NP-2589, September, 1982.
129. R.W. Staehle, Fundamental Aspects of Stress Corrosion Cracking, pp. 3-14.
130. A.P. Bond, J.P. Dundas, Stress Corrosion Cracking and Hydrogen Embrittlement of Iron Base Alloys, pp. 1136-1148.
131. E.N. Pugh, J.V. Craig, J.A. Sedricks, Fundamental Aspects of Stress Corrosion Cracking, pp. 118-158.
132. E.N. Pugh, The Theory of Stress Corrosion Cracking of Alloys, pp. 418-441.
133. H.W. Pickering, Fundamental Aspects of Stress Corrosion Cracking, pp. 159-177.
134. R.M. Latanision, R.W. Staehle, Scripta Metall. 2(1968) p 667
135. R.M. Latanision, R.W. Staehle, Fundamental Aspects of Stress Corrosion Cracking, pp. 215-307.
136. J.R. Galvele, Corros. Sci. 27(1987): pp 1-33
137. H.K. Birnbaum, M. Grossbeck, S. Gahr, Hydrogen in Metals, pp. 303-323.
138. G.A. Nelson, Petrol. Refiner. 29(1950): p. 104.
139. M. Ransick, P.G. Shewmon, Hydrogen Effects in Metals, pp 895-902.
140. J.H. Payer, R.W. Staehle, Corrosion 32, 10(1976): pp. 418-420.
141. N.A. Nielsen, Corrosion 20(1964): p. 105t.
142. M.F. Long, A.K. Agrawal, R.W. Staehle, High Temperature, High Pressure Electrochemistry in Aqueous Solutions, ed. D. de G. Jones, J.E. Slater, R.W. Staehle (Houston, TX: NACE, 1976), pp 524-531.
143. M. Henthorne, R.N. Parkins, Corros. Sci. 6(1966): p. 357.
144. W.E. Berry, Proceedings of the 5th Symposium on Line Pipe Research, Vol. 1, held November 20-22, Houston, TX, 1974.
145. G.M. Ugiansky, J.H. Payer, eds., Stress Corrosion Cracking—The Slow Strain Rate Technique, ASTM STP 665 (Philadelphia, PA: ASTM, 1979).
146. B.F. Brown, Stress Corrosion Cracking Control Measures (Houston, TX: NACE, 1981).
147. Fracture Toughness Testing and its Applications, ASTM STP 381 (Philadelphia, PA: ASTM, 1965).
148. S.W. Dean, E.N. Pugh, G.M. Ugiansky, eds., Environment-Sensitive Fracture: Evaluation and Comparison of Test Methods, ASTM STP 821 (Philadelphia, PA: ASTM, 1984).
149. M.O. Speidel, Predictive Methods For Assessing Corrosion Damage to BWR Piping and PWR Steam Generators, ed. H. Okada, R.W. Staehle (Houston, TX: NACE, 1982), pp. 31-44.
150. M.E. Indig, A.R. McIlree, Corrosion 35, 7(1979): pp. 288-295.
151. G.E. Kerns, R.W. Staehle, Scripta Metall. 6(1972): pp. 631-634.
152. D.J. Duquette and H.H. Uhlig, Trans. ASM 61(1968): p. 449.
153. J.E. Campbell, W.W. Gerberich, J.H. Underwood, eds., Application of Fracture Mechanics for Selection of Metallic Structural Materials (Metals Park, OH: ASM International, 1982), p. 18.
154. B.F. Jones, Embrittlement by the Localized Crack Environment, ed. R.P. Gangloff (New York, NY: AIME, 1984), p. 457.
155. G.P. Airey, Proceedings of the International Symposium on the Degradation of Materials in Nuclear Power Systems—Water Reactors (Houston, TX: NACE, 1984), p. 475.
156. T.B. Cassagne, "Oxide Formation and Transgranular Stress Corrosion Cracking of Copper" (Ph.D. diss., The Johns Hopkins University, 1988).
157. E.N. Pugh, W.G. Montague, A.R.C. Westwood, Corros. Sci. 6(1966): p. 345.
158. M.T. Wang, R.W. Staehle, Hydrogen in Metals, International Conference, held May-June, 1972 (Paris, France: Editions Science and Industry, 1972), p. 346.
159. E.N. Pugh, W.G. Montague, A.R.C. Westwood, Trans. ASM 58(1965): p. 665.
160. W.L. Clarke, G.M. Gordon, Corrosion 29(1973): p. 4.
161. M.O. Speidel, A. Atrens, Corrosion in Power Generating Equipment, Proceedings of the 8th International Brown Boveri Symposium on Corrosion in Power Generating, held Sept. 19-20, 1983, Switzerland (New York, NY. Plenum Press, 1984), pp. 88, 343.
162. R.M. Rentler, I.H. Welinksy, "Effect of HNO_3-HF Pickling on Stress Corrosion Cracking of Ni-Cr-Fe Alloy 600 in High-Purity Water at 600°F," Bettis Atomic Power Laboratory Report WAPD-TM-944, October, 1970.
163. R.W. Cochran, R.W. Staehle, Corrosion 24, 11(1968): pp 369-378.
164. J. Congleton, T. Shoji, R.N. Parkins, Corros Sci 25(1985) p 646.
165. T.R. Pinchback, S.P. Clough, L.A. Heldt, Corrosion 32(1976): p. 469.
166. T.B. Cassagne, W.F. Flanagan, B.D. Lichter, Chemistry and Physics of Fracture, p. 659.
167. H. Nagano, K. Yamanaka, K. Tokimasa, H. Miyuki, this proceedings.
168. A. Kishida, H. Takamatsu, S. Isobe, K. Arioka, T. Tsuruta, Symposium on Chemistry in High-Temperature Aqueous Solutions, Provo, Utah, held August 25-27, 1987.
169. N. Pessall, G.P. Airey, B.P. Lingenfelter, Corrosion 35, 3(1979): pp. 100-107.
170. R. Bandy, D. van Rooyen, Symposium on Environmental Degradation of Materials in Nuclear Power Systems—Water Reactors, pp. 763-774.
171. G. Economy, R.J. Jacko, J.A. Begley, F.W. Pement, EPRI Report NP-5987-SP, "Proceedings of the 1987 Workshop on the Mechanism of Primary H_2O IGSCC," 1987, Appendix B-1.
172. J.F. Newman, EPRI Report NP-3043, 1983.
173. D. van Rooyen, Proceedings of the First International Conference on Stress Corrosion Cracking (London, England: Butterworths, 1961).
174. H.H. Uhlig, Stress Corrosion Cracking and Hydrogen Embrittlement of Iron Base Alloys, pp. 174-179.
175. T.W. Crooker, E.A. Lange, Effects of Environment and Complex Loading History on Fatigue Life, ASTM STP 462 (Philadelphia, PA: ASTM, 1970), p. 258.
176. U.R. Evans, An Introduction to Metallic Corrosion, 3rd ed (Metals Park, OH: ASM International 1982), p. 165.
177. R.P. Wei, J.D. Landes, Mater. Res. Std. ASTM 9(1969) p 25

178. R.P. Wei, Environmental Degradation of Engineering Materials in Aggressive Environments (Blacksburg, VA: VPI, 1981), p. 79.
179. R.R. Fessler, Pipe Line Industry 44(1976): p. 37.
180. R.N. Parkins, "Environment-Sensitive Fracture. Evaluation and Comparison of Test Methods," ASTM STP 821, p. 23.
181. M.O. Speidel, Predictive Methods for Assessing Corrosion Damage to BWR Piping and PWR Steam Generators, ed. H. Okada, R.W. Staehle (Houston, TX: NACE, 1982), p. 36.
182. W.W. Gerberich, Hydrogen Degradation of Ferrous Alloys, ed. R.A. Oriani, J.P. Hirth, M. Smialowski (Park Ridge, NJ: Noyes, 1985), pp. 366-413.
183. H. Spaehn, G.H. Wagner, U. Steinhoff, Stress Corrosion Cracking and Hydrogen Embrittlement of Iron Base Alloys, pp. 80-110.
184. S.H. Bush, R.L. Dillon, Stress Corrosion Cracking and Hydrogen Embrittlement of Iron Base Alloys, pp. 61-79.
185. J.E. Campbell, W.W. Gerberich, J.H. Underwood, Application of Fracture Mechanics for Selection of Metallic Materials (Metals Park, OH: ASM International, 1982).
186. J.M. Wells, J.D. Landes, Fracture: Interaction of Microstructure, Mechanisms and Mechanics (New York, NY: AIME, 1984).
187. Fracture Analysis, ASTM STP 560, 1974.
188. H.G. Nelson, D.P. Williams, Stress Corrosion Cracking and Hydrogen Embrittlement of Iron Base Alloys, pp. 396-398.
189. T.P. Hoar, Corros. Sci. 7(1967): p. 341.
190. F. Mazza, N.D. Greene, Proceedings 2nd International Congress on Corrosion Inhibitors, held Sept. 22-24, 1965, Italy, pp. 401-415.
191. R.W. Staehle, The Theory of Stress Corrosion Cracking in Alloys, p. 255.
192. D.V. Subrahmanyam, A.K. Agrawal, R.W. Staehle, Proceedings 7th International Congress on Metallic Corrosion (Houston, TX: NACE 1978), p. 786.
193. Y.S. Park, A.K. Agrawal, R.W. Staehle, Corrosion 35(1979). pp. 333-339.
194. M. Pourbaix, Lectures on Electrochemical Corrosion (New York, NY: Plenum Press, 1973), p. 270.
195. M F. Ashby, B. Tomkins, Mechanical Behavior of Materials, Vol. 1, ed. K.J. Miller, R.F. Smith (Oxford, England: Pergamon Press, 1980), p. 57.
196. C.M. Chen, "Computer-Calculated Potential pH Diagrams to 300°C, Volume 2. Handbook and Diagrams," EPRI Report NP-3137, 1983.
197. R.E. Barlow, F. Proschan, Statistical Theory of Reliability Testing (Silver Spring, MD. McArdle Press, 1975).
198. J.S. Bendat, A.G. Piersol, Random Data Analysis and Measurement Procedures, 2nd ed. (New York, NY: Wiley, 1986).
199. N.R. Mann, R E. Schafer, N.D. Singpurwalla, Methods for Statistical Analysis of Reliability and Life Data (New York, NY: Wiley, 1974).
200. C. Lipson, N.J. Sheth, Statistical Design and Analysis of Engineering Experiments (New York, NY: McGraw-Hill, 1973).
201. J.F. Lawless, Statistical Models and Methods for Lifetime Data (New York, NY: Wiley, 1982).
202. S. Shimada, M. Nagai, Reliability Eng. 9(1984): p. 19.
203. T. Shibata, T. Takeyama, J.I.S.I. Japan 66(1980): pp. 693-701.
204 T Shibata, T. Takeyama, Corros. Eng. 30(1981): pp. 47-53.
205 H Coriou, L. Grall, P. Olivier, H. Willermoz, Fundamental Aspects of Stress Corrosion Cracking, pp. 352-360.
206. J. Blanchet, H. Coriou, L. Grall, C. Mattieu, C. Otter, G. Turler, Stress Corrosion Cracking and Hydrogen Embrittlement of Iron Base Alloys, pp. 1149-1160.

Bibliography

1. Hydrogen Embrittlement and Stress Corrosion Cracking Meetings

Bastien, P., ed. *L'Hydrogene dans les Metaux, Congres International*, held 29 mai-2 juin, 1972. Paris, France: Editions Science et Industrie, 1972.
Devereux, O., A.J. McEvily, R.W. Staehle, eds. *Corrosion Fatigue: Chemistry, Mechanics and Microstructure*. Houston, TX. National Association of Corrosion Engineers, 1972.
Gangloff, R.P., ed. *Embrittlement by the Localized Crack Environment, Proceedings of an International Symposium*, held October 4-5, 1983. New York, NY: AIME, 1984.
Henthorne, M., ed. *Localized Corrosion—Cause of Metal Failure*, held June 27-July 2, 1971. ASTM STP 516, Philadelphia, PA: ASTM, 1972.
Jones, G., J.E. Slater, R.W. Staehle, eds. *High Temperature, High Pressure Electrochemistry in Aqueous Solutions*, International Corrosion Conference Series, NACE-4. Houston, TX: NACE, 1976.
Louthan, M.R. R.P. McNitt, eds. *Environmental Degradation of Engineering Materials—Proceedings of Conference*, held October 10-12, 1977. Blacksburg, VA: Virginia Polytechnic Institute, 1977.
Louthan, M.R., R.P. McNitt, R.D. Sisson, eds. *Environmental Degradation of Engineering Materials in Aggressive Environments, Proceedings of the Second International Conference on Environmental Degradation of Engineering Materials*, held September 21-23, 1981. Blacksburg, VA: Virginia Polytechnic Institute.
Louthan, M.R., R.P. McNitt, R.D. Sisson, eds. *Environmental Degradation of Engineering Materials in Hydrogen, Proceedings of the Second International Conference on Environmental Degradation of Engineering Materials*, held September 21-23, 1981. Blacksburg, VA: Virginia Polytechnic Institute.
Rhodin, T., ed. *Physical Metallurgy of Stress Corrosion Fracture*. New York, NY: Interscience, 1959.
Robertson, W.D., ed. *Stress Corrosion Cracking and Embrittlement*, held October, 1954. New York, NY. John Wiley & Sons, 1956.
Salesse, M., M. Chaudron, eds. *Stress-Corrosion, Delayed Failures, Fatigue-Corrosion and Relations Between These Phenomena*, 8th Colloque de Metallurgie, held June 25-26, 1964. Paris, France: Presses Universitaires de France, 1965.
Scully, J.C., ed. *The Theory of Stress Corrosion Cracking in Alloys*, NATO Science Committee Research Evaluation Conference, held March 29-April 2, 1971. Brussels, Belgium: NATO Scientific Affairs Division, 1971.
Staehle, R.W., A.J. Forty, D. van Rooyen, eds. *Fundamental Aspects of Stress Corrosion Cracking*. Houston, TX: NACE, 1969.
Staehle, R.W., J. Hochmann, R.D. McCright, J.E. Slater, eds. *Stress Corrosion Cracking and Hydrogen Embrittlement of Iron Base Alloys*. Houston, TX: NACE, 1977.
Staehle, R.W., B.F. Brown, J. Kruger, A. Agrawal, eds. *U.R. Evans Conference on Localized Corrosion*, held December 6-10, 1971, International Corrosion Conference Series, NACE-3. Houston, TX: NACE, 1971.
Symposium on Stress-Corrosion Cracking of Metals, held November 29-30 and December 1, 1944, ASTM and AIME.
Thompson, A.W., I.M. Bernstein, eds. *Effect of Hydrogen on Behavior of Materials; Proceedings of an International Conference*, held September 7-11, 1975. Warrendale, PA: The Metallurgical Society of AIME, 1976.
Thompson, A.W., I.M. Bernstein, eds. *Hydrogen in Metals, Proceedings of an International Conference on the Effects of Hydrogen on Materials Properties and Selection and Structural Design*, held September 23-27, 1973. Metals Park, OH: ASM International, 1974.
Thompson, A.W., I.M. Bernstein, eds. *Hydrogen Effects in Metals, Proceedings of the Third International Conference on Effect of*

Hydrogen on Behavior of Materials, held August 26-31, 1980. New York, NY: AIME, 1981.

Wicke, E., ed *Wasserstoff in Metallen*, Berichte der Bunsen Gesellschaft fur Physikalische Chemie, held March 20-24, 1972. Julich, Germany: 1972.

2. Techniques

Dean, S.W , E N. Pugh, G.M. Ugiansky, eds. *Environment-Sensitive Fracture: Evaluation and Comparison of Test Methods, ASTM STP 821*. Philadelphia, PA: ASTM, 1984.

Fracture Toughness Testing and its Applications, A Symposium Presented at the Sixty-Seventh Annual Meeting, ASTM STP 381. Philadelphia, PA: ASTM, 1965.

Ugiansky, G.M., J.H. Payer, eds. *Stress Corrosion Cracking—The Slow Strain Rate Technique, ASTM 665*. Philadelphia, PA: ASTM, 1979.

Raymond, L.E., ed. *Hydrogen Embrittlement Testing, ASTM STP 543*, held June 25-30, 1972. Philadelphia, PA: ASTM, 1974.

3. Basic Science

Latanision, R.M., J.R. Pickens, eds. *Atomistics of Fracture*. New York, NY: Plenum Press, 1983.

Latanision, R.M., J.T. Fourie, eds. *Surface Effects in Crystal Plasticity*. Leyden, The Netherlands. Noordhoff, 1977.

Latanision, R.M., R.H. Jones, eds. *Chemistry and Physics of Fracture*. Dordrecht, The Netherlands. Martinus Nijhoff, 1987.

Westwood, A.R.C., N.S. Stoloff, eds. *Environment Sensitive Mechanical Behavior*. New York, NY. Gordon and Breach, 1966.

4. Power Industry Applications

Ianniello, L C , ed *Stress Corrosion Cracking Problems and Research in Energy Systems*, held February 24-25, 1976. Washington, DC· U S Energy Research and Development Administration, (ERDA) 1976.

Okada, H., R.W. Staehle, eds. *Predictive Methods for Assessing Corrosion Damage to BWR Piping and PWR Steam Generators*. Houston, TX: NACE, 1982.

Roberts, J.T.A., W. Berry, eds. *Proceedings of the International Symposium on Environmental Degradation of Materials in Nuclear Power Systems—Water Reactors*, held August 22-25, 1983. Houston, TX: NACE 1984.

Speidel, M O , A Atrens, eds. *Corrosion in Power Generating Equipment, Proceedings of the Eighth International Symposium on Corrosion in Power Generating Equipment*, held September 19-20, 1983. New York, NY: Plenum Press, 1984.

Roberts, J T A , J R Weeks, G J Theus, eds. *Proceedings of the Second International Symposium on Environmental Degradation of Materials in Nuclear Power Systems—Water Reactors*, held September 9-12, 1985 LaGrange Park, IL: ANS, 1985.

Theus, G J , J R Weeks, eds. *Proceedings of the Third Symposium on Environmental Degradation of Materials in Nuclear Power Systems-Water Reactors*, held August 30-September 3, 1987. Warrendale, PA: The Metallurgical Society, 1988.

5. Fracture and Fatigue Meetings

Environment Sensitive Fracture of Metals and Alloys, Proceedings of the Office of Naval Research Workshop on Environment Sensitive Fracture of Metals and Alloys held at the Naval Research Laboratory, held June 3-4, 1985. Arlington, VA. U.S. Office of Naval Research, 1987.

Environmentally Induced Cracking. The Interaction Between Mechanisms and Design, Proceedings of the CORROSION/86 Symposium on Environmental Cracking, The Interaction Between Mechanisms and Design. Houston, TX. NACE, 1988.

Goel, V.S., ed. *Corrosion Cracking, Proceedings of the Corrosion Cracking Program and Related Papers presented at the International Conference and Exposition on Fatigue, Fracture Mechanics and Failure Analysis*, held December 2-6, 1985. Metals Park, OH: ASM International, 1986.

Miller, K.J., R.F. Smith, eds. *Mechanical Behaviour of Materials, Proceedings of the Third International Conference*, held August 20-24, 1979. Oxford, UK: Pergamon Press, 1980.

Osborn, C.J., R.C. Gifkins, eds. *Effects of Chemical Environment on Fracture Processes, Proceedings of the Third Tewksbury Symposium on Fracture*, held June 4-6, 1974.

Pratt, P.L., ed. *Fracture 1969, Proceedings of the Second International Conference on Fracture*, held April, 1969. London, UK. Chapman and Hall, 1969.

Third International Congress on Fracture, held April 8-13, 1973, Dusseldorf, FDR: V. Deutch. Eisenhuttenleute, 1973.

6. Texts

Beachem, C.D., ed. *Hydrogen Damage*. Metals Park, OH: ASM International, 1977.

Brown, B.F., ed. *Stress Corrosion Cracking Control Measures*, Houston, TX: NACE, 1981.

Davis, J.R., ed. *Metals Handbook*, Ninth Edition, Vol. 13, *Corrosion*. Metals Park, OH: ASM International, 1987.

Evans, U.R., ed. *The Corrosion and Oxidation of Metals. Scientific Principles and Practical Applications*. London, UK, Edward Arnold, 1960.

Fontana, M.G., *Corrosion Engineering*, Third Edition. New York, NY. McGraw-Hill, 1986.

Logan, H.L., ed. *The Stress Corrosion of Metals*. New York, NY. John Wiley and Sons, 1966.

Oriani, R.A., J.P. Hirth, M. Smialowski, eds. *Hydrogen Degradation of Ferrous Alloys*. Park Ridge, NJ: Noyes Publications, 1985.

Shreir, L.L., ed. *Corrosion*. London, UK: Newnes-Butterworths, 1965.

Tetelman, A.S., A.J. McEvily, eds. *Fracture of Structural Materials*. New York, NY: Wiley, 1967.

Uhlig, H.H., ed. *Corrosion Handbook*. New York, NY: Wiley, 1948.

Uhlig, H.H., R.W. Revie, eds. *Corrosion and Corrosion Control*. New York, NY: Wiley, 1985.

Discussion

B.D. Lichter (Vanderbilt University, USA): I am sure that I am expressing the sentiments of others here today by thanking you for a very impressive and synthesized account of the subject we have been discussing this week. I certainly intend to use your ideas in the classroom. I like the concept of situation-dependent strength (SDS). I also am taken by the point you made early on, and reiterated at the end, namely, the concept that materials are to be considered 'guilty' until proven "innocent." This is an important policy statement with ethical implications and relates to the professional responsibility of corrosion engineers and scientists.

In your survey of the history of this field, do you have any examples of the consequences of not applying this *caveat*? Can you give us a notion of a systematic framework for applying the *caveat* in future materials—system design? In particular, could you comment on the U.S. National Aerospace Plane (NASP) Project, where it would seem that a commitment to the use of "guilty" Ti-Al alloys has been made in 1988 with expected system implementation in 1994. This is being done prior to the solution of serious problems with this material.

R.W. Staehle. With respect to the guilty until proven innocent idea, there are two responses. First, I do not want this idea to be the basis for alarmist notions about the integrity of engineering systems and components since, in many cases, they operate reliably for their intended life in spite of the abuse inherent during operations. However, second, I intend this idea to identify the fact that all engineering materials are reactive chemicals and, in many of the environments to which the materials are exposed, engineering materials are extremely reactive chemically. The reason that such

reactive materials work is usually attributable to the formation of protective layers. The specific image I wish to portray is one in which this great chemical reactivity of engineering solids is a persistent force determined to get out by whatever avenue is available. There are many avenues by which such a persistent force can, and often does, prevail for a single alloy: stress corrosion cracking, dissolution in acidic and caustic environments, dissolution by complex-forming species, evaporation via reactions that produce volatile species, hydriding, high-temperature oxidation, and so on. With such inherent reactivity, it is incumbent upon designers and materials people together to exercise prudent care in the application of materials.

Further, the surprise should never be that materials fail, the surprise is that they work! Such a view engenders a more appropriately respectful point of view. Concerning the question of the titanium-aluminum alloy for the National Aerospace Plane, I have two ideas. One is that similarly reactive materials have been developed and used reliably in aggressive environments, but only after a very large amount of very good engineering. A good example is zirconium-base alloys, which are used as cladding for uranium in nuclear reactors. Another good example is the use of aluminum in the aerospace industry. In the latter case, it is sobering to realize that powdered metallic aluminum is used as a propellant for solid rocket motors because of its high reactivity and energy release, while the metal in bulk form is used for structural applications. The second point of view here is the example of the molybdenum, tungsten, tantalum, and niobium alloys, which cannot provide designers with the advantages inherent in their high melting points because of the volatility of their oxides at relatively low temperatures.

R.L. Jones (Pacific Northwest Laboratories, USA). I agree with you regarding the need to identify the situation-dependent performance of materials, although I would choose a term other than strength. Strength refers to intrinsic material properties, while you are using the term to indicate the extrinsic properties of materials. Fracture toughness is a better description of the extrinsic properties of materials.

I would also like to add to your excellent summary of where the environment-induced crack growth community has come since 1960. In the last 10 years or so, I feel that major progress has been made in local effects on crack growth. Evaluations of crack-tip chemistry and mechanics (local stress, strain, film-induced cleavage) and material microchemistry and microstructural effects on crack growth are examples of some crack-tip effects that have received considerable emphasis. A challenge for the future is to link these crack-tip processes to external loading and chemical conditions. Also, I feel we should be applying our knowledge of environment-induced crack growth mechanisms to newer materials, such as metal and ceramic matrix composites and intermetallic materials.

R.W. Staehle: First, regarding your question of "intrinsic" strength, it seems to me that what we know about engineering strength comes from tests conducted in nominally benign environments—but nonetheless "environments." In such environments, the strength itself is a statistical property and well known to be distributed about some mean (depending on the statistical correlation used). Further, the strength is very sensitive to metallurgical conditions resulting from the processing history and details of alloy chemistry. It seems to me that one can use the term "intrinsic" only for such structure-insensitive properties as modulus, density, specific heat.

Regarding the question of whether the strength term in my strength -dependent formulation should be strength, toughness, crack velocity, K_{Iscc}, or another is not clear to me at this time. For example, the SCC of stainless steels has very little to do with toughness. Further, I am not sure of the simplest means to portray the effects of time. Many experimentalists have found that, for very long times, there are no minima in K_{Iscc} or in endurance limits. As I refine my approach to this concept, I look forward to the suggestions of those, like you, who have wrestled with such issues.

Concerning the important contributions that are inevitable from the intersection of experiment and theory as both approach the atomistic dimensions with greater precision, I am optimistic. However, from a practical point of view, I question whether the results of such work at the atomistic level will ever really define the dependencies on material, environment, stress, geometry, temperature, and time that are necessary for the design of reliable structures. However, fundamental work continues to stimulate the community and will inevitably provide successively higher levels of rationality to engineering correlations.

F.P. Ford (General Electric R&D, USA). One of the rate-determining steps in the process of transmitting our mechanistic knowledge to life prediction is persuading the design and operating engineer to use these ideas. Do you have any ideas on how to accelerate this "engineer education" phase?

R.W. Staehle: I especially appreciate that you have raised this important question of how we all communicate effectively among the materials, design, and operating communities. One needs only to look at the persistence of failure phenomena via modes that have, for many years, been well documented in the public literature to realize that our communication is not satisfactory. In the past, means of handling the communication among these three key communities—materials, design, operator—have included codes, specifications, safety factors, interdisciplinary groups, and task forces. Whatever is implied or hoped for from such efforts has been somewhat effective but is still inadequate. I often wonder why anyone would so wantonly avoid knowing that his machine or design is clearly headed for failure, when the information that would prevent such failure is so abundant, or so predictable, or so easily obtained.

There are probably some good reasons for what has always seemed to me to be this technical masochism. One is that the inherent chemical reactivity of engineering solids is never understood nor appreciated by the design and operating communities. Incidentally, many of the materials community itself do not appreciate this fact either. This inherent chemical reactivity as an engineering reality is taught in neither mechanics or mechanical engineering courses. Second, there is the naturally human reaction to assume that these shiny metals like stainless steel and titanium have some impregnability associated with their shiny appearance! Third, it is quite unreasonable to most engineers that pure water could be an aggressive environment. Fourth, the materials community has really misled the design and operating communities with the conceptual framework of SCC and related phenomena. While such misleading has certainly not been malicious, I think that it really occurs. Let me illustrate with the following:

(1) The concept of susceptibility has been and continues to be very misleading. Charts abound with susceptible "material–environment couples." Such a concept obscures the fact that all materials in all heat treatments undergo SCC. Only the intensity of SCC changes. The concept of susceptibility has led many designers to assume that a material was not susceptible if it were not listed on a "susceptibility" table!

(2) The materials community continues to wrangle concerning the details of the "mechanism(s)" of SCC, as many of us here have been doing this week, while the designer cares only about usable strength or other indicators of mechanical performance. This endless public debate about the details has obscured the needs of the design community.

(3) The experimental testing to determine susceptibility has focused on narrowly conceived environments, assuming that such tests defined or did not define SCC in other environments. This approach has obscured the "field dependence" of SCC.

No doubt there are many other similar illustrations.

One of my reasons for proposing the concept of situation-dependent strength is to place the emphasis upon parameters that the three communities – materials, design, operator – understand. strength and measurable environmental qualities. Further, this approach makes explicit considerations that have in the past been implicit, e.g., the safety factor. For example, to the extent that strength is portrayed over a broader environmental panorama, it should be clear to the designer that sharp changes in strength may occur within the possible operating domain. Thus, rather than relying on the imprecise safety factor to catch such surprises, they can be predicted explicitly.

My primary objective in formulating the concept of situation-dependent strength is to provide a framework within which the following can be accomplished:

(1) The materials design and operating communities can communicate in a single and nonmagical language.
(2) The work of scientists studying mechanisms will have a set of objectives with respect to materials, environments, stresses, designs, temperature, and times that the scientists' proposed mechanisms must satisfy.

H. Kaesche (Freidrich Alexander University of Erlangen-Nurnburg, Federal Republic of Germany): Staehle's argument that a material should be considered guilty unless proven innocent is certainly interesting in the context of expert exchange of opinions. Since it leaves the meaning of either guilt or innocent open to speculation, it may, especially in cases of safety considerations during nonexpert exchange of opinions, become misleading. There then may be no end of claims of still unproven innocence, which of course is what is presently happening to, for instance, nuclear energy. On the other hand, the body of experts indeed tends to underestimate the degree and the impact of political decisions, of public opposition to nuclear energy. We must, of course, also be aware of the consequences of previous expert errors.

On the whole, Staehle certainly makes a number of thoroughly interesting points. He is right when he claims that, in comparison to the situation as it prevailed in the early 1960s, the field of environment-sensitive cracking has expanded far beyond what was then separately considered as being stress corrosion cracking and corrosion fatigue. At the same time, the issue of environment-sensitive cracking has become rather less mysterious, in the sense that it now seems quite obvious that the thermodynamic drive to relieve stresses by propagating cracks can operate through a number of kinetic mechanisms. Of these, some are by now well known, while others are under study. The situation is thus one of advanced knowledge, provided that the multiplicity of possible crack propagation mechanisms is properly taken into account, which of course does require quite an effort on the part of the materials scientist.

R.W. Staehle: This question of the political vs the expert s views is an important one to raise, because of the public arenas in which highly vulnerable materials operate, e.g., commercial aircraft and nuclear power. Despite the nominal sophistication of the engineers in all aspects of these and similar industries, SCC and related failures continue to occur. Therefore, those of us in the interior of the materials community look for means to call the attention of designers to the vulnerability of materials. To say that a material is guilty until proven innocent is the same as I have already noted that engineering materials are, in fact, inherently reactive. Specifically, to be "guilty" implies that the material will react, as indeed it is predisposed to do, unless it has been specifically shown by experience or testing to be stable under exactly the conditions expected in service. Conversely, to assume that the material is going to perform reliably without a prior well-established record of satisfactory performance is an unwarranted presumption of innocence.

My suggestion that guilt is a better presumption than innocence is a device to put the design and operations communities on notice that they have no basis for expecting satisfactory performance without explicit proof that the material will not degrade under the expected normal and accidental conditions. This guilty/innocent approach will force designers and operators, as well as the public, to ask more serious and relevant questions than they seem to have asked in the past I believe that by keeping these ideas of vulnerability and inherent reactivity within the confines of the technical inner circle, we have come to believe our own propaganda to the detriment of satisfactory designs This has led to insufficient money allocated to materials, prototype, scale-up, and full-scale testing. It has lead designers to believe in the invulnerability of their materials.

Concerning the major advances in understanding, I agree. Some very fine work has been conducted in many laboratories, and many of the past uncertainties have indeed been resolved. However, despite these advances, not a single modeling effort permits any prediction of the six factors of SDS.

J.M. Sarver (Babcock and Wilcox, USA): The search for SCC mechanisms and models is important; however, unless these models can be related to actual engineering problems, their practical use will be minimal. Do you believe that this link has been made adequately?

R.W. Staehle: I would refer you to my earlier response to the comments of Jones (above).

S.M. Bruemmer (Pacific Northwest Laboratories): An important aspect of the "lessons learned" you touched upon is the realization that materials selection alone cannot ensure immunity. The nuclear industry is a good example where material replacement [e g , low-carbon instead of high-carbon stainless steel in piping and higher chromium-nickel alloys instead of alloy 600 (UNS N06600) in steam generator tubing] has not ensured problem-free performance without addressing other critical aspects such as environment, stress, etc Even though "easy" material solutions to environment-induced cracking is being asked for by the design engineer, I believe we have achieved a consensus that such solutions are not possible. Total system control is necessary. As you noted, defining the limits of necessary control and selling this total concept to the designer are essential at this time.

R.W. Staehle: I agree. Starting with the basic idea that all engineering materials are reactive chemicals, the only means by which engineering materials can function as intended is to orchestrate the design and control of the environment in such a way as to account for the vulnerability of the materials. This means, as your question points out, that all aspects of entire operating systems have to be controlled vigilantly. This, incidentally, places responsibility in the hands of both the designer and the operator. The designer must have thoroughly defined the regimes of high SCC intensity and must have communicated such information clearly and persuasively to the operator.

R. Griffin (Texas A&M University, USA): This is a suggestion. Instead of "situation strength," I would suggest using "situation toughness." I think toughness is a more useful descriptor of a material's resistance to environmental cracking.

R.W. Staehle: The suggestion makes sense to me. At present, as I said earlier in response to Jones, I am not sure of the best formulation for the mechanical property that is situation dependent. It could be the yield strength, the flow stress, K_{Iscc}, crack velocity, or some other indicator

SECTION X

Final Discussion Session

Co-Chairmen's Introduction

R.P. Gangloff
University of Virginia
Charlottesville, Virginia, USA

M.B. Ives
McMaster University
Hamilton, Ontario, Canada

The final session of the conference was devoted to a general review and discussion of the events of the week, with emphasis on audience participation. Although the express purpose of the conference was to discuss and evaluate the mechanisms of environment-induced cracking, the ability of such mechanisms to provide a practical and predictive capability is clearly an important measure of the success of the research. We were therefore particularly interested in learning the views of those delegates who are responsible for combating environmental cracking in practice and for applying the results of laboratory research.

Other issues also surfaced in the session, these are recorded below, along with excerpts from the written submissions of the participants. Our goal in providing this wrap-up session and in soliciting and recording written comments was to provide all participants with a forum for their views apart from the often hectic and tumultuous sessions earlier in the week.

Views of the Participants

M.M. Hall (Westinghouse Electric Corporation, USA): Our failure-prevention design philosophy currently places heavy emphasis on the prevention of crack initiation. Unhappily, I find that there is significant variability in stress corrosion cracking initiation times for every materials application of interest to us. Conservative design practice results in large design margins (safety factors as great as 100 or more in some cases) to ensure acceptable low probabilities of component failure (viz., crack initiation). This approach can severely limit the useful lifetime of otherwise acceptable materials.

Our approach has been to seek materials and heat treatments that improve median crack initiation times. We find that, although median failure times have been significantly improved, these improvements have been accompanied in many cases by large increases in variability. This situation often results in only moderate increases in the useful lifetime of a material when much larger increases in median lifetimes have been attained. The situation is worsened by the fact that good failure statistics are difficult to obtain because of the long time required to get failures, even in accelerated tests. We need, therefore, a better understanding of the sources of variability in stress corrosion cracking initiation times, particularly in actual plant components.

Another approach that we often consider is the prevention of crack growth to critical flaw sizes whenever crack initiation prevention cannot be acceptably demonstrated. However, we just as often find that there is variability in thresholds for crack growth and crack growth rates, although we find these variabilities to be generally smaller than for stress corrosion cracking initiation times. An added problem is that design choices, which set stress and temperature levels for lowering the susceptibility to stress corrosion cracking initiation, may increase the susceptibility to crack growth. We need, therefore, a better understanding of the relationship between the conditions promoting initiation and those favoring nonpropagating cracks. The trade-offs between initiation prevention and crack growth control need to be better understood.

H.G. Nelson (NASA-Ames, USA): Considering life prediction, most engineering structures contain pre existing cracks. Emphasis in our research must address crack growth behavior. Understanding initiation contributes little to life prediction. If quantitative crack growth can be defined, both in magnitude and in terms of causal conditions (with limits of applicability), then a major contribution to life prediction will result.



Photos: M.B. Ives

D.I. Morton (Caterpillar Inc., USA): We in industry need help in avoiding stress corrosion cracking and corrosion fatigue. For example, there is a great need for higher strength fasteners. In my mind, the development of a practical economical bolt of 1350 to 1725 MPa ultimate tensile strength that will not suffer stress corrosion is of more value than knowing the exact mechanism of how stress corrosion cracking works.

J. Stewart (Harwell Laboratory, UK): This is a comment on the design engineer's plea for help in finding relevant information when trying to identify potential cracking problems in a given material/environment application. My suggestion is that knowledge-based systems can provide the database and consultancy he seeks. One such system is under development at Harwell on localized corrosion (called "Achilles"). At present it is being developed for pitting, but in the future the system will include environment-induced cracking. However, a word of caution is in order. Such systems must be developed with corrosion and computer experts working closely together.

F.P. Ford (General Electric Corporate R&D, USA): Referring to "expert systems," General Electric has developed a life-prediction system for stainless steels and nickel-base alloys in high-temperature water that relies on the integration of system monitors and modeling knowledge. The monitors essentially define the real system conditions, and the model predicts the present and future extent of cracking in that system. Such an integrated approach, known as a SMART monitor, is being used in boiling water reactors for both optimization of operating conditions (*vis à vis* cracking resistance) and for development of life-extension decisions.

H.G. Nelson (NASA-Ames, USA): Bringing material behavior into design requires the development of a trust between the materials scientist or engineer and the designer. The initial interaction between the two must come from us—we know what we can do and they do not! Once we demonstrate our contributions, our ideas will be used.

R. Griffin (Texas A&M University, USA): Design programs at universities are undergoing considerable self-examination with respect to the process of teaching design. There is a National Science Foundation-funded cooperative program at Texas A&M University that will attempt to integrate design, manufacturing, and materials. Students from mechanical, industrial, and materials engineering will have classes together. The necessary information will be given to the students as they need it and in these integrated rather than separate classes. There will be an attempt to present classroom information so that students will see that the integrated whole is more than the sum of the parts, and so that they will see how the individual parts fit together.

R.N. Parkins (University of Newcastle upon Tyne, UK). I think that to assume we can always design our way out of the environment sensitive cracking problem is a mistake. If we take the six parameters listed by Staehle earlier this morning and require that all six need to be conjointly met if cracking is to occur, this total probability can vary enormously. If one operates an ammonium nitrate evaporating tank fabricated from nonstress relieved mild steel, the probability of cracking is unity. If we take the high pressure gas pipeline cracking problem, the chances of each of the controlling parameters being met is probably about one in ten, so that the probability of a joint of pipe failing is about 1 in 105. In some cases, that probability may be even less. In such circumstances, even if the problem could be identified at the design stage, it may not be economically worthwhile to do other than live with the problem – that is, to accept that cracking will occur. In other cases, it may be that the probability of cracking cannot be anticipated at the design stage, for example, because the structure is exposed to an environment not anticipated by the designer.

In those circumstances in which living with cracking has to be accepted, remaining life prediction becomes very important. For the latter, reliable information is required on crack growth rates, and that is where knowledge of crack growth mechanisms becomes important. If the appropriate measurements are to be made, what is also needed in relation to life prediction is a much better understanding of slow crack coalescence and of the effective fracture toughness of structures containing colonies of cracks that are not coplanar and are of different sizes.

D. Hardie (University of Newcastle upon Tyne, UK). With regard to standard tests, it is important to have a mechanistic back-up. As Parkins pointed out, such understanding is essential in choosing a material for particular conditions. The standardization may not cover some particular combination of conditions. It is well known, for instance, by people working with aluminum alloys that application of a potential of 250 mV_{SCE} in an aqueous environment will bring about rapid failure in any of these alloys, yet, at one time, this was considered by some as a suitable test for selection.

M.M. Hall: I consider the slow-strain-rate method to be a useful test that could be made more useful by improvements in the mechanical aspects and understanding of these tests. My inclination is to apply strain energy concepts to the initiation and growth of stress corrosion cracking cracks and to apply the slow-strain-rate test to accelerate stress corrosion cracking initiation and growth. The slow-strain-rate test equipment being used in our laboratory (and apparently in many others) has significant limitations to determine the stress and strain rates applied to the specimen. This is due to the fact that the machines are not very good mechanical test beds. The load train is compliant and is subject to large load variation because of variations in temperature between the specimen and load frame. This uncertainty could be reduced by the use of a stiff load frame and better temperature control and temperature compensation of the applied displacements. *In situ* strain and crack monitors are needed to improve our knowledge of specimen strain and crack length. Smooth specimens may be suitable for stress corrosion cracking initiation studies using crack monitoring methods, but may be unsuitable for crack growth studies because of the difficulty of monitoring the length of multiple cracks. Effort should be applied to the development of these improved equipment and test specimen designs.

T. Murata (Nippon Steel, Japan): Extensive studies on the cracking behavior of steels in anhydrous ammonia have been done in Japan. We believe that for low- and medium-strength steels, active path corrosion is the dominant mechanism of cracking, but hydrogen-assisted cracking may occur in high-strength steel. The difficulty in obtaining a quantitative understanding of liquid ammonia cracking is the variation of chemical composition in ammonia and obtaining dynamic measurements *in situ*. However, we have some consensus on how this cracking may be prevented through the control of residual stresses, temperature, and chemistry of liquid ammonia.

R.P.M. Procter (University of Manchester Institute of Science and Technology, UK): The cracking of carbon-manganese steels in anhydrous ammonia is one important specific industrial problem that merits further basic research. At UMIST we are doing some work in this environment using a slow-strain-rate test rig/autoclave assembly. However, anhydrous liquid ammonia is an extremely difficult and potentially dangerous system to work with. One way of circumventing some of these difficulties and dangers is to work with anhydrous methanol-ammonia solutions. These will cause transgranular cracking of carbon-manganese steels at ambient temperatures and pressures, they are much less hazardous, and there are many similarities (effects of contaminants, potential, etc.) between the two environments.

B. Cox (University of Toronto, Canada). The fundamental mechanistic questions seem to remain the same from conference to conference, but perhaps of more concern, so do the experimental techniques. There seems to remain a reluctance to use modern physical techniques for investigation. Perhaps they are inappropriate if they cannot give *in situ* information. Nonetheless, as in many other fields, there seems to be a growing emphasis on modeling, and again, as in other fields, this seems to be regarded as a substitute for experimentation.

R. Jones (Pacific Northwest Laboratories, USA). There are advances being made in the area of *in situ* surface probes, such as laser Raman and nonlinear optical techniques. The nonlinear optical technique has the potential to measure monolayer surface chemistry

on a surface in an aqueous/liquid environment. The need for these measurements is obvious, since the transfer of a sample from the environment of interest to a remote analytical instrument may affect surface reaction products.

T. Murata: With respect to future measurement systems to be used in corrosion science and technology, I would strongly suggest consideration of the importance of *in situ* measurements with two-dimensional variation Such techniques will enable us to assess the heterogeneity of a corroding surface or corrosion products. Examples include laser-enhanced ellipsometry and laser Raman spectroscopy.

R.W. Staehle (University of Minnesota, USA): Rather than thinking only of a single mechanism for propagating cracks, we might think of simultaneous processes For example, a combination of dealloying, hydrogen, and induced slip. We could then allocate different fractions of the effect of the multiple mechanisms, depending on changes in alloy and environment.

Regarding the future· I believe that intelligent people will continue to do the research that is demanded by the state of knowledge and will develop good approaches. I believe that the future will be more defined by creating institutional approaches and by building better connections between the materials and the design communities and between engineers and scientists.

Suggestions for Specific, Unanswered Fundamental Questions and New Research Directions

R Martin (Petrolite Corporation, USA): The reasons for the failure of most tests to predict the service life of metal components must be explained.

R. Griffin: Environmental cracking methodologies must be applied to characterize advanced materials, including composites, plastics and metal matrix composites Environmental cracking studies and information must be coupled with designers and specific engineering applications.

D. Hardie: Attempts must be made to bridge the gap between atomistic models and practical situations, particularly with respect to metallurgical considerations More information is required about the constitution character, and properties of passive films and dealloyed layers, as well as the detailed structure of the substrate.

M.N. Hall: Greater emphasis should be placed on establishing stress or stress-related parameters for correlation of stress corrosion cracking initiation and crack growth with material microstructures and environmental conditions The designer has the tools to calculate elastic and elastic-plastic stress and strain parameters. I view the mistrust by some of the stress-intensity factor as an unfortunate failure to focus on the strain energy foundations that support this and all other fracture criteria The transition between deep-notched and precracked test results and those obtained on smooth specimens can be more easily made if one focuses on elastic strain energy density (viz., K^2/E) as the driving force for crack initiation and growthin cases of limited plasticity. A problem exists in relating results obtained in deep-notched specimens, which are predominantly elastic, with smooth specimens such as slow-strain-rate specimens, which are grossly plastic. There is a need to develop an appropriate strain energy fracture criterion (both initiation and crack growth) for the slow-strain rate and statically loaded smooth specimen, and to relate this to the stress-intensity factor parameters used for deep-notched and precracked specimens. Ranges of validity must be established for each.

K.L. Wrisley (Rensselaer Polytechnic Institute, USA): Techniques must be developed and standardized for determining the environment at and near the crack tip.

L. Germeys (Avesta A B, Sweden): Much more emphasis has to be put on crack initiation and the design of experiments that provide reliable data for service conditions.

F.P. Ford: Environmental cracking mechanisms must be quantified and validated. The hydrogen embrittlement models must be made quantitative if they are to be useful.

R.L. Sindelar (E.I. du Pont de Nemours Co. Inc., USA): The connection between laboratory tests and service experience needs to be established. Environmental-cracking-resistant alloys must be designed and demonstrated.

R. Oltra (Universite de Bourgogne, France): The effect of dissolution on the relief of strain hardening must be determined. Strain rate at the crack tip and micromechanical studies of crack-tip processes are required.

M.R. Jarrett (Alcan International Limited, UK): The interaction of hydrogen with the mechanical fracture process leading to failure in bulk specimens must be defined.

A. Turnbull (National Physical Laboratory, UK): The need exists to define the details of the electrochemical kinetics at the crack tip. This information is essential to both the qualitative and quantitative predictions of cracking.

We need to move forward from qualitative explanations of cracking behavior to the development of quantitative predictive models in relation to (1) hydrogen cracking associated with enhanced localized plasticity and (2) film-induced cleavage. The development of such models, and the application to experimental data, will help resolve the relevance of competing mechanisms.

L.E. Willertz (Pennsylvania Power and Light Company, USA): Fracture morphology and how it is affected by environment appears to be one area that will provide research opportunities and practical applications for those doing failure analysis.

J. Stewart: Crack initiation in many systems has not been satisfactorily addressed.

H.-J. Engell (Max Planck Institut fur Eisenforchung, Federal Republic of Germany): We must develop better methods for experimental investigations of mechanical and electrochemical conditions and processes immediately at the crack tip.

R. Jones: It is necessary to provide better analytical characterizations of dealloyed layers, using methods such as scanning tunneling microscopy. It is also important to seek better measurements and analytical descriptions of crack-tip strain rates and chemistry.

D.B. Kasul (Michigan Technological University, USA): The effects of microplasticity, either preceding or accompanying environmental cracking, must be specifically characterized.

Author Index

A

Atrens, A. 513

B

Ballinger, R.G. 241
Bertocci, U. 273
Beitscher, S. 429
Birnbaum, H.K. 21
Blondeau, R. 531
Boukerrou, A. 223
Bruemmer, S.M. 287
Burnette, C.C. 401

C

Charles, J. 531
Chatterjee, U.K. 397
Chen, S. 167
Cheviet, A. 531
Clarke, C.F. 419
Cottis, R.A. 223
Coudreuse, L. 531
Crompton, J.S. 383

D

Desai, V. 549
Desestret, A. 207
Duffo, G.S. 261
Duquette, D.J. 45

E

Elboujdaini, M. 365
Elliott, C.K. 241
Erlings, J.G. 229

F

Festen, M.M. 229
Flanagan, W.F. 251
Ford, F.P. 139
Fransz, R.A. 229
Friedersdorf, F. 549

G

Galibois, A. 365
Galvele, J.R. 261
Gangloff, R.P. 55,233
Gates, J.D. 513
Garud, Y.S. 415
Gerberich, W.W. 167
Ghali, E. 365

H

Haritopoulos, P. 223
Hardie, D. 347,419
Hehemann, R.F. 527
Heldt, L.A. 219
Hepples, W. 383
Hochman, R.F. 541
Holroyd, N. 311,371,383
Hwang, I.S. 241

I

Ikeda, B.M. 419
Iyer, R.N. 527,545

J

Jani, S.C. 541
Jarrett, M.R. 383
Jones, D.A. 265
Jones, R.H. 287
Joosten, M.W. 401

K

Kassner, M.E. 429
Kasul, D.B. 219
Kim, Y.S. 371
Kolts, J. 401
Komai, K. 213

L

Lee, J.B. 251
Lewandowski, J.J. 371
Liao, C.-M. 379
Lichter, B.D. 251

M

McIlree, A.R. 415
Marek, M. 541
Markfield, A. 223
Mehta, A. 489
Meletis, E.I. 541
Minoshima, K. 213
Miyuki, H. 407
Murata, T. 437

N

Nagano, H. 407
Nakasa, K. 537
Newman, R.C. 489,555

O

Oltra, R. 207
Oriani, R.A. 439

P

Parkins, R.N. 1
Piascik, R.S. 233
Pineau, A. 111
Pound, B.G. 203
Procter, R.P.M. 555
Pugh, E.N. 273

R

Ramamurthy, S. 513
Ricker, R.E. 273
Rieck, R.M. 513
Rosen, R. 429

S

Saenz de Santa
Maria, M. 193,523
Scott, P.M. 517
Shaw, T. 549
Shih, H.C. 389
Sieradzki, K. 125
Sircar, S.C. 397
Smith, I.O. 513
Spaehn, H. 449
Staehle, R.W. 561
Stewart, J. 517
Stoloff, N.S. 31
Suzawa, M. 537

T

Tokimasa, K. 407
Turnbull, A. 193,523
Tzou, R.J. 389

V

Vereecken, J. 425

W

v.d. Wekken, C.J. 197
Wenyue, Z. 555
White, C.L. 219
Wells, B. 517

Y

Yamanaka, K. 407

Z

Zhang, X.G. 425
Zhu, M. 251

Chairmen/Rapporteur Index

Asphahani, A.I. 271
Briant, C.L. 511
Bruemmer, S.M. 189
Engell, H.-J. 435
Ford, F.P. 435
Gangloff, R.P. 559,613
Heldt, L.A. 363
Ives, M.B. vii,559,613
Kaesche, H. 435
Komai, K. 43
Lichter, B.D. 363
Mazza, F. 271
Pelloux, R. 43
Procter, R.P.M. 511
Pugh, E.N. vii
Turnbull, A. 123
Wei, R.P. 189

Subject Index

304: 3, 18, 22, 23, 28, 64, 84, 92, 96, 148, 150, 157, 164, 165, 176, 261, 265, 291, 293, 296, 363, 418, 429, 436, 492, 493, 494, 495, 497, 498, 500, 501, 502, 507, 508, 509, 512, 517, 520, 543
304L: 430, 500, 512, 541
316: 22, 23, 32, 33, 148, 291, 293, 364, 401, 402, 418, 470, 471, 473, 494, 498, 499, 507, 512, 543, 549, 550, 552
316L: 113, 207, 229, 231, 460, 461, 499, 549, 570
310: 22, 176, 274, 284, 345, 452, 494, 498, 499, 500, 507, 509, 543, 549, 600
316L: 113, 207, 229, 231, 460, 461, 499, 549, 570
316: 22, 23, 32, 33, 148, 291, 293, 364, 401, 402, 418, 470, 471, 473, 494, 498, 499, 507, 512, 543, 549, 550, 552
410: 401, 450, 451, 452, 454, 479, 481, 523
430: 13, 252, 254, 255, 259, 478
600: 58, 77, 91, 113, 203, 287, 288, 289, 290, 291, 292, 293, 295, 296, 297, 299, 300, 302, 303, 305, 309, 310, 350, 364, 407, 408, 409, 410, 413, 415, 416, 417, 418, 429, 436, 450, 451, 478, 479, 480, 501, 502, 503, 507, 508, 509, 550, 564, 568, 569, 570, 571, 573, 576, 583, 584, 586, 587, 588, 591, 592, 593, 594, 596, 598, 599, 601, 612
800: 34, 169, 293, 305, 350, 356, 458, 459, 483, 570
825: 34, 309, 364, 403, 404
1020: 62, 67, 74, 344
1095: 171
2000 series: 62, 74, 233, 239
2024: 34, 314
2090: 62, 74, 233, 235, 236, 237, 238, 239
2XXX: 311, 313, 319, 330, 331, 333, 334, 345
4130: 61, 99, 444
4140: 31, 32, 74
4340: 32, 57, 58, 75, 169, 173, 175, 178, 181, 203, 204, 205, 299, 443, 445, 534, 537, 538, 539
5XXX: 311, 319
6061: 35, 365, 366, 368, 369
7000 series: 62, 70, 74, 79, 80, 93, 235, 237, 238, 345, 379
7075: 23, 34, 35, 40, 70, 74, 93, 94, 96, 233, 235, 237, 238, 239, 314, 316, 318, 326, 574
7079-T651: 58, 74, 182, 320, 321, 322, 323, 324, 325, 326, 330, 333, 335
718: 23, 111, 113, 114, 116, 117, 118, 120, 121, 122, 288, 289, 290, 291, 292
7XXX: 311, 313, 314, 319, 320, 322, 323, 324, 325, 326, 327, 328, 330, 331, 333, 334, 335, 338, 339, 343, 344, 345, 385
Al 6351: 365, 368, 369
API 5L X60: 229, 231
X-750: 241, 242, 247, 248, 288, 289, 290, 291, 292, 293, 295, 296, 297, 303, 305, 504

A

absorption: 2, 114, 141, 143, 151, 189, 241, 298, 299, 300, 344, 351, 529
acetate(s): 9, 88, 203, 278, 389, 475, 494
acid, hydrochloric: 242, 351, 361, 401, 402, 405
acid, nitric: 190, 219, 336, 347, 352, 402, 403, 410, 438, 456, 468, 470, 486, 512, 527, 529, 572, 594
acid, polythionic: 418, 502, 503, 588
acid, salts: 14, 95, 141, 163, 262, 264, 326, 327, 358, 402, 476, 523, 587
acid, sulfuric: 190, 402, 403, 410, 438, 456, 468, 470, 486, 512, 527, 529
acoustic emission(s): 2, 34, 40, 123, 143, 173, 177, 183, 186, 281, 305, 309, 331, 333, 344, 508
adsorption: 33, 38, 41, 60, 81, 128, 133, 134, 136, 141, 153, 221, 266, 267, 280, 281, 284, 358, 361, 397, 398, 399, 404, 422, 427, 429, 439, 441, 444, 446, 492, 537, 539, 540, 564, 576, 586
alloy(s): See specific alloys
alloying: 4, 5, 17, 18, 86, 140, 164, 181, 268, 275, 287, 288, 289, 290, 303, 351, 352, 356, 357, 358, 365, 383, 399, 407, 419, 436, 455, 460, 468, 474, 483, 489, 500
aluminum-lithium: 239, 331
ammonia: 6, 10, 17, 18, 144, 164, 187, 192, 268, 271, 273, 274, 275, 276, 277, 278, 279, 280, 281, 282, 285, 330, 393, 398, 452, 489, 496, 507, 549, 555, 557, 568, 569, 572, 574, 587, 598, 614
ammonium chloride: 3, 4, 6, 8, 14, 17, 18, 136, 141, 163, 165, 199, 268, 327, 330, 339, 353, 389, 438, 451, 493, 494, 508, 570, 587, 614
anion(s): 5, 147, 149, 152, 190, 276, 320, 421, 502
anodic attenuation: 265, 268, 269
anodic dissolution: 2, 17, 47, 51, 59, 60, 62, 74, 79, 81, 82, 83, 86, 88, 91, 106, 127, 135, 163, 164, 190, 207, 208, 209, 210, 226, 239, 251, 252, 257, 259, 264, 265, 266, 267, 268, 269, 273, 280, 285, 296, 303, 311, 313, 316, 319, 322, 324, 330, 335, 336, 340, 343, 344, 345, 347, 353, 354, 355, 358, 361, 363, 364, 365, 368, 385, 389, 392, 393, 394, 397, 410, 425, 427, 438, 450, 451, 460, 465, 472, 479, 484, 486, 502, 508, 511, 513, 520, 543, 555
anodic protection: 465, 474, 487, 519, 520
ASTM: 19, 33, 64, 66, 191, 194, 233, 235, 273, 383, 389, 419, 420, 517, 523, 567, 574, 575, 609, 610
atomistic: 59, 107, 123, 125, 127, 128, 134, 135, 137, 143, 167, 183, 190, 302, 512, 541, 574, 575, 611, 615
attack, intergranular: 1, 2, 3, 4, 5, 6, 9, 10, 17, 18, 24, 25, 29, 33, 34, 51, 62, 71, 77, 79, 80, 81, 89, 90, 95, 96, 98, 108, 111, 112, 113, 114, 117, 121, 123, 125, 127, 129, 134, 135, 136, 137, 140, 142, 143, 150, 156, 163, 165, 167, 171, 173, 174, 177, 178, 182, 191, 192, 220, 233, 235, 237, 238, 241, 242, 243, 246, 248, 251, 259, 261, 262, 263, 264, 268, 269, 271, 273, 276, 277, 280, 281, 283, 284, 285, 287, 288, 289, 290, 291, 293, 294, 295, 298, 299, 300, 301, 302, 303, 305, 309, 310, 311, 317, 319, 330, 333, 339, 343, 344, 345, 348, 351, 353, 354, 355, 356, 358, 359, 361, 363, 364, 365, 366, 368, 369, 371, 373, 376, 379, 380, 381, 383, 384, 392, 393, 394, 395, 397, 398, 399, 401, 403, 405, 407, 413, 415, 418, 433, 436, 437, 438, 448, 449, 450, 451, 452, 454, 455, 461, 481, 482, 491, 493, 494, 495, 496, 497, 498, 499, 500, 501, 502, 503, 504, 508, 509, 511, 513, 515, 517, 520, 527, 528, 529, 533, 539, 541, 542, 549, 552, 555, 556, 558, 562, 564, 568, 569, 570, 571, 572, 573, 574, 576, 578, 579, 583, 584, 586, 587, 591, 593, 594, 595, 596, 614
Auger method: 3, 4, 66, 67, 93, 114, 191, 192, 259, 294, 309, 316, 371, 372, 373, 420, 422, 443, 456, 490, 507

B

base(s): 25, 98, 114, 235, 277, 278, 328, 352, 355, 358, 437, 467, 476, 486, 550, 575, 579, 586, 596, 609
body-centered cubic: 2, 23, 25, 125, 178, 181, 186, 442, 444, 541, 568, 585
boiler(s): 1, 452, 476
boiling water reactor(s): 80, 289, 290, 418, 570, 574, 591, 610
bonding: 25, 75, 123, 127, 130, 143, 302, 430, 448
brass: 3, 5, 6, 10, 12, 17, 18, 31, 37, 140, 165, 172, 174, 183, 192, 219, 221, 251, 262, 266, 268, 273, 275, 276, 277, 278, 279, 280, 281, 282, 283, 284, 285, 363, 389, 390, 391, 392, 393, 394, 395, 397, 398, 399, 491, 496, 497, 498, 501, 509, 574
brass, 70/30: 23, 37, 59, 62, 73, 91, 92, 144, 171, 172, 175, 177, 208, 242, 255, 257, 280, 285, 290, 291, 294, 297, 313, 314, 318, 322, 335, 336, 352, 371, 389, 392, 393, 394, 418, 445, 446, 450, 451, 452, 454, 458, 461, 470, 476, 477, 480, 481, 498, 517, 556, 574, 596, 598, 599, 600, 601, 603
brass, admiralty: 174, 183, 393, 574

C

cadmium: 32, 33, 34, 40
carbide precipitation: 79, 113, 289, 291, 303, 305, 410, 413, 503, 511, 520
carbon: 4, 17, 28, 31, 49, 59, 61, 62, 69, 70, 75, 77, 99, 117, 140, 141, 147, 268, 291, 330, 361, 372, 401, 413, 436, 437, 438, 440, 453, 455, 461, 479, 482, 502, 507, 555, 556, 568, 570, 580, 583
carbonate: 18, 88, 147, 165, 229, 237, 326, 328, 399, 438
cathodic protection: 109, 195, 246, 347, 351, 353, 355, 357, 419
458, 465, 481, 483, 555
cation(s): 60, 86, 87, 147, 163, 164
caustic embrittlement: 1, 164, 287, 289, 291, 292, 293, 303, 305, 332, 407, 409, 410, 413, 456, 489, 500, 501, 503, 568, 570, 572, 593, 611
cavitation: 111, 112, 113, 121, 453, 464, 480, 483
charge density: 10, 13, 126, 127, 142, 150, 152, 304, 361, 507, 578

charging: 21, 22, 23, 24, 27, 37, 169, 176, 181, 193, 194, 195, 203, 204, 205, 243, 257, 269, 281, 285, 293, 294, 295, 298, 300, 302, 303, 311, 318, 352, 403, 439, 440, 442, 443, 500, 511, 525, 526, 527, 528, 529, 531
chemisorption: 51, 75, 81, 333
chloride: 6, 7, 17, 18, 27, 58, 59, 60, 62, 64, 66, 67, 68, 69, 70, 71, 72, 73, 74, 76, 77, 79, 80, 81, 86, 87, 88, 89, 90, 91, 93, 95, 96, 97, 98, 99, 106, 108, 136, 140, 144, 147, 163, 164, 199, 207, 208, 217, 225, 227, 233, 235, 238, 251, 252, 258, 259, 268, 269, 270, 273, 278, 281, 282, 285, 293, 319, 320, 321, 322, 324, 327, 328, 329, 330, 333, 338, 343, 345, 347, 351, 352, 353, 354, 355, 356, 357, 363, 364, 365, 389, 393, 395, 399, 407, 419, 421, 436, 437, 438, 449, 450, 451, 454, 455, 456, 458, 461, 476, 477, 479, 480, 481, 482, 483, 484, 486, 487, 489, 490, 491, 492, 494, 495, 496, 497, 498, 499, 500, 501, 502, 507, 508, 509, 512, 523, 541, 543, 545, 546, 548, 549, 550, 552, 566, 568, 569, 570, 571, 572, 580, 581, 591, 602
chloride ions: 199, 329, 345, 352, 399, 461, 481, 494, 495, 498, 502
chlorine: 28, 40, 135, 136, 353, 439, 440, 568, 569, 573, 586
chromium: 79, 86, 87, 99, 122, 140, 156, 164, 195, 243, 291, 436, 450, 451, 452, 453, 454, 455, 456, 460, 461, 468, 471, 476, 478, 479, 481, 483, 484, 486, 487, 490, 492, 500, 503, 517, 520, 523, 524, 577
cladding: 32, 290, 573, 611
cleavage mechanism(s): 18, 22, 142, 282, 285, 436, 508, 556
cold work: 1, 31, 288, 289, 295, 298, 300, 310, 397, 399, 401, 435, 494, 496, 499, 509, 586
combustion, gases: 55, 60, 64, 74, 75, 76, 85, 88, 89, 90, 95, 97, 117, 319, 365, 523, 565, 592
conductivity: 55, 64, 68, 92, 148, 152, 156, 157, 195, 242, 248, 274, 304, 326, 383, 384, 385, 490, 517, 555, 566
constant-extension-rate testing: 293, 295, 296, 297, 298, 305, 363
copper: 6, 10, 12, 13, 31, 43, 46, 47, 48, 49, 50, 51, 79, 108, 177, 186, 191, 192, 251, 252, 257, 259, 261, 265, 273, 274, 275, 276, 277, 278, 280, 281, 282, 283, 284, 285, 313, 314, 315, 316, 317, 318, 331, 337, 343, 345, 363, 383, 386, 389, 393, 398, 399, 403, 404, 440, 446, 455, 481, 489, 568, 574, 578, 579, 584, 587, 588, 602
copper-gold: 144
corrosion fatigue: 1, 7, 14, 43, 45, 46, 48, 49, 50, 51, 52, 55, 56, 57, 58, 59, 60, 61, 62, 64, 66, 67, 68, 69, 70, 71, 72, 73, 74, 75, 76, 77, 79, 80, 81, 82, 83, 84, 85, 86, 87, 88, 89, 90, 91, 92, 93, 94, 95, 96, 97, 98, 99, 101, 106, 107, 108, 109, 114, 118, 120, 139, 140, 141, 144, 149, 150, 155, 156, 157, 158, 168, 193, 194, 195, 197, 198, 199, 200, 201, 213, 217, 223, 224, 226, 227, 233, 235, 236, 237, 238, 239, 241, 242, 243, 246, 249, 265, 269, 284, 331, 335, 336, 339, 345, 351, 358, 361, 436, 437, 449, 450, 458, 459, 461, 464, 465, 467, 468, 469, 470, 471, 472, 474, 475, 476, 477, 478, 479, 480, 481, 482, 483, 484, 486, 487, 498, 561, 566, 568, 574, 584, 589, 590, 609, 612, 614
corrosion product(s): 96, 163, 224, 227, 238, 436, 438, 507, 565
crack branching: 2, 508, 512, 537, 538, 539, 540, 543
crack closure: 43, 55, 61, 62, 64, 66, 68, 69, 75, 77, 86, 92, 94, 95, 96, 97, 101, 118, 122, 223, 227, 233, 237, 238
crack growth data: 43, 117, 120, 243, 289, 297, 323, 351
crack initiation: 5, 6, 13, 37, 38, 43, 45, 46, 47, 49, 50, 51, 52, 56, 60, 73, 74, 79, 99, 107, 108, 111, 113, 114, 117, 121, 122, 139, 140, 143, 154, 165, 167, 168, 169, 172, 173, 175, 187, 189, 190, 191, 207, 213, 214, 215, 216, 217, 220, 221, 223, 226, 229, 231, 254, 256, 267, 275, 277, 284, 289, 295, 296, 297, 299, 321, 331, 336, 337, 350, 355, 371, 373, 376, 397, 398, 418, 425, 426, 427, 438, 443, 450, 452, 455, 461, 468, 470, 471, 472, 473, 474, 475, 479, 481, 483, 486, 490, 492, 494, 502, 511, 512, 513, 517, 518, 519, 520, 524, 545, 613, 615
crack mechanics: 68, 77, 84, 86, 94, 97, 106
crack propagation databases: 62, 106
crack propagation rate: 57, 70, 81, 83, 88, 89, 111, 119, 139, 140, 141, 142, 143, 144, 147, 150, 151, 152, 153, 154, 155, 156, 158, 163, 164, 187, 247, 248, 259, 261, 262, 263, 408, 435, 464, 465, 483, 549, 552
crack velocity: 10, 11, 13, 14, 15, 18, 40, 164, 165, 178, 187, 195, 219, 220, 259, 261, 273, 282, 295, 296, 297, 298, 304, 305, 320, 321, 323, 324, 333, 335, 336, 338, 340, 350, 351, 353, 354, 356, 361, 371, 379, 438, 439, 446, 492, 493, 494, 513, 514, 515, 562, 563, 568, 582, 588, 611, 612
cracking: See specific entries
cracking, Stage I: 40, 46, 51, 71, 80, 107, 108, 120, 178, 219, 220, 221, 294, 295, 296, 297, 298, 304, 305, 363, 435, 439, 446, 543, 549, 550, 582
creep: 11, 17, 28, 41, 43, 50, 51, 111, 112, 113, 114, 119, 120, 121, 122, 126, 127, 141, 153, 155, 157, 165, 187, 191, 229, 230, 231, 232, 263, 264, 265, 269, 284, 314, 344, 353, 356, 371, 376, 377, 429, 430, 431, 455, 482, 513, 514, 515, 527, 528, 529, 531, 545, 546, 547, 566, 600
crevice(s): 147, 235, 355, 364, 403, 419, 420, 421, 422, 423, 424, 427, 453, 459, 464, 465, 476, 479, 481, 483, 484, 490, 491, 492, 494, 496, 508, 509, 573, 583, 591
current density: 7, 8, 10, 18, 47, 92, 107, 141, 147, 150, 151, 152, 163, 165, 193, 194, 243, 246, 247, 248, 257, 262, 263, 268, 274, 294, 295, 298, 299, 302, 303, 304, 305, 352, 354, 365, 366, 368, 426, 449, 468, 483, 486, 492, 493, 502, 515, 523, 527, 555, 577
cyclic plastic strain: 43, 46, 49, 56, 57, 76, 79, 82, 84, 89, 97, 99, 107, 122, 142, 464, 465, 481

D

deaeration: 147, 156, 197, 200, 203, 233, 235, 237, 252, 261, 287, 289, 290, 291, 293, 296, 303, 352, 366, 401, 402, 491, 523, 527, 545, 584, 598, 599
dealloying: 10, 18, 123, 125, 134, 135, 136, 137, 143, 165, 178, 179, 190, 191, 192, 251, 252, 253, 257, 258, 259, 268, 273, 276, 278, 280, 281, 282, 284, 285, 309, 359, 361, 436, 489, 490, 491, 492, 494, 496, 497, 498, 499, 501, 503, 507, 508, 509, 615
decohesion: 21, 24, 25, 27, 28, 31, 34, 37, 38, 39, 40, 59, 171, 172, 176, 177, 178, 181, 183, 237, 299, 301, 302, 309, 332, 333, 371, 373, 435, 438, 439, 440, 441, 442, 443, 445, 446, 448, 481, 576, 578, 580
density: 13, 28, 31, 43, 50, 83, 85, 91, 92, 126, 127, 129, 142, 146, 199, 203, 204, 205, 219, 220, 221, 222, 269, 289, 290, 347, 349, 361, 444, 486, 507, 524, 545, 547, 548, 578, 611, 615
depassivation: 49, 207, 208, 209, 210, 449, 460, 461, 473, 483, 486
desorption: 299, 397, 422, 444
dezincification: 251, 280, 281, 285, 363, 393, 397, 578
diffusion: 4, 13, 14, 21, 22, 23, 24, 27, 28, 31, 38, 39, 43, 59, 61, 70, 72, 86, 89, 90, 91, 95, 99, 108, 114, 116, 142, 143, 146, 147, 148, 150, 151, 152, 163, 164, 169, 175, 189, 192, 195, 197, 198, 199, 201, 203, 204, 210, 261, 262, 263, 264, 267, 268, 269, 274, 275, 278, 291, 300, 301, 322, 324, 325, 332, 334, 335, 336, 338, 350, 351, 352, 353, 354, 355, 356, 361, 371, 373, 376, 420, 422, 424, 429, 439, 440, 444, 445, 446, 449, 452, 454, 455, 482, 496, 498, 499, 508, 520, 523, 524, 525, 527, 539, 543, 566, 579
dislocation: 2, 3, 5, 6, 18, 21, 23, 24, 27, 28, 29, 31, 33, 34, 36, 37, 39, 41, 43, 46, 48, 49, 50, 51, 59, 60, 66, 74, 79, 94, 96, 101 107, 112, 113, 125, 129, 133, 134, 136, 137, 141, 142, 144, 145, 153, 154, 155, 164, 165, 167, 169, 171, 173, 174, 177, 178, 179, 180, 181, 182, 183, 186, 187, 219, 220, 221, 222, 232, 238, 252, 264, 265, 268, 269, 276, 282, 283, 284, 288, 289, 290, 299, 300, 301, 302, 303, 308, 309, 310, 314, 317, 318, 324, 333, 354, 361, 364, 397, 399, 416, 425, 427, 428, 435, 441, 442, 443, 446, 448, 449, 454, 458, 472, 479, 482, 511, 512, 513, 514, 515, 524, 527, 528, 529, 530, 533, 541, 542, 543, 545, 547, 578
dissolution: 1, 3, 4, 5, 6, 7, 9, 10, 13, 18, 31, 45, 46, 48, 49, 50, 55, 56, 70, 72, 77, 85, 87, 92, 93, 96, 98, 99, 108, 125, 139, 140, 141, 142, 147, 149, 150, 152, 153, 156, 158, 165, 167, 177, 178, 179, 189, 192, 200, 221, 227, 233, 236, 237, 238, 247, 258, 276, 277, 278, 281, 282, 284, 289, 304, 305, 314, 317, 329, 366, 384, 399, 401, 407, 409, 422, 428, 436, 468, 474, 475, 483, 489, 490, 491, 492, 493, 497, 498, 499, 500, 501, 512, 515, 545, 547, 568, 576, 577, 578, 579, 580, 586, 596, 603, 604, 611, 615
duplex steel: 207, 208, 209, 210, 211, 229, 449, 458, 460, 470, 486

E

electrolyte(s): 9, 55, 58, 60, 68, 73, 74, 79, 84, 85, 86, 87, 88, 89, 98, 189, 190, 203, 208, 235, 238, 242, 243, 245, 246, 248, 298, 299, 303, 334, 366, 425, 427, 438, 518
embrittlement, hydrogen: 2, 13, 21, 22, 23, 24, 25, 37, 55, 56, 59, 71, 72, 74, 82, 83, 85, 86, 87, 88, 89, 95, 106, 107, 109, 125, 139, 141, 143, 167, 189, 190, 203, 207, 208,

209, 210, 213, 217, 229, 233, 235, 237, 238, 239, 249, 261, 271, 273, 278, 279, 280, 281, 282, 284, 309, 311, 318, 334, 344, 347, 353, 359, 361, 363, 364, 365, 368, 385, 401, 403, 419, 423, 425, 427, 429, 435, 436, 439, 440, 441, 442, 443, 448, 450, 451, 454, 455, 482, 486, 489, 509, 511, 512, 513, 527, 528, 530, 531, 534, 555, 561, 568, 569, 578, 580, 603, 604, 609, 610, 615
embrittlement, liquid-metal: 13, 31, 32, 40, 107, 136, 137, 167, 172, 181, 183, 186, 261, 281, 320, 357, 440, 442, 448, 511, 512, 561, 568, 604
embrittlement, solid-metal: 31, 34, 285, 334, 588
energy: 1, 2, 6, 14, 23, 24, 25, 27, 28, 29, 40, 41, 46, 49, 51, 60, 61, 112, 116, 125, 127, 128, 129, 130, 131, 132, 133, 134, 136, 153, 157, 164, 169, 171, 173, 179, 183, 186, 190, 222, 242, 251, 252, 273, 281, 282, 284, 295, 296, 298, 299, 300, 301, 302, 306, 309, 322, 329, 332, 333, 334, 344, 348, 349, 350, 361, 372, 377, 383, 397, 398, 433, 437, 439, 440, 442, 443, 444, 446, 448, 449, 452, 455, 464, 465, 482, 512, 515, 524, 538, 541, 542, 543, 566, 575, 606, 610, 611, 612, 614, 615
evolution: 45, 60, 74, 96, 139, 279, 280, 328, 345, 347, 352, 355, 368, 421, 449, 455, 467, 482, 489, 527, 531, 532, 543, 545, 547, 548
examination, metallographic: 352, 384, 420, 424, 461, 468
exfoliation: 336, 337, 338, 343, 345, 383, 384, 387

F

fabrication(s): 1, 113, 292, 312, 317, 349, 350, 389, 417, 456, 531 562, 581
face-centered cubic: 2, 6, 22, 23, 25, 37, 80, 114, 129, 167, 178, 182, 187, 241, 251, 252, 268, 273, 281, 284, 302, 498, 541, 585
fast fracture: 164, 380, 574
fatigue: 1, 7, 17, 32, 33, 34, 35, 47, 49, 50, 55, 56, 58, 59, 66, 67, 69, 70, 71, 72, 74, 75, 76, 77, , 82, 83, 87, 88, 89, 90, 91, 92, 96, 98, 101, 107, 109, 112, 114, 116, 123, 136, 137, 139, 141, 144, 147, 149, 150, 155, 156, 157, 158, 175, 178, 186, 187, 191, 193, 194, 197, 199, 213, 214, 219, 224, 225, 227, 241, 242, 243, 247, 248, 265, 276, 284, 294, 302, 310, 331, 345, 351, 358, 361, 435, 436, 437, 441, 449, 450, 453, 461, 465, 468, 471, 472, 474, 475, 498, 520, 531, 532, 533, 561, 566, 568, 574, 584, 589, 609, 610, 612, 614
fatigue crack growth: 14, 43, 51, 52, 57, 60, 61, 62, 64, 68, 80, 81, 84, 85, 86, 93, 94, 95, 97, 106, 108, 111, 113, 117, 118, 120, 121, 122, 142, 168, 181, 195, 223, 226, 233, 235, 236, 237, 238, 239, 298, 301, 479, 588
fatigue crack initiation: 43, 45, 46, 51, 99, 108, 121, 140, 217, 299, 479
fatigue, Mode I: 94, 108, 167, 169, 171, 172, 173, 174, 181, 183, 215, 335, 344, 440, 464, 465, 467, 476, 483, 484, 513, 582, 590
fatigue, Mode II: 94, 171, 173, 181, 442, 443, 449, 464, 465, 467, 468, 472, 474, 475, 476, 479, 481, 483, 484, 486
fatigue, Mode III: 37, 171, 172, 173, 335, 364, 442, 464, 476, 484, 487, 513, 515
fatigue, Mode IV: 464, 476, 477, 479, 480, 481, 484, 487
film formation(s): 62, 93, 192, 239, 247, 248, 251, 262, 267, 268, 270, 275, 276, 285, 304, 305, 309, 399, 419, 435, 490, 499, 512, 566
film rupture: 1, 2, 18, 49, 56, 59, 60, 70, 72, 82, 83, 85, 88, 91, 92, 93, 97, 101, 106, 127, 141, 142, 153, 167, 187, 190, 191, 237, 238, 265, 266, 267, 268, 269, 270, 273, 280, 303, 305, 309, 352, 404, 449, 455, 482, 545, 576, 578
fluoride(s): 164, 363, 389, 390, 391, 392, 393, 394, 395
fractography: 2, 3, 22, 23, 27, 28, 33, 34, 36, 41, 55, 68, 80, 83, 101, 143, 169, 236, 237, 239, 268, 277, 280, 285, 305, 314, 316, 333, 334, 336, 358, 363, 365, 373, 392, 442, 500, 509, 527, 528, 529, 538, 556, 579
fracture mechanics: 43, 46, 55, 56, 57, 60, 61, 62, 64, 66, 68, 73, 74, 75, 82, 83, 86, 92, 94, 99, 101, 106, 107, 108, 109, 117, 122, 125, 153, 154, 155, 165, 195, 215, 223, 233, 311, 437, 448, 450, 452, 479, 494, 523, 525, 526, 531, 532, 533, 574, 575, 582, 583, 584, 588, 589, 610
free-corrosion potential: 49, 208, 233, 323, 324, 327, 328, 336, 555

G

galvanic action: 4, 5, 241, 247, 248, 268, 303, 398, 479, 484, 566, 570, 588, 591, 592, 598
galvanic coupling: 249, 265, 266, 267, 269, 295, 305, 352, 420, 423, 481, 583, 594, 601
generator(s): 292, 417, 418, 503, 569, 570, 589, 591, 598, 612
glass: 1, 135, 136, 197, 365, 430, 527, 545, 550
gold: 31, 192, 251, 252, 253, 257, 258, 277, 278, 280, 507
grain boundary: 1, 3, 4, 5, 6, 18, 24, 25, 29, 31, 34, 37, 38, 39, 41, 43, 45, 46, 51, 59, 71, 72, 77, 107, 108, 112, 113, 114, 116, 117, 118, 129, 150, 163, 164, 165, 174, 175, 176, 205, 217, 223, 226, 227, 237, 241, 242, 243, 247, 249, 264, 268, 277, 280, 289, 290, 291, 293, 294, 298, 299, 300, 301, 302, 303, 304, 305, 309, 310, 315, 317, 345, 354, 355, 357, 363, 365, 368, 371, 372, 373, 376, 380, 383, 385, 386, 387, 393, 398, 407, 409, 410, 413, 435, 438, 440, 441, 444, 445, 446, 449, 451, 452, 455, 460, 461, 481, 482, 496, 502, 503, 508, 515, 517, 519, 520, 524, 528, 529, 530, 538, 539, 549, 552, 564, 568, 569, 570, 573, 576, 580, 584, 586
grain-boundary segregation: 134, 311, 312, 313, 314, 316, 317, 318, 319, 322, 331, 333, 334, 335, 336, 338
graphite: 252, 291, 294, 402, 507

H

halide(s): 7, 319, 320, 322, 324, 339, 347, 354, 355, 361
halogen(s): 55, 58, 68, 73, 361
Hastelloy: 287, 295
heat-affected zone(s): 343, 450, 452, 458, 461
heat treatment: 4, 36, 77, 89, 213, 233, 241, 242, 243, 246, 247, 248, 249, 289, 291, 297, 312, 317, 347, 350, 356, 358, 383, 422, 425, 428, 449, 451, 453, 455, 478, 482, 503, 523, 527, 531, 533, 556, 564, 569, 574, 581, 584, 586, 592, 596, 598
helium: 60, 61, 62, 74, 75, 80, 93, 233, 235, 243, 246, 249, 252, 377
hexagonal closed-packed: 23, 27, 40, 178, 182, 541
humidity: 181, 233, 319, 429, 433
hydride(s): 2, 21, 22, 23, 25, 27, 28, 29, 129, 182, 271, 301, 302, 303, 347, 348, 349, 350, 351, 352, 354, 356, 358, 361, 422, 423, 424, 429, 440
hydrogen: See specific entries
hydrogen entry: 23, 28, 81, 189, 203, 204, 205, 209, 210, 238, 316, 325, 344, 345, 352, 361, 419, 421, 461, 483, 500, 523, 524, 525, 526, 527, 543, 568, 573, 580
hydrogen-induced cracking: 287, 288, 289, 290, 291, 437
hydrogen permeation: 74, 194, 207, 208, 209, 309, 334, 438, 523, 524, 526, 543
hydrogen recombination: 210, 241, 248, 328, 344
hydrogen sulfide(s): 75, 144, 187, 193, 195, 352, 364, 438, 443, 511, 580
hydrogen uptake: 18, 74, 75, 77, 79, 81, 87, 101, 164, 165, 195, 301, 309, 332, 334, 344, 347, 351, 352, 355, 364, 419, 424, 435, 451, 523, 525, 526
hydroxide(s): 58, 62, 95, 108, 199, 238, 309, 327, 329, 330, 352, 389, 436, 490, 545
hysteresis: 11, 22, 27, 350, 440

I

impedance: 85, 207, 208, 209, 470, 496, 499, 512
impurity: 32, 34, 37, 38, 45, 55, 68, 75, 77, 123, 129, 130, 131, 132, 164, 288, 289, 290, 291, 292, 294, 298, 299, 300, 301, 302, 303, 304, 305, 306, 309, 310, 312, 356, 407, 438, 440, 442, 446, 480, 503, 509, 529, 530, 568, 571, 572, 576, 580, 587, 602
Incoloy: 34, 293, 570
Inconel: 58, 111, 113, 114, 116, 117, 118, 120, 121, 122, 309, 504, 564, 568, 569, 570, 571, 573, 574, 576, 583, 584, 586, 587, 588, 591, 592, 593, 594, 596, 598, 599, 600, 601
Industry: 31, 32, 37, 111, 139, 157, 287, 347, 389, 401, 404, 450, 454, 456, 482, 483, 500, 509, 545, 561, 568, 569, 575, 590, 604, 610, 611, 612, 614
Inhibition: 247, 389, 394, 401, 403, 404, 405, 409, 494, 572, 591
Inhibitor(s): 220, 320, 351, 391, 399, 402, 403, 404, 405, 567
Inhomogeneous: 45, 99, 146, 168, 208, 274, 289, 313, 314, 315, 440, 445, 512, 541, 566
Initiation vs propagation: 108, 139
Interaction(s): 24, 29, 31, 37, 41, 47, 50, 56, 57, 59, 62, 77, 79, 82, 85, 98, 106, 108, 111, 113, 118, 123, 125, 129, 143, 144, 167, 173, 181, 189, 197, 207, 208, 217, 221, 248, 266, 284, 300, 301, 302, 308, 314, 357, 364, 422, 438, 446, 449, 454, 472, 482, 533, 539, 549, 562, 566, 569, 573, 574, 578, 584, 592, 601, 603, 604, 610, 614, 615

interface(s): 1, 5, 29, 51, 89, 107, 114, 125, 129, 132, 134, 143, 152, 164, 175, 179, 181, 190, 203, 204, 205, 207, 237, 251, 257, 263, 274, 275, 278, 281, 302, 344, 363, 364, 366, 422, 429, 430, 431, 433, 435, 438, 440, 444, 446, 473, 484, 486, 527, 590
interstitial(s): 21, 94, 129, 132, 143, 191, 350, 351, 438, 441, 442, 449, 451, 455, 456, 479, 481, 482, 483, 484, 523, 581, 602
iodine: 262, 357, 568, 569, 573, 586, 600
IR drop(s): 241, 248, 303, 495, 543, 545
iron: 4, 5, 14, 17, 23, 24, 27, 29, 31, 32, 34, 77, 86, 95, 125, 134, 136, 167, 171, 179, 181, 186, 190, 191, 226, 309, 338, 352, 419, 420, 438, 440, 441, 442, 443, 444, 456, 486, 493, 525, 555, 568, 580, 586, 598, 599, 609
iron, Armco: 5, 34
irradiation: 111, 150, 164, 289, 290, 291, 305, 377

K

kinetic: 1, 10, 15, 21, 109, 140, 144, 163, 167, 175, 179, 193, 264, 274, 275, 279, 282, 300, 329, 397, 398, 435, 439, 440, 443, 444, 445, 446, 491, 494, 499, 502, 593, 612

L

laser(s): 508, 614, 615
lead: 2, 17, 23, 24, 31, 32, 33, 34, 37, 38, 40, 41, 43, 45, 60, 75, 85, 93, 107, 109, 118, 123, 132, 136, 145, 147, 149, 151, 155, 163, 167, 173, 175, 181, 191, 194, 203, 238, 251, 253, 254, 256, 258, 261, 264, 266, 280, 281, 283, 285, 289, 290, 291, 301, 309, 312, 316, 320, 332, 334, 344, 351, 363, 371, 372, 376, 377, 383, 390, 435, 438, 449, 450, 454, 458, 471, 474, 479, 484, 490, 492, 525, 527, 571, 580, 587, 590, 591, 594, 612
LEFM: 43, 155, 165, 448
light water reactor(s): 158, 241, 242
liquid metals: 13, 31, 37, 40, 107, 136, 137, 167, 182, 261, 281, 320, 357, 440, 448, 511, 512, 539, 561, 571, 588, 604
lithium: 31, 32, 34, 38, 136, 237, 238, 239, 328, 331, 332, 377, 503, 512, 545, 549, 550, 552, 598
localization: 1, 2, 5, 6, 7, 8, 18, 23, 25, 27, 28, 33, 45, 49, 52, 56, 59, 60, 74, 79, 80, 85, 86, 97, 139, 143, 144, 153, 155, 163, 165, 169, 190, 191, 195, 208, 210, 232, 235, 237, 238, 239, 241, 265, 266, 267, 268, 269, 270, 273, 280, 284, 289, 290, 299, 301, 302, 303, 305, 310, 311, 314, 336, 338, 344, 345, 350, 351, 355, 364, 365, 366, 368, 369, 383, 384, 386, 393, 419, 424, 427, 438, 439, 440, 442, 450, 452, 455, 460, 461, 472, 482, 483, 492, 496, 502, 508, 509, 518, 520, 523, 524, 525, 526, 529, 574, 609, 614, 615
localized slip: 34, 186, 285, 333, 435, 446
localized surface plasticity: 191, 265, 267, 268, 269
long crack(s): 73, 98, 107, 108, 150, 226, 437
long-range ordering: 288, 301, 305, 306

M

macrocrack(s): 28, 56, 175, 177
magnesium: 17, 32, 33, 34, 40, 62, 72, 95, 191, 313, 316, 317, 331, 338, 347, 348, 351, 352, 353, 355, 356, 357, 358, 359, 361, 386, 508, 509, 512, 549, 550
manganese: 4, 5, 11, 114, 147, 164, 312, 313, 345, 351, 371, 373, 376, 379, 381, 442, 481, 502, 517, 541, 556
maraging steel(s): 9, 57, 475, 476
martensitic: 21, 22, 56, 77, 88, 97, 98, 195, 356, 435, 436, 449, 450, 451, 452, 453, 454, 464, 467, 468, 476, 477, 478, 479, 480, 481, 482, 484, 511, 523, 526, 541
matrix: 4, 5, 27, 29, 51, 114, 116, 137, 141, 142, 143, 144, 151, 153, 179, 187, 241, 242, 243, 247, 248, 249, 251, 265, 271, 278, 281, 282, 284, 285, 289, 290, 294, 302, 303, 305, 311, 314, 316, 317, 318, 319, 331, 348, 349, 356, 361, 363, 366, 372, 373, 384, 385, 387, 425, 438, 454, 471, 473, 479, 481, 482, 484, 504, 580, 611, 615
mechanisms, active path: 141, 303, 304, 305, 314, 332, 436, 437, 450, 451, 482, 508, 580, 614
mercury: 31, 32, 33, 34, 35, 37, 40, 136, 172, 182, 320, 357, 539
metal(s): See specific metals
metal cation(s): 147, 163
metallurgy: 18, 45, 55, 58, 68, 77, 79, 80, 83, 91, 92, 111, 118, 139, 150, 152, 153, 154, 191, 207, 210, 264, 268, 273, 283, 287, 288, 311, 319, 330, 338, 352, 436, 450, 453, 455, 481, 482, 548, 559, 562, 577, 588, 591, 593, 609, 610, 611, 615
metals, liquid: 13, 31, 37, 40, 107, 136, 137, 167, 182, 261, 281, 320, 357, 440, 448, 511, 512, 539, 561, 571, 588, 604
metals, powder metallurgy: 118, 311, 338
microcrack(s): 34, 56, 73, 107, 117, 175, 178, 251, 284, 303, 543
microstructure(s): 18, 31, 55, 56, 64, 68, 77, 79, 82, 89, 97, 98, 99, 106, 107, 109, 112, 114, 120, 121, 142, 164, 167, 174, 183, 204, 233, 235, 242, 243, 246, 248, 271, 287, 288, 289, 290, 291, 292, 293, 295, 303, 305, 311, 317, 318, 319, 322, 331, 333, 338, 339, 343, 345, 350, 356, 357, 358, 371, 372, 383, 385, 387, 422, 439, 443, 444, 450, 453, 458, 459, 479, 481, 482, 520, 523, 556, 585, 609
microvoid(s): 22, 167, 182, 316, 333, 345, 371, 373, 441, 556
mode intensity: 598, 599, 600, 601, 602, 603, 605
molybdenum: 419, 454, 456, 486, 578, 611
morphology: 17, 18, 23, 25, 46, 50, 60, 83, 93, 96, 114, 135, 142, 144, 145, 152, 153, 155, 164, 165, 233, 237, 238, 241, 249, 251, 278, 279, 282, 288, 289, 300, 302, 316, 319, 331, 359, 365, 368, 369, 371, 380, 386, 389, 392, 397, 425, 426, 427, 428, 437, 438, 496, 515, 541, 550, 555, 556, 569, 576, 615

N

NACE: 108, 158, 163, 190, 195, 208, 209, 295, 402, 438, 454, 458, 460, 461, 486, 508, 509, 523, 525, 533, 574, 609, 610
NACE standard(s): 208, 402, 458, 460, 461, 523, 525
nickel: 23, 24, 27, 28, 32, 33, 34, 37, 38, 46, 47, 50, 108, 140, 171, 174, 176, 183, 191, 203, 284, 285, 291, 294, 295, 296, 309, 310, 352, 364, 372, 403, 404, 410, 419, 436, 441, 442, 443, 449, 450, 451, 453, 454, 455, 456, 461, 480, 481, 482, 483, 486, 489, 490, 494, 498, 501, 503, 504, 507, 543, 569, 576, 578, 580, 586, 593, 594, 598
nickel martensitic: 449, 450, 453, 454, 480, 481, 482
niobium: 350, 440, 611
notch(es, -ed): 3, 28, 31, 34, 46, 74, 88, 91, 99, 112, 123, 139, 140, 167, 169, 172, 175, 181, 182, 187, 190, 219, 226, 233, 242, 296, 328, 331, 332, 334, 335, 344, 350, 355, 389, 401, 403, 429, 442, 443, 464, 465, 475, 476, 477, 537, 568
nuclear reactor(s): 62, 73, 92, 164

O

overvoltage: 263, 275
oxidation: 43, 72, 75, 81, 91, 93, 94, 95, 111, 112, 113, 114, 116, 117, 118, 120, 121, 122, 136, 139, 140, 141, 142, 143, 144, 145, 146, 147, 150, 151, 152, 153, 158, 163, 164, 264, 276, 278, 303, 438, 507, 523, 524, 555, 573, 578, 604, 610, 611
oxide(s): 1, 5, 6, 7, 28, 43, 45, 47, 50, 51, 52, 60, 62, 75, 93, 95, 108, 111, 114, 116, 117, 118, 120, 121, 122, 137, 140, 142, 143, 147, 150, 151, 152, 153, 154, 155, 158, 163, 165, 177, 178, 179, 187, 192, 209, 226, 251, 252, 257, 271, 273, 275, 276, 278, 285, 309, 316, 327, 345, 347, 352, 355, 358, 363, 391, 392, 393, 398, 407, 409, 410, 416, 418, 419, 422, 423, 424, 427, 428, 429, 430, 431, 438, 443, 481, 486, 490, 499, 507, 545, 578, 604
oxygen: 27, 28, 43, 58, 60, 62, 64, 73, 80, 85, 86, 87, 89, 92, 93, 94, 98, 99, 113, 114, 116, 117, 120, 135, 136, 137, 147, 150, 164, 174, 208, 235, 238, 246, 266, 273, 274, 275, 276, 277, 292, 299, 321, 330, 351, 355, 356, 361, 419, 421, 422, 423, 424, 429, 431, 437, 438, 439, 440, 441, 443, 477, 486, 491, 494, 502, 504, 507, 555, 562, 570, 572, 573, 581, 583, 591, 592, 598, 599, 601, 602

P

passivation: 7, 13, 49, 56, 117, 164, 178, 190, 247, 303, 352, 355, 368, 391, 419, 426, 449, 456, 464, 467, 468, 470, 473, 474, 476, 483, 484, 486, 507, 543, 580
passivity: 7, 13, 14, 45, 46, 49, 50, 52, 56, 62, 86, 91, 107, 117, 120, 164, 167, 178, 190, 192, 195, 207, 208, 209, 210, 235, 238, 247, 252, 265, 266, 267, 268, 269, 271, 275, 280, 281, 291, 303, 304, 309, 345, 347, 351, 352, 353, 354, 355, 356, 357, 358, 361, 364, 365, 368, 391, 393, 403, 404, 409, 419, 424, 426, 436, 438, 449, 450, 452, 453, 456, 460, 461, 464, 465, 467, 468, 470, 471, 472, 473, 474, 475, 476, 478, 479, 481, 483, 484, 486, 487, 489, 490, 491, 492, 494, 496, 499, 507, 515, 523, 524, 526, 543, 555, 557, 578, 580, 591, 593, 594, 615
passivity breakdown: 17, 262, 285
pearlitic: 77, 217, 435, 438
permeation: 74, 81, 151, 194, 207, 208, 209, 210, 300, 301, 309, 334, 438, 511, 523, 524, 525, 526
persistent slip band(s): 46, 47, 49, 50, 51, 108, 473, 476
phosphorus: 77, 205, 309, 436, 438, 495, 496, 500, 515, 530, 568, 580
pickling: 430, 431, 458, 586
planar slip: 46, 60, 79, 80, 95, 112, 113, 167, 181, 182, 186, 276, 288, 301, 303, 345, 542
plastic(s): 2, 5, 23, 24, 25, 27, 33, 34, 43, 46, 47, 49, 56, 57, 59, 60, 61, 68, 70, 74, 76,

79, 81, 82, 83, 84, 89, 90, 91, 93, 94, 96, 97, 99, 106, 107, 108, 111, 116, 117, 121, 122, 126, 142, 153, 154, 155, 164, 165, 168, 169, 171, 174, 178, 181, 182, 186, 209, 221, 222, 224, 226, 229, 231, 232, 235, 238, 242, 252, 256, 262, 263, 265, 266, 267, 268, 273, 276, 280, 282, 284, 285, 288, 298, 299, 300, 302, 305, 309, 314, 318, 344, 348, 350, 351, 352, 361, 365, 397, 417, 426, 427, 430, 431, 436, 439, 440, 442, 443, 446, 449, 464, 465, 468, 473, 475, 481, 483, 498, 512, 514, 515, 529, 537, 538, 539, 549, 556, 615

plastic strain: 2, 46, 47, 49, 68, 76, 83, 84, 89, 96, 99, 106, 107, 108, 116, 122, 126, 168, 186, 318, 348, 361, 417, 430, 465, 473

plastic zone: 23, 33, 56, 59, 70, 76, 79, 81, 84, 89, 90, 91, 93, 94, 96, 97, 107, 108, 126, 154, 168, 174, 178, 186, 235, 238, 298, 299, 351, 475, 514, 515

plasticity: 2, 17, 22, 23, 25, 28, 29, 33, 34, 37, 45, 51, 59, 60, 67, 68, 75, 77, 80, 83, 93, 94, 95, 96, 97, 101, 106, 107, 108, 109, 111, 143, 144, 155, 157, 164, 168, 169, 174, 177, 179, 182, 187, 191, 219, 237, 265, 267, 268, 269, 284, 285, 298, 299, 300, 302, 309, 332, 430, 436, 439, 440, 442, 449, 468, 483, 513, 514, 575, 578, 615

platinum: 233, 252, 402, 403, 517, 527

polarization: 5, 62, 70, 73, 74, 76, 77, 80, 86, 87, 88, 91, 95, 99, 109, 195, 197, 200, 201, 233, 235, 236, 237, 238, 239, 241, 242, 243, 245, 246, 247, 248, 252, 257, 268, 269, 289, 316, 322, 323, 324, 325, 327, 328, 329, 330, 336, 338, 352, 355, 361, 363, 364, 366, 368. 369, 389, 391, 393, 394, 397, 398, 399, 401, 402, 403, 404, 405, 408, 421, 423, 437, 438, 450, 451, 461, 476, 484, 492, 494, 500, 507, 509, 523, 524, 543, 591, 593

polycrystalline: 5, 38, 43, 46, 50, 108, 111, 132, 219, 220, 280, 299, 300, 301, 397

polyethylene: 429, 430, 431

porosity: 136, 167, 177, 178, 397, 436, 496, 501, 507

potassium: 18, 38, 165, 320, 322, 324, 325, 328, 352, 353, 357, 442

potential-pH diagram(s): 1, 9, 140, 146, 147, 151, 190, 590, 596

potentiostatic: 151, 203, 209, 233, 252, 266, 345, 365, 366, 368, 389, 420, 449, 450, 455, 465, 467, 468, 469, 470, 472, 475, 483, 492, 520

Pourbaix diagram: 147, 450, 583, 586, 593

power generation: 139, 165, 450

precipitate-free zone: 311, 314, 316, 318, 373, 376, 384, 385

precracking: 32, 45, 50, 52, 332, 355, 481, 525, 537, 538

pressure vessel: 62, 79, 92, 157, 191, 350

propagation: 2, 3, 5, 6, 10, 17, 18, 21, 22, 23, 25, 28, 31, 34, 37, 39, 40, 43, 45, 46, 51, 55, 56, 57, 59, 60, 61, 62, 64, 66, 67, 68, 69, 70, 71, 72, 73, 74, 75, 76, 77, 79, 80, 81, 82, 83, 84, 85, 86, 88, 89, 90, 91, 92, 93, 94, 95, 96, 97, 99, 101, 106, 107, 108, 109, 111, 114, 117, 119, 120, 122, 135, 136, 139, 140, 141, 142, 143, 144, 145, 147, 150, 151, 152, 153, 154, 155, 156, 158, 162, 163, 164, 165, 167, 172, 173, 176, 187, 190, 191, 192, 221, 223, 226, 229, 231, 232, 233, 235, 237, 238, 239, 247, 248, 251, 252, 258, 259, 261, 264, 267, 268, 271, 273, 275, 276, 277, 278, 280, 281, 282, 284, 285, 296, 297, 309, 310, 311, 314, 321, 322, 323, 324, 325, 326, 330, 331, 332, 333, 334, 335, 336, 337, 339, 340, 344, 345, 348, 353, 354, 355, 356, 357, 368, 369, 371, 376, 379, 380, 381, 383, 385, 397, 398, 407, 408, 409, 410, 419, 423, 424, 425, 427, 428, 429, 435, 436, 437, 438, 439, 440, 441, 443, 444, 446, 449, 450, 454, 461, 464, 465, 467, 468, 469, 470, 471, 481, 483, 489, 491, 508, 509, 512, 513, 517, 518, 519, 520, 521, 524, 531, 532, 533, 537, 538, 539, 540, 541, 542, 543, 546, 549, 550, 551, 552, 555, 556, 557, 558, 561, 564, 573, 577, 578, 580, 582, 588, 590, 612

Q

quantum: 127, 130, 135, 441, 442, 443

R

radiation: 92, 139, 284, 289, 290, 419, 561

reaction rate: 61, 71, 72, 83, 85, 88, 90, 91, 106, 140, 143, 144, 146, 151, 152, 157, 423, 429

reactor(s): 32, 62, 73, 92, 156, 158, 164, 241, 290, 377, 418, 570, 573, 575

retrogression: 317, 345, 363, 383, 384, 386

S

saline solution(s): 322, 333, 338, 419, 524, 545

salt(s): 88, 140, 147, 148, 187, 190, 199, 252, 276, 304, 309, 419, 476, 524, 545, 550, 584

salts, molten: 358, 587

segregant(s): 4, 134, 280, 290, 302

sensitization: 64, 79, 92, 148, 152, 156, 157, 164, 165, 243, 291, 303, 305, 309, 336, 436, 450, 455, 461, 489, 494, 495, 501, 502, 503, 504, 511, 517, 520, 566, 569, 570, 576, 577, 584, 586, 589

shear stress: 29, 222, 267, 376, 427, 429, 430, 433, 443

short crack(s): 43, 56, 61, 87, 97, 98, 99, 108, 117, 122, 123, 150, 153, 155, 165, 223, 224, 226, 227, 233, 235, 238, 331, 517, 518

short-range ordering: 288

shot peening: 122, 310, 337, 474, 481

silicon: 179, 181, 197, 338, 425

silver: 31, 163, 164, 261, 262, 329, 337, 343, 429, 430, 431, 574

situation-dependent strength: 562, 563, 564, 565, 566, 568, 576, 580, 584, 586, 588, 590, 591, 600, 603, 610, 612

slip dissolution: 2, 139, 141, 152, 156, 158, 436, 489, 491, 493, 497, 501, 504, 512, 545, 547, 548, 555, 576, 577, 578, 580, 586

sodium hydroxide: 58, 108, 199, 327

soluble: 9, 92, 95, 136, 147, 163, 164, 261, 274, 275, 276, 281, 289, 290, 291, 300, 320, 334, 347, 348, 350, 351, 358, 361, 373, 386, 422, 424, 438, 454, 455, 476, 482, 502, 507, 508, 533, 568, 580, 586

solution anneal: 28, 79, 156, 219, 220, 229, 252, 276, 277, 293, 298, 299, 309, 310, 350, 354, 355, 357, 377, 383, 389, 397, 398, 402, 407, 422, 425, 428, 449, 450, 453, 455, 458, 459, 460, 482, 483, 494, 496, 499, 502, 517, 527, 545, 546, 547, 548, 550

specificity: 6, 17, 35, 268, 586

sponge(s): 251, 252, 253, 277, 278, 284, 508

stacking fault energy: 6, 112, 113, 153, 181, 186, 273, 284, 288, 301, 303, 397, 512, 541, 542, 543

steam generator(s): 292, 417, 418, 503, 569, 570, 591, 598, 612

steel(s): See specific entries

steel, carbon: 61, 62, 70, 141, 268, 437, 438, 570, 583

steel, chromium: 79, 86, 87, 99, 122, 140, 156, 164, 243, 291, 436, 452, 455, 460, 461, 468, 471, 481, 483, 486, 487, 490, 492, 500, 503, 517, 520, 523, 524, 577

steel, maraging: 9, 57, 450, 455, 475, 476, 480, 481

steel, molybdenum: 419, 454, 456, 486, 578, 611

steel, nickel: 23, 24, 27, 28, 32, 33, 34, 37, 38, 46, 47, 50, 108, 140, 171, 174, 176, 183, 191, 203, 284, 285, 291, 294, 295, 296, 309, 310, 352, 364, 372, 403, 404, 410, 419, 436, 441, 442, 443, 449, 450, 451, 453, 454, 455, 456, 461, 480, 481, 482, 483, 486, 489, 490, 494, 498, 501, 503, 504, 507, 543, 569, 576, 578, 580, 586, 593, 594, 598

steel, silicon: 179, 181, 197, 338, 425

steel, stainless: See specific steels

stochastic: 437, 438, 449, 450, 469, 470, 471, 473, 483

strain, constant: 47, 51, 353, 568, 570, 584

strain hardening: 168, 169, 191, 265, 266, 267, 268, 269, 270, 301, 469, 520, 528, 615

strain rate: 3, 7, 10, 11, 12, 13, 15, 17, 19, 21, 22, 31, 33, 36, 37, 38, 49, 52, 59, 60, 70, 72, 84, 91, 92, 97, 107, 142, 145, 150, 152, 153, 154, 155, 156, 158, 164, 165, 189, 191, 219, 229, 230, 231, 232, 238, 252, 255, 261, 262, 266, 270, 276, 278, 284, 293, 294, 295, 296, 298, 304, 305, 306, 309, 317, 318, 331, 333, 344, 352, 353, 354, 363, 372, 373, 389, 390, 395, 408, 415, 416, 418, 420, 425, 426, 427, 428, 437, 470, 496, 511, 513, 514, 515, 517, 518, 520, 523, 525, 527, 528, 529, 543, 577, 578, 581, 588, 610, 615

strain, slow: 3, 4, 8, 11, 12, 19, 70, 153, 191, 229, 230, 231, 363, 389, 394, 395, 407, 408, 410, 517, 518, 519, 520, 549, 550, 552, 553, 610

stress corrosion: 1, 2, 3, 4, 6, 7, 8, 9, 10, 11, 14, 18, 19, 27, 52, 56, 57, 58, 61, 62, 73, 74, 82, 96, 118, 120, 123, 125, 127, 136, 139, 140, 141, 142, 147, 149, 153, 155, 156, 157, 158, 162, 163, 165, 167, 178, 182, 190, 191, 192, 195, 197, 207, 209, 213, 214, 215, 216, 217, 219, 221, 229, 232, 237, 238, 241, 251, 261, 263, 265, 273, 283, 284, 287, 290, 296, 303, 304, 305, 309, 311, 313, 345, 347, 352, 353, 354, 355, 356, 357, 358, 363, 364, 365, 366, 368, 377, 379, 380, 383, 389, 393, 395, 397, 401, 407, 415, 416, 425, 429, 430, 435, 436, 437, 439, 442, 446, 449, 452, 455, 461, 476, 482, 486, 489, 502, 508, 509, 511,

512, 513, 514, 517, 519, 520, 539, 541, 543, 545, 549, 550, 552, 553, 555, 556, 557, 558, 561, 562, 573, 576, 577, 579, 580, 603, 604, 606, 609, 610, 611, 612, 613, 614, 615
stress corrosion cracking: 1, 6, 7, 9, 11, 13, 14, 15, 16, 17, 18, 19, 27, 52, 56, 57, 58, 59, 60, 62, 64, 68, 74, 79, 81, 82, 123, 125, 126, 134, 135, 136, 137, 141, 149, 156, 162, 163, 164, 167, 168, 169, 171, 172, 174, 179, 181, 182, 183, 186, 187, 190, 191, 192, 195, 197, 207, 208, 209, 213, 219, 220, 221, 222, 229, 231, 232, 237, 238, 241, 259, 261, 262, 263, 264, 265, 266, 267, 268, 269, 270, 271, 276, 283, 284, 285, 287, 295, 296, 297, 309, 311, 312, 313, 314, 315, 316, 320, 321, 323, 324, 325, 326, 327, 328, 329, 330, 332, 334, 335, 336, 338, 339, 340, 343, 344, 345, 347, 351, 352, 353, 355, 356, 359, 361, 363, 364, 365, 366, 368, 369, 377, 379, 380, 381, 383, 385, 386, 387, 389, 390, 391, 392, 393, 394, 395, 397, 398, 399, 401, 402, 403, 404, 405, 413, 425, 427, 428, 429, 431, 433, 435, 436, 437, 438, 439, 446, 449, 450, 451, 452, 453, 454, 455, 456, 458, 459, 460, 461, 465, 482, 483, 486, 489, 490, 491, 492, 494, 495, 498, 499, 500, 502, 504, 507, 508, 509, 511, 512, 513, 514, 515, 539, 545, 546, 547, 548, 549, 552, 553, 555, 556, 557, 561, 562, 563, 564, 565, 566, 567, 568, 569, 570, 571, 572, 573, 574, 575, 576, 577, 578, 579, 580, 581, 582, 583, 584, 585, 586, 587, 588, 589, 590, 591, 592, 593, 594, 595, 596, 598, 599, 600, 601, 602, 603, 604, 606, 609, 610, 611, 612, 613, 614, 615
stress corrosion cracking, intergranular: 3, 4, 5, 273, 275, 280, 282, 288, 289, 290, 291, 292, 293, 303, 304, 317, 318, 319, 322, 331, 333, 407, 408, 410, 415, 416, 417, 418, 493, 496, 497, 501, 503, 517
stress corrosion cracking, transgranular: 2, 3, 4, 5, 10, 12, 178, 251, 252, 253, 254, 256, 257, 258, 273, 275, 277, 278, 280, 281, 282, 288, 289, 290, 291, 292, 293, 303, 304, 305, 317, 318, 319, 322, 331, 333, 407, 408, 410, 415, 416, 417, 418, 493, 496, 497, 501, 503, 517, 541, 542, 543
stress intensity: 7, 10, 14, 21, 36, 38, 55, 56, 57, 64, 66, 68, 69, 70, 75, 82, 83, 85, 89, 91, 94, 95, 96, 97, 99, 101, 109, 125, 133, 137, 144, 153, 156, 169, 171, 174, 178, 181, 182, 186, 219, 220, 222, 232, 233, 235, 236, 237, 273, 276, 280, 296, 304, 351, 355, 366, 371, 379, 397, 416, 437, 440, 444, 446, 448, 496, 513, 514, 515, 528, 569, 582, 584, 590
stress-strain curve: 46, 49, 229, 256, 390, 391, 405
stress, residual: 156, 157, 167, 181, 289, 349, 431, 563
stress, tensile: 21, 24, 28, 31, 33, 34, 37, 39, 49, 74, 93, 113, 114, 118, 151, 153, 154, 156, 171, 172, 173, 174, 191, 208, 213, 214, 215, 216, 217, 219, 221, 224, 225, 229, 230, 231, 232, 251, 252, 261, 263, 264, 266, 267, 268, 269, 277, 298, 302, 305, 316, 318, 331, 334, 335, 348, 349, 350, 353, 356, 359, 363, 365, 366, 371, 372, 373, 376, 377, 379, 389, 390, 395, 402, 403, 419, 420, 421, 423, 424, 425, 427, 429, 430, 433, 437, 440, 441, 442, 445, 450, 453, 456, 458, 470, 480, 482, 486, 487, 497, 503, 508, 511, 512, 513, 517, 527, 531, 533, 537, 539, 545, 547, 550, 555, 556, 581, 596, 600, 603, 614
sulfate(s): 10, 88, 92, 93, 96, 147, 154, 243, 246, 248, 289, 291, 327, 329, 330, 339, 352, 361, 389, 393, 399, 436, 452, 494, 498, 501, 502, 503, 507, 509, 580, 591, 602
sulfide(s): 28, 55, 68, 75, 79, 81, 144, 164, 187, 193, 195, 208, 209, 210, 217, 223, 229, 290, 295, 302, 352, 364, 401, 402, 403, 438, 443, 450, 452, 454, 456, 458, 459, 460, 461, 479, 481, 484, 502, 509, 511, 523, 525, 573, 580
sulfide stress cracking: 208, 229, 295, 402, 450, 454
sulfur: 24, 73, 79, 80, 81, 123, 174, 205, 226, 285, 309, 310, 410, 438, 452, 502, 520, 530, 568, 576, 580, 602
superposition: 51, 57, 58, 69, 76, 82, 83, 92, 98, 122, 129, 335, 336, 464, 465, 476, 481, 484
surface film(s): 2, 5, 10, 12, 13, 74, 143, 191, 192, 207, 210, 265, 267, 268, 281, 309, 345, 347, 351, 352, 354, 355, 356, 361, 377, 397, 409, 419, 437, 507, 523
surface film effects: 60, 75, 89, 93, 94, 106, 238
surface mobility: 13, 40, 135, 163, 259, 261, 264, 579
susceptibility: 3, 4, 5, 17, 18, 21, 31, 32, 34, 36, 37, 38, 39, 40, 58, 62, 139, 140, 141, 144, 145, 153, 155, 157, 165, 169, 172, 176, 181, 229, 238, 239, 241, 242, 261, 265, 267, 268, 269, 284, 287, 288, 289, 290, 291, 292, 293, 294, 295, 297, 299, 301, 305, 309, 311, 312, 313, 314, 316, 317, 318, 319, 320, 321, 323, 324, 331, 334, 335, 337, 338, 339, 343, 345, 347, 348, 350, 351, 355, 356, 358, 359, 361, 363, 365, 366, 369, 379, 380, 383, 385, 389, 390, 392, 393, 394, 395, 397, 398, 401, 403, 404, 405, 409, 410, 419, 429, 433, 436, 437, 449, 450, 451, 452, 455, 458, 459, 481, 482, 483, 489, 496, 503, 509, 512, 520, 525, 527, 529, 531, 533, 541, 542, 543, 545, 546, 548, 555, 561, 562, 563, 568, 586, 591, 600, 611, 613
sustained load: 37, 66, 120, 141, 153, 156, 169, 173, 176, 178, 179, 190, 213, 214, 217, 219, 231, 265, 276, 389, 408, 443, 446, 527, 528, 545, 549, 568, 570, 584, 588
synergistic: 24, 56, 57, 58, 59, 108, 217, 321, 339, 446, 509, 569

T

thermodynamic: 1, 7, 132, 140, 144, 163, 164, 167, 190, 252, 264, 285, 435, 439, 440, 446, 448, 489, 572, 593, 612
thermomechanical: 99, 287, 290, 312, 349, 356, 512, 545
thiosulfate: 292, 303, 305, 502, 503, 517, 518, 520
threshold stress: 56, 75, 96, 137, 169, 182, 186, 223, 236, 296, 351, 353, 355, 379, 415, 416, 418, 448, 451, 454, 456, 458, 460, 461, 513, 582, 588, 590, 591
tin: 31, 32, 33, 38, 354, 356
titanium: 31, 59, 64, 68, 91, 93, 101, 147, 167, 174, 191, 219, 242, 243, 247, 347, 348, 349, 350, 351, 352, 353, 354, 355, 356, 357, 358, 361, 364, 393, 419, 420, 421, 422, 423, 424, 425, 427, 428, 567, 571, 572, 574, 575, 611
torsion: 37, 38, 172, 173, 213
transient dissolution: 56, 60, 70, 72, 82, 83, 88, 91, 106, 238, 257, 577
trapping: 59, 89, 143, 167, 182, 203, 204, 300, 306, 309, 317, 318, 444, 445, 511, 523, 524. 528, 530, 531, 533
tungsten: 452, 458, 611
tunneling: 6, 174, 190, 332, 490, 580, 615
turbine(s): 111, 113, 158, 450, 476, 479, 480, 481, 482, 484, 487, 566, 574, 590
turbines, steam: 158, 476, 479, 480, 481

U

ultimate tensile strength: 229, 268, 372, 373, 389, 390, 391, 392, 395, 556, 614
Unieux-Firminy Conference: 55, 57, 58, 83, 106, 107, 125, 167, 186, 448, 497, 559, 567, 574
uranium: 28, 363, 389, 429, 430, 431, 433, 570, 573, 611

V

valve(s): 389, 452, 602
vanadium: 28, 354, 356, 440, 442, 511, 531, 533, 534

W

Waspaloy: 113
water: See specific entries
water cooling: 541, 581
water, pure: 62, 71, 80, 86, 93, 197, 407, 413, 501, 502, 503, 515, 564, 568, 569, 570, 571, 572, 574, 586, 593, 611
water quench: 203, 383, 455, 527
water, sea: 62, 64, 67, 70, 71, 77, 81, 86, 87, 90, 91, 95, 99, 109, 147, 193, 194, 195, 197, 200, 201, 217, 334, 335, 352, 355, 356, 478, 479, 480, 523, 524, 525, 526, 555, 584
wave form: 55, 58, 68, 69, 70, 86, 87, 98, 99, 106, 198, 213, 233
weld(s, -ed, -ing): 1, 3, 61, 62, 97, 109, 118, 156, 157, 336, 337, 338, 343, 350, 355, 363, 364, 401, 429, 435, 436, 450, 452, 453, 456, 458, 459, 460, 461, 480, 483, 570, 590

Y

yield strength: 32, 55, 58, 68, 71, 73, 75, 76, 77, 79, 81, 82, 83, 84, 85, 86, 91, 98, 99, 101, 106, 107, 111, 126, 154, 167, 168, 169, 171, 174, 176, 179, 182, 183, 186, 203, 207, 268, 295, 296, 301, 401, 402, 403, 416, 417, 418, 439, 443, 450, 451, 453, 454, 455, 458, 460, 461, 481, 513, 514, 517, 527, 528, 529, 537, 545, 555, 556, 580, 600, 612

Z

zinc: 2, 3, 31, 32, 34, 38, 40, 62, 144, 219, 273, 275, 276, 277, 278, 281, 284, 316, 317, 337, 345, 361, 383, 385, 386, 389, 393, 397, 476
zinc, liquid: 512, 537, 538, 539, 540
Zircaloy: 28, 32, 40, 348, 349, 355, 357, 358, 377
zirconium: 28, 32, 164, 347, 348, 349, 350, 351, 353, 356, 357, 358, 361, 377, 393, 422, 440, 568, 573, 586, 600